FISCAL YEAR 1985 DEPARTMENT OF ENERGY AUTHORIZATION

(High Energy and Nuclear Physics)

HEARING

BEFORE THE

SUBCOMMITTEE ON
ENERGY DEVELOPMENT AND APPLICATIONS

OF THE

COMMITTEE ON SCIENCE AND TECHNOLOGY U.S. HOUSE OF REPRESENTATIVES

NINETY-EIGHTH CONGRESS

SECOND SESSION

FEBRUARY 22, 1984

[No. 117]

VOLUME II-B

Printed for the use of the
Committee on Science and Technology

U.S. GOVERNMENT PRINTING OFFICE
39-587 O WASHINGTON : 1984

H701-24

COMMITTEE ON SCIENCE AND TECHNOLOGY

DON FUQUA, Florida, *Chairman*

ROBERT A. ROE, New Jersey
GEORGE E. BROWN, JR., California
JAMES H. SCHEUER, New York
RICHARD L. OTTINGER, New York
TOM HARKIN, Iowa
MARILYN LLOYD, Tennessee
DOUG WALGREN, Pennsylvania
DAN GLICKMAN, Kansas
ALBERT GORE, JR., Tennessee
ROBERT A. YOUNG, Missouri
HAROLD L. VOLKMER, Missouri
BILL NELSON, Florida
STAN LUNDINE, New York
RALPH M. HALL, Texas
DAVE McCURDY, Oklahoma
MERVYN M. DYMALLY, California
PAUL SIMON, Illinois
NORMAN Y. MINETA, California
RICHARD J. DURBIN, Illinois
MICHAEL A. ANDREWS, Texas
BUDDY MacKAY, Florida
TIM VALENTINE, North Carolina
HARRY M. REID, Nevada
ROBERT G. TORRICELLI, New Jersey
FREDERICK C. BOUCHER, Virginia

LARRY WINN, JR., Kansas
MANUEL LUJAN, JR., New Mexico
ROBERT S. WALKER, Pennsylvania
WILLIAM CARNEY, New York
F. JAMES SENSENBRENNER, JR., Wisconsin
JUDD GREGG, New Hampshire
RAYMOND J. McGRATH, New York
JOE SKEEN, New Mexico
CLAUDINE SCHNEIDER, Rhode Island
BILL LOWERY, California
ROD CHANDLER, Washington
HERBERT H. BATEMAN, Virginia
SHERWOOD L. BOEHLERT, New York
ALFRED A. (AL) McCANDLESS, California
TOM LEWIS, Florida

HAROLD P. HANSON, *Executive Director*
ROBERT C. KETCHAM, *General Counsel*
REGINA A. DAVIS, *Chief Clerk*
DAVID S. JEFFERY, *Minority Staff Director*

SUBCOMMITTEE ON ENERGY DEVELOPMENT AND APPLICATIONS

DON FUQUA, Florida, *Chairman*

RICHARD L. OTTINGER, New York
TOM HARKIN, Iowa
RALPH M. HALL, Texas
PAUL SIMON, Illinois
RICHARD J. DURBIN, Illinois
FREDERICK C. BOUCHER, Virginia
ROBERT A. ROE, New Jersey
JAMES H. SCHEUER, New York
MARILYN LLOYD, Tennessee
ROBERT A. YOUNG, Missouri
BILL NELSON, Florida
DAVE McCURDY, Oklahoma
NORMAN Y. MINETA, California

F. JAMES SENSENBRENNER, JR., Wisconsin
CLAUDINE SCHNEIDER, Rhode Island
BILL LOWERY, California
HERBERT H. BATEMAN, Virginia
TOM LEWIS, Florida
WILLIAM CARNEY, New York
JUDD GREGG, New Hampshire

ROBERT S. KRIPOWICZ, *Staff Director*
HARLAN L. WATSON, *Technical Consultant*

CONTENTS

Page

Appendix I: Questions and answers submitted for the record—Continued:
Dr. Alvin W. Trivelpiece—Continued
Nuclear physics—Continued
C. Facilities—Continued
5.0 Los Alamos National Laboratory, Clinton P. Anderson Meson Physics Facility (LAMPF) 1
6.0 Massachusetts Institute of Technology, William H. Bates Linear Accelerator Center 287
7.0 Oak Ridge National Laboratory, Holifield Heavy Ion Research Facility (HHIRF) 432
8.0 Texas A&M University, Texas A&M Cyclotron 609
9.0 University of Washington, Three-stage Tandem Van de Graaff Accelerator Facility. 759
10.0 Yale University, A.W. Wright Nuclear Structure Laboratory Model MP Tandem Van de Graaff Accelerator 885
D. Construction 939
1.0 Project 85-R-201, General Plant Projects 939
2.0 Project 85-R-203, Continuous Electron Beam Accelerator Facility (CEBAF) 941
3.0 Project 84-R-123, Tandem/AGS Heavy Ion Transfer Line 942
4.0 Project 84-ER-110, University Accelerator Upgrade at the University of Washington and Yale University 942
Appendix II: Additional materials for the record:
"Report of the Panel on Electron Accelerator Facilities," April 1983, DOE/NSF Nuclear Science Advisory Committee, U.S. Department of Energy, Office of Energy Research, Division of Nuclear Physics and National Science Foundation, Division of Physics, Nuclear Science Section, DOE/ER-0164 945
"A Long Range Plan for Nuclear Science: A Report by the DOE/NSF Nuclear Science Advisory Committee," December 1983, U.S. Department of Energy, Office of Energy Research, Division of Nuclear Physics and National Science Foundation, Division of Physics, Nuclear Science Section 1024
Department of Energy, fiscal year 1985 congressional budget request:
General Science and Research, Volume 4 1117
Appropriation Language 1118
Summary of Estimates by Major Category 1119
Program Overview 1120
High Energy Physics 1120
General Science Program Direction 1123

5.0 Los Alamos National Laboratory
Clinton P. Anderson Meson Physics Facility (LAMPF)

1. **What new science is being explored by this facility? What scientific opportunities are being exploited?**

   Answer: LAMPF is the most powerful facility in the world for exploring physics in the energy region 200 - 800 MeV. One scientific opportunity that is being vigorously exploited is the use of the pion as a unique probe of the architecture of the nucleus and of nuclear reactions. The valuable and unique features of the pion are its small size compared to the nucleus, its spinless nature, the fact that it comes in three charge states, and the fact that its interaction with the nucleon has a very strong peak at about 180 MeV, right in the middle of the energy range of LAMPF pions. A number of spectrometers have been built to exploit the uniquely powerful pion beams at LAMPF including EPICS, a high resolution, higher energy pion spectrometer and the neutral pion spectrometer, the major instrument in the world for measuring the energy and direction of neutral pions. Other major facilities are HRS, a high resolution proton spectrometer, an intense beam of very low energy muons, excellent capabilities in polarized proton beams and in polarized targets, and two locations for neutrino experiments.

   With these tools, new collective modes of excitation of the nucleus are being studied. New nuclei far from the maximum stability region are being created via the double charge-exchange reactions--a LAMPF specialty. Precision measurements of nucleon-nucleon amplitudes are being determined. A wealth of detail is emerging about nuclear states as seen in proton scattering.

   A number of tests of the nature of fundamental interactions of particles are being carried out. These bear, in some cases, on aspects of particle interactions that otherwise can be checked only in high energy experiments which often are orders of magnitude more expensive.

   In addition to basic research in nuclear and particle physics, a variety of applied and interdisciplinary programs are in progress, including muon spin rotation experiments to investigate selected areas in solid state physics, radiation-effects studies using protons and neutrons, atomic and molecular physics using H^- ions and muons, radiobiology using pions, and radioisotope production using protons.

2. **How does this facility's accelerator (or accelerators) performance compare with any other in the world that are operating, under construction, or planned?**

   Answer: The major unique features of LAMPF are: (1) high intensity of primary and secondary beams; (2) multiple and simultaneous use of primary and secondary beams; (3) extreme versatility in duty factor (up to 10%), pulse structure, energy variability, and polarization parameters.

   LAMPF has demonstrated operational capability at 1.2 milliampere (mA) average current, 20% above its design goal of 1.0 mA. LAMPF now generates higher intensity than the sum of intensities of all the world's proton accelerators which operate above the pion production threshold.

The meson factory in the U.S.S.R., now nearing completion, is designed to operate at 1 mA average current at 600 MeV. Modifications to the Swiss meson factory (SIN) are designed to raise their intensity to 3 mA average current at 650 MeV. In Germany, there are plans to build a 1 GeV accelerator with an average current of 5 mA, mainly for pulsed neutron research.

LAMPF has 12 channels, aside from the WNR neutron beam lines, which provide simultaneous beams of protons (polarized and unpolarized), high energy neutrons (polarized and unpolarized), pions, muons, neutrinos, and the capability for radioisotope production and radiation damage studies induced by neutrons and protons.

Including WNR, about 500 scientists from approximately 100 institutions are accommodated each year. A list of last year's participants and their institutions are included in the LAMPF annual report. No other nuclear physics facility in the world accommodates as many simultaneous experiments or as many scientists per year.

To date, approximately 1,000 papers on LAMPF research have been published in refereed journals. Also, 100 theses have been completed or are in progress.

3. **What types of research instrumentation/experimental devices are available at this facility, and what are their capabilities?**

Answer:

Research Instrumentation and Experimental Devices

Research facilities and experimental devices available at LAMPF include primary beams (protons and H- ions, both polarized and unpolarized), secondary beams (neutrons, pions, muons, and neutrinos), particle spectrometers, target systems, computer systems, electronics equipment, electromagnets, and a wide variety of additional apparatus used in modern nuclear and particle physics research.

Primary Beams
Particles

H+	900 microampere at 9% duty factor
H-	3-5 microampere at 6% duty factor
H- (polarized)	5 nanoampere at 3% duty factor with 80% polarization

(Dual energy operation is routine for H- beam energies of 212 to 800 MeV and H+ beam energy of 800 MeV; requires time sharing of duty factor)

Secondary Beams
Particles

pions (+ and -)	Four beams; up to 109 pions/sec; 100-700 MeV/c
muons (+ and -)	Two beams; more than 107 muons/sec; 0-250 MeV/c
protons	Four beams; 650-1500 MeV/c
neutrons	One beam; 600-1500 MeV/c
neutrinos	One beam; 20-50 MeV/c

(These beams can be operated simultaneously. In regular operation, LAMPF provides primary or secondary beam to 12 or more experiments simultaneously.)

Spectrometer Systems

Designation	
High Resolution Spectrometer (HRS)	30-50 kiloelectron volts (keV) energy resolution; 2 milliradian (mrad) angular resolution; high efficiency focal plane polarimeter
Energetic Pion Channel Spectrometer (EPICS)	150 keV energy resolution. 10 mrad angular resolution; handles 10^8 pions/sec
Neutral Pion	2 MeV energy resolution; large solid angle

(Other permanent facilities are available at LAMPF, but these three are the premier facilities of their type at any laboratory in the world.)

Target Systems

Cryogenic liquid and gas targets of hydrogen, deuterium, tritium, helium, nitrogen, oxygen, and neon.

Polarized proton targets in both transverse and longitudinal configurations.

Computer Systems

For data acquisition: 9 PDP-11 computers, each with maximum memory, 2 tape drives, and 120 megabytes of disk storage.

For data analyses: four VAX-11/780 computers with peripheral equipment.

Electronics Equipment

The electronic equipment pool consists of 3,783 items valued at $3.12 million. Items stocked include NIM and CAMAC modules, test and measuring equipment, power supplies, etc.

Magnets

A substantial pool of electromagnets of various types is maintained.

4. **What have been the facility's research highlights for the period FY 1981 - present, and what are anticipated for the remainder of FY 1984 and FY 1985?**

Answer: Research Highlights from FY 1981 through FY 1984, more or less chronologically, include the following:

-- Measurement of double-isobaric-analog states in heavy nuclei, October 1980.

-- New and order-of-magnitude improved measurement of the pion beta decay process: improved test of the conserved vector current hypotheses, November 1980.

-- First observation in pion single charge exchange reactions of the Giant Dipole resonance, March 1981.

-- Demonstration of nonexistence of the critical opalescence phenomenon in nuclei, September 1981.

-- Production of exotic nuclei far from the valley of stability using pion double charge exchange reactions.

-- D-T fusion catalyzed by muons, November 1982.

-- Excitation of very high angular momentum (8^-) "stretched" states in ^{54}Fe by inelastic scattering of pions. (A "stretched" state is a shell-model state which has the maximum angular momentum possible for a certain excitation.) Excitation in ^{26}Mg of a 6^-, T = 2 state, FY 1984.

-- Excitation of Giant Resonances in ^{208}Pb with inelastic pion scattering.

-- Measurement of inelastic scattering of protons in medium weight nuclei, FY 1983.

-- Measurement of the depolarization parameter in proton-nucleus scattering at high energy, FY 1983.

-- Measurement of spin excitations in Ca and in Zr by proton scattering, FY 1983.

-- Giant resonances in heavy nuclei excited by medium energy protons: the isoscalar high energy octopole resonance, the giant quadrupole resonance, FY 1983.

-- Excitation of very high angular momentum, "stretched," states in ^{208}Pb in proton scattering. States up to 14^- were observed, FY 1983.

-- Excitation of isobaric analog states across the periodic table by pion charge exchange scattering, FY 1983.

-- Program of pion scattering experiments on ^{14}C: elastic, single charge exchange, and double charge exchange, FY 1983. Excitation of isobaric analog states.

-- New limit for parity nonconserving pp scattering, FY 1984.

-- Observation of about 65 neutrino-electron scattering events is expected in FY 1984.

For the remainder of FY 1984 and FY 1985, the following accomplishments are expected:

Crystal Box

A long data-taking run will occur in summer 1984. The analysis of data acquired in January 1984 should be completed before the summer run begins. These data should result in improved limits for all three decay modes.

Neutrino-Electron Scattering

Data taking will continue in an experiment to achieve an accurate measurement of electron neutrino-electron elastic scattering, the first measurements of neutrino-carbon reactions, and more sensitive searches for muon-neutrino oscillations, neutrino decay, and axion production. To reduce the accelerator-associated and cosmic-ray neutron backgrounds, experimenters will try to improve the passive shielding surrounding the neutrino area. In particular, a high-density (lead and tungsten) section of shielding is being designed for the beam stop. This would produce a significant reduction of backgrounds for the neutrino oscillation and decay experiments.

The goals of this experiment remain of strong interest to the fields of physics, astrophysics, and cosmology. The measurement of the scattering of electron-neutrinos from electrons is still the only feasible measure of weak charged-current and neutral-current interference. The size and sign of this interference term is directly connected to the vector boson content of the Weinberg-Glashow-Salam standard model: it is a measure of the number of bosons and the relative strengths of their interactions. As the interest rises in unified models, so it does in the understanding of this basic structural component.

Neutrino Oscillations and Neutrino Nucleus Interactions

The program of muon-neutrino induced charge-current reactions on carbon, aluminum, and lead will continue. In addition, sensitive search will be made for neutrino oscillations in the muon neutrino to electron neutrino channel.

During the winter shutdown, some changes will be made in Line E to increase the proton current above 20 microamperes. Two new large-aperture bending magnets will replace existing magnets, and more extensive diagnostics will be added. The neutrino-production target and beam stop will be rebuilt to handle higher currents.

An experimental team will begin construction and testing of a horn as a pulsed focusing device for the pion beam used to produce muon-neutrinos. Such a device will increase the intensity of the 150 MeV muon-neutrino beam by a factor of 10.

Low-Energy Pion-Nucleus Interations

A concentrated program of low energy pion inelastic scattering will proceed using the Clamshell spectrometer. Study of inelastic scattering from 16O and from the 0^+ states in 28Si and 90Zr is expected to be pursued. Additional proposals for the study of isospin dependence of transition amplitudes and for locating and studying M1 strengths are anticipated. An improvement program for the Clamshell will continue.

A new pion scattering program, elastic positive- and negative-pion scattering from deuterium, will be undertaken by the Virginia Polytechnic Institute and State University, Oak Ridge National Laboratory, the University of South Carolina, University of Maryland, and Los Alamos National Laboratory collaboration. This experiment is designed to measure the differential cross sec-

tion with good absolute accuracy over the energy range 30-80 MeV. Such measurements will provide excellent data with which to test the current models of the pion-nucleon-nucleon interaction. In particular, data of good absolute accuracy will enable quantitative measurements of charge symmetry violations in the pion-nucleon-nucleon system. This is currently thought to be a promising testing ground for nuclear quark bag models.

Energetic Pion Channel and Spectrometer (EPICS)

The next beam-production period at EPICS will see time devoted to two feasibility studies. One will look at the (pi-, p) reaction on heavy targets such as 50Ti and 50Cr. The reaction with incident negative pions and outgoing protons involves at least two active nucleons and is potentially a rich source of information about pion and delta dynamics. The other feasibility study will look at the pion double charge exchange reaction. Pions will be detected in the spectrometer and protons will be detected in a scintillator telescope. This study could provide useful new information about the basic double charge exchange mechanism.

The study of giant resonances by means of inelastic pion scattering has provided valuable information about these fundamental nuclear excitations. The comparison of negative pion and positive pion cross sections in 40Ca, 118Sn, and 208Pb with neutron excesses has shown ratios considerably larger than those expected from simple models. An experiment on 90Zr will complete the investigation of the neutron excess dependence. In addition, an experiment will study the energy dependence of pion excitation of the giant resonance region in 208Pb.

High Resolution Spectrometer (HRS)

The next beam production period at the HRS will have time devoted to the polarized target facility. The forward-angle measurements of the spin-transfer observable A_{LL} in elastic scattering will be made. Experimenters also plan to measure the spin-transfer observables in the scattering of polarized protons (in the transverse, sideways transverse, and longitudinal directions) from a vector polarized deuteron target of the S type (sideways transverse). Both of these experiments will complement existing data taken in the Nucleon Physics Laboratory (NPL) area at LAMPF at moderate scattering angles. The HRS facility with its good energy and angular resolution will enable the measurement of these spin-transfer observables at very forward angles.

Very recently, the HRS facility was used to measure the complete set of polarization transfer observables for quasi-elastic scattering of 500 MeV protons from lead and deuterium. This leads to a direct comparison of the axial-longitudinal and axial-transverse responses of a heavy nucleus to those for essentially free nucleons. For momentum transfer q = 1.75 fm-1 there is complete disagreement with currently fashionable theories for the nuclear response. Additional time will be used to extend this experiment to other momentum transfers to confirm and/or augment these important results.

Nucleon-Nucleon Program

Plans are being made for a major upgrade of nucleon-nucleon facilities, primarily for the polarized neutron program. At a workshop held in November 1983, it was concluded that the isospin-zero nucleon-nucleon phase shifts

and amplitudes could not be adequately determined without a new intense polarized ion source. Current plans indicate that such a source would give an increase of one and possibly two orders of magnitude in the polarized neutron beam intensity, and so allow measurements that previously have been performed only at forward angles and with marginal statistical precision. To make optimum use of this new source, plans are being developed for improved polarized target facilities, new spin precessors, and additional or alternative neutron-production targets.

In the shorter term, work will continue on the second phase of the np elastic experiment using the new large-acceptance spectrometer. The spin-correlation parameter will be measured over part of the angular range. Measurement of A_{LL} in pp scattering at small angles will allow direct extraction of the forward pp amplitudes.

With pp elastic scattering measurements essentially complete, the primary effort in the EPB line is concentrated on the inelastic reactions. It is clear that "dibaryons" (if they exist) couple strongly to the inelastic channels, so that a study of the energy dependence of pp inelastic scattering should provide a clear indication for or against such exotic resonances. The D_{LL}, A_{SL}, and A_{NO} are the most sensitive probes (being sensitive to interference between the relevant partial waves). In 1984, experimenters will attempt to measure the energy dependence of D_{LL}, and in 1985 the energy dependence of A_{SL} and A_{NO} will be studied over a wide region of phase space.

Investigation of the three body problem continues with a measurement of eight more spin parameters in pd elastic scattering. These additional measurements should allow, for the first time at any energy, the (first order) extraction of the complete set of 12 pd-scattering amplitudes.

Large-Aperature Spectrometer (LAS)

The LAS will be used in a number of important experiments: (1) a first attempt to study the production of eta mesons at LAMPF in the scattering of pions from 3He using the LAS to detect forward-going tritons; (2) a study of the nucleon-delta interactions in pion-deuterium reactions; (3) coincidence studies in pion-3He and pion 4He reactions; and (4) the completion of the study of pion absorption in 3He.

5. **What facility changes and additions have occurred or are anticipated for the period FY 1981 - FY 1985?**

Answer: During the period FY 1981 through FY 1985, the major changes and additions have been or will be:

- Routine operation at currents of 900 - 1000 microamperes.
- Replacement/rebuilding of main beam target cells and beam stop.
- Construction of a polarized proton target facility at the High Resolution Spectrometer.
- Construction and utilization of a new Time-of-Flight-Isochronous spectrometer for nuclear chemistry research and a new Low-Energy Pion spectrometer for pion research.

- Significant physical construction includes a new staging building for the experimental areas, a new Stopped Muon Channel counting house, completion of the enclosure of the AE beam line support area, and initiation of construction of a new office building.

- Construction and implementation of a Data Analysis Center.

- Enhanced operation for H- areas including focal plane polarimeter at the High Resolution Spectrometer. Spin precession apparatus and improved dual-energy capabilities.

6. **For the period FY 1981 - FY 1985, please provide actual and estimated budget profiles for operations, in-house research, out-of-house research, other operating expenses, Capital Equipment, General Plant Projects, In-House Energy Management, and any other specific construction projects attributable to the facility. Please indicate the source of these funds (i.e., Medium Energy Nuclear Physics, Heavy Ion Nuclear Physics, Low Energy Nuclear Physics, High Energy Physics, Basic Energy Sciences, etc.).**

Answer:

LAMPF Budget Profiles
(B/A in thousands of dollars)

	FY 1981	FY 1982	FY 1983	FY 1984	FY 1985
Operating Expenses					
Operations					
Medium Energy	$23,460	$24,272	$29,334	$30,475	$36,480
Defense Programs		2,000	3,000	3,000	
Research (In-House)					
Medium Energy	6,000	6,300	6,500	6,600	6,800
Life Sci. & Nuc. Med.	385	408	408	373	373
LANL Int. R&D	223	466	605	264	200
Research (Out-of-House)					
Medium Energy	91	110	80	119	149
Subtotal	$30,159	$33,556	$39,927	$40,831	$44,002
Plant and Capital Equipment					
Capital Equipment					
Medium Energy	2,000	2,094	2,500	2,640	2,640
Life Sci. & Nuc. Med.	16	15	14	15	15
LANL Int. R&D	0	0	0	200	
General Plant Projects					
Nuclear Physics	400	400	200	500	950
In-House Energy Mgt.					
Energy Management	0	101	0	0	0
Acc. Improvemenmt Proj.					
Nuclear Physics	600	700	200	500	1,100
Subtotal	$ 3,016	$ 3,310	$ 2,914	$ 3,855	$ 4,705
Total	$33,175	$36,866	$42,841	$44,686	$48,707

7. **How much funding for FY 1981 - FY 1985 has been or is expected to be provided by other federal agencies such as the National Science Foundation or by State agencies?**

Answer:

Support from Other Federal Agencies
(in thousands of dollars)

	FY 1981	FY 1982	FY 1983	FY 1984	FY 1985
Nat. Inst. of Health	935	506	96	57	37

8. **For the period FY 1981 - FY 1985, please provide actual and estimated staffing levels.**

Answer:

LAMPF Staffing Levels
(Man-Years)

	FY 1981	FY 1982	FY 1983	FY 1984	FY 1985
Scientific	113.5	109.7	112.1	113.0	113.0
Other Direct	210.4	211.4	217.4	216.0	216.0
Total	323.9	321.1	329.5	329.0	329.0

9. **What is the actual and estimated facility utilization for the period FY 1981 - FY 1985? What would be defined as "full" utilization of the facility?**

Answer: For the period FY 1981 - FY 1985, actual and estimated utilization of LAMPF is:

LAMPF Utilization
(Beam Hours for Research)

FY 1981	FY 1982	FY 1983	FY 1984	FY 1985
3100	3095	3153	3100	2450

For LAMPF, we estimate full utilization to be 4,500 beam hours for research per year.

10. **For the period FY 1981 - FY 1985, how many experiments will have been started, continued, and completed?**

Answer: The following table gives count of experiments by category for period starting on October 1, 1980 (beginning of FY 1981) and projecting through September 30, 1985 (end of FY 1985).

Experiments at LAMPF

	ACTUAL Oct. 1980 - Nov. 1983	PROJECTED Dec. 1983 - Sept. 1985
Experiments started (received first beam)	91	39
Experiments run but not complete	75	32
Experiments completed	155	67

This does not include WNR.

11. What is this facility's user policy?

Answer: LAMPF is a national accelerator facility open to all the Nation's scientists on the basis of scientific merit and technical feasibility of proposals reviewed by a peer committee called the LAMPF Program Advisory Committee. The LAMPF Program Advisory Committee is appointed by and reports to the director of LAMPF.

12. For the period FY 1981 - FY 1985, how much reimbursable research has taken place or is estimated to take place? What revenues have been involved?

Answer: None.

13. What is the mechanism by which specific research proposals for experiments at the facility are considered?

Answer: Beam time at LAMPF is available to all the Nation's scientists on the basis of scientific merit and technical feasibility of proposals reviewed by a peer committee called the Program Advisory Committee (PAC). The LAMPF Program Advisory Committee is appointed by and reports to the Director of LAMPF. On the average, LAMPF provides to outside, university-based user scientists 60% of the total beam time which is available for research. Typically, such an outside university-based group plans experiments and fabricates detectors and other instrumentation at the home institution, executes and partially analyzes experiments at the national facility, and completes analyses and publication of results at the home institution.

The PAC is organized into eight subcommittees which review proposals in the various subfields of physics research conducted at LAMPF. The entire PAC meets for one week twice each year. The new written proposals (numbering about 50 for each of the last few sessions) are received by PAC members about 1 month prior to the biannual meeting. Oral presentations are made by the proposal spokespersons during the meeting. Competition is keen as the total amount of beam time requested far exceeds that available. In executive sessions, the PAC makes recommendations (approve, reject, defer) for each proposal and for priorities in connection with use of beam time. These recommendations are reviewed by the Director of LAMPF who makes the final determination.

14. How many research proposals have been submitted over the past five years, and how many of these have been approved?

Answer: Starting in January 1979 through November 1983, 407 proposals were submitted and 206 were approved.

Please note that most of the disapproved proposals represented good physics. However, they did not have high enough relative priority to be addressed within a two or three year time interval.

15. **How many university personnel (i.e., faculty and students) have utilized the facility over the past five years?**

Answer: There were 469 participants from 83 universities (includes both United States and foreign) using the facility over the past 5 years. This does not include use of WNR.

16. **How many industrial researchers have utilized the facility over the past five years?**

Answer: Eleven participants from seven United States industries utilized the facility over the past five years.

17. **How many researchers from foreign institutions have utilized the facility over the past five years?**

Answer: Seventy-five participants from forty foreign institutions utilized the facility over the past five years.

18. **How many researchers from other agencies have utilized the facility over the past five years?**

Answer: One participant from another agency utilized the facility during this period.

19. **What are the future development possibilities for this facility (including research instrumentation/experimental devices), what plans are being made to exploit these possibilities, and what are the budgetary implications?**

Answer: There are many potential future development possibilities for this accelerator facility, but there are currently no approved plans to undertake any of them beyond the activities identified in the FY 1985 budget request. New research instruments and experimental devices will be developed as the physics research program progresses. We intend to give high priority to the exploitation of the facility's unique capabilities.

20. **Please provide a copy of the facility's latest annual report.**

Answer: The attached, just completed LAMPF annual progress report is appended. Please note the appendices which summarize LAMPF milestones and document the names of those who participated in LAMPF programs last year and also their institutions. **(Note: Excerpts from this report follow.)**

PREPRINT. IN PRESS.

LA-10070-PR
Progress Report

UC-28
Issued: April 1984

Progress at LAMPF

January—December 1983
Clinton P. Anderson Meson Physics Facility

Editor

John C. Allred

Scientific Editorial Board

Olin B. van Dyck
Richard L. Hutson
M. Stanley Livingston
Mario E. Schillaci

Production Staff

Kit Ruminer
Beverly H. Talley

ABSTRACT

Progress at LAMPF is the annual progress report of the MP Division of the Los Alamos National Laboratory. The report includes brief reports on research done at LAMPF by researchers from other institutions and Los Alamos divisions.

Los Alamos Los Alamos National Laboratory
Los Alamos, New Mexico 87545

PROMISES vs ACHIEVEMENTS

This year marks the fifteenth anniversary of the publication of a paper in Science Journal [Science J. 5A, No. 1, 39 (1969)] in which I documented our hopes for the construction and operation of LAMPF. It is interesting to compare what we promised more than 15 years ago with what we actually achieved. A forthcoming paper will make this comparison in some detail, but a simple table shows many of the salient points.

The following table does not show how our research program has evolved compared to initial predictions, or how LAMPF has served the national scientific and academic communities. Here too, we need make no apologies.

As the realization that basic science and derivative technologies are absolutely vital to our Nation's well being continues to invade our civilization's consciousness the scientific community's obligations toward its credibility and responsibilities becomes even more important. Making worthwhile promises that can be kept and then keeping them are two ways we can achieve those goals.

L Rosen

Louis Rosen
Director, LAMPF

LAMPF PROMISES vs ACHIEVEMENTS

Parameter	Promised	Achieved
• Energy	Variable up to 800 MeV	Variable up to 800 MeV
• Intensity	1 mA	>1 mA
• Extraction efficiency	>99%	>99.8%
• Energy spread at ½ max	0.5%	0.15%
• Duty factor	>5%	>9%
• rf power sources	Computer-controlled rf power sources, modulators, and switch gear	Computer-controlled reliable and stable rf power >80% beam availability
• Accelerator structures	High-efficiency accelerator structures	At 1 mA, 30% of rf power is converted to beam power
• H^+ and H^- beams	Simultaneous beams	Simultaneous dual-beam operation and energy variability, 20-nA average 90% polarized H^-
• Secondary beams	Six beam lines	12 experimental ports plus 6 neutron lines at WNR
• Practical applications	National defense Isotope production Radiation damage Radiobiology	WNR Isotope production Pion therapy (successfully initiated, now in abeyance)

39-587 O - 84 - 2

Experimental Areas

Primary beam lines in experimental areas:

Line A — Main Beam Line for Pion and Muon Channels
Line B — Neutron and Proton Beams and Nuclear Chemistry Facility
Line C — High-Resolution Proton Spectrometer
Line D — Weapons Neutron Research Facility

Experimental beam lines:

Area A:

BSA — Beam Stop A
EPICS — Energetic Pion Channel and Spectrometer
LEP — Low-Energy Pion Channel
P³ — High-Energy Pion Channel
SMC — Stopped Muon Channel
TTA — Thin Target Area

Area B (AB or Nucleon Physics Facility):

BR — Neutrons and Protons
EPB — External Proton Beam
LB-NC — Line B, Nuclear Chemistry

Area C:

CCH — Area C Control and Counting House
HRS — High-Resolution Proton Spectrometer

Area A-East:

Biomedical Pion and Muon Channel
TA-5 — Target A-5
ISORAD — Isotope Production and Radiation Effects Facility
Neutrino Area

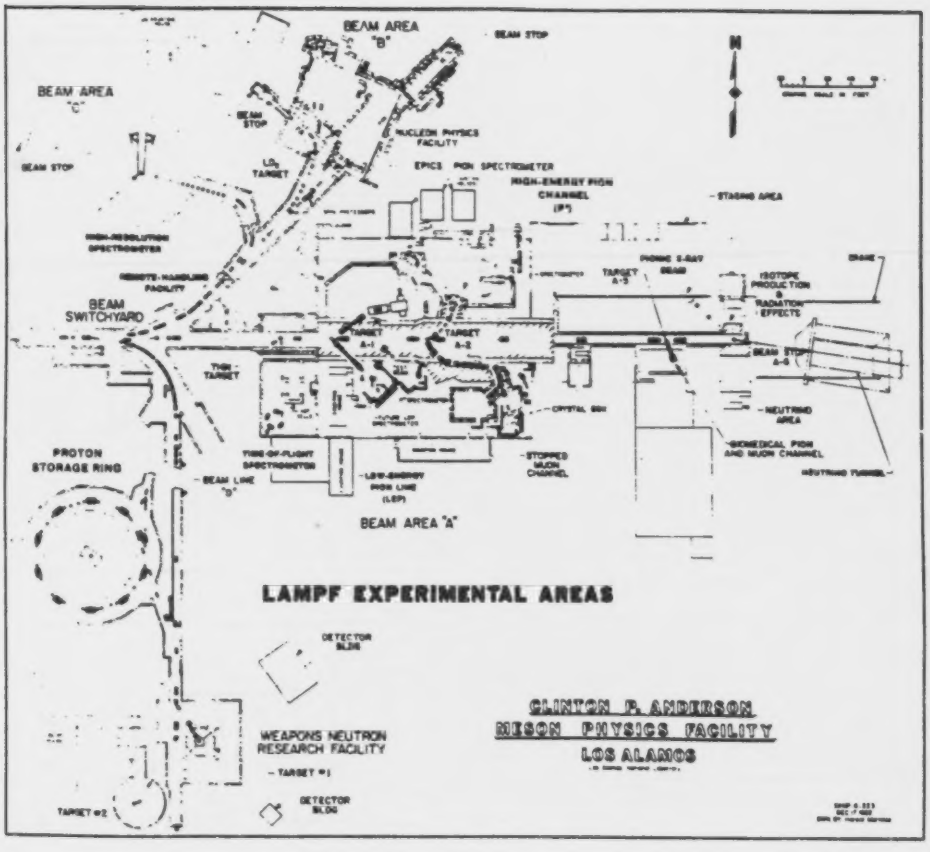
BEAM AREA "B"
BEAM STOP
BEAM AREA "C"
BEAM STOP
BEAM STOP
LH2 TARGET
NUCLEON PHYSICS FACILITY
EPICS PION SPECTROMETER
HIGH-ENERGY PION CHANNEL (P3)
STAGING AREA
HIGH-RESOLUTION SPECTROMETER
REMOTE-HANDLING FACILITY
BEAM SWITCHYARD
TARGET A-1
TARGET A-2
PRIME 0-DEG BEAM
TARGET A-3
ISOTOPE PRODUCTION & RADIATION EFFECTS
DUMP
BEAM STOP A-3
THIN TARGET
CRYSTAL BOX
NEUTRINO AREA
BIOMEDICAL PION AND MUON CHANNEL
NEUTRINO TUNNEL
PROTON STORAGE RING
TIME-OF-FLIGHT SPECTROMETER
BEAM LINE "A"
LOW-ENERGY PION LINE (LEP)
STOPPED MUON CHANNEL
BEAM AREA "A"
LAMPF EXPERIMENTAL AREAS
DETECTOR BLDG
WEAPONS NEUTRON RESEARCH FACILITY
TARGET #1
TARGET #2
DETECTOR BLDG
N
CLINTON P. ANDERSON
MESON PHYSICS FACILITY
LOS ALAMOS

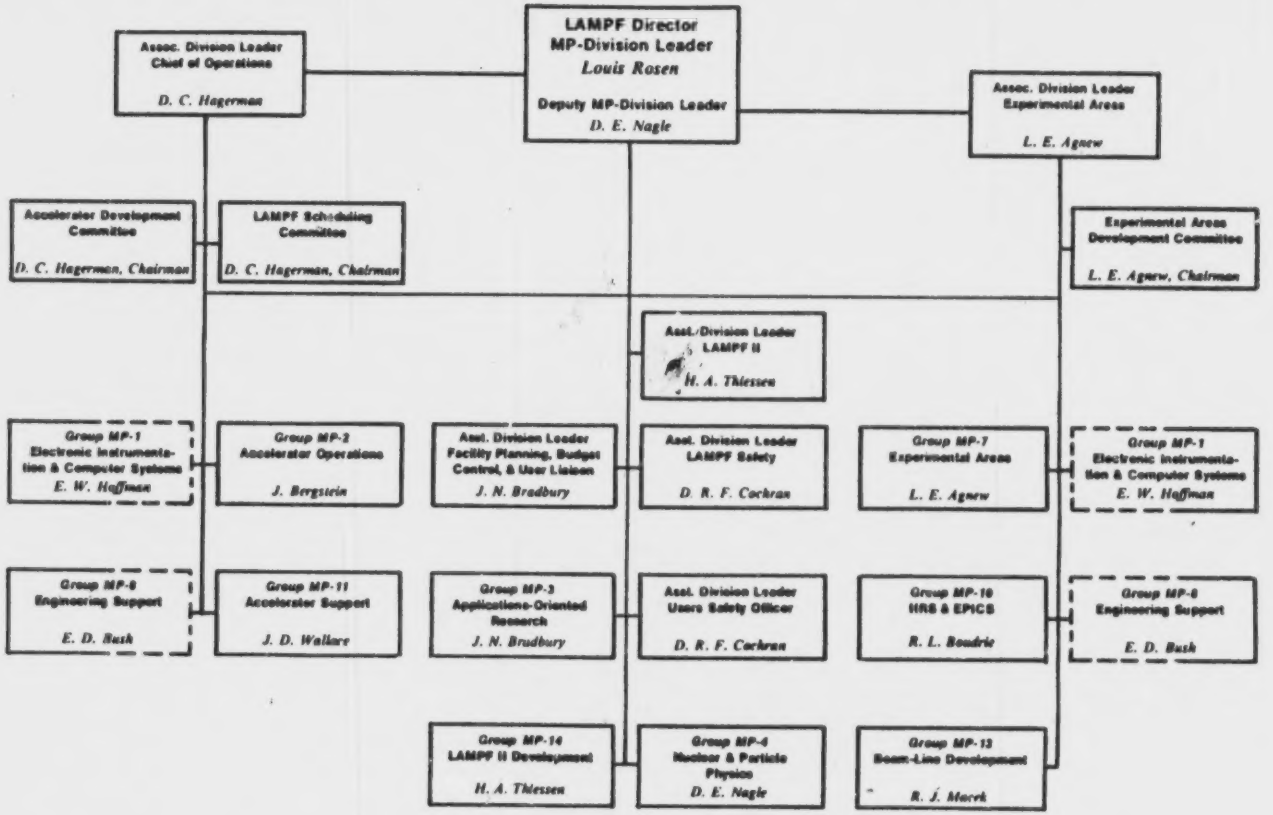

LAMPF ORGANIZATION

December 1983

PROGRESS AT LAMPF

JANUARY — DECEMBER 1983

CLINTON P. ANDERSON MESON PHYSICS FACILITY

I. LAMPF NEWS

• At its March 1983 meeting, the Board of Directors of the LAMPF Users Group, Inc., established a new award, the Louis Rosen Prize. This prize, consisting of $1000 and a certificate, is awarded annually for the outstanding Ph.D. thesis based on LAMPF research. Judging is done by the Board of Directors. Theses should be submitted to the Users Group Office at LAMPF by August 31 for consideration. To be eligible, a thesis must have been completed since the previous August. Announcement of the winner of the prize is made at the annual Users Meeting in November.

• At the Users Meeting of November 7, 1983, Chairman George Igo announced the award of the first Louis Rosen Prize to Stephen A. Wood for his thesis entitled "An Experimental Study of Inclusive Pion Double-Charge-Exchange Reactions in the Delta-Resonance Region."

• On February 7, 1983, at the end of a production run, the LAMPF accelerator was tested for maximum proton beam current. An average current of 1.2 mA, 20% above design, was produced for several hours.

On behalf of the LAMPF Users Group, Inc., Director Andy Bacher presents to Stephen Wood the Louis Rosen Prize. Left to right: Rosen, Wood, Bacher.

George J. Krausse, MP-4, with the prototype H^- beam modulator he designed and built. The beam modulator will shape the beam pulse for injection into the PSR. Extended-life tests were performed successfully in December 1983; the slew rate of the modulator is 500 kV/μs.

• With the Proton Storage Ring (PSR) coming on line in 1985, major necessary modifications of the LAMPF accelerator are proceeding. (1) An H^- beam modulator prototype that will shape the beam pulse for injection into the PSR (see photograph above) has been designed, built, and tested; (2) a new high-intensity H^- ion source has been designed and a prototype built; and (3) components are being built for a new injector and for a reconfigured switchyard.

During summer/fall of 1983 a collaboration (Japan, UCLA, University of Minnesota, Los Alamos) worked at the HRS making nucleon-nucleon measurements in the Coulomb-nuclear interference region at forward-scattering angles. Polarized beam struck polarized $\vec{p}$ and $\vec{d}$ targets cooled to 25-50 mK by a dilution ^{3}He/^{4}He refrigerator furnished by KEK. Shown in the photograph, left to right, are George Igo (UCLA), Hiromi Hasai (Hiroshima University), Akira Masaike (KEK), Steven Greene (Los Alamos), and Yuji Ohashi (Nagoya University).

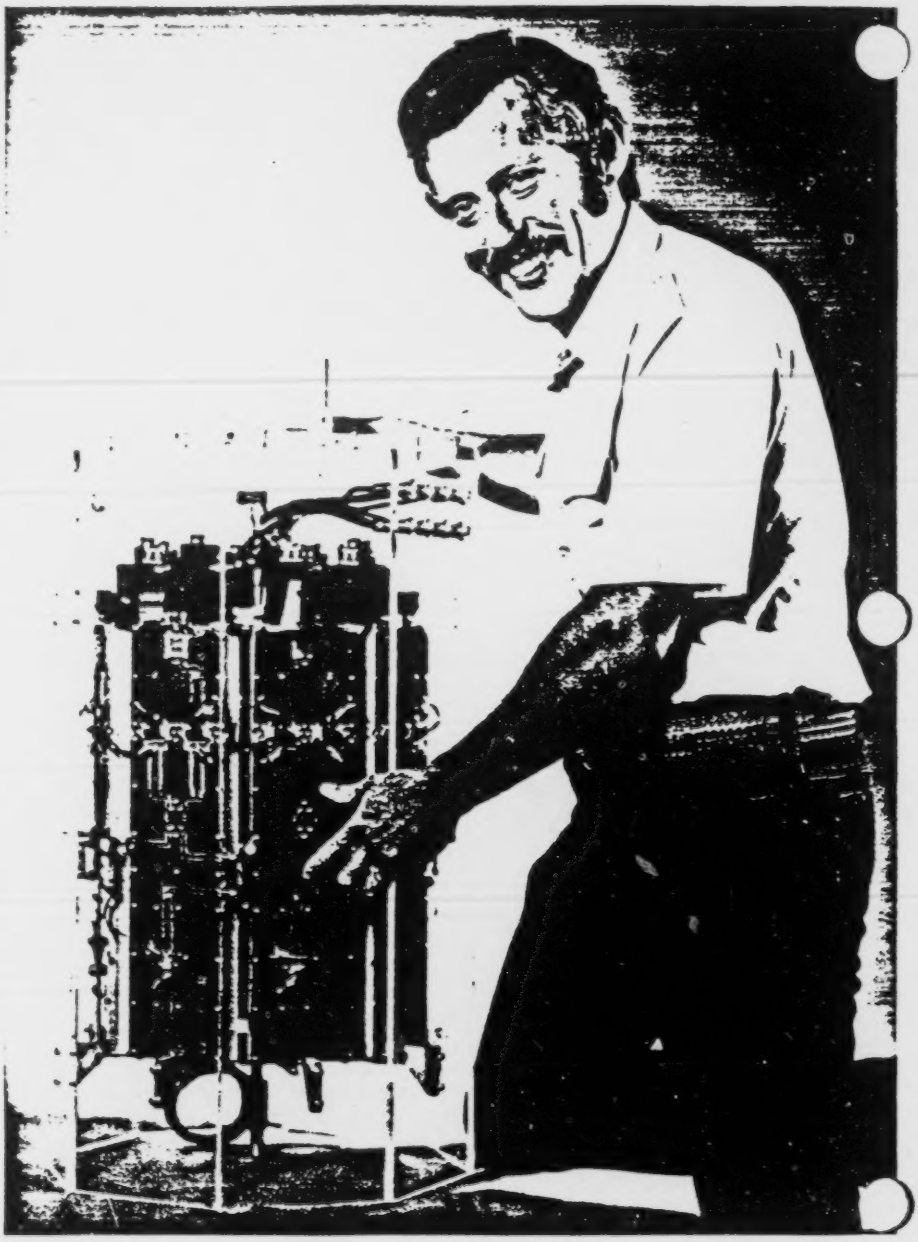

LAMPF Satellite? Jerry Davis, MP-11, displaying the 805-MHz intermediate driver amplifier he designed. This amplifier, with an output power of 1 kW, drives a vacuum-tube amplifier which in turn drives the klystrons of the side-coupled-cavity linac.

• On August 5, 1983 a serious electrical accident occurred at LAMPF. Three technicians from MP-8 began what they thought was routine maintenance of a portion of the power supply to the klystron test stand at the Engineering Test Laboratory.

Through an unexpected sequence of circumstances — things that "could not happen" — a key interlock was unknowingly by-passed and a hand-held grounding hook contacted an energized 4160-V, 60-Hz power bus. The resulting fireball caused burns to all three persons exposed; the person holding the grounding hook was painfully burned. Injuries were fortunately much less serious than they might have been.

Of greater interest than the actual details are the boundary conditions. The person closest to the accident was a senior, skilled technician, who believed (as did his supervisors) that he understood the hazards and how to manage them. All three persons involved believed, without doubt, that the circuit in question was de-energized. The mechanical and key interlocks were in

place and were functioning properly, but the system was by-passed. It is now clear that none of the people involved realized the seriousness of the risks associated with the operation.

The hazards at LAMPF are many — electrical, chemical, cryogenic, radiation and radioactive materials, pressurized and evacuated systems, and magnets — practically every hazard that can be imagined. Experimental areas can be especially hazardous because conditions are constantly changing. Even for a single experiment, in a matter of weeks an experimental area may undergo a drastic rearrangement.

An accident such as the one of August 5 must remind all of us that safety is always paramount. The safety record at LAMPF is outstanding because all the people here, Users and lab employees alike, work at safety. Safety requires continuous vigilance; it is not a matter of good luck.

• The radiation monitoring system at the entrance to the LAMPF site paid an unexpected dividend. A truck carrying construction steel from Mexico independently wandered onto the LAMPF site and triggered our radiation alarm system. Sure enough, the entire load of steel was sufficiently radioactive to set off a search in the United States and Mexico for other steel from the same mill. Once again LAMPF served the national interest in an unexpected way.

II. MEETINGS

LAMPF Users Group, Inc.

Seventeenth Annual LAMPF Users Group Meeting

The LAMPF Users Seventeenth Annual Meeting was held in Los Alamos on November 7-8, 1983, with 222 attendees. Chairman George Igo (UCLA) presided at the first session, which opened with a welcoming address by Warren F. Miller, Associate Director of Los Alamos National Laboratory. The session continued with a LAMPF Status Report presented by Louis Rosen, Director of LAMPF, and a report on LAMPF operations by Andrew A. Browman.

During the second portion of the morning session, George Igo gave the Annual Users Group Report, followed by a presentation of the election results. Robert Redwine (MIT) is the Chairman-Elect of the Board of Directors, and new members are Peter D. Barnes (Carnegie-Mellon University), Barry Preedom (University of South Carolina), and John D. Walecka (Stanford University). Members whose terms continue in 1984 are Charles Glashausser, Chairman, and George Igo, Past-Chairman. A presentation was given by Charles Bowman (Los Alamos) on Proton Storage Ring Research.

The afternoon session was conducted by incoming Chairman Charles Glashausser (Rutgers University). The following talks were given during this session:

"*New Approach to Polarized-Proton Scattering Based on Dirac Dynamics*," Steven J. Wallace (University of Maryland),

"*Progress Report—LAMPF II*," Henry A. Thiessen (Los Alamos), and

"*Muon Neutrino Physics Before the PSR*," Gerard Stephenson (Los Alamos).

The afternoon session concluded with a panel discussion on the present LAMPF II concept in the context of nuclear and particle physics needs of the 1990s.

Talks given during the Tuesday morning session, presided over by Igo, were

"*Energy and Angular Dependence of the Tensor Polarization T20 in π Elastic Scattering*," Willi Grüebler (FTH),

"*Tensor Polarization in Pion-Deuteron Elastic Scattering*," Roy Holt (Argonne),

"*Simple Features of (pπ⁻) Reactions Near Threshold*," Steven Vigdor (Indiana University),

"pp *and* np *Phase Shifts up to 800 MeV*," Catherine Lechanoine-LeLuc (University of Geneve), and

"*Status of Exp. 225, A Study of Neutrino-Electron Elastic Scattering*," Herbert Chen (University of California, Irvine).

Working group meetings were held the rest of the day.

Visitors Center

During this report period, 572 research guests worked on LAMPF-related activities or participated in experiments at LAMPF; of these, 126 were foreign visitors. A total of 656 check-ins and 625 check-outs were processed by the Visitors Center.

• MEMBERSHIP

Non-Los Alamos National Laboratory	706
Los Alamos National Laboratory	171
TOTAL	877

• INSTITUTIONAL DISTRIBUTION

Membership by Institutions

Los Alamos National Laboratory	171
National or Government Laboratories	96
U.S. Universities	364
Industry	41
Foreign	162
Hospitals	30
Nonaffiliated	13
TOTAL	877

Number of Institutions

National or Government Laboratories	19
U.S. Universities	108
Industry	30
Foreign	82
Hospitals	25
Nonaffiliated	7
TOTAL	271

• REGIONAL BREAKDOWN

East (Pennsylvania, New Jersey, Delaware, Washington DC, Massachusetts, New York, Connecticut, Vermont, Rhode Island, New Hampshire, Maine)	132
Midwest (Ohio, Missouri, Kansas, Indiana, Wisconsin, Michigan, Illinois, North Dakota, South Dakota, Nebraska, Iowa, Minnesota)	102
South (Maryland, Virginia, Tennessee, Arkansas, West Virginia, Kentucky, North Carolina, South Carolina, Alabama, Mississippi, Louisiana, Georgia, Florida)	71
Southwest, Mountain (Montana, Idaho, Utah, Wyoming, Arizona, Colorado, New Mexico, Oklahoma, Texas) (excluding Los Alamos)	128
West (Alaska, Hawaii, Nevada, Washington, Oregon, California)	110
Foreign	163
Los Alamos National Laboratory	171
TOTAL	877

1984 WORKING GROUP CHAIRMEN

High-Resolution Spectrometer (HRS)
M. Gazzaly
University of Minnesota

Neutrino Facilities
Thomas A. Romanowski
Ohio State University

Stopped-Muon Channel (SMC)
Fesseha Mariam
Los Alamos National Laboratory

Nuclear Chemistry
Yoshitaki Ohkubo
Los Alamos National Laboratory

Energetic Pion Channel and Spectrometer (EPICS)
William Cottingame
New Mexico State University/
Los Alamos National Laboratory

High-Energy Pion (P^3) Channel
Jon Engelage
University of California,
Los Angeles

Nucleon Physics Laboratory (NPL)/ Polarized Facilities
Tarlochan Bhatia
Texas A&M University/
Los Alamos National Laboratory

Computer Facilities
James F. Amann
Los Alamos National Laboratory

Solid-State Physics and Materials Science
Walter F. Sommer
Los Alamos National Laboratory

Muon-Spin Rotation (μSR)
Art Denison
University of Wyoming

Low-Energy Pion (LEP) Channel
Michael J. Leitch
Los Alamos National Laboratory

LAMPF PROGRAM ADVISORY COMMITTEE (PAC)

The PAC consists of about 25 members appointed for staggered 3-year terms. Members advise the Director of LAMPF on the priorities they deem appropriate for the commitment of beam time and the allocation of resources for the development of experimental facilities. The PAC meets twice each year for 1 week during which time all new proposals that have been submitted at least 2 months before the meeting date are considered. Old proposals, and the priorities accorded to them, may also be reviewed.

Terms Expiring 1983

Richard Arndt
Virginia Polytechnic Inst. and State University

Robert Redwine
Massachusetts Institute of Technology

S. Peter Rosen
Los Alamos National Laboratory

Dieter Kurath
Argonne National Laboratory

Louis Remsberg
Brookhaven National Laboratory

Stephen J. Wallace
University of Maryland

Terms Expiring 1984

Franz L. Gross
College of William & Mary

Leonard S. Kisslinger
Carnegie-Mellon University

Darragh Nagle
Los Alamos National Laboratory

Barry Holstein
University of Massachusetts

June L. Matthews
Massachusetts Institute of Technology

Bruce VerWest
Arco Oil and Gas Company

Sheldon B. Kaufman
Argonne National Laboratory

Daniel W. Miller
Indiana University

Robert Lee Walker
Tesuque, New Mexico

Terms Expiring 1985

David Axen
TRIUMF

Frieder Lenz
SIN

Victor E. Viola, Jr.
Indiana University

Barry Barish
California Institute of Technology

Harold M. Spinka, Jr.
Argonne National Laboratory

Larry Zamick
Rutgers University

Dietrich Dehnhard
University of Minnesota

1984 TECHNICAL ADVISORY PANEL (TAP) OF THE LAMPF USERS GROUP, INC.

The TAP provides technical recommendations to the Board of Directors and LAMPF management about the development of experimental facilities and experiment support activities. The TAP has 12 members, appointed by the Board of Directors, serving 3-year staggered terms. The Chairman of the Board of Directors serves as TAP chairman. The TAP membership and term expiration dates are listed below.

1984 Billy E. Bonner
Los Alamos National Laboratory

1984 Thomas J. Bowles
Los Alamos National Laboratory

1986 George R. Burleson
New Mexico State University

1984 Gerald Dugan
Fermi National Accelerator Laboratory

1985 Donald Geesaman
Argonne National Laboratory

1985 Kazuo Gotow
Virginia Polytechnic Institute and State University

1985 C. L. Morris
Los Alamos National Laboratory

1986 Michael A. Oothoudt
Los Alamos National Laboratory

1984 Barry Preedom
University of South Carolina

1985 Thomas A. Romanowski
Ohio State University

1986 Gary Sanders
Los Alamos National Laboratory

1986 Charles A. Whitten
University of California, Los Angeles
Los Angeles

SCIENCE POLICY ADVISORY COMMITTEE (SPAC)

A Science Policy Advisory Committee was formed during 1983 to advise the Board of Directors on the long-term development of research and facilities at LAMPF. The first charge to the SPAC was the examination of the LAMPF II concept and justification in the context of nuclear and particle physics needs of the 1990s.

Barry C. Barish
California Institute of Technology

Leonard S. Kisslinger
Carnegie-Mellon University

Alan D. Krisch
University of Michigan

Malcolm MacFarlane
Indiana University

Sydney Meshkov
National Bureau of Standards

Frederick Reines
University of California, Irvine

S. Peter Rosen
Los Alamos National Laboratory

Lee C. Teng
Fermi National Accelerator Laboratory

Akihiko Yokosawa
Argonne National Laboratory

John D. Walecka
Stanford University

1984 BOARD OF DIRECTORS OF THE LAMPF USERS GROUP, INC.

The Board of Directors consists of seven members elected by the LAMPF Users Group, Inc., whose interests they represent and promote. They concern themselves with LAMPF programs, policies, future plans, and especially with how users are treated at LAMPF. Users should address problems and suggestions to individual Board members.

The Board also nominates new members to the Program Advisory Committee (PAC).

The 1983 membership and term expiration dates are listed below.

1985 Charles Glashausser (Chairman)
Rutgers University

1986 Robert Redwine (Chairman-Elect)
Massachusetts Institute of Technology

1984 George Igo (Past-Chairman)
University of California, Los Angeles

James Bradbury (Secretary/Treasurer)
Los Alamos National Laboratory

1984 Andrew D. Bacher
Indiana University

1985 Peter D. Barnes
Carnegie-Mellon University

1985 Barry Preedom
University of South Carolina

1985 John D. Walecka
Stanford University

LAMPF USERS GROUP, INC., (LUGI)

BOARD OF DIRECTORS

The LAMPF Users Group Board of Directors (BOD) met on March 6-7, July 20-21, and November 8, 1983. All meetings were chaired by George Igo; selected topics of discussion are provided below.

The 1983 Annual Users Meeting was very successful. There were 222 registrants of whom 119 were from ouside the Laboratory. The panel discussion about LAMPF II involving the BOD, the Science Policy Advisory Committee (SPAC), and the attending users, received favorable comments for being stimulating and informative. A summary of the discussion is provided in these proceedings.

Sixty-one new proposals were received for review by the Program Advisory Committee (PAC) at the January 1984 meeting. The breakdown by channel is: EPICS - 15, HRS - 10, NPL - 7, LEP - 12, P^3 - 11, SMC - 3, Neutrino - 1, Radiation Effects - 1, and Nuclear Chemistry - 1. Because of the proposal load, the Low-Energy Pion Channel (LEP) and High-Energy Pion Channel (P^3) PAC subcommittees will be augmented by one member (either from the Laboratory or from another subcommittee) for the January meeting.

Those PAC members whose terms nominally expire in 1983 have been asked, as usual, to serve in January and also to serve at the summer meeting in 1984, as there was no meeting in the summer of 1983. The summer 1984 meeting will thus be the "overlap" meeting. New PAC members will be recommended by the BOD at their next meeting.

Four new members were appointed to the Technical Advisory Panel from the lists provided by the LUGI working groups. The appointees are: Michael Oothoudt, Computer Facilities; Gary Sanders, Stopped-Muon Channel (SMC); George Burleson, Energetic Pion Channel and Spectrometer (EPICS); and Charles Whitten, High-Resolution Spectrometer (HRS).

The Board agreed to employ Users Group funds to establish and support a new award, the Louis Rosen Prize. This prize, consisting of $1000 and a certificate, is to be awarded annually for the outstanding Ph.D. thesis based on LAMPF research. The judging is to be done by the Board of Directors. For consideration, theses should be submitted to the Users Group Office at LAMPF by August 31; announcement of the winner will be made at the Users Meeting in November. To be eligible, a thesis must have been completed since the previous August.

The criteria for thesis evaluation were discussed. In addition to intellectual content, quality of presentation, and significance of results, the level of the contributions to the work by the student is obviously important. Contributions to the experiment design, data analysis, and data interpretation are to be assessed by requiring explanatory letters from both student and advisor.

The BOD selected Stephen A. Wood as the recipient of the Louis Rosen Prize for 1983. The title of the thesis is "An Experimental Study of Inclusive Pion Double-Charge-Exchange Reactions in the Delta Resonance Region."

MP-Division has purchased a 10-ft. by 55-ft. trailer to be equipped as a User lounge. The trailer will be located to the east of the Data-Acquisition Center and will arrive about December 1, 1983. The lounge will contain space for a library, kitchen, and computer terminal as well as a large open area; some landscaping in the vicinity is planned. User representatives will be asked to consider furnishings for the lounge and arrange for their purchase with User funds available for this purpose.

George Igo announced the formation of a Science Policy Advisory Committee (SPAC) whose role is to advise on the long-term development of research and facilities at LAMPF. The following persons participated in an organizational meeting on July 26, 1983.

Barry Barish	Caltech
Leonard Kisslinger	Carnegie-Mellon University
Alan Krisch	University of Michigan
Sydney Meshkov	National Bureau of Standards
Fredrick Reines	University of California/Irvine
Peter Rosen	Los Alamos National Laboratory
Dirk Walecka	Stanford University
Akihiko Yokosawa	Argonne National Laboratory

The first charge to the SPAC is to examine the present LAMPF II concept and physics justification in the context of nuclear and particle physics needs of the 1990s. The committee is to advise the LUGI-BOD on:

- specific strengths and weaknesses in the LAMPF II concept and justification,
- the highest priority experimental programs and facilities to be developed at LAMPF II, and
- the best strategies for advancing the case and developing support for LAMPF II in the nuclear and particle physics communities.

The SPAC met on October 22, 1983 at UCLA. Preliminary reports were presented on four topics important to the LAMPF II concept: accelerator design (Alan Krisch), experimental facilities (Akihiko Yokosawa), and physics justification and community support (Barry Barish). George Igo will assemble the written reports and send them, together with a summary of the panel discussion during the Annual Users Meeting, to the Users. This is a crucial period for LAMPF II because the concept and justification must become firm very soon in order to produce a proposal by the end of 1984. Strong support of physicists in both nuclear and particle physics must be garnered and maintained. Consequently the BOD feels that the SPAC should be requested to continue to provide input to the LAMPF II plan. A nuclear physics subcommittee of the SPAC will be organized by C. Glashausser to define more precisely the potential of LAMPF II in this area.

Following a suggestion by Louis Rosen, plans are being made to hold a comprehensive workshop on the interface between particle and nuclear physics, in May of 1984. Two members of the SPAC, Alan Krisch and Malcolm MacFarlane, have agreed to head an organizing committee for this workshop. A one-half-day session of invited papers on the interface region will be held at the spring APS meeting.

To bolster the case for LAMPF II, it is important to publicize the achievements of existing meson factories and their impact on the development of nuclear physics. Members of LUGI are encouraged to give presentations at universities and an article should be prepared for *Physics Today*. A semitechnical brochure on LAMPF accomplishments could also be prepared for widespread distribution.

The annual user meeting in 1984 will be held on October 29-30 (November 6 is election day). The next BOD meeting will be on February 17, 1984 at LAMPF.

TECHNICAL ADVISORY PANEL

The Technical Advisory Panel (TAP) met on July 29 and November 6, 1983. Some excerpts of the minutes are presented below. After noting that the budgetary position of LAMPF appears reasonable for FY 1984, Louis Rosen made some general comments about the LAMPF neutrino program. The proposed neutrino program using the Proton Storage Ring (PSR) is in abeyance at this time primarily because the neutron scattering and defense programs have first priority on PSR beam and it is not clear that an adequate amount of current will be available for the neutrino program. However, as neutrino physics is an important component of LAMPF research, experiments are being conducted at the beam stop and Line E. At Line E, neutrino cross sections will be measured using a 5-ton liquid scintillator detector (Exp. 764). LAMPF will provide up to $200 thousand to prepare Line E, which is expected to be ready to receive beam in January 1984. If approved by PAC, a modular detector may be constructed, which might eventually be used at LAMPF II.

Louis Rosen commented that for long-term survival, LAMPF needs a major upgrade. He feels that the Laboratory top management will support such a project, as it clearly will provide important opportunities for performing high-quality research and for extending the base for education of young scientists. Interested members of the scientific community must make the DOE and Congress aware that they need and will use a LAMPF II. In addition to the in-house work of Los Alamos in terms of proposal preparation, there must be a well-established effort by external users to define and support LAMPF II.

Richard Boudrie reported that the new Low-Energy Pion Channel (LEP) spectrometer project is proceeding very well. The spectrometer will be useful for pion-inelastic scattering in the 20- to 80-MeV range and will provide <0.1% resolution with large acceptance. The pole pieces and yoke are presently being machined at a cost much less than anticipated; the vacuum can has been cast and vacuum tests will soon be performed. It is expected that the poles, yoke, and vacuum can will be assembled and doweled at the machine-shop facility by late September. One coil has been fabricated and the second coil is expected by October.

A conceptual design and drawing have been completed for the scattering chamber and target mechanism. Comments are being solicited from potential users and engineers. Studies have been made regarding the relative merits of the vertical drift (VDC) and MP-10 drift chambers for the focal plane. Tests of the MP-10-style chambers at a 45° angle of incidence for the incoming particle will be made at the end of Cycle 38 to evaluate their performance. The project is on schedule and within the budget of $350 thousand. A working system ready to accept beam is expected by April 1984.

Helmut Baer reviewed the development history and current performance characteristics of the π^0 spectrometer. Highlights of the research program include the studies of isobaric analogs to determine the isovector component of the optical potential, and the studies of giant resonances with $(\pi^\pm,\pi^0)$ reactions. Of particular significance is the presence of the nuclear monopole signal.

The π^0 spectrometer is capable of obtaining a resolution of 2-MeV FWHM, although 4 MeV is more typical. To make a significant improvement in resolution, the γ-ray energy resolution must be improved. If the photon resolution were 5% FWHM at 100 MeV, the π^0 energy resolution could be improved to approximately 0.5 MeV FWHM. Monte Carlo design studies are being performed to determine the advantages of replacing the lead-glass photon detectors with either NaI or BGO modular arrays. Such an improvement might cost about $1 million. If the modification project is deemed worthwhile, the group will prepare a detailed proposal for evaluation by the TAP.

LAMPF may be able to acquire a new polarized ion source with 1 to 2 orders of magnitude higher intensity than the present source at a cost of several million dollars and several man-years of effort. Perhaps Accelerator Improvements Project (AIP) funds (estimated to be about $1 million per year after FY 1984) could be used. It is necessary, however, to evaluate the physics justification for such a source, and a workshop will be convened for that purpose in November.

Billy Bonner discussed his investigation of new polarized ion source possibilities for LAMPF. The National Laboratory for High-Energy Physics in Japan (KEK) has developed an optically pumped source with demonstrated output of 10-25 μA and an anticipated output of about 60 μA. An atomic beam ion source (Gruebler, SIN) has produced 6 μA with projections (perhaps optimistic) of 100 μA. A 20-μA source would provide an increase in intensity by a factor of 50-100 over the present LAMPF source.

Lewis Agnew reported on experimental-area development projects. The A-2 target cell was rebuilt during the 1983 shutdown. Production currents up to 900 μA have been achieved on Line A. Replacement of the A-1 target cell is planned for the 1984 spring shutdown. Both the LEP and TOFI spectrometers are making reasonable progress; first use of the LEP spectrometer is planned for next summer.The polarized-target program at the High-Resolution Spectrometer (HRS) was successful; plans for the 1984 continuation of this program are being reviewed. Design work for the HRS focal-plane shielding is complete, but installation in 1984 will be in conflict with the polarized-target setup. The shielding will be deferred until 1985 if the polarized-target program is scheduled for 1984.

Planned modifications to the beam-stop area were presented by Walter Sommer. The major design considerations and goals are to provide:

- improved environment for beamline diagnostics,
- improved shielding and elimination of cracks to reduce leakage of activated gas,
- new facility for proton- and neutron-radiation-effects studies that allows multiple bulk samples and control of irradiation parameters,
- improved facility for high-speed and ultra-high-speed isotope transport and identification,
- access for additional experiment initiatives in nuclear and solid state physics,
- remote handling and shielded transport of radioactive material, and
- one-day repair/replacement of components or experimental hardware.

Design of the new facility is nearing completion and accelerator improvement funds are available for the project. Material procurement and fabrication have been initiated, and a schedule calling for completion in the spring of 1985 has been established.

A status report on the Long-Range Planning Committee for LAMPF Computing Needs was presented by Martha Hoehn. The committee met for 3 days, October 24-26, 1983.

The committee generally discussed topics in two areas: data acquistion and data analysis. A few notable points in each section were presented to the TAP.

Five topics were discussed for data acquisition: (1) front-end processing, (2) hardware standards, (3) buffer processors, (4) data-acquisition program Q, and (5) networks in the experimental area. These are briefly summarized below.

1. *Front-end processing.* The committee heard a presentation by James Amann summarizing the status of the committee looking into this topic. The microprogrammable branch driver (MBD) does not satisfy all the needs of the users, but there is no obvious candidate for a replacement. It appears that auxiliary crate controllers may solve some problems for some applications. A new high-speed flexible electronics system, FASTBUS, looks like a promising technology to pursue, and the committee recommended that Group MP-1 should do that.

2. *Hardware standards.* The committee felt that we should be moving toward 32-bit VAX-class machines for data acquisition, primarily to solve the 16-bit address space problem with PDP-11s. The committee also felt that LAMPF should begin upgrading tape units to 6250/1600 bpi.
3. *Buffer processors.* Michael Oothoudt presented to the committee a simple idea for taking advantage of the processing capabilities of the new machines without adding overhead from peripherals. The basic idea is to attach multiple processors to a central unit. As an event comes in, it is sent to the first processor, the second event to the second, and so on. Thus, the analysis of events would be carried on in parallel and increase the computing capacity of the central unit.
4. *Data-acquisition system Q.* The committee identified a few Q projects that should be completed, for example, VAX data acquisition and documentation of internals of Q. However, they felt that the Q programmers should not spend time adding "bells and whistles" to Q but should direct their efforts in more productive areas such as FASTBUS and buffer processors.
5. *Networks.* Networks to the experimental area are long overdue and should be implemented with a high priority.

Three topics were discussed under data analysis: (1) Data-Analysis Center (DAC) functions, (2) problems, and (3) external networks. Each of these areas is discussed below.

1. *DAC functions.* The committee discussed at some length the functions that the DAC can serve, and those that should be addressed elsewhere. Specifically, the DAC should provide interactive graphics capabilities, should be able to handle tapes effectively, and should serve as a convenient computing tool for the LAMPF community. However, it should be recognized that the DAC cannot necessarily satisfy all the needs of the users and that LAMPF should be willing to use other resources at this Laboratory, namely the Central Computing Facility (CCF).
2. *Problems.* Two main problem areas were identified:
   (1) unacceptable interactive response time on the current systems, and
   (2) inadequate disk space.
   These problems are being addressed.
3. *External networks.* The committee recognized a need to provide convenient communications with other locations. Specifically, MP-1 should investigate implementation of a network system such as Telenet and should provide a convenient method to dial out of the DAC. This communication enhancement can, for example, facilitate distribution of drafts of papers.

The TAP members had several comments and questions concerning this presentation. These questions are listed here.

- Did the committee consider small (personal) computers as a standard for data acquisition?
- Has parallel processing been considered for the DAC?
- Has the committee properly considered options for the long term; specifically, writing data-acquisition systems in portable languages?
- Has the committee considered other standard operating systems, such as UNIX?

These points will be brought up at the Long-Range Planning Committee meeting before the final report is prepared.

III. RESEARCH

Nuclear and Particle Physics

Transverse Spin Dependence of the Proton-Proton Total Cross Section
(Exps. 504/505, EPB)

(Rice Univ., Univ. of Houston, Institute "Ruđer Bošković," Univ. of Bonn, Los Alamos)
Spokesman: G. C. Phillips (Rice Univ.)
Participants: W. P. Madigan, D. A. Bell, J. A. Buchanan, M. M. Calkin, J. M. Clement, M. D. Corcoran, K. A. Johns, J. D. Lesikar, H. E. Miettinen, G. S. Mutchler, C. J. Naudet, G. P. Pepin, G. C. Phillips, J. B. Roberts, S. E. Turpin, A. D. Hancock, B. W. Mayes, L. S. Pinsky, K. K. Sekharan, M. Furic, V. Valkovic, W. von Witsch, J. C. Allred, B. E. Bonner, and C. Hollas

Final analysis of the total-cross-section difference data $\Delta\sigma_T = \sigma(\uparrow\downarrow) - \sigma(\uparrow\uparrow)$ for proton-proton scattering with the protons in transverse spin states has been completed. The measurements were made for 12 incident proton energies from 300 to 800 MeV. The experiment was performed during the period from June to November 1980, using the LAMPF variable-energy polarized proton beam and the Rice University polarized proton target. The detectors were precision ionization chambers.

The measurements were made by holding the spin orientation of the target constant and reversing the spin orientation of the beam every minute. Thus a measurement of $\Delta\sigma_T$ is made every 2 min. The target polarity was reversed every hour, and in this way 60-80 values of $\Delta\sigma_T$ were obtained for each target polarity. As a result of the current- and position-dependent responses of the ionization chambers, the $\Delta\sigma_T$ values were systematically dependent on the changes of beam position and current, which we found were correlated with the beam spin reversals.

These dependences were removed by regressions against the measured changes in vertical position, horizontal position, and beam current. The remaining small systematic dependences were adequately randomized by the target polarity reversals to produce nearly complete cancellation on averaging the positive- and negative-target polarity data. This procedure was applied to the data from each of the six transmission chambers (each subtending a different solid angle). Coulomb-nuclear interference corrections were applied at each solid angle, and an extrapolation to zero solid angle was made.

The results are tabulated in Table I. The total error is the pure statistical error added in quadrature with the systematic errors in the target polarization, beam polarization, and the target constant, which is the reciprocal of the target density and target length. The last column lists the Coulomb-nuclear interference corrections.

Figure 1 is a plot of $\Delta\sigma_T$ (mb) vs T (MeV), the kinetic energy of the incident proton. All the published data[1-5] in this energy range are plotted. The four experimental groups used a variety of techniques: Rice University at LAMPF (this experiment) used ionization chambers; Rice University at ZGS[1] and Bugg et al.,[2] scintillators; Bystricky et al.,[3] Gray-encoded scintillators with a frozen-spin target; and Ditzler et al.,[4] scintillators with a frozen-spin target. The Rice data indicate a sharper structure at $T = 562$ MeV than that previously observed.

These results were reported at the 1983 meeting of the Division of Particles and Fields, Blacksburg, Virginia. A Ph.D. thesis based on this work is in preparation.

REFERENCES

1. J. D. Lesikar, Ph.D. thesis, 1981.

2. D. V. Bugg et al., TRIUMF Annual Report, June 1983.

3. J. Bystricky et al., preliminary results of $\Delta\sigma_T$ at Saclay, Commissariat a L'Energie Atomique note CEA-N-2276, ISSN 0750-6678, 1980-1981.

4. W. R. Ditzler et al., Phys. Rev. D 27, 680 (1983).

5. R. A. Arndt et al., Phys. Rev. D 28, 97 (1983).

Table I. Summary of Results from LAMPF Exp. 504, a Measurement of the Total Cross-Section Difference ($\Delta\sigma$) for Transversely Polarized Protons. The energies quoted are the laboratory beam energies at the center of the target. The $\Delta\sigma$'s are final values, corrected for Coulomb-Nuclear Interference (CNI). The total error is the pure statistical error added in quadrature with the systematic errors in the target polarization, beam polarization, and target constant C (the reciprocal of the product of the target density and target length). The CNI corrections are tabulated in the last column.

Energy (MeV)	Momentum (GeV/c)	$\Delta\sigma$(mb)	Errors (mb)					
			Total	Statistical	Target Polarization	C	Beam Polarization	CNI
304	0.81	−0.2976	1.0010	0.5486	0.8302	0.1011	0.0404	1.7236
436	1.00	5.8415	0.7296	0.3051	0.6132	0.2334	0.0934	1.1729
485	1.07	8.3381	0.9669	0.2816	0.8375	0.3646	0.1459	1.0452
519	1.12	8.6139	1.1843	0.2106	1.0950	0.3705	0.1482	1.2042
536	1.14	10.4697	0.8767	0.2056	0.6888	0.4661	0.1864	1.1486
571	1.18	12.2696	1.4226	0.2079	1.2698	0.5634	0.2254	1.0014
587	1.20	9.8386	1.2944	0.6410	1.0153	0.4489	0.1796	0.8607
620	1.24	7.8671	0.4935	0.0778	0.3079	0.3507	0.1403	0.8522
637	1.27	7.1526	1.0763	0.2184	0.9954	0.3216	0.1286	0.7207
689	1.33	5.6256	0.5337	0.1191	0.4498	0.2427	0.0971	0.7712
741	1.39	5.6360	0.3122	0.1006	0.1299	0.2464	0.0986	0.7072
791	1.45	5.8884	1.0627	0.1231	1.0177	0.2604	0.1041	0.6809

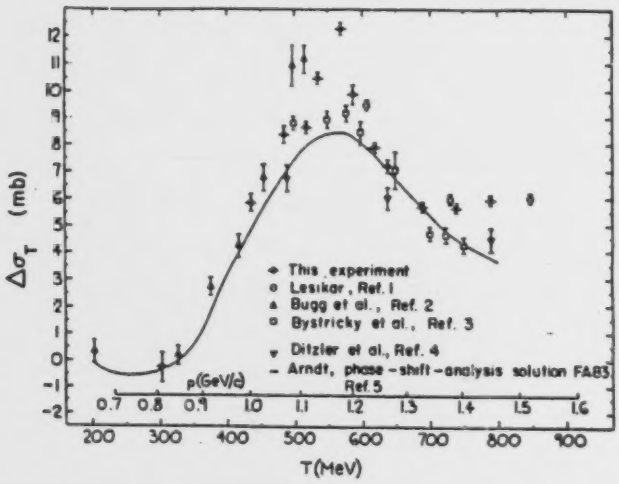

Fig. 1.

Plot of $\Delta\sigma_T$ (mb) vs T (Mev), the kinetic energy of the incident proton. Error bars show statistical errors only.

Measurements of the Spin-Rotation Parameters for $\bar{p}d \rightarrow \bar{p}d$ Elastic Scattering at 496, 647, and 800 MeV

(Exp. 635, EPB)

(Los Alamos, UCLA, Univ. of Texas at Austin, Rice Univ.)

Spokesmen: B. E. Bonner (Los Alamos) and G. J. Igo (UCLA)

This collaboration has completed $\bar{p}d \rightarrow \bar{p}d$ elastic-scattering experiments at 500, 650, and 800 MeV[1-3] at the EPB area. These experiments used a polarized proton beam and an unpolarized liquid-deuterium target, and measure the outgoing proton polarization in the "Janus" polarimeter, which incorporates a carbon analyzer (efficiency ~10%). A two-arm counter system is used to obtain a clean two-body trigger.

A publication is in progress on the 1981 measurements of D_{NN}, D_{SS}, D_{LS}, P, and A_N at 500 and 800 MeV[1] (D is the polarization memory parameter). In 1982 we remeasured the above parameters with a faster data-acquisition system, thereby obtaining smaller statistical errors in addition to measuring D_{SL} and D_{LL} at 500 and 800 MeV. The measurement of L in the final state required a bending magnet to precess the outgoing proton spin direction sideways (S) in order that it be observable; the magnet also serves as an analyzer for momentum.

In August 1983 we measured D_{NN}, D_{SS}, D_{LS}, D_{SL}, D_{LL}, P, and A at 650 MeV for the four-momentum transfer range $-t = 0.4\text{-}1.18$ (GeV/c)^2 (30-60° lab).

All the data taken since September 1982 have been analyzed and a compilation has been submitted to Physical Review C. The EPB experiments complement HRS experiments at smaller angles.

REFERENCES

1. A. Rahbar, Ph.D. thesis, University of California at Los Angeles, 1982, unpublished.

2. Sun Tsu-hsun et al., submitted to Phys. Rev. C.

3. Sun Tsu-hsun et al., in Proc. of the 10th Int. Conf. on Few-Body Problems, Karlsruhe, Germany (1983), p. 233.

Studies of the Spin Dependence of $p \uparrow p \rightarrow \pi X$

(Exp. 336, EPB)

(Rice Univ., Univ. of Houston, Los Alamos)

Spokesmen: G. S. Mutchler (Rice Univ.) and L. S. Pinsky (Univ. of Houston)

Participants: S. D. Baker, J. A. Buchanan, J. M. Clement, M. D. Corcoran, I. M. Duck, M. Furic, G. P. Pepin, G. C. Phillips, E. A. Umland, A. D. Hancock, E. V. Hungerford, B. W. Mayes, Y. Xue, J. C. Allred, T. M. Williams, M. W. McNaughton, and C. Hwang

Analysis of the $pp \rightarrow pp\pi^0$ data from Phase II of this experiment has been completed. In Phase II the spin-dependent cross section $d^3\sigma/dp_1 d\Omega_1 d\Omega_2$ for the reactions $p \uparrow p \rightarrow p\pi^+ n$ and $pp\pi^0$ were measured at EPB at 500 and 647 MeV, along with some repeated measurements at 800 MeV. This was a kinematically complete experiment using a liquid-hydrogen target and a polarized beam. The angles θ_1 and ϕ_1 and momentum p_1 of the proton were measured in a magnetic spectrometer, in coincidence with the angles θ_2 and ϕ_2 of the pion (second proton) in a time-of-flight arm. The data were taken during the summer of 1982.

Of the 17 angle pairs measured in Phase II, 14 have good statistics for the reaction $pp \rightarrow pp\pi^0$. There are six angle pairs at 800 MeV and four each at 500 and 647 MeV. The asymmetries and fifth-order differential cross section $d^3\sigma/dp_1 d\Omega_1 d\Omega_2$ are plotted against p_1, the momentum of the proton in arm 1 in Figs. 1-3. The data appear as dots; errors are small on the scale of the figures.

The solid lines are the predictions of Dubach et al.,[1] who have provided us with their nucleon-nucleon computer code, which incorporates a relativistic, unitary, three-body pion-exchange model. Since the system had a solid-angle acceptance of 9 × 10 sr or more in each arm, it was necessary to average the theoretical predictions over the actual geometry used. The theoretical curves shown in the figures thus have been averaged over the system acceptance using a Monte Carlo program.

Comparison of the data with theory shows excellent agreement at 800 MeV. At lower energies the general shape of the asymmetries is reproduced, but the cross

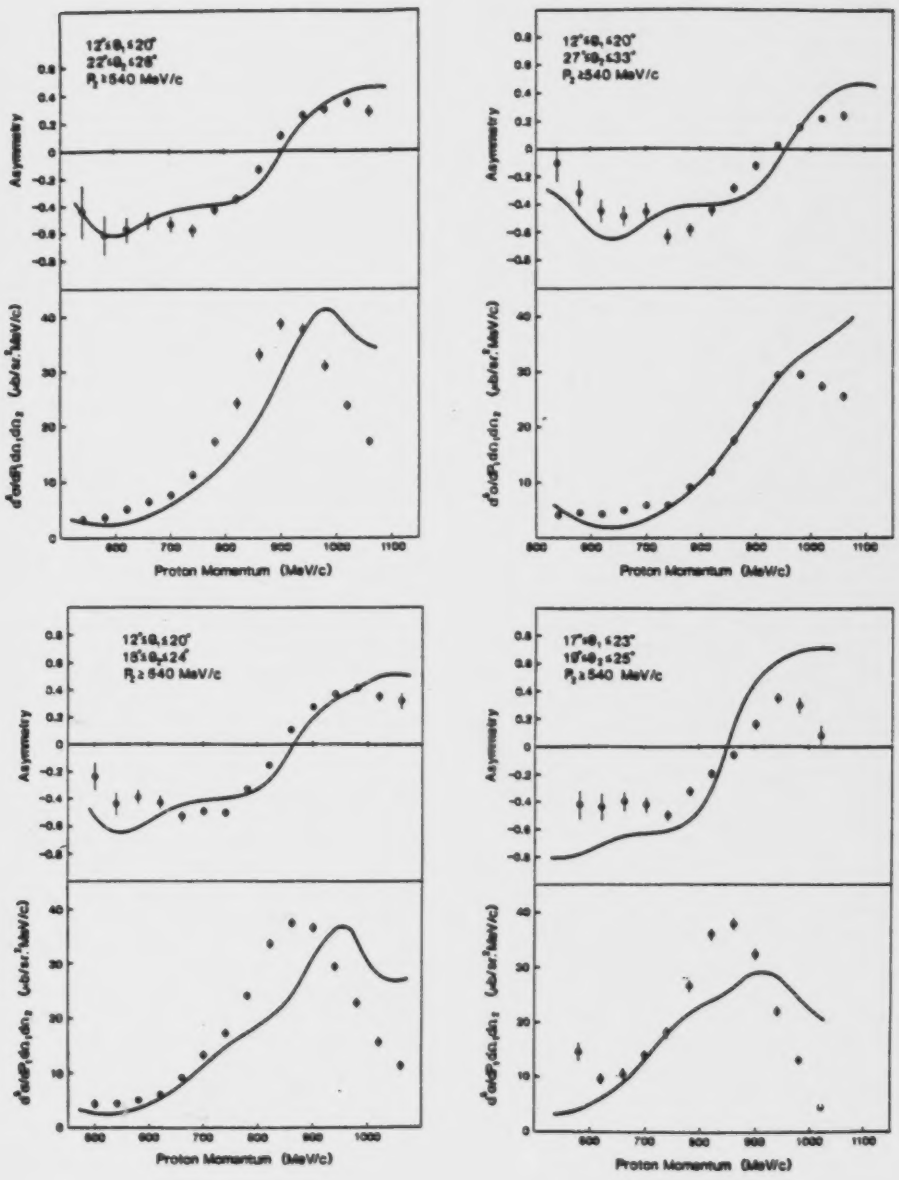

Fig. 1.
Cross sections and asymmetries $p \uparrow p \rightarrow pp\pi^0$ at 800 MeV.

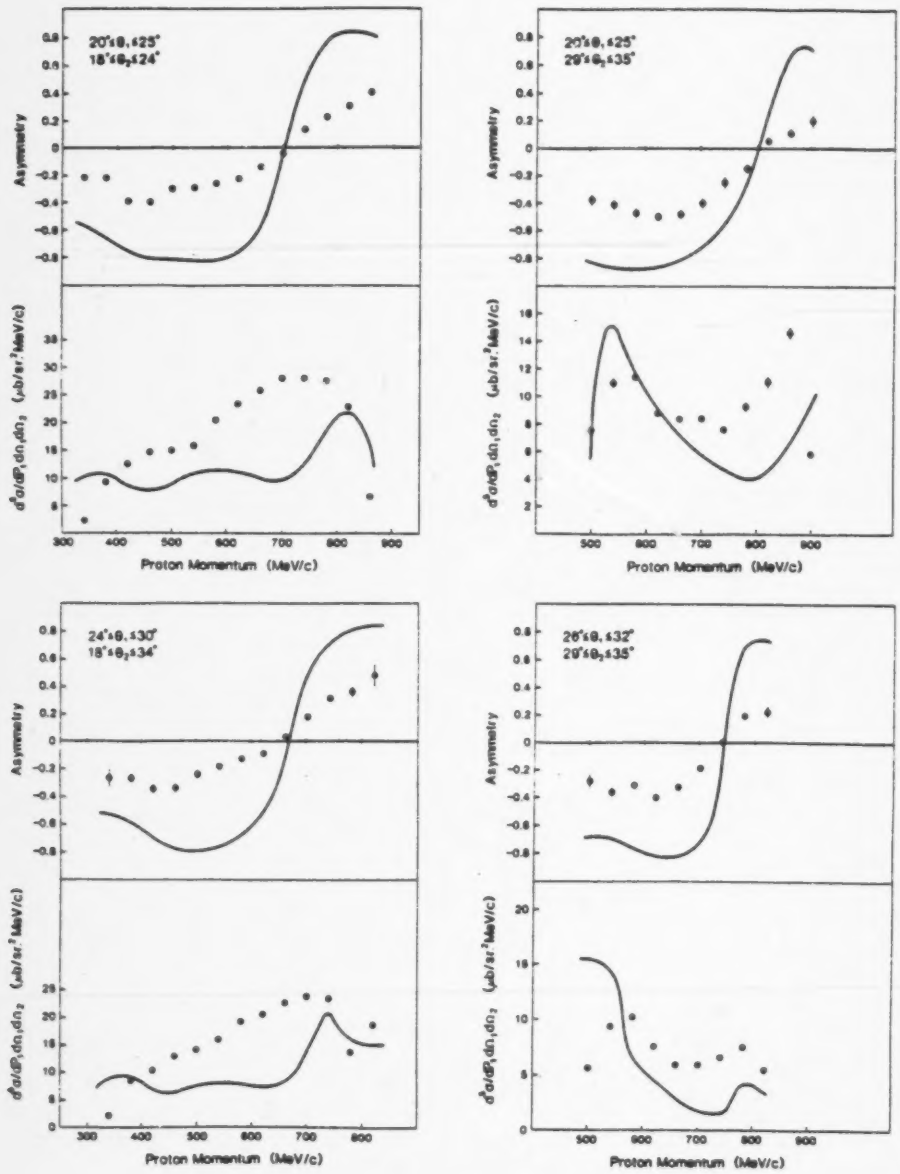

Fig. 2.
Cross sections and asymmetries $p \uparrow p \rightarrow pp\pi^0$ at 647 MeV.

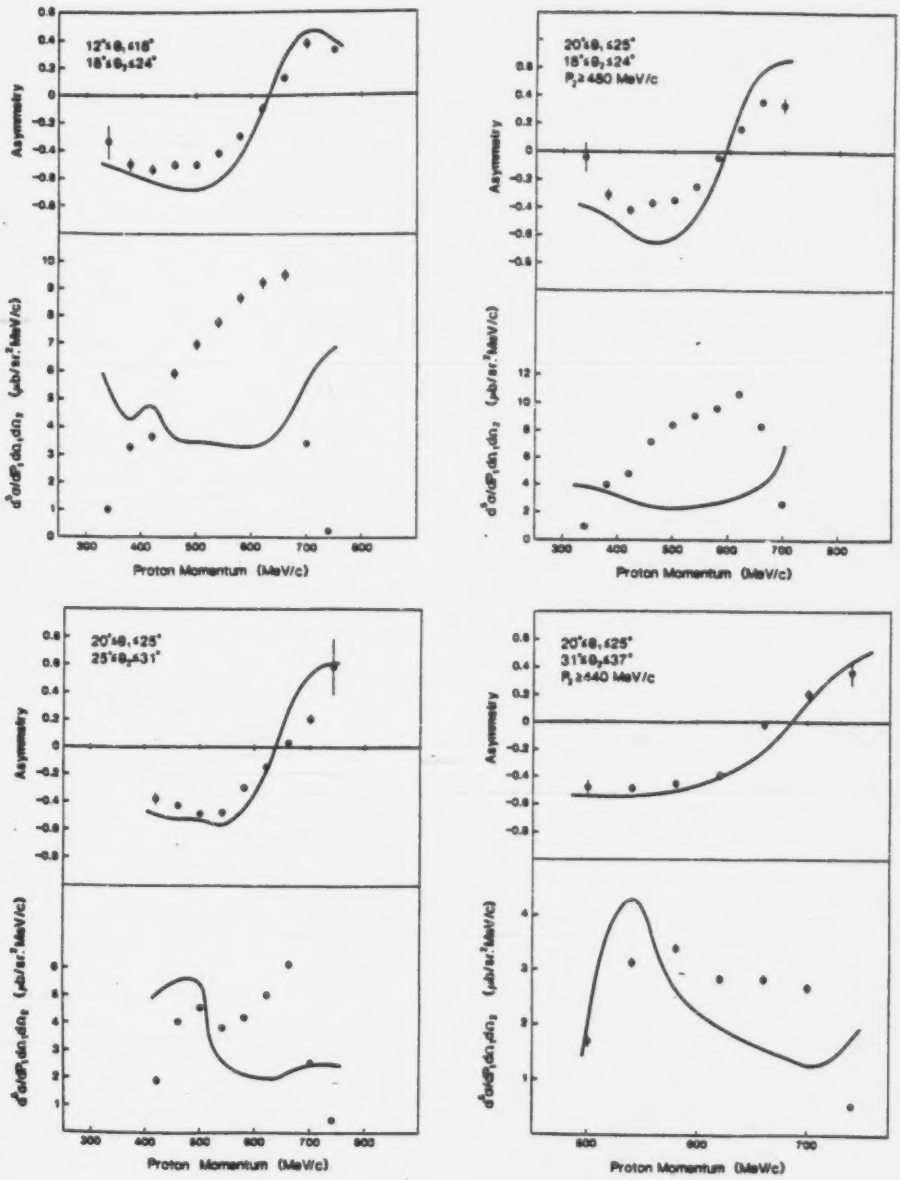

Fig. 3.
Cross sections and asymmetries $p \uparrow p \rightarrow pp\pi^0$ at 500 MeV.

sections are underestimated, with the discrepancy getting worse at the lower energy.

Preliminary results of this work were presented in April at the American Physical Society meetings in Baltimore.

REFERENCE

1. J. Dubach, W. M. Kloet, A. Cass, and R. R. Silbar, Phys. Lett. 106B, 29 (1981), and J. Phys. C (Nucl. Phys.) 8, 475 (1982); and W. M. Kloet and R. R. Silbar, "Nucleus-Nucleon Dynamics at Medium Energies" (I and II), Nucl. Phys. A 338, 231 (1980).

Measurement of Parity Violation in the *pp* and *p*-Nucleus Total Cross Sections at 800 MeV (Exp. 792, EPB)

(Los Alamos, Univ. of Illinois, Princeton Univ., Univ. of Maryland)

Spokesman: V. Yuan (Los Alamos)

Participants: J. D. Bowman, R. Carlini, D. MacArthur, R. E. Mischke, D. E. Nagle, H. Frauenfelder, R. W. Harper, A. B. McDonald, and R. L. Talaga

The goal of Exp. 792 is to measure the contribution of the weak force to nucleon-nucleon scattering at 800 MeV. Although the scattering is dominated by strong and electromagnetic interactions, the weak interaction may be identified by the signature of parity violation.

In the experiment, longitudinally polarized protons are scattered from an unpolarized target; parity violation manifests itself as a small helicity dependence in the total cross section. A longitudinal asymmetry can be defined as $A_L = (\sigma_+ - \sigma_-)/(\sigma_+ + \sigma_-)$, where $\sigma_+(\sigma_-)$ is the total cross section for positive- (negative-) helicity protons on the target.

Experiment 792 was active for two run periods during the second half of 1983: a 1-week run in August, which served as a tuneup to test several important improvements to the experiment, was followed by a 2-week-long data run in November with a liquid-hydrogen target. In the November run a statistical sensitivity in A_L of 1.5×10^{-7} was achieved.

This experiment is one of a series to measure the contribution of the weak force to nucleon-nucleon scattering as a function of energy. At 15 and 45 MeV, the experiments[1-3] yield $A_L = -(1.7 \pm 0.8) \times 10^{-7}$ and $A_L = -(3.2 \pm 1.1) \times 10^{-7}$, respectively, in good agreement with theoretical predictions based on a meson-exchange model[4-6] and a hybrid quark model.[7] In contrast, for 6-GeV/c protons on a water target, a value of $A_L = (2.65 \pm 0.60) \times 10^{-6}$ has been reported.[8] This value is larger than the meson-exchange prediction by more than an order of magnitude.[9] It is in agreement, however, with recent calculations that treat wave-function renormalization[10] and the parity-violating effects of the quark constituents of nucleons.[11]

The basic experimental layout is shown in Fig. 1. The experiment uses the LAMPF polarized proton beam at an intermediate energy of 800 MeV, with polarization reversed at a rate of 30 Hz at the injector. Two low-noise ion chambers[12] determine the cross section by measuring the transmission of the polarized beam incident on the target. By analyzing the signal for a component correlated with the 30-Hz polarization-reversal frequency, we can determine the magnitude of any helicity dependence of the total cross section. Auxiliary detectors monitor 30-Hz changes in beam properties that may

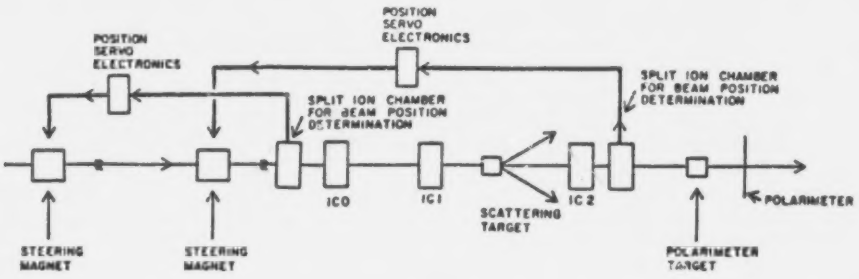

Fig. 1.
Schematic of experimental apparatus.

Table I. Results for November 1983 Run.

	Data	A_L	Chi-Squared	Number of Runs
Normal	Raw	$(-1.9 \pm 1.7) \times 10^{-7}$	79.5	74
	Corrected	$(0.3 \pm 2.1) \times 10^{-7}$	64.4	74
Reverse	Raw	$(-7.2 \pm 1.6) \times 10^{-7}$	200.0	83
	Corrected	$(-2.1 \pm 1.9) \times 10^{-7}$	85.6	83

Combined Result $\left(\frac{NN - RR}{2}\right)$: $A_L = (1.2 \pm 1.4) \times 10^{-7}$.

mimic a true parity-violation signal. The beam properties monitored include intensity modulation, position motion, residual transverse polarization, and a phase-space distribution of residual transverse polarization across the profile of the beam.

In August 1983 we implemented and tested two important improvements to the experiment. The first was to supplement our split-foil position monitors with new position/size detectors of multiwire design. Not only did we obtain pulse-by-pulse information on beam size for the first time, but we were able to calculate beam position in a way that takes the beam spot size into account. The second improvement was to use the EPB precessor to provide longitudinal polarization in EPB. In the November data run that followed, this change greatly improved the compatibility of Exp. 792 with other experiments running concurrently in Line C.

Following the successful conclusion of the August tests, an extensive data run on hydrogen was undertaken in November. In this run, a third important improvement was introduced: a rotating stripper wheel that gave a better measurement of our sensitivity to intensity modulation. With proper synchronization of the rotating wheel, the effects of intensity changes correlated to the polarization reversal could, for the first time, be examined directly.

Sufficient LH_2 data were taken in the November run to reach a statistical error limit of 1.5×10^{-7} in A_L for hydrogen. As had been done in the past, equal amounts of data were taken in both the "normal" and "reverse" configurations of the polarized source. By using the dual source configurations, we can measure and remove systematic contributions not included in the corrections that are applied for systematics of known origin.

Obtaining final results for the November run is under way, but awaits completion of a careful determination of systematic corrections. However, an initial estimate of the asymmetry has been made, based on a rough calculation of the systematic corrections.

Table I shows the results for "normal" and "reverse"; the combined value is $A_L = (1.2 \pm 1.4) \times 10^{-7}$. Such a value is consistent with predictions for 800 MeV based on the meson-exchange[9] and hybrid quark[7] models. It disagrees, however, with the large value predicted by the wave-function-effect analysis of Nardulli et al.[13] We point out that all errors quoted are based only on statistical uncertainties and do not include any nonstatistical contributions.

Systematic corrections used in the calculation of A_L are listed in Table II. The nonstatistical uncertainties in the determination of systematic corrections are estimated to be 10-15% as large as those corrections.

Table II. Systematic Contributions to A_L.

Quantity	Source	Contribution to A_L
Intensity	Normal	-3.7×10^{-7}
	Reverse	-7.0×10^{-7}
Position	Normal	1.6×10^{-7}
	Reverse	1.3×10^{-7}
Polarization		$\leq 9 \times 10^{-8}$

REFERENCES

1. D. E. Nagle et al., in *High Energy Physics with Polarized Beams and Targets*, G. H. Thomas, Ed., AIP Conf. Proc. 51, 224 (1978).
2. R. Balzer et al., Phys. Rev. Lett. 44, 699 (1980).
3. M. Simonius, in *High Energy Physics with Polarized Beams and Targets*, C. Joseph and J. Soffer, Eds., Experientia, Suppl. No. 38 (International Symposium, Lausanne, 1980), p. 355.
4. V. R. Brown, E. M. Henley, and F. R. Krejs, Phys. Rev. C 9, 935 (1974).
5. M. Simonius, Nucl. Phys. A 220, 269 (1974).
6. B. Desplanques, J. F. Donoghue, and B. R. Holstein, Ann. Phys. 124, 449 (1980).
7. L. S. Kisslinger and G. A. Miller, Phys. Rev. C 27, 1602 (1983).
8. N. Lockyer et al., Phys. Rev. Lett. 45, 1821 (1980).
9. E. M. Henley and F. R. Krejs, Phys. Rev. D 11, 605 (1975).
10. G. Nardulli and G. Preparata, Phys. Lett. 117B, 445 (1982).
11. T. Goldman and D. Preston, Nucl. Phys. B 217, 61 (1983).
12. J. D. Bowman et al., Nucl. Instrum. Methods 216, 399 (1983).
13. G. Nardulli, E. Scrimeri, and J. Soffer, Centre de Physique Théorique, CRNS, Marseille, France, preprint CPT-82, p. 1420 (to be published in Z. Phys. Chem.).

Inelastic Pion Scattering from ^{17}O and ^{18}O (Exp. 369, EPICS)

(Univ. of Minnesota)

Spokesman: D. Dehnhard (Univ. of Minnesota)

The analysis of data taken during Exp. 369 has been completed and a manuscript is being prepared for publication. The π^+ and π^- scattering cross sections were measured on ^{17}O, using version I of the EPICS cooled-gas target. Because the gas was made up of ≃50% ^{17}O, 25% ^{18}O, and 25% ^{16}O, extensive ^{18}O runs were made for background subtraction. Here, we report on some of the results of the analysis of the ^{17}O and ^{18}O data.

Octupole transitions in ^{17}O had been studied before by inelastic electron scattering[1,2] and the strength had followed approximately the rules of a weak-coupling model assuming a

$$\left[^{16}\mathrm{O}(3^-) \times 1d^n_{5/2}\right]_{J^\pi = (\frac{1}{2})^- \ldots (^{11}/_2)^-}$$

multiplet.

In this work the angular distributions (Fig. 1) for the 4.55-MeV $[(\frac{1}{2})^-]$, 3.85-MeV $[(\frac{1}{2})^-]$, 5.69-MeV $[(\frac{5}{2})^-]$, 5.22-MeV $[(\frac{5}{2})^-]$, and 7.76-MeV $[(^{11}/_2)^-]$ states in ^{17}O closely resemble those of the 3^- states in ^{16}O (6.13 MeV) and ^{18}O (5.09 MeV), even though the transitions in ^{17}O can proceed by other than the total angular momentum transfer $J = 3$, as in ^{16}O and ^{18}O. For example, the $(\frac{7}{2})^-$ state can be reached by $J = 1$, 2, 3, 4, 5, and 6. Nevertheless, judging by the similarity of all angular distributions, the contributions with $J \neq 3$ appear to be not very important for these states in ^{17}O. An exception might be the $(\frac{1}{2})^-$ state, for which $J = 1$ is predicted to be quite important, but the data are not sufficiently good to extract the relative contributions from $J = 1$ and 3. [No cross sections could be extracted for the very weakly excited $(\frac{1}{2})^-$ state.]

If we compare the relative cross section for these transitions with the prediction of the simple version of the $[3^- \times 1d^n_{5/2}]$ model (that is, without proper antisymmetrization), we find that the octupole strength is not split among the states according to this model. For instance, for the $(^{11}/_2)^-$state we observe only about 50% of the predicted strength (Table I).

To analyze the data in the distorted-wave impulse approximation (DWIA), calculations were done with the code ARPIN.[3] Microscopic transition densitites from three different models were used. Here, we report the results that were obtained using the large-space shell-model

Table I. Renormalization factor $R^\pm = \sigma^\pm_{\mathrm{exp}}/\sigma^\pm_{\mathrm{DWIA}}$ at $\theta_{\mathrm{c.m.}} = 44°$ for Octupole Transitions in ^{17}O and ^{16}O Calculated Without ($\delta = 0$) and With ($\delta = 0.6$) Polarization Charges.

			($\delta = 0$)		($\delta = 0.6$)	
	J_f	E_x (MeV)	R^+	R^-	R^+	R^-
	$(^{11}/_2)^-$	7.76	3.5	8.0	1.0	1.2
	$(\frac{5}{2})^-$	5.22	6.0	12.0	1.1	1.0
^{17}O	$(\frac{5}{2})^-$	5.69	10.0	9.0	1.2	1.0
	$(\frac{1}{2})^-$	3.84	3.5	2.5	0.8	0.8
	$(\frac{1}{2})^-$	4.55	5.0	4.5	1.1	0.9
^{16}O	3^-	6.13	4.0	4.0	1.0	1.0

calculations.[6] Both the $1p \rightarrow 2s1d$ and $2s1d \rightarrow 1f2p$ excitation amplitudes are included for the transitions to low-lying negative-parity states in ^{17}O and ^{18}O. The DWIA curves for ^{17}O (π,π'), with these transition densities and without any effective charge enhancements, are shown in Fig. 1 as broken lines.

For all states, the predicted cross sections are significantly smaller than the data because these transitions are collectively enhanced. The ratios of experimental and theoretical cross sections, $R^{\pm} = \sigma^{\pm}_{\rm exp}/\sigma^{\pm}_{\rm DWIA}$, are given in Table I, columns 2 and 3. Clearly, there is no systematic behavior in R. Next, the $\{LSJ\} = \{303\}$ parts of the neutron and proton transition densities ρ_n and ρ_p were multiplied by enhancement factors E_n and E_p, respectively—that is, $\rho_n' = E_n\rho_n$ and $\rho_p' = E_p\rho_p$. (Here, L, S, and J are, respectively, the transferred orbital, spin, and total angular momenta.) This calculation has been done in Ref. 3 for the $\{202\}$ parts of the $L = 2$ transitions in the p shell. For the $(^{11}/_{2})^-$ state, we found that $E_n = 4.7$ and $E_p = 1.7$ are needed to fit the data. For the other states, very different factors were necessary, which makes this approach quite unattractive. Similar erratic behavior in the enhancement factor was found for the $[3^- \times 1d^0_{5/2}]$ model, even when the wave functions were properly antisymmetrized.

A consistent description of the data was obtained by enhancing only the isoscalar, spin-independent part of the transition density. Use of $\delta_n = \delta_p = 0.6$, or equivalently $\delta_0 = 1.2$ and $\delta_1 = 0$, resulted in the absolute cross sections shown as solid lines in Fig. 1. The ratios are now strikingly close to 1. The same isoscalar enhancement factor $(1 + \delta_0) = 2.2$ gave a good fit to the pion data for ^{16}O $(3^-, 6.13$ MeV).

We have used the same parameters for the DWIA analysis as in Ref. 4. The oscillator parameter, $b = 1.63$ fm, is smaller than the value ($b = 1.76 - 1.78$ fm) needed to fit the ground-state densities of ^{17}O (Refs. 1 and 3). Using $b = 1.76$ fm results in smaller polarization charges, slightly larger π^+/π^- asymmetries, and a slight shift of the angular distribution toward smaller angles—that is, the fit to the pion data is not as good as with $b = 1.63$ fm. It is worth mentioning that $b = 1.63$ fm and $\delta_p = \delta_n = 0.6$ give good agreement (just as $b = 1.76$ and $\delta_p = \delta_n = 0.35$ do) between the large-space shell-model calculations and the experimental $B(E3)$ values. An exception is the value for the $(\frac{11}{2})^-$ state, for which the (e,e') data[1] are suspect.

[6]The large-space shell-model calculations used in this experiment are from D. J. Millener, private communication.

Cross sections for ^{18}O(π,π') were extracted for the first three 2^+ (1.98-, 3.92-, and 5.26-MeV) states, the 1^- (4.45-MeV) state, and the 3^- (5.10-MeV) state. In the previous ^{18}O experiment,[5] cross sections for the second and third 2^+ states could not be extracted because of poor energy resolution. Figure 2 shows the π^+ and π^- data for the three lowest 2^+ states. The ratio $R = \sigma(\pi^-)/\sigma(\pi^+) = 2.1$ for the 2^+ (1.98-MeV) state is consistent with that previously measured for this transition by Iversen et al.[5] For the second 2^+ (3.92-MeV) state, the π^+ and π^- cross sections are more nearly equal, $R = 1.27$. The third 2^+ (5.26-MeV) state is somewhat surprising in that the cross section is much larger than most models predict for ^{18}O wave functions and there is a large π^+ enhancement, $R = 0.2$.

The π^+ and π^- cross sections for the 3^- state at 5.10 MeV are essentially equal. The dashed curves are DWIA calculations using the transition densities of the full $1\hbar\omega$ shell-model calculations of Millener. The predicted cross sections are too small, and the π^+/π^- asymmetry is not observed in the data. The data can be reproduced by enhancing the isoscalar $J(LS) = 3(30)$ amplitude by a factor of 2 and completely omitting the isovector amplitude. This implies a very large neutron polarization change, which indicates a lack of understanding of the neutron components in the wave function of ^{18}O.

The data obtained for the 1^- state at 4.45 MeV were initially very surprising. The π^+ and π^- angular distributions are very similar, with the π^+ being slightly larger than the π^-. The angular-distribution shapes are completely out of phase with calculations using simple single particle-hole transition densities, such as $1p_{1/2} \rightarrow 2s_{1/2}$ or $1p_{3/2} \rightarrow 1d_{3/2}$. The DWIA calculations, using one-body density-matrix elements (from shell-model calculations) as transition densities,[4] produce angular-distribution shapes closer to that of the data. The magnitudes for both π^+ and π^- are more than an order of magnitude smaller than the data [Fig. 3(a) and (b)].

The two calculations use the full $1\hbar\omega$ shell-model calculation of Millener (solid curve) and the *p-sd* calculations of Brown.[6] The addition of the *sd-fp* components in the full $1\hbar\omega$ calculation decreased the large ratio $\sigma(\pi^+)/\sigma(\pi^-)$, but it is still much larger than experimentally observed. It should be noted that a calculation using an ^{16}O shell-model calculation that included core polarization in pertubation theory produces agreement with the data for both the ^{18}O, 1^- (4.45-MeV) and ^{16}O, 1^- (7.12-MeV) states.

[6]B. A. Brown, private communication.

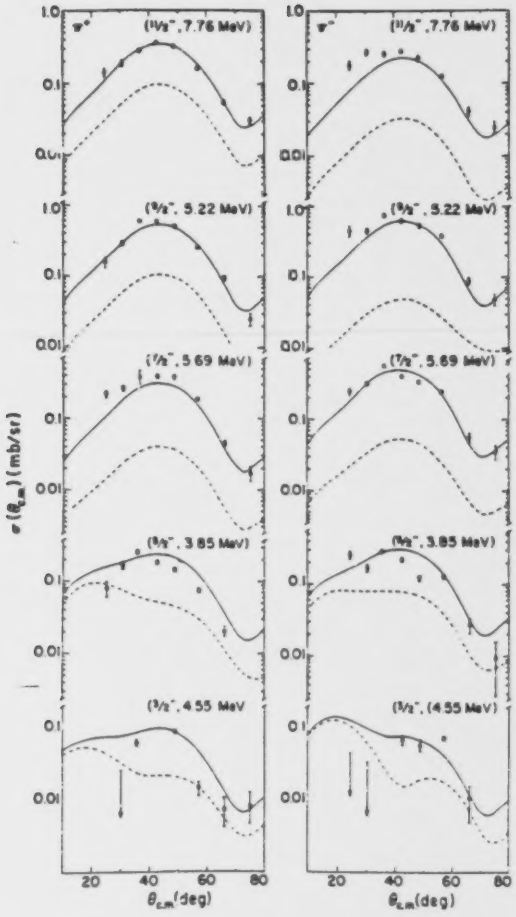

Fig. 1.
Angular distributions for states in ^{17}O. The curves are DWIA calculations with (solid-line) and without (broken-line) effective charge enhancements.

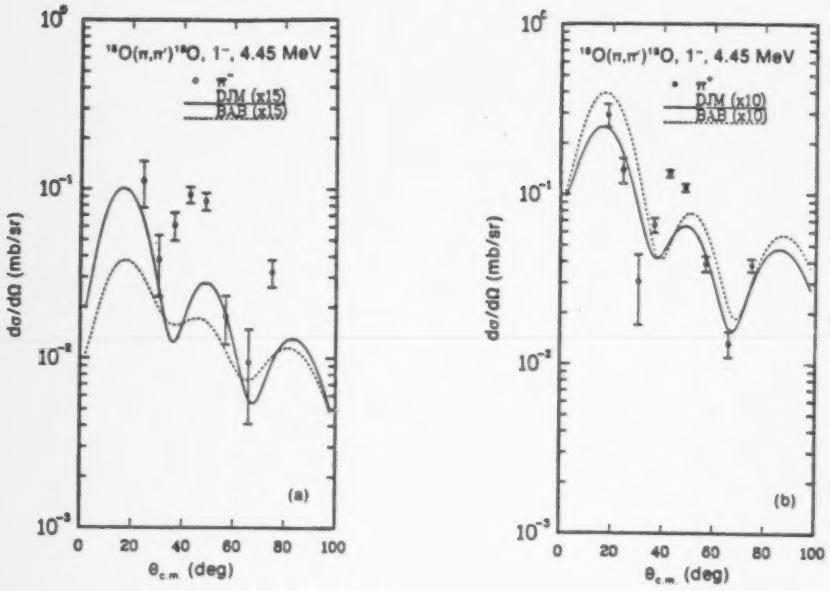

Fig. 3(a) and (b).
Angular distributions for the 1^- state in ^{18}O for (a)π^- and (b) π^+ scattering. The curves are described in the text.

REFERENCES

1. J. C. Kim et al., Phys. Lett. 57B, 341 (1975), and Nucl. Phys. A 297, 301 (1978).

2. J. Kelly et al., Bull. Am. Phys. Soc. 25, 575 (1980).

3. T.-S. H. Lee and D. Kurath, Phys. Rev. C 21, 293 (1980).

4. T.-S. H. Lee and R. D. Lawson, Phys. Rev. C 21, 679 (1980).

5. S. Iverson et al., Phys. Rev. Lett. 40, 227 (1978).

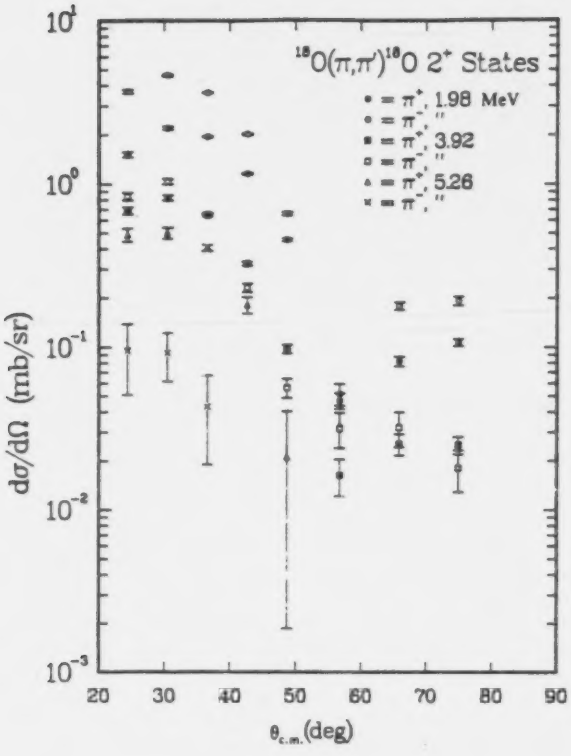

Fig. 2.
Angular distributions for the three lowest 2$^+$ states in ^{18}O.

Excitation of 8⁻ States in ^{54}Fe (Exp. 565, EPICS)

(Argonne National Lab.; Univ. of Birmingham, United Kingdom; Indiana Univ.; New Mexico State Univ; Los Alamos; Univ. of Massachusetts; Montana State Univ.; Northwestern Univ.; Oregon State Univ.)
Spokesman: B. Zeidman (Argonne National Lab.)

We have investigated the excitation of 8⁻ states in ^{54}Fe with 162-MeV pions at EPICS. At large momentum transfer, such high-spin particle-hole (stretched) states are selectively excited in pion inelastic scattering.[1] By combining the analysis of the pion data and previously published electron data, isoscalar and isovector transition strengths were extracted for each 8⁻ state.

The selectivity of pion inelastic scattering for isoscalar spin-flip strength is particularly valuable because no other probe shares this selectivity. This fact makes pion scattering a natural complement to 180° electron scattering, which selectively excites isovector spin-flip states.

With the ^{54}Fe results obtained in this work, it is clear that in high-spin particle-hole states much less isoscalar spin-flip strength has been identified than isovector spin-flip strength. This phenomenon persists from *p*-shell nuclei, at least up to the middle of the *f*-*p* shell. It is already well known that the isovector spin-flip strength to such high-spin states is only 30-50% of simple single-particle estimates.[2] This amount of quenching also has been observed for Gamow-Teller resonances ($L = 0$, isovector spin-flip excitations),* where it has been interpreted as evidence for non-nucleonic degrees of freedom, and in particular isobar-hole states.[4] Since non-nucleonic degrees of freedom contribute only weakly to isoscalar excitations, the large unexplained relative quenching of the isoscalar strength compared to the isovector strength implies that the nuclear-structure input must be examined more critically for both modes of the nuclear response.

The experiment was carried out on the EPICS channel and spectrometer system. A large (10- by 20-cm) isotopically enriched (>97%, ^{54}Fe, 151-mg/cm^2) target was used. Spectra with π^+ were accumulated in 10° steps from 40 to 100°; π^- spectra were accumulated at 70, 80, and 90°. Short runs were taken at 5° intervals to establish the elastic-scattering yields. The channel and spectrometer were used in the conventional fashion. In addition to the 8⁻ states at 8.31, 8.95, 9.97, 10.68, and 13.26 MeV identified in electron scattering, two new 8⁻ states at 9.80 ± 0.05 and 11.65 ± 0.05 MeV excitation were observed.

The inelastic yields to the different 8⁻ states differ greatly for π^+ and π^-. This difference is the result of interference of isoscalar and isovector amplitudes, since for a transition with a pure isospin structure (either pure $\Delta T = 0$ or pure $\Delta T = 1$) the π^+ and π^- yields must be equal, as they are for the 13.26-MeV $T = 2$ state. By combining the pion data with the electron inelastic-scattering results,[5] it is possible to separate the isospin amplitudes for each state. The experimental cross sections and $B(M8)$ satisfy the following relations for each state f:

$$\sigma^f_{\pi^-}(\theta) = [Z^f_0 M^{-}_0(\theta) + Z^f_1 M^{-}_1(\theta)]^2 ,$$

$$\sigma^f_{\pi^+}(\theta) = [Z^f_0 M^{-}_0(\theta) - Z^f_1 M^{-}_1(\theta)]^2 ,$$

$$B^f(M8)_e = (Z^f_0 M^{+}_0 + Z^f_1 M^{+}_1)^2 .$$

In these equations, M^+_0 (M^+_1) is the square root of the cross section for exciting an isoscalar (isovector) transition to a pure one-particle one-hole state in a closed-shell nucleus by π^- inelastic scattering. The M^+_0 and M^+_1 are similar amplitudes $[B(M8)]^{1/2}$ for electron inelastic scattering. The coefficients Z_0 and Z_1 contain the nuclear-structure amplitudes of isoscalar and isovector excitation of each state. The reaction dynamics is contained in the M factors, which can be obtained from distorted-wave impulse approximation (DWIA) calculations. Based on the free-nucleon properties,

$$M^-_0 \approx 2M^-_1 ,$$

$$M^+_0 = \left(\frac{\mu_n + \mu_p}{\mu_n - \mu_p}\right) M^+_1 = -0.187\ M^+_1 ,$$

where μ_n and μ_p are the neutron and proton magnetic moments, respectively.

For electron scattering, the absolute values of M^+_0 and M^+_1 can be obtained from DWIA. However, the uncertainties in the reaction dynamics make the DWIA calculation of the absolute values of M^+_0 and M^+_1 more

*See, for example, Ref. 3 and references therein.

uncertain. To avoid this uncertainty, M_0^π can be obtained for the $T = 2$ state, since Z_1 is determined by the electron-scattering data. Then, only the ratio M_0^π/M_1^π need be extracted from the DWIA calculations.

This procedure renders the results insensitive to the exact choice of the radial form factor or the pion optical potential. Because the ratio of isoscalar to isovector cross sections is determined essentially by an isospin Clebsch-Gordan coefficient, it is not expected to be sensitive to the reaction dynamics. This is particularly true for high-spin states where the transition density is surface localized. Recent calculations indicate that although medium corrections may modify the ratio of M_0^π/M_1^π for low-spin states, they have little effect for high-spin states, thereby supporting the procedure used here. It should also be noted that in the few cases where the isoscalar pion results have been checked with proton inelastic scattering, the results have agreed very well,[2] although there are considerable uncertainties in the reaction dynamics in the proton case.[6]

The structure coefficients Z_0 and Z_1 for each 8^- state are tabulated in Table I. For comparison, the coefficients obtained in a $[(f_{7/2}^{-2}) \times g_{9/2}]_{8^-}$ calculation are also given. In this model space, the structure coefficients satisfy a sum rule — that is,

$$\sum_i (Z_0^i)^2 = \frac{7}{8}$$

and

$$\sum_i (Z_1^i) = \frac{7}{8} .$$

The isovector strength can be further subdivided into strength in $T = 2$ states,

Table I. Isospin Amplitudes for ^{54}Fe 8^- States.

Experiment			Theory[a]		
Excitation Energy	Z_0	Z_1	Excitation Energy	Z_0	Z_1
8.31	$0.12 \pm {0.02 \atop 0.04}$	0.24 ± 0.02	8.31	0.336	0.444
8.95	0.02 ± 0.04	0.20 ± 0.04			
9.80	$0.16 \pm {0.02 \atop 0.04}$	0.04 ± 0.04	9.58	0.226	0.193
9.97	0.08 ± 0.04	-0.20 ± 0.02	10.37	0.312	−0.349
			10.80	0.204	0.202
10.68	$0.20 \pm {0.04 \atop 0.02}$	-0.14 ± 0.04	11.014	0.432	−0.192
11.65	$0.12 \pm {0.03 \atop 0.06}$	0.04 ± 0.08	11.57	0.353	0.125
			11.98	0.380	0.064
13.26	0	0.44 ± 0.02	13.26	0	0.601
$\sum_i Z^2$	0.102	0.354		0.759	0.815
$1p$-$3h$ sum rule	0.875	0.875			
Fraction of $1p$-$3h$ sum	12%	40%			

[a]Only the eight states with the largest expected cross sections in pion or electron inelastic scattering are listed.

$$\sum_i (Z_i')^2 = \frac{3}{8}$$

and $T = 1$ states,

$$\sum_i (Z_i')^2 = \frac{4}{8} .$$

The sum of the experimental isoscalar strength is only 12% of this limit, and the sum of the isovector strength is only 40% of this extreme three-hole one-particle calculation.

It is significant that the quenching of the particle-hole strengths is similar to the values obtained in other nuclei for high-spin particle-hole states. The ratio of the summed isoscalar strength to the summed isovector strength for all cases of stretched particle-hole states, where information on the isoscalar strength exists, exhibits a consistent trend in which the isoscalar strength is more strongly quenched than the isovector strength. (A stretched state is one that has the maximum angular momentum available for a $1\hbar\omega$ excitation—that is, 4^- in the $0p$ shell, 6^- in the $1s$-$0d$ shell, and 8^- in the $0f$-$1p$ shell.) The present data therefore give a clear indication that the strong quenching of isoscalar spin-flip strength is a rather general phenomenon.

In summary, data for pion inelastic scattering to 8^- levels in ^{54}Fe have been presented. By combining these data with previous electron-scattering data, isoscalar and isovector transition amplitudes were extracted for each 8^- state. Only 12% of the simple one-particle three-hole strength was observed for the isoscalar excitations, and only 40% of the one-particle three-hole strength was observed for the isovector excitations. This stronger quenching of the isoscalar spin-flip strength compared to the isovector strength appears to be a general feature for high-spin particle-hole states; the present case represents the heaviest nucleus where such an isospin decomposition has been done thus far.

REFERENCES

1. C. Olmer, B. Zeidman, D. F. Geesaman, T.-S. H. Lee, R. E. Segel, L. W. Swenson, R. L. Boudrie, G. S. Blanpied, H. A. Thiessen, C. L. Morris, and R. E. Anderson, Phys. Rev. Lett. 43, 612 (1979).

2. R. A. Lindgren, W. J. Gerace, A. D. Bacher, W. G. Love, and F. Petrovich, Phys. Rev. Lett. 42, 1524 (1979).

3. C. Goodman, Nucl. Phys. A 374, 241c (1982).

4. M. Ericson, A. Figureau, and C. Thevenot, Phys. Lett. 45B, 19 (1973); E. Oset and M. Rho, Phys. Rev. Lett. 42, 47 (1979); A. Bohr and B. Mottelson, Phys. Lett. 100B, 10 (1981); and R. D. Lawson, Phys. Lett. 125B, 255 (1983).

5. R. A. Lindgren, J. B. Flanz, R. S. Hicks, B. Parker, G. A. Peterson, R. D. Lawson, W. Teeters, C. F. Williamson, S. Kowalski, and X. K. Maruyama, Phys. Rev. Lett. 46, 706 (1981).

6. C. Olmer et al., to be published in Phys. Rev. C.

Inelastic Pion Scattering from ^{24}Mg and ^{26}Mg: The New Year's Experiment (Exp. 573, EPICS)

(Univ. of South Carolina, Univ. of Texas, Univ. of Pennsylvania, Los Alamos, Drexel Univ., Univ. of Massachusetts)

Spokesman: G. Blanpied (Univ. of South Carolina)

This experiment first ran at EPICS during New Year's Day 1983, using about one-half of the allotted time. The second half is scheduled for New Year's, 1984.

In the first run, π^+ and π^- data were taken on ^{24}Mg at three energies. Angles were chosen to provide steps of momentum transfer $\hbar \sim qR$, where R was determined by the ratio $A^{1/3}$ for ^{28}Si and compared with π^+ data on ^{28}Si (Refs. 1-3). Data were obtained at scattering angles corresponding to $qR \sim 2$, 3, 4, and 6 at 116 and 292 MeV, and $qR \sim$ 2-8 at 180 MeV, where $R \sim 3.3$ fm. Inelastic spectra up to an excitation of more than 20 MeV were acquired with a resolution of better than 250 keV at most angles. The normalization was done relative to $\pi^{\pm}p$ scattering. Of interest is the comparison of the relative π^-/π^+ strengths for the excitation of $J^\pi = 2^+$, 3^-, and 4^+ collective states to shell-model predictions.

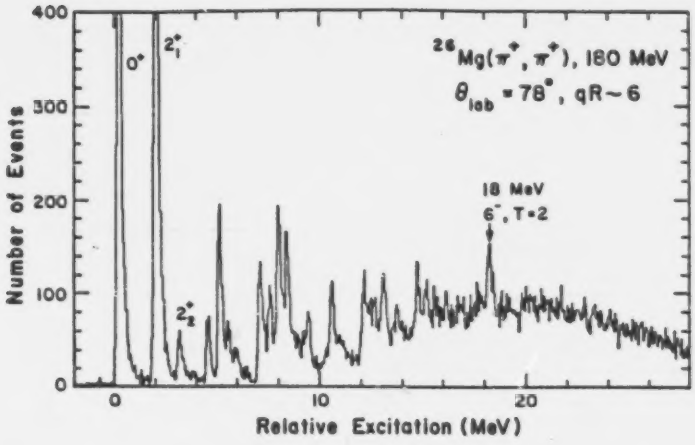

Fig. 1.
Spectrum of π^+ scattering from ^{26}Mg at a laboratory angle of 78° where the momentum transfer is relatively large.

Seen in the π^+ spectrum (Fig. 1), obtained at an angle corresponding to $qR \sim 6$, is the (6^-, $T=2$) state at 18 MeV. This state also has been seen in 180° electron scattering[4] at Bates and with (p,p') at the Indiana University Cyclotron Facility (IUCF).* The π^+ and π^- cross sections are approximately equal, as expected for a pure isovector transition, and are equal to 11 μb/sr at the peak. The same cross section for the ($T=1$, 6^-) state in ^{28}Si excited by 162-MeV pions was observed to be 24 μb/sr (Ref. 2).

*D. F. Geesaman et al., Ref. 5, and private communication.

REFERENCES

1. B. M. Preedom et al., Nucl. Phys. A 236, 385 (1979).

2. C. Olmer et al., Phys. Rev. Lett. 43, 612 (1979).

3. B. Zeidman et al., Phys. Rev. Lett. 40, 1539 (1978).

4. R. A. Lindgren et al., Bull. Am. Phys. Soc. 27, 697 (1982); and Long Don Pham, University of Massachusetts B.S. thesis, May 1983, unpublished.

5. D. F. Geesaman et al., Bull. Am. Phys. Soc. 27, 697 (1982).

Isovector Properties of Collective States and the Interacting Boson Approximation Model
(Exp. 671, EPICS)

(Northwestern Univ.)
Spokesmen: A. Saha and K. K. Seth (Northwestern Univ.)

Isovector (or, equivalently, proton-neutron) properties of nuclear states provide extremely sensitive tests of nuclear-structure models.[1,2] For heavy nuclei, one model, which has gained increasing attention in recent years, is the Interacting Boson Approximation (IBA) model.[3] In the latest version of this model, called the IBA-2 model,[4] the active part of the nucleus (outside a supposedly inert core) is described in terms of a small number of mutually interacting proton and neutron bosons that can be either in the *s* or *d* state. This model can make explicit predictions regarding the isovector properties of nuclear transitions. Here we report on the first successful experiment specifically designed to test these predictions.

We have measured differential cross sections for elastic and inelastic scattering of 180-MeV π^+ and π^- from enriched targets (≥95%) of ^{104,106,108,110}Pd at the EPICS facility. As illustrated in Fig. 1, the energy resolution obtained was ≃165 keV. To extract M_n and M_p from our data, we have made distorted-wave impulse approximation (DWIA) calculations with the coordinate-space computer code DWPI[5] using a Kisslinger-type optical potential and collective form factors. As is well known, the proton transition matrix element M_p is related to β_p as

$$B(E\ell\uparrow) \equiv M_p^2 \equiv (3ZR^\ell/4\pi)^2 \beta_p^2 \quad .$$

The M_n is defined in exactly the same manner in terms of N and β_n. We note that our values of M_p for the 2_1^+ states agree well within errors (≤5%) with those from lifetime measurements.[6] For the 3_1^- states, no other direct results for M_p are available for comparison.

In the IBA-2 model the neutron and proton quadrupole transition matrix elements are defined[7] as

$$Q_p = \alpha_p A_p + \beta_p B_p \quad ,$$

and

$$Q_n = \alpha_n A_n + \beta_n B_n \quad ,$$

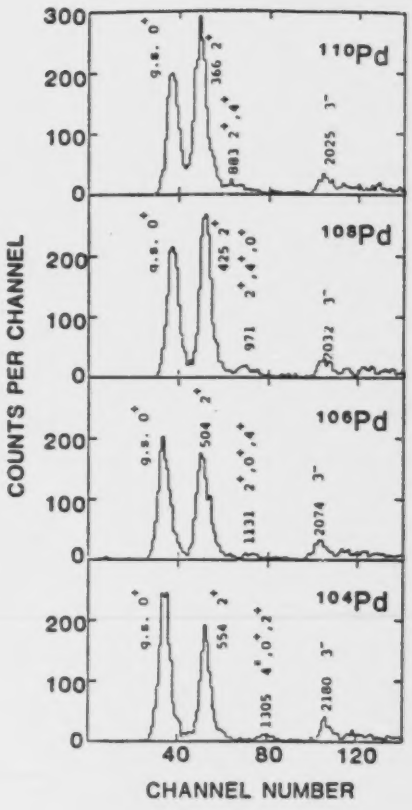

Fig. 1.
Excitation-energy spectra for the reaction Pd(π,π′) at $\theta_{lab} = 42.5°$.

The nuclear-structure information is contained in the reduced boson proton-neutron transition matrix elements, $A_{p,n}$ and $B_{p,n}$, for the *d*-boson nonconserving and *d*-boson conserving parts, respectively. The $\alpha_{p,n}$ and $\beta_{p,n}$ are the corresponding values of the quadrupole operators.

We relate our experimental results to the IBA-2 model at two different levels, with or without core polarization. Further, we can treat $\alpha_{n,p}$ and $\beta_{n,p}$ as adjustable parameters, as was done in Ref. 7, or we can use the values calculated in a generalized seniority scheme using

a surface delta interaction.[8] These calculations for palladium give the following results.

	^{104}Pd	^{106}Pd	^{108}Pd	^{110}Pd
	(fm^2)			
α_n	18.5	16.6	15.6	14.8
β_n	−8.2	−8.2	−3.7	2.4
α_p	14.7	15.1	15.3	15.6
β_p	−4.3	−3.9	−2.6	−3.3

In all these comparisons we take A_l and B_l from Ref. 7.

We first consider the IBA-2 model without core polarization. If we follow the phenomenological procedure, using $\chi_p \equiv \alpha_p/\beta_p$ and $\chi_n = \alpha_n/\beta_n$, as optimized in Ref. 7, and setting $M_n = eQ_n$ and $M_p = eQ_p$ for the 2_1^+ states, we obtain the average values $\langle\alpha_n\rangle = 21.2$ fm^2 and $\langle\alpha_p\rangle = 38.8$ fm^2. These lead to a constant $M_p \approx 86$ e-fm^2 and to the rapidly changing M_n/M_p, shown by the thin solid curve in Fig. 2. Neither of these results is in agreement with the data. Further, the M_p for the 2_2^+ states are predicted to be ≈2.5 times larger than the experimental results. If we use the calculated values of α and β, we obtain even poorer agreement with the data. We obtain M_n, which are ≈75 (±8)% of the experimental results; M_p, which are ≈41 (±4)%; and M_n/M_p, which are a uniform factor of ~2 larger than the experimental results (thin dashed curve in Fig. 2). The M_p for the 2_2^+ states fare better, being only ≈21 (±5)% smaller than the experimental values.

From the above results, we conclude that irrespective of what approach is adopted toward α's and β's, we must compensate for the truncation of the valence boson space by including core polarization. As in the shell model, one can do this by introducing "effective" charges e_p and e_n for proton and neutron bosons and note that for a self-conjugate core (here $N = Z = 50$),

$$M_p = e_p Q_p + e_n Q_n \ ,$$

$$M_n = e_n Q_p + e_p Q_n \ .$$

For a given nucleus, once Q_p and Q_n are known, e_p and e_n are determined uniquely by fitting the measured values of M_n and M_p. We first use χ's, as empirically optimized in Ref. 7, and $\langle\alpha_n\rangle = 16.4$ fm^2, $\langle\alpha_p\rangle = 15.2$ fm^2 (which are averages of the calculated results) to obtain Q_p and Q_n for each isotope. Comparison with M_p and M_n then leads to a set of e_p and e_n that is essentially the same (within ≈±5%) for all isotopes: $\langle e_p\rangle = 1.13e$, $\langle e_n\rangle = 0.49e$. The results for M_p and M_n/M_p obtained by using these effective charges are shown in Table I and by the thick solid curve in Fig. 2. The fit to the data is quite good. The same effective charges (Table I) predict M_p for the 2_2^+ states, which are in fair agreement with the data. In addition, they lead to very distinctive predictions for M_n/M_p that should be tested in future experiments.

Unfortunately, if we use α's and β's, as obtained from the microscopic calculations referred to earlier, the results are much poorer. Individual e_n are fairly constant ($e_n = 0.46e \rightarrow 0.50e$), but e_p show an unacceptable amount of variation ($e_p = 1.02e \rightarrow 1.35e$) in going from ^{104}Pd to ^{110}Pd. Equivalently, we note that if we use the average values, $\langle e_n\rangle = 0.48e$ and $\langle e_p\rangle = 1.17e$, we fail to reproduce the trend of M_p and M_n individually,

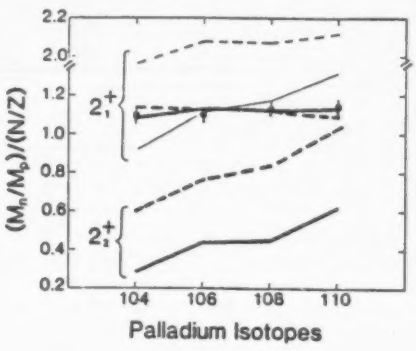

Fig. 2.
The $(M_n/M_p)/(N/Z)$ for the 2^+ states in palladium isotopes. The curves refer to IBA-2 calculations described in the text.

Without core polarization: thin solid line for empirically adjusted $\langle\alpha\rangle$, $\langle\beta\rangle$; thin dashed line for microscopically calculated α, β.

With core polarization: thick solid line for empirically adjusted $\langle\alpha\rangle$, $\langle\beta\rangle$ and $\langle e_p\rangle = 1.12e$, $\langle e_n\rangle = 0.49e$; thick dashed line for microscopically calculated α, β and $\langle e_p\rangle = 1.17e$, $\langle e_n\rangle = 0.48e$.

Table I. Summary of Results for Excitation of 2^+ States in Palladium Isotopes.[a]

		Experimental Results					Model Predictions			
		Ref. 6	(π,π')				IBA-2			
J^π	A	M_p	M_p	M_n	M_n/M_p	N/Z	M_n[b]	M_p[b]	M_n[c]	M_p[c]
2_1^+	104	74(2)	77(2)	106(3)	1.38(5)	1.26	108	79	119	83
	106	83(3)	83(2)	118(3)	1.43(5)	1.30	125	85	126	86
	108	88(3)	89(2)	136(3)	1.52(5)	1.35	135	89	129	87
	110	94(3)	98(2)	156(4)	1.59(6)	1.39	150	95	136	90
2_2^+	104	16(1)					6	17	13	17
	106	13(1)					10	18	19	19
	108	13(1)					9	15	21	18
	110	11(1)					14	16	30	21
3_1^-	104		365(9)	542(14)	1.49(5)	1.26				
	106		360(9)	533(13)	1.48(5)	1.30				
	108		334(8)	539(13)	1.61(6)	1.35				
	110		315(8)	523(13)	1.66(6)	1.39				

[a] $M_{p,n}$, in units of e-fm^2 for 2^+, and e-fm^3 for 3^-.
[b] Average $\langle e_p\rangle = 1.13e$, $\langle e_n\rangle = 0.49e$, and empirical α's and β's.
[c] Average $\langle e_p\rangle = 1.17e$, $\langle e_n\rangle = 0.48e$, and calculated α's and β's.

although M_n/M_p agree with the data (thick dashed curve in Fig. 2). For the 2_2^+ states, the predicted M_p differ from the experimental ones by 43 ($\pm$23)% and the predicted M_n/M_p differ by a factor of 2 from those with empirically adjusted α's and β's.

Because of the limited success obtained above with the IBA-2 model without empirically adjusted parameters, it is instructive to examine what other simple phenomenological models predict. In the hydrodynamical model, nuclei in the palladium region are well described as vibrational nuclei, with

$$E(\lambda) = \hbar^{-2}\langle C_\lambda/B_\lambda\rangle^{1/2} ,$$

$$M_p^2 = \hbar^{-2}(\lambda + 1/2)\,[(3/4\pi)ZeR_p^\lambda]^2/(B_\lambda C_\lambda)_p^{1/2} .$$

By analogy, M_n is defined in terms of N, R_n, and $(B_\lambda,C_\lambda)_n$. The parameters B_λ (related to the mass transport associated with the vibration), C_λ (related to the effective surface tension or restoring force), and R, in principle, can vary from nucleus to nucleus and between neutron and proton fluids, but generally are considered constant in a small region of N and Z. Thus, this model predicts M_p = constant for a series of isotopes and $M_n/M_p = N/Z$. As seen in Table I, the experimental M_p increased by ~25% from ^{104}Pd to ^{110}Pd. Also, the experimentally observed ratios of M_n/M_p for the 2_1^+ and 3_1^- states are, respectively, ~12 and ~18% higher than N/Z (see Table I). Better agreement with the experimental results can be obtained by treating B_λ, C_λ, and R as adjustable parameters. For example, we can obtain excellent fits to the measured M_p by simply varying C_2 with neutron number. Similarly, the experimental M_n/M_p for both 2_1^+ and 3_1^- can be fitted perfectly by assuming either that the effective-radius parameters R_n and R_p are different, or that $(B_\lambda,C_\lambda)_p$ and $(B_\lambda,C_\lambda)_n$ are different.

We can summarize our results as follows. The IBA-2 model without core polarization is clearly unsuccessful in explaining the experimental results. By including core-polarization effects, using effective charges, the IBA-2 model can provide a good description of the data if one allows empirical adjustment of its parameters. However,

at this level, it is worthwhile to remember that other, even simpler models, also can explain the experimental results, provided that their parameters are also adjusted from isotope to isotope. Our first attempts to calculate some of the IBA-2 parameters on a microscopic basis have so far been unsuccessful. Clearly more theoretical work is required. At the experimental front, measurement of M_n/M_p for other quadrupole transitions, particularly 0_1^+ to 2_2^+, would help narrow the range of alternative explanations.

REFERENCES

1. A. Saha et al., Phys. Lett. 114B, 419 (1982), and references therein.

2. S. G. Iversen et al., Phys. Rev. Lett. 40, 17 (1978); and S. G. Iversen et al., Phys. Lett. 82B, 51 (1979).

3. A. Arima and F. Iachello, Phys. Rev. Lett. 35, 1069 (1975); and F. Iachello, in "Interacting Bosons in Nuclear Physics" (Plenum Press, New York, 1979), p. 1.

4. T. Otsuka, A. Arima, F. Iachello, and I. Talmi, Phys. Lett. 76B, 139 (1978); and T. Otsuka, A. Arima, and F. Iachello, Nucl. Phys. A 309, 1 (1978).

5. R. A. Eisenstein and G. A. Miller, Comput. Phys. Commun. 11, 95 (1976).

6. Nuclear Data sheets, 18, 125 (1976); 30, 305 (1980); B7, 33 (1972); and 22, 135 (1977).

7. P. Van Isacker and G. Puddu, Nucl. Phys. A 238, 125 (1980).

8. O. Scholten, Michigan State University preprint #MSUCL-416 (1983).

Studies of Giant Resonances in ^{208}Pb with Inelastic Pion Scattering
(Exp. 672, EPICS)

(Los Alamos, Univ. of Minnesota)

Spokesmen: T. A. Carey and J. M. Moss (Los Alamos) and S. Seestrom-Morris (Univ. of Minnesota)

To broaden our base for investigating the high-lying nuclear response, we have used 162-MeV inelastic pion scattering to study giant resonances in ^{208}Pb at excitations <40 MeV.

Pions cause isovector transitions relative to isoscalar ones much more strongly than do either 200- or 800-MeV protons, so (π,π') should be better for exciting the isovector giant quadrupole resonance. Comparisons of π^+ and π^- scattering are also a powerful tool for identifying the isospin character of specific transitions. Furthermore, in view of the intrinsic energy dependences of Coulomb excitation, we expect that this mechanism will be much weaker in the excitation of giant resonances with 162-MeV pions than is the case with 800-MeV protons. In general, then, (π,π') should nicely complement our (p,p') studies and be most helpful in unraveling the specific natures of the observed resonances.

High-precision data were acquired in November 1982 at LAMPF. Replay of these data is now complete and several avenues of theoretical analysis currently are being pursued. Both π^+ and π^- spectra exhibit a definite resonance at $E_x \simeq 21$ MeV. Analysis thus far suggests that its quantum numbers are $J^\pi,T = 1^-,0$, but conclusive assignments await ongoing considerations of Coulomb excitation and the underlying continuum. Still, we may have the first strong evidence for a surface-compressional mode as opposed to the volume-compressional mode associated with the isoscalar giant monopole resonance.

To date the most extensive analysis has concentrated on the lower lying isoscalar giant quadrupole resonance (ISGQR) and 3_1^- states because they have been thoroughly studied with other probes and because the extraction of precise absolute yields for them is less hindered by underlying backgrounds. These excitations are believed to involve strongly collective, isoscalar transitions. The generally successful pure collective model predicts $R = \alpha(\pi^-)/\alpha(\pi^+) \simeq N/Z = 1.5$ for such states in ^{208}Pb. Surprisingly, we find that our data give $R = 1.8 \pm 0.1$ for the 3_1^-, whereas for the ISGQR $R = 3.0 \pm 0.5$.

The data for ISGQR transitions, shown in Fig. 1, indicate an even more serious discrepancy than that recently reported for the ISGQR from an independent ^{118}Sn(π,π') experiment.[1] Also, a preliminary analysis of our data for the isoscalar high-energy octupole resonance gives $R = 3.3 \pm 1$. These results could imply the presence

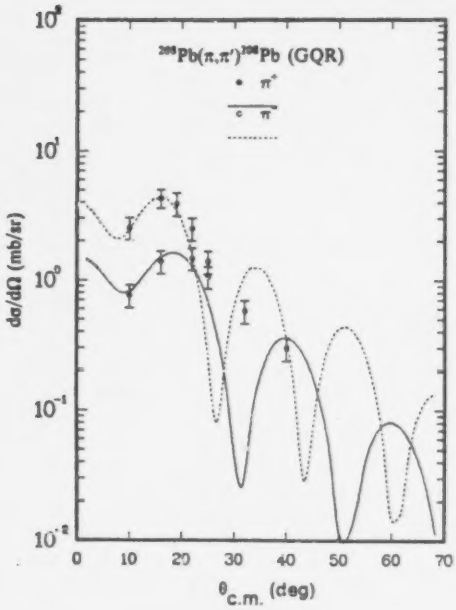

Fig. 1.
The π^+ and π^- angular distributions and collective-model calculations for the giant quadrupole resonance in ^{208}Pb.

of substantial isovector contributions to these purportedly isoscalar transitions, but the rather systematic nature of the disagreement between experiment and theory for more than one giant resonance in more than one nucleus may also be indicative of a breakdown in the standard collective model. Further analysis is in progress.

REFERENCE

1. J. L. Ullman et al., Phys. Rev. Lett. 51, 1038 (1983).

Measurements of Large-Angle Pion-Nucleus Scattering
(Exp. 681, EPICS)

(New Mexico State Univ., Univ. of Texas, Univ. of Minnesota, Los Alamos)
Spokesman: G. Burleson (New Mexico State Univ.)

The motivation for this experiment was to explore possible systematics of pion-nucleus scattering in the large-angle region, where the behavior is poorly known from an experimental point of view and poorly understood from a theoretical point of view. In general, there are many models of pion-nucleus scattering that give a good description of elastic and inelastic scattering over the angular range for which data are abundant (to ~100°) but that diverge drastically for large angles. For a realistic description of pion-nucleus scattering, a fair amount of data is required in the backward hemisphere to constrain the calculations. The results of this first experiment on large-angle pion-nucleus scattering at LAMPF have begun to reveal some of these features.

The experimental configuration is as follows. Basically, a circular magnet is placed at the EPICS pivot point, which is displaced laterally from its normal position. The incident pion enters parallel to a line through the center of the magnet, effectively bends through the arc of a circle, and is incident upon the scattering target at the center of the magnet. A pion scattered at a large angle is bent so as to enter the spectrometer when it is positioned within its normal operating angular range. With this design, the effective solid angle of the spectrometer should be independent of the scattering angle.

Wire-orbit measurements of the magnet were made in place before the experiment began. No indication of azimuthal asymmetry was found over the angular region of the scattered pion. During the experiment, the yield of pions scattered from protons tracked the pion-proton cross section calculated from the phase shifts of Rowe et al.[1] to within ±5% over the full range of scattering angles, 115-180°, confirming the design characteristics of the system.

Some of the preliminary results are shown in Figs. 1-4. All data points were normalized to pion-proton scattering

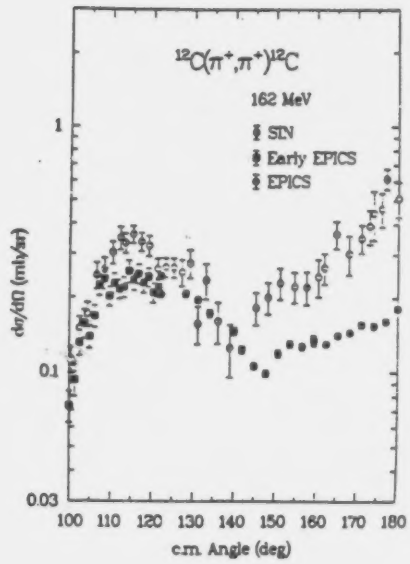

Fig. 1.
Preliminary results for the π^+-^{12}C angular distribution at 162 MeV, compared with previous data (Ref. 2).

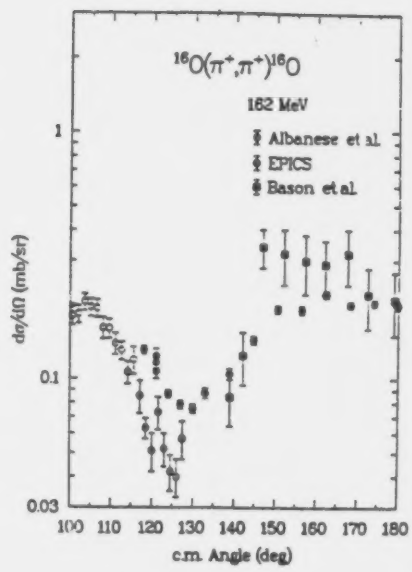

Fig. 2.
Preliminary results for the π^+-^{16}O angular distribution at 162 MeV, compared with previous data (Ref. 3).

measured under spectrometer conditions identical in angle and magnetic-field settings with those used for the pion-nucleus scattering measurements. The experimental differential cross sections for π^+-^{12}C scattering at 162 MeV are shown in Fig. 1. The agreement with previous EPICS data is good, but there is a disagreement with the previous SIN backward data[2] in that the SIN results show a fairly strong backward peaking, whereas the new results do not, and in that there is a difference in absolute value of about a factor of 2.

The results for π^+-^{16}O scattering at 162 MeV are shown in Fig. 2, with previous data from SIN[3] and CERN.[4] The agreement with the CERN results is satisfactory, considering the large error bars, but there is again a disagreement with some previous results from SIN, this time with data taken with the "normal" spectrometer setup.

An excitation function for π^+-deuteron scattering at 176° is shown in Fig. 3 and compared with previous data[5-7] at 180°. There is disagreement with the absolute values of some of the previously measured cross sections, but the new data points join smoothly onto the recent data from KEK.[7] An excitation function for π^+-^{12}C scattering is shown in Fig. 4, with a prediction of the optical model of Cottingame and Holtkamp.[8] It is interesting that this model, which has had good success in predicting pion-nucleus cross sections at angles up to ~100°, makes a fairly good prediction of the structure observed between 130 and 170 MeV, even though it misses the magnitude of the cross sections.

Further studies of these results are in progress.

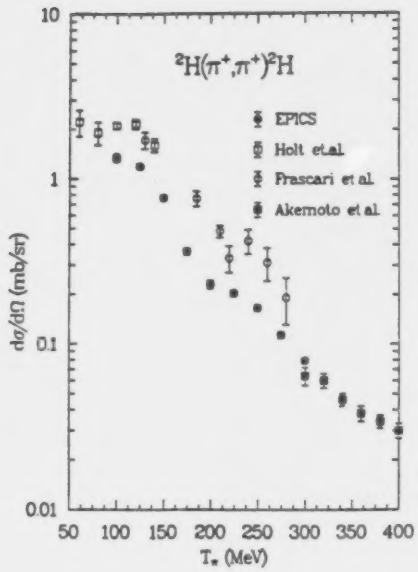

Fig. 3.
Preliminary results for the π^+-deuteron excitation function at 176°, compared with previous data (Refs. 5-7) at 180°.

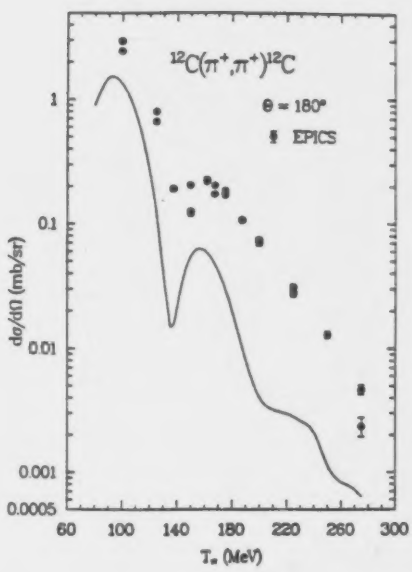

Fig. 4.
Preliminary results for the π^+-^{12}C excitation function at 180°, compared with the prediction of the model of Cottingame and Holtkamp (Ref. 8).

REFERENCES

1. G. Rowe, M. Saloman, and R. H. Landau, Phys. Rev. C 18, 584 (1978).

2. B. Chabloz et al., Phys. Lett. 81B, 143 (1979).

3. J. P. Albanese et al., Nucl. Phys. A 350, 301 (1980).

4. E. Bason et al., contribution to the Ninth Int. Conf. on High-Energy Physics and Nuclear Structure, Versailles, France, 1981.

5. R. J. Holt et al., Phys. Rev. Lett. 43, 1229 (1979).

6. R. Frascaria et al., Phys. Lett. 91B, 345 (1980).

7. M. Akemoto et al., Phys. Rev. Lett. 50, 400 (1983).

8. W. B. Cottingame and D. B. Holtkamp, Phys. Rev. Lett. 45, 1828 (1980).

π^+/π^- on ^{15}N
(Exp. 703, EPICS)
(Univ. of Minnesota, Los Alamos, Univ. of Texas)
Spokespersons: D. B. Holtkamp (Los Alamos) and S. J. Seestrom-Morris (Univ. of Minnesota)

Experiment 703 ran during January 1983, measuring π^+ and π^- cross sections for excitation of states in ^{15}N. Replay of the data is complete, as is the peak stripping for states below about 8-MeV excitation energy. Calculation of the absolute normalization of the data is currently under way.

Figure 1 shows spectra of π^+ and π^- scattering at $T_\pi = 164$ MeV near the maximum in the angular distribution for $M4$ transitions. Arrows indicate those groups that have been identified as due to $M4$ transitions, $(\frac{9}{2})^+$ states; π^+/π^- asymmetries have been observed for some of these transitions, for example,

$$\frac{\sigma(\pi^+)}{\sigma(\pi^-)} > 3 \text{ for } 10.6 \text{ MeV},$$

$$\frac{\sigma(\pi^+)}{\sigma(\pi^-)} \simeq 5 \text{ for } 12.5 \text{ MeV}.$$

Although the $M4$ transitions were the primary goal of this experiment, interesting data also were obtained on the low-lying excited states. One example is the transition from the $(\frac{1}{2})^-$ ground state to the $(\frac{1}{2})^-$ state at 6.32 MeV. In the extreme shell model, the ^{15}N ground state can be described as a single proton hole in the $1p_{1/2}$ shell and the $(\frac{1}{2})^-$ state as a single proton hole in the $1p_{3/2}$ shell. In this model the transition from $(\frac{1}{2})^- \rightarrow (\frac{1}{2})^-$ would be a pure proton $p_{3/2} \rightarrow p_{1/2}$ single-particle transition. Such a transition would yield a ratio of $R = \sigma(\pi^+)/\sigma(\pi^-) = 9$.

The preliminary data of Exp. 703 for this transition show a significantly smaller value of $R = 1.5$. This difference probably is due to contributions of collective electric quadrupole components. To try to account for this, distorted-wave impulse approximation (DWIA) calculations were performed using a combination of a pure proton $p_{3/2} \rightarrow p_{1/2}pn$ component and a $J(LS) = 2(20)$ component scaled by neutron and proton polarization changes $(1 + \delta_n)$ and $(1 + \delta_p)$. The data and resulting calculations are displayed in Fig. 2. These values of $\delta_p = 0.3$ and $\delta_n = 1.0$ and an additional renormalization of the DWIA amplitude by 1.13 produce electromagnetic properties in agreement with those measured using other probes.

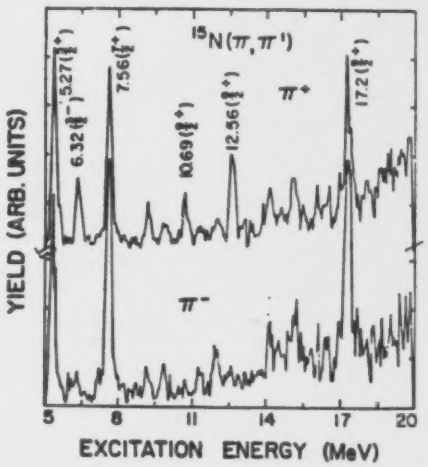

Fig. 1.
The π^+ and π^- spectra for ^{15}N at a scattering angle where the momentum transfer for $M4$ transitions is maximum. States labeled have been identified as $M4$ transitions.

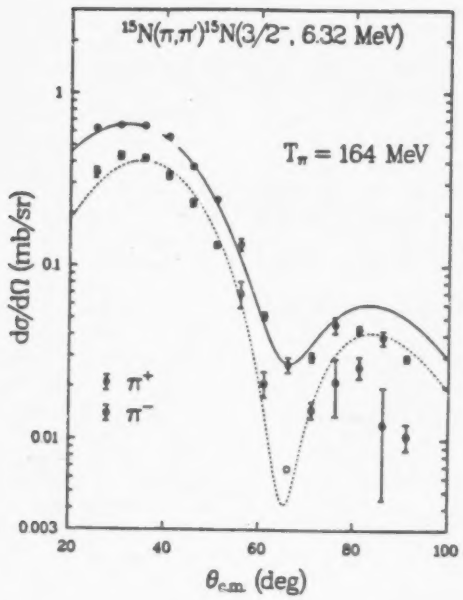

Fig. 2.
The π^+ and π^- angular distributions for the $(\frac{1}{2})^-$ state at 6.32 MeV in ^{15}N. The curves are DWIA calculations described in the text.

Energy Dependence of Pion Double-Charge-Exchange Angular Distributions for the Reaction $^{16}O(\pi^+,\pi^-)^{16}Ne$ (g.s.)
(Exp. 749, EPICS)
(Univ. of Texas, Los Alamos, New Mexico State Univ., Univ. of Pennsylvania)
Spokesmen: L. C. Bland and H. T. Fortune (Univ. of Pennsylvania)

Experiment 749 is one of a series of EPICS experiments, including Exps. 310, 448, 577, and 701, that have investigated the features of nonanalog pion double-charge-exchange (DCX) transitions between ground states of $T=0$ and $T=2$ nuclei. The previous experiments have measured $\theta=5°$ excitation functions, $T_\pi=164$-MeV angular distributions, and the mass dependence of nonanalog DCX. The observed systematics included the following.

(1) Forward-angle excitation functions show a peaked energy dependence.
(2) The peaks all have similar widths.
(3) Angular distributions at $T_\pi=164$ MeV are consistent with being diffractive.
(4) The target-mass dependence of $\theta=5°$ cross sections at $T_\pi=164$ MeV is approximately $A^{-4/3}$.

The proposal for Exp. 749 suggested that these features are consistent with a single-step process leading to $\Delta(3,3)$ components of the residual nuclear wave function. The explanation included the following.

(1) The rapid energy dependence results from the intermediate Δ propagator.
(2) The shape of the angular distributions follows from the surface domination of the single-step process.
(3) The single step should lead to an $A^{-4/3}$ mass dependence.
(4) The deduced size of the Δ-component admixture in ^{16}Ne (g.s.) is reasonable.

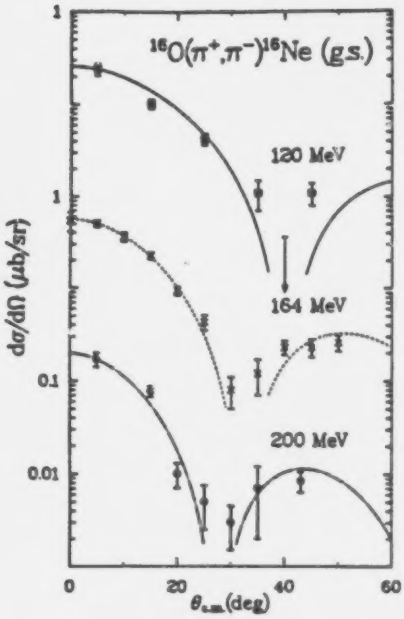

Fig. 1.
Comparison of angular distributions at three energies for the DCX reaction $^{16}O(\pi^+,\pi^-)^{16}Ne$ (g.s.). The curves are described in the text.

Experiment 749 was designed to investigate the energy dependence of the $^{16}O(\pi^+,\pi^-)^{16}Ne$ (g.s.) angular distributions to see if they changed in a diffractive manner. The experiment was run during cycle 39 (replay and analysis are continuing). Some on-line results for the two angular distributions obtained are displayed in Fig. 1 along with the previously measured (Exp. 577) angular distribution for $^{16}O(\pi^+,\pi^-)^{16}Ne$ (g.s.) at $T_\pi = 164$ MeV. The curves presented are damped Bessel functions,

$$\sigma = N J_0^2(qR)\, e^{-qd} \quad ,$$

where the radius $R = 3.3$ fm and damping length $d = 1.2$ fm are independent of energy. The quantity N is an energy-dependent normalization factor. The results appear consistent with a diffractive process.

Isospin Dependence of Nonanalog Pion Double Charge Exchange
(Exp. 780, EPICS)

(Univ. of Texas, Los Alamos, New Mexico State Univ., and Univ. of Pennsylvania)
Spokesmen: R. Gilman (Univ. of Pennsylvania) and P. A. Seidl (Univ. of Texas)

Experiment 780, which was run during cycle 38, is the most recent in a series of experiments that have investigated the features of nonanalog pion double-charge-exchange (DCX) reactions. Previous experiments, including Exps. 310, 448, 577, and 701, have measured $\theta = 5°$ excitation functions, $T_\pi = 164$-MeV angular distributions, the mass dependence of nonanalog DCX, and recently in Exp. 749 (this Progress Report, above), the energy dependence of the angular distributions. All of these measurements were made for transitions between J^π, $T = 0^+,0$ and J^π, $T = 0^+,2$ ground states.

These experiments had determined that the target-mass dependence of $\theta = 5°$ cross sections for nonanalog transitions is approximately $A^{-4/3}$. Experiment 780 proposed to measure transitions between $T = 1$ and $T = 3$ nuclei to investigate possible effects of isospin dependence or nuclear structure on the size of the cross section. Data obtained include

(1) a $\theta = 5°$ excitation function for the reaction $^{18}O(\pi^-,\pi^+)^{18}C$ ground state (g.s.);
(2) a $T_{\pi^-} = 164$-MeV angular distribution for the reaction $^{18}O(\pi^-,\pi^+)^{18}C$ (g.s.);
(3) a $\theta = 5°$, $T_{\pi^-} = 164$-MeV cross section obtained for the reaction $^{14}C(\pi^-,\pi^+)^{14}Be$ (g.s.); and
(4) a $\theta = 5°$, $T_{\pi^-} = 164$-MeV cross section obtained for the reaction $^{58}Ni(\pi^-,\pi^+)^{58}Fe$ (g.s.).

Figure 1 compares the ^{18}O angular distribution to a fit with earlier measurements (Exp. 577) of the $^{16}O(\pi^+,\pi^-)^{16}Ne$ (g.s.) reaction; Fig. 2. compares the ^{18}O excitation function to a fit to earlier measurements (Exps. 310/448/577) of the same reaction. The energy and the angular dependence of nonanalog DCX are obviously similar in the two cases. Figure 3 compares $\theta = 5°$, $T_\pi = 164$-MeV, on-line cross sections for the $T = 1$ to $T = 3$ transitions of Exp. 780 with an $A^{-4/3}$ fit to the $T = 0$ to $T = 2$ cross sections. There is an enhancement of the $T = 1$ to $T = 3$ transitions of about 30% over the fit to the $T = 0$ to $T = 2$ transitions. Thus, we may have evidence for an isospin dependence or nuclear-structure effects in the nonanalog reaction mechanism.

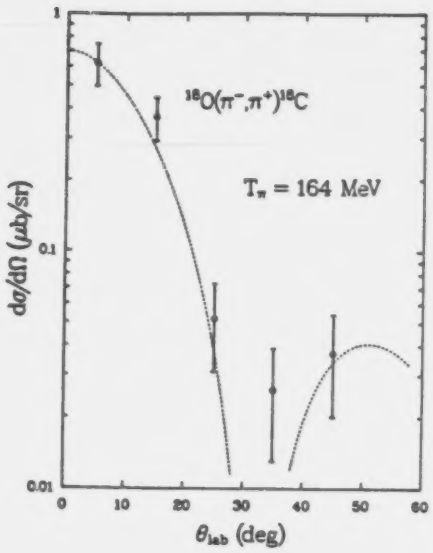

Fig. 1.
Comparison of on-line angular distribution for the reaction $^{18}O(\pi^-,\pi^+)^{18}C$ (g.s.) with a fit to the previously measured angular distribution of $^{16}O(\pi^+,\pi^-)^{16}Ne$ (g.s.). The fit has been renormalized to the value of the $\theta = 5°$ point.

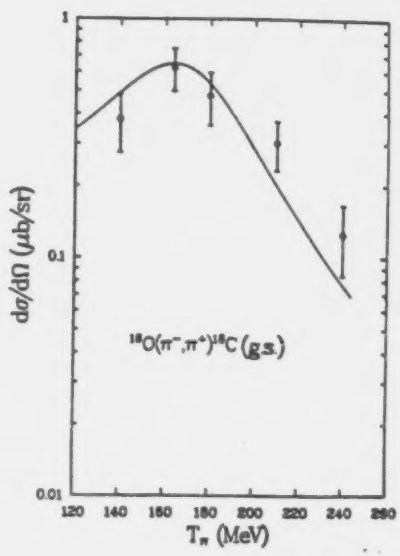

Fig. 2.
Comparison of on-line excitation function for the reaction $^{18}O(\pi^-,\pi^+)^{18}C$ (g.s.) with a Breit-Wigner fit to the previously measured excitation function for $^{16}O(\pi^+,\pi^-)^{16}Ne$ (g.s.). The fit has been renormalized by 30%.

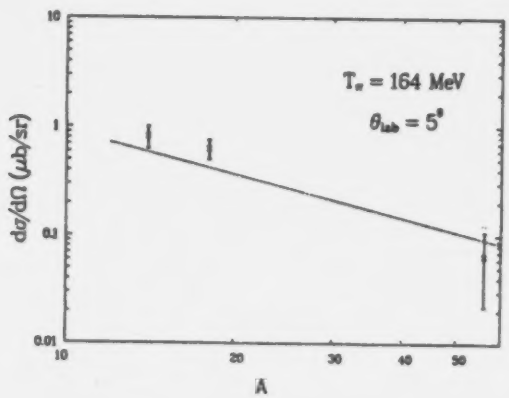

Fig. 3.
Comparison of on-line $\theta = 5°$, T_π = 164-MeV data from Exp. 780 with best-fit $A^{-4/3}$ curve for $T = 0$ to $T = 2$ transitions.

Inelastic Scattering from ^{12}C at Intermediate Energies

(Exps. 432 and 531, HRS)

(Rutgers Univ., Los Alamos, Univ. of Minnesota, Saclay, Univ. of Texas, UCLA, Univ. of Pittsburgh)

Spokesmen: C. Glashausser (Rutgers Univ.) and J. Moss (Los Alamos)

Analysis of the data from Exps. 432/531 is in the final stages, and some results have already been published. We present here a brief summary of the current status of this work.

Differential cross-section and analyzing-power angular distributions spanning the momentum transfer range from 0.3 to 2.4 fm^{-1} have been obtained for elastic and inelastic (up to an excitation energy of 21 MeV) proton scattering from ^{12}C at 398, 597, and 698 MeV. Analysis of the data has been performed using the recently improved version of the nucleon-nucleon t matrix of Love and Franey. This analysis has yielded several interesting results, both for the energy dependence of various components of the interaction and in the identification of the 2^- strength in the high-excitation region (18-20 MeV) of ^{12}C (Ref. 1).

Carbon-12 is a nucleus well suited to the study of systematic effects as it provides a full complement of well-resolved states excited by all possible combinations of spin transfer ($\Delta S = 0,1$) and isospin transfer ($\Delta T = 0,1$). Microscopic wave functions for these levels, such as those derived by Cohen and Kurath and Millener, have been tested extensively in inelastic electron scattering, which also establishes oscillator parameters for bound-state orbitals.

Cross-section and analyzing-power data for the 4.44- and 12.71-MeV states are shown in Fig. 1 at a variety of incident energies. Typical data for the states at 15.11, 16.11, and 16.58 MeV are shown in Fig. 2. The most striking feature of the data is the energy independence of the cross section (both the absolute magnitude and the angular distribution) for all classes of transitions except isoscalar states of natural parity. The solid curves in the figures show the results of distorted-wave impulse approximation (DWIA) calculations. Renormalization factors required to bring the calculations into agreement with the data are included and are listed in Table I. These factors necessarily include some arbitrariness because of imperfect fits.

The analysis shows that there is considerable room for improvement in the DWIA description of the energy dependence of the cross sections and analyzing powers. Whereas the shapes of the angular distributions for the cross sections are generally adequately predicted at 400 MeV and above, the angular distributions for $A_y(A_N)$, with the exception of the 12.71-MeV state, are not. In addition, normalization factors required to match theory and experiment show substantial variation with energy. The origin of these problems is not clear. Certainly, the wave functions may be partly responsible. A detailed examination of the effect of coupled-channels corrections and of changes in the optical potentials and single components in the NN force is currently under way. Furthermore, it will be useful to determine whether density-dependent forces or relativistic theories yield significant improvements.

Analysis of the 18- to 20-MeV region of excitation for the beam energies mentioned previously has yielded interesting results. States at 18.30 and 19.40 MeV of excitation with widths of 380 ± 30 and 480 ± 40 keV

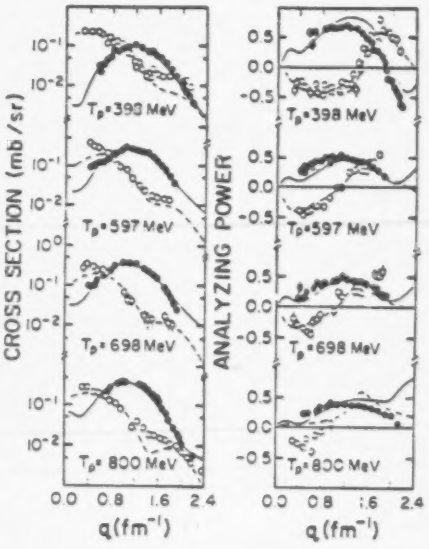

Fig. 1.
Cross-section and analyzing-power data for the 4.44- (solid circles) and 12.71- (open circles) MeV states at a variety of incident energies. Solid and dashed curves are DWIA calculations for these states.

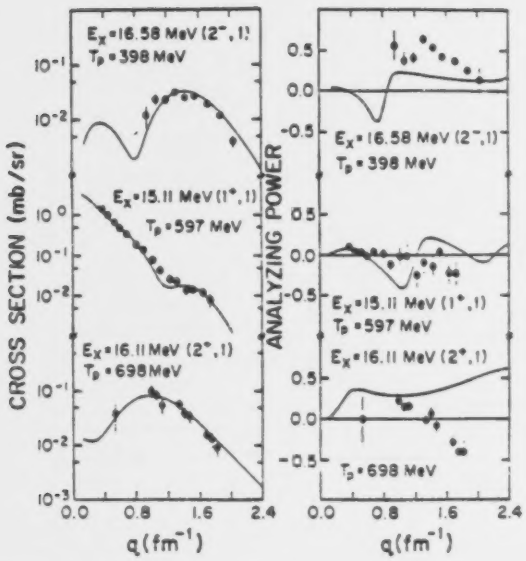

Fig. 2.
Cross-section and analyzing-power data for the states at 15.11, 16.11, and 16.58 MeV at a variety of incident energies. Solid curves are DWIA calculations.

Table I. Renormalization Factors. The theoretical cross sections were multiplied by the factors shown below to achieve the best fit to the experimental cross sections. See text for additional factors for the 16.11-MeV state.

			(p, p')				
E_x (MeV)	$J^\pi; T$	(e, e')	200 MeV	398 MeV	597 MeV	698 MeV	800 MeV
4.44	2⁺, 0	2.0	1.0	2.0	2.68	3.0	2.65
12.71	1⁺, 0	---	0.3	1.0	1.40	1.30	1.15
15.11	1⁺, 1	1.0	1.0	1.0	1.44	1.15	1.38
16.11	2⁺, 1	1.0	0.60	0.78	1.32	0.90	1.15
16.58	2⁻, 1	0.67	0.20	0.30	0.50	0.58	0.38

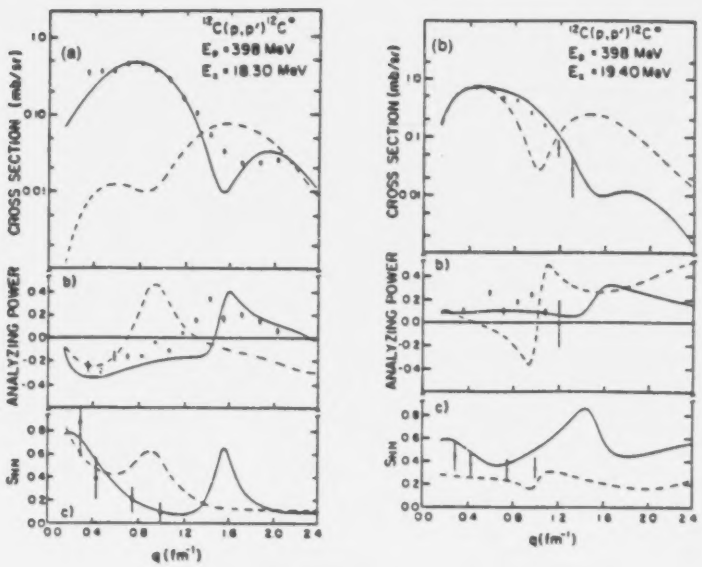

Fig. 3(a) and (b).
Cross-section, analyzing-power, and spin-flip data for the 2^-,0 and 2^-,1 states at (a) 18.30 and (b) 19.40 MeV. Solid curves are renormalized DWIA calculations for 2^-,0(2) and 2^-,1(2) configurations, as discussed in the text. Dashed curves are 2^-,0(1) and 1^-,1 configurations for the 18.30- and 19.40-MeV states, respectively.

have been identified. Angular distributions of cross sections, analyzing powers, and spin-flip probabilities are shown in Fig. 3. Analysis of the data in the DWIA, using the Love-Franey t matrix and transition densities of Millener, have permitted identification of these two states to be 2^-,0 and 2^-,1, respectively. In particular, the state at 18.30 MeV is very well described by the second transition density predicted by Millener. This state is dominated by the $(1d_{3/2}, 1p_{3/2}^{-1})$ configuration, whereas the remaining states, such as the third shown as the dotted line in the figure, are dominated by the $(2s_{1/1}, 1p_{3/2}^{-1})$ configuration. A renormalization factor of about 0.7 is required at all energies to bring the calculations into agreement with the data. The 19.40-MeV state is best described by the second $(2^-,1)$ transition density of Millener. Renormalization by factors of 0.33 is required to bring the calculations into agreement with the data. In general, 1^-,0 and 1^-,1 transitions may be ruled out because of poor agreement with the data. The results of this work substantiate and verify previous ambiguous assignments of spin, parity, and isospin in this region.

REFERENCE

1. K. W. Jones et al., Phys. Lett. 128B, 281 (1983).

Proton Scattering from ^{20}Ne and ^{22}Ne at 0.8 GeV (Exp. 475, HRS)

(Univ. of South Carolina, Univ. of Texas, Drexel Univ.)
Spokesman: G. Blanpied (Univ. of South Carolina)

In several recent publications,[1-6] coupled-channel analyses of ~1-GeV proton inelastic scattering from *s-d* shell nuclei and heavy rare-earth nuclei have been shown to be generally successful, provided deformation and multistep processes are properly treated. These collective rotational-model calculations provide an excellent description of the data for the lowest 0^+, 2^+, and 4^+ states in ^{24,26}Mg and ^{20}Ne (Refs. 6 and 7). The results of the first half of this experiment confirmed the large hexadecapole deformation of ^{20}Ne. Data on the negative-parity rotational bands in ^{20}Ne also were explained in the coupled-channels framework.

These results motivated the measurement of (p,p') inelastic scattering from ^{22}Ne. The experiment consisted of scattering 0.8-GeV protons from a ^{22}Ne gas target enriched to 99%. Angular distributions were obtained using the high-resolution spectrometer (HRS). Data were acquired for ^{20}Ne and ^{14}N using a gas target of identical geometry and were compared to the data from the previous run. The absolute cross section is obtained relative to a solid melamine target and a ^{208}Pb foil. The resulting angular distributions are given in Fig. 1.

Coupled-channel calculations using a deformed optical potential have been performed using the code ECIS.[8] in which the 0^+, 2^+, and 4^+ states, and a 6^+ state that is not available, are treated as members of the ground-state rotational band and are coupled with deformation up to β_6. The results are given in Fig. 1, using $\beta_2 = +0.42$, $\beta_4 = +0.10$, and $\beta_6 = 0.0 \pm 0.05$. This range for β_6 is larger than that observed for other 6^+ states in this mass region, although in general the 6^+ data are poorly explained. This range in β_6 has no effect on the 0^+ and 2^+ angular distributions, although the results for the 4^+ are small, as seen in Fig. 1. The values for the multipole moments of

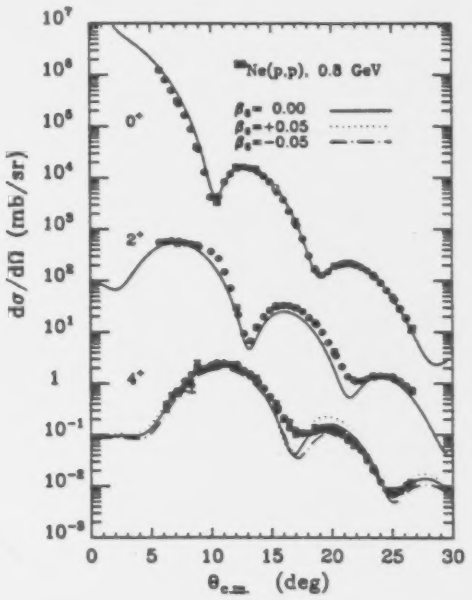

Fig. 1.
Angular distributions of ^{22}Ne (p,p) at 0.8 GeV for the 0^+, 2^+, and 4^+ members of the ground-state rotational band. The curves result from coupled-channel calculations, as discussed in the text.

Table I. Deformation Moments of Some Neon and Magnesium Isotopes.

	Matter $M(E2)$ (eb)	Charge $B(E2)$ (eb)	Neutron $M_N(E2)$ (eb)	Matter $M(E4)$ (eb^2)
^{20}Ne	0.164	0.171(11)	0.155	+0.0253
^{22}Ne	0.132	0.151(3)	0.135	+0.0109
^{24}Mg	0.187	0.207(2)	0.162	+0.0073
^{26}Mg	0.152	0.174(4)	0.150	−0.0025
^{22}Ne/^{20}Ne	0.80	0.88	0.87	Difference = 0.0144
^{24}Mg/^{26}Mg	0.81	0.84	0.93	Difference = 0.0098

the matter distribution, the known $B(E2)$ charge moments, the inferred neutron moments $[M_N(E2)]$, and the matter $M(E4)$ are given in Table I for ^{20,22}Ne and ^{24,26}Mg. In both elements, the $M(E2)$ and $M(E4)$ deformations decrease when adding a neutron pair to the $N = Z$ isotope. The inferred neutron deformations are essentially equal to that of the protons in the cases studied. Calculations are under way for other excited states in ^{20}Ne and ^{22}Ne.

REFERENCES

1. L. Ray et al., Phys. Rev. Lett. 40, 1547 (1978).
2. G. S. Blanpied et al., Phys. Rev. C 23, 2599 (1981).
3. G. S. Blanpied et al., Phys Rev. C 20, 1490 (1979).
4. L. Ray, G. S. Blanpied, and W. R. Coker, Phys. Rev. C 20, 1236 (1979).
5. M. Barlett et al., Phys. Rev. C 22, 1168 (1980).
6. G. S. Blanpied et al., Phys. Rev. C 25, 422 (1982).
7. G. S. Blanpied et al., submitted to Phys. Rev. C.
8. J. Raynal, International Atomic Energy Agency report IAEA-SWR-918, 281 (1972).

Measurement of Spin-Dependent Observables for $\vec{p}d \to \vec{p}d$ Elastic Scattering at 500, 650, and 800 MeV

(Exp. 540, HRS)

(UCLA, Los Alamos)

Spokesmen: G. J. Igo and M. Bleszynski (UCLA)

An extensive program for measuring the spin-dependent observables in $\vec{p}d \to \vec{p}d$ elastic scattering at intermediate energies continues at LAMPF at the HRS and EPB experimental areas.

A UCLA-Los Alamos collaboration is measuring the complete set of proton spin-transfer observables for $\vec{p}d \to \vec{p}d$ elastic scattering at 500, 650, and 800 MeV at the HRS using the focal plane polarimeter (FPP). In September 1982, we measured D_{NN}, D_{SS}, D_{SL}, D_{LL}, D_{LS}, P, and A_y at 800 MeV over the four-momentum transfer range $-t = 0.006 - 0.46$ (GeV/c)^2 (3-28° lab). These data have been analyzed and are being prepared for publication.

As an example, the preliminary results for D_{LL} and A_y are shown in Figs. 1 and 2. As seen, the multiple-scattering calculation[1,2] is not in good agreement with the data. The multiple-scattering calculation includes noneikonal and several kinematic corrections and has the nucleon-nucleon (NN) amplitudes and the deuteron wave function as input. Energy dependence in the NN amplitudes has been included. Further work with this calculation is in progress.

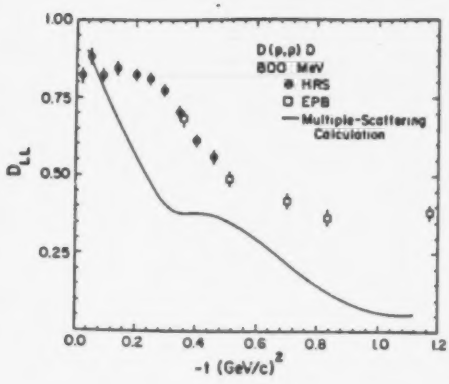

Fig. 1.
Spin-transfer parameter D_{LL} at 800 MeV for the $D(\vec{p},\vec{p})D$ reaction compared to multiple-scattering calculation.

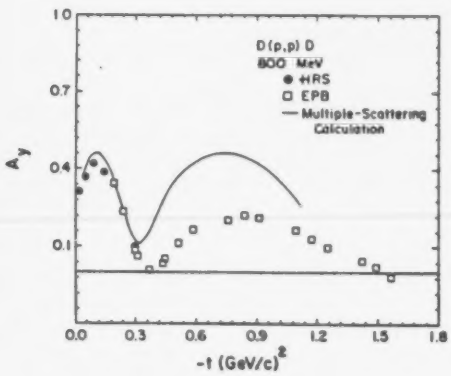

Fig. 2.
Asymmetry parameter A_y at 800 MeV for the $D(\vec{p},p)D$ reaction compared to multiple-scattering calculation.

In November 1983, the same experiment was done at 500 MeV, again using an unpolarized liquid-deuterium target. A proposal has been submitted to measure the same spin-transfer parameters at the HRS with a 650-MeV incident proton beam over the same four-momentum transfer range.

REFERENCES

1. G. Alberi, M. Bleszynski, and T. Jaroszewicz, Ann. Phys. 142, 299 (1982).

2. M. Bleszynski, Phys. Lett. 92B, 91 (1980).

Measurement of the Depolarization Parameters in Proton-Nucleus Scattering to Very High Excitation Energies
(Exp. 626, HRS)

(Rutgers Univ., Los Alamos, Univ. of Texas at Austin)
Spokesmen: J. A. McGill and C. Glashausser (Rutgers Univ.)

During cycle 35 (1982), data were taken for the inclusive reaction $^{12}C(\vec{p},\vec{p}')X$ for $D_{NN'}$, $D_{LL'}$, $D_{SS'}$, and $D_{SL'}$ at laboratory angles of 5, 11, 15, and 20°. The momentum of the outgoing protons extended from the quasi-elastic peak to ~600 MeV/c at each angle. Interpretation of these data, however, awaited the corresponding data for the reactions $^1H(\vec{p},\vec{p}')X$ and $^2H(\vec{p},\vec{p}')X$.

In cycle 39 (1983), the data for hydrogen and deuterium were taken at comparable lab angles and momenta. The experiment ran for approximately 120 h. Normally polarized beam was delivered in the usual slow-reversal mode, but both longitudinal and sideways polarizations came during the rapid-reversal mode of the polarized source. The RR mode precludes a regular quench measurement of the beam polarization, so that P_B cannot be monitored when longitudinal polarized beam is delivered. The experiment therefore ran with orthogonal spin directions, precessed about 40° from sideways and longitudinal directions, respectively. This provided some sideways component to the beam polarization for both spin directions, which was monitored with the Line C polarimeter. The arrangement was a first for the HRS.

With the exception of a few minor problems in the double-flask cryogenic target (another first), the run went smoothly. The data are in the process of being analyzed now.

Work for this experiment was supported by the National Science Foundation, the USDOE, and the Robert A. Welch Foundation.

Inclusive (p,p') Cross Sections and Analyzing Powers for ^1H and ^{12}C in the Delta Region (Exp. 642, HRS)

(Rutgers Univ. and Univ. of Texas at Austin)
Spokesmen: G. W. Hoffmann (Univ. of Texas) and J. A. McGill (Rutgers Univ.)

The delta isobar plays an important role as an intermediate state in pion-nucleus scattering to low-lying excited states; it has also been suggested that excitation of the isobar leads to quenching of Gamow-Teller and $M1$ transition strengths observed in (p,n) and (p,p') reactions. Yet, the region of nuclear excitation around 300 MeV, where the direct excitation of the delta resonance can be seen as a (decaying) final state, has been little explored thus far in intermediate-energy proton scattering.

Thus, to examine the spin structure of the $NN \rightarrow N\Delta$ interaction and to investigate deviations from quasi-free scattering, we have carried out experiments using the HRS in which the inclusive (p,p') cross sections and analyzing power were measured for $^1H(p,p'X)$ and $^{12}C(p,p'X)$. An 800-MeV proton beam was scattered from either a 267-mg/cm^2 liquid-hydrogen target or a 174-mg/cm^2 ^{12}C foil. Cross sections and analyzing powers were measured between 5 and 20°. At each angle, the HRS fields were changed by 20-30 MeV/c to search for detailed structure in the delta region. In the figures presented here, each point represents a single spectrometer setting, corresponding to a momentum acceptance of ±1%. The cross-section data were normalized to the $^1H(p,p)$ elastic data of Barlett et al.[1]

Figure 1 shows the hydrogen cross sections at 5, 11, and 15° plotted vs the laboratory momentum of the outgoing proton. The cross sections agree with our earlier work,[2] but show the structure, particularly near pion threshold, in greater detail. The solid lines in the figure are the result of a calculation carried out with the code by VerWest,[3] which uses a Born approximation treatment of NN scattering and includes π and ρ exchange.

The analyzing powers in Fig. 1 fall from a maximum value of about 0.3 at threshold to small values with little structure at low outgoing momenta. When the product of σ and A_y is formed, an interesting feature is observed — a clear peak, which crosses zero at the maximum of the

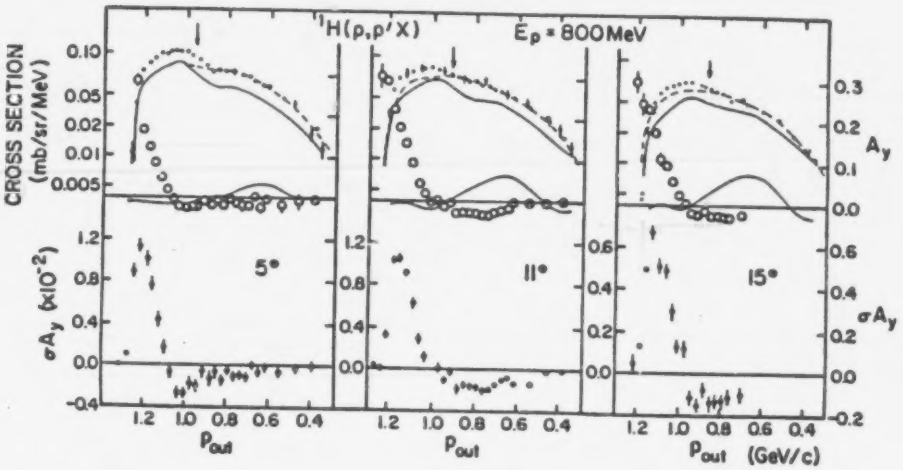

Fig. 1.
Differential cross sections, analyzing powers, and the products σA_y for inclusive (p,p') scattering from ^1H at lab angles of 5, 11, and 15°. The abscissa is the laboratory momentum of the outgoing proton. The solid curves are from a Born calculation of σ and A_y (Ref. 3). The dashed curves are the phase space available to a nucleon in the $NN \rightarrow NN\pi$ reaction. The arrows correspond to an excitation energy of 300 MeV.

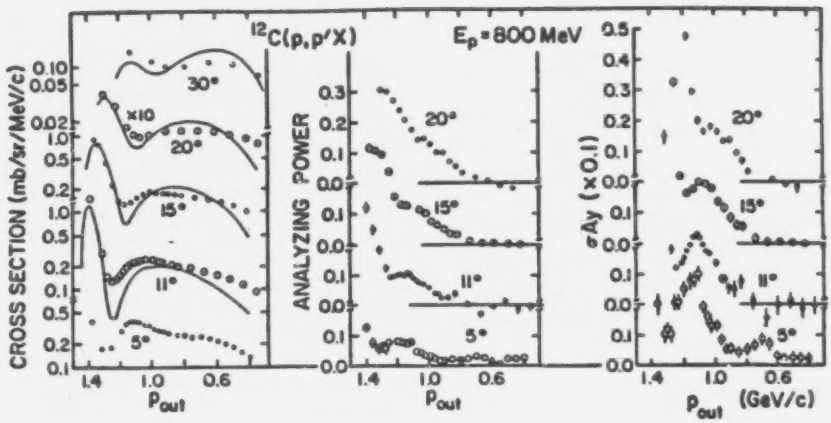

Fig. 2.
Differential cross sections, analyzing powers, and the products σA_y for inclusive (p,p') scattering from ^{12}C at lab angles of 5, 11, 15, and 20°. The curves for σ are taken from Ref. 6.

cross section. In fact, the σA_y spectrum resembles the logarithmic derivative of the cross section with respect to outgoing proton momentum; such a relation is surprisingly simple for an inclusive reaction. (Note that the product σA_y eliminates processes with zero analyzing powers and so can be a sensitive indicator of weak processes.) An attempt to predict A_y with the VerWest model fails badly, as shown in Fig. 1. A unitary-model calculation recently has been shown to be more successful in predicting spin-observables for exclusive final states; it is currently being adapted for application to these inclusive data.[4]

Examples of corresponding data for ^{12}C are shown in Fig. 2. Even with the greater accuracy of these measurements, they are strikingly similar to those for ^1H, as in the earlier work.[2] The cross sections for ^{12}C are about 7 times larger than for ^1H; the value of σA_y at the maximum in ^{12}C is 3 times larger.

It is important to note that the peak in the σA_y data for ^{12}C moves with angle approximately according to ^1H, not ^{12}C, kinematics, even though it is shifted down by about 50 MeV/c from the ^1H peak position. A smaller shift would be expected from binding-energy effects. We also note that at 5° the peak in the cross section is shifted by ~100 MeV/c to higher outgoing momenta. Fermi broadening can be expected to lower the threshold and wash out the structure of the nucleon-nucleon spectrum. Also, a peaking of the nucleon-nucleon cross section at some energy away from the incident beam energy can cause such a "Fermi shift" (as has been suggested[5] for the quasi-free $pp \rightarrow d\pi^+$ reaction), but the pion-production cross sections involved here are relatively flat above 750 MeV.

The solid curves in Fig. 2 have been calculated in a plane wave impulse approximation using an isobar-doorway model by Alexander et al.[6] The curves are arbitrarily normalized in the region of the quasi-elastic peak. Some of the discrepancies between the data and these curves, particularly at low outgoing momentum, can be attributed to the absence of distortions in the calculation. It would be useful to have a more detailed calculation of the theoretical expectations, including distortions. No calculations at all are available for the analyzing power in ^{12}C, partly because the pp data are themselves not explained.

In summary, we have reported the measurement of cross sections and analyzing powers for inclusive (p,p') reactions on ^1H and ^{12}C at 800 MeV. The cross sections, but not the analyzing powers, for ^1H can be reasonably explained in the Born-approximation model of VerWest. The data for ^{12}C are qualitatively similar to those for ^1H. A narrow peak is observed in the σA_y spectrum for both nuclei; even in ^{12}C, it moves with ^1H kinematics. Nevertheless, there are differences in detail, notably energy shifts, between the data for ^1H and ^{12}C.

This work was supported by the National Science Foundation, the USDOE, and the Robert A. Welch Foundation.

REFERENCES

1. M. L. Barlett et al., Phys. Rev. C 27, 682 (1983).

2. J. A. McGill et al., Phys. Rev. C (to be published).

3. B. J. VerWest, Phys. Lett. 3B, 61 (1979).

4. W. M. Kloet and R. R. Silbar, Nucl. Phys. A 338, 231 (1980); and J. Dubach, W. M. Kloet, A. Cass, and R. R. Silbar, Phys. Lett. 106B, 29 (1981).

5. H. Toki, to be published in Phys. Lett. B.

6. Y. Alexander, J. W. VanOrden, E. F. Redish, and S. J. Wallace, Phys. Rev. Lett. 44, 1579 (1980).

The $^9Be(\vec{p},\pi^+)^{10}Be$ and $^9Be(\vec{p},\pi^-)^{10}C$ Reactions at 650 MeV

(Exp. 649, HRS)

(Los Alamos, Univ. of California, Univ. of Minnesota, Univ. of South Carolina, Univ. of Texas at Austin)

Spokesman: Bo Höistad (Univ. of Texas at Austin)

Tentative results from the differential cross section as well as the analyzing power for the $^9Be(\vec{p},\pi^+)^{10}Be$ and $^9Be(\vec{p},\pi^-)^{10}C$ reactions are now available at 650 MeV. The angular distribution of the analyzing power A_y is presented in Fig. 1. The $(\vec{p},\pi^+)$ data from 10 to 30° were obtained in April 1981 and the rest of the data are from a run between December 28, 1983 and January 3, 1984. In addition, this experiment will receive beam time January 12-16, 1984, during which time more $(\vec{p},\pi^-)$ data will be collected.

From the present data, the salient features of A_y appear clearly. The $A_y(\pi^+)$ is negative out to ~35°, where it becomes positive. This trend is the same as observed previously for the $^{3,4}He(\vec{p},\pi^+)^{4,3}He$ reactions at 800 MeV.[1] Also, there is an indication of nuclear-structure dependence in the detailed shape of A_y.

The present data represent the first measurement of $A_y(\pi^-)$ far above the energy threshold. We note with interest that $A_y(\pi^-)$ has opposite sign compared to $A_y(\pi^+)$ in the observed angular range. In fact, this general behavior was predicted from a "pion knockout model" and was used as an argument to measure $A_y(\pi^-)$ as a test of this reaction model.

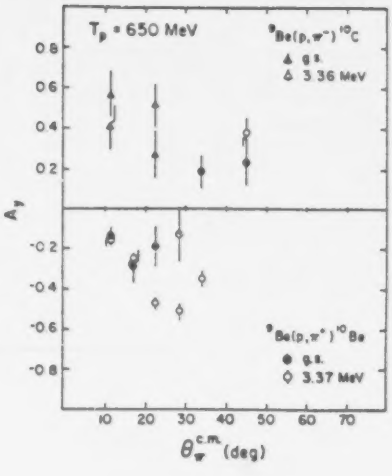

Fig. 1.
Analyzing power as a function of scattering angle in the center-of-mass system for both $^9Be(p,\pi^+)$ and $^9B(p,\pi^-)$ going to the ground state and first excited state.

A diagram of the model is shown in Fig. 2. In this process, a virtual pion is emitted from the target nucleus and knocked out by the incident proton. Since the upper vertex in the diagram corresponds to $\vec{p}\pi^+$ scattering for the $(\vec{p},\pi^+)$ and $\vec{p}\pi^-$ scattering for the (p,π^-) reaction, we can use A_y data from elastic πN scattering to predict $A_y(\pi^\pm)$ for ^9Be. A procedure for how this can be done is given in Ref. 1. If the large momentum transfer involved in the (p,π) reaction is assumed to be equally shared between the two lower vertices in Fig. 2, and if the captured proton is assumed to be on its mass shell (that is, the emitted pion is off shell), we get a shape of A_y for

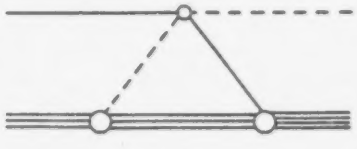

Fig. 2.
Diagram for pion knockout in the (p,π) reaction.

$^{9}Be(p,\pi^{+})^{10}Be$ that is in qualitative agreement with the experimental data. Moreover, A_y for $^{9}Be(\vec{p},\pi^{-})^{10}C$ is positive up to ~45°, which is consistent with the two data points available.

A further analysis will be performed when the data from the run in the middle of January 1984 can be included.

REFERENCE

1. B. Höistad et al., Phys. Rev. C 29, to be published.

Measurement of Spin Excitations in the $^{48}Ca(\vec{p},\vec{p}')^{48}Ca$ and $^{90}Zr(\vec{p},\vec{p}')^{90}Zr$ Reactions (Exp. 660, HRS)

(Rutgers Univ., Los Alamos, Arizona State Univ., Northwestern Univ., Tokyo Institute of Technology)

Spokesman: C. Glashausser (Rutgers Univ.)

The $M1$ transition in ^{48}Ca is an excellent test case for the study of magnetic dipole transitions because of the expected simple shell structure and the small fragmentation of the observed $M1$ strength. A strong $M1$ state was first observed at an excitation energy of 10.23 MeV in inelastic electron scattering[1]; the analog of this state has been observed in (p,n) measurements.[2] Previous (p,p') experiments with proton energies in the range of 45-200 MeV also have reported observation of this state, which is believed to be mostly a pure neutron $(\nu f_{7/2}^{-1} \cdot f_{5/2})_{1^+}$ configuration. The experimentally observed strength for the 10.23-MeV transition is approximately 30% of the predicted theoretical value obtained from the pure independent-particle model with bare g factors.

We have measured the cross section $\sigma(\theta)$, the analyzing power $A_y(\theta)$, and the spin-flip probability $S_{NN}(\theta)$ for the 10.23-MeV state in the $^{48}Ca(p,p')^{48}Ca^*$ reaction at 319 MeV. The data were taken at the HRS with a vertically polarized (N) proton beam. The polarization of the outgoing particles was measured with the focal plane polarimeter. An isotopically enriched ^{48}Ca (94.7%) target 100 mg/cm^2 thick was used; the total energy resolution was 120 keV. The data were taken at 3.5 and 5.0° laboratory angles.

Angular distributions for $\sigma(\theta)$, A_y, and S_{NN} are shown in Fig. 1. The shape of the σ angular distribution plotted vs momentum transfer q agrees well with the 200-MeV data[3]; the absolute cross section is about 10% higher. The curves represent distorted-wave impulse approxima-

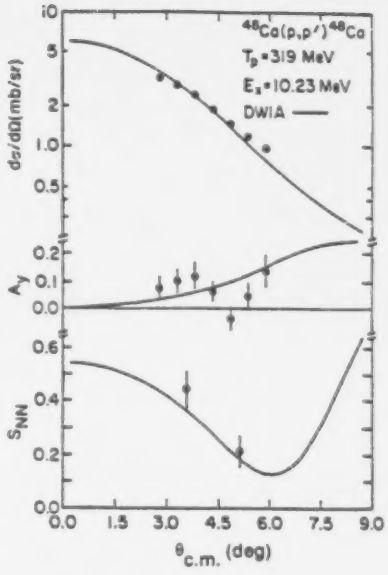

Fig. 1.
Measured values of $\sigma(\theta)$, A_y, and S_{NN} for the 10.23-MeV $M1$ transition in $^{48}Ca(p,p')^{48}Ca^*$ at 319 MeV. The solid curves correspond to DWIA calculations described in the text.

tion (DWIA) predictions with the code DW81 for the $M1$ transition assuming a $(\nu f_{7/2}^{-1} \cdot f_{5/2})_{1^+}$ transition; exchange was included exactly. The 325-MeV t matrix of Love and Franey was used; optical parameters were extrapolated from nearby energies. The σ angular distribution is well described by the DWIA calculation. The absolute cross section is about 28% of the DWIA prediction, which is consistent with the quenching observed in the (e,e') results of Ref. 1 and the previous (p,p') results at 200 MeV of Ref. 3.

The values of A_y for the 10.23-MeV state shown in Fig. 1 are small and mostly positive, similar to those measured for the 15.11-MeV 1^+ state in ^{12}C at energies from 400 to 800 MeV. There is a hint of structure in the ^{48}Ca data that has not been observed in ^{12}C. The DWIA calculations for ^{48}Ca agree reasonably well with the data; there is no indication of structure. Note that the pure neutron transition assumed here has equal amplitudes of isovector and isoscalar components in the wave function.

A pure isoscalar transition yields a negative A_y of about −0.30 at these q values, both in data for the 12.71-MeV 1^+, $T = 0$ state between 400 and 800 MeV and in calculations for ^{12}C and ^{48}Ca at 319 MeV. The A_y for the pure neutron transition is very similar to the A_y for a pure $\Delta T = 1$ transition, however, because of the weakness of the $\Delta T = 0$ components in the effective interaction at these energies.

In the plane-wave impulse approximation using only central forces and excluding exchange effects in the reaction, an $L = 0$, 0^+ to 1^+ transition should yield an S_{NN} value of 2/3, independent of q. Distortion effects, noncentral forces, and exchange effects tend to produce structure in the angular distribution of S_{NN}. In contrast, transitions with $\Delta S = 0$ yield S_{NN} values close to zero. Our measured values of S_{NN} are 0.44 ± 0.08 at 3.5° and 0.20 ± 0.07 at 5.0° for the 10.23-MeV state; the angular distribution is in good agreement with the DWIA predictions.

In summary, our measurements at small q for the 10.23-MeV transition in ^{48}Ca show large values of S_{NN} and small values of A_y, in good agreement with the DWIA. The measured σ is about 28% of the single-particle DWIA prediction, consistent with previous work. The results support the usefulness of S_{NN} measurements in searching for $M1$ strength in heavy nuclei, as well as the validity of a DWIA description of such data.

To determine whether significant unnatural-parity strength exists at excitations above the $M1$ giant resonance in ^{90}Zr, we measured $\sigma(\theta)$, $A_y(\theta)$, and $S_{NN}(\theta)$ in the $^{90}Zr(p,p')^{90}Zr$ reaction at 319 MeV. As with back-angle electron-scattering cross sections, the spin-flip cross section σS_{NN} is a measure of $\Delta S = 1$ excitations, whereas σ data by themselves can seldom distinguish between $\Delta S = 0$ and $\Delta S = 1$. The data were taken at the HRS, as described above. A thick target (250 mg/cm^2) was required, so the energy resolution was 180 keV and the instrumental background was significant.

Shown in Fig. 2 are the spectra of S_{NN} and σS_{NN} at 3.5° without background subtraction; data at 5° are similar, but they extend only to 16 MeV. As expected, spin-flip cross sections are small at low-excitation energy in the region of isolated states; they rise to significant values around 8 MeV. Compared to the higher excitation energy region, however, the region around 9 MeV is in no way remarkable. Rather, spin excitations are observed up to at least 25 MeV where only natural-parity states previously have been seen.

If a simple background is drawn in the 9-MeV region, a value of 0.62 ± 0.20 is obtained for S_{NN}, but because of

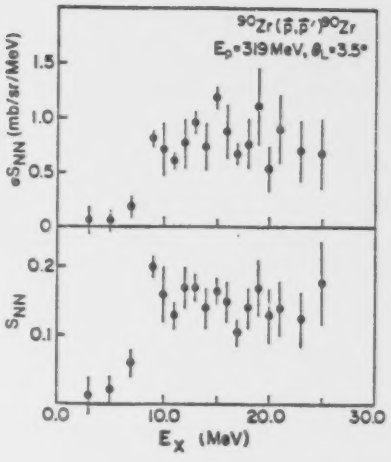

Fig. 2.
Spectra of S_{NN} and σS_{NN} for the $^{90}Zr(p,p')^{90}Zr^*$ reaction at 3.5°.

the uncertainty in the background, the systematic error in this value is large. To calibrate the value expected for a pure $M1$ transition, S_{NN} was measured for the $^{48}Ca(p,p')^{48}Ca^*$ reaction to the 10.23-MeV 1^+ state as described above. The value obtained, 0.44 ± 0.08 at 3.5°, is consistent with an $M1$ assignment for the 9-MeV bump in ^{90}Zr. The poor resolution of the present S_{NN} data does not permit isolation of individual $E1$ states.

We have closely examined many possible sources of error in obtaining the spectra of Fig. 2, but because of the uniform spreading of the spin-flip strength, it is difficult to be certain that all sources of error have been eliminated. Nevertheless, our results strongly suggest that the spin-flip cross section at 3.5° is approximately 0.8 mb/sr/MeV throughout the region from 8- to 25-MeV excitation.

Although no spin excitations previously have been observed above 10 MeV, it is important to note that no experiments really sensitive to such strength have been performed. The uniform spreading of the σS_{NN} strength is suggestive of the apparent quasi-free background observed in the (p,n) reaction; Osterfeld explains this as $\Delta S = 1$ excitations up to spin 3$^+$ even at 0°. It is interesting to observe that the S_{NN} predicted by Arndt's phase-shift solutions at 3.5° are 0.37 and 0.20 for free pp and pn scattering, respectively. Comparison with the S_{NN}

values in Fig. 2 shows that the nuclear response is not dramatically different from that of a Fermi gas, even though this is a region of high natural-parity collectivity. This result disagrees with the conclusions of Moss et al.[4] for ^{208}Pb at 400 MeV.

REFERENCES

1. W. Steffen et al., Phys. Lett. 95B, 23 (1980).

2. B. D. Anderson et al., Phys. Rev. Lett. 45, 699 (1980); and C. D. Goodman, Nucl. Phys. A 374, 241 (1982).

3. G. M. Crawley et al., Phys. Lett. 127B, 322 (1983).

4. J. M. Moss et al., Phys. Rev. Lett. 48, 789 (1982).

Giant Resonance Studies with Medium-Energy Protons

(Exp. 670, HRS)

(Los Alamos, Univ. of South Carolina)

Spokesmen: T. A. Carey and J. M. Moss (Los Alamos) and G. S. Adams (Univ. of South Carolina)

Our efforts in the development of unique small-angle scattering techniques for the exploration of $M1$ strength at the HRS have proved equally fruitful in searches for new giant resonances (GRs).

Starting with our discovery[1] of an isoscalar high-energy octupole resonance (ISHEOR) occurring systematically at $E_x \simeq 110A^{-1/3}$ in heavy nuclei, increased attention has been focused on the high-excitation spectrum of ^{208}Pb. In addition to the ISHEOR at $E_x \simeq 19$ MeV, theoretical calculations have predicted the existence of both isoscalar giant dipole resonances (ISGDRs) and isovector giant quadrupole resonances (IVGQRs) at about 22 MeV of excitation in ^{208}Pb. Since they are isospin partners of the well-known isovector giant dipole resonances (IVGDRs) and isoscalar giant quadrupole resonances (ISGQRs), an experimental determination of their existence and properties would place important general constraints on theoretical models of the nuclear response and of the residual interaction in nuclei. Previous investigations of this region have led to strongly conflicting interpretations; a group from Jülich using 172-MeV α particles favors the ISGDR at $E_x \simeq 21$ MeV, whereas a group from Orsay has claimed strong excitation of the IVGQR near $E_x \simeq 22$ MeV with 200-MeV protons.

In our opinion, both of these experiments suffered from low sensitivity because of large backgrounds and neither provided adequate evidence to support their respective conclusions. On the other hand, the small-angle system at the HRS is virtually free of instrumental background. Furthermore, we have previously shown[2] that in 800-MeV proton inelastic scattering the nuclear continuum is dominated by quasi-free scattering, and at small momentum transfers, Pauli-blocking suppresses it in such a way as to considerably enhance the signals of weakly excited GR.

Exploiting these two facts in a February 1983 run, we obtained GR data of the unparalleled quality illustrated in Fig. 1. At the larger scattering angles the previously observed ISGQR ($\Delta L = 2$) and ISHEOR ($\Delta L = 3$) are clearly evident, and as we move to very forward angles we see the definite appearance of other broad structures near 13 and 22 MeV of excitation in ^{208}Pb. The dominantly isoscalar character of 800-MeV protons, in conjunction with the angular distribution of the high-excitation bump as compared with that for the ISGQR, strongly suggests an isoscalar dipole ($\Delta L = 1$) assignment.

We have identified similar structures in comparable data for ^{144}Sm and ^{116}Sn, and together their excitation energies exhibit a target-mass dependence close to that predicted for the ISGDR. The peak near $E_x = 13$ MeV in ^{208}Pb that is strong at $\theta_{lab} = 1.8°$ and completely disappears by $\theta_{lab} = 2.5°$ might tentatively be identified with the isoscalar giant monopole ($\Delta L = 0$) resonance (ISGMR), but such extreme forward peaking could also be indicative of Coulomb excitation of the standard isovector dipole mode. Therefore, a considerable fraction of the concentrated strength seen near $E_x = 22$ MeV at the smallest angles may be due to Coulomb excitation of the IVGQR. Theoretical analysis of these possibilities employing microscopic transition densities in extensive inelastic-scattering calculations is in progress.

To further aid us in sorting out this region of the ^{208}Pb spectrum, we have also explored it with pion inelastic scattering, since (π,π') incorporates an isospin selectivity fundamentally different from that of (p,p').

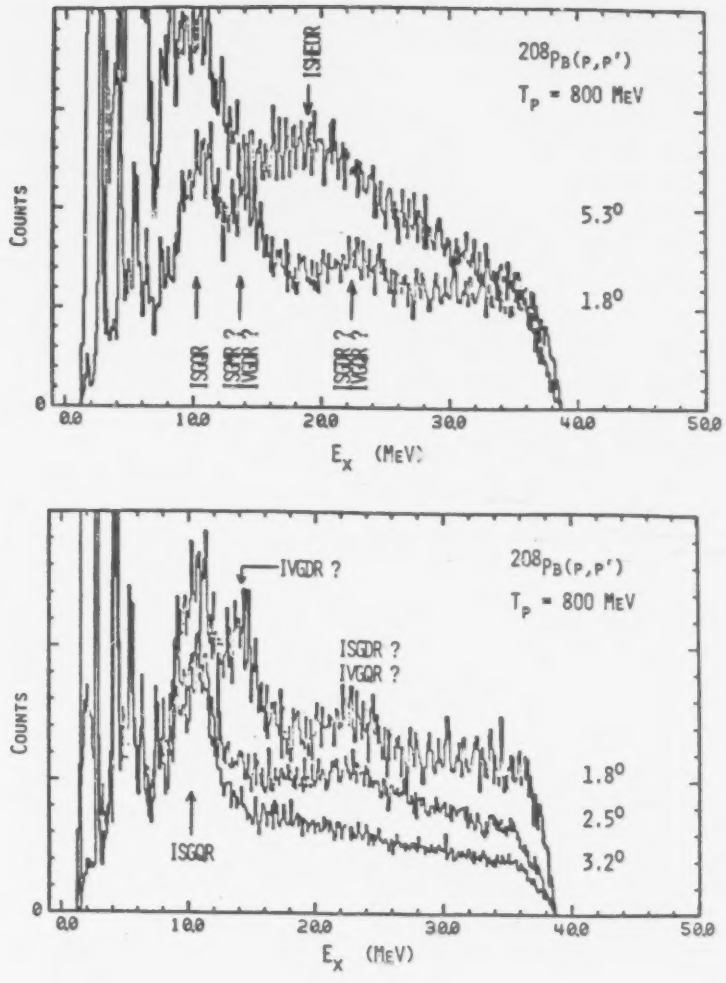

Fig. 1.
On-line excitation spectra for ^{208}Pb at various laboratory scattering angles. The relative normalizations between different angle bins were arbitrarily selected for display purposes only.

REFERENCES

1. T. A. Carey et al., Phys. Rev. Lett. 45, 239 (1980).

2. J. M. Moss et al., Phys. Rev. Lett. 48, 789 (1982).

Measurement of the Third-Order Spin-Dependent Observables for the $\vec{p}\vec{d} \rightarrow \vec{p}d$ at 800 MeV with a Polarized Deuterium Target

(Exp. 685, HRS)

(UCLA; Los Alamos; KEK Lab.; Hiroshima Univ.; Kyoto Univ. of Education, Japan; Univ. of Minnesota)
Spokesmen: G. J. Igo and M. Bleszynski (UCLA)

A collaboration has measured some third-order spin-dependent observables for $\vec{p}\vec{d} \rightarrow \vec{p}d$ elastic scattering at 800 MeV at the HRS. This experiment uses a polarized proton beam and a polarized deuterium target while measuring the polarization of the scattered proton. During the period September-October 1983 we used an *N*-type (perpendicular to the scattering plane) polarized deuterium target. By using an *N*-type polarized target with all three independent proton beam spin directions, we plan to extract roughly 14 observables that have never been measured for the spin-1/2 on spin-1 system at 800 MeV. The analysis of these data has just started, so no results are available yet.

To completely determine the *pd* scattering amplitude, 23 independent observables must be measured.[1] During the next 2 years, we plan to complete the measurement of these third-order $\vec{p}\vec{d} \rightarrow \vec{p}d$ observables with *L*- and *S*-type polarized deuterium targets using a superconducting magnet. This should allow us to completely determine the *pd* scattering amplitude at 800 MeV for the four-momentum transfer range $-t = 0.03\text{-}0.22$ $(\text{GeV/c})^2$ (7-19° lab). As a result of this work, we also hope to better understand the multiple-scattering theory.

In these experiments with a polarized deuteron target, we use a horizontal dilution refrigerator,[2,3] thus pumping on the ^{3}He/^{4}He dilution phase. The propanediol-D8 target can be cooled to ~20 mK and can be polarized using microwaves (~69 GHz) to ~30% deuteron vector polarization (tensor polarization ~7%) in a 25-kOe magnetic field. Because of the low temperature attainable, we operate the polarized target in a spin-frozen mode using a holding magnetic field of 10 kOe and still have a deuteron spin-relaxation time > 100 h. A drawing of the experimental floor layout is shown in Fig. 1. After the scattering target, the HRS was used in its standard configuration with the focal-plane polarimeter. Wire chambers C1 and C2 and scintillators M1 through M8 make up the monitor telescope used to measure the target and beam polarizations.

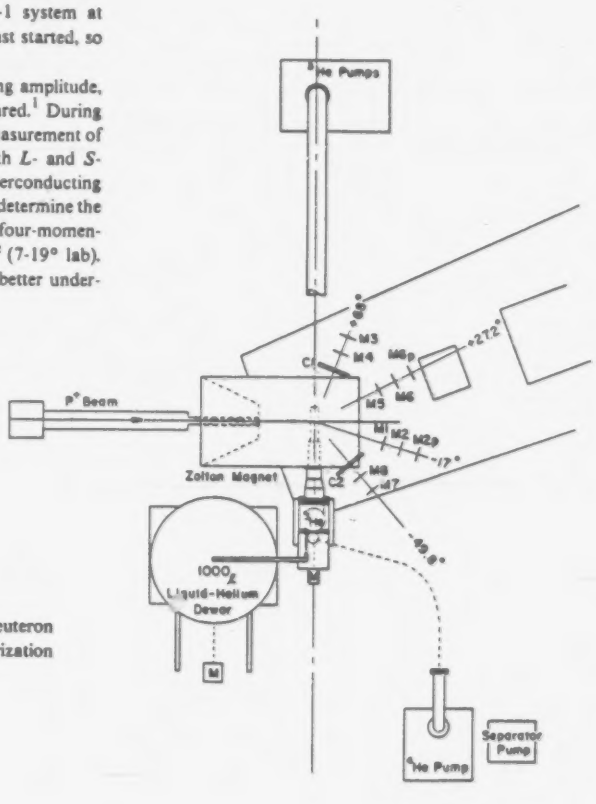

Fig. 1.
Experimental floor layout for polarized deuteron target, including layout of target polarization monitor.

We hope to measure the deuteron target polarization in three ways. The first technique involves measuring left/right (±22° c.m., near maximum of deuteron analyzing power) with the HRS. Using the proton analyzing power with the deuteron vector and tensor analyzing powers previously measured[4] allows one to extract the target and beam polarizations. The second method uses the monitor telescope. By monitoring the *pp* quasi-free scattering asymmetry from the deuterium target, we hope to determine both the target and beam polarizations. In addition to these scattering asymmetry measurements, a third method uses coils positioned around the target flask to obtain deuteron magnetic resonance (DMR) data, which determine the average target polarization throughout the target flask. This method should provide a relative measure of the target polarization. All three of these techniques are presently being pursued.

REFERENCES

1. G. Alberi, M. Bleszynski, T. Jaroszewicz, and S. Santos, Phys. Lett. 92B, 41 (1980).

2. S. Ishimoto et al., Nucl. Instrum. Methods 171, 269 (1980).

3. A. Masaike, "Polarized Target with Dilution Refrigerator," Argonne National Laboratory report ANL-HEP-PR-77-88.

4. M. Bleszynski et al., Phys. Lett. 87B, 198 (1979).

Neutron Transition Densities in ^{208}Pb (p,p') at 318 MeV

(Exp. 686, HRS)

(Univ. of Minnesota, Los Alamos, Univ. of Texas)

Spokesman: N. Hintz (Univ. of Minnesota)

The purpose of this experiment was to obtain high-resolution (ΔE = 35- to 45-keV) data on inelastic proton scattering to the low-lying "collective" states and the high-spin particle-hole states of ^{208}Pb. From these data we plan to extract neutron transition densities, making use of collective or microscopic models and proton densities from electron scattering.

In our earlier experiment (Exp. 347) at 800 MeV, the high-spin natural-parity states (10^+, 12^+) were poorly resolved, and the unnatural-parity states (12^-, 14^-) were not seen above background. However, at 318 MeV, because of improved resolution and the increased ratio of the spin-dependent to spin-independent parts of the *NN* force, the high-spin states are better (though not completely) resolved. In January 1983, data were obtained up to an excitation energy of $E^* \simeq 12$ MeV over an angular range of θ_L = 3-40°. A spectrum at θ_L = 28° is shown in Fig. 1.

The ground-state angular distribution is shown in Fig. 2. The absolute normalization is still tentative but is believed to be good to ±10%. The elastic angular distribution was fit with a 2PF phenomenological optical

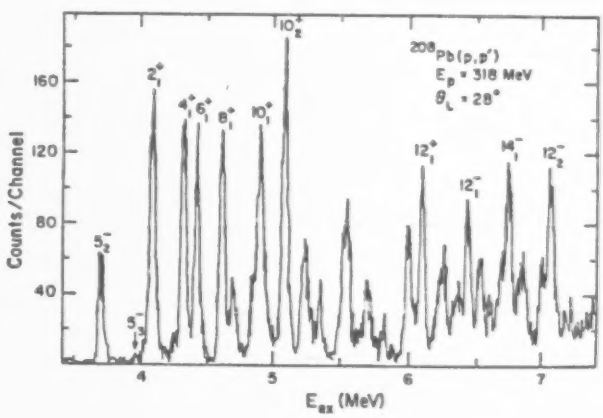

Fig. 1.
Spectrum for proton scattering from ^{208}Pb at an incident energy of 318 MeV.

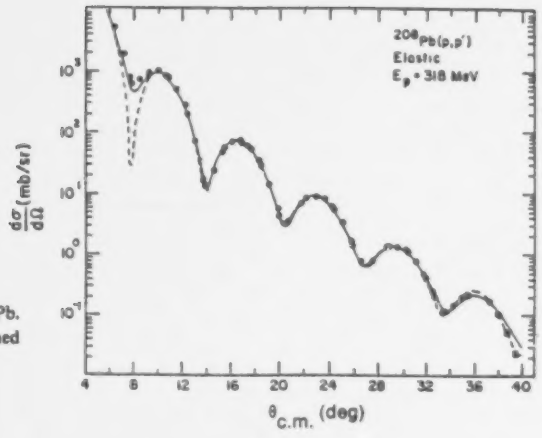

Fig. 2.
Elastic-scattering angular distribution for ^{208}Pb. The curves are with (solid line) and without (dashed line) a spin-orbit potential.

potential by searching with the program RELOM, both with and without a spin-orbit potential. The results are not completely satisfactory, even with the spin-orbit potential included, in contrast to the situation at 800 MeV where excellent fits were obtained both with and without spin orbit. We are now attempting, with folded [first-order Kerman-McManus-Thaler (KMT)] and with phenomenological optical potentials with repulsive real cores, to obtain a better representation of the elastic data for the inelastic analysis.

For the low-spin states, we have, as a first step, used collective form factors (vibrating potential model) to obtain deformation lengths δ_λ for comparison with those obtained at other energies. Figure 3 shows predictions (theory normalized to data to obtain β_λ) for the 3^- state (using the optical potential with a spin-orbit term) with the spin-orbit deformation β_s varied. The best fit is for β_c (central potential deformation) = β_s. However, as Fig. 4 shows, there is some indication that the fits improve for higher spin collective states ($J \geq 6$) with $\beta_s > \beta_c$. Our

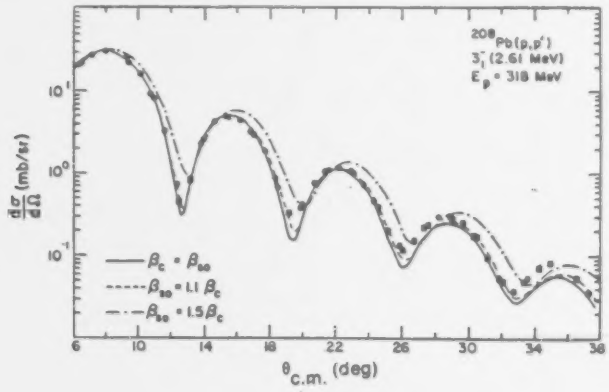

Fig. 3.
Angular distribution for the 3^- state in ^{208}Pb. The curves are described in the text.

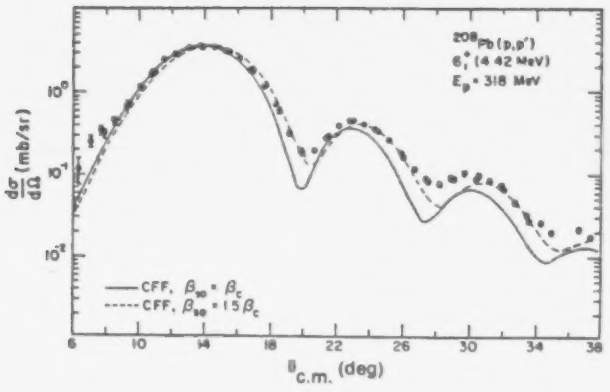

Fig. 4.
Angular distribution for the 6^+ state in ^{208}Pb. The curves are described in the text.

tentative fits are not of the same quality as the 800-MeV fits.[1]

Another purpose of this experiment was to examine high-spin "stretched configuration" states in ^{208}Pb. In Fig. 5 the angular distribution for the 14^- (6.74-MeV) state is shown. The calculation was done in the distorted-wave impulse approximation (DWIA) with bound-state Woods-Saxon wave functions ($r = 1.2$, $a = 0.65$) for a pure $\nu(i_{13/2}^{-1}, j_{15/2})$ configuration, using the free Love-Franey *NN* force to represent the interaction. The theoretical curve has been normalized to the data, with $\sigma_{EXP}/\sigma_{THEO} = 0.25$. However, as can be seen in Fig. 1, there is significant background under this peak, which leads to an uncertainty in σ_{EXP} well above that resulting from the absolute normalization alone.

REFERENCE

1. M. Gazzaly et al., Phys. Rev. C 25, 408 (1982).

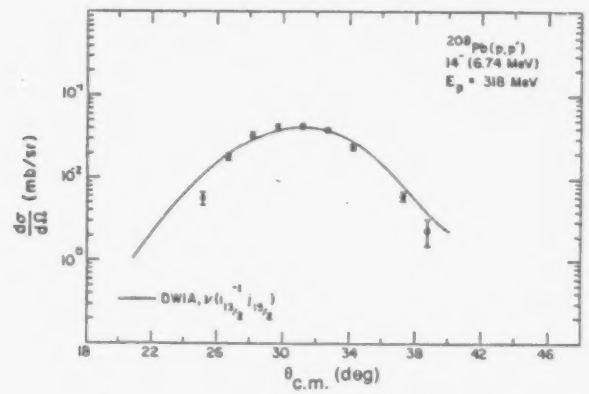

Fig. 5.
Angular distribution for the stretched 14^- state in ^{208}Pb. The curve is described in the text.

Measurement of A_{NN} for $\bar{p}p$ Elastic Scattering in the Coulomb-Nuclear Interference Region at 650 and 800 MeV

(Exp. 709, HRS)

(Univ. of Minnesota; UCLA; Los Alamos; KEK Lab.; Hiroshima Univ.; Kyoto Univ. of Education, Japan)

Spokesmen: M. Gazzaly (Univ. of Minnesota), G. Pauletta (UCLA), and N. Tanaka (Los Alamos)

The first of a series of experiments to measure the real parts of the forward, double spin-flip amplitudes at intermediate energies was completed in September 1983. Measurements were made at 650 and 800 MeV with an *N*-polarized proton beam and *N*-polarized frozen-spin target on HRS. The dilution refrigerator and polarized target expertise were provided by a team from KEK Laboratory, Hiroshima University, and Kyoto University of Education, Japan.

Whereas the imaginary parts of the forward, double spin-flip *pp* amplitudes at intermediate energies have been determined by measurements of the total *pp* cross sections (σ_{tot}, $\Delta\sigma_L$, $\Delta\sigma_T$) with polarized beam and target combinations,[1] we still rely on the semiphenomenological predictions of the forward dispersion relations[2] (FDRs) for our knowledge of the real parts. These predictions are used as constraints on current phase-shift analyses. The experimental determination of the real parts by measurements of A_{NN}, A_{LL}, A_{SS}, and A_{LS} in the Coulomb-nuclear interference region are therefore desirable, but have not yet been attempted because of experimental difficulties. At intermediate energies, the motivation for experimental data is enhanced by the observation of energy dependence in the imaginary parts.[2] This structure leads to similar structure in the FDR predictions of the real parts and to counterclockwise rotations of their Argand diagrams, which have been interpreted as evidence for the existence of dibaryon resonances.

Motivated by the interests outlined above, a series of experiments to determine the real parts of the forward *pp* double spin-flip amplitudes at 650 and 800 MeV has been initiated. Here we report on the first of these measurements, namely, that of A_{NN}.

To extend such measurements to small angles, one must be able to distinguish between scattering from the heavier target and cryostat components and scattering from hydrogen. Since the energy of the recoil proton is too small to allow detection, one must rely entirely on momentum resolution for the forward-scattered proton to separate out the hydrogen elastic-scattering component. The intrinsic momentum resolution of the HRS is more than adequate, so that the total experimental momentum resolution is determined by the combined thickness of the polarized target and the cryostat walls.

For our experiment, the outermost and thickest of the cryostat walls was modified so that the incident beam and the scattered protons passed through thin (0.2-mil) titanium windows and so that the effective target thickness was 0.5 cm. The polarizing field of 25 kG was provided by a *C*-type magnet (Zoltan) obtained from Lawrence Berkeley Laboratory. After the target polarization had been frozen, the field was reduced to 3 kG to minimize deflections of the incident and scattered protons in the field of Zoltan. Using calculations based on field maps, the scattering angle measured by the HRS was corrected for these deflections.

Spectrometer calculations were performed using a series of wire targets, and the beam position on target was determined by inserting a phosphor at the target position. The cryostat could be removed from the target position and replaced reproducibly by means of a system of synchronized servo-motors that moved the cryostat and associated liquid helium dewar in unison. The target position was checked by x-ray photographs. Upstream and downstream wire chambers were used to monitor beam profiles, which were typically 3 mm (horizontally) by 4 mm (vertically) FWHM. At larger angles, where momentum and angular resolution were not critical, the beam was wiggled $\sim\pm 3$ mm about its central horizontal position, with a frequency of $\sim$60 Hz to reduce the incident beam density, permitting higher beam currents with acceptable target depolarization. A beam flux of $\sim 2 \times 10^6$/s in a stationary spot of size given above produced an $\sim$5 h target polarization relaxation time.

Mean target polarizations were measured by NMR, but since the polarization in the target volume illuminated by the beam varied more rapidly than the average polarization, it was necessary to measure and monitor the relevant target polarization by other means. A polarimeter made up of two scintillation counter telescopes at $\pm 18.5°$ and two conjugate recoil telescopes at $\sim\pm 61.5°$ was used to monitor both beam and target polarization. Each of the recoil arms consisted of a multiwire proportional chamber (MWPC) and two scintillators. The scattering-angle information from the MWPCs was used to distinguish between elastic *pp* scattering and quasi-free *pp* scattering from bound protons in the nuclei of the target material and cryostat

windows. Since A_N is known to $\sim\pm 3\%$ for 800-MeV elastic scattering at 18.5°, the beam and target polarizations could be determined to this accuracy. The beam polarization also was obtained independently by the quench method.[3] The beam intensities were monitored by means of high-gain ion chambers filled with xenon and krypton gas, respectively, at 2-atm pressure.

Four independent measurements were made at each spectrometer angle: $Y(\uparrow\uparrow)$, $Y(\downarrow\uparrow)$, $Y(\uparrow\downarrow)$, and $Y(\downarrow\downarrow)$, where the first arrow in the parentheses refers to the direction of the beam polarization relative to the scattering plane, and the second arrow refers to that of the target. The target polarization was reversed once at each angle, whereas the beam polarization was reversed every 120 s in a repetitive cycle: up-quench-down-quench.... From the above measurements, four independent quantities were calculated:

$$\epsilon_1 = Y(\uparrow\uparrow) - Y(\downarrow\uparrow) - Y(\uparrow\downarrow) + Y(\downarrow\downarrow) = 4Y_0 P_B P_T A_{NN} ,$$

$$\epsilon_2 = Y(\uparrow\uparrow) + Y(\downarrow\uparrow) - Y(\uparrow\downarrow) - Y(\downarrow\downarrow) = 4Y_0 P_T A_N ,$$

$$\epsilon_3 = Y(\uparrow\uparrow) - Y(\downarrow\uparrow) + Y(\uparrow\downarrow) - Y(\downarrow\downarrow) = 4Y_0 P_B A_N ,$$

$$\epsilon_4 = Y(\uparrow\uparrow) + Y(\downarrow\uparrow) + Y(\uparrow\downarrow) + Y(\downarrow\downarrow) = 4Y_0 .$$

where Y_0 is the spin-averaged yield, P_T is the target polarization, and P_B is the beam polarization. Since both the beam and target polarizations were determined independently as described above, values of A_{NN} and A_N could be extracted at each angle. A more sophisticated analysis that takes into account differences in the values of the beam and target polarizations as a function of the polarization direction is needed to eliminate spurious asymmetries; such an analysis is in progress.

REFERENCES

1. I. P. Auer, Nucl. Phys. A 335, 193 (1980); and D. Bugg, Nucl. Phys. A 374, 95 (1982).

2. W. Grein and P. Kroll, Nucl. Phys. B 136, 425 (1978).

3. M. A. McNaughton et al., Phys. Rev. C 23, 1128 (1981).

Development of 0° Capabilities at the HRS Facility (Exp. 768, HRS)

(Los Alamos, Univ. of Minnesota, Rutgers Univ.)
Spokesmen: J. B. McClelland and T. A. Carey, (Los Alamos) and S. Seestrom-Morris (Univ. of Minnesota)

A great deal of time and effort has been devoted in the past several years to obtaining very forward-angle inelastic proton spectra on medium to heavy nuclei at different medium-energy facilities. The thrust of this effort has been directed toward the identification of giant monopole and dipole excitation in these nuclei. The most successful measurements have been made at low energies (200-300 MeV) where the interaction causes a selectivity of spin-flip over non-spin-flip transitions, especially for low momentum transfer to the nucleus.

The ultimate goal of this experiment is to obtain high-quality spectra on medium to heavy nuclei in an effort to identify $M1$ strength systematically. The added selectivity of 0° measurements might disentangle the question of $M1$, $E1$, and $M2$ assignments.

We have recently run this experiment at 318 MeV on a variety of targets, and show here some preliminary on-line spectra taken during this run. This is the lowest energy at which 0° spectra have successfully been acquired at HRS. These spectra were taken without the use of either the active collimator system or focal-plane beam-pipe setup. The primary source of background was due to rescattering of particles from the exit flange of the spectrometer, provided that all other parameters had been optimized.

The quality of the preliminary spectra is good. The ^{12}C spectrum [Fig. 1(a)] is comparable to the best obtained at $T_p = 500$ MeV [Fig. 1(b)]. The 1^+ state in ^{48}Ca is clearly seen in Fig. 2, and the periodic structure seen in these spectra likely will be removed when calibrations are optimized. Evidence for increased Coulomb scattering because of the heavier mass target may be seen at low excitation in the ^{48}Ca spectrum.

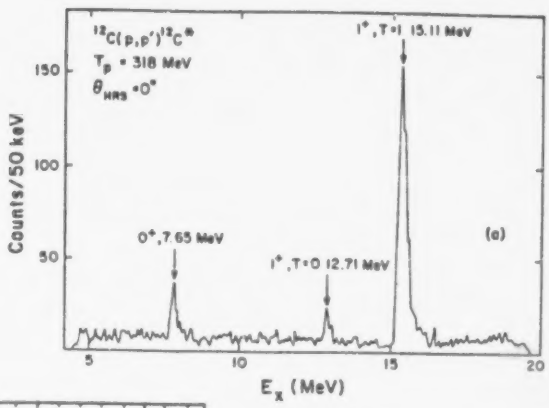

Fig. 1(a) and (b).
Spectra for ^{12}C at a 0° scattering angle for incident proton energies of (a) 318 MeV, and (b) 500 MeV.

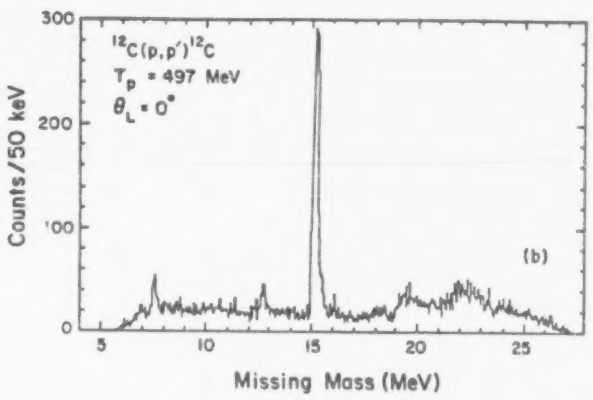

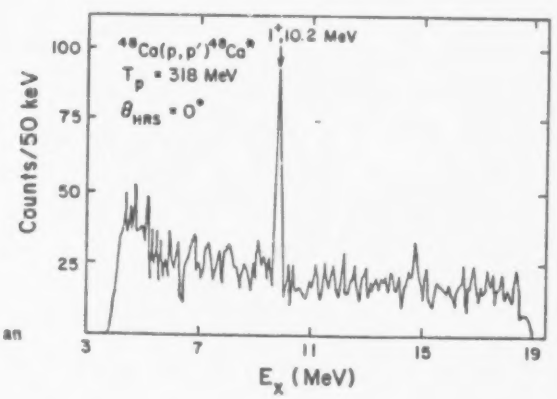

Fig. 2.
Spectrum for ^{48}Ca at a 0° scattering angle for an incident proton energy of 318 MeV.

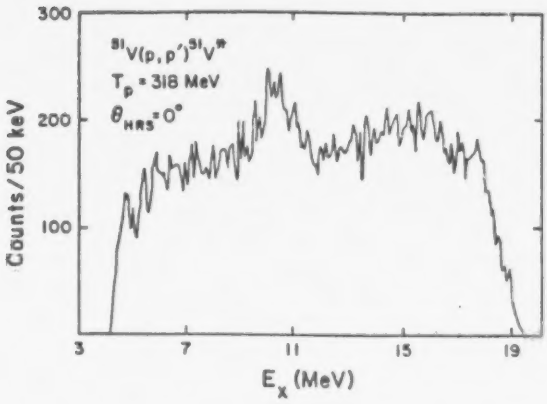

Fig. 3.
Spectrum for ^{51}V at a 0° scattering angle for an incident proton energy of 318 MeV.

Figure 3 shows a spectrum for ^{51}V at 0°. The quality of this spectrum is comparable to, if not better than, small-angle spectra taken at Orsay at 200 MeV. Furthermore, preliminary results show that the resonance is at about the same excitation energy as that seen at 200 MeV. Inadequate calibrations preclude any statement about fine structure in the resonance at this stage. Absolute normalization data have been taken, and it is hoped that absolute cross sections with reasonable error bars may be extracted from these data.

Measurement of A_{NN} for the $\bar{p}\bar{p} \rightarrow d\pi^+$ Reaction at 650 and 800 MeV (Exp. 790, HRS)

(UCLA; Univ. of Minnesota; Los Alamos; KEK Lab.; Hiroshima Univ.; Kyoto Univ. of Education, Japan)
Spokesmen: G. Pauletta (UCLA), M. Gazzaly (Univ. of Minnesota), and N. Tanaka (Los Alamos)

The $A_{NN}(\bar{p}\bar{p} \rightarrow d\pi^+)$ was measured at 650 and 800 MeV for laboratory angles of 2, 3.5, 5.5, and 7.5°. The aim of the experiment is to measure A_{NN}, A_{LL}, A_{SS}, and A_{LS} for this reaction at angles not previously accessible. When combined with measurements from previous experiments, complete angular distributions will be obtained. This can be integrated to obtain $\Delta\sigma_L(\bar{p}\bar{p} \rightarrow d\pi^+)$ and $\Delta\sigma_T(\bar{p}\bar{p} \rightarrow d\pi^+)$. The decomposition of the total cross sections $\Delta\sigma_L(\bar{p}\bar{p})$ and $\Delta\sigma_T(\bar{p}\bar{p})$ into their inelastic components will be obtained by further combination of these data with complete elastic $\bar{p}\bar{p}$ angular distributions (Exps. 583 and 709). The measurement of A_{LL} at 0 and 180° is of particular interest since it will provide the only measurements for the deuteron tensor polarization T_{20}. These data will contribute to our general understanding of the $I = 1$ nucleon-nucleon interaction and of the specific problem of the reaction mechanism involved in the $pp \rightarrow d\pi^+$ reaction.

This experiment was performed at the HRS using the same experimental setup as Exp. 709. Figure 1 presents a dot plot of energy loss vs time of flight. Since the deuteron momenta are greater than any proton momenta from the beam-target interactions, a clear deuteron group is observed in Fig. 1 along with a proton group caused by protons that scatter off the spectrometer magnet pole faces. Figure 2 presents a missing-mass spectrum for the deuterons. A clear peak is observed that corresponds to the $pp \rightarrow d\pi^+$ reaction. The data from this experiment are being analyzed.

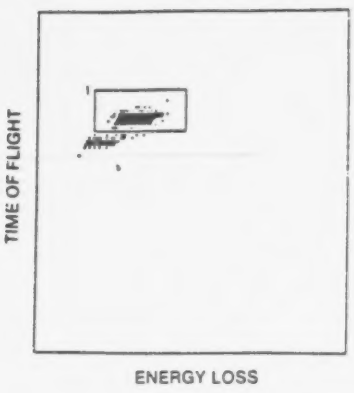

Fig. 1.
A dot plot of energy loss vs time of flight measured by the detector array at the focal plane of the HRS. Deuterons are designated by the box.

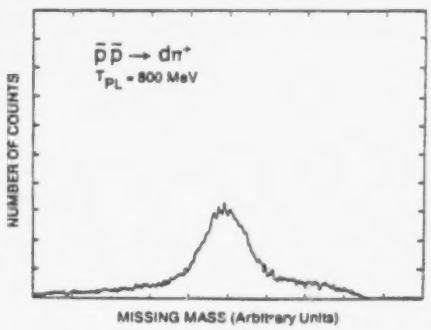

Fig. 2.
A deuteron missing-mass spectra measured at the HRS focal plane. A clear peak corresponding to the $pp \rightarrow d\pi^+$ reaction is observed.

Spin-Depolarization Measurements on the Oxygen Isotopes
(Exp. 643, HRS)

(MIT, Indiana Univ., UCLA, Lawrence Livermore Lab., Los Alamos)
Spokesmen: James J. Kelly (MIT) and M. V. Hynes and B. Aas (Los Alamos)

This experiment will use measurements of the spin-depolarization coefficients D_{as} to enhance the study of the two-nucleon effective interaction in the nuclear medium and to improve the precision with which nuclear-structure comparisons can be made among the oxygen isotopes. Ultimately, we wish to obtain spin-rotation measurements for elastic scattering by $^{14-18}$O and spin-depolarization measurements for as many inelastic excitations of all three isotopes as possible. Data taking has been completed for ^{16}O, but has not yet begun for ^{17}O or ^{18}O.

The central data-analysis problem is to apply line-shape analysis techniques to many spectra simultaneously and to obtain the maximum statistical precision without introducing bias. Because we believe that the techniques currently available are inadequate, we have formulated the maximum-likelihood estimators for the observables of interest and are studying the application of these estimators to line-shape fitting. An extensive Monte Carlo simulation program for the HRS and focal-plane polarimeter has been written, but the optimal data-reduction strategy has not yet been decided. It is clear from the volume of magnetic tape requiring processing that a careful decision is advisable before replaying the data.

A preliminary analysis of the cross-section and analyzing-power data obtained with *N*-type beam has been performed. These data have been compared with impulse-approximation calculations. Qualitatively, the same systematics is observed at 500 MeV as was observed at 318 MeV, with a somewhat stronger enhancement of the interior states over the predictions.

Energy Dependence of the Two-Nucleon Effective Interaction
(Exp. 718, HRS)

(MIT, Indiana Univ., UCLA, Lawrence Livermore Lab., Los Alamos)

Spokesmen: James J. Kelly (MIT) and M. V. Hynes (Los Alamos)

The two-nucleon effective interaction is modified in the nuclear medium by the local density in the vicinity of the interacting nucleons. These modifications have been most carefully studied for incident proton energies between 100 and 200 MeV.

The magnitude of these medium corrections is expected to decrease slowly with energy. To study this energy dependence, we have measured the cross section and analyzing power for the excitation of all narrow states of ^{16}O below 13-MeV inelasticity by 318-MeV protons. These data will be combined with comparable 135- and 180-MeV data taken at the Indiana University Cyclotron Facility (IUCF) and 500-MeV data taken at LAMPF (Exp. 643).

Approximately one-half of the data has been reduced, forming angular distributions with twice the expected final-step size. These data have been compared with impulse-approximation calculations based on the Love-Franey interaction, and with local density approximation calculations using a G matrix based on the Paris potential. The nuclear structure was specified by transition densities fitted to electron-scattering data.

To summarize the comparisons between theory and experiment, it is convenient to divide the states into two classes: (1) interior states whose transition densities peak in the high-density nuclear interior, and (2) surface states whose transition densities peak in the low-density nuclear surface. The predicted cross sections for surface states agree well with the data at the peak of the angular distributions. For interior states the predicted peak cross sections are about 30% below the data. The high momentum-transfer (q) predictions for all states are substantially below the data.

These results allow us to draw several conclusions about the 318-MeV effective interaction. First, the low-q amplitude is approximately correct for small density. Second, the strength of the dominant imaginary part of the isoscalar spin-independent central component is enhanced as the density increases. And third, the high q interaction needs to be enhanced, but it is not yet clear whether this effect depends on density. These conclusions will be quantified using the modeling techniques briefly described below.

Direct Reaction Analysis with Linear Expansions

James J. Kelly (MIT)

A general modelling technique has been developed that can fit a variety of linear expansions to any set of direct reaction observables. This technique has been implemented for nucleon-nucleus scattering, but can be readily expanded to include electron scattering and pion scattering.

If we expand the scattering operator U in a linear basis such that

$$U = \sum_n a_n U_n \ ,$$

the distorted-wave matrix element for the reaction $A(\bar{a},\bar{b})B$ may be written

$$T = \sum_n a_n \langle \bar{k}_f \, {}^{J_B J_b}_{m_B m_b} \left| \, U_n \, \right| \, {}^{J_A J_a}_{m_A m_a} \bar{K}_i \rangle$$

$$= \sum_n a_n H^n_{m_B m_b m_A m_a}(\theta) \ ,$$

where the $(j_i m_i)$'s are the spins and spin projections of the particles involved, and $\sigma_{s m_s}$ represent the Pauli spin operators for the projectile. It is convenient to construct the quadratic forms

$$X^{nn'}_{ab}(\theta) = \sum_{m_B m_b m_A m_a} H^n_{m_B m_b m_A m_a}(\theta) \, \sigma_{m_a m'_a} \, H^{n'}_{m_B m_b m'_A m'_a}(\theta) \, \sigma_{b m'_b m_b}$$

The observables are then contractions of these quadratic forms (sum on six repeated indices):

$$\sigma_0(\theta) = \frac{\mu_a \mu_b}{(2\pi)^2} \frac{k_b}{k_a} I_0(\theta) ,$$

$$I_0(\theta) = \frac{1}{2} \sum_{n n'} a_n X^{n n'}_{00}(\theta) a^*_{n'} ,$$

$$I_0 A_y = \frac{1}{2} \sum_{n n'} a_n X^{n n'}_{y0}(\theta) a^*_{n'} ,$$

$$I_0 \ldots = \frac{1}{2} \sum_{n n'} a_n X^{n n'}_{\sigma y}(\theta) a^*_{n'} ,$$

$$I_0 D_{0\theta} = \frac{1}{2} \sum_{n n'} a_n X^{n n'}_{0\theta}(\theta) a^*_{n'} .$$

A very simple search algorithm can minimize the total χ^2 for an arbitrary set of observables with respect to the expansion coefficients a_n. Several applications that have used this technique follow.

(1) Effective Interactions. We expand medium corrections to the effective interaction in the form

$$t_{eff} = t_{free} + \sum_{n=1}^{N} a_n t_n(q, \rho) .$$

For a given projectile energy, the effective interaction is common to all transitions excited. The maximum sensitivity to the density (ρ) and momentum transfer (q) dependence of the medium corrections is obtained in a simultaneous fit to the cross-section and analyzing-power data for many multipolarities. We have performed this type of fit at several projectile energies using the 0^+_1, 1^-_1, 2^+_1, 3^-_1, and 4^+_1 states of ^{16}O.

(2) Neutron Densities. For normal parity transitions whose spin and current contributions are negligible, the proton distribution can be fully specified by electron-scattering measurements. The neutron distribution ρ_n can then be fit to proton-scattering data using linear expansions of the form

$$\rho_n^{(n)} = \sum_n a_n f_n(r) ,$$

where $f_n(r)$ are any convenient complete set of radial functions. We have used both Fourier-Bessel expansions and polynomial-times-Gaussian expansions. The error envelope $S_{nn}(r)$ is obtained from the covariance matrix ν_{ij} using

$$[S_{nn}(r)]^2 = \sum_{ij} f_i(r) V_{ij} f_j(r) .$$

Fits have been made for several states of ^{18}O and ^{88}Sr. Pseudodata studies also have been made.

(3) Longitudinal Spin Density. The 0^+ to 0^- transitions are driven by the longitudinal spin density, which can be expanded as above. The ^{16}O(p,p') 0^-, $T=0$ reaction has been studied at 135 MeV.

Study of Isobaric-Analog States in (π^+,π^0) Reactions (Exp. 412, LEP)

(Los Alamos, Tel Aviv Univ., Arizona State Univ.)
Spokesmen: H. W. Baer and J. D. Bowman (Los Alamos)

We completed[1] a series of measurements of 0° differential cross sections for isobaric-analog states (IASs) on nuclei ranging from ^{7}Li to ^{208}Pb. The measurements were performed with the π^0 spectrometer at the LEP channel at four energies between 100 and 300 MeV. The A dependence at each energy is shown in Fig. 1. These data showed that 0° IAS cross sections follow a remarkably regular pattern when plotted against $g(E)(N-Z)A^{-\alpha(E)}$.

Using the determined parameters $g(E)$ and $\alpha(E)$, it appears first that one can estimate a 0° IAS cross section on any nucleus in the periodic table to an average accuracy of 20% for beam energies between 100 and 300 MeV. Second, the regular pattern in the data established that the parameters g and α constitute a good meeting ground for comparisons between experiments and theories, particularly those theories that attempt to describe the general features of π-nucleus scattering. For example, the data show that α decreases from 1.35 at the resonance energy (165 MeV) to 1.10 at 295 MeV (Fig. 2). Generally, this reflects the changing nature of pion single-charge-exchange (SCX) scattering, going from approximately black-disk scattering at 165 MeV (a value of $\alpha = \frac{1}{2}$ is given in Ref. 2) to increased volume scattering at higher energies. A third consequence of these measurements is that it now becomes possible to recognize with some degree of confidence an "anomalous" 0° IAS cross section.

At resonance energies, deviations from the general trends are expected to arise primarily from unusual neutron-proton density distributions in the surface region; ^{90}Ar appears to be such a case.[1] Since it is generally believed that pion SCX to the IAS is one of the most sensitive tools available to study the relative neutron-to-proton density distributions ($\Delta\rho$) in nuclei, determining the systematic features is particularly desirable.

Figure 3 presents $\sigma_{IAS}(0°)$ as a function of incoming pion kinetic energy. For comparison we show in Fig. 3 the energy dependence of the free cross section $\sigma_{\pi^-p\to\pi^0n}(0°)$. In general, the maximum of the 0° IAS cross section is observed on the (3,3) resonance energy. It drops quickly when below and slowly when above the resonance. These trends follow the shape of the free cross section but are less pronounced.

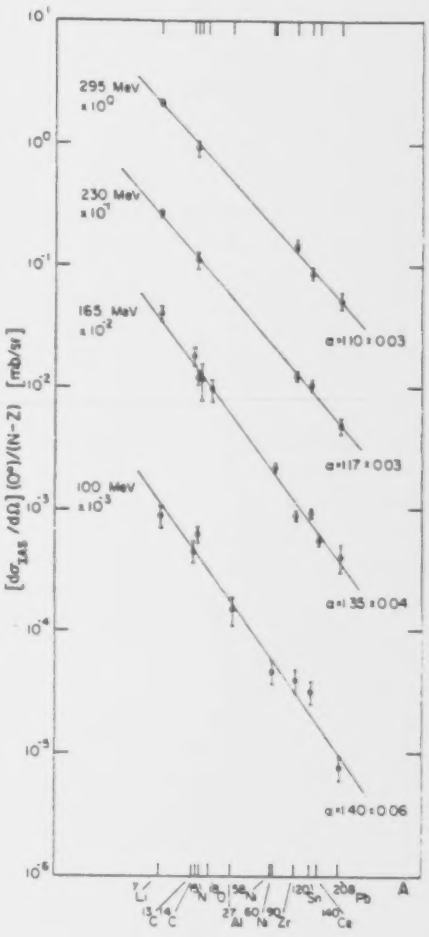

Fig. 1.
Measured (Ref. 1) $\sigma_{IAS}(0°)$. The straight lines represent $g(E)(N-Z)A^{-\alpha}$.

An anomalous behavior is observed for the ^{90}Zr nucleus where the cross section is monotonically increasing with the energy and does not reflect the (3,3) resonance as do the other nuclei. This effect might be related to the neutron-proton density difference at the surface. In general, the ratio of the number of neutrons to protons, evaluated as

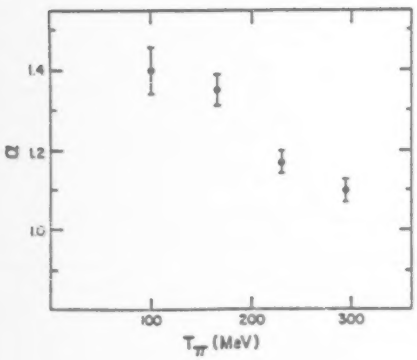

Fig. 2.
The energy dependence of the exponent α in the function $g(N-Z)A^{-\alpha}$ deduced from the measurements shown in Fig. 1.

$$\frac{\int_R^\infty \rho_n \, d\tau}{\int_R^\infty \rho_p \, d\tau}$$

with the use of density-matrix expansion or Hartree-Fock Skyrme III force densities,[3,4] exceeds the N/Z ratio in the surface region probed by the strongly absorbed pions; ^{90}Zr is an exception, as the calculated ratio is very close to N/Z. This means that for ^{90}Zr the SCX cross section around the (3,3) resonance is relatively suppressed because the interaction occurs near the surface, which has a comparatively low neutron density. At higher energies with a larger penetration depth, the behavior is closer to that of an average nucleus. This interpretation agrees with the observation that the reduced cross section (see Fig. 1) of ^{90}Zr at 165 MeV is lower than the fitted line whereas that of ^{120}Sn (a nearby nucleus with a large "neutron halo") is higher.

We have proposed (Exp. 728) to extend the (π^+,π^0) IAS measurements into the 300- to 500-MeV region using the π^0 spectrometer at the P^3 pion channel. A major motivation is to see whether the remarkably regular patterns found for the 0° cross sections in the 100- to 300-MeV region continue at the higher energies. A second goal is to provide more evaluation of the distorted-wave impulse approximation (DWIA) theory. If the DWIA theory is more accurate at higher energies, $\sigma_{IAS}(0°)$ should increase* in the 300- to 500-MeV interval. If this behavior is not observed, it will show unequivocally that a major ingredient is missing in the theoretical description.

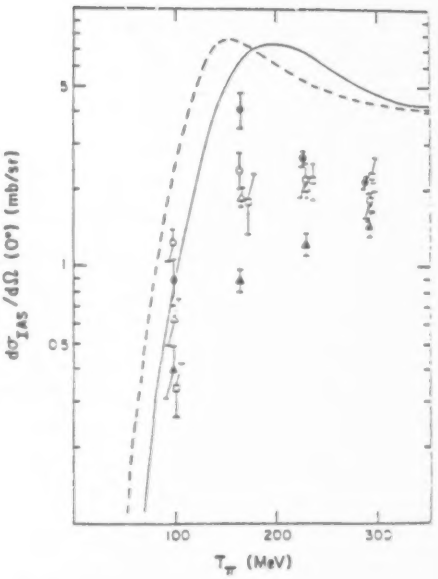

Fig. 3.
Excitation function of the 0° IAS cross sections (c.m. system) for ^{7}Li (solid circles), ^{14}C (open circles), ^{90}Zr (solid triangles), ^{120}Sn (open triangles), and ^{208}Pb (open squares). The solid line represents the c.m. cross section of the free charge-exchange reaction $\pi^+ + n \rightarrow \pi^0 + p$ plotted vs the laboratory kinetic energy; the dashed line, vs the c.m. kinetic energy (Ref. 9).

If $\sigma_{IAS}(0°)$ continues to follow the shape of the free $\sigma(\pi N)$, the excitation functions for most nuclei should follow the shape shown in Fig. 4. The $\sigma(\pi N)$ curve was normalized to the 295-MeV data point.

It is our belief that the experimental determination of the systematics for IAS excitation as a function of E and

*See, for example, LAMPF proposal 728, where calculations performed with the code PIESDEX are presented.

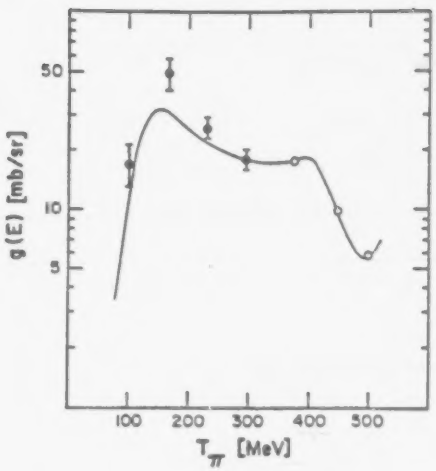

Fig. 4.
The deduced values of $g(E)$ obtained by fitting $g(E)(N-Z)A^{-\alpha}$ to the measured $\sigma_{IAS}(0°)$. The curve represents the shape of $\sigma(\pi^- p \to \pi^0 n)$ at 0°; it is normalized to the 295-MeV data point.

A constitutes a basic characterization of the π-nucleus interaction between 100 and 500 MeV. We have completed the first half of this study at the LEP and plan to perform the high-energy half of the study at P[3] in 1984.

REFERENCES

1. U. Sennhauser et al., Phys. Rev. Lett. 51, 1324 (1983).

2. M. B. Johnson, Phys. Rev. C 22, 192 (1980).

3. J. W. Negele and D. Vautherin, Phys. Rev. C 5, 1472 (1972).

4. M. Beiner et al., Nucl. Phys. A 238, 29 (1975).

Pion Elastic-Scattering Single- and Double-Charge-Exchange Reactions on ^{14}C
(Exp. 523, LEP)
(Los Alamos, Univ. of Colorado, Arizona State Univ., Tel Aviv Univ.)
Spokesmen: H. W. Baer (Los Alamos) and J. L. Ullmann (Univ. of Colorado)

(Exp. 539, EPICS)
(Los Alamos, Univ. of Minnesota)
Spokesmen: H. W. Baer (Los Alamos) and D. B. Holtkamp (Univ. of Minnesota)

(Exp. 558, EPICS)
(Los Alamos, New Mexico State Univ., Univ. of Texas, Univ. of Minnesota)
Spokesmen: H. W. Baer (Los Alamos) and G. R. Burleson (New Mexico State Univ.)

This set of experiments is intended to provide complete data on a single nucleus for pion reactions that are related by isospin invariance: π^+ and π^- elastic scattering (π^+,π^0) to the isobaric-analog state (IAS), and (π^+,π^-) to the double-isobaric-analog state (DIAS). Carbon-14 was chosen because it has the most favorable level separations among the $T \geq 1$ nuclei.

The measurements are being made at various energies between 35 and 300 MeV. These data should provide a good picture of the changing nature of the pion-nucleus interaction. Specifically, comparisons will be made with theories that attempt to describe in a continuous manner the dynamical changes that occur in the pion-nucleus interaction at energies below, on, and above the Δ resonance.

Elastic-scattering data now have been measured at 164 MeV (Exp. 539) and at 80 and 65 MeV.[1] The 164-MeV data are shown in Fig. 1. The difference in the angle of the first minimum between π^+ and π^- scattering is approximately 2.5°, indicating a slightly larger effective radius for neutrons than for protons in ^{14}C.

Forward-angle single-charge-exchange (SCX) cross sections have been measured at 35, 50, 65, 80, 100, 165, 230, and 295 MeV. The dramatic energy dependence in the forward-angle IAS cross sections is exhibited in Figs. 2 and 3. At energies between 100 and 300 MeV, the

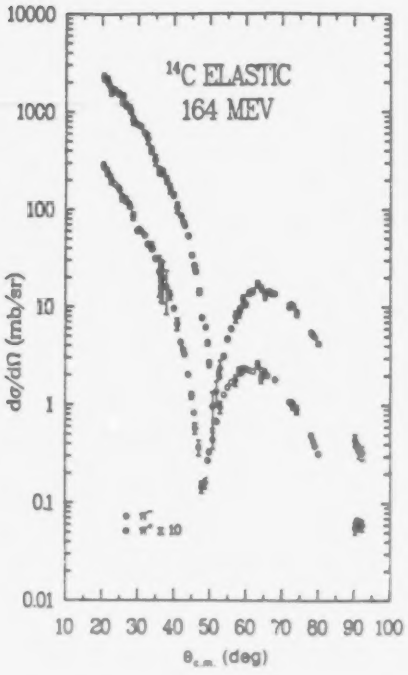

Fig. 1.
Elastic-scattering cross sections for π^+ and π^- on ^{14}C.

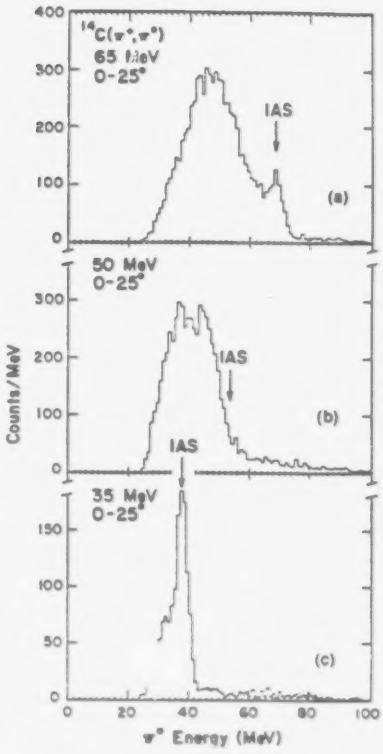

Fig. 3(a)-(c).
Measured spectra for the ^{14}C(π^+,π^0) reaction at low energies.

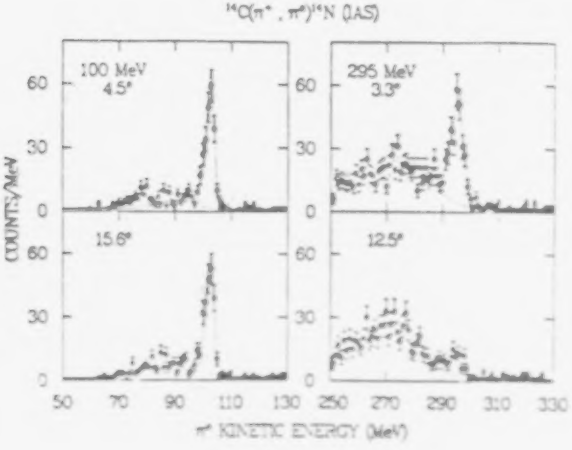

Fig. 2.
Measured π^0 spectra for the ^{14}C(π^+,π^0) reaction.

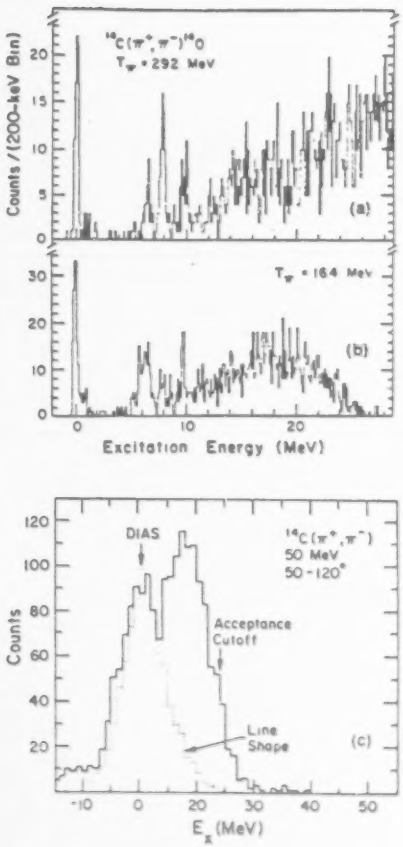

Fig. 4(a)-(c).
Measured spectra for the $^{14}C(\pi^+,\pi^-)$ reaction at (a) 292 MeV, EPICS; (b) 164 MeV, EPICS; and (c) 50 MeV, TRIUMF-TPC.

IAS is a prominent feature of forward-angle (π^+,π^0) reactions. At 50 MeV the IAS vanishes. An upper limit on the 0° cross section, based on the data of Fig. 3(b), is 5 μb/sr. At 35 MeV the IAS is again a prominent feature of the spectrum [Fig. 3(c)].

The deep minimum in the 0° cross section near 50 MeV would seem to be a direct reflection of the corresponding deep minimum in the $\pi^- p \to \pi^0 n$ reaction. However, calculations by Siciliano[2] have shown that sizable isovector-correlation (ρ^2) terms are required to obtain a deep minimum in the 0° cross section at 50 MeV for the $^{15}N(\pi^+,\pi^0)$ reaction. The ^{14}C data are being analyzed in the framework of the Johnson-Siciliano[3] theory and the Kauffman-Gibbs[4] multiple-scattering theory.

The first double-charge-exchange (DCX) cross sections for a DIAS transition at 50 MeV were measured in 1983 using the time-projection chamber (TPC) at the M9 channel at TRIUMF.* These measurements at a low energy were made possible by a large solid-angle detector (TPC) and a sufficient quantity (7 g) of ^{14}C packaged into suitable target cells. In Fig. 4 the spectrum measured with the TPC at 50 MeV is compared with spectra measured at EPICS at 165 and 292 MeV. The measured angular distributions at these energies are shown in Fig. 5. The high resolution in the EPICS data is attractive, but not necessary, to measure $^{14}C(\pi^+,\pi^-)^{14}O$ (DIAS) because the first excited state in ^{14}O is at 5.9 MeV.

EPICS, because of its long length, is not well suited to measure 50-MeV cross sections. It is interesting to see that the 50-MeV cross sections for angles $\theta \geq 50°$ are larger than the cross sections at 165 and 295 MeV for $\theta \geq 20°$.

This first measurement of DCX at low energy should put constraints on the very uncertain theoretical calculations. The main features that can be observed in the results follow.

- The shape of the angular distribution has some resemblance to the shape of elastic scattering, but the minimum at 70° is much shallower.
- The angular-distribution seems to increase at small angles, unlike SCX,[3] which has a minimum at 0°.

Optical-model calculations, using a modified version of the code PIESDEX, were done by E. Siciliano. The parameters were the same ones that gave good agreement with the 50-MeV SCX of ^{15}N (Ref. 3) and 50-MeV elastic scattering on ^{16}O. The results of the calculations with and without the isotensor Lorentz-Lorenz term are shown with the experimental data in Fig. 5(c).

The calculations have the right magnitude, but the shape has only a modest resemblance to the data. Clearly a better theoretical understanding and more data are desirable.

*Experiment TPC-DCX at TRIUMF, "Pion Double Charge Exchange at Low Energy," by a TRIUMF collaboration and H. W. Baer of Los Alamos as Spokesmen.

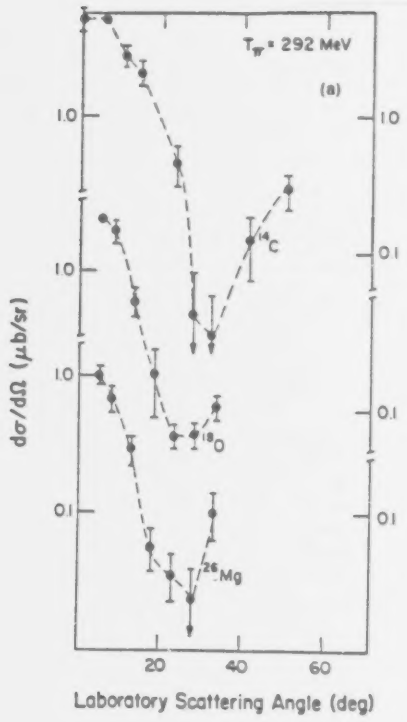

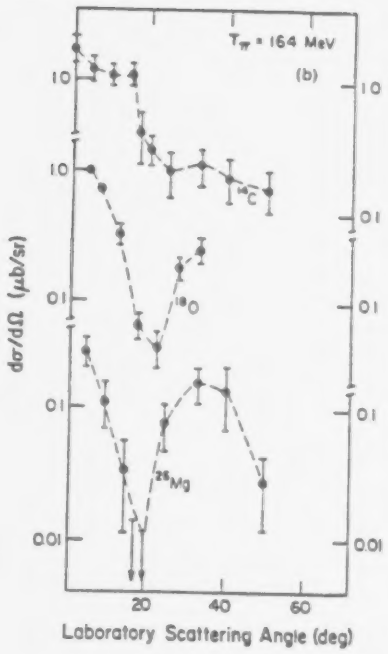

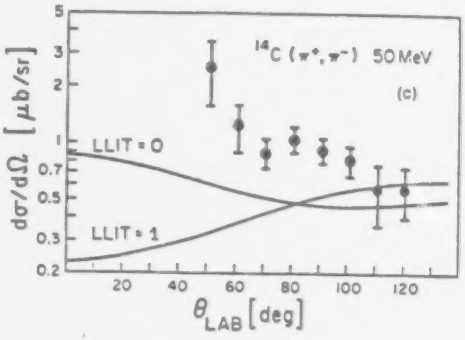

Fig. 5(a)-(c).
Differential cross sections for the reaction $^{14}C(\pi^+,\pi^-)$ at (a) 292 MeV, EPICS; (b) 164 MeV, EPICS; and (c) 50 MeV, TRIUMF-TPC.

REFERENCES

1. M. Blecher et al., Phys. Rev. C 28, 2033 (1983).

2. M. D. Cooper et al., submitted to Phys. Rev. Lett.

3. M. B. Johnson and E. R. Siciliano, Phys. Rev. C 27, 720 (1983).

4. W. Kaufmann and W. R. Gibbs, Los Alamos National Laboratory document LA-UR-83-736 (1983).

A Dependence of the Excitation Energy, Width, and Cross Section of the Isovector Monopole Resonance (Exp. 607, LEP)

(Los Alamos, Tel Aviv Univ., Arizona State Univ., SIN)
Spokesmen: J. D. Bowman and H. W. Baer (Los Alamos) and J. Alster (Tel Aviv Univ.)

We have used the (π^-,π^0) charge-exchange reaction at 165-MeV kinetic energy to study the $T+1$ component of the isovector monopole resonance (IVM). The nuclei ^{40}Ca, ^{60}Ni, ^{90}Zr, ^{120}Sn, ^{140}Ce, and ^{208}Pb were used as targets. We also observed the $T+1$ component of the giant dipole resonance (GDR) in the lighter targets. The (π^+,π^0) reaction cross sections showed the presence of the $T-1$ component of the IVM and GDR in ^{40}Ca, ^{60}Ni, and ^{90}Zr.

Pion charge exchange is well suited to the study of the isovector giant resonance, and particularly the IVM, for a number of reasons. The pion is spinless, and at forward angles the excitation of spin-flip states is strongly inhibited. The charge-exchange reactions proceed through the $T\cdot\tau$ piece of the π-nucleon t matrix; hence, charge-exchange reactions must excite isovector states. This is in contrast to inelastic hadron scattering, which strongly excites isoscalar states.

Giant resonances have large transition densities in the nuclear surface. Because 165-MeV π's are strongly absorbed, they couple efficiently to these surface-peaked transition densities. This point is crucial for monopole modes where the volume integral of the transition density vanishes. The excitation of a monopole mode by a weakly absorbed probe therefore is strongly suppressed at forward angles. The angular distributions produced by the strongly absorbed 165-MeV π's are sharply diffractive and allow a direct determination of the angular momentum of the final states. Finally, the Coulomb energy shifts the $T+1$ component of the IVM to a low-excitation energy in the (π^-,π^0) daughter nucleus. The decay width of this state therefore is reduced.

Figure 1 shows plots of doubly differential cross sections for the (π^-,π^0) reaction vs the kinetic energy of the detected π^0s. Representative targets, ^{60}Ni and ^{140}Ce, are shown. The top spectra are for a scattering angle of 4° near the forward direction where the IVM cross section is largest; the middle spectra are for 15° where the IVM cross section is small and that of the GDR is largest; and the bottom spectra are for 33° where both the IVM and GDR have small cross sections. The dashed lines represent a smoothly interpolated background.

In Fig. 2 we plot the normalized cross section S in the monopole region of the spectra vs momentum transfer squared ($q = k_\pi \sin\theta$). The monopole-region cross sections were divided by the observed differential cross section

$$S = \frac{\int \frac{d^2\sigma}{d\Omega dT} dT \text{ (monopole region)}}{\int \frac{d^2\sigma}{d\Omega dT} dT \ (E_x < 70 \text{ MeV})} .$$

It is the excess of cross section above the linearly extrapolated background that we identify as caused by the IVM. The first minimum of the IVM angular distribution occurs where $qR = \pi/2$, where R is the π-absorption radius. This point is indicated on Fig. 2. The observed break points between the background and the forward-peaked IVM feature are near the $\pi/2$ point for each nucleus.

Angular distributions, excitation energies, and widths were extracted by fitting the doubly differential cross sections to a sum of IVM, GDR, and nonresonant background components. The background was smoothly interpolated under the resonances as a function of q^2 and T_{π^0}. The angular distribution for the IVM and GDR peaks in the ^{60}Ni(π^-,π^0) data is shown in Fig. 3. The solid lines are the angular distribution of Auerbach and Klein[1] normalized to the data.

In Fig. 4(a) we show the extracted maximum monopole and dipole cross sections compared to calculations of Auerbach and Klein for the different targets.

In Fig. 4(b) we show excitation energies and widths, again compared to the random-phase-approximation (RPA) theory of Auerbach and Klein. The agreement is remarkable.

We observed no hint of isovector quadrupole signal. For example, in the ^{60}Ni (π^-,π^0) data where we observe 70% of the IVM and GDR cross sections predicted by the RPA distorted-wave impulse approximation (DWIA) theory, we observe <25% (90% confidence level) of the isovector quadrupole predicted cross section.

Our conclusions are that the IVM is a systematic feature of nuclei from ^{40}Ca to ^{208}Pb. Its excitation energy and width are well reproduced by RPA calculations. Its cross section is large, indicating the collective nature of

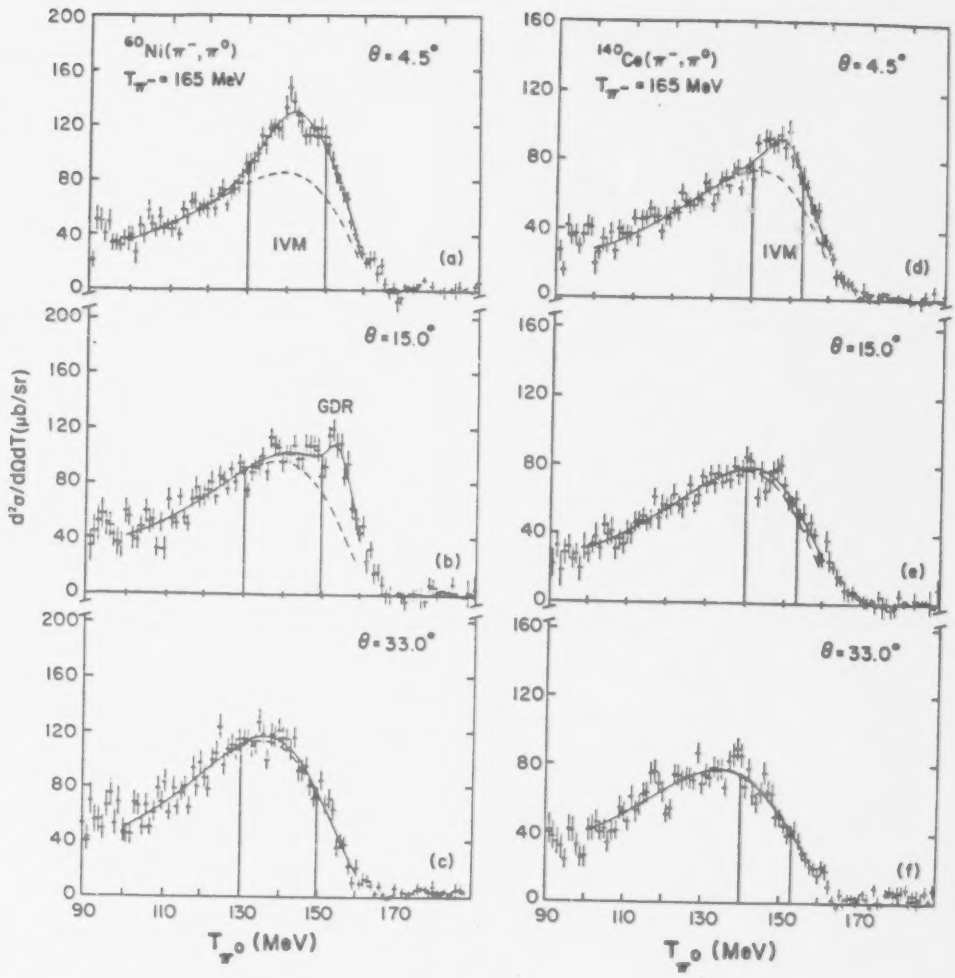

Fig. 1.
Doubly differential cross sections vs π^0 kinetic energy for $^{60}Ni(\pi^-,\pi^0)$ and $^{140}Ce(\pi^-,\pi^0)$ at laboratory angles of 4.5, 15.0, and 33.0°.

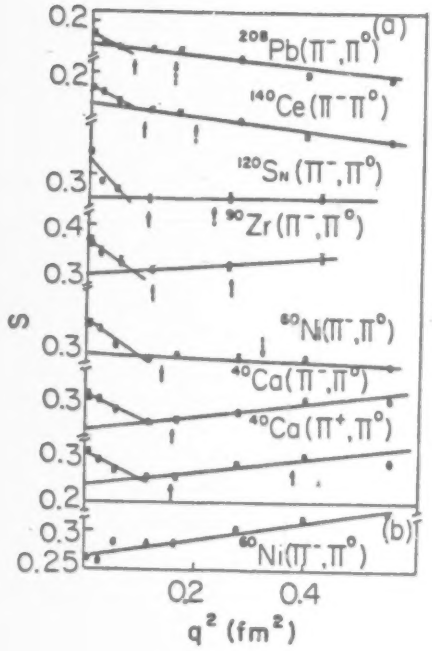

Fig. 2(a) and (b).
The ratio S plotted vs momentum-transfer squared. The region of integration is (a) centered on the expected IVM energy, and (b) centered above the IVM energy.

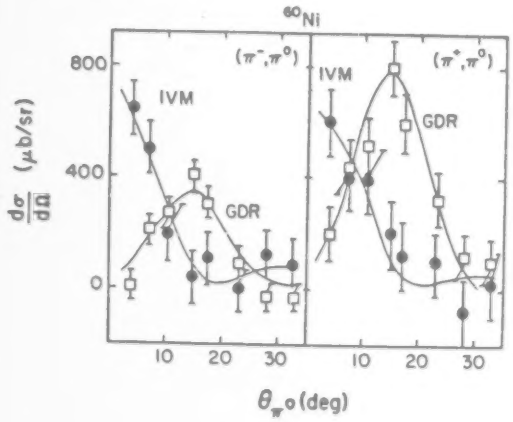

Fig. 3.
Angular distribution for the IVMs and GDRs in $^{60}Ni(\pi^{\pm},\pi^0)$.

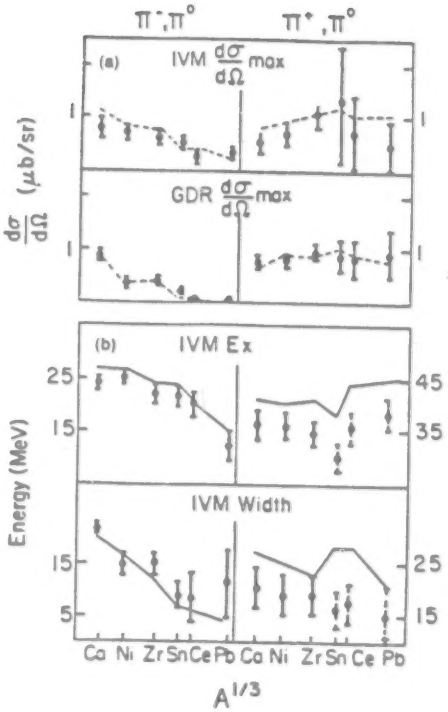

Fig. 4(a) and (b).
(a) Maximum cross section for the isovector monopole and giant dipole resonances in the $(\pi^{\pm},\pi^0)$ reactions, and (b) excitation energies and widths of the isovector monopole resonance in the $(\pi^{\pm},\pi^0)$ reaction. The (π^-,π^0) reaction excites the $T+1$ component and the (π^+,π^0) excites the $T-1$ component of each resonance.

the state, and is in qualitative agreement with RPA-DWIA theory. The IVM and GDR cross sections deviate from RPA-DWIA theory by the same ratio. The absence of the isovector quadrupole resonance poses an interesting problem.

REFERENCE

1. N. Auerbach, Proc. of the Conf. on Highly Excited States and Nuclear Structure (HESANS), 1983 Int. Symp., Orsay, France, September 5-8, 1983.

Study of the Mass and Energy Dependence of Low-Energy Pion Single Charge Exchange (Exp. 688, LEP)

(Los Alamos, Tel Aviv Univ., TRIUMF, Arizona State Univ.)

Spokemen: M. D. Cooper and M. J. Leitch (Los Alamos)

At low energies the free-nucleon charge-exchange angular distribution is strongly backward peaked with a deep forward minimum. Furthermore, phase-shift analyses predict that the 0° excitation function has a minimum around 50 MeV. These minima are the result of a near perfect cancellation of *s*- and *p*-wave π-nucleon amplitudes. If the nucleus is transparent, the nuclear single-charge-exchange (SCX) reaction to the isobaric-analog state (IAS) should show the same features. Of course, in nuclear matter these features will be distorted by effects such as absorption and Pauli blocking.

In this experiment we have measured forward-angle differential cross sections for ^{7}Li(π^+,π^0)(IAS) at the 33.5-, 41.1-, 48.5-, and 58.8-MeV incident pion energy. Also, angular distributions for ^{39}K(π^+,π^0)(IAS) and ^{48}Ca(π^+,π^0)(IAS) were measured at 48-MeV incident pion energy. The experiment was performed at the LEP channel using the π^0 spectrometer.[1]

Typical π^0 spectra for incident pion beam energies of 33.5, 41.1, 48.7, and 58.8 MeV on the ^{7}Li target are shown in Fig. 1. The π^0 energy resolution (FWHM) in these measurements was 3.0-3.5 MeV. In the analysis of the data, angle-dependent line shapes, together with kinematic constraints on the energies of states in residual nuclei and three-body thresholds, were used to separate the IAS peak from continuum charge exchange and background. The line shapes were obtained by Monte Carlo simulation of the beam, target, and spectrometer conditions.[1]

The decomposition of the spectra into background and the IAS peak for the ^{7}Li(π^+,π^0) measurement can be seen from the dashed lines in Fig. 1. The data were fitted by the maximum-likelihood method described in Ref. 2. The statistical and instrumental error in the extraction of the IAS area was 20-30%; the error caused by the unfolding of the IAS peak was typically 50% of the statistical error. The normalization procedure is described in detail in Ref. 3.

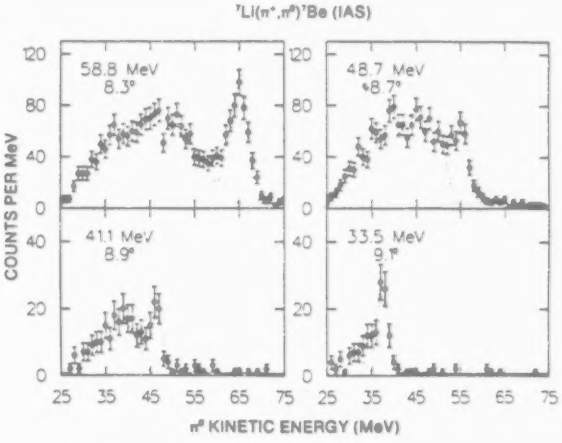

Fig. 1.
Measured π^0 spectra for the ^{7}Li(π^+,π^0) (IAS) reaction at 33.5-, 41.1-, 48.7-, and 58.8-MeV incident pion energy. The dashed curves show the fits to the IAS and to the second excited state.

In Fig. 2 we show the measured cross sections for ^{7}Li, ^{39}K, and ^{48}Ca taken near 50-MeV incident pion beam energy, and for comparison we also include the ^{15}N(π^{+},π^{0}) (IAS) data of Cooper et al.[3] taken at 48-MeV pion energy. These data show that as we increase nuclear size, the shape of the angular distribution continues to reflect the forward-angle minimum and backward-angle peaking nature of the free-nucleon charge-exchange cross section. Also shown in Fig. 2 is the prediction of the PIESDEX code* for SCX on ^{15}N at 48 MeV. In this calculation, second-order terms representing isovector true pion absorption and the Lorentz-Lorenz effect are included in the optical potential; optical-model calculations without second-order terms are unable to reproduce the deep minimum at 0° seen for ^{15}N (Ref. 3).

*E. R. Siciliano and M. B. Johnson, private communication, 1983.

For ^{7}Li data, the 0° cross sections were extrapolated by fitting the angular distributions with $A + B\theta^{2}$ functional form. This is based on expansion of angular distribution at small angles in terms of the Legendre polynomials. The measured 0° excitation function for ^{7}Li is shown in Fig. 3. The error bars are the combined error from the extrapolation to 0°, the uncertainty in the normalization, and the statistical fluctuations. The data points at 70 and 98 MeV were taken previously with the π^{0} spectrometer. To estimate the location of the minimum, we fit the four data points with a parabola (Fig. 3). The minimum of the parabola is at 42.3 ± 1 MeV. It is interesting to note that the minimum in ^{7}Li data obtained in this work is different by 3-8 MeV from predictions of different phase shifts for the minimum in a free πN excitation function. For comparison we show only the prediction of Rowe et al.[4] in Fig. 3.

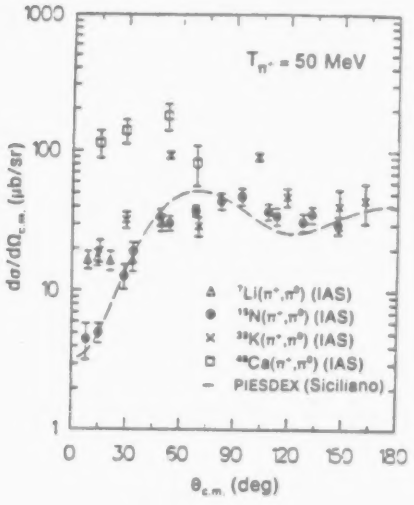

Fig. 2.
Angular distributions for the ^{7}Li(π^{+},π^{0}) (IAS), ^{15}N(π^{+},π^{0}) (IAS), ^{39}K(π^{+},π^{0}) (IAS), and ^{48}Ca(π^{+},π^{0}) (IAS) at incident pion energy near 50 MeV. The solid curve is an optical-model calculation that includes the second-order isovector terms described in the text.

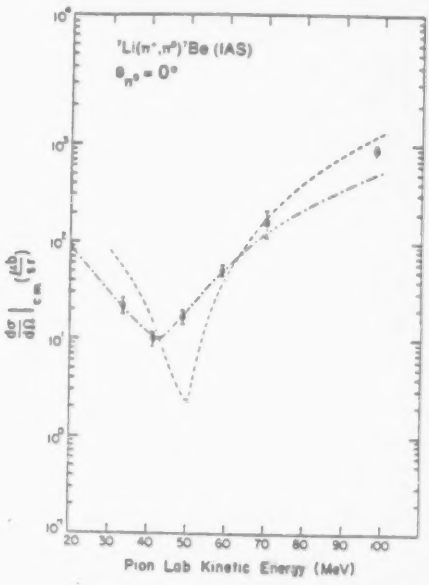

Fig. 3.
The ^{7}Li(π^{+},π^{0}) (IAS) excitation function. The dot-dashed curve is a least squares fit to the data. The dashed curve represents the free πN cross sections (Ref. 4).

The differences in forward-angle behavior among ^{7}Li, ^{13}N, ^{39}K, and ^{48}Ca indicate that π-nucleus charge exchange is sensitive to the medium effects. These medium effects cause changes in the delicate cancellation between π-nucleon s- and p-wave amplitudes that result in a shift in position of the minimum of the excitation function with increasing nuclear size (A), or alternatively in a change in the depth of the 0° minimum for different nuclei at a particular energy.

Presently there are very few low-energy SCX data, with the exception of several angular distributions near 50 MeV and one excitation function. To understand the effect of the second-order terms and establish the systematics of the A dependence and energy dependence of forward-angle SCX at low energies, a larger body of data is needed. Future experiments using the π^0 spectrometer are planned to study the mass and energy dependence of low-energy SCX.

REFERENCES

1. H. W. Baer et al., Nucl. Instrum. Methods 180, 495 (1981).

2. M. D. Cooper et al., Phys. Rev. C 25, 438 (1982).

3. M. D. Cooper et al., "Angular Distribution for ^{13}N(π^+,π^0)^{13}O (g.s.) at T_π = 48 MeV," submitted to Phys. Rev. Lett.

4. G. Rowe et al., Phys. Rev. C 18, 546 (1987).

Muon Decay Spectrum
(Exp. 455, P³-West)

(Los Alamos; Univ. of Chicago; National Research Council, Canada)
Spokesmen: H. L. Anderson and W. Wayne Kinnison (Los Alamos)

The measurement of the positron spectrum of muon decay is one of the most fundamental experiments in particle physics because it is the best way to determine the attributes and magnitudes of the weak interaction. We are making a new measurement to improve the existing accuracy by a factor of 5. The spectrum can be calculated precisely from the accepted theory, based on a simple symmetry proposed by Feynman and Gell-Mann, in which the neutrinos are massless, with two rather than four components. The theory also is characterized by the fact that the only interactions entering are vector and axial-vector interactions, of equal magnitude and opposite sign, referred to as $V-A$. In this theory the currents are purely left-handed. All searches to date to find right-handed currents or massive neutrinos have been unsuccessful. (We discount the Russian experiment, which has reported a finite neutrino mass, because of doubts about the correctness of the result.)

The weak-interaction theory is beautiful in its simplicity, but we do not know whether that beauty is more than skin deep; that is the purpose of this experiment. We plan to measure the spectrum with high resolution and statistics 100-fold greater than previously obtained. We will compare the spectrum with its well-known theoretical value.

As part of the comparison of the spectrum to theory, the experiment first will attempt to improve the high-energy shape parameter ρ to a new level of precision, nearly ± 0.0003. This will represent an improvement in the existing limits on this parameter by about a factor of 10. Beg et al.[1] have shown that such an improvement in ρ can place a constraint on possible left-right weak-interaction theories. In such theories, there are two charged intermediate-vector bosons, W_L and W_R, that couple to left- and right-handed currents, respectively. These bosons are not necessarily themselves eigenstates of the mass matrix. Instead, the mass eigenstates W_1 and W_2 may be expressed as Cabibbo-like mixtures of W_L and W_R,

$$W_1 = W_L \cos\zeta - W_R \sin\zeta \ ,$$

$$W_2 = W_L \sin\zeta + W_R \cos\zeta \ .$$

Thus, it is of interest to place limits on $\kappa \equiv [M(W_2)/M(W_1)]^2$, the mass-squared ratio, and ζ, the mixing angle. An improved measurement of ρ can reduce the allowable range of ζ almost independently of the value of κ. This is shown in Fig. 1, where the current limits on κ

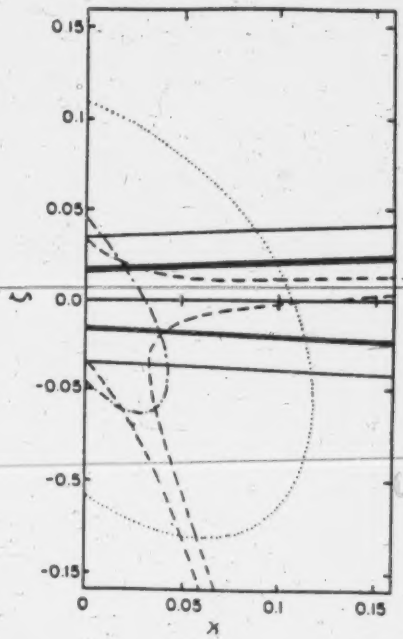

Fig. 1.
Experimental 90% confidence-limit contours on the mass-squared ratio, $\kappa \equiv [M(W_2)/M(W_1)]^2$, and mixing angle ζ for possible left-right symmetric weak-interaction theories. The two bold solid lines represent the constraint that would result from this experiment's improved 0.03-per-millimeter (0.3-per-mil) measurement of ρ. The current limits are from the recently improved measurement of the end-point spectrum ξP_μ (dot-dashed curve, Ref. 2); the previous measurement of ξP_μ (dotted curve, Ref. 3); the present value for the ρ parameter (solid curve, Ref. 4); and a comparison between Fermi and Gamow-Teller β polarization (dashed curve, Ref. 3). In all cases, the allowed regions are those that include the origin, $\zeta = \kappa = 0$.

and ζ are given.* As seen in the figure, these limits currently come predominantly from the recently improved measurement of ξ by Mark Strovink and group[2] at TRIUMF. The figure also shows how the limit on ζ will be improved by the proposed 0.03-per-millimeter (0.3-per-mil) measurement of ρ, which is the immediate goal of Exp. 455. Figure 2 shows a schematic view of the Exp. 455 apparatus. The major component of the detector is a time-projection chamber (TPC), which has a sensitive volume 52 cm in length and 122 cm in diameter. The TPC magnetic field is provided by an iron-enclosed solenoid that supplies a maximum field of 0.7 T, which is uniform to better than 0.6% over the entire TPC sensitive volume. Such a magnetic field will allow a precision measurement of the positron momentum absolutely.

*References 2-5. The dotted and solid curves in Fig. 1 represent world-average values, with primary contributions from Refs. 3 and 4, respectively.

The muons for the experiment, which are from a surface muon beam in P^3-West, are brought to rest in the TPC gas at the center of the chamber. An event trigger requires that a muon enter the TPC [as determined by the 0.25-mm (10-mil) muon transmission scintillator at the TPC entrance] during the LAMPF beam gate, and that this muon stop in the central 10 cm of the TPC gas, as determined by signals from the TPC sense wires. When a muon enters the chamber, the deflector/separator is used to turn off the beam. In this manner, the experiment looks at events that have one, and only one, muon in the chamber. The momentum of the decay positron is then measured by analysis of its helical track in the known magnetic field.

Figure 3 shows the three plane projections and a three-dimensional view of a typical event. In the figure the incoming muon is indicated by coordinates drawn with the letter *M*, and the helical trajectory of the decay positron is indicated by coordinates drawn with a small

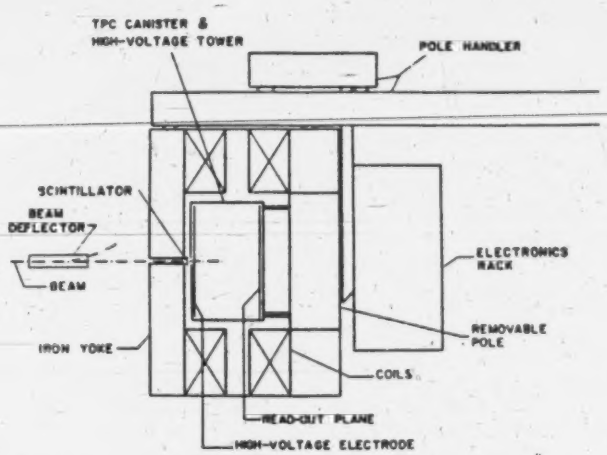

Fig. 2.
A pictorial view of the LAMPF Exp. 455 experimental apparatus. The detector consists of a 122-cm-diam by 52-cm-long TPC inside an iron-enclosed solenoid. This TPC drift region, which is filled with an 80-20 Ar-CH_4 gas mixture, is bounded on one end by a high-voltage electrode and on the other end by the read-out plane. The read-out plane consists of 21 modules, each of which has 15 sense wires spaced on 1-cm centers. Under each sense wire there are seventeen 0.8- by 0.8-cm pads spaced on 1-cm centers for determination of coordinate positions along the sense wires. The muons enter the TPC through a hole in the magnet pole after passing through a deflector/separator that is used to turn off the surface muon beam when a muon enters the TPC, as determined by a coincidence signal from the phototubes attached to the 0.25-mm- (10-mil-) thick scintillator covering the TPC entrance hole.

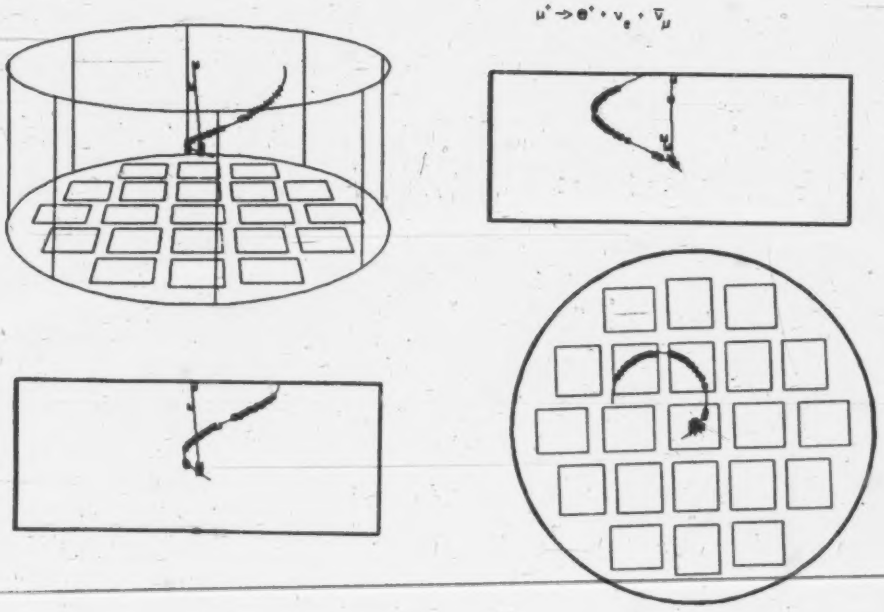

Fig. 3.
Three plane projections and a three-dimensional view of a typical muon decay event, as measured in the TPC apparatus. The entering muon coordinates, indicated by the letter *M*, are fitted to a straight line, as shown in three of the views. (No attempt is made to fit them to their actual helical track.) The decay positron coordinates, which are fitted with a helix, are indicated by square boxes.

box. To obtain the necessary experimental precision, about 10^9 such events will be analyzed. The experimental apparatus is designed to collect events at a rate of 1 per LAMPF macropulse (usually 120 per second).

In 1983, Exp. 455 had two data-collection runs. During the first run, the high-speed data-acquisition electronics was not in place and the resulting event rate was approximately 1 per second. About 4×10^5 events were collected during the 4-week running period and these data were analyzed to study the TPC resolutions and acceptance. It was found that the coordinate resolution along the drift direction was about 900 μm, more than a factor of 2 better than the proposed value of 2 mm, and that the resolution along the wire direction, uncorrected for known systematic errors, was about 600 μm. The resulting positron momentum resolution was 0.6% rms averaged over the Michel spectrum, which is only slightly worse than the proposed resolution of 0.5%. However, the combination of detector acceptance and software cuts resulted in only about 25% of all triggers being analyzed. Some of the rejected events will be recoverable by more sophisticated software algorithms, but mostly the acceptance is limited because of the length of detector. Ways of getting around this problem are currently under investigation.

The second data-collection run during 1983, of 1-week duration, was devoted to the development of the high-speed data-acquisition electronics. This new electronics, which consists primarily of three asynchronous, bit-slice computers in the read-out system, was installed and successfully tested during the run. It was found that a maximum event rate of about 50 per second could be

handled. This was somewhat below the 120-per-second goal, but the test run was limited by diagnostic codes that were in the bit-slice computers.

In the coming year, two large data-collection periods are planned and considerably more time will be spent optimizing the detector parameters, such as drift electric field voltage, gas mixtures, and magnetic field settings. We expect to achieve, or in some cases surpass, the design goals for the detector.

REFERENCES

1. M. A. B. Beg, R. V. Budny, R. Mohapatra, and A. Sirlin, Phys. Rev. Lett. 38, 1252 (1977).

2. J. Carr, G. Gidal, B. Gobbi, A. Jodidio, C. J. Oram, K. A. Shinsky, H. M. Steiner, D. P. Stoker, M. Strovink, and R. D. Tripp, Phys. Rev. Lett. 51, 627 (1983).

3. V. V. Akhmanov, I. I. Gurevick, Yu. P. Dobretsov, L. A. Makarina, A. P. Mishakova, B. A. Nikolskii, B. V. Sokolov, L. V. Surkova, and V. D. Shestakov, Yad. Fiz. 6, 316 (1977).

4. J. Peoples, Nevis Cyclotron report 147, 1966 (unpublished).

5. J. Van Klinken, K. Stam, W. Z. Venema, V. A. Wickers, and D. Atkinson, Phys. Rev. Lett. 50, 97 (1983).

Tensor Polarization in πd Scattering (Exp. 673, P^3)

(Argonne National Lab., Indiana Univ. Cyclotron Facility, Los Alamos, MIT)

Spokesman: R. J. Holt (Argonne)

Participants: W. S. Freeman, D. F. Geesaman, J. R. Specht, E. Ungricht, B. Zeidman, E. J. Stephenson, J. D. Moses, M. Farkhondeh, S. Gilad, and R. P. Redwine

The prospect of measuring the quadrupole form factor or D-state probability of the deuteron by observing the tensor polarization t_{20} in πd scattering led to an early interest in measuring t_{20} at backward angles.[1] During the past few years this interest has been spurred by questions regarding true pion absorption in nuclei and the possible existence of dibaryon resonance in the πd system.

In this experiment the angular dependence of t_{20}^{lab} for recoiling deuterons in πd elastic scattering was measured as a function of incident pion energy in the range 134-256 MeV. No evidence was found for rapid energy or angular dependences in t_{20}, contradicting recent publications[2] that claim the observation of dibaryon resonances in t_{20}. Our results agree most favorably with theoretical calculations in which the P_{11} πN amplitude has been removed altogether. This suggests that pion absorption has a small effect on t_{20} in the elastic channel.

The experimental apparatus used to measure t_{20} is illustrated in Fig. 1. Pions from the P^3-East channel at LAMPF were focused onto a liquid-deuterium target of 5 mm thickness. Scattered pions were detected in an array of three plastic scintillators, in coincidence with the

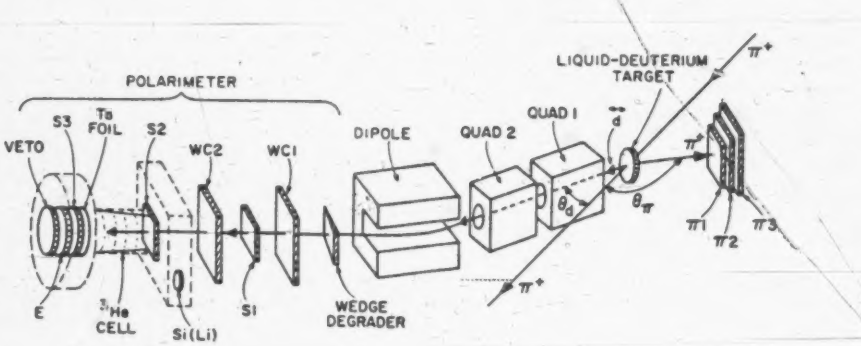

Fig. 1.
Apparatus to measure t_{20} in πd scattering (not to scale).

recoil deuterons that were focused onto the polarimeter with a QQD system.

The key feature for performing measurements of t_{20} in πd scattering is the development of a high-efficiency deuteron tensor polarimeter. The polarimeter employs the ^{3}He(d,p)^{4}He reaction, which has a large cross section and tensor-analyzing power T_{20} at forward angles, and a large Q value, 18.4 MeV.

The polarimeter was calibrated in a separate experiment at the Berkeley 88-in. cyclotron. The calibration of the polarimeter was determined as a function of incident deuteron energies, position, and angle of incidence on the polarimeter. The calibration was checked 2 years after the primary calibration by measuring the efficiency ϵ_0 again at the Los Alamos three-stage tandem Van de Graaff. We conclude from this test that the measurement of the efficiency ϵ_0 is reproducible to ~2%. The same polarimeter was used in previous measurements of the tensor polarization in πd scattering at 142 MeV[3] and in an ed scattering experiment.[4]

As shown in Fig. 2, our excitation function at $\theta^*_{c.m.} \approx 144°$ differs from recent data of Grüebler et al.[2] In that experiment the deuteron beam size, when the effects of second-order beam optics are taken into account, is comparable with the size of the polarimeter aperture (30 mm). This problem is not encountered in the present work because the deuteron beam size is 20 mm (FWHM) but the polarimeter aperture is 89 mm. Clearly, there are no dramatic energy or angular dependences

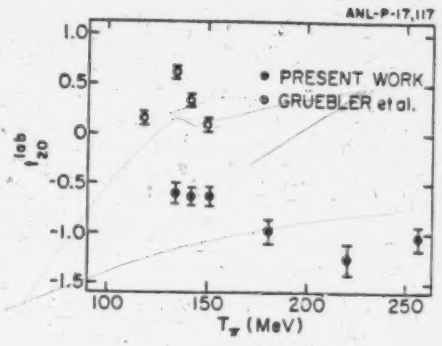

Fig. 2.
Excitation function at $\theta_d = 18°$ (solid dots) compared with the results of Grüebler et al. (Ref. 2) at $\theta_d = 15°$ (open circles). The angular acceptances are ±1.5 and ±2.5°, respectively.

observed in our work, so there is no apparent evidence for dibaryon-resonance effects.

Angular distributions at pion energies of 142, 180, 220, and 256 MeV are compared with recent theoretical predictions in Fig. 3. Presently, the theoretical calculations of the πd system have achieved a high level of sophistication. These calculations are typically three-body in nature and include both the absorptive channel

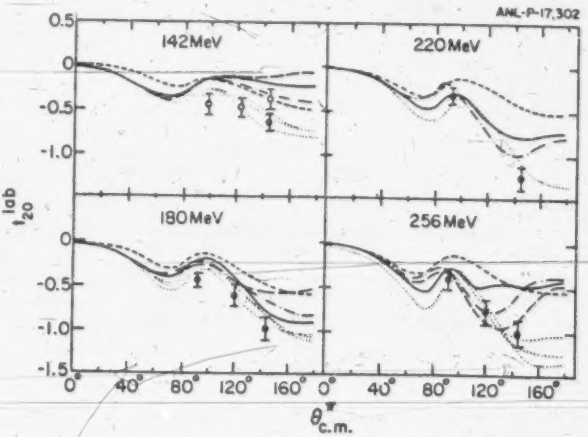

Fig. 3.
Angular distributions at pion energies of 142, 180, 220, and 256 MeV (open circles are from the previous experiment) (Ref. 3). The calculations are solid line, from Blankleider and Afnan (Ref. 6); long-dashed line, from Betz and Lee (Ref. 7); short-dashed line, from Fayard, Lamot, and Mizutani (Ref. 8); and dot-dashed line, from Rinat and Starkand (Ref. 9), all including true pion absorption. The dotted lines are results without P_{11} amplitude, that is, without pion absorption.

$\pi d \rightarrow NN$ and pion scattering. All calculations without a P_{11} πN amplitude give very similar results (dotted curves in Fig. 3) and are remarkably close to the present experimental data.

Omitting the P_{11} channel has the effect of both removing pion absorption and P_{11} πN rescattering from the calculation. Although omitting the P_{11} channel from the calculation is a somewhat drastic measure, especially since absorption is removed, it may not be as unreasonable as it appears. Afnan and Blankleider[5] have shown that the dominant absorptive effects in $\pi d \rightarrow \pi d$ and $\pi d \rightarrow pp$ occur in different spin-isospin channels. Therefore, it seems possible that the absorption amplitudes can be adjusted to improve t_{20} without worsening the results for other observables. Since it appears that absorption affects the elastic amplitudes far less than previously predicted, the chance for constraining the deuteron quadrupole form factor has improved, but more theoretical and experimental work must be done.

We are grateful to S. J. St. Lorant for the loan of the ^{3}He gas and to N. Jarmie and R. Martinez for assistance during the calibration at the Los Alamos tandem. In addition, we thank K. Stephenson, J. S. Frank, and M. J. Leitch for their substantial part in developing the new polarimeter.

This research was supported by the USDOE and the National Science Foundation.

REFERENCES

1. W. R. Gibbs, Phys. Rev. C 3, 1127 (1971).

2. W. Grüebler, J. Ulbricht, V. König, P. A. Schmelzbach, K. Elsener, C. Schweizer, M. Merdzan, and A. Chisholm, Phys. Rev. Lett. 49, 444 (1982); and 5th Int. Symp. on High-Energy Spin Particles, Brookhaven, New York (1982).

3. R. J. Holt, J. R. Specht, K. Stephenson, B. Zeidman, J. S. Frank, M. J. Leitch, J. D. Moses, E. J. Stephenson, and R. M. Laszewski, Phys. Rev. Lett. 47, 472 (1981).

4. M. E. Schulze, D. Beck, M. Farkhondeh, S. Gilad, S. Kowalski, R. P. Redwine, W. Turchinetz, R. J. Holt, J. R. Specht, K. Stephenson, B. Zeidman, R. M. Laszewski, E. J. Stephenson, J. D. Moses, M. J. Leitch, R. Goloskie, and D. P. Saylor, Tenth Int. Conf. on Few-Body Problems in Physics, Karlsruhe, Germany, 1983.

5. I. R. Afnan and B. Blankleider, Phys. Lett. 93B, 367 (1980).

6. B. Blankleider and I. R. Afnan, Phys. Rev. C 24, 1572 (1981).

7. M. Betz and T.-S. H. Lee, Phys. Rev. C 23, 375 (1981).

8. C. Fayard, G. H. Lamot, and T. Mizutani, Phys. Rev. Lett. 45, 524 (1980).

9. A. S. Rinat and Y. Starkand, Nucl. Phys. A 397, 381 (1983).

Pion-Induced Pion Production on the Deuteron (Exp. 783, P^3-West)

(Los Alamos, Univ. of Wyoming, Colorado College, MIT, Tel Aviv Univ.)

Participants: E. Piasetzky, P. A. M. Gram, D. W. MacArthur, G. A. Rebka, Jr., C. A. Bordner, S. Høibråten, E. R. Kinney, J. L. Matthews, S. A. Wood, D. Ashery, and J. Lichtenstadt

One way to characterize the study of pion-nucleus reaction mechanisms is to say that we are trying to find out how many nucleons it takes to scatter a pion. For example, pion quasi-free scattering appears to be almost entirely a single-scattering process, but even in this reaction the single-scattering peak in the momentum spectrum is thought to exist only because multiply scattered pions tend to be absorbed. Thus, information about pion multiple scattering is difficult to extract from the rather extensive measurements of quasi-free scattering that have been performed.

Recent editions of *Progress at LAMPF*[1,2] have presented our observations of inclusive pion double charge exchange. In this reaction a pion must interact with at least two nucleons and then escape from the nucleus. Comparisons of the momentum spectra of double charge exchange with the low-energy tail of quasi-free scattering are beginning to shed light on the contribution of multiple scattering to pion reactions.[3]

Another reaction in which the participation of more than one nucleon might be seen is in pion-induced pion production. Because the intermediate states that may contribute to $(\pi,2\pi)$ reactions are different from those that contribute to either quasi-free scattering or to double charge exchange, the balance between single and multiple scattering may be altered in an observable way.

Pion-induced pion production on the proton has been studied* systematically to obtain $\pi\pi$-scattering parameters, but there is virtually no information about this process in nuclei. The simplest system in which multiple-nucleon processes may occur is the deuteron. The reactions

*A bibliography of previous work is given in Ref. 4.

$\pi^- d \rightarrow \pi^+ \pi^- nn$

and

$\pi^+ d \rightarrow \pi^- \pi^+ pp$

can be studied and compared with $\pi^- p \rightarrow \pi^+ \pi^- n$ to search for two-nucleon mechanisms.

One two-nucleon mechanism for $(\pi,2\pi)$ was proposed by Brown et al.[5] who predicted, based on the $SU(4)$ quark model, the existence of a strong $\Delta N \rightarrow \Delta\Delta$ transition in systems of two or more nucleons. Subsequent decay of the two Δ's contributes to the $(\pi,2\pi)$ reaction. The $\pi^- nn$ or the $\pi^+ pp$ component of the final state has $T = 2$. If the NN system is formed at low momentum, it is likely to be in a $^1S_0$ state with $T = 1$. The pion may then be attracted to it through the P_{33} interaction to form a state that may be considered an off-shell ΔN.

In heavier nuclei these $T = 2$, ΔN states can be doorways to the formation of $T = 2$, $\Delta\Delta$ states. Since a ΔN state cannot decay by either the strong or the electromagnetic interaction, it may appear in the reactions studied here as a narrow resonance or even as a bound state. This subject was recently discussed by Garcilazo,[6] who showed that with certain parameterizations of the πN and NN interactions, the calculations predict the existence of a bound state. However, the uncertainties in our knowledge of these parameterizations, and in particular of the πN effective range, leave ample room to doubt its existence.

We report an experimental study of the $\pi^{\mp} d \rightarrow \pi^{\pm} \pi^{\mp} NN$ reactions that was performed at the high-energy pion channel (P^3). The doubly differential cross section $d^2\sigma/d\Omega dT$ for the production of pions with charge opposite to that of the incident beam was measured at uniformly distributed locations in barycentric T-cos θ phase space. Double charge exchange is impossible on the deuteron, so this method unambiguously identifies pion production. Measurements were made with π^+ and π^- beams at an incident kinetic energy of 256 MeV and with a π^- beam at 331 MeV. The momentum spread of the beams was $\Delta p/p = 4\%$ FWHM and their intensities were approximately 2×10^8 π^-/s and 10^9 π^+/s.

Outgoing particles were detected by a 180° double-focusing magnetic spectrometer[3,7] (the "Little Yellow Spectrometer") with a solid angle of 15 msr and momentum acceptance of 9.5%. The detector system consisted of a multiwire proportional chamber between the two dipole magnets of the spectrometer, a pair of multiwire proportional chambers immediately behind the focal plane, a 1.6-mm-thick plastic scintillation detector, a fluorocarbon (FC-88) threshold Čerenkov counter, and last, an Aerogel ($n = 1.055$) Čerenkov counter.

A quadruple coincidence among signals from the three-wire-chamber delay lines and the scintillator defined an acceptable event. The last two-wire chambers established the trajectory of a particle as it crossed the focal plane. For events that corresponded to an allowable trajectory, pulse heights from the scintillator and Čerenkov detectors and the time of flight through the second bending magnet discriminated against electrons or, when set for positive charge, positrons, protons, and other light nuclei. Corrections for pions decaying in the relatively short 3.5-m flight path and for muons that were recorded as good events were calculated with the Monte Carlo simulation DECAY TURTLE.[3]

A cylindrical target flask 2.5 cm in diameter, which was concentrically mounted on the axis of rotation of the spectrometer, contained liquid deuterium (99.83% deuterium) for observing pion production or liquid hydrogen for calibration. Background from the 50-μm Mylar walls was observed with the flask empty. The incident pion flux was measured with an ionization chamber as well as with a scattering monitor downstream from the spectrometer.

The measured pion-production cross sections were normalized to πp elastic scattering. At each incident energy, relative πp elastic cross sections were measured at several angles and the angular distribution was normalized to fit the "known cross sections" with a scale factor that calibrated the system as a whole. Below 300 MeV, known cross sections were derived from the phase-shift analysis of Carter, Bugg, and Carter[8] using the routine SCATPI.[9] Above this energy, they were interpolated directly from the measurements.[10] The interpolation procedure is described in detail in Ref. 4 and is the same procedure used to normalize the $\pi^- p \rightarrow \pi^- \pi^- n$ cross sections of Ref. 1.

Figure 1 shows the doubly differential cross sections for the $\pi^- d \rightarrow \pi^+ \pi^- nn$ reaction at 256 and 331 MeV. At 256 MeV the measured cross sections for the $\pi^+ d \rightarrow \pi^- \pi^+ pp$ reaction are equal to those for the $\pi^- d \rightarrow \pi^+ \pi^- nn$ reaction within the experimental uncertainties. To this accuracy the Coulomb force appears to have no influence on this reaction. The errors shown in the figure represent the combination of statistical uncertainty and those systematic uncertainties that depend on the outgoing momentum. Overall normalization is uncertain by a further 4%.

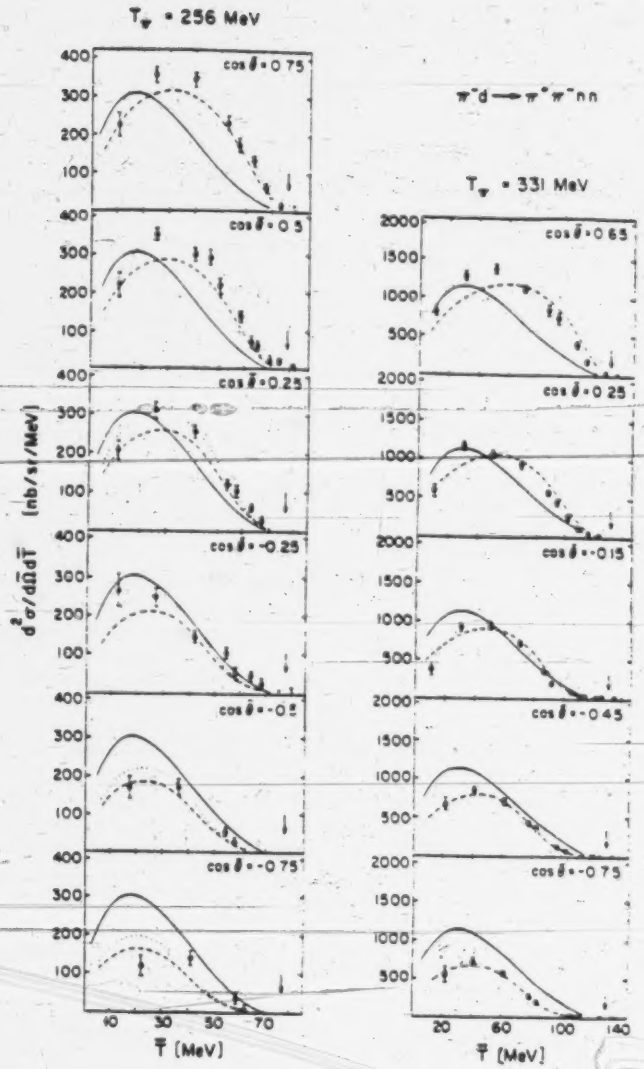

Fig. 1.

Doubly differential cross section for the $\pi^- d \rightarrow \pi^+ \pi^- nn$ reaction at 256 and 331 MeV. $\bar{T}$ and $\bar{\theta}$ are the outgoing π^+ kinetic energy and angle in the center-of-mass system. The arrows mark the energy corresponding to the two-body $\pi(\pi NN)$ production, with zero binding energy for the πNN system. The solid curves represent four-body phase space normalized to the data. The dashed and dotted lines are quasi-free calculations in plane-wave Born approximation (see text).

The solid curves in Fig. 1 represent the distribution of events in four-body phase space, normalized so that its integral over energy and angle will equal the integrated reaction cross section determined from the data. The dashed curves are the predictions of a simple calculation,[11] in plane-wave Born approximation, of quasi-free pion production on the one-nucleon using phenomenological on-shell amplitudes deduced from the $\pi^- p \rightarrow \pi^+ \pi^- n$ data.[4]

The quasi-free calculation is in good agreement with the general features of the data, although some discrepancies do exist. At 256 MeV the quasi-free calculation reproduces the shape of the spectra very well, but the absolute value of the cross section is 20% below the measured result. The dotted curve in Fig. 1 is the quasi-free calculation normalized by the ratio of the measured and calculated integrated cross sections. At 331 MeV the integrated reaction cross section obtained from the quasi-free calculation is in agreement with that measured, within the experimental uncertainty, but a slight discrepancy exists between the measured and calculated shape of the spectra at forward angles. These effects could be attributed either to rescattering of the pion by the second nucleon or to the formation of πNN systems.

In pion production on protons, the average squared modulus of the matrix element[4,7] increases by a factor of 2 at forward angles and low outgoing pion energies, presumably because of the onset of significant contribution from a $\pi\Delta$ intermediate state. Indeed, in an isobar-model analysis of $\pi^- p \rightarrow \pi^- \pi^+ n$, the P_{33} partial wave first becomes important above 300 MeV.[7] One is tempted to speculate that a two-nucleon-reaction mechanism, either the $N\Delta \rightarrow \Delta\Delta$ transition or a rescattering process, would become significant where the $\pi\Delta$-state formation is most pronounced.

The measured doubly differential cross sections were integrated over the energy and angle of the produced pion to determine an integrated reaction cross section. To estimate the contribution from the unobserved kinematic range, we assumed the form of the cross section given by the plane-wave Born approximation and assigned a 25% uncertainty to the contribution from the extrapolated region. The integrated-reaction cross sections for $\pi^- d \rightarrow \pi^+ \pi^- nn$ are 160 ± 10 μb at 256 MeV and 1000 ± 100 μb at 331 MeV. The corresponding cross sections for $\pi^- p \rightarrow \pi^+ \pi^- n$ are 166 ± 6 μb and 1160 ± 50 μb at 256 and 331 MeV, respectively.[4]

In October 1983 we continued these measurements at an incident energy of 450 MeV, including a measurement of $\pi^- p \rightarrow \pi^+ \pi^- n$, which had not previously been done, for comparison. These data are presently being analyzed.

We intend to extend these observations to the ^{3}He nucleus in the next series of experiments, studying $\pi^+ {}^3\text{He} \rightarrow \pi^- \pi^+ ppp$. The ^{3}He nucleus differs from the deuteron by the addition of a proton, but also and more importantly because it is a much denser structure. The density of ^{3}He approaches that of normal nuclear matter, and one expects that two-nucleon effects will be stronger in ^{3}He than in deuterium. The second proton in ^{3}He does not contribute to the quasi-free part of the interaction, and the proton pair cannot contribute to the two-nucleon mechanism of pion production.

As for $\pi^+ d \rightarrow \pi^- \pi^+ pp$, the quasi-free pion production is only from the neutron, and the two-nucleon mechanism can only be attributed to the np pair. To first order, the quasi-free contribution in ^{3}He is expected to be equal to that in the deuteron, whereas the two-nucleon contributions are expected to be twice as large. The advantage of and interest in obtaining a larger and clearer signal for the two-body mechanism is obvious. Even if, disappointingly, no large two-nucleon contribution is found for pion production on ^{3}He, this result itself would be critical for possible application of the $(\pi,2\pi)$ reaction to nuclear-structure studies[5] in the future and for understanding the $N\Delta \rightarrow \Delta\Delta$ process.

REFERENCES

1. Los Alamos National Laboratory report LA-9256-PR (March 1982), p. 55.

2. Los Alamos National Laboratory report LA-9709-PR (March 1983), p. 57.

3. S. A. Wood, Ph.D. thesis, Massachusetts Institute of Technology, 1983 (unpublished).

4. C. W. Bjork et al., Phys. Rev. Lett. 44, 62 (1980).

5. G. E. Brown, H. Toki, W. Weise, and A. Wirzba, Phys. Rev. Lett. 118B, 39 (1982).

6. H. Garcilazo, Phys. Rev. C 26, 2685 (1982).

7. A. T. Oyer, Los Alamos National Laboratory report LA-6599-T (1976); J. B. Walter, Los Alamos National Laboratory report LA-8377-T (1979); and D. Manley, Los Alamos National Laboratory report LA-9101-T (1981).

8. J. R. Carter, D. V. Bugg, and A. A. Carter, Nucl. Phys. B 58, 378 (1973).

9. J. B. Walter and G. A. Rebka, Jr., Los Alamos National Laboratory report LA-7731-MS (1979).

10. P. J. Bussey et al., Nucl. Phys. B 58, 363 (1973); H. R. Rugge and O. T. Vik, Phys. Rev. 129, 2300 (1963); and Philip M. Ogden et al., Phys. Rev. 137, B1115 (1965).

11. L.-C. Liu, R. S. Bhalerao, and E. Piasetzky, contribution to the Symp. on Delta-Nucleus Dynamics, Argonne, Illinois, 1983.

The Crystal Box Experiments (Exps. 400/445 and 726, SMC)

(Los Alamos, Univ. of Chicago, Stanford Univ., Temple Univ.)

Spokesmen: (Exps. 400/445) — C. M. Hoffman, J. D. Bowman, and H. S. Matis (Los Alamos); (Exp. 726) — V. L. Highland (Temple Univ.) and G. H. Sanders (Los Alamos)

Discussions of these experiments have been presented in the past several Progress Reports. The aim of these experiments is to search with unprecedented sensitivity for several rare decay modes of the muon and the pion. Experiments 400/445 are searching for the muon-number-violating decays $\mu^+ \to e^+e^+e^-$, $\mu^+ \to e^+\gamma$, and $\mu^+ \to e^+\gamma\gamma$, with branching ratios somewhat smaller than 10^{-11}. Experiment 726 will search for the charge-conjugation-violating decay $\pi^0 \to 3\gamma$ with a sensitivity to a branching ratio as low as 10^{-9}.

Experiments 400/445

A schematic of the apparatus is shown in Fig. 1. The detector consists of a modular array of 396 NaI(Tl) crystals that surround an array of plastic scintillation counters and a high-resolution drift chamber. Approximately 5×10^5 μ^+/s are stopped in a thin target located in the center of the apparatus. The major source of backgrounds is the random coincidence of e^+'s and γ's from the uncorrelated decays of several muons. These backgrounds are eliminated by requiring that the detected particles be in time coincidence and satisfy the conservation of energy and momentum. For the $\mu^+ \to e^+e^+e^-$ mode, there is the additional constraint that the three tracks must emerge from a common vertex. To reject the backgrounds to an adequate level, excellent resolutions in timing, energy, and position are required.

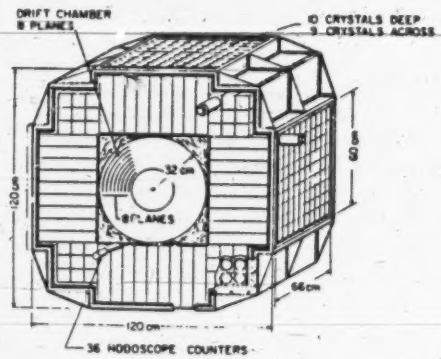

Fig. 1.
Schematic of the Crystal Box detector.

A short tuneup run was taken in January 1983, with two of the four NaI(Tl) quadrants instrumented. The purpose of this run was to measure trigger rates and check all parts of the system. Several problems were uncovered. The $\mu^+ \to e^+e^+e^-$ trigger rate was unacceptably high because of particles that trigger the scintillation counters but that deposit little or no energy in the sodium iodide; some of these are from low-energy particles present in the electromagnetic showers in the crystals. After analyzing data tapes, it was determined that the best way to eliminate these triggers is to require at least one discriminator from the crystals behind the scintillator fire. The electronics needed to implement this logic was constructed in the spring and summer and installed this fall; it performed according to expectations. The photon definition in the tune-up run also was found to be inadequate (a photon is defined as a quadrant with a sodium iodide discriminator firing but no scintillator firing). The major improvement needed here was the installation of separate leading-edge discriminators for the scintillators to provide the photon veto. Other changes involved minor improvements in how the corner crystals were apportioned between the two quadrants straddling the corner, and the removal of the most upstream and downstream rows from the photon definition.

The final major problem uncovered was the need for a more sophisticated system to detect pileup in the NaI(Tl). The system we designed to detect pileup was not efficient enough at detecting low levels of pileup and also rejected many events that were, in fact, not piled up. A compact CAMAC-based sample-and-hold system was purchased and installed to solve this problem. It also was necessary to modify the circuits that clip the NaI(Tl) output pulses and to use higher quality delay lines to shorten the length of the pulse at the circuit that measures the pulse area (for the energy determination). All these improvements and modifications were installed by the fall of 1983.

As discussed in the last Progress Report, the method used to mount photomultiplier tubes on the first two quadrants led to several vacuum leaks in the hermetically sealed container housing the crystals. An alternative mounting scheme that subjects the container to much

smaller stresses was designed and has been used on all four quadrants. In the 5 months since this was done, no vacuum leaks have occurred and we believe the problem is solved.

During several test runs in the fall, the entire system was connected, timed, calibrated, and debugged. This included all the electronics and the on-line data-acquisition code. A nagging problem in the LSI-11-based system, which reads out the NaI(Tl) pulse height and timing information, was fixed with the aid of Jerry Potter, Group MP-1; this system now works flawlessly. We also installed a crystal calibration system that uses a xenon flash tube and fiber optics cables; this system is working quite well.

In addition to all the above hardware changes, substantial progress was made in our analysis programs. For example, the track reconstruction efficiency in the drift chamber has risen from 86 to 97%. This is due to a combination of improvements in the software and hardware.

During our last run in 1983, we took 5 days of data at a reduced muon rate of $2 \times 10^5\ \mu^+/s$, and we are now analyzing these data. A typical $\mu \rightarrow e\gamma$ candidate is shown in Fig. 2. At the end of this run, the drift chamber was removed, a small liquid-hydrogen target was inserted, and data were taken with incident π^-. Figure 3 shows a spectrum from π^0's produced in the reaction $\pi^- p \rightarrow \pi^0 n$ at rest. These data are used to help calibrate the apparatus.

Plans call for a 3-week data run in January 1984 and more runs next summer.

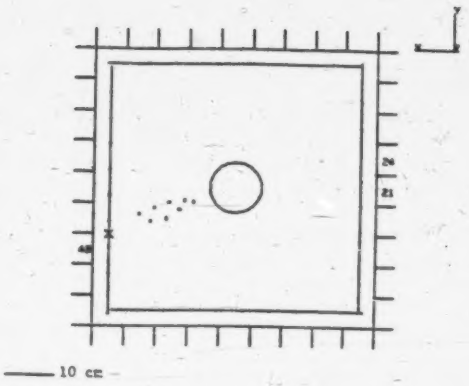

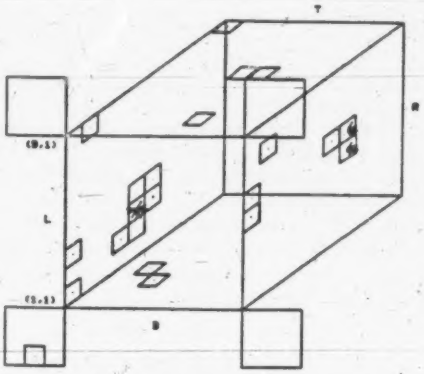

Fig. 2(a) and (b).
A typical $\mu \rightarrow e\gamma$ event: (a) view along beam line showing drift chamber wire hits, the struck scintillator, and the sodium iodide row sum energies; and (b) a three-dimensional view of the sodium iodide.

Experiment 726

During the aforementioned running with a π^- beam and a liquid-hydrogen target, a data tape was taken while triggering on $\pi^0 \rightarrow 3\gamma$. A study of this tape will be invaluable for designing the details of the trigger electronics.

Data taking for this experiment will take place after the muon data have been obtained.

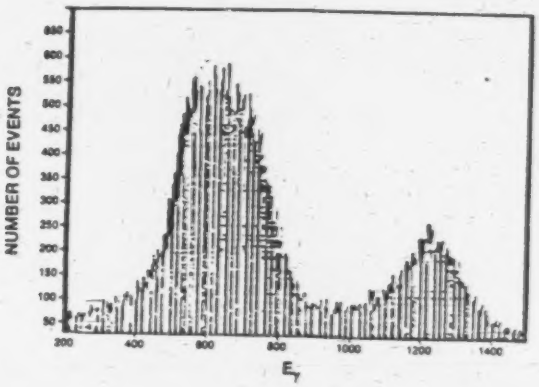

Fig. 3.
An on-line spectrum of single γ-ray energies from stopping π^- in hydrogen. The units for the abscissa are not MeV.

Deformation of Rare-Earth Nuclei and the Sternheimer Effect
(Exp. 698, SMC)

(Purdue Univ., Los Alamos, Princeton Univ.)
Spokesmen: R. M. Steffen (Purdue Univ.) and E. B. Shera (Los Alamos)
Participants: Y. Tanaka, W. Reuter, M. V. Hoehn, and J. D. Zumbro

Values of nuclear quadrupole moments Q_1 deduced from electronic-atom hyperfine measurements are rather uncertain even though measurements of optical hyperfine-splitting energies are very precise. The reason lies in the difficulty of exactly calculating the electrostatic gradient at the nucleus produced by the multielectron environment. In general, the nonspherical shape of the nuclear quadrupole field causes a nonspherical distribution of the core electrons (the Sternheimer effect) that in turn affects the electronic valence states.

In a muonic atom, however, the (single) muon is overwhelmingly responsible for the field gradient at the nucleus, allowing nuclear quadrupole moments to be precisely extracted from measurements of the hyperfine-splitting energies of muonic $3d$ and $4f$ states (that is, by observation of the muonic-M x rays).

We have measured the ground-state quadrupole moments of 11 odd-A nuclei in the region from $Z = 63$ to 77 by observing the hyperfine structure of their muonic-M x rays. The total errors of the present quadrupole moments, including the uncertainty arising from the model assumed for the radial quadrupole charge distribution within the nuclear volume, are less than 1%.

Our data for the odd-A nuclei demonstrate that, after the abrupt onset of deformation at $N = 90$, the deformation parameters β_2 vary smoothly with neutron number (see Fig. 1). Contrary to the rather scattered electronic-atom results (see Fig. 2), the present results indicate that the deformations of the odd-A nuclei are quite consistent with those of the adjacent even-A neighbors.

We expect that our precise new quadrupole-moment values will stimulate theoretical calculation of the ground-state deformation of odd-A nuclei. Correct prediction of the equilibrium deformation of the ground state is a central issue in gauging the success of mean-field theories of nuclear structure.

By comparing our muonic-atom quadrupole-moment values with electronic-atom values, we have computed experimental Sternheimer shielding factors for several electronic orbitals relevant to rare-earth atoms. We are thus led to the following conclusions.

1. The shielding factors have the same value for isotopes of the same element, even though the nuclear quadrupole moments may be quite different (by almost a factor of 3 for europium isotopes).
2. The $R(5d)$ shielding factors vary irregularly from $-0.16(13)$ to $-0.75(17)$, in serious disagreement with the theoretical estimate of $R(5d) = -0.25(5)$. Whereas the $R(4f)$ shielding factors for terbium, dysprosium, and erbium, and the $R(6p)$ shielding factors for europium and gadolinium, are close to

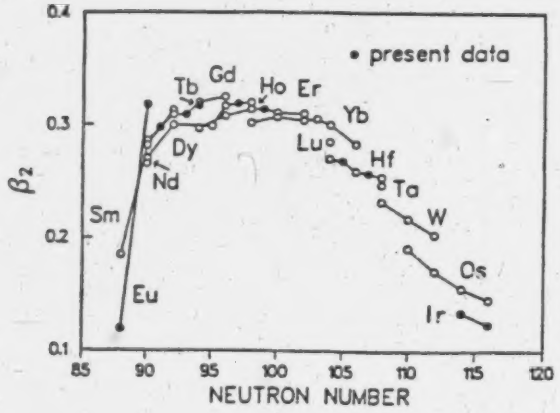

Fig. 1.
Systematics of the deformation parameter β^2 in the rare-earth region. The new muonic data for odd-A nuclei are shown as solid dots.

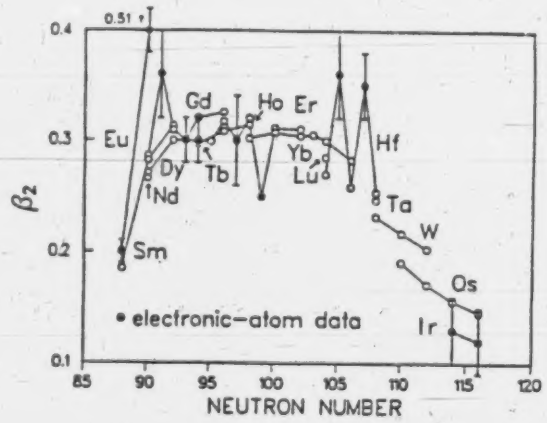

Fig. 2.
Similar to Fig. 1, except that the widely scattered optical data are shown for the odd-A nuclei.

the theoretical values, the $R(6p)$ value for dysprosium is several times smaller than the theoretical value. Clearly, the theory of the Sternheimer shielding effect in the $5d$ and $6p$ electronic valence states of rare-earth atoms must be reexamined.

Although our understanding of the electronic electrostatic gradients at the nucleus in rare-earth atoms is far from complete, it seems that no matter which effects contribute to the shielding phenomena, the same shielding factor is valid for all isotopes of a particular element regardless of the value of the nuclear quadrupole moment. Hence electronic-atom hyperfine measurements, which require only small amounts of target material, are well suited for determining accurate ratios of ground-state nuclear quadrupole moments of different isotopes of the same element. Furthermore, if the appropriate muonic-atom data are available for empirical calibration of the Sternheimer effect, the electronic-atom measurements can furnish absolute measurements of the quadrupole moments of otherwise inaccessible nuclei.

Further information concerning this work can be obtained from Phys. Lett. 108B, 8 (1982) and Phys. Rev. Lett. 51, 1633 (1983).

Formation of Muonium in the $2S$ State and Observation of the Lamb-Shift Transition (Exp. 724, SMC)

(Yale Univ., Univ. of Heidelberg, College of William and Mary, Los Alamos, Univ. of Mississippi)

Spokesmen: P. O. Egan and V. W. Hughes (Yale Univ.), and M. Gladisch (Univ. of Heidelberg)

Participants: A. Badertscher, S. Dhawan, P. O. Egan, V. W. Hughes, D. C. Lu, M. W. Ritter, K. A. Woodle, M. Gladisch, H. Orth, G. zu Putlitz, M. Eckhause, J. Kane, F. G. Mariam, and J. Reidy

Muonium (M) is an atom consisting of a positive muon and an electron and is an ideal system to test quantum electrodynamics (QED).[1] High-precision measurements of the hyperfine-structure interval $\Delta\nu$ and of the Zeeman effect in its ground state have provided very sensitive tests of QED, as well as precise values of the fine structure constant α and the ratio of the muon and proton magnetic moments.[2,3] In these experiments muonium was formed by stopping μ^+ in gaseous targets.

Another important QED test would be a precise measurement of the Lamb shift in muonium in the $n=2$ state, since it would be free of the effects of proton structure that complicate the interpretation of the Lamb shift in hydrogen.[4] For this measurement muonium in the $2S$ state must be obtained in vacuum to avoid collisional quenching of $M(2S)$ atoms. Using a method similar to beam neutralization in proton beam foil spectroscopy,[5] we have shown that muonium in its ground state is formed by passing a μ^+ beam through a thin foil in vacuum.[6] From proton data[7] we expect that metastable $M(2S)$ atoms will be formed as well, and that $M(2S)/M(1S)$ will be about 0.1. Higher excited states will also be formed, but their formation probabilities are lower and most of these excited-state atoms will decay rapidly.

Here we report on further developments for producing muonium in vacuum, detecting $M(2S)$ by a static electric-field quenching method, and observing the Lamb-shift transition $2S \rightarrow 2P$ induced by an electric rf field of about 1140 MHz.

Our experiment was done at the SMC at LAMPF. Figure 1 shows a diagram of our apparatus.

Figure 2 is the energy-level diagram for muonium in its $n=1$ and $n=2$ states, including fine structure, Lamb shift, and hyperfine structure. The value of the Lamb-shift interval of $2S_{1/2}$ to $2P_{1/2}$ for muonium has been calculated from QED.[8] The $2S$ atomic state is metastable with the mean lifetime of 1/7 s for two-photon decay to the $1S$ state; however, the mean life of 2.2 μs for μ^+ decay determines the lifetime of $M(2S)$. Our first approach to observation of $M(2S)$ was to detect the static electric-field quenching of $M(2S)$.

We searched for $M(2S)$ by modulating the static electric field between on (600 V/cm) and off and by looking for a difference in the event rate due to Lyman α photons emitted during the field on phase. An event required a triple coincidence between an incoming muon, a delayed Lyman α photon in one of the four ultraviolet phototubes, and a further-delayed $M(1S)$ atom detected in the microchannel plate. The time gates were set to accept $M(2S)$ atoms with kinetic energies between 4 and 26 keV. The asymmetry between quenching field on and field off, defined with the events (E) normalized to the number of incoming muons,

$$A = \frac{(E/\mu)_{on} - (E/\mu)_{off}}{(E/\mu)_{on} + (E/\mu)_{off}},$$

was $A = (41.5 \pm 5.8)\%$.

The next step in establishing the formation of $M(2S)$ atoms was to search for the Lamb-shift transition $2S_{1/2}$-

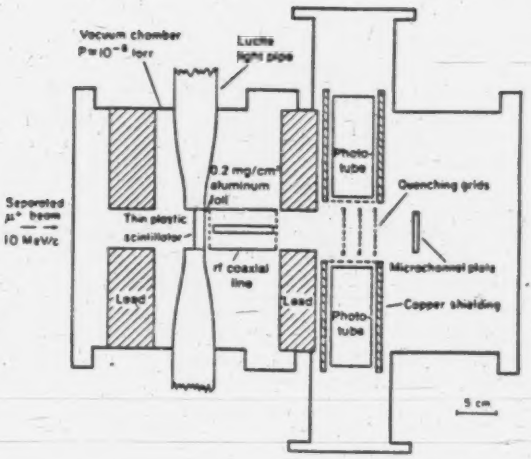

Fig. 1.
Diagram of the apparatus.

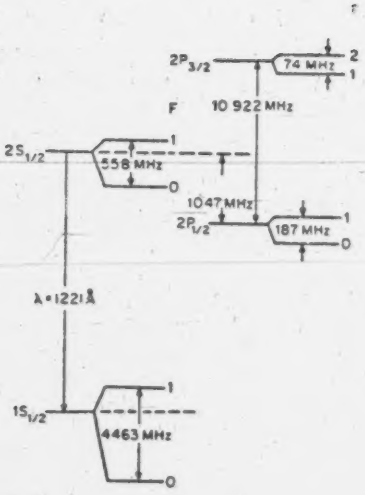

Fig. 2.
Energy-level diagram of the $n = 1$ and $n = 2$ states of muonium.

$F = 1 \rightarrow 2P_{1/2}$, $F = 1$ driven with an electric rf field. In Fig. 3 the solid curve shows the theoretical non-power-broadened resonance lines for two transitions between the hyperfine sublevels of the $2S_{1/2}$ and $2P_{1/2}$ states. The natural linewidth of 100 MHz (FWHM) is due to the

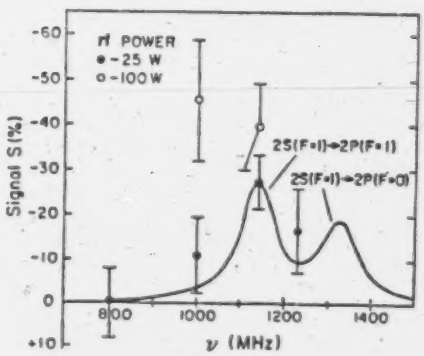

Fig. 3.
Muonium $2S_{1/2} - 2P_{1/2}$ resonance lines. The solid curve shows the theoretical non-power-broadened resonance line shape. The data points for 100- and 25-W rf input power are shown.

lifetime of the $2P_{1/2}$ state. Our rf interaction region (Fig. 1) consisted of a coaxial line. The experimental data are shown.

We conclude from our data that we have formed muonium in the $2S$ state with the expected rate and that we have observed the Lamb-shift transition. We are making measurements of the $2S_{1/2} \rightarrow 2P_{1/2}$ transitions to determine the Lamb shift and hfs intervals.

REFERENCES

1. V. W. Hughes and T. Kinoshita, in *Muon Physics I*, V. W. Hughes and C. S. Wu, Eds. (Academic Press, New York, 1977), p. 12.

2. F. G. Mariam et al., Phys. Rev. Lett. 49, 993 (1982).

3. J. R. Sapirstein et al., Phys. Rev. Lett. 51, 982 and 985 (1983).

4. S. R. Lundeen and F. M. Pipkin, Phys. Rev. Lett. 46, 232 (1981).

5. H. G. Berry, Rep. Prog. Phys. 40, 155 (1977).

6. P. R. Bolton et al., Phys. Rev. Lett. 47, 1441 (1981).

7. G. Gabrielse, Phys. Rev. A 23, 775 (1981).

8. D. A. Owen, Phys. Lett. 44B, 199 (1973).

$E2$ and $E4$ Moments in $^{233,234,235,238}U$ (Exp. 745, SMC)

(Princeton Univ., Los Alamos, Purdue Univ., Oak Ridge National Lab.)

Spokesmen: J. D. Zumbro (Princeton Univ.) and E. B. Shera (Los Alamos)

Participants: Y. Tanaka, C. E. Bemis, Jr., R. A. Naumann, M. V. Hoehn, W. R. Reuter, and R. M. Steffen

The rigid-rotor model postulates that the low-lying excited nuclear states arise from rotations of an intrinsically deformed ground state. With this model the quadrupole and hexadecapole moments of the low-lying states are related by well-known geometrical factors (Clebsch-Gordon coefficients). In a heavy, highly deformed nucleus like uranium it is possible to test the (adiabatic) rotational-model predictions by studying the interaction of the nucleus with a bound muon. This is possible because in heavy nuclei several excited nuclear states are mixed appreciably in the muonic $3d$ and $2p$ states. By simultaneously analyzing the muonic $2p \rightarrow 1s$ (K), $3d \rightarrow 2p$ (L), and $4f \rightarrow 3d$ (M) x-ray transitions, a large number of $E2$ matrix elements can be independently determined. We therefore are able, for the first time, to make a detailed electromagnetic test of a principal underlying assumption of the rotational model.

Figure 1 summarizes our results for ^{233}U. The upper section of the figure shows the $E2$ matrix elements that were independently determined; the lower part of the figure indicates that the measured matrix elements are consistent with an adiabatic intrinsic state at the level of a few per cent.

The present muonic-atom experiments on uranium also represent the first direct measurement of spectroscopic hexadecapole ($E4$) nuclear moments. The measurements are direct in the sense that the hyperfine splitting produced by the interaction of the nuclear $E4$ moment with the (readily computed) electric-field gradient at the nucleus is observed directly.

The muonic-atom method stands in contrast to previous methods that have employed strongly interacting probes and that have sometimes yielded inconsistent results, presumably from model dependence or interference from strong-interaction effects. Discrepancies between different types of experiments have suggested[1]

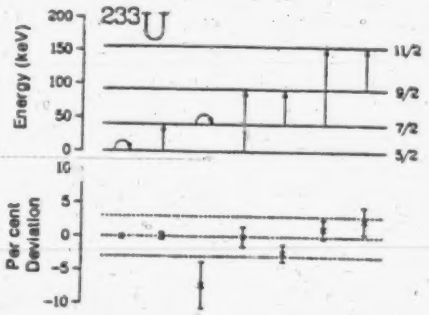

Fig. 1.

Results for $E2$ matrix elements in ^{233}U that were independently determined. The upper part of the figure indicates the $E2$ moments that also were independently determined. A line between two levels indicates a dynamic $E2$ moment [$B(E2)$], and the circular line closing on a level indicates a static $E2$ moment. In the lower part of the figure the deviation of each moment from the rotational-model value is shown; these deviations indicate that the measured matrix elements are consistent with an adiabatic intrinsic state at the level of a few per cent. The dashed lines are ±3%.

that nuclear shapes depend somehow on the probe or reaction mechanism used to explore them.

The results of our muonic $E4$ measurements are shown in Fig. 2. These results, while more precise, are in reasonable agreement with the Coulomb excitation work of Bemis et al.[2] The hexadecapole moments have approximately the same value (~2.5 eb^2) for all four uranium isotopes that we have studied. This result is in agreement with equilibrium shapes of the uranium isotopes predicted by Brack et al.[3] using the Strutinsky shell-correction method with a Woods-Saxon potential. We are now using the Hartee-Fock deformed density-matrix-expansion theories from Negele and Rinker[4] to perform calculations for these nuclei.

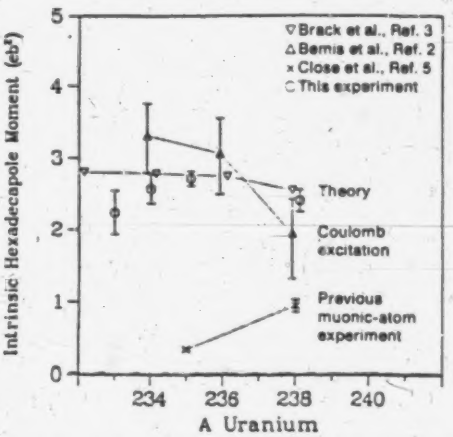

Fig. 2.
Intrinsic hexadecapole moment vs A for the uranium isotopes.

The early muonic-atom results of Close et al.[5] are in serious disagreement with the present results, with Coulomb excitation, and with theoretical calculations (see Fig. 2). The present work indicates that a carefully analyzed muonic-atom experiment produces results in agreement with other methods, thereby removing one piece of evidence for probe dependence of nuclear shapes.

REFERENCES

1. V. A. Madsen, V. R. Brown, and J. D. Anderson, Phys. Rev. Lett. 34, 1038 (1975); and V. A. Madsen et al., Phys. Rev. C 12, 1205 (1975).

2. C. E. Bemis, Jr., F. K. McGowan, J. L. C. Ford, Jr., W. T. Milner, P. H. Stelson, and R. L. Robinson, Phys. Rev. C 8, 1466 (1973).

3. M. Brack, T. Ledergerber, H. C. Pauli, and A. S. Jensen, Nucl. Phys. A 234, 185 (1974).

4. J. W. Negele and G. Rinker, Phys. Rev. C 15, 1499 (1977).

5. D. A. Close, J. J. Malanify, and J. P. Davidson, Phys. Rev. C 17, 1433 (1978).

Atomic and Molecular Physics

Theory of Muon-Catalyzed *dt* Fusion: Resonant Mesomolecule Formation (Biomed)

Spokesman: M. Leon (Los Alamos)

Muon catalysis of deuterium-tritium fusion has recently become a topic of widespread interest. On one hand, experiments probing this process under a variety of conditions are being performed at several muon facilities.[1,2] On the other, the sustained assault mounted by Ponomarev and his colleagues on many of the theoretical problems involved has made impressive progress in removing many of the gaps in our understanding.*

The most crucial and perhaps the most fascinating aspect of the muon-catalysis cycle is the role played by the resonant formation of the $dt\mu$ molecule.[5] This resonant formation occurs because of the existence of a very loosely bound $J=1$, $v=1$ excited state in the $dt\mu$ mesomolecule. The binding energy ($\simeq 0.64$ eV) is small enough that the energy released in the $dt\mu$ formation from the $t\mu + d$ state can go into vibration and rotation of the resulting $dt\mu$-d (or $dt\mu$-t) molecule instead of into Auger emission. The resulting molecular-formation rates are at least two orders of magnitude larger than the nonresonant (Auger) rates.[5,6]

In developing the theory of resonant $dt\mu$ formation, we have generalized the calculation of Vinitsky et al.[6] (hereafter referred to as VP) to include the very important effects of the (1) orbital angular momentum carried into the reaction by the $t\mu$-D_2 (or DT) relative motion, and (2) initial D_2 (DT) angular momentum $K_i > 0$. We show as a result that, rather than a single resonance as in VP, the molecular formation reactions are dominated by a plethora of resonances, with a variety of initial and final molecular angular momenta. We also find that both the $v=2$ and $v=3$ vibrational levels of the final $dt\mu$-d molecule contribute significantly. Our final calculations for the molecular-formation rates as functions of temperature therefore include contributions from about 500 individual resonances.

The matrix element of the transition is written by VP as

$$T_{fi} = \int d\bar{R}\, d\bar{r}\, d\bar{\rho}\; \psi_f^*(\bar{r},\bar{R})\; \psi_f^*(\bar{\rho})\; H \psi_i(\bar{\rho}) \psi_i(\bar{r},\bar{R}) \quad ,$$

where $\Psi(\bar{r},\bar{R})$ are the wave functions of the internal coordinates of the mesosystem $t\mu + d$ and where $\psi(\bar{\rho})$ are that of the motion of the mesosystem with respect to the spectator nucleus (see Fig. 1). The $t\mu + d$ collision time (at thermal energies) is estimated to be $\sim 10^{-15}$ s, which means that whereas the collision is sudden for the D_2 (DT) molecule, it is adiabatic for the electrons. Hence no electron excitation takes place during the "compound-molecule" formation. However, it is important that the next stage, deexcitation of the compound molecule by Auger emission, is much more probable than dissociation.

For the wave function $\psi_i(\bar{\rho})$, VP simply use the ground-state wave function of the target D_2 molecule (for $K_i = 0$ and vibrational $v_i = 0$):

$$\psi_i(\bar{\rho}) = \frac{y_0(\rho)}{\sqrt{4\pi}\,\rho} \quad .$$

An obvious generalization is to replace

$$1/\sqrt{4\pi} \qquad [\equiv Y_{00}(\hat{\rho})]$$

with

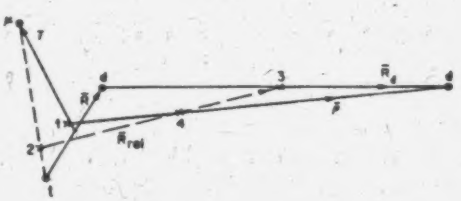

Fig. 1.
Vectors involved in the molecular-formation calculation: $\bar{r}$ goes from the midpoint of $\bar{R}$ to μ, $\bar{\rho}$ from the $dt\mu$ c.m. (marked 1) to the spectator d, and $\bar{R}_{rel}$ goes from the c.m. of the $t\mu$ (marked 2) to that of the D_2 (marked 3). The overall c.m. is marked 4.

*References 3 and 4. For a readily accessible review, see Bracci and Fiorentini, Ref. 4.

$Y_{K_i M_i}(\hat{\rho})$.

However, it is also necessary to include a factor to express the motion of the $t\mu$ atom and the D_2 molecule with respect to the overall center of mass (c.m.). This implies the factor $\exp(i\vec{p}\cdot\vec{R}_{cm})$, which introduces the dependence on the orbital angular momentum L; here $\vec{p}$ is the c.m. momentum (Fig. 1). Because of the small size of the $t\mu$ atom, interaction takes place when $r,R \ll \rho$. Then $\vec{R}_{cm} \simeq \eta\vec{\rho}$, where $\eta = 1/2$ for D_2, 3/5 for DT. Thus the VP expression is replaced by

$$\psi_i(\vec{\rho}) \simeq e^{i\eta\vec{p}\cdot\vec{\rho}}\, y_0(\rho)\, Y_{K_i M_i}(\hat{\rho})/\rho$$

$$= \sum_L (2L+1)\, i^L j_L(\eta p\rho)\, P_L(\cos\theta_{\vec{p}})$$

$$\times y_0(\rho)\, Y_{K_i M_i}(\hat{\rho})/\rho \quad . \qquad (1)$$

The interaction Hamiltonian is approximated by

$$H \simeq \frac{\vec{d}\cdot\rho}{\rho^3}\left(\frac{4\pi d}{3\rho^2}\right)\sum_{m=-1}^{1} Y^*_{1m}(\vec{d})\; Y_{1m}(\hat{\rho}) \quad ,$$

where $\vec{d}$ is the dipole moment of the $dt\mu$ system.[6] The angular factors are now separated so that the angular integrals can be performed and the results expressed in terms of 3-J coefficients.[7] Taking the absolute square of T_{fi} and averaging over M_i and summing over M_f, we find the factor

$$F(K_i, K_f) = (2K_f+1)\sum_L (2L+1)\; J^2_{L\nu}$$

$$\times\left\{(2L+3)\left[\begin{pmatrix} K_i & L+1 & K_f \\ 0 & 0 & 0\end{pmatrix}\begin{pmatrix} L & 1 & L+1 \\ 0 & 0 & 0\end{pmatrix}\right]^2\right.$$

$$\left.+(2L-1)\left[\begin{pmatrix} K_i & L-1 & K_f \\ 0 & 0 & 0\end{pmatrix}\begin{pmatrix} L & 1 & L-1 \\ 0 & 0 & 0\end{pmatrix}\right]^2\right\} . \qquad (2)$$

The

$$\begin{pmatrix} K_i & L\pm1 & K_f \\ 0 & 0 & 0\end{pmatrix} \quad \text{etc.}$$

are 3-J coefficients,[7] and the second term in the $\{\ \}$ is absent for $L = 0$. (The ±1 arises from the $J = 1$ of the loosely bound $dt\mu$ state.) The factor

$$J_{L\nu} \equiv \int d\rho\, y_0(\rho)\, y_\nu(\rho)\, j_L(\eta p\rho)\rho^{-2}$$

replaces the vibrational matrix element I_ν of VP. Since the vibrational motion is of rather small amplitude around the equilibrium value $\rho_0 \simeq 1.4\, a_0$ (Ref. 8), for a rough approximation we can replace ρ with ρ_0 in the argument of the spherical Bessel function j_L, and therefore get

$$J_{L\nu} \simeq j_L(\eta p\rho_0) I_\nu ,$$

where, as in VP,

$$I_\nu \equiv \int d\rho\, y_0(\rho)\, y_\nu(\rho)\rho^{-2} \quad .$$

For $p \to 0$, only the S wave survives and $j_0 \to 1$; then for $K_i = 0$, only $K_f = 1$ is possible and $F \to I^2_\nu$. Thus

$$\bar{F}(K_i, K_f) \equiv \frac{F(K_i, K_f)}{I^2_\nu}$$

is precisely the factor that corrects the VP result for the incoming orbital angular momentum and $K_i > 0$. Orbital angular momentum $L > 0$ obviously allows a much greater variety of K_f values, not just $K_f = K_i \pm 1$, and therefore greatly increases the number of resonances contributing to molecular formation. For any fixed collision energy, however, the centrifugal barrier factor $j^2_L(\eta p\rho_0)$ will limit the number of partial waves contributing to the sum in Eq. (2).

The incoming $t\mu$ atom can be in the singlet ($S = 0$) or triplet ($S = 1$) spin state. Because the deuteron has spin 1,

the singlet $t\mu$ can only give the $S = 1$, $dt\mu$ mesomolecule, whereas triplet $t\mu$ can give rise to $S = 0$, 1, or 2. The $dt\mu$ hyperfine splittings have been calculated by Bakalov et al.[9] For our purposes, we can ignore the energy splitting between the three hyperfine states formed from triplet $t\mu$; then the hyperfine shifts mean that the effective $dt\mu$ binding energy is decreased by 38 meV for singlet $t\mu$ and increased by 13 meV for triplet $t\mu$.

Consider collisions of singlet $t\mu$ with D_2 molecules. Angular momentum conservation requires that the $L = 0$ partial wave have $K_f = K_i \pm 1$; then the corresponding $\nu \leq 2$, K_f states have energies below the initial-state threshhold and hence cannot contribute to resonant mesomolecule formation. Thus only $\nu \geq 3$ formation can occur, which (it turns out) requires at least 0.27 eV in initial kinetic energy. Therefore $L = 0$ can contribute significantly to the molecular-formation rate $\lambda^0_{dt\mu-d}$ only at extremely high temperature (T).

In contrast, when $L > 0$ is permitted, K_f can be as large as $K_i + L + 1$, adding a significant amount of rotational energy and thus moving several $\nu = 2$ levels above threshhold. In this way, $K_i \rightarrow K_f$ transitions of $2 \rightarrow 4$, $3 \rightarrow 5$, ... (requiring $L = 1$), and $0 \rightarrow 3$, $1 \rightarrow 4$, ... (requiring $L = 2$), etc., produce resonances at energies of tens of milli-electron-volts or less. These terms are dominant not only because the resonant energies are extremely low, but also because I_2 is significantly larger than I_1 (Ref. 6).

These very low energy resonances produce a $\lambda^0_{dt\mu-d}$ that is very sensitive to the precise value of the $dt\mu$ excited-state binding energy. Changing this number by 10 meV, which is the present limit of accuracy of the calculation,[3] will drive several of the resonances below threshold or introduce new ones. The temperature dependence comes not only from the positions and strengths of the resonances, which determine the contribution of different parts of the Maxwell-Boltzmann distribution of initial $t\mu$ energies[6] (the $t\mu$ is assumed thermalized), but also from the Boltzmann factor for the initial molecular excitation.

The calculated temperature dependences of the four molecular-formation rates are shown in Fig. 2, including for $\lambda^0_{dt\mu-d}$ the effect of varying the $dt\mu$ binding energy. These results make use of the $\lambda_{dt\mu-d}$ value computed by VP for $L = 0$ and resonance energy 0.07 eV. For D_2 collisions of singlet $t\mu$ atoms, the $\nu = 2$ contribution is strongly dominant, as stated above; the extreme sensitivity to the $dt\mu$ excited-state binding energy seen in Fig. 2(b) and its qualitatively different behavior both come from the low-energy resonances (indicated schematically). For triplet $t\mu$, an additional 51 MeV of rotational excitation is needed for resonant formation with $\nu = 2$; this requires a larger increase in rotational angular momentum (for example, $2 \rightarrow 6$ rather than $2 \rightarrow 4$) and therefore larger L ($L = 3$ rather than $L = 1$),

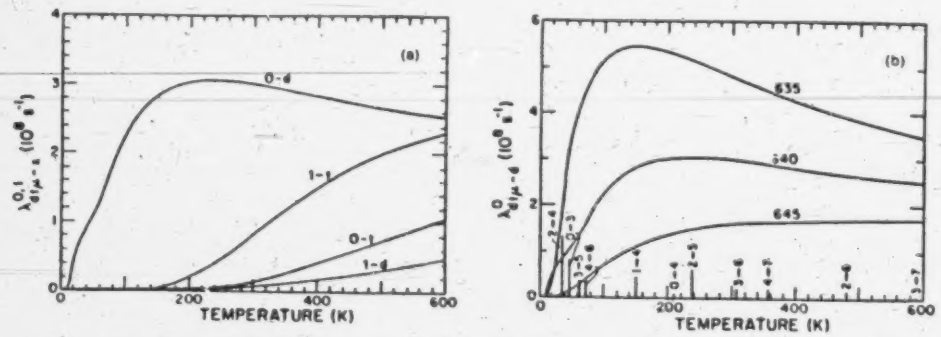

Fig. 2.

(a) The four molecular-formation rates, calculated for $dt\mu$ binding energy 640 meV; 0-d indicates $\lambda^0_{dt\mu-d}$, etc.

(b) The variation of $\lambda^0_{dt\mu-d}$ with binding energy, marked in milli-electron-volts. The variation with binding energy of the other three molecular-formation rates is rather small. For 640-meV binding energy, the positions and approximate strengths of the important low-energy resonances are shown as vertical bars, with the $K_i \rightarrow K_f$ values marked.

For DT collisions, the greater reduced mass lowers the vibrational levels so that the $v = 2$ contribution is completely negligible and only $v = 3$ is significant. Here the majority of important resonant contributions involve a reduction in rotational energy. For $dt\mu$-t, the vibrational energies and matrix elements are scaled from the $dt\mu$-d values of VP using harmonic oscillator behavior.

To make contact with experiment, we must consider how the four molecular formation rates contribute to the experimentally determined (normalized) muon-cycling rate λ_c. Introducing the effective (singlet or triplet) molecular-formation rates, which depend on the atomic concentrations C_d and C_t (see Refs. 1 and 10),

$$\lambda^{0,1}_{dt\mu} = \lambda^{0,1}_{dt\mu-d}\, C_d + \lambda^{0,1}_{dt\mu-t}\, C_t \quad ,$$

it can be seen that

$$\frac{1}{\lambda_c} = \frac{P_d}{\lambda_{dt} C_t} + \frac{3}{4}\,\frac{1}{\lambda_{10} + \lambda^1_{dt\mu}\, C_d} + \frac{\frac{1}{4} + \frac{3}{4}\,\chi}{\lambda^0_{dt\mu}\, C_d} \quad . \tag{3}$$

P_d is the probability for a ground-state $d\mu$ atom; because transfer to tritium can take place during the $d\mu$ deexcitation, this can be significantly less than C_d (Ref. 3). We use $P_d = C_d \exp(-\alpha C_t)$ to express this effect. Furthermore, λ_{dt} is the $d \rightarrow t$ ground-state transfer rate. The branching ratio χ is given by

$$\chi = \frac{\lambda_{10}}{(\lambda_{10} + \lambda^1_{dt\mu}\, C_d)} \quad ;$$

λ_{10} is the effective triplet-quenching rate, which has contributions from both d and t collisions

$$\lambda_{10} = \lambda^d_{10}\, C_d + \lambda^t_{10}\, C_t \quad .$$

The rate λ^t_{10} has been predicted to be very large: $9 \times 10^8\ s^{-1}$ (Ref. 11). If this is indeed the case, the second term of the right-hand side of Eq. (3) is always dominated by either the first or third term, and only the singlet molecular-formation rates can be easily extracted from experiment.

We show in Fig. 3 the data of Jones et al.[2] and two sets of calculated curves for $\lambda_c(T)$. Although parameters to give good agreement for $C_t = 10$, 20, and either 50 or 80% can readily be found (including increasing the rate given by VP by an overall factor β), we have not been able to fit all of the data simulaneously. Although our exploration of the six-dimensional parameter space certainly has not been exhaustive, we strongly suspect that this represents a real discrepancy. To pin down the source of this discrepancy, we urge the experimenters to

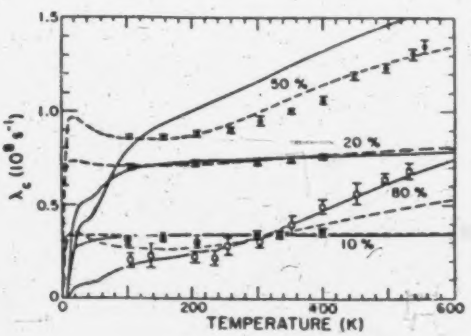

Fig. 3.
Theoretical and measured cycling rates λ_c for the C_t values marked. The curves were calculated using the following parameter values.

Solid curves:
Binding energy = 641 meV,
$\lambda_{dt} = 2.8 \times 10^8\ s^{-1}$,
$\alpha = 2.0$,
$\lambda^d_{10} = 5 \times 10^8\ s^{-1}$,
$\lambda^t_{10} = 0$, and
$\beta = 2.5$.

Dashed curves:
Binding energy = 628 meV,
$\lambda_{dt} = 2.6 \times 10^8\ s^{-1}$,
$\alpha = 3.3$,
$\lambda^d_{10} = 1.75 \times 10^8\ s^{-1}$,
$\lambda^t_{10} = 0$, and
$\beta = 1.6$.

measure as many of the various rates and parameters as possible.

REFERENCES

1. S. E. Jones et al., Phys. Rev. Lett. 51, 1757-1760 (1983).
2. Proceedings of the Third Int. Conf. on Emerging Nuclear Energy Systems, Helsinki, Finland, June 6-9, 1983, Atomkernenergie-Kerntechnik 43, No. 3 (1983).
3. L. I. Ponomarev, Proc. of the Third Int. Conf. on Emerging Nuclear Energy Systems, Helsinki, Finland, June 6-9, 1983, Atomkernenergie-Kerntechnik 43, No. 3 (1983); Proc. of the 10th European Conf. on Controlled Fusion and Plasma Physics (Moscow, 1981), Vol. II, p. 66; and S. I. Vinitsky and L. I. Ponomarev, Sov. J. Part. Nucl. 13, 557 (1982) [Fiz. Elem. Chastits At. Yadra 13, 1336 (1982)].
4. L. Bracci and G. Fiorentini, Phys. Rep. 86, 169 (1982).
5. S. S. Gershtein and L. I. Ponomarev, Phys. Lett. 72B, 80 (1977).
6. S. I. Vinitsky et al., Sov. Phys.-JETP 47, 444 (1978) [Zh. Eksp. Teor. Fiz. 74, 849 (1978)].
7. A. R. Edmonds, *Angular Momentum in Quantum Mechanics* (Princeton Universsity Press, 1957).
8. D. Rapp, *Quantum Mechanics* (Holt Rinehart, and Winston, New York, 1971).
9. D. D. Bakalov et al., Sov. Phys.-JETP 52, 820 (1980) [Zh. Eksp. Teor. Fiz. 79, 1629 (1980)].
10. S. S. Gershtein et al., Sov. Phys.-JETP 51, 1053 (1980) [Zh. Eksp. Teor. Fiz. 78, 2099 (1980)].
11. A. V. Matveenko and L. I. Ponomarev, Sov. Phys.-JETP 32, 871 (1971) [Zh. Eksp. Teor. Fiz. 59, 1593 (1970)].

Experimental Investigation of Muon-Catalyzed *dt* Fusion

(Exp.727, Biomed)

(Idaho National Engineering Lab., Los Alamos)
Spokesman: S. E. Jones (Idaho Engineering Lab.)

Because the dimensions of a muonic-hydrogen molecule are about 200 times smaller than those of an ordinary hydrogen molecule, negative muons stopped in a mixture of hydrogen isotopes can rapidly bring about fusion reactions. Muon-catalyzed fusion was first seen by Alvarez et al.[1] in 1957 but had been predicted even earlier by Frank and others.[2]

The recent revival of interest in the *dd* and *dt* reactions is mainly due to the discovery of a resonant molecular-formation process that precedes the fusion reactions.[3] For *dt*, this allows the formation of a loosely bound excited state of the $dt\mu$ mesomolecule, with the released energy going into vibration and rotation of the resulting large molecule (of which the $dt\mu$ is one nucleus) rather than electron emission (see Fig. 1). This resonant process is predicted to enhance the molecular-formation rate by two orders of magnitude and to induce a strong temperature dependence. In dense *dt* mixtures this opens the interesting possibility of a single negative muon catalyzing ~100 fusions.[4–6]

An experiment to measure the parameters governing muon-catalyzed fusion in deuterium-tritium mixtures is being carried out at the Biomed channel. The processes involved are shown schematically in Fig. 2. Of the rates defined there, only the transfer rate λ_{dt} and a lower limit on the molecular-formation rate $\lambda_{dt\mu}$ had been determined previously.[7] We have now measured λ_{dt}, $\lambda_{dt\mu}$ as a function of temperature in the range 100-540 K, the sticking probability ω_s, and the ^{3}He scavenging parameters (see below). (The fusion rate λ_f and the atomic capture rate λ_a are too fast to be measured.) Furthermore, we are also able to separate the two constituents[8] of $\lambda_{dt\mu}$:

$$\lambda_{dt\mu-d}: \quad t\mu + D_2 \rightarrow [(dt\mu)\, d\, 2e^-]^* \,, \tag{1a}$$

$$\lambda_{dt\mu-t}: \quad t\mu + DT \rightarrow [(dt\mu)\, t\, 2e^-]^* \,. \tag{1b}$$

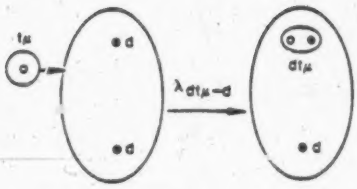

Fig. 1.
Resonant production of $dt\mu$ molecules.

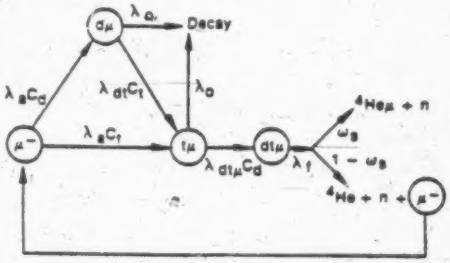

Fig. 2.
Muon catalysis in a mixture of deuterium and tritium.

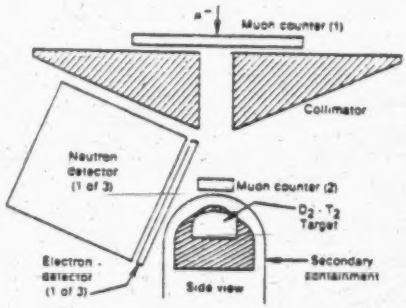

Fig. 3.
Layout of the experiment.

The apparatus is sketched in Fig. 3. The deuterium-tritium mixtures (0.45 and 0.60 of liquid-hydrogen density) are contained in gold-lined stainless steel vessels that can be heated or cooled.[9] Entering negative muons are registered by a scintillator telescope, the 14-MeV fusion neutrons by three liquid scintillators, and the muon-decay electrons by the combination of plastic scintillation counters plus the liquid scintillators. An accepted event requires, in sequence, (1) entry of a single muon, (2)

detection of one or more neutrons, and (3) detection of the muon-decay electron.

The times between neutron and e^- pulses following muon arrival are recorded. Neutron and γ events in the neutron detectors are distinguished by fast pulse-shape discrimination. These methods reduce background to acceptable levels. The neutron detector efficiencies are determined using the Los Alamos Van de Graaff accelerator as a 14-MeV neutron source in conjunction with Monte Carlo calculations that incorporate geometrical acceptance.[10] Overall neutron detection efficiency ϵ is $3.4 \pm 0.4\%$.

For any set of conditions there are two basic quantities to be determined: $\bar{n}$, the average number of neutrons produced per muon stopped in the gas, and λ_n, the rate associated with the time dependence of the appearance of the neutrons. The equations relating $\bar{n}$, λ_n, and the muon-cycling rate λ_c to the fundamental rates can easily be deduced from some simple considerations. Because λ_γ and λ_e are very large,[5] the cycling time ($1/\lambda_c$) of the muon is simply the sum of the time spent waiting to transfer from d to t for that fraction captured in deuterium C_d, plus the time the $t\mu$ atom waits for molecular formation. Therefore,

$$\frac{1}{\lambda_c} = \frac{C_d}{\phi\lambda_{dt}\, C_t} + \frac{1}{\phi\lambda_{dt\mu}\, C_d} . \qquad (2)$$

(By convention, the fundamental rates are normalized to liquid-hydrogen density, hence the density factor ϕ, which is the ratio of the actual number density to liquid-hydrogen density.) Rate λ_n depends on all the processes that remove muons from the cycle; for small ^{3}He concentrations,

$$\lambda_n = \lambda_0 + \omega_s\lambda_c\left(\omega_{He} + \frac{C_d}{C_t}\frac{\lambda_{dHe}}{\lambda_{dt}} + \frac{\lambda_{tHe}}{C_d\lambda_{dt\mu}}\right) , \qquad (3)$$

where ω_{He} is the probability for initial capture on ^{3}He plus the probability of transferring to ^{3}He during the muonic-hydrogen cascade, and where λ_{dHe} and λ_{tHe} are the rates for transfer from the ground state of the muonic-hydrogen atoms. Finally, as indicated by reactions of Eq. (1), there are two components of $\lambda_{dt\mu}$:

$$\lambda_{dt\mu} = \lambda_{dt\mu-d}\, C_d + \lambda_{dt\mu-t}\, C_t . \qquad (4)$$

Our principal experimental results obtained so far are displayed in Figs. 4 and 5 and Table I; the error bars in

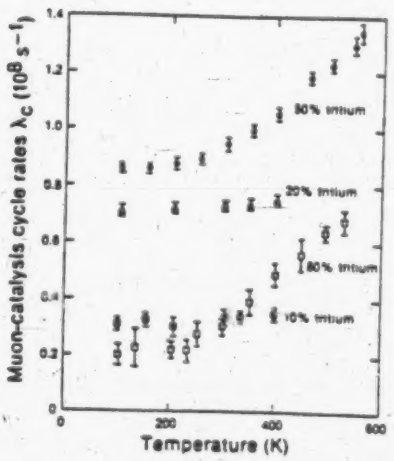

Fig. 4.
Muon-cycle rate λ_c normalized to liquid-hydrogen density as a function of temperature.

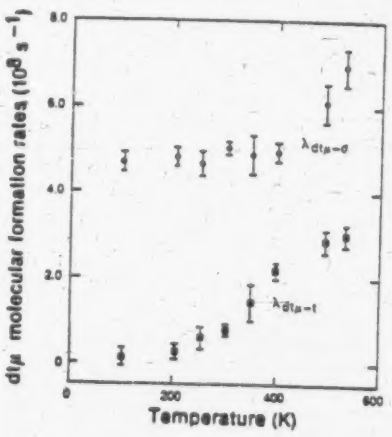

Fig. 5.
Mesomolecular formation rates as functions of temperature.

Table I. Parameters of Muon Catalysis in Deuterium-Tritium Mixtures.

Parameter	Theory	Reference	Previous Experiment[a]	This Experiment
λ_{dt}	$2 \times 10^8\ s^{-1}$	8	$(2.9 \pm 0.4) \times 10^8\ s^{-1}$	$(2.8 \pm 0.3) \times 10^8\ s^{-1}$
$\lambda_{dt\mu}$	$\sim 10^8$	5	$> 10^8\ s^{-1}$	see Fig. 5
ω_s	0.86%	11	—	$(0.77 \pm 0.08)\%$
	0.91%	12		
$\omega_{^3He}$	~ 1	14	—	1 ± 1
λ_{d^3He}	$1.5 \times 10^8\ s^{-1}$	13	—	$(2 \pm 1) \times 10^8\ s^{-1}$
λ_{t^3He}	$5.6 \times 10^8\ s^{-1}$	13	—	$(7 \pm 2) \times 10^8\ s^{-1}$
$\bar{n}$	$\sim 10^2$	5	—	90 ± 10

[a]Reference 7.

the figures are statistical, whereas the errors quoted in the table include systematic errors. Figure 4 shows the temperature dependence of λ_c for four concentration ratios. Whereas the low C_t data show no significant temperature dependence, in agreement with the experiment of Bystritsky et al.,[7] the temperature dependence for the higher tritium concentrations is quite striking. The low tritium concentration data are flat because the cycling time is dominated by the $d \rightarrow t$ transfer time $(1/C_t\lambda_{dt})$. The rate λ_{dt} (assumed to be independent of temperature) extracted from our data agrees very well with that reported in Ref. 7 (see Table I).

Once λ_{dt} is determined, $\lambda_{dt\mu}$ can be obtained using Eq. (2). From the concentration dependence of Eq. (4), the separate components of $\lambda_{dt\mu}$ are found (Fig. 5). Both of these components appear to be resonant. However, whereas $\lambda_{dt\mu-1}$ has the expected property of approaching zero as $T \rightarrow 0$, the $\lambda_{dt\mu-0}$ surprisingly appears to be constant in the temperature range 100-400 K.

The experiment also determines the sticking probability ω_s [see Eq. (3)]. The result for ω_s $(0.77 \pm 0.08)\%$ is in fair agreement with the two calculations.[11,12] (High-Z contamination of our target gas, which could produce an artificially large value of ω_s, was calculated to be less than 2 ppm and therefore negligible, but so far has not been measured.)

The final results concern the scavenging of muons by ^{3}He produced from tritium decay. The three contributions to this scavenging have been separated roughly by their λ_c and C_t dependence [see Eq. (3)]; the results are shown in Table I. The λ_{d^3He} and λ_{t^3He} values agree quite well with the calculations of Aristov et al.,[13] and the $\omega_{^3He}$ value is quite reasonable.[14]

In summary, this first investigation of muon-catalyzed fusion in high-density dt mixtures has produced a number of new results. Formation rates for $dt\mu$ molecules have been observed to be large and dependent on temperature, and quite different for the two molecular species involved (D_2 and DT). The measured sticking probability ω_s is consistent with calculation. The cycle rates and neutron yields demonstrate that a significant number of dt fusions per muon can be realized. Indeed, our measurements indicate that an average of 90 ± 10 fusions per muon will be produced in an equimolar deuterium-tritium mixture at $\phi = 1$ and 540 K.

REFERENCES

1. L. W. Alvarez et al., Phys. Rev. 105, 1127 (1957).
2. F. C. Frank, Nature 160, 525 (1947); A. D. Sakharov, Report of the Physics Institute, Academy of Sciences (1948); and Ya. B. Zeldovitch, Dokl. Akad. Nauk SSSR 95, 493 (1954).
3. E. A. Vesman, Sov. Phys.-JETP Lett. 5, 113 (1967).
4. S. S. Gershtein and L. I. Ponomarev, Phys. Lett. 72B, 80 (1977).
5. L. I. Ponomarev, Proc. of the 10th European Conf. on Controlled Fusion and Plasma Physics (Moscow, 1981), Vol. II, p. 66.
6. L. I. Ponomarev, Proc. of the 6th Int. Conf. on Atomic Physics, R. Danberg, Ed. (Plenum Press, New York, 1978), p. 182.
7. V. M. Bystritsky et al., Sov. Phys.-JETP 53, 877 (1981).
8. S. S. Gershtein et al., Sov. Phys.-JETP 51, 1053 (1980).
9. A. J. Caffrey, S. E. Jones, and K. D. Watts, Bull. Am. Phys. Soc. 28, 646 (1983).

10. N. R. Stanton, Ohio State Research Foundation report COO-1545-92 (1971); and A. J. Caffrey and S. E. Jones, to be published.

11. S. S. Gershtein et al., Sov. Phys.-JETP 53, 872 (1981).

12. L. Bracci and G. Fiorentini, Phys. Rep. 86, 169 (1982).

13. Yu. A. Aristov et al., Sov. J. Nucl. Phys. 33, 564 (1981).

14. J. S. Cohen, R. L. Martin, and W. R. Wadt, Phys. Rev. A 27, 1821 (1983).

Materials Science

Dilution Refrigerator for μSR Measurements (Exps. 499, 640, 771, SMC)

(Los Alamos, Rice Univ., Univ. of California at Riverside)

Spokesman: D. Wayne Cooke (Los Alamos)

The potential of muon spin rotation (μSR) as a condensed matter probe has been well established. Recent experiments have shown that such phenomena as fluctuation dynamics near spin-glass transition temperatures and muon motion in noble metals, for example, are amenable to study by muon-spin rotation and relaxation techniques. It is expected that potentially exciting physics occurs at temperatures below 4 K and that future μSR experiments will thus require cryogenic apparatus that can attain temperatures in the millikelvin region.

Accordingly, Group MP-3, assisted by Group P-10, has undertaken the task of designing and constructing a ^{3}He/^{4}He dilution refrigerator suitable for use in μSR studies. In addition to the temperature requirements, the refrigerator also must satisfy space requirements — namely, it must fit inside the existing μSR high-field Helmholtz coil.

Such a refrigerator has been designed and constructed, and initial testing has indicated the need for several modifications. During the past year these modifications have been made and tested, and include

- an improved method of mounting the refrigerator so that thermal isolation between the 1 K cold plate and 4 K heat shield is assured;
- the installation of a larger diameter heat shield to minimize risk of thermal shorts between the mixing chamber and heat shield;
- the construction and installation of a new counterflow heat exchanger that provides the proper pressure gradient between the still and mixing chamber; and
- an improved method of connecting the still and mixing chamber so that the thermal link between the two is minimized for temperatures below 1 K.

To date the minimum temperature attained by operating in a continuous mode has been 235 mK. It is expected that replacement of a faulty ^{4}He dewar will lower this temperature further to the design value of 50 mK. The present experimental effort is directed toward designing a suitable target chamber and devising a sample temperature control scheme in anticipation of performing μSR experiments with the dilution refrigerator.

Muon Longitudinal and Transverse Relaxation Studies in Systems with Random Exchange (Exp. 499, SMC)

(Rice Univ.; Los Alamos; UC, Riverside; Univ. of Leiden, The Netherlands)

Spokesmen: S. A. Dodds (Rice Univ.), R. H. Heffner (Los Alamos), and D. E. MacLaughlin (UC, Riverside)

Silver-Manganese Spin Glasses

Progress has been made in understanding the field dependence of zero- and longitudinal-field muon-spin relaxation (μSR) in *Ag*Mn spin-glass alloys at temperatures well below the freezing or "glass" temperature T_g (Ref. 1). These experiments provide a direct measurement of spin-glass dynamics, which is quite different in *Ag*Mn spin glasses than in their ordered counterparts (ferromagnets, antiferromagnets). In particular, the local spin correlations die off as $t^{-\nu}$; that is, the correlations possess "long-time tails." This is in contrast to the behavior of correlations in comparable nonrandom systems, which typically decay with an exponential time dependence.[2] Recent theories,[3] which use Langevin equations to represent the dynamics of the spin glass, also give this result, with $\nu \simeq \frac{1}{2}$, when applied to a mean-field model of the spin-glass state.

Our results may be summarized as follows.

1. Over a wide range of magnetic fields for $0.3 < T/T_g < 0.7$, and for several manganese concentrations, the positive-muon (μ^+) spin-lattice relaxation rate $\lambda_{\|}$ varies with effective applied field as $H^{\nu-1}$, with $\nu \simeq 0.54 \pm 0.05$. On general grounds we expect $\lambda_{\|} \propto J(\omega_\mu)$, where $J(\omega)$ is the noise spectrum of fluctuating fields produced at μ^+ sites by manganese spins and where ω_μ is the μ^+ Larmor frequency. Thus the field dependence of $\lambda_{\|}$ gives the functional form of $J(\omega)$, *if* the external field (1) dominates ω_μ, and (2) does not affect the functional form of $J(\omega)$ directly.

Static internal field distributions are known from μSR measurements in zero- and transverse-applied fields, so corrections can be made. Confirmation that the manganese-spin dynamics is indeed independent of applied field comes from ^{63}Cu and ^{109}Ag nuclear-magnetic-resonance experiments[4] in *Cu*Mn and *Ag*Mn alloys for $T \ll T_g$, which directly demonstrate the absence of a field

dependence of $J(\omega)$. Our data therefore provide the first experimental evidence that spin correlations decay algebraically and not exponentially in spin glasses below T_g. The observed value of ν is within experimental error of that obtained from dynamic theories.

2. For T near T_g we obtain $\nu \simeq 0.2$, which is not in agreement with the dynamic theories. Here, however, $J(\omega)$ may be directly affected by the applied field. The data are shown in Fig. 1.

3. A scaling law of the form

$$\lambda_{\parallel} = x^2 f(T/T_g, H/T_g)/T_g \ , \qquad (1)$$

where x is the manganese concentration and $f(u,v)$ is a dimensionless function, is obeyed. This form is expected for dilute spin glasses, where the dipolar coupling scales as x and spin-glass energies (and frequencies) scale as T_g (Ref. 5).

These results call for further theoretical work. It is important to know, for example, how much intrinsic field dependence of $J(\omega)$ is to be expected from current theory. The most fundamental question, perhaps, is whether power-law correlation decays can be obtained from more realistic models than have been studied up to the present time.

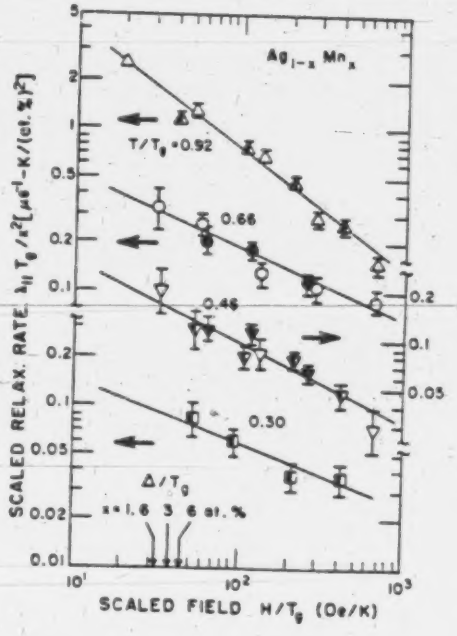

Fig. 1.
Scaled isotherms of μ^+ spin-lattice relaxation rate $\lambda_{\parallel}$ vs effective longitudinal field H for temperatures below T_g in $Ag_{1-x}Mn_x$ spin glasses.
Open symbols: $x = 0.016$,
Half-filled symbols: $x = 0.03$,
Filled symbols: $x = 0.06$.
Least squares fits to a power law are shown for each scaled temperature T/T_g. Scaled widths Δ/T_g of the μ^+ dipolar field distributions for the various manganese concentrations are shown by arrows on the horizontal axis.

Palladium Manganese

The $Pd_{1-x}Mn_x$ system has been widely studied, both as an example of a non-RKKY spin glass and as a dilute ferromagnet. A competition between direct antiferromagnetic couplings and long-range ferromagnetic couplings leads to a complicated phase diagram[6] with a ferromagnetic phase for $x \lesssim 3$ at.% and a spin-glass phase for $x \gtrsim 5$ at.%. In addition, manganese in palladium possesses a giant moment described by spin $S = \frac{5}{2}$ and effective g factor $g_{eff} \simeq 2.7$. Both the $x = 0.02$ ferromagnetic ($T_c = 5.8$ K) system and $x = 0.07$ spin-glass ($T_g = 5$ K) system have been studied using μSR as a microscopic probe of magnetic ordering and dynamics. Measurements were carried out in zero-applied field and with both transverse- and longitudinal-applied fields. The data were analyzed using standard expressions[7] for the μSR linewidths. The data analysis and sample characterization are described in Ref. 8 for *Pd*Mn (2 at.%) and in Ref. 9 for *Pd*Mn (7 at.%).

Ferromagnetic *Pd*Mn (2 at.%)

It was determined that the transverse-field relaxation-rate data $\lambda_{\perp}$ were much larger than the longitudinal-field rates $\lambda_{\parallel}$ for nearly all temperatures and fields. Furthermore, measurements of muon diffusion in palladium with gadolinium impurities indicate a negligible

muon diffusion rate below about 100 K. Thus the $\lambda_\perp$ data reflect the distribution of quasi-static internal fields.

Walstedt and Walker (WW) have treated[10] the problem of local-field distributions at spin-probe sites in dilute magnetic alloys and find a Lorentzian line shape with a width $\lambda_\perp$ given by

$$\lambda_\perp/\lambda_{\perp 0} = \begin{cases} \langle |S_z| \rangle_{\rm th} & \text{(quasi-static limit)} \\ \langle S_z \rangle_{\rm th} & \text{(rapid limit)} \end{cases}, \quad (2)$$

where $\lambda_{\perp 0}$ denotes the dilute-limit dipolar coupling and the brackets refer to a thermal average of the Z component of spin S. This can be generalized in cases where the impurity spins possess randomly distributed values of $\langle S_z \rangle_{\rm th}$, as discussed in Ref. 8.

In Fig. 2 we compare our transverse-field relaxation rates $\lambda_\perp$ to the linewidth computed using the WW coupling scheme. The quantity $\langle S_z \rangle_{\rm th}$ is given by (1) a uniform mean-field model, and (2) the measured magnetization data of Star et al.[11] We used $g_{\rm eff} = 2$ because the induced conduction-electron polarization cloud about the manganese spins is comparable to the average manganese-manganese spacing, thus giving rise to a uniform magnetization density that does not contribute greatly to the spread in local fields sensed by the muon. For $T \gtrsim 1.5\ T_c$ both the mean-field model and the magnetization data give excellent fits to $\lambda_\perp$. This is in contrast to the spin-glass *Pd*Mn (7 at.%) discussed below.

Below T_c, however, the homogeneous mean-field model overestimates both $\lambda_\perp$ (Fig. 2) and the zero-field inhomogeneous linewidth $\sigma(T)$ (Fig. 3). These data therefore are compared to the infinite-range mean-field Ising model of Sherrington and Kirkpatrick (SK).[12] In spite of a great deal of theoretical work, this is the only model that explicitly accounts for the disorder in a random magnet. In the SK model, impurity spins ($S_i = \pm 1$) are coupled by random interactions with mean and variance given by J_0/N and J^2/N, respectively. Here N is the number of spins and $J_0 = k_B T_c$. Figures 2 and 3 show that the SK model yields a better description of both the zero- and transverse-field ferromagnetic linewidths than does the mean-field model. The "shortfall" in μSR linewidths in the ferromagnetic state is thus qualitatively explained in the SK model by including antiferromagnetic coupling ($J_0/J = 1.1$).

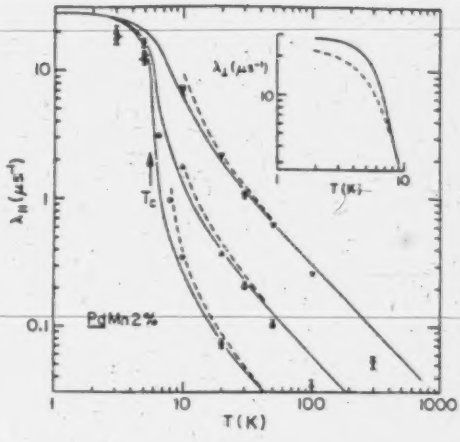

Fig. 2.
Temperature and field dependence of the transverse μ^+ relaxation rate $\lambda_\perp(H,T)$ in Pd + 2.0 at.% Mn.
Circles: H = 200 Oe,
Upright triangles: H = 1 kOe,
Inverted triangles: H = 5 kOe.
The dashed curves were obtained from susceptibility data. The solid curves are obtained from the uniform mean-field model. The inset shows the temperature dependence of $\lambda_\perp$ in the SK model with H = 5 kOe.
Dashed curve: J_0 = 5.8 K, J_0/J = 1.1,
Solid curve: J_0 = 5.8 K, J = 0.

The muon spin-lattice relaxation rate $\lambda_\parallel$ is shown in Fig. 4. The data show a sharp cusp in the zero-field $\lambda_\parallel$ at $T = T_c$ that is completely destroyed by a 5-kOe applied field. This cusp presumably is due to critical spin fluctuations; the broad temperature range is larger than usually observed in ordered ferromagnets, however. Similar results are seen in neutron-scattering data on ferromagnetic *Pd*Mn.

Ramon-magnon scattering[13,8] can explain the order of magnitude of $\lambda_\parallel$ well below T_c, as shown in Fig. 4. This is in contrast to spin-glass *Ag*Mn where the observed $\lambda_\parallel$ at $T \sim T_g/2$ are almost two orders of magnitude larger than estimates obtained from simulated low-temperature magnon spectra. In ferromagnetic *Pd*Mn there appears to

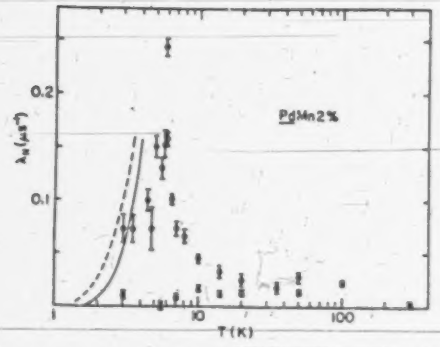

Fig. 3.
Temperature dependence of the zero-field μ^+ quasi-static field distribution width $a(T)$ (in frequency units) in Pd + 2.0 at.% Mn.
Solid curve:
SK model with $J_0 = 5.8$ K, $J_0/J = 1.1$,
Dashed curve:
SK model, $J_0 = 5.8$ K, $J_0/J = 1.5$,
Dash-dot curve:
Homogeneous mean-field model, $S = \frac{1}{2}$.

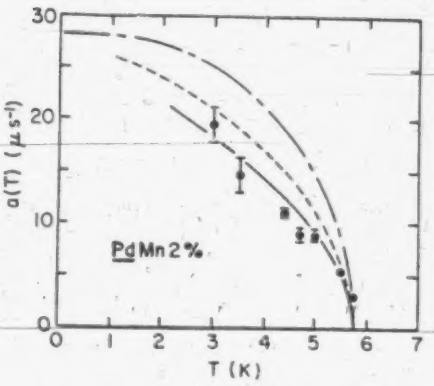

Fig. 4.
Temperature dependence of the μ^+ spin-lattice relaxation rate in Pd + 2.0 at.% at zero field (circles) and 5 kOe (triangles). The curves are predictions of the two-magnon (Ramon) scattering mechanism (see text).
Solid curve:
Anisotropy energy $\hbar\omega_A = 0.3\, k_B T_c$.
Dashed curve:
$\hbar\omega_A = 0.2\, k_B T_c$.

be no additional relaxation mechanism caused by the random nature of the spin system.

Spin-Glass *Pd*Mn (7 at.%)

The main goal of this is to measure the temperature and field dependence of both the quasi-static local-field distribution at the muon site and the muon's dynamic spin-lattice relaxation. Theories of linewidths and relaxation mechanisms in dilute alloys have been used to infer features of the impurity spin configuration. Comparisons with ferromagnetic *Pd*Mn (2 at.%), discussed above, are useful to show how the difference in magnetic ordering brought about by a change in concentration influences microscopic properties.

Figure 5 shows measured transverse-field exponential relaxation rates $\lambda_\perp$ for applied fields of 200 G, 1 kG, and 5 kG. Measured spin-lattice relaxation rates (discussed below) indicate that the nonsecular contribution to $\lambda_\perp$ is small. Thus the rates shown in Fig. 5 represent only the quasi-static field distribution in *Pd*Mn (7 at.%).

The observed paramagnetic susceptibility in a *Pd*Mn (5 at.%) sample is well described by a $g = 2$, $S = \frac{1}{2}$ Curie law for $T \gtrsim 3\, T_g$ and low field.[14] Using this Curie law for $\langle S_z \rangle_{th}$ in Eq. (2) gives the lines shown in Fig. 5. At low temperatures, we simulate the spin-glass state by assuming spins to be quasi-static and equally distributed among the $2S + 1$ M_S states in calculating the order parameter $\langle |S_z| \rangle_{th}$. Equation (2) then gives the high-field frozen-spin linewidth $(\lambda_\perp)_{frozen} = 57.1\ \mu s^{-1}$. A concentration of 7 at.% is not ordinarily considered to be in the dilute limit, so we have calculated a polycrystalline-averaged line shape numerically; the result differs in width from the WW result by no more than 7%.

The discrepancy in Fig. 5 between the $\lambda_\perp$ data and the WW prediction using a Curie law well above T_g is not understood. Similar data on the disordered ferromagnet *Pd*Mn (2 at.%) show very good agreement with the WW result. Since our numerical work indicates that the WW result should still be valid at this higher concentration, we conclude that the observed discrepancy is due to the spin-glass ordering and is present for T well above T_g. Transverse-field μSR results in spin-glass *Ag*Mn show an increase above the WW result, however, to at least 10 T_g.

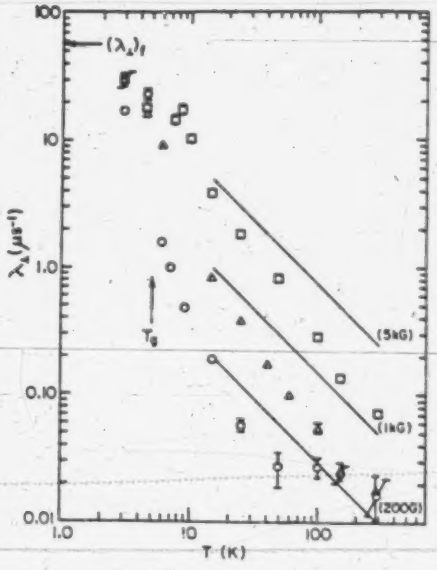

Fig. 5.
Temperature and field dependence of the transverse muon relaxation rate $\lambda_\perp$ in *Pd*Mn (7 at.%).
Circles: 200 G,
Triangles: 1 kG,
Squares: 5 kG.
The solid lines are from Eq. (2) using a Curie law for $<S_z>$; $(\lambda_\perp)_f$ is the frozen-spin rate.

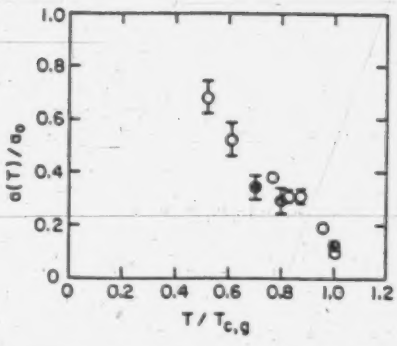

Fig. 6.
Reduced temperature dependence of the zero-field quasi-static field distribution width $\sigma(T)$, normalized to the theoretical zero-field frozen rate σ_0.
Open circles:
*Pd*Mn (2 at.%), $\sigma_0 = 28\ \mu s^{-1}$, $T_c = 5.8$ K.
Filled circles:
*Pd*Mn (7 at.%), $\sigma_0 = 85\ \mu s^{-1}$, $T_g = 5$ K.

The zero-field muon-relaxation function[7] allows a separation between the quasi-static field distribution of width $\sigma(T)$ and relaxation from dynamic spin-lattice relaxation (rate $\lambda_\parallel$). In zero-applied field the WW result is no longer valid, however, because all three components of the local-field distribution contribute to the muon relaxation. Including this effect,[16] one obtains the zero-field frozen-spin linewidth $\sigma_0 = 85\ \mu s^{-1}$ for *Pd*Mn (7 at.%). The temperature dependence of $\sigma(T)$, normalized by σ_0, shows a temperature dependence similar to ferromagnetic *Pd*Mn (2 at.%), as shown in Fig. 6. Thus the development of a static field distribution is independent of the character of the magnetic ordering.

Figure 7 presents measured muon-spin-lattice relaxation rates in zero and applied longitudinal fields above and below T_g. Above T_g the relaxation was fit to the "root exponential" form[7] appropriate for rapidly fluctuating (paramagnetic) spins in a dilute alloy. Fits of the data to a simple exponential form for $G_z(t)$ yield a similar χ^2 value, so that we have not explicitly demonstrated the root exponential form. Below T_g we expect that fluctuations will remain rapid, since this has been observed by μSR in spin-glass *Ag*Mn (Ref. 7). Thus a root exponential decay of the dynamical component of the relaxation function was used to fit the low-temperature data for $\lambda_\parallel$.

The peak in the zero-field spin-lattice relaxation rate at T_g is interpreted as being due to a change in the power spectrum of manganese spin fluctuations near the glass transition. Note that a relaxation mechanism is still effective near T_g in an applied field of 5 kG, whereas in ferromagnetic *Pd*Mn (2 at.%) an applied field of 5 kG completely suppresses the fluctuation-induced relaxation.

At temperatures well below T_g, spin-lattice relaxation presumably is due to spin wave-like excitations of the ground state.[17] Walker and Walstedt[18] have computed the spectrum of excitation frequencies numerically for a

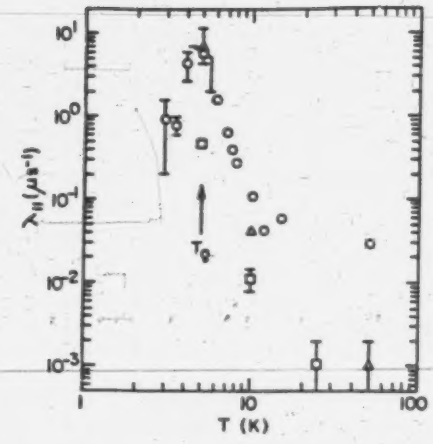

Fig. 7.
Temperature and field dependence of the muon-spin lattice relaxation rate in spin-glass *Pd*Mn (7 at.%).

Circles:	Zero field,
Triangles	200 G,
Squares:	5 kG.

Fitting functions used are described in Ref. 7.

realistic model of a ground state of a *Cu*Mn spin glass. These excitations are localized (nonpropagating) modes of the linearized equations of motion. A similar calculation[19] for spin-glass *Pd*Mn (10 at.%) has shown a more complicated three-peak structure for the excitation spectrum, with the mean spectral weight at a frequency $\sim 5 \times 10^{12}\ s^{-1}$. Because these fluctuations are much too fast to cause depolarization through the dipolar interaction in the lifetime of the muon, the observed relaxation must be due to some other (other than WW) lower frequency component of the excitation spectrum.

Recent analytic theories of spin-wave excitations in spin glasses predict that small k magnons can propagate through the system with a dispersion relation linear in k (Ref. 20). Further evidence for propagating modes has been seen in recent computer simulations.[21] These excitations are at frequencies lower than the localized modes and may be responsible for the relaxation observed at low temperatures. Future zero-field μSR studies in spin glasses at lower temperatures may provide useful data on relaxation for comparison with these theories.

In conclusion, the transverse-field relaxation rate $\lambda_\perp$ in *Pd*Mn (7 at.%) is not proportional to the observed Curie law magnetization for temperatures as high as 100 K (20 T_g), where the onset of muon diffusion makes interpretation of $\lambda_\perp$ difficult. This result is especially surprising because $\lambda_\perp$ in ferromagnetic *Pd*Mn (2 at.%) is proportional to a Curie-Weiss magnetization over a wide temperature range, indicating that the observed reduction in $\lambda_\perp$ below the Curie law prediction may be a high-temperature precursor of the spin-glass phase. We know of no satisfactory explanation for this effect nor for the increase in $\lambda_\perp$ above the measured magnetization in spin-glass *Ag*Mn (1.6 at.%).

In zero field we observe the onset of a quasi-static field distribution below T_g with a similar temperature dependence to that observed in *Pd*Mn (2 at.%). Spin-lattice relaxation near T_g shows a strong cusp, indicating a change in the spectrum of manganese-spin fluctuations. These fluctuations continue to induce relaxation in a large applied field, in contrast to *Pd*Mn (2 at.%).

REFERENCES

1. D. E. MacLaughlin, L. C. Gupta, D. W. Cooke, R. H. Heffner, M. Leon, and M. E. Schillaci, Phys. Rev. Lett. 51, 927 (1983).
2. S.-K. Ma, *Modern Theory of Critical Phenomena* (Benjamin, Reading, Massachusetts, 1976), pp. 442-444.
3. H. Sompolinsky and A. Zippelius, Phys. Rev. Lett. 47, 359 (1981); Phys. Rev. B 25, 6860 (1982); and J. Phys. C 40, L1059 (1982).
4. H. Alloul, S. Murayama, and M. Chapellier, J. Magn. Magn. Mater. 31-34, 1353 (1983).
5. J. Souletie and R. Tournier, J. Phys. (Paris) Colloq. 32, C1-172 (1971).
6. H. A. Zweers and G. J. van den Berg, J. Phys. F 5, 555 (1975); and B. R. Coles, H. Jamieson, R. H. Taylor, and A. Tari, J. Phys. F 5, 565 (1975).
7. R. H. Heffner, M. Leon, M. E. Schillaci, D. E. MacLaughlin, and S. A. Dodds, J. Appl. Phys. 53, 2174 (1982).
8. S. A. Dodds, G. A. Gist, D. E. MacLaughlin, R. H. Heffner, M. Leon, M. E. Schillaci, G. J. Nieuwenhuys, and J. A. Mydosh, Phys. Rev. B 28, 6209 (1983).
9. R. H. Heffner, M. Leon, M. E. Schillaci, S. A. Dodds, G. A. Gist, D. E. MacLaughlin, J. A. Mydosh, and G. J. Nieuwenhuys, in Proc. of the 29th Magnetism and Magnetic Materials Conf., Pittsburgh, Pennsylvania, 1983, to be published in J. Appl. Phys.

10. R. E. Walstedt and L. R. Walker, Phys. Rev. B 9, 4587 (1974).

11. W. M. Star, S. Foner, and E. J. McNiff, Phys. Rev. B 12, 2690 (1975).

12. D. Sherrington and S. Kirkpatrick, Phys. Rev. Lett. 35, 1792 (1975); and S. Kirkpatrick and D. Sherrington, Phys. Rev. B 17, 4384 (1978).

13. E. A. Turov and M. P. Petrov, *Nuclear Magnetic Resonance in Ferro- and Antiferromagnets* (Halsted Press, New York, 1972), p. 93.

14. B. R. Coles, H. Jamieson, R. H. Taylor, and A. Tari, J. Phys. F 5, 565 (1975).

15. J. A. Brown, R. H. Heffner, T. A. Kitchens, M. Leon, C. E. Olsen, M. E. Schillaci, S. A. Dodds, and D. E. MacLaughlin, J. Appl. Phys. 52, 1766 (1981).

16. A. T. Fiory, Hyperfine Interactions 8, 777 (1981).

17. D. Beeman and P. Pincus, Phys. Rev. 166, 359 (1968); and A. H. Mitchell, J. Chem. Phys. 27, 17 (1957).

18. L. R. Walker and R. E. Walstedt, Phys. Rev. B 22, 3816 (1980).

19. W. Y. Ching, D. L. Huber, and B. H. Verbeek, J. Appl. Phys. 50, 1715 (1979).

20. B. I. Halperin and W. M. Saslow, Phys. Rev. B 16, 2154 (1977); W. M. Saslow, Phys. Rev. B 22, 1174 (1980); K. H. Fischer, Z. Phys. B 39, 37 (1980); and S. E. Barnes, J. Phys. F 11, L249 (1981).

21. D. L. Huber, W. Y. Ching, and M. Fibich, J. Phys. C 12, 3535 (1979).

Fusion Materials Neutron Irradiations (Exp. 545, Radiation Effects Facility)

(Los Alamos, Arizona State Univ.)
Spokesman: R. D. Brown (Los Alamos)

Toroids wound from strips of the soft magnetic alloys Mumetal (crystalline) and 2605S-3 (amorphous) were neutron irradiated at the LAMPF Radiation-Effects Facility. The initial magnetic permeability values for both materials decreased during irradiation. The permeability of the Mumetal decreased more rapidly than that for the amorphous alloy, resulting in the 2605S-3 having the higher permeability for neutron fluences exceeding about 3×10^{21} n/m^2. At the beginning of the irradiation the Mumetal had permeability of 23 000 and the 2605S-3 had permeability of 5000. Four months later, after irradiation to 2×10^{23} n/m^2, the permeability of the Mumetal approached unity, whereas that for the 2605S-3 was about 2000.

We have reported similar results for a comparative irradiation of Permalloy and the amorphous alloy 2605S-3 (Ref. 1). For both the crystalline Mumetal and the amorphous 2605S-3, the drop in permeability was very rapid initially, followed by a slow decrease that appeared to continue to the maximum fluence.

A quantitative analysis of the permeability decay curves was made using the direct spectrum analysis method,[2] which is capable of determining a good approximation of the spectrum of relaxation constants for a process involving first-order kinetics, without requiring initial assumptions as to the nature of the spectrum. Analysis of our data in terms of a relaxation fluence (analogous to a relaxation time) showed that both the Mumetal and the amorphous 2605S-3 alloy exhibited virtually identical spectra. Each spectrum consisted of two discrete peaks, one centered at a fluence of about 1×10^{21} n/m^2 and the second at a fluence of about 4×10^{22} n/m^2. The two widely separated peaks provide evidence for the permeability decay occurring in two stages, each associated with a particular mechanism.

Our interpretation of the data[3] assumes that the first stage is governed by short-range ordering because of excess point defects introduced during the irradiation, whereas the second stage is dependent on agglomerations of these point defects, such as dislocation loops and voids that pin the magnetic domain walls. The finding that the relaxation fluences are virtually identical for the crystalline Mumetal and the amorphous 2605S-3 was surprising. Although it was not totally unexpected that defect agglomerates could pin domain walls, the presence or absence of short-range ordering in amorphous alloys has been the subject of controversy.

Further work is planned to obtain more information on these stages observed during irradiation. The effects of the initial heat treatment on the permeability of several 2605 amorphous alloys will be studied. This alloy system may be suitable, because of its relative stability under irradiation, as a replacement for the present Mumetal toroids used upstream of the beam stop, where radiation damage results in a rapid decay in permeability, requiring frequent replacement.

REFERENCES

1. R. D. Brown, J. R. Cost, and J. T. Stanley, "Effects of Neutron Irradiation on Magnetic Permeability of Amorphous and Crystalline Magnetic Alloys," to be published in J. Appl. Phys., Suppl. Part 2 (March 1984).

2. J. R. Cost, J. Appl. Phys. 54, 2137 (1983).

3. R. D. Brown, J. R. Cost, and J. T. Stanley, "Irradiation-Induced Decay of Magnetic Permeability of Metglas 2605S-3 and Mumetal," submitted to J. Nucl. Mater.

Muon-Spin-Rotation (μSR) Studies of Dilute Magnetic Alloys
(Exp. 571, SMC)

(Los Alamos, Rice Univ., Univ. of California at Riverside, Sandia National Lab.)

Spokesmen: S. A. Dodds (Rice Univ.) and R. H. Heffner and M. E. Schillaci (Los Alamos)

Experimental Program

Experiment 571 is designed to measure muon diffusion in fcc materials other than copper and aluminum. The resulting diffusion data will provide a basis for understanding the apparently anomalous motion of muons in copper, aluminum, and bcc materials. In addition, knowledge of muon mobility is needed to properly interpret data from the other muon-spin-rotation (μSR) experiments being undertaken by our group.

Our muon-diffusion measurements have exploited the impurity-doping technique first applied[1] to μSR at LAMPF. As noted in the previous report,[2] we have extensive data on the field and temperature dependence of the muon depolarization rate in silver, gold, and palladium doped with gadolinium, erbium, and manganese. We have extracted the muon-diffusion rate from these data with a model that treats the muon hopping, muon-impurity interaction, and impurity spin-flip time rather simply.[1,3] This model gives a reasonable account of the observed temperature dependence in the systems studied, but it is not able to account for the magnetic-field dependence of the depolarization rate, as shown by the dashed lines in Fig. 1.

Several features of the simple model have been examined to determine the cause of the problem. We have been able to show that the muon-impurity interaction is weak enough that "strong-collision" effects as seen in NMR[4] are unimportant here. We have also shown that the effective correlation time approximation used in our model yields the same results as a near-exact treatment of the combined muon hopping and impurity spin flipping, at least in the parameter region of interest.

Our next approach was to examine the effect of host or muon-induced electric fields on the impurity relaxation. The simplest case, an axial field gradient, improves the agreement between the model and the data considerably,[5] as shown by the solid lines in Fig. 1.

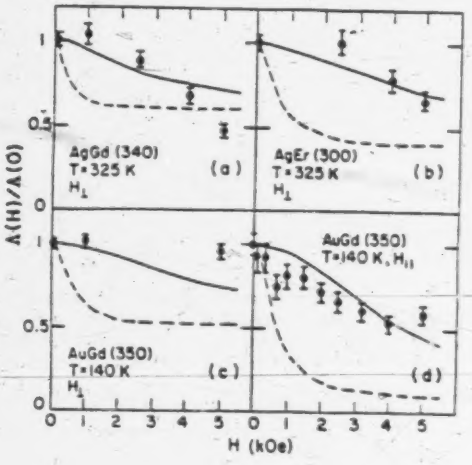

Fig. 1.
Magnetic-field dependence of muon depolarization rates for the alloys listed. Rare-earth concentrations are in parts per million (atomic). Data are shown for both transverse ($H_\perp$) and longitudinal ($H_\parallel$) applied fields. The curves are fits to the two models described in the text.

At the temperatures of interest, all of the crystal-field levels are populated, so the cubic fields of the host must be considered together with the axial field due to the muon. We have reformulated a theory[6] for spin dynamics of a multilevel system and have carried out numerical calculations for erbium [$J = (^{15}/_{2})$] in silver and gold. To the best of our knowledge, this is the first calculation that treats a high-spin system in an unsymmetric electric-field environment with arbitrary applied magnetic field. Preliminary results show that the muon-induced axial field has a profound effect on the erbium fluctuation rate that leads to an enhanced depolarization rate for the muon. Yet to be done is incorporating this model into our hopping model, so that muon diffusion and muon-ion interaction are treated together.

Theory: Calculaton of Muon Polarization Function

P. F. Meier (Univ. of Zürich) and M. E. Schillaci (Los Alamos)

The spin dynamics of a muon localized at an interstitial site interacting with nearest neighbor nuclear spins is being investigated. Kubo and Toyabe[7] studied the spin-relaxation process in zero or weak external magnetic field by approximating the influence of the surrounding nuclear spins by a random local field.

For a static muon in zero external field the muon polarization decreases from its initial value of unity, passes through a minimum, and smoothly reaches a value of one-third asymptotically with time. Recently, Celio and Meier[8,9] reported on exact numerical calculations for $N = 4$ nuclear spins with angular momentum $J = \frac{1}{2}$ and $J = 1$, and for $N = 6$ with $J = \frac{1}{2}$. Both dipolar and quadrupolar interactions with the muon were incuded. Their principal result is that the muon polarization function continues to oscillate with time, contrary to the smooth, asymptotic behavior predicted by the Kubo-Toyabe theory.

The critical limitations in these investigations are the time and memory required to diagonalize very large Hamiltonian matrices. Using a Cray-1 computer at Los Alamos, we were able to study $N = 4$ nuclear spins with $J = \frac{1}{2}$, which corresponds, for example, to a muon localized in a tetrahedral site in copper. Dipolar and quadrupolar interactions between the nuclei and the muon were included, and applied fields in transverse and longitudinal orientations, as well as zero field, were treated. Including isotope effects (for example, copper) and internuclear dipolar interactions had little effect on the results.

Recently, Holzschuh and Meier[10] gave an analytic zero-field approximation for $J = \frac{1}{2}$ and $N = 4,6,8$ corresponding to tetrahedral, octahedral, and cubic arrangements, respectively. For $J = \frac{1}{2}$, $N = 4$, their solution is in good agreement with our exact numerical result. Also, they find that with increasing N the oscillations of the muon polarization function are reduced and the minimum is shifted to shorter times.

We have started numerical calculations for $N = 8$, $J = \frac{1}{2}$ and have begun preparations for $N = 6$, $J = 1$, corresponding to cubic and octahedral arrangements, respectively. The dimension of the state space is given by $2(2J + 1)^N$; consequently, we are nearing the 4×10^7 word capacity of our largest Cray-1. In some cases, group-theoretical reduction techniques can be applied to reduce the maximum dimension; however, for zero external field, the approximation scheme given in Ref. 10 is better suited for studying larger systems (for example, the effects of next-nearest neighbor nuclear spins).

REFERENCES

1. J. A. Brown, R. H. Heffner, R. L. Hutson, S. Kohn, M. Leon, C. E. Olson, M. E. Schillaci, S. A. Dodds, T. L. Estle, D. A. Vanderwater, P. M. Richards, and O. D. McMasters, Phys. Rev. Len. 47, 261 (1981).

2. "Progress at LAMPF, January–December 1982," J. C. Allred, Ed., Los Alamos National Laboratory report LA-9709-PR (March 1983), p. 70.

3. M. E. Schillaci, R. L. Hutson, R. H. Heffner, M. Leon, S. A. Dodds, and T. L. Estle, Hyperfine Interactions 8, 663 (1981).

4. S. P. Vernon, P. Thayamballi, R. D. Hogg, D. Hone, and V. Jaccarino, Phys. Rev. B 24, 3756 (1981).

5. M. E. Schillaci, R. H. Heffner, R. L. Hutson, M. Leon, D. W. Cooke, S. A. Dodds, P. M. Richards, D. E. MacLaughlin, and C. Boekema, Proc. of the Third Int. Conf. on Muon Spin Rotation, Tokyo, Japan, April 1983 (to appear in Hyperfine Interactions).

6. K. W. Becker, P. W. Fulde, and J. Keller, Z. Phys. B 28, 9 (1977).

7. R. Kubo and T. Toyabe, in *Magnetic Resonance and Relaxation*, R. Blinc, Ed. (North-Holland, Amsterdam, 1966).

8. M. Celio and P. F. Meier, Phys. Rev. B 27, 1908 (1983).

9. M. Celio and P. F. Meier, "Exact Calculation of the Muon Polarization Function," Yamada Conference on Muon Spin Rotation and Associated Problems, Shimoda, Japan, April 1983 (to be published in Hyperfine Interactions).

10. E. Holzschuh and P. F. Meier, "Zero-Field Spin Relaxation of Positive Muons," University of Zürich preprint (1983).

Muon-Spin-Rotation Study on Muon Bonding and Motion in Select Magnetic Oxides (Exp. 639, SMC)

[Los Alamos; Texas Tech Univ.; Univ. of Wyoming; Atomic Energy Research Establishment (AERE), Harwell, United Kingdom; Technical Univ., Eindhoven (NL)]

Spokesmen: C. Boekema (Texas Tech Univ.), D. W. Cooke (Los Alamos), and A. B. Denison (Univ. of Wyoming)

Muon-spin-rotation (μSR) studies on select magnetic oxides are nearing completion. Detailed knowledge and better understanding of muon behavior, especially bonding and localization, have been obtained.[1,2] These results are based primarily on work done at LAMPF, with contributions from experiments at SIN to complete the overall picture.

Our most recent efforts were directed to the sesquioxides, with emphasis on Al_2O_3 and V_2O_3. In addition to these experiments, efforts have been made to integrate the μSR data, taken on a larger set of (magnetic) oxides, into a consistent model of the muon in oxides.

Al_2O_3 (corundum) is a structure model for a set of magnetic oxides studied or currently under study [α-Fe_2O_3, Cr_2O_3, $FeTiO_3$ (Ref. 3), and V_2O_3]. This diamagnetic material has been examined with μSR to see if the muon behaves in a similar manner in the nonmagnetic host as it does in magnetic crystals of the same corundum structure. This question carries two aspects: (1) do we see free muon-like behavior, or is muonium (also) formed, as has been reported earlier[4]; and (2) if a μ-oxygen complex exists, what can we say about its mobility in these materials, particularly at low temperatures?

In zero-field measurements recorded between 50 and 200 K, a weak μSR signal is seen with an asymmetry of 0.04 and a constant relaxation rate of 0.05 μs^{-1}. This weak signal could be identified as the "1/3 component" of muon polarization, indicating strongly that the muon is localized. Above 200 K the signal disappears because of increasing relaxation effects, probably muon diffusion; below 50 K the signal strength increases as a result of an increasing asymmetry. Because ^{27}Al nuclear moments will fluctuate slower at decreasing temperatures, the muon polarization at short times (0.2-1.0 μs) therefore will increase.

Of special interest is the transverse field dependence of the relaxation rate (λ) at 5 K, illustrated in Fig. 1; λ decreases very rapidly by a factor of 2 for the first 100 G of externally applied field, then at higher fields remains constant within experimental error. This figure may be compared with Fig. 2 of Ref. 4, where the longitudinal field dependence of the muon polarization is depicted. A striking similarity can be seen.

From these experimental data we estimate that the effective local fields at the muon site are of the order of 100 Oe and may be caused by the ^{27}Al nuclear moments through superhyperfine effects. Here we assume that the muon is localized at low temperatures, as indicated by zero-field measurements and observed for similarly structured magnetic oxides.

Vanadium oxide V_2O_3 also possesses the corundum structure and is therefore isostructural with α-Fe_2O_3, $FeTiO_3$, and Cr_2O_3, which have been recently reviewed.[3] Of main interest is that a metal insulator (MI) as well as a magnetic transition occurs at 150 K. Below this temperature, V_2O_3 is an insulator and is antiferromagnetic, whereas above the transition temperature it is conducting and paramagnetic.

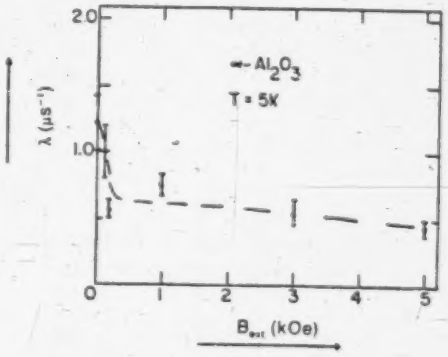

Fig. 1.
The muon-relaxation rate measured at 5 K for a single refined crystal of α-Al_2O_3 as a function of a transverse externally applied field.

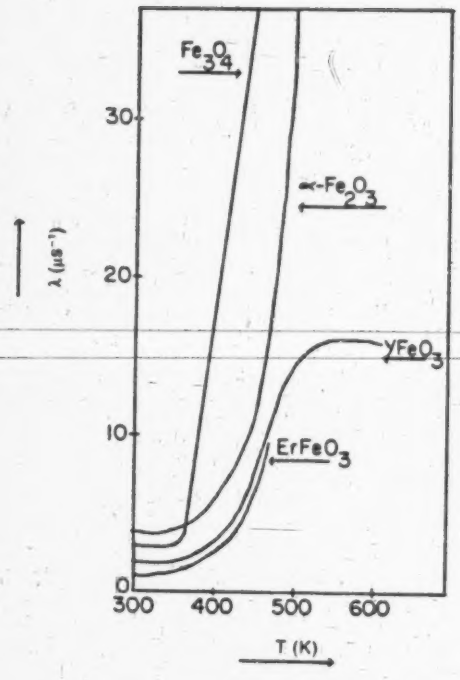

Fig. 2.
The temperature dependences of the relaxation rate (λ) in the temperature region (300-600 K) for the magnetic oxides. For comparison the data have been smoothed. Data are from Refs. 1, 2, and 8. The flattening of the $\lambda(T)$ curve above 500 K for the orthoferrites is due to decreasing magnetization (Ref. 8).

Of additional interest in the light of other oxides investigated is the fact that the conduction in V_2O_3 is bandlike, whereas in Fe_3O_4 conduction is most likely due to phonon-assisted electron hopping above the (Verwey) MI transition[5] (the other oxides are insulating). Also, V_2O_3 is an end member of two most interesting mixed sesquioxide systems $(Ti_{1-x}V_x)_2O_3$ and $(V_{1-x}Cr_x)_2O_3$. The former is known because of remarkable spin-glass properties,[6] the latter, for interesting changes in conductive and magnetic properties.[7]

To date the temperature dependences of the μSR frequency and relaxation rate (λ) have been traced. Above the MI transition a strong μSR signal is seen at the free muon frequency with a low Gaussian λ of 0.06 μs^{-1}. Most likely this Gaussian behavior indicates local diffusive behavior. Below the transition temperature a strong signal was seen in zero field at 15 MHz, corresponding to a muon site with an internal field of 1.1 kOe. Presently we are pursuing a study of the phase transition in more detail and trying to determine the muon stop site from crystal-oriented transverse-field measurements.

A consistent picture of the muon behavior in (magnetic) oxides is developing, and a general model based on the collective knowledge of the different oxides appears to be emerging.[1,2] In this examination it is most helpful to consider μSR results from the rare-earth orthoferrites.[8]

Basically, it was found that in $RFeO_3$ the muon localizes near oxygen and engages in a muon-oxygen bond. These results are in agreement with those obtained earlier for α-Fe_2O_3, which showed for the first time that muon-oxygen bonding occurs in oxides and also that long-lived metastable muon states may be present in (magnetic) oxides well below room temperature.[9]

If one compares the muon-relaxation rates as a function of temperature for magnetically and structurally different oxides (α-Fe_2O_3, Fe_3O_4, $ErFeO_3$, and $YFeO_3$), it can be seen (Fig. 2) that the λ increase starts above 360 K. These combined-relaxation data also suggest that the muon is behaving similarly in various magnetic oxides.

Generally, at temperatures below 100 K the muon appears to find itself in several inequivalent magnetic sites. As proposed by Stoneham,[9] the muon is trapped in a metastable state longer-lived than the muon decay time. Going up in temperature, local diffusion sets in; above 500 K, global diffusion through the whole lattice takes place.

With the chemical and physical muon behavior becoming understood the muon can now be used as a *bona fide* magnetic probe of the sample under investigation. The observation, for instance, of the anomalous behavior of the μSR frequency at 250 K in the Verwey transition temperature region is a good example.[1,2] Moreover, preliminary μSR measurements on V_2O_3 point in the same direction.

REFERENCES

1. C. Boekema, in the Proc. of the Yamada Conf. on Muon Spin Rotation and Associated Problems, Shimoda, Japan, April 1983 (to be published in Hyperfine Interactions).

2. A. B. Denison, Proc. of the 29th Annual Conf. on Magnetism and Magnetic Materials, Pittsburgh, Pennsylvania, November 1983.

3. C. Boekema, A. B. Denison, K. J. Rüegg, J. Magn. Magn. Mat. 36, 111 (1983).

4. E. V. Minaichev et al., Sov. Phys.-JETP 31, 849 (1970).

5. J. M. Honig, J. Solid State Chem. 45, 1 (1982).

6. J. Dumas and C. Schlenker, J. Phys. C 12, 2381 (1979).

7. H. Kuwamuto et al., Phys. Rev. B 22, 2626 (1980).

8. E. Holzschuh et al., Phys. Rev. B 27, 5294 (1983).

9. A. Browne and A. M. Stoneham, J. Phys. C 15, 2709 (1982).

Effects of Superconductivity on Rare-Earth Ion Dynamics in $(Ho_xLu_{1-x})Rh_4B_4$ (Exp. 640, SMC)

(Rice Univ., Los Alamos, and UC, Riverside)

Spokesmen: S. A. Dodds (Rice Univ.), R. H. Heffner (Los Alamos), and D. E. MacLaughlin (Univ. of California at Riverside)

Our previous μSR studies[1,2] in the rare-earth rhodium borides[3,4] $Ho_xLu_{1-x}Rh_4B_4$, for $x = 1.0$, 0.7, 0.35, and 0.0, have revealed a sharp shoulder in the temperature dependence of the muon-spin-lattice relaxation rate at the temperature T_s corresponding to the onset of superconductivity. Here we report zero-field measurements in $Ho_{0.02}Lu_{0.98}Rh_4B_4$, which becomes superconducting at $T_s = 11.3$ K.

Three distinct forms for the normalized muon-spin-relaxation function[1,5] $G_z(t)$ were observed in different temperature regimes (Fig. 1). At 50 K the $G_z(t)$ was found to be well described by the static zero-field relaxation function derived by Kubo and Toyabe,[6] which is appropriate for a time-independent Gaussian distribution of local magnetic fields at μ^+ sites.

The measured width of the field distribution, about 4 Oe, indicates that the μ^+ spin relaxation is caused primarily by μ^+ precession about the host nuclear dipolar fields. As the temperature is lowered, the form of $G_z(t)$ changes, until at 15 K the relaxation function can be approximated by a simple exponential $G_z(t) = \exp(-\lambda_1 t)$ (Fig. 1), where λ_1 is the μ^+ spin-lattice relaxation rate. At $T \leq 11$ K, the form of the relaxation function again changes, exhibiting the two-component form shown in Fig. 1 for $T = 6$ K. These data were fit with the function

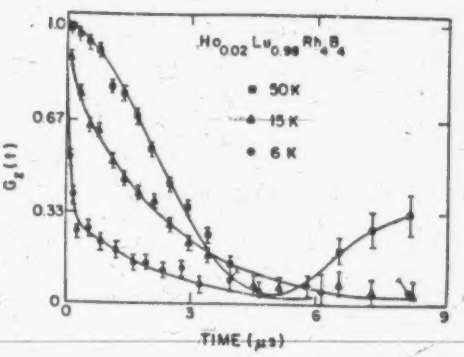

Fig. 1.
Zero-field muon-spin-relaxation function $G_z(t)$ at representative temperatures in $Ho_{0.02}Lu_{0.98}Rh_4B_4$. The curves are fits to the appropriate functions as discussed in the text.

$$G_z(t) = [1 - a]\exp(-\sigma t) + a\exp(-\lambda_2 t)\ , \qquad (1)$$

with $\sigma \gg \lambda_2$. One finds that

(1) σ is essentially independent of temperature, with an average value of $11.5 \pm 0.6\ \mu s^{-1}$;

(2) a is about 0.6 at $T = 11$ K, and falls to one-third for $T \leq 8$ K; and

(3) λ_2 falls exponentially with decreasing temperature below T_s, with an activation energy $\Delta = 9.8 \pm 1.3$ K (Fig. 2).

From these results we conclude that the stochastic motion of the Ho^{3+} moments becomes quasi-static below ~11 K. The value of one-third for a at low temperatures is itself indicative of a random, quasi-static field distribution.[1,5,6] Furthermore, the temperature independence of σ is evidence that the local field $h_L(t)$ reorients completely in a time τ_m such that $\sigma\tau_m \gg 1$, whence $\lambda_2 = 2/(3\tau_m)$ (Refs. 5 and 6).

A two-component form for $G_z(t)$ also can be due to limited-amplitude fluctuations of $h_L(t)$ around a static or quasi-static average value,[7] but in such a case σ increases markedly with decreasing temperature as the fluctuation amplitude decreases. This is not observed in $Ho_{0.02}Lu_{0.98}Rh_4B_4$, and we conclude that $h_L(t)$ reorients completely below 8-10 K.

The value of σ can be estimated using the formalism of Walstedt and Walker[8] for dipolar coupling and the holmium two-level Ising-like ground state discussed

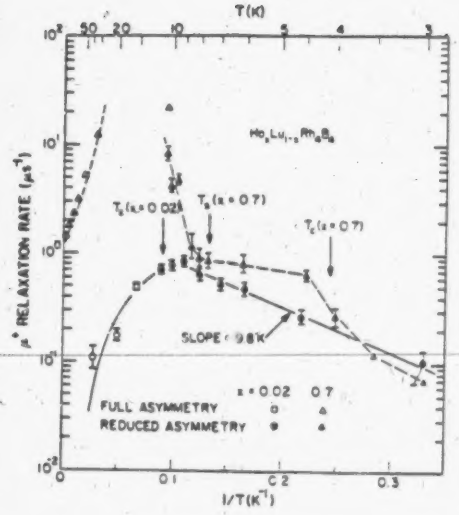

Fig. 2.

Temperature dependence of the zero-field μ^+ spin-lattice relaxation rate in $Ho_xLu_{1-x}Rh_4B_4$, $x = 0.02$ (circles and solid curves) and 0.7 (triangles and dashed curves).

Open symbols: relaxation rate of the full μ^+ asymmetry (relaxation rate λ_1).

Filled symbols: relaxation rate of the reduced-asymmetry component of the μ^+ polarization below ~11 K (relaxation rate λ_2).

Superconducting (T_s) and ferromagnetic (T_c) transition temperatures are indicated. The curves are guides to the eye.

below, with a magnetic dipole moment of ~10 μ_B (Ref. 9). For randomly oriented holmium moments this calculation yields $\sigma = 6.7\ \mu s^{-1}$, which indicates a significant dipole coupling to the μ^+ and is consistent with identification of the two-component structure of $G_z(t)$ with quasi-static inhomogeneous broadening.

Two basic processes, Korringa scattering of conduction electrons[10] and indirect exchange (RKKY) coupling between Ho^{3+} spins,[11] should be important in dilute magnetic alloys. For the Korringa mechanism the μ^+ spin-lattice relaxation rate λ should be proportional to x^2 at high temperatures, whereas $\lambda \propto x$ for the RKKY process. At 100 K our measured values of λ_1 for $x \geq 0.35$ are proportional to x^2, which indicates that the Korringa mechanism is dominant in this temperature regime. The concentration dependence of λ_1 for $x \geq 0.35$ cannot be determined in the temperature range $11\ K < T < 50\ K$ because λ_1 is too large.

We have calculated crystalline-electric-field (CEF) energies and wave functions for rare-earth (RE) 3+ ions in the RE Rh_4B_4 structure by diagonalizing the Hamiltonian for $\bar{4}2m$ point symmetry, using the crystal-field parameters of Dunlap and Niarchos.* For Ho^{3+} the ground and first excited states are each doubly degenerate, with nearly pure $|J_z = \pm 8\rangle$ and $|\pm 7\rangle$ wave functions, respectively. The first excited states occur at $\delta \simeq 55$ K. Allowed transitions from $|\pm 8\rangle$ to $|\mp 8\rangle$ therefore can occur only through small admixtures of different J_z eigenfunctions in the ground and excited states, which are separated by at least 55 K. The slow Ho^{3+}-moment fluctuations at low temperatures then can be accounted for by a combination of the large ground-state isolation and the weakness of $\Delta J_z = \pm 1$ transitions within the ground-state doublet.

Below ~9 K the values of λ_2 for $x = 0.02$ and $x = 0.7$, shown in Fig. 2, are remarkably similar considering the large difference in holmium concentrations. This observation can be understood if the dominant Ho^{3+}-moment relaxation mechanism is again Korringa scattering, as at 100 K. At least one source of difference in the temperature dependence of λ_2 between $x = 0.02$ and $x = 0.7$ is the onset of ferromagnetism below the Curie temperature $T_c = 4.1$ K at the latter concentration.

Below T_s the temperature dependence of λ_2 for $x = 0.02$ indicates an activation energy $\Delta \simeq 10$ K, which is much smaller than the CEF ground-state isolation δ. Since $\Delta \simeq 1.8\ T_s$, interpretation of Δ as a superconducting gap parameter yields a value considerably smaller than the BCS gap parameter $\Delta_{BCS} = 3.5\ T_s$. Such an interpretation is, however, speculative at this time, because it is not clear how the superconducting state could reduce the activation energy for Ho^{3+} fluctuations to a value much less than δ.

*See Ref. 12. The actual parameters used vary somewhat from this reference, and were obtained from B. D. Dunlap, private communication.

REFERENCES

1. C. Boekema, R. H. Heffner, R. L. Hutson, M. Leon, M. E. Schillaci, J. L. Smith, S. A. Dodds, and D. E. MacLaughlin, J. Appl. Phys. 53, 2625 (1982).

2. D. E. MacLaughlin, S. A. Dodds, C. Boekema, R. H. Heffner, R. L. Hutson, M. Leon, M. E. Schillaci, and J. L. Smith, J. Magn. Magn. Mat. 31-34, 497 (1983).

3. B. T. Matthias, E. Corenzwit, J. M. Vandenberg, and E. Barz, Proc. Natl. Acad. Sci. USA 74, 1334 (1977).

4. *Proceedings of the Int. Conf. on Ternary Superconductors*, G. K. Shenoy, B. D. Dunlap, and F. Y. Fradin, Eds. (North Holland, New York, 1981).

5. R. S. Hayano, Y. J. Uemura, J. Imazato, N. Nishida, T. Yamazaki, and R. Kubo, Phys. Rev. B 20, 850 (1979).

6. R. Kubo and T. Toyabe, in *Magnetic Resonance and Relaxation*, R. Blinc, Ed. (North Holland, Amsterdam, 1967), p. 810.

7. R. H. Heffner, M. Leon, M. E. Schillaci, D. E. MacLaughlin, and S. A. Dodds, J. Appl. Phys. 53, 2174 (1982).

8. R. E. Walstedt and L. R. Walker, Phys. Rev. B 9, 4857 (1974).

9. H. R. Ott, L. O. Woolf, M. B. Maples, and D. C. Johnson, J. Low Temp. Phys. 39, 383 (1980).

10. H. Hasegawa, Prog. Theor. Phys. 21, 483 (1959).

11. M. R. McHenry, B. G. Silbernagel, and J. H. Wernick, Phys. Rev. B 5, 2958 (1972).

12. B. D. Dunlap and D. Niarchos, Solid State Commun. 44, 1577 (1982).

Biomedical Research and Instrumentation

Instrumentation

J. D. Doss (Los Alamos)

Ophthalmology

This year has seen significant improvements in both instrumentation and treatments techniques in the thermokeratoplasty program. This work involves using shaped rf fields to thermally shrink the human cornea to alter shape and improve vision. Because the work done in the previous year to increase heat transfer at the corneal endothelium proved successful in animal experiments, human trials were resumed.

Introduction of a "triad" treatment, that is, three symmetric applications around the pupil—have proved very effective, both in shrinkage and, so far, in stability. Several patients have experienced dramatic clinical benefits, which will be observed for long-term stability.

A private corporation is seeking an exclusive license on the two USDOE patents that cover this technology. A version of the ray-trace program LENS has been supplied to the Doheny Eye Institute, University of Southern California, where it is expected to be used to evaluate animal experiments involving modification of the eye.

Hyperthermia

The hyperthermia unit loaned to China has been used to treat seven cases of human brain cancer, with some evidence of beneficial effect in two of the three cases where the highest dose was applied. This program will continue, with treatment of 30 patients planned. Additional instrumentation was supplied to China during 1983, following the initial treatments.

A protocol for treatment[1] of cervical intraepithelial neoplasia (CIN) has been approved and special electrodes have been designed for use at the University of Kansas. The field-calculating software FIELD has been supplied to the United States Environmental Protection Agency office in Las Vegas, Nevada. Work to develop less expensive, more efficient rf sources for hyperthermia continues.

Microwave Dosimetry

Several passive resonant microwave dosimeters[2] have been constructed and tested, in the frequency range from 50 to 1000 MHz. Maximum useful sensitivity is about 10 $\mu W\ cm^{-2}$. A patent[3] will be filed by the USDOE; two private companies are planning to develop the device for commercial production.

Microsurgery

An applicator for microclips used in blood vessel surgery has been developed, in collaboration with the University of New Mexico (UNM) School of Medicine. Initial tests indicate that the device will enable more effective and rapid anastomoses (joining) of small blood vessels. This work has implications for stroke victims, hand surgery, and a variety of related procedures. A joint UNM/USDOE patent is expected to be filed.

REFERENCES

1. C. J. Sternhagen and J. D. Doss, "Combined Radiation Therapy and Localized Current Field Hyperthermia with a 13-MHz Applicator in Head and Neck and Gynecological Cancer Therapy," in the Proc. of the meeting of the Radiation Research Society, San Antonio, Texas, February 28, 1983.

2. J. D. Doss, "Passive Dosimeters for rf and Microwave Fields," accepted for publication in Rev. Sci. Instrum.

3. J. D. Doss, "Multipolar Corneal-Shaping Electrode with Flexible Removable Skirt," U.S. Patent No. 4,381,007, issued April 26, 1983.

Nuclear Chemistry

Time-of-Flight Isochronous (TOFI) Spectrometer for the Mass Measurements of Nuclei Far from Stability

D. J. Vieira, J. M. Wouter, G. W. Butler (Los Alamos), H. Wollnik (Univ. of Giessen), L. P. Remsberg (Brookhaven), and D. S. Brenner (Clark Univ.)

Introduction

In recent years there has been a rapid increase in our knowledge of the atomic-mass surface far from the valley of β stability.[1,2] However, even with these advances there remain more than 60 neutron-rich nuclei with $A < 70$ for which the only known information is that they are stable with respect to neutron emission. Clearly, more detailed information about these nuclei is essential.

Especially important are the measurements of ground-state atomic masses, because the ground-state mass is one of the most fundamental properties of a nucleus. A comparison of measured masses with those predicted by various mass models not only is a test of these models but is a serious test of our understanding of nuclear interactions in general.

Because the binding energy, and hence the mass, of a nucleus is dependent on the exact details of the nuclear force, its prediction requires an understanding of these details. In a strong sense, an atomic-mass model includes everything that we know about the nuclear force and nuclear interactions. A systematic study of accurately determined masses encompassing a wide variety of nuclei far from β stability would provide a most challenging test of current atomic-mass theories and should yield new insight into the nuclear structure of such exotic nuclei.

During discussions in 1979 with Hermann Wollnik of the University of Giessen concerning the limitations of performing direct mass measurements using a total kinetic-energy, time-of-flight measurement technique, the idea of building a recoil time-of-flight spectrometer was conceived and developed.[3]

Such a spectrometer, which we call the time-of-flight isochronous (TOFI) spectrometer, has vastly improved the ability to make direct mass measurements, overcoming to a large extent the limitations of the above approach. Moreover, this new type of recoil spectrometer has all the advantages of other direct mass measurement approaches, but with the added features of being both fast and universal (that is, all reaction products with half-lives greater than ~2 μs could be studied). Thus, with the development of the TOFI spectrometer, one expects for the first time to be able to systematically and globally investigate the entire nuclear-mass surface up to $A = 70$.

In this report we outline the basic features of the TOFI spectrometer and its associated transport line, discuss the mass measurement capabilities of the system, highlight progress during 1983, and review future plans.

TOFI Spectrometer

The basic principle of the TOFI spectrometer is that it is designed to be isochronous (the TOF is velocity independent). This means that the measured transit time of an ion through the system provides a precise measurement of the mass-to-charge ratio. Because charge is a quantized entity, only moderately accurate measurements (at the 1-2% level) of the energy and free-space time of flight, together with the known momentum acceptance of the spectrometer, are necessary to uniquely define the charge state. Having thus determined the charge, the mass can be deduced from the mass-to-charge ratio as obtained from the measured transit time of the ion through the spectrometer.

Another important feature of the spectrometer is that it can be focused in both energy and angle, thus allowing a long flight path (~13 m) with a relatively large solid angle (2.5 msr) and momentum acceptance (±2%). Because the spectrometer is nondispersive, there is no physical separation between different ions, allowing the simultaneous measurement of many nuclei (especially important are isobaric members with well-known masses that will be used as internal calibration points). Since approval of the funding proposal[4] to DOE, extensive work has gone into improving the design of the spectrometer, and during the last year significant engineering progress has been made (see section under Progress in 1983 in this report, p.). Figure 1 shows a sketch of the current system, which consists of a transport line and the TOFI spectrometer.

Through discussions with Karl Brown of SLAC, an improved version of the TOFI spectrometer has been developed that is optically superior to the original design. Applying Brown's ideas of an achromatic system consisting of identical unit cells,[5] the spectrometer is envisioned to consist of four integrated-function dipoles. Each dipole bends the beam by ~81° such that sufficient dispersion is produced to make the overall system isochronous (that is, ions of higher momentum are made to follow a longer flight path than those with lower momentum so that all ions take the same amount of time to traverse the

spectrometer). Edge angle focusing at the entrance and exit boundaries of the magnets is used to produce an intermediate image of the beam spot exactly at the midpoint of the system. Here the beam is dispersed and a momentum collimator defines the momentum acceptance of the spectrometer, after which the dispersion is removed by the last two dipoles.

The beauty of this system is its symmetry. Because of this symmetry, all first- and second-order geometric optical terms are identically zero, and because the system is made to be isochronous, all first- and second-order achromatic optical terms are essentially zero. Beyond second order, the symmetry of the system ensures that higher order terms should be small as well. This has been confirmed in RAYTRACE calculations performed by Harald Enge (MIT), who has consulted with us on the optics of both the spectrometer and the transport line and who has greatly assisted with the engineering and construction details. Thus, to the extent that the magnets follow design, no ray tracing of particle trajectories employing position-sensitive detectors will be necessary, and the mass resolution will be limited only by the timing between the start and stop signals.

In summary, the important features of the spectrometer are

(1) isochronicity;
(2) 1:1 imaging, nondispersive at focus;
(3) acceptance $\Delta\Omega = 2.5$ msr, $\Delta p = \pm 2.5\%$; and
(4) resolution $M/\Delta M = 2000$.

The first two features enable the time-of-flight technique to determine the mass of the ion, using small state-of-the-art timing counters to obtain the ultimate in mass resolution while simultaneously maintaining a large solid angle and momentum acceptance. Incorporating all these features, this unique spectrometer will make possible a series of direct atomic-mass measurements involving a large number of previously unmeasured nuclei that lie far from β stability.

Transport Line

Another important development is the idea of moving the spectrometer out of the LAMPF switchyard into a more accessible area with the reaction products being transported to the spectrometer via a secondary beam line. In the Thin Target Area there has always been provision for a 90° port and a pipe through the switchyard wall that leads to the basement area of the hot cells. This location has recently been vacated with the move of the machine shop to a new building. Working around the constraints of not disturbing the nuclear chemistry rabbit system and the hot water resin filters, we developed the layout shown in Fig. 1 for a secondary beam line connecting to the Thin Target Area scattering chamber. The advantages of incorporating such a transport line into the design include the ability to

(1) accept a larger phase space with better matching to the spectrometer acceptance,
(2) use a dedicated start-time counter to sharpen time-of-flight resolution (and thus mass resolution) independently of the primary beam timing,
(3) eliminate high-yield light ions before they enter the spectrometer, and
(4) work on the system during LAMPF beam operation.

Mass Measurement Capabilities

The TOFI spectrometer will greatly advance direct measurements of atomic masses of numerous light nuclei that lie far from stability. With a mass resolving power of $M/\Delta M = 2000$, an $A = 40$ reaction product would have a linewidth of ~19 MeV (FWHM) and a centroid uncertainty of

$$\sigma_A = \frac{A}{2.35\sqrt{N}} \frac{\Delta M}{M} ,$$

where N is the number of events in the mass line. This centroid uncertainty, which represents the mass measurement accuracy, can be minimized by good mass resolution and large sample size, both of which the TOFI spectrometer and high-intensity LAMPF beam can provide.

In the above case with an accumulation of 10^4 events, a mass accuracy of 80 keV can be achieved. Systematic errors, which also contribute to the overall uncertainty of the determination, are dramatically reduced ($\lesssim$30 keV), as our technique would take advantage of the fact that several members of an isobar (which are resolved in Z by a thin dE/dx detector) with accurately known masses would be measured simultaneously at each mass position. Thus, mass measurement accuracies ranging from 30 keV to 1 MeV are expected, depending on the production rates of these nuclei.

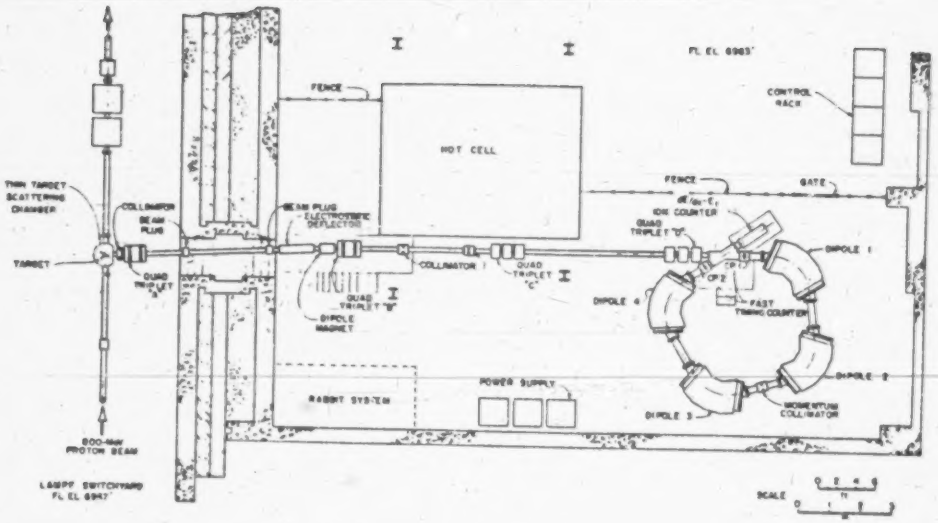

LAMPF TOFI SPECTROMETER

Fig. 1.
Layout of the TOFI spectrometer and transport line.

Scaling from the neutron-rich isotopic yields that we have observed in the nitrogen through chlorine region,[6] we estimate that the TOFI spectrometer can measure some 30 new or improved atomic masses with accuracies of 100 keV or better together with some 15 additional new measurements with accuracies ranging between 100 keV and 1 MeV. Outside this region, numerous mass measurements of other neutron-rich nuclei in the argon-to-zinc region appear feasible, where adequate Z resolution can still be obtained. Moreover, the masses of a limited number of neutron-deficient nuclei could also be measured.

In summary, the TOFI spectrometer will be able to measure the masses of from two to five new isotopes per element from $Z = 7$ to $Z = 30$. Development of such a spectrometer at LAMPF will provide a unique opportunity to systematically study the atomic-mass surface throughout the light mass region. Such measurements will permit a critical test for a variety of atomic-mass models, sufficiently constraining these theories to such a degree that significant advances in our understanding of the light nuclear-mass surface can be expected.

Progress in 1983

During the past year the TOFI spectrometer project has made significant progress in three major areas. First, detailed optical studies of the spectrometer and transport line have resulted in final designs. Second, the spectrometer dipoles have been designed, modeled (using the POISSON magnet code), and sent out for fabrication. And third, the first half of the transport line has been engineered and all four quadrupole triplets needed for the line have been refurbished.

In addition, conceptual layouts and engineering details of various other components of the spectrometer and transport line (magnet stands, vacuum tanks, collimators, control system, and beam boxes) have been developed. Finally, the room in which the spectrometer will reside has been prepared and fitted with water-cooling lines.

These undertakings have been carried out with the assistance of several MP-Division groups. In particular, we would like to acknowledge Jim Sims, Don Clark, and Joe Van Dyke (MP-8); Jim Little and Del Kercher (MP-1); Ed Schneider and Harold Ferguson (MP-11); and Dick Werbeck (MP-7). We greatly appreciate this essential LAMPF support.

Future Plans

During the 1984 winter/spring shutdown of LAMPF, the first of half of the transport line will be installed, which will enable the characterization and performance optimization of one of the key transport-line components: the mass-to-charge filter. Moreover, the first half of the transport line will be used to test and develop new detectors needed for the TOFI spectrometer. Finally, once this section of the transport line is operational, the remaining part of the transport line and the spectrometer can be assembled and tested independently of LAMPF beam operations.

The spectrometer dipole components are scheduled for delivery in early summer, at which time they will be assembled and the initial field mapping will take place. After one dipole has been thoroughly tested and optimized, the other dipoles will be trimmed in like fashion. Configuration of the four dipoles into final spectrometer form is planned for the fall when off-line testing using alpha and fission sources will begin. After optimization of the spectrometer performance and the completion of the secondary beam transport line in early 1985, the TOFI spectrometer is scheduled to undertake its first on-line experiment.

REFERENCES

1. W. Benenson and J. Nolen, Eds., "Proceedings of the Sixth International Atomic Mass Conference," East Lansing, Michigan, September 1979 (Plenum Press, New York, 1980).

2. "Proceedings of the Fourth International Conference on Nuclei Far From Stability," Helsingor, Denmark, June 1981, CERN report 81-09 (1981).

3. H. Wollnik and T. Matsuo, Int. J. Mass Spectrom. Ion Phys. 37, 209 (1981); and J. M. Wouters, D. J. Vieira, H. Wollnik, H. A. Enge, S. B. Kowalski, and K. L. Brown, in preparation.

4. D. J. Vieira, G. W. Butler, L. P. Remsberg, A. M. Poskanzer, and H. Wollnik, "LAMPF Time-of-Flight Magnetic Spectrometer for Precision Mass Measurements of Very Neutron-Rich Light Nuclei," in the INC-Division proposal to DOE, WPAS-FY84 (1980), pp. 41-73.

5. K. L. Brown, IEEE Trans. Nucl. Sci. NS-26, 3490 (1979); and Stanford Linear Accelerator Center report SLAC-PUB-2257 (1979).

6. G. W. Butler, D. G. Perry, L. P. Remsberg, A. M. Poskanzer, J. B. Natowitz, and F. Plasil, Phys. Rev. Lett. 38, 1380 (1977).

Helium-Jet Transport of Fission and Spallation Reaction Products

(Exp. 629, AB-Nucchem)

(Los Alamos, Idaho National Engineering Lab., Univ. of Oklahoma)

Spokesmen: M. E. Bunker and W. L. Talbert, Jr., (Los Alamos) and R. C. Greenwood (Idaho National Engineering Lab.)

Introduction

A unique opportunity exists at LAMPF for the production and study of nuclei far from stability. The properties of these highly unstable nuclei are of great interest to theorists, largely because they constitute an important extension of the systematic base of data that is used to test nuclear models and thus to improve our understanding of nuclear forces.

Approximately 3 years ago, advances in helium-jet technology, especially the coupling of helium-jet systems to isotope separators, suggested a relatively simple method of gaining access to the short-lived reaction products producible at LAMPF. The helium-jet technique, as a method for transporting radioisotopes to an isotope separator, has three main advantages:

(1) it provides access to many isotopes of a number of elements that cannot be efficiently extracted for study at any of the present or proposed on-line facilities;

(2) it allows transport of recoil reaction products over distances of many meters in fractions of a second, thus providing access to very short-lived activities; and

(3) it has a relatively low cost.

Except for gaseous products, all elemental species are transported efficiently with a helium-jet system, including the refractory metals such as zirconium, niobium, molybdenum, technetium, palladium, ruthenium, and rhodium. In contrast, the relatively massive targets that must be used (because of low beam currents) at other major on-line separator facilities almost completely retain the refractory-metal radionuclides, making these activities unavailable for study. Use of the thin targets required in the helium-jet method requires a very large incident beam current, of the order of that available at LAMPF, to get a sufficient yield of individual radioisotopes for detailed study.

The helium-jet technique involves stopping the atoms that recoil from the thin targets in aerosol-loaded helium, with subsequent attachment of the radioisotopes to the aerosol particles. The transport of the activity-laden gas from the target chamber to an evacuated collection chamber or mass-separator ion source then takes place through a long, small-diameter capillary, at velocities approaching sonic.

The separated ion beams extracted from the isotope separator would be directed to various experimental devices capable of determining basic nuclear properties such as half-life, spin, nuclear moments, mass, and nuclear structure. The data acquired would have broad application to theories of nuclear matter and such related topics as nucleosynthesis of the elements. Emphasis initially would be on the study of short-lived, neutron-rich fission products. Fission is the only way to reach very neutron-rich nuclei, and among the refractory metals alone it appears that we would have a good chance of identifying and making measurements on at least 150 previously unobserved isotopes, a prospect that would inevitably attract a sizable international user group.

Our studies of helium-jet systems at LAMPF were initiated in FY 1981. These initial experiments, which used a rather crude target chamber and activity collection arrangement, yielded very promising results on the activity transport efficiency for both fission and spallation products. The experiments were carried out with little flexibility; only one target chamber pressure was used, and the beam current and aerosol furnace temperature were not widely varied. Hence, additional experiments were outlined to better investigate the influences of beam-current variations, aerosol furnace temperatures, and target chamber pressures. Since the first experiments employed only NaCl as the aerosol, it was also considered important that another aerosol, namely $PbCl_2$, be studied in the next set of experiments.

For the second set of experiments at LAMPF, a new target chamber design was needed to determine pressure effects on transport efficiency and transport time. With assistance from Los Alamos Technical Associates, a new concept was developed that facilitated changes in chamber thickness for the pressures of interest (to keep the chamber thickness approximately equal to the fission-product range in helium when different pressures were used). Also, analytical calculations were made to predict the transit times through the capillary.

The above preparations were accompanied by a series of discussions with MP-Division staff, which resulted in including a helium-jet target in the plans to reconstruct the beam-stop area of LAMPF and in providing space in the LAMPF staging area for an on-line separator system.

Experimental Results

Much of our experimental effort has been directed toward (1) establishing whether a helium-jet system can be operated successfully when an 800-MeV, ~750-μA proton beam is incident on the target chamber, and (2) establishing whether transport times of <1 s for the reaction products can be achieved. Not until these questions were satisfactorily resolved could we consider that the planned facility is viable.

Because of the great difficulty of using the main beam (Line A) for our feasibility experiments, we chose instead to use the beam available in the Nuclear Chemistry cave on Line B, where the maximum beam current is only about 6 μA. However, since the beam-current densities on Lines A and B are comparable, many of the data obtained on Line B should be representative of what we can expect on Line A. In addition to the on-line LAMPF experiments, we have conducted on-line experiments at the Omega-West Reactor, as well as various bench-type experiments on helium-jet configurations, to study variations in performance caused by changes in critical design and operating parameters.

The second set of LAMPF experiments was performed in November 1982. The operations staff provided an intense, steady, tightly focused beam, which in effect made unnecessary the plans to continue these studies with a future Line A experiment. The major results of the experiments are summarized below.

The target chamber contained two 7.6-cm-diam depleted-uranium foils, of thickness ~10 mg/cm², situated facing each other across the chamber volume. At the collection chamber, we used a moving tape collector to rapidly transport collected samples of activity to a well-shielded Ge(Li) gamma-ray detector. The tape collector allowed us to observe short-lived activities, of half-life 1-5 s. The observed counting rates of $^{238}U(p,f)$ products were very high, and in the resulting spectra many of the gamma-ray peaks could not be identified from previously reported studies. The transport efficiencies for all non-gaseous-element activities averaged about 60%, measured absolutely. At higher target chamber pressures (up to 600 kPa), the short-lived activity levels were much higher than those observed at 200 kPa, in keeping with faster transport caused by higher flow rates.

Transit-time measurements were performed for various conditions, with the best result being 230 ms for a target chamber pressure of 500 kPa. The data are shown in Fig. 1. The calculated prediction of this transit time for a capillary length of 22 m is 320 ms. Since the calculation is based on an average flow velocity in the capillary, the experimental result illustrates that the aerosols are "herded" into the central part of the capillary during the flow, thus acquiring a larger-than-average flow velocity. The transit-time measurements provide convincing evidence that activities as short as 300 ms can be studied with the proposed helium-jet on-line mass-separator system.

The Line B current was varied over a range from 1.5 to 6.1 μA. The transport efficiency did not vary over this range. Postexperiment scans of the beam-induced activity in the ^{238}U target foils indicated that at the highest

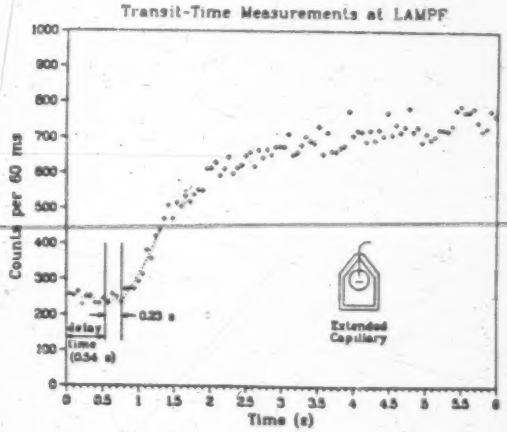

Fig. 1.
Activity transit-time measurements at LAMPF. Beam is turned on at 0 s, tape transport delay is 0.54 s. The target chamber is illustrated, and beam spot is the horizontal line across the circular target foil.

current, a beam-current density of 45 $\mu A/cm^2$ had been achieved, about twice that expected for Line A. We conclude that the gas-transport system should function satisfactorily in the intense Line A beam.

The highest target chamber pressures used (500 and 600 kPa) resulted in capillary flow for which the Reynolds number exceeded conventional design limits (value of 2200). However, the activity rate continued to increase when these pressures were used. The conclusion was that any turbulence resulting from the flow did little to disturb the transport of the heavy aerosols.

The temperature dependence of the amount of activity transported verified that the activity attaches to the aerosols according to the total aerosol surface area, which had been indicated in other, unrelated studies at laboratories for aerosols in the size range employed here (less than 0.1 μm). Samples were collected for electron microscopy, and aerosol size distribution measurements were made on activity-loaded aerosols. The $PbCl_2$ aerosols were seen to be chain-like aggregates with a large resulting surface area.

The availability of a several-micro-amp beam on Line B is too rare to make systematic studies of design parameters to optimize the configuration of a Line A target chamber. We therefore have installed a neutron beam shutter at the Omega-West Reactor to continue these studies and to arrive at an optimum configuration regarding these questions:

1. What will be the effect of using multiple capillaries rather than only one?
2. What design of capillary and helium supply-line placement will result in the highest target-volume sweep rate?
3. Which of the three candidate aerosol materials will provide the highest transport efficiency—NaCl, KCl, or $PbCl_2$?

The test target chamber has a number of possible configurations for gas inlet and exit ports. Preliminary results indicate that, for a circular target chamber (such as would be installed at Line A), a single capillary outlet line, opposite from two inlet lines 90° apart, would provide an optimum configuration. Multiple capillary outlets appear not to improve the flow characteristics, but two inlets provide improved performance over one or three inlets. $PbCl_2$ appears to be the most efficient aerosol for activity transport.

We have developed a series of figures showing the limits of known properties for nuclei and graphically depicting the large regions of nuclei that are unknown and yet have half-lives larger than 300 ms, consistent with the capabilities of the proposed helium-jet system. The illustrations for mass and ground-state spin are shown in Figs. 2 and 3, in which some of the regions that are available only with the use of a helium jet are highlighted. The neutron-rich regions are accessible by fission of ^{238}U, and the neutron-deficient regions are accessible by use of appropriate spallation targets.

The experimental results from the LAMPF experiments have been reported at APS meetings[1-3] and at the Organization for Economic Cooperation and Development, Nuclear Energy Agency (OECD/NEA), Nuclear

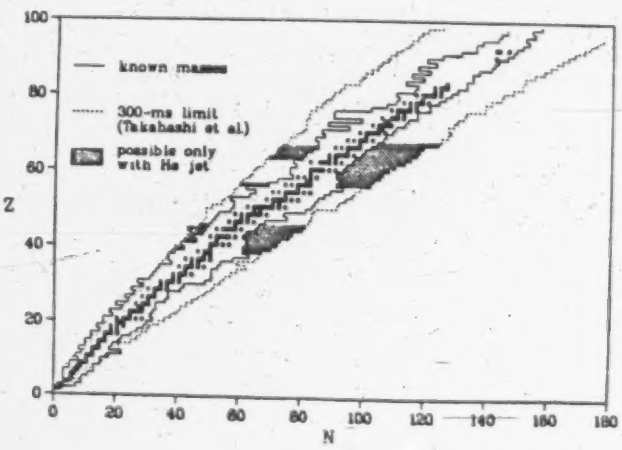

Fig. 2.
Chart of nuclides showing limit of known masses and predicted 300-ms half-life boundaries. The shaded areas are some of the regions where a helium-jet/isotope-separator system can uniquely provide separated isotopes for on-line study.

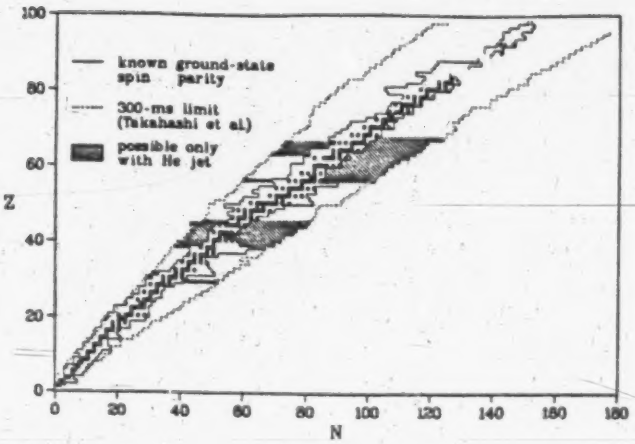

Fig. 3.
Chart of nuclides showing limit of known spin-parity assignments and predicted 300-ms half-life boundaries. The shaded areas are some of the regions where a helium-jet/isotope-separator system can uniquely provide separated isotopes for on-line study.

Data Committee Specialists' Meeting on Yields and Decay Data for Fission Product Nuclides.[4] At the Third LAMPF II Workshop, a presentation was made of the results of Exp. 629, and the merits of a helium-jet system at a thin target area at LAMPF II were discussed.[5]

We are confident that the results obtained in Exp. 629 establish the feasibility of a helium-jet activity transport system at LAMPF, and no further beam requests are contemplated. A proposal for funding a helium-jet coupled mass separator at LAMPF is in preparation and will be submitted to the USDOE Division of High Energy and Nuclear Physics in early 1984.

REFERENCES

1. W. L. Talbert, Jr., M. E. Bunker, B. J. Dropesky, J. W. Starner, P. C. Greenwood, R. J. Gehrke, and V. J. Novick, Bull. Am. Phys. Soc. 26, 1156 (1981).

2. W. L. Talbert, Jr., M. E. Bunker, J. W. Starner, S. C. Soderholm, V. J. Novick, and R. F. Petry, Bull. Am. Phys. Soc. 28, 646 (1983).

3. W. L. Talbert, Jr., M. E. Bunker, J. W. Starner, and M. E. Schaffner, Bull. Am. Phys. Soc. 28, 990 (1983).

4. W. L. Talbert, Jr., M. E. Bunker, and J. W. Starner, in "Proceedings of the OECD/NEA Nuclear Data Committee Specialists' Meeting on Yields and Decay Data for Fission Product Nuclides" (October 1983).

5. D. J. Vieira and W. L. Talbert, Jr., in "Proceedings of the Third LAMPF II Workshop," Los Alamos National Laboratory report LA-9933-C (1983), Vol. II, p. 886.

Radioisotope Production

David C. Moody

During 1983 the Medical Radioisotopes Research Group (INC-3) substantially increased the quantity of radioisotopes made available to the nuclear medicine community (22 Ci in 1982 vs 35 Ci in 1983). This increase is tied directly to requests from the nuclear medicine community in general, but also can be linked to major new emphases in our own radiopharmaceuticals research program at Los Alamos, as well as new collaborative research directions.

Isotope Production and Separation

Table I shows radioisotope shipments made during FY 1983. Although this presents a reasonable summary of our production and separation activities, two areas of emphasis during 1983 warrant more detailed discussion (these are grouped under the principal isotopes involved, ^{123}I and ^{67}Cu, in the sections that follow).

Iodine-123

J. W. Barnes, M. A. Ott, K. E. Thomas, and P. M. Wanek

Current brain perfusion agents under development indicate a need for amounts of ^{123}I that far surpass the present supply. To evaluate LAMPF as a potential new source for this radioisotope, we have developed a batch process and are initiating the design and implementation of an on-line ^{123}Xe recovery system that is expected to substantially increase the ^{123}I yield and improve its radionuclidic purity.

At LAMPF, ^{123}I is produced through the decay of ^{123}Xe formed by spallation of cesium in CsCl. The batch process currently in use involves transferring of ^{123}Xe after irradiation to a generator where it is held for an appropriate decay period for the formation of ^{123}I. A proposed on-line process uses the same generator system, but differs from the currently used process in that the xenon is continuously transferred to the generator during irradiation.

The development of a reliable target container and a trouble-free vacuum system for ^{123}I production was reported in the INC-Division Annual Report in 1982. Additional experiments were performed to demonstrate the maximum production capability of the batch process at LAMPF. A target containing 175 g of CsCl was irradiated for 4 h and subjected to a 4-h growth period. The quantity of ^{123}I recovered, corrected to the end-of-growth period, was 850 mCi with a 0.4% contamination by ^{125}I. The surface of the void above the salt was washed with dilute NaOH to extract the ^{123}I that resulted from the decay of ^{123}Xe during irradiation. The resultant solution contained 900 mCi of ^{123}I, corrected to the end-of-growth period, with a 0.5% contamination by ^{125}I. The ^{123}I in this last solution represents a proof of principle for the on-line process, but is not a usable product from the batch method because it contains undesirable spallogenic iodine species that were extracted from the surface of the solid CsCl block. However, the sum of the two solutions, 1750 mCi of ^{123}I, represents a conservative approximation of the 8-h production from the on-line operation.

Copper-67

G. Bentley and W. Taylor

A new separation method for ^{67}Cu has been developed, based on a novel electrochemical technique. The product from the separation is free from radioactive contaminants, with the exception of ^{64}Cu, and has minimal quantities of stable materials present as impurities.

The zinc oxide target is dissolved in 3*M* sulfuric acid. Following dissolution of the target material, the solution is transferred to an electrolytic cell that consists of a platinum working electrode, a platinum counter electrode that is isolated from the bulk of the solution by a glass frit, and a silver/silver chloride reference electrode. The electrodes are connected to a potentiostat that maintains a controlled potential at the working electrode. A potential of –0.35 V (all potentials are vs Ag/AgCl) is applied to the working electrode. This potential is sufficiently cathodic to result in the reduction of copper. Zinc, lead or cadmium (both of which are present in the zinc oxide as impurities), or nuclides other than copper formed during the irradiation are not reduced at this potential.

Following deposition of the copper onto the platinum electrode, the electrode is rinsed and the solution is replaced with a clean 0.1*M* sulfuric acid solution. A +0.1-V potential is applied to the working electrode and the copper is stripped off the electrode into the solution. The potential of the working electrode is again changed to –0.35 V and the copper replated onto it. This second plating operation affords additional decontamination of the copper from any zinc that is carried along with the copper product. The sulfuric acid solution is replaced

Table I. Medical Radioisotope Shipments—FY 1983.

Isotope	Institution	Number of Shipments	Amount (mCi)
^{26}Al	Oak Ridge National Laboratory, EPRI	1	0.004
	TOTAL	1	0.004
^{77}Br	George Washington University	4	624
	Johns Hopkins Medical Institute	4	955
	Los Alamos National Laboratory, Group INC-3	8	963
	Los Alamos National Laboratory, Group INC-7	1	1
	TRIUMF	1	50
	University of New Mexico	6	511
	Washington University	2	339
	TOTAL	26	3 443
^{77}Br Estradiol	University of Massachusetts	2	52.6
	Northeastern University	1	3
	University of New Mexico	1	1.36
	TOTAL	4	56.96
^{67}Cu	California State University, Fullerton	4	2 030
	Columbia University	1	5
	Hospital for Sick Children, Toronto, Canada	4	493
	Johns Hopkins Medical Institute	2	148.4
	Los Alamos National Laboratory, Group INC-3	1	2.4
	Los Alamos National Laboratory, Group LS-3	3	30
	Mayo Clinic	1	15
	University of California, Davis	5	1 083
	TOTAL	21	3 806.8
^{59}Fe	Los Alamos National Laboratory, Group INC-11	2	0.0042
	TOTAL	2	0.0042
^{148}Gd	Lawrence Livermore National Laboratory	2	10.8
	TOTAL	2	10.8
^{68}Ge	Brookhaven	1	10.12
	Medical Research Council, Hammersmith Hospital, London	2	11
	Mt. Sinai Medical Center, Florida	1	3
	Oak Ridge Associated Universities	2	11
	Office des Rayonnement Ionisant, France	1	20
	Oak Ridge National Laboratory/DOE	1	253
	University Hospital/The Netherlands	1	5
	University of Chicago	2	4
	University of Liege, Belgium	1	25.4
	Washington University	2	15.06
	TOTAL	14	357.58

Table I. Cont.

Isotope	Institution	Number of Shipments	Amount (mCi)
^{123}I	Benedict Nuclear	1	248
	Medi-Physics	1	31
	TOTAL	2	279
^{172}Lu	VA Hospital, San Diego	2	17.6
	TOTAL	2	17.6
^{173}Lu	Los Alamos National Laboratory, Group INC-11	1	0.8
	Los Alamos National Laboratory, Group INC-7	1	0.16
	TOTAL	2	0.96
^{86}Rb	New England Nuclear, University of South Carolina	1	0.04
	New England Nuclear	1	0.236
	University of South Carolina	1	0.04
	TOTAL	3	0.316
^{82}Sr	Medical Research Council, Hammersmith Hospital, London	4	550
	E. R. Squibb & Sons	5	3 392
	E. R. Squibb & Sons/Mt. Sinai and University of Texas	1	340
	E. R. Squibb & Sons/National Institutes of Health	1	125
	E. R. Squibb & Sons/Sloan Kettering Institute	2	310
	University of California, Donner Laboratory	4	1 031
	University of Liege, Belgium	4	432
	TOTAL	21	6 180
^{158}Tb	Los Alamos National Laboratory, Group INC-11	1	0.010
	TOTAL	1	0.010
^{44}Ti	Los Alamos National Laboratory, Group INC-DO	1	0.013
	TOTAL	1	0.013
^{48}V	California State University, Northridge	4	24.7
	Los Alamos National Laboratory, Group HSE-8	1	0.067
	Los Alamos National Laboratory, Group INC-11	1	0.15
	TOTAL	6	24.92
^{127}Xe	Brookhaven	5	20 820
	TOTAL	5	20 820
^{88}Y	Hybritech Inc., San Diego	1	10
	New England Nuclear	2	16
	VA Hospital, San Diego	1	10
	TOTAL	4	36

Total Shipments: 117
Total Curies Distributed: 35.03

with a 2*M* HCl solution and the copper is again removed from the electrode by applying an anodic potential. The solution is passed through an anion-exchange resin column to remove any remaining zinc contamination. Quantities of ^{67}Cu that have been recovered using this technique have been as large as 5-6 Ci.

Radiopharmaceutical Labeling Research

Our radiopharmaceutical labeling program is made possible by the availability of isotopes from LAMPF. These efforts continue to emphasize the use of silane intermediates to achieve regiospecific labeling with ^{77}Br and ^{123}I. This expertise in no-carrier-added radiochemistry is currently being applied to monoclonal-antibody labeling for radioimmunoimaging and therapy. We are evaluating direct halogenation coupling reactions of small labeled precursors and complexing agents, such as metallochelates. These areas are briefly outlined below.

Radiohalogen Labeling: Brain and Heart Agents

D. S. Wilbur and Zitta V. Svitra

Brain. Amines play a major role in regulation of brain activities. Although many molecules circulating in the blood cannot cross the blood-brain barrier,[1] a variety of amines can pass readily into the cerebral cavity. The ability of some amines to pass through the blood-brain barrier makes these compounds attractive for radiolabeling. For example, an amine labeled with a gamma-emitting radionuclide might find wide use in single-photon-emission computed tomography (SPECT) for evaluation of the 400 000 hospitalized stroke patients in this country.[2] In addition to the benefits derived from the measurement of cerebral blood flow, radiolabeled amines might be used to measure brain amine metabolism and to quantify amine protein receptors in different regions of the brain. Metabolism of amines and amine receptor concentrations have been implicated in a number of mental disorders,[3] such as schizophrenia, manic-depressive psychoses, and parkinsonism.

Blau and Kung have studied several different amine-containing compounds that were able to cross the blood-brain barrier.[4-6] However, they found that only a few of the compounds stayed in the brain long enough to permit study of the regional blood flow. From their studies they have postulated that the difference in the intracellular brain pH (~7.0) and the blood pH (~7.4) is enough to retain some amines in the brain for extended periods of time. In one study[7] they were able to demonstrate that [^{125}I]-iodoxyldiamine, 1, would stay in the brain for hours ($T_{1/2}$ = 18 h), whereas [^{125}I]-iodobenzylamine, 2, came out of the brain within minutes ($T_{1/2}$ = 15 min). Despite the fact that 1 appeared to be a promising blood flow agent, the investigators chose to study other compounds[8] because the radiolabeling yields obtained for 1 were very poor.

Our model compound studies[9] using simple compounds similar to 1 and 2 had shown that aryltrimethylsilanes could be used to regiospecifically introduce radiobromine and radioiodine into such molecules. Therefore, a chemical study to investigate the use of arylsilanes in radiolabeling 1 and a benzylamine similar to 2 was carried out (for specific details, see the 1983 INC-Division Annual Report).

Another class of amines that is interesting with respect to brain studies is the phenethylamines. These compounds are congeners of the naturally occurring catecholamine, dopamine. Changes in substituents on the phenethylamine backbone yield a variety of compounds that produce physiological responses from a light euphoria (caused, for example, by amphetamines) to hallucinations (for example, from mescaline or the more potent DOM). The interest in radiolabeling these compounds comes from the fact that they most likely interact with dopaminergic or other catecholaminergic systems. Studies of the interactions may ultimately help delineate how these systems work and thus how malfunctions of the systems might be treated.

Preliminary radiobromination studies of benzylamines and phenethylamines demonstrate that the aryltrimethylsilane intermediates should work well for radiohalogenations of amines for brain studies. Collaborative studies with C.-Y. Shuie and A. Wolf (Brookhaven) are under way to determine if radiofluorinations might also be accomplished using arylsilanes. Applications of aryltrimethylsilanes and pentafluorosilicates[10] in radiohalogenations will continue to be studied since the results thus far have been very encouraging.

REFERENCES

1. H. Davson, "The Blood-Brain Barrier," J. Physiol. 225, 1-28 (1976).

2. T. C. Hill, "Single-Photon Emission Computed Tomography to Study Cerebral Function in Man," J. Nucl. Med. 21, 1197-1199 (1980).

3. P. L. McGeer, J. C. Eccles, and E. G. McGeer, *Neurobiology of the Mammalian Brain* (Plenum Press, New York, 1978), Chap. 8, pp. 493-500.

4. K. M. Tramposch, H. F. Kung, and M. Blau, "Radioiodine Labeled Amines as Brain Imaging Agents," *Applications of Nuclear and Radiochemistry*, R. Lambrecht and N. Morcos, Eds. (Pergamon Press, New York, 1982).

5. H. F. Kung and M. Blau, "Regional Intracellular pH Shift: A Proposed New Mechanism for Radiopharmaceutical Uptake in Brain and Other Tissues," J. Nucl. Med. 21, 147-152 (1980).

6. H. F. Kung and M. Blau, "Synthesis of Selenium-75 Labeled Tertiary Diamines: New Brain Imaging Agents," J. Med. Chem. 23, 1127-1130 (1980).

7. K. M. Tramposch, H. F. Kung, and M. Blau, "Synthesis and Tissue Distribution Study of Iodine-Labeled Benzyl- and Xylylamines," J. Med. Chem. 25, 870-873 (1982).

8. H. F. Kung, K. M. Tramposch, and M. Blau, "A New Brain Perfusion Agent: [I-123] HIPDM: N,N,N'Trimethyl-N'-[2-Hydroxy-3-Methyl-5-Iodobenzyl]-1,3-Propanediamine," J. Nucl. Med. 24, 66-72 (1983).

9. D. S. Wilbur, K. W. Anderson, W. E. Stone, and H. A. O'Brien, Jr., "Radiohalogenation of Non-Activated Aromatic Compounds Via Aryltrimethylsilyl Intermediates," J. Labelled Compd. Radiopharm. 19, 1171-1188 (1982).

10. D. S. Wilbur and Z. V. Svitra, "Organopentafluorosilicates: Reagents for Rapid and Efficient Incorporation of No-Carrier-Added Radiobromine and Radioiodine," J. Labelled Compd. Radiopharm. 20, 619-626 (1983).

Heart. An accurate assessment of the extent of the damage in myocardial infarcts or ischemia is critically important to heart patients. One method of evaluating damage to the myocardial tissue is to study the metabolic processes in that tissue. Because the major metabolic process in the heart is degradation of non-esterified fatty acids, it is not surprising that researchers from many different groups have been exploring radiolabeled fatty acids as a noninvasive method for evaluating regional myocardial metabolism.

The radionuclide of choice for metabolic studies using labeled fatty acids is carbon,[1] but as a positron emitter its application is limited to only a few institutions. Radiofluorinated fatty acids also have been studied,[2] but this label has the same shortcoming. Radioiodine- and radiobromine-labeled fatty acids have been studied as the best alternatives.[3,4]

Studies of radiolabeled fatty acids that encompassed modifying the fatty acids chain length,[4-6] degree of unsaturation,[7] and position of radiohalogen attachment[4,8] have been carried out. Researchers have found that long-chain fatty acids, 16-22 carbons in length, are most effectively extracted, and unsaturation appears to be unimportant. The most important factor appears to be the position of the label within the molecule. Addition of bulky halogens to unsaturations within the fatty acid chain or halogenation at the carbon adjacent to the carboxylic acid functionality has led to dramatic decreases in the extraction from the blood. Contrary to this, radiohalogen labeling at the carbon farthest from the carboxylic acid functionality (ω carbon) has shown little difference in extraction from that of the [^{11}C]-labeled analogs.[3,9]

Radiohalogen labeling at the ω carbon has been accomplished in high radiochemical yields by exchange reactions.[9-11] Despite this fact, problems still exist for the ω-radiohalogenated fatty acids. One of the problems arises because haloacetic acids are produced as metabolites of ω-radiohalogenated fatty acids and these compounds are extremely toxic substances. A solution to this problem can be obtained by making a very high specific-activity radiohalogen-labeled fatty acid. Unfortunately, this is not readily accomplished through exchange reactions.[12-13] A second problem arises because ω-radiohalogenated fatty acids are not very stable *in vitro* or *in vivo*, which seriously affects the blood activity for imaging studies. Stabilization of the radiohalogen label has been accomplished by attaching the radiohalogens to phenyl or vinyl substituents on the ω carbon. Although there are some questions about using these agents to measure metabolism,[14,15] a large effort has been devoted to the synthesis and evaluation of these compounds.[16-19]

The problems with obtaining high specific activities, long reaction times, and low radiochemical yields have led to an investigation of organosilanes as intermediates[20-22] to radiohalogen-labeled fatty acids. The investigation has been directed toward the synthesis of key precursor compounds that could be used to make

a series of ω-silylated fatty acids. Several intermediates necessary to the synthesis of these precursor compounds have been prepared. Synthesis procedures for converting these intermediates into the desired precursors and ultimately into the ω-silylated fatty acids are being developed.

REFERENCES

1. E. S. Weiss, E. F. Hoffman, M. E. Phelps, M. J. Welch, P. D. Henry, M. M. Ter-Pogossian, and B. E. Sobel, "External Detection and Visualization of Myocardial Ischemia with ^{11}C-Substrates In Vitro and In Vivo," Circ. Res. 39, 24-32 (1976).

2. E. J. Knust, M. Schüller, and G. Stöcklin, "Synthesis and Quality Control of Long-Chain ^{18}F-Fatty Acids," J. Labelled Compd. Radiopharm. 17, 353-363 (1979).

3. N. D. Poe, G. D. Robinson, and N. S. MacDonald, "Myocardial Extraction of Labeled Long-Chain Fatty Acid Analogs," Proc. Soc. Exp. Biol. Med. 148, 215-218 (1975).

4. H. J. Machulla, G. Stöcklin, C. Kupfernagel, C. Freundlieb, A. Höck, K. Vyska, and L. E. Feinendegen, "Comparative Evaluation of Fatty Acids Labeled with C-11, Cl-34m, Br-77, and I-123 for Metabolic Studies of the Myocardium: Concise Communication," J. Nucl. Med. 19, 298-302 (1978).

5. C. A. Otto, L. E. Brown, D. M. Wieland, and W. H. Bierwaltes, "Radioiodinated Fatty Acids for Myocardial Imaging: Effects of Chain Length," J. Nucl. Med. 22, 613-618 (1981).

6. E. J. Knust, C. Kupfernagel, and G. Stöcklin, "Long-Chained ^{18}F-Labeled Fatty Acids for the Study of Myocardial Metabolism: Odd-Even Effects," J. Labelled Compd. Radiopharm. (Abstract) 16, 143-144 (1978).

7. W. H. Beierwaltes, R. D. Ice, M. J. Shaw, and U. Y. Ryo, "Myocardial Uptake of Labeled Oleic and Linoleic Acids," J. Nucl. Med. 16, 842-845 (1975).

8. G. D. Robinson and A. W. Lee, "Radioiodinated Fatty Acids for Heart Imaging: Iodine Monochloride Addition Compared with Iodine Replacement Labeling," J. Nucl. Med. 16, 17-21 (1975).

9. G. D. Robinson, "Synthesis of ^{123}I-16-Iodo-9-Hexadecanoic Acid and Derivatives for Use as Myocardial Perfusion Imaging Agents," Int. J. Appl. Radiat. Isotop. 28, 149-156 (1977).

10. P. Laufer, H.-J. Machulla, H. Michael, H. H. Coenen, A. S. El-Wetery, G. Kloster, and G. Stöcklin, "Preparation of ω-^{123}I-Labeled Fatty Acids by ^{123}I-For-Br Exchange: Comparison of Three Methods," J. Labelled Compd. Radiopharm. 18, 1205-1214 (1980).

11. H.-J. Machulla, K. Dutschka, and C. Astfalk, "Improved Synthesis of 17-^{123}I-Heptadecanoic Acid for Routine Preparation," Radiochem. Radioanal. Lett. 47, 189-192 (1981).

12. H.-J. Machulla and K. Dutschka, "Iodination Methods for Routine Preparation of 17-^{123}I-Heptadecanoic Acid and 15-(^{123}I-Phenyl)Pentadecanoic Acid," J. Radioanal. Chem. 65, 122-130 (1981).

13. M. Argentini, M. Zahner, and P. A. Schubiger, "Comparison of Several Methods for the Synthesis of ω-Iodine-123-Heptadecanoic Acid," J. Radioanal. Chem. 65, 131-138 (1981).

14. H.-J. Machulla, M. Marsmann, and K. Dutschka, "Biochemical Concept and Synthesis of a Radioiodinated Phenylfatty Acid for *In Vivo* Metabolic Studies of the Myocardium," Eur. J. Nucl. Med. 5, 171-173 (1980).

15. H. H. Coenen, M.-F. Harmand, G. Kloster, and G. Stöcklin, "15-(p-[^{77}Br]Bromophenyl)Pentadecanoic Acid: Pharmacokinetics and Potential as a Heart Agent," J. Nucl. Med. 22, 891-896 (1981).

16. H.-J. Machulla, M. Marsmann, K. Dutschka, and D. van Beuningen, "Radiopharmaceuticals. II. Radiobromination of Phenylpentadecanoic Acid and Biodistribution in Mice," Radiochem. Radioanal. Lett. 42, 243-250 (1980).

17. H.-J. Machulla, M. Marsmann, and K. Dutschka, "Synthesis of Radioiodinated Phenylfatty Acids for Studying Myocardial Metabolism," J. Radioanal. Chem. 56, 253-261 (1980).

18. H.-J. Machulla, K. Dutschka, D. van Beuningen, and T. Chen, "Development of 15-(p-^{123}I-Phenyl)Pentadecanoic Acid for *In Vivo* Diagnosis of the Myocardium," J. Radioanal. Chem. 65, 279-286 (1981).

19. G. W. Kabalka, S. A. R. Sastry, and K. Muralidhar, "Synthesis of Iodine-125 Labeled Aryl and Vinyl Iodides," J. Labelled Compd. Radiopharm. 19, 795-799 (1982).

20. D. S. Wilbur, K. W. Anderson, W. E. Stone, and H. A. O'Brien, "Radiohalogenation of Non-Activated Aromatic Compounds Via Aryltrimethylsilyl Intermediates," J. Labelled Compd. Radiopharm. 19, 1171-1188 (1982).

21. D. S. Wilbur, W. E. Stone, and K. W. Anderson, "Regiospecific Incorporation of Bromine and Iodine into Phenols Using (Trimethylsilyl)-Phenol Derivatives," J. Org. Chem. 48, 1542-1544 (1983).

22. D. S. Wilbur and Z. V. Svitra, "Organopentafluorosilicates: Reagents for Rapid and Efficient Incorporation of No-Carrier-Added Radiobromine and Radioiodine," J. Labelled Compd. Radiopharm. 20, 619-626 (1983).

Monoclonal-Antibody Labeling: ^{123}I, ^{77}Br, and ^{67}Cu

R. S. Rogers, J. A. Mercer-Smith, and W. A. Taylor

Monoclonal antibodies are produced using the hybridoma technique developed by Kohler and Milstein in which spleen cells from an immunized animal are fused with myeloma cells and the resulting hybrid cells are cloned.[1] The explosive growth in this field is due to the utility of the resulting homogeneous antibodies.[2] Labeled antibodies made to a specific tumor antigen may provide a highly specific way of delivering radionuclides to a tumor for diagnosis by radioimmunoassay or radioimmunoimaging and for radioimmunotherapy.[3,4] We are working to develop chemical methods of labeling antibodies in high radiochemical yield with high specific activity that result in biologically active antibodies for medical use. It is also important that the antibodies have good *in vivo* stability. We are collaborating with S. DeNardo's group at the University of California, Davis. We will examine the labeling chemistry and they will provide the monoclonal antibodies and do the biological testing. We are interested in three approaches to the radiolabeling of antibodies: radiohalogenation, chelate conjugation, and linking of tagged organic molecules to the proteins.

Methods for radioiodination have been used extensively for many years and are well characterized.[5-7] In general, electrophilic reagents are generated *in situ* through oxidation of iodide by chloramine-T, iodogen, enzymes, electrolysis, or iodine monochloride.[8-10] Iodination occurs primarily on tyrosyl residues.[6] Radiochemical yields vary from 75 to 100%. Unfortunately, iodinated proteins are not extremely stable *in vivo*, liberating free iodide on degradation. Though radioiodinated proteins have been used widely, free iodide increases background, thus limiting contrast in radioimmunoimaging and increasing whole-body dose in radioimmunotherapy.

The bromine carbon bond is stronger than the iodine carbon bond and should be more stable *in vivo*. Also important is the fact that bromine does not concentrate in the thyroid. Radiobromination offers high lethality for radiotherapy of tumors because the Auger electrons produced in the decay of ^{77}Br deposit their energy over a small distance.[11] For these reasons radiobromination of antibodies is of great interest.

The literature and our own preliminary work have shown that for the most part methods developed for iodination are not applicable to bromination. Some methods for bromination have been published, but in general they suffer from low yields, harsh conditions, or low availability of starting materials.[12-14] We have radioiodinated a model protein, ovalbumin, and an ascites mixture (the proteins isolated from the peritoneal cavity of a mouse in which a hybridoma is grown) in high yield using iodogen, enzymobeads (immobilized lactoperoxidase), and iodobeads (immobilized chloramine-T). However, radiobromination with ^{77}Br with these methods was unsuccessful. We have been successful in brominating ovalbumin in a buffered system (pH = 6.8) in 20% radiochemical yield with ^{77}Br and sodium hypochlorite, although an excessive amount of protein degradation was seen by high-performance liquid chromatography (HPLC). With ^{82}Br of low specific activity and iodobeads as oxidant, we found that some labeling had occurred with no observable protein degradation.

Neither of these methods is useful as they stand, but they suggest that two questions must be addressed: the first is the oxidation of radiobromide to an electrophilic form suitable for aromatic substitution, and the second is the stability of the proteins in the presence of the oxidizing agent. Our experience with the labeling of small molecules and model systems will allow us to optimize oxidation.[15-17] The denaturation of the antibodies may then be addressed by sequestering the oxidizing agent, thereby preventing direct oxidation of the protein. For example, we are examining different methods of forming the hypochlorite of a hydroxyl-containing resin with pores too small to allow the proteins to diffuse into the resin. We have found that t-butyl hypochlorite oxidizes radiobromide to bromine monochloride in solution, and we hope to be able to form BrCl in the pores of the resin from the reaction of the resin hypochlorite and bromide (which would freely diffuse into the resin). The BrCl so formed would then be able to diffuse out of the resin to react with the excluded protein. Our preliminary results using a Sephadex resin are promising.

Conjugation of chelating agents with proteins is another important method of labeling.[18-21] For this method a ligand that has a high binding affinity for the nuclide of choice is derivatized to allow covalent bonding to the protein. The activated ligand is then reacted with the protein, linking the ligand and protein. Radiolabeling is accomplished by adding the nuclide to the derivatized protein. This method is promising in that a number of different nuclides could be chelated by the same conjugated protein, allowing optimization of decay characteristics for different purposes. We are studying

the binding properties of porphyrins for nuclides that we produce, such as ^{67}Cu and ^{65}Zn, and we will then develop methods to conjugate the porphyrins and other chelating ligands to our antibodies.

In the area of ^{67}Cu-metalloporphyrin research, initial studies appear quite promising. Copper (II) mesotetra (4-carboxyphenyl) porphine (CuTCPP) was prepared from $CuCl_2$ and mesotetra (4-carboxyphenyl) porphine (H_2TCPP). A study of the effect of solvent on the metallation reaction indicates that dimethylformamide (DMF) is by far the best solvent tested for this reaction. ZnTCPP was prepared from $ZnCl_2$ and H_2TCPP, since Zn^{2+} is present in the ^{67}Cu hot cell preparation and can readily metallate H_2TCPP under the same conditions used for the copper metallation reaction. Conditions were developed to separate H_2TCPP, CuTCPP, and ZnTCPP by HPLC.

Once the methods of metallation and separation of H_2TCPP and CuTCPP were developed, carrier-added radiolabeling of H_2TCPP was performed. The $^{67}Cu^{2+}$ usually is supplied in 2*M* HCl. The HCl presents a problem because it protonates the pyrrole nitrogens of the porphyrin: this pyrrole protonation retards the metallation reaction. Therefore, a series of $^{67}Cu^{2+}$ solutions in different solvents was prepared. These solvents were used to optimize the carrier-added metallation reaction. Neutralizing the HCl solution increased the radiolabeling yield from 61 to 76%, but the phosphate buffer was only slightly soluble in DMF. The best radiolabeling yield, 93%, was obtained when the HCl solution was removed by evaporation and $^{67}Cu^{2+}$ was redissolved in DMF before initiation of the chelation reaction. This yield was obtained after 45 min of refluxing the porphyrin and $^{67}Cu^{2+}$. In the analogous no-carrier-added reaction, a radiolabeling yield of 76% was obtained. Two additional porphyrin bands could be seen by HPLC and radio-HPLC under no-carrier-added conditions; these are under study to determine their identity.

REFERENCES

1. G. Kohler and C. Milstein, "Continuous Culture of Fused Cells Secreting Antibody of Predefined Specificity," Nature 265, 495 (1975).

2. D. E. Yelton and M. D. Scharff, "Monoclonal Antibodies: Powerful New Tool in Biology and Medicine," Ann. Rev. Biochem. 50, 657-680 (1980).

3. V. R. McCready, "Tumour Localization," Br. Med. Bull. 36(3), 209 (1980).

4. T. Ghose, A. Guclu, J. Tai, A. S. MacDonald, S. T. Norvell, and J. A. Aquino, "Antibody as Carrier of ^{131}I in Cancer Diagnosis and Treatment," Cancer 36, 1648 (1975).

5. W. C. Eckelman, C. H. Paik, and R. C. Reba, "Radiolabeling of Antibodies," Cancer Res. 40, 3036-3042 (1980).

6. K. A. Krohn, K. C. Knight, J. F. Harwig, and M. J. Welch, "Differences in the Sites of Iodonation of Proteins Following Four Methods of Radioiodination," Biochim. Biophys. Acta 490, 497 (1977).

7. L. R. Chervu and D. R. K. Murty, "Radiolabeling of Antigens: Procedures and Assessment of Properties," Semin. Nucl. Med. 5(2), 157 (1957).

8. K. A. Krohn, L. Sherman, and M. Welch, "Studies of Radioiodinated Fibrinogen. I. Physicochemical Properties of the ICl, Chloramine-T, and Electrolytic Reaction Products," Biochim. Biophys. Acta 285, 404 (1972).

9. P. R. P. Salacinski, C. McLean, J. E. C. Sykes, V. V. Clements-Jones, and P. J. Lowery, "Iodination of Proteins, Glycoproteins, and Peptides Using a Solid-Phase Oxidizing Agent, 1,3,4,6-Tetrachloro-3, 6-Diphenyl Glycoluril (Iodogen)," Anal. Biochem. 117, 136 (1981).

10. A. Sinda, B. Lucka, and K. Russin, "Enzymatic Labeling of Carcinoembryonic Antigen with Iodine-125," J. Labelled Compd. Radiopharm. 18(12), 1797 (1981).

11. A. I. Kassis, S. J. Adelstein, C. Haydock, K. S. R. Sastry, K. D. McElvany, and M. J. Welch, "Lethality of Auger Electrons from the Decay of Bromine-77 in the DNA of Mammalian Cells," Radiat. Res. 90, 362 (1982).

12. L. Knight, K. A. Krohn, M. J. Welch, and B. Spomer, "LPH, ^{77}Br: A New Protein Label," in *Radiopharmaceuticals*, G. Subramanian, B. A. Rhodes, J. F. Cooper, and V. J. Sodd, Eds. (Soc. Nucl. Med., New York, 1975), pp. 149-154.

13. K. D. McElvany, J. W. Barnes, and M. J. Welch, "Characterization of Bromine-77-Labeled Proteins Prepared Using Myeloperoxidase," Int. J. Appl. Radiat. Isotop. 31, 679 (1980).

14. G. Petzold and H. H. Coenen, "Chloramine-T for 'No-Carrier-Added' Labeling of Aromatic Biomolecules with Bromine-75,77," J. Labelled Compd. Radiopharm. 18, 1319 (1981).

15. D. S. Wilbur and K. W. Anderson, "Bromine Chloride from N-Chlorosuccinimide Oxidation of Bromide Ion. Electrophilic Addition Reactions in Protic and Aprotic Solvents, "J. Org. Chem. 47(2), 358 (1982).

16. D. S. Wilbur and H. A. O'Brien, "A-Ring Bromination of Estradiol and 17α-Ethynylestradiol with N-Chlorosuccinimide and Bromide Ion. Possible Evidence for Hybromite Intermediates," J. Org. Chem. 47(2), 359 (1982).

17. D. S. Wilbur, K. W. Anderson, W. E. Stone, and H. A. O'Brien, "Radiohalogenation of Non-Activated Aromatic Compounds Via Aryltrimethylsilyl Intermediates," J. Labelled Compd. Radiopharm. 19, 1171 (1982).

18. G. E. Krejcarek and K. L. Tucker, "Covalent Attachment of Chelating Groups to Macromolecules," Biochem. Biophys. Res. Commun. 77(2), 581 (1977).

19. M. W. Sundberg, C. F. Meares, D. A. Goodwin, and C. I. Diamanti, "Chelating Agents for the Binding of Metal Ions to Macromolecules," Nature 250, 587 (1974).

20. M. W. Sundberg, C. F. Meares, D. A. Goodwin, and C. I. Diamanti, "Selective Binding of Metal Ion to Macromolecules Using Bifunctional Analogs of EDTA," J. Med. Chem. 17(12), 1304 (1974).

21. C. F. Meares, D. A. Goodwin, C. S.-H. Leung, A. G. Girgis, D. J. Silvester, A. D. Nunn, and P. J. Lavender, "Covalent Attachment of Metal Chelates to Proteins: The Stability In Vivo and In Vitro of the Conjugates of Albumin with a Chelate of Indium-111," Proc. Nat. Acad. Sci. USA 73(11), 3803 (1976).

Group INC-3 Publications

J. W. Barnes, M. A. Ott, P. M. Wanek, G. E. Bentley, K. E. Thomas, F. J. Steinkruger, and H. A. O'Brien, Jr., "Iodine-123 Yields from 800-MeV Proton Irradiation of CsCl Target," Proc. Thirtieth Annual Meeting of the Society of Nuclear Medicine, St. Louis, Missouri, June 7-10, 1983, J. Nucl. Med. (Abstract) 24, P24 (1983).

W. Cole, S. DeNardo, C. Meares, G. DeNardo, and H. O'Brien, "Development of Copper-67 Chelate Conjugated Monoclonal Antibodies for Radioimmunotherapy," Proc. Thirtieth Annual Meeting of the Society of Nuclear Medicine, St. Louis, Missouri, June 7-10, 1983, J. Nucl. Med. (Abstract) 24, P30 (1983).

R. E. Gibson, W. C. Eckelman, B. Francis, H. A. O'Brien, J. K. Mazaitis, D. S. Wilbur, and R. C. Reba, "[^{77}Br]-17-α-Bromoethynylestradiol: *In Vivo* and *In Vitro* Characterization of an Estrogen Receptor Radiotracer," Int. J. Nucl. Med. Biol. 9, 245-250 (1982).

R. A. Goldstein, N. A. Mullani, D. J. Fisher, S. K. Marani, H. A. O'Brien, and K. L. Gould, "Quantification of Regional Myocardial Flow with Rb-82 Despite Pharmacologic Intervention," Proc. Thirtieth Annual Meeting of the Society of Nuclear Medicine, St. Louis, Missouri, June 7-10, 1983, J. Nucl. Med. (Abstract) 24, P30 (1983).

D. A. Miller, P. M. Grant, J. W. Barnes, G. E. Bentley, and H. A. O'Brien, Jr., "Research-Scale Experimentation on the Production and Purification of Spallogenic Germanium-68 at Los Alamos for Nuclear Medicine Applications," in *Applications of Nuclear and Radiochemistry*, R. M. Lambrecht and N. Morcos, Eds. (Pergamon Press, New York, 1982), Chap. 4, pp. 37-44.

H. A. O'Brien, Jr., and P. M. Grant, "Biomedical Positron Generators," in *Applications of Nuclear and Radiochemistry*, R. M. Lambrecht and N. Morcos, Eds. (Pergamon Press, New York, 1982), Chap. 6, pp. 57-68.

A. P. Selwyn, R. M. Allan, A. L'Abbate, P. Horlock, P. Camici, J. Clark, H. A. O'Brien, Jr., and P. M. Grant, "Relation Between Regional Myocardial Uptake of Rubidium-82 and Perfusion: Absolute Reduction of Cation Uptake in Ischemia," Am. J. Cardiol. 50, 112-121 (1982).

D. S. Wilbur, K. W. Anderson, W. E. Stone, and H. A. O'Brien, Jr., "Radiohalogenation of Non-Activated Aromatic Compounds Via Aryltrimethylsilyl Intermediates," J. Labelled Compd. Radiopharm. 19, 1171-1186 (1982).

D. S. Wilbur, W. E. Stone, and K. W. Anderson, "Regiospecific Incorporation of Bromine and Iodine into Phenols Using Trimethylsilylphenol Derivatives," J. Org. Chem. 48, 1542-1544 (1983).

D. S. Wilbur and Z. V. Svitra, "Organopentafluorosilicates: Reagents for Rapid and Efficient Incorporation of No-Carrier-Added Radiobromine and Radioiodine," J. Labelled Compd. Radiopharm. 20, 619-626 (1983).

D. S. Wilbur, Z. V. Svitra, and H. A. O'Brien, Jr., "Applications of Aryltrimethylsilanes in Radiobrominations," J. Nucl. Med. (Abstract) 24, P43 (1983).

D. S. Wilbur, Z. V. Svitra, and H. A. O'Brien, Jr., "Applications of Aryltrimethylsilanes in Radiobrominations," Proc. Thirtieth Annual Meeting of the Society of Nuclear Medicine, St. Louis, Missouri, June 7-10, 1983, J. Nucl. Med. (Abstract) 24, P43 (1983).

Papers Accepted for Publication

G. E. Bentley, F. J. Steinkruger, and P. M. Wanek, "Electrochemistry as a Basis for Radiochemical Generator Systems," Proc. of the Symp. on New Radionuclide Generator Systems for Nuclear Medicine, 185th American Chemical Society National Meeting, Seattle, Washington, March 20-25, 1983 (in press); Los Alamos National Laboratory document LA-UR-83-898.

D. T. Cromer, R. R. Ryan, and D. S. Wilbur, "Structure of 1-H-Azepine- 2-1-5-Methoxime, $C_7H_9N_2O_2$," Acta Crystallogr. Sect. C (in press); Los Alamos National Laboratory document LA-UR-83-2303.

H. A. O'Brien, Jr., "Overview of Radionuclides Useful for Radioimmunoimaging and Current Status of Preparing Radiolabeled Antibodies," in *Radioimmunoimaging* (Elsevier Biomedical Press, New York, in press); Los Alamos National Laboratory document LA-UR-83-154.

H. A. O'Brien, Jr., J. W. Barnes, G. E. Bentley, F. J. Steinkruger, K. E. Thomas, M. A. Ott, F. H. Seurer, and W. A. Taylor, "The Development of Short-Lived Radionuclides at Los Alamos," Proc. of the Int. Symp. on the Developing Role of Short-Lived Radionuclides in Nuclear Medical Practice, Washington, DC, May 3-5, 1982 (in press); Los Alamos National Laboratory document LA-UR-83-791.

F. J. Steinkruger, G. E. Bentley, H. A. O'Brien, Jr., M. A. Ott, F. H. Seurer, W. A. Taylor, and J. W. Barnes, "Production and Recovery of Large Quantities of Radionuclides for Nuclear Medicine Generator Systems," Proc. of the Symp. on New Radionuclide Generator Systems for Nuclear Medicine, 185th American Chemical Society National Meeting, Seattle, Washington, March 20-25, 1983 (in press); Los Alamos National Laboratory document LA-UR-83-835.

K. E. Thomas, "Recovery and Isolation of Curie Quantities of Hafnium and the Lanthanides from LAMPF-Irradiated Tantalum Targets," Radiochim. Acta (in press); Los Alamos National Laboratory document LA-UR-83-579.

K. E. Thomas, "Proposal for the Production of Carrier-Free Osmium-191," Proc. of the Int. Conf. on Single Photon Ultra-Short-Lived Radionuclides, Pan American Health Organization, Washington, DC, May 9-10, 1983; Los Alamos National Laboratory document LA-UR-83-1367 (in press).

K. E. Thomas and J. W. Barnes, "Large Scale Isolation of Strontium-82 for Generator Production," Proc. of the Symp. on New Radionuclide Generator Systems for Nuclear Medicine, 185th American Chemical Society National Meeting, Seattle, Washington, March 20-25, 1983 (in press); Los Alamos National Laboratory document LA-UR-83-939.

D. S. Wilbur, Z. V. Svitra, R. S. Rogers, and W. E. Stone, "Radiohalogen Labeling Studies at Los Alamos," Proc. of the Int. Symp. on the Developing Role of Short-Lived Radionuclides in Nuclear Medical Practice, Washington, DC, May 3-5, 1982 (in press).

Papers Submitted for Publication

K. W. Thomas and the Los Alamos Medical Radioisotopes Group, "Production of Microcurie Amounts of Carrier-Free Aluminum-26," Los Alamos National Laboratory document LA-UR-83-1413 (submitted to Radiochim. Acta).

D. S. Wilbur, "Structural Determinations of Some Chloroazepin-2,5-Diones Using a Lanthanide Shift Reagent," Los Alamos National Laboratory document LA-UR-83-2233 (submitted as a Note to J. Org. Chem.).

Theory

Spin Dependence of NN and $NN\pi$ Reactions and the Question of Dibaryon Resonances*

Richard R. Silbar (Los Alamos)

Abstract

Recent experiments on the spin dependence of the coupled NN and $NN\pi$ systems are reviewed and compared with theory. Conventional models involving the usual interactions of mesons and nucleons appear to explain the rich spin dependence observed.

Introduction

The experimental information on spin dependence in the coupled NN and $NN\pi$ systems for medium energies has mushroomed in the past few years. The energies involved run from pion-production threshold (around 300-MeV incident nucleon laboratory energy) to about 1500 MeV (where two-pion production becomes important).

At the same time theoretical models for the coupled NN and $NN\pi$ systems have undergone vigorous development. Both experiment and theory have been much stimulated by the observation of relatively sharp energy-dependent structures.[1] It was quickly recognized that these might be manifestations of new degrees of freedom, such as the dibaryon resonances suggested by the quark bag model.[2]

This report summarizes recent experimental progress in this field** and discusses to what extent the new data require an interpretation of new quark substructures.

What is a Dibaryon Resonance?

A resonance is more than just a bump in a cross section. The classic example of an elastic resonance is provided by a Breit-Wigner amplitude

$$T_J = \frac{1}{2}\,\frac{\Gamma}{E_R - E - i\Gamma/2}\ ,$$

where J denotes the partial-wave amplitude that is resonating. Such a structure has a pole in the complex energy plane at $E = E_R - i\Gamma/2$, that is, "on the second sheet." As the energy increases through E_R, the complex amplitude T_J traces a counterclockwise path along a circle of radius $\frac{1}{2}$ centered at $+\frac{1}{2}$, the so-called unitarity circle. In this example without any background, the partial-wave amplitude reaches the top of the circle ($+i$) at the resonance energy E_R and moves around into the left half plane for energies above E_R. This counterclockwise motion on an Argand diagram is typical of a resonance. However, a warning is definitely in order: such motions can arise from other kinds of analytical structures, as well as from resonance poles.

In the presence of inelasticity (that is, coupling to other open channels), the scattering amplitude becomes a matrix, and a resonance shows up as a pole in each matrix element. As the energy increases, the path traced by the elastic amplitude T_J is still counterclockwise, but the conservation of probability (unitarity) constrains it only to be somewhere within the unitarity circle.

At least two such counterclockwise looping behaviors deep inside the unitarity circle have been found in phase-shift analyses for NN elastic scattering.[4] These occur in the $^1D_2$ and $^1F_3$ partial waves, the two prime candidates for dibaryon resonances. One needs a model to extrapolate the physical amplitude into the complex energy plane and search for resonance poles. There is an extensive theoretical literature that deals with whether the looping behavior is due to resonance poles (that is, dibaryons).* The issue is not settled, but it is clear from simple models that coupled-channel resonance poles certainly can be present. On the other hand, the cut from the $NN \to N\Delta$ threshold also produces a resonance-like behavior, and it could be the combined effect of poles and the $N\Delta$ cut that causes the structures seen in the observables.

The existence of dibaryons was first suggested in 1977 by the energy-dependent structures found in spin-dependent total cross-section differences.[6] These and other structures go hand in hand with inelasticity, which in this energy region means single-pion production,

---

*To be published in Comments on Nuclear and Particle Physics 12(4), 177-189 (March 1984).

**Experiments involving electromagnetic probes are not discussed; references in this subfield may be traced, for example, from K. Baba et al., Ref. 3.

*Recent literature may be traced from W. M. Kloet and J. A. Tjon, Ref. 4.

$NN \rightarrow NN\pi$. If dibaryons are actually given by resonance poles, the next questions are: What is their origin? Can they be explained by conventional models of mesons interacting with nucleons? Or, does their existence imply a new underlying hadronic structure, such as that associated with quarks and color degrees of freedom?

Theoretical Framework

In the energy region under discussion, the standard description of the $NN \rightarrow NN\pi$ or $\pi d \rightarrow \pi d$ scattering amplitudes uses the isobar model,[7] as illustrated by the graphs in Figs. 1(a) and (b). Originally, the isobar amplitudes (the "blobs" in the figure) were simply fit to the available data or calculated in the Born approximation. Today, however, these amplitudes are calculated in a unified and unitary way. There are two approaches.

(1) The coupled two-body channel approach involves solving coupled scattering equations with transition potentials between the NN, $N\Delta$, and πd two-body channels. This method has been applied to calculate inelasticity parameters and phase shifts for NN scattering above the pion-production threshold[8-10] and spin observables for the $pp \rightarrow d\pi$ reaction.[11]

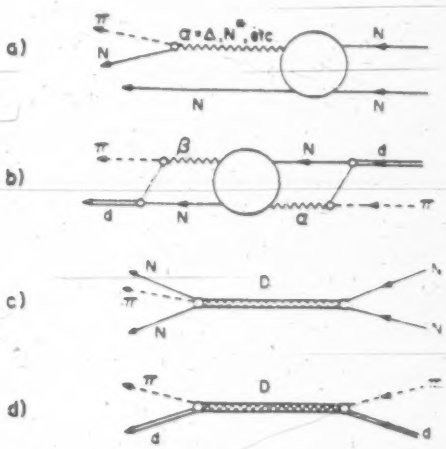

Fig. 1.
Four Feynman graphs: (a) and (b) show graphs for the isobar-model treatment of the $NN \rightarrow NN\pi$ and $\pi d \rightarrow \pi d$ reactions, respectively, and (c) and (d) indicate explicit dibaryon-resonance graphs.

(2) The three-body-equation approach has been the most realistic path to the elastic scattering of pions by deuterons, with important work being done by Rinat and Thomas,[12] Garcilazo,[13] and the Lyon group.[14] Garcilazo has extended his calculations to the breakup process $\pi d \rightarrow \pi NN$ with good success.[15] The other two groups have emphasized the treatment of NN intermediate states, which is closely connected to an alternative approach and which involves the truncation of an underlying field theory to consider, at any given time, only two nucleons or two nucleons and a pion. The original work was by Afnan and Thomas.[16] Later developments[17-20] vary in their details and philosophical basis. The major emphasis of Refs. 18-20 so far has been on the $pp \rightarrow d\pi$ reaction, whereas the authors of Ref. 17 have concentrated on calculating spin observables for the three-body final state, $NN \rightarrow NN\pi$ (Ref. 21).

All these models, two-body as well as three-body, are conventional in that they involve only the known mesons and nucleons interacting in the usual way. If there are explicit dibaryon resonances—that is, resonances *not* generated by the conventional meson-nucleon dynamics—these models must be supplemented by contributions that look like Figs. 1(c) and (d). Incorporating such graphs without destroying the unitarity of the conventional models is slightly problematical. One way of doing this has been discussed by Locher and co-workers.[22]

Recent Experiments

It is convenient to discuss separately five kinds of spin-observable experiments: (1) πd elastic scattering, (2) $pp \rightarrow d\pi$ (and its inverse), (3) spin-dependent total cross sections, and (4) inclusive and (5) exclusive experiments on the $NN \rightarrow NN\pi$ reaction. Table I gives definitions for these different spin observables.

(1) Elastic pion-deuteron scattering. Two different spin observables are measured for this reaction. The sharp angular oscillations in the vector polarization (iT_{11}), found[23] at $T_{\pi,lab} = 256$ MeV, have been particularly suggestive of a $^1G_4$ dibaryon resonance. The extant (conventional) three-body calculations (see, for example, Ref. 14) give rather smooth angular variations for iT_{11}. By incorporating explicit dibaryon-resonance

Table I. Definitions of Spin Observables.

$\pi d + \pi d$:

$$iT_{11}(\theta) = (\sqrt{3/2})\ [\sigma(M_d = +1) - \sigma(M_d = -1)] \Big/ \Big[\sum_{M_d = -1,0,1} \sigma(M_d) \Big] ,$$

$$T_{20}(\theta) = (1/\sqrt{2}) [\sigma(+1) - 2\sigma(0) + \sigma(-1)] \Big/ \Big[\sum_{M_d = -1,0,1} \sigma(M_d) \Big] .$$

The deuteron spin is quantized normal to the scattering plane.

Total Cross-Section Differences:

$$\Delta\sigma_T = \sigma(\uparrow\downarrow) - \sigma(\uparrow\uparrow) .$$

Initial nucleon spins are quantized in a direction transverse to the beam direction; $\Delta\sigma_L$ is defined likewise, but with spins quantized along the beam direction (longitudinal).

$NN \to NN\pi$ (or $d\pi$):

$$A_N(\theta,\ldots) = [\sigma(\uparrow) - \sigma(\downarrow)]/[\sigma(\uparrow) + \sigma(\downarrow)] ,$$

$$A_N^{(\mathrm{tgt})}(\theta,\ldots) \neq A_N^{(\mathrm{beam})}(\theta,\ldots) ,$$

$$A_{NN} = [\sigma(\uparrow\uparrow) - \sigma(\uparrow\downarrow) - \sigma(\downarrow\uparrow) + \sigma(\downarrow\downarrow)]/\text{ sum} .$$

Initial nucleon spins are quantized normal to the reaction plane. Similar formulae define A_{LL}, A_{SS}, A_{LS}, and $A_{SL} \neq A_{LS}$, but with longitudinal and sideways quantization axes; likewise for spin-transfer observables D_{NN}, K_{LL}, etc., except that one spin is for an initial nucleon, the other for a final nucleon.

graphs, as in Fig. 1(d), Locher et al.[22] could predict oscillatory behavior very much like that observed.

Recently, however, Gibbs* noticed that the three-body calculations are quite sensitive to the small πN interactions that enter as input. The vector polarization is basically an interference effect between the dominant P_{33} πN interaction and the smaller contributions. In particular, the earlier three-body calculations used input πN potentials, which were in fact unsupported by the πN experimental data. Gibbs and Gibson[24] have shown that a single-scattering-approximation calculation with πN input directly related to the πN phase shifts can do a reasonable job of reproducing the 256-MeV iT_{11} angular distribution, with the exception of a singularly negative datum at 135°. That datum, in the meantime, has been remeasured and was found to be positive.** Thus, on the whole, the experimental data set for iT_{11}, over the whole energy range measured, now seems not to require (explicit) dibaryon resonances.

The other spin observable of current interest in πd scattering is the tensor polarization T_{20} of the recoil deuteron. Two groups have obtained very different experimental results. The Argonne group[25] finds T_{20}'s in agreement with conventional expectations—that is, predictions of the three-body models. In contrast, the ETH group obtained data[26] sufficiently oscillatory that, if correct, may demand an interpretation involving explicit dibaryon resonances. In view of the present discrepancy in the T_{20} data, it is difficult at this time to draw any conclusions about the existence of dibaryon resonances.

*Reference 24. A similar observation was evidently made earlier by J. Arvieux and A. S. Rinat (unpublished).

**Private communication to W. R. Gibbs, spring 1983, from Dubach et al., authors of Ref. 21.

(2) The reaction $pp \to d\pi$ *and its inverse.* Because the two-body final state is easier to deal with experimentally than the three-body state, there is already an extensive data set for this reaction from threshold to above 1000 MeV. Three kinds of spin observables have been measured: polarization asymmetries, spin-spin correlations, and polarization transfers.[27]

The data, especially for the asymmetries A_N, are smoothly varying with energy and generally have very small error bars. At the moment, no conventional theoretical model[11,18,20] does a very good job. However, the models do reproduce the general trends of the data. To judge from the differences among the various models, which are big compared with the experimental errors, it is reasonable to presume that a conventional model can someday fit this data set.

Incidentally, the spin-spin correlations A_{NN} for $pp \to d\pi$ are large and negative, $A_{NN} \simeq -0.8$, a result that comes from conventional models quite easily since the reaction is dominated by $N\Delta$ intermediate states with orbital angular momenta $L' = 0$. These states are produced in the initial NN state from the $^1D_2$ partial wave. Thus, the basic negativeness of A_{NN} is largely determined by nearly model-independent considerations (see definition, Table I).

(3) Spin-dependent total cross sections. It was the Argonnne ZGS measurements of the cross-section differences $\Delta\sigma_L$ and $\Delta\sigma_T$ that created the great interest in dibaryons.[1] These quantities have since been remeasured at all the meson factories. The sharp energy-dependent structures in $\Delta\sigma_L$ and $\Delta\sigma_T$ have been confirmed, although there is not yet complete agreement as to what the magnitudes of the cross-section differences are.

The peak in $\Delta\sigma_T$ and $\Delta\sigma_L$ at 550 MeV is related to the resonance-like structure of the $^1D_2$ amplitude, whereas the dip in $\Delta\sigma_L$ near 750 MeV is related to the $^3F_3$ amplitude ($\Delta\sigma_L$ contains contributions from the $L = J$ triplet partial waves but $\Delta\sigma_T$ does not). From the point of view of conventional models, these structures to a large extent are due to the onset of the $NN \to N\Delta$ reaction as it opens up in the s and p waves of the $N\Delta$ state, respectively. However, none of the conventional models has as yet reproduced the details of the experimentally observed structures. As an example, Fig. 2 compares the predictions of Ref. 28 with the data.

Conventional models also might be running into trouble with the inelastic part of the longitudinal cross-section difference $\Delta\sigma_L^{\text{inel}}$, which is negative ($-3.5 \pm 1$ mb) at 800 MeV.[29] Three different conventional

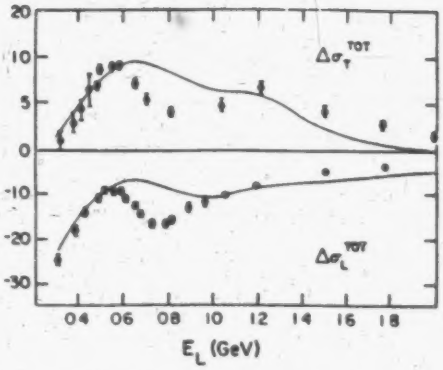

Fig. 2.
Experimental data for $\Delta\sigma_T$ and $\Delta\sigma_L$ (in millibarns), compared with the conventional model prediction of Ref. 28 (from which this figure was taken).

models[17,30,31] give positive ($\simeq$7-mb) predictions for this quantity at that energy. Even the shape of the energy dependence differs markedly between the models and data. It should be pointed out that extracting $\Delta\sigma_L^{\text{inel}}$ is difficult, involving the difference of two large numbers obtained from two different experiments. The results of Ref. 29 should be checked.

The above remarks all refer to $I = 1$ cross sections. Little is known about the $I = 0$ cross-section differences, although a flat $\Delta\sigma_L$ observed in pd interactions has been interpreted as requiring a $^1F_3$ "antidip" to compensate for the $^3F_3$ dip at 750 MeV.[32] Such a structure, if it exists, would be very difficult to interpret in terms of conventional models.

(4) Inclusive $NN \to NN\pi$ *reactions.* In these reactions, typically, only one particle in the three-body final state is detected. Such experiments are more easily performed and more precise than exclusive experiments, which use detectors in coincidence to determine the momentum and direction of every final-state particle. The results of inclusive experiments measuring spin observables are just now appearing in the literature.

One such experiment measures the analyzing power A_N in the reaction $\vec{p}p \to pX$ ($X = n\pi^+$ or $p\pi^0$) at 800 MeV.[33] The prominent feature in the data is a sharp rise to a value of 0.3 at the upper end of the outgoing proton momentum spectrum (Fig. 3). This feature can be

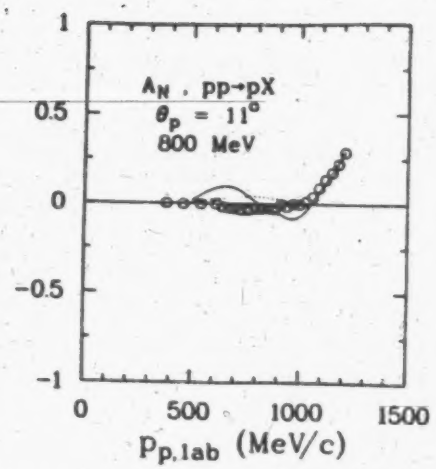

Fig. 3.
Asymmetry for the inclusive reaction $\bar{p}p \to pX$, $X = n\pi^+$ or $p\pi^0$. Data are from Ref. 33 and the curves are the unitary (solid) and Born approximation (dashed) predictions from Ref. 34.

reproduced in a unitary model[34] (the solid line in Fig. 3) but appears difficult to explain using a Born approximation approach[35] (dashed line). Spin observables such as A_N result from interference between different complex amplitudes and thus are sensitive to unitarization.

Another group has measured the polarization transfers K_{NN} and K_{LL} in the $\bar{p}p \to \bar{\Lambda}X$ reaction, $X = p\pi^+$, again at 800 MeV.[36] There are as yet no unitary model predictions for these quantities, but a Born approximation calculation[35] fails to reproduce the features of the data entirely. It will be interesting to see if unitarity alone can cure the disagreement.

(3) Exclusive NN → NNπ *reactions.* Until recently, kinematically complete information about this fundamental pion-production process came mostly from a small number of bubble chamber experiments performed in the 1960s. The data base was therefore embarrassingly small. With the advent of meson factories, however, there are now counter experiments that measure complete kinematics for the reaction (although usually only for in-plane geometry). Two particles (at least) must be measured in coincidence to determine five kinematical quantities: for example, p_p, θ_p, ϕ_p, θ_n, and ϕ_n.

The first such experiment[37] measured the polarization asymmetry in $\bar{p}p \to p\pi^+ n$ at 800 MeV, and it established the crucial importance of dealing with unitarity properly. As the first data were being processed, Umland, Duck, and Mutchler[38] made Born approximation predictions of A_N as a function of the outgoing proton momentum for the various angle pairs measured. Not surprisingly, since A_N depends on the relative phases between complex amplitudes, the agreement with the data was quite poor. They then tried including explicit dibaryon-resonance graphs [Fig. 1(c)], fitting a free phase between those graphs and the usual isobar graphs [Fig. 1(a)]. The agreement with the experimental A_N was much improved, but still not remarkably good.

Soon after this, Dubach et al.[21] applied the unitary model of Ref. 17 to the problem, using the no-free-parameter version of the model based solely on one-pion exchange (OPE). These predictions, although still not agreeing very well with the data of Ref. 37, were qualitatively much more like the data than the Born approximation results. Considering the simple nature of the model (only OPE forces between the nucleons and isobars, only P_{33} and P_{11} πN input forces, etc.), one can be optimistic that a more complete model eventually might be able to explain these data.

The asymmetry experiment[37] also was able to record data at the same time for the reaction $\bar{p}p \to pp\pi^0$. It is curious that the predictions of the unitary model[21] seem to fit these data much better than the data* for $np\pi^+$. It is not clear why this happens.

Another set of exclusive experiments measures spin-spin correlations A_{NN}, A_{LL}, etc., for the reaction $\bar{p}\bar{p} \to np\pi^+$ at three energies near 500 MeV[39] and at 650 and 800 MeV.[40] The no-free-parameter OPE predictions of Ref. 21 are compared with preliminary data at 500 MeV in Fig. 4. The agreement is quite good—that is, these data provide no surprises in comparison with a conventional model. All the spin-spin correlation coefficients in Fig. 4 are large and negative, again reflecting the dominance of the $NN(^1D_2) \to N\Delta(^3S_1)$ partial-wave amplitude.

The experiment on A_{NN} and A_{LL} at 650 and 800 MeV[40] has fewer data points (but smaller errors). These data also are in agreement with the predictions of Ref. 21. At 800 MeV, A_{LL} has become slightly positive, indicating a cancellation between the $^1D_2$ and $^3F_3$ partial waves for this quantity (see definition in Table I).

*G. S. Mutchler, private communication.

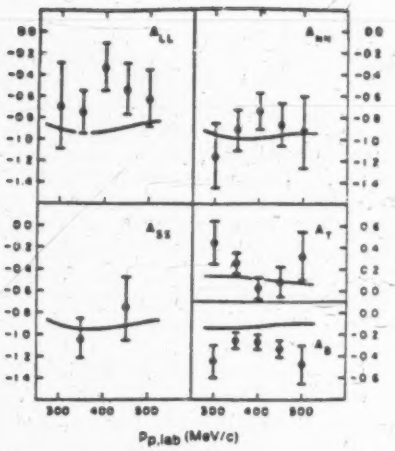

Fig. 4.
Spin-spin correlation coefficients for $\bar{p}\bar{p} \rightarrow np\pi^+$ at 500 MeV. Data are from Ref. 39 and the curves were calculated as in Ref. 21. This figure is a corrected version of one appearing in Ref. 39.

It is curious that in both experiments (and in the calculations) the beam and target particle asymmetries for a given angle pair are approximately equal and opposite in sign. There is no evident simple reason for this. (Identical-particle symmetry gives exact equalities between *different* angle pairs.)

A third kind of experiment involves the measurement of the polarization transfer coefficient D_{NN}, for the reaction $\bar{p}p \rightarrow n\bar{p}\pi^+$ at 800 MeV.[41] The one data point measured (right at the peak of the Δ^{++} resonance) is also in good agreement with the prediction of Ref. 21. The differential cross-section data elsewhere indicate the presence of a strong final-state interaction between the outgoing nucleons. One naturally wonders how well the unitary models (which generally do not contain such interactions in their input) will compare with a more extensive D_{NN} data set.

Conclusions

In general, we have seen that conventional models of mesons and nucleons, so far, are able to explain a substantial amount of new experimental data on the rich spin dependence of the coupled NN and $NN\pi$ interactions. Not all predictions agree perfectly, but that is to be expected at this stage. It seems a little peculiar that the gross quantities (total cross-section differences) are harder to understand in this picture than the detailed ones (exclusive cross sections). Nonetheless, the major point to be emphasized is that there is no obvious need at this time to invoke new quark substructures to explain the present data.

So where, then, are the effects of the quarks and gluons in the $A = 2$ interacting systems to be seen? It may simply be that the present round of experiments is not very sensitive to quark degrees of freedom.[42] To find out what experiments *are* sensitive, perhaps of this type or perhaps of some totally different kind, will probably require a lot more experimental and theoretical work.

Acknowledgments

I wish to thank the many experimentalists who have discussed with me their data, often while still preliminary. My colleagues J. Dubach and W. M. Kloet have contributed greatly to my understanding of the theory, and T. S. Bhatia urged me to write this summary of the rapidly changing experimental situation.

This work was supported by the USDOE.

REFERENCES

1. A. Yokosawa, Phys. Rep. 64, 47 (1980); and D. V. Bugg, Nucl. Phys. A 374, 95c (1982).
2. A. Aerts et al., Phys. Rev. Lett. 40, 1543 (1978).
3. K. Baba et al., Phys. Rev. C (July 1983).
4. R. A. Arndt, phase-shift analysis WI82 (winter 1982).
5. W. M. Kloet and J. A. Tjon, Nucl. Phys. A 392, 271 (1983).
6. K. Hidaka et al., Phys. Lett. 70B, 479 (1977).
7. S. J. Lindenbaum and R. M. Sternheimer, Phys. Rev. 105, 1874 (1957); and 123, 333 (1961).
8. A. M. Green, J. A. Niskanen, and M. E. Sainio, J. Phys. G (Nucl. Phys.) 4, 1055 (1978).
9. E. L. Lomon, Phys. Rev. D 26, 576 (1982).

10. E. E. van Faassen and J. A. Tjon, Phys. Lett. 120B, 39 (1983); and Phys. Rev. C (August 1983).

11. J. A. Niskanen, Santa Fe Polarization Conf., AIP Conf. Proc. 69, 62 (1981).

12. A. S. Rinat and A. W. Thomas, Nucl. Phys. A 282, 365, (1977); and A. S. Rinat, Y. Starkand, and E. Hammel, Nucl. Phys. A 364, 486 (1981).

13. H. Garcilazo, Phys. Rev. Lett. 45, 780 (1980).

14. C. Fayard, G. H. Lamot, and T. Mizutani, Phys. Rev. Lett. 45, 524 (1980).

15. H. Garcilazo, Phys. Rev. Lett. 48, 577 (1982).

16. I. R. Afnan and A. W. Thomas, Phys. Rev. C 10, 109 (1974).

17. W. M. Kloet and R. R. Silbar, Nucl. Phys. A 338, 281 and 317 (1980); and A 364, 346 (1981).

18. B. Blankleider and I. R. Afnan, Phys. Rev. C 24, 1572 (1981).

19. M. Betz and T.-S. H. Lee, Phys. Rev. C 23, 375 (1981).

20. A. S. Rinat, Nucl. Phys. A 397, 381 (1983).

21. J. Dubach et al., Phys. Lett. 106B, 29 (1981); and J. Phys. G (Nucl. Phys.) 8, 475 (1982).

22. K. Kubodera et al., J. Phys. G (Nucl. Phys.) 6, 171 (1980).

23. J. Bolger et al., Phys. Rev. Lett. 46, 167 (1981); and 484, 1667 (1982).

24. W. R. Gibbs, invited talk, Baltimore APS Meeting, April 1983, Los Alamos National Laboratory preprint LA-UR-83-245 (1983).

25. R. J. Holt et al., Phys. Rev. Lett. 47, 472 (1981).

26. W. Grüebler et al., Phys. Rev. Lett. 49, 444 (1982).

27. P. Walden et al., Phys. Lett. 81B, 156 (1979); E. Aprile et al., Nucl. Phys. A 335, 245 (1980); R. Bertini et al., "High Energy Spin Physics," AIP Conf. Proc. 95, 231 (1982); A. Saha et al., submitted to Phys. Lett. B; M. D. Corcoran et al., Phys. Lett. 120B, 309 (1983); and W. B. Tippens et al., to be published.

28. T.-S. H. Lee, Argonne preprint (June 1983).

29. I. P. Auer et al., Argonne preprint ANL-HEP-PR-83-27 (July 1983).

30. A. S. Rinat and R. S. Bhalerao, Weizmann preprint WIS-82 155 (1982).

31. A. König and P. Kroll, Nucl. Phys. A 356, 345 (1981).

32. I. P. Auer et al., Phys. Rev. Lett. 46, 1177 (1981).

33. J. A. McGill et al., submitted to Phys. Lett. B, July 1983.

34. R. R. Silbar et al., contribution to the Few-Body Conf., Karlsruhe, Germany, August 1983.

35. B. J. VerWest, Phys. Lett. 83B, 161 (1979).

36. G. Glass et al., Phys. Lett. B (to be published).

37. A. D. Hancock et al., Phys. Rev. C 27, 2742 (1983).

38. E. A. Umland, I. M. Duck, and G. S. Mutchler, Santa Fe Polarization Conf., AIP Proc. Conf. 69, 172 (1981).

39. R. Shypit et al., Phys. Lett. 124B, 314 (1983).

40. T. S. Bhatia et al., Phys. Rev. C (to be published).

41. B. E. Bonner et al., contribution to the Few-Body Conf., Karlsruhe, Germany, August 1983.

42. P. J. Mulders, Phys. Rev. D 25, 1269 (1982).

Medium-Energy Probes and the Interacting Boson Model

J. N. Ginocchio (Los Alamos)

Introduction

In medium and heavy nuclei far from closed shells, the number of shell-model degrees of freedom in the low-lying spectrum of nuclei becomes enormous. For example, the number of shell-model $J^\pi = 2^+$ states with only the valence nucleons active for ^{154}Sm is of the order of 10^{14}. Hence, spherical shell-model calculations of these nuclei are impossible. The collective model of Bohr and Mottelson can explain spectroscopic properties of the most interesting collective states for nuclei that have a very stable equilibrium deformation, but most nuclei do not have a stable equilibrium deformation. Such nuclei are called *transitional* nuclei. The series of samarium isotopes from ^{148}Sm to ^{154}Sm, for example, fall into this category.

Recently the interacting boson model (IBM) of the nucleus,[1] which is an approximation to the shell model, has been able to describe these transitional nuclei. This model has three basic assumptions. One is that the low-lying spectra of nuclei are composed primarily of collective pairs of valence nucleons coupled to angular momentum 0 and 2 moving about a spherical doubly magic core. The second is that these collective monopole and quadrupole nucleon pairs are approximated as bosons. And the third assumption is that the effect of the Pauli principle and other degrees of freedom, such as excitations of other pairs and excitations of the core, are assumed to be taken into account through a renormalized effective boson Hamiltonian and transition operators.

There are two versions of the IBM. The original version, called IBM-1, does not distinguish between neutrons and protons. This version has had phenomenological success in many regions of the periodic table, and can be related to the geometrical Bohr-Mottelson model.[2] In Fig. 1 we show a comparison of the spectrum of ^{168}Er produced by IBM-1 along with the spectrum seen in (n,γ) experiments.[3] These experiments measure not only the ground state band but the sidebands as well. The IBM-1 with three parameters gives a remarkable reproduction of this pattern of excited states, as well as reproducing transition rates.[3]

The second version, called IBM-2, distinguishes between neutrons and protons. This model has been used to study a number of different types of nuclei. A few examples are the samarium and thorium isotopes,[4] the palladium isotopes,[5] xenon, barium, and cesium isotopes,[6] platinum and osmium isotopes,[7] and the tungsten isotopes.[8]

Although IBM-1 is relatively simple, IBM-2 is necessary to develop a deep understanding of nuclei for several reasons. First, we have learned through phenomenological studies of the shell model that the effective interaction between like nucleons inside the nucleus is

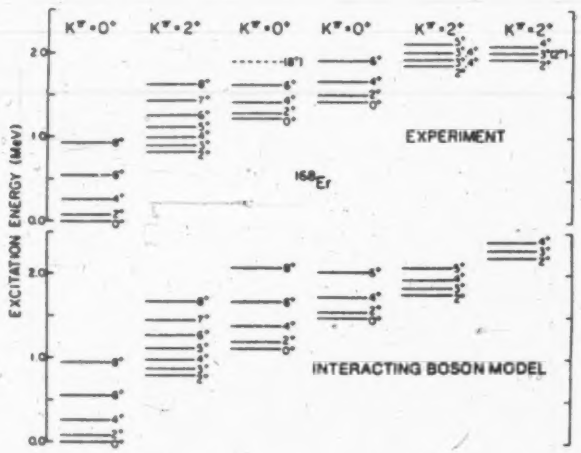

Fig. 1.
The experimental and IBM-1 spectrum for ^{168}Er from Ref. 3.

dominated by the pairing interaction and tends to make nuclei spherical. On the other hand, the effective neutron-proton interaction is dominated by a quadrupole interaction and produces nuclear deformation. Furthermore, IBM-2 has additional states that can be excited that are not in the IBM-1 space.

The states in IBM-2 that correspond to those in IBM-1 are the ones most symmetric in the neutron-proton degrees of freedom. However, the less symmetric states also may occur in the low-lying spectrum. The combined use of medium-energy electrons, pions, and protons can sort out the nature of the neutron and proton excitations in nuclei. Finally, the parameters of IBM-2 may be derived from an underlying fermion many-body system.

Here we review some of these aspects of the IBM, particularly as they apply to medium-energy scattering.

The Boson Hamiltonian

The boson Hamiltonian reflects the properties of the effective nucleon-nucleon interaction mentioned above:

$$H = \epsilon_\nu N_\nu + \epsilon_\pi N_\pi - \kappa Q_\nu \cdot Q_\pi \quad , \tag{1}$$

where ν refers to neutron bosons and π refers to proton bosons. The operators N_ν and N_π count the number of neutron and proton quadrupole bosons, respectively,

$$N_\sigma = \sum_m d^\dagger_{m\sigma} d_{m\sigma} \quad ; \quad \sigma = \nu,\pi \quad , \tag{2}$$

where $d^\dagger_{m\sigma}(d_{m\sigma})$ creates (destroys) a quadrupole boson: $m = 2, 1, 0, -1, -2$; and $\sigma = \pi$ or ν. The energies ϵ_σ are the excitation energies of the quadrupole boson with respect to the monopole boson. This part of the Hamiltonian reflects pairing between like nucleons. The second part reflects the quadrupole interaction between neutrons and protons. The operator $Q_{m\sigma}$ is the quadrupole operator and is given by

$$Q_{m\sigma} = d^\dagger_{m\sigma} s_\sigma + s^\dagger_\sigma \tilde{d}_{m\sigma} + \chi_\sigma (d^\dagger_\sigma \tilde{d}_\sigma)^{(2)}_m \quad ; \quad \sigma = \pi,\nu \quad , \tag{3}$$

where $\tilde{d}_m = (-1)^m d_{-m}$ and $s^\dagger(s)$ creates (destroys) a monopole pair. The quadrupole transition operator is

$$T_m = \sum_{\sigma=\pi,\nu} e^B_\sigma Q_{m\sigma} \quad . \tag{4}$$

where e^B_σ is the boson effective charge.

The quadrupole operator in Eq. (3) has two parts. The first changes a monopole boson into a quadrupole boson, and the second reorients the quadrupole boson. The attractive ($\kappa > 0$) quadrupole interaction reflects the neutron-proton quadrupole interaction, with the monopole-changing component producing deformed nuclei. Hence, the pairing interaction and the quadrupole interaction compete with each other. As neutrons are added to a given nucleus, the role of the proton-neutron interaction becomes more important and mixes more quadrupole bosons into the low-lying spectrum, inducing deformation.

The samarium isotopes illustrate this effect very well. The isotope ^{144}Sm is semimagic, having the neutron shells closed at magic number 82 and having no valence neutrons. The excitation energy of the first $J^\pi = 2^+$ is 1660 keV. As neutrons are added, the number of interactions between valence neutrons and protons increases, resulting in a decrease of the $J^\pi = 2^+$ excitation energy to 73 keV in ^{158}Sm.

Figure 2 shows this dramatic drop in excitation energy. Furthermore, since the pairing interaction favors pairs of protons coupled to angular momentum 0, or monopole pairs, the lowest $J^\pi = 4^+$ state in ^{144}Sm is primarily composed of monopole proton pairs, with one pair coupled to $J^\pi = 4^+$.

However, the IBM does not have such a state in its space. The only way to produce a $J^\pi = 4^+$ in the IBM space is to have two quadrupole pairs couple to angular momentum $J^\pi = 4^+$. Such a state has two broken monopole pairs; hence in a semimagic nucleus these will lie higher in energy than the one broken-pair state. However, the implicit assumption in the IBM is that the quadrupole interaction lowers the energy of the state with the quadrupole pairs more than that of the states with pairs with higher angular momentum.

In Fig. 2, calculated results are shown that illustrate this point. A schematic fermion model was used that has an SO_6 dynamical symmetry,[9] but otherwise has many features in common with the IBM-2. With only three

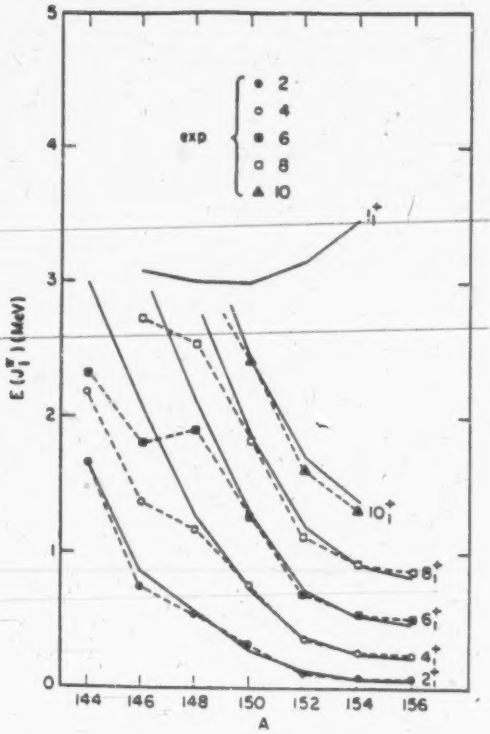

Fig. 2.
Excitation energy for some low-lying states in the samarium isotopes vs mass number. The solid lines are calculated (Ref. 9), the symbols are empirical.

parameters, the dramatic decrease in energy for the yrast levels is reproduced for the isotopes $^{148\text{-}156}$Sm. However, for the lighter isotopes the calculated levels with $J > 2$ rise much higher than the measured excitation energy.

As suggested in the previous paragraphs, the explanation for this is that for the isotopes with neutron number close to magic, the pairing interaction favors states with the fewest broken pairs. Hence the $J^\pi = 4^+$ state, for example, with one $J^\pi = 4^+$ pair, will lie lower in energy than the $J^\pi = 4^+$ state with two quadrupole pairs. Thus the $J^\pi = 4^+$ state in the IBM space, which must have at least two quadrupole pairs, will rise in energy as the nucleus becomes more nearly singly magic. Investigations are under way[10] to determine whether medium-energy scattering to high momentum transfer can help sort out these different parts of the nuclear wave function and thereby test this basic premise of the IBM.

The first $J^\pi = 1^+$ state that is predicted by this model is also plotted in Fig. 2, although experimentally no such state has yet been detected. This state is of special interest because within IBM-1 it cannot exist. This follows from the fact that identical quadrupole bosons cannot couple to angular momentum $J^\pi = 1^+$, which is obvious for two quadrupole bosons, but it turns out to be true no matter what the number of identical quadrupole bosons. However, for nuclei with neutron and proton quadrupole bosons that are active, such a state is possible. For ^{144}Sm, which has only valence protons, we see that this state does not exist, but as neutrons are added, this state appears at about 3 MeV in excitation energy. This energy prediction is a by-product of the model. Recently such a $J^\pi = 1^+$ state has been observed in electron scattering in the neighboring $^{156}_{64}$Gd nucleus at an excitation energy of about 3 MeV.[11] These types of neutron-proton excitations are of interest to probe further.

Microscopic Basis of IBM

As we stated in the Introduction, the IBM is an approximation to the nuclear shell model. How, then, do we produce a boson Hamiltonian and transition operators from a fermion Hamiltonian and transition operators?

This question is actually an old one in nuclear physics and was originally stimulated by the quadrupole vibrator model. However, there has not been a satisfactory resolution of this problem. The most difficult point is to determine the coordinate-space wave function of the monopole and quadrupole bosons. The reason for the difficulty is that this wave function varies with mass number because the renormalization effects due to the Pauli principle and the excluded pair and core excitations vary with mass number.

For nuclei near closed shells there has been some success. The procedure here is to diagonalize the shell-model Hamiltonian in the two-nucleon space and to take as the collective monopole and quadrupole pair the lowest $J^\pi = 0^+$ and 2^+ pairs. The boson Hamiltonian and transition operators are then determined by calculating matrix elements of the fermion Hamiltonian and transition operators in the subspace of fermion states with only monopole and quadrupole pairs. These matrix elements are then equated to the corresponding boson matrix elements. Since a transition operator is at most a one-boson operator, only the matrix elements with at most one quadrupole pair need be mapped, whereas for the Hamiltonian, only the matrix elements with at most two quadrupole pairs need to be mapped.[12-14] This method is called the OAI method, using the initials of the original authors[12] (the first initial belongs to Takaharu Otsuka, at present a postdoctoral fellow in T-5, who continues to pursue the microscopic understanding of the IBM).

For highly deformed nuclei there also has been some success.[15] In this case the collective pair is determined by a Hartree-Fock-Bolgolubov minimization of the fermion Hamiltonian. Because the nucleus is deformed, this pair will be an admixture of different angular momenta. About 90% of the pair is made up of a $J^\pi = 0^+$ and $J^\pi = 2^+$ pair, with the remaining 10% being a $J^\pi = 4^+$ pair.[16] The matrix elements between many collective fermion pairs are then set equal to the matrix elements between many collective bosons, with the collective boson having the same angular-momentum composition as the collective fermion pair. The effects of the $J^\pi = 4^+$ boson, or g boson, are removed by renormalizing the resulting boson Hamiltonian and transition operators.

Using this procedure, the parameters of the boson Hamiltonian [Eq. (1)] and transition operator [Eq. (4)] are determined for the nucleus ^{158}Gd (Ref. 15). The microscopic results are given in Table I. Phenomenological parameters determined by fitting spectra and transition rates of ^{158}Gd are listed in the fourth column. We see that agreement between the microscopic and phenomenologically determined parameters is very good. The last column gives the parameters determined by the OAI method, valid near spherical nuclei but invalid for a deformed nucleus like ^{158}Gd. In fact, the parameters derived by the OAI method do not produce a stable equilibrium deformation because the absolute magnitudes of χ_π and χ_ν are too small. The third column gives the

Table I. Parameters in the Boson Quadrupole Interaction and in the Boson $E2$ Operator for ^{158}Gd. The second column shows calculations obtained using the mapping method described in the text with renormalization resulting from the elimination of the g boson; the unrenormalized result is shown in the next column in parentheses. Parameters obtained by a phenomenological calculation and those by the OAI method are also shown (from Ref. 15).

Parameter	Microscopic Calculation	Unrenormalized Result	Phenomenological Parameters	OAI Method
κ (MeV)	0.094	(0.12)	0.08 ~ 0.09	0.19
χ_π	−0.86	(−0.80)	−0.8 ~ −0.9	0.04
χ_ν	−1.18	(−1.03)	−1.1 ~ −1.2	−0.55
e_π^B (e-fm^2)	12.0	(10.6)	12 ~ 14	14.3
e_ν^B (e-fm^2)	10.0	(6.7)	12 ~ 14	8.4

results before renormalization. In each case the renormalization improves agreement, but is not too large a correction—less than 35% for all parameters.

The difficult task is to handle the transitional nuclei, those between spherical and deformed. The search for a unified mapping procedure continues.

Transition Densities

The range of momentum transfer involved in medium-energy electron and proton scattering provides a tool for probing the nuclear transition density. Within the IBM, the quadrupole transition density operator is a generalization of the transition operator given in Eq. (4):

$$\hat{T}_m(r) = \sum_{\text{pairs } \nu} [\alpha_\nu(r)\,(d^\dagger_m s_\nu + s^\dagger_\nu \tilde{d}_m) + \beta_\nu(r)\,(d^\dagger_\nu \tilde{d}_\nu)^{(2)}_m] \quad . \tag{5}$$

The boson wave transition densities $\alpha_\nu(r)$ and $\beta_\nu(r)$ can be determined phenomenologically or from a microscopic theory.

Recently the $0^+_g \rightarrow 2^+_1$ transition densities for $^{134}_{56}Ba_{78}$, $^{138}_{56}Ba_{82}$, and $^{124}_{50}Sn_{74}$ were measured in electron scattering.[17] The nucleus $^{138}_{56}Ba_{82}$ has a closed neutron shell, hence the density is due primarily to the valence protons. Furthermore, since it is singly magic, the ground state is primarily monopole bosons. Hence the matrix element of $(d^\dagger_\nu \tilde{d}_\nu)^{(2)}_m$ to the first $J^\pi = 2^+$ state will vanish. Therefore the transition density will depend predominantly on $\alpha_\nu(r)$. Consequently, this function can be determined phenomenologically. Likewise, $\alpha_\nu(r)$ can be determined from the transition density for $^{144}_{50}Sn_{74}$.

Because $^{132}_{56}Ba_{76}$ has both valence neutrons and protons, it is more complicated than either ^{138}Ba or ^{124}Sn, but the wave functions have been determined in IBM-2 (Ref. 6). To determine the transition density for ^{134}Ba, we need to know $\beta_\nu(r)$. It turns out, however, that the matrix elements of $(d^\dagger_\nu \tilde{d}_\nu)^{(2)}_m$ between 0^+_g and 2^+_1 is 1% or less of the matrix element of $s^\dagger \tilde{d}_m + d^\dagger_m s$ between these two states.[17] Hence the transition density will not be sensitive to β_ν.

Ignoring β_ν, we can determine the transition density of ^{134}Ba from the phenomenologically determined α_ν and the IBM-2 wave functions. Of course we must assume that the structure of the monopole and quadrupole pair does not change appreciably between ^{138}Ba (^{134}Sn) and ^{134}Ba. In Fig. 3 the empirical transition density is given by the hatched line, where the hatches measure the uncertainty in experimental analysis. The solid line is the IBM-2 transition density, determined by combining the phenomenologically determined α_ν's and the IBM-2 wave functions. On the surface the measured and IBM-2 transition densities overlap and are undistinguishable.[17]

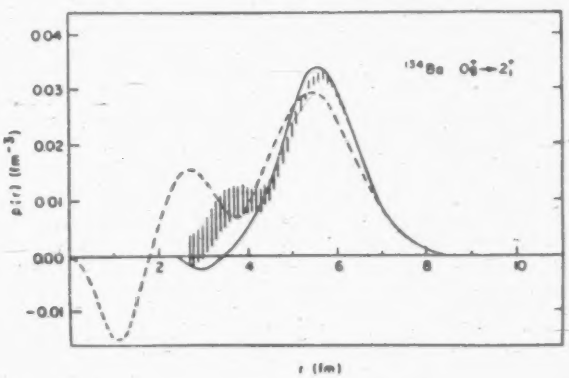

Fig. 3.
The transition density $p(r)$ for the $0^+_g \rightarrow 2^+_1$ transition in ^{134}Ba. The hatched line is the empirical transition density, the solid line is the phenomenological IBM-2 density, and the dashed line is the microscopic IBM-2 density, as explained in the text.

In the interior region there seems to be some disagreement. However, since the phenomenologically determined $\alpha_\sigma(r)$ is less certain in the interior, the extent of real disagreement is unclear. Further, since the IBM-2 transition density becomes small for $r \sim 3.5$ fm, the neglected effects such as β_σ and renormalization of α_σ may be important. Although not shown on the curve, the Tassie transition density extends further out on the surface, in disagreement with the empirical transition density.

The functions $\alpha_\sigma(r)$ can be determined microscopically as well. The structure of the monopole pair has been determined from a BCS calculation for both ^{124}Sn and ^{138}Ba within one major shell using harmonic oscillator wave functions. The quadrupole pair is determined by operating on the monopole pair with the (fermion) quadrupole operator.[17] The result is given by the dashed line in Fig. 3. The microscopic result is shifted to a lower radius than that of the empirical transition density (hatched line). However, core polarization was neglected in the microscopic transition density; this could reduce the wiggles. Improved calculations are under way in which core polarization and more realistic single-nucleon wave functions can be included in the microscopic transition density.*

Glauber Approximation and IBM

Because the interaction of electrons with nuclei is weak, medium-energy electron scattering can be analyzed using the distorted-wave Born approximation (DWBA). For hadronic probes this is not necessarily the case. For 800-MeV protons, multiple scattering is important at high momentum transfer.[18,19] One approach for taking multiple scattering into account is to solve a set of coupled-channel equations.[18] Another approach is to calculate the transition matrix to all orders in the Glauber approximation.[20] Although the physics content of these two approaches is similar, the Glauber approximation gives more insight and is numerically simpler.[19]

For a strongly deformed nucleus such as ^{154}Sm, the Bohr-Mottelson model can be used to evaluate the Glauber transition matrix to all orders.[19] In Fig. 4 the results of this calculation are shown for 800-MeV proton elastic and inelastic scattering from ^{154}Sm (solid line) and

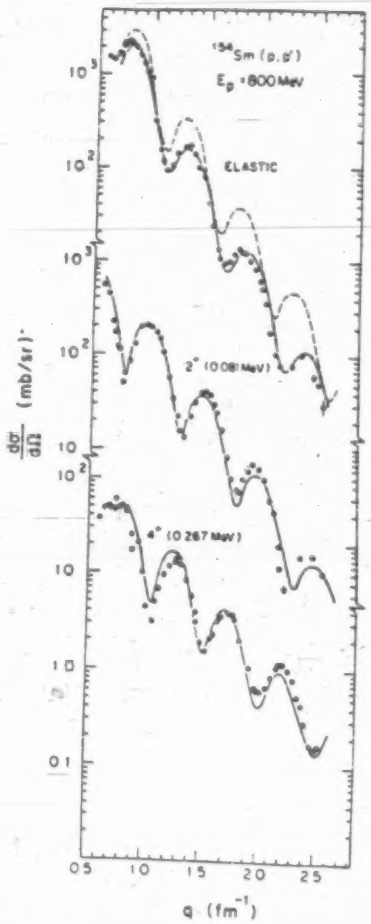

Fig. 4.
The differential cross section vs momentum transfer for 800-MeV proton elastic and inelastic scattering from ^{154}Sm. The dots are the data (Ref. 18), the solid line is the Glauber approximation using a deformed density (Ref. 19), and the dashed line is the distorted-wave approximation to the elastic scattering.

*T. Otsuka, private communication.

are compared to the experimental data.[18] The agreement is very good. The dashed line shows the DWBA prediction for elastic scattering. One sees the inadequacy of the DWBA in reproducing the phase and amplitudes of the differential cross section at high momentum transfer.

Recently we have realized that the Glauber approximation can be combined with the IBM such that the transition matrix can be evaluated to all orders in closed form.[10] This combination arises from the fact that the Glauber transition operator is a linear rotation in the IBM space. For example, if the incoming projectile has a quadrupole interaction with the target, the Glauber transition matrix for scattering a projectile with momentum $\vec{k}$ to $\vec{k}'$ with resulting momentum transfer,

$$\vec{q} = \vec{k}' - \vec{k} \quad , \tag{6a}$$

is

$$\langle f|T|i\rangle = \frac{k}{2\pi i}\int d^2b \;\; e^{i\vec{q}\cdot\vec{b}}\,(U_{fi}^{(\pi)}U_{fi}^{(\nu)} - \delta_{fi}) \quad , \tag{6b}$$

where

$$U_{fi}^{(\sigma)} = e^{i\eta_\sigma} M_{fi}^{(\sigma)} \tag{6c}$$

and the reduced transition matrix is

$$M_{fi}^{(\sigma)} = \langle f_\sigma | e^{i\psi_\sigma C^{(2)}(\vec{b})\cdot Q_\sigma} | i_\sigma \rangle \quad . \tag{6d}$$

In the above, f and i label the final and initial states, respectively. Denoting the positon of the incoming projectile as $\vec{r}$, the two-dimensional impact radius $\vec{b}$ is

$$\vec{r} = \vec{b} + k\hat{z} \quad , \tag{7}$$

where $\hat{k}$ is the unit vector of the projectile momentum. Within an optical-model approximation, the Glauber phases are

$$\eta_\sigma = \frac{2\pi f_\sigma}{k}\int_{-\infty}^{\infty} \rho_\sigma[(b^2+z^2)^{1/2}]\,dz \quad , \tag{8a}$$

$$\psi_\sigma = \frac{2\pi f_\sigma g_\sigma}{k}\int_{-\infty}^{\infty} \frac{r\,d\rho_\sigma}{dr}\,dz \quad , \tag{8b}$$

where f_σ is the forward-scattering amplitude of the projectile and proton ($\sigma = \pi$) or neutron ($\sigma = \nu$); g_σ is the quadrupole coupling strength between the projectile and target nucleon; $C_m^{(\ell)}(\hat{b})$ is the projectile unit spherical tensor of rank ℓ,

$$C_m^{(\ell)}(\hat{b}) = \left(\frac{4\pi}{2\ell+1}\right)^{1/2} Y_m^{(\ell)}(\hat{b}) \quad , \tag{9}$$

and $\rho_\sigma(r)$ is the proton ($\sigma = \pi$) or neutron ($\sigma = \nu$) matter density.

Because the operator in the matrix element [Eq. (6d)] is an exponential function of the boson quadrupole operator [Eq. (3)], this operator has the effect of rotating the bosons in the initial nuclear wave function into those of the final nuclear wave function. For the example of a quadrupole vibrator, this transition matrix from the ground state can be simply derived.[10]

The ground state of the quadrupole vibrator is a boson condensate of N monopole bosons, where N is one-half the number of valence nucleons. Excited states are labeled by the number n of quadrupole bosons, or "phonons," with the energy of the states increasing approximately linearly with n. For a given n there is a multiplet of states, with the quantum number τ designating the number of quadrupole bosons not coupled, in pairs, to angular momentum 0, the quantum number n_Δ designating the number of quadrupole bosons coupled in triplets to angular momentum 0, and of course the angular momentum J and its projection M. The allowed values of these quantum numbers are

$$\tau = n \;,\quad n-2 \;,\quad \ldots \;, \text{ and finally 1 or 0} \quad , \tag{10a}$$

and for each τ the allowed angular momenta and n_Δ are determined by all possibilities of partitioning τ,

$$\tau = 3n_\Delta + \lambda \quad , \tag{10b}$$

where n_Δ and λ are integers. Then the allowed J are

$$J = 2\lambda \ , \ 2\lambda - 2 \ , \ 2\lambda - 3 \ , \ \ldots \ , \ \lambda \ . \tag{10c}$$

The reduced transition matrix for scattering from the initial ground state ($n = \tau = n_\Delta = J = M = 0$) to an excited final state with quantum numbers n, τ, n_Δ, J, M is

$$M_{fi}^{(\sigma)} = \left[\frac{N!(2\tau+3)!!}{(N-n)!(n+\tau+3)!!(n-\tau)!!} \right]^{1/2} \times e^{iN\tilde{\chi}_\sigma} W_\sigma^{(N-n)} X_\sigma^n A_{\tau n_\Delta J} C_M^{(J)}(\hat{b})^* \quad . \tag{11}$$

where $A_{\tau n_\Delta J}$ is a constant that is independent of the Glauber phase ψ_σ. The functions W, X are

$$W_\sigma = \cos\psi_\sigma [1+\tilde{\chi}_\sigma^2]^{1/2} - \frac{i\tilde{\chi}_\sigma}{[1+\tilde{\chi}_\sigma^2]^{1/2}} \sin\psi_\sigma [1+\tilde{\chi}_\sigma^2]^{1/2} \quad , \tag{12a}$$

$$X_\sigma = i \frac{\sin\psi_\sigma [1+\tilde{\chi}_\sigma^2]^{1/2}}{[1+\tilde{\chi}_\sigma^2]^{1/2}} \quad , \tag{12b}$$

and

$$\tilde{\chi}_\sigma = -\left(\frac{1}{14}\right)^{1/2} \chi_\sigma \quad . \tag{12c}$$

The coefficients $A_{\tau n_\Delta J}$ are given in Table II for the lowest values of τ.

In Fig. 5 an example of the elastic differential cross section for the scattering of 800-MeV protons from a vibrational nucleus is shown as a function of the momentum transfer. The solid line is the differential cross section given by the transition matrix of Eq. (11), which includes all the multiple scattering. The dashed line does not include the multiple scattering but is the DWBA elastic differential cross section. We see that for high momentum transfer the higher order multiple scattering makes a substantial difference even in the elastic channel, particularly in the phase relationship between maxima and minima.

Table II. Coefficients $A_{\tau n_\Delta J}$ for the Lowest Values of τ.

τ	n_Δ	J	A
0	0	0	1
1	0	2	1
2	0	2	$-[1/7]^{1/2}$
2	0	4	$[9/35]^{1/2}$
3	0	6	$[3/77]^{1/2}$
3	0	4	$-(1/7)[6/5]^{1/2}$
3	0	3	0
3	1	0	$-[1/105]^{1/2}$

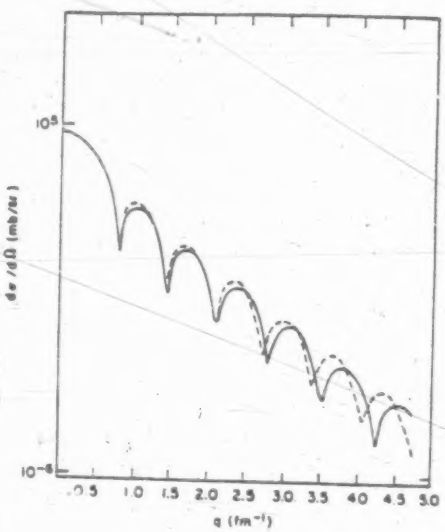

Fig. 5.
The differential cross section vs momentum transfer for 800-MeV proton scattering from a typical quadrupole vibrator in the Glauber approximation (Ref. 10). The dashed line is the distorted-wave approximation to the elastic scattering.

Summary

Because medium-energy projectiles can probe the nucleus at high momentum transfer, detailed information about static and transition densities can be determined. The IBM gives a framework to study these derived densities both phenomenologically and microscopically. Of particular interest is the transition from spherical to deformed nuclei. Furthermore, because of the algebraic nature of the IBM, multiple scattering in the Glauber approximation, which becomes important at high momentum transfer, can be treated exactly to all orders.

Also, because medium-energy probes have varieties of electromagnetic and hadronic charge, the neutron and proton static and transition densities can be disentangled. These neutron and proton degrees of freedom can be analyzed in IBM-2.

Although in this review we have restricted ourselves to even-even nuclei, odd nuclei can be studied in a similar manner in the interacting boson-fermion model.[21]

REFERENCES

1. A. Arima and F. Iachello, Ann. Rev. Nucl. Part. Sci. 31, 75 (1981).
2. J. N. Ginocchio and M. W. Kirson, Nucl. Phys. A 350, 31 (1980).
3. D. D. Warner, R. F. Casten, and W. F. Davidson, Phys. Rev. C 24, 1713 (1981).
4. O. Scholten, "A Phenomenological Study of Even-Even Nuclei in the Neutron-Proton IBM," in *Interacting Bosons in Nuclei*, F. Iachello, Ed. (Plenum Press, New York, 1979), pp. 17-35.
5. P. van Isacker and G. Puddu, Nucl. Phys. A 348, 125 (1980).
6. G. Puddu, O. Scholten, and T. Otsuka, Nucl. Phys. A 348, 109 (1980).
7. R. Bijker, A. E. L. Dieperink, O. Scholten, and R. Spanhoff, Nucl. Phys. A 344, 207 (1980).
8. B. R. Barrett and P. D. Duval, "Recent IBM-2 Calculations," in *Interacting Bose-Fermi Systems in Nuclei*, F. Iachello, Ed. (Plenum Press, New York, 1981), pp. 47-52.
9. A. Arima, J. Ginocchio, and N. Yoshida, Nucl. Phys. A 384, 112 (1982).
10. J. N. Ginocchio, in the Proc. of the Workshop on Nuclear Collective States, Suzhow University, China, L. M. Yang, G. O. Zhou, S. S. Wu, Z. Q. Zhou, and D. H. Feng, Eds., (1983); Los Alamos National Laboratory document LA-UR-83-3638; and to be published in a special issue of Nucl. Phys. A (1984).
11. A. Richter, in the Proc. of the Int. Conf. on Nuclear Physics, Florence, Italy (1983), Vol. 2.
12. T. Otsuka, A. Arima, and F. Iachello, Nucl. Phys. A 309, 1 (1978).
13. T. Otsuka, Phys. Rev. Lett. 46, 710 (1981).
14. S. Pittel, P. D. Duval, and B. R. Barrett, Ann. Phys. 144, 168 (1982).
15. T. Otsuka, Los Alamos National Laboratory document LA-UR-83-1744, to be published in Phys. Lett. (1984).
16. T. Otsuka, A. Arima, and N. Yoshinaga, Phys. Rev. Lett. 48, 387 (1982).
17. T. Otsuka, K. Mori, Y. Mizuno, T. Terasawa, and Y. Torizuka, "Test of the Interacting Boson Model by Inelastic Electron Scattering for the 2^+ State of ^{134}Ba," to be published in Phys. Lett. (1984).
18. M. L. Barlett, J. A. McGill, L. Ray, M. M. Barlett, G. W. Hoffman, N. M. Hintz, G. S. Kyle, M. A. Franey, and G. Blanpied, Phys. Rev. C 22, 1168 (1980).
19. R. D. Amado, J. A. McNeil, and D. A. Sparrow, Phys. Rev. C 23, 13 (1982).
20. R. J. Glauber, "High-Energy Collision Theory," in *Lectures in Theoretical Physics*, Vol. 1, W. E. Britin and L. G. Dunham, Eds. (Interscience Publishers, Inc., New York, 1959), pp. 315-414.
21. F. Iachello, "Present Status of the Interacting Boson-Fermion Model," in *Interacting Bose-Fermi Systems in Nuclei*, F. Iachello, Ed. (Plenum Press, New York, 1981), pp. 273-283.

Implications of Using Approximate Chiral-Dynamics $\pi N \to \pi\pi N$ Amplitude in the Calculation of $A(\pi,2\pi)$ Cross Sections

R. S. Bhalerao and L.-C. Liu (Los Alamos)

We have completed a study of the relative importance of the diagrams contributing to the $\pi N \to \pi\pi N$ reaction in the framework of the Weinberg effective Lagrangian theory. Various approximate schemes in the recent literature used to calculate the $\pi N \to \pi\pi N$ amplitude and thus the $A(\pi,2\pi)$ cross sections have been found to be inadequate. Besides the total cross sections, we have studied for the first time the angular correlations of the outgoing pions and the energy spectrum of the outgoing nucleon in the $\pi N \to \pi\pi N$ reaction. A brief description of this investigation, which we think is of vital importance for theoretical interpretation of the $A(\pi,2\pi)$ experiments planned at LAMPF, is given here. (Details can be found in a paper, with the same title as this experiment, to be submitted to Phys. Rev. C.)

For definiteness, we consider the reaction

$$\pi^-(Q) + p(p_i) \to \pi^+(q_1) + \pi^-(q_2) + n(p_f) \quad , \qquad (1)$$

with the four-momenta of the respective particles written in parentheses. The invariant amplitude T for this reaction, which can be calculated using Weinberg's effective Lagrangian[1,2] in the lowest order perturbation theory, and has the form[3]

$$T = T^{(1)} + T^{(2)} + T^{(3)} + T^{(K)} \quad . \qquad (2)$$

$T^{(1)}$ is composed of the pion-pole term and the contact term. $T^{(2)}$ and $T^{(3)}$ are the so-called two- and three-point diagrams with one- and two-nucleon propagators, respectively. $T^{(K)}$ is the anomalous magnetic-moment term. Various approximations to the above amplitude have been proposed in the literature. We describe them briefly in the following paragraphs.

Olsson and Turner[2] (OT) have neglected the contributions of $T^{(3)}$ and $T^{(K)}$ and have calculated $T^{(1)}$ and $T^{(2)}$ in the threshold approximation defined by $q_1 = q_2 = (m_\pi, \vec{0})$, $p_f = (m_N, \vec{0})$, $Q = Q_{thr}$, and $p_i = p_{i\,thr}$. They have made this approximation also in the invariant phase space and have calculated $\pi N \to \pi\pi N$ cross sections up to $T_\pi = 300$ MeV.

Rockmore[4] (R1) has neglected $T^{(2)}$, $T^{(3)}$, and $T^{(K)}$ and has calculated $T^{(1)}$ and the invariant phase space in the threshold approximation defined above. He has used this procedure to calculate $A(\pi,2\pi)$ cross sections up to $T_\pi = 290$ MeV.

Recently, Rockmore[5] (R2) has neglected $T^{(2)}$, $T^{(3)}$, $T^{(K)}$, and the contact term in $T^{(1)}$, made the threshold approximation, and thus calculated $A(\pi,2\pi)$ cross sections up to $T_\pi = 280$ MeV.

Eisenberg and Cohen[6] (EC) retained the contributions of $T^{(1)}$ and $T^{(2)}$, made the threshold approximation, and used the center-of-mass amplitude in the laboratory frame to calculate the $A(\pi,2\pi)$ cross sections.

In spite of the diversity of these approximations, we note that as soon as the threshold approximation is invoked, the amplitude T becomes independent of the energy and momentum of the particles in the final state. As a consequence, these different approximate calculations differ from each other and from the phase space only by constant multiplicative factors. That is to say, they all have the same energy and angular dependence as that predicted by the phase space.

Figures 1 and 2 show the relative importance of the various terms in Eq. (2), with and without the threshold approximation. It is evident from Fig. 1 that even at $T_\pi = 190$ MeV the contact term and $T^{(2)}$ are far from negligible with respect to the pion-pole term. $T^{(3)}$, however, is relatively less important until $T_\pi \sim 240$ MeV; $T^{(K)}$ is negligible over the entire energy region considered.

It is clear from Fig. 2 that even in the near-threshold region there are sizable differences among the exact and the approximate curves. The relatively close agreement of the curve labeled R2 with the low-energy data is somewhat fortuitous in that this curve is based on the most extreme of the approximations—that which neglects all but the pion-pole term in Eq. (2).

The remaining curves tend to underestimate the exact theoretical cross sections significantly. Considering that the exact theoretical cross sections in turn are much smaller than the experimental data, the approximate amplitudes for $\pi N \to \pi\pi N$ (except R2), when used in the calculation of $(\pi,2\pi)$ cross sections on nuclei, tend to underestimate the $A(\pi,2\pi)$ data, in some cases by an order of magnitude. Results in Refs. 4-6 should be viewed in light of these remarks. (Incidentally, our remark above concerning the essential phase-space nature of the calculations in Refs. 2 and 4-6 is borne out by Fig. 2.)

It has been suggested in Ref. 6 that the existence of pion condensation precursor phenomena would enhance the $A(\pi,2\pi)$ cross sections considerably above what would be observed otherwise, and that such an enhancement could provide partial evidence in support of such

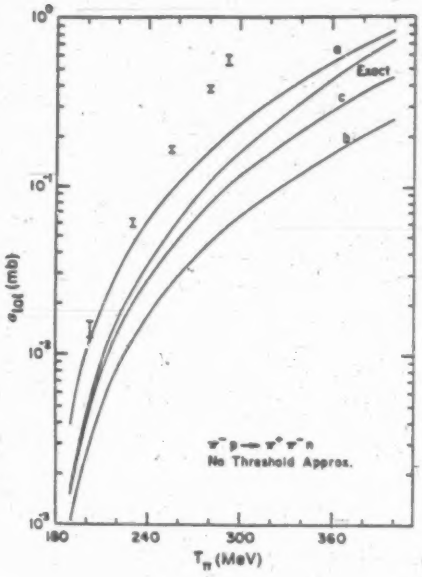

Fig. 1.
Total cross section for the reaction $\pi^- p \to \pi^+ \pi^- n$ as a function of the incident pion kinetic energy in the lab frame. The curve based on the full amplitude [Eq. (2)] is labeled *Exact*. The remaining curves include only some of the terms: (a) pion-pole term, (b) $T^{(1)}$, and (c) $T^{(1)} + T^{(3)}$. The curve based on $T^{(1)} + T^{(2)} + T^{(3)}$ is practically indistinguishable from the exact curve and hence is not shown. Experimental data are from Ref. 7.

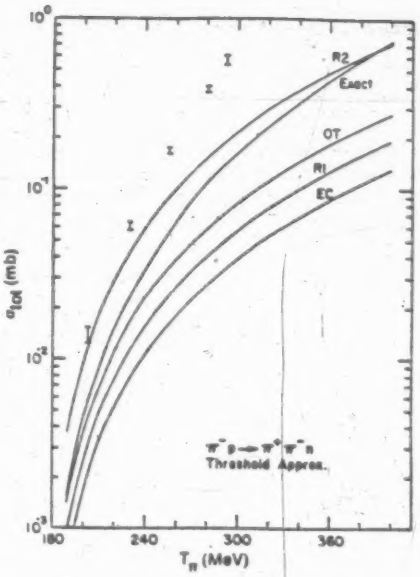

Fig. 2.
Total cross section for the reaction $\pi^- p \to \pi^+ \pi^- n$ as a function of the incident pion kinetic energy in the lab frame. Curve labeled *Exact* is the same as in Fig. 1. The remaining curves represent the four approximate schemes described in the text: OT (Ref. 2), R1 (Ref. 4), R2 (Ref. 5), and EC (Ref. 6). Experimental data are from Ref. 7.

phenomena. However, it is evident from the inspection of curves EC and *Exact* in Fig. 2 that a similar large enhancement can be achieved by simply making an exact calculation of the $\pi N \to \pi\pi N$ amplitude. Interpretation of future $A(\pi,2\pi)$ data will have to bear this in mind.

In Figs. 3 and 4 we present our results for the energy spectrum of the outgoing neutron for fixed directions of the outgoing pions (chosen to be $\theta_{\pi^+} = \theta_{\pi^-} = 35°$, $\phi_{\pi^+} = 0°$, $\phi_{\pi^-} = 180°$) and for angular correlations of the outgoing pions. These results are compared with those obtained using the approximate scheme of Eisenberg and Cohen.[6] Results based on other approximate schemes—namely R1, R2, OT, and the phase-space distribution—will be identical in shape, differing only in size. In this respect, these theories have only a minimal dynamical content. Obviously, the exact and approximate curves in Figs. 3 and 4 are quite different in shape and size.

In this work we paid particular attention to the various approximate schemes in the recent literature used to calculate the $\pi N \to \pi\pi N$ amplitude. We did not consider other approximations that the authors of Refs. 4-6 have made in the calculation of $(\pi,2\pi)$ cross sections on nuclei—for example, neglect of the off-shell behavior of the basic production amplitude. In fact, the expressions for T used in Refs. 4-6 are valid only if all the external particles are on-mass shell, which is not the case if the reaction takes place in a nuclear medium. Moreover, unlike the fully on-shell case, the off-shell amplitude can be singular.

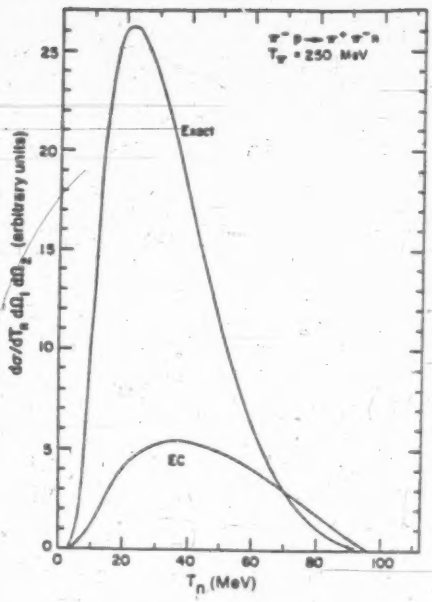

Fig. 3.
Energy spectrum of the outgoing neutron in the reaction $\pi^- p \to \pi^+ \pi^- n$ in the lab frame, directions of the outgoing pions being fixed ($\theta_{\pi^+} = \theta_{\pi^-} = 35°$, $\phi_{\pi^+} = 0°$, $\phi_{\pi^-} = 180°$). The curve labeled *Exact* represents an exact calculation that includes all the terms in Eq. (2). Curve EC is based on the Eisenberg-Cohen (Ref. 6) approximate procedure.

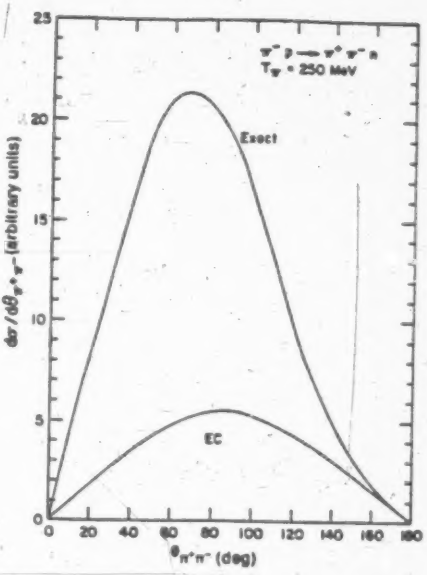

Fig. 4.
Angular correlations of the outgoing pions in the reaction $\pi\pi^- p \to \pi^+ \pi^- n$ in the lab frame. Meaning of the curves is the same as in Fig. 3.

In summary, the following comments can be made.

1. Contributions made by the contact term and $T^{(2)}$ to the total cross section are far from negligible compared with the contribution of the pion-pole term.

2. With the exception of the curve labeled R2 (Fig. 2), approximate calculations of $\pi N \to \pi\pi N$ cross sections tend to greatly underestimate the exact theoretical cross sections. Disagreement between the approximate calculations and the experimental data is even more marked. The curve R2 is based on the most extreme approximation—all terms but the pion-pole term in Eq. (2) are neglected. Hence we regard its better agreement with the experimental data as fortuitous.

3. Approximate schemes described above have only a minimum dynamical content in that their predictions differ from the phase-space prediction only by a multiplicative constant.

4. Cross sections for the $A(\pi.2\pi)$ reaction predicted in the literature suffer from these drawbacks. In particular, if the existence of the pion condensation precursor phenomena is to be tested in $A(\pi.2\pi)$ reactions, the calculation of the basic $\pi N \to \pi\pi N$ amplitude will have to be done more accurately than has been reported in the literature. Otherwise, the importance of the precursor phenomena, if they exist at all, would be overestimated because they will be required to simulate the greater strength of the exact theoretical cross sections relative to the approximate[4-6] theoretical cross sections.

5. Angular correlations of the outgoing pions and the energy spectrum of the outgoing neutron calculated in the exact theory and with the approximate schemes of Refs. 4-6 differ significantly in size and shape, indicating the additional inadequacies of the latter calculations.

REFERENCES

1. S. Weinberg, Phys. Rev. Lett. 18, 188 (1967).
2. M. G. Olsson and L. Turner, Phys. Rev. Lett. 20, 1127 (1968).
3. R. A. Arndt et al., Phys. Rev. D 20, 651 (1979).
4. R. Rockmore, Phys. Rev. C 11, 1953 (1975).
5. R. Rockmore, Phys. Rev. C 27, 2150 (1983).
6. J. M. Eisenberg, Phys. Lett. 93B, 12 (1980); J. Cohen and J. M. Eisenberg, Nucl. Phys. A 395, 389 (1983), and Nuovo Cimento 76A, 488 (1983); and J. Cohen, J. Phys. G 9, 621 (1983).
7. C. W. Bjork et al., Phys. Rev. Lett. 44, 62 (1980).

Report of the T-5 Theoretical Group

T. Goldman (Los Alamos)

This is a brief summary of some of the T-5 research activities relevant to LAMPF and LAMPF II. Because this report is included in a basically experimental document, items of a primarily technical nature have been omitted.

While continuing their research role, T-5 staff members have invested a substantial amount of time and effort to further the LAMPF II project, including preparing for and running conferences and workshops, reporting at plenary sessions, and contributing to and editing the resulting proceedings. Major efforts included the Theoretical Symposium on Intense Medium-Energy Sources of Strangeness at the University of California, Santa Cruz, and the Third LAMPF II Workshop at Los Alamos. Material in the Santa Cruz[1] and Los Alamos[2] Proceedings is not repeated here. In addition, T-5 staff members have argued the physics justification for LAMPF II in public forums and in the LAMPF II proposal.

Research Related to LAMPF

We have made several developments in the code PIPROD. Motivated by the imminence of a number of experiments at LAMPF and elsewhere, we have extended PIPROD to calculate spin-transfer coefficients (Wolfenstein parameters, D_{LL}, etc.) that measure the dependence of the $NN \to NN\pi$ reaction on the spin directions of one initial and one final nucleon. We have numerically integrated exclusive cross-section predictions from PIPROD to produce inclusive cross sections and spin observables. Our parameter-free prediction (using only one-pion-exchange forces) for the polarized beam asymmetry in the reaction $\vec{p} + p \to p' + X$ is in good agreement with a recent HRS experiment. Our preliminary results on the spin-transfer coefficients for $\vec{p} + p \to \vec{n} + X$, however, do not agree so well with another recent experiment. This is perhaps an indication that a dibaryon resonance can show up in this particular spin observable but not in others.

We have also employed PIPROD to calculate the relative absorption rates of pions on a pair of (free) nucleons, using a relativistic isobar model for the coupled NN and $NN\pi$ systems that respects two- and three-body unitarity. In contrast with an earlier calculation that only considered $N\Delta$ intermediate states, we found that much of the absorption takes place through an intermediate state involving a nucleon and a (nonresonant) interacting pion-nucleon pair with the same quantum numbers as the nucleon. Moreover, this effect was able, for the first time, to explain qualitatively the order-of-magnitude changes in the proton-proton to proton-neutron suppression as the incident pion energy increases from zero (capture at rest) to above the Δ resonance. In general, for the inverse reaction $NN \to NN\pi$, this mechanism is rather unimportant compared with the $N\Delta$ state. Thus, the experimental investigation of two-nucleon pion absorption in light nuclei may clarify details of the weaker πN interactions. Much of our $NN\pi$ work is summarized in the preceding report in this section by R. Silbar.

Configuration-space, local-potential Faddéev calculations were extended to the Coulomb problem of elastic scattering of protons by deuterons at zero incident energy. We found that the spin-doublet scattering length a_2^{pd} was approximately zero. This differs substantially from (1) the accepted experimental value, (2) theoretical estimates using approximation schemes to combine Coulomb effects with known neutron-deuteron amplitudes to obtain a_2^{pd}, and (3) intuitive estimates based on the established linear relationship between the triton binding energy and the neutron-deuteron doublet scattering length. (The fact that the binding energy of ^{3}He is smaller than that of ^{3}H led people to expect that a_2^{pd} would be larger than $a_2^{nd} \cong 0.7$ fm.) However, the qualitative features of the Coulomb correction to the doublet scattering length are analogous to Coulomb corrections in the two-body scattering problem when the scattering length is small (as for pion-nucleon scattering). Thus, although novel, the results of our Faddéev calculations are *a posteriori* quite understandable.

Eikonal expansions were developed for the amplitudes in the scattering of Dirac particles (protons) by central scalar and vector potentials, and for the corresponding Schrödinger case with central and spin-orbit potentials. The eikonal phases were calculated through second-order corrections. Our motivation was to correlate the Dirac and Schrödinger approaches to proton-nucleus scattering, to develop systematically a practical formalism for calculation, and to provide insight into the scattering process. Recently, the Dirac phenomenology approach to optical potentials has given a more economical description of spin-dependent observables in medium-energy proton-nucleus scattering than the usual Schrödinger approach. Our analysis elucidates the simple physical reasons for this.

The $\pi^0 \rightarrow \mu^{\pm} e$ decays were investigated and an experimental upper limit of

$$\frac{1}{2}\,\frac{\Gamma(\pi^0 \rightarrow \mu^+ e^-) + \Gamma(\pi^0 \rightarrow \mu^- e^+)}{\Gamma(\pi^0 \rightarrow all)}$$

$$< 7 \times 10^{-8} \text{ (90\% confidence level)}$$

was deduced from available data. We also considered the existing constraints on the underlying muon-number-violating interaction. We found that the present experimental information on $\mu^- \rightarrow e^-$ conversion in sulfur implies an upper bound on the individual $\pi^0 \rightarrow \mu^{\pm} e$ branching ratios of about 10^{-13}.

Research Relevant to LAMPF II

Study of K^+-nucleus elastic scattering has been pursued. Comparison with the available data on ^{12}C and ^{40}Ca shows no conflicts with the scattering theory. We conclude that the goal of precision measurements of the nuclear density, as seen by a K^+, can be achieved as soon as accurate data on the fundamental K^+-nucleon system can be obtained.

A new investigation of the Λ lifetime in nuclear matter has been completed. The free decay $\Lambda \rightarrow \pi N$ is severely inhibited in nuclei because of Pauli blocking of the nucleon, and the weak nonleptonic transition $\Lambda N \rightarrow NN$ dominates the decay process. The long-standing discrepancy between the calculation of Adams ($\Gamma_{nm}/\Gamma_{free} = 0.06$) and the single experimental value for ^{16}O, which was determined by only 22 events ($\Gamma_{nm}/\Gamma_{free} = 3 \pm 1$), has been resolved; an incorrect coupling constant was used in the earlier theoretical investigation. Including model estimates of the effects of short-range correlations, tensor forces, and heavy-meson exchange in the weak interaction (in addition to one-pion exchange), and allowing for uncertainties in the various coupling constants and the vertex form factors, we estimate the ratio by $\log_{10}(\Gamma_{nm}/\Gamma_{free}) = 0 \pm 0.3$.

Detailed studies of the muon-number-violating decay modes of hyperons were carried out, both in a phenomenological framework and in considering some possible sources of muon-number violation. We find that branching ratios as large as 10^{-4} cannot be excluded by available data and that they are consistent with some extensions of the three-generation minimal (standard) electroweak model. However, such branching ratios require the muon-number-violating interaction to be of a very special structure.

The experimental limit of $d_n \lesssim 6 \times 10^{-25}$ e-cm for the electric-dipole moment of the neutron has ruled out some of the many theories proposed to explain the CP and T violation observed in kaon decays. We have demonstrated that many-body effects can lead to large enhancements of nuclear electric-dipole moments, which in certain cases fully compensate for the effects of atomic shielding; thus, the latter need no longer limit measurements of the proton electric-dipole moment d_p. The recent development of experimental techniques to measure atomic-dipole moments at levels well below the limit on d_n leads us to conclude that comparable stringent new limits on both d_n and d_p may be obtained with significant implications for predictions in the kaon system.

Anyone wishing further information on these subjects may contact Group T-5 members J. L. Friar, W. R. Gibbs, B. F. Gibson (Group Leader), J. N. Ginocchio, T. Goldman, W. C. Haxton, L. Heller, P. Herczeg, R. R. Silbar, or G. J. Stephenson, Jr. (Acting P-3 Group Leader).

REFERENCES

1. T. Goldman, H. E. Haber, and H. F.-W. Sadrozinski, Eds., *Intense Medium-Energy Sources of Strangeness*, University of California, Santa Cruz, 1983, AIP. Conf. Proc. No. 102. Particles and Fields Subseries No. 31 (American Institute of Physics, New York, 1983).

2. "Proceedings of the Third LAMPF II Workshop," Vols. I and II, Los Alamos National Laboratory report LA-9933-C (1983).

Group T-5 Publications

J. L. Friar, B. F. Gibson, and G. L. Payne, "Three-Nucleon Forces and Meson-Exchange Currents in the Trinucleon," Comments Nucl. Part. Phys. 11, 51 (1983).

J. L. Friar, "Classification of Exchange Currents," Phys. Rev. C 27, 2078 (1983).

J. L. Friar and E. L. Tomusiak, "Threshold Pion Photoproduction from the Trinucleon," Phys. Lett. 122B, 11 (1983).

J. L. Friar and B. H. J. McKellar, "Pion Exchange Contributions to the Lobashov Experiment," Phys. Lett. 123B, 284 (1983).

J. L. Friar, S. Fallieros, E. L. Tomusiak, D. Skopik, and E. G. Fuller, "Electric Polarizability of the Deuteron," Phys. Rev. C 27, 1364-1366 (1983).

J. L. Friar, "Three-Body Forces," Indiana University Cyclotron Facility (IUCF) Workshop on the Interaction Between Medium-Energy Nucleons in Nuclei—1982, H. O. Meyer, Ed., AIP Conf. Proc. 97, 378 (1983).

J. L. Friar, B. F. Gibson, and G. L. Payne, "The Proton-Deuteron Scattering Length," Phys. Lett. 124B, 287 (1983).

B. F. Gibson, C. B. Dover, G. Bhamati, and D. R. Lehman, "Binding Energy Estimates for Charmed Few-Body Systems," Phys. Rev. C 27, 2085 (1983).

B. F. Gibson, W. M. Kloet, G. J. Stephenson, Jr., and E. M. Henley, "Parity Nonconserving Asymmetry in Neutron-Deuteron and Proton-Deuteron Scattering," Phys. Rev. C 27, 2529 (1983).

J. L. Friar, B. F. Gibson, and G. L. Payne, "Configuration-Space Faddéev Calculations: VI. Triton Wave Function," Z. Phys. A 312, 169 (1983).

J. L. Friar, B. F. Gibson, and G. L. Payne, "Configuration-Space Faddéev Calculations: *pd s*-Wave Scattering Length," Phys. Rev. C 28, 983 (1983).

B. F. Gibson and D. R. Lehman, "Structure of the $^3H \rightarrow nd\,(d^*)$ Vertices," Los Alamos National Laboratory document LA-UR-83-2960 (to be published in Phys. Rev. C).

W. C. Haxton and E. M. Henley, "Enhanced T-Nonconserving Nuclear Moments," Phys. Rev. Lett. 51, 1937 (1983).

W. C. Haxton, "Double Beta Decay," Comments Nucl. Part. Phys. 11, 41 (1983).

W. C. Haxton, "Double Beta Decay," in the *McGraw-Hill 1984 Yearbook of Science and Technology*.

E. G. Adelberger, W. C. Haxton, M. M. Hindi, C. D. Hoyle, and R. D. Von Lintig, "The Beta Decays of ^{18}Ne and ^{19}Ne and their Relation to Parity Mixing in ^{18}F and ^{19}F," Phys. Rev. C 27, 2833 (1983).

G. A. Cowan, M. Goldhaber, and W. C. Haxton, "A Radiochemical Test of Double Beta Decay," Phys. Rev. C 28, 467 (1983).

W. C. Haxton and G. J. Stephenson, Jr., "A Comment on 'Nilsson-Pairing Model for Double Beta Decay,'" Phys. Rev. C 28, 458 (1983).

W. C. Haxton et al., "Neutron and Proton Transition Matrix Elements for ^{90}Zr from a Microscopic Analysis of 0.8-GeV Proton Inelastic Scattering," Phys. Rev. C 28, 294 (1983).

P. Herczeg and T. Oka, "Study of Muon-Number-Violating Hyperon Decays" (to be published in Phys. Rev. D, February 1984).

P. Herczeg and C. M. Hoffman, "Study of $\pi^0 \rightarrow \mu^{\pm}e$ Decays" (submitted to Phys. Rev. D).

Dean Preston and T. Goldman, "The Strangeness-Conserving Effective Weak Interaction in the Quark Basis," Nucl. Phys. B 217, 31 (1983).

T. Goldman and Dean Preston, "A Quark Model Calculation of the Weak Parity-Violating Asymmetry in High-Energy Proton-Nucleon Scattering," Nucl. Phys. B 217, 61 (1983).

R. R. Silbar and E. Piasetzky, "Isospin Dependence of Pion Absorption on Nucleon Pairs," Los Alamos National Laboratory document LA-UR-83-1883 (to be published in Phys. Rev. C).

R. R. Silbar and E. Piasetzky, "Ratio of Pion-Induced Nucleon Removal Cross Section Involving Charge Exchange," Phys. Rev. C 27, 894 (1983).

T. S. Bhatia, J. G. J. Boissevain, J. J. Jarmer, J. E. Simmons, G. Glass, J. C. Hiebert, R. A. Kenefick, L. C. Northcliffe, W. B. Tippens, R. R. Silbar, W. M. Kloet, and J. Dubach, "Analyzing Powers and Spin Correlations A_{NN} and A_{LL} for $pp \rightarrow np\pi^+$ at 650 and 800 MeV" (to be published in Phys. Rev. C).

J. N. Ginocchio, "A Class of Exactly Solvable Potentials: I. One-Dimensional Schrödinger Equation" (to be published in Ann. Phys. 152, 1984).

J. N. Ginocchio, "An SO_8 Model of Collectivity in Nuclei," in *Bosons in Nuclei*, D. H. Feng, M. Vallieres, and S. P. Hel. Eds. (World Scientific Publishers Press, Singapore, 1984).

W. R. Gibbs, J. Kogut, M. Stone, H. W. Wyld, J. Shigemitsu, S. H. Shanker, and D. K. Sinclair, "Deconfinement and Chiral Symmetry Restoration at Finite Temperatures in $SU(2)$ and $SU(3)$ Gauge Theories," Phys. Rev. Lett. 50, 393 (1983).

W. R. Gibbs, "Analytic Structure of the $\bar{p}$-Nucleus Optical Potential," Phys. Rev. C 27, 408 (1983).

W. R. Gibbs and W. B. Kaufmann, "Nuclear Medium Effects in Pion Elastic Scattering and Charge Exchange," Los Alamos National Laboratory document LA-UR-83-736 (Phys. Rev. C, in press).

B. F. Gibson, "Hyperon and Hypernuclear Physics with Intense Beams," in *Intense Medium Energy Sources of Strangeness*, T. Goldman, H. E. Haber, and H. F.-W. Sadrozinski, Eds., AIP Conf. Proc. 102, 43 (1983).

B. F. Gibson, "Electromagnetic and Weak Interactions in Few Nucleon Systems," in the Proc. of the 10th Int. Conf. on Few-Body Problems in Physics, Karlsruhe, Germany, August 21-27, 1983.

M. M. Nieto, W. C. Haxton, C. M. Hoffman, E. W. Kolb, V. D. Sandberg, and J. W. Toevs, Eds., *Science Underground*, AIP Conf. Proc. No. 96 (American Institute of Physics, New York, 1983).

T. Goldman, H. E. Haber, and H. F.-W. Sadrozinski, Eds., *Intense Medium Energy Sources of Strangeness*, University of California, Santa Cruz, 1983, *AIP Conf. Proc. No. 102*, Particles and Fields Subseries No. 31 (American Institute of Physics, New York, 1983).

MP-Division Publications; Papers Submitted for Publication and Papers Presented

S. Adachi and N. Auerbach, "Widths of Isovector Monopole Resonances," Phys. Lett. 131B, 11 (1983). Los Alamos National Laboratory document LA-UR-83-1811

L. Agnew, D. Grisham, R. J. Macek, W. F. Sommer, and R. D. Werbeck, "Design Features and Performance of the LAMPF High-Intensity Beam Area," presented at ICANS VII meeting, Chalk River Nuclear Laboratories, Ontario, Canada, September 12-16, 1983, Los Alamos National Laboratory document LA-UR-83-2693.

J. F. Amann, R. J. Macek, T. W. L. Sanford, H. A. Thiessen, O. van Dyck, et al., "Measurement of Production Cross Sections for Negative Pions, Kaons, and Protons at 10, 18, and 24 GeV," Los Alamos National Laboratory report LA-9486-MS (1982).

G. Anderson, M. Oothoudt, J. Amann, and T. Kozlowski, "Dynamic Parameter Array System," IEEE Trans. Nucl. Sci. NS-30, 3975 (1983).

I. P. Auer, W. R. Ditzler, D. Hill, K. Imai, H. Spinka, R. Stanek, K. Toshioka, D. Underwood, R. Wagner, A. Yokosawa, E. W. Hoffman, J. J. Jarmer, G. R. Burleson, W. B. Cottingame, S. J. Greene, and S. Stuart, "Measure of $\Delta\sigma_L$ and D_{LL} = (L,L;O,O) in Proton-Proton Scattering Between 300 and 800 MeV," submitted to Phys. Rev., Los Alamos National Laboratory document LA-UR-83-3612.

N. Auerbach, "Coulomb Effects in Nuclear Structure," Phys. Rep. 98, 273 (1983), Los Alamos National Laboratory document LA-UR-83-535

N. Auerbach, J. D. Bowman, M. A. Franey, and W. G. Love, "(p,n) and (n,p) Reactions as Probes of Isovector Giant Monopole Resonances," Phys. Rev. C 28, 280 (1983).

N. Auerbach and A. Klein, "Excitation of Giant Electric Isovector Resonances in Pion Charge Exchange Reactions," Phys. Rev. C 28, 2075 (1983), Los Alamos National Laboratory document LA-UR-1810 (1983).

N. Auerbach and A. Klein, "Excitation of Giant Resonances in the Ca Isotopes in (π^+,π^0) Reactions," to be published in Nucl. Phys. A, Los Alamos National Laboratory document LA-UR-83-2978.

N. Auerbach and A. Klein, "The Structure of Isovector Spin Excitations in Nuclei," submitted to Phys. Rev. C, Los Alamos National Laboratory document LA-UR-83-2943.

H. W. Baer, J. A. Bistirlich, K. M. Crowe, W. Dahme, C. Joseph, J. P. Perroud, M. Lebrun, C. J. Martoff, U. Straumann, and P. Truöl, "Study of the $T = 2$ States in $A = 14$ Nuclei with the $^{14}C(\pi^-,\gamma)^{14}B$ Reaction," submitted to Phys. Rev. C, Los Alamos National Laboratory document LA-UR-83-170.

H. W. Baer, J. A. Bistirlich, K. M. Crowe, W. Dahme, C. Joseph, J. P. Perroud, M. Lebrun, "Isovector $M2$ State Observed in the $^{14}C(\pi^-,\gamma)$ Reaction," Phys. Rev. C 28, 761 (1983).

R. D. Bolton, R. D. Carlini, M. D. Cooper, J. S. Frank, V. E. Hart, H. S. Matis, R. E. Mischke, V. D. Sandberg, and U. Sennhauser, "A Stereo, Cylindrical Drift Chamber for Muon Decay Experiments at LAMPF," presented at the Wire Chamber Conf., Vienna, Austria, February 15-18, 1983; Nucl. Instrum. Methods 217, 173 (1983); Los Alamos National Laboratory document LA-UR-83-796.

R. L. Boudrie, "Spectrometers at LAMPF," invited talk at Magnetic Spectrometer Workshop, College of William and Mary, Williamsburg, Virginia, October 10-12, 1983, Los Alamos National Laboratory document LA-UR-83-3294

J. D. Bowman and M. D. Cooper, "Pion Charge Exchange and Nuclear Structure," submitted to Comments on Nucl. Part. Phys., Los Alamos National Laboratory document LA-UR-83-3097.

D. J. Brenner and M. Zaider, "The Applications of Track Calculations to Radiobiology. II. Calculations of Microdosimetric Quantities," Rad. Res. 98 (in press), Los Alamos National Laboratory document LA-UR-83-809

D. J. Brenner and M. Zaider, "Soft X Rays as a Tool to Investigate Radiation-Sensitive Sites in Mammalian Cells," presented at Conf. on Advances in Soft X-Ray Science and Technology, Brookhaven National Laboratory, Long Island, New York, October 17-19, 1983; Los Alamos National Laboratory document LA-UR-83-3156

R. D. Brown, J. R. Cost, and J. T. Stanley, "Effects of Neutron Irradiation on Magnetic Permeability of Amorphous and Crystalline Magnetic Alloys," presented at the 29th Ann. Conf. on Magnetism and Magnetic Materials, Pittsburgh, Pennsylvania, November 1983; to be published in J. Appl. Phys. Magnetism and Magnetic Materials Conf., 1983, Los Alamos National Laboratory document LA-UR-83-2718.

R. D. Brown and D. L. Grisham, "Graphite Targets at LAMPF," presented at the 1983 Particle Accelerator Conf., Santa Fe, New Mexico, March 21-23, 1983; IEEE Trans. Nucl. Sci. NS-30, 2801 (1983); Los Alamos National Laboratory document LA-UR-83-956.

S. K. Brown, "The Use of a Commercial Data Base Management System in the LAMPF Control System," presented at the 1983 Particle Accelerator Conf., Santa Fe, New Mexico, March 21-23, 1983, IEEE Trans. Nucl. Sci. NS-30, 2302 (1983).

R. D. Carlini, H. A. Thiessen, and J. M. Potter, "A High-Q Perpendicular Biased Ferrite-Tuned Cavity," presented at the 12th Int. Conf. on High-Energy Accelerators, Fermi National Accelerator Laboratory, Batavia, Illinois, August 1983; Los Alamos National Laboratory document LA-UR-83-2445 and LA-9946-MS (1983).

R. D. Carlini and G. J. Stephenson, "On the Feasibility of Performing Neutrino Experiments at an Intense Source of Strangeness," presented at the Conf. on Intense Medium Energy Sources of Strangeness, University of California, Santa Cruz, March 1983, AIP Conf. Proc. No. 102, Particle and Field Subseries No. 31, pp. 170-180; Los Alamos National Laboratory document LA-UR-83-1788.

E. P. Chamberlin, J. F. Benage, Jr., and H. E. Williams, "Developing a 500-eV Proton Beam," presented at the 1983 Polarized Ion Workshop, Vancouver, B.C., May 23-28, 1983 (American Institute of Physics) and to be published in its Proceedings; Los Alamos National Laboratory document LA-UR-83-1466

E. P. Colton, "Beam Transfer and Extraction at LAMPF II," presented at the 12th Int. Conf. on High-Energy Accelerators, Fermi National Accelerator Laboratory, August 1983, and to be published in its Proceedings; Los Alamos National Laboratory report LA-9878-MS (1983).

E. P. Colton, "4-GeV Preaccelerator for LAMPF II." Los Alamos National Laboratory report LA-9889-MS (1983).

I. P. Auer, E. Colton, W. R. Ditzler, D. Hill, R. Miller, H. Spinka, G. Theodosiou, J. J. Tavernier, N. Tamura, K. Toshioka, D. Underwood, R. Wagner, A. Yokosawa, P. Kroll, and W. Jauch, "Measurement of Spin Parameters for a Decisive Clarification of the Structure Observed in the *p-p* System,"
Phys. Rev. Lett. 51, 1411 (1983).

E. P. Colton, "Simulation of Betatron-Synchrotron Coupling," Los Alamos National Laboratory report LA-9901-MS (1983).

E. P. Colton, "SSC rf Design Example," presented at the SSC Workshop, University of Michigan, Ann Arbor, Michigan, December 12-17, 1983, to be published in the Proceedings; Los Alamos National Laboratory document LA-UR-84-327 (in press).

E. P. Colton, "A Staged Approach for LAMPF II." Los Alamos National Laboratory report LA-9946-MS (1983).

J. K. Corley and S. C. Schaller, "Particle Accelerator Control and Data Acquisition in the Context of VAX-VMS," presented at the Digital Equipment Computer Users Society Symp., Las Vegas, Nevada, October 23-28, 1983, to be published in the Proceedings; Los Alamos National Laboratory document LA-UR-83-3444.

J. F. Dicello, C. W. McCabe, J. D. Doss, and M. Paciotti, "The Relative Efficiency of Soft-Error Induction in 4K Static RAMs by Muons and Pions," IEEE Trans. Nucl. Sci. NS-30, 4613 (1983).

J. B. Donahue, "Power Deposition of LAMPF Proton Beam in Various Materials," Group MP-7 Technical Note 9MP-7-TN-14, October 1980, Los Alamos National Laboratory document LA-UR-83-2769.

J. D. Doss, "Passive Dosimeters for rf and Microwave Fields," Rev. Sci. Instrum. (in press); Los Alamos National Laboratory document LA-UR-83-2333

L. M. Earley, H. A. Thiessen, R. Carlini, and J. M. Potter, "A High-Q Ferrite-Tuned Cavity," presented at the 1983 Particle Accelerator Conf., Santa Fe, New Mexico, March 21-23, 1983, IEEE Trans. Nucl. Sci. NS-30, 3469 (1983), Los Alamos National Laboratory report LA-9823-MS (1983).

R. A. Fisher, M. M. Nieto, and V. D. Sandberg, "Non-existence of the Naive Generalization of Many-Photon Coherent States," submitted to Phys. Rev.; Los Alamos National Laboratory document LA-UR-84-21.

D. L. Grisham and J. E. Lambert, "Applying Accelerator Remote Technology to Fusion Devices," presented at the American Nuclear Society annual meeting, Detroit, Michigan, June 12-15, 1983; Los Alamos National Laboratory document LA-UR-83-1558.

D. L. Grisham and J. E. Lambert, "Human Factors Considerations in the Monitor System," presented at the American Nuclear Society annual meeting, Detroit, Michigan, June 12-15, 1983; Los Alamos National Laboratory document LA-UR-83-1559.

D. L. Grisham and J. E. Lambert, "Monitor 1983," presented at the Particle Accelerator Conf., Santa Fe, New Mexico, March 21-23, 1983, IEEE Trans. Nucl. Sci. NS-30, 2267 (1983), Los Alamos National Laboratory document LA-UR-83-955.

D. L. Grisham and J. E. Lambert, "Remote Handling at LAMPF," presented at the ICANS VII meeting, Chalk River Nuclear Laboratories, Chalk River, Ontario, Canada, September 12-16, 1983; Los Alamos National Laboratory document LA-UR-83-2692.

D. L. Grisham and J. E. Lambert, "Remote Handling Experience at LAMPF," to be presented at the American Ceramic Society meeting May 1984; Los Alamos National Laboratory document LA-UR-83-3613.

D. Grisham and J. Lambert, "Water-Cooled Target Box Design at LAMPF," presented at the Particle Accelerator Conf., Santa Fe, New Mexico, March 21-23, 1983, IEEE Trans. Nucl. Sci. NS-30, 2270 (1983), Los Alamos National Laboratory document LA-UR-83-954.

P. Herczeg and C. M. Hoffman, "Study of $\pi^0 \rightarrow \mu^{\pm}e^{\mp}$ Decays," submitted to Phys. Rev. D, Los Alamos National Laboratory document LA-UR-83-3573.

C. M. Hoffman, "LAMPF II," invited talk at the Theoretical Symp. on Intense Medium-Energy Sources of Strangeness, Universityof California, Santa Cruz, California, March 1983, AIP Conf. Proc. No. 102, Particle and Field Subseries, No. 31; Los Alamos National Laboratory document LA-UR-83-795.

J. W. Hurd, "Solution to the Transverse Phase Space-Time Dependence Problem with LAMPF's High-Intensity H^+ Beam," presented at the 1983 Particle Accelerator Conf., Santa Fe, New Mexico, March 21-23, 1983, IEEE Trans. Nucl. Sci. NS-30 No. 4 (1983), p. 2487.

G. C. Idzorek and L. G. Atencio, "Fabrication of a Hermetically Sealed Connector," Los Alamos National Laboratory report LA-9849-MS (1983).

T. Kozlowski, J. Amann, G. Anderson, R. Floyd, J. Harrison, and M. Oothoudt, "Performance Results for the New RSX-11M Q System," IEEE Trans. Nucl. Sci. NS-30, 3998 (1983).

R. W. Lourie, W. Bertozzi, T. N. Buti, J. M. Finn, F. W. Hersman, C. Hyde, J. Kelly, M. A. Kovash, S. Kowalski, M. V. Hynes, B. E. Norum, and B. L. Berman, "Inelastic Electron Scattering from ^{9}Be," Phys. Rev. C 28, 489 (1983).

R. J. Macek, D. L. Grisham, J. E. Lambert, and R. Werbeck, "Radiation-ResistantBeam-Line Components at LAMPF," presented at the ICANS VII Conf., Chalk River Nuclear Laboratories, Chalk River, Ontario, Canada, September 13-16, 1983, to be published in the Proceedings; Los Alamos National Laboratory document LA-UR-83-2736.

Y. Mori, K. Ikegami, A. Takagi, Z. Igarashi, S. Fukumoto, W. Cornelius, and R. York, "Optically Pumped Polarized H^- Ion Source," to be published in the Proc. of the 3rd Symp. on the Production and Neutralization of the Negative Hydrogen Ions and Beams, Brookhaven National Laboratory, Upton, New York, November 14-17, 1983.

M. Oothoudt and T. Kozlowski, "ALECS: Assembly Language Extensions and Control Structures," Proc. Digital Equipment Users Society (1982), p. 537; Los Alamos National Laboratory document LA-UR-82-3334.

M. Oothoudt, J. Amann, R. Floyd, J. Harrison, and T. Kozlowski, "The Q Memory Resident Histogramming System," IEEE Trans. Nucl. Sci. NS-30, 3838 (1983).

G. C. Phillips, E. A. Umland, G. S. Mutchler, J. B. Roberts, M. Duong-Van, J. A. Buchanan, J. B Donahue, J. C. Allred, B. W. Noel, T. A. Mulera, B. Aas, and B. W. Mayes, "A Novel Neutrino Detection System," to be published in Nucl. Instrum. Methods; Los Alamos National Laboratory document LA-UR-83-2519

W. Reuter, E. B. Shera, M. V. Hoehn, F. W. Hersman, T. Milliman, J. M. Finn, C. Hyde-Wright, R. Lourie, B. Pugh, and W. Bertozzi, "Nuclear Charge Densities in the Transition Region ^{192}Os," to be published in Phys. Rev. Lett.; Los Alamos National Laboratory document LA-UR-83-3313.

L. Rosen, "The Pros and Cons of a Nuclear Freeze," invited talk at Trinity on the Hill Episcopal Church, Los Alamos, New Mexico, March 15, 1983.

V. D. Sandberg, "An Heuristic Introduction to Gravitational Waves," Proc. Workshop on Science Underground, Los Alamos National Laboratory, Los Alamos, New Mexico, September 27-October 1, 1982, Los Alamos National Laboratory document LA-UR-83-333.

G. H. Sanders, "The Imagery of Physics in Psychology: A Physicist's Reactions," presented at the Conf. on Nuclear Reactions: A Three-Day Dialogue Between Physicists and Psychologists, University of New Mexico, Albuquerque, New Mexico, November 1983, to be published in the Proceedings; Los Alamos National Laboratory document LA-UR-83-744.

S. C. Schaller and P. A. Rose, "Data-Acquisition Software for the LAMPF Control System," presented at the 1983 Particle Accelerator Conf., Santa Fe, New Mexico, March 21-23, 1983; IEEE Trans. Nucl. Sci. NS-30, 2308 (1983); Los Alamos National Laboratory document LA-UR-83-744.

P. Schuler, K. Hardt, C. Gunther, K. Freitag, P. Herzog, H. Niederwestberg, H. Reif, E. B. Shera, and M. V. Hoehn, "Experimental Investigation of Low-Lying Excited States in ^{201}Hg," Z. Phys. A. 313, 305 (1983).

C. J. Sternhagen and J. D. Doss, "Combined Radiation Therapy and Localized Current Field Hyperthermia with a 13-MHz Applicator in Head and Neck and Gynecological Cancer Therapy," in the Proc. of the meeting of the Radiation Research Society, San Antonio, Texas, February 28, 1983.

R. R. Stevens, Jr., and R. L. York, "A Cusped Field H^- Ion Source for LAMPF," presented at the 1983 Particle Accelerator Conf., Santa Fe, New Mexico, March 21-23, 1983, Los Alamos National Laboratory document LA-UR-83-815.

G. W. Swift, A. Migliori, J. Wheatley, C. R. Waller, and G. Suazo, "Fabrication and Leak-Tight Furnace Brazing of Intricate Objects," submitted to Rev. Sci. Instrum.; Los Alamos National Laboratory document LA-UR-83-3455.

H. A. Thiessen and E. J. Scheidker, "Production of Pions, Kaons, and Muons by 16-GeV Protons," Los Alamos National Laboratory report LA-9587-MS (1983).

H. A. Thiessen, "A Reference Design for LAMPF II," Proc. of the 12th Int. Conf. on High-Energy Accelerators, Fermi National Accelerator Laboratory, August 11-16, 1983; Los Alamos National Laboratory document LA-UR-83-2426.

J. L. Warren and H. A. Thiessen, "Simulation of Transition Crossing in LAMPF II," Proc. of the 12th Int. Conf. on High-Energy Accelerators, Fermi National Accelerator Laboratory, August 11-16, 1983; Los Alamos National Laboratory document LA-UR-83-2367.

R. R. Wilson, "Acceleration in a Synchrotron by Harmonic Hopping," Los Alamos National Laboratory report LA-9904-MS (1983).

A. Yaouanc, "Correlation Functions, Generalized Susceptibility, and μSR Spectroscopy," submitted to J. Phys. Lett., Los Alamos National Laboratory document LA-UR-83-664.

R. L. York and R. R. Stevens, Jr., "A Cusped Field H^- Ion Source for LAMPF," IEEE Trans. Nucl. Sci. NS-30, 2704 (1983).

R. L. York and R. R. Stevens, Jr., "Development of a Multicusp H^- Ion Source for Accelerator Applications," to be published in the Proc. of the 3rd Int. Symp. on the Production and Neutralization of Negative Ions and Beams, Brookhaven National Laboratory, Upton, New York, November 14-17, 1983; Los Alamos National Laboratory document LA-UR-83-3273.

R. L. York, R. R. Stevens, Jr., K. N. Leung, and K. W. Ehlers, "Extraction of H^- Beams from a Magnetically Filtered Multicusp Source," to be published in Rev. Sci. Instrum., Los Alamos National Laboratory document LA-UR-83-3098.

LAMPF Experimental Program Reports and Publications

(EXP. 2) R. H. Jeppesen, M. J. Jakobson, M. D. Cooper, D. C. Hagerman, M. B. Johnson, R. P. Redwine, G. R. Burleson, K. F. Johnson, R. E. Marrs, H. O. Meyer, I. Halpern, and L. D. Knutson, "Pion-Nucleus Forward Scattering Amplitudes from Total Cross Section Measurements," Phys. Rev. C 27, 697 (1983).

(EXP. 9) K. G. Boyer, W. J. Braithwaite, W. B. Cottingame, S. J. Greene, L. E. Smith, C. F. Moore, C. L. Morris, H. A. Thiessen, G. S. Blanpied, G. R. Burleson, J. F. Davis, J. S. McCarthy, R. C. Minehart, and C. A. Goulding, "Pion Elastic and Inelastic Scattering from ^{40,42,44,48}Ca and ^{54}Fe," Phys. Rev. C. 29, 182 (1984); Los Alamos National Laboratory document LA-UR-82-3171.

(EXPS. 9, 310, 401, 412, 448, 523, 680, 716) M. B. Johnson, "Recent Developments in the Understanding of Pion-Nucleus Scattering," lectures presented at the 1983 Int. Symp. on Nucleon-Nucleon Interaction and Nuclear Many-Body Problems, Beijing, China, September 1983; Los Alamos National Laboratory document LA-UR-83-2851

(EXP. 12) C. Gunther, E. B. Shera, M. V. Hoehn, H. D. Wohlfahrt, R. J. Powers, Y. Tanaka, and A. R. Kunselman, "Muonic X-Ray Study of ^{199}Hg and ^{200}Hg," Phys. Rev. C 27, 816 (1983).

(EXP. 15) G. Pauletta, G. Adams, S. M. Haji-Saeid, G. J. Igo, J. B. McClelland, A. T. M. Wang, C. A. Whitten, Jr., A. Wriekat, M. M. Gazzaly, and N. Tanaka, "Differential Cross Section and Analyzing Powers for pp Elastic Scattering at 1.46 GeV/c in the Coulomb-Nuclear Interference Region," Phys. Rev. C 27, 282 (1983).

(EXP. 22) R. Kunselman, R. J. Powers, M. V. Hoehn, and E. B. Shera, "Pionic $3d \rightarrow 2p$ X-Ray Measurements in ^{50,52,54}Cr, ^{45}Sc, ^{51}V, ^{55}Mn, and Fe," Nucl. Phys. A 405, 627 (1983).

(EXP. 31) J. S. Frank, R. L. Burman, D. R. F. Cochran, P. Nemethy, S. E. Willis, V. W. Hughes, R. P. Redwine, J. Duclos, H. Kaspar, C. K. Hargrove, and U. Moser, "Reply to Direct Comparison Between the γ-Ray Fluxes from Proton Beam Dumps at LAMPF and SIN," submitted to Phys. Rev. D; Los Alamos National Laboratory document LA-UR-83-1345

(EXP. 32) W. K. McFarlane, L. B. Auerbach, F. C. Gaille, V. L. Highland, E. Jastrzembski, R. J. Macek, F. H. Cverna, C. M. Hoffman, G. E. Hogan, R. E. Morgado, J. C. Pratt, and R. D. Werbeck, "New Measurement of the Rate for Pion Beta Decay," Phys. Rev. Lett. 51, 249 (1983).

(EXP. 87) J. Källne, R. C. Minehart, R. R. Whitney, R. L. Boudrie, J. B. McClelland, and A. W. Stetz, "Pion Scattering and Absorption Contributions to Proton Emission from Pion-Nucleus Collisions at T_π = 50-295 MeV," Phys. Rev. C 28, 304 (1983).

(EXP. 96) J. S. Frank, A. A. Browman, P. A. M. Gram, K. A. Klare, R. E. Mischke, D. C. Moir, D. E. Nagle, R. H. Heffner, J. M. Potter, R. P. Redwine, and M. A. Yates, "Measurement of Low-Energy Elastic $\pi^{\pm}p$ Differential Cross Sections," Phys. Rev. D 28, 1569 (1983); Los Alamos National Laboratory document LA-UR-83-1490.

(EXPS. 120, 363) D. H. Fitzgerald, "πN Scattering at LAMPF: Baryon Spectroscopy at 1200-1500 MeV/c," presented at the University of Colorado, April 25, 1983, Los Alamos National Laboratory document LA-UR-83-1179.

(EXPS. 120, 363) D. H. Fitzgerald, "πN Scattering at LAMPF: Natural Baryon Spectroscopy at 1200-1500 MeV/c^2," presented at George Washington University, Washington, D.C., March 11, 1983; Los Alamos National Laboratory document LA-UR-83-635.

(EXP. 249) B. Höistad, M. Gazzaly, B. Aas, G. Igo, A. Rahbar, C. Whitten, G. S. Adams, and R. Whitney, "^{3,4}He$(\vec{p},\pi^+)^{4,5}$He$_{g.s.}$ Reactions at 800 MeV," Phys. Rev. C 29, 553 (1984).

(EXP. 298) F. Irom, G. J. Igo, J. B. McClelland, C. A. Whitten, Jr., and M. Bleszynski, "Measurements of Small-Angle Elastic $\vec{p}$-d Scattering at 796 MeV Using a Recoil Method," Phys. Rev. C 28, 2380 (1983).

(EXP. 309) S. A. Wood, "An Experimental Study of Inclusive Pion Double Charge Exchange Reactions in the Delta Resonance Region," Ph.D. thesis, Massachusetts Institute of Technology, Cambridge, Massachusetts, 1983; Los Alamos National Laboratory report LA-9932-T (1983).

(EXP. 333) M. J. Leitch, R. L. Burman, R. Carlini, S. Dam, V. Sandberg, et al., "Pion-Nucleus Elastic Scattering at 80 MeV," Phys. Rev. C 29, 561 (1984); Los Alamos National Laboratory document LA-UR-83-2569

(EXP. 335) D. B. Laubacher, Y. Tanaka, R. M. Steffen, E. B. Shera, and M. V. Hoehn, "Muonic X-Ray Measurement of the Monopole and Quadrupole Charge Parameters of ^{154,155,156,157,158,160}Gd," Phys. Rev. C 27, 1772 (1983).

(EXP. 336) A. D. Hancock, R. W. Hackenburg, E. V. Hungerford, B. W. Mayes, L. S. Pinsky, J. C. Allred, T. M. Williams, S. D. Baker, J. A. Buchanan, J. M. Clement, M. Copel, I. M. Duck, G. S. Mutchler, G. P. Pepin, E. A. Umland, G. C. Phillips, M. W. McNaughton, C. Hwang, and M. Furic, "Asymmetries and Cross Sections for the Reaction $\vec{p} + p \rightarrow p + \pi^+ + n$ at 800 MeV," Phys. Rev. C 27, 2742 (1983).

(EXP. 348) C. J. Martoff, J. A. Bistirlich, C. W. Clawson, K. M. Crowe, M. Kroike, J. P. Miller, S. S. Rosenblum, W. A. Zajc, H. W. Baer, A. H. Wapstra, G. Strassner, and P. Truöl, "Spin-Flip Transitions in ^{13}C^{19}F Probed with the (π^-,γ) Reaction," Phys. Rev. C 27, 1621 (1983).

(EXP. 357) J. D. Knight, C. J. Orth, M. E. Schillaci, R. A. Naumann, F. J. Hartmann, and H. Schneuwly, "Target-Density Effects in Muonic-Atom Cascades," Phys. Rev. A 27, 2936 (1983).

(EXPS. 385, 563) M. L. Barlett, G. W. Hoffmann, J. A. McGill, B. Höistad, L. Ray, R. W. Fergerson, E. C. Milner, J. A. Marshall, J. F. Amann, B. E. Bonner, J. B. McClelland, G. S. Blanpied, and R. A. Arndt, "Forward-Angle Elastic and Quasi-elastic Proton-Nucleon Cross Sections and Analyzing Powers at 0.8 GeV," Phys. Rev. C 27, 682 (1983).

(EXP. 389) D. F. Geesaman, D. Kurath, G. C. Morrison, C. Olmer, B. Zeidman, R. E. Anderson, R. L. Boudrie, H. A. Thiessen, G. S. Blanpied, G. R. Burleson, R. E. Segel, and L. W. Swenson, "Inelastic Scattering of 162-MeV Pions by ^{14}N," Phys. Rev. C 27, 1134 (1983); Los Alamos National Laboratory document LA-UR-82-3258.

(EXP. 390) S. M. Levenson, D. F. Geesaman, E. P. Colton, R. J. Holt, H. E. Jackson, J. P. Schiffer, J. R. Specht, K. E. Stephenson, B. Zeidman, R. E. Segel, P. A. M. Gram, and C. A. Goulding, "Inclusive Pion Scattering in the $\Delta(1232)$ Region," Phys. Rev. C 28, 326 (1983).

(EXP. 400) R. Bolton, R. Carlini, J. D. Bowman, M. Cooper, A. Hallin, J. Frank, C. Hoffman, H. Matis, R. Mischke, D. Nagle, F. Mariam, V. Sandberg, U. Sennhauser, G. Sanders, R. Werbeck, R. Williams, R. Hofstadter, E. Hughes, S. Wilson, J. Rolfe, S. Wright, D. Grosnick, G. Hogan, V. Highland, and M. Van, "The Crystal Box: Rare Decays of the Muon," presented at the Blacksburg, Virginia, Workshop on Low-Energy Tests of Conservation Laws in Particle Physics, September 11-15, 1983; Los Alamos National Laboratory document LA-UR-83-2908.

(EXP. 400) J. P. Sandoval, L. Bayliss, T. Gordon, G. Hart, C. M. Hoffman, G. E. Hogan, V. D. Sandberg, G. H. Sanders, and S. L. Wilson, "Alternatives to Coaxial Cable for Delaying Analog and Digital Signals in a Particle Physics Experiment," Nucl. Instrum. Methods 216, 171 (1983); Los Alamos National Laboratory document LA-UR-83-967.

(EXP. 401) M. D. Cooper, H. W. Baer, R. D. Bolton, J. D. Bowman, F. H. Cverna, N. S. P. King, M. Leitch, J. Alster, A. Doron, A. Erell, M. A. Moinester, E. Blackmore, and E. Siciliano, "Angular Distribution for $^{13}N(\pi^{+1},\pi^{0})^{13}O(g.s)$ at T_{π} = 48 MeV," submitted to Phys. Rev. Lett.; Los Alamos National Laboratory document LA-UR-83-1030.

(EXP. 407) D. J. Farnum, W. F. Sommer, and O. T. Inal, "A Study of Defects Produced in Tungsten by 800-MeV Protons Using Field Ion Microscopy," presented at the Third Topical Meeting on Fusion Reactor Materials, Albuquerque, New Mexico, September 19-22, 1983, to be published in J. Nucl. Mater.; Los Alamos National Laboratory document LA-UR-83-2572

(EXP. 407) W. F. Sommer, D. S. Phillips, W. V. Green, L. W. Hobbs, and C. A. Wert, "Proton Irradiation Damage in Cyclically Stressed Aluminum," J. Nucl. Mater. 114, 267 (1983).

(EXPS. 412, 523, 827) N. Auerbach, M. B. Johnson, A. Klein, and E. R. Siciliano, "Nuclear Structure Effects in Pion Single Charge Exchange," Phys. Rev. C 29 526 (1984); Los Alamos National Laboratory document LA-UR-83-2699.

(EXPS. 412, 607) A. E. Erell, J. Alster, J. Lichtenstadt, M. A. Moinester, J. D. Bowman, M. D. Cooper, F. Irom, H. S. Matis, E. Piasetzky, U. Sennhauser, and Q. Ingram, "Properties of the Isovector Monopole and Other Giant Resonances in Pion Charge Exchange," submitted to Phys. Rev. Lett.; Los Alamos National Laboratory document LA-UR-84-599

(EXP. 412) U. Sennhauser, E. Piasetzky, H. Baer, J. D. Bowman, M. D. Cooper, H. S. Matis, H. J. Ziock, J. Alster, A. Erell, M. A. Moinester, and F. Irom, "Isobaric Analog States in Pion Single-Charge-Exchange Reactions On and Above the (3,3) Resonance Energy," Phys. Rev. Lett. 51, 1324 (1983).

(EXP. 452) S. Seestrom-Morris, C. L. Morris, R. L. Boudrie, H. A. Thiessen, D. Dehnhard, and M. A. Franey, "Analysis of Elastic and Inelastic Scattering of 162-MeV Pions from ^{12}C by an Optical Potential and a Collective Model," Phys. Rev. C 28, 1301 (1983); Los Alamos National Laboratory document LA-UR-83-452.

(EXP. 479) D. L. Adams and M. Bleszynski, "On the Relevance of the Dirac Equation to the Scattering of Medium-Energy Nucleons from Nuclei," submitted to Phys. Lett.; Los Alamos National Laboratory document LA-UR-83-2749

(EXP. 484) C. L. Morris, S. J. Seestrom-Morris, P. A. Seidl, R. R. Kiziah, and S. J. Greene, "Pion Elastic and Inelastic Scattering from ^{152}Sm," Phys. Rev. C 28, 2165 (1983); Los Alamos National Laboratory document LA-UR-82-2542.

(EXP. 495) C. L. Morris, N. Tanaka, R. L. Boudrie, L. C. Bland, H. T. Fortune, R. Gilman, S. J. Seestrom-Morris, C. F. Moore, and D. Dehnhard, "Small Angle Pion Inelastic Scattering from ^{12}C at 162 MeV," submitted to Phys. Rev. C; Los Alamos National Laboratory document LA-UR-84-16.

(EXP. 498) I. P. Auer, W. R. Ditzler, D. Hill, K. Imai, H. Spinka, R. Stanek, K. Toshioka, D. Underwood, R. Wagner, A. Yokosawa, E. W. Hoffman, J. J. Jarmer, G. R. Burleson, W. B. Cottingame, S. J. Greene, and S. Stuart, "Measure of $\Delta\sigma_L$ and C_{LL} in Proton-Proton Scattering Between 300 and 800 MeV," submitted to Phys. Rev. D; Los Alamos National Laboratory document LA-UR-83-3612.

(EXP. 498) G. R. Burleson, W. B. Cottingame, S. J. Greene, S. Stuart, E. W. Hoffman, J. J. Jarmer, I. P. Auer, W. R. Ditzler, D. Hill, K. Imai, H. Spinka, R. Stanek, K. Toshioka, D. Underwood, R. Wagner, and A. Yokosawa, "$C_{LL} = (L,L;0,0)$ Measurements and a Structure Due to a P Partial Wave in the pp System," Nucl. Phys. B 213, 365 (1983).

(EXP. 517) W. B. Tippens, "Measurement of A_N and A_{NN} for the Reaction $pp \rightarrow d\pi^+$ at Six Energies from 500 to 800 MeV," Ph.D. thesis, Texas A&M University, College Station, Texas, 1983; Los Alamos National Laboratory report LA-9909-T (1983).

(EXPS. 517, 518) T. S. Bhatia, J. G. J. Boissevain, J. J. Jarmer, R. R. Silbar, J. E. Simmons, G. Glass, J. C. Hiebert, R. A. Kenefick, L. C. Northcliffe, W. B. Tippens, W. M. Kloet, and J. Duback, "Analyzing Powers and Spin Correlations A_{NN} and A_{LL} for $pp \rightarrow np\pi^+$ at 650 and 800 MeV," Phys. Rev. C 28, 2071 (1983).

(EXP. 523) F. Irom, J. R. Comfort, R. Jeppeson, J. J. Kraushaar, R. A. Ristinen, W. Tew, J. L. Ullmann, H. W. Baer, J. D. Bowman, M. D. Cooper, A. Erell, M. A. Moinester, E. Piasetsky, U. Sennhauser, and E. R. Siciliano, "Pion Single Charge Exchange on ^{14}C," Phys. Rev. C 28, 2568 (1983).

(EXP. 545) R. D. Brown, J. R. Cost, and J. T. Stanley, "Effects of Neutron Irradiation on Magnetic Permeability of Amorphous and Crystalline Magnetic Alloys," presented at the 29th Ann. Conf. Magnetism and Magnetic Materials, Pittsburgh, Pennsylvania, November 8-11, 1983, to be published in J. Appl. Phys.; Los Alamos National Laboratory document LA-UR-83-2718.

(EXP. 558) P. A. Seidl, R. R. Kiziah, M. K. Brown, C. F. Moore, C. L. Morris, H. Baer, S. J. Greene, G. R. Burleson, W. B. Cottingame, L. C. Bland, R. Gilman, and H. T. Fortune, "Observation of Analog and Nonanalog Transitions in the Reaction ^{58}Fe(π^+,π^-)^{58}Ni," Phys. Rev. Lett. 50, 1106 (1983); Los Alamos National Laboratory document LA-UR-83-248.

(EXP. 558) P. A. Seidl, M. D. Brown, R. R. Kiziah, C. F. Moore, H. Baer, C. L. Morris, G. R. Burleson, W. B. Cottingame, S. J. Greene, L. C. Bland, R. Gilman, and H. T. Fortune, "Pion Double Charge Exchange on $T = 1$ Nuclei," submitted to Phys. Rev. C; Los Alamos National Laboratory document LA-UR-84-17.

(EXP. 561) M. Blecher, K. Gotow, R. L. Burman, M. V. Hynes, M. J. Leitch, N. S. Chant, L. Rees, P. G. Roos, F. E. Bertrand, E. E. Gross, F. E. Obenshain, T. P. Sjoreen, G. S. Blanpied, B. M. Preedom, and B. G. Ritchie, "Isospin Effects in $\pi^{\pm}$ Elastic Scattering from ^{12}C, ^{13}C, and ^{14}C at 65 and 80 MeV," Phys. Rev. C 28, 2033 (1983).

(EXP. 601, 659) C. L. Morris, S. J. Seestrom-Morris, and L. C. Bland, "Excitation of Giant Resonances in Pion Inelastic Scattering," invited talk at the HESANS '83 Int. Symp., Orsay, France, September 5-8, 1983; Los Alamos National Laboratory document LA-UR-83-3237.

(EXP. 606) M. O. Kaletka, "Core Excitation Effects in Pion Double Charge Exchange," Ph.D. thesis, Northwestern University, Evanston, Illinois, 1983; Los Alamos National Laboratory report LA-9947-T.

(EXP. 607) J. D. Bowman, H. W. Baer, M. D. Cooper, H. S. Matis, F. Irom, E. Piasetzky, U. Sennhauser, N. S. P. King, J. Alster, A. Erell, M. A. Moinester, J. Lichtenstadt, and C. H. Q. Ingram, "A Dependence of the Excitation Energy, Width, and Cross Section of the Isovector Monopole Resonance," presented at the HESANS '83 Int. Symp., Orsay, France, September 5-8, 1983; Los Alamos National Laboratory document LA-UR-83-2924

(EXP. 616) J. B. McClelland, J. M. Moss, B. Aas, A. Azizi, E. Bleszynski, M. Bleszynski, J. Geaga, G. Igo, A. Rahbar, J. B. Wagner, G. S. Weston, C. Whitten, Jr., K. Jones, S. Nanda, M. Gazzaly, and N. Hintz, "Complete Measurement of Polarization Transfer Observables for the ^{12}C(p,p')^{12}C*," Phys. Rev. Lett. 52, 98 (1984); Los Alamos National Laboratory document LA-UR-83-3292.

(EXP. 625) J. L. Ullmann, J. J. Kraushaar, T. G. Masterson, R. J. Peterson, R. S. Raymond, R. A. Ristinen, N. S. P. King, R. L. Boudrie, C. L. Morris, W. W. True, R. E. Anderson, and E. R. Siciliano, "Excitation of the Isoscalar Giant Quadrupole Resonance in ^{116}Sn ($\pi^{\pm},\pi^{\pm}$)," Phys. Rev. Lett. 51, 1038 (1983); Los Alamos National Laboratory document LA-UR-83-2226.

(EXP. 627) R. A. Riskinen, A. M. Bernstein, B. Quinn, S. A. Wood, G. S. Blanpied, B. G. Ritchie, and V. R. Brown, "DWIA Predictions of (p,p') Data Using Electromagnetically Constrained Densities," Phys. Lett. 131B, 26 (1983).

(EXP. 634) J. D. Bowman, R. Carlini, R. Damjanovich, R. W. Harper, R. E. Mischke, D. E. Nagle, R. Talaga, and V. Yuan, "Low-Noise Ionization Chambers for Use in Transmission Measurements with Medium- and High-Energy Beams," Nucl. Instrum. Methods 216, 399 (1983).

(EXP. 635) S. Tsu-hsun, B. E. Bonner, M. W. McNaughton, O. B. van Dyck, G. S. Weston, B. Aas, E. Bleszynski, M. Bleszynski, G. J. Igo, H. Ohnuma, D. J. Cremans, C. L. Hollas, K. H. McNaughton, P. J. Riley, R. F. Rodebaugh, S. Zu, and S. E. Turpin, "Measurements of the Spin-Rotation Parameters for $\bar{p}d \rightarrow \bar{p}d$ Elastic Scattering at 496, 647, and 800 MeV," submitted to Phys. Rev. C; Los Alamos National Laboratory document LA-UR-83-3484.

(EXP. 659) L. C. Bland, "Forward-Angle Pion Inelastic Scattering," Ph.D. thesis, University of Pennsylvania, Philadelphia, 1983; Los Alamos National Laboratory report LA-6022-T (1983).

(EXP. 659, 659U) L. C. Bland, R. Gilman, G. S. Stephans, G. P. Gilgoyle, H. T. Fortune, C. L. Morris, S. J. Seestrom-Morris, S. J. Greene, P. A. Seidl, R. R. Kiziah, and C. F. Moore, "Forward-Peaked Angular Distributions Observed in (π,π') on Light Nuclei," submitted to Phys. Rev.; Los Alamos National Laboratory document LA-UR-83-3086.

(EXP. 660) J. B. McClelland, "Spin Excitation Studies via (p,p') at the HRS," invited talk at the Int. Symp. on Electromagnetic Properties of Atomic Nuclei, Tokyo, Japan, November 9-12, 1983; Los Alamos National Laboratory document LA-UR-83-3236.

(EXP. 698) Y. Tanaka, R. M. Steffen, E. B. Shera, W. Reuter, M. V. Hoehn, and J. D. Zumbro, "Muonic X-Ray Study of ^{151}Eu and ^{153}Eu," to be published in Phys. Rev. C; Los Alamos National Laboratory document LA-UR-84-22

(EXP. 698) Y. Tanaka, R. M. Steffen, E. B. Shera, W. Reuter, M. V. Hoehn, and J. D. Zumbro, "Precision Muonic-Atom Measurements of Nuclear Quadrupole Moments and the Sternheimer Effect in Rare-Earth Atoms," Phys. Rev. Lett. 51, 1633 (1983).

(EXP. 701) L. C. Bland, R. Gilman, M. Carchidi, K. Dhuga, C. L. Morris, H. T. Fortune, S. J. Greene, P. A. Seidl, and C. F. Moore, "Systematics of Pion Double-Charge-Exchange Reactions on $T = 0$ Nuclei," Phys. Lett. 128B, 157 (1983); Los Alamos National Laboratory document LA-UR-83-1195.

(EXP. 705) R. R. Silbar and E. Piasetzky, "Isospin Dependence of Pion Absorption on Nucleon Pairs," to be published in Phys. Rev. C; Los Alamos National Laboratory document LA-UR-83-1883

(EXP. 720) C. L. Morris, J. F. Amann, S. J. Seestrom-Morris, J. A. McGill, C. Glashausser, K. Jones, S. Nanda, M. Barlett, G. W. Hoffman, C. Milner, C. F. Moore, J. R. Comfort, L. C. Bland, and R. Gilman, "Low-Momentum Delta Production in the $^{12}C(p,d)^{11}C^*$ Reaction," Phys. Lett. 123B, 37 (1983); Los Alamos National Laboratory document LA-UR-82-2877.

(EXP. 727) S. E. Jones, A. N. Anderson, A. J. Caffrey, J. B. Walter, K. D. Watts, J. N. Bradbury, P. A. M. Gram, M. Leon, H. R. Maltrud, and M. A. Paciotti, "Experimental Investigatioin of Muon-Catalyzed d-t Fusion," Phys. Rev. Lett. 51, 1757 (1983).

(EXPS. 727, 745) M. A. Paciotti, J. N. Bradbury, and O. M. Rivera, "Muon Beams at the LAMPF Biomedical Channel," presented at the Particle Accelerator Conf., Santa Fe, New Mexico, March 21-23, 1983, IEEE Trans. Nucl. Sci. NS-30, 2359 (1983).

(EXP. 780) R. Gilman, H. T. Fortune, L. C. Bland R. R. Kiziah, C. F. Moore, P. A. Seidl, C. L. Morris, and W. B. Cottingame, "Nonanalog (π^-,π^+) Double Charge Exchange on ^{18}O," submitted to Phys. Rev. Lett.; Los Alamos National Laboratory document LA-UR-84-436.

(EXP. 783) E. Piasetzky, P. A. M. Gram, D. W. MacArthur, G. A. Rebka, Jr., C. A. Bordner, S. Hoibraten, E. R. Kinney, J. L. Matthews, S. A. Wood, D. Ashery, and J. Lichtenstadt, "Pion-Induced Pion Production on the Deuteron," submitted to Phys. Rev. Lett.; Los Alamos National Laboratory document LA-UR-84-231

IV. PROTON STORAGE RING CONSTRUCTION AND RESEARCH PROGRAM DEVELOPMENT

Overview

C. D. Bowman

A world-class facility is under development on Line D for pulsed neutron and other research. The principal elements in this facility are the Proton Storage Ring (PSR) now under construction and the existing Weapons Neutron Research (WNR) facility target and experimental areas. The storage ring will convert the long LAMPF macropulses into short, intense proton bursts for a variety of experimental programs. Two pulse structures will be provided: the long-burst, low-frequency (LBLF) mode with 270-ns pulses at 12 Hz for an average current of 100 μA, and the short-burst, high-frequency (SBHF) mode with 1-ns pulses at 720 Hz for an average current of 12 μA.

The long-burst mode will be devoted primarily to condensed matter research using pulsed neutron scattering techniques and will be the major facility for this type of pulsed neutron research in the United States. A User program is being developed under the auspices of the Division of Materials Science of the USDOE, which should grow to more than 100 Users annually when the PSR becomes operational. This User program began in calendar year 1983 with the availability of pulsed neutrons produced by 5-μs bursts of LAMPF beam on the present WNR target-moderator system. More than 100 visitors from 30 institutions participated in the pulsed-neutron planning and research in 1983.

Plans also were completed for a major increase in experimental space around the WNR target area to accommodate as many as 15 spectrometers for this research. Funds were received in FY 1983 for a $2.7-million 3-year WNR program to upgrade the target area and beam-transport system to handle the required current and to improve the neutron-production target and shielding.

Research in the field of neutron-nuclear physics will receive a major boost from the short, intense bursts of neutrons produced from the PSR, the extension of useful neutron energies up to several hundred MeV, and the absence of an intense gamma flash associated with the neutron burst. Neutron physics experiments were performed this year at the WNR using sub-micro-amp currents of LAMPF micropulses. Although these experiments are unsurpassed in intensity and resolution, orders-of-magnitude improvements will be possible when the PSR short-pulse mode becomes operational.

The low duty cycle and high-current capacity of the PSR almost certainly will be major advantages for low-energy neutrino research. In anticipation of such a program, a new beam line (Line E) has been assembled parallel to Line D and in the Line D channel, with a pulsed magnet for multiplexing LAMPF beam between Lines D and E. Neutrino experiments requiring an unshared target will be conducted on this line using a target and detector area now under construction.

The rapid progress on the installation of Line E, carried out by a collaboration of Los Alamos Groups P-3, P-9, P-14, and MP Division, the University of New Mexico, University of California at Riverside, and Temple and Valparaiso Universities, should enable measurements on ν_μ-nucleus charged-current cross sections during the summer of 1984. These data are crucial for the design of future detectors for use with any Los Alamos neutrino source. This measurement also will provide data on possible $\nu_\mu \rightarrow \nu_e$ oscillations with a sensitivity of about 10^{-3}, although this is far from the limit ultimately achievable at LAMPF.

The construction of the PSR is supported by Laboratory Defense Program Funding. A substantial defense research program will be conducted using the PSR and associated facilities. On infrequent occasions, defense

---

The WNR/PSR facility, located south of the LAMPF switchyard, accepts 800-MeV proton beam pulses from the LAMPF accelerator. Its design was accomplished in large part by the Accelerator Technology (AT) Division of Los Alamos National Laboratory.

The research program at WNR/PSR is managed by the Physics (P) Division at Los Alamos and is supported jointly by Laboratory internal funding and the Office of Energy Research of the USDOE. Researchers from P Division collaborate with other Los Alamos staff and outside Users in their experiments.

Progress at LAMPF thanks the management of P Division, especially Charles Bowman, for this section of reports on developments and research at WNR/PSR.

programs will require the unshared use of the PSR, but the typical defense experiment will only require the use of one or more of the many neutron drift tubes that view a common pulsed source of neutrons.

Participation in the PSR research programs is encouraged. Interested individuals should contact Richard N. Silver for condensed matter physics, and Gerard J. Stephenson for neutron or neutrino physics.

PSR Construction

G. A. Sawyer

The PSR is a major addition to the WNR facility at LAMPF. It will be a bunch compressor for the relatively long linac macropulses from LAMPF, tailoring them into short, intense pulses ideally suited for neutron-scattering research.

The PSR is located in a tunnel adjacent to, and below the level of, the existing beam line (Line D) that serves the WNR facility. A plan view of the ring and tunnel, showing component locations, is given in Fig. 1. Beam enters the ring from Line D; after accumulation, it returns to Line D, through which it is transported to the WNR neutron-production target. Connections with Line D are made by short, sloped, beam-transport channels. Located above the ring tunnel and on top of a 4.9-m-thick earth shield are service and assembly buildings.

The ring operates in two accumulation modes, each independently optimized to provide the desired neutron-source pulse structure for nuclear physics and materials research programs.

Operational characteristics of the two PSR storage modes are summarized in Table I. In the short-bunch high-frequency (SBHF) mode, protons are accumulated in six equally spaced 1-ns bunches during each LAMPF macropulse. The bunches are individually extracted by a fast kicker during the 8.2-ms interval between injection pulses. Because the linac macropulse frequency is 120 Hz, this program produces an extraction rate of 720 pps. For PSR injection, the final 108 μs of each macropulse is modified by a chopper-buncher system in the linac low-energy transport to form a sequence of micropulses spaced at 60-ns intervals. The ring circulation period is chosen so that this injected pulse train is synchronized with the six bunches already stored. Each incoming micropulse, containing 3.3×10^8 protons, merges with a ring bunch; 300 micropulses are accumulated in each ring bunch. The narrow bunch width in this mode is maintained by a high-frequency buncher located in the ring.

In the long-bunch low-frequency (LBLF) mode, the ring accumulates complete linac macropulses (5.2×10^{13} protons) in a single 270-ns bunch. Each stored bunch is extracted after completion of the injection cycle, with a maximum delay of 4 ms. The cycle repetition rate is 12 Hz. Peak current, assuming a parabolic longitudinal charge distribution, is 46.3 A; average circulating current is 100 μA. For injection, a slow-wave chopper in the linac low-energy transport carves 90 ns out of each 360 ns throughout the macropulse, permitting entering pulses to be overlapped with those that are already stored in the 360-ns circulation period. A first-harmonic buncher keeps the 90-ns gap clear of protons to facilitate low-loss

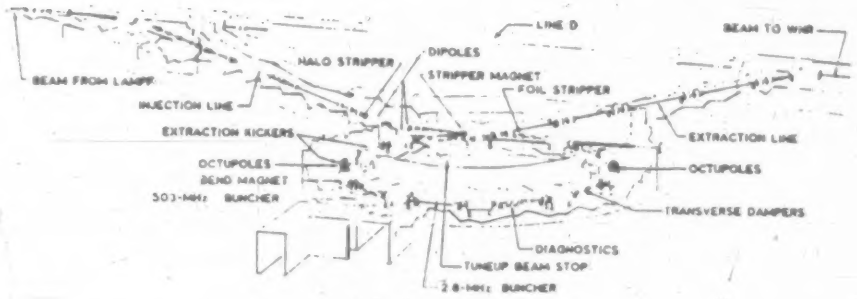

Fig. 1.
Plan view of the Proton Storage Ring.

Table I. PSR Operating-Mode Characteristics.

	Short Bunch, High Frequency	Long Bunch, Low Frequency
Parameter	Nuclear physics	Materials science
Number of bunches in ring	6	1
Bunch length in ring	1 ns	270 ns
Bunch interval in ring	59.63 ns	—
Buncher frequency	603.75 MHz	2.795 MHz
Protons/bunch accumulated	1×10^{13}	5.2×10^{13}
Accumulated turns	300	2100
Injection rate	120 bursts/s	12 pps
Filling time	108 μs	750 μs
Extraction rate	720 pps	12 pps
Peak circulating current	24.0 μA	100 μA

extraction. After accumulation is complete, the ring is emptied in a single turn by the fast-extraction kicker.

The PSR was authorized as a $21.8-million construction project in FY 1981, and a staging building for development and assembly of equipment was built by the end of that year. Construction of the main-ring tunnel and its associated equipment building started in May 1982 and is now complete.

It was necessary to develop specialized equipment systems for the PSR, including an intense negative-ion source, a beam chopper to provide the desired beam-bunch pattern, kicker magnets to deflect the beam into and out of the ring, and beam bunchers to compress the beam into well-defined short pulses. These developments have been under way for several years and satisfactory designs are proven for all systems. Final component assembly is in progress.

Procurement of standard equipment, such as magnets and vacuum components, is nearly complete and installation in the ring has started.

First operation of the PSR is expected on schedule in the spring of 1985. At first the beam current will be small, but as tuneup proceeds, the beam current will increase and we expect to reach the 100-μA level at the end of FY 1986.

WNR Upgrade

R. Woods

The WNR upgrade will raise beam-handling capability to the 100-μA level of the PSR design. The project requires improvements to the proton beam-transport line and the target-moderator-reflector (TMR) system.

To allow continuing hands-on maintenance of the proton beam-transport line under higher current conditions, beam losses must be kept low, requiring a larger aperture in the beam-transport system. The change from H^+ to H^- and the revamping of the switchyard also require reworking the beginning of Line D. There are time-sharing modes in which some beam will be going to the PSR and other beam pulses will be going either to the WNR or to the neutrino facility. A kicker magnet and stripper foil will be mounted in Line D to permit this time sharing.

The major thrust of the upgrade will be seen in the TMR. The increased current, from 10 to 100 μA, must be dissipated in the new design. We are also planning for a depleted uranium target and designing to permit the installation of a boosted target in the future.

The new concept for the TMR is shown in Fig. 2. The concept is a split target with a void between and moderators located around this void in an arrangement termed the flux trap geometry. The neutron flight paths that view these moderators thus will not "see" the neutron target itself. This arrangement significantly reduces the background of unwanted high-energy neutrons.

The existing WNR flight paths will view these moderators. The upper target will be provided with wing moderators that can be viewed by future flight paths. In this design the target and moderators are surrounded by a 1-mm-diam cylinder of material that reflects neutrons back into the moderators and also adds to the shielding.

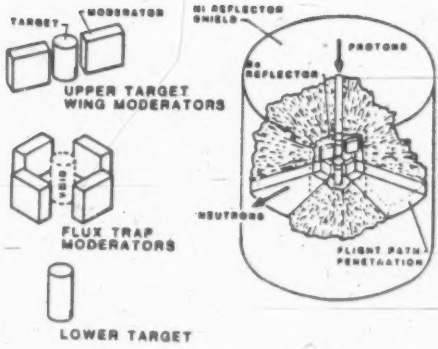

Fig. 2.
New concept for target-moderator-reflector (TMR) system.

The installation of a depleted uranium target in the spring of 1985 will give a factor of ~2 in useful neutron production. A liquid-hydrogen moderator also will be installed at that time to provide a source of cold and ultracold neutrons. A separate insertable target with little or no moderation will be provided for higher energy neutron experiments.

The increased neutron flux resulting from these improvements requires an additional 0.6 m of iron shielding above the WNR target for equipment protection; additional shielding and a water-cooled beam stop also will be provided below the WNR target.

Experimental Halls Expansion

H. Robinson

The original plan for the existing WNR experimental hall did not contemplate the 100-fold increase in neutron source capability made possible by the PSR. This greater intensity and optimized pulse structure from the PSR transforms the source into the most intense spallation neutron source in the nation, and perhaps in the world. These extraordinary capabilities have proved attractive not only to the Los Alamos National Laboratory staff, but to a large contingent of researchers from universities and industry. Soon after the PSR becomes operational, the facility expects to host approximately 100 visiting experimenters each year.

To provide an adequate experimental area to accommodate the User community and permit the full use of the neutron source, construction funding of $15.7 million is requested for FY 1985 to expand the present experimental hall and support facility.

This funding will provide a 929-m², pre-engineered, high-bay structure attached to the east side of the existing hall on the existing grade. The hall will be equipped with the full complement of services required for six major neutron-scattering spectrometers. A 186-m² pre-engineered wing attached to this structure, shown in Fig. 3, will house quiet rooms, set-up areas, and restroom facilities.

In addition, a 1115-m² reinforced concrete subterranean structure attached to the west side of the existing hall at the same floor elevation will be built. The complement of mechanical and electrical services provided in the east hall will be installed here for six more experiments.

A 745-m², two-story, reinforced concrete and pre-engineered laboratory and support complex will adjoin the present control room and the west experimental hall. This building, shown in Fig. 4, will be equipped for offices and used for data collection and technician work space.

Modifications will be made to the existing hall to allow better access and control of experiments and to provide penetrations for additional neutron-beam tubes from the target crypt. The proposed project includes funding for the construction of three new spectrometers especially designed to make optimum use of the intense pulsed-neutron beam, plus funding for six additional data-collection computers and a hub computer for data analysis.

In summary, the combined floor space of the experimental halls (2230 m²) will more than quadruple the space available for the spectrometers and staging of experiments, thus assuring full use of the source for the national neutron-scattering program. The 743 m² of support area on the west side will provide adequate room for data collection and light technician service to experimenters using this world-class facility.

Line E for Neutrino Physics

T. Domeck and G. J. Stephenson, Jr.

The neutrino beam line designated Line E lies to the south of the LAMPF switchyard in the WNR complex, as shown schematically in Fig. 5. A kicker magnet was

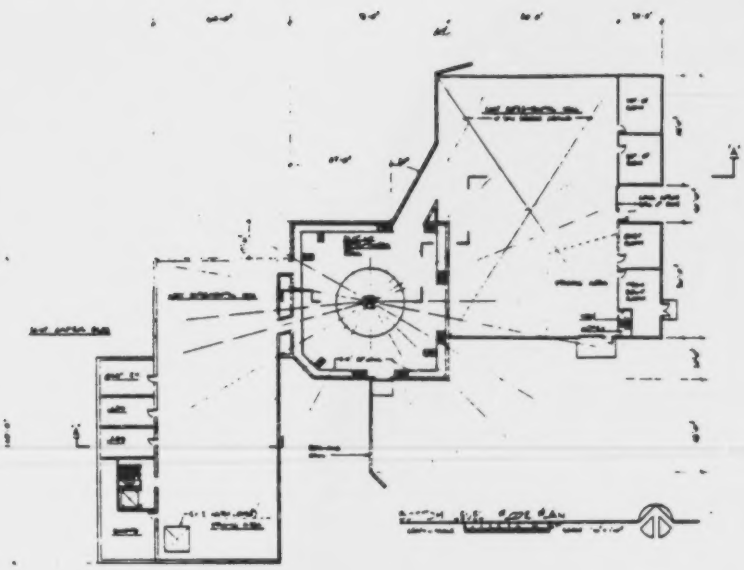

Fig. 3.
Lower level floor plan for experimental halls.

inserted into Line D to divert LAMPF 800-MeV macropulses into Line E with current initially at ~20 μA, upgradable to perhaps 200 μA. The beam line consists of four quadrupole doublets, two bending dipoles, a graphite target, and a tungsten beam stop. The target station is followed by a 12-m-long, 4-m-diam pion-decay tunnel and an iron-concrete shield approximately 9 m thick. The detector sits on a concrete pad beyond the iron shield in a concrete blockhouse used for cosmic-ray attenuation. Biological shielding is provided by concrete and earth overburden.

The target and beam-stop areas are water cooled and designed for remote handling. Iron shielding around the target allows manual maintenance to within a few feet of the target. The target is viewed by a beam pipe at 9° that allows one to monitor the pion flux continuously during the run.

Engineering for the construction and beam-line components was performed by Los Alamos Groups ENG-2 and P-12, construction was carried out by the Zia Corporation, and alignment was done by the Antares alignment crew (Group P-5). Beam-line magnets and power supplies were provided by LAMPF. Various beam components were fabricated or provided by university groups: vacuum pieces and electronics trailer (New Mexico State University); harp boxes (Temple University); target and computer (University of California, Riverside); and pion monitor (UCLA). Shielding material was provided by LAMPF and P Division.

A number of features incorporated into Line E will be used in future beam lines. The kicker magnet, its power supply, and the vacuum fan-out pipe will be duplicated for the PSR. The skew in Line E is a first at LAMPF and required a novel method of alignment, sighting along the bore tubes of the magnets. The harps for beam monitoring in Line E also are of a new design that will be duplicated for use in the PSR and other LAMPF beams.

The expected flux of muon neutrinos in the detector for a current of 20 μA is shown in Fig. 6. Provision has been made for a magnetic pion-focusing device that will be inserted just downstream of the target; it will enhance the neutrino flux by an order of magnitude. Flux calculations were performed using two Monte Carlo programs based on pion yields that were measured for carbon targets.

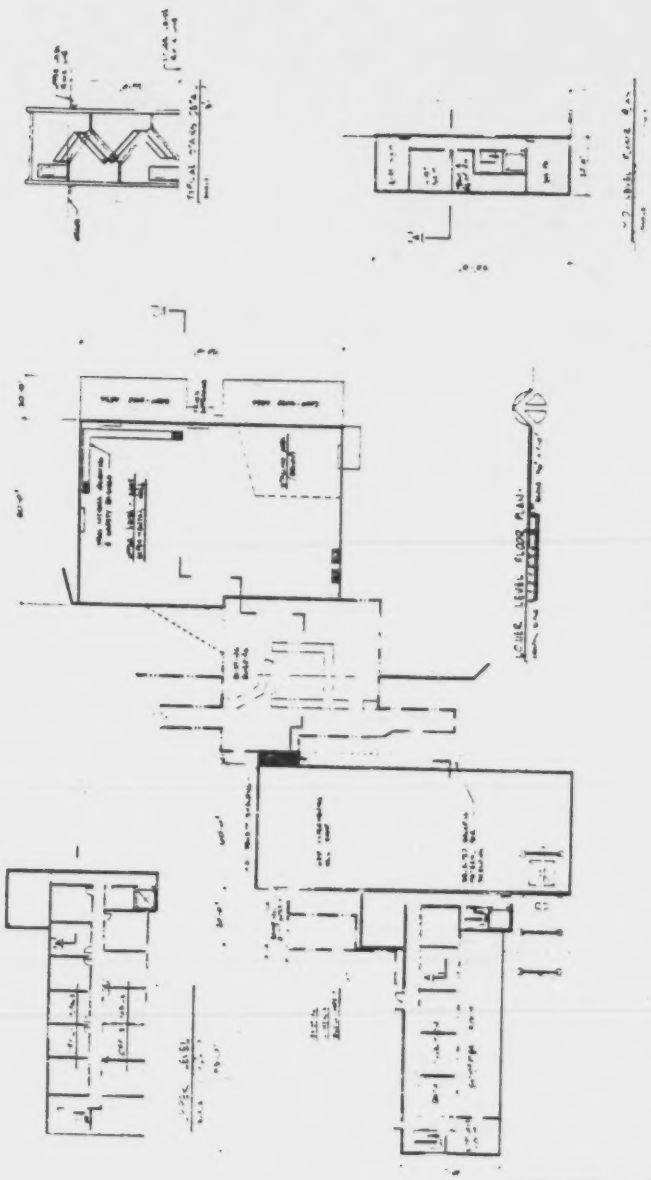

Fig. 4.
Upper level floor plan for experimental halls.

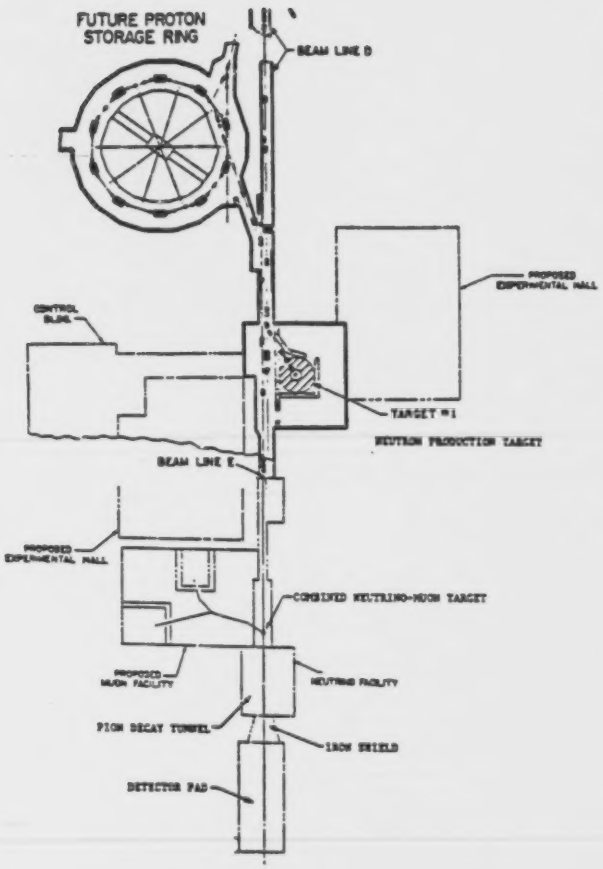

Fig. 5.
Layout of the WNR/PSR complex showing location of neutrino beam line (Line E), neutrino-production target, pion decay channel, shielding, and neutrino detector.

At the end of 1983, the construction is approximately two-thirds complete. Beam-line magnet elements and a vacuum system are installed and tested, and alignment is complete, as are the wire connections. A test to transport a small proton current was successfully performed in January 1984.

Publication

1. P. Denes et al., Phys. Rev. C 27, 1339 (1983).

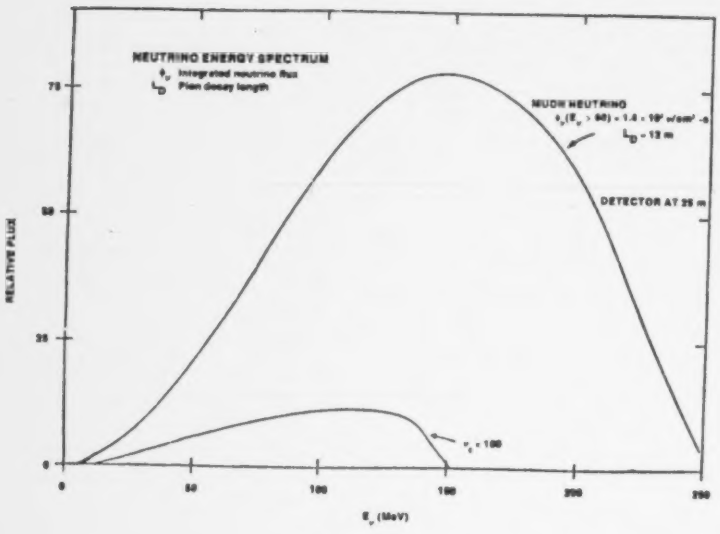

Fig. 6.
Calculated neutrino energy spectrum. Calculated flux is for a bare target with 20-μA beam of 800-MeV protons.

Research Programs

WNR/PSR Neutron Scattering Research

R. N. Silver, R. Alkire, G. Christoph, J. Eckert, J. Goldstone, A. Larson, R. Robinson, P. Seeger, P. Vergamini, and A. Williams

In 1983 the neutron-scattering group (P-8) announced a National User Program at the WNR/PSR facility. This announcement formally opened the facility to the national and international scientific communities in solid-state physics, chemistry, materials science, and biology. Proposals for the use of neutron-scattering instrumentation are reviewed by a nationally appointed Program Advisory Committee, which also reviews proposals for the Intense Pulsed Neutron Source (IPNS) at the Argonne National Laboratory. Proposals are reviewed on the basis of scientific excellence and optimal use of WNR/PSR characteristics.

The first two instruments in the formal User program are the Be-BeO Filter Difference Spectrometer (FDS) and the Single-Crystal Diffractometer (SCD). The FDS, shown in Fig. 7, is used for chemical spectroscopy, localized modes, and phonon density-of-state measurements. The FDS instrument is the responsibility of J. Eckert. The SCD, shown in Fig. 8, uses the Laue-TOF technique and is the responsibility of P. Vergamini. In 1983, 24 proposals for experiments were received and 15 were approved by the Program Advisory Committee.

In 1984 the Neutron Powder Diffractometer (NPD) will join the User program. The NPD is used for neutron powder diffraction by the Rietveld profile-refinement technique. The scientist responsible for the NPD is G. Christoph.

In 1983 major progress was made in the construction of neutron-scattering instrumentation. The present arrangement of instrumentation at the WNR is shown in Fig. 9.

(1) The prototype FDS and SCD instruments were completely rebuilt into well-engineered instruments suitable for the National User Program. These modifications greatly improved instrument performance and reliability.

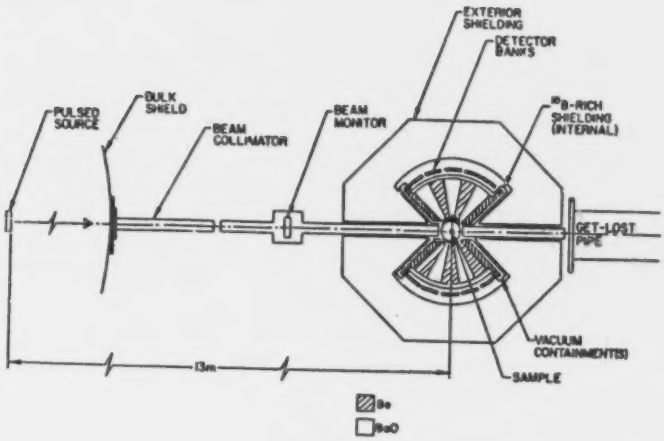

Fig. 7.
Filter Difference Spectrometer.

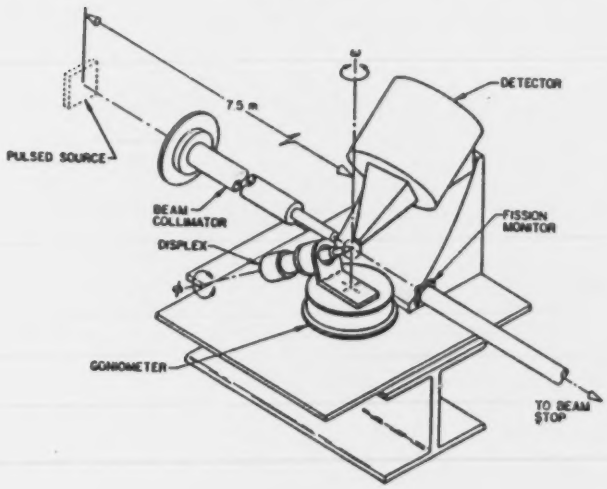

Fig. 8.
Single-Crystal Diffractometer.

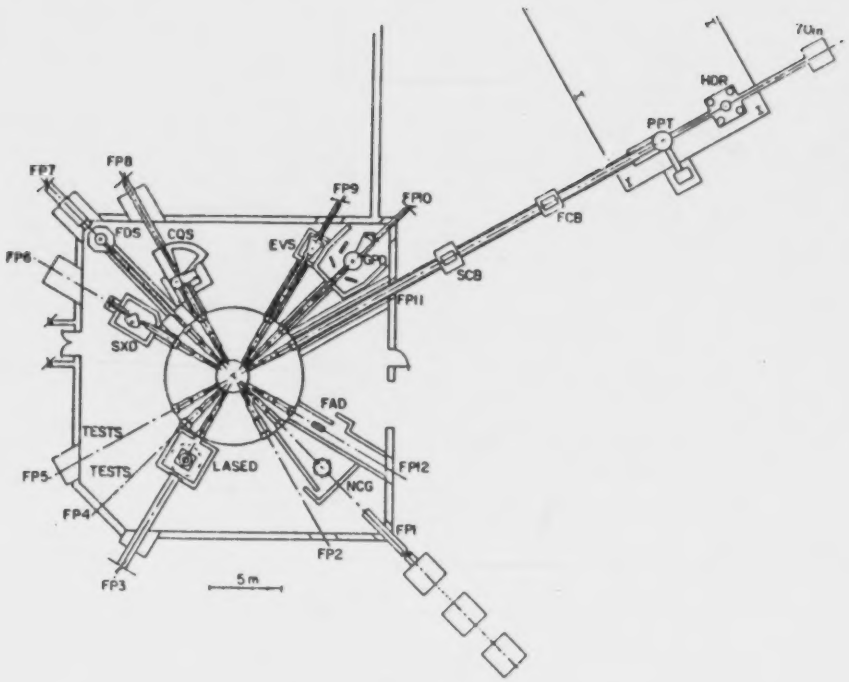

Fig. 9.
WNR layout of instrumentation.

(2) A prototype Constant-Q Spectrometer (CQS) began operation. The CQS, shown in Fig. 10, will be used to study elementary excitations, such as phonons and magnons in single-crystal samples.

(3) The nuclear-resonance-filter difference technique for electron-volt spectroscopy was extended to low-Q measurements appropriate for the study of magnetic and electronic excitations. In a collaboration with the Rutherford Appleton Laboratory, a prototype low-Q electron-volt spectrometer (EVS) was constructed and brought into initial operation at the WNR.

(4) An instrument optimized for low-angle diffractive scattering with epithermal neutrons at high intensities and low resolution is required for diffraction of liquids and amorphous materials. Such an instrument requires special attention to keep backgrounds low. A protoype diffractometer for liquid, amorphous, and special-environment materials (LASED) built with these goals in mind began operation at the WNR.

(5) A new sample environment container was constructed for the NPD, and additional detectors were installed.

Some highlights of neutron-scattering research in 1983 included the following.

- ***First Molecular Hydrogen Complex***
  P. Vergamini and A. Larson (P-8) and H. Wasserman and R. Ryan (INC-4)

  The structure of the first complex that reversibly binds molecular hydrogen was determined by single-crystal neutron diffraction at the WNR facility. This is an intermediate species in the catalysis of hydrogen, a long-sought missing link. The structure is shown in Fig. 11.

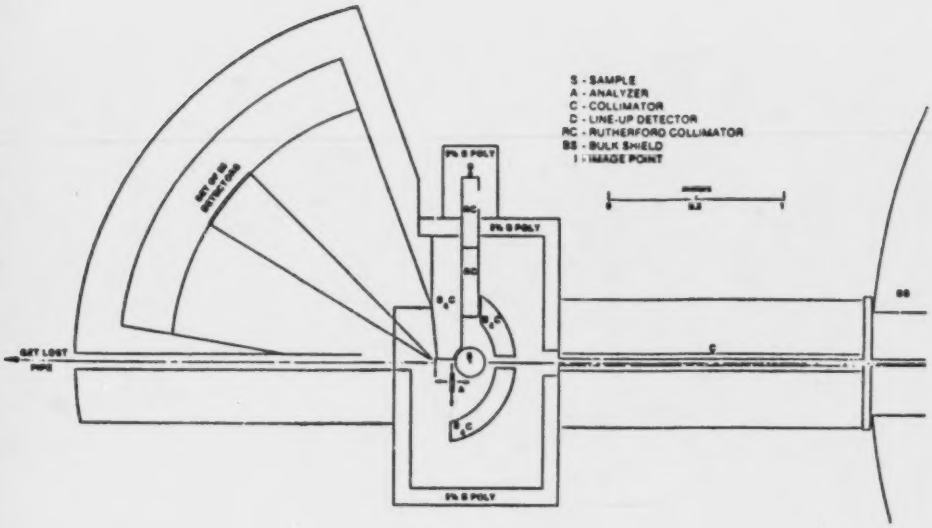

Fig. 10.
Schematic of the Los Alamos Constant-Q Spectrometer.

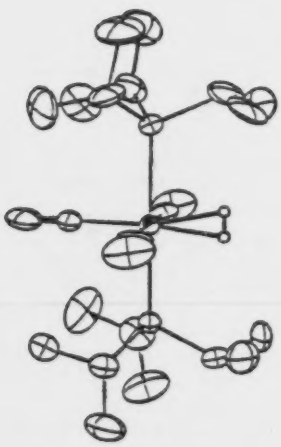

Fig. 11.
Molecular hydrogen complex.

- *High-Pressure Structure of ReO_3*
  R. Alkire, A. Larson, J. Schirber, and B. Morosin (Sandia National Labs.)

  ReO_3 is an unusual material because it undergoes a "compressibility collapse" at high pressures with a factor-of-10 decrease in compressibility above 10 kbar. The long-sought structure of the high-pressure phase has finally yielded to a time-of-flight neutron-scattering experiment in which one can take advantage of the strong penetrating power of the neutron and its ability to Bragg scatter at fixed angles with a white neutron beam in a high-pressure (15-kbar) cell using the SCD.

- *Hydrogen Sites in PbO_2 Battery-Plate Material*
  J. Eckert, J. Goldstone, J. Jorgensen, and R. Varma (Argonne National Lab.)

  The problem of hydrogen bonding in electrochemical cells is of immense practical interest. The strong penetrating power of the neutron, its sensitivity to hydrogen, and the high epithermal flux of the WNR facility make it a very suitable probe for addressing practical problems of this sort. Figure 12 shows inelastic neutron spectra taken with the Filter Difference Spectrometer of PbO_2 before and after

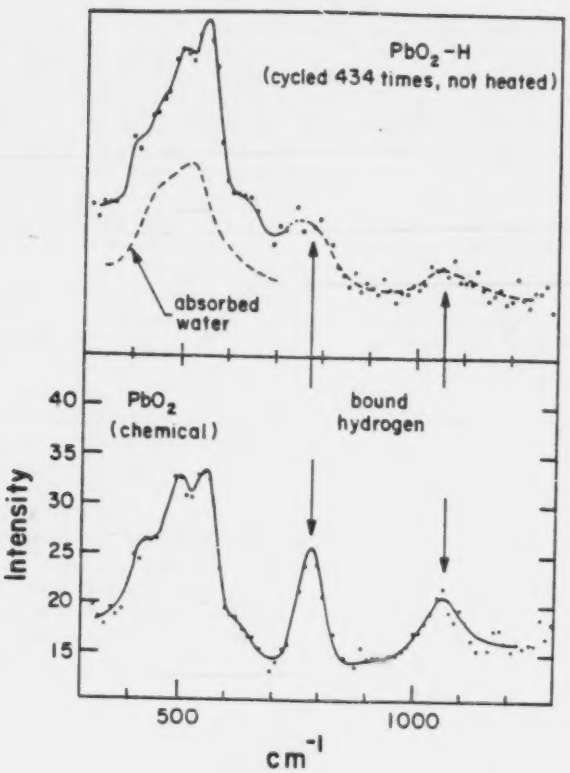

Fig. 12.
Inelastic neutron spectra of lead dioxide PbO_2 battery-plate material.

cycling. The spectra clearly show that the hydrogen introduced in the cells appears as vibrational modes of water H_2O and not as increased bound-hydrogen modes.

- ***Octahedral-Site Occupancy in Rare-Earth Hydrides*** *J. Goldstone, J. Eckert, G. Venturini, and P. Richards (Sandia National Labs.)*

In LaH_x, CeH_x, and other rare-earth hydrides, the hydrogen atoms primarily occupy tetrahedral sites until $x > 2$ is reached, at which point octahedral sites begin to be filled. The relative occupancy of these sites can be determined by the differing vibrational modes in inelastic neutron scattering and by powder diffraction. In YH_x, octahedral sites were found to be occupied before $x = 2$ composition was reached, and the occupation of these sites increased with decreasing temperature, in contradiction to expectations of increasing order at low temperatures. Experiments at the WNR using the FDS and NPD instruments showed that the "octahedral" sites were not quite octahedral as the temperature decreased, leading to an increased degeneracy that could explain the observed temperature dependence.

Other important activities in the neutron-scattering group in 1983 included the following.

- ***Development of a Proposal for the Expansion of the Experimental Halls at the WNR Facility.*** In accordance with the recommendations of the DOE review committees (Brinkman I and II, and Rowe), a proposal has been developed and submitted to the

DOE for expansion of the experimental halls, computer support, and instrumentation in order for the WNR/PSR to serve as a national User facility. This proposal was submitted for FY 1985 funding.

- ***Workshops and Conferences.*** A workshop was held in September 1983 on "Frontiers in Condensed Matter Physics with the WNR/PSR Pulsed Neutron Source," chaired by R. Birgeneau of MIT. A mini-workshop was held in November on "Biological Applications of the WNR/PSR Facility." Planning was carried out for a conference to be held in February 1984 on "High-Energy Excitations in Condensed Matter," and commitments were made to sponsor an "International Conference on Neutron Scattering" in August 1985 in Santa Fe.

WNR/PSR Nuclear Science

Search for Resonance Structure in Few-Nucleon Systems

P. W. Lisowski and G. F. Auchampaugh (P-3); M. Moore and G. Morgan (P-15); and R. Shamu (Western Michigan Univ.)

During the past few years, both experimental claims and theoretical predictions for the existence of dibaryon resonances have been made. The conventional meson approach interprets observed structure in the nucleon-nucleon system as resulting from inelastic channels in various partial waves. A more exciting possibility is that the resonances may result from six-quark bound states. In this model the nucleons are pictured as two bags of quarks, with the resulting overlap producing a rich density of dibaryon states. Before experiments performed at Los Alamos in 1982 and 1983, there was no undisputed picture of the energy or width of the proposed resonances. In fact, searches at LAMPF and elsewhere had insufficient energy resolution to observe the narrow structure predicted by some models.

A search for resonance structure in the nucleon-nucleon system was completed by performing a high-resolution, high-precision *np* total cross-section measurement over the entire range of interest. These data showed no evidence for narrow structure. A broad anomaly previously seen in the *np* system, attributed to an $I = 1$, $^3F_3$ dibaryon resonance, was confirmed. An $I = 0$, $^1F_3$ state proposed by other authors was not observed. From 200 to 700 MeV, our data (Fig. 13) indicate that existing cross sections may be as much as 6% too low.

A second set of measurements searching for resonance effects in the nine-quark system *nD* was partially completed in 1983. These data will provide accurate cross sections to test both the theory of binding effects in the

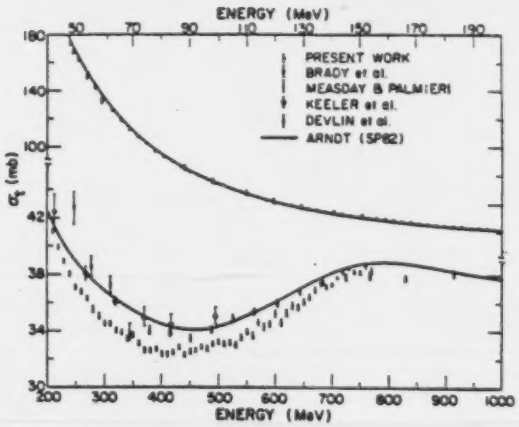

Fig. 13.

Comparison of present results with selected high-accuracy *np* total cross-section data and with phase-shift predictions. The upper (lower) data correspond to the upper (lower) energy scale. Note that the cross-section scale for the upper data is a factor of 10 smaller than that for the lower data.

deuteron and charge-symmetry effects in the three-nucleon system.

REFERENCE

1. P. W. Lisowski, R. E. Shamu, G. F. Auchampaugh, N. S. P. King, M. S. Moore, and T. S. Singleto... "Search for Resonance Structure in the *np* Total Cross Section Below 800 MeV," Phys. Rev. Lett. 49, 255 (1982).

High-Resolution Nucleon-Induced Charge-Exchange Reaction Studies at 800 MeV

P. Lisowski (P-3); G. Morgan and N. King (P-15); and P. Craig, D. Lind, R. Jeffesen, J. Shepard, J. Ullman, and C. Zafiratos (Univ. of Colorado)

Nucleon-induced charge-exchange reactions at bombarding energies of several hundred MeV have indicated that there are interesting but poorly understood processes involved. For example, in (p,n) reactions the strength of Gamow-Teller (GT) transitions may be computed from a simple sum rule. Recent data near 200 MeV indicate that approximately 30% of the expected GT strength is missing.

One exciting possibility is that the GT strength is "quenched" because of appreciable delta-isobar, nucleon-hole (Δ-hole) components in the low-lying GT levels. Such a theory, if correct, would imply that nucleon excitations such as the Δ, which have been considered to be too high in energy to be of importance in the low-energy domain, must be considered. Alternative conventional nuclear-structure effects also have been proposed to account for the GT quenching effect. Our studies of (p,n) reactions at the WNR will permit a search for the transfer of GT strength directly.

To study this and other aspects of nucleon-induced charge-exchange, we are using a 213-m-long 0° reaction angle flight path at the WNR, the only facility in the world capable of neutron energy resolution sufficient to permit the observation of nuclear-structure effects at 800 MeV. Preliminary results thus far obtained for (p,n) indicate that we can obtain information addressing four areas of interest: (1) the excitation of discrete levels leading to unique information on the isovector and isovector spin-flip parts of the effective *NN* interaction; (2) the nature of the Pauli-blocked quasi-elastic knock-on peak; (3) the nature of the broad resonances associated with the Δ and the possible implications for Δ-hole configurations in nuclear spectra; and (4) the excitation of charge-exchange analogs specifically using (n,p) reactions.

As an example of the above, we have compared our spectra for $^{13}C(p,n)$, shown in Fig. 14, with those available at lower energies and have conclusively identified GT and Fermi transitions, thus greatly extending the energy range over which these transitions have been studied.

To obtain angular distributions, we plan to install a beam swinger to change the angle of incidence of the proton beam and thereby obtain angular distributions using the existing equipment.

Neutron-Induced γ-Ray Processes

S. A. Wender and G. F. Auchampaugh (P-3); L. R. Nilsson (Tandem Accelerator Lab., Uppsala, Sweden); and N. R. Roberson (Triangle Universities Nuclear Lab., Duke Univ.)

Experiments that study γ rays in the energy range from 4 to 30 MeV produced by fast-neutron-induced reactions have been hampered by low data-acquisition rates, restricted neutron energy ranges, and high backgrounds. Typical systems for studying fast-neutron-capture reactions, for example, have been located at Van de Graaff accelerators and have used large-volume NaI detectors with massive active and passive shielding. These detector systems have been limited to one or two detectors because of their large size and high costs. The neutron sources have been limited in their energy range and resolution because they usually relied on secondary production targets [for example, the $D(d,n)$ reaction with gas cells].

During FY 1983 we developed a unique system to study high-energy γ rays produced by neutron-induced reactions. This system consists of five bismuth germanate (BGO) scintillators used in conjunction with a pulsed spallation neutron source at the WNR. The simultaneous acquisition of γ-ray excitation functions and angular distributions for incident neutrons in the energy range from 1 to 200 MeV is possible with this system (a paper describing this method has been accepted for publication in Nuclear Instruments and Methods). Figure 15 shows a diagram of the apparatus.

The physics program based on this system is being formulated as the particular parameters and capabilities of the system are determined. The program presently

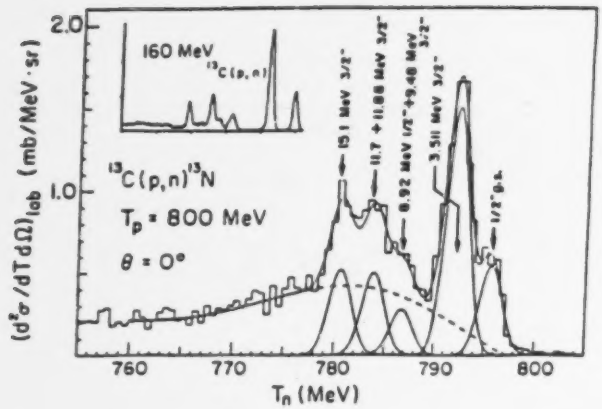

Fig. 14.
An 800-MeV $^{13}C(p,n)$ TOF spectrum at $\theta = 0°$. Overall resolution is approximately 2.5 MeV (FWHM). Arrows indicate expected locations of peaks observed in the 160-MeV spectrum shown in the inset. The smooth curves indicate best fits to the background and peaks.

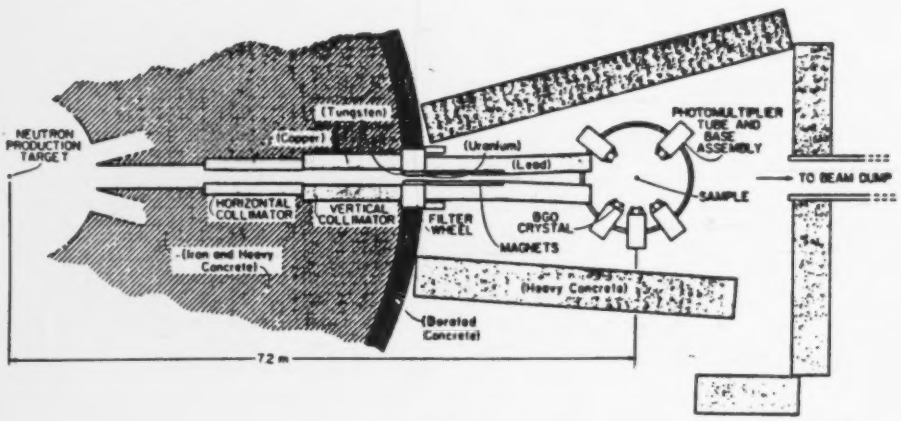

Fig. 15.
Experimental setup showing neutron collimators, shielding, and detector assembly.

consists of studying two broad areas: (1) inelastic neutron excitation of γ rays from bound states using the (n,n') reaction, and (2) fast-neutron-capture reactions into the giant-resonance region of nuclei.

In addition to these two programs we are also investigating the properties of the BGO detectors to optimize their characteristics.

Inelastic γ-Ray Production. As an initial test of the system, we measured the $^{12}C(nn'\gamma = 4.44\text{-MeV})$ reaction cross section for incident neutron energies from threshold (4.9 MeV) to 100 MeV. This reaction previously has been studied up to 20 MeV. Figure 16 shows the results of our measurements. These data represent approximately 13 h of beam time.

In this run we used only four BGO detectors at $\theta_{lab} = 55$, 90, 125, and 140°. The data from these detectors were fitted to an expansion in Legendre polynomials,

$$d\sigma(\theta)/d\Omega = A_0 \{ 1 + \Sigma a_k P_k |\cos(\theta)| \} .$$

The a_2 coefficient to the order of $k = 2$ as a function of neutron energy agrees well with previous results, and is shown in Fig. 17. However, the data show the need for terms to the order of $k = 4$, consistent with the results of the $^{12}C(p,p'\gamma = 4.44\text{-MeV})$ reaction. Because only four detectors were used and two of them were at symmetric angles, the errors in the Legendre coefficients are large when the expansion includes $k = 4$ terms; a remeasurement is planned.

Fast-Neutron Capture. For our first fast-neutron-capture experiment we studied the $^{40}Ca(n,\gamma_0)$ reaction. Because the cross section for this reaction in the giant-resonance region is only on the order of 10 μb, we used a relatively large sample of natural calcium (500 g, 7.6 cm long by 7.6 cm diameter). Data were acquired for approximately 50 h. Preliminary analysis of the ground-state γ-ray yield as a function of neutron energy, corrected for incident neutron flux and neutron energy bin size, is

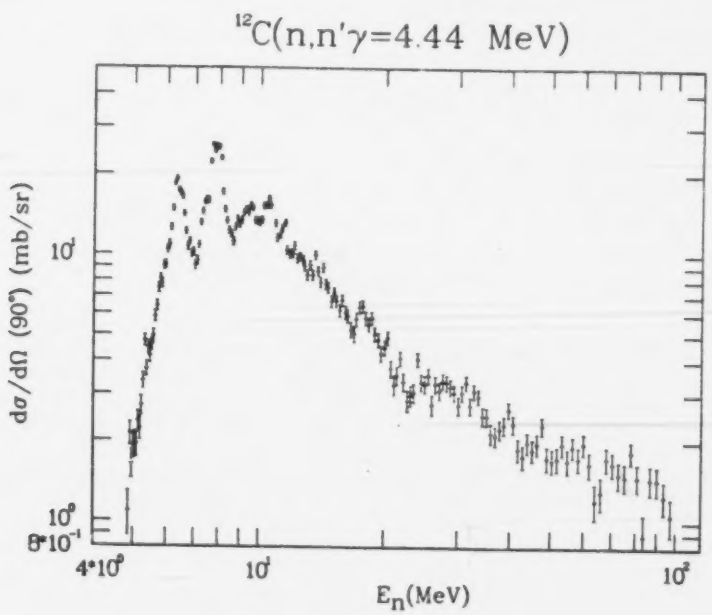

Fig. 16.
The 90° differential cross section for the $^{12}C(n,n'\gamma) = 4.44$-MeV reaction as a function of neutron energy.

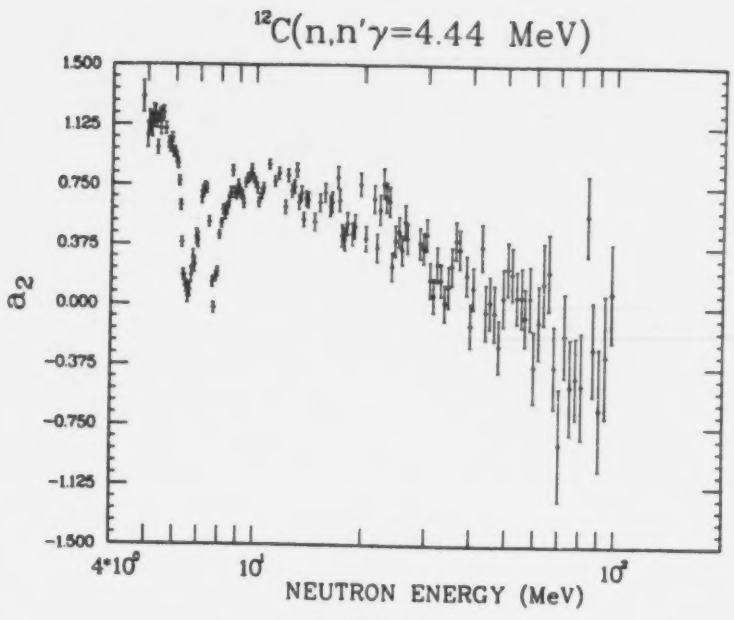

Fig. 17.
The A_2 Legendre polynomial coefficient for the 4.44-MeV γ ray from the $^{12}C(n,n'\gamma)$ reaction. The plot corresponds to fitting the data to A_0 and A_2 only.

shown in Fig. 18. The absolute cross section was obtained by normalizing to previous results. The maximum in the yield curve at $E_n = 11$ MeV corresponds to the peak of the giant dipole resonance in ^{41}Ca. The shape of this excitation function is in good agreement with previous results.

BGO Detector Development. The use of BGO scintillators to detect high-energy γ rays is a relatively recent development. We therefore have spent some time studying their characteristics and have considered methods to improve their performance.

In a paper submitted to Nuclear Instruments and Methods, we report the measurement of absolute efficiency of a 7.6- by 7.6-cm BGO detector at 15 MeV. We used the $^{13}C(p,\gamma_0)$ reaction at $E_p = 14.2$ MeV and determined the efficiency to be (51 ± 4)%. We expect to obtain response functions and efficiencies over the energy range 1-30 MeV.

Planned Work. We plan to continue our study of the $^{12}C(n,n'\gamma)$ reaction to improve the quality of the preliminary data, and to study ^{11}B, which shows several isolated resonances in the γ-ray yield for the 2.0- and 4.4-MeV states. In addition, we plan to measure the γ-ray production cross section of ^{14}N and ^{15}N.

The fast-neutron-capture program will continue the study of the giant-resonance region of nuclei — in particular, the search for the isovector $E2$ resonance in ^{208}Pb. In addition, we plan to search for giant resonances built on excited states in ^{14}C using the $^{13}C(n,\gamma)$ reactions. Such resonances previously have been seen in proton-capture studies. Visitors interested in participating in this research are welcome.

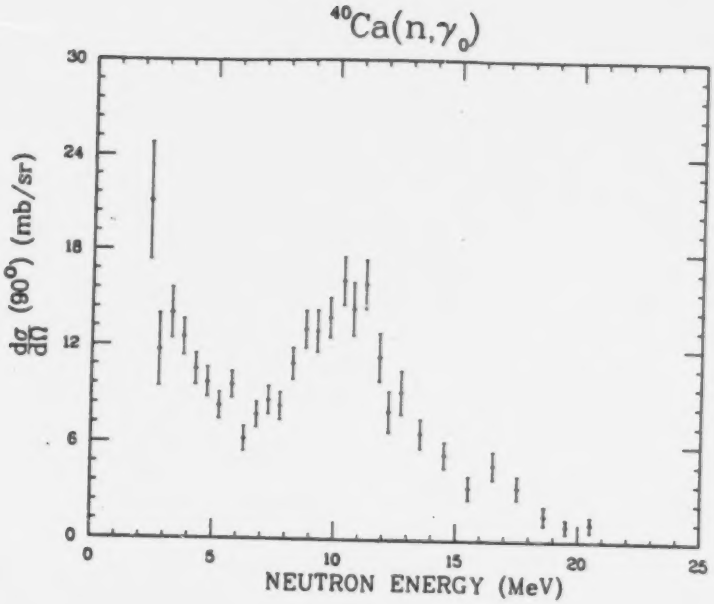

Fig. 18.
The 90° differential cross section for the $^{40}Ca(n,\gamma_0)$ reaction as a function of incident neutron energy.

Fission Fragment Angular and Kinetic Distributions for Actinide Nuclei

G. F. Auchampaugh (P-3); M. S. Moore (P-15); C. E. Olsen (MST-13); C. Goulding (Q-2); N. W. Hill (Oak Ridge National Lab.); and R. White (Lawrence Livermore National Lab.)

Angular, kinetic-energy, and mass distributions as functions of excitation energy play an important role in revealing the physics of the fission process. Answers to questions such as the importance of shell effects and angular momentum on the potential energy surface, the nature of vibration and complex structures associated with this surface, and the time scale and energy dissipation mechanism in fission are all addressed by such measurements. The paucity of high-quality data in this area opens a rich field of research in neutron physics.

During the past year we developed a double-volume Frisch-grid ionization chamber that permits simultaneous measurements of the angular, kinetic-energy, and mass distributions of each fragment as a function of neutron energy for low α-active targets. A detector with cathode foils of $^{233,238}U$ and ^{232}Th was used to obtain data from 0.8 to 20 MeV at the WNR facility. The ^{233}U data have been examined in detail and show systematic effects that are attributed to nonuniformity in the conductivity of the foils and base-line shifts because of pulse pileup from charged particles in the neutron beam. Further development and measurements are planned.

On the Nature of the Coupling in Subthreshold Fission of ^{238}Np

G. F. Auchampaugh and J. D. Moses (P-3); M. S. Moore (P-15); R. O. Nelson (P-9); R. C. Extermann (P-3 Visiting Staff Member); C. E. Olsen (MST-13); and N. W. Hill and J. A. Harvey (Oak Ridge National Lab.)

Although intermediate structure in subthreshold fission was first observed in the neutron-induced fission of ^{237}Np (Refs. 1 and 2), and the structure at 40 eV has been

extensively studied,[3,4] the nature of the coupling between the first and second wells of the ^{238}Np fission barrier remains unknown.

Inspection of high-resolution fission data[4] reveals that several levels are strongly enhanced in the fission channel, so that the mixing between the class II level underlying the intermediate structure and the class I background is neither extremely weak nor very strong. The mixing can, however, be attributed to two very different physical causes, as discussed by Bjørnholm and Lynn.[5] In the simplest case, the two classes of states may be weakly mixed because of a high intermediate barrier. Bjørnholm and Lynn refer to this kind of mixing as moderately weak mixing to a narrow class II state. Alternatively, the class II state may have a very large fission width that leads to weak mixing because of rapid decay of the class II state. This is known as very weak mixing to a broad class II state. The data for ^{237}Np have not clearly distinguished between these alternatives.

Our work was an attempt to resolve this question by measuring the fission and total cross sections with very good energy resolution (1) to expose any underlying broad resonance near 40 eV, if possible; and (2) to obtain good enough resonance parameters to permit detailed analysis of the fine structure of the class II fission resonances at 40 and 120 eV.

The total cross section was measured at the Oak Ridge Electron Linear Accelerator using a 78-m flight path and metallic samples cooled to liquid-nitrogen temperature (~77 K) to reduce Doppler broadening. The fission cross section was measured at the WNR using a 30-m flight path and a unique cryogenic ionization chamber that maintained the samples at a temperature of 84 K. Both experiments were designed to achieve the highest statistical accuracy and the smallest possible neutron resolution at the 40- and 120-eV class II states.

We attempted to determine the relative sizes of the coupling and fission widths of the subthreshold resonances in ^{238}Np by measuring and analyzing the fission and total cross sections with great care and by analyzing the resulting resonance parameters by a varicty of techniques. We believe we succeeded to the extent that we carried these techniques as far as they can reasonably be taken with current technology. We did not succeed in providing a clear answer to the nature of the coupling in ^{238}Np.

The multilevel analysis neither requires nor precludes the presence of a broad resonance underlying the 40-eV structure. The statistical analysis of the resonance-spacing distribution gives some indication that an anomalous intruder level is present at 40 eV, but the data also permit the alternate hypothesis. We believe that this problem will not be resolved by precise measurements of the type described here, but by a more sensitive measurement of a different type that can be carried out at the WNR.

V. STATUS OF LAMPF II*

H. A. Thiessen
(Los Alamos)

I will give you a report on progress since the beginning of the summer, including the physics that we learned at the July workshop. One way of organizing the physics we would like to do at LAMPF II is to order it by the needed energy of the proton beam. This list is presented in Table I.

One of the stars of the LAMPF II program will be muon-neutrino physics, which would be quite interesting if we had a 5-GeV proton beam. We could make a better muon factory than LAMPF, even with the 5-GeV beam. We would get variable-energy polarized protons, higher energy pions, and most likely the nuclear chemists would see the bulk of the changes in the reaction mechanism that occur between 1 and 10 GeV in the first 5 GeV.

At 12 GeV we get kaon physics; charge-parity (CP) violation is one of the important things—the study of the rare decays, the hypernuclei. We get kaon-nucleon scattering; we get a way to study the spectrum of the hadrons, some of which are missing, and the low-energy K-N scattering has lots of holes in the data. We get kaon-nucleus scattering, and we get more flux of pions, muons, and neutrinos. If we get up to a 32-GeV class of machine, then we have a decent antiproton factory, we get much higher-energy kaons and pions, and we have a much higher flux of low-energy kaons than we would have with lower-energy protons. And if we get above Brookhaven, then we begin to get into new territory; we could have a machine with the capability of the highest-energy polarized protons available anywhere, as well as improved kaon and antiproton flux.

Table I. Physics at Various Proton Energies.

5 GeV	Neutrino physics
	Improved muon physics
	Polarized protons
	High-energy pions
	Nuclear chemistry
10 GeV	Kaon physics: charge-parity violation
	Rare decays
	Hypernuclei
	Kaon-nucleus scattering
	More flux of pions and muons
30 GeV	Antiproton physics
	Higher energy K's
	More kaon flux
50 GeV	Higher energy polarized P
	Better antiproton beams

What I saw in the July Workshop was the best workshop ever held here on any subject. We brought in some new physics topics, including the high-$p_\perp$ exclusive processes that Glynnis Farrar talked about. We had some fine talks on high-energy antiproton physics; high energy means well above LEAR but nowhere near the collider energies. We briefly discussed extending the energy range of polarized protons, and we talked about glueballs. We learned that the long lifetime of the B meson and the apparent large mass of the top quark may make some huge differences in the details of our write-up of the kaon decays, but they may in fact make it even more interesting.

You should receive the Proceedings of the Third LAMPF II Workshop about January 1. I would like to thank Tarlochan Bhatia (he managed to solicit from you every talk save one, which was held up in the French postal strike) and the Proceedings production staff. It is a beautiful job—this is the best workshop we have ever had, and the best documented one.

At the end of the workshop, we were talking about a 32-GeV machine, something like the biggest machine at 12 kG that will fit on the mesa. This machine is shown in Fig. 1. It would be injected by H^- beam; it would be tunneled under the existing machine and would have four major experimental areas: a neutrino pulsed-muon area and three slow-extractive beam areas with a thin target upstream.

Our cost estimate for the 32-GeV machine was started before the workshop, but the numbers came out later. We had a machine that cost about $130 million. We had a stretcher that might cost half that, thus the total was $200 million for the machine and stretcher. We had four experimental areas at about $50 million each, with beams and detectors. So that gave us $400 million, and adding 20% extra for contingencies raised the total to roughly

*This report is excerpted from a presentation to the Seventeenth LAMPF Users Group Inc., Meeting, November 7-8, 1983. The full text is available in report LA- .

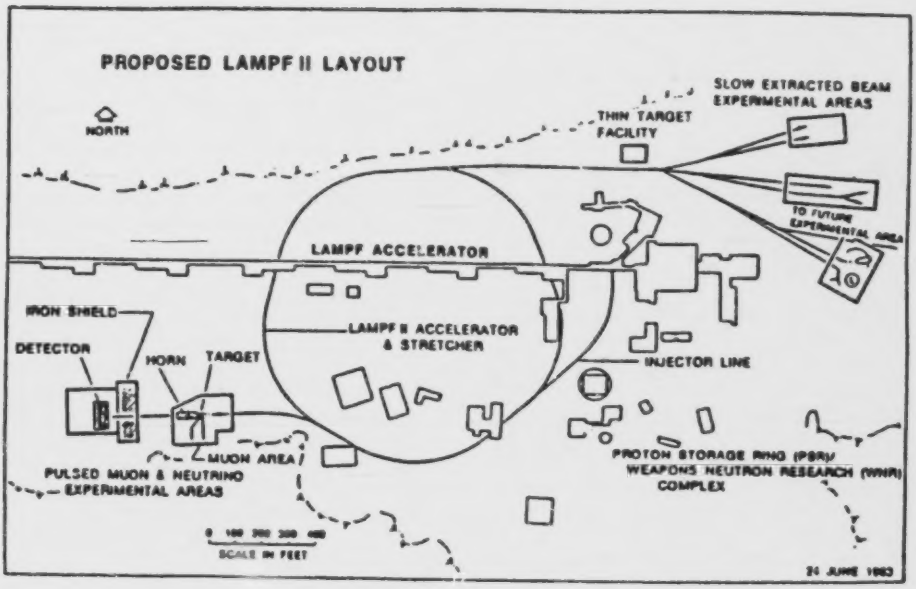

Fig. 1.
LAMPF II site layout

$500 million. We had a very expensive proposal as shown in Fig. 1, and that did not include cooled antiprotons, which may cost, as a wild guess, another $100 million.

At the end of the summer, the system consisted of the following: we had a 32-GeV accelerator and its stretcher, but we also had a booster. We did not know exactly what energy booster we wanted, and still do not, but the proposal included a booster, and because of a need for polarized beam, it had a stretcher on the booster so the unused pulses of the booster could be used for variable-energy polarized proton beam. We have not carefully priced this, but it costs about the same to build a 32-GeV machine with a booster or without. The big machine gets cheaper if we have a booster, but first we have to make up the additional cost of the booster.

The last day of the workshop I talked about a staged proposal; we would build the facility in several stages. The first stage, for example, might be just the injection line in the neutrino area. The second stage might be a booster that could feed that neutrino area, and maybe it would have one experimental area in addition, with the booster set up so that the next stage, which would be a higher energy machine, could use the same experimental area. And then we would add experimental areas and probably add the $\bar{p}$'s last. So, the features were: we had a booster, we had a higher energy machine, we had several experimental areas, and we build them one at a time.

Just before the workshop, the news hit that the Nuclear Science Advisory Committee group making a long-range plan decided that there should be a heavy-ion collider, and that such a collider represented a unique opportunity in the area of nuclear physics. And, given the constraints of that report, it is not possible to have two expensive facilities. And so LAMPF II was postponed for a very long time. I see no way, as the committee is now constituted and the ground rules are now set up, to build the full facility, even in stages, because it is recognized that the whole accelerator is going to be very expensive in the end, and what difference does it make if it is staged?

We must step back and ask, in some order, what does the country need? Let us say that it needs a next-generation e^+e^- or $\mu^+\mu^-$ collider somewhere. It needs a Desertron. I think we need some kind of a factory for fixed-target physics that includes the physics we have

been talking about. We appear to need a heavy-ion collider, and we are already committed to a 4-GeV electron machine.

At present, we are trying to come up with the minimum factory that we could build here. It would be at least a 12-GeV, 100-μa kaon factory. We have several ideas for reducing the cost. We can reduce the energy, which means reducing the counting rate, and thus it may be possible to eliminate the stretcher. Eliminating the stretcher would dictate that the duty factor be one-third instead of 1, but that goes with the counting rate, and so it is probably acceptable. And as you saw, if we had no money in the accelerator, it would still cost $200 million for the experimental areas, so we are thinking about ways to run with about half the number of beams talked about at the workshop. (I think we had 15 or 16 beams at the end of the workshop.) And we may be able to save some money by reconfiguring the existing experimental areas.

I remind you about the flux arguments. Figure 2 shows a plot on linear paper of the kaon yield at fixed 1.4-GeV

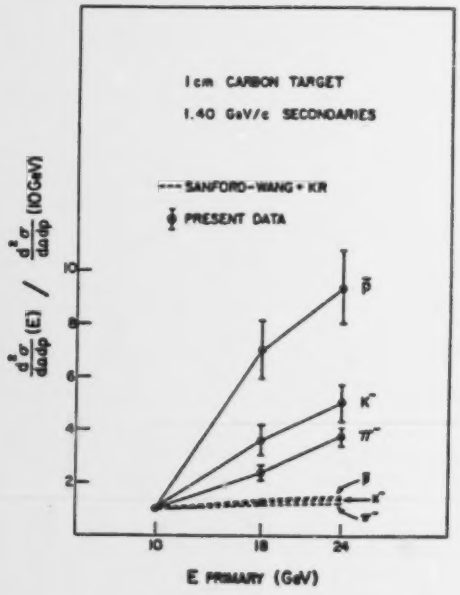

Fig. 2.
Energy dependence of production cross sections on 1-cm carbon target normalized to 10-GeV cross section.

secondary energy as a function of proton energy. You can see that there is no sharp structure in the region proposed. The kaon yield is about 5 times more at 24 GeV than at 10 GeV, so the first factor we have lost in lowering the energy is the beam power. And then maybe another factor of 2 at most. It is a penalty we have to pay if we lower the beam energy, but it is not a dramatic one, and there is no clear threshold in the region 10-24 GeV for kaons. For $\bar{p}$'s it is different. If we go down much below 32 GeV, we lose fast on the $\bar{p}$'s.

Suppose we propose a 12-GeV machine like the one shown in Fig. 3. It would have 10 times the flux of the existing Brookhaven AGS slow-extracted beam, 20 times the flux of kaons below 1 GeV, and of course at Brookhaven they have to divide the beam many ways. We have to divide the beam many ways; let us call that even. So as a kaon factory, it is 20 Brookhavens. A 12-GeV machine is smaller, there may be a cheaper site, and we have a way to do it with no interference with PSR. Figure 3 is a scheme in which we reconfigure Area A; that means at least a shutdown like the Great Shutdown for Area A. And in that picture, Areas B and C are not easily used after we go to LAMPF II.

To see this concept in its simplest form, let us put a ring as shown, where it does not cross through the forest of existing buildings. It could be built at the same elevation as the present linac, and it could be injected off the present Line B and reinjected into the switchyard with minimum trouble. We could then reconfigure Area A to have some very useful beams in it. Should we decide to have a booster for such a machine, there is a natural location for it in the present parking lot for Area B, and there could be an experimental area for the booster.

Figure 4 is a blown-up drawing of Area A reconfigured for 12 GeV. It is conceptual only. The idea is to extract from the accelerator at one point and to provide, down a single line, the capability of alternating pulses of a fast-extracted beam and a slow-extracted beam. On the slow-extracted pulses, which would have duty factor of about one-third, the beam would hit the first three targets.

The first target might be used for making a stopping K^+ and K^- beam off the same target, with a first magnet being a bending magnet common to both. This system gives very clean beams, and it is clear that there is a need for stopping K^+ beams and stopping K^- beams, both. When there are stopping beams, the energy is rarely varied. So this scheme might work for kaons even though they are coupled and even though it is an awkward arrangement for muon beams at existing meson factories.

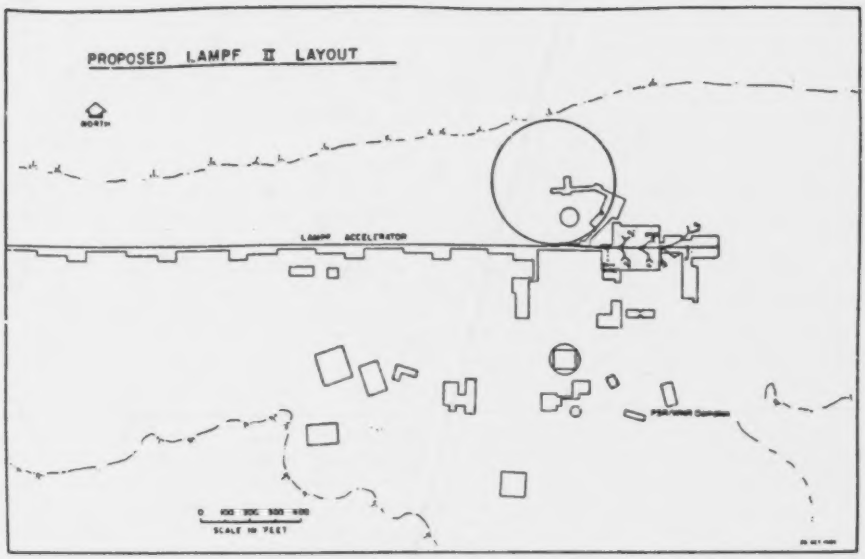

Fig. 3.
A scheme for a 12-GeV machine.

The new target cell might include two medium-energy beams, and two examples might be an EPICS II and the 1.8-GeV kaon beam. Anything could go there, but, looking at that target, they may have to be nonzero-degree beams independent of each other.

The third target cell would contain the high-energy beam. If the machine is only 12 GeV, then the beam would be about a 6-GeV $\pi,K,\bar{p}$ beam and it could share that target with a K^0 beam. Bob Macek has suggested putting a bending magnet right upstream of the target and aiming the proton beam toward the south side of the building so that 0° for K^0s points into a useful experimental area, and then bend it back to get onto the dump. There could be a muon beam produced at this thick target. We would have the best duty factor and the best muon rate. There could also be a test beam at this target. So for the slow-extracted beams, we would get a nice set containing most of the secondary-beam physics shown in the proposal.

Another idea for the fast-extracted beam is to let it go on down the same beam line, either with rotating targets with holes, or the beam kicked around the upstream targets, or slow and fast-extracted beam scheduled during different time periods. In any case, there is a fourth target, which is used as a neutrino target and a pulsed-muon target. For neutrinos, there is a horn with the existing Line A as the decay region, putting the neutrino area downstream of the present beam stop. We might even be able to use the Biomed beam as a pulsed-muon beam if we add a vacuum chamber. So we have beautiful neutrino physics, beautiful pulsed-muon physics, beautiful kaon physics up to 6 GeV, and somewhere else where we can get a not-too-expensive, low-energy, variable-energy polarized beam. If we choose to have no booster, we could put a jet target in Area B. Polarized proton experiments could be done at variable energy by just watching what happens as the circulating beam energy changes. The beam could be polarized; we will certainly design the accelerator for polarized protons.

What does this scenario cost? Table II shows the accelerator cost estimate. We scaled the cost estimate we had for the 32-GeV machine and came up with the following set of numbers, which says that for about $60 million, we could build such a machine. We made a guess,

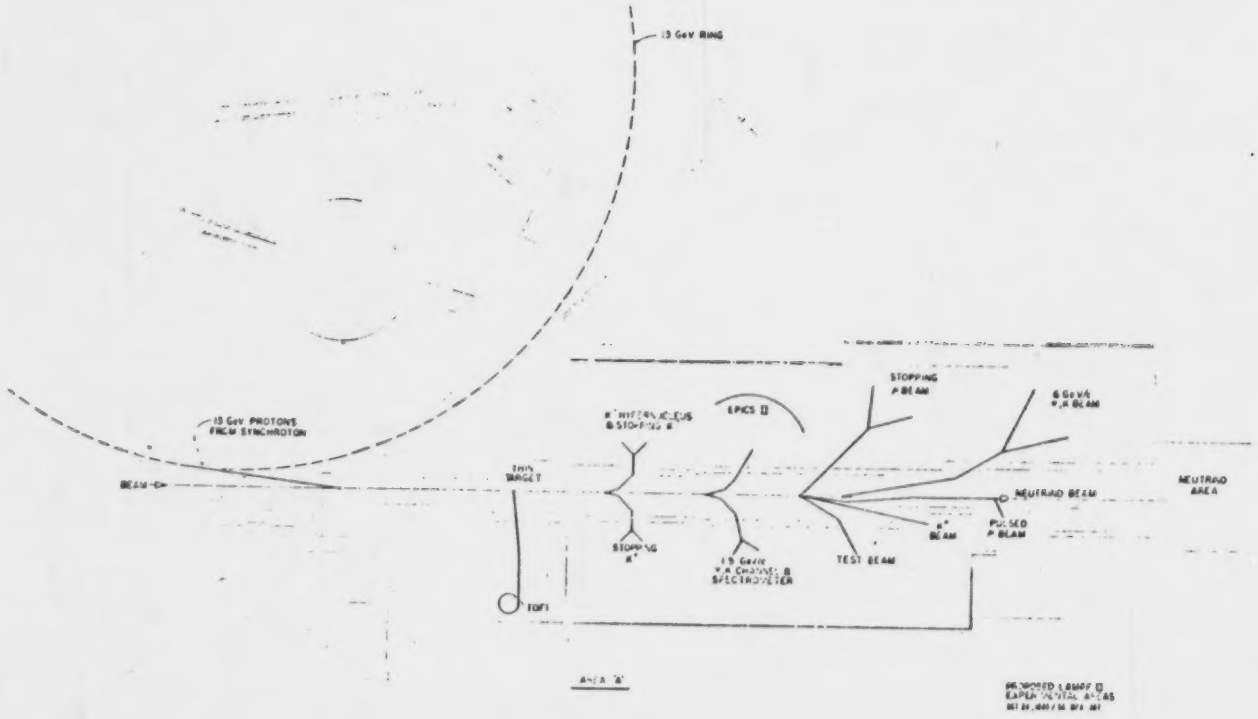

Fig. 4.
A conception of Area A reconfigured for 12 GeV

Table II. Accelerator Cost Estimate 10/28/83.

		Dollars (in Millions)
Accelerator		
	Magnets and power supplies	$ 15.8
	rf system	13.6
	Diagnostic and controls	12.0
	Vacuum	6.0
	Extraction systems	2.0
	Fast dampers	1.5
	Injection	1.4
	Fast abort and dump	1.0
	Collimator system	1.0
	Bucket rotator	1.0
	LAMPF injector mods	0.3
	Installation	7.5
		$ 63.1
Buildings		
	3 electromechanical equipment	5.4
	1500-ft tunnel @ $2000/ft	3.0
	Support lab	2.0
	Office for 100 people	2.0
	Control building expansion	1.3
	Ring entrance building	0.2
		$ 13.9
Experimental-area mods		
	See Table III	68.0
	TOTAL	145.0
	Contingency +20%	29.0
	TOTAL (in 1984 dollars)	174×10^6

not yet verified, that we really can have efficient slow extraction from single ring that goes along with a lower intensity overall, a lower beam power overall. It may have a booster with a similar total cost. We have not proved that we can do it, but we are working on it.

The buildings are mostly mechanical equipment buildings for this new ring. We are making very good use of what we already have, so we need only a small number of additional buildings.

Table III shows the cost of the experimental area. Macek suggests reworking about two-thirds of the steel and concrete that we already have. We add 10 kilotons (kt) of new steel, some train—or canyon—fill (filling the trains containing the secondary beam lines out to a standardized cross section), and some new concrete. The costs for shielding, beam transport, etc., are shown. The biggest single item is the beams, seven beams guessed at $5 million apiece.

So we have a rather cost-effective experimental area where at least half of the funds go directly into things we want, namely, into the beams. By using Area A, we save shielding, beam transport, water, power, and buildings, and we can use the existing remote handling equipment; the final savings is over $30 million. The total cost, including a contingency in this year's dollars, is about $175 million, which is sufficiently close to Louis Rosen's guideline of $150 million to meet his request.

Table III. LAMPF II Experimental Area Cost Estimates 10/28/83.

				Dollars (in Millions)
Shielding installed				$18
		Cost		
	(Kilotons	Per ton	Total (in Millions)	
Reworked steel	20	$ 200	$ 4	
New steel	10	800	8	
Train fill	4	1000	4	
New concrete	10	200	2	
			$18	
Primary beam transport				6
Primary beam tunnel rework				1
Targets and target chambers (4 targets)				4
Rework beam-stop area and neutrino-area construction				5
Secondary beam lines (7)				35
Extend building				2
TOTAL				$71

VI. FACILITY AND EXPERIMENTAL DEVELOPMENT

The New Transition Region

A. A. Browman

Introduction

The first 100 MeV of energy gain at the LAMPF facility is provided by an Alvarez-type[1] accelerating structure operating at 201.25 MHz. The remaining acceleration is provided by the side-coupled linac,[2] which operates at 805 (≡4 × 201.25) MHz. The transition region (TR) connects these two types of accelerating structures and provides proper phase-space adjustments of the 100-MeV beams so they can be accelerated without loss in the side-coupled linac.

The original TR (Ref. 3) was unable to provide correct matching of H^+ and H^- (P^-) beams simultaneously without causing unacceptable beam losses. When only one high-current beam was being run at a time, the TR could be adjusted to handle it properly by allowing the other (low-current) beam to be not as well matched. The necessary "compromise tunes" were time consuming to achieve, and often did not result in very good beam quality for the low-current beams. In addition, the new Proton Storage Ring (PSR) was designed to use high-current H^- beams, so LAMPF will be required to operate with two high-current beams when the PSR comes on line in 1985. Thus, the decision was made to replace the TR.

Features of the TR

The most obvious requirement of the TR arises because the operating frequency of the side-coupled linac is an *even* multiple (4) of that in the Alvarez linac. Thus, for dual-beam operation the phase of one of the beams must be changed relative to the other one by 180° (805 MHz) (see Fig. 1). In the TR this is achieved by separating the beams and causing the paths followed by the two beams to differ in length by 8 cm (nominally) before they are recombined. Other functions that the TR must perform are the correct steering and matching of both beams. Detailed descriptions of these requirements may be found in Refs. 4 and 5.

Both the original and new TR are shown schematically in Fig. 2. In addition to the features described, the new TR includes larger apertures, additional diagnostics, a "straight-through" path, beam-path-length adjustment, quadrupole and steering magnets on all beam lines for independent control of each beam, and a much neater installation, as shown in Fig. 3. Considerable effort was

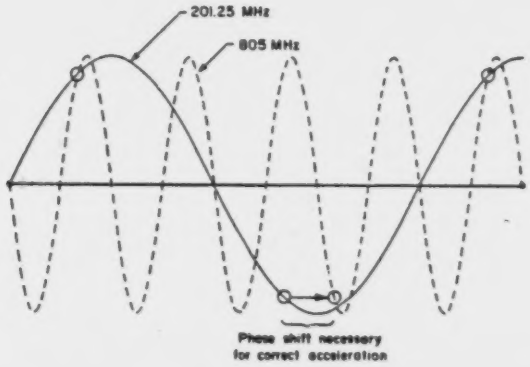

Fig. 1.
Representation of 201.25- and 805-MHz accelerating fields. The circles on the 201.25-MHz trace show the approximate location of the different sign beam bunches. Note that the 805-MHz wave would decelerate one bunch of particles if their phase were not shifted.

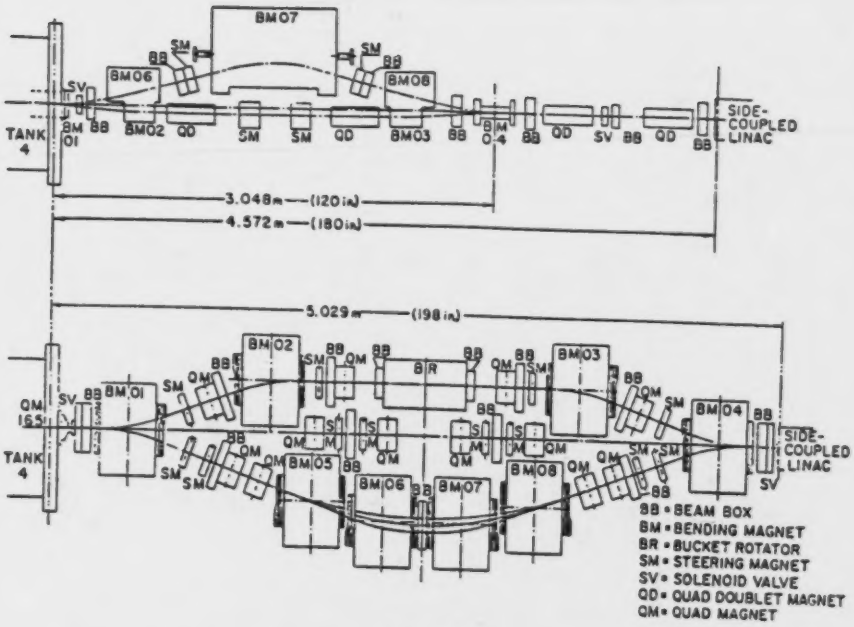

Fig. 2.
Original TR (top) and new TR (bottom). The first module in the side-coupled linac was moved to obtain more room. Each beam line in the new TR has its independent quadrupole and steering magnets. Space was allowed for longitudinal matching (bucket rotator) in the new TR.

expended to make the TR installation as uncluttered and serviceable as possible (see Ref. 6 for a detailed description of the mechanical fabrication of the TR, as well as a list of the drawings used in the TR construction).

To minimize beam loss in the side-coupled linac caused by "emittance growth" in the TR, field quality in the magnetic elements must be quite good. The magnets used in the TR were extensively mapped and trimmed (see Refs. 7 and 8 for a detailed report of the methods used and the results obtained). The final TR design enabled a single type of bending magnet, quadrupole magnet, and steering magnet to be used. This approach allowed spares for all elements to be built and mapped during construction of the TR.

Because the entire LAMPF facility would be rendered inoperable during the removal of the old TR and installation of the new one, extensive planning was necessary before the work began. Most major components were assembled and staged at the Equipment Test Laboratory (ETL) during production running and then moved to the beam channel during the shutdown period. As a result, we were able to resume operation with a new working TR by the end of the same shutdown period that was scheduled for experimental area maintenance and repairs.

Operation of the TR

Approximately 1 month was used to commission the new TR. During this time beams were run through all three beam lines, matched, steered, and checked for beam quality. A major effort was needed to get the diagnostic equipment checked out, but everything was working in time for production running.

By the end of 1983 we had run for several months with high-current H^+ beam (up to 900 μA) and low-current

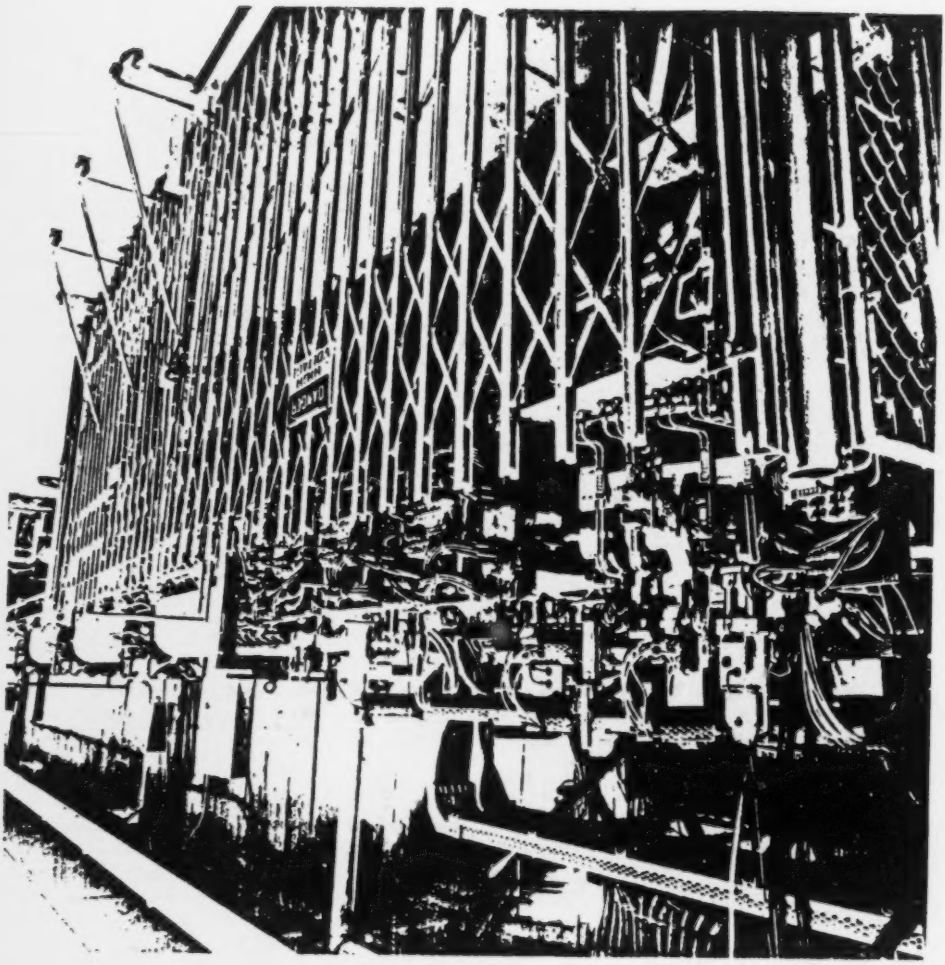

Fig. 3.
Photograph of the new TR. Note success achieved in cleaning up the installation; maintenance is considerably easier.

polarized H^- beams. Beam quality is improved, tuning is easier and faster, and the beams are stable.

At this time no changes to the TR have been necessary and we believe the TR will satisfactorily handle the high-current H^- beam when it becomes available in early 1985.

REFERENCES

1. D. A. Swenson, E. A. Knapp, J. M. Potter, and E. J. Schneider, "Stabilization of the Drift-Tube Linac by Operation in the π/2 Cavity Mode," R. A. Mack, Ed., Sixth Int. Conf. on High-Energy Accelerators, Cambridge, Massachusetts, September 11-15, 1967, Cambridge Electron Accelerator report CEAL-2000 (1967), pp. 167-173.

2. E. A. Knapp, "High-Energy Structures," in *Linear Accelerators*, P. O. Lapostolle and A. L. Septier, Eds. (North-Holland, Amsterdam, 1970), pp. 601-616.

3. D. A. Swenson, "The Transition Region," Los Alamos National Laboratory Group MP-3 document MP-3-75, February 24, 1969.

4. O. R. Sander, "LAMPF Transition Region," Los Alamos National Laboratory report LA-9315-MS (June 1982).

5. O. R. Sander, A. A. Browman, and E. D. Bush, "Redesign of the LAMPF Transition Region," in Proc. of the 1981 Particle Accelerator Conference, Washington, DC, IEEE Trans. Nucl. Sci. NS-28, 2914-2915 (1981).

6. E. D. Bush, Jr., J. D. F. Gallegos, R. Harrison, V. E. Hart, W. T. Hunter, S. E. Rislove, J. R. Sims, and W. J. Van Dyke, "LAMPF Transition Region Mechanical Fabrication," to be available in a Los Alamos National Laboratory LA-UR document.

7. A. A. Browman, "TR Bending Magnet Description," Los Alamos National Laboratory Group MP-DO memo, August 18, 1983.

8. A. A. Browman, "TR II Quadrupole Magnets," Los Alamos National Laboratory Group MP-DO memo, April 7, 1983.

New Experimental Staging Area

The Experimental Staging Area was completed and in use in September 1983. The primary purpose of this 9000-sq-ft facility is to provide an area for experimental teams to assemble and test their experiments before installation in the experimental caves.

The facility is equipped with a 30-ton bridge crane and ample utilities for User requirements. In addition, an office is available, as well as power pedestals adjacent to the Staging Area to accommodate trailers.

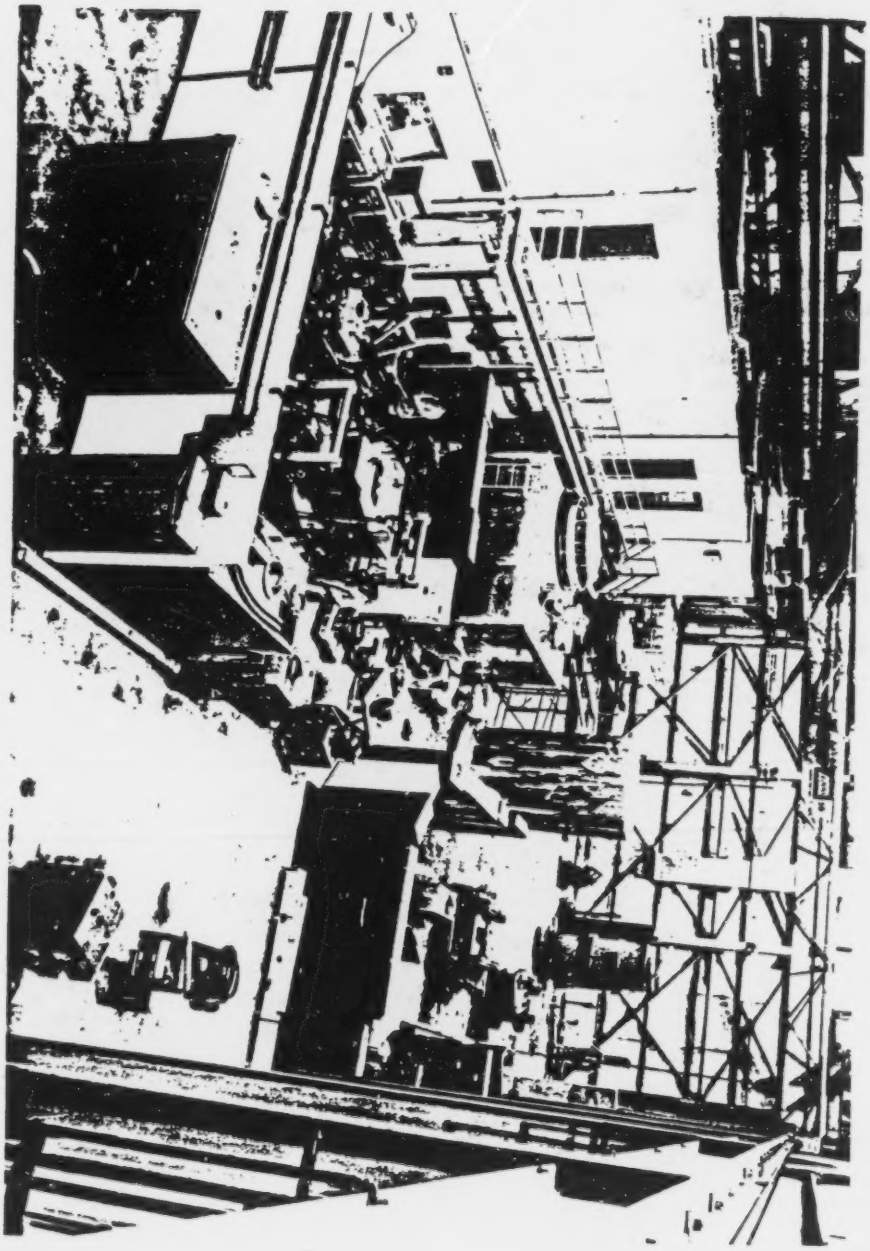

Fig. 1.
New Experimental Staging Area.

EPICS and HRS Data Systems

Group MP-10 spectrometer software has been rewritten in the conversion from RSX-11D to -11M operating systems. In addition, some special features from the old spectrometer software are now available in the new standard Q program from MP-1. Improvements include core histogram storage, easier implementation of data cuts, data reduction before taping, and batch replay on VAXes with spooled tapes.

An array processor (a used AP-120B) has been acquired for EPICS and upgraded to be compatible with the two in place at the HRS, but software conversion to RSX-11M is still in progress. The HRS array processors have developed problems that have been difficult to resolve during production.

Other planned upgrades include the addition of a VAX-11/730 to replace the on-line PDP-11/45 at either HRS or EPICS, and higher density tape drives to reduce the number of tapes used by a factor of 3 or 4.

Instrumentation Technology Developments in MP-4

Vernon Sandberg

The instrumentation developments in MP-4 during 1983 have been to

- design a magnetic horn and pulser for a high flux neutrino facility;
- develop a high-speed, high-voltage, variable-width pulser for beam chopping;
- construct a CAMAC-controlled pulser monitor for the flash chamber system used in Exp. 225;
- construct a computer-controlled test and repair station for the multiwire proportional chamber (MWPC) input electronics used in Exp. 225;
- design and fabricate the signal-processing electronics for the drift chamber and the sodium iodide detectors used in Exp. 400;
- develop and build a variety of control systems for Exp. 634;
- upgrade the chamber wire-winding shop with new controllers; and
- provide miscellaneous support to LAMPF facilities and experiments.

A brief description and a few highlights of some of these instruments follows.

Portions of a design have been done for a neutrino horn system. The system consists of a capacitor bank, horn, and silicon control rectifier (SCR) switches. The capacitor bank energy is switched into the horn, which acts as a resonating inductor. The current flow recharges the capacitors through a bridge rectifier circuit, thus completing one-half of a sinusoidal cycle. The horn size is 2 m in diameter and 4 m in length; its capacitance is 0.1 F. The peak voltage is 500-800 V, and the peak current is 300 kA.

A high-voltage pulser for the injector beam-chopper system has been built. It produces a positive pulse of adjustable amplitude from 1 to 15 kV, adjustable pulse width from 40 ns to ∞, and rise and fall times of 20 ns across a 1-MΩ load shunted by 150 pF. The pulse is "flat" to within 5% of its peak voltage and recovers to within ±10 V of ground potential. The pulser is a hybrid system composed of hard triode vacuum tubes, MOSFET power transistors, bipolar microwave transistors, integrated circuits, and fiber optics systems. The pulser, which is mounted in a cylinder 1 m in diameter and 1.5 m in length, will be installed in the injector area in 1984.

In support of Exp. 225 a system to monitor the high-voltage pulsers that drive the detector flash chambers has been built. The monitor watches several key parameters in the flash chamber system (for example, the charging voltage and current, the trigger pulser waveform, and the main pulser waveform) and reports their status to the experiment computer. When a major fault is detected (such as a capacitor failure), the monitor compares the pulser-system status with its past history and then takes appropriate action (such as disconnecting the high-voltage charging power supply from the shorted capacitor bank). The monitor is fabricated with TTL logic and communicates with the experiment's computer through CAMAC.

To facilitate testing and repair of the electronics used in the cosmic-ray anticoincidence system for Exp. 225, we have built a computer-controlled test station that tests the memory, logic, and shift registers of the input cards, the PAL layer logic, and the control-test cards. It is based on a Hewlett-Packard HP-85 portable computer and standard CAMAC-control modules. Its software is very flexible and can be easily adapted to changing requirements encountered in diagnosing problems in the anticoincidence system.

In support of Exp. 400, a system of amplifiers, analog delay lines, and pulse-shaping circuits has been developed and fabricated. To run the Crystal Box detector at an instantaneous muon stopping rate of 5-million muon stops per second, the sodium iodide signals must be clipped to reduce pileup and improve energy resolution.

The photomultiplier-tube base and amplifier system used on the Crystal Box sodium iodide detectors clips the signal (to a 100-ns-wide pulse) and then amplifies and further shapes the pulse leading edge with a pole-zero filter. The processed signal is then split three ways and sent to a constant fraction discriminator, an analog summing circuit, and into a 450-ns-wide bandwidth delay line, after which the analog signal is further split and sent to two parallel integrating analog-to-digital (ADC) channels. Before clipping, the sodium iodide pulses have 250-ns decay time; after processing, the pulses are approximately square and 100 ns wide. This system has 432 such amplifier cards and each card is independently accessible.

Group MP-1 Electronic Instrumentation and Computer Systems

Computer Maintenance Section

Since its inception 3 years ago, the MP-1 Computer Maintenance (COMAINT) section has grown from six to its current staff of eight technicians. Meanwhile, the maintenance value of the equipment maintained by the section has increased 60%. The increase in maintenance efficiency is largely due to three factors: (1) replacement and/or redesign of older more troublesome hardware; (2) increased experience and training within the section; and

Martha Hoehn and Elvira Martinez working at a VAX-11/780 console.

Sharon Lisowski and Mark Kaletka shelving magnetic tapes in the Data Analysis Center tape library.

(3) more efficient utilization of manpower by using split shifts, with reduced on-call and overtime hours.

The COMAINT section is responsible for the maintenance of more than 50 computer systems and 200 computer terminals at LAMPF. During operating cycles, the section is staffed from 7 a.m. to 12 p.m. midnight, Monday through Friday, with weekends and early mornings covered by assigned on-call duty. The section handles more than 100 trouble calls per month and counts most of the personnel at LAMPF among its clientele.

Data Analysis Center (DAC)

The year 1983 brought several changes to the LAMPF Data Analysis Center (DAC). In cooperation with the Medium-Energy Physics Theory Group (T-5), MP-1 purchased and installed a new VAX-11/780 system (MPBG1), bringing the total number of VAX computers in the DAC to four. Delivered as part of this new system were two 125-in./s, 6250-bits/in. TU-78 tape drives, an

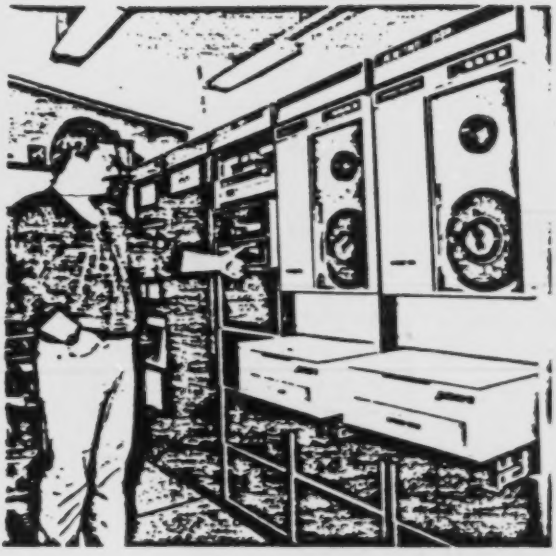

Tony Gonzales making adjustments to MPSERF in the Data Analysis Center.

Andy Steck, Gerry Maestas, and Jim Santana performing routine maintenance on the Data Analysis Center computer MPSERF.

Leon Guerin and Kelly Blount at the Computer Maintenance section repair facility.

Bob Critchfield inspecting a removable disk system in the computer maintenance shop.

Bryan O'Malley and Boyd Cummings testing the operation of a line printer.

HSC-50 disk and tape controller, four RA-81 Winchester-type disk drives, and an RP-07 Winchester-type disk drive.

The VAX systems are now connected to each other via a CI-780 computer interconnect, a high-speed (70-megabit/s) bus link that replaces the slower DMR-32 hardware for network links. The CI-780 hardware also forms the basis for a future VAX-cluster architecture, a closely cooperating network of VAX computers that shares common resources, such as disk storage, batch queues, and print queues. Because full software support for the VAX-cluster features is not available with the current (version 3.4) release of the VMS operating system, MP-1 is acting as a test site for a pre-release of VMS version 4.0. The pre-release was installed on MPBG1 in December 1983 and will be extended to the other three VAX systems during the early months of 1984. The test phase will run until the official release of VMS version 4.0 in mid-1984.

The year also saw the completion of the LAMPF terminal network, with the Micom Micro-600 port selector system becoming fully operational. All terminals connected to the DAC are now routed through this sytem, which allows flexible terminal switching between computers. The system is undergoing its first expansion, with equipment on order to service the new VAX MPBG1, provide additional terminals in the Laboratory Office Building, and possibly expand access to terminals at the experimental areas.

A committee convened for 3 days during October 1983 to consider long-range (5- to 10-year) computing needs at LAMPF. This committee consisted of representatives from MP Division and LAMPF Users, and was chaired by Martha Hoehn of MP-1. The committee heard presentations on topics including parallel and front-end processing, computer networks, word processing, and new central processing unit (CPU) standards, while considering future directions for both data acquisition and analysis at LAMPF. Presentations were made by speakers from SLAC, Fermilab, and TRIUMF on the computer facilities and philosophies of those institutions. The final report of the committee should be available in early 1984.

Design for a Muon Channel Based on the Proton Storage Ring

A muon channel using the proton beam from the LAMPF Proton Storage Ring (PSR) would provide pulsed muon beams uniquely applicable to a wide class of experiments. Beam-optics studies led to a design for such a PSR-based channel capable of providing either decay muon beams, with momenta as high as 80 MeV/c, or surface muon beams at 30 MeV/c.

The design incorporates a superconducting solenoid as a pion decay section for producing decay muons, and includes an electrostatic chopper for short-pulse surface muon beams. The PSR is designed to run at 100 μA average in the long-bunch mode at 12 Hz with 270-ns proton bunches or at 10 μA average in the short-bunch mode at 720 Hz with 1-ns pulses.

In the long-bunch mode, the chopper selects a small interval of the surface beam to produce intense 5- to 10-ns pulses of surface muons at 12 Hz. In the short-bunch mode of PSR operation, the surface beam will not be chopped; then the muon pulses are approximately 30 ns wide at 720 Hz. In neither mode of PSR operation will the higher momentum decay beams be chopped. Calculated positive muon fluxes range from $\simeq 1 \times 10^4$/s for chopped long-bunch-mode surface beams to $\simeq 8 \times 10^7$/s for long-bunch-mode decay beams.

VII. ACCELERATOR OPERATIONS

This report covers operating cycles 37 through 39. The accelerator was in operation from December 30, 1982 through February 8, 1983, and again from August 1 through December 1, 1983. Beams were provided for research for 136 days, and for facility development for 11 days. A summary of information on beams provided for research is given in Table I.

Machine operation continued to be reliable and stable. The H^+ beam intensity was increased to the 800- to 900-μA range for routine production, and the beam duty factor was increased to 10.5%.

As noted in LAMPF News in this report, the H^+ average beam intensity reached and exceeded the design level of 1 mA for the first time on February 1. In a 3-h demonstration run, 1.2 mA of 800-MeV beam was delivered to Area A at 10.5% duty factor.

Installation of the new transition region between the drift-tube and side-coupled linacs during the February-to-July shutdown has made the machine-tuning task much easier. Dual-beam operation with no steering magnets energized in the 805-MHz linac has become routine.

A summary of unscheduled facility downtime during research shifts is given in Table II. Because some of the outages are concurrent, the total is greater than the beam downtime.

Accelerator development efforts concentrated on making the new transition region operational and on improving the H^+ beam deflector in the low-energy transport.

Table I. Beam Statistics for Cycles 37 Through 39.

		Cycle 37	Cycle 38	Cycle 39
Number of experiments served		33	33	23
H^+	scheduled beam (h)	860	884	792
H^-	scheduled beam (h)	276	200	----
P^-	scheduled beam (h)	588	1356	784
H^+	beam availability (%)	89	80	87
H^-	beam availability (%)	80	86	----
P^-	beam availability (%)	90	80	82
H^+	average current (μA)	625	770	825
H^-	average current (μA)	1	2	----
P^-	average current (nA)	~10	~10	~10
H^+	beam duty factor (%)	6-9	6-9	7-10.5
H^-, P^-	beam duty factor (%)	3-9	3-9	3.5-10.5

Table II. Unscheduled Machine Downtime from December 30, 1982 to December 1, 1983.

Category	Downtime (h)	Per Cent of Total
201-MHz amplifiers and transmission lines	86	14
805-MHz amplifier systems	96	16
Vacuum systems	69	12
Magnets	36	6
Magnet power supplies	48	8
Interlocks	16	3
Ion sources and Cockcroft-Walton hv supplies	170	29
Cooling water systems	18	3
Computer control and data acquisition	23	4
Production targets	26	4
Miscellaneous (utilities, ligtning)	7	1
TOTAL	595	

CLINTON P. ANDERSON MESON PHYSICS FACILITY

MILESTONES

Official Ground Breaking	February 15, 1968
Spinoff: Adoption of LAMPF Accelerating Structure for X-Ray Therapy and Radiography Machines	ca 1968
5-MeV Beam Achieved	June 10, 1970
Adoption of a LAMPF-Standard Data-Acquisition System	August 1970
100-MeV Beam Achieved	June 21, 1971
211-MeV Beam Achieved	August 27, 1971
800-MeV Beam Achieved	June 9, 1972
Spinoff: First Use of Electrosurgical Forceps in Open-Heart Surgery (University of New Mexico)	September 13, 1972
Discovery of ^{235}Th (Experiment Zero)	September 25, 1972
Dedication to Senator Clinton P. Anderson	September 29, 1972
Spinoff: First Hyperthermic Treatment of Animal Tumors	October 1972
First H^- Injector Beam	March 28, 1973
First Simultaneous H^+ and H^- Beams	May 4, 1973
Beam to Area B	July 15, 1973
First Experiment (#56) Received Beam	August 24, 1973
First Meson Production, Beam to Area A	August 26, 1973
Beam to Area A-East	February 6, 1974
First Medical Radioisotope Shipment	July 30, 1974
Usable 100-μA Beam to Switchyard	September 5, 1974
Pi-Mesic Atoms with "Ticklish" Nuclei	October 13, 1974
First Experimental Pion Radiotherapy	October 21, 1974
First Tritium Experiment (80 000 Ci)	November 1974
Start of Great Shutdown	December 24, 1974
New Precise Measurements of Muonium Hyperfine-Structure Interval and μ^+ Magnetic Moment	1975-77-80
Q Data-Acquisition Software Operational	June 1975
Spinoff: First Use of ^{82}Rb for Myocardial Imaging in Humans (Donner Laboratory, Lawrence Berkeley Laboratory)	June 1975
Spinoff: First Hyperthermic Treatment of Human Cancer (University of New Mexico)	July 11, 1975
Accelerator Turn On	August 1, 1975
Acceptable Simultaneous 100-μA H^+ and 3-μA H^- Beams to Switchyard	September 14, 1975
Production Beam to Area B	October 7, 1975
First Pions Through EPICS Channel	March 18, 1976
Production Beam in Areas A and A-East: End of Great Shutdown	April 5, 1976
Muon-Spin-Rotation Program	June 1976
Spinoff: First Hyperthermic Treatment of "Cancer Eye" in Cattle (Jicarilla Reservation)	June 3, 1976
100-μA Production Beam in Area A	August 1976

MILESTONES

(Continued)

Experiment in Atomic Physics (H^- + laser beam): Observation of Feshbach and Shape Resonances in H^-	October 1976
Double Charge Exchange in ^{18}O: LEP Channel	October 5, 1976
Start Up of Isotope Production Facility	October 15, 1976
HRS Operation Begins	November 1976
Maintenance by "Monitor" System of Remote Handling	Fall 1976
Proton Beam to WNR	March 12, 1977
Polarized Proton Beam Available	April 1977
Spinoff: First Practical Applications Patent Licensed to Private Industry	April 12, 1977
Pion Radiotherapy with Curative Intent	May 1977
Proton-Computed Tomography Program	June 1977
Experimental Results at Neutrino Facility	July 1977
Cloud and Surface Muon Beams: SMC Channel	July 1977
EPICS Operation Begins	August 1977
300-μA Production Beam in Area A	Fall 1977
AT Division Established	January 1, 1978
π^0 Spectrometer Begins Operation	February 1978
Operation of Polarized-Proton Target	Spring 1978
Successful Water-Cooled Graphite Production Target	November 1978
Spinoff: First Thermal Modification of Human Cornea (University of Oklahoma)	July 11, 1979
600-μA Production Beam in Area A	November 1979
New Limit on $\mu \rightarrow e\gamma$	December 1979
Experimental Measurement of the Strong-Interaction Shift in the $2p$-$1s$ Transition for Pionic Hydrogen	1980-81-82
Commercial Production of Radioisotopes	January 1980
Spin Precessor Begins Operation	February 1980
Data-Analysis Center Operational	April 1980
Variable-Energy Operation	June 1980
Single-Isobaric-Analog States in Heavy Nuclei	June 1980
Spinoff: First Use of ^{82}Rb for Brain Tumor Imaging in Humans (Donner Laboratory, Lawrence Berkeley Laboratory)	September 1980
Production of Fast Muonium in Vacuum	Fall 1980
Double-Isobaric-Analog States in Heavy Nuclei	October 1980
Focal-Plane Polarimeter Operational at HRS	October 1980
Safety Award to LAMPF Users Group, Inc., for Working One Million Man-Hours Since 1975 Without a Disabling Injury	October 27, 1980
New Measurement of Pion Beta Decay — Improved Test of Conserved Vector Current	November 1980
First Excitation of Giant Dipole Resonance by Pion Single-Charge Exchange	March 1981
First Excitation of Isovector Monopole Resonance in ^{120}Sn and ^{90}Zr by Pion Single-Charge Exchange	March 1981

MILESTONES

(Continued)

Search for Critical Opalescence in ^{40}Ca	September 1981
Average Beam Current of LAMPF Accelerator Established at 750 μA	1982
Staging Area Constructed	1982
Particle Separator Installed at Stopped Muon Channel	1982
"Dial-A-Spin" Capability on Line B Permits Different Spin Orientations for HRS, Line B, and EPB Simultaneously	1982
Time-Projection Chamber in Operation	1982
Improved Test of Time-Reversal Invariance in Strong Interactions	January 1982
Search for Parity Nonconservation in *p-p* Scattering	November 1982
d-t Fusion Catalyzed by Muons	November 1982
LAMPF Accelerator Produces Proton Beam of 1.2 mA	February 7, 1983
First Observation of ν_e-e^- Scattering	October 1983

APPENDIX A

EXPERIMENTS RUN IN 1983

Exp. No.	Experiment Title	Channel	Beam Hours
106	Proton-Induced Spallation Reactions Related to the Isotope Production Program at LAMPF	AB-Nuccham	7.0
190	A Precision Measurement of the $\pi^- - \pi^0$ Mass Difference	LEP	133.0
225	A Study of Neutrino-Electron Elastic Scattering	Neutrino Area	692.0 709.0
267	Preparation of Radioisotopes for Medicine and the Physical Services Using the LAMPF Isotope Production Facility	ISORAD	709.0 692.0
294	High-Energy Nuclear Reactions	AB-Nuccham	16.0
308	An Attempt to Make Direct Atomic Mass Measurements in the Thin Target Area	Thin Target Area	70.0 692.0
392	A Measurement of the Triple-Scattering Parameters D, R, A, R', and A' for Proton-Proton and Proton-Neutron Scattering at 800 MeV	HRS	104.0
400	Search for the Rare Decay $\mu^+ \rightarrow e^+e^+e^-$	SMC	402.0 329.0
449	Survey of the Single and Double Photodetachment Cross Section of the H^- Ion from 14 to 21.8 eV	SMC	112.0
455	High-Precision Study of the μ^+ Decay Spectrum	P3	95.0
465	Radiochemical Study of Pion Single Charge Exchange	LEP	8.0
470	Reactive Content of the Optical Potential	HRS	70.0
474	A Measurement of Spin-Dependent Effects in P + D Elastic and Inelastic Scattering	HRS	60.0
523	Study of the $^{14}C(\pi^+,\pi^0)^{14}N$ Reaction	LEP	64.0
545	Fusion Materials Neutron Irradiations — A Parasite Experiment	RADAMAGE-1	260.0
553	Study of Target Thickness Effects in the Cross-Section Measurement of the Pion Single-Charge-Exchange Reaction $^{13}C(\pi^+,\pi^0)^{13}N$ (g.s.) from 50 to 350 MeV	LEP	15.0
571	Muon Spin Rotation Studies of Dilute Magnetic Alloys	SMC	17.0
587	Fundamental Experiments with Relativistic Hydrogen Atoms: Exploratory Work	EPB	400.0

Exp. No.	Experiment Title	Channel	Beam Hours
601	Determination of Isoscalar and Isovector Transition Rates for Low-Lying Collective States in ^{90}Zr and ^{208}Pb by π^+ and π^- Inelastic Scattering	LEP	414.0
626	Measurement of the Depolarization Parameters $D_{NN'}$, $D_{LS'}$, and $D_{SS'}$ in Proton-Nucleus Scattering at Very High Excitation Energies	HRS	154.0
635	Spin Measurements in pd Elastic Scattering	EPB	166.0
639	Muon-Spin-Rotation Study of Muon Bonding and Motion in Selected Magnetic Oxides	SMC	44.0
640	Transverse and Longitudinal Field μSR Measurements in Selected Ternary Metallic Compounds	SMC	102.0
654	Measurement of the Spin-Rotation Parameter Q for 800-MeV p + ^{16}O, ^{40}Ca, and ^{208}Pb Elastic Scattering	HRS	153.0
665	The Measurement of the Initial-State Spin-Correlation Parameters C_{LL} and C_{SL} in n-p Elastic Scattering at 500, 650, and 800 MeV	A3-Nucchem	727.0 175.0
675	Nuclear Distributions from the Study of the 2p States of Pionic Atoms	Biomed	126.0
681	Measurements of Large-Angle Pion-Nucleus Scattering with EPICS	EPICS	266.0
685	Spin Correlations in the Reaction $\vec{p}(\vec{d},d)\vec{p}$ at 500 MeV	HRS	447.0
698	Ground-State Quadrupole Moments of Deformed Nuclei	Biomed	157.0
705	Study of Pion Absorption in ^3He On and Above the (3,3) Resonance	P3	283.0
708	A Measurement of the Depolarization, the Polarization, and the Polarization Rotation Parameters and the Analyzing Power for the Reaction $\vec{p}\vec{p} \rightarrow \vec{p}\pi^+n$	EPB	608.0 43.0 43.0
709	Measurements of A_{NN}, A_{SS}, and A_{SL} in the Coulomb-Interference Region at 650 and 800 MeV	HRS	522.0
724	Measurement of the Lamb Shift in Muonium	SMC	380.0
727	Measurement of the Efficiency of Muon Catalysis in Deuterium-Tritium Mixtures at High Densities	Biomed	341.0
728	Study of Pion Charge-Exchange Mechanisms by Means of Activation Techniques	P3	88.0 51.0
730	Pion Production in Pion-Nucleon and Pion-Nucleus Interactions	P3	16.0
735	Pion-Induced Emission of Light Nuclear Fragments	LEP	173.0
741	Investigation of the Longitudinal-Spin Response of ^{208}Pb and Implications of Spin-Transfer Form Factors for Non-Nucleon Degrees of Freedom in Nuclei	HRS	189.0

Exp. No.	Experiment Title	Channel	Beam Hours
745	Hexadecapole Moments in Uranium: ^{233}U and ^{234}U	Biomed	284.0
749	$^{18}O(\pi^+,\pi^-)^{18}Ne$ (g.s.) Angular-Distribution Measurements at T_π = 120 MeV and T_π = 200 MeV	EPICS	357.0
750	Inclusive π^+ and π^- Double Charge Exchange on ^4He	P3	641.0
765	800-MeV Proton Irradiation of Materials for the SIN Beam Stop	ISORAD	570.0 652.0
780	A Study of the Double-Charge-Exchange Reactions $^{14}C(\pi^-,\pi^+)^{14}Be$ and $^{18}O(\pi^-,\pi^+)^{18}C$	EPICS	220.0
783	Pion-Induced Pion Production on Deuterons	P3	242.0
789	Two-Nucleon-Out Products Following the Absorption of of 10-MeV π^+ in ^{26}Mg and ^{74}Ge	LEP	7.9
792	Measurement of Parity Violation in the $\bar{p}$-p and $\bar{p}$-Nucleon Total Cross Sections at 600 MeV	EPB	176.0 351.0
798	Core Excitation Effects in Pion Double Charge Exchange	EPICS	328.0
798	Fission Induced by Energetic $\pi^\pm$ Particles	LEP	61.0
808	0° Excitation Functions for $\pi^-p \rightarrow \pi^0 n$	LEP	71.0

APPENDIX B

NEW PROPOSALS

Proposal No.	Title	Spokesmen	Institutions
808	0° Excitation Function for $\pi^- p \rightarrow \pi^0 n$	M. Cooper D. Fitzgerald	Los Alamos Los Alamos
809	Study of π^-, p and π^+, p Reactions with EPICS	G. S. Blanpied J.-P. Egger	Univ. of South Carolina Univ. of Neuchatel, Switzerland
810	Test Channel		
811	Study of Unnatural-Parity States in Nuclei Using Low-Energy Pions	B. G. Ritchie	Univ. of Maryland
812	Back-Angle Charge Asymmetries for Elastic π-Deuteron Scattering	R. J. Peterson	Univ. of Colorado
813	Pion Charge Asymmetries for ^{12}C at Low Beam Energies on the LEP Spectrometer	J. J. Kraushaar R. J. Peterson	Univ. of Colorado Univ. of Colorado
814	$\pi^{\pm}$-Nuclear Elastic Scattering from Nickel and Tin Isotopes at Energies Between 30 and 80 MeV	M. Blecher M. Hynes	VPI and State Univ. Los Alamos
815	Measurement of A_{no}, A_{kk}, and A_{ll} in $\bar{p}\vec{p} \rightarrow p\pi^+$ at 500, 580, 650, 720, and 800 MeV	D. V. Bugg	Queen Mary College, London
816	Radiation Effects on the Field Strength of Samarium-Cobalt Permanent Magnets	R. D. Brown	Los Alamos
817	I. Elastic Scattering of Polarized Protons from ^3H at Intermediate Energy	A. Azizi M. Bleszynski G. Igo	UCLA UCLA UCLA
818	Proton-Deuteron Elastic Scattering at 800-MeV Two- and Three-Spin Observables	G. Igo	UCLA
819	II. Elastic Scattering of Polarized Protons from ^3H at Intermediate Energy	A. Azizi M. Bleszynski G. Igo	UCLA UCLA UCLA
820	Pion-Induced Pion Production on ^3He	E. Piasetzky P. A. M. Gram G. A. Rebka, Jr. J. Lichtenstadt	Los Alamos Los Alamos Univ. of Wyoming Tel Aviv Univ.
821	Pion Charge Exchange to Delta-Hole States of Complex Nuclei	R. J. Peterson	Univ. of Colorado
822	Inelastic π^+ and π^- Scattering on ^{48}Ca at 50 and 75 MeV	J. J. Kraushaar J. L. Ullmann	Univ. of Colorado Univ. of Colorado
823	Development of an (n,p) Reaction Capability at Area B or Beam Line D	N. S. P. King P. Lisowski J. D. Bowman J. Shepard	Los Alamos Los Alamos Los Alamos Univ. of Colorado

Proposal No.	Title	Spokesmen	Institutions
824	A Study of Low-Energy Pion Scattering as a Probe of Nuclear Magnetic Dipole Excitation	H. E. Jackson	Argonne
825	Investigation of the $N\Delta$ Interaction Via $\pi^+ d \rightarrow pn^+ n$	G. S. Mutchler	Rice Univ.
826	Isospin Dependence of Nonanalog Pion Double Charge Exchange	C. L. Morris C. Fred Moore R. Gilman	Los Alamos Univ. of Texas Univ. of Pennsylvania
827	Study of Isobaric-Analog States in Pion Single-Charge-Exchange Reactions in the 300- to 500-MeV Region	J. Alster H. W. Baer E. Piasetzky U. Sennhauser	Tel Aviv Univ. Los Alamos Los Alamos Los Alamos Natl. Lab.
828	Total and Differential Cross Sections for $\pi^+ d \rightarrow pp$ Below 20 MeV	K. Gotow R. C. Minehart	VPI and State Univ. Univ. of Virginia
829	A Measurement of the Width and Position of the Δ^{++} Resonance in ^{6}Li and ^{12}C	K. Ziock	Univ. of Virginia
830	The Reaction $(\pi,\pi p)$ on ^{3}He and ^{4}He at Energies Above the (3,3) Resonance	R. Minehart	Univ. of Virginia
831	The $[\pi^+, p(pp)]$ Reaction on Light Nuclei	C. F. Perdrisat R. Minehart	College of William & Mary Univ. of Virginia
832	Gamma-Ray Angular Correlation from $^{12}C(\vec{p},p')^{12}C^*(15.11$ MeV)	B. J. Lieb C. F. Perdrisat H. O. Funsten	George Mason Univ. College of William & Mary College of William & Mary
833	Continuation of the Investigation of Large-Angle Pion-Nucleus Scattering	G. R. Burleson	New Mexico State Univ.
834	The Pion-Nucleus Interaction Studied with the $4f \rightarrow 3d$ Transition of Rare-Earth Pionic Atoms	Y. Tanaka R. M. Steffen E. B. Shera	Purdue Univ. Purdue Univ. Los Alamos
835	Target Mass Dependence of the Isovector Contribution to the Giant Quadrupole Resonance	S. J. Seestrom-Morris	Univ. of Minnesota
836	Energy Dependence of Pion Scattering to the Giant Resonance Region of ^{208}Pb	S. J. Seestrom-Morris	Univ. of Minnesota
837	Measurement of Spin-Flip Cross Sections up to 40-MeV Excitation in ^{58}Ni and ^{90}Zr	C. Glashausser S. Nanda	Rutgers Univ. Rutgers Univ.
838	Pion-Induced Pion Production on Nuclei at 400 MeV	M. J. Leitch E. Piasetzky	Los Alamos Los Alamos
839	Pion Inelastic Scattering from the 1$^+$ Doublet in ^{12}C	C. F. Moore C. L. Morris	Univ. of Texas Los Alamos
840	Inelastic Pion Scattering from ^{16}O at T_π = 120 and 200 MeV	L. C. Bland H. T. Fortune	Univ. of Texas, Austin Univ. of Pennsylvania
841	Forward-Angle Pion Inelastic Scattering on Light Nuclei	L. C. Bland C. F. Moore H. T. Fortune	Univ. of Texas, Austin Univ. of Texas, Austin Univ. of Pennsylvania
842	μSR Shift and Relaxation Measurements in Itinerant Magnets	L. C. Gupta R. H. Heffner D. E. MacLaughlin	Tata Inst., India Los Alamos Univ. of Calif., Riverside

Proposal No.	Title	Spokesmen	Institutions
843	A Search for $\Delta_{3,3}$ Components of Ground-State Nuclear Wave Functions	C. L. Morris C. F. Moore	Los Alamos Univ. of Texas
844	Measurement of A_{ss}, A_{ll}, and A_{ls} for the Reaction $\vec{p}\vec{p} \rightarrow p + n + \pi^+$ at 800 MeV	G. Paulenta M. Gazzaly N. Tanaka	UCLA Univ. of Minnesota Los Alamos
845	Pion Inelastic Scattering from ^{9}Be	J. J. Kelly	Los Alamos
846	$NN \rightarrow NN\pi$: Cross Sections and Analyzing Powers for the 800-MeV $\vec{p}p \rightarrow \pi^+(np)$ and $\vec{p}n \rightarrow \pi^-(pp)$ Inclusive Reactions	T. S. Bhatia G. Glass	Texas A&M Univ. Texas A&M Univ.
847	A Precision Test of Nuclear Charge Symmetry	T. S. Bhatia J. C. Hiebert	Texas A&M Univ. Texas A&M Univ.
848	In-Flight Absorption of Low-Energy Negative Pions	Y. Ohkubo	Los Alamos
849	A. Measurement of the Differential Cross Section for $\pi^-p \rightarrow \pi^0 n$ at 0 and 180° in the Momentum Region 471-687 MeV/c B. Test of Isospin Invariance in πN Scattering at 180° in the Momentum Region 471-687 MeV/c	D. H. Fitzgerald W. J. Briscoe M. E. Sadler	Los Alamos George Washington Univ. Abilene Christian Univ.
850	Study of the Mass and Energy Dependence of Low-Energy Pion Single Charge Exchange at 0°	F. Irom M. J. Leitch	Los Alamos Los Alamos
851	Search for Recoil-Free Δ Production and High-Spin States in the ^{208}Pb$(p,t)^{206}$Pb Reaction at $E_p \simeq 400$ MeV	N. M. Hintz	Univ. of Minnesota
852	Measurements of $(\pi^\pm,n)$ Reactions on Nuclear Targets to Study the Production and Interaction of η Mesons with Nuclei	J. C. Peng	Los Alamos
853	Measurement of Wolfenstein Parameters at 650 MeV and $d\sigma/d\Omega$ at 500, 650, and 800 MeV for $\vec{p}d \rightarrow \vec{p}d$ Elastic Scattering	G. S. Weston G. J. Igo	UCLA UCLA
854	Muon Spin Research in Oxide Spin Glasses	C. Boekema D. W. Cooke	Texas Tech Univ. Los Alamos
855	Measurement of ^{208}Pb-^{206}Pb Ground-State Neutron Density Difference	N. Hintz	Univ. of Minnesota
856	Comparison of Double Charge Exchange and Inclusive Scattering in ^{3}He	P. A. M. Gram J. L. Matthews G. A. Rebka, Jr.	Los Alamos MIT Univ. of Wyoming
857	Inelastic Pion Scattering from ^{16}O at $T_\pi = 50$ MeV	L. C. Bland C. F. Moore	Univ. of Texas, Austin Univ. of Texas, Austin
858	Additional Measurements of ^{18}O$(\pi^+,\pi^-)^{18}$Ne(g.s.)	H. T. Fortune R. Gilman	Univ. of Pennsylvania Univ. of Pennsylvania
859	Study of the A Dependence of Inclusive Pion Double Charge Exchange in Nuclei	P. A. M. Gram J. L. Matthews G. A. Rebka, Jr.	Los Alamos MIT Univ. of Wyoming
860	Inelastic $\pi^\pm$ Scattering to Excited 0$^+$ States at Energies Between 30 and 80 MeV	B. M. Preedom C. S. Whisnant	Univ. of South Carolina Univ. of South Carolina

Proposal No.	Title	Spokesmen	Institutions
861	Measurements of the Spin-Correlation Parameter $A_{nn}(\theta)$ for n-p Elastic Scattering at 800 MeV	L. C. Northcliffe	Texas A&M Univ.
862	Study of the $M1$ Transition in ^{88}Sr by the Inelastic Scattering of π^+ and π^-	S. K. Nanda D. K. Dehnhard	Univ. of Minnesota Univ. of Minnesota
863	Study of Giant Resonances in the Palladium Isotopes Via Pion Scattering	A. Saha K. K. Seth	Northwestern Univ. Northwestern Univ.
864	Study of Deeply Bound Hole States in the Tin Isotopes Via the $(\vec{p}, d)$ Reaction	A. Saha K. K. Seth	Northwestern Univ. Northwestern Univ.
865	Spin-Rotation Measurement of ^4He at 320, 500, and 800 MeV	B. Aas M. Bleszynski G. Igo	UCLA UCLA UCLA
866	Neutrino Source Calibration	R. Hausammann J. Donahue	Univ. of Calif., Irvine Los Alamos
867	Measurement of Isovector Quadrupole Transition Densities in the Palladium Isotopes	A. Saha K. K. Seth	Northwestern Univ. Northwestern Univ.
868	An Experimental Test of the Δ-Hole Model of Nonanalog Double Charge Exchange	K. K. Seth	Northwestern Univ.
869	Higher Precision Measurement of the Lamb Shift in Muonium	V. W. Hughes A. Badertscher M. W. Gladisch	Yale Univ. Yale Univ. Heidelberg Univ.
870	Search for New Magic Numbers: Direct Mass Measurements of the Neutron-Rich Isotopes with $Z = 4$ to 9	J. M. Wouters	Los Alamos
871	Coincident Nuclear γ-Ray and Pionic X-Ray Study of π Absorption at Rest on ^{12}C	E. J. Lieb H. O. Funsten	George Mason Univ. College of William & Mary
872	Direct Atomic Mass Measurements of Neutron-Rich Isotopes in the Region $Z = 13$-17 Using the Time-of-Flight Isochronous Spectrometer	D. S. Brenner	Clark Univ.
873	Pionic X-Ray Study of the Carbon Isotopes	E. B. Shera A. R. Kunselman	Los Alamos Univ. of Wyoming
874	Elastic Scattering of π^+ from Deuterium in the Region of the $^3F_3$ Dibaryon Resonance	C. L. Blilie D. Dehnhard	Univ. of Minnesota Univ. of Minnesota

APPENDIX C

ACTIVE AND COMPLETE EXPERIMENTS BY CHANNEL

BR NEUTRONS AND PROTONS

Exp. No.	Title	Spokesman	Phase No. * = Complete	Beam Hours
56	STUDY OF NEUTRON SPECTRUM FROM PROTON BOMBARDMENT OF DEUTERIUM IN THE 300-600-MeV REGION	NORTHCLIFFE SIMMONS	1 * 2 *	0.0 0.0
65	NEUTRON-PROTON POLARIZATION MEASUREMENTS USING A POLARIZED TARGET — PHASE I: THE n-p POLARIZATION OBSERVABLE P(θ)	SIMMONS	1 *	996.8
66	NEUTRON-PROTON POLARIZATION MEASUREMENTS WITH A POLARIZED TARGET — PHASE II: THE n-p SPIN-CORRELATION OBSERVABLE	SIMMONS	1 * 2 *	343.4 472.0
125	ELASTIC NEUTRON-PROTON BACK-ANGLE DIFFERENTIAL CROSS-SECTION MEASUREMENTS 300-800 MeV	DIETERLE	1 *	0.0
129	PION PRODUCTION IN NEUTRON-PROTON COLLISIONS	WOLFE	1 *	319.0
189	SEARCH FOR CONDENSED NUCLEAR STATES AND STUDY OF HIGH-q^2 LOW-ν NUCLEAR INTERACTIONS	VAN DYCK	1 *	0.0
193	MEASUREMENT OF SMALL-ANGLE NEUTRONS ELASTIC SCATTERING FROM PROTONS	DIETERLE McFARLANE	1 * 2 *	1091.1 0.0
205	(n,p) CHARGE-EXCHANGE AND NEUTRON-INDUCED QUASI-FREE SCATTERING	KENEFICK RILEY	1 *	38.5
255	MEASUREMENT OF $\sigma(\theta)$ FOR n-p ELASTIC SCATTERING AT 460 MeV	NORTHCLIFFE	1 *	5.0
262	TEST OF ISOSPIN INVARIANCE IN THE REACTION $np \rightarrow d\pi^0$	BONNER	1 *	304.8
263	MEASUREMENT OF THE ENERGY AND ANGULAR VARIATION OF THE np CHARGE-EXCHANGE CROSS SECTIONS	BONNER	1 *	237.1
264	MEASUREMENT OF THE ENERGY VARIATIONS OF THE nd ELASTIC DIFFERENTIAL CROSS SECTIONS NEAR 180°	BONNER	1 *	473.1
279	TEST OF CHARGE SYMMETRY IN nd AND pd SCATTERING	DIETERLE McFARLANE	FS*[a]	101.0
360	THE MEASUREMENT OF THE POLARIZATION TRANSFER COEFFICIENT D_t AND A_t AT 800 MeV FOR THE REACTIONS d(p,n)2p, ^{6}Li(p,n)^{6}Be, AND ^{9}Be(p,n)^{9}B	RILEY SIMMONS	1 *	493.5
366	NONRESONANT PION PRODUCTION IN THE REACTION $np \rightarrow n^+pp$	MAYES MUTCHLER	1 *	427.7

[a]FEASIBILITY STUDY.

Exp. No.	Title	Spokesman	Phase No. *—Complete	Beam Hours
402	A MEASUREMENT OF THE POLARIZATION TRANSFER COEFFICIENTS $D_{\vec{L}}(0°)$ AND $A_{\vec{L}}'(0°)$ IN THE REACTION $\vec{p}\vec{p} \rightarrow nX$ AT 800 MeV	GLASS SIMMONS	1 * 2 *	166.1 83.8
403	A MEASUREMENT OF THE TRIPLE-SCATTERING PARAMETER D_t FOR THE CHARGE-EXCHANGE REGION IN np SCATTERING	SONNER	1 * 2 *	0.0 223.8
457	MEASUREMENT OF THE QUASI-FREE pn AND pp AND FREE pp ANALYZING POWERS 500-800 MeV	BHATIA SIMMONS	1 *	785.0
492	POLARIMETER CALIBRATIONS AND SEARCH FOR ENERGY-DEPENDENT STRUCTURE IN pp ELASTIC SCATTERING VIA CROSS SECTION, ANALYZING POWER, AND WOLFENSTEIN PARAMETER MEASUREMENTS	McNAUGHTON WILLARD	1 *	860.2
504	MEASUREMENT OF THE TOTAL CROSS-SECTION DIFFERENCE FOR PROTON-PROTON AND PROTON-NEUTRON SCATTERING IN PURE TRANSVERSE INITIAL SPIN STATES IN THE 400-800-MeV REGION	PHILLIPS	1 *	1568.0
505	MEASUREMENT OF THE TRANSVERSE SPIN-SPIN ASYMMETRY IN THE REACTION $pp \rightarrow d\pi^+$ IN THE 500-800-MeV REGION	PHILLIPS	1 * 2	860.2 0.0
517	POLARIZED BEAM AND TARGET EXPERIMENTS IN THE p-p SYSTEM. PHASE 1. A_y AND A_{yy} FOR THE $d\pi^+$ CHANNEL AND A_{yy} FOR THE ELASTIC CHANNEL FROM 500-800 MeV	SIMMONS JARMER NORTHCLIFFE	1	1294.9
518	POLARIZED BEAM AND TARGET EXPERIMENTS IN THE p-p SYSTEM. PHASE 2. MEASUREMENTS OF A_{zz} AND A_{xz} FOR THE $d\pi^+$ CHANNEL AND FOR THE ELASTIC CHANNEL FROM 500-800 MeV	SIMMONS JARMER NORTHCLIFFE	1	1409.0
589	FREE FORWARD np ELASTIC-SCATTERING ANALYZING POWER MEASUREMENTS AT 800 MeV	GLASS NORTHCLIFFE	1	0.0
590	MEASUREMENT OF $d(\theta)$ IN p-n AND n-p SCATTERING AT 800 AND 650 MeV AND OTHER ENERGIES WITH ASSOCIATED p-p MEASUREMENTS	SIMMONS NORTHCLIFFE	1 2	330.0 0.0
664	THE MEASUREMENT OF THE POLARIZATION TRANSFER COEFFICIENTS $A_{\vec{t}}'$ AND $D_{\vec{t}}$ AT 500, 650, AND 800 MeV FOR THE REACTION $D(\vec{p},\vec{n})2P$	GLASS STANEK	1	426.0
665	THE MEASUREMENT OF THE INITIAL-STATE SPIN-CORRELATION PARAMETERS C_{LL} AND C_{SL} IN n-p ELASTIC SCATTERING AT 500, 650, AND 800 MeV	BURLESON WAGNER	1	1258.0
683	MEASUREMENT OF $\Delta\sigma_L$ IN FREE NEUTRON-PROTON SCATTERING AT 500, 650, AND 800 MeV	DITZLER SIMMONS	F S	0.0
739	P-A FOR 800-MeV SCATTERING: TEST OF TIME-REVERSAL INVARIANCE IN STRONG INTERACTIONS	BHATIA KENEFICK	1	0.0
770	THE MEASUREMENT OF np ELASTIC-SCATTERING SPIN-CORRELATION PARAMETERS WITH L- AND S-TYPE POLARIZED BEAM AND TARGET BETWEEN 500 AND 800 MeV	SPINKA BURLESON	1	0.0

Exp. No.	Title	Spokesman	Phase No. * = Complete	Beam Hours
847	A PRECISION TEST OF NUCLEAR CHARGE SYMMETRY	BHATIA HIEBERT	1	0.0
861	MEASUREMENTS OF THE SPIN-CORRELATION PARAMETER $A_{NN}(\theta)$ FOR np ELASTIC SCATTERING AT 800 MeV	NORTHCLIFFE	1	0.0

AREA B NUCLEAR CHEMISTRY (AB-Nucchem)

Exp. No.	Title	Spokesman	Phase No. * = Complete	Beam Hours
103	SPALLATION YIELD DISTRIBUTIONS FOR PION INTERACTIONS WITH COMPLEX NUCLEI	HUDIS	2 *	0.4
104	PROPOSAL FOR LAMPF EXPERIMENT: STUDIES OF THE PROTON- AND PION-INDUCED FISSION OF MEDIUM-MASS NUCLIDES	PATE	1 * 2 *	0.0 5.0
105	NUCLEAR SPECTROSCOPY STUDIES OF PROTON-INDUCED SPALLATION PRODUCTS	BUNKER	1 * 2 *	10.0 58.6
106	PROTON-INDUCED SPALLATION REACTIONS RELATED TO THE ISOTOPE PRODUCTION PROGRAM AT LAMPF	O'BRIEN	1 * 2	0.7 46.1
118	FRAGMENT EMISSION FROM PION INTERACTIONS WITH COMPLEX NUCLEI	PORILE	1 * 2	0.0 0.0
119	CROSS SECTIONS OF SIMPLE NUCLEAR REACTIONS INDUCED BY π^- MESONS	KAUFMAN	2 *	15.2
123	NUCLEAR STRUCTURE EFFECTS IN PION-INDUCED NUCLEAR REACTIONS	KAROL	1 * 2 *	0.0 1.0
150	SEARCH FOR POLYNEUTRON SYSTEMS	TURKEVICH	1 * 2 *	0.0 14.2
169	PROTON IRRADIATIONS FOR PROJECT JUMPER	ORTH SATTIZAHN	1 *	0.0
243	RECOIL STUDIES OF DEEP SPALLATION AND FRAGMENTATION PRODUCTS FROM THE INTERACTION OF 800-MeV PROTONS WITH HEAVY ELEMENTS	PORILE	1 *	55.8
282	MEASUREMENT OF CROSS SECTIONS FOR PROTON-INDUCED FORMATION OF SPALLATION PRODUCTS IN COPPER BY ACTIVATION ANALYSIS	DONNERT	1 * 2 * 3 *	0.6 1.5 0.1
294	HIGH-ENERGY NUCLEAR REACTIONS	KAROL	1	134.2
301	IMPAIRMENT OF SUPERCONDUCTING CHARACTERISTICS BY PROTON IRRADIATION	WILSON	1 *	185.0
349	NUCLEAR REACTIONS OF ^{127}I WITH PIONS	PORILE	3 *	3.6
407	THE EFFECT OF DISLOCATION VIBRATION ON VOID GROWTH IN METALS DURING IRRADIATION	SOMMER PHILLIPS	1 * 2	516.2 0.0

Exp. No.	Title	Spokesman	Phase No. * = Complete	Beam Hours
410	RADIATION EFFECTS IN AMORPHOUS METALS DUE TO 800-MeV PROTONS	COST	1 *	583.0
424	PRELIMINARY EXPERIMENTS FOR DOUBLE CHARGE EXCHANGE AND (μ^-,e^+) SEARCHES	TURKEVICH WARREN	1 *	8.0
465	RADIOCHEMICAL STUDY OF PION SINGLE CHARGE EXCHANGE	RUNDBERG	1 *	0.5
579	A RADIOCHEMICAL STUDY OF NEUTRON-DEFICIENT PRODUCTS FROM 500 MeV AND ^{238}U	FAUBEL	1	0.8
603	SEARCH FOR DELTAS IN A COMPLEX NUCLEUS BY A RADIOCHEMICAL TECHNIQUE	TURKEVICH	1 * 2	38.5 234.0
610	USE OF LAMPF BEAM STOP TO OBTAIN ^{60}Fe	HENNING KUTSCHERA	1	0.0
629	FEASIBILITY OF HELIUM-JET TECHNIQUES FOR STUDYING SHORT-LIVED NUCLEI PRODUCED AT LAMPF	GREENWOOD BUNKER TALBERT, J.	1 * 2	47.5 135.0
679	A RADIOCHEMICAL STUDY OF THE $^{209}Bi(p,\pi^0)^{210}Po$, $^{209}Bi(p,\pi^-xn)^{210}At$, AND $^{209}Bi(p,p2\pi^-xn)^{209}At$ PION PRODUCTION REACTIONS AT 500-800 MeV	DAURIA WARD	1	9.4
690	SIMULATIONS OF COSMIC-RAY-PRODUCED GAMMA RAYS FROM THICK TARGETS	REEDY	1	0.0
728	STUDY OF PION CHARGE-EXCHANGE MECHANISMS BY MEANS OF ACTIVATION TECHNIQUES	GIESLER	1 1 2	52.0 58.0 0.0
762	COMPONENT IRRADIATION	HOLTKAMP JOSEPH	1	0.0
789	TWO-NUCLEON-OUT PRODUCTS FOLLOWING THE ABSORPTION OF 10-MeV π^+ in ^{26}Mg AND ^{74}Ge	OHKUBO	1	0.0

BIOMEDICAL PION AND MUON CHANNEL (BIOMED)

Exp. No.	Title	Spokesman	Phase No. * = Complete	Beam Hours
44	RADIOBIOLOGY OF π^- MESONS, A PRELIMINARY STUDY	CARLSON	1 *	75.0
84	QUALITY OF MESON RADIATION FIELDS	PHILLIPS	1 *	0.0
143	STUDY OF THE RADIOBIOLOGICAL PROPERTIES OF NEGATIVE PIONS	KLIGERMAN KNAPP	1 * 2 * 3 *	0.0 0.0 0.0
151	AN INVESTIGATION OF PION DOSIMETRY BY PASSIVE PARTICLE DETECTORS	KNOWLES	1 *	8.0
167	HEAVY FRAGMENT FORMATION FOLLOWING THE ABSORPTION OF π^- IN ^{12}C	ZIOCK	1 *	0.0

Exp. No.	Title	Spokesman	Phase No. * = Complete	Beam Hours
171	STUDY OF NEGATIVE PION BEAMS BY MEANS OF PLASTIC NUCLEAR TRACK DETECTORS	BENTON	1	0.0
187	NUCLEAR GAMMA RAYS PRODUCED BY NEGATIVE PIONS STOPPING IN CARBON, NITROGEN, OXYGEN, AND TISSUE	REIDY	1	21.6
195	NUCLEAR RESONANCE EFFECT IN PIONIC ATOMS	LEON REIDY	1 * 2 *	0.0 155.2
196	A VISUALIZATION EXPERIMENT WITH CHARGED PARTICLES	DANIEL REIDY	1 *	0.0
198	EFFECTS OF PIONS ON DNA OF NONDIVIDING CELL SYSTEMS	POWERS	1 *	0.0
207	MEASUREMENT OF NEUTRON SPECTRUM AND INTENSITY RESULTING FROM π^- CAPTURE IN WATER PHANTOM AND HUMAN TISSUE	BRADBURY ALLRED	1 *	0.0
209	PION INTERACTIONS IN NUCLEAR EMULSIONS	BRADBURY ALLRED	1 *	0.0
212	COMPARATIVE EFFECTIVENESS OF NEGATIVE PIONS vs ^{252}Cf IN A TUMOR ANIMAL SYSTEM	MEWISSEN	1 *	0.0
215	VISUALIZATION OF STOPPING PION DISTRIBUTION	PEREZ-MENDEZ BRADBURY	1	172.1
217	π^- PRODUCTION CROSS SECTIONS	PACIOTTI	1	5.9
218	PION DOSIMETRY WITH NUCLEAR EMULSIONS AND ALANINE	KATZ	1	0.0
235	RADIATION REPAIR OF NORMAL MAMMALIAN TISSUES	GILLETTE	1 *	68.4
236	BIOLOGICAL EFFECTS OF NEGATIVE PIONS	RAJU	1	556.0
239	STUDY OF ^{11}C AND ^{13}N PRODUCTION BY π^- IRRADIATION OF CARBON, NITROGEN, OXYGEN, AND TISSUE FOR RADIOTHERAPY MONITORING	FRIEDLAND MAUSNER	1 * 2 *	55.0 8.0
242	SURVIVAL OF SYNCHRONIZED CULTURED HUMAN KIDNEY T-1 CELLS EXPOSED TO STOPPING PIONS AND X RAYS AT VARIOUS TIMES AFTER MITOSIS	TODD	1 *	105.5
244	SYSTEMS DEVELOPMENT FOR EFFICIENT UTILIZATION OF HIGH-PURITY GERMANIUM MOSAIC DETECTORS FOR TUMOR UTILIZATION	BRILL	1 *	0.0
270	THERAPY BEAM DEVELOPMENT — BIOMEDICAL CHANNEL TUNING	PACIOTTI	1	992.8
271	THERAPY BEAM DEVELOPMENT — DOSIMETRY	SMITH	1	3225.1
272	THERAPY BEAM DEVELOPMENT — MICRODOSIMETRY	DICELLO	1 *	566.2
273	THERAPY BEAM DEVELOPMENT — LET MEASUREMENTS		1 *	783.7
274	PION RADIOBIOLOGY	BUSH	1 *	2910.0

Exp. No.	Title	Spokesman	Phase No. * = Complete	Beam Hours
275	PION CLINICAL TRIALS	BUSH	1 *	7297.4
285	MIGRATION OF ^{11}C AND ^{13}N RADIOACTIVITY PRODUCED *IN VIVO* BY π^-	MAUSNER	1 *	13.0
300	NEGATIVE PIONS COULOMB CAPTURE AND NEGATIVE PIONS TRANSFER IN TISSUE, TISSUE-EQUIVALENT LIQUID, AND SIMPLE COMPONENTS	DANIEL LEON	1 *	37.0
304	STUDY OF THE AUGER PROCESS IN PIONIC ATOMS	LEON MAUSNER	1 *	9.2
380	RBE AND OER FOR NORMAL AND TUMOR TISSUE	PHILLIPS GOLDSTEIN	1 *	52.1
384	PF USING MOUSE TESTES AS A BIOLOGICAL TEST SYSTEM	GERACI	1 *	23.7
675	NUCLEAR DISTRIBUTIONS FROM THE STUDY OF THE 2P STATES OF PIONIC ATOMS	KUNSELMAN	1	126.0
698	GROUND-STATE QUADRUPOLE MOMENTS OF DEFORMED NUCLEI	STEFFEN SHERA	1 * 3	305.0 0.0
727	MEASUREMENT OF THE EFFICIENCY OF MUON CATALYSIS IN DEUTERIUM-TRITIUM MIXTURES AT HIGH DENSITIES	JONES	1 2	919.0 341.0
732	HEAVY ELEMENT FISSION INDUCED BY ENERGETIC PIONS	PETERSON RISTINEN	1 * 2	271.0 0.0
745	HEXADECAPOLE MOMENTS IN URANIUM: ^{233}U AND ^{234}U	ZUMBRO SHERA	1 4	565.0 0.0
763	NATURE OF OXYGEN CONTAMINATION IN TITANIUM WITH STOPPED MUONS	TAYLOR	1	259.0
787	MUON CHANNELING FOR SOLID-STATE PHYSICS INFORMATION	MAIER PACIOTTI FLIK	1	0.0
834	THE PION-NUCLEUS INTERACTION STUDIED WITH THE 4f → 3d TRANSITION OF RARE-EARTH PIONIC ATOMS	TANAKA STEFFEN SHERA	1	0.0

BEAM STOP A RADIATION (BSA-RAD)

Exp. No.	Title	Spokesman	Phase No. * = Complete	Beam Hours
45	RADIATION-DAMAGE STUDIES — HIGH-TEMPERATURE REACTOR MATERIALS AND TYPE II SUPERCONDUCTORS	DUDZIAK GREEN GIORGI	1 * 2 *	0.0 1833.0
111	SEARCH FOR NEW NEUTRON-RICH NUCLIDES PRODUCED BY FAST NEUTRONS	HILL	1 * 2 *	0.0 10.8

Exp. No.	Title	Spokesman	Phase No. *–Complete	Beam Hours
113	RADIATION DAMAGE AND HELIUM EMBRITTLEMENT IN ELEVATED TEMPERATURE REACTOR STRUCTURAL ALLOYS	MICHEL	1	0.0
161	THE MICRODISTRIBUTION OF THORIUM IN METEORITES	BURNETT	1	11.7
174	INVESTIGATION OF THE CHEMICAL REACTIONS OF ATOMIC ^{18}F AS A MEANS FOR DIRECT SYNTHESIS OF ^{18}F-LABELED COMPOUNDS	ROWLAND MILLER	1 * 2 *	0.0 7.0
326	ELECTRICAL COMPONENT RADIATION EFFECTS STUDY	HARVEY	1 1	179.9 294.5
406	NEUTRON FLUX CHARACTERIZATION AT A-6 RADIATION EFFECTS FACILITY	HARVEY	1	1306.3
415	TWO-NUCLEON-OUT PRODUCTS FROM STOPPED π^- INTERACTIONS	ORTH	1 *	0.0
467	IRRADIATION IN SUPPORT OF FERFICON STUDIES	GILMORE	1	0.4
542	FEASIBILITY STUDY — USING AN EXISTING NEUTRON BEAM PIPE AT LAMPF BEAM STOP FOR CRYSTAL DIFFRACTION SPECTROMETER EXPERIMENTS	LU	1 * 2	699.7 0.0
545	FUSION MATERIALS NEUTRON IRRADIATIONS — A PARASITE EXPERIMENT	BROWN	1 2	0.0 0.0
554	IRRADIATION OF TECHNOLOGICALLY IMPORTANT METALS WITH 800-MeV PROTONS USING THE ISOTOPE PRODUCTION FACILITY AT LAMPF	BROWN COST	1 1 2	0.0 75.2 0.0
560	STUDY OF NEUTRON-IRRADIATION-INDUCED GROWTH OF METALS AT RADIATION EFFECTS FACILITY	HARVEY	1	63.4
691	SIMULATION OF COSMIC-RAY PRODUCTION OF NUCLIDES BY SPALLATION-PRODUCED NEUTRONS	REEDY	1	0.0
769	PROTON IRRADIATION EFFECTS ON CANDIDATE MATERIALS FOR THE GERMAN SPALLATION NEUTRON SOURCE (SNQ)	LOHMANN SOMMER	1	0.0
816	RADIATION EFFECTS ON THE FIELD STRENGTH OF SAMARIUM-COBALT PERMANENT MAGNETS	BROWN	1	0.0
587	FUNDAMENTAL EXPERIMENTS WITH RELATIVISTIC HYDROGEN ATOMS: EXPLORATORY WORK	SMITH DONAHUE	3	0.0

EXTERNAL PROTON BEAM (EPB)

Exp. No.	Title	Spokesman	Phase No. *–Complete	Beam Hours
26	NEUTRON TIME-OF-FLIGHT EXPERIMENT AT BEAM STOP	VEESER	1 *	0.0
27	p-p SPIN-CORRELATION EXPERIMENTS	WILLARD	1 * 2 *	0.0 1141.8
42	BREAKUP OF FEW-NUCLEON SYSTEMS AND NUCLEI	COLE	1 *	530.8

Exp. No.	Title	Spokesman	Phase No. * = Complete	Beam Hours
81	STUDY OF NEUTRON-PROTON AND PROTON-PROTON COINCIDENCE SPECTRA FROM p + d — n + p + p REACTION	PHILLIPS	1 * 2 *	0.0 600.5
128	WNR STORAGE RING STRIPPER EXPERIMENT	HAYWARD	1 *	0.0
137	SEARCH FOR PARITY-VIOLATING CONTRIBUTION TO SCATTERING OF HADRONS	NAGLE MISCHKE FRAUENFELDER	1 * 2 * 3 *	316.6 363.4 346.5
153	INVESTIGATION OF NUCLEAR GAMMA RAYS RESULTING FROM IN-FLIGHT PION AND PROTON REACTIONS	EISENSTEIN	1 *	0.0
159	CHARGED-PARTICLE EMISSION IN PROTON-INDUCED REACTIONS AS A FEASIBILITY STUDY IN THE USE OF INTRINISIC GERMANIUM DETECTORS WITH THE PRIMARY LAMPF BEAM	EISENSTEIN	1 *	0.0
176	p-NUCLEUS TOTAL AND TOTAL REACTION CROSS-SECTION MEASUREMENTS	ANDERSON	1 * 2 *	0.0 296.6
192	MEASUREMENT OF THE EMITTANCE GROWTH IN H^- STRIPPING	HAYWARD	1 *	70.0
194	p-p, D, R, AND A MEASUREMENTS	McNAUGHTON	1 * 2 *	185.2 498.5
197	INVESTIGATION REACTION $p + d \rightarrow {}^3He + \pi^0$ AT LAMPF ENERGIES	HUNGERFORD	1 *	363.0
200	STUDY OF THE PHOTODETACHMENT SPECTRUM OF H^- IN THE VICINITY OF 11 eV	BRYANT	1 *	128.8
219	DOUBLE PION PRODUCTION IN PROTON-PROTON SCATTERING	BEVINGTON	1 *	422.0
223	STUDIES OF THE (p,np) CHARGE-EXCHANGE REACTION	HOFFMANN	F S*	66.3
241	DIRECT LEPTON PRODUCTION AT LAMPF ENERGIES	HOFFMAN MISCHKE	1 *	531.2
278	STUDY OF REACTION MECHANISMS USING INTERNAL CONVERSION TECHNIQUES	HOFFMANN MOORE	1 *	53.0
279	TEST OF CHARGE SYMMETRY IN nd AND pd SCATTERING	DIETERLE McFARLANE	F S* 1 *	67.0 0.0
289	MEASUREMENT OF THE PHASE OF THE FORWARD NUCLEON-NUCLEON SPIN-INDEPENDENT ELASTIC-SCATTERING AMPLITUDE AT 800 MeV	WHITTEN	1 *	354.6
323	STARK EFFECT QUENCHING OF RESONANCES IN THE PHOTODISINTEGRATION OF THE H^- ION	BRYANT GRAM	1 *	350.6
336	STUDY OF THE SPIN DEPENDENCE OF PROTON-PROTON PION PRODUCTION REACTIONS	MUTCHLER PINSKY	1 * 2 *	419.4 747.0
339	SURVEY OF PHOTODETACHMENT CROSS SECTION OF H^- FROM THRESHOLD TO 15 eV AND ITS DEPENDENCE UPON ELECTRIC FIELD	BRYANT GRAM	1 *	1363.1
341	STUDY OF pd — dm^+n REACTION MECHANISMS	PHILLIPS	1 *	229.0

Exp. No.	Title	Spokesman	Phase No. * = Complete	Beam Hours
392	A MEASUREMENT OF THE TRIPLE-SCATTERING PARAMETERS D, R, A, R', AND A' FOR PROTON-PROTON AND PROTON-NEUTRON SCATTERING AT 800 MeV	HOFFMANN BONNER	5 *	87.0
449	SURVEY OF SINGLE AND DOUBLE PHOTODETACHMENT CROSS SECTION OF THE H^- ION FROM 14 TO 21.8 eV	BRYANT DONAHUE	1 * 2 *	570.7 229.9
468	MECHANISMS OF LUMINESCENCE INDUCED BY PROTONS INCIDENT OF ULTRAVIOLET GRADE OPTICAL MATERIALS	BECHER	1 *	70.8
492	POLARIMETER CALIBRATIONS AND SEARCH FOR ENERGY-DEPENDENT STRUCTURE IN pp ELASTIC SCATTERING VIA CROSS SECTION, ANALYZING POWER, AND WOLFENSTEIN PARAMETER MEASUREMENTS	McNAUGHTON WILLARD	1 *	0.0
498	MEASUREMENTS OF LONGITUDINAL CROSS-SECTION DIFFERENCE FOR LONGITUDINAL POLARIZED BEAM AND TARGETS (pp, pd, np)	WAGNER BURLESON	1 * 2 3	1664.5 0.0 0.0
512	PROTON-PROTON ELASTIC-SCATTERING MEASUREMENTS OF THE $A_{SS}\theta$), $A_{LL}\theta$), AND $A_{SL}\theta$) SPIN-CORRELATION PARAMETERS AT 500, 650, and 800 MeV	GREENE IMAI	–NU –NU 1 *	0.0 0.0 835.0
530	H^- MAGNETIC STRIPPING RATES	JASON	1 *	237.2
586	A STUDY OF THE EFFECTS OF VERY STRONG ELECTRIC FIELDS ON THE STRUCTURE OF THE H^- ION	BRYANT GRAM	1 2	517.0 0.0
587	FUNDAMENTAL EXPERIMENTS WITH RELATIVISTIC HYDROGEN ATOMS EXPLORATORY WORK	SMITH DONAHUE	1 * 2 * 4	400.0 0.0 0.0
588	A SEARCH FOR LONG-LIVED STATES OF THE H^- ION	CLARK BRYANT	1	0.0
591	AN INVESTIGATION OF INCLUSIVE ONE-PION PRODUCTION IN PROTON-NUCLEUS COLLISIONS	DEVRIES DIGIACOMO	1 * 2	651.1 243.0
592	AN INVESTIGATION OF TWO-PION PRODUCTION AND CORRELATIONS IN PROTON-NUCLEUS COLLISIONS AT 800 MeV	DEVRIES DIGIACOMO	1	0.0
633	MEASUREMENT OF p-p ELASTIC SCATTERING IN THE COULOMB INTERFERENCE REGION BETWEEN 300 AND 800 MeV	PAULETTA IROM	1	0.0
634	MEASUREMENT OF PARITY VIOLATION IN THE p-NUCLEUS TOTAL CROSS SECTIONS AT 800 MeV	CARLINI TALAGA YUAN	1 * 2	299.2 471.0
635	SPIN MEASUREMENTS IN pd ELASTIC SCATTERING	BONNER IGO BLESZYNSKI	1 2	507.7 622.0
636	A MEASUREMENT OF THE WOLFENSTEIN POLARIZATION PARAMETERS D_{LL}, D_{SL}, K_{LL}, AND K_{SL} FOR p-p ELASTIC SCATTERING	HOLLAS	1	683.0
637	A MEASUREMENT OF THE VECTOR POLARIZATION OF THE DEUTERON IN THE REACTION $pp \rightarrow d\pi^+$	BONNER	1	430.0

Exp. No.	Title	Spokesman	Phase No. * = Complete	Beam Hours
708	A MEASUREMENT OF THE DEPOLARIZATION, THE POLARIZATION, AND THE POLARIZATION ROTATION PARAMETERS AND THE ANALYZING POWER FOR THE REACTION $pp \rightarrow pn^+n$	HOLLAS	1 2	651.0 0.0
792	MEASUREMENT OF PARITY VIOLATION IN THE $\bar{p}p$ AND $\bar{p}$-NUCLEON TOTAL CROSS SECTIONS AT 800 MeV	YUAN	1	527.0
815	MEASUREMENT OF A_{NO}, S_{SL}, AND A_{LL} IN $\bar{p}\bar{p} \rightarrow pn\pi^+$ AT 500, 580, 650, 720, AND 800 MeV	BUGG	1	0.0
817	ELASTIC SCATTERING OF POLARIZED PROTONS FROM 3M AT INTERMEDIATE ENERGY	BLESZYNSKI AZIZI IGO	1	0.0
818	PROTON-DEUTERON ELASTIC SCATTERING AT 800-MeV TWO- AND THREE-SPIN OBSERVABLES	IGO	1	0.0
832	GAMMA-RAY ANGULAR CORRELATION FROM $^{12}C(\bar{p},p')^{12}C$ (15.11 MeV)	LIEB PERDRISAT FUNSTEN	1	0.0
866	NEUTRINO SOURCE CALIBRATION	HAUSAMMANN DONAHUE	1	0.0

ENERGETIC PION CHANNEL SPECTROMETER (EPICS)

Exp. No.	Title	Spokesman	Phase No. * = Complete	Beam Hours
9	ELASTIC AND INELASTIC PION SCATTERING FROM CALCIUM ISOTOPES	McCARTHY MORRIS	1 *	646.7
13	STUDY OF π^+-INDUCED DOUBLE-CHARGE-EXCHANGE REACTIONS	SETH	1 *	334.5
14	π^+ AND π^- ELASTIC AND INELASTIC SCATTERING FROM ^{18}O	THIESSEN	1 * 2 *	798.8 218.0
18	SURVEY OF π SCATTERING BY COMPLEX NUCLEI	ZEIDMAN	1 * 2 * 3 *	289.8 198.4 54.3
23	A SURVEY OF PION-NUCLEUS ELASTIC AND INELASTIC SCATTERING AT 180 MeV	WHARTON	1 *	300.5
39	SEARCH FOR (π,p) REACTIONS WITH EPICS	MACEK THIESSEN	1 *	295.5
74	STUDY OF PION-INDUCED DOUBLE-CHARGE-EXCHANGE REACTIONS ON LOW-Z ELEMENTS	PEREZ-MENDEZ STETZ	1 *	346.0
87	π^+ AND π^- SCATTERING FROM ^3He AND ^4He	McCARTHY	1 *	358.1
130	EPICS TUNEUP PROPOSAL: PION CARBON SCATTERING	THIESSEN	1 * 2 *	221.0 674.4
133	PRELIMINARY PION CHANNELING EXPERIMENTS	GEMMELL	1 *	200.9

Exp. No.	Title	Spokesman	Phase No. * = Complete	Beam Hours
156	SURVEY OF QUASI-ELASTIC PION SCATTERING	SWENSON	1 *	190.0
229	π^+ vs π^- INELASTIC EXCITATION OF LOW-LYING COLLECTIVE STATES IN ^{28}N NUCLEI	BRAITHWAITE MOORE	1 *	281.8
245	STUDY OF THE (π^-,n) AND (π,πp) REACTIONS IN ^{3,4}He AND HEAVIER NUCLEI BY DETECTING RECOILING TRITONS OR DEUTERONS	KALLNE THIESSEN	1 *	943.9
246	STUDIES OF π^+ SCATTERING AT 50 MeV FROM LIGHT NUCLEI	EISENSTEIN	1 *	564.0
265	STUDY OF PROMPT NUCLEAR DEEXCITATION GAMMA RAYS FROM PION INTERACTIONS WITH ^{6,7}Li AND ^{12}C	MORRIS BRAITHWAITE	1 *	319.0
310	(π^+,π^- DOUBLE-CHARGE-EXCHANGE REACTIONS USING CORE 2n TARGETS	BRAITHWAITE MORRIS	1 *	265.2
317	INELASTIC PION SCATTERING TO THE 1$^+$ STATES OF ^{12}C	PETERSON	1 *	246.5
325	PION AND MUON MULTIPLE COULOMB-SCATTERING EXPERIMENT ON THE EPICS BEAM LINE	HANSON	1 *	69.7
342	STUDY OF THE (π^+,p) REACTION IN ^{12}C	McCARTHY KALLNE	1 *	151.2
368	ELASTIC PION SCATTERING TO THE 19.2 $\pm$ 0.3 MeV STATE IN ^{12}C	MOORE	1 *	246.5
369	INELASTIC PION SCATTERING BY ^{17}O, ^{18}O, AND ^{19}F	DEHNHARD	1 *	318.1
389	INELASTIC PION SCATTERING FROM LIGHT NUCLEI ^{10}B, ^{11}B, ^{14}N, AND ^{15}N	MORRISON ZEIDMAN	1 * 2 * 3 *	685.0 0.0 132.0
391	INELASTIC $\pi^\pm$ SCATTERING ON ^{7}Li	PETERSON	1 *	201.7
413	MASS MEASUREMENT OF ^{26}Ne AND ^{48}Ar BY THE (π^-,π^+ REACTION	SETH NANN	1 *	0.0
419	π^+ vs π^- INELASTIC EXCITATION OF SINGLE-PARTICLE AND CORE-COUPLED STATES IN ^{207}Pb AND ^{209}Bi	BRAITHWAITE MORRIS MOORE	1 *	25.3
442	STUDY OF THE INCLUSIVE PION DOUBLE-CHARGE-EXCHANGE REACTION	KALLNE	1 *	124.7
446	STUDY OF E0 GIANT RESONANCES	HALPERN EISENSTEIN THIESSEN	1	0.0
448	STUDY OF π^+ DOUBLE-CHARGE-EXCHANGE SCATTERING AT SMALL ANGLES ON VARIOUS NUCLEI	BURLESON	1 *	399.7
452	ELASTIC AND INELASTIC SCATTERING OF $\pi^\pm$ BY ^{13}C	DEHNHARD	1 *	219.5
456	THE (π,d) REACTION ON ^{12}C AT 60 MeV	HOISTAD	1	0.0
460	AN INVESTIGATION OF THE STABILITY OF ^{6}H, ^{7}H, AND ^{9}He BY (π^-,π^+ REACTIONS	SETH	1 *	444.7

Exp. No.	Title	Spokesman	Phase No. *=Complete	Beam Hours
463	COMPARATIVE STUDY OF THE $(\pi^+,\pi^-$ AND $(\pi^-,\pi^+$ REACTIONS ON ^{12}C	NANN SETH	1 *	444.7
478	$\pi^\pm$ ELASTIC SCATTERING FROM DEUTERIUM	MASTERSON	1 *	148.3
481	EXCITATION OF HIGH-SPIN STATES IN $T_z = 0$ s-d SHELL NUCLEI BY PION ELASTIC SCATTERING	GEESAMAN	1 *	134.7
484	INELASTIC PION SCATTERING FROM ^{148}Sm AND ^{152}Sm	MORRIS	1 *	70.7
495	ISOSPIN MIXING IN ^{12}C	MORRIS BRAITHWAITE	1 *	424.1
506	INELASTIC PION SCATTERING TO THE UNNATURAL PARITY LEVELS IN ^{12}C AND ^{6}Li	COTTINGAME BRAITHWAITE	1 *	0.0
510	ENERGY DEPENDENCE OF ELASTIC AND INELASTIC SCATTERING OF $\pi^\pm$ BY ^{13}C BETWEEN 116 AND 280 MeV	DEHNHARD	1 * 2 *	61.1 239.0
516	THE (π^+,p) REACTION OF $^{16,18}O$	ANDERSON HOISTAD	1 *	36.0
522	EXCITATION OF GIANT RESONANCE STATES IN ^{90} AND ^{208}Pb WITH 150-MeV PIONS	KING ANDERSON PETERSON	1 *	198.6
539	SEARCH FOR PURE NEUTRON/PROTON TRANSITIONS IN ^{14}C	BAER HOLTKAMP	1 *	345.7
546	INVESTIGATION OF THE SPIN FORM FACTOR OF TRITIUM AND ^{3}He	BRISCOE NEFKENS	F S* 1 *	60.9 240.0
549	A STUDY OF THE DCX REACTION MECHANISM THE $^{42}Ca(\pi^-,\pi^-)^{42}Ti$ REACTION	SETH	1 *	349.3
550	EXCITED-STATE SPECTRA OF THE EXOTIC NUCLEI ^{18}C AND ^{28}Ne BY (π^-,π^-) DCX REACTIONS	SETH	1	0.0
558	MEASUREMENT OF (π^+,π^-) REACTIONS ON $^{13,14}C$ AND ^{26}Mg	BAER BURLESON	1 *	432.0
565	EXCITATION OF HIGH-SPIN PARTICLE-HOLE STATES IN ^{54}Fe AND ^{58}Ni	ZEIDMAN GEESAMAN	1 *	209.0
570	INVESTIGATION OF THE STRUCTURE OF ^{16}O WITH PION INELASTIC SCATTERING	HOLTKAMP FORTUNE	1 *	325.0
572	A-DEPENDENCE OF THE (π^+,π^-) REACTION AND THE WIDTH OF A DOUBLE ISOBARIC ANALOG STATE IN HEAVY NUCLEI	GREENE MOORE MORRIS	1 2	0.0 0.0
573	PION SCATTERING FROM ^{24}Mg AND ^{26}Mg	BLANPIED	1	159.0
577	MEASUREMENT OF ANGULAR DISTRIBUTIONS FOR $^{16}O(\pi^+,\pi^-)^{16}Ne$	GREENE FORTUNE	1 *	237.0
581	$\pi^\pm$ ELASTIC SCATTERING FROM DEUTERIUM AT 237 MeV	MASTERSON BOUDRIE	1 * 2 *	193.0 236.0

Exp. No.	Title	Spokesman	Phase No. * = Complete	Beam Hours
597	THE STUDY OF BROAD-RANGE PION INELASTIC SCATTERING SPECTRA (WITH EMPHASIS ON THE EXCITATION OF THE GIANT MONOPOLE RESONANCE)	HALPERN EISENSTEIN	1 *	190.0
598	INELASTIC PION SCATTERING TO THE UNNATURAL PARITY LEVELS IN ^{6}Li	COTTINGAME KIZIAH	1	332.0
601	DETERMINATION OF ISOSCALAR AND ISOVECTOR TRANSITION RATES FOR LOW-LYING COLLECTIVE STATES IN ^{90}Zr AND ^{208}Pb BY π^+ AND π^- INELASTIC SCATTERING	HINTZ	1	0.0
602	NEUTRON-PROTON COMPONENTS OF INELASTIC TRANSITIONS IN PION SCATTERING ON ^{23}Na AND ^{25}Mg	HARVEY DEHNHARD	1	0.0
604	AN INVESTIGATION OF THE NEAR STABILITY OF ^{5}H	SETH	1 *	254.8
605	A DIBARYON SEARCH AT EPICS	SETH	1 *	107.0
606	TESTS OF THE (N − Z) DEPENDENCE OF PION DOUBLE CHARGE EXCHANGE	SETH	1 *	431.0
617	A STUDY OF THE (3/2,3/2) RESONANCE IN LIGHT NUCLEI	ZIOCK	1 * 2 *	321.0 0.0
619	INELASTIC PION SCATTERING TO 0^+ AND 2^+ STATES IN ^{40}Ca AND ^{42}Ca	MOORE FORTUNE MORRIS	1 *	136.6
622	INVESTIGATION OF THE STRONG CANCELLATIONS OF NEUTRON-PROTON TRANSITION AMPLITUDES IN ^{14}C	HOLTKAMP BAER	1 *	138.1
625	INELASTIC SCATTERING OF PIONS TO GIANT RESONANCES	KING ANDERSON PETERSON	1 *	162.0
651	MEASUREMENT OF A LOWER LIMIT FOR THE SUBTHRESHOLD PRODUCTION OF KAONS WITH 800-MeV PROTONS	MORRIS	1	0.0
657	INELASTIC $\pi^{\pm}$ SCATTERING FROM THE N = 26 ISOTONES	SEIDL MOORE	1	0.0
659	SPIN-FLIP GIANT RESONANCE EXCITATION	BLAND MOORE	1 * 2 *	174.0 108.0
661	GOOD-RESOLUTION STUDY OF ^{18}O(π,π')	MORRIS BLAND	1	0.0
662	ELASTIC AND INELASTIC π^- AND π^+ SCATTERING FROM ^{32}S, ^{31}P AND ^{90,89}Y	KRAUSHAAR PETERSON	1	0.0
671	EXPERIMENTAL INVESTIGATIONS OF ISOVECTOR PROPERTIES OF COLLECTIVE TRANSITIONS	SAHA SETH	1	271.0
672	STUDY OF GIANT RESONANCES IN ^{90}Zr, ^{116}Sn, AND ^{208}Pb WITH π^+ AND π^- INELASTIC SCATTERING	CAREY MOSS	1 *	233.0
677	A DETERMINATION OF $\Delta S = 1$ CONTRIBUTIONS IN INELASTIC PION SCATTERING FROM ODD-A NUCLEI	HOLTKAMP FUNSTEN	1	0.0

Exp. No.	Title	Spokesman	Phase No. * = Complete	Beam Hours
678	STUDY OF THE M1 TRANSITION IN ^{48}Ca BY INELASTIC SCATTERING OF π^+ AND π^-	DEHNHARD MORRIS	1 *	281.0
681	MEASUREMENTS OF LARGE-ANGLE PION-NUCLEUS SCATTERING WITH EPICS	BURLESON	1	266.0
701	PION DOUBLE CHARGE EXCHANGE ON SELF-CONJUGATE NUCLEI	MORRIS FORTUNE	1 *	314.0
702	NUCLEAR STRUCTURE EFFECTS IN PION SCATTERING FROM $^{92\text{-}100}Mo$	COMFORT	1	0.0
703	STUDY OF M4 STRENGTH IN ^{15}N BY π^+ AND π^- INELASTIC SCATTERING	HOLTKAMP SEESTROM-MORRIS	1 *	245.0
716	PION DOUBLE CHARGE EXCHANGE ON HEAVY NUCLEI	SETH	1 * 2	120.0 0.0
717	PION SCATTERING TO COLLECTIVE STATES IN SELENIUM ISOTOPES	BLAND MORRIS GREENE	1	0.0
723	MEASUREMENT OF THE NEUTRON AND PROTON CONTRIBUTIONS TO EXCITED STATES IN ^{39}K BY π^+ AND π^- INELASTIC SCATTERING	HARVEY FORTUNE	1	0.0
744	PION INELASTIC SCATTERING FROM ^{20}Ne	MOORE FORTUNE	1	0.0
746	PION INELASTIC SCATTERING FROM ^{6}Li	KIZIAH COTTINGAME	1 * 2	114.0 0.0
748	MEASUREMENT OF $(M_n/M_p)^2$ FOR 2^+ TRANSITIONS IN T = 1 NUCLEI	SEESTROM-MORRIS	1	0.0
749	$^{18}O(\pi^+,\pi^-)^{18}Ne$ (g.s.) ANGULAR DISTRIBUTION MEASUREMENTS AT T_π = 120 MeV AND T_π = 200 MeV	BLAND FORTUNE	1 *	357.0
755	MEASUREMENT OF M1 GIANT RESONANCES IN PION INELASTIC SCATTERING	SEESTROM-MORRIS BLAND	1 *	169.0
756	$\pi^\pm$ INELASTIC SCATTERING FROM ^{4}He: AN EXAMINATION OF ISOSPIN-SYMMETRY BREAKING	HOLTKAMP COTTINGAME	1	0.0
772	NEUTRON-PROTON COMPOSITION OF TRANSITIONS IN ^{23}Na AND ^{25}Mg FROM INELASTIC SCATTERING OF π^+ AND π^-	HARVEY DEHNHARD	1	0.0
773	MEASUREMENTS OF (π^+,π^-) ANGULAR DISTRIBUTIONS ON ^{56}Fe AT 164 AND 292 MeV	SEIDL BURLESON	1	0.0
777	ANGULAR DISTRIBUTIONS FOR DCX ON ^{14}C AND ^{18}O	SEIDL FORTUNE BAER	1	0.0

Exp. No.	Title	Spokesman	Phase No. * = Complete	Beam Hours
778	CONTINUATION OF THE STUDY OF THE M1 TRANSITION IN ^{48}Ca BY THE INELASTIC SCATTERING OF π^+ AND π^-	DEHNHARD MORRIS	1	0.0
780	A STUDY OF THE DOUBLE-CHARGE-EXCHANGE REACTIONS $^{14}C(\pi^-,\pi^+)^{14}Be$ AND $^{18}O(\pi^-,\pi^+)^{18}C$	BAER SEIDL GILMAN	1	220.0
782	ELASTIC SCATTERING OF π^+ AND π^- FROM ^3He AND ^4He BETWEEN 88.5 AND 194.3 MeV	DEHNHARD SEESTROM-MORRIS	1	0.0
791	ISOSCALAR QUENCHING IN THE EXCITATION OF 8^- STATES IN ^{52}Cr	ZEIDMAN MORRISON	1	0.0
793	PION DOUBLE CHARGE EXCHANGE ON SELF-CONJUGATE NUCLEI (CONTINUED)	BLAND MOORE MORRIS	1	0.0
796	CORE EXCITATION EFFECTS IN PION DOUBLE CHARGE EXCHANGE	SETH	1 *	328.0
797	THE STUDY OF GIANT RESONANCES AND LOW-LYING COLLECTIVE STATES IN ^{90} BY INELASTIC π^- AND π^+ SCATTERING	ULLMANN KING	1	0.0
800	INELASTIC PION SCATTERING FROM ^{22}Ne	FORTUNE	1	0.0
809	STUDY OF π^-,p AND π^+,p REACTIONS WITH EPICS	EGGER BLANPIED	1	0.0
812	BACK-ANGLE CHARGE ASYMMETRIES FOR ELASTIC PI-DEUTERON SCATTERING	PETERSON	1	0.0
826	ISOSPIN DEPENDENCE OF NONANALOG PION DOUBLE CHARGE EXCHANGE	MORRIS MOORE GILMAN	1	0.0
833	CONTINUATION OF THE INVESTIGATION OF LARGE-ANGLE PION-NUCLEUS SCATTERING	BURLESON	1	0.0
835	TARGET MASS DEPENDENCE OF THE ISOVECTOR CONTRIBUTION TO THE GIANT QUADRUPOLE RESONANCE	SEESTROM-MORRIS	1	0.0
836	ENERGY DEPENDENCE OF PION SCATTERING TO THE GIANT RESONANCE REGION OF ^{208}Pb	SEESTROM-MORRIS	1	0.0
839	PION INELASTIC SCATTERING FROM THE 1^+ DOUBLET IN ^{12}C	MOORE MORRIS	1	0.0
840	INELASTIC PION SCATTERING FROM ^{16}O AT T_π = 120 AND 200 MeV	BLAND FORTUNE	1	0.0
841	FORWARD-ANGLE PION INELASTIC SCATTERING ON LIGHT NUCLEI	BLAND MOORE FORTUNE	1	0.0
843	A SEARCH FOR $\Delta_{3,3}$ COMPONENTS OF GROUND-STATE NUCLEAR WAVE FUNCTIONS	MORRIS MOORE	1	0.0
845	PION INELASTIC SCATTERING FROM ^9Be	KELLY	1	0.0

Exp. No.	Title	Spokesman	Phase No. * = Complete	Beam Hours
858	ADDITIONAL MEASUREMENTS OF $^{18}O(\pi^+,\pi^-)^{18}Ne$ (g.s.)	FORTUNE GILMAN	1	0.0
862	STUDY OF THE M1 TRANSITION IN ^{88}Sr BY THE INELASTIC SCATTERING OF π^+ AND π^-	NANDA DEHNHARD	1	0.0
863	STUDY OF GIANT RESONANCES IN THE PALLADIUM ISOTOPES VIA PION SCATTERING	SAHA SETH	1	0.0
868	AN EXPERIMENTAL TEST OF THE Δ-HOLE MODEL OF NONANALOG DOUBLE CHARGE EXCHANGE	SETH	1	0.0
874	ELASTIC SCATTERING OF π^+ FROM DEUTERIUM IN THE REGION OF THE $^3F_3$ DIBARYON RESONANCE	BLILIE DEHNHARD	1	0.0

HIGH-RESOLUTION SPECTROMETER (HRS)

Exp. No.	Title	Spokesman	Phase No. * = Complete	Beam Hours
4	LARGE ANGLE ELASTIC SCATTERING OF PROTONS FROM HELIUM AND QUASI-ELASTIC KNOCKOUT OF ALPHA PARTICLES BY 800-MeV PROTONS	IGO	1 *	458.0
5	INELASTIC SCATTERING OF 800-MeV PROTONS FROM NUCLEI TO STUDY QUASI-FREE MODES	CHRIEN PALEVSKY	1 *	532.7
10	SEARCH FOR (p,π) REACTIONS WITH HRS	SPENCER	1 *	167.9
15	ELASTIC SCATTERING AND TOTAL CROSS-SECTION MEASUREMENTS OF PROTON ON HYDROGEN, DEUTERIUM, AND HELIUM	IGO TANAKA	1 * 2 * 3 *	0.0 75.0 249.0
49	ELASTIC AND INELASTIC PROTON SCATTERING FROM THE NICKEL ISOTOPES AND FROM ^{89}Y	PETERSON	1 *	68.3
117	HIGH-RESOLUTION STUDY OF THE NEUTRON PICK-UP REACTION	IGO	1 *	273.2
138	INELASTIC PROTON SCATTERING AND EXCITATION OF STATES OF INTERMEDIATE COLLECTIVITY IN OPEN-SHELL NUCLEI	McDANIELS SWENSON	1 *	184.2
139	PRELIMINARY PROTON SCATTERING SURVEY WITH HRS	SPENCER TANAKA	1 *	695.1
178	PROTON SCATTERING SURVEY ON s-d SHELL NUCLEI	SPENCER HINTZ	1 *	209.3
183	PROTON SCATTERING SURVEY ON HEAVY DEFORMED NUCLEI	HINTZ SPENCER	1 *	382.1
204	EXCITATION AND ASYMMETRY MEASUREMENT OF T ≈ 1, HIGH-SPIN, NONNORMAL PARITY PARTICLE-HOLE STATE BY (p,p') SCATTERING IN THE INTERMEDIATE-ENERGY RANGE	IGO	1 *	127.0
223	STUDIES OF THE (p,np) CHARGE-EXCHANGE REACTION	HOFFMANN	F S*	0.0

Exp. No.	Title	Spokesman	Phase No. * = Complete	Beam Hours
233	SEARCH FOR DELTA-CONFIGURATIONS NUCLEI	SETH SPENCER	1 *	167.9
249	THE (p,π⁺) REACTION ON ^{4}He WITH 800-MeV PROTONS	WHITTEN	1 *	296.7
256	p-NUCLEUS ELASTIC SCATTERING AT $q^2 = 8$ GeV^2 IN Be, C, AND THE STUDY OF p-NUCLEUS INTERACTIONS IN COBALT AND GOLD UP TO $m^* = q^2/2\nu \cong 20$	FRANKEL	1 *	107.6
258	STUDY OF MECHANISMS FOR THE EJECTION OF HIGH-MOMENTUM PARTICLES FROM NUCLEI BY STUDY OF THE COINCIDENCE SPECTRUM IN p + a → (p,d,t) + (p,d,t) + X	FRANKEL FRATI	1 * 2	178.7 0.0
261	INTERMEDIATE-ENERGY (p,d) REACTION MECHANISM STUDIES	RICKEY SHEPARD PETERSON	1 *	0.0
311	ELASTIC-SCATTERING SURVEY USING POLARIZED PROTONS	HOFFMANN	1 * 2 *	715.3 245.6
346	STUDY OF HIGH-MOMENTUM COMPONENTS IN NUCLEI USING A POLARIZED PROTON BEAM	FRANKEL	1 *	209.8
347	SEARCH FOR ORBIT-FLIP STATES BY INELASTIC PROTON SCATTERING	HINTZ	1 *	209.3
352	DETERMINATION OF NEUTRON-MASS DISTRIBUTION FROM ELASTIC PROTON MEASUREMENTS [P(t) AND dσ/dt] ON ISOTOPES IN THE CALCIUM REGION	WHITTEN	1 *	204.8
354	SCATTERING OF 800-MeV PROTONS FROM ^{12}C AND ^{13}C AT MOMENTUM TRANSFER > 4 F^{-1}	BLANPIED	1 *	324.1
355	FURTHER ELASTIC SCATTERING CROSS SECTION AND ANALYZING POWER MEASUREMENTS ON ^{208}Pb AND ^{118,124}Sn	HOFFMANN	1 * 2 *	130.0 55.0
356	ANALYZING POWER AND CROSS-SECTION MEASUREMENTS FOR INELASTIC PROTON EXCITATION OF SIMPLE STATES	GLASHAUSSER BAKER SCOTT	1 * 2 *	199.9 88.1
385	MEASUREMENT OF THE POLARIZED PROTONS + NEUTRONS ANALYZING POWER $A_y(\theta)$ FROM $\theta_{c.m.}$ 10-70°	HOFFMANN	1 * 2 *	140.6 108.8
386	TOTAL REACTION CROSS SECTIONS FOR p⁻ NUCLEI AT 800 MeV	HOFFMANN BURLESON YOKOSAWA	1 * 2 * 3 * 4 *	404.0 113.5 113.5 0.0
392	A MEASUREMENT OF THE TRIPLE-SCATTERING PARAMETERS D, R, A, R′, AND A′ FOR PROTON-PROTON AND PROTON-NEUTRON SCATTERING AT 800 MeV	HOFFMANN	1 * 2 * 3 * 4 5 *	208.6 491.0 146.0 0.0 104.0
395	THE (p,π⁺) REACTION ON ^{16}O AND ^{40}Ca	BAUER HOISTAD NANN	1 *	195.8

Exp. No.	Title	Spokesman	Phase No. * = Complete	Beam Hours
399	EXCITATION OF GIANT MULTIPOLE RESONANCES BY 200-400-MeV PROTONS	BERTRAND	1 * 2 *	40.0 144.0
405	THE (p,π^-) REACTION ON ^{12}C AND ^{13}C	HOISTAD BAUER SETH	1 *	271.7
411	MEASUREMENT OF SPIN-FLIP PROBABILITIES IN PROTON INELASTIC SCATTERING AT 800 MeV AND SEARCH FOR COLLECTIVE SPIN-FLIP MODES. PRELIMINARY SURVEY	HINTZ MOSS	1 *	247.0
425	PROTON ELASTIC SCATTERING AT ~600 MeV BY ^{40,42,44,48}Ca, ^{90}Zr, AND ^{208}Pb	SETH HOFFMANN	1 *	283.2
431	CROSS SECTION AND ANALYZING POWER FOR INELASTIC PROTON EXCITATION OF UNNATURAL PARITY STATES IN ^{6}Li, ^{12}C, ^{14}N, AND ^{16}O	GLASHAUSSER MOSS	1 *	181.0
432	CROSS SECTION FOR EXCITATION OF UNNATURAL PARITY STATES IN ^{12}C AT E_p < 800 MeV	GLASHAUSSER MOSS	1 *	148.9
433	ELASTIC SCATTERING DIFFERENTIAL CROSS SECTIONS AND ANALYZING POWERS FOR POLARIZED p + ^{40,48}Ca, ^{90}Zr, AND ^{208}Pb AT ~400 MeV	HOFFMANN SETH	1 *	0.0
438	THE (p,α) REACTIONS ON ^{12,13}C, ^{7}Li, ^{18}O, ^{25}Mg, ^{28}Si, AND ^{40}Cu BETWEEN 650 AND 800 MeV	IGO	1 *	249.5
451	INELASTIC PROTON SCATTERING IN THE RANGE 300 TO 500 MeV	HINTZ	1 2	221.3 0.0
462	ANALYZING POWER AND DIFFERENTIAL CROSS SECTIONS FOR THE REACTIONS p + p — d + π^+ AND p + d — t + π^+ AT ~600 AND 400 MeV	SETH NANN	1 *	118.0
470	REACTIVE CONTENT OF THE OPTICAL POTENTIAL	BARLETT HOFFMANN	1 * 2 *	247.5 83.0
472	STUDY OF THE (p,d) REACTION ON ^{90}Zr, ^{140}Ce, AND ^{208}Pb AT 800 MeV	WHITTEN	1 *	79.5
473	STUDY OF GIANT MULTIPOLE RESONANCES WITH 800-MeV PROTONS	MOSS ADAMS CAREY	1 * 2 *	110.8 197.7
474	A MEASUREMENT OF SPIN-DEPENDENT EFFECTS IN p + d ELASTIC AND INELASTIC SCATTERING	CORNELIUS	1 * 2 *	71.0 60.0
475	SCATTERING OF 0.8-GeV PROTONS FROM ^{20}Ne AND ^{22}Ne	BLANPIED	1 * 2 *	154.9 133.0
476	THE ANALYZING POWER FOR POLARIZED PROTONS + ^{24,26}Mg AT 500 AND 800 MeV	BLANPIED	1 *	147.6
485	THE ENERGY DEPENDENCE IN THE (p,π^-) REACTION	HOISTAD SHEPARD	1	0.0
486	INELASTIC SCATTERING OF PROTONS POPULATING THE 4$^-$ (3.44-MeV) LEVEL OF ^{208}Pb — A SEARCH FOR CRITICAL OPALESCENCE	IGO GLASHAUSSER MOSS	1 *	65.6

Exp. No.	Title	Spokesman	Phase No. * = Complete	Beam Hours
489	SEARCH FOR M1 GIANT RESONANCES IN THE (p,p') REACTION AT E_p = 800 MeV	MOSS	1 *	63.9
508	DIBARYON RESONANCES IN PION PRODUCTION	SETH	1 *	178.0
			2 *	171.0
			3	0.0
			4	0.0
519	STUDY OF THE REACTION p(pol) + d — (p,π) + X TO MEASURE THE ANALYZING POWER AND STRUCTURE FUNCTION FOR BACKWARD PARTICLES	FRANKEL	1 *	130.3
520	STUDY OF THE REACTION p(POLARIZED) + ^{3,4}He — (p,d,π..) + X TO MEASURE THE ANALYZING POWER STRUCTURE FUNCTIONS FOR BACKWARDS PARTICLES	VAN DYCK	1 *	127.0
531	EXCITATION OF UNNATURAL PARITY STATES IN ^{12}C AT 500 MeV	GLASHAUSSER MOSS	1	101.3
532	MEASUREMENTS OF CROSS SECTIONS AND ANALYZING POWER IN THE (p,2p) REACTION ON DEUTERIUM	VAN DYCK	1	0.0
533	THE ASYMMETRY IN THE (p,π) REACTION ON ^{6}Li AT 800 MeV	HOISTAD SETH	1	0.0
535	A STUDY OF THE RELATION BETWEEN THE (p,d) AND (π,p) REACTION IN A PION EXCHANGE MODEL	ANDERSON HOISTAD	1	0.0
538	ANALYZING POWER AND CROSS-SECTION MEASUREMENTS OF THE ^{4}He(p,d)^{3}He REACTION	SHEPARD KING	1 *	43.0
			2	0.0
540	ELASTIC SCATTERING FROM LIGHT NUCLEI	IGO BLESZYNSKI	1 *	0.0
556	A PROPOSAL TO STUDY THE (p,p') PROCESS LEADING TO π-ATOMIC STATES	BERTOZZI	1 *	52.6
563	p + p ELASTIC SCATTERING AT 800 AND 500 MeV	HOFFMANN	1 *	143.3
580	CROSS SECTIONS AND ANALYZING POWERS FOR ELASTIC AND INELASTIC SCATTERING OF 515-MeV PROTONS FROM ^{13}C	SEESTROM-MORRIS DEHNHARD	1	43.6
583	MEASUREMENT OF C_{LL} IN THE COULOMB INTERFERENCE REGION	PAULETTA GAZZALY	1	0.0
			2	0.0
585	MEASUREMENT OF p-p AND p-d ELASTIC SCATTERING IN THE COULOMB INTERFERENCE REGION BETWEEN 500 AND 800 MeV	PAULETTA	1 *	106.0
616	MEASUREMENT OF THE WOLFENSTEIN PARAMETERS FOR THE 1^{+} STATES OF ^{12}C	BLESZYNSKI McCLELLAND HINTZ MOSS	1 *	324.4
			2 *	0.0
623	MEASUREMENT OF CROSS SECTION, ANALYZING POWER, AND DEPOLARIZATION PARAMETERS IN THE ^{28}Si(p,p')^{28}Si (6^{-}, T = 0 AND T = 1) REACTION AT 400 MeV	GLASHAUSSER	1	0.0

Exp. No.	Title	Spokesman	Phase No. * = Complete	Beam Hours
626	MEASUREMENT OF THE DEPOLARIZATION PARAMETERS $D_{NN'}$, $D_{LS'}$, AND $D_{SS'}$ IN PROTON-NUCLEUS SCATTERING AT VERY HIGH EXCITATION ENERGIES	GLASHAUSSER McGILL	1 *	208.0
627	MEASUREMENT OF THE RELATIVE SIGN OF NEUTRON AND PROTON TRANSITION MATRIX ELEMENTS IN (p,p') REACTIONS	HYNES BERNSTEIN	1 *	64.0
630	A STUDY OF PROTON INELASTIC SCATTERING AT 0° AND A SEARCH FOR GIANT MONOPOLE AND GIANT MAGNETIC DIPOLE EXCITATIONS	CAREY HINTZ McCLELLAND MOSS	1 * 2 3	133.0 76.0 0.0
632	CAN PROTON DENSITY DIFFERENCES BE EXTRACTED FROM MEDIUM-ENERGY p-NUCLEUS ELASTIC-SCATTERING DATA	BARLETT HOFFMANN	1	0.0
642	REACTIVE CONTENT OF THE OPTICAL POTENTIAL — PHASE 2	McGILL HOFFMANN	1 *	151.3
643	STRUCTURE OF STATES IN THE OXYGEN ISOTOPES VIA MEASUREMENTS OF THE SPIN DEPOLARIZATION AND SPIN-ROTATION OBSERVABLES	AAS HYNES	1 * 2 *	20.0 325.0
644	TESTS OF THE POLARIZATION-ANALYZING POWER EQUALITY IN ELASTIC SCATTERING OF INTERMEDIATE-ENERGY PROTONS FROM NUCLEI	IGO	1	0.0
649	$^{9}Be(p,\pi^{\pm})$ REACTION AT 650 MeV	HOISTAD	1 * 2	85.9 0.0
654	MEASUREMENT OF THE SPIN-ROTATION PARAMETER Q FOR 800-MeV p + ^{16}O, ^{40}Ca, AND ^{208}Pb ELASTIC SCATTERING	HOFFMANN	1 *	400.0
658	STUDY OF THE SPIN-FLIP PROBABILITY FOR ELASTIC AND INELASTIC SCATTERING FROM ODD-MASS NUCLEI	SEESTROM-MORRIS CAREY MOSS DEHNHARD	1	0.0
660	MEASUREMENT OF POLARIZATION PARAMETERS FOR M1 TRANSITIONS IN THE $^{90}Zr(p,p')^{90}Zr^{*}$ AND $^{116}Sn(p,p')^{116}Sn^{*}$ REACTIONS AT 500 MeV	GLASHAUSSER	1	156.0
663	ELASTIC SCATTERING OF POLARIZED PROTONS FROM ^{3}H AND ^{3}He AT INTERMEDIATE ENERGIES	IGO BLESZYNSKI	1 *	205.0
668	THE $^{12}C(p,p'\pi)^{12}C$ REACTION AND THE SEARCH FOR COHERENT ISOBAR-HOLE RESONANCES	GLASHAUSSER WHITTEN	1	0.0
669	INVESTIGATION OF THE N = 28 NEUTRON SHELL CLOSURE BY ELASTIC SCATTERING OF 800-MeV POLARIZED PROTONS	SHERA	1	0.0
670	CONTINUATION OF GIANT RESONANCE STUDIES AT THE HRS	MOSS CAREY ADAMS	1 *	116.0
685	SPIN CORRELATIONS IN THE REACTION $\vec{p}(\vec{d},d)\vec{p}$ AT 500 MeV	BLESZYNSKI IGO	1 2	447.0 0.0

Exp. No.	Title	Spokesman	Phase No. *—Complete	Beam Hours
686	DETERMINATION OF NEUTRON TRANSITION DENSITIES IN ^{16}O AND ^{208}Pb BY INELASTIC SCATTERING OF ~400-MeV PROTONS	HINTZ	1 *	105.0
687	MEASUREMENT OF THE SPIN-ROTATION PARAMETERS IN ^{208}Pb AND IN ^{40}Ca AT 400 MeV	AAS IGO	1 *	134.0
709	MEASUREMENTS OF A_{NN}, A_{SS}, AND A_{SL} IN THE COULOMB INTERFERENCE REGION AT 650 AND 800 MeV	GAZZALY PAULETTA TANAKA	1 2	0.0 522.0
712	INELASTIC PROTON SCATTERING ON ^{48}Ca AND ^{50}Ti — AN ATTEMPT TO IDENTIFY MESONIC EFFECTS AS THE CAUSE OF M1 QUENCHING	SEGEL COMFORT	1	0.0
718	ENERGY DEPENDENCE OF THE TWO-NUCLEON EFFECTIVE INTERACTION	KELLY HYNES	1 *	143.0
720	RECOILLESS DELTA PRODUCTION IN THE REACTION $^{13}C(p,d)^{12}C\Delta$	MORRIS McGILL	1 * 2 *	218.0 140.0
722	MEASUREMENT OF CROSS SECTIONS AND ANALYZING POWERS FOR ELASTIC AND INELASTIC SCATTERING OF 400-500-MeV PROTONS FROM ^{14}C	HARVEY SEESTROM-MORRIS	1	0.0
736	STUDIES OF MULTIPLE-SCATTERING THEORY, THE EFFECTIVE INTERACTION AND Δ-HOLE INTERMEDIATE STATES IN 300-MeV p-NUCLEUS ELASTIC SCATTERING	HOFFMANN	1 2	0.0 0.0
740	LARGE-ANGLE ELASTIC SCATTERING OF PROTONS FROM ^{90} AND ^{208}Pb	AAS BLESZYNSKI IGO	1	0.0
741	INVESTIGATION OF THE LONGITUDINAL-SPIN RESPONSE OF ^{208}Pb AND IMPLICATIONS OF SPIN-TRANSFER FORM FACTORS FOR NONNUCLEON DEGREES OF FREEDOM IN NUCLEI	CAREY McCLELLAND	1 *	189.0
758	TO CATCH A DEMON. . .	SETH	1	0.0
760	PROTON ELASTIC SCATTERING ON ^{40}Ca AND ^{208}Pb	HOFFMANN	1 *	44.0
761	Q MEASUREMENTS AT 650 MeV ON ^{40}Ca	IGO	1 * 2	65.0 0.0
766	ASYMMETRY MEASUREMENT OF THE p-^{9}Be — dπX REACTION AT 800 MeV	HOISTAD	1 *	89.0
768	DEVELOPMENT OF 0° CAPABILITIES AT THE HRS FACILITY	McCLELLAND CAREY SEESTROM-MORRIS	1	0.0
774	EXCITATION OF GIANT MULTIPOLE RESONANCES IN sd-SHELL NUCLEI VIA MEDIUM-ENERGY PROTON INELASTIC SCATTERING	BERTRAND	1	0.0
775	SEARCH FOR M1 RESONANCES IN HEAVY NUCLEI USING SMALL-ANGLE PROTON SCATTERING	MOSS HINTZ	1	0.0

Exp. No.	Title	Spokesman	Phase No. * = Complete	Beam Hours
784	CROSS SECTION AND ANALYZING POWER MEASUREMENTS FOR THE (p,d) REACTIONS ON ^{18}O, ^{56}Fe, AND ^{90}	OHNUMA WHITTEN	1	0.0
785	ELASTIC SCATTERING OF POLARIZED PROTONS FROM ^{3}H AT INTERMEDIATE ENERGY	AZIZI BLESZYNSKI	1	0.0
788	STUDY OF ISOSCALAR M(1) EXCITATIONS IN LIGHT NUCLEI BY PROTON INELASTIC SCATTERING	HINTZ	1	0.0
790	I = 1 NN INELASTIC CROSS SECTIONS AND AND FIRST MEASUREMENTS OF T_{20} FOR THE $pp \rightarrow dn^{+}$ REACTION AT 800 AND 650 MeV	PAULETTA GAZZALY TANAKA	1	0.0
795	A PRECISION TEST OF CHARGE INDEPENDENCE	SETH	1	0.0
799	LARGE-MOMENTUM TRANSFER MEASUREMENTS OF A_y FOR 800-MeV p + ^{208}Pb ELASTIC SCATTERING	BLESZYNSKI WHITTEN	1	0.0
801	A MEASUREMENT OF THE WOLFENSTEIN PARAMETERS FOR $^{48}Ca(p,p')^{48}Ca(1^{+}, 10.2\ MeV)$	JONES McCLELLAND IGO BLESZYNSKI	1	0.0
803	CROSS-SECTION AND ANALYZING-POWER MEASUREMENTS IN THE M1,M2 REGION IN ^{90}Zr AND ^{88}Sr AT 318 MeV	GLASHAUSSER McCLELLAND NANDA	1	0.0
819	II. ELASTIC SCATTERING OF POLARIZED PROTONS FROM ^{3}H AT INTERMEDIATE ENERGY	AZIZI BLESZYNSKI IGO	1	0.0
837	MEASUREMENT OF SPIN-FLIP CROSS SECTIONS UP TO 40-MeV EXCITATION IN ^{58}Ni AND ^{90}Zr	GLASHAUSSER NANDA	1	0.0
844	MEASUREMENT OF A_{NN}, A_{SS}, AND A_{LS} FOR THE REACTION $\vec{p}\,\vec{p} \rightarrow p + n + \pi^{+}$ AT 800 MeV	PAULETTA GAZZALY TANAKA	1	0.0
846	NN → NNπ: CROSS SECTIONS AND ANALYZING POWERS FOR THE 800-MeV $\vec{p}p \rightarrow \pi^{+}np$) AND $\vec{p}n \rightarrow \pi^{-}(pp)$ INCLUSIVE REACTIONS	BHATIA GLASS	1	0.0
851	SEARCH FOR RECOIL-FREE Δ PRODUCTION AND HIGH-SPIN STATES IN THE $^{208}Pb(p,t)^{206}Pb$ REACTION AT $E_p \simeq 400$ MeV	HINTZ	1	0.0
855	MEASUREMENT OF ^{206}Pb-^{208}Pb GROUND-STATE NEUTRON DENSITY DIFFERENCE	HINTZ	1	0.0
864	STUDY OF DEEPLY BOUND HOLE STATES IN THE TIN ISOTOPES VIA THE $(\vec{p},d)$ REACTION	SAHA SETH	1	0.0
865	SPIN-ROTATION MEASUREMENT ON ^{4}He AT 320, 500, AND 800 MeV	AAS BLESZYNSKI IGO	1	0.0
867	MEASUREMENT OF ISOVECTOR QUADRUPOLE TRANSITION DENSITIES IN THE PALLADIUM ISOTOPES	SAHA SETH	1	0.0

ISOTOPE PRODUCTION AND RADIATION-EFFECTS FACILITY (ISORAD)

Exp. No.	Title	Spokesman	Phase No. *=Complete	Beam Hours
184	PRODUCTION OF ^{82}Sr	O'BRIEN	1 *	0.0
210	ISOTOPE PRODUCTION FACILITY IRRADIATION VANADIUM, MOLYBDENUM, AND LANTHANUM TARGETS	O'BRIEN	1 *	0.0
211	NEUTRON IRRADIATION OF COPPER SINGLE CRYSTALS	GREEN	1 *	0.0
267	PREPARATION OF RADIOISOTOPES FOR MEDICINE AND THE PHYSICAL SCIENCES USING THE LAMPF ISOTOPE PRODUCTION FACILITY	O'BRIEN	1 1 1	643.0 19889.3 709.0
407	THE EFFECT OF DISLOCATION VIBRATION ON VOID GROWTH IN METALS DURING IRRADIATION	SOMMER PHILLIPS	3	0.0
725	THE EFFECT OF RARE-EARTH ADDITIONS ON RADIATION DAMAGE IN ALLOY HT-9 (FERRITIC/MARTENSITIC) ALLOY STEEL	DAVIDSON WECHSLER SOMMER	1	0.0
765	800-MeV PROTON IRRADIATION OF MATERIALS FOR THE SIN BEAM STOP	BROWN	1 1 1	692.0 0.0 570.0

LOW-ENERGY PION (LEP)

Exp. No.	Title	Spokesman	Phase No. *=Complete	Beam Hours
2	TOTAL PION CROSS SECTIONS	JAKOBSON	2 *	663.4
25	PION DOUBLE-CHARGE-EXCHANGE REACTION	BURMAN	1 * 2 * 3 *	0.0 681.2 268.2
28	STUDIES OF THE π^+,π^0 REACTION	YAVIN	1 *	195.0
29	ELASTIC SCATTERING OF π^+ AND π^- AT 10-30 MeV	PREEDOM	1 * 2 *	0.0 0.0
35	CLUSTER EFFECTS IN NUCLEAR PION CAPTURE	ZIOCK	1 *	297.5
50	RADIATIVE PION CAPTURE IN LIGHT NUCLEI	CROWE ROWE	1 * 2 *	0.0 460.3
54	ELASTIC SCATTERING OF MESONS IN THE ENERGY RANGE 20-60 MeV	PREEDOM	1 * 2 *	264.6 707.4
67	DEVELOPMENT OF PION BEAM-MONITORING TECHNIQUES	DROPESKY	1 * 2 *	0.0 87.5
79	CALIBRATION OF THE PION BEAM TRANSPORT SYSTEMS AND A PION BEAM MONITOR	PHILLIPS	1 *	0.0
96	SCATTERING OF 20-50-MeV $\pi^\pm$ BY HYDROGEN AND DEUTERIUM	NAGLE	1 * 2 *	0.0 728.0
102	EXCITATION FUNCTIONS AND ANGULAR DISTRIBUTION RECOIL STUDIES OF SIMPLE PION-INDUCED NUCLEAR REACTIONS	MARKOWITZ	1 *	0.0

Exp. No.	Title	Spokesman	Phase No. * = Complete	Beam Hours
121	PION-INDUCED NUCLEAR REACTIONS	SEGEL	1 * 2 *	0.0 150.0
122	PIONIC ATOM X RAYS AND NUCLEAR DISTRIBUTIONS	KUNSELMAN	1 *	0.0
123	NUCLEAR- STRUCTURE EFFECTS IN PION-INDUCED NUCLEAR REACTIONS	KAROL	5 *	25.0
131	A STUDY OF THE $\pi^+ + d \rightarrow p + p$ REACTION AT PION ENERGIES 10-60 MeV	PREEDOM	1 * 2 *	0.0 260.0
140	STUDY OF THE $(\pi^{\pm},d)$ REACTION WITH AN INTRINSIC GERMANIUM DETECTOR	BARNES	1 * 2 * 3 *	0.0 385.0 0.0
144	SEARCH FOR THE C-VIOLATING DECAY $\pi^0 \rightarrow 3\gamma$	HIGHLAND MACEK	1 *	333.0
162	STUDIES OF THE $(\pi^+,\pi^0$ REACTION ON LIGHT ELEMENTS	YAVIN ALSTER	1 *	0.0
164	PION TOTAL CROSS-SECTION MEASUREMENTS WITH AN ORIENTED ^{165}Ho TARGET	FISHER MARSHAK	1 *	88.0
170	STUDY OF REACTION $^{13}C(\pi^+,\pi^0)^{13}N$ (GROUND STATE)	ALSTER	1 *	0.0
180	ELASTIC AND INELASTIC π^+ NUCLEUS SCATTERING AT 25, 50, AND 75 MeV	EISENSTEIN	1 * 2 *	0.0 191.3
181	MEASUREMENTS OF THE $\pi^-p \rightarrow \pi^0n$ ANGULAR DISTRIBUTION AT LOW ENERGIES AND CALIBRATION OF THE π^0 SPECTROMETER	ALSTER BOWMAN	1 * 2 *	346.0 859.2
190	A PRECISION MEASUREMENT OF THE $\pi^- - \pi^0$ MASS DIFFERENCE	ZIOCK	1	133.0
191	π^- NUCLEUS INELASTIC SCATTERING TO GIANT RESONANCES	HALPERN	1 * 2 * 3 * 4 *	0.0 292.7 484.4 284.4
209	PION INTERACTIONS IN NUCLEAR EMULSIONS	BRADBURY ALLRED	1 *	0.0
234	A STUDY OF THE INELASTIC PION SCATTERING REACTION AT PION ENERGIES 10-100 MeV	GOTOW	1 *	436.3
247	DISTRIBUTION OF PRODUCTS FROM INTERACTIONS OF STOPPED π^- WITH SEVERAL MEDIUM- AND HEAVY-MASS NUCLEI	ORTH	1 * 2 *	35.6 59.5
284	MEASUREMENT OF THE $^3He(\pi^-,\pi^0)^3He$ ANGULAR DISTRIBUTION	COOPER WHITNEY	1 2 *	209.0 0.0
293	STUDY OF THE DOMINANT REACTION MODES FOR PIONS INTERFACING WITH COMPLEX NUCLEI	SEGEL	1 *	151.0
295	STUDY OF THE PION-DEUTERON SINGLE-CHARGE-EXCHANGE REACTION $d(\pi^-,\pi^0)2n$	BOWMAN MOINESTER	1	75.8

Exp. No.	Title	Spokesman	Phase No. * = Complete	Beam Hours
299	AN INVESTIGATION OF THE REACTION ($\pi^+,\pi^+ + p$)	ZIOCK	1 *	0.0
			2 *	960.1
			3 *	0.0
303	A SURVEY OF PION SINGLE-CHARGE-EXCHANGE SCATTERING USING BACK-ANGLE GAMMA SPECTROSCOPY	JACKSON	1 *	152.8
			2 *	290.9
			3 *	304.0
315	HIGH-RESOLUTION STUDY OF THE (π^+,2p) REACTION	WHARTON	1 *	0.0
			2 *	338.1
			3 *	862.4
316	π^-NUCLEUS ELASTIC SCATTERING BETWEEN 20 AND 50 MeV	SETH	1 *	699.6
		BURLESON	2 *	0.0
320	A COMPARISON OF (π^+,xn) AND (π^-,xn) REACTIONS	CHURCH	3 *	33.0
			4	0.0
322	SYSTEMATIC STUDY OF PION-INELASTIC SCATTERING AT ENERGIES BELOW 100 MeV	BERTRAND GOTOW	1 *	877.1
324	PRECISION MEASUREMENT OF RATIOS OF CERTAIN LIGHT ELEMENT PION EXCITATION FUNCTIONS	HALPERN	1 *	118.6
333	$\pi^\pm$NUCLEAR ELASTIC SCATTERING AT ENERGIES BETWEEN 50 AND 100 MeV	GOTOW	1 *	512.2
348	STUDY OF GIANT RESONANCES WITH RADIATIVE PION CAPTURE ON MEDIUM-Z NUCLEI AT LEP	CROWE	1 *	761.7
349	NUCLEAR REACTIONS OF ^{127}I WITH PIONS	PORILE	2 *	25.0
			3 *	28.0
350	STUDY OF PION-ABSORPTION MECHANISMS IN NUCLEI	SEGEL SCHIFFER	1 *	225.8
388	LOW-ENERGY PION ELASTIC SCATTERING FROM THE PROTON AND DEUTERON AT 180°	HOLT	1 *	392.2
393	ANGULAR DISTRIBUTION MEASUREMENTS OF THE PION SINGLE-CHARGE-EXCHANGE REACTION ON ^{13}C	ALSTER MOINESTER	1	279.8
401	STUDY OF THE ISOBARIC ANALOG CHARGE-EXCHANGE REACTION ^{15}N(π^-,π^0)^{15}O	BOWMAN COOPER	1 *	357.1
			2	0.0
412	SEARCH FOR ANALOG STATE TRANSITIONS IN (π^-,π^0) REACTIONS ON ^{7}Li, ^{27}Al, ^{93}Zr, ^{120}Sn, AND ^{208}Pb AND FOR COLLECTIVE ISOVECTOR STATES IN THE (π^-,π^0 REACTION ON ^{93}Zr	BAER BOWMAN CVERNA	1 *	270.6
			2 *	224.0
415	TWO-NUCLEON-OUT PRODUCTS FROM STOPPED π^- INTERACTIONS	ORTH	1 *	121.6
416	STUDY OF FAST PION-INDUCED FISSION OF URANIUM	DROPESKY	3 *	15.0
			4 *	11.0
465	RADIOCHEMICAL STUDY OF PION SINGLE CHARGE EXCHANGE	RUNDBERG	1 *	46.0
			2	61.4
483	MEASUREMENT OF THE ANGULAR DEPENDENCE OF TENSOR POLARIZATION IN THE ^{2}H(π^+,π^+)^{2}H REACTION	HOLT	1 *	478.3

Exp. No.	Title	Spokesman	Phase No. * = Complete	Beam Hours
487	MEASUREMENT OF THE NUCLEAR RESONANCE EFFECT IN SOME PIONIC ATOMS	REIDY LEON	1 *	202.8
523	STUDY OF $^{14}C(\pi^+,\pi^0)^{14}N$ REACTION	GOODMAN BAER	1 * 3 3	103.4 154.0 0.0
524	STUDY OF THE ISOVECTOR TERMS IN π-NUCLEUS INTERACTIONS WITH (π^+,π^0) REACTIONS ON $^{40,42,44,48}Ca$ AND $^{112,118,124}Sn$	BAER BOWMAN CVERNA	1 *	243.9
525	EXCITATION OF ISOVECTOR TRANSITIONS WITH PION SINGLE CHARGE EXCHANGE ON ^{12}C	KING MOINESTER	1	24.2
527	STUDY OF THE $^{10}B(\pi^-,\pi^0)^{10}B$ REACTION	BAER BOWMAN	1	0.0
536	EFFICIENCY MEASUREMENTS FOR π^+ IDENTIFICATION IN THE PLASTIC BALL DETECTOR	GUTBROD	1 *	106.7
541	A SEARCH FOR NUCLEAR CRITICAL OPALESCENCE USING THE REACTION $^{40}Ca(\pi^+,2\gamma)$	COOPER	1 *	773.7
543	A PRODUCT RECOIL STUDY OF THE $(\pi^\pm,\pi^\pm n)$ REACTION	CARETTO	1 2	7.8 51.5
544	SEARCH FOR A FAST FISSION PROCESS	WILHELMY	1 * 2 *	48.0 76.0
553	STUDY OF TARGET THICKNESS EFFECTS IN THE CROSS-SECTION MEASUREMENT OF THE PION SINGLE-CHARGE-EXCHANGE REACTION $^{13}C(\pi^+,\pi^0)^{13}N$ (g.s.) FROM 50 TO 350 MeV	RUNDBERG	1 * 2 * 3	69.0 14.0 100.0
557	EXPOSURE, IN A PARASITIC MODE, OF A 3-cm BY 3-cm BY 1-cm STACK OF SOLID-TRACK DETECTORS TO A π^- BEAM	COWSIK	1 *	0.0
561	$\pi^\pm$-NUCLEAR ELASTIC SCATTERING AT ENERGIES BETWEEN 30 AND 80 MeV	BLECHER OBENSHAIN HYNES	1 * 2 *	241.0 294.0
567	A STUDY OF THE $\pi^+ + d \rightarrow p + p$ REACTION AT PION ENERGIES 5-200 MeV	GOTOW MINEHART RITCHIE	1 *	503.0
578	STUDY OF THE $(\pi^+,2p)$ AND $(\pi^-,2p)$ REACTIONS ON THE ISOTOPIC PAIRS ^{16}O-^{18}O AND ^{40}Ca-^{48}Ca	ROOS PREEDOM CHANT	1	246.0
595	AN ON-LINE GAMMA-RAY STUDY OF PION-INDUCED SINGLE-NUCLEON-REMOVAL REACTIONS ON ^{13}C AND ^{48}Ca	ORTH VIEIRA	1	34.0
601	DETERMINATION OF ISOSCALAR AND ISOVECTOR TRANSITION RATES FOR LOW-LYING COLLECTIVE STATES IN ^{90}Zr and ^{208}Pb BY π^+ AND π^- INELASTIC SCATTERING	HINTZ	1	414.0
607	STUDY OF ISOVECTOR GIANT RESONANCES WITH PION CHARGE EXCHANGE	ALSTER BAER BOWMAN	1 * 2 * 3	259.5 774.0 0.0

Exp. No.	Title	Spokesman	Phase No. *—Complete	Beam Hours
611	EXCITATION FUNCTIONS OF THE FOUR $^{130}Te(\pi^{\pm},\pi^{\pm}n)$ REACTIONS	HOGAN	1	0.0
650	A SEARCH FOR NEUTRINO MIXING VIA NONEXPONENTIAL $\pi \rightarrow \mu\nu$ DECAY	BOWMAN MOINESTER	1 *	249.0
675	NUCLEAR DISTRIBUTIONS FROM THE STUDY OF THE 2p STATES OF PIONIC ATOMS	KUNSELMAN	1	0.0
676	STUDY OF PION ABSORPTION ON ^{58}Ni AT T_π = 160 MeV	CHANT REDWINE ROOS	1	557.0
688	STUDY OF THE MASS AND ENERGY DEPENDENCE OF LOW-ENERGY PION SINGLE CHARGE EXCHANGE	LEITCH COOPER	1	157.0
732	HEAVY ELEMENT FISSION INDUCED BY ENERGETIC PIONS	PETERSON RISTINEN	1 *	0.0
735	PION-INDUCED EMISSION OF LIGHT NUCLEAR FRAGMENTS	KAUFMAN	1	173.0
738	ANALOG STATE CROSS SECTIONS OF THE $^{92,96,100}Mo(\pi^+,\pi^0)$ REACTION	COMFORT	1	0.0
767	$\pi^{\pm}$ DEUTERON ELASTIC SCATTERING AT THREE ENERGIES BETWEEN 30 AND 80 MeV	GOTOW	1	0.0
776	STUDY OF THE $^{16}O(\pi^-,\pi^0p)$ REACTION	GILAD PIASETZKY ALSTER	1	0.0
789	TWO-NUCLEON-OUT PRODUCTS FOLLOWING THE ABSORPTION OF 10-MeV π^- IN ^{25}Mg AND ^{74}Ge	OHKUBO	1	100.0
794	$\pi^{\pm}$-NUCLEAR ELASTIC SCATTERING AT ENERGIES BETWEEN 30 AND 65 MeV	BLECHER HYNES OBENSHAIN	1	452.0
798	FISSION INDUCED BY ENERGETIC $\pi^{\pm}$ PARTICLES	HICKS PETERSON RISTINEN	1	61.0
808	0° EXCITATION FUNCTION FOR $\pi^-p \rightarrow \pi^0n$	COOPER FITZGERALD	1	71.0
811	STUDY OF UNNATURAL-PARITY STATES IN NUCLEI USING LOW-ENERGY PIONS	RITCHIE	1	0.0
813	PION CHARGE ASYMMETRIES FOR ^{13}C AT LOW BEAM ENERGIES ON THE LEP SPECTROMETER	KRAUSHAAR PETERSON	1	0.0
814	$\pi^{\pm}$-NUCLEAR ELASTIC SCATTERING FROM NICKEL AND TIN ISOTOPES AT ENERGIES BETWEEN 30 AND 80 MeV	BLECHER HYNES	1	0.0
822	INELASTIC π^+ AND π^- SCATTERING ON ^{48}Ca AT 50 AND 75 MeV	KRAUSHAAR	1	0.0
824	A STUDY OF LOW-ENERGY PION SCATTERING AS A PROBE OF NUCLEAR MAGNETIC DIPOLE EXCITATION	JACKSON	1	0.0

Exp. No.	Title	Spokesman	Phase No. * = Complete	Beam Hours
828	TOTAL AND DIFFERENTIAL CROSS SECTIONS FOR $\pi^+ - pp$ BELOW 20 MeV	GOTOW MINEHART RITCHIE	1	0.0
829	A MEASUREMENT OF THE WIDTH AND POSITION OF THE Δ^{++} RESONANCE IN ^{6}Li AND ^{12}C	ZIOCK	1	0.0
848	IN-FLIGHT ABSORPTION OF LOW-ENERGY NEGATIVE PIONS	OHKUBO	1	0.0
850	STUDY OF THE MASS AND ENERGY DEPENDENCE OF LOW-ENERGY PION SINGLE CHARGE EXCHANGE AT 0°	IROM LEITCH	1	0.0
857	INELASTIC PION SCATTERING FROM ^{16}O AT T_π = 50 MeV	BLAND MOORE	1	0.0
860	INELASTIC $\pi^\pm$ SCATTERING TO EXCITED 0° STATES AT ENERGIES BETWEEN 30 AND 80 MeV	PREEDOM WHISNANT	1	0.0
871	COINCIDENT NUCLEAR γ-RAY AND PIONIC X-RAY STUDY OF π ABSORPTION AT REST ON ^{12}C	LIEB FUNSTEN	1	0.0

LINE B (LB)

Exp. No.	Title	Spokesman	Phase No. * = Complete	Beam Hours
179	DIFFERENTIAL PRODUCTION CROSS SECTIONS OF MULTIPLY CHARGED FRAGMENTS IN PROTON- AND PION-INDUCED SPALLATION OF LIGHT NUCLEI	BOWMAN	1 *	1341.4

LINE X BEAM STOP (LX-BS)

Exp. No.	Title	Spokesman	Phase No. * = Complete	Beam Hours
184	PRODUCTION OF ^{82}Sr	O'BRIEN	1 *	0.0

NEUTRINO AREA (Neutrino-A)

Exp. No.	Title	Spokesman	Phase No. * = Complete	Beam Hours
31	A NEUTRINO EXPERIMENT TO TEST MUON CONSERVATION	NEMETHY	1 * 2 *	6713.2 1097.4
148	NEUTRINO-ELECTRON ELASTIC SCATTERING AT LAMPF (A FEASIBILITY STUDY)	CHEN REINES	1 * 2 *	0.0 1132.0
225	A STUDY OF NEUTRINO-ELECTRON ELASTIC SCATTERING	CHEN	1 1	709.0 3213.0
254	FEASIBILITY STUDY FOR THE MEASUREMENT OF THE INELASTIC NEUTRINO-SCATTERING CROSS SECTIONS IN ^{39}K	FIREMAN	1 *	1026.0

Exp. No.	Title	Spokesman	Phase No. * = Complete	Beam Hours
638	A SEARCH FOR OSCILLATIONS USING MUON-NEUTRINOS	DOMBECK	1	0.0
645	A SEARCH FOR NEUTRINO OSCILLATIONS AT LAMPF	LING	1	0.0
		ROMANOWSKI	2	0.0
647	A NEUTRON OSCILLATION EXPERIMENT AT LAMPF	ELLIS	1	0.0
708	A MEASUREMENT OF THE DEPOLARIZATION, THE POLARIZATION, AND THE POLARIZATION ROTATION PARAMETERS AND THE ANALYZING POWER FOR THE REACTION $\vec{p}p \rightarrow \vec{p}n$	HOLLAS	3	0.0
764	SEARCH OF NEUTRINO OSCILLATIONS AND MEASUREMENT OF CROSS SECTIONS USING A LIQUID SCINTILLATOR DETECTOR IN A MUON-NEUTRINO BEAM AT THE LINE D STUB	DOMBECK KRUSE	1	0.0
823	DEVELOPMENT OF AN (n,p) REACTION CAPABILITY AT AREA B OR BEAM LINE D	KING LISOWSKI BOWMAN SHEPARD	1	0.0

PROTON IRRADIATION PORT (PIP)

Exp. No.	Title	Spokesman	Phase No. * = Complete	Beam Hours
298	MEASUREMENT OF LIGHT OUTPUT vs ENERGY FOR VARIOUS SCINTILLATORS	SELOVE	1 *	0.0
302	800-MeV PROTON IRRADIATION OF AN ALUMINUM SAMPLE	GREEN	1 *	326.6
327	PIP, PROTON IRRADIATION PORT	WILSON	1 *	16.9

PION PARTICLE PHYSICS (P^3)

Exp. No.	Title	Spokesman	Phase No. * = Complete	Beam Hours
32	PRECISION MEASUREMENT OF THE PROCESSES $\pi^{\pm} \rightarrow \pi^0 + e^{\pm} + \nu$	McFARLANE	1 *	0.0
		MACEK	2 *	1092.2
34	ELASTIC SCATTERING OF $\pi^{\pm}$ ON DEUTERONS	MINEHART	1 *	0.0
58	MEASUREMENT OF $\pi^- + p \rightarrow \gamma + n$	NEFKENS	1 *	0.0
		FITZGERALD		
67	DEVELOPMENT OF PION BEAM MONITORING TECHNIQUES	DROPESKY	1 *	0.0
			2 *	220.2
			3	6.3
79	CALIBRATION OF THE PION BEAM TRANSPORT SYSTEMS AND A PION BEAM MONITOR	PHILLIPS	1 *	0.0

Exp. No.	Title	Spokesman	Phase No. * – Complete	Beam Hours
80	FORWARD ELASTIC SCATTERING OF π^+ AND π^- FROM ^{12}C, ^{13}C, ^{18}O, ^{40}Ca, AND ^{208}Pb	PHILLIPS	1 * 2 *	0.0 528.8
82	INVESTIGATION OF PION-INDUCED REACTIONS ON LIGHT ELEMENTS WITH THREE PARTICLES IN THE FINAL STATE	PHILLIPS	1 *	425.3
90	A TEST OF THE REVERSAL INVARIANCE IN SINGLE-PION PHOTOPRODUCTION THROUGH A STUDY OF RECIPROCITY IN THE REACTIONS $\pi^- {}^3He \simeq \gamma$ (AND ITS INVERSE) AND π^0 / γ $^3He\gamma$ (AND ITS INVERSE)	SHERMAN SHIVELY GLODIS SPENCER WADLINGER NEFKENS	1 * 2 *	0.0 806.9
99	MEASUREMENT OF THE CROSS SECTION FOR $\pi^- + p \rightarrow \pi^- + \pi^+ + n$ WITH A MAGNETIC SPECTROMETER	REBKA GRAM	1 * 2 *	0.0 648.0
102	EXCITATION FUNCTIONS AND ANGULAR DISTRIBUTION RECOIL STUDIES OF SIMPLE PION-INDUCED NUCLEAR REACTIONS	MARKOWITZ	1 *	0.0
103	SPALLATION YIELD DISTRIBUTIONS FOR PION INTERACTIONS WITH COMPLEX NUCLEI	HUDIS	1 * 2 *	0.0 295.7
104	PROPOSAL FOR LAMPF EXPERIMENT: STUDIES OF THE PROTON- AND PION-INDUCED FISSION OF MEDIUM-MASS NUCLIDES	PATE	1 * 2 *	0.0 118.7
118	FRAGMENT EMISSION FROM PION INTERACTIONS WITH COMPLEX NUCLEI	PORILE	1 * 2 *	0.0 97.0
119	CROSS SECTIONS OF SIMPLE NUCLEAR REACTIONS INDUCED BY π MESONS	KAUFMAN	1 * 2 *	27.8 186.8
120	MEASUREMENT OF THE POLARIZATION ASYMMETRY AND THE DIFFERENTIAL CROSS SECTION OF PION-NUCLEON CHARGE EXCHANGE FROM 160 TO 500 MeV	NEFKENS FITZGERALD	1 * 2 * 3 *	870.2 90.3 1543.0
121	PION-INDUCED NUCLEAR REACTIONS	SEGEL	1 * 2 *	0.0 0.0
123	NUCLEAR STRUCTURE EFFECTS IN PION-INDUCED NUCLEAR REACTIONS	KAROL	1 * 2 * 3 * 4 * 5	0.0 75.0 135.1 0.0 21.0
144	SEARCH FOR THE C-VIOLATING DECAY $\pi^0 \rightarrow 3\gamma$	HIGHLAND MACEK	2 *	602.1
153	INVESTIGATION OF NUCLEAR GAMMA RAYS RESULTING FROM IN-FLIGHT PION AND PROTON REACTIONS	EISENSTEIN	1 *	0.0
154	ELASTIC SCATTERING OF π^+ AND π^- FROM THE HELIUM ISOTOPE	MINEHART McCARTHY	1 * 2 *	7.2 316.0
181	MEASUREMENTS OF THE $\pi^- p \rightarrow \pi^0 n$ ANGULAR DISTRIBUTION AT LOW ENERGIES AND CALIBRATION OF THE π^0 SPECTROMETER	ALSTER BOWMAN	2 *	204.3

Exp. No.	Title	Spokesman	Phase No. *=Complete	Beam Hours
195	NUCLEAR RESONANCE EFFECT IN PIONIC ATOMS	LEON	2 *	0.0
		REIDY	3 *	163.1
201	THE $\pi^- d \rightarrow 2d$ REACTION AT 100-500 MeV	MINEHART	1 *	338.0
214	PIONIC X-RAY ABSOLUTE YIELDS AS A FUNCTION OF Z	HARGROVE	1 *	199.1
		LEON		
221	PRECISION MEASUREMENT OF THE DECAY RATE FOR THE DALITZ DECAY MODE OF THE π^0 MESON	HOFFMAN	1 *	351.5
222	MEASUREMENT OF THE DECAY RATE FOR $\pi^0 \rightarrow e^+e^-$	MISCHKE	1 *	945.8
247	DISTRIBUTION OF PRODUCTS FROM INTERACTIONS OF STOPPED π^- WITH SEVERAL MEDIUM- AND HEAVY-MASS NUCLEI	ORTH	2 *	28.0
248	STUDY OF THE (π,π), (π,Δ), (π,B_Δ), AND (π,n) REACTIONS IN $^{3,4}He$ AND ^{6}Li BY MEASURING RECOIL SPECTRA	KALLNE	1 *	674.4
		McCARTHY		
		GUGELOT		
283	CHARGED-PARTICLE EMISSION FOLLOWING μ^- CAPTURE	KRANE	1 *	31.0
		SHARMA		
286	PROTON AXIAL TOMOGRAPHY	HANSON	1 *	345.5
304	STUDY OF THE AUGER PROCESS IN PIONIC ATOMS	LEON	1 *	78.6
		MAUSNER		
309	INCLUSIVE π^+ AND π^- DOUBLE CHARGE EXCHANGE ON ^{16}O AND ^{40}Ca	REBKA	1 *	594.0
319	DETERMINING THE MECHANISM FOR MULTINUCLEON AND CLUSTER REMOVAL IN 200-MeV π-NUCLEAR INTERACTIONS	LIND	1 *	283.0
320	A COMPARISON OF (π^+,xn) AND (π^-,xn) REACTIONS	CHURCH	1 *	57.8
			2 *	170.1
337	MEASUREMENT OF THE CROSS SECTION FOR $\pi^- p \rightarrow \pi^-\pi^+ n$ AT 200 AND 229 MeV	REBKA	1 *	999.8
		GRAM		
349	NUCLEAR REACTIONS OF ^{127}I WITH PIONS	PORILE	1 *	74.5
			2 *	55.2
			3 *	9.0
358	ELASTIC SCATTERING OF PIONS FROM DEUTERIUM	MINEHART	1 *	514.0
363	MEASUREMENT OF $\pi^\pm + p$ ELASTIC SCATTERING	SADLER	1 *	700.5
		NEFKENS	2 *	844.5
373	A COMPARISON OF RESIDUAL NUCLEI YIELDS FROM π^- ABSORPTION IN ^{112}Cd (GROUND STATE) AND ^{112}Cd (FIRST EXCITED STATE)	REIDY	1 *	94.1
		LEON		
390	A STUDY OF INCLUSIVE INELASTIC PION SCATTERING NEAR THE $\Delta(3/2,3/2)$ RESONANCE	JACKSON	1 *	453.0
394	APPLICATION OF PROTON-COMPUTED TOMOGRAPHY	HANSON	1 *	195.3

Exp. No.	Title	Spokesman	Phase No. * = Complete	Beam Hours
396	COMPARISON OF MEASURED PIONIC-ATOM CASCADE INTENSITIES WITH THEORETICAL INTENSITIES OBTAINED USING PARAMETERS FROM MUONIC-ATOM STUDIES	REIDY	1 *	110.9
400	SEARCH FOR THE RARE DECAY $\mu^+ \rightarrow e^+e^+e^-$	HOFFMAN	1 *	156.8
404	A KINEMATICALLY COMPLETE STUDY OF THE $(\pi,\pi'p)$ REACTION ON ^{16}O ABOVE THE RESONANCE BY DETECTING PIONS AND PROTONS IN COINCIDENCE	HAMM SWENSON	1 *	401.5
418	STUDY OF FAST PION-INDUCED FISSION OF URANIUM	DROPESKY	1 * 2 * 3 * 4 *	141.0 17.0 26.2 0.0
455	HIGH-PRECISION STUDY OF THE μ^+ DECAY SPECTRUM	ANDERSON KINNISON	1 2	1739.3 95.0
458	THE EXCITATION FUNCTION FOR THE SINGLE-CHARGE-EXCHANGE REACTION $^{65}Cu(\pi^-,\pi^0)^{65}Ni$	KAUFMAN	1 *	80.4
459	CROSS-SECTION MEASUREMENTS OF THE $^{14}N(\pi^+,\pi^0)^{14}O$ (g.s.) REACTION	VIEIRA	1 *	96.0
465	RADIOCHEMICAL STUDY OF PION SINGLE CHARGE EXCHANGE	RUNDBERG	1 * 2	99.1 104.4
466	NUCLEAR CONFIGURATION OF INDIVIDUAL CORE-COUPLED STATES IN ^{209}Bi FROM INELASTIC $\pi^\pm$ SCATTERING	FUNSTEN PLENDL	1 *	219.6
500	FISSION FRAGMENT DISTRIBUTIONS IN FAST PION-INDUCED FISSION OF ^{238}U	RUNDBERG	1 * 2	72.2 0.0
513	$\pi^\pm$ QUASI-FREE SCATTERING FROM THE HELIUM ISOTOPES	McCARTHY MINEHART	1 * 2 *	0.0 557.7
543	A PRODUCT RECOIL STUDY OF THE $(\pi^\pm,\pi^\pm n)$ REACTION	CARETTO	1	95.5
553	STUDY OF TARGET THICKNESS EFFECTS IN THE CROSS-SECTION MEASUREMENT OF THE PION SINGLE-CHARGE-EXCHANGE REACTION $^{13}C(\pi^+,\pi^0)^{13}N$ (g.s.) FROM 50 TO 350 MeV	RUNDBERG	1 * 2 *	61.3 37.5
555	TOTAL CROSS-SECTION MEASUREMENTS OF THE SINGLE-CHARGE-EXCHANGE REACTION $^{12}C(\pi^+,\pi^0)^{12}N$ (g.s.)	IMANISHI VIEIRA	1 *	139.0
562	STUDY OF THE PION ABSORPTION MECHANISM THROUGH THE A(π,p)X REACTION AT $T_\pi = 500$ MeV	JACKSON SCHIFFER	1 *	428.0
564	STUDY OF SMALL-ANGLE $^4He(\pi^-,\pi^+)$ REACTION	McKEOWN	1 *	435.5
595	AN ON-LINE γ-RAY STUDY OF PION-INDUCED SINGLE-NUCLEON-REMOVAL REACTIONS ON ^{13}C AND ^{48}Ca	ORTH VIEIRA	1	89.0
603	SEARCH FOR DELTAS IN A COMPLEX NUCLEUS BY A RADIOCHEMICAL TECHNIQUE	TURKEVICH	2	13.0
611	EXCITATION FUNCTIONS OF THE FOUR $^{130}Te(\pi^\pm,\pi^\pm n)$ REACTIONS	HOGAN	1	8.5

Exp. No.	Title	Spokesman	Phase No. *—Complete	Beam Hours
617	A STUDY OF THE (3/2,3/2) RESONANCE IN LIGHT NUCLEI	ZIOCK	1	0.0
628	STUDY OF THE (π,πp) REACTION AND QUASI-FREE SCATTERING IN ^{4}He	JACKSON	1 0.0	
673	MEASUREMENTS OF THE ANGULAR DEPENDENCE OF TENSOR POLARIZATION IN THE ^{2}H(π+,π+)^{2}H REACTION AT T_π = 180 AND 256 MeV	HOLT	1	534.0
674	MEASUREMENTS OF PION-NUCLEUS ELASTIC AND DOUBLE-CHARGE-EXCHANGE SCATTERING AT ENERGIES ABOVE 300 MeV	BURLESON MORRIS	1	0.0
682	SEARCH FOR DIBARYON RESONANCES IN THE REACTION πD → ppn AT P_π^- = 200 TO 600 MeV/c	IMAI GREENE	1	0.0
689	A. NEUTRON COUNTER CALIBRATION USING TAGGED NEUTRONS FROM THE REACTION π^-d → nn. B. FEASIBILITY STUDY: MEASUREMENTS OF THE DIFFERENTIAL CROSS SECTION FOR π^-d → nn TO TEST CHARGE SYMMETRY AND ISOSPIN INVARIANCE	NEFKENS FITZGERALD	1 *	332.0
705	STUDY OF PION ABSORPTION IN ^{3}He ON AND ABOVE THE (3,3) RESONANCE	ASHERY	1	283.0
728	STUDY OF PION CHARGE-EXCHANGE MECHANISMS BY MEANS OF ACTIVATION TECHNIQUES	GIESLER	1	160.0
730	PION PRODUCTION IN PION-NUCLEON AND PION-NUCLEUS INTERACTIONS	SAGHAI FREEDOM DROPESKY	1 2	168.5 0.0
734	PION PRODUCTION IN PION-NUCLEUS COLLISIONS	PIASETZKY DiGIACOMO LICHTENSTADT	1	0.0
750	INCLUSIVE π+ AND π− DOUBLE CHARGE EXCHANGE ON ^{4}He	GRAM MATTHEWS REBKA	1	641.0
753	RECOILLESS Δ PRODUCTION IN THE REACTION ^{13}C(π+,p)^{12}CΔ	AMANN MORRIS McGILL	1	0.0
783	PION-INDUCED PION PRODUCTION ON DEUTERONS	GRAM PIASETZKY REBKA LICHTENSTADT	1	622.0
804	MEASUREMENT OF THE ASYMMETRY PARAMETER IN π− + p → γ + n USING A TRANSVERSE POLARIZED TARGET	NEFKENS	1	0.0
806	MEASUREMENT OF SPIN ROTATION PARAMETERS "A AND R" IN π+p → π+p AND π−p → π−p	NEFKENS BRISCOE SADLER	1	0.0
807	AN ABSOLUTE CALIBRATION OF A PROTON POLARIMETER BETWEEN 90 AND 250 MeV	BRISCOE	1	0.0

Exp. No.	Title	Spokesman	Phase No. * = Complete	Beam Hours
820	PION-INDUCED PION PRODUCTION ON ^{3}He	PIASETZKY REBKA GRAM LICHTENSTADT	1	0.0
821	PION CHARGE EXCHANGE TO DELTA-HOLE STATES OF COMPLEX NUCLEI	PETERSON	1	0.0
825	INVESTIGATION OF THE NΔ INTERACTION VIA $\pi^+ \rightarrow \pi^- n$	MUTCHLER	1	0.0
827	STUDY OF ISOBARIC-ANALOG STATES IN PION SINGLE-CHARGE-EXCHANGE REACTIONS IN THE 300- TO 500-MeV REGION	ALSTER BAER PIASETZKY SENNHAUSER	1	0.0
830	THE REACTION ($\pi,\pi p$) ON ^{3}He AND ^{4}He AT ENERGIES ABOVE THE (3,3) RESONANCE	MINEHART	1	0.0
831	THE [π^+,p(pp)] REACTION ON LIGHT NUCLEI	PERDRISAT MINEHART	1	0.0
838	PION-INDUCED PION PRODUCTION ON NUCLEI AT 400 MeV	LEITCH PIASETZKY	1	0.0
849	A. MEASUREMENT OF THE DIFFERENTIAL CROSS SECTION ON $\pi^- p \rightarrow \pi^0 n$ AT 0° AND 180° IN THE MOMENTUM REGION 471-687 MeV/c B. TEST OF ISOSPIN INVARIANCE IN πN SCATTERING AT 180° IN THE MOMENTUM REGION 471-687 MeV/c	FITZGERALD BRISCOE SADLER	1	0.0
852	MEASUREMENTS OF ($\pi^\pm$,η) REACTIONS ON NUCLEAR TARGETS TO STUDY THE PRODUCTION AND INTERACTION OF η MESONS WITH NUCLEI	PENG	1	0.0
856	COMPARISON OF DOUBLE CHARGE EXCHANGE AND INCLUSIVE SCATTERING IN ^{3}He	GRAM MATTHEWS REBKA	1	0.0
859	STUDY OF THE A DEPENDENCE OF INCLUSIVE PION DOUBLE CHARGE EXCHANGE IN NUCLEI	GRAM MATTHEWS REBKA	1	0.0

RADIATION DAMAGE A-1 (RADAMAGE-1)

Exp. No.	Title	Spokesman	Phase No. * = Complete	Beam Hours
302	800-MeV PROTON IRRADIATION OF AN ALUMINUM SAMPLE	GREEN	1 *	0.0
545	FUSION MATERIALS NEUTRON IRRADIATIONS — A PARASITE EXPERIMENT	BROWN	1	3821.8

STOPPED MUON CHANNEL (SMC)

Exp. No.	Title	Spokesman	Phase No. * = Complete	Beam Hours
7	NUCLEAR-STRUCTURE PHYSICS USING STOPPED MUONS	SHERA	1 * 2 *	0.0 617.3
12	MUONIC X RAYS AND NUCLEAR CHARGE DISTRIBUTIONS	POWERS KUNSELMAN	1 * 2 *	173.0 141.9
37	ULTRA-HIGH-PRECISION MEASUREMENTS OF MUONIUM GROUND-STATE ENERGY LEVELS: HYPERFINE STRUCTURE INTERVAL AND MUON MAGNETIC MOMENT	HUGHES CRANE	1 *	0.0
51	TECHNIQUES FOR MATERIALS IDENTIFICATION AND ANALYSIS	MALANIFY	1 *	119.3
60	CHEMICAL EFFECTS IN THE CAPTURE OF NEGATIVE MESONS IN MATTER	KNIGHT SCHILLACI	1 * 2 *	0.0 451.5
76	SEARCH FOR MUONIUM-ANTIMUONIUM TRANSITION	CHANG KANE	1 *	0.0
85	GAMMA-NEUTRINO CORRELATION AFTER NEGATIVE-MUON CAPTURE	WELSH	1 *	193.6
100	TISSUE CHEMICAL ANALYSIS WITH MU-MESIC X RAYS	HUTSON	1 * 2 *	0.0 187.0
101	FEASIBILITY STUDIES: MEASUREMENT OF MUONIC X RAYS AND NUCLEAR GAMMA RAYS WITH CRYSTAL DIFFRACTION SPECTROMETERS AT LAMPF	BOEHM LU	F S*	103.0
122	PIONIC-ATOM X RAYS AND NUCLEAR DISTRIBUTIONS	KUNSELMAN	2 *	84.8
142	NEGATIVE-MUON-INDUCED FISSION IN THE ACTINIDE ELEMENTS	HUIZENGA	1 * 2 *	0.0 520.3
163	INVESTIGATION OF CHANGES IN CHARGE DISTRIBUTIONS FOR NUCLEI NEAR Z = 28 BY ELECTRON SCATTERING AND MUONIC X RAYS	PERKINS SHERA	1 *	0.0
165	MUONIUM FORMATION IN HELIUM AND OTHER RARE GASES	HUGHES	1 *	0.0
166	MUONIC X RAYS AND NUCLEAR CHARGE DISTRIBUTIONS ELECTRIC QUADRUPOLE MOMENTS OF $_{67}Ho^{165}$ AND $_{73}Ta^{181}$	POWERS	1 *	0.0
173	PHYSICS OF THE PION AND THE PIONIC ATOM	BOEHM VOGEL	1 * 2 *	600.9 309.6
175	SEARCH FOR THE FORMATION OF MUONIC HELIUM ($\alpha\mu^-e$)	HUGHES	1 *	0.0
206	SEARCH FOR THE 2S METASTABLE STATE OF MUONIC HYDROGEN	HUGHES EGAN	1 *	497.0
213	MUON-TRANSFER STUDY	SHERA STEFFEN	1 *	50.9
240	ISOTOPE AND ISOTONE SHIFTS IN THE $1f_{7/2}$ SHELL	SHERA	1 *	294.1

Exp. No.	Title	Spokesman	Phase No. * – Complete	Beam Hours
266	TRAPPING OF POSITIVE MUONS AT DEFECTS IN METALS	GAUSTER HEFFNER	1 * 2 * 3 *	223.0 106.1 9.0
268	MEASUREMENT OF THE GROUND-STATE HYPERFINE STRUCTURE INTERVAL OF THE MUONIC HELIUM ATOM ($\alpha\mu^-e^-$)	SOUDER HUGHES	1 *	518.6
276	PERTURBED CIRCULAR POLARIZATION OF MUONIC X RAYS	YAMAZAKI	1 * 2 * 3 *	0.0 183.6 235.1
277	MUONIC X-RAY ANALYSIS OF CORE SAMPLES FROM OIL-BEARING FORMATIONS	ALLRED	1 *	33.0
283	CHARGED-PARTICLE EMISSION FOLLOWING μ^- CAPTURE	KRANE SHARMA	1 * 2 *	138.3 88.6
288	STUDIES OF μ^- CAPTURE PROBABILITIES FOR SOLID-STATE SOLUTIONS	NAUMANN	1 *	180.1
292	NEUTRON EMISSION FROM MUON-INDUCED REACTIONS ON ACTINIDE ELEMENTS	HUIZENGA	1 * 2 *	196.2 138.3
297	A BICENTENNIAL PROPOSAL TO STUDY THE BEHAVIOR OF POSITIVE MUONS IN SOLIDS	BROWN	1 * 2 * 3 *	144.1 137.1 47.1
328	MEASUREMENT OF THE DECAY RATE AND PARITY-VIOLATING ASYMMETRY FOR $\mu^+ \rightarrow e^+\gamma$	BOWMAN COOPER	1 *	1668.3
330	FUNDAMENTAL MUONIC X-RAY MEASUREMENTS OF INTEREST TO MATERIALS ANALYSIS	HUTSON YATES-WILLIAMS	1 * 2 *	90.4 67.8
331	FAST MUON REACTIONS WITH ^{12}C, ^{48}Ti, AND ^{58}Ni	ORTH	1 * 2 *	97.2 78.0
334	NUCLEAR CHARGE PARAMETERS OF ^{41}Ca AND STABLE CADMIUM AND TELLURIUM ISOTOPES	SHERA	1 * 2 *	162.4 170.3
335	MONOPOLE AND QUADRUPOLE CHARGE DISTRIBUTIONS IN THE SAMARIUM AND GADOLINIUM ISOTOPES	SHERA YAMAZAKI	1 * 2 * 3 *	298.7 65.0 0.0
344	HIGHER PRECISION MEASUREMENT OF MUON MAGNETIC MOMENT AND OF MUONIUM hfs INTERVAL	HUGHES	1 *	425.6
357	MUONIC X-RAY SPECTRA OF GASES: 1. DENSITY AND ADMIXTURE EFFECTS	KNIGHT	1 *	145.1
364	SEARCH FOR THE EXCITED 2S STATE OF MUONIUM	EGAN DENISON HUGHES	1 * 2 *	535.8 167.7
371	MUONIC X-RAY SPECTRA OF GASES: 2. CAPTURE PROBABILITIES IN MIXTURES	HUTSON	1 *	122.7
374	μ^- CAPTURE PROBABILITIES FOR SELECTED SOLID BINARY COMPOUNDS	SCHILLACI	1 *	161.7

Exp. No.	Title	Spokesman	Phase No. *—Complete	Beam Hours
375	μSR STUDY OF DIFFUSION IN METALS IN THE PRESENCE OF PARAMAGNETIC IONS	SCHILLACI	1 * 2 * 3 *	194.6 287.0 45.0
377	INVESTIGATION ON THE EFFECT OF GRAIN SIZE IN MUON CAPTURE IN INHOMOGENEOUS SYSTEMS	REIDY	1 *	28.0
382	A μSR INVESTIGATION OF THE EFFECTS OF IMPURITIES ON THE TRAPPING AND DIFFUSION OF μ^+ PARTICLES IN bcc METALS	KOSSLER	1 *	111.4
400	SEARCH FOR THE RARE-DECAY $\mu^+ \rightarrow e^+e^+e^-$	HOFFMAN	1 2	651.4 1297.9
408	MACROSCOPIC DIFFUSION STUDIES IN METALS	HEFFNER LEON	1 *	81.0
414	BONE CALCIUM ASSAY WITH MUONIC X RAYS — SIGNAL/NOISE AND REPRODUCIBILITY STUDIES	HUTSON REIDY	1 *	118.6
421	SENSITIVE SEARCH FOR $\mu^- \rightarrow e$ CONVERSION	SOUDER FRANKEL HUGHES	1	42.0
427	MAGNET RESONANCE STUDIES OF μ^+-ELECTRON DEFECT COMPLEXES IN NONMETALS	ESTLE	1 * 2 3	253.3 161.4 24.0
436	NEGATIVE MUON SPIN ROTATION AND RELAXATION IN MAGNETIC MATERIALS	YAMAZAKI HAYANO	1 *	196.2
444	SEARCH FOR THE DECAY $\mu \rightarrow e\gamma$	BOWMAN HOFSTADTER	1	0.0
445	SEARCH FOR THE LEPTON-FLAVOR-VIOLATING DECAY $\mu^+ \rightarrow e^+\gamma\gamma$	MATIS BOWMAN	1	54.4
449	SURVEY OF SINGLE AND DOUBLE PHOTODETACHMENT CROSS SECTION OF THE H− ION FROM 14 TO 21.8 eV	BRYANT DONAHUE	3	112.0
464	RADIATIVE MUON CAPTURE IN GASEOUS ^{3}He	ROBERTS MILLER	1	0.0
491	EXPERIMENTAL DETERMINATION OF THE STRONG INTERACTION SHIFT IN THE 2p-1s TRANSITION OF PIONIC DEUTERIUM AND HYDROGEN ATOMS	LEE FORSTER	1 * 2 * 3 * 4 *	646.6 376.1 306.0 0.0
494	NUCLEAR CHARGE PARAMETERS OF THE STABLE RUTHENIUM AND PALLADIUM ISOTOPES	HOEHN	1	169.0
499	MUON LONGITUDINAL AND TRANSVERSE RELAXATION STUDIES IN SPIN-GLASS SYSTEMS	DODDS MacLAUGHLIN HEFFNER	1 * 2 3 4	329.6 456.0 0.0 0.0
517	POLARIZED BEAM AND TARGET EXPERIMENTS IN THE p-p SYSTEM: PHASE I. A_y AND A_{yy} FOR THE $d\pi^+$ CHANNEL AND A_{yy} FOR THE ELASTIC CHANNEL FROM 500 TO 800 MeV	SIMMONS JARMER NORTHCLIFFE	2	0.0

Exp. No.	Title	Spokesman	Phase No. * = Complete	Beam Hours
529	PART 1: MEASUREMENT OF THE RESIDUAL MUON POLARIZATION IN ^3He MUONIC ATOM (A FEASIBILITY TEST FOR PART 2), AND PART 2: ANGULAR CORRELATIONS IN THE CAPTURE OF POLARIZED MUONS IN GASEOUS ^3He	WU DUGAN HUGHES	1 * 2	136.0 765.0
547	SEARCH FOR FAST MUONIUM IN VACUUM	EGAN HUGHES KANE	1 * 2 * 3 *	231.4 144.0 100.1
552	ULTRA-HIGH-PRECISION MEASUREMENTS ON MUONIUM	HUGHES EGAN	1	0.0
571	MUON-SPIN-ROTATION STUDIES OF DILUTE MAGNETIC ALLOYS	DODDS HEFFNER SCHILLACI	1 2	359.4 110.0
594	PRECISION DETERMINATIONS OF SOME RELATIVE MUONIC COULOMB-CAPTURE RATIOS IN OXIDES OF DIFFERENT VALENCES	REIDY	1 *	93.0
639	MUON-SPIN-ROTATION STUDY OF MUON BONDING AND MOTION IN SELECT MAGNETIC OXIDES	BOEKEMA DENISON COOKE	1 2	144.0 44.0
640	TRANSVERSE AND LONGITUDINAL FIELD μSR MEASUREMENTS IN SELECTED TERNARY METALLIC COMPOUNDS	DODDS HEFFNER MacLAUGHLIN	1 * 2	246.0 177.0
648	HYPERFINE STRUCTURE OF MUONIC ^3He AND MUONIC ^4He ATOMS	HUGHES EGAN	1 * 2	414.0 0.0
653	THE ^{241}Am AND ^{243}Am MUONIC ATOM STUDIES	SHERA JOHNSON NAUMANN	1 *	151.1
693	INVESTIGATION OF THE TWO-PHOTON DECAY RATE FROM THE $(\mu^4He)^+_{2S}$ STATE AS A FUNCTION OF PRESSURE	REIDY	1	0.0
698	GROUND-STATE QUADRUPOLE MOMENTS OF DEFORMED NUCLEI	STEFFEN SHERA	1 * 2	0.0 0.0
724	MEASUREMENT OF THE LAMB SHIFT IN MUONIUM	EGAN GLADISCH HUGHES	1 * 2 *	786.0 380.0
726	SEARCH FOR THE C-NONINVARIANT DECAY $\pi^0 \rightarrow 3\gamma$	HIGHLAND SANDERS	1	0.0
727	MEASUREMENT OF THE EFFICIENCY OF MUON CATALYSIS IN DEUTERIUM-TRITIUM MIXTURES AT HIGH DENSITIES	JONES	1 2	0.0 0.0
742	SEARCH FOR THE NEGATIVE MUONIUM ION	EGAN SOUDER	1	0.0
745	HEXADECAPOLE MOMENTS IN URANIUM: ^{233}U AND ^{234}U	ZUMBRO SHERA	1 3	0.0 0.0
763	NATURE OF OXYGEN CONTAMINATION IN TITANIUM WITH STOPPED MUONS	TAYLOR	1	0.0

Exp. No.	Title	Spokesman	Phase No. * = Complete	Beam Hours
771	MUON DIFFUSION IN fcc METALS	COOKE HEFFNER	1	0.0
842	μSR SHIFT AND RELAXATION MEASUREMENTS IN ITINERANT MAGNETS	GUPTA HEFFNER MacLAUGHLIN	1	0.0
854	MUON-SPIN RESEARCH IN OXIDE SPIN GLASSES	BOEKEMA COOKE	1	0.0
869	HIGHER PRECISION MEASUREMENT OF THE LAMB SHIFT IN MUONIUM	BADERTSCHER GLADISCH HUGHES	1	0.0
873	PIONIC X-RAY STUDY OF THE CARBON ISOTOPES	SHERA KUNSELMAN	1	0.0

SWITCHYARD LINE A BEAM STOP (LA-BS)

Exp. No.	Title	Spokesman	Phase No. * = Complete	Beam Hours
105	NUCLEAR SPECTROSCOPY STUDIES OF PROTON-INDUCED SPALLATION PRODUCTS	BUNKER	1 *	0.0
118	FRAGMENT EMISSION FROM PION INTERACTIONS WITH COMPLEX NUCLEI	PORILE	1 *	0.0
259	800-MEV PROTON IRRADIATION OF METAL SAMPLES	GREEN	1 *	4.5
381	ALUMINA CERAMIC RADIATION EFFECTS STUDY	HARVEY	1 *	0.0
648	TEST OF EQUIPMENT FOR THE MEASUREMENT OF THE Σ^- FOR THE MAGNETIC MOMENT AT BNL	MILLER	1	0.0
652	TESTS OF PROTOTYPE SEMICONDUCTOR DETECTORS	SKUBIC	1	0.0

THIN TARGET AREA (TTA)

Exp. No.	Title	Spokesman	Phase No. * = Complete	Beam Hours
88	COUNTER EXPERIMENTS IN THE THIN TARGET AREA	POSKANZER	1 *	0.0
			2 *	743.0
			3 *	1129.0
308	AN ATTEMPT TO MAKE DIRECT ATOMIC MASS MEASUREMENTS IN THE THIN TARGET AREA	BUTLER POSKANZER	1 * 2	7692.4 762.0
592	GERMANIUM-DETECTOR LOW-LEVEL RADIATION-DAMAGE EQUILIBRATION EXPERIMENT	REEDY	1	0.0
752	TUNEUP OF THE TIME-OF-FLIGHT SPECTROMETER DIRECT ATOMIC MASS MEASUREMENTS	VIEIRA	1	0.0

Exp. No.	Title	Spokesman	Phase No. * = Complete	Beam Hours
870	SEARCH FOR NEW MAGIC NUMBERS. DIRECT MASS MEASUREMENTS OF THE NEUTRON-RICH ISOTOPES WITH Z = 4-9	WOUTERS	1	0.0
872	DIRECT ATOMIC MASS MEASUREMENTS OF NEUTRON-RICH ISOTOPES IN THE REGION Z = 13-17 USING THE TIME-OF-FLIGHT ISOCHRONOUS SPECTROMETER	BRENNER	1	0.0

APPENDIX D

ACTIVE SPOKESMEN, INSTITUTIONS, AND EXPERIMENTS

SPOKESMEN	INSTITUTIONS	EXPERIMENTS
ANDERSON, H. L.	LOS ALAMOS	455
ANDERSON, R. E.	UNIV. OF NORTH CAROLINA	535
BAER, H. W.	LOS ALAMOS	523 527
BARLETT, M. L.	UNIV. OF TEXAS, AUSTIN	632
BENTON, E. V.	UNIV. OF SAN FRANCISCO	171
BLANPIED, G. S.	UNIV. OF SOUTH CAROLINA	475 573
BLESZYNSKI, M.	UCLA	635
BOEKEMA, C.	TEXAS TECH UNIV.	639
BONNER, B. E.	LOS ALAMOS	635 637
BOWMAN, J. D.	LOS ALAMOS	295 401 444 445 527
BRADBURY, J. N.	LOS ALAMOS	215
BROWN, R. D.	LOS ALAMOS	545 554
BRYANT, H. C.	UNIV. OF NEW MEXICO	586 588
BUNKER, M. E.	LOS ALAMOS	629
BURLESON, G. R.	NEW MEXICO STATE UNIV.	498
BURNETT, D. S.	CALTECH	161
BUTLER, G. W.	LOS ALAMOS	308
CARETTO, A. A.	CARNEGIE-MELLON UNIV.	543
CAREY, T. A.	LOS ALAMOS	630
CARLINI, R. D.	LOS ALAMOS	634
CHANT, N. S.	UNIV. OF MARYLAND	576
CHEN, H. H.	UNIV. OF CALIFORNIA, IRVINE	225
CLARK, D. A.	LOS ALAMOS	588
COOKE, D. W.	MEMPHIS STATE UNIV.	639
COOPER, M. D.	LOS ALAMOS	401
COST, J. R.	LOS ALAMOS	554
COTTINGAME, W. B.	NEW MEXICO STATE UNIV.	598
DEHNHARD, D. K.	UNIV. OF MINNESOTA	580 602
DENISON, A. B.	UNIV. OF WYOMING	639
DEVRIES, R. M.	LOS ALAMOS	591 592
DIGIACOMO, N.	LOS ALAMOS	591 592
DODDS, S. A.	RICE UNIV.	499 571 640
DOMBECK, T. W.	UNIV. OF MARYLAND	638
DONAHUE, J. B.	LOS ALAMOS	587
DUGAN, G.	COLUMBIA UNIV.	529
EGAN, P. O.	YALE UNIV.	552 646
ELLIS, R. J.	LOS ALAMOS	647
ESTLE, T. L.	RICE UNIV.	427
FAUBEL, W.	KARLSRUHE	579
FRANKEL, S.	UNIV. OF PENNSYLVANIA	421
GAZZALY, M. M.	UNIV. OF MINNESOTA	583
GILMORE, J. S.	LOS ALAMOS	487
GLASHAUSSER, C.	RUTGERS UNIV.	531 623
GLASS, G.	TEXAS A&M UNIV.	589
GOODMAN, C. D.	INDIANA UNIV.	523
GRAM, P. A. M.	LOS ALAMOS	586

SPOKESMEN	INSTITUTIONS	EXPERIMENTS
GREENE, S. J.	LOS ALAMOS	572
GREENWOOD, R. C.	IDAHO NATIONAL ENGINEERING LAB.	629
HARVEY, A.	LOS ALAMOS	326 406 560
HARVEY, C. J.	UNIV. OF TEXAS, AUSTIN	602
HEFFNER, R. H.	LOS ALAMOS	499 571 640
HENNING, W.	ARGONNE	610
HINTZ, N. M.	UNIV. OF MINNESOTA	601 630
HOEHN, M. V.	LOS ALAMOS	494
HOFFMAN, C. M.	LOS ALAMOS	400
HOFFMANN, G. W.	UNIV. OF TEXAS, AUSTIN	632
HOFSTADTER, R.	STANFORD UNIV.	444
HOGAN, J. J.	McGILL UNIV.	611
HOISTAD, B.	UNIV. OF TEXAS, AUSTIN	456 485 533 535 649
HOLLAS, C. L.	UNIV. OF TEXAS, AUSTIN	636
HUGHES, V. W.	YALE UNIV.	421 529 552 648
IGO, G. J.	UCLA	635 644
IROM, F.	ARIZONA STATE UNIV.	633
JACKSON, H. E.	ARGONNE	628
JARMER, J. J.	LOS ALAMOS	518
KAROL, P. J.	CARNEGIE-MELLON UNIV.	294
KATZ, R.	UNIV. OF NEBRASKA	218
KING, N. S. P.	LOS ALAMOS	525 538
KINNISON, W. W.	LOS ALAMOS	455
KIZIAH, R. R.	UNIV. OF TEXAS, AUSTIN	598
KUTSCHERA, W.	ARGONNE	610
LING, T. Y.	OHIO STATE UNIV.	645
LU, D. C.	YALE UNIV.	542
MacLAUGHLIN, D. E.	UNIV. OF CALIFORNIA, RIVERSIDE	499 640
MATIS, H. S.	LAWRENCE BERKELEY	445
McCLELLAND, J. B.	LOS ALAMOS	630
MICHEL, D. J.	NAVAL RESEARCH LAB.	113
MILLER, J.	BOSTON UNIV.	648
MILLER, J. P.	BOSTON UNIV.	464
MOINESTER, M. A.	LOS ALAMOS/TEL AVIV UNIV.	295 525
MOORE, C. F.	UNIV. OF TEXAS, AUSTIN	572
MORRIS, C. L.	LOS ALAMOS	572 651
MOSS, J. M.	LOS ALAMOS	531 630
NORTHCLIFFE, L. C.	TEXAS A&M UNIV.	518 589 590
O'BRIEN, H. A.	LOS ALAMOS	106 267
ORTH, C. J.	LOS ALAMOS	595
PACIOTTI, M. A.	LOS ALAMOS	217 270
PAULETTA, G.	UCLA	583 633
PEREZ-MENDEZ, V.	LAWRENCE BERKELEY	215
PHILLIPS, D. S.	UNIV. OF ILLINOIS	407
POSKANZER, A. M.	LAWRENCE BERKELEY	308
PREEDOM, B. M.	UNIV. OF SOUTH CAROLINA	576
RAJU, M. R.	LOS ALAMOS	236
REIDY, J. J.	UNIV. OF MISSISSIPPI	187
ROBERTS, B. L.	BOSTON UNIV.	464
ROMANOWSKI, T.	OHIO STATE UNIV.	645
ROOS, P. G.	INDIANA UNIV. CYCLOTRON FACILITY	576

SPOKESMEN	INSTITUTIONS	EXPERIMENTS
RUNDBERG, R. S.	LOS ALAMOS	465 553
SCHILLACI, M. E.	LOS ALAMOS	571
SEESTROM-MORRIS, S. J.	UNIV. OF MINNESOTA	580
SETH, K. K.	NORTHWESTERN UNIV.	508 533 550
SHEPARD, J. R.	UNIV. OF COLORADO	485 538
SIMMONS, J. E.	LOS ALAMOS	518 590
SKUBIC, P.	UNIV. OF OKLAHOMA	652
SMITH, A. R.	UNIV. OF NEW MEXICO	271
SMITH, W. W.	UNIV. OF CONNECTICUT	587
SOMMER, W. F.	LOS ALAMOS	407
SOUDER, P. A.	YALE UNIV.	421
TALAGA, R. L.	UNIV. OF MARYLAND	634
TALBERT, JR., W. L.	LOS ALAMOS	629
TURKEVICH, A. L.	UNIV. OF CHICAGO	603
VAN DYCK, O. B.	LOS ALAMOS	532
VIEIRA, D. J.	LOS ALAMOS	595
WAGNER, R.	ARGONNE	498
WU, C. S.	COLUMBIA UNIV.	529
YUAN, V.	UNIV. OF ILLINOIS	634
ZIOCK, K. O. H.	UNIV. OF VIRGINIA	190

APPENDIX E

VISITORS TO LAMPF DURING THE PERIOD
JANUARY 1 — DECEMBER 31, 1983

Bjarne Aas . . . . . UCLA
Daniel S. Acton . . . . . Abilene Christian Univ.
David L. Adams . . . . . UCLA
Gary S. Adams . . . . . Univ. of South Carolina
Steven D. Adrian . . . . . Abilene Christian Univ.
Douglas M. Alde . . . . . Columbia Univ.
Richard C. Allen . . . . . UC, Irvine
John C. Allred . . . . . Consultant, New Mexico
Peter W. F. Alons . . . . . Univ. of Colorado
Jonas Alster . . . . . Tel Aviv Univ.
Aharon Amittay . . . . . Yale Univ.
Adam W. Anderson . . . . . Yale Univ.
Alan N. Anderson . . . . . EG&G, Idaho
Bryon D. Anderson . . . . . Kent State Univ.
Daniel H. Anderson . . . . . UCLA
Konrad A. Aniol . . . . . TRIUMF
Hans-Jurgen Arends . . . . . Catholic Univ.
Richard A. Arndt . . . . . Virginia Poly. Inst./State Univ.
Daniel Ashery . . . . . Tel Aviv Univ.
Leonard B. Auerbach . . . . . Temple Univ.
Naftali Auerbach . . . . . Tel Aviv Univ.
David A. Axen . . . . . TRIUMF
Alireza Azizi . . . . . UCLA
Andrew D. Bacher . . . . . Indiana Univ.
Mark G. Bachman . . . . . Univ. of Texas
Andreas Badertscher . . . . . Univ. of Berne
Leonard J. Balka . . . . . Argonne
Martin L. Barlett . . . . . Univ. of Texas
David B. Barlow . . . . . Northwestern Univ.
Charles A. Barnes . . . . . Caltech
Bernd Bassalleck . . . . . Univ. of New Mexico
Thomas S. Bauer . . . . . SIN
Stephen C. Bayliss . . . . . Univ. of New Mexico
Frederick D. Becchetti . . . . . Univ. of Michigan
T. H. Bergeman . State Univ. of New York, Stony Brook
Michael G. Burlein . . . . . Univ. of Pennsylvania
Barry L. Berman . . . . . Lawrence Livermore Lab.
Raimondo P. M. Bertini . . . . . CEN, Saclay
William Bertozzi . . . . . MIT
Vinod K. Bharadwaj . . . . . UC, Irvine
Tarlochan S. Bhatia . . . . . Texas A&M Univ.
Hans Bichsel . . . . . Univ. of Washington
Leslie C. Bland . . . . . Univ. of Texas
Gary S. Blanpied . . . . . Univ. of South Carolina
Marvin Blecher . . . . . Virginia Poly. Inst./State Univ.
Marek Bleszynski . . . . . UCLA
Charles L. Blilie . . . . . Univ. of Minnesota
Carolus Boekema . . . . . Texas Tech Univ.
Joseph E. Bolger . . . . . Univ. of Texas
Joe H. Booth . . . . . Abilene Christian Univ.
Michael J. Borden . . . New Mexico Inst. of Mining Tech.
Charles A. Bordner . . . . . Colorado College
William J. Briscoe . . . . . George Washington Univ.
Mark D. Brown . . . . . Univ. of Texas
Paul A. Bruhwiler . . . . . Univ. of Virginia
Howard C. Bryant . . . . . Univ. of New Mexico
William J. Burger . . . . . MIT
George R. Burleson . . . . . New Mexico State Univ.
Marshall Burns . . . . . Univ. of Texas
Mary J. Burns . . . . . Univ. of New Mexico
Kenneth B. Butterfield . . . . . Univ. of New Mexico
Karen L. Byrum . . . . . Argonne
Augustine J. Caffrey . . . . . EG&G, Idaho
Nicholas S. Chant . . . . . Univ. of Maryland
Herbert H. Chen . . . . . UC, Irvine
Huan-Ching Chiang . . . . . Inst. of High-Energy Phys.
Katherine W. C. Choi . . . . . Louisiana State Univ.
Gheorghe Ciangaru . . . Boston Univ./Univ. of Maryland
David A. Clark . . . . . Univ. of New Mexico
Nance L. Colbert . . . . . UC, Irvine
Joseph R. Comfort . . . . . Arizona State Univ.
Genevieve R. Comtet . Centre Nat. de la Recherche Sci.
Dominic C. Constantino . . . . . Yale Univ.
David C. Cook . . . . . Univ. of Minnesota
D. Wayne Cooke . . . . . Memphis State Univ.
William Cottingame . . . . . New Mexico State Univ.
John B. Coxe . . . . . Temple Univ.
David J. Crabtree . . . . . Abilene Christian Univ.
Donna J. Cremans . . . . . Univ. of Texas
Gerald G. Crough . . . . . UCLA
David J. Cunningham . . . . . Abilene Christian Univ.
James A. Dalton . . . . . Abilene Christian Univ.
Gourisankar Das . . . . . Univ. of Virginia
Sunayana Datta . . . . . Temple Univ.
Dorothy R. Davidson . . . . . Iowa State Univ.
John K. Dayton . . . . . Univ. of Connecticut
Dietrich Dehnhard . . . . . Univ. of Minnesota
Peter P. Denes . . . . . Univ. of New Mexico
Arthur B. Denison . . . . . Univ. of Wyoming
Burton A. Devolk . . . . . Univ. of New Mexico
Satish Dhawan . . . . . Yale Univ.
Kalvir Singh Dhuga . . . . . Univ. of Pennsylvania

Byron D. Dieterle . . . . . Univ. of New Mexico
W. Rodney Ditzler . . . . . Argonne
Stanley A. Dodds . . . . . Rice Univ.
George W. Dodson . . . . . MIT
Peter J. Doe . . . . . UC, Irvine
Argyrios Doumas . . . . . Texas A&M Univ.
Minh V. Duong-Van . . . . . Rice Univ.
Morton Eckhause . . . . . Coll. of William & Mary
Patrick O. Egan . . . . . Lawrence Livermore Lab.
Andrew D. Eichon . . . . . UCLA
Judah M. Eisenberg . . . . . Tel Aviv Univ.
Mohammed Emadi-Babaki . George Washington Univ.
Jon M. Engelage . . . . . UCLA
Peter A. J. Englert . . . . . Univ. of Koln
Adoram Erell . . . . . Tel Aviv Univ.
David J. Ernst . . . . . Texas A&M Univ.
Jorge A. Escalante . . . . . Univ. of South Carolina
Monouchehr Farkhondeh . . . . . MIT
David J. Farnum . . . . New Mexico Inst. of Mining Tech.
John A. Faucett . . . . . Univ. of Oregon
Ali Fazely . . . . . Louisiana State Univ.
Raymond W. Fergerson . . . . . Univ. of Texas
Brian E. Fick . . . . . Virginia Poly. Inst./State Univ.
John M. Finn . . . . . MIT
David B. Fisher . . . . . Ohio State Univ.
Steven B. Fisher . . . . . Ohio State Univ.
Donald G. Fleming . . . . . TRIUMF
Gottfried Flik . . . . . Max-Planck Inst.
Carlos A. Fontenla . . . . . New Mexico State Univ.
Irene Forster . . . . . Univ. of Koln
H. Terry Fortune . . . . . Univ. of Pennsylvania
Barnhard J. Franczak . . . . . Gsellsch. für Schwerionf.
Michael Franey . . . . . Univ. of Minnesota
Dan M. Fraser . . . . . Utah State Univ.
Hans Frauenfelder . . . . . Univ. of Illinois
Stuart J. Freedman . . . . . Argonne
William S. Freeman . . . . . Argonne
Hiroshi Fujisawa . . . . . Univ. of Minnesota
Avraham Gal . . . . . Hebrew Univ.
Mehryar K. Garakani . . . . . Univ. of Minnesota
Robert W. Garnett . . . . . New Mexico State Univ.
Albert G. Gay . . . . . Abilene Christian Univ.
M. Magdy Gazzaly . . . . . Univ. of Minnesota
Donald F. Geesaman . . . . . Argonne
David R. Giebink . . Texas A&M Univ./Univ. of Maryland
Shalev Gilad . . . . . MIT
Gerard P. Gilfoyle . . . . . Univ. of Pennsylvania
Ronald A. Gilman . . . . . Univ. of Pennsylvania
Grant A. Gist . . . . . Rice Univ.
Michael Gladisch . . . . . Univ. of Heidelberg
Charles Glashausser . . . . . Rutgers Univ.
George Glass . . . . . Texas A&M Univ.
Roy J. Glauber . . . . . Harvard Univ.
A. S. Goldhaber . State Univ. of New York, Stony Brook

Peggy A. Goldman . . . . . Univ. of New Mexico
Dudley T. Goodhead . . . Medical Res. Council, Harwell
Kazuo Gotow . . . . . Virginia Poly. Inst./State Univ.
Charles A. Goulding . . . . . EG&G, Los Alamos
Scott C. Graessle . . . . . Abilene Christian Univ.
Michael C. Green . . . . . Argonne
Ray E. L. Green . . . . . Simon Fraser Univ.
Steven J. Greene . . . . . New Mexico State Univ.
Chilton B. Gregory . . . . . Univ. of New Mexico
David P. Grosnick . . . . . Univ. of Chicago
Franz L. Gross . . . . . Coll. of William & Mary
Willi Grübler . . . . . Lab. Fur Kernphysik
Laxmi Chand Gupta . Tata Inst. of Fund. Research, India
William Haberichter . . . . . Argonne
Jeffrey A. Hall . . . . . Abilene Christian Univ.
Hisashi Harada . . . . . Columbia Univ.
Serge Haroche . . . . . Univ. of Paris
Ronnie W. Harper . . . . . Univ. of Illinois
Margye P. Harrington . . . . . Univ. of New Mexico
Benjamin L. Harris . . . . . Northwestern Univ.
Carol J. Harvey . . . Univ. of New Mexico/Univ. of Texas
Hiromi Hasai . . . . . Hiroshima Univ.
Rene Hausammann . . . . . Univ. of Geneva/UC, Irvine
John Walker Heimaster . . . . . Ohio State Univ.
Dale J. Henderson . . . . . Argonne
Jose Luis Hernandez . . . . . Univ. of South Carolina
Kenneth H. Hicks . . . . . Univ. of Colorado
John C. Hiebert . . . . . Texas A&M Univ.
Virgil L. Highland . . . . . Temple Univ.
Daniel A. Hill . . . . . Argonne
Roger E. Hill . . . . . Univ. of New Mexico
Norton M. Hintz . . . . . Univ. of Minnesota
Gerhard W. J. Hoehler . . . . . Univ. of Karlsruhe
Gerald W. Hoffmann . . . . . Univ. of Texas
John H. Hoftiezer . . . . . Argonne
Gary E. Hogan . . . . . Temple Univ.
Steinar Hoibraten . . . . . MIT
Bo Hoistad . . . . . Univ. of Texas
Karl F. Holinde . . . . . Univ. of Bonn
Charles L. Hollas . . . . . Univ. of Texas
Barry R. Holstein . . . . . Univ. of Massachusetts
James A. Holt . . . . . UCLA
Roy J. Holt . . . . . Argonne
Masaharu Hoshi . . . . . Hiroshima Univ.
David Huang . . . . . Temple Univ.
E. Barrie Hughes . . . . . Stanford Univ.
Vernon W. Hughes . . . . . Yale Univ.
Jon R. Hurd . . . . . Univ. of Virginia
George J. Igo . . . . . UCLA
C. H. Quentin Ingram . . . . . SIN
Farokh Irom . . Arizona State Univ./Arizona State Univ.
Shigeru Isagawa . . . . . KEK
Shigaru Ishimoto . . . . . KEK
Vincent Jaccarino . . . . . UC, Santa Barbara

Harold E. Jackson . . . . . Argonne
Mark J. Jakobson . . . . . Univ. of Montana
Randolph H. Jeppesen . . . . . Univ. of Montana
Robert S. Johnson . . . . . Argonne
Wayne A. Johnson . . . . . UC, Irvine
Garth Jones . . . . . TRIUMF
Kevin W. Jones . . . . . UCLA
Steven E. Jones . . . . . EG&G, Idaho
William P. Jones . . . . . Indiana Univ.
Richard J. Joseph . . . . . U.S. Air Force Academy
Donald Joyce . . . . . Coll. of William & Mary
Jan Kalina . . . . . JET/Harvard Smithsonian
John R. Kane . . . . . Coll. of William & Mary
Ju Hwan Kang . . . . . Univ. of New Mexico
Paul J. Karol . . . . . Carnegie-Mellon Univ.
Thomas E. Kasprzyk . . . . . Argonne
Sheldon Kaufman . . . . . Argonne
Robert A. Kenefick . . . . . Texas A&M Univ.
George J. Kim . . . . . UCLA
Edward R. Kinney . . . . . MIT
Leonard S. Kisslinger . . . . . Carnegie-Mellon Univ.
Rex R. Kiziah . . . . . Univ. of Texas
Todd E. Kiziah . . . . . Univ. of Texas
Harrold B. Knowles . . . . . Univ. of New Mexico
James N. Knudson . . . . . Arizona State Univ.
Lawrence J. Kocenko . . . . . Argonne
Dale S. Koetke . . . . . Valparaiso Univ.
Donald D. Koetke . . . . . Valparaiso Univ.
Donald K. Kohl . . . . . Consultant, New Mexico
Norman R. Kolb . . . . . Valparaiso Univ.
Kathryn L. Kolsky . . . . . Carnegie-Mellon Univ.
Ralph G. Korteling . . . . . Simon Fraser Univ.
Robert S. Kowalczyk . . . . . Argonne
Daniel A. Krakauer . . . . . Univ. of Maryland
Jack J. Kraushaar . . . . . Univ. of Colorado
Raymond Kunselman . . . . . Univ. of Wyoming
Dieter Kurath . . . . . Argonne
Peter H. Kutt . . . . . Univ. of Pennsylvania
Gary Kyle . . . . . SIN
Chris P. Leavitt . . . . . Univ. of New Mexico
Samuel M. Levenson . . . . . Northwestern Univ.
Jechiel Lichtenstadt . . . . . Tel Aviv Univ.
Roger L. Lichti . . . . . Texas Tech Univ.
Chung-Yi Lin . . . . . Ohio State Univ.
David A. Lind . . . . . Univ. of Colorado
Richard A. Lindgren . . . . . Univ. of Massachusetts
Ta-Yung Ling . . . . . Ohio State Univ.
Jerry E. Lisantti . . . . . Univ. of Oregon
Stanley Livingston . . . . . Consultant, New Mexico
Earle L. Lomon . . . . . MIT
David Lopiano . . . . . UCLA
Daniel C. J. Lu . . . . . Yale Univ.
Henry J. Lubatti . . . . . Univ. of Washington
Donald R. Machen . . . . . Sci. Systems Int.

Douglas Maclaughlin . . . . . UC, Riverside
Richard Madey . . . . . Kent State Univ.
Kazushige Maeda . . . . . Tohoku Univ.
Hansjuerg Mahler . . . . . UC, Irvine
Jill Ann Marshall . . . . . Univ. of Texas
Richard M. Marshall . . . . . Univ. of Virginia
Akira Masaike . . . . . KEK
Terrence S. Mathis . . . . . UNM Cancer Center
June L. Matthews . . . . . MIT
Arthur B. Mcdonald . . . . . Princeton Univ.
James E. Mcdonough . . . . . Temple Univ.
John A. Mcgill . . . . . Rutgers Univ.
Carl Mchargue . . . . . Oak Ridge
Robert D. Mckeown . . . . . Caltech
Kok-Heong Mcnaughton . . . . . Univ. of Texas
Daniel W. Miller . . . . . Indiana Univ.
Cas Milner . . . . . Univ. of Texas
Richard G. Milner . . . . . Caltech
Ralph C. Minehart . . . . . Univ. of Virginia
Ricardo T. Miranda . . . . . Ohio State Univ.
Rachel E. Mischke . . . . . Univ. of Illinois
Chandrashekhar Mishra . . . . . Univ. of South Carolina
Joseph H. Mitchell . . . . . Univ. of Colorado
Joseph W. Mitchell . . . . . Ohio State Univ.
Murray Moinester . . . . . Tel Aviv Univ.
Alireza Mokhtari . . . . . UCLA
C. Fred Moore . . . . . Univ. of Texas
C. Fred Moore Sr . . . . . Univ. of Texas
Shaul Mordechai . . . . . Univ. of Pennsylvania
William G. Morterer . . . . . Louisiana State Univ.
Sanjoy Mukhopadhyay . . . . . Northwestern Univ.
Takemi Nakagawa . . . . . Tohoku Univ.
Sirish K. Nanda . . . . . Rutgers Univ.
James J. Napolitano . . . . . Argonne
Subrata Nath . . . . . Texas A&M Univ.
Robert A. Naumann . . . . . Princeton Univ.
B. M. K. Nefkens . . . . . UCLA
Ted E. Neil . . . . . Abilene Christian Univ.
Ronota A. Newberry . . . . . Abilene Christian Univ.
Charles Newsom . . . . . UCLA
Fumitaka Nishiyama . . . . . Hiroshima Univ.
Lee C. Northcliffe . . . . . Texas A&M Univ.
David S. Oakley . . . . . Univ. of Texas
Yuji Ohashi . . . . . UCLA
Hajime Ohnuma . . . . . Tokyo Inst. of Tech.
Pedro Oillataguerre . . . . . UCLA
Akira Okihana . . . . . Kyoto Univ. of Educ.
Glenn A. Olah . . . . . Abilene Christian Univ.
Hikonojo Orihara . . . . . Tohoku Univ.
Herbert Orth . . . . . Univ. of Heidelberg
Gianni Pauletta . . . . . UCLA
Judith D. Pelzer . . . . . Univ. of New Mexico
Benjie M. Peterson . . . . . Ohio State Univ.
Roy J. Peterson . . . . . Univ. of Colorado

Fred L. Petrovich . . . . . Florida State Univ.
Alan Picklesimer . . . . . Case Western Reserve Univ.
Chandra Pillai . . . . . Oregon State Univ.
Michael E. Potter . . . . . UC, Irvine
David H. Potterveld . . . . . Caltech
Barry M. Preedom . . . . . Univ. of South Carolina
Arthur M. Rask . . . . . Argonne
Mohini W. Rawool . . . . . New Mexico State Univ.
Glen A. Rebka . . . . . Univ. of Wyoming
Robert P. Redwine . . . . . MIT
James J. Reidy . . . . . Univ. of Mississippi
Louis P. Remsberg . . . . . Brookhaven
James H. Richardson . . . . . Consultant, New Mexico
Kenneth P. Riley . . . . . Univ. of Texas
Peter J. Riley
Robert A. Ristinen . . . . . Univ. of Colorado
Barry G. Ritchie . . . . . Univ. of Maryland
Michael W. Ritter . . . . . Yale Univ.
Warren M. Roane . . . . . Abilene Christian Univ.
Donald A. Roberts . . . . . Univ. of Wyoming
John P. Roberts . . . . . Abilene Christian Univ.
Raymond F. Rodebaugh . . . . . Univ. of Texas
Urs C. Rohrer . . . . . SIN
Sayed H. Rokni . . . . . Utah State Univ.
Joseph Rolfe . . . . . Stanford Univ.
Thomas A. Romanowski . . . . . Ohio State Univ.
Philip G. Roos . . . . . Univ. of Maryland
S. Peter Rosen . . . . . Purdue Univ.
Serge L. Rudaz . . . . . Rice Univ.
Michael E. Sadler . . . . . Abilene Christian Univ.
Arunava Saha . . . . . Northwestern Univ.
David P. Saunders . . . . . Univ. of Texas
John P. Schiffer . . . . . Argonne
S. Seestrom-Morris . . . . . Univ. of Minnesota
Colin J. Seftor . . . . . George Washington Univ.
Ralph E. Segel . . . . . Northwestern Univ.
Peter A. Seidl . . . . . Univ. of Texas
Roger V. Servrancks . . . . . Univ. of Saskatchewan
Kamal K. Seth . . . . . Northwestern Univ.
Stephen L. Shaffer . . . . . Abilene Christian Univ.
Tomikazu Shima . . . . . Argonne
Hajime Shimizu
Frank T. Shively . . . . . Lawrence Berkeley Laboratory
Edward R. Siciliano . Univ. of Georgia/Univ. of Colorado
Robert T. Siegel . . . . . Coll. of William & Mary
Terrence P. Sjoreen . . . . . Oak Ridge
Daniel M. Slate . . . . . Univ. of New Mexico
Elton S. Smith . . . . . Ohio State Univ.
Kaleen J. Smith . . . . . Abilene Christian Univ.
L. Cole Smith . . . . . Univ. of Virginia
Robert W. Smith . . . . . Abilene Christian Univ.
Winthrop W. Smith . . . . . Univ. of Connecticut
W. Rodman Smythe . . . . . Univ. of Colorado
Daniel I. Sober . . . . . Catholic Univ.

James R. Specht . . . . . Argonne
Franz Sperisen . . . . . UCLA
Brian M. Spicer . . . . . Univ. of Melbourne
Harold M. Spinka . . . . . Argonne
Robert W. Stanek
Rolf M. Steffen . . . . . Purdue Univ.
George S. F. Stephans . . . . . Argonne
Edward J. Stephenson . . . . . Indiana Univ.
Morton M. Sternheim . . . . . Univ. of Massachusetts
Tsu-Hsun Sun . . . . . Institute of Atomic Energy, PRC
Frank Tabakin . . . . . Univ. of Pittsburgh
Terry N. Taddeucci . . . . . Ohio Univ.
Richard L. Talaga . . . . . Univ. of Maryland
Yasutoshi Tanaka . . . . . Purdue Univ.
Peter C. Tandy . . . . . Kent State Univ.
Robert L. Tanner . . . . . Consultant, New Mexico
Morton F. Taragin . . . . . George Washington Univ.
Scott Taylor . . . . . Abilene Christian Univ.
Raphael M. Thaler . . . . . Case Western Reserve Univ.
Terry L. Thode . . . . . UCLA
T. Neil Thompson . . . . . UC, Irvine
Mark Timko . . . . . Ohio State Univ.
W. Bradford Tippens . . . . . Texas A&M Univ.
Benjamin Titov . . . . . UC, Irvine
Michael J. Tobin . . . . . Carnegie-Mellon Univ.
Gerald E. Tripard . . . . . Washington State Univ.
Stephen E. Turpin . . . . . Rice Univ.
John L. Ullmann . . . . . Univ. of Colorado
Ernst Ungricht . . . . . Argonne
Albert Van Der Kogel . . . . . UNM Cancer Center
Kamran Vaziri . . . . . Utah State Univ.
Bruce J. Ver West . . . . . Arco Oil/gas Company
Roberta J. Wade . . . . . Univ. of New Mexico
Robert G. Wagner . . . . . Argonne
John D. Walecka . . . . . Stanford Univ.
Robert L. Walker . . . . . Consultant, New Mexico
Thad G. Walker . . . . . Abilene Christian Univ.
Stephen J. Wallace . . . . . Univ. of Maryland
Russell E. Walstedt . . . . Bell Laboratories/murray Hill
John B. Walter . . . . . EG&G, Idaho
Angel T. M. Wang . . . . . UCLA
Jiunn-Ming Wang . . . . . Brookhaven
Keh-Chung Wang . . . . . UC, Irvine
Zhao-Min Wang . . . . . Univ. of Maryland
Cary M. Warren . . . . . UC, Riverside
John W. Watson . . . . . Kent State Univ.
Monroe S. Wechsler . . . . . Iowa State Univ.
Charles A. Wert . . . . . Univ. of Illinois
Christopher Wesselborg . . . . . Univ. of Koln
Gary S. Weston . . . . . UCLA
C. Steven Whisnant . . . . . Univ. of South Carolina
D. Hywel White . . . . . Brookhaven
R. Roy Whitney . . . . . Univ. of Virginia
Charles A. Whitten . . . . . UCLA

Robert J. Whyley . . . . . Coll. of William & Mary
Jay A. Wightman . . . . . .UCLA
Bruce D. Wilkins . . . . . Argonne
Kentner B. Wilson . . . . . .Remotion Co.
Robert R. Wilson . . . . . .Columbia Univ.
Steven L. Wilson . . . . . Stanford Univ.
Andreas Wirzba . State Univ. of New York, Stony Brook
Stephen A. Wood . . . . . Tel Aviv Univ./MIT
Kim A. Woodle . . . . . Yale Univ.
H. G. Worstell . . . . . Consultant, New Mexico
Bryan K. Wright . . . . . .Univ. of Virginia
Dennis H. Wright . . . . . .Virginia Poly. Inst./State Univ.
S. Courtenay Wright . . . . . Univ. of Chicago
Shen-Wu Xu . . . . . .Univ. of Texas
Shuheng Yan . . . . . Inst. of Atomic Energy, PRC
Ming-Jen Yang . . . . . Univ. of Chicago
Wilox Yang . . . . . .Fermilab
Alain J. Yaouanc . . . . . .CEN, Grenoble
Akihiko Yokosawa . . . . . Argonne
Vincent Yuan . . . . . Univ. of Illinois
Larry Zamick . . . . . Rutgers Univ.
Benjamin Zeidman . . . . . Argonne
John J. Zimerle . . . . . Ohio State Univ.
Sandra R. Zink . . . . . .UNM Cancer Center
Hans J. Ziock . . . . . .UCLA
Klaus O. H. Ziock . . . . . .Univ. of Virginia
Gisbert zu Putlitz . . . . . Univ. of Heidelberg
John D. Zumbro . . . . . .Princeton Univ.

39-587 O - 84 - 19

INFORMATION FOR CONTRIBUTORS

Progress at LAMPF is the progress report of MP Division of Los Alamos National Laboratory. In addition it includes brief reports on research done at LAMPF by researchers from other institutions and Los Alamos National Laboratory divisions.

Progress at LAMPF is published annually on April 1. This schedule requires that manuscripts be received by January 1.

Published material is edited to the standards of the *Style Manual* of the American Institute of Physics. Papers are not refereed, hence presentation in this report does not constitute professional publication of the material nor does it preempt publication in other journals. Readers should recognize that results reported in *Progress at LAMPF* are sometimes preliminary or tentative and that authors should therefore be consulted in the event that these results are cited.

Contributors can expedite the publication process by giving special care to the following specifics:

1. When possible, furnish computer files together with hardcopy of paper. *Progress at LAMPF* can accept files from DEC computers and word processors, Wang, and IBM System 6.

2. Drawings and figures submitted should be of quality suitable for direct reproduction after reduction to single-column width, 83 mm (3-1/4 in.).

3. Figure captions and table headings should be furnished.

4. References should be complete and accurate.

5. Abbreviations and acronyms should be avoided if possible (in figures and tables as well as text), and when used must be defined.

6. All numerical data should be given in SI units.

7. Authors are reminded that it helps the reader to have an introduction, which states the purpose(s) of the experiment, before presentation of the data.

Research reports should be brief but complete. A list of recent publications relating to the experiment, for separate tabulation in this report, is much appreciated.

Contributors are encouraged to include as authors all participants in experiments so that they may receive credit for authorship and participation.

Questions and suggestions should be directed to John C. Allred, Los Alamos National Laboratory, MS H850, Los Alamos, NM 87545.

6.0 Massachusetts Institute of Technology
William H. Bates Linear Accelerator Center

1. **What new science is being explored by this facility? What scientific opportunities are being exploited?**

Answer: The Bates facility is involved in frontier research across a broad range of issues in nuclear science.

1. Nuclear structure. Bates is unmatched in energy resolution (4×10^{-5}) for intermediate energy electron scattering. This capability, together with high intensity and the clarity of the electromagnetic coupling, has led to a blossoming of the field with a new spectroscopy going far beyond location and classification of nuclear states to a determination of the dynamical structure at distance scales small compared with the size of the nucleon itself. The special character of individual nuclear shapes, both spherical and deformed, is determined. The motions of individual nucleons are observed revealing the coupling to complex nuclear modes. Collective modes and their dynamical coupling to specific decay channels are mapped out. These data push theoretical models of nuclear structures to and beyond their present limits.

Determination of the electromagnetic current in few nucleon systems provides stringent tests of microscopic calculations based upon the most current ideas about the strong interaction. With the kinematic range available at Bates, the role of mesonic degrees of freedom is seen clearly.

2. Short-range structure. The short-range structure of nuclei is probed in reactions with large energy transfer to the nucleus. In particular, experiments detecting final state nucleons in kinematical situations in which one-nucleon processes are unfavored show clearly the breakdown of the mean field approach which underlies most nuclear models. Quantitative characterization of the nuclear-pair wavefunction has long been a primary goal of nuclear physicists. These studies are facilitated by the large solid angle, broad range spectrometers now available at Bates and will develop fully with a future upgrade to CW operation.

3. Subnucleon degrees of freedom. Nuclear physics has changed profoundly in the last decade in admitting nonnucleonic degrees of freedom as central to our understanding of nuclear structure forces and reactions. Bates is heavily involved in this physics in many ways. Examples are demonstration of the role of meson currents in large momentum transfer electron scattering and determination of a systematic reduction of magnetic strength. The propagation of pions and interactions of nucleon isobars have been studied showing a strong coupling between mesonic and nuclear modes. Multinucleon processes, the analogs of many-body forces at low energies, are central for extrapolating into new regimes such as high density.

4. Electroweak interaction. With completion of a polarized electron source, the Weinberg-Salam model and the quark structure of the electroweak current will be tested unambiguously by measuring the left-right asymmetry of elastic electron scattering from a spin-zero target. This experiment is unique in measuring coherent scattering from the quarks. It leads to a different combination of electroweak coupling constants than can be investigated at higher energy facilities.

2. **How does this facility's accelerator (or accelerators) performance compare with any other in the world that are operating, under construction, or planned?**

Answer: The Bates Accelerator is one of only three electron accelerators dedicated to research in intermediate energy nuclear physics. The other two are at NIKHEF-K (Amsterdam) and Saclay (France). Each of these accelerators is designed to operate at beam energies in the range 100 to 750 MeV, at high average currents (up to 100 microamperes), and moderate duty factor (1 to 2%).

The advances in electro-nuclear physics made at Bates and elsewhere have pointed to the importance of coincidence measurements for addressing a range of fundamental questions in nuclear structure and reactions. Limited coincidence programs have begun at all three laboratories, but duty factor approaching 100% is needed to pursue this physics vigorously. Technological developments have brought this objective within reach at reasonable cost, and so all three laboratories mentioned above plus several others are planning CW capability at intermediate energy. The approach planned at Bates is addition of a pulse stretcher ring.

3. **What types of research instrumentation/experimental devices are available at this facility, and what are their capabilities?**

Answer: The Bates laboratory operates six major spectrometer systems. The energy loss spectrometer system (ELSSY), located in the North Experimental Hall, utilizes the dispersion matching technique to achieve the extraordinary momentum resolution of 4×10^{-5}. Although the design of this instrument is now widely copied, this high resolution capability remains unmatched and has proved crucial for advancing a variety of nuclear structure studies. The South Hall contains three magnetic spectrometers, MEPS, OHIPS and BIGBITE. These spectrometers emphasize large solid angle and/or momentum acceptance. Any pair of these spectrometers can be used in coincidence on Beam Line B, providing a product of solid angles one order of magnitude higher than that for coincidence spectrometers at comparable facilities. The further possibility of using all three spectrometers in coincidence is unique to Bates. Beam Line C is currently used for photoreaction studies. The neutral pion spectrometer is located at this beam line. It has achieved an energy resolution of a few MeV, allowing the first reliable measurements of coherent neutral pion photoproduction from nuclei at intermediate energies. A high intensity photon beam is being developed for Beam Line C. The BIGBITE spectrometer can be moved without disassembly between Beam Lines B and C, allowing its use for both electron scattering and photon reactions (for example, the intermediate energy nuclear photoeffect). Finally, a pair of quadrupole spectrometers with resolution adequate to detect elastic scattering from carbon is positioned along the accelerator axis. The spectrometers will be used to measure the asymmetry in elastic scattering of polarized electrons, thereby providing a new test of the unified theory of electromagnetic and weak interactions.

4. **What have been the facility's research highlights for the period FY 1981 - present, and what are anticipated for the remainder of FY 1984 and FY 1985?**

Answer: The Bates research program deals with a variety of important questions about nuclear structure, forces, and reactions. A few highlights are:

1. High resolution studies of nuclear structure: The power of electron scattering as a probe of nuclear structure lies in its providing a precise model independent measure of the nuclear charge, current, and magnetization. This is exploited through high resolution, in which Bates is unmatched, and through kinematic range, where Bates energies allow investigations down to distance scales a fraction of the size of the nucleon.

Charge scattering has led to precise determination of the nuclear shape, with neither simple phenomenological representations nor sophisticated theoretical models (e.g., density-dependent Hartree-Fock) able to reproduce the charge density systematically. The intrinsic shapes of deformed nuclei have been determined with the surprising result that these shapes are complex and have a different character with the addition of only a few nucleons. The transition densities of vibrations built upon the deformed shape have shown directly the geometrical nature of these quantum states, e.g., vibration about the long and short areas of an axially symmetric deformed nucleus.

Magnetization studies focus upon the distribution of valence nucleons. While the single-particle nature of the magnetization is confirmed qualitatively, particle-core coupling is evidenced strongly in the magnetic strength (e.g., in ^{207}Pb) and in the differing behaviors of multipoles (e.g., quenching of the octupole strength in ^{17}O).

The study of nuclear "elementary excitations" has proved very profitable. Stretched states have been studied at Bates across the Periodic Table. These are states at fairly large excitation energy which support the maximum angular momentum transferrable to the nucleus in one step and, for this reason, are expected to be simple modes. However, the strength of these states is substantially less than expected with coupling to nucleon excited states offering one possible explanation and admixture with multinucleon configurations another. These are basic questions in probing the limits of single-particle behavior in the nucleus. This work has had, together with other Bates experiments, an important connection with hadronic studies of nuclei. Electron scattering provides the benchmark for all reaction processes mediated by one-body densities; a unified analysis of Bates and Indiana Cyclotron data on elastic and inelastic scattering from ^{16}O has led to a determination of the density dependence of intermediate energy nucleon interactions inside the nucleus.

Cross section measurements for magnetic transitions out to large momentum transfer (i.e., with high spatial resolution) have revealed the presence of meson currents in the nucleus. For example, the cross section for ^{13}C was found to be more than an order of magnitude larger at a momentum transfer of 3 fm^{-1} than that expected in the absence of mesons. Quantitative understanding of the role of subnucleon degrees of freedom in the nucleus comprises a central program in nuclear science.

Coincidence measurements mark a new direction in nuclear structure studies at Bates. Both proton emission from and fission of nuclear collective states are being investigated. These data are expected to advance substantially an understanding of fundamental collective nuclear modes by determining the spatial distribution for coupling into specific decay channels.

2. Electromagnetic structure of few-body systems: The few-body systems have a special interest in that detailed microscopic calculations of their structure are available. Thus, one can test precisely our understanding of the nuclear force and, indeed, of the relevant underlying degrees of freedom at different scales.

The first separation of the deuteron monopole and quadrupole charge distributions has been carried out at Bates. This separation requires measurement of an appropriate spin observable; the Bates experiment accomplished this by measuring the tensor polarization of the recoil deuteron in coincidence with the elastically scattered electron. The measurements were performed at a momentum transfer of about 2 fm^{-1} and ruled out certain classes of nuclear force models. Extension to larger momentum transfer, say 5 fm^{-1}, will provide stringent tests of theory in a regime where subnucleon degrees of freedom are very important.

Later this year, the charge and magnetization distributions of tritium will be measured. Together with data already in hand for ^3He, the mirror to ^3H, an isospin decomposition of the three-nucleon bound state electromagnetic current will be provided. This is important because meson and nucleon isobar currents are expected to have a strong isospin signature. Learning about this in the few-body system will enable us to progress towards a fuller understanding of hadronic degrees of freedom in nuclei.

3. Nuclear reaction mechanisms: The manner in which the nucleus absorbs large energy (i.e., an energy significantly greater than that needed to eject nucleons) is very sensitive to the short-range structure of the nucleus. Several surprising results have emerged from Bates studies over the last few years. For example, the inclusive cross section (i.e., measuring only the scattered electrons) at large energy transfer shows, for charge scattering, a substantial spreading of the strength compared with expectations of the single-particle or shell-model picture. To understand the physical origin of this behavior, one must examine explicitly the dominant reaction channels. The photo-proton cross section, which is proportional to the nuclear spectral function in the single particle picture, has been measured at Bates. This is a kinematically mismatched reaction and the data indicate an important role for multinucleon processes with mesonic effects. As in the ^3H - ^3He case mentioned above, isospin decomposition of the cross section is crucial for achieving a quantitative understanding. To accomplish this, the complementary photo-neutron cross section will be measured at Bates during 1985.

The full power of the electromagnetic probe is brought to bear on this problem through coincidence studies in which the scattered electron is detected in coincidence with an ejected nucleon. The first measurement of this process for energy transfers, large compared to that defined by single nucleon scattering, has been carried out at Bates. The resulting spectrum clearly shows the failure of the one-body model and may provide a quantitative measure of the pair wavefunction in the nucleus. Further experimental work and more refined theoretical analysis will be carried out in the next year.

Studies of deuteron photodisintegration will be prominent in the Bates research program over the next years. Measurement of neutron polarization in breakup and coincidence studies in pion production will be carried forward. These reactions, particularly at photon energies of several hundred MeV, are sensitive to nuclear modes built upon nucleon internal degrees of freedom.

4. Pion and nucleon propagation in nuclei: The propagation of pions through the nucleus and the interactions of deltas (the first excited state of the nucleon) are not yet understood adequately. These questions will continue to receive considerable attention at intermediate energy facilities because of their bearing upon a host of fundamental issues.

Coherent photoproduction of neutral pions from nuclei has been measured at Bates. The data indicate strong damping of delta propagation consistent with that found in pion reactions. This damping appears to be largely connected with the pion annihilation process which lies at the origin of the intermediate range nuclear force. A new program at Bates, to be carried out over the next year, is the measurement of elastic photon scattering from nuclei in the energy region corresponding to delta excitation. This process is sensitive to the spin dependence of the delta-nucleus interaction. Systematic studies of charged pion photoproduction from nuclei, now possible with the development of appropriate detectors, are being carried out. In the region close to threshold, the photo-production process couples mainly to the nuclear spin-isospin response. The relative simplicity of the process and the weak interaction of the photon makes this reaction attractive for learning about the pion optical potential at low energies.

5. Electroweak interactions: A unique test of the unified theory of electromagnetic and weak interactions is planned at Bates for the coming year. The left-right asymmetry in polarized electron scattering from a spin-zero nucleus will be measured. This test is unique in that coherent scattering from the quarks is involved and in that, given the quark structure of electroweak currents, the asymmetry is independent of nuclear or atomic models. The linear combination of electroweak coupling constants measured is completely different from that already measured in inelastic scattering. The asymmetry predicted by the Weinberg-Salam model is 2×10^{-6}; the experiment is designed to achieve an order of magnitude greater sensitivity.

5. What facility changes and additions have occurred or are anticipated for the period FY 1981 - FY 1985?

Answer: The following facility changes and additions have occurred in the period FY 1981 - FY 1985.

1981 - 1982: Energy doubling by means of recirculation of the beam for a second pass through the accelerator. Maximum beam energy increased from 410 MeV to 800 MeV.

1981 - 1982: Completion of construction of MEPS, OHIPS, and neutral pion spectrometers.

1981 - 1984: Design and fabrication of a polarized electron source. (A collaboration of Yale, MIT, Syracuse, and City University of New York.)

1981 - 1985: Continuous upgrade of data acquisition/computing facilities including dual VAX-780/82 on campus, surplus VAX-750, augmented mass storage, and PDP-11/44 at Bates.

1982 - 1984: Design and construction of BIGBITE spectrometer.

1982 - 1984: Design and construction of high resolution neutron spectrometer.

1983 - 1984: Extension of Utility Building by the addition, on two floors, of a total of approximately 12,000 square feet of shop, laboratory, and office space.

1983 - 1985: Fabrication and installation of a sixth RF transmitter and rework of modulators 2 through 5 to increase maximum energy to 1060 MeV.

1984 - 1985: Modification of Beam Line C to provide high intensity pure photon beam.

6. **For the period FY 1981 - FY 1985, please provide actual and estimated budget profiles for operations, in-house research, out-of-house research, other operating expenses, Capital Equipment, General Plant Projects, In-House Energy Management, and any other specific construction projects attributable to the facility. Please indicate the source of these funds (i.e., Medium Energy Nuclear Physics, Heavy Ion Nuclear Physics, Low Energy Nuclear Physics, High Energy Physics, Basic Energy Sciences, etc.).**

Answer:

Bates Linear Accelerator Center
(B/A in thousands of dollars)

Source of Funding (All Medium Energy NP)	FY 1981	FY 1982	FY 1983	FY 1984	FY 1985
Operations	$ 4,162	$ 4,603	$ 4,738	$ 5,360	$ 5,750
Research					
In-house	$ 1,083	$ 1,447	$ 1,544	$ 2,016	$ 2,091
Out-of-house	100	150	205	159	174
Subtotal	$ 1,183	$ 1,597	$ 1,749	$ 2,175	$ 2,265
Equipment	$ 1,510	$ 1,200	$ 950	$ 1,015	$ 1,000
GPP	$ 300	$ 100	$ 500	$ 200	$ 50
Accel. Improv. & Mod.	$ 0	$ 0	$ 500	$ 650	$ 340
Bates Recirculator	$ 0	$ 0	$ 115	$ 0	$ 0
Energy Management	$ 0	$ 0	$ 72	$ 0	$ 0

7. **How much funding for FY 1981 - FY 1985 has been or is expected to be provided by other federal agencies such as the National Science Foundation or by State agencies?**

Answer: None.

8. **For the period FY 1981 - FY 1985, please provide actual and estimated staffing levels.**

Answer:

Statfing Associated with the Bates Linac Fiscal Year	Man Years
1981	109
1982	102
1983	102
1984	103
1985	102

9. What is the actual and estimated facility utilization for the period FY 1981 - FY 1985? What would be defined as "full" utilization of the facility?

Answer: For the period FY 1981 - FY 1985, actual and estimated utilization of the Bates facility is given in the following table:

Bates Linear Accelerator Center

	FY 1981	FY 1982	FY 1983	FY 1984	FY 1985
Beam Hours for Research	3165	1620	2105	2460	2400

For the Bates facility, we estimate full utilization to be 5000 beam hours for research per year.

10. For the period FY 1981 - FY 1985, how many experiments will have been started, continued, and completed?

Answer:

Experiments with the Bates Facility

	FY 1981	FY 1982	FY 1983	FY 1984	FY 1985
No. Started	10	12	14	15	15
No. Continued	27	21	30	22	27
No. Completed	9	9	10	10	10

11. What is this facility's user policy?

Answer: The Bates Linear Accelerator Center has a strong user program. Approximately 60% of the research carried out at Bates involves non-MIT users. The user community has a variety of formal mechanisms for communicating concerns and desires to the Laboratory management. The user group is incorporated (Bates Laboratory User Group Incorporated) in the Commonwealth of Massachusetts, and the elected Board of Directors meets with the Bates Director a few times per year. The Board appoints a Technical Advisory Panel which makes recommendations on operations and future developments in the Laboratory. The Laboratory provides logistical support for the publication of a newsletter and for the support of workshops.

All experimental facilities are available to users, with experiments evaluated by a Program Advisory Committee purely on the basis of scientific merit. A variety of materials and services are provided to users for approved experiments. A number of major equipment developments have taken place with varying degrees of Bates-user collaboration: the 180 degree scattering facility (University of Massachusetts, Amherst); the neutral pion spectrometer (Boston University); the Medium Energy Pion Spectrometer (Rensselaer Polytechnic Institute); the polarized electron source (Yale University).

Modest accommodations are provided on-site for experimenters during their running periods.

12. For the period FY 1981 - FY 1985, how much reimbursable research has taken place or is estimated to take place? What revenues have been involved?

Answer: None.

13. **What is the mechanism by which specific research proposals for experiments at the facility are considered?**

Answer: Proposals are submitted to the Director, who solicits the opinion and recommendation of a Program Advisory Committee (PAC). The PAC meets twice a year and hears oral presentations from the proposers. All meetings of the PAC, including executive sessions, include an observer from the Bates User Group Board of Directors. The PAC both recommends beam time allocations and assigns scientific priorities for the various proposed experiments.

14. **How many research proposals have been submitted over the past five years, and how many of these have been approved?**

Answer:

TABLE I: NEW PROPOSALS

Year	Submitted	Accepted	Hours Requested	Hours Granted
1979	20	7	4012	1396
1980	24	11	4319	1435
1981	12	4	2324	380
1982	16	10	4949	1286
1983	29	18	5283	1704

TABLE II: UPDATES REQUESTING ADDITIONAL TIME

	Submitted	Accepted	Hours Requested	Hours Granted
1979	22	16	4404	1641
1980	14	13	3460	1055
1981	10	5	3751	445
1982	26	5	3868	1191
1983	21	13	5316	1828

15. **How many university personnel (i.e., faculty and students) have utilized the facility over the past five years?**

Answer: The number of university personnel who have utilized the facility over the past five years is given in the following table.

Year	University Users
FY 1979	86
FY 1980	94
FY 1981	103
FY 1982	103
FY 1983	106

16. **How many industrial researchers have utilized the facility over the past five years?**

Answer: None.

17. How many researchers from foreign institutions have utilized the facility over the past five years?

Answer: The number of researchers from foreign institutions who have utilized the Bates facility over the past five years is given in the following table.

Year	Foreign Users
FY 1979	2
FY 1980	2
FY 1981	5
FY 1982	13
FY 1983	14

18. How many researchers from other agencies have utilized the facility over the past five years?

Answer: The number of researchers from other agencies who have utilized the Bates facility over the past five years is given in the following table.

Year	Other Agency Users
FY 1979	2
FY 1980	2
FY 1981	5
FY 1982	5
FY 1983	5

19. What are the future development possibilities for this facility (including research instrumentation/experimental devices), what plans are being made to exploit these possibilities, and what are the budgetary implications?

Answer: There are many potential future development possibilities for this accelerator facility, but there are currently no approved plans to undertake any of them beyond the activities identified in the FY 1985 budget request. New research instruments and experimental devices will be developed as the physics research program progresses. We intend to give high priority to the exploitation of the facility's unique capabilities.

20. Please provide a copy of the facility's latest annual report.

Answer: The Laboratory's first annual report will be prepared in May 1984. Attached is a Bates facility status report prepared for the February 1984 meeting of the DOE/NSF Nuclear Science Advisory Committee and a research summary taken from last year's budget submission. **(Note: Excerpts from these documents follow.)**

Presented to NSAC (Feb. 1984)

BATES LINEAR ACCELERATOR CENTER

Laboratory for Nuclear Science
Massachusetts Institute of Technology

The current status of and near future developments at the Bates Linear Accelerator Center are summarized. We start with a brief review of accelerator and experimental facilities development. This will be followed by more detailed discussions. Finally, a few experimental results, indicative of the breadth of the research program made possible with the new facilities, are indicated.

Figure 1 shows the facility site plan as of December 1983. A two-story 70'x85' extension of the utility/data assembly building is under construction, to be completed in June 1984. This project will provide office, lab, shop, and equipment assembly space.

The accelerator comprises 160M of S Band waveguide powered by 10 klystrons rated at 4MW peak and 100kW average. The maximum energy, for one pass, is 400 MeV at 8mA peak current, and a recently completed recirculator (Figure 2) has resulted in 750 MeV. A project, now in progress, will add two more klystrons to the RF system and result in about 840 MeV maximum energy by early 1985. In FY85, the existing transmitters will be upgraded to increase peak power capability to 5.4MW per klystron. The major modification required is a change of the magnetic confinement field for the switch tubes from permanent magnets to solenoids. With this upgrade, the maximum recirculated energy will be about

1 GeV. In one-pass operation, 80μA of average current is available, but more typical is 40 to 50μA. At recirculated energies (400-750 MeV), 28μA has been provided to date and 40μA will be available during the coming running period.

A more secure protective collimator system will be installed during the next shutdown which will allow an increase in average current capability. The accelerated beam lies within 0.3% of momentum spread. The maximum duty factor used to date has been 1.7%, with 0.75% being more typical.

A polarized electron source has been under construction at Yale University. The source is based on laser excitation of a GaAs crystal and is expected to provide average currents of about 50μA with a polarization of about 40%. Final development and assembly of the source will take place at Bates during 1984.

Figure 3 shows schematically the layout of the beam switchyard and experimental halls. Table I lists the design specifications of the spectrometer systems.

In the North Hall is located the energy loss spectrometer system (ELSSY) which is used mainly for high resolution electron scattering from complex nuclei. The resolution available today is routinely less than 10^{-4}, with special care has been as good as 4×10^{-5}, and further improvements are being pursued. In addition to the high resolution, this facility has a number of auxiliary features which should make it possible to perform absolute measurements with high precision. These include:

a) a low emittance ($\lesssim 10\pi/\gamma$ mm-mr) incident beam, b) high precision, redundant monitoring of beam intensity, c) extensive internal baffling in the dipoles, d) a long distance (2M) between the target and solid angle defining slits, and e) capability to measure the absolute beam energy with a precision of $< 10^{-3}$. Attempts to realize this potential in routine operation would be greatly aided by the addition of an auxiliary spectrometer located at small angles to measure the luminosity of the experiment. The beam transport system to ELSSY may be operated as an achromat, but is usually tuned to provide a beam dispersed in momentum (7cm/%) in the vertical direction, with a space focus for a monochromatic component. An auxiliary chicane makes possible detection of 180° scattering.

In the South Hall, which was completed in 1979, there is a complex of five spectrometers on three beam lines. The design objectives for these spectrometers emphasized solid angle and momentum range at the cost of resolution.

On the B line, which is a 90° achromat, there is located a target region at the common pivot of three spectrometers: OHIPS, MEPS and BIGBITE. These spectrometers may be used singly, in pairs or in triple coincidence. To date only the first two possibilities have been required. The first two spectrometers are mounted on air pads, and preparations are underway similarly to equip BIGBITE. It will be possible to move BIGBITE, without disassembly, between beam lines B and C. Beam line C is also a 90° achromat and has been used, to date, to produce a collimated

photon beam to a π^0 opening angle spectrometer. A low intensity γ-tagger ($\sim 10^4$ sec^{-1}) is available for calibration and test purposes. This beam line will be further developed this coming year to produce a high intensity photon beam ($\sim 5 \times 10^{11}$ photons/sec/50 MeV). This beam is needed for experiments in high resolution photo-neutron spectroscopy and for measurement of the neutron polarization in $D(\gamma,\vec{n})p$.

On the Z line, which is at zero degrees to the accelerator axis, there is a pair of quadrupole spectrometers, with a total solid angle of about 30msr and adequate resolution to detect elastic scattering in ^{12}C at energies of about 250 MeV. These spectrometers are intended to be used in an experiment to measure the asymmetry in the elastic scattering of polarized electrons as predicted by electro-weak theory. This experiment will require control of systematic asymmetries at the level of 10^{-7}. To facilitate this objective, the angle of incidence of the beam is measured within 5×10^{-6} radians, the centroid energy within 10^{-4}, and the relative beam intensity within 10^{-4}. These are correlated with the scattered flux and the polarization state which may be randomly changed on a pulse-to-pulse basis. Most of the detector and beam line hardware has been installed and checked out, indicating that the design objectives listed above have been met.

The beam monitoring capability of this accuracy, while essential for the parity experiment, can also contribute to the precision of many other experiments, and will be installed on the other beam lines as needed.

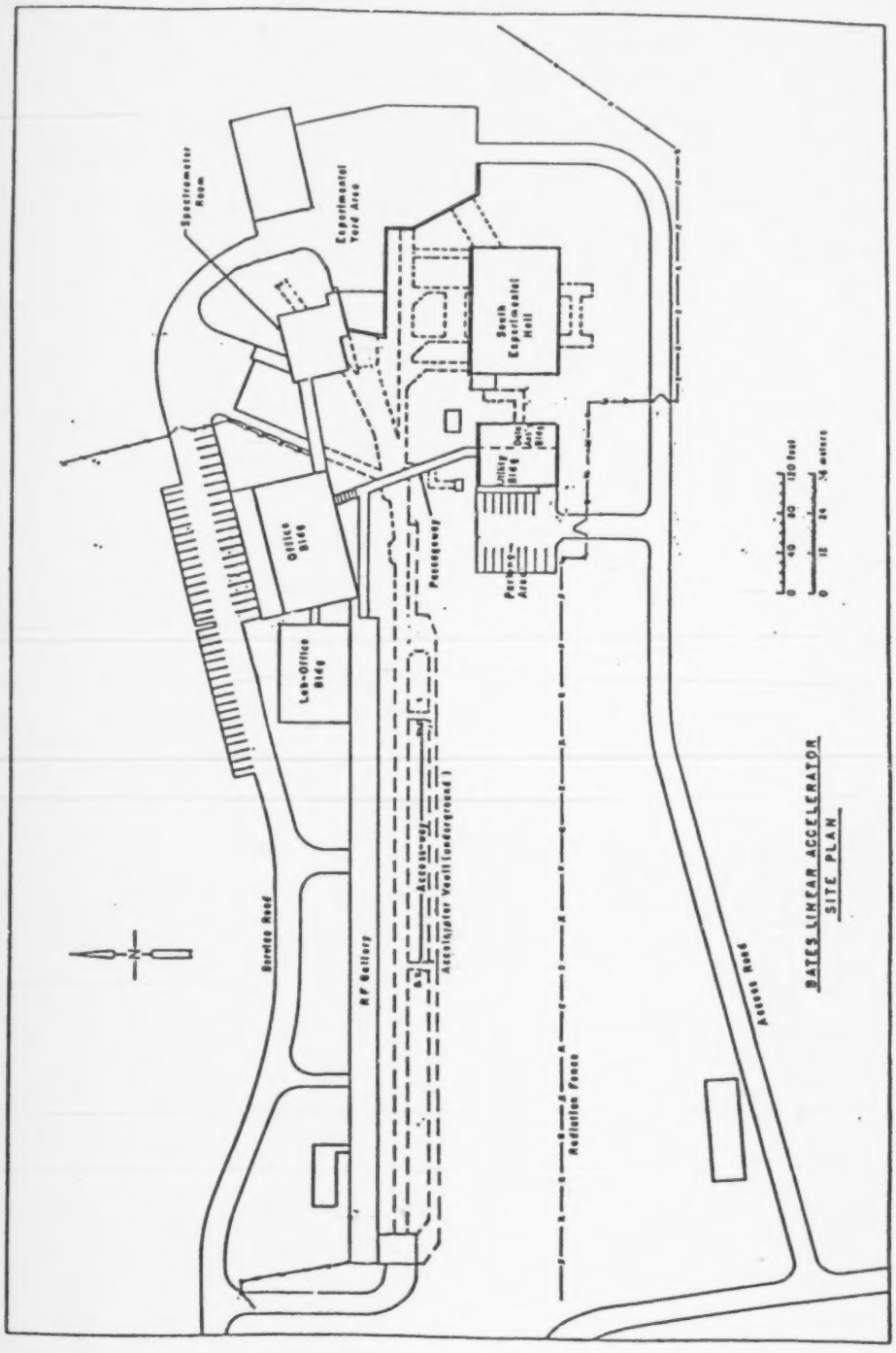
Spectrometer Room
Experimental Yard Area
South Experimental Hall
Office Bldg
Lab-Office Bldg
Passageway
Parking Area
Boreham Road
RF Gallery
Accelerator Vault (underground)
Radiation Fence
Access Road
BATES LINEAR ACCELERATOR
SITE PLAN

Fig. 1

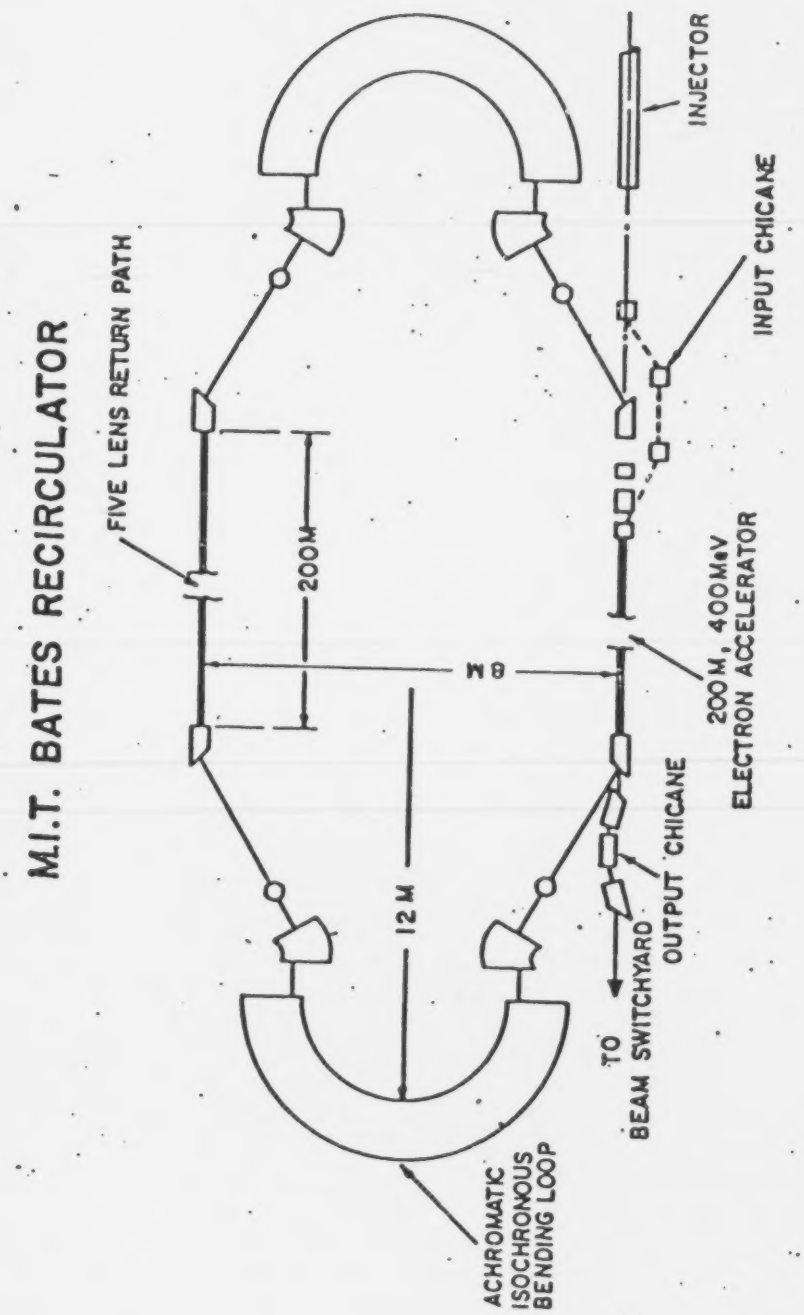
M.I.T. BATES RECIRCULATOR
FIVE LENS RETURN PATH
200M
8M
12M
ACHROMATIC ISOCHRONOUS BENDING LOOP
TO BEAM SWITCHYARD
OUTPUT CHICANE
200M, 400MeV ELECTRON ACCELERATOR
INPUT CHICANE
INJECTOR

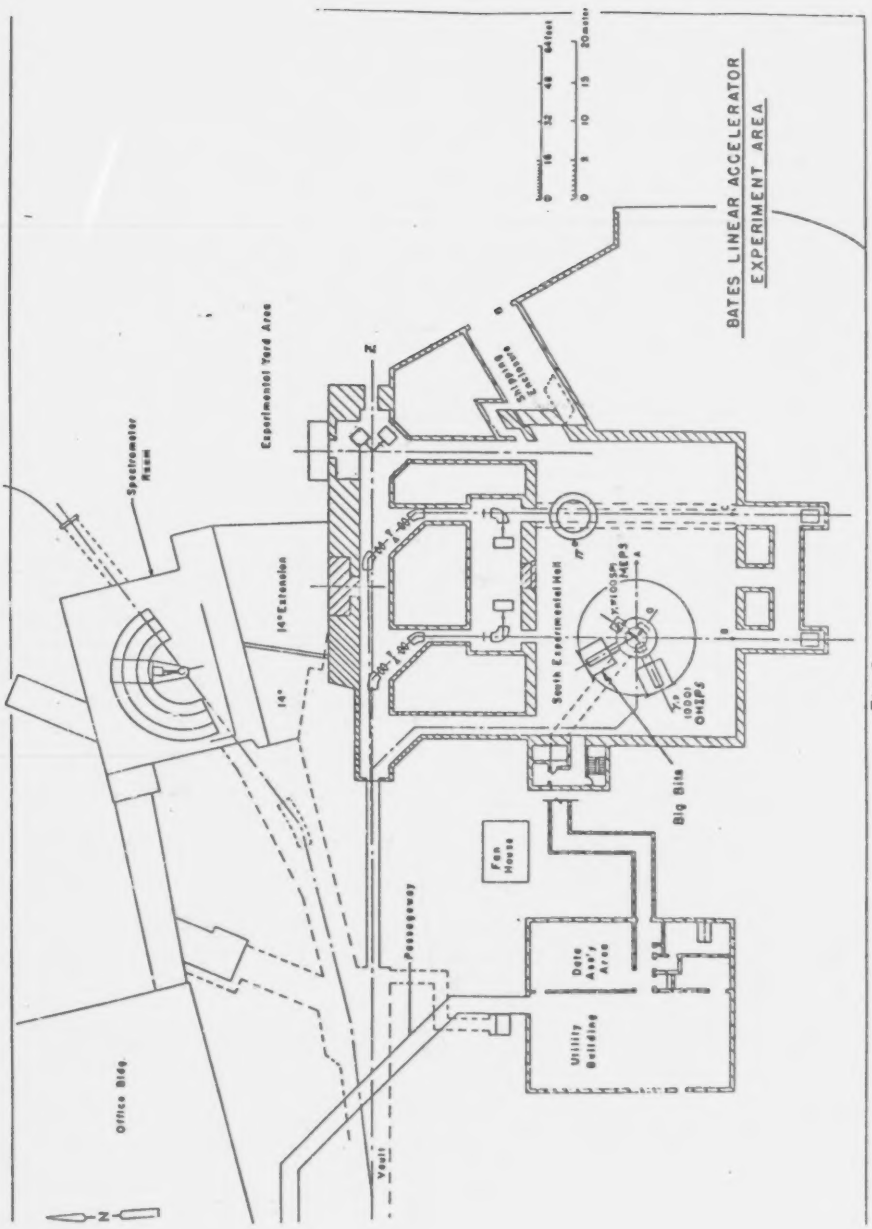
BATES LINEAR ACCELERATOR
EXPERIMENT AREA
Experimental Yard Area
Spectrometer Room
14° Extension
14°
South Experimental Hall
Big Bite
Fan House
Data Ass'y Area
Utility Building
Passageway
Vault
Office Bldg.
N

Fig. 3

TABLE I. DESIGN SPECIFICATIONS FOR BATES SPECTROMETERS

	ELSSY	MEPS[a]	OHIPS[a,b]	BIGBITE[a,c]	QUADS	π^0
SOLID ANGLE (msr)	5.4	30	20	2-15	15	~0.5
MOMENTUM ACCEPTANCE (%)	10	20	16	50-10	25	15
RESOLUTION ($\delta p/p$)	$<4\times10^{-5}$	5×10^{-4}	5×10^{-4}	10^{-3}-10^{-2}	3×10^{-2}	10^{-1}-10^{-2}
ANGULAR RANGE	20°-180°	0°;30°-150°	30°-150°	30°-150°	30°-150°	0°-180°
FLIGHT PATH (m)	11	5	9	4	3.5	-
MAXIMUM MOMENTUM (meV/c)	900	400	1300	800	600	~350
RADIUS OF CURVATURE (m)	2.2	0.75	2.54	2	-	-
CONFIGURATION	DD	QQSP	QQD	QQD	Q	-
MINIMUM ENERGY (MeV)						160
MAXIMUM ENERGY (MeV)						350

[a] All of these spectrometers feature a variable first drift space; a large angular range is then possible with reduced solid angle and incresed flight path.

[b] The characteristics shown anticipate the procurement of specially designed quadrupoles.

[c] This spectrometer is in fabrication and expected to be put into operation during FY/84. The other systems are now operational but in frequent reconfiguration according to specific experimental needs.

I. Accelerator/Recirculator

A. THE MIT-BATES BEAM RECIRCULATION SYSTEM

Introduction

The beam energy capability of the Bates electron linear accelerator has been increased from 400 MeV to 750 MeV by the addition of a recirculation system. This recirculator is a transport system which returns the beam to the injector end of the accelerator after it passes once through the accelerator and then reinjects it to allow a second pass. Construction was completed in early 1982 and the system has since been furnishing beam to nuclear structure experiments. This report summarizes the design requirements of the recirculator, the magneto-optical design and performance, and the operating history and present status.

Design Requirements

The Bates accelerator is a long (160m active length), high-impedance (2.5 MeV/mA beam-loading characteristic) accelerator designed to furnish high-quality, high-duty (~ 1%) beam for nuclear structure research. The laboratory is currently equipped to handle safely average beam currents up to about 80μA. The part of the accelerator which carries both the first-pass low energy beam and the second-pass recirculated beam begins after the 20-MeV injector and contains 21 accelerating guides, which are numbered from 2 through 22. The first three are each four meters in length, and the remainder eight meters. Beam focussing along the accelerator is accomplished by six quadrupole doublets

located at guides numbered 5, 7, 9, 11, 15, 19. There are 11mm diameter protective collimators at the four central quadrupoles. There are also solenoid focussing fields over guides 2 and 3. Normal output beam pulse length is about 15μsec with pulse repetition frequency about 500Hz, although pulse lengths to more than 20μsec and PRF to at least 1000Hz are possible (although not possible simultaneously, at least at higher energy). Normal peak beam current is less than 10mA, as required by experiment.

The requirement that beam duty factor (pulse length) be maintained dictates that the recirculation system operate in the simultaneous rather than the head-to-tail mode, with both first and second pass beams present simultaneously in the accelerator. This in turn, along with the pulsed nature of the beam, requires that the recirculator transport system be highly achromatic over as wide an accelerator energy pass band as possible in order to accommodate the full peak current range. When the returned beam first enters the accelerator on its second pass the energy of the first pass beam begins to decrease, reaching equilibrium only after a change determined by the beam current and accelerator impedance. If stable operation is to result, the beam must successfully pass through the accelerator on its second pass as energy varies over this range. For example at 300 MeV, in the middle of the required recirculator dynamic range (200-400 MeV/pass), and at 6mA current the beam must pass through the accelerator twice over a 5% pass band, from 315 MeV to 300 MeV. The current range, limited by the pass band, can be extended by

increasing the accelerator energy simultaneous with the entry of the second-pass beam. This "beam-loading compensation" is accomplished by shifting the phase of the accelerating RF relative to the beam over a part of the accelerator. To date the system has successfully accelerated 7mA at 300 MeV without compensation, and 11mA with compensation. Figure 1 illustrates the transient behavior of the energy as a function of time and current in the accelerator as described above.

The second important system requirement, that the transport be isochronous, derives from the need to preserve a narrow energy spread (100% of current in less than 0.3% in energy). The path length of the returned beam can be adjusted to optimally phase the beam with respect to the RF on its second pass. The velocity of both first and second pass beams are sufficiently close to c so th .his control and optimum phasing of the first pass over the length of the accelerator assures optimal phasing of second pass. This is true provided that variation of path length with energy of the return-path magnetic optics is sufficiently small. If the return-path consisted simply of a 180° bend at each end of the accelerator with bending radius appropriate to the energy, the path length variation would be several centimeters per percent in energy and more than an order of magnitude too large. Small variations of path length (phase) with energy, of order a mm/%, can be useful in minimizing energy spread. But the most stable operation with respect to RF phase variations is obtained with isochronous operation and the charge bunches riding on the crest of the RF wave.

The Bates system is the only pulsed recirculator operating at realtively high peak currents. The Stanford superconducting recyclotron was designed for CW and is not isochronous. The Darmstadt superconducting 3-pass CW recirculating linac now under construction will be isochronous.

Design and Performance

The considerations leading to the particular choice of a magneto-optical design and the details of the system have been previously described.[1] Only a general description will be given here, along with mention of how the system as-built differs from the system as-designed.

The magnetic system uses reverse bends to achieve isochronicity. It consists of five parts (see Fig. 2). Starting at the accelerator output, the first system is the "output chicane", to separate the first-pass low energy beam to be recirculated from the high-energy second pass beam to be transported to an experimental target. The first magnet of this chicane bends the low energy beam 20°, and is also the first of five dipoles and two sextupoles comprising the second part of the system, which we call a "recirculation loop". The loop is itself achromatic and isochronous and its symmetry corrects the second-order chromatic aberration θ/δ^2. All focussing and most sextupole correction

---

[1] J. B. Flanz, S. Kowalski, C. P. Sargent, IEEE Trans. N.S. 28, 2847 (1981); J. B. Flanz, C. P. Sargent, Recirculator Reports 1-7, Bates Linac Internal Reports (1979-1983).

within the loop is built in as edge rotation and curvature. Figure 3 illustrates the principal orbits for the loop as defined from the end of the accelerator (beginning of the loop). The third part of the system is the 170m long return path housed in a separate tunnel 8m offset from the accelerator. The magnetic elements in this part are five quadrupole triplets operated so that there is a single betatron wavelength in the bend plane (less in the transverse plane) between the first and the fifth. Fig. 4 shows the design principal orbits through the return path. Fourth, there is a second loop identical to the first which returns the beam to the accelerator line. Finally, there is a small chicane which joins the return beam with the 20 MeV beam from the injector.

The entire system is designed to have unity transfer matrix from accelerator output to input, with four betatron wavelengths in the bend plane and one in the transverse. The orbit-shifting chromatic aberrations (x/δ^2), (θ/δ^2) are symmetry corrected, with sextupole strengths chosen to optimize the remaining second-order chromatics. Matching of accelerator output emittance to accelerator input admittance is accomplished with the last two quadrupoles along the accelerator, the first four being operated as strong as is possible (consistent with the low energy beam) to provide as much focussing as possible for the high energy beam. Typically, in the region of strongest focus about a third of the way down the accelerator, the energy of the two passes differ by about a factor of four. Predicted performance, limited by third

and higher order chromatic aberrations, is illustrated in Figure 5. The prediction is that one should be able to pass beam through the accelerator a second time which varies in energy from -3% to +5% around a central energy. Energy-defining slits which cover ±3% were installed within the loops, and an energy pass band covering this range has been achieved.

The as-built system does differ from the designed system. There is a small (1°) edge error in the reverse bend magnets, and all the magnets have small gradients. These errors have insignificant effect on the bend plane orbits within the loop which determine the important chromatic and isochronous properties. A small gradient ($n \approx .03$) in the 180° magnets does have an important effect in the transverse plane, requiring the addition of one-half (or one) betatron wavelength to the design in this plane. These effects are accommodated by operating the quadrupoles in the return path at values which differ from the design values. The only practical solution which adds one-half to the transverse "tune" has been investigated to date. It has been found entirely adequate.

Figures 6A and 6B illustrate the chosen solution (to be compared with Figure 4). The points in Figure 6 represent measurements made during a run which recirculated 295 MeV to produce a 570 MeV output beam. Figure 7 illustrates the beam size (full diameter) in centimeters for the matching conditions which were used. The last column in Table 1 lists beam transfer matrix elements from accelerator output to input measured during this run.

These are compared in the first two columns of Table 1 with elements predicted for the system as designed and also with elements predicted for the system as built incorporating our best knowledge of system construction errors and using the return path optics illustrated in Figure 6. The single sextupole family (the four sextupoles) which can be controlled was set to null (θ/δ^2) aberrations arising from small asymmetries within each loop. Trimming the sextupoles, one relative to another, or separately controlling them, could eliminate the small (x/δ^2) aberration arising from a lack of symmetry between the first and second loops and could better optimize the transverse plane chromatics, but this has not yet been done. Figure 8 shows a simulation of the predicted performance limited by higher order aberrations. Figure 9 illustrates the measured beam size and location during this run of the second pass beam at the limiting aperture along the accelerator for three different energies. This aperture is the 11mm diameter collimator at guide 7. The effective aperture is only 11mm x 8.8mm because of a misalignment. Each rectangle represents an area containing about 65% of the beam and is measured by displacing the second-pass beam at the aperture such as to lose 10% of the beam. The observed transverse dependence of the beam position on energy comes from a small rotational misalignment of some recirculator dipole which has a curved pole edge. The effect of the third and fourth order chromatic aberrations in the bend plane, which are predicted to limit the pass band, are not observed. The entire 6% slit width was used to

pass beam during this run, allowing 7mA without compensation at 570 MeV (see Photos # 3A and 3B).

The highest energy obtained to date was 783 MeV during an early run to test component range. The highest peak current (11mA) has already been mentioned. The highest average current (28μA) was run for an experiment. The limitations on average current will be discussed below. There has never been a problem in obtaining full transmission of the output beam through 0.3% energy slits, and on some occasions at high energy the energy spectrum width has been very small (<0.1%), probably because of the use of a small phase-energy correlation to "compress" energy changes caused by current variations (see Photo 1A).

Recently the head-to-tail mode of recirculation has been successfully attempted, with 40mA accelerated to 570 MeV with 100% transmission (see Photos 4A,B,C). Pulse width in this mode is limited by the total recirculator-accelerator path length to 1.3μsec. Beam emittance in each dimension is about a factor three larger at 40mA than the 10π mm-mrad (normalized to $\beta\gamma=1$) obtained at low current. Gun optics have not been optimized for the high current. 0.6% energy slits were required to contain the 40mA output beam in head-to-tail mode for reasons which are not yet understood, since all of the 40mA single-pass beam was within 0.3%.

Operating History and Present Status

The first recirculated beams were delivered to experiment late in 1982. These were limited to two experiments which could obtain useful data at very low current (< 5μA) and were essential in accumulating the experience necessary to allow the recirculator to play a major role during the Spring 1983 running cycle.

The first 1983 running cycle scheduled 550 hours of recirculator time, about 25% of the total. Experiments requiring low current were scheduled early in the period and, as experience allowed, recirculator current was increased from 8μA for the first experiments to 25μA at the end of the cycle. Tuning time and other down time also decreased by a similar factor, until at the end of the period efficiency records were comparable to those for unrecirculated beam (70%). During this period only two of the four 11mm beam-limiting protective collimators were water-cooled. All the collimators were the original collimator design and unsuited to high energy use. At the higher currents beam loss too small to detect on beam-monitoring toroids produced unacceptably high rates of accelerator guide outgassing. This experience was however essential in determining proper apertures of the final collimators. It was found that the limiting aperture was at guide 7 at recirculated beam energies of 300 MeV and below, moving down to guide 11 at the upper end of the range. The aperture at guide 15 was never touched. The permanent collimators have now been built and are being installed during the

present shutdown. They consist of a water-cooled collimator followed by a water cooled shower-scraper. Apertures have been increased in 1/16" steps from 9/16 at quide 11 to 11/16" at guide 7, which should allow safe operation at high current, but much cleaner operation from a radioactivity point of view, and should also operate to much lower energy should that be necessary.

During the Fall 1983 cycle the scheduling anticipated that operation would be similar to that prevailing at the end of the previous cycle. However there were difficulties in delivering adequate beam, particularly early in the period. The operational problems had little to do with the recirculator. They were the direct and indirect result of a contaminated accelerator guide discovered at the beginning of the period. The recovery took some time and forced cancellation of the tuneup-shakedown period which normally precedes a running period. Accelerator operation was very unstable for several weeks as hardware and procedural problems were discovered. Misaligned collimators had reduced the effective aperture of the accelerator for recirculated beams to 6mm x 6mm. There were however successful runs. Particularly noteworthy was a remarkably stable 12μA (limited by the coincidence nature of the experiment) for 48 hours at 463 MeV, even though this beam was through the 6mm aperture.

At present the recirculator system is believed to be well understood. Developments for insuring reliable and systematic operation have been scheduled during the next year. The developments are in the two areas of operability and stability.

With the operating experience of Spring 1983 a systematic tuning procedure was developed. Until that time recirculator tuning had been done by accelerator physicists, with the regular operator maintaining the beam. Unfortunately the experience of Fall 1983 required the continued assistance of accelerator physicists. However much progress has been made in the past few months and a program of operator training is underway. Some of this progress in operability has been hardware. A small quadrupole has been added near the beginning of each loop to trim the achromaticity. Two Rawson probes now allow precise settings of the dipole supplies. Most important has been the greater understanding and resulting confidence in the system which allows simple check measurements to be made which insure proper setting of quadrupoles, for example. During the next cycle we anticipate that the operators will do much of the tuning and that tuning in general will be much faster.

The recirculator places higher demands on accelerator stability than does single-pass operation. When the accelerator is running well, as is normally the case, this is not a critical problem, but it does merit serious attention. The important instabilities involve either the phasing of RF sources or guide tuning, particularly early in the accelerator where such effects couple to beam steering. When the beam drifts off-energy, the operator restores it by phasing a klystron which is intentionally run slightly off-crest in order to serve as control. In fact the

problem is that another klystron, or the temperature of some guide, has wandered. In this way the system can walk out of tune. Phase bridge investigations of these effects have top priority during the coming running cycle. The addition of RF phase-amplitude measuring equipment to the control system will be important in solving the problem. Such equipment, based on a recent SLAC design, is budgeted over the next two years and procurement has begun.

During the Spring 1984 cycle the recirculator will furnish current to 40μA. There are not many experiments which can use more current, but there are some. To increase current beyond 40μA at the higher energies (80μA in the accelerator) will require a better beam-loss protection system not only along the accelerator, but in the entire laboratory. Such a system, using secondary-emission control apertures, is being developed. A prototype will be tested at a critical point in the beam switchyard this spring. The full system will probably be installed during the summer shutdown.

Attached to this report are a collection of photos taken during recirculator operation. Some were already referred to above.

TABLE I

RECIRCULATOR OPTICS

		Installed System	
	Ideal	Calculated	Measured
ρ	1.33	1.33	
β_1	2.054°	2.1°	
n_1	0	.2	
α_2	-14.798°	-15.7°	
n_2	0	.025, .035	
α_3	13.156°	13.16°	
n_3	0	.025, .035	
$1/R_2$	.0142cm^{-1}	.013cm^{-1}	
$1/R_3$	.0257cm^{-1}	.026cm^{-1}	
SEXT	-3.908 G/cm^2 @500 MeV/C	-2.3	
(x/x)	1	1	1.04
(x/θ)	0	0.25	0.24
(y/y)	1	-1	-0.71
(y/ϕ)	0	0	.31
(x/δ)	0	0	0
(θ/δ)	0	0	0
(z/δ)	0	0.12	0.04
$(x/x\delta)$	-	2.35(-2)	-1.6(-1) *
$(x/\theta\delta)$	-1.95(-1)	-2.36(-1)	-2.6(-1) *
$(\theta/x\delta)$	4.84(-2)	1.43(-1)	
$(\theta/\theta\delta)$	-	1.24(-2)	
$(y/y\delta)$	-	-2.37(-2)	1.5(-1) *
$(y/\phi\delta)$	-1.71(-1)	1.31(0)	3.6(-1) *
$(\phi/y\delta)$	-7.60(-3)	-2.10(-2)	
$(\phi/\phi\delta)$	-	2.37(-2)	
(θ/δ^2)	-	7.07(-2)	
(x/δ^2)	-	1.25(-2)	8.1(-3) *
(z/δ^2)	-4.81(-3)	-1.63(-2)	<5.2(-3)
(x/δ^3)	-6.15(-4)	-1.82(-3)	
(x/δ^4)	2.10(-4)	8.56(-4)	
(θ/δ^3)	-1.56(-3)	-4.08(-3)	
(θ/δ^4)	4.79(-4)	2.74(-4)	
(z/δ^3)	-8.70(-3)	-9.31(-3)	
(z/δ^4)	-1.67(-4)	-2.36(-4)	

* Preliminary -
May include higher order components

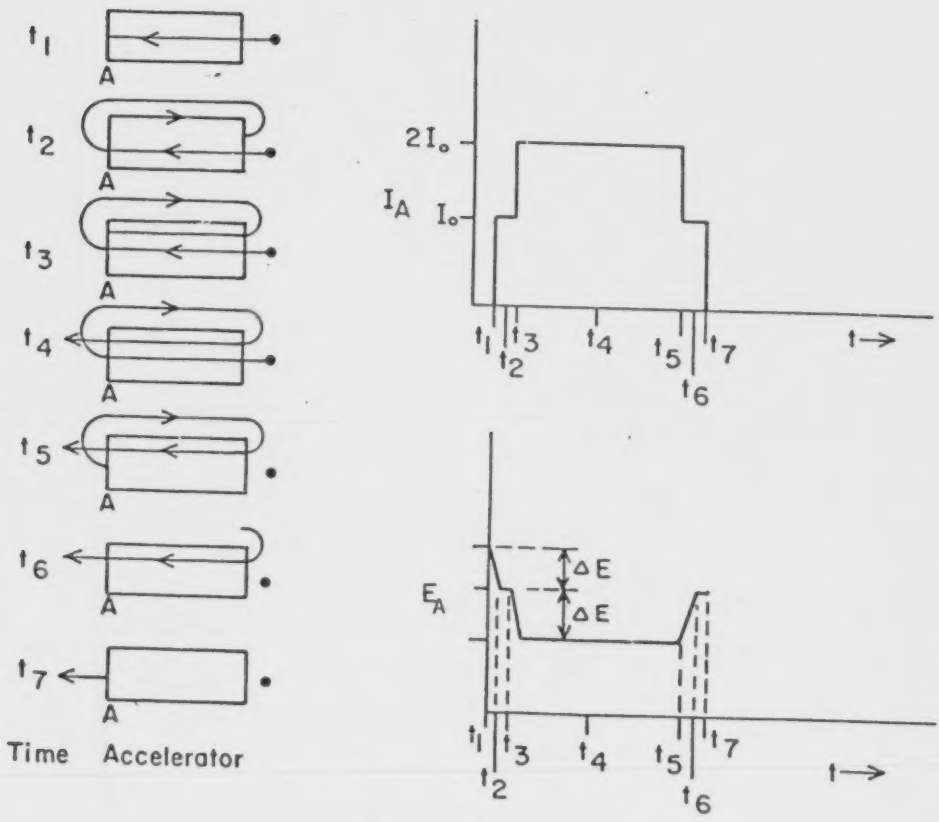

FIGURE 1

TIME DEPENDENCE OF CURRENT (I_A) AND FIRST PASS ENERGY (E_A) FOR SIMULTANEOUS RECIRCULATION. I_A AND E_A ARE MEASURED AT POSITION A IN ACCELERATOR AS SHOWN AT LEFT.

M.I.T. BATES RECIRCULATOR

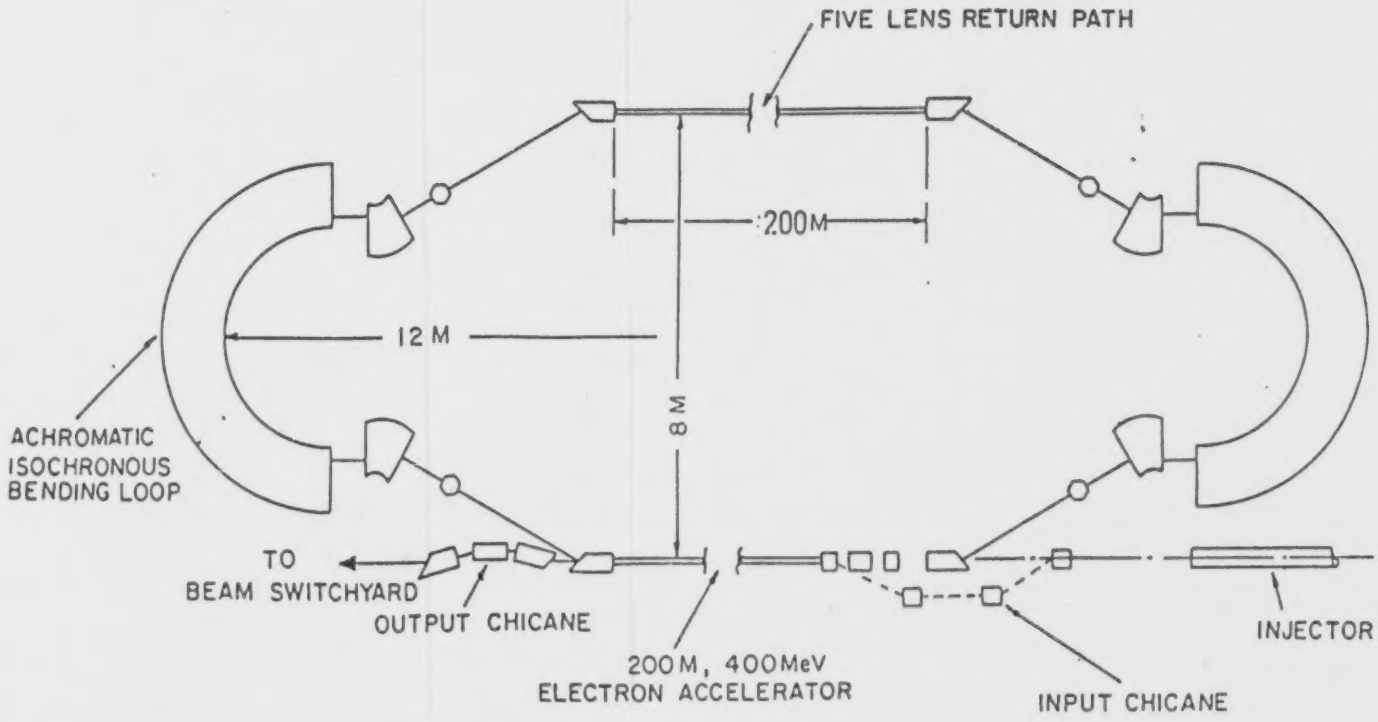

FIGURE 2 - THE COMPONENTS OF THE RECIRCULATION SYSTEM

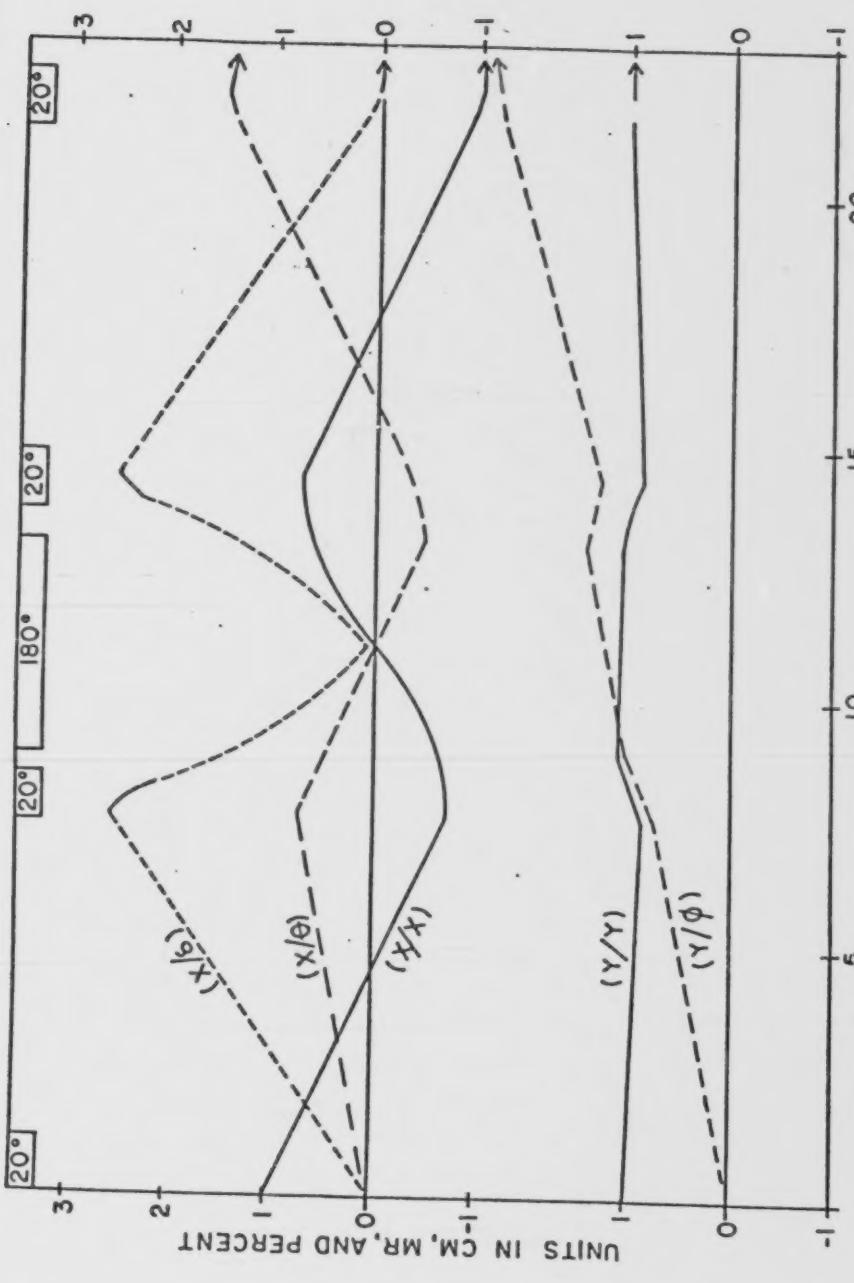

Figure 3 - Design First Order Orbits In Loop

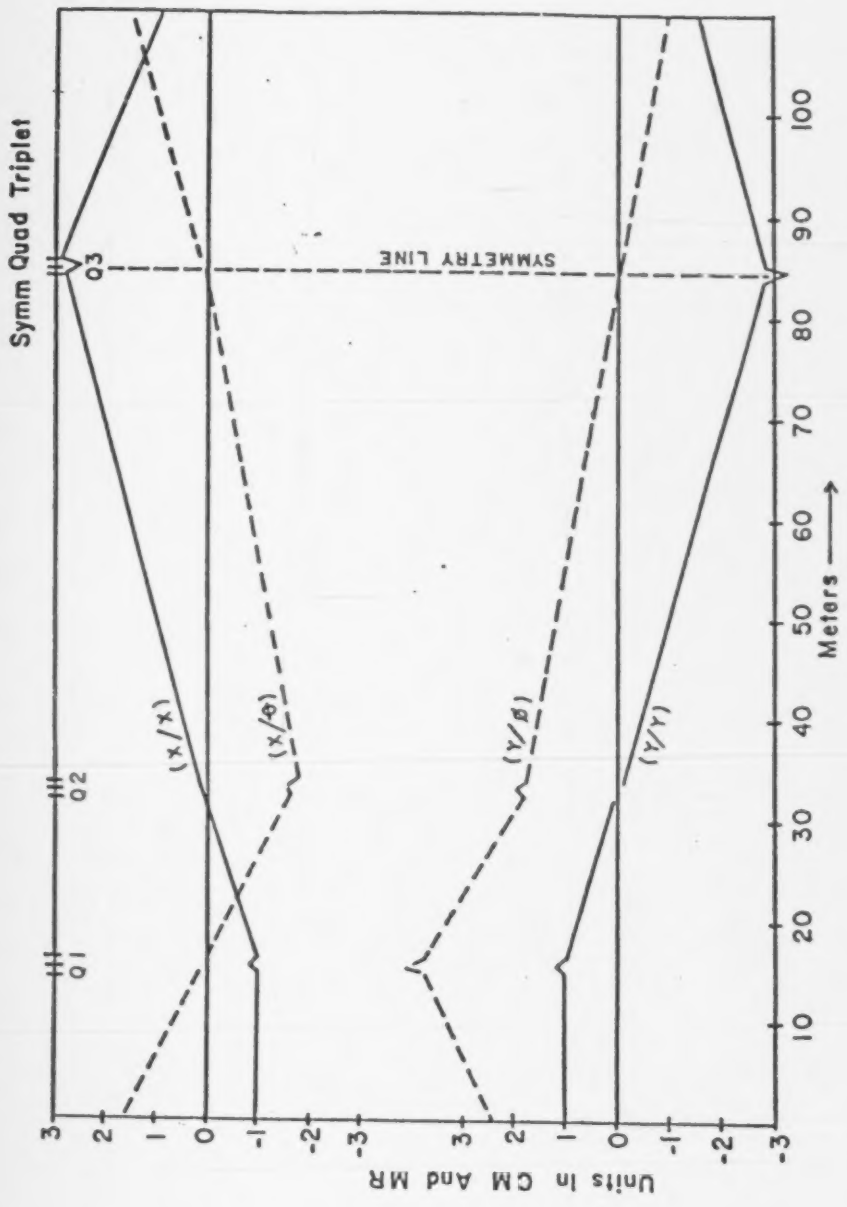

Figure 4 - Design First Order Orbits In Return Path

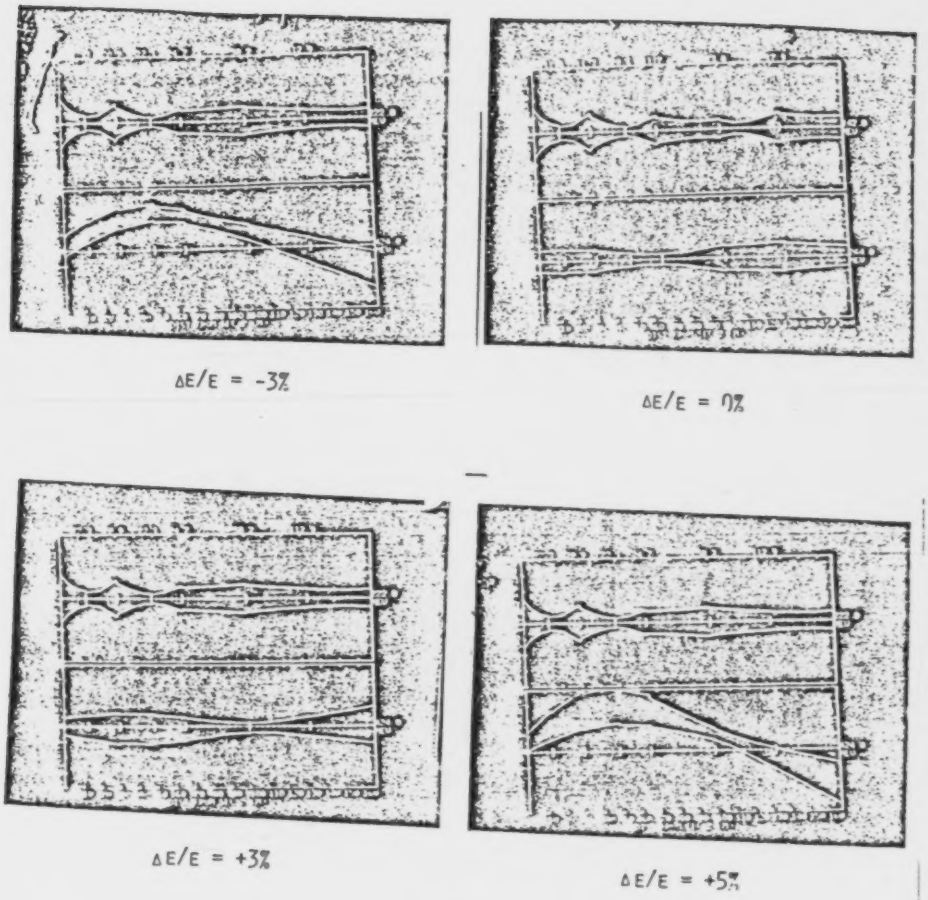

FIGURE 5

HORIZONTAL BEAM ENVELOPE THROUGH ACCELERATOR FOR BEAMS WITH ENERGY DEVIATIONS (ΔE/E) FROM THE RECIRCULATOR CENTRAL ENERGY. UPPER TRACE IN EACH PHOTO IS FIRST PASS BEAM, LOWER TRACE IS SECOND PASS BEAM. FULL SCALE ON EACH TRACE IS 8MM. HORIZONTAL AXIS SHOWS DISTANCE FROM ACCELERATOR SECTION 2. CENTRAL ENERGY FOR THIS EXAMPLE IS 222 MEV.

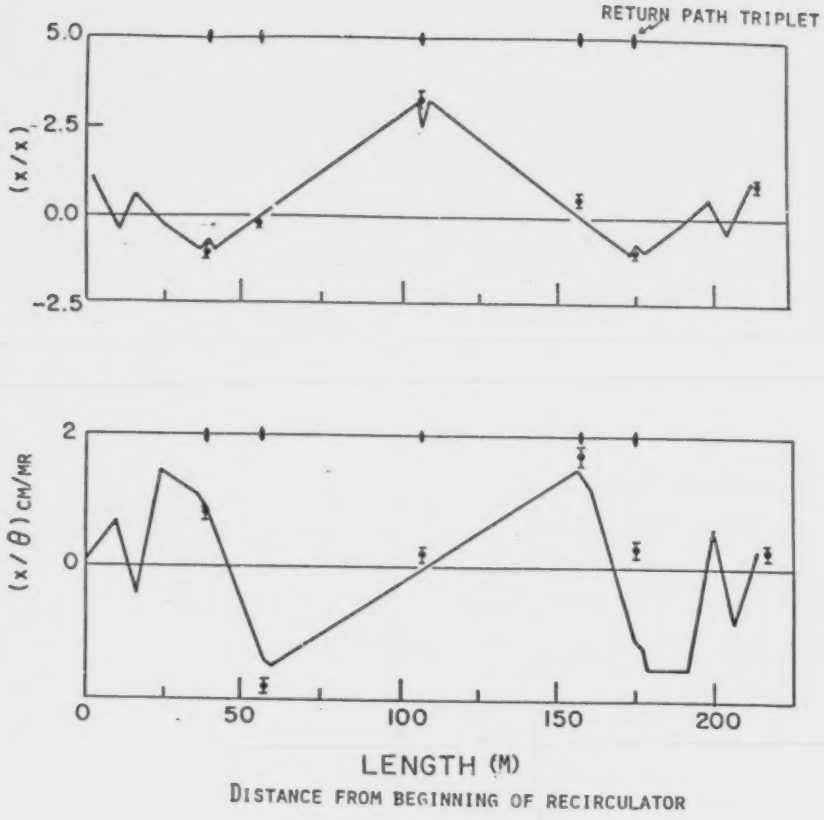

FIGURE 6A

HORIZONTAL PRINCIPLE ORBITS FOR AS-INSTALLED AND AS-OPERATING SYSTEM. LINES REPRESENT CALCULATED OPTICS. POINTS REPRESENT MEASURED VALUES.

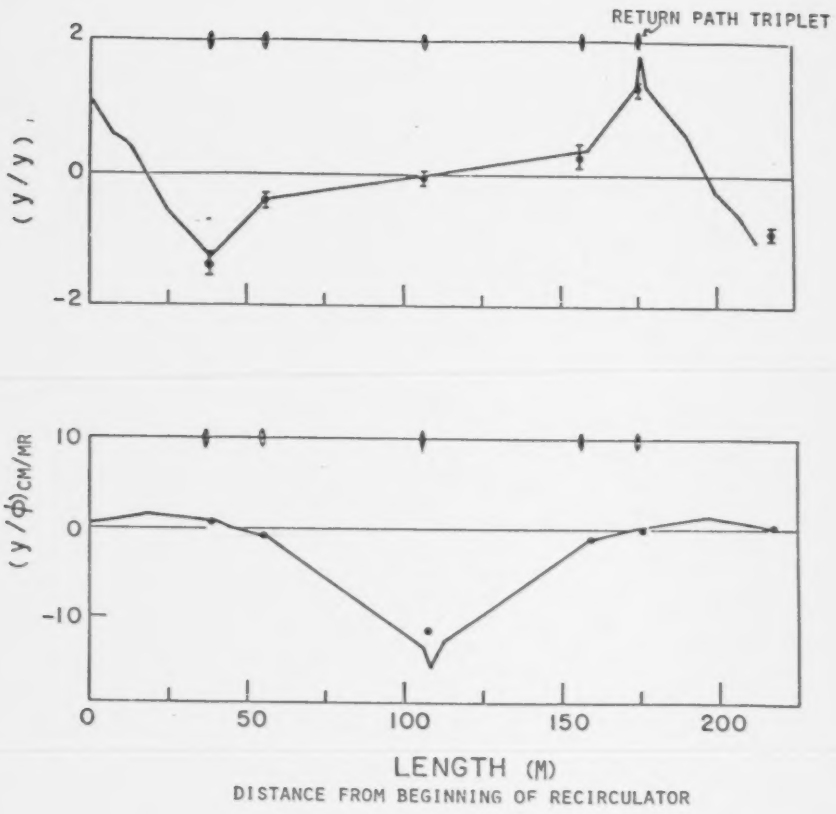

FIGURE 6B

VERTICAL PRINCIPLE ORBITS FOR AS-INSTALLED AND AS-OPERATED SYSTEM. LINES REPRESENT CALCULATED OPTICS. POINTS REPRESENT MEASURED VALUES.

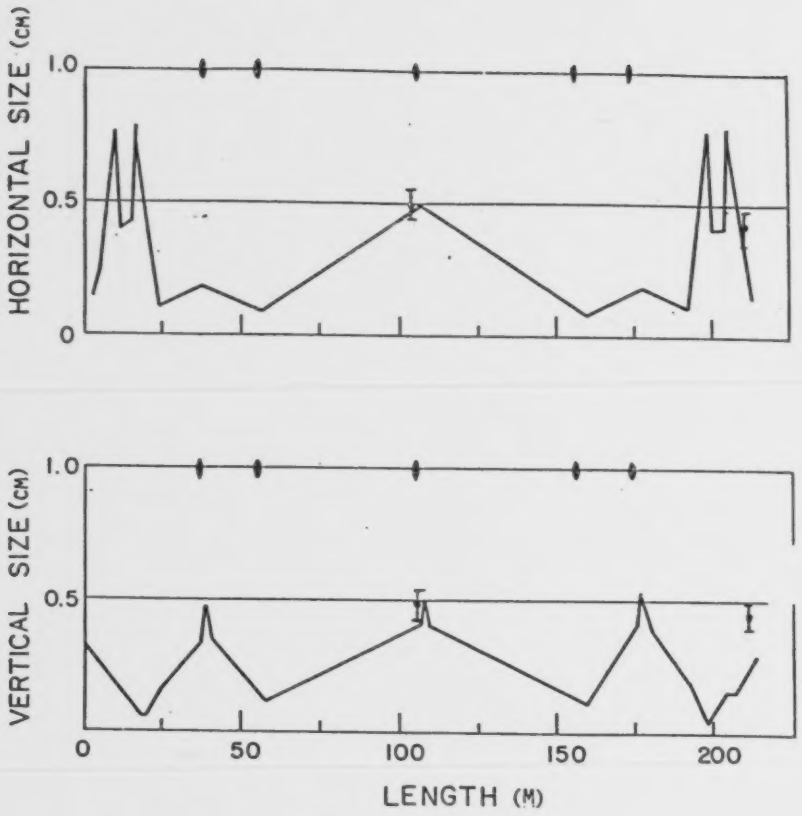

FIGURE 7

FULL BEAM SIZE THROUGH RECIRCULATOR SYSTEM.
HORIZONTAL SIZE INCLUDES 0.3% ENERGY SPREAD

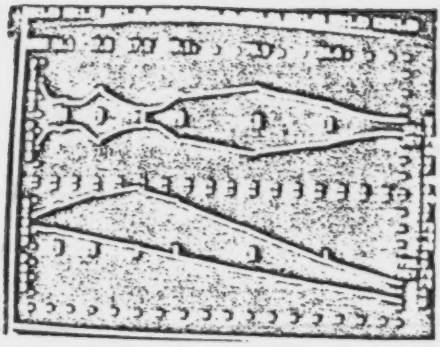

$\Delta E/E = +4\%$

distance (M)

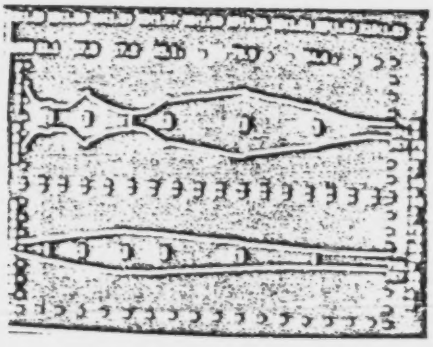

$\Delta E/E = 0\%$

FIGURE 8

CALCULATED HORIZONTAL BEAM ENVELOPE THROUGH ACCELERATOR FOR AS-INSTALLED SYSTEM AT DIFFERENT ENERGIES. UPPER TRACE IS FIRST PASS BEAM, LOWER TRACE IS SECOND PASS. FULL SCALE OF EACH VERTICAL TRACE IS 8MM. HORIZONTAL AXIS SHOWS DISTANCE FROM ACCELERATOR SECTION 2. CENTRAL ENERGY OF FIRST PASS BEAM IS 374 MEV.

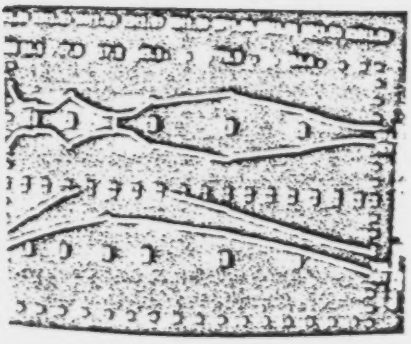

$\Delta E/E = -2\%$

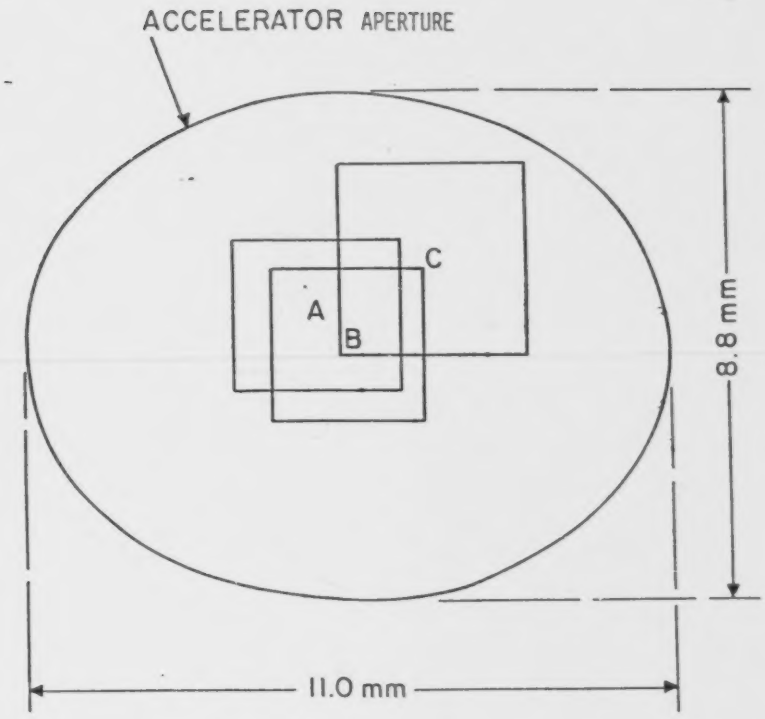

BEAM A: $E_o + 1.7\ \%$

BEAM B: E_o

BEAM C: $E_o - 2.3\ \%$

FIGURE 9 - RECIRCULATED BEAM SIZE AND POSITION RELATIVE TO ACCELERATOR LIMITING APERTURE FOR 3 DIFFERENT ENERGIES. MEASURED RESULTS.

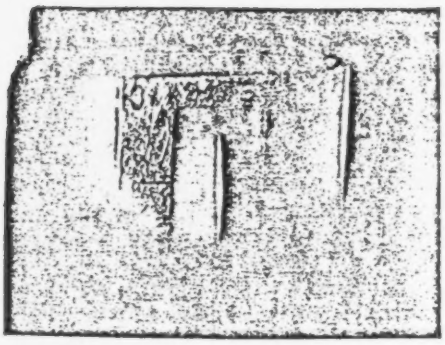

PHOTO 1A

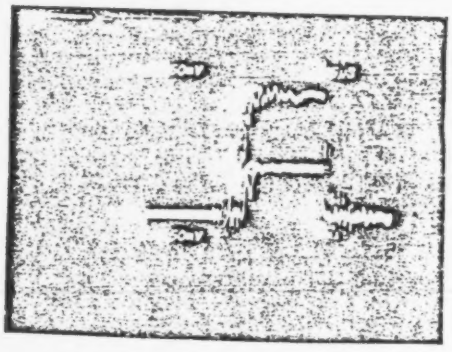

PHOTO 1B

PHOTO 1A - RECIRCULATED BEAM SPOT ON TARGET. FULL LENGTH REPRESENTS 0.3% ENERGY WIDTH. 90% OF BEAM IS IN BRIGHT SPOT AT CENTER WITHIN 0.1%

PHOTO 1B - LARGER SIGNAL IS CURRENT AT END OF ACCELERATOR SHOWING BOTH PASSES. LOWER TRACE IS ENERGY ANALYZED RECIRCULATED BEAM. PULSE WIDTH IS 15 μSEC CONDITIONS ARE THE SAME AS IN PHOTO 1A.

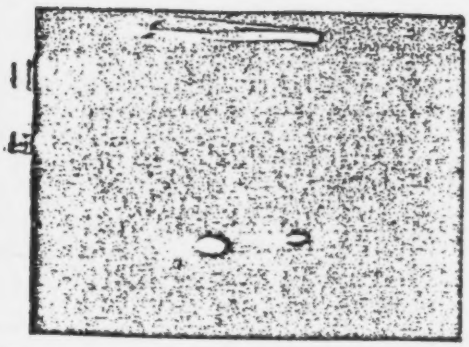

PHOTO 2A - SYNCHROTRON LIGHT FROM RECIRCULATOR DURING TYPICAL RUN. HORIZONTAL POSITION REPRESENTS ENERGY. RIGHT HAND SPOT IS FIRST PASS BEAM BEFORE SECOND PASS IS REINJECTED. LEFT HAND SPOT IS SAME BEAM AT LOWER ENERGY AFTER SECOND PASS BEAM IS REINJECTED.

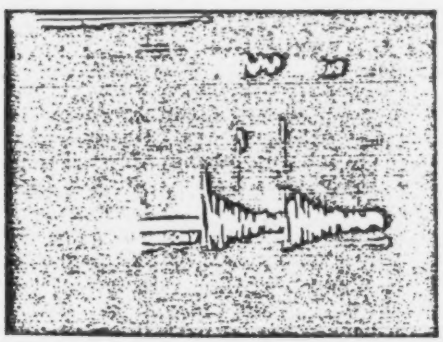

PHOTO 2B - CURRENT PULSE AT END OF ACCELERATOR FOR ABOVE CONDITIONS. CURRENT STEP AT LEFT HAND SIDE OF SIGNAL CAN BE SEEN WHEN SECOND PASS IS REINJECTED. (TOTAL CURRENT IN ACCELERATOR IS 6.4 mA FROM BOTH BEAMS) FINAL ENERGY IN THIS CASE IS 460 MeV.

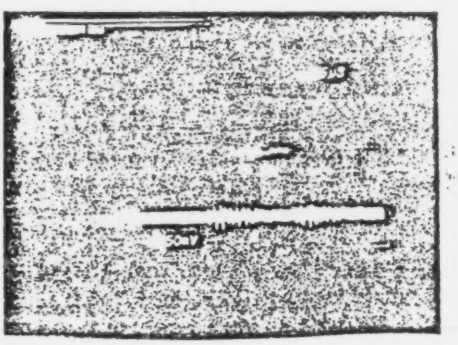

PHOTO 2C - ENERGY ANALYZED RECIRCULATED BEAM FOR ABOVE CONDITIONS.

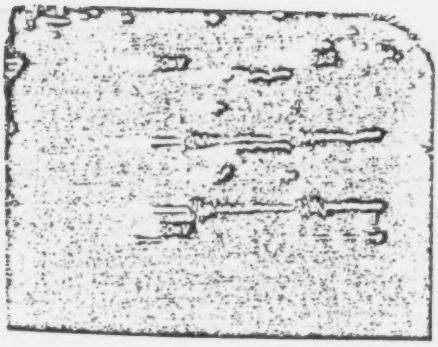

PHOTO 3A

7MA RECIRCULATED CURRENT AT 295 MEV
UPPER TRACE IS FRONT END OF ACCELERATOR
LOWER TRACE IS END OF ACCELERATOR

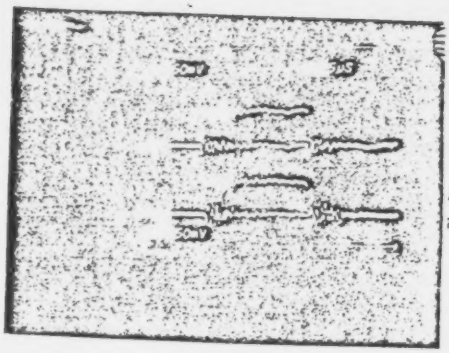

PHOTO 3B

SAME CONDITIONS AS PHOTO 3A
WITHOUT SECOND PASS BEAM

14MA TOTAL IN ACCELERATOR, FINAL ENERGY IS 570 MEV

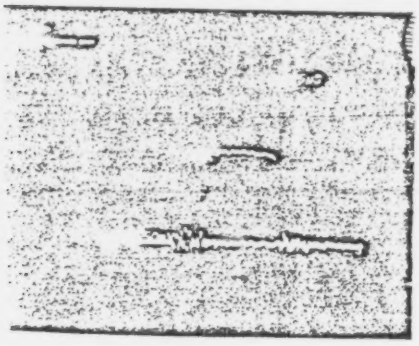

PHOTO 3C

11MA RECIRCULATED CURRENT WITH PHASE SHIFT COMPENSATION (570 MEV FINAL ENERGY)

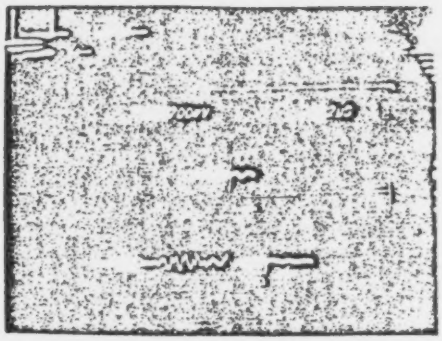

PHOTO 4A - 40mA NARROW PULSE SINGLE PASS BEAM AT END OF ACCELERATOR. NOTE THIS PULSE INCLUDES THE 1μSEC TRANSIENT PART OF THE PULSE WITH ABOUT 100 MEV OF ENERGY SPREAD.

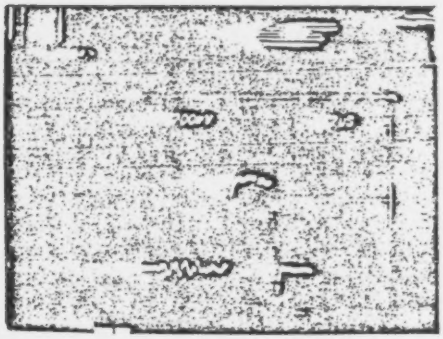

PHOTO 4B - HEAD-TO-TAIL STYLE OF RECIRCULATION SHOWING THE FIRST PASS BEAM AS IN PHOTO 4A FOLLOWED BY THE 40mA RECIRCULATED BEAM.

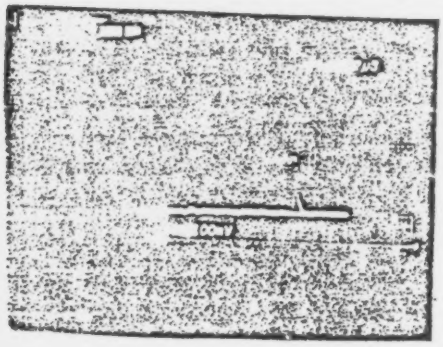

PHOTO 4C - ENERGY ANALYZED BEAM RECIRCULATED HEAD-TO-TAIL STYLE. 40mA THROUGH 0.6% ENERGY DEFINING SLITS. FULL WIDTH IS 1.3 μSEC.

B. Beam Sharing

Entry into the South Hall switchyard is through a small chicane which both separates South Hall and North Hall beams and defines the energy of the South Hall beam. The first magnet of this chicane is a small-angle (0.5°) bend. This spring this magnet will be replaced by a pulsed kicker magnet which will allow pulse-to-pulse beam sharing (at the same energy) between the two experimental areas. Testing will be done during the spring running period, and it is expected that scheduling for the fall period will be done to accommodate those situations for which this beam sharing is efficient.

A more useful form of beam sharing would provide a non-recirculated low energy beam to the North Hall and a recirculated high energy beam to the South Hall (or vice versa). The energy ratio could be varied over a wide range. Switching would be done on a pulse-to-pulse basis. Two kicker magnet systems and modifications of the recirculator output chicane system are required and preliminary plans have been developed for possible implementation during FY/85.

C. RF Upgrades

Sixth Modulator:

A sixth modulator is currently being installed at Bates. The present system contains five modulators. The first powers the injector and one accelerator section. The second, third and fourth each power four accelerating waveguides and the fifth modulator feeds 8 accelerating sections. The sixth modulator will power the last four guides and leave the fifth to power the other four sections. In this way the energy capability will be increased to 840 MeV.

In this first year of construction just concluding the modulator tank is in place, and we are acquiring the high-voltage power supply components. The tank will be filled with oil and will be capable of high voltage testing with our spare modulator and switchtube components.

In the coming year the remainder of the transmitter components will be assembled and installed. These include the modulator, switchtube racks, controls, RF drives, and microwave transmission lines. Checkout of the modulator will occur during the normal running schedule, and we expect the final connection of the waveguide to the accelerator to occur during the winter shutdown in December 1984.

Switchtube Modifications:

Presently each main klystron is driven by a pair of switchtubes. Although indiviudally they achieve their design

specifications, together the output current is limited by coupling between them. Installation of separately controlled solenoidal focussing rather than the presently used permanent magnet focussing will decouple the tubes and allow full output current. This will increase the peak power capability of each klystron to 5.4MW. The sixth modulator will be used to test the procedure and the FY/85 retrofit to modulators 2-5 is expected to proceed during the summer and winter shutdowns of 1985.

With the above schedule a 1 GeV capacity may be available early in 1986.

D. Control System

The growth of the laboratory in recent years has brought with it a large number of components and fifteen operating modes. The accelerator was designed for operation without a computer controlled system by virtue of its excellent stability. However due to the increase in complexity of the additional system and to allow the operators to concentrate on the important aspects of beam tuning, we have begun a program of developing a computer controlled operating system. Presently we have the first stage of this system in operation. It is based on a LSI 11/2 microprocessor and is used to set, monitor and log switchyard magnetics. It also monitors and displays toroid beam position monitor mesurements in the accelerator and switchyard.

The full system to be implemented is shown in Figure 1. The present system is basically the left hand side of the figure with the user interface incorporated in that computer. At this time the full control system is being developed. It will include the ability to detect phase and amplitude of the accelerator RF. In addition certain steering will be computer controlled. An additional two micro PDP-11 computers are now in-house and the control system using MICROPOWER Pascal is being programmed. It is expected that the system will be implemented in stages in the summer and the winter shutdowns of 1984.

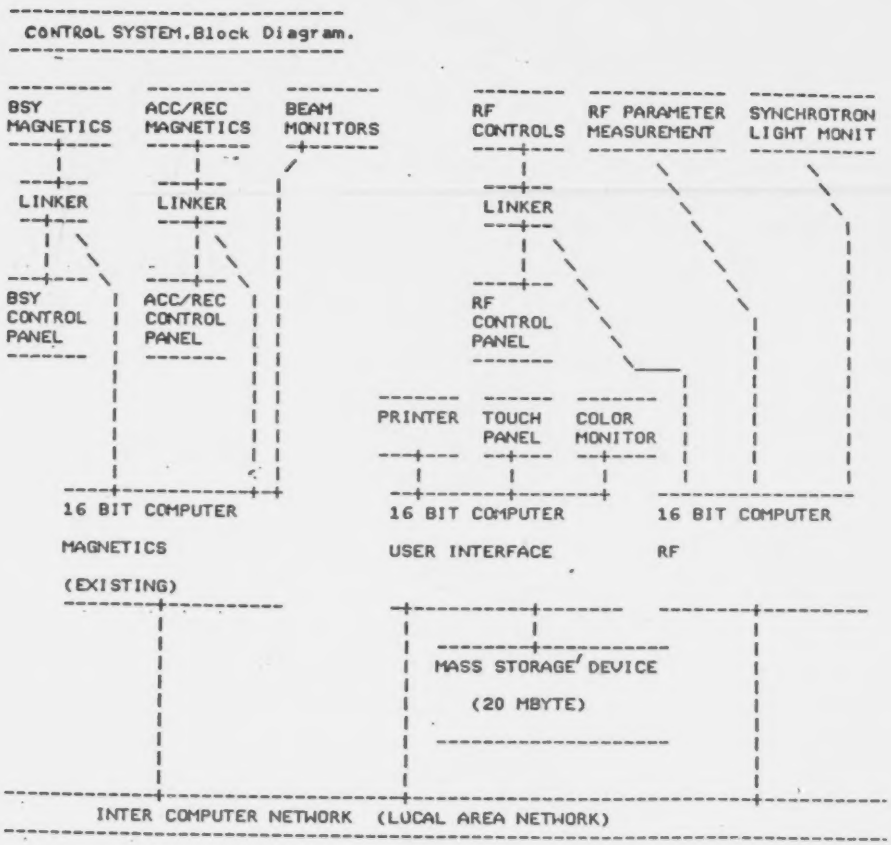

FIGURE 1 - CONTROL SYSTEM

E. POLARIZED ELECTRON SOURCE

A polarized electron source has been under development at Yale for the MIT Bates Linear Accelerator Center. The ability to accelerate polarized electrons will extend the physics capabilities of the facility and allow the measurement of spin related effects. One important measurement of this type will be the study of parity violating interference effects due to the weak neutral currents in the elastic scattering from ^{12}C. Future experiments might include the use of polarized targets and/or the study of polarization transfer to the nucleon and to the two body system. The latter measurements would provide important information on the neutron charge form factor and the deuteron wavefunction.

The polarized electron source must provide high intensity, high polarization, and, for the parity experiment, stability under helicity reversal in order to achieve the required statistical accuracy with minimal systematic uncertainties in a reasonable time. It must be compatible with the existing injector with respect to phase space and injection energy considerations. Table I lists the design goals for the polarized source.

The source is based on photoemission from a GaAs crystal. A continuous wave Kr ion laser operating at 752nm is used to produce the polarized photoemission. An electro-optical shutter (Pockels cell) chops the light to provide the 20 μsec pulses to match the accelerator macroscopic pulse width. A circular polarizing Pockels cell is used to randomly reverse the helicity

of the laser beam, and thus the polarization of the electrons on a pulse to pulse basis.

The design incorporates a gun chamber which contains an extraction electrode assembly, an accelerating column and a preparation chamber used for activating the GaAs cathodes (Fig. 1.) The entire source assembly is contained in a Faraday cage at 335Kv. High voltage insulation between the cage and the accelerating column is provided by a fiberglass bushing filled with SF_6. At ground potential the beam passes through focus coils, a Wien filter and two 45° dipole magnets which transport the low energy beam into the accelerator.

Preliminary testing of the source has been completed at Yale. Crystal lifetimes of ~ 200 hours have been measured at low light intensity (emission < 1μA). A new room temperature electrode assembly is currently being designed at MIT for the extraction of the high intensity beam (emission ~ 300μA). At present the source is being disassembled at Yale for its transportation to Bates. Installation of the new electrode and reassembly of the source with some planned modifications should be completed within 6 to 8 months.

Table I

Design Goals for Polarized Electron Source

Intensity	20 mA peak: 300 μA average
Duty Factor	20 μsec long pulses; 720 Hz
Polarization	0.4
Injection Energy	365 kV
Phase Space	$<10^{-3}\pi$ mc-cm
Intensity Stability	<0.5% jitter
	$<10^{-4}$ correlated with helicity

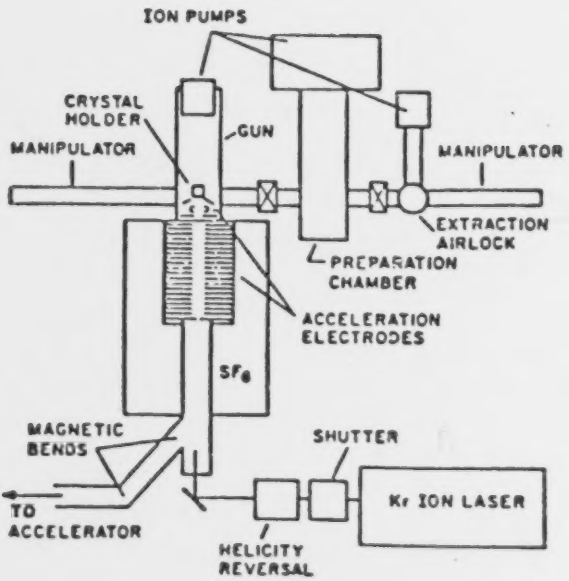

Figure 1. Schematic layout of the source.

II. Experimental Facilities

A. ENERGY LOSS SPECTROMETER SYSTEM

Over the past five years, significant efforts have been directed towards improving the Energy Loss Spectrometer System (ELSSY) at Bates. We have now observed resolution of 4×10^{-5} and our experience, although limited, points to a normally available resolution of 7×10^{-5}. Along with the improved resolution, a reduction has been achieved in the detector response nonuniformity by an order of magnitude. This high resolution capability has an important impact on the physics program. For example, the sample spectrum shown in Figure 1 for electron scattering from ^{154}Gd, taken with resolution 6×10^{-5}, shows that the resolution is crucial for extracting the cross section to weakly excited states such as the 2^+ beta vibration at 816 keV. The extracted cross section for this state is shown in Figure 2.

These improvements are the result of two major hardware modifications to the focal plane itself, substantial changes to the data acquisition software, and assorted hardware conveniences. The dacron/mylar spectrometer exit window was replaced by a kevlar/mylar window that reduced its thickness a factor of 3.5 and reduced the deflection a factor of two. This reduced the multiple scattering contribution to the resolution almost a factor of three and is especially noticeable when taking data at low energies. The other major change in hardware was the installation of a second VDC into the focal plane array. By providing a second precise measure of the electron track position, the additional chamber allowed more precise determination of the track

angle. Since the angle is important for several aberrative corrections, the improved precision also contributed to improved resolution. Perhaps equally important is the elimination of systematic wire-by-wire errors in the determination of this angle with only one chamber. These had been responsible for sharp spectrum nonuniformities that imitated weak transitions. These nonuniformities have effectively been eliminated. Substantial changes in software have both increased the ultimate resolution through improved algorithms, and also facilitate tune-up procedures with more convenient and informative diagnostics.

Continuing development is planned, emphasizing improved resolution and reliability and increased data rates. It is anticipated that a resolution of 2×10^{-5} may be possible. Achieving this goal may require a more complete understanding of beam transport aberrations and instabilities, and a more refined tuning of the spectrometer magnetics to reduce important aberrative terms.

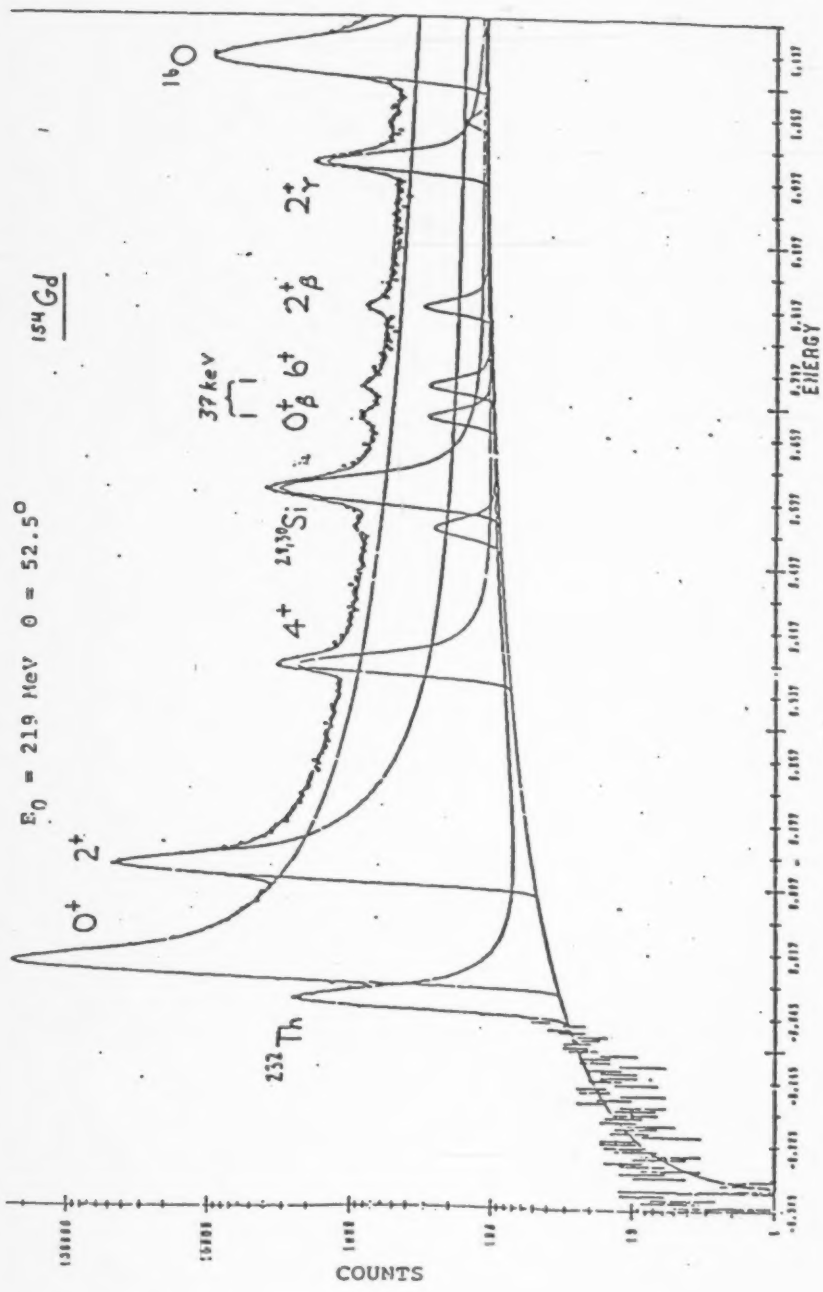
^{16}O
2^+_γ
2^+_β
0^+_β 6^+
37 keV
4^+ $^{29,30}Si$
^{154}Gd
E_0 = 219 MeV θ = 52.5°
0^+ 2^+
^{232}Th
COUNTS
ENERGY

Fig. 1

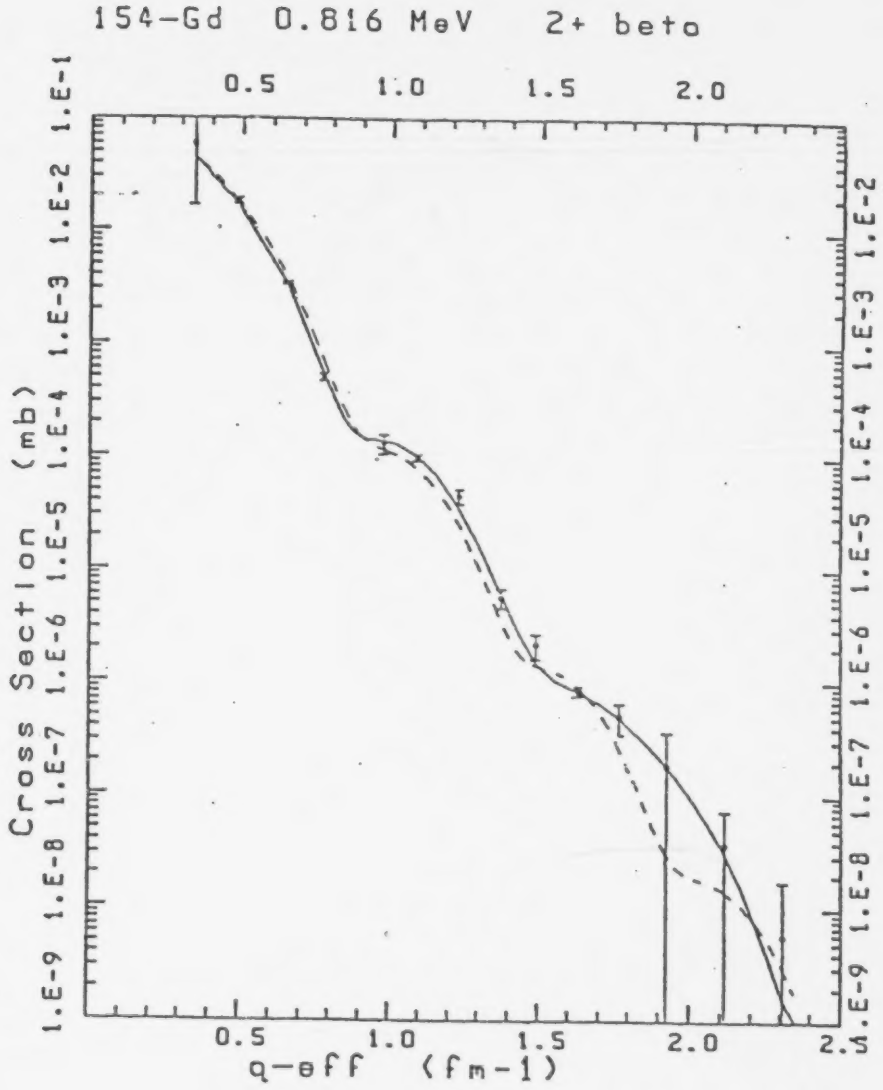
154-Gd 0.816 MeV 2+ beta
Cross Section (mb)
1.E-1 1.E-2 1.E-3 1.E-4 1.E-5 1.E-6 1.E-7 1.E-8 1.E-9
0.5 1.0 1.5 2.0
q-eff (fm-1)

B. MEDIUM ENERGY PION SPECTROMETER

The design criteria for the Medium Energy Pion Spectrometer (MEPS) were a large solid angle (35msr), good resolution ($<5 \times 10^{-4}$ with software correction), relatively large momentum acceptance (20%), good angular resolution (< 5 mrad) and ability to operate in the energy loss mode. The magnet layout, shown in Figure 1, is QQDD with a total angle of bend of 110° and the two dipoles joined together in the form of a splitpole. The spectrometer has been in use for about one year for measurements of differential cross sections for (γ,π^+)-reactions in complex nuclei and together with OHIPS for measurements of the $^{12}C(e,e'p)$-reaction in the quasifree region.

The focal plane detector consists of two crossed vertical drift chambers able to measure both the position and direction of a particle traversing the focal plane. The chambers are read out with a newly developed TIRUS system using a 0.8GHz scaler for each wire. This system gives a much improved immunity to background events in the chambers. The particle identification system consists of four thin scintillators in coincidence with each other and an Aerogel counter with an index of refraction of 1.05 to distinguish between electrons and pions.

In Figure 2 is shown a spectrum of 200 MeV electrons scattered through 60° from a CH_2 target taken with a solid angle of 2.5msr. The three strong peaks are ^{12}C(elastic), ^{12}C(4.4 MeV), and ^{1}H(elastic). After correction for kinematic broadening, we obtain

a resolution of 2×10^{-3} FWHM, equal to the resolution of the incident beam. Figure 3 shows a spectrum of π^+ produced at 120° by a 200 MeV bremsstrahlung beam incident on a ^{14}N-target taken with a solid angle of 26msr and a resolution of 3×10^{-3}. We see the transition to the ground state of ^{14}C and transitions to the many states above 6 MeV excitation energy in ^{14}C. The cross section for the ground state transition is shown in Figure 4.

Presently the efficiency of the Aerogel counter is being optimized to allow measurements of (γ,π^-)-reactions and a vacuum dump line is under design to reduce the general background level. We are presently limited to a momentum resolution of $2\text{-}3 \times 10^{-3}$, but the upgrade of Beam Line B to allow energy loss operations, tentatively scheduled for FY85, will allow MEPS to reach its design resolution of 5×10^{-4}.

FIGURE CAPTIONS

Figure 1 - Layout of the MEPS magnet system.

Figure 2 - Spectrum of 200 MeV electrons scattered through 60° by a CH_2-target. Spectrometer solid angle 2.5msr.

Figure 3 - Spectrum of π^+ from ^{14}N produced at 120° by a 200 MeV bremsstrahlung beam. Spectrometer solid angle 26msr.

Figure 4 - Preliminary cross sections for the reaction $^{14}N(\gamma,\pi^+)^{14}C(g.s.)$.

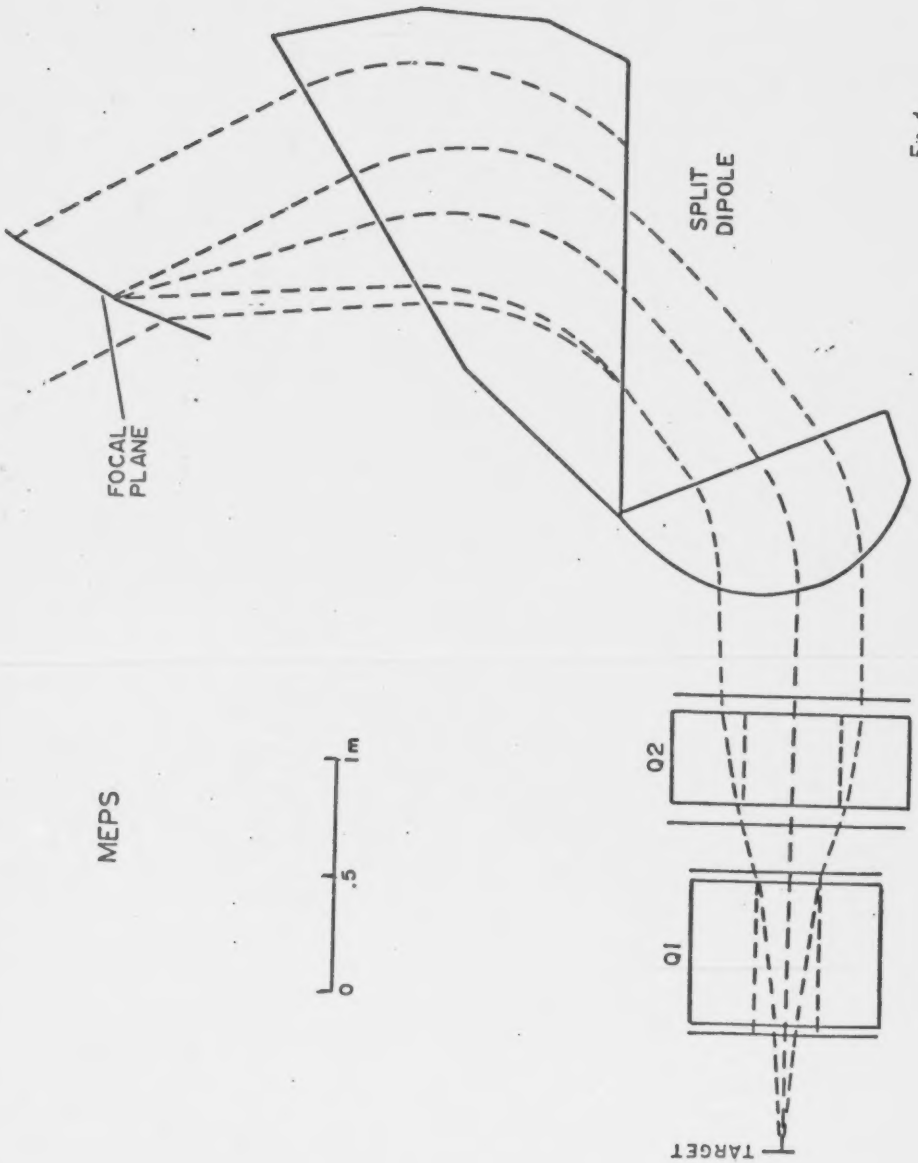

Fig. 1

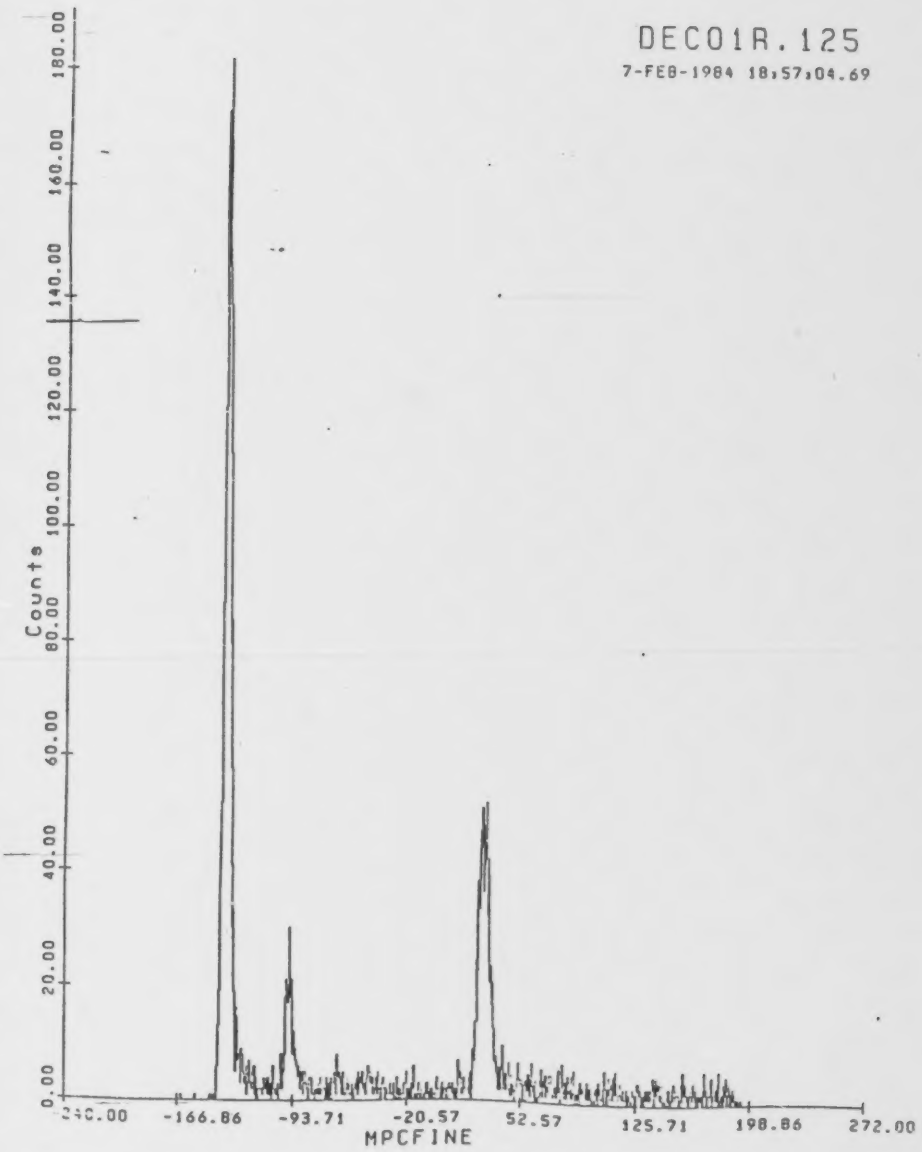
DEC01R.125
7-FEB-1984 18:57:04.69
Counts
0.00
20.00
40.00
60.00
80.00
100.00
120.00
140.00
160.00
180.00
-240.00
-166.86
-93.71
-20.57
52.57
125.71
198.86
272.00
MPCFINE

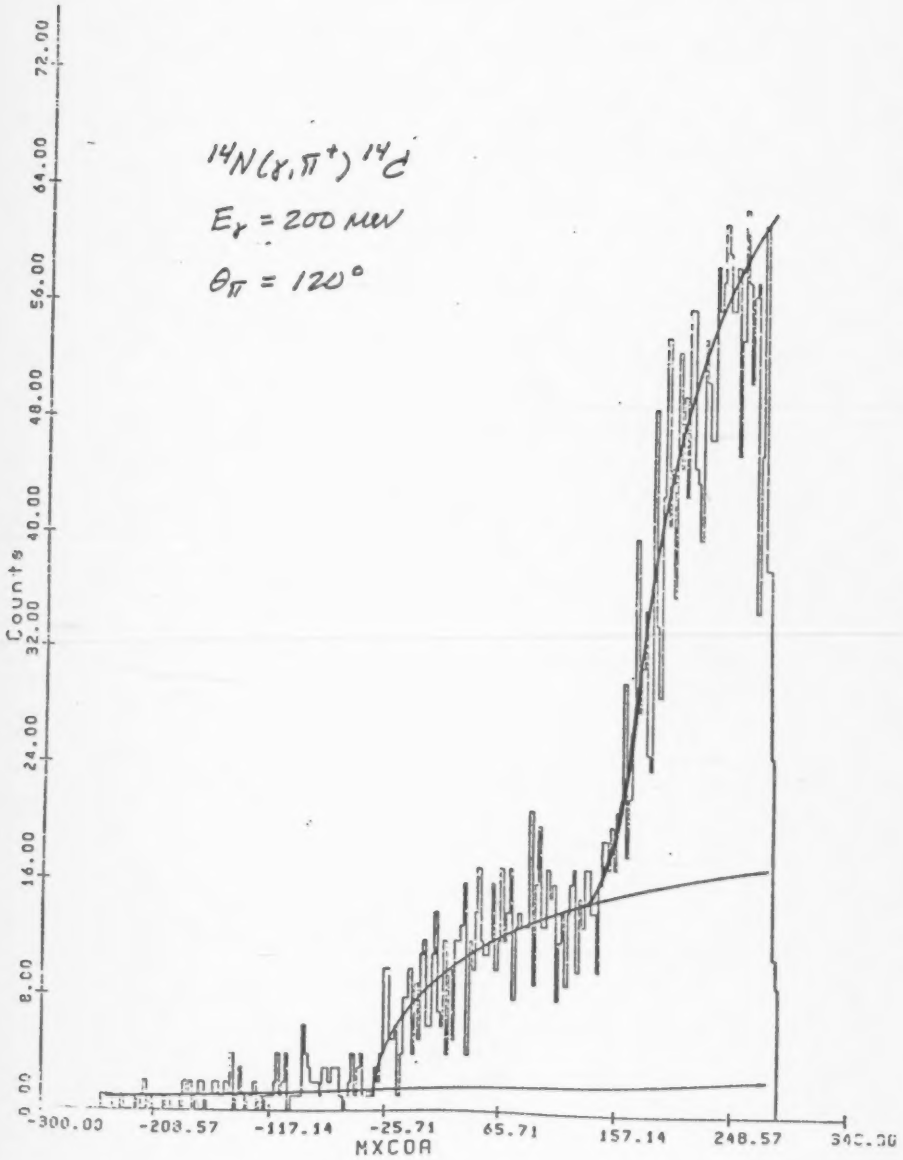
$^{14}N(\gamma,\pi^+)^{14}C$
$E_\gamma = 200$ MeV
$\theta_\pi = 120°$
Counts
0.00
8.00
16.00
24.00
32.00
40.00
48.00
56.00
64.00
72.00
-300.00
-208.57
-117.14
-25.71
65.71
157.14
248.57
MXCOA

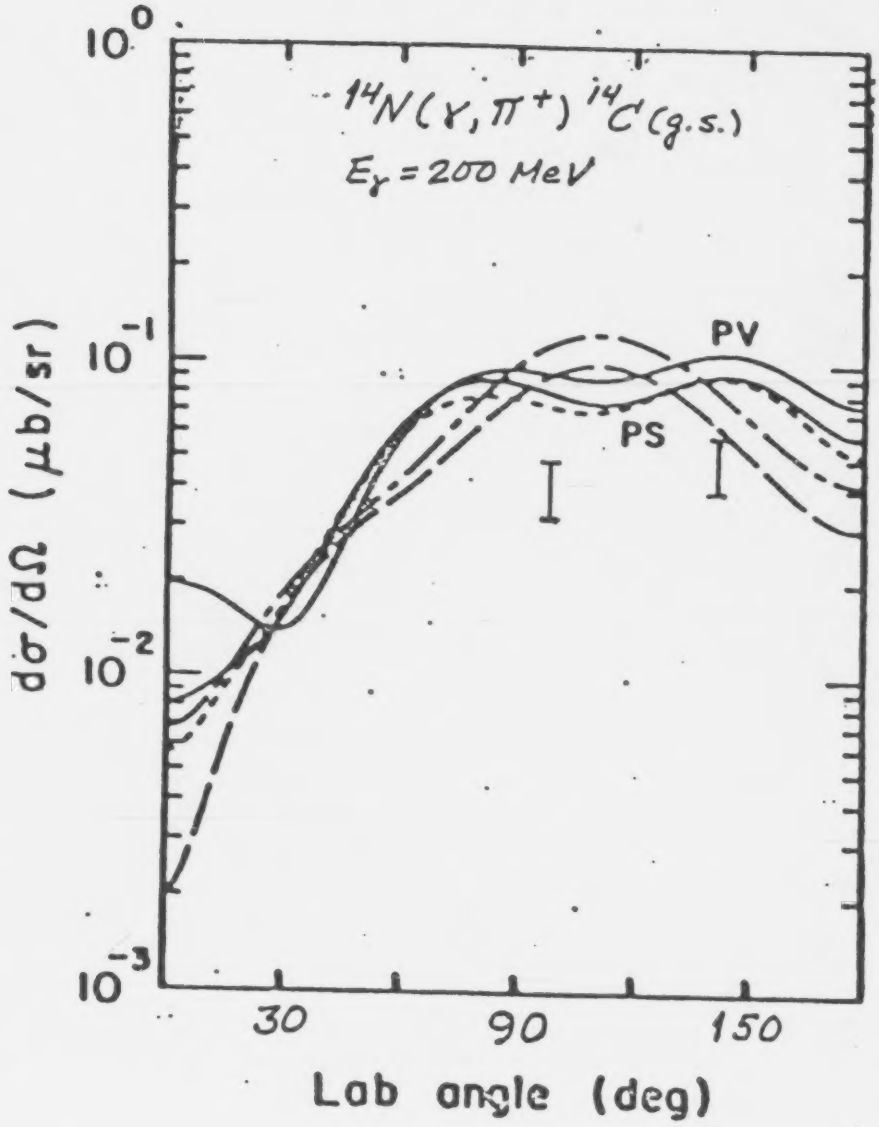
$^{14}N(\gamma,\pi^+)\,^{14}C(g.s.)$
$E_\gamma = 200$ MeV
PV
PS
$d\sigma/d\Omega$ (μb/sr)
10^0
10^{-1}
10^{-2}
10^{-3}
30
90
150
Lab angle (deg)

Fig. 4

C. ONE HUNDRED INCH PROTON SPECTROMETER

Introduction and Overview:

The One Hundred Inch Proton Spectrometer (OHIPS) is a moderate resolution (measured $\delta p/p \sim 0.14\%$), high momentum (1.3 GeV/c) device with a maximum solid angle acceptance of about 20 msr at about 500 MeV/c. (see tables I & II) The construction phase of the project using surplus magnets was completed in 1982. Since that time, the philosophy has been to let the improvements be determined by the experimental program while maintaining enough configuration stability to facilitate on-going experiments. For example, the variable first drift space D_1 has been held constant for the last two running periods and probably will not be changed until the summer shutdown.

Status:

The present configuration is shown in Figure 1. The detectors still consist of the prototype VDCX (wire chamber) and scintillation trigger counters which were available at the laboratory. After the floor in the experimental hall was covered with aluminum sheets, the air pads have been largely trouble-free and angle changes can be made in approximately 30 minutes, including realignment. Measurements have been made as far forward as 20° (the practical limit is approximately 17°). The breadth of the program using this spectrometer is indicated by the list of approved experiments in Table III. Examples of data taken with this instrument are shown in Figures 2-4. Note in Figure 2 the acceptably low background above the bremsstrahlung

endpoint obtained with the provisional shielding enclosure; the relatively large number of angular positions at which measurements were made (Figure 3) was greatly facilitated by the rapid-angle-change capability. In Figure 4 is shown the coincidence timing spectrum for the $^{12}C(e,e'p)$ experiment; MEPS was used for the electron arm and OHIPS for the proton. Here again the signal-to-noise ratio is quite acceptable.

Near-term Developments:

Highest on the priority list is the installation of certain safety features, associated primarily with access to the electronics platform at the rear of the spectrometer and to the detector region immediately above it.

Experience gained with the existing, simple alignment aids indicates that an upgrade would be very cost effective in terms of saving talented manpower. With coincidence experiments an important part of the program, an additional premium is placed on rapidly aligning the spectrometers such that both instruments view the same interaction region.

On a somewhat longer time scale, but still in 1984, it is hoped to acquire wire-chamber readout electronics for the entire focal plane and build dedicated detectors to cover the full solid angle and momentum bite. A mechanism for remotely changing solid angle defining apertures is also foreseen.

The basic design exists for two new quadrupoles which should make possible a momentum resolution of 5×10^{-4} (software corrected) and maximum momentum of 1300 MeV/c both at large solid angle. They are physically narrower than the present magnets and will permit measurements at more extreme angles. The quadrupoles for MEPS, while smaller, are of similar design and may be considered successful prototypes for these new magnets. This higher resolution capability responds to growing interest in good resolution coincidence measurements.

TABLE I: Initial operating parameters for OHIPS in -Q+Q (highest resolution) mode. Note that the present detector size limits $\Delta p = \pm 2.5\%$.

D1 (m)	ϕ_o, Spect.Ang. (deg)	$\Delta\phi$ (deg)	$\Delta\theta$ (deg)	$\Delta\Omega$, Elliptical (msr)	$\frac{\langle x/x \rangle}{\langle x/\delta \rangle}$, ± 0.5cm tgt. (%)	P_{max} (MeV/c)
0.4	55-125	± 10.7	± 2.2	23.0	0.15	537
0.5	49-131	9.5	2.2	19.8	0.15	604
1.0	28-152	6.0	1.9	10.8	0.13	907
2.0	16-164	3.4	1.5	4.7	0.10	1300

TABLE II: Initial operating parameters for OHIPS in +Q-Q (largest $\Delta\theta$) mode.

D1 (m)	θ_o, Spect.Ang. (deg)	$\Delta\phi$ (deg)	$\Delta\theta$ (deg)	$\Delta\Omega$, Elliptical (msr)	$\frac{\langle x/x \rangle}{\langle x/\delta \rangle}$, ± 0.5cm tgt. (%)	P_{max} (MeV/c)
0.4	55-125	± 2.1	±11.1	22.4	1.3	508
0.5	49-131	2.0	9.9	19.3	1.1	569
1.0	28-152	1.8	6.2	10.4	0.68	838
2.0	16-164	1.4	3.5	4.5	0.35	1280

TABLE III

OHIPS EXPERIMENTS

#79-20	Deuteron Form Factors by Tensor Polarization of Recoil Deuterons (T_{20}) MIT; TRIUMF; ANL; WPI; LANL; U.Ill.
#81-01	$^{16}O(\gamma,p_0)^{15}N$ Angular Distributions MIT; U.So.Car.; Glasgow
#81-06	A Measurement of the Deuteron S- and D-State Interference Amplitudes by the D(e,e'n) Reaction MIT; RPI; UNH
#82-03	The ^{12}C(e,e'p) Reaction Mechanism MIT; RPI; UNH
#83-15	Measurement of the Reaction $D(\gamma,pp)\pi^-$ RPI; LSU; MIT; Saclay
#83-17	The A Dependence of the (e,e'p) Reaction on the Quasi-free Region: A Study of the Nucleon Mean Free Path ANL; NW; MIT; NBS

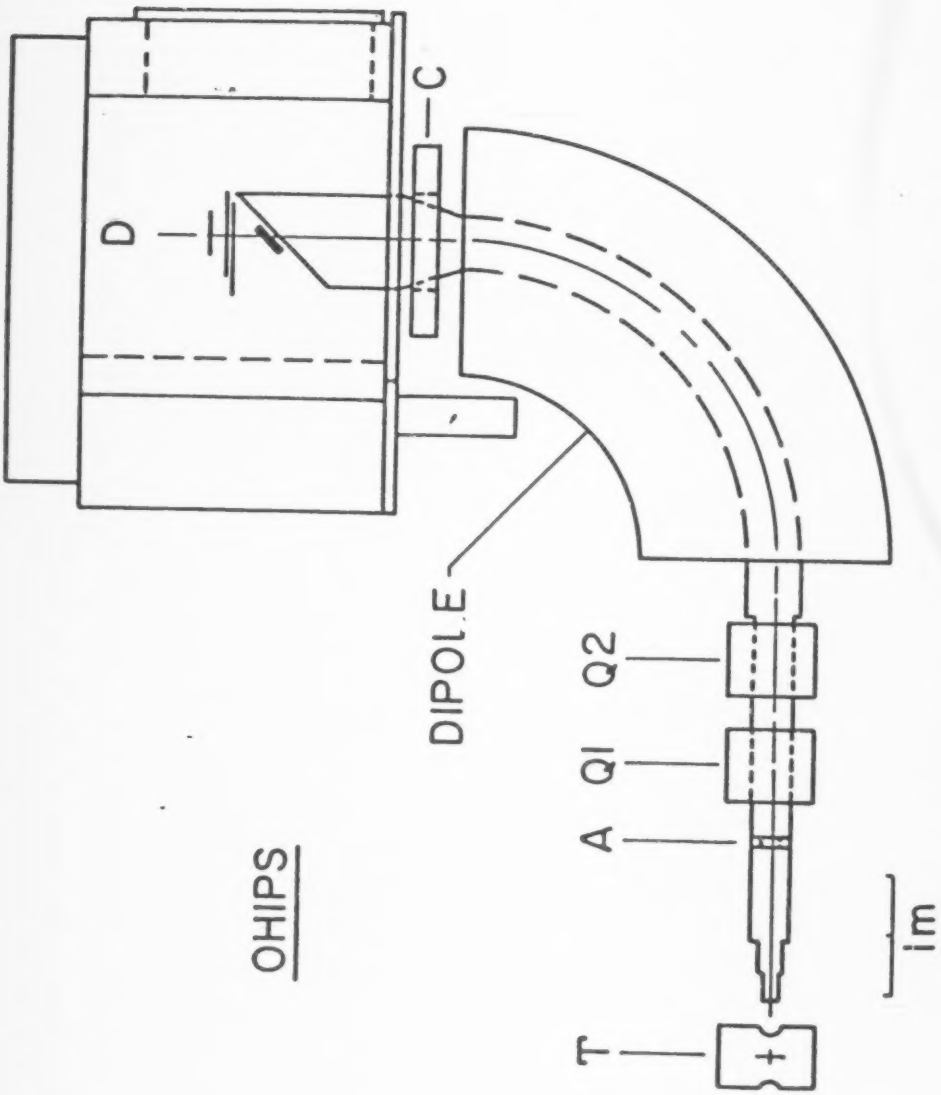

Fig. 1

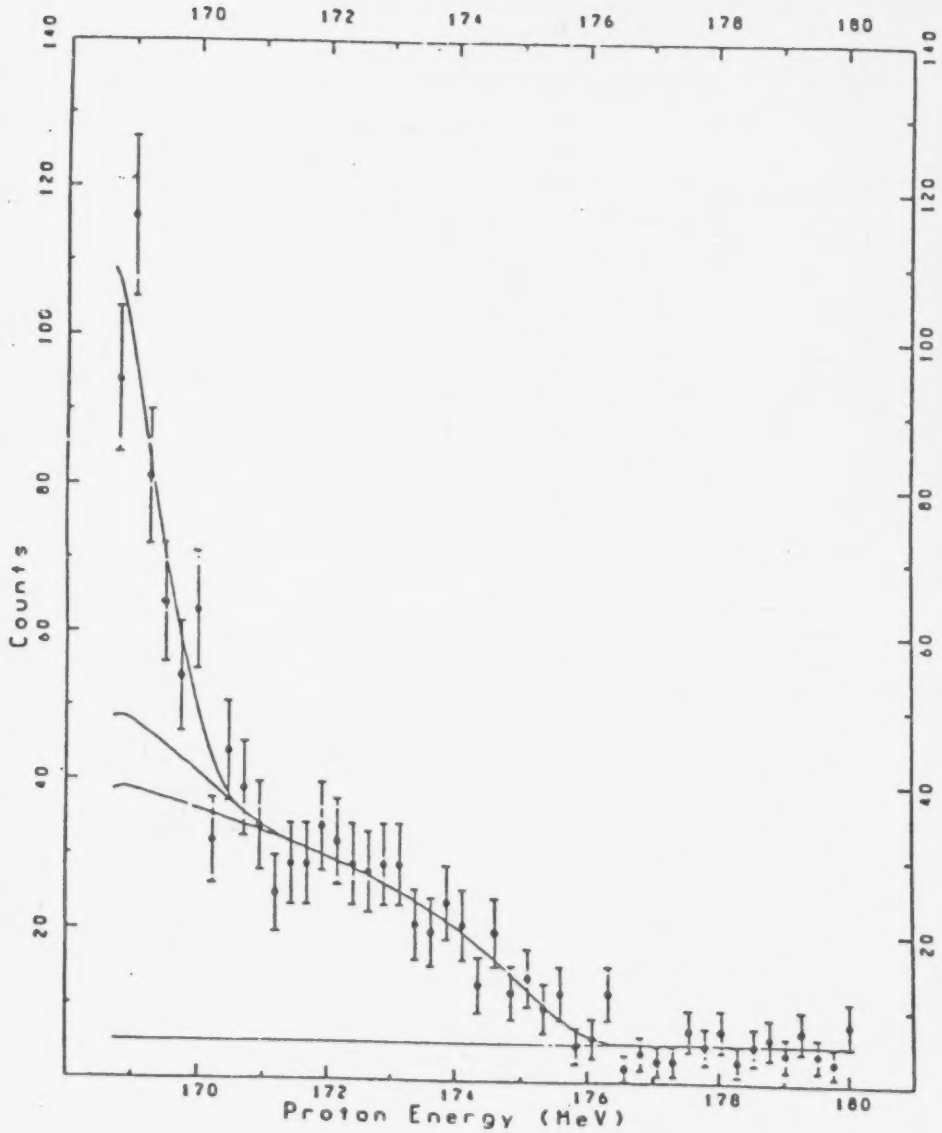

Figure 2. 70 degree cross section fit to data obtained with a 195 MeV bremsstrahlung beam.

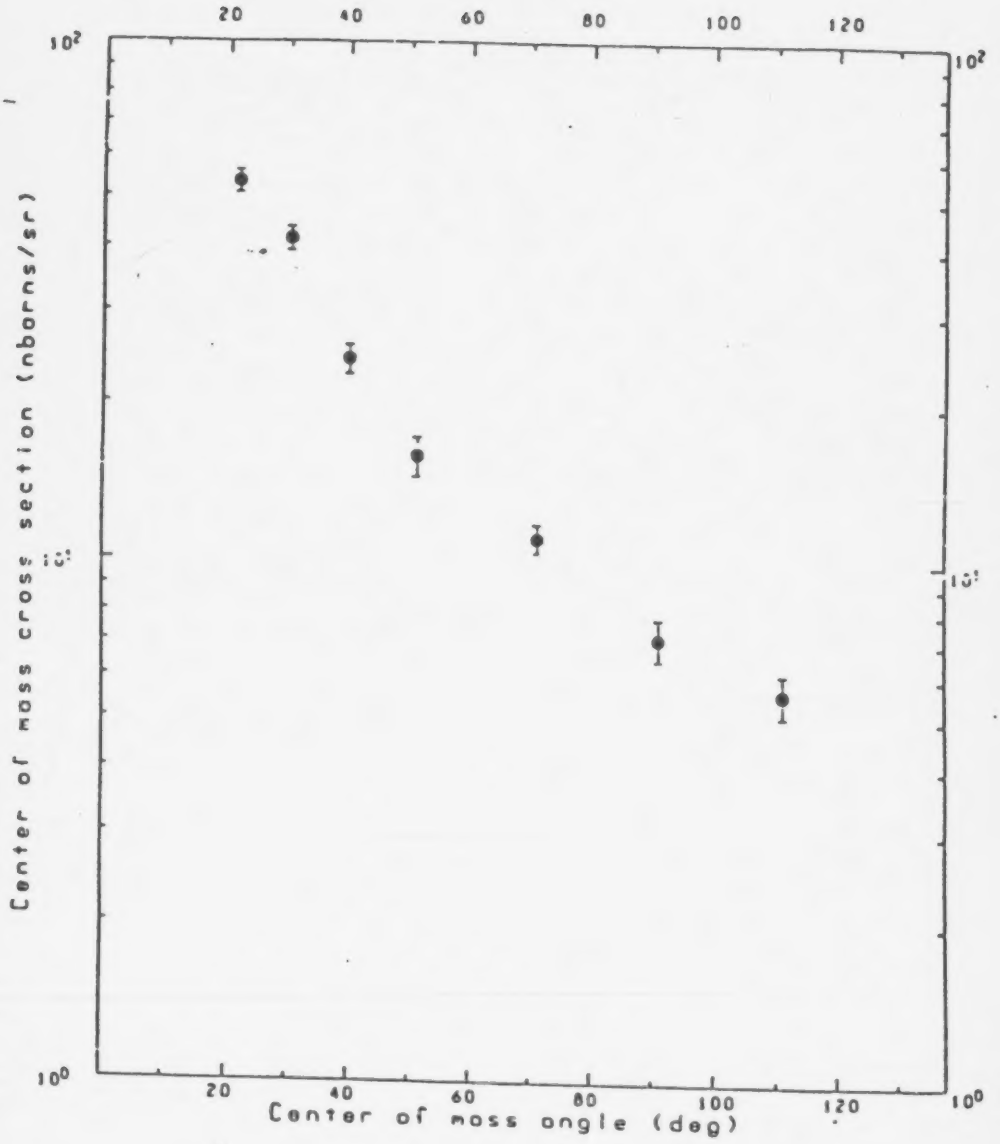

Figure 3. Ground state center of mass cross section at 195 MeV. The error bars are only statistical.

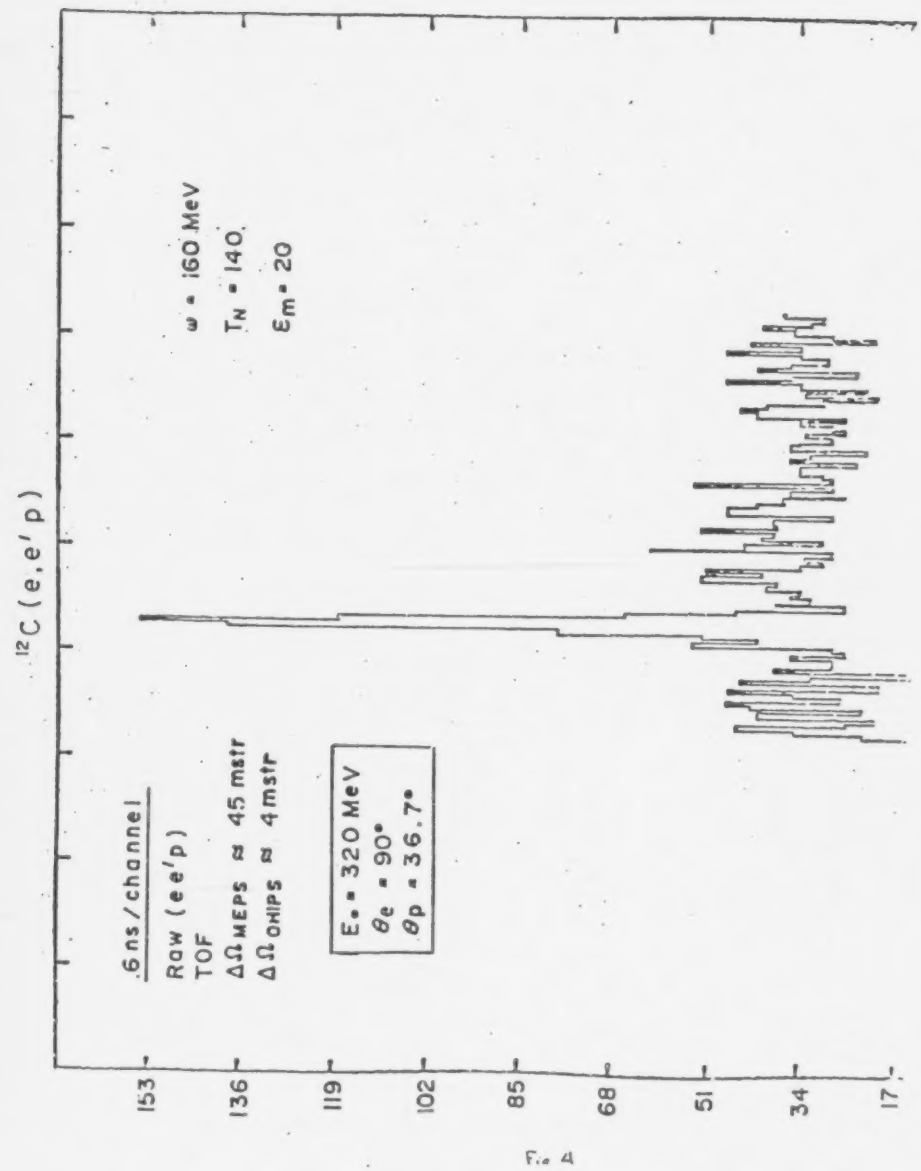
$^{12}C(e,e'p)$
.6 ns/channel
Raw (e e' p)
TOF
$\Delta\Omega$ HEPS ≈ 45 mstr
$\Delta\Omega$ OHIPS ≈ 4 mstr
E_e = 320 MeV
θ_e = 90°
θ_p = 36.7°
ω = 160 MeV
T_N = 140
ε_m = 20
153
136
119
102
85
68
51
34
17

Fig. 4

D. BIGBITE SPECTROMETER

The BIGBITE spectrometer, as its name suggests, was originally conceived as a very broad range (~ ±25% in momentum) spectrometer of modest solid angle (~ 3msr) and resolution (~ 1%) to serve the needs of the Bates program in deep inelastic electron scattering. As the design developed it became clear that with careful design the needs of other experimental programs might also be served with the same instrument. In particular, the QQD design decided upon was very compatible with the needs of the deuteron transport arm in the T_{20} experiment. In this application one moves the spectrometer closer to the target to achieve a larger solid angle at the expense of reduced useful momentum range.

Another experimental program that will be served by this instrument is the high-resolution (γ,n) studies. In this manifestation the QQ of the QQD would be replaced by a neutron converter scintillator and two x-y wire chamber arrays.

The BIGBITE spectrometer has been developed as a flexible instrument with interchangeable, self-aligning input and focal plane modules. The dipole sits on the front of a platform approximately 13½ft. wide by 20ft. long. Upon this platform is built a 3ft. concrete enclosure to shield the focal plane detectors. The entire system is moved on an air flotation system. The present mechanical tether is specifically designed for the beam line "B" pivot point in the South Hall. However, the system

is designed in such a manner that it can be moved in its air flotation pads to beam line "C", where it is foreseen that the (γ,n) experiments will be performed.

This system has already been used in a temporary setup with Ω = 17 msr for the first phase of the deuteron T_{20} experiment, so some operational experience has been obtained. The dipole has been field mapped, and the QQ module has been magnetically aligned. The main support system, air pad structure, and tether are complete; and assembly and alignment are underway. The focal plane detection system is about 80% complete, and the (γ,n) front end is nearing design completion with some parts already manufactured. The vacuum system is 95% complete, and all necessary elements of the PICOS-3 readout system and all required CAMAC modules have been purchased. The Los Alamos "Q" software will be used in BIGBITE data acquisition, and this system is now available at Bates.

It is forseen that all mechanical assembly, with the exception of the shielding enclosure, will be complete by April 1, 1984. Final bench testing of the detection system should be complete by May 1, 1984, and it is planned to request a short beam test run in June.

The following is a brief summary of the vital statistics of this system:

Dipole:

Maximum Field - 14.5 kG*

Power Supply - 1600 A @ 175 V

Pole Gap Volume - 29" wide x 10" high x 40" deep

Nominal Bend Angle - 35° (central ray)

Maximum Central Momentum - 800 MeV/c

Weight - 36 tons

Quadrupoles:

Maximum Pole Tip Field - 10 kG

Bore Radius - 4"

Length - 16"

System:

Total Weight - ~/70 tons

Angular Range (Beam Line B) - 30°-150°

*Limited by temperature rise in the coils.

E. π^0 SPECTROMETER

The Bates π^0 spectrometer (a collaborative effort by Boston University and MIT) was completed in 1982 and has been used to acquire data on the following reactions: $^{1}H(\gamma,\pi^0)^{1}H$, $^{4}He(\gamma,\pi^0)^{4}He$, and $^{12}C(\gamma,\pi^0)^{12}C$. The spectrometer is similar in principle to the LAMPF π^0 spectrometer. Two independent photon detectors, each consisting of two Pb-glass converter/multiwire proportional chamber arrays followed by total absorption Pb-glass blocks, provide a precise determination of the two π^0 decay photon conversion points and a rough measurement of the photon energies. By restricting events to those where the two photons had roughly equal energies (the preferred region of phase space) the π^0 energy is determined primarily by the measured opening angle of the photons. The ultimate π^0 energy resolution is then sensitive to the photon beam spot size and target thickness. The best resolution achieved so far under running conditions is 6 MeV.

Because the spectrometer acceptance is quite energy dependent and because a bremsstrahlung photon spectrum is used, it is important that the spectrometer performance is well-understood. We have therefore measured the π^0's produced at a laboratory angle of 72.5° in the reaction $\gamma+p\rightarrow\pi^0+p$ by a bremsstrahlung beam with a tip energy of 298 MeV. The spectrum of π^0's is shown in Figure 1; on the abscissa is plotted the photon energy corresponding to a π^0 from the $\gamma+p\rightarrow\pi^0+p$ process. The cutoff on the low-energy side is due to spectrometer acceptance; on the

high energy side it is due to the bremsstrahlung shape. The curve in the figure is the expected yield of π^0's calculated by convoluting the bremsstrahlung shape, the π^0 spectrometer acceptance, and previously measured cross sections from Bonn. The agreement between the measured and calculated yield curves, with no normalization factor applied, is excellent. The $^4He(\gamma,\pi^0)^4He$ data at 290 MeV are shown in Figure 2, together with the Δ-hole model prediction.

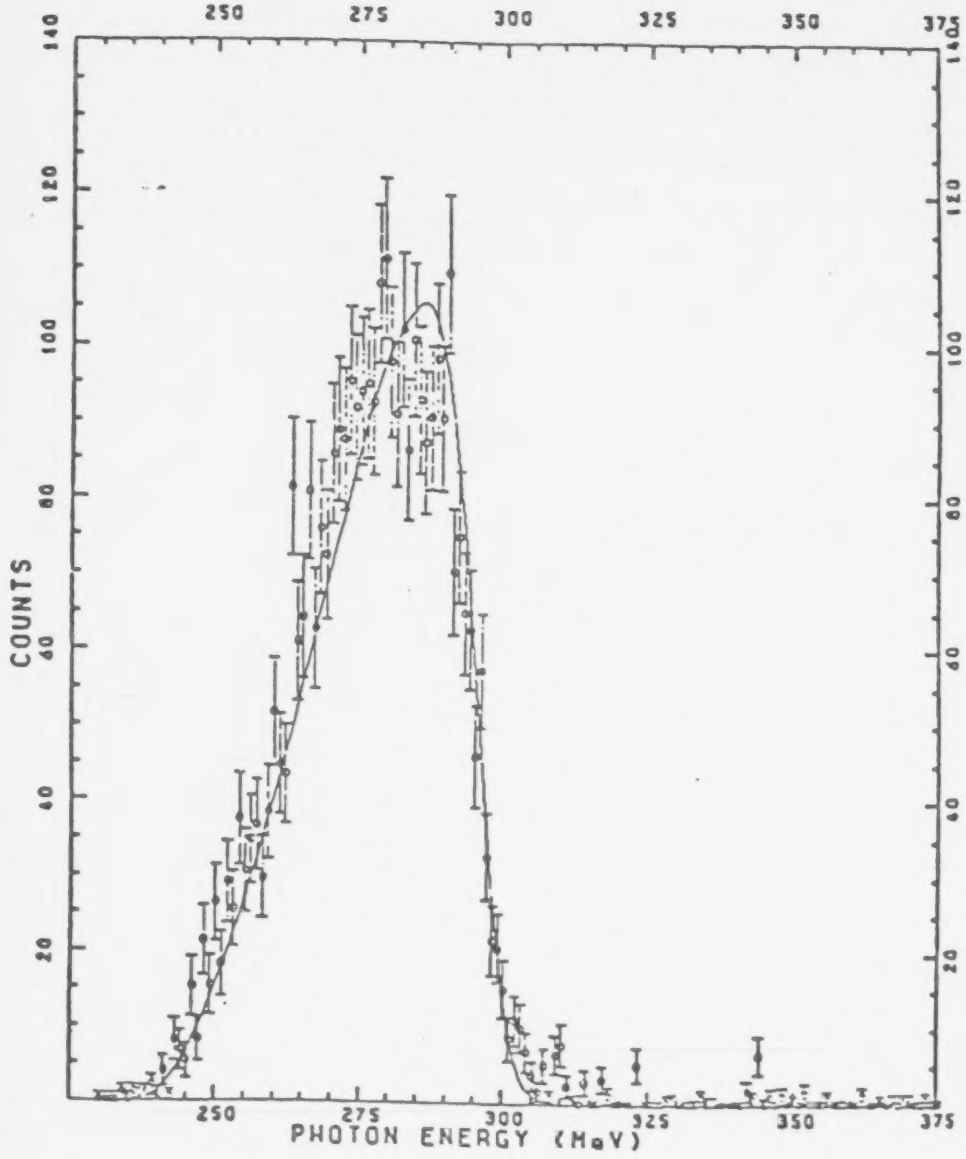
250
275
300
325
350
375
140
120
100
80
60
40
20
COUNTS
PHOTON ENERGY (MeV)

Fig. 1

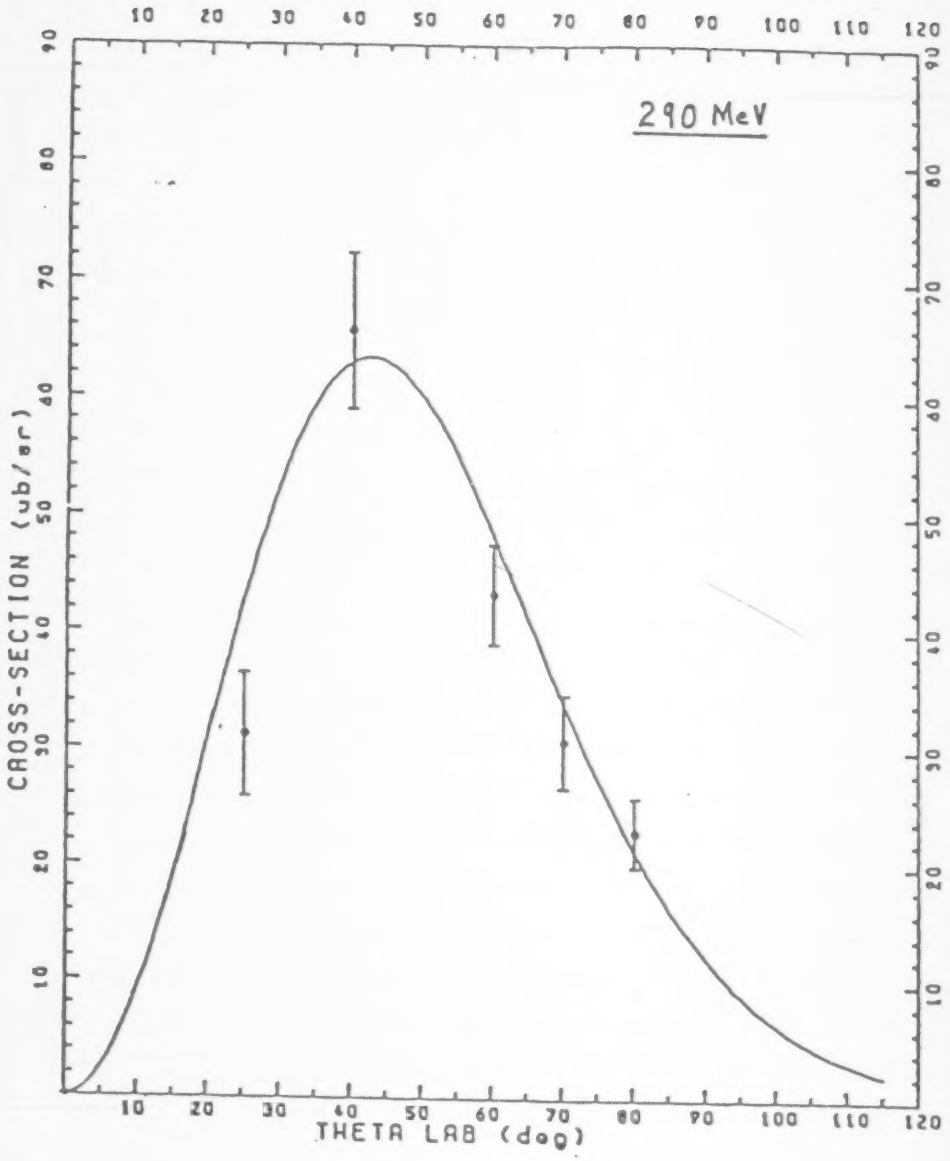

Fig. 2

39-587 O - 84 - 24

F. HIGH FLUX PURE PHOTON FACILITY ON BEAM LINE C

We presently have a pure photon beam on Beam Line C this has been used for (γ,π^0) and (γ,γ) experiments. The flux available (0.2% radiator, 5.5m distance from radiator to target) is sufficient for these experiments, which are limited in any case by target-associated background, but not for experiments such as (γ,p_0) on complex nuclei. Until now, experiments which needed a higher flux of real photons at Bates have used the radiator in/radiator out technique, with the electron beam passing through the target.

To provide a high flux pure photon beam for upcoming (γ,n_0) and $\gamma + d \rightarrow \vec{n} + p$ experiments, we have designed a facility on Beam Line C which will combine a thick radiator, short radiator to target distance, and excellent electron beam dumping capabilities. The radiator will be immediately upstream of a C-magnet which will bend the electron beam into a trench dug in the South Hall floor. The radiator to target distance can be as short as one meter, thus allowing use of up to 4% radiators while still maintaining a reasonable photon beam spot size on target. Use of a C-magnet will mean that the low energy tail of the beam will be dumped well away from the radiator/target area. It also allows for future installation of a tagging hodoscope when the beam duty factor is increased. Dedicated shielding blocks to cover the trench will allow dumping of the beam at different angles depending on experimental requirements. The C-magnet which will be constructed will be capable of dumping electron beams up to

400 MeV. The magnet could be replaced in the future by a larger one (with some increase in radiator to target distance) if higher energy beams are used.

We hope to do the excavation and concrete work during the summer 1984 shutdown and to have the facility ready for initial tests in late 1984.

III. The Research Program - Some Recent Results

With the development of the experimental facilities outlined above, the Bates research program has expanded quickly to exploit the full range of new capabilities to their limits. To demonstrate the breadth of this program, we present here a few examples of recent experimental results. Many of these are preliminary results obtained within the last six months and represent only the initial stage of an experimental program.

1. Nuclear Spectroscopy

The research program continues to reflect a strong commitment to precision nuclear spectroscopy through electron scattering. Measurements of nuclear form factors over a large range of momentum transfer yield precise representations of the nuclear charge, current and magnetization densities free of the uncertainties introduced by the use of hadronic probes.

This program is very extensive, addressing fundamental issues in nuclear spectroscopy across the Periodic Table. We shall discuss here only one example, electron scattering from the deformed nucleus ^{154}Gd (MIT, UNH, Illinois). As seen in Figure II.A.1, this experinent needed the extremely high resolution available only on ELSSY. The transition densities for the ground state rotational band are shown in Figure 1. Assuming a stable axially symmetric intrinsic shape, these densities determine the multipoles $\rho_J(r)$, $J = 0, 2, 4, 6, \ldots$, allowing reconstruction of the intrinsic shape

$$\rho(\vec{r}) = \Sigma_J \hat{J} Y_{J0}(\Omega)\rho_J(r) \ .$$

The isodensity contours are shown in Figure 2, demonstrating the precise determination of nuclear shapes in electron scattering. Going beyond this, the collective motions of this nucleus are studied by comparing the transition densities for the three lowest 2^+ states (ground state, β, and γ bands); see Figure 3. The 816 keV and 996 keV state transition densities peak farther out and closer in, respectively, than does the transition density for the lowest 2^+, in agreement with expectations for β- and γ-vibrations, respectively. Further, the amplitudes for exciting the three 2^+ states were found to be linearly independent, while a simple interpretation of the interacting boson model (with s- and d-bosons only) would lead to an expectation of linear dependence.

The high energy capability now available is also important for nuclear structure studies. For example longitudinal form factors can now be measured to large momentum transfer. This is a necessary complement to the transverse form factors available from low energy, back-angle scattering for developing quantitative spectroscopic models (the University of Massachusetts group is heavily involved in these studies). Also, measurements in the few body system can now be pushed to large momentum transfer; for example, the ^{3}H form factors will be measured out to $q \sim 5$ fm^{-1} during 1984 (MIT, Virginia, Saskatchewan, Worcester Polytechnic Institute, N.B.S.). These data, together with ^{3}He data, are considered crucial for reaching a better understanding of meson exchange currents.

2. Single Particle Response and Intermediate Energy Reaction Mechanisms

The nuclear single particle response is measured directly in inclusive, deep inelastic electron scattering. The longitudinal and transverse response functions for ^{40}Ca (Figure 4) were recently measured in the quasielastic region (MIT, Louisiana State University, Virginia, Mount Holyoke). The physics is thought to be quite different in each of the response functions. The longitudinal response function should be fairly insensitive to mesonic effects in this kinematical range but shows a substantial spreading of strength compared to that expected on the basis of simple mean-field ideas. The transverse response function is clearly very sensitive to mesonic effects and indeed there is a large excess cross section on the high energy loss side of the quasielastic peak (but still below the Δ). These are fundamental issues in nuclear physics. The higher energy now available and the BIGBITE spectrometer now in assembly will allow efficient further investigation over a broader range of targets and kinematics (e.g., over the Δ peak). Clearly, the physics here also points to the need for measuring hadrons in coincidence with the scattered electron; we shall return to this below.

Absorption of intermediate energy photons probes the nuclear spectral function in a very different way, since the reaction is kinematically mismatched. That is, absorption on a single nucleon requires that the nucleon have an extremely high momentum in the nuclear ground state (e.g. p ~ 600 MeV/c for 200 MeV

photons). The $^{16}O(\gamma,p_o)^{15}N$ angular distribution taken with OHIPS, is shown in Figure II.C.3 (MIT, South Carolina, Glasgow). These data follow earlier measurements of excitation functions taken on ELSSY. As is well known, the interpretation of the intermediate energy $^{16}O(\gamma,p_o)^{15}N$ is not yet clear, with a variety of mechanisms (including single proton absorption and intermediate Δ excitation) under consideration. The theoretical disarray is indicated in Figure 5. These studies address the issue of short range hadronic interactions in the nucleus and will be pursued further. For example, the isospin structure of the reaction will be probed through high resolution (γ,n_o) work using the Beam Line C high flux photon facility and BIGBITE.

3. Pion-nucleus Physics and Δ-Propagation

The interplay of nuclear and nucleon degrees of freedom presents one of the basic issues in nuclear physics. The electromagnetic probe is very important in the drive for a quantitative understanding of the associated phenomena. This has been alluded to above in the studies of meson exchange currents and of the nuclear response in the Δ-region. Photopion studies, both $(\gamma,\pi^{\pm})$ with MEPS (RPI, MIT) Fig. II.B.3,4 and (γ,π°), Fig. II.E.2, are now an important part of the Bates research program. These reactions are complementary to pion induced reactions in that the photon is weakly absorbed and couples to the nucleon quite differently (e.g., transverse $\gamma N\Delta$ coupling versus longitudinal $\pi N\Delta$ coupling).

At low energies the program aims to extract clearly the pion wavefunction in the nucleus; this addresses the poorly understood nature of the pion nucleus optical potential below resonance. In the Δ-region, the strong damping of Δ propagation in nuclei is seen in the comparison of the $^4He(\gamma,\pi^0)^4He$ data, Fig. II.E.2 (Boston University, MIT) with Δ-hole calculations. Elastic Compton scattering is now being pursued by this group; the (γ,γ) reaction is sensitive to spin-dependence in the Δ-nucleus interaction.

4. Parity Violation

The asymmetry in elastic scattering of polarized electrons from ^{12}C will be measured at Bates (Yale, MIT, Syracuse, C.U.N.Y., Harvard) when the polarized electron source is operational. The asymmetry expected in the standard model is $\sim 2\times10^{-6}$ for the relevant kinematics. This experiment is unique in probing coherent scattering from the nuclear constituents (i.e., quarks). Consequently, a very different combination of coupling constants is probed when compared with deep inelastic scattering experiments (basically $(g_{AV}^{eu} + g_{AV}^{ed})$ in the elastic scattering versus $(2/3\ g_{AV}^{eu} - 1/3\ g_{AV}^{ed})$ in deep-inelastic scattering). Also, q^2-independence of the asymmetry on a spin-zero target provides a test of the quark structure of the electroweak current.

5. Coincidence Measurements

Despite the ~ 1% duty factor now available at Bates, there is a growing program of coincidence measurements taking advantage of

the new South Hall capabilities. For example, see Table II.C.3. While this duty factor is comparable to that at Saclay and at NIKHEF, the considerably larger solid angle spectrometers at Bates (an order of magnitude larger in the product) extend the kinematic range over which these studies are possible. (NIKHEF presently has the advantage of very high resolution in missing mass at the expense of solid angle).

An experiment was performed in the South Hall to measure the tensor polarization of recoil deuterons in elastic electron scattering (MIT, Argonne, WPI, Los Alamos, Illinois, Indiana, TRIUMF). This measurement allows one to separate the monopole and quadrupole charge distributions of the deuteron for the first time. The scattered electrons were detected in OHIPS, while the recoil deuterons were selected with a primitive version of BIGBITE and focussed onto a polarimeter. BIGBITE operated with an acceptance and dispersion of 15 msr and 1.7 cm/%, while OHIPS operated with 20 msr and 4.5 cm/%. The data, for $q = 1.74$ fm^{-1} and 2.03 fm^{-1}, are shown in Figure 6, together with the predictions of various potential models. Clearly, it is important to extend these data to large momentum transfer to distinguish between "realistic" models and to confirm the presence of relativistic and meson exchange current effects.

As discussed above, the nuclear response function is not understood at large energy transfer. A program (MIT, UNH, RPI) has recently been initiated at Bates to clarify the nature of the

(e,e') inclusive process via the more specific information contained in the (e,e'p) component. A first measurement was completed in December 1983, focussing on the "dip" region between the quasielastic and Δ peaks. Preliminary analysis of these data (Figure 7) for $q = 400$ MeV/c and energy transfer $\omega = 200$ MeV indicates a prominent, broad structure peaking at about 50 MeV missing energy with significant strength extending to the lowest measured proton energy of 60 MeV. The distribution of strength appears inconsistent with one-body knockout. Further studies will examine the kinematical behavior of this structure and the transverse/longitudinal character.

The experiments referred to above capture the flavor and breadth of the current research program at Bates; the full active program as of the last PAC meeting (Nov. 1983) is attached. There will be increasing pressure from the physics to expand future capabilities for coincidence measurements. The completion of the energy extension to 1 GeV is eagerly awaited. Clearly, high duty factor would be the most crucial next development at Bates for studying new physics.

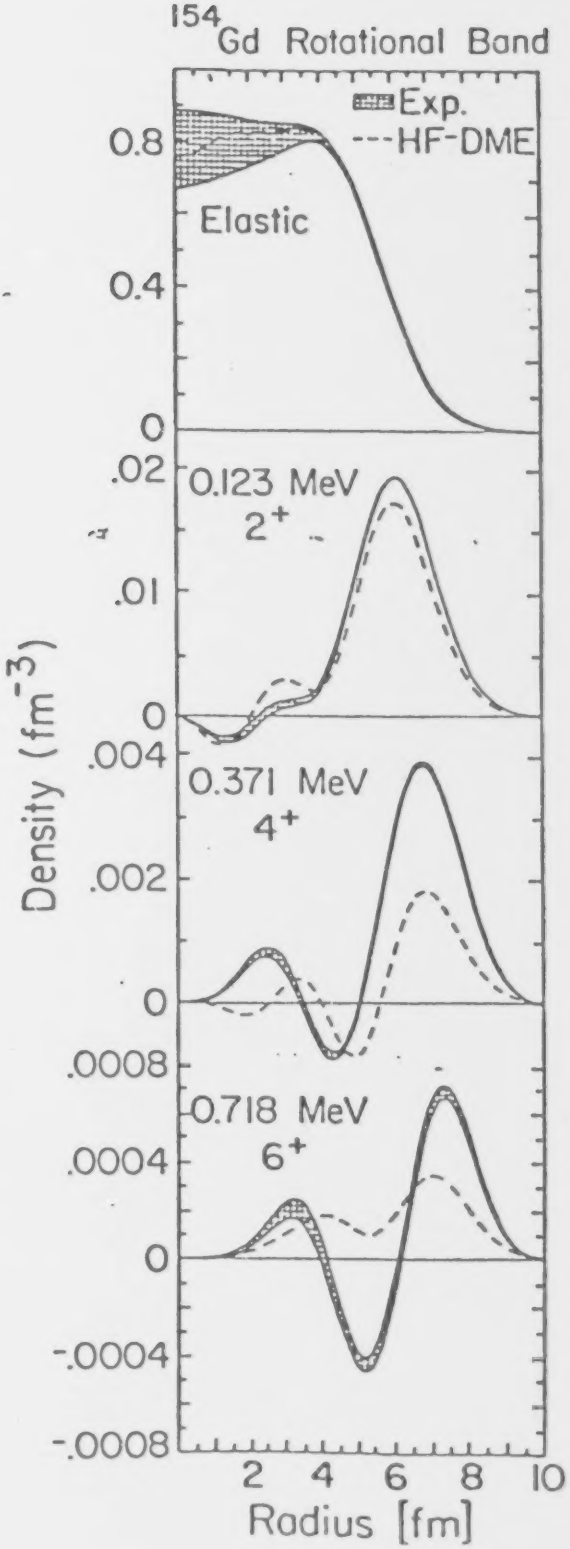
154Gd Rotational Band
Exp.
---HF-DME
Elastic
0.123 MeV
2+
0.371 MeV
4+
0.718 MeV
6+
Density (fm-3)
Radius [fm]

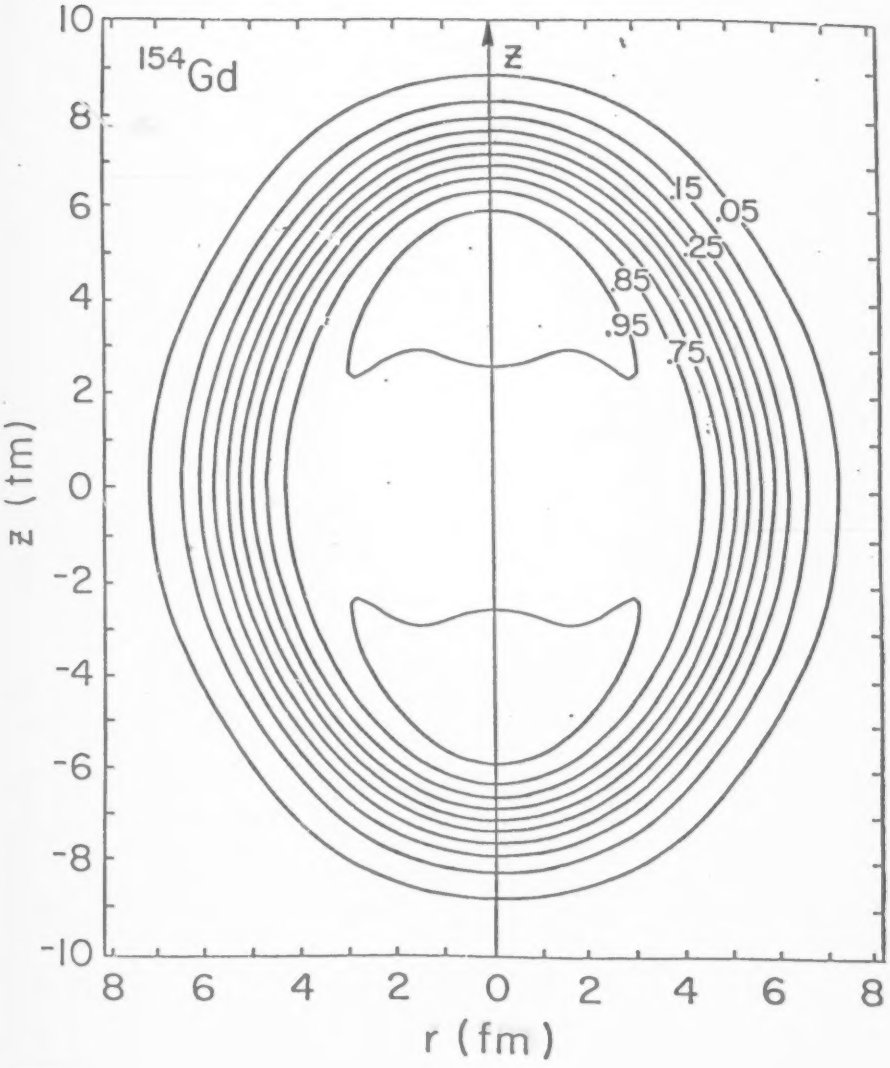

Fig. 2

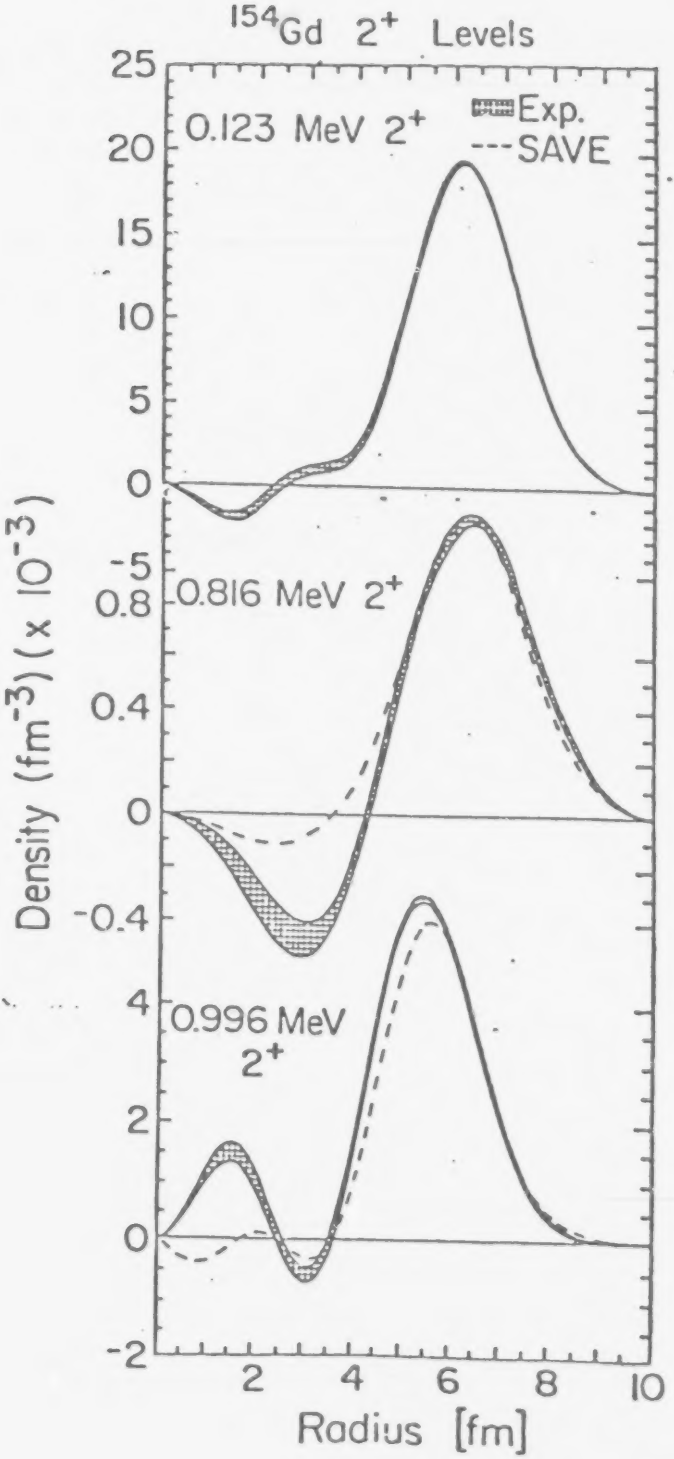
154Gd 2+ Levels
0.123 MeV 2+
Exp.
---SAVE
0.816 MeV 2+
0.996 MeV
2+
Density (fm-3) (x 10-3)
Radius [fm]

^{40}Ca

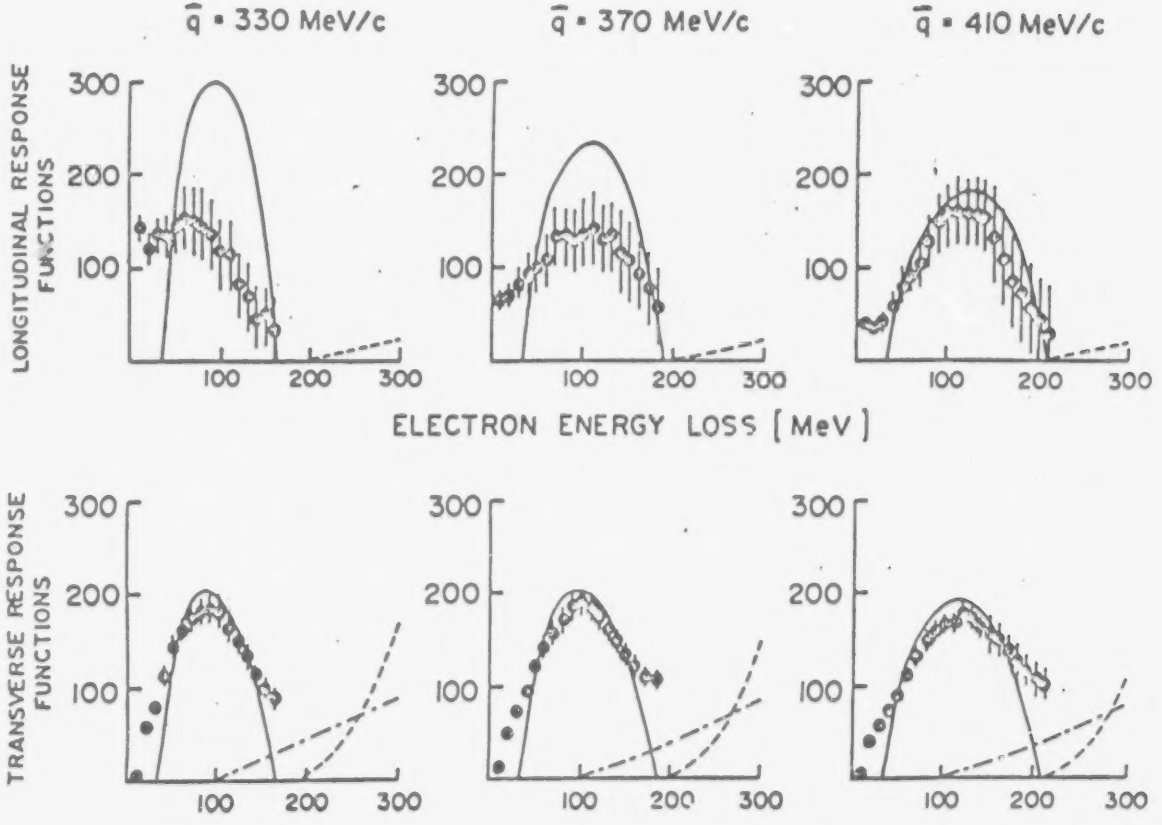
$\bar{q}$ = 330 MeV/c
$\bar{q}$ = 370 MeV/c
$\bar{q}$ = 410 MeV/c
LONGITUDINAL RESPONSE FUNCTIONS
TRANSVERSE RESPONSE FUNCTIONS
300
200
100
100
200
300
ELECTRON ENERGY LOSS [MeV]

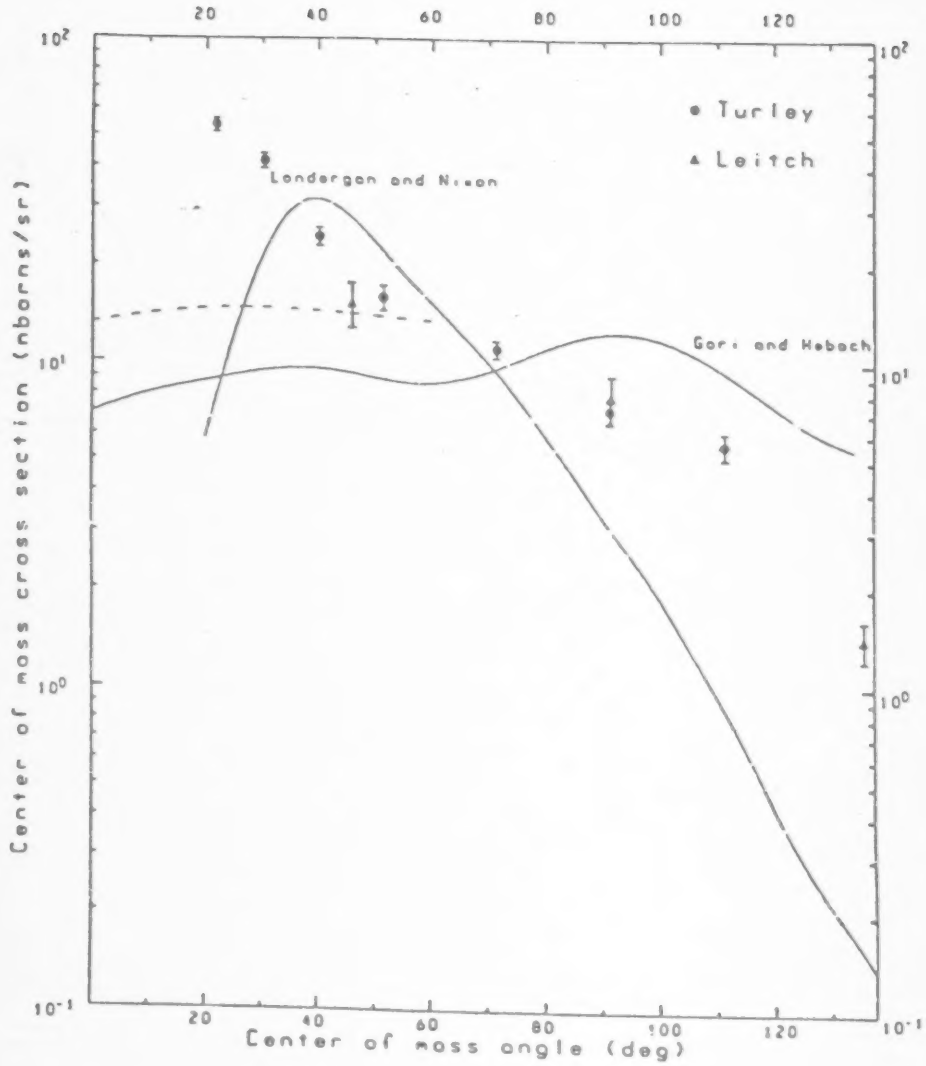
20
40
60
80
100
120
10^2
10^1
10^0
10^{-1}
• Turley
▲ Leitch
Londergan and Nixon
Gari and Hebach
Center of mass cross section (nbarns/sr)
Center of mass angle (deg)

Fig. 5

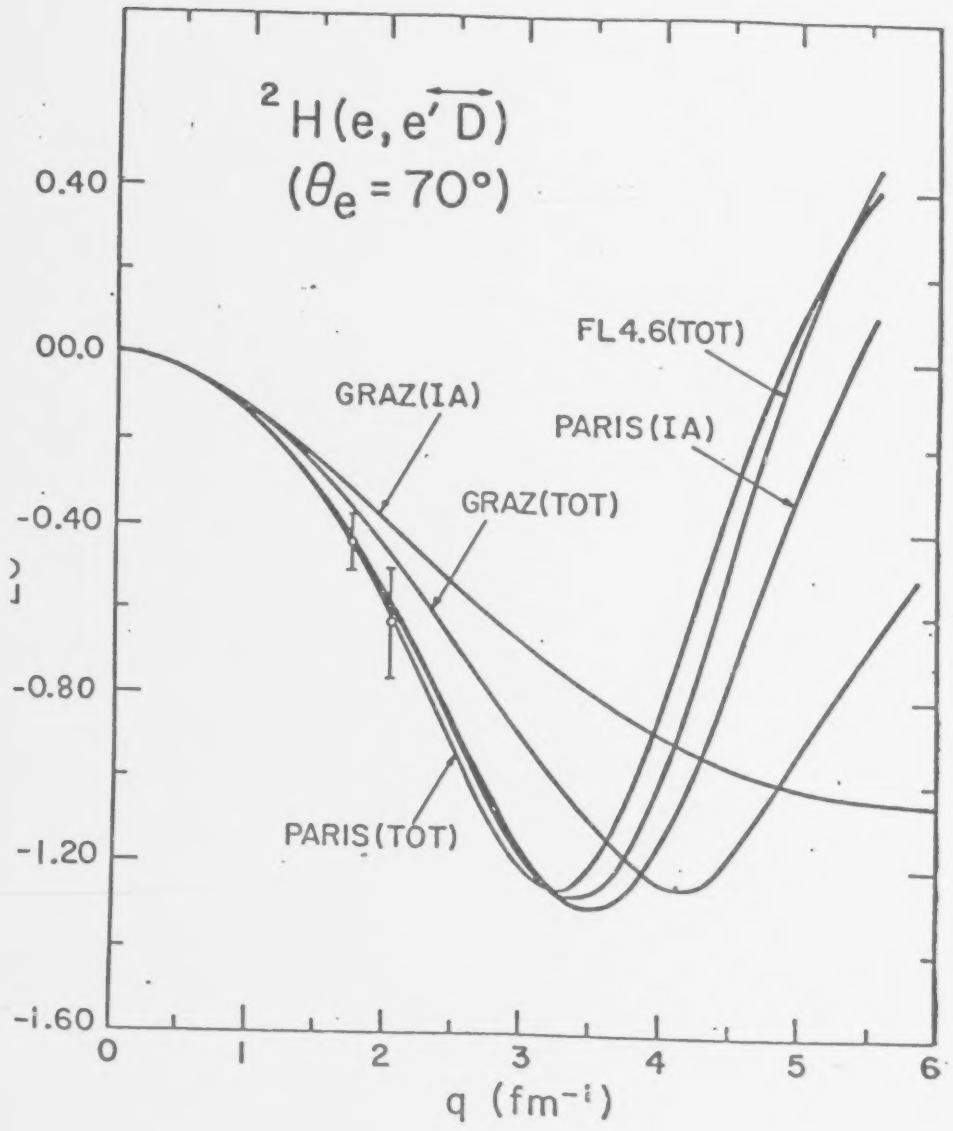
$^2H(e,e'\overleftrightarrow{D})$
$(\theta_e = 70°)$
0.40
00.0
-0.40
-0.80
-1.20
-i.60
FL4.6(TOT)
GRAZ(IA)
PARIS(IA)
GRAZ(TOT)
PARIS(TOT)
0
1
2
3
4
5
6
q (fm^{-i})

Fig. 6

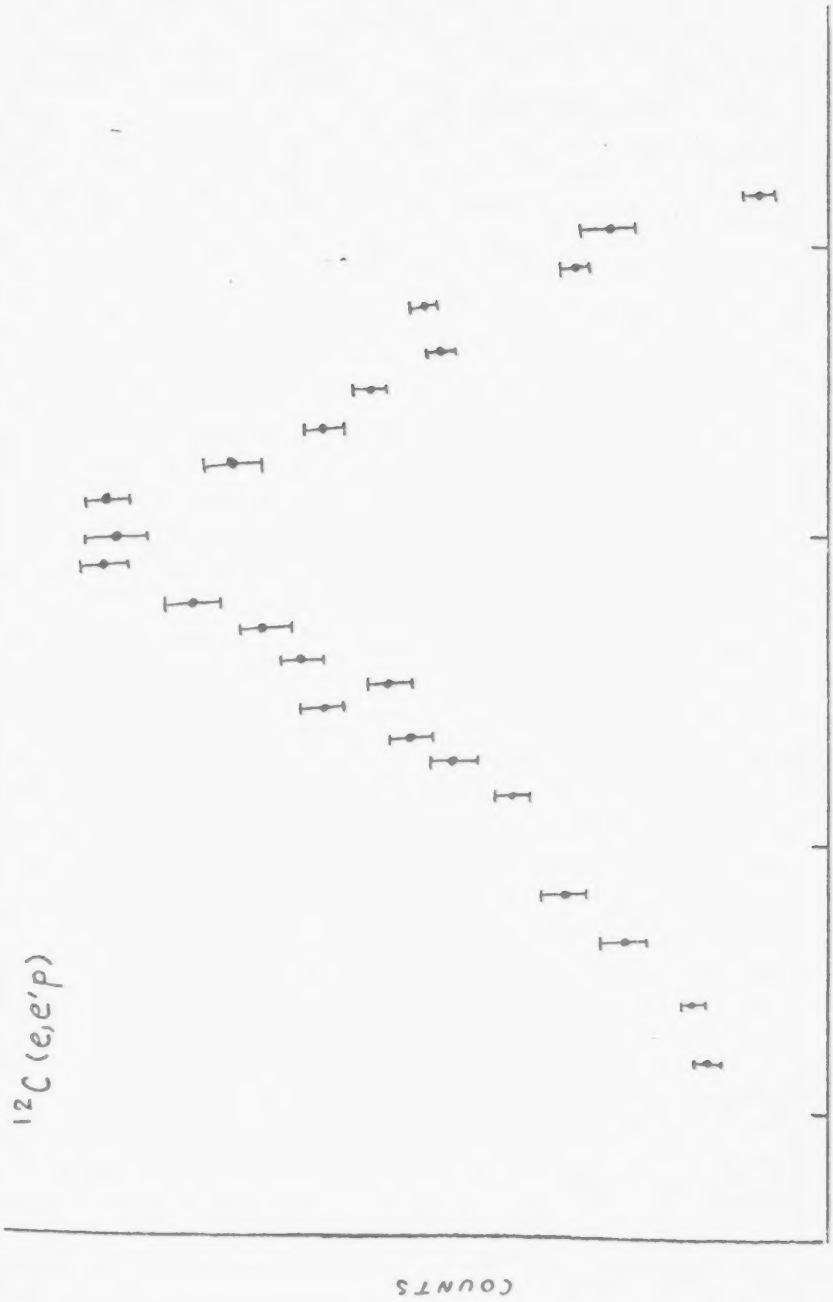

Fig 7

BATES LINEAR ACCELERATOR CENTER
PROGRAM ADVISORY COMMITTEE MEETING
NOVEMBER 1983

ACTIVE PROGRAM

SUMMARY OF PHYSICS PRIORITIES

I. NUCLEAR STRUCTURE

#	Title	Spokesman	Hours Available Oct. 31, 1983	Recommended New Allocation (hours)	Recommended Total Allocation (hours)
83-10	^{205}Tl(ee')180°	Papanicolas	200.0		200.0
*82-11	^{13}C(ee')M1	Hicks	56.5		56.5
*82-13	^{92}Mo(ee')	Milliman	6.3	198	204.3
*83-05	^{4}He(ee')180°	Peterson	11.0		11.0
*82-02	^{7}Li(ee')Trans.	Lichtenstadt, Peterson	129.2		129.2
83-07	^{7}Li(ee')Long.	Lichtenstadt, Peterson	29.5		29.5
83-02	^{208}Pb(ee')	Heisenberg	1.6	100	101.6
83-23	^{17}O(ee')Mag.	Bertozzi	-	175	175.0
81-04	^{140}Ce(ee')	Heisenberg, Papanicolas	0	24	24.0
83-03	^{10}B(ee')M3	Hicks, Singhal	42.0		42.0
83-12	^{86}Sr(ee')	Hersman	142.5		142.5
*83-13	^{12}C(e,e'p)GR [Phase I]	Calarco	50.0		50.0
82-14	^{238}U(e,e'f)	Papanicolas	48.0		48.0
80-01	^{14}N(ee')	Hicks	17.0		17.0
*80-03	^{52}Cr(ee')	Lightbody	24.5		24.5
82-08	^{26}Mg(ee')	Lindgren	0		0
83-04	^{28}Si(ee')M6	Lindgren, Ryan, Singhal	43.5		43.5
			801.6	497	1298.6

(Hours in * Category: 475.5)

In addition Proposal #83-18 was rejected and Proposal #83-24 was placed in the Action Deferred Category.

II. DEEP INELASTIC SCATTERING

#	Title	Spokesman	Hours Available Oct. 31, 1983	Recommended New Allocation (hours)	Recommended Total Allocation (hours)
*82-03	$^{12}C, ^{2}H(e,e'p)$	Bertozzi	256.1	0	256.1
81-08	$X(ee')\Delta$	Blomqvist, O'Connell	32.6		32.6
82-06a	$^{1}H, ^{4}He(ee')$	Bernstein, Quinn	32.6		32.6
80-17a	$^{3,4}He$(High E)	Whitney	124.4		124.4
*80-15a	$^{40,48}Ca, ^{238}U$ (low q)	Zimmerman	100.0	50	150.0
80-15b	^{40}Ca(high q)	Zimmerman	0	100	100.0
83-09	$^{238}U(e,e'f)$	O'Connell, Blomqvist	50.0		50.0
82-06b	Long.p.Resp.Fn.	Bernstein, Quinn	100.0		100.0
*80-19	$^{56}Fe(ee')180°$	Peterson, Singhal	20.0		20.0
83-17	(e,e'p)QF	Geesaman, Segel	-	100	100.0
			715.7	250	965.7

(Hours in * Category: 426.1)

In addition Proposal #83-26 was placed in the Action Deferred Catgegory.

III. PHOTOPRODUCTION

#	Title	Spokesman	Hours Available Oct. 31, 1983	Recommended New Allocation (hours)	Recommended Total Allocation (hours)
83-01	$d(\gamma,n)p$ [Phase I]	Firk, Matthews	100.0		100.0
*83-08	Tagged γ Tests	Miller	12.3		12.3
83-19	$^4He(\gamma\pi^0)$	Dodson, Miller, Tieger	-	200	200.0
83-06	$^4He(\gamma\gamma)^4He@\Delta$	Miller	0	150	150.0
*80-22	$^6Li,^{10}B(\gamma\pi^+)$	Bernstein, Blomqvist	137.4		137.4
80-20	$^{14}N(\gamma\pi^+)$	Stoler	70.7		70.7
83-20	$^{14}N(\gamma\pi^+)@\Delta$	Stoler	-	150	150.0
83-11	$^3He(\gamma\pi^+)^3H$	Dytman, Bernstein	135.0		135.0
82-10	$^{16}O(\gamma n_0)^{15}O$ [Phase I]	Redwine	41.0		41.0
83-15	$D(\gamma,pp)\pi^-$ [Phase I]	Stoler	100.0		100.0
*77-12	$d(\gamma p)n$	Matthews	27.9	85	112.9
*81-01	$^{16}O(\gamma p_0)$	Adams, Matthews	31.7	0	31.7
			656.0	585	1241.0
				(Hours in * Category:	294.3)

In addition Proposals #83-21, 83-22, 83-25 and 83-28 were placed in the Action Deferred Category.

IV. SPECIAL

#	Title	Spokesman	Hours Available Oct. 31, 1983	Recommended New Allocation (hours)	Recommended Total Allocation (hours)
*77-14	Parity	Kowalski, Souder	373.6		373.6
*82-17	^{3}H(ee')elastic	Turchinetz, Whitney	394.2	425	819.2
80-17b	^{3}H(ee')inelastic	Whitney		0	0
*79-20	Tensor Polar.	Holt, Turchinetz	26.2		26.2
*81-06	D(e,e'n) [Phase I]	Bertozzi, Finn, Kovash	33.8		33.8
*78-18	Brem. Spectrum	Matthews	50.3	50	100.3
			878.1	475	1353.1
				(Hours in * Category:	1353.1)

In addition Proposal #83-27 was placed in the Action Deferred Category.

U.S. DEPARTMENT OF ENERGY

FIELD TASK PROPOSAL/AGREEMENT

WP B.N NUMBER	2. TASK NO.	3. REV. NO.	4. PROJECT NO.	5. DATE PREPARED	6. CONTRACTOR NUMBER
E-AC02-76-ERO-3069	--	--	--	April 10, 1983	CH-3069-002(ME)-BATES

TASK TITLE	8. WORK PACKAGE TITLE
MEDIUM ENERGY RESEARCH OPERATIONS	Same as Item 7.

BUDGET AND REPORTING CODE	10. TASK TERM	11. CONTRACTOR NAME	12. CODE
KB 0101	Open	M.I.T./ Laboratory for Nuclear Science, Cambridge, MA 02139	--

CONTRACTOR TASK MANAGER (Name, FTS no.)	14. PRINCIPAL INVESTIGATORS
Supervisors LNS Directorate, Bates Directorate + PI's	W. C. Barber, A. Bernstein, W. Bertozzi, P. Demos, S. Kowalski, J. Matthews, R. Redwine, C. P. Sargent, W. Turchinetz, C. Williamson, W. Donnelly

WORK LOCATION (SEE INSTRUCTIONS): NAME OF FACILITY, CITY, STATE, ZIP CODE	16. Does this task include any management services effort
M.I.T. CAMBRIDGE, MASSACHUSETTS 02139 M.I.T./BATES LINEAR ACCELERATOR, MIDDLETON, MASSACHUSETTS 01949-2846 ALSO OTHER ACCELERATOR FACILITIES AS DESCRIBED HEREIN	☐YES ☐NO

TASK DESCRIPTION (Approach, relation to work package, in 200 words or less)

This category covers the research program in medium-energy nuclear structure physics at the M.I.T. Laboratory for Nuclear Science. The research at Bates is carried out in part by individuals of the M.I.T. group as independent programs and some is carried out in collaboration with scientists, faculty and research staff at other institutions. Some of the research at Bates is also being carried out by user groups from other institutions with only little or no direct participation by M.I.T. research staff, but using Bates facilities, and supported with appropriate on-site services by Bates personnel. Some medium-energy research is being carried out by the M.I.T. groups at other accelerator facilities.

CONTRACTOR TASK MANAGER

(SIGNATURE) (DATE)

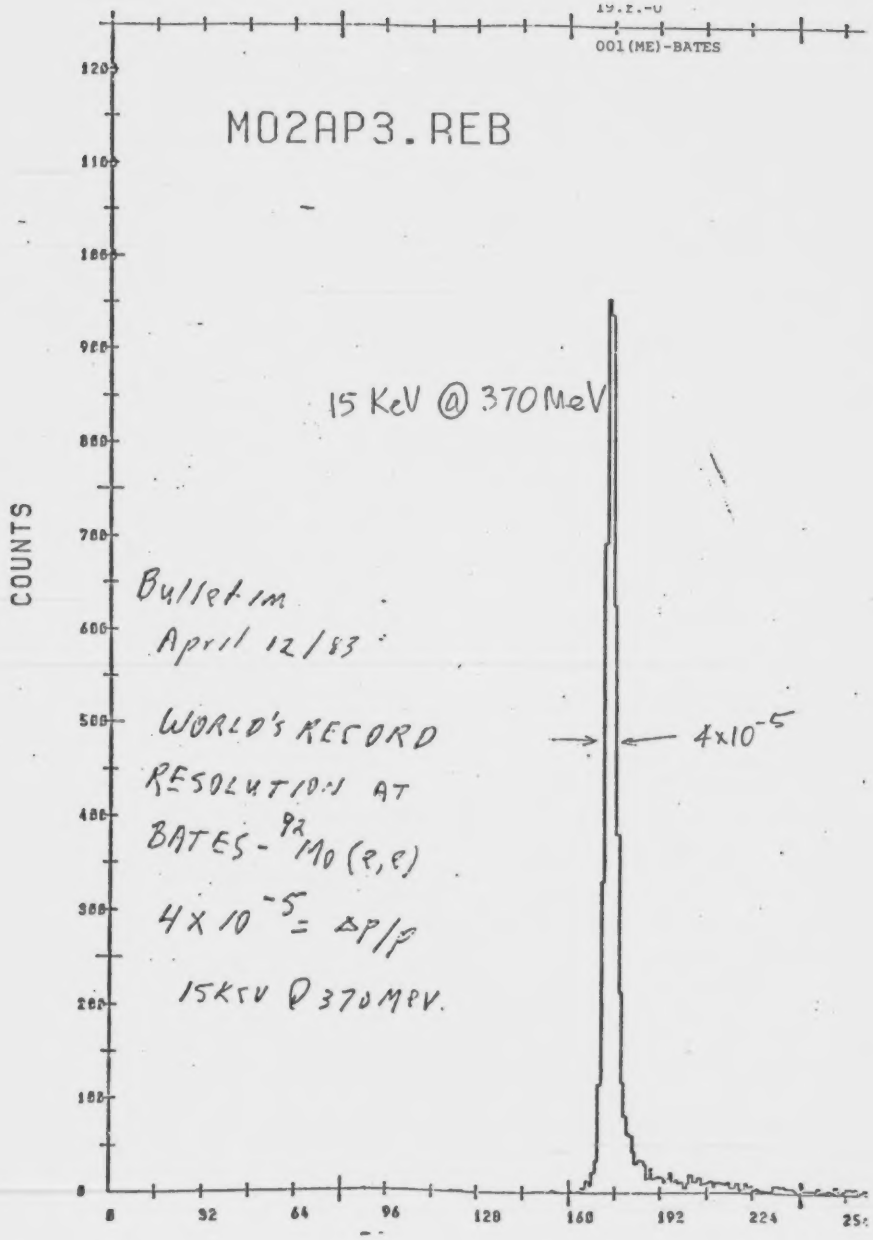
001(ME)-BATES
M02AP3.REB
COUNTS
15 KeV @ 370 MeV
Bulletin
April 12/83:
WORLD'S RECORD
RESOLUTION AT
BATES - ^{92}Mo (p,p)
$4 \times 10^{-5} = \Delta p/p$
15KeV @ 370MeV.
4×10^{-5}
0
32
64
96
128
160
192
224

TABLE 19.b.-I

PRESENT ACTIVE USERS OF THE BATES FACILITY

PRESENT ACTIVE USERS OF THE BATES FACILITY

AMERICAN UNIVERSITY
ARGONNE NATIONAL LABORATORY
BOSTON COLLEGE
BOSTON UNIVERSITY
CALIFORNIA LOS ANGELES, UNIVERSITY OF
CATHOLIC UNIVERSITY
FREE UNIVERSITY OF AMSTERDAM
GLASGOW (SCOTLAND), UNIVERSITY OF
HARVARD UNIVERSITY
ILLINOIS, UNIVERSITY OF
INDIANA UNIVERSITY
LOS ALAMOS NATIONAL LABORATORY
LOUISIANA STATE UNIVERSITY
LOWELL (MASSACHUSETTS), UNIVERSITY OF
LUND (SWEDEN), UNIVERSITY OF
MAINZ (GERMANY), UNIVERSITY OF
MARYLAND, UNIVERSITY OF
MASSACHUSETTS (AMHERST), UNIVERSITY OF
MICHIGAN STATE UNIVERSITY
MOUNT HOLYOKE COLLEGE
NATIONAL BUREAU OF STANDARDS
NEW HAMPSHIRE, UNIVERSITY OF
NORTHWESTERN UNIVERSITY
PITTSBURGH, UNIVERSITY OF
RENSSELAER POLYTECHNIC INSTITUTE
SACLAY (FRANCE)
SASKATCHEWAN (CANADA), UNIVERSITY OF
SHIZUOKA UNIVERSITY (JAPAN)
SOUTH CAROLINA, UNIVERSITY OF
STANFORD UNIVERSITY
TEL AVIV (ISRAEL), UNIVERSITY OF
TOHOKU (JAPAN), UNIVERSITY OF
VANDERBILT UNIVERSITY
VIRGINIA, UNIVERSITY OF
WORCESTER POLYTECHNIC INSTITUTE
YALE UNIVERSITY

TABLE 19.b.-II

PUBLICATIONS

I. ARTICLES & LETTERS

"Isospin Effects in Pion Single-Charge-Exchange Reactions" - D. Ashery, D. F. Geesaman, R. J. Holt, H. E. Jackson, J. R. Specht, K. E. Stephenson, ANL; R. E. Segel, P. Zupranski, NWU; H. W. Baer, J. D. Bowman, M. D. Cooper, LANL; M. Leitch, TRIUMF; A. Arel, R. Chefety, Tel Aviv U; J. Comuzzi, R. P. Redwine, MIT; D. R. Tieger, BU. Phys. Rev. Lett. 50, 482 (1983).

"Determination of Relative Signs of Neutron and Proton Transition Matrix Elements: Strong Cahcellation Observed for the $^{34}S(0^+ \rightarrow 2_2^+)$ Transition" - A. M. Bernstein, R. A. Miskimen, B. Quinn, S. A. Wood, MIT; M. V. Hynes, LANL; G. S. Blanpied, B. G. Ritchie, U. South Carolina; V. R. Brown, LLNL. Phys. Rev. Lett. 49, No. 7 (1982).

"Electron Scattering from Complex Nuclei" - W. Bertozzi, MIT. Nucl. Phys. A374, 109C (1982).

"Pion-Nucleus Inelastic Scattering at 80 MeV" - M. Blecher, K. Gotow, R. Ng, VPI&SU; R. L. Burman, R. Carlini, S. Dam, M. V. Hynes, V. Sandberg, LANL; M. J. Leitch, TRIUMF; R. Auble, F. E. Bertrand, E. E. Gross, F. E. Obenshain, S. Wu, ORNL; G. S. Blanpied, B. M. Preedom, B. G. Ritchie, U. South Carolina; W. Bertozzi, M. A. Kovash, R. P. Redwine, MIT. Phys. Rev. C25, 2554 (1982).

"Isovector E2 Matrix Elements from Electromagnetic Transitions in the s-d Shell: Experiment and Shell-Model Calculations" - B. A. Brown, S. E. Massen, Oxford U; M. Bernas, Orsay; A. M. Bernstein, R. Miskimen, MIT; V. R. Brown, V. A. Madsen, LLNL; B. H. Wildenthal, Mich. St. U. Phys. Rev. C26, 2247 (1982).

"Elastic Scattering of π^+ and π^- from ^{40}Ca at 64.8 MeV" - S. H. Dam, R. L. Burman, R. Carlini, M. Hamm, M. A. Yates, LANL; R. D. Edge, B. M. Preedom, U. South Carolina; R. P. Redwine, MIT; M. Blecher, K. Gotow, VPI&SU; F. E. Bertrand, E. E. Gross, ORNL. Phys. Rev. C25, 2574 (1982).

"Threshold Region Photoproduction of Neutral π Mesons off Complex Nuclei" - G. W. Dodson, E. C. Booth, F. L. Milder, B. E. Parad, B. L. Roberts, D. R. Tieger, BU; J. Comuzzi, MIT. Phys. Rev. C26, No. 6 (1982).

"^{3}He Magnetic Form Factor" - P. C. Dunn, S. B. Kowalski, F. N. Rad, C. P. Sargent, W. E. Turchinetz, MIT; R. Goloskie, D. P. Saylor, WPI. Phys. Rev. C27, No. 1 (1983).

"Spectroscopy of ^{16}F from the $^{16}O(p,n)^{16}F$ Reaction at 99 and 135 MeV" - A. Fazely, B. D. Anderson, M. Ahmad, A. R. Baldwin, A. M. Kalenda, R. J. McCarthy, J. W. Watson, R. Madey, Kent State; W. Bertozzi, T. N. Buti, J. M. Finn, M. A. Kovash, B. Pugh, MIT; C. C. Foster, IUCF. Phys. Rev. C25, 1760 (1982).

"Elastic Magnetic Scattering of Electrons from ^{13}C" - R. S. Hicks, J. Dubach, R. A. Lindgren, B. Parker, G. A. Peterson, UMass. Phys. Rev. C26, 339-347 (1982).

"Inelastic Electron Scattering from ^{208}Pb at 180°" - R. S. Hicks, R. L. Huffman, R. A. Lindgren, B. Parker, G. A. Peterson, UMass; S. Raman, ORNL; C. P. Sargent, MIT. Phys. Rev. C26, 920-930 (1982).

"Quasi-free (e,e'p) Reaction on ^{3}He" - E. Jans, NIKHEF; P. Barreau, M. Bernheim, J. Morgenstern, J. Mougey, D. Tarnowski, S. Turck-Chieze, CEN Saclay; J. M. Finn, MIT; S. Frullani, F. Garibaldi, ROMA; G. P. Capitani, E. de Sanctis, Frascati; M. K. Brussel, U.Ill; I. Sick, Basel. Phys. Rev. Lett. 49, 974 (1982).

"Pion-Nucleus Forward Scattering Amplitudes from Total Cross Section Measurements" - R. H. Jeppesen, M. J. Jakobson, UMontana; M. D. Cooper, D. C. Hagerman, M. B. Johnson, LANL; R. P. Redwine, MIT; G. R. Burleson, K. F. Johnson, New Mexico St.U; I. Halpern, R. E. Marrs, Wash.U; H. O. Meyer, Ind.U; L. D. Knutson, UWisc. Phys. Rev. C27, 697 (1983).

"π^{+} Photoproduction from ^{13}C" - J. LeRose, K. Min, D. Rowley, B. O. Sapp, P. Stoler, P. K. Teng, E. J. Winhold, P. F. Yergin, RPI; A. M. Bernstein, K. I. Blomqvist, S. A. Dytman, G. Franklin, M. Pauli, MIT; H. S. Caplan, USask; K. Shoda, M. Yamazaki, Tohoku U. Phys. Rev. C26, 2554 (1982).

"Anomalously Low Cross Section in $^{13}C(\gamma,\pi^{-})^{13}N_{g.s.}$" - J. LeRose, K. Min, D. Rowley, B. O. Sapp, P. Stoler, E. J. Winhold, P. F. Yergin, RPI; A. M. Bernstein, K. I. Blomqvist, S. Dytman, G. Franklin, M. Pauli, MIT. Phys. Rev. C25, No. 3 (1982).

"Analyzing Power for the $^{16}O(\vec{p},n)^{16}F(4^{-},6.37\ MeV)$ Reaction at 134 MeV" - R. Madey, B. D. Anderson, A. R. Baldwin, A. Fazely, A. M. Kalenda, R. J. McCarthy, P. C. Tandy, J. W. Watson, Kent St; W. Bertozzi, T. Buti, J. M. Finn, M. Kovash, B. Pugh, MIT; C. C. Foster, IUCF. Phys. Rev. C25, 1715 (1982).

"Nuclear Momentum Distributions from (γ,p) and (e,e'p) Reactions" - J. L. Matthews, MIT. In Momemtum Wave Functions-1982, Erich Weigold, ed. (AIP, New York, 1982), p. 57.

"Charged Pion Photoproduction from ^{10}B" - D. Rowley, J. LeRose, K. Min, B. O. Sapp, P. Stoler, E. J. Winhold, P. F. Yergin, RPI; A. M. Bernstein, K. I. Blomqvist, S. A. Dytman, G. Franklin, M. Pauli, MIT; H. S. Caplan, USask. Phys. Rev. C25, 2652 (1982).

"Pion Angular Distribution in $^{13}C(\gamma,\pi^{+})^{13}B_{g.s.}$" - K. Shoda, M. Torikoshi, H. Tsubota, M. Yamazaki, Tohoku U; K. Min, J. Winhold, RPI; A. M. Bernstein, MIT. Phys. Rev. C27, No. 1 (1983).

"Reaction $^{9}Be(\gamma,\pi^{+})^{9}Li(g.s.)$ at $\theta_{\pi}=90°$" - P. K. Teng, A. Chaudhury, J. LeRose, K. Min, D. Rowley, B. O. Sapp, P. Stoler, E. J. Winhold, P. F. Yergin, RPI; A. M. Bernstein, K. I. Blomqvist, G. Franklin, N. Paras, M. Pauli, B. Schoch, MIT. Phys. Rev. C26, No. 3 (1982).

"Proton Capture to Bound and Unbound States of ^{12}C" - H. R. Weller, B. Hasan, S. Manglos, G. Mitev, N. R. Roberson, Duke; S. L. Blatt, H. J. Hausman, R. G. Seyler, R. N. Boyd, T. R. Donoghue, Ohio St. U; M. A. Kovash, MIT; A. D. Bacher, C. C. Foster, Ind. U. Phys. Rev. C25, 2921 (1982).

ARTICLES & LETTERS - LATE ADDITIONS

"Two-Body Photodisintegration of ^{3}He between 150 and 350 MeV" - W. J. Briscoe, D. H. Fitzgerald, B. M. K, Nefkens, UCLA; H. Crannell, D, I. Sober, Cath. U; R. Goloskie, WPI; W. W. Sapp, MIT. Phys. Rev. Lett. 49, 187 (1982).

"The Low Lying Levels of ^{7}Li Studied by Electron Scattering" - J. Lichtenstadt, J. Alster, M. A. Moinester, Tel-Aviv U; J. Dubach, R. S. Hicks, G. A. Peterson, UMass; S. Kowalski, MIT. Phys. Lett. 121B, 377 (1983).

"Inelastic Electron Scattering from ^{18}O" - B. E. Norum, W. Bertozzi, M. V. Hynes, J. Kelly, S. Kowalski, H. Miska, F. N. Rad, C. P. Sargent, T. Sasanuma, W. Turchinetz, MIT; B. L. Berman, LLNL. Phys. Rev. C25, 1778 (1982).

II. CONFERENCE PROCEEDINGS - INVITED PAPERS

"Determination of the Relative Signs of Neutron and Proton Transition Matrix Elements" - A. M. Bernstein, MIT. Division of Nuclear Physics, APS, Amherst, Mass. (Oct. 1982).

"Electromagnetic Production of Hypernuclear States" - A. M. Bernstein, MIT. International Conference on Hypernuclear and Kaon Physics, Heidelberg, Germany (June 1982); Proceedings of the International Conference on Hypernuclear and Kaon Physics, B. Povh, editor, Max-Planck Institut für Kernphysik Report, MPI H-1982-V20.

"Measurements of the Relative Signs of Neutron and Proton Transition Matrix Elements" - A. M. Bernstein, MIT. Division of Nuclear Physics, APS, Amherst, Mass. (Oct. 1982).

"Electron Scattering from Complex Nuclei" - W. Bertozzi, MIT. Proceedings of the International Conference on High Energy Nuclear Physics, Versailles, France (July 1981).

"Experimental Perspectives of the Conference" - W. Bertozzi, MIT. International Conference on Spin Excitations in Nuclei, Telluride (March 1982).

"Synthesis of Hadronic and Electromagnetic Studies of Nuclei and Effective Interactions" - W. Bertozzi, MIT. Gordon Conference on Nuclear Structure (June 1982).

"The Independent Pair Wave Function at 150 MeV as Observed in a Synthesis of Electromagnetic and Hadronic Studies of Nuclear Structure" - W. Bertozzi, MIT. Bates Theory Workshop (Dec. 1982).

"The Common Ground Between Hadronic and Electromagnetic Probes of Nuclei" - W. Bertozzi, J. J. Kelly, MIT. Conference on New Horizons in Electromagnetic Physics at the University of Virginia (May 1982).

"Physics in a Stretcher Ring" - E. C. Booth, BU. International Conference on New Horizons in Electromagnetic Physics, University of Virginia (April 1982).

"Coherent (γ,γ) Reactions in the Resonance Region" - E. C. Booth, J. Miller, BU. International Conference on Electron Rings for Nuclear Physics Research, Lund (Oct. 1982).

"Intermediate-Energy Elastic Neutrino Scattering from Nuclei" - T. W. Donnelly, MIT. Proceedings of the Los Alamos Neutrino Workshop, Los Alamos Report LA-9358-C.

"The Search for M1 Strength" - R. S. Hicks, G. A. Peterson, UMass. Proceedings of the Telluride International Conference on Spin Excitations in Nuclei (March 1982).

"Implications of Density Dependence in the Effective Interaction for the Excitation of Spin Modes" - J. J. Kelly, MIT; J. A. Carr, FSU. International Conference on Spin Excitations in Nuclei, Telluride (March 1982).

"Nuclear Models, Successes and Problems via a Unified Use of Hadronic and Electromagnetic Probes" - W. Bertozzi, MIT. International School on Intermediate Energy Nuclear Physics, Verona, Italy (Jul. 1982).

"The Role of Electromagnetic Interactions in the Future of Nuclear Physics" - W. Bertozzi, MIT. Symposium on the Future of Electromagnetic Physics, Montreal (Jan. 1981).

"Proton Scattering to Collective States: What We Learn About the Effective Interaction in the Nuclear Medium" - J. J. Kelly, MIT. IUCF Workshop (Oct. 1982).

"Comparative Studies with Different Probes" - R. A. Lindgren, UMass. Proceedings of the Telluride International Conference on Spin Excitations in Nuclei (March 1982).

"Undergraduate Curricula" - J. L. Matthews, MIT. Presentation in panel discussion on "The Teaching of Physics" at Meeting of the New England section of the American Association of Physics Teachers (May 1982).

"Photonuclear Experiments at Intermediate Energies" - J. L. Matthews, MIT. Seminar on Electromagnetic Interactions of Nuclei at Low and Medium Energies, Moscow (1981). Proceedings p.202 (1982).

"Measurement of the $^{12}C(\gamma,\pi^0)^{12}C$ Reaction" - R. P. Redwine, MIT. Nuclear Structure Gordon Conference (1982).

"Low Energy Pion-Nucleus Elastic Scattering" - R. P. Redwine, MIT. SIN Workshop on Low Energy Pion Nucleus Physics (Sep. 1982).

"Polarized Electron Source for Parity Experiment at Bates" - P. Souder, Yale. Fifth International Conference on Spin Physics, Brookhaven National Laboratory, (1982).

"Quasi Elastic (e,e') Scattering on Nuclei" - C. F. Williamson, MIT. American Physical Society Meeting, Washington, D.C. (April 1982).

LATE ADDITIONS

"Concluding Remarks" - K. I. Blomqvist, MIT. Workshop on the Use of Electron Rings in Nuclear Physics Research, Lund, Sweden (Oct. 1982).

"The Common Ground Between Hadronic and Electromagnetic Probes of Nuclei" - W. Bertozzi, J. Kelly, MIT. Conference on New Horizons in Electromagnetic Physics, University of Virginia (Apr. 1982).

"Hadronic and Electromagnetic Probing of Nuclei: The Common Ground" - W. Bertozzi, MIT; S. J. Wallace, U. Maryland. Conference on New Horizons in Electromagnetic Physics, University of Virginia (Apr. 1982).

"Experiments Using an Electron Storage Ring - Stretcher" - E. C. Booth, BU. Conference on New Horizons in Electromagnetic Physics, University of Virginia (Apr. 1982).

"Detectors and Spectrometers" - S. B. Kowalski, MIT. Conference on New Horizons in Electromagnetic Physics, University of Virginia (Apr. 1982).

"Physics, Technology and Cost of the New Facilities - A World-Wide Roundup" - W. Turchinetz, MIT. Conference on New Horizons in Electromagnetic Physics, University of Virginia (Apr. 1982).

III. CONTRIBUTED PAPERS

"Virtual Photon Spectra from $H(e,\pi^+)n,e'$" - A. M. Bernstein, K. I. Blomqvist S. A. Dytman, R. A. Miskimen, B. Quinn, MIT; B. O. Sapp, P. F. Yergin, RPI. Bull. Am. Phys. Soc. 27, 719 (1982).

"Deep-Inelastic Electron Scattering from Uranium: First Look" - C. C. Blatchley, J. LeRose, O. E. Pruet, P. Sioshansi, P. D. Zimmerman, LSU; C. F. Williamson, M. W. Deady, MIT. Bull. Am. Phys. Soc. 27, 530 (1982).

"The ^{7}Li 0.478 MeV Transition Form Factor at Low Momentum Transfer" - P. E. Burt, L. W. Fagg, H. Crannell, Cath. U. Bull. Am. Phys. Soc. 27, 529 (1982).

"Measurement of $^{12}C(\gamma,\pi^0)^{12}C$ at E_γ=250 MeV" - J. Comuzzi, W. J. Burger, G. W. Dodson, R. P. Redwine, MIT; R. Becker, Boston Coll; E. C. Booth, J. P. Miller, B. L. Roberts, D. R. Tieger, BU. Bull. Am. Phys. Soc. 27, 468 (1982).

"Total Cross Section Measurements of (γ,π) for ^{10}B, ^{14}N and ^{16}O" - B. Cottman, A. M. Bernstein, K. I. Blomqvist, S. A. Dytman, J. Nelson, MIT. Bull. Am. Phys. Soc. 27, 709 (1982).

"Shell Model Studies of the Low-Lying Nuclear Structure in the Zirconium Region" - J. F. Dawson, J. Heisenberg, UNH. Bull. Am. Phys. Soc. 27, 726 (1982).

"Microscopic Optical Model for Nucleon Elastic Scattering on ^{208}Pb" - F. S. Dietrich, LLNL; R. W. Finlay, R. G. Kurup, S. Mellema, G. Randers-Pehrson, Ohio U; F. Petrovich, J. A. Carr, FSU; W. G. Love, U. Ga; J. J. Kelly, MIT. Bull. Am. Phys. Soc. 27, 722 (1982).

"A High Speed Drift Chamber Readout System: TIRUS" - J. H. J. Distelbrink, B. H. Cottman, MIT. Wire Chamber Conference, Vienna, Austria (Feb. 1983).

"A Test of the Interacting Boson Approximation Using Electron Scattering" - F. W. Hersman, UNH; W. Bertozzi, T. N. Buti, J. M. Finn, C. Hyde, J. Kelly, M. A. Kovash, S. Kowalski, R. Lourie, B. Murdock, B. Pugh, C. P. Sargent, W. Turchinetz, MIT; M. V. Hynes, LANL; J. Lichtenstadt, Tel Aviv U; F. N. Rad, Fermilab; J. B. Bellicard, CEN-Saclay. Bull. Am. Phys. Soc. 27, 726 (1982).

"Elastic and M1 Scattering of Electrons from $5<A<28$ Nuclei" - R. S. Hicks, UMass. Bull. Am. Phys. Soc. 27, 694 (1982).

"Transverse Quasi-elastic Electron Scattering from ^{56}Fe at 180°" - A. Hotta, Shizuoka; R. P. Singhal, U. Glasgow; R. S. Hicks, B. Parker, G. A. Peterson, M. A. Plum, UMass. Bull. Am. Phys. Soc. 27, 718 (1982).

"180° Electron Scattering from ^{14}N" - R. L. Huffman, J. Dubach, R. S. Hicks, R. A. Lindgren, B. Parker, G. A. Peterson, M. A. Plum, UMass; R. P. Singhal, U. Glasgow. Bull. Am. Phys. Soc. 27, 530 (1982).

"Differential Cross Sections for the ^{6,7}Li$(\gamma,d)^{4,5}$He Reactions at E_γ=100 and 150 MeV" - E. R. Kinney, G. S. Adams, J. L. Matthews, W. W. Sapp, MIT. Bull. Am. Phys. Soc. 27, 708 (1982).

"Nuclear Structure of ^{7}Li by Transverse Electron Scattering" - J. Lichtenstadt, J. Alster, M. A. Moinester, Tel Aviv U; J. F. Dubach, R. S. Hicks, G. A. Peterson, UMass; S. Kowalski, MIT. Bull. Am. Phys. Soc. 27, 718 (1982).

"Measurements of Transverse Electron Scattering Cross Sections in ^{26}Mg" - R. A. Lindgren, M. A. Plum, R. L. Huffman, R. S. Hicks, UMass; X. K. Maruyama, NBS; A. D. Bacher, C. Olmer, Ind. U; D. F. Geesaman, ANL; B. H. Wildenthal, Mich. St. Bull. Am. Phys. Soc. 27, 697 (1982).

"Excited States in ^{89}Y" - T. Milliman, J. Heisenberg, J. Dawson, O. Schwentker, J. Robb, UNH; J. Lichtenstadt, Tel Aviv U; C. N. Papanicolas, U. Ill; J. Wise, J. S. McCarthy, UVa; L. T. Van der Bijl, H. P. Blok, Frije U. Bull. Am. Phys. Soc. 27, 719 (1982).

"Proton Scattering at 650 and 800 MeV on ^{30}Si, ^{34}S and ^{42}Ca" - R. A. Miskimen, A. M. Bernstein, B. Quinn, S. A. Wood, MIT; M. V. Hynes, LANL; G. S. Blanpied, B. G. Ritchie, U. South Carolina; V. R. Brown, LLNL. Bull. Am. Phys. Soc. 27, 730 (1982).

"A Coulomb Sum Rule Test at Low Momentum Transfer" - J. S. O'Connell, J. W. Lightbody, E. Hayward, X. K. Maruyama, NBS; K. I. Blomqvist, MIT; G. Franklin, Carn-Mell. U; P. Bosted, Amer. U; J. O. Adler, K. Hansson, B. Schroder, U. Lund. Bull. Am. Phys. Soc. 27, 530 (1982).

"A Measurement of 180° Electron Scattering Cross Sections for the Deuteron" - B. Parker, R. S. Hicks, R. L. Huffman, R. Lindgren, G. A. Peterson, M. A. Plum, UMass; R. P. Singhal, U. Glasgow. Bull. Am. Phys. Soc. 27, 529 (1982).

"Inelastic Electron Scattering on ^{14}C" - M. A. Plum, R. A. Lindgren, R. S. Hicks, R. L. Huffman, G. A. Peterson, UMass; J. Lichtenstadt, M. A. Moinester, J. Alster, Tel Aviv U; H. Baer, LANL. Bull. Am. Phys. Soc. 27, 530 (1982).

"(π^+,xx) Reactions on Light Nuclei with x=p,d,t or He" - R. Rieder, P. D. Barnes, R. A. Eisenstein, G. Franklin, R. Grace, C. Maher, P. Pile, J. Szymanski, W. R. Wharton, Carn-Mell. U; J. Amann, LANL; B. Bassalleck. U. New Mexico; J. Comfort, U. Arizona; M. Doss, U. Wash; S. Dtyman, MIT, F. Takeutchi, Kyoto-Sangyo U. Bull. Am. Phys. Soc. 27, 469 (1982).

"High Resolution Study of ^{16}O$(\pi^+,2p)^{14}$N" - R. Rieder, P. D. Barnes, R. A. Eisenstein, G. Franklin, R. Grace, C. Maher, P. Pile, J. Szymanski, W. R. Wharton, Carn-Mell. U; J. Amann, LANL, B. Bassalleck, U. New Mexico; J. Comfort, U. Arizona; M. Doss. U. Wash; S. Dytman, MIT; F. Takeutchi, Kyoto-Sangyo U. Bull. Am. Phys. Soc. 27, 468 (1982).

"Electroexcitation of Even-Parity States in ^{27}Al" - P. J. Ryan, R. S. Hicks, J. Dubach, G. A. Peterson, UMass; S. Jain, India; A. Hotta, Shizuoka. Bull. Am. Phys. Soc. 27, 530 (1982).

"Inclusive Pion Double Charge Exchange (DCX) on ^{16}O and ^{40}Ca Between 120 and 270 MeV" - S. A. Wood, J. L. Matthews, MIT; G. A. Rebka, U. Wyoming; P. A. M. Gram, H. J. Ziock, LANL; D. A. Clark, U. New Mexico. Bull. Am. Phys. Soc. 27, 721 (1982).

IV. SEMINARS & COLLOQUIA

"Energetic Photons and Fast Protons: A Tail Not Told by Fermi" - J. L. Matthews, MIT. University of Arizona, Tucson (April 1982).

"Photon Interactions with Few Body Systems and Complex Nuclei" - J. L. Matthews, MIT. Arizona State University, Tempe (April 1982).

"Photonuclear Reaction Mechanisms at Intermediate Energies" - J. L. Matthews, MIT. LAMPF, Los Alamos (June 1982).

"Energetic Photons and Fast Protons" - J. L. Matthews, MIT. Harvard University (Nov. 1982)

"Results of the Recent d(γ,p)n Experiments at Bonn and MIT" - W. W. Sapp, MIT. University of Saskatoon (May 1982).

"Summary Talk" - W. Turchinetz, MIT. Gordon Photonuclear Conference (Aug. 1982).

LATE ADDITIONS

"Low Energy Photonuclear Physics" - K. I. Blomqvist, MIT. University of Montreal, Montreal, Canada (Nov. 1982).

"Radiative Capture into the Continuum" - M. A. Kovash, MIT. University of Kentucky (Jun. 1982).

"Probing the Nucleus with Real and Virtual Photons" - M. A. Kovash, MIT. Indiana University (Mar. 1982).

"Is There a Second-Harmonic Giant Resonance?" - M. A. Kovash, MIT. University of Colorado (Mar. 1982).

V. THESES

"Electron Scattering from Silicon 30" - George Paul Bernhardt, IV, M.S. MIT January 1983.

"π^0 Photoproduction on ^{12}C in the $\Delta(1232)$ Region" - Joseph J. Comuzzi, Ph.D. MIT February 1983.

"The Measurement of Total Cross Sections for Charged Pion Photoproduction" - Bruce Cottman, M.S. MIT August 1982.

"The Photodisintegration of the Deuteron, E_γ= 50 to 350 MeV" - Benjamin Cole Craft, III, Ph.D. MIT September 1982.

"Application of an Optical Model to Alpha Particle Elastic Scattering" - Peter M. Dick, B.S. MIT February 1983.

"Inelastic Electron Scattering from ^9Be" - R. W. Lourie, S.B. MIT June 1982.

"Proton-Neutron Transition Differences in Inelastic Proton Scattering from Oxygen - 18" - J. J. Pekar, S.B. MIT June 1981.

"Electroexcitation of Unnatural Parity States in ^{40}Ca" - Justin Wai-Chow Wong, M.S. MIT January 1983.

U.S. DEPARTMENT OF ENERGY
FIELD TASK PROPOSAL/AGREEMENT

WP BIN NUMBER	2. TASK NUMBER	3. REV. NUMBER	4. PROJECT NUMBER	5. DATE PREPARED	6. CONTRACTOR NUMBER
-AC02-76-ERO-3069	--	--	--	April 10, 1983	CH-3069-002 (ME)-BATES

Item: 19.f. & 19.g. TECHNICAL PROGRESS & FUTURE ACCOMPLISHMENTS

Page(s): 19.f.&g.-1 - 19.f.&g.-32

A. Pion Production

1. Total Cross Section Measurements in the Δ Energy Region (MIT)

The measurement of the total cross sections for the $^{10}B(\gamma,\pi^-)^{10}C(0^+,2^+)$, $^{16}O(\gamma,\pi^+)^{16}N(2^-,0^-,3^-,1^-)$ and $^{14}N(\gamma,\pi^+)^{14}O(0^+)$ reactions has been performed by detecting the residual radioactivity of the daughter nucleus. The results are not in agreement with Distorted Wave Impulse Approximation (DWIA) calculations. A paper is presenbly being written. This work is the subject of a M.S. thesis.

2. Bremsstrahlung and Virtual Photon Spectra from the $\gamma p \rightarrow n\pi^+$ Reaction (MIT)

The real and virtual photon spectra have been measured near the endpoint with good energy resolution. The results are in reasonable agreement with theory and are being written up for publication.

3. Medium Energy Pion Spectrometer (MEPS) in the South Hall (MIT,RPI)

The spectrometer was completed in the fall running period. The first tests with electron scattering and (γ,π) reactions were successful with reasonably low background levels. The spectrometer optics are being studied and data acquisition will commence in the spring. The first scheduled experiments are on the $^{10}B(\gamma,\pi^+)^{10}Be$ and $^{14}N(\gamma,\pi^+)^{14}C$ reactions. The newly-approved experiment on the $^3He(\gamma,\pi^+)^3H$ mirror transition which is expected to run this fall (MIT - UPitt) collaboration). Gas targets for this and other reactions are being developed. Future plans include proposals to measure mirror transitions via the (γ,π^-) reaction and to study the (γ,π) reaction in heavier nuclei.

4. MIT-RPI-Tohoku University Collaboration

Professor Shoda and a student from Sendai are visiting Bates this spring and collaborating on MEPS tune up runs. This visit completes the presently funded collaboration. A paper on the $^{13}C(\gamma,\pi^+)^{13}B$ reaction previously performed at Sendai has been published.

5. $^{12}C(\gamma,\pi^0)^{12}C$ (BU,MIT)

The $^{12}C(\gamma,\pi^0)^{12}C$ high resolution data was taken at E_γ = 240 MeV. This data is still undergoing evaluation. A short calibration test run of 32 hours (also required for the $^4He(\gamma,\pi^0)^4He$ experiment) remains. This will be done in March 1983. The spectrometer development for this experiment was the subject of a PhD thesis awarded this year.

6. $^4He(\gamma,\pi^0)^4He$ (BU,MIT)

The $^4He(\gamma,\pi^0)^4He$ high resolution data was taken at E_γ = 300 MeV. This experiment has a higher counting rate than the $^{12}C(\gamma,\pi^0)^{12}C$ data because of the 20 MeV gap between ground state and inverted state, permitting a wider range of coherent π^0 to be measured. This work is the subject of a PhD thesis.

7. Parasite Test Facility (BU)

A parasite test beam is being developed for the South Hall which is adequate for spectrometer testing using electrons and bremsstrahlung. The parasite beam will also be used for tagged photon testing of NaI detectors from 100 to 600 MeV.

B. Nuclear Compton Scattering (BU,MIT,BC)

Nuclear Compton Scattering will be carried out this year in Beam Line C using a 12" by 12" NaI detector. Differential coherent (γ,γ) cross sections will be measured in ^1H, ^4He, and ^{16}O at energies of 130 to 160 MeV. A high resolution NaI detector will be used to carry out (γ,γ) measurements from 200 to 400 MeV in 1984-1985.

C. Photonuclear Reaction Studies

Research Completed and In Progress (FY83)

1. d(γ,p)n and d(e,p)e'n (MIT,Glasgow,U.S.Carolina)

Data have been taken at six angles (20°, 40°, 60°, 90°, 140°, 160°); the analysis of some of the data is complete and the remainder is in progress. We intend to make measurements at 120° to complete the angular distribution and to perform some auxiliary studies of the shape of the bremsstrahlung spectrum.

2. $^4He(\gamma,^3He)n$ and $^4He(\gamma,^3H)p$ (MIT,U.S.Carolina,Glasgow)

Two good-resolution gas proportional chambers have been built for the detection of the recoiling ^3He's to allow the extension of the (γ,n) measurements to as low a photon energy as possible. Data have been taken at two angles (θ_{CM} = 90° and 120°) and a run is planned at 60° to complete the experiment. In addition, more limited measurements of the (γ,p) cross section have been performed, by detecting the ^3H recoils. A direct comparison of (γ,p) and (γ,n) cross sections will thus be possible, as well as comparisons of both with theory. The results are expected to elucidate the role of meson exchange currents in intermediate energy photonuclear reaction mechanisms.

3. ^{3,4}He(γ,p)X (MIT,Glasgow,U.S.Carolina)

A measurement of inclusive photoproton spectra for E_γ = 300 MeV has been proposed. The data may be interpreted in terms of a two-nucleon absorption process, and should provide information on the distribution of momenta exchanged between the two nucleons. Comparisons between the results for ^{3}He and ^{4}He, nuclei of quite different density for which the wave functions are relatively well known, are expected to be of particular interest. In addition, comparison of the ^{4}He(γ,p) cross section with similar ^{4}He(π,p) results should shed additional light on both reaction mechanisms in the Δ(1232) region.

4. ^{16}O(γ,p$_0$)^{15}N (MIT,U.S.Carolina,Glasgow)

Preparations are in progress for the performance of a measurement of the angular distribution of the ^{16}O(γ,p$_0$) cross section in fine angular steps for three photon energies (E_γ = 140, 220, 320 MeV) using the OHIPS spectrometer. The angular distributions predicted by theoretical calculations exhibit narrow structures due to the interference between various single- and two-particle terms in the photoreaction amplitude.

Research Proposed for FY84 and FY85

1. d(γ,$\vec{n}$)p for E_γ = 50-750 MeV (Yale,MIT)

A measurement of the neutron polarization in the photodisintegration of the deuteron over a broad photon energy range will be performed using a liquid He spectrometer-polarimeter. The results are expected to be sensitive to meson exchange currents at low energies and possible dibaryonic effects at high energies.

2. Measurement of the Spectral Function S(p,E) (MIT)

The (γ,p) reaction can be used to extend to high momentum our knowledge of the nuclear spectral function (the probability of finding a proton of momentum p and energy (-E) within the nucleus). These measurements will provide information complementary to that obtained from (e,e'p) experiments. It is proposed to investigate the photoproton spectrum from ^{6}Li and ^{16}O for several photon energies in the 100-300 MeV range, using a bremsstrahlung difference technique and the OHIPS spectrometer.

3. A High-Flux Real Photon Facility in the South Hall (MIT)

The present bremsstrahlung beam line in the South Hall, Beam Line C, provides a well-collimated, well-shielded, γ-ray beam to the π^0 spectrometer. The flux of photons is, however, several orders of magnitude lower than will be needed by experiments such as the (γ,n$_0$) project. We are therefore planning to put together at least an initial version of a high flux photon facility. This will involve bringing an electron beam onto the South Hall floor in Beam Line C,

a thick (~ 1%) radiator, approximately 1 meter radiator to target distance, and dumping facilities for the electron beam. Backgrounds from the electron beam will be of prime concern and eventually a sophisticated dumping system will be required. The preliminary design and costs for this are detailed elsewhere in this document. To learn quickly about the difficulties of such a system, we are proceeding now to put together a dumping system using as much as possible existing magnets and shielding. This will be used then for the initial (γ,n_o) measurements.

4. Good Resolution Photoneutron Experiments at Bates (MIT,Glasgow)

Photonucleon experiments have played a major role in investigations of electromagnetic interactions with nuclei, especially in providing information on high-momentum components of nuclear wave functions. Data from Bates on the (γ,p_o) reaction, where the residual nucleus is left in its ground state, have provided much of our knowledge of this reaction in the intermediate energy region (100-300 MeV). From these data and other photonucleon experiments at lower energies, important questions concerning the reaction mechanism have emerged. For example, while the (γ,p_o) data show much of the character of one-body knockout, (γ,p_o) and (γ,n_o) cross sections at ~ 100 MeV are approximately the same size, contrary to expectations of a simple one-body knockout picture.

It is clear that a very important contribution to understanding the photonucleon process at intermediate energies can be made by (γ,n_o) data. We are presently preparing to take such data on ^{16}O using a recoil proton spectrometer to detect the neutrons. The protons produced at forward angles will have their momentum vectors determined by deflection in a large gap dipole magnet. We will use the BIGBITE dipole to demonstrate the feasibility of this approach. As much as possible we are making the BIGBITE system compatible with its use as a neutron spectrometer. We plan to measure $^{16}O(\gamma,n_o)^{15}O$ cross sections as several angles between 30° and 120° and at energies between 150 and 300 MeV. This will provide important information on the photonucleon reaction process, especially when the results are compared to the existing (γ,p_o) data.

5. Photodisintegration of ^3He (CUA,UCLA,WPI,MIT)

Differential cross sections for $^3He(\gamma,d)p$ have been measured at θ_p(c.m.) ~ 60° and 90° for photon energies between 150 and 350 MeV. The final analysis of this data is complete. Results have been published in letter form and a more complete paper is being prepared for publication. The data have an absolute normalization uncertainty of 6% and provide absolute differential cross sections suitable for a test of time reversal invariance when used in conjunction with comparable data on the inverse reaction.

D. Polarized Electrons

1. Polarized Electron Source (MIT,Yale)

The polarized electron source is a joint MIT/Yale project. Yale is responsible for the source itself, and MIT will provide support services and the injector transport system into the accelerator. The source is completely assembled and is currently being tested at Yale. Emission has been observed in the preparation chamber. Tests of emission and polarization will continue at Yale for two more months. The injection room is ready to receive the source at Bates. It is expected that the source will be delivered and installed during the Summer of 1983. The Moller apparatus is installed, has been tested, and is operational. The parity quadrupole spectrometers are basically complete, lacking only final detector arrays. The homodyne beam position monitors are currently being assembled and tested. Components are on order to allow the monitors to be converted to superheterodyne receivers if we find that it is necessary to do so.

2. Neutral Current Parity Experiment (MIT,Yale,Harvard)

This experiment will measure the parity violating asymmetry (10^{-6}) in the elastic scattering of longitudinally polarized electrons from carbon. The asymmetry is due to the existence of weak neutral currents as originally predicted by a variety of SU(2) x U(1) gauge theories - the standard model being that due to Weinberg-Salam.

This is a collaborative effort involving researchers from MIT, Yale and Harvard. The construction of the polarized source is funded under a separate DOE contract and is nearing completion at Yale. MIT will provide support services and the injector transport system into the accelerator. The source is completely assembled and is currently being tested. The vacuum integrity of the system has been checked and is satisfactory. Mechanical testing of the crystal transfer mechanism is completed. The optical components, including the laser system, have been procured and are under assembly and test at Yale. Emission has been observed in the preparation chamber. Low voltage emission and polarization tests are expected to be underway at Yale by the end of the month. The working source is scheduled to be installed at Bates by mid-summer.

The room for housing the source is completed along with all of the power and water requirements. The lower injector line assembly is completed and installed. Some elements of the upper injector line have been completed. Work is also underway on the optical design and construction of a Wein filter to be located in the injection line. This will then give us additional capability for flipping the electron polarization, as well as provide a means of making transversely polarized electron beams. These will be required in possible future storage ring devices and for making use of high energy recirculated beams and/or polarization experiments in other experimental halls. This effort should be completed this year.

The Moller apparatus, required to measure the polarization of the electrons leaving the accelerator, is assembled and tested. Only the magnetization measurements on the Fe foil targets remain to be completed.

The homodyne beam position monitors are currently being assembled and tested. Components are on order to allow the monitors to be converted to superheterodyne receivers if we find that it is necessary to do so. Toroid measurements made during the last run cycle indicate that the stability and linearity of the beam current monitors are adequate.

The parity quadrupole spectrometers are nearing completion. Beam tests indicate that the necessary resolution and solid angle are realistically achievable and will be studied during the Spring 1983 running cycle. Experimental tests last fall indicate a reduced background with the newly installed beam dump.

E. Electron Scattering

1. ^{180}Hf(e,e') (MIT,Vanderbilt)

Motivated by the earlier Coulomb excitation and α inelastic scattering studies which indicated an unusually large β_4 deformation for ^{180}Hf, measurements of the electroexcitation of ^{180}Hf were begun at Bates in June 1982. Although only 50 hours were available, data were obtained at five different energies including two very low momentum transfer points crucial to extrapolating for the static B(E2) value. The data are still being analyzed, but the preliminary cross sections are higher than those of nearby ^{176}Yb indicating a significantly large β_4 value which is inconsistent with the near zero value expected by certain theoretical calculations, but consistent with the Coulomb excitation results.

2. ^{16}O(e,e') (MIT,LLNL)

Final data production runs for this experiment occurred in September of this past year. Final cross-sections for all natural parity states below 12.5 MeV have been extracted from the data, which spans a region of momentum transfer from 0.8fm^{-1} to 2.5fm^{-1}. Work is now proceeding with a model-independent-analysis of the charge distributions of these states. Analysis of all states observed with electron scattering in ^{16}O below 22 MeV is nearly complete. Over 30 discrete transitions in ^{16}O below 22 MeV have been identified in the (e,e') data, and it has been determined that the ^{16}O continuum plays a negligible role below 16 MeV.

These electron scattering measurements in ^{16}O are part of a larger program of study of the structure of ^{9}Be and ^{16,17,18}O and of the intermediate energy nucleon-nucleus reaction mechanism. In addition to electron scattering, our measurements include proton scattering

at 135, 180, 312, and 500 MeV, and the (p,n) reaction at 80 MeV and 135 MeV. It is remarkable that the (p,p') probe at these energies excites precisely the same (except for $0^+ \rightarrow 0^-$ transitions) collection of states as the (e,e') probe, in spite of the fact that a recent compilation (Ref. A-S NP A375 (1982) 21) lists over 100 states in the same excitation region. The entire assembly of data has demonstrated both qualitatively and quantitatively that intermediate energy nucleon-nucleus scattering is a one-body process. This conclusion is unaffected by the important role of distortions in proton-nucleus scattering, and is reinforced by the fact that this collection of states in ^{16}O spans a very wide range of structures.

3. $^{9}Be(e,e')$ (MIT,LLNL)

As part of the combined study of the oxygen isotopes using BeO targets, ^{9}Be elastic and inelastic form-factors for the ground state and several excited states in ^{9}Be have been measured at Bates. Momentum transfers ranged from 0.9 to 2.5fm^{-1}. The analysis of the data on the four narrow transverse states at 14.393 (T=3/2), 16.671, 16.976 (T=3/2) and 17.490 MeV (T=1/2) was the subject of a senior thesis. The two T=3/2 states exhibit considerably more low momentum transfer strength than is predicted using the wavefunctions of Cohen and Kurath. These results indicate the necessity of enlarging the model space beyond the 1p shell to provide an adequate description of these states. A paper presenting these results has been accepted by Physical Review C.

Analysis of the data on the broader states, including those at 1.68, 3.05, and 6.76 MeV is nearly complete. There is strong indication from both (e,e') and (p,p') data of a new broad (decay width = 1 MeV) state at 6.36 MeV.

4. $^{192}Os(e,e')$ (LANL,UNH,MIT)

^{192}Os is an example of a transitional nucleus at the boundary between prolate and oblate nuclei, thus it presents an important test of the IBA model. A very strong and uniform Os target has been fabricated at LANL after considerable effort. The target has been used during a 40 hour run at Bates in December 1982. Usable data were obtained at several angles at a single energy of 150 MeV. In view of the limited q-range of the data, they have been analyzed using model-dependent methods. This analysis has confirmed the self-consistency of the data. As more data are acquired in future runs, a model-independent Fourier-Bessel analysis that includes the muonic atom data will be performed.

5. $^{167}Er(e,e')$ at 180° (MIT,UNH,UMass)

In the Fall of 1983 a study was made of the feasibility of measuring the elastic and inelastic magnetic scattering from the ground state rotational band of ^{167}Er, an odd-neutron deformed nucleus. Count

rates for the highest multipole components of these transitions were extremely low, and it will require two to three thousand hours of beam time to carry out the original proposal with the available facilities. There are no present plans to continue this work.

6. ^{154}Gd(e,e') (MIT,Saclay)

Included in this study were the rotational bands built on the ^{154}Gd ground state, as well as the beta and gamma vibrational states. The difficulty of making measurements on the small beta transition required that improvements be made to the already good response of the Bates energy loss spectrometer focal-plane detectors. These efforts resulted in a factor of two improvements in resolution and an order of magnitude improvement in uniformity of response.

Results obtained in this experiment demonstrated that the geometrical theory of Bohr and Mottelson provides a good description of both vibrational-type transitions, whereas the Interaction Boson Approximation (IBA) does not. A publication has been submitted comparing the experimental results to the IBA. A complete paper is in preparation.

7. Improvements to High-Resolution-Spectrometer (MIT,UNH)

Over the past year, the high resolution electron scattering system has been upgraded to improve resolution and spectrum uniformity. A new detector carriage has been installed in the focal plane pit to allow reproducible placement and movement of the wire chambers. A new data acquisition program and accompanying documentation has been written with a "conversational" environment which uses a more systematic approach to the data treatment.

8. A Study of the (e,e'p) Reaction Mechanism (MIT,RPI,UNH)

An experiment to explore the microscopic character of the electromagnetic current operator using the (e,e'p) probe in the deep inelastic continuum has been approved by the PAC. The initial phase of this experiment will focus on 1) obtaining the first longitudinal/transverse separation of the coincidence response functions as a function of missing mass and 2) coincidence measurements in the dip region between the quasi-elastic and delta resonance structures where there is strong evidence that two-, and possibly many-body components of the electromagnetic current operator play a major role. These measurements will be made with parallel kinematics, i.e., with the momentum vector of the detected proton parallel to the virtual photon direction. This eliminates ambiguities due to contributions from interference amplitudes. Extension of this experiment to the delta resonance regions of carbon and deuterium is anticipated and will explore the medium modifications to the delta isobar propagator as well as multi-body and relativistic effects such as pion

rescattering, MEC's, and isobar configurations. Studies are being undertaken of how best to exploit the content of the coincidence interference amplitudes that mix the various virtual photon polarizations. A complete set of measurements for these terms will require the construction of a beam swinger for out of plane measurements.

A successful feasibility study was undertaken in December of 1982 exploring the suitability of using the new spectrometers (MEPS and OHIPS) on Beam Line B for this work. Although the kinematics were far from optimal, coincidence rates of hundreds per hour were observed in the dip region with uncorrected signal-to-noise ratios ranging from 3:1 to 1:3 as the missing energy was varied from 20 to 80 MeV. The raw time-of-flight spectrum for a carbon target using the full acceptances of MEPS and OHIPS (~ 45 mstr and 5 mstr, respectively) was approximately 2 ns FWHM. For the kinematically constrained reaction H(e,e'p) using modest apertures (~ 2 mstr in MEPS), 1.2 ns FWHM was observed. With ray tracing this latter timing resolution is expected to be generally available over the full acceptances of the spectrometers. The combination of large solid angle and momentum acceptances, together with the ability to reach small forward angles with OHIPS (< 20°) and excellent timing resolution, makes the new spectrometers of Beam Line B an ideal tool for (e,e'p) reaction studies where only modest energy resolution (~ 1-2 MeV) is required.

9. Electron-Neutron Coincidence Measurements at Bates (MIT)

During the last year the development of an electron-neutron coincidence capability has continued at Bates. The current status of this effort is as follows:

a. An (e,e'n) coincidence measurement of the electro-disintegration of the deuteron in the quasi-elastic regime has been proposed. A major element of this proposal is the development of a neutron hodoscope array which will allow the detection of neutrons in directions out of the (e,e') scattering plane. Contributions to the cross-sections due to interference between the various virtual photon polarizations (two transverse and one longitudinal) can be extracted by a harmonic analysis of the azimuthal dependence of the cross-sections relative to a neutron detection plane perpendicular to the virtual photon direction. In particular, the transverse-transverse interference part of the total cross-section is directly proportional to the S- and D-state interference amplitude in the impulse approximation. Thus a measurement of the D- to S-state amplitude ratio can be carried out in a manner that is insensitive to most sources of experimental error, and to the neutron's electromagnetic form-factor as well. The magnitude of the effect to be measured is on the order of a ± 10%

oscillation of the interference part relative to the averaged cross-sections. Although the first part of this experiment involves events near the quasi-elastic peak, the program will be extended to regions distant from the quasi-elastic peak, where mesonic effects have been demonstrated to play an important role.

b. A feasibility study of the above reaction has been approved by the PAC. Two prototype scintillators of $^{10?}$Ne coupled to fast Amperex photomultiplier tubes have been built for these tests. Since n-gamma discrimination is not possible with this fast scintillator material, an RF beam pulse will be used to chop the linac beam at 20 MHz. Prompt gamma-rays from the target arrive at the detector separated in time from the neutrons of interest. A fast amplifier of 100V output has been bought for driving a pair of deflection plates in the linac injector to produce the beam modulation. To handle the high pulse currents in the photomultiplier dynode structure at the occurrence of each "gamma-flash", active stabilized divider chains have been built and tested. These units, incorporating a parallel transistorized divider network, have been tested at rates to 30 MHz. A fast LED pulser has also been assembled and is used to monitor gain stability at high rates.

10. Measurement of Tensor Polarization in Elastic Electron-Deuteron Scattering (MIT,ANL,LANL,UIll,UInd,TRIUMF,WPI)

The tensor polarization (T_{20}) of the recoiling deuterons following elastic scattering of electrons has been measured at two values of momentum transfer: $q^2 = 3.1$ and $4.2 fm^{-2}$. The experiment was performed in the South Hall using electron energies of 313 and 375 MeV and a coincidence was required between a scattered electron and a recoiling deuteron, each of which was momentum analyzed in a magnetic spectrometer. The deuteron target was a laminar flow of heavy water, and the polarimeter was the same as the one used in earlier experiments in πD elastic scattering at LAMPF. The results are in good agreement with predictions based on phase-shift-equivalent potential models with relativistic and exchange corrections. Calibration measurements on the polarimeter were carried out at LBL and LANL. To extend these measurements to higher q, a more efficient higher energy deuteron polarimeter is desirable. Survey measurements of the deuteron analyzing power T_{20} are underway at IUCF with this end in mind. Elastic scattering of deuterons from the proton looks like a promising reaction. This experiment is the subject of a PhD discertation.

11. Tritium Electromagnetic Form Factors (MIT,NBS,USask,UVa,WPI)

a. Low q

The charge form factor of ^3H has been measured at 8 points between $q^2 = 0.0477$ and $2.96fm^{-2}$. The magnetic form factor has been measured at 4 points between $q^2 = 0.0931$ and $2.96fm^{-2}$. These measurements were made at Bates and NBS with elastic electron scattering. The target was a solid tritide of Ti with a tritium thickness of $0.226\ mg/cm^2$. Its thickness was calibrated independently using elastic proton scattering at TUNL. Preliminary analysis shows the magnet form factor to agree with that of Collard et al, Phys. Rev. 138, 1357 (1965). However, a power series fit to the charge form factor indicates a radius of 1.54 ± .05fm as compared with 1.70 ± .05fm in Collard et al. This result bears on the current shortfall in calculations of the binding energy difference between ^3H and ^3He. Specifically, the Coulomb energy difference between ^3He and ^3H is reduced, increasing the anomaly in the calculated binding energy difference. J. Friar of LANL is recalculating the Coulomb energy difference based on the new data.

b. High q

Future plans include the measurement of the charge and magnetic form factors of ^3H at Bates in the range of $q = 2.0$ to $5.5fm^{-1}$. 500 hours has already been allocated by the PAC for this experiment. A ^3H target is presently being designed. It will contain 50 to 100 kCi of ^3H gas at 45K and 15 atm giving a target density of $25\ mg/cm^3$. It is similar to a ^2H gas cell used for the $^2H(\gamma,p)$ experiment at Bates which has withstood currents of 25μA. This target may be used for (or readily adapted to) several other experiments either proposed or contemplated including $^3H(e,e')$, $^3H(e,e'2n)$, $^3H(e,e'd)$ and $^3H(\gamma,\pi)$. An identical ^3He cell has been included in the design to provide a reference especially useful for the (e,e') experiment.

At present it has not been decided whether to do the elastic scattering with the energy loss spectrometer or using two spectrometers on the B line in the South Hall to measure an e-t coincidence. The background and resolution with the energy loss spectrometer will be examined to determine if the single arm measurement is feasible. The experiment will otherwise be delayed while the B line large momentum bite spectrometer is completed.

12. Electron Scattering from ^{30}Si (MIT)

An electron scattering experiment was performed at the MIT Bates Linear Accelerator facility on a target of naturally occurring silicon. Several of the low-lying inelastic states of ^{30}Si were examined to determine the single-particle transitions which contribute to the states.

The levels examined were the second, third, eleventh, twelfth, and thirteenth levels. Form factors for each of these states were determined experimentally and the appropriate harmonic oscillator polynomial was then extracted from the form factors. Derived polynomials, using a harmonic oscillator model, for single-particle transitions were then compared to the fitted polynomials.

The second and twelfth levels, $J^\pi = 2^+$, were found to be mostly a 2S-1d transition while the third level, also $J^\pi = 2^+$, was found to be mostly a 1d-1d transition. The eleventh state, $J^\pi = 3^-$, was found to be approximated best by a 1d-1f transition. The thirteenth level, $J^\pi = 4^+$, led to the possibility of 1f strength in the ^{30}Si ground state as other possible transitions are unlikely.

13. Electroexcitation of Unnatural Parity States in ^{40}Ca (MIT)

Electron scattering on ^{40}Ca has been performed at the MIT Bates Linear Accelerator from 81 to 379 MeV and angles of 45°, 90°, and 160°. Form factors for the low-lying states were extracted berween momentum transfers of 0.4fm^{-1} to 2.9fm^{-1}. Three unnatural parity states at 6.7509 MeV 2^-, 8.4242 MeV 2^-; T=1 and 8.5511 MeV $(4^-,5^-)$; T=1 were studied. A way of fitting the form factors with polynomials in the basis of harmonic oscillator wave functions suggested by Donnelly and Haxton were used in the data analyses. Transition strengths, harmonic oscillator length parameters, and the coefficients of the polynomials were extracted. The 8.5511 MeV level was found not to be a high-spin 6^- candidate, but appears more likely to be a 5^- state with unusual cancellation of the convection current part of the form factors, leaving an almost purely spin-flip E5 transition. Good form factors are also available for the first 0^+ level which indicate substantial $2\hbar\omega$ contributions. Both the unusual 5^- structure and the 0^+ indicate strong coupling of the particle-hole excitations to multi-particle multi-hole configurations in the ground state.

14. NBS-MIT-LUND Collaboration

a. The experiment "Total Nuclear Inelastic Electron Scattering Cross Sections Compared to Sum Rule Calculations" has been completed and the results are in press in Physical Review C. The nuclear response to 200/350 MeV electrons inelastically scattered at 20° for six nuclei ranging from A = 9 to 181 is given. An excitation energy integral is formed and compared with three theoretical calculations of the total inelastic scattering cross section.

b. The experiment "Measurement of Photon Cross Sections in the Delta Region" is scheduled during May 1983. A new Cereknov detector system has been designed and is now being constructed for use in this experiment. The (e,e') cross section in the region of the delta resonance (E_x = 140-450 MeV) will be measured at forward angles near the kinematic condition $k_\mu^2 = 0$ to obtain the total photon absorption cross section. Targets of Be and BeO will be used.

15. ^{40,48}Ca(e,e') and ^{238}U(e,e') in the Quasi-Elastic Region (MIT, UVa,LSU)

Deep inelastic electron scattering cross sections have been measured from ^{48}Ca at energies between 100 and 375 MeV and at scattering angles of 90° and 140°. Longitudinal and transverse response functions at three-vector momentum transfers of 330, 370, and 410 MeV/c were extracted from these data using a Rosenbluth separation. The integrated longitudinal response functions for the three momentum transfers are found to have, respectively, 65%, 75%, and 90% of the longitudinal strength predicted by the Fermi gas model.

Data are also available over the same kinematic range for deep inelastic scattering from ^{40}Ca, and these are undergoing analysis. About 70% of the data for a similar experiment on ^{238}U are in hand, and this will be completed in the next running period. Future plans call for extension of this work for all three of these nuclei with the recirculated beam at Bates to obtain data that will allow transverse longitudinal separations for a momentum transfer approximately three times the Fermi momentum. Along with the Saclay data on deep inelastic scattering from ^{12}C, this wil complete a rough survey in mass number of quasi-elastic scattering with transverse-longitudinal separations over the entire momentum transfer range for which the experiment is feasible. The future extensions of this experiment will also provide transverse-longitudinal separations in the Δ-excitation region over a limited kinematic range.

16. D,^{3,4}He(e,e') in the Quasi-Free Region (MIT,UVa)

Two PhD theses are involved in this project to measure the quasi-free and dip regions in D and ^{3,4}He. A longitudinal-transverse separation of the data will be made. As part of this experiment the radiation tail of the proton will be examined. Data acquisition is expected to be completed in the Spring and Fall 1983 running periods.

17. Deep Inelastic Scattering in p,^{4}He (MIT)

This experiment, which uses recirculator energies (~ 700 MeV), will examine the Δ region of the inelastic electron scattering at 35°; this physics is similar to a measurement of the total photon absorption cross section and should give a measure of the shift in energy and width of the Δ excitation from the proton to ^{4}He. This experiment is expected to begin in the Spring running period.

The separate measurements of the longitudinal and transverse spectral functions for inelastic electron scattering from the proton just above the pion threshold is planned to start in the Fall running period. It is also planned to study the feasibility of coincidence experiments to extend the sensitivity of this measurement. This represents an initial experimental entry into the field of quark-nuclear dynamics.

18. D, ^{3,4}He(e,e') at High Energies (UVa)

An experiment has been approved to examine the delta production region of D and ^{3,4}He at high electron energies and forward angles and the low energy loss (scaling) region at backward angles. This experiment will run in Spring and Fall of 1983 and will form part of a PhD thesis.

19. Inelastic Electron Scattering from ^{13}C (CUA,MIT)

An extensive set of measurements on the longitudinal and transverse form factors for transitions to inelastic states in ^{13}C have been completed. The analysis of all these data is now finished and a paper reporting these results is in the final stages of preparation.

20. Electron Scattering Investigations of M1 States in ^{32}S (CUA,NBS,MIT)

Four M1 states have been observed and investigated in a 180° (e,e') experiment using a natural Li_2S target. Transverse form factors and transition widths for these states have been extracted. A draft of a paper reporting these results has been prepared.

21. ^{7}Li(e,e') (CUA,MIT)

As a by-product of the ^{32}S(e,e') experiment using the 180 MeV scattering system, data on the ^{7}Li state at 0.478 MeV have been extracted and published in Phys. Rev. C during the past year.

22. ^{52}Cr(e,e') at 180° (NBS,CUA,UMass)

An experiment to study convection current contributions to low lying E2 strength in ^{52}Cr is in progress. Analysis of the existing data is underway.

23. ^{40}Ca(e,e') at 180° (CUA,NBS,UMass)

An experiment to examine the M1 strength of ^{40}Ca has been completed. A paper presenting the results for the 1^+ state at 10.32 MeV has been published in Phys. Rev. C during the last year.

24. Inelastic Electron Scattering from the Pb Isotopes (UNH)

This experiment has been completed for several years now. Even though many papers have come out of this effort, much of the data, containing additional information, have not yet been published. The continuing work on this project is concentrated almost entirely on finding good theoretical models for the even Pb isotopes.

In ^{208}Pb, work is continuing on a general analysis of the data, in order to correlate the transition strength seen in the experiment with that predicted from RPA calculations. Several corrections into these calculations (such as the Coulomb corrections) are being incorporated which modify the results significantly and, thus, are essential in such a comparison. The hope is that such comparisons improve the understanding of the structure of several unresolved complexes and

will permit the identification of the various levels involved. Preliminary comparisons have already helped to identify several levels previously unknown.

With the new shell-model RPA (SMRPA) a powerful method exists to predict the excitation energies and transition densities of the low-lying levels in ^{204}Pb and ^{206}Pb. It is planned that this work will be carried out as part of a Master's thesis. This will allow a meaningful comparison to the (e,e') data for these nuclei and should lead to a publication of the experimental results.

The data for the lowest 2^+ and 4^+ levels in these nuclei have been analyzed resulting in the extraction of transition charge densities which are being compared to theoretical predictions. A short paper on that subject is in preparation.

25. 180° Scattering from ^{207}Pb (UNH,UIll,UMass,UVa)

This experiment is almost completed, with the remaining 76 hours of beam time scheduled for at least two additional data points. The measurement of the M1 elastic scattering form factor is sensitive to several effects. The single particle strength is due to the neutron $3p_{1/2}$ orbit only. Since this is the last neutron orbit filled, it should be most strongly affected by the softening of the Fermi surface. In addition there are strong contributions from exchange currents and nuclear core-polarization. Several predictions have been made for the resulting form factor including an unpublished prediction of Hamamoto that fits the data rather well.

26. ^{90}Zr and ^{88}Sr(e,e') (UNH,Vrije,UMinn,UVa,UIll)

The data acquisition was completed during the past year, and most of the levels have been analyzed. The analysis of the ^{90}Zr levels is being carried out at UNH, while the analysis of the ^{88}Sr levels is being done at Amsterdam and constitutes a major part of a PhD thesis.

In ^{90}Zr the studies were split up into the study of the positive parity states and the negative parity states. With the positive parity states one studies the effects of the pairing that lead to partial occupations. On a more quantitative level, the analysis leads to a testing of shell model wave functions. The large spread of the observed multipolarities in ^{90}Zr is an ideal example to study the q-dependence of the spin-independent part of the residual interaction. A paper on these results is in preparation.

In the negative parity transitions one finds strong transverse electric form factors. Thus for these transitions one can determine two independent densities from the experiment and from these learn much more about the microscopic form of these transitions.

For ^{88}Sr the initial interest was in the study of the low-lying positive parity excitations. A paper on the comparison of the E2 excitations in the nuclei ^{88}Sr, ^{89}Y, and ^{90}Zr has been submitted to Phys. Rev. Letters. Considerable interest exists in the excitation of the 1^+ and 3^+ states in ^{88}Sr. This data extends the low q data from Darmstadt to q = 2.7fm. The form factor of the 1^+ level can probably be taken as the strongest evidence for delta-hole components in the nuclear transitions since these components modify the q-dependence of the form factor in a way that improves the agreement with the experiment. This subject was extensively discussed at the Amsterdam meeting as well as most recent conferences, and thus it is in the main stream of current interest.

Another surprise was the discovery of an 8^+ state in ^{88}Sr with the configuration $(1g_{9/2})^2$. The excitation strength of this level allows one to determine the occupation probability of the $1g_{9/2}$ orbit in the nuclear ground state similar to the case of ^{90}Zr.

The results from these nuclei have stimulated a strong theoretical effort that has led to the development of the SMRPA model.

27. ^{87}Sr and ^{89}Y

The data from ^{89}Y are essentially complete. For ^{87}Sr enough data exists to extract the most important results from these experiments. However, more data may be needed at high momentum transfer.

The results from the excitation of the 0.909 MeV level in ^{89}Y in comparison to the lowest 5^- excitation in ^{90}Zr have already been published. This comparison allowed for the first time a determination of the size of the ground state correlations as pointed out in several subsequent publications.

At the present time the analysis is concentrated on the weak-coupling aspect of these nuclei. In ^{87}Sr, the multiplets originating from the coupling of the neutron $1g_{9/2}$ hole to the collective 2^+ and 3^- core excitations have been identified already in proton scattering. Form factors have been measured for the various members of these multiplets.

In ^{89}Y, the doublet from the coupling of the $2p_{1/2}$ proton to the E7 core excitation has been identified. The resulting states can be compared to the predictions using the shell model. Since the E7 core excitation is essentially a pure $1g_{9/2}\,(1f_{5/2})^{-1}$ ph excitation, the energies and transition strengths measured in ^{89}Y give a very good measure of the matrix elements of the residual interaction.

28. Electron Scattering from ^{92}Mo (UNH)

This experiment has been accepted at the Bates Accelerator. Beam time is scheduled for early December 1982.

In view of the recent results from ^{90}Zr and ^{88}Sr the prime interest is in the positive parity transitions. It is hoped that using the SMRPA calculations, agreement can be produced for the whole region of N=50.

29. Electron Scattering from the Ce Isotopes (UNH)

Beam time is scheduled for this experiment together with the experiment on ^{92}Mo. Since for these nuclei resolution is the most important factor in the success of the experiment, UNH has a strong involvement in the upgrade of the high resolution spectrometer at the Bates Accelerator. W. Hersman is spending considerable time at Bates in developing the new software for the on-line data taking capability with two chambers in the focal plane. Up to now most data have been taken with only one chamber. Significant improvement is expected with the two chamber system.

30. Electron Scattering from ^{27}Al (UMass)

Data-taking for this experiment was concluded in 1979, and electron scattering form factors have now been extracted for status up to 8 MeV excitation energy. Previous electron scattering experiments lacked the resolution to cope with the high level-density above 4 MeV, whereas almost all levels were resolved in this experiment up to 8 MeV.

A paper on the negative-parity states[1] has been published. In that paper it was necessary to use weak-coupling and strong-coupling of single-particle excitations to collective modes. Although shell-model calculations of the positive parity states can be made within the sd-shell configuration space, a calculation of the negative-parity states would have to include the 1p and 2p-1f shells, thus vastly complicating the problem. It was shown that the weak-coupling model can provide a good understanding of the level scheme of negative-parity states up to 7.5 MeV, although the deduced transition strengths are only approximately given by this model.

Experimental (e,e') form factors were extracted for most of the ^{27}Al positive-parity states below 7 MeV. The availability of these comprehensive data provides a detailed test of shell model calculations. It is found that the longitudinal form factors of the low-lying excited states are well-described providing C2 and C4 effective charges are introduced. These effective charges seem to show little dependence on momentum transfer as far as $q \simeq 2fm^{-1}$. The procedure is less successful for higher-lying excited states. Comparisons of theoretical and experimental transverse form factors are also being made for states below about 3.8 MeV.

Also, the longitudinal and transverse elastic form factors for ^{27}Al have been deduced from measurements performed at Mainz and Bates. These data are sensitive to both many-particle and single-particle properties: Collective aspects such as ground state multipole moments

and charge density distribution, and single particle properties such as the radial distribution of valence orbits, and the relative differences in subshell occupation numbers with neighboring nuclei.

[1]R. S. Hicks, et al., Phys. Rev. C 21, 2177 (1980).

31. Deuteron Electrodisintegration at 180° (UMass,MIT,NRL)

The primary objective of this experiment is to examine the break-up of the deuteron at high excitation energies and at moderate momentum transfers. Subsidiary objectives are to measure the elastic magnetic scattering and the threshold electrodisintegration. The high-excitation data should yield information on the role of isobar configurations according to Fabian and Arenhovel.[1] The included the NΔ(1232), the NN'(1470), and the Δ(1232)Δ(1232) configurations in an impulse approximation calculation by using π- and ρ- exchange for the appropriate transition potentials. A substantial enhancement of the 180° cross section is expected. For example, at $q = 2fm^{-1}$ and an excitation energy of 120 MeV, an enhancement of about a factor of two is expected. On the other hand, large enhancements of the threshold M1 break-up are expected due to meson exchange currents.[1,2] Furthermore, a measurement of the elastic electron-deuteron magnetic form factor should greatly narrow down the allowable range of the percentage of D-state in the deuteron. At this time there is no other measurement of the transverse (180°) form factor at high-excitation energies.

A liquid-nitrogen cooled gas-target system was built which uses a 11.4 cm long cylindrical cell containing deuterium gas at about 150 psi, and an identical cell containing hydrogen gas at about the same pressure. A remotely-controlled target changing mechanism, and temperature and pressure monitors were interlocked to the accelerator. All of this equipment was built in the UMass Nuclear Physics Shop.

Measurements have been made using incident beam energies up to 320 MeV and break-up energy transfers as large as 175 MeV. Several measurements were made at lower beam energies in order to get information necessary for radiation tail subtractions. It is hoped that this experiment may be analyzed and completed during the coming year.

The SLAC radiation tail code of Guthrie Miller has been made to operate on the UMass Cyber 175 Computer. This code should be useful for both this experiment and experiment 80-19, quasielastic electron scattering from ^{56}Fe.

[1]W. Fabian and H. Arenhovel, Nucl. Phys. A258, 461 (1976).
[2]D. O. Riska and G. E. Brown, Phys. Lett. 38B, 193 (1972).

32. $^{12}C(e,e')$ at 180° (UMass)

This experiment is complete except for the reporting of all of the results in the literature. Two papers have been published, namely, "Convection Currents and Spin Magnetization in E2 Transitions in ^{12}C" and "Electron Scattering, Isospin Mixing, and the Structure

of the 12.71- and 15.11 MeV Levels in ^{12}C ". A first draft of a paper on the transverse form factors of the rest of the levels below 19 MeV has been written, and a second paper is nearing completion on the M4 transitions in the 19 MeV region, which will also include M4 form factors for the other p-shell nuclei ^{13}C and ^{15}N.

33. Backward-Angle Electron Scattering from ^{13}C (UMass)

The elastic magnetic dipole form factor has been measured in the momentum transfer range from 0.7 to 3.2fm^{-1}. There is a considerable enhancement of the experimental results over those of simple shell model calculations in the highest momentum transfer region, and the height of the second maxima in the cross section is a factor of ten smaller than the value of the extreme single-particle picture. This difficulty has stimulated considerable theoretical interest in the problem. Lin and Zamick[1] have made Nilsson model calculations, Suzuki et al.[2] have computed the core-polarization terms, J. Delorme et al.[3] have considered pion condensate effects, and Dubach[4] has made a large-basis shell model calculation including exchange currents in a full $2\hbar\omega$ space, and a particle in the p-f shell. None of the calculations come close to explaining the data. These data have clearly pointed out theoretical problems that need to be investigated. A paper[5] has been published describing the experimental results and comparing them to the various theoretical calculations.

The data-taking and the analysis phases of this experiment for inelastic scattering are also complete. Transverse form factors have been determined for states up to 22 MeV in excitation energy. Strong M4 transitions to states at 9.5, 16.2, and 21.4 MeV have been found. These states are formed by coupling an odd neutron to the "stretched" 4^- states of ^{12}C. Such stretched configurations are of general interest because the number of configurations entering into their excitation matrix elements is severely restricted, and hence their interpretation is less model dependent. The total observed M4 strength in ^{13}C is essentially the same as that measured in ^{12}C: about 25% of the value indicated by a simple $(p^{-1}_{3/2}, d_{5/2})$ model calculation. Comparisons of inelastic π^+ and π^- scattering show that the 9.4 MeV transition is dominated by neutron components, and that the 16.2 MeV transition represents proton excitations.[6] Shell model calculations agree with the excitation energies, relative transition strengths, and the isospin structure.[4]

[1]C. K. Lin and L. Zamick, preprint, July 1981.
[2]T. Suzuki, et al, Nucl. Phys. A358, 421 (1981).
[3]J. Delorme et al., Phys. Lett. 89B, 327 (1980); 91B, 328 (1980).
[4]J. Dubach, UMass, private communication.
[5]R. S. Hicks et al., Phys. Rev. C 26, 339 (1982).
[6]D. Dehnhard et al., Phys. Revl Lett. 43, 1091 (1979); S.U. Seestron-Morris et al., Phys. Rev. Lett. 46, 1447 (1981).

34. Inelastic Electron Scattering from ^{208}Pb (UMass,ORNL,MIT)

This experiment involved a search for M1 strength and the measurement of the transverse form factors of the low-lying collective states. This work has been reported in the physics literature.[1]

[1]R. S. Hicks et al., Phys. Rev. C 26, 920 (1982).

35. ^{29}Si, ^{31}P(e,e) Elastic Magnetic Scattering (UMass,Mainz,MIT,LLNL)

This experiment was the thesis topic of Helmut Miessen of Mainz.[1] Data above momentum transfers of about 1.8fm^{-1} were obtained using the Mainz linear accelerator, and lower momentum transfer data were taken at Bates by utilizing 180° scattering so as to suppress Coulomb scattering. The data taken at the two laboratories are consistent. A paper is being written.

[1]H. Miessen, PhD Thesis, University of Mainz, Mainz, West Germany

36. Electron Scattering from ^{15}N at 180° (UMass,Glasgow)

Through the use of a gas target cell designed for 180° scattering, transverse cross sections have been measured for the complete ^{15}N level spectrum up to about 30 MeV. Interpretation of the inelastic cross sections is in progress. As may be seen, the elastic M1 form factor lies in reasonable agreement with shell-model predictions for $q \leq 2.4\text{fm}^{-1}$, but shows an unexplained enhancement at higher momentum transfers. A similar effect has previously been observed in ^{13}C. At low q the ^{13}C and ^{15}N form factors are very different, but tend to merge together above $q = 3\text{fm}^{-1}$. Lin and Zamick[1] have surmised that this convergence might indicate that the high-q cross sections are dominated by isovector core polarization and meson exchange effects, rather than simple p-shell one-body transitions.

[1]C. K. Lin and L. Zamick, Bull. Am. Phys. Soc. 27, 530 (1982).

37. Elastic and Inelastic Electron Scattering from ^{14}N (UMass,Mainz,USask)

Transverse M1 form factors for transition in ^{14}N have been measured between momentum transfers of 0.8 and 3.0fm^{-1}. In the case of the elastic scattering, comparisons are made with the $0\hbar\omega$ shell-model form factors computed using harmonic oscillator radial wave functions. Cohen-Kurath shell model wave functions lie in good agreement with the data, however the phenomenological wave functions of Ensslin et al.[1] lead to cross sections that are too low. Unlike the elastic T=0 form factor, the data for the transition to the T=1 first-excited state at 2.313 MeV shows a large relative enhancement at high-momentum transfer. This enhancement cannot be accounted for by any p-shell calculation using one-body operators and reasonable radial wave functions. Similar unexplained enhancements have also been observed in other isovector M1 transitions in p-shell nuclei. The fact that the purely isoscalar elastic form factor lies in good agreement with

theoretical predictions suggests that the isovector transition operator is less well understood than the isoscalar transition operator, particularly at shorter distances. A paper is in preparation.

[1]N. Ensslin et al., Phys. Rev. C 9, 1705 (1974).

38. Transverse Electron Scattering from ^{14}C (UMass,TelAviv,LANL,MIT)

During the past year a double-containment cell was constructed for eight Curie's of radioactive ^{14}C. Numerous safety precautions have been taken including the use of a secondary emission-fast-trip system in order to keep the beam from striking the target frame. Several runs were made on mock targets using beams up to 35 μA before a successful target configuration was found.

To date five spectra have been obtained at 180° for incident electron energies between 110 and 225 MeV. Additional data will be obtained in the near future. Transitions were measured for the previously observed 1^- state at 6.09 MeV, the 3^- state at 6.73 MeV, the 2^+ state at 7.01 MeV, and the 2^+ state at 8.32 MeV. In addition candidates for transitions to stretched-spin T $1,4^-$ states at 11.7 and 17.3 MeV have been found. Two previously unobserved states were seen at excitation energies of 22.1 and 24.3 MeV, and are tentatively identified as 2^- and 4^- T=2 states, respectively. The 22.1 MeV state was previously unobserved by (e,e'), probably because of an interference which causes the form factor to peak at an unexpectedly high momentum transfer. The 24.3 MeV state had not been observed with pion scattering due to the nature of the pion-nucleus interaction. The electron T=1 data can be combined with pion data to predict the cross section of the excitation of the 4^-, T=2 state for pion scattering. The predictions agree with the latest pion scattering data. Predictions have also been made for proton scattering, and work is now underway to predict (p,n) cross sections.

39. ^{56}Fe Transverse Quasi-elastic Electron Scattering (UMass,Glasgow,UVa, Shizuoka,MIT)

The objective of this experiment is to measure the transverse quasi-elastic structure function for ^{56}Fe at 180° so as to avoid the need of a Rosenbluth separation of the longitudinal response function from the transverse response function. There are uncertainties in the data analysis which will thus be avoided. If the longitudinal response function behaves normally, there should appear in the transverse response function features of interest such as exchange current and delta resonance enhancements, which are not present to first order in the longitudinal response function.

Data were acquired in 1981 for three different incident energies, and in 1982 for seven different incident energies so that two quasi-elastic spectra may be plotted for constant momentum transfers of 1.5 and 2.0fm^{-1}. The data are essentially reduced to cross sections at this time, but radiation tail unfolding still is needed. The results will eventually be compared with calculations by E. Moniz of MIT.

40. The Structure of ^{7}Li by Elextriexcitation (UMass,TelAviv,MIT)

The transverse form factors of the ^{7}Li ground and first excited states have been measured. When combined with existing low-q data, the measurements now span the momentum transfer range of q = 0.2 to 3.0fm^{-1}. The data lie in good agreement with calculations using Cohen-Kurath amplitudes, but are less well described by Hartree-Fock predictions. The agreement with the Cohen-Kurath calculation contrasts shaprly with other p-shell nuclei, where the shell model fails to fit the transverse form factors measured throughout an extended range of momentum transfer. A paper has been accepted for publication in Physics Letters. A run has been scheduled for the near future to extend the momentum transfer range to higher values through the use of the recirculated beam for the first time in a nuclear structure experiment. At higher momentum transfers a deviation from the Cohen-Kurath predictions is expected.

41. Transverse Electroexcitation of ^{26}Mg (UMass,UInd,ANL,NBS,Mich.St.)

Several runs were carried out on ^{26}Mg, in conjunction with other 180° experiments, so as to isolate these transitions that had large transverse components, and those transitions that are likely M6 candidates for $f_{7/2}d_{5/2}^{-1}$ particle-hole excitations. Spectra rich with excitations were found, and one particular high-energy state appears to be a very strong M6. This will be the first M6 stretched particle-hole transition found in a nucleus with $T_z \geq 1$. In ^{24}Mg and ^{28}Si, the M6 transition strength is concentrated in a single transition in each case and is about 0.5 of that predicted by RPA calculations. In ^{26}Mg both T=1 and T=2 6^{-} states should be found. It is likely that the strong high-energy excitation is the T=2 M6 excitation. Measurements of the M6 form factor should permit the extraction of information on the isoscalar and isovector parts of the tensor force in the effective interaction used in describing the proton scattering from ^{26}Mg.

42. Elastic Magnetic Scattering from ^{13}C (UMass)

This is an extension to higher momentum transfers by using the recirculated beam in order to find out if the form factor remains high as the momentum transfer is increased. This is an especially favorable case for higher momentum transfer studies because the expected very low cross sections can be compensated for by the use of an especially thick target placed in a transmission geometry at 150°. The large ionization losses in the thick target are allowable since the first excited state lies rather high in energy at 3.09 MeV.

The isotope has a T=1/2 ground state, and hence can have both isoscalar and isovector components in the elastic magnetic scattering. Experiment 80-1 involving ^{14}N, has only an isoscalar component in the ground state scattering and isovector in that from the first excited state. Measurements of all of these cases should help to elucidate the reasons for the enhanced form factors at large momentum transfers. This experiment on elastic magnetic scattering on ^{13}C is the highest rated experiment in the nuclear structure class approved for beam time at Bates.

43. ^{4}He(γ,^{3}He)n (U.S.Carolina,MIT,Glasgow)

This experiment is to compare exclusive (γ,n) and (γ,p) cross sections at E_γ = 170-360 MeV. We had a test run and a longer run in 1982. We have accumulated data at nucleon cm angles equal to 90° and 120°. Our preliminary findings show that the (γ,p) and (γ,n) cross sections are nearly equal and that there is a serious discrepancy with the published Bonn ^{4}He(γ,p) data at 120°.

In order to measure low energy ^{3}He's, it was necessary to build two large area MWPC's for particle identification in the 900 MeV/c - spectrometer focal plane. These were built at MIT. The cooled gas target that was developed for the ^{2}H(γ,p)n experiment was used for this experiment also.

44. Systematics of M8 Strength in ^{54,56}Fe and ^{58,60}Ni (UMass,NBS)

The main focus of the work is to obtain systematics on the fragmented ($g_{9/2}f_{7/2}^{-1}$) M8 strength in ^{54,56}Fe and ^{58,60}Ni. Because the 8^- states are excited exclusively through the "stretched" particle-hole configurations, determination of the multipolarity and strength of the $g_{9/2}f_{7/2}^{-1}$ component is unambiguous and direct. Excitation energies, form factors, multipole assignments, spectroscopic amplitudes, reduced B(M8)'s, isospin assignments, and symmetry energies are extracted from the data. These results are compared to nuclear structure calculations and information extracted from inelastic proton scattering. The goal is to test nuclear structure model calculations and the effective nucleon-nucleon force used in inelastic hadron scattering. Efforts are directed towards obtaining a complete self-consistent interpretation of (e,e'), (p,p'), (π,π'), and model calculations for these M8 excitations. For example, one result reported in the past pertained to information acquired about the tensor force in the effective interaction for hadron scattering.[1] Since the number of terms contributing to the amplitude for the stretched-spin case for both (e,e') and hadron scattering is severely limited, the interpretation of results is less model-dependent than for lower multipoles. Also, previous results have been reported[2] on the fragmentation of M8 transition strength in ^{58}Ni. This case should be constrasted with ^{54}Fe where a large fraction of the strength resides in one strong transition.[3] Shell model calculations have been made by Lawson and Teeters pertaining to this latter case. Symmetry energies can also be deduced from the isospin splitting into T_o and T_o + 1 components[4] of the states identified as having $J^\pi = 8^-$. Data acquisition and data analysis for the isotopes ^{54}Fe, ^{58,60}Ni are essentially complete. Data acquisition for ^{56}Fe is not yet complete. A paper has been published this past year on the isospin splitting of these states in non-self-conjugate nuclei.[5]

[1]R. A. Lindgren, et al., Phys. Rev. Lett. 42, 1850 (1979).
[2]R. A. Lindgren, et al., Phys. Rev. Lett. 40, 504 (1978).
[3]R. A. Lindgren, et al., Phys. Rev. Lett. 46, 706 (1981).
[4]R. A. Lindgren, et al., Phys. Rev. Lett, 47, 1266 (1981).
[5]R. A. Lindgren, et al., Phys. Rev. Lett. 47, 1266 (1981).

e. Precision Experiments with Low Energy Pions (MIT,LAMPF,SIN)

Both LAMPF and SIN are in the process of constructing Low Energy Pion Spectrometers. These devices will be high resolution facilities with large solid angles and momentum acceptances. They will allow for the first time the precision study of low energy pion-nucleus interactions. Since the character of the interaction is rather different at low energy from that observed near the $\Delta(3,3)$ resonance, this should prove to be a rich field of study. We have for the past few years been advising both LAMPF and SIN on the optimal parameters for the Spectrometers. As the projects near completion, it is likely that we will become involved in the experimental programs. Inclusive and exclusive pion double-charge-exchange especially appears to be a potentially rich and certainly unexplored field at low energy.

Study of the $(\pi^+,\pi^\circ p)$ Reaction (MIT,LANL,TelAviv)

There has been considerable progress in recent years in the attempt to understand the interactions of pions with nuclei. Much of this progress has come through the detailed study of specific reaction channels, such as inelastic scattering and single-charge-exchange. For example, comparison of single-arm and coincidence quasi-free pion scattering data has yielded insight into the nature of this process. Coupling to other reaction channels is of great importance and has been studied as well.

While a significant amount of pion single-charge-exchange data has been accumulated during the past several years, mostly using the LAMPF π° spectrometer, there are as yet no coincidence measurements. We plan to study the reaction $^{16}O(\pi^+,\pi^\circ p)$ at 165 and 245 MeV using the aforementioned spectrometer and an array of plastic scintillators for detection of the protons. The experiment was approved with high priority by the LAMPF Program Advisory Committee in January and should run during the Fall of 1983. These data, when compared to the inelastic scattering data and single-arm charge exchange data described previously, should contribute substantially to our knowledge of pion-nucleus reactions, especially the isospin structure of the interaction.

Measurement of the Tensor Polarization of Recoil Deuterons in π^+-d Elastic Scattering at Intermediate Energies at LAMPF (MIT,ANL, IUCF,LANL,UIll)

One of the most interesting puzzles in intermediate energy nuclear physics in recent years has been the general question of polarization observables in the pion-deuteron system. It was realized several years ago that such observables should be sensitive to the presence of dibaryon resonances. Even without such "exotic" phenomena, it is expected that experiments of this type will show large sensitivity to pion absorption mechanisms.

There have recently become available on both the π-d T_{11} analyzing power and the tensor polarization (T_{20}) of recoil deuterons from π^+-d elastic scattering. The T_{11} data (from SIN) show structure at forward angles for pion energies around 250 MeV. Two groups have published results on T_{20}. This collaboration measured T_{20} at T_π = 142 MeV and obtained values which were negative and relatively structureless as a function of angle. More recently a SIN group has published T_{20} data at T_π = 134 MeV which show large oscillations as a function of angle.

In an attempt to provide more information for this puzzling picture, we have recently (December 1982, January 1983) taken more T_{20} data at 134, 180, 220 and 256 MeV. As with previous runs, the ^{3}He(d,p) reaction at forward angles was used as an analyzer. The deuterons were magnetically analyzed and required to be in coincidence with a scattered pion. The results are still preliminary, but it is clear that at none of the energies is structure of the kind reported by the SIN group seen. The angular distributions do show systematic behavior with energy, but they tend to be smooth and have negative T_{20} values. The data are now undergoing final analysis.

h. Measurement of ($\pi^\pm$,pp) and ($\pi^\pm$,np) Reactions in Complex Nuclei (MIT,U.Md,VPI,U.S.Carolina,LANL)

As part of a continuing program of studies of pion absorption in nuclei, we have recently (December 1982, January 1983) taken a significant amount of data at LAMPF on the ^{58}Ni(π^-,pp) reaction at 160 MeV and studied the feasibility of measuring the ($\pi^\pm$,np) reaction. Although some previous (π,pp) and (π,np) data exist, the energy resolution is significantly poorer than one would like. The thrust of this experiment is to provide data with total energy resolution on the order of 5 MeV. To this end we employed plastic scintillator/NaI(Tl) telescopes arranged around a thin ^{58}Ni target. The ^{58}Ni target was chosen because this mass region has been well studied in previous experiments on pion absorption, especially those involving proton-singles measurements. The detector systems were arranged so that essentially the full angular range of coincidence events was studied. A strong angular correlation of 2-proton events for (π^+,pp) reactions was detected, indicating pion absorption on n-p pairs. This finding is consistent with previous experiments.

We were also able to run a few days with a π^- beam and in fact did observe a clear (π^-,pp) signal, although at a much reduced rate from the (π^+,pp) data. We also spent some time looking at the feasibility of neutron measurements to look at (π,np) and (π,nn) reactions. All of the data are currently under analysis. It is certainly possible that follow-up experiments may be indicated, especially if (π^-,pp) events rates are as promising as our first look showed.

i. Study of the π^+-d→pp Reaction at Energies below the Δ(3,3) Resonance (MIT,UMd,UVa,VPI)

The π^+d→pp reaction is the basic starting point for experimental and theoretical studies of pion absorption. We have previously studied this reaction at energies up to 70 MeV. There are high-quality data available for energies above 150 MeV. The purpose of the experiment performed in July 1982 at LAMPF was to provide high-quality data in the intermediate region. In fact, there has been some hints that structure might exist around T_π = 80 MeV.

During this recent run we measured π^+d→pp differential cross sections at pion energies of 65, 72.5, 80, 95, 110, 125 and 140 MeV and at laboratory angles between 93° and 165°. Analysis of these data is now complete. The dependence on energy is smooth, so no anomalous structure appears to be present. There now exists a complete set of π^+d→pp cross sections from 20 MeV to well over the Δ(3,3) resonance for comparison with detailed pion absorption models and as input to calculations of pion absorption in nuclei. A paper containing all of the results of the recent run has been accepted for publication.

j. (π,π') at LAMPF (LEP Channel) (MIT,VPI,LAMPF,ORNL,U.S.Carolina)

Positive and negative pions of 80 MeV, scattered inelastically from targets of ^{12}C and ^{40}Ca, have been studied at laboratory angles between 50° and 120° using the low energy pion channel at LAMPF. The rapid change of the π-N amplitudes in the energy range of 50 to 100 MeV is well suited for studies of isospin effects and optical potentials used in distorted wave calculations. Furthermore, at low energies, pions penetrate further into the nuclear interior making the pion probe an interesting alternative for the study of nuclear structure. A paper presenting the angular distributions for the 4.44 MeV (2^+) state in ^{12}C and the 3.17 MeV 3^-, 13.4 MeV giant quadrupole resonance, and the 17.5 MeV states in ^{40}Ca has appeared in Physical Review C. A further paper covering elastic scattering from various nuclei is being prepared. The MIT group was responsible, in part, for the development and winding of the vertical drift chamber used in the LEP channel at LAMPF.

2. Hadron Scattering

a. Determination of Nuclear Densities from Elastic α Particle Scattering (MIT,UIll)

Theoretical Hartree-Fock densities have been used to predict the cross sections for elastic α particle scattering. In particular the densities of Gogny for the Ca isotopes through the Ni isotopes give predictions which are in reasonable agreement with experiment, indicating a proper description of both the neutron and proton densities in the surface region. These densities are also in agreement with electron scattering and with 800 MeV proton scattering results. We are presently writing papers on these results.

b. Neutron and Proton Transition Matrix Elements from Inelastic Hadron Scattering (MIT,LANL,UOregon)

We were invited to write a review for Comments in Nuclear and Particle Physics of our work on the determination of neutron and proton transition matrix elements from a comparison of inelastic hadron scattering and electromagnetic results. We are presently preparing a general discussion of measurements of the relative signs of neutron and proton matrix elements. We are also extending our work on nuclear models, core polarization, and inelastic hadron scattering.

c. Measurements of (p,p') Reactions at Intermediate Energies (MIT, LANL,U.S.Carolina)

We have finished analyzing our data for the inelastic scattering of 650 and 800 MeV protons from ^{30}Si, ^{34}S and ^{42}Ca. A paper on the relative signs of neutron and proton matrix elements has been published. Predictions of the observed cross sections using parameter-free distorted wave impulse approximation have been made in which the neutron and proton transition matrix elements were taken from mirror electromagnetic decay rates. A paper on this subject is almost finished. We plan to use shell model plus core polarization transition densities to predice the scattering cross sections.

d. (p,p') Studies of ^{9}Be and ^{16,17,18}O (MIT,IUCF,LAMPF,LLNL,UCLA)

Significant theoretical and experimental progress has been made in advancing knowledge of both the nuclear structure of these isotopes and the effective nucleon-nucleus interaction at intermediate energies. Most of the effort in the past year has concentrated on the ^{16}O nucleus because of its importance for testing the theoretical framework of the Local Density Approximation (LDA). Two new experiments have been carried out at LAMPF to test the energy dependence of the interaction at higher energies. Data analysis programs have been developed to new levels of sophistication enhancing the speed and accuracy of the analysis techniques. Specific points of progress include the following:

i) (p,p') Experiments at IUCF (MIT,IUCF,LLNL,LAMPF)

Analysis of the 180 MeV proton scattering experiment on ^{16}O is nearly complete. Cross-sections and analyzing powers of all resolvable states below 14 MeV have been extracted. The results of LDA calculations on natural parity transitions where the electron scattering determines the nuclear structure uniquely are in excellent agreement with the earlier data at 135 MeV and with the LDA predictions. The data for the low-lying abnormal-parity states exhibit a significant energy dependence between 135 and 180 MeV. The structure of the 4^+ state at 11.096 MeV is considerably different at these two energies, indicating the presence of either a strong unresolved doublet or of a multi-step reaction process. The LDA calculations are sensitive to the choice of nucleon-nucleon

potential, and prefer a potential whose core is intermediate between the hard core Hamada-Johnston potential and the softer core Paris potential. Analysis of higher energy excitations to 22 MeV is in progress.

ii. $^{16}O(p,p')$ at LAMPF (MIT,LAMPF,IUCF,UCLA,LLNL)

Data was obtained in January 1983 on ^{16}O covering the range of states and momentum transfers (less than $3.3fm^{-1}$) observed in the lower energy work at IUCF. Data analysis has commenced. The work at 312 MeV is particularly interesting since this energy corresponds with the minimum of the central iso-scalar interaction and thus represents the energy at which the impulse approximation is most likely to be valid. LDA and impulse approximation calculations give similar predictions in this energy range.

iii. Wolfenstein Parameters for (p,p') at 500 MeV (MIT,LAMPF,IUCF, UCLA,LLNL)

Progress is being made in the analysis of the Wolfenstein parameters for the strongest low-lying states in ^{16}O and ^{9}Be. Emphasis is being placed on development of statistical methods for maximizing the information that can be extracted from the focal-plane-polarimeter measurements. The fitting code ALLFIT is being modified to permit simultaneous determination of the spin transfer observables. Extraction of analyzing powers and cross sections is underway and will add to the knowledge of the energy dependence of the proton-nucleus interaction gained from the lower energy work.

e. (p,n) Measurements at IUCF (MIT,KSU,IUCF,LAMPF)

i. (p,n) Studies on Isotopes of Si, O and Be

The (p,n) collaboration was initiated as part of the unified approach to the study of the oxygen isotopes. Two papers on the (p,n) work at 135 MeV have been published in PRC on Si and O isotopes and a third paper has been submitted. The work on ^{17}O is the subject of a PhD thesis and is expected to be completed this summer. As a by-product of the Oxygen studies, ^{9}Be spectra have been obtained as well. Analysis of these spectra at forward angles gives the first clear measurement of the $p_{3/2}$ to $p_{1/2}$ spin flip transition to ^{9}B.

ii. D(p,n)

Time has been approved for a study of the D(p,n) reaction at IUCF. Preliminary data obtained as part of a feasibility study have been analyzed and form part of a Master's Thesis to be completed this Spring. Theoretical modeling of the singlet two proton state at threshold and of the quasi-elastic continuum has begun.

iii. $^{16}O(p,n)\ 0^+ \rightarrow 0^-$ Longitudinal Spin Flip Transition

The $^{16}O(p,n)$ reaction to the ground state of ^{16}F presents a rare opportunity to study the $0^+ \rightarrow 0^-$ pure longitudinal spin transfer transition. This experiment is important since the zero degree measurement can be incorporated with other data to help extract the effective weak pseudo-scalar coupling constant in the nuclear medium. It is also important for nuclear structure reasons since it yields information on a unique and seldom-measured nuclear transition density, and also because its pion-like quantum numbers may help to shed light on precursor phenomena to pion condensation. This experiment is difficult since the transition is weak and good resolution is required. A feasibility study was approved by the IUCF PAC and 5 shifts of beam time were successfully used in February of 1983 to study this reaction. An energy resolution of 125 keV was achieved for 80 MeV incident protons. Measurements of the transition to ten percent were obtained at several angles. With an improved target and anticipated improvements in pulse selection techniques, the prognosis of this experiment is excellent.

f. Spin-Flip and P-A in $^{12}C(p,p\gamma)$ (MIT,OSU,IUCF)

Because of the sensitivity of the spin-flip variable S to the tensor force between nucleons, careful measurement of S will provide a stringent test of this component of the nucleon-nucleon force as it is presently used in microscopic scattering theories. Furthermore, the nature of the mechanism responsible for nonzero values of P-A for inelastic processes is not at present well known. There is, however, some indication that the exchange components of the tensor force are primarily responsible. One aim of the present program is to provide precise measurements of S and P-A over a broad range of momentum transfers to that a careful test of reaction mechanisms can be made.

The first measurements using the $^{12}C(p,p\gamma)$ reaction have just been completed, where the state of primary interst is the $J^\pi = 1^+$, $T = 1$ excitation at 15.11 MeV. This experiment used a beam of 150 MeV polarized protons from IUCF. The QDDM magnetic spectrograph was used for detection of the scattered protons. A large NaI crystal mounted at 90°, perpendicular to the scattering plane was used to detect the coincident de-excitation gamma rays. These initial measurements have yielded data over the q range from 200 to 400 MeV/c with a true/accidental ratio better than 10:1. These data are presently being analyzed. The gamma detector, shielding, and support structure were designed and fabricated at MIT.

g. $^{12}C(\alpha,\alpha)$ and $^{12}C(\alpha,\gamma\gamma)$ (MIT,OSU)

An experimental attempt was made to resolve a possible doublet at 9.85 MeV in ^{16}O using the $^{12}C(\alpha,\gamma\gamma)$ reaction at low energies. This work is being done at the Van de Graaff Laboratory of the Ohio State University in Columbus, Ohio. Resonant capture gamma rays decaying to the 2^+ state at 6.92 MeV are observed in coincidence with the photons subsequently emitted by this intermediate level. No direct evidence for a doublet is observed in the gamma decay data. A simultaneous measurement was also performed of the elastic scattering yield at 4 angles, where only an $\ell=2$ component can be observed. A careful correlation of the results from these two measurements is underway to investigate whether it might reveal an energy shift of the weak photon decay resonance energy from the 2^+ position, as determined from the elastic scattering results.

h. $\overleftrightarrow{H(d,P)}$ at IUCF (MIT,IUCF,ANL)

$\overleftrightarrow{H(d,P)}$ elastic scattering will be studied at 80 MeV at IUCF to ascertain the feasibility of constructing a higher energy deuteron polarimeter for use in the Bates d(e,e'd) T_{20} experiment.

3. Channeling of Electrons, and Coherent Radiation (MIT,LAMPF,LLNL)

Channeling of electrons and positrons in single crystals has been the subject of an exploratory computational effort. The work has been stimulated by experimental ideas for (e,e') photon coincidence work using the high resolution energy-loss spectrometer at Bates. A quantum mechanical model of axial channeling of electrons has been developed in order to understand the gamma-ray line structure observed experimentally. It has been possible to reproduce the energies and relative intensities of the radiation lines observed in crystal-line channeling. The observed widths are considerably greater than the natural widths for electric dipole radiation. The results indicate that the interaction of the channeled particle with the thermally vibrating crystal lattice is responsible for limiting the lifetime of the channeling state. The temperature and energy dependence of the linewidths is predicted by the model, and experimental investigation of these effects is planned in collaboration with the LLNL group in the near future.

The most recent efforts have studied the possibility of optical pumping to alter the population of channeling states. The frequency of a visible laser, entering the crystal anti-parallel to the electron or positron beam, will be greatly Doppler shifted in the particle's rest frame. This offers the possibility of matching the energy of some transitions with visible photons which are of order 50 eV in the rest frame. Calculations of necessary laser power levels, population densities of channeling states, and stimulated and spontaneous emission rates are in progress to study the feasibility of an optical pumping experiment.

4. Data Analysis Techniques (MIT,LAMPF)

A powerful lineshape fitting code, ALLFIT, has been developed which is capable of analyzing the spectra resulting from any binary reaction. The code is routinely used to analyze electron scattering spectra collected at Bates, proton scattering and charge exchange spectra collected at IUCF, and proton scattering spectra collected at HRS. It has also been used for transfer reactions at IUCF.

The code uses a maximum likelihood optimization criterion based upon Poisson statistics. The code is able to convolute a sophisticated multiparameter resolution function with an intrinsic lineshape. The intrinsic lineshape may be chosen as Gaussian, Breit-Wigner, or Lorentzian. Neglect of the intrinsic width of inelastic states can make large (50%) errors. The Lorentzian lineshape includes the proper threshold behavior. The electron scattering radiative response function may be either included in the empirical lineshape, or calculated theoretically. Radiative corrections can be applied separately. The background function consists of a continuous, piecewise smooth polynomial portion, including thresholds, and is supplemented, if desired, by an external spectrum.

Developments are in progress that will enable one to fit focal plane polarimeter data taken at the LAMPF HRS. For each incident beam polarization, the polarimeter measures the scattered beam polarization. These data form several spectra of polarization estimators. Simultaneous lineshape analysis of these several spectra will provide a more reliable treatment of the lineshapes of low statistics spectra, thereby maximizing productivity while minimizing systematic uncertainties.

U.S. DEPARTMENT OF ENERGY
FIELD TASK PROPOSAL/AGREEMENT

1. WP BIN NUMBER	2. TASK NUMBER	3. REV. NUMBER	4. PROJECT NUMBER	5. DATE PREPARED	6. CONTRACTOR NUMBER
AC02-76-ERO-3069	--	--	--	April 10, 1983	CH-3069-002(ME)-BATES

Item: 19.h. RELATIONSHIP TO OTHER PROJECTS

Page(s): 19.h.1

The work of the laboratory either directly or indirectly derives from the requirements of the experimental program. Through personal contact, at conferences, and inter-lab visits, attempts are made to coordinate materials, equipment standards, and research programs. This is especially important in this era of limited resources and in view of the growing use of a few central facilities by user groups from various institutions. Part of the program of the MIT Center for Theoretical Physics is directed to problems which are to be studied experimentally at Bates.

7.0 Oak Ridge National Laboratory
Holifield Heavy Ion Research Facility (HHIRF)

1. What new science is being explored by this facility? What scientific opportunities are being exploited?

Answer: The research capabilities of the Holifield Heavy Ion Research Facility (HHIRF) are being used to increase our knowledge of the behavior of nuclear matter under ever increasing conditions of temperature, pressure, spin, deformation, and neutron to proton ratio. A large effort is presently devoted to understanding a new time scale for nuclear reactions that appears to be characteristic of heavy ion collisions. This new time scale is rich in interesting phenomena which go by the names of nuclear orbiting, deep inelastic scattering, projectile excitation and decay, pre-equilibrium emission, and "fast" fission. Crystal blocking is one of the techniques being used to explore this time region. The effect of spin on nuclear structure and shape as well as its effect on the ultimate stability of nuclear matter is studied with the unique combination of HHIRF beams and the Spin Spectrometer. The stability and structure of nuclear matter far from the "valley of stability" and close to the proton drip line are studied with an on-line isotope separator, UNISOR, another unique facility. The production of neutral pions in heavy ion collisions is being studied at HHIRF to understand if collective pion production, as opposed to nucleon-nucleon production, is a real process. Using the broad-range spectrograph equipment at HHIRF, the interaction between colliding nuclei is being explored in new regions of mass, charge, energy, and angular momentum. The HHIRF facility is ideal for studying the giant resonance behavior of nuclei. Experiments in progress promise to provide the detailed information necessary to test the microscopic theories of giant resonances.

Energetic heavy ion projectiles also provide a source of atoms with few (or no) orbital electrons. Atomic structure under relatively simple conditions can then be explored. Electron transfer cross sections can be obtained by matching the velocity of the accelerated stripped atom to that of the orbital electron velocities. Crystalline structure of materials can be investigated through resonant excitation of an atomic projectile when its velocity is appropriately related to the lattice spacing of the crystal.

The x-rays resulting from multiple inner-shell ionizations of energetic heavy ions with target material depend on the environment of the target atoms. The x-ray energies are correlated with bulk chemical properties such as valence electron densities, effective charge, and covalencies. Future investigations should provide chemical information on implanted materials and on metal alloys.

2. How does this facility's accelerator (or accelerators) performance compare with any other in the world that are operating, under construction, or planned?

Answer: The 25 MV Tandem Electrostatic Accelerator - With a design terminal potential of 25 MV, the Holifield Heavy Ion Research Facility (HHIRF) tandem accelerator is one of two existing electrostatic accelerators designed to operate at terminal potentials in excess of 20 MV. The other such accelerator is located at the Daresbury Laboratory in England and is comparable in size to the HHIRF accelerator. Since the achievable energy for partially stripped heavy ions is a strong function of terminal potential, the beam energy performance of the HHIRF and Daresbury accelerators is better than all other tandem accelerators. Of the tandem accelerators now under construction or planned, only one is larger than the HHIRF accelerator. This is a 35 MV accelerator now being planned for the Nuclear Research Center at Strasbourg, France.

Oak Ridge Isochronous Cyclotron (ORIC) - The cyclotron may be used to accelerate ions from an internal ion source (stand-alone operation) or to boost the energy of beams injected from the 25 MV tandem accelerator (coupled operation). Stand-alone operation is seldom used at present because higher energies and improved beam quality are obtained in the coupled mode. In coupled operation, the cyclotron provides energies of 25 MeV/amu in the mass range up to sulfur (A=32), energies exceeding 6 MeV/amu for ions of $A \leq 160$ and about 3 MeV/amu for the heaviest ions. The beams from the cyclotron are of very high quality with energy spread of 1/1000 and emittance (approximately the product of spot size and angular divergence) of about 3 mm-mrad.

3. **What types of research instrumentation/experimental devices are available at this facility, and what are their capabilities?**

Answer: The facility is equipped with 14 experimental stations. These are discussed below and grouped according to the accelerators to which they have access:

Tandem-only beam lines:

Velocity filter. By means of a separated element Wien filter, this device can remove the primary beam through velocity dispersion, permitting observation of reaction products at and near 0°.

Gamma-ray spectrometer station. This is a flexible system that allows for various combinations of Ge and NaI detectors and special devices such as a lifetime plunger.

High resolution split-pole magnetic spectrometer with provision for windowless gas targets by use of a supersonic gas jet.

Atomic physics station which can be adapted to a variety of existing devices. This line is also used for other portable equipment set up for specific experiments.

Coupled accelerators:

Gamma-ray station similar to the one on the tandem.

Two beam stations for temporary setups. Currently, these support atomic physics and pion experiments.

0.8-m-diameter scattering chamber.

Accessible from both tandem-only and coupled accelerators:

High-resolution (Elbek) magnetic spectrometer with multi-element gas detector for simultaneous measurement of Z, A, time-of-flight, E, position and direction of emerging charged particles.

Time-of-flight system (normal flight path of 1.2 m) with large area ionization chambers.

1.6-m-diameter scattering chamber.

Mass separator (UNISOR) for on-line study of short-lived radioactive nuclei produced in heavy ion induced reactions.

Spin spectrometer. This 4-pi spectrometer, composed of 70 tightly packed NaI detectors which encompass a 14-in-diam scattering chamber, measures the total gamma-ray multiplicity and energy associated with each nuclear event.

The data acquisition/reduction system utilizes three nearly identical computers, each with a Perkin-Elmer 3230 CPU and typical ancillary equipment. Communication with experimental devices is via CAMAC branch and serial highways. There is also a VAX 11/780 computer with an array processor that is used principally for calculations. The electronic pool contains about 800 modules.

4. What have been the facility's research highlights for the period FY 1981 - present, and what are anticipated for the remainder of FY 1984 and FY 1985?

Answer: The angular distribution of evaporated alpha particles were measured relative to the spin direction of a highly excited ^{170}Yb compound system. The nuclear spin direction was determined from the E2 gamma-ray cascade angular distribution detected by the 70 NaI detectors of the Spin Spectrometer. The measurements showed that the low energy alpha particles are primarily evaporated at 90° to the spin direction and that this effect is an increasing function of nuclear spin. The most reasonable interpretation of these results is that the alpha-emitting nuclei are oblate spheroids rotating about the symmetry axis and that their deformation increases with spin.

Also by use of the Spin Spectrometer, for the first time the gamma-decay from the giant quadrupole, giant monopole, and giant hexadecapole resonances in ^{208}Pb have been observed and their various decay branches have been measured. This information will be very useful in testing microscopic theories of nuclear structure.

With a diamond crystal target and a 120 MeV ^{16}O beam, the crystal blocking technique (channeling) was used to successfully measure deexcitation times of 4×10^{-19} sec for Mg products to 4×10^{-18} sec for N products. These values are consistent with statistical model predictions and demonstrate the sequential decay nature of the deexcitation process in heavy ion fusion reactions. They also represent some of the shortest deexcitation times measured by the blocking technique.

The optical isomer shift experiments for the spontaneous fission isomer, 0.94-ms ^{240m}Am, have been completed. The data from three separate and independent experiments have been analyzed. In these experiments, the symmetry axis of the deformed isomer was aligned by a laser-induced nuclear polarization technique. All three experiments yielded the same optical shift. When combined with the mu-mesic x-ray shift results for ^{241}Am and ^{243}Am, which were used as a calibration for the ^{240m}Am optical isomeric shift, an intrinsic quadrupole moment of 33.5 ± 1.5 eb for ^{240m}Am was obtained.

A systematic study of angular-momentum-dependent fission barriers has been carried out. Fission and, in some cases, evaporation residue excitation functions were measured for the compound nuclei ^{153}Tb, ^{158}Er, ^{181}Re, ^{186}Os, and $^{204,206,208,210}Po$. Except in the case of some of the Po systems, two to five different reactions were used to produce the same compound nucleus, with projectiles ranging from ^{9}Be to ^{64}Ni, thus isolating angular momentum effects over a large range of both excitation energy and angular momentum. Analysis of the data was carried out by means of statistical model calculations in which calculated fission barriers from the newly developed rotating finite-range model (RFRM) were incorporated. The RFRM takes into account effects of the finite range of the nuclear force, as well as surface diffuseness effects. Very good agreement between experiment and theory was found without any adjustment of the calculated RFRM barriers. Previous discrepancies between the rotating liquid-drop model (RLDM) and experimental results were explained. It was concluded that the RFRM should replace the frequently used RLDM in interpretations of data from heavy ion reactions and in making predictions of angular momentum effects.

Correlations of two protons emitted with small relative momentum ($dP < 80$ MeV/c) in reactions of 25-MeV/amu $^{16}O + ^{197}Au$ were measured. An enhancement in yield over that expected from uncorrelated emission was found at $dP = 25$ MeV/c; this enhancement goes to zero for $dP > 80$ MeV/c. An analysis indicates that less than 40 nucleons participate in the heated zone. For larger total proton energies, the apparent source size shrinks, indicating these correlated protons are emitted in a very early stage of the reaction before the energy deposited by the projectile has time to be shared among a large number of nucleons.

To date, the lowest energy per amu used to observe pion production is 35 MeV/amu ^{14}N at the MSU superconducting cyclotron laboratory. An attempt will be made to lower this limit to 22-25 MeV/amu using 400 MeV 160 and 200 MeV ^{32}S beams from HHIRF. These data will test theoretical calculations of pion production in heavy nucleus collisions.

The construction of a polarized gas-jet target will be completed and the device will be used to measure the dependence of fusion probability on the direction of the target symmetry axis relative to the incoming beam direction.

Sub-barrier and near-barrier fusion will also be studied using the newly commissioned velocity separator.

Many of the BGO Compton suppression elements for the Spin Spectrometer should be available in FY 1985. This upgrade of the device will greatly enhance its capabilities for nuclear spectroscopy of high-spin states and for studies of nuclear reaction mechanisms.

5. **What facility changes and additions have occurred or are anticipated for the period FY 1981 - FY 1985?**

Answer:

(1) Completion of the Holifield Heavy Ion Research Facility (HHIRF) construction project (FY 1982; $18,000,000).

(2) Buildings, building additions or modifications

a. Joint Institute for Heavy Ion Research - Bldg. I (FY 1981; $439,000; funding included $100,000 from Vanderbilt University and $100,000 from State of Tennessee).

b. Detector Laboratory (FY 1982; $50,000).

c. HHIRF South Research Addition (FY 1983; $435,000).

d. Joint Institute for Heavy Ion Research - Bldg. II (FY 1983; $394,000; $350,000 from State of Tennessee and $44,000 from Oak Ridge Associated Universities).

e. Applications and Atomic Physics Research Addition (planned; $425,000).

(3) Accelerator improvement or modification projects or major accelerator equipment acquisitions (year completed, cost).

a. Improved negative ion sources (FY 1983; $200,000).
b. Improved beam buncher system (FY 1985; $450,000).
c. ORIC control computer (FY 1985; $250,000).

(4) Major experimental apparatus.

a. Spin spectrometer (FY 1981; $370,000).
b. Gamma-ray spectrometer (FY 1981; $55,000).
c. VAX computer (FY 1982; $400,000).
d. Beam line to three major devices (FY 1983; $280,000).
e. Focal plane detector for magnetic spectrometer (FY 1983; $130,000).
f. Gas target for magnetic spectrometer (FY 1983; $40,000).
g. Velocity filter (FY 1983; $165,000).
h. Data acquisition/reduction computer (FY 1983; $1,130,000).
i. Polarizer for gas target for magnetic spectrometer (FY 1984; $115,000).
j. He transport system for UNISOR (FY 1984; $45,000).
k. UNISOR laser (FY 1984; $90,000).
l. BGO Compton suppression system - phase I (FY 1985; $800,000).
m. UNISOR nuclear orientation facility (FY 1985; $240,000).

6. For the period FY 1981 - FY 1985, please provide actual and estimated budget profiles for operations, in-house research, out-of-house research, other operating expenses, Capital Equipment, General Plant Projects, In-House Energy Management, and any other specific construction projects attributable to the facility. Please indicate the source of these funds (i.e., Medium Energy Nuclear Physics, Heavy Ion Nuclear Physics, Low Energy Nuclear Physics, High Energy Physics, Basic Energy Sciences, etc.).

Answer:

Hollfield Heavy Ion Research Facility
(B/A in thousands of dollars)

	FY 1981	FY 1982	FY 1983	FY 1984	FY 1985
Operations					
Heavy Ion Nuclear Physics	$ 3,525	$ 4,100	$ 4,408	$ 4,700	$ 4,905
Low Energy Nuclear Physics	40	40	49	50	50
Total	$ 3,565	$ 4,140	$ 4,457	$ 4,750	$ 4,955
In-House Research					
Heavy Ion Nuclear Physics	$ 2,539	$ 2,688	$ 2,564	$ 2,874	$ 2,890
Low Energy Nuclear Physics	147	184	477	364	456
Total	$ 2,686	$ 2,872	$ 3,041	$ 3,238	$ 3,346
Out-of-House Research					
Medium Energy	$ 84	$ 88	$ 0	$ 0	$ 0
Heavy Ion	456	379	531	736	884
Total	$ 540	$ 467	$ 531	$ 736	$ 884
Capital Equipment					
Nuclear Physics	$ 1,020	$ 1,010	$ 990	$ 1,290	$ 1,250
Accel. Improv. & Mod.					
Nuclear Physics	$ 200	$ 450	$ 0	$ 0	$ 0
General Plant Projects					
MFE	$ 435	$ 0	$ 0	$ 0	$ 425
UNISOR*					
Heavy Ion Nuclear Physics	$ 315	$ 345	$ 345	$ 345	$ 380
Capital Equipment	50	50	50	20	20
In-House Energy Mgmt.	$ 80	$ 0	$ 0	$ 0	$ 0

* University Isotope Separator - Oak Ridge (UNISOR) is operated by a consortium of universities under the auspices of Oak Ridge Associated Universities. The UNISOR project is an integral component of Hollfield.

7. **How much funding for FY 1981 - FY 1985 has been or is expected to be provided by other federal agencies such as the National Science Foundation or by State agencies?**

Answer: In FY 1981, the first users' building was completed. This building provides support space for short-term visiting users of the Holifield Heavy Ion Research Facility. The funding for this building included $100,000 contributed by the State of Tennessee through the University of Tennessee and $100,000 from Vanderbilt University.

In FY 1984, a second users' building was completed. This building (6,000 ft^2) contains office, laboratory, and auditorium space. The funds for this building ($394,000) were provided by the State of Tennessee ($350,000) and by Oak Ridge Associated Universities ($44,000).

The Joint Institute for Heavy Ion Research (JIHIR) will be housed in the two users' buildings. The JIHIR will be managed by a three-person committee with one representative each from the University of Tennessee, Vanderbilt University, and Oak Ridge National Laboratory. Beginning in late FY 1984, the committee will request operating funds of $165,000 per year from the State of Tennessee for the support of the JIHIR. In addition, Vanderbilt will provide $12,000. These funds will provide for operation of the second building, and will support distinguished scientists who will be brought as guests of the JIHIR.

About $65,000 per year of the support of UNISOR, which is one of the major experiment devices at Holifield is provided by a consortium of ten universities. In addition, these universities spend about $25,000 per year fabricating and procuring equipment which is placed at UNISOR.

8. **For the period FY 1981 - FY 1985, please provide actual and estimated staffing levels.**

Answer:

Holifield Heavy Ion Research Facility
Staffing Levels (Man Years)

	FY 1981	FY 1982	FY 1983	FY 1984	FY 1985
Operations	25.3	25.5	27.6	29.9	29.9
Research	25.5	27.8	26.5	28.9	29.2
UNISOR	4.0	4.5	4.5	4.6	4.6

9. **What is the actual and estimated facility utilization for the period FY 1981 - FY 1985? What would be defined as "full" utilization of the facility?**

Answer: For the period FY 1981 - FY 1985, actual and estimated utilization of the Holifield Heavy Ion Research Facility is given in the following table:

Holifield Heavy Ion Research Facility Utilization

	FY 1981	FY 1982	FY 1983	FY 1984	FY 1985
Beam Hours for Research	1,980	1,525	3,249	3,350	4,000

For the Holifield facility, we estimate full utilization to be 6,000 beam hours for research per year.

10. For the period FY 1981 - FY 1985, how many experiments will have been started, continued, and completed?

Answer: The number of experiments that have been run or are projected to be run in the period FY 1981 to FY 1985 is indicated below.

	FY 1981	FY 1982	FY 1983	FY 1984	FY 1985
Number of Experiments	40	44	53	54	65

Since the lifetime of a typical experiment is less than one year, the above numbers represent closely the experiments started and completed during this period. The total number of experiments performed in this 5-year cycle will thus be about 256.

11. What is this facility's user policy?

Answer: Use of the facility is open to all scientists with an approved research program. Such approval is obtained through formal submission of research proposals to a Program Advisory Committee (PAC). This committee, constituted of knowledgeable scientists representing the entire research community, reviews proposals and recommends approval or disapproval to the facility director. A formal solicitation for proposals is issued and meetings of the PAC are held on a semi-annual schedule.

The Holifield Heavy Ion Research Facility has a formal users organization which elects annually its own Executive Committee and Chairman. This group interacts directly with the facility management through the Facility Liaison Officer. In 1984, there were 470 members of the HHIRF Users Group.

12. For the period FY 1981 - FY 1985, how much reimbursable research has taken place or is estimated to take place? What revenues have been involved?

Answer: None.

13. What is the mechanism by which specific research proposals for experiments at the facility are considered?

Answer: Formal written research proposals are submitted to a Program Advisory Committee (PAC). This committee is constituted of knowledgeable scientists selected to represent the breadth of the research community interested in the capabilities of this facility. The PAC reviews proposals and recommends approval or disapproval to the facility director.

The PAC is appointed by Oak Ridge National Laboratory management from suggestions provided by the Executive Committee of the HHIRF Users Group and by interested users. The PAC has a rotating membership of 7 to 8 members with the restriction that no more than two may be from the same institution.

A call for research proposals is made, and the PAC meets to review these proposals, on a twice-per-year schedule. Announcement of the call for proposals is made by mailings to each member of the users organization (about 470 members) and through a newsletter published by the facility.

14. How many research proposals have been submitted over the past five years, and how many of these have been approved?

Answer: The Holifield Heavy Ion Research Facility began operation as a formal user facility with the initial operation of the 25 MV tandem in FY 1981. In the commissioning period, extending from FY 1981 through mid-FY 1984, the HHIRF Program Advisory Committee considered proposals for 154 experiments requesting a total of 15,848 research hours. From these, the PAC recommended approval of 67 for a total of 5,168 research hours.

The most recent request for proposals was issued in January 1984. Proposals for 57 experiments totaling 5,288 research hours were received. Of these, the PAC has been requested to recommend the best experiments totaling to no more than 2,200 hours.

Based on experience to date, it is anticipated that about 120 proposals for experiments totaling 11,000 research hours will be submitted each year. Of these, about 55 will be recommended for approval, amounting to about 4,400 hours of running time. It is expected that the total research time requested will average two to three times the amount that the facility can accommodate.

15. How many university personnel (i.e., faculty and students) have utilized the facility over the past five years?

Answer: The tandem accelerator of the Holifield Facility first became operational in June 1981. Between then and the present, there have been 87 persons (25 of these are students) from American universities who have participated in 1 or more experiments at the Holifield. However, because this period was also used to commission the accelerator system, there were several major blocks of time devoted to bringing the accelerator system up to its full operational capability. A more representative measure of normal operation would be a 12-month period of accelerator operation that ended August 31, 1983. In that period, 76 university personnel participated in the experimental program at the Holifield facility.

16. How many industrial researchers have utilized the facility over the past five years?

Answer: Since the tandem accelerator of the Holifield Facility first became operational in June 1981, there have been three researchers from the industrial sector.

17. How many researchers from foreign institutions have utilized the facility over the past five years?

Answer: Since the Holifield tandem accelerator first became operational in June 1981, there have been 18 researchers from foreign institutions who have participated in experiments at the Holifield facility. In the 12-month period of accelerator operation ending August 31, 1983, there were 14 researchers from foreign institutions.

18. How many researchers from other agencies have utilized the facility over the past five years?

Answer: Since the tandem accelerator of the Holifield facility first became operational in June 1981, there have been three researchers from agencies of the United States Government other than DOE.

19. What are the future development possibilities for this facility (including research instrumentation/experimental devices), what plans are being made to exploit these possibilities, and what are the budgetary implications?

Answer: There are many potential future development possibilities for this accelerator facility, but there are currently no approved plans to undertake any of them beyond the activities identified in the FY 1985 budget request. New research instruments and experimental devices will be developed as the physics research program progresses. We intend to give hign priority to the exploitation of the facility's unique capabilities.

20. Please provide a copy of the facility's latest annual report.

Answer: The annual report for the facility forms a portion of the Physics Division Progress Report. The latest report (ORNL-6004, December 1983) is attached. **(Note: Excerpts from this report follow.)**

ORNL-6004
Distribution Category
UC-34

Contract No. W-7405-eng-26

PHYSICS DIVISION

PROGRESS REPORT

for Period Ending September 30, 1983

J. B. Ball, Director

Date Published: December 1983

OAK RIDGE NATIONAL LABORATORY
Oak Ridge, Tennessee 37831
operated by
UNION CARBIDE CORPORATION
for the
DEPARTMENT OF ENERGY

1. HOLIFIELD HEAVY ION RESEARCH FACILITY

HOLIFIELD HEAVY-ION RESEARCH FACILITY

OVERVIEW

J. B. Ball
C. M. Jones
J. A. Martin
R. L. Robinson

Although interrupted by two periods required for commissioning and development work on the tandem accelerator, the Holifield Facility has been in operation (beginning June 17, 1981) throughout this report period providing beams for scheduled experiments with tandem-only, ORIC-only, and coupled operation. As shown in Fig. 1.1, reliability has steadily improved for tandem and coupled accelerator operation so that in the first seven months of 1983, an average of 400 research hours per month were provided. Since June 1, 1981 there have been 6549 hours for research divided as follows: tandem-only, 2621 h; ORIC-only, 1847 h; and coupled operation, 2081 h. Statistical information on research activities and research participation is given in Tables 1.1, 1.2, and 1.3.

Noteworthy achievements during the period include routine coupled operation and provision of beams of 36 ion species ranging in mass from H to ^{197}Au at energies up to 1000 MeV. A major disappointment has been failure of the tandem accelerator to reach its design terminal potential of 25 MV, a failure ascribed to damaged tube sections which are now being replaced. The highest value reached thus far is 22 MV without beam and 20 MV with beam.

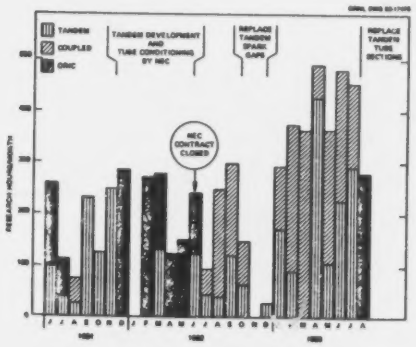

Fig. 1.1. Research hours per month for experiments utilizing the HHIRF accelerators.

Table 1.1. Division of research hours by research activities for period of June 1, 1981 to August 31, 1983

Activity	Research Hours			
	Tandem	Coupled	ORIC	Total
High-spin states	783	124	158	1065
Non-equilibrium processes	384	294	225	903
Energetic light-particles emission		333	121	454
Giant multipole resonances		435		435
Fusion	200	155	35	390
Detector tests	105	96	188	389
Transfer reactions	231	146		377
Decay of neutron deficient nuclei	86		291	377
Tests of experimental devices	120	49	195	364
Fission	55	65	206	326
Atomic physics	110	172		282
Scattering	145	67		212
Crystal blocking	115		67	182
Applications	86		50	136
Continuum γ rays	100		28	128
Nuclear shapes		83	20	103
Coulomb excitation	101			101
Pion production		62		62
Other			263	263
Total	2,621	2,081	1,847	6,549

New major experimental devices brought into operation during the period of this report were the velocity filter and the gas target assembly for the split-pole magnetic spectrometer. Other devices under development are a He gas transport system and an atomic hyperfine structure spectrometer, both part of the UNISOR mass spectrometer system, and a laser-pumped polarized-target assembly to be incorporated into the gas target of the split-pole magnetic spectrometer. Capabilities of many of the experimental devices have been substantially improved by a major effort of the Physics Division Nuclear Research Section to develop a variety of gas filled charged particle detectors. An outstanding accomplishment has been

Table 1.2. Number of researchers from different institutions who participated in experiments at the HHIRF in the fourteen month period between July 1, 1982 and August 31, 1983

Institutions	Number of Researchers
UNIVERSITIES	
Emory Univ.	1
Georgia State Univ.	1
Georgia Inst. of Tech.	7
Indiana Univ.	3
Jyvaskala Univ. (Finland)	1
Kansas State Univ.	3
Louisiana State Univ.	2
McMaster Univ.	1
Massachusetts Inst. of Tech.	1
Michigan State Univ.	7
Murray State Univ.	1
Niels Bohr Inst. (Denmark)	1
ORAU	3
Oregon State Univ.	1
Research Inst. of Phys. (Sweden)	2
Tennessee Tech. Univ.	1
Texas A&M Univ.	1
Univ. of Chicago	1
Univ. of Colgne (Germany)	1
Univ. of Frankfurt (Germany)	2
Univ. of Kentucky	1
Univ. of Maryland	4
Univ. of Mexico (Mexico)	2
Univ. of Rochester	3
Univ. of South Carolina	1
Univ. of Tennessee	13
Univ. of Virginia	2
Univ. of Washington	6
Univ. of Witwatersrand (South Africa)	2
Vanderbilt Univ.	9
Washington Univ.	5
Yale Univ.	1
	90
NATIONAL LABORATORIES	
AERE (Harwell)	1
BNL	2
Centro Atomico Baralache (Argentina)	1
LANL	5
NASA/Goddard	3
ORNL	45
Orsay (France)	1
	58
INDUSTRY	
Aerospace Corp.	3

Table 1.3. Use of experiment target stations for period of June 1, 1981 to August 31, 1983

Target Station	Number of Runs			
	Tandem	Coupled	ORIC	Total
γ-ray spectrometer (tandem)	8	na	na	8
γ-ray spectrometer (ORIC)	na[a]	1	3	4
Velocity filter	3	na	na	3
Atomic physics (tandem)	3	na	na	3
Atomic physics (ORIC)	na	2	1	3
Split-pole magnet	5	na	na	5
Applications (Beam line 31)	4	na	na	4
Beam line C-9	na	2	3	5
0.8-m chamber	na	3	4	7
Broad-range magnet	1	5	2	8
Time-of-flight system	2	4	4	10
1.6-m chamber	5	7	1	13
UNISOR	7	0	13	20
Spin spectrometer	10	3	6	19
Total	48	27	37	112

a) na = not accessible to beam

completion of a multi-element detector system for the broad-range magnetic spectrometer that has a position resolution of 0.1 mm.

The data acquisition/data reduction system is now composed of three, essentially identical computers with sufficient capacity to permit data acquisition by two experimental groups while at the same time allowing data reduction by one or more other researchers. A complete package of software for handling histograms has been developed. An additional, "calculational" computer centered around a VAX 11/780 main frame with an array processor was brought into service.

A 3400-ft^2 annex was completed that will satisfy a variety of space needs for the experimental facility and, in particular, makes space available for one and possibly two new target rooms. A second building for the Joint Institute for Heavy Ion Research was begun in May 1983. This will provide offices and laboratories for HHIRF users from the universities of Tennessee, guest appointees of the Institute, and staff persons of UNISOR.

The HHIRF, as one means to determine how to best use its resources in fulfilling its mission as a user facility, requests regular reviews by a panel of distinguished scientists. This Policy Review Committee last met with the ORNL management on October 21-22, 1982 and provided valuable recommendations on operating strategies, composition of the Program Advisory Committee, future directions, and experimental

instrumentation. Members of the Committee that took part in the review were W. L. Brown (Bell Laboratories), J. H. Hamilton (Vanderbilt University), T. A. Tombrello (California Institute of Technology), J. P. Unik (Argonne National Laboratory), and H. E. Wegner (Brookhaven National Laboratory).

Probably the most unusual occurrence during the period of this report was the rupture of a 41-cm-diam water main just behind the HHIRF building. Before appropriate valves could be closed, about four million liters of water spewed out, and were largely collected in the ground floor of the HHIRF building. The short-lived flood crested at about 70 cm in the UNISOR and spin spectrometer areas.

ACCELERATOR OPERATIONS

N. F. Ziegler	P. K. Kloeppel[1]
C. L. Viar	R. C. Juras[2]
P. T. Singley	C. M. Jones
E. G. Richardson	N. L. Jones
S. N. Murray	F. Irwin
S. W. Mosko	E. D. Hudson
G. D. Mills	C. L. Haley
C. A. Maples	H. D. Hackler
J. E. Mann	R. H. Enix
C. A. Ludemann	B. J. Casstevens[3]
R. S. Lord	J. A. Biggerstaff
C. T. LeCroy	J. A. Benjamin
S. N. Lane	G. D. Alton

Although hampered by commissioning and development work on the tandem accelerator, the Holifield Facility has been in almost continuous operation throughout the period covered by this report, providing beams with tandem-only, ORIC-only, and coupled operation. Two milestones are of special importance: In June 1982, the installation phase of the National Electrostatics Corporation (NEC) contract and the construction phase of the facility were completed and the facility began routine operation. In January 1983, the facility scheduling basis was changed from 15 shifts/week to 21 shifts/week - a change which has resulted in a noticeable improvement in efficiency.

Electric power budgetary limitations continue to restrict ORIC operation to about 2500 hours per year. Efficient accelerator utilization has been achieved by using the tandem accelerator in stand-alone mode whenever possible and using ORIC almost exclusively in the booster mode to reach beam energies beyond the capability of the tandem accelerator.

Utilization analyses for the tandem accelerator and ORIC are presented in Tables 1.4 and 1.5, respectively. Table 1.4 covers the period which begins with routine operation on June 7, 1982 and ends with the start of the maintenance period which is now in progress. Table 1.5 covers the period of this report.

An important contribution to efficient operation of the Facility is a formal operator training and certification program which began in October 1982 and ended in July 1983. This program, which focused primarily on operation of the tandem accelerator, utilized almost 60 hours of video taped lectures prepared by Facility staff members. At this time, eight members of the operations staff have been formally certified for tandem accelerator operation and five members are certified for ORIC operation.

Table 1.4. Tandem accelerator utilization for the period June 7, 1982 through July 31, 1983

	Hours	Percent
Beam available for research (tandem-alone and coupled operation)	3760	37
Beam available during ORIC tuning (coupled operation)	599	6
Accelerator tuning (includes scheduled startup-shutdown and conditioning)	1872	19
Machine studies	726	7
Unscheduled maintenance	856	8
Scheduled maintenance	895	9
Scheduled shutdown	1371	14

Table 1.5. Cyclotron accelerator utilization for the period June 1, 1981 through September 30, 1983

	Hours	Percent
Beam available for research (cyclotron-alone and coupled operation)	3928	20
Beam available during tandem tuning (coupled operation)	417	2
Accelerator tuning (includes scheduled startup-shutdown)	980	5
Machine studies	549	3
Unscheduled maintenance	1830	9
Scheduled maintenance	1272	6
Scheduled shutdown	10734	54

1. Guest scientist from Monmouth College, Monmouth, IL.
2. Instrumentation and Controls Division.
3. UCCND Computer Sciences Division.

TANDEM ACCELERATOR

N.F. Ziegler
E.G. Richardson
J.E. Mann
R.C. Juras[1]
C.M. Jones
J.A. Biggerstaff
J.A. Benjamin
G.D. Alton

Introduction

The period covered by this report has seen a concerted effort by NEC and ORNL staff members to complete commissioning of the tandem accelerator and to prepare the accelerator for routine operation in the facility experimental program. The first part of the period, July 1981 through May 1982, was devoted to work by NEC and to two interim periods of operation: July 1981 through mid-November 1981 and the month of March 1982. The second part of the period, which began after completion of the installation phase of the NEC contract in June 1982, has been devoted to routine operation, interrupted by one long maintenance period: mid-October 1982 through mid-January 1983. In the remainder of this contribution we will discuss several aspects of this work, with emphasis on voltage performance and our experience in routine operation.

Voltage Performance

Tests of the voltage holding capability of the column structure before installation of acceleration tubes were performed by NEC in May 1979. The essential result of these tests[2,3] is that the column structure appears to be easily capable of operation at potentials near 30 MV. Furthermore, although operation at this level was quite limited in time, there was no evidence of significant spark induced damage to the column structure.

Voltage performance of the accelerator with acceleration tubes has been less encouraging. Although, on isolated occasions, the accelerator has been conditioned to 22 MV without beam and operated with beam at a potential of 20 MV, a more typical limit to terminal potential under normal operating conditions has been 18 MV. At higher voltages, there has been a tendency for the accelerator to spark and in some cases for such sparks to cause the acceleration tube conditioning threshold to be reduced (spark-induced deconditioning). Tests of individual 61-cm units show that typically a number of units tend to spark at gradients well below their nominal maximum operating gradient of 1 MV - at times at gradients as low as 0.7 MV/unit.

In some cases, the resistance of individual acceleration tube gaps has been lowered to values as low as a few GΩ. Physical examination of 20.3-cm acceleration tube sections removed from the accelerator indicates that lowered gap resistance is caused by metalization of the inside surface of the insulator due to apparent insulator flashover. These effects are typically most pronounced at end gaps (with the most severe damage occurring at the negative end of the section).

Our response to this problem has been influenced, in part, by the special situation which results from our ability to use the ORIC as an energy booster for tandem beams. Specifically, with the ORIC as an energy booster, we may produce beams whose energy far exceeds that which could be obtained from the tandem accelerator operating alone at 25 MV. Furthermore, as shown in Fig. 1.2, the maximum energy of beams which may be obtained from tandem-ORIC coupled operation is sensitive to the maximum tandem terminal potential only for higher masses. Since the beams which may be produced in tandem-ORIC coupled operation represent an almost unique capability at this time, our primary focus in the past two years has been on utilization of the tandem accelerator rather than achievement of ultimate voltage performance. Specifically, it was these considerations which motivated us to negotiate with NEC two periods of interim usage prior to completion of the installation phase of the contract and our decision to operate the tandem accelerator for a period of approximately one year (June 1982 - July 1983) before beginning a significant acceleration tube replacement program.

Initial attempts to solve our voltage performance problems focused on two areas: spark gaps and hydrogen glow discharge cleaning. In December 1980, the end spark gaps of each 20.3-cm acceleration tube section were readjusted by NEC to reduce the average gap spacing by about 20%. Eight 20.3-cm acceleration tube sections were also replaced at that time. In November 1981 and April 1982, NEC performed a hydrogen glow discharge cleaning procedure on the

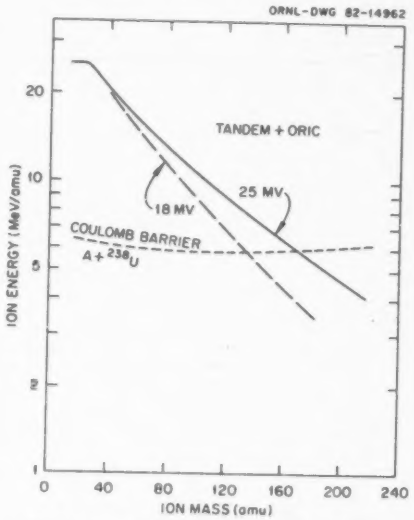

Fig. 1.2. Ion energy performance functions for coupled operation with two assumed values of maximum tandem accelerator terminal potential.

acceleration tubes using a technique similar to that described by Isoya et al.[4] Four 20.3-cm acceleration tube sections were also replaced in April 1982. Finally, in November 1982, all of the acceleration tube spark gaps were replaced with gaps provided by NEC which had been manufactured to the design used in previously built NEC accelerators. (The Oak Ridge accelerator had originally been equipped with spark gaps of a "new" design.) Unfortunately, none of these measures resulted in significantly improved voltage performance.

Since other large accelerators manufactured by NEC have shown satisfactory voltage performance,[5] the question remains as to the source of the difficulties in the Oak Ridge accelerator. Our present thoughts on this problem are strongly influenced by the observation that pathological acceleration tube behavior in the Oak Ridge accelerator is almost wholly confined to the upper two-thirds of the column and tends to be found on the low-energy side. Two hypotheses have been suggested. The first is based on the fact that the Oak Ridge accelerator was equipped with permanent magnet electron traps in each of the five dead sections. Although the field in these traps is adjustable, it is not possible to adjust the field to zero value. We note also that maximum beam transmission in the low-energy acceleration tube varies approximately linearly from about 60% for light ions (^{16}O) to almost 100% for ^{197}Au. This behavior is consistent with steering of the beam or elements of the beam in the low-energy acceleration tube by residual magnetic fields. We therefore hypothesize that part of the beam (typically 50%) is chronically lost in the low-energy acceleration tube and that, for reasons not understood, this lost beam has a deleterious effect on the acceleration tube. This hypothesis is supported by the observation that only the JAERI 20-MV accelerator and the Oak Ridge accelerator were equipped by NEC with electron traps and that the JAERI accelerator, which is operating much closer to its design voltage[6] than the Oak Ridge accelerator, was equipped with only four electron traps, one of which (the first one on the low-energy side) was removed early in the installation. The other hypothesis is based on the fact that the Oak Ridge accelerator has had a relatively large number of vacuum leaks which allowed SF_6 to be admitted into the column vacuum system. These have ranged from small, chronic leaks of long duration to catastrophic leaks which, in at least one case, pressurized the acceleration tubes to more than two atmospheres (absolute) of SF_6. Specifically, we note a correlation between the location of small leaks of long duration (many months) and the location of pathological acceleration tube behavior. We thus hypothesize that SF_6 has a deleterious effect on acceleration tube performance, an hypothesis which is supported by detailed observations of the response of the JAERI 20-MV accelerator to small SF_6 leaks.[6]

Since removal of the magnetic electron traps involves a significant perturbation of the column vacuum system, our short term response to the hypotheses described above has been to make a strenuous effort to eliminate all SF_6 leaks into the column vacuum system. Unfortunately, the removal of significant SF_6 leaks has not resulted in improved voltage performance. We therefore have concluded that either (1) the deflected beam effect is the more important, (2) the acceleration tubes have been permanently damaged (by metalization of the insulators), or (3) other effects, not yet completely understood, are operative.

As the next step in our efforts to improve voltage performance, we are now engaged in a maintenance period (which began August 1, 1983) in which all electron traps have been removed and all apparently defective acceleration tube sections have been replaced. We then expect that by operating the accelerator only in the absence of SF_6 leaks we can more accurately test the hypotheses described above.

Routine Operation

As indicated above, the installation phase of the NEC contract was completed in June 1982. Since that time, with the exception of one scheduled maintenance period, the tandem accelerator has been operated continuously for the facility experimental program. The first period of operation, on a nominal fifteen 8-hour shift per week basis, extended from June 1982 to October 1982. During this interval, there was one tank opening and the time in which beam was available for experiment in stand-alone operation or for ORIC injection averaged 65 hours/week. The second period of operation, on a nominal twenty-one 8-hour shift per week basis, began January 1983 and continued until the end of July 1983. During this period, there were three short tank openings and the time in which beam was available for experiment or ORIC injection averaged 112 hours/week. Beam time available for experiment or ORIC injection since June 1982 is shown in Fig. 1.3.

The maintenance period which began in November 1982 was scheduled primarily for the purpose of replacing the acceleration tube spark gaps and elements of the terminal water cooling system (pump, distribution system, and associated instrumentation). This time was also used to replace all corona points in the column, to replace the SF_6 vacuum pump oil mist eliminators, and to make a number of other changes and improvements.

In broad perspective we have, with the exception of voltage performance, been pleased with the performance and reliability of the accelerator. After some initial problems resulting from misalignment, the column rotating shafts are now performing well and have accumulated more than 16,500 operating hours without requiring general bearing replacement. After more than 13,000 operating hours, the six Pelletron charging chains have performed almost flawlessly and have required only replacement of a few idler wheels. With the exception of one quadrupole lens which malfunctioned due to apparently defective feedthrough couplings and column Faraday cups and variable apertures whose bellows failed prematurely, virtually all major components of the accelerator have performed as designed. We believe that it has been clearly demonstrated

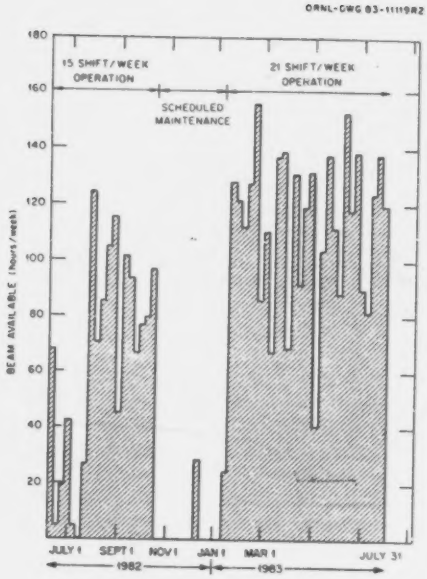

Fig. 1.3. Tandem accelerator beam time available for experiment or ORIC injection June 7, 1982 – July 31, 1983.

Table 1.6. HHIRF beams provided for scheduled experiments

Beams	Source	Maximum Energy (MeV)	Comments
^{9}Be	A	158*	BeH_3 - injected
^{11}B	S	93	
^{12}C	A	126	
^{16}O	A, S	405*	
^{17}O	A	381*	Separated isotope probe
^{18}O	A	348*	Separated isotope probe
^{19}F	A	190	
^{24}Mg	A	129	MgH_3 - injected
^{25}Mg	A	132	MgH_3 - injected
^{26}Mg	A	132	MgH_3 - injected
^{28}Si	A	200	
^{32}S	A	679*	
^{34}S	A	143	
^{35}Cl	A	680*	
^{37}Cl	A	160	
^{46}Ti	A	229	TiH_3 - injected
^{50}Ti	A	230	TiH_3 - injected
^{56}Fe	A	821*	FeH - injected
^{58}Ni	A	896*	
^{60}Ni	A, S	228	
^{64}Ni	A	285	Separated isotope probe
^{63}Cu	A	189	
^{79}Br	A	1000*	
^{107}Ag	A	233	
^{109}Ag	A	733*	
^{116}Cd	A	495*	CdO - injected, separated isotope probe
^{116}Sn	A	631*	Separated isotope probe
^{120}Sn	A	240	
^{197}Au	A	100	28+ charge state provided with post-accelerator stripper

*Coupled operation.

that the accelerator, although complex, can function well in the real world of scheduled experiments in a national user facility.

Ion Sources

As indicated above, the tandem accelerator was first used to provide beam for scheduled experiments in June 1981. Table 1.6 summarizes the beams which have been provided since that time. Although a modified General Ionex Corporation Model 834 sputter source (indicated by "S" in the table) has been used to produce several of these beams, the source used for virtually all scheduled operation to date is a version of the Aarhus radial extraction Penning source which has been further modified and developed at ORNL by Alton[7] (indicated by "A" in the table). We have used this source for two basic reasons: (1) It is a versatile, prolific source and (2) it exhibits good stability in both intensity and position. Two especially notable achievements have been development of intense Mg beams using CuMg alloy probes and development of ^{17}O and ^{18}O beams using copper oxide probes fabricated with ^{17}O and ^{18}O enriched gas.

SF_6 Handling System

The SF_6 handling system was commissioned in May 1979 and has been in almost continuous use since February 1980. At this time, 55 complete transfers (storage to accelerator to storage) have been accomplished without major incident or significant SF_6 loss. The observed average SF_6 inventory loss of 1.9% per year since February 1980 is attributed primarily to loss during transfers with some additional loss due to leakage through small leaks. The observed increase in air concentration of about 0.6% is attributed wholly to transfers.

We have reported previously a problem which occurred when carbon steel piping components immediately downstream from the SF_6 vaporizer were excessively cooled by liquid SF_6 droplets which passed through the vaporizer.[2] This problem has been solved through installation (by

NEC) of an entrainment separator downstream from the vaporizer. Other significant changes to the system included installation of new oil mist eliminators (which may be evacuated) for the SF_6 vacuum pumps and a scavenge compressor for the crank cases of the two large SF_6 compressors.

Although we have experienced some corrosion problems due to water introduced into the SF_6 by leakage from the terminal cooling system, we have experienced no problems which may clearly be attributed to SF_6 breakdown products.

---

1. Instrumentation and Controls Division.
2. C.M. Jones, Nucl. Instrum. and Methods 184 (1981) 145.
3. C.M. Jones, Proceedings of the Third Conference on Electrostatic Accelerator Technology, Oak Ridge, Tennessee, April 13-16, 1981, p. 23.
4. A. Isoya et al., Ibid., p. 98.
5. D.C. Weisser, Ibid., p. 31.
6. G.A. Norton et al., Proceedings of the 1982 Symposium for Northeastern Accelerator Personnel, Seattle, Washington, October 6-8, 1982, p. 32; and G.A. Norton, private communication.
7. G.D. Alton and G.C. Blazey, Nucl. Instrum. and Methods 166 (1979) 105.

TANDEM ACCELERATOR CONTROL SYSTEM AND COMPUTER BASED AIDS TO OPERATION

R.C. Juras[1] K.A. Erb
J.A. Biggerstaff P.K. Kloeppel[2]
R.O. Sayer[3]

The digital control system provided by NEC is a CAMAC based system employing bit-serial highways. An essential feature of the system is a 32kb "shared" memory which contains virtually all control and monitoring information and which may be accessed by each of two computers. As provided by NEC, the system employed two Perkin-Elmer 7/32 computers. The first was used as a controller and interface between the shared memory and the CAMAC highways and the second served to perform more sophisticated functions such as monitoring, logging, diagnostics, and control. The latter computer was named the control and supervisory computer (CSC).

Since initial installation of the control system, the CSC has been replaced by a Perkin-Elmer 8/32 computer which has also been provided with memory and disc-storage expansions. This computer, which is equipped with a multi-user, multi-task operating system, now performs its original functions and also is used for calculation of initial operating parameters for ORIC operation. In addition, it supports software development for both accelerators. Other significant improvements made since initial installation include a complete rewriting of the operating system software, expansion of the system to include control of beam lines contiguous to the tandem accelerator, and incorporation of software based monitoring and alarm functions.

An interesting development has been the use of the CSC to actively control elements of the accelerator system. The first example of this type of application is a group of programs which are used to control the three dipole magnets of the tandem accelerator system. Specific applications are: (1) Control of the 90° injector magnet to measure and record mass spectra of beams from the injector, (2) control of the 180° terminal magnet to measure and record mass and charge state spectra of beams transmitted through the terminal region, and (3) automatic recycling of the 90° energy analyzing magnet to minimize energy calibration errors due to differential hysteresis effects. The second example is a group of programs which perform two important functions related to routine operation. In the first, ion-optic parameters from selected runs may be stored in memory and after appropriate editing serve as a reference for future setup functions. In the second, ion-optic parameters from a run in progress or a run recalled from memory can be scaled to serve as the parameters for a new run. With one command, these new parameters can be written into the control system shared memory, thus setting all ion-optic component power supplies (except two dipole magnets). We find this program useful for changing energies, charge states, etc., and for set up of new beams.

The CSC is also being used for more passive functions. These include parameter logging (both upon request and automatically), diagnostic functions such as mass and charge state identifications, and calculation of both equilibrium charge state fractions and setup parameters dependent on these fractions.

---

1. Instrumentation and Controls Division.
2. Guest scientist from Monmouth College, Monmouth, Ill.
3. UCCND Computer Sciences Division.

CARBON STRIPPER FOIL PERFORMANCE

R.L. Auble D.M. Galbraith

The operating period from November 1982 to July 1983 saw the first large scale use in the tandem accelerator of carbon stripper foils made by the glow discharge process.[1] Foils made by this process have been found to be less susceptible to radiation induced failure than those made by vapor deposition and should provide a longer period of operation before reloading of the foil changer is required. The foils were made by dc-cracking of an ethylene-10% argon mixture at 0.2 Torr and 3 kV, for times of 10, 15, 30, and 45 seconds. Fourteen of the 30-s foils were mounted on aluminum rings to produce "slackened" foils.[2] A total of 158 glow discharge and 18 vapor deposited (5 $\mu g/cm^2$) foils were loaded in the changer. These foils were used to strip beams of ^{11}B, ^{16}O, ^{28}Si, ^{35}Cl, ^{48}Ti, ^{50}Ti, ^{58}Ni, and ^{64}Ni. The lifetimes of the glow discharge foils, relative to the vapor deposited foils, followed the trends expected

from reported foil lifetime studies.[3] Average lifetimes of the glow discharge foils, relative to the vapor deposited foils, were: $T(10\ s + 15\ s)/T_{VD} = 1$, $T(30\ s + 45\ s)/T_{VD} = 9$, $T(30\ s\ slackened)/T_{VD} = 40$. It should be noted that there were large variations in the lifetimes of the glow discharge foils, several of which had negligible lifetimes. These variations were not as evident for the slackened foils.

The need to extend foil lifetime also became apparent. For example, in one run covering ~4 days of operation with a ^{58}Ni beam, 51 foils were consumed. The enhanced lifetimes found for slackened glow-discharge foils makes their use highly desirable. Unfortunately, the method commonly used to slacken foils, which requires reducing the diameter of a soft aluminum ring, becomes very costly and time-consuming when applied to large scale foil production; therefore, a simpler technique was developed. Briefly, the foil is picked up on a conventional frame and immediately placed foil side up over a cavity into which dry nitrogen is flowed. The pressure under the foil is increased until the foil slides on the frame to produce a 2-3-mm-high "bubble". The gas flow is then reduced to the point where it just prevents the bubble from collapsing and is maintained until the foil is completely dry (~2 min.). This method is fast and easy; however, the amount of slackening is not as consistent as with the "ring-shrink" technique. One question which remains is whether the stress applied to the foil during slackening causes damage which might affect its lifetime. This question should be answered during the next operating cycle since approximately one-half of the foils used in the present loading (September 1983) were slackened using this technique. Slackened glow-discharge foils, fabricated with the technique described above, have also been provided for use in the EN tandem accelerator where their lifetimes will be studied under somewhat different conditions.

---

1. D.S. Whitmell et al., Nucl. Instrum. and Methods 159 (1979) 605.
2. B.H. Armitage et al., Nucl. Instrum. and Methods 155 (1978) 565.
3. R.L. Auble, Proceedings of the Third International Conference on Electrostatic Accelerator Technology, April 1981, p. 158.

ORIC OPERATION AND DEVELOPMENT

E. D. Hudson, R. S. Lord, C. A. Ludemann, S. W. Mosko, C. L. Viar, R. L. Auble, C. E. Bemis, Jr., B. J. Casstevens[1], F. Irwin, P. K. Kloeppel[2]

Coupled Operation

Routine coupled operation of the tandem accelerator and ORIC commenced July 29, 1982. Since then, beams up to mass 116 have been accelerated. The most frequently used beam was 400-MeV $^{16}O^{8+}$ (maximum attainable energy per nucleon). The highest total energy achieved was 1 GeV (^{79}Br).

The tandem voltage for most coupled operation beams was between 12 and 16 MV. In many cases this is sufficient for optimum performance; however, for the higher mass beams, optimum intensity will not be achieved until higher injection energies are available. During the first period of operation in 1981, beams of especially high energy resolution were obtained. It has not been possible to consistently reproduce beams of this quality, and the reasons for loss of resolution are not fully understood. A systematic investigation of the problem is in progress.

Stripping foil lifetime in the cyclotron has exceeded expectations. Only a few foils have failed during operation. It has been found, however, that beam intensity for nickel and iron beams increases by 20-40% if foils are changed about once in 24 hours.

Beam losses occur at several points in the coupled configuration. If we consider only losses occurring after the beam exits the tandem accelerator, the principal reasons for loss are: (1) only about half the bunched beam is within the ±3-degree window needed for acceleration with energy spread of 1:1000; (2) the fraction of beam in the desired charge state after stripping in the cyclotron is typically less than 30%, and even less than 5% in extreme cases; (3) the efficiency of beam extraction from the cyclotron varies between 30 and 80% depending on turn spacing, beam phase width, beam centering, etc. Beam loss due to interaction with residual gas has not been measured but seems to be quite small. Pressure in the injection line is about 5×10^{-8} Torr. Pressure in the cyclotron is about 10^{-6} Torr.

Table 1.7 gives the measured beam intensity at various points for several typical runs. Predicted intensities with 50% bunching efficiency assumed are also tabulated. The differences between actual and predicted beam intensities may be attributed to inexact knowledge of the charge fraction, bunching efficiency, and charge exchange. A detailed study has not been undertaken since all available accelerator time has been allocated to experimental physics and to developing new beams.

Residual Radiation

During a routine radiation survey when the cyclotron extraction system was removed for repair, alpha activity was discovered on the extraction elements and other nearby components. The sources were identified as ^{208}Po, ^{209}Po, and ^{210}Po through measurement of the alpha-particle energies.

For a variety of projectile-target combinations, many different multinucleon transfer reactions and subsequent radioactive decay-chains can lead to these Po isotopes. An experimental measurement of the cumulative production cross sections for these Po isotopes in reactions of 820-MeV ^{56}Fe with Ta was subsequently performed using the stacked foil

Table 1.7. Typical ion beam intensities as measured at the tandem exit, cyclotron internal, and cyclotron exit

Ion	Beam from Tandem (pnA)	Cyclotron Circ. Beam Meas. (pnA)	Cyclotron Circ. Beam Pred. (pnA)	Extracted Beam Meas. (pnA)	Extracted Beam Pred.* (pnA)	Extracted Beam Max.** Observed (pnA)
^{9}Be	9	3	4.7	2.3	3.5	3.3
^{16}O	18	3.2	2.3	1.9	1.4	60
^{17}O	8	1.1	0.44	3.3	1.7	3.3
^{58}Ni	29	1.4	1.6	0.43	0.48	1.3
^{116}Cd	5	0.32	0.53	0.16	0.27	0.5

* The predicted currents include factors for bunching efficiency (assumed to be 0.5) and stripping efficiency (assuming a foil of equilibrium thickness). The observed extraction efficiency was used.

**Record maximum intensity observed for this ion. The other values are self consistent.

technique. Production cross sections of ~100 mb were obtained. These long-lived, alpha-active nuclides presumably may be formed when: (1) the sum of nucleons in the target and projectile exceeds 210-230; (2) the total number of protons is at least 84, and (3) the projectile energy is sufficient to produce the required multinucleon transfer (~10 MeV/amu).

To avoid the potential health hazard of alpha-contaminated accelerator components, we have substituted molybdenum for tantalum and tungsten wherever these metals are exposed to the high energy beam - principally the tungsten septum and tantalum extraction system shields. The effect of this substitution on polonium production is shown in Fig. 1.4.

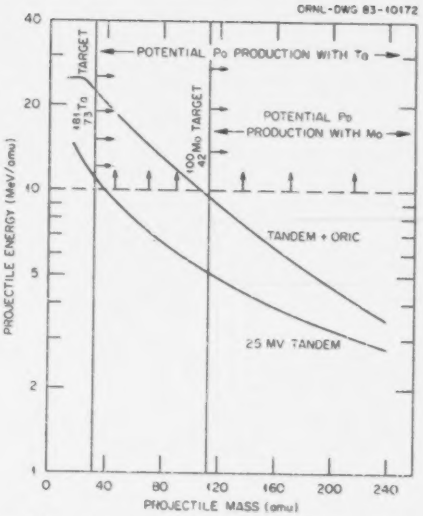

Fig. 1.4. The potential for producing polonium exists to the right of the target lines (^{181}Ta, ^{100}Mo) and above the energy threshold (~10 MeV/amu). Substituting molybdenum for tantalum and tungsten shields and septum moves the polonium production potential effectively out of range of MHIRF capability if 10 MeV/amu is the threshold energy.

Dual Arc Chamber Heavy Ion Source

A dual-arc chamber, heavy-ion source for stand-alone operation has been tested on ORIC. The source offers improvement in performance for beams below mass 20. A 42-μA beam of $^{16}Ne^{5+}$ was extracted from ORIC using the dual-arc-chamber source and a 1.5-μA beam of $^{20}Ne^{5+}$ was obtained 1.5 min after turning on the arc voltage.

Most cyclotron internal heavy-ion sources are of the Penning cold cathode type. The maximum charge obtainable from these sources, at intensities sufficient for useful experiments, is limited partly by how low the arc chamber pressure can be maintained while achieving sufficient ion bombardment of the cathode to sustain an arc discharge. Previously, the use of a heavy support gas such as krypton or xenon had proved to be very successful in improving performance of the ORIC ion source by increasing the intensity of the higher charge states for ion masses of 20 or less. In the new source, an auxiliary arc chamber has been added to the cold cathode Penning ion source, Fig. 1.5. This chamber is separated from the main arc chamber by a 0.5-mm-wall tantalum sleeve which forms the

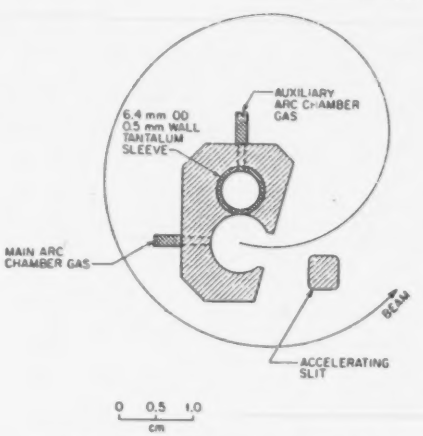

Fig. 1.5. Median plane cross section of the dual arc chamber source.

liner of the auxiliary arc chamber. Support gas is supplied directly to the auxiliary arc chamber rather than to the main chamber, as is done with the regular ORIC ion source. The only connections between the two arc chambers are at the ends next to the cathodes.

The new source appears to be more stable and to have the capability of producing larger beam currents of the higher charge state ions for masses up to 20. It has been demonstrated that two arcs can be operated in parallel and that one of the arcs can be used to influence the output of the other arc (probably by influencing the temperature of the common cathodes). It is possible that, to some degree, these positive results may be due directly to the introduction of the support gas in a region where it interacts with the cathodes before it reaches the extraction region of the main arc chamber. Further tests are planned to determine if the dominant characteristics of the dual arc chamber source are due to the cathode temperature control, to the placement of the support gas, or to some as yet undetermined factor.

Extraction System Improvements

Several extraction system modifications were implemented to improve extraction efficiency and to increase the reliability of component position sensing. The 1.5-mm graphite slotted septum of the electrostatic deflector was replaced with a 0.25-mm nonslotted metal septum, and the shape of the septum was made to conform more closely with the known orbit shape. These changes resulted in a septum with a greater effective length and smaller effective thickness. The gradient was also increased by reducing the deflector-septum gap. The maximum gradient is now ~100 kV/cm at 50 kV.

Linear position sensing potentiometers were installed on both magnetic extraction channels, and position readings are available in computer scanned data channels. Previously, the extraction channel position data was obtained from synchro readouts which were coupled to positioner drive systems. These synchros were subject to calibration loss each time the drive systems were uncoupled for maintenance.

Power Supply Improvements

A power supply upgrade program is continuing for magnet coil power sources associated with the cyclotron and with beam line components. All obsolescent power supplies which use germanium transistors and/or vacuum tube amplifiers are to be replaced with modern equipment. Many of the new power supplies have SCR regulators instead of the traditional series transistor regulators. The SCR units are much less expensive since they are typically available in "off the shelf" configurations while the series transistor units are typically custom designed. In order to achieve acceptable current regulation with typical SCR units, it is necessary to provide an external high stability shunt or other current sensor for incorporation in the regulator loop. Loss of bandwidth is not a problem, since most magnet coil loads have sufficient inductance to reduce current ripple and noise to acceptable levels. Eight units ranging in size from 250 A to 1000 A have been installed since 1982.

Control System Development

One of the early successes of the computer control system was in the tuning of the harmonic coil currents to cancel imperfections in the magnetic field caused by asymmetric cyclotron elements such as the extraction system. Rather than tune individual power supply currents, the operator is provided with controls which represent coefficients in trigonometric relationships. The operator is able to tune each set of harmonic coil currents in such a manner that their contribution to the azimuthally averaged field is a constant while their resultant cancellation field can be altered in strength and azimuth. The computer's computational capability provided a significant increase in reliability, reproducibility, and control resolution in comparison with that which was obtained by electromechanical means.

The approach to tuning the four sets of harmonic coils has changed with the advent of the capability to compute magnet settings and extraction system parameters of the ORIC. In order to provide a systematic approach to the verification of our computational model (and in turn, the development of new ion beams from this model), an attempt has been made to restrict operator tuning of machine elements to only small excursions from computed values. In practice, this is difficult to do with the original harmonic controls. An additional set of controls has been created in order to assist the operator. These are called "micro-harmonics." The operator can add a small harmonic strength vector to the original harmonic vector and vary its azimuth through 360 degrees. The computer calculates the vector sum with its appropriate cancellation currents and a systematic sweep can be accomplished. If no improvement in tuning is found, the operator simply resets the "micro-vector" to zero amplitude and the coil currents return to their prescribed values.

Functional control of the inside and outside coil currents of the lower channel extraction element has been coded and will be implemented at the end of the present shutdown period. Here "strength" and "balance" controls determine the coil currents which the computer calculates from a polynomial representation of a model relationship. These control functions will permit independent adjustment of the internal field of the channel as seen by the extracted beam, and the external field of the channel (ideally zero) as seen by the circulating beam. It is expected that this capability will make optimization of extracted beam easier and more straightforward.

A multi-task monitor program for microprocessors was written for the Intel 8085, incorporating features that would be beneficial in other microprocessors used in controlling and monitoring experiments and accelerators.[3] The monitor places permanent programs (tasks) located arbitrarily through ROM in a priority ordered queue. The programmer is provided with

the flexibility to add new tasks or modified versions of existing tasks, without having to comply with previously defined task boundaries or having to reprogram all of ROM. Scheduling of tasks is triggered by timers, outside stimuli (interrupts), or inter-task communications. Context switching time is of the order of tenths of a millisecond.

The first application of the monitor was the replacement of a digital voltmeter and mechanical cross-bar scanner with a faster, more modern scanning system. The system permits the control computer to continuously scan 96 data channels at a 100 Hz rate (the old system scanned one channel every two seconds and could not be operated continuously). A manual control panel and LED display are provided for off-line operation. The actual digitization of the analog signals is performed by integrating ADCs at 15 Hz. These are incorporated into eight commercial scanners[4] that provide information in ASCII form over a 9600-baud, 20-mA current loop. The command-reply sequence to poll each of the scanners and the structure of the messages is such as to keep almost continuous traffic on the loop. The monitor not only controls the flow of information from the transducers but significantly expands the system capability by producing, in conjunction with the control computer, optional local or public address system voice-synthesized alarms for up to 64 parameters.

The monitor also has been used to control beam emittance measurements[5] and will make possible a considerable cost saving by emulating stepper motor controllers for the planned rf improvement.

---

1. UCCND Computer Sciences Division.
2. Monmouth College, Monmouth, IL.
3. C.A. Ludemann, "A Microprocessor Multi-Task Monitor," presented at the 3rd Biennial Conference on Real-Time Computer Applications in Nuclear and Particle Physics, Berkeley, CA, May 16-19, 1983.
4. Manufactured by Analog Devices, Norwood, MA.
5. C. E. Bemis, Jr. et al., ORIC Beam Emittance Measurements, this report.

ORIC BEAM-EMITTANCE MEASUREMENTS

C. E. Bemis, Jr.[1] J. A. Biggerstaff
C. A. Ludemann[2] J. W. McConnell
P. A. Kloeppel[1] J. W. Johnson

A beam-emittance-measurement instrumentation system has been installed in the ORIC extracted beam line to provide on-line diagnostic information for accelerator tuning and to provide ion-optical information required for subsequent beam transport. This commercially available system[2] is described elsewhere in detail.[3] Two orthogonal stepper-motor-driven arms, each containing a plate with a 0.1 x 40 mm slit and a 32-channel detector assembly located 40 cm downstream, are moved sequentially across the ion beam. At selected positions in the ion beam profile, either vertical or horizontal measurements of the slit-transmitted beamlet are made with the 32-channel detector. The beamlet angular divergence and angular extent at selected beamlet current profile levels are readily determinable. The motor drive, control, status, and multiplexed slit/detector readout electronics are accessible via standard CAMAC hardware. Local crate control of the emittance measurements is accomplished using an 8085 microprocessor. Software for control of the emittance equipment and the acquisition of the emittance data executes efficiently under a multitasking monitor executive.[4] The raw emittance data, after a complete measurement, are passed via the CAMAC serial highway to the HHIRF Data Acquisition Computer where data manipulation, calculations, and the generation of color displays are performed.

Initial measurements with the device were made on a $^{160+5}$ beam at 130.2 MeV from ORIC using an internal ion source. The results are shown in Fig. 1.6 for the entire angular extent of transmitted beamlets, i.e., the emittance at the 100% beam contour level. In ORIC, the horizontal direction (X) is the axial direction, and the vertical direction (Y) is the radial or energy dispersive direction. Both the horizontal and vertical beam profiles and corresponding emittance diagrams are shown. An upstream quadrupole doublet presents a converging beam in X (horizontal) and slightly converging beam in Y (vertical) to the emittance equipment. No attempt, in these brief, initial measurements, was made to investigate the wide range of ORIC parameters which could affect the exit beam emittance.

As these emittance measurements on ORIC were the first ever performed with heavy ions, a few features should be noted. Currently used values of the ORIC exit emittances for ion-transport calculations are 10π mm-mrad horizontal and 20π mm-mrad vertical, as based on earlier measurements with protons.[5] We expect the transverse emittances for ions of mass A and energy E to scale as the longitudinal momentum, i.e., $\varepsilon = \sqrt{E/A}$. For heavy ions in ORIC, transverse emittances should be larger than those measured earlier for protons for the same cyclotron parameters, dimensions, and tuning. This is clearly not the case, especially for the vertical, since the vertical emittance is at least a factor of 4 smaller than expected.

The vertical emittance and profile displayed in Fig. 1.6 also shows the clear presence of two separate beams. Multi-turn extraction, i.e., beams with different energies, is the most plausible and attractive explanation (ΔE would be ~800 keV for adjacent orbits for this case), although other explanations have been proffered.

Some improvements in the equipment, particularly in improving the angular resolution, are being implemented. Full integration of the emittance-measurement equipment into the control system is contemplated. We expect the emittance on-line diagnostic to be a useful tool in routine

HHIRF accelerator operations and development, particularly for coupled accelerator operations.

---

1. Monmouth College, Monmouth, IL.
2. NTG Nucleartechnic, GmbH Am Spielacker, 6460 Gelnhaussen, West Germany.

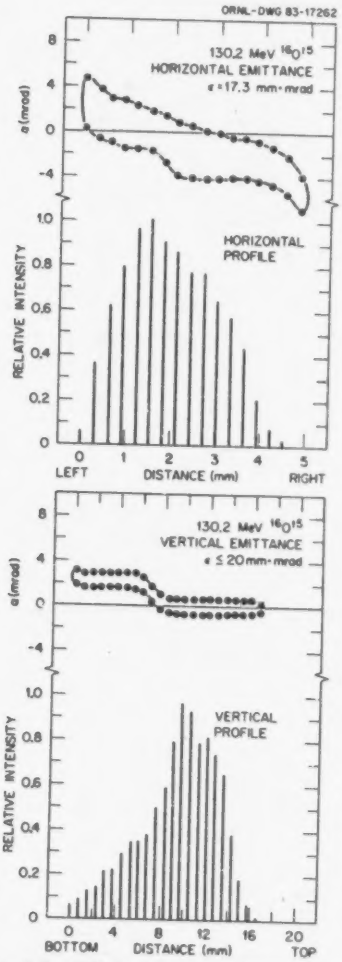

Fig. 1.6. ORIC horizontal emittance and beam profile (upper curves) and vertical emittance and beam profile (lower curves) measured for a 130.2 MeV $^{16}O^{5+}$ beam.

3. A. Ehrlich, J. Glatz, and P. Strehl, Gesellschaft für Schwerionenforschung Report, GSI-PB-3-74, pp. 19-26 (1974).
4. C. A. Ludemann, "A Microprocessor Multi-Task Monitor," Proceedings of the Third Biennial Conference on Real-Time Computer Applications in Nuclear and Particle Physics, Berkeley, California, May 1983 (to be published); also, C. A. Ludemann DVM Replacement using a Microprocessor Multitask Monitor (this report).
5. Electronuclear Division Annual Report, ORNL-3630 (1963), pp. 54-57.

NEW SOURCES AND SOURCE CONCEPTS

G.D. Alton R.M. Beckers[1] J.W. Johnson

Negative ion source research and development activities during the past months have centered around design, fabrication, and preliminary evaluation of additional cesium plasma sputter ion sources and modification of a high intensity He^- charge exchange source so that it can be used to produce a wide spectrum of negative ions. In the remainder of this contribution we give a brief discussion of each of these sources.

The Radial Geometry Cesium Plasma Ion Source

The basic principles underlying ion formation in this source are identical to those of the original modified University of Aarhus geometry source which has been used for almost all routine operation of the tandem accelerator.[2] However, efforts have been made to improve mechanical design features of the source in order to facilitate maintenance and rapid change of degradable components, as well as to provide better thermal isolation between the cesium reservoir and the plasma generation region of the source. For example, the cesium oven in the new source is mounted externally, permitting easy access for servicing while effecting excellent thermal isolation between the plasma discharge chamber and the oven, thus alleviating thermal feedback to the oven due to changes in discharge power. In addition, the main source subassembly can be quickly and easily withdrawn from the freon cooled housing to facilitate rapid replacement of ionization filaments. An important design feature allows removal and replacement of the boron-nitride sputter probe insulator without major disassembly of the ion source. Thus, insulators which have been contaminated during source operation can be quickly replaced without prolonged down time. A schematic drawing of the new source is shown in Fig. 1.7.

Preliminary operational experience indicates that the source has improved stability, better thermal isolation, and higher beam intensities than its predecessor. For example, total negative ion beam intensities from Ni and Cu probes have exceeded 80 μA and 140 μA, respectively.

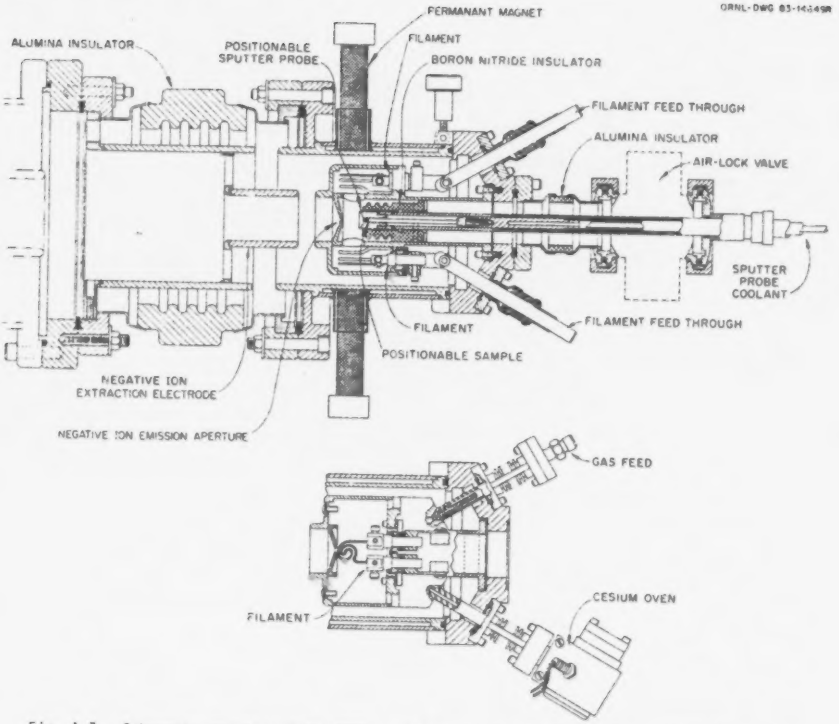

Fig. 1.7. Schematic drawing of the ORNL radial geometry cesium-plasma negative ion source.

The Axial Geometry Cesium Plasma Ion Source

Conversion of the radial geometry source discussed above to an axial geometry source is easily accomplished by mounting an annular surface ionizer on the axis of negative ion extraction. Such sources have been previously developed at the University of Wisconsin,[3] ORNL,[4] and, more recently, at the University of Pennsylvania.[5] The surface ionizer is usually a helically wound tungsten or tantalum wire but may be a continuous surface such as that described in this report.

Because of the annular geometries of surface ionizers usually utilized in the axial geometry sources, the sputter probe is bombarded nonuniformly, resulting in a strong wear pattern on or near the probe axis surrounded by a more diffuse pattern. As a consequence of the continued erosion of the sample surface, the negative ion extraction optics also change continually. This problem has been reduced substantially in the present design by incorporation of a linear sample feed mechanism shown schematically in Fig. 1.8.

The new source concept was optimized by performing detailed calculations of positive and negative ion trajectories. The annular surface ionizer is made of solid tungsten and heated by a noninductively wound tungsten filament. Thus, the cesium plasma source may be operated in the axial or radial modes by an almost trivial modification. Future comparative performance studies are planned so that an objective decision can be made as to which configuration is best in terms of intensity, number of species, operational stability, reliability, and emittance properties.

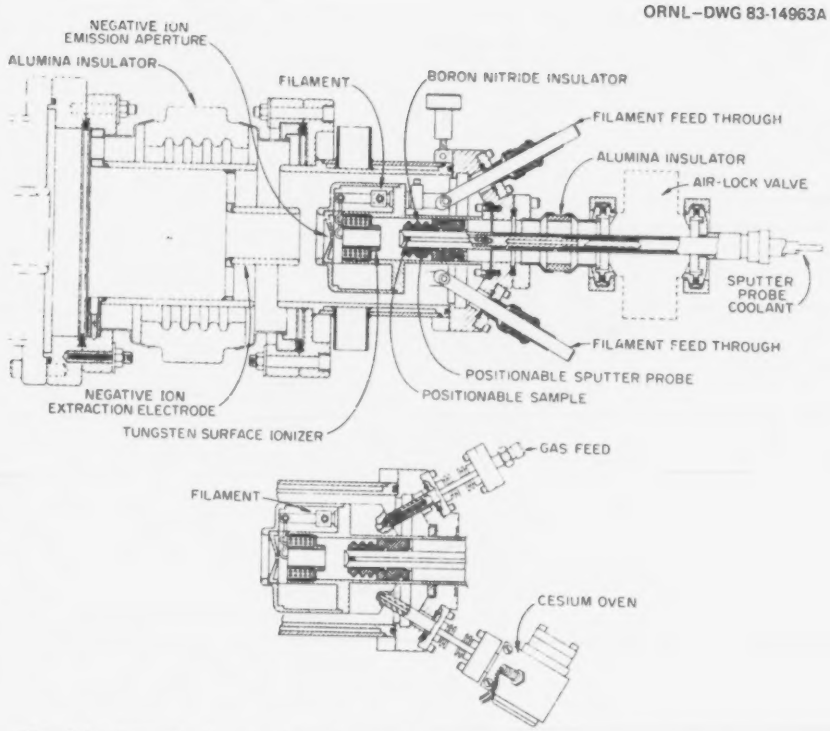

Fig. 1.8. Schematic drawing of the ORNL axial geometry cesium-plasma negative ion source.

The Universal Charge Exchange Source

Negative ion conversion from an initially positive ion beam interacting with a low ionization potential vapor can take place with high probability. The charge exchange mechanism is therefore a practical method for the production of negative ion beams and has been utilized for this purpose for several years.

Production efficiencies depend primarily on ion energy, the electron affinity of the element under consideration, and the electron binding energy of the donor material. For efficient ion production, members of the Groups IA and IIA elements are usually utilized as donor materials.

Extensive and systematic investigations of the exchange production of many ions in sodium and magnesium vapors have been reported in recent years.[6,7] These investigations show production efficiencies ranging from ~0.5 to >90% for the elements considered. These studies indicate that Mg is a more effective electron donor for high electron affinity elements while Na vapor is desirable for the production of beams from low affinity materials.

The gaseous feed positive sources (duoplasmatrons or radiofrequency sources) usually utilized restrict the number of species that can be produced. Incorporation of a universal type positive ion source permits generation of negative ions from any element which has a positive electron affinity as well as a number of metastable ions. The ORNL universal source is illustrated schematically in Fig. 1.9. This source employs a hollow cathode positive ion source and a recirculating lithium charge exchange canal developed for use in high intensity He^- ion sources.[8]

The source has been installed on the negative ion test facility and is in the initial stages of evaluation. The source will be used

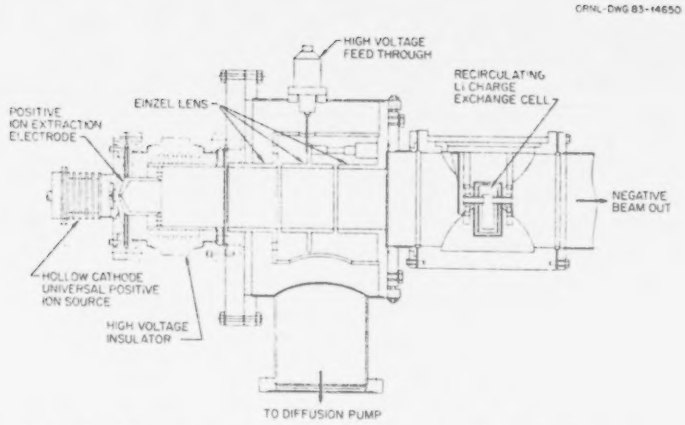

Fig. 1.9. Schematic diagram of the ORNL universal charge exchange source.

primarily in attempts to form difficult negative ion beams such as Group IA and IIA elements.

---

1. UCC-ND Engineering Division.
2. G.D. Alton and G.C. Blazey, Nucl. Instrum. and Methods **166**, 105 (1979).
3. G.T. Caskey, et al., Nucl. Instrum. and Methods **157**, 1 (1978).
4. G.D. Alton, IEEE Trans. Nucl. Sci. **NS-26**, 3708 (1979).
5. R. Middleton, Proceedings of the Symposium of Northeastern Accelerator Personnel, University of Wisconsin, Oct. 13-15, 1980, p. 134.
6. J. Heinemeier and P. Hvelplund, Nucl. Instrum. and Methods **148**, 65 (1975).
7. Ibid., p. 425.
8. T.J.L. Greenway, Oxford University Report 85/77 (1977), unpublished.

PROGRESS TOWARD GENERATION OF NEGATIVE ION BEAMS FROM DIFFICULT ELEMENTS

G. D. Alton J. A. Benjamin

The group IIA elements (Be, Mg, Ca, Sr, and Ba) have negative ground state electron affinities and thus do not form stable ground-state atomic negative ions. Therefore, other techniques must be employed for the production of these elements in order to meet the intensity requirements of tandem accelerator applications. For example, some of these elements (Be^- and Ca^-) can be formed through charge exchange in metastably bound, autoionizing states which have lifetimes long enough to be of practical value.[1,2]

The metastable characteristics of other members of the group have not been investigated at this time and therefore it is unclear whether the charge exchange technique can be employed for their production. Charge exchange sources are typically more complex in design and operation and many such sources also have relatively short operational lifetimes due to high rates of exchange vapor expenditure. However, operational lifetimes can be extended considerably by incorporating a recirculating exchange vapor cell.[3]

These elements can also be formed as molecular negative ions (usually in the form of oxides or hydrides) in conventional Middleton-Adams geometry sources or other sources utilizing the principle of this source. The hydride is preferred due to the mass partition of energy in the low energy stage of the tandem accelerator. In these sources, the hydride is most efficiently produced by introducing ammonia (NH_3) onto the cone surface rather than hydrogen (H_2) due to the greater reactivity of NH_3 for hydride formation with these elements. However, observed negative ion intensities usually fluctuate widely with time when ammonia is used for their production - resulting in erratic and unpredictable behavior. The problem is due in part to the difficulty of precisely metering ammonia into the source by means of conventional leak valves and therefore controlling the chemical reaction rate between ammonia and the sputter sample. Ammonia may also be chemically deleterious to component parts of the source due to its very active nature.

The ORNL modified University of Aarhus geometry source,[4] has been used recently in conjunction with the Holifield tandem accelerator to produce μA intensities of the Group IIA elements. The intensities and operational stabilities associated with the production of these beams are such that the new method can be viewed

as a significant advancement for the generation of molecular hydride negative ions with these difficult elements. The method is a particularly effective means of producing high intensity beams of MgH_3^-.

During initial investigations involving the production of magnesium hydride beams from elemental Mg sputter probes, beam intensities exceeding 5 μA MgH^- were realized. However, these intensities rapidly decreased due to excessive reaction and sublimation rates, and resulting probe shape degradation. In an attempt to control this deleterious effect, a 76% Mg-24% Ni (atomic percentages) sputter probe was prepared. A yield of ~3 μA MgH_3^- was observed which declined with time as well, but over a substantially longer time period. Observation of the probe wear pattern indicated that the alloy was effective in eliminating the problem previously experienced with elemental Mg probes. The decrease in observed intensity in this case was believed to be associated with the low Ni sputtering rate relative to the chemical erosion and sublimation rates of Mg, subsequently producing an almost pure nickel probe surface. In order to test this conjecture, a 60% Mg – 40% Cu alloy probe was procured. Copper was chosen because its sputtering rate is higher than that of nickel at the same ion energy. This approach proved successful, producing analyzed MgH_3^- negative ion beams in excess of 12 μA.

During these tests, both H_2 and NH_3 reactants were used. The negative ion yield decreased when Cs was introduced into the source with H_2 reactant gas, while Cs was required for optimization when NH_3 was used.

A list of momentum analyzed, negative ion yields produced during extended periods of source operation is shown in Table 1.8. A single attempt was made to generate beams of BaH_n^- from 50% Ba-50% Cu alloy. Beam intensities were <100 nA, presumably due to a very thick oxide layer which formed during transfer into the vacuum system. Further development efforts regarding this element (Ba) as well as the other members of the group are planned. Increased yields from most of the elements are expected as more time is given to their generation.

The technique of employing alloys is useful in controlling sublimation and excessive chemical reaction rates during source operation for the more active Group IIA elements. Their use also has the attractive advantage of providing other ion beams such as Cu^- from a single probe as well. This suggests the use of composite alloy probes for generating several different ion beams from the same probe, obviating the necessity of changing probes during specific accelerator runs. The chemical effects, if any, of the alloy constituent Cu on the negative ion yield are not known at this time. Interesting intermetallic alloy negative ion beams from all of the Group IIA elements have also been observed - a discovery which may have future implications for providing negative ion beams from other difficult elements.

Table 1.8. Momentum analyzed negative hydride ion yields of the Group IIA elements

Element	Discharge Gas	Probe Material	Principal Negative Ion Species	Intensity (μA)
Be	H_2	Be	BeH_3^-	0.6-4
Mg	H_2	60% Mg-40% Cu	MgH_3^-	2-12
Ca	H_2	50% Ca-50% Cu	CaH_3^-	0.5-2
Sr	H_2	50% Sr-50% Cu	SrH_3^-	0.4
Ba	H_2	50% Ba-50% Cu	BaH_3^-	<0.1

1. J. Heinemeier and P. Tykesson, Nucl. Instrum. and Methods 141 (1977) 183.
2. W. Kutschera and G. Korschinek, Proc. Second International Conference on Ion Sources, Vienna, Austria (1972) p. 908.
3. T.J.L. Greenway, Oxford University Report 85 (1977), unpublished.
4. G.D. Alton and G.C. Blazey, Nucl. Instrum. and Methods 166, 105 (1979).

EXPERIMENTAL STUDIES OF THE REFOCUS SPUTTER NEGATIVE ION SOURCE

G. D. Alton

Progress derived from both experiment and theory has been made in recent years toward a better understanding of the basic processes which underlie negative ion formation by sputtering in the presence of Group IA adsorbates. The dependence of negative ion yield on alkali metal surface coverage was first demonstrated experimentally by Abdullayeva et al.,[1] while more recently a direct or nearly direct correlation between negative ion yield and surface work function was made by Yu.[2]

Quantum mechanical treatment of the non-thermodynamic equilibrium secondary ion emission problem has been made by Norskov and Lundqvist in the first order time dependent perturbation theory approximation.[3] The probability of electron attachment at distances far from the metal is found to be exponentially dependent on the difference between the electron affinity E_A and the work function ϕ with the denominator in the exponential term proportional to the velocity of the sputtered particle. Thus, higher velocity particles are more efficiently ionized in this model. We note that the negative ion yield in the adiabatic approximation to the model is similar to the modified surface model used at ORNL to compute relative negative ionization probabilities.[4,5] Because of both the interrelationship between source operational parameters and the inability to directly monitor certain functions, interpretation of yield data from negative sputter sources has proved to be difficult. In the present work, experiments have been performed which were designed to establish more directly the correlation between positive cesium ion current utilized to sputter the material of interest and the resulting

observed negative ion yields from conventional refocus geometry sputter sources.

Studies were made of the dependence of Cs^+ ion current on ionizer porosity for each of two porosities with respective densities $\rho_0 = 0.7\ \rho_0$ and $\rho = 0.8\ \rho_0$, where ρ_0 is the theoretical density of tungsten. The positive ion current under temperature-limited conditions for the $\rho = 0.7\ \rho_0$ ionizer is ~5 times that of the $\rho = 0.8\ \rho_0$. The $\rho = 0.7\ \rho_0$ ionizer produces positive ion currents equivalent to those of the conventionally used $\rho = 0.8\ \rho_0$ ionizer at ~60°C lower cesium oven temperatures. Figure 1.10 shows the relationship between cesium ion current I^+ and extraction voltage V_{ex} at several cesium oven temperatures obtained with the $\rho = 0.7\ \rho_0$ ionizer.

Total negative ion yields from carbon and copper samples were also measured as a function of extraction voltage for various cesium oven temperatures. The maxima in the yield versus extraction voltage for Cu^- were found to occur at ~8 kV, while those from C^- were observed at ~20 kV. The maxima in the negative ion current were found to occur at positive cesium ion currents of ~0.4 mA for Cu^- and 2 mA for C^-. Negative ion yields were also found to initially increase in close correlation with the product of sputter coefficient and cesium ion current for both samples. Total Cu^- negative ion yield I^- versus extraction voltage V_{ex} data are shown in Fig. 1.11.

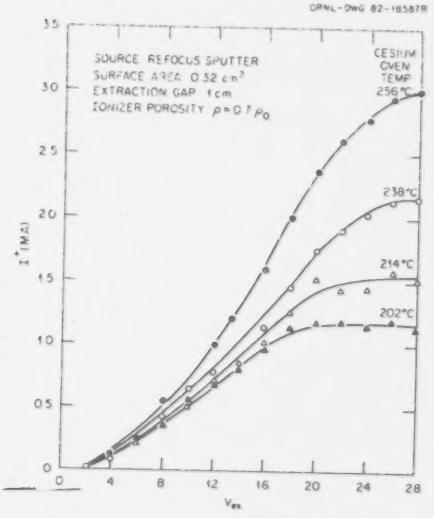

Fig. 1.10. Cesium surface ionization source positive ion current I^+ versus extraction voltage V_{ex} for several cesium oven temperatures.

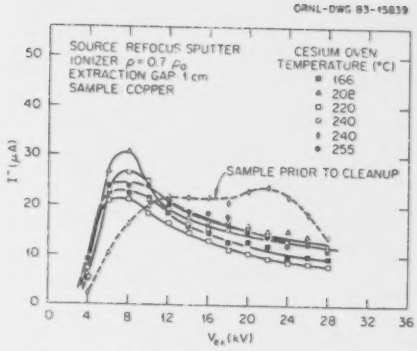

Fig. 1.11. Total Cu^- negative ion yields I^- versus extraction voltage V_{ex}.

Experimental measurements of the dependence of negative ion yield on sample temperature were also performed. The results show that Cu^- ion yields are independent of sample temperature over a temperature range 40°C < T < 200°C and that C^- yields are affected only marginally. These findings are commensurate with the constant temperature values required to fit the modified surface ionization theoretical model to observed negative-ion yield data.[4,5] These findings also support recent first order perturbation theoretical predictions that the negative ion generation by sputtering process depends on the velocity of the sputtered particles and not on the sample temperature.[3] The results for Cu^- are shown in Fig. 1.12.

1. M.K. Abdullayeva, A.K. Ayukhanov, and V.G. Shamsiyev, Determination of the Negative Ion Yield of Copper Sputtered by Cesium Ions in Ion

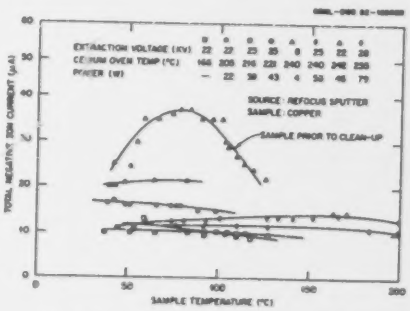

Fig. 1.12. Dependence of total Cu^- negative ion yields on sample temperature.

Surface Interactions, Sputtering and Related Phenomena, eds, R. Behrish, W. Hieland, W. Poschanvieder, P. Staib, and H. Verbeek (Gordon Breach, London, 1973).
2. M.L. Yu, Phys. Rev. Lett. 40, 574 (1978).
3. J.K. Norskov and B.I. Lundqvist, Phys. Rev. B 19, 5661 (1979).
4. G.D. Alton, Proceedings of Third International Conference on Electrostatic Accelelerator Technology, Oak Ridge, TN, 1981, p. 228.
5. G.D. Alton, IEEE Trans. Nucl. Sci. NS-30, No. 2, 1480 (1983).

REFLECTED BEAM ION OPTICAL STUDIES: REFOCUS SPUTTER NEGATIVE ION SOURCE

G. D. Alton

The refocus type source can be operated in the reflected beam mode by steering the beam at a slight angle with respect to the axis of symmetry while allowing the beam to pass through an aperture into the deceleration field. The action of the field reflects the beam backward along the initial direction of motion. By properly positioning the aperture with respect to the axis of symmetry, the cesium beam can be steered so that it impacts a sample mounted on axis. This mode of operation has found practical use in production of beams from small isotopically enriched samples and as a concept useful in tandem mass spectrometry applications.[1] The final results of ion optic calculations for this mode of operation are shown in Fig. 1.13. The beam size on impact was found to be sensitively dependent on angle of entrance and included angle of the beam itself as well as position of entrance into the retarding field.

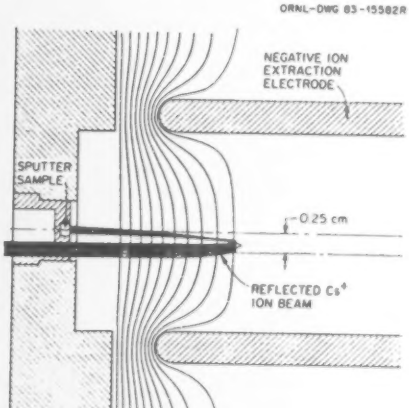

Fig. 1.13. Ion optics of the reflected beam sputter source.

1. K. Brand, Nucl. Instrum. and Methods 154, 595 (1978).

PROGRESS TOWARD UNDERSTANDING THE NEGATIVE ION GENERATION VIA SPUTTERING MECHANISM

G. D. Alton

Quantitative understanding of work function changes $\Delta\phi_m$ due to adsorption has been seriously impeded by the lack of accurate theoretical or semiempirical analytical expressions for relating changes in work function to surface coverage. In order to predict maximum negative ion generation probabilities from work function dependent models, it is necessary to know or be able to calculate the value of the work function at its minimum. A semiempirical relation has been found which reproduces with good accuracy maximum work function changes for alkali metal adsorption on polycrystalline materials.[1,2] The expression is:

$$\Delta\phi_m \text{ (eV)} = -1.24\ [\phi_o - 1/2(I_a + E_a)]\ . \qquad (1)$$

where ϕ_o is the intrinsic work function of the surface and I_a, E_a are respectively the ionization and electron affinity of the adsorbate material.

Experimental and calculated values using Eq. (1) for changes in work function due to various electropositive adsorbates are compared in Table 1.9. Experimental values were taken from the indicated references. A number of the values shown in Table 1.9 were derived from ORNL modified University of Aarhus geometry negative ion source data by assuming negative ion generation through a surface ionization mechanism. The agreement of calculated and experimental values is taken as evidence of the appropriateness of Eq. (1) for calculating $\Delta\phi_m$ and also that surface ionization is the mechanism for negative ion production for the cases considered.

1. G.D. Alton, Proc. of the Third International Conference on Electrostatic Accelerator Technology, Oak Ridge, TN, 1981, p. 228.
2. G.D. Alton, IEEE Trans. Nucl. Sci. NS-30, No. 2, 1480 (1983).
3. J.J. Broeder et al., Z. Electrochem 60, 838 (1956).
4. R. Suhrmann, Z. Electrochem 60, 804 (1956).
5. Taken from ORNL modified University of Aarhus geometry negative ion source data.
6. D.L. Fehrs and R.E. Stickney, Surface Science 24, 309 (1971).
7. M. Blaszczyszyn, Surface Science 59, 533 (1976).
8. M.L. Yu, Phys. Rev. Lett. 40, 574 (1978).

Table 1.9. Comparison of calculated and experimentally determined work function changes $\Delta\phi_m$

Adsorbant	Intrinsic Work Function eV	Adsorbate	$\Delta\phi_m$ eV	$\Delta\phi_{cal}$ eV	Ref.
W	4.52	Cs	-2.90	-2.89	3
W	4.52	Cs	-2.83	-2.89	4
Pt	5.29	Cs	-3.76	-3.84	5
C	4.39	Cs	-2.72	-2.73	5
Ni	4.84	Cs	-3.35	-3.35	5
Cu	4.47	Cs	-2.89	-2.88	5
Ag	4.28	Cs	-2.54	-2.65	5
Mo	4.27	Cs	-2.65	-2.59	8
W(100)	4.51	Cs	-2.89	-3.06	6
Ta(110	4.94	Cs	-3.42	-3.44	6
Ta(110)	4.94	Na	-2.68	-2.68	6
Ta(112)	4.93	K	-3.12	-3.11	7
Ta(100)	4.52	K	-2.59	-2.60	7
Ta(111)	3.73	K	-1.52	-1.63	7
Ta(011)	4.76	K	-2.89	-2.90	7
Mo(100)	4.27	K	-2.29	-2.39	7
Mo(112)	4.40	K	-2.58	-2.50	7
Mo(011)	4.89	K	-2.99	-3.06	7
Mo(111)	4.10	K	-2.06	-2.08	7

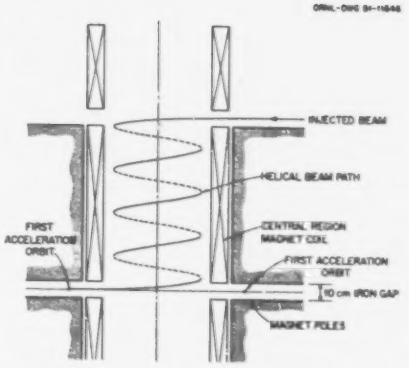

Fig. 1.14. Elevation view of the injected beam as it enters the central region of the cyclotron. The incoming beam is in a plane parallel to, and 1 m from, the median plane. It is deflected into a helical path, transported to the median plane, and inflected into the first acceleration orbit. The elements that direct the beam into and out of the helical path are not shown.

HELICAL AXIAL INJECTION CONCEPT FOR CYCLOTRONS

E. D. Hudson

During a study of injection from ORIC into a heavy-ion cyclotron with circular coils and an energy constant of K=3200 ($B\rho$ = 8.1 Tm), it became apparent that injection could not be achieved by the conventional method (capture by stripping); a higher energy injector or a different injection system would be needed.

The concept of a helical path injection system was developed which may provide a solution to this type of injection problem. Instead of injecting the beam along the cyclotron axis and bending with 90° elements into the median plane, the beam would follow a helical path around the axis, as shown in Fig. 1.14. This is feasible when the field along the helical path is made about a factor of two higher than the average magnetic field at the first acceleration orbit. A series of magnetic and electric deflectors position the beam on the acceleration orbit, as in Fig. 1.15.

This system may prove useful in many applications where it is necessary to inject beam from a small cyclotron or other accelerator into a very large cyclotron.

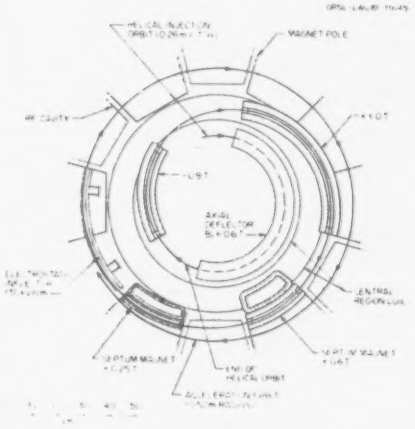

Fig. 1.15. View at the median plane of the system for deflecting the beam from a helical orbit and inflecting it onto an acceleration orbit.

EXPERIMENTAL APPARATUS

J. L. C. Ford
R. L. Robinson
R. A. Auble
C. B. Fulmer
E. E. Gross
M. L. Halbert
J. W. Johnson
N. R. Johnson
H. J. Kim
C. D. Moak
F. E. Obenshain
E. H. Spejewski[1]

A wide variety of state of the art and often unique experimental devices are available at the Holifield Heavy Ion Research Facility. The locations of these instruments are shown in Fig. 1.16 which displays the layout of the experimental areas. The design and implementation of this equipment represents a major investment of time and effort by the ORNL staff along with significant contributions by the HHIRF Users Group. The status of each experimental station will be briefly reviewed. If further development work involving a particular piece of apparatus is described elsewhere in this progress report the pertinent section is given in parenthesis.

Gamma-Ray Spectrometers

Beam lines 23 and C7 (see Fig. 1.16), accessible to the tandem and cyclotron (or coupled accelerator) beams respectively, lead to general purpose gamma-ray stations. A variety of different detector configurations, including NaI, Ge and avalanche counters, can be mounted for experiments involving gamma-ray or particle-gamma detection.

Velocity Filter

This instrument (Fig. 1.17) was designed by Harald Enge of the Massachusetts Institute of Technology, fabricated at MIT, and shipped to the HHIRF in the spring of 1982 where it was installed on a new beam line built for the velocity filter. This line has a 3° bend to eliminate particles scattered from the slit edges of the tandem energy-magnet stabilizer. Major elements of the device are shown in Fig. 1.18. The velocity filter permits detection of reaction products near and at 0° relative to the beam. Separated electric and magnetic fields disperse the velocities at the focal plane within a velocity acceptance of ±5% and a solid angle of 2 msr. The device is designed to give maximum separation for nuclei with energies up to 9.6 MeV/q (see Sect. 2).

Split-Pole Spectrometer

This magnetic spectrometer located on beam line 33 and so available to the tandem beams

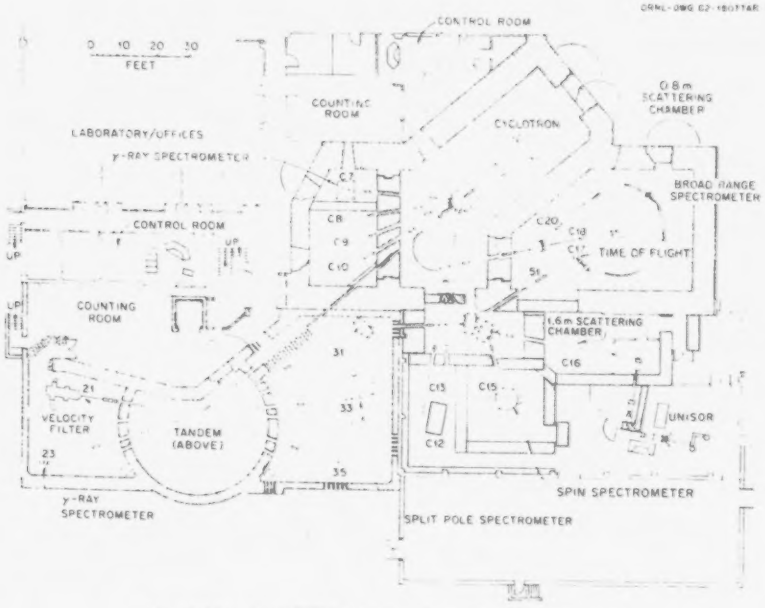

Fig. 1.16. Experimental layout of the Holifield Facility.

ORNL PHOTO 5570-83

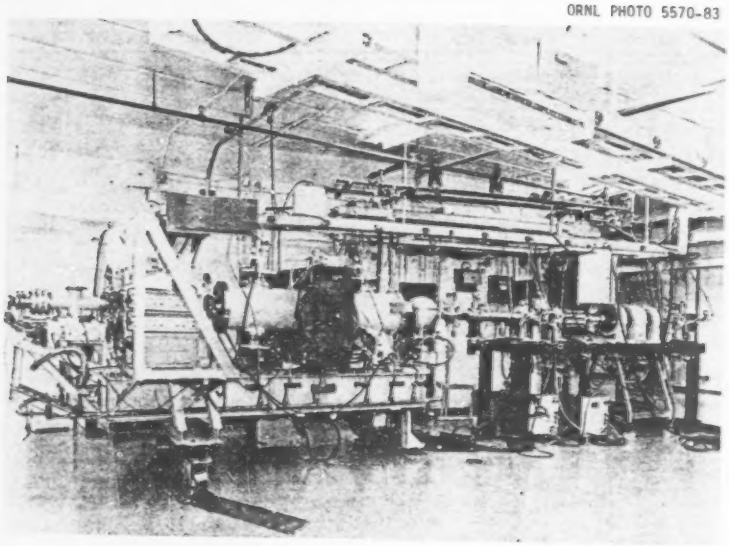

Fig. 1.17. The velocity filter.

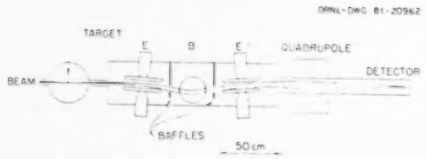

Fig. 1.18. Schematic view of the velocity filter. E represents the electrostatic deflectors and B the dipole magnet.

only, has a mass-energy product of ~100. The present focal plane counter is a hybrid-ionization chamber providing ΔE and E information as well as two position measurements for ray tracing purposes.[2] The split-pole spectrometer has been equipped with a windowless target[3] producing thin, contaminant-free targets (Fig. 1.19). This device requires no windows because of the combination of a well defined target, as obtained with a supersonic jet flowing through a convergent-divergent Laval nozzle, with four stages of pumping (see Sect. 2). Modifications now being made to the gas jet will provide optical pumping by a laser of material seeded into the gas jet stream.[4] This technique should yield a target with ~90% spin alignment and a thickness in excess of 10^{15} atoms/cm^2 (see Sect. 2).

Broad-Range Spectrometer

The magnetic spectrometer is an Elbek spectrometer (Fig. 1.20) preceded by a quadrupole lens to increase the solid angle of the instrument. Beams from either accelerator can be used with this magnet which has a mass-energy product of ~240. The spectrometer was vastly improved by the addition of the multiple-detector focal plane counter system consisting of two parallel plate avalanche counters, a vertical drift chamber, and an ionization chamber with a segmented anode. Time-of-flight, ΔE, and E information are obtained as well as the position along the focal plane with approximately 0.1 mm resolution (see Sect. 2). Because of the superior position resolution, the contribution to the energy resolution that had resulted previously because of the small dispersion of the magnet (about 2 cm/%p), has been essentially eliminated. This new detector system required that the vacuum chamber containing the focal plane be enlarged by the addition of a detector box. Improvement of the pumping system by the addition of two cryopumps is in progress.

ORNL PHOTO 3714-82

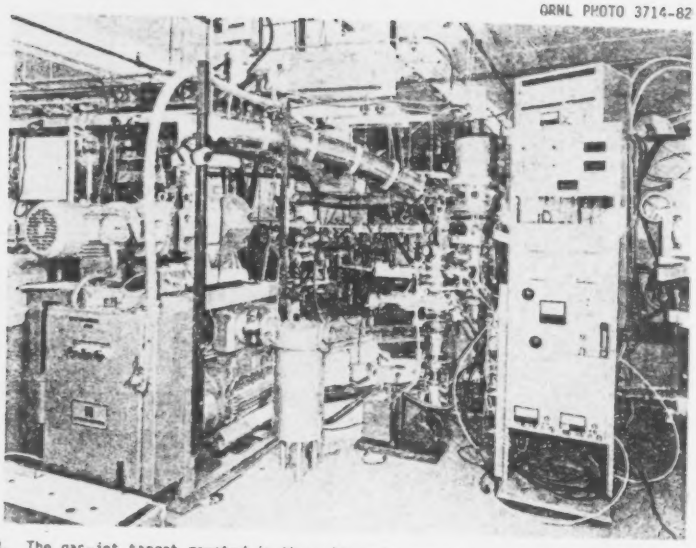

Fig. 1.19. The gas-jet target mounted in the split-pole magnetic spectrometer scattering chamber. The laser and the spectrometer are out of view to the left and right of the photograph, respectively.

ORNL PHOTO 5572-83

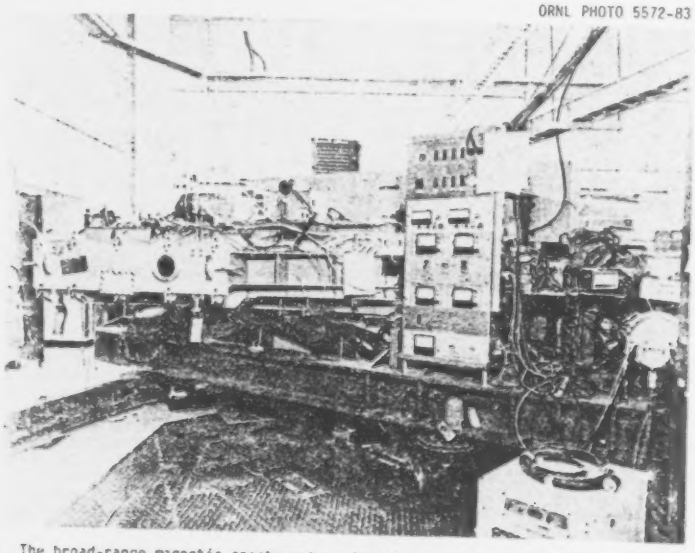

Fig. 1.20. The broad-range magnetic spectrometer with the new detector box for the multiple-detector focal plane counter system.

Scattering Chambers

Two general purpose scattering chambers are available: one 0.8 m in diameter (on beam line C20, accessible only to the cyclotron beam) and the other 1.6 m in diameter (on beam line C16) accessible to either accelerator. The apparatus at the 1.6-m chamber includes dedicated gas handling equipment for gaseous counters. Recently the target ladder mechanism and control and readout systems for the detector mounting rings within the 1.6-m chamber were upgraded.

Time-of-Flight Facility

The TOF spectrometer (see Fig. 1.21) consists of a 30.5-cm inside diameter scattering chamber to which is attached a flight tube whose length can be varied but, to date, has typically been about 1 m. Timing counters, either carbon foils viewed by microchannel plates or parallel plate avalanche detectors, can be mounted on the flight tube to provide start and stop signals for the time-of-flight measurement. A large ionization chamber with segmented anode and cathode structures may be attached to the end of the flight tube to determine the energy loss and total energy of the reaction products. In addition, a second large ionization chamber (volume ~1 m^3) can view the target through a port in the scattering chamber to provide a large solid angle detector for looking at particles in coincidence with those detected by the TOF leg of the system.

Spin Spectrometer

The spin spectrometer[5] is a closely packed array of 72 18-cm-deep, equal area, NaI detectors used to make total energy and gamma-ray multiplicity measurements on an event by event basis. Demetrios Sarantites and his collaborators at Washington University, St. Louis played a lead role in the design and construction of this instrument. Various solid state and avalanche counters have been mounted within the 17-cm-radius spherical scattering chamber, inside the NaI array, to perform particle-gamma ray coincidence measurements. Future plans call for replacement of some segments of the NaI array with Ge counters in BGO shrouds to add high resolution energy channels with Compton suppression.

On-Line Isotope Separator

The University Isotope Separator at Oak Ridge (UNISOR)[6] is operated by the Oak Ridge Associated Universities to support the research of a consortium of universities. However, this facility like others at HHIRF is available to all users. The UNISOR consists of electric and magnetic filters to enable the study of neutron-deficient nuclei far off the stabilty line. Three beam lines following the electric and

ORNL PHOTO 5571-83

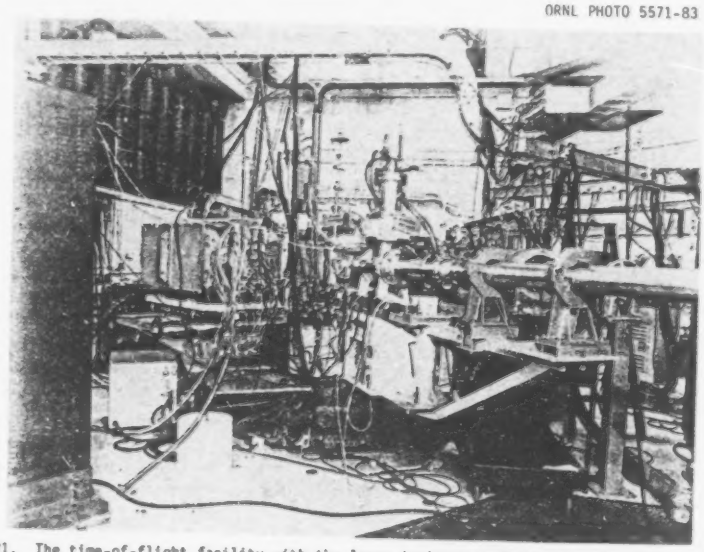

Fig. 1.21. The time-of-flight facility with the large ionization chamber in place (to the left) and flight tube (to the right).

magnetic analysis allow the collection of the nuclei under investigation. One beam line is designed for experiments in which ground-state spins and nuclear moments will be measured through atomic excitation with a laser. The standard ion sources used to inject reaction products into the separator have been augmented by a helium jet transport[7] system thus expanding the number of elements available for study (see Sect. 9).

Atomic and Molecular Physics

Beam lines CB, 31 and 35 lead to stations primarily intended for atomic and molecular physics and applications of heavy ions. These stations can be adapted to a variety of existing devices.

---

1. Oak Ridge Associated Universities.
2. D. Shapira et al., Nucl. Instrum. & Methods **169**, 77 (1980).
3. J. L.C. Ford et al., Physics Division Progress Report, December 31, 1978, ORNL-5498 p. 45; J. L. C. Ford et al., Physics Division Progress Report, June 30, 1981, ORNL-5787 p. 128; and to be published.
4. B. Shivakumar et al., Proceedings of the Conference on Lasers in Nuclear Physics, Oak Ridge, April 1982, edited by C. E. Bemis, Jr. and H. K. Carter (Harwood Academic Press, New York 1982) p. 384.
5. M. Jaaskelainen et al., Nucl. Instrum. & Methods **204**, 385 (1983).
6. E. H. Spejewski, R. L. Mlekodaj, and H. K. Carter, Nucl. Instrum. & Methods **186**, 71 (1981).
7. D. M. Moltz, Nucl. Instrum. & Methods **186**, 135 (1981).

DATA HANDLING

J. A. Biggerstaff
W. H. Atkins[1]
J. R. Beene
D. C. Hensley
W. T. Milner
R. O. Sayer[1]
R. P. Cumby
C. N. Thomas[2]
J. W. McConnell

HHIRF Data Acquisition/Reduction System[3]

As a national facility, the HHIRF serves a large and diverse group of experimentalists who require a flexible and easy to use data acquisition system. The system must serve typically two simultaneous on-line experiments while providing additional capability for experiment set-up and calibration. In addition, facilities for interactive off-line data processing must be provided.

The system, shown in Fig. 1.22, is based on three Perkin-Elmer model 3230 "super-mini" computers supporting independent but identical

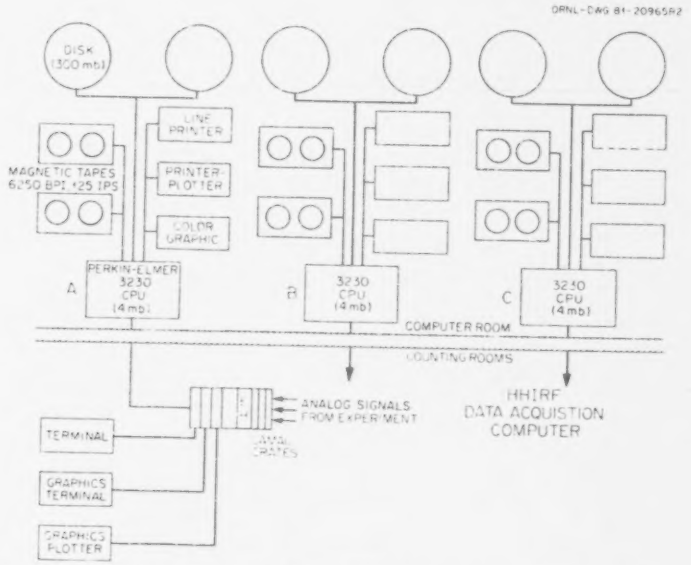

Fig. 1.22. Hardware configuration of the HHIRF data acquisition/reduction computer.

environments. Each system can comfortably support one experiment and several general computing tasks without degrading time-critical operations. Major items of peripheral equipment associated with each CPU include two 300 Mb disk drives, two 6250 bpi/125 ips tape drives, two color graphics terminals, color printer/plotter, line printer, six or more alphanumeric video terminals, and CAMAC interfaces providing "branch" and "serial" highways to CAMAC crates located in the various experimental stations. Many of the peripherals are interfaced through CAMAC enabling them to be sited conveniently near the experimenters' work station.

The software structure of the data acquisition/reduction system is summarized in Fig. 1.23. The system makes effective use of the powerful multi-tasking and real-time features of the Perkin-Elmer operating system. The software shown in Fig. 1.23 is flexible enough to support essentially all of the data acquisition performed at HHIRF; the system is easily customizable by means of "hooks" in the histogramming program that provide an easy-to-use interface to (optional) user-supplied software and by means of a user-supplied (at run-time) gating and histogramming specification list. Off-line data processing is performed with essentially the same software system, except that (1) data comes from tape instead of CAMAC, (2) only one user interface is supported, and (3) the display program is not imbedded in the processing system. Histogramming speeds into arrays up to 16 megachannels vary from a few hundred counts/s to nearly 10,000 counts/s depending on the complexity of the gating and other transformations required to generate the address of each count. During data acquisition, histogramming can take place on an "as time permits" basis permitting an unimpeded flow of data from the experiment to the magnetic tape.

The input data stream for data acquisition is generated, using user-supplied software, by a CAMAC auxilliary processor called the "Event Handler[4]". This processor reacts to a primary event trigger by performing simple tests on event parameter flags which it reads from CAMAC modules, reading appropriate CAMAC ADC's and TDC's, and putting the resulting information into a format suitable for the host processor software.

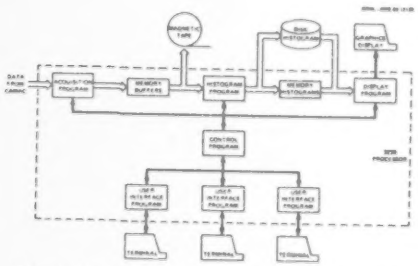

Fig. 1.23. Software configuration of the HHIRF data acquisition/reduction computer.

RIP - General Purpose Interactive Display At HHIRF[5]

RIP is a general purpose interactive code for display and analysis of data. The HHIRF data acquisition system includes a version of RIP for on-line display of one- and two-dimensional histograms on color graphic terminals and hard copy on color printer/plotters. General features of the program are:

1. Input consists of simple commands or directives followed by data items in free form. Help messages are built into the program.
2. Up to 8 one-dimensional histograms may be stacked or overlaid on the screen simultaneously in a given window; up to four windows are permitted. A given histogram may be displayed in any of 7 colors.
3. Linear or logarithmic intensity versus channel number or energy in keV may be selected.
4. A histogram may be searched for peaks, and peak centroids may be marked with either channel number or energy in keV.
5. Up to 4 two-dimensional histograms may be displayed simultaneously with intensity mapped into color.
6. Gates may be set on either axis of a two-dimensional histogram, and projections on the other axis may be displayed.
7. "Free-form" gates may be specified in an interactive mode and saved on disk. Counts within a gate boundary may be summed, and projections on either axis may be displayed (see Fig. 1.24).
8. A fitting procedure may be employed to fit one-dimensional histograms to a polynomial background plus a series of gaussians in order to obtain estimates of peak areas, centroids, and widths. A display of fit results is produced.
9. Color or monochrome "hard copies" of the screen display may be generated on the Tektronix color plotter.
10. The sum, centroid, and width may be calculated for a region of channels selected interactively.
11. Repetitive "pseudo-live" display of in-core histograms is provided.

Data Acquisition Electronics Development

A number of electronic modules for use in the HHIRF data acquisition system have been developed and are briefly described below.

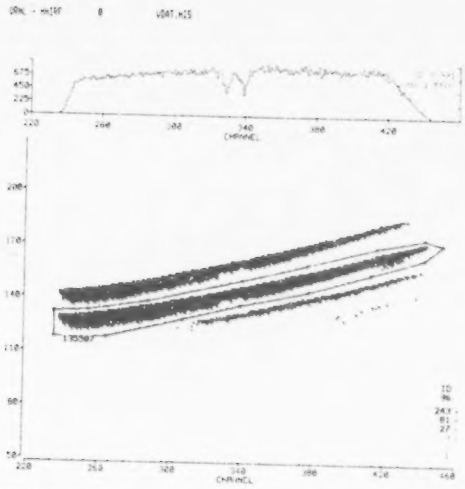

Fig. I.24. Two-dimensional display with free-form gate produced by RIP. The x projection of the counts in the gate is shown above.

M68000 Development Station - Intelligent Branch Driver. A Motorola 68k microprocessor and system hardware have been obtained, and a cross-assembler for the microprocessor has been installed on the data acquisition/reduction computer system. An "intelligent" CAMAC branch driver has been designed, fabricated, and partially tested. These components are for a system that is intended for future use in experiments requiring more than two front-end CAMAC crates (a limitation of the existing Event Handler), to develop techniques for more sophisticated front-end processing, and to provide stand-alone capability for setup and for simple acquisition tasks.

ADC Interface. A CAMAC interface for up to 16 NIM or free-standing ADC's has been commissioned. The system appears to the user to be very similar to standard CAMAC ADC modules but also supports independent "singles" operations. At present six Canberra ADC's are available. A Nuclear Data 16k-channel fixed-deadtime ADC will be added to this system.

Printer Interface. A buffered CAMAC line-printer interface suitable for most commercially available line printers, including our TRILOG's has been built and tested. This module gives much greater flexibility in placing the printers where they are needed without burdensome cabling problems. Its greatest advantage, however, lies in the load it can take off the CPU's; it actually takes about 25% of the CPU's time to drive a TRILOG in plot mode. We will soon have all of our printer-plotters interfaced to CAMAC using these modules and have already implemented, via a shared CAMAC crate, access to one of the plotters from any of the three Perkin-Elmer CPU's of the HHIRF computer.

Totalizer. A module has been designed which can assist in the processing of spin-spectrometer type data. The module can count bits in gated-latch words as they are being read by the Event Handler. For example, this could be used to reject low-multiplicity events. In addition the module will contain two normal summation accumulators. One of these could be used to calculate total energy while the other is used to sum TDC outputs as the first step in calculating "T-zero." All these calculations are performed without slowing down data acquisition because the module "snoops" on data being read by the Event Handler.

Electronics

Ever expanding numbers of detectors, many with multiple outputs, utilized in experiments place growing demands on the electronics. The HHIRF electronic pool has been increased to about 700 modules and is usually sufficient, at present, to handle situations requiring simultaneous setups of two complex systems with some modules remaining for off-line use. In addition, several of the major experimental devices have dedicated electronic systems for detectors which are a permanent part of these instruments. Such systems exist for the focal plane multi-element detector of the broad-range

magnetic spectrometer, for the 72-NaI crystals of the spin spectrometer, for the fast-timing detectors in the flight arm of the time-of-flight facility, and for the focal plane detector of the split-pole magnetic spectrometer.

The VAX-FPS Dual Processor Computer System

A Digital Equipment Corporation VAX 11/780 computer with a Floating Point Systems FPS-164 attached processor (AP) has been installed to provide support for large scale scientific calculations (Fig. 1.25). The VAX system currently consists of a 11/780 processor with 4 Mb of memory, 640 Mb of disk storage, a 800/1600-bpi, 125-ips tape drive, together with a line printer, a high resolution dot matrix color plotter/printer, and 16 serial (RS232C) communication ports mostly connected to DEC VT100 or VT100 compatible terminals. Interactive graphics is provided by a Tektronix 4014 and two 4105 terminals, together with VT100 terminals retrofitted for graphics, all compatible with the Tektronix software on which our graphics programs are based.

The FPS-164 AP is a special purpose high speed "number cruncher" with parallel architecture, and multiple floating point arithmetic elements designed to perform matrix and vector operations at up to 12 million floating point operations per second (MFLOPS). Modern general purpose mini computers typically achieve speeds much less than 1 MFLOP. The FPS-164 is attached to the VAX via the unibus. The AP currently has 2 Mb of memory and 270 Mb of local disk storage. It operates under the FPS single job executive which enables complete jobs to execute independently in the AP once loaded down and initiated by the VAX. (Performance of this computer is discussed in Sect. 2.)

---

1. UCC-ND Computer Sciences Division.
2. Oak Ridge Associated Universities.
3. Summary of paper to be published: W. H. Atkins, Proceedings of the Conference on Real-Time Computer Applications in Particle and Nuclear Physics, Berkeley, California, 1983.
4. D. C. Hensley, IEEE Transactions on Nuclear Science, NS-26, No. 4, 1979.
5. Summary of paper to be published: R. O. Sayer, Proceedings of the Conference on Real-Time Computer Applications in Particle and Nuclear Physics, Berkeley, California, 1983.

ORNL PHOTO 2556-82

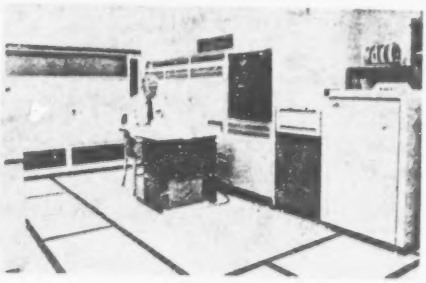

Fig. 1.25. The VAX computer system.

FACILITIES

R. L. Robinson

A 3400-ft^2 addition to the HHIRF building, just south of the UNISOR area (see Fig. 1.16), was completed and opened for occupancy in April 1983. Figure 1.26 shows the planned use of this new area as well as plans for reconfiguring the existing area made possible by relocating some of UNISOR equipment in the new south addition. The new configuration allows for an additional target room between the spin spectrometer room and UNISOR that is large enough, for example, to house a 3- to 4-m-diam vacuum vessel that in turn could house many large detectors. This target room is in prime space since there can be access to beams from either accelerator along the same beam line. The layout illustrated in Fig. 1.26 is now being implemented. Thus far, UNISOR has relocated support equipment in the new south addition, three cubicles have been set up as small laboratories for off-line testing of equipment, plans have been developed for the new counting room, and reconfiguration of the stacked blocks around the spin spectrometer has been initiated.

An in-house committee chaired by F. E. Bertrand was set up to review counting rooms and establish layouts that would best meet the needs of the researchers. This committee submitted a plan for the ORIC counting room (the counting room near the top of Fig. 1.16) and the plan has

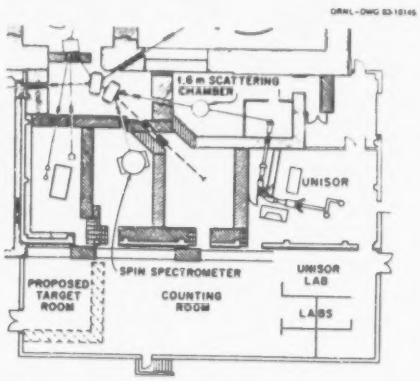

Fig. 1.26. Planned use of the new south addition and proposed reconfiguration to provide a new target room between the spin spectrometer and UNISOR.

been fully implemented. Basically, it allows for two counting stations, back to back, each with three fixed electronic racks, and space for three additional portable racks. Each station has a graphics terminal, two CRT terminals, and access to a nearby lineprinter. There are CAMAC highways from this room to two of the computers of the data acquisition/reduction system. This committee is now reviewing the layout of the counting room near the tandem and the proposed counting room for the south addition. The latter will service the spin spectrometer, the 1.6-m-diam scattering chamber, UNISOR, and any future device located between the spin spectrometer and UNISOR.

Construction of the second building for the Joint Institute for Heavy Ion Research (JIHIR) began in May 1983. Figure 1.27 illustrates a model of this 6000-ft^2, one story structure, and Fig. 1.28 shows the floor plan. Construction is scheduled for completion in January 1984. Funds for the design and construction of the building are being provided by the State of Tennessee ($350,000) and by UNISOR ($44,000). The building is on land that will be leased by DOE to the State of Tennessee.

USERS SUPPORT

J. L. C. Ford
W. T. Milner
J. A. Biggerstaff
R. P. Cumby
R. W. Miles
C. A. Reed
R. L. Robinson
C. N. Thomas
J. W. Johnson

Support for users of the Holifield heavy Ion Research Facility is provided by various sources. Each of the major experimental stations shown in Fig. 1.16 has an ORNL staff physicist assigned to it as the mentor for that station. The mentor is then responsible for maintaining and upgrading the experimental apparatus and for assisting users in implementing experiments which use that apparatus. The major equipment and assigned mentors are listed in Table 1.10.

In addition four technicians are available to support users during setup of experimental equipment and while the experiment is in progress. R. W. Miles and C. A. Reed are laboratory technicians each of whom is assigned to specific experimental stations. They assist with setting up and aligning apparatus, solving

ORNL PHOTO 4025-82

Fig. 1.27. Model of the second building of the JIHIR. It adjoins the existing JIHIR building which is shown on the left.

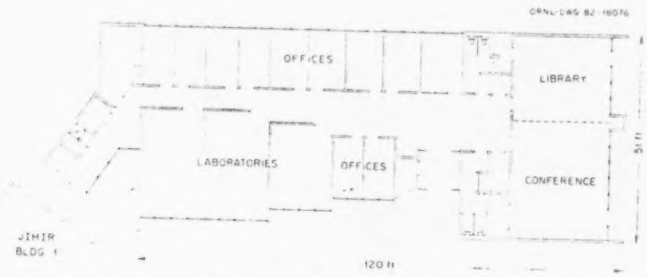

Fig. 1.28. Floor plan of the second building of the JIHIR.

Table 1.10 Major apparatus available for experiments at HHIRF and mentors responsible for each device

Device	Accelerator[a]	Mentor
76-cm-diam Scattering Chamber	O	E. E. Gross
1.6-m-diam Scattering Chamber	O,T	C. B. Fulmer
Split-Pole Magnetic Spectrometer	T	J. L. C. Ford
Broad-Range Magnetic Spectrometer	O,T	R. L. Auble
Time-of-Flight Spectrometer	O,T	F. E. Obenshain
UNISOR Facility	O,T	E. H. Spejewski
γ-ray Spectrometer Systems	O,T	N. R. Johnson
Spin Spectrometer	O,T	M. L. Halbert
Velocity Filter	T	H. J. Kim
Atomic Physics Beam Line	T	C. D. Moak

a) T = Tandem Accelerator, O = ORIC or coupled accelerators

vacuum problems, locating hardware for the beam lines and experimental chambers, and generally helping with mechanical aspects of an experiment. R. P. Cumby, the electronic technician, assists in locating electronic modules and components and in setting up electronics. He also takes responsibility for repair of malfunctioning modules, and in general will provide assistance with the detector and electronic systems. The computer technician, C. N. Thomas, helps researchers in interfacing the electronics with the computer, and, in general, assists in use of the computer for data acquisition and data reduction.

Because the HHIRF data acquisition/reduction computer system must support experiments which vary widely in type and complexity, the system is rather complex. For this reason, several research personnel denoted as "computer nannies", have been designated to help the novice user, deal with the system. Each local research group has one such nanny. Current nannies are: J. D. Cole, R. L. Ferguson, T. P. Sjoreen and Y. S. Schutz. Outside groups with no local collaboration are provided "nannyship" and training by members of the computer group.

JOINT INSTITUTE FOR HEAVY ION RESEARCH

R. L. Robinson R. T. Webber

The Joint Institute for Heavy Ion Research became defined in an Agreement entered into by the Department of Energy, Nuclear Division of the Union Carbide Co., the University of Tennessee, and Vanderbilt University in June 1982. The mission of the JIHIR as stated in the Agreement is:

> "to promote and support heavy-ion research at the HHIRF by providing an intellectual center and physical support for researchers who work at the HHIRF to the mutual benefit of all sponsors and participants in the field of heavy-ion research."

This mission is to be accomplished by (1) providing a physical environment that will enable visitors and users of the HHIRF to be more effective and efficient in the use of HHIRF, and (2) arranging financial support for visiting scientists with expertise in nuclear and atomic physics and other fields related to heavy-ion research programs that can be carried out at the HHIRF.

The policies of the JIHIR will be determined by a three-person Policy Council, one person each from the University of Tennessee, Vanderbilt University, and ORNL. The first meeting of the Council took place on May 5,1983. Members are W. G. Holladay (Vanderbilt University), L. L. Riedinger (University of Tennessee), and R. L. Robinson (ORNL). J. H. Hamilton will serve as the first Director of the JIHIR.

The first building of the JIHIR was to provide offices, dormitory rooms, and kitchen facilities for outside users of the HHIRF. The original number of overnight accommodations for four persons has proven often to be inadequate for the large number of outside researchers either taking or reducing data and has now been increased to eight. In the first two and one half years of operation, 370 visitors have made use of the dormitory facility with an average length of stay of 6 nights.

The second building of the JIHIR (see Figs. 1.27 and 1.28), now under construction, contains offices and laboratories to be assigned to HHIRF users from the universities of Tennessee, to guests of the JIHIR, and to staff persons of UNISOR. The 80-person auditorium will be available for seminars and workshops of ORNL, the JIHIR, or the HHIRF Users Group.

USERS ACTIVITIES

R. L. Robinson. J. L. C. Ford

In order to keep the membership list of the HHIRF Users Group up to date, membership must be renewed by written request every third year. Since the beginning of the last triennial period, January 1, 1982, 465 persons from over 150 institutions have become members.

The Users Group is represented by an Executive Committee with 6 members. Members of the Executive Committee who served in 1981-1983 are listed in Table 1.11. These were elected by members of the Users Group from candidates selected by a Nomination Committee. Members of the Nomination Committee are also listed in Table 1.11.

The Executive Committee, which met about four times a year, provided valuable discussion and

Table 1.11. Members of the Committees of the HHIRF Users Group

Executive Committee

1980-1981

J. V. Maher (University of Pittsburgh)
L. L. Riedinger* (University of Tennessee)
D. Ward (Chalk River Nuclear Laboratories)

1981-1982

P. D. Bond* (Brookhaven National Laboratory)
P. Braun-Munzinger (SUNY at Stony Brook)
M. L. Halbert (Oak Ridge National Laboratory)

1982-1983

H. C. Britt (Los Alamos National Laboratory)
J. B. Natowitz (Texas A&M University)
E. H. Spejewski* (Oak Ridge Associated Univ.)

1983-1984

C. K. Gelbke (Michigan State University)
D. C. Hensley (Oak Ridge National Laboratory)
D. G. Sarantites (Washington University)

Nomination Committee

1981

D. Cline (University of Rochester)
J. D. Fox (Florida State University)
B. D. Kern (University of Kentucky)
F. Plasil* (Oak Ridge National Laboratory)
V. E. Viola (Indiana University)

1982

S. G. Steadman (Mass. Institute of Technology)
D. G. Sarantites (Washington University)
C. D. Moak (Oak Ridge National Laboratory)
L. L. Riedinger* (University of Tennessee)
R. G. Stokstad (Lawrence Berkeley Laboratory)

1983

F. T. Avignone (University of South Carolina)
A. I. Gavron (Los Alamos National Laboratory)
M. L. Halbert* (Oak Ridge National Laboratory)
C. F. Maguire (Vanderbilt University)
A. C. Mignerey (University of Maryland)

*Chairman

recommendations in several areas including experimental apparatus, computer equipment, scheduling policies for approved experiments, and names of persons to serve on the Program Advisory Committee and the Policy Review Committee. They also recommended a change in the Users Group Charter, that was later approved by the members of the Users Group, increasing the term of office for an Executive Committee member from two to three years.

In response to users interest in multiple charged particle detector arrays, the Executive Committee recommended that a workshop be held with the goal of providing direction on such a device to the Holifield Facility. This meeting was organized primarily through the efforts of H. C. Britt (Los Alamos National Laboratory) and was held December 2-4, 1982 at the Holifield Facility. It was attended by sixteen persons from outside the laboratory and a similiar number from within. The first day and a half were spent on presentations and discussions of a variety of charged particle detectors. The remaining day was devoted to an open forum that led ultimately to a proposed detector array with the acronym SPIDAR (Simultaneous Particle Identification Detector ARray).

PROGRAM ADVISORY COMMITTEE

J. B. Ball R. L. Robinson

The Program Advisory Committee met June 5, 1981 (PAC-1A) and March 1, 1983 (PAC-2). Members of this Committee were K. Gelbke (Michigan State University), E. E. Gross (Oak Ridge National Laboratory), F. Iachello (Yale University), P. Richard (Kansas State University), P. H. Stelson (Oak Ridge National Laboratory), F. Stephens (Lawrence Berkeley Laboratory), and K. Wolf (Texas A&M University). PAC-1A was called to review principally proposals for coupled operation since this mode of operation became routine earlier than expected. PAC-1A recommended that 129 of the 273 shifts requested for that cycle be approved, and PAC-2 recommended 219 of the requested 587 shifts.

FUTURE DIRECTIONS

ORIC K-140 Superconducting Conversion

E. D. Hudson S. W. Mosko
R. S. Lord R. L. Brown[1]
J. A. Martin M. S. Lubbell[1]
G. A. Byington[2]

Providing superconducting main magnet coils for the ORIC is an attractive option for improvement of the Holifield Facility to increase beam energies and to reduce electrical energy consumption. During the past two years we have developed the conceptual design of a conversion that will increase the energy of the cyclotron by 40% for all ion species. The criterion for this design was achievement of the largest

energy increase compatible with straightforward and minor changes in the cyclotron beam extraction system and in the beam transport and analysis systems. An earlier conversion design (1980)[3] to increase the cyclotron energy by a factor of three required stiffening of the magnet yoke, a superconducting magnetic beam extraction channel, and major modification of the beam transport system. The estimated cost of this conversion, ~ $10,000,000 as an FY 1983 project, was deemed too large for the improvement which would have been obtained. In addition, there were unresolved technical uncertainties in the design of the beam extraction system.

The new design for the conversion will increase the maximum average magnetic field from 1.9 to 2.3 T to give an increase in the mass energy product (ME/q^2) from 100 to 140. The improvement of energy performance for the modified cyclotron is illustrated in Fig. 1.29.

The superconducting coils are of much smaller size than the existing aluminum coils (Fig. 1.30), allowing ample space for the coil cryostat, suspension system, thermal insulation, and vacuum chamber. The new system, Figs. 1.31 and 1.32. will fit in the space now occupied by the aluminum coils and will use the existing coil mounting holes.

Coil forces for the K-140 coils are much smaller than for the K-300 version, 534,000 N (120,000 lb) versus 4,000,000 N (900,000 lb), allowing use of a much simpler suspension system. Axial forces on the coils are supported by 24 stainless steel links; radial forces are carried by eight stainless-steel adjustable support rods. Cryogenic requirements for the system are about 16 L/h of liquid helium and 10 L/h of liquid nitrogen.

Superconducting coil design is based on providing a fully cryostable coil. The present concept is based on the use of seven strands of 54-filament, 0.5-mm-diam, NbTi conductor with a Cu/NbTi ratio of 1.5:1. The NbTi/Cu strands are compacted in copper to form a 0.95 cm x 0.32 cm composite with a Cu/NbTi ratio of 50:1. Each

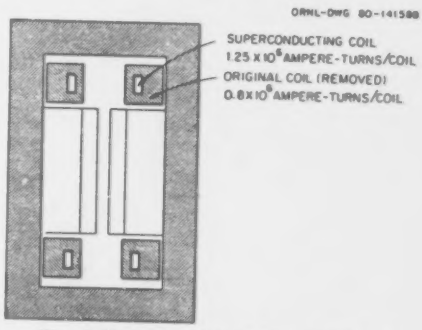

Fig. 1.30. Comparison of coil geometry for ORIC aluminum coils and superconducting coils.

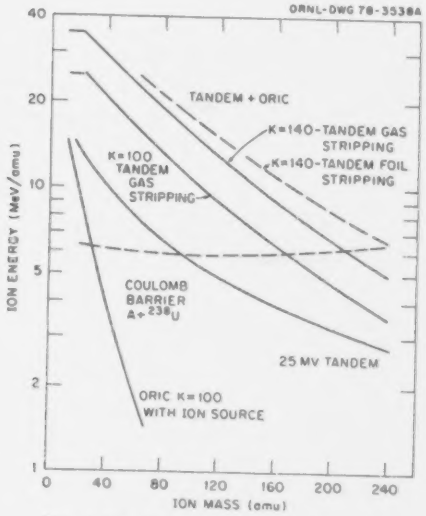

Fig. 1.29. Energy performance for K-140 conversion.

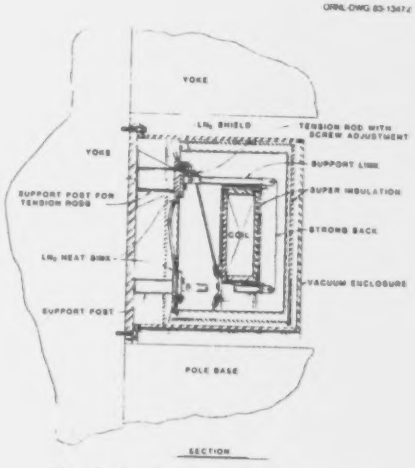

Fig. 1.31. Coil assembly cross-section

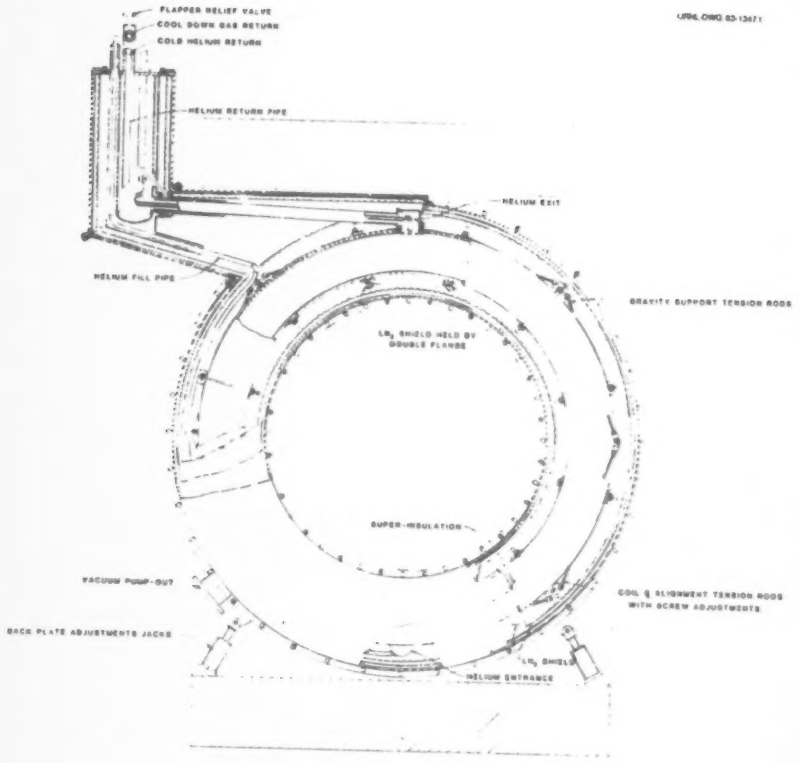

Fig. 1.32 Side view of coil assembly

coil is formed of four double-pancake windings with 78 radial turns. Epoxy fiberglass insulation (G-10), 0.5 mm between layers and 2.4 mm between pancakes, is used. The conductor current required for this configuration, 2000 A, is 60% of the critical current at a magnetic field of 30 T (the maximum value in the winding pack).

The conversion will provide a very significant decrease in electrical power usage, from an average of approximately 2.5 MW to 1.0 MW. With a limited power budget (as we now operate) the operating hours of the cyclotron could be increased by a factor of 2.5. In FY 1983, 1500 h of beam time for research utilizing the ORIC were provided; with the conversion, 3800 h could have been provided.

The estimated cost of the superconducting coil system for K-140 conversion (as a three-year FY 1986 project including allowance for contingencies) is $4,200,000. Improvements to the beam extraction and beam transport system (~$250,000) will be done separately as part of the continuing improvement program.

---

1. Fusion Energy Division.
2. UCC-ND Engineering.
3. Physics Division Progress Report, ORNL-5787 (1980), p. 22.

K-1200 Booster Cyclotron

J. B. Ball
E. D. Hudson
R. S. Lord
C. A. Ludemann
J. A. Martin
S. W. Mosko
W. T. Milner
R. L. Robinson

In 1978, a proposal was presented to the Nuclear Science Advisory Committee for addition

of a K-1200 superconducting cyclotron booster to the facility and rearrangement of the research areas to be compatible with the higher energy beams. In late 1981 that plan was reexamined with a view toward reducing costs and minimizing development. It was decided that, in view of the advanced state of development of the MSU - Phase II Cyclotron concept, the design could be adapted for the Holifield Facility with minimal changes.

Principal characteristics of the MSU - Phase II Cyclotron and modifications proposed for the Holifield version are given in Table 1.12. The only change envisioned is a reduction in frequency range of the resonators from 9-32 MHz to 15-32 MHz. This is possible because beam injection from the 25-MV tandem accelerator eliminates requirements that were imposed on the MSU design by coupling to the K-500 injector cyclotron. The reduction in frequency range reduces the half-height of the resonators from 5.9 m (19.3 ft) to 3.7 m (12 ft) and permits a corresponding reduction in the height of the cyclotron vault.

The energy performance of the facility, taking into account injection limitations derived from information supplied by MSU, is shown in Fig. 1.33. Beam energies from the HHIRF K-1200 facility would be slightly lower than MSU-II, up to about A = 80 and significantly higher for the heaviest ions. For some experiments, total energy may be more important than energy per nucleon. The energy performance is replotted in Fig. 1.34 to show the total energy as a function of ion mass. This capability to produce the heaviest ions with large total energy is enhanced by the ready availability of a rich selection of negative ions from the tandem ion source.

The facility plan, Fig. 1.35 was designed to minimize bend angles in the beam transport system (to allow use of existing bending magnets), to make beams from either the tandem or coupled accelerators available to all experiment stations, and to provide for beam splitting to serve several experiments simultaneously. The beam splitting system, Fig. 1.36, was based on the use of rf deflectors operating at a subharmonic of the cyclotron rf. When operated at one-quarter the cyclotron frequency, the system will deliver beam to three experiments; at one-half frequency, beam may be delivered to any two experiments. A possible alternate to the rf beam splitting system would be a thin septum electrostatic deflector as developed at the Swiss Institute for Nuclear Research (SIN).[1]

Table 1.12. MSU-Phase II/HHIRF-Phase II Cyclotron Characteristics

Pole radius	1.07 m
Sectors	3
Spiral	3.03 radians/m
Minimum hill gap	9.6 cm
Maximum valley gap	0.91 m
Average field range	3.0-5.0 T
Yoke height	2.92 m
Yoke inner-outer diameters	3.0-4.4 m
RF frequency range	9-32 MHz*
Harmonic modes	1st, 2nd**
Peak dee voltage	200 kV
Number of trimming coils	22
Max. total trim coil power	70 kW
K_B at 5.0 T	1200 MeV/amu
K_f	400 MeV/amu

* 15-32 MHz for the HHIRF version

** 1st, 2nd, 3rd for the HHIRF version

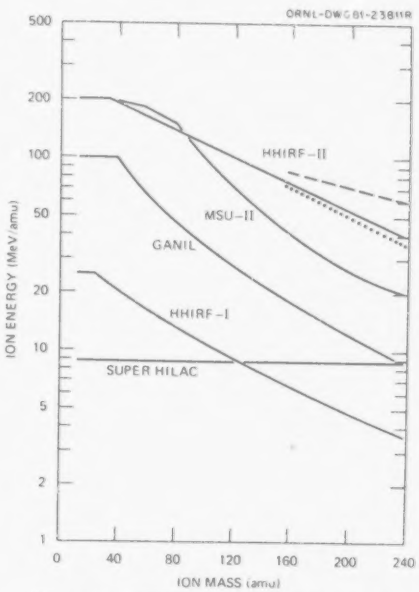

Fig. 1.33. Energy performance (MeV/amu) for HHIRF - Phase II and other accelerators. Dashed line is for foil stripping in the tandem.

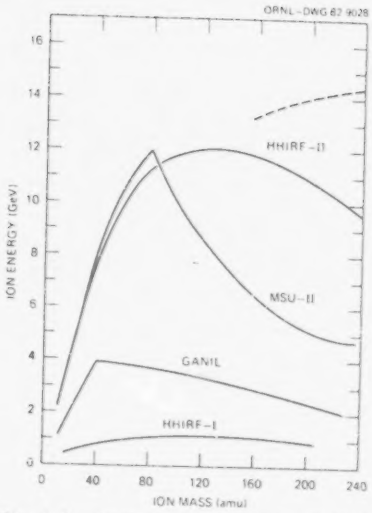

Fig. 1.34. Total energy performance (MeV) for HHIRF - Phase II and other accelerators. Dashed line is for foil stripping in the tandem.

The estimated cost of the K-1200 facility was 22.5 million dollars (1983).

---

1. M. Olivo, "The Electrostatic Channel for the S.I.N. 590 MeV Ring Cyclotron," Proceedings of the Conference on Cyclotrons and Their Applications, Birkhauser, Basel (1975).

Experimental Facilities

R. L. Robinson
D. C. Hensley
J. W. Johnson
P. D. Miller
C. D. Moak
F. Plasil
M. R. Johnson

The staff of the Holifield Facility has recognized a need to improve the experimental facilities for atomic physicists. Currently, the Facility offers one short beam line from each of the two accelerators for their use. These lines are, in general, available to all users with portable apparatus that need to be installed for a short period for a particular experiment. Specific requirements to better serve atomic physicists are: a target station with sufficient space to allow for a distance of 10- to 20-m between the target and detector that makes feasible small angle scattering studies; a bending magnet following the target to permit separation of beam ions of different charge

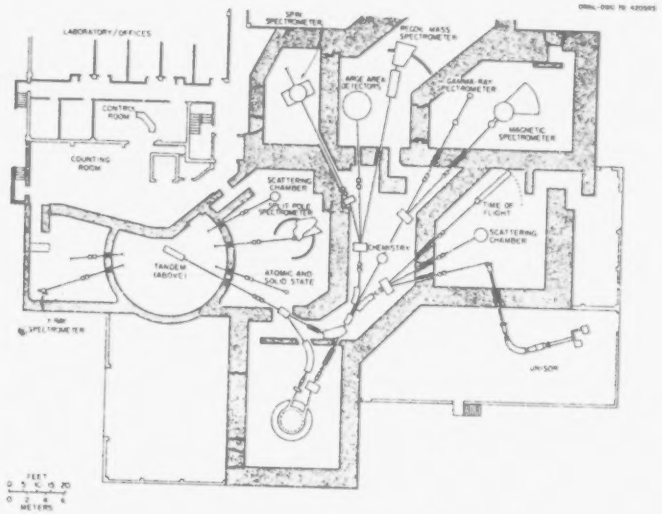

Fig. 1.35. Facility plan.

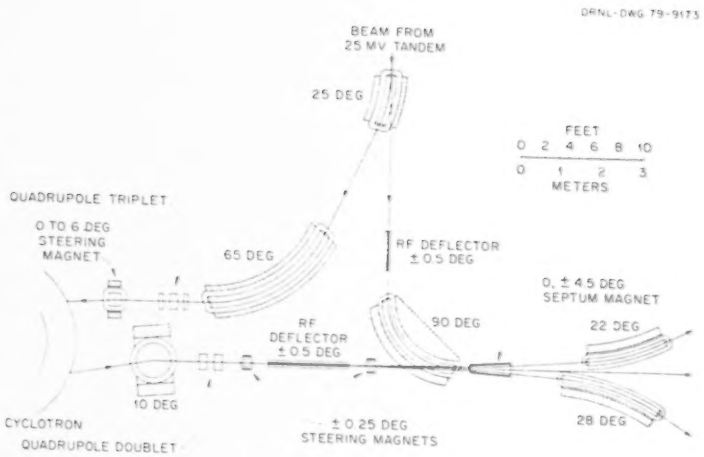

Fig. 1.36. Beam splitting system.

states; and several target stations dedicated to permanently installed complex atomic physics apparatus. For example, one such target station would involve a beam collimation system which would pass a small amount of beam through two 0.5-mm apertures set 3-5 m apart to a crystal goniometer mount for channeling experiments. Following the goniometer another set of apertures, which could be swung through a few degrees around the forward direction, would be used to select various portions of the so-called "channeling-pattern" of particles emerging from the crystal. The different portions of the emergent pattern would show differences in the charge-state distribution. The crystal could be replaced by a differentially-pumped gas cell and the same collimation system utilized. The semi-permanent nature of the station would conserve the very tedious and complex setup and alignment work required for such a collimation system.

To remedy these Facility deficiencies, and to also provide space for the anticipated growth of applications physics, a request has been made for a new building addition as illustrated in Fig. 1.37. A conceptual design has been completed. This 2400-ft^2 addition has sufficient space for at least four target stations on beam lines from the tandem accelerator. Funds have already been identified to obtain one beam line. The present schedule for this annex, if approved in October 1983, would call for completion by the end of 1985.

A substantial upgrade to the spin spectrometer has been proposed by Noah Johnson and collaborators. This upgrade, estimated to cost 1.4 million dollars, would replace 17 of the

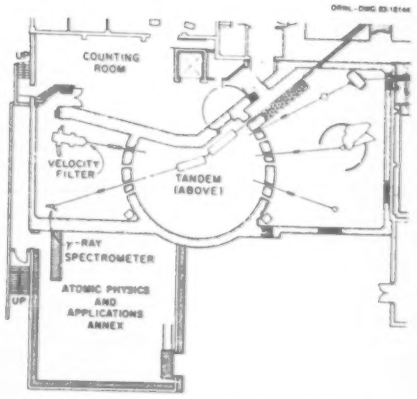

Fig. 1.37. Proposed annex for atomic physics and applications target room.

spin-spectrometer NaI elements with high resolution γ-ray modules that consist of a Ge detector shielded by an annulus made of a composite of bismuth germanate (BGO) and sodium iodide. The shields are split into five or six optically-isolated segments that can function as a

Compton-suppression spectrometer and/or a γ-ray polarimeter. Contribution of Compton scattered γ rays to the spectra should be reduced by about a factor of 9. This major upgrade retains the unique power of the spin spectrometer for selectiny the spin and energy of the entry state into the residual nucleus while at the same time permits measurement of γ rays with high resolution in double and triple coincidences. Because the whole system encompasses a 33-cm-diam spherical scattering chamber, which has been proven in a variety of experiments to be adequate for containing various types of charged-particle detectors (e.g., ΔE - E Si telescopes, avalanche detectors, telescopes with NaI for energetic light ions), this device will be an extremely powerful tool for study of reaction mechanisms as well as high-spin states through discrete and continuum γ-ray spectroscopy.

Another new experimental device under consideration is a large vacuum vessel with diameter of about 3.7 m (see Fig. 1.38). The trend in macroscopic reaction studies is to move toward more complex detector arrays which can measure many properties (A, Z, energy, angle) of many particles emitted simultaneously from a given event. This vacuum vessel would provide an environment in which different configurations of detectors, that in some cases are already exceeding a meter in depth, could be set up. The proposed chamber is simple in design in order to minimize cost. There is a manway in the wall of the vessel but for major work on interior components the bell could be removed by on overhead crane.

A major use of the data acquisition/data reduction computer is scanning of the event-by-event data tapes. For example, some spin

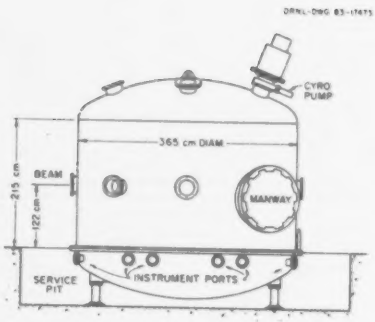

Fig. 1.38. Proposed 3.7-m-diam vacuum vessel for housing large arrays of detectors.

spectrometer experiments generate of the order of 200 high density (6250 bpi) tapes and a pre-scan of each tape requires two hours. The next major challenge for the computer group is to reduce this scanning time. One proposed solution is to develop a data tape pre-processor whose heart would be a set of parallel microprocessors. A multiplexer would route different events to available processors so that data manipulation can be done on several events simultaneously. Design of such a system has been initiated and, concurrently, an approach using commercial hardware is being explored.

2. NUCLEAR PHYSICS

The following short accounts represent contributions to our knowledge and understanding of nuclear structure and nuclear reaction mechanisms as achieved by the experimental nuclear research section during the past two years. The main emphasis of the program is heavy-ion physics conducted at the Holifield Heavy Ion Research Facility where our staff also provides mentorship for most of the large scale equipment. In addition we carry out research programs in medium energy physics at LAMPF, IUCF and TRIUMF, as well as a neutron physics program at ORELA.

This period has been noteworthy for the initial experiments with the Spin Spectrometer. This unique device has produced qualitatively new information about nuclear structure and behavior: (1) alpha particle emission from high-spin nuclei has been measured relative to the spin direction showing an excess yield of low-energy alphas along the spin direction; (2) decay paths from high excitation and high spin have been followed to the yrast entry point in much more detail than ever before; and (3) gamma and neutron decay from giant dipole, giant quadrupole and giant monopole states have been observed and measured, thus providing the information needed to test microscopic descriptions of giant resonances. Also noteworthy in this period has been the measurement of very short nuclear reaction times using the crystal blocking technique and the observation of π^0 production in heavy-ion collisions down to 25 MeV/amu beam energies.

Equipment development continues to be an essential part of our research activities. In this period, an impressive focal plane detector for the broad range spectrograph has been completed and tested, the recoil mass separator has likewise been commissioned, and the development of a polarized target assembly has progressed to the point of readiness for testing.

DIRECT REACTIONS

LIGHT-HEAVY-ION SCATTERING

C. B. Fulmer
R. L. Auble
J. B. Ball
F. E. Bertrand
K. A. Erb
E. E. Gross
D. C. Hensley
G. R. Satchler

The importance of the scattering of light heavy ions ($4 < A < 12$) was discussed in the last Physics Division Progress Report.[1] Since that time, analyses and publication[2] of $^{10,11}B$ scattering data have been completed and elastic and inelastic scattering measurements were performed with 158 MeV ^{9}Be ions (from coupled-machine operation) on a number of targets of a wide range of mass. Results of analyses of some of the ^{9}Be data were published,[3] and a journal article[4] of the full range of data and analyses was written.

Table 2.1 lists all reported light-heavy-ion scattering measurements (except for ^{7}Li ions) at incident particle energies greater than 50 MeV. Approximately half of these measurements were performed at HHIRF. ^{9}Be scattering measurements have been previously reported for only two targets at other laboratories (at beam energies > 50 MeV).

The scattering of light heavy ions is said to exhibit a transition[11] between that characteristic of light ions ($A \leq 4$) and that characteristic of heavy ions ($A \geq 12$). For light ions (at lower scattering energies) the elastic scattering is characterized by incomplete absorption and can be well described by the optical model using a Woods-Saxon form factor for both real and imaginary parts of the potential, albeit with an ambiguity of discrete families of real potential well depth. Heavy-ion elastic scattering differs in that it is characterized by almost complete absorption of lower partial waves and by good optical model fits, with Woods-Saxon and other form factors for the real well, that exhibit continuous ambiguities in the potential and little or no energy dependence. Heavy-ion elastic scattering is also well described by the double-folding optical model[18] with a semirealistic interaction to generate the real part of the nucleus-nucleus potential.

The optical model analyses[4] of our 158 MeV ^{9}Be elastic scattering data reveal features of both light and heavy ion scattering, but the results do not fit the usual pattern of either. Except for the lightest targets (^{12}C and ^{16}O) there is almost complete absorption of the lower partial waves. This results in a continuous ambiguity in the real well depth (for a Woods-Saxon form factor) which is characteristic of heavy ion scattering. For example Woods-Saxon potentials with real well depths fixed at values from 15 to 150 MeV give equivalent fits to the ^{26}Mg data and even putting $V = 500$ MeV results in only a small increase in χ^2. The folding model potentials, however, require renormalization by $N \approx 0.5$ to 0.6 (characteristic of light ion scattering) and for the lighter targets give distinctly poorer agreement with the data; for the ^{26}Mg data χ^2 is more than a

Table 2.1. Elastic scattering measurements with light heavy ions at incident beam energies > 50 MeV. The numbers are beam energies in MeV. Those underlined were performed at the HHIRF.

	Projectile[a]			
Target	^{6}Li	^{9}Be	^{10}B	^{11}B
^{12}C	99,[5] 156[6]	158[3,4]	100[7]	100[7]
^{14}N	--	--	100[7]	100[7]
^{16}O	50.6[8]	158[3,4]	--	69.5[9]
^{24}Mg	88[10]	--	87.5[2]	79.6[2]
^{25}Mg	88[10]	--	87.5[2]	79.6[2]
^{26}Mg	88[10]	158[4]	--	79.6[2]
^{27}Al	88[10]	158[4]	--	79.6[2]
^{28}Si	99,[5] 135[11]	121,[12] 201.6[12]	--	--
^{40}Ca	50.6,[8] 88,[10] 99,[5] 156[6]	60,[13] 158[4]	--	51.5[14]
^{44}Ca	88[10]	--	--	--
^{48}Ca	156[6]	--	--	--
^{58}Ni	50.6,[8] 73.7,[15] 99[5]	--	--	--
^{59}Co	88[10]	--	--	79.6[2]
^{60}Ni	88[10]	158[4]	87.5[2]	79.6[2]
^{74}Ge	50.6[8]	--	--	--
^{90}Zr	73.7,[15] 99[5]	--	--	--
^{124}Sn	73.7[15]	--	--	--
^{166}Er	50.6[8]	--	--	--
^{197}Au	88[10]	158[4]	--	79.6[2]
^{208}Pb	88[10]	--	--	--
^{208}Pb	50.6,[8] 23.7,[15] 88[10] 99,[5] 156[6]	--	--	71.2[16]
^{209}Bi	--	--	--	74.5[17]

a) Inasmuch as no measurements have been made with ^{7}Li beams from HHIRF, data for that ion are not listed in the table.

factor of 2 larger for fits with the folding model than with the Woods-Saxon form factor for the real potential.

In Fig. 2.1 we compare real and imaginary well depths of representative 6-parameter Woods-Saxon potentials that fit elastic scattering of ^{6}Li, ^{9}Be, and ^{11}B from ^{26}Mg. While the imaginary well depths are similar for the three projectiles, we see a distinctly larger diffuseness in the real well for ^{9}Be scattering than for the other projectiles. The real well for the folding model potential has a less diffuse surface than the best-fit Woods-Saxon potentials and hence the shapes, as well as the strengths, are unsatisfactory for describing ^{9}Be elastic scattering. This suggests that break-up (^{9}Be is particle unstable in the lowest excited state) is an important influence.[21]

Elastic scattering angular distributions for ^{9}Be on ^{12}C and ^{16}O are presented in Fig. 2.2. Both show interference oscillations at the more forward angles. These are damped for $\theta \gtrsim 35°$, where the cross sections show a steady decrease with increasing angle with a significant change of slope at ~ 45° for both targets. An optical model analysis of the ^{12}C and ^{16}O data is discussed in detail in ref. 3 where the shoulder beginning at ~ 45° is identified as a residuum of a nuclear rainbow.

This observation is significant because it seems to be the first case of a true rainbow phenomenon in heavy ion scattering. Previous cases cited[7,22,23] as evidence for rainbow scattering do not show this structure. Instead, a structureless exponential-like falloff in cross section is observed which is due to the dominance by the tail of the farside amplitude. This is itself an indication of refractive effects, but as discussed in detail elsewhere,[3,24] a true rainbow arises from inter-

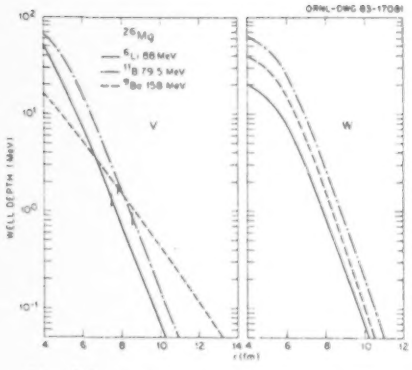

Fig. 2.1. Real and imaginary well depths vs. radius for a variety of light heavy ions elastically scattered from ^{26}Mg. The six parameter Woods-Saxon potentials were obtained from fitting data obtained at HHIRF.

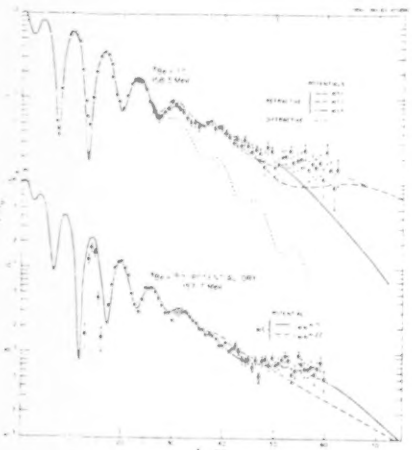

Fig. 2.2. Elastic scattering of 158 MeV ^{9}Be from ^{12}C and ^{16}O. Parameters for optical model potentials are listed in ref. 3.

ference between partial waves with L values above and below the rainbow L_R. The lower partial waves are too strongly absorbed in the other heavy ion cases[7,22,23] for this interference to be visible. However, the potentials obtained from the present data (ref. 3) result in somewhat weaker absorption for the lower partial waves that allows a remnant of the rainbow structure to be seen.

It is apparent in Fig. 2.2 that extending the measurements to larger angles would give more definitive information about the rainbow phenomenon.

1. C. B. Fulmer et al., Phys. Div. Prog. Rep. June 30, 1981, ORNL-5787, p. 30 (1981).
2. C. B. Fulmer et al., Nucl. Phys. A385, 83 (1982).
3. G. R. Satchler et al., Phys. Lett. 128B, 147 (1983).
4. C. B. Fulmer et al., to be submitted to Nuclear Physics A.
5. D. P. Stanley, F. Petrovich and P. Schwandt, Phys. Rev. C 22, 1357 (1980).
6. J. Cook et al., Nucl. Phys. A388, 173 (1982).
7. C. W. Glover et al., Nucl. Phys. A337, 520 (1980).
8. L. T. Chua et al., Nucl. Phys. A373, 243 (1976).
9. L. A. Parks et al., Phys. Lett. 70B, 27 (1977).
10. C. B. Fulmer et al., Nucl. Phys. A356, 235 (1981).
11. R. M. DeVries et al., Phys. Rev. Lett. 39, 450 (1977).
12. M. S. Zisman et al., Phys. Rev. C, 2398 (1980).
13. J. S. Eck et al., Nucl. Phys. A334, 529 (1980).
14. O. Huizdo, C. W. Clover and K. W. Kemper, Phys. Rev. C 23, 236 (1981).
15. P. Schumacher et al., Nucl. Phys. A212, 573 (1973).
16. J. L. C. Ford et al., Phys. Rev. C 10, 1429 (1974).
17. K. S. Toth et al., Phys. Rev. C 14, 1471 (1976).
18. G. R. Satchler and W. G. Love, Phys. Rep. 55, 183 (1979).
19. I. J. Thompson and M. A. Nagarajan, Phys. Lett. 168, 163 (1981).
20. R. S. Mackintosh and A. M. Kobas, Phys. Lett. 116B, 95 (1982).
21. Y. Sakuragi, M. Yahiro and M. Kamimura, Prog. Theor. Phys. 79, ___ (1983).
22. M. E. Brandan, Phys. Rev. Lett. 49, 1132 (1982).
23. H. E. Bohlen et al., Z. Phys. A308, 121 (1982).
24. K. W. McVoy and G. R. Satchler, submitted to Nuclear Physics.

COULOMB-NUCLEAR INTERFERENCE STUDIES[1]

E. E. Gross
F. T. Baker
J. R. Beene
C. R. Bingham[2]
T. P. Cleary[3]
K. A. Erb
M. P. Fewell
J. L. C. Ford, Jr.
D. C. Hensley
M. J. Rhoades-Brown[4]
G. R. Satchler
A. Scott[5]
D. Shapira
C. E. Thorn[6]
K. S. Toth
J. A. Vrba[2]

Coupled-channels analyses of heavy-ion inelastic-scattering data at energies slightly

above the Coulomb barrier have proven useful in providing information on collective nuclear-structure properties as well as providing information on the ion-ion optical potential near the nuclear surface. Examples include quadrupole, octupole and hexadecapole deformations of the charge distribution,[7] triaxial shape parameters,[8] static quadrupole moments of 2^+ states,[7,9] and the value of the real potential near the strong absorption radius.[10] Continuing this program, we have applied these methods to the interesting nucleus ^{18}O[11,12] as well as to ^{22}Ne[13] where a comparison to a previous study[9] on ^{20}Ne was made.

^{18}O Scattering from ^{208}Pb at 120 MeV Lab[11,12]

Elastic scattering data and ^{18}O 2_1^+ state differential cross section data from 120 MeV ^{18}O incident on ^{208}Pb are shown in Fig. 2.3. These data were supplemented by m-substate populations for the 2_1^+ state obtained from detailed line shape analysis.[11] The measurements were made at the BNL Tandem Laboratory. A two-level (0^+-2_1^+) rotational model analysis[11] of these data revealed the need for a large static hexadecapole moment for the ^{18}O 2_1^+ state to account for the deep minimum in the differential cross section near 50° c.m. (Fig. 2.3b). The m-substate populations could not be adequately accounted for unless a small negative spin orbit term was added to the optical potential.

A three level coupled channels analysis[12] including the effect of the second 2^+ state

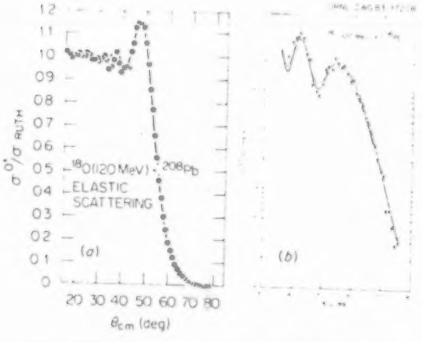

Fig. 2.3. Elastic ratio-to-Rutherford (2.3a) and ^{18}O 2_1^+ inelastic cross section (2.3b) for 120 MeV ^{18}O scattering from ^{208}Pb. The solid curves are minimum χ^2 coupled-channels fits in a three level calculation including the ground state and the first two 2^+ states in ^{18}O. The dashed curve in 2.3b illustrates the deterioration of the fit as the coupling between the two 2^+ states, $M_{2_1 2_2}$, and the self coupling of the 2_1^+ state, $M_{2_1 2_1}$, are allowed to vary from their minimum χ^2 values.

(0^+-2_1^+-2_2^+) revealed a sensitivity to the sign of $P_4 = M_{1_1 2_1} M_{0_1 2_2} M_{2_1 2_2} M_{2_1 2_1}$ where $M_{ij} = \langle i \| M(E2) \| i \rangle$. The previous ambiguity in the sign of P_4 was reflected in a factor of two uncertainty in the static quadrupole moment of the ^{18}O 2_1^+ state as deduced from Coulomb reorientation measurements.[14] The sensitivity of the above-the-barrier data (Fig. 2.3b) to the sign of P_4 is illustrated in Fig. 2.4 which establishes $P_4 > 0$. The three level analysis which accounts for the influence of the 2_2^+ state on the 2_1^+ state also resolves a previous discrepancy in the value of $Q_{2_1^+}$ obtained from a 2-level analysis of above-the-barrier inelastic scattering[15] as compared to the Coulomb reorientation result.[14]

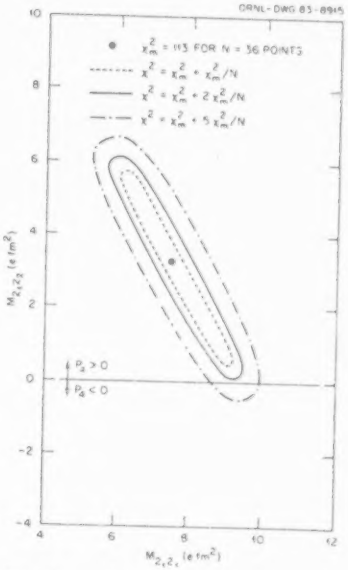
ORNL-DWG 83-8845
χ_m^2 = 113 FOR N = 36 POINTS
$\chi^2 = \chi_m^2 + \chi_m^2/N$
$\chi^2 = \chi_m^2 + 2\chi_m^2/N$
$\chi^2 = \chi_m^2 + 5\chi_m^2/N$
$P_4 > 0$
$P_4 < 0$
$M_{2_1 2_1}$ (e fm^2)
$M_{2_1 2_2}$ (e fm^2)

Fig. 2.4. χ^2 contours in the $M_{2_1 2_1}$, $M_{2_1 2_2}$ plane for a three level, 0^+-2_1^+-2_2^+, coupled-channels fit to the data of Fig. 2.3. The region within the solid-line contour is considered the region of acceptable fits. This entire region lies in the domain $P_4 > 0$.

^{22}Ne Scattering from ^{208}Pb at 132 MeV[13]

Elastic scattering and inelastic excitation of the first collective 2^+ state in ^{22}Ne were measured[13] for 132 MeV ^{22}Ne incident on a ^{208}Pb target to supplement previous data[3] with a ^{20}Ne beam at the same c.m. energy. Elastic scattering data are compared in Fig. 2.5a and inelastic scattering data are compared in Fig. 2.5b.

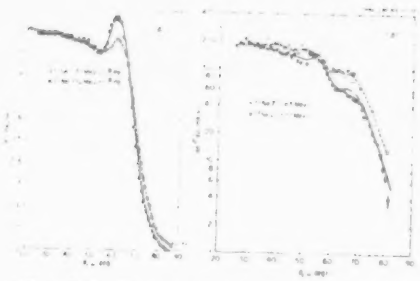

Fig. 2.5. Elastic ratio-to-Rutherford (2.5a) and the differential cross section for exciting the 2_1^+ state (2.5b) of ^{22}Ne (•) and ^{20}Ne(o) by scattering from a ^{208}Pb target at 120 MeV c.m. The curves are coupled-channels fits including the ground state, first 2^+ state and first 4^+ states of the neon nuclei.

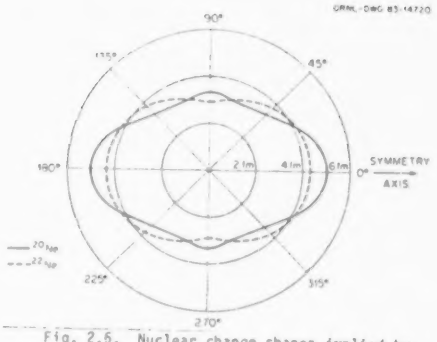

Fig. 2.6. Nuclear change shapes implied by the rotational-model fits to the data of Fig. 2.5.

The data were subjected to a three-level 0^+-2^+-4^+, rotational-model coupled-channels calculation to extract charge distributions and matrix elements. The dashed curves are the best fits to the ^{20}Ne data and the solid curves are the best fits to the ^{22}Ne data. A small negative spin orbit potential ($V_{L\cdot S}$ = -0.15 MeV) was included in the ^{22}Ne + ^{208}Pb optical potential. Without the spin-orbit potential term, the best fit to the ^{22}Ne 2^+ differential cross section is shown as the dot-dashed curve in Fig. 2.5b. The extracted charge distributions for ^{20}Ne and ^{22}Ne are compared in Fig. 2.6. The addition of two neutrons to ^{22}Ne is seen to eliminate the equatorial hexadecapole bulge.

1. Summary of 1 published paper, ref. 11, and 2 submitted papers, refs. 12 and 13.
2. Guest scientist from the University of Tennessee.
3. Present address: World Information and Technology Systems Corp., Willowdale, Ontario, Canada.
4. Present address: State University of New York at Stony Brook.
5. Guest scientist from the University of Georgia.
6. Guest scientist from Brookhaven National Laboratory.

7. D. L. Hillis et al., Phys. Rev. C 16, 1467 (1977).
8. F. T. Baker et al., Nucl. Phys. A321, 222 (1979).
9. E. E. Gross et al., Phys. Rev. C 17, 1665 (1978).
10. P. R. Christensen et al., Nucl. Phys. A207, 433 (1973).
11. E. E. Gross et al., Nucl. Phys. A401, 362 (1983).
12. E. E. Gross and M. P. Fewell, Nuclear Physics, to be published.
13. E. E. Gross et al., submitted to Physical Review.
14. M. P. Fewell et al., Nucl. Phys. A321, 457 (1979).
15. F. Videbaek et al., Nucl. Phys. A256, 301 (1976).

ELASTIC AND INELASTIC SCATTERING OF ^{60}Ni BY ^{60}Ni, ^{58}Ni, AND ^{56}Fe

K. A. Erb
D. Shapira
J. Gomez del Campo
R. Novotny
C. B. Fulmer
J. L. C. Ford
E. E. Gross
M. Rhoades-Brown
G. R. Satchler

The high resolution beams from the new high energy tandem accelerators make it possible to study the interactions of medium mass nuclei (A $\lesssim$ 50) with a precision that reveals unexpected and puzzling behavior. Collisions of nickel isotopes at sub and near Coulomb-barrier energies are a case in point. Measurements by Beckerman et al.,[1] show that the sub-barrier fusion yields from ^{64}Ni + ^{64}Ni, ^{64}Ni + ^{58}Ni, and ^{58}Ni + ^{58}Ni interactions differ unaccountably from one another. Balantekin, Koonin and Negele[2] demonstrated that these measurements rule out any description of the fusion process in terms of a standard one-dimensional barrier penetrability treatment, in contrast to the situation for lighter systems such as ^{12}C + ^{12}C, ^{16}O + ^{16}O, etc. Additional but unidentified degrees of freedom thus influence strongly the evolution of reactions involving heavier nuclei, even at energies as low as 2-4 MeV/nucleon.

Surface reactions, such as elastic and inelastic scattering and rearrangement processes, are likely candidates. However, the lack of systematic data in which individual exit channels are cleanly resolved, for projectiles and targets heavier than silicon, has prevented an assessment of the role of these degrees of freedom.

In the present work elastic and inelastic scattering yields were measured for collisions of ^{60}Ni beams with ^{60}Ni, ^{58}Ni, and ^{56}Fe targets. Measurements were made at laboratory energies of 198 MeV--close to the Coulomb barrier--and at 228 MeV. Reaction products were detected in kinematic coincidence in two silicon position-sensitive detectors placed on opposite sides of the beams, with an angular resolution of 0.1°. Two-body kinematic reconstructions were made on an event-by-event basis to separately identify

scattered beam nuclei and recoiling target nuclei. Angular distributions were obtained for the elastic and the inelastic yields over the angular range $60° \leq \theta_{cm} \leq 115°$.

The large magnitudes of the inelastic yields are a dominant feature of the data. For collisions of relatively light nuclei the total reaction cross section near the Coulomb barrier is dominated by the fusion cross section, while for Ni + Ni interactions we found that flux removed from the elastic channels appears almost entirely (~ 95%, at the Coulomb barrier) in elastic channels. The strong coupling between elastic and inelastic channels implied by these results could be important for descriptions of the evolution of medium mass collision complexes, particularly since the coupling implies non-local effects which would be difficult to mimic in standard one-channel models.

We have begun to probe these possibilities in several ways. Coupled-channels calculations incorporating the ground and first-excited states in each collision partner were carried out using the code PTOLEMY. These calculations provide a generally satisfactory account of the data, using previously measured BE2 values to describe the coupling to excited states. However, it was found necessary to modify the optical potential on a target-by-target basis to achieve this result, despite the apparent macroscopic similarity of the three targets treated. Potentials adequate for one projectile-target combination provide poor fits to data for the others, raising the possibility that degrees of freedom in addition to those describing the inelastic channels are important.

Folded potentials will be used in the optical channels to further investigate the differences outlined above. In addition, we are constructing and examining local potentials for one-channel calculations that yield wave functions equivalent to those arising from the coupled-channels calculations, to try to understand the origin of these differences. Finally, work has begun to investigate the extent to which polarization potentials[3] can mimic the long-range absorption associated with the Coulomb interaction in these Coulomb-dominated collisions.

1. M. Beckerman et al., Phys. Rev. Lett. 45, 1472 (1980).
2. A. B. Balentekin, S. E. Koonin and J. W. Negele, Phys. Rev. C 27, 17611 (1983).
3. W. G. Love, T. Terasawa and G. R. Satchler, Nucl. Phys. A291, 183 (1977); Phys. Rev. Lett. 39, 6 (1977).

SYSTEMATIC ANALYSIS OF HEAVY ION INELASTIC SCATTERING

M.W. Guidry[1] D. Cline[2]
L.L. Riedinger[1] A. Bakleen[2]
C.R. Bingham[1] D. Kotlinski[2]
A. Larabee[1] P. Bond[3]
C. Baktash P. Butler[4]
I.Y. Lee

In conjunction with the heavy ion transfer reactions discussed in a separate section, we are accumulating very large amounts of high quality inelastic scattering data. These data involve extensive heavy-ion angular distributions with resolution approximately 2°, and in some cases at more than one beam energy. They undoubtedly constitute the best data available on inelastic scattering of very heavy ions. A number of ground band states are populated, and gamma-ray intensities and angular distributions are being recorded in coincidence with the scattered particles. The systems for which we have data thus far are $^{58}Ni + {}^{161,162,163}Dy$, $^{113,114}Cd$; $^{116}Sn + {}^{161,162,163}Dy$, ^{166}Er, ^{158}Gd; and $^{161}Dy + {}^{208}Pb$.

We are, therefore, in a position to systematically analyze inelastic scattering of very heavy ions on heavy deformed and vibrational nuclei along the lines of our previous work in this area,[5,6] but at a much more ambitious level. As we have discussed in detail before, coupled channels and semiclassical calculations fitted simultaneously to the large number of states populated provide a far more detailed picture of the surface of collective nuclei than do reactions such as elastic scattering or fusion reactions.

The analysis of this inelastic scattering data will be important because of its intrinsic nuclear structure information and because its understanding is a required input for making sense of any more complicated heavy-ion reaction. For example, quasielastic reactions such as transfer, and deep inelastic reactions, must proceed appreciably through the doorway of these collective states, since their excitation can hardly be avoided in a heavy ion collision.

1. University of Tennessee, Knoxville, TN.
2. University of Rochester, Rochester, NY.
3. Brookhaven National Laboratory, Upton, NY.
4. Liverpool University, Liverpool, United Kingdom.

5. R. E. Neese et al., Phys. Lett. 85B, 209 (1979).
6. M. W. Guidry, et al., Phys. Rev. Lett. 40, 1016 (1978).

HEAVY ION TRANSFER REACTIONS FOPULATING HIGH-SPIN STATES

M. W. Guidry[1] D. Cline[2]
L. L. Riedinger[1] A. Bakleen[2]
C. R. Bingham[1] D. Kotlinski[2]
A. Larabee[1] P. Bond[3]
C. Baktash P. Butler[4]
I. Y. Lee D. Sarantites[5]
M.L. Halbert

Heavy ion transfer reactions populating strongly collective states represent a potentially rich field of study for nuclear physics. With rapid advances in theoretical methods to handle the coupled-channels problem, and sophisticated particle-γ coincidence experiments we finally have the tools to explore the new physics of this area.[5]

In recent particle-γ coincidence experiments with Ni and Sn beams on rare earth targets, and rare earth beams on lead targets, the population

of high spin states has been seen with large cross section in one- and two-neutron transfer channels. The Ni data have been taken at Brookhaven, the Sn data at Oak Ridge, and the Pb data at GSI, Darmstadt. For scattered particles near the grazing angle the intensity of lines in the rotational bands of transfer products are comparable to those for direct Coulomb excitation of the target. Fig. 2.7 illustrates the detector arrangement, and Fig. 2.8 shows a typical spectrum.

ORNL-DWG 83-17490

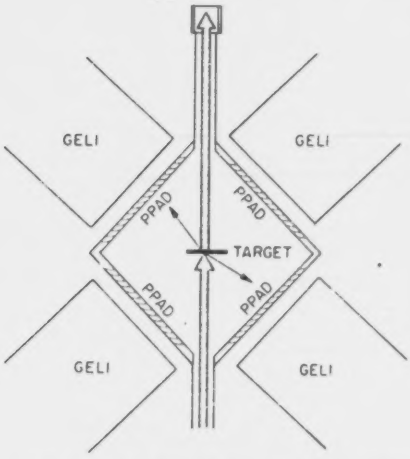

Fig. 2.7 The detector system used to acquire the data in Fig. 2.8. The PPAD's are parallel plate avalanche detectors, used for position-sensitive particle detection. Gamma rays are detected in the GeLi detectors in coincidence with the beam-like and target-like fragments.

In more recent experiments these studies have been performed inside the Spin Spectrometer at HHIRF. The total energy and multiplicity for γ-rays in the transfer reaction ^{161}Dy(^{58}Ni,^{59}Ni)^{160}Dy to high spin states demonstrate that 1) the multiplicity of the transfer reaction is considerably larger than for the corresponding inelastic reactions. 2) The major portion of the transfer reaction is populating states on or near the yrast line. 3) There is significant population by the transfer reaction up to ~4 MeV above the yrast line. These results demonstrate the possibility of a direct reaction probe of highly excited, discrete collective states along the yrast line and a highly selective method to populate the energy-angular momentum plane a few MeV above the yrast line.

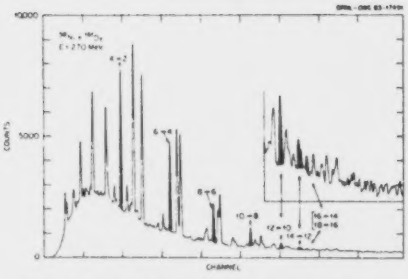

Fig. 2.8 Particle-particle-gamma coincidence spectra taken using GeLi detectors operated in coincidence with position sensitive parallel plate avalanche detectors. The peaks in the gamma-ray spectra correspond to transitions following the inelastic reaction ^{161}Dy(^{58}Ni,^{58}Ni)^{161}Dy* and the 1-neutron pickup reaction ^{161}Dy(^{58}Ni,^{59}Ni)^{160}Dy* for E_{LAB} = 270 MeV. Lines in the ^{160}Dy transfer product ground band are labeled and shaded. The strong unmarked peaks correspond to transitions in the inelastic product ^{161}Dy. The spectrum corresponds to an integrated 20° range around the grazing angle (approximately 130°) and peaks in the 1-neutron transfer channel (ground state band of ^{160}Dy) appear with intensities comparable to the inelastic transitions. These peaks are identified as transfer lines from the known transition energies in ^{160}Dy and from the particle angular distribution which was measured with an angular resolution of approximately 2°. Transitions are seen clearly to the 14+12 and possibly to the 16+14, 18+16 doublet. ^{160}Dy backbends beginning at the 14+12 transition.

Quantitative calculations for these kinds of reactions have yet to be done. However, all the necessary ingredients are available, relatively well understood, and at least partially implemented. The reader may consult Ref. 6 for discussions of how the requisite calculations can be done and examples of some simple initial computations. It is expected that the recently acquired data of the kind in Fig. 2.7 will stimulate considerable theoretical activity along these lines.

---

1. University of Tennessee, Knoxville, TN.
2. University of Rochester, Rochester, NN.
3. Brookhaven National Laboratory.
4. Liverpool University, Liverpool, U.K.
5. Washington University, St. Louis, MO
6. M. W. Guidry, T. L. Nichols, R. E. Neese, R. Donangelo, L. Oliviera, and J. O. Rasmussen, Nucl. Phys. A361, 275 (1981).

SEARCH FOR SPIN-ORBIT EFFECTS IN THE $^{28}Si(^{11}B,^{10}B)$ REACTIONS

C. F. Maguire[1] F. E. Bertrand
Zhao Kui[1] E. E. Gross
K. Teh[1] R. O. Sayer
J. L. C. Ford, Jr. D. Shapira
T. P. Sjoreen

There has been a growing interest in the topic of spin effects in heavy-ion reactions.[2] Information on these effects can best be gleaned with the use of polarized beams or targets which can give direct evidence on the significance of the spin-orbit coupling term in the heavy-ion optical potential. Polarizations induced in the outgoing channel can also be investigated by measuring the spin-alignment of excited ejectile states in a transfer reaction.

From an analysis of the m-substate populations in the $^{88}Sr[^{16}O,^{15}N^*(6.33\ MeV)]^{89}Y$ reaction at E_{lab} = 96 MeV, Wüst et al.[3] concluded that a sizeable spin-orbit term was present. This term in the optical potential is parameterized in a Thomas form:

$$V_{SO}(r) = V_{SO}^{o} \times \frac{\hbar^2}{m_\pi c} \times \frac{1}{r}\frac{d}{dr} f(r,R_o,a) \times \hat{\sigma}\cdot\hat{L}$$

In this representation, R_o and a are the nuclear radius and diffuseness of the Woods-Saxon function f, m_π is the pion mass, and L is the orbital angular momentum of the heavy ion. The strength scaling term V_{SO}^{o} was determined for this reaction to be 1.5 MeV, which is an order of magnitude or larger than expected based on folding model type calculations.[4]

As a means of testing the presence of such a term in heavy-ion transfer reactions, we devised an experiment at HHIRF using a 93 MeV ^{11}B beam. Three simple, single-neutron transfer reactions were measured using a 300 $\mu g/cm^2$ natural silicon target with the ^{10}B ejectiles momentum analyzed in a magnetic spectrometer. Reaction product identification was accomplished using the new focal plane counter system developed at ORNL[5] (see Equipment Development Section, this report). In this experiment the primary reactions of interest were:

$^{28}Si[^{11}B,^{10}B(0.000\ MeV, 3^+)]^{29}Si(0.0\ MeV, \frac{1}{2}^+)$

$^{28}Si[^{11}B,^{10}B(0.718\ MeV, 1^+)]^{29}Si(0.0\ MeV, \frac{1}{2}^+)$

$^{28}Si[^{11}B,^{10}B(1.740\ MeV, 0^+)]^{29}Si(0.0\ MeV, \frac{1}{2}^+)$.

In each case the residual nucleus final bound state is the same, specifically ^{29}Si in a $2s_{1/2}$ neutron configuration. According to the DWBA transfer selection rules, all the ℓ transfers for these reactions are uniquely ℓ = 1 since in each case a p-shell neutron is being stripped out of the projectile ^{11}B. In the absence of any spin-orbit coupling effects, the differential cross sections for the above three reactions should have almost precisely the same shapes because there is only a small (compared to the incident energy) Q-value change between the reactions. On the other hand, with the introduction of a spin-orbit term, modifications in the angular distributions might be introduced for the reactions leading to the $^{10}B(3^+)$ and to the $^{10}B(1^+)$ final states, but not to the spin zero $^{10}B(0^+)$ final state. With this theoretical perspective in mind, we illustrate in Figs. 2.9 and 2.10 the $^{28}Si[^{11}B,^{10}B(0.0\ MeV, 3^+)]\ ^{29}Si(0.0\ MeV, \frac{1}{2}^+)$ and $^{28}Si[^{11}B,^{10}B(0.718\ MeV, 1^+)]^{29}Si(0.0\ MeV, \frac{1}{2}^+)$ DWBA angular distribution predictions with and without a spin-orbit coupling potential term of the size prescribed by Wüst et al.[3] Without a spin-orbit term, the predicted angular distributions have almost exactly the same shape over the entire angular range. However, with the 1.5 MeV spin-orbit potential, the two predictions become noticeably different.

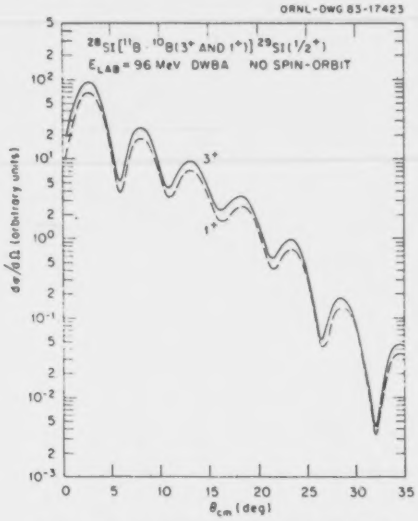

Fig. 2.9. DWBA predicted angular distributions for the $^{28}Si(^{11}B,^{10}B)^{29}Si(g.s.)$ single neutron transfer reaction. Standard optical model potential parameters were used while a spin-orbit coupling term was not included.

This experiment was carried out in early July, 1983 and represented one of the first "live" tests of the new vertical drift chamber system. Data were taken with the full angular opening (4° lab) of the magnetic spectrometer, and subsequently software algorithms resolved the data into 0.5° bins according to reaction product identification. Overall the system worked extremely well, although there were still some relative angle efficiency normalizations to be determined. In addition to measuring the above three reaction groups, data were also obtained for the elastic and inelastic scattering of ^{11}B + ^{28}Si. These scattering data

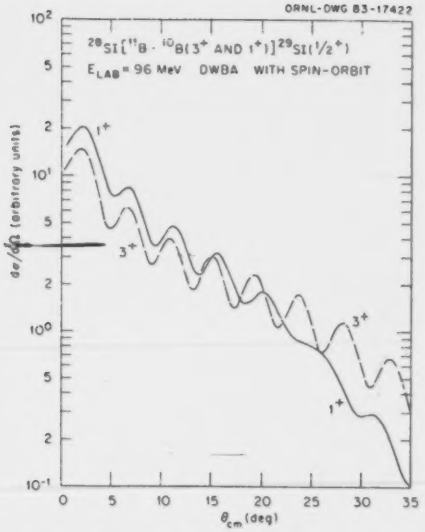

Fig. 2.10. As in Fig. 2.9 except a 1.5 MeV deep spin-orbit coupling term was added. The different ejectile final states now have very different shapes for their differential cross sections.

will enable us to deduce a "baseline" optical potential and also to place limits on coupled-channels effects which might interfere with the one-step DWBA analysis of the reactions. A preliminary analysis of the transfer reaction data appears to indicate that there are pronounced oscillations in the ^{10}B(3$^+$) reaction group but that these oscillations are damped out in the ^{10}B(1$^+$) reaction, much as illustrated in Fig. 2.10. Further analysis will be required to ascertain whether and what size spin-orbit terms can reproduce these angular distributions.

---

1. Vanderbilt University, Nashville, Tennessee 37235.
2. D. Fick, "Polarization in Heavy-Ion Reactions" and references therein, ORNL TM-8816 (1983), unpublished.
3. P. Wüst et al., Z. Physik A291, 151 (1979).
4. F. Petrovich et al., Phys. Rev. C 17, 1042 (1978).
5. M. V. Hynes et al., Nucl. Instrum. Methods; and T. P. Sjoreen et al., Nucl. Instrum. Methods, to be published.

QUASI-ELASTIC TRANSFER REACTIONS INDUCED BY ^{56}Fe ON ^{58}Ni, ^{64}Ni, AND ^{122}Sn[1]

S. Pontoppidan[2] Y. Patin[3]
P. R. Christensen[2] R. H. Stokes[3]
O. Hansen[2] M. P. Webb[3]
F. Videbaek[2] R. L. Ferguson
H. C. Britt[3] F. Plasil
B. H. Erkkila[3] G. R. Young

Differential cross sections, $\sigma(Z,A,E,\theta)$, for the quasi-elastic projectilelike reaction products from reactions of ^{56}Fe with ^{58}Ni, ^{64}Ni, and ^{122}Sn nuclei have been measured with a channel plate time-of-flight system, followed by a ΔE gas ionization chamber and a silicon E detector. The ^{56}Fe projectiles were obtained from the LBL SuperHILAC at laboratory energies of 320 and 460 MeV. In the case of the ^{56}Fe + ^{64}Ni reaction, data were obtained only at 460 MeV. Angular intervals of 10°-15°, centered at the grazing angles, were covered in 2°-4° steps. Single-mass and single-charge resolution was achieved.

A sample of the extensive data obtained is shown in Fig. 2.11. For each of the five reactions, Q-value spectra obtained at the grazing

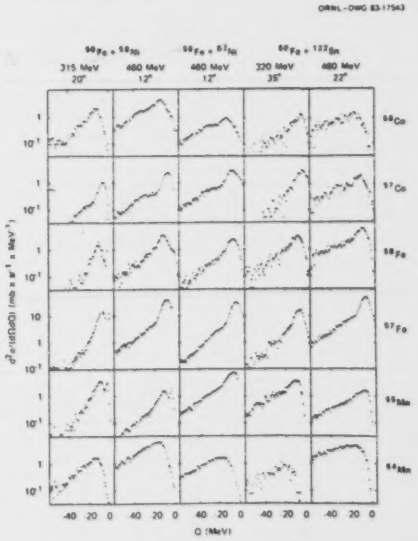

Fig. 2.11. Q-value spectra for the quasi-elastic region of six different projectilelike fragments. The grazing angles of the five different reactions are indicated, and the cross sections refer to the laboratory system. Each point corresponds to a Q-bin size of 1 MeV.

angles are shown for six different projectile-like products. A number of substructures (bumps) are evident, with perhaps the most prominent ones being located at Q ≈ -25 MeV in the spectra of ^{57}Co produced in the 460-MeV bombardments. The angular distributions were observed to have a Guassian shape for Q ≥ -60 MeV. With increasing energy loss, the angle of maximum yield was found to move forward, and the width of the distributions was found to increase. The differential cross sections for one-proton transfer were analyzed with the DWBA. It was possible to account for the shape of the angular distributions and, to better than a factor of 5, for the absolute cross sections, in the Q-value range from zero to -10 MeV.

A model for unfolding the effects of particle evaporation from the reaction products was developed[4] and applied to the data in order to see whether the observed substructures can be accounted for. The formalism employed was similar to that used to unfold effects of detector response in γ-ray spectra. With reasonable assumptions regarding the sharing of excitation energy between the two primary products, it was shown that the observed bumps cannot be due to evaporation effects alone and must be present in the primary distributions.

Effective optimum Q values of individual products were defined as the Q values at which maxima are observed in the energy spectra in the quasi-elastic region, after Q values are corrected for differences in the potential barriers in the entrance and exit channels. They were found to vary roughly linearly with the number of transferred nucleons. For a given reaction, this implies a fixed energy loss per transferred nucleon. The general trends of the observed effective optimum Q values can be understood within the simple classical Brink[5] picture combined with the effect of Pauli blocking.[6] Reasonable agreement between experiment and theory was obtained when the magnitude of Pauli blocking was determined not by the global Fermi momentum of the nucleus, but by the local Fermi momentum in the region of the nuclear surface, where the transfer process is localized.

---

1. Summary of paper: Physical Review C (in press).
2. Niels Bohr Institute, University of Copenhagen, Copenhagen, Denmark.
3. Los Alamos National Laboratory, Los Alamos, New Mexico.
4. This approach was suggested by Th. Døssing.
5. D. M. Brink, Phys. Lett. 40B, 37 (1972).
6. J. Randrup, Nucl. Phys. A307, 319 (1978); A327, 498 (1979).

CALCULATION OF THE ENERGY-AVERAGED SCATTERING FUNCTION FROM HIGH RESOLUTION LOW-ENERGY NEUTRON SCATTERING DATA[1]

C. H. Johnson N. M. Larson,[2]
C. Mahaux,[3] R. R. Winters[4]

Most optical model analyses of nucleon-nucleus scattering involve data representing not only averages over energies but also sums over partial waves. However, individual partial waves can be studied by scattering neutrons at low energies with good resolution. One fits the resonances to obtain the energy dependent scattering function S(E) for each partial wave and then averages over energy for the purpose of comparing to the model. In Fig. 2.12 the solid curves show averages versus the average energy E for $p_{3/2}$ neutrons[5] on ^{32}S.

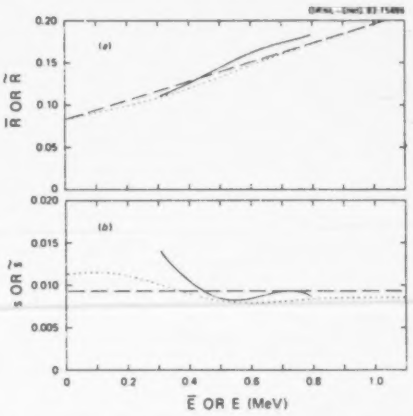

Fig. 2.12. Average scattering function for $p_{3/2}$ neutrons on ^{32}S. The solid curves are numerical R and s versus E for I=300 keV. The dotted curve is the analytic approximation versus E. Long dashed curves show R and s.

Averaging was done with a normalized Lorentzian weight function of width 2I = 600 keV truncated at the energy limits of the data, E_ℓ = 0 to E_u = 1100 keV. The plots show the quantities R and s defined by the relation

$$\langle S(E)\rangle_I = e^{-2i\phi(E)}\,\frac{1+iP(E)\mathcal{R}(E)}{1-iP(E)\mathcal{R}(E)} \qquad (1)$$

where $\mathcal{R}(E) = \bar{R}+is$ and where P and φ are the penetrability and hard-sphere phase shift.

Averaging was done numerically using selected quadrature schemes. In order to make a simpler analytic approximation we first parametrize S(E) using the R-matrix formalism;

$$S(E) = e^{-2i\phi(E)}\,\frac{1+iP(E)R(E)}{1-iP(E)R(E)} \qquad (2)$$

$$\text{with}\quad R(E) = R^{ext}(E) + \sum_\lambda \frac{\gamma_\lambda^2}{(E_\lambda - E)} \qquad (3)$$

where the summation is over the observed resonances and $R^{ext}(E)$ is a smoothly increasing parametric function which accounts for resonances outside the observed region.

A good approximation can be obtained and justified if R^{ext} is parametrized as

$$R^{ext}(E) = \tilde{R}(E) + \tilde{s}\ln\frac{E_u-E}{E-E_\ell} \qquad (4)$$

where $\tilde{R}$ is a simple function, say linear, and $\tilde{s}$ is the strength $\langle\gamma^2\rangle/D$ for the observed levels. The approximation is given by Eq. (1) with $\tilde{R}(E)$ replaced by

$$\tilde{R}(E) + i\pi\tilde{s} + R^f(E+iI) \qquad (5)$$

where R^f is a term which fluctuates about zero;

$$R^f(E) = \sum_\lambda \frac{\gamma_\lambda^2}{E_\lambda-E-iI} - \int_{E_\ell}^{E_u} \frac{\tilde{s}dE'}{E'-E-iI} \qquad (6)$$

The resulting average, as shown by the dotted curves in Fig. 2.12, agrees well with the numerical average. If we omit R^f we have simply R and s, as shown by the long-dashed curves. This also is a good approximation which is particularly easy to use.

---

1. C. H. Johnson et al., Phys. Rev. C 27, 1913 (1983).
2. Computer Science Division.
3. Institut de Physique, Université de Liège, 4000 Liège, Belgium.
4. Denison University, Granville, Ohio.
5. C. H. Johnson and R. R. Winters, Phys. Rev. C 21, 2196 (1980).

OPTICAL MODEL POTENTIALS FOR s- AND p-NEUTRONS ON ^{30}Si, ^{32}S, ^{34}S, ^{40}Ca AND ^{60}Ni

C. H. Johnson R. F. Carlton[1]
J. A. Harvey[2] C. Mahaux[3]
R. R. Winters[4]

We have extended to higher energies and higher partial waves some concepts that are well known for very low energy neutron scattering. Familiar quantities for low energy s-waves are the potential scattering radius R', which is found from the off-resonance scattering and the strength function $\tilde{s}_0$, which is the ratio $\langle\gamma^2/D\rangle$ of the average reduced width to spacing. The quantities R' and $\tilde{s}_0$ are closely related respectively to the real and imaginary parts of an optical model potential (OMP).

With a high resolution facility such as the Oak Ridge Electron Linear Accelerator (ORELA), measurements related to the OMP can be extended to several hundred keV, not only for s-waves but also in favorable cases to p- and d-waves. The simplest data are total cross sections for spin-zero targets at energies below the inelastic threshold. In the analysis one makes a multilevel R-matrix fit to find the detailed scattering function $S_{\ell J}(E)$ for each partial wave ℓ J and then averages over energy, as discussed in the preceding report,[5] for comparison to the S^{OMP} of the model.

The R-function for the multilevel analysis is written $R^{ext}(E) + R^{int}(E)$ where R^{int} is the sum over resonances within the region of measurement, E_ℓ to E_u, and R^{ext} is a smoothly increasing function that accounts for all external levels. Various parametric forms could be used for R^{ext}; however, a simple analytic approximation to the average of $S_{\ell J}$ can be made if one chooses the parametrization

$$R^{ext}(E) = \tilde{R}_{\ell J}(E) - \tilde{s}_{\ell J}\ln\frac{E_u-E}{E-E_\ell}, \qquad (1)$$

where $\tilde{s}_{\ell J}$ is the observed strength and $R_{\ell J}$ is a simple function, say a+bE. The last term in Eq. (1) is equivalent to a distribution of strength $\tilde{s}_{\ell J}$ everywhere outside the measured region. The quantity $\tilde{s}_{\ell J}$ is closely related to the imaginary part of the OMP, and $\tilde{R}_{\ell J}$ is related to the real part. At low energies for s-waves, R' = a(1-$\tilde{R}$) where a is the boundary radius.

We begin with the R-matrix parameters obtained by other workers[6-10] at ORELA for ^{30}Si, ^{32}S, ^{34}S, ^{40}Ca, and ^{60}Ni. For ^{30}Si and ^{60}Ni we convert R^{ext} from the published multipole parametrization to Eq. (1). In Fig. 2.13 the solid curve is calculated from the tabulation[7] of ten s-wave poles for ^{60}Ni; the short dash curve is our fit of Eq. (1) to the solid curve. The long dash line is the resulting $\tilde{R}$.

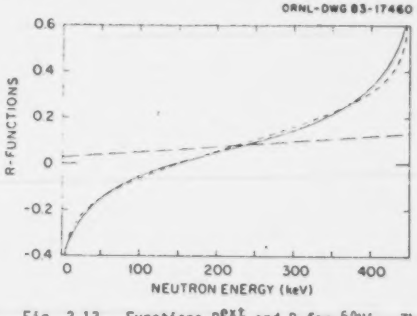

Fig. 2.13. Functions R^{ext} and R for ^{60}Ni. The solid curve is R^{ext} from ref. 7 and the short-dash curve is a refit using Eq. (1) with R given by the long dash line.

For each nuclide we averaged $S_{\ell J}(E)$ using an analytic approximation.[5] To show these results we adopt the procedure[6] of plotting the shape elastic and compound nucleus cross sections, σ_{se} and σ_c. Figure 2.14 shows these functions (divided by 2) for $p_{3/2}$ neutrons[8] on ^{30}Si. The long dash curves result from the analytic approximation for I=300 keV; the curve for σ_c shows a peak at the energy of two strong resonances which are located at the energies of the arrows. The solid curves were calculated from R and s with the fluctuating term omitted. The short dash curves show the visual OMP fit discussed below.

For each nuclide we fit σ_{se} and σ_c by adjusting the depths V_0 and V_{so} for the real part and W_D for the imaginary part for an OMP of fixed geometry.

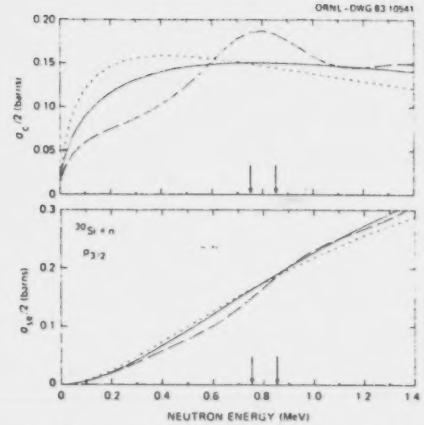

Fig. 2.14. Cross sections for the average scattering function for n+^{30}Si. The long dash curve is from the analytic approximation for I=300 keV and the solid line is the approximation with the fluctuating term omitted. The best visual fit for the OMP is the short dash curve. Arrows indicate energies of prominent resonances.

Our OMP has a Woods-Saxon real well and surface-derivative spin-orbit and imaginary wells, all with radius r_0 = 1.21 fm. The real wells had diffuseness a_0 = 0.66 fm, and the imaginary well had a_D = 0.48 fm.

Table 2.2 lists the results. Within the uncertainties the values of V_0 for ℓ=0 are all about the same, about 52 MeV. However, the p-wave wells are much deeper for ^{30}Si, ^{32}S and ^{34}S. Those differences are attributed to vibrational[12] effects in those nuclei. The imaginary depths average about 3 MeV; however, a very small depth of 0.6 MeV is found for p-waves on ^{40}Ca and a large depth of 29 MeV for s-waves on ^{60}Ni. This suggests that the effects of collective excitation should be studied in relation to the absorptive potential.

These results are published[6,11] for ^{32}S, submitted for publication[13] for ^{30}Si and ^{34}S and in progress for ^{40}Ca and ^{60}Ni.

Table 2.2. Neutron optical model potential well depths.

Nucleus	ℓ	V_0	V_{so}	W_D
^{30}Si	0	48 ± 1.7		4.5 ± 1.5
	1	62 ± 2.5	7[a]	4.5 ± 2.5
^{32}S	0	51.5 ± 0.4		6.0 ± 3.0
	1	61.4 ± 1.1	11 ± 3	2.7 ± 1.5
^{34}S	0	51.5 ± 1.1		3.0 ± 2.0
	1	58.5 ± 1.2	6 ± 3.5	3.5 ± 1.9
^{40}Ca	0	53.6 ± 1.0		6.7 ± 0.3
	1	56.1 ± 1.0	6 ± 7	0.6 ± 0.3
^{60}Ni	0	48 ± 5		29 ± 5

a. Assumed value.

10. J. L. Fowler, C. H. Johnson and N. W. Hill, (unpublished).
11. C. H. Johnson and R. R. Winters, Phys. Rev. C 27, 416 (1983).
12. A. D. MacKellar and B. Castel, Phys. Rev. C 28, 441 (1983).
13. R. F. Carlton, J. A. Harvey, and C. H. Johnson, submitted to Phys. Rev. C.

STUDY OF THE ORIGINS OF THE ℓ-DEPENDENCE OF THE SPHERICAL OPTICAL POTENTIAL DERIVED FROM LOW ENERGY NEUTRON SCATTERING

A. D. MacKellar[1] B. Castel[2]
C. H. Johnson

As discussed in the preceding report, an analysis of neutron-nucleus scattering data in the low energy resonance region (100-1200 keV) has resulted in optical potentials with quite different s- and p-wave well depth parameters.[3,4,5] That analysis involves R-matrix analysis of high-resolution resonance data, energy averaging, and calculation of an average S-matrix.[6] This leads to the average partial wave shape elastic and compound cross sections.

In both the preceding and present reports these cross sections are considered the "experimental" results. Previously these data were fitted with a standard spherical optical model potential to obtain the potential parameters listed in Table 2.3 for ^{30}Si, ^{32}S, ^{34}S, and ^{40}Ca. Clearly the real potential well depths are much larger for p-waves than for s-waves. The limitation of that analysis is that it assumes 1) that the nucleus is spherical and does not couple to vibrational or rotational collective modes and 2) the optical

1. Middle Tennessee State University, Murfreesboro, Tennessee.
2. Now in Engineering Physics Division.
3. Institut de Physique, Université de Liège, Liège, Belgium.
4. Denison University, Granville, Ohio.

5. Preceding report and C. H. Johnson et al., Phys. Rev. C 27, 1913 (1983).
6. C. H. Johnson and R. R. Winters, Phys. Rev. C 21, 2190 (1980).
7. C. M. Perey et al., Phys. Rev. C 27, 2556 (1983).
8. J. A. Harvey et al., Phys. Rev. C 28, 24 (1983).
9. R. F. Carlton et al., submitted to Phys. Rev. C.

Table 2.3.[a] Optical model potentials for ^{30}Si, $^{32,34}S$ and ^{40}Ca. (See text for definition of quantities listed.)

Target	ℓ	V(MeV) sph	V(MeV) cc	W_D(MeV) sph	W_D(MeV) cc	V_{SO}(MeV) sph	V_{SO}(MeV) cc
^{30}Si	0	48	49.5	2	1		
	1	62	51.5	4.5	2	7	3.3
^{32}S	0	51.5	50.8	6	4		
	1	61.4	50.8	2.7	0.8	11	5.3
^{34}S	0	51.5	50.5	3	2.5		
	1	58.5	51	3.5	2.5	6	3.5
^{40}Ca	0	53.6	51	6.7	7		
	1[b]	56.1	53	1.3	0.1	6	4
	1[c]	56.1	53	0.65	0.1	6	4

a. Geometric parameters: $r_o = r_D = 1.21$ fm, $a_o = 0.66$ fm, $a_D = 0.48$ fm.
b. $p_{1/2}$ case
c. $p_{3/2}$ case

Table 2.4. Description of target and neutron states used in coupled-channel calculations.

Channel Spin J^π	Target State	Neutron ℓ	State J	Parity of Optical Potential Used
$1/2^+$	0^+	0	1/2	+
	3^-	3	5/2	-
	3^-	3	7/2	-
	2^+	2	3/2	+
	2^+	2	5/2	+
$1/2^-$	0^+	1	1/2	-
	3^-	2	5/2	+
	3^-	2	7/2	+
	2^+	1	3/2	-
	2^+	3	5/2	-

potential is local. In this report we focus on the effects of dynamic and static deformations of the target nuclei on the optical model potential parameters. We employ the standard coupled channels analysis as discussed by Tamura.[7] The results for ^{32}S have been published.[8]

The ^{32}S, ^{34}S, and ^{40}Ca nuclei are treated in a one phonon vibrational model. For ^{32}S and ^{34}S we have coupled together the 0^+-2^+-3^+ states, while for ^{40}Ca we have studied the effect of the giant resonances, using a 0^+-3^--5^--GQR-HEOR coupling scheme. We treated ^{30}Si as a rotational nucleus, coupling the 0^+-2^+-4^+ states. The deformation parameters β were taken whenever possible from other experimental analyses and were not treated as free parameters. We used the same fixed geometries as were used for the spherical analysis, and varied only the well depth parameters $V^{\ell=0}$, $W_D{}^{\ell=0}$, $V^{\ell=1}$, $W_D{}^{\ell=1}$, and V_{SO}. We used the coupled channels code[9] ECIS79, which allows for the use of different potentials for different collective target modes. For instance, for coupling to 0^+-2^+-3^- states Table 2.4 gives the target and neutron states which are coupled together for a given channel spin and parity. For each set of potential parameters two calculations were made. For the $s_{1/2}$ wave partial cross sections we choose the potential parameters appropriate to the channel spin $1/2^+$, which contains the ℓ=0 scattering, while for $p_{1/2}$ and $p_{3/2}$ we choose potential parameters appropriate to the channel spin $1/2^-$ and $3/2^-$, respectively. Since only the ℓ=0 and ℓ=1 data are known, in practice we use positive (negative) parity potentials $V^+(V^-)$ instead of $V^{\ell=0}$ ($V^{\ell=1}$).

In Fig. 2.15a we plot the $s_{1/2}$ shape elastic cross section for the n-^{30}Si reaction at E_n = 500 keV as a function of V^+, the real positive parity potential well depth whose predominant component for the $J^\pi = 1/2^+$ channel is ℓ=0. The $p_{1/2}$ and $p_{3/2}$ cross sections (Figs. 2.15b and c) are plotted as a function of V^-, the real negative parity potential well depth. The horizontal lines represent the "experimental" values obtained by Carlton et al.[4] The potential parameters, other than the one varied, were kept the same for the vibrational (0^+-2^+-3^-), and rotational (0^+-2^+-4^+) coupling schemes as for the spherical case. It can be seen that for s-waves, the best values for V^+ are 48.5, 47.5, and 49.5 MeV for spherical, vibrational, and rotational models respectively. Therefore the effect of coupling on s-wave scattering is small. However for $p_{1/2}$ the best values for V^- are [illegible], 54, and 51 MeV, and for $p_{3/2}$ the best values for V^- are 62, 54, and 52 MeV, respectively. Therefore the difference in the V^+ and V^- well depth is about 13 MeV for the spherical model, 6.5 MeV for the vibrational model, and 2 MeV for the rotational model. Both types of coupling drastically reduce the ℓ or parity dependence of the real well depths, an effect which shows up also for ^{32}S and ^{34}S. Since ^{30}Si probably is a rotational nucleus, and the potential parameters other than V^+ and V^- were obtained by a vibrational model fit to the six partial wave cross sections vs. energy, the 2 MeV difference between V^+ and V^- could possibly be reduced.

The best well depth parameters obtained for ^{30}Si, ^{32}S, ^{34}S, and ^{40}Ca using the coupling schemes described are given in Table 2.3 along with the corresponding spherical parameters. The calculations for ^{40}Ca are in progress and the results are preliminary.

The coupled channels V_{SO} well depths are less than the spherical values but follow the same trend as a function of A, a result which also occurs for W^+ and W^-. However, the differences between W^+ and W^- are not removed by treatment of deformations. The difference between W^+ = 7 MeV and W^- = 0.1 MeV for ^{40}Ca is striking, but is consistent with a factor of about 20 between the s- and p-wave strength functions. It would be interesting to check for this ℓ-dependence in a partial wave equivalent local imaginary potential obtained from a self-consistent RPA calculation. The influence of coupling to the giant quadrupole and high energy octupole resonances of ^{40}Ca on low energy scat-

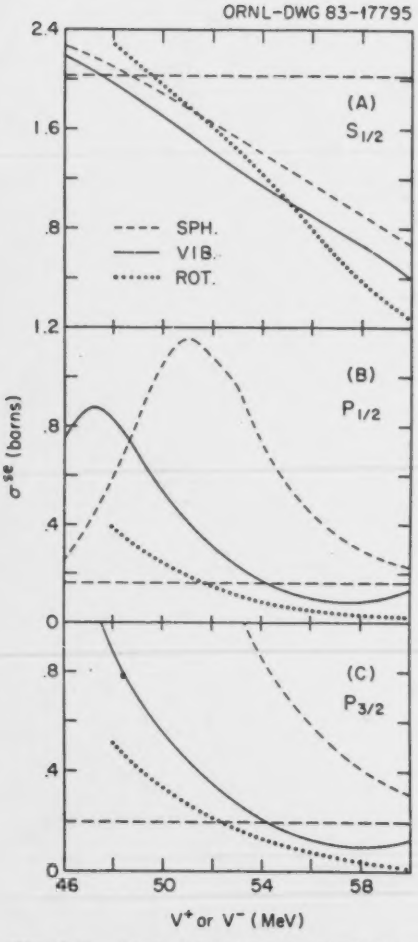

Fig. 2.15. Shape elastic cross section for 600 keV neutrons on ^{30}Si versus V^+ for $s_{1/2}$ and versus V^- for $p_{1/2}$ or $p_{3/2}$. The horizontal dashed line in each figure is the experimental value from ref. 4.

tering has been emphasized by Delaroche et al.[10] However they used the same potential for both s and p waves and did not obtain the correct experimental results for the s and p wave strength functions. Although we did not attempt a fit, at E = 10 keV we obtained values of $S_0 = 2.3 \times 10^{-4}$ and $S_1 = 0.25 \times 10^{-4}$ compared to the experimental values of 2.6×10^{-4} and 0.12×10^{-4} respectively. We obtained differences of up to approximately 10% in the shape elastic cross sections between a calculation with 0^+-3^--5^- coupling and one with 0^+-3^--5^--GQR-HEOR coupling.

It can be seen that a proper treatment of the deformed nature of the target nucleus reduces the difference in s and p wave real well depths to at most 2 MeV. Since this difference is within the limits of experimental error, the need for introduction of ℓ-dependence is not pressing. However, the argument would not be conclusive without some mention of the effects of non-locality on ℓ-dependence. Studies employing different local approximations to several non-local potentials show a large decrease with ℓ in the well depth at small radial distances, with this effect moving to larger radii for larger ℓ values. Recent calculations[11] employing two different equivalent local potential approximations to the Perey-Buck[12] non-local potential for n-^{40}Ca scattering at 24 MeV show this interior damping of the ℓ=0 potential compared to the ℓ=2 potential inside r=1.5 fm. The question arises as to whether this difference will affect scattering at energies below 1 MeV. As a test we have fitted the experimental n-^{32}S partial-wave cross sections in the energy region 100-1000 keV using a non-local potential with β=0.85, as suggested by Perey-Buck. A fit as good as that for the spherical local potential was obtained with parameters (in Perey-Buck form): $V^{\ell=0} = 72$ MeV, $V^{\ell=1} = 90$ MeV, $W^{\ell=0} = 7$ MeV, $W^{\ell=1} = 5$ MeV, and $V_{SO} = 13$ MeV. We see that both the local and non-local potentials required the same 20% increase in p-wave over s-wave real well depth. Therefore, for ^{32}S we attribute a major portion of the 20% difference to the vibrational character of ^{32}S rather than to non-locality.

---

1. Consultant from University of Kentucky, Lexington, Kentucky 40506.
2. Consultant from Queen's University, Kingston, Ontario, Canada K76 3N6.
3. C. H. Johnson and R. R. Winters, Phys. Rev. C 27, 416 (1983).
4. R. F. Carlton, J. A. Harvey, and C. H. Johnson, to be published.
5. R. R. Winters, C. H. Johnson, and C. Mahaux, unpublished.
6. C. H. Johnson et al., Phys. Rev. C 27, 1913 (1983).
7. T. Tamura, Rev. Mod. Phys. 37, 679 (1965).
8. A. D. MacKellar and B. Castel, Phys. Rev. C 28, 441 (1983).
9. J. Raynal, private communication.
10. J. P. Delaroche et al., Nucl. Phys. A390, 541 (1982).
11. H. Fiedeldey and S. A. Sofianos, Z. Phys. A 311, 339 (1983).
12. F. Perey and B. Buck, Nucl. Phys. 32, 353 (1962).

DOORWAY STATES IN ^{208}Pb+n REACTION

D. J. Horen C. H. Johnson
J. L. Fowler[1]

In studies of the ^{206,207}Pb+n reactions Horen et al.[2] have reported the presence of doorway states in the s-, p- and d-wave neutron channels

which were interpreted as arising from the coupling of particle states to collective excitations of the core (i.e., particle-core excitations). The presence of such doorway states could play a prominent role in determining the spreading width of p-h states in the continuum. In fact, such a case has been reported[3] in ^{208}Pb where a doorway in the g-wave channel arising from coupling of a d5/2 p1/2 p-h with the 3$^-$ core state occurs at nearly the same excitation as a fragment of the M1 p-h excitation.

We have performed high resolution neutron transmission and elastic scattering measurements on targets of ^{208}Pb using the 200-m flight path at ORELA. The transmission data were taken with an in-beam sample of ^{208}Pb enriched to 72.4% and a combined out of beam sample consisting of a piece of natural lead and a piece of lead enriched in ^{208}Pb. The latter were chosen so as to compensate for the non-^{208}Pb in the in-beam sample. For the scattering we used a hollow cylinder of ^{208}Pb (enriched to 99.14%). The cylinder was located at the center of a 143-cm scattering chamber in which there were five neutron detectors located at angles of 39°, 55°, 90°, 120°, 140° and 160° with respect to the incident neutron beam. Each detector consisted of a 7.62-cm long by 4.32-cm diameter cylinder of NE-110 which was viewed at each end by an RCA-8850 photomultiplier. The threshold for each phototube was set at the single photoelectron level, and a fast coincidence between the two tubes was required to define an event. The system was operated such that a maximum of one event per detector per machine burst could be accepted. Time-of-flight spectra were recorded in two pulse-height bins of 45000 channels each for each detector. The relative efficiencies of the six detectors were essentially identical. Data were also taken with one detector placed in the direct beam and this was used to remove the energy dependence of the incident neutron flux and detector efficiency (i.e., $F(E)\varepsilon(E)$).

The data were analyzed by examining the scattering spectra to determine the L-transfer (and possibly J-value) associated with each resonance, and using this information as input to an R-matrix code for fitting transmission data. The resonance parameters obtained from the fits to the latter, were then used in another R-matrix code to calculate the differential scattering cross sections for comparison with the data. The experimental data and calculated cross sections were normalized in an energy region void of resonances.

The data have been analyzed over a neutron energy range of 50-1005 keV in which we find about 63 resonances. Resonance parameters have been deduced for most of these. In Fig. 2.16 are shown the data and analyses for the interval 220-400 keV. We believe the resonance located at 351 keV (d3/2) represents a doorway state in the 3/2$^+$ channel which arises from a $g_{9/2}\times 4^+$ particle-core excitation. The 1/2$^+$ member is the well known s-wave resonance at 505 keV. Our data indicate a doorway in the 5/2$^+$ channel centered at about 750 keV, which is probably another member of the same multiplet.

Doorways are also seen in the 1/2$^-$ and 3/2$^-$ channels analogous to those reported for other lead isotopes. Calculations are in progress to test the particle-core interpretation of these doorway states.

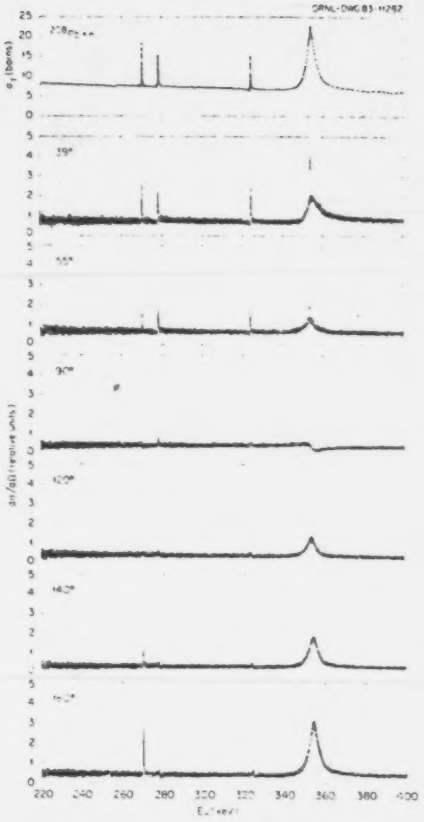

Fig. 2.16. Total (top) and differential elastic scattering cross sections at 39°, 55°, 90°, 120°, 140°, and 160° for ^{208}Pb+n reaction. The data are represented by the points and the calculated curves by solid lines.

---

1. University of Tennessee, Knoxville, Tennessee 37916.
2. D. J. Horen, J. A. Harvey, and N. W. Hill, Phys. Rev. C 18, 722 (1978); Phys. Rev. C 20, 478 (1979); Phys. Rev. C 24, 1961 (1981).
3. D. J. Horen, J. A. Harvey, and N. W. Hill, Phys. Rev. Lett. 38, 1344 (1977).

SMALL ANGLE 334-MeV POLARIZED PROTON SCATTERING FROM ^{40,42,48}Ca

D. J. Horen — L. W. Swenson[4]
F. E. Bertrand — J. B. McClelland[3]
E. E. Gross — T. A. Carey
T. P. Sjoreen — S. J. Seestrom-Morris[3]
D. K. McDaniels[1] — K. Thomas[3]
J. Lisantti[1] — E. G. Behrens[4]

Recent studies of the (p,n) reaction at intermediate energies (100-200 MeV) have revealed much information on the distribution and strength of Gamow-Teller (GT) transitions throughout the periodic table. These transitions (which involve L=0, S=1, ΔT=0,±1) dominate the small angle (θ~10°) spectra because at these energies the $v_{\sigma\tau}$ component of the effective nucleon-nucleon interaction is dominant. This implies that isovector M1 transitions should also be strongly excited at small angles in the (p,p') reaction. The cross section for exciting an isovector M1 state with isospin T in the target by (p,p') should be related to the excitation of its analogue via (p,n) by

$$\sigma_{pp'} = \frac{T_o}{2}\,\sigma_{pn}\ (T=T_o)$$

$$= \frac{2T_o+1}{2}\,\sigma_{pn}\ (T=T_o+1),$$

where T_o is the isospin of the target and the cross sections are measured at the same momentum transfer. Analogous relations should hold for other states which are excited via a spin-isospin operator.

We are studying the ^{40,42,48}Ca(p,p) reactions to investigate the relation of the cross sections excited by (p,p') with those to the same states by (e,e') or analogue states by (p,n) reactions. Data have been obtained using 334-MeV polarized proton beams from LAMPF in conjunction with the HRS facility. Targets consisted of self supported foils of 46.9 mg/cm^2, 50.7 mg/cm^2 and 100 mg/cm^2 for ^{40}Ca, ^{42}Ca, and ^{48}Ca, respectively.

A particular point of interest is the 1$^+$ state in ^{42}Ca at 11.24 MeV which is the strongest M1 state excited in the (e,e') reaction,[5] but only weakly seen[6] in the (p,n) work where a strong peak is observed at 10.2 MeV. As pointed out by Horen[7] the deduced GT strength[6] for the latter is in good agreement with what one would calculate assuming the 10.2 MeV peak seen in (p,n) represents the analogue of a group of M1 states seen[8] in (e,e') at about the same excitation energy, if these have T=1. Then, if the 11.24-MeV state has T=2, its cross section would be reduced in the (p,n) reaction because of the isospin Clebsch-Gordon coefficient and would become comparable to that of the continuum cross section.[7] In Fig. 2.17 is shown a ^{42}Ca(p,p') spectrum obtained at θ_L = 2.7° for the excitation region near 10 MeV. Preliminary analyses of the data show two peaks which have an L=0 angular distribution and energies of 9.96 MeV and 11.06 MeV. Although our preliminary energies differ somewhat from those for the M1 states

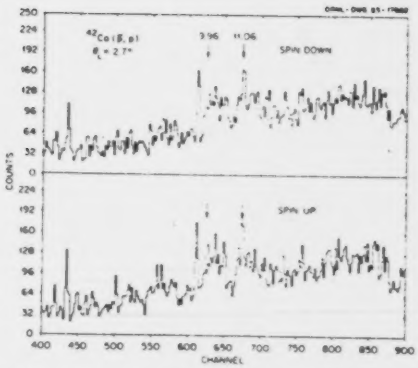

Fig. 2.17. Spectrum of inelastically scattered protons from the ^{42}Ca(p,p') reaction. The bottom figure is for spin up and the top for spin down. The arrows indicate peaks which have an L=0 angular momentum transfer and are assigned $J^\pi = 1^+$.

reported[5,6] in (e,e') work, we believe them to be the same. The ratio of the cross sections for the 11.06-MeV to 9.96-MeV states is ~2.1 versus a value of ~3.3 for the ratio of B(M1)'s. Since the isospin C-G coefficient is the same for a transition in ^{42}Ca to a T=1 or 2 state, one would expect these ratios to be the same for pure $\sigma\tau$ transitions. However, one must remember that the (e,e') experiment samples the total M1 operator, i.e., both the $\sigma\tau$ and orbital components which add coherently, whereas the (p,p') reaction excites mainly the $\sigma\tau$ component.

In addition to observing the excitation of the strong 1$^+$ state at 10.32 MeV in ^{40}Ca, we have obtained partial angular distributions (out to θ_{cm} ~9° which is close to the peak for L=2) for nine 2$^+$ states. In Table 2.5 we tabulate the peak cross sections and relative ratios and compare the latter to relative B(E2) values deduced[10,11] from photon work. The agreement between the relative cross section and B(E2) ratios is seen to be excellent. The state at 9.869 MeV has been observed in (e,e') studies[5,9] where it was suggested as a 1$^+$, 2$^+$ doublet. In this work it is excited predominantly by L=2, with little if any L=0 contribution. Our relative cross section for this state is in excellent agreement with the relative B(E2) ratio deduced from the Γ_{γ_o} reported by Rangen et al.[11] who studied the ^{39}K(p,γ_o)^{40}Ca reaction. DWBA calculations are in progress to deduce δ_2 values for comparison with reported B(E2)'s.

Asymmetries have been determined for many of the levels observed in this work. In general, the asymmetry for 3$^-$ excitations is found to be ~+.4 over the angular region investigated. That for 2$^+$ states goes from ~0.0 toward ~+.4, whereas asymmetries for spin-flip transitions (i.e., 1$^+$ or 2$^+$ states) hovers near A_y ~0.0 except for the 1$^+$

Table 2.5. Peak cross sections (and ratios) for 2^+ states in ^{40}Ca excited in 334-MeV inelastic proton scattering. Also shown are relative ratios for B(E2) values.

E_x	σ_{peak}(mb/sr)	σ_{rel}	$B(E2)_{rel}$[a]
3.904	3.1	1.0	1.0
5.249	0.20	0.065	0.07
5.630	0.30	0.097	0.083
6.909	3.15	1.02	0.82
7.873	1.17	0.38	0.42
8.091	0.61	0.20	0.29
8.580	0.41	0.13	0.14
8.748	0.23	0.074	0.085
9.869	0.33	0.11	0.13

a. From Ref. 9 except for the 9.869-MeV state which comes from Ref. 10.

state in ^{48}Ca which increases toward a value of +0.3 near 9°.

1. University of Oregon, Eugene, Oregon 97403.
2. Oregon State University, Corvallis, Oregon 97330.
3. Los Alamos National Laboratory, Los Alamos, New Mexico.
4. Oak Ridge Associated Universities, Summer Student (Southern Oklahoma State University, Durant, Oklahoma 74701).
5. W. Steffen et al., Phys. Lett. 95B, 23 (1980).
6. C. D. Goodman et al., Phys. Lett. 107B, 406 (1981).
7. D. J. Horen, BAPS 27, 732 (1982).
8. A. Richter, Nucl. Phys. A374, 177C (1982).
9. P. E. Burt et al., Phys. Rev. C 25, 2805 (1982).
10. R. Moreh et al., Phys. Rev. C 25, 1824 (1982).
11. Rangen et al., Phys. Rev. 127, 2180 (1962).

INELASTIC ELECTRON SCATTERING FROM ^{208}Pb AT 180°[1]

R. S. Hicks[2] R. L. Huffman[2]
R. A. Lindgren[2] B. Parker[2]
G. A. Peterson[2] S. Raman
C. P. Sargent[3]

Inelastic cross sections for 180° electron scattering from ^{208}Pb have been measured at incident energies of 40.5, 50.4, 60.3, and 75.2 MeV. Transverse electric form factors have been determined for the 3^- state at 2.614 MeV, the 5^- states at 3.198 and 3.708 MeV, the 2^+ states at 4.085 and 6.21 MeV, the 4^+ state at 4.323 MeV, and the 6^+ state at 4.422 MeV. The results for these natural parity states are compared to the predictions of an incompressible, irrotational current model, and of a particle-hole model. All transverse electric form factors show strong contributions from intrinsic magnetization currents. Transverse form factors were obtained for the proposed 1^+ state at 4.84 MeV, for the group of 1^+ states at 7.48 MeV, and for several proposed 2^- states. A search for M1 transition strength was made up to excitation energies of 19 MeV. The future of electron scattering as a tool for probing M1 strength in ^{208}Pb is discussed.

1. Abstract of paper: Phys. Rev. C 26, 920 (1982).
2. Department of Physics and Astronomy, University of Massachusetts, Amherst, Massachusetts.
3. Laboratory for Nuclear Science, Massachusetts Institute of Technology, Cambridge, Massachusetts.

ISOSPIN EFFECTS IN $\pi^{\pm}$ ^{12}C, ^{13}C, and ^{14}C ELASTIC SCATTERING AT 65 AND 80 MeV[1]

F. E. Bertrand M. V. Hynes[3]
E. E. Gross M. J. Leitch[3]
F. E. Obenshain N. S. Chant[4]
T. P. Sjoreen L. Rees[5]
M. Blecher[2] P. G. Roos[4]
K. Gotow[2] G. S. Blanpied[5]
R. L. Burman[3] B. M. Preedom[5]
B. G. Ritchie[5]

Low-energy pion-nucleus elastic scattering data have been obtained for positive-pion scattering from nuclear targets spanning a wide range of the periodic table, and the general features of the elastic scattering have been mapped out in terms of an optical model potential.[6-12] The isospin part of the pion-nucleus reaction mechanism has received very little attention for low-energy pions. Single and double pion-charge-exchange reactions depend specifically on the isospin term. A successful general theory of pion-nucleus reactions should yield cross sections in agreement with both elastic scattering and charge-exchange data.

Another long-standing problem in nuclear physics is the determination of neutron densities. Since, at low energies, the π^+p and π^-p angular distributions are different, the scattering of charged pions from isotopes appears to be a fruitful way of attacking the problem. The data obtained at TRIUMF for negative-pion scattering from two isotopes of carbon and oxygen indicated a sensitivity to the neutron radius, but more data were needed in order to draw any conclusions.

We have measured elastic scattering of positive and negative pions from ^{12}C, ^{13}C, and ^{14}C. Data were obtained for pion energies of 65 and 80 MeV for scattering angles between 20° and 120° at LAMPF. These data are shown in Fig. 2.18, along with the theoretical model calculations based on the phenomenological Kisslinger optical potential (solid curves). The errors

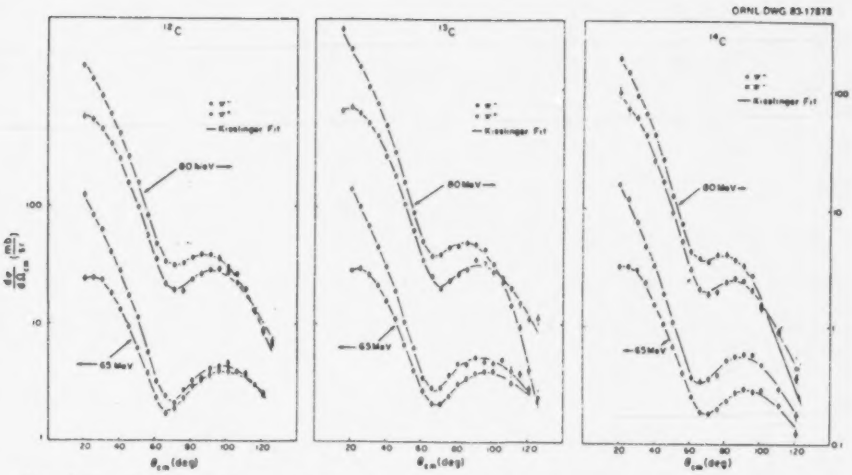

Fig. 2.18. The center-of-mass elastic scattering cross sections versus center-of-mass angle are shown for (a) $^{12}C(\pi^{\pm},\pi^{\pm})^{12}C$; (b) $^{13}C(\pi^{\pm},\pi^{\pm})^{13}C$; and (c) $^{14}C(\pi^{\pm},\pi^{\pm})^{14}C$.

shown are statistical. The cross sections are larger at forward angles for 80 MeV than for 65 MeV, but fall more rapidly at backward angles. This effect is due to the earlier onset of the first diffraction minimum for the higher energy.

The potential strength parameters, as a function of the isospin parameter (N - Z)/A, have been obtained from fitting our data. These parameters are then compared with strength parameters obtained from an impulse approximation calculation, which used the latest values for the π-nucleon phase shifts as input parameters. At 65 MeV there is agreement with the general trends of the two sets of parameters, but they do not agree in magnitude, except for the imaginary part of the p-wave strength parameter. At 80 MeV the agreement with the trends disappears, which suggests that a complex energy dependence for the isospin part of the Kisslinger potential may be required.

The optical model potential of Siciliano[13] includes isoscalar, isovector, and isotensor parts. He has included the isospin dependence of the Lorentz-Lorenz-Ericson-Ericson effect,[14] which enters to all orders in the nuclear density. Since this model, because of its parameters, appears appropriate for analysis of the charge-exchange data, we have also used it to calculate the cross sections for our data. With no adjustable parameters, other than the absorption term, the cross sections obtained with this model do not fit the magnitude of our measured cross sections, but they do show the same trends. This demonstrates the necessity to include the energy dependence of the absorptive term since this model correctly predicts the cross sections for our data at 30 MeV.

The elastic scattering cross sections for positive and negative pions from these three isotopes of carbon give information about the surface densities for the neutron and proton distributions. There is an excess neutron density near the nuclear surface for ^{13}C, but for ^{12}C and ^{14}C the neutron and proton densities are approximately the same to within our statistical errors.

---

1. Summary of paper: Physical Review C (in press).
2. Virginia Polytechnic Institute and State University, Blacksburg, Virginia.
3. Los Alamos National Laboratory, Los Alamos, New Mexico.
4. University of Maryland, College Park, Maryland.
5. University of South Carolina, Columbia, South Carolina.
6. M. Blecher et al., Phys. Rev C 20, 1884 (1979).
7. B. M. Preedom et al., Phys. Rev. C 23, 1134 (1981).
8. S. A. Dytman et al., Phys. Rev. C 19, 971 (1979).
9. R. R. Johnson et al., Phys. Rev. Lett. 43, 844 (1979); R. R. Johnson, private communication.
10. S. H. Dam et al., Phys. Rev. C 25, 2574 (1982).
11. M. Blecher et al., Proc. IX Int. Conf. on High Energy Physics and Nuclear Structure (Versailles, France, July 1981).
12. F. E. Obenshain et al., Proc. IX Int. Conf. on High Energy and Nuclear Structure (Versailles, France, July 1981).

13. E. Siciliano, private communication. For the general information, see also M. B. Johnson and E. R. Siciliano, Phys. Rev. C 27, 730 (1983); Phys. Rev. C 27, 1647 (1983).
14. M. Ericson and T.E.O. Ericson, Ann. Phys. (N.Y.) 36, 323 (1965).

GIANT RESONANCES

GIANT RESONANCE EXCITATION BY MEDIUM ENERGY PROTON INELASTIC SCATTERING

F. E. Bertrand J. E. Lisantti[1]
E. E. Gross D. K. McDaniels[1]
D. J. Horen L. W. Swenson[2]
T. P. Sjoreen J. R. Tinsley[2]

Since 1971 several non-dipole giant resonances of different multipolarity (L) have been observed.[3] The L=2 isoscalar giant quadrupole resonance (GQR) at ~ 63 $A^{-1/3}$ MeV the L=0 isoscalar giant monopole resonance (GMR) at ~ 80 $A^{-1/3}$ MeV and the $3\hbar\omega$ component of the L=3 giant octupole resonance (GOR) at ~ 120 $A^{-1/3}$ MeV have been well established in nuclei spanning much of the periodic table. In addition, some evidence for excitation of the isovector quadrupole[4,5] and isoscalar dipole[6] (^{208}Pb only) resonances has been suggested.

The observation of higher multipolarity giant resonances (L > 3) is made difficult by the fact that the strength for each multipole may be split among several classes of excitations.[3] For example, the L=4 hexadecapole (GHR) strength should be distributed among $0\hbar\omega$, $2\hbar\omega$ and $4\hbar\omega$ transitions, while L=6 strength could be located at $0\hbar\omega$, $2\hbar\omega$, $4\hbar\omega$ and $6\hbar\omega$. This is to be contrasted with the giant dipole resonance (GDR) strength which is localized entirely in $1\hbar\omega$ transitions at ~ 77 $A^{-1/3}$ MeV and quadrupole strength which is found in low-lying, $0\hbar\omega$ states and higher-lying, $2\hbar\omega$ excitations.

Further complicating the observation of higher multipolarity giant resonances (GR) is the fact that the $2\hbar\omega$ strengths of the even multipole resonances are expected[3] at nearly the same excitation energy. A similar situation holds for $3\hbar\omega$ strength of the odd L resonances.

These considerations imply that in order to observe experimentally high-L giant resonances they must be excited with a probe that provides both multipole selectivity and as clean an underlying continuum as possible. Intermediate energy protons provide such a probe. Figure 2.19 shows a plot of calculated (DWBA) angular distribution for the reaction ^{208}Pb(p,p') at E_p = 200 MeV. Unlike the case with alpha-particles or with heavy ions, significant differences exist between the angular distributions of neighboring L-transfer values. For example, the difference between the angular distribution for a pure L=2 giant resonance and a mixed L=2+4 (even for only 15-20% L=4 EWSR) is very large. An additional feature lies in the fact that Coulomb excitation provides nearly all of the small angle cross section for the L=1 (isovector GDR) excitation. For angles greater than ~ 5 degrees (Fig. 2.19) the GDR cross section is predicted to be as much as thirty times smaller

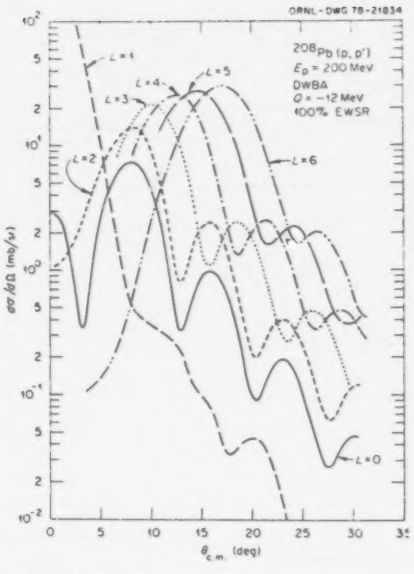

Fig. 2.19. DWBA calculations for excitation of various multipoles (all isoscalar except L=1 is isovector) by the reaction ^{208}Pb(p,p') for E_p = 200 MeV.

than the L=0 cross section, while at small angles the GDR should be the dominate peak in the GR excitation energy region.

In addition, we have found the inelastic proton continuum to be unstructured and to have a generally smoothly varying magnitude as a function of angle. This is to be contrasted with the continuum problems encountered with projectile excitation or the decay of pickup reaction products for inelastic alpha-particle or heavy-ion scattering.

In the last Physics Division Progress Report[7] we reported on our initial measurements[8] using the 200 Mev (p,p') reaction. Since then we have continued to pursue vigorously this area of study. Measurements have been made using 200 and 300-MeV proton beams from the TRIUMF accelerator in Vancouver, British Columbia, Canada and 334-MeV protons from LAMPF. The inelastically scattered protons are detected using magnetic spectrographs. At TRIUMF the MRS magnetic spectrometer facility provides a large excitation energy range ($\Delta E/E$ ~ 25% in practice) for a single setting of the spectrograph – a very desirable feature for GR studies. However, the energy resolution from the MRS facility is at present rather poor (500-1100 keV) which often precludes observation of low-lying collective states. At LAMPF the HRS spectrometer facility provided extremely high energy resolution (70 keV at 334 MeV), but the usable excita-

tion energy range for a given magnet setting is only ~ 12 MeV at 334 MeV. Furthermore, the HRS provides an extremely clean beam which allowed data to be taken at angles as small as ~ 2 degrees.

Typical beam intensities at each facility ranged from 0.1-1.5 nA. At TRIUMF the absolute beam current was determined using a calibrated monitor of proton-proton scattering from a thin CH_2 target located upstream of the spectrograph. At the HRS data are normalized to hydrogen scattering from a CH_2 target using phase-shift calculated[9] p-p cross sections.

Observation of $2\hbar\omega$ Hexadecapole Giant Resonance Strength in Lead Nuclei[13]

Inelastic proton scattering spectra at 200 MeV for ^{208}Pb and ^{206}Pb at an angle for which the L=2 angular distribution should be maximized (8 deg.) and at angles where any L=4 contribution should be maximized relative to the GQR (14, 16 deg.) are shown in Fig. 2.20. The spectra were analyzed by assuming, as shown on the figure, a smooth shape for the nuclear continuum, and by fitting the resonance peaks with Gaussian shapes. Parameters for each peak were determined where the cross section is largest for a given peak and those parameters were then used for peak extraction at all other angles.

Clearly visible in the 8 degree spectrum for both nuclei are a 2.4 MeV wide peak at 10.6 MeV from excitation of the GQR and a 3.4 MeV wide peak at 13.8 MeV, which arises from combined excitation of the GMR and GDR. The width and location of the GQR and GMR + GDR peaks extracted in these data are in excellent agreement with previous measurements. Another, broader, peak is observed at ~ 20 MeV. This peak is from excitation of the $3\hbar\omega$, T=0, GQR.

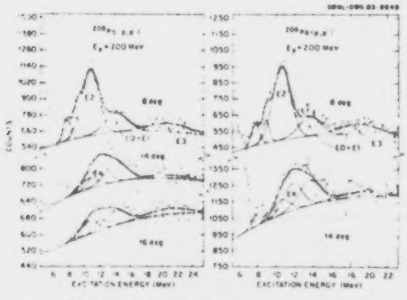

Fig. 2.20. Giant resonance spectra from inelastic scattering of 200 MeV protons from ^{208}Pb and ^{206}Pb. The multipolarities shown for the resonance peaks are discussed in the text. The smooth solid curve under the resonance peaks shows the shape and magnitude assumed for the nuclear continuum underlying the resonances. The shapes of the individual resonance peaks and the sum of the assumed continuum and peak shapes are shown.

The giant resonance spectrum in the 9-16 MeV region at 8 degrees is fitted very well by inclusion of only the GQR and GMR + GDR peaks. However, the spectra in the 9-16 MeV region at larger angles cannot be fitted by inclusion of only the GQR and GMR + GDR peaks with centroids and widths determined at the smaller angles. The overall centroid of the peak strength in the 9-16 MeV region shifts to a higher excitation energy. We find that consistently good fits to the larger angle (≥ 12 degrees) data can be achieved with the inclusion of a 2.7 ± 0.3 MeV wide peak located at 12.0 ± 0.3 MeV in both ^{208}Pb and ^{206}Pb.

Figure 2.21 shows the angular distribution for the 12.0 MeV peak extracted from the ^{208}Pb data. The uncertainties in the data are largely determined by the uncertainty in the assumed magnitude and shape of the underlying nuclear continuum and in the peak fitting procedure. Although data were taken at angles smaller than 10 degrees, extraction of a statistically significant peak at 12.0 MeV is not possible because of the very large GQR cross section.

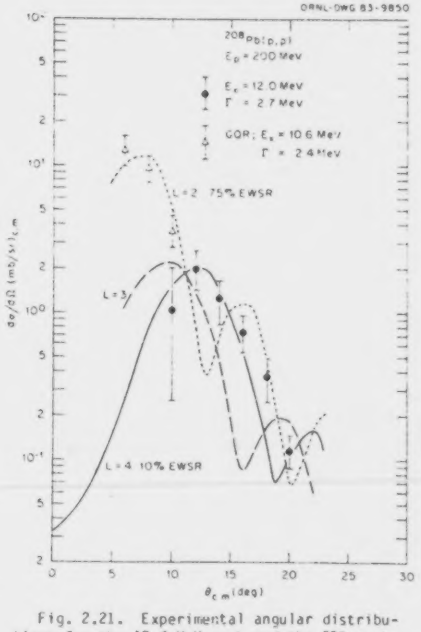

Fig. 2.21. Experimental angular distributions for the 12.0 MeV peak and the GQR peak (forward angles only) compared with L=2, 3 and 4 DWBA calculations which are denoted by the solid, long-dash and short-dash curves, respectively. The EWSR depletions shown were obtained by normalizing the L=2 calculation to the GQR cross section as discussed in the text.

The curves shown on Fig. 2.21 are distorted-wave Born approximation (DWBA) calculations with a collective model form factor for isoscalar, L=2, 3 and 4 excitations near 12 MeV in ^{208}Pb. The L=4 and L=3 calculated angular distributions are normalized to the measured cross sections for the 12.0 MeV peak. The L=2 calculation is normalized to the measured cross section for the GQR peak and is in excellent agreement with the measured GQR angular distributions at all angles. (Not all the L=2 data is shown for clarity.) The data for the 12.0 MeV peak agree with the shape of only the calculated L=4 angular distribution. Because of present problems of normalization in the DWBA for medium energy proton inelastic scattering, we have normalized our results to a value of 75% for the GQR, EWSR depletion in ^{208}Pb. This normalization then yields a value of 10% ± 3% for the EWSR depletion of the L=4 strength at 12.0 MeV.

Cross Section and Analyzing Power Measurements for the Giant Resonance Region in ^{208}Pb[11]

During the past two years, differential cross sections for the excitation of giant resonances in ^{208}Pb by 200-MeV protons have been studied at TRIUMF as part of our overall program to show the feasibility and utility of medium energy protons as a probe for giant resonance investigations. Our measurements cover a large angle range, 6 to 20°, and a large excitation energy range, about 40 MeV. Recently, these data have been supplemented with analyzing power measurements on ^{208}Pb at 200 MeV.

A typical spectrum for the inelastic protons scattered at 8° is shown in Fig. 2.22. The multipolarities of the giant resonance peaks, are indicated on the figure. The 8° spectrum was chosen to emphasize the presence of a peak at about 21 MeV of excitation, which our results indicate is produced by excitation of the GQR resonance. The decomposition of the spectrum into the different peaks was done with the aid of a peak fitting program. A summary of the giant resonance peaks found in the present study is given in Table 2.6. Most of the error in the individual peak determinations arises from the choice for the underlying continuum. Typically, this leads to an uncertainty of the order of 20-30% in the final cross section value.

The measured angular distribution for the strong peak at 10.6 ± 0.5 MeV is shown in Fig. 2.23. The cross section data, which are indicated by solid points, are averages of measurements taken with both polarized and unpolarized beams. The solid line is the result of a standard DWBA calculation for an L=2 tran-

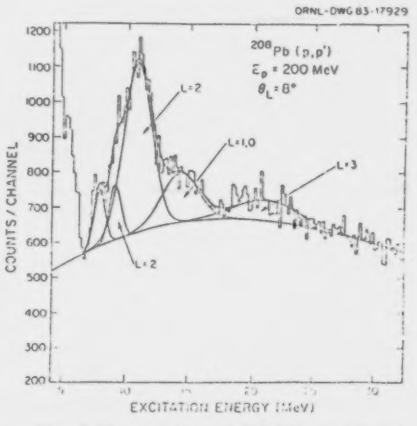

Fig. 2.22. Spectrum of 200-MeV unpolarized protons scattered from a ^{208}Pb target at a laboratory angle of 8°.

Table 2.6. Giant resonance parameters measured in the present experiment for ^{208}Pb.

J^π	E_x (MeV)	E_x from Systematics[a]	Width (MeV)	EWSR[b] (%)
2^+	8.9 ± 0.7	—	1.2 ± 0.6	11 ± 6
2^+	10.6 ± 0.5	11.0	2.6 ± 0.8	69 ± 15
4^+	12.0 ± 0.7	—	2.7 ± 1.0	10 ± 3
1^-	13.5 ± 0.5	13.2	3.4 ± 0.8	100 ± 25
0^+	14.1 ± 0.5	13.5	3.4 ± 0.8	90 ± 45
3^-	20.9 ± 1.0	20.3	6.0 ± 1.0	30 ± 9

[a]See Ref. 3.

[b]All EWSR values were obtained by multiplying the values obtained from a comparison with DWBA analysis by a factor of 3.

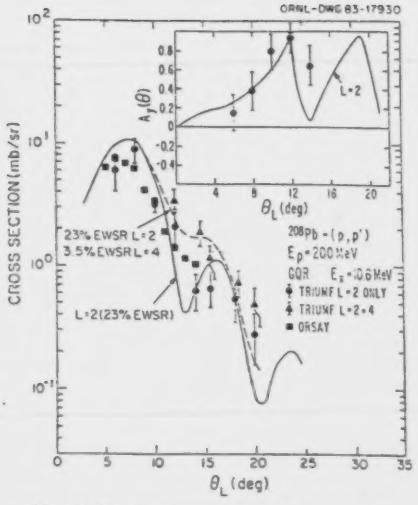

Fig. 2.23. Angular distributions for the peak near 11.0 MeV in excitation. The solid circles are the measured absolute cross section for the strong GQR peak at 10.6 MeV, whereas the solid triangles are the combined cross section for the peaks at 10.6 and 12.0 MeV. The solid curve is the L=2 DWBA calculation; the dashed curve represents a DWBA calculation including L=4 strength. the insert shows our measured Ay(θ) data along with a DWBA calculation for a multipolarity of L=2.

sition using a collective form factor. Optical model parameters were chosen to provide the best fit to the elastic-scattering data at 200 MeV. Because of present problems of normalization in the DWBA calculations we have normalized the calculations to the measured cross sections for the low-lying 2.615 MeV, 3⁻ state. The normalization required was a factor of 3. Using this normalization we extract ~ 70% of the T=0, L=2 EWSR depleted in the GQR peak. We are currently reinvestigating the DWBA calculations used at medium energies.

As described in the previous section we have found $2\hbar\omega$, L=4 strength at 12.0-MeV in ^{208}Pb. The solid circles on Fig. 2.23 show the sum of the measured cross sections for both the 10.6 and 12.0-MeV peaks. The dashed curve is the DWBA prediction assuming an L=4 EWSR strength of 3.5% (corresponding to a normalized EWSR strength of 10%). The analyzing power data for the GQR peak at 10.6 MeV is shown in the inset of Fig. 2.23. The solid curve corresponds to the DWBA fit, which includes a deformed spin-orbit interaction.

Evidence for a $3\hbar\omega$ GQR with strength concentrated at about 120 $A^{-1/3}$ MeV has come from several inelastic-scattering experiments[4]. In ^{208}Pb, all of the experiments are in rough agreement that the T=0, L=3 giant resonance is localized near 20 MeV of excitation energy, however, there is no consistent agreement about the precise location. The values span the region of 16-21 MeV.

In our data we find a broad peak centered at about 20.9 ± 1.0 MeV with a width of about 6.0 ± 1.0 MeV which we interpret as the $3\hbar\omega$ GQR. This peak stands out very clearly in the 8° spectrum, as shown in Fig. 2.22. The angular distribution measured for this peak is shown in Fig. 2.24. The data for the peak found at 21.5 MeV by the authors of Ref. 5 are also shown. The data of Ref. 5 show a rapid rise in cross section at forward angles, which they interpret as evidence for excitation of the isovector GQR. Our measurements were limited to a smallest angle of 6°, however our measured cross section at 6° is approximately a factor of 2 lower than the cross section value quoted in Ref. 5.

The solid curve in Fig. 2.24 is a DWBA calculation for an L=3 transition, corresponding to a strength of 10% for the ESWR which we renormalized to 30%. The results of our analyzing power measurements for the 20.9-MeV peak are presented in the inset of Fig. 2.24

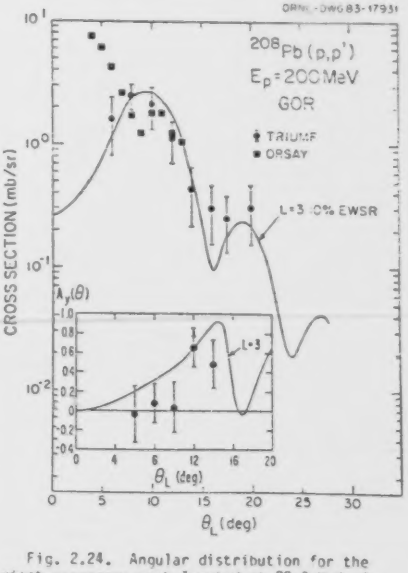

Fig. 2.24. Angular distribution for the giant resonance peak located at 20.9 MeV of excitation. The solid curve is the DWBA prediction for an L=3 transition. The insert shows our measured Ay(θ) data along with a DWBA calculation for a multipolarity of L=3.

Search for High Angular Momentum Giant Resonance Strength Using 200-MeV Proton Inelastic Scattering

While our knowledge of giant resonance excitation in nuclei has been expanded greatly through the use of direct reactions, the observations have mostly been confined to low multipole giant resonances, except for the recent L=4 observation.[13] This situation is not surprising since as the angular momentum increases, the resonance strength can be fragmented among several classes of excitations with overlapping energies. We have used the very characteristic shape of the angular distribution for various L-transfers in medium energy proton inelastic scattering to search for high-L ($L \geq 4$) giant resonance strength.

Figure 2.25 shows spectra from ^{60}Ni, ^{90}Zr, ^{120}Sn, and ^{208}Pb at angles chosen to emphasize both the GQR peak and GDR peak. The spectra are shown over an excitation energy range of ~ 5 MeV to ~ 40 MeV. These spectra were obtained with a single setting of the spectrograph magnetic field. The decomposition of the spectrum into the different peaks was done with the aid of the peak fitting program. The spectra all show the presence of peaks from excitation of giant resonances. The largest peak (shown shaded on Fig. 2.25) located at 16.5 MeV in ^{60}Ni, 14.1 MeV in ^{90}Zr, 13.2 MeV in ^{120}Sn, and 10.6 MeV in ^{208}Pb is predominately from excitation of the GQR. Also evident in ^{208}Pb is a peak at ~ 14 MeV which arises from excitation of the GMR and GDR. Excitations of these latter two resonances are assumed to be present in the other nuclei, but because the width of the giant resonances increases as $A^{-2/3}$, their presence is not as clear as for ^{208}Pb. The peak observed at high excitation energies (cross hatched on Fig. 2.25) is predominately from excitation of the $3\hbar\omega$, giant octupole resonance. In the present analysis for ^{208}Pb we have not separated the L=4 strength from the GQR peak as we did in an earlier publication.[13]

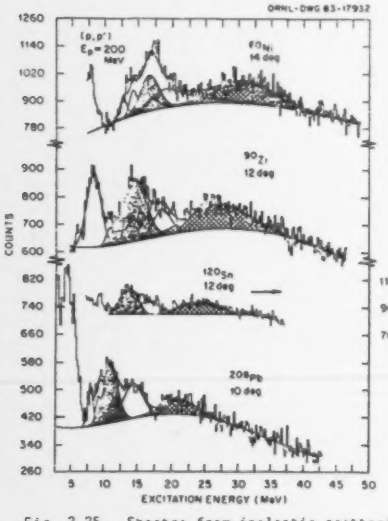

Fig. 2.25. Spectra from inelastic scattering of 200-MeV protons on ^{60}Ni, ^{90}Zr, ^{120}Sn and ^{208}Pb. Giant resonance peaks are shown fitted with Gaussian shaped curves except for the giant dipole resonance which is fitted with the peak shape from (γ,n) measurements. The shaded peak is located at ~ 63 x $A^{-1/3}$ MeV, the GQR, and the cross-hatched peak is located at ~ 120 x $A^{-1/3}$ MeV, the GDR. The shape assumed for the underlying nuclear continuum is shown by the smooth solid curve.

We concern ourselves with the question of multipole purity of the peaks generally referred to as the GQR or GDR peaks (see Fig. 2.25). We address the question of possible $2\hbar\omega$ L=4 and L=6 strength located within the GQR peak region (shaded peak in Fig. 2.25) and $3\hbar\omega$ L=5 strength located within the GDR peak (cross-hatched peak in Fig. 2.25).

In order to avoid the uncertainties in B(EL) extraction in the 200 MeV (p,p') reaction, we have normalized the L=2 and L=3 calculations to the measured GQR and GDR angular distributions for values of the GQR and GDR EWSR's shown on the various calculated curves in Figs. 2.26 and 2.27. The EWSR values used were adopted from previous studies.[3] The normalization factors needed to fit the DWBA to the accepted L=2 and L=3 EWSR values was used as the normalization factor for the L=4, 5 and 6 calculations. The L=2 and L=3 normalization factors were found to be the same within the uncertainty in the data.

Figure 2.26 shows the measured cross sections and DWBA calculations for the GQR peak, i.e., the peak in ^{60}Ni, ^{90}Zr, ^{120}Sn, ^{208}Pb and ^{238}U at ~ E_x = 63$A^{-1/3}$ MeV. The L=2 calculations describe the shape of the data in the peak of the angular distribution very well. The calculations have been normalized to the data for EWSR strengths shown in parenthesis in the figure. The dotted curves in Fig. 2.26 show the sum of the L=2 calculation and an L=4 calculation which depletes 10% of the L=4 EWSR. For ^{120}Sn, ^{208}Pb and ^{238}U, the data are much better fitted by dashed curve. The results in ^{208}Pb are in excellent agreement with our previous results[10] in which we decomposed the "GQR" peak into peaks from L=2 and L=4 excitation. The zirconium data are best fitted with the sum of 60% L=2 and 5% L=4. Although the ^{60}Ni are better described with 10% L=4 added to the L=2 curve, it should be noted that the shape of the angular distribution for the low-lying, 1.33-MeV, 2^+ state in ^{60}Ni also describes the giant resonance angular distribution shape.

Even though, as shown in Fig. 2.26, the data can be very well described by use of L=2 and 4 angular distributions alone, we examine in Fig. 2.27 the effect that only a small admixture of L=6 strength,would have in the "GQR" cross sections. The same data are shown in Fig. 2.27 as in Fig. 2.26, and the solid curves show L=2 calculations as in Fig. 2.26 but now L=4 and L=6

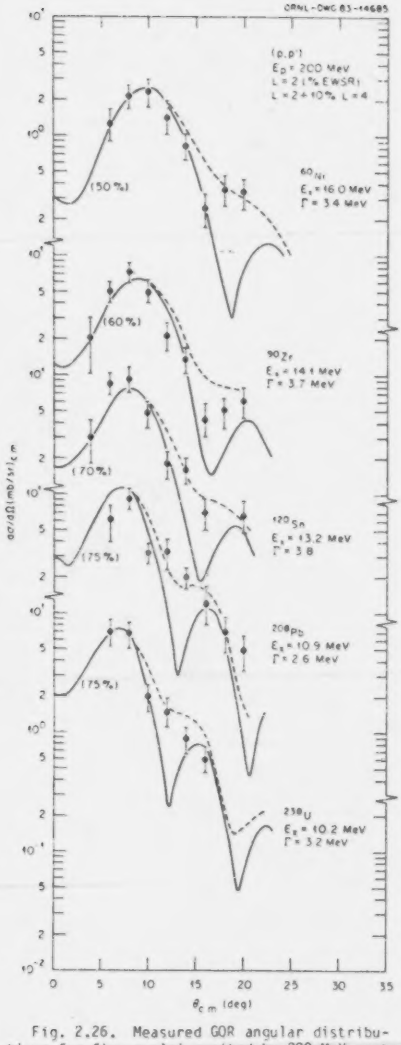

Fig. 2.26. Measured GOR angular distributions for five nuclei excited by 200 MeV protons compared with DWBA calculations for L=2 and L=2+4 excitations.

calculations are shown with EWSR depletions suggested by recent calculations.[12] The figure shows the separate angular distributions and the sum of the L=2, 4 and 6 calculations. As expected from Fig. 2.26, the addition of some L=4 strength to the L=2 calculation improves the

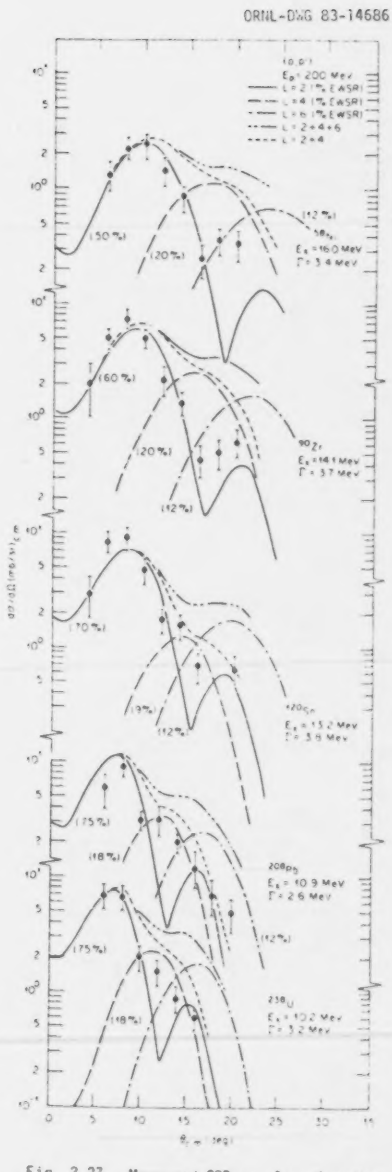

Fig. 2.27. Measured GOR angular distributions for five nuclei excited by 200 MeV protons compared with DWBA calculations for L=2, L=4, L=6 and sums of those calculations.

fit for the heavy nuclei. However, the addition of L=6 strength, at least in the amounts indicated, seems to be unsupported by the data.

The measured angular distributions for the peak found at ~ 120 $A^{-1/3}$ MeV, the GDR peak, are shown in Fig. 2.28 along with DWBA calculations for L=3 and L-5 excitations which are normalized to the data at forward angles. The percentage of EWSR strength is given in parenthesis. For ^{60}Ni, ^{90}Zr, and ^{120}Sn the data are well described by the pure L=3 curve, yielding no evidence for L=5 excitation. On the other hand, the data for the heavier nuclei, ^{208}Pb and ^{238}U, are better described by a sum of L=3+5 than the pure L=3 calculation although the evidence is not conclusive.

It is to be noted that our observation or lack of observation of certain multipolarity strength refers only to the location of such strength within the peaks as defined in Fig. 2.25. The fact that we do not observe L=5 strength in the light nuclei or L=6 strength in any of the nuclei may be understood by the increasing width expected[3] for giant resonances as the nuclear mass decreases and as the excitation energy of the resonance increases. The high-L resonance strength in light nuclei may be too spread in excitation energy to provide any significant angular distribution differences from the dominate resonance angular momentum shape. At best we believe the data indicate there is some evidence in heavier nuclei for the presence of L=4 and L=5 strength at high excitation energies, but no evidence for the existence of localized L=6 strength.

The experimental results have been analyzed and are now being compared with calculations.

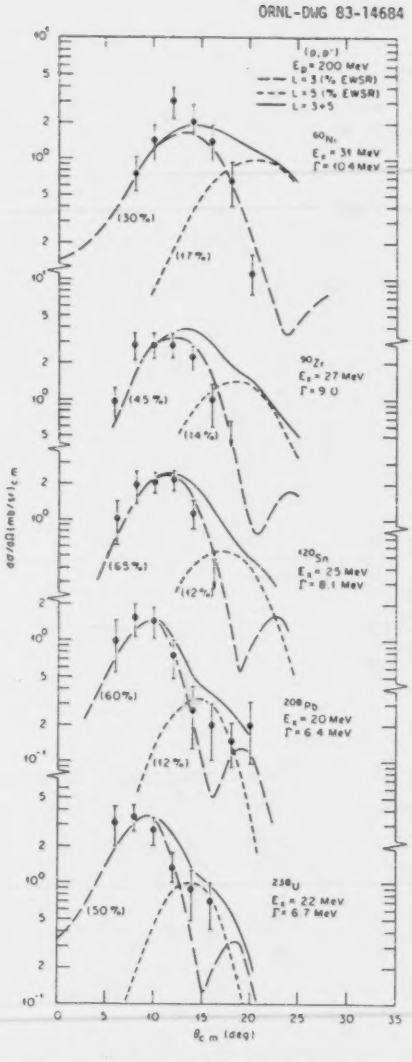

Fig. 2.28. Measured GDR angular distributions for five nuclei excited by 200 MeV protons compared with DWBA calculations for L=3 and L=5 excitations.

1. University of Oregon.
2. Oregon State University.
3. F. E. Bertrand, Ann. Rev. Nucl. Sci. 26, 457 (1976). Giant multipole resonances – perspectives after ten years, Proc. Intern. Conf. on Nuclear Physics (Berkeley, 1980), Nucl. Phys. A345, 153c (1981).
4. M. Nagao and Y. Torizuka, Phys. Rev. Lett. 30, 1068 (1973).
5. C. Djalali et al., Nucl. Phys. A380, 42 (1982).
6. H. P. Morsch et al., Phys. Rev. Lett. 45, 337 (1980).
7. Phys. Div. Prog. Rep. for Period Ending June 30, 1981, ORNL-5787, p. 118 (1931).
8. F. E. Bertrand et al., Phys. Lett. 103B, 326 (1981).
9. R. A. Arndt et al., Phys. Rev. C 9, 555 (1974).
10. J. R. Tinsley et al., Phys. Rev. C 28, 1417 (1983).
11. To be published in Phys. Rev. C.
12. F. E. Serr, P. F. Bortignon and R. A. Broglia, Nucl. Phys. A393, 109 (1983).
13. For these measurements the author list should include: T. A. Carey, K. Jones, J. B. McClelland and S. Seestrom-Morris, Los Alamos National Laboratory.

Evidence for Quasifree Proton Scattering at 200 MeV

One of the most important uncertainties in the study of giant resonances has to do with the determination of the nuclear continuum underlying the resonance peaks. To understand and calculate, rather than estimate, the shape of this underlying continuum is a high priority task which so far has been unsuccessful. A detailed description of the continuum depends on our knowledge of the basic reaction mechanism. It is important to experimentally evaluate the role of single-scattering processes in the case of medium-energy inelastic proton scattering.

We present evidence for the dominance of the quasifree process for 200-MeV protons scattered at small angles (< 20 degrees). Inelastic proton spectra were measured from 6° to 20° using the MRS facility at TRIUMF. The availability of a high-quality polarized beam at TRIUMF allowed us to obtain analyzing power [Ay(θ)] using the following relation,

$$Ay(\theta) = \frac{\sigma+(\theta) - \sigma+(\theta)}{P+\sigma+(\theta) + P+\sigma+(\theta)} ,$$

where σ+(θ) and σ+(θ) represent the spin up and down differential cross sections and P+ and P+ are the spin up and down beam polarizations, respectively. Beam polarization for the Ay(θ) measurements, obtained with an in-beam polarimeter, varied from | 0.72 | to | 0.75 | . The uncertainty of an individual determination was ±0.005. Data with unpolarized beam incident on the targets were taken for angles between 6 and 20° in 2° steps, whereas that with polarized beam ranged between 6 and 16° in 2° steps.

All of our spectra show peaks from the excitation of several giant resonances. The continuum underlying the resonances exhibits a broad peaked structure which we attribute to quasifree scattering. This broad structure is illustrated in Fig. 2.29 for the ^{208}Pb target. The centroid of this broad structure shifts monotonically to higher excitation energy as the scattering angle is increased. The spectra for ^{60}Ni and ^{90}Zr are similar in appearance and the broad structure shows the same kinematical shift as scattering angle is increased.

The kinematical shifting of the quasifree peak is shown in detail in Fig. 2.30 for all three targets. Each point of the angular distribution was obtained by determining the excitation energy at which the continuum cross section is a maximum. For each target the curves were calculated utilizing free nucleon-nucleon (NN) kinematics. An additional amount of energy was added to the difference between the incident proton energy and the scattered energy at each angle to represent an average binding of the proton in the nuclear potential. From Fig. 2.30 it is seen that the kinematic plots are best fit by modifying the free NN kinematics to include binding energy shifts of 9 MeV for ^{208}Pb, 15 MeV for ^{90}Zr and 16 MeV for ^{60}Ni. The large uncertainties in the individual centroid determinations render average binding energy shifts uncertain by at least ±2 MeV.

ORNL-DWG 83-17933

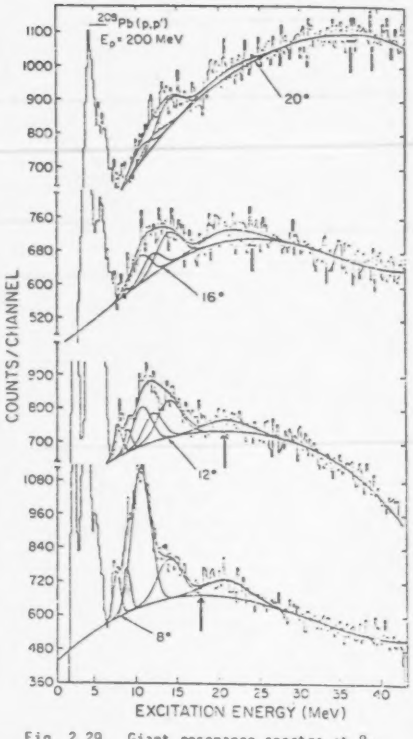

Fig. 2.29. Giant resonance spectra at 8-, 12-, 16-, and 20-degrees for the reaction ^{208}Pb(p,p') at E_p = 200 MeV. The arrows indicate the maxima in the broad continuum peaks.

The analyzing power data present a further test of the quasifree hypothesis. Analyzing powers measured near the centroids of the broad structure are plotted in Fig. 2.31 for all three targets. Within the uncertainty of the data, the values for ^{60}Ni and ^{208}Pb are identical, while there is a slight dip in the Ay(θ) values for ^{90}Zr at 10 and 12 degrees. For comparison the Ay(θ) values for all three targets at 40 MeV excitation are also plotted in Fig. 2.31. No apparent angular dependence is present for the higher excitation data.

We find that the observed shape of the continuum spectra is in accordance with what is expected if single-scattering processes dominate at low excitation energies. The continuum shapes follow quasifree kinematics quite well, providing account is taken of an average binding energy shift. The analyzing power data for a

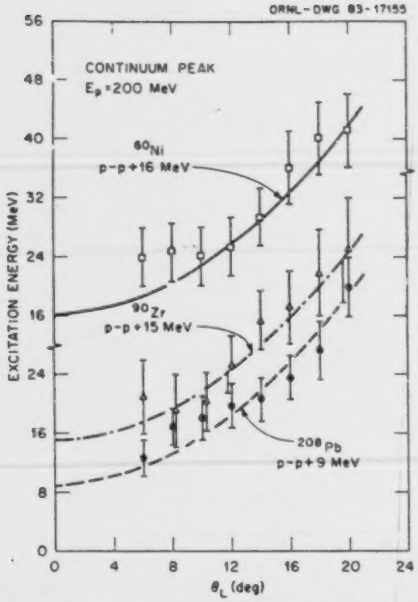

Fig. 2.30. Plot of the excitation energy of the quasi-elastic structure as a function of scattering angle for ^{60}Ni, ^{90}Zr, and ^{208}Pb targets. The smooth curves were calculated assuming NN kinematics and subtracting an average binding energy as indicated.

3-MeV region of the continuum centered on the quasifree peak exhibit an angular dependence similar to free NN scattering. In magnitude the Ay(θ) values are close to the free PP values and somewhat below those for the free PN case. Ay(θ) values at higher excitation energies do not show an angular dependence characteristic of free particle scattering and are quite small for a heavy target such as ^{208}Pb. This result is to be expected if a simple single-scattering process no longer dominates.

High Resolution Study of Giant Resonances in ^{208}Pb Using 334-MeV Proton Inelastic Scattering[13]

Although the use of 200 MeV inelastic proton scattering at TRIUMF has provided a great deal of new information on giant resonances, the analyses have suffered from very poor energy resolution. While the giant resonances are broad states there have long been suggestions and some observations[3] of fine structure located within and below the giant quadrupole resonances. Furthermore, in order to test the DWBA calculations data must be taken for low-lying states of known spin and parity.

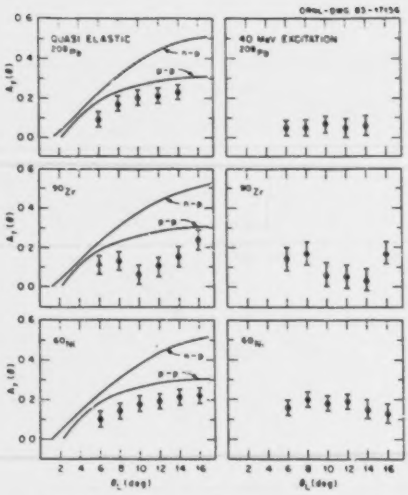

Fig. 2.31. Plots of Ay(θ) versus scattering angle for the region near the centroid of the quasifree peak and for an excitation energy of 40 MeV. The curves show the phase shift predictions of PP and NP scattering.

Using inelastic scattering of 334-MeV polarized protons and the HRS facility at LAMPF, we have measured spectra from ^{208}Pb. This unique facility provided an energy resolution of 70 keV (FWHM) for 334-MeV protons. Data were obtained for angles between 2.25 and 13.5 degrees, with no observable "bogus" background. Three settings of the spectrometer magnetic field were required to obtain composite spectra covering an excitation energy angle from 0 to ~ 27 MeV.

Figure 2.32 shows a spectrum at 6.25 degrees for spin-up protons inelastically scattered from ^{208}Pb. The data are shown fitted with several Gaussian peaks on top of a continuum background. (The background shape varies as a function of angle.) The prominent peak at ~ 10.5 MeV excitation energy is from excitation of the GQR while the peak at ~ 13.9 MeV is assumed to arise from excitation of the GDR and GMR. The excellent energy resolution permits the resolution of several separate peaks at excitation energies just below the GQR.

INELASTIC EXCITATION OF GIANT RESONANCES BY 400 MeV ^{16}O

T. P. Sjoreen
F. E. Bertrand
R. L. Auble
D. W. Wright[1]
E. E. Gross
D. J. Horen
D. Shapira

Giant resonances were excited in ^{90}Zr and ^{208}Pb by inelastic scattering of 350- and

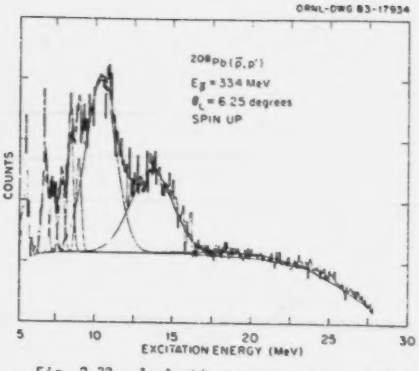

Fig. 2.32. Inelastic proton spectrum from 334-MeV spin-up, protons on ^{208}Pb for θ_L = 6.25 degrees.

400-MeV ^{16}O beams from the coupled operation of the tandem and cyclotron at HHIRF. The scattered charged particles were detected by cooled, silicon, surface-barrier, detector telescopes consisting of 500 μm ΔE and 1500 μm E detectors. The excitation energy range of these telescopes for 400-MeV ^{16}O ions was about 80-MeV in the inelastic channel, and the mass resolution was ~ 0.25 amu FWHM. The overall energy resolution was typically about 550 keV FWHM.

Figure 2.33 is the ^{16}O inelastic scattering spectrum obtained at 12° (lab) with a 2.0 mg/cm^2 ^{208}Pb target at 400 MeV bombarding energy. The peak on the far right is from the tail of the elastic peak. The peak at 2.6 MeV is the 3$^-$ state, and that at 4.1 MeV should be a combination of the 4.08 MeV 2$^+$ state and 4.32 MeV, 4$^+$ state. The broad structure between 5- and 10-MeV excitation is due to excitation of both the target and the ^{16}O projectile. The latter are Doppler broadened with widths of ~ 3 MeV.

The structure between 9 and 20 MeV excitation above the flat estimated "background" has been decomposed into three Gaussian shaped peaks, with centroids at 10.9-, 13.7-, and 17.6-MeV excitation. The peak at 10.9 MeV is assumed to be the isoscalar quadrupole resonance (GQR), while the peak at 13.7 MeV is assumed to arise from both the isoscalar monopole resonance (GMR) and the Coulomb excited isovector giant dipole resonance (GDR). A broad structure is also evident between 22- and 45-MeV excitation. However, similar measurements made at 350-MeV bombarding energy showed this same broad structure shifted lower in excitation by ~ 2.5 MeV. This shift with bombarding energy indicates that the broad structure between 22 and 45 MeV is not an excitation of ^{208}Pb but rather is due to the particle decay of the (^{16}O,^{17}O) and (^{16}O,^{17}F) pickup reactions.

The angular distributions for ^{208}Pb and ^{90}Zr from the present measurements are shown as a function of center-of-mass angle in Figs. 2.34 and 2.35, respectively. Figure 2.34 includes the results for the 3$^-$ state at 2.61-MeV excitation, as well as those for the GQR at 10.9 MeV

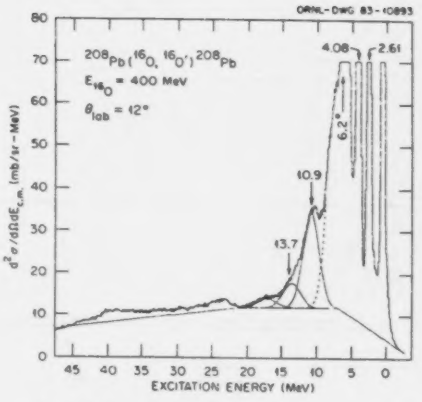

Fig. 2.33. Inelastic scattering spectrum at 12 degrees from the ^{208}Pb (^{16}O,^{16}O') reactions at 400 MeV. The solid curves show a decomposition of the spectrum into resonance peaks and an underlying continuum.

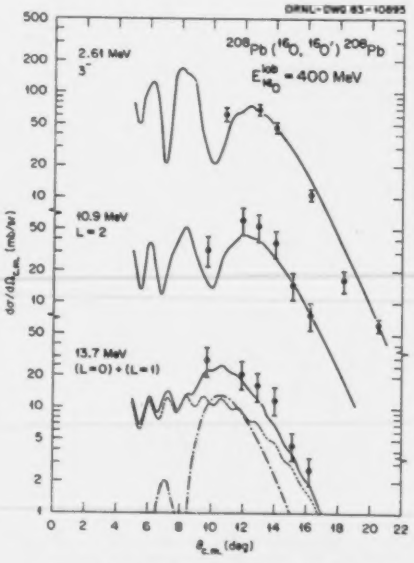

Fig. 2.34. Measured and calculated angular distributions for indicated states in ^{208}Pb. The 3$^-$ calculation is normalized to the B(E3) values measured in Coulomb excitation. The L=2 calculation is normalized to 80% of the T=0, L=2 EWSR. The L=0 (short-dash) and L=1 (dash-dot) calculations are normalized to 100% of their respective sum rule.

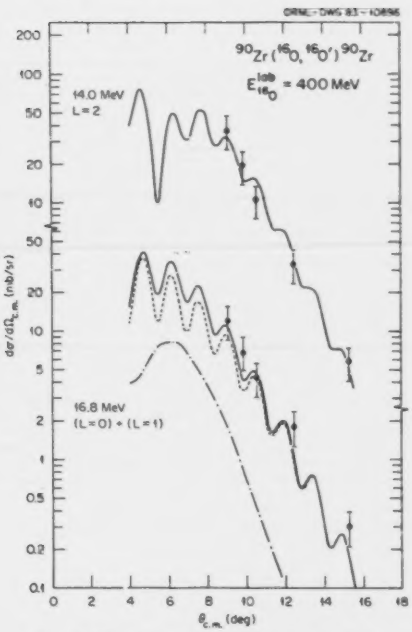

Fig. 2.35. Measured and calculated angular distributions for indicated giant resonance states in ^{90}Zr. The L=2 calculation is normalized to 60% of the T=0 EWSR, while the T=1, L=1 (dash-dot) and T=0, L=0 (short-dash) calculations are normalized to 100% of their respective sum rules.

and the sum of the GMR and GDR at 13.7 MeV. Figure 2.35 shows the results for ^{90}Zr peaks at 14.0- and 16.8-MeV excitation, which we assume are the GQR and GDR + GMR sum, respectively. The curves in these two figures are the results of DWBA calculations in which standard collective model form factors are used. A set of optical model parameters was obtained from the elastic data.

The DWBA calculations for the 3$^-$ state in ^{208}Pb were made with a deformation of $\beta = 0.110$, which corresponds to B(E3) = 0.600 e^2b^3 — a value which agrees well with experimental B(E3) values. As shown in Fig. 2.34, there is good agreement between the experimental and calculated angular distributions for the 3$^-$ state, which indicates that giant resonance sum rule strength can be properly deduced. The giant resonance calculations shown in Figs. 2.34 and 2.35 are normalized to EWSR strengths. For the GQR we used 80% and 60% of the EWSR for ^{208}Pb and ^{90}Zr respectively. For the remaining resonances, we used 100% of the appropriate EWSR. For ^{208}Pb it is clear that the L=0 calculation with 100% EWSR cannot account for the measured cross sections at all angles. However, inclusion of 100% of the L=1 calculation provides excellent agreement with the data. In the case of ^{90}Zr however, the data can be explained equally well by either the L=0 calculation alone or by the sum of L=0 and L=1.

One of the disadvantages of heavy-ion, inelastic excitation of giant resonances is that the shapes of the low-L transfer angular distribution are nearly identical, hence, identification of resonance multipolarity is not possible. Moreover, the angular distribution of the "background" is nearly the same as the resonances. Because of these two features we have not been able to determine whether the 17.6-MeV peak (see Fig. 2.33), which persists at all angles measured, is a giant resonance or due to decay of pickup products. However, the energy (17.6 MeV) and width (4.0 MeV) of this peak agrees with an (α,α') study[2] at E_α = 172 MeV, in which strength at 17.6 MeV is interpreted as the $3\hbar\omega$ isoscalar octupole resonance (GOR), depleting about 60% of the EWSR. If we interpret the 17.6 MeV peak in our data as arising from excitation of the GOR, then the peak cross section accounts for ~ 40% of the EWSR, a value not inconsistent with the (α,α') results. Note, however, that medium energy proton inelastic scattering measurements[3,4] in ^{208}Pb find the GQR at ~ 19-20 MeV.

The most important and positive features of heavy-ion inelastic excitation of giant resonances are the large resonance cross sections and the large peak-to-continuum ratios. As shown in Fig. 2.34, the GQR cross section reaches ~ 60 mb/sr at the grazing angle, and as shown in Fig. 2.33 the peak-to-continuum ratio for the GQR is ~ 2.2 to 1. Both of these values are better, by at least factors of 2, than those obtained by light ion excitation of giant resonances. Hence heavy-ion excitation of giant resonances offers significant advantages for measurements of the decay of the giant resonances (see following two articles).

---

1. Present address: Computer Science Department, University of Illinois. Oak Ridge Summer Research Participant.
2. H. P. Morsch et al., Phys. Rev. Lett. 45, 337 (1980).
3. T. A. Carey et al., Phys. Rev. Lett. 45, 239 (1980).
4. D. K. McDaniels et al., to be published in Phys. Rev. C.

ELECTROMAGNETIC DECAY OF GIANT RESONANCES

J. R. Beene
R. L. Auble
F. E. Bertrand
M. L. Halbert
D. C. Hensley
D. Horen
R. L. Robinson
R. O. Sayer[1]
T. P. Sjoreen
G. Ball[2]

Coincidence studies of the decay of giant resonances (GR) offer the possibility of probing the microscopic structure of the resonances and

the details of their damping or spreading into the continuum.[3-5] Studies of the electromagnetic decay are especially interesting for a number of reasons, the most obvious being that the familiar (E1, E2, E0, etc.) GR are conventionally defined in terms of the action of electromagnetic transition operators on the nuclear ground state.[4] The study of electromagnetic transitions from the GR to the ground state directly probes this simple relationship.

In heavy nuclei the electromagnetic decay branch of states in the GR region is $\sim 10^{-4}$. Consequently, a successful experiment requires a large excitation cross section, a good resonance-to-continuum ratio, and a very efficient gamma-ray detection system. We have performed such an experiment using inelastic scattering of 380-MeV ^{17}O ions from the coupled HHIRF accelerators to provide the necessary excitation conditions[6] and the ORNL Spin Spectrometer,[7] a modular, almost 4π, NaI detector system, to provide the gamma detection. Experiments on ^{208}Pb and ^{90}Zr have been carried out. Only the ^{208}Pb data have been analyzed sufficiently to be discussed.

The experiment on ^{208}Pb was performed using six Si surface-barrier telescopes to detect inelastically scattered ^{17}O ions at $\theta = 13°$. The telescopes together subtended 22.6 msr. Neutrons and gamma rays from the subsequent decay of the excited reaction products were detected in 70 NaI detectors of the Spin Spectrometer.

Lead-208, excited to the GR region (10-20 MeV), has a neutron decay branch in excess of 99.9%. Thus, isolation of decays in which only gamma rays are emitted is a challenging problem. Neutron-gamma discrimination by time of flight can be done effectively in the Spin Spectrometer;[7] however, this alone is of little use in the present context since the total neutron detection efficiency of the spectrometer is $\lesssim$70%. The following requirements were applied to identify purely gamma decays: (a) No delayed (i.e., n) pulse was present in the event. (b) The projectilelike particle was identified as ^{17}O. (c) The excitation energy in ^{208}Pb as determined from the energy of the inelastically scattered ^{17}O was equal, within the resolution of the detectors, to the total energy emitted as gamma radiation (sum of gamma-ray pulse heights in the Spin Spectrometer). The requirement (c) is particularly effective since a minimum of 7.4 MeV (the n binding energy) is missing from the total gamma energy in those events in which a neutron was emitted. From these purely gamma-decay events, it was necessary to select those which were due to a single high-energy gamma ray directly to the ground state. The number of detectors triggered in an event does not provide the necessary information, since a 10- to 20-MeV gamma ray has a high probability of triggering three to five detectors. An effective and efficient technique[8,9] for selecting single gamma events was developed and tested on 12.7- and 15.1-MeV gamma rays produced in the $^{12}C(p,p'\gamma)$ reaction (which also provided energy and response calibration data).

Figure 2.36 shows results of the analysis. The solid line is the yield of purely gamma decays as a function of excitation energy (E^*) in ^{208}Pb. (Note that the condition $E^* = \text{Sum } E_\gamma$ has been applied.) The dashed curve shows the

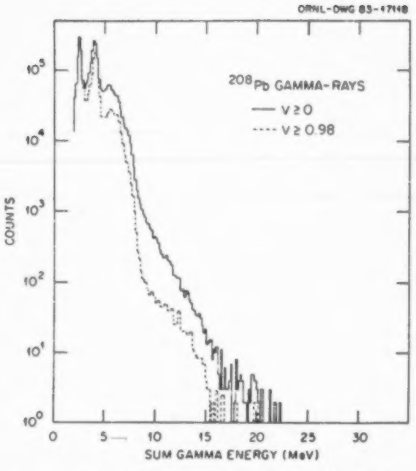

Fig. 2.36. Gamma-ray spectra from ^{208}Pb for $V > 0$ (all gamma rays) and $V > 0.98$ (only ground-state gamma rays). See Refs. 6 and 7 for a discussion of the parameter V.

yield of direct ground-state decays. The plot in Fig. 2.37 is the ratio of the curves in Fig. 2.36 and gives the fraction of all gamma decays which went to the ground state. The structures below the neutron binding energy can be understood in terms of known discrete levels of ^{208}Pb. The clear enhancement in the $E^* = 10$-15 MeV region is a graphic illustration of the special relationship the states in this region have to the ground state. Multipolarities other than E1 and E2 are extremely unlikely to contribute to the direct decay above 10 MeV. We expect analysis of angular distribution data to provide a rigorous separation of these components. For the present, we assume that the structure between 10 and 15 MeV is composed of an E2 part, reflecting the accepted position (10.9 MeV) and shape of the giant quadrupole resonance (GQR), and an E1 part due to the 13.7-MeV giant dipole resonance (GDR). We are thereby able to obtain the following results: (1) The ground state to gamma-ray branching ratio for the GQR is $\Gamma_{\gamma 0}/\Gamma_\gamma = 30\%$. (2) The data in Fig. 2.36, together with the inclusive ^{17}O inelastic spectrum, give $\Gamma_{\gamma 0}/\Gamma_{TOTAL} \sim (1.1 \pm 0.2) \times 10^{-4}$ for the GQR. (3) Making standard assumptions about the decay of giant resonances,[3] we deduced a $B(\hat{E}2)\uparrow$ from the GQR region of 21 ± 4 W.u. or $81 \pm 15\%$ of the energy-weighted sum rule (EWSR). (4) The yield in the vicinity of the GDR is consistent with a $B(E1)\uparrow$ corresponding to the full EWSR strength of the GDR.

Cascade decay properties can also provide important data. The analysis to date has produced the following results: (1) The branch to the 3^- (2.6-MeV) state is $\sim$15-30% of all gamma

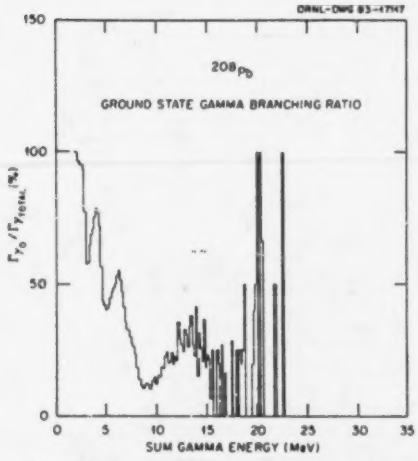

Fig. 2.37. Ground-state gamma-ray branching ratio (%) as a function of sum gamma-ray energy (or excitation energy in ^{208}Pb).

decays at 11 MeV, falling to less than 5% above 12.5 MeV. (2) Significant cascade branches to 4^- and 5^- states are seen in the $E^* \approx 8.5$-12 MeV region, consistent with the presence of 4^+ or 6^+ strength in this region. (3) The only cascade decays of sufficient intensity to be identified in the $E^* \approx 12.5$-15.5 MeV region are two-step processes through known 1^- states in ^{208}Pb between 5.3 and 7.4 MeV of excitation energy. This is the expected gamma-decay mode for the monopole (0^+) resonance which has been found in this excitation region.

We expect further analysis of the data discussed here, together with the more extensive data recently acquired, to improve the quality of the numerical results quoted and cast new light on the details of GR structure and damping.

---

1. Computer Sciences Division, ORNL.
2. Chalk River Nuclear Laboratories, Chalk River, Ontario.
3. L. S. Cardman, Nucl. Phys. A354, 173c (1981) and G. J. Wagner, Giant Multipole Resonaces, edited by F. E. Bertrand, Harwood Academic, New York, 1980, p. 251
4. F. E. Bertrand, Nucl. Phys. A354, 129c (1981); Giant Multipole Resonances, edited by F. E. Bertrand, Harwood Academic, New York, 1980; F. E. Bertrand, Annu. Rev. Nucl. Sci. 26, 457 (1976).
5. F. Bortignon and R. A. Broglia, Nucl. Phys. A317, 405 (1981).
6. T. P. Sjoreen et al., "Inelastic Excitation of Giant Resonances by 400-MeV ^{16}O," this report.
7. M. J. Jääskeläinen et al., Nucl. Instrum. Methods. Phys. Res. 204, 385 (1983).
8. J. R. Beene et al., in Proceedings of the Conference on Physics with Heavy Ions (Stony Brook, New York, April 1983), Harwood Academic, New York, in press.
9. F. E. Bertrand, J. R. Beene, and T. P. Sjoreen, in Proceedings of the International Symposium of Highly Excited States and Nuclear Structure (Orsay, France, September 1983), to be published.

NEUTRON DECAY OF GIANT RESONANCES

J. R. Beene
R. L. Auble
F. E. Bertrand
M. L. Halbert
D. C. Hensley
D. Horen
R. L. Robinson
R. O. Sayer[1]
T. P. Sjoreen
G. Ball[2]

One of the principal aims of experimental nuclear structure physics has been an understanding of simple nuclear excitations, such as single-particle states and giant resonances (GR). The theory of such states, in the absence of coupling to more complex degrees of freedom, seems to be reasonably well understood in terms of mean-field theories, e.g., for GR the random phase approximation.[3,4] However, at the excitation energies where most GR are observed, particularly in heavy nuclei, the simple modes are embedded in a complex background of states with which they mix. The understanding of this mixing, or damping, requires a level of theory beyond mean-field approximations, and it is this aspect that is the focus of current theoretical work on the GR.[5] More sophisticated experiments, in particular, coincidence experiments of GR decay, are required to provide constraints on and guidance to this theoretical work.

Following conventional terminology,[6] we consider inelastic excitation of the GR to proceed via a highly coherent 1p-1h state (primary doorway), which we identify with the undamped GR. This state may decay directly into the continuum by nucleon emission, leaving a 1h state in the A-1 nucleus; this process is referred to as "direct emission" with a width $\Gamma^\uparrow$. This state may also decay into (i.e., mix with) more complex np-nh ($n > 1$) states (compound states) in the same energy region. The corresponding width, $\Gamma^\downarrow$, is referred to as a spreading or damping width. The decay of the GR will proceed with a probability $\Gamma^\uparrow/\Gamma$ by "direct emission" of particles from the primary doorway and by damping into the continuum with subsequent equilibrium evaporation of particles with probability $\Gamma^\downarrow/\Gamma$. The giant dipole resonance and giant quadrupole resonance are expected to have $\Gamma^\downarrow \gg \Gamma^\uparrow$; however, there is a suggestion that "direct escape" could play a larger role in the decay of the monopole resonance.[5]

We have performed experiments to study the neutron decay of GR in ^{208}Pb and ^{90}Zr, using inelastic scattering of 381-MeV ^{17}O beams from the HHIRF coupled accelerators to excite the resonances and the ORNL Spin Spectrometer to identify neutron decays. Some details of the

experimental setup are discussed in another contribution to this report.[7] Pulses due to neutrons in the NaI detectors of the Spin Spectrometer can be separated from gamma rays by time of flight.[8] Unfortunately, the flight path is too short, compared to the detector thickness, to provide much neutron energy resolution. However, over most of the excitation energy region of interest (e.g., up to >16 MeV in ^{208}Pb), single neutron emission dominates. Hence, neutron energies can be determined very accurately from the target excitation energy obtained from the kinetic energy of the outgoing ^{17}O, together with the total energy of the gamma radiation emitted following the neutron emission. This sum gamma energy, in fact, gives directly the excitation energy of the state populated in the daughter nucleus by the neutron emission process. Figure 2.38 shows data obtained with the ^{208}Pb(^{17}O,^{17}O') reaction. It is a two-dimensional histogram of ^{17}O kinetic energy (and hence ^{208}Pb excitation) against sum gamma-ray energy (~residual ^{207}Pb excitation energy) for events in which a delayed (i.e., neutron) pulse was detected. The upper diagonal line in Fig. 2.38 indicates the locus of points for which $E^*(^{208}Pb) = \text{Sum } E_\gamma$. This can only be the case if no neutrons are emitted; hence, data in this region represent random coincidences with very intense gamma radiation from states below the neutron threshold. The lower line is drawn shifted from the upper line by S_n (the neutron binding energy in ^{208}Pb). The true neutron decay events lie below this line. The gamma-ray sum energy resolution is sufficient (though it is not apparent in Fig. 2.38) to separate individual excited states of ^{207}Pb.

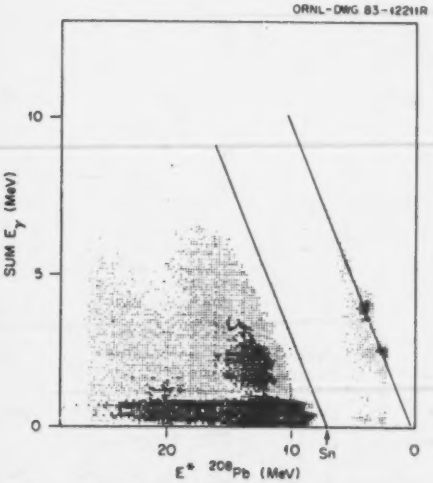

Fig. 2.38. Coincidence yield as a function of ^{17}O kinetic energy (^{208}Pb excitation energy) and the total gamma-ray energy, i.e., residual excitation in ^{207}Pb. The solid lines are discussed in the text.

The analysis of the data is in an early stage. We intend to investigate the distribution of excited-state population in ^{207}Pb resulting from neutron decay of the GR region in ^{208}Pb and to investigate simultaneously the complete angular distributions of the corresponding decay neutrons. This data should show any significant direct escape ($\Gamma^\downarrow$) and enable us to study it in detail. The main goal, however, is to investigate the structure of the states which play a major role in the damping of the GRs. This study is motivated by the work of Broglia and collaborators.[9] Some preliminary analysis on ^{208}Pb decay is complete. As yet, we see no compelling evidence for direct emission in the 8-to 16-MeV excitation energy region. There does seem to be clear evidence for substantial high-spin strength (e.g., 4$^+$, 6$^+$) in the 10- to 13-MeV excitation energy region. The evidence for this is substantial yield to states with $J > 9/2$ in ^{207}Pb.

---

1. Computer Sciences Division, ORNL.
2. Chalk River Nuclear Laboratories, Chalk River, Ontario.
3. K. Goeke and J. Speth, Annu. Rev. Nucl. Part. Sci. 32, 65 (1982).
4. F. E. Bertrand, Nucl. Phys. A354, 129c (1981).
5. G. F. Bertsch, P. F. Bortignon, and R. A. Broglia, Rev. Mod. Phys. 55, 287 (1983).
6. G. J. Wagner in Giant Multipole Resonances, edited by F. E. Bertrand, Harwood, Academic, New York, 1980, p. 251
7. J. R. Beene et al., "Electromagnetic Decay of Giant Resonances," this report.
8. M. Jääskeläinen et al., Nucl. Instrum. Methods Phys. Res. 204, 385 (1983)
9. F. Bortignon and R. A. Broglia, Nucl. Phys. A317, 405 (1981) and references therein.

COLLECTIVE SPIN-ISOSPIN EXCITATIONS OBSERVED IN THE (p,n) REACTION[1]

D. E. Bainum[2] D. Horen
S. D. Bloom[3] P. Koncz[9]
C. C. Foster[4] J. Larsen[5]
C. Gaarde[5] T. Masterson[10]
C. D. Goodman[4] J. R. McGrory
C. A. Goulding[6] J. Rapaport[8]
M. B. Greenfield[7] E. Sugarbaker[9]
S. Grimes[8] T. N. Taddeucci[8]
T. P. Welch[8]

The selectivity of the (p,n) reaction at intermediate proton energies (~100-200 MeV) to study spin-isospin excitations has been pursued at the Indiana University Cyclotron Facility (IUCF) using the beam-swinger system.[11] Following studies on targets of ^{90}Zr[12] and ^{208}Pb[13] where only about 50% of the Gamow-Teller (GT) strength was found and a new L=1, S=1, T=1 resonance was observed, data have been recorded for a number of nuclei spanning the periodic table. The energy systematics of the GT and L=1, S=1, T=1 resonances were reported previously.[14]

Two time-of-flight detector stations were used. One was positioned on the 0° line (with respect to the incident proton direction) at a distance between 60-100 m, and the other on the 24° line at a

distance of about 40 m. These allowed measurements over an angular range of 0°-48° with the beam swinger. The neutron detectors were used in a time-compensated mode[15,16] and were 15 cm x 15 cm x 1 m long. Two or more detectors were located at each station. Further details pertaining to the experimental conditions and data reduction can be found in the referenced works.

Gamow-Teller Resonances

Neutron energy spectra[17] for targets of ^{40}Ca, ^{90}Zr, ^{112}Sn, ^{124}Sn, ^{169}Tm and ^{208}Pb taken at 0° with protons of incident energy 200 MeV are shown in Fig. 2.39. As can be seen, the spectra are dominated by the GT resonance. The resolution is not sufficient to resolve the IAS peak for ^{124}Sn, ^{169}Tm and ^{208}Pb, which, however, is quite small. In Fig. 2.40 we show energy spectra for ^{208}Pb at several angles out to 18.7°. The individual spectra, were decomposed in several ways in order to extract cross sections for the L=0, L=1 and L=2 components. Angular distributions for ^{208}Pb are shown in Fig. 2.41, along with DWIA calculations for typical single-particle transitions using the Love-Franey[18] interaction and DWBA70.

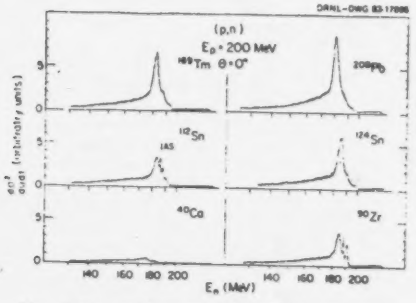

Fig. 2.39. Neutron time-of-flight spectra at θ=0° for an incident proton energy of 200 MeV. The spectra are normalized to show relative cross sections.

In the low momentum transfer limit the zero degree cross section in the impulse approximation can be reduced[19] to

$$\frac{d\sigma}{d\Omega}(0°) = \frac{\mu}{\pi\hbar^2}\frac{k_f}{k_i}\left(N_T J_\tau^2 B(F) + N_{\sigma\tau} J_{\sigma\tau}^2 B(GT)\right).$$

Here, μ and k are the relativistic reduced mass and wave number, respectively, N_T and $N_{\sigma\tau}$ are distortion factors which can be calculated, and J_τ and $J_{\sigma\tau}$ are volume integrals of the effective isospin and spin-isospin interactions, respectively. The nuclear structure factors θ=0° where the momentum transfer q=0 become the Fermi and GT β-decay matrix elements, i.e.,

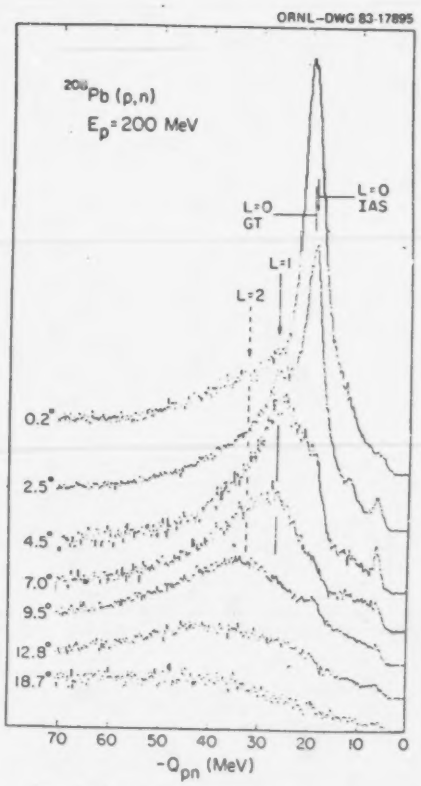

Fig. 2.40. Neutron energy spectra for ^{208}Pb(p,n)^{208}Bi at E_p = 200 MeV.

$$B(F) = \frac{1}{2J_i+1}\langle f\|\sum_k t_-(k)\|i\rangle^2 \text{ and}$$

$$B(GT) = \frac{1}{2J_i+1}\langle f\|\sum_k \sigma(k)t_-(k)\|i\rangle^2.$$

For a transition which has a measured β-decay lifetime, one has

$$B(F) + \left(\frac{g_A}{g_V}\right)^2 B(GT) = \frac{(6163.4\pm3.8)}{ft}.$$

By measuring 0° cross sections for known β-decay transitions one can deduce values for the volume integral for comparison with those deduced by Love and Franey. Or one can normalize the (p,n) data to the DWBA calculations. This normalization is then used to extract B(F) and B(GT) for transitions not accessible by β-decay measurements.

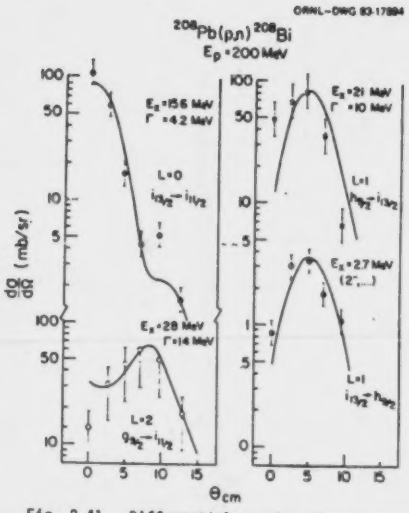

Fig. 2.41. Differential angular distributions for $^{208}Pb(p,n)^{208}Bi$ at E_p = 200 MeV. Calculated angular distributions are shown for typical single particle-hole transitions with arbitrary normalizations. The cross section for the GT transition (E_x = 15.6 MeV) includes a small contribution from the IAS (E_x = 15.2 MeV).

One can derive general sumrules for charge exchange modes using commutator relations for operators involving t_+ and t_-, which for GT transitions leads[20] to

$$S_{\beta^-} - S_{\beta^+} = \sum_f \sum_u \left| \langle f | \sum_{k=1}^{A} \sigma_u(k) t_-(k) | i \rangle \right|^2$$

$$- \sum_{f'} \sum_u \left| \langle f' | \sum_{k=1}^{A} \sigma_u(k) t_+(k) | i \rangle \right|^2$$

$$= 3(N-Z).$$

This says that the difference between the sum of the β_- and β_+ GT strength from an initial state $|i\rangle$ to all final states is equal to 3(N-Z), where N and Z refer to the target nucleus.

The fraction of the GT sum rule deduced from our data for several target nuclei is shown in Fig. 2.42. It is apparent from this figure that only about 40-60% of the expected GT strength is observed. Two ideas have been proposed that might lead to quenching of the GT strength: a) configuration mixing and b) mixing of the GT resonance with the ΔN^- (i.e., internal degrees of freedom of the nucleon) which can also be effected by a $\sigma\tau$ operator. Even though the latter resonance lies at an excitation energy of ~300 MeV (compared

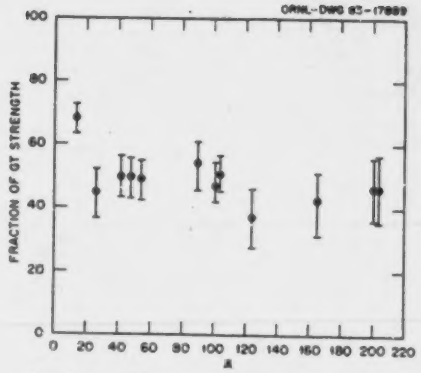

Fig. 2.42. Fraction of GT sum rule strength observed in the (p,n) reaction.

e.g., to ~20 MeV for the nuclear GT resonance for lead) it has considerably more strength. The net effect of a calculation which includes the ΔN^{-1} interaction is that about 36% of the GT strength from the nuclear excitation region is moved up to the ΔN^{-1} region. Configuration mixing also causes an upward shift in some of the GT strength, and there has been considerable theoretical controversy as to which of these effects (or possibly both) is responsible for quenching of the GT strength (see, e.g., refs. 21, 22, 23, and 24). Although this question is not yet resolved it is interesting to note that the ΔN^{-1} theory provides some rather nice features. Since it is not excitable by a Fermi operator, it cannot effect the Fermi strength. In addition, the ΔN^{-1} resonance would have the effect of reducing the GT strength in the nuclear region by about 69% independent of A.

Dipole Spin Resonances

The dipole spin resonance has been identified from its differential angular distribution which indicates an L=1 angular momentum transfer,[12,13] and its increase[13] in cross section with higher incident energy protons which is a signature of the spin-isospin interaction. This resonance would be related to the dipole spin resonance of the target in a manner similar to the relation of the GT with respect to the M1 resonance. The form of an operator which could give rise to such transitions is

$$r(Y_1 \times \sigma)_{\lambda=0,1,2}\, \tau_{-1},$$

and thus acting on a 0^+ target state would lead to final states with $J^\pi = 0^-$, 1^- and 2^-. Angular distributions are not capable of distinguishing between these J-values. The width of the observed L=1, S=1 resonance is Γ~10 MeV.

Peak cross sections (at θ=4.5°) for L=1 resonance at E_p = 200 MeV for some targets with A>40 are shown in Fig. 2.43. A sum rule for the dipole

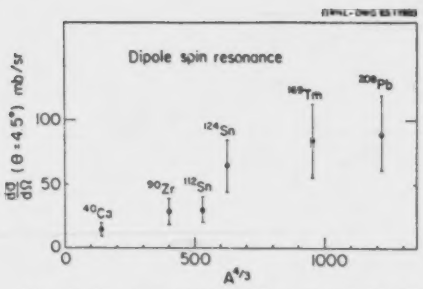

Fig. 2.43. Peak cross sections at θ=4.5° and E_p = 200 MeV for the L=1 resonance.

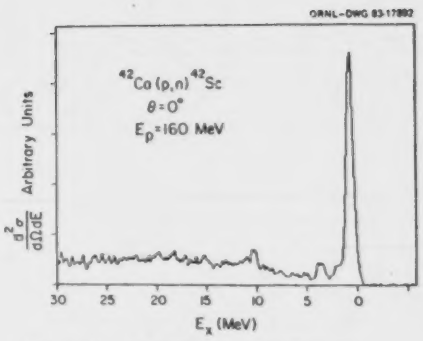

Fig. 2.44. Neutron energy spectrum for ^{42}Ca(p,n)^{42}Sc taken at θ=0° with E_p = 160 MeV.

spin excitation can be derived in a manner analogous to that for the GT resonance. For details the reader is referred to ref. 17. The dipole strength that we observe in the (p,n) reaction is also about 50% of the calculated value. The latter can be estimated by calculating DWIA cross sections using the Love-Franey interaction[18] for representative single particle transitions and forming the ratio

$$d\sigma/d\Omega(\text{DWIA};\ i\to f)/B(i\to f),$$

where

$$B(i\to f) = \left| \langle f \left| r(Y_1 \times \sigma)\tau_{-1} \right| i \rangle \right|^2,$$

This ratio can be considered as the cross section per unit strength for a spin dipole transition. Division of the observed cross section by this latter ratio yields a measure of the observed strength. From a comparison of the observed strengths derived in this manner with those predicted with a Tamm-Dancoff calculation, it thus appears that the L=1, S=1 resonance is quenched to about the same extent as the GT strength.

Some Comparisons of Observed GT Strength with Shell-Model Calculations

In this section we present a few selected studies of GT strength observed via the (p,n) reaction as compared to strength calculated utilizing a shell model theory.

^{42}Ca(p,n)^{42}Sc. A neutron energy spectrum[25] for ^{42}Ca(p,n)^{42}Sc taken at θ=0° with E_p = 160 MeV is shown in Fig. 2.44. The spectrum is dominated by a transition to a state in ^{42}Sc at 0.61 MeV with $J^\pi = 1^+$ (T=0) which is the analogue of the beta-decay transition from the g.s. of ^{42}Ti to the same level in ^{42}Sc. One can use these transitions to normalize the (p,n) data B(GT) values to compare with shell model calculations. The latter were carried out using an f,p model space with the PWM residual force[26] and the results are compared with the data in Table 2.7. The agreement between the observed and the β-decay normalized calculated values in both magnitude and distribution is quite remarkable.

^{58}Ni(p,n)^{58}Cu. The GT strength for the ^{58}Ni(p,n)^{58}Cu reaction has been identified by its L=0 angular distribution using proton beams of 120 and 160 MeV. The GT strength distribution is shown in Fig. 2.45 along with M1 strength as observed in the (e,e') reactions. The deduced B(GT) strength distribution is summarized in Table 2.7. Unfortunately, the experimental resolution is not sufficient to resolve individual states in the excitation region above ~7 MeV so that comparison could be made with analogue states of known isospin.

Shell model calculations for ^{58}Ni and ^{58}Cu have been carried out in a $f_{7/2}$ $(p_{3/2}, p_{1/2}, f_{5/2})^{2+n}$ configuration space with n=0 and 1, i.e., a closed shell ^{56}Ni plus states with one particle excited from the $f_{7/2}$ orbit to a $p_{3/2}$, $p_{1/2}$ and $f_{5/2}$ level. This model space can be considered as a reasonable approximation for the wave functions for a single one-body operator, $\Sigma\sigma\tau$, needed here. A Kuo-Brown interaction was used for the residual two-body force. The interaction was constructed for a ^{40}Ca core but with a size parameter relevant to ^{56}Ni. Single-particle energies were adjusted to fit the spectrum of ^{57}Ni.

In Fig. 2.46 histograms of the calculated GT strength for each isospin component as well as the total are plotted in 1 MeV bins versus excitation energy in ^{58}Cu. The calculations indicate that above about 7 MeV there is overlapping of strength from the different isospin components. Experimentally we find ΣB(GT) = 7.3±1.3 versus a calculated value of 13.8, i.e., about 53% of the theoretical value. Note that for this case, the theoretical value is considerably greater than the minimum value of 3(N-Z) due to the fact that β_+ transitions are not blocked.

From ^{58}Ni(e,e') measurements, Lindgren et al.[27] report ΣB(M1)$_+$ = 1.89 μ_0^2 for T=2. The model calculations (which include both spin and orbital operators) gives 2.83 μ_0^2. However, if we quench the $\sigma\tau$ part of the M1 operator by 0.8 (as indicated by the (p,n) data) we find the calculated strength for T=2 reduces to ΣB(M1)$_+$ = 1.7 μ_0^2, in good agreement with the reported value.

Table 2.7. Gamow-Teller strengths.

Calculation (1^+ levels)				Beta decay		(p,n)		
Calculation	T	B(GT)	B(GT)[b]	E_x (MeV)	B(GT)	E_x (MeV[a])	$(d\sigma/d\omega)0°$	B(GT)[b]
0.6	0	4.92	2.67	0.6	2.67	0.6	15.3 ± 0.9	2.67
4.2	0	0.06	0.03			~2.1	1.2 ± 0.2	0.21
5.6	0	0.06	0.03			~3.6	1.2 ± 0.2	0.21
7.5	0	0.12	0.06					
7.9	1	0.03	0.02					
8.0	0	0.01	0.003					
9.3	0	0.01	0.01					
11.1	1	0.78	0.43					
15.4	0	0.01	0.01					
c)								
		6.00	3.26					3.24

a) Energies are determined by assuming the first 1^+ state to be the 0.61-MeV level in ^{54}Sc.
b) Normalized to the beta decay value.
c) A tenth state of the configuration $(p_{3/2})(f_{5/2})$ contains no GT strength and therefore does not appear in our calculation.

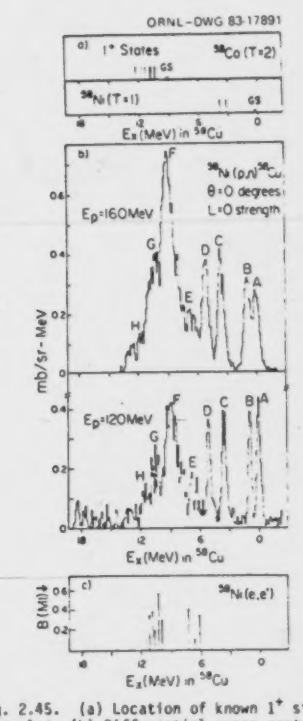

Fig. 2.45. (a) Location of known 1^+ states in A=58 nuclei. (b) Differential cross section of L=0 strength observed at θ=0° for ^{58}Ni(p,n)^{58}Cu at E_p = 126 and 160 MeV. (c) Distribution of reported M1 strength in ^{58}Ni.

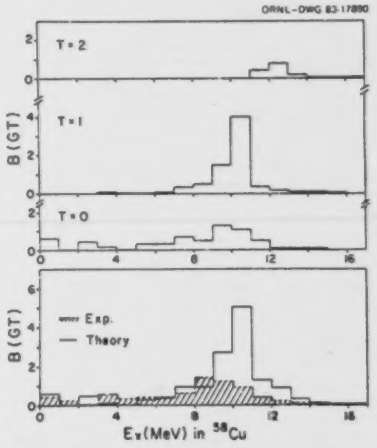

Fig. 2.46. Gamow-Teller strength in ^{58}Cu. The strength (in energy bins of 1 MeV) $\Sigma B(GT) = \Sigma(2J_i+1)^{-1} \times |\langle 1^+, T \| \sigma\tau_- \| 0^+, T_0 \rangle|^2$ is plotted versus excitation energy in ^{58}Cu for each T value. The summed total is compared with the experimentally deduced strength in the bottom part of the figure.

$^{54+56}$Fe(p,n)$^{54+56}$Co and ^{60}Ni(p,n)^{60}Co. Experiments similar to that for ^{58}Ni(p,n)^{58}Cu discussed above have been performed.[2B] Deduced GT strength has been compared with shell model calculations (where available) with results similar to those for ^{58}Ni.

---

1. Summary of work published or in press.
2. Emporia State University, Emporia, Kansas 66801.

3. Livermore Lawrence Laboratory, Livermore, California 94550.
4. Indiana University, Bloomington, Indiana 47405.
5. Niels Bohr Institute, Copenhagen, Denmark.
6. EG&G, Los Alamos, New Mexico 87544.
7. Florida A&M University, Tallahassee, Florida 32307.
8. Ohio University, Athens, Ohio 45701.
9. Ohio State University, Columbus, Ohio 43210.
10. University of Colorado, Boulder, Colorado 80309.
11. C. D. Goodman et al., IEEE Trans. Nucl. Sci. NS-26, 2248 (1979).
12. D. E. Bainum et al., Phys. Rev. Lett. 44, 1751 (1980).
13. D. J. Horen et al., Phys. Lett. 95B, 27 (1980).
14. D. J. Horen et al., Phys. Lett. 99B, 383 (1980).
15. C. D. Goodman et al., Nucl. Instrum. Methods 151, 125 (1978).
16. C. D. Goodman et al., IEEE Trans. Nucl. Sci. NS-25, 577 (1979).
17. C. Gaarde et al., Nucl. Phys. A369, 258 (1981).
18. W. G. Love and M. A. Franey, Phys. Rev. C 24, 1073 (1981).
19. C. D. Goodman et al., Phys. Rev. Lett. 44, 1755 (1980).
20. C. Gaarde et al., Nucl. Phys. A334, 248 (1980).
21. A. Bohr and B. R. Mottelson, Phys. Lett. 100B, 10 (1981).
22. M. Rho, in Spin Excitations in Nuclei, ed. F. Petrovich et al., Plenum (New York) to be published.
23. A. Arima, loc. cit.
24. I. S. Towner and F. C. Khanna, Nucl. Phys. A399, 334 (1983).
25. C. D. Goodman et al., Phys. Lett. 107B, 406 (1981).
26. F. Petrovich et al., Phys. Rev. Lett. 22, 895 (1969).
27. R. A. Lindgren et al., Phys. Rev. C 14, 1789 (1976).
28. J. Rapaport et al., Nuclear Physics, (to be published).

SEARCH FOR GAMOW TELLER STRENGTH USING THE $^{18}O+^{18}F$ CHARGE EXCHANGE REACTION

D. J. Horen, R. L. Auble, F. E. Bertrand, J. L. Blankenship, J. L. Ford, Jr., E. E. Gross, D. C. Hensley, R. O. Sayer, D. Shapira, T. P. Sjoreen

In the last few years, the use of intermediate energy protons to locate and measure Gamow-Teller (GT) strength utilizing the (p,n) reaction has been highly successful. The results of this work indicate that the observed strength represents only about 50% of the GT sum rule which can be expressed as

$$\Sigma S_{\beta-} - \Sigma S_{\beta+} = 3(N-Z),$$

where the summations extend over all the GT transitions. For heavy targets such as ^{208}Pb, Pauli blocking prevents β^+ transitions, and thus the $\Sigma S_{\beta-}$ which is measured by the (p,n) reaction should be equal to 3(N-Z). Deviations from this value can possibly arise from configuration mixing or coupling to the ΔN^{-1} excitation of the nuclear constituents. To date there is little measured data available for $S_{\beta+}$. Hence, for target nuclei where N and Z are comparable, in order to deduce the fraction of GT strength observed in the (p,n) measurements, one must resort to some type of model calculation.

In view of the above, we have undertaken to determine whether the heavy-ion charge exchange reaction at ~22 MeV/A would be sufficiently selective so as to allow measurement of $S_{\beta+}$. As a first case, we have chosen to study the $^{28}Si(^{18}O,^{18}F)^{28}Al$ reaction using 340-MeV ^{18}O ions provided by the coupled machine operation of the Holifield Heavy Ion Research Facility (HHIFR). The ^{28}Si target was a self-supported foil of 265 $\mu g/cm^2$. The reaction products were detected with the broad-range spectrograph focal plane detector system (described elsewhere in this report) which provided position information and particle-identification. Fluorine ions from the $^{18}O(^{28}Si,^{27}Al)^{19}F$ reaction were recorded simultaneously.

Preliminary spectra measured at θ=3° and 5° for the charge-exchange reaction are shown in Fig. 2.47. Peaks indicated by arrows correspond to excitation energies of 1^+ states in ^{28}Al (which are analogues of 1^+ states in ^{28}Si for which B(M1) values have been reported) and might be expected to be excited in the charge-exchange reactions. Although these preliminary results are very encouraging, we will require higher beam currents and thinner ^{28}Si targets to obtain definitive results. Further measurements are planned.

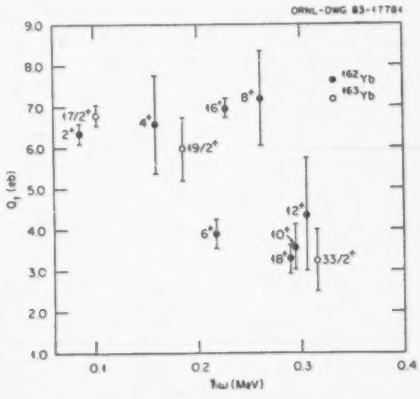

Fig. 2.47. Spectrum of ^{18}F ions from the $^{28}Si(^{18}O,^{18}F)^{28}Al$ reaction at θ_L = 2.3°. The arrows indicate positions of excited states in ^{28}Al known to have $J^\pi = 1^+$ and which would be expected to be excited in this reaction.

SPIN TRANSFER IN (p,n) REACTIONS

T. N. Taddeucci[1] E. Sugarbaker[3]
J. Rapaport[1] P. Koncz[3]
C. D. Goodman[2] C. Gaarde[4]
C. C. Foster[2] J. S. Larsen[4]
D. J. Horen

The (p,n) reaction at intermediate energies has become an important probe of spin-excitation ($\Delta S=1$) strength in nuclei. The circumstance responsible for this development is the dominance at energies larger than about 50 MeV of the isovector spin-flip component $v_{\sigma\tau}$ over the non-spin-flip component v_{τ}.[5,6] This dominance causes $\Delta S=1$ excitation to be favored over $\Delta S=0$ excitations by a ratio of 13:1 at 200 MeV.[5]

Identification of spin-flip excitation strength has been made largely on the basis of the observed energy dependence and shape of differential-cross-section angular distributions. Despite the apparently successful application of such inferential evidence, some important ambiguities remain in trying to characterize features observed in (p,n) spectra. In spectra obtained with medium and heavy-mass nuclei the excited states and giant resonances ride on a large continuum background. The large widths (several MeV) of the resonances make it difficult to separate these excitations from the underlying continuum. The problem is further complicated by the changing shape of the continuum as a function of angle.

While it is not possible to gain a complete understanding of the giant resonances and the continuum by using differential cross sections alone, measurements of spin-dependent quantities should help to sort things out. For angles larger than 0°, measurements of the analyzing power appear to provide valuable information despite the lack of a unique signature for $\Delta S=1$ and $\Delta S=0$ excitations.[7] A quantity that does uniquely characterize $\Delta S=1$ and $\Delta S=0$ transitions is the transverse-polarization-transfer coefficient $D_{NN}(\theta)$. At $\theta=0°$ this quantity is simply the ratio of outgoing to incoming projectile polarization: $D_{NN}(0°) = P_f/P_i$. Non-spin-flip transitions such as $0^+ \rightarrow 0^+$ IAS reactions will have $D_{NN}(0°) = 1$, while $0^+ \rightarrow 1^+$ spin-flip excitations will have the distinctly different value $D_{NN}(0°) = -1/3$.

Direct measurement of the spin transfer in (p,n) reactions at intermediate energy should help to establish the magnitude and nature of the continuum and answer the question of whether or not it contains previously undetected GT strength.

Spin transfer measurements are useful not only for the nuclear structure information they provide but are crucial for obtaining a better understanding of the effective interaction that mediates intermediate-energy inelastic nucleon-nucleus scattering. Transitions for which nuclear structure or transition strength information is available from other probes are useful tools for studying the effective interaction and the applicability of the impulse approximation at intermediate energies. Nuclear-medium effects that modify the free nucleon-nucleon interaction are more susceptible to understanding when information in addition to cross sections is available.[8] The importance of such effects is clearly evident in the comparison of the $v_{\sigma\tau}/v_{\tau}$ ratio determined from (p,n) measurements and that predicted from free nucleon-nucleon interaction studies.[5]

We have initiated a program of (p,n) spin transfer measurements employing the neutron polarimeter configuration illustrated in Fig. 2.48. The polarimeter consists of six standard large-volume (15 x 15 x 100 cm, NE102) neutron detectors arranged in three stacks of two detectors. The detector stacks are oriented perpendicular to the incident neutron flux and are separated by a distance of about 1.4 m. The two forward-most detectors serve as active analyzers, while the middle two detectors can be either analyzers or polarimeter "arms." Time signals derived from both ends of each detector are combined to yield position and time-of-flight information for each event. A valid event consists of a coincidence between any two detectors that are not in the same stack. The event is characterized as a "left" scatter or a "right" scatter by utilizing the position information from each detector.

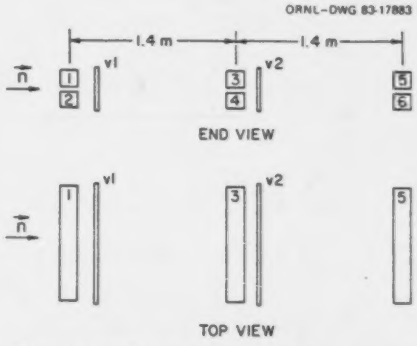

Fig. 2.48. Schematic diagram of the neutron polarimeter to be used for spin transfer measurements at IUCF. The neutron flux is incident from the left. The veto scintillators v1 and v2 eliminate false coincidences caused by forward-scattered protons from $^1H(n,p)n$ reactions.

The primary analyzing reaction is $^1H(n,n)^1H$, which has an average analyzing power of $A(\theta) = 0.3$ for $10° \leq \theta_{lab} \leq 40°$ and $E_p = 160$ MeV. The inclusive reaction $^{12}C(n,n'x)$ has a similar analyzing power[9] over the range $6° < 25°$.

The effective analyzing power and instrumental asymmetry of the polarimeter are determined by calibration runs with the incident proton beam in different polarization states. In terms of the yield of neutrons scattered to the left (Y_L) and to the right (Y_R), the neutron polarization p_n is given by

$$p_n = \frac{1}{A}\frac{Y_L - (\epsilon_L/\epsilon_R)Y_R}{Y_L + (\epsilon_L/\epsilon_R)Y_R} , \qquad (1)$$

where $\epsilon_L(\epsilon_R)$ is the relative efficiency for detection of left(right)-scattered neutrons and A is the effective analyzing power. The polarimeter constants A and ϵ_L/ϵ_R) are determined by measuring the left and right yields of neutrons produced by the $0^+ \rightarrow 0^+$ $^{14}C(p,n)^{14}N(2.31\ MeV)$ reaction for two different proton-beam polarization states. The neutrons produced by this reaction have the same polarization as the incident protons.

The polarimeter configuration described here has been tested using the beam swinger at the Indiana Cyclotron Facility (IUCF) with 160-MeV protons. Polarized beam currents of ~30 na and $|P_y| \sim 0.7$ were delivered on target. Targets of $^{13+14}C$ and ^{6+7}Li and ^{90}Zr were investigated. Runs were also made with unpolarized beam in order to check for instrumental asymmetries.

In the first attempt, the veto counters only had phototubes at one end and the optical coupling was poor. Preliminary analyses of the data from this run indicated a veto counter rejection efficiency of ~93%, ϵ_L/ϵ_R =1.06, and A ~0.19. Part of the left-right asymmetry can be ascribed to the veto detector. The deduced D_{NN} for a number of pure GT transitions were found to be in the range minus 0.29-0.37 in excellent agreement with expectations.

The veto detector was modified in a second run and had phototubes on both ends. Here, the veto efficiency was determined to be ~100%. Analyses of these data are in progress.

1. Ohio University, Athens, Ohio 45701.
2. Indiana University, Bloomington, Indiana 47405.
3. Ohio State University, Columbus, Ohio 43212.
4. Niels Bohr Institute, Copenhagen, Denmark.
5. T. N. Taddeucci et al., Phys. Rev. C 25, 1094 (1982).
6. W. G. Love and M. A. Franey, Phys. Rev. C 24, 1973 (1981).
7. E. Sugarbaker et al., Proceedings of the International Conference on Nuclear Structure, Amsterdam, 30 August-3 September 1982, Vol. I, p. 77.
8. J. M. Moss, Phys. Rev. C 26, 727 (1982).
9. R. D. Ransome et al., Nucl. Instrum. Methods 201, 315 (1982).

ASYMMETRY MEASUREMENTS IN THE $^{90}Zr(\vec{p},n)^{90}Nb$ AND $^{208}Pb(\vec{p},n)^{208}Bi$ REACTIONS

E. Sugarbaker[1] P. Welch[3]
P. Koncz[1] D. Horen
D. Krofcheck[1] C. Gaarde[4]
C. D. Goodman[2] J. Larsen[4]
C. C. Foster[2] S. Austin[5]
J. Rapaport[3] A. Galonsky[5]
T. Taddeucci[3] T. Masterson[6]

We have found that at IUCF energies the forward angle neutron energy spectra for (p,n) reactions on medium and heavy nuclei are characterized by spinflip, isovector collective states riding on a large continuum. Concentrations of Gamow-Teller (GT) strength have been identified via angular distributions of differential cross sections consistent with a $\Delta L=0$ transition and a bombarding energy dependence characteristic of a transition mitigated by the $\sigma\cdot\sigma$ $\tau_-\tau$ operator. This strength is fragmented in the $^{90}Zr(p,n)^{90}Nb$ reaction, in which 1^+ strength is located at 2.33 and 8.7 MeV.[7] In the $^{208}Pb(p,n)^{208}Bi$ reaction only the dominant "giant" GT state can be identified at an excitation energy above that of the IAS.[8] An additional feature of these (p,n) data is that a $\Delta L=1$, $\Delta S=1$ resonance has also been identified at an even higher excitation energy.[9]

During the past year we have extended our study of these isovector modes of excitation to the measurement of vector analyzing powers (A_y) for the (p,n) reaction on targets of ^{90}Zr and ^{208}Pb. For the ^{90}Zr target, angular distributions of A_y have been measured in the angular range from 0° and 24° to 48° using two neutron detector stations having neutron flight paths of 100 and 39 m, respectively. For the ^{208}Pb target, measurements at only a few angles have been obtained. In the present work, spectra have been measured at E_p = 160 MeV in order to further investigate the nature of these excitations and of the continuum.

Figure 2.49 shows a sample A_y spectrum for the $^{90}Zr(\vec{p},n)^{90}Nb$ reaction at θ=4.2°. The indicated excitation regions associated with each previously identified state have distinct values of A_y. At these forward angles the continuum, does not appear to have a significantly non-zero A_y. Preliminary extraction of the A_y data for the lower 1^+ state differ from that for the giant GT, possibly reflecting the expected difference in the dominant particle-hole configurations. Alternately the A_y of the broad $\Delta L=1$ resonance do not appear to exhibit a strong excitation energy dependent variation consistent with discrete concentrations of 0^-, 1^-, and 2^- strengths.[10] The back angle A_y spectra are dominated by the continuum. Data have been obtained over an excitation range of 0 to 60 MeV. In Fig. 2.50 it can be seen that as the angle increases from 15° to 48°, the A_y becomes increasingly more positive. The largest A_y at each angle are associated with the

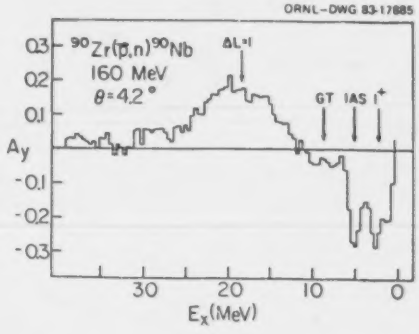

Fig. 2.49. Analyzing power for the $^{90}Zr(\vec{p},n)^{90}Nb$ reaction at 4.2°. The uncertainty in A_y is about ±0.02.

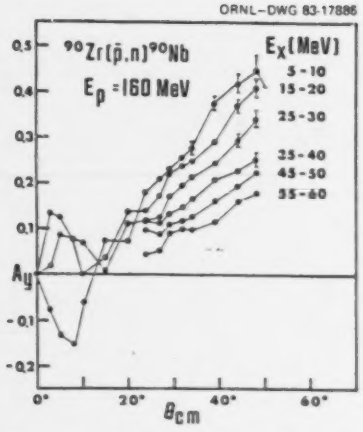

Fig. 2.50. Analyzing power for 5-MeV energy bins for the ^{90}Zr(p⃗,n)^{90}Nb reaction as a function of angle.

lowest excitation energies, with the maximum A_y reaching a value of about +0.5 at θ=48°.

Further reduction of the data and DWIA calculations are in progress.

1. Ohio State Univesity, Columbus, Ohio 43210.
2. Indiana University, Bloomington, Indiana 47405.
3. Ohio University, Athens, Ohio 45701.
4. Niels Bohr Institute, Copenhagen, Denmark.
5. Michigan State University, East Lansing, Michigan 48824.
6. University of Colorado, Boulder, Colorado 80309.

7. D. E. Bainum et al., Phys. Rev. Lett. 44, 1751 (1980).
8. D. J. Horen et al., Phys. Lett. 95B, 27 (1980).
9. D. J. Horen et al., Phys. Lett. 99B, 383 (1981).
10. F. Osterfeld et al., Phys. Lett. 105B, 257 (1981).

ENERGY DEPENDENCE OF THE RATIO OF ISOVECTOR EFFECTIVE INTERACTION STRENGTHS $|J_{\sigma\tau}/J_\tau|$ [1]

T. N. Taddeucci[2] C. Gaarde[5]
J. Rapaport[4] J. Larsen[5]
D. E. Bainum[3] C. A. Goulding[6]
C. D. Goodman[+] D. J. Horen
C. C. Foster[+] T. Masterson[7]
E. Sugarbaker[8]

The L=0, θ=0° (p,n) differential cross section can be expressed in terms of a factorized distorted-wave impulse approximation (DWIA) as

$$\sigma_\alpha(q) = K_\alpha(E_p)N_\alpha(q)\,|\,J_\alpha(q)\,|^2\,B(\alpha,q),$$

where $K_\alpha(E_p) = (E_iE_f/\pi^2)(k_f/k_i)$ and E and k are the total energy and wave number respectively. $N_\alpha(q)$ is a distortion factor and $J_\alpha(q)$ is the Fourier transform of the effective nucleon-nucleon interaction. $B(\alpha,q)$ is a nuclear structure factor, and $\alpha=\sigma\tau(\tau)$ for spin-flip (nonspin-flip) transitions, respectively. At θ=0° and q=0, $B(\alpha,q)$ are equal to β-decay matrix elements for Gamow-Teller ($\alpha=\sigma\tau$) and Fermi ($\alpha=\tau$) transitions.

The (p,n) reaction in even-A, T≠0 targets excite such transitions and one can define an empirical ratio for θ=0°, q=0 as

$$[R(E_p)]^2 = \frac{\sigma_{GT}(0^\circ)/B(GT)K_{GT}(E_p}{\sigma_F(0^\circ)/B(F)K_F(E_p)}.$$

In terms of the quantities discussed above, this can be written as

$$R(E_p) = |\,J_{\sigma\tau}/J_\tau\,|\,(N_{\sigma\tau}/N_\tau)^{1/2}.$$

DWIA calculations indicate that at intermediate energies the distortion factor ratio is approximately independent of energy with a value $N_{\sigma\tau}/N_\tau$ =1.2 for GT and F transitions not widely separated in energy. Hence, the empirical ratio defined above approximates the ratio of the interaction strengths $|\,J_{\sigma\tau}/J_\tau\,|$ at q=0. A similar type ratio can be formed for odd-A targets.

The specific transitions considered here are listed in Table 2.8. The empirical quantity $R(E_p)$ for even and odd A is plotted in Fig. 2.51, where it can be seen that $R(E_p) = a\,E_p$ for E_p >50 MeV with a = (54.9±0.9 MeV)$^{-1}$ for the even-A targets.

Comparison of the empirical results with some theoretical predictions for effective interactions is shown in Fig. 2.52. The line labeled EXPT is our average value for $R(E_p)$ divided by $\sqrt{1.2}$ to account for the distortion factor. An interesting feature is that above ~140 MeV the empirical ratio is still increasing whereas the Love-Franey[12] and PW[11] t-matrix interaction exhibits a plateau.

Further work is required to map out the energy dependence of the effective interactions for spin-isospin and isospin, respectively.

1. Summary of paper: Phys. Rev. C 25, 1094 (1981).
2. Ohio University, Athens, Ohio 45701.
3. Emporia State University, Emporia, Kansas 66801.
4. Indiana University, Bloomington, Indiana 47405.
5. Niels Bohr Institute, Copenhagen, Denmark.
6. EG&G, Los Alamos, New Mexico 87544.
7. University of Colorado, Boulder, Colorado 80309.
8. Ohio State University, Columbus, Ohio 43214.

9. C. D. Goodman, in the (p,n) Reaction and the Nucleon-Nucleon Force, ed. by C. D. Goodman et al. (Plenum, New York 1980).
10. G. Bertsch et al., Nucl. Phys. A284, 399 (1977); W. G. Love in Ref. 9.
11. A. Picklesimer and G. E. Walker, Phys. Rev. C 17, 237 (1978).

Table 2.9. Targets, final-state spin parities and excitation energies, and GT transition strengths for the (p,n) transitions studied in this work. Transition strengths are from the references indicated.

Target	J^π	E_x (MeV)	B(GT)	Ref.
^{7}Li	3/2⁻	0.000	1.25 ± 0.01	a
	1/2⁻	0.429	1.11 ± 0.01	a
^{13}C	1/2⁻	0.000	0.209 ± 0.003	b
	3/2⁻	3.511	0.85 ± 0.03	c
^{14}C	0⁺	2.313	0	
	1⁺	3.948	2.81 ± 0.11	d,e
^{26}Mg	0⁺	0.228	0	
	1⁺	1.058	1.11 ± 0.03	d
^{37}Cl	3/2⁺	0.000	0.031 ± 0.001	f
	3/2⁺	4.993	0.052 ± 0.004	f
^{42}Ca	0⁺	0.000	0	
	1⁺	0.611	2.67 ± 0.10	f

a. F. Ajzenberg-Selove, Nucl. Phys. A320, 1 (1979).
b. F. Ajzenberg-Selove, Nucl. Phys. A268, 1 (1976).
c. Obtained by normalizing to $R(Ep)/E_p$ = (54.9 MeV)$^{-1}$ at E_p = 120 and 160 MeV.
d. H. S. Wilson, R. W. Kavanaugh, and F. M. Mann, Phys. Rev. C 22, 1969 (1980).
e. A. M. Hernandez and W. W. Daehnick, Phys. Rev. C 24, 2235 (1981).
f. P. M. Endt and C. Van der Leun, Nucl. Phys. A310, 1 (1978).

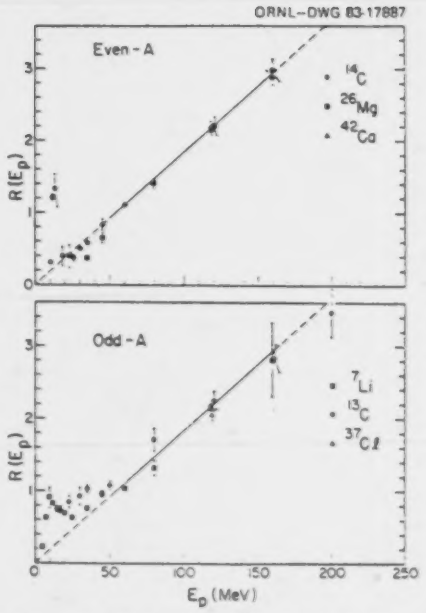

Fig. 2.51. Empirical quantity $R(E_p)$ for odd- and even-A targets. The solid line represents the average value of $R(E_p)/E_p$ = (54.9±0.9 MeV)$^{-1}$ determined from the even-A targets with $E_p \geq 50$ MeV.

12. W. G. Love and M. A. Franey, Phys. Rev. C 24, 1073 (1981).
13. G. E. Brown, J. Speth, and I. Wambach, Phys. Rev. Lett. 46, 1057 (1981). In a private communication from G. E. Brown it was learned that a "screening factor" was omitted from the $J_{\sigma\tau}$ calculations, inclusion of which would bring their calculation closer to our empirical curve.

SOLAR NEUTRINO DETECTOR GT STRENGTH DISTRIBUTIONS via (p,n) REACTIONS

J. N. Bahcall [1]
J. Rapaport[2]
T. N. Taddeucci[2]
P. Welch[2]
E. Sugarbaker[3]
C. D. Goodman[4]
C. C. Foster[4]
D. J. Horen
C. Gaarde[5]
J. Larsen[5]
T. Masterson[6]
S. Austin[7]
C. A. Goulding[8]

The observed and predicted capture rates for the chlorine solar neutrino experiment indicate a large discrepancy. This has stimulated new efforts to establish empirically whether this disagreement is caused by inadequate solar models

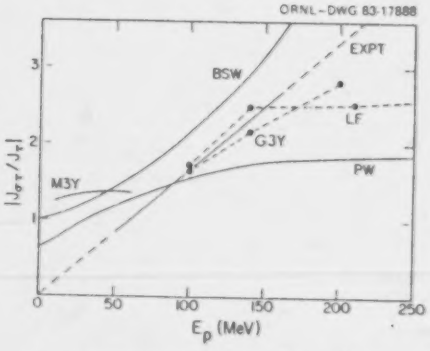

Fig. 2.52. Comparison of experimental and theoretical values of $|J_{\sigma\tau}/J_\tau|$ versus E_p. The theoretical lines are from interactions described in Ref. 9 (G3Y), Ref. 10 (M3Y), Ref. 11 (PW), Ref. 12 (LF), and Ref. 13 (BSW).

or by a decrease in the detectable neutrino flux in transit from the sun. The most recent experimental results[9] for the capture rate (2.1±0.3)SNU, are very different from the model predictions,[10] (8±3.5)SNU.

In addition to the use of ^{37}Cl, four new detectors are presently being considered as most likely candidates for solar neutrino experiments. The latter are ^{71}Ga, ^{81}Br, ^{98}Mo and ^{115}In. The ^{71}Ga and ^{115}In detectors are primarily sensitive to the flux of proton-proton neutrinos, while the ^{81}Br is most sensitive to the neutrino line arising from electron capture in ^{7}Be. The reaction ^{98}Mo(ν,e$^-$)^{98}Tc will determine the average ^{8}B neutrino flux over the past several million years by analyzing neutrino absorption products in deeply buried molybdenum ore.

For all these cases the cross section for capture of neutrinos by these detectors must be known accurately in order to interpret the results of these expensive and difficult experiments. One method of doing so is to determine the β-decay matrix elements from the measurement of L=0 (p,n) cross sections at θ=0°.

Measurements have been performed and reported[11] for the ^{37}Cl(p,n)^{37}Ar reaction. The p-p chain involving the β decay of ^{8}B (maximum neutrino energy ~14 MeV) is the most important solar neutrino source when ^{37}Cl is used as a detector. These neutrinos excite the strong Fermi transition to the 4.99-MeV IAS in ^{37}Ar which dominates the neutrino capture. Bachcall[12] used data obtained from the delayed proton spectrum following β decay of ^{37}Ca to deduce the GT information for neutrino reactions on the mirror nucleus ^{37}Cl. Our measurements were made using 120-MeV protons and a Ca^{37}Cl$_2$ target. The large difference in the (p,n) Q-values (i.e., 13.5 MeV) between the ^{40}Ca and ^{37}Cl nuclei allowed a clear observation of ^{37}Ar states up to ~13 MeV. A target of ^{40}Ca was also run and its normalized spectrum was subtracted from that for the combined target. The resulting spectrum is shown in Fig. 2.53. The extracted 0° cross sections and B(GT) values deduced therefrom for the peaks shown in Fig. 2.53 are tabulated in Table 2.9. This study indicates that the 1.4-MeV state in ^{37}Ar is very weakly excited, and that the distribution of GT strength ^{37}Ar is slightly different than that to its mirror nucleus ^{37}K.

The cross sections for absorption of ^{8}B neutrinos by ^{37}Cl can be calculated using the logft values given in Table 2.9 for excited states below the particle emission threshold of 8.6 MeV using an expression[12] given by Bahcall. These are listed in Table 2.10. The total cross section that we obtain for neutrino capture on ^{37}Cl is $\sigma(^{37}\text{Cl}) = (0.98 \pm 0.07)\times10^{-42}$ cm^2 which is in excellent agreement with a value of $(1.08 \pm 0.1)\times10^{-42}$ cm^2 previously estimated[12] by Bahcall. Hence, the observed discrepancy between the measured[9] and predicted capture rates will not be affected by our data.

Preliminary measurements on ^{69}Ga, ^{71}Ga, ^{81}Br, ^{98}Mo, and ^{115}In have been made using protons with incident energies of 120 and 200 MeV. Analyses of these data are in progress. The targets with Ga were made as an alloy of ^{24}Mg because of its large negative Q-value (Q=14.67 MeV). The ^{81}Br target was fabricated from a compound with natural Ca for similar reasons.

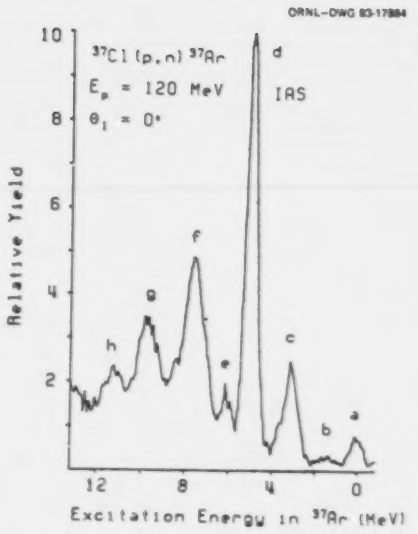

Fig. 2.53. Neutron time-of-flight subtracted spectra for ^{37}Cl(p,n)^{37}Ar at θ_L = 0° and E_p = 120 MeV. Cross sections for neutron groups as labelled in the figure are presented in Table 2.9.

Table 2.9. Results of reaction ^{37}Cl(p,n)^{37}Ar. E_p = 120 MeV. L=0 transitions. Rows 1-8 correspond to peaks a-h in Fig. 2.53, respectively.

$E_x(^{37}\text{Ar})^a$ (MeV)	$\sigma_{cm}(0°)^b$ (mb/sr)	G(GT)	Log/ft
gs	0.20±0.04	0.034±0.007	5.06±0.09
1.4	<0.05	<0.009	>5.64
3.1	1.3±0.2	0.23±0.04	4.23±0.08
4.99[c]	4.8±0.7	0.08±0.08[d]	3.29±0.02
6.1	0.53±0.1	0.10±0.02	4.60±0.09
7.65	4.7±0.7	0.87±0.13	3.66±0.06
9.65	3.3±0.6	0.64±0.12	3.79±0.08
11.5	2.3±0.4	0.47±0.08	3.92±0.08

a. Uncertainty estimated to be less than 0.2 MeV. Instrumental full width at half maximum resolution 0.6 MeV.
b. Estimated absolute uncertainties which are also propagated to the B(GT) and logft calculated values.
c. IAS.
d. A value B(F) = 3.0 was assumed for this transition.

1. Institute for Advanced Study, Princeton University, Princeton, New Jersey 08540.
2. Ohio University, Athens, Ohio 47501.
3. Ohio State University, Columbus, Ohio 43212.
4. Indiana University, Bloomington, Indiana 47405.
5. Niels Bohr Institute, Copenhagen, Denmark.
6. University of Colorado, Boulder, Colorado 80309.

7. Michigan State University, East Lansing, Michigan 48824.
8. EG&G, Los Alamos, New Mexico 87545.
9. B. T. Cleveland, R. Davis, Jr. and J. K. Rowley, in "Weak Interactions as Probes of Unification", ed. by Collins, Chang and Ficence (AIP Conf. Proc. #72, 1981), p. 322.
10. J. N. Bahcall et al., Phys. Rev. Lett. 45, 945 (1980).
11. J. Rapaport et al., Phys. Rev. Lett. 47, 1518 (1981).
12. J. N. Bahcall, Rev. Mod. Phys. 50, 881 (1978).

Table 2.10. Individual ft values and cross section for ^{8}B neutrinos on ^{37}Cl.

E_x (MeV)	$10^5 S/ft^a$	$\sigma(^{37}Cl) \times 10^{-46}$ (cm^2)
0.0	0.86±0.17	650±130
1.4	0.23	≤115
3.1	5.9±0.9	1660±250
4.99	50.7±1.5	6530±130
6.1	2.5±0.5	190±40
7.65	22±3	610±100
		$\sum$: (0.98±0.07)x10^{-42}

a. Values from Table 2.9.

CORE EXCITATIONS AND M1 STRENGTHS IN THE Ca ISOTOPES[1]

B. A. Brown[2] B. Castel[3]
D. J. Horen H. Toki[2]

The existence of strong M1 transitions from T=1 and T=2 states in ^{40}Ca provides an interesting challenge to nuclear structure models. We show that the recent M1 data can be reconciled with a shell model study of ^{40}Ca and that the fragmentation and disappearance of strengths in ^{42}Ca and ^{44}Ca is consistent with a weak-coupling extension of the ^{40}Ca system in which the M1 strength is divided among T_z and T_{z+1} components.

1. Abstract of paper: Phys. Lett. 127B, 151 (1983).
2. Michigan State University, East Lansing, Michigan 48824.
3. Queen's University, Kingston, Canada.

A TEST OF THE PARTICLE-ASYMMETRIC RIGID ROTOR MODEL AND THE INTERACTING BOSON-FERMION MODEL DESCRIPTION OF THE STATES FROM COULOMB EXCITATION OF ^{191}Ir[1]

F.K. McGowan N.R. Johnson
I-Y. Lee W.T. Milner
M.W. Guidry[2] C. Roulet[3]
R.M. Diamond[4] F.S. Stephens[4]
J.X. Saladin[5] A.A. Hussein[5]
M.P. Fewell J. Hattula[6]
Y. A. Ellis-Akovali

We have observed Coulomb excitation of states in ^{191}Ir up to J = 21/2 with 617-MeV ^{136}Xe ions from SuperHILAC and 160-MeV ^{40}Ar ions from ORIC. At the University of Pittsburgh Coulomb excitation measurements from the reaction (α,α') have been done with the EN tandem. Most of the states in ^{191}Ir are grouped into three rotational-like bands based on the $3/2^+$ ground state, the $1/2^+$ first excited state, and the $7/2^+$ γ-vibrational-like state at 686.3 keV. We have compared the experimental γ-ray yields with the predictions of two models, viz., the particle-asymmetric rigid rotor model[7] and the interacting boson-fermion model.[8] The Coulomb excitation yields are calculated using the program of Winther and deBoer. For the input of the program, we use the experimental level energies and a set of theoretical E2 matrix elements. The latter, for example, were obtained from calculations using the particle-triaxial rigid rotor model program.[7] The deformation parameters ϵ and γ were adjusted to give the best agreement between theoretical and experimental excitation energies. The average deviation between experimental and theoretical energies is 30 keV for a fit to 14 state energies in ^{191}Ir with ϵ = 0.168, γ = 24.5°, and E(2+) = 200 keV. These parameters are very close to those for the (A-1) core ^{190}Os, viz., ϵ = 0.157, γ = 22.0°, and E(2+) = 187 keV. This choice of deformation parameters in the calculations reproduces the B(E2) values deduced from light-ion Coulomb excitation for transitions within the K = $3/2^+$ band presented in Table 2.11. For transitions originating in the K = $1/2^+$ and $7/2^+$ bands the particle-triaxial rigid rotor model predicts the overall trend of the B(E2) values.

The average deviation between experimental and theoretical energies from the interacting boson-fermion model is 125 keV. The model reproduces the B(E2) values for the stronger (collective) transitions. However, this model tends to underestimate the B(E2) values for the less collective transitions by an order of magnitude. The input to the calculations of Coulomb excitation probabilities involved 38 states and 173 E2 matrix elements. Fifteen of these E2 matrix elements were fixed by results deduced from light-ion direct E2 Coulomb excitation and nuclear spectroscopic information for the decay modes of these states. The remaining E2 matrix elements were taken from the model calculations.

The γ-ray yields for transitions within the rotational-like band based on the $3/2^+$ ground state are presented relative to the γ-ray yields for the $7/2^+ \rightarrow 3/2^+$ transition. The overall agreement of both model predictions with the experimental results is quite good. The comparison between the experimental and calculated results from the particle-asymmetric rigid rotor model for the transitions from decay of the K_i, J_i^π = 7/2,$7/2^+$ state at 686.3 keV is good. However, the interacting boson-fermion model predictions are in very poor agreement with the data. It is not at all clear whether or not the discrepancies are related to the breakdown of the supersymmetry itself or to the fact that this observed J = 7/2 state does not belong to the lowest representation of the supersymmetry structure.

The deformation parameter γ of the particle-asymmetric rigid rotor model is sharply defined in the fit to the K,J = 7/2,7/2 level position. This contradicts microscopic collective model

TABLE 2.11. EXPERIMENTAL AND MODEL-PREDICTED B(E2) VALUES FOR ^{191}Ir

Initial State		Final State			B(E2,$J_i \to J_f$) (e^2b^2)		
J_i	K_i	J_f	K_f	E_γ(keV)	Experiment	Triaxial Rotor	IBA
11/2	3/2	7/2	3/2	489	0.469 ± 0.026	0.524	0.527
9/2		5/2		373.1	0.663 ± 0.021	0.513	0.485
7/2		3/2		343.2	0.278 ± 0.006	0.302	0.360
7/2		5/2		213.8	0.227 ± 0.006	0.173	0.268
5/2		3/2		129.4	0.598 ± 0.017	0.575	0.623
5/2		1/2	1/2	47.0	0.043 ± 0.022	0.078	0.020
3/2		3/2	3/2	0.0	$0.326 \begin{smallmatrix}+0.191\\-0.147\end{smallmatrix}$	0.137	0.451
5/2	1/2	3/2	3/2	351.1	0.020 ± 0.005	0.029	0.0035
5/2		1/2	1/2	268.6	0.62 ± 0.20	0.316	0.313
5/2		3/2	1/2	172.1	0.090 ± 0.011	0.014	0.0013
3/2		3/2	3/2	179.0	0.108 ± 0.009	0.224	0.013
3/2		1/2	1/2	96.5	0.59 ± 0.15	0.213	0.249
1/2		3/2	3/2	82.5	0.136 ± 0.016	0.117	0.186
7/2	7/2	3/2	3/2	686.3	0.063 ± 0.002	0.023	0.0079
7/2	7/2	5/2	3/2	556.8	0.095 ± 0.004	0.091	0.223

calculations of potential energy surfaces which predict considerable γ softness (shallow deformation potentials).

In addition to the positive states, seven negative parity states appear to be Coulomb excited in ^{191}Ir with ^{136}Xe and ^{40}Ar ions. Complex spectra of unique-parity states in the odd-A Ir nuclei have been rather successfully described by the coupling of the $h_{11/2}$ hole to a rotating triaxial core by Meyer-ter-Vehn.[9] We have observed states in the $h_{11/2}$ hole band up to J=19/2⁻.

1. Summary of paper published in Proc. of on High Angular Momentum Properties of Nuclei, Oak Ridge, TN, November 1982, Vol. 1, Abstracts, p. 36.
2. University of Tennessee, Knoxville, TN.
3. Institut de Physique Nucleaire, Orsay, France.
4. Lawrence Berkeley Laboratory, Berkeley, CA.
5. University of Pittsburgh, Pittsburgh, PA.
6. University of Jyvaskyla, Jyvaskyla, Finland.

7. Ch. Vieu et al., Z. Physik A290, 301 (1979).
8. F. Iachello, Phys. Rev. Lett. 44, 772 (1980).
9. J. Meyer-ter-Vehn, Nucl. Phys. A249, 111 and 141 (1975).

COULOMB EXCITATION OF STATES IN ^{229}Th[1]

C. E. Bemis, Jr. W. T. Milner
F. K. McGowan R. L. Robinson
J.L.C. Ford, Jr. P. H. Stelson
C. W. Reich[2]

The Coulomb excitation of states in ^{229}Th using 17.0-MeV $^4He^{++}$ ions has been observed by measuring the elastically and inelastically scattered particles at a laboratory angle of 150° with a magnetic spectrometer (see Fig. 2.54). Excitation probabilities, relative to the elastic peak, have been determined for members of the 5/2⁺[633] ground-state rotational band through the 13/2⁺ member and for several other weakly excited states in the energy range 250-650 keV. Large contributions from E4 excitations are observed in the ground-state band; we

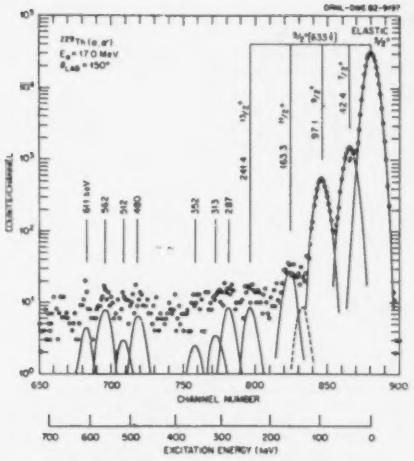

Fig. 2.54. Spectrum of elastically and inelastically scattered 17.0-MeV ^{4}He ions from ^{229}Th at a laboratory angle of 150°. The $5/2^+[633]$ ground-state rotational band through the $13/2^+$ member is indicated, as well as other states at higher excitation energies.

deduce an intrinsic quadrupole moment, Q_{20}, of 8.816 ± 0.090 eb and an intrinsic hexadecapole moment, Q_{40}, of 3.69 ± 0.72 eb^2. This Q_{40} value for ^{229}Th is nearly 50% larger than that for the even-even neighbor, ^{230}Th. Ground-band g factors, B(M1) values, and $3/2^+[631] \updownarrow 5/2^+[633]$ interband M1 and E2 transition probabilities have also been derived. A summary of our results for the ground-state band is given in Table 2.12.

Weakly excited states, known from previous work (Ref. 3), are observed at 287, 313, 352, and 480 keV and are most probably excited by direct E2 Coulomb excitation. States at 512, 562, and 611 keV are also weakly excited in our experiments. Based on previous assignments (Ref. 4) of $5/2^-$, $7/2^-$, and $9/2^-$, i.e., a $K^\pi = 0^-$ octupole band built on the $5/2^+[633]$ ground state, we have assumed E3 excitation to these states and derived the corresponding reduced transition probabilities. A summary of our experimental excitation probabilities and resultant $B(E\lambda;5/2 \rightarrow I)$ values is given in Table 2.13.

---

1. Summary of paper to be published.
2. Idaho National Engineering Laboratory, Idaho Falls, Idaho.
3. K. S. Toth, Nucl. Data Sheets 24, 263 (1978).
4. I. Ahmad et al., Bull. Am. Phys. Soc. 26, 1118 (1981); I. Ahmad, private communication, 1982.

Table 2.12. Summary of measured and deduced ground-band moments and interband transition probabilities for ^{229}Th.

Quantity[a]	Value
Q_{20}	8.816 ± 0.090 eb
Q_{40}	3.69 ± 0.72 eb^2
$Q_{2,5/2}$	3.149 ± 0.032 eb
$Q_{4,5/2}$	0.088 ± 0.017 eb^2
$Q_{20}/\lvert g_K - g_R\rvert$	48.7 ± 1.3 eb
$g_K - g_R$	-(0.181 ± 0.005)
g_R	^.309 ± 0.016
g_K	+0.128 ± 0.017
B(E2; 9/2 5/2 → 5/2 3/2)	0.042 ± 0.005 eb^2
B(M1; 9/2 5/2 → 7/2 3/2)	0.032 ± 0.006 $(e\hbar/2Mc)^2$

[a] Intraground-band E2, E4, and M1 transition probabilities may easily be evaluated using

$$B(E\lambda;I_iK \rightarrow I_fK) = \frac{2\lambda+1}{16\pi} Q_{\lambda 0}^2 \langle I_i 2K0 | I_i 2 I_f K\rangle^2 e^2 b^\lambda$$

and

$$B(M1;I_iK \rightarrow I_fK) = \frac{3}{4\pi} (g_K - g_R)^2 K^2 \langle I_i 1K0 | I_i 1 I_f K\rangle^2$$

in $(e\hbar/2Mc)^2$ units, with the moments given above.

Table 2.13. Experimental excitation probabilities for states in ^{229}Th populated in the ^{229}Th(α,α') reaction with 17.0-MeV alpha particles (θ_{LAB} = 150°) and resultant B(Eλ; 5/2 → I) values

K, I^π	E(I)[a] (keV)	$10^3[\sigma(I)/\sigma_{elastic}]$	Reduced transition probability B(Eλ; 5/2⁺ → I) (e^2b^λ)
5/2, 5/2⁺	0	1000	
5/2, 7/2⁺	42.44	47.06 ± 1.11	B(E2) = 3.691 ± 0.089
5/2, 9/2⁺	97.13	16.58 ± 0.62	B(E2) = 1.281 ± 0.048
5/2, 11/2⁺	163.25	0.83 ± 0.11	
5/2, 13/2⁺	241.45	0.27 ± 0.06	
5/2, 15/2⁺	327	<0.06	
5/2, 17/2⁺	(424)[b]	<0.06	
(?, 3/2⁺, 7/2⁺, 9/2⁺)	287 ± 5	0.26 ± 0.06	B(E2) = 0.023 ± 0.005
(?, 5/2⁺)	313 ± 5	0.11 ± 0.05	B(E2) = 0.010 ± 0.005
(?)	352 ± 5	0.08 ± 0.04	B(E2) = 0.008 ± 0.004
(?)	480 ± 5	0.20 ± 0.05	B(E2) = 0.021 ± 0.006
			or B(E3) = 0.15 ± 0.04
(5/2, 5/2⁻)	512 ± 5	0.10 ± 0.04	B(E3) = 0.076 ± 0.030
(5/2, 7/2⁻)	562 ± 5	0.25 ± 0.05	B(E3) = 0.195 ± 0.039
(5/2, 9/2⁻)	611 ± 5	0.14 ± 0.04	B(E3) = 0.114 ± 0.033

[a] Ground-state band energies from Ref. 3.

[b] Estimated from $E = E_0 + A[(I)(I+1)] + B[(I)(I+1)]^2$ with A = 6.257 keV and B = −4.09 eV.

COULOMB EXCITATION OF GROUND-BAND ROTATIONAL STATES IN ^{249}Bk[1]

C. E. Bemis, Jr.
F. K. McGowan
J.L.C. Ford, Jr.
W. T. Milner
R. L. Robinson
P. H. Stelson

Coulomb-excitation probabilities for the first few members of the 7/2⁺[633↑] ground-state rotational band in ^{249}Bk have been determined with 17.06-MeV ^{4}He ions. These previously known excited states include the 9/2⁺ (41.8-keV), 11/2⁺ (93.7-keV), and 13/2⁺ (155.8-keV) members of the 7/2⁺[633↑] band. Within experimental uncertainties, the Coulomb-excitation probabilities for these rotational states are reproduced by calculated values when only E2 excitations are considered with an intrinsic quadrupole moment, Q_{20}, of 12.70 ± 0.24 eb in the rigid rotor limit. The deduced ground-state spectroscopic quadrupole moment is 5.93 ± 0.11 eb. Intraband M1 transition rates have also been deduced by combining the Q_{20} result with other experimental data. Within the rotational model, a ground-state magnetic moment of +3.45 ± 0.10 nm is indicated.

1. Abstract of paper: Phys. Rev. C 25, 1637 (1982).

THE COLLECTIVITY OF LIGHT Yb NUCLEI AT HIGH SPIN[1]

M.P. Fewell[2]
J.S. Hattula[3]
C. Baktash
J.W. Johnson
J.C. Wells[5]
A. Larabee[6]
S.C. Pancholi[7]
F.K. McGowan
I.Y. Lee
Y. Schutz[4]
N.R. Johnson
L.L. Riedinger[6]
M.W. Guidry[6]
D.R. Haenni[8]

It is generally thought that many nuclei which have prolate shapes in their ground states will have a tendency to move toward oblate shapes at higher spins, in part due to the alignment of angular momentum along the rotation axis. At these higher spins such a nucleus would exhibit yrast structures which are more single-particle than collective in nature. The E2 matrix elements along the yrast line should reflect such a loss of collectivity. Indeed, recently it has been found that the s-bands of $^{156-158}$Dy seem to have a reduced collectivity compared with the ground bands of these nuclei.[9] A study of the light ytterbium nuclei can be instructive in this context because they are known[10,11] to have a number of well-aligned sidebands, presenting the possibility of examining the effects of different quasiparticle

configurations on collectivity. Also, nuclei in the N = 88-90 region are known to be soft with respect to deformation changes and thus should respond easily to any polarizing forces generated by the aligned quasiparticles.

To search for possible shape changes as a function of rotational frequency, we have measured the lifetimes of high-spin states of zero-, one-, two-, and three-quasiparticle bands in the nuclei $^{159-163}$Yb by means of the recoil-distance method. The nuclei were populated by reactions ^{116}Cd(^{50}Ti,xn), ^{116}Cd(^{48}Ti,xn) and ^{48}Ti(^{116}Cd,xn), at a center-of-mass energy of about 145 MeV in each case. The recoil-distance device was designed to fit in the annular opening of a 25-cm x 25-cm NaI crystal which acts as a total-energy filter and thus provides some selectivity of reaction channel (see Ref. 12). Lifetimes were extracted from the resulting decay curves by a computer program, originally due to Emling,[13] but extensively modified by Fewell and Wells.[14] The program applies all of the usual corrections to the data and handles the crucial problem of feeding by direct solution of the Bateman equations.

The analyses of data on some of these nuclei are still incomplete. However, we discuss all of the results available at this time, even if preliminary in nature. Some basic problems that often make it impossible to extract reliable lifetimes for states are lack of information on transitions feeding the level of interest, inability to resolve overlapping transitions in the spectrum, and the situation where the feeding transition is longer-lived than the transition of interest. For example, in ^{160}Yb we were unable to get reliable lifetime values for the 8$^+$, 10$^+$, and 12$^+$ states because of the relatively long lifetime of the 14$^+$ state and the strong sidefeeding into the 8$^+$ and 10$^+$ states.

Reduced transition probabilities were extracted from the lifetimes and, from these, we have calculated transition quadrupole moments, Q_t, according to the expression

$$B(E2;I\to I-2) = \frac{5}{16\pi} \langle I\ 2\ 0\ 0 \mid I-2\ 0\rangle^2\ Q_t^2 .$$

In Fig. 2.55, the Q_t values for ^{159,160,161}Yb are plotted versus the rotational frequency which is one-half the I → I-2 transition energy for K=0 bands. (We emphasize that the results on ^{159,162,163}Yb are to be considered as very preliminary in nature.)

The most conspicuous feature in Fig. 2.55 is that the quasiparticle bands in each of these nuclei appear to have reduced collectivity at large rotational frequencies. A second striking feature of the data presented here is that the behavior of Q_t with ω seems to be insensitive to the details of quasiparticles involved. For ^{160}Yb we have three different two-quasiparticle bands with each showing Q_t values varying similarly as a function of the rotational frequency. Likewise, ^{161}Yb shows one- and three- quasiparticle bands with similar behavior. The common aligned quasiparticle in all of these bands is the lowest energy $i_{13/2}$ orbital with parity and signature $(-,\alpha) = (+,+\tfrac{1}{2})$. In ^{160}Yb, this quasiparticle is coupled to the $(-,+\tfrac{1}{2})$ and $(-,-\tfrac{1}{2})$ $h_{9/2}$ orbitals to form two side bands.

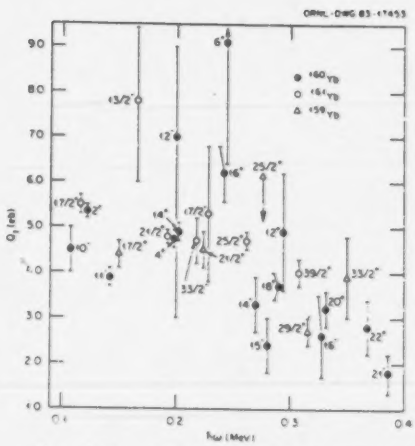

Fig. 2.55. Transition quadrupole moments of states in ^{159,160,161}Yb plotted as a function of the rotational frequency.

These negative parity orbitals are mainly $h_{9/2}$, but contain admixtures of $f_{7/2}$. The similarities in the behavior of Q_t with ω for these bands suggest the possibility that the $(+,+1/2)$ quasineutron has a dominant influence on the core. In Fig. 2.56 we show preliminary Q_t values for some of the states in ^{162,163}Yb. Again, there is evidence for reduced collectivity in the quasiparticle states (involving the $i_{13/2}$ orbital) at larger ω values.

There are several groups carrying out theoretical calculations that speak to the effects observed in these nuclei near N = 90. Recently, a group at Lund has reported[15] preliminary results of some self-consistent cranked Hartree-Fock-Bogoliubov (HFB) calculations of the shape of the N = 90 nucleus ^{160}Yb as a function of angular momentum. They find that, in the s-band, ε_2 remains approximately constant while γ shows a steady increase, reaching about 10° by I = 18$^+$, the highest spin they[15] considered. (In the Lund convention, γ = 0° corresponds to collective rotations of a prolate ellipsoid and γ = 60° corresponds to noncollective rotations of an oblate ellipsoid.) This theory accounts qualitatively for the observed behavior, but falls short quantitatively. From the Q_t value of the 18$^+$ state in ^{160}Yb we extract a value of 21° for the deformation parameter γ if it is assumed that ε_2 remains constant in the s band.

A second theoretical approach involves a more phenomenological examination of the effects of the γ degree of freedom on the energy of the quasiparticles and the core.[16,17] The energy of the core is described as the sum of two terms, one involving the prolate-oblate energy difference V_{PO}, and the other involving the energy based on the frequency dependent moment

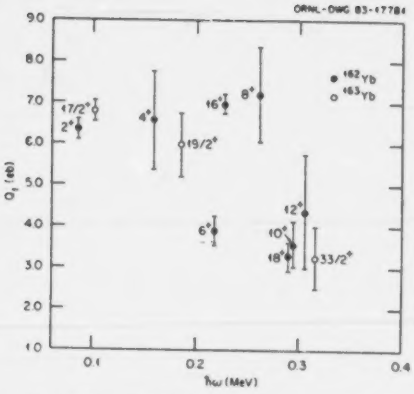

Fig. 2.56. Transition quadrupole moments of states in ^{162,163}Yb plotted as a function of the rotational frequency.

of inertia. The energy of the quasiparticles is calculated with the cranked shell model. In this picture, the equilibrium γ value adopted by a nucleus with excited quasiparticles depends on an interplay between the driving forces of the quasiparticles, the hydrodynamic behavior of the core, and the prolate-oblate energy difference. In particular, nuclei with relatively small values of γ_{pot}, for example those with N ~ 90, should have quasiparticle bands with deformations which reveal the imprint of the quasiparticles. This theory also gives a reduction in Q_t at large ω, but it likewise fails to account for the large effect observed.

It is anticipated that, when the data analyses for ^{159,162,163}Yb are completed and planned lifetime measurements on other nuclei in this region are performed and when all of the data are compared with ongoing theoretical developments, we will have a good picture of shape evolution in these γ-soft nuclei.

---

1. Summary of paper to be published in part.
2. Present address: Australian National University, Canberra, Australia.
3. Present address: University of Jyväskylä, Jyväskylä, Finland.
4. On leave from CRN, Strasbourg, France.
5. Tennessee Technological University, Cookeville, TN.
6. University of Tennessee, Knoxville, TN.
7. Guest Scientist from the University of Delhi, India, and Vanderbilt University, Nashville, TN.
8. Present address: Texas A&M University, College Station, TX.
9. H. Emling, Proc. XIV Masurian Summer School on Nuclear Physics, Mikolajkni, Poland, 1981, to be published in Nukleonika; H. Emling, et al. Phys. Lett. 98B, 169 (1981).
10. L.L. Riedinger et al., Phys. Rev. Lett. 44, 568 (1980); to be published in Nucl. Phys.
11. L.L. Riedinger et al., Proc. Int. Conf. on Nuclear Physics, Berkeley, Vol. 1, ed. by R.M. Diamond and J.O. Rasmussen (North-Holland, Amsterdam, 1981); to be published in Nucl. Phys.
12. N.R. Johnson et al., ORNL Phys. Div. Prog. Report, November 1981, ORNL-5787, p. 147.
13. H. Emling, private communication.
14. M.P. Fewell and J.C. Wells, to be published; also see separate paper in this report.
15. R. Bengtsson, Proc. Conf. on High Angular Momentum Properties of Nuclei, Vol. IV, Nuclear Science Research Conference Series, ed. by N.R. N.R. Johnson (Harwood Academic Publishers, New York, 1983) p. 161.
16. G.A. Leander, S. Frauendorf and F.R. May, Proc. Conf. on High Angular Momentum Properties of Nuclei, Vol. IV Nuclear Science Research Conference Series, ed. by N.R. Johnson (Harwood Academic Publishers, New York, 1983) p. 281.
17. S. Frauendorf and F.R. May, submitted to Phys. Lett.

HIGH-SPIN STATES IN THE MASS REGION AROUND A = 70

A. Y. Ahmed[1]
M. E. Barclay[2]
G. L. Bomar[2]
L. Cleeman[3]
J. D. Cole[4]
A. P. de Lima[5]
J. Eberth[6]
J. H. Hamilton[2]
H. J. Kim
W. C. Ma[2]
C. F. Maguire[2]
W. T. Milner
S. C. Pancholi[2]
R. B. Piercey[7]
S. Ramavataram[8]
A. V. Ramayya[2]
R. L. Robinson
R. Soundranayagam[2]
X. J. Sun[2]
J. C. Wells[9]
H. Yamada[10]
Z. Z. Zhao[2]

Nuclei in the A = 60 - 84 region have proven to be rich in a variety of collective motions and structure, and, as a result, the region has become an important testing ground for many types of nuclear structure models. Shape coexistence with bands of levels built on quite different deformation have been found; rotational-like bands analogous to those in very deformed nuclei have been seen; and quasiparticle degrees of freedom, which are responsible for backbending of the moment of inertia in well deformed rare earth nuclei, have also been established in this region both for positive and negative parity states.

A program of investigating high-spin states through in-beam γ-ray spectroscopy that began on the ORNL EN tandem several years ago is being continued on the HHIRF tandem accelerator. The nuclei investigated are produced through fusion reactions resulting from bombarding targets with heavy ions with energies just above the Coulomb barrier. A wide variety of types of measurements have been employed in this program: γ-ray angular distributions, γγ angular correlations, γγ coincidences, linear polarization, nγ coincidences (to favor reaction products associated with neutron emission), Doppler broadened line shapes, line shapes as a function of recoil distance, and transient magnetic field technic for determining gyromagnetic ratios.

Studies of specific isotopes are discussed in the following subsections.

^{66}Ge[11]

The levels of ^{66}Ge were excited through the ^{58}Ni(^{10}B,pn) reaction. Level properties are summarized in Fig. 2.57. The band built on the (8^+) state at 5535 keV is attributed to alignment of the angular momentum of two quasiparticles in the $g_{9/2}$ orbital. The remaining positive-parity band beginning with the 2^+ state at 1693 keV has features of a quasigamma band. Levels of this band and those of the yrast band are reproduced excellently by predictions of an interacting-boson-model calculation.

Calculations were also made with a two-quasiparticle-plus-rotor model. They indicate that the 7^- and (9^-) levels have about 86% contribution from the $(g_{9/2}, f_{5/2})$ proton configuration, and the 5^- state at 3684 keV has about a 97% $(g_{9/2}, p_{3/2})$ proton configuration.

Three close lying 8^+ levels have been observed in ^{68}Ge decaying into the 6^+ level at 3696 keV. The origin suggested earlier for these three was (1) two aligned $g_{9/2}$ quasineutron state, (2) two aligned $g_{9/2}$ quasiproton state, and (3) a member of the yrast ground-state band. A possible way to check the interpretation for these states is to measure their gyromagnetic ratio g. The quasiparticle-plus-rotor model gives approximate values for the g factor of 0.4 for collective rotation, 1.2 for proton orbitals and -0.2 for neutron orbitals. The g factor has been measured for the lowest two 8^+ levels at 4838 and 5050 keV in ^{68}Ge by using a transient magnetic field technic. The nuclei were made through the reactions of ^{40}Ca(^{32}S, 4p), and ^{12}C(^{58}Ni, 2p). The target, which was a sandwich of the target material, a ferromagnetic foil, and a stopping material, was placed in the gap of a magnet. The g factors were deduced from the perturbation in the angular distribution of γ rays from recoil nuclei in the ferromagnetic material with the magnetic field alternately up and down.

The g factors obtained for the 8^+ states at 4838 and 5050 keV are, respectively, -0.04 ± 0.05 and $+0.11 \pm 0.08$. Comparison of these to the model predictions suggests both of these states are in fact due to alignment of two neutrons. The magnitude of the g factors indicates the alignment is more complete for the 4838-keV state.

^{76}Kr[12]

Figure 2.58 shows the level structure found for ^{76}Kr. This nucleus was produced through the reaction ^{66}Zn(^{12}C, 2n) with $E_{^{12}C}$ = 39 MeV.

^{76}Kr can be understood in a shape coexistence picture where the ground state is deformed and the 0_2^+ state at 770 keV is near spherical. Evidence for such includes the energy spacing and B(E2)'s of levels of the ground-state band. The B(E2)'s, which are the largest known for a ground-state band in this mass region, range from 59 single-particle units (spu) for the $2 \rightarrow 0$ transition to 129 spu for the $10 \rightarrow 8$ transition.

The measured lifetimes for states in the negative-parity bands built on the 5^- and (6^-) levels yield B(E2)'s that are exceptionally large (e.g., B(E2)'s for the $7^- \rightarrow 5^-$ and $(11^-) \rightarrow 9^-$ transitions are, respectively, 863 $^{+178}_{-128}$ and 264 $^{+34}_{-26}$spu). The origin of such large B(E2)'s is not understood.

The positive parity band with even- and odd-spin members to (6^+) and (9^+) is interpreted as a $\Delta J = 1$ quasigamma band. B(E2)'s for γ rays in these bands are of the order of 80 spu. The presence of vibrational levels underscores the importance of strong deformation in this nucleus.

Two Quasiparticle-Plus-Rotor Model Calculations of ^{76,78,80}Kr[13]

Two-quasiparticle-plus-rotor calculations have been performed for Kr nuclei to study the systematics of their high-spin states. The moment of inertia parameter appearing in the potential energy term of the Hamiltonian was determined by fitting the ground-state bands with the variable moment of inertia model. It is evidence from the fit that the ground-state bands are rotational-like. The effect of

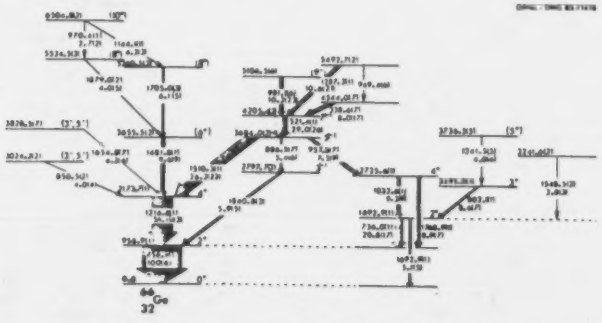

Fig. 2.57 The energy level diagram of ^{66}Ge.

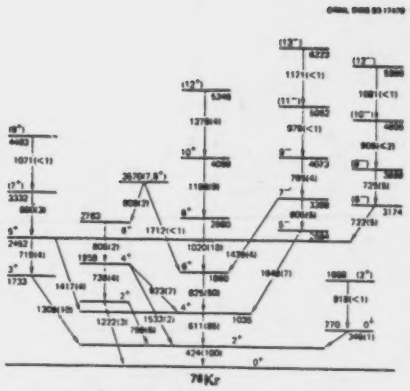

Fig. 2.58 Level scheme of ^{76}Kr.

approaching the closed shell is seen in ^{80}Kr where for this nucleus, the moment of inertia drops to almost one fourth of that in ^{78}Kr.

The best fits indicate that the negative parity states built on bands beginning at 4$^-$ and 5$^-$, with the exception of the second 6$^-$ state of ^{80}Kr contain up to 99% of the ($g_{9/2}$, $f_{7/2}$) configuration. The configuration of the 6$^-$ exception is 92% ($g_{9/2}$, $f_{5/2}$) and 8% ($g_{9/2}$, $p_{3/2}$). The contribution of the octupole vibration to these states is very small. Fits of the positive parity band built on the 8$^+$ level in ^{80}Kr [2] indicate it has very little mixing of zero quasiparticles states. Another result from these fits is that the quasiparticles of the negative parity states have large alignments while the two quasiproton-positive-parity states are not completely aligned.

^{80}Sr

Levels in ^{80}Sr were excited through the reaction ^{51}V(^{32}S, p2n) using projectiles from the HHIRF tandem accelerator with energies of 120, 137, and 159 MeV. States of the yrast band have been observed at energies (in keV) of 385(2$^+$), 981(4$^+$), 1763(6$^+$), 2699(8$^+$), and 3766(10$^+$). The energy of the 2$^+$ state continues the systematic trend of decreasing energy from ^{86}Sr to ^{82}Sr. These data support the earlier conclusion that as both N and Z approach 38, the nuclear ground states approach deformation.

---

1. University of Alfeath, Tripoli, Libya.
2. Vanderbilt University, Nashville, TN.
3. University of Koln, West Germany.
4. Louisiana State University, Baton Rouge, LA.
5. University of Coiimbra, Portugal.
6. University of Koln, West Germany.
7. University of Florida, Gainesville, FL.
8. Brookhaven National Laboratory, Upton, NY.
9. Tennessee Technological University, Cookeville, TN.
10. Univeristy of Melbourne, Australia.
11. R. Soundranayagam et al., Phys. Rev. C 25, 1575 (1982).
12. R. B. Piercey et al., Phys. Rev. C 25, 1941 (1982).
13. R. Soundranayagam et al., Phys. Rev. C 25, 2983 (1982).

EVIDENCE FOR COLLECTIVE BEHAVIOR IN ^{128}Ce FROM LIFETIME MEASUREMENTS[1]

J.C. Wells[2] J. Hattula[3]
M.P. Fewell[4] D.R. Haenni[5]
N.R. Johnson I.Y. Lee
F.K. McGowan L.L. Riedinger[6]

As pointed out elsewhere in this report,[7] we have carried out measurements on light cerium nuclei, searching for collective behavior indicative of strong deformation. In doing this we have measured lifetimes of yrast states of ^{128}Ce by using a newly-constructed recoil-distance device which fits inside a 25cm x 25cm NaI total-energy detector to provide some selectivity of the desired reaction channel.

Excited ^{128}Ce nuclei were produced via the ^{92}Zr(^{40}Ar,4n)^{128}Ce reaction by bombarding an enriched ^{92}Zr target with 159-MeV ^{40}Ar ions from the Oak Ridge Isochronous Cyclotron. Shifted and unshifted γ-ray energies and intensities were measured with a large-volume Ge(Li) detector for ten recoil flight distances, ranging from 9.3 μm to 2.03 mm. The recoil velocity, determined from the energy shifts, was 7.26 μm/ps (0.0242 c).

The γ-ray intensities were normalized to the total γ-ray intensity in the energy range 1500-2000 keV, a region in which there were very few discrete γ-rays. The shifted and unshifted intensities were analyzed with a computer code which performs a least-squares fit in which initial level populations and transition probabilities are the variable parameters. The standard corrections were applied to the data.

Data were obtained for transitions from the 2$^+$ through 16$^+$ members of the yrast band. Two-step feeding was assigned to the 2$^+$, 6$^+$, 8$^+$, 10$^+$, 12$^+$, 14$^+$, and 16$^+$ states. No feeding was assigned into the 4$^+$ state because the intensity balance did not require it. In addition, the 16$^+$, 18$^+$, 20$^+$, 22$^+$, and 24$^+$ states were assumed to be members of a rotational band with constant intrinsic quadrupole moment Q_0 and experimentally known level energies and to have lifetimes given by the expression

$$\frac{1}{\tau} = 1.22\, E_\lambda^5\, Q_0^2\, (J_I\ 200 \mid J_I 2\ J_F 0)\,\mathrm{ps}^{-1}.$$

The lifetimes and B(E2) values determined from these measurements are summarized in Table 2.14.

In Table 2.15 are given the ratios of experimental B(E2) values to rotational B(E2) values for yrast transitions in light cerium nuclei. In each case the data are normalized to the 2$^+$→0$^+$ state. Results for ^{128}Ce are from the present work, and the values for ^{130,132,134}Ce

TABLE 2.14. LIFETIMES OF YRAST STATES OF ^{128}Ce.

E_γ(keV)	J^π	τ(ps)	B(E2) (e^2b^2)
207	2^+	423±34	0.42±0.03
400	4^+	10.8±2.0	0.73±0.13
551	6^+	2.9±0.5	0.56±0.10
663	8^+	>1.2	>0.5
712	10^+	0.9±0.3	0.50±0.17
576	12^+	0.9±0.3	1.4 ±0.5
561	14^+	1.9±0.5	0.78±0.20

are from the work of Husar et al.[8] and Nolan et al.[9]

Reference to Table 2.15 reveals that ^{130}Ce, ^{132}Ce and ^{134}Ce exhibit some dropoff in B(E2) strength up to the backbend at 10^+ at which point they reach their minimum values in transition strengths. On the other hand, ^{128}Ce data show no significant dropoff in the ratio of experiment to theory all the way through the 14^+ state.

In an attempt to understand the behavior in this region, Leander et al.[10,11] have carried out cranked Hartree Fock-Bogoliubov (HFB) calculations up to moderately high spin (see Fig. 2.59). In addition, Chen, Frauendorf and Leander[12] have carried out cranked shell model calculations in which they were able to fit their parameters from the ^{130}Ce data of Nolan et al.[9] The net result is that the balance between prolate-driving aligned protons and oblate-driving aligned neutrons in this nucleus falls in favor of the prolate shape. Thus, it is probable that the large collectivity in ^{128}Ce results from a prolate nucleus rotating collectively about an axis perpendicular to its symmetry axis. The more unusual negative γ-aligned nuetron configuration might still be observed in nearby nuclei.

ORNL-DWG 83-18053

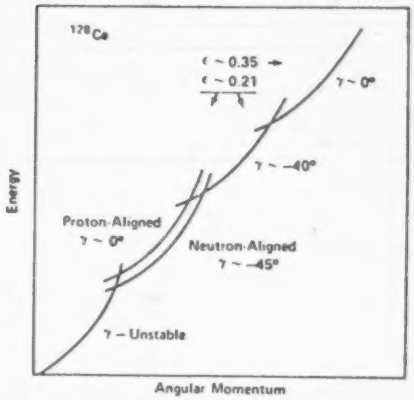

Fig. 2.59. Schematic picture of differently structured bands along the yrast line of ^{128}Ce, obtained by minimization of a cranking Hamiltonian with respect to shape and pairing coordinates (Ref. 10).

1. Summary of paper to be published.
2. Tennessee Technological University, TN.
3. On leave from the University of Jyväskylä, Jyväskylä, Finland.
4. Present address: Australian National University, Canberra, Australia.
5. Present address: Texas A&M University, College Station, TX.

TABLE 2.15. $B(E2)_{exp}/B(E2)_{rot}$ FOR YRAST TRANSITIONS OF LIGHT Ce ISOTOPES.

	$B(E2)_{exp}/B(E2)_{rot}$ (Normalized)						
	$2^+\to0^+$	$4^+\to2^+$	$6^+\to4^+$	$8^+\to6^+$	$10^+\to8^+$	$12^+\to10^+$	$14^+\to12^+$
^{128}Ce	1.0	1.2±0.2	0.85±0.15	>0.7	0.7 ±0.2	1.9±0.7	1.1±0.3
^{130}Ce	1.0	1.2±0.2	0.6 ±0.3	>0.7	$0.5\ ^{+0.5}_{-0.2}$	0.6±0.1	$2\ ^{+3}_{-1}$
^{132}Ce	1.0	0.7±0.2	$0.9\ ^{+0.9}_{-0.3}$	>0.4	0.14±0.04	>1.6	0.7±0.2
^{134}Ce	1.0	0.6±0.1	$0.2\ ^{+0.2}_{-0.1}$	>0.3	0.04±0.01	0.6±0.1	$0.6^{+0.4}_{-0.2}$

6. University of Tennessee, Knoxville, TN.
7. J.L.S. Carvalho et al., contribution in this report.
8. D. Husar et al., Nucl. Phys A292, 267 (1977).
9. P.J. Nolan et al., Proc. Conf. on High Angular Momentum Properties of Nuclei, Vol. 4, Nuclear Science Research Conference Series, ed. by N.R. Johnson (Harwood Academic Publishers, New York, 1983) p. 8.
10. G.A. Leander et al., Nucl. Phys. A400, 97 (1983).
11. G.A. Leander et al., Proc. Conf. on High Angular Momentum Properties of Nuclei, Vol. 4, Nuclear Science Research Conference Series, ed. by N.R. Johnson (Harwood Academic Publishers, New York, 1983) p. 10.
12. Y.S. Chen, S. Frauendorf and G.A. Leander, submitted to Phys. Rev. C.

HIGH SPIN STATES IN ^{128}Ce[1]

J.L.S. Carvalho[2] N.R. Johnson
R.M. Ronningen[3] J.S. Hattula[4]
I.Y. Lee M.P. Fewell
F.M. Bernthal[5] J.C. Wells[6]
L.L. Riedinger[7] H. Ower[7]

From both the spacings of the energy levels and the lifetimes[8] of the excited states, there come the indications of increasing collectivity in progressing through the series of nuclei ^{134}Ce, ^{132}Ce, ^{130}Ce. To see if this evolving pattern signifies that we are moving to a region of strong deformation, we initiated studies of the 70-neutron nucleus, ^{128}Ce.

High-spin states in ^{128}Ce were populated via the bombardment of ^{112}Cd with a 103-MeV beam of ^{20}Ne ions from ORIC. Efficient γ-γ coincidence measurements were carried out by utilizing seven large-volume Ge detectors in the horizontal plane. Two 10-in. x 10-in. NaI detectors located above and below the reaction chamber served as a total γ-ray energy spectrometer and, thus, provided a means to enhance the desired 4n reaction channel.

Since ^{128}Ce lies somewhat close to the proton drip line, we had to contend with several charged particle reaction channels. In spite of these complications, it was possible to develop the yrast sequence up to I=24$^+$ and to assign with less certainty two partially developed side bands. The level scheme shown in Fig. 2.60 summarizes these results. Angular distribution results showed that the yrast sequence in this scheme consisted of stretched E2 transitions, as does sideband 1. However, decay of sideband 1 into the ground band is of undetermined multipolarity. The data were not of sufficient statistical quality for a determination of the multipolarities in sideband 2.

At spin 10$^+$ in this nucleus we see a backbend similar to that seen in ^{130,132,134}Ce. Aligned angular momentum (I_x) plots for all four of these nuclei are shown in Fig. 2.61. In moving to lower A it is seen that the backbending sets in at lower rotational frequency, ω. However, ^{128,130,132,134}Ce show very similar crossing frequencies of ~0.3 MeV and have very similar

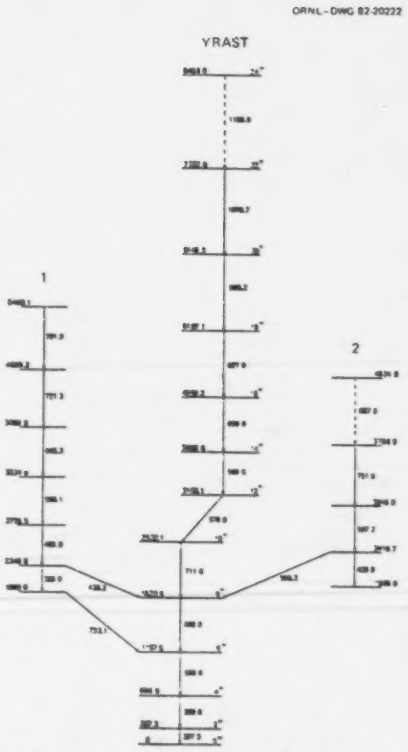

Fig. 2.60. Level Scheme of ^{128}Ce determined from the reaction ^{112}Cd(^{20}Ce,4n)^{128}Ce.

alignment gain (ΔI_x) values of 8, 9, 10 and 9.3, respectively. It apears that the alignments all come from a strongly decoupled high-j orbit. This is thought to be $h_{11/2}$ protons which are just below the Fermi surface in these nuclei.

One should be able to carry out blocking experiments in this region to demonstrate the orbitals involved in these backbends. Indeed, Ward et al.[8] have done just this for ^{127}La and ^{129}La and concluded that $h_{11/2}$ protons were responsible. (They saw no backbend in the $h_{11/2}$ band in either nucleus.) Recently, Nolan and collaborators[9] looked at the nuclei ^{127}La and ^{130,131}Ce. They measured ^{130}Ce up to I=26 and saw, as did we in ^{128}Ce, a sharp backbend at I=10; in addition, they saw at spin 26$^+$ what looks like the beginning of a second backbend. In ^{131}Ce, they observed alignment in both the positive and negative parity bands, indicating that neutron configurations 7/2 + [404] on which they are based are not active in the yrast band alignment of ^{130}Ce, i.e., their data are con-

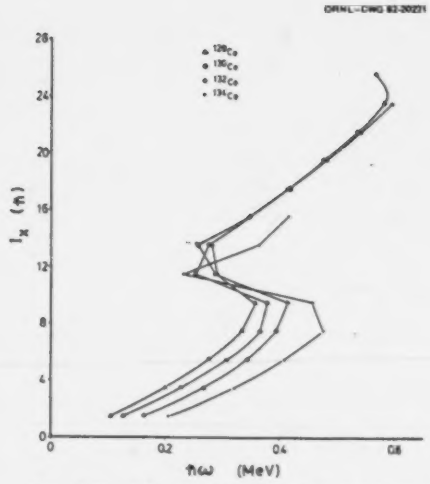

Fig. 2.61. Plot of aligned angular momentum (I_x) vs. rotational frequency ($\hbar\omega$) for $^{128-134}$Ce.

sistent with a first backbend in ^{130}Ce due to $h_{11/2}$ protons. Further, we have carried out cranked shell model (CSM) calculations for ^{128}Ce, as did Nolan et al.[9] for ^{130}Ce, and in both cases the alignment gains and crossing frequencies are consistent with alignment by $h_{11/2}$ protons. (In these calculations the nucleus was assumed to be prolate, i.e., $\gamma = 0°$.) However, in the case of ^{128}Ce the $h_{11/2}$ neutrons are also just below the Fermi surface. So in spite of the evidence that $h_{11/2}$ protons play the dominant role in this region, we must reserve the possibility that the neutrons could be instrumental in the first backbend in this nucleus. In another report[10] in this volume there are lifetime results which are not fully inconsistent with either interpretation.

---

1. Summary of paper to be published; a fuller account of this work appears in the Ph.D. thesis of J.L.S. Carvalho, 1982 (unpublished).
2. Michigan State University, East Lansing, Michigan. Part of thesis research carried out at the Oak Ridge National Laboratory.
3. Michigan State University, East Lansing, Michigan.
4. University of Jyväskylä, Jyväskylä, Finland.
5. Michigan State University and U. S. Senate Staff.
6. Tennessee Technological University, Cookeville, Tennessee.
7. University of Tennessee, Knoxville, Tennessee

8. D. Ward, H. Hertschat, P. A. Butler, P. Colombani, R. M. Diamond and F. S. Stephens, Phys. Lett. 56B, 139 (1975).
9. P. J. Nolan, D. M. Todd, P. J. Smith, D.J.G Love, P. J. Twin, O. Andersen, J. D. J. D. Garrett, G. B. Hagemann and B. Herskind, Phys. Lett. 108B, 269 (1982).
10. J. C. Wells, et al., separate paper in this volume.

HIGH-SPIN PROPERTIES OF ^{130}Ce FROM CONTINUUM γ-RAY STUDIES USING THE SPIN SPECTROMETER[1]

I.Y. Lee — N.R. Johnson
C. Baktash — F.K. McGowan
J.R. Beene — W.T. Milner
H. Kim — D.G. Sarantites[2]
R.O. Sayer — M. P. Fewell
M. L. Halbert — J. S. Bull[3]

With the spin spectrometer, which covers nearly 4π solid angle, measurement with very good resolution in both spin and excitation energy can be achieved. It is therefore possible to study the change of nuclear properties as a function of both spin and excitation energy. We have carried out an experiment on the continuum γ rays of ^{130}Ce from the reaction induced by a 144-MeV ^{34}S beam on a ^{100}Mo target. The beam was obtained from the Holifield Heavy Ion Research Facility. In the experiment, we used two Ge detectors as trigger detectors which replaced two pentagonal elements in the spin spectrometer.

One-dimensional and two-dimensional NaI spectra were obtained by sorting events according to total γ-ray pulse height H and fold K values. The pileup and Compton contribution in the spectra were removed by a deconvolution and an unfolding procedure, and the spectra were normalized using the average multiplicity values corresponding to the (H,K) values.

For a quantitative study of the K, H and angular dependence of the one-dimensional spectra, we subtracted the low K spectra from the high K spectra with the same excitation energy above the yrast line. Since these spectra are all properly normalized, the difference spectra give the energy distribution of the additional γ rays on the top of the cascade. Figure 2.62 shows the difference spectra at 24.4° and 87.3°. Several features become very clear in these spectra. The discrete lines are all subtracted out, which indicates that there is no direct feeding to these states at high spin. Therefore, we can analyze the low energy part of the spectrum without the interference of discrete lines. There are two broad peaks in all the spectra. From these spectra, we determined the area, centroid position and the width of these peaks. The anistropy [w(24°)/w(87°)] of the high peaks has a value ~ 1.6, which is consistent with the stretched quadrupole decay, and the value 0.64 for the low peaks is consistent with the stretched dipole decay. Using the measured angular distribution, we can derive the number of quadrupole and dipole γ rays. The

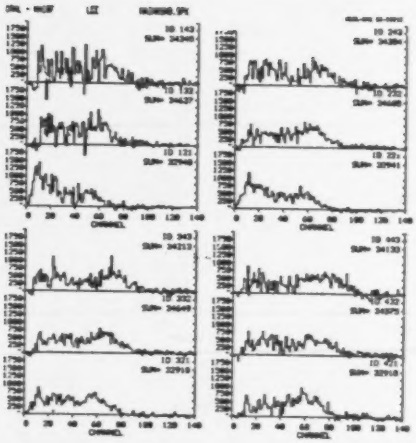

Fig. 2.62. Difference spectra for 24.4° obtained by subtracting low fold spectra from high fold spectra of the same entry energy region above the yrast line. The upper left block is for H* = 0-3 MeV and from bottom to top its three spectra correspond to K differences of 17-14, 20-17 and 23-20. The spectra in the upper right block are for H* = 3-6 MeV; lower left 6-9 MeV and lower right 9-12 MeV.

position of the quadrupole peak moves up in energy with increasing fold and the dipole peak stays at the same energy, around 0.5 MeV. It is well known that the stretched quadrupole γ rays are associated with decay along the yrast line. Therefore, from its centroid energy and the spin value derived from the multiplicity, we can determine the effective moment of inertia, $\mathcal{I}^{(1)}_{eff}$ defined as

$$2\,\mathcal{I}^{(1)}_{eff}/\hbar^2 = 2\,\frac{I}{\omega} \quad ,$$

where

$$\omega = \frac{E_\gamma \text{centroid}}{2} \quad .$$

To derive spin from the fold, we first obtained from K the multiplicity (M) using the response of the spin spectrometer. Then the spin was determined using the formula

$$I = (M - M_{stat})\cdot(2\cdot f_Q + f_D) \quad ,$$

where M_{stat} is the number of statistical γ rays which is calculated using the program JULIAN-PACE.[4] The f_Q and f_D are the measured fraction of stretched quadrupole and dipole γ rays in the decay. This calculation was carried out for each fold and entry energy region. The $\mathcal{I}^{(1)}_{eff}$ obtained are plotted in Fig. 2.63, together with the value of the yrast line derived from the discrete line study of

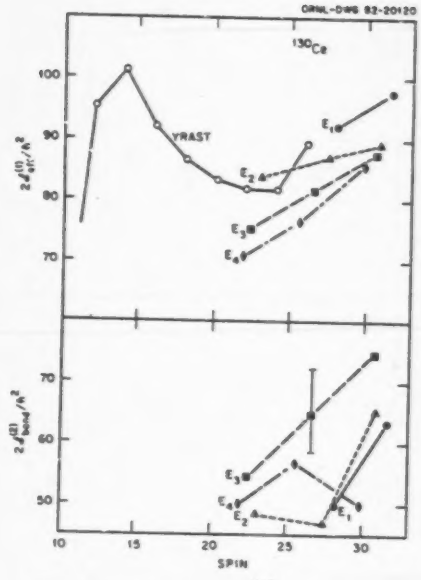

Fig. 2.63. Effective $[\mathcal{I}^{(1)}_{eff}]$ and collective $[\mathcal{I}^{(2)}_{band}]$ moments of inertia derived from the present experiment. The results of Nolan et al.[3] on the yrast line are also plotted. The entry regions are the same as in Fig. 2.62.

Nolan et al.[5] We see the increase of $\mathcal{I}^{(1)}_{eff}$ as the spin increases and the decrease of $\mathcal{I}^{(1)}_{eff}$ as the entry energy increases. The entry energy dependence is very interesting. It indicates that the cascades started at different entry energies go through nuclear states with different properties. Most likely the population with the higher initial entry energy decays through states with higher excitation energy above the yrast line, i.e., states with higher temperature.

To further investigate these effects, the two-dimensional energy-energy correlation was studied. Shown in Fig. 2.64 are the correlation maps obtained after applying the one-step Copenhagen subtraction method[5] to the unfolded two-dimensional spectra. The valley along the diagonal is quite distinct. From the width of the valley, W, the second moment of inertia $\mathcal{I}^{(2)}_{band}$ can be determined as

$$2\,\mathcal{I}^{(2)}_{band}/\hbar^2 = \frac{16}{W} \quad .$$

Also plotted in Fig. 2.63 are the $\mathcal{I}^{(2)}_{band}$ values determined from the maps at γ-ray energies corre-

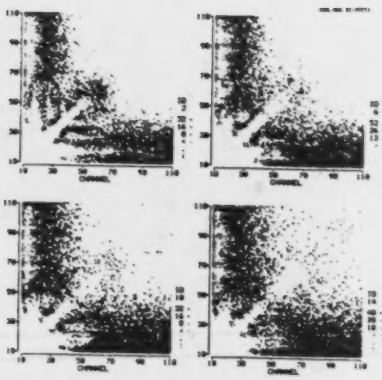

Fig. 2.64. Gamma-ray energy-energy correlation spectra for $H^* = 3$-6 MeV. The upper left spectrum is for K = 14, upper right K = 17, lower left K = 20, and lower right K = 23. The energy scale is 50 channels = 1 MeV.

sponding to the centroid of the quadrupole transition of the particular (H,K) gate. Due to the low statistics, the uncertainty of $\mathcal{J}^{(2)}_{band}$ is large. However, the increasing of $\mathcal{J}^{(2)}_{band}$ as a function of spin is quite clear and is similar to that of $\mathcal{J}^{(1)}_{eff}$. The change as a function of entry energy is not so obvious. It seems that either the change is small or it reduces at high excitation energy. These observations may indicate that the deformation of the nucleus increases as spin increases, but the spin alignment is reduced at high temperature.

---

1. Summary of paper to be published.
2. Washington University, St. Louis, MO.
3. Participating student from Southern College and Universities Union/Oak Ridge Science Semester.
4. M. Hillman and Y. Eyal, Code JULIAN, unpublisned; A. Gavron, modification PACE, Phys. Rev. C21, 230 (1980).
5. P.J. Nolan et al., Phys. Lett. 108B, 269 (1982).
6. O. Andersen et al., Phys. Rev. Lett. 43, 687 (1979).

SEARCH FOR SUPERDEFORMED SHAPES IN ^{154}Er

C. Baktash
J.X. Saladin[1]
O.C. Kistner[2]
I.Y. Lee
E. der Mateosian[2]
A.W. Sunyar[2]

Study of the interplay between the macroscopic and microscopic effects in nuclei as a function of angular momentum has become the focus of nuclear structure studies in recent years. On the basis of the Liquid Drop model, nuclei are expected to become oblate at spins I ≥ 40 under the stress of the centrifugal force. At yet higher angular momentum, they gradually change over to a triaxial shape before fissioning. This general behavior, however, could be modified by the shell effects.

Shell model calculations by the Lund group (Ref. 3) predict shape transition patterns which depend sensitively on the neutron number. For example, the Er isotopes with N ≤ 86 are predicted to have nearly spherical shapes at low spins and gradually become obate at higher angular momenta (Fig. 2.65). In contrast, for neutron numbers N > 90, the equilibrium shapes are expected to change from prolate at spins I ≤ 40 to triaxial at I ≥ 50. Of particular interest is the predicted transition to superprolate (β = 0.6) shapes for N = 82 isotopes at very high spins (I ≥ 50). Such large deformations correspond to a major-to-minor axis ratio of nearly 2:1 and have been observed only in the fission isomers. Experimental verification of these predictions provides a very stringent test of the validity of these calculations, which have been very successful in describing the nuclear behavior at high angular momenta.

One possible method of investigation of the shape changes is to study the changes in the moment of inertia and the nuclear excitation mode. As the nucleus undergoes a transition from oblate to superprolate shapes, the nuclear excitation mode changes from a noncollective rotation around the major (symmetry) axis to a collective rotation around the minor axis. The

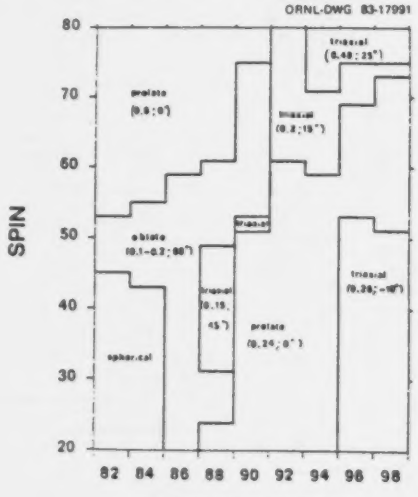

Fig. 2.65. Predicted equilibrium shapes as a function of angular momentum for Er-isotopes (Ref. 1).

large moment of inertia associated with the latter mode may be inferred from the study of the γ rays deexciting the corresponding collective rotational bands.

The recently developed γ-γ energy correlation technique is particularly suited for the study of the moments of inertia. Since, for an ideal rigid rotor, no two γ rays have the same energy, one gets a valley separating the two ridges (formed by the neighboring γ rays) that run along the diagonal ($E_{\gamma 1} = E_{\gamma 1}$) of the two-dimensional γ-γ coincidence map. The moment of inertia is then related to the width of this valley, W, through $(2\mathcal{J}/\hbar^2) = 16/W$. In the case of superdeformed shapes where the moment of inertia $(2\mathcal{J}/\hbar^2)$ may assume values as large as 200 MeV^{-1}, the valley width may be as small as 80 keV. Thus, in the region where superdeformations are expected to set in, namely γ rays of nearly 1.4-MeV energy, one needs detectors with resolutions better than a few per cent in order to clearly resolve the two ridges. Therefore, while NaI detectors are well suited for the task of establishing the existence of the correlated events (ridges), they lack adequate resolution to measure the width of the valley. The Ge detectors, on the other hand, while offering superior resolution, suffer from having a relatively small (typically 15-20%) photopeak-to-total ratio. Thus, only less than 4% of the total counts in a two-dimensional γ-γ coincidence map are useful. This problem could be partially rectified by fitting the Ge detectors with anti-Compton shields.

Using two Ge(Li) counters, both equipped with 25-cm x 25-cm NaI anti-Compton shields (suppression factors of ≈ 4), we have obtained γ-γ coincidence data for the ^{154}Er nucleus. The high-spin states of this nucleus were populated via the ^{96}Zr(^{64}Ni, 4n) reactions, using a 275-MeV ^{64}Ni beam from the tandem accelerator. In 2½ days of running time, we collected nearly 0.7 million coincidence events. Figure 2.66 shows the raw E_γ-E_γ correlation spectrum. A newly developed background subtraction technique (Ref. 4) was used to subtract nearly 90% of the Compton events present in the matrix. The resulting unsymmetrized matrix is shown in Fig. 2.67. Unfortunately, lack of adequate statistics prevented us from drawing any conclusions regarding the presence or absence of correlated γ rays at ~ 1.4 MeV, the predicted energy for transitions originating from superdeformed states. This is largely due to (a) the low efficiency of Ge crystals for detection of relatively high-energy γ rays and (b) the small solid angles (0.5% of 4π) subtented by the Ge detectors because of the geometrical constraints imposed by the use of anti-Compton shields. To partially circumvent these problems, we are planning to use six Ge detectors which are equipped with somewhat smaller anti-Compton shields to repeat this experiment in the near future.

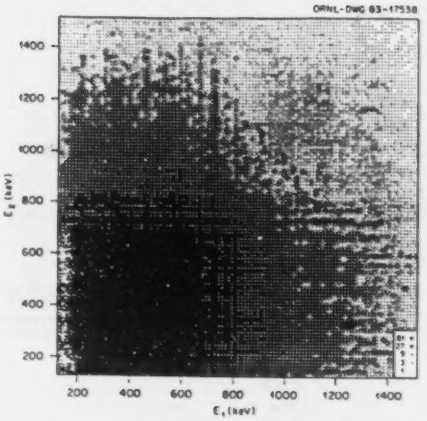

Fig. 2.66. Gamma-Gamma energy correlation map for ^{154}Er constructed from the raw data.

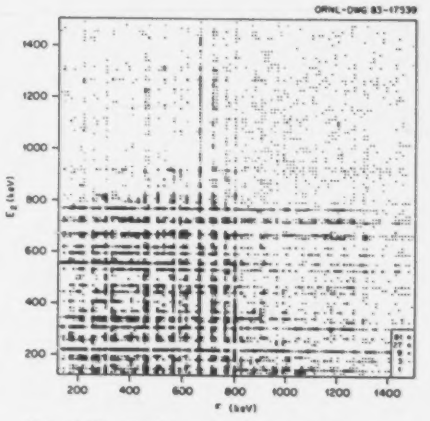

Fig. 2.67. Background subtracted, but not symmetrized γ-γ energy correlation map for ^{154}Er.

STUDY OF THE SPIN-INDUCED SHAPE CHANGES IN ^{158}Yb[1]

C. Baktash
I.Y. Lee
Y. Schutz
F.K. McGowan
L.L. Riedinger[2]
D.G. Sarantites[3]
D.C. Hensley
L. Courtney[2]
A.J. Larabee[2]
N.R. Johnson
M.P. Fewell
M.L. Halbert

According to shell model calculations, rare earth nuclei with N >88 neutrons undergo a tran sition from prolate shapes at low spins

---

1. University of Pittsburgh, Pittsburgh, PA.
2. Brookhaven National Laboratory, Upton, NY.
3. I. Ragnarsson et al., Nucl. Phys. A347, 287 (1980).
4. Y. Schutz (see contribution in this report.)

to oblate shapes at high spins. The corresponding modes of generation of angular momentum are collective rotations and single-particle excitations, respectively. The study of these shape changes and the associated excitation modes, therefore, provides valuable insight into the question of the interplay between collective and single-particle degrees of freedom in nuclear systems.

To investigate these effects, we have studied the high spin states in ^{158}Yb, which is predicted to have softer potential energy surfaces compared to its lighter N=88 isotopes. The high spin states in ^{158}Yb were populated via (HI, 4n) reactions in two different experiments using ^{20}Ne(E=115 MeV) and ^{64}Ni(E=285 MeV) beams.

The ^{20}Ne beam run utilized an array of six Ge counters, along with two large (25cm x 25cm) NaI crystals that served as a total energy spectrometer. Nearly 200 million events, defined by coincident firing of both of NaI detectors and a minimum of 2 Ge counters, were collected in this mode. Analysis of these data resulted in the identification of the yrast sequence up to spin I=34.

The ^{64}Ni beam run was carried out in the spin spectrometer, with six portable Ge counters replacing four hexagonal and two pentagonal elements of the system. By demanding a coincident firing of a minimum of 22 NaI detectors, we emphasized collection of those events which were rich in multiplicity content. This requirement also resulted in the enhancement of the 4n channel (nearly 75% of the collected events). In the first phase of this run, the recoiling residual nuclei were allowed to decay in flight. However, despite a relatively large target-to-detector distance (≈ 15cm), Doppler broadening posed a serious problem. We, therefore, changed to a Pb-backed target after collection of 135 high density (6250 BPI) tapes of data. No noticeable Doppler broadening effects were observed in this mode, which indicates existence of long feeding times even for the highest spin states populated in this reaction. Another 95 tapes of data were collected in this mode.

Off-line analysis of the above data started with gain matching of all the NaI elements and separating neutron signals from the gamma rays'. The corrected data were then scanned to generate several E_γ-E_γ matrices that were gated with various total pulse height-multiplicity, (H,K), cuts. A newly developed background subtraction technique* was used to subtract nearly 90% of the Compton events present in these matrices before generating gated coincidence spectra.

A preliminary analysis of the data has so far revealed several new yrast transitions. The resulting tentative decay scheme is shown in Fig. 2.68. Since we have not yet analyzed our angular distribution and angular correlation data, the spin assignments in this figure should be viewed with caution. However, assuming stretched E2 character for all the observed yrast transition γ rays, we have plotted the effective moment of inertia ($\mathcal{J}_{eff}$) of the yrast band in Fig. 2.69. While the deduced $\mathcal{J}_{eff}$ for ^{158}Yb follows the general trend of those of its isotones ^{154}Dy (Ref. 5) and ^{156}Er (Ref. 6) up to spin I = 32, it differs significantly from them in details.. First, compared to its isotones,

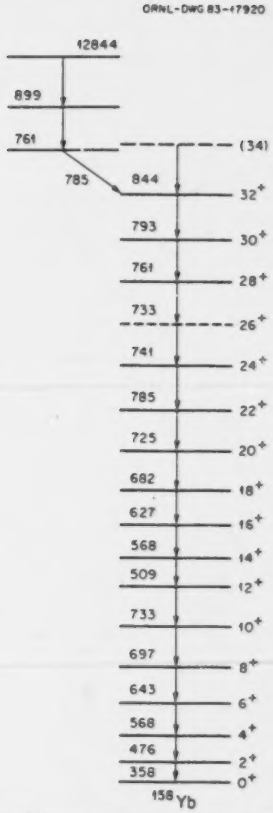

Fig. 2.68. A tentative decay scheme for ^{158}Yb.

although ^{158}Yb shows the least stretching effect in the ground band, it exhibits considerable stretching after the first backbending at spin 14. In contrast, after the first backbending, $\mathcal{J}_{eff}$ remains nearly constant in ^{154}Dy and ^{156}Er and generally decreases in the more deformed nuclei. Secondly, beginning with the second discontinuity in the $_{eff}$ at spin 24, $_{eff}$ rises sharply and, after undergoing yet a third discontinuity at spin 32, exceeds the rigid rotor value by nearly 40% at its maximum. Such a large effective moment of inertia has not been previously observed in a rotational nucleus and, if true, is reflective of a change in the excitation mode of this nucleus. The fact that the γ-ray energies are all concentrated in the narrow 730- to 790-keV range may indicate that the nucleus is rapidly becoming triaxial, thus giving rise to many band intersections.

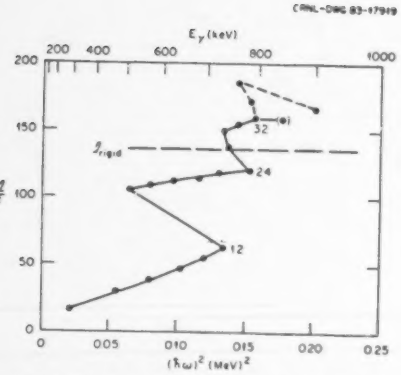

Fig. 2.69. The effective moment of inertia as a function of $(\hbar\omega)^2$ for ^{158}Yb. The yrast transitions were assumed to be stretched E2 in character.

On the other hand, the yrast γ rays may not all be stretched E2 in character, as assumed above. For example, presence of some dipole transitions would invalidate the above picture. Interestingly, Jääskeläinen et al. have recently reported that, starting with spin ≈ 40, a strong stretched dipole (presumably M1) component develops around $E_\gamma \sim 700$ keV in their continuum spectra (Ref. 7). However, this alternative picture would also entail a change in the shape and excitation mode of ^{158}Yb at high spins. Our observation of long feeding times for the highest spin states indicates loss of collectivity and, hence, a gradual change toward oblate (γ = +60°) shapes at the highest angular momentum.

At present, one could only speculate about the nature of yrast states at high spins in ^{158}Yb. Various possibile excitation modes include: (a) the wobbling mode, (b) the vibrational mode of a soft triaxial nucleus, and (c) the band termination mechanism (Ref. 8). To provide some answere to these questions, we shall analyze the continuum γ-ray data that were simultaneously collected. Since the spin spectrometer allows the determination of the spin alignment, we shall construct various E_γ-E_γ matrices to study the dipole-dipole, dipole-quadrupole and quadrupole-quadrupole correlations for the γ rays that deexcite the near-yrast bands in this nucleus.

---

1. Summary of paper to be published.
2. University of Tennessee, Knoxville, TN.
3. Washington University, St. Louis, MO.
4. Y. Schutz (see contribution in this report.
5. A. Pakkanen et al., Phys. Rev. Lett. 48, 1530 (1982).
6. T. Byrski et al, Phys. Lett. 102B, 235 (1981).
7. M. Jääskeläinen et al., Phys. Lett. 119, 65 (1982).
8. T. Bengtsson and I. Ragnarsson, Physica Scripta (in press).

SHAPE EFFECTS IN $h_{11/2}$ AND $g_{7/2}$ BANDS IN ^{159}Tm

A. J. Larabee[1] L. H. Courtney[1]
S. Frauendorf[2] L. L. Riedinger[1]
J. C. Waddington[3] M. P. Fewell[4]
N. R. Johnson I. Y. Lee
F. K. McGowan

The differing influences of the various quasiparticle orbits on the shape of the nuclear core for the rather soft N = 90 transitional nuclei are quite effectively demonstrated by a comparison of the $h_{11/2}$ and $g_{7/2}$ proton band structures observed in ^{159}Tm.

The alignment of two $i_{13/2}$ neutrons, indicated by the sharp backbend at the rotational frequency of $\omega = 0.26$ MeV/ħ, results in deformation changes. A dramatic increase in the B(M1; I → I-1)/B(E2: I → I-2) ratio is also found to occur after the backbend and can be attributed to both an increase in the M1 rate as a result of the neutron alignment, and a decrease in the E2 rate due to deformation changes.

The level scheme for ^{159}Tm shown in Fig. 2.70 has been constructed based upon experiments involving the ^{148}Sm(^{14}N,3n) reaction with a bombarding energy of 68 MeV at the McMaster University tandem accelerator[5] and the ^{141}Pr(^{22}Ne,4n) reaction with a bombarding energy of 113 MeV at the Oak Ridge Isochronous Cyclotron. In the Oak

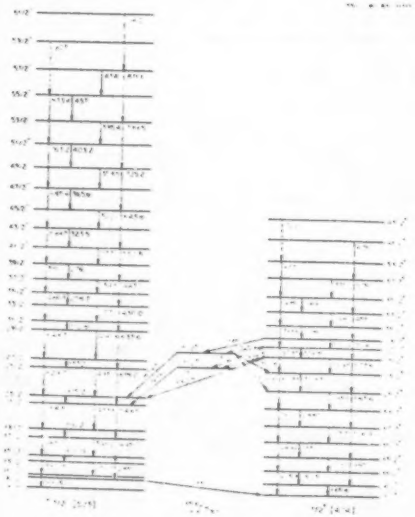

Fig. 2.70. Level scheme for ^{159}Tm.

Ridge measurement, the γ-rays emitted in the neon-induced reaction were detected in an array consisting of two large NaI counters used as a total energy filter and 7 Ge counters for the primary γ-γ coincidence data. Triple coincidences between the Ge detectors were accumulated and subsequently analyzed to give approximately 240 million γ-γ pairs in coincidence with the total energy range which emphasizes the ^{159}Tm reaction product. The higher angular momentum input in the Oak Ridge experiment allowed the construction of the yrast-band up to spin I = 61/2. Angular distribution and angular correlation data were analyzed to assign spins and extract multipole mixing ratios. The lowest levels observed in each band were both assigned I = 7/2 based primarily upon the systematics of these structures in odd-Z isotopes and isotones in this region.

A comparison of the 7/2[523] and 7/2[404] bands in ^{159}Tm reveals striking differences in the signature splitting (that is, the energy shift of the unfavored relative to the favored part of the band). Above the backbend both bands are similar in structure with only a small signature splitting being present. However, below the backbend, the 7/2[523] band has a large degree of signature splitting, while the 7/2[404] band has virtually none. This difference is easily seen in Fig. 2.70, where the ΔI = 1 transitions in the 7/2[523] band up to I = 31/2 alternate between small and large energy transition, while no such staggering effect is observed in the 7/2[404] band.

Cranked Shell Model (CSM) calculations show that the large signature splitting in the 7/2[523] band can be accounted for by allowing a large negative γ-deformation.[6-9] This push towards triaxiality is determined by the driving influence of the quasiparticle configuration, where the strength and direction of the driving force depends on the position of the fermi surface in the quasiparticle shell[10]. In ^{159}Tm, the 7/2[523] band corresponds to a Fermi surface near the middle of the $h_{11/2}$ shell and this quasiparticle is expected to exert a strong drive to large negative γ values, resulting in a large degree of signature splitting. The fermi surface for the 7/2[404] band lies at the top of the $g_{7/2}$ shell and there should thus be virtually no driving force in γ for moderate values of γ. In this case the equilibrium γ-deformation simply corresponds to the core deformation. After the backbend, the driving influence of the $i_{13/2}$ neutrons dominates. The orbitals involved here lie at the bottom of the $i_{13/2}$ shell and therefore should drive to slightly positive values of γ. This picture is consistent with the observed differences in the signature splitting among the various quasiparticle configurations.

Figure 2.71 shows the measured values of the ratio R = B(M1; I → I-1)/B(E2; I → I-2). Below the backbend, the value of R in the 7/2[523] band appears to be signature-dependent, while in the 7/2[404] band the ratio is essentially constant. In both bands a large decrease in the ratio is observed after the backbend. A geometrical model has been developed by Dönau and Frauendorf[11], in order to examine the effect of quasiparticle alignment on the B(M1) values.

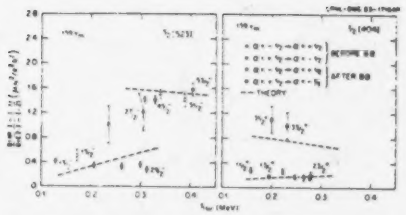

Fig. 2.71. Ratio of the stretched M1 to stretched E2 reduced transition probabilities of members of the 7/2[523] band (left) and the 7/2[404] band (right) in ^{159}Tm. Experimental values come from observed branching ratios, the theoretical values from Donau and Frauendorf.[11] Theoretical parameters used were: $(g_1-g_R) = .92$, $i_1 = 4\hbar(h_{11/2}$ protons); $(g_1-g_R) = .42$, $i_1 = 2\hbar$, $\gamma = -9°$ ($g_{7/2}$ protons); $(g_1-g_R) = -.52$, $i_2 = 9.5\hbar$, $\gamma = 0°$($i_{13/2}$ neutrons); and $Q_0 = 5$eb. For the 7/2[523] band, the signature-averaged values were used below the backbend where $\gamma = -25°(\alpha = -1/2)$ and $-14°(\alpha = +1/2)$.

For bands with a definite value of K, the projection of I on the symmetry axis, the time-dependent component of K perpendicular to the I axis gives rise to the M1 transitions between the two signatures of the high-K band. For an odd-proton nucleus like ^{159}Tm, the neutron alignment along the rotation axis in the backbend process increases this time-dependent component of the magnetic moment, leading to a large increase in the M1 transition probabilities. The B(M1)/B(E2) equation of ref. 11 has been modified to account for γ changes (which affects the B(E2) value) and is given by:

$$\frac{B(M1;\ I\to I-1)}{B(E2;\ I\to I-2)} = \frac{12}{5Q_0^2\cos^2(30°+\gamma)}$$

$$\left[1-\frac{K^2}{(I-1/2)^2}\right]^{-2}\frac{K^2}{I^2}\left[(g_1-g_R)(\sqrt{I^2-K^2}-i_1)-(g_2-g_R)i_2\right]^2$$

The equilibrium γ-values used in the calculation are given in the figure caption and were derived using CSM calculations to determine the driving force of the quasiparticle configurations. The theory reproduces quite nicely the qualitative pattern of the observed B(M1)/B(E2) ratio, showing the large increase in R after the backbend, due both to a decrease in the B(E2) value (based upon γ changing from negative to positive through the backbend) and to an increase of the B(M1) value as a result of the aligning $i_{13/2}$ neutrons. It thus appears that the branching ratios in these high-K bands contain structure information which is understood in this case.

---

1. University of Tennessee, Knoxville, TN.
2. University of Tennessee, Knoxville, TN. Permanent Address: Central Institute for Nuclear Research, Rossendorf, E. Germany.
3. McMaster University, Hamilton, Ontario.

4 Permanent Address: Australian National University, Canberra Australia.
5. A.J. Larabee and J.C. Waddington, Phys. Rev. C24, 2367 (1981).
6. R. Bengtsson, F.R. May and J.A. Pinston, Proc. XX International Winter Meeting on Nuclear Physics, Bormio, Italy, Jan. 25-30, 1982.
7. L.L. Riedinger, Nordic Meeting on Nuclear Physics, Fuglso, Denmark, Aug. 16-20, 1982.
8. S. Frauendorf and F. R. May, Phys. Lett. 125B, 245 (1983).
9. R. Holzmann et.al, Phys. Rev. Lett. 50, 1834 (1983).
10. G.A. Leander, S. Frauendorf and F. R. May, Proc. Conf. on High Angular Momentum Properties of Nuclei, Vol. 4, Nuclear Science Research Conference Series, ed. N.R. Johnson (Harwood Academic Publishers, 1983).
11. F. Donau and S. Frauendorf, Proc. Conf. on High Angular Momentum Properties of Nuclei, Vol. 4, Nuclear Science Research Conference Series, ed. N.R. Johnson (Harwood Academic Publishers, 1983).
12. I. Hamamoto, Phys. Lett. 102B, 225 (1981); I. Hamamoto, Phys. Lett. 106B, 281 (1981).

THE SPECTROSCOPY OF ^{159,160}Yb USING THE SPIN SPECTROMETER

L.L. Riedinger[1] L.H. Courtney[1]
C.R. Bingham[1] A.J. Larabee[1]
C. Baktash M.L. Halbert
D.C. Hensley N.R. Johnson
I.Y. Lee Y. Schultz
B. Herskind[2] S.A. Hjorth[3]
A. Johnson[3] A. Dilmanian[4]
M. Rajagopalan[4] D. Sarantites[4]
D.R. Haenni[5] J.C. Waddington[6]
J. S. Hattula[7]

A high-spin γ-ray spectroscopy experiment has been performed using the filtering power of the spin spectrometer in an effort to study the discrete structure in the I = 35ħ - 45ħ region. The experiment performed involved 220 MeV ^{48}Ti bombarding a ^{116}Cd target, making equal amounts of the 4n(^{160}Yb) and 5n(^{159}Yb) products. Six of the NaI counters in the spin spectrometer were replaced by Ge detectors positioned at 10-15 cm from the target. At least 18 of the remaining 65 NaI counters and two of the six Ge counters were required to fire before the event was accepted. Around 200 million pairs of Ge-Ge coincidences were thus accumulated for later analysis.

Portions of the Ge spectra from the spin spectrometer experiment are shown in Fig. 2.72 for 8 different (H,K) gates. A comparison of the spectra 6, 7 and 8 to spectra 1, 2 and 3 show quite a clean separation between the dominating 4n and 5n reaction channels. Since ^{160}Yb is already a well-studied case,[8-10] the purpose of the current study was to push the discrete-line spectroscopy up to higher spins. So far, the analysis of the data has yielded discrete lines up to 38$^+$ in the yrast-structure of ^{160}Yb, as well as a tentative assignment for the 40$^+$-38$^+$ transition. Also, 3 more transitions

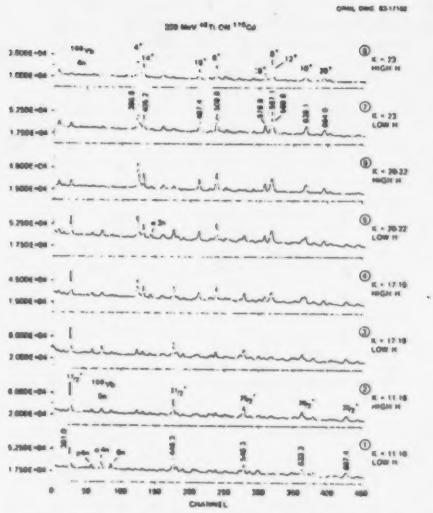

Fig. 2.72. Ge spectra from Spin-Spectrometer measurement. These eight spectra result from gates on the fold (K) and total energy (H) detected in the 65 NaI counters. The ridge of the total energy projections was used to define the division between the low and high H gates.

were added to a negative-parity side band, (π,α) = (-,1), pushing it up to a spin of 33$^-$. Angular momentum, I_x, is plotted as a function of rotational frequency, ω, for both of these bands in Fig. 2.73.

The yrast sequence of levels is plotted in Fig. 2.72 only above I=12, that is, above the first backbend which corresponds to an alignment of $i_{13/2}$ quasineutrons. The second backbend occurs at $\hbar\omega$ = .42 MeV and results from the alignment of $h_{11/2}$ quasiprotons, based upon the blocking experiment on the $h_{11/2}$ 7/2[523] band performed on ^{159}Tm by our group (another contribution to this report) and by Holzmann et al.[11] The (π,α) = (-,1) band is a two quasiparticle structure composed of an $i_{13/2}$ and $h_{9/2}$ neutron. This band experiences an $i_{13/2}$ alignment process at $\hbar\omega$ = 0.37 MeV, followed by the proton crossing at $\hbar\omega$ = 0.44 MeV. This latter frequency is somewhat higher than that for the same backbend in the yrast band, and the difference probably is related to slightly different shape parameters in the two bands.

The yrast-band for ^{160}Yb is seen to continue quite smoothly up to spin 38$^+$, and possibly to 40$^+$. The structure of the isotone ^{158}Er is currently being studied by the Liverpool group,[12] who find a drastic structure change in ^{158}Er above I = 38$^+$, where the yrast band splits into two different cascades. If a similar structure change exists in ^{160}Yb, it does not appear to occur below I = 38$^+$.

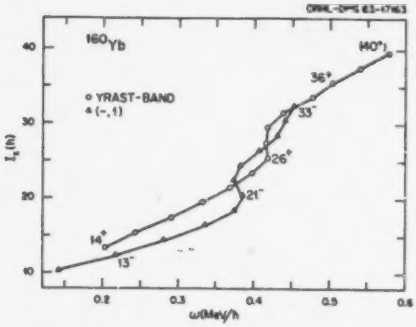

Fig. 2.73. Plot of the total angular momentum along the rotation axis, I_x, versus the rotational frequency ω for the yrast-band and a negative-parity side band in ^{160}Yb.

The bottom three spectra in Fig. 2.72 show a portion of the data collected for ^{159}Yb. Very little information is known about this nucleus and it is clear that the data collected on the spin spectrometer should yield a considerable amount of new information on this structure. The analysis of these data is currently in progress.

Besides the discrete γ-ray data, this spin spectrometer experiment should enable us to examine the feeding patterns from the entry region to the yrast high spin states. A preliminary analysis indicates that the feeding of the yrast line is relatively independent of the (H,K) gate selected. For example, an examination of spectra 5 to 8 in Fig. 2.72 shows that the intensity of the $34^+ \rightarrow 32^+$ transition relative to the $4^+ \rightarrow 2^+$ transition is the same for all five. There is also an indication that more side-feeding occurs to the yrast-line below $I = 28^+$ for spectra 4 and 5 than is found in spectra 6, 7 and 8. In attempting to understand this behavior it becomes clear that a more careful examination of the feeding patterns is required. It is necessary to examine the discrete-line intensities with finer (H,K) gates than used so far. Also, it would be informative to look at the relative intensities of the discrete lines when gating by one, two or three statistical transitions in the NaI counters. Such an analysis of the current data is under way.

---

1. University of Tennessee, Knoxville, TN.
2. Niels Bohr Institute, Copenhagen, Denmark.
3. Institute of Atomic Physics, Stockholm, Sweden.
4. Washington University, St. Louis, MO.
5. Texas A&M University, College Station, TX.
6. McMaster University, Hamilton, Ontario.
7. Jyväskylä University, Jyväskylä, Finland.

8. L.L. Riedinger et al., Phys. Rev. Lett. 44, 568 (1980).
9. L.L. Riedinger, Physica Scripta 42, 312 (1981).
10. L.L. Riedinger, Nucl. Phys. A347, 14 (1980).
11. R. Holzmann et al., Phys. Rev. Lett. 50, 1834 (1983).
12. M. A. Riley et al., to be published.

γ-γ ENERGY CORRELATIONS AND THE MOMENTS OF INERTIA IN ^{176}W[1]

I.Y. Lee C. Baktash[2]
J.X. Saladin[3]

The behavior of ^{176}W at high angular momentum was investigated through both spectroscopy of the discrete and correlation measurements of the continuum γ rays. The γ-γ coincidence data were taken with a detection system consisting of two Ge(Li) counters, both equipped with 10-in. x 10-in. NaI anti-Compton shields which gave suppression factors of ≈ 4. In a complementary experiment, the multiplicity of γ rays deexciting the same compound system was measured by using an array of 4 (3-in. x 3-in.) NaI detectors in coincidence with either a Compton-suppressed Ge(Li), or a 5-in. x 5-in. NaI counter.

The high-spin states of the nucleus ^{176}W were populated via the ^{154}Sm(^{26}Mg,4n) reaction using a 120-MeV ^{26}Mg from the tandem accelerator at Brookhaven National Laboratory. The yrast states in ^{176}W have been established up to $I^\pi = 18^+$ by Dracoulis et al.[4] We have identified three new transitions, tentatively assigned as the $20^+ \rightarrow 18^+$ (612 keV), $22^+ \rightarrow 20^+$ (687 keV) and $24^+ \rightarrow 22^+$ (753 keV) members of the yrast cascade. The deduced effective moment of inertia, $\mathcal{J}^{(1)}_{eff}$, backbends at $(\hbar\omega)^2 = 0.1$ (MeV)^2. This band crossing also appears as a bridge in the continuum γ-γ energy correlation matrix shown in Fig. 2.74. The accuracy of the correlated events in this matrix was significantly improved because of the 16-fold relative enhancement of the photo-photo coincidence events, resulting from the use of anti-Compton shields.

To be noted in Fig. 2.74 is the persistence of a clear diagonal valley with well-defined ridges up to about 1 MeV, indicating collective motion beyond the last known discrete transition at $E_\gamma = 0.75$ MeV. Also present are some fillings of the valley beyond the first band crossing frequency. The second moment of inertia, $\mathcal{J}^{(2)}_{band} = dI/d\omega$, is related to the valley width (W) by $[2\mathcal{J}^{(2)}_{band}/\hbar^2] = 16/W$. Therefore, the observed smooth decrease of W indicates a gradual increase of $\mathcal{J}^{(2)}_{band}$ with frequency, $\omega = E_\gamma/2$, as shown in Fig. 2.75.

The first moment of inertia, $\mathcal{J}^{(1)}_{band} = I/\omega$, was obtained from the $\mathcal{J}^{(2)}_{band}$ values by numerical solution of the differential equation $(\omega - d\mathcal{J}^{(1)}_{band}/d\omega) + \mathcal{J}^{(1)}_{band} = \mathcal{J}^{(2)}_{band}$. The resulting values (squares in Fig. 2.75) may be used to deduce the noncollective component of the angular momentum, i, from $(i/I) = 1 - [\mathcal{J}^{(1)}_{band}/\mathcal{J}^{(1)}_{eff}]$.

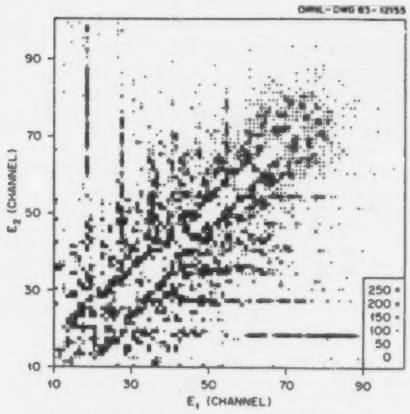

Fig. 2.74. Correlation spectrum from $^{154}Sm + ^{26}Mg$ reaction at 120 MeV. The energy scale is 80 channels = 1 MeV.

At the highest frequency, $(E_\gamma/2)_{max}$ = 0.5 MeV, $\mathcal{J}^{(1)}_{eff}$ was estimated to be 174 MeV^{-1} from the γ-ray multiplicity data. This indicates ≈ 30% noncollective contribution to the total angular momentum at the maximum spin of 40 produced in this reaction.

In the cranking model the value of $\mathcal{J}^{(2)}$ depends explicitly on the rotational frequency and implicitly on nuclear deformation parameters and the pairing correlation. If we only consider quadrupole deformations (β and γ), then a large β value leads to a large $\mathcal{J}^{(2)}$ if γ is near zero. When the value of γ changes from 0° to 60°, the nuclei become less collective, and more angular momentum is carried by single-particle motion and $\mathcal{J}^{(2)}$ will decrease. Similarly, the rotational alignment of high-j orbitals will also decrease the value of $\mathcal{J}^{(2)}$. Therefore, as more orbitals are aligned at high ω, $\mathcal{J}^{(2)}$ will decrease if deformation and pairing correlation remain constant. Pairing is another important factor. When pairing is reduced by Coriolis anti-pairing effect, both $\mathcal{J}^{(1)}$ and $\mathcal{J}^{(2)}$ will increase.

A cranked shell model calculation[5] of the potential energy function of ^{176}W in the (β,γ) plane shows a constant deformation up to spin 50. If this calculation is realistic, then the observed increase of $\mathcal{J}^{(2)}$ is not likely to be due to the change of the deformation. Similarly, since the effect of rotational alignment causes a reduction of the second moment of inertia, neither can it be a major effect. Therefore, it is likely that the increase of $\mathcal{J}^{(2)}$ is due to a reduction in the pairing correlation. As has been pointed out by Bohr and Mottelson,[6] the value of $\mathcal{J}^{(2)}$ will increase and exceed the rigid rotor value before the collapse of pairing and will be reduced to the rigid rotor value afterward. However, our measured value of $\mathcal{J}^{(2)}$ does not exceed the rigid rotor value of 165 MeV^{-1} up to ħω = 0.47 MeV. This may indicate that the pairing correlation has not completely vanished at this frequency.

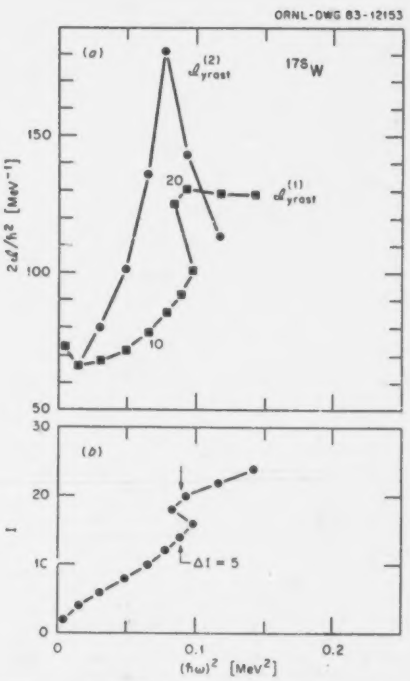

Fig. 2.75. (a) The first and second moments of inertia for ^{176}W derived from discrete yrast transition. (b) Spin of the yrast states as a function of the square of rotation frequency.

---

1. Summary of a paper to be published.
2. Brookhaven National Laboratory and Oak Ridge National Laboratory.
3. University of Pittsburgh, Pittsburgh, PA.
4. G.D. Dracoulis et al, J. Phys. G: Nucl. Phys. 4, 713 (1978).
5. S. Åberg, Phys. Scrip. 25, 23 (1983).
6. A. Bohr and B. Mottelson, Phys. Scrip. 24, 71 (1981).

NUCLEAR STRUCTURE

PRECISION MASS DIFFERENCE MEASUREMENTS IN LIGHT RUBIDIUM AND KRYPTON ISOTOPES UTILIZING BETA ENDPOINTS[1]

D.M. Moltz[2] K.S. Toth
F.T. Avignone, III[2] H. Noma[2]
B.G. Ritchie[2] B.D. Kern[3]

Many mass measurements have been made utilizing direct reaction measurements and discrete energy charged-particle spectroscopy. However, mass determinations on a vast majority of nuclides far from stability require accurate spectroscopic information combined with mass differences derived from β-endpoint measurements. These are fraught with inconsistencies due to the continuous nature of β spectra. A technique for precise determination of β endpoints with an intrinsic germanium detector[4] has been developed and checked with ^{27}Si and ^{58}Cu sources.

Beta-gamma coincidence data were obtained, along with the singles spectra for mass separated samples of ^{77}Rb, ^{76}Rb and ^{77}Kr. A typical gamma-gated beta spectrum is shown in Fig. 2.76. By deriving endpoints from several such spectra, composite Q values were obtained. Q_{EC} values of 5277 ± 26, 8063 ± 44, and 2760 ± 42 keV were determined for ^{77}Rb, ^{76}Rb, and ^{77}Kr. These values were combined with known daughter masses to provide new determinations for comparison with the direct rubidium mass measurements[5] and with various mass formulae. Within error bars, our measured values agree well with previous measurements, but do not necessarily agree with the various mass formula predictions. Some ideas concerning these discrepancies have been presented elsewhere.[6]

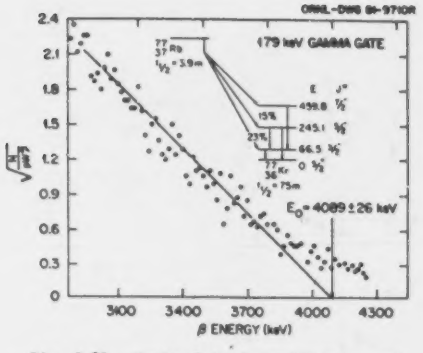

Fig. 2.76. Kurie plot of the 179-keV gated data from the decay of ^{77}Rb. Only one-third of the data points have been plotted.

Such ideas, however, require large quantities of systematic data or, as in this case, many new mass measurements. A recent foray into this region consisted of direct mass measurements[4] for most of the light rubidium isotopes. More recently, we have begun a systematic study[5] of the light neutron-deficient isotopes of rubidium and krypton to determine accurate beta endpoints with an intrinsic germanium detector. Not all of the light krypton isotopes, however, were suitable for beta endpoint analysis. It was thus decided to employ reaction studies to measure several light krypton masses.

Alpha-particle beams from the Texas A&M University 224-cm cyclotron were incident upon enriched krypton gas targets. The masses of ^{76}Kr and ^{74}Kr were determined by measuring the Q values for the ^{78}Kr(^{4}He,^{6}He)^{76}Kr reaction at $E_{^4He}$ = 79.7 MeV and for the ^{78}Kr(^{4}He,^{8}He)^{74}Kr at $E_{^4He}$ = 102.7 MeV. The spectrum arising from the former reaction is shown in Fig. 2.77. The final mass excesses of -68971 ± 13 and -62210 ± 75 keV for ^{76}Kr and ^{74}Kr, respectively, were found to compare favorably with some mass formulae predictions but not with others. These differences have been postulated as arising to the strong prolate deformation[6] known to exist in this region.

1. Summary of published paper; D.M. Moltz et al., Phys. Lett. 113B, 16 (1982).
2. University of South Carolina, Columbia, SC.
3. University of Kentucky, Lexington, KY.
4. F.T. Avignone, III, et al., Nucl. Instrum. Meth. 189, 453 (1981).
5. G. Audi et al., Nucl. Phys. A378, 443 (1982).
6. D.M. Moltz et al., Phys. Rev. C26, 1914 (1982).

MASSES OF ^{76}Kr AND ^{74}Kr[1]

D.M. Moltz[2] K.S. Toth
R.E. Tribble[3] R.E. Neese[3]
J.P. Sullivan[3]

A study of the mass systematics of nuclei far from stability is a sensitive way of comparing nuclear models. It also presents an interesting method for demonstrating specific nuclear phenomena. For instance, model-independent two-neutron separation energies (S_{2n}) readily exhibit the standard nuclear shell structure.

1. Summary of published paper; D.M. Moltz et al., Phys. Rev. C16, 1914 (1982).
2. University of South Carolina, Columbia, SC.
3. Texas A&M University, College Station, TX.
4. G. Audi et al., Nucl. Phys. A378, 443 (1982).
5. D.M. Moltz et al., Phys. Lett. 113B, 16 (1982).
6. C.J. Lister et al., Phys. Rev. Lett. 49, 308 (1982).

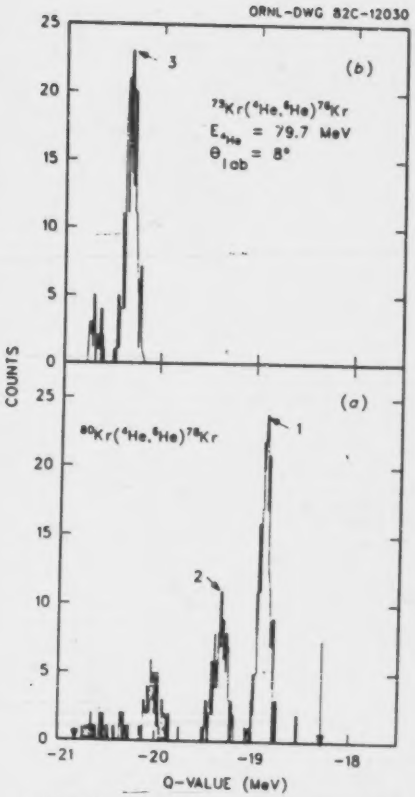

Fig. 2.77. Gated ^{6}He positron spectra at $E_{^4He}$ = 79.7 MeV for the reactions: (a) ^{80}Kr(^{4}He,^{6}He)^{78}Kr and (b) ^{78}Kr(^{4}He,^{6}He)^{76}Kr. Large arrows indicate detector limits. Peaks labeled by numerals correspond to: (1) ^{76}Kr ground state, (2) first 2^+ excited state in ^{78}Kr, and (3) ^{76}Kr ground state.

BETA DECAY OF ^{75}Rb TO LOW-LYING LEVELS IN ^{75}Kr[1]

B.D. Kern[2] K.S. Toth
D.M. Moltz[3] J. Lin[4]
F.T. Avignone, III[3] H. Noma[3]
G.A. Leander[5]

Recent spectroscopy on nuclei surrounding ^{75}Kr in the N vs. Z plane indicate that this is a collective phase transition region.[6,7] Some nuclei located closer to stability, like ^{78}Kr and the selenium isotopes, exhibit the characteristics of large-amplitude anharmonic collective motion. However, as the neutron number goes down toward N = 40, the effective quadrupole deformation increases for Z = 35 (Ref. 6) and Z = 38 (Ref. 7), although it does not do so for Z = 34 and below. In the Z = 36 isotopes ^{74,76}Kr, two low-lying K = 0 bands have been inferred from available data,[8] one with a large moment of inertia, which suggests that a second distinct intrinsic structure comes down in energy with decreasing neutron number. Spectroscopy on the nucleus ^{75}Kr should help to probe the nature of the structure in the neighboring cores.

The isotope ^{75}Rb was produced via the ^{58}Ni(^{20}Ne,p2n) reaction and mass separated with the UNISOR on-line separator. Its half-life was determined to be 21.4 ± 1.0 sec. Twenty-one γ rays were placed in a partial decay scheme (Fig. 2.78) with levels in ^{75}Kr up to 1042.4 keV in excitation. The data are consistent with the existence of previously proposed[9,10] bands built on the $5/2^+$ ground and $3/2^-$ first-excited states in ^{75}Kr.

A theoretical analysis of the ^{75}Kr spectrum was made within the framework of core-particle coupling. The effective quadrupole field of the core was simulated by a triaxial rotor, adiabatic odd-nucleon orbitals near the Fermi level were calculated via the Nilsson model, and the rotational couplings diagonalized as in Ref. 11. Parameters were varied to see which values were compatible with the experiment.

The possibility of a negative intrinsic quadrupole moment, or oblate shape, is definitely excluded. Even a triaxial shape, which can be used to account for the spectra of ^{75,77}Se and ^{79}Kr (Ref. 11), is unlikely because it would imply additional low-spin states of low excitation energy which are not observed in the β-decay scheme (Fig. 2.78). Below about 500 keV in both ^{75}Kr and ^{77}Kr (Ref. 12), which have rather similar spectra, there is evidence for

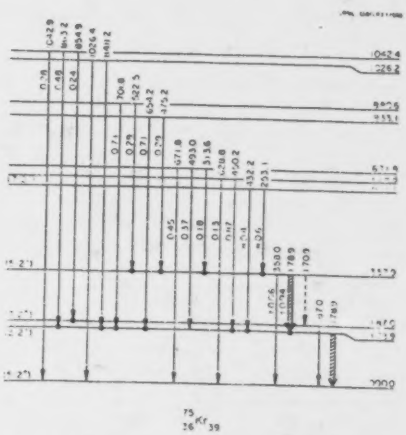

Fig. 2.78. Partial decay scheme of ^{75}Rb. Energies are expressed in keV. Dots indicate observed coincidence sequences.

only two rotational bands. This indicates a prolate shape and likely Nilsson assignments are 3/2⁻[301] and 5/2⁺[422]. The positive-parity band can be identified from higher spin states observed in-beam as being of high-j ($g_{9/2}$) origin. The nonobservation of other bands also constrains the magnitude of the quadrupole deformation to $\varepsilon = 0.35 \pm 0.05$ for ^{75}Kr, and somewhat smaller ε or more triaxiality for ^{77}Kr.

The experimental moment-of-inertia parameters, $\hbar^2/2\mathcal{I}_0$, for the 5/2⁺ bands are 26.6 and 17.4 keV in ^{75}Kr and ^{77}Kr, respectively, and for the 3/2⁻ bands 36.0 and 34.9 keV, respectively. The values in ^{74,76}Kr deduced by Piercey et al.[8] are <40 keV and >70 keV for the two coexisting 0⁺ bands. The theoretical 3/2⁻[301] band is hardly influenced by Coriolis coupling to other one-quasiparticle bands, so these moments of inertia may be taken to suggest that the 3/2⁻ band arises from coupling to the more deformed core configuration. The further lowering of $\hbar^2/2\mathcal{I}_0$ for the 5/2⁺ bands is readily accounted for by single-particle alignment in the $g_{9/2}$ shell.

---

1. Summary of paper to be published.
2. University of Kentucky, Lexington, KY.
3. University of South Carolina, Columbia, SC.
4. Present address: Hewlett-Packard Corp., Palo Alto, CA.
5. UNISOR, Oak Ridge, TN.
6. G. Winter et al., Nucl. Phys. A367, 95 (1981).
7. C.J. Lister et al., Phys. Rev. Lett. 49, 308 (1982).
8. R.B. Piercey et al., Phys. Rev. C25, 1941 (1982); R.B. Piercey et al., Phys. Rev. Lett. 47, 1524 (1982).
9. A.V. Ramayya and J. Eberth, Lecture Notes in Physics No. 168: Heavy Ion Collisions, ed. by G. Madurga and M. Lozano (Springer, Berlin, 1982).
10. G. Winter et al., Z. Phys. A309, 243 (1983).
11. S.E. Larsson, G. Leander and I. Ragnarsson, Nucl. Phys. A307, 189 (1978).
12. E. Nolte and P. Vogt, Z. Phys. A275, 33 (1975).

LEVELS IN ^{76}Kr[1]

D.M. Moltz[2] K.S. Toth
H. Noma[2] F.T. Avignone, III[2]
B.D. Kern[3] R.E. Tribble[4]
R.E. Neese[4] J.P. Sullivan[4]
J. Lin[5]

As part of our program[6,7] to measure masses in the region of A = 75 to A = 80 the beta decay of mass-separated ^{76}Rb and the ^{78}Kr(^{6}He,^{6}He) reaction at E_{lab} = 102.7 MeV were used to investigate levels in ^{76}Kr. For a more complete picture of ^{76}Kr level structure these two sets of data were then compared and combined with results from the extensively publicized[8] ^{66}Zn(^{12}C,2n) in-beam γ-ray investigation and from the recent ^{78}Kr (p,t) reaction study.[9]

The decay information was used to construct a decay scheme (Fig. 2.79) for ^{76}Rb which incorporates 38 transitions and 16 excited levels.

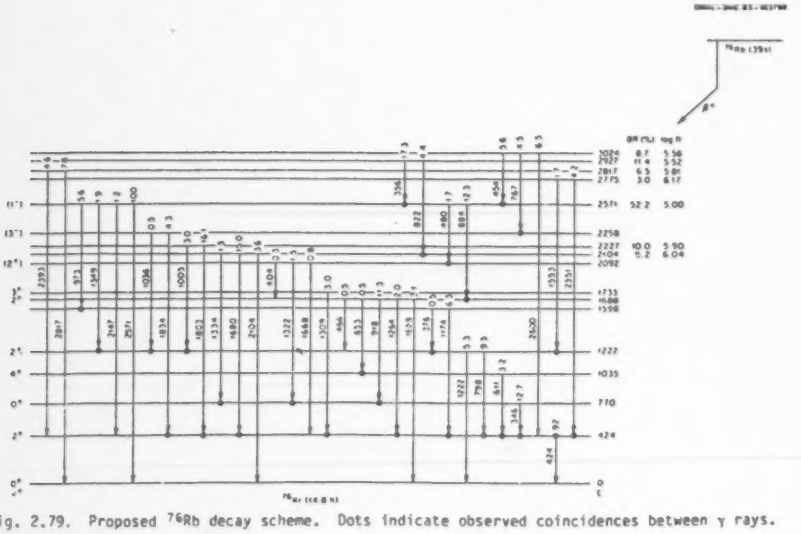

Fig. 2.79. Proposed ^{76}Rb decay scheme. Dots indicate observed coincidences between γ rays.

This scheme is much more complete than the adopted one.[10] In addition, our data show that most of the beta-decay strength proceeds to levels above 2 MeV in contrast to the earlier proposition[10] that ^{76}Rb decay populates primarily the ground-and first-excited states in ^{76}Kr.

Data obtained from the ^{78}Kr(^{4}He,^{6}He) reaction were compared with the ^{78}Kr(p,t) results.[9] On a relative basis the cross sections from these two-neutron-transfer reactions are in general agreement. Within our statistics we did not observe the 0_2^+ state at 770 keV. The (p,t) reaction[9] does excite this state but with an intensity of only ~1% of the ground state transition indicating very different wave functions for the 0_1^+ and 0_2^+ states. Indeed this 0_2^+ level has been suggested to be a β vibrational state. Because of the physical limitations of our focal plane detector, we were unable to check the enhanced transition strengths observed[9] to populate 3^- levels above 2.2 MeV in excitation.

Table 2.16 summarizes the properties of ^{76}Kr levels (up to ~ 3 Mev) as observed in Refs. 8 and 9 and in the present investigation. The final column in the table lists the J^π assignments that we adopt for levels seen in ^{76}Rb decay. Based on these decay data we propose a 1^- $\frac{3}{2}$[312], $\nu 5/2$[422]) configuration for the ^{76}Rb ground state. This combination of Nilsson orbitals agrees with the measured spin value[11,12] of 1 and a magnetic moment[12] of -0.548 μ_N for ^{76}Rb.

---

1. Summary of paper to be published.
2. University of South Carolina, Columbia, SC.
3. University of Kentucky, Lexington, KY.
4. Texas A&M University, College Station, TX.
5. Tennessee Technological University, Cookeville, TN.
6. D.M. Moltz et al., Phys. Lett. 113B, 16 (1982).
7. D.M. Moltz et al., Phys. Rev. C26, 1914 (1982).
8. R.B. Piercey et al., Phys. Rev. C25, 1941 (1982) and references therein.
9. S. Matsuki et al., Nucl. Phys. A370, 1 (1981).
10. F.E. Bertrand and R.L. Auble, Nucl. Data Sheets 19, 507 (1976).
11. H. Fischer et al., Z. Phys. A284, 3 (1978).
12. C. Thibault et al., Phys. Rev. C23, 2720 (1981).

Table 2.16. Levels in ^{76}Kr (all energies are expressed in keV).

^{66}Zn(^{12}C,2nγ)a)		^{78}Kr(p,t)b)		^{78}Kr(^{4}He,^{6}He)c)	^{76}Rb Decay c)	
E_{level}	J^π	E_{level}	J^π	E_{level}	E_{level}	Adopted J^π
0.0	0^+	0.0	0^+	0.0	0.0	0^+
423.9	2^+	424	2^+	424	424.0	2^+
769.6	0^+	762	0^+		770.0	0^+
1034.7	4^+	1041	4^+		1034.8	4^+
1221.5	2^+	1218	2^+	1214	1221.8	2^+
					1598.3	
1688		1681	2^+	1693	1687.7	2^+
1732.6	3^+				1732.9	3^+
1859.5	6^+					
1957.6	4^+					
		2079	$2^+,3^-,4^+$	2095	2091.6	(2^+)
					2104.4	
		2260	3^-		2227.3	
2451.8	(5^+)				2257.6	(3^-)
					2571.3	(1^-)
		2601	$3^-,4^+$			
2683.5	5^-					
		2697	2^+			
2762.8	6^+					
					2775.0	
		2872	3^-		2816.7	
2879.6	8^+					
					2926.9	
					3024.5	

a)Ref. 8.
b)Ref. 9.
c)Present study.

OVERLAPPING β DECAY AND RESONANCE NEUTRON SPECTROSCOPY OF LEVELS IN ^{87}Kr[1]

S. Raman B. Fogelberg[2]
J. A. Harvey[3] R. L. Macklin[3]
P. H. Stelson A. Schröder[4]
K.-L. Kratz[4]

Energy levels in ^{87}Kr have been studied, with special emphasis on the unbound region, using two different methods. The first method comprises neutron capture and transmission measurements on an enriched gas target of ^{86}Kr using neutron time-of-flight techniques. In this way, neutron widths were determined for 39 resonances below 400 keV and capture areas for 14 resonances below 90 keV. The second method is a decay study of 56-s ^{87}Br in which a level scheme for ^{87}Kr has been established that shows 126 levels in the bound and 12 levels in the unbound region. A detailed comparison amongst the neutron resonance, the γ-ray decay, and available delayed neutron results has been made. Almost a one-to-one correspondence exists between the currently observed p-wave resonances below 250 keV and levels in ^{87}Kr studied through delayed neutron emission. The overall β-strength distribution derived from the present data shows broad resonance like structures. However, no marked selectivity is observed in the β decay to individual levels in the unbound region of ^{87}Kr. The neutron capture cross section of ^{86}Kr is found to be about 5 mb for 30-keV neutrons with a Maxwellian energy distribution. The future of delayed neutron spectroscopy as a new tool for obtaining level-density information is discussed.

---

1. Abstract of paper: Phys. Rev. C 28, 602 (1983).
2. Guest scientist from the Studsvik Science Research Laboratory, S-611 82 Nyköping, Sweden.
3. Engineering Physics Division, ORNL.
4. Institut für Kernchemie, Universität Mainz, D-65 Mainz, Federal Republic of Germany.

EXCITED STATES OF ^{96}Ru[1]

T. A. Walkiewicz[2] S. Raman
J. B. McGrory

The nuclear excited states of ^{96}Ru were studied by means of the decays of 9.25-min and 1.55-min ^{96}Ru isomers, and the ^{93}Nb(^{6}Li,3nγ) reaction. Approximately 140 γ rays measured in these experiments were incorporated into a level scheme consisting of approximately 50 excited states. The experimental level scheme is compared with a level scheme calculated on the basis of the shell model.

---

1. Abstract of paper: Phys. Rev. C 27, 1710 (1983).
2. Edinboro State College, Edinboro, Pennsylvania.

LOW-LYING 1^+ AND 2^- STATES IN DOUBLY-ODD TERBIUM, HOLMIUM AND THULIUM NUCLEI[1]

K.S. Toth D.M. Moltz[2]
Y.A. Ellis-Akovali R.L. Mlekodaj[3]

In the electron-capture plus positron (E.C.+β^+) decays of ^{148,150,152}Dy only one γ ray has been observed.[4-7] This concentration of decay strength results in β transitions which are allowed, log ft ~ 4.0, and which populate single 1^+ levels in the respective terbium daughters. The lone γ rays that deexcite these 1^+ states have E1 multipolarities[5,7] so that the connected levels are either 0^-, 1^-, or 2^-. Because other coincident transitions have not been seen, these final levels are assumed[4-7] to be the low-spin isomers in ^{148,150,152}Tb whose decay patterns are most consistent with 2^- assignments.

The existence of similar levels in nuclei with N=83, 85, and 87 raises questions concerning the nature of their configurations. To provide additional insight, we investigated the (E.C.+β^+) decay properties of ^{150,152,154}Er and ^{156}Yb. Once again, only single γ rays were identified in each of the four decays. The resultant log ft values range from 3.7 to 4.2, so that the levels in the daughter nuclei are fed by allowed β transitions and therefore have 1^+ assignments. In addition, the multipolarities of the ^{152}Er and ^{156}Yb γ rays were determined to be E1. It therefore appears that the levels fed by these single γ rays are the known 2^- isomers in ^{150,152,154}Ho and ^{156}Tm.

In Fig. 2.80 the excitation energies of the 1^+ states relative to those of the 2^- levels are plotted as a function of neutron number. For holmium and terbium nuclei there is a regular compression in energy spacing both as N and Z increase; it would thus appear that these levels have similar configurations.

Nuclei with a few nucleons beyond closed shells are usually regarded as being spherical. In the rare earth region there is a closure at Z=64 after the $g_{7/2}$ and $d_{5/2}$ orbitals have been filled, so that for terbium, holmium, and thulium nuclei these orbitals are hole states, while the $h_{11/2}$, $s_{1/2}$, and $d_{3/2}$ orbitals lie above the Fermi surface. Beyond N=82, the first available neutron orbitals are $f_{7/2}$, $h_{9/2}$ and $f_{13/2}$. While the 1^+ states can be expressed as $1^+\{\pi h_{11/2}, \nu h_{9/2}\}$, no reasonable combination of low-lying spherical shell model states can couple to 2^-.

Small quadrupole deformations in these N>83 nuclei were considered to describe the 1^+ and 2^- level structures and decay properties. A search for possible descriptions by oblately deformed configurations yielded negative results. For ^{148}Tb and ^{150}Ho the $1^+\{\pi 3/2[541], \nu 1/2[541]\}$ and $2^-\{\pi 5/2[402], \nu 1/2[541]\}$ configurations corresponding to a prolate deformation can explain the level properties adequately. The β decays

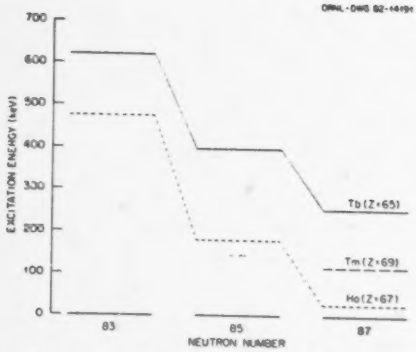

Fig. 2.80. Excitation energies of 1^+ levels relative to the low-spin isomers in doubly-odd terbium, holmium, and thulium nuclei with N=83, 85, and 87.

of ^{148}Dy and ^{150}Er to the 1^+ levels would involve $\pi 3/2[541] \rightarrow \nu 1/2[541]$ transitions. There are two sets of probable quasiparticle configurations which, as the main components for the 1^+ and 2^- in the N=85 and N=87 nuclei, can explain their properties: $1^+\{\pi 3/2[541], \nu 1/2[530]\}$, $2^-\{\pi 5/2[402], \nu 1/2[530]\}$; and, $1^+\{\pi 5/2[532], \nu 3/2[532]\}$, $2^-\{\pi 7/2[404], \nu 3/2[532]\}$. The β decays then occur through either $\pi 3/2[541] \rightarrow \nu 1/2[530]$ or $\pi 5/2[532] \rightarrow \nu 3/2[532]$ transitions, respectively. In all cases, the E1 transitions from the 1^+ to 2^- states involve a change in proton orbitals.

We conclude that the properties of 1^+ and 2^- states in doubly-odd terbium, holmium, and thulium isotopes with only a few nucleons above the closed proton Z=64 and neutron N=82 shells can be explained by invoking prolate deformations for these nuclei. The excitation energies of the 1^+ states for isotopes with the same neutron number (Fig. 2.80) can be considered as an indication of a gradual change in the nuclear deformations.

---

1. Summary of paper: Phys. Lett. 117B, 11 (1982).
2. Guest Scientist from the University of South Carolina., Columbia, SC.
3. UNISOR, Oak Ridge, Tennessee.
4. K.S. Toth, C.R. Bingham and W.-D. Schmidt-Ott, Phys. Rev. C10, 2550 (1974).
5. M.D. Devous, Sr., and T.T. Sugihara, J. Inorg. Nucl. Chem. 36, 1697 (1974).
6. K.S. Toth et al., Phys. Rev. C11, 1370 (1975).
7. K.Ya. Gromov et al., Acta Phys. Pol. B6, 421 (1975).

FIRST-EXCITED 0^+ STATE IN ^{144}Nd[1]

K. S. Krane[2] S. Raman
F. K. McGowan

Gamma-ray angular correlation measurements have led to a definite identification of the 2084.5-keV level as the first-excited 0^+ state in ^{144}Nd. This level is in good accord with the predictions of both the unified model and the interacting boson approximation model.

---

1. Abstract of paper: Phys. Rev. C 27, 2863 (1983).
2. Department of Physics, Oregon State University, Corvallis, Oregon.

SINGLE-PROTON STATES IN ^{147}Tb[1]

K.S. Toth C.R. Bingham[3]
D.M. Moltz[2] M.D. Cable[4]
Y.A. Ellis-Akovali R.F. Parry[4]
J.M. Wouters[4]

Nuclei in the vicinity of N=82 have low-lying levels which are describable in terms of the spherical shell model. Of particular interest are the 82-neutron isotones, since their low-energy structure should arise mainly from excitations of proton orbitals beyond Z=50. In addition, because of the Z=64 subshell closure[5,6] these isotones provide an opportunity for the study of the proton shell structure in a mass region almost midway between Z=50 and Z=82. One nucleus, ^{147}Tb, is especially interesting since its low-lying states should be describable in terms of a proton added to the ^{146}Gd core. With the aid of an on-line isotope separator the decay of ^{147}Dy to levels in ^{147}Tb was investigated in a series of heavy-ion bombardments of rare earth targets. These data allow us to identify the $s_{1/2}$, $d_{3/2}$, $d_{5/2}$ and $g_{7/2}$ (but not the $h_{11/2}$ proton orbitals in ^{147}Tb.

The level order in ^{147}Tb is very different from those in odd-Z N=82 nuclei with Z<63 (Ref. 7) where the $g_{7/2}$ and $d_{5/2}$ orbitals are below the $s_{1/2}$, $d_{3/2}$ and $h_{11/2}$ states. One must remember, however, that the $g_{7/2}$ orbital is a hole state for Z>59 and that the $d_{5/2}$ orbital becomes a hole state in ^{147}Tb. Bearing this in mind, we show in Fig. 2.81 the systematics of single proton levels for N=82 nuclei with hole states indicated as having negative energies. One then sees that the ^{147}Tb levels are not discontinuous with respect to the energies of the $s_{1/2}$, $d_{3/2}$, $d_{5/2}$ and $g_{7/2}$ orbitals in the lower-Z isotones. (There is an indication that the two hole states are more tightly bound in ^{147}Tb.) A concurrent study[8] of ^{147}Tb arrived at the same low-lying structure. However, the investigators, in contrast to our conclusion,

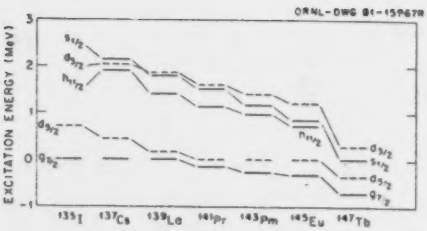

Fig. 2.81. Energy systematics of single-proton states in odd-Z N=82 isotones from ^{135}I to ^{147}Tb.

interpreted the transition between ^{145}Eu and ^{147}Tb as a pronounced discontinuity that lends strong support for a large energy gap in the single-proton spectrum at Z=64. To understand more fully the influence of the Z=64 gap on the quasiparticle energies, levels in the ^{149}Ho need to be investigated.

---

1. Summary of paper: Phys. Rev. C25, 667 (1982).
2. Guest Scientist from University of South Carolina, Columbia,SC.
3. University of Tennessee, Knoxville, TN.
4. Lawrence Berkeley Laboratory, Berkeley, CA.
5. K.S. Toth et al., Phys. Rev. C2, 1480 (1970).
6. W.D. Schmidt-Ott and K.S. Toth, Phys. Rev. C13, 2574 (1976).
7. E. Newman et al., Phys. Rev. C1, 1118 (1970).
8. Y. Nagai et al., Phys. Rev. Lett. 47, 1259 (1981).

INVESTIGATION OF SHORT-LIVED ERBIUM NUCLIDES; SEARCH FOR ^{149}Er

K.S. Toth Y.A. Ellis-Akovali
D.M. Moltz[1] J.D. Cole[2]
D.C. Sousa[3]

Recently we reported[4] on single-proton levels in ^{147}Tb populated in the decay of ^{147}Dy. These data, combined with information on levels in other odd-Z, N = 82 isotones, indicated that the ordering of the $s_{1/2}$, $d_{3/2}$, $d_{5/2}$, $g_{7/2}$, and $h_{11/2}$ proton orbitals behaves smoothly from ^{135}I to ^{147}Tb. There is, however, an indication that they are more tightly bound in ^{147}Tb, perhaps as a result of the Z = 64 closure.

To explore more fully single-particle states in this region, we extended our overall study of low-lying levels near N = 82 to holmium nuclei. Targets of ^{144}Sm and ^{147}Sm were bombarded with ^{12}C ions to produce erbium isotopes. A helium gas-jet system was utilized to transport the radioactive products to a shielded area suitable for γ-ray assay.

A new isotope ^{150}Er ($T_{1/2}$ = 20 ± 2 sec) was identified and found to be associated with only one transition, 476.0 ± 0.1 keV. Similarly, ^{152}Er and ^{154}Er, known previously from their α-decay properties, were also found to have single transitions, 179.3 ± 0.1 and 26.9 ± 0.2 keV, respectively, associated with their (ε.C. + β^+) decays. Up to now the existence of ^{151}Er had been deduced[5] only from an observed growth period in the decay curve of the ^{151}Ho low-spin isomer α group. In the present investigation we confirm its half-life to be 23 sec. Its decay scheme is more complicated than that of the doubly-even erbium nuclides discussed above, with at least three transitions identified so far, 100, 257 and 667 keV.

No γ rays could be ascribed to ^{149}Er decay, despite the fact that ^{149}Ho transitions were observed. There are three possible explanations: (1) The maximum on-target 125-MeV ^{12}C bombarding energy was insufficient to reach the peak of the $^{144}Sm(^{12}C,7n)$ excitation function. (2) The ^{149}Er half-life is much less than the move time, ~ 4s, of the tape collector used to transport the radioactive products to the counting station. (3) Most of the ^{149}Er positron decay strength is concentrated at or near the ^{149}Ho ground state. (4) Erbium-149 has a large probability for β^+-delayed proton emission. (Recent results[6] attribute a delayed-proton branch to ^{147}Dy and the proton binding energy in ^{149}Ho is estimated to be 1 MeV less than that in ^{147}Tb).

---

1. University of South Carolina, Columbia, SC.
2. Louisiana State University, Baton Rouge, LA.
3. Eastern Kentucky University, Richmond, KY.
4. K.S. Toth et al., Phys. Rev. C25, 667 (1982).
6. K.S. Toth et al., Phys. Rev. C2, 1480 (1970).
7. O. Klepper et al., Z. Phys. A305, 125 (1982).

ELECTRIC DIPOLE TRANSITIONS FROM NEUTRON CAPTURE IN ^{167}Er RESONANCES[1]

S. Kahana[2] S. Raman
G. G. Slaughter C. Coceva[3]
M. Stefanon[3]

Primary neutron capture γ rays have been studied from 86 neutron resonances in ^{167}Er in the 5-600 eV energy range. The spins of these resonances are assigned as I=3 or I=4 on the basis of the intensity ratios of suitable pairs of low-energy γ rays. The measured intensities of the high-energy primary γ rays have been converted to partial radiation widths and further analyzed to obtain average E1-gamma strength. Individual γ spectra from I=3 and I=4 resonances were summed separately after appropriate normalization. The resulting average radiation widths (and hence the gamma ray strength function) were in good agreement with the Axel-Brink predictions based on a giant dipole resonance model. These widths were also consistent with the assumption that the γ-strength is independent of the initial spin. The

partial E1 radiation widths were subjected to a distribution analysis yielding the result that these widths had a slightly narrower distribution than that predicted by the Porter-Thomas law. The ratio of the average population of a particular low-lying level from I=4 resonances to its population from I=3 resonances was found to be in good agreement with a five-step cascade model. The populations of successive spins within a rotational band lie on smooth curves which, for different bands, are nearly parallel. A level scheme for ^{169}Er was constructed and the neutron separation energy for this nucleus was deduced as 7771.6±1.0 keV.

---

1. Abstract of paper to be published.
2. Guest scientist from the Nuclear Research Centre-Negev, Beer Sheva, Israel.
3. ENEA, CRE "E-Clementel," Bologna, Italy.

POPULATION OF ENTRY STATES FOLLOWING HEAVY-ION FUSION REACTIONS

ENTRY-STATE POPULATIONS IN FUSION OF Ne + Nd AND THE HIGH-SPIN STRUCTURE OF $^{157-161}$Yb

D. G. Sarantites[1] J. R. Beene
M. Jääskeläinen[1,2] D. C. Hensley
F. A. Dilmanian[1,3] M. L. Halbert
R. Woodward[1] W. T. Milner
H. Puchta[1,4] J. H. Barker[5]
J. Hattula[2]

The Spin Spectrometer is a 4π array of NaI detectors[6] designed to measure the number, energy, angle, and timing of all γ rays associated with a nuclear reaction. The population of the entry states, that is, the states in which the residual nuclei are left after all particles have been emitted, may be deduced from measurements of the total pulse height H and the γ-ray coincidence fold k since these quantities are closely related to the excitation energy E* and the spin I of the entry state.

The first use of the Spectrometer was for studies with ORIC of the fusion-evaporation reaction ^{146}Nd + ^{20}Ne at 136 MeV.[7] One of the NaI detectors was replaced by a Ge counter which served as the trigger for recording events on magnetic tape. Off-line selection of exit channels for xn and αxn evaporation was made by gating on known γ transitions in the corresponding product nuclei. The (H,k) entry-state distributions for 6n product, ^{160}Yb, are shown in Fig. 2.82a. These and similar distributions were transformed to (E*,M_γ) space on the basis of responses measured with γ-ray sources. Figure 2.82b shows the results for the strongest xn channels.

To compare these results with expectations from the statistical model, the Monte-Carlo code JULIAN-PACE[8] was modified to include a more realistic treatment of γ decay.[7] In particular, the E1 decay probability included the giant resonance with a strength equal to the energy-weighted sum rule. The results of a typical calculation in (E*,I) space are shown in Fig. 2.82c and in (E*,M_γ) space by Fig. 2.82d.

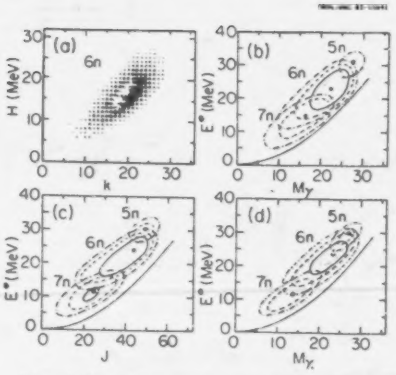

Fig. 2.82. Entry-state distributions for xn products from 136-MeV ^{20}Ne on ^{146}Nd. (a) Experimental density map in (H,k) space for the 6n channel. (b) Contour maps of experimental results in (E*,M_γ) space for the strongest xn channels. (c) Contour maps of calculated results in (E*,I) space from the statistical model. (d) Contour map of results in (E*,M_γ) space from the same calculations as in (c). The cross-section contours in (b), (c) and (d) decrease going outward by the factors of 1.4, 2.0, 4.0, and 8.0 relative to the peak value of the 6n channel and are represented by the dotted, full, dashed and dash-dotted curves, respectively. The heavy dots locate the maximum intensity for each channel. The ^{160}Yb yrast line used in the calculations is shown by the curve below the contours.

Comparison of Fig. 2.82d with 2.82b shows clearly that the data are well represented by the statistical model with these realistic γ-decay parameters.

The experimental entry lines (average E* vs. M_γ) for ^{160}Yb and ^{161}Yb show a bending down from the calculated lines at large M_γ which suggested that ΔI = 1 transitions might be important for I ≳ 45. Additional experiments were run in which ^{20}Ne at 149 MeV bombarded ^{146}Nd and ^{144}Nd.[9,10] Similar bending of the entry lines was found for $^{158-161}$Yb, commencing at lower M_γ for the lighter isotopes (see Fig. 2.83). In ^{158}Yb, the bend straightens out at still higher M_γ, signifying the disappearance of the excess ΔI = 1 transitions.

Unfolded γ-ray energy spectra are shown in Fig. 2.84 for a number of M_γ bins for these five nuclei. In ^{161}Yb, the incremental yield with increasing M_γ appears at higher and higher E_γ except for the M_γ = 29 bin, where most of the increment appears at ~ 0.7 MeV. The same thing occurs in the lighter isotopes of Yb for progressively lower M_γ bins. In ^{158}Yb, the increment from M_γ = 25 to 28 is localized again primarily at high E_γ (~ 1.3 MeV).

The γ-ray angular distributions show that the peak at ~ 0.7 MeV is consistent with stretched

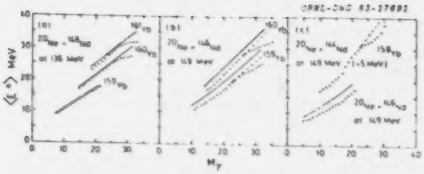

Fig. 2.83. Experimental (data points) and calculated (solid curves) entry lines $\langle E^x \rangle$ vs. M_γ, for $^{159-161}$Yb from (a) 136-MeV and (b) 149-MeV reactions of ^{20}Ne + ^{146}Nd, and (c) for ^{158}Yb from 149-MeV reactions of ^{20}Ne on ^{144}Nd (shifted by +5 MeV) and on ^{146}Nd. The dashed lines are empirical curves showing extrapolations of smooth curves through the data in order to locate the positions of the change in slope. They are nearly parallel to the calculated entry lines.

dipole emission while the higher energy region is stretched quadrupole. This may be demonstrated by the anisotropies shown in Fig. 2.85. The dip near E_γ = 0.6-0.7 MeV indicates the presence of stretched dipole radiation at high M_γ. This dip is absent or seen only weakly at the low M_γ. For E_γ from ~ 0.8 to ~ 1.4 MeV, the anisotropy is ~ 1.4, characteristic of the stretched quadrupoles expected in the "yrast bump." Above E_γ = 1.4 MeV, the data approach the isoptropy expected for a statistical mixture of stretched and unstretched E1 radiation.

Our observations may be summarized as follows. At low spin, these nuclei are known to be prolate rotors, and the spectra show only stretched quadrupoles being added as the spin increases. Some evidence for possible non-collective effects appears at moderate spins, but a most dramatic change occurs at high spins (I ~ 40 in ^{158}Yb, I ~ 45 in ^{160}Yb). A strong stretched-dipole component appears at about half the energy of the quadrupole edge, accounting for ~ 50% of the additional transitions that cause the flattening of the entry lines. At still higher spins, these dipoles disappear (I ~ 49 in ^{158}Yb). The stretched-quadrupole component continues to evolve in the normal way over the entire range of spins and becomes the sole component for I > 49 in ^{158}Yb.

These observations are consistent with theoretical predictions by Bengtsson et al.,[11] for the even Yb isotopes. The nuclei are prolate at low spin and become oblate as their spin increases. In such nuclei the yrast states are expected to be members of high-K bands connected by M1 transitions having half the energy of the E2 transitions. The disappearance of the dipole transitions in ^{158}Yb may be due to a move toward a triaxial shape. Further details on the data and this possible interpretation may be found in Refs. 9 (for ^{160}Yb), Ref. 10 (for ^{158}Yb), and Ref. 12 (for the evolution from ^{157}Yb to ^{161}Yb).

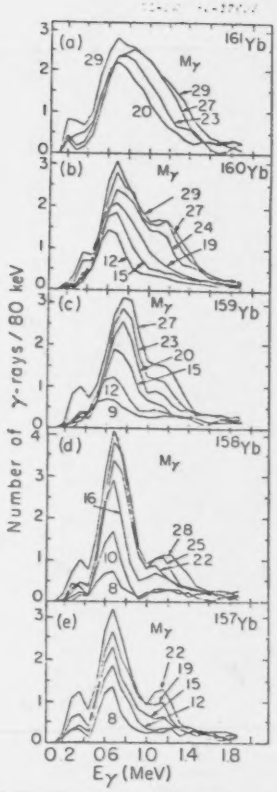

Fig. 2.84. Continuum γ-ray spectra for $^{157-161}$Yb for bins centered on the indicated values of M_γ. The beams and targets were (a): 136-MeV ^{20}Ne on ^{146}Nd, (b)-(c): 149-MeV ^{20}Ne on ^{146}Nd, (d)-(e): 149-MeV ^{20}Ne on ^{144}Nd.

1. Washington University, St. Louis, Missouri 63130.

2. Present address: Department of Physics, University of Jyväskylä, Finland.

3. Present address: Elscint Ltd., Haifa 310501, Israel.

4. Present address: Sektion Physik, Universität München, 8046 Garching, West Germany.

5. Present address: South Carolina Electric & Gas Company, P.O. Box 764, Columbia, South Carolina 29218.

6. M. Jääskeläinen et al., Nucl. Instrum. Methods 204, 385 (1983).

7. D. G. Sarantites et al., Phys. Lett. 115B, 441 (1982).

8. A. Gavron, Phys. Rev. C 21, 230 (1980).

9. M. Jääskeläinen et al., Phys. Rev. Lett. 49, 1387 (1982).

10. M. Jääskeläinen et al., Phys. Lett. 119B, 65 (1982).
11. R. Bengtsson et al., Phys. Lett. 57B, 301 (1975).
12. M. Jääskeläinen et al., Dynamics of Nuclear Collective Motion, ed. K. Ogawa and K. Tanabe, (Institute for Nuclear Study, University of Tokyo, 1982), p. 51.

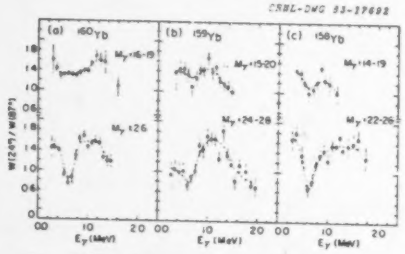

Fig. 2.85. Anisotropies of the γ-ray continuum as a function of E_γ for (a) ^{160}Yb, (b) ^{159}Yb, and (c) ^{158}Yb. The M_γ values give the half maximum limits of the corresponding k bins. The dashed lines guide the eye.

ENTRY STATE DISTRIBUTIONS OF DISCRETE YRAST TRANSITIONS IN HEAVY ION INDUCED FUSION REACTIONS[1]

I.Y. Lee, C. Baktash, J.R. Beene, M.P. Fewell, M.L. Halbert, N.R. Johnson, F.K. McGowan, W.T. Milner, H. Kim, D.G. Sarantites, R.O. Sayer

The compound nucleus formed in a heavy ion induced fusion reaction usually has a large amount of excitation energy and angular momentum. The emission of particles proceeds immediately and brings the nuclear excitation energy down to about one neutron binding energy above the yrast line. From there, γ-decay removes the rest of the excitation energy and angular momentum. The point at which γ-ray emission begins is called the entry state and it has a wide distribution both in angular momentum and excitation energy.

Entry state distribution for various residual nuclei in a fusion reaction have been measured by Sarantites et al.[2] They found that different Xn channels had different entry state distributions, and that usually the channel emitting the least number of neutrons, had highest angular momentum and excitation energy. On the surface it seems reasonable to expect that for a given residual nucleus, the entry state distributions will also depend on the fine details of the regions of H and K selected for the gating process. However, it is important that we make measurements of these distributions to establish how the yrast states are populated from the entry region. Also, if large differences in entry distributions are observed between the low spin and the high spin states, then this becomes a valuable mechanism to enhance the population of high spin states for discrete line spectroscopy.

The present experiments were carried out by using the spin-spectrometer with two of its NaI elements replaced by high resolution Ge detectors. Coincidence data between either of the Ge detectors and the spin spectrometer were taken. In the off-line analysis, the total pulse height (H) and coincidence fold (K) were obtained for each event from the pulse height of the individual NaI detectors, after energy calibration and the removal of neutron pulses. The two dimensional distribution of (H,K) were then obtained by sorting events in coincidence with discrete transitions and correcting this with data from several background regions of the Ge spectra. These corrected data provide the information necessary to determine the entry distributions of the discrete yrast transitions.

From these (H,K) distributions, the average values of H and K can be calculated. These values for the yrast states of ^{158,159}Er from the ^{150}Sm(^{12}C,Xn) reaction and for ^{130}Ce from the ^{100}Mo(^{34}S,4n) reaction are plotted in Figs. 2.86 and 2.87, respectively.

In Fig. 2.86, it can be seen as expected that the 4n channel which produces ^{159}Er has lower

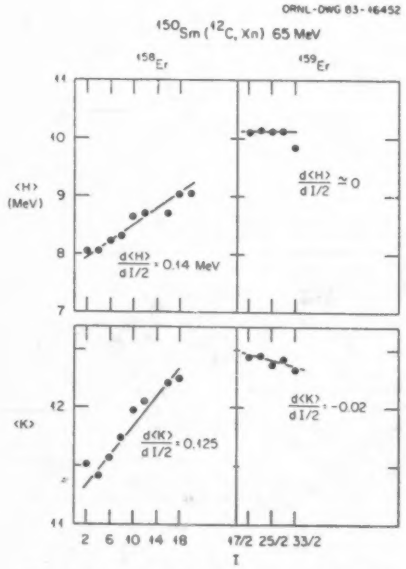

Fig. 2.86. The average total pulse height <H> and coincidence fold <K> of the entry state distribution for yrast states of ^{158}Er and ^{159}Er populated in the ^{150}Sm(^{12}C,Xn) reaction.

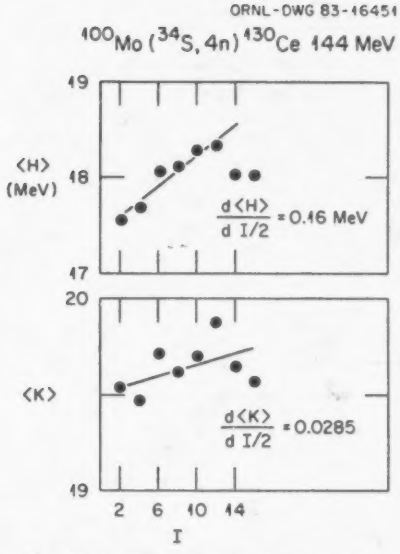

Fig. 2.87. The average total pulse height <H> and coincidence fold <K> of the entry state distribution for yrast states of ^{158}Er and ^{159}Er populated in the reaction ^{100}Mo(^{34}S, 4n) ^{130}Ce.

<H> and <K> values than the 3n channel (^{159}Er). The change of <H> and <K> as a function of the spin of the yrast state is rather small for ^{158}Er; the percentage changes for ^{158}Er per yrast state $\frac{d\langle H\rangle}{dI/2}\frac{1}{\langle H\rangle}$ and $\frac{d\langle K\rangle}{dI/2}\frac{1}{\langle K\rangle}$ are about 2%. For ^{159}Er there is no appreciable change at all. In Fig. 2.87, the results are shown for ^{130}Ce which is formed with heavier ions; thus, it has higher average H and K values. However, the percentage changes of <H> and <K> per yrast state are less than one percent.

From the present results, it can be concluded that when the nucleus is formed with higher angular momentum, the sensitivity of entry state population on the spin of the yrast transition is reduced. This probably is due to the mixing of the nuclear decay pathways between the entry region and the yrast line. The higher the initial angular momentum the longer the decay path will be; hence, there is more mixing of decay paths resulting in less sensitivity. With the low sensitivity observed in the present experiments, it would be very ineffective to attempt to use H and K selection to enhance the population of these high spin states. Whether this is true in general has to be determined from the study of many more reaction systems.

---

1. Summary of paper to be published.
2. D.G. Sarantites et al., Phys. Lett. 115B (1982) 441.

DETERMINATION OF THE SPIN DIRECTION IN HEAVY-ION REACTIONS: ALPHA-PARTICLE ANGULAR DISTRIBUTIONS WITH RESPECT TO SPIN

J. R. Beene
F. A. Dilmanian[1]
M. L. Halbert
D. C. Hensley
M. Jääskeläinen[1]
S. Pontoppidan[2]
H. Puchta[1]
D. G. Sarantites[1]
R. Woodward[1]

The Spin Spectrometer can be used to determine both the magnitude and direction of the spin on an event-by-event basis.[3] The magnitude of the spin can, as is well known, be determined from the gamma-ray multiplicity, M_γ. The determination of the spin direction is made from the distribution in space of the gamma rays detected in each event. The technique works best in situations where a single multipolarity dominates the gamma-ray cascade (for example, reactions that produce predominantly rotational residual nuclei in which stretched E2 gamma rays dominate). It is straightforward to handle strongly mixed cascades; however, the effectiveness of the spin-finding algorithms is reduced.

Two methods for finding the spin direction have been developed. In method one, developed by Dilmanian,[3,4] the spin direction is located by an iterative search procedure, in which the theoretical gamma-ray distributions are employed explicitly. The search procedure works effectively only if the initial spin direction is assumed to be confined to a plane, so that the search need locate it in only two dimensions. For fusion reactions in which the compound nucleus spin is known to lie in the plane perpendicular to the beam, this results in no loss of generality. Method two, due to Pontoppidan,[5] involves an application of numerical techniques adapted from the analysis of hadron jets in high-energy e^+e^- collider experiments[6] and high-energy heavy-ion experiments.[7] An ellipsoid is fit to the pattern of detected gamma rays in a single-step diagonalization of the photon "covariance tensor." For a cascade dominated by stretched E2 decays, the spin direction is identified with the eigenvector corresponding to the smallest eigenvalue found. This procedure works, in principle, in three dimensions, but it is clearly advantageous, if possible, to reduce the problem to two dimensions.

One of the first experiments to employ the spin direction techniques was a study of the angular distribution with respect to the spin direction of alpha particles emitted in the ^{20}Ne on ^{150}Nd reaction at 176.6 MeV.[3] Such alpha-particle angular distributions were obtained as a function of alpha-particle energy for various M_γ (spin) bins. These angular distributions were fit to an even-order Legendre polynomial expansion. The resulting best fit second-order coefficients (A_2) are shown in Fig. 2.88. (We find $|A_4| \ll |A_2|$.) The solid lines on the figure indicate the range of results which are obtained in statistical model calculations for various reasonable values of model parameters. The large increase in anisotropy near and below the expected Coulomb barrier for alpha emission by a spherical ^{170}Yb nucleus ($E_\alpha \approx 18$ MeV) is not accounted for by the calculations. The low E_α anisotropy is seen to increase with M_γ and

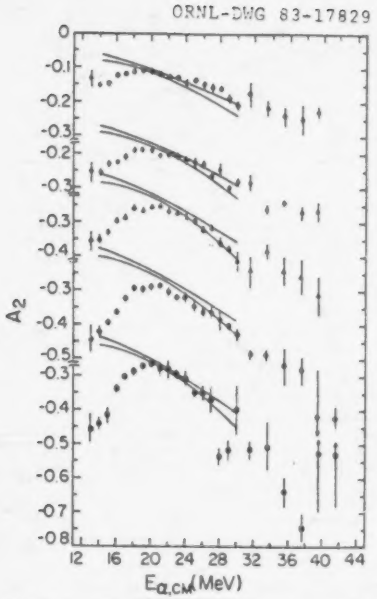

Fig. 2.88. The A_2 coefficients as a function of E_α. The points represent experimental results. Closed and open circles correspond to k bins of 11-14 and 15-18 (I ~ 34 and 43), respectively. The closed triangles, closed large circles, and closed squares correspond to the k bins of 19-22, 23-26, and 27-32 (I ~ 51, 59, and 64), respectively. The curves are theoretical A_2 coefficients which use $T_\ell(E_\alpha)$ from a spherical optical potential. The double lines in each case reflect the statistical uncertainties due to the Monte Carlo simulation.

hence with spin. In Ref. 3 a possible explanation for this result is given in terms of deformation of the compound nucleus at high excitation energy, perhaps increasing with increasing spin. Other experiments are planned to study the systematics of this effect as a function of spin, mass, and excitation energy of the compound system. Experiments have also been proposed to test for the existence of other effects which could produce similar experimental results.

---

1. Wasnington University, St. Louis, Missouri.
2. On leave from Niels Bohr Institute, University of Copenhagen, Copennagen, Denmark.
3. F. A. Dilmanian et al., Phys. Rev. Lett. 49, 1909 (1982).
4. F. A. Dilmanian, unpublished.
5. S. Pontoppidan, unpublished.
6. P. Duinker, Rev. Mod. Phys. 54, 325 (1982) and references therein.
7. M. Gyulassy, K. A. Frankel, and H. Stocker, Phys. Lett. 110B, 185 (1982).

ENTRY-STATE POPULATION AND DECAY IN ^{48}Ti- and ^{50}Ti-INDUCED REACTIONS

D. G. Sarantites[1]
F. A. Dilmanian[1]
M. Jääskeläinen[1]
H. Puchta[1]
R. Woodward[1]
M. Rajagopalan[1]
K. Honkanen[1]
T. Semkow[1]
B. Herskind[2]
G. B. Hagemann[2]
G. Sletten[2]
J. J. Gaardhoje[2]
J. D. Garrett[2]
S. Pontoppidan[2]
P. Nolan[3]
Th. Lindblad[4]
J. R. Beene
M. L. Halbert
D. C. Hensley
I. Y. Lee
W. T. Milner
F. Plasil
J. Hattula

The desire to investigate in greater detail the distribution of entry-state population in excitation energy and spin following fusionlike reactions was one of the principal motivations for the construction of the Spin Spectrometer[5] and formed the basis for the first program of study to which it was applied upon its completion. The first generation of entry-state experiments is described elsewhere in this report.[6] Here, more recent experiments are discussed, including a survey experiment in which 50 targets were bombarded with a 230-MeV ^{50}Ti beam from the HHIRF tandem electrostatic accelerator, and higher statistic, more nearly exclusive, experiments were undertaken to follow leads suggested by the survey. The latter experiments included 225-MeV ^{50}Ti bombardment of ^{110}Pd and ^{130}Te; 225-MeV ^{48}Ti bombardment of ^{126,130}Te, ^{108}Pb, ^{124}Sn, and ^{68}Zn; and 205-MeV ^{48}Ti bombardment of ^{108}Pd. In all these cases, data were obtained in coincidence with Ge detectors so that the final residues populated can be identified. In addition, coincidences with Si surface-barrier fission fragment detectors and light-particle telescopes were obtained.

The basic piece of experimental data obtained from the Spin Spectrometer in these experiments is a bivariate distribution in H (sum gamma-ray pulse height) and k (number of NaI detectors triggered by gamma rays, or "fold") of population in the entry states. The entry states are those states in the residual nucleus populated by the final charged-particle or neutron evaporation in the cascade from the excited primary reaction products. This distribution in H and k is closely related[5] to the distribution in excitation energy and spin (E^*,I), which is the real goal of the experiments. To a first approximation, the relationship between (H,k) and (E^*,M) spaces is a simple linear mapping. An approximate transformation to entry-state distribution in (E^*,I) is easily performed by assuming that the parameters of this mapping remain constant to high spins and excitations. However, for many purposes this is inadequate. Variations in the dominant structure of excited states, with spin and excitation energy, can lead to local variations in the parameters of the (H,k) to

(E*,I) mapping.[6-8] These structure effects can sometimes masquerade as reaction mechanism effects, and vice versa. It is generally essential that both be studied together.

Once the (E*,I) distributions have been obtained, important questions can be addressed; examples include: (1) What is the Z and N dependence of the spin distributions in the residues? (2) Have interesting variations in the dominant gamma-decay mode been observed as a function of spin or temperature (T)? (3) Are there important particle emission effects (e.g., preequilibrium emission or "alpha pinch-off" limiting the range of angular momenta populated in the final residues? (4) Can inferences be made concerning the distribution of entrance-channel angular momenta leading to fusion and fusionlike processes?

In order to transform M_γ distributions [the relation of (H,k) to (E^*,M_γ) depends on the properties of the spectrometer only[5]] to spin distributions in a rigorous and reliable way, it is necessary to study the multipolarity of gamma rays emitted in the cascades deexciting the entry states. This has been pursued by using the spin-alignment technique[10,11] to enhance angular distribution effects. Extensive studies of gamma-ray angular distributions with respect to the spin direction, as a function of both spin and excitation energy, are now available for the data acquired in the survey experiment. We find a number of new effects. One of the most interesting is the observation of gamma radiation at energies well above the normal "quadrupole bump"[6-8,12] region, yet having an angular distribution indistinguishable from that of a stretched quadrupole decay. One interesting possibility is that these transitions are unstretched M1 transitions. Such transitions have been predicted[13] to occur at high temperatures between one-quasi-particle states of the same signature.

In some cases, particularly interesting decay modes are found to play a dominant role in determining the entry-state distributions. For heavy systems or high spins, fission can play this role. In favorable cases, information on angular momentum effects in the fission process can be inferred from the entry-state distribution in nonfissioning residue nuclei. An interesting example, taken from the multitarget survey, is presented in Fig. 2.89. These data were obtained with 230-MeV ^{50}Ti incident on a range of Sn, Cd, and Te targets which produce various Yb, Hf, and W compound systems, as indicated in the figure. The distribution of entry-state population as a function of gamma-ray multiplicity, M_γ, is shown. It is apparent that higher spin residue states are populated in the heavier, less fissile (smaller Z^2/A), compound systems for each of the three species. Statistical model calculations are found to reproduce the observed results reasonably well and indicate that the variation in the upper edge of the M_γ distribution is determined by the spin dependence of the fission probability in the various isotopes. (The large bump in M_γ yield near $M_\gamma \sim 9$ is found by coincidence with fission fragments to be consistent with gamma decay from fission fragments.) These results suggest that carefully acquired, sufficiently exclusive data can be used to measure the fission probability

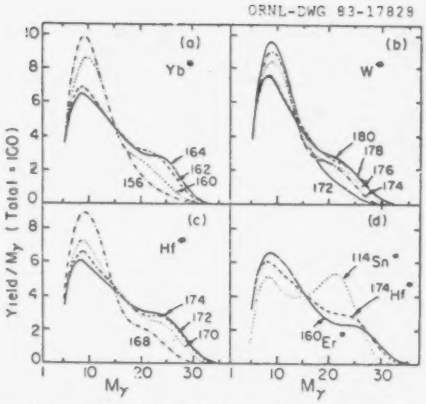

Fig. 2.89. Multiplicity distributions from the entry-state populations from the 230-MeV ^{50}Ti-induced reactions producing the compound systems indicated. All the distributions were normalized to the same total area to facilitate comparison.

of the compound systems as a function of spin and neutron number. This possibility was pursued in the follow-up experiments outlined above. The data analysis is in progress.

Only two examples of the many interesting observations obtained from the extensive survey experiment have been discussed. We expect the more complete data taken in follow-ups to the survey to provide much richer and more definitive information on these points, as well as many others only alluded to, or skipped completely, in this limited space.

---

1. Washington University, St. Louis, Missouri.
2. Niels Bohr Institute, Copenhagen, Denmark.
3. Liverpool University, Liverpool, U.K.
4. Research Institute for Physics, Stockholm, Sweden.

5. M. Jääskeläinen et al., Nucl. Instrum. Methods Phys. Res. 204, 385 (1983).
6. D. G. Sarantites et al., "Entry-State Populations in Fusion of Ne + Nd and the High-Spin Structure of $^{157-161}$Yb," this report.
7. M. Jääskeläinen et al., Phys. Rev. Lett. 49, 1387 (1982).
8. D. G. Sarantites et al., Phys. Lett. 115B, 441 (1982).
9. J. R. Grover and J. Gilat, Phys. Rev. 157, 823 (1967).
10. F. A. Dilmanian et al., Phys. Rev. Lett. 49, 1909 (1982).
11. J. R. Beene et al., "Determination of the Spin Direction in Heavy-Ion Reactions: Alpha-Particle Angular Distributions with Respect to Spin," this report.

12. F. S. Stephens and R. M. Diamond, Annu. Rev. Nucl. Part. Sci. 30, 85 (1980).
13. Y. S. Chen and G. A. Leander, in High Angular Momentum Properties of Nuclei, Harwood Academic, New York, 1983, p. 327.

SPIN-SPECTROMETER STUDIES OF ^{19}F + ^{159}Tb AT 9.5 MeV/NUCLEON

M. L. Halbert G. R. Young
J. R. Beene H. Puchta[1,2]
R. L. Ferguson F. A. Dilmanian[1,3]
D. C. Hensley M. Jääskeläinen[1,4]
D. G. Sarantites[1]

A 1.45-mg/cm^2 target of ^{159}Tb was bombarded in the Spin Spectrometer by ^{19}F at a mean energy of 180.2 MeV. Eleven Si surface-barrier (ΔE,E) telescopes were placed at angles from 15° to 150°. Two single Si detectors were placed at 8° to detect evaporation residues (ER). Whenever one or more of the 11 E counters was triggered, the pulse heights and times of the corresponding telescopes, ER counters, and all nonzero NaI information were recorded on magnetic tape. All of the telescopes could measure protons and α particles. In addition, those at 20°, 30°, 40°, and 50° provided data on heavy ions. The resolution at 20° and 30° was adequate to resolve isotopes.

A sample of the heavy-ion data at 40°, well beyond the grazing angle (29.5° lab), is shown in Fig. 2.90. The intense group of N ions at about 120 MeV is centered a little below the beam velocity. The arrow marks the optimum Q value for particle transfer conserving linear and angular momentum along the classical trajectory.

A second group is centered at the Coulomb barrier for N + Ho and is probably due to fully-damped deep-inelastic products. The number of γ rays detected, k, is lower for the first group, indicating that the beam-velocity ions carry away a significant amount of angular momentum. There is a third group at low k and low particle energy that is most likely due to target impurities such as C or O.

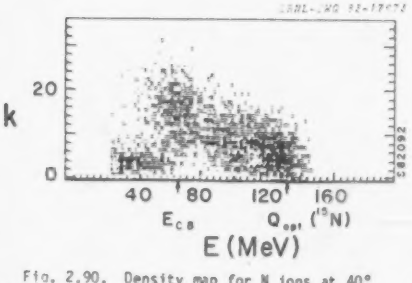

Fig. 2.90. Density map for N ions at 40° from 180-MeV ^{19}F on ^{159}Tb as a function of particle energy, E, and γ-ray coincidence fold, k.

Figure 2.91 shows the average γ-ray multiplicity, $\langle M_\gamma \rangle$, deduced from the measured k distributions at 20° and 30°, presented as a function of ejectile mass, A. The overall linear decrease of $\langle M_\gamma \rangle$ with increasing A may be explained by the incomplete-fusion picture[5] in which the projectile is thought to break up as it interacts with the target and only a part of it fuses with the target. The remainder escapes with essentially its original velocity and carries away angular momentum proportional to its mass. Most of the angular momentum transferred to the partially-fused nucleus is dissipated by γ-ray emission. The decrease of $\langle M_\gamma \rangle$ with A follows naturally from this picture since the transferred angular momentum is small when the escaping mass A is large.

The approximately linear dependence of $\langle M_\gamma \rangle$ on mass may be represented by $1.9\ A_c = 2\ (\langle M_\gamma \rangle - 3.4)$, where $A_c = 19 - A$ is the mass captured by the target in the partial fusion. This expression resembles the well-known relation between multiplicity and angular momentum in rare-earth fusion products, leading us to conclude that on the average the captured nucleons each transfer about 1.9 units of angular momentum.

The sum-rule model is a semiclassical model of incomplete fusion developed by Wilczynski et al.[5] and applied successfully by them to reactions of 10-MeV/nucleon ^{14}N on ^{159}Tb. To provide a more quantitative check of the model, a series of calculations was made for incomplete

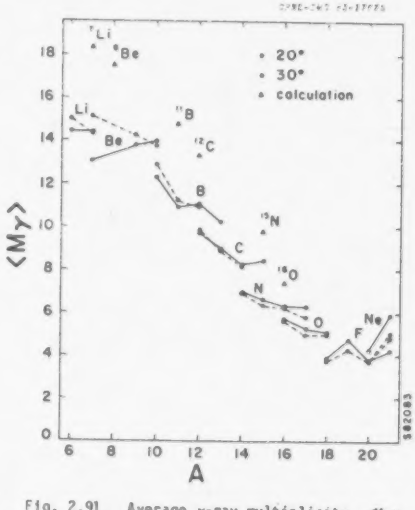

Fig. 2.91. Average γ-ray multiplicity, $\langle M_\gamma \rangle$, of heavy ions of mass A from 180-MeV ^{19}F on ^{159}Tb at 20° (•) and 30° (○). The results of statistical-model calculations using the sum-rule model (Ref. 5) for the initial ℓ distributions are shown by the triangles.

fusion leading to most of the products shown in Fig. 2.91. In each case the entrance-channel ℓ-distribution predicted by the sum-rule model was taken as the starting point for statistical evaporation of particles followed by γ-ray deexcitation calculated with JULIAN-PACE[6] as modified by J. R. Beene.[7] All the excitation energy available was assumed to be taken up by the partially-fused product. This is a reasonable assumption if thermal equilibrium is established in the initial stages of the reaction so that the energy is shared among the partners according to their masses. We will return to this point, but we note here that $\langle M_\gamma \rangle$ is insensitive to the excitation energy since it is principally dependent on the initial ℓ distribution.

Samples of the results are given by the triangles in Fig. 2.91. For A ~ 18 the agreement is satisfactory, but for lighter products the predicted $\langle M_\gamma \rangle$ exceeds the observed values. One important effect has not been taken into account here, namely particle decay of excited primary ejectiles. For example, if ^{16}O is excited to or above its 9.632-MeV level, it will most likely decay to $^{12}C + \alpha$. Such a large excitation cannot occur if the assumption of early thermal equilibrium is valid, but the data of T. Awes et al. presented elsewhere in this report[8] indicate that for undamped reaction products the energy tends to be shared equally between the partners. In this case, the average ^{16}O excitation would be 12.6 MeV, more than enough for α decay of the ^{16}O. The γ multiplicity associated with these secondary ^{12}C particles would be that characterizing ^{16}O, which is lower than for primary ^{12}C. For lighter ejectiles, the energy available on the equal-sharing hypothesis is so large that very few of the observed particles are likely to be primaries. For A = 17 and 18, the available energy is insufficient to lead to much particle decay. Thus we may say that the calculations are in quantitative agreement with the model at the highest masses, and the discrepancies for lower A are qualitatively understood. It should be kept in mind, however, that the sum-rule model involves touching of the nuclear matter, and thus will not include transfers occurring in the nuclear halo that may contribute significantly to the yields near A ~ 18.

The relative widths of the $\langle M_\gamma \rangle$ distributions also point out the importance of these secondaries. The predicted widths are approximately equal to the observed widths for A ~ 18 and A ~ 7, but are as much as twice as large for intermediate masses. The processes leading to the intermediate masses must therefore originate from a wide range of entrance-channel angular momenta. This observation is consistent with the particle-decay hypothesis.

Studies of particle-particle coincidences should shed further light on the role of particle decay. In the meantime, it is fair to say that the basic premises of the incomplete-fusion picture apply to this reaction. A more complete report on this experiment, with data also on particle angular distributions and cross sections, is found in a conference report.[9]

---

1. Washington University, St. Louis, Missouri 63130.
2. Present address: Sektion Physik, Universität München, 8046 Garching, West Germany.
3. Present address: Elscint Ltd., Haifa 310501, Israel.
4. Present address: Department of Physics, University of Jyväskylä, Jyväskylä, Finland.

5. J. Wilczynski et al., Nucl. Phys. A373, 109 (1982).
6. A. Gavron, Phys. Rev. C 21, 230 (1980).
7. D. G. Sarantites et al., Phys. Lett. 115B, 441 (1982), and private communication.
8. T. C. Awes et al., elsewhere in this report.
9. M. L. Halbert et al., Phys. Scripta T5, 91 (1983).

LIGHT HEAVY-ION REACTIONS

FUSION CROSS SECTION MEASUREMENTS FOR LIGHT SYSTEMS

J. Gomez del Campo, Y.D. Chan[1], J.L.C. Ford, Jr., M.E. Ortiz[4], D. Shapira, D. DiGregorio[2], R. Novotny[3], F. Pougheon[5]

The fusion cross sections for the $^{17}O + ^{10}B$[6], $^{15}N + ^{12}C$[7] and $^{14}N + ^{13}C$[8] leading to the same compound nucleus ^{27}Al, were measured to investigate the effects of entrance channel or compound nucleus mechanisms as determining factors in the fusion of "light" heavy-ion systems.

The $^{17}O + ^{10}B$[6] system was studied for E(^{17}O) bombarding energies of 54 to 124 MeV, with beams extracted from the BNL MP-Tandem facility and the $^{14}N + ^{13}C$[8] system was measured for E(^{14}N) = 86 to 178 MeV with beams extracted from the Oak Ridge Isochronous Cyclotron (ORIC). In both of these measurements self-supporting targets of 140 $\mu g/Cm^2$ ^{10}B and 57 and 125 $\mu g/Cm^2$ ^{13}C were used. The measurements for the $^{15}N + ^{12}C$[7] system were done using a gas cell target[9] containing 99% ^{15}N gas and ^{12}C beams extracted ORIC. In all cases, reaction products from Li to Mg were detected in a E(PSD)-ΔE (ionization chamber) counter telescope in the laboratory angular range of 4° to 30°. Reaction products were analyzed in terms of kinematical considerations and Hauser-Feshbach Monte-Carlo calculations using the code LILITA.[10] The evaporation residues were clearly identified. The extracted fusion cross sections were transformed in angular momentum cut-off using the sharp cut-off relation of $\sigma = \pi\lambda^2(J+1)^2$. The deduced angular momenta values are plotted against the excitation energy in ^{27}Al in Fig. 2.92. The fact that all values of the angular momenta define a common band clearly indicates that for these systems the limitation on fusion is determined by the properties of the compound nucleus. The solid line through the data points in a least square fit of $E^* = E_0 + (\hbar^2/2\mathcal{I})J(J+1)$ where the bandhead $E_0 = 27.4$ and $\mathcal{I}/\hbar^2 = 5.5$ MeV^{-1}. It is important to point out that the value of $\mathcal{I}/\hbar^2$ extracted from the fusion data is within uncertainties the same as that obtained by the coherence width analysis of the $^{12}C(^{15}N,\alpha)$ reaction data at lower energies indicating that,

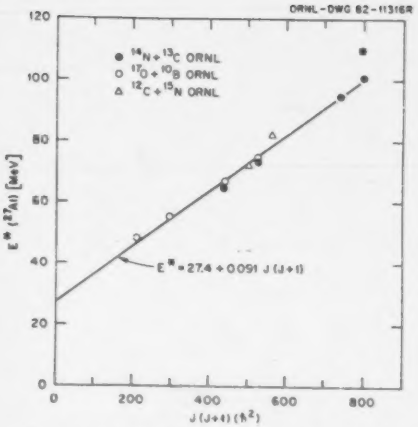

Fig. 2.92. Plot of the excitation energy in ^{27}Al vs. $J(J+1)$. The value of the compound nucleus angular momentum J is extracted from the fusion measurements using the relation $\sigma_{fus} = \pi \lambda^2 (J+1)^2$.

indeed, the extracted moment of inertia is that of the compound nucleus ^{27}Al.

---

1. Present address: Lawrence Berkeley Laboratory, Berkeley, CA.
2. Doctoral research student from the Comision Nacional de Energia Atomica, Argentina.
3. Present address: Second Physikalische Institute Gissen, West Germany.
4. Guest scientist from Universidad Nacional Autonoma de Mexico, Mexico.
5. Guest scientist from the Institute de Physique Nucleaire, Orsay, France.
6. Y. D. Chan et al., Phys. Rev. C25, 1410 (1982).
7. R. Novotny et al., Phys. Rev. C26, 2554 (1982).
8. D. E. DiGregorio et al., Phys. Rev. C26, 1490 (1982).
9. D. Shapira et al., Nucl. Instrum. Methods 163, 325 (1979).
10. J. Gomez del Campo and R. G. Stokstad, ORNL Report No. TM-7295, 1981.
11. J. Gomez del Campo et al., Nucl. Phys. A297, 125 (1978).

CRYSTAL BLOCKING MEASUREMENTS IN HEAVY-ION REACTIONS[1]

J. Gomez del Campo — R.W. Fearick[2]
J.A. Biggerstaff — C.D. Moak
P.D. Miller — N. Neskovic[3]
D. Shapira — J.P.F. Sellschop[4]

The crystal blocking technique offers the unique possibility of a direct measurement of reaction times for cases where the decaying products are charged particles. This technique has been used primarily in the past to study light-ion-induced resonance reactions,[5,6] although some measurements exist for the case of heavy-ion-induced fission reactions.[7,8] In this work,[1] we extend such measurements to heavy-ion reactions, in particular to the $^{16}O + ^{12}C$[9] (diamond) and $^{16}O + ^{nat}Ge$ systems. One of the motivations for the study of the $^{16}O + ^{12}C$[9] system is to test, through the blocking measurements of the evaporation residues (ER), our ideas of compound nucleus formation and equilibrium decay. In the statistical theory of decay of an equilibrated system, the ER are produced in a sequential decay of the compound nucleus by the emission of light particles (mostly α,p,n), where this sequence proceeds through states of well-defined spin parities and total widths Γ. This process, if it occurs, introduces a time delay τ associated to the production of a given ER. This characteristic time is, in general, a convolution of more than one nuclear lifetime. In this work, we present for the first time the measurements of τ using the crystal blocking technique while bombarding a diamond crystal (98.9% ^{12}C) with a 120 MeV ^{16}O beam.

Measurements for the elastic scattering and those for reaction for 120-MeV ^{16}O on ^{nat}Ge were also carried out, mainly to test our equipment and data acquisition system, but also to lay the groundwork for future efforts in the study of equilibration effects in deep inelastic collisions and fusion in medium mass systems.

Beams of ^{16}O were extracted from the tandem accelerator at the Holifield Heavy-Ion Research Facility to bombard in a random direction a 12-μm-thick diamond crystal and an 8-μm Ge crystal. The crystals were mounted in a high-precision goniometer and the <110> axis was found by channeling the beam, observing the typical star patterns on a phosphor screen. Once the alignment of the crystal was established, the <110> axis was rotated to the angle where the detector was located. The detector system consisted of a position sensitive gas proportional wire, a ΔE (ionization chamber) and E (solid state) elements. The vertical position is determined by measuring the drift time of the electrons to the proportional wire.

Figure 2.93 shows the blocking pattern of the elastic scattering measured in the bombardment of a Ge crystal with 103-MeV ^{16}O ions. The detection angle was 22.3°. In the center of the figure one can see clearly the blocking effects of the <110> axis; the thin lines emerging from the center of the figure indicate the blocking of the {111}, {100} and {110} planes. The angular resolution of the detector was 0.04°, consistent with a position resolution of 0.8 mm with the detector placed at 109 cm from the target.

After integrating the blocking patterns over the polar angle and normalizing to the random yield, the blocking angular distributions are obtained and used to extract the time information. For the case of the projectile-like fragments in the 103-MeV ^{16}O + Ge and assuming a minimum sensitivity for the recoil distance in Ge of 0.1 A, an upper limit of the reaction time

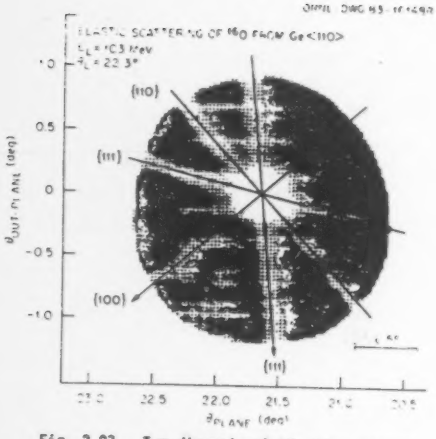

Fig. 2.93. Two-dimensional blocking pattern for the elastic scattering of ^{16}O on Ge at E(^{16}O) = 103 Mev. The angles are measured along the reaction plane or perpendicular to the reaction plane and the axis <110> is centered at 22.3°.

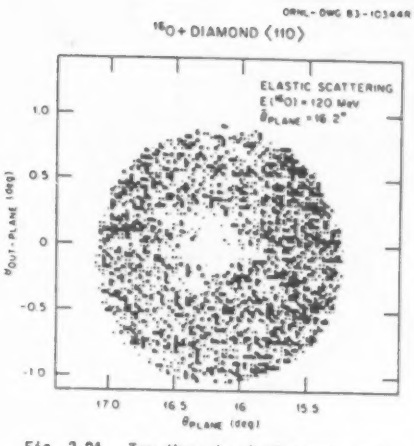

Fig. 2.94. Two-dimensional blocking pattern for the elastic scattering of ^{16}O on diamond at E(^{16}O) = 120 MeV. The angles are measured along the reaction plane or perpendicular to the reaction plane, and the <110> axis is centered at 16.2°.

was found to be < 6 x 10^{-19} sec, indicating the "fast" direct reaction nature of the DIC process.

Figure 2.94 shows a typical two-dimensional blocking pattern for the elastic scattering of 120-MeV ^{16}O on diamond. Similar patterns were taken for the elastic scattering at 80 MeV bombarding energy and nuclear reaction fragments from B to Mg for the bombardment at 120 MeV. The axial blocking dip can be seen clearly in the center of the figure, although the planar blocking dips, similar to those in Fig. 2.93, are not seen due to thickness effects and crystal defects.

From analysis of the blocking angular distributions for the evaporation residues of ^{16}O on diamond, deexcitation times were obtained[1] and they ranged from 4 x 10^{-19} sec for Mg isotopes to 4 x 10^{-18} sec for N isotopes. These values are consistent with statistical model predictions and demonstrate in a direct way the sequential decay nature of the deexcitation process in heavy-ion fusion reactions.

---

1. Summary of paper published in Proc. of 6th Ann. Symp. on Nuclear Physics, Oaxtepec, Mexico, January 1983 (Notas de Fisica, 1983).
2. On leave from the University of Witwatersrand, Johannesburg, SA.
3. Fullbright Fellow from Boris Kidric Institute, Belgrade, Yugoslavia.
4. Guest scientist from the University of Witwatersrand, Johannesburg, SA.
5. W.M. Gibson et al., Nucl. Phys. A317, 313 (1979).
6. E. Fuschini et al., Phys. Rev. C27, 1332 (1983).
7. J.U. Andersen et al., Phys. Rev. Lett. 36, 1539 (1976).
8. J.U. Andersen et al., Dan. Vidensk. Selsk. Mat. Fys. Medd. 40:F, 1 (1980).
9. J. Gomez del Campo et al., Phys. Rev. Lett. 51, 451 (1983).

ORBITING AND DEEP INELASTIC SCATTERING IN COLLISIONS BETWEEN LIGHT HEAVY IONS

D. Shapira
K. A. Erb
J. L. C. Ford, Jr.
J. Gomez del Campo
B. Shivakumar
S. T. Thornton[1]
R. L. Parks[1]
R. Cecil[1]

The measurement of reaction products at backward angles on several light heavy-ion systems revealed large yields of highly excited, two-body reaction products emitted with kinetic energies equal to the combined Coulomb and centrifugal barrier of a rotating dinuclear system. The angular distributions were isotropic as a function of $d\sigma/d\theta$. The magnitude of the yields from this process is very large precluding its interpretation as asymmetric fission of a statistical compound nucleus formed in the collision.[2-6]

We carried out further investigation of this process with the ^{28}Si + ^{12}C system. These proceeded along two lines: a) More first generation singles measurements extended to higher energies. b) "Second generation" coincidence experiments with multiparticle detector systems. The purpose of the latter is to verify the two-body-like nature of this reaction and to study how angular momentum and excitation energy are

shared between the two final fragments. Some results from these new measurements and their interpretation will be discussed below.

Studies of $^{28}Si + ^{12}C$ at Higher Energies

Figure 2.95 shows spectra of recoiling carbon ions at two energies — the shapes of the energy spectra are similar. Figure 2.96 shows that the constancy of the average excitation energy with angle, a characteristic of complete energy damping, persists at these higher bombarding energies. The angular distributions also continue to show a $1/\sin\theta_{c.m.}$ angular dependence. The dependence of the fragments' kinetic energy for deep inelastic scattering products in the collisions between light heavy-ions has long been recognized to reflect angular momentum contributions to the ion-ion potential barrier. Figure 2.97 shows a dramatic and fairly sudden departure from this behavior. The obvious interpretation of such a sudden transition can be made in terms of a ceiling on the orbital angular momenta (partial waves) that contribute to deep inelastic scattering in this system. This maximum or critical angular momentum is reached when the centrifugal and Coulomb barrier overcome the nuclear attraction at the contact

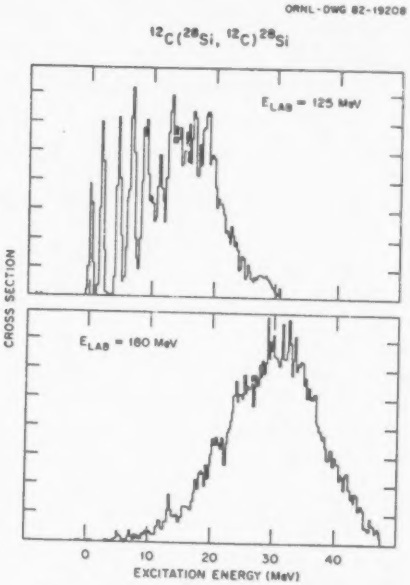

Fig. 2.95. Energy spectra for outgoing carbon nuclei — the abscissa is transformed to excitation energy assuming a two-body $^{12}C(^{28}Si, ^{12}C)^{28}Si$ process has occurred.

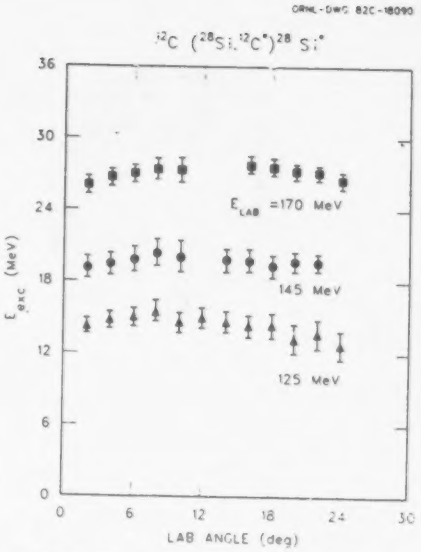

Fig. 2.96. Most probable Q value (a excitation energy) deduced from the centroids of spectra similar to those shown in Fig. 1. Plotted as a function of angle for several bombarding energies. Clearly one can associate a single most probable Q value with each bombarding energy.

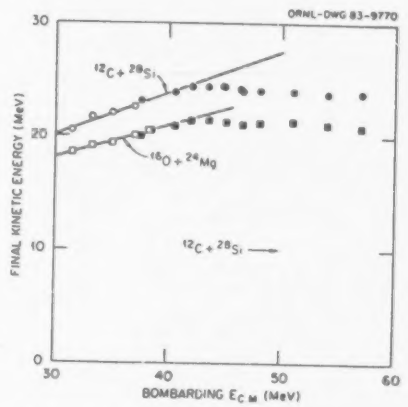

Fig. 2.97. The most probable Q value plotted as a function of bombarding energy for two-exit channels.

configuration. For higher angular momenta the two nuclei briefly in contact feel a net repulsion and cannot orbit. The reaction kinematics at which this critical angular momentum occurs, together with the related cross sections, should yield quantitative information on the nucleus-nucleus potential and critical angular momentum for orbiting processes.

Coincidence Measurements

In the first coincidence measurement performed, 150 MeV ^{28}Si ions from the HHIRF tandem were used to bombard a ^{12}C target. Heavy fragments that are associated with the emission of the target-like recoil were detected over a wide angular range in coincidence with the target-like recoil nucleus. Results of preliminary scans of these data aimed solely at confirming the two-body nature of this process are shown in Fig. 2.98. At the bottom of the figure is a schematic in-plane view of the experimental setup, while above are recoiling carbon spectra recorded with and without an associated particle detected in the counter on the opposite side of the beam. The very small number of products recorded without an associated particle detected on the opposite side of the beam bears evidence to the two-body nature of this reaction. A more detailed kinematic analysis of these data is now in progress. The second coincidence experiment was performed at the Max Planck Institute at Heidelberg and involved one medium sized and two large (1 m deep) gas ionization chambers. The experiment was performed at 180 MeV ^{28}Si bombarding energy and the analysis of these data is now in progress.

---

1. University of Virginia, Charlottesville, Virginia 22901.
2. ORNL Progress Report 1981, p. 39, ORNL/TM-5787.

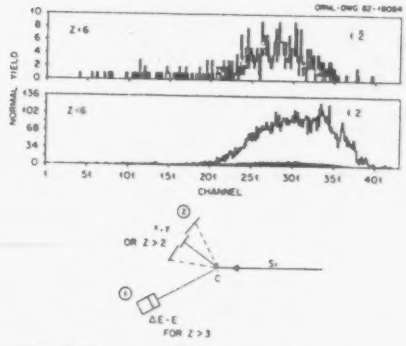

Fig. 2.98. Spectra of recoiling carbon products with (12) and without ($\overline{12}$) an associated product detected.

3. D. Shapira et al., Phys. Rev. Lett. 43, 1781 (1979).
4. D. Shapira et al., Phys. Lett. 114B, 111 (1982).
5. D. Shapira et al., Phys. Rev. C 21, 1824 (1980).
6. D. Shapira et al., submitted to Phys. Lett.

HIGHLY DAMPED PROCESSES IN THE MEDIUM MASS HEAVY-ION RANGE

INCLUSIVE SPECTRA OF Z = 1,2 PARTICLES FROM HEAVY ION REACTIONS

R. L. Auble
J. B. Ball
F. E. Bertrand
C. B. Fulmer
R. L. Robinson
C. Y. Wong
D. C. Hensley
I. Y. Lee
P. H. Stelson
R. L. Ferguson
G. R. Young
D. L. Hendrie[1]
J. D. Silk[2]
H. D. Holmgren[2]

The aim of this study is to search for clues which may lead to a better understanding of the processes responsible for the emission of energetic charged particles in heavy ion induced reactions. To this end, we have examined the spectra of Z = 1 and 2 particles as a function of projectile energy and target mass. Measurements using 7.5-16 MeV/nucleon ^{12}C projectiles were reported in the previous progress report and have been published.[3] The projectile energy dependence has been extended using 52-, 100-, and 147 MeV/nucleon ^{16}O beams from the Bevalac.[4] The data were analyzed by fitting the spectra using various semi-empirical formulations. Parameters derived using the simplest model, a single heated moving source, are displayed in Fig. 2.99. The "source temperature", T, is observed to increase smoothly with projectile energy, while the ratio of "source velocity" to the projectile velocity, V_s/V_{proj}, remains nearly constant. These results suggest that there are no abrupt changes in the light ion emission process over this energy range.

At the higher projectile energies, the data were not well represented by this simple model, and a two-component model having "peripheral fragmentation" and "central collision" components was applied. In this model, each source is described in terms of a momentum distribution with independent longitudinal and transverse components. This formulation provides good fits to the proton and deuteron data. The fits to the ^3He and ^4He spectra were somewhat poorer, possibly due to target fragmentation contributions, especially at the lower particle energies. The momentum distribution for the fragmentation component was found to be essentially isotropic, with momentum widths ranging from σ_0 = 69 MeV/c for protons to 80 MeV/c for heavier particles. The central collision term was found to require an anisotropic momentum distribution and much larger widths indicating that the central "source" is not an equilibrated system of nucleons.

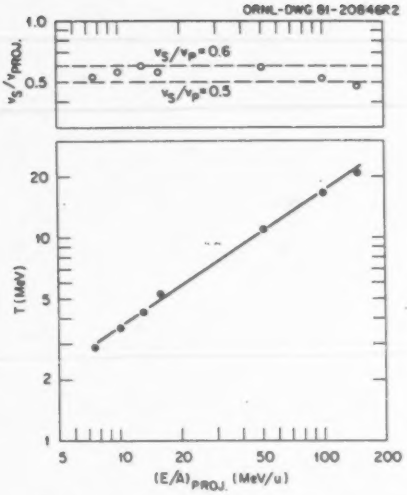

Fig. 2.99. Temperature and velocity parameters obtained by fitting energetic proton spectra with a heated moving source model.

Dependence on target size was examined at 100 MeV/nucleon, and it was found that the yield of light particles increases as $\propto A_T^{1/3}$ at small angles and changes smoothly to an $\propto A_T^{2/3}$ dependence at larger angles.[5] This is illustrated, for proton emission, in Fig. 2.100. Such a behavior is consistent with the conjecture that the small angle emissions arise from interactions occurring on the periphery of the target nucleus, while at larger angles, smaller impact parameters are involved. These results are quite different from those obtained at lower projectile energies. In studies[6] with 208 MeV ^{16}O on ^{12}C, ^{56}Fe, and ^{91}Zr, the yields were found to have a very weak dependence on A_T. Measurements with 140, 215, and 310 MeV ^{16}O on Al, ^{90}Zr, and Au suggested that the light ion yields were related to the amount of energy above the Coulomb barrier.[7] We have examined the A_T - dependence in more detail using 190 MeV ^{12}C projectiles. Preliminary results, for energetic proton emission, are shown in Fig. 2.101. The rapid drop near A_T = 100, and the small yield for ^{46}Ti, indicate that factors other than the Coulomb barrier are important at this projectile energy. Thus far, no mechanism has been found to explain this A_T dependence. Additional studies are planned to determine if this behavior is observed with other projectiles and at other projectile energies.

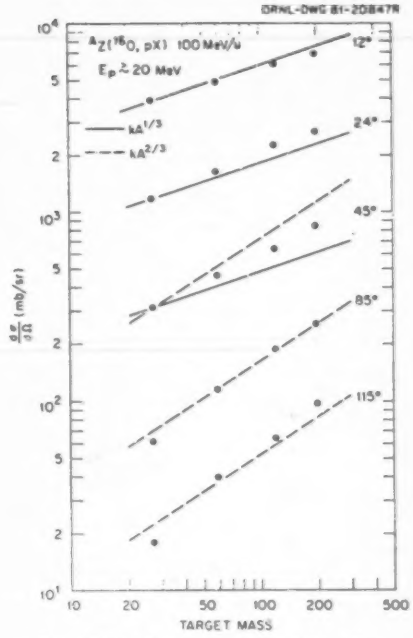

Fig. 2.100. Target mass dependence of energetic proton yields, for various detection angles, obtained with 100 MeV/nucleon ^{16}O projectiles.

4. R. L. Auble et al., Phys. Rev. C, to be published.
5. R. L. Auble et al., Phys. Rev. Lett. 49, 441 (1982).
6. C. B. Fulmer et al., Phys. Lett. 100B, 305 (1981).
7. T. C. Awes et al., Phys. Rev. C. 25, 2361 (1982).

ENERGETIC LIGHT IONS FROM HEAVY ION INDUCED REACTIONS

R. L. Robinson
W. Rauch[1]
R. L. Auble
T. C. Awes
J. B. Ball
F. E. Bertrand
R. L. Ferguson
C. B. Fulmer
J. Gomez del Campo
M. L. Halbert
D. C. Hensley
I. Y. Lee
R. W. Novotny[2]
D. G. Sarantites[3]
G. R. Young
J. C. Wells[4]
C. F. Maguire[5]
H. Yamada[6]

The spectra of high-energy light ions resulting from reactions produced with intermediate-energy heavy ions extend to energies that exceed those expected for evaporation from a completely fused system. Thus these

1. Lawrence Berkeley Laboratory.
2. University of Maryland.
3. R. L. Auble et al., Phys. Rev. C 25, 2504 (1982).

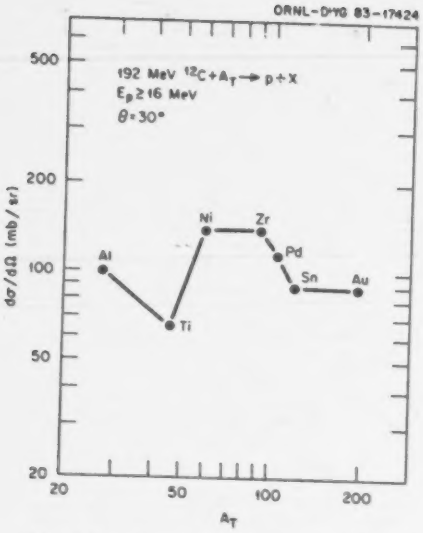

Fig. 2.101. Target mass dependence of proton yields from 190 MeV ^{12}C induced reactions.

particles provide a means to study reaction mechanisms other than complete fusion (CF) and to determine the contribution of these mechanisms as a function of target mass, and of projectile mass and energy. In an effort to identify the reaction mechanisms that yield energetic light ions in heavy-ion induced reactions, we have performed two types of coincidence measurements as described in the following subsections.

Nucleon Multiplicity Associated With Energetic Protons From The $^{12}C + ^{60}Ni$ Reaction[7]

We measured Z = 1-7 particles emitted in coincidence with energetic protons when ^{60}Ni was bombarded with 191-MeV ^{12}C projectiles. The energetic protons were detected in six ΔE (Si) - E (NaI) telescopes placed at angles from 7° to 62°. Coincident particles with Z = 1 to 7 were detected in 17 ΔE (Si) - E (Si) telescopes, fourteen in plane with angles from 7° to 140°, and three out of plane.

The multiplicity of Z = 1-7 particles integrated over all angles and energies in coincidence with the energetic protons was determined. The multiplicities of Z = 3-7 particles are typically a few percent of the multiplicities of the Z = 1-2 particles. The total number of all nucleons emitted in a given event in which one is an energetic proton was deduced from the multiplicities. (The number of emitted neutrons was assumed to be equal to the number of protons.) These are plotted in Fig. 2.102 as a function of the energy and angle of the energetic proton.

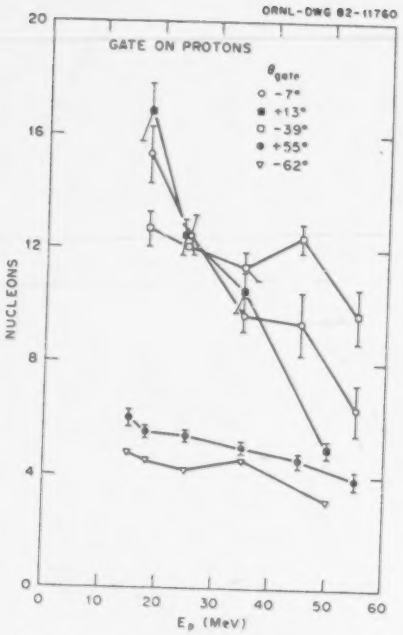

Fig. 2.102. Average number of nucleons N emitted from an event in which one particle is an energetic proton detected at the angle noted. E_p is the energy of the gating proton.

The results summarized in Fig. 2.102 were compared to predictions for CF made with the statistical-model program LILITA[8]. It was concluded that, for example, CF contributes <5% of the 16-MeV protons emitted at all angles, and <1.4% of the 30-MeV protons. An upper limit of the deep inelastic collision process which is accompanied by an energetic proton, or any other process in which a projectile-like fragment (PLF) is emitted, was obtained from the multiplicity of PLF's (Z = 3-7). For example, only 7% of 20-MeV protons are emitted with a PLF; this decreases to 2% for 50-MeV protons.

The results in Fig. 2.102 can be explained if there are two major reaction processes associated with energetic proton emission. The first is disintegration of the projectile into a number of particles most of which have atomic mass of 4 or less. This would explain the large number of nucleons observed when the energetic proton is detected at a forward angle. The second process, to explain the larger angle results, must be associated with emission of few nucleons, and thus much of the projectile mass must fuse with the target but under conditions such that substantially fewer nucleons are emitted than predicted for CF. An interesting unanswered question in this nonequilibrium process is where does much of the energy go.

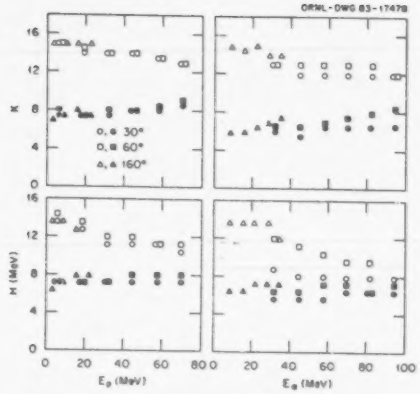

Fig. 2.103. The number K of NaI crystals triggered by a γ ray and total γ-ray energy H deposited in the NaI crystals when gating on an energetic proton or alpha particle at the angle noted. The open symbols are for ^{120}Sn, the closed symbols for ^{60}Ni.

We estimate that about 40% of the energetic protons are associated with projectile disintegration and 60% with nonequilibrium emission.

Multiplicity of γ Rays Emitted with Energetic Protons and Alpha Particles

In this study the multiplicity of γ rays emitted in coincidence with energetic light ions was determined using the spin spectrometer. Energetic light ions were detected with three ΔE-E telescopes placed in the scattering chamber of the spin spectrometer. Two telescopes at 30° and -60° (Δθ = ±8°) were each composed of a 200-μm Si detector and a 2-cm deep NaI crystal; the third at -160° was two Si detectors with thicknesses of 72 and 1500 μm. The projectiles were 194-MeV ^{12}C and the targets were ^{60}Ni and ^{120}Sn. The 30° and -60° detectors, given the results of the previous report emphasize, respectively, energetic protons associated with projectile disintegration and nonequilibrium emission. The back angle detector should strongly favor complete fusion.

Figure 2.103 shows the average number of NaI γ-ray detectors of the spin spectrometer that triggered (denoted as K in the figure) in coincidence with an energetic proton or alpha particle, and the total energy H in MeV deposited by the γ rays. K and H are related, respectively, to the γ-ray multiplicity and total γ-ray energy associated with a given event. It can be seen that K for each target is essentially independent of the angle of the gating light ion. H for protons is also independent of gating angle. However, for alpha particles the total γ-ray energy does increase with increasing angle for the Sn target although not for the Ni.

In brief, these results suggest, at least for the projectile-target combinations investigated here, that multiplicity of γ rays observed in coincidence with energetic protons and α particles is about the same whether the reaction process is projectile disintegration, nonequilibrium emission, or complete fusion, and thus is not a good signature of the reaction process.

---

1. Centre De Recherches Nucleaires, B.P. 20, 23, Rue Du Loess, 67037 Strasbourg Cedex, France.
2. Physikalisches Institut, Universitaet Heidelberg, Philosophenweg 12, D-6900 Heidelberg, West Germany.
3. Washington University, St. Louis, MO 63130.
4. Tennessee Technological University, Cookeville, TN 38501.
5. Vanderbilt University, Nashville, TN 37235.
6. University of Melbourne, Australia.
7. R. L. Robinson et al., Phys. Rev. C27, 3006 (1983).
8. J. Gomez del Campo and R. G. Stokstad, Oak Ridge National Laboratory Report TM-7295 (1981).

LIGHT-PARTICLE EMISSION IN DEEPLY INELASTIC REACTIONS OF 13-MeV/u ^{16}O WITH ^{93}Nb

B. Cheynis[1] D. Pelte[3]
R. L. Ferguson F. Plasil
A. Gavron[2] R. L. Robinson
I. Y. Lee G. R. Young
R. Novotny[3] C. F. Maguire[4]
F. E. Obenshain G. A. Petitt[5]

The emission of fast light particles is thought to provide a means of probing early stages in the time development of heavy-ion reactions. It is important to extract first the contribution from statistical emission before ascribing any yield to exotic mechanisms. Statistical emission must be searched for in both its equilibrium and preequilibrium forms. The experimental situation is confused for deeply inelastic reactions. Claims have been made that nonequilibrium components do and do not exist in reactions involving similar projectile and target masses and bombarding energies. For cases involving neutron emission, there does seem to be a trend towards an increasing fraction of nonequilibrium neutrons with increasing bombarding energy, with no such neutrons being found for reactions between heavy ions ($A > 80$) at energies below 10 MeV/u. For proton and alpha-particle emission, no clear trends are yet established.

To improve upon previous work for the system ^{16}O + ^{93}Nb, a new experiment was carried out at HHIRF in the 1.6-m scattering chamber. Eighteen ΔE-E telescopes were arrayed about a 1-mg/cm^2 ^{93}Nb target, which was bombarded with 13-MeV/u ^{16}O. Six of the telescopes, placed at ±7°, ±13°, 21°, and 39°, were used to detect both light ($A < 4$) and heavy ($A > 7$) ions, up to and including evaporation residues. Projectilelike fragments (PLFs) were identified by the ΔE-E method; evaporation residues were identified by energy and flight time relative to the cyclotron

RF. The other twelve telescopes recorded light ions only. Four were placed on an out-of-plane ring intersecting the reaction plane at 23°. The others were positioned at several angles between -140° and +160° in the reaction plane and were moved in angle from time to time. Seven of the telescopes had NaI(Tl) third elements to detect fast light ions. All possible heavy ion-light ion coincidences were recorded on magnetic tape for subsequent analysis.

From the measured quantity

$$A = \frac{d\sigma(E_{HI}, \Omega_{HI}, E_{LI}, \Omega_{LI})}{dE_{HI}\, d\Omega_{HI}\, dE_{LI}\, d\Omega_{LI}}\Bigg|_{\substack{Z_{HI} \\ Z,M_{LI}}},$$

we obtain light-ion energy spectra

$$\frac{dM}{dE_{LI}d\Omega_{LI}}\Bigg|_{\Omega_\alpha}$$ and angular distributions $$\frac{dM}{d\Omega_{LI}}$$

(where M is multiplicity) by normalizing to the heavy-ion singles counts, which were also recorded during the experiments. In some cases we found it useful to transform the results to the form $$\frac{d^6\sigma}{dv^3_{HI}\, dv^3_{LI}}$$, which is a Galilean invariant quantity. Experimental results were compared (in the laboratory frame) to results of Monte Carlo calculations which were designed to model statistical emission of light particles from fully accelerated projectilelike and targetlike fragments produced in deeply inelastic collisions.

The variation of $dM/d\Omega_\alpha$ with alpha-particle detection angle for carbon-alpha particle coincidences is shown in Fig. 2.104a. These results correspond to detecting the carbon nucleus at 21°, about 11° outside the grazing angle, and were obtained by summing over all observed kinetic energies of the carbon.

The solid line is the result of a Monte Carlo calculation which employs the observed kinetic energy spectrum of carbon as input. Two regions of discrepancy can be found, one at forward angles (near $\theta_\alpha = 0°$) and another at large angles ($\theta_\alpha \sim 40°$-$140°$) on the opposite side of the beam axis from the detected carbon.

The excess near $\theta_\alpha = 0°$ can be shown to arise from events in which the projectile dissociates into a carbon and an alpha particle with a three-body Q value near zero. These "projectile breakup" events produce a PLF and alpha particle with velocities near that of the projectile. They leave little or no excitation in the target nucleus and correspond to low (~20-MeV) excitations of the primary PLF that, however, do populate particle unstable states. Inclusion of such processes in the Monte Carlo calculation reproduces the forward-angle excess in $dM/d\Omega_\alpha$. This also removes the discrepancy between measured and calculated kinetic energy spectra of light ions in these detectors, as seen in Fig. 2.104b.

The origin of the excess at large angles is more elusive. Its character is best seen by examining maps of $$\frac{dM}{v_\alpha{}^2 dv_\alpha d\Omega_\alpha}\Bigg|_{\Omega_{HI},Q_3}$$. Two such maps are shown in Fig. 2.105 for the exit channel carbon + alpha particle for two slices in

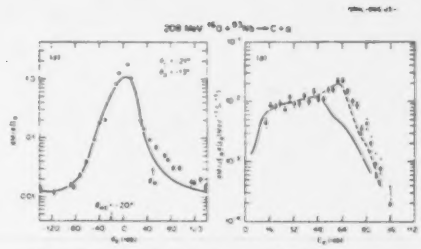

Fig. 2.104. (a) Variation of $dM/d\Omega_\alpha$ with θ_α for carbon-alpha particle coincidences. (b) Kinetic energy spectra of alpha particles detected in coincidence with carbon; solid line: Monte Carlo result without breakup contribution; dashed line: breakup contribution added.

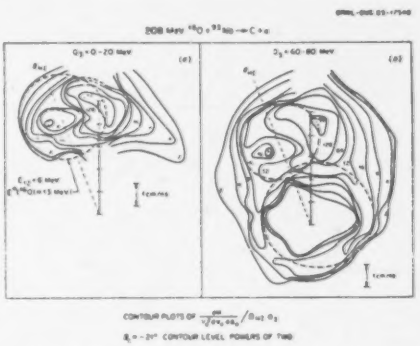

Fig. 2.105. Two-dimensional maps of $$\frac{dM}{v_\alpha{}^2 dv_\alpha d\Omega_\alpha}\Bigg|_{\Omega_{HI},Q_3}$$ for carbon-alpha particle coincidences for the Q_3 ranges given.

the three-body Q value, Q_3 = 0-20 MeV (quasi elastic) and Q_3 = 60-80 MeV (deeply inelastic). In addition to the expected ridges resulting from PLF and TLF decay (with the expected angular asymmetry in that of the PLF due to recoil and primary angular distribution effects), an excess of yield is found, which rapidly decreases in magnitude with increasing angular separation from the PLF direction. Such an excess is also found for protons and was seen for the neutrons in this same reaction. Such an excess has been suggested as evidence for formation of a "hot spot" on the target. Before such an explanation is adopted, it is useful to search for less exotic explanations. One such explanation is preequilibrium emission (in the statistical model sense) from broad states ($\Gamma \sim 1$ MeV) which have mean decay times on the order of the rotational time of the dinuclear

complex and/or Coulomb reseparation times of the projectilelike and targetlike nuclei. The resulting lower source velocity for alpha particles emitted by the PLF causes their emission into a broader angular range than that expected for emission from fully accelerated PLF, i.e., PLF which have reached their asymptotic velocity. Schematic calculations which employ a three-body Coulomb trajectory code suggest that the expected fall off in yield of such alpha particles with increasing laboratory angle is similar to that observed. This ensures treatment of, e.g., proximity effects, such as Coulomb effects, in the model. This is required before a meaningful comparison with experiment can be made.

---

1. Guest scientist from Institut de Physique Nucléaire de Lyon, Villeurbanne, France.
2. Los Alamos National Laboratory, Los Alamos, New Mexico.
3. On leave from Physical Institute, University of Heidelberg, Heidelberg, West Germany.
4. Vanderbilt University, Nashville, Tennessee.
5. Georgia State University, Atlanta, Georgia.

NONEQUILIBRIUM PROTON AND ALPHA-PARTICLE EMISSION IN FUSIONLIKE REACTIONS OF 206-MeV ^{16}O AND ^{93}Nb

C. F. Maguire[1] F. E. Obenshain
B. Cheynis[2] D. Pelte[3]
R. L. Ferguson F. Plasil
I-Y. Lee R. L. Robinson
M. Novotny[3] G. R. Young

The study of the emission of energetic light particles (typically protons, neutrons, and alphas) is aimed at illuminating the dynamics of a heavy-ion collision at its earliest stages. We have studied the energy and angular correlations of protons and alpha particles emitted in coincidence with fusionlike residues from reactions of 206-MeV ^{16}O with ^{93}Nb. All the reaction products were detected in an array of 18 silicon surface-barrier detector double telescopes. Six of these, which were in the forward direction, were backed by NaI(Tl) detectors capable of stopping up to 50-MeV protons. The particles (light ions and evaporation residues) were identified by standard ΔE-E and E-TOF techniques. The data were reduced to differential multiplicity spectra, i.e., the number of protons (alphas) per unit energy per detected residue, for a given pair of light-particle and residue detector angles. Sample differential multiplicity spectra of protons are shown in Fig. 2.106 for four widely spaced angular positions of the light-ion detectors. The residue detector was fixed at $\theta_{ER} = -7°$.

The system we have studied in coincidence is quite similar to one of three studied in singles over a range of incident energies by Awes et al.[4] This systematic study led to the conclusion that the major fraction of the inclusive

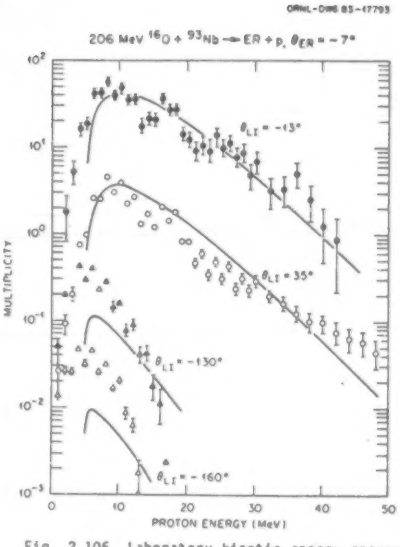

Fig. 2.106. Laboratory kinetic energy spectra of protons emitted at selected angles in coincidence with evaporation residues detected at $\theta_{ER} = -7°$. The curves are calculated using the moving-source parameters listed in Ref. 4 for 215-MeV ^{16}O + ^{90}Zr.

light-particle data (including protons, deuterons, tritons, and alphas) could be parameterized with a single moving source emitting according to a Maxwell-Boltzmann distribution. In the lab the differential cross section for particle emission is given by

$$\frac{d^2\sigma}{dE d\Omega} = N_0\sqrt{E - ZE_C} \qquad (1)$$

$$\times \exp \frac{-[E - ZE_C + E_1 - 2E_1^{1/2}(E - ZE_C)^{1/2}\cos\theta]}{T} ,$$

where N_0 is the source strength, E_C is the Coulomb repulsion per unit charge after emission, E_1 is the source kinetic energy per nucleon (MeV/u), θ the lab detection angle, Z the light-ion charge, and T the source temperature. The inclusive emission function, Eq. (1), can be integrated over energy and angle to yield the total production cross section,

$$\sigma = 2N_0(\pi T)^{3/2} . \qquad (2)$$

For the system ^{16}O + ^{90}Zr at 215-MeV incident energy, the following source parameters for the proton spectra extracted in Ref. 4: E_1 = 1.31 MeV/u (= 1.59 cm/ns), T = 4.54 MeV, σ = 1368 mb. For comparison, the compound nucleus recoil velocity is 0.77 cm/ns; the compound nucleus

temperature is 3.5 MeV; and the projectile (lab) velocity is 4.99 cm/ns. From this comparison and also from the comparison of their data for other systems, the authors of Ref. 4 concluded that there appeared to be evidence of emission from a source, moving faster than the compound nucleus but at only one-third of the projectile velocity, whose velocity and temperature were consistent with thermalization among a subset of nucleons. If these parameters are correct, one has the interesting possibility that something similar to a hot spot is being created at these incident energies, perhaps precursors of the "fireballs" being created at relativistic bombarding energies.

With our new data, we are able to test the moving-source hypothesis further because we gate on residues, and the light-particle energy cutoffs here are much lower (1.5 vs 12 MeV for the protons) than in the experiment of Ref. 4. These advantages enable us to resolve the fusion-evaporation component which is present in any singles spectrum. The moving-source function of Eq. (1), with the velocity and temperature parameters deduced for 215-MeV $^{16}O + ^{90}Zr$, was used to fit the spectra shown in Fig. 2.106. In particular, the normalization constant was obtained by fitting on the most forward-angle spectrum. It can be seen that, while that moving-source function fits the entire kinetic energy range of the spectra at forward angles, it underpredicts the data as one moves into the backward hemisphere. In fact, fitting the entire forward-angle spectra is not a boon, since it implies that the evaporation component must be being fit by a source that manifestly does not resemble an evaporation source. In fact, there are at least two components present in these spectra. This can be seen in Fig. 2.107 which displays the same data, but with fits extracted by using the back-angle spectra to determine the yield due to a source with velocity and temperature expected for a compound nucleus. With a normalization as given by fitting the backward-angle spectra, the projected evaporation yield at forward angles reproduces the data in the 3- to 15-MeV region. There remains a high-energy component which is concentrated at forward angles in these spectra. That component can be fitted with a high temperature source which has a velocity only slightly less than the original projectile velocity. One interpretation of this is that the fast protons are emitted from the projectile as it is slowing down in the Coulomb field of the target, but before a large fraction of the projectile momentum is deposited in the compound system being formed. The integrated yield of these fast particles corresponds to about 10% of the yield of the fusion-evaporation protons, being about 0.24 nonequilibrium protons per fusion event.

We have analyzed the alpha-particle multiplicity spectra in the same fashion and come to the conclusion that the vast majority of the alpha yield (>95%) is simply due to fusion evaporation. The small remainder arises from projectile breakup, followed by fusion of the projectile remnan Thus, none of the alpha yield seems to be amenable to the moving-source description of Eq. (1), a conclusion at variance with that of Ref. 4.

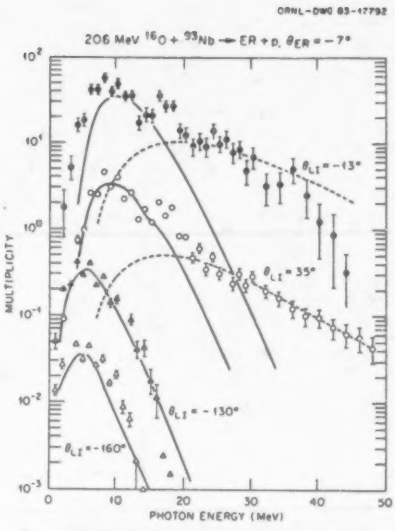

Fig. 2.107. Spectra as described in Fig. 1. The solid lines are the result of an evaporation model fit to the back-angle data and projected onto the forward-angle data. The dashed line represents the additional contribution from a thermal source with temperature 4.5 MeV, lab velocity 4.2 cm/ns along the projectile direction, and multiplicity 0.24 proton per evaporation residue.

---

1. Vanderbilt University, Nashville, Tennessee.
2. Guest from Institut de Physique Nucléaire de Lyon, Villeurbanne, France.
3. On leave from Physical Institute, University of Heidelberg, Heidelberg, West Germany.
4. T. C. Awes et al., Phys. Rev. C 25, 2361 (1982).

TWO-PROTON CORRELATION MEASUREMENTS AT 25 MeV/u[1]

W. G. Lynch[2] G. R. Young
C. B. Chitwood[2] T. C. Awes
M. B. Tsang[2] R. L. Ferguson
D. J. Fields[2] F. E. Obenshain
D. R. Klesch[2] F. Plasil
C. K. Gelbke[2] R. L. Robinson
A. D. Panagiotou[3]

Of the many differing theoretical approaches to nonequilibrium particle emission, the concept

of a spatially localized region of high excitation ("hot spot"), first suggested by Bethe in 1938,[6-7] has received support from the comparisons of inclusive light-particle spectra and multiplicities with statistical predictions.[8-9] While these comparisons test the thermal assumptions of the "hot spot" picture, until now the particular aspect of spatial localization has lacked direct experimental verification.

A gold target of 8.6 mg/cm^2 was bombarded with ^{16}O ions of 400-MeV incident energy obtained from HHIRF. Single and coincident protons were detected with 13 ΔE-E telescopes consisting of silicon ΔE and NaI(Tl) E detectors. Small-angle correlations were measured with six telescopes having individual solid angles of 0.76 msr. The telescopes were mounted in a closely packed hexagonal array that was centered at a scattering angle of 15°. The angular resolution and the angular separation between adjacent telescopes were 1.6° and 5.1°, respectively. Large-angle correlations were measured with seven telescopes of solid angles between 13 and 41 msr. Three of these telescopes were mounted in the plane of the small angle hodoscope (ϕ = 0°) at scattering angles of θ = 40°, 70°, and 130°, where θ and ϕ denote the polar and azimuthal angles measured with respect to the beam axis. The remaining four telescopes were positioned at polar angles of θ = 40°, 70°, 130°, and 160°; their azimuthal angle was varied between 50° and 180°. Absolute cross sections accurate to 10% were obtained from the integrated beam current, the target thickness, and the solid angles of the telescopes. Energy calibrations accurate to 3% were obtained by measuring the energies of recoil protons from a Mylar target bombarded by a 200-MeV ^{16}O beam.

Information regarding the space-time localization of the emitting source is contained in the magnitude of the final-state correlations between light particles emitted at small relative momenta. For the case of two protons emitted at close proximity in space and time, the strong attractive nuclear interaction in the singlet-s partial wave causes a characteristic increase in the two-proton correlation at relative momenta of about 20 MeV/c.[10] Emission from a source of large dimensions or long lifetime results in a weakened final-state effect and subsequent decrease in their correlation.

The two-proton correlation function, $R(\vec{p}_1,\vec{p}_2)$, is defined in terms of the singles cross sections, $\sigma(\vec{p}_1)$, $\sigma(\vec{p}_2)$, and coincidence cross sections, $\sigma(\vec{p}_1,\vec{p}_2)$, by

$$\sigma(\vec{p}_1,\vec{p}_2) = C\sigma(\vec{p}_1)\sigma(\vec{p}_2)[1 + R(\vec{p}_1,\vec{p}_2)],$$

where $\vec{p}_i$ indicates the momentum of particle i and the normalization constant C is experimentally determined by the condition $R(\vec{p}_1,\vec{p}_2) = 0$ for sufficiently large relative momenta, where final-state interactions are very small. In Fig. 2.108 the experimental correlation function is shown as a function of the magnitude of the relative momentum $\Delta p = (|\vec{p}_1 - \vec{p}_2|)/2$. The curves shown in the figure are the results of model calculations[10] for the case of incoherent emission from a source of negligible lifetime and Gaussian spatial distribution of rms radius $\sqrt{(3/2)}\, r_0$. The correlations observed experimentally are slightly larger than those calculated

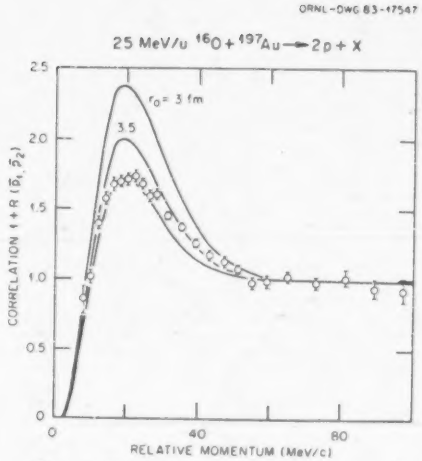

Fig. 2.108. The experimental correlation function $1 + R(\vec{p}_1,\vec{p}_2)$ is plotted as a function of the proton relative momentum. The errors are purely statistical. See the text for a discussion of the curves.

for a source with r_0 = 4 fm. Nonnegligible decay times will reduce the correlations; therefore, values for r_0 deduced by comparison with the present calculations represent upper limits on the average source sizes.

Further insight may be gained by investigating the dependence of the measured correlation function $1 + R(\vec{p}_1,\vec{p}_2)$ on the total energy of the two coincident protons. This energy dependence is shown in Fig. 2.109 for the relative momentum intervals of Δp = 15-25 MeV/c [where $R(\vec{p}_1,\vec{p}_2)$ is predicted to reach a maximum] and Δp = 50-80 MeV/c [where $R(\vec{p}_1,\vec{p}_2)$ is predicted to be near zero]. For the lowest sum proton energies observed, no substantial differences in the correlations of the two regions are observed, which indicates that these protons are predominantly emitted from a source of rather large space-time extent, e.g., a long-lived compound nucleus. With increasing sum proton energies, the differences between the measured correlations become more pronounced, which indicates that high-energy protons are emitted primarily from a short-lived and spatially localized region of high excitation, in qualitative agreement with the concept of formation and decay of a "hot spot." For sum proton energies above E1 + E2 = 90 MeV, the measurement of $R(\Delta p)$, provided by the ratio of the two measured correlations, yields an upper limit of r_0 = 3.1 fm. With the assumption of normal nuclear matter density (0.15 fm^{-3}), a maximum number of 25 participating nucleons is estimated.

In conclusion, two-proton correlations measured for ^{16}O-induced reactions on ^{197}Au at 400 MeV provide evidence for the formation and decay

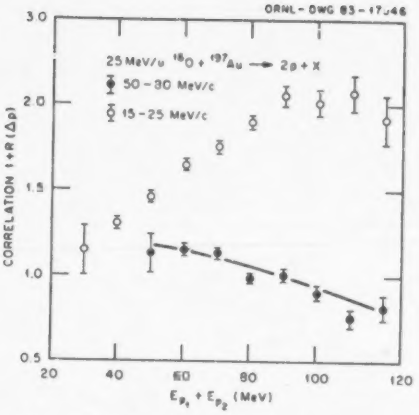

Fig. 2.109. The correlation function $1 + R(\vec{p}_1, \vec{p}_2)$, gated on relative momentum for 15-25 MeV/c and 50-80 MeV/c, is plotted as a function of the sum energy of the two protons. The errors are purely statistical. The solid line gives the correlation calculated for a set of nucleons recoiling at 0.084 c and emitting protons with a Maxwell-Boltzmann spectrum of temperature 7.1 MeV.

of a localized region of high excitation. High-energy protons sample the early stages of the reaction characterized by a rather small space-time extent of the emitting source. Low-energy protons, on the other hand, are primarily emitted at later stages of the reaction corresponding to an emitting source consistent with the compound nucleus.

---

1. Summary of paper to be published.
2. Michigan State University, East Lansing, Michigan.
3. Michigan State University, East Lansing, Michigan, and University of Athens, Athens, Greece.
4. H. A. Bethe, Phys. Rev. 53, 675 (1938).
5. R. Weiner and M. Westrom, Nucl. Phys. A286, 282 (1977).
6. P.-A. Gottschalk and M. Westrom, Nucl. Phys. A314, 232 (1979).
7. S.I.A. Garpman, D. Sperber, and M. Zielinska-Pfabe, Phys. Lett. 90B, 53 (1980); Phys. Lett. 92B, 56 (1980).
8. C. K. Gelbke, Comments Nucl. Part. Phys. 11, 259 (1983) and references given therein.
9. T. C. Awes et al., Phys. Rev. C 25, 2361 (1982).
10. S. E. Koonin, Phys. Lett. 70B, 43 (1977).

ENERGY DIVISION IN DAMPED REACTIONS[1]

T. C. Awes, R. L. Ferguson, R. Novotny[2], F. E. Obenshain, F. Plasil, S. Pontoppidan[3], V. Rauch[4], H. Sann[5], G. R. Young

We have investigated ^{58}Ni-induced reactions by using the 889-MeV ^{58}Ni beam produced by coupled operation of the tandem electrostatic and cyclotron accelerators of the Holifield Heavy Ion Research Facility at Oak Ridge. Projectilelike fragments resulting from interactions with targets of ^{58}Ni (1.9 mg/cm^2) and of ^{197}Au (1.2 mg/cm^2) were identified by their nuclear charge with a large-area position-sensitive gas ionization chamber located 1 m from the target.

The centroids of the angle-integrated charge distributions are presented in Figs. 2.110a and 2.110b for reactions on ^{58}Ni and ^{197}Au, respectively. The most striking feature of these distributions is the strong drift of the charge centroids, with increasing energy loss, toward charges smaller than that of the projectile. We have performed an evaporation calculation to determine whether the observed drift is consistent with equilibrium evaporation. For this calculation we have used a modified form of the evaporation code LILITA,[6] which allows a chosen primary distribution to be sampled in all variables. The primary distribution is specified by an excitation energy distribution and, at each excitation energy, by a bivariate distribution in proton and neutron number, a Gaussian distribution in dissipated angular momentum, and a Gaussian distribution in the relative sharing of the excitation energy. The energy loss is calculated with binary kinematics and uses the secondary PLF; i.e., the evaporation results are treated in the same manner as the experimental data.

Primary distributions predicted by Randrup's transport model[7] were used as input for the calculations of Fig. 2.110. In this model the relative kinetic energy of the two nuclei is dissipated by the stochastic transfer of nucleons. The nucleon transfer is driven by the available phase space as determined by the dinuclear potential energy surface and the finite-temperature Fermi-Dirac statistics. For the heavy solid curves of Fig. 2.110, it was assumed that the excitation energy is shared according to mass and that the dissipated angular momentum increases linearly from zero at zero energy loss to the sticking limit at the interaction barrier. For the ^{58}Ni + ^{58}Ni reaction the calculation is shown to reproduce the observed widths and centroids quite well, up to the largest energy losses where the charge distributions become asymmetric due to fissionlike decay of the PLF.[8] This suggests that equilibrium evaporation is the dominant source of the drift toward smaller charges.

For the ^{58}Ni + ^{197}Au reaction the values of the predicted charge centroids (heavy solid

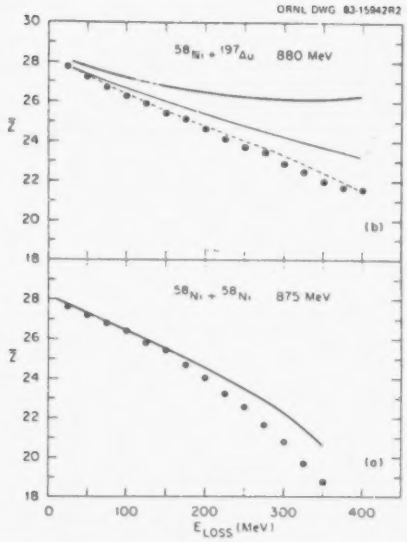

Fig. 2.110. Centroids of the angle-integrated charge distributions for (a) $^{58}Ni + ^{58}Ni$, integrated over the angular range $4 < \theta < 38.5$ ($\theta_{gr} = 7.2$), and (b) $^{58}Ni + ^{197}Au$, integrated over the angular range $6 < \theta < 38.5$ ($\theta_{gr} = 18.6$). The centroids have been extracted by a moment analysis with a smooth interpolation through $Z = 28$ at large energy losses to avoid the influence of possible beam tail. The calculations are described in the text.

curve) are larger than those observed, which indicates a deficiency in the assumed primary distribution. A possible explanation for this discrepancy is that, at high bombarding energy, the interaction time is too short to permit an equilibrium division of the excitation energy between the PLF and TLF. If the excitation energy is assumed to be shared equally between the two fragments (light solid curve), rather than according to mass (heavy solid curve), then Randrup's model is found to provide an acceptable description of the observed charge distributions. It is interesting that if, in addition, the primary N and Z centroids are fixed at ^{58}Ni, then the agreement is improved further (dashed curve).

Although the assumption of equally shared excitation energy is in contradiction to conclusions reached in experiments at lower incident energies, a careful analysis of such results suggests otherwise. In Fig. 2.111 we show the neutron multiplicities and the measured N and Z centroids from Refs. 9 and 10, respectively. Three calculations are shown in Fig. 2.111 for the assumptions that (1) the excitation energy is shared according to mass (long dashed curve),

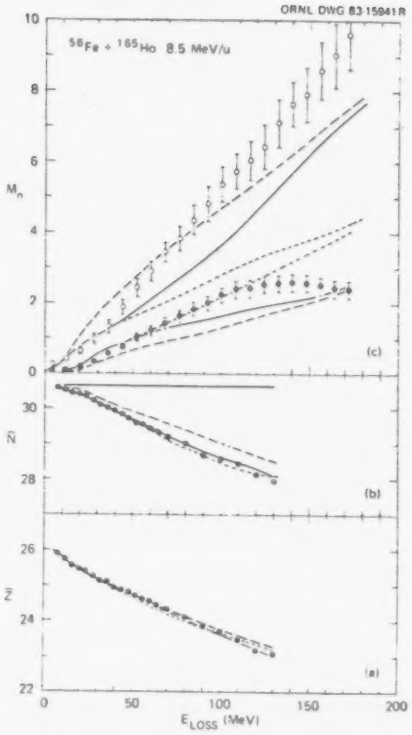

Fig. 2.111. Centroids of the (a) charge and (b) neutron number distribution of PLFs for the $^{56}Fe + ^{165}Ho$ reaction at 8.5 MeV/u incident energy (Ref. 10). Note: A small correction for neutron evaporation was made to the energy loss in Ref. 10. (c) Average multiplicity of neutrons emitted from the TLF (open circles) and PLF (filled circles) (Ref. 9). The calculations are described in the text.

(2) the excitation energy is shared equally (short dashed curve), and (3) the excitation energy division makes a smooth transition from equal sharing at small energy loss to equal temperatures at large energy loss (solid curve). For each calculation the primary distributions were allowed to vary freely within the constraint given below. Since there is no constraint on the primary Z distribution, all three calculations are able to reproduce the observed charge centroids (Fig. 2.111a). The primary N distribution is weakly constrained by the fact that at a given energy loss, the primary N centroid must be greater than the observed centroid plus the average multiplicity of emitted neutrons (see light line, Fig. 2.111b). This limit

can be extracted only approximately due to the uncertain relationship between calculated energy loss and excitation energy. With this constraint and the assumption of thermal equilibrium, it is not possible to reproduce the observed N centroids. In Fig. 2.111c it is shown that, for energy losses less than about 50 MeV, the assumption of thermal equilibrium yields too little neutron emission from the PLF and too much emission from the TLF. The multiplicities are predicted correctly here if the excitation energy is shared equally between the fragments. On the other hand, at the largest energy losses the assumption of thermal equilibrium gives results which best reproduce the observed multiplicities. It follows that a smooth transition from the limit of equal sharing of the dissipated energy at small energy loss to the limit of equal temperatures at large energy loss gives the best overall description of the data. For the calculation of Fig. 2.111 (solid curve), a linear transition was assumed to occur from the limit of equal sharing at excitation energies of 30 MeV or less to the equal temperature limit for excitation energies of greater than 130 MeV. Although qualitatively correct, this transition cannot be accurately determined since the calculation underpredicts the neutron multiplicity from both fragments for large energy losses. Finally, it should be remarked that the primary N and Z distributions used for the calculation with the transitional energy division evolve in a manner which is in reasonable agreement with expectations based upon the potential energy surface.

---

1. Summary of paper to be published.
2. On leave from Physical Institute, University of Heidelberg, Heidelberg, West Germany.
3. On leave from Niels Bohr Institute, University of Copenhagen, Copenhagen, Denmark.
4. Present address: Centre de Rechearches Nucléaries, Strasbourg, France.
5. Gesellschaft für Schwerionenforschung, Darmstadt, West Germany.
6. Program LILITA, J. Gomez del Campo et al., Phys. Rev. C 19, 2170 (1979). Modified by S. Pontoppidan, Ph.D. thesis, NBI, University of Copenhangen, June 1981.
7. J. Randrup, Nucl. Phys. A327, 490 (1979).
8. T. C. Awes et al., "Fissionlike Decay of Projectilelike Fragments in ^{58}Ni-Induced Reactions at 15.3 MeV/u," this report.
9. D. Hilscher et al., Phys. Rev. C 20, 576 (1979).
10. H. Breuer et al., Phys. Rev. C 28, 1080 (1983).

QUASI-ELASTIC STRUCTURE IN THE REACTION ^{56}Fe + ^{56}Fe AT 14.6 MeV/NUCLEON

A. C. Mignerey[1] J. D. Silk[1]
C. Merouane[1] K. Kwiatowski[2]
S. O. Bradley[1] V. E. Viola, Jr.[2]
D. Benton[1] T. C. Awes
H. Breuer[1] F. E. Obenshain
S. Pontoppidan[3]

Symmetric and near-symmetric product nuclides from reactions in the mass ranges of Ca and Fe have shown structure in the quasi-elastic regions of the kinetic energy spectra of isotopically separated product nuclides. In the ^{56}Fe + ^{56}Fe reaction studied previously at 8.3 MeV/nucleon, only the ^{57}Co product nuclide showed clear indications of structures. These appeared at total excitation energies of ~30, 45, and 60 MeV. While the 30-MeV structure may originate from evaporation, calculations have shown that this is not true for the higher excitation energy peaks.[4]

Indications that the structure is enhanced for higher bombarding energies led to the study of the ^{56}Fe + ^{56}Fe reaction at the HHIRF with the 14.6-MeV/nucleon ^{56}Fe beam. A time-of-flight system, with a 1.5-meter flight path and with channel-plate fast timing devices as start and stop detectors, was employed for mass identification. A large four-element ΔE-E ion chamber, known after its creator as the Snell chamber, was used for Z identification and total energy measurement. The resulting charge and mass resolutions were <0.4 charge units and ~0.8 mass units, respectively. The use of an internal Faraday cup allowed measurements of projectilelike fragments down to laboratory angles of 3°. The large ion chamber was filled with CF_4 at a pressure of 140 torr and, with a total depth of 70 cm, was capable of stopping the majority of the observed projectilelike fragments.

A distinctive feature of the reaction is the lack of cross section at the lower kinetic energies for the products with Z > 27. This can be seen in Fig. 2.112 where the laboratory kinetic energy spectra for projectilelike products, with Z = 27 measured at 3° and 7°, are shown. Unfortunately, the statistics for these two angles were not sufficient to produce energy spectra separated according to product masses with great statistical significance (see Fig. 2.113). After summing over all masses, the 7° spectrum shows two major peaks corresponding to excitation energies of approximately 20 and 50 MeV. The 20-MeV peak is greatly reduced in the 3° spectrum, while the broader, higher energy peak seems to have shifted to an excitation energy of ~60 MeV. There are indications in both spectra

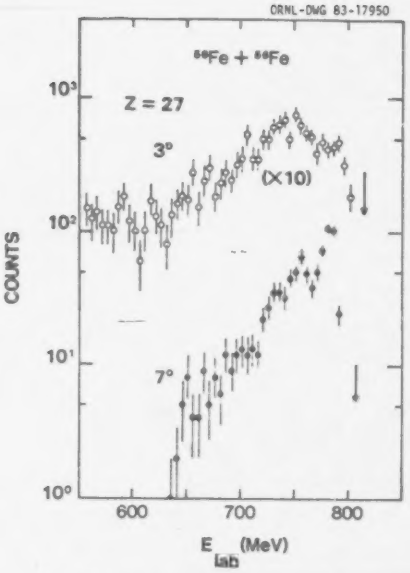

Fig. 2.112. Laboratory kinetic energy spectra for the cobalt product nuclides from the reaction of 817-MeV ^{56}Fe with ^{56}Fe. The open and filled points are data taken at θ_{lab} = 3° and 7°, respectively. The arrows indicate the energies for elastically scattered ^{56}Fe at each angle.

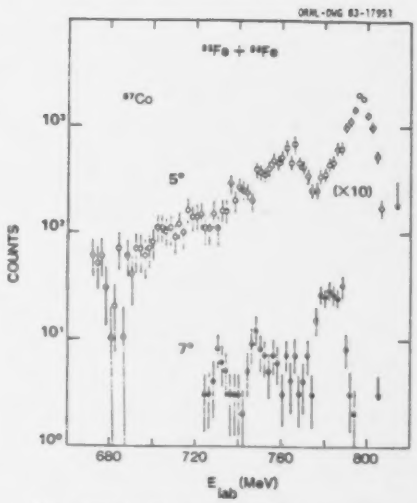

Fig. 2.113. Laboratory kinetic energy spectra for the ^{57}Co product nuclide measured at θ_{lab} = 5° and 7° for the reaction $^{56}Fe + ^{56}Fe$ at E_{lab} = 817 MeV. The open and filled circles are data taken at θ_{lab} = 5° and 7°, respectively. As in Fig. 2.112, the arrows indicate the energies of elastically scattered ^{56}Fe.

that the broad peak may be a superposition of two peaks, perhaps due to the different contributing cobalt isotopes.

Sufficient statistics were obtained at θ_{lab} = 5° to produce energy spectra for individual product nuclides. The laboratory energy spectrum of the dominant nuclide ^{57}Co is shown in Fig. 2.113. As seen at 7°, there are two major peaks corresponding to excitation energies of approximately 20 and 50 MeV. Note that the energy scale has been expanded relative to that of Fig. 2.112. The 20-MeV peak has a width of ~10 MeV and does not seem to change position with angle. However, the intensity is quite angle dependent, which suggests a direct reaction that may involve the proton pickup channel.

The lower excitation energy peak appears at all three angles. The significance of the apparent shift in excitation energy at θ_{lab} = 3° is hard to judge from the present data since two peaks may be contributing, as appears to be the case from the 7° data. What is clear is that this structure has a behavior different from that of the 20-MeV peak and deserves further investigation. Calculations are presently being performed to rule out the possibility of particle evaporation.

---

1. University of Maryland, College Park, Maryland.
2. Indiana University Cyclotron Facility, Bloomington, Indiana.
3. On leave from Niels Bohr Institute, University of Copenhagen, Copenhagen, Denmark.
4. A. C. Mignerey et al., University of Maryland Nuclear Chemistry Progress Report ORO-5172-0019, 1981, p. 20, and to be published.

SYSTEMATICS OF NONEQUILIBRIUM NEUTRON EMISSION[1]

A. Gavron[2] G. R. Young
J. R. Beene G. A. Petitt[4]
B. Cheynis[3] C. F. Maguire[5]
R. L. Ferguson D. G. Sarantites[6]
F. E. Obenshain M. Jääskeläinen[6]
F. Plasil K. Geoffroy-Young[7]

Energy spectra and angular distributions of neutrons associated with evaporation residues were measured in the reactions $^{12}C + ^{158}Gd$, $^{13}C + ^{157}Gd$, and $^{20}Ne + ^{150}Nd$ at energies between 4 and 11 MeV/u. The data were analyzed

in terms of a moving hot-source model,[8] and multiplicities of neutrons resulting from nonequilibrium neutron emission (NNE) were deduced. These are shown, as a function of the energy per nucleon above the Coulomb barrier, in Fig. 2.114. The trends of the NNE multiplicities can be seen to be similar for the three reactions. The slightly higher values for NNE in the ^{13}C reaction may be due to a small breakup contribution in which the ^{13}C fragment resulting from the breakup is absorbed by the target nucleus. The lines represent multiplicities predicted from the preequilibrium Boltzmann-master-equation (BME) model of Blann,[9] on the assumption that the number of excitons is equal to the number of particles in the projectile. It can be seen that the BME model does not predict correctly the projectile dependence of NNE.

The temperatures of the hot sources, as deduced from the data, were found to be constant when plotted as a function of the energy per nucleon above the Coulomb barrier. In contrast, a linear correlation is observed between the velocity of the hot source in the target frame of reference and the relative velocity of the target and the projectile at the Coulomb barrier, which implies an increase in the temperature of the hot source with bombarding energy. This apparent inconsistency raises a question as to whether the moving-source model has an underlying physical justification or is just a convenient parametrization.

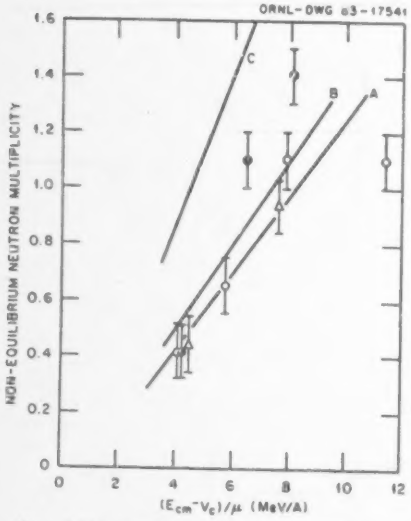

Fig. 2.114. Nonequilibrium neutron multiplicity as a function of energy per nucleon above the Coulomb barrier. Hollow circles: ^{12}C data; full circles: ^{13}C data; triangles: ^{20}Ne data. The lines marked A, B, and C are obtained from the BME model for ^{12}C, ^{13}C, and ^{20}Ne, respectively.

---

1. Summary of paper: Phys. Rev. C 27, 450 (1983).
2. Los Alamos National Laboratory, Los Alamos, New Mexico.
3. Guest from Institut de Physique Nucléaire de Lyon, Villeurbanne, France.
4. Georgia State University, Atlanta, Georgia.
5. Vanderbilt University, Nashville, Tennessee.
6. Washington University, St. Louis, Missouri.
7. Washington University, St. Louis, Missouri. Present address: Fusion Energy Division, ORNL.
8. A. Gavron et al., Phys. Rev. C 24, 2048 (1981).
9. M. Blann et al., Phys. Rev. C 23, 205 (1981).

HEAVY-ION-INDUCED FISSION AND FUSION

FISSIONLIKE DECAY OF PROJECTILELIKE FRAGMENTS IN ^{58}Ni-INDUCED REACTIONS AT 15.3 MeV/u[1]

T. C. Awes
R. L. Ferguson
R. Novotny[2]
F. E. Obenshain
F. Plasil
V. Rauch[3]
H. Sann[4]
G. R. Young

This study was motivated by reports[5,6] of the observation of ternary events in Kr- and Xe-induced reactions corresponding to the fast fission, or "splitting," of projectilelike products.

The present study was intended to determine if such three-body events also occur in reactions with lighter projectiles and to establish the extent of charge transfer and energy loss in the first step of the reaction. The experimental configuration was optimized for the detection of three-body events over the full range of possible energy losses. The detector arrangement included a large-area ionization chamber capable of measuring the energy, E, and the energy loss, ΔE, of reaction products as well as their (x,y) position. A second detector was operated in coincidence on the other side of the beam. It consisted of an ionization ΔE section backed by a position-sensitive silicon counter. This detector covered a fixed in-plane angular range of -12° to -32°, while the large-area ionization chamber was operated at three angles, covering the angular range of 4° to 39°.

The inclusive charge distributions measured with the large-area ionization chamber were found to be dominated by products with $Z < 28$, and very little yield was observed for nuclei with charges greater than that of the projectile. It has been shown[7] that most of the shift toward lighter products is consistent with the effects of equilibrium evaporation.

In Fig. 2.115a the distribution of coincident events is shown as a function of $Z_1 + Z_2$ and of $E_1 + E_2$. A strong cluster of events appears centered at $Z_1 + Z_2 \approx 40$ and $E_1 + E_2 \approx 440$ MeV. Events in this region can be shown to originate from binary events. They involve large energy losses and, therefore, large amounts of charged-particle emission. The peak represents only a small portion of all binary events due to phase-space restrictions resulting from our experimental configuration. In contrast, events with $10 \lesssim Z_1 + Z_2 \lesssim 30$ and $200 \lesssim E_1 + E_2 \lesssim 750$ MeV (see Fig. 2.115a) are not due to binary reactions between ^{58}Ni nuclei, but must originate either from three-body sequential fission events or from binary reactions between ^{58}Ni projectiles and light target contaminants.

Several arguments can be presented for the three-body interpretation of the events with $Z_1 + Z_2 \lesssim 30$. First, the rest frame velocity of these events is centered near 3.8 cm/ns, which is consistent with a fully damped two-body reaction on ^{58}Ni followed by a sequential fission process. For comparison, the velocity of the center of mass of the ^{58}Ni + ^{58}Ni system is 2.7 cm/ns, and the c.m. velocity of the ^{58}Ni + ^{12}C system (^{12}C contaminant) is 4.5 cm/ns. Second, a comparison of the $E_1 + E_2$ vs. $Z_1 + Z_2$ distribution from ^{58}Ni + ^{58}Ni reactions (see Fig. 2.115a) can be made with that obtained from reactions between ^{58}Ni and ^{12}C under identical experimental conditions (see lower half of Fig. 2.116). From Fig. 2.116 it is clear that reactions on a light target contaminant would result in a coincidence distribution which might be interpreted as resulting from three-body sequential fission occurring after very little charge transfer and energy loss. In contrast, we observe that energy losses of at least 200 MeV are required in the first step of the reaction before symmetric fission products are observed. We conclude that possible contributions from light target contaminants are less than 5%, as might have been expected, since a thick ^{58}Ni foil of 1.9 mg/cm^2 was used.

The relatively small amount of energy loss and charge transfer preceding fission, suggested by Fig. 4 of Ref. 5, is in contradiction with the present results and the results of von Harrach et al.[6] Although the experimental geometry and the systems studied were rather different, there is an obvious qualitative similarity between our results on ^{12}C (see Fig. 2.116) and the ^{86}Kr + ^{89}Y coincidence measurements presented in Ref. 5. The strong similarity suggests that the bulk of the coincidence events in the region of small, apparent energy loss and charge transfer may arise from reactions on a light target contaminant.

Further direct evidence for the three-body interpretation of our results is shown in Fig. 2.115b by the correlation between coincident charges, Z_1 and Z_2, obtained with the lower and upper halves of the large-area ionization chamber. Thus, both of the detected fragments were observed on the same side of the beam. The concentration of events along the lines $Z = 28$ is obviously due to random coincidences with elastically scattered ions. However, those events in the region $Z_1 + Z_2 \lesssim 28$ are primarily valid coincidences. Simple considerations of momentum conservation immediately rule out any kind of binary events and imply that a third large reaction product must be present on the other side of the beam.

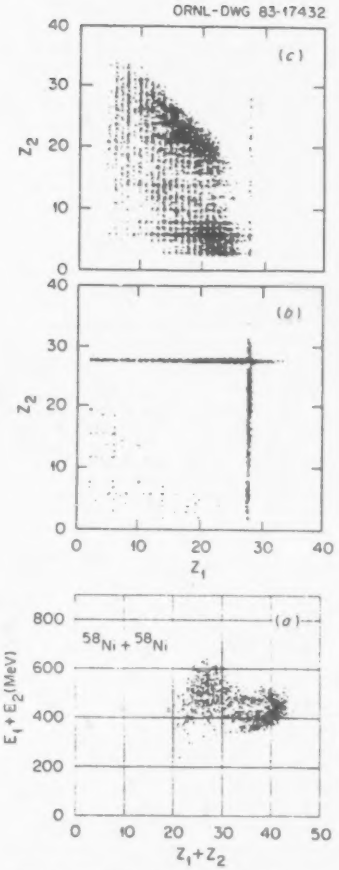

Fig. 2.115. Distributions of coincident products for reactions of ^{58}Ni + ^{58}Ni at 15.3 MeV/u. (a) Summed charge versus the summed laboratory energy. (b) Charge of fragment observed in lower half versus that observed in upper half of ionization chamber. Both fragments are observed on the same side of the beam axis. (c) Correlation between fragment charges observed on opposite sides of the beam by two different ionization chambers.

In Fig. 2.115c the correlation between the nuclear charge, Z_1, observed in the large ionization chamber is shown versus the nuclear charge, Z_2, observed in the small detector. In

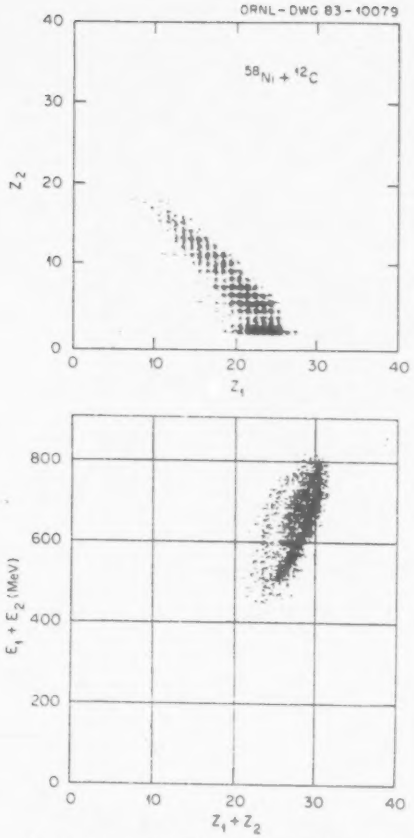

Fig. 2.116. Distributions of coincident products for reactions of $^{58}Ni + ^{12}C$ at 15.3 MeV/u. The upper part of the figure shows the correlated charge distribution for products detected by two ionization chambers on opposite sides of the beam axis. The lower part of the figure shows the summed charge versus the summed laboratory energy of the coincident fragments.

this case the line of random coincidences at $Z_2 = 28$ is absent since this detector was located beyond the grazing angle and, thus, was not exposed to a large flux of elastically scattered particles. The concentration of yield at $Z_1 + Z_2 = 40$ due to binary events is again clearly observed. A striking feature of Figs. 2.115b and 2.115c is the very broad distribution of the three-body events over nearly all possible Z_1, Z_2 combinations having sum charge less than or about equal to ^{58}Ni. In fact, since the sum charge is generally less than 28, it is most likely that there are more than three large fragments in the final state. There also appear to be indications of an enhanced probability for an asymmetric split of the nickellike fragment.

---

1. Summary of paper: Proc. Int. Winter Meeting on Nuclear Physics, Bormio, Italy, January 1983, Universitá and Istituto Nazional di Fisica Nucleare, Milano, Italy, 1983, p. 425.
2. On leave from Physical Institute, University of Heidelberg, Heidelberg, West Germany.
3. On leave from Centre de Rechearches Nucléaries, Strasbourg, France.
4. Gesellschaft für Schwerionenforschung, Darmstadt, West Germany.
5. A. Olmi et al., Phys. Rev. Lett. **44**, 383 (1980).
6. P. Glässel et al., Phys. Rev. Lett. **48**, 1089 (1982); D. v. Harrach et al., Phys. Rev. Lett. **48**, 1093 (1982).
7. T. C. Awes et al., "Energy Division in Damped Reactions," this report.

ANGULAR-MOMENTUM-DEPENDENT FISSION BARRIERS IN THE MASS REGION FROM A = 153 TO A = 210

T. C. Awes
H. C. Britt[1]
B. Cheynis[2]
D. Drain[2]
R. L. Ferguson
M. M. Fowler[4]
Z. Fraenkel[3]
A. Gavron[1]
F. E. Obenshain
F. Plasil
A. J. Sierk[1]
S. G. Steadman[4]
J. van der Plicht[1]
J. B. Wilhelmy[1]
G. R. Young

In most studies of angular-momentum-dependent fission barriers, fission excitation functions have been measured and analyzed within the framework of the statistical model by means of two-parameter fits. Typically, one of these parameters is related to the fission barrier, B_f, and the other is the ratio of the Fermi-gas level density parameter for fission to that for particle emission, a_f/a_ν. The values of the parameters are determined by the slopes and the magnitudes of the excitation functions and are valid in the region of angular momentum where the fission barrier is in the same energy range as the binding energies of the evaporated particles. Due to this constraint, it is not possible to extract the angular momentum dependence of the fission barriers over a large range, in a model independent manner, and reference must be made to theoretical calculations.

Until recently the only calculated angular-momentum-dependent fission barriers available were those obtained from the rotating liquid drop model, RLDM.[5] These liquid drop fission barriers, $B_f^{LD}(J)$, were used in the statistical model calculations and were adjusted with angular-momentum-independent parameters, such as k_f, defined by $B_f(J) = k_f B_f^{LD}(J)$. For an adequate description of the measured excitation functions, $B_f(J)$ values smaller than $B_f^{LD}(J)$ have

been found in almost all cases. This basic conclusion was not surprising since more realistic calculations, which take into account the finite range of the nuclear force and the diffuseness of the nuclear surface,[6] result in lower calculated fission barriers. The finite-range model of Ref. 6, however, applies only to nonrotating nuclei, and direct comparison of theory with experiment requires the development of a rotating finite-range model, RFRM. Recently, calculations of fission barriers as a function of angular momentum have been performed with such a model.[7] We have reexamined our earlier results for the ^{153}Tb system, in the context of these calculations, and have obtained new results for ^{158}Er, ^{181}Re, ^{186}Os, and ^{210}Po compound nuclei.

In order to apply a statistical model treatment to heavy-ion-induced fission excitation functions, the total fusion cross sections must be known. Thus it is necessary either to measure or to estimate evaporation residue cross sections, σ_{ER}. In addition, in order to explore angular momentum effects adequately, two or more reactions leading to the same compound nucleus must be investigated. The reactions studied are given in Table 2.17. Measurements for the ^{153}Tb and ^{181}Re systems[8] were performed at the Oak Ridge Isochronous Cyclotron, while those for the ^{158}Er, ^{186}Os, and ^{210}Po systems[9] were carried out at the Brookhaven National Laboratory tandem Van de Graaff accelerator.

Determinations of σ_{ER} were made in the cases of ^{153}Tb and ^{181}Re. A time-of-flight method was used. The results were found to be consistent with fusion cross section values calculated with the 1977 version of the Bass model,[10] and σ_{ER} values deduced from the Bass model were, therefore, used in all cases where evaporation residue measurements were not made. The fission cross sections, σ_f, were measured by means of surface barrier semiconductor detectors in the ^{153}Tb case and by means of ultrathin multiwire counters in all other cases, except that, for ^{12}C + ^{169}Tm and ^{22}Ne + ^{159}Tb, σ_f values of Sikkeland[11] were used. We have remeasured σ_f in the cases of ^{16}O + ^{170}Er, ^{12}C + ^{174}Yb, and ^{12}C + ^{169}Tm and have obtained good agreement with the results of Ref. 11.

Table 2.17. Reactions investigated.

Compound system	Reaction
^{153}Tb	^{12}C + ^{141}Pr
	^{20}Ne + ^{133}Cs
^{158}Er	^{16}O + ^{142}Nd
	^{24}Mg + ^{134}Ba
	^{32}S + ^{126}Te
	^{64}Ni + ^{94}Zr
^{181}Re	^{12}C + ^{169}Tm
	^{22}Ne + ^{159}Tb
^{186}Os	^{9}Be + ^{177}Hf
	^{12}C + ^{174}Yb
	^{16}O + ^{170}Er
	^{26}Mg + ^{160}Gd
^{210}Po	^{12}C + ^{198}Pt
	^{13}O + ^{192}Os

Statistical model fits to the data were performed with PACE, which is a modified version of the computer code JULIAN.[12] The single adjustable parameter was the ratio of the level density parameters, a_f/a_ν. The value of this parameter was, of course, constrained to a single value for the two reactions leading to the same compound nucleus. The angular-momentum-dependent fission barriers, $B_f(J)$, of Sierk,[7] calculated with the RFRM, were incorporated into PACE without any adjustments.

The fission barrier calculations used here include, in addition to corrections to the surface energies discussed above, corrections to the rotational energies due to the diffuseness of the matter distribution, as well as corrections to the Coulomb energies due to the diffuseness of the charge distribution. The calculated $B_f(J)$ values are shown as a function of angular momentum for ^{153}Tb in Fig. 2.117. The RLDM values[5] are also shown, and as expected, the RFRM values lie significantly below the RLDM values. The relative positions of the two curves for the other cases studied are similar to those for ^{153}Tb.

The fission excitation functions, together with the statistical model fits, are shown for ^{158}Er in Fig. 2.118, for ^{181}Re in Fig. 2.119, and for ^{210}Po in Fig. 2.120. Fermi-gas level densities were used in most of the fits (Fig. 2.119 and solid lines in Figs. 2.118 and 2.120).

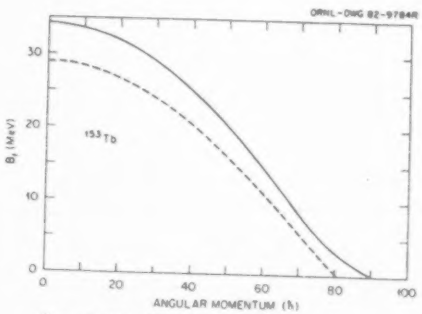

Fig. 2.117. Calculated fission barriers, B_f, for ^{153}Tb as a function of angular momentum. The solid curve represents values from the rotating liquid drop model.[5] The dashed curve represents values calculated by Sierk in the rotating finite-range model.[7]

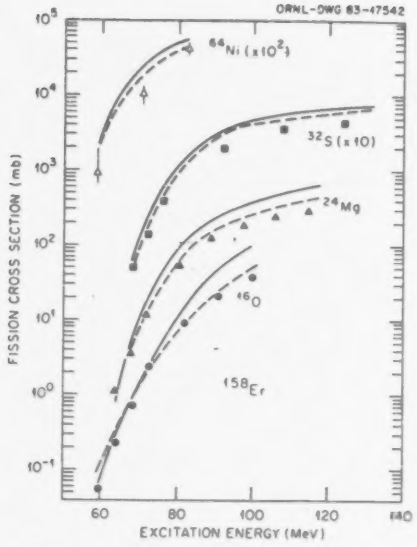

Fig. 2.118. Measured (points) and calculated fission excitation functions for the ^{158}Er system. Solid lines were obtained with Fermi-gas level densities. Dashed lines were obtained with microscopic level densities.[13]

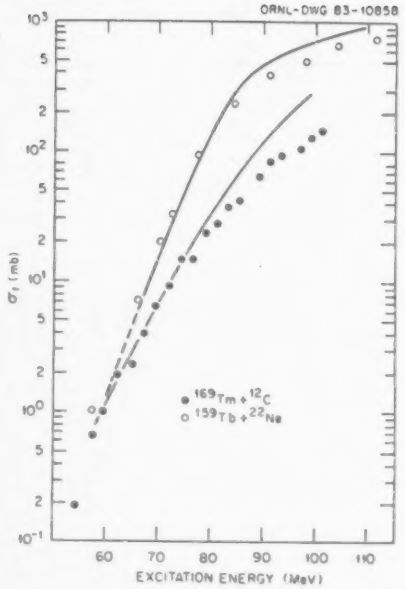

Fig. 2.119. Measured (circles) and calculated fission excitation functions for two reactions leading to the ^{181}Re compound nucleus. Results of the calculations are depicted by the solid and dashed curves. The fission data are from Ref. 11. The dashed portion of the ^{22}Ne + ^{159}Tb curve indicates the region where extrapolated values of evaporation residue cross sections had to be used in the calculations.

The values of a_f/a_ν were found to range from 1.0 to 1.08. In the steep portions of the excitation functions, which are most sensitive to variations in the fission barrier, the calculated curves represent the measurements very well. This indicates that the calculated barriers of the RFRM agree with experiments in the mass range from 150 to 210 amu and in a range of angular momenta from about 30 to 75 ħ.

At the highest excitation energies, significant deviations can be seen between measured excitation functions and those calculated with Fermi-gas level densities. The agreement between experiment and theory can be improved in this region by the use of microscopic level densities,[13] indicated by dashed lines in Figs. 2.118 and 2.120. It is also possible that effects of incomplete fusion may contribute to the divergence of the theoretical and experimental excitation functions at the highest energies. The conclusions regarding the fission barriers are not modified either by changes in level densities or by the consideration of incomplete fusion. We conclude that the RFRM adequately represents the experimental fission cross sections without any arbitrary adjustments and that the new calculated fission barriers are valid in this broad mass region. Thus the RFRM should replace the widely used RLDM in interpretations of data obtained from heavy-ion reactions and in making predictions of various angular momentum effects.

---

1. Los Alamos National Laboratory, Los Alamos, New Mexico.
2. Guest from Institut de Physique Nucléaire de Lyon, Villeurbanne, France.
3. Weizmann Institute, Rehovot, Israel.
4. On leave from Massachusetts Institute of Technology, Cambridge, Massachusetts.

5. S. Cohen, F. Plasil, and W. J. Swiatecki, Ann. Phys. (N.Y.) 82, 557 (1974).
6. H. J. Krappe, J. R. Nix, and A. J. Sierk, Phys. Rev. C 20, 992 (1979).
7. A. J. Sierk, unpublished results.
8. F. Plasil et al., submitted to Phys. Rev. C.
9. J. van der Plicht et.al., submitted to Phys. Rev. C.
10. R. Bass, Phys. Rev. Lett. 39, 265 (1977).
11. T. Sikkeland, Phys. Rev. 135, B669 (1964).

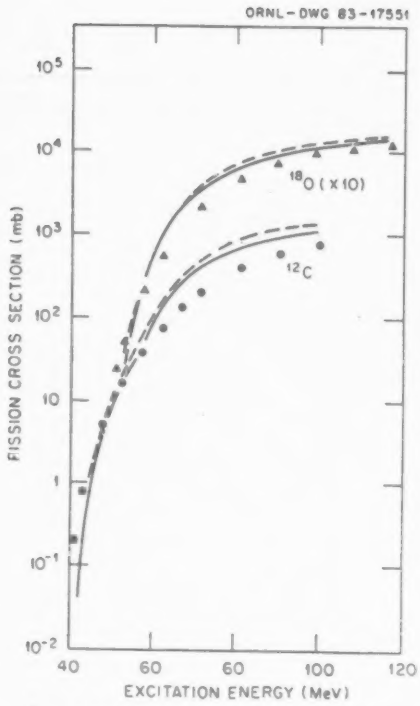

Fig. 2.120. Similar to Fig. 2.118, but for the ^{210}Po system.

12. A. Gavron, Phys. Rev. C 21, 230 (1980).
13. S. G. Nilsson et al., Nucl. Phys. A13, 1 (1969) and J. R. Nix, private communication.

PARAMETER SCALING TEST OF A DYNAMIC NUCLEUS-NUCLEUS COLLISION THEORY[1]

B. Sikora[2]
J. Bisplinghoff[3]
M. Blann[4]
W. Scobel[5]
M. Beckerman[6]
F. Plasil
R. L. Ferguson
J. Birkelund[7]
W. Wilcke[7]

A dynamic theory of macroscopic aspects of nucleus-nucleus collisions at moderate energies has been developed by Swiatecki.[8] The model involves a liquid-drop potential-energy component, macroscopic energy dissipation, and a simplified inertial force treatment. Reactions are treated by means of scaling parameters, in terms of which a single parameter set should describe reactions over a broad range of targets, projectiles, and bombarding energies.

At GSI, fusion measurements have been made with a ^{208}Pb beam on targets ranging from ^{24}Mg through ^{64}Ni (Ref. 9). Swiatecki has analyzed those results and has deduced values for his scaling parameters.[8] A value of 33 ± 1 was obtained for $(Z^2/A)_{\text{eff thr}}$, the critical threshold above which a system requires additional energy ("extra push") in order to fuse. A value of 12 ± 2 was obtained for the parameter $\underline{a}$, a quantity related to the amount of extra push required. The appropriate moment of inertia for the model was found from the data analysis to be consistent with that of two spheres rolling on each other.

In this work, we test the universality of the scaling parameters by using the parameter results of Ref. 8 in an entirely different target-projectile mass range. The results to be tested involve fusion excitation functions for ^{35}Cl + ^{62}Ni, ^{35}Cl + ^{116}Sn, and ^{35}Cl + ^{141}Pr. Results at the lower energies discussed here have been published.[10] To these data we add not-yet-published results obtained at ^{35}Cl energies of 200, 215, 256, and 300 MeV.

We have used Swiatecki's extra-push model with his parameters to calculate fusion excitation functions for these reactions, and we present the results in Fig. 2.121. Moments of inertia were computed both for rolling motion of spheres and for rigidly sticking spheres. Interaction barriers and radii used were the experimentally deduced values summarized in Ref. 11.

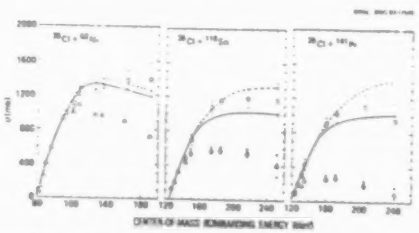

Fig. 2.121. Calculated fusion excitation functions and experimental excitation functions for evaporation residues (ER) and for fission-like fragments. Triangles represent ER cross sections. Circles represent the sum of ER-plus-fissionlike-fragment cross sections. The solid curves are results of the "extra-push" model calculation with moments of inertia for rolling spheres; the dashed curves, for sticking spheres.

The success of the model in reproducing the experimental results is clear. This agreement lends support both to the validity of the underlying assumptions and to the universality of the scaling parameters. However, because the theory makes use of a schematic model with many simplifications, deviations of experimental results from its detailed predictions should be expected. Such deviations can be used to deduce

detailed aspects of the physics involved in collisions of nuclei.

---

1. Summary of paper: Phys. Rev. C 25, 686 (1982).
2. Warsaw University, Warsaw Poland.
3. Bonn University, Bonn, West Germany.
4. Lawrence Livermore National Laboratory, Livermore, California.
5. University of Hamburg, Hamburg, West Germany.
6. Massachusetts Institute of Technology, Cambridge, Massachusetts.
7. University of Rochester, Rochester, New York.
8. W. J. Swiatecki, Nucl. Phys. A376, 275 (1982).
9. H. Sann et al., in Proc. Int. Conf. on Nuclear Physics, August 24-30, 1980, Lawrence Berkeley Laboratory Report LBL-11118 (1980), p. 570; H. Sann et al., Phys. Rev. Lett. 47, 1248 (1981).
10. J. Bisplinghoff et al., Phys. Rev. C 17, 177 (1978); P. David et al., Nucl. Phys. A287, 179 (1977).
11. B. Sikora et al., Phys. Rev. C 21, 614 (1980).

SATURATION ANALYSIS AS A TEST OF STATISTICAL FISSION IN HEAVY-ION REACTIONS[1]

M. Blann[2] J. G. Woodworth[2]
D. Akers[2] W. Scobel[3]
T. A. Komoto[2] J. Bisplinghoff[4]
F. S. Dietrich[2] B. Sikora[5]
L. F. Hansen[2] F. Plasil
R. L. Ferguson

In this work, we demonstrate that evaporation residue excitation functions, for systems which fulfill a "saturation" requirement, can be used to determine statistical model fission parameters. This saturation condition is one that exists when the contribution of high-angular-momentum partial waves to evaporation residue formation is limited only by competition from equilibrium fission in the deexcitation process.

For the reactions $^{56}Fe + ^{120,122}Sn$ we have measured evaporation residue excitation functions and, in this report, use them, along with data for other entrance channels leading to Os nuclei[6-9] and with data from reactions that produce Tb nuclei,[10] to illustrate that statistical model fits to saturation data are quite sensitive to the choice of statistical fission parameters.

Reduced cross sections ($\sigma/\pi\lambda^2$, where λ^2 is the reduced de Broglie wavelength in the entrance channel) are plotted in parts (c) and (d) of Fig. 2.122 for the Os compound nuclei and in parts (a) and (b) for the Tb compound nuclei. Note that the data do not exhibit entrance-channel correlations, an indication that they fulfill the saturation condition. The curves are results of calculations made with the computer program ALERT.[11] The solid lines in parts (a) and (c) were obtained with a value of 1.02

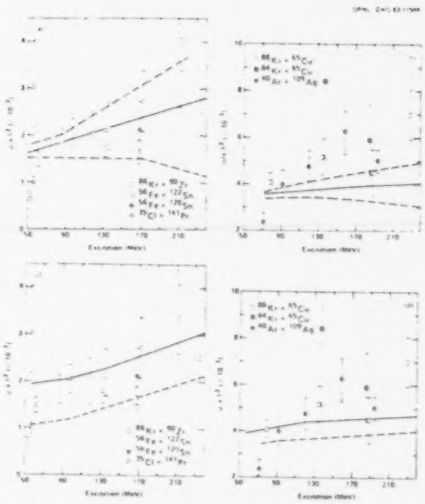

Fig. 2.122. Reduced evaporation residue cross sections as a function of excitation energy for several entrance channels leading to Tb compound nuclei [(a) and (b)] and to Os compound nuclei [(c) and (d)]. The curves in parts (a) and (c) show the effect of varying the parameter a_f/a_ν in a statistical model calculation, and those in parts (b) and (d), the effect of varying the fission barrier height.

or 1.03 for a_f/a_ν in the Tb or Os systems, respectively. Here, a_f is the level density parameter for fission and a_ν, for particle emission. The dashed curves were obtained with a_f/a_ν 2% smaller or larger. Thus, the sensitivity for this parameter is of the order of ±1%. Sensitivity to fission barrier height is shown in parts (b) and (d) of the figure. For the solid curves, fission barriers predicted by the rotating liquid drop model[12] were used directly, and for the dashed curves, those values were reduced by 3 MeV. A best-fit value could be selected to within ±1 to 1.5 MeV. Finally, note that variation in a_f/a_ν results in changes in slope of the curves, whereas changes in fission barriers cause a parallel displacement. This implies that analysis of saturation data, as outlined here, may be useful in deducing values for both parameters simultaneously.

---

1. Summary of paper: Phys. Rev. C 26, 1471 (1982).
2. Lawrence Livermore National Laboratory, Livermore, California.
3. University of Hamburg, Hamburg, West Germany.
4. Bonn University, Bonn, West Germany.
5. Warsaw University, Warsaw, Poland.
6. J. R. Huizenga, R. Chaudhry, and R. Vandenbosch, Phys. Rev. 126, 210 (1962).

7. M. Beckerman and M. Blann, Phys. Rev. C 17, 1615 (1978), and references therein.
8. B. Sikora et al., Phys. Rev. C 25, 1446 (1982).
9. F. Plasil et al., Phys. Rev. C 18, 2603 (1978).
10. H. C. Britt et al., Phys. Rev. C 13, 1483 (1976).
11. M. Blann and T. Komoto, University of California Radiation Laboratory Report UCID 19390, 1982 (unpublished).
12. S. Cohen, F. Plasil, and W. J. Swiatecki, Ann. Phys. (N.Y.) 82, 557 (1974).

FUSION OF ^{16}O WITH ^{182}W, ^{184}W, AND ^{186}W

H. J. Kim
C. E. Bemis, Jr.
F. K. McGowan
R. L. Robinson
S. G. Steadman[1]
F. Plasil
R. L. Ferguson
T. C. Awes
F. E. Obenshain
J. R. Beene
V. Rauch[2]

The cross sections for heavy-ion fusion reactions at near-barrier energies depend critically on static deformation and orientation effects and on the dynamic effects in the interplay between repulsive Coulomb and attractive nuclear forces of target/projectile (see, e.g., Ref. 3). Dramatic target static quadrupole deformation effects have been observed (Ref. 3), and large static hexadecapole deformation effects have been predicted (Ref. 4).

Comparative fusion cross section studies with ^{16}O projectiles on targets of ^{182}W, ^{184}W, and ^{186}W are expected to reveal the influences of large static negative hexadecapole deformation. We have measured both the evaporation residue excitation functions and the fission excitation functions for ^{16}O ions in the energy range 70-120 MeV incident on targets of ^{182}W, ^{184}W, and ^{186}W. The evaporation residue cross sections were determined with the HHIRF Recoil Mass Selector (RMS) in an inaugural experiment (Ref. 5). Absolute evaporation residue cross sections were derived from the number of detected recoils; the integrated beam flux; the measured solid angle of the instrument; and the measured evaporation residue angular, velocity, and charge-state distributions for the ^{16}O + W systems together with known target thicknesses. The influence of short-lived isomeric states, which decay by internal conversion and thus modify the emergent recoil charge-state distributions, was reduced by using a carbon "charge reset" foil at the spectrometer entrance (~20 cm downstream of the target). Longer-lived isomeric states in the range $50 \lesssim \tau_{1/2} \lesssim 500$ ns are known among the Pb isotopes and could affect our evaporation residue results. Although this latter effect remains unaddressed at present, we expect the influence to be $\lesssim 5\%$.

Complementary fission cross sections for the ^{16}O + $^{182,184,186}W$ systems were determined at selected energies in the range 70-120 MeV in a separate experiment by using large-area position-sensitive proportional detectors. These multiwire proportional detectors and operating characteristics are the subject of Ref. 6. Preliminary analyses of the fission experiments have been performed. The fusion cross section (compound nucleus), as a function of incident ^{16}O energy, is the sum of the evaporation residue cross section and the fission cross section. Fission accounts for more than ~80% of the total fusion cross section at the highest energy of 120 MeV for all targets.

Our preliminary total fusion cross sections are displayed graphically in Fig. 2.123. The fusion cross sections at all energies are largest for ^{182}W and smallest for ^{186}W. Attempts to understand these effects will be made after the data analyses are completed.

---

1. Massachusetts Institute of Technology, Cambridge, Massachusetts.
2. On leave from Centre de Recherches Nucléaires, Strasbourg, France.
3. R. G. Stokstad and E. E. Gross, Phys. Rev. C 23, 281 (1981).
4. M. J. Rhoades-Brown and V. E. Oberacker, Phys. Rev. Lett. 50, 1435 (1983).
5. H. J. Kim, "Installation and Calibration of the Recoil Mass Spectrometer," this report.
6. F. E. Obenshain and J. L. Blankenship, "Development of Multiwire Proportional Detectors for Fission Measurements," this report.

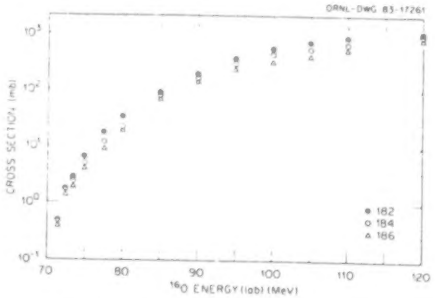

Fig. 2.123. Complete fusion cross section for ^{16}O projectiles on targets of ^{182}W, ^{184}W, and ^{186}W as a function of incident ^{16}O energy.

DIVERSE STUDIES

PRECISION K, L, and M MUONIC X-RAY STUDIES IN THE ACTINIDE REGION

E. B. Shera[1]
J. D. Zumbro[2]
C. E. Bemis, Jr.
M. V. Hoehn[1]
M. W. Johnson[1]
R. A. Naumann[2]
W. Reuter[1,3]
R. M. Steffen[4]
Y. Tanaka[4]

Muonic x-ray measurements can provide detailed information on the monopole and multipole charge distribution parameters for the nuclear ground state. In strongly deformed

nuclei, such as those in the actinide region, the coupling of the ground-band rotational members via E2 and E4 interactions is sufficiently large that details (energies and intensities) of the muon deexcitation between coupled muon-nucleus hyperfine states show unique sensitivities to these interactions. The M1, E2, and E4 muonic hyperfine interactions yield complex and extremely fragmented patterns which may be analyzed to yield both static and transition moments, in addition to the charge distribution parameters.

We have performed high resolution measurements of the muonic K, L, and M x-ray spectra for the nuclides $^{233,234,235,236,238}U$, $^{241,243}Am$, and recently for $^{239,240,242}Pu$. Nearly isotopically pure targets of these nuclides, in oxide form, were used. One-gram targets of the Am isotopes and ten-gram targets of the U and Pu isotopes, with the exception of ^{236}U, were sealed in aluminum cans for safety and used in these experiments. All experiments were performed at the stopped muon channel at the Los Alamos Meson Physics Facility (LAMPF) using a Ge(Li) spectrometer. Details of the target arrangements, data acquisition, energy calibrations, and descriptions of the analysis procedures may be found in Refs. 5-8. The electric monopole and electric quadrupole charge parameters were extracted from the spectra with a two-parameter deformed Fermi distribution by direct fitting of the K and L spectra with computed theoretical line patterns. The computed spectra involve numerical solutions of the Dirac equation (see, e.g., Ref. 9) with corrections for the radiative (QED) shifts and for nuclear polarization effects. The computed line pattern is broadened with a Lorentz line profile and with the semi-Gaussian response profile measured for the Ge(Li) detector and then compared directly to the experimental spectra.

The studies with the $^{241-243}Am$ isotopic pair have provided the monopole and quadrupole charge distribution parameters necessary for the detailed interpretation of the laser-optical isomer/isotope shift measured for the fission isomer ^{240m}Am. Analysis of the ^{240m}Am laser-optical experiments, as based on the muonic calibration, has been presented by Beene et al. (Ref. 10).

The muonic M x-ray spectrum (4f → 3d) is particularly valuable for the extraction of nearly model independent nuclear quadrupole and hexadecapole parameters. For the less penetrating M orbits, the muon-generated potential exhibits a nearly r^2 radial dependence (point moment) and thus does not require a model for the radial dependence of the nuclear quadrupole or hexadecapole charge distributions. To illustrate the sensitivity of the actinide muonic M x-ray spectra to E2 and E4 nuclear interactions, both static and dynamic, we display in Fig. 2.124 the experimental and calculated M x-ray spectra for ^{233}U. The analysis was performed with the monopole parameters, C and a, fixed from analyses of the K spectrum, and with $\beta_2 = 0.24$ and $\beta_4 = +0.09$. All possible muon-nuclear states coupled by M1, E2, and E4 interactions for the muon 3d, 4f, and 5g levels, and the nuclear states 5/2 through 13/2 of the ground-state rotational band were included. The calculations were performed in the rigid-rotor or strong coupling limit,

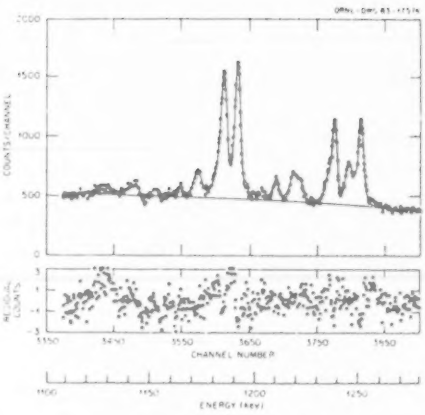

Fig. 2.124. The experimental muonic M x-ray spectrum for ^{233}U. Satisfactory agreement between the experimental data (points) and the calculated spectrum (solid) is achieved by including both E2 and E4 moments.

which is applicable to strongly deformed axially symmetric nuclei. All possible E2 nuclear couplings, both static and dynamic, corresponding to an intrinsic quadrupole moment of 10.32 ± 0.01 eb were included. To obtain satisfactory agreement between the experimental spectrum and the calculated spectrum, it is necessary to include also the E4 nuclear couplings. We deduce a preliminary value for the intrinsic hexadecapole moment of $+2.4 \pm 0.3$ eb^2 for ^{233}U defined as $Q_{40} = \sqrt{16\pi/9}\,\langle r^4 Y_{40}(\theta)\rangle$. More refined analyses are in progress (Ref. 11).

---

1. Los Alamos National Laboratory, Los Alamos, New Mexico.
2. Princeton University, Princeton, New Jersey.
3. University of Mainz, Mainz, West Germany.
4. Purdue University, West Lafayette, Indiana.

5. E. B. Shera et al., Phys. Rev. C 14, 731 (1976).
6. L. K. Wagner et al., Phys. Rev. C 16, 1549 (1977).
7. Y. Yamazaki et al., Phys. Rev. C 18, 1474 (1978).
8. D. B. Laubacher et al., Phys. Rev. C 27, 1772 (1983).
9. G. A. Rinker, Comp. Phys. Commun. 16, 221 (1979).
10. J. R. Beene et al., in Lasers in Nuclear Physics, edited by C. E. Bemis, Jr., and H. K. Carter, Harwood Academic, New York, 1982, pp. 171-82.
11. J. D. Zumbro et al., Bull. Am. Phys. Soc. 28 688 (1983).

NEUTRON-ANTINEUTRON OSCILLATIONS

H. O. Cohn[1] J. A. Brau[2]
T. A. Gabriel[1] W. M. Bugg[2]
R. A. Lillie[1] G. T. Condo[2]
F. E. Obenshain T. A. Handler[2]
P. D. Miller H. J. Hargis[2]
R. R. Spencer[1] E. L. Hart[2]
G. R. Young M. S. Goodman[3]
R. Wilson[3]

Current theories, attempting to unify the strong, electromagnetic, and weak interactions[4-8] in a single framework based on the successful unification of electricity and magnetism in the 19th century, and more recently, the unification of electromagnetism and weak interactions[9-12] have led to predictions that baryon number is not a strictly conserved quantity. The hypothesis that baryons obey an absolute conservation law was advanced many years ago to account for the experimental observation that the lowest mass baryon (the proton) appeared to be absolutely stable. The best available results on stability of matter indicate the proton lifetime is greater than 10^{32} years.[13] One of the startling results of some recent models[4,5,8] of grand unified theories (GUTs) and partially unified theories (PUTs) of strong and electroweak interactions is that neutrons can change into antineutrons, possibly with oscillation times as short as 10^6 seconds, and still not be in disagreement with the experimental data for matter stability.

Some of the abovementioned unified theories also predict the existence of $\Delta B = 1$ baryon number nonconserving interactions, such as proton decay. Since neutron oscillation and proton decay experiments test different possibilities from amongst the proposed unified theories, the results of the proposed experiment to search for neutron → antineutron $\Delta B = 2$ transitions and those of experiments already in progress to search for $\Delta B = 1$ proton decay together can serve as a powerful discriminator among possible physical theories.

Ever since Dirac predicted the existence of positrons or antielectrons, all electrically charged particles have been found to have an associated antiparticle of oppositely signed charge. Neutral particles may have a separate and distinct antiparticle [$(n,\bar{n})$, $(\Lambda^0,\bar{\Lambda}^0)$, $(K^0,\bar{K}^0)$, etc.], or they may be identical to their own antiparticle [γ, π^0, η, ρ^0, etc.]. It is clear that the concept of particle-antiparticle oscillations is only meaningful for the former category of neutral particles. The first confirmed observation of this phenomenon involved $K^0 \leftrightarrow \bar{K}^0$ transitions,[14,15] which had the far-reaching consequence that CP invariance had to be discarded as a property of the weak interaction. More recently, experimental results have been presented relating to the search for the existence of neutrino flavor oscillations ($\nu_e \leftrightarrow \nu_\mu \leftrightarrow \nu_\tau$).[16-18] The experimental results are sufficiently ambiguous to cause extensive experimental activity to be devoted to this question.

The presently known "families" of baryons and mesons have masses in the range 0.1-10 GeV. The grand unification model involving the symmetry SU(5) suggests that there exist particles of masses 10^{14} GeV which are exchanged in the proton decay process. This leaves a desert between known and expected particles with masses of the order of 1-100 GeV and the grand unification mass scale of 10^{14} GeV. The discovery of neutron-antineutron mixing times of $\sim 10^7$ seconds would imply the existence of particle masses around 10^4 GeV, which would fill in this mass region to some extent. Indeed, this may be the best way to search for particles in this energy region, which is inaccessible to present accelerators, but might be accessible to accelerators in the 1- to 10-TeV range in the future.

We have proposed to search for the predicted $\Delta B = 2$ oscillations of a neutron into an antineutron. The experiment would be implemented by allowing a very large number of thermal neutrons to exit the Oak Ridge Research Reactor and traverse an evacuated, magnetic-field-free region for 20 meters. The sensitivity of an experiment searching for n-$\bar{n}$ oscillations is enhanced by using the largest number of lowest energy neutrons that can be obtained, subject to the constraint of maximizing Nt^2, defined below. An oscillation region in which the earth's magnetic field has been degaussed by 1000 must be set up for the neutrons to pass through; the length of this region is constrained by the requirements of lowest possible neutron source background at the detector, which lengthens it, and by the need to degauss the earth's magnetic field and control costs, which shortens it. Detection of any antineutrons present in the beam at this point would be accomplished by allowing the neutrons to pass through a thin target and searching for antineutron annihilation products (see Fig. 2.125). This technique makes use of the fact that antineutrons have a very high probability of annihilating with normal matter in the target, thereby releasing $2M_nc^2$ (~2 GeV) of energy in the form of a number of energetic pions. From past work on $p\bar{p}$, $p\bar{n}$, and $n\bar{n}$ annihilations, we expect, on the average, 3 charged pions and 1.5 neutral pions to be emitted per event. Using a detector consisting of an array of lead glass Čerenkov counters and proportional counters, we expect to detect over half of the annihilation products leaving the target.

The principal background events at a reactor that can simulate an $\bar{n}$ annihilation are cosmic-ray events. This background can be reduced with 1.5 meters of nickel absorber and an anticoincidence veto array. Further background reduction involves use of event topology, multiplicity, time-of-flight, and energy deposition cuts. Our test measurements show that the large background of neutrons and gamma rays of energy below 10 MeV which issue from the reactor will not cause any insurmountable problems. The use of a thin target and appropriate types of shielding between the target and detector will minimize the effects of this radiation.

An appropriate figure of merit to describe the sensitivities of the various, proposed, direct searches for neutron-antineutron oscillations is Nt^2, where N is the number of neutrons and t is the time of observation of the neutrons. This experiment will have a sensitivity

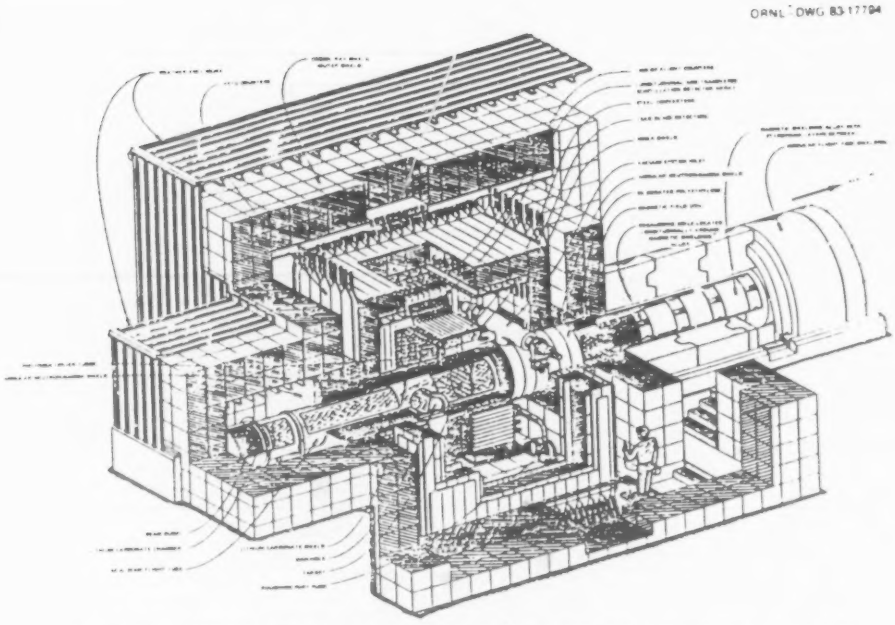

Fig. 2.125. Isometric view of the target and $n + \bar{n}$ detector area, together with associated shielding and veto counters, for the proposed $n + \bar{n}$ experiment.

more than ten times greater than that of any proposed experiment of which we are aware (see Table 2.18). We anticipate that in a run of 120 days, we will detect neutron + antineutron mixing if the transition time for this process is less than 2×10^8 seconds. Current direct measurements of neutron-antineutron mixing give a mixing time of at least two orders of magnitude less than this figure.

---

1. Engineering Physics Division, ORNL.
2. University of Tennessee, Knoxville, Tennessee.
3. Harvard University, Cambridge, Massachusetts.

4. S. L. Glashow, Harvard preprints HUTP 79/A059 and HUTP 79/A029.
5. J. C. Pati and A. Salam, Phys. Rev. Lett. 31, 661 (1973); Phys. Rev. D 10, 275 (1974).
6. H. Georgi and S. L. Glashow, Phys. Rev. Lett. 32, 438 (1974).
7. D. V. Nanopoulos, Harvard preprint HUTP 78/A062.
8. R. N. Mohapatra and R. E. Marshak, Phys. Rev. Lett. 44, 1316 (1980).
9. S. L. Glashow, Nucl. Phys. 22, 579 (1961).
10. S. Weinberg, Phys. Rev. Lett. 19, 1264 (1967).
11. A. Salam, in Elementary Particle Theory, ed. N. Svartholm, Almqvist and Wiksell, Stockholm, 1968.
12. S. L. Glashow, J. Iliopoulos, and L. Maiani, Phys. Rev. D 2, 1285 (1970).
13. R. Bionta et al., Phys. Rev. Lett. 51, 27 (1983).
14. P. K. Kabir, The CP Puzzle, Academic Press, New York, 1968.
15. R. P. Feynmann, Lectures on Physics, Vol. III, Chapter II, Addison-Wesley, Reading, Massachusetts, 1964.
16. F. Reines, H. W. Sobel, and E. Pasierb, Phys. Rev. Lett. 45, 1307 (1980).
17. F. Bochum et al., Phys. Lett. 97, 310 (1980); Phys. Rev. D 24, 1097 (1979).
18. N. Ushida, Phys. Rev. Lett. 47, 1694 (1981).

Table 2.18. Possible neutron sources.

Source	ϕ (n/cm^2 sec x 10^{13})	A (cm^2)	Ω (fraction of 4π x 10^{4})	$\overline{t^2}$ (sec^2)	$\overline{Nt^2}$ (sec)
		Considered			
MIT	10	100	10	2×10^{-5}	2×10^{8}
BSR	3	2000	8	3×10^{-5}	7×10^{8}
HFIR	10	80	6	1.5×10^{-4}	5×10^{8}
ORELA		10^{14} sec	2	3×10^{-5}	6×10^{5}
ORR Poolside	15	4000	6	3×10^{-5}	1×10^{10}
ILL Bottle	10^2 n/cm^3	3×10^5 cm^3		V = 5 m/sec	1×10^{7}
		Running or Projected			
ILL H18*		2×10^{9}/sec		6×10^{-4}	1×10^{6}
Pavia	0.2	800	1.5	1×10^{-4}	2.5×10^{7}
LAMPF	1	3777	0.5	2×10^{-4}	4×10^{8}
Omega West					1.5×10^{8}
ORR "Goat Hole"	7	1400	2	1×10^{-4}	2×10^{9}
ILL New Source	for 20-m flight path				8×10^{8}
	for 40-m flight path				5×10^{9}

*For ILL H18, the effective beam intensity is given.

SEARCH FOR AXIONS IN THE DECAY OF ^{65}Zn[1]

F.P. Calaprice[2] R.W. Dunford[2]
F.T. Avignone,III[3] D. Kahana[4]
C. Baktash R.T. Kouzes[2]
R. Davis[4] D. Moltz[3]

The axion is a neutral, pseudoscalar particle proposed by Weinberg[5] and Wilczek[6] in 1978 to prevent CP violation in strong interactions. Axions couple to quarks and leptons semiweakly and can be created in competition with γ rays in radioactive decay. They can decay into two photons and can interact semiweakly with electrons and nuclei. The present effort involves searching for axions, using (a) multiple NaI (Tl) detectors to search for decay into γ rays and (b) a low background/intrinsic Ge detector to detect direct interactions with electrons in processes analgous to photoelectric absorption and Compton scattering. The experimental setup is schematically shown in Fig. 2.126. The average activity of the ^{65}Zn source was about 40 μCi during the initial phase of the experiment.

In the standard treatment, the expressions for the photon and axion production rates in radioactive decay are similar[7,8] and the correspondence between the axion and γ ray operators is given by Donnelly et al.[7] Using our best knowledge of the nuclear structure of ^{65}Cu, we arrive at the following expression for the production ratio of axions to γ rays for the 1115.5 keV transition

$$\omega_a/\omega_\gamma = (9 \times 10^{-6})\, X^2\, (0.45 + 1.0\, X^{-2})^2. \quad (1)$$

The mixing angle parameter X is the ratio of the vacuum expectation values of the two Higgs fields introduced when chiral symmetry is imposed on the Lagrangian. Placing experimental limits on the ranges of X imposes limits on the properties of the axion such as mass, lifetime, etc. We should caution, however, that the expression given above for ω_a/ω_γ has nuclear structure uncertainties as large as a factor of 4 and hence we use it very cautiously.

The cross section for the interaction $ae \to e\gamma$ depends directly on X^2, hence the detection rate in the vicinity of the radioactive source

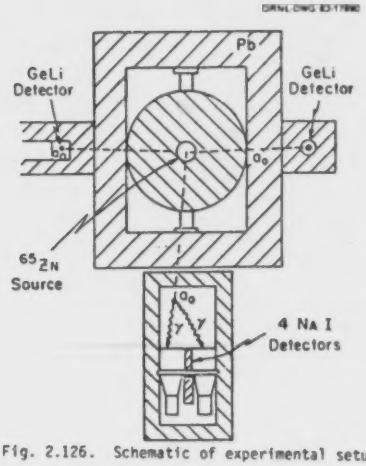

Fig. 2.126. Schematic of experimental setup.

depends on X^{-2} and X^{-4}. This provides a particularly sensitive test for small values of X. The cross section $\sigma(ae \to e\gamma)$ rises slowly and peaks at an axion energy of 1 MeV, finally reaching zero near 100 MeV. In the first phase of the experiment, we counted for 83 days and placed a limit of < 4 axions per day in a peak at 1115.5 keV. This places a limit of $X > 1$ if we accept the results of eq. (1), or a limit of $X > 0.7$ using a conservative factor of 4 on the theoretical uncertainties in ω_a/ω_γ. A new version of the experiment with the shielded detector on wheels has been constructed and is running.

The coincidence search for γ-ray pairs from axion decay consists of an array of four 7.62 cm x 7.62 cm NaI(Tℓ) detectors located approximately 65 cm from the source and inside a Pb shield box which provides approximately 40 cm of decay path length. Plastic scintilator counters, placed above the Pb shield box, provide veto signals for cosmic rays entering the cavity from above. The data, acquired through a CAMAC-based electronics system, were stored on floppy disks on an event-by-event basis. The data were later scanned to search for evidence of $a \to \gamma\gamma$ decays which would give rise to a coincidence sum energy of 1115 keV, corresponding to the $(5/2^- \to 3/2^-)$ transition energy in ^{65}Zn.

A typical sum spectrum $(E_{\gamma_1} + E_{\gamma_2})$ for one of the six pairs of detectors is illdstrated in Fig. 2.127. The events shown are genuine coincidences but there is no evidence for a peak at 1.1 MeV, indicated by an arrow in Fig. 2.127. The average rate per pair for all six pairs is less than 7×10^{-5} coin/sec/pair, with 95% confidence. The rates expected from axions vary strongly with the axion mass m_a and mixing angle parameter X. The present experimental limit allows us to rule out all values of X for 100

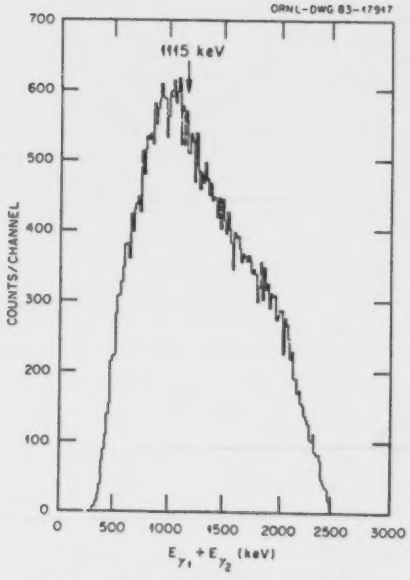

Fig. 2.127. A typical sum spectrum for one of six possible detector pairs and 25 days of running time. The arrow indicates the expected peak position at 1115 keV.

keV < m_a < 1000 keV. The rate expected from m_a = 250 keV and X = 3, which are parameters suggested from the experiment of Faissner et al.[9], is ~ 1 coin/sec/pair. Thus, this combination of parameters is strongly ruled out by our data.

The expected rate due to axion decays drops off fast below 100 keV. The lowest rate occurs for X ~ 1, which implies that for m_a < 100 keV our data rule out only large X or small X. These limits are better than those achieved in other axion "decay" experiments.[10,11]

At present, we are planning to continue data collection to improve statistical accuracy while also investing a significant effort to increase our theoretical understanding of the nuclear structure of ^{65}Cu. We also intend to place limits on the larger values of X using the Primakoff effect conversion of γ rays by the coherent interaction with the nucleus.[12] A conservative preliminsry result from this effort, coupled with the lower limit quoted above, is $0.7 < X < 7$. Our results also rule out all values of X for 100 keV < m_a < 1000 keV.

---

1. Summary of paper to be published.
2. Princeton University, Princeton, NJ.
3. University of South Carolina, Columbia, SC.
4. Brookhaven National Laboratory, Upton, NY.
5. S. Weinberg, Phys. Rev. Lett. 40, 223 (1978).

6. F. Wilczek, Phys. Rev. Lett. 40, 279 (1978).
7. T.W. Donnelly et al., Phys. Rev. D18, 1607 (1978).
8. Barroso and N.C. Mukhopadhyay, Phys. Rev. C24, 2382 (1981).
9. H. Faissner, E. Frenzel, W. Heinrigs, A. Prenssger, D. Samm and U. Samm, Phys. Lett. 103B, 234 (1981).
10. A. Zehnder, Phys. Lett. 104B, 494 (1981).
11. P. Lehmann, E. Lesqnoy, A. Muller and S. Zylberajch, Phys. Lett. 115B, 270 (1982).
12. S. Barshay et al., Phys. Rev. Lett. 46, 1361 (1981).

MEASUREMENT OF THE ^{241}Am NEUTRON FISSION CROSS SECTION[1]

J. W. T. Dabbs[2] C. H. Johnson
C. E. Bemis, Jr.

The fission cross section of ^{241}Am has been measured from 0.02 eV to 20 MeV using time-of-flight techniques at the Oak Ridge Electron Linear Accelerator. Approximately 700 h of data were obtained at a flight path distance of 9.1 m, primarily with 40-ns bursts. A "honeycomb" fission ionization chamber contained six deposits totaling 14.3 mg of ^{241}Am, a single deposit of ^{252}Cf, and six deposits totaling 116 mg of ^{235}U, which served as a standard for energies above 101 keV, while ^{6}Li(n,α), normalized to ^{235}U fission in the 7.8-11.0-eV interval, served as a shape standard below 101 keV.

The fission chamber plates necessarily subtended large solid angles in order to obtain adequate statistics with the small fission cross section of ^{241}Am. As a result there were significant corrections for backgrounds by neutron scattering from parts of the chamber to the ^{241}Am target. In Fig. 2.128 the lower curve shows the calculated inscattering correction and the upper curve is the corrected fission cross section. Even though the corrections are large for some valleys between resonances, the resulting valleys agree well with other work[3] in the literature.

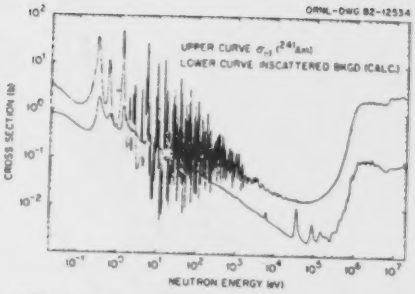

Fig. 2.128. An overview of the ^{241}Am fission cross section for the full energy region of the experiment. The lower curve is the largest background component, the inscattered background, shown as a cross section.

1. J. W. T. Dabbs, C. H. Johnson, and C. E. Bemis, Jr., Nucl. Sci. Eng. 83, 22 (1983).
2. Now in Engineering Physics Division.
3. H. Derrien and B. Lucas, Proc. Conf. Nuclear Cross Sections and Technology, NBS Special Publication 425, Vol. VII, p. 637, U. S. National Bureau of Standards (1975).

MEASUREMENT OF THE ^{242m}Am NEUTRON FISSION CROSS SECTION[1]

J.W.T. Dabbs[2] S. Raman
C. E. Bemis, Jr. R. J. Dougan[3]
R. W. Hoff[3]

The fission cross section of ^{242m}Am (141 ± 2 yr) has been measured from 0.005 eV to 20 MeV by using time-of-flight techniques at the Oak Ridge Electron Linear Accelerator. A hemispherical plate fission ionization chamber with five pairs of plates contained three deposits totaling 507 μg of ^{242m}Am, one deposit of 168 μg of ^{235}U, and a "weightless" deposit of ^{252}Cf, which served as a monitor of chamber performance. The fission of ^{235}U served as the cross section standard for energies above 101 keV, while ^{6}Li(n,α), normalized to ^{235}U fission in the 7.8- to 11.0-eV interval, served as a shape standard below 101 keV. Approximately 360 h of data was obtained at a flight path distance of 9.1 m, primarily with 40-ns bursts. Particular attention was paid to correction of backgrounds, especially inscattered-neutron-induced events.

An overall graphical representation of our final results is given in Fig. 2.129, which spans nine decades in energy and four decades in cross section. For comparison, the ENDF/B-V fission cross section is shown, as well as our calculated inscattering corrections which were applied to our experimental data. We derive a

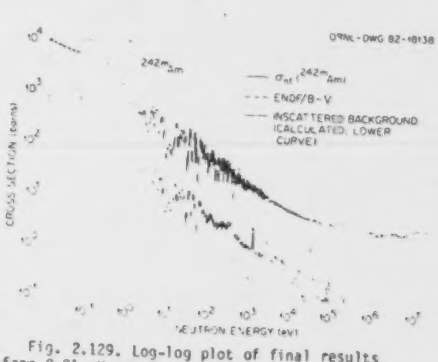

Fig. 2.129. Log-log plot of final results from 0.01 eV to 20 MeV. The dashed curve is ENDF/B-V; the calculated inscattered background is shown for comparison (lower curve). The result curve is an 1346-point average approximation to 14,620 actual data points.

0.0253-eV fission cross section of 6950 ± 250 barns and a fission resonance integral, I_f = 20 MeV / 0.5 eV $\int \sigma_f dE/E$, of 1800 ± 65 b. An 1846-point reduced data set representing our final results [$\sigma_{n,f}(\epsilon)$, uncertainties, corrections, etc.] is available in EXFOR format from the National Nuclear Data Center (NNDC).

---

1. Summary of paper: Nucl. Sci. Eng. 84, 1 (1983).
2. Now in Engineering Physics Division, ORNL.
3. Lawrence Livermore National Laboratory, Livermore, California.

SUBTHRESHOLD NEUTRAL PION PRODUCTION WITH HEAVY IONS

P. Braun-Munzinger[1], P. Paul[1], L. Ricken[1], J. Stachel[1], P-M. Zhang[1], T. C. Awes, R. L. Ferguson, F. E. Obenshain, S. Pontoppidan[2], V. Rauch[3], G. R. Young

Surprisingly large cross sections have been measured for the production of pions in nucleus-nucleus collisions at E_{lab} < 80 MeV/u. In particular, spectra and angular distributions obtained[4,5] at 84, 74, and 60 MeV/u for π^+ and π^0 production indicate that pions are produced from a source moving much more slowly than the nucleon-nucleon c.m. system. Furthermore, analysis[6] of the cross sections and spectral shapes supports the assumption that the cooperative action of many nucleons is required to produce the observed pions. With even smaller beam energy, one expects that this collectivity will increase until, near absolute threshold, π production is accompanied by fusion of the target and projectile (pionic fusion).

We have measured π^0 production in reactions of ^{14}N with Al, Ni, and W at E_{lab} = 35 MeV/u (at MSU) and in reactions of ^{16}O with Au at E_{lab} = 25 MeV/u (at ORNL). The neutral pions were detected by measuring in coincidence the angle and energy of their decay photons in a Pb-glass Cerenkov counter array consisting of ten converters and ten absorbers. The array is arranged as ten pairs of counters, with each pair having one converter and one absorber counter. The converters are 4" x 4" x 2" blocks of F2 lead glass, viewed from a 4" x 2" side by a 2" photomultiplier tube. The absorbers are 5.8" x 5.8" x 14" blocks of SF5 lead glass viewed from the rear 5.8" x 5.8" face using 5" photomultiplier tubes. The total efficiency of this array, which consists of the geometrical efficiency and the probability for photon to e^+e^- pair conversion in the converters, is of the order of 0.5%, depends slightly on π^0 kinetic energy, and has been calculated in detail using Monte Carlo techniques and the "EGS" shower development code. Using this array, we can detect π^0's at the level of nb cross sections. In Fig. 2.130 data are presented for the system ^{14}N + ^{27}Al at 35 MeV/u as a histogram of invariant mass,

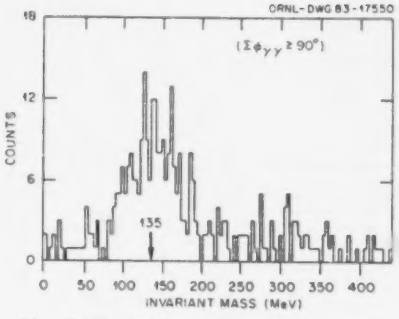

Fig. 2.130. Spectrum of invariant mass for high-energy two-fold gamma-ray events seen in the reaction 35-MeV/u ^{14}N + ^{27}Al.

$M_{inv} = 2\sqrt{E_{\gamma 1} E_{\gamma 2}}\ \sin(\phi/2)$. A clear peak is observed near M_{inv} = 135 MeV, uniquely identifying the pion events. Background due to cosmic rays and from the gamma-ray flash of the beam in the targets is quite small, even at this cross section level (σ_{total} = 42 nb). The former is suppressed by its very large energy deposition; the latter, by its very small energy deposition. Preliminary results for total π^0 production cross sections are shown in Fig. 2.131a for the three targets studied at 35 MeV/u. The inclusive π^0 production cross section is of the order of 40-100 nb, increasing with target mass roughly as AT**0.7. With the assumption that this dependence holds for both projectile and target, we can extrapolate to the system C + C, which has been studied elsewhere at higher bombarding energies. Figure 2.131b shows an excitation function of inclusive π^0 and π^+ production in the energy range 35 < E_{lab} < 700 MeV/u. None of the cross sections at E_{lab} < 100 MeV/u can be explained in a single collision picture invoking colliding Fermi spheres[6] (with or without sharp surface). It has been suggested recently that the trend of the data can be reproduced by assuming that the pions are produced in a process analogous to bremsstrahlung. Various other models, such as pionic instability of compressed nuclear matter[8] or freezing of degrees of freedom[6] (composite nucleus formation), may also be responsible for the observed rather large cross section. The laboratory angular distributions $d\sigma/d\Omega_\pi$ found at 35 MeV/u are nearly flat, arguing against models (such as Fermi-gas models) producing a strong forward peaking, or forward + backward peaking, of the π^0 yield.

---

1. State University of New York, Stony Brook, New York.
2. On leave from Niels Bohr Institute, University of Copenhagen, Copenhagen, Denmark.
3. On leave from Centre de Recherches Nucléaires, Strasbourg, France.
4. Grenoble-Lund-Saclay-CERN Collaboration, Phys. Lett. 48, 732 (1982); B. Jakobsson, Proc. Nordic Meeting on Nuclear Physics, Fuglso,

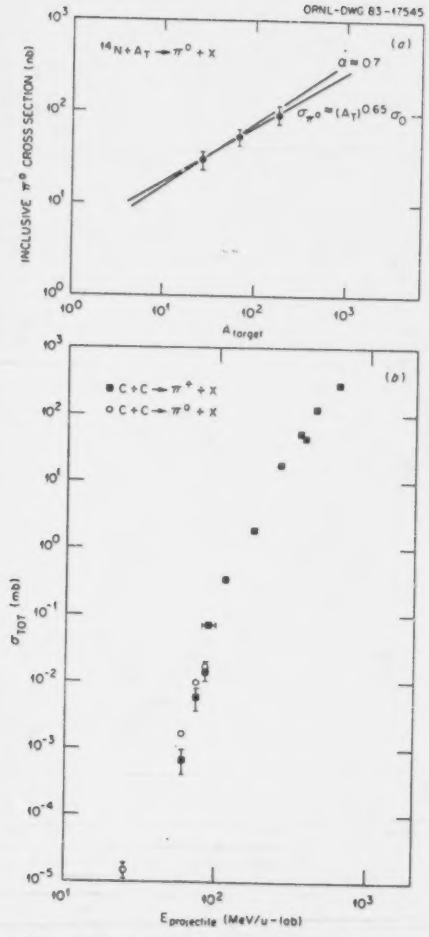

Fig. 2.131. (a) Total cross section at 35 MeV/u (lab) for ^{14}N bombardment of Al, Ni, and W targets. (b) Excitation function for inclusive π^0 and π^+ production in C + C reactions at bombarding energies between 35 and 700 MeV/u.

Denmark, August 1982 (unpublished); C. Guet, Nucl. Phys. A400, 191c (1983).

5. GSI-Frankfurt-Darmstadt-SUNY(SB) Collaboration; E. Grosse et al., GSI Annual Report 1982; C. Michel et al., Proc. 1982 Winter Meeting, Hirschegg, Austria (unpublished).

6. R. Shyam and J. Knoll, GSI preprint, June 1983.

7. D. Vasak et al., Phys. Lett. 93B, 243 (1980).

8. M. Gyulassy, Nucl. Phys. A354, 395 (1981).

^{34}Cl SUPERALLOWED β DECAY[1]

S. Raman
E. T. Jurney[2]
D. A. Outlaw[3]
I. S. Towner[4]

The neutron separation energy of ^{34}S and the proton separation energy of ^{34}Cl have been measured accurately via the ^{33}S(n,γ)^{34}S and the ^{33}S(p,γ)^{34}Cl reactions. The measured values imply a Q value of 5492.48±0.20 keV for the total decay energy of ^{34}Cl if the calibration is based on the "mass doublet standard" and a Q value of 5492.42±0.23 keV if based on the 411.8044±0.0011 keV line in ^{198}Au. If the conserved vector current hypothesis is valid and the electromagnetic corrections are made properly, the ft values for superallowed $0^+ \rightarrow 0^+$ β decays should all be the same. The ft values for the superallowed ^{34}Cl and ^{14}O decays were found to be equal to better than (4±16) parts in 10^4, in agreement with the expectations.

---

1. Abstract of paper: Phys. Rev. C 27, 1188 (1983).

2. Los Alamos National Laboratory, Los Alamos, New Mexico.
3. Duke University and Triangle Nuclear Laboratory, Duke station, Durham, North Carolina.
4. Chalk River Nuclear Laboratories, Chalk River, Ontario, Canada.

RELIABILITY OF RESONANCE-AVERAGED NEUTRON-CAPTURE MEASUREMENTS[1]

S. Raman
O. Shahal[2]
M. J. Kenny[3]
R. E. Chrien[4]

We show that well established levels (within a limited spin range) in ^{146}Nd below 2.2 MeV are indeed populated by primary transmission in "2 keV neutrons" resonance-averaged capture (RAC) measurements. Therefore, an apparent failure to identify crucial levels in ^{146}Nd from previous 'reactor-neutrons' RAC measurements is not a valid basis for questioning the general reliability of the RAC method for level identification.

---

1. Abstract of paper: J. Phys. G:Nucl. Phys. 9, L137 (1983).

2. Guest scientist from the Nuclear Research Centre-Negev, Beer Sheva, Israel.
3. Guest scientist at BNL from the Lucas Heights Research Laboratories, Lucas Heights, Australia.
4. Brookhaven National Laboratory.

FUTURE DIRECTIONS FOR PHYSICS DIVISION RESEARCH

C. Baktash
J. R. Beene
C. E. Bemis, Jr.
K. A. Erb
J. Gomez del Campo
G. A. Leander
I-Y. Lee
D. Shapira
G. R. Young

Introduction

In late 1982 a group of nine members of the ORNL Physics Division was asked to consider the field of nuclear physics in a broad manner and to explore possible long-term directions for nuclear physics research at ORNL, with a specific directive not to limit the discussion to those future possibilities requiring present ORNL facilities as a base. The group was asked to determine what sorts of major, national-type facilities would be needed to explore the areas of nuclear physics that we felt were interesting and held promise. The history of past facilities in the division and the lengthy effort required to obtain approval for, and then construct, the Holifield Heavy Ion Research Facility were reviewed first, before delving into other areas.

The present facility, HHIRF, lends itself well to investigations requiring beams, of nuclear projectiles with $A > 4$, of high intensity or small momentum spread. Kinetic energy constraints imposed by the bending power of the ORIC mean all research is carried out with projectile energies per nucleon no greater than 25 MeV, which is less than the nuclear Fermi energy. Accordingly, research concentrates on those aspects of nuclear structure and macroscopic behavior best described by mean-field theories, although the theoretical models run the gamut from the shell model, the sine qua non of structure work, to time-dependent Hartree-Fock and less formal variants, which form the theoretical underpinnings of much fission and reaction mechanism work. At such energies, only virtual (or collective) excitations of the pion field enter, in contrast to the case at intermediate-energy or relativistic hadron machines.

The group invested some time reviewing past and present research and plans for immediate-future research at HHIRF. A survey of publicly and privately discussed plans for future facilities at other laboratories, both in the U.S. and abroad, was made, followed by a lengthy period of reading and discussion about present and planned research at existing and proposed facilities. The varied interests of the group led to one or more persons researching the areas of electron scattering and quark degrees of freedom, high-energy light-ion and hypernuclear physics, weak interaction physics, intermediate-energy heavy-ion physics, atomic physics with few-electron atoms of all elements, exotica such as X-ray and gamma-ray lasers, relativistic heavy-ion physics, high-energy collider physics (embracing e^+e^-, $p\bar{p}$, and AA colliders), and low-energy "fundamental" physics that would benefit from a national laboratory's resources. A sampling of some research possibilities is given below.

Intermediate-Energy Heavy-Ion Physics

Intermediate-energy heavy-ion physics, loosely defined as covering the projectile energy range 20-1000 MeV/amu, deals with phenomena expected in crossing several energy thresholds. These thresholds include the velocity of sound in nuclear matter, the Fermi energy, the nucleon-nucleon thresholds for meson and strangeness production, and the onset of strong nuclear compression ($\rho > 2\rho_0$). One looks for effects of nucleon nucleon, as opposed to nucleus-nucleus, interactions in gross quantities, such as the decrease in the nucleus-nucleus total reaction cross section found around 100 MeV/nucleon which parallels a similar decrease in the nucleon-nucleon cross section. Conversely, one can search for collective production of, e.g., pions, or look for large-scale collective effects such as creation of a pion condensate. The onset of strong compression will allow a determination of the density dependence of the nuclear equation of state and will allow an extraction of a value for the nuclear compressibility complementary to those determined from giant monopole resonance parameters.

This is also the energy region which spans the onset of fragmentation processes. Dynamical limits to linear and angular momentum transferred in a reaction can be mapped out. These limits ultimately result in production of a fireball-like participant zone in a reaction, whose parameters can be determined by performing multiparticle correlation experiments. The fragmentation process also opens the possibility of producing very neutron-rich isotopes. These can be used either to explore the neutron drip line or to produce neutron-rich secondary beams for use as projectiles in further reactions.

Secondary-Beam Physics

Secondary-beam physics in the meson factory sense, wherein secondary beams of pions, kaons, muons, and neutrinos, among others, are employed, concerns itself with the physics of few-quark systems, the properties of hypernuclei, and the testing of weak interaction theories with high precision. Baryon spectroscopy involves the study of baryons and their excited states, such as the delta resonance for the nucleon. It yields information about the many-body physics of systems subject to strong decay. From that, it may be possible to refine SU(3) theory and perhaps identify predicted exotica such as multiquark states or glueballs (strongly interacting objects with no quark content, comprised only of gluons). By implanting one or more strange particles into a nucleus, a spectroscopy can be established for the resulting hypernucleus. Depending on quark structure involved, a different interaction and, therefore, spectroscopy is expected for each type of strange particle implanted in a nucleus. Since

K^+ interact weakly with nuclei, the multiple scattering series for its interactions should converge rapidly, providing an excellent testing ground for reaction theory.

Searches for rare, weak decays can provide a measurement of the mixing angles in Weinberg-Salam theory, information which is lacking at present. This work can also place limits on effects due to right-handed intermediate vector bosons, a crucial test of basic assumptions in Weinberg-Salam theory. Neutrino scattering experiments can establish whether the neutrino is a Dirac or Majorana (self-conjugate) particle and can limit the neutrino mass. Whether or not the (V - A) form of weak interaction theory can account for all results can also be tested.

High-Energy Electron Physics

High-energy electron scattering from nuclei can be used to study small enough distance scales to probe the quark constituents of hadrons comprising nuclei. As electrons interact only electroweakly and are pointlike, their scattering can be interpreted readily. As they penetrate the nuclear volume uniformly, they are an excellent complement to hadronic probes. The ability to vary independently the energy and momentum transferred in electron-nucleus scattering allows the entire nuclear response to be mapped. This, coupled with coincidence experiments involving emitted nucleons and mesons, will allow studying how nucleons deform as they approach one another and how the confined quarks in each hadron can interact to build up light nuclei. Production of strange mesons can be used to explore the sea quark distribution in nucleons, as strange mesons are involved.

A high duty-factor electron machine allows performance of coincidence experiments. The study of giant resonances could be thus advanced by study of the angular correlations of their decay products; charge and current transition densities could be separated using the out-of-plane information. Tagged photon experiments, such as (γ,np), give information on relative nucleon momenta in complex nuclei. Vector meson photoproduction can explore the relation of photons and vector mesons and study interactions of mesons and isobars.

Such a machine can also be used to test fundamental symmetries, such as time reversal, and to make high statistics tests of parity-violating terms in electroweak theory. Parity nonconservation studies for discrete states in the Δ-resonance region will help determine nonleptonic weak currents and the weak interactions of mesons and resonances.

Relativistic Heavy-Ion Physics

Relativistic heavy-ion reactions can be used to study nuclei under extreme conditions of temperature, pressure, and density. These conditions may be so extreme as to approximate the behavior of neutron star matter in the laboratory. In the most exciting limit, the conditions existing less than 10 μs after the "Big Bang" might be reproduced and studied. These speculations rest on the recent discovery that lattice gauge calculations of the behavior of quarks, as given by quantum chromodynamics, indicate that a phase transition in the behavior of nuclear matter occurs at sufficiently high temperatures and densities. The phase transition results in a deconfinement of the quarks and the associated vector bosons of the strong interaction, the gluons, from the hadrons in which they reside in normal, cold nuclei into an extended region of space. The new phase of matter formed is called a quark-gluon plasma. Much experimentation would be required to understand the plasma and establish its properties for comparison with theory. The formation of the plasma is a basic prediction of QCD, at present the only viable theory of the strong interactions. New types of stable objects composed of quarks and/or gluons might be formed in such collisions, in analogy to the discovery of new chemical compounds, solid state devices, and radioisotopes.

Collisions of relativistic nuclei provide a laboratory for studying nuclei under extreme conditions akin to those occurring in dense stellar environments. This forges a further link between nuclear physics and astrophysics. Models abound for the existence of other stable phases of nuclear matter; these usually involve extremes in temperature or density and thus can be tested by studying relativistic heavy-ion collisions. The extremely large energy deposits in such reactions manifest themselves in large numbers of mesons produced. The study of these by multiparticle coincidence methods will elucidate shapes, sizes, and energy densities of emitting zones. The production conditions for the anomalous projectile fragments found at the Bevalac can be established, and the decay and/or interaction modes of the same elucidated.

Atomic Physics with Relativistic Heavy-Ion Beams

Atomic physics of one- or few-electron atoms becomes possible for all elements in the periodic table once a relativistic heavy-ion accelerator is available to boost the atoms to kinetic energies where K-shell electrons can be stripped off. QED effects, such as Lamb shifts in hydrogenic atoms, can be measured for such atoms. As the usual perturbative expansion in powers of $Z\alpha$ converges very slowly for elements such as Pb and U, nonperturbative theoretical calculations are needed for comparison to experiment. Such a development in field theory could serve as primary intuition on how to proceed in the much more difficult quantum chromodynamic case. Rydberg atoms ($n > 10$) could be made of single-electron atoms of any element using beam foil techniques. This would allow study of truly large, fragile atoms (the radius of an orbital scales as n^2), which would allow large distance tests of Coulomb's law through determination of energy levels by laser methods.

Relativistic effects could be used to produce motional $\vec{E}$ fields of several MV/cm causing strong Stark mixing of levels. Very large transient $\vec{B}$ fields would permit study of hyperfine structure of all atoms and measurement of

nuclear g factors for states with lifetimes as short as 10^{-14} seconds. It could prove possible to produce a coherent X-ray source by optically pumping a relativistic heavy-ion beam with a visible laser; pumping would be obtained by Doppler upshifting. Such a source might even prove to be tunable.

Fundamental Physics Experiments

Fundamental experiments which could be pursued depend on the availability of intense radioactive sources or intense sources of neutrons or neutrinos. Included in the list are improved searches for: the electric dipole moment of the neutron, axions, nonzero neutrino mass, exotic superheavy particles, and neutrino and neutron oscillations. The given choice of experiments is dictated by sources readily available at the laboratory. Equally interesting experiments requiring work at other facilities include searches for rare μ- and K-decay modes, for example.

Options Pursued

At the end of this study, it was decided to pursue construction of a relativistic heavy-ion collider (see Section 10), since this option allows pursuing three of the areas mentioned above, namely, relativistic heavy-ion physics, intermediate-energy heavy-ion physics, and atomic physics of one- or few-electron atoms of all elements. Recent decisions by the National Science Advisory Committee and DOE to recommend to Congress the construction of a 4-GeV CW electron machine by the Southeastern Universities Research Association (SURA) effectively eliminates the option of proposing an electron machine. It is most likely that the secondary-beam physics is best carried out at LAMPF or the AGS at BNL, if the former gained a synchrotron or the latter had a booster synchrotron added to its linac injector.

The most compelling reason for choosing the collider option is the possibility of investigating the physics of quark-gluon plasmas. This will yield further insight into quantum chromodynamics, the theory underlying nuclear physics. Further discussion of this topic is given in Section 10.

INSTRUMENTATION

MULTIPARAMETER FOCAL PLANE DETECTOR SYSTEM FOR THE BROAD RANGE SPECTROMETER

J. L. C. Ford, Jr.
R. L. Auble
F. E. Bertrand
J. L. Blankenship
T. P. Sjoreen
E. E. Gross
R. O. Sayer
D. Shapira

The good resolution, higher energy heavy ion beams from the HHIRF tandem and coupled accelerators offer new possibilities for charged particle spectroscopy with heavy ions. However, full exploitation of these capabilities requires magnetic spectrometers with advanced focal plane detector systems. The energies available, particularly from the coupled accelerators (up to 25 MeV/amu) together with the dispersion of the present ORNL spectrometers, demand a focal plane counter with a position resolution of at least a few tenths of a millimeter. The heart of the new system which has been installed in the BRS is a vertical drift chamber (VDC) having an intrinsic position resolution of about 0.1 mm and able to measure the angle of the particle trajectory at the focal plane to within about 10 mrad. This counter covers about 40 cm of the focal plane corresponding to ~120 MeV in excitation energy for an incident 400 MeV beam. The design and performance of this counter is described in further detail in the following contribution.

An adequate focal plane system must also identify the type of particle detected at the focal plane. In the most general case at least four parameters must be measured since the energy, mass number, atomic number, and charge state (E, A, Z, q) of the heavy ion must be determined. The position sensitive detector (the vertical drift chamber) provides one measured parameter; namely $B\rho$ (B = magnetic field, ρ = radius of curvature in the field B).

The other necessary parameters to completely determine the identity of the detected nuclei are obtained by three additional counters:

1) Start detector - a 2.5 cm x 2.5 cm parallel plate avalanche detector near the exit of the scattering chamber provides one of the fast timing signals used to measure the flight time of reaction products through the spectrometer. The detector consists of 1.5 μm mylar gas windows and ~ 100 μg/cm^2 electrodes (total thickness ~ 600 μg/cm^2) and did not affect the resolution of particles detected at the focal plane in tests with 400 MeV ^{16}O ions.

2) Stop detector - A second timing signal is obtained from a 40 cm long parallel plate avalanche detector which is mounted directly on the back of the vertical drift chamber. This counter furnishes the event signal used to initiate the analysis of an event in the multidetector system, the timing signal with which to measure the electron drift times in the vertical drift chamber, and the second timing signal necessary to determine the time-of-flight (TOF) through the spectrometer. Comparison of the count rates in this detector with those in the ionization chamber discussed below indicate a detector efficiency of essentially 100% for 400 MeV ^{16}O ions when using 7 torr of isobutane and a bias of 600 V.

3) Ionization chamber - The final detector in the system following the avalanche and vertical drift chambers is a large 40 cm deep ionization chamber with a 40 cm long entrance window. A segmented anode structure makes it possible to measure the energy loss (ΔE) and total energy (E) of the particles with $\lesssim$ 2% and $\lesssim$ 1% resolution, respectively.

By measuring TOF, ΔE, and E in addition to the $B\rho$ value the parameters of detected nuclei can be completely determined. In addition, by measuring the trajectory angle at the focal plane it is possible to determine the angle at which the particle entered the spectrometer.

Thus structured angular distributions can be measured across the spectrometer entrance window so that the full solid angle of the spectrometer can be utilized without loss of angular resolution. Furthermore, measurements of the electron drift times in the ionization chamber yields a constant monitor of the position and vertical height of the beam spot at the target. Thus one can avoid vertical beam shifts which may reduce the effective solid angle. Figure 2.132 is a photograph showing the ionization chamber, the vertical drift chamber and the second parallel plate avalanche counter (see figure caption).

Although this counter system has only recently become operational it already has been used in a number of experiments. Results (described elsewhere in this report) from a ^{28}Si (^{11}B, ^{10}B) experiment at 93 MeV using the direct tandem beam, and from a $^{28}Si(^{18}O, ^{18}F)$ measurement at 348 MeV using the coupled accelerators are shown in Figs. 2.133 and 2.134, respectively. These two figures illustrate the power of the focal plane system as a tool for investigating direct reactions with heavy ions.

ORNL-PHOTO 4670-83

Fig. 2.132. The three counters used at the focal plane of the BRS. The ionization chamber is on the left, the vertical drift chamber on the right (with attached ribbon cables), and the parallel plate avalanche counter is next to the centimeter scale.

THE VERTICAL DRIFT CHAMBER AS A HIGH RESOLUTION FOCAL PLANE DETECTOR FOR HEAVY IONS

T. P. Sjoreen
R. L. Auble
F. E. Bertrand
J. L. Blankenship
J. L. C. Ford, Jr.
E. E. Gross
D. C. Hensley
M. V. Hynes[1]
D. Schull[2]

Measurements made during beam development of the coupled operation of the tandem and cyclotron have indicated that a focal-plane detector system for the Elbek broad range spectrometer (BRS) will require a position resolution of ≤ 0.25 mm FWHM if we are to exploit fully the high-quality heavy-ion beams at HHIRF. A detector which could possibly meet our dual requirements of 1) submillimeter position resolution and 2) an active focal plane length of ~ 35 cm (10% range in momentum) was the vertical drift chamber (VDC).[3] This detector had the additional capability to measure trajectory angles. In order to determine the performance of the VDC as a heavy-ion detector, we have designed, constructed, and tested a detector similar to the original,[3] but suitable for use at gas pressures ≤ 200 torr while operating in a high vacuum chamber.

The VDC is a multiwire proportional counter, which consists of an anode wire plane symmetrically placed between high voltage cathode planes spaced 2.4 mm apart. The wire plane consists of 51 active sense wires 20 μm in diameter each separated from its neighbor by two guard wires 50 μm in diameter. All wires are

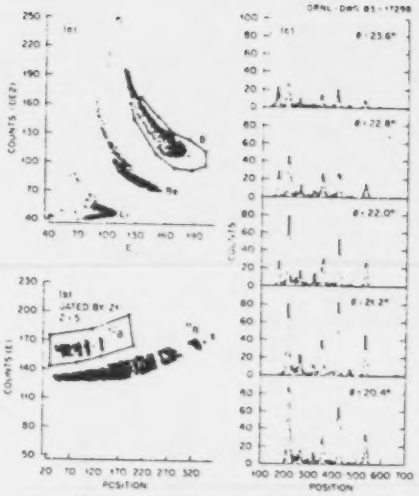

Fig. 2.133. Spectra from a study of spin-orbit effects in the $^{28}Si(^{11}B, ^{10}B)^{29}Si$ reaction at 93-MeV bombarding energy. Part (a) shows the correlation between the total energy loss (E) and the energy loss in the second anode (dE2) for reaction products in the ionization chamber. This correlation separates the reaction products into their respective atomic numbers (i.e. element identification). As indicated, the B, Be, and Li products are well separated. Part (b) shows the correlation between focal plane position and E for those boron products which fall inside the contour shown in part (a). This correlation separates the isotopes for a given element (i.e. mass identification). Part (c) shows those ^{10}B reaction products, which fall inside the contour of part (b), as a function of focal plane position binned into 5 angles. Each angle bin has an acceptance of 0.8°. These spectra were obtained with one angle setting of the BRS spectrometer. The 150-keV line widths (FWHM) are due almost entirely to target thickness effects and the energy spread in the incident beam.

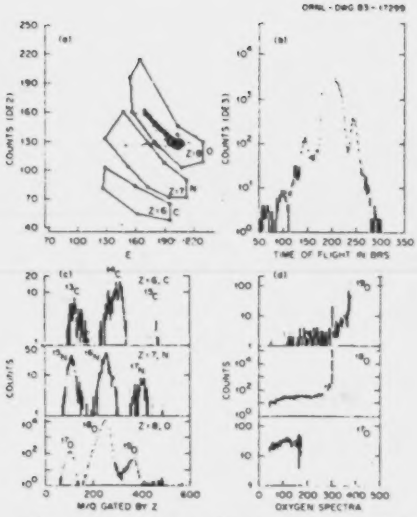

Fig. 2.134. Spectra from the study of single charge exchange with heavy ions using the (^{18}O, ^{18}F) reaction at 348-MeV bombarding energy. These spectra were taken from a "tune up" run with a Au target and demonstrate the time-of-flight (TOF) capability. Part (a) is an E-dE2 correlation (see Fig. 1 for explanation). Part (b) is the TOF spectrum through the BRS. Resolution is about 800 ps (FWHM). Part (c) shows mass spectra for each of three elements (O,N,C) using the element identification contours of part (a). The mass spectra were calculated with TOF, Bρ, and trajectory angle information. Part (d) shows focal plane position spectra for the oxygen mass spectrum of part (c).

evenly spaced at 2.54 mm. The low-gain guard wires effectively serve to divide the electrostatic volume of the counter into a series of drift cells, each centered on a sense wire. The VDC is designed for use with spectrometers in which the focal plane is at an oblique angle with respect to the particle trajectories. Because the particle trajectories pass through the counter at an oblique angle as well, several adjacent drift cells are activated. Hence, the sense wire number and the corresponding drift times for each of several cells is obtained and transformed into coordinates from which the intersection and the angle of the trajectory with the focal plane is computed. In our application the heavy ions typically pass through the counter at angles ranging between 30° and 44° -- intersecting 4 or 5 drift cells in the process. For more information, ref. 3 contains a detailed description of the operating principle of the VDC, while ref. 4 briefly details the construction of the ORNL counter.

The performance of the VDC as a heavy-ion detector was tested in the BRS with 129-MeV ^{12}C, 176-MeV ^{14}N, and 140-MeV ^{16}O ions from ORIC. Measurements were made with isobutane at pressures of 200, 100, and 50 torr, for which the best operating cathode biases were found to be 4.4, 3.7, and ~ 3.2 kV, respectively. The results of these measurements show that the VDC is an excellent counter for use with heavy ions. We estimate that the position resolution of the VDC is ~ 0.1 mm FWHM and that the angular resolution is about 10.5 msr FWHM. Because the BRS has an angular magnification of about 3.5, the value of 10.5 msr corresponds to ~ 3 msr (~ 0.2°) in scattering angle.

Figure 2.135 illustrates the usefulness of the VDC for heavy-ion research. This figure shows the ^{148}Nd inelastic spectrum obtained at 15° lab by scattering 129-MeV ^{12}C ions from 140 μg/cm^2 of ^{148}Nd mounted on a 40 μg/cm^2 ^{12}C backing.

The ability to measure trajectory angles accurately will enable us to operate the modified Elbek spectrometer with a larger acceptance angle (α) than previously used. Earlier measurements without angle measuring capability had to restrict the range of values of α so that magnet aberrations did not degrade the focal plane resolution. The effect of these aberrations is shown in Fig. 2.136c, which shows an uncorrected distribution of elastically scattered ^{14}N particles along the focal plane when the α acceptance slits were set at ± 37 mrad.

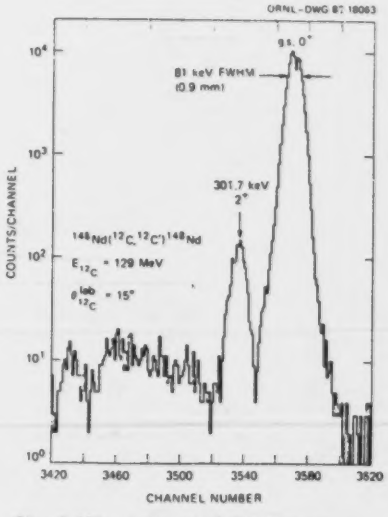

Fig. 2.135. Inelastic ^{148}Nd spectrum obtained by scattering 129-MeV ^{12}C ions from 140 μg/cm^2 of ^{148}Nd on a backing of 40 μg/cm^2 of ^{12}C.

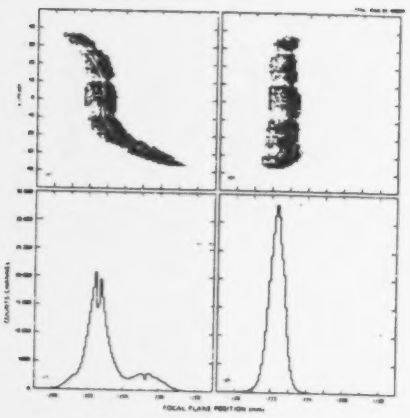

Fig. 2.136. Elastic scattering spectra obtained with the entrance angle (α) aperture of the spectrometer set at ±37 mr. These figures are discussed in the text.

The tail on the left side of the main peak and the satellite peak on the right are due to magnet aberrations. (The narrow valleys in each peak are the detectors response to the 50 μm field shaping wires and the broad valley between the two peaks is an artifact of a wire mask in front of the entrance aperature.) That the poor resolution in Fig. 2.136c is due to those events with large values of $|\alpha|$ is indicated in the correlation between focal plane position and α shown in Fig. 2.136a. The solid line drawn in Fig. 2.136a is the calculated central image position computed by a geometrical ray tracing program.[5] The calculation does not include the sources of finite resolution from the beam and target which dominate the spread in the line shape seen in the data. The horizontal separations of the image seen in Fig. 2.136a and 2.136b again result from the wire mask placed between the scattering chamber and the spectrometer entrance window.

Previously, in order to avoid limiting the experimental resolution, it was necessary to reduce the angular opening of the spectrometer to cut out the wings observed in Fig. 2.136a. This, of course, reduced the solid angle of the instrument. However, the VDC makes it possible to correct empirically for the α dependence in the focal plane position. Results of the correction are shown in Fig. 2.136b. The position resolution is recovered over the entire range of α as is made apparent in the corrected distribution shown in Fig. 2.136d.

---

1. Los Alamos National Laboratory.
2. Visiting scientist from GSI, Darmstadt, Germany.

3. W. Bertuzzi et al., Nucl. Instrum. Methods 141, 457 (1977).
4. J. L. C. Ford, Jr. et al., Phys. Div. Prog. Rep. June 30, 1981, ORNL-5787, p. 142.
5. J. B. Ball, private communication.

THE Q-5921 FAST TIMING AMPLIFIER

J. L. Blankenship[1]

A fast pulse amplifier was designed to provide the gain and fast risetime needed for use with parallel plate avalanche detectors (PPAD), multiwire proportional detectors, and thin silicon detectors in timing applications. The circuit design is similar to that of Stelzer[2] but utilizes hybrid microcircuit components mounted on a conventional printed circuit board. Up to eight amplifier channels are incorporated in a single-width NIM module. Each amplifier can be assembled as either inverting or non-inverting, so that a single NIM module can accept signals from the anode, cathodes, and/or sense wire planes of a PPAD, for example.

Each amplifier channel has an input impedance of 50 ohms and has diode overload protection. Amplifier gain is 200, and the unipolar output pulse has a risetime of 1 ns, a decay time of 40 ns, and an amplitude of 0 to -5 volts across 50 ohms. Amplifier noise is < 10 μV rms referred to the input. Coaxial cable lengths are matched to within ±3 mm between channels. Crosstalk between channels is less than -60 db.

---

1. Instrumentation and Controls Division.
2. H. Stelzer, Nucl. Instrum. Methods 133, 409 (1976).

THE Q-5927 FAST PULSE GENERATOR

J. L. Blankenship[1]

A sub-nanosecond-risetime pulse generator was designed for development and testing of fast-timing-pulse amplifiers which are used with microchannel plate and parallel plate avalanche detectors. The fastest commercially available pulse generator is the Model BL-2 made by BNC and has a 3 ns risetime. The response of an amplifier to a positive step function can be obtained with the 7S12 sampling oscilloscope module made by Tektronix, using the S-52 pulse generator head and the S-4 sampling head. However, the response of an amplifier which requires a negative-input pulse, or a narrow pulse cannot be obtained with the sampling oscilloscope pulser.

The Q-5927 fast pulse generator has both positive and negative output pulses available, with risetimes of ~ 150 ps, pulse width adjustable from 3 to 30 ns, and an amplitude of ~ 0.25 volts. Pulse repetition rate is variable from 100 Hz to 10^5 Hz. A trigger pulse is available in advance of the test pulse, with time advances variable from 0 to 80 ns. The short delays are useful for real-time

oscilloscope displays, and the 80 ns delay is matched to the Tektronix 7S12 pretrigger requirement. This pretrigger eliminates the use of an 80 ns delay line in the signal path, which would degrade the pulse risetime. The pulse generator design is based on ECL logic and the Tektronix part number 152-0177-22 tunnel diode.

---

1. Instrumentation and Controls Division.

POSITION-SENSITIVE PARALLEL PLATE AVALANCHE COUNTER DEVELOPMENT

R. L. Auble I. Y. Lee J. L. Blankenship[1]

In the last progress report, a parallel plate avalanche counter (PPAC) was described which had position sensitivity in one direction. In order to obtain both x and y coordinates, two counters oriented at 90° to each other were required. The additional electrodes introduced by such stacking limit the energy-mass range of the particles which can be detected. These detectors have now been modified to provide both x and y position information from a single detector volume.

The overall construction is similar to that previously used, with the exception that the anode has been divided into 0.25 cm wide strips. The new counter is shown schematically in Fig. 2.137. The anode and cathode are made of 1.5 μm thick mylar, with a thin (~ 50 μg/cm²) vapor deposited coating of aluminum or gold. To form the anode, the metal coating was deposited through a wire grid consisting of 0.025 cm diameter wires spaced 0.25 cm apart. The sense wires are 20 μm diameter gold coated tungsten

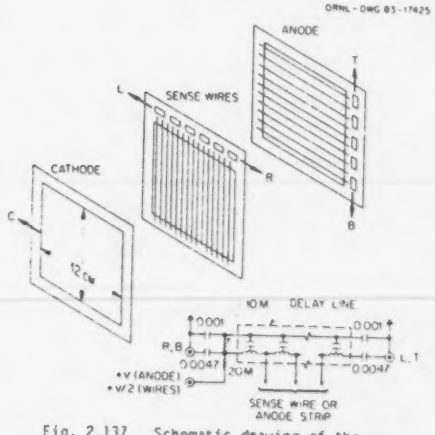

Fig. 2.137. Schematic drawing of the x-y position sensitive parallel plate avalanche counter.

spaced 0.2 cm apart. The various planes are separated by 1.6mm. Delay line "chips", each having ten 2 ns delay lines,[2] are used to encode each sense wire or anode strip. The sense wire and anode signals are amplified and then analyzed in a time-to-digital converter.

The cathode is connected to ground via the 50 Ω input of the amplifier and this signal is used to provide fast timing and pulse height information. Typical operating pressures have been 600-1300 Pa of isobutane, with anode voltages in the range of 500V to 600V. Breakdown, at a pressure of 7 torr, is approximately 650V and care must be exercised since sparking has been found to cause removal of the metal coating on the cathode.

The detectors have been tested with 5.8 MeV alpha particles and with ^{252}Cf fission fragments with good results: no "cross-talk" has been observed between signals from the different planes, the position resolution is equal to or better than the sense wire or anode strip spacing, the timing resolution using the cathode signal is better than 0.5 ns, and the amplitude of the cathode signal provides a reasonable ΔE measurement. These detectors have been used in a study of the focusing properties of the Velocity Filter using elastically scattered 100 MeV ^{197}Au and will be used in a study of the fission decay of the giant quadrupole resonance in heavy nuclei.

---

1. Instrumentation and Controls Division.
2. Rhombus Industries Inc., Model TZB12-5.

DEVELOPMENT OF MULTIWIRE PROPORTIONAL DETECTORS FOR FISSION MEASUREMENTS

J. L. Blankenship[1] F. E. Obenshain

Two multiwire proportional detectors were designed to measure fission products following heavy ion fusion. One design has a sensitive area of 2 x 2 cm² and provides a fast timing pulse, typically the start signal. The other design has an 8 x 10 cm² working area and provides both a fast timing signal and 2-dimensional position information.

The 2 x 2 cm² detector shown in Fig. 2.138 has four polypropylene foils of ~ 50 μg/cm² each in the beam path. Two foils are windows, and two foils are coated with 20 μg/cm² aluminum and are used as cathodes. The anode plane consists of 20-μm-diameter tungsten (6% gold coated) wires spaced 1 mm on center. Typical operating conditions are: pressure, 1.5 torr of isobutane; and 400 volts on the anode. The output pulses have a risetime of ~ 2 ns and pulse widths (FWHM) of 3 to 4 ns.

Timing performance was evaluated by accumulating the time-of-flight distribution (TOF) of fission fragments from ^{252}Cf for a 2.1 cm flight path. A thin, over-biased silicon surface barrier detector provided the stop pulse. Precision measurements by Schmitt et al.[2] demonstrate an intrinsic width of 167 ps for the

ORNL-PHOTO 5439-83

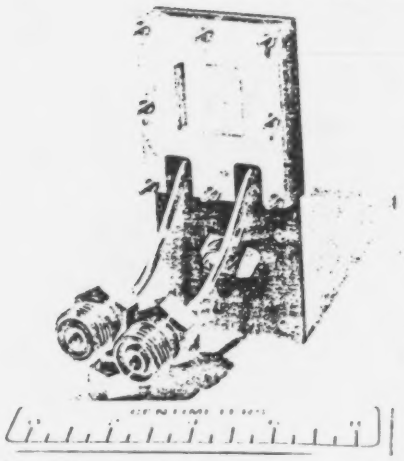

Fig. 2.138. The 2 x 2 cm² multiwire proportional counter for fast timing.

ORNL-PHOTO 5440-83

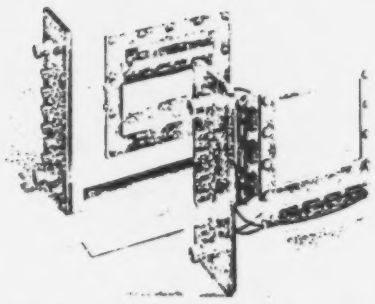

Fig. 2.139. The 8 x 10 cm² position-sensitive, multiwire proportional detector. A complete detector mounted in the housing is shown at left. The gas window and supporting wires are shown in this view. The detector assembled to a mounting flange is shown on the right. Note the stripes of aluminum on the cathode and the seven dip chips which are tapped, lumped-element delay lines. This flange-mounted assembly design provides for quick access for service.

lighter fragment group. The 2 x 2 cm² detector timing distribution was 400 ps FWHM. If the silicon detector is assumed to contribute 100 ps, then the 2 x 2 cm² detector timing performance was 349 ps FWHM.

Breskin[3] has achieved a timing spread of 200 ps FWHM for a similar detector under comparable operating conditions, but using 27 MeV ^{16}O particles.

The 8 x 10 cm² detector shown in Fig. 2.139 has the same construction materials (windows, cathodes, anode wires) as the 2 x 2 cm² except that the cathodes have segmented, 3-mm-wide stripes of aluminum each of which is connected to a tap on a set of lumped-element delay-line chips to provide position encoding. The delay line dip chips are tested to obtain tap-to-tap delay and are sorted into sets with closely matching properties and minimum spread in delays per taps. The orientation of the stripes on the two cathodes is orthogonal to provide x-y coordinate readout. The timing signal is taken from the anode and has a risetime of ~ 3 ns (10-90 percent) and a pulse width of 12 ns (FWHM). Timing resolution was evaluated from the ^{252}Cf fission fragments TOF over a 6 cm flight path. The timing distribution was 830 ps FWHM, and an intrinisic width of 466 ps is obtained from the work of Schmitt.[2] The start pulse was furnished by a 2 x 2 cm² detector which has an estimated timing width of 349 ps. Thus, the intrinsic timing performance of the 8 x 10 cm² detector was 591 ps (FWHM). Typical gas pressures are 2 to 4 torr of isobutane and bias voltages are 420 to 480 volts. Position resolution is limited by the discrete width of the aluminum stripes, and position linearity is determined by the uniformity of delay increments between taps.

---

1. Instrumentation and Controls Division.
2. H. W. Schmitt et al., Phys. Rev. 137, B837 (1965).
3. A. Breskin, R. Chechik and N. Zwang, IEEE Trans. Nucl. Sci. NS27, 133 (1980).

LARGE IONIZATION DETECTORS FOR HEAVY ION REACTIONS

J. L. Blankenship[1] F. E. Obenshain
A. H. Snell

The Time-of-Flight (TOF) facility is instrumented with a start detector, a position sensitive stop detector, and an 80-cm-deep ion chamber to obtain E and ΔE. The stop detector and ion chamber window assemblies have been replaced with new designs which enable ease of replacement or repair to the stop detector. The window design provides a more uniform electric field and a better measurement of ΔE with the first anode segment.

The original parallel plate avalanche detector (PPAD) provided good timing performance but did not provide for x- and y-coordinate readout. The new stop detector is an 8 x 10 cm² multiwire proportional detector (MWPD) with position encoding from the striped cathodes, and is identical in design to the detector described in the previous article for use in fission measure-

ments. This design requires an additional window of 50 μg/cm² in the particle path, but prevents gas contamination of the stop detector by gas leaking or diffusing from the ion chamber. Freon is frequently used in the ion chamber, and small leaks had caused several PPAD failures in the original design. An adapter and housing for the MWPD was designed which connects the flight tube to the front flange of the ion chamber. This housing has a rectangular mounting flange on the side to receive the MWPD and enables easy replacement of the MWPD.

The ion chamber entrance window now projects into the region between cathode and Frisch grid and has a graded electric field which ensures proper charge collection from all particle entrance points.

---

1. Instrumentation and Controls Division.

A GAS HANDLING SYSTEM FOR HEAVY ION DETECTORS

J. L. Blankenship[1] C. A. Reed[2]

A high-stability, pressure-regulated, variable-flow gas handling system has been developed for general use with gas-filled heavy ion detectors. This design features a graphic front panel which illustrates the function of each valve and control. The vacuum manifold is 1.9 cm in diameter and is connected to the gas handling system by three valves to enable the pumpout of the system by section.

The absolute gas pressure is measured by a capacitance manometer made by MKS Instruments, Inc., and is displayed on a 4½ digit readout; the pressure setpoint is adjusted by a ten-turn potentiometer in conjunction with a 3-position decade switch on the pressure controller. Pressure transducers with full-scale ranges from 10 torr to 10,000 torr are interchangeable, and therefore the gas handling system can accommodate, for example, a PPAD operating at 1.5 torr for one experiment, and an ion chamber operating at 1000 torr for another. The gas flow rate is controlled by the manual setting of a sensitive needle valve, and therefore, a large range of flow rates can be achieved, including a static gas-filled system.

---

1. Instrumentation and Controls Division.
2. Guest assignee from Oak Ridge Associated Universities.

THE WINDOWLESS, SUPERSONIC GAS JET TARGET

J. L. C. Ford, Jr. B. Shivakumar[1]
D. Shapira S. T. Thornton[2]

The windowless, supersonic gas jet target[3] now installed at the split-pole magnetic spectrometer at HHIRF is an instrument capable of high resolution experiments with high purity gaseous targets. The schematic of this device, shown in Fig. 2.140, illustrates how the gas flows through a convergent-divergent Laval nozzle to form a film-like sheet before being recaptured by a multi-stage pumping system (~ 90% of the gas is pumped by the first stage 600 ℓ/sec roots blower). The incident beam enters through a set of slits, intersects the gas foil just above the Laval nozzle, and the reaction products exit through a second slit system which can be rotated between 0 and 60° in the horizontal reaction plane. The detector system is the split-pole spectrometer[4] capable of high resolution measurments over an extended range of excitation energies.

By adjusting the pressure and flow rate of the gas at the inlet to the Laval nozzle the thickness of the gas target can be easily changed. The available pumping speeds of the four-stage differential pumping system allow the target thickness to be varied between a fraction of a μgm/cm² up to about 30 μgm/cm².

Figure 2.141 demonstrates the capabilities of this device for nuclear physics as it displays a $^{40}Ar(^{16}O, ^{17}O)$ spectrum measured at 100 MeV and at 13°. The target thickness was 10.5 μgm/cm² and the resolution of ~150 keV ($\Delta E/E$ = 0.15%) was limited by the position resolution of the hybrid-ionization chamber[5] used as the focal plane detector. Tests with a position sensitive solid state detector yielded an energy resolution of 50 keV at 100 MeV ($\Delta E/E$ = 0.05%). A vertical drift chamber, such as described elsewhere in this section, will be constructed for this spectrometer in order to fully expoit the capabilities of the gas jet.

Future experiments planned with this apparatus include; a) the study of orbiting processes in ^{28}Si + ^{14}N collisions to investigate the effect of non-alpha conjugate nuclei in such reactions, b) the elastic and inelastic scattering, fusion, and transfer channels in ^{12}C + ^{20}Ne and ^{16}O + ^{20}Ne interactions where both nuclei are alpha conjugate systems, and c) reaction mechanism and high spin states populated by reactions such as $^{16}O(^{12}C,\alpha)^{24}Mg$.

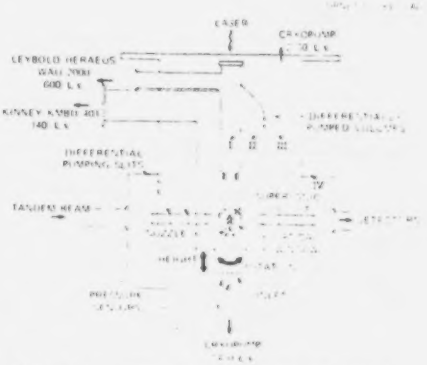

Fig. 2.140. Schematic of the gas jet target.

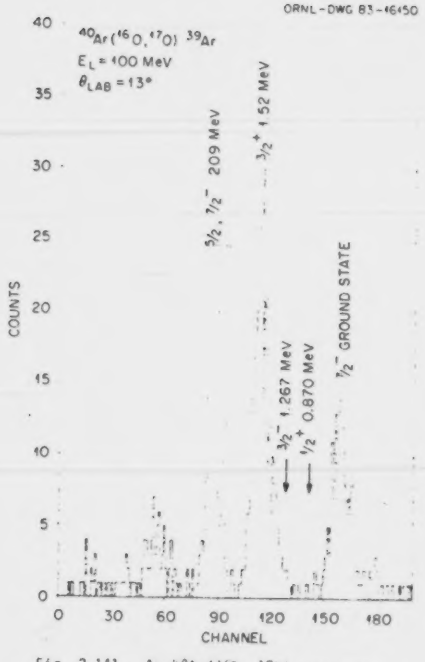

Fig. 2.141. An $^{40}Ar(^{16}O, ^{17}O)$ spectrum measured[3] with a 10.5 μgm/cm² thick target from the gas jet.

The advantages offered by the gas jet target include: 1) availability of targets which cannot be obtained as solids, 2) a target thickness which can be minimized and varied at will, 3) the target contamination can be minimized, 4) entrance and exit windows are absent, thus minimizing the energy degradation of the incident beam and the reaction products, 5) ray tracing measurements at the focal plane when using the gas jet demonstrate good focusing of the reaction products indicating a highly localized jet permitting kinematic compensation with a magnetic spectrometer, 6) the target is indestructible, thus permitting the use of high beam currents, 7) the gas jet can be seeded with materials available as solids or liquids at room temperature but from which it would be difficult to fabricate targets as thin foils, 8) it is possible, in cases, to illuminate the gas jet with lasers in order to optically pump the gas or material seeded into the gas to produce a polarized target (see following article).

---

1. Permanent address: A. W. Wright Nuclear Structure Laboratory, Yale University, New Haven, Connecticut 06511.

2. University of Virginia, Charlottesville, Virginia 22901.

3. J. L. C. Ford et al., Phys. Div. Ann. Prog. Rep. Dec. 31, 1978, ORNL-5498 (June 1979) p. 45; J. L. C. Ford et al., Phys. Div. Ann. Prog. Rep. June 30, 1981, ORNL-5787 (Nov. 1981) p. 128; and to be published.

4. J. E. Spencer and H. A. Enge, Nucl. Instr. Meth. 49, 181 (1967).

5. D. Shapira et al., Nucl. Instr. Meth. 169, 77 (1980).

DEVELOPMENT AND CONSTRUCTION OF A POLARIZED Eu TARGET

B. Shivakumar[1] J. L. C. Ford, Jr.
J. R. Beene D. Shapira
C. E. Bemis, Jr. J. W. Johnson
R. H. Ward

A nuclear spin polarized Eu target is being constructed[2,3] to facilitate the explicit determination of important microscopic and macroscopic details of heavy ion reactions. The operation of the target is based on laser depopulation optical pumping of Eu atoms seeded into a gas jet.[4] A target of Eu atoms (seeded in an Ar carrier gas) of thickness ~ 10^{15} atoms/cm² with a polarization of ~ 90% is expected.

A schematic of the setup is shown in Fig. 2.142 The gas-jet target (GJT) assembly has been modified, by the addition of an optical window,

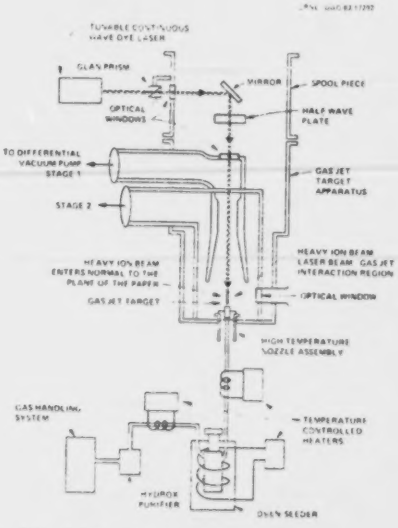

Fig. 2.142. Polarized target apparatus. The details of laser diagnostics, three axis degaussing and "keeper" field coils and nuclear reaction detection devices are not shown.

to allow for the admission of a polarized laser beam into the region of the target. A spool piece has been constructed and placed immediately above the GJT assembly in order to carry the laser transport and polarization optics. The entrance anti-reflection coated window is provided with a mount carrying a glan prism. A mirror on an adjustable mount, at the center of the spool piece, helps in the positioning of the laser beam at the gas jet. A half-wave plate is mounted on a rotatable table immediately below this mirror and allows for remote changing of the laser's plane of polarization. An optical window has been provided at 90° to the heavy ion beam in the horizontal reaction plane to facilitate optical monitoring, using a narrow band single frequency laser, of the polarization of the target. A removable mirror assembly has been constructed to allow positioning of a mirror at the nozzle site. Using this device, a collimated laser beam can be directed with accuracy to the position of the target.

The optical pumping cycle employed to polarize the Eu jet places severe constraints on the characteristics of the pumping laser. In order to polarize the Eu efficiently on a time scale comparable to the flight time of atoms from the nozzle to the accelerator ion beam we require large CW laser powers with a bandwidth as nearly matched as possible to the absorption profile of the Eu transitions to be pumped. We have achieved laser operation satisfying these criteria and are currently implementing a system to insure that the laser frequency spectrum, within the nominal bandwidth, is free of pronounced fine structure when averaged over the ~ μs timescale of the Eu optical pumping cycle.

Stray magnetic fields present in the vicinity of the target can have a substantial effect on the maximum polarization achievable through optical pumping. The magnetic field in the scattering chamber has been mapped in detail as a function of the current energizing the Enge spectrometer, the fringe field of the cyclotron at various excitations, and as a function of the angular position of the Enge magnet. From these measurements, the total field at the region of the target can be predicted to within 100 mG. Three pairs of coils have been constructed and mounted along mutually orthogonal axes to allow for the cancellation of stray magnetic fields, and to provide a "keeper" field of 1-2 gauss.

Experiments have been performed to investigate gas jets seeded with I_2 via laser fluorescence spectroscopy. Similar measurements will be used to test the performance of the new nozzles and the associated assembly designed for use with Eu at temperatures up to 1000°C. The new assembly has a water cooled outer jacket separated from the central nozzle and gas line section by a ceramic insulator. The seeding of the carrier gas with Eu atoms will be done at a high temperature (~ 900°C) in an oven that has been designed specifically for this purpose. The oven incorporates a valve of novel design, capable of operating at high temperatures and allowing for isolation of the Eu containing portions of the oven.

Experiments planned with the apparatus will investigate in detail the effects of static and dynamic nuclear deformations on elastic and inelastic scattering, transfer reactions, fusion and the role of limiting angular momentum in fusion-fission reactions.

---

1. Permanent address: A. W. Wright Nuclear Structure Laboratory, Yale University, New Haven, Connecticut 06511.
2. J. R. Beene et al., Phys. Div. Annu. Prog. Rep. June 30, 1982, ORNL-5787 (Nov. 1981) p. 132.
3. B. Shivakumar et al., p. 385 in Lasers in Nuclear Physics, Nuclear Science Research conference series, Vol. 3, edited by C. E. Bemis, Jr. and H. K. Carter (Harwood Academic Publishers, 1982).
4. J. L. C. Ford, Jr. et al., this report and Phys. Div. Annu. Prog. Rep. June 30, 1981, ORNL-5787 (Nov. 1981) p. 128.

AFTERPULSES FROM DETECTORS FOR LOW ENERGY NEUTRONS

N. W. Hill[1] J. A. Harvey[2]
D. Horen C. H. Johnson

At the ORELA time-of-flight facility we have extended the energy for neutron detection down to about 10 keV for liquid and plastic scintillators by accepting pulses corresponding to a few photoelectrons. At such low levels there is a background of afterpulses which originate either in the scintillator or in the photomultiplier, a 5-inch RCA-8854 PMT, but appear several μsec after the earlier detection of a neutron or γ-ray. Here we investigate the afterpulsing phenomenon.

We have studied four RCA-8854 PMT's: one coupled to a BIBUQ liquid scintillator, one to plastic NE-110, and the two others to a single NE-110 scintillator such that they could also be operated in coincidence. We used a two dimensional analyzer to record not only the time spectrum of afterpulses but also their pulse height spectra in 220 selected time bins. The initial events in the scintillator and the start pulses for the time spectrum were generated not by neutrons but by γ-rays or x-rays from one of three radioactive sources: a ^{60}Co source with a detector bias corresponding to an average 830-keV Compton electron, a ^{137}Cs source biased for 380-keV, and a Ag x-ray source biased for the full 22.6-keV photoelectron. The calibration for the pulse heights in units of electrons from the photo cathode was deduced from the thermal one- and two-electron distributions. We then observed the mean number of electrons from the Ag x-ray source and calculated the means for the Co and Cs sources using their relative energies. The lower bias for the afterpulses was set to accept the upper 5% of the predominantly thermal one-electron distribution. We corrected for thermal and source background using the spectra observed at very late times.

Figure 2.143 shows time spectra plotted in terms of afterpulses per initial photoelectron versus the delay time. The lower curve is for the multiplier coupled to BIBUQ and the upper curve is for one of the two coupled to NE-110. These spec-

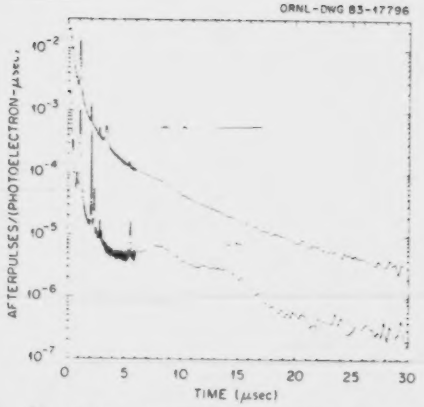

Fig. 2.143. Afterpulse time spectra for RCA-8854 multipliers coupled to a NE-110 scintillator (upper curve) and to a BIBUQ scintillator (lower curve).

tra were obtained using Co, but spectra nearly identical to these were also found using Cs and Ag.

Each spectrum shows a decaying background underlying narrow peaks. This background is 20 to 50 times smaller for the tube coupled to BIBUQ than for the one coupled to NE-110. About the same difference was observed between BIBUQ and the other tube for that NE-110 and an even larger difference was observed relative to the single tube coupled to NE-110. We attribute this background to delayed light in the scintillators and we conclude that the intensity of that light is much less for BIBUQ than for NE-110.

The spectra in Fig. 2.143, as well as those for the other two multipliers, each show relatively narrow peaks superimposed on the background. The intensity of a peak with a given delay varies from one spectrum to another and some peaks are not present in all spectra.

We interpret these peaks as resulting from positive ions of various masses, which are formed by electron bombardment in the residual gas of the cathode-dynode region and accelerated back to the cathode where they eject "ion-electrons" to produce afterpulses with amplitudes and time delays depending on the abundances and masses of the gas atoms. The peaks are relatively narrow because the transit time for an ion in the cathode-dynode region is nearly independent of the point of origin.[3] Some spectra, such as the lower one in Fig. 2.143, also showed broad peaks near 8 and 14 usec.

In Fig. 2.144 the smooth curve is the pulse height spectrum, with the off-peak background subtracted, for the 1.1-usec peak seen in the upper curve of Fig. 2.143. This group, which was present with similar intensities for all four multipliers results from a light ion, probably H_2^+. The curve shows the number of ions or afterpulses

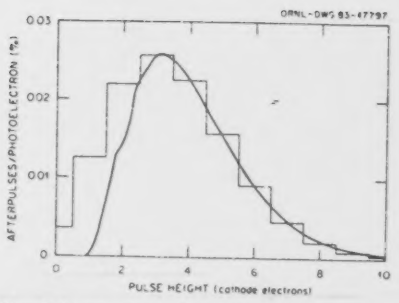

Fig. 2.144. Pulse height distribution for afterpulses in the 1.1-μsec peak for a particular RCA-8854 photomultiplier.

per initial photoelectron versus the number of ion-electrons ejected by the ion at the cathode. The curve falls to zero at the lower bias.

The figure includes a Poisson histogram which has been parametrized with a mean value of 3.5 electrons in order to give a good visual fit to the observed distribution. From the histogram we find a 0.12% probability that a photoelectron produces a 1.1-μsec afterpulse in this multiplier. For the NE-110 scintillator that was mounted on this multiplier the mean afterpulse height corresponds to 70-keV neutron pulses and the probability for the afterpulse is about 14, 0.6 and 0.02 percent, respectively, for incident 1-MeV, 100-keV and 10-keV neutrons.

With the knowledge gained at the completion of this study we aim to adopt a particular detector system in order to make measurements with negligible afterpulse backgrounds at low neutron energies.

---

1. Instrumentation and Controls Division.
2. Now in Engineering Physics Division.
3. G. A. Morton, H. M. Smith and R. Wasserman, IEEE Trans. on Nucl. Sci. NS-14, 443 (1967).

EVENT HANDLER DRIVEN DATA ACQUISITION

D. C. Hensley

Most major nuclear physics laboratories have chosen to incorporate CAMAC into their data acquisition systems. This decision is based on two perceived benefits. First that the systems will be largely computer independent, in as much as CAMAC is standardized and its computer interfacing requirements clearly defined. Second, that many support modules for data acquisition, communications, and equipment control will be available off-the-shelf. This implies that much of the time which might be spent in redesigning the wheel can be invested into research. On the other hand, much of the support for CAMAC has

come from industrial applications and from business uses, so that in fact much of equipment available is only marginally useful for nuclear physics. In particular, many of the CAMAC manufacturers have concentrated on μP applications and equipment control. Fortunately, many of the basic building blocks of a nuclear physics data acquisition system are available, ADCs, TDCs, latches, and input and output registers, but a controller which can manage the data flow at the crate level with a speed matching that of CAMAC has not been generally available.

The Event Handler[1,2] a fast, programmable CAMAC based processor with auxiliary crate controller capability, was designed to fit into this very niche. It has a basic speed of 400 ns which comfortably matches that of CAMAC (1 μs), it has special direct interfacing to the experiment in order to best aid the experimenter, and it has logic capability which helps to enhance the quality of the data flow to the computer. While it possesses no computational capability, its ability to manage data acquisition exceeds that of the remote host computer and far exceeds that of local microprocessor systems. Its greatest competition lies in Fastbus where applications with local 16-bit μPs are being implemented.

The Event Handler is programmable with a current memory size of 2048 instructions. Typical large experiments currently use fewer than 1024 of the available memory space. The device is downloaded from the host computer via the CAMAC dataway -- it appears as a simple 24-bit wide memory to the host. The Event Handler can access any "legal" module in either of two crates and can pass the result on the CAMAC dataway or out its own special front-panel FIFO output. The latter method allows data input and output to be separated so that contention for the dataway is kept to a minimum. Although the full 24 bit capability of CAMAC is supported by the Event Handler, it has been optimized for 16-bit transfers, since such transfers fit best the structure of the current 16 and 32 bit mini-computers. It is capable of placing into the data stream various arbitrary 16-bit words which may be used for data acquisition indexing or control by the host computer.

Data acquisition with the Event Handler as the front-end manager is quite straight forward for most applications. Whatever pattern of ADCs, TDCs, etc. is desired is written into the program for the Event Handler and downloaded from the host computer. Then whenever an event is detected, the appropriate pattern is read and transmitted to the computer with whatever indexing or tag words necessary inserted by the Event Handler. Because the processor is relatively simple, the instructions are nearly as simple as "read" and "transmit". The major complexity has to do with how the various parameters are scattered throughout the CAMAC modules, but from the computer's point of view there is simply a continuous stream of data appearing as if out of a single FIFO. The Event Handler has the necessary "hooks" to let it know when the computer is busy and thus when the data acquisition should be suspended.

Data rates achievable with this system are usually limited principally by the detectors, the ADCs, or the accelerator beam. The standard ADC or TDC modules have conversion times near 100 μs, and the use of these devices of necessity holds the event rate below 10 kHz. The time required for the Event Handler to service a given parameter is of the order of a few microseconds, so that a 10 parameter experiment might require some 30 μs of Event Handler time. In this case, an average event rate of 5 kHz could be sustained with a load on the computer of about 120 kBytes/s data rate. Since the computer has a rate limitation at the 500 kBytes/s level imposed by its CAMAC branch highway and a rate limitation of 700 kBytes/s imposed by its 6250 BPI magnetic tape drives, the computer generally does not limit the event rate for most experiments. The one exception is for the Spin Spectrometer which can have quite high raw event rates coupled with very long events. In some cases, the branch highway may then be the limiting factor, but in few cases has that limitation been approached.

One of the special features of the Event Handler is that it can perform sparse data scans, that is, it can transmit to the computer only those parameters which are judged to be relevant, irrelevant parameters can be skipped. In many experiments, the detectors making up the overall system are uncorrelated, and there is no need for a given event to record any data from those detectors which are uninvolved. For the Spin Spectrometer with its 70 detectors, transmitting 70*3 words/event to the computer would soon bog down the computer and greatly increase the number of magnetic tapes used for data storage. For this device, a sparse data scan gives a savings of approximately a factor of 2. The traditional way to perform a sparse data scan quickly is to use a gated latch module (or coincidence buffer) which generates a bit pattern which indicates which detectors or detector systems are relevant. The Event Handler is specially structured so that it can make optimal use of such a pattern register -- it takes it about 1 μs to check a given bit in a register.

Another special feature of the Event Handler is its ability to reject certain classes of events. It is able to make either arithmetic or logic checks on various parameters or front panel inputs and to reject events based on these checks. Experiments involving elastic scattering have been optimized by having the Event Handler decide whether a particular event was an elastic event and rejecting it if it was. It is capable of making this decision within about 10 μs, and by doing so it both frees up the front end data acquisition and reduces that load to the data spooling device. Or it may decide on the basis of the pattern in the gated latch that this particular event should be scrapped. In any case, this particular feature has greatly enhanced the quality of several experiments and is a feature which is simply not available with computer driven CAMAC data acquisition systems.

The decision to implement data acquisition in CAMAC based systems has been a valuable one for the HHIRF as it has allowed an orderly progress to complicated, multi-parameter experiments. Only with the Event Handler can we fully utilize

this capability, and with it we have been able to improve many of our standard experiments.

---

1. D. C. Hensley, IEEE Trans. Nucl. Sci. NS-26, 710 (1979).
2. D. C. Hensley, IEEE Trans. Nucl. Sci. NS-26, 4454 (1979).

SPIN SPECTROMETER ELECTRONICS

D. C. Hensley

The timing, logic, and linear shaping electronics for the Spin Spectrometer[1,2] were designed with the overall objectives of convenience, a minimum of interconnections, fast access to event timing logic, and ease of control. The electronics can conveniently be treated in logical groups; the constant fraction discriminators (CFD), the strobe control, the clear control, and the gated latch interface (GLI).

The constant fraction discriminators are of a standard design where a fraction of the signal is compared with the original signal delayed by the approximate rise time. Because such a system might multiple trigger on the very long pulse tail generated by a NaI(Tl) detector, the output of the CFD comparator circuit triggers a D-style flip-flop whose D-input is the logical AND of a lower level discriminator and a similar CFD circuit. This edge-triggered flip-flop can set only once during a pulse -- its output triggers a precise RC delay one-shot which provides an adjustable delay (20 to 500 ns) for the logic pulse. At the end of this delay time, two fast logic signals are generated, one to an internal gated latch and the other to the time digitizing module (TDC) in the CAMAC crate. The enabling strobe for the internal gated latch is brought in from a back card edge connector.

The CFDs attain an average time resolution for the NaI detectors for the Spin Spectrometer of 2 ns. The walk can be minimized over the full dynamic range of the input. The threshold for the CFDs can run as low as 40 keV (<20 mV), but cross-talk in the units has dictated that the thresholds be set above 100 keV for some of the units, a condition that has a small but nagging effect on the multiplicity resolution of the device. The resolving time of the gated latches is approximately 30 ns, minimum.

In addition to the CFD circuit which samples the front edge of the pulse, there is a similar circuit which compares the time at which the front edge, delayed by 160 ns, crosses the tail of the pulse. This circuit allows one to have a measure of possible pulse pile-up, whenever that pile-up takes place at least one rise-time after the initial pulse. This rather simple circuit is intended to allow one to reject large pulses associated with the capture of relatively slow neutrons (<5 MeV). For experiments involving the search for high energy γ rays, the effect of captured neutrons must be minimized, and this pile-up circuit allows one to detect these events, particularly when the detector in question has already been triggered by a prompt low energy γ ray.

The CFD, pile-up, and gated latch circuits are packaged 4 to a unit. This unit then has front panel connectors for signal input, TDC output, pile-up output, and prompt CFD output. The back panel has a mother board which brings in the gated latch strobe and clear strobe and which takes the output of the gated latch circuits to the Gated Latch Interface module.

In order to simplify and reduce the number of interconnectors, a Strobe module, Clear module, and Gated Latch Interface module were constructed such that all communications with the 72 CFD circuits could be handled over the back mother-board bus. In addition, since many dedicated gating, clearing, and timing signals would be necessary, the modules were constructed in such a way that these signals were taken directly off the circuit boards into a cable bundle; front panel connectors were avoided as much as possible. This both simplifies the set-up and makes it less susceptible to problems of bad connectors or innovative physicists.

The Strobe module accepts a NIM-fast EVENT trigger signal and uses the front edge of this signal to generate gates for the ADCs, strobes for the TDCs, and strobes for the gated latches. It immediately generates a BUSY signal which can be cleared only by the Clear module. Since the data acquisition electronics depend on the integrity of the front edge of the input EVENT signal to the strobe module, this module does not allow the BUSY to go away or strobes to be generated during a subsequent EVENT trigger. Separate "gate/delay" generators are provided for the gated latches, the NaI-energy ADCs, the pile-up ADCs, the TDCs, user ADCs, and user TDCs. Thus the strobe module acts as a very compact fanout for the incoming EVENT trigger. A special feature of the user ADC strobe is that it will fail to appear if a clear pulse is provided before the end of the delay for this strobe. This permits slower or more complex ADC systems to remain unstrobed for events rejected during the user strobe delay time.

The Clear module accepts either TTL or NIM-fast inputs. It then generates clear strobes for all ADCs, TDCs, gated latches, and user systems. The width of the clear strobe is determined by an internal one-shot or by the width of the input clear pulse, whichever is longer. The internal width is set to about 1 μs, sufficiently wide that CAMAC ADCs and TDCs will have totally recovered and be ready for the next input. The Clear module also has a gated input. This particular input is ANDed with a "Wallace Tree" strobe (WTS), a strobe which is generated about 150 ns after the end of the strobe to the gated latches. The WTS is designed to appear after the Wallace Tree Adders have counted all of the active NaI detectors. Then, if the user desires to reject an event which has too few or too many active detectors, the WTS can be ANDed with any logic condition which requests a clear, such as an undesired multiplicity condition or other condition.

The Gated Latch Interface (GLI) module interfaces the full 72 gated latch bits from the CFDs to the CAMAC data acquisition system. These bits are grouped into 5 16-bit words -- the last word has as its top 8 bits the raw multiplicity from the Wallace Tree Adders. A 6th word gives the acquisition system access to a 16 bit Users'

Gated Latch, a module integrated into the overall system and provided to make the inclusion of user electronics as convenient as possible. The GLI has three front panel dials which allow the user to set conditions on the raw multiplicities from the 72 gated latch bits or on the 16 user gated latch bits. These conditions can be cabled to the Clear module in order to reject unwanted events.

The linear signals from the NaI detector tube bases are amplified by a factor of ten and are sent both to the CFD modules and to linear shaping circuits. These circuits passively shape the pulses so as to remove the long tail -- the shaped pulses are then delayed by about 240 ns, are attenuated by about 30, and are then input into LeCroy (2249) integrating ADCs. The energy resolution attained depends solely on the quality of the NaI detectors and averages about 6% for ^{60}Co. The shaping circuit allows integration times of less than a microsecond and minimizes any affect from time jitter of the input gate.

The data acquisition is controlled by the Event Handler, a device described elsewhere. For that part of the data acquisition involving just the Spin Spectrometer, the Event Handler checks the 72-bit gated latch pattern to find out which detectors were involved. Uninvolved detectors are ignored. It outputs an index appropriate to the detector it is then servicing, reads and transmits the energy ADC, the TDC, and the pile-up ADC. It then finds the next relevant detector and services it. At the end of this procedure, it checks to see if the computer is accepting new events. If so, it clears the acquisition system and waits for the next event. If not, it holds the acquisition system busy and waits for the computer to recover. It takes up to 300 µs to handle a typical event; of this time 100 µs is taken up by the conversion of the ADCs/TDCs. Event rates approaching 3 kHz have been achieved, though the typical high rate is usually less than 2 kHz. For high multiplicities, a 2 kHz rate implies a data rate of approximately 500 kBytes/s which is about the maximum rate that the CAMAC branch highway to the host computers can handle. Typical experiments may write as many as 2 to 6 tapes per hour of beam-on-target time.

---

1. D.G. Sarantites et al., Journal De Physique, Colloque C10, Supplement au n° 12, 41, C10-269 (1980).

2. M. Jääskeläinen et al., Nucl. Instrum. Methods 204, 385 (1983).

DATA ACQUISITION SUPPORT ELECTRONICS

D. C. Hensley

Pace Interface

The PACE based ADC system has been a powerful and useful component of the data acquisition hardware of the HHIRF. The system which is based on Tennelec stretchers and ADCs has served for many years in Tennecomp Data Acquisition systems, dedicated PDP-11 based systems. As the data acquisition has moved to the Perkin-Elmer computers, the PACE system has become somewhat less useful. For this reason, a CAMAC interface to the PACE was developed which allows it to be used in the HHIRF CAMAC based data acquisition system.

The interface accepts directly the output of the PACE controller and provides the necessary handshaking signals. The ADC outputs are memory mapped into a 16 word file register which are then available over the CAMAC dataway. Special error correction logic has been built into the interface to overcome bugs which have infested the PACE controller from day one. Sequencing problems are fully corrected, and special CAMAC "hooks" have been included such that other problems can be recognized and attended to.

A special feature of the implementation is that the PACE data may now be interrogated randomly. That is, the ADC values may be read out in any order and any number of times. This is especially useful to Event Handler driven data acquisition where acceptance criteria are placed on one or more of the ADC values.

The unusual and rather unique feature of the PACE system which allows it to handle a mixture of singles and coincidence inputs has been preserved. Separate CAMAC ports allow one to service these two acquisition modes independently. A 2 deep FIFO on the singles port helps to avoid data being lost by the host handler.

Some of the CAMAC functions for the interface are listed below.

F(0) A(0-15)	read coincidence ADCs
F(2) A(0)	read singles ADC
F(10) A(0)	clear coincidence LAM
F(10) A(1)	clear single LAM

The PACE system has now been used in a number of CAMAC linked experiments, either as the sole digitizing device or as simply a part of the overall system.

Cassette Tape Mass Storage System

A cassette tape system from 3M company has been assembled in order to provide a new and flexible method for data logging of large quantities of data or large numbers of files.

The device consists of a formatter and 2 cassette tape drives; a CAMAC interface is under development. The system allows one to write up to 67 MBytes on a formatted, 600 foot, 1/4 inch cassette tape at an average speed of 37 kBytes/s. The capacity compares favorably with that of our 6250 BPI tape drives which achieve some 120 MBytes per reel. The speed is only 1/20 of the 700 kBytes/s capability of the larger tape drives.

In addition to its mass storage capability, the cassette system can be used for random access, because it uses a formatted medium. Unlike a standard tape system, the cassette system allows one to position anywhere readily and to update or replace existing records. Average latency of 40 seconds, while not competitive with disks, does allow the device to be used as a file storage device for many large

files with easy access. In particular, a directory structure for the system is planned which should make file manipulation especially pleasant.

The planned CAMAC interface will allow the cassettes to be accessed both by the computer and by the Event Handler. This will allow the data acquisition stream to be spooled directly to the cassette. Since the system is small and portable, the experimenter will be able to have local tape storage, if he so desires. If an experiment producing some 10 bytes per event is assumed, maximum event rates of 3.7 kHz could be accommodated.

Fast Countdown Module

One of the capabilities desired in many experiments is the ability to countdown (scale-down) some particular counting rate. For example, one may wish merely to sample the elastic scattering but not have this sampling dominate the counting rate. Most commercially available countdown modules accept a slow logic signal and produce an output pulse when the countdown is satisfied. Generally the appearance of this countdown-pulse is too slow to be useful in normal data acquisition -- the analog pulses of interest have disappeared before one knows that they are to be analyzed.

For this reason, a fast countdown module was developed which introduces a nominal fast-logic delay of 15 ns or less. This allows a possible acquisition gating signal to be counted down while allowing the result to be available essentially without delay. This minimal delay time is essential for allowing one to mix this logic directly in with any other event-trigger logic.

The box has a built in deadtime of approximately 400 ns, to accommodate the TTL countdown circuitry and allows countdowns by 2**N, where N is set via a front panel dial to be from 0 to 15. Thus countdowns from 1 to 32768 may be used.

The output, when present, follows the input; that is, a 30 ns wide logic pulse will be 30 ns on the output, but with an overall delay of about 15 ns. A front panel LED indicates when the unit is at a count down stage.

PREPARATION OF TARGETS AND DETECTOR WINDOWS FOR NUCLEAR PHYSICS RESEARCH

D.M. Galbraith F.K. McCowan

The SPUTTERBELL (focused ion beam sputtering system) has been used in the preparation of a number of targets for nuclear physics research. Focused ion beam sputtering differs from thermal deposition methods in several fundamental ways: The deposition of target atoms does not depend on the vapor pressure of the target material; it is a high vacuum process; it is very economical of bulk material; and it is a "cool" process in the sense that substrate heating during deposition is negligible and sputtering source heating can be controlled.

A list of targets prepared by the sputtering method are given in Table 2.19. The sputter samples of $^{182-186}W$ were prepared by sintering metallic powders at room temperature under a pressure of 5 tons/cm^2. The tungsten targets used in an experiment with the recoil mass spectrometer were first analyzed with backscattered 2-MeV ^4He ions from a 2-MV Van de Graaff accelerator. They were found to be uniform to better than 2% over an area comparable to that of the 1- to 2-mm-diameter beam from the HHIRF tandem.

To produce self-supporting foils of ^{238}U, it is absolutely essential to pre-etch the ^{238}U sample by sputtering to remove surface oxides of uranium before collecting the incoming ^{238}U atoms on the substrate. Otherwise, the sputtered oxides of uranium react by chemical adsorption with the NaCl release agent. It appears that this reaction leads to compounds which are soluble in H_2O during the release step from the substrate. As a result, the ^{238}U foils are not free of holes. But, with the pre-etch step, the ^{238}U foils are free of pinholes and oxides.

In principle, the focused ion beam sputtering system should be useful in making self-supporting targets of many elements. We have found, however, that release or parting agents commonly used in the evaporation method are not successful in the sputtering method. For many elements, the release agents BaCl and NaCl provide no perceptible release action at all.

Table 2.19 also contains examples of targets prepared by the evaporation method. In addition, ten targets each of ^{197}Au, ^{181}Ta, In, Zr, and Cu, with thickness 80-100 µg/cm^2 on 30 µg/cm^2 C backing, were prepared for the heavy-ion applications group in the study of ion-induced x ray and x-ray satellite spectroscopy. Many productions of detector windows and planes for avalanche counters were also done.

INSTALLATION AND CALIBRATION OF RECOIL MASS SEPARATOR

H. J. Kim J. W. Johnson
S. G. Steadman[1] R. W. Miles
R. P. Cumby

The recoil mass separator (RMS), which was designed by H. Enge, was completed early spring of 1982 at Massachusetts Institute of Technology and shipped to the Holifield facility. It was assembled under the combined supervision of S. Steadman from MIT and H. J. Kim of the Holifield facility, and was installed on a new beam line from the 25 MV tandem accelerator. The major elements of the RMS are illustrated in Fig. 2.145. The device allows selective detection of recoil nuclei up to an energy of E_L = 8.4 MeV/q, where q is the ionic charge of the recoil nuclei, at angles near to and 0° relative to the incident beam. Recoil nuclei with greater E_L/q can be accommodated by having a smaller deflection angle through the device.

Trajectories of incident beam particles and recoil nuclei in a typical fusion experiment ($^{48}Ca + ^{197}Au \rightarrow ^{245}Es$ at E_L = 209 MeV) are shown in Fig. 2.146. Trajectories of recoiling fusion products having velocity Vo are folded out in

TABLE 2.19. TARGETS AND DETECTOR WINDOWS FOR NUCLEAR PHYSICS RESEARCH.

Element	Weight	Backing	Method	Remarks
Si	0.2-1.3 mg/cm^2	None	Sputtering	Cr plated steel substrate; 30 ug/cm^2 NaCl release agent
Ru	425 ug/cm^2	None	Sputtering	Glass substrate; 100 ug/cm^2 NaCl release agent
^{165}Ho	55 ug/cm^2	30 ug/cm^2 C	Sputtering	
^{182}W	50-90 ug/cm^2	30 ug/cm^2 C	Sputtering	Recoil mass spectrometer
^{184}W	50-80 ug/cm^2	30 ug/cm^2 C	Sputtering	Recoil mass spectrometer
^{186}W	50-80 ug/cm^2	30 ug/cm^2 C	Sputtering	Recoil mass spectrometer
^{238}U	0.7-2.65 mg/cm^2	None	Sputtering	Glass substrate; 100 ug/cm^2 NaCl release agent
Ca		1.5 mg/cm^2 Fe	Evaporation	Transient magnetic field for magnetic moment measurements
$^{170}Er_2O_3$	200 ug/cm^2	20 ug/cm^2 C	Evaporation Electron gun	
Pb	30 mg/cm^2	2.5 um Ni	Evaporation Mo boat	Stopper for recoil distance device
Pb	13 mg/cm^2	1 mg/cm^2 ^{98}Mo	Evaporation Mo boat	Pb-backed target for γ-ray spectroscopy of ^{150}Yb
^{208}Pb	0.47-2.0 mg/cm^2	None	Evaporation Mo boat	Glass substrate dipped in solution 50% polystyrene Q-dope and 50% toluene release agent; foils parted after being in toluene for several hours and are free of oxidation
^{27}Al	15 ug/cm^2	Stretched Polypropylene	Evaporation W filament	Large detector windows
^{27}Al	15 ug/cm^2	Stretched Polypropylene	Evaporation W filament	Anode and cathode planes for large parallel-plate avalanche counters

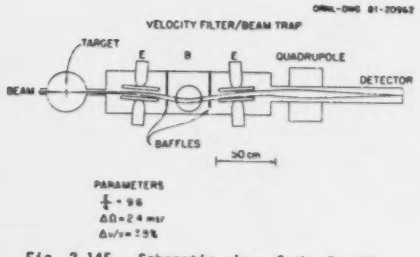

Fig. 2.145. Schematic view of the Recoil Mass Separator.

this figure such that they are shown as straight lines. The main beam and beam "tail" particle having V-Vo are trapped on the second baffle, as shown and the elastic scattered particles having $E_L'/q' = E_L/q$ are trapped on the third baffle in this illustration.

Following the installation a series of calibration runs was performed to determine the intrinsic solid angle, velocity response, charge-state response, and scale factors for setting the E and B fields. The measured solid angle, responses, and scale factors are in good accord with the expected results based on the design specifications.[2]

The first experiment incorporating the routine use of Recoil Mass Separator (RMS) was successfully performed in the last week of July

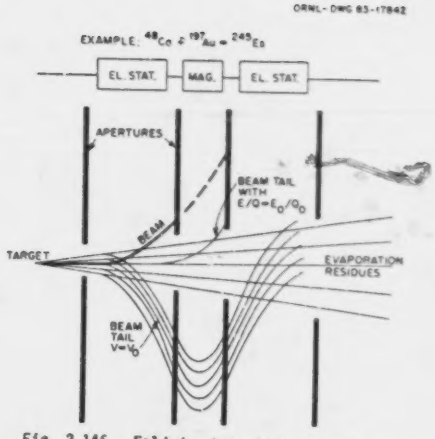

Fig. 2.146. Folded out trajectories for a typical fusion reaction.

1983. For the inaugural experiment, we chose to study the fusion of ^{16}O projectiles with $^{182,184,186}W$ targets well below, near, and above the Coulomb barrier.[3] Zero-degree excitation functions, angle, velocity, and charge-state dependences of fusion-evaporation residues were studied for the incident energy range 68-120 MeV. The low-energy residues ($E \approx 0.08\ E_L$) were completely separated from the incident beam and other reaction products by the RMS and were counted by a Si surface barrier detector. The various E and B field settings of the RMS required for these low-energy heavy residues scaled exactly as q/E_L for electrostatic (E) and q/mv for magnetic (B) settings which allowed the rapid initialization of the RMS using the calibration constants based on off-line measurements with α-sources. Furthermore, this adherence to the scaling laws allowed the determination of relative excitation functions to be a very simple and beam-time efficient procedure (the acquisition times for the bulk of data were about 200s/datum with ~5 pnA incident ^{16}O beam on ~50 ugr/cm^2 targets). The RMS operated easily and reliably throughout the experiment amply demonstrating that the separation of evaporation residues is indeed a very appropriate application of the RMS.

Implementing a microprocessor based control and monitoring of all power supplies and a large area gas filled start detector are nearly complete, and a new set of electrostatic deflector plates, which should improve the performance of the RMS, will be installed in the fall of 1983.

1. Massachusetts Institute of Technology.
2. H. A. Enge, DOE/ER/10767-1, Agreement No. DE-AC02-80ER10767.M001, 1982.
3. This activity is described elsewhere in this report.

THE HELIUM-JET COUPLED MASS SEPARATOR PROJECT

D.M. Moltz[1] K.S. Toth

In the previous Physics Division Progress Report[2] we discussed the desirability of constructing a helium-jet system and coupling it to an ion source operable with the UNISOR isotope separator. While the premises behind such a coupling are based upon rather straightforward ideas (see e.g. Ref. 3) various problems, as in most projects, have arisen that have slowed things down. Nevertheless, significant progress has been made during the past two years.

The helium-jet system has now been assembled and tested. The unique design[3] of a pressure chamber within a vacuum vessel permits effective operating temperature variation to be made independent of surrounding environmental conditions. Both the two- and four-target systems have been found to meet or exceed expectations. Published results[4,5] now exist which demonstrate the versatility and utility of this helium-jet system. A new window arrangement has recently been installed to eliminate much of the drift helium volume which caused severe energy losses for ions such as ^{32}S and ^{35}Cl.

A more serious redesign has occurred with the ion source. A planned change in the hollow-cathode ion source to eliminate all high-temperature insulators, was hastened by the quick (< 3 h) demise of several boron nitride insulators by a coating of a molybdenum-boron-nitrogen compound that becomes conducting at temperatures above 1700 C. Figure 2.147 depicts the hollow-cathode ion source; it has not yet been tested, but only a few minor adjustments are anticipated. Additionally, Fig. 2.147 shows a rudimentary Bernas source which could well be the best ion source for coupling the helium-jet to a mass separator. Unfortunately, a major

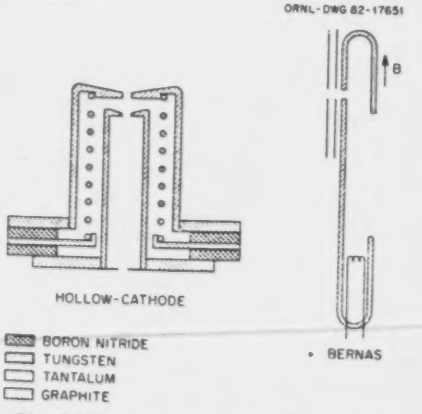

Fig. 2.147.- Schematic diagram of new hollow-cathode and Bernas type ion sources.

redesign of the UNISOR separator may be required to accommodate this source.

The most radical change in the entire system has occurred with the high voltage stepdown system. Originally, in order to conserve funds, a simple system was designed to slip inside the main pumping tube. After much work it was discovered that it was not feasible to place the resistance chain within the vacuum chamber. After studying designs in Jyväskylä[6] and Chalk River,[7] a hybrid system was constructed. The design and normal operating characteristics are shown in Fig. 2.148. Although five sections are adequate to stepdown the 50-kV operating potential, eight sections are normally used with the remaining sections not connected. The reverse bias voltage has been optimized for this particular arrangement and grid spacing. A 50% mixture of neon and helium has also been successfully run with flow rates in the 15 Torr-ℓ/s range.

Full testing of the complete coupled helium-jet separator system with accelerator-produced radioactivity is imminent.

---

1. University of South Carolina, Columbia, SC.
2. Phys. Div. Annu. Prog. Rep. June 1981, ORNL-5787, pp. 149-151.
3. D.M. Moltz, Nucl. Instrum. Meth. 186, 135 (1981).
4. D.M. Moltz et al., Phys. Rev. C26, 1316 (1982).
5. K.S. Toth et al., Phys. Lett. 117B, 11 (1982).
6. J. Äystö, private communication.
7. H. Schmeing, private communication.

ORNL-DWG 83 11870

HIGH VOLTAGE STEPDOWN SYSTEM

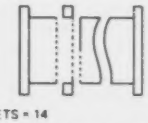

NUMBER OF GRID SETS = 14

THREE GRIDS/SET FIRST TWO GRIDS WITH 4 WIRES/cm
LAST GRID WITH 8 WIRES/cm

MAIN GRID SPACING = 8 mm

REVERSE BIAS GRID SPACING = 6 mm

MAIN RESISTANCE = 320 M Ω

REVERSE BIAS RESISTANCE = 4.7 MΩ

NUMBER OF SECTIONS	BREAKDOWN VOLTAGE (kV) UNDER NORMAL CONDITIONS (HELIUM FLOW RATE = 15–20 Torr-ℓ/s)
2	23
3	32
4	40
5	53
6	62
7	69

Fig. 2.148. Design and operation of the high voltage stepdown system.

BACKGROUND SUBTRACTION METHODS FOR γ-RAY ENERGY-ENERGY CORRELATIONS SPECTRA

Y. Schutz[1]

The study of the unresolved continuum γ rays emitted in heavy-ion-induced fusion reactions is a unique way to investigate nuclear structure in the region with spins as high as 60 ħ and with excitation energy 10 MeV above the yrast line. The γ-ray energy-energy corelations technique introduced[2] a few years ago enables us to characterize the properties of the γ cascades building up the γ-ray continuum. In a E_{γ_1}-E_{γ_2} correlations map, a rotational band will show up as a valley-like structure along the diagonal $E_{\gamma_1} = E_{\gamma_2}$. The width of this valley is directly related to the moment of inertia. A major problem is that the characteristic structure, which is built from photopeak-photopeak coincidences, represents less than 1.5% of the total number of coincidences for a Ge(Li) detector with a peak-to-total ratio of 0.12.

Several methods to suppress or reduce the uncorrelated background have been proposed. The aim of this work is to compare the performance of the existing subtraction methods. As a test case, the various methods were applied to a Monte-Carlo simulated deexcitation spectrum of ^{152}Dy. We used the code GAMBLE[3] and the results of a cranked Wood-Saxon calculation[4] which indicates the coexistence of a triaxial and a superdeformed shape above the yrast line at spins higher than 50 ħ. This calculation reproduces the experimentally observed[5] intensities of the discrete lines in a ^{32}S induced reaction. Figure 2.149a shows the result of the simulation when only photopeak events are considered, whereas Fig. 2.149b includes the response function of a Ge(Li) detector.

The most obvious method is to remove exactly the contribution of the Compton-scattered γ rays. This supposes the knowledge of the response function of the γ detectors in situ, which can be simulated by an analytical function whose parameters vary with the energy of the incoming γ rays. This method, by definition, does not modify the photopeak-photopeak correlation pattern and leads to the true intensities of the γ-ray transitions. Figure 2.150a shows the result of this procedure.

Two statistical methods have been proposed by the Copenhagen group. For both methods, one assumes that the probability P_{ij} to have a count in (i,j) is the probability P_i to have a count in column i times the probability P_j to have a count in raw j. In the so-called "first Copenhagen Method",[2] one calculates the deviation from P_{ij} normalized to the total number of counts. In order to avoid handling low and high statistics regions together, we treat the spectrum of Fig. 2.149b in three steps, considering three different regions of the spectrum. The result is shown in Fig. 2.150b. Whereas the valley-like structure and especially the second ridge due to the triaxial deformation are drastically enhanced, one cannot recognize the structure (stripes) of Fig. 2.149a.

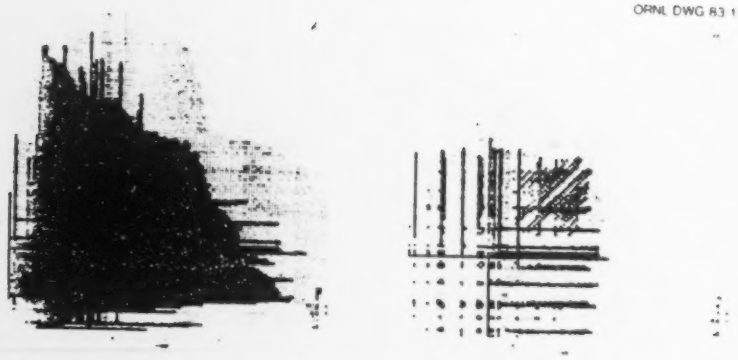

Fig. 2.149. E_γ-E_γ correlations spectra for the deexcitation of ^{152}Dy simulated by the program GAMBLE.
(a) photopeaks only
(b) true response function of a Ge(Li) detector

The Copenhagen group has recently proposed[5] a more sophisticated method, the so-called "Maximum Matrix Method". This method assumes that the uncorrelated background is a matrix M_{ij} whose elements are equal to $P_i \times P_j$. This matrix will have a zero determinant, and all the terms of the determinant will be equal but with alternate signs. The addition of correlated events will give rise to a number of terms with much larger value than the average. One can then, using these properties, evaluate statistically the background to be removed. The result of this procedure is shown in Fig. 2.150c. The overall structure of the original spectrum is reproduced, together with the relative intensities of the discrete lines. Since this method requires a lot of computer time, we have sought a simplified version. Because no correlated events are expected along the diagonal (except in the case of a relatively sharp band crossing), one can calculate the background by considering only the events on or in the vicinity of the diagonal. The result of this procedure, which is comparable in time to the first Copenhagen method, is shown in Fig. 2.150d. No major differences from the Maximum Matrix Method are observed.

In conclusion, whereas the real subtraction of the Compton events gives the most accurate result, the first Copenhagen method and the simplified version of the Maximum Matrix Method give quickly an idea of the correlation pattern. The latest method has, in addition, the enormous advantage of preserving the relative intensities.

---

1. On leave from CRN, Strasbourg, France.
2. O. Andersen et al., Phys. Rev. Lett. 43, 687 (1979).
3. G. Leander, Physica Scripta 34, 164 (1981).
4. Y. Schutz et al., Phys. Rev. Lett. 48, 1534 (1982); Y. Schutz, Thèse de Doctorat d'Etat, not published.
5. B. Herskind, private communication.

A COMPUTER PROGRAM FOR ANALYZING RECOIL-DISTANCE LIFETIME DATA[1]

J.C. Wells[2] M.P. Fewell
N.R. Johnson

The program LIFETIME has been developed to extract lifetimes of nuclear levels from Doppler-shift recoil-distance experiments by performing a least-squares fit to the experimental data (shifted and unshifted photopeak intensities). Initial populations of levels and transition rates for transitions between levels are treated as variable parameters. In terms of these parameters, the population of each level as a function of time is calculated by the Bateman equations using an algorithm by H. Emling[3] and, from these, the calculated values of the shifted and unshifted intensities are obtained. The shifted and unshifted intensities are fitted separately rather than in the form of the ratio of unshifted-to-total intensity, as is usually done. This often makes it possible to include data where one of the peaks is masked by an impurity.

A number of corrections to the data are incorporated in the program. These include (a) the change in solid angle as a function of position along the flight path, (b) the relativistic dependence of solid angle on velocity, (c) modifications of the intensities to account for effects of the Doppler-broadened line shape of the unshifted peak occurring as a result of the finite slowing down time in the stopper, and (d) the change in angular distribution due to the

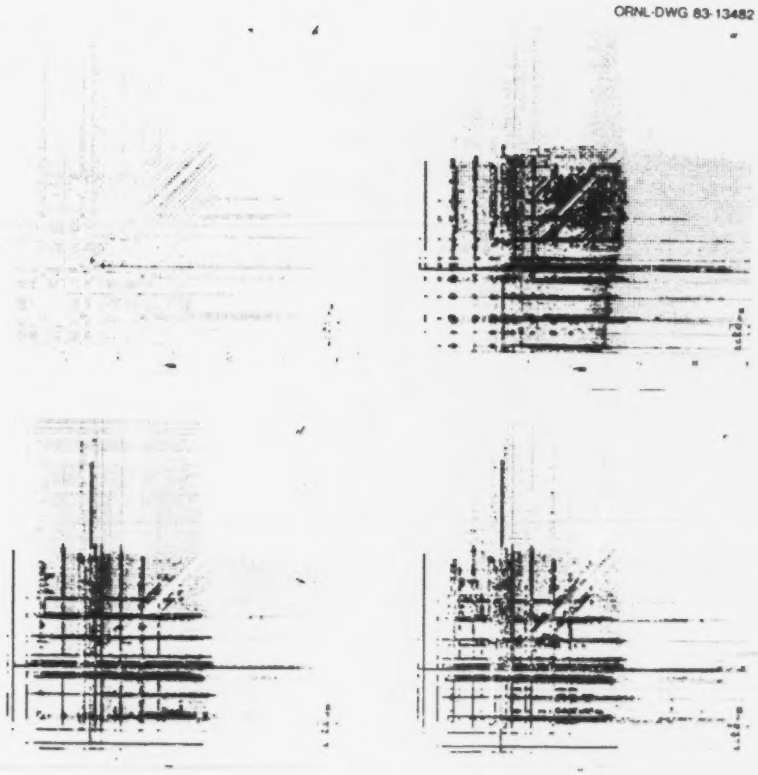

Fig. 2.150. Spectrum obtained after background subtraction from Fig. 2.148b.
(a) unfolding
(b) first Copenhagen Method
(c) Maximum Matrix Method
(d) simplified Maximum Matrix Method

loss of alignment caused by electronic hyperfine interactions during flight.

Since one generally does not know the side-feeding pattern to the levels of interest, it is possible to define additional levels in multi-step cascades from which feeding transitions occur. The initial population and transition rate of each of these feeder levels are also treated as variable parameters.

The least-squares fit is performed by the program MINUIT, developed by James and Roos.[4] It includes three minimization algorithms: (a) a Monte Carlo search, (b) the simplex method of Nelder and Mead,[5] and (c) a variable metric method of Fletcher.[6] It computes the covariance matrix and confidence intervals for the parameters.

LIFETIME is designed to be used interactively. Thus, from the terminal one can fix or free parameters, include or exclude data, recalculate corrections, and choose which minimization routine to use, while observing the progress of the fit. It includes an interrupt feature which allows one to check the progress of a fit without stopping it and to stop a particular fit without terminating the job.

LIFETIME can accommodate both experiments in which the recoil nucleus stops in the plunger and those in which it is slowed by a foil. It computes the stopping or slowing down time and calculates the recoil velocity from shifted and unshifted energies. It can include branching ratios as additional data and can handle

doublets or multiplets in the experimental data by summing the calculated intensities.

With overlays, LIFETIME uses 264 kilobytes of memory on the Perkin-Elmer 32/30 computer. It also has been adapted for use on the VAX 780 computer.

---

1. Summary of paper to be published.
2. Tennessee Technological University
3. H. Emling, private communication.
4. F. James and M. Roos, Computer Physics Communications 10, 343 (1975).
5. J. A. Nelder and R. Mead, Comput. J. 7, 308 (1965).
6. R. Fletcher, Comput. J. 13, 370 (1970).

INITIAL EXPERIENCE WITH THE VAX-AP COMPUTER SYSTEM

J. R. Beene K. T. R. Davies
K. A. Erb J. B. McGrory

The VAX-AP system, described elsewhere in this progress report, is used almost exclusively to carry out calculations and data analyses (other than primary acquisition and reduction) in support of theoretical and experimental physics programs. One of the prime motivations for acquisition of the system was to facilitate large scale time dependent Hartree-Fock (TDHF) studies of nuclear reactions. These codes have been successfully implemented on the AP. A carefully documented test case (see Chapter 5) was found to run, at the present state of development approximately 25% faster on the AP than on the CSD IBM-3033 computers at ORNL. A large number of other codes including standard nuclear physics statistical model codes, direct reaction codes, coupled channels codes, as well as many special purpose programs have been successfully implemented on either the VAX alone or the VAX-FPS system. In addition two standard high quality scientific numerical analysis libraries, several graphics libraries, the SPEAKEASY[1] program together with other software tools suited to our needs, have been installed on the system.

We view the first full year of operation of the VAX-FPS system as an unqualified success. The usage of the system of both the AP and the VAX alone, has risen steadily throughout the year thanks largely to the large body of relevant software available and to the reliable, easily used, program development tools on the VAX. Most significant however, is that the dual processor system gives the user an extremely powerful facility for carrying out large computation intensive calculations in an extremely cost effective way. Complex, exploratory calculations are now being undertaken which simply would not have been done previously.

---

1. Trademark of Speakeasy Computing Corporation, Chicago Illinois.

8.0 Texas A&M University Texas A&M Cyclotron

1. **What new science is being explored by this facility? What scientific opportunities are being exploited?**

Answer: At Texas A&M, new science is being explored experimentally in five areas and theoretically over an even broader range. In several experiments, the properties of the force which holds nuclei together is being explored. For example, one experiment investigates hadronic parity violation which should provide key information on how quark-quark interactions lead to the nuclear force. In essence, this experiment should provide a better understanding of how the force which holds the atomic nucleus together can be understood from the viewpoint of the unified theories of all matter developed in the last few years.

The general properties of nuclei, when they are subjected to extreme conditions, are being explored through studies of nucleus-nucleus collisions. Questions being explored include: How much excitation energy and angular momentum (spin) can a nucleus possess before it breaks up or disintegrates? The mechanisms operating in the disassembly of the nuclear system are being investigated, including the shapes and the types of motion through which the system evolves, and the possible occurrence of phase transitions. The entire range of de-excitation processes and correlations is utilized, including nucleon, alpha-particle and light fragment emission, fission, and gamma-ray decay. In these studies pion emission has been observed in reactions induced by 20 MeV/nucleon oxygen ions.

Two particular aspects of nuclear structure are being studied. New methods of studying the vibrations in nuclei known as "giant resonances" are being employed. These oscillations provide a sensitive test of theories of nuclear structure. A new reaction called "massive transfer", has been investigated to determine the structure of nuclei which are naturally highly deformed. This reaction is being used at Texas A&M to study nuclei previously inaccessible to studies of these kinds.

The properties of the atom, molecule, and associated electrons are being explored in several ways. The mechanisms for transfer of electrons between atoms are being explored by studies of collisions of high-speed ionized atoms from the cyclotron with stationary target atoms. Detailed investigations of electron binding in molecules are being carried out through studies of x-rays emitted when ion beams pass through a material.

Techniques are being developed to use cyclotron beams to perform analytical chemistry on trace contaminants in materials at extremely low concentrations. There are two present objectives: (1) detection of elements (from hydrogen to uranium) at the femtogram level; and (2) microscopic chemical analysis on submicron size spots.

In conjunction with the experimental program, the development of new approaches to explaining nuclear phenomena is underway. The implications and signatures for new states of nuclear matter (liquid-gas mixtures, quark matter) are being explored. The connections between the nuclear vibrations (giant resonances) and properties of nuclear matter are being studied and new types of calculations are relating these properties to the observed data. The properties of nuclear matter revealed by relativistic heavy ion collisions are also under theoretical investigation.

2. **How does this facility's accelerator (or accelerators) performance compare with any other in the world that are operating, under construction, or planned?**

Answer: Texas A&M has one accelerator in operation (K=155 cyclotron) and a second under construction (K=500 superconducting cyclotron), which is projected to be operational for experiments in 1986. The two accelerators will be coupled to produce higher energy beams of heavier nuclei. The ATLAS facility now under construction at Argonne National Laboratory will have more precision but lower energies. Internationally, GANIL in France will be more powerful. Facilities at Grenoble, France; Groningen, Netherlands and Osaka, Japan will be considerably less powerful.

The performance of the present Texas A&M cyclotron is in the mid to upper range of accelerators of light and heavy ions. The existing K=155 cyclotron is a versatile accelerator, producing both polarized and unpolarized beams of protons and deuterons, as well as heavy ion beams as heavy as argon for nuclear science experiments and as heavy as xenon for atomic experiments. Higher energy light ion beams are available only at Indiana University in the United States and at Saclay in France.

3. **What types of research instrumentation/experimental devices are available at this facility, and what are their capabilities?**

Answer: The laboratory has several high-resolution, high-efficiency germanium detectors, several x-ray detectors, many silicon particle detectors of different thicknesses, and a variety of electronics modules necessary at any nuclear facility. There are two general purpose scattering chambers and a number of smaller chambers designed for specific tasks. The laboratory also has a well-equipped machine shop and well-equipped electronic construction and repair shops.

Major pieces of research instrumentation:

1. Enge Split Pole Spectrograph - A magnetic spectrograph capable of bending any particle accelerated by the K=155 cyclotron, processing excellent energy resolution, a moderately large solid angle, and the capability for correcting for kinematic dispersion of reaction products. It is excellent for studies of nuclear structure and identification of nuclear species produced in two-body nuclear reactions. Several different detectors are available for the focal plane, allowing "live" particle identification for a variety of particles from protons to heavy ions.

2. Focal Plane Polarimeter - A polarimeter for the focal plane of the Enge spectrograph which allows measurement of the alignment of the spin of particles after nuclear reactions. This allows studies of spin transfer for discrete levels in the target nucleus.

3. Sixteen Segment Sodium Iodide Crystal - A segmented NaI(Tl) detector having a diameter of 21 inches and a length of 16 inches (active material) with 16 individual segments. It has a total efficiency for 1.3 MeV gamma rays of about 75%. It can be configured in a number of ways to study reaction mechanisms as well as nuclear spectroscopy. It has been used as a single, large, high solid-angle, highly efficient detector; as a multiplicity detector, and to supplement high resolution germanium detectors in other experiments.

4. Large Position Sensitive Ionization Chamber (GSI design) - An ionization chamber which allows simultaneous measurement of energy, position, and angle of emission of a wide range of heavy ion reaction products over a large solid angle. Elements up to and including uranium can be resolved. A powerful tool for the study of complex reactions providing sufficient information to deduce processes occurring in these complex reactions.

5. Superconducting Solenoid and Longitudinal Beam Polarizer - A solenoid, bending magnet, and sets of horizontal and vertical polarimeters capable of rotating a transversely polarized proton beam to a longitudinally polarized one. Designed for measuring parity violation in the hadronic weak interaction.

6. Two Digital Equipment Corporation VAX 11/780 Computers - One VAX provides a modern high-rate data acquisition system based on the CAMAC standard for use with cyclotron experiments. Events with up to 75 input parameters have been accepted, and acquisition rates of 50,000 words per second are practical. The second VAX serves as the general computational facility of the laboratory and is equipped with two tape drives, 700 megabytes of disk storage, 6 megabytes of memory, 4 graphics terminals, and 30 user terminals.

7. A Plane Crystal X-Ray Spectrometer; a 12.5 cm curved-crystal x-ray spectrometer; and a 1.0 m grazing-incidence xuv spectrometer. These x-ray detectors are all designed for in-beam use. The plane crystal spectrometer is unique in its rotation capability, which permits its use for angular distribution measurements.

4. What have been the facility's research highlights for the period FY 1981 - present, and what are anticipated for the remainder of FY 1984 and FY 1985?

Answer: Brief descriptions of highlights of the research programs for the period FY 1981 - FY 1983 are given below. It is difficult to predict what new discoveries will be made over the remainder of the period through FY 1985; however, some experiments which may lead to important results are mentioned.

In studies of the behavior of nuclei under extreme conditions, the production of pions has been observed, the existence of two different components of non equilibrium particle emission was established, and the limits to nucleus-nucleus fusion were determined in heavy ion reactions at 20 MeV/nucleon. Nuclei were found to deform under conditions of high angular momentum and the asymptotic limit in fragment momentum width was achieved at projectile velocities comparable to the Fermi velocity. Evidence for enhanced fragment spins and shell effects in heavy ion induced fission has been obtained from studies of the energy dependence of gamma ray multiplicities. A detailed picture of the magnitude and alignment of angular momentum transfer has been obtained for deep-inelastic reactions and this picture suggests that angular momentum fluctuations do not reach equilibrium even for the largest total energy losses. Measurements of gamma-ray multiplicities have shown that one can distinguish between transfer and fragmentation processes.

Studies of nuclear structure have revealed the systematic existence of the monopole resonance in nuclei as light as zirconium. This important nuclear vibration was also identified in zinc nuclei and, more recently, in silicon, where it occurs at an unexpectedly low energy. Experiments and accompanying theoretical calculations suggest that the apparent absence of the monopole resonance in lighter nuclei may be due to the use of incorrect models to predict its strength. This resonance was also found to be split into two resonances in nuclei with deformed ground states. The "massive transfer" reaction has been shown to be a new and promising tool for the study of nuclear structure in naturally deformed nuclei. Backbending in transitional rubidium nuclei has been shown through blocking experiments to be due to the neutrons. Heavy ion reactions previously thought to populate molecular resonances were shown to be due to breakup instead, destroying some of the evidence for so-called nuclear molecules.

In studies of the nuclear force, a measurement of parity violation in the hadronic weak interaction was obtained which yielded a result in agreement with present theories. This experiment continues with improvements in techniques and within the next year should improve the test of theory by a factor of five. The first test of isobarics mass multiplet equation in nuclei has been completed and the production of He-8 particles in reactions induced by Li-6 particles has been observed for the first time.

In studies of the interactions of ions with atoms and molecules, a new inter-atomic electron transfer mechanism (resonant transfer) has been discovered. Polarized x-ray emission from helium-like sulphur ions has been observed and the subshell cross section ratio determined for capture to the 2p level. A new grazing incidence spectrometer will be applied to the search for additional radiative interatomic electron transfers, which is likely to lead in the near future to the identification of a number of cases where this newly discovered mechanism occurs. Studies of the use of cyclotron beams for ultrasensitive chemical analysis demonstrated that hydrogen impurities can be identified at concentrations 100 times lower than with any other technique. Using heavy ion backscattering, the presence of 10^{10} atoms/cm^2 of gold diffused in silicon could be identified. The measurements of thickness variations as small as 50 angstroms on spots as small as 1 micrometer in diameter were accomplished through heavy ion absorptiometry. The feasibility of chemical analysis of 1 micrometer spots with a detection sensitivity of 10s atoms was demonstrated. By FY 1985, the development of a truly unique chemical microscopy and imaging capability with submicron spatial resolution is expected. Also, an ultratrace analysis procedure suitable for detection of as little as 10^5 to 10^7 atoms of any given element should be perfected in this time period.

In theoretical efforts, a prediction of the giant quadrupole resonance in uranium was the first true continuum calculation for a deformed nucleus. Predictions of yields of heavy nuclear fragments at cyclotron energies led to the deduction of properties of nuclear matter needed for understanding supernovae.

5. What facility changes and additions have occurred or are anticipated for the period FY 1981 - FY 1985?

Answer: In 1982, construction began on a new superconducting cyclotron having an energy constant nearly four times larger than the present cyclotron. A 7,000 square foot building addition has been constructed to house

the new cyclotron and to provide an additional experimental area. The construction of the new cyclotron and building addition was funded by Texas A&M University ($6,260,152), and the Robert A. Welch Foundation provided $1,000,000. First beam from the new cyclotron is expected in FY 1986.

When completed, the new cyclotron will be used both alone and as an injector for the existing cyclotron to provide very energetic beams of light ions such as heavy hydrogen (deuterium) and helium, light-heavy ions such as carbon, oxygen, and neon through medium-heavy ions (argon, copper, krypton). Heavier ions such as uranium will be available at energies sufficient to study nuclear reactions occurring when two uranium nuclei collide.

The new cyclotron has a superconducting main magnet coil which results in a very powerful but compact cyclotron. Low initial cost (due to small size and a relatively small amount of iron) and very low electricity consumption are major advantages of this type of cyclotron. The Texas A&M cyclotron would be the second such cyclotron in the United States, and one of five in the world.

The new building was completed in July 1983 and is now in use as a construction area for the new cyclotron. Many of the components for the new cyclotron are completed or nearly so. Of the major components, the iron yoke was delivered in July 1983 and the helium refrigerator in October 1983. The superconducting coil was finished in mid-March 1984 and testing of the entire superconducting magnet should begin this June.

6. **For the period FY 1981 - FY 1985, please provide actual and estimated budget profiles for operations, in-house research, out-of-house research, other operating expenses, Capital Equipment, General Plant Projects, In-House Energy Management, and any other specific construction projects attributable to the facility. Please indicate the source of these funds (i.e., Medium Energy Nuclear Physics, Heavy Ion Nuclear Physics, Low Energy Nuclear Physics, High Energy Physics, Basic Energy Sciences, etc.).**

Answer:

Texas A&M Cyclotron
(B/A in thousands of dollars)

	FY 1981	FY 1982	FY 1983	FY 1984	FY 1985
Operations					
Heavy Ion Nuclear Physics	$ 135	$ 150	$ 200	$ 225	$ 230
Low Energy Nuclear Physics	230	270	385	415	420
	$ 365	$ 420	$ 585	$ 640	$ 650
Research					
Heavy Ion Nuclear Physics	$ 195	$ 200	$ 150	$ 175	$ 160
Low Energy Nuclear Physics	230	270	265	265	240
Basic Energy Sci.	45	50	55	61	65
	$ 470	$ 520	$ 470	$ 501	$ 465

7. **How much funding for FY 1981 - FY 1985 has been or is expected to be provided by other federal agencies such as the National Science Foundation or by State agencies?**

Answer:

Texas A&M Cyclotron
(B/A in thousands of dollars)

	FY 1981	FY 1982	FY 1983	FY 1984	FY 1985
WELCH Foundation	$ 124	$ 144	$ 114	$ 157	$ 157
State of Texas	1,418	1,654	1,734	1,790	1,900
NSF Chemistry	73	76	112	94	102
NSF Theory	0	96	110	122	128

The Robert A. Welch Foundation is a private foundation that supports chemical research within the State of Texas. The State contribution includes payment of utilities for operation and an annual appropriation for partial support of facility operation.

8. **For the period FY 1981 - FY 1985, please provide actual and estimated staffing levels.**

Answer:

Operations and Administrative Staff
(Man Years)

	FY 1981	FY 1982	FY 1983	FY 1984	FY 1985
Operations	38	37	36*	35	37*
Administrative	4	4	4	4	4

* Includes staff constructing new cyclotron.

9. **What is the actual and estimated facility utilization for the period FY 1981 - FY 1985? What would be defined as "full" utilization of the facility?**

Answer: For the period FY 1981 - FY 1985, actual and estimated utilization of the Texas A&M Cyclotron is given in the following table:

Cyclotron Utilization

	FY 1981	FY 1982	FY 1983	FY 1984	FY 1985
Beam Hours for Research	3200*	6000	5500	5000	5000

* The facility was shut down for 6 months for a major overhaul in FY 1981. For the Texas A&M Cyclotron, we estimate full utilization to be 6000 beam hours for research.

10. **For the period FY 1981 - FY 1985, how many experiments will have been started, continued, and completed?**

Answer: The Texas A&M facility is a university laboratory where faculty, students, and staff carry out programs of research according to their interests. Much of the program, as at any university laboratory, is carried out by students working on thesis projects which, by their nature, require a relatively large amount of time to complete.

As there are no formal proposals to count for most experiments, the figures provided below were obtained by asking the individuals who use the facility to each tell how many experiments they have started, are continuing, or have completed using their own definition of just what constitutes an experiment.

Experiments Started:	160
Experiments Completed:	100
Experiments Continuing:	60

11. What is this facility's user policy?

Answer: The cyclotron facility at Texas A&M is not a national user facility but, rather, a university facility utilized largely by Texas A&M faculty and students. The facility, however, is available to other users on the basis of the scientific merit of their proposed work, and a formal procedure is in place to review such proposals. Proposals for facility use by non-Texas A&M scientists are encouraged. The facility, however, does not have available the support staff or equipment required to properly support large outside user experiments, so that outsiders coming to the facility typically attempt to arrange an inside collaboration to accommodate logistics problems. No scientific staff with the primary task of assisting these users is available.

12. For the period FY 1981 - FY 1985, how much reimbursable research has taken place or is estimated to take place? What revenues have been involved?

Answer: During the period FY 1981 - FY 1984, two outside groups used the facility and paid for the beam time. The total fee collected was $4,005; $1,055 in FY 1983 and $2,950 in FY 1981. For the balance of FY 1984 and for FY 1985 no reimbursable research is scheduled. It is possible that small uses, such as those above, will reoccur. The facility does not derive any substantial support from selling time or research services.

13. What is the mechanism by which specific research proposals for experiments at the facility are considered?

Answer: Proposals for the use of the facility are submitted to the Institute Director and must contain the scientific motivation, a short vita of each of the proposers, the resources (beam time, type and energy, electronics, detectors, etc.) required from the facility, and the usual safety and logistics information. Proposals are considered at any time. There are no formal calls for proposals or deadlines. The facility is scheduled on a monthly basis so a prospective user need not submit a proposal many months in advance, which can provide an advantage for some fast moving experiments.

The proposals are evaluated by the Institute Steering Committee (a committee of senior Institute researchers) with assistance from others outside the Institute as needed. About one proposal in four requires input from outside reviewers. The Steering Committee then makes a recommendation to the Institute Director of the scientific merit, the technical feasibility, and the amount of beam time (if any) that should be allocated for the proposed experiment. The Institute Director makes an appropriate allocation considering the overall demands on the facility and notifies the proposer of the allocation and provides information on scheduling.

14. How many research proposals have been submitted over the past five years, and how many of these have been approved?

Answer: Since 1979, there have been 17 proposals submitted for use of the Texas A&M facility by prospective outside users. Of the 17, 1 has been temporarily withdrawn, 1 has been permanently withdrawn, 1 has been turned down, and 3 users' runs are pending. One was cancelled due to a long term cyclotron problem (in 1979). The remainder have been carried out. Formal proposals for beam time use are not required of Cyclotron Institute staff, students, and faculty.

15. How many university personnel (i.e., faculty and students) have utilized the facility over the past five years?

Answer: The Texas A&M facility is a university laboratory, so most of the users are faculty, staff, and students at Texas A&M. The numbers of each who used the facility in the last five years are given below.

Faculty	24
Graduate Students	34
Undergraduate Students	55
University Research Staff	38

16. How many industrial researchers have utilized the facility over the past five years?

Answer: Three industrial researchers have used the facility in the last five years.

17. How many researchers from foreign institutions have utilized the facility over the past five years?

Answer: During the last 5 years, 35 foreign researchers have used the Texas A&M facility. These were individuals either at Texas A&M for a short visit or on leave from their institution for an extended period. A number of other foreign researchers have chosen to receive their postdoctoral training at the Texas A&M facility.

18. How many researchers from other agencies have utilized the facility over the past five years?

Answer: There have been two users from NASA and one from the Naval Research Laboratory in the last five years.

19. What are the future development possibilities for this facility (including research instrumentation/experimental devices), what plans are being made to exploit these possibilities, and what are the budgetary implications?

Answer: There are many potential future development possibilities for this accelerator facility, but there are currently no approved plans to undertake any of them beyond the activities identified in the FY 1985 budget request. New research instruments and experimental devices will be developed as the physics research program progresses. We intend to give high priority to the exploitation of the facility's unique capabilities.

20. Please provide a copy of the facility's latest annual report.

Answer: Attached is a copy of the latest annual report from the Cyclotron Institute, Texas A&M University: "Progress in Research: April 1, 1982 - March 31, 1983."

PROGRESS IN RESEARCH

April 1, 1982 - March 31, 1983

Prepared by

The Cyclotron Institute Staff

Texas A&M University

College Station, Texas 77843

July 1983

INTRODUCTION

This report contains descriptions of the activities of the research programs at the Institute and the progress on construction of the new cyclotron facility over the past year. In the period April 1, 1982 to March 31, 1983 the cyclotron provided beam for experiments, beam tuning, and beam development a total of 6633 hours or 76% of the available calender hours. Research programs in nuclear science scheduled 78% of the time, with atomic physics and activation analysis programs scheduling 11% each and the balance going primarily to beam development.

A wide variety of both experimental and theoretical programs were underway and brief descriptions of recent progress in some areas of current interest are given below.

1. The first measurement of parity violation in the H(p,p) reaction has been completed at Ep = 47 MeV; the result including statistical and measured systematic errors is $(-4.6 \pm 2.6) \times 10^{-7}$.

2. Measurements of the vector and tensor analyzing powers $A_y(18°)$, $A_{yy}(18°)$, and A_{zz} (0°) for the $^2H(d,n)^3He$, $^2H(d,n)X$ and $^1H(d,n)2p$ reactions at E_d = 46 MeV have shown that while these parameters are generally quite small, $A_{yy}(18°) = 0.54 \pm 0.07$ for the first reaction.

3. The giant monopole resonance has been identified in ^{28}Si at $E_x = 55/A^{1/3}$ MeV by small angle inelastic alpha scattering measurements where approximately 60% of the E0 energy weighted sum rule has been located at approximately 18 MeV. This contrasts to heavier nuclei where the GMR is at about $80/A^{1/3}$ MeV.

4. Further evidence for the proton character of levels causing second backbending in the Yb region has been obtained through the use of in-beam spectroscopy combined with a total multiplicity filter.

5. Measurements of the energy spectra of H and He isotopes from the fragmentation of 320 MeV ^{10}B projectiles in the system $^{10}B + ^{181}Ta$ lead to low momentum widths (σ_0 = 54 MeV/c) suggesting a rapid transition in momentum width between 32 and 43 MeV/nucleon.

6. Evidence for enhanced fragment spins and shell effects in heavy-ion induced fission have been obtained from studies of the energy dependence of gamma ray multiplicities.

7. High resolution fluorine x-ray spectra of ionic solids excited by 80 MeV Ar ions have provided evidence of rapid electron transfer from the outer levels of surrounding atoms to energy matched high n states of highly ionized fluorine target atoms.

8. In theoretical efforts, the transition from fusion and deep inelastic reactions at low energies to spectator/participant and fireball pictures at high energies has been clarified in relation to nuclear matter properties, with predictions of a multifragmentation region in between. Additionally the study of short-lived nuclear fragments in high-energy heavy-ion collisions via pionic atom formation is shown to be feasible.

The research programs at the Institute during this period were funded by the Department of Energy under Contracts DE-AS05-80ER10565 (nuclear) and DE-AS05-78ER06036 (atomic); by the National Science Foundation under grants PHY-8109019 (theory) and CHE-7927157 (activation analysis); and by the Robert A. Welch Foundation under grants A-330, A-355, A-558, and A-692. Operation of the facility is also supported by the university.

Much progress has occurred in construction of the new cyclotron facility. The building addition has been completed, the magnet yoke, superconductor, bobbin and helium compressor have been delivered and the trim coils fabricated. The coil tank and pole tips are nearing completion. We are awaiting our turn on the winding equipment at Michigan State University, where our magnet will be wound following completion of the MSU K800 magnet. The new facility, which will provide light ions to 80 MeV/nucleon, heavy ions for A<20 to 60 MeV/nucleon, heavy ions for 20<A<40 to 37 MeV/ nucleon and up to 8 MeV/nucleon for heavy beams, is scheduled for initial operation in 1986.

An annual report such as this will contain some preliminary data or speculative conclusions; these provide a general picture of the current research program. Until the research is published, however, we request that work described in this report not be cited in the literature without the express consent of the investigators.

Comments about the work described in this report or about our programs in general are welcome. While we have only limited facilities to assist outside users, we invite inquiries about use of the cyclotron.

D. H. Youngblood

NUCLEAR STRUCTURE

Backbending

Cluster Transfer

Giant Resonances

IN-BEAM γ-RAY SPECTROSCOPY FOLLOWING MASSIVE TRANSFER REACTIONS; BACKBENDING AND BLOCKING AROUND ^{102}Ru

D. R. Haenni, H. Dejbakhsh, R. P. Schmitt, and G. Mouchaty

A major effort of the γ-ray spectroscopy program has been to develop techniques for in-beam γ-ray spectroscopy following the so called "massive transfer" reactions. Some of the benefits which accrue from the use of massive transfer reactions include exit channel selectivity, preferential populations of high-spin states, and in some cases the ability to obtain the equivalent of reactions induced by exotic neturon rich beams.

As an initial test of these features, massive transfer reactions induced by ^{7}Li beams on ^{100}Mo have been studied. The ^{7}Li beam provides the equivalent of ^{3}H and ^{6}He beams through (^{7}Li,pxn) and (^{7}Li,αxn) reactions. The residual products from these reactions lie on the edge of the region of deformation centered around N = 66 and Z = 39. Our knowledge of high-spin states in these neutron rich nuclei is somewhat limited particularly since they are not readily accessible with accelerator based in-beam γ-ray spectroscopy. Through the observation of transitional nuclei surrounding this region perhaps some insight can be gleaned into any special characteristics of these deformed nuclei.

Experimentally, a self-supporting ^{100}Mo foil was irradiated with a beam of 45 MeV ^{7}Li. High resolution Ge(Li) detectors were used to observe γ-rays in coincidence with energetic forward peaked p,d,t,α, and ^{6}He ejectiles at 20° in the laboratory. Details of the experimental apaparatus and discussions of product selectivity, population of high-spin states, and production of residual nuclei at low excitation energy can be found elsewhere.[1,2]

Results from the analysis of the γ-γ coincidence data will be presented here. The processing of these data are in some respects similar to that for the study of ^{161}Yb using the total energy crystal as a filter (p. 5). The γ-γ coincidence events are separated on the basis of type and energy of the associated light particle. Data from two measurements were combined through the construction of 7 symmetrized matrices which maximized the yields of ^{101,102,103,104}Ru and ^{101,102,103}Tc, respectively. Coincidence spectra were then extracted for all observable peaks in the projection of each matrix.

Partial level schemes for ^{102,103,104}Ru and ^{101,102,103}Tc deduced from these coincidence spectra are presented in Fig. 1. The results from gates on transitions in ^{101}Ru confirmed but

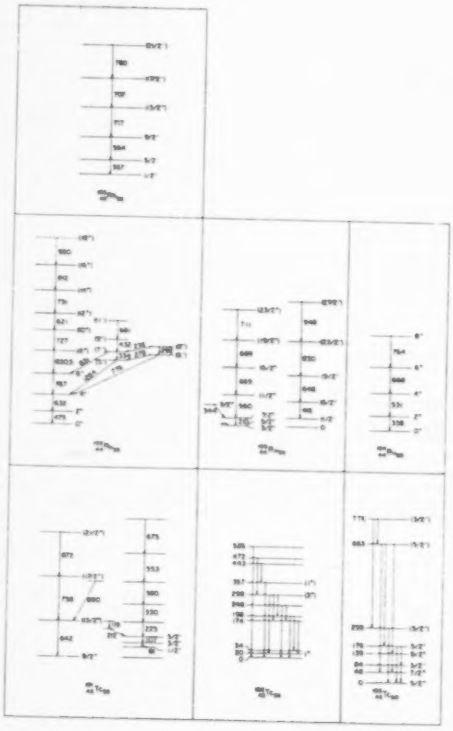

Fig. 1. Partial level schemes for ^{102,103,104}Ru and ^{101,102,103}Tc from in-beam spectroscopy following massive transfer reactions. The scheme for ^{103}Rh is from the (^{7}Li, 4nγ) reactions.

could not extend the results reported by Klamra et al.[3] The ground state band in ^{104}Ru has also been observed up to the 8^{+} level in recent Coulomb excitation studies.[4] The level schemes for ^{102,103}Tc represent the first in-beam γ-ray data for these isotopes and agree with previous particle spectroscopy results.[5,6] In Fig. 2, summed coincidence spectra are presented for the 9/2^{+} band in ^{101}Tc and the 11/2^{-} band in ^{103}Ru.

One of the interesting features of these level schemes is the backbend in the yrast cascade in ^{102}Ru. Having observed the backbend, the next

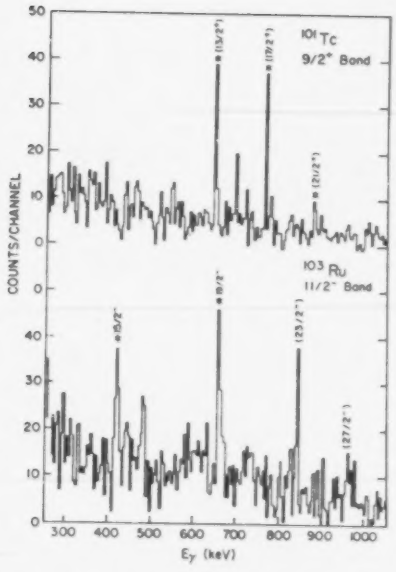

Fig. 2. Summed coincidence spectra for the band built on the 9/2$^+$ level in ^{101}Tc and the 11/2$^-$ level in ^{103}Ru. Gated transitions are indicated with an (*).

problem is to determine which particles are aligning. Experimentally this can be accomplished through "blocking" arguments. Essentially, one observes the effect on the backbending of the core as one blocks various orbitals by placing an odd nucleon in them. This is accomplished through the study of the odd A neighbors of the backbending nucleus. With data collected simultaneously with that for ^{102}Ru, three of its odd A neighbors, ^{101}Tc, ^{101,103}Ru can be observed. In addition, from (^{7}Li,xn) data collected during a portion of the massive transfer experiments a band based on the ground state of ^{103}Rh has been identified and included in Fig. 1.

The backbending and blocking information for these nuclei is summarized in Fig. 3 in terms of alignment vs. rotational frequency plots. Bands based on 7/2$^+$ states in ^{101}Ru and ^{103}Ru and a band based on the 1/2$^-$ ground state of ^{103}Rh upbend or backbend at about the same frequency as ^{102}Ru. However, bands built on 11/2$^-$ states in ^{101,103}Ru are not observed to backbend at this frequency. One can conclude from Fig. 3 that the backbend in ^{102}Ru is a result of the alignment of a pair of $h_{11/2}$ neutrons. Furthermore, this provides evidence that the $h_{11/2}$ neutrons play a role in this deformed region, similar to that of the $i_{13/2}$ neutrons in the deformed rare earths.

Preliminary results[7] from cranked shell model[8] calculations also indicate that the $h_{11/2}$ neutrons are responsible for the backbend in ^{102}Ru. More calculations, however, are required before a detailed comparison of the data and model predictions can be made.

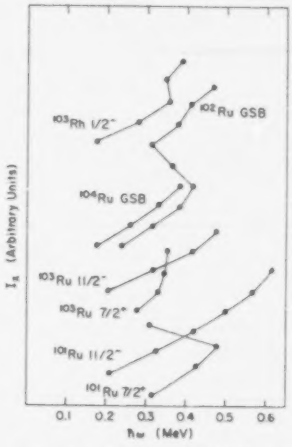

Fig. 3. Alignment (In) vs. rotational frequency ($\hbar\omega$) plots for bands in ^{101,102,103}Ru, ^{101}Tc, and ^{103}Rh. The data for ^{101}Ru is from Ref. 3.

References

[1]D. R. Haenni, T. T. Sugihara, R. P. Schmitt, G. Mouchaty, and U. Garg, Phys. Rev. C 25, 1699 (1982).

[2]D. R. Haenni, P. Bogucki, U. Garg, G. Mouchaty, R. P. Schmitt, and T. T. Sugihara, Progress in Research 1981-1982, Cyclotron Institute, Texas A&M University, pp. 12-16.

[3]W. Klamra, K. Fransson, B. Sundstrom, M. Branner, S. Engman, and R. Kuarnstrom, Nucl. Phys. A376, 463 (1982.)

[4]J. Stachel, W. Kaffrell, E. Grosse, H. Emling, H. Folger, R. Kulessa, and D. Schwalm, Nucl. Phys. A383, 429 (1982).

[5]P. DeGelde, D. DeFrenne, E. Jacobs, K. Heyde, S. Fortier, J. M. Maison, M. N. Rao, and C. P. Massolo, Phys. Rev. C 25, 146 (1982).

[6]E. R. Flynn, F. Ajzenberg-Selove, R. E. Brown, J. A. Cizewski, and J. W. Sunier, Phys. Rev. C 24, 902 (1981).

[7]S.Frauendorf, private communication.

[8]R. Bengtsson and S. Frauendorf, Nucl. Phys. A316, 27 (1979) and Nucl. Phys. A327, 139 (1979).

EXTENSION OF SPECTROSCOPY USING MASSIVE TRANSFER REACTIONS WITH PROJECTILES HEAVIER THAN Li

D. R. Haenni, H. Dejbakhsh, R. P. Schmitt, and G. Mouchaty

Massive transfer reactions with ^{7}Li beams have proven to be an excellent tool for studying nuclei which are more neutron rich than those normally available for in-beam γ-ray spectroscopy (p. 2). It is desirable to extend the use of massive transfer reactions to heavier projectiles so as to produce higher-spin states and open other mass regions for study. To probe the highest spin regions now observed by discrete-line spectroscopy with fusion reactions, one may need to transfer ~40 amu from the projectile to the target.

Initial tests with beams from B to F have revealed some practical problems which must be overcome. One is the need for a relatively high geometry for particle detection. The design of a new 290 msr detector was already discussed in a previous report.[1] The 12 elements of this 4 stack detector are shown in Fig. 1.

The second problem arises from the need to provide a technique for discrimination against reactions which produce energetic light particles. One of these, especially noticeable with the beams tested thus far, is inelastic scattering from light impurities either in the target or implanted on it during irradiation. The energetic light particles are forward peaked and often in coincidence with γ rays from the excited projectile. Secondly, with heavier beams it is possible to observe in-flight particle decay from excited fragments formed in deep inelastic or quasi elastic reactions. All of these processes, however, should usually have a lower γ-ray multiplicity than that associated with massive transfer reactions.

From our discrete line spectroscpy studies using the total energy crystal (TEC) (p. 5) it has been observed that the TEC is an excellent device for discriminating between high and low multiplicities on an event-by-event basis. A combination of the TEC with massive transfer spectroscopy measurements should provide the desired discrimination against non-massive transfer reactions. A schematic drawing of a possible experimental arrangement is shown in Fig. 2. This apparatus would consist of 27 detectors: 8 surface barrier and 4 NaI for particle detection, 4 Ge(Li) for high resolution γ-ray detection and 11 segments from the TEC.

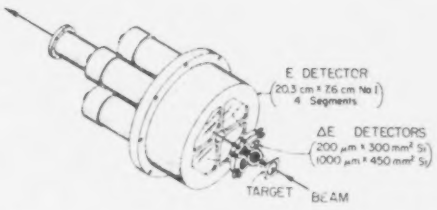

Fig. 1. Configuration of the 4 stack light ion detector.

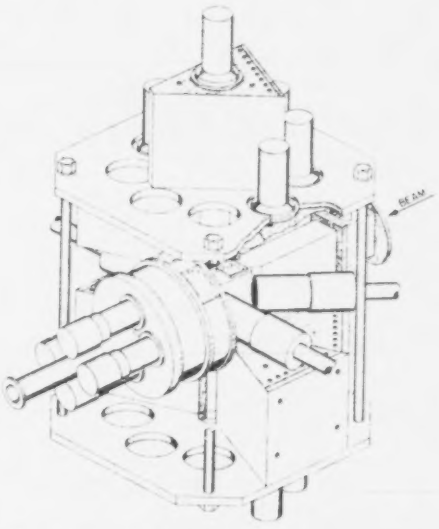

Fig. 2. Experimental configuration for spectroscopic studies following massive transfer reactions including the TEC.

Since fewer elements are used from the TEC, an estimate of the ability of this system to discriminate between high and low multiplicities has been made using the model of Sarantites et al.[2] and scaling the necessary parameters from those obtained in the study (p. 5) of ^{161}Yb. The plot in Fig. 3 in analogous to Fig. 6 (p. 8). While the cut in multiplicities is not as good as for the system with more detectors, it still should be sufficient for structure studies with massive transfer reactions.

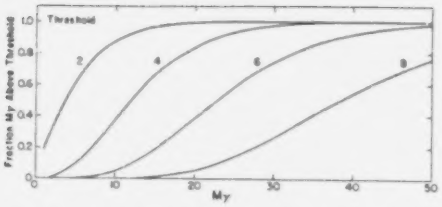

Fig. 3. Calculated multiplicity selection resulting from various fold thresholds for 11 segments of the TEC to be used with the massive transfer experiments.

References

[1]D. R. Haenni, Progress in Research 1981-1982, Cyclotron Institute, Texas A&M University, p. 106.

[2]D. G. Sarantites, R. Lovett, and R. Woodward, Nucl. Instrum. Methods 191, 503 (1980).

TESTING COMBINED TOTAL ENERGY - MULTIPLICITY FILTERS AS A TOOL FOR DISCRETE LINE γ-RAY SPECTROSCOPY: SECOND BACKBENDING IN ^{161}Yb

D. R. Haenni, H. Dejbakhsh, R. P. Schmitt, G. Mouchaty, L. R. Riedinger,* and M. P. Fewell**

The study of high-spin states through in-beam γ-ray spectroscopy has been enhanced during the past few years by the addition of either total γ-ray energy[1] or γ-ray multiplicity[2] selection to the usual spectroscopy experiment. Combining total energy and multiplicity selection could, in principle, allow even greater selectivity by providing the opportunity to bias the entry state population in both E* and J. The benefits of such a filter have not been well documented due to a lack of suitable multi-segmented, high-geometry γ-ray detector systems. Spin spectrometers which represent the ultimate in such 4π γ-ray detection systems are just now beginning to provide results. The 16-segment total energy crystal (TEC) at Texas A&M represents a system intermediate to the simple filters and spin spectrometers. Since the TEC can supply both total energy and multiplicity information on an event-by-event basis, it should be a useful filter for in-beam spectroscopy experiments.

We have initiated a study of ^{161}Yb both to explore the capabilities of the TEC as a filter and to learn more concerning "second backbends" in this odd neutron nucleus. The interest in ^{161}Yb arises from the fact that it has one neutron more than ^{160}Yb which is well known for its "second backbend". A knowledge of the ^{161}Yb level scheme at rotational frequencies corresponding to the second backbend in ^{160}Yb should help to determine the character of the bands which cross in this region through blocking arguments. Currently, ^{159}Tm, the odd proton neighbor of ^{160}Yb is being studied at ORNL.[3] Knowledge of ^{161}Yb will therefore help complete the set of blocking information for both protons and neutrons in ^{160}Yb.

The experimental set up, shown in Fig. 1, consisted of 3 Ge(Li) detectors, the TEC and 6 additional NaI detectors. The halves of the TEC were placed above and below the target chamber. The segments were separated slightly to permit the placement of 4 mm of Pb betwen them. The 3 Ge(Li) and five 7.6 x 7.6 cm NaI were placed in the median plane and the large hole in the upper half of the TEC was partially filled by a spare wedge for the TEC. In this configuration the TEC augmented by the additional NaI detectors had an overall efficiency of 56% at 1.17 MeV. The counter-to-counter scattering was measured to be 8.6% at this same energy. The target consisted of four ^{125}Te foils (400-500 μg/cm^2 on 10-20 μg/cm^2 carbon) separated by ~2 mm to allow for in-flight decay of short lived states in the recoiling nucleus. The target stack was irradiated by 180 MeV ^{40}Ar. Since this energy is below the Coulomb Barrier for Pb, the beam could be stopped in a Pb foil placed behind the target.

The energy signals from the individual NaI crystals were electronically summed to produce a total γ-ray pulse height while the fold (i.e. number of detectors firing) was determined by feeding NaI discriminator outputs into a multiplicity logic unit. Events consisting of these signals and the energies from two of the three Ge(Li) detectors was recorded in an event-by-event mode for subsequent analysis.

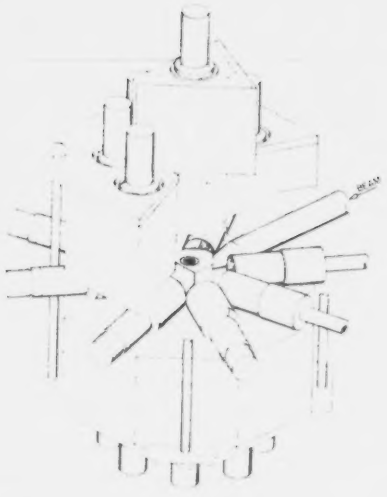

Fig. 1. Experimental configuration for γ-γ coincidence measurements using the TEC as a filter.

The response of this system to the various exit channels is illustrated in Fig. 2. Here the total pulse height vs. fold distributions are plotted for the major reaction products; ^{160,161,162}Yb. These were produced by gating appropriate discrete γ rays in the Ge(Li) detector spectra. Projections of these distributions onto the pulse height and fold axes are shown in Fig. 3. As expected from statistical model calculations, the products from the (^{40}Ar, 3n) reaction peak at highest folds and pulse heights, implying the largest spin. The mean M_γ inferred from the measured fold distributions agree with those obtained in other ^{40}Ar induced reactions.[4] However, the widths of the distributions are relatively large.

An estimate of the instrumental fold resolution can be obtained from the simple model of Sarantites et al.[5] using the measured efficiency and counter-to-counter scattering. In Fig. 4(a), calculated fold distributions are plotted for several M_γ with the assumption that four neutrons are emitted with the γ-ray cascade and that they have a detection efficiency of 0.5 relative to the γ-rays. Except for unphysically large M_γ's ($\geq$ 50), the fold distributions are reasonably well

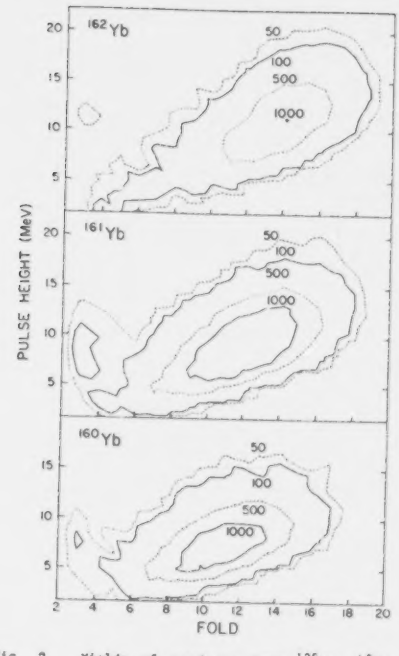

Fig. 2. Yields of products from ^{125}Te (^{40}Ar, Xn)$^{165-x}$Yb at 180 MeV plotted as a function of fold vs. total pulse height in the TEC.

separated. In contrast, a similar calculation for the eight-detector array of 7.6 x 7.6 cm NaI's (10% efficiency, 1.5% scattering) used for multiplicity measurements on page 51 offers rather poor spin selection on an event by event basis.

To provide further insight into product selectivity, the distributions in Figs. 2 and 3 were searched to find the best "window" for the yields of ^{160,161,162}Yb under the constraint that at least 50% of the total yield for the product was included in the window. Table I summarizes the results for each product and either total pulse height (E), fold (M), or two dimensional (EM) gates. For comparison, values for the "total data" (T), i.e. all events with at least 2 Ge(Li) and 2 NaI responding, are also included. For this particular data set, there does not seem to be much advantage for using EM gates over either E or M gates for exit channel selection. Portions of the γ-ray spectra projected by the EM gates for ^{160,161,162}Yb are shown in Fig. 5. These

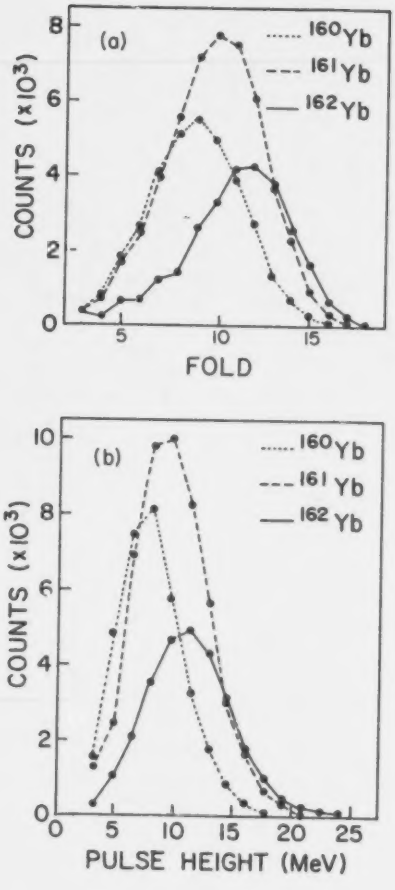

Fig. 3. Projections of the product distributions shown in Fig. 2 onto the (a) fold and (b) pulseheight axes.

permit one to compare graphically the exit channel selection and relative yields of the various reaction products.

Instead of product selectivity, one could also employ the TEC as a spin filter. In this case, a threshold in the fold could be used to discriminate between high and low multiplicity (angular momentum) events. An estimate of the ability of the TEC to make such a discrimination can be seen in Fig. 6. Here the results of the calculation discussed

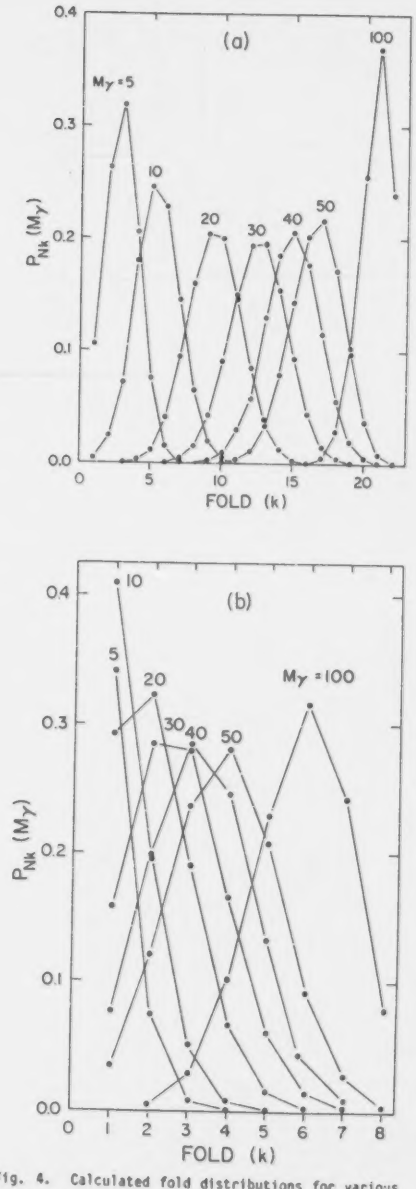

Fig. 4. Calculated fold distributions for various multiplicities for (a) the augmented TEC used for γ-ray spectroscopy measurements and (b) the 8 detector system used on page .

Table I. Relative product yields for various one- and two-dimensional gates. See text for more details.

Nucl	Gate	R(^{160}Yb)	R(^{161}Yb)	R(^{162}Yb)
^{160}Yb	T	1.0	1.5	0.8
	E	1.0	1.0	0.3
	M	1.0	1.1	0.4
	EM	1.0	1.0	0.3
^{161}Yb	T	0.7	1.0	0.6
	E	0.6	1.0	0.5
	M	0.6	1.0	0.5
	EM	0.6	1.0	0.4
^{162}Yb	T	1.2	1.8	1.0
	E	0.4	1.0	1.0
	M	0.4	1.0	1.0
	EM	0.3	1.0	1.0

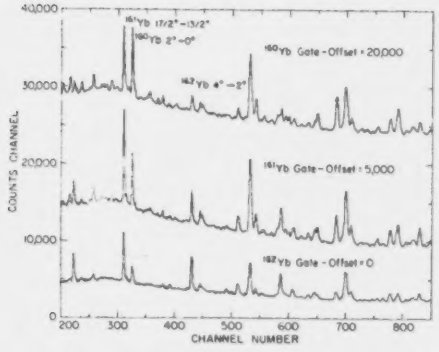

Fig. 5. Projected γ-γ coincidence spectra gated by the two dimensional EM Gates in Table I.

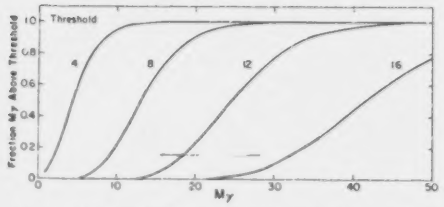

Fig. 6. Calculated multiplicity selection resulting from various thresholds in fold.

above are plotted to show the fractional yield of each multiplicity above various fold thresholds. At a moderate threshold value, the TEC provides a reasonably sharp cut in multiplicity thereby allowing one to make a good separation between low and high multiplicity events. Coincidence spectra summed on low-lying members of various bands in ^{160,161,162}Yb were extracted for thresholds at 2, 8 and 12 fold. The relative intensity enhancement for the transitions in these bands is plotted as a function of spin. It should be noted that these enhancements are obtained at a sizeable loss in counting statistics. Thresholds at 8 and 12 fold pass 55% and 12% of the 2 fold coincidence events, respectively. The variations in the enhancements between the different isotopes and bands may be a consequence of either structure effects, instrumental resolution or the relative position of the threshold in the fold distributions (Fig. 3a).

To obtain sufficient statistics for the study of ^{161}Yb, it was necessary to combine the results from two essentially identical measurements.

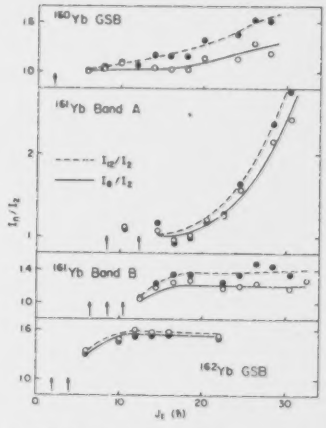

Fig. 7. Relative intensity enhancement for transitions in bands in ^{160,161,162}Yb from summed coincidence spectra gated by 8 and 12 fold thresholds relative to a 2 fold threshold. The initial J for the transitions gated in each band are indicated by vertical bars. Bands (a) and (b) in ^{161}Yb are identified in Fig. 9. Lines are drawn to guide the eye.

Initially, all events having a fold of 8 or above were sorted into a "symmetrized matrix" in the following way. The γ-γ coincidence events meeting the fold threshold for each Ge(Li) detector pair (3 in each measurement) were sorted into a 2048 x 2048 matrix. The six matrix were then combined into a single symmetrized one by converting the energy calibration for each detector to a common value followed by summing the six gain shifted matrices with their transposes. From this symmetrized matrix, a single coincidence "gate" returns all of the γ-γ coincidence information available for the transition in the gate.

Examples of summed coincidence spectra for 3 major bands in ^{161}Yb are shown in Fig. 8. The lower part of the partial level scheme for ^{161}Yb (Fig. 9) agrees well with that reported in Ref. 6. The bands a, b and c have been extended by 4, 3, and 2 transitions, respectively. Plots of alignment vs. rotational frequency for the three bands in ^{161}Yb are compared with the ground state band (GSB) in ^{160}Yb in Fig. 10. All three bands show an "up-bend" between $\hbar\omega$ of 0.41 - 0.45 MeV. This would indicate that the second backbend in ^{160}Yb is not "blocked" by the addition of a neutron and therefore results from the alignment of a proton pair. The differences in the frequencies of the "up-bends" in the three bands in ^{161}Yb are not yet fully understood. A comparison of the levels in ^{161}Yb with the results of cranked shell model calculations[7] is in progress.

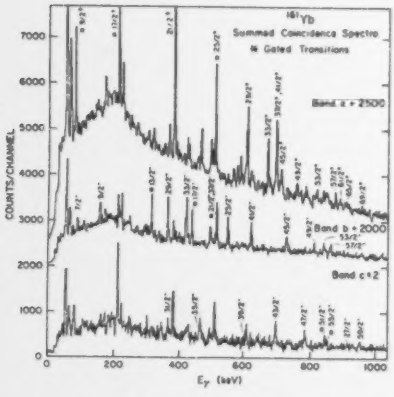

Fig. 8. Summed γ-γ coincidence spectra for the three strong bands in ^{161}Yb. The gated transitions are denoted by a (*).

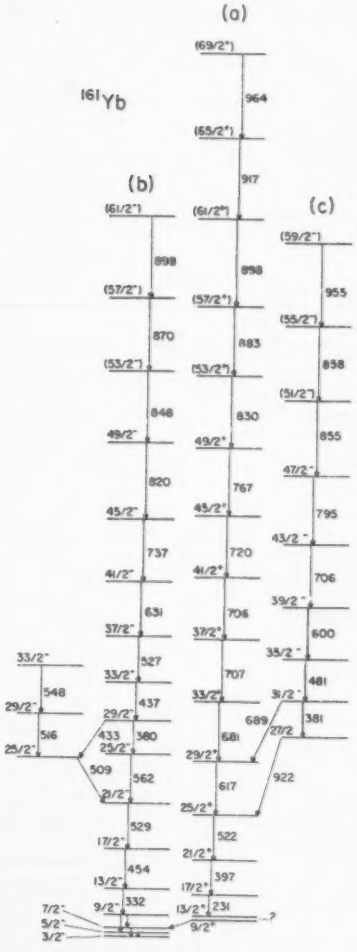

Fig. 9. Partial level scheme for ^{161}Yb from ^{125}Te(^{40}Ar, 4nγ) ^{161}Yb reaction at 180 MeV.

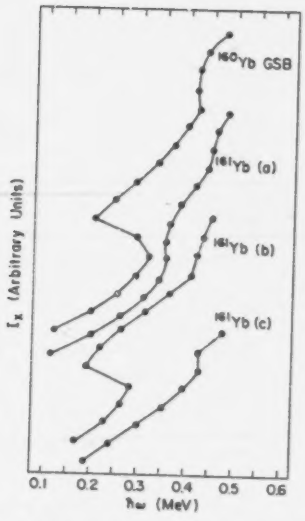

Fig. 10. Alignment vs. rotational frequency plots for the three bands in ^{161}Yb compared with the GSB in ^{160}Yb.

*University of Tennessee, Knoxville, TN.

**Oak Ridge National Laboratory, Oak Ridge, TN.

References

[1] L. L. Riedinger, Physics Scripta 24, 312 (1981).

[2] J. Burde, E. L. Dines, S. Shih, R. M. Diamond, J. E. Draper, K. H. Lindenberger, C. Schuck, and F. S. Stephens, Phys. Rev. Lett. 48, 539 (1982).

[3] L. L. Riedinge, L. H. Courtney, A. J. Larabee, J. C. Waddington, M. P. Fewell, N. R. Johnson, I. Y. Lee, F. K. McGowan, Conference on High Angular Momentum Properties of Nuclei, Oak Ridge Tennessee, Nov. 1982. Proceedings Vol. 1, p. 8.

[4] D. L. Hillis, J. D. Garrett, O. Christensen, B. Fernandez, G. B. Hagemann, B. Herskind, B. B. Back, and F. Folkmann, Nucl. Phys. A325, 216 (1979).

[5] D. G. Sarantites, R. Lovett, and R. Woodward, Nucl. Instrum. Methods 171, 503 (1980).

[6] J. J. Gaardhbje Thesis, The Niels Bohr Institute, University of Copenhayen, 1980. Also reported in L. L. Riedinger, Nucl. Phys. A347, 141 (1980).

[7] R. Bengtsson and S. Frauendorf, Nucl. Phys. A314, 27 (1979); Nucl. Phys. A327, 139 (1979).

HIGH LYING PROTON STATES IN HEAVY NUCLEI

E. Takada, Y. -W. Lui, Y. Mihara, T. Murakami, Y. Toba, R. Tribble, and M. Ishihara*

Proton stripping reactions were used to study high-lying proton states in ^{209}Bi and other nuclei. Especially of interest are the location, width and strength of high angular momentum states, such as $j_{15/2}$, $i_{11/2}$ in ^{209}Bi. This information will provide an important testing ground for various aspects of theory, such as the shell structure at $2\hbar\omega$ excitation and the origin of the ℓ-s coupling through spin-orbit splitting. While there are numerous experiments aimed at understanding the structures of deep hole states, no study of these configurations has been carried out.[1] Although the strength is spread over a wide range of excitation for high-lying states in general, one can expect a relatively small spreading for these high spin states because of their high angular momentum. The high spin selectivity of the (α,t) reaction, as well as some heavy ion reactions are expected to provide a good tool to study these states.

A 50 MeV α beam was used to bombard self-supporting ^{208}Pb foils, which were isotopically enriched to more than 99% ^{208}Pb. The outgoing tritons were detected at the focal plane of the ESP-110 spectrograph by a position-sensitive gas proportional counter. Typical solid angle was 1.6 msr, and the angular opening was 1.7°. The energy calibration was obtained from the low lying states of ^{209}Bi. Spectra spanning E_x = 0 to 18 MeV were measured at several angles. Cross sections for the low lying states were consistent with the results of Perry et al.[2] within experimental errors. A typical spectrum at 14° is shown in Fig. 1a.

Also measured were the (^{3}He,d) reaction at E(^{3}He)= 75 MeV with the spectrograph, and the (^{12}C,^{11}B) reaction at E(^{12}C)= 180 and 300 MeV using solid-state counter telescopes. These measurements were performed in hopes that they would help delineate the nature of the observed spectra.

The triton spectrum in Fig. 1a shows the anticipated high-spin selectivity in the low-lying states of $h_{9/2}$(0.0 MeV) and $i_{13/2}$(1.6 MeV). Also several bumps are prominent at higher excitation. Preliminary DWBA calculations suggest high ℓ dominance for these bumps. A deuteron spectrum from the ^{208}Pb(^{3}He,d) reaction at 5° is shown in Fig. 1b. The spectrum has a large contribution from the ^{3}He breakup process and tends to favor lower spin final states such as the $p_{3/2}$(3.1 MeV) and $f_{7/2}$(0.9 MeV) levels.

Although the poor statistics prevent us from making any definite assessment, the (^{12}C,^{11}B) reaction at 25 MeV/n seems to have better matching for the higher excitation region than at 15 MeV/n, which shows more or less the same selectivity as the (α,t) reaction at 15 MeV/n.

Further analyses are now in progress.

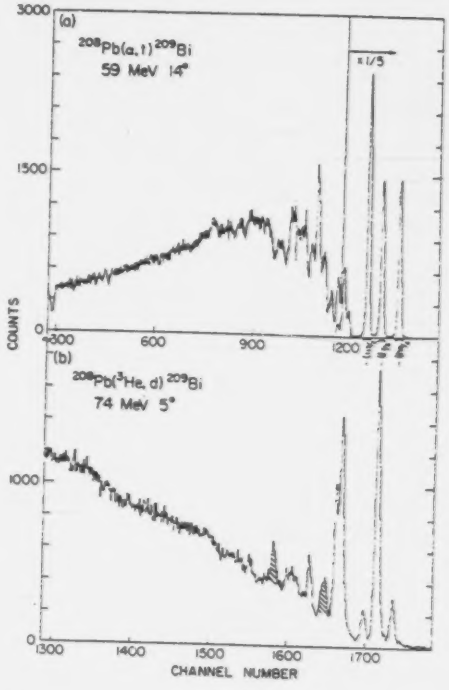

Fig. 1. Typical spectra of (a) ^{208}Pb(α,t)^{209}Bi reaction and (b) ^{208}Pb(^{3}He,d)^{209}Bi reaction. High-spin selectivity of the (α,t) reaction is clearly shown for low lying states and bumps at high excitation region are being analyzed to study high-spin proton strength. The deuteron spectrum shows contrasting feature that the (^{3}He,d) reaction favors lower spin. Shadows in the figure indicate contamination in target.

References

*Institute of Physical and Chemical Research, Japan.

[1] S. Galès, C. P. Massolo, S. Fortier, E. Gerlic, J. Guillot, E. Hourani, J. M. Maison, J. P. Schapira, S. Zwieglinski, P. Martin, and V. Comparat, Phys. Rev. Lett. 48, 1593 (1982).

[2] R. Perry, A. Nadasen, D. L. Hendrie, P. G. Roos, and N. S. Chant, Phys. Rev. C 24, 1471 (1981).

THE $^{20}Ne(^{6}Li,d)^{24}Mg$ REACTION AT 72 MeV

E. Ungricht, Y.-W. Lui, Y. Mihara, T. Murakami, R. E. Neese, E. Takada, N. Takahashi,* R. Tribble and K. Nagatani

The (^{6}Li,d) alpha stripping is one of the most useful alpha-transfer reactions and has been used as a spectroscopic tool for more than a decade.[1,2] Most of the work has been limited to bombarding energies around ~30 MeV,[3,4] where high excited states are weakly populated and obscured by deuterons from the breakup of ^{6}Li. The extraction of reliable spectroscopic factors at such low energies is difficult since the compound cross section can be a considerable fraction of the cross section for any state, especially if the spin is large. Recent experiments have shown a much more favorable situation at higher energies with clean experimental spectra and essentially no compound contribution.[5]

This makes the $^{20}Ne(^{6}Li,d)^{24}Mg$ reaction very attractive to study the structure of ^{24}Mg. Rotational bands are better developed in ^{24}Mg than in any other sd-shell nucleus and some of them are known up to spins $8\hbar$ or $9\hbar$ and excitation energies around 15 MeV.[6] The test case used often for theoretical calculations is ^{24}Mg. The results of the SU(3) calculations show that the spectroscopic strength for the (8,4) symmetry is concentrated at low spins for the $K = 0^+$ ground state band and at successively higher spins for higher K-bands. If supported experimentally, this would allow the identification of unknown high-spin members of high K-bands.

A 72.6 MeV $^{6}Li^{2+}$ beam was used together with a 2 in. diameter gas cell for the ^{20}Ne target. The beam intensity after the target was 200 ~ 300 nA $^{6}Li^{3+}$, limited by the neutron count rate in the detector. The target pressure was set to 50 torr at forward angles and 100 torr at backward angles. The target temperature and pressure were monitored throughout the experiment. The outgoing deuterons were analyzed by an Enge split-pole spectrograph. The focal plane detector consisted of a position-sensitive proportional counter with two resistive wires, three additional wires for energy loss measurement, and a plastic scintillator.[7] The bias of the proportional counter was carefully adjusted for optimum resolution which was about 130 keV for the deuterons. The angular resolution was ±0.8°.

Well known levels of ^{24}Mg below 11 MeV were used to obtain an energy calibration. Absolute cross sections were obtained from the target pressure, the beam current and the slit geometry, using the formulae of Silverstein.[8] The error of the absolute cross sections is 25%, but errors from peak identification are often larger. A small contamination of ^{16}O in the target obscured some of the weaker peaks.

A deuteron spectrum from the $^{20}Ne(^{6}Li,d)^{24}Mg$ reaction is compared with a spectrum from $^{16}O(^{6}Li,d)^{20}Ne$ in Fig. 1. The spectra are shifted so that deuterons of the same momentum are aligned. The vertical scaling is chosen so that the same peak height corresponds to a cross section approximately five times larger in the $^{16}O(^{6}Li,d)^{20}Ne$ reaction. It is evident that the cross sections for the most prominent peaks are about five times larger in the latter reaction than in the former one. The total strength to a given bin of excitation energy, however, is fairly comparable. In $^{20}Ne^*$, this strength is concentrated in a very few states up to excitation energies of 12 MeV while in $^{24}Mg^*$ the strength is distributed among several states at excitation energies as low as 6 MeV. Below 12 MeV in $^{20}Ne^*$, only the $K = 0^+$ and 0^- bands are strongly excited, but in $^{24}Mg^*$ the $K = 0^+$, 2^+, 0^+_2 and 1^- bands are excited with cross sections ~10 μb/sr and the $K = 0^-$ band is strongly populated with ~ 50 μb/sr. In view of the strong configuration mixing found in shell model calculation for ^{24}Mg,[9] the observed spread of the transition strength among several rotational bands is not surprising.

The $K = 0^+$ and 2^+ bands in ^{24}Mg are well established. In the SU(3) model, the bands have the symmetry $(\lambda,\mu) = (8,4)$ and this strength is concentrated in $J = 0^+$, 2^+, or 4^+, 6^+ respectively.[10] The shell model calculations show that the leading SU(3) component of the high spin states is rather small, but the alpha-structure amplitudes are similar to those of the SU(3). In our experiment we find a rather strong peak at 14.15 MeV which is the energy of the $J,K = 8^+,2^+$ state. Our resolution is not sufficient to separate the states at 14.08 (6^+), 14.10 (4^+), 14.15 (4^+), and 14.19 MeV (8^+) found in a $^{20}Ne(\alpha,\gamma)^{24}Mg$ experiment.[11] Those states may be more strongly populated than the 8^+ state of the $K = 2^+$ band.

While Fifield et al.[11] found no hint for a $K = 4^+$ band with symmetry (8,4) in their $^{20}Ne(\alpha,\gamma)^{24}Mg$ work, they found two states at 9.30 (4^+) and 12.86 (6^+) MeV with a somewhat enhanced γ-transition rate. We also find peaks at these energies and in addition we find a distinct peak at 17.5 MeV. If we speculate that these three peaks

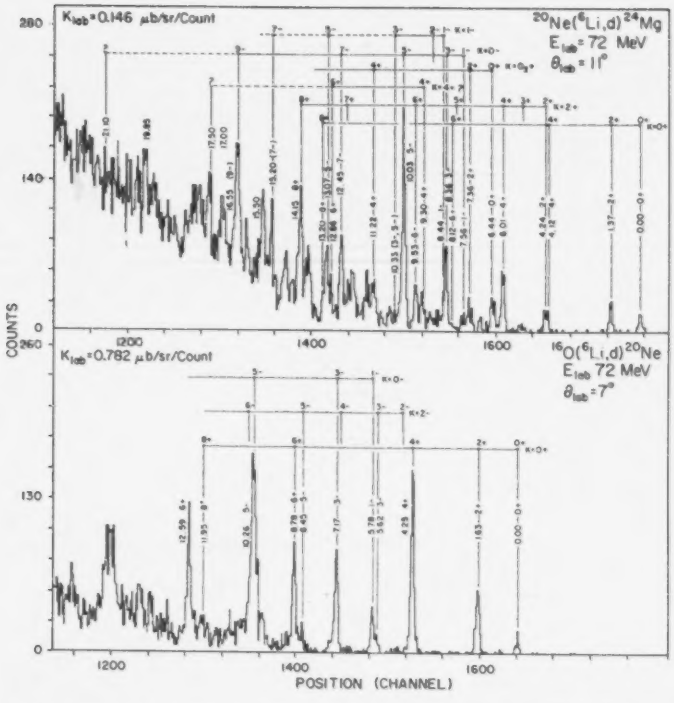

Fig. 1. Deuteron momentum spectra from ^{20}Ne(^{6}Li,d)^{24}Mg and ^{16}O(^{6}Li,d)^{20}Ne. The vertical scales are adjusted so that the same height corresponds to a five times larger cross section for the lower spectrum.

form the K = 4$^+$ band we get a moment of inertia for this band which is very similar to that of the K = 0$^+$ and 2$^+$ bands. According to SU(3), the alpha strength in the K = 4$^+$ band should be concentrated in the J = 8$^+$ state[10] which would agree with our spectra. However, to confirm this, it is necessary to know the spin of the state (or states) around 17.5 MeV.

The bandhead for the second K = 0$^+$ band is thought to be the 6.44 (0$^+$) MeV state. For the 2$^+$ state, however, different assignments exist to either the 7.35 MeV state[12] or the 8.65 MeV state.[13] We find peaks at 6.44, 7.35 and 11.22 MeV (there is a 4$^+$ state at 11.22 MeV[6]) which could form the K = 0^+_2 band. However, we do not find candidates for high spin members of this band.

The K = 0$^-$ band is the strongest populated band in the ^{20}Ne(^{6}Li,d)^{24}Mg reaction at 72 MeV. This band has a (9,4) symmetry in SU(3). All states of the K = 0$^-$ band up to the 16.55 (9$^-$) MeV state are strongly populated, but there is no indication of a strong peak around 21.1 MeV where a 11$^-$ state with the same moment of inertia should be.

The K = 1$^-$ band starting at 8.44 MeV is suggested from a (^{3}He,d) study[12] and might have an (11,3) symmetry corresponding to a $(sd)^7f^1$ structure.[13] We see peaks at excitation energies corresponding to this band. However, there is some confusion about the states belonging to the band. Proposed members are at 8.44(1$^-$), 8.86(2$^-$), 10.33(3$^-$, 5$^-$), 13.07(5$^-$) and 15.15(7$^-$) MeV.[13] The moment of inertia in this band would be very different from state-to-state if these states really form the K = 1$^-$ band.

The grazing angular momenta in the incident and exit channels of the (^{6}Li,d) reaction are not

well matched, being 24ħ and 12ħ, respectively for $^{20}Ne(^{6}Li,d)^{24}Mg$ at 72 MeV. Any reaction localized to the nuclear surface, or more accurately to angular momenta around the grazing angular momentum, should therefore strongly prefer high spin states. Even then, such reactions will have only small cross sections due to the angular momentum mismatch.

The cross section from a compound nucleus process was calculated with the program STATIS.[14] The compound nucleus formation is limited by the yrast line to $\ell \leq 20\hbar$, resulting in a fusion cross section of 1080 mb compared to reaction cross section of 1860 mb. The cross sections for the interesting states in ^{24}Mg are of the orders of 1-10 nb/sr, roughly 1000-times smaller than the experimental results.

Zero-range DWBA calculations were performed with the code DWUCK4[15] using a parameter set 2 (Table I) fitted to the elastic scattering of ^{6}Li + ^{20}Ne and the parameters of Daehnick et al.[16] for d + ^{24}Mg. The zero-range normalization for ^{6}Li was obtained from the bound state potential of Kubo and Hirata[17] as $D_0^2 = 0.85 \times 10^{-4}$ MeV^2 fm^3, and the spectroscopic factor for ^{6}Li was set to one. The bound state potential depth for ^{24}Mg was fitted to the binding energy with a usual Woods-Saxon geometry (Table I). The number of nodes was given by the Moshinsky relation. The results were completely different from the experimental data in shape and about three orders of magnitude larger.

The good agreement between experimental and exact finite range DWBA calculations for $^{16}O(^{6}Li, d)^{20}Ne$ at nearby energies[5] led us to expect similar agreement for $^{20}Ne(^{6}Li,d)^{24}Mg$. We used the code, SATURN-MARS,[18] with the same parameters as above (Table I).

Unfortunately, the transfer cross section in the EFR-DWBA depends strongly on the choice of the potentials for the elastic scattering. The optical potential, sets 1 and 2, (Table I) give two orders of magnitude difference in transfer cross sections, while the predicted elastic scattering is not very different. A more detailed analysis suggests that this arises entirely from differences in the overlap integral below 3 fm which is far inside the nuclear surface. The overlap integral is large around 3 fm because neither the form factor nor the distorted wave is dropping rapidly in the interior of the nucleus. Since the form factor is large and oscillating, any change in the phase of the distorted wave has a dramatic effect on the overlap integral. Rather than being a pure numerical problem, this unusual form factor may be the result of a basic shortcoming in the DWBA treatment.

Thus, even though we find several distinct peaks at excitation energies of 15-20 MeV, no suggestions for spin assignments can be made at this time because the angular distributions are insensitive to the spin within the experimental errors.

References

* Present address: Dept. of Physics, University of Tokyo, Tokyo, Japan.

[1] K. Bethge, Ann. Rev. Nucl. Sci. 20, 255 (1970).

[2] H. W. Fulbright, Ann. Rev. Nucl. Sci. 29, 161 (1979).

[3] N. Anantaraman, H. E. Gove, J. Toke, and J. P. Draayer, Nucl. Phys. A279, 474 (1977); N. Anantaraman, H. E. Gove, R. A. Lindgren, J. Toke, J. P. Trentelman, J. P. Draayer, F. C. Jundt, and G. Guillaume, Nucl. Phys. A313, 445 (1979).

[4] F. D. Becchetti, D. Overway, J. Jänecke, and W. W. Jacobs, Nucl. Phys. A344, 336 (1980).

Table I. Elastic scattering and bound state parameters used in DWBA calculations for the ^{24}Mg ground state.

System		V (MeV)	R_r (fm)	A_R (fm)	W (MeV)	W_D (MeV)	R_i (fm)	A_I (fm)	R_c (fm)
$^{6}Li+^{20}Ne$	1	187.7	3.53	0.70	31.4		4.61	0.90	3.80
	2	116.1	3.53	0.81	49.5		3.42	1.16	3.53
d + ^{24}Mg		74.4	3.37	0.83	5.24	8.74	3.82	0.73	3.75
^{6}Li		77.2*	1.90	0.65					1.90
^{24}Mg		120.0*	3.53	0.65					3.53

Set 1 is from Tanabe et al.[5] and not fitted.
*Fitted to the binding energy.

[5]T. Tanabe, M. Yasue, K. Sato, K. Ogino, Y. Kadota, Y. Taniguchi, K. Obori, K. Makino, and M. Tochi, Phys. Rev. C 24, 2556 (1981).

[6]P. M. Endt and C. Van der Leun, Nucl. Phys. A310, 1 (1978).

[7]N. Takahashi, T. Yamaya, E. Takada, Y.-W. Lui, and K. Nagatani, Nucl. Instrum. Methods 196, 253 (1982).

[8]E. A. Silverstein, Nucl. Instrum. Methods 4, 53 (1959).

[9]M. Conze & P. Manakos, J. Phys. G5, 671 (1979).

[10]J. P. Draayer, Nucl. Phys. A237, 157 (1975).

[11]L. K. Fifield, M. J. Hurst, T. J. M. Symons, F. Watt, C. H. Zimmerman, and K. W. Allen, Nucl. Phys. A309, 77 (1978).

[12]J. D. Garrett, H. T. Fortune, R. Middleton, and W. Scholz, Phys. Rev. C 18, 2032 (1978).

[13]Y. Fujiwara, H. Horiuchi, K. Ikeda, M. Kamimura, K. Kato, Y. Suzuki, and E. Uegaki, Suppl. of Prog. Theor. Phys. (Kyoto) 68, 22 (1980).

[14]R. Stokstad, Internal Report 52, Wright Nuclear Structure Laboratory, Yale Univ., (unpublished), 1972.

[15]P. D. Kunz, Univ. of Colorado 1972 (unpublished).

[16]W. W. Daehnick, J. D. Childs and Z. Vrcelj, Phys. Rev. C 21, 2253 (1980).

[17]K.-I. Kubo and M. Hirata, Nucl. Phys. A187, 186 (1982).

[18]T. Tamura and K. S. Low, Comp. Phys. Comm. 8, 349 (1974); T. Tamura, T. Udagawa, K. E. Wood, and H. Amakawa, Comp. Phys. Comm. 18, 163 (1979). Some modifications were made to avoid numerical problems pertinent to VAX11.

$^{16}O(^{12}C,^{8}Be)^{20}Ne$ REACTION

T. Murakami, E. Ungricht, Y.-W. Lui, Y. Mihara, E. Takada, and R. Tribble

As we reported earlier,[1] the reaction mechanism in the $^{12}C(^{16}O,\alpha)$ reaction is complicated. Sequential decay via inelastic $^{16}O^*$ and α-transfer $^{20}Ne^*$ processes were suggested. The results of coincidence measurements of $^{12}C(^{16}O,\alpha^{12}C)$ and $^{13}C(^{16}O,\alpha^{12}C)$ reactions[2] showed, however, only a small difference (less than a factor of three) in the cross section, while $^{12}C(^{16}O,\alpha)$ and $^{13}C(^{16}O,\alpha)$ reactions showed a prominent difference. In order to check the α transfer process, we must compare the $^{16}O(^{12}C,^{8}Be)$ and $^{16}O(^{13}C,^{9}Be)$ reactions. However, only data for $^{16}O(^{13}C,^{9}Be)$ at $E(^{13}C)$=105 MeV have been published.[3] Therefore, we measured the $^{16}O(^{12}C,^{8}Be)$ reaction at 109 MeV. This reaction is also of great interest from both the reaction mechanism and spectroscopic viewpoint.

The beam energy was selected so that center-of-mass energy of the ^{12}C + ^{16}O system matched to the $^{12}C(^{16}O,\alpha)$ at 145 MeV. A self supporting Al_2O_3 foil was used as a target. To measure two α-particles decaying from ^{8}Be, two counter telescopes were set 3.44° apart from each other, perpendicular to the reaction plane. The detection efficiency was calculated to be typically 0.075 msr. Spectra were measured at four angles (5°, 7.5°, 10° and 12.5°).

A typical ^{8}Be spectrum is shown in Fig. 1, together with a spectrum from an ^{27}Al target.

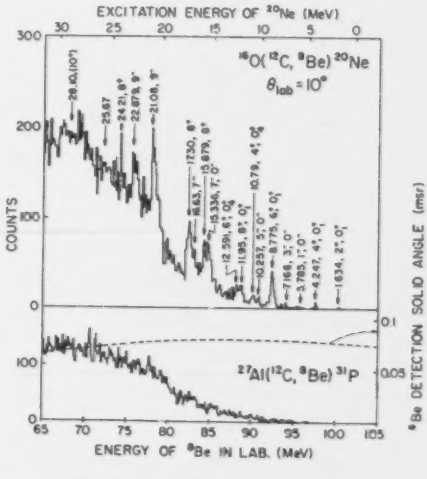

Fig. 1. Energy spectrum of ^{8}Be detected at θ_{lab} = 10°. The peaks are identified by their energies, J^{π} and K^{π} values if previously known.[4] The dashed curve indicates the detection efficiency as a function of the ^{8}Be energy and corresponds to the right-hand scale in the figure.

Several sharp peaks can be identified on the continuum background. Energies, J^π, and K^π values are taken from Ref. 4. Of the more than 150 known levels below $E_x(^{20}Ne) = 25$ MeV, the $(^{12}C,^{8}Be)$ reaction populates only members of the $K^\pi = 0^+_1$, 0^-, and 0^+_4 bands. These bands are indeed expected to be populated strongly by a direct α-transfer reaction. The population of the 0^- band is surprisingly large compared to the other reactions, and 9^- states at 21.1 and 22.9 MeV are both strong candidates for the 9^- member of this band. Also, strongly populated 8^+ states at 15.9 and 17.3 MeV are candidates for the 8^+ member of the 0^+_4 band.

Angular distributions to the several states were measured and showed a strong decrease in the cross section with angle in most cases. They were analyzed with EFR-DWBA assuming a one-step α-cluster transfer. The calculation reproduced the general tendency of the angular distributions. Comparison of the present $^{16}O(^{12}C,^{8}Be)^{20}Ne$ reaction and the results of $^{16}O(^{13}C,^{9}Be)^{20}Ne$ reaction revealed two large differences. First, as the spin value of the residual ^{20}Ne is getting larger, the cross section of the $(^{12}C,^{8}Be)$ reaction became significantly larger than those of the $(^{13}C,^{9}Be)$ reaction. In fact, the 15.4 (7^-) and 21.1 (9^-) MeV states show at least one order of magnitude larger cross sections in the $(^{12}C,^{8}Be)$ reaction than in the other, while 1.63 (2^+) and 4.25(4^+) MeV states have similar cross sections in both reactions. Second, the angular distributions of the $(^{12}C,^{8}Be)$ reaction are much steeper than those of the $(^{13}C,^{9}Be)$ reaction in the forward angle region. These differences can explain the fact that the $^{12}C(^{16}O,\alpha)$ reaction shows distinct structures while the $^{13}C(^{16}O,\alpha)$ reaction does not. Further investigations are in progress.

References

[1] T. Murakami, E. Ungricht, N. Takahashi, Y.-W. Lui, Y. Mihara, R. E. Meese, E. Takada, D. M. Tanner, R. E. Tribble, and K. Nagatani, Phys. Lett. B 120, 319 (1983).

[2] W. D. Rae, R. G. Stokstad, B. G. Harvey, A. Dacal, R. Legrain, J. Mahoney, M. J. Murphy, and T. J. M. Symons, Phys. Rev. Lett. 45, 884 (1980).

[3] H. S. Bradlow, W. D. M. Rae, P. S. Fisher, N. S. Godwin, G. Proudfoot, and D. Sinclair, Nucl. Phys. A314, 171 (1979).

[4] F. Ajzenberg-Selove, Nucl. Phys. A300, 1 (1978).

THE GIANT MONOPOLE RESONANCE IN TRANSITIONAL AND DEFORMED NUCLEI

U. Garg*, P. Bogucki, J. D. Bronson, Y. -W. Lui, M. Parkin, J. A. Sullivan, and D. H. Youngblood

In continuation of our earlir work[1,2] on the effects of the ground state deformation on the giant monopole (GMR) and giant quadrupole (GQR) resonances, we have performed small-angle inelastic α-scattering measurements on $^{142,146,150}Nd$. Data were obtained for 129 MeV α-particles at several angles between 0° and 6°, using an 86 cm resistive-wire proportional counter in the focal plane of the Enge split-pole spectrograph. Details of the experimental techniques including data handling and analysis procedures have been described previously.[3,4]

Figure 1 shows the "raw" spectra for the aforementioned nuclei as well as for the previously reported[3] $^{144,148}Sm$. The giant resonance (GR) regions, after subtraction of a smooth continuum background (the assumed shapes of which are displayed in Fig. 1), were analyzed in the usual way,[4] assuming two (2) Gaussian components in the GR peak and performing multi-spectrum fits. The resonance parameters extracted from this data are summarized in Table I. For ^{142}Nd and ^{150}Nd, the relative cross section data are presented in Table II for 0° and 5° where the GMR is maximal. The angular distributions for the GR components for $^{142,150}Nd$ are shown in Fig. 2(a).

Table I. Parameters obtained for GR peaks in $^{142,146,150}Nd$.

Nucleus	LE Peak		HE Peak	
	E(MeV)	Γ(MeV)	E(MeV)	Γ(MeV)
^{142}Nd	12.1±0.2	2.9±0.3	14.8±0.3	3.3±0.2
^{146}Nd	12.2±0.2	3.3±0.3	15.1±0.3	3.5±0.2
^{150}Nd	12.2±0.2	3.8±0.3	15.4±0.3	3.4±0.2

$E_{HE} - E_{LE} = 2.7 \pm 0.4$ MeV for ^{142}Nd
$= 3.2 \pm 0.4$ MeV for ^{150}Nd.

$\Gamma_{LE}(^{150}Nd) - \Gamma_{LE}(^{142}Nd) = 0.9 \pm 0.4$ MeV.

Table II. GR cross sections relative to (σ^{LE} + σ^{HE}) in ^{142}Nd.

Angle	Nucleus	σ_{LE}	σ_{HE}	$\sigma_{LE} + \sigma_{HE}$
0°	^{142}Nd	.36 ± .07	.64 ± .09	1.0
0°	^{150}Nd[a]	.70 ± .10	.52 ± .07	1.22 ± .14
		(.57 ± .08)	(.43 ± .06)	(1.00± .10)
5°	^{142}Nd	.57 ± .06	.43 ± .06	1.0
5°	^{150}Nd[a]	.82 ± .09	.29 ± .05	1.11 ± .10
		(.74 ± .08)	(.26 ± .05)	(1.00± .10)

[a]Numbers in parenthesis correspond to normalization of σ_{LE} + σ_{HE} to 1.0.

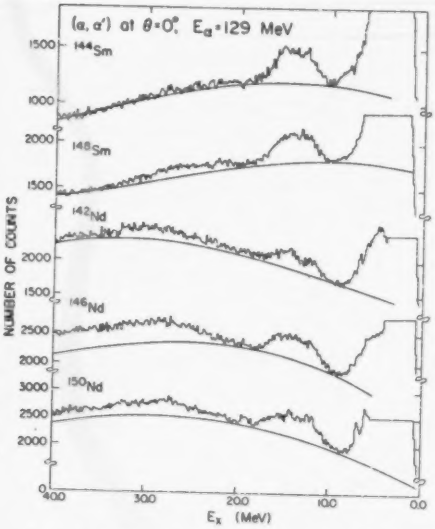

Fig. 1. Inelastic α-scattering spectra at 0° for ^{144}Sm, ^{148}Sm, ^{142}Nd, ^{146}Nd, and ^{150}Nd. The solid lines show the assumed shape of the background for subtraction.

The splitting of the GMR is evident from Table II: while the total cross section of the low-energy (LE) and high-energy (HE) components is practically the same in ^{142}Nd and ^{150}Nd, there is a definite "shift" of strength from the HE to LE component in ^{150}Nd. The extent of this shift for the Nd nuclei is smaller than that for the Sm nuclei. Nevertheless, in all other relevant respects viz the angular distribution of the LE component, and the relative energy separation of two components, the Nd data is qualitatively similar to the Sm data reported in Ref. 2.

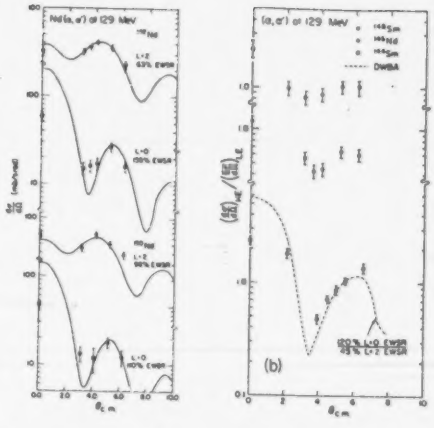

Fig. 2. (a) Angular distribution for the components of the giant resonances in ^{142}Nd and ^{150}Nd. The DWBA calculations are shown superimposed; (b) Angular distributions for the ratio R, described in the text, for ^{144,148}Sm and ^{146}Nd. The DWBA calculation for R is shown superimposed on the ^{144}Sm data.

The "splitting" of the GMR has been explained in RPA calculations of Kishimoto,[1,5] Abgrall et al.,[6] and Zawischa et al.[7] In a nucleus with a deformed ground state, the L = 0 and L = 2 oscillations mix, resulting in two K = 0 states which share the L = 0 strength between them. In the model of Abgrall et al.,[6] the GQR splits into two components, the axial β and non-axial γ where the K = 0 and 2 components coincide with β and γ, respectively. In the models of Kishimoto[1,5] and Zawischa et al.,[7] the GQR splits into three components corresponding to K = 0, 1, and 2. The coupling of L = 0 and L = 2 modes leads to a redistribution of L = 0 and L = 2 strengths as shown for the model of Abgrall et al.[5] in Fig. 3 for a hypothetical nucleus with deformation ε = 0.3. In all three models, the extent of this sharing of strengths depends on the deformation of the nucleus. This feature would explain the smaller amount of "shifted" GMR strength in the Nd nuclei when compared to the Sm nuclei; the deformation ε for ^{150}Nd is 0.236 while that for ^{154}Sm is 0.284.[8] However, the observed "shift" of strength from GMR

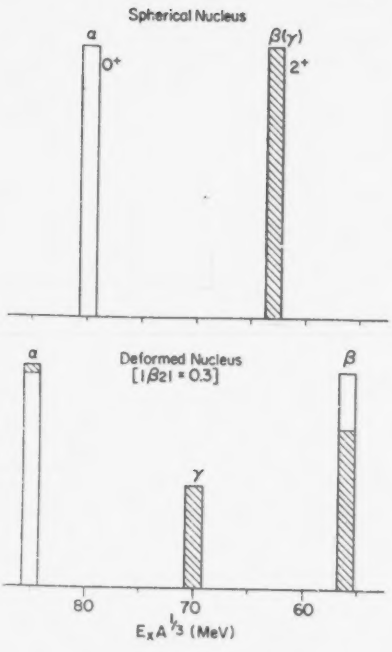

Fig. 3. Schematic strength distribution of the giant resonances in a deformed nucleus according to the model of Abgrall et al. (Ref. 5). α, β, γ are respectively, the monopole, axial and non-axial components.

strength from GMR to GQR in both cases is larger than that predicted by the theoretical models and this discrepancy between the theoretical and experimental results needs to be further explored.

For the transitional nuclei ^{148}Sm and ^{146}Nd, the ratios, R, of the cross sections for the high- (HE) and low-energy (LE) components ($R = (d\sigma/d\Omega)_{HE}/(d\sigma/d\Omega)_{LE}$) were extracted. The angular distribution for this ratio is displayed in Fig. 2(b) and compared with that for ^{144}Sm. Note that for the spherical nucleus ^{144}Sm, the HE and LE components correspond to the GMR and GQR, respectively. Also shown in Fig. 2(b) is a DWBA calculation for R for ^{144}Sm. While the values of R for ^{144}Sm very closely follow the DWBA predictions, they exhibit a strikingly different angular distribution in the case of ^{148}Sm. In fact, for ^{148}Sm, this ratio is more-or-less constant over the angular range 2° - 6°.

On the other hand, the observed ratio, R, for ^{146}Nd exhibits an angular distribution which is different from both ^{144}Sm (spherical) and ^{148}Sm (transitional) and appears to be in between these two nuclei. This somewhat puzzling feature could probably be understood in terms of the relative "softness" of ^{146}Nd, as explained below. On the other hand, this might be merely an experimental effect, arising from the errors introduced in the cross sections in the background subtraction procedure since the peak-to-valley ratios in the angular distributions are particularly sensitive to the details of the continuum background.

Although none of the aforementioned theoretical models dealing with the effects of deformation on collective vibrations has explicitly treated the transitional nuclei, certain predictions can be made for ^{148}Sm in the approach developed by Kishimoto.[4,5] In this model, a rigorous self consistency is applied which leads to a modification of the usual quadrupole-quadrupole interaction; this approach has successfully explained the broadening of GQR and the splitting of GMR in the deformed nuclei. In the transitional nucleus ^{148}Sm, the L = 0 and L = 2 modes are predicted to be in a phase of extensive mixing which arises from a combination of the splitting of the GMR and successive couplings of the GQR with the low-lying collective 2^+ state (E_x = 0.55 MeV) in ^{148}Sm. As a result, both components of the GR peak would share the L = 0 and L = 2 strengths and the two "usual" components of the GR peak would show more-or-less identical angular distributions - a combination of the L = 0 and L = 2 angular behaviors. The experimental observations for ^{148}Sm are consistent with these predictions. The ^{146}Nd data, however, does not show similar agreement; it might be attributable to the relative "softness" of ^{146}Nd. This nucleus probably lies just on the verge of transition from spherical to deformed shape, and, accordingly, its behavior is closer to that of a spherical nucleus. In a similar way, an "incomplete" mixing of L = 0 and L = 2 modes would explain the increase in the value of R for ^{148}Sm at 0° since the L = 0 character of the HE component would strongly manifest itself at 0°.

It is clear from the above discussion that a considerable amount of additional theoretical and experimental effort is required to fully understand the behavior of collective modes in the transitional nuclei. It is hoped that the measurements reported herein would encourage further exploration

of this important aspect of the collective behavior of nuclei. Measurements on other transitional nuclei, specifically ^{146,150}Sm and ^{148}Nd might be particularly instructive.

References

*Presently at the University of Notre Dame, Notre Dame, IN.

[1]T. Kishimoto, J. M. Moss, D. H. Youngblood, J. D. Bronson, C. M. Rozsa, D. R. Brown and A. D. Bacher, Phys. Rev. Lett. 35, 552 (1975).

[2]U. Garg, P. Bogucki, J. D. Bronson, Y. -W. Lui, C. M. Rozsa, and D. H. Youngblood, Phys. Rev. Lett. 45, 1670 (1980).

[3]U. Garg, P. Bogucki, J. D. Bronson, Y. -W Lui, and D. H. Youngblood, Progress In Researc 1981-1982, Cyclotron Institute, Texas A&I University, p. 2.

[4]C. M. Rozsa, D. H. Youngblood, J. D. Bronson, Y. -W. Lui, and U. Garg, Phys. Rev. C 21, 125 (1980).

[5]T. Kishimoto, (unpublished).

[6]Y. Abgrall, B. Morand, E. Caurier, and B. Grammaticos, Nucl. Phys. A346, 431 (1980).

[7]D. Zawischa, J. Speth, and D. Pal, Nucl. Phys. A311, 445 (1978).

[8]K. E. G. Lobner, M. Vetter, and V. Honig, Nucl. Data Tables A7, 495 (1970).

GIANT RESONANCES IN ^{24}Mg AND ^{28}Si

Y. -W. Lui, J. D. Bronson, U. Garg*, M. Parkin and D. H. Youngblood

Only a small portion of the total monopole strength has been identified in nuclei with A < 64. Lebrun et al.[1] studied the giant resonance region in ^{27}Al, ^{40}Ca, ^{56}Fe and ^{58,60}Ni using inelastic scattering of 108.5 MeV ^{3}He particles at small angles and reported a small amount (<10% EWSR) of concentrated monopole strength situated close to the excitation energy of the giant quadrupole resonance (GQR). Van der Borg et al.[2] have performed a detailed study of the isoscalar strength distributions in ^{24,26}Mg, ^{28}Si and ^{40}Ca; they found a large amount of the E2 EWSR exhausted between 14 and 27 MeV, consistent with earlier studies by Youngblood et al.[3] who investigated ^{24}Mg, ^{27}Al, and ^{28}Si with 126 MeV inelastic alpha scattering at angles larger than 10°. Some evidence of E0 strength was also found; however, there are uncertainties in most of the $J^{\pi} = 0^{+}$ assignments due to lack of data points at very forward angles ($\theta < 6°$) in their experiment.

We have investigated the GR region of ^{24}Mg and ^{28}Si using inelastic scattering of 129 MeV alpha particles over the angular region of 0°-10° to identify monopole strength by its distinctive signature near 0°.[4] The experimental setup and beam preparation methods were similar to those discussed in detail in Ref. 4. Considerable care was taken to minimize spurious contributions from the beam as well as slit scattering. The ^{24}Mg target was an isotopically enriched (>99%) metallic foil with thickness of 1 mg/cm^2. The ^{28}Si target was dismounted from a 8.8 μm thick silicon detector and the corresponding thickness was 2.05 mg/cm^2. The inelastically scattered alpha particles were detected in the focal plane of the Enge Split-Pole spectrograph with a 40-cm long resistive wire proportional counter backed by an NE102 plastic scintillator. Details of the electronic setup, the data acquisition system, and the distorted wave Born approximation (DWBA) calculations are discussed in Ref. 4.

Data were taken at twelve angles between θ_{lab} = 0° and 12° for ^{24}Mg and at nine angles between θ_{lab} = 0° and 8.6° for ^{28}Si. Sample ^{24}Mg and ^{28}Si spectra are shown in Fig. 1. The background-subtracted spectra for both nuclei are shown in Fig. 2. In ^{28}Si, a distinct difference between 0° and 4° spectra in the GR region indicates the presence of substantial monopole strength in this nucleus. In ^{24}Mg, although some E0 strength was identified in the GR region, it is not as concentrated as in ^{28}Si.

Analyses of ^{28}Si data were done by integrating two regions between 15.3 MeV and 23.0 MeV as labeled in Fig. 1. The angular distributions of these two regions and the two low-lying 3-states at 6.88 MeV and 10.17 MeV, respectively, are shown in Fig. 3 along with the corresponding DWBA calculations.[5] The optical potentials used for these calculations were taken from Ref. 6. The DWBA calculations for the low-lying 3-states are in good agreement with the experimental data. The

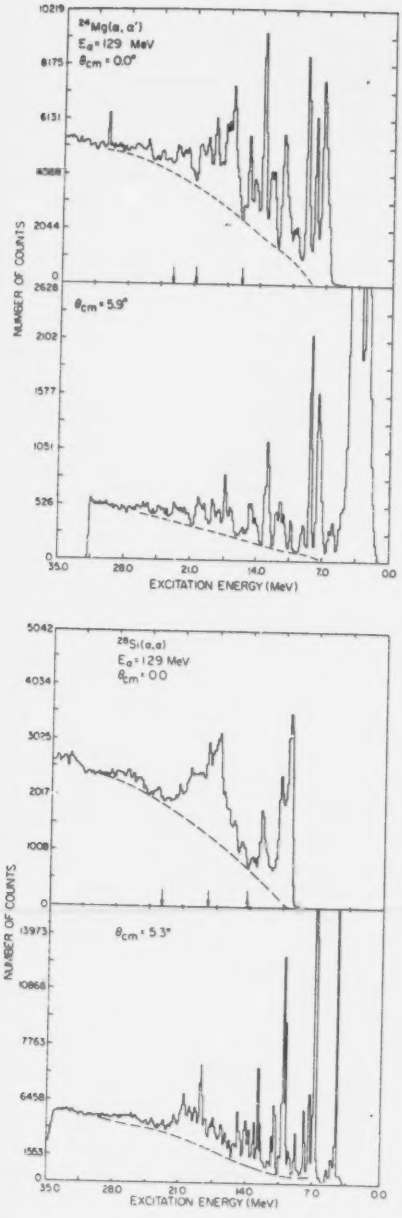

Fig. 1. Energy spectra of ^{24}Mg and ^{28}Si at 0° and 4°.

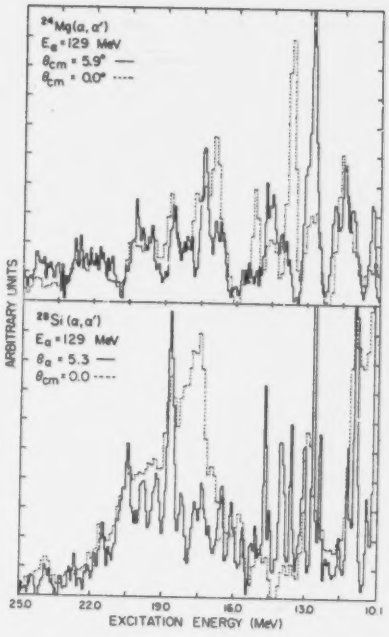

Fig. 2. Background subtracted spectra of ^{24}Mg and ^{28}Si at 0° and 4°.

experimental data of the two regions are also in resonable agreement with a combination of L = 0 and L = 2 calculations. A similar analysis was performed for the ^{24}Mg data; the angular distributions of the 8.36 MeV 3^- state and the GR region are shown together with the DWBA calculations in Fig. 4. Comparison between the experimental data and the calculations shows that multipolarities other than L = 2 may be present in the GR region. Table I shows the J^π assignment and the EWSR strengths of the structures in the GR region. Unlike ^{28}Si, the E0 strength found in ^{24}Mg is spread over several groups.

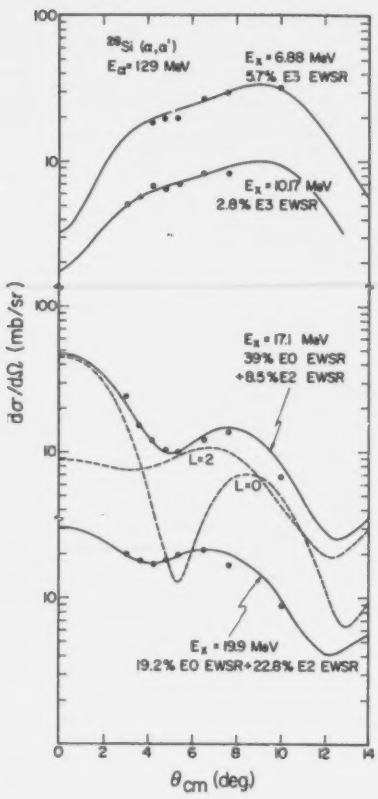

Fig. 3. Angular distributions obtained for the 6.88 MeV state, 10.17 MeV state, and the 17.2 MeV and 19.9 MeV groups of ^{28}Si. The curves are DWBA calculations for the ℓ-transfer indicated.

Table I. J^π assignments and EWSR strengths obtained for ^{24}Mg and ^{28}Si.

Nucleus	E_x(MeV)	J^π	EWSR(%)*
^{24}Mg	8.36	3^-	4.2
	16.0-20.8	0^+	13.0
		2^+	10.0
	20.8-23.1	4^+	3.0
		0^+	3.0
		2^+	2.2
		4^+	1.4
^{28}Si	6.88	3^-	5.7
	10.17	3^-	2.8
	15.48-17.9	2^+	8.5
		0^+	39.0
	17.9-23.0	2^+	22.8
		0^+	19.2

*EO EWSR were based on Satchler version 2 form factor.[7]

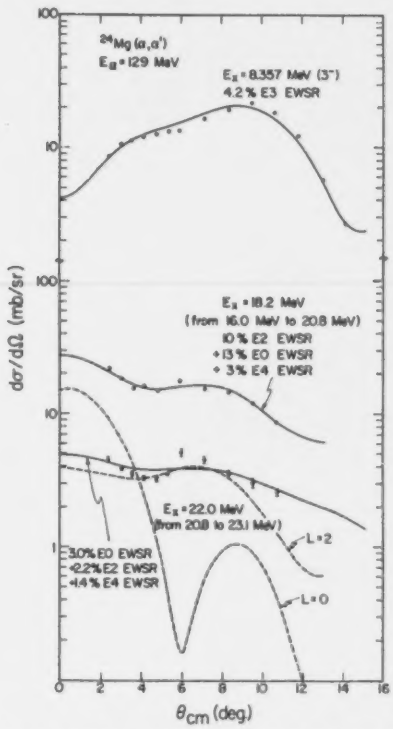

Fig. 4. Angular distributions obtained for the 8.36 MeV state and several other groups in the GR region of ^{24}Mg. The curves are DWBA calculations for the ℓ-transfer indicated.

References

*Presently at University of Notre Dame, Notre Dame, IN 46556.

[1]D. Lebrun, M. Buenerd, P. Martin, P. de Saintignon, and G. Perrin, Phys. Lett. 97B, 358 (1980).

[2]K. van der Borg, M. N. Harakeh, and A. van de Woude, Nucl. Phys. A365, 243 (1981).

[3]D. H. Youngblood, C. M. Rozsa, J. M. Moss, D.R. Brown, and J.D. Bronson, Phys. Rev. C 15, 1644 (1977).

[4]D. H. Youngblood, P. Bogucki, J. D. Bronson, U. Garg, Y. -W. Lui, and C. M. Rozsa. Phys. Rev. C 23, 1997 (1981).

[5]Program DWUCK, received from P. D. Kunz, University of Colorado.

[6]D. H. Youngblood, J. M. Moss, C. M. Rozsa, J. D. Bronson, A. D. Bacher, and D. R. Brown, Phys. Rev. C 13, 994 (1976).

[7]G. R. Satchler, Nucl. Phys. A195, 1 (1972).

FUNDAMENTAL INTERACTIONS AND FEW NUCLEON STUDIES

PARITY VIOLATION IN PROTON-PROTON SCATTERING

D. M. Tanner, R. E. Tribble, C. A. Gagliardi, Y. Mihara, R. Neese, and J. Sullivan

In previous progress reports, we discussed the experimental setup which we have developed to search for parity violation in proton-proton scattering. During the past year, we have tested all of the system components and performed our first measurement of the longitudinal analyzing power at an incident beam energy of 50 MeV. A preliminary analysis of the experiment has been completed. We present below results of the analysis along with a discussion of various systematic effects which either have been estimated or measured.

Several improvements are underway which should help to reduce substantially some of the dominant systematic effects that plagued us during the last experiment. The beam line polarimeter just after the solenoid has been modified to scan for both P_x and P_y components of polarization. This polarimeter will be relocated after the 47° bending magnet thus giving us two polarimeters in the drift space between the bending magnet and the scattering chamber. The bases on the phototubes have been rebuilt to reduce any nonlinearities inherent in the original bases. Also the electronics modules are being improved to reduce d.c. offsets to less than 1 mV. In addition to the polarimeter, we are now testing some centroid monitors that would remain fixed in the beam. These monitors ultimately can be used to correct for small position changes by feedback loops coupled to a bending magnet. A feedback loop connected to the axial line buncher has been tested and found to reduce substantially the difference in beam intensity for the + and - helicities. Finally, a number of modifications of the polarized ion source are underway. These are detailed in a separate section of this report.

For reference, a layout of the experimental apparatus is shown in Fig. 1. The data collected in the parity-violation experiment consist of two types, polarimeter data and chamber data. The polarimeters yield information on the beam's intensity profiles and polarization profiles. In order to provide statistical accuracy in the polarization profiles, the data from the polarimeters were summed over the entire run. POL. 1 was used to determine the average polarization during the run. POL. 3, which is located near the entrance to the chamber, measured the transverse polarization components in the longitudinally polarized beam. The polarization profiles, $P_y(x)$ and $P_x(y)$, for

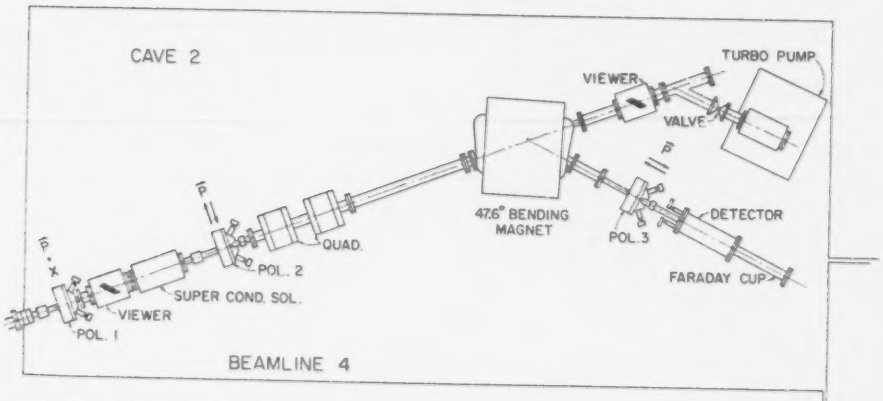

Fig. 1. Experimental arrangement for the parity-violation measurement. P represents the orientations of the beam polarization as the beam traverses the precession elements, superconducting solenoid and 47.6° bending magnet.

POL. 3 (3X and 3Y) and their corresponding intensity profiles, IP(x) and IP(y) are shown in Figs. 2 and 3. The effect of these polarization profiles on the measurement of $p_z A_z$ is discussed below.

The chamber data yield measurements of $p_z A_z$, $-p_y A_y$, $-p_x A_x$, and beam modulation (FC). The spectra shown in Figs. 4, 5, 6, and 7 represent $p_z A_z$, $-p_y A_y$, $-p_x A_x$ and FC, respectively. The analysis of the spectra is as follows. The spectra are used to generate centroids and uncertainties in the centroids using standard statistical equations.[1] The centroid is then compared to a null measurement. The null measurement is the centroid of the spectra with a null signal (93Ω terminator) acting as input into the LIAs. A simple conversion calculation yields the number desired, N, where N = $p_z A_z$, $-p_y A_y$, $-p_x A_x$, or FC. The expression for the calculation is:

$$N = (\text{centroid-null})(\text{RIA-C})(\text{FSS})(\text{GAIN})^{-1}(1.11)^{-1} \quad (1)$$

where RIA-C is the rotary integration amp calibration factor and is 1.14×10^{-3}/channel, FSS is full-scale sensitivity of the LIA used (FSS =50 μV for $p_z A_z$ and FSS = 250 μV for the other three), GAIN is the the gain of the analog dividers (GAIN = 1 v for $p_z A_z$ and FC, and GAIN = 2.5 v for $p_y A_y$ and $p_x A_x$), and the factor $(1.11)^{-1}$ is from a dc amplification built into the LIA units.

Using Eq. (1) for the four spectra of interest lead to the result,

$$p_z A_z = (2.0 \pm 1.2) \times 10^{-7},$$
$$-p_y A_y = -(7.5 \pm 1.5) \times 10^{-7},$$
$$-p_x A_x = -(7.5 \pm 1.6) \times 10^{-7},$$

and $$FC = (24.6 \pm 0.5) \times 10^{-6}.$$

In a separate measurement we find that $A_y = A_x = 1.1 \times 10^{-2}$ for the hydrogen target.

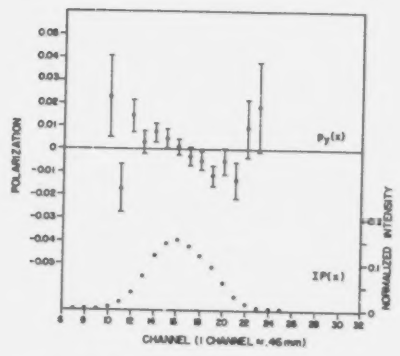

Fig. 2. Polarization and intensity profiles of the longitudinally polarized beam measured with POL. 3 X-scan.

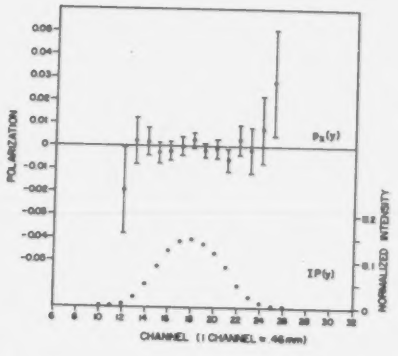

Fig. 3. Polarization and intensity profiles of the longitudinally polarized beam measured with POL. 3 Y-scan.

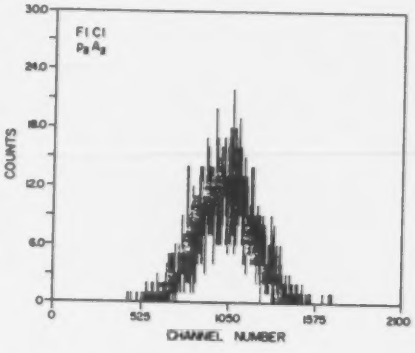

Fig. 4. The $p_z A_z$ spectrum.

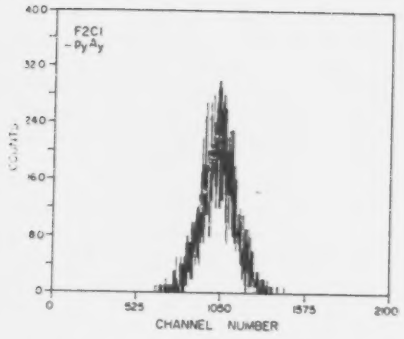

Fig. 5. The p_yA_y spectrum.

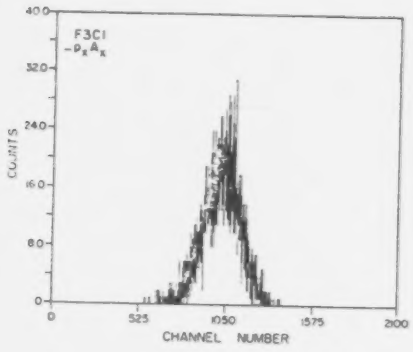

Fig. 6. The p_xA_x spectrum.

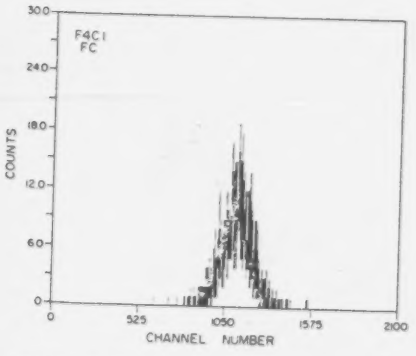

Fig. 7. The FC spectrum.

The uncertainties calculated above assume that the distribution is Gaussian and that the fluctuations in the data are statistical. In order to investigate any fluctuations, the data were reanalyzed as a function of time. The data were separated into ≈ 20 minute intervals producing 48 measurements of p_zA_z, $-p_yA_y$, $-p_xA_x$ and 22 measurements of FC. For each interval (run), centroids were calculated and the value of the centroid-null was determined. A calculation of weighted means and reduced χ_ν^2 for each signal yield

p_zA_z = (1.6 ± 1.1) x 10^{-7}, χ_ν^2 = 2.8,
$-p_yA_y$ = -(6.0 ± 1.3) x 10^{-7}, χ_ν^2 = 7.0,
$-p_xA_x$ = -(4.3 ± 1.3) x 10^{-7}, χ_ν^2 = 23.2,
and FC = (25.3 ± 0.2) x 10^{-6}, χ_ν^2 = 5.6,

where each uncertainty quoted is determined using the uncertainty of each data point to estimate the uncertainty in the mean. The large values of χ_ν^2 indicate that nonstatistical fluctuations are sizeable.

An investigation of the sources of these fluctuations was necessary. The fluctuations in the p_yA_y and p_xA_x measurements were due to actual changes in the average polarization through the course of the experiment. Any $p_x(p_z)$ component of polarization in the initial beam can be precessed into a $p_y(p_x)$ component in the chamber. These components could fluctuate with drifts in the magnetic elements of the ion optics system and changes in the cyclotron. Another possibility would be drifts in the spin precession elements. For example, a drift in the 47.6° bending magnet would introduce a change in the p_x component of polarization. The superconducting solenoid is not expected to drift (this would introduce a p_y component), but it was periodically powered down and back up again which could result in a change in p_y. A complete analysis of the effect of the average polarization component on the measurement of p_zA_z will be discussed below.

The most disturbing fluctuations are those present in the measurement of p_zA_z. Whether these fluctuations are due to polarization effects or some other systematic effect is a matter which warrants further investigation.

A separate test was performed using a completely unpolarized beam. Data were collected for about four and one-half hours and analyzed in the same manner as the p_zA_z experiment. The results of the weighted means and reduced χ_ν^2 for 14 points are:

$p_z A_z$ = -(1.9 ± 2.7) x 10^{-7}, χ_ν^2 = 1.8,
$-p_y A_y$ = (0.2 ± 2.3) x 10^{-7}, χ_ν^2 = 1.6,
$-p_x A_x$ = -(2.0 ± 2.2) x 10^{-7}, χ_ν^2 = 1.6,
FC = -(0.9 ± 1.3) x 10^{-7}, χ_ν^2 = 0.8,

where the uncertainties are statistical. The large values of χ_ν^2 indicate that fluctuations are present in the unpolarized beam also.

To study the matter further, a noise signal (=300 mV peak-to-peak) was input the LIA used for the $p_z A_z$ measurement. The noise source was the output of two amplifiers in series where the first amplifier had no input. This generates a noise signal that can be adjusted in amplitude and is composed of many frequencies. Data were collected for about 24 hours which resulted in 71 20-minute measurements. The same analysis as before resulted in a χ_ν^2 = 1.5 for the noise data. The calculation of the uncertainty in each data point was rechecked and verified following this measurement. The large χ_ν^2 is puzzling and likely indicates that the fluctuations are a result of noise in the signal frequency near the reference frequency (23.8 Hz) that enter into the LIAs phase-sensitive detector and produce spurious results. The solution to this problem is not easy for it involves reducing the low frequency components of noise in the beam. These low frequency components are likely introduced in the polarized ion source and during acceleration in the cyclotron.

The noise characteristics of the unpolarized beam data should be equivalent to that of the polarized beam data. For this reason, the χ_ν^2 for the unpolarized beam data provide the "best estimate" of a correction factor for the uncertainty in the polarized data. If we multiply each uncertainty in the polarized data by the square root of the corresponding χ_ν^2 for the unpolarized data, the raw data values then become,

$p_z A_z$ = (1.6 ± 1.5) x 10^{-7},
$p_y A_y$ = -(6.0 ± 1.6) x 10^{-7},
$p_x A_x$ = -(4.3 ± 1.6) x 10^{-7},
and FC = (25.3 ± 0.2) x 10^{-6}.

A number of systematic effects have been investigated. Of these, the beam intensity modulation yields the largest correction factor. Using an unpolarized beam, the beam intensity was artificially modulated and the false asymmetry A_F was measured. The average beam modulation during the run, FC = (25.3 ± 0.2) x 10^{-6}, was used to determine the effect on $p_z A_z$ with a result of A_F = (4.8 ± 0.3) x 10^{-7}.

The effect of a possible dc offset in the I signal divided by a modulating FC signal is present in the beam intensity modulation test. It is estimated that the dc offset effect could change A_F by as much as 20%; the uncertainty in A_F should be increased to reflect this. Combining both the beam intensity modulation and the dc offset effect yields an estimate of the false asymmetry in $p_z A_z$ of A_F = (4.8 ± 1.0) x 10^{-7}.

A test was performed with the longitudinally polarized beam to determine the effect of a beam misalignment. Using the 47.6° bending magnet, the beam was displaced 0.6 mm (1.2 mm) to the left (right) as measured in POL3, corresponding to an angle change of -0.03°(+0.06°). The false asymmetry (corrected for beam intensity modulation) measured for the left and right displacement was -(8 ± 6) x 10^{-7} and (22 ± 12) x 10^{-7}, respectively. Using these results, one can predict that an angle change of ±0.03° will result in a false effect in $p_z A_z$ of ±(10 ± 13) x 10^{-7}. The angle information was obtained by measuring the change in the beam's position in POL3 (a change in the centroid of the intensity profile) and then calculating the angle using the known distance between POL3 and the center of the 47.6° magnet. Unfortunately, two beam position monitors located in separate planes in front of the detector system are needed to correctly predict the beam's angle of entrance into the detector. However, the use of only one monitor will yield an upper limit on the effect of $p_z A_z$ due to a possible beam misalignment. An analysis of the intensity profiles in POL3 throughout the entire run resulted in a possible angle change of ±0.2 x 10^{-2} degrees. However, since the angle could change and not be detected, a more conservative estimate of the angle change might be ±0.4 x 10^{-2} degrees (twice what was seen during the run). This yields a false effect in $p_z A_z$ of ±(1.3 ± 1.7) x 10^{-7}.

The angle of entrance into the chamber is expected to fluctuate throughout the run (due mainly to drifts in beam focusing and steering elements). An estimate of the upper limit (at one standard deviation) for the effect is 3 x 10^{-7} which assumes the worst case of an angle misalignment of 0.4 x 10^{-2} degrees for the entire run. The average uncertainty in the $p_z A_z$ measurement due to this effect is estimated to be no more than 1/3 of this upper limit.

The effect of an average p_y polarization component was investigated by adjusting the current in the solenoid to yield an average p_y of $\pm(1.7 \pm 0.02) \times 10^{-2}$. Combining the results of the two cases (+ and -) leads to an effect on $p_z A_z$ of $+(1.4 \pm 0.8) \times 10^{-7}$. The actual polarization during the measurement of $p_z A_z$ averaged to $p_y = (5.5 \pm 1.2) \times 10^{-5}$ with a largest single value of $p_y = (7.6 \pm 0.8) \times 10^{-4}$. Using the larger value, the upper limit of the effect on $p_z A_z$ is estimated to be $(6 \pm 3) \times 10^{-9}$. The effect of an average p_x component was determined by using results of an earlier experiment where $p_x = -(8.7 \pm 0.1) \times 10^{-3}$. An analysis of the earlier experiment taking into account beam intensity modulation leads to a possible effect of $-(4 \pm 6) \times 10^{-7}$. During the $p_z A_z$ measurement, the average p_x was $(5 \pm 6) \times 10^{-5}$ with a largest single value of $(1.0 \pm 0.1) \times 10^{-3}$. Using the larger value, the upper limit of the effect on $p_z A_z$ is estimated to be $\pm(0.5 \pm 0.8) \times 10^{-7}$.

The effect of a non-uniform polarization profile can be estimated by using $A_{FY} = a_{y1} \overline{p_y(x)x}$ where $a_{y1} = 4 \times 10^{-5}$ mm^{-1} and $\overline{p_y(x)x}$ is the first moment of the polarization profile.[2] Using the measured first moment value for the 3X scan yields $A_{FY} = -(2.0 \pm 0.6) \times 10^{-7}$. A similar expression for the 3Y scan ($A_{FX} = a_{x1} \overline{p_x(y)y}$) yields $A_{FX} = (0.2 \pm 0.6) \times 10^{-7}$, assuming $a_{x1} = a_{y1}$. For both A_{FY} and A_{FX} the value of a_{y1} is a calculated estimate. Because the a_{x1} and a_{y1} could not be measured with the present setup, the effect of A_{FX} and A_{FY} is not corrected in our data but an uncertainty is added to reflect the effect.

The beam position modulation effect was monitored by calculating the centroid in the intensity profiles for + and - polarization states. If the beam position modulation is estimated to be 0.023 mm (half of 0.1 channel), then using the result that a 0.6 mm displacement in POL3 gave a $(10 \pm 13) \times 10^{-7}$ effect in $p_z A_z$ yields an upper limit estimate of $(0.4 \pm 1.0) \times 10^{-7}$ for the position modulation.

To test the overall stability of the electronic equipment, constant current sources were used as input into the current-to-voltage convertors and data were taken in the same manner as during an experiment. This resulted in a value of $(2 \pm 4) \times 10^{-9}$ for the LIA monitoring $p_z A_z$. This implies that there are minimal false asymmetries due to electronic instability and ground loop effects.

Table I lists all of the systematic effects and the uncertainty assigned to each. The raw data value of $p_z A_z = (1.6 \pm 1.5) \times 10^{-7}$ can be corrected for the beam intensity modulation by using the predicted effect of $(4.8 \pm 1.0) \times 10^{-7}$. This yields $p_z A_z = -(3.2 \pm 1.8) \times 10^{-7}$. All the other uncertainties are then added in quadrature to yield a more conservative result $p_z A_z = -(3.2 \pm 2.9) \times 10^{-7}$. The value of p_z is determined from the value of p_y in POL1 which was (0.69 ± 0.02). The final results for the longitudinal analyzing power are then

$$A_z = -(4.6 \pm 2.6) \times 10^{-7}$$

after a beam intensity modulation correction only. For a more conservative estimate of the uncertainties,

$$A_z = -(4.6 \pm 4.2) \times 10^{-7}.$$

The range of the first result (where only the beam intensity modulation was used as a correction) is probably a more acceptable range. The second result involves uncertainties that are likely over estimated.

Table I. Systematic effects in the measurement of $p_z A_z$.

Systematic Effect	Effect on $p_z A_z$ ($\times 10^{-7}$)	Uncertainty ($\times 10^{-7}$)
Beam Modulation	$+(4.8 \pm 1.0)$†	1.0
Beam Misalignment	3.0††	1.0
Average Polarization		
$\overline{p_y}$	(0.06 ± 0.03)††	<0.1
$\overline{p_x}$	(0.5 ± 0.8)††	<0.5
Polarization Profile		
$\overline{p_y(x)x}$	$-(2.0 \pm 0.6)$†††	2.0
$\overline{p_x(y)y}$	$+(0.2 \pm 0.6)$†††	0.2
Beam Position Modulation	$\pm(0.4 \pm 1.0)$††	<0.4
Electronics Effects	(0.02 ± 0.04)†	0.04

†Measured effect
††Upper limit for effect
†††Calculated effect

The result agrees with the measurement at SIN where a final value $A_z = -(2.3 \pm 0.8) \times 10^{-7}$ for 45 MeV protons has resulted from a series of experiments.[3] We also find agreement with a first result from Berkeley of $A_z = -(1.3 \pm 2.3) \times 10^{-7}$ at 46 MeV.[4]

References

[1]P. R. Bevington, Data Reduction and Error Analysis for the Physical Sciences, (McGraw-Hill, New York, 1969).

[2]M. Simonus, R. Henneck, Ch. Jacquemart, J. Lang, W. Haeberli, and Ch. Weddigen, Nucl. Instrum. Methods 177, 471 (1980).

[3]W. Haeberli, in Polarization Phenomena in Nuclear Physics - 1980, edited by G. G. Ohlsen et al., AIP Conf. Proc. No. 69 (American Institute of Physics, New York, 1981), p. 1340.

[4]P. von Rossen, U. von Rossen, and H. E. Conzett, in Polarization Phenomena in Nuclear Physics - 1980, edited by G. G. Ohlsen et al., AIP Conf. Proc. No. 69 (American Institute of Physics, New York, 1981), p. 1442.

BETA DECAY OF N = Z NUCLEI

C. A. Gagliardi, R. E. Tribble and E. Takada

The ft values of the $0^+ \rightarrow 0^+$ superallowed Fermi transitions provide the most sensitive measurement of the vector coupling constant in nuclear β decay. Eight cases, from ^{14}O to ^{54}Co, have been measured to an accuracy of <0.3%. "Outer" radiative corrections δ_R and charge-dependent corrections δ_C must be applied to the measured ft values before G_V may be extracted. Theoretical uncertainties in the radiative corrections, which are independent of the structure of the individual nuclear states, are <0.1%. The charge-dependent corrections, which depend upon the nuclear structure, are considerably less certain. Two approaches have been taken to determine them. In one approach,[1] they are calculated separately for each decay, and the corrected ft values, $Ft = ft(1 + \delta_R)(1 - \delta_C)$, are compared. In the second approach,[2] the charge-dependent corrections are treated in a average way by fitting $ft(1 + \delta_R) = (ft)_{Z=0} + aZ^{1.86}$. In either case, the corrections increase approximately as Z^2, so it is of interest to measure heavier cases in order to test our understanding of these effects. The highest Z $0^+ \rightarrow 0^+$ Fermi transition whose ft value has been measured to date is ^{62}Ga. We are attempting to extend the series to include ^{66}As and ^{70}Br. Only half-lives have been reported[3] for these two decays.

We are beginning with a measurement of the half-lives using a different technique. The activities are produced in the $^{58}Ni(^{10}B,2n)^{66}As$ and $^{58}Ni(^{14}N,2n)^{70}Br$ reactions, using pulsed beams from the cyclotron. The beam irradiates the target for 130 msec, and then is turned off for 1.3 sec by clamping the cyclotron dee voltage. During the beam-off period, high-energy β rays emitted from the target are multiscaled. High-energy β rays emitted are identified by their range in the four-element plastic scintillator telescope shown in Fig. 1. The anode output of the four detectors feed directly into fast discriminators whose thresholds are set at <1/2 of minimum ionizing. A four-fold coincidence with a 20 nsec resolving time selects the β rays. Absorbers placed between the detectors determine the telescope threshold by ranging out low-energy β rays. The scintillators are thin (≈ 1 mm thick each) in order to minimize

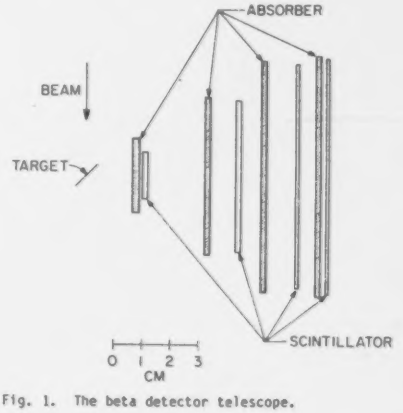

Fig. 1. The beta detector telescope.

the background due to Compton-scattered γ rays. The fast electronics and low thresholds guarantee that systematic errors due to rate-dependent effects, such as pile up and gain shifts, are negligible. This is a substantial improvement over the previous experiment, that used a large-volume plastic scintillator to detect β rays and pulse-height discrimination to separate high-energy positrons from the intense background due to low-energy β rays and Compton-scattered γ rays.

Figure 2 shows the beta-decay rate as a function of time for an ^{66}As measurement. The results were obtained in a 2 hour run with a 250 nA $^{10}B^{2+}$ beam and an effective β ray energy threshold of 4.8 MeV. At present, the data is being fit to extract the lifetime.

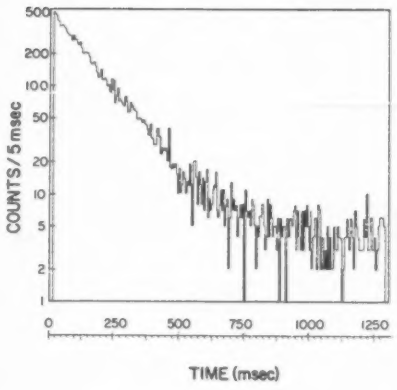

Fig. 2. An ^{66}As beta-decay rate as a function of time during a preliminary run.

References

[1] J. C. Hardy and M. Harvey, Nucl. Phys. A284, 269 (1977).

[2] D. H. Wilkinson, A. Gallmann and D. E. Alburger, Phys. Rev. C 18, 401 (1978).

[3] D. E. Alburger, Phys. Rev. C 18, 1875 (1978).

VECTOR AND TENSOR ANALYZING POWERS FOR THE CONTINUUM NEUTRONS FROM THE REACTION D($\vec{d}$,$\vec{n}$)ppn AT LAB ANGLES 0° AND 18°

W. F. Woodward, S. Nath, L. C. Northcliffe, J. C. Hiebert, J. Doumas, W. M. Schmidt, and W. D. Cash

We report here on the measurement of vector and tensor analyzing powers, A_y (θ_{lab} = 18°), A_{zz} (0°) and A_{yy} (18°) for the ^{2}H($\vec{d}$,n)ppn reaction at E_d = 45.5 MeV as a function of the breakup neutron energy. Details on the technique of measurement and analysis have been reported in last year's progress report.[1] Polarized deuterons from the cyclotron were focused onto a deuterium target, contained in a high pressure (200 psig), liquid-nitrogen-cooled gas cell with HAVAR foil entrance and exit windows. A 90° bending magnet situated directly behind the target gas cell deflected the charged particles out of the cell into a heavily shielded Faraday cup.

Neutrons from the reaction entered collimators oriented at 0° and 18° and were detected by NE102 scintillators positioned 6.0 m from the neutron production target. Appropriately tagged time and pulse-height signals for each event were acquired by a computer and written onto a magnetic tape for subsequent off-line analysis. A time-of-flight spectrum for neutrons from the D(d,n)x reaction at 0° is shown in Fig. 1. During data acquisition, the beam polarization was switched between each of four polarization states in a cycle of approximately 0.5 sec duration by switching the rf transitions at the ion source. The clock driving the polarization controller was free running so that each polarization state was effective for the same average period. An upper limit on any correlation between beam current and beam polarization state is of the order 10^{-5}.

The beam polarization was measured before the experiment by a method similar to that described by Collins and Glavish.[3] A 45 keV polarized deuteron beam from the ion source was focused onto a tritiated target and the asymmetry of neutrons produced via the ^{3}H($\vec{d}$,$\vec{n}$)^{4}He reaction yielded values of p_{zz} for each of the two rf transitions operated one at a time. The overall uncertainty in the value of p_{zz} was estimated to be ±0.03.

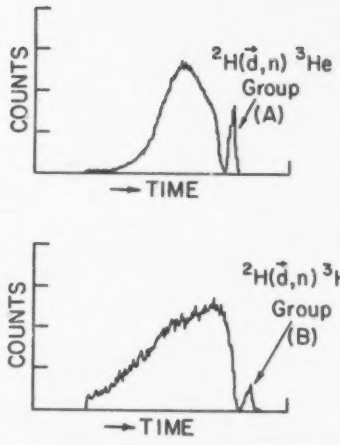

Fig. 1. Background subtracted time of flight spectrum for neutrons from the $^2H(\vec{d},n)X$ reactions at 0°(A) and 18°(B).

The measured analyzing power values for the breakup neutrons are shown in Figs. 2, 3 and 4. Since the uncertainty in the beam polarization was much smaller than statistical uncertainties in the measured asymmetries, only statistical errors are shown in the plots. The larger error bars for the values at lower neutron energies are a result of the relatively high pulse-height threshold set during off-line analysis to exclude background. The $^2H(\vec{d},n)$ breakup reaction produces neutrons in an energy continuum up to 40 MeV at θ_n = 0° and 38 MeV at θ_n = 18°. The A_y (18°) values are

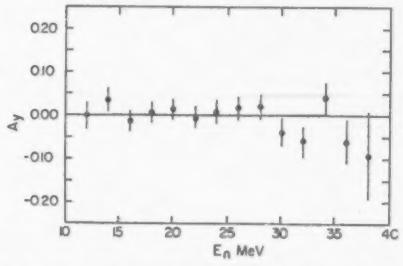

Fig. 2. Measured vector analyzing power Ay for the $^2H(\vec{d},n)2pn$ reaction at θ_n = 18°.

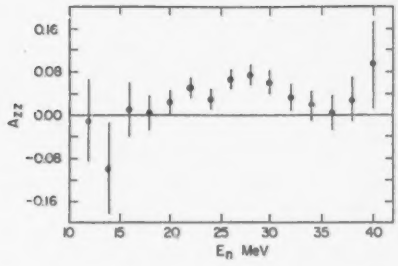

Fig. 3. Measured tensor analyzing power A_{zz} for the $^2H(\vec{d},n)2pn$ reaction at θ_n = 0°.

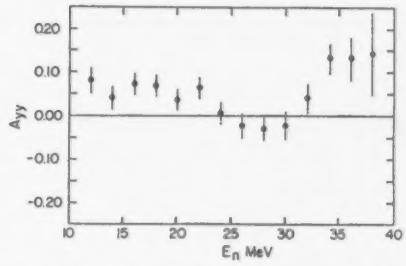

Fig. 4. Measured tensor analyzing power A_{yy} for the $^2H(\vec{d},n)2pn$ reaction at θ_n = 18°.

consistent with zero below about 30 MeV, but above that energy become increasingly negative. The tensor analyzing powers show more interesting behavior. The dip in A_{yy} (18°) betwen 24 and 32 MeV (Fig. 4) seems to correspond to a rise in A_{zz} (0°) (Fig. 3). between 26 and 34 MeV. The A_y, A_{yy} and A_{zz} values for the neutrons from the two-body reaction channel $D(d,n)^3He$ obtained in the same experiment are discussed elsewhere in this report (p. 30).

References

[1]W. F. Woodward, S. Nath, L. C. Northcliffe, M. J. Marolda, K. Washington, A. Doumas, W. D. Cash, Progress in Research 1981-82, Cyclotron Institute, Texas A&M University, p. 28.

[2]D. P. May, R. E. Tribble, and J. M. Moss, Nucl. Instrum. Methods 174, 167 (1980).

[3]E. R. Collins and H. F. Glavish, Nucl. Instrum. Methods 30, 245 (1964).

VECTOR AND TENSOR ANALYZING POWERS FOR THE $^2H(\vec{d},n)^3He$ REACTION AT LAB ANGLES 0°, 1°, AND 18°

W. F. Woodward, J. C. Hiebert, W. D. Cash, J. Doumas, S. Nath, W. M. Schmidt, and L. C. Northcliffe

In conjunction with the measurements of analyzing powers at θ_{lab} = 0°, 18° for the $^2H(\vec{d},n)$ breakup reactions at Ed = 45.5 MeV reported above, data were also obtained for the $^2H(\vec{d},n)^3He$ reaction. In a subsequent measurement, data were obtained for these same reactions at E_d = 52 MeV. In the latter experiment, the 0° neutron collimator was utilized for measurements at θ_{lab} = 1° with a left-right pair of 2"D x 3" NE102 scintillators and an up-down pair of 1"D x 2" NE102 scintillators. With these detectors A_{xx} and A_{yy} could be measured and thereby A_{zz} (1°) is also determined.

Other than the four detectors at 1° lab and the removal of the steel inserts for the 0° neutron collimator, the experimental setup was the same as for the 45.5 MeV experiment. An event descriptor word containing detector and beam polarization state identification was read into the computer together with ADC words containing scintillator pulse height and neutron time of flight. A beam line polarimeter utilizng d-^{12}C elastic scattering at ± 60°(lab) was located just upstream of the $^2H(d,n)$ target. The elastic deuterons at 60° were degraded with 0.125 in. of aluminum and detected by 150 micron surface barrier ΔE detectors followed by NE102 stopping counters.

Roughly half of the 52 MeV data have been analyzed at this time. The measured vector analyzing power for 52 MeV d + ^{12}C scattering at 60° (lab) of Mairle et al.,[1] has been used to determine the rf transition efficiencies at the PIS; α for the 2-6 transition and β for the 3-5 transition. Typical values measured during one run were α = 0.886 ± 0.070 and β = 0.805 ± 0.070 which lead to a predicted p_y (both transitions on) = -0.560 ± 0.051 versus the measured value - 0.526 ± 0.07. The errors quoted are statistical. We note that when only the 2-6 transition is on, $p_y = -\alpha/3$ and $p_{yy} = +\alpha$, while when the 3-5 transition is on, $p_y = -\beta/3$ and $p_{yy} = -\beta$ (the solenoid being in the antiparallel mode).

The measured analyzing powers are shown in Table I. The values quoted at 45.5 MeV represent a completed analysis of these data. The 52 MeV analysis is still being refined and about half of the data acquired are not included in these preliminary results. The value of $A_{zz}(1°)$ is obtained from the measured quantities A_{xx} and A_{yy} through the relation $A_{xx} + A_{yy} + A_{zz} = 0$. Data at 18° and 52 MeV and at 1°, 18° and 30 MeV have also been acquired and will be analyzed in the near future.

Table I. Analyzing powers for the $^2H(\vec{d},n)^3He$ reaction.

En(MeV)	θ_{lab}	A_y	A_{yy}	A_{xx}	A_{zz}
45.5	0°	0.00±0.02	0.18±0.02	0.18±0.02	-0.36±0.04
45.5	18°	0.00±0.06	0.54±0.07		
52.0	1°	0.008±0.	0.178±0.083	0.19±0.13	-0.37±0.15

References

[1]G. Mairle, K. T. Knopfle, H. Riedesel, G. J. Wagner, V. Bechtold and L. Friedrich, Nucl. Phys. A339, 61 (1980).

HEAVY ION REACTIONS

Complete Fusion

Fragmentation

Collective Modes

PARTICLE EMISSION IN THE REACTIONS OF ^{32}S WITH ^{27}Al

K. Hagel, P. L. Gonthier, J. B. Natowitz, M. N. Namboodiri, L. Adler,
R. Choudhury, S. Simon, S. Kniffen and G. Berkowitz

Often the emission of light particles from compound nuclei produced in heavy ion reactions has been interpreted in light of comparisons with the statistical model predictions. Recently, Blann and Komoto[1] have studied the effects of the deformation of the shape of compound nuclei which result from high angular momentum states on the ratios of various decay channels and on the energy spectra of emitted light particles. In these statistical model calculations the transmission coefficients and the yrast energies were modified in various ways to take into account the deformation of the decaying nuclei. The cross sections and energy spectra of the emitted light particles were shown to depend strongly on the different assumptions for the transmission coefficients and the yrast energies.

We have continued to pursue the investigation of deformation effects on the α-particle emission from compound nuclei formed in the reactions of ^{32}S with ^{27}Al at the projectile energies of 105, 130, 147, 160, and 214 MeV. At the projectile energy of 105 MeV the measured total fusion cross section leads to a critical angular momentum in the sharp cutoff model of 29 ħ. According to the rotating liquid drop model[2] (RLDM) compound nuclei having angular momenta up to this value are nearly spherical with a predicted ratio of the major axis to the radius of the spherical nucleus of 1.1. This ratio increases to 1.8 for compound nuclei with an angular momentum of 45 ħ. The critical angular momentum extracted from the total fusion cross section at the projectile energy of 214 MeV is 45 ħ. Therefore the energy range from 105 MeV to 214 MeV allows us to study the effects of deformation on the emission of α particles.

The light particles were detected in three-detector telescopes consisting of Si detectors and the heavy products were detected in a telescope which employed a gas-ionization chamber as the ΔE detector backed by an E Si detector. Both singles and coincidence data were recorded event-by-event and later analyzed off line.

A version of the statistical model code CASCADE[3] has been modified and converted into a Monte Carlo program in order to calculate angular distributions and energy spectra in the laboratory frame of reference. A event-by-event file containing the information for each decay is analyzed, and correlations are then constructed. Default values of all parameters[3] were used in the calculations with the exception of the radius parameter, ROLDM, for the spin cutoff factor and for calculating the moment of inertia. A value of 1.4 was used for this parameter.

In Fig. 1, we compare the singles energy spectra of α particles at 25° and 45° to the calculated energy spectra for the projectile energy of 105 MeV. The calculated spectra shown as histograms are normalized to the data. The most probable energies agree with those calculated; however, the calculated energy spectra are slightly narrower than those observed especially in the lower portion of the spectra. Perhaps a small adjustment in the parameters could improve the agreement.

Using the same parameters, we have performed a calculation at the projectile energy of 214 MeV. Figure 2a presents the singles energy spectra of α particles together with the calculated spectra (histograms) assuming a spherical, rigid moment of

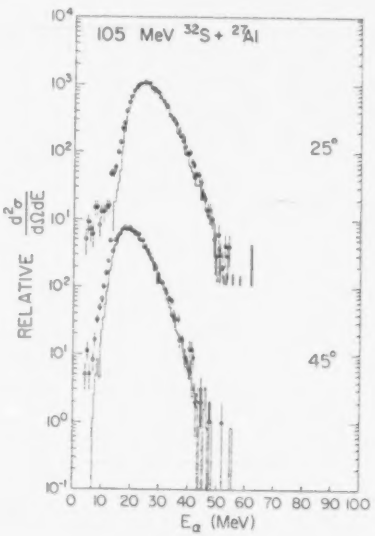

Fig. 1. Singles energy spectra of α-particles observed at 25° and 45° in the reactions of 105 MeV ^{32}S with ^{27}Al. The histograms are calculated spectra using a Monte Carlo version of the code CASCADE.

inertia. The calculated spectra are broader, extending to higher energies, and have most probable energies which are slightly higher than those observed. This is especially noticeable at 60°. In Fig. 2b, we compare the singles data to the calculated spectra using a moment of inertia predicted by the RLDM. From this comparison, it can be seen that a deformed shape results in calculated spectra which are more consistent with the data. The high energy portions of the calculated spectra become narrower agreeing with the experimental spectra. However, the calculated most probable energies are still higher than the observed ones and the lower portions of the calculated energy spectra do not agree with the data.

In order to make certain that the observed single α particles come from fusion reactions and not from other processes, we have performed a coincidence measurement between fusion residues at +6° and +15° and α particles on the opposite side of the beam from the detected fusion residues at angles of -15°, -30°, -45°, -60°, and -90°.

In Figs. 3a and 3b, we compare the experimental spectra of α particles in coincidence with fusion residues at +6° and +15°, respectively, with those calculated assuming a spherical, rigid moment of inertia. The calculated spectra were normalized in each case to the peak of the experimental spectra at -90°. The experimental spectra are normalized with respect to each other. As in the case of the singles, the calculated spectra at all angles appear to be broader extending to higher

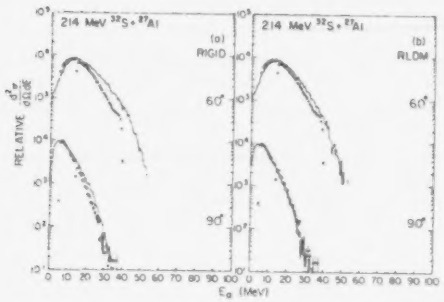

Fig. 2. Singles energy spectra of α-particles observed at 60° and 90° in the reactions of 214 MeV ^{32}S with ^{27}Al. The histograms are calculated spectra using a Monte Carlo version of the code CASCADE. The calculation assumes (a) a spherical rigid moment of inertia; and (b) the RLDM moment of inertia.

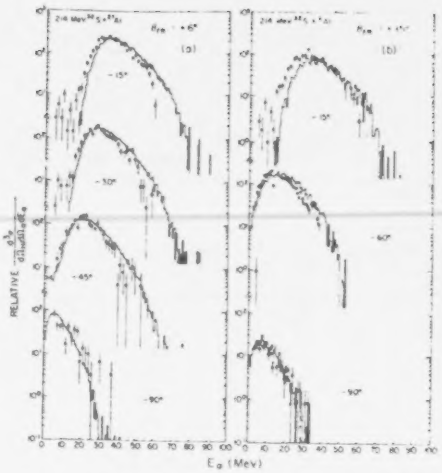

Fig. 3. Energy spectra of α particles in coincidence with fusion residues observed at (a) +6° and (b) +15° from the reactions of 214 MeV ^{32}S with ^{27}Al. The lab angles of the α telescope are indicated. The histograms are the calculated coincidence spectra using a Monte Carlo version of the code CASCADE assuming a spherical, rigid moment of inertia.

energies than the measured spectra, and the calculated most probable energies are higher than those observed, especially in the forward direction. The calculated most probable energies agree better in the case of fusion residues at +6° than for fusion residues at +15°.

In Figs. 4a and 4b, we compare the same experimental data as in Fig. 3a and 3b with calculated spectra assuming a moment of inertia as predicted by the RLDM. Here the high energy portions of the α spectra are in better agreement with the data. However, the calculated most probable energies are still higher than those observed, especially for α particles in coincidence with fusion residues at +15° (Fig. 4b).

Figure 5 shows a plot of the excitation energy for a ^{59}Cu nucleus as a function of its angular momentum. The dashed curve represents the rotational energy for a spherical, rigid moment of inertia, and the dotted curve represents the rotational energy for the nucleus with the moment of inertia as predicted by the RLDM. Also shown in this figure are the entrance channel partial cross sections as a function of angular momentum for both

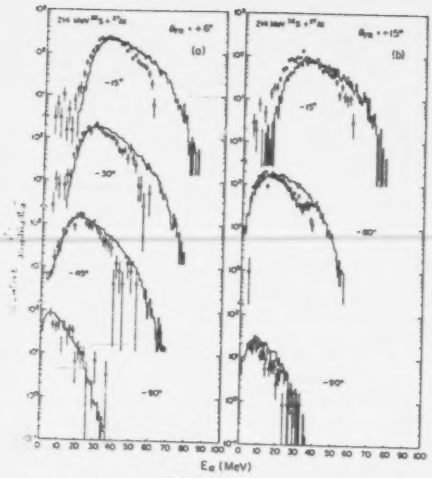

Fig. 4. Energy spectra of α particles in coincidence with fusion residues observed at (a) +6° and (b) +15° from the reactions of 214 MeV ^{32}S with ^{27}Al. The lab angles of the α telescopes are indicated. The histograms are the calculated coincidence spectra using a Monte Carlo version of the code CASCADE assuming a RLDM moment of inertia.

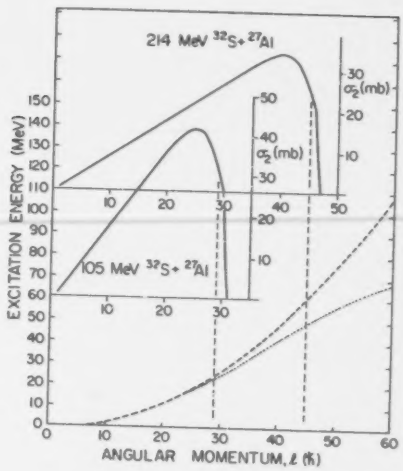

Fig. 5. Excitation energy as a function of the initial angular momentum for a ^{59}Cu nucleus. The rotational energy for a spherical nucleus is represented by a dashed curve. The rotational energy for a nucleus with a RLDM moment of inertia is shown as a dotted curve. The entrance channel partial cross sections as a function of angular momentum are shown for the projectile energies of 105 and 214 MeV.

projectile energies. For the projectile energy of 105 MeV, there is little deformation, and the deformed moment of inertia is nearly that of a spherical nucleus. However, at the projectile energy of 214 MeV, the compound nuclei can have angular momenta up to 45 $\hbar$. At this value the RLDM moment of inertia is quite different than the spherical moment of inertia. With the spherical, rigid moment of inertia the calculation predicts a larger probability of high energy α particles than in the case assuming the RLDM moment of inertia, since the emitted α particles must remove more orbital angular momenta. Therefore, the spectra are broader extending to higher energies than those α spectra calculated with the RLDM moment of inertia. For the first chance α particles the calculation predicts most probable decay energies of 22 MeV and 18.5 MeV assuming a spherical, rigid moment of inertia and a RLDM moment of inertia, respectively.

However, the most probable energies and the lower portion of the α-energy spectra are not reproduced by the calculation with a moment of inertia predicted by the RLDM. Some other effect must be included in order to reproduce the data. If the compound nuclei are deformed as suggested by the calculation, then the Coulomb barrier for the α particles would be altered. The probability of α emission is largest at the tips or larger axis of the deformed nucleus than emission along the smaller axis or the "waist" of the deformed nucleus. The Coulomb barriers are expected to be reduced by 30% at the tips or larger axis of the nuclei. As Blann and Komoto[1] have shown, this effect leads to an enhancement of the lower portion of the α-energy spectra relative to the spherical calculation.

We are currently exploring ways to take into account deformation by varying various parameters in an attempt to understand better the experimental observations.

References

[1]M. Blann and T. T. Komoto, Phys. Rev. C 24, 426 (1981).

[2]S. Cohen, F. Plasil, and J. W. Swiatecki, Ann. Phys. (N.Y.) 82, 557 (1974).

[3]F. Pühlhofer, Nucl. Phys. A280, 267 (1977).

LIGHT PARTICLE EMISSION IN THE REACTIONS 310 MeV ^{16}O WITH Ti

P. L. Gonthier, H. Ho, M. N. Namboodiri, J. B. Natowitz, L. Adler,
S. Simon, K. Hagel, S. Kniffen, and A. Khodai

Over the past several years, we have continued to investigate nonequilibrium phenomena manifested in fusion-like and binary collisions in the reactions of 310 MeV ^{16}O with Ti. Experimental details and much of the results have been previously reported.[1,2] Recently, we have used schematic calculations to model kinematic effects of nonequilibrium emission and of sequential emission to further our understanding of the nature of these reactions.

In Figs. 1a and 1b, we present the experimental energy spectra of α particles in coincidence with fusion-like residues (FLR), $Z \geq 16$, detected at +20° on the opposite side and on the same side of the beam, respectively. The LILITA[3] calculation assumes a critical angular momentum of 69 ħ and includes the experimental energy thresholds for the FLR. The apparent structures in the calculated spectra are a result of poor statistics in the Monte Carlo calculation. In the sharp cutoff approximation, this critical angular momentum corresponds to the total cross section of 1130 ± 80 mb for the observed group of FLR. Comparisons of the observed and calculated spectra reveal that at forward angles the bump in the lower portion of the energy spectra seems to be approximately consistent with evaporation of the compound system. However, the experimental spectra show an additional large probability of α particles with energies much greater than those predicted by the calculation. It appears then that the experimental spectra contain a high-energy, nonequilibrium component and a low-energy component. The most probable energies of the lower energy component are smaller than those predicted by the calculation especially in the forward direction. At the most backward angle of -130° in Fig. 1a, the slope of the experimental spectrum is steeper than the one calculated.

Integrating over the α-energy spectra, we obtain the angular correlations shown in Fig. 2 for FLR at +20° and +40°. The calculation (dashed curves) has the same normalization factors as in the energy spectra. The calculated yields at -130° and +140° for FLR at +20° are higher than the experimental ones since the α-energy thresholds were not included in the calculation. The excess yield in the experimental correlations in the forward direction results from the high-energy α particles.

The estimated average multiplicities of the low-energy, equilibrium component and the high-energy, nonequilibrium component of α particles and protons are tabulated in Table I.

Table I. Average multiplicities of light particles in coincidence with heavy residues

θ_{FLR}	High E_α	Low E_α	High E_p	Low E_p
+20°	0.4±0.1	1.6±0.3	0.3±0.1	0.6±0.3
+40°	1.1±0.2	1.3±0.1	0.2±0.1	0.5±0.3

The data indicate that there is a significant fraction of collisions producing FLR in which high-energy α particles and protons are emitted. Further, the comparison of the low-energy component in the coincidence energy spectra of α with the calculated spectra indicates that the most probable energies in the experimental spectra are smaller than those calculated and that the experimental spectra are steeper than the calculated spectra at the most backward angles. Fast ejectiles emitted at the early stages of incomplete fusion processes would remove energy and angular momentum from the composite system and less linear momentum would be transferred than in complete fusion processes. The energy spectra of particles evaporated from the incompletely fused system would be steeper and would have smaller most probable energies in the lab system. Thus the data suggest an incomplete fusion or massive transfer mechanism analogous to the type studied by several groups with different techniques.[4]

In order to study further the kinematic effects of such a mechanism, we have performed a calculation which allows the emission of a fast particle and then follows the statistical decay of the residual composite system. The observed energy and angular distributions of the ejectiles were parametrized with simple functions. The parameters were adjusted to fit the high energy portion of the α-particle spectra. The calculations were done for both ^{4}He and ^{8}Be as fast ejectiles. For each calculation a multiplicity of one was assumed for the fast ejectile. The transfer of ^{4}He to the target nucleus with ^{12}C as a fast ejectile is not expected to contribute to the observed FLR, since for these

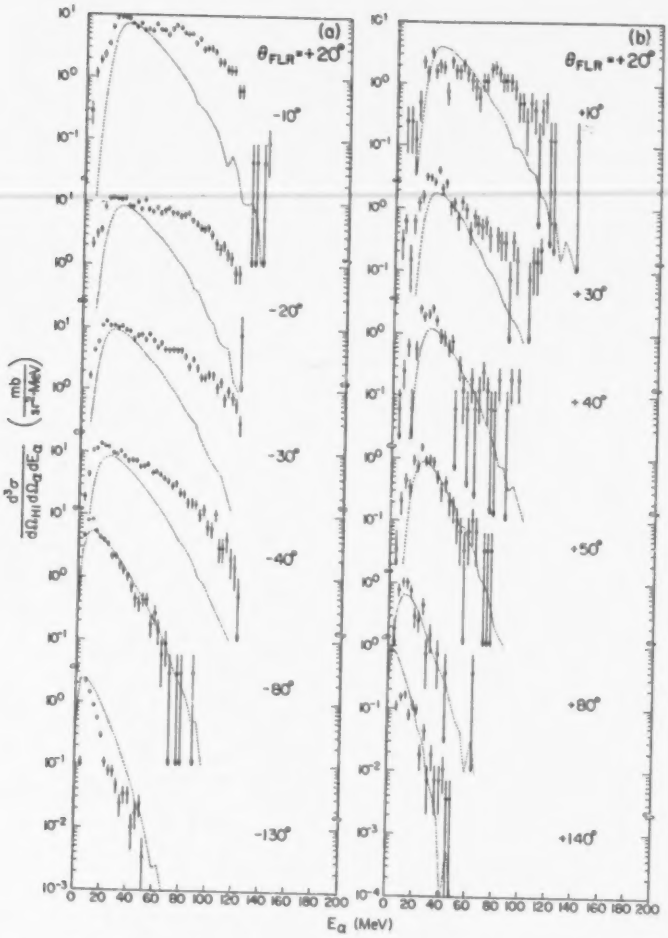

Fig. 1. Energy spectra of α particles detected in coincidence with heavy products (Z > 16) observed at +20° from the reactions of 310 MeV ^{16}O with Tl. Error bars represent the statistical errors. Spectra on the (a) opposite side of the beam from the detected heavy products and (b) on the same side of the beam at the indicated angles. The calculated spectra are represented by dashed curves and have been normalized to the data at -80°.

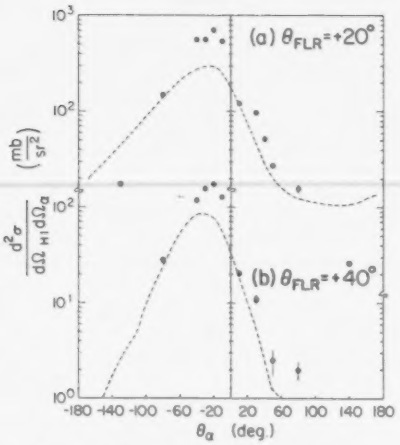

Fig. 2. Angular correlations of α particles in coincidence with heavy products (Z > 16) from the reactions of 310 MeV ^{16}O with Ti observed at (a) +20° and (b) +40°. The calculated correlations are shown as dashed curves. The same normalization factor was used as in Fig. 1.

collisions there would be insufficient momentum transfer for the FLR to be detected above the energy threshold of our HI detector.

The singles energy spectra of the FLR are compared to the calculated spectra in Fig. 3. The apparent structures in the calculated spectra are a result of poor statistics in the Monte Carlo calculation. As the transferred mass decreases the energy spectra shift downward. The discrepancy between the data and the calculated for the complete fusion (solid curves) is always in the lower portion of the energy spectra. The comparisons reinforce the conclusion that both fusion and incomplete fusion are contributing to the production of FLR. From the normalization of the calculated energy spectrum assuming complete fusion, we derive an upper limit to the total fusion cross section of 265 mb. This upper limit corresponds to 12% of the total reaction cross section.

The kinematic effects of the emission of high-energy particles cause the angular distribution of the FLR to broaden as shown in Fig. 4 in which the experimental singles angular distribution of FLR is compared to the calculated angular distributions resulting from complete and incomplete fusion processes. The solid curve represents the calculation for complete fusion. The dashed curve is the cal-

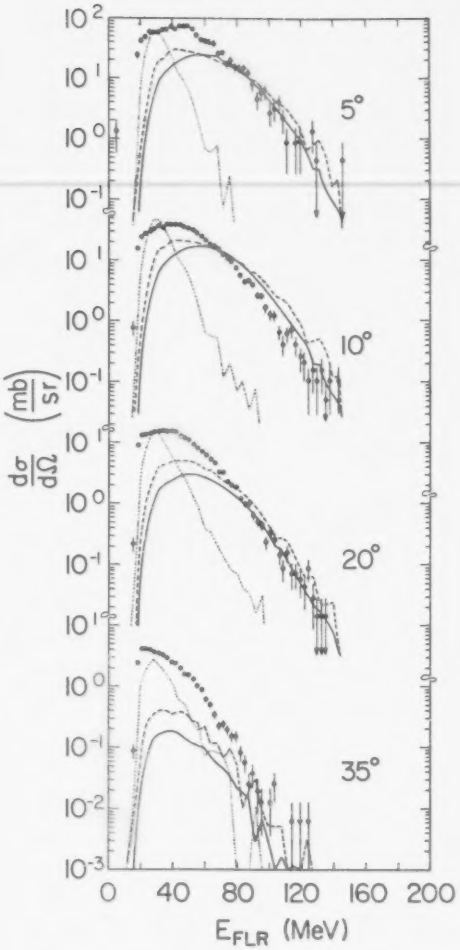

Fig. 3. Singles energy spectra of heavy products (Z > 16) from the reactions of 310 MeV ^{16}O with Ti observed at the indicated angles. The solid curves are the predictions of the code LILITA for complete fusion. The dashed curves are the calculated spectra assuming that a fast ^{4}He is ejected and that a ^{12}C fuses with the Ti nucleus. The dotted curves are the calculated spectra assuming that a fast ^{8}Be is ejected and that a ^{8}Be fuses with the Ti nucleus. The calculated spectra were normalized to the data at 5°.

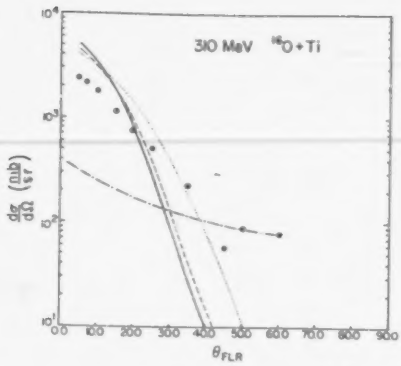

Fig. 4. Singles angular distributions of heavy products (Z > 16) from the reactions of 310 MeV ^{16}O with Ti. The solid curve is the prediction of the code LILITA for complete fusion. The dashed curve is the calculated distribution assuming that a fast ^{4}He is ejected and that a ^{12}C fuses with the Ti nucleus. The dotted curve is the calculated distribution assuming that a fast ^{8}Be is ejected and a ^{8}Be fuses with the Ti nucleus. The dot-dashed curve is the singles angular distribution of aluminum normalized to the distribution of heavy products at 50.

culation for the massive transfer of ^{12}C and a fast ^{4}He ejected. The dotted curve is the calculation for the massive transfer of ^{8}Be and a fast ^{8}Be ejected. To estimate the maximum contribution of heavy products resulting from deep-inelastic collisions, we have normalized the singles angular distribution of Z = 13 (shown as a dot-dashed curve) to the singles angular distribution of FLR at 50°. Products of atomic number 13 are representative[2] of the group of target-like fragments which result from deep-inelastic collisions. Although at the most backward angles, target-like fragments from deep-inelastic collisions may dominate, their contribution cannot be greater than 360 mb or 30% of the total cross section of FLR. With this upper limit together with the upper limit of the total fusion cross section, we extract a lower limit of 505 mb for the cross section of incomplete fusion processes.

The shape of the calculated angular distribution resulting from a ^{8}Be ejected (dotted curve) is similar to the shape of the experimental distribution. The total multiplicity of 1 assumed for the fast ^{8}Be would produce two fast α particles per collision. This multiplicity is consistent with the measured average multiplicities of one for high-energy alphas and protons. On the basis of these studies, we can conclude that a major fraction of the total cross section of fusion-like residues results from incomplete fusion or massive transfer reactions indicating that the complete fusion cross section is very small at 20 MeV/u for this light system.

We have also observed nonequilibrium emission of α particles in coincidence with projectile-like fragments (PLF). Since the coincidence data are very similar for all PLF, we have combined the data to improve the statistics by adding the data for PLF ranging in atomic number from 4 to 10. The energy spectra of α-particles in coincidence with quasi-elastic PLF (QE-PLF) at +20° are shown in Figs. 5a and 5b and in coincidence with deep-inelastic PLF (DI-PLF) at +20° are shown in Figs. 5c and 5d. The presence of high-energy α particles in coincidence with PLF does not necessarily imply that they have a nonequilibrium origin, since sequential emission from the PLF also may lead to high energy α particles in the beam direction.

In order to estimate how much of the α particle cross section can in fact be explained in terms of the sequential decay of both PLF and target-like fragments (TLF), we have performed simple schematic calculations. The α-decay energies are parametrized with Boltzmann distributions and the primary energy and angular distributions in the laboratory frame of the decaying PLF are parameterized with Gaussians and exponentials whose means and widths vary smoothly with the laboratory angle of the primary PLF. Because of the two-body intermediate state, the primary distributions of the PLF determine the spacial distribution of the TLF prior to their decay. The emission of the light particles is assumed to be isotropic in the reaction plane defined by the HI-detector and the beam direction. The two cases considered are :

1) $^{16}O + {}^{48}Ti \longrightarrow {}^{16}O^{*} + {}^{48}Ti \longrightarrow {}^{12}C + \alpha + {}^{48}Ti$

2) $^{16}O + {}^{48}Ti \longrightarrow {}^{12}C + {}^{52}Cr^{*} \longrightarrow {}^{12}C + {}^{48}Ti + \alpha$

A simple analytical expression for the cross section can be obtained because of the assumption of the three-body final state. Case 1 provides the contribution to the α distributions from the decay of the ^{16}O and case 2 from the decay of the ^{52}Cr.

It is clear that, in reality, with 200 MeV excitation energy there will be many particles in the final state. The effect of multiple particle emission leads to broader angular correlations and broader α spectra and PLF spectra. The parameters are adjusted to fit the data at selected angles in which sequential decay processes are expected to dominate. After the shapes of the calculated energy spectra of both α particles and PLF reproduce the experimental spectra, then the calculated spectra are normalized to the data. Although many particles might be emitted in these collisions, with this procedure we are able on the average to account for the effects of multiple particle emission. In what follows we will be comparing the calculated energy spectra from this model for the above two cases to the α particle and PLF energy spectra obtained by adding together the spectra for the PLF of atomic numbers from 4 to 10. The experimental light particle energy thresholds have not been included in the calculation.

The dashed curves in Fig. 5 are the calculated α-energy spectra arising from the decay of the PLF (case 1) and the dotted curves are the result of the decay of the TLF (case 2). The solid curves are the sum of the two contributions.

The parameters for the decay of the TLF are adjusted to best describe the spectra at the backward angles of -80° and -130° where the decay of the PLF is not expected to contribute due to the kinematic restrictions and also where nonequilibrium effects are minimal. The decay energy distributions are adjusted to reproduce the shape of the α spectra at -80° and -130° in Figs. 5a and 5c. The contribution to the energy spectra from the decay of the TLF is adjusted to the tails in the spectra at -130° in Figs. 5a and 5c. This provides the normalization factor to be applied to other α angles for both α-energy spectra and PLF-energy spectra. The parameters for the primary energy distributions are adjusted to fit the PLF-energy spectrum at -80°.

The parameters for the contribution to the α distributions from the decay of the PLF are adjusted to reproduce the data at +50° together with the contribution from the decay of the TLF. At this angle the contribution of the PLF is normalized to the tails of the α-energy spectra at +50° in Figs. 5b and 5d. This factor for the PLF contribution is common to all other angles for both α spectra and PLF spectra. The assumption then is that at +50° the α-energy spectra can be explained entirely in terms of sequential emission processes. Therefore, the calculation gives an upper limit for the contribution of sequential emission processes.

For the decay of the quasi-elastic PLF (QE-PLF), one can observe that the forward emission is distinctly separated from the backwards emission in the calculated α-energy spectra at +10° and +30° in Fig 5b. Comparing these spectra to the same spectra for DI-PLF in Fig. 5d, we note that the separation is not as great since the emitting PLF are not moving as fast. This effect is manifested in the data at both +10° and +30°. However, the exnerimental spectra are not exhausted by the calculated spectra presumably because at these forward angles, sources of nonequilibrium α particles contribute to the spectra.

Comparing the calculation to the α-energy spectra on the opposite side of the beam, we find that the decay of the QE-PLF can contribute significantly to the higher energy portion of the spectra at forward angles (-10° in Fig. 5a) whereas the decay of the DI-PLF contribute to the lower portion of the spectra (-10° in Fig. 5c). This also is the effect of different source velocities. From these comparisons, most of the high energy α particles from -10° to -40° are not accounted for in terms of the sequential decay of both PLF and TLF.

It is also interesting to note that the lower portion of the energy spectra from -10° to -80° is not all accounted for by the calculation, especially notable in Fig. 5a. It would seem that after subtracting the calculated spectra for the sequential decay of both fragments from the experimental spectra, a broad high-energy component would remain and extend to low energy. This would indicate that the excess yield in the lower portion of the energy spectra might arise from a mechanism similar to the one which leads to the emission of high-energy α particles. However, if this is the case, then one would also expect a similar excess yield in the lower portion of the energy spectra for α particles in coincidence with FLR (Fig. 1). The absence of the excess in case of FLR suggests that these lower energy α particles are a result of some mechanism other than the one that leads to high-energy α particles.

In a similar manner, the calculation was performed for the α particles in coincidence with PLF at +40°. At this angle the contribution from

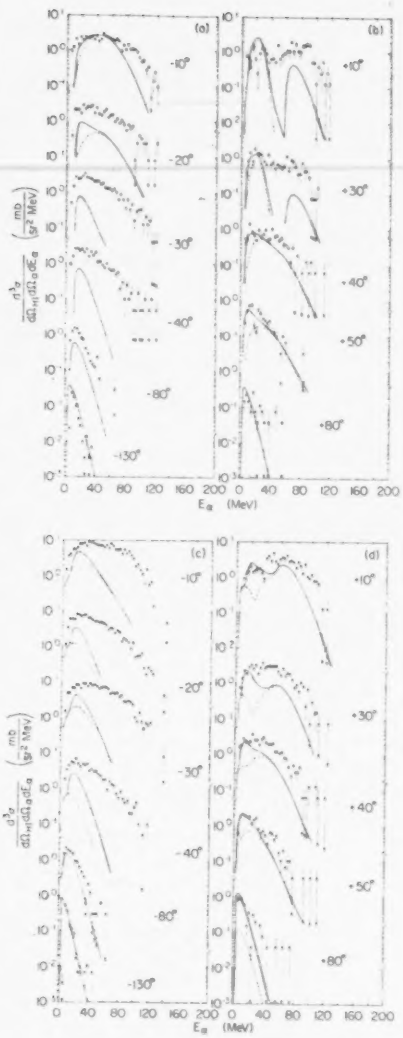

Fig. 5. Energy spectra of α-particles in coincidence (a) with quasi-elastic products (Z = 4 - 10); (b) and with deep-inelastic products (Z = 4 - 10); and (c) and (d) observed at +20°. The dashed curves are the calculated spectra for the decay of the PLF, the dotted curves for the decay of the TLF, and the sum of both contributions is represented by solid curves.

the quasi-elastic component is gone. Figures 6a and 6b show the α-energy spectra on the opposite side of the beam and on the same side of the beam as the detected PLF, respectively. As before, the calculation cannot explain the high-energy portion of the spectra in the forward direction from -10° to -40° on the opposite side of the beam in Fig. 6a. The calculation is in much better agreement on the same side of the beam in Fig. 6b with the exception of +10° where the calculation overestimates the data.

Figures 7a, 7b and 7c show the evolution of the angular correlations from low to high velocity α particles in coincidence with QE-PLF at +20°, with DI-PLF at +20° and with DI-PLF at +40°, respectively. Windows have been placed on the laboratory velocity of the α particles, and the average velocities are indicated. At the bottom of these figures are the angular correlations integrated over the whole energy spectrum of the α particles. The calculated contributions from the sequential decay of the PLF, from the decay of the TLF and the total contributions are indicated as dashed, dotted and solid curves, respectively. Since the experimental energy thresholds for α particles have not been included in the calculation, the experimental points at -130° and +140° fall below the calculated correlations.

The correlations with an average velocity of 5 cm/ns are representative of α particles with beam velocity. In the case of the QE-PLF, this angular correlation is symmetric with respect to the beam direction, whereas in the case of DI-PLF at both +20° and +40°, the correlations are asymmetric peaking at -10° regardless of the detection angle of the PLF. This indicates that these high velocity α particles are emitted during the early stages of the collision before the two nuclei have interacted strongly.

The component of the lower velocity α particles is represented by the correlations with an average velocity of 3 cm/ns. In these correlations, there is good agreement on the same side of the beam as the detected PLF. However, on the opposite side of the beam between -10° and -40° the calculation underestimates the experimental points. In case of the PLF at +40°, the peak of the contribution from the decay of the PLF has moved from -10° for the PLF at +20° to +10°. The shape of the experimental correlation on the

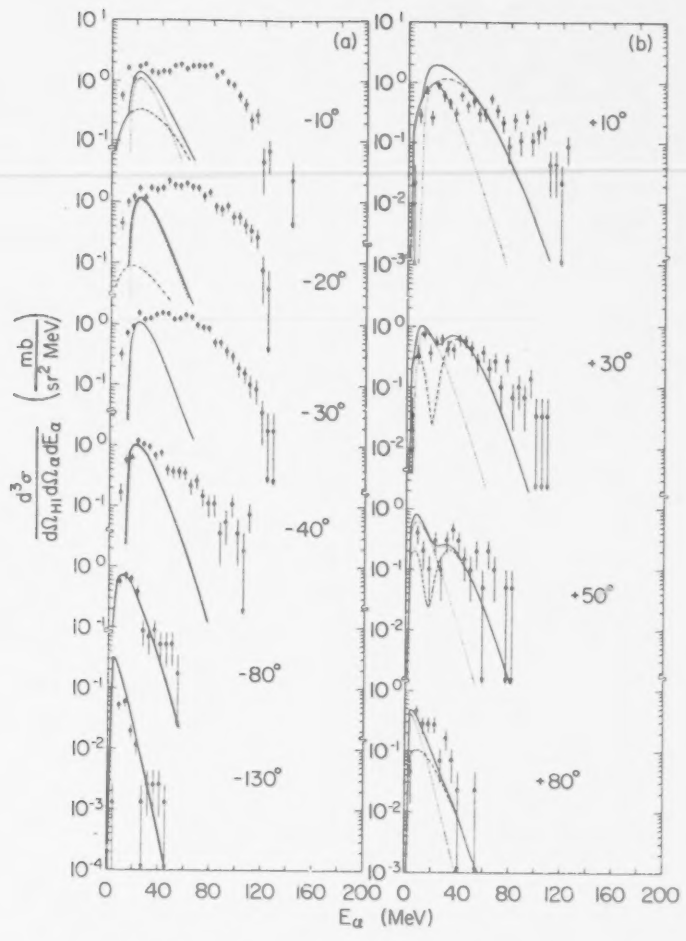

Fig. 6. Energy spectra of α particles in coincidence with deep-inelastic products (Z = 4 - 10) observed at +40°. The dashed curves are the calculated spectra for the decay of PLF, the dotted curves for the decay of the TLF, and the sum of both contributions is represented by solid curves.

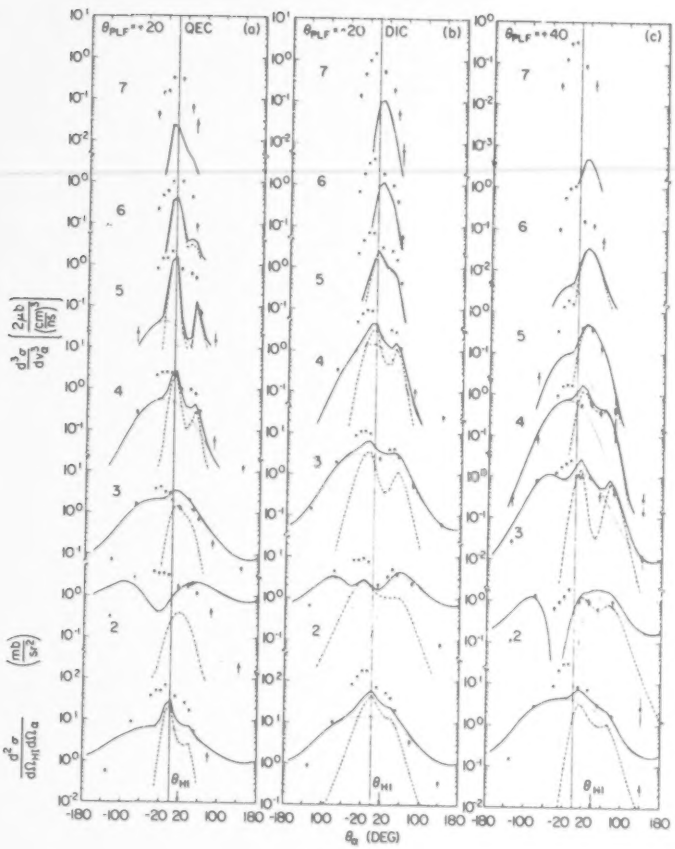

Fig. 7. Angular correlations of α particles in coincidence with (a) quasi-elastic products (Z = 4 - 10) observed at +20°; (b) with deep-inelastic products (Z = 4 - 10) observed at +20°; and (c) with deep-inelastic products (Z = 4 - 10) observed at +40. The correlations are plotted for different velocity windows in the laboratory velocity of the α particles. The average velocity for each window is indicated in units of cm/ns. At the bottom of the figures, the total correlations integrated over the entire velocity spectra of the α particles are shown.

opposite side of the beam becomes skewed in (c) as compared to (b). This dependence on detection angle of PLF might suggest that these lower velocity α particles are emitted during the interaction time but prior to the full acceleration of the two heavy fragments.

Integrating over the out-of-plane correlations, we have estimated the average multiplicities of α particles and protons in coincidence with PLF. The average multiplicities of the low-energy component and the high-energy, nonequilibrium component of α particles and protons are tabulated in Table II. Also listed in this table are the average multiplicities accounted for in terms of the sequential model calculations and those which are not accounted for by sequential emission processes. It should be noted, that the portion of the average multiplicities explained by sequential emission processes is an upper limit.

We can conclude that emission of high energy α particles and protons is observed to be a characteristic feature of quasi-elastic, deep-inelastic

Table II. Average multiplicities of light particles in coincidence with projectile-like fragments.

θ_{PLF}	High E_α	Low E_α	High E_p	Low E_p
+ 20° QE[a]	0.17 ± 0.03	1.4 ± 0.5	≈0.2	≈0.4
+ 20° DI[b]	0.28 ± 0.05	1.9 ± 0.5	0.51 ± 0.08	1.0 ± 0.1
+ 40° DI[b]	0.31 ± 0.06	2.1 ± 0.6	0.19 ± 0.03	0.78 ± 0.09

θ_{PLF}	SEQ. α	NONSEQ. α	SEQ. p	NONSEQ. p
+ 20° QE[a]	.63 TLF[c] .35 PLF[d]	.60	.35 TLF[c] .16 PLF[d]	0.1
+ 20° DI[b]	.44 TLF[c] .26 PLF[d]	1.5	.70 TLF[c] .26 PLF[d]	0.55
+ 40° DI[b]	.80 TLF[c] .19 PLF[d]	1.4	.74 TLF[c] .34 PLF	0

a) Quasi-elastic products Z = 4 - 10
b) Deep-inelastic products Z = 4 - 10
c) Sequentially Emitted From Target-like Fragments
d) Sequentially Emitted From Projectile-like Fragments

and fusion-like reactions. Average multiplicities of the order of one for these fast, high-energy α particles and protons in coincidence with any HI at +20° or +40° were estimated. The energy spectra of these fast particles are broad and extend to the lower portion of the spectra where sequential processes contribute. The angular correlations of high-energy light particles are narrow and asymmetric with respect to the beam direction peaking on the opposite side of the beam at -10° or -20°. These correlations are also independent of the identity of the coincident heavy ion and the heavy-ion detection angle indicating that these fast particles are emitted during the early stages of the collision.

The fast particles are emitted during the early phases of the interaction and remove energy and angular momentum, and the two fragments will either fuse resulting in incomplete fusion processes or undergo inelastic scattering resulting in incomplete deep-inelastic processes. The process responsible for the prompt emission of light particles appears to be the principal mechanism which limits complete fusion and leads to the observation of fusionlike residues. This is in contrast to the predictions of dynamic model calculations which predict the increase of deep-inelastic processes as the mechanism reducing the compound nuclear cross section.

Schematic calculations which model the sequential decay of projectile-like and target-like fragments have allowed us to observe a second component of α particles in coincidence with deep-inelastic and quasi-elastic projectile-like fragments. This component has an intermediate velocity between the velocities of the beam and the center-of-mass, appears as an excess yield in the direction of the recoiling target-like fragments and cannot be accounted for in terms of the sequential decay of both primary fragments. The lower ties of these light particles (as compared to the high velocity component) and their angular correlations indicate that these particles result from stronger interactions than those producing the fast particles and are emitted during the interaction but prior to the full acceleration of the two outgoing fragments. These particles may not necessarily have to be characterized as pre-equilibrium or nonequilibrium as in the case of the high velocity component. During the interaction a large amount of the relative kinetic energy may be converted into excitation energy and may be even fully dissipated due to short internal equilibration time. As a result, the lifetime for light particle emission becomes of the order of the interaction time.

References

[1]H. Ho, P. Gonthier, M. N. Namboodiri, J. B. Natowitz, L. Adler, S. Simon, K. Hagel, R. Terry, and A. Khodai, Phys. Lett. 96B, 51 (1980); P. Gonthier, H. Ho, M. N. Namboodiri, L. Adler, J. B. Natowitz, S. Simon, K. Hagel, R. Terry, and A. Khodai, Phys. Rev. Lett. 44, 1378 (1980).

[2]P. L. Gonthier, Ph.D. Dissertation, Texas A&M University (1980); P. L. Gonthier, H. Ho, M. N. Namboodiri, J. B. Natowitz, L. Adler, S. Simon, K. Hagel, S. Kniffen and A. Khodai, Submitted to Nucl. Phys.

[3]J. Gomez del Campo and R. G. Stokstad (unpublished) ORNL/TM-7295; J. Gomez del Campo, R. G. Stokstad, J. A. Biggerstaff, R. A. Dayras, A. H. Snell, and P. H. Stelson, Phys. Rev. C 19, 2170 (1979).

[4]T. Inamura, M. Ishihara, T. Fukuda, T. Shimoda, and H. Hiruta, Phys. Lett. 68B, 51 (1977); D. R. Zolnowski, H. Yamada, S. E. Cala, A. C. Kahler, and T. T. Sugihara, Phys. Rev. Lett. 41, 92 (1978); Yamada, D. R. Zolnowski, S. E. Cala, A. C. Kahler, J. Pierce, and T. T. Sugihara, Phys. Rev. Lett. 43, 605 (1979); K. Siwek-Wilczynska, E. H. du Marchie van Voorthuysen, J. van Popta, R. H. Siemssen, and J. Wilczynski, Phys. Rev. Lett. 42, 1599 (1979); Nucl. Phys. A330, 150 (1979); J. Wilczynski, K. Siwek-Wilczynska, J. van Driel, S. Gonggrijp, D. C. J. M. Hageman, R. V. F. Janssen, J. Lukasiak and R. H. Siemssen, Phys. Rev. Lett. 45, 606 (1980); Nucl. Phys. A373, 109 (1982).

MOMENTUM WIDTHS IN THE FRAGMENTATION OF 32 MeV/u ^{10}B

M. N. Namboodiri, R. K. Choudhury*, J. B. Natowitz, K. Hagel, L. Adler, P. L. Gonthier, H. Simon, S. Kniffen, R. Patton, B. Sterling, E. Tomasi†, C. Ngô†, C. Mazur† and M. Ribrag†

The characteristics of projectile fragmentation in peripheral heavy ion collisions in the intermediate energy range of 20-100 MeV/u has been the subject of several recent studies.[1-4] The interest in this process results from the expected occurrence of transitions in the nature of nuclear collisions from low-energy to high-energy behavior in this energy range. In the reactions of 860 Mev ^{20}Ne with Ni, Ag and Ta targets we observed[1] that the forward angle spectra of H and He isotopes exhibited fragmentation components which can be characterized by apparent nucleon momentum widths σ_0 = 85.1 MeV/c, essentially identical to those found at relativistic energies,[5] and much larger than the value of about 40 Mev/c obtained in reactions at 20 MeV/u.[2] Recently, we have extracted nucleon momentum widths from H and He spectra observed in the reactions of 320 Mev ^{10}B projectiles with ^{181}Ta. The widths are only slightly greater than those observed at 20 MeV/u, indicating that the transition to asymptotic high energy behavior occurs quite rapidly between 32 and 43 MeV/u.

The spectra of H isotopes and ^4He measured at θ_{lab} = 6° are shown in Figs. 1a - 1d. The spectra are dominated by a component peaking at energy-per-nucleon close to the value for the incident projectile. This component is especially distinct in the case of protons and ^4He. We interpret this component as originating from the fragmentation of the projectile.

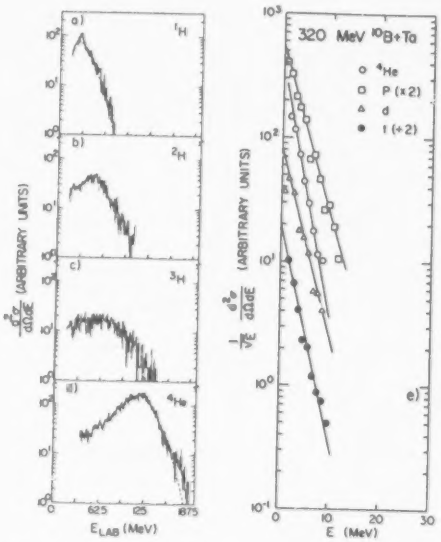

Fig. 1. Energy spectra of light particles observed at θ_{lab} = 6°; (a) protons; (b) deuterons; (c) tritons; (d) α particles. In parts (a) and (d), the fits to the fragmentation model are also shown as dashed lines; (e) plot for extracting momentum widths from light particle spectra. θ_{lab} = 6°. The spectra have been transformed to a moving frame with V = 0.95 x V_{proj}.

In the simple fragmentation picture developed by Goldhaber[6] one assumes that the fragment momentum distribution in the projectile rest frame is a Gaussian, with a width given by

$$\sigma^2 = \sigma_0^2 \frac{(A - F)F}{A - 1}$$

where A and F are the projectile and fragment mass number respectively, and σ_0 is the width of the momentum distribution of individual nucleons in the projectile. Alternatively, the fragment energy distribution can be parametrized in terms of a temperature T which is related to the reduced width σ_0 by the equation, $T = A\,\sigma_0^2/m(A-1)$, where m is the nucleon mass.

We have fitted the high energy part of the proton and ^{4}He spectra to the above fragmentation model.

The velocity of the projectile undergoing fragmentation and the momentum width σ_0 were treated as free parameters. The fits shown in Fig. 1(a) and (d) yield σ_0 values of 50.6 and 50.8 MeV/c for protons and ^{4}He respectively. By fitting the entire ^{4}He spectrum including the lower energies to a sum of the fragmentation component and a second component arising from another moving thermal source, one obtains the slightly lower value of 45 MeV/c for σ_0 for the fragmentation component. These fits resulted in a value for the velocity of the fragmentation source equal to 0.95 times the incident projectile velocity.

An alternative method for obtaining σ_0 is given in Fig 1(e). Here we have plotted the quantity, $\log (d^2\sigma/\sqrt{E}dEd\Omega)$ in the projectile frame against E extracted values of σ_0 and T from the slopes of the straight lines (Table I). The reduced widths for the three H isotopes and for ^{4}He are essentially identical and average to 54.0 MeV/c, corresponding to an average T of 3.5 MeV.

Table I. Reduced width σ_0, and temperature, T extracted from the forward angle spectra of light particles in the system 320 MeV ^{10}B + ^{181}Ta.

Particle	σ_0(MeV/c)	T (MeV)
p	54.0 ± 1.5	3.5 ± 0.2
d	53.5 ± 2.0	3.4 ± 0.3
t	54.2 ± 1.5	3.5 ± 0.2
^{4}He	54.3 ± 1.0	3.5 ± 0.2

The variation of the fragmentation component with angle is depicted in Fig. 2, where ^{4}He spectra taken at five angles in the range from 3 to 19 degrees are shown. The five spectra in Fig. 2 were fitted together to a sum of two components as described before. In the present case, the longitudinal and transverse momentum widths of the fragmentation component, $\sigma_\parallel$ and $\sigma_\perp$ respectively, were allowed to vary independently in addition to the velocity of the projectile undergoing fragmentation. The fits, shown in Fig. 2, give $\sigma_\parallel$ = 84.4 MeV/c (corresponding to reduced width, σ_0 = 52.3) and $\sigma_\perp$ = 113 MeV/c for the fragmentation component. Thus, no large anisotropy in σ is indicated by our data for ^{4}He. For fragments close to the projectile, Van Bibber et al. observed $\sigma_\perp$ values twice as large as $\sigma_\parallel$ in the system ^{16}O + Au and ^{16}O + Al at 90 and 125 MeV/u and interpreted the results as due to orbital deflection of the projectile.[3] This effect is expected to be small for fragments much lighter than the projectile.

Forward angle spectra of Li and Be isotopes also exhibit peaks very close to the projectile velocity (Fig. 3). The data suffer from poor statistics and do not allow us to extract the widths unambiguously. The dashed curves in Fig. 3 represent the spectra calculated from the Goldhaber model with σ_0 = 54.0 MeV/c and $V = V_{proj}$. Although the experimental spectra peak close to the velocity of the projectile, they are somewhat broader than the calculated ones. This suggests, perhaps, that the energy spectra of all fragments cannot be accounted for by a constant σ_0 parameter.[6] It is also possible that mechanisms involving significant energy loss are contributing to the observed spectra.

In Fig. 4 the nucleon momentum widths obtained in the present work and in some other recent studies are plotted against the energy per nucleon above the Coulomb barrier. It is seen that σ_0 for 32 MeV/u ^{10}B fragmentation is clearly lower than the result obtained for 43 MeV/u ^{20}Ne in Ref. 1, the latter value being essentially identical to the result at relativistic energies. Thus, a rapid transition in σ_0 or T occurs just above the projectile energy employed in the present experiment.

The Fermi energies of nucleons in ^{10}B and ^{20}Ne are about 25 and 29 MeV respectively[7] (see Fig. 4). As pointed out in Ref. 1, it is possible that the Fermi energy may reoresent an approximate boundary between low- and high-energy phenomena and

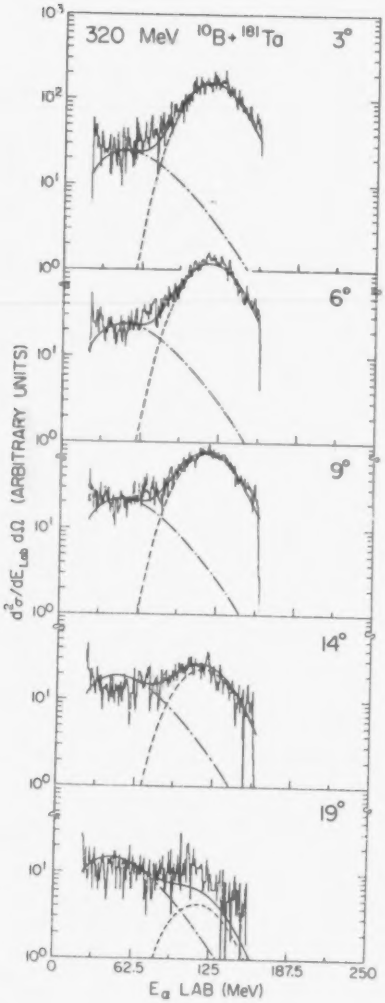

Fig. 2. Spectra of ^{4}He observed at forward angles. The solid curve is a fit of all the spectra together to a sum of two components. (1) dashed line, fragmentation component: $\sigma_\parallel$ = 85.5 MeV/c, $\sigma_\perp$ = 113.5 MeV/c, v/v_{proj} = 0.95; (2) dot-dashed line: T = 8.9 MeV, v/v_{proj} = 0.56

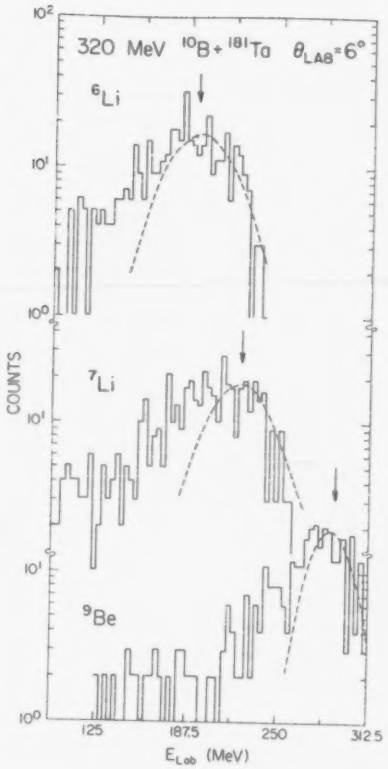

Fig. 3. Energy spectra of various fragments measured at lab angle = 6°. The dashed lines show fragmentation model calculations with σ_0 = 54 MeV/c. The arrows represent fragment energies corresponding to the incident projectile velocity.

that as the projectile energy per nucleon exceeds the Fermi energy, projectile fragmentation is characterized by the statistically dominated limiting behavior observed at relativistic energies. In Fig. 4, we have also indicated the energy corresponding to the velocity of sound in nuclear matter (derived from the value of nuclear matter incompressibility[8]) which may be another relevant quantity in defining the boundary between low- and high-energy behavior.

Recently, Friedman[9] has proposed a peripheral model to account for the parallel momentum widths observed in the fragmentation process. The model

that takes into account the absorptive effect of the optical potential and relates the momentum widths to the separation energies of the fragments from the projectile and to a cut-off radius. Satisfactory agreement is obtained with momentum width data at high energies. Variation of the width with projectile energy is attributed to Coulomb effects and the trend of the data for ^{16}) fragmentation from 7 to 20 MeV/u is reasonably well reproduced (Fig. 4). However, the widths predicted for ^{4}He fragments from ^{10}B and ^{20}Ne projectiles do not correspond to our results. Additional measurements on all fragments with the same projectile over the entire energy range from 20 to 40 MeV/u will be useful and are planned for the near future.

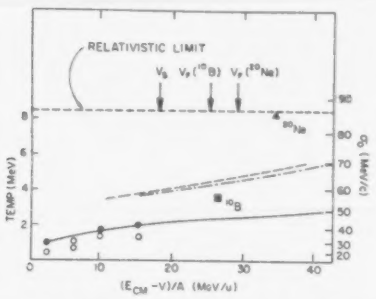

Fig. 4. Reduced width, σ_0 and temperature, T, plotted as a function of the energy per nucleon over the coulomb barrier: Square represents work; Triangle results from Ref. 1 for 43 MeV/u ^{20}Ne; Closed and open circles results from Ref. 2 for ^{16}O and ^{12}C reactions. The Fermi energies of nucleons in ^{20}Ne and ^{10}B are indicated by arrows. V_s represents the energy corresponding to the velocity of sound in nuclear matter. The prediction of the model of Ref. 9 are shown as follows: dashed and dot-dashed lines for ^{4}He from ^{10}B and ^{20}Ne projectiles and solid lines for ^{12}C from ^{16}O projectiles.

References

*Permanent address: Nuclear Physics Division, Bhabha Atomic Research Centre, Trombay, Bombay

†Permanent address: DPh-N/MF, CEN saclay, 91191 Gif-sur-Yvette Cedex, France

[1] J. B. Natowitz, M. N. Namboodiri, L. Adler, R. P. Schmitt, R. L. Watson, S. Simon, M. Berlander, and R. K. Choudhury, Phys. Rev. Lett. 47, 1114 (1981).

[2] Ch. Egelhaaf, G. Bohlen, H. Fuchs, A. Gamp, H. Homeyer, and H. Kluge, Phys. Rev. Lett. 46, 813 (1981).

[3] K. Van Bibber, D. L. Hendrie, D. K. Scott, H. H. Wieman, L. S. Schroeder, J. V. Geaga, S. A. Chessin, R. Treuhaft, J. Y. Grossiord, J. O. Rasmussen, and C. Y. Wong, Phys. Rev. Lett. 43, 840 (1979).

[4] J. Mougey, Nucl. Phys. A387, 109c (1982).

[5] D. E. Greiner, P. J. Lindstrom, H. Heckman, B. Cork, F. S. Bieser, Phys. Rev. Lett. 35, 152 (1975).

[6] A. S. Goldhaber, Phys. Lett. 53B, 306 (1974).

[7] E. J. Moniz, I. Sick, R. R. Whitney, J. R. Ficenec, R. D. Kephart, and W. P. Trower, Phys. Rev. Lett. 26, 445 (1971).

[8] D. H. Youngblood, P. Bogucki, J. D. Bronson, U. Garg, Y. -W. Lui, and C. M. Roszca, Phys. Rev. C 23, 1997 (1981).

[9] W. A. Friedman, Phys. Rev. C 27, 569 (1983).

^{12}C ON ^{12}C AT 300 MeV

S. H. Simon, R. K. Choudhury, J. B. Natowitz, P. L. Gonthier, L. A. Adler, and K. Hagel

By comparing experimental results with model calculations, it is possible to draw conclusions about the various mechanistic contributions to a particular reaction. A series of four experiments using the 300 MeV ^{12}C^{5+} beam have been completed and the data have been processed in order to probe the reaction mechanism of carbon on carbon at 25 MeV/N. Energy spectra, angular distributions, and yield distributions have been plotted and compared with data reported in the literature and with model calculations for complete and incomplete fusion reaction mechanisms. The total reaction cross section has been measured yielding a value of 1174 +100/-50 mb as compared with the value of 1315 +/- 40 mb which was reported in the literature for this system at 30 MeV/n (Fig. 1).[1] Note that the value

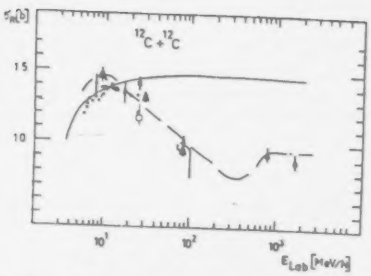

Fig. 1. Total reaction cross section for $^{12}C + ^{12}C$ collisions as a function of incident energy. Solid triangles are from Ref 2. Solid circles were obtained from parametrized phase-shift analysis (Ref. 4) of data from Ref. 3. The other data points labeled open circles, crosses, plusses, and open triangles are from Refs. 4, 5, 6, and 7, respectively. Our direct measurement is indicated by an open square. The agreement with other data is apparent. There is experimental evidence for the deviation of σ_R ($^{12}C + ^{12}C$) from the geometrical cross section which is illustrated by a solid curve (Ref. 8).

indicated by the solid circle just below 25 MeV/n is in agreement with our data point. The value for the experimental cross section was arrived at by considering conservation of charge. Products ranging from Z = 1 - 9 were observed. The summation of each Z multiplied by its respective cross section was divided by 12 to account for all possible protons in the reaction. This value (1174 mb) differed little from the value 1152 mb, which was obtained by summing the cross sections for $Z \geq 3$ products. This may mean that there is no double counting for the products $Z \geq 3$.

Cross sections and energy spectra for N product nuclei at various angles are shown in Fig. 2. The angular distribution of the heavier fragments is very forward peaked. Comparisons with the statistical model calculations obtained using the Lilita code[1] of Gomez del Campo and Stokstad indicate that very little of the cross section for this reaction is due to fusion. In Fig. 3 yield calculations in the region $Z > 6$ imply an $L_{crit} < 15$ $\hbar$, which suggest a fusion cross section < 170 mb.

A major portion of the reaction cross section appears to be due to incomplete fusion. Model calculations are shown in Fig. 4 for evaporation residues resulting from fast emission of an alpha particle and a beryllium ion. As can be seen in Fig. 5, yield distributions obtained from calcu-

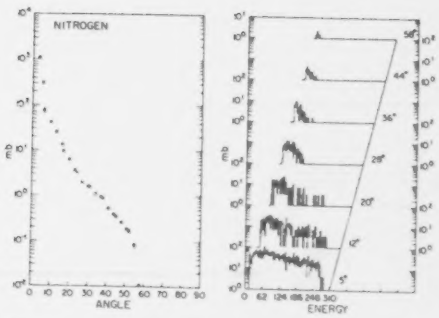

Fig. 2. Cross section and angular distributions for nitrogen data.

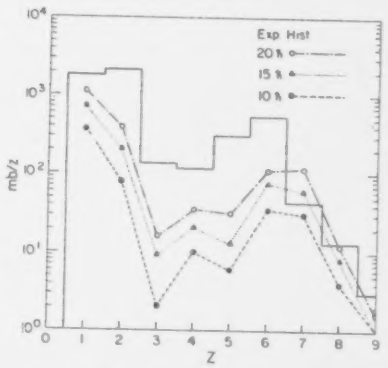

Fig. 3. Comparison of the yield data (histogram) with statistical model calculations for fusion of 12C with 12C at 300 MeV for different values for L_{crit} with L_{crit} = 20 $\hbar$ (broken line), 15 $\hbar$ (dotted line), and 10 $\hbar$ (dashed line). The trends for $Z > 7$ suggest the maximum angular momentum cutoff for fusion to be between 10 $\hbar$ and 15 $\hbar$.

lations for a fast alpha emitted follow a similar trend as the experimental data. Note that the cross section in the calculation for alphas includes an extra 1214 mb for fast alphas and an extra 2428 mb for alphas due to ^{8}Be emission and decay.

These mechanisms do not account for all of the observed features. Further studies involving coincident fragment detection may be undertaken to determine the various mechanistic contributions in greater detail.

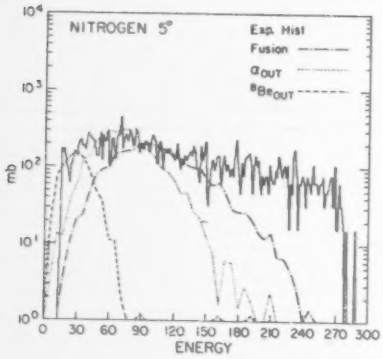

Fig. 4. Nitrogen energy spectrum at 5° with model calculations. Fusion is indicated by the broken line. Incomplete fusion is indicated by the dotted line for the prompt emission of a fast alpha and by a dashed line for the prompt emission of a ^{8}Be. The calculations have been normalized to the data.

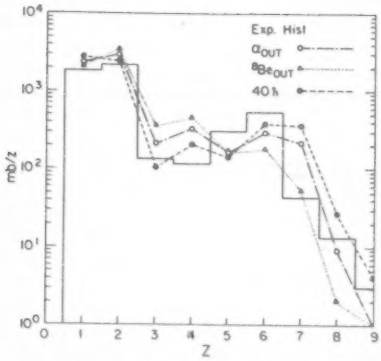

Fig. 5. Comparison of the yield data (histogram) with statistical model calculations for fusion with L_{crit} = 40 ħ (dashed line), and incomplete fusion: α emission (broken line) and ^{8}Be emission (dotted line). Note that the cross sections for alpha products in incomplete fusion include 1214 mb for fast alphas and an extra 2428 mb for alphas due to ^{8}Be emission and decay.

References

[1]J. Gomez del Campo, R. A. Dayras, G. A. Biggerstaff, D. Shapira, A. H. Snell, P. M. Stelson and P. G. Stokstad, Phys. Rev. Lett. 43, 26 (1979).

[2]C. Perrin, S. Kox, N. Longequeue, J. B. Viano, M. Buenerd, R. Cherkaoui, A. J. Cole, A. Gamp, J. Hemet, and R. Ost, Phys. Rev. Lett. 49, 1905 (1982).

[3]R. G. Stokstad, R. M. Wieland, G. R. Satchler, C. B. Fulmer, D. C. Hensley, S. Raman, L. D. Rickerston, A. H. Snell, and P. H. Stelson, Phys. Rev. C 20, 655 (1979).

[4]A. J. Cole, W. D. M. Kae, M. E. Brandan, A. Dacal, B. G. Harvey, R. Legrain, M. J. Murphy, and R. G. Stokstad, Phys. Rev. Lett. 47, 1705 (1981).

[5] H. G. Bohlen, M. R. Clover, G. Ingold, H. Letteau, W. von Oertzen, Z. Phys. A308, 121 (1982).

[6]M. Buenard, P. Martin, R. Bertholet, C. Guet, M. Maurel, J. Mougey, H. Nifenecker, J. Pinston, P. Perrin, F. Schussler, J. Julien, J. P. Bondorf, L. Carlen, H. A. Gustafsson, B. Jakobsson, T. Johansson, P. Kristiansson, O. B. Nielson, A. Oskarsson, I. Otterlund, H. Ryde, B. Schroder, and G. Tibell, Phys. Rev. C 26, 1299 (1982).

[7]J. Jaros, A. Wagner, L. Anderson, O. Chamberlain, R. Z. Fuzesy, J. Gallup, W. Gorn, L. Schroeder, S. Shannon, G. Shapiro, H. Steiner, Phys. Rev. C 18, 2273 (1978).

[8]R. M. DeVries and J. C. Peng, Phys. Rev. Lett. 43, 1373 (1979).

POSSIBLE EVIDENCE FOR THE STATISTICAL EXCITATION OF COLLECTIVE MODES IN HEAVY ION INDUCED FISSION

R. P. Schmitt, G. Mouchaty, D. R. Haenni, and P. Bogucki

Experiments have shown that considerable spin is imparted to the fragments in spontaneous fission.[1] A variety of mechanisms have been proposed to explain this effect, including Coulomb excitation of the fragments and the excitation of angular-momentum-bearing collective modes. In an effort to explore this effect more thoroughly, we have investigated the angular momentum transfer in heavy-ion-induced fission. We find evidence that the fragment spins are enhanced with respect to rigid rotation. The magnitude of this spin enhancement appears to be in reasonable agreement with the predictions of a simple model which assumes the statistical excitation of collective modes.

Thin, self-supporing foils of $^{182}WO_3$ and ^{154}Sm were bombarded with beams of 140 MeV $^{12}C^{4+}$ and 240 MeV $^{40}Ar^{8+}$, respectively. Coincident fission fragments from the ^{194}Hg system formed in these reactions (E^* = 115 MeV) were detected with a

pair of solid state counters (see schematic in Fig. 1). In the ^{12}C experiment, the detectors were placed at 55° and 95° in the laboratory system. Both of the detectors were positioned at 60° during the ^{40}Ar study. These angles correspond to the maxima of the angular correlations for symmetric decay. One of the detectors had a relatively small angular acceptance (about 6°). The angular acceptance of the second detector was much larger (approximately 18°) to ensure that a broad range of masses could be detected in coincidence. Gamma-rays were detected utilizing a multiplicity filter consisting of eight 7.6 x 7.6 cm NaI counters, which were shielded with lead to minimize crystal-to-crystal scattering (<2%). The thresholds in the NaI detectors were adjusted to 120 keV. The absolute efficiency of the multiplicity filter was determined in coincidence with sources of ^{60}Co, ^{88}Y, ^{207}Bi, and ^{152}Eu using a Ge(Li) detector as a trigger. The total detection efficiency of the NaI array was slightly less than 10%.

Fission events were easily separated from other processes (such as deep-inelastic reactions) in the ^{12}C experiments. While some overlap between fission and deep-inelastic reactions occurred in the ^{40}Ar data, the fission component was, nevertheless, well defined. After correcting for the energy loss in the target and the pulse-height defect of the particle detectors, the pre-evaporative masses of the fission fragments were calculated from two-body kinematics using an iterative procedure. The gamma-ray multiplicities (M_γ) were calculated from the n-fold data for various bins of mass and total kinetic energy.

In Fig. 2, the average M_γ is shown for the two reactions as a function of fragment mass. Note that the data are symmetric with respect to half the compound nucleus mass (symmetry has not been forced). For both reactions the M_γ's are quite large. At symmetry $M_\gamma \approx 13$ for $^{12}C + ^{182}W$ and $M_\gamma \approx 15$ for $^{40}Ar + ^{154}Sm$. Anomolously large multiplicities have also been recently observed in studies of Pb-induced reactions.[2] The ^{12}C data is relatively independent of the exit channel of mass asymmetry. In contrast, the ^{40}Ar data show a rather pronounced minimum at symmetry. This trend is suggestive of that observed in multiplicity studies of deep inelastic reactions with light projectiles. At extreme mass asymmetries, M_γ for the $^{40}Ar + ^{154}Sm$ reaction drops off very abruptly due to the overlap between fission and transfer reactions.

Using γ-ray multiplicity systematics,[3,4] we have estimated the total fragment spins (S_T) for these reactions. In Fig. 2, the estimated S_T for the $^{182}W + ^{12}C$ reaction is plotted as a function of fragment mass. The shading gives an indication of the uncertainty in the transformation from M_γ to S_T. The dashed curve represents the fragment spin expected for a system consisting of two rigidly-rotating, touching spheres for $\ell \approx 43\ \hbar$. This is the average ℓ-value leading to fission as estimated from fission and evaporation residue

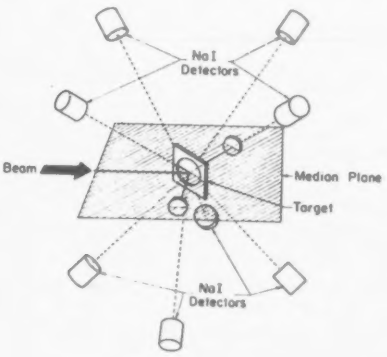

Fig. 1. Schematic of the experimental apparatus used in the γ-ray multiplicity measurements.

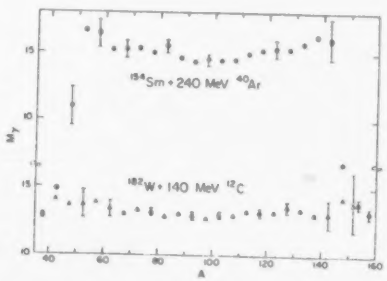

Fig. 2. Average γ-ray multiplicity as a function of fission fragment mass for the reaction ^{182}W 140 Mev ^{12}C (triangles) and ^{154}Sm + 240 MeV ^{40}Ar (points). Statistical errors are shown for selected points.

cross section measurements[5,6] assuming sharp cutoffs. Note that the predicted spin near symmetry is only about 12 $\hbar$, considerably less than that deduced from M_γ. Similarly, the spins extracted from the ^{40}Ar data (Fig. 4) are also generally larger than those expected from rigid rotation ($\langle \ell \rangle$ = 67 $\hbar$ is estimated from experiment).[6]

Although there are uncertainties in the transformation from M_γ to spin, errors in this transformation can not entirely explain the deviations from rigid rotation, especially in the ^{12}C data. It is unlikely that errors in the cross section data used to define the ℓ range for fission could account for this effect. For example, in the ^{12}C reaction a 20% increase in both the evaporation residue and fission cross sections would increase $\langle \ell \rangle$ by about 5 units, but the total fragment spin at symmetry would increase by only 1.4 units. It is also not possible to explain the fragment spins by using smoothed ℓ boundaries at the evaporation residue and fission borders. One might be tempted to attribute the deviations to deformations of the fragments. However, prolate deformations of the fragments actually tend to decrease the intrinsic spins. While oblate deformations increase the fragment spin, such deformations seem unlikely in view of the sub-barrier kinetic energies of the fragments. Thus, it appears that the fragments' spins are enhanced with respect to rigid rotation.

We have performed calculations for the two reactions using a simple model,[7] which assumes the thermal excitation of collective modes (bending, wriggling, twisting, and tilting) for a system consisting of two touching spheres. In this model calculation, the temperature of the system is determined from the excitation energy of the rigidly rotating spheres assuming a level density parameter, a = A/8. For simplicity, we present the model calculations for the average ℓ waves quoted above. Including the whole ℓ range leading to fission does not affect the results appreciably.

The results of the model calculations are shown by the solid curves in Figs. 3 and 4. Considering the simplicity of the model and the absence of adjustable parameters, the magnitude of the spin enhancement is reasonably well reproduced for both reactions. In the ^{12}C + ^{182}W reaction, the model predicts the rather weak dependence of the fragment spin on mass asymmetry, which is evident in the data. In the calculation, this weak dependence on asymmetry is the result of two opposing tendencies: the increase in the spin from rigid rotation with increasing asymmetry and the decrease in the spin generated by collective modes with increasing asymmetry. The calculation exhibits a stronger variation of S_T with fragment mass for the ^{40}Ar reaction, as does experiment.

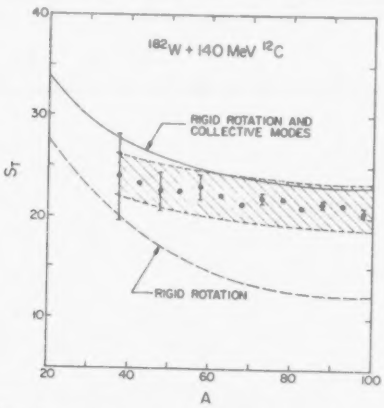

Fig. 3. Average total fragment spin (S_T) as a function of fragment mass (A) for the ^{182}W + 140 MeV ^{12}C reaction. The error bars reflect statistical uncertainties. The shading gives an indication of the errors in the transformation from M_γ to S_T. The curves are calculated values (see text).

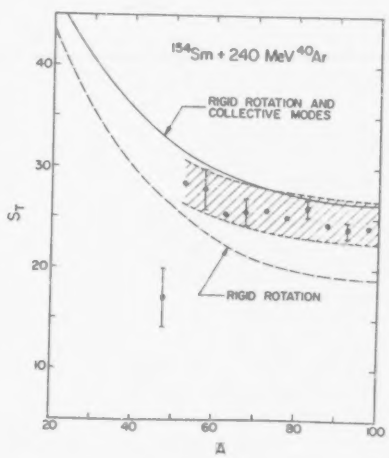

Fig. 4. Average total fragment spin as a function of mass for the reaction ^{154}Sm + 240 MeV ^{40}Ar. Representative statistical errors are shown.

This stronger dependence on fragment mass reflects the larger angular momenta in the ^{40}Ar reaction, which tend to overpower the effect of the collective modes. One should note that the ^{40}Ar results deviate from the calculation below mass 50 due to the large contribution from other processes (mostly quasi-elastic transfer) in this mass region. The reasonable agreement with model calculations suggests the excitation of a variety of collective modes which enhance the fragment spins. Because of uncertainties in the transformation from M_γ to spin, however, this conclusion should be regarded as somewhat tentative. Further investigations are in progress to more thoroughly test this hypothesis.

References

[1]J. B. Wilhelmy, E. Cheifetz, R. C. Jared, S. G. Thompson, H. R. Bowman, and J. O. Rasmussen, Phys. Rev. C 5, 2041 (1972).

[2]R. Boch, Y. T. Chu, M. Dakowski, A. Gobbi, E. Grosse, A. Olmi, H. Sann, D. Schwalm, U. Lynen, W. Muller, S. Bjornholm, H. Esbensen, W. Wolfi and E. Morenzoni, Nucl. Phys. A388, 344 (1982).

[3]J. B. Natowitz, M. N. Namboodiri, P. Kasiraj, R. Eggers, L. Adler, P. Gonthier, C. Cerruti, and T. Alleman, Phys. Rev. Lett. 40, 751 (1978).

[4]J. J. Simpson, G. B. Hagemann, B. Herskind, and M. Neiman, Nucl. Phys. A287, 362 (1977).

[5]J. M. Miller, D. Logan, G. L. Catchen, M. Rajagopalan, M. J. Alexander, M. Kaplan, J. W. Ball, M. S. Zisman and L. Kowalski, Phys. Rev. Lett. 40, 1074 (1978).

[6]H. Delagrange, D. Logan, M. F. Rivet, M. Rajagopalan, J. M. Alexander, M. S. Zisman, M. Kaplan, and J. W. Ball, Phys. Rev. Lett. 43, 1490 (1979).

[7]R. P. Schmitt and A. J. Pacheco, Nucl. Phys. A379, 313 (1982).

THE BOMBARDING ENERGY DEPENDENCE OF THE GAMMA-RAY MULTIPLICITIES IN ^{12}C-INDUCED FISSION

R. P. Schmitt, D. R. Haenni, G. Mouchaty, S. Nath and M. Tirion

Recent Y-ray multiplicity studies[1,2] have provided evidence for enhanced fragment spins in fission and fission-like reactions induced with heavy ions. While some studies[2] suggest this effect may arise from the statistical excitation of a number of angular momentum bearing collective modes,[3] the origin of the spin enhancement is still uncertain. Further measurements are needed to elucidate the mechanism. To shed light on the matter, we have investigated the Y-ray multiplicities associated with ^{12}C-induced fission at a number of bombarding energies.

In the experiments thin, self-supporting foils (typically about 400 $\mu g/cm^2$) were bombarded with 100, 140 and 180 MeV ^{12}C ions. Table I summarizes the systems studied in these measurements. Fission fragments were detected in coincidence with a pair of solid-state counters which were positioned at the kinematically correlated angles for symmetric fission. Gamma rays were detected using a multiplicity filter consisting of eight 7.6 x 7.6 cm NaI detectors. In the off-line analysis, the pre-evaporative mass distributions were reconstructed from the fission fragment energies and emission angles using two-body kinematics. The data were sorted into 5 or 10 amu wide mass bins and the Y-ray multiplicities (M_γ) were determined using standard algorithms. Additional details regarding the experiments and analysis may be found elsewhere[2] (see also page 48).

Table I. Summary of the reactions investigated.

Projectile	Target	Compound System	Excitation Energy
100 MeV ^{12}C	^{174}Yb	^{186}Os	80 MeV
100 MeV ^{12}C	^{197}Au	^{209}At	76 MeV
100 MeV ^{12}C	^{209}Bi	^{221}Ac	62 MeV
140 MeV ^{12}C	^{174}Yb	^{186}Os	117 MeV
140 MeV ^{12}C	^{182}W	^{194}Hg	115 MeV
140 MeV ^{12}C	^{197}Au	^{209}At	114 MeV
180 MeV ^{12}C	^{154}Sm	^{166}Er	160 MeV
180 MeV ^{12}C	^{174}Yb	^{186}Os	154 MeV
180 MeV ^{12}C	^{197}Au	^{209}At	151 MeV
180 MeV ^{12}C	^{209}Bi	^{221}Ac	137 MeV

In general, the particle data from these studies are consistent with full momentum trans-

fer. The mass distributions all are highly symmetric and peak within a few amu of half the compound system mass. This does not mean that incomplete fusion is negligible in these reactions. On the contrary, there is likely to be a significant incomplete fusion component particularly at the highest bombarding energy. However, the experimental geometry is biased against such processes due to the angles of the detectors (incomplete fusion changes the folding angle) and the requirement of coplanar fragment emission. Moreover, the high fission barriers of the target-like fragments tend to inhibit fission following incomplete fusion. With the possible exception of the ^{209}Bi + 180 MeV ^{12}C, fission following incomplete fusion probably contributes less than 10% to the experimental data.

In Figs. 1-3, the γ-ray multiplicities (M_γ) are plotted as a function of the mass of one of the fragments. Symmetry has not been forced in any of these data sets. Thus, the observed symmetry reflects the symmetry of the data. Two general trends are evident: First, for a given system, M_γ increases (except for 180 MeV ^{12}C + ^{174}Yb) with bombarding energy; and second, at a fixed bombarding energy, M_γ increases with the mass of the compound system. Both of the trends could be due to changes in the ℓ distribution leading to fission. For instance, one can argue that as the bombarding energy is increased, progressively higher ℓ waves contribute to fission. Similarly, for a given incident energy, slightly more angular momentum may be invovled for the heavier systems.

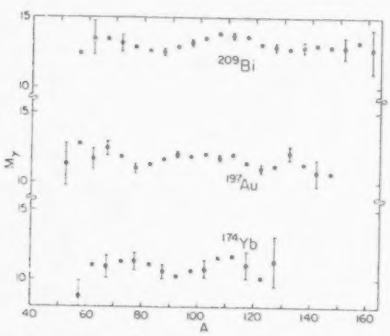

Fig. 1. Gamma-ray multiplicities as a function of fission fragment mass for 160 MeV ^{12}C-induced fission of the indicated targets. Representative statistical error bars are shown.

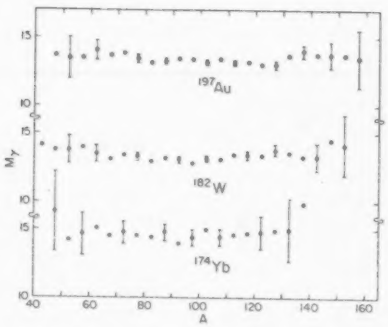

Fig. 2. Gamma-ray multiplicities as a function of fission fragment mass for 140 MeV ^{12}C-induced fission of the indicated targets. Representative statistical error bars are shown.

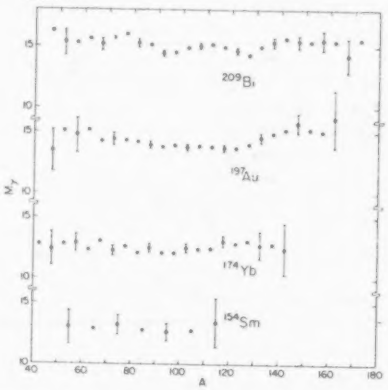

Fig. 3. Gamma-ray multiplicities as a function of fission fragment mass for 180 MeV ^{12}C-induced fission of the indicated targets. Representative statistical error bars are shown.

However, the magnitudes of M_γ suggest that these arguments are incomplete.

As an example, let us consider the data for the reaction ^{209}Bi + 180 MeV ^{12}C. The value of M_γ in the vicinity of symmetry is approxiamtely 15. If one assumes five statistical gamma-rays which remove no angular momentum, this M_γ corresponds to a total spin of about 2(15-5) = 20 ħ. The estimated neutron multiplicity for this system is about 14. Assuming that the neutrons remove 0.5 ħ on the average implies an average total fragment spin of roughly 27 ħ at symmetry which corresponds to $\langle \ell \rangle_{fiss}$ = 95 ħ for touching spheres (prolate

deformations would increase the estimate of $\langle \ell \rangle_{fiss}$. Since ℓ_{max} is only ≈ 93 ħ for this reaction, the value of $\langle \ell \rangle_{fiss}$ is surely an overestimate.

While the example considered above was obviously an extreme case, it emphasizes the fact that the M_γ's are generally larger than expected solely on the basis of rigid rotation, implying considerable spin enhancement. While we are not yet in a position to give a detailed analysis of this spin enhancement for all the reactions, we should mention that the gross trends in the data are in qualitative agreement with statistical excitation of collective modes. For example, the increase in M_γ with bombarding energy could reflect the increase in the temperature of the system. The increase in M_γ with the total mass of the system would also be predicted by the excitation of collective modes due to the increase of the moments of inertia of the fragments.[3] In order to make a detailed comparison with theory, it is necessary to pin down the range of ℓ-values leading to fission, which requires a knowledge of the evaporation residue and fission cross sections. Since these data are not available for all the systems, we will have to use fusion cross section systematics and statistical model calculations to estimate $\langle \ell \rangle_{fiss}$.

So far, we have concentrated only on the gross trends in M_γ. As the readers have surely noticed, there is also some rather interesting fine structure in M_γ, particularly in the 100 MeV ^{12}C induced reactions. Rather well-defined local minima in M_γ are observed at A = 88 and 132 for ^{209}Bi + 100 MeV ^{12}C, A = 83 and 126 for ^{197}Au + 100MeV ^{12}C, A = 93 for ^{174}Yb + 100 MeV ^{12}C, and A = 94 and 127 for ^{209}Bi + 180 MeV ^{12}C. Note that in all cases, the minima correspond to complimentary fragments.

Similar structure in M_γ has also been observed in spontaneous and neutron induced fission[4] and which may arise from shell effects in the products after neutron emission. Near shell closures, the level density is generally lower which tends to decrease the average number of γ-rays (and increase the average γ-ray energy). This explanation probably holds for the current data. To see this consider the reaction ^{209}Bi + 100 MeV ^{12}C. Assuming equilibrium of the charge and excitation energy of the fragments and neglecting second and higher chance fission, one possible scenario is

$$^{209}Bi + {}^{12}C \rightarrow {}^{221}Ac^* \rightarrow \begin{cases} {}^{88}Kr^* + {}^{86}_{36}Kr_{50} + 2n \\ {}^{133}I^* + {}^{129}_{53}I_{76} + 4n. \end{cases}$$

In this case, the N = 50 shell would be responsible for minima in M_γ. Other scenarios involving the N = 50 and the Z = 50 closures are also possible.

Generally speaking, the structures in M_γ tend to wash out at the higher bombarding energies, possibly due to the larger dispersion in the product mass and charge distributions which result from more extensive evaporation. The system ^{209}Bi + 180 MeV ^{12}C is an interesting exception. It is possible that the minima in M_γ at A = 94 and 127 in this reaction could result from shell closures in both fragments. In support of this conjecture, one could consider scenarios of the following type:

$$^{221}Ac^* \rightarrow \begin{cases} {}^{95}Y^* + {}^{89}_{39}Y_{50} + 6n \\ {}^{126}Sn^* + {}^{119}_{50}Sn_{68} + 8n. \end{cases}$$

The observation of shell effects in heavy ion induced fission offers some interesting possibilities. For example, because a broad range of products are formed, one can obtain an overview of the dependence of M_γ and E_γ for many different nuclei which are not easily accessible using conventional techniques. We are currently exploring this and other possibilities.

References

[1] R. Boch, Y. T. Chu, M. Dakowski, A. Gobbi, E. Grosse, A. Olmi, H. Sann, D. Schwalm, U. Lynen, W. Muller, S. Bjornholm, H. Esbensen, W. Wolfi, and E. Morenzoni, Nucl. Phys. A388, 344 (1982).

[2] R. P. Schmitt, G. Mouchaty, D. R. Haenni and P. Bogucki, Phys. Lett. B. (In Press).

[3] R. P. Schmitt and A. J. Pacheco, Nucl. Phys. A379, 313-329 (1982).

[4] F. Pleasonton, R. L. Ferguson, and H. W. Schmitt, Phys. Rev. C. 6, 1023 (1972).

ANGULAR MOMENTUM ALIGNMENT IN THE REACTION ^{154}Sm + 214 MeV ^{32}S

G. Mouchaty, D. R. Haenni, S. Nath, U. Garg† and R. P. Schmitt

Measurements of the angular momentum transferred in heavy-ion collisions have proved to be of great importance in unraveling the complex dynamics of these reactions. One aspect of the angular momentum transfer process currently under investigation is the alignment of the fragments' spin vectors. A number of experiments have demonstrated the existence of fluctuations in the spin direction.[1-4] Several mechanisms have been suggested to explain this spin depolarization effect, including particle level transfer[5] and the excitation of collective modes.[6] However, the mechanism for this effect is still largely an open question.

In an effort to obtain further information on fragment spin alignment, we have undertaken a detailed study of the reaction ^{154}Sm + 214 MeV ^{32}S. This system was chosen because deep-inelastic scattering is expected to be well developed with ^{32}S and because the resulting target-like fragments are expected to be good rotors. The alignment was investigated by measuring the anisotropies of known discrete γ rays. This technique avoids problems connected with the unknown γ-ray multipolarities which arise in continuum studies. While other techniques such as the sequential fission method can provide somewhat more information concerning the alignment, they do not yield the precise exit channel definition available in discrete-line studies.

A 1.38 mg/cm^2 thick, self-supporting foil of ^{154}Sm (99% enrichment) was bombarded with 214 MeV $^{32}S^{7+}$ ions. Projectile-like fragments emitted at θ_{lab}=47° were detected and identified in Z using a pair of three element, solid state telescopes (thicknesses approximately 15 μm, 75 μm and 1 mm), which had opening angles of about ±4°. As shown in the schematic at the top of Fig. 1, the telescopes were mounted in perpendicular planes. Two high-resolution Ge(Li) detectors were placed in the horizontal plane about 7 cm from the target. One of these detectors was positioned at 90° with respect to the beam axis while the second was placed to 120°. Copper absorbers (2 mm thick) were mounted on the detectors to reduce the x ray counting rate.

During the measurements all particle-γ and particle-γ-γ events were recorded on tape in an event-by-event format. Scaled-down particle singles were also recorded simultaneously for both telescopes. The beam intensity was controlled to minimize accidental coincidences (<8%) and count rate instabilities in the Ge(Li) detectors (the average instantaneous rate was about 20 kHz). While the intrinsic resolution of the Ge(Li)'s was <1.9 keV at 1.33 MeV, the resolution (FWHM) integrated over eight days of running time was 3.5-4.0 keV due to doppler broadening and some small, long term instabilities. The Ge(Li) detectors were calibrated *in situ* using ^{152}Eu and ^{133}Ba sources. In related experiments the continuum γ-ray multiplicities (M_γ) were studied for the same reaction using an array of eight 7.6 x 7.6 cm NaI detectors.

In the off-line analysis, the Ge(Li) data were sorted into a Z, E_{part}, E_γ arrays. Because the measurements were made at an energy relatively close to the interaction barrier (E_{cm}/B_{coul} = 1.5) and near the grazing angle, the best statistics were obtained for Z = 14, 15 and 16 at small and moderate energy losses. In these regions the data were compressed into 5 MeV wide bins. At larger energy losses, it was necessary to use bins 10-25 MeV wide.

Representative, random-corrected γ-ray spectra are shown in Fig. 1 for Z = 14 and 16 fragments for the indicated energy ranges. Some of the assignments are indicated. Most of the peaks which could be confidently assigned were stretched quadrupole γ rays from even-even target-like fragments (a few γ rays from the projectile were visible, but were so broad that they could not be assigned unambiguously). The spectra associated with Z = 15 fragments are difficult to interpret because they are largely associated with odd A and odd-odd nuclei. In view of these observations, we have focussed on stretched E2 γ-rays associated with Z = 14 and 16 fragments.

Scanning the spectra in Fig. 1 gives an indication of the evolution of the reaction mechanism with energy loss and mass transfer. For Z = 16, at the highest kinetic energies, inelastic excitation of the target is the dominant process. Weaker transitions in ^{152}Sm are visible which probably arise from two nucleon transfer. As the fragment energy decreases, the ^{154}Sm lines quickly diminish in intensity and γ rays from more complex processes appear. The strongest transitions are associated with A ≤ 154 as expected from neutron evaporation and equilibrium of the N/Z ratios of the fragments. The spectra for Z = 14 show similar trends.

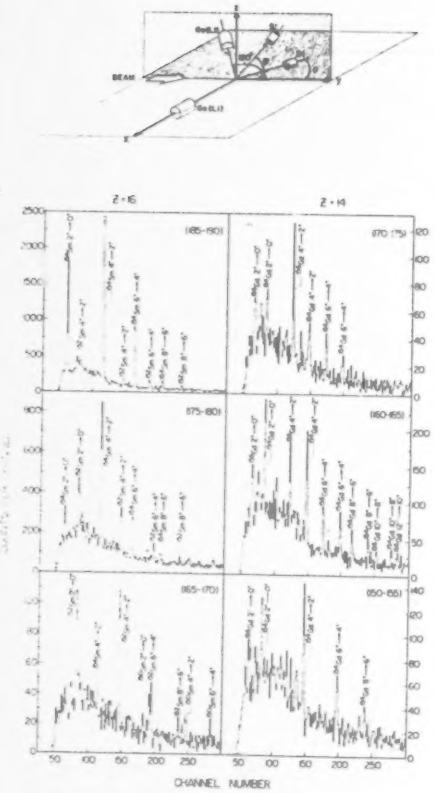

Fig. 1. (Top) Schematic of the apparatus used in the discrete line studies. (Bottom) Gamma-ray energy spectra for various laboratory kinetic energy bins (given in KeV in parenthesis) for Z = 14 and 16 fragments.

Although some Sm transitions are seen in coincidence with Z = 14, these peaks are rather weak, implying that neutron emission from the fragments is probably the dominant de-excitation process.

Peak intensities were extracted for all assigned transitions using linear backgrounds. Because the background subtraction is a major source of error, the spectra were analyzed twice to check consistency. The area of each γ peak was normalized by dividing it by the particle singles in the coincident telescope. Points in the γ-ray angular distributions were then obtained by comparing these normalized yields for the various telescope-Ge(Li) pairs.

A comparison of the normalized yields for coincidences for the in-plane telescope and the two in-plane Ge(Li)'s showed that the in-plane γ-ray angular distributions are isotropic to within 10%. In contrast, the in-plane to out-of-plane anisotropies (W_{in}/W_{out}) obtained by comparing the normalized coincidence yields of the two telescopes are frequently quite large, especially at large energy losses. In a number of cases the ratio W_{in}/W_{out} for a given isotope, Z gate and energy bin depends on the spin; that is, γ-rays from low lying states (especially $2^+ \rightarrow 0^+$ transitions) sometimes have small anisotropies while the higher spin transitions show large anisotropies. This effect is generally observed when the low lying states have relatively long lifetimes and thus may be due to the hyperfine interaction. These anomolous points were rejected and the remaining values were averaged.

In Fig. 2, the ratio W_{in}/W_{out} for some Gd isotopes are plotted as a function the lab kinetic energy of Z = 14 fragments. The error bars include uncertainties associated with counting statistics and background subtraction and reflect the averaging over the γ-ray cascades. At the very highest energies, large anisotropies are sometimes observed (e.g. ^{158}Gd and ^{156}Gd). This could imply that some direct process (perhaps α transfer, 2p transfer) leads to large alignment. However, this is rather speculative. At slightly lower energies, the anisotropies are all rather small. However, as the energy decreases further, the anisotropy increases steadily and eventually reaches a value of about three. The trend is quite similar for the Sm isotopes associated with Z = 16 fragments.

The anisotropy of the γ-ray continuum was obtained by integrating over E_γ. While the continuum anisotropies exhibit the same general trend with energy loss as the discrete γ ray anisotropies, the continuum anisotropies are significantly smaller. Over most of the particle energy range, W_{in}/W_{out} is less than 1.5. Anisotropies of about two are observed as the largest energy losses.

We shall assume that the fragment spin alignment is governed by a probability distribution of the form

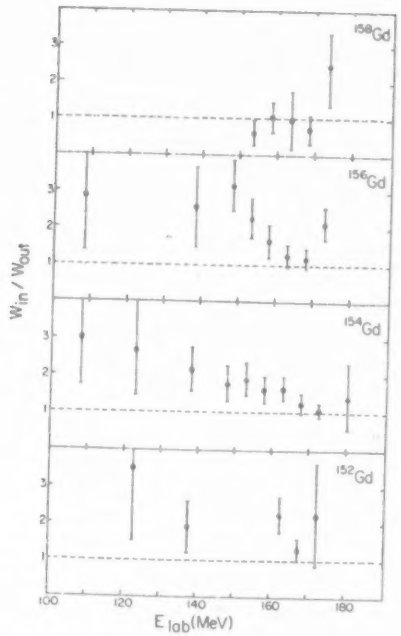

Fig. 2. Gamma-ray anisotropies for various Gd isotopes as a function of laboratory kinetic energy of Z = 14 projectile-like fragments.

$$P(\vec{I}) = \exp[-(I_x^2/2\sigma_x^2 + I_y^2/2\sigma_y^2 + (I_z-\langle I_z\rangle)^2/2\sigma_z^2)], \quad (1)$$

where $\langle I_z\rangle$ is the average aligned spin of the heavy fragment. While this equation contains four unknowns, only two quantities can be reliably extracted from the current data. Thus we have assumed that $\sigma_x = \sigma_y = \sigma_z = \sigma$. Using this assumption we have determined the quantity P_{zz} from the discrete line anisotropies. The values of P_{zz} were averaged over the Gd and the Sm isotopes for the Z = 14 and Z = 16 particle gates, respectively. The results are shown in Fig. 3(a) as a function of total kinetic energy loss (TKEL) estimated from two body kinematics. The alignment is small at the small TKEL but increases steadily with increasing TKEL and reaches about 0.7 at the largest TKEL. The apparent lack of dependence on the exit channel seems to argue against a particle

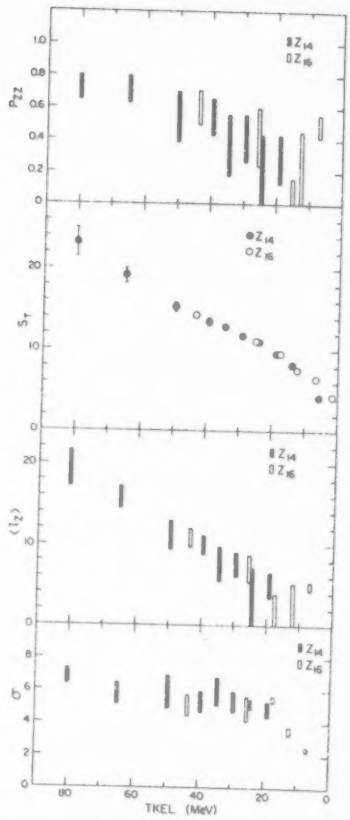

Fig. 3. (a) Plot of P_{zz} as a function of total kinetic energy loss (TKEL); (b) Plot of S_T (= 1.8 M_γ) as a function of total kinetic energy loss; (c) Aligned spin (I_z) as a function of TKEL; and (d) Misalignment parameter (σ) as a function of TKEL.

transfer mechanism for the spin depolarization. However, detailed calculations are needed before any definitive conclusions can be drawn.

The values of σ and $\langle I_z\rangle$ were obtained in the following way. First, the ratio $\sigma/\langle I_z\rangle$ was determined from the anisotropies of discrete lines. The total fragment spin $S_T = \langle|\vec{S}_1|+|\vec{S}_2|\rangle$ was obtained from the γ ray multiplicities (M_γ) using the parameterization $S_T = 1.8\ M_\gamma$ [Fig. 3(b)]. The heavy fragment spin was estimated using $S_H = S_T \mathcal{J}_H/\mathcal{J}_T$, where $\mathcal{J}_H$ and $\mathcal{J}_T$ are the moments

of inertia of the heavy fragment and the dinuclear system respectively (spheres were assumed). Using the probability distribution given in Eq. (1) and the values of S_H and $\sigma/\langle I_z\rangle$, the quantities σ and $\langle I_z\rangle$ were determined. The results are plotted in Fig. 3(c) and (d). The error bars reflect the uncertainties in the anisotropies and M_γ.

The aligned component of the angular momentum, $\langle I_z\rangle$, increases smoothly with TKEL suggesting a good correlation between the initial orbital angular momentum and energy loss. In contrast, σ initially increases quite rapidly with TKEL and then varies slowly with TKEL. The maximum value of about seven is reached at 80 MeV of energy loss.

The experimental results can be most readily compared with a statistical model which assumes the excitation of a variety of angular momentum bearing collective modes.[6] In this model

$$\sigma_x^2 = \sigma_y^2 = \frac{\mathcal{J}_1(\mathcal{J}_2 + \mathcal{J}_r)T}{\mathcal{T}},$$

and

$$\sigma_z^2 = \frac{\mathcal{J}_1(\mathcal{J}_2 + \mathcal{J}_r)T}{r},$$

where $_r$ is the relative moment of inertia and T is the temperature. At 80 MeV TKEL the model predicts $\sigma_x = \sigma_y = 7.9$ and $\sigma_z = 13.5$. These three values yield the same anistoropy (for stretched E2's) as $\sigma_x = \sigma_y = \sigma_z = 8.5$, which is about 20% larger than the value extracted from experiment. This difference could be taken as an indication that equilibrium has not been achieved. However, this is not the only explanation. The model assumes for simplicity that the fragments are spherical. If instead the fragments are deformed, the tilting mode would be supressed, which could bring the statistical prediction into better agreement with experiment. We are currently investigating the effect of fragment deformation on the spin alignment.

References

[1]G. J. Wozniak, R. P. Schmitt, P. Glassel, R. C. Jared, G. Bizard and L. G. Moretto, Phys. Rev. Lett. 40, 1436 (1978).

[2]D. v. Harrach, P. Glassel, Y. Civelekoglu, R. Manner, and H. J. Specht, Phys. Rev. Lett. 42, 1728 (1979).

[3]P. Dyer, R. J. Puigh, R. Vandenbosch, T. Thomas and M. S. Zisman, Phys. Rev. Lett. 39, 392 (1977).

[4]D. J. Morrissey, G. J. Wozniak, L. G. Sobotka, J. Pacheco, C. C. Hsu, R. J. McDonald, and L. G. Moretto, Z. Phys. A305, 131 (1982).

[5]R. Vandenbosch, Phys. Rev. C 20, 171 (1979).

[6]R. P. Schmitt and A. J. Pacheco, Nucl. Phys. A379, 313 (1982).

NUCLEAR THEORY

STRUCTURAL AND DYNAMICAL EFFECTS OF TWO-BODY COLLISIONS IN NUCLEAR MANY-BODY SYSTEMS

H. H. K. Tang and P. J. Siemens

Research in the last few years seems to indicate that the mean-field theory, with the use of appropriate effective interactions, may be able to account for many bulk features of nuclear structure and dynamics at low excitation energy of up to a few MeV per particle. The key concept here is the Pauli principle, by which scatterings due to the residual interaction are prohibited, so that the original many-body problem is assumed to be well approximated by a one-body theory.

However, from a few MeV per particle up to tens of MeV per particle, there is a large range of excitation energies over which the pure mean-field picture is certain to be modified in a non-trivial manner. To facilitate the study of nuclear dynamics over such energy range, we consider a framework[1,2] which includes both the mean field effects and two-body collisions. The basic dynamical equations are

$$ih\frac{\partial}{\partial t}\hat{\rho}^{>}<(t,t') - [\hat{h}_{MHF}, \hat{\rho}^{>}<](t,t') = \int_{t_0}^{t} d\bar{t}\, \hat{M}_c(t,\bar{t})\,\hat{\rho}^{>}<(\bar{t},t') \qquad (1)$$

and their adjoints. Here, the two-time density matrices in coordinate space are defined as

$$\langle x|\hat{\rho}^{<}(t,t')|x'\rangle \equiv \langle\phi_{in}|\hat{\psi}^{+}(x't')\hat{\psi}(xt)|\phi_{in}\rangle \qquad (2a)$$

and

$$\langle x|\hat{\rho}^{>}(t,t')|x'\rangle \equiv \langle\phi_{in}|\hat{\psi}(xt)\hat{\psi}^{+}(x't')|\phi_{in}\rangle \qquad (2b)$$

where $|\phi_{in}\rangle$ is some appropriate N-particle initial state corresponding to the boundary conditions. The mean-field is contained in the Hartree-Fock-like Hamiltonian $\hat{h}_{MHF}$, whereas the particle-particle collision is contained in the mass operator $\hat{M}_c$. In general, the collision kernel is non-Markovian in the sense that past history of the density matrices must be integrated over. It is the understanding of this non-Markovian feature which leads to new results in our investigations.

Equation (1) is, in principle, exact if we iterate the residual interaction to all orders. But in the present work, we use phenomenological forces so that it suffices to consider up to the Born term in the collision integral.

I. ANALYSIS OF THE COLLISION KERNEL

Invoking simplifying assumptions about the mean-field propagation of the system, we are able to derive useful forms of the collision kernel. For example, the integration over past history can be replaced by approximate analytic expressions under many conditions. Transforming the dynamical equation to the Wigner space, we arrive at a quantum Boltzmann-like equation which is much more general than the usual Uehling-Uhlenberg equation. We parametrize the residual interaction in momentum space and have found that the zero-range part leads to a term which resembles the Uehling-Uhlenberg collision kernel, whereas the finite-range parts give rise to correction terms.

II. SIMPLE SYSTEMS AND ANALYTIC SOLUTIONS

We consider the case of nuclear matter from the framework of this theory. We attempt to make contact with the Landau theory of Fermi liquids, since there is formal resemblance between the two theories. The general dynamical equation (1) is expanded around Hartree-Fock configuration and is linearized, so that the dynamics of small amplitude oscillations can be studied. In the case of infinite nuclear matter the linearized equation can be solved analytically, from which we obtain results which are generalizations of the usual random phase approximation. We analyze the dispersion relation and stability of such solutions and the nature of the correlated ground state. Results of such investigations may also be useful in the study of giant resonances.

References

[1]H. H. K. Tang, Ph.D. Dissertation, Yale University (1979).

[2]C. Y. Wong and H. H. K. Tang, Phys. Rev. C 20, 1419 (1979).

SINGLE PARTICLE RESPONSE FUNCTION IN FINITE NUCLEI

S. Shlomo

The single-particle response function S(E,q) is an important ingredient utilized in theoretical descriptions[1] of properties of a many-body system, such as excited states and the scattering of an interacting particle from the system. In this work I will first derive expressions for S(E,q) and the Pauli blocking (PB) factor P(q) = $\int$dE S(E,q), in terms of the Wigner transforms (WTs) of the single-particle wave functions $\psi_i(\vec{r})$ and the scattering probe $\sigma(\vec{q},\vec{r})$, and discuss the results. Then using the Born approximation for $\sigma(\vec{q},\vec{r})$, I will derive simple analytic expressions for S(E,q) and P(q) for finite nuclei, assuming independent nucleons in a harmonic-oscillator (HO) potential well, and compare the results with the well-known response function for an infinite Fermi gas (FG).

I first recall some basic definitions. Within the independent-particle model, the response of the nucleus to the projectile scattering probe $\sigma(\vec{q},\vec{r})$ is defined by,

$$S(E,q) = \frac{1}{N}\sum_{i,f} |\langle\psi_f|\sigma|\psi_i\rangle|^2 \delta(E_f-E_i-E), \quad (1)$$

where ψ_i and ψ_f are occupied and unoccupied states, respectively, and $N = \sum \langle\psi_i|\sigma^*\sigma|\psi_i\rangle$ is the normalization factor. The Pauli blocking (PB) factor is defined as the sum rule,

$$P(q) = \int dE\ S(E,q). \quad (2)$$

For a given wave function $\psi(\vec{r})$, the corresponding Wigner transform (WT) is defined[2] as the shifted Fourier transform of the density matrix $\rho(\vec{r},\vec{r}') = \psi^*(\vec{r})\psi(\vec{r}')$ by,

$$f(\vec{r},\vec{p}) = \frac{1}{(2\pi)^3}\int d\vec{s}\ e^{i\vec{p}\cdot\vec{s}}\ \psi^*(\vec{r}+\vec{s}/2)\psi(\vec{r}-\vec{s}/2), \quad (3)$$

with $\hbar = 1$. The inverse transform is,

$$\rho(\vec{r},\vec{r}') = \int d\vec{p}\ e^{-i\vec{p}\cdot(\vec{r}-\vec{r}')}\ f(\frac{\vec{r}+\vec{r}'}{2},\vec{p}) . \quad (4)$$

To express S(E,q) in terms of the WTs of $\psi_i(\vec{r})$, $\psi_f(\vec{r})$, and $\sigma(\vec{q},\vec{r})$, I first note the following property: If f_1 and f_2 are the WTs which correspond to ψ_1 and ψ_2, respectively, then the WT f_{12} which corresponds to $\psi_{12}(\vec{r}) = \psi_1(\vec{r})\psi_2(\vec{r})$ is given by a convolution in momentum space of f_1 and f_2,

$$f_{12}(\vec{r},\vec{p}) = \int d\vec{p}'\ f_1(\vec{r},\vec{p}-\vec{p}')\ f_2(\vec{r},\vec{p}') . \quad (5)$$

This is easily proved using the definition (3) and employing (4) for $\psi_2^*(\vec{r}+\vec{s}/2)\psi_2(\vec{r}-\vec{s}/2)$. Utilizing (5) together with the well-known property,[3]

$$\left|\langle\psi_1|\psi_2\rangle\right|^2 = (2\pi)^3\int d\vec{r}\ d\vec{p}\ f_1(\vec{r},\vec{p})\ f_2(\vec{r},\vec{p}) , \quad (6)$$

S(E,q) can be written in the form,

$$S(E,q) = \frac{1}{N}\sum_{i,f} I_{if}(q)\ \delta(E_f-E_i-E) , \quad (7)$$

with,

$$I_{if}(q) = (2\pi)^3\int d\vec{r}\ d\vec{p}\ d\vec{p}'\ f_\sigma(\vec{r},\vec{p}') * f_i(\vec{r},\vec{p})\ f_f(\vec{r},\vec{p}+\vec{p}') \quad (8)$$

where $f_\sigma(\vec{r},\vec{p})$ is the WT of $\sigma(\vec{q},\vec{r})$ as a function of $\vec{r}$. Utilizing the completeness of the single-particle basis, one finds that,

$$\sum_f f_f(\vec{r},\vec{p}) = \sum_{k=1}^{\infty} f_k(\vec{r},\vec{p}) - \sum_i f_i(\vec{r},\vec{p}) = \frac{1}{(2\pi)^3} - F_a(\vec{r},\vec{p}) \quad (9)$$

where

$$F_a(\vec{r},\vec{p}) = \sum_i f_i(\vec{r},\vec{p})$$

is the WT of the one-body density matrix $\rho_a(\vec{r},\vec{r}')$ of the system with a nucleons. Using (8) and (9), P(q) can be written in the interesting form,

$$P(q) = \frac{1}{N}\sum_{i,f} I_{if}(q) = \frac{1}{N}\int d\vec{r}\ d\vec{p}\ d\vec{p}'\ f_\sigma(\vec{r},\vec{p}')\ F_a(\vec{r},\vec{p}) * [1-(2\pi)^3 F_a(\vec{r},\vec{p}+\vec{p}')] . \quad (10)$$

For simplicity, the spin-isospin degeneracy factor of 4 is omitted (A = N + Z = 4a).

The WT $f(\vec{r},\vec{p})$ may be considered as the quantum-mechanical analog of the classical phase-space distribution function.[3-8] However, it should be noted here that $f(\vec{r},\vec{p})$ is a "quasi-probability" function since it may acquire negative values in

certain regions.[8] With this in mind, the basic results of (8) and (10) have the following interpretation, in the semi-classical sense. The integrand in (8) is just the product of the probability density for $(\vec{r},\vec{p})$ in the occupied state, i, the probability density of $(\vec{r},\vec{p}+\vec{p}')$ in the unoccupied state f (note the momentum transfer $\vec{p}'$) and the probability density of $(\vec{r},\vec{p}')$ in the phase space of the scattering probe $\sigma(\vec{q},\vec{r})$. Similarly, the result (10) for the Pauli blocking factor P(q) is of the form that one may write down under the assumption that $F_a(\vec{r},\vec{p})$ is the probability density for finding a nucleon at the position $\vec{r}$ with momentum $\vec{p}$.

To evaluate S(E,q), a model for $\sigma(\vec{q},\vec{r})$ and $\psi_i(\vec{r})$ should be specified. In the Born approximation for σ one has,

$$\sigma(\vec{q},\vec{r}) = e^{i\vec{q}\cdot\vec{r}} \quad \text{and} \quad f_\sigma(\vec{r},\vec{p}') = \delta(\vec{p}' - \vec{q}) \tag{11}$$

where q is the momentum transfer. In this case the normalization N = a, and (8) and (10) can be simplified to read,

$$S(E,q) = \frac{(2\pi)^3}{a} \sum_{i,f} \delta(E_f - E_i - E) \int d\vec{r}\, d\vec{p}\, f_i(\vec{r},\vec{p}) \cdot f_f(\vec{r},\vec{p}+\vec{q}), \tag{12}$$

$$P(q) = \frac{1}{a}\int d\vec{r}\, d\vec{p}\, F_a(\vec{r},\vec{p})[1 - (2\pi)^3 F_a(\vec{r},\vec{p}+\vec{q})]. \tag{13}$$

For the Fermi-gas model one recovers the Lindhard function[9,10] using (12). Substituting

$$F_{FG}(\vec{r},\vec{p}) = \frac{1}{(2\pi)^3}\, \theta(P_F^2 - p^2)$$

in (13), one get the well-known results,

$$P(q) = \begin{cases} \frac{3}{4}\, x\, (1 - x^2/12), & x \le 2 \\ 1, & x > 2 \end{cases} \tag{14}$$

where $x = q/p_F$ and p_F is the Fermi momentum.

To evaluate (12) and (13) for the HO model, I utilize the result,[8]

$$F_a(\vec{r},\vec{p}) = \sum_{K=0}^{M} f_K(\vec{r},\vec{p}) = \sum_{K=0}^{M} \frac{(-1)^K}{\pi^3}\, e^{-\epsilon}\, L_K^2(2\epsilon), \tag{15}$$

where $f_K(\vec{r},\vec{p})$ is the sum over the WFs of all degenerate states with $E_K = (K + 3/2)\hbar\omega$, and M is the highest occupied shell. In (15), ϵ is a dimensionless energy, $\epsilon = p^2 + r^2 = 2E/\hbar\omega$, where p and r are in units of $\hbar\sqrt{\nu}$ and $1/\sqrt{\nu}$, respectively ($\nu = m\omega/\hbar$) and $L_K^2(x)$ is the associated Laguerre polynomial defined by,[11]

$$L_n^a(x) = \sum_{k=0}^{n} \binom{n+a}{n-k} \frac{(-1)^k}{k!}\, x^k . \tag{16}$$

Using the result that for $n \ge m$,

$$\int_{-\infty}^{\infty} dp\, e^{-[p^2 + (p+q)^2]}\, L_n^{-1/2}(2(p+q)^2)\, L_m^{-1/2}(2p^2) = (-1)^{n+m}\, \left(\frac{\pi}{2}\right)^{1/2} \frac{m!}{n!}\, L_m^{-1/2}(0)\, (q^2/2)^{n-m} \cdot e^{-q^2/2}\, L_{2n}^{2n-2m}(q^2),$$

together with the addition theorem for the associated Laguerre polynomials, the integral

$$I_{K_1K_2}(q) = (2\pi)^3 \int d\vec{r}\, d\vec{p}\, f_{K_1}(\vec{r},\vec{p})\, f_{K_2}(\vec{r},\vec{p}+\vec{q}), \tag{17}$$

reduces to

$$I_{K_1K_2}(q) = (q^2/2)^k\, e^{-q^2/2} \sum_{n+m=K_1} \frac{n!}{(n+k)!} \cdot L_m^{3/2}(0)\, L_n^{-1/2}(0)\, L_{2n}^{2k}(q^2) , \tag{18}$$

with $k = K_2 - K_1 \ge 0$. I then obtain for S(E,q) and P(q) of (12) and (13), respectively, the explicit forms,

$$S(E,q) = \frac{1}{a} \sum_{k=1}^{\infty} \delta(k\hbar\omega - E)\, (q^2/2)^k\, e^{-q^2/2} \cdot \left[\sum_{n=0}^{M} \frac{n!}{(n+k)!}\, L_{M-n}^{5/2}(0)\, L_n^{-1/2}(0)\, L_{2n}^{2k}(q^2) - \sum_{n=0}^{M-k} \frac{n!}{(n+k)!}\, L_{M-k-n}^{5/2}(0)\, L_n^{-1/2}(0)\, L_{2n}^{2k}(q^2) \right] , \tag{19}$$

$$P(q) = 1 - \frac{1}{a} \sum_{k=0}^{M} \frac{2}{1+\delta_{k0}}\, (q^2/2)^k\, e^{-q^2/2} \sum_{n=0}^{M-k} \frac{n!}{(n+k)!} \cdot L_{M-k-n}^{5/2}(0)\, L_n^{-1/2}(0)\, L_{2n}^{2k}(q^2) , \tag{20}$$

where $a = L_M^3(0) = \binom{M+3}{3}$, and q is in units of $\hbar/\sqrt{\nu}$.

Since, for example, M=1, 2, and 3 for ^{16}O, ^{40}Ca, and ^{88}Zr, respectively, the sums over n in (19) and (20) are quite limited. Eq. (19) is very much simpler than the expression (involving a Clebsch-Gordan coefficient and a sum over 8 indices) that one may derive[12] by a straightforward

evaluation of (1) utilizing the explicit form for the HO wave functions. Several interesting features of S(E,q) and P(q) are easily obtained from (19) and (20), respectively. The response S(E,q) vanishes when one of the arguments equals 0 or ∞. For a fixed k (E = kħω), S is given by $e^{-q^2/2}$ times a polynomial of $(q^2/2)$ of order 2N + k with coefficients of alternating sign. For very small values of q, S(E,q) has a maximum at E = ħω with the strength at higher energies (k > 1) decreasing as $1/(k!2^k)$. For larger q, S tends toward a symmetric distribution with the maximum shifted to a higher E. Compared with the Lindhard function, (19) exhibits detailed shell structure which is more pronounced for q < 1/2, since the nuclear radius R = $2/\sqrt{\nu}$. As an example, Fig. 1 shows a comparison between the Fermi gas response (Lindhard function) and S(E,q) of (19) for a nucleus with A = 224, for q = 0.2 and 0.6 fm^{-1}.

Recently, there has been considerable interest concerning the Pauli suppression effect in the analysis of forward angles of inelastic scattering of protons with E > 200 MeV from nuclei. The experimental results indicate[10,13] that for low q, the values of P(q) obtained from (14) are too small to explain the data. A similar conclusion is obtained from time dependent Hartree-Fock (TDHF) calculations[14] of mass transfer between heavy ions colliding at low energy (E/A = 1 - 2 MeV). Figure 2 shows the results for P(q) in (20) for nuclei with A = 16 and 224 compared to the infinite Fermi-gas results of (14) using P_F = 1.37 fm^{-1}. One may conclude from Fig. 2 that the disagreement between theory and experiment can not be attributed to finite size effects. In fact, it was shown by Bertsch and Scholten,[10] using a semi-infinite slab model, that a better approximation (DWBA) for $\sigma(\vec{q},\vec{r})$ leads to an agreement with experiment. Eq. (10) offers a rather simple explanation. In the more realistic approximation for $\sigma(\vec{q},\vec{r})$, which accounts for the absorption, $f_\sigma(\vec{r},\vec{p}')$ is of finite size in momentum space. This in turn produces an averaging over P(q) in (20), which results in P(0)≠0. It would be interesting to carry out a detailed calculation of (10) using a 3-dimensional model for the wave-functions.

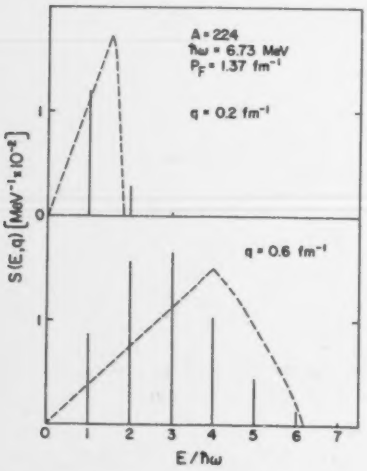

Fig. 1. The single particle response for the harmonic-oscillator model compared with the Fermi-gas model (dashed curve).

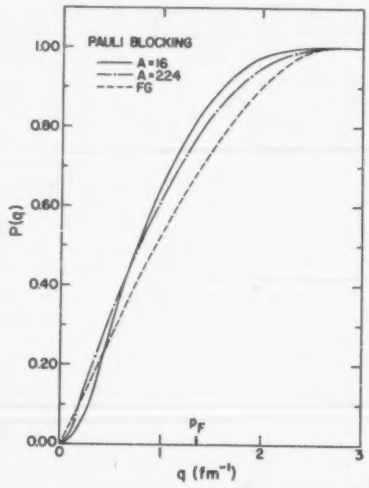

Fig. 2. The Pauli blocking factor for A = 16 (ħω = 13.92 MeV) and A = 224 (ħω = 6.73 MeV), compared with the Fermi-gas model (P_F = 1.37 fm^{-1}).

References

[1]A. L. Fetter and J. D. Walecka, Quantum Theory of Many-Particle Systems (McGraw-Hill, N.Y. 1971).

[2]E. P. Wigner, Phys. Rev. 40, 749 (1932).

[3]R. F. O'Connell and E. P. Wigner, Phys. Lett. 85A, 121 (1981).

[4]N. L. Balazs and G. G. Zipfel, Jr., Ann. Phys. 77, 139 (1973).

[5]P. Ring and P. Schuck, The Many-Body Problem (Springer-Verlag, N.Y. 1980), Chap. 13.

[6]P. Carruthers and F. Zachariasen, Caltech Preprint CALT-68-856, (1982).

[7]R. F. O'Connell and A. K. Rajagopal, Phys. Rev. Lett. 48, 525 (1982).

[8]S. Shlomo and M. Prakash, Nucl. Phys. A357, 157 (1981).

[9]J. Lindhard, K. Dan Videnak, Selsk. Mat. Fys. Medd. 28, No. 8. (1954).

[10]G. F. Bertsch and O. Scholten, Phys. Rev. C 25, 804 (1982).

[11]W. Magnus, F. Oberhettinger and R. P. Soni, Formulas and Theorems for Special Functions of Mathematical Physics, 3rd ed. (Springer, N.Y. 1966).

[12]W. M. Alberico, R. Cerni, V. R. Manfredi and A. Molinari, Nuovo Cimento 40A, 449 (1977).

[13]J. M. Moss et al., Phys. Rev. Lett. 48, 789 (1982).

[14]M. Prakash, S. Shlomo, B. S. Nilsson, J. P. Bondorf and F. E. Serr, Nucl. Phys. A385, 483 (1982).

SUM RULES FOR HARMONIC-OSCILLATOR BRACKETS

S. Shlomo

It is well known that harmonic-oscillator wave functions (HOWF) have the property that a product of two wave functions can be transformed from the single-particle coordinates to the relative and the center-of-mass coordinates.[1] This is known as the Talmi transformation and the transformation coefficients are called the oscillator-brackets or the Talmi-Brody-Moshinsky (TBM) coefficients.[2,3] This transformation simplifies the calculation of two-body matrix elements and the coefficients are widely used in nuclear structure calculations.[4] Various methods for the calculation of these coefficients and several explicit expressions for the coefficients are described in the literature.[5] The brackets satisfy the standard orthogonality relations and have some simple symmetries. In this paper I derive a class of sum rules for the HO brackets. These are new interesting relations that can also provide independent checks for any calculation of the brackets.

I first consider the one-dimensional case. The harmonic-oscillator (HO) Hamiltonian can be written in the form

$$H = \frac{1}{2}(p^2 + x^2)\,\hbar\omega\,, \qquad (1)$$

where p and x are in units of $\hbar/\sqrt{\nu}$ and $1/\sqrt{\nu}$, respectively, and $\nu = m\omega/\hbar$. The eigenvalues of (1) are of the form $(K + 1/2)\hbar\omega$, where K is a positive integer; the corresponding eigenfunctions are

$$\phi_K(x) = [\sqrt{\pi}\,2^K\,K!]^{-1/2}\,e^{-x^2/2}\,H_K(x), \qquad (2)$$

where $H_K(x)$ is the Hermite polynomial,

$$H_K(x) = K!\sum_{m=0}^{[K/2]}(-1)^m\frac{(2x)^{K-2m}}{m!\,(K-2m)!}\,. \qquad (3)$$

Here [K/2] equals K/2 or (K-1)/2 if K is even or odd, respectively. The HO brackets $\langle kK|K_1K_2\rangle$ are defined by,

$$\phi_{K_1}(x_1)\,\phi_{K_2}(x_2) = \sum_{k+K=K_1+K_2}\langle kK|K_1K_2\rangle\phi_k(x)\phi_K(X), \qquad (4)$$

where x is the relative coordinate and X is the center-of-mass coordinate, given by

$$x = (x_1 - x_2)/\sqrt{2}\,,\quad X = (x_1 + x_2)/\sqrt{2}. \qquad (5)$$

Using (2) to (5),[6]

$$\langle kK|K_1K_2\rangle = \left(\frac{k!K!}{K_1!K_2!}\right)^{1/2}2^{-(K_1+K_2)/2} \times\sum_n(-1)^n\binom{K_1}{k-n}\binom{K_2}{n}. \qquad (6)$$

The HO brackets (6) obey the orthogonality relations and the symmetry relations,

$$\langle kK|K_1K_2\rangle = (-1)^k\langle kK|K_2K_1\rangle = (-1)^{K_2}\langle Kk|K_1K_2\rangle. \qquad (7)$$

To derive the sum rules for the HO brackets, I first Fourier transform Eq. (4) over the relative coordinate x. This is also known as the Wigner transform.[7] One can utilize the Rodrigues' formulae for the Hermite and the associated Laguerre polynomials[8] to carry out the Wigner transform of the left hand side (l.h.s.) and obtain[9]

$$f_{K_1K_2}(x,p) = \frac{1}{2\pi}\int_{-\infty}^{\infty} ds\, e^{ips}\, \phi^*_{K_1}(x + s/2)\, \phi_{K_2}(x - s/2)$$

$$= \frac{(-1)^{K_2}}{\pi}\left(\frac{K_2!}{K_1!}\right)^{1/2} 2^{(K_1 - K_2)/2} e^{-(x^2 + p^2)}$$

$$* (x + ip)^{K_1 - K_2}$$

$$* L^{K_1 - K_2}_{K_2}(2x^2 + 2p^2)\ , \qquad (8)$$

where $L^{\alpha}_{K}(x)$ is the associated Laguerre polynomial,

$$L^{\alpha}_{K}(x) = \sum_{\ell=0}^{K} \binom{K+\alpha}{K-\ell} \frac{(-1)^{\ell} x^{\ell}}{\ell!}\ . \qquad (9)$$

Substituting (9) in (8) and using,

$$\sum_{n} (-1)^n \binom{K_1 - K_2}{N-2n}\binom{K_2}{n} = \sum_{n} (-1)^n \binom{K_1}{N-n}\binom{K_2}{n}\ , \qquad (10)$$

together with (6) and (7), I find that,

$$f_{K_1K_2}(x,p) = \frac{1}{\pi}\, e^{-(x^2 + p^2)} \sum_{N,M} C^{K_1K_2}_{NM}$$

$$* \langle NM \left| \frac{N+M+K_1-K_2}{2}\ \ \frac{N+M-K_1+K_2}{2} \right\rangle (2ip)^N (2x)^M\ , \qquad (11)$$

where the coefficient C is defined by

$$1 / C^{K_1K_2}_{NM} = (-1)^{(K_1+K_2-N-M)/2} \left(\frac{K_1+K_2-N-M}{2}\right)!$$

$$* \left[\frac{N!M!}{K_1!K_2!}\left(\frac{N+M+K_1-K_2}{2}\right)!\left(\frac{N+M-K_1+K_2}{2}\right)!\right]^{1/2}\ . \qquad (12)$$

The sum in (11) is limited by $|K_1-K_2| \le N+M \le K_1+K_2$ and $N+M+K_1+K_2$ must be even, i.e., $N+M = |K_1-K_2|, |K_1-K_2|+2, \ldots, K_1+K_2$. Note that in (8) and (11) $f_{K_1K_2}(x,p) = f^*_{K_2K_1}(x,p) = f_{K_2K_1}(x,-p)$. This can be verified using (7) and the fact that $C^{K_1K_2}_{NM}$ in (12) is symmetric under the interchange of K_1 and K_2 or N and M.

Utilizing (11) together with the transform

$$\frac{1}{\sqrt{2\pi}}\int_{-\infty}^{\infty} dx\, e^{ipx}\, \phi_k(x) = i^k\, \phi_k(p)\ , \qquad (13)$$

for the right hand side (r.h.s.) of (4) I find, using (2) that

$$\sum_{k+K=K_1+K_2} \langle kK \left| K_1K_2 \right\rangle [k!K!2^{(K_1+K_2)}]^{-1/2}$$

$$* i^k H_k(\sqrt{2}p)\, H_K(\sqrt{2}x)$$

$$= \sum_{NM} C^{K_1K_2}_{NM} \langle NM \left| \frac{N+M+K_1-K_2}{2}\ \ \frac{N+M-K_1+K_2}{2} \right\rangle$$

$$* (2ip)^M (2x)^M \qquad (14)$$

Substituting the explicit expression (3) for the Hermite polynomial in (14) and equating the coefficients of $(ip)^N x^M$, I find the sum rule,

$$\sum_{k+K=K_1+K_2} \langle kK \left| K_1K_2 \right\rangle (-1)^{(K-M)/2}$$

$$* [k!K!]^{1/2} / [(\tfrac{k-N}{2})!(\tfrac{K-M}{2})!]$$

$$= 2^{(K_1+K_2-N-M)/2}\, N!M!\, C^{K_1K_2}_{NM}$$

$$* \langle NM \left| \frac{N+M+K_1-K_2}{2}\ \ \frac{N+M-K_1+K_2}{2} \right\rangle \qquad (15)$$

for each pair (N,M) that satisfies $N+M \le K_1+K_2$ with $N+M+K_1+K_2$ even. The sum over k and K is further limited by the requirements that k-N and K-M are non-negative even integers. It should be noted that for $N+M < |K_1-K_2|$, the r.h.s. of (15) vanishes and the sum rule has a simple form.

Sum rules for the brackets of a HO of higher dimensions can be derived in a similar way by using the transformation coefficients of the HOWF from the chosen coordinate system to the Cartesian coordinate system. I will now consider in some detail the three-dimensional case in spherical coordinates. In this case x and p in (1) should be replaced by the vectors $\vec{r} = (x,y,z)$ and $\vec{p} = (p_x, p_y, p_z)$, respectively. The eigenvalues of the HO Hamiltonian are $E_{n\ell} = (2n+\ell+3/2)\hbar\omega$ with the corresponding wave-functions,

$$\phi_{n\ell m}(\vec{r}) = U_{n\ell}(r)\, Y_{\ell m}(\theta,\phi)\ , \qquad (16)$$

where $Y_{\ell m}(\theta,\phi)$ are the spherical harmonics and

$$U_{n\ell}(r) = \left[\frac{2(n!)}{\Gamma(n+\ell+3/2)}\right]^{1/2} r^{\ell}\, e^{-r^2/2}\, L_n^{\ell+1/2}(r^2). \qquad (17)$$

As before, r is in units of $1/\sqrt{\nu}$. The TBM coefficients $(n\ell NL\lambda|n_1\ell_1 n_2\ell_2\lambda)$ are defined by,[3]

$$\sum_{m_1+m_2=\mu} \langle \ell_1 m_1 \ell_2 m_2|\lambda\mu\rangle\, \phi_{n_1\ell_1 m_1}(\vec{r}_1)$$

$$\cdot\ \phi_{n_2\ell_2 m_2}(\vec{r}_2) = \sum_{n\ell NL} \sum_{m+M=\mu} (n\ell NL\lambda|n_1\rho_1 n_2\ell_2\lambda)$$

$$\cdot\ \langle \ell m L M\,\lambda\mu\rangle \phi_{n\ell m}(\vec{r})\phi_{NLM}(\vec{R}) \qquad (18)$$

where $\vec{r} = (\vec{r}_1-\vec{r}_2)/\sqrt{2}$, $\vec{R} = (\vec{r}_1+\vec{r}_2)/\sqrt{2}$ and $\langle \ell_1 m_1 \ell_2 m_2|\lambda\mu\rangle$ is the Clebsch-Gordan coefficient. The sum over n, ℓ, N, and L in (18) is restricted by the energy-conservation condition $2n+\ell+2N+L = \rho = \rho_1+\rho_2$, where $\rho_1 = 2n_1+\ell_1$ and $\rho_2 = 2n_2+\ell_2$. The TBM coefficients obey the orthogonality relations and some symmetry relations that can be found in Ref. 3).

The transformation coefficients $\langle K_1K_2K_3|n\ell m\rangle$ from spherical coordinates system to the Cartesian coordinates system are defined by,[3]

$$\phi_{n\ell m}(\vec{r}) = \sum_{K_1+K_2+K_3=2n+\ell} \langle K_1K_2K_3|n\ell m\rangle \phi_{K_1}(x)$$

$$\cdot\ \phi_{K_2}(y)\phi_{K_3}(z) \qquad (19)$$

where $\phi_K(x)$ is given by (2). The explicit expression for the coefficient $\langle K_1K_2K_3|n\ell m\rangle$, the orthogonality relations, and the properties given by Chasman and Wahlborn (1967), will be used in the following. To derive the sum rule for the TBM the relative coordinate, r, using (19). This leads to

$$\frac{1}{\pi^{3/2}} \sum_{m+M=\mu} \sum_{n\ell NL} \langle \ell m L M|\lambda\mu\rangle\, (n\ell NL\lambda|n_1\ell_1 n_2\ell_2\lambda)$$

$$\cdot\ i^{2n+\ell}\, \phi_{n\ell m}(\sqrt{2}\,\vec{\beta})\, \phi_{NLM}(\sqrt{2}\,\vec{R})$$

$$= \sum_{m_1+m_2=\mu} \sum_{K_1,K_1'} \langle \ell_1 m_1 \ell_2 m_2|\lambda\mu\rangle \langle K_1K_2K_3|n_1\ell_1 m_1\rangle$$

$$\cdot\ \langle K_1'K_2'K_3'|n_2\ell_2 m_2\rangle f_{K_1K_1'}(X,\rho_x)$$

$$\cdot\ f_{K_2K_2'}(Y,\rho_y) f_{K_3K_3'}(Z,\rho_z), \qquad (20)$$

where the sums over K_i and K_i' are limited by $K_1+K_2+K_3 = 2n_1+\ell_1$ and $K_1'+K_2'+K_3' = 2n_2+\ell_2$. Eq. (20) holds for any value of $n_1,\ell_1,n_2,\ell_2,\lambda$ and μ. Utilizing (19) for $\phi_{n\ell m}$ and ϕ_{NLM} and using (2), (3) and (11) in (20), a sum rule is obtained for each set of (r,s,t,u,v,w) by comparing the coefficients of $(ip_x)^r\,(ip_y)^s\,(ip_z)^t\,(X)^u\,(Y)^v\,(Z)^w$. Note that if $r+s+t+u+v+w < |\rho_1-\rho_2|$ the corresponding coefficient in the r.h.s. of (20) vanishes, leading to a particularly simple sum rule. For special values of r, s, t, u, v, and w, the sum rule can be simplified by employing well-known properties of the Clebsch-Gordan coefficients and the transformation coefficients $\langle K_1K_2K_3|n\ell m\rangle$.

The general expression of the sum rules for the TBM coefficients is somewhat complicated and is not given here. Instead, as an example, I now present the relatively simple results for the case in which r=s=u=v=0, i.e., $\vec{\beta}=(0,0,p)$ and $\vec{R}=(0,0,Z)$. In this case m=M=μ=0 in (20). Using (11) for f and (16) and (17) for $\phi_{n\ell 0}$ and ϕ_{NL0} in (20) and equating the coefficients of $(ip)^t\,(Z)^w$, I obtain the sum rule,

$$\sum_{n\ell NL} \langle \ell 0 L 0|\lambda 0\rangle\, D_{tw}^{n\ell NL}\, (n\ell NL\lambda|n_1\ell_1 n_2\ell_2\lambda)$$

$$= 2^{(t+w)/2} \left\langle tw\middle|\frac{t+w+\rho_1-\rho_2}{2}\ \ \frac{t+w-\rho_1+\rho_2}{2}\right\rangle$$

$$\cdot \sum_{K_1,K_3'} \sum_{m_1} (-1)^{\ell_1-m_1} \langle \ell_1 m_1 \ell_2 -m_1|\lambda 0\rangle\, (-1)^{K_3} C_{tw}^{K_3K_3'}$$

$$\cdot\ \langle K_1K_2K_3|n_1\ell_1 m_1\rangle \langle K_1K_2K_3'|n_2\ell_2 m_2\rangle^*, \qquad (21)$$

where,

$$D_{tw}^{n\ell NL} = (-1)^{(2n+w-L)/2} \left[\frac{\pi(2\ell+1)(2L+1)(n!)(N!)}{4\Gamma(n+\ell+3/2)\Gamma(N+L+3/2)}\right]^{1/2}$$

$$\cdot \binom{n+\ell+1/2}{(2n+\ell-t)/2} \binom{N+L+1/2}{(2N+L-w)/2} \Big/ \left[\left(\frac{t-\ell}{2}\right)! \left(\frac{w-L}{2}\right)!\right]. \qquad (22)$$

In (21), the sums over ℓ and L are restricted by the requirement that $(t-\ell)/2$ and $(w-L)/2$ are non-negative integers (see (22)), and the sums over K_1 and K_3' are limited by $K_1+K_2+K_3 = \rho_1$ and $K_1+K_2+K_3' = \rho_2$. The sum t+w must have the same parity as $\ell_1+\ell_2$. Using the properties of the coefficients $\langle K_1K_2K_3|n\ell m\rangle$ given by Ref. 6, the r.h.s. of (21) could be simplified further.

A particularly simple sum rule is obtained from (21) for the case t=w=0. This leads to ℓ=L=0

and therefore to $\lambda=0$ and $\ell_1=\ell_2$. Using the relation $\langle \ell m \ell -m | 00\rangle = (-1)^{\ell-m}/\sqrt{2\ell+1}$ and the orthogonality relation for $\langle K_1K_2K_3 | n_1\ell_1 m_1\rangle$, I find the sum rule,

$$\sum_{n+N=n_1+n_2+\ell_1} (-1)^n \left[\frac{4\,\Gamma(n+3/2)\,\Gamma(N+3/2)}{\pi(n!)(N!)}\right]^{1/2} * (n_1\ell_1 N\ell 0 | n_1\ell_1 n_2\ell_1 0)\,\delta_{\ell 0} = \delta_{n_1 n_2}\sqrt{2\ell_1+1}\ . \tag{23}$$

For the special case of $n_1=n_2$, the sum rule in (23) can be written in a different form. Utilizing the orthogonality relation for the TBM coefficients and summing over n_1 and ℓ_1 with the restriction $2n_1+\ell_1=\rho_1$, I find that

$$\sum_{2n_1+\ell_1=\rho_1} \sqrt{2\ell_1+1}\ (n_1\ell_1 N\ell 0 | n_1\ell_1 n_1\ell_1 0) = (-1)^n \left[\frac{4\,\Gamma(n+3/2)\,\Gamma(N+3/2)}{\pi(n!)(N!)}\right]^{1/2}\delta_{\ell 0}\ . \tag{24}$$

This is the same expression derived earlier in Ref. 10, Eq. (33).

Sum rules involving the sum over the rows and columns indices of the TBM coefficients can be obtained by summing over n_1,ℓ_1,n_2,ℓ_2 in (20) (or (21)) with the restrictions that $2n_1+\ell_1=\rho_1$ and $2n_2+\ell_2=\rho_2$. The resulting sum-rules can be simplified for certain values of (r,s,t,u,v,w), using the orthogonality relations and the explicit expressions for the coefficients appearing in the sum rules. A particularly simple form is found from (21) for the case $(n_1\ell_1) = (n_2\ell_2)$. By multiplying (21) by $(-1)^{\ell_1-m}\langle \ell\, m\ell -m | \lambda 0\rangle$, using the relation $(-1)^{\ell_1-m} = \sqrt{2\ell_1+1}\,\langle \ell_1 m \ell_1 -m | 00\rangle$, summing over λ and m, and employing the orthogonality relationsfor the Clebsch-Gordan coefficients, one finds that the l.h.s. vanishes unless $\lambda=0$. Finally the expression,

$$\sum_{2n_1+\ell_1=\rho_1}\ \sum_{n+N+\ell=\rho_1} (-1)^{\ell}\,\frac{2\ell_1+1}{2\ell+1}\,D^{n\ell N\ell}_{tw} * (n\ell N\ell 0 | n_1\ell_1 n_1\ell_1 0) = (-1)^{w/2}\,\frac{\rho_1+2}{(2\rho_1-t-w)/2}\,/[(\tfrac{t}{2})!\,(\tfrac{w}{2})!] \tag{25}$$

is found by taking the sum over $(n_1\ell_1)$. The simple expression for the r.h.s. of (25) follows from the orthogonality relation for $\langle K_1K_2K_3 | n\ell m\rangle$ and the results of (9) to (12). The sum over ℓ in (25) is restricted by t-ℓ = even and the r.h.s. is replaced by zero if t is odd.

In summary, I have derived a new class of sum rules for the HO brackets given by (15) for the one-dimensional case and by (20), (21), and (25) for the three-dimensional case.

References

[1] I. Talmi, Helv. Phys. Acta 25, 185 (1952).

[2] M. Moshinsky, Nucl. Phys. 13, 104 (1959).

[3] T. A. Brody and M. Moshinsky, Tables of Transformation Brackets for Nuclear Shell-Model Calculations (Gordon and Breach, New York, 1967).

[4] A. de-Shalit and I. Talmi, Nuclear Shell Theory (Academic Press, New York, 1963).

[5] L. Trlifaj, Phys. Rev. C 5, 1534 (1972) and references therein.

[6] R. R. Chasman and S. Wahlborn, Nucl. Phys. A90, 401 (1967).

[7] E. P. Wigner, Phys. Rev. 40, 749 (1932).

[8] W. Magnus, F. Oberhettinger and R. P. Soni, Formulas and Theorems for the Special Functions of Mathematical Physics 3rd ed. (Springer, New York, 1966).

[9] M. S. Bartlett and J. E. Moyal, Proc. Cambridge Phil. Soc. 45, 545 (1949).

[10] S. Shlomo and M. Prakash, Nucl. Phys. A357, 157 (1981).

EXOTIC PIONIC ATOMS IN HEAVY-ION COLLISIONS

C. M. Ko

Two years ago, we proposed the possibility of producing pionic atoms in heavy-ion collisions.[1] The motivation then was the hope to use it as a means to study the critical opalescence effect associated with the pion condensation in normal nuclear matter.[2] Letting the target nucleus be excited to the pion condensed state, it is possible to emit a pion directly into the atomic orbits of the projectile nucleus. Unfortunately, because of the strong interaction widths in pionic atoms, none of the pion atomic states which have a production cross section above 0.1 μb can decay electromagnetically to lower levels.[3] This makes it very hard to verify experimentally the existence of the pionic atom.

The effects of the Coulomb field on the pion spectra in heavy-ion collisions have been shown to be very prominent.[4] It is therefore very possible that the pions produced by nuclear collisions may be captured into the atomic orbits of the projectile fragments in peripheral collisions. Shor has suggested that by studying the strong interaction shifts and widths of the pionic x-rays in this system, one can thus probe the properties of the exotic projectile fragments which exist longer than 10^{-16} seconds.[5]

To find out how feasible this process is, we have been carrying out a model calculation of its cross section. For a projectile nucleus with N neutrons and Z protons, the probability for the aberation of n neutrons and z protons can be obtained from the abration-ablation model of Hufner et al.[6]

$$P_{nz}(\underline{b}) = \binom{N}{n}\binom{Z}{z} [1-P(\underline{b})]^{n+z} P(\underline{b})^{A_p-n-z} \qquad (1)$$

where $(1 - P(\underline{b}))$ is the probability to find a projectile nucleon in the overlap region of the projectile and the target nuclei when the impact parameter of the collision is $\underline{b}$. The probability function $P(\underline{b})$ can be calculated from the Glauber theory applicable for high energy collisions.

$$P(\underline{b}) = \int d^2\underline{s}\, dz\, \rho_p(\underline{s},z) e^{-A_T \sigma_{NN}^{tot} \int_{-\infty}^{\infty} \rho_T(\underline{s}+\underline{b},z')dz'} \qquad (2)$$

where ρ_p and ρ_T are the density distributions of the projectile and the target nuclei, respectively. The target atomic number is denoted by A_T while σ_{NN}^{tot} is the nucleon-nucleon total cross section. For peripheral collisions which are dominated by the fragmentation processes that we are interested in, the exponent in Eq. (2) is small. We therefore have,

$$P(\underline{b}) = 1 - A_T \sigma_{NN}^{tot} \int d^2\underline{s}\, dz\, \rho_p(\underline{s},z)\, \rho_T(\underline{s}+\underline{b}, z')dz' \cdot \rho_T(\underline{s}+\underline{b}, z')dz' \qquad (3)$$

The integral is essentially the overlap of the projectile and target densities for impact parameter, $\underline{b}$.

The number of pions produced from the overlap region and their momentum distributions can be approximately determined either by the fireball model[8] or the nucleon-nucleon collision model.[9] Denoting this quantity by $\Pi_{\underline{p}}(\underline{b})$, the production cross section for a pionic atom in the (NL) orbit of the projectile fragment (Z-z, N-z) is given by

$$\sigma_{NL} = 2\pi \int d\underline{b}\, \underline{b}\, P_{nz}(\underline{b}) \int d^3\underline{p}\, \Pi_{\underline{p}}(\underline{b})\, C_{\underline{p}}(NL) \qquad (4)$$

The capture probability $C_{\underline{p}}(NL)$ of a pion with momentum $\underline{p}$ in the rest frame of the projectile fragment (Z-z, N-n) into its atomic orbit (N,L) is related to the capture cross section via

$$C_{\underline{p}}(NL) = \sum_{\ell} \frac{p^2}{\hbar^2} \frac{\sigma_{\ell}(NL)}{v(2\ell+1)} \qquad (5)$$

In the above, the radiative capture cross section for the ℓth partial wave in the dipole approximation is given by

$$\sigma_{\ell}(NL) = \frac{4\omega^3}{3c^2v} \frac{1}{2\ell+1} \sum_{M,m} \left| \langle NLM | \underline{r} | \ell m \rangle \right|^2 \qquad (6)$$

where v is the velocity of the pion in the projectile frame. The dipole matrix element is taken between the continuum and bound state Coulomb wave functions. The frequency of the emitted photon is given by

$$\hbar\omega = m_\pi v^2/2 + m_\pi \alpha^2 c^2/2N^2 \qquad (7)$$

from the energy conservation.

Neglecting the Coulomb distortion on the pion, and the finite size of the projectile fragment, then

$$\sigma_\ell = \frac{4\omega^3}{3c^2v}\left[\frac{(L+1)/(2L+1)}{L/(2L+1)}\right]\left|\int_{-\infty}^{\infty} dr r^2\, R_{NL}(r)\, j_\ell\left(\frac{pr}{\hbar}\right)\right|^2$$

$$\text{for } \ell = \begin{cases} L+1 \\ L-1 \end{cases} \qquad (8)$$

where j_ℓ is the spherical Bessel function and $R_{NL}(r)$ is the radial hydrogen-like atomic wave function.

Work is in progress to evaluate Eqs. (4) and (8).

References

[1]C. M. Ko and P. J. Siemens, Progress in Research 1980-1981, Cyclotron Institute, Texas A&M University, p. 42; Nucl Phys. A367, 496 (1981).

[2]T. Izumoto, M. Ichimura, C. M. Ko, and P. J. Siemens, Phys. Lett. B 112, 315 (1982).

[3]G. Backenstoss, Ann. Rev. Nucl. Sci. 20, 467 (1970).

[4]G. Bertsch, Nature 283, 280 (1980).

[5]A. Shor, private communication.

[6]J. Hufner, K. Schafer, and B. Schurmann, Phys. Rev. C 12, 1888 (1975).

[7]J. I. Kapusta, Phys. Rev. C 16, 1493 (1977).

[8]G. F. Bertsch, Phys. Rev. C 15, 713 (1977).

MAGNETIC MONOPOLE INTERACTS WITH NUCLEI

C. M. Ko

The grand unified theory of strong, weak, and electromagnetic interactions predicts the existence of massive magnetic monopoles.[1] This has revived the interests of people to study the interactions of the magnetic monopole with matter. The scattering of a charged Dirac particle by a magnetic monopole has been studied in Ref. 2. Possible bound states for a charged spin-1/2 particle with an extra magnetic moment in the field of a magnetic monopole has also been investigated by Kazama and Yang.[3] More recently, the exact solution of the Dirac equation for an I = 1/2 fermion in the field of a 't Hooft-Polyakov monopole has been studied,[4] confirming the Rubakov conjecture for the monopole catalysis of proton decays.[5] On the other hand, the stopping power of slowly moving magnetic monopoles in condensed materials has been studied in Ref. 6. These studies are relevant to the evaluation of the response of particle detectors to slow and massive monopoles. Bracci and Fiorentini[7] discussed the possibility that magnetic monopoles can form electromagnetically bound systems with atomic nuclei.

We are studying the interaction of slowly moving monopoles with nuclei, taking into account the effects of the monopole magnetic field on the nuclear energy levels. The motivations for this study are two-fold. First of all, we want to see how important are nuclear excitations in the stopping of a magnetic monopole in matter. Secondly, we would like to determine the probability for the capture of a nucleus by a slowly moving magnetic monopole via inelastic nuclear excitations.

To study the effects of the monopole magnetic field on the nuclear energy levels, we have examined a simple model. In this model, the nucleus is described by a three-dimensional harmonic oscillator in which nucleons move freely. Let a magnetic monopole be situated in the center of the harmonic well, the single-particle Hamiltonian is thus

$$H = \frac{1}{2m}(\hat{p} - e\hat{A})^2 + \frac{1}{2}m\omega^2 r^2 - \hat{\sigma}\cdot\hat{B} \qquad (1)$$

where e and m are, respectively, the charge and mass of the nucleon; ω is the frequency of the harmonic potential. The gyromagnetic ratio of the nucleon is denoted by γ. The vector potential due to a magnetic monopole is given by[2]

$$A_r = A_\theta = 0$$

$$A_\rho = -\frac{g}{r}\frac{1+\cos\theta}{\sin\theta} \qquad (2)$$

where g is the monopole magnetic charge with magnitude determined by the Dirac quantization

condition ge = hc/2. The magnetic field due to the magnetic monopole is then

$$\vec{B} = \frac{\vec{r}}{r^2} \tag{3}$$

The eigenvalues of H can be straightforwardly found to be

$$E = (2N + S + \tfrac{3}{2})\,\hbar\omega \tag{4}$$

where

$$S = \frac{-1 + (1 + 4\lambda)^{1/2}}{2} \tag{5}$$

with

$$\lambda = J(J+1) \pm [J(J+1) + \tfrac{1}{4}(\tfrac{\gamma}{2} + 1)^2]^{1/2} \tag{6}$$

for protons, and

$$\lambda = (J + \tfrac{1}{2})^2 \pm [(J + \tfrac{1}{2})^2 + \tfrac{\gamma^2}{16}]^{1/2} \tag{7}$$

for neutrons. In the above, the principal quantum number N has the value of positive integers; the angular momentum J is a positive integer for protons and a positive half-integer for neutrons. Without the magnetic monopole, the quantity S in Eq. (4) is the orbital angular momentum. When the magnetic monopole is present, the orbital angular momentum ceases to be a conserved quantity so that S is no longer an integer. For neutrons, the gyromagnetic ratio $\gamma = -3.82$, the quantity S is tabulated in Table I against the total angular momentum J. There are two allowed values for each J except for J = 1/2. In the latter case, S can be complex and this is due to the fact that the effective potential becomes too singular at the origin. For protons, the gyromagnetic ratio $\gamma = 5.6$, the quantity S is also shown in Table I. However, the proton angular momentum is an integer since the interaction of a charged particle with the magnetic field of the magnetic monopole introduces an extra angular momentum of magnitude eg/c = h/2. Again,

Table I. The effective angular momentum S versus the total angular momentum J.

Neutrons			Protons		
J		S	J		S
1/2		1.13	0		0.966
3/2	0.92	2.05	1		1.649
5/2	1.97	3.02	2	1.275	2.558
7/2	2.98	4.01	3	2.381	3.525

we encounter the situation that the effective potential is too singular at the origin for J = 0 and 1. To remove this singular behavior requires either to include the relativistic effects or a cutoff distance such that the wave function vanishes inside.

Eventually, we wish to determine in the adiabatic approximation the cross section for exciting nucleus by slowly moving magnetic monopoles. Also, we shall study the nuclear capture probability via inelastic excitations. When this has happened, the energy loss rate of the bound monopole-nucleus system would be ~1 GeV/cm which offers a distinct signature for its identification.

References

[1] G. 't Hooft, Nucl. Phys. B79,. 276 (1974); A. M. Polyakov, JETP Lett. 20, 194 (1974).

[2] J. Schwinger, K. A. Milton, W. Y. Tsai, L. L. DeRaad, and D. C. Clark, Ann. of Phys. 101, 451 (1976); Y. Kazama, C. N. Yang, and A. S. Goldhaben, Phys. Rev. D15, 2287 (1977).

[3] Y. Kazama and C. N. Yang, Phys. Rev. D 15, 2300 (1977).

[4] W. J. Marciana and L. J. Muzinich, Phys. Rev. Lett. 50, 1035 (1983).

[5] V. A. Rubakov, JETP Lett. 33, 645 (1981) and Nucl. Phys. B203, 311 (1982).

[6] S. P. Ahlen and K. Kinoshita, Phys. Rev. D26, 2347 (1982); S. D. Drell, N. M. Kroll, M. Y. Mueller, S. J. Parke, and M. Ruderman, Phys. Rev. Lett. 50, 644 (1983).

[7] L. Bracci and G. Fiorentini, Phys. Lett. B 124, 493 (1983).

ROLE OF PIONS IN STRANGE PARTICLE PRODUCTIONS IN RELATIVISTIC HEAVY-ION COLLISIONS

C. M. Ko

In last year's report,[1] we estimated the contribution to K^- production at subthreshold energy in high-energy heavy-ion collisions from the secondary process, $\pi Y \to K^- N$, where Y denotes either Λ or Σ particles. For the reaction ^{28}Si on ^{28}Si at 2.1 GeV/nucleon, the ratio of the number of K^- to that of π^- is predicted to be ~1/3000 which is comparable to the observed ratio of ~1/2000.[2]

Since the K^- has a short mean free path ($\lesssim$ 2 fm) in normal nuclear matter, we expect that its momentum distribution is equilibrated on its way out of the reaction region. For collisions with equal mass projectile and target, the K^- inclusive cross section in the laboratory is then

$$E\frac{d^2\sigma}{p^2dpd\Omega} = \gamma(E - \beta p\cos\theta)e^{-[\gamma(E-p\cos\theta)-m_k]/T} \cdot (2\pi m_k T)^{3/2} \cdot \sigma_{K^-} \qquad (1)$$

Here, p and E are the momentum and energy of K^-, respectively; β is the velocity of the fireball, and γ is the Lorentz factor. The temperature of the fireball is denoted by T. The total inclusive K^- cross section σ_{K^-} is computed according to the strangeness-exchange reaction, $\pi Y \to K^- N$. For the reaction ^{28}Si on ^{28}Si at 2.1 GeV/nucleon, we have $\sigma_{K^-} \sim 0.6$ mb. The calculated K^- spectra are shown in Fig. 1 by the solid curves and can explain a large fraction of the experimental cross section.

The production of K^- at subthreshold energy in high-energy heavy-ion collisions offers the possibility of studying the nuclear collective effects. Muller[3] has suggested that the decay of the coherently produced ϕ-meson into K^+K^- pair is responsible for the enhancement of the subthreshold K^- production. Whether this is indeed so depends on a careful study of non-collective contributions to the K^- production. Besides the strangeness-exchange reactions we mentioned previously, one other possible mechanism has been suggested to be the reaction $NY \to NNK$. Using the one-pion exchange model as shown by the Feynman diagram in Fig. 2, approximating the vertex on the right by the on-shell one, the cross section for $NY \to NNK^-$ can be related to that of $\pi Y \to NK^-$. After averaging over the isospin, we obtain the cross section

$$\sigma(NY \to NNK^-) \sim A(T - T_{thr})\text{mb}$$

where T is the nucleon kinetic energy in MeV in the hyperon frame. The threshold energies T_{thr} are ~455 MeV and ~635 MeV for $\Sigma N \to NNK^-$ and $\Lambda N \to NNK^-$, respectively. The constant, A is ~0.0004

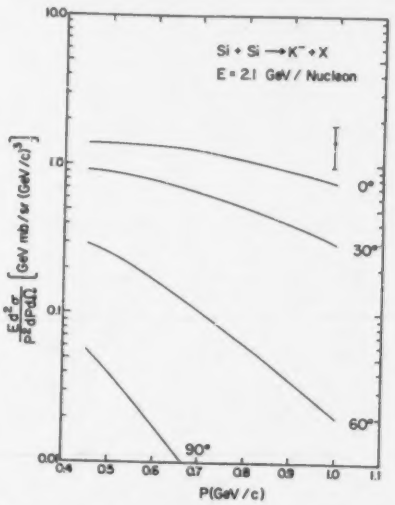

Fig. 1. K^- inclusive spectra. Solid lines are contributions from the reaction $Y\pi \to K^- N$. The experimental data are from Ref. 2.

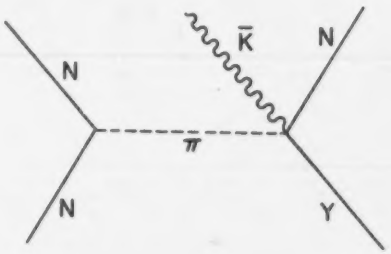

Fig. 2. Feynman diagram for the process $NY \to NNK$ in the one-pion exchange model.

and 0.0006, respectively, for Y = Λ and Y = Σ. It is seen that the cross sections are very small for nucleon kinetic energies below 1.5 GeV, compared with the strangeness-exchange reactions $\pi Y \to NK^-$ which are about a few mb.

We have started microscopic cascade calculations for K^- production. The main input to such a calculation is the cross sections for the strangeness-exchange reactions. According to the analysis of Martin and Gross[4] the experimental data on K^-p and K^0p reactions below 280 MeV/c can be parametrized in terms of nine S-wave K-matrix elements in the space of the three channels K^-N, $\Sigma\pi$ and $\Lambda\pi$. Among them, three are for isospin I = 0 and six are for I = 1, i.e.,

$$K_0 = \begin{pmatrix} \alpha_K & \alpha_{K\Sigma} \\ \alpha_{K\Sigma} & \alpha_\Sigma \end{pmatrix}, \qquad K_1 = \begin{pmatrix} \beta_K & \beta_{K\Sigma} & \beta_{K\Lambda} \\ \beta_{K\Sigma} & \beta_\Sigma & \beta_{\Sigma\Lambda} \\ \beta_{K\Lambda} & \beta_{\Sigma\Lambda} & \beta_\Lambda \end{pmatrix} \tag{3}$$

In units of fm, they have the following values,

α_K = -2.40, $\alpha_{K\Sigma}$ = -1.21, α_Σ = -1.05

β_K = -0.01, $\beta_{K\Sigma}$ = -0.71, $\beta_{K\Lambda}$ = -0.38

β_Σ = 0.34, $\beta_{\Sigma\Lambda}$ = -0.21, β_Λ = 0.17

The T-matrix is related to the K-matrix via the relation

$$T^{-1} = K^{-1} - iq \tag{4}$$

where q is a diagonal matrix of the channel center-of-mass momenta, i.e.,

$$q = \begin{pmatrix} q_K & 0 & 0 \\ 0 & q_\Sigma & 0 \\ 0 & 0 & q_\Lambda \end{pmatrix} \tag{5}$$

corresponding to K^-N, $\Sigma\pi$, and $\Lambda\pi$ channels, respectively. The isospin-averaged cross section can then be written as

$$\sigma_{i\to f} = \frac{2\pi(q_f/q_i)}{(2I_1+1)(2I_2+1)} \sum_I (2I+1)\left|T_I(i \to f)\right|^2 \tag{6}$$

where I_1 and I_2 are the isospins of the two particles in the initial channel. The calculated isospin-averaged cross sections are shown in Fig. 3.

Work is in progress to extend the cascade code of Cugnon[5] to include the processes of strange particle productions. In particular, the strangeness-exchange reactions are being investigated.

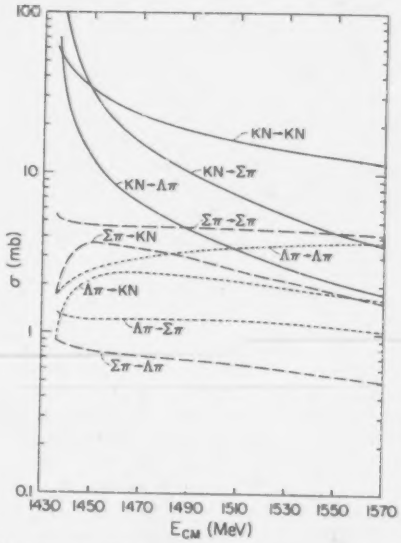

Fig. 3. Strangeness-exchange cross sections as functions of the total center-of-mass energy.

References

[1] C. M. Ko, Progress In Research 1981-1982, Cyclotron Institute, Texas A&M University, p. 66; Phys. Lett. B 120, 294 (1983); Proc. of the Inter. Conf. on Hypernuclear and Kaon Physics, Heidelberg, MPIH-1982-V20, p. 34.

[2] A. Shor, K. Ganazer, S. Abachi, J. Carroll, J. Geega, G. Igo, P. Lindstrom, T. Mulera, V. Perez-Mendez, A. Sagle, D. Woodard, and F. Zarbakhash, Phys. Rev. Lett. 48, 1592 (1982).

[3] K. H. Muller, Nucl. Phys. A395, 509 (1983).

[4] A. D. Martin and G. Ross, Nur' Phys. B16, 479 (1970).

[5] J. Cugnon, Phys. Rev. C 22, 1885 (1980).

ATOMIC STUDIES AND ACTIVATION ANALYSIS

MICROBEAM STUDIES

L. M. Divis,* P. E. Filpus-Luyckx,* D. J. Keith,* A. O. Sanni,†
J. A. Scheer,†† E. A. Schweikert,* and W. R. Summers*

The purpose of this project is to evaluate high energy heavy ions for the physico-chemical characterization of thin films, particles, and surfaces. The experimental effort utilizes microbeams (1-10 μm diameter) of ions with $E \geq 0.5$ MeV/amu and $Z > 5$. Three specific topics studied in the past year are summarized below. More detailed descriptions can be found in Refs. 1-4.

I. Microabsorptiometry

The experimental setup consists of a pinhole collimator in front of a thin target mounted on a high precision positioning and translation device. The energy of the ions emerging from the target is measured either with a surface barrier detector or a time-of-flight setup. Heavy ion absorptiometry can achieve high spatial resolution; x-ray resolution of ~ 1 μm, and a thickness resolution of ~90Å in materials with densities of 1-2 g/cm³ have been obtained (Fig. 1). Overall, this 3D resolution results in a sensitivity to mass differences of ~ 10^{-14} g. Our current capabilities in microabsorptiometry are illustrated in Fig. 2.

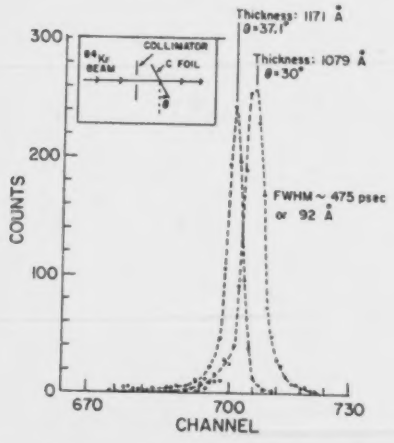

Fig. 1. Thickness resolution of 92 Å demonstrated with a 39.6 MeV $^{84}Kr^{5+}$ beam on a carbon foil (ρ = 1.82) with thicknesses of 1079 Å and of 1171 Å when tilted at 30° and at 37.1°, respectively. The peaks shown are time-of-flight signals of the Kr beam.

II. Imaging

The objective is to generate images using the secondary electrons emitted during heavy ion bombardment, an approach similar to that used in scanning electron microscopy. In preliminary work, the feasibility of this technique has been verified with line scans across a carbon foil mounted on a 100 mesh electron microscopy grid (Fig. 3). To maximize topographical contrast, the electron detector must be at an angle approaching 90° with

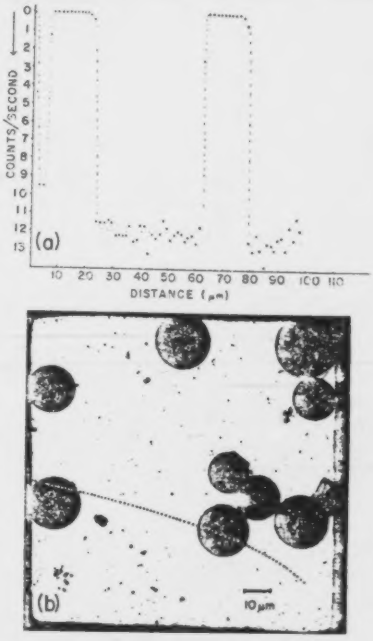

Fig. 2. Microabsorptiometry scan of latex spheres (nominal average diameter ~16 μm) supported by a formvar film and mounted on a 200 mesh EM grid; (a) shows the intensity of the transmitted ion beam (15.3 MeV ^{40}Ar using a 1 μm collimator) versus the distance scanned. Data points are scaled in size (1 μm collimator) and located at positions during scan. Spatial resolution is ~ 1.5 μm; (b) shows a TEM photomicrograph of the same sample. The scan is indicated with dots again scaled to collimator size and located at scan positions.

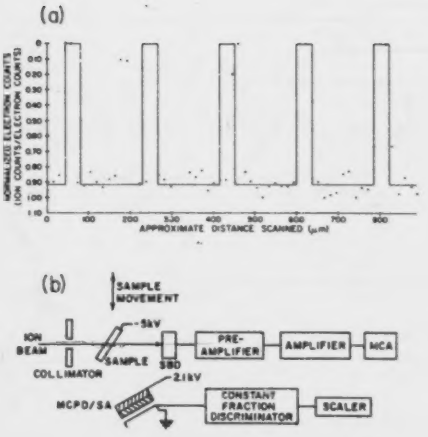

Fig. 3. (a) Heavy-ion induced secondary electron emission from a ~ 40 μg/cm^2 C foil mounted on a 100 mesh Cu electron microscopy grid. Beam: 84 MeV $^{84}Kr^{+7}$. Beam current: ~1 ion/sec. The solid line shows the theoretical results based on a scanning electron micrograph of a 100 mesh grid similar to the one examined with the ion beam; (b) Schematic diagram of the present experimental set-up for heavy-ion induced scanning electron microscopy. SBD - surface barrier detector. MCA - multichannel analyzer. MCPD/SA - microchannel plate detector with solid anode.

respect to the incident beam axis; such a setup has been successfully tested. In addition to using a suitable sample/detector geometry, amplitude information must be extracted from the electron signal to obtain accurate morphological information from surfaces of complex texture and composition. Efforts to develop the imaging capability are continuing.

III. Ion-Induced Microscopic Mass Spectrometry

The goal is to carry out comprehensive chemical analysis on a microscopic scale. Our approach is to identify, via time-of-flight mass spectrometry, the molecular fragments desorbed from a surface spot bombarded with a microbeam of high-energy heavy projectiles.

We have examined thin alkali halide targets (~ 100 μg/cm^2 on a 500 μg/cm^2 aluminized mylar backing) with an 84 MeV $^{84}Kr^{+7}$ beam collimated to a 10 μm diameter. The spectra obtained with CsI, KCl, and NaCl targets are shown in Fig. 4. Each spectrum shows the ubiquitous H^+ peak characteristic of plasma desorption MS spectra, as well as the alkali cation peak.[5] The relationship between time-of-flight and the square root of the mass can be clearly seen in the spacing in the mass series from ^{133}Cs to ^{39}K to ^{23}Na, as well as in the spacing between the K_2Cl^+ cluster ion from the KCl target and the Na contamination of the CsI salt. Also, we have examined a RbCl target and have collimated the Kr beam down to 1 μm. Further work will entail combination of Ion Induced Microscopic

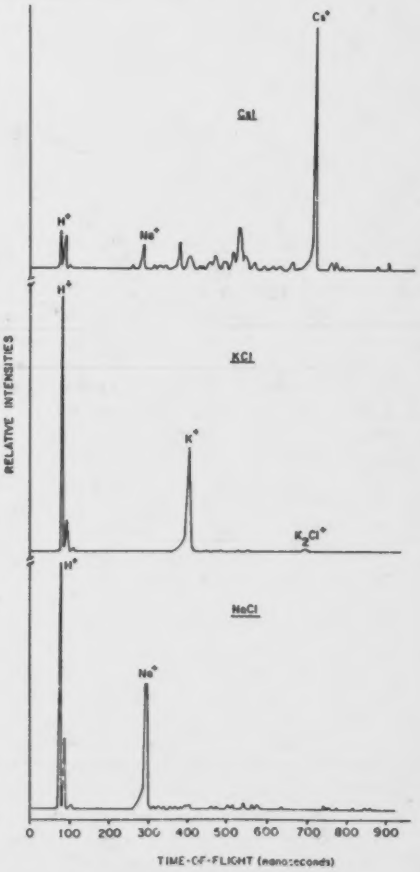

Fig. 4. Time-of-flight IMMS spectra of CsI, KCl, and NaCl targets (~100 μg/cm^2 on a 500 μg/cm^2 aluminized mylar backing) with a +5000 volt acceleration potential and a 6 cm drift length. The primary ion beam was an 84 MeV $^{84}Kr^{+7}$ beam collimated to 10 μm.

MS (IMMS) with the scanning capability developed in our laboratory[2] to study the spatially-resolved mass analysis of samples that are heterogeneous on a microscale. This work will allow us to examine the capabilities of IMMS as a microprobe.

References

[1]D. J. Keith, E. A. Schweikert, J. Trace and Microprobe Techn. 1, 187 (1982).

[2]D. J. Keith, Ph.D. Dissertation, Texas A&M University (1983).

[3]D. J. Keith, P. E. Filpus-Luyckx, E. A. Schweikert, to appear in J. Trace and Microprobe Techn. (1983).

[4]P. E. Filpus-Luyckx, W. R. Summers, E. A. Schweikert, to appear in Int. J. Mass Spectrom. and Ion Physics (1983).

[5]R. D. Macfarlane, Acc. Chem. Res. 15, 268 (1982).

ACTIVATION ANALYSIS

C. Friedli,* J. R. Joyce,† E. A. Schweikert,† and M. E. Vargast

*Center for Trace Characterization

†Department of Physics, University of Ibadan, Nigeria.

††Department of Physics, University of Bremen, F.R.G.

I. Proton Activation

As a complement to earlier work[1] we are examining proton activation with the aim of producing a single radioisotope decaying by x-ray emission. In cases where this requirement is met, the combination of proton activation and autoradiography will provide sensitive, accurate, and quantitative positional analysis. Surveys employing proton beams of 3.6, 5.0, and 6.0 MeV have been completed. X-ray emitting radionuclides have been observed from (p,n) reactions on Cl, Ti, V, Fe, Cu, Zn, Ga, Ge, As, Rb, Sr, Y, Zr, Mo, and Pd. Interference-free detection limits calculated using Currie's criterion[2] are presented in Table I. For $E_p \leq 5$ MeV, only ^{51}V and ^{71}Ga result in detectable activity at concentration levels $\leq$ 500 ppm.

To test this procedure, analyses were performed on a series of NBS steel samples and on a series of NBS glass samples doped with 62 different trace elements at nominal 500 and 50 ppm levels. Results from the glass samples are presented in Table II.

Having confirmed the selectivity of the technique with the NBS glasses, an attempt was then made to determine the capability of the technique for spatially resolved quantitative analysis. This capability was tested using a Ga doped Si sample (obtained from Hughes Laboratories, Santa Barbara, CA). Irradiation with 5 MeV protons followed by x-ray counting indicated an average Ga concentration of 8.48 ppt. The autoradiograph shown in Fig. 1 was produced by exposing double emulsion x-ray film to the sample until 10^6 cts/cm^2 were accumulated. The light areas represent regions of Ga concentration indicating the inhomogeneity of the Ga doping. From the 1 mm spacing of the calibration bars, a 50-100 μm grain limited resolution can be inferred; this resolution can be improved to 3-10 μm with the use of single emulsion x-ray film.

Table I. Interference-free detection limits for proton activation

Reaction	Interference-free Detection Limits (μg)*			
	3.6 MeV	5.0 MeV	6.0 MeV	20 MeV**
^{37}Cl(p,n)^{37}Ar	1.20 E-2	4.58 E-1	4.89 E-1	---
^{49}Ti(p,n)^{49}V	---	1.85	---	---
^{51}V(p,n)^{51}Cr	1.47	7.88 E-2	7.27 E-2	---
^{57}Fe(p,n)^{57}Co	5.4 E-1	1.33 E-1	6.38	---
^{65}Cu(p,n)^{65}Zn	---	2.21 E-1	1.30 E-1	---
^{67}Zn(p,n)^{67}Ga	2.87 E-1	8.65 E-2	4.37 E-2	---
^{71}Ga(p,n)^{71}Ge	4.75 E-2	9.18 E-3	4.14 E-3	---
^{73}Ge(p,n)^{73}As	---	4.14 E-3	2.85 E-2	---
^{75}As(p,n)^{75}Se	5.35 E-1	8.12 E-2	---	1.49 E-2
^{85}Rb(p,n)^{85}Sr	1.36	1.25 E-2	5.34 E-2	4.43 E-2
^{88}Sr(p,n)^{88}Y	---	1.26 E-1	3.17 E-2	---
^{89}Y(p,n)^{89}Zr	---	1.93 E-2	2.30 E-3	7.4 E-4
^{92}Zr(p,n)^{92m}Nb	---	---	2.38	---
^{95}Mo(p,n)^{95}Tc	---	---	5.40 E-2	1 E-4
^{105}Pd(p,n)^{105}Ag	9.26 E-2	5.08 E-2	1.61 E-2	---

*Normalized to 3 μA irradiation for 3 hr or 1 half-life (whichever is shorter) and a count time of 1 half-life of product nuclide.
**McGinley et al.[3]

II. Ultratrace Determination of Hydrogen

Based on a survey of heavy-ion reactions on hydrogen, two reactions have been chosen to be studied: ^{1}H(^{7}Li,n)^{7}Be and ^{1}H(^{10}B,α)^{7}Be. Their

Table II.

Sample	Element	Concentration Found (ppm)	Other Methods (ppm)
SRM 610*	V	494.2 ± 54.1	No data available
SRM 610*	Ga	431 ± 21	423 ± 15**
SRM 612†	V	42.0 ± 4.2	No data available
SRM 612†	Ga	44.9 ± 11.0	44 ± 10**

*Irradiated at 200 nA for 1 hr.
**McGinley[1].
†Irradiated at 200 nA for 2 hrs.

Fig. 1. Autoradiograph of Ga doped Si sample, after 5 MeV proton irradiation (2 hr at 200 nA). Light areas represent regions of Ga concentration. Scale bars at base of picture are 1 mm apart.

cross sections for energies up to 3 MeV/amu are in the range of hundreds of mb, and they yield a long-life radionuclide (53.4 d). Thus, radiochemical separations can easily be accomplished.

The specific activities achieved with both reactions have been determined to be (4.4 ± 0.6) x 10^7 Bq/μC and (1.5 ± 0.2) x 10^7 Bq/μC for ^{7}Li and ^{10}B beams, respectively (specific activities for 1 g of hydrogen). With the Li beam, 31 potentially interferring elements have been irradiated, typically for 20 minutes, with a 5-10 nA beam intensity. Only boron, magnesium, scandium, and zinc present a small interference as shown in Table III together with those results from ^{10}B bombardment.

To test the validity of the activation technique, hydrogen determinations have been carried out with both beam on two samples. Preliminary results obtained with ^{7}Li activation are presented in Table IV. The discrepancy between our data and the certified value for the NBS standard is believed to be due to surface contamination.

Table III. Nuclear interferences in the determination of hydrogen via ^{1}H(^{7}Li,n)^{7}Be and ^{1}H(^{10}B,α)^{7}Be using 3 MeV/amu heavy ions.

Element	Reaction	Specific Activity Bq/μC/g	% Interference
H	^{1}H(^{7}Li,n)^{7}Be	4.4 x 10^7	---
B	^{10}B(^{7}Li,^{10}Be)^{7}Be		
	^{11}B(^{7}Li,^{11}Be)^{7}Be	1.3 x 10^5	0.3%
Mg	^{24}Mg(^{7}Li,^{24}Na)^{7}Be		
	^{25}Mg(^{7}Li,^{25}Na)^{7}Be	1.7 x 10^5	0.4%
	^{26}Mg(^{7}Li,^{26}Na)^{7}Be		
Sc	^{45}Sc(^{7}Li,^{45}Ca)^{7}Be	3.0 x 10^4	0.07%
Zn	^{66}Zn(^{7}Li,^{66}Cu)^{7}Be	1.8 x 10^4	0.04%
H	^{1}H(^{10}B,α)^{7}Be	1.5 x 10^7	---
B	^{10}B(^{10}B,^{13}C)^{7}Be		
	^{11}B(^{10}B,^{14}C)^{7}Be	7.0 x 10^4	0.5%
Mg	^{24}Mg(^{10}B,^{27}Al)^{7}Be		
	^{25}Mg(^{10}B,^{28}Al)^{7}Be	2.0 x 10^4	0.1%
	^{26}Mg(^{10}B,^{29}Al)^{7}Be		

Table IV. Preliminary results of hydrogen determinations using ^{1}H(^{7}Li,n)^{7}Be

Sample	Concentration of Hydrogen (ppm) Calculated/Certified	Found
Cellulose	5.6 x 10^4	Standard
SRM-1086 (NBS)	116	156 ± 30
Lead Bronze	---	137 ± 27

References

*Center for Trace Characterization

†Institut d'electrochimie et de radiochimie, Swiss Federal Institute of Technology in Lausanne, Switzerland.

[1]J. R. McGinley and E. A. Schweikert, Anal. Chem. 48, 429 (1976).

[2]L. A. Currie, Anal. Chem. 40, 586 (1968).

[3]B. D. Lass, Ph.D. Dissertation, Texas A&M University (1981).

K X-RAY SPECTRA OF SOLID AND GASEOUS FLUORINE COMPOUNDS EXCITED BY 80 MeV Ar AND 48 MeV Mg IONS

O. Benka, R. L. Watson, and B. Bandong

Systematic measurements of the spectra of fluorine Kα x rays produced by the bombardment of alkali and alkaline earth fluorides with 5.5 MeV He and 22 MeV C ions have been reported previously.[1,2] The spectra obtained with He-ions provided clear evidence of resonant electron transfer to the fluorine L-shell following 1s2p ionization in the compounds KF and SrF_2. In this study, it was shown that such state selective electron transfer processes result from close energy matches between the pre- and post-transfer metal fluoride electron configurations. The spectra excited with C-ions revealed that when higher stages of ionization are created, rapid electron transfer to the fluorine L-shell occurs largely via a mechanism that is not state selective. Consequently, an overall depression of the intensities of the KL^n x-ray satellites for $n > 2$ is observed.

The exact nature of the mechanism for electron transfer in highly ionized atoms is still unknown. The fact that the effects of electron transfer are readily visible in K x-ray spectra means that the transfer process effectively competes with K vacancy decay on a time scale of the order of 10^{-13} sec. Thus, these transfer times are much shorter than typical valence electron transition lifetimes. They are, however, quite comparable to the the plasma frequencies of the solids involved.

It is of interest to extend the investigations mentioned above to states of higher excitation. This is readily accomplished by examining the x-ray spectra produced by projectiles having charges significantly greater than the atomic number of the target. The measurements of Beyer et al.[3], as well as those presented in Ref. 4, demonstrate that when a 2 MeV/amu Ar ion undergoes a K-shell ionizing collision with a Ne atom, all but one or at most two electrons are stripped from the Ne atom. In the measurements to be presented herein, beams of 2 MeV/amu Mg and Ar ions were used to excite K x-ray emission in the series of alkali and alkaline earth fluorides studied previously with considerably lighter ions. In addition, measurements were performed on a number of gaseous fluorine compounds to investigate electron transfer in single molecules, and on HF to obtain spectra characteristic of free F^- ions.

The experiments were performed using beams of 48 MeV Mg^{3+} and 80 MeV Ar^{5+} ions provided by the Texas A&M variable energy cyclotron. The Ar beam was used to obtain the spectra for the solid fluorine compounds whereas the Mg beam was used for the gas spectra because, at the gas pressures employed, interfering L-radiation from Ar was produced at intensities comparable to the fluorine intensities. Targets of LiF, NaF, KF, MgF_2, CaF_2, CaF_2, and BaF_2 were made by vacuum evaporation onto 20 $\mu g/cm^2$ carbon backing foils. The thickness of target material was 10 $\mu g/cm^2$ or less as discussed previously in conjunction with the C-projectile measurements. The x-ray spectrometer was a Johansson type having a 12.7 cm focal circle radius and a curved thallium acid phthalate (TAP) crystal. The geometry and other details were the same as described previously.[2]

Repetitive measurements with the same target showed that, during each measurement, the target became thinner. This effect was not found for C^- projectiles and is probably due to sputtering. Extremely high sputter rates have been observed recently for alkali halides under bombardment by high energy heavy ions.[5] Only the total x-ray intensities changed in the repeated measurements; the relative intensities of the individual satellite lines were not affected.

The gas measurements were performed on HF, SiF_4, SF_6, C_2F_6, CHF_3 and CHF_2CH_3 using a closed gas cell. The beam entrance window was a 1.9 mg/cm^2 havar foil and the x-ray exit window consisted of 65 $\mu g/cm^2$ stretched polypropylene. In order to minimize self absorption of the fluorine x rays in the gas, the distance between the beam axis and the x-ray window was 2.5 mm. The gas pressure varied between 5 and 50 mbar, as measured by a mechanical diaphragm gauge, to check on self absorption effects. The fluorine hypersatellites were measured using thick solid targets, since disturbing effects from the absorption edge were not expected. No sputtering effects were observed with the thick targets.

The spectra obtained for the alkali and alkaline earth fluorides from thin targets are compared in Fig. 1. The X-ray groups KL^0 to KL^7 appear in order of increasing energy. Rather large relative intensity differences occur for the first three satellite lines (KL^0 to KL^2) among the various compounds, whereas the higher satellite groups are rather similar.

In Fig. 2, a complete satellite and hypersatellite spectrum of KF, obtained with a thick

target, is shown. As can be seen by comparison with the thin target spectrum, the influence of the absorption edge is not very great for this compound because of the high absorption coefficient of potassium. For all the other compounds, the absorption of the metal ion is, in general, lower

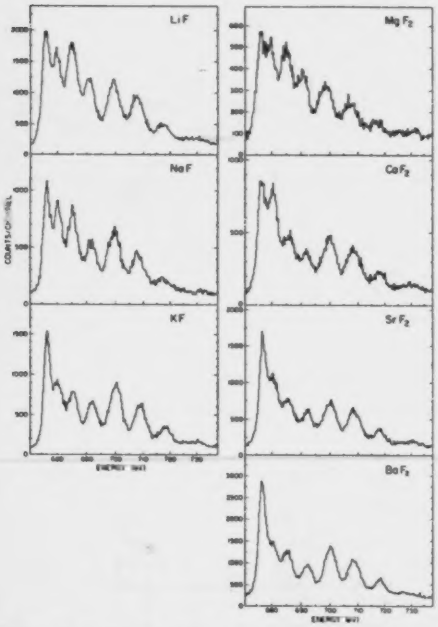

Fig. 1. Comparison of fluorine Kα x-ray satellite spectra, excited by 80 MeV Ar ions in thin targets of alkali and alkaline earth fluorides.

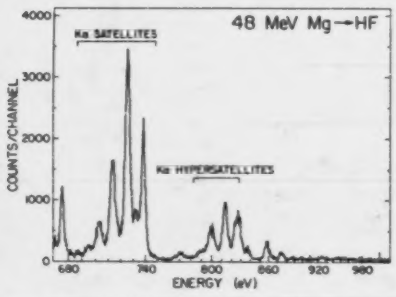

Fig. 2. Spectrum of fluorine K x rays excited by 80 MeV Ar ions in a thick KF target.

and the effect of the absorption edge is more significant. In the Kα hypersatellite region, the line of highest intensity is the K^2L^5 group. The K^2L^6, K^2L^1 and K^2L^2 groups are of such low intensity that their peaks are not distinguishable. The Kα hypersatellite peaks have about the same relative intensity distribution for all of the compounds. The broad peaks above the Kα hypersatellites are attributed to Kβ hypersatellite transitions from $n \geq 3$ states. They are discussed on page 79. Kα satellite spectra for the gases are compared in Fig. 3. The low energy end of each spectrum was observed by the presence of Mg-projectile lines measured in second order. This region is shown in the spectrum for SiF_4, but has been removed from the other spectra to facilitate comparison of the fluorine Kα satellite peaks. The most intense satellite peak in the gas spectra is KL^5.

A spectrum of fluorine K x rays excited by 48 MeV Mg ions in (gaseous) HF is shown in Fig. 4. The average state of ionization associated with this spectrum is much higher than those associated with the other gas spectra (Fig. 3). Here, the most prominent peaks are KL^6 and KL^7, and both the ^3P and ^1P components of KL^7 are readily distinguishable. This spectrum is very similar to that obtained for Ne using the same projectile.

All spectra were analyzed by means of a least squares peak fitting program employing Voigt functions (FACELIFT). The procedure was the same as that described previously.[2] The peak intensities were corrected for crystal reflectivity and for absorption in the proportional counter window. The intensities obtained for the thin target spectra were corrected for intensity loss due to sputtering by assuming a linear decrease between repetitive measurements. In addition, components attributed to Ar projectile L x rays were subtracted from the thin target spectra using a spectrum of the projectile x rays excited during passage through a thin carbon foil. The Kα hypersatellite intensities obtained from the thick target spectra were corrected for self absorption by the target. In the case of the gas spectra, only the satellite groups KL^4 to KL^7 were used for the evaluation to follow. These groups are well above the absorption edge and self absorption corrections were negligible. Only corrections for absorption in the gas cell x-ray window were required in addition to the corrections mentioned above. The corrected intensities are listed in Table I.

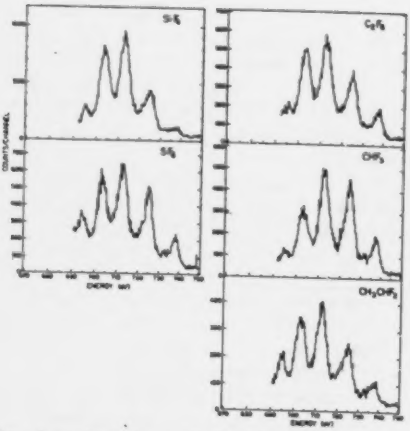

Fig. 3. Comparison of fluorine Kα satellite spectra excited by 48 MeV Mg ions on a variety of gaseous compounds.

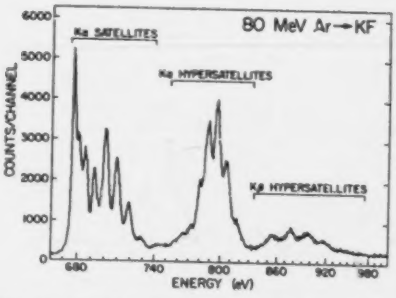

Fig. 4. Fluorine K x-ray spectrum excited by 48 MeV Mg ions in (gaseous) HF.

Table I: Experimental fluorine K x ray relative intensities for satellite and hypersatellite groups.

A. Kα Satellites

Compound	KL^0	KL^1	KL^2	KL^3	KL^4	KL^5	KL^6	$KL^7(^3P)$	$KL^7(^1P)$
Solids									
LiF	0.165	0.112	0.191	0.137	0.138	0.119	0.055		0.026
NaF	0.162	0.137	0.177	0.135	0.171	0.119	0.056		0.035
KF	0.177	0.148	0.126	0.139	0.188	0.138	0.056		0.017
MgF_2	0.131	0.147	0.221	0.135	0.144	0.120	0.062		0.039
CaF_2	0.189	0.173	0.150	0.101	0.158	0.147	0.061		0.021
SrF_2	0.212	0.147	0.157	0.121	0.155	0.135	0.058		0.013
BaF_2	0.252	0.107	0.153	0.110	0.170	0.142	0.054		0.012
Gases									
HF				0.005	0.049	0.225	0.400	0.118	0.219
SiF_4					0.340	0.419	0.208	0.013	0.021
SF_6					0.362	0.377	0.266	0.025	0.071
C_2F_6					0.306	0.388	0.231	0.022	0.054
CHF_3					0.229	0.373	0.301	0.027	0.069
CHF_2CH_3					0.337	0.372	0.233	0.022	0.037

B. Kα Hypersatellites

Compound	K^2L^0	K^2L^1	K^2L^2	K^2L^3	K^2L^4	K^2L^5	K^2L^6	K^2L^7
LiF	0.006	0.020	0.063	0.120	0.272	0.239	0.183	0.096
NaF	0.005	0.014	0.049	0.117	0.270	0.259	0.189	0.098
KF	0.011	0.026	0.035	0.117	0.279	0.238	0.185	0.064
MgF_2	0.009	0.027	0.071	0.135	0.277	0.235	0.154	0.093
CaF_2	0.014	0.030	0.048	0.116	0.277	0.259	0.180	0.076
SrF_2	0.010	0.031	0.050	0.125	0.289	0.284	0.154	0.059

Discussions of the various spectra are presented below.

A. $K\alpha$ satellite spectrum of HF

Since there are no extra-atomic electrons available to F^- in this gas, no L-vacancy filling processes are expected. The primary L-vacancy yield distribution was obtained (as for neon in Ref. 5) by correcting the satellite intensities for fluorescence yield.[6] The distribution so obtained was nearly binomial with a p_L value of 0.70. The corresponding p_L value for Ne (0.66) is slightly lower; as is to be expected since p_L decreases with increasing Z. The fact that the p_L values are nearly the same for Ne and HF is confirmation of the previous assumption[2] that the primary vacancy distribution of F^- can be accurately estimated from that for Ne.

B. $K\alpha$ satellite spectra of solid compounds

The intensity distributions in the spectra of Fig. 1 give the appearance of being composed of contributions from two different mechanisms. The lower n satellites (KL^0, KL^1, and KL^2) are greatly enhanced compared to the higher n satellites. Therefore, an analysis similar to that described in Ref. 2 was performed using only the intensities for KL^3 to KL^7. In this analysis, it was assumed that the primary L-vacancy distribution is binomial with a p_L value of 0.78, as determined from the previous data obtained for 80 MeV Ar on Ne.[5] Applying the formalism detailed in Ref. 2, values of the rate constants for electron transfer to the L-shell λ_t were determined. They are listed in Table II. The error associated with each value is roughly estimated to be about $\pm 5 \times 10^{-4}$ a.u.

The calculated x-ray distributions for KL^3 to KL^7, obtained using the λ_t from Table II, and the experimental distributions were in good agreement, and the individual peak intensities agreed to within 10%. As expected from the appearance of the spectra, the experimental KL^0, KL^1, and KL^2 intensities were considerably larger than those predicted from the above analysis. The magnitude of this effect can be shown by calculating the excess yield $E(n) = y(n) - n(n)$ for each peak (KL^0, KL^1, and KL^2) where $y(n)$ is the experimental relative yield of the KL^n peak and $n(n)$ is its calculated relative yield. The total enhancements

$$E = \sum_{n=0}^{2} E(n)$$

are listed in the third column of Table II. Unlike the enhancements observed for the KL^0 in the carbon ion work (Ref.2), the present enhancements do not show a discernable dependence on stopping power. About all that can be said is that the enhancements for the alkaline earth fluorides are somewhat larger than those for the alkali fluorides. It was found that the enhancement of KL^0 was always the largest contributor to the total enhancement, and that E(o) was particularly large for the compounds KF, SrF_2, and BaF_2, where contribution from resonant electron transfer is expected.

Table II. Rate constants for electron transfer to the L-shell $\lambda_t(10^{-4}$ a.u.) and enhancements E (see text).

Compound	λ_t	E
LiF	33.2	0.27
NaF	28.3	0.30
KF	26.2	0.27
MgF_2	29.5	0.33
CaF_2	18.7	0.42
SrF_2	24.3	0.37
BaF_2	23.4	0.38
SiF_4	10.2	
SF_6	3.8	
C_2F_6	6.2	
CHF_3	3.0	
CHF_2CH_3	8.1	

C. $K\alpha$ satellite spectra of gaseous compounds

An analysis similar to that described above was performed on the intensity distributions (KL^4 to KL^7) obtained for the gaseous compounds. The resulting λ_t values are listed in Table II. Compared with the solids, the rate constants for the gases are much lower. Also, significant differences in the rate constants occur among the various gases. It is not obvious, however, what causes these variations and a more systematic investigation will be necessary to shed further light upon this question.

References

[1]O. Benka, R. L. Watson, and R. A. Kenefick, Phys. Rev. Lett. 47, 1202 (1981).

[2]O. Benka, R. L. Watson, K. Parthasaradhi, J. M. Sanders, and R. J. Maurer, Phys. Rev. A 27, 149 (1983).

[3]H. F. Beyer, R. Mann, and F. Folkmann, J. Phys. B 14, L377 (1981).

[4]R. L. Watson, O. Benka, K. Parthasardhi, R. J. Maurer, and J. M. Sanders, J. Phys. B 16, 835 (1983).

[5]J. P. Biersack and E. Santner, Nucl. Instrum. Methods 198, 29 (1982).

ELECTRON TRANSFER TO N $\geq$ 3 STATES OF FLUORINE FOLLOWING K-PLUS L-SHELL IONIZATION BY HEAVY IONS

O. Benka, R. L. Watson, T. Ritter, B. Bandong, and K. Parthasaradhi

The intensity distributions displayed by ion-excited Kα satellite and hypersatellite spectra of gaseous and solid fluorine compounds were discussed on page 75. In the present article, attention is focused on a comparison of the energies of these satellite and hypersatellite groups in gases and solids, and upon an analysis of the series of broad peaks appearing above the Kα hypersatellites in the spectra for solid compounds excited by 80 MeV Ar ions. As will be seen, both of these considerations lead to the conclusion that, on average, several electrons occupy n $\geq$ 3 states at the time of K-vacancy decay.

I. Kα Satellite and Hypersatellite Energies

Listed in Table I are the experimental Kα satellite and hypersatellite energies obtained for the solid and gaseous fluorine compounds. Within experimental error, which is estimated to be ±0.3 eV for the satellites and ±0.5 eV for the hypersatellites, all of the solid compounds studied gave the same energies. The energies obtained from the spectra for the gases were likewise essentially the same except for HF, which gave slightly different values for KL^5, KL^6, and $KL^7(^3P)$. As may be seen from Table I, however, the solid compounds energies are significantly lower than the gaseous compound energies, and the deviation increases steadily as the number of L-vacancies increases. This trend is shown graphically in Fig. 1 where the energy differences E(HF) - E(solid) are plotted versus the number of L-vacancies.

An absolute comparison of the measured satellite and hypersatellite energies with the energies predicted by Hartree-Fock or Dirac-Fock calculations is complicated by the fact that the experimental energies are averages of the energies of the many multiplet transitions which comprise each satellite and hypersatellite group. In order to calculate properly averaged theoretical energies, each multiplet transition energy must be computed and its relative intensity estimated from theoretical fluorescence yields and initial satellite population probabilities. This laborious procedure was recently carried out for neon and the calculated average energies agreed to within 0.5 eV for the satellites and to within 1.7 eV for the hypersatel-

Table I. Experimental fluorine Kα satellite and hypersatellite energies for gases and solids (in eV).

A. Kα Satellites

	Solids	HF	Other Gases
KL^0	676.8		
KL^1	680.5		
KL^2	685.5		
KL^3	692.1	694.4	694.0
KL^4	699.9	702.3	702.2
KL^5	708.5	712.8	711.6
KL^6	717.9	724.2	723.3
$KL^7(^3P)$		731.2	732.1
$KL^7(^1P)$	728.7	737.2	737.1

B. Kα Hypersatellites

	Solids	HF	Other Gases
K^2L^0	761.2		
K^2L^1	764.9		
K^2L^2	771.8		
K^2L^3	779.3		
K^2L^4	787.3		
K^2L^5	796.1	799.1	
K^2L^6	805.3	812.9	
K^2L^7	816.5	827.2	

lites, on average.[1] For the present purposes, it is sufficient to make a relative comparison between the corresponding energies of fluorine and neon. This procedure is advantageous because all relative energies, whether they are computed from individual multiplet term energies or from average of configurations energies, lie along a single smooth curve. Such a comparison is shown for the Kα satellites in Fig. 2a and for the Kα hypersatellites in Fig. 2b. The solid squares in these figures are plotted at the intersection points of corresponding fluorine and neon multiplet transition energies, as computed using the Hartree-Fock program of Fischer.[2] The solid line was constructed by drawing a smooth curve through the intersection points of corresponding fluorine and neon transition energies computed from average of configurations initial and final state energies.

The above comparison indicates that as long as the fluorine and neon energies are averaged in the same way, their relative energies should lie along smooth curves in Fig. 2. The experimental energies are shown in Fig. 2 by the open circles for the solid fluorine compounds. It is apparent that the HF energies agree very well with the Hartree-Fock values. Therefore, it must be concluded that the energies for the solid compounds are lowered by some effect associated with the solid state environment.

One possible cause of the observed energy shifts in the solid compounds might be screening arising from the presence of electrons in n = 3 states. Since the L-shell is the outermost shell of a ground state F^- ion, such electrons are normally unbound. Following K-p¹us L-shell ionization, however, the $n \geq 3$ states drop out of the continuum and can accomodate bound electrons. To test this hypothesis, the average enegies of the initial and final state configurations were calculated for the various satellite and hypersatellite configurations in the presence of 1 to 4 M shell (3p) electrons. The transition energy differences are plotted versus the corresponding energy differences for neon without 3p electrons in Fig. 3. Also shown are the experimental energies for HF gas and the

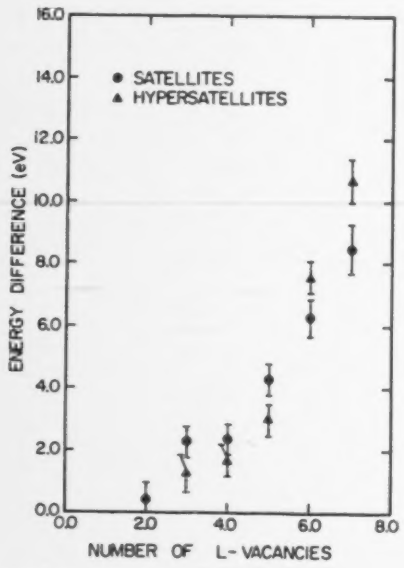

Fig. 1. The energy differences E(HF) - E(solid) for fluorine satellites and hypersatellites as a function of the number of the L-vacancies.

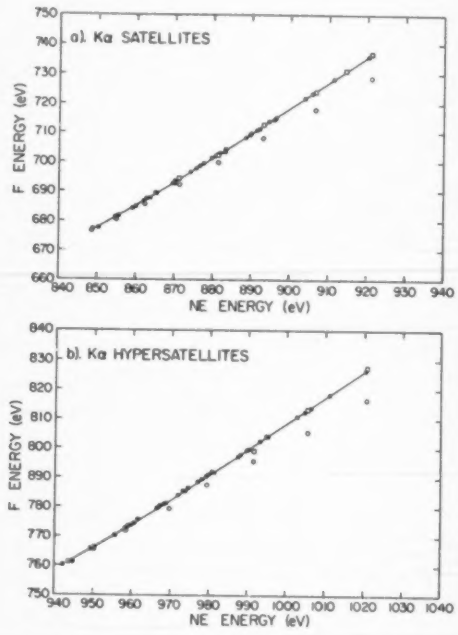

Fig. 2. Calculated (solid squares and solid line) and experimental (open squares for HF and open circles for solid compounds) Kα satellite and hypersatellite energies plotted against the corresponding values for neon (Ref. 1.).

solid fluorine compounds, as in Fig. 2. It may be seen that satellite energies for the solid compounds all line up closely with the curve corresponding to 3 M-shell electrons. The hypersatellite energies for n > 4 lie along the m = 3 line while those for n 4 lie along the m = 4 line. Hence, the observed energy decreases for the solid fluorine compounds are consistent with the presence of 3 to 4 M-shell electrons at the time of K-vacancy decay.

II. Kα Hypersatellites

In Fig. 4 a comparison is shown between a spectrum of fluorine K x-rays excited in solid LiF by 80 MeV Ar ions and a spectrum obtained for gaseous HF using 48 MeV Mg ions. In addition to the very different satellite and hypersatellite structure displayed by the spectrum for the solid (as was discussed on page 75 and in section I of the present article), there is a series of broad peaks

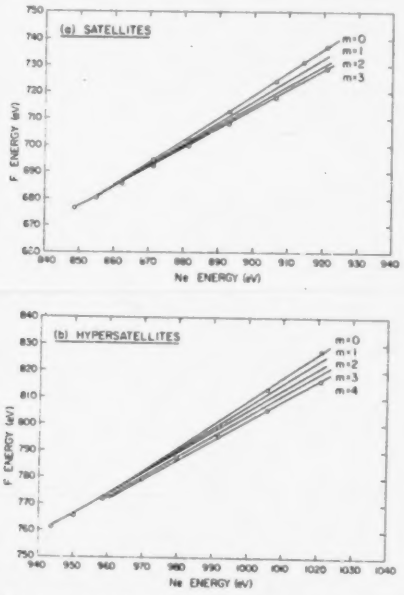

Fig. 3. Calculated (solid lines) average of configurations energy differences for fluorine containing 0 to 4 electrons in 3p levels plotted versus the corresponding energy differences for neon without 3p electrons. The open squares are the experimental values for HF gas and the open circles are the experimental values for the solid fluorine compounds.

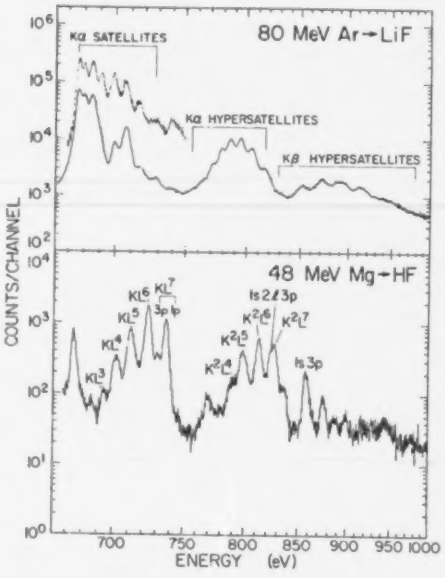

Fig. 4. Comparison of the spectra of fluorine K x rays excited in solid LiF by 80 MeV Ar ions and in gaseous HF by 48 MeV Mg ions, showing the presence of Kα hypersatellites in the LiF spectrum but not in the HF spectrum.

spanning the energy region 820 to 970 eV which are not present in the spectrum for the gas. Based upon the evidence presented in section A for the presence of 3 or 4 M-shell electrons at the time of K-vacancy decay in solids it is likely that these peaks are K hypersatellites arising from np→1s transitions where $n \geq 3$.

The experimental energies of the peaks tentatively identified as Kβ hypersatellites are listed in Table II. As may be seen in Table II, the peak energies vary considerably among the various compounds. (Because of the large uncertainities associated with peaks B1 and B7, only average energies are given for them). In Table III are listed 3p-1s transition energies calculated from Hartree-Fock average of configurations initial and final state energies. The value of m in this table indicates the number of 3p electrons present in the initial state configuration. Based on these numbers, which are not expected to be accurate to better than ±5eV, the following assignments are made:

Table II. Experimental Kβ hypersatellite energies for fluorine in eV

Peak	LiF	NaF	KF	MgF_2	CaF_2	Avg.
B1						833±5
B2	853.5	853.4	855.9	852.6	856.0	854.3±1.6
B3	872.4	873.2	876.3	872.5	879.5	874.0±1.8
B4	893.2	894.2	896.9	892.9	894.9	894.4±1.6
B5	914.7	917.4	917.2	915.1	916.5	916.2±1.2
B6	935.9	943.5	938.9	938.1	943.7	940.6±2.7
B7						959±5

Table III. Hartree-Fock 3p-1s Transition Energies (eV) for fluorine atoms having initial states with 1 to 4 electrons in 3p levels.

	m=1	m=2	m=3	m=4
K^2L^2	816	815	812	812
K^2L^3	837	834	831	830
K^2L^4	861	856	853	850
K^2L^5	887	881	879	873
K^2L^6	915	907	906	899
K^2L^7	946	941	933	927
K^2L^8	980	971	964	957

peak	initial configuration	m
B1	K^2L^3	2-3
B2	K^2L^4	3-4
B3	K^2L^5	4

peak	initial configuration	m
B4	K^2L^6	4
B5	K^2L^7	5
B6	K^2L^8	5-6
B7	K^2L^8	(transition from $\geq$ 4)

Additional support for the hypothesis that the peaks B1 to B7 arise from np-1s transitions, where $n \geq 3$, is provided by a comparison of their intensities with the intensities of the Kα hypersatellite peaks for the corresponding L-vacancy configurations. The intensities for these sets of peaks are listed in Table IV. They have been corrected for self absorption, crystal reflectivity variation, and proportional counter window absorption. The ratios of these intensities may be compared with those predicted by the semiempirical scaling law;

Table IV. Corrected Kα and Kβ hypersatellite peak areas for the solid compounds.

	LiF	NaF	KF	MgF_2	CaF_2
K^2L^0	48	34	33	28	29
K^2L^1	153	98	81	85	63
K^2L^2	676	331	110	227	101
K^2L^3	897	790	363	429	241
K^2L^4	2043	1831	868	879	577
K^2L^5	1792	1753	881	747	539
K^2L^6	1372	1279	557	488	376
K^2L^7	721	664	200	295	158
B1	15	65	47	48	21
B2	283	175	151	140	78
B3	546	331	194	186	145
B4	512	408	168	204	119
B5	298	237	85	100	96
B6	167	121	31	64	76
B7	74	18	13	18	17

$$R(\beta/\alpha) = \frac{N(n''l'')}{N(n'l')} \left[\frac{Zeff(n''l'')}{Zeff(n'l')}\right]^2 \frac{T(n''l''\rightarrow nl)}{T(n\ l\ \ nl)}$$

In the above equation

$R(\beta/\alpha)$ = ratio of the Kβ hypersatellite intensity to the corresponding Kα hyper satellite intensity.

$N(nl)$ = number of electrons in the level from which the transition occurs.

$Zeff(nl)$ = screened atomic number for the level from which the transition occurs as calculated from Slater's rules.

$T(n'l'\rightarrow nl)$ = theoretical hydrogen atom transition probability from level n'l' to nl.

As will be shown on page 83, this scaling law yields values which in, general, agree with theoretical transition probability ratios to better than 20%.

The results are shown in Fig. 5. The solid curves are drawn through the values of the 3p-1s/2p-1s transition intensity ratios calculated with the above equation for a 3p electron population ranging from 1 to 5. The value of L indicates the number of L-vacancies, which are assumed to be statistically distributed between the 2s and 2p

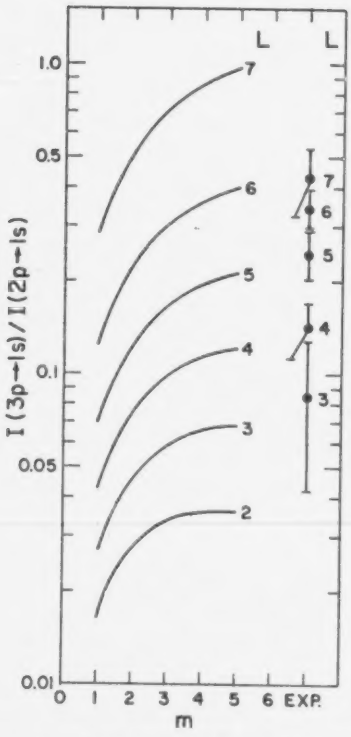

Fig. 5. Comparisons of the predicted (3p-1s)/(2p-1s) intensity ratios (solid curves) with those determined from the spectra. The value of L indicates the number of L-shell vacancies and the value of m indicates the number of 3p electrons assumed present.

levels. Along the right side of Fig. 5 are plotted the experimental values obtained using the peak assignments deduced from the peak energies. The filled circles show the averages of the ratios for all the solid compounds and the error bars show their standard deviations. It is apparent that, overall, the experimental ratios are fairly consistent with those expected for 3p electron populations of 2 to 5, and are therefore in general agreement with the conclusions reached in the peak energy comparison. The experimental vaues for n = 7, however, are conspicuously low. A possible explanation for this might be that when L becomes >7, the repopulation process may begin to shift from the M-shell to the N-shell. A reduction in the number of 3p electrons would account for the low ratio observed for peak B5 while addition of electrons to the N-shell would maintain the degree of screening necessary to account for the peak energy. A 4p-1s transition intensity arising from electron transfer to the N-shell would show up in the higher energy peaks B6, B7, and B8. In fact, peak B8 must arise entirely from $n \geq 4$ transitions.

References

[1]R. L. Watson, O. Benka, K. Parthasaradhi, R. J. Maurer, and J. M. Sanders, J. Phys. B 16, 835 (1983).

[2]C. F. Fischer, Comput. Phys. Commun. 1, 151 (1969).

SEMI-EMPIRICAL SCALING LAW FOR np-1s TRANSITION INTENSITY RATIOS OF MULTIPLY IONIZED ATOMS

O. Benka and R. L. Watson

Numerous measurements of the Kβ/Kα x-ray intensity ratios for atoms with single K-vacancies are recorded in the literature,[1] and Scofield[2] has shown that relativistic Hartree-Fock-Slater calculations yield values for these ratios which are in fair agreement with the accepted experimental ratios. Unfortunately, the calculation of accurate theoretical transition probabilities is a laborious and time consuming process. Consequently, very few calculations have been carried out for multiply ionized atoms. The purpose of the present report is to outline a simple semi-empirical scaling procedure which permits the estimation of intensity ratios for np-1s transitions in multiply ionized atoms with a precision of 2% or better.

The probability of a radiative (electric dipole) transition from an initial state having quantum numbers n'l' to a final state having quantum numbers nl is given by the well known formula

$$T(n'l' \; nl) = kN(n'l') \; E^3(n'l'-nl) \; D^2(n'l'-nl) \quad (1)$$

where N(n'l') is the number of electrons in the n'l' level; E(n'l'-nl) is the transition energy; and D(n'l' nl) is the electric dipole matrix element. For hydrogen-like atoms, the transition energy and dipole matrix element reduce to[3]

$$E(n'l'-nl) = A(n'l'-nl)Z^2 \quad (2)$$

$$D(n'l'-nl) = g(n'l'-nl)(a_0/Z) \quad (3)$$

where A and g are factors which depend on the initial and final state quantum numbers, and a_0 is the Bohr radius (0.529A). As a first approximation for the estimation of electric dipole transition probabilities in multielectron atoms, one might simply replace Z in equations (2) and (3) with a screened atomic number $Z_{eff}(n'l')$. The ratio of probabilities for transitions n"l"-nl and n'l'-nl would then become

$$\frac{T(n"l"-nl)}{T(n'l'-nl)} = \frac{N(n"l")}{N(n'l')} \left[\frac{Z_{eff}(n"l")}{Z_{eff}(n'l')}\right]^4 \frac{T_h(n"l"-nl)}{T_h(n'l'-nl)} \quad (4)$$

where $T_h(n'l'-nl)$ is the transition probability for a hydrogen atom.

Employing Slater's screening rules[5] to calculate Z_{eff}, it is found that Eq. (4) does not, in fact, provide reliable estimates of np-1s transition probability ratios. As an example, the experimental value of the ratio T(3p-1s)/ T(2p-1s) for a Zn atom (Z=30) having a single K-vacancy is 0.14, whereas the value given by Eq. (4) is 0.078. Surprisingly, however, a slight modification of Eq. (4) involving the replacement of Z_{eff}^4 by Z_{eff}^2, such as

$$\frac{T(n"l"-nl)}{T(n'l'-nl)} = \frac{N(n"l")}{N(n'l')} \left[\frac{Z_{eff}(n"l")}{Z_{eff}(n'l')}\right]^2 \frac{T_h(n"l"-nl)}{T_h(n'l'-nl)} \quad (5)$$

brings the estimates into close agreement with experiment throughout the whole periodic table.

In Fig. 1, the transition probability ratios predicted by eq (5) are compared with the relativistic Hartree-Slater results of Scofield[2] and available experimental data[1] for atoms having a single vacancy in the K-shell. The solid curves are drawn through the theoretical values, the experimental values are shown by the open circles and the values obtained with Eq. (5) are indicated by crosses since the experimental ratios for M_3/L_3

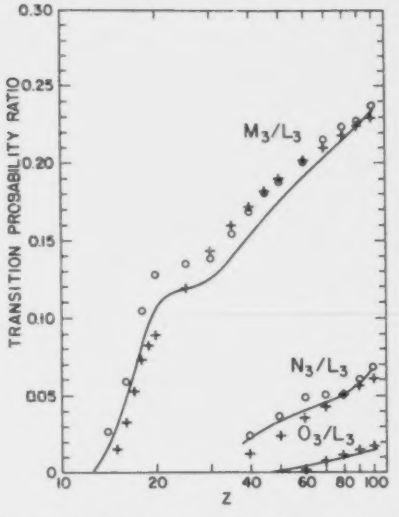

Fig. 1. Comparison of the transition probability ratios for transitions to the K-shell insingly ionized atoms obtained from Eq. (5) (crosses) with theoretical (solid curves) and experimental (open circles) values.

(i.e. $T(3p_{3/2}\text{-}1s)/T(2p_{1/2}\text{-}1s)$) have only been measured for Z > 60, the values plotted in Fig. 1 were obtained by multiplying the experimental $K_\beta bn_\alpha$ ratio times the theoretical ratio $(K_{\beta_1}/K_{\alpha_1})/(K_\beta/K_\alpha)$ obtained from Schofield's calculations. Similar corrections were applied to the experimental $K_{\beta_2}'/K_{\alpha_1}$ ratios to remove contributions from levels other that N_3. The agreement of the values obtained by this simple scaling law with the experimental and theoretical transition probability ratios is remarkable.

The reliability of Eq. (5) for the estimation of (3p-1s)/(2p-1s) transition probability ratios in atoms having single K plus multiple L-shell vacancies was tested using the Hartree-Fock-Slater results for Ti reported in Ref. 6. It was found that Eq. (5) gives values for K_β/K_α that are about 10% lower than those obtained from the Hartree-Fock-Slater calculations and the variation of K_β/K_α with increasing numbers of L-vacancies was well reproduced.

In conclusion, the scaling relationships given by Eq. (5) provides a simple means of estimating transition probability ratios for radiative (dipole) transitions to the K-shell in multiply

ionized atoms. The values obtained in this way are expected to be accurate within 10 to 20%.

References

[1]S. I. Salem, S. L. Panossian, and R. A. Krause, At. Data and Nucl. Data Tables 14, 91 (1974).

[2]J. H. Scofield, At. Data and Nucl. Data Tables 14, 121 (1974).

[3]See for example Masataka Mizushima, Quantum Mechanics of Atomic Spectra and Atomic Structure, (W. A. Benjamin, Inc., N.Y., 1970) p. 121 and 131.

[4]H. A. Bethe and E. E. Salpeter, Quantum Mechanics of One and Two Electron Atoms, (Springer-Verlog, 1957).

[5]J. C. Slater, Phys. Rev. 36, 57 (1930).

[6]T. K. Li and R. L. Watson, Phys. Rev. A9, 1574 (1974).

SPECTRA OF np-1s TRANSITIONS EXCITED DURING THE PASSAGE OF 48 MeV Mg IONS THROUGH THIN AND THICK CARBON TARGETS

R. J. Maurer, R. L. Watson, and G. J. Pedrazzini

The x-ray spectra of few electron ions have been studied extensively in recent years in connection with solar,[1-3] plasma,[4-6] and beam-foil[7-11] investigations of highly ionized atoms. Most of the prominent features of these spectra are well understood and the line assignments are substantiated by theoretical transition energy calculations based upon Z expansion or relativistic self-consistent field methods. However, a number of questions still remain concerning the assignments of certain core transitions occurring in the presence of an outer level "spectator" electron. Also, the effects of screening on x-ray emission from highly stripped heavy ions inside a high electron density medium, such as a fusion plasma or a solid, continues to be of interest.[12-14]

The present work was performed to further investigate np-1s transitions from H-like and He-like Mg ions traveling in solids. Detailed comparisons of the spectra obtained in thin and thick carbon targets have revealed several puzzling structural features, and the screening shifts expected in the thick target spectra appear to be anomalously small.

Beams of 48 MeV Mg^{3+} were extracted from the Texas A&M variable energy cyclotron, focused, and directed through a 2 mm diameter collimator located 2 cm in front of the target. The beam intensity was monitored by measuring the current produced in an 8 $\mu g/cm^2$ carbon foil located directly behind the collimator. Targets consisted of 8 $\mu g/cm^2$ and 800 $\mu g/cm^2$ carbon foils, and a 3 mm thick disc of amorphous carbon. The targets were positioned at a 45° angle with respect to the beam.

The spectral measurements were performed with a 12.7 cm Johansson-type curved crystal spectrometer employing an ammonium dihydrogen phosphate (ADP) diffraction crystal. The resolution (FWHM) for the 1253.6 ev $K_{\alpha_{1,2}}$ transition measured for a Mg target was 1.7 eV. Further details of the spectrometer system are given in Ref. 11.

Presented in Fig. 1 is a spectrum of the np-1s transitions resulting from the passage of 48 MeV Mg ions through an 8 $\mu g/cm^2$ carbon foil. The most prominent lines are identified by their initial state electron configurations. These assignments were made on the basis of transition energy calculations performed with Dirac-Fock[15] and non-relativistic Hartree-Fock[16] computer codes. They are in agreement with the assignments reported previously by Armour et al.[17] Numerical results are listed in Table I.

It is interesting to note that all of the observed transitions originate from Li-, He-, or H-like states. Since the incident beam is Mg^{3+}, and because the foil is much thinner than that required to achieve charge state equilibrium, it may be concluded that at least nine electrons are

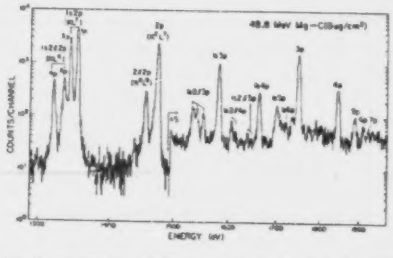

Fig. 1. Spectrum of Mg K x rays excited during the passage of 48 MeV Mg ions through a thin carbon foil.

Table I. Transition energies (eV units) for the lines appearing in Fig.1.

Initial State	Present Work	Ref[.7]	Dirac-Fock	Hartree-Fock
1s2p(^{3}P)	1343.4	1343.1	1342.2	1340.2
1s2p(^{1}P)	1352.5	1352.5	1351.5	1349.5
2p	1472.3	1472.3	1472.2	1469.4
1s2l3p(l=p)	1532.7	1531.8	1534.4	1531.5
- (l=s)	1539.3	1538.6	1542.7	1539.9
	1550.5	1550.5		
1s3p(^{1}P)	1579.5	1579.4	1578.4	1572.2
1s2l4p(l=p)	1604.3	1603.3	1604.3	1600.5
(l=s)		1612.2	1612.9	1608.9
1s4p(^{1}P)	1659.4	1659.1	1658.1	1654.0
1s5p(^{1}P)	1696.9	1696.1	1695.0	1691.7
3p	1744.6	1744.8	1745.1	1741.5
4p	1839.5	1840.4	1840.1	1836.9
5p	1883.3	1884.3	1884.2	1880.9
6p	1909.3	1909.8	1908.2	1904.8

removed in a single K-shell ionizing collision at 2 MeV/amu.

Three regular sequences of lines of the type $1s2lnp\text{-}1s^22l$, $lsnp\text{-}1s^2$, and np-1s appear in Fig. 1. For all except the 1s2lnp series, clearly distinguishable members are present up to and including those for n = 6. Several relatively long-lived (metastable) transitions are also present in this spectrum. In particular, the $(1s2p)\ ^4P$ transitions having $\tau = 4.1 \times 10^{-9}$ sec[18-20] and the $(1s2p)\ ^3P$ transition having $\tau = 2.94 \times 10^{-11}$ sec[21] are quite intense.

A spectrum obtained using the thick carbon target is shown in Fig. 2. (The Si lines are caused by contamination of the target with pump oil). It is apparent that the Mg lines are considerably broader here than they are in the thin target spectrum. Doppler broadening increases the thin target line widths by only 0.4 eV and this effect is not expected to broaden the thick target line widths by more than about 1 eV. As will be shown below, most of the broadening in the thick target spectrum is associated with the Lorentzian component of the peak shape. This implies that collision broadening is the principal contributor. The observed Lorentzian widths are consistent with previous results for sulfur ions.[10]

The metastable lines mentioned above are almost entirely absent in the thick target spectrum. The reason for this is that the cross sections for collisionally destroying the ^4P and ^3P states are large compared to their radiative decay cross sections. In this regard, it is surprising to find lines present in the thick target spectrum arising from initial states involving n = 3 and 4 to find lines present in the thick target spectrum

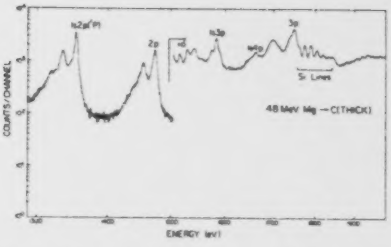

Fig. 2. Spectrum of Mg x rays emitted during the passage of 48 MeV ions through a thick carbon target.

arising from initial states involving n=3 and 4 electrons. The radius of the 4p electron in a 1s4p He-like Mg ion is about 0.7Å. Assuming that the cross section for stripping a 4p electron is nearly geometrical at 2 MeV/amu yields a value of 1.5×10^{-16} cm^2. Such a large cross section would require that the radiative lifetime of the $1s4p\text{-}1s^2$ transition be approximately 5×10^{-18} sec in order for radiative decay to compete significantly with excitation and ionization. This lifetime is roughly four orders of magnitude shorter than that expected for the $1s4p\text{-}1s^2$ transition occurring in vacuum.

Detailed peak fitting analyses employing Voigt functions were performed on the 1s2p, 2p, and 1s3p peaks appearing in the spectra obtained with the 8 μg/cm^2, 800 μg/cm^2, and thick carbon targets. The results are shown in Figs. 3, 4, and 5. In the case of the $1s2p(^1P)$ peak shown in Fig. 3, it may be seen that a small satellite peak appears on the low energy side of the main peak, and that the relative intensity of this satellite increases steadily in going from the thin target to the thick target. The Lorentzian width of the main peak increases from 0 in the thin target to 3.5 eV in the thick target while the Gaussian width remains nearly constant at 2.6 eV.

The peak resulting from the 2p-1s H-like Mg transition shown in Fig. 4 behaves in a fashion similar to that displayed by the 1s2p peak. Here, however, the satellite peak is much more prominent in the thick target spectrum. The 1s3p peak shown in Fig. 5 developes a satellite component on both the high and low energy sides.

Listed in Table II are the differences between the observed energies of the satellite peaks and the main peaks appearing in the thick target spectra, and the differences between the observed

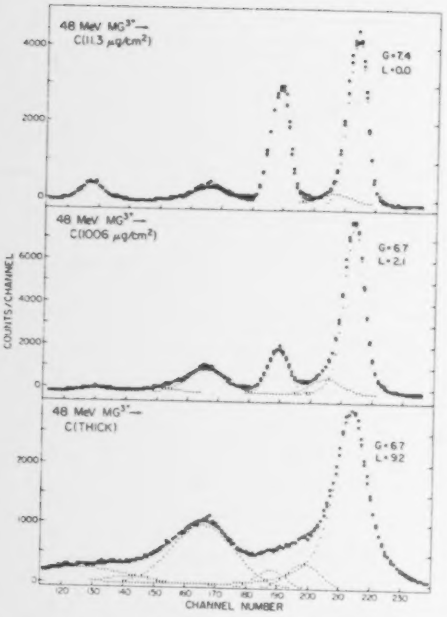

Fig. 3. Peak fitting analysis of the Mg $1s2p(^1P)$-$1s^2$ transition region for three carbon targets. The filled circles are the data points and the open circles are the least-squares calculated points.

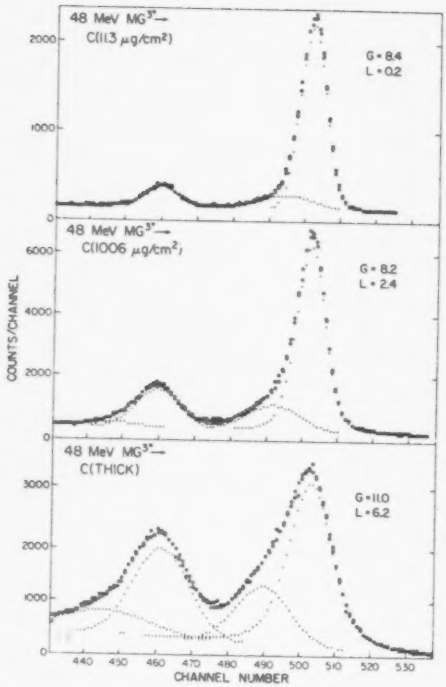

Fig. 4. Peak fitting analysis for the Mg 2p-1s transition region for three carbon targets. The filled circles are the data points and the open circles are the least-squares calculated points.

energies of the main peaks in the thick and thin targets. On the basis of absorption considerations, the average projectile energies for the detection of x rays from the 1s2p, 2p, and 1s3p states in the thick carbon target are estimated to be 39, 37, and 35 MeV, respectively. Correcting the observed thick target x-ray energies for Doppler shift yields the values -0.3, -0.3, and -0.5 eV for the energy shifts of the 1s2p, 2p, and 1s3p lines caused by dynamic screening. These values are consistent with those estimated earlier,[11] but are much smaller than the shifts observed for 2 MeV/amu sulfur ions.[14]

The identities of the satellite peaks are still uncertain. Similar peaks have been observed in plasma[4,5] and solar[2] spectra, and have been attributed to core electron transitions in the presence of outer level "spectator" electrons. Presented in Table III is a comparison of experimental and calculated satellite transition energies measured relative to the transition energy with the spectator electron absent. In the $1s2p3p$-$1s^23p$ case, there are 18 dipole allowed transitions between the various initial and final state terms. The energies of these transitions cluster together in three groups whose average calculated displacements from the $1s2p(^1P)$-$1s^2$ transition energy are the values given in the second column of Table III. The agreement between the calculated energy differences and those observed in the plasma and solar spectra is not good, as may be seen by referring to columns 2 and 3. Also, it is apparent that the satellite energy differences observed in the present experiment (column 1 of Table II) do not correspond at all well with those observed in the plasma and solar experiments. The present energy differences are, however, in reasonable agreement with the values calculated for 1s2p3p and 2s3p spectator satellites.

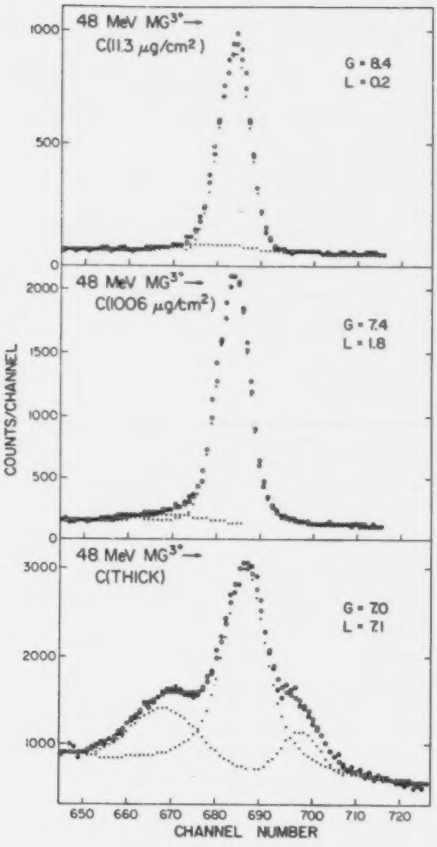

Fig. 5. Peak fitting analysis of the Mg 1s3p 1s transition region for three carbon targets. The filled circles are the data points and the open circles are the least-squares calculated points.

Further questions are raised by the fact that the satellites observed in the present work are more intense relative to the main peaks in the thick target spectra than in the thin target spectra. If these satellites are indeed caused by the presence of n = 3 or 4 spectator electrons, it is hard to understand how their relative intensities can increase with target thickness. Such a behavior would require that the transition lifetime be substantially reduced by the presence of the spectator electron. A detailed investigation of the target thickness dependence of these satellites is currently in progress.

Table II. Differences between the observed energies (uncorrected for Doppler shift) of the satellite peaks and the main peaks in the thick target spectra, and of the main peaks in the thick and thin targets, in units of eV.

Peak	Satellite-Main	Peak	Thick-Thin
$1s2p(^1P)$	-4.0	$1s2p(^1P)$	0.4
2p	-4.7	2p	0.8
1s3p	-9.1	1s3p	0.9

Table III. Energy shifts caused by the presence of an n = 3 or 4 spectator electron.

Satellite Transition	ΔE(Dirac-Fock)	ΔE(expt)	
	-10.9	-1.3	Ref[4],plasma
$1s2p3p-1s^2 3p$	-4.8	-3.4	
	-2.7	-3.5	Ref[2],solar
$1s2p4l-1s^2 4l$		-1.6	
2p3p-1s3p	-4.3	-1.7	Ref[5],plasma
		-2.4	
$1s3p4p-1s^2 4p$	-3.8		

Comparisons of the spectra of K x rays emitted by 48 MeV Mg ions during their passage through thin and thick carbon targets have revealed a number of features which are, as yet, not well understood. Although the magnitude of the line broadenings observed for the 1s2p-1s[1] and 2p-1s transitions are consistent with those observed previously with 65 MeV sulfur ions, the energy shifts attributable to dynamic screening are much smaller than expected. Satellite peaks associated with the main transitions do not appear at the same energies that have been observed for transitions in the presence of an n = 3 "spectator" electron in plasma and solar spectra. Moreover, their intensities increase relative to the main peaks in going from thin to thick targets, in opposition to the behavior expected for spectator satellites.

References

[1]A. B. Walker and H. R. Rugge, Astrophys. J. 164, 181 (1971).

[2]J. H. Parkinson, Solar Physics 42, 183 (1975).

[3]A. Gabriel and K. Phillips, Mon. Not. R. Astron. Soc. 189, 319 (1979).

[4]E. V. Aglitskii, V. A. Boiko, S. M. Zakharov, S. A. Pikuz, and A. Ya Faenov, Sov. J. Quantum Electron. 4, 500 (1974).

[5]V. A. Boiko, A. Ya Faenov, S. A. Pikuz, and U. I. Sofronova Mon. Not. R. Astron. Soc. 187, 107 (1977).

[6]E. Kallne and J. Kallne, Phys. Rev. Lett. 49, 330 (1982).

[7]C. F. Moore, H. H. Wolter, R. L. Kauffman, J. McWherter, J. E. Bolger, and C. P. Browne, J. Phys. B 5, L262 (1972).

[8]P. Richard, R. L. Kauffman, F. F. Hopkins, C. W. Woods, and K. A. Jamison, Phys. Rev. Lett. 30, 888 (1973).

[9]H. Panke, F. Bell, H.-D. Betz, and W. Stehling, Nucl. Instrum. Methods 132, 25 (1976).

[10]R. L. Watson, J. R. White, A. Langenberg, R. A. Kenefick, and C. C. Bahr, Phys. Rev. A 22, 582 (1980).

[11]R. J. Maurer, R. L. Watson, O. Benka, J. M. Sanders, and D. M. Oldham, Nucl. Instrum. Methods 202, 193 (1982).

[12]A. Langenberg, R. L. Watson, and J. R. White, J. Phys. B 13, 4193 (1980).

[13]F. Bell, H.-D. Betz, H. Panke, and W. Stehling, J. Phys. B 9, L443 (1976).

[14]R. L. Watson, A. Langenberg, R. A. Kenefick, C. C. Bahr, and J. R. White, Phys. Rev. A 23, 2471 (1981).

[15]J. P. Desclaux, Comput. Phys. Commun. 9, 31 (1975).

[16]C. Froese Fischer, Comput. Phys. Commun. 1, 151 (1969).

[17]I.A. Armour, B. C. Fawcett, J. D. Silver, and E. Trabert, J. Phys. B 13, 2701 (1980).

[18]C. L. Cocke, B. Curnutte, and R. Randall, Phys. Rev. A 9, 1823 (1973).

[19]B. Donnally and W.W. Smith, Phys. Rev. A 4, 122 (1971).

[20]I. S. Dimitriev, V. S. Nikolaev, and Y. A. Teplova, Phys. Lett. 26A, 122 (1968).

[21]C.D. Lin, W.R. Johnson, and A. Dalgarno, Phys. Rev. A 15, 154 (1977).

DIRAC-FOCK ENERGIES FOR $1s^2 3p - 1s^2 21$ TRANSITIONS IN He-LIKE Mg

B. Bandong, R. J. Maurer, G. J. Pedrazzini, and R. L. Watson

Over the last few years, the lines from helium-like ions have been a subject of interest, and recently, much attention has been focused on satellite lines of the type $(1s2p)nl - (1s^2)nl$, $n > 2$. A high resolution investigation of the solar x-ray spectrum of Mg has been reported by Parkinson.[1,2] Many of the observed lines were attributed to 2p-1s transitions in the presence of n=3 or 4 spectator electrons. Positive identification of the observed lines, however, is only possible by comparison with accurate theoretical transition energies. In the present work, results of Dirac-Fock calculations of $1s2p3l - 1s^2 3l$ transition energies in Mg are reported. These results are also relevant to our current investigation of foil excited Mg K x rays, where low energy components have been observed below the main resonance lines (see page 85).

The calculated multiplet transition energies for Mg XI with initial configurations of 1s2p3p, 1s2p3d and 1s2p3s are presented in Table I. They were obtained using the Dirac-Fock program of Desclaux[3] by taking the differences in total energies between the final and initial states. (A description of this program has been given by Grant[4]). Only electric dipole allowed transitions have been considered here.

The Mg solar x-ray spectrum obtained by Parkinson[1] is shown in Fig. 1a. The resonance, intercombination and forbidden lines are labeled by R, I, and F, respectively. The energies and tentative identifications given for these lines are listed in Table II. Note that peak R2 is attributed to a spectator transition of the type under consideration here. In Fig. 1 the spectator line energies predicted by the Dirac-Fock calculations are compared with the experimental spectrum. Since the calculated energy of the resonance line $1s2p(^1P)-1s^2(^1S)$ was 0.7 eV lower than that given by Parkinson, the lines appearing in Fig. 1b-d were shifted up in energy by this amount to make the comparison as accurate as possible. It is apparent that a number of the 1s2p3d -1s 3d lines match up with peak R1, and the 1s2p3s-1s 3s lines match up with peaks R2 and I2. None of the calculated line energies closely coincide with peak R3, however, and none of the predicted structure resulting from 1s2p3p-1s 3p transitions is present in the measured spectrum.

Table I. Theoretical transition energies (eV) for Mg XI with initial configurations of 1s2p3s, 1s2p3p, and 1s2p3d.

1s2p3p-1s 3p Transition	Energy	1s2p3d-1s 3d Transition	Energy	1s2p3s-1s 3s Transition	Energy
$^2P_{3/2}$-$^2P_{3/2}$	1337.5	$^2D_{3/2}$-$^2D_{3/2}$	1339.8	$^2P_{1/2}$-$^2S_{1/2}$	1341.6
$^2P_{3/2}$-$^2P_{1/2}$	1337.7	$^2D_{3/2}$-$^2D_{5/2}$	1339.9	$^2P_{3/2}$-$^2S_{1/2}$	1342.0
$^2P_{1/2}$-$^2P_{3/2}$	1337.8	$^2D_{5/2}$-$^2D_{5/2}$	1339.9	$^2P_{1/2}$-$^2S_{1/2}$	1348.2
$^2P_{1/2}$-$^2P_{1/2}$	1337.9	$^2D_{5/2}$-$^2D_{3/2}$	1340.0	$^2P_{3/2}$-$^2S_{1/2}$	1349.8
$^2D_{3/2}$-$^2P_{3/2}$	1338.9	$^2F_{5/2}$-$^2D_{5/2}$	1340.6		
$^2D_{3/2}$-$^2P_{1/2}$	1339.1	$^2F_{7/2}$-$^2D_{3/2}$	1340.6		
$^2D_{5/2}$-$^2P_{3/2}$	1340.5	$^2F_{7/2}$-$^2D_{5/2}$	1342.8		
$^2S_{1/2}$-$^2P_{3/2}$	1342.5	$^2P_{3/2}$-$^2D_{5/2}$	1343.0		
$^2S_{1/2}$-$^2P_{1/2}$	1342.7	$^2P_{3/2}$-$^2D_{3/2}$	1343.0		
$^2D_{5/2}$-$^2P_{3/2}$	1346.5	$^2P_{1/2}$-$^2D_{3/2}$	1344.0		
$^2D_{3/2}$-$^2P_{3/2}$	1346.9	$^2F_{7/2}$-$^2D_{5/2}$	1349.0		
$^2D_{3/2}$-$^2P_{1/2}$	1347.1	$^2D_{3/2}$-$^2D_{5/2}$	1349.4		
$^2P_{1/2}$-$^2P_{3/2}$	1348.1	$^2D_{3/2}$-$^2D_{3/2}$	1349.4		
$^2P_{1/2}$-$^2P_{1/2}$	1348.3	$^2F_{5/2}$-$^2D_{5/2}$	1349.6		
$^2P_{3/2}$-$^2P_{3/2}$	1348.8	$^2F_{5/2}$-$^2D_{3/2}$	1349.6		
$^2P_{3/2}$-$^2P_{1/2}$	1349.0	$^2D_{5/2}$-$^2D_{5/2}$	1350.2		
$^2S_{1/2}$-$^2P_{3/2}$	1349.4	$^2D_{5/2}$-$^2D_{3/2}$	1350.3		
$^2S_{1/2}$-$^2P_{3/2}$	1349.5	$^2P_{3/2}$-$^2D_{5/2}$	1351.1		
		$^2P_{3/2}$-$^2D_{3/2}$	1351.2		
		$^2P_{1/2}$-$^2D_{3/2}$	1351.4		

Table II. Parkinson's assignments and energies (in eV) for the peaks in Fig. 1a.

Line	Transition		Energy
R	1s2p $-1s^2$	($^1S_0$ $-^1P_1$)	1352.2
R1	1s2p4l $-1s^24l$		1350.6
R2	1s2p3l $-1s^23l$		1348.7
I1	1s2p $-1s^22p$	($^2P_{1/2}$-$^2S_{1/2}$)	1344.3
		($^2P_{3/2}$-$^2S_{1/2}$)	
I	1s2p $-1s^2$	($^1S_0$-$^3P_1$)	1343.0
		($^1S_0$-$^3P_2$)	
I2	1s2p(^{3}P)2s $-1s^22s$	($^2S_{1/2}$ $-^2P_{3/2}$)	1342.3
		($^2S_{1/2}$ $-^2P_{1/2}$)	
R3	1s2p(^{1}P)2s $-1s^22s$	($^2S_{1/2}$-$^2P_{3/2}$)	1335.6
		($^2S_{1/2}$-$^2P_{1/2}$)	1335.2
F	1s2s $-1s^2$	($^1S_0$-$^3S_1$)	1331.0
R4	1s2p^2-1s^{2}2p	($^2P_{1/2}$-$^2D_{3/2}$)	1330.5
		($^2P_{3/2}$-$^2D_{3/2}$)	1329.9

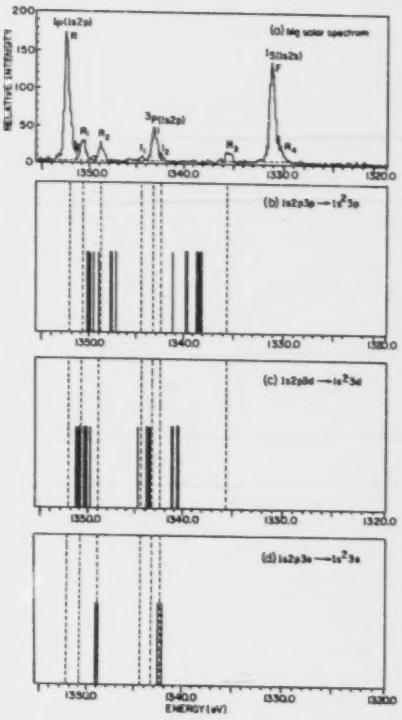

Fig. 1. (a) Solar x-ray spectrum of Mg from Parkinson; (b-d) Calculated line positions for 1s2p3l-1s^{2}el spectator transitions.

References

[1]J. H. Parkinson, Nature Phys. Sci. 233, 44 (1971).

[2]J. H. Parkinson, Nature Phys. Sci. 236, 68 (1972).

[3]J. P. Desclaux, Computer Phys. Commun. 9, 31 (1975).

[4]I. P. Grant, Adv. Physics 19, 747 (1970).

ION EXCITED K X-RAY SPECTRA OF SODIUM

K. Parthasaradhi, J. M. Sanders, and R. L. Watson

Systematic studies of the energies of the $K\alpha$ satellites and hypersatellites of neon and fluorine were recently completed.[1,2] Similar measurements are now being performed for sodium excited by 5.5 MeV He, 22 MeV C, and 48 MeV Mg ions. The sodium K x-ray spectra are measured in second order using a TAP crystal, which gives a resolution of 0.7 eV (FWHM) for the 1041 eV $K\alpha_{1,2}$ peak.

Sample spectra are shown in Figs. 1, 2, and 3. As may be seen in these figures, the resolution is good enough to display some of the multiplet structure. The fifth peak in Fig. 2 and Fig. 3 (KL^4) is distorted by the absorption edge of sodium, since these spectra were taken with a thick target. Accurate peak positions were determined by means of a least-squares peak fitting program and the resultant average satellite and hypersatellite energies are listed in Table I.

Moore et al.[3] measured spectra of sodium with a KAP crystal using beams of H, He, and O ions. They reported an energy of 1136 eV for the K^2L^0 peak. Later, Nagel et al.[4] reanalyzed the same spectrum and concluded that a peak at 1151 eV was the K^2L^0 peak. Analysis of our higher resolution spectra yields the value 1145.5 ± 0.3 eV for the K^2L^0 peak energy. Also, a new peak was found at 1195.2 eV. On the basis of these observations, the peak assignments listed in Table II were made. Also listed in Table II are the calculated energies obtained using the Hartree-Fock program of Fischer.[5] To get the peak energies given here, the individual multiplet transition energies were averaged using the procedure outlined in Ref. 2. The agreement between theory and experiment is quite reasonable for the lower n satellites and hypersatellites, but it becomes increasingly worse as the number of L-vacancies increases. This is the same behavior as was observed for fluorine (p. 79), where it was concluded that electron transfer to $n > 3$ states lowers the K x-ray energies via screening.

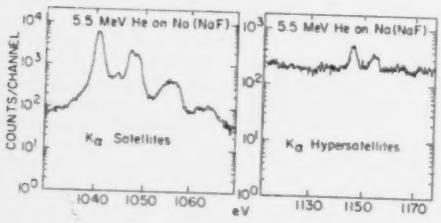

Fig. 1. Sodium K x-ray spectrum excited in NaF by 5.5 MeV He ions.

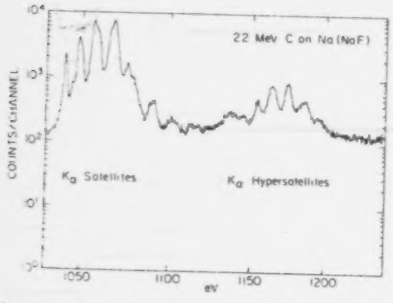

Fig. 2. Sodium K x-ray spectrum excited in NaF by 22 MeV C ions.

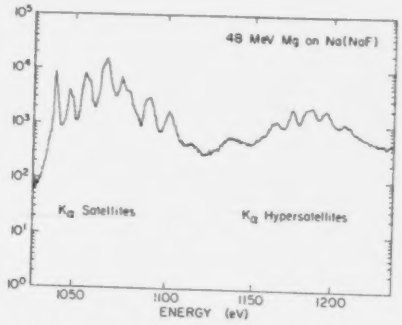

Fig. 3. Sodium K x-ray spectrum excited in NaF by 48 MeV Mg ions.

Spectra were also taken for a variety of sodium compounds to look for chemical effects. Preliminary results for NaOH, Na_2S, NaF, NaCl, NaBr, and NaI indicate that chemical effects are quite small. Furthurmore, no evidence of RET has been found. The largest differences are seen in comparisons of the spectrum for Na metal with the other spectra. Such a comparison of spectra excited by 5.5 MeV He ions is shown in Fig. 4. A significantly different KL^1 structure is observable for Na metal in this figure. Also, the P_L value for the Na metal spectrum is 0.082 whereas it is 0.067 for the NaF spectrum, and the $K\alpha_3/K\alpha_4$

Table I. Na Kα x-ray satellite and hypersatellite energies (eV)

Peak No.	Projectile		
	He	C	Mg
1	1041.0	1041.0	1041.0
2	1043.1	1043.0	1042.8
	1045.3	1045.0	1044.9
	1048.4	1047.9	1047.8
	1049.9	1049.6	1049.6
3	1052.9	1052.8	1052.6
	1055.7	1055.9	1055.8
	1058.2	1058.4	1058.2
4	1061.6	1061.9	1061.7
	1064.6	1065.1	1064.9
		1067.5	1067.3
		1070.9	1070.8
5		1074.8	1074.7
		1078.2	1078.4
		1081.6	1082.0
6		1089.3	1089.2
7		1101.2	1101.0
8			1114.6
9	1145.4	1145.5	
10	1154.0	1154.2	
11		1163.5	1163.2
12		1173.0	1173.7
13		1184.2	1181.3
14		1195.1	1195.2
15			1207.3
16			1218.2

intensity ratios are 1.50 and 1.23, respectively. This kind of change in the $K\alpha_3/K\alpha_4$ intensity ratio in going from the metal to a compound has been observed previously,[6,7] but its cause is still not well understood.

A comparison of Kα satellite spectra for Na metal and NaF excited by 22 MeV C ions is shown in Fig. 5. Both the overall intensity distributions (P_L is 0.273 for Na metal and 0.270 for NaF) and the $K\alpha_3/K\alpha_4$ intensity ratios (3.0 for Na metal and 2.7 for NaF) are quite similar for these spectra. Large structural changes were observed in the KL^4 peak due to changes in the energy of the sodium absorption edge.

Table II. Average energies of the Na K x-ray satellite and hypersatellite peaks (eV).

Peak	Experiment	Hartree-Fock
KL_1^0	1041.0	1041.2
KL_2	1048.2	1048.9
KL_3	1056.8	1057.9
KL_4	1066.6	1066.5
KL_5	1076.0	1080.6
KL_6	1089.2	1093.0
KL_7	1101.1	1108.8
KL	1114.6	1124.7
$K_2^2L_1^0$	1145.5	1144.6
K_2L_2	1154.2	1153.5
K_2L_3	1163.4	1163.5
K_2L_4	1173.4	1175.3
K_2L_5	1184.2	1187.7
K_2L_6	1195.2	1202.4
K_2L_7	1207.3	1218.3
K^2L	1218.2	1234.7

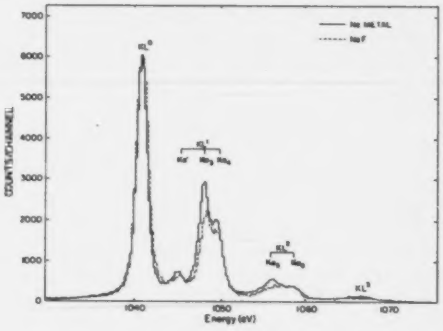

Fig. 4. Comparison of Na metal and NaF spectra excited by 5.5 MeV He ions.

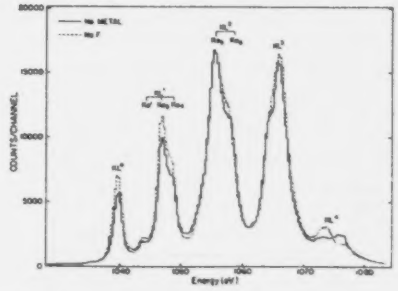

Fig. 5. Comparison of Na metal and NaF spectra excited by 22 MeV C ions.

References

[1]O. Benka, R. L. Watson, K. Parthasaradhi, J. M. Sanders, and R. J. Maurer, Phys. Rev. A 27, 149 (1983).

[2]R. L. Watson, O. Benka, K. Parthasaradhi, R. J. Maurer, and J. M. Sanders, J. Phys. B 16, 835 (1983).

[3]C. F. Moore, D. K. Olson, B. Hodge and P. Richards, Z. Phys. 257, 288 (1972).

[4]D. J. Nagel, A. R. Knudson and P. G. Burkhalter, J. Phys. B 8, 2779 (1975).

[5]C. F. Fischer, Comput. Phys. Commun. 1, 15 (1969).

[6]V. F. Demekhin and V. P. Sachenko, Bull. Acad. Sci. USSR Phys. Ser. 31, 921 (1967).

[7]A. Langenberg and R. L. Watson, Phys. Rev. A 23, 1177 (1981).

SYSTEMATICS OF K_α X-RAY SATELLITE AND HYPERSATELLITE ENERGIES

K. Parthasaradhi and R. L. Watson

When heavy projectile ions are employed to ionize K-shell electrons in low to intermediate Z elements, the process is usually accompanied by multiple ionization of the L-shell as well. In measurements with high resolution crystal spectrometers, L-vacancies give rise to satellite peaks in the K x-ray spectrum occuring at energies above the single K-vacancy diagram line.

The accumulation of a relatively large volume of experimental data on K x-ray satellites over the past ten years now allows one to examine the systematics of the satellite energies (i.e., line spacings and assignments) in considerable detail. Jundt et al.[1] have reported that the spacings of the first three satellite groups predicted by Hartree-Fock-Slater calculations are significantly smaller than the experimental values. Kauffman et al.,[2] on the other hand, contend that both HFS and HF (Hartree-Fock) calculations yield similar values, and, except for the higher order satellites, these values are in good agreement with the experimental data. The applicability of a Moseley type formula to the task of predicting accurate KL^0-K^2L^0 energy intervals has been discussed by Nagel et al.[3]

In all of the foregoing work, no attempt was made to discriminate between the average satellite energies measured with solid as opposed to gaseous targets. In a case where the average satellite energies for solid and gaseous targets were studied in detail,[4] the discrepancies were attributed to differences in the numbers of M-shell vacancies present at the time of K x-ray emission. The current work was performed in an attempt to clarify the situation with regard to the elements fluorine through potassium.

The average satellite energies for F, Na, Mg, Al, Si, Cl, and K, excited by beams of 22 MeV C, 48 MeV Mg, and 80 MeV Ar ions were measured with a 12.7 cm curved crystal spectrometer. The gas spectra were obtained with a closed gas cell and the solid spectra were recorded using targets in the form of compressed pellets or, where possible, metallic foils. Other experimental details are given elsewhere.[5,6] The spectra were analyzed with an nonlinear least-squares fitting program (FACELIFT) and the resulting energies, including some obtained previously,[4] are listed in Table I.

The differences between the average energies of the various satellite groups and that of the diagram line are plotted in Fig. 1 as a function of Z. The dashed lines have been drawn smoothly through the solid target data. It is apparent that, especially at low Z, the values for gaseous targets are significantly larger than those for solid targets.

A comparison of the experimental energy differences for gases with those obtained from Hartree-Fock calculations is shown in Fig. 2. These energy differences were calculated from weighted averages of the multiplet transition energies for Ne-like ions. The weighting factors used were products of the statistical population probabilities of the initial states times the transition fluorescence yields. It may be seen that good agreement exists between the measured and calculated energy differences for 0 through 4 L-vacancies, but the agreement worsens considerably above KL^5 for the higher Z elements.

Using the gas data, fits were made to a Moseley type formula of the form

Table I. K_α satellite energies for Z= 9 to 19 (eV).

A. Solids	KL^0	KL^1	KL^2	KL^3	KL^4	KL^5	KL^6	KL^7
F	676.8	680.5	685.4	691.9	699.9	708.6	717.9	728.7
NA	1041.0	1048.2	1056.8	1066.6	1076.0	1089.6	1101.1	1114.6
MG	1253.9	1262.8	1272.7	1283.9	1296.6	1308.5	1324.1	1342.1
AL	1486.7	1496.8	1508.0	1521.0	1534.9	1549.8	1566.9	1584.7
SI	1739.8	1751.0	1763.4	1778.4	1793.8	1810.8	1829.8	1852.3
Cl	2622.2	2641.4	2660.4	2680.7	2701.6	2724.6	2748.2	2772.8
K	3313.2	3338.4	3360.2	3383.3	3408.6	3435.0	3461.9	3485.1

B. Gases		KL^0	KL^1	KL^2	KL^3	KL^4	KL^5	KL^6	KL^7
(HF)	F	676.8	680.5	686.4	694.3	702.4	712.5	724.2	737.1
	Ne	848.6	854.9	862.3	871.3	881.4	893.0	906.5	921.0
(SiH_4)	Si	1739.6	1754.3	1768.0	1783.6	1799.4	1815.4	1831.2	
(H_2S)	S	2308.7	2325.8	2343.7	2361.8	2380.0	2398.5		
	Cl	2622.3	2640.7	2660.1	2680.5	2700.7	2721.7		
	Ar	2957.0	2975.8	2996.5	3018.3	3041.2	3061.9		

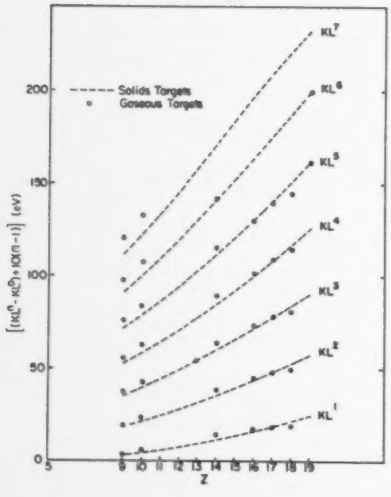

Fig. 1. Comparison of satellite energy differences (relative to the diagram line) for solid (dashed lines) and gaseous (data points) targets. The factor of 10(n-1) added to the energy difference is to separate the groups for easier viewing.

$$E = a(Z - b)^2$$

where E is the satellite energy and b is a screening constant. These fits are shown in Fig. 3. The resulting values of a and b are listed in Table II, along with the mean deviations of the energies calculated using them from the experimental energies.

Table II. Moseley parameters.

	a	b	ΔE (eV)
KL^0	9.95	0.765	1.3
KL^1	10.01	0.757	0.4
KL^2	10.06	0.741	0.5
KL^3	10.10	0.711	0.5
KL^4	10.13	0.673	0.2
KL^5	10.13	0.613	0.2
KL^6	10.08	0.522	0.5

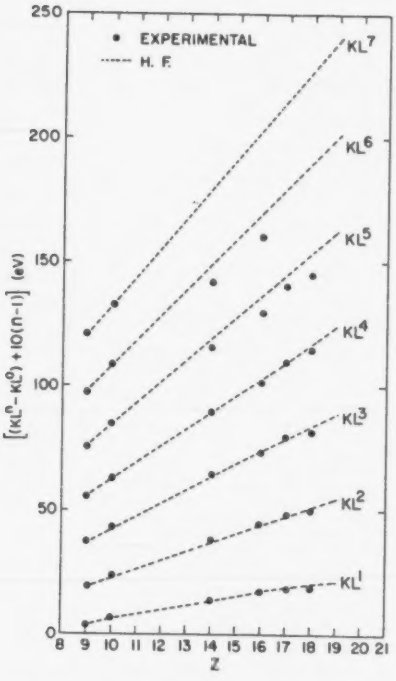

Fig. 2. Comparison of satellite energy differences (relative to the diagram line) for gaseous targets with Hartree-Fock results for Ne-like ions. The factor of 10(n-1) added to the energy difference is to separate the groups for easier viewing.

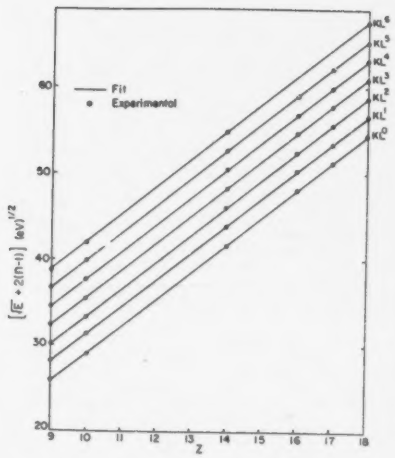

Fig. 3. Moseley type plots using the satellite energies for gaseous targets. The added factor of 2(n-1) is to separate the groups for easier viewing.

References

[1]F. C. Jundt and D. J. Nagel, Phys. Lett. 50A, 179 (1974).

[2]R. L. Kauffman and P. Richards, Methods of Experimental Physics 13, 148 (1976); 17, 390 (1980).

[3]D. J. Nagel, A. R. Kundson and P. G. Burkhalter, J. Phys. B. 8, 2779 (1975).

[4]J. A. Demarest and R. L. Watson, Phys. Rev. A 17, 1302 (1978).

[5] R. L. Watson, O. Benka, K. Parthasaradhi, J. M. Sanders and R. J. Maurer, J. Phys. B 16, 835 (1983).

[6]O. Benka, R. L. Watson, K. Parthasaradhi, J. M. Sanders and R. J. Maurer, Phys. Rev. A 27, 149 (1983).

[7]E. Clementi and D. L. Raimandi, J. Chem. Phys. 38, 2686 (1963).

INSTRUMENTATION AND SYSTEMS DEVELOPMENT

Cyclotron Operation

Detector Systems

Polarized Source

Computer Systems

Superconducting Cyclotron

STATISTICS OF CYCLOTRON OPERATION

April 1, 1982 - March 31, 1983

During the past year the cyclotron operated normally, with no major failures, and experimental runs were scheduled 20 shifts per week, with one shift set aside for routine maintenance. A number of technical staff members have been reassigned from routine maintenance of the 88" cyclotron to construction of the new cyclotron, and this has increased somewhat the time required for maintenance. No extended shutdowns were required for cyclotron maintenance, although three were required for a total of 366 hours because of construction of the building addition to house the new cyclotron.

Beam was available for experiments 6422 hours in the period April 1, 1982 - March 31, 1983 or 73% of the calender hours in the year. Beam time continues in great demand, and all available time was scheduled for experiments. Operational statistics are summarized in Table I. A significant portion of non-scheduled maintenance is now the changing of heavy-ion sources during runs; this required 339 hours in the year, while other non-scheduled maintenance required 688 hours. The combined total for these last year was 545 hours, the increase reflecting largely the decreased manpower available for maintenance. Beam development was carried out 211 hours, down considerably from 286 hours last year due to staff efforts on the new project.

In 1982-83 5815 hours (78%) of the 7449 hours scheduled for use by experimental programs were for nuclear science investigations by resident staff. Atomic physics programs scheduled 793 hours (11%), while applied programs scheduled 833 hours (11%). Details are presented in Table II. Nuclear physics and chemistry are distinguished by the academic department in which a group leader teaches.

The distribution of beam on target time by projectile is given in Table III. During the year, heavy-ion beams accounted for approximately two-thirds of the time or 2978 hours, while polarized light ions were used 785 hours (18%) of the time and unpolarized ions 891 hours (19%). The beams listed are those actually run during the period; many other beams are available.

Table I. Operation of the cyclotron during the period April 1, 1982 - March 31, 1983.

	Hours	%
Normal Operation[a]		
Beam on target	4654	53.1
Extraction, tuning, optics	1768	20.1
Maintenance		
Scheduled[b]	744	8.5
Nonscheduled	688	7.9
Ion source change	339	3.9
Beam Development	211	2.4
University Holidays	356	4.1
	8760	100.0

[a]Beam under control of experimenter.
[b]366 hours due to new building construction.

Table II. Distribution of scheduled time among users April 1, 1982 - March 31, 1983.

	Hours	%
Resident Staff		
Nuclear Physics	3196	36.5
Nuclear Chemistry	2619	29.9
Atomic Physics	793	9.0
Users Group		
Naval Research Lab	8	0.1
Activation Analysis	833	9.5
Beam Development	211	2.4
Maintenance Scheduled	744	8.5
Holidays	356	4.1
	8760	100.0

Table III. Distribution of beam on-target time among particles accelerated.

Particle	Hours	%
p	301	6.5
$\vec{p}$	582	12.5
d	49	1.1
$\vec{d}$	203	4.4
α	439	9.4
^{3}He	35	0.8
^{4}He	67	1.4
^{6}Li	151	3.2
^{7}Li	64	1.4
^{10}B	303	6.5
^{12}C	437	9.4
^{14}N	21	0.5
^{16}O	902	19.4
^{19}F	69	1.5
^{20}Ne	90	1.9
^{24}Mg	220	4.7
^{32}S	239	5.1
^{40}Ar	430	9.2
^{63}Cu	1	0.02
^{84}Kr	51	1.1
	4654	100.0
Light Ions, Unpolarized	891	19.1
Light Ions, Polarized	785	16.9
Heavy Ions	2978	64.0
	4654	100.0

LARGE POSITION-SENSITIVE IONIZATION CHAMBER

M. N. Namboodiri, S. Kniffen, G. M. Berkowitz, J. B. Natowitz, K. Hagel, R. Patton, R. K. Choudhury, P. L. Gonthier, H. S. Simon, L. Adler, and H. Sann*

The large position-sensitive ionization chamber (IC) described previously[1,2] is now operational. An existing 43 cm scattering chamber was modified for use in conjunction with the IC. The scattering chamber has a number of ports to which the IC can be connected successively so that angular distribution measurements are possible between 0° and 90° with respect to the beam. The IC is connected to the scattering chamber through an intermediate box so that the IC window is approximately 120 cm from the target in the present configuration. The IC and the intermediate box are mounted on a cart that moves on the floor in a circle with the target axis as the center. A cryopump is installed on the intermediate box to maintain a good vacuum even in the presence of small leaks in the IC window.

As described previously,[1,2] the IC consists of a large 1.2 m deep vacuum chamber containing two symmetric independent ionization chambers with a common central cathode, each half having a Frisch grid, a θ grid for measuring the in-plane scattering angle and an anode which is divided into three ΔE sections and an E section. The details of the operation of the device have been described before.[1,2]

Recently, the IC has been used in a number of experiments and the data are presently being analyzed. A few of the results are shown here to demonstrate the performance of the device. The chamber was filled with methane at 200 torr in these experiments.

Figure 1 demonstrates the excellent Z resolution that can be obtained. Data from the reactions of 240 Mev ^{40}Ar with ^{27}Al are presented in this figure. In Fig. 2, a position spectrum for the elastic scattering of 80 MeV ^{40}Ar from ^{197}Au is shown. Figure 3 shows some results at a beam energy of 180 KeV in an experiment performed to

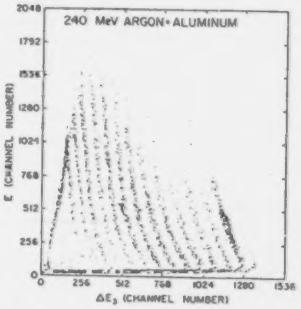

Fig. 1. Plot of ΔE_3 (pulse height in the third anode) vs E_4 (pulse height in the fourth anode) for products from 240 Mev ^{40}Ar + ^{27}Al detected in the top half of the IC. The mean angle of the IC was 40°. The intense band at the extreme right is Z = 18.

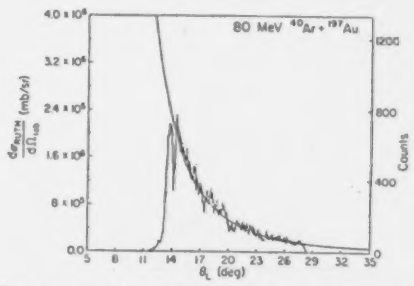

Fig. 2. Position spectrum from the top half of the IC for the elastic scattering of 80 Mev ^{40}Ar from ^{197}Au. The angle scale was obtained by fitting the spectrum to the calculated Rutherford cross section, which is shown by the solid curve. The IC was positioned at a mean angle of 20° with respect to the beam. The minima in the spectrum at θ = 14, 17 etc. are due to partitions in the window frame.

study the excitation function for fission in the system ^{10}B + 197 Au. The fission fragments are seen as a broad group with large ΔE and E values in Fig. 3(a). In Fig. 3(b), projectile-like fragments are seen, the most intense band being ^{10}B. These light fragments are too energetic to be stopped in the chamber at this pressure.

With its large solid angle, excellent resolution and large dynamic range, the IC will be very useful in a variety of coincidence experiments we wish to undertake in our study of heavy-ion reactions. We are at present constructing additional trigger detectors such as position-sensitive parallel plate counters for use in such experiments.

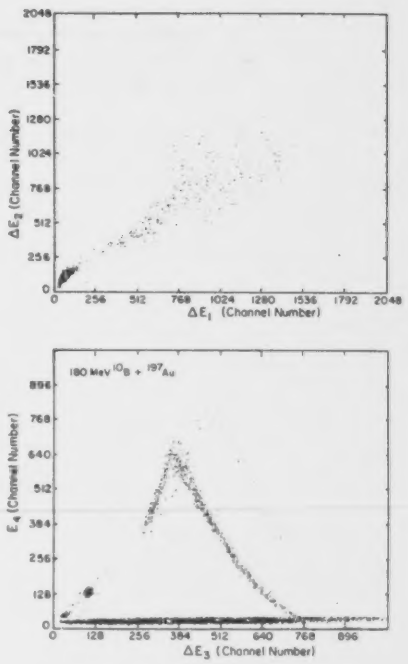

Fig. 3. ΔE-E distributions for different products from the reactions of 180 Mev ^{10}B with ^{197}Au.

References

*Permanent address: Gesellschaft fur Schwerimenforschung, Darmstadt, W. Germany.

[1]H. Sann, H. Damjantschitsch, D. Hebbard, J. Junge, D. Pelte, B. Povh, D. Schwalm, and D. B. Tran Thoai, Nucl. Instrum. Methods 124, 509 (1975).

[2]M. N. Namboodiri, J. B. Natowitz, R. Patton, K. Hagel, W. Chapman, D. Crocker, H. O'Neill, F. Abegglen and L. Duel, Progress in Research 1980-1981, Cyclotron Institute, Texas A&M University, p.76.

DEVELOPMENT OF AN IN-BEAM GRAZING INCIDENCE SPECTROMETER SYSTEM

J. A. Demarest, G. J. Pedrazzini, R. A. Kenefick, and R. L. Watson

For many years, spectroscopists using crystal spectrometers and Si(Li) detectors have studied radiation from ion-atom collisions in the x-ray region of the electromagnetic spectrum (0.1 to ~30A). Similarly, chemists and astrophysicists have studied optical transitions at wavelengths greater than 500A.

Only recently have ion-beam spectroscopists begun to investigate seriously the soft x-ray/extreme ultra-violet region of wavelengths from 30A to 500A. Additional motivation for studying this difficult region is provided by recent technological advances in detectors and components.[1] In the soft x-ray region, conventional crystal spectroscopy suffers from the attenuation of long wave-length reflection at normal incidence. Organo-metallic or pseudo crystals with large lattice spacings used for soft x-rays also suffer from lattice abberations and temperature effects. On the other hand, grazing incidence spectrometers perform admirably in this region by utilizing the specular reflection of soft x-rays at angles larger than possible for hard x-rays and at an order of magnitude improvement in resolution over crystal spectrometers. In addition, the inherent low sensitivity of grazing incidence spectrometers can now be compensated by the availability of low noise, moderately high quantum efficiency detectors such as channel electron multipliers. Recent reviews of the latest techniques adapted for use in beam-foil

spectroscopy are given in Refs. 2 and 3.

Figure 1 depicts the geometry of the grazing incidence condition. An entrance slit, grating and detector/exit slit all lie on the arc of a Rowland circle. Photons enter the entrance slit at a fixed angle ϕ with respect to the grating surface. The diffraction angle ε is defined by the angle from the surface of the grating to the detector. Motion of the detector is restricted to movement along the arc of the Rowland circle.

The grating equation is given by:

$$m\lambda = d\sin\alpha - d\sin\beta \qquad (1)$$

or

$$m\lambda = d\cos\phi - d\cos\varepsilon \qquad (2)$$

where m is the order of reflection, λ is the wavelength of the photon, d is the grating spacing and angles α, β, ϕ and ε are as shown in Fig. 1. The term $d\sin\alpha$ is a constant whereas $d\sin\beta$ varies over the detector angle and position. The distance from the exit slit to the grating, X, is a chord of the arc defined by 2ε so that

$$X = R\sin\varepsilon \qquad (3)$$

but

$$\varepsilon = 90° - \beta \qquad (4)$$

so

$$X/R = \cos\beta \qquad (5)$$

Substituting $\sin^2\beta = 1-\cos^2\beta$,

so that $\sin\beta = [1-(X/R)^2]^{1/2}$, reduces Eq. (1) to

$$m\lambda = d\sin\alpha - d[1-(X/R)^2]^{1/2} \qquad (6)$$

Shown in Fig. 2 is a plot of Eq. (5) for a 1200g/mm grating. The chord length X (counter number) is expressed in inches.

Our recently acquired Minuteman 1-meter grazing incidence spectrometer has been adapted for in-beam use. Figure 3 displays the top and aft views of the essential components of this system. All chambers, valves, and ports are made from stainless steel. The spectrometer chamber is coupled directly to a Leybold-Heraeus TURBOVAC 150 turbomolecular pump which is also coupled to a Leybold-Heraeus TRIVAC dual-stage direct drive pump. Shut off valves allow the vacuum in the spectrometer to be isolated from the target chamber. Sources, targets and collimators can be

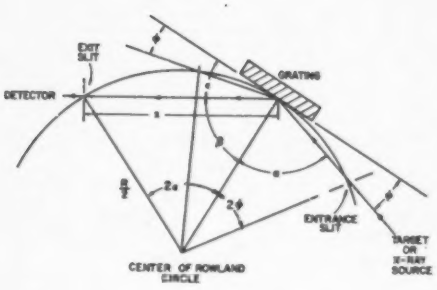

Fig. 1. Grazing incidence geometry.

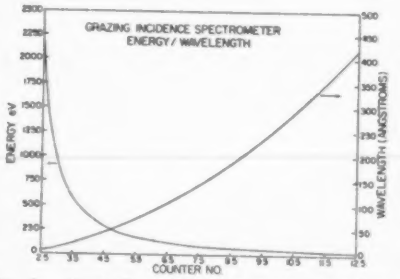

Fig. 2. Spectral region of a grazing incidence spectrometer with a 1200g/mm grating. The left scale is photon energy (eV) and the right scale is wavelength (A). The count number is the chord length X in inches.

changed without bringing the entire system up to atmospheric pressure. The detector system automatically steps a given interval along the Rowland circle track by a motor that receives signals based upon a preset number of beam monitor counts.

Alignment and calibration of the spectrometer will be accomplished off line initially by means of a Manson Ultra-Soft X-Ray Source. This source produces beams of Al, Mg, O, N, C, B and Be K x rays at a photon flux of the order of approximating 10^{11} photons per second per sterradian. These lines will calibrate the shorter wavelength region of the spectrometer. Under construction is a photon source that will excite lines of ionized He, Ne or Ar gas, with which the long wavelength region of the spectrometer will be calibrated.

The spectrometer system will use two primary detection devices. The first of these is a flow proportional counter which will be used in various

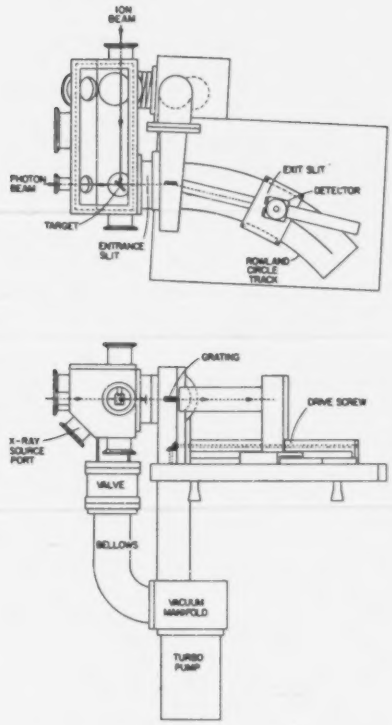

Fig. 3. Top and aft views of the in-beam grazing incidence spectrometer system.

testing modes. The proportional counter has a 65 $\mu g/cm^2$ stretched polypropylene window.

The second detection device is a Galileo Channel Electron Multiplier Array (CEMA) Model 3508. The CEMA is a chevron two-stage plate with an approximate electron gain of 10 when operated at 1kV. The CEMA is assembled with a Resistive Anode Encoder (RAE) that provides an electrical image of output events. The CEMA/RAE will be mounted tangent to the Rowland circle in place of the exit slit. The RAE yields positional information with resolutions of up to 60 m when used with either pulse-height-rise-time or charge division electronics. A recent application of the pulse height rise time method is given in Ref. 4. The charge division method is described in Ref. 5 and results of its ion-beam application are given in Ref. 3.

References

[1]D. T. Attwood and B. L. Henke, in Low Energy X-Ray Diagnostics-1981 (ed. by Attwood and Henke, AIP, N.Y., 1981).

[2]D. J. Pegg, in Methods of Experimental Physics (ed. by P. Richard, Academic Press, N.Y., 1980) Vol. 17, p.541.

[3]B. M. Johnson, K. W. Jones, D. C. Gregory, T. H. Kruse and E. Trabert, Phys. Lett. 86A, 285 (1981).

[4]O. Benka, Nucl. Instrum. Meth. 203, 547 (1982).

[5]G. M. Lawrence and E. J. Stone, Rev. Sci. Instrum. 46, 432 (1975).

DEVELOPMENT OF A SYSTEM FOR THE STUDY OF POLARIZED X-RAY EMISSION FROM LOW ENERGY RECOILS PRODUCED IN ION-ATOM COLLISIONS

G. J. Pedrazzini, D. A. Church, R. A. Kenefick, and R. L. Watson

The recently completed measurements of the polarization of excited states of helium-like sulfur,[1] and studies of highly ionized magnesium which are in progress, support the hypothesis that symmetry considerations play a dominant role in the production of inner-shell excited-state population distributions. The importance of the geometry of the ion-target orientation has been well established for the case of outer-shell excitation,[2] and has revealed useful information about the interaction itself. On the basis of the strong observable effect on the projectiles involved in these interactions, it is reasonable to assume that correspondingly strong polarizations may be induced in the excited states of the target atoms. This has been confirmed for the case of light ion projectiles on solid magnesium targets.[3] The importance of the inceraction history of the target atoms has been further emphasized in recently published results,[4,5] in which the highly charged, low energy recoil ions produced in heavy-ion/gas-target interactions have been observed. The results are

strongly indicative of selective electron capture processes occurring in secondary interactions involving the recoil ions, thus implying the necessity of exercising discrimination in using target x-ray studies to support inferences about the initial projectile-target interaction. A detailed study of the polarization of the excited states of these low energy recoils for a number of projectile/target combinations will provide information about aspects of the collision dynamics which affect the production of these states. In order to implement this study we have constructed a target chamber and spectrometer mounting assembly shown schematically in Fig. 1. The spectrometer and its coupling assembly can be rotated through 90 degrees about the axis of the cylindrical target chamber as indicated in the figure, thus allowing for the direct measurement of the alignment of any selected transitions of interest.

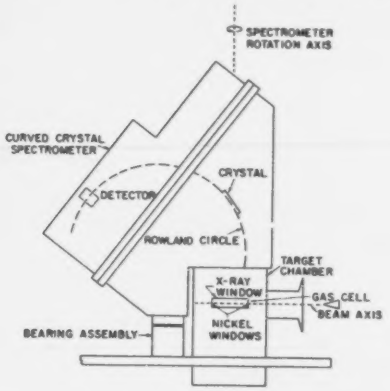

Fig. 1. Schematic view of spectrometer and target chamber to be used to study the alignment of highly charged - low energy recoil ions.

The schematic details of the experimental geometry are also indicated in the figure. The target gases will be introduced into an enclosed cell sealed by a mesh-supported stretched polypropelene window, and the projectile beam will pass into and exit the cell in the direction indicated through thin nickel foils. The excited target recoil ions have trajectories that are essentially perpendicular to the beam axis and hence the decay of these excited ions will be readily observed with the spectrometer mounted in this orientaton. The crystal is inherently polarization sensitive, so that by measuring the intensity of a transition in two orientations i.e., parallel and perpendicular to the beam direction, enables a direct estimate of the alignment of the excited level that gives rise to the transition of interest.

References

[1] D. W. Wang, R. L. Watson, R. A. Kenefick and D. A. Church, Nucl. Instrum. Meth. 202, 355 (1982).

[2] D. A. Church, M. C. Michel and W. Kolbe, Phys. Rev. Lett. 34, 1140 (1975).

[3] K. A. Jamison and Patrick Richard, Phys. Rev. Lett. 38, 484 (1977).

[4] H. F. Beyer, R. Mann and F. Folkmann, J. Phys. B 14, L377 (1981).

[5] H. F. Beyer, K-H. Schartner, F. Folkmann, J. Phys. B 13, 2495 (1980).

ALPHA PARTICLE TELESCOPE WITH PLASTIC SCINTILLATOR

Y. -W. Lui, J. D. Bronson, J. P. Sullivan, Y. Toba, and D. H. Youngblood

Semiconductor detectors, such as silicon surface-barrier detectors and lithium-drifted silicon detectors have a number of advantages in detecting alpha particles in the range 50-150 MeV. Most important are their excellent resolution and their ease of use. However, silicon detectors are not well suited to experiments requiring large solid angles and/or special geometries because they generally have a relatively small active area. Special shapes or multiple arrays are very expensive. Furthermore, Si(Li) detectors, which are much cheaper than surface barrier detectors in the thicknesses required for these beams, are quite susceptible to radiation damage. Plastic scintillators have long been used for particle detection in long-range particles where silicon detectors are impractical. Various combinations of different scintillators have been used at several laboratories.[1]

We report here the results of explorations

aimed at identifying a large solid-angle detector system capable of separating Z = 1 and Z = 2 particles and hopefully separating ^{3}He and ^{4}He. This detector would be used in measuring gamma decay from isoscalar giant resonances where large solid angles, but only modest resolution, are required. Since the giant resonances have a width around 3 to 4 MeV,[2] a resolution of 2 MeV would be adequate. In experiments with alpha beam at incident energies of 20 and 40 MeV/nucleon,[3] there is a large flux of Z = 1 particles which would cover up the giant resonances if Z identification were not accomplished. There are three criteria on the performance of this detector. It must have 1) a large active area, 2) separate Z = 1 and Z = 2 particles, and 3) sufficient energy resolution to observe giant resonances.

A detector telescope consisting of a 2.75 mm thick BC400[4] plastic scintillator (δE) and a 10 mm thick BC400 plastic scintillator (E) has been tested and the configuration is shown in Fig. 1. This detector is one segment, six of which will form a ring detector for detecting alphas over the range $12° < \theta < 20°$ for all ϕ. Each scintillator was coupled to a light guide which was coupled to a photomultiplier tube. Each counter was wrapped with thin aluminum foil to provide light shielding from external light sources. Initially, a collimator with a small angular opening (around 1°) was used to insure that edge effects were negligible. Figure 2a shows a two-dimensional plot of particle identification vs total energy and Fig. 2b shows the particle identification spectrum obtained for 100 MeV alphas on ^{12}C. A simple algorithim where PI = (AE + B(δE) + C)(δE) was applied to the E and δE signals on-line to obtain the PI channel number for each event. Separation between Z = 1 and Z = 2 particles is very good and identification of p, d

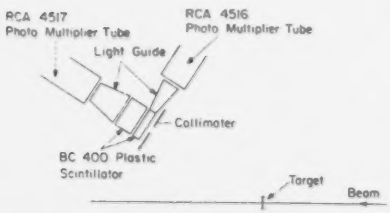

Fig. 1. Configuration of the detector telescope.

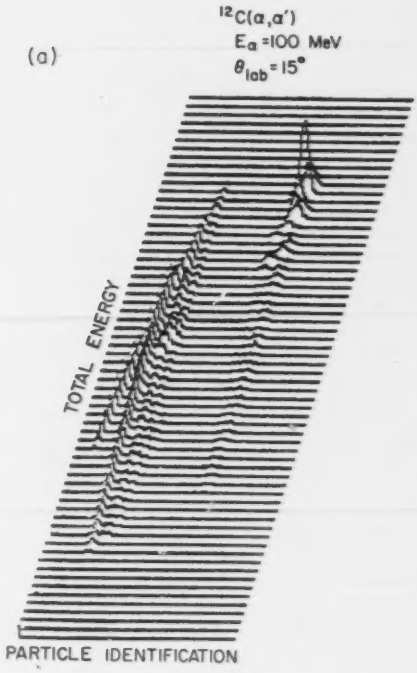

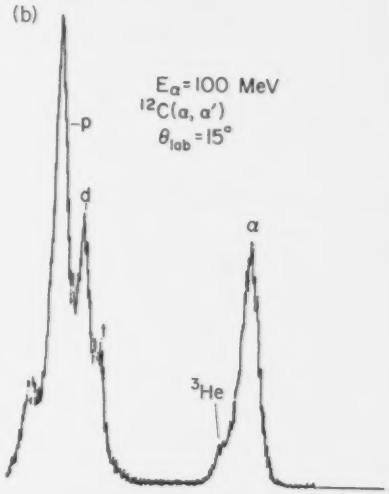

Fig. 2. a) Two-dimensional plot of particle identification vs total energy; b) Spectrum of particle identification of 100 MeV alphas on ^{12}C.

and t as well as ^{3}He and ^{4}He can be made. The bump in the left corner is from protons which penetrate the detector. The total energy spectrum of alpha particles is shown in Fig. 3 and the resolution is sufficient to separate the ^{12}C 4.44 MeV excited state from the ground state. The energy resolution of the elastic peak is about 2% of the beam energy. In a separate run, a collimator with an angular opening which uses the full area of the detector (about 10°) was placed in front of the detector. Some resolution degradation was apparent as ^{3}He and ^{4}He particles could not be completly separated. However, separation of Z = 2 from Z = 1 is still very good. An alpha energy spectrum obtained in the full geometry with 100 MeV alphas on ^{90}Zr is shown in Fig. 4 and the giant quadrupole resonance (GQR) is clearly observed.

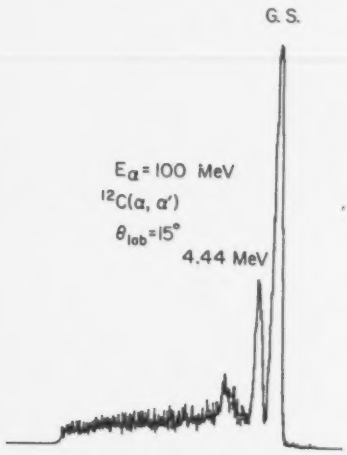

Fig. 3. The total energy spectrum of alpha particles from 100 MeV alphas on ^{12}C.

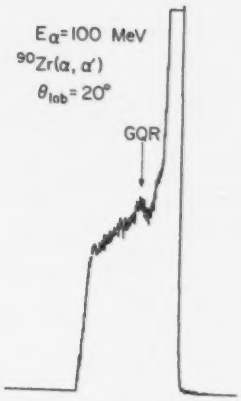

Fig. 4. The total energy spectrum of alpha particles from 100 MeV alphase on ^{90}Zr.

Preliminary tests using a CaF_2 phoswich counter[5] which results in a simpler counter geometry (half as many phototubes) has shown as good particle identification as the ΔE - E scintillator counter. Further tests are planned on both systems.

References

[1]R. L. Craun and D. L. Smith, Nucl. Instrum. Meth. 80, 239 (1970); F. Ashton, H. J. Edwards and G. N. Kelly, Nucl. Instrum. Meth. 95, 109 (1971); H. A. Enge, IEEE Trans. Nucl. Sci. NS-26, No. 2, 2420 (1979).

[2]D. H. Youngblood, P. Bogucki, J. D. Bronson, U. Garg, Y. -W. Lui, and C. M. Rozsa, Phys. Rev. C 23, 1997 (1981).

[3]J. R. Wu, C. C. Chang, H. D. Holmgren, and R. W. Koontz, Phys. Rev. C 20, 1284 (1979).

[4]Same as NE102.

[5]M. R. Maier, H. G. Ritter, and H. H. Gutbrod, IEEE Trans. Nucl. Sci. NS-27, No.1 (1980).

MODIFICATIONS OF THE POLARIZED ION SOURCE

R. E. Tribble, C. A. Gagliardi, and D. Semon

During the past year, we have undertaken several modifications on the polarized ion source (PIS) to increase the beam intensity and reduce the noise on the beam. Both of these aspects of the PIS operation are important for the experiment looking for parity violation in proton-proton scattering. An increase in beam intensity also will be useful for many other experiments using polarized beams that are either underway or being planned.

Over the last several years, the beam intensity for the source has steadily declined. In order to understand this, we tested several different filament shapes including both large and small Ω's. The results from these tests were very inconsistent, indicating that an important characteristic of the filament geometry was being ignored. After several trials, we ascertained that the distance between the filament and the first electrode was varying by as much as 0.030 in. when the filament was changed. This distance is critical to the electron current produced with the ionizer. In our tests with Ω shapes of approximately 1/4" in. diameter, we found that a distance of ~0.020 in. between the filament and this electrode was optimum. By doubling this distance, the beam intensity dropped a factor of 2.

Noise on the polarized ion beam was traced to several sources. One of these was the filament supply. Originally, it was an a.c. supply that was rectified to be d.c. The filtering was not sufficient to eliminate the 60 cycle ripple, however. A new d.c. supply has been acquired to replace the existing one. The HV supply for the first set of electrodes was found to be another source of noise. With a filament emission current of more than 30 mA, the voltage on the third electrode would not remain constant. The effect on the beam was to have large (fast) fluctuations from a maximum intensity to near zero intensity. This modulation overwhelms any other noise on the beam. Three supplies have been acquired to replace the single supply now used on the electrodes. In addition to being higher current HV supplies, they will allow independent adjustment of these electrodes.

The extraction voltage for the source is limited to 20 kV by the existing supply. This voltage appears to be optimum for injection and acceleration of ~35 MeV protons. In recent tests on the 45 MeV d beam, we added another HV supply and boosted the extraction voltage up to 28 kV. We found a factor of 2 improvement in the extracted beam intensity by increasing the voltage to 28 kV. Further tests with both proton and deuteron beams will be required in order to determine the optimum operating conditions.

During this next year, we shall implement a system to cool the dissociator gas bottle to LN temperatures. Tests performed at other laboratories[1] indicate that this should result in a substantial improvement in the beam intensity. Construction of the parts to implement LN cooling is now underway. Also, a new first electrode has been constructed that will allow us to insert a grid structure across the opening to the solenoid. We expect to improve the efficiency of the electron beam by directing most of it into the center of the solenoid. After the grid system is installed, we plan to conduct tests of filament shapes and the grid to filament distance to optimize the source performance.

References

[1]W. Gruebler and P. A. Schmelzback, Proc. Fifth International Symposium on Polarization Phenomena in Nuclear Reactions, G. G. Ohlsen et al. [editors], AIP Conference Proceedings No. 69 (1981).

AUTOMATIC CYCLING OF DEUTERON BEAM POLARIZATION

W. F. Woodward, L. C. Northcliffe, J. C. Hiebert, and S. Nath

The addition of a weak-field rf transition to supplement the strong-field transition (or transitions) of a polarized ion source increases the flexibility of its operation. Spin manipulation of proton beams with weak and strong field transitions has been in routine use here for several years, but full exploitation of both weak and strong field transitions for deuteron beams required a source modification, to make space available for the three transition regions required. A test of the weak field transition was reported in the 1978-79 progress report[1] and the required source modification was also accomplished.

In earlier experiments done here with polarized deuteron beams, two strong field transitions were used; the 3-5 transition produced deuterons with nominal vector polarization $p_z = 1/3$ and nominal tensor polarization $p_{zz} = -1$, while the 2-6 transition produced deuterons with $p_z = 1/3$ and $p_{zz} = 1$. Together they produced deuterons with $p_z = 2/3$ and $p_{zz} = 0$. The vector polarization was reversed by reversing the magnetic field in the strong-field ionizer solenoid. This magnetic field reversal caused undesirable changes in the beam optics, was difficult to make automatic and was incompatible with rapid reversal.

In a first attempt to reduce these systematic errors, we presented in last year's report preliminary results of anlayzing power remeasurements for the $^1H(d,n)$ reaction at 42.4 MeV in which the polarization of the beam was cycled automatically through the four states available with different on-off combinations of the two strong field transitions. The nominal polarizations were those given above, and also p_z; $p_{zz} = 0;0$. Since the solenoid field in the ionizer was not changed, the beam optics remained essentially constant throughout the cycle. Additional analyzing power results obtained with this automatic cycling technique are presented elsewhere in this report. The internal consistency of the measurements has been improved considerably by implementation of this technique. Despite this, the need remains for a further improvement: cyclic reversal of the vector polarization, so as to permit use of the ratio method of asymmetry determination, a very effective method for the elimination of instrumental asymmetries.

The weak-field (1-4) transition produces deuterons with nominal polarization $p_z = -2/3$ and $p_{zz} = 0$. Thus, beam polarization reversal can be achieved by switching between the weak field and the two strong field transitions. Since the transition oscillators can be turned on or off rapidly by external gating signals, automatic spin reversal becomes feasible.

Actually, the presence of three transitions, each of which produces a different polarization state, makes possible a large variety of automatic cyclic changes of beam polarization. A few such cycles of special interest are shown in Fig. 1. The nominal values of p_z and p_{zz} for each stage of each cycle are indicated in the figure. In practice, the rf transitions are not 100% efficient and the p_z and p_{zz} values obtained when the efficiencies are α, β, and γ (typically each ~0.8 - 0.9) for the 2-6, 3-5 and 1-4 transitions, respectively are also indicated in the figure. In addition, all polarizations are further diluted by the factor $1-2\varepsilon$, where ε is the fraction of the beam emerging from the sextupole magnet which remains in unwanted atomic states (typically, $\varepsilon = 1\%$). (The polarization is further diluted by depolarizing collisions of the atomic beam with source components and by ionization of background gas in the strong field ionizer.)

Cycle A is the one mentioned in the paragraph above. It provides automatic reversal of the atomic beam vector polarization. It suffers from two drawbacks, however: the transition efficiencies α and β must be carefully matched if p_{zz} is to vanish, and it does not permit automatic determination of instrumental asymmetries, which requires unpolarized beam. The latter drawback is eliminated by use of cycle B, but not the former. Cycle D has the further advantage of providing additional information on the efficiency γ. For tensor analyzing power measurements, cycle C is particularly useful because the sign of p_{zz} is reversed periodically and the efficiencies α and β are monitored continuously and independently. It is less useful for vector analyzing power measurements because the sign of p_z is not reversed. This drawback can be overcome partially by use of cycle E, and totally by use of cycle F, which makes numerous internal consistency checks available.

A circuit has been built which is capable of providing the gating pulses needed for the automatic cycles shown in Fig. 1. The changes in polarization state can be triggered by an external pulse to the circuit or by an internal pulser

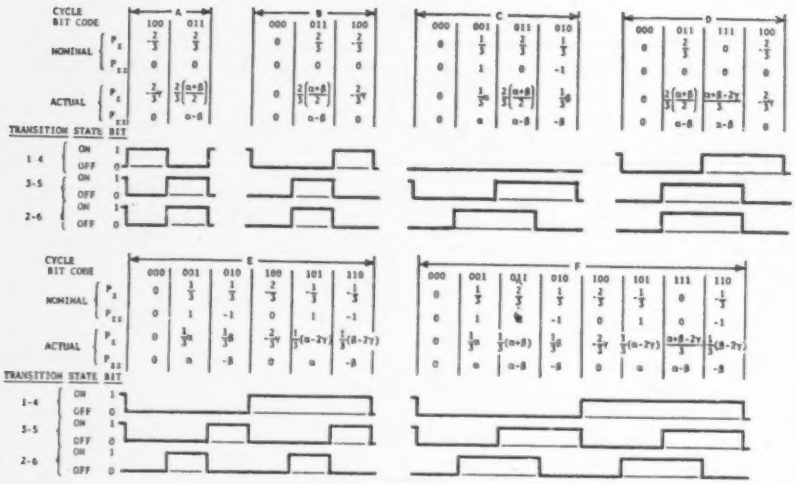

Fig. 1. Some automatic polarization cycles and the polarization values achieved with them (nominal and actual). The quantities, α, β and γ are the efficiencies, respectively of the 2-6, 3-5 and 1-4 rf transitions.

(clock) of variable frequency. If the time interval between pulses is fixed, the amount of time spent in each phase of the cycle is the same. An alternate way of operation is to trigger the circuit by output pulses from a current integrator, which insures that each phase of the cycle receives an equal amount of beam.

This circuit was used successfully, utilizing a cycle equivalent to cycle C, in the measurements of vector and tensor analyzing powers A_y and A_{yy} presented in this year's and last year's progress reports. An interesting example of the power of the automatic cycling technique occurred during the 0° measurements for the $^1H(d,n)2p$ breakup reaction at 42.4 MeV. The 0° measurement was of particular interest because the asymmetry between phase 1 (p_z = 0, p_{zz} = 0) and phase 3 (p_z = 2/3, p_{zz} = 0) of cycle C should be zero. The fact that it differed from zero by 2-3% early in the run was a sign of trouble, which ultimately led to the discovery and replacement of a malfunctioning electronic module which might not otherwise have been found. The internal consistency of the measurements obtained with automatic cycling has been clearly improved over that which we had achieved previously.

An attempt to use cycle A in a first test of a three-transition cycle was only partially successful. Although the weak field (1-4) transition had worked well in a previous test[1] showing a broad plateau of high efficiency, the plateau in the recent run had narrowed to a sharp peak and the efficiency was less than expected. This was attributed to a change in transition region design which permitted the fringing B-field of the strong field transitions to dominate the weak field transition region, and a design modification was made which placed magnetic shielding between the strong and weak field regions. A test of the new system will be made soon, and we hope to use cycle F in our next series of analyzing power measurements.

References

[1]W. D. Cornelius, R. L. York and L. C. Northcliffe, Progress in Research 1978-1979, Cyclotron Institute, Texas A&M University, p. 105.

DEVELOPMENT OF POLARIMETER INSTRUMENTATION

L. C. Northcliffe, S. Nath J. C. Hiebert, C. A. Gagliardi, W. F. Woodward, A. Doumas, W. M. Schmidt and W. D. Cash

Some time ago, we began a series of few-nucleon charged-particle polarization transfer experiments which exploited a technique developed at this laboratory,[1] in which a proton polarimeter is used on the focal plane of the split-pole spectrograph, permitting measurements to be made at small angles, including $\theta_{lab} = 0°$ ($\theta^* = 180°$).[2] Results obtained for $K_y^{y'}$ (180°) for the $H(\vec{d},\vec{p})D$ reaction[3] and the $D(\vec{d},\vec{p})T$ reaction[4] were presented at the Santa Fe Polarization Symposium. An investigation of $K_y^{y'}(\theta^*)$ for the first of these reactions in the angular region $120° < \theta^* \leq 180°$, devoid of data, was begun by calibrating the focal plane polarimeter (FPP) for proton energies 30-44 MeV.[5] Results of the first of these $K_y^{y'}$ measurements were presented last year.[5] This series of experiments was brought to a halt by the deterioration of the set of five Si(Li) detectors used in the FPP and the set of four used in the beam-line monitor polarimeter (BMP). Replacement of these detectors was precluded by their cost (over $10,000), prohibitive in these economic times, as well as their unavailability. As a long-term solution to this problem, we have undertaken a redesign of both polarimeters, in which the Si(Li) detectors have been replaced by plastic scintillators and photomultiplier tubes (PMTs).

Since both polarimeters are located in a confined space, in vacuum, compactness is important. Therefore, the PMT chosen was a small ten-stage tube (RCA 4517), and a compact PMT base capable of operating in vacuum was designed. The scintillator material used was NE102.

A sketch of the original FPP is shown in Fig. 1. The first modification tried was to replace the E counter of the Si(Li)ΔE-E telescope with a plastic scintillator of appropriate thickness. In test runs with this configuration we were unable to distinguish the coincident signal for scattered protons from the huge background of accidental coincidences. The modification which proved to be successful was to replace the polystyrene foam target of the original FPP by a scintillator target, an NE102 cylinder of height 2 in. and diameter 0.25 in. located just downstream of the target collimator. The scintillator light was conducted by a cylindrical light guide through a hole bored in the polarimeter pivot to the PMT, which was clamped to the underside of the polarimeter platform. The

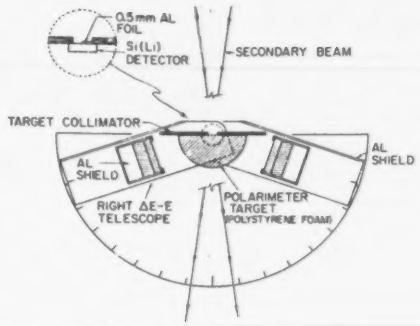

Fig. 1. Original design of spectrograph focal plane polarimeter. Modifications are discussed in text.

signal provided by coincidences between the target scintillator and the E scintillator (with or without use of a ΔE counter) was clearly distinguishable from background. While the calibration needs to be redone fo this new polarimeter configuration, it is not expected to differ significantly from the old calibration.

The detectors for the BMP have been a problem for years because of their short life in the high flux area and the expense of their periodic replacement. After several attempts, we have developed a scintillator telescope that works well in the region $29 < E_d < 53$ MeV. The ΔE scintillator thickness is 0.062 in. and the E scintillator thickness is 0.75 in. The reaction used thus far is elastic d-^{12}C scattering from a polyethylene target. At 52.6 MeV the d-C analyzing power near $\theta_{lab} = 60°$ is substantial (0.46) and slowly varying with angle.[6] The elastically scattered deuterons are clearly resolved if an Al absorber of 0.125 in. thickness is placed in the detector arm, either upstream or downstream of the ΔE scintillator. At $E_d = 29.5$ MeV, a more suitable angle has been found to be $\theta_{lab} = 90°$, where A_y is large (0.46) and relatively independent of angle.[7] There the elastic signal is clearly resolved with no absorber in the detector arm. At $E_d = 45$ MeV, we conjectured that Ay should be substantial and slowly varying with angle near $\theta_{lab} = 60°$, as was verified in a recent run.

References

In the following, "Santa Fe-1980" is an abbreviation for Polarization Phenomenon in Nuclear Physics - 1980 (Fifth International Symposium, Sante Fe) AIP Conf. Proc. No. 69.

[1]J. M. Moss, D. R. Brown and W. D. Cornelius, Nucl. Instrum. Meth. 135, 139 (1976).

[2]W. D. Cornelius and R. L. York, Santa Fe - 1980, p. 994.

[3]W. D. Cornelius, R. L. York, L. C. Northcliffe and J. C. Hiebert, Santa Fe-1980, p. 1223.

[4]R. L. York, W. D. Cornelius, L. C. Northcliffe and J. C. Hiebert, Sante Fe-1980, p. 1461.

[5]W. D. Cornelius , R. L. York, L. C. Northcliffe, S. Nath, J. C. Hiebert, W. F. Woodward, A. Doumas, M. J. Marolda and K. Washington, Progress in Research 1981-1982, Cyclotron Institute, Texas A&M University, p. 25.

[6]G. Mairle, K. T. Knopfle, H. Riedesel, G. J. Wagner, V. Bechtold and L. Friedrich, Nucl. Phys. A339, 61 (1980).

[7]G. Perrin, N. Van Sen, J. Arvieux, R. Darves-Blanc, J. L. Durand, A. Fiore, J. C. Gondrand, F. Merchez and C. Perrin, Nucl. Phys. A282, 221 (1977).

VACUUM IMPROVEMENT ON THE 88" CYCLOTRON WITH A 35-INCH TITANIUM SUBLIMATION PUMP

A. Horbowa and H. Peeler

The 35" diffusion pump installed at the bottom of the resonator tank is providing a vacuum pressure of about 2 x 10^{-6} torr. Because of the limited conductance between the resonator tank and the dee tank, a 10" and a 6" diffusion pump has been installed on the side of the dee tank. This pumping geometry produced a lower limit pressure of about 1.2 x 10^{-6} torr in the accelerator chamber, and 2.2 x 10^{-6} torr in the resonator tank.

To further improve the vacuum, a titanium sublimation pump (TSP) has been constructed and installed on the spare 35" diameter port on the bottom of the resonator tank. The pumping action of a TSP by the process of chemisorption is well known. Furthermore, it is an efficient pumping system for N_2, CO, CO_2, O_2 and H_2 which are the main residual gases evolving continuously from the stainless steel and copper of the vacuum system. This technique provides a high pumping speed for such gases and a contaminant free vacuum but is limited in its ability to adsorb noble gases such as He, Ne, Ar, and hydrocarbons as CH_4, C_3H_8, etc.

Figure 1 shows the schematic arrangement of the TSP system used for testing the pump prior to its installation on the cyclotron.

The steel vacuum vessel is cylindrical and has a volume of about 670 liters. The pump is installed vertically with the 35" inlet on the top. The titanium is sublimated onto a water cooled cylindrical copper liner. This getter surface has an area of about 20,000 cm^2.

An electron bombardment sublimator provides the gettering film by evaporating 0.1 to 0.5 grams

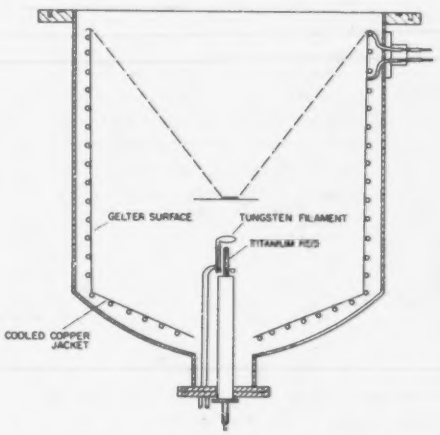

Fig. 1. Schematic diagram of titanium sublimation pump.

per hour of titanium. First measurements of pumping speeds on nitrogen gas (Fig. 2) showed that the TSP worked well enough to warrant further investigation.

For testing on the 88" cyclotron, the TSP, cooled by city water was attached to the spare 35" port near the 35" diffusion pump. The vacuum in the resonator tank improved by more than a factor of two after only half an hour of pumping. However, a pressure lower than 8.5 x 10^{-7} could not be achieved in the accelerator chamber. This indicated that an important partial pressure of

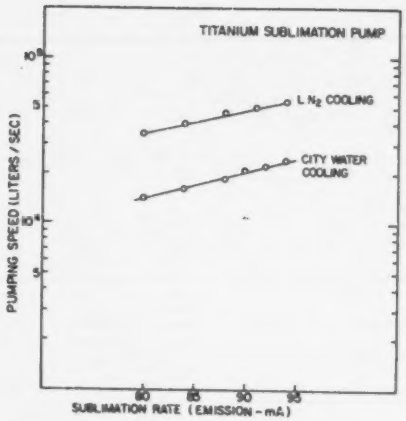

Fig. 2. Measured pumping speeds of titanium sublimation pump.

non-getterable gases was still in the chamber. This lower-limit pressure appears to be determined by residual non-getterable gases rather than by remaining noble gases (as ion source residual gas flow) and is therefore independent of the TSP pumping speed. This limiting partial pressure is probably composed of hydrocarbon gases from the large diffusion pump, non-getterable gases introduced by ion source changing, and outgassing from the inner walls (H_2 reacting with residual carbon in the system forms methane gas (CH_4) which is hard to adsorb while H_2O reacting with H_2 and carbon can also form CH_4 and C_3H_8).

Tests and improvements are continuing at the present and a lowering of the diffusion pump limit pressure is expected to bring more efficacy to the TSP.

An expected improvement of 2 to 3 times on the cyclotron lower pressure and when running with gases N_2, H_2, and CO_2, seems reasonable with such a system.

References

[1]R. P. Henry, Cours de Sciences et Techniques du Vide T2 (SFITV 1972).

[2]EURATOM CEA, Une pompe a sublimation de titane a grande dimensions, (1971).

[3]L. Shen, (The design and performance of a high speed economical ultrahigh vacuum chamber utilizing titanium sublimation), Rev. of Sci. Instrum. (1972).

TESTING A BEAM PROFILE MONITOR

Y. Tsien, G. Derrig, B. Laune, F. Abegglen, D. May

In an effort to develop diagnostic equipment for the transfer line between the K500 and 88" cyclotrons, a beam profile monitor has been built and tested in the existing beam lines.

The device is a secondary emission multiwire monitor.[1] The principle is that wires will intercept the beam causing secondary emission. The resulting current is then amplified and measured.

Two monitors have been built. They are made of 61 gold coated wires, 20 μm diameter, 1 mm apart, soldered on a G-10 board with a 20 mg tension. On both sides of the wires plane, two aluminium electrodes are used to collect the secondary emission. A +100 V is applied to these electrodes. The device can be inserted or removed pneumatically in the beam line.

A scanning system allows the connection of an amplifier to the wires. The signal can be read directly or sent to an X-Y plotter. In the preliminary tests we have performed so far, only a portion of the wires were connected: the area used was 30 mm wide and the resolution 2 mm. Figure 1 shows a picture of the multiwire device.

Tests were performed with beams ranging from protons to argon, intensities from 20 nA to 10 μA, energies from 9 MeV protons to 127 MeV alphas. The response from the device is linear with the current as measured on a Faraday cup. In Fig. 2 an example of a profile is shown as recorded on the X-Y plotter.

The beam emittance of the 88" cyclotron was measured using the three gradients method.[2] It was

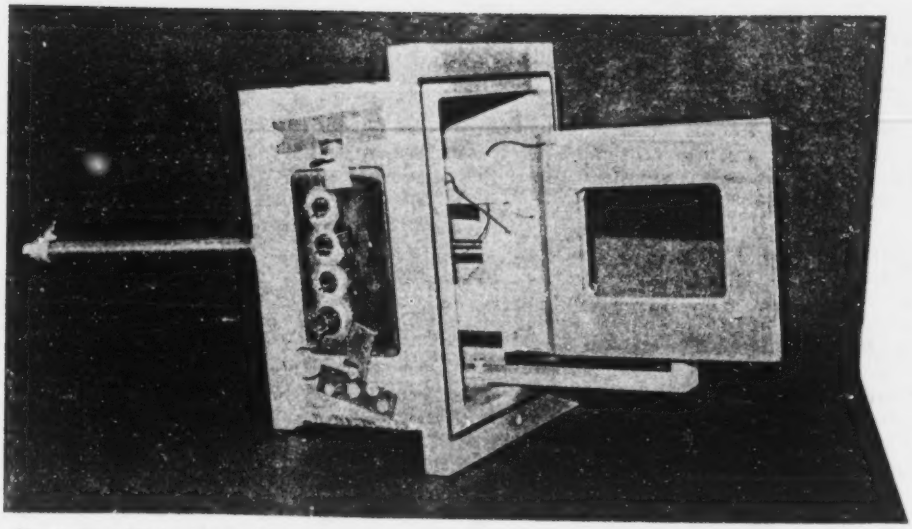

Fig. 1. The multiwire beam profile monitor.

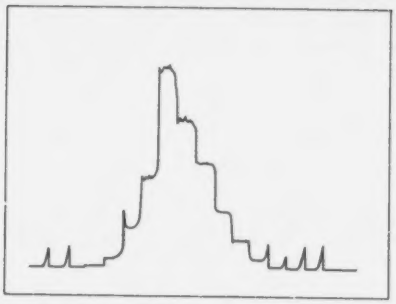

Fig. 2. Example of a beam profile as recorded on a X-Y plotter.

found to be in the order of 50 mm.mrad for the horizontal emittance (127 MeV alpha) and 60-70 mm.mrad for the vertical one (23 MeV alpha). The beam width was determined by fitting the profile with a Gaussian. The given emittances are those containing 90% of the particles. The present off-line technique of calculating the emittance is very slow. We intend to hook up the monitor to the VAX, so that the signals from the wires could be read directly. The emittance would then be calculated. This fast capability will also allow a better precision since more measurements could be performed in a short time.[2]

As a miscentering of the beam out of the 88" in the vertical plane was occurring, a study is underway to understand this beam behavior with the help of the monitor. For that purpose, a program has been written to calculate the location of the beam center from its measured position as the field of a quadrupole magnet is varied. As for the emittance measurements, several points are measured to increase the precision.

In order to couple the K500 and the 88" cyclotrons, it is necessary to bring the beam achromatic. A minimum of the beam emittance is the indication of the achromatic condition. To gain time in this process, one can measure the beam width and the beam angle (by difference of beam widths in two different positions) and it can be shown by TRANSPORT[3] calculations that a simultaneous minimum of width and angle corresponds to the achromatic condition. Next, we intend to put two multiwire devices, separated by a drift length, after the first quadrupole doublet following the analyzing magnet which we will use to cancel the beam dispersion. The two doublets before the analyzing magnet will be adjusted to produce the minimum beam width and angle.

References

[1]R. Anne and M. Van den Bossche, IEEE Trans. Nucl. Sci. NS-26, Vol. 2, 1979.

[2]Y. L. Tsien and B. Launé, Progress in Research 1981-1982, Cyclotron Institute, Texas A&M University, p. 101.

[3]K. L. Brown, SLAC Report 91, July 1970.

COMPUTER SYSTEMS

E. Basilier, F. Blando, J. D. Bronson and D. R. Haenni

The primary data acquisition computer for the laboratory is a VAX 11/780 from Digital Equipment Corporation; - 90% of all data acquisition tasks are run on this system. The remaining data acquisition is handled by a vintage 1970 PDP-15. Both machines are operated in a single user mode when data acquisition is occurring. For the rare occasions when the data acquisition VAX (ACQ VAX) fails, its workload can readily be switched over to a second VAX 11/780. This is done by redirecting three cables. This second computational VAX (COMP VAX) has all the equipment present on the ACQ VAX plus some additions that make it more convenient for data analysis work, which is its principal application. The present configuration of the two VAX computers is summarized in Fig. 1.

During the past year, the COMP VAX has been equipped with an additional 2 Megabytes of main memory, a 414 Megabyte Winchester disk subsystem and an RX02 floppy disk subsystem. The new hard disk subsystem has its own interface to the main computer bus (SBI). This allows higher total throughput than would have been possible had the new disk shared a "channel" with other peripherals. The bus interface came with a CPU expansion cabinet which provides yet further space for expansion. The new floppy disk subsystem permits users to easily transfer files to and from hard disk without resorting to the use of magnetic tape. Thus the amount of hard disk space assigned to individual users can be reduced to provide large amounts of disk space for the use of currently running programs. The number of DZ11-type asynchronous terminal ports has been increased from 32 to 40 by moving 8 unused lines from the ACQ VAX to the COMP VAX. This minimizes the need for changing connections between terminals and ports. Currently 30 alphanumeric CRT terminals and 4 assorted graphics terminals are attached to these lines.

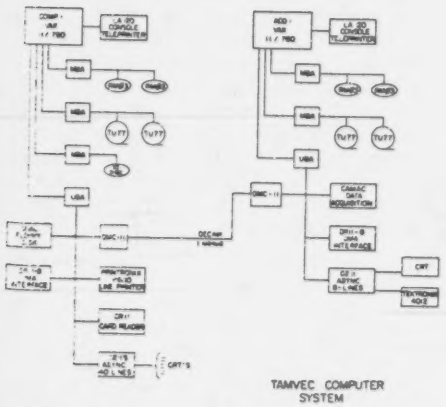

Fig. 1. Schematic of computer system.

Each VAX can be connected to the data acquisition hardware, which presently consists of one CAMAC crate with a crate controller driven directly off the UNIBUS, as well as an old hardwired interface for up to 7 fast ADCs that connects to the DR11-B. For the CAMAC crate, 28 low-resolution/low-speed ADCs are available, as well as 36 TDCs, 24 scalers and several miscellaneous control and input modules are available and heavily used. An interface is being constructed to interface up to 16 high-speed ADCs to the CAMAC. At present, 6 8192-channel Canberra 8080 ADCs are available for use with this unit when completed. There are also some older Canberra 8060 ADCs and Geoscience ADCs which will be compatible with this new interface.

Data acquisition on the VAX presently utilizes one of two software systems: a slightly modified version of ACQUIRE, a flexible data acquisition program written in FORTRAN by Dr. Richard Kouzes of Princeton University, and a highly modified version called VULCAN that is more suitable for experiments with a large number of input parameters. However, the flexibility of these programs is provided by built-in "features" rather than by structural flexibility. This not only limits the options available, but limits execution speed as well.

Work has begun on a new data acquisition system which will provide both more flexibility in experiment design and the capability of higher data acquisition rates than now possible. The hardware to do this will offload part of the task from the VAX by providing a front-end device capable reading sets of ADCs etc. based on its own stored program, and transfer the data to the VAX via a FIFO and the DR11-B. The device selected is the "Event Handler" developed by Dr. Dave Hensley at the Oak Ridge National Laboratory[1] which is implemented as an Auxiliary Crate Controller within the CAMAC crate. A new software system will also be introduced,

borrowing ideas and parts from the XSYS system developed at the Triangle Universities Nuclear Laboratory (TUNL).[2] It will be adapted to utilize features of the new acquisition hardware and will incorporate other improvements to better serve our diverse local needs.

References

[1]D. C. Hensley, IEEE Trans. Nucl. Sci. NS-26, 4454 (1979).

[2]C. R. Gould, L. G. Holzweig, S. E. King, Y. C. Lau, R. U. Poore, N. R. Roberson and S. A. Wender, IEEE Trans. Nucl. Sci. NS-28, 3708 (1981).

CYCLOTRON EXPANSION STATUS

G. Derrig and P. Smelser

Construction of an additional 7000 sq. ft. of vault and experimental area is nearing completion and is expected to be finished by late June. This will represent an early completion compared to the scheduled completion date of July 15, 1983.

On March 28, 1983 the temporary cooling tower was taken out of service and the newly completed ceramic cooling tower was tied on to the building's low conductivity water system.

Operations resumed on April 12, 1983 when the Institute accepted the tower and a major portion of the electrical equipment needed to operate the tower.

Figure 1 shows the interior of the building addition looking north from the new experimental area into the new vault area where the K500 cyclotron will be installed.

The concrete roof planks that will span the

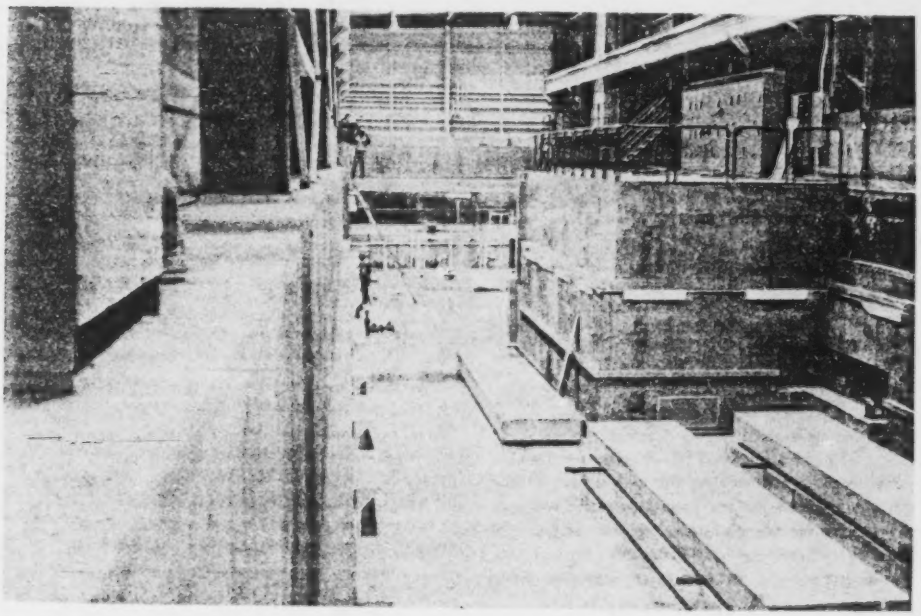

Fig. 1. Building addition looking from experimental area into vault area.

walls of the vault and experimental area are about 50% complete and will be stored off-site until roof shielding is required.

Major components of the cyclotron itself are starting to arrive. The helium storage tank and compressor system are on hand. The remainder of the refrigeration system is scheduled for shipment at the end of July 1983. Installation of the refrigerator will start as soon as the building is finished.

The magnet iron, Fig. 2, is scheduled for shipment from Japan at the end of May.

The bobbin, conductor and outer banding for the magnet coil are on hand, and winding of the coil is scheduled to start in September 1983.

The coil tank and pole tips, which are being manufactured in Houston, are expected to arrive in July 1983.

Fig. 2. K500 cyclotron magnet iron at final inspection in Japan Steel Works, Muroran, Japan.

K500 DEE STEM DESIGN STUDY

R. C. Rogers

A study has been made of the K500 cyclotron resonant structure from the point at which the coaxial line attaches to the dee to the point where it joins with the section of line containing the sliding short. The design of this short (1.2 m) section of line, the dee stem, has significant consequences in the power consumption and voltage holding capabilities of the rf system.

Figure 1 shows a possible configuration of a coaxial line which has a well defined characteristic impedance taper $Z_0(x)$ through that portion of line which has an outer conductor of constant diameter. (The taper of the line in the region of the insulator is a continuation of the same mechanical taper but $Z_0(x)$ varies widely because of the change in outer conductor dimensions.) Through the section of line which is well defined, the impedance taper is given by:

$$Z_0(x) = 45.1 - 8x^3 \text{ ohms},$$

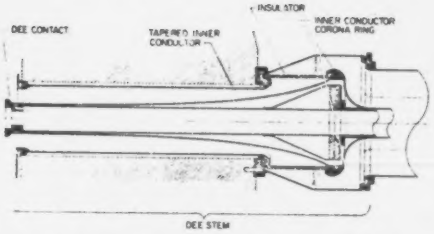

Fig. 1. Coaxial line dee stem with a tapered characteristic impedance.

where x is the distance along the line from the point of entry into the coaxial section and δ is a factor which fits the taper to the desired endpoint impedances.

Tapering of the line impedance gives the designer a measure of control over the current and voltage distribution along the line. Hence, some control is also gained over both the power consumption of the system and the current which must be handled by the sliding short. Since analytic solutions of the transmission line equations do not exist for a general tapered line, numerical methods were used to find the voltage, current and power distributions. The numerical technique was tested for lines for which analytic solutions exist and was found to be in good agreement. Figure 2 shows the peak voltage and rms current distributions along the line at f = 32 MHz and V_d = 100 kV; for these values, the power consumption is calculated to be 65 kW per dee.

The maximum dee voltage which can be achieved is determined in part by the voltage holding capability of the inner conductor corona ring. Since the K500 cyclotron has a constant-turn orbit geometry, the required dee voltage (V_d) varies with frequency as shown in Figure 3. The voltage which appears across the insulator (V_{ins}) and also on the corona ring is shown in the same figure. It can be seen that if the corona ring can hold a maximum voltage of 70 kV then the required dee voltages can be obtained. Figure 4 is a plot of the electric field gradient at the surface of the corona ring for a voltage of 70 kV. The two highest gradients are well below the 30 kV/cm breakdown limit for dry air so no sparking problems should be encountered.

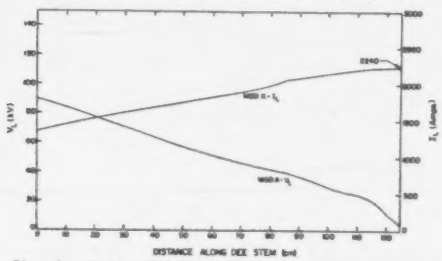

Fig. 2. Peak voltage and rms current distribution along the tapered line.

While tapering of coaxial lines for impedance matching purposes is well known, use of this technique in the design of resonators has been little explored. However, our investigations have led us to believe that power savings of 10% to 20% can usually be achieved by selecting a proper taper. Furthermore the use of tapers to avoid step changes in characteristic impedance may also avoid spurious resonances.

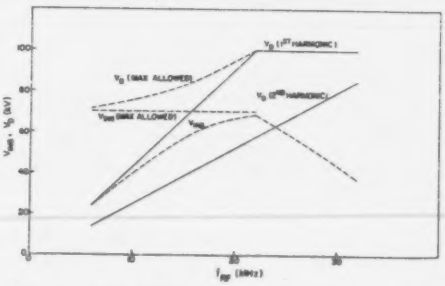

Fig. 3. K500 cyclotron dee voltage and insulator voltage.

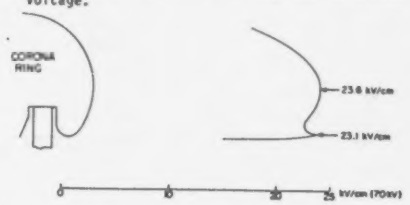

Fig. 4. Electric field gradient at the surface of the inner conductor corona ring.

TRANSFER LINE BETWEEN THE K500 AND THE 88" CYCLOTRONS: HIGH ORDER EFFECTS

B. Laune

The design of the transfer line is described in Ref. 1. However, the study was limited to the first order. The program TRANSPORT[2] has been used to calculate the second-order matrix, enabling estimation of the second-order aberrations. TURTLE[3] was also used: this is a Monte Carlo program which simulates the beam line performance by pseudo ray-tracing. It includes higher order terms and generates histograms at any point of the line. Reference 2 also provides a theory of second order transport and shows that for a fixed location of a sextupole component, the partial derivative of any second order matrix element with respect to the strength of the sextupole component is a constant and depends only on first order matrix elements. This coupling coefficient can be calculated anywhere in the line. It makes understanding of the second order aberrations easier and reduces their correction to a first order problem.

The calculation was performed for the two following representative cases

- Beam #4 → (2,1) SR=4.
- Beam #3 → (1,1) SR=4.

No significant aberrations appear if perfect elements are assumed. However, a huge vertical aberration (x,y^2) is present in the first case if a small sextupole component is assumed in the bending magnets. In this case, the dispersion element R_{16} has to be inverted to bring the beam to achromaticity, and that makes the transport solution more complicated. The large value of the first order matrix coefficient (y,y) at the first bending magnet (BM1) is responsible for this aberration. Since no chromatic aberration arises, the sextupole magnet needed to correct this aberration should be located in the achromatic section and where the coupling coefficient is maximum for this aberration and minimum for the others. Furthermore, the double waist is strongly affected, and for tuning purposes, the waist distortion has to be eliminated. Two sextupole magnets are needed: one before the double waist, in section D2B,[1] the other in section D3D. It was checked with the program TURTLE that the aberration was effectively reduced to an acceptable level by the use of these sextupole magnets and that no other significant aberration was present.

Since the large value of (y,y) is responsible for this aberration, the transfer line was redesigned. Changing the location of the third quadrupole magnet, Q1C, is sufficient to reduce the value of (y,y) at BM1: it was relocated 0.4 m from the fourth one, whose position remains unchanged. This increases the required gradient in Q1D, making the use of a non-standard quadrupole magnet necessary. There is no change in the tuning of the transfer line for beams one and three, since Q1C quadrupole magnet was not turned on for these beams.[1] This new arrangement will effectively reduce the vertical aberration by a factor of ten. This is not enough to avoid the use of a sextupole magnet, however, but only one located in section D2B is necessary. It corrects the double waist and no additional sextupole magnet is required farther down. Figure 1 shows the TURTLE printouts of the emittance at the double waist location when the sextupole magnet is on or off, assuming a positive or negative sextupole component in BM1. The latter is more favorable because in the former case some horizontal aberrations will appear. Note that the

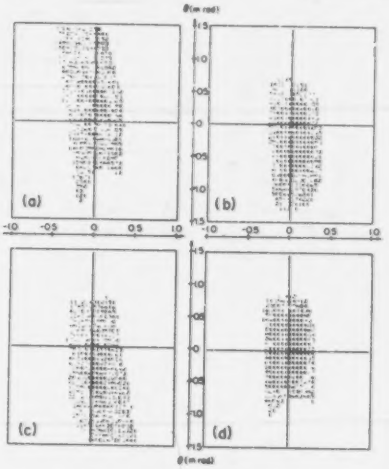

Fig. 1. Horizontal emittance of the achromatic double waist as produced by TURTLE. The first order size is ±0.3 cm by ±0.74 mrad. 10,000 rays have been tracked. The number of rays falling in a given bin (here 0.05 cm for x, 0.075 mrad for θ) is printed directly for 1-9 rays, by letters A-Z for 10-35 rays and by a $ sign for more than 35 rays; a) β = +1.15, sextupole off; b) β = +1.15, sextupole on; c) β = -1.15, sextupole off; d) β = -1.15, sextupole on. Note that a significant number of rays (15-20%) falls out of the shown window in the cases where the sextupole magnet is turned off.

defect assumed in BM1 is small: $\beta = 1.15$, that is $(\delta)B/B_0 = 5.10^{-4}$ at x=5 cm. β is defined as follows:

$$B/B_0 = 1 - n\,(x/R) + \beta(x/R)^2 + \ldots$$

where B_0 is the central magnetic field, R is the radius of curvature, and x is the distance from the reference trajectory.

Using TURTLE, sextupole and octupole components were introduced in the quadrupole magnets. As expected, the quadrupole magnets Q2A, Q2B, Q3C and Q3D were those where such field defects have the largest effect. The field quality in these quadrupoles is more important than in the others. Again, moving Q1C reduces the aberrations due to these defects.

This study has shown how a first order design could strongly influence the second order aberrations and how these can be minimized by the use of well-placed sextupole magnets and by an adequate design of the bending and quadrupole magnets.

References

[1]B. Laune and D. P. May, Progress in Research 1981-1982, Cyclotron Institute, Texas A&M University, p. 92.

[2]K. L. Brown, SLAC Report #91, July 1970.

[3]D. C. Carey, NAL Report #64, May 1978.

USE OF THE K500 CYCLOTRON WITH EXISTING BEAM LINES

B. Laune

The transfer line between the K500 and the 88" cyclotrons is configured to allow the transport of beams from the K500 cyclotron into the present caves 3 and 4.[1] Transport calculations have been performed in order to check that satisfactory solutions can be found from the exit of the K500 cyclotron up to the target stations. As an example, the following case will be described: K500 cyclotron and Enge split-pole spectrograph coupled in the "energy-loss" mode.[2] The good quality of the beams from the K500 cyclotron will allow a high resolution spectrometry.

In the energy-loss mode, the beam dispersion on the target has to be matched to that of the spectrometer. The split-pole spectrometer has the following matrix elements at mid-range: $(x,x) = 0.35$, $(x,\delta p/p) = 1.75$ cm/%. For elastically scattered particles, the dispersion on the target should be $R_{16} = (x,\delta p/p) = 1.75/0.35 = 5.0$ cm/%. This value, as well as a double waist on target, has to be provided by the line.

It was found that no additional element was needed, other than the existing elements in the present line or those planned for the coupling between the K500 and the 88" cyclotrons. Furthermore, a significant part of the resolution power has to be provided by the switching magnet which bends the beams from the K500 into line 5. The beam is wide (±2 cm) in this circular pole switching magnet which introduces a sextupole component into the phase ellipse of the beam. It may be necessary to cancel this component by a sextupole magnet. But for the present study, only the first order was considered.

Calculations were performed for two beams of different characteristics at the exit of the K500 cyclotron. (Beams 5 and 6, Ref. 3). Table I shows the properties of the beams at different positions along the line: exit of the K500, intermediate double waist (at the same location that was used for the coupling), and, finally, at the spectrograph target.

References

[1]B. Laune and D. P. May, Progress in Research 1981-1982, Cyclotron Institute, Texas A&M University, p. 92.

[2]H. G. Blosser and al., NIM 91, 61-65 (1971).

[3]J. Kasagi and al., IEEE Trans. Nucl. Sci. NS-28, No. 3, (1981).

TABLE I.

Beam	Q/A	W/A (MeV/A)	Location	x (cm)	θ (mrad)	y (cm)	φ (mrad)	R_{16} (cm/%)	R_{26} (mrad/%)
5	0.322	49.9	exit K500	0.49	0.85	0.12	3.25	-18.1	15.0
			inter. waist	0.056	5.17	0.083	3.61	-1.6	-40.9
			target	0.066	4.36	0.20	1.51	5.0	-8.6
6	0.332	22.2	exit K500	0.34	0.89	0.36	2.5	-0.96	21.4
			inter. waist	0.075	3.265	0.28	1.62	-2.0	-34.0
			target	0.061	3.99	0.22	2.10	5.0	12.6

PUBLICATIONS

Published April 1982—March 1983

Submitted

ABSTRACTS OF PAPERS PUBLISHED
April 1982 -- March 1983

Spectra of Ne K_α X-ray Satellites and Hypersatellites Excited by 1.2-1.4 MeV amu^{-1} He, C, Mg and Ar Ions
R. L. Watson, O. Benka, K. Parthasaradhi, R. J. Maurer, and J. M. Sanders
J. Phys. B 16, 835 (1983)

The sepctra of Ne K x-rays excited by beams of 4.7 MeV He ions, 16.7 MeV C ions, 32.4 MeV Mg ions and 54.0 MeV Ar ions have been measured with a curved crystal spectrometer. A detailed analysis of the multiplet line structure contributing to the K_α satellites and hypersatellites was performed and comparisons with the experimental spectrum excited by C ions yielded quite good agreement with the theoretical predictions. The correspondence of the ratios of the hypersatellite to satellite relative intensity ratios to those predicted by the ratios of the average theoretical fluorescence yields was investigated. The dependence of the average L-vacancy fraction for Ne on the ratio of the projectile velocity to average charge was extended beyond the region previously explored and large deviations from the original linear function were found.

Radioactive Implant Induced X-Ray Emission
J. R. Joyce, A. O. Sanni[1] and E. A. Schweikert
Nucl. Instrum. Methods 193, 21 (1982)

Two approaches with X-ray excitation sources directly inside a sample have been examined: mixing a sample in solution with a radioisotope or bombardment of a solid specimen with a radioactive ion beam. The radioisotopes used were ^{3}H, ^{35}S, ^{125}I, with detection limits of, for example, 20 μg/g for Ag excited by a ^{125}I implant of ~75kBq; 100 μg/g for Ti excited by a ^{3}H implant of ~7MBq. For comparable detection limits, the source strengths required are ~10^{3} less than that needed with external sources. The elemental coverages and the capabilities for simultaneous multielement detection are similar to "conventional" XES. In the beam implant mode, the spot size and energy of the beam provide for spatially resolved in situ X-ray excitation at a desired location inside a solid.

[1]University of Ibadan, Nigeria.

Analyzing Power for $^{4}He(n,n)^{4}He$ Elastic Scattering at 50.4 MeV
R. L. York, J. C. Hiebert, N. L. Woolverton, and L. C. Northcliffe
Phys. Rev. C 27, 46 (1983)

The analyzing power $A_y(\theta)$ for elastic scattering of neutrons by ^{4}He has been measured for eight angles in the range $80° < \theta_{lab} < 150°$ at 50.4 MeV. A polarized neutron beam (p_n = 0.50) was produced through bombardment of a high-pressure deuterium target by a 50 MeV polarized deuteron beam (p_d = 0.55) and by collimation of the neutrons in the 0° direction. A liquid-helium polarimeter placed in the neutron beam was used to measure asymmetries for left and right elastic scattering, with cyclic beam polarization reversal. Multiparameter methods of data acquisition and analysis were used to discriminate against backgrounds from ^{4}He breakup reactions and from interactions with the target-cell walls. The extracted A_y values exhibit the large positive maximum at backward angles and the smaller negative minimum at more forward angles typical of n-^{4}He scattering at lower energies. The n-^{4}He A_y values are compared with p-^{4}He results at a nearby energy by means of a phase-shift analysis and are found to be in good agreement (except perhaps in the negative minimum) when Coulomb corrections to the phase shifts are taken into account.

Masses of ^{76}Kr and ^{74}Kr
D. M. Moltz,[1] K. S. Toth,[1] R. E. Tribble, R. E. Neese, and J. P. Sullivan
Phys. Rev. C 26, 1914 (1982)

The masses of ^{76}Kr and ^{74}Kr were measured utilizng the $^{78}Kr(^{4}He,^{6}He)$ and $^{78}Kr(^{4}He,^{8}He)$ reactions. Mass excesses of -68971 ± 13 and -62210 ± 7 keV were obtained for ^{76}Kr and ^{74}Kr, respectively, and found to compare favorably with some mass formulae preidcitons, but not with others. Speculations about shape differences in light krypton and rubidium isotopes are presented as they relate to various mass formulae.

[1]Oak Ridge National Laboratory, Oak Ridge, Tennessee 37830.

Energy Dependence of the $^{12}C(^{16}O, \alpha)$ Reaction

T. Murakami, E. Ungricht, N. Takahashi, Y.-W. Lui, Y. Mihara, R. E. Meese, E. Takada,[1] D. M. Tanner, R. E. Tribble, and K. Nagatani

Phys. Lett. 120B, 319 (1983)

The energy dependence of the $^{12}C(^{16}O, \alpha)$ reaction was measured at incident energies of E_{lab} = 112-191 MeV. In the range of $E_x(^{24}Mg)$ = 30-56 MeV, the excitation energies of the structures in the inclusive α spectrum were found to vary continuously as a function of incident energy in this region. This fact indicates that these structures do not represent excitations in ^{24}Mg, but rather that they originate from a different process such as a sequential ejectile decay.

[1]Supported by Japan-US collaboration program of the Institute of Physical and Chemical Research, Wako-shi 351, Japan

Electron Transfer in Ionic Flourine Compounds Following Multiple Ionization by 22-MeV Carbon Ions

O. Benka, R. L. Watson, K. Parthasaradhi, J. M. Sanders, and R. J. Maurer

Phys. Rev. A 27, 149 (1983)

The spectra of K x rays emitted by thin targets of the alkali-metal and alkaline-earth flourides under bombardment with 22-MeV carbon ions were measured with a curved crystal spectrometer. Comparison of the satellite intensity distributions with that obtained for neon under similar conditions revealed that electron transfer within the K-hole lifetime ($\sim 10^{-13}$ sec) is highly probable even for these highly ionic compounds. A detailed analysis of the satellite intensity distribution obtained for LiF yielded a rate constant for KL^1-KL^0 transfer equal to 30% that for K-vacancy decay. The spectra for KF, SrF_2, and BaF_2 show evidence of resonant electron transfer (RET) associated with the matching of the 2p binding energies of flourine atoms in KL^1 states with the outer np binding energies of adjacent metal ions, in agreement with previous findings. Also, an anomalously low KL^2 intensity, indicative of RET in association with this double L-hole state, was observed for CaF_2. An additional component contributing to the enhancement of the KL^0 peak was attributed to secondary-electron ionization.

High Resolution K X-ray Angular Distribution Measurements

D. -W. Wang,[1] R. L. Watson, R. A. Kenefick, and D. A. Church

Nucl. Instrum. Methods 202, 355 (1982)

The angular distribution of K x-rays produced by highly-stripped fast ions is measured in high resolution with a rotatable Bragg plane-crystal spectrometer pivoted about a vertical axis through the target carbon foil. The helium-like and lithium-like spectra of 64 MeV sulfur ions are obtained at observation angles ranging from 20 to 160 degrees using a NaCl crystal. The collected x-ray count is normalized to the incident beam flux, and the spectra are fit with Voigt functions. Due to the Doppler effect, the spectra are recorded at Bragg angles ranging from 57 to 72 degrees. Thus, for absolute intensity measurements, the variation of crystal absorption and reflectivity with Bragg angle are significant. The theoretical curves for crystal reflectivity for both perfect and mosaic crystals, which have different angular dependences, can be generated for different x-ray polarizations, and compared with angular distribution data. The total beam x-ray intensities measured as a function of observation angle are corrected for relativistic effects and proportional counter efficiency dependences, and compared with the polarization-dependent theoretical curves to determine the optimum x-ray polarization value.

[1]Physics Dept., Peking Normal University, Peking, China.

Dissipation of Nuclear Collective Motion

P. J. Siemens

Nucl. Phys. A387, 247c (1982)

The collective transport theory provides a framework for understanding dampled collective motion. The irreversibility of collective motion is traced to the fact that the nuycleus is an open system. The finite lifetime of single-particle excitations causes the relaxation of the nuclear collective response. Both vibrational states and damped heavy-ion collisions can be understood quantitatively by computations without free parameters.

Alignment of the 2P State of 2-MeV/amu Heliumlike Sulfur

D. A. Church, R. A. Kenefick, D. -W. Wang,[1] and R. L. Watson

Phys. Rev. A 26, 3093 (1982)

The 2^1P and 2^3P levels of two-electrons S xv have been aligned by collision at 2 MeV/amu with carbon atoms in a foil. The degree of alignment is obtained by analysis of the normalized angular distribution of K x-ray radiation measured in high resolution with a pivoted plane-crystal Bragg spectrometer. The mean cross-section ratio σ_0/σ_1 for population of the m=0 sublevel relative to the m = ±1 sublevels of the 2P parent state is obtained by analysis of the 1^1S-2^1P and 1^1S-2^3P transition intensities. The result $\sigma_0/\sigma_1 = 1.79 \pm 0.1$ leads to the polarization fractions $P(^1P) = 0.28 \pm 0.05$, and $P(^3P) = -0.16 \pm 0.03$, in good agreement with results obtained by an independent analysis, and in excellent agreement with coupled-states calculations of Reading et al.[2] Comparison with other theories is also made.

[1]Physics Dept., Peking Normal University, Peking, China.

Dynamic Screening Energy Shifts and Collision Broadening of 2p→1s Transitions in 2-MeV/amu H- and He-like Ne, Mg and S Ions

R. J. Maurer, R. L. Watson, O. Benka, J. M. Sanders, and D. M. Oldham

Nucl. Instrum. Methods 202, 193 (1982)

The spectra of K x-rays emitted by 2 MeV/amu Ne, Mg, and S ions in a thick carbon target were measured with a curved-crystal spectrometer. Energy shifts of the hydrogen-like ion 2^2P→1^2S transition and the helium-like ion 2^1P→1^1S transition were determined by means of energy calibrations obtained from thin target spectra, for which x-ray emission occurred almost entirely in vacuum. The spectra were fit with a least-squares program employing Voigt functions to extract accurate peak centriods and, in the thick target cases, Lorentzian widths. The energy shifts were compared to those determined previously for S ions and found to be much smaller then expected on the basis of a dynamic screening model. The lorentzian widths were found to increase slowly with decreasing projectile Z, and those for the ^2P transition were ~50% smaller than those for the ^1P transition.

Single-Particle Response Function in Finite Nuclei

S. Shlomo

Phys. Lett. 118B, 233 (1982)

I derive expressions for the single-particle response (structure) function $S(E,q)$ and its sum rule, (Pauli blocking factor) $P(q) = \int dE\ S(E,q)$, in terms of the Wigner transforms (WTs) of the single-particle wave functions and the scattering probe $\sigma(q,r)$ and discuss the semi-classical phase-space interpretation of the results. For $\sigma(q,r) = e^{iq\cdot r}$, I derive simple expressions for $S(E,q)$ and $P(q)$ for finite nuclei within the harmonic-oscillator model and compare the results with the well-known results of the Fermi-gas model.

Reaction Mechanisms of 10 to 43 MeV/u Heavy Ions

J. B. Natowitz

Nucl. Phys. A387, 65c (1982)

Measurements of particle emission, linear momentum transfer and angular momentum transfer have been used to explore reaction mechanisms in the intermediate energy range where qualitatively different nuclear processes may be observable. The current status of our understanding of heavy ion reaction mechanisms with projectiles having velocities comparable to the velocity of sound and the Fermi velocity is summarized.

Pairing in Collective Transport Theory

A. S. Jensen,[1] J. Leffers,[1] K. Reese,[1] and P. J. Siemens

Phys. Lett. 117B, 157 (1982)

The introduction of pairing enters the collective transport theory treatment in two ways. The independent particle model results for the ordinary collective coordinates are modified and a new coordinate appears and results in new response functions. The general theory is sketched and the results obtained by using the new coordinate is investigated by numerical computaions. Friction, mass and stiffness coefficients and widths of the pairing distributions are given. The number of pairs broken during the descent from saddle to scission is estimated.

[1]Institute of Physics, University of Aarhus, DK-8000 Aarhus C, Denmark.

Pionic Modes of Excitation in Continuum from (p,n) Reaction

T. Izumoto, M. Ichimura,[1] C. M. Ko, and P. J. Siemens

Phys. Lett. 112B, 315 (1982)

The continuum spectra of the $^{90}Zr(p,n)$ reaction at E_p = 200 MeV are studied in the DWBA up to high excitation $\hbar\omega$(<60 MeV) and large momentum transfer $q(<3\mu_\pi)$. The response function is obtained in a local-density approximation, taking into account p-h and Δ-h excitations and the short-range correlation g' between them. For small g' < 0.5, a broad bump due to the opalescence effect can be seen in the calculated cross section at rather low excitation and near $q\sim 2.2\mu_\pi$. However, for larger g', this effect is suppressed, and a broader bump in cross section is located at higher excitation.

[1]Institute of Physics, University of Tokyo, Komaba, Tokyo.

Matter, Momentum and Energy Flow in Heavy-Ion Collisions

M. Prakash,[1] S. Shlomo, B. S. Nilsson,[2] J. P. Bondorf[2] and F. E. Serr[3]

Nucl. Phys. A385, 483 (1982)

We study the flow of matter, momentum and energy in low-energy heavy-ion collisions. This is done by using the Wigner phase space distribution function to calculate quantum mechanical analogs of the classical distributions of the observables. We apply the Wigner transformation to time-dependent Hartree-Fock calculations of $^{16}O + ^{16}O$ and $^{40}Ca + ^{40}Ca$ reactions. Both static and dynamic features of the distribution functions are demonstrated. We find a significant energy flow perpendicular to the beam direction. The one-way matter current obtained from time-dependent Hartree-Fock calculations is reproduced well by a combination of two simplified models for the relative motion and tunneling.

[1]Department of Physics, State University of New York at Stony Brook, Stony Brook, New York.
[2]The Niels Bohr Institute, University of Copenhagen, DK-2100 Copenhagen O, Denmark.
[3]Center for Theoretical Physics, Laboratory for Nuclear Science and Department of Physics, Massachusetts Institute of Technology, Cambridge, Massachusetts.

Core Polarization and Coulomb Displacement Energies

S. Shlomo, and W. G. Love[1]

Phys. Scripta 26, 280 (1982)

The contributions of core polarization terms (other than the Auerbach-Kahana-Weneser (AKW) effect) to Coulomb displacement energies of mirror nuclei near A = 16 and A = 40 are examined within the particle-vibration coupling model. The parameters of the model are determined using updated data on the locations and strengths of multipole core excitations. In the absence of relevant data an energy-weight sum rule (EWSR) is exploited. Taking into account multipole excitations up to L = 5 and subtracting the contributions which are due to short-range correlations, significant contributions (1 - 3%) to δE_C are found. These corrections arise from particle coupling to low-lying collective states (long-range correlations). The implications of these results on the Coulomb energy problem are discussed.

[1]Cyclotron Laboratory and Department of Physics, Michigan State University, Department of Physics and Astronomy, University of Georgia.

Comment on the Evidence for a Monopole Resonance at Approximately 20 MeV in ^{58}Ni

U. Garg, P. Bogucki, J. D. Bronson, Y.-W. Lui, C. M. Rozsa[1], and D. H. Youngblood

Phys. Rev. C 25, 3204 (1982)

Small-angle inelastic α scattering data for ^{58}Ni at 129 MeV have been reanalyzed with the giant resonance (GR) peak parameters suggested by Bertrand et al. The two components of the GR peak, assumed by them to correspond to L = 0 and L = 2, respectively, are found to have similar angular distributions between 0° - 8° where large differences between these multipolarities should exist. This is not in agreement with their interpretation of (p,p') and large-angle (α,α') data wherein a concentration of L = 0 strength was suggested at 20 MeV in ^{58}Ni. Their data for the assumed L = 0 component are shown in our analysis to be consistent with an L = 2 transfer.

[1]Harshaw Chemical Company, Solon, Ohio 44139.

Breakup Dominance at Higher Incident Energy In the $^{40}Ca(^{16}O,^{12}C)$ Reaction

E. Takada,[1] N. Takahashi, T. Murakami, Y. -W. Lui, T. Yamaya, and K. Nagatani

Phys. Lett. 118B, 307 (1982)

Incident energy dependence of $^{40}Ca(^{16}O,^{12}C)$ inclusive spectra was studied, and it was found that the projectile breakup process prevails at ~20 MeV/A. Coincidence measurement was then carried out between ^{12}C and α-particle, and the experimental results confirmed the dominance of the elastic-breakup process in the forward angles. A significant contribution of the inelastic ^{16}O breakup into $^{12}C^*(2^+,4.44MeV)$ and α particles is also found, proving a general trend that the lower energy portion in the inclusive spectrum is composed of the more complicated process.

[1]Supported by Japan-US collaboration program of the Institute of Physical and Chemical Research, Wako-shi 351, JAPAN.

Alpha-Particle Angular Distributions with Respect to Spin Direction

F. A. Dilmanian,[1] D. G. Sarantites,[1] M. Jaaskelainen,[1] H. Puchta,[1] R. Woodward,[1] J. R. Beene,[2] D. C. Hensley,[2] M. L. Halbert,[2] R. Novotny,[2] L. Adler, R. K. Choudhury, M. N. Namboodiri, R. P. Schmitt, and J. B. Natowitz

Phys. Rev. Lett. 49, 1909 (1982)

Angular distribution of alpha particles with respect to spin directon of residual nuclei from fusion of 176-MeV ^{20}Ne with ^{150}Nd has been measured with the spin spectrometer. Below the Coulomb barrier, the ratio of the 90° to 0° yields with respect to spin direction increase with decreasing E_α. This effect is not shown by a statistical-model calculation using penetrabilities for spherical potentials, which suggests that the α-emitting nuclei are deformed with their longest axis perpendicular to the spin direction. If so, the deformation increases as the spin rises from ~34 to 64 h.

[1]Department of Chemistry, Washington University, St. Louis, Missouri.
[2]Oak Ridge National Laboratory, Oak Ridge, Tennessee.

Quadrupole Vibrations of ^{238}U in Collective Transport Theory

A. S. Jensen,[1] J. Leffers,[1] K. Reese,[1] H. Hofmann,[2] and P. J. Siemens

Phys. Lett. 117B, 5 (1982)

The collective transport theory is applied to vibrational degrees of freedom. The general theory is briefly sketched and the relevant quantities introduced. Numerical results for the quadrupole vibrations of ^{238}U are presented for temperatures larger than 1 MeV. The beta vibration and the giant quadrupole resonance are identified, their positions and widths calculated and found in good agreement with available experimental numbers. Two new collective quadrupole resonances are predicted. The friction and mass coefficients describing motion of the quadrupole degree of freedom are calculated together with the width of the corresponding probability distribution.

[1]Institute of Physics, University of Aarhus, DK-8000 Aarhus C, Denmark

A Long Focal-Plane Detector with a Hybrid Structure

N. Takahashi, T. Yamaya, E. Takada,[1] Y. -W. Lui and K. Nagatani

Nucl. Instrum. Methods 196, 253 (1982)

A 1.2 m long position sensitive detector has been constructed to detect light and light-heavy ions over a wide momentum range with large vertical acceptance in the focal plane of the Texas A&M Enge split-pole spectrograph. The detector consists of a stack of five single-wire proportional counters in combination with another ionization and drift domain. The front two counters provide information about the energy loss and the position of the incident particles, and the others given only energy loss information. Separation of ionization and multiplication regions using the drift mechanism enables a large vertical acceptance, i.e. 27 mm. A position resolution better than 1.2 mm is obtained for 50 MeV alpha particles. Particle identification can easily be obtained for light and light-heavy ions.

[1]Supported by Japan-US collaboration program of the Institute of Physical and Chemical Research, Wako-shi 351, JAPAN.

Giant Spin-Isospin Vibrations and the Continuum Spectra from the (p,n) Reaction at Forward Angles
T. Izumoto
Nucl. Phys. A395, 189 (1983)

The giant Gamow-Teller (GT) resonance and the spin-isospin multipole vibrations are calculated in terms of the continuum RPA. The effective particle-hole interaction consists of the Migdal paramter g' = 0.7 (in units of f^2/μ^2=390MeV·fm^3) and the one-pion exchange potential. The RPA response functions are obtained withinthe full 1p-1h space. In addition to the natural excaping width of the single particle, a constant spreading width for 1p-1h states is incorporated into the correlation function, which makes numerical calculations fast and feasible. The giant GT resonances in ^{90}Zr and ^{208}Pb collect, respectively about 80% and 93% strengths of the sum-rule limit within the nculeon degrees of freedom. It is found that the strengths are further quenched by about 30% due to the coupling with the isobar Δ(1230)-hole configuration. The total quenching thus amounts to -45% and -40% respectively in two cases, which is in fair agreement with experiment. The continuum cross sections of the ^{90}Zr(p,n) reaction at forward angles are calculated for spins up to J = 4 with both parities in the distorted-wave Born approximation. While the giant GT resonance is located at a low excitation energy, ħω-17 MeV, the broad peaks of the dipole and quadrupole modes are found to dominate at ħω-25 and 35 MeV, respectively. The calculation fairly reproduces the experimental inclusive cross sections up to ħω-50 MeV.

Equilibrium Treatment of Spin-Depolarizing Modes in Mass Asymmetric Heavy-Ion Systems
R. P. Schmitt and A. J. Pacheco[1]
Nucl. Phys. A379, 313 (1982)

A two-sphere model is developed for the thermal excitation of spin-depolarizing modes in mass asymmetric heavy-ion systems. The effect of these modes on the spin distributions and the spin alignment of the fragments is investigated.

[1]Nuclear Science Division, Lawerence Berkeley Laboratory, University of California; Comision Nacional de Energia Atomica, Buenos Aires, Argentina

Comparative Study of Compound Components in ^{14}N(^{14}N,α), and ^{12}C(^{16}O,α) Reactions
N. Takahashi, E. Ungricht, T. Murakami, Y.-W. Lui, R. Neese, D. Tanner, R. Tribble, and K. Nagatani
Phys. Lett. 110B, 445 (1982)

Experimental spectra of the reaction ^{14}N(^{14}N,α) were measured at 111 MeV. Continuum spectra extending to high excitation energy of ^{24}Mg do not show any structure which is completely at variance with the reaction ^{12}C(^{16}O,α). A compound evaporation calculation reproduces the smooth components of the spectra of both reactions. The same theoretical prediction, however, seems to contradict the conjecture that the compound process yields the broad peaks in the ^{12}C(^{16}O,α) reaction.

Subthreshold K$^-$ Production in High Energy Heavy Ion Collisions
C. M. Ko
Phys. Lett. 120B, 294 (1983)

We show that an important contribution to subthreshold K$^-$ production in high energy heavy ion collision is the strangeness exchange reactions Y_π+K-N between the hyperons and pions initially produced in the collision. Estimates are given for the number of K$^-$ produced via this mechanism and it accounts for a large fraction of the experimental observation.

Comparison of Alpha Spectroscopic Factors on ^{24,26}Mg: The (^{14}N,^{10}B) Reaction
A. F. Zeller,[1] L. H. Harwood,[1] R. E. Tribble, Y. -W. Lui, and N. Takahashi
Phys. Rev. C 26, 2035 (1982)

Cross sections for states populated in the ^{24}Mg(^{14}N, ^{10}B) ^{28}Si and ^{26}Mg(^{14}N, ^{10}B)^{30}Si reactions at 83 MeV were measured. Equal strengths for population of ^{28}Si and ^{30}Si ground states were observed, in contrast to (^{16}O, ^{12}C) and (^{12}C, ^{8}Be) reactions, but in agreement with (^{6}Li, d) results and with theoretical predictions.

[1]National Superconducting Cyclotron Laboratory, Michigan State University, East Lansing, Michigan 48824.

Electron Transfer to the L-Shell Following Double K-Shell Ionization of Fluorine in Ionic Solids

O. Benka and R. L. Watson

Phys. Lett. 94A, 143 (1983)

Spectra of Kα hypersatellite x-rays excited in alkali and alkaline earth fluorides by 22 MeV carbon ions have been measured and used to deduce average probabilities for electron transfer to the L-shell. It was found that the average electron transfer probabilities for the double K-vacancy states are about a factor of 2 lower than those for the single K-vacancy states.

Heavy Ion Activation Analysis

B. D. Lass, N. G. Roche, A. O. Sanni,[1]
E. A. Schweikert, and J. F. Ojo

J. Radio. Chem. 70, 251 (1982)

A report on radioactivation with ion beams of $3 \leq Z \leq 8$ and energies of ~ 1 MeV/amu is presented.

a. Activation with ^{6}Li and ^{14}N. Among the analytical applications noted are: the determination of C via $^{12}C(^{6}Li,\alpha n)^{13}N$ with a limitation in Be-containing specimens due to $^{9}Be(^{6}Li,2n)^{13}N$; the determination of Li and Be, using ^{14}N activation [$^{6}Li(^{14}N,d)^{18}F$, $^{7}Li(^{14}N,t)^{18}F$ and $^{9}Be(^{14}N,\alpha n)^{18}F$ respectively], with limitations in selectivity as the ^{18}F yields are about the same for equal amounts of Li and Be. The detection limits using a 1 μA-h irradiation are 5 ppm for C and 1 ppm for Li or Be.

b. Activation with ^{9}Be. Two reactions on B and N are suitable for analytical applications: $^{10,11}B(^{9}Be,xn)^{18}F$ and $^{14}N(^{9}Be,\alpha n)^{18}F$. Assuming the 1 μA-h irradiation, the detection limits for N and B are 1.5 ng and 0.5 ng, respectively with 7.8 MeV ^{9}Be beam.

c. Activation with ^{12}C. Experimental results with 12 MeV ^{12}C beam demonstrate that the beam is best suited for ^{7}Li analysis by the reaction $^{7}Li(^{12}C,n)^{18}F$. The detection limit for a 1 μa-h irradiation is 1 ng and the only other low Z elements activated are B and C which produce 5% and 0.01% interferences respectively for equal weights.

d. Autoradiography. ^{12}C radioactivation was further combined with autoradiography for positional analysis. The spatial resolution of the technique was estimated by irradiating an NBS 610 sample with an 80 mesh grid on top and then taking an autoradiograph with a Kodak x-ray film. The resolution was estimated to be 40 μm for an exposure corresponding to 6×10^{5} disintegrations. As little as 10^{-12}g of Li was readily detected by autoradiography.

[1]University of Ibadan, Nigeria.

Mechanisms for Rapid Electron Transfer in Ionic Solids Following Multiple Ionization by Heavy-Ion Impact

R. L. Watson, O. Benka, K. Parthasaradhi,
R. A. Kenefick, R. J. Maurer, J. M. Sanders,
B. Bandong, and T. Ritter

IEEE Trans. Nucl. Sci. NS-30, No. 2, 919 (1983)

Systematic measurments of the spectra of fluorine Kα x-rays produced by the bombardment of alkali and alkaline earth fluorides with 2-MeV/amu ions ranging from He to Ar have given new information on the mechanisms for rapid electron transfer with the K-hole lifetime (~10^{-13} sec.). Spectra obtained with He ions provide clear evidence of the occurrence of resonant electron transfer (RET) following 1s2p ionization of F^{-} in the compounds KF and SrF_2. Calculations employing a point-charge model support the conclusion that the anomalously low KL^{1} x-rays satellite intensities observed for these two compounds are the result of a resonant exchange of an electron between the outermost p level of the metal ion and the 2p level of the fluorine ion. Such a transfer mechanism requires a close match between the energies of the two levels involved. Recent measurements using 22-MeV carbon ions have revealed that the KL^{2} satellite intensity in CaF_2 is much lower than that displayed by any of the other group II fluorides, thereby suggesting RET also occurs in association with this double L-hole state. When high staes of ionization are produced, rapid electron transfer to the fluorine L-shell becomes highly probable even in the absence of level matching. The mechanism for this probably involves collision induced transitions from the fluorine 2p band. At the same time, population of the M-shell levels of the ionized fluorine occurs, as is evidenced by the observation of large x-ray energy shifts and intense Kβ hypersatellite structure.

Mass of ^{16}Ne

C. J. Woodward, R. E. Tribble, D. M. Tanner

Phys. Rev. C 27, 27 (1982)

The mass of ^{16}Ne has been measured using the ^{20}Ne(^{4}He,^{8}He)^{16}Ne reaction. The Q-value of the reaction was determined to be -60.197 ± 0.023 MeV which corresponds to a mass excess of 23.984 ± 0.024 MeV. The weighted average of this result with two previous measurements yields a mass excess of 23.994 ± 0.020 MeV. This value is in reasonable agreement with the quadratic isobaric multiplet mass equation. The four parameter IMME suggests a cubic or quartic coefficient of 4 ± 3 keV for the A=16 multiplet.

Nuclear Fragmentation

G. Bertsch[1] and P. J. Siemens

Phys. Lett. B 126, 9 (1983)

We consider the conditions under which nuclei will fragment into smaller pieces. We argue that fragmentation will occur when the nuclear matter has expanded adiabatically to the onset of hydrodynamic instability, $\partial P/\partial V\big|_S = 0$. We discuss the conditions of initial heating and/or compression which lead to fragmentation, and argue that the resulting fragmented matter will be composed mainly of alpha-particles and nucleons.

[1]Physics Department, Michigan State University, E. Lansing, MI.

ABSTRACTS OF PAPERS SUBMITTED FOR PUBLICATION OR IN PRESS
April 1982 -- March 1983

Sum Rules for Harmonic-Oscillator Brackets
Shalom Shlomo
Jour. of Phys. A

A new class of sum rules is derived for the coefficients of the Talmi transformation of the harmonic-oscillator wave functions from the single particle coordinates to the relative and the center-of-mass coordinates.

Possible Evidence for the Statistical Excitation of Collective Modes in Heavy Ion Induced Reactions
R. P. Schmitt, G. Mouchaty, D. R. Haenni, and P. Bogucki
Phys. Lett. B

Angular momentum transfer in heavy-ion-induced fission has been studied utilizing gamma-ray multiplicity techniques. The results indicate that the fragment spins are considerably larger than expected from rigid rotation. The data are successfully compared with the predictions of a simple model which assumes the statistical excitation of a variety of collective modes.

Momentum Widths in the Fragmentation of 32 MeV/u ^{10}B
M. N. Namboodiri, R. K. Choudhury, J. B. Natowitz, K. Hagel, L. Adler, P. L. Gonthier, H. Simon, S. Kniffen, R. Patton, E. Thomasi, C. Ngo, C. Mazur and M. Ribrag
Phys. Rev. C (in press)

Momentum widths of fragments produced in the reactions of 320 MeV ^{10}B with ^{181}Ta have been measured. At forward angles the energy spectra of light particles (Z=1,2) exhibit energy peaks characterized by a reduced momentum width σ_0 =54 MeV/c, which is well below the values near 85 MeV/c observed in the reactions of 43 MeV/u ^{20}Ne with ^{181}Ta and in reactions induced by relativistic heavy ions. These results suggest a rapid increase in momentum widths, or apparent temperature, in the 32 to 43 MeV/u range.

Theoretical Relaxation Parameters for New Degrees of Freedom
P. J. Siemens, A. S. Jensen,[1] and H. Hofmann[2]
Nucl. Phys. (in press)

The application of Collective Transport Theory to quantifying an intuitive picture of nuclear collective motion is described in simple terms. Emphasis is laid on the connection to established phenomenology of nuclear structure and elementary excitations. By way of example, the "wall formula" of Swiatecki, Randrup and Koonin is cited, along with the damping of giant resonances.

[1]Fysisk Institut, Aarhus Universitet, 8000 Aarhus C, Denmark
[2]Physik-Department, Technische Universitat Muenchen, 8046 Garching, West Germany

Measurement of the $^1H(\vec{d},\vec{n})pp$ Transverse Polarization Transfer Coefficient at 42.8 MeV
Subrata Nath, R. G. Graves, J. C. Hiebert, L. C. Northcliffe, H. L. Woolverton, and R. L. York
Phys. Rev. C

The transverse polarization transfer coefficient $K_y^{y'}$ has been measured for the reaction $^1H(\vec{d},\vec{n})pp$ at 0° for E_d = 42.8 MeV as a function of breakup neutron energy. For the high-energy neutrons (E_n > 28 MeV) the average value for $K_y^{y'}$ is close to 0.6, in conformity with the prediction of simple stripping or spectator model for polarization transfer in deuteron stripping reactions.

APPENDIX

Oral Presentations

Staff and Students

Institute Colloquium Series

(753)

TALKS PRESENTED

April 1982 - March 1983

1. Effect of Relaxation on the K X-ray Spectra of Light Elements Following Multiple Ionization by Heavy Ion Impact, R. L. Watson, O. Benka, K. Parthasaradhi, J. Sanders, B. Bandong, G. Pedrazzini, US/Japan Summer Conference, Hawaii (April 1983).

2 Probing Spin-Isospin Modes in Nuclei by the (p,n) Reaction, C. M. Ko, Invited Talk, Conference on Nuclear Reaction Mechanisms, Varenna, Italy (June 1982).

3. Kaon Production in Relativistic Heavy Ion Collisions, C. M. Ko, Invited Talk, International Conference on Hypernuclear and Kaon Physics, Heidelberg, Germany (June 1982).

4. Spin Alignment in Mass Asymmetric Heavy-Ion Reactions, R. P. Schmitt, Invited Talk, Nuclear Chemistry, Gordon Conference, New London, New Hampshire (June 1982).

5. Dissipation of Nuclear Collective Motion, P. J. Siemens, Invited Talk, International Conference on Selected Aspects of Heavy Ion Reaction, Saclay, France (May 1982).

6. Future of Nuclear Reactions, P. J. Siemens, Invited Talk, Fifth Oaxtepec Symposium on Nuclear Physics, Oaxtepec, Mexico (January 1982).

7. Clusters in Nuclear Matter, P. J. Siemens, Invited Talk, Sixth Pan American Workshop on Condensed Matter Theories, St. Louis, Missouri (September 1982).

8. Structure of the $\pi^+ - \pi_0$ Continuum, P. J. Siemens, Invited Talk, Isovector Giant Resonances Workshop, Los Alamos, New Mexico (February 1982).

9. Reaction Mechanisms of 10 to 43 MeV/u Heavy Ions, J. B. Natowitz, Invited Talk, International Conference on Selected Aspects of Heavy Ion Reaction Mechanisms, Gif-sur-yvette, France (May 1982).

10. Matter, Momentum, and Energy Flow in Heavy Ion Collisions, M. Prakash, S. Shlomo, B. S. Nilsson, J. P. Bondorf, and F. E. Serr, Invited Talk, Workshop on Time Dependent Hartree-Fock and Beyond, Bad-Honnef, West Germany (June 1982).

11. Study of Nuclear Static and Dynamics Using the Wigner Transform, S. Shlomo, Invited Talk, Nuclear Fluid Dynamics, Treiste, Italy (October 1982).

12. The Texas A&M Coupled-Cyclotron System, D. H. Youngblood, Invited Talk, Seventh Conference on the Application of Accelerators in Research and Industry, North Texas State University, Denton, Texas (November 1982).

13. Resonant Electron Transfer in Ionic Compounds Following Inner-Shell Ionization, R. Watson, Invited Talk, Seventh Conference on the Application of Accelerators in Research and Industry, North Texas State University, Denton, Texas (November 1982).

14. Streamer Chambers for Intermediate Energy Heavy Ion Research, K. L. Wolf, Invited Talk, Workshop on Phase II Devices, Michigan State University, East Lansing, Michigan (December 1982).

15. Evidence for Statistical Excitation of Angular Momentum-Bearing Modes In Heavy Ion Induced Fission, R. P. Schmitt, D. R. Haenni, and G. Mouchaty, Spring Meeting of the American Physical Society, Baltimore (April 1983).

16. Angular Momentum Transfer and Alignment in the Reaction 214 MeV $^{32}S + ^{154}Sm$, G. Mouchaty, D. R. Haenni, S. Nath, U. Garg, and R. P. Schmitt, Spring Meeting of the American Physical Society, Baltimore (April 1983).

17. Difference between P and A for 800 MeV n-p Elastic Scattering: Test of Time-Reversal Invariance, L. C. Northcliffe, T. S. Bhatia, G. Glass, J. C. Hiebert, W. B. Tippens, B. E. Bonner, J. E. Simmons, C. L. Hollas C. R. Newsom, P. J. Riley, and R. D. Ransome, Bulletin of the American Physical Society 27, 47 (1982).

18. Study of ^{16}O-induced Transfer Reactions on Heavy Nuclei, E. Takada, Y. -W. Lui, T. Murakami, R. Tribble, and E. Ungricht, Bulletin of the American Physical Society 27, 714 (1982).

19. Masses of ^{76}Kr and ^{74}Kr, D. M. Moltz, K. S. Toth, R. E. Tribble, R. E. Neese, and J. P. Sullivan, Bulletin of the American Physical Society 27, 713 (1982).

20. Attenuation of the Giant Gamow-Teller Resonance, T. Izmoto, Bulletin of the American Physical Society, 27, 510 (1982).

21. Measurement of the Beta Decay of $^{16}N(0^-, 120\ keV)$: The Need for Meson Exchange Currents and the Value of g_p, C. A. Gagliardi, G. T. Garvey, S. J. Freedman, and J. R. Wrobel, Bulletin of the American Physical Society 27, 492 (1982).

22. What We Learn From Nuclear Collisions, P. J. Siemens, Spring Meeting of the American Physical Society, Washington, D. C. (April 1982).

23. First Experiments on Few-Nucleon Problems at the Karlsruhe Polarized Neutron Facility, P. Doll, B. Haesner, J. Hansmeyer, J. C. Hiebert, H. -O Klages, H. Krupp, M. Oexner, P. Plischke, P. Schwarz, and J. Wilczynski. Bulletin of the German Physical Society 6/1982, 1128 (1982).

24. Lifetimes of Yrast States of ^{128}Ce, J. C. Wells, J. Hattula, M. P. Fewell, D. R. Haenni, N. R. Johnson, I. Y. Lee, F. K. McGowan, L. L. Riedinger, Spring Meeting of the American Physical Society, Washington, D.C. (April 1982).

25. Lifetimes of Yrast States of ^{160}Yb, M. P. Fewell, J. Hattula, D. R. Haenni, N. R. Johnson, J. W. Johnson, I. Y. Lee, F. K. McGowan, L. L. Riedinger, J. C. Wells, S. C. Pancholi, Spring Meeting of the American Physical Society, Washington, D.C. (April 1982).

CONFERENCE PROCEEDINGS

April 1982 - May 1983

1. Effect of Delta-Hole States on Giant Spin-Isospin Vibrations, T. Izumoto, Proceedings of the 1982 INS International Symposium on Dynamics of Nuclear Collective Motion, Japan p. 74, (July 1982).

2. Single Particle Response in Finite Nuclei, S. Shlomo, Proceedings of the International Conference on Nucleus-Nucleus Collisions, Michigan State University (September 1982).

3. In-Beam Spectroscopy of ^{101,102,103}Tc Via Massive Transfer Reactions, D. R. Haenni, R. P. Schmitt, G. Mouchaty, T. T. Sugihara, and U. Garg, Proceedings of the International Conference on Nucleus-Nucleus Collisions, Michigan State University (September 1982).

4. Nucleon Exchange in ^{56}Fe-Induced Reactions at 8.3 MeV/Nucleon, H. Breuer, A. C. Mignerey, V. E. Viola, Jr., K. Kwiatkowski, K. L. Wolf, J. Birkelund, D. Hilscher, J. R. Huizenga, W. U. Schroder, and W. Wilcke, Proceedings of the International Conference on Nucleus-Nucleus Collisions, Michigan State University (September 1982).

5. Study of the Gamma Decay of States Excited Via Inelastic Scattering of α and ^{16}O Beams, J. P. Sullivan, R. K. Choudhury, U. Garg, L. Adler, J. D. Bronson, P. Gonther, D. Haenni, Y. -W. Lui, G. Mouchaty, T. Murakami, M. N. Namboodiri, J. B. Natowitz, M. Parkin, R. P. Schmitt, S. Simon, and D. H. Youngblood, Proceedings of the International Conference on Nucleus-Nucleus Collisions, Michigan State University (September 1982).

6. Nucleon Momentum Widths in ^{10}B For Projectile Fragmentation at 32 MeV/u, R. K. Choudhury, M. N. Namboodiri, J. B. Natowitz, K. Hagel, L. Adler, P. Gonthier, H. Simon, S. Kniffen, R. Patton, E. Tomasi, C. Ngo, C. Mazur, and M. Ribrag, Proceedings of the International Conference on Nucleus-Nucleus Collisions, Michigan State University (September 1982).

7. Excitation of Collective States in Transitional Nuclei by Massive Transfer, T. T. Sugihara, D. R. Haenni, R. P. Schmitt, G. Mouchaty, and U. Garg, Proceedings of the 1982 INS International Symposium on Dynamics of Nuclear Collective Motion - High Spin States and Transitional Nuclei, Japan (July 1982).

8. A Second Neutron Alignment in Yrast Spectra for N = 90, L. L. Riedinger, S. Fravendorf, H. Ower, L. H. Courtney, M. P. Fewell, D. R. Haenni, J. S. Hattula, S. A. Hjorth, N. R. Johnson, and I. Y. Lee, Conference on High Angular Momentum Properties of Nuclei, Oak Ridge, Tennessee (November 1982).

9. Product Selectivity of a Combined Total Energy Multiplicity Filter for In-Beam Gamma-Ray Spectroscopic Studies, D. R. Haenni, R. P. Schmitt, L. L. Riedinger, G. Mouchaty, and M. P. Fewell, Conference on High Angular Momentum Properties of Nuclei, Oak Ridge, Tennessee (November 1982).

10. Injection from the K500 Superconducting Cyclotron into the 88" Cyclotron at Texas A&M, B. Laune, D. P. May, W. C. Chapman, W. J. Walterscheid, G. Derrig, Y. L. Tsein, P. Smelser, and D. H. Youngblood, Proceedings of 1983 Particle Accelerator Conference, Santa Fe, New Mexico (March 1983).

RESEARCH PERSONNEL AND ENGINEERING STAFF

FACULTY AND RESEARCH GROUP LEADERS

Carl A. Gagliardi,[1] Assistant Professor of Physics
David R. Haenni, Research Scientist
Jack C. Hiebert, Professor of Physics
Che Ming Ko, Assistant Professor of Physics
Ken Nagatani, Professor of Physics
Joseph B. Natowitz, Professor of Chemistry, Head, Department of Chemistry
Lee C. Northcliffe, Professor of Physics
Emilie Schweikert, Professor of Chemistry
Richard P. Schmitt, Assistant Professor of Chemistry
Philip J. Siemens, Professor of Physics
Robert E. Tribble, Associate Professor of Physics, Head, Department of Physics
Rand L. Watson, Professor of Chemistry, Associate Dean of Science
Kevin L. Wolf,[2] Professor of Chemistry
D. H. Youngblood, Professor of Physics, Director

VISITING SCIENTISTS

Gert Hansen,[3] University of Aarhus, Denmark
Helmut Hofmann,[4] Technische Universitat, Munchen, Germany
Munetake Ichimura,[5] Institute of Physics, University of Tokyo, Komaba, Japan
Yasuo Mihara, Tokyo Institute of Technology, Tokyo, Japan
Tetsuya Murakami,[6] Kyoto University, Japan
Eiichi Takada,[7] Institute of Physical and Chemical Research, Waki-Kami, Japan
Yun-lung Tsien, Institute of Nuclear Research, Academy of Science of China, Shanghi, Peoples Republic of China

PERMANENT RESEARCH STAFF

Jeff Bronson, Senior Scientist
Toshiaki Izumoto,[8] Research Scientist
Bernard Launé, Accelerator Physicist
Yiu-Wing Lui, Research Scientist
Donald May, Accelerator Physicist
Neil Namboodiri, Senior Scientist
Shalom Shlomo, Research Scientist

RESEARCH ASSOCIATES

Michael Akanni[9]
Haydeh Dejbakhsh[10]
Oswald Benka[11]
Gary Berkowitz[12]
R. Choudhury[13]
Umesh Garg[14]
Peter Gonthier
Georges Mouchaty
Subrata Nath
Richard Neese[15]
K. Parthasaradhi
Greg Pedrazzini[16]
Yoshiyuki Toba[17]
John Sullivan
Ernst Ungricht[18]

GRADUATE STUDENTS

Chemistry

Lee Adler
Bryan Bandong
John Demarest
John Joyce
Lynne Divis
Janice Epstein[19]
Paul Filpus
David Keith
Richard Maurer
Solomon Simon
William Summers
Maria Vargas

Physics

Argyrios Doumas
Jorge Lopez
Mark Parkin
William Schmidt
Danelle Tanner
Cathleen Woodward[20]
Warren Woodward[21]

ENGINEERING STAFF

Erik N. Basilier, Assistant Research Engineer
Walter Chapman, Mechanical Engineer
Gary DeHaven, Operations Chief
Greg Derrig, Mechanical Engineer
Robert C. Rogers, Chief Engineer Cyclotron
Peter Smelser, Cryogenics Engineer
James Reimund,[22] Electrical Engineer

THESES COMPLETED

W. F. Woodw[illegible]	M.S., Physics	12/82	Vector and Tensor Analyzing Powers for $^{1}H(\vec{d},n)2p$ and $^{2}H(\vec{d},n)X$ at E_d = 45.5 MeV	Northcliffe

[1]From 8-16-82
[2]From 8-9-82
[3]Through 1-31-83
[4]Through 5-31-82
[5]Through 4-13-82
[6]Through 12-31-82
[7]From 4-8-82
[8]Through 11-30-82
[9]Through 11-30-82
[10]From 1-7-83
[11]Through 7-31-82
[12]From 11-22-82
[13]Through 8-31-82
[14]Through 5-31-82
[15]Through 10-31-82
[16]From 10-1-82
[17]From 9-1-82
[18]Through 10-31-82
[19]From 9-2-82
[20]Through 7-31-82
[21]Through 12-31-82
[22]From 5-10-82

INSTITUTE COLLOQUIUM SERIES

Apr. 1	P. T. DeBevec, University of Illinois	Shedding Light on Nuclei: Electron and Photon Interactions
Apr. 12	P. Wurm, Max-Planck-Institute Fur Kernphysik, Heidelberg	Proximity Effects in Heavy-Ion Collisions
Apr. 12	H. Ho, Max-Planck-Institute Fur Kernphysik, Heidelberg	Nonequilibrium α Emission in $^{16}O + ^{58}Ni$ Collisions
Apr. 13	J. Schiffer, Argonne National Laboratory	Delta Propagation in Nuclei
Apr. 15	T. Humanic, Argonne National Laboratory	Reactions to Resolved States and to Non-Fusion Channels for $^{16}O + ^{48}Ca$ at 158 MeV
Apr. 16	M. Ichimura, University of Tokyo, Japan	A Formalism for Inclusive Breakup Reactions and Validity of the Surface Approximation
Jun. 9	G. Berkowitz, S.U.N.Y. at Stony Brook	Systematic Study of Heavy-Ion Fusion Between Medium Mass Heavy Ions
Jun. 17	N. Carjan, Centre d' Etudes Nucleaires, Bordeaux, France	Recent Results on α-Particle Emission During Fission
Jun. 24	T. Gray, Kansas State University	Atomic Physics with Recoil Ions
Jul. 13	C. Ngô, Saclay, France	Heavy Ion Interaction Potential at Finite Temperature
Jul. 27	H. Dejbakhsh, University of Oklahoma	Nuclear Spectroscopy of Neutron-Rich Nuclei in the A = 100 Region
Aug. 16	F. Folkmann, University of Aarhus, Denmark	Selective Electron Capture into Highly Charged Ions
Sep. 6	M. Uda, The Institute of Physical and Chemical Research, Wako-shi, Saitama, Japan	Chemical Effects on X-Ray Satellite Spectra
Oct. 4	K. Nakai, University of Tokyo	Recent Experimental Results from KEK
Oct. 5	A. Fleury, Centre D'etudes Nucleaires, de Bordeaux-Gradignan	Properties of Heavy Recoil Nuclei in ^{12}C Induced Reactions at 86 MeV/Nucleon
Oct. 7	R. Dayras, Centre d' Etude Nucleaires de Saclay	Light Particle Emission in Light Heavy Ion Induced Reactions
Oct. 8	J. L. Adler, University of Mexico	An Alpha Plus Boson Model of Nuclear Structure
Oct. 11	S. Yamaji, Institute of Physical and Chemical Research, Wako-shi, Saitama, Japan	Two-Particle, Two Hole Effects on the Mass Distributions in Deep Inelastic Collisions
Oct. 25	D. Hensley, Oak Ridge National Laboratory	Data Acquisition with the Event Handler
Nov. 4	H. Sann, GSI & Berkeley	Music at Hiss Experiment
Nov. 5	C. Rolfs, Universitat Muenster	$^{3}He(^{4}He,\lambda)^{7}Be$ and the Solar Neutrino Problem
Nov. 11	H. Frohlich, Universitat Erlangen/ Nurnberg	Experimental Evidence for Dinuclear Structure of $^{16}O + ^{12}C$ Resonances
Nov. 12	S. Hjorth, Research Institute of Physics, Stockholm, Sweden	Energy-Energy Correlations
Nov. 16	D. Machen, Director of Engineering-Scientific Systems International	Front-End Processing for Physics Data Acquisition
Jan. 27	J. Wesick, University of Maryland	Continuum Spectra from Few Nucleon Targets Using 100-150 MeV Polarized Protons
Feb. 8	P. McIntyre, Texas A&M University	The Texatron: A Proposal for a Major New Accelerator Laboratory
Feb. 21	P. Siemens, Texas A&M University	Heavy Ion Collisions at Intermediate Energy
Mar. 1	K. Grotowski, Jagellonian University, Cracow, Poland	Fission-like Phenomena Around A = 50 and the Kinematics of Hot Fragments

9.0 University of Washington
Three-Stage Tandem Van de Graaff Accelerator Facility

1. What new science is being explored by this facility? What scientific opportunities are being exploited?

Answer: The basic research activities of the University of Washington Nuclear Physics Laboratory (NPL) can be roughly divided into seven major areas of investigation: nuclear astrophysics, light ion reactions, fundamental symmetries, giant resonances, heavy ion reactions, medium energy physics, and accelerator radiochronology.

Nuclear astrophysics exploits the facilities and techniques of nuclear physics to simulate the environment which was present in the early universe to test current ideas of cosmology, star formation, and the production in stars of the chemical elements and isotopes; to measure the detailed properties of nuclei which are needed to accurately formulate astrophysical theories; and to interpret the measurements made with new astrophysical instruments (x-ray and gamma-ray space telescopes). This area of nuclear research is an example of the cross-fertilization which frequently occurs between nuclear science and related fields (e.g., astrophysics) through an exchange of ideas, techniques, and information.

A special feature of the NPL accelerator facility is the availability of intense energy-variable polarized beams of protons and deuterons, i.e., projectiles with "spins" or internal rotations prepared so as to point in a particular spatial direction which can be varied. This capability has provided an excellent opportunity for the study of light-ion-induced nuclear reactions and, particularly, the spin dependence of these reactions. Such measurements in resonant and direct nuclear reactions have proved to be powerful probes for gaining information on the structure of nuclei and insights into the dynamics of nuclear reactions.

The investigation of fundamental symmetries probes the symmetry properties of the forces which bind nuclei, particularly the property of "parity" or space reversal (as in a mirror image) and the property of time reversal. High precision measurements of carefully selected nuclear reactions can reveal small violations of these symmetry properties, giving important clues to the origins and interrelations of the fundamental forces of nature. The University of Washington Nuclear Physics Laboratory is continuing to exploit the capabilities of its accelerator facility to produce beams of spin-polarized protons for the investigation of these symmetry properties.

One of the most remarkable general properties of nuclei is the phenomenon of "giant resonances," the very simple vibrational modes of the nucleus as a whole which occur at relatively high excitation energies. These resonances may be excited by reactions involving both light and heavy projectiles, and they may deexcite by the emission of gamma rays or particles. The simplicity of the giant resonances can be exploited to gain insights into the dynamic behavior of nuclei and the action of nuclear forces in a simple but unusual situation. The capabilities of the Nuclear Physics Laboratory for producing intense polarized proton beams and beams of heavy ions with easy variation of beam energy along with the facilities for detection of energetic gamma rays with good energy resolution are being exploited to investigate this phenomenon.

The investigation of the structure and dynamic behavior of nuclei with reactions involving the collision of two complex nuclei has proved in recent years to be a very rich field of study. Such reactions can prepare the nucleus in excitation modes which are not accessible to other techniques, particularly those in which the nucleus is rotating very rapidly or has been very severely deformed from its normal shape. The operation of the nuclear force in these reactions is also of particular interest because it exhibits a behavior which is altered and "filtered" by the presence of the large number of nucleons in the reaction and therefore can exhibit properties which do not manifest themselves in simpler situations. In these investigations, the scientists of the Washington Nuclear Physics Laboratory use the laboratory accelerator facilities for these investigations and also function as users at national facilities (Lawrence Berkeley Laboratory, Oak Ridge National Laboratory, Michigan State University) where more energetic beams of heavy ions are available.

The work in medium energy physics by scientists of the Nuclear Physics Laboratory is also performed primarily in the user mode, using the Laboratory as a base providing technical resources for experiments performed at the "meson factory" facilities at Los Alamos National Laboratory and the University of British Columbia. This work has primarily focused on the interactions of pi-mesons with nuclei and on the nuclear excitations which are produced in these interactions.

The work in accelerator radiochronology is another example of the cross-fertilization of nuclear science with related disciplines--in this case, the geological and archaeological sciences. The thrust of this work is to provide archaeological and geological "clocks" for dating artifacts and objects. These clocks are radioactive isotopes (e.g., ^{14}C and ^{10}Be) which are identified not by conventional radioactive counting but, rather, by accelerating them through an accelerator. This permits the use of isotopes with very long half lives and requires only very small samples of the materials to be dated. The excellent stability of the FN tandem of the Nuclear Physics Laboratory and the ability of the sputter ion source to produce intense beams of carbon and beryllium ions are exploited for this research which is performed in collaboration with scientists from the Quaternary Research Center of the University of Washington.

2. **How does this facility's accelerator (or accelerators) performance compare with any other in the world that are operating, under construction, or planned?**

Answer: The accelerator facility at the University of Washington Nuclear Physics Laboratory (NPL) is currently undergoing a major upgrade. The "injector" FN Van de Graaff of the present three-stage facility will no longer be used (except possibly for gas storage), while the "tandem" FN accelerator of the present facility will become the injector for a new superconducting linac accelerator presently under construction. This new facility will be completed in 1986-1987. The effect of the accelerator upgrade will be to approximately double the energies of light ion beams available from the facility and to quadruple the energies of heavy ion beams. This will provide proton and deuteron beams of up to 40 MeV and heavy ion beams of 10-20 MeV/nucleon. These energy domains will provide access to a field rich in opportunities for the exploration and investigation of nuclear phenomena.

With the addition of the superconducting linac booster mentioned above, the NPL accelerator facility joins a select group of "booster-enhanced" tandems. This group includes completed and operating facilities at Heidelberg (West Germany), Argonne National Laboratory, and the State University of New York at Stony Brook as well as projects under construction at Florida State University, Oxford University (United Kingdom), the Weizmann Institute (Israel), and ANU Canberra (Australia).

It is unique among these facilities in its ability to provide significant acceleration for "light" ion beams (protons, deuterons, tritons, and helium isotopes) as well as "heavy" ion beams (from lithium to zirconium). The facility will also be unique in having a high-current ion source producing intense beams of spin-polarized protons and deuterons.

3. **What types of research instrumentation/experimental devices are available at this facility, and what are their capabilities?**

Answer: The University of Washington Nuclear Physics Laboratory (NPL) accelerator facility, in its present configuration, has a number of features and major items of research instrumentation which offer advantages for research in nuclear physics. The accelerator is equipped with a terminal stabilization system which, by means of a light beam sent to the tandem terminal, regulates the energy of the tandem beam to high precision and removes the high frequency components of energy fluctuation providing very stable accelerator operation. The tandem is equipped with several kinds of ion sources for the production of negative ions including a "direct extraction" source for producing beams from gases (e.g., hydrogen, oxygen), a "sputter" ion source for producing beams from solid materials (e.g., carbon, silicon), and a "Lamb shift" polarized ion source for producing spin-polarized beams of protons and deuterons. The facility also has a "buncher" for altering the continuous time structure of beams so that the stream of ions is compressed into "bunches" with a time width of about one one-billionth of a second.

The facility also has available a number of major items of instrumentation for use with the beams produced by the accelerator. There are two general purpose scattering chambers for use in the detection of particles produced in nuclear reactions. The largest of these chambers is 60 inches in diameter and provides remote control of two rotatable detector-support arms, a rotatable floor, and target rotation and positioning. This chamber offers a very large internal volume for complex experimental setups and a relatively long permanent setup for the 10 inch diameter by 10 inch long NaI scintillation spectrometer system with a plastic anti-Compton shield for the detection and analysis of energetic gamma rays. On another beam line, a "momentum filter" magnetic spectrometer system has recently been installed. This system, a QDD-DDQ configuration, is essentially a conventional magnetic spectrograph feeding into its own mirror reflection. It can be used as a large solid angle (10 msr) medium-resolution spectrograph and also has important applications for eliminating or tagging particle groups in its focal plane before coincidence or measurements are made at its second focus. It also has important applications by providing a long (5.7 m) large solid angle flight path for time-of-flight measurements of charged particles.

For data collection, the laboratory operates a DEC PDP-11/60 computer system which is equipped with 12 ADC's, 15 computer-readable scalers, and a fast MBD-controlled CAMAC interface to assorted data acquisition modules. The system can collect data at rates of about 70 event-kHz in singles mode and about 30 parameter-kHz in multiparameter mode. The laboratory also operates a DEC VAX-11/780 computer system for off-line data analysis, scientific calculations, and scientific text processing.

With the upgrading of the facility will come a number of changes in the experimental apparatus. The buncher will be upgraded to meet the requirements of the booster, and bunch time widths of less than 100 psec will become available. The Lamb-shift polarized source is being replaced with a colliding beam polarized source which provides more than an order of magnitude increase in intensity. The crystal of the NaI spectrometer is being replaced with a somewhat larger one of improved resolution. We also anticipate that other improvements in and additions to the experimental equipment will be possible before the booster becomes operational.

4. **What have been the facility's research highlights for the period FY 1981 - present, and what are anticipated for the remainder of FY 1984 and FY 1985?**

Answer: The basic research activities of the University of Washington Nuclear Physics Laboratory (NPL) can be roughly divided into seven major areas of investigation: nuclear astrophysics, light ion reactions, fundamental symmetries, giant resonances, heavy ion reactions, medium energy physics, and accelerator radiochronology.

For nuclear astrophysics, the nucleosynthesis of the rare isotope ^{26}Al is currently a topic of great interest in astrophysics because it is the signature of a key step in the synthesis of light elements. Understanding of the synthesis of this element requires measurement of the cross sections for both its formation and its destruction (primarily by fast neutrons). The latter cross sections have proved elusive because ^{26}Al is not stable and cannot be used as a target. This problem has recently been overcome at Washington's Nuclear Physics Laboratory by measuring cross sections for the time reversed processes which may then be directly related to the cross sections of interest.

A new window has opened on the universe as space-mounted gamma ray telescopes have come into operation. However, the interpretation of data from gamma ray line astronomy (GRLA) with such instruments requires a data base detailing which gamma rays are produced by what stellar constituents under which conditions. At the NPL, a systematic catalog has been assembled of gamma rays arising from nuclear processes in the principal medium-weight isotopes found in stars based on measurements made at this Laboratory. These data are proving to be of great value in interpreting recent GRLA observations.

For light ion reactions, the detailed structure of the double closed shell nucleus ^{208}Pb and its neighboring nuclei is of considerable interest because the nuclear shell model is expected to work very well in this region. Detailed spectroscopic information on nuclear excited states in ^{207}Bi and ^{209}Bi has been obtained. These measurements used spin-polarized protons to excite isobaric analog resonances which then decayed by proton emission.

The technique provided independent information on cross sections (i.e., yield) and analyzing power (i.e., yield change with beam polarization) which allowed good accuracy in the extraction of parameters to be compared with theory.

By studying how the spin-polarization of a beam of deuterons is altered in a nuclear reaction (using a polarized beam and measuring final particle polarization), it has been possible to identify effects in polarized reactions arising from breakup of the deuteron by the nuclear forces as it passes through the target nucleus.

For fundamental symmetries, two very demanding measurements of parity violations (the breakdown of mirror reflection symmetry), one in a nuclear system and the other in an atomic system, are being pursued to test the current understanding of the unification of the "weak" force (the force responsible for radioactivity in light nuclei) and the electromagnetic force through the Weinberg-Salam theory.

A major effort has been initiated to measure the parity mixing in a pair of excited states of the ^{14}N nucleus. The experiment will use a new technique (helicity dependence of resonant proton scattering) and will provide fundamental information on the part of the weak force which involves the protons and neutrons symmetrically.

The limits of sensitivity for parity violation studies are being pressed in the most fundamental atomic system, the hydrogen atom, with detailed studies of small systematic errors in the measurement of small interference effects in atomic transitions using apparatus developed as an offshoot of nuclear physics oriented technical developments. The next few years should see improved limits for this atomic case and a positive measured effect for the nuclear case.

Recently, a whole new family of giant resonances has been discovered at very high energies in nuclei, corresponding to giant "electric dipole" vibrations of excited or "hot" nuclei. Work at the University of Washington Nuclear Physics Laboratory in the past three years has made a major contribution in this new area, demonstrating that these vibrations are a general feature of excited nuclei and that they may be excited in several different ways (by "direct" collisions induced by nucleon projectiles and by equilibrated collisions induced by complex projectiles). The properties of these vibrations in highly excited nuclei (vibrational energy, lifetime, and strength) are giving important new clues about the nature of highly excited nuclei. During the next two years, the systematics of these vibrations in different nuclei will be established, from which more general conclusions may be drawn. Also, new information is currently being obtained in lead nuclei on the nature of the high energy giant electric quadrupole resonance.

With regard to heavy ion reactions, as mentioned previously, nuclear reactions involving the collision of two complex nuclei have proved to be a powerful tool for the investigation of the structure and dynamic behavior of nuclei. Such reactions prepare the nucleus in excitation modes in which the nucleus is rotating very rapidly (corresponding to high spin states) or has been severely deformed from its normal shape. The distribution of spins of nuclear energy levels at energies just above the Coulomb barrier have been measured for the system $^{160} + {}^{154}Sm$. To describe such systems, a new model has been developed including both centrifugal barrier penetration and target deformation. This model is capable of describing both spin distributions and absolute fusion cross sections.

The electrical repulsion between colliding heavy ions has been used as a "depth gauge" by carefully adjusting the energy to keep the ions' distance of closest approach large enough that subtle and very fundamental effects arising from the theory of relativity can be identified and tested.

For medium energy physics, mechanisms by which pi-mesons lose energy when they are scattered by nuclei are being explored. These mechanisms are usually described in terms of primary processes involving one or two nucleons and are not well understood. This problem is being systematically studied by looking at pi-meson scattering from the neighboring light nuclei hydrogen, deuterium, helium-3, and helium-4.

A program of accelerator development needed to provide definitive and reproducible results in the determination of isotopic concentrations of ^{14}C and ^{10}Be for radiochronology has been completed. A program has been developed to measure both ^{14}C and ^{10}Be in environmental samples and, in particular, to determine ^{14}C abundance in small segments of single tree rings formed during the nuclear weapons testing period of 1962 to 1964 (the so-called Bomb Spike). For ^{10}Be, concentration in precipitation samples collected at latitudes from 46°N to 71°N has been determined to study both temporal and latitude variations.

5. **What facility changes and additions have occurred or are anticipated for the period FY 1981 - FY 1985?**

Answer: The University of Washington Nuclear Physics Laboratory (NPL) facility presently has a major facility upgrade in progress. The "injector" FN Van de Graaff of the present three-stage facility will no longer be used (except possibly for gas storage), while the "tandem" FN accelerator of the present facility will become the injector for a new superconducting linac accelerator presently under construction. This new facility will be completed in 1986-1987. The effect of the accelerator upgrade will be to approximately double the energies of light ion beams available from the facility and to quadruple the energies of heavy ion beams. This will provide proton and deuteron beams of up to 40 MeV and heavy ion beams (lithium to sulfur) of 10-20 MeV/nucleon. Beams of heavier ions (calcium to zinc) will be available at 5-10 MeV/nucleon. These energy domains will provide access to a field rich in opportunities for the exploration and investigation of nuclear phenomena.

6. **For the period FY 1981 - FY 1985, please provide actual and estimated budget profiles for operations, in-house research, out-of-house research, other operating expenses, Capital Equipment, General Plant Projects, In-House Energy Management, and any other specific construction projects attributable to the facility. Please indicate the source of these funds (i.e., Medium Energy Nuclear Physics, Heavy Ion Nuclear Physics, Low Energy Nuclear Physics, High Energy Physics, Basic Energy Sciences, etc.).**

Answer:

University of Washington Tandem
(B/A in thousands of dollars)

	FY 1981	FY 1982	FY 1983	FY 1984	FY 1985
Accelerator Operations					
Heavy Ion Nuclear Physics	$ 120	$ 125	$ 245	$ 325	$ 315
Low Energy Nuclear Physics	275	300	365	390	405
Total	$ 395	$ 425	$ 610	$ 715	$ 720
In-House Research					
Heavy Ion Nuclear Physics	$ 395	$ 417	$ 251	$ 356	$ 316
Low Energy Nuclear Physics	450	1,039*	603	645	670
Total	$ 845	$1,456	$ 854	$1,001	$ 986
Out-of-House Research					
Medium Energy Nuclear Physics	$ 135	$ 115	$ 125	$ 105	$ 65
Heavy Ion Nuclear Physics	15	33	54	44	44
Total	$ 150	$ 148	$ 179	$ 149	$ 109
Construction					
Nuclear Physics	$ 0	$ 0	$ 0	$4,000	$4,000

* Includes $548,000 for a polarized ion source.

7. How much funding for FY 1981 - FY 1985 has been or is expected to be provided by other federal agencies such as the National Science Foundation or by State agencies?

Answer: No direct support was received from Federal agencies other than the Department of Energy. The following table gives State of Washington support, including support provided for the superconducting booster project in FY 1984 and FY 1985.

Nuclear Physics Laboratory State Funding
(dollars in thousands)

	FY 1981	FY 1982	FY 1983	FY 1984	FY 1985
State of Washington	$ 251	$ 340	$ 326	$ 648	$ 706

8. For the period FY 1981 - FY 1985, please provide actual and estimated staffing levels.

Answer:

Nuclear Physics Laboratory Staffing Levels

	FY 1981	FY 1982	FY 1983	FY 1984	FY 1985
Total Full Time Equivalents	45	42	46	47*	49*

* Includes staff working on superconducting booster project.

9. **What is the actual and estimated facility utilization for the period FY 1981 - FY 1985? What would be defined as "full" utilization of the facility?**

Answer: For the period FY 1981 - FY 1985, actual and estimated utilization of the University of Washington tandem accelerator facility is given in the following table.

University of Washington
Tandem Utilization

	FY 1981	FY 1982	FY 1983	FY 1984	FY 1985
Beam Hours for Research	4,620	4,270	3,780	4,200	3,500

For the tandem facility, we estimate full utilization to be 7,000 beam hours for research per year.

10. **For the period FY 1981 - FY 1985, how many experiments will have been started, continued, and completed?**

Answer:

University of Washington

	FY 1981	FY 1982	FY 1983	FY 1984	FY 1985
Experiments started	28	29	30	28	26
Experiments continued	20	15	16	18	16
Experiments completed	24	26	27	27	25
Total	72	70	73	73	67

11. **What is this facility's user policy?**

Answer: Collaborative users (that is, scientists collaborating with Nuclear Physics Laboratory staff) are treated essentially the same as in-house users. They receive the same priority for beam time, technical support, and computer time as in-house users and are not charged for these services. They are also provided office space if needed and if available. Collaborative users may be asked to contribute to the financial support of their projects.

12. **For the period FY 1981 - FY 1985, how much reimbursable research has taken place or is estimated to take place? What revenues have been involved?**

Answer: None.

13. **What is the mechanism by which specific research proposals for experiments at the facility are considered?**

Answer: Research proposals from in-house users and collaborative users are submitted for approval to either the Accelerator Scheduling Committee, the Laboratory Director, or the Laboratory Faculty Committee, depending on the size of the time and financial commitment required from the Laboratory.

In each case, proposals are evaluated on whether or not the project is appropriate for the facilities of the Laboratory and whether or not the proposer is likely to be able to complete the project successfully.

14. **How many research proposals have been submitted over the past five years, and how many of these have been approved?**

    Answer: Approximately 150 research proposals have been submitted. All have been approved, occasionally after some modification of the proposal.

15. **How many university personnel (i.e., faculty and students) have utilized the facility over the past five years?**

    Answer: Over the past 5 years, 25 faculty (including a postdoctoral research associate) and 22 graduate students from the University of Washington Physics and Chemistry Departments utilized the Nuclear Physics Laboratory. Fourteen other University of Washington faculty and graduate students and nine other faculty and graduate students from other universities also utilized the facility.

16. **How many industrial researchers have utilized the facility over the past five years?**

    Answer: Over the past 5 years, 20 industrial researchers have used the facility.

17. **How many researchers from foreign institutions have utilized the facility over the past five years?**

    Answer: Over the past 5 years, 14 researchers from foreign institutions used the facility.

18. **How many researchers from other agencies have utilized the facility over the past five years?**

    Answer: None.

19. **What are the future development possibilities for this facility (including research instrumentation/experimental devices), what plans are being made to exploit these possibilities, and what are the budgetary implications?**

    Answer: There are many potential future development possibilities for this accelerator facility, but there are currently no approved plans to undertake any of them beyond the activities identified in the FY 1985 budget request. New research instruments and experimental devices will be developed as the physics research program progresses. We intend to give high priority to the exploitation of the facility's unique capabilities.

20. **Please provide a copy of the facility's latest annual report.**

    Answer: Attached is a copy of the "Annual Report 1984" from the Nuclear Physics Laboratory of the University of Washington.

ANNUAL REPORT

Nuclear Physics Laboratory
University of Washington
April, 1984

Supported in part by the United States Department of Energy
under contract DE-AC06-81ER40048

INTRODUCTION

This Report summarizes all work during the year ending in April, 1984 done in the Nuclear Physics Laboratory or by our staff at other research institutions. Most staff projects are supported by the Laboratory's Department of Energy contract, two major projects are supported in part by the Murdock Charitable Trust, and outside users receive support from a variety of sources.

The big news this year is certainly the start of the booster LINAC project. Money began to flow late in 1983. In April, 1984, after a little suspense, our low-β prototype resonator was successfully tested at Stony Brook signalling the start of full-scale production for the low-β portion of the LINAC. Construction noise, concrete dust and new staff members are increasingly in evidence as production deadlines begin to loom on the horizon.

The saga of the new polarized ion source has entered another chapter with receipt of existing hardware from Auckland in October. This followed efforts over the summer, first to negotiate a new contract with ANAC (in receivership), and when that failed, to legally secure our property and ship it to Seattle. Remaining construction and assembly are now well underway.

In the field of nuclear astrophysics we note that recent measurements made here seem to eliminate both s- and r-process flow through $^{180}Hf^{m}$ as possible sources for nucleosynthesis of $^{180}Ta^{m}$. So there remains a puzzle: Where does the observed $^{180}Ta^{m}$ come from?

We have made careful measurements of certain isospin-forbidden Fermi β decays in order to test new shell-model codes which employ much larger bases for calculation. When the accuracy of the calculation is not dominated by use of a restricted basis, such decays provide very sensitive tests of the charge-dependent interaction.

We have greatly expanded our program to understand giant dipole resonances built on excited nuclear states (e.s.-GDR). We have confirmed in detail in (p,γ) reactions the simple one-step semidirect GDR excitation mechanism which populates the same residual states made in proton stripping. Our statistical GDR decay studies of C + C and C + O provide new information on compound nuclear isospin mixing in light nuclei. Some of our statistical studies in the mass-60 region have revealed a new puzzle-namely, that the average e.s.-GDR decay strength required is only a fraction of the classical dipole sum rule. And, we are very excited to observe splitting of the e.s.-GDR in alpha plus samarium, providing indication of the persistence of nuclear deformation at elevated temperature.

We have initiated a new program to look for isovector quadrupole and higher multipolarity giant resonances with the (γ,n) reaction. This complements our previous (n,γ) work and offers a particularly clean way to observe the collective excitations free of masking direct-reaction effects.

Using the mass asymmetry of sequential fission fragments we have determined the division of excitation energy in partially damped collisions between heavy ions. In contrast to earlier results with other methods we find that the excitation energy is divided almost equally between the two fragments rather than according to the mass ratio. This means that the collision time is shorter than the thermalization time.

In the area of heavy ion collisions at intermediate energies we have identified a new mode of dissociation for the heavy-ion projectile - the decay of the relatively light excited nucleus into multiple heavy fragments, with a probability higher than previously expected.

Development work continues on hardware for the ^{14}N nuclear parity mixing experiment. This experiment is sensitive to $\Delta I=0$ mixing between $I=1$, 0^+ and 0^- levels in ^{14}N near $E_x = 8.7$ MeV. The longitudinal analyzing power A_L for elastic proton scattering is measured over the narrow 0^+ level. To date the beam line hardware and electronic systems are complete. Systematic asymmetries with unpolarized beam are less than a statistical upper limit of 8×10^{-6}. We are continuing to study systematics and refine our beam stabilization system while awaiting installation of the new polarized ion source.

A new solenoid for the hydrogen atom parity experiment has required very accurate physical measurements and careful assembly this year to insure our required $1/10^5$ field homogeneity. The new magnet plus better vacuum and gold-plated rf cavities should, we expect, bring our systematic errors down by a factor of 100.

It is generally accepted that inelastic pion scattering from nuclei proceeds mainly via single scattering from constituent nucleons. In order to study the departures from free pion-nucleon scattering caused by the nuclear medium we have compared spectra for the four lightest target nuclei and find that, even in the simplest composite systems, there are some fairly complicated medium effects.

A new NMR-controlled isotope switching system has allowed us to measure the ^{14}C distribution across a single Sitka spruce tree ring and show a definite correlation with the ^{14}C atmospheric abundance history of that year, 1963, when nuclear weapons testing was at its peak.

One of our biggest outside user programs was terminated in February. The Fast Neutron Radiotherapy Program has moved to its own quarters in the University Medical Center and is preparing to begin patient therapy with its own new cyclotron. A very interesting and novel outside user program carried out this year has been a study of cosmic-ray induced integrated circuit bit errors simulated by charge deposition by fast heavy ions passing through integrated circuits.

Our data acquisition and analysis systems continue to proliferate in greed and flexibility, both because of creative in-house hardware and software development and also because of extensive software exchange with other

laboratories, thanks to increasing world-wide hardware compatibility.

We close this introduction with a reminder that the articles in this report describe work in progress and are not to be regarded as publications or quoted without permission of the investigators. In each article the names of the investigators have been listed alphabetically, but where appropriate the names of those primarily responsible for the report have been underlined.

As always, we welcome applications from outsiders for the use of our facilities. As a convenient reference for potential users, the table on the following page lists the vital statistics of our accelerators. For further information please write or telephone Dr. W.G. Weitkamp, Technical Director, Nuclear Physics Laboratory, University of Washington, Seattle, WA 98195; (206) 543-4080.

The editors are grateful to Barbara Fulton for keeping this project together in the face of many new demands, and to Maria Ramirez who, among many other things, made sure the figures figured.

Thomas A. Trainor
Scientific Editor

William G. Weitkamp
Technical Editor

THREE STAGE TANDEM VAN DE GRAAFF ACCELERATOR

A High Voltage Engineering Corp. Model FN purchased in 1966 with NSF funds; operation funded primarily by the U.S. Department of Energy. See W.G. Weitkamp and F.H. Schmidt, "The University of Washington Three Stage Van de Graaff Accelerator," Nucl. Instrum. Meth. 122, 65 (1974).

Available Energy Analyzed Beams:

Ion	Max. Current 2 Stage (pμA)	Max. Practical Energy 2 Stage (MeV)	Max. Current 3 Stage (pμA)	Max. Practical Energy 3 Stage (MeV)
p,d	20	18	5	24
polarized p,d	0.1	18		
He	1.5	27		
Li	0.2	36		
C	1.8	63		
N	0.2	62	0.2	67
O	1	72	0.5	78
Si	0.1	90		
Cl	0.2	90	0.02	114
Ni	0.005	99		
Br	0.05	108		
Ag	0.001	108		

60-INCH CYCLOTRON

A fixed energy cyclotron constructed in 1950-52 with State of Washington funds; operated with income from outside users. See F.H. Schmidt, G.W. Farwell, J.E. Henderson, T.J. Morgan, and J.F. Streib, "The University of Washington Sixty-Inch Cyclotron," Rev. Sci. Instrum. 25, 499 (1954).

Available Target Box Beams:

Ion	Maximum Current (μA)	Energy (MeV)
p	100	11
d	150	22
^{4}He	30	42

1. ASTROPHYSICS AND COSMOLOGY

1.1 Alpha-Particle Cross Sections Relevant to Gamma-Ray Astronomy

D. Bodansky, P. Dyer,* D.D. Leach, E.B. Norman, and A.G. Seamster

The analysis of gamma-ray production cross sections for alpha-particle induced reactions[1] on light nuclei (^{12}C, ^{14}N, and ^{16}O) is nearing completion. The cross section for production of the 4.44-MeV line in (α,α') reactions on ^{12}C is found to exceed 200 mb for incident energies from E_α = 10 Mev to the maximum energy studied, E_α = 27 Mev, and exceeds 400 mb at some points. These cross sections are somewhat greater than those for producing the 4.44-MeV line in (p,p') reactions on ^{12}C.[2] Similarly the cross sections for the production of the 1.63-MeV and 2.31-MeV lines in (α,α') reactions on ^{14}N slightly exceed those for the corresponding (p,p') lines.[2]

The analysis of the cross sections for alpha-particle induced reactions on heavier abundant nuclei (^{20}Ne, ^{24}Mg, ^{27}Al, ^{28}Si, and ^{56}Fe) has been completed.[3]

References:

* Los Alamos National Laboratory, Los Alamos, NM 87545.

1. Nuclear Physics Laboratory Annual Report, University of Washington (1983) p. 4.
2. P. Dyer, D. Bodansky, A.G. Seamster, E.B. Norman, and D.R. Maxson, Phys. Rev. C 23, 1865 (1981).
3. A.G. Seamster, E.B. Norman, D.D. Leach, P. Dyer, and D. Bodansky, Phys. Rev. C 29, 394 (1984).

*****

1.2 Gamma-Ray Lines from SS433.

D. Bodansky and E.B. Norman

The interpretation of observed gamma-ray lines from the astronomical source SS433[1] was examined in the light of gamma-ray production cross sections measured at the University of Washington[2] and elsewhere.[3] It had been initially suggested by Lamb et al.[4] that the observed lines were the blue- and red-shifted components of the 1.369-MeV line from the ^{24}Mg(p,p')^{24}Mg reaction between ^{24}Mg nuclei in the jet of SS433, moving at a speed equivalent to 33 MeV per nucleon, and ambient protons. However, this explanation implied that the shifted components of the doublet at 1.64 MeV from the ^{24}Mg(p,pα)^{20}Ne and ^{24}Mg(p,2p)^{23}Na reactions should be seen with nearly the same intensity.[4] The apparent absence of these lines argued against the original simple interpretation.

It has been subsequently proposed by Ramaty, Kozlovsky, and Lingenfelter[5] that the 1.369-MeV line could be produced by a combination of the $^{24}Mg(p,p')^{24}Mg$ and $^{28}Si(p,p\alpha)^{24}Mg$ reactions taking place in collisions between grains in the jet and ambient protons. The addition of the $^{28}Si(p,p\alpha)^{24}Mg$ somewhat relieves the constraint imposed by the upper limit on the observed flux for the 1.64-MeV line but suggests the presence of the 1.779-Mev line from ^{28}Si at slightly reduced intensity. A test of the model of Ramaty et al.[5] can in principle be provided by further examination of the gamma-ray spectra from SS433. The uncertainties in this test would be reduced were measured cross sections available for gamma-ray production at 33 Mev per nucleon, but at present it is still necessary to rely largely on extrapolations from data near 24 Mev.

References:

1. R.C. Lamb, J.C. Ling, W.A. Mahoney, G.R. Riegler, W.A. Wheaton, and A.S. Jacobson, Nature 305, 37 (1983).
2. P. Dyer, D. Bodansky, A.G. Seamster, E.B. Norman, and D.R. Maxson, Phys. Rev. C 23, 1865 (1981).
3. W. Zobel, F.C. Maienschein, J.H. Todd, and G.T. Chapman, Nucl. Sci. Eng. 32, 392 (1968).
4. E.B. Norman and D. Bodansky, Nature 308, 212 (1984).
5. R. Ramaty, B. Kozlovsky, and R.E. Lingenfelter, preprint (1984).

*****

1.3 Searches for $\beta^+\beta^+$, β^+/EC and EC/EC Decays

M.A. Nelson and E.B. Norman

As described in last year's Annual Report,[1] we have begun a search for $\beta^+\beta^+$, β^+/EC, and EC/EC decays using a 4π NaI detector system. In an attempt to reduce the background counting rate due to cosmic rays, we installed a large plastic scintillator veto paddle above the detector. However, this was found to produce no observable decrease in the background rate. Thus it appears that the origin of our background must be radioactive impurities in the detector itself and in the shielding material. For the immediate future, in order to obtain greater sensitivity for detecting $\beta^+\beta^+$, β^+/EC, and EC/EC decays we simply plan to count for long periods of time.

Reference:

1. Nuclear Physics Laboratory Annual Report, University of Washington (1983) p. 36.

*****

1.4 Search for ^{92}Nb in Nature

E.B. Norman

Apt et al.[1] have reported the observation of the $t_{1/2} = 3.5 \times 10^7$ year ^{92}Nb in a sample of natural niobium. Although the inferred abundance ratio of ^{92}Nb/^{93}Nb is only 2×10^{-13}, it is far larger than can be accounted for by any conventional nucleosynthetic process. Because of the difficulty in accounting for the presence of ^{92}Nb in terrestrial material, it was felt that a remeasurement of ^{92}Nb abundance should be performed. To do so, two ~1 kg samples of Nb were acquired. Using the 4π NaI detector system at the UW Laboratory for Radiation Ecology, searches are currently being made for the 561- and 935-keV γ rays known to be emitted in the decay of ^{92}Nb. To date, no positive evidence of these two γ rays has been observed.

Reference:

1. K.E. Apt et al., Geochim. Cosmochim. Acta 38, 1485 (1974).

*****

1.5 Equilibration of ^{176}Lu^{g,m} Under Stellar Conditions

T. Bertram, S. Gil, S.E. Kellogg, E.B. Norman, and P. Wong

As discussed in previous Annual Reports,[1] we are studying processes that can occur in stellar environments by which ^{176}Lu^g and ^{176}Lu^m could come into thermal equilibrium. From our observation of the photoactivation of ^{176}Lu^g - ^{176}Lu^m using a large ^{60}Co γ-ray source, we have found that in environments in which the temperature is $\geq 4 \times 10^8$ °K photoexcitation alone guarantees thermal equilibrium. By including the effects of positron-annihilation-excitation we find that even at the canonical s-process temperature of 3.5×10^8 °K ^{176}Lu^{g,m} are in equilibrium. Thus ^{176}Lu is probably not a reliable cosmochronometer but instead may be useful as a stellar thermometer.

Reference:

1. Nuclear Physics Laboratory Annual Report, University of Washington (1983) p. 2; ibid. (1982) p. 3.

*****

1.6 Nucleosynthesis of ^{180}Ta^m

S.E. Kellogg and E.B. Norman

Our interest in the nucleosynthetic mechanism responsible for the production of the naturally occurring isomer, ^{180}Ta^m continues unabated. Beer and Ward[1] suggested that ^{180}Ta^m may in fact be produced in stars by the

standard s and/or r neutron capture processes through the fractional β decay, f_β, of 5.5 hr $^{180}Hf^m$ directly to $^{180}Ta^m$. As described in last year's Annual Report,[2] we have been using a VETO technique to suppress the dominant and rich spectrum of conversion electrons which masks the 204 keV endpoint β continuum. We successfully suppressed contaminant β decays from ^{181}Hf by introducing a 50 usec software delay in the MBD code to allow an 18 usec level in ^{181}Ta to γ decay and be eligible for vetoing (see Sec. 12.1). Our new limit, $f_\beta \leq 0.6\%$, implies that the s process alone is insufficient by a factor of 5 in explaining the observed $^{180}Ta^m$ abundance.

We also searched for β decays to excited states above the long-lived isomer by replacing our e^- detector with a high-resolution GeLi detector and looking for single γ events in our VETO arrangement. Our observation of a 100.8 keV γ ray following a 2×10^{-4} β-decay branch of $^{180}Hf^m$, though too small to be astrophysically important, nevertheless represents the first observed gamma transition that feeds the long-lived isomer in ^{180}Ta. Log-ft considerations lead us to conclude that the nuclear structure of the Hf isomer is principally that of a broken proton pair ($9/2^-[514] + 7/2^+[404]$). Further, we verify Naumann's[3] objection to Warde's[4] placement of the low-lying 7^- level in ^{180}Ta.

Beer and Ward identified the possibility of an r-process contribution through the fractional β decay, f_{m} of 5.7 min ^{180}Lu to $^{180}Hf^m$. We repeated our radiochemical separation of ^{180}Lu from a cyclotron activated Hf sample described in last year's Annual Report. We increased our sensitivity by using ^{181}Hf as a radiochemical tracer and have established a firm upper limit of $f_m \leq 0.06\%$. If we exclude the possible existence of a high-spin short-lived isomer in ^{180}Lu, less than 10% of the observed abundance of $^{180}Ta^m$ can be produced through the r process.

While our work virtually closes the s- and r-process paths through $^{180}Hf^m$, recently Yokoi and Takahashi[5] suggested that a tiny s-process branch proceeding through ^{179}Ta may be the preferred route for the stellar production of $^{180}Ta^m$. If $^{180}Ta^m$ is to be produced in a hot star, then possible destruction mechanisms must be considered. We established limits on the photodeactivation cross section of $^{180}Ta^m$ to 8.1 hr $^{180}Ta^g$ by exposing natural Ta foils to kilocurie strength hospital sources of ^{137}Cs and ^{60}Co γ rays. A paper based on this work and describing the effects of stellar temperatures and densities on the destruction rates of $^{180}Ta^{g,m}$ has been accepted for publication.

References:

1. H. Beer and R. Ward, Nature 291, 308 (1981).
2. Nuclear Physics Laboratory Annual Report, University of Washington (1983) p. 1.
3. R. Dewberry and R. Naumann, Phys. Rev. C 28, 2259 (1983).
4. E. Warde et al., Phys. Rev. C 27, 98 (1983).
5. K. Yokoi and K. Takahashi, Nature 305, 198 (1983).

2. NUCLEAR STRUCTURE

2.1 The β^+ Decays of ^{34}Ar, ^{34}Cl and ^{38}K

E.G. Adelberger, J.L. Osborne, H.E. Swanson, and V.J. Zeps

We have performed a series of preliminary experiments using the gas-transfer system to investigate the feasibility of measuring weak branches in the β^+ decays of ^{34}Ar, ^{34}Cl and ^{38}K. As in previous experiments,[1] the activities of interest were produced by bombarding a gas target and transporting the gas to a well shielded counting station where the decay γ rays were counted by a large GeLi detector. A 2.5-cm lead 'hardener' was placed in front of the detector to reduce the counting rate of annihilation radiation relative to the more energetic beta-delayed γ rays. The 0.845s ^{34}Ar activity was produced by the ^{32}S(^{3}He,n) reaction on H_2S gas at a bombarding energy of 14.5 MeV. At the same time, the 1.526s positron decay of the daughter nucleus, ^{34}Cl was also investigated. The 3^+ ground state of ^{38}K and its 0^+ isomer, the analogue of the ground state of ^{38}Ar, were produced by the reaction ^{35}Cl(α,n) at a bombarding energy of 11 MeV, using Freon-11 ($CFCl_3$) as the target gas.

These decays are of interest for several reasons. Recent $0\hbar\omega$ shell model calculations in a complete $(2s\text{-}1d)^n$ space predict the M(GT) values for most of these decay branches.[2] In general, the theory does extremely well in reproducing the observed ft values for all but the weakest transitions. The largest discrepancy between the calculated values and experimental data for any strong Gamow-Teller transition in the 2s-1d shell occurs in the decay of ^{34}Ar to the 3128 keV state in ^{34}Cl, for which the measured branch is nearly twice the calculated value. We therefore felt it would be interesting to check the experimental branching ratio. In the short preliminary runs we were able to identify all of the previously known branches from these positron decays. With a few days of data collection it should be possible to improve the statistical accuracy of these ratios branching and to extend the search to other allowed decay channels.

In the ^{34}Ar and ^{34}Cl decays and in the decay of the 0^+ isomer in ^{38}K, there is the possibility of observing isospin-forbidden T=1 → T=1, $0^+ \rightarrow 0^+$ Fermi transitions. Superallowed $0^+ \rightarrow 0^+$ decays in light nuclei have been used to measure the vector coupling constant, but charge-dependent mixing alters these analogue states and necessitates small theoretical corrections. The $0^+ \rightarrow 0^+$, T=1 → T=1 isospin-forbidden decays proceed only through charge-dependent mixing and thereby provide a stringent test of the calculations of charge-dependent corrections. To date, the only decay of this type that has been observed is in ^{42}Sc.[3] However, it is difficult to do a good shell model calculation of the expected effects in A = 42. B.A. Brown[4] has developed a shell model treatment of charge dependent mixing in the 2s-1d shell using the known mass splitting of isobaric multiplets to fix the parameters of the charge-dependent interaction. With these fitted charge-dependent matrix elements, Brown predicts that the T=1 → T=1 forbidden Fermi transitions in ^{34}Cl or ^{34}Ar should have branchings ratio of $<10^{-7}$. Unreasonable increases in running time or decreases in γ-ray background would be needed to detect such a

small branch.

Finally, in the decay of ^{38}K there is a first-forbidden $3^+ - 3^-$ transition to the 3810 keV state in ^{38}Ar. Using the prescription of Wilkinson and Macefield[5] to calculate f(E), and assuming a log(ft) value similar to that measured for the $0^+ - 0^-$ branch in ^{18}Ne,[6] we may roughly estimate a branching ratio of 10^{-4} for this transition. This should be detectable.

References:

1. Nuclear Physics Laboratory Annual Report, University of Washington (1981) p. 201.
2. B.A. Brown and B.H. Wildenthal, to be published in At. Data and Nucl. Data Tables.
3. P.D. Ingalls, J.C. Overley, and H.S. Wilson, Nucl. Phys. A 293, 117 (1977)
4. B.A. Brown, Bull. Am. Phys. Soc. 29, 678 (1984).
5. D.H. Wilkinson and B.E.F. Macefield, Nucl. Phys. A 232, 58 (1974).
6. E.G. Adelberger, C.D. Hoyle, H.E. Swanson, and R.D. Von Lintig, Phys. Rev. Lett. 46, 695 (1981).

3. GIANT RESONANCES

3.1 Schematic Model Calculations of Nucleon Decay Strengths from Giant Dipole Resonances Built on Excited States

J.A. Behr and K.A. Snover

A simple relation between experimental (p,γ) giant dipole resonance integrated strengths and spectroscopic factors from proton stripping reactions has been noted.[1] This relation has been explained within the context of an independent-particle direct emission model; it also follows from the simple schematic model of the GDR in the limit of equal decay penetrabilities for all decay channels.[2] We have now used the schematic model to calculate nucleon decay branching ratios to various excited states following photoexcitation of the GDR; the effects of Coulomb plus centrifugal barrier penetration have now been explicitly included.

The schematic model, in the extreme limit in which we employ it, treats the GDR as a sum of 1p-1h dipole excitations in a harmonic oscillator basis. We identify residual configurations produced by nucleon decay of these 1p-1h excitations directly with excited states in the daughter nucleus. Escape probabilities of the excited nucleons are treated using Coulomb penetrabilities in an R-matrix formalism. Branching ratios are calculated by integrating over the shape of the GDR.

Branching ratios calculated for ground-state ^{16}O and ^{28}Si (γ,nucleon) reactions have been compared with experiment. For ^{16}O, the relative branching ratios to $p_{3/2}$ and $p_{1/2}$ neutron and proton hole states are calculated correctly within experimental error. In this case, barrier penetration effects are essential; if they are not included, the model predicts far too much $p_{3/2}$ strength. For ^{28}Si, calculated decays to eight proton hole states produce fair agreement with experiment. However, the dominant branch, proton decay to the ground state of ^{27}Al, is calculated to be a factor of two too strong, independent of the details of the calculation. This over-predicted p_0 strength appears to be a clear indication of the need for a statistical component of the ground-state GDR in ^{28}Si with a relative strength (spreading width)/(total width) of about 50%.

The calculation is currently being extended to (nucleon,γ) reactions populating GDR's on excited states, where much more experimental data exist.

References:

1. D.H. Dowell, G. Feldman, K.A. Snover, A.M. Sandorfi, M.T. Collins, Phys. Rev. Lett. 50, 1191 (1983).
2. Nuclear Physics Laboratory Annual Report, University of Washington (1983) p. 18. See also "Giant Resonances Built on Highly Excited States," K.A. Snover, Proceedings of the International Symposium on Highly Excited States and Nuclear Structure, Orsay, France, Sept. 1983, Editions de Physique, to be published.

3.2 Compound Nuclear Isospin Purity and the Statistical Decay of the GDR in Light Nuclei

D.H. Dowell, G. Feldman, M.N. Harakeh, C.A. Gossett, R. Loveman, T. Murakami, J.L. Osborne, and K.A. Snover

In light self-conjugate nuclei the study of statistical excited-state GDR decays can provide a sensitive measure of compound nuclear isospin purity at moderate excitation energies. This follows from the well-known selection rule for N=Z nuclei that E1 decays must change isospin; hence an E1 decay from a T=0 state must go to a T=1 final state, and vice versa. Thus, if isospin is good, one expects an inhibition for statistical GDR decays from a T=0 entrance channel, since the density of T=1 final states at moderate excitation energies is much less than the density of T=0 states. The sensitivity to the isospin purity in such an experiment scales as the final-state level density ratio $\rho(T=0)/\rho(T=1)$, which can easily be greater than a factor of 10, making this method much more sensitive than many other types of experiments which have been previously employed. The restriction to moderate energies follows from two considerations: If the energy is too high, then 1) the level density ratio $\rho(T=0)/\rho(T=1)$, and hence the sensitivity, drops, and 2) high energy γ-ray decays from daughter nuclei become important, further washing out the effect. This limits the sensitivity to E_x (initial) $\lesssim$ 30 MeV + E_{GDR} ~50 MeV in light nuclei.

We have made two different types of measurements of these effects in the A = 24 - 28 mass region. The first is ^{12}C + ^{16}O at excitation energies similar to those studied in ^{25}Mg + ^{3}He (see last year's Annual Report[1]). Here, one directly sees the effect of isospin purity in the strong inhibition of high energy γ-ray production in ^{12}C + ^{16}O (T=0 entrance channel) relative to ^{25}Mg + ^{3}He (T=0 + T=1). The spectrum shape and a preliminary analysis for 40 MeV ^{12}C + ^{16}O are shown in Fig. 3.2-1. For E_γ > 13 MeV the yield comes

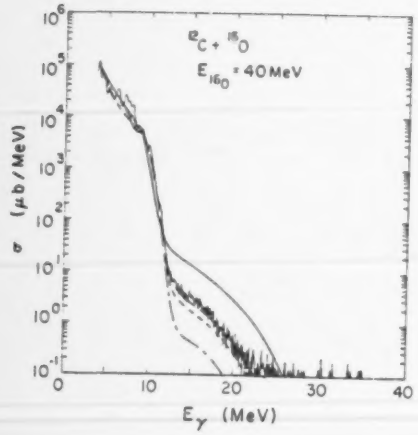

Fig. 3.2-1 Gamma rays from ^{12}C + ^{16}O, E(^{16}O) = 40 MeV, E($^{28}Si^*$) = 34 MeV. Cascade calculations: solid line - completely mixed isospin; long dash - 3% isospin mixing; short dash - pure isospin, all curves E1 + E2; long-short dash - E2 only.

mainly from the initial compound nucleus and is much less than the mixed isospin limit. However, the measured yield is somewhat larger than the pure isospin calculation, requiring about 3% isospin mixing in the initial compound nucleus. This is about five times less than other experiments have indicated for lower excitation energies.

The second type of measurement consists of comparing $^{12}C + {}^{12}C$, $^{12}C + {}^{13}C$ and $^{13}C + {}^{13}C$ reaction yields. The latter two reactions lead to N≠Z compound nuclei and hence have "normal" γ-ray yields, whereas high energy γ-ray yields from $^{12}C + {}^{12}C$ are again observed to be strongly inhibited. Spectrum shape analyses for all of these reactions, including $^{12}C + {}^{16}O$ and $^{25}Mg + {}^{3}He$, lead to similar GDR energies and widths. Quantitative analysis of the C + C data is complicated by the presence of strong individual lines at low (E_γ ~ 4-7 MeV) gamma ray energy. Preliminary fits indicate somewhat less isospin inhibition for $^{12}C + {}^{12}C$ than for $^{12}C + {}^{16}O$, but this conclusion is sensitive to details of the statistical analysis. Final analysis for the various isotopes is in progress including all the effects of individual level densities, GDR parameters and isospin mixing in a proper, self-consistent manner.

References:

1. Nuclear Physics Laboratory Annual Report, University of Washington (1983) p. 16.

*****

3.3 Statistical GDR Decays over a Wide Range of Energy from the $^{63}Cu^*$ Compound Nucleus

E.F. Garman, J. Gundlach, G. Feldman, M.N. Harakeh, J.A. Behr, J.L. Osborne, and K.A. Snover

As a follow-up investigation of statistical GDR emission from highly excited states in medium mass nuclei,[1] we have made a study of $^{63}Cu^*$ over a wide range of excitation energy. We have formed this compound nucleus via $\alpha + {}^{59}Co$ for a range of different initial excitation energies E_x = 16.9 to 28.2 MeV, and via $^{12}C + {}^{51}V$ for E_x = 34.7 to 52.3 MeV.

The experiments were performed using pulsed ^{4}He and ^{12}C beams, which permitted the direct measurement of the inclusive γ-ray production cross section. Neutron-induced events from the target were eliminated by time-of-flight (time resolution was 3-4 nsec). And γ-rays were detected in the large NaI spectrometer. All spectra have an apparently statistical shape, with an exponentially falling intensity between 6 and 10 MeV and a broad bump in the region of the GDR (E_γ ~ 10-20 MeV).

The data have been fitted to obtain the GDR strength function using a modified version of the statistical code Cascade. The excitation energy,

width and strength of the GDR were extracted, the GDR being parameterized as a Lorentzian. Preliminary results indicate a confirmation of the small (~5-10%) downward shift in the resonance energy of the excited-state GDR decays, as compared to the ground-state GDR. Also apparent is the surprising feature that the excited state GDR strength is significantly less than one Energy Weighted Sum Rule (EWSR). In this mass region the ground state GDR is known experimentally to exhaust approximately one EWSR. The reduced strength for the excited state GDR decays depends quantitatively on knowledge of the accuracy of the Cascade description of the statistical process. This is confirmed in detail by the data of Parker *et al.*[2] This puzzling strength reduction is not understood.

Reference:

1. E.F. Garman, K.A. Snover, S.H. Chew, S.K.B. Hesmondhalgh, W.N. Catford, and P.M. Walker, Phys. Rev. C 28, 2554 (1983).
2. D. Parker, J. Asher, T.W. Conlon, and I. Naqib, Harwell Internal Report AERE-R-10408 and private communication.

*****

3.4 Statistical GDR Decays in ^{16}O + Ni for Various Ni Isotopes

E.F. Garman, J. Gundlach, G. Feldman, M.N. Harakeh, J.A. Behr, J.L. Osborne, and K.A. Snover

In addition to studying $^{63}Cu^*$ decays over a wide excitation energy range, as described in the preceeding section of this report, we are also examining the inclusive γ-ray production cross section for ^{16}O + ^{x}Ni - induced reactions over a wide range of nickel isotope number (x = 58 to 64). Results have been obtained to date for 60-MeV ^{16}O + $^{58,61,64}Ni$. Preliminary Cascade fits to the ^{61}Ni and ^{64}Ni data indicate similar GDR parameters: GDR resonance energies $E_G \cong 15.5$ MeV, widths $\Gamma \cong 5.5$ MeV and strengths $S_{E1} \cong 0.33$ in units of the classical dipole sum rule. The resonance energies are similar to, and the widths somewhat narrower than the ^{16}O + ^{58}Ni results previously reported.[1] This pulsed-beam singles experiment, in contrast to the previous coincidence experiment,[1] has a well-determined absolute cross section, and thus is sensitive to S_{E1}, the average GDR strength built on excited states. These results, as with the $^{63}Cu^*$ study (see Sec. 3.3), indicate a surprisingly small value for S_{E1}: a typical value for ground-state GDR strength in this region is $S_{E1} \cong 1$. The accuracy of essential aspects of the Cascade calculation pertinent to extracting this strength, such as reasonable values for the fusion cross section, is substantiated by comparison with ^{16}O + Ni reaction data in the literature.

Reference:

1. E.F. Garman, K.A. Snover, S.H. Chew, S.K.B. Hesmondhalgh, W.N. Catford, and P.M. Walker, Phys. Rev. C 28, 2554 (1983).

*****

3.5 Study of Excited-State GDR's in the 1f-2p Shell Nuclei

J.A. Behr, D.H. Dowell, G. Feldman, E.F. Garman, C.A. Gossett, J. Gundlach, M.N. Harakeh, R.A. Loveman, J.L. Osborne, and K.A. Snover

An earlier study of the $^{27}Al(p,\gamma)^{28}Si^*$ reaction revealed a series of GDR's built upon excited states in ^{28}Si up to E_x^f = 14.36 MeV.[1,2] We are continuing our investigation of the properties of excited-state GDR's by studying (p,γ) reactions in the $f_{7/2}$ nuclei (A = 45-60). Our emphasis is on understanding how the (p,γ) GDR capture strength is related to the single-proton stripping spectroscopic factors $C^2S_p^+$ for states in these nuclei up to E_x^f = 8 MeV. We will also study statistical γ-ray spectra from heavy-ion fusion reactions forming the same compound system to determine the extent to which the observed (p,γ) strength comes from statistical decay of a thermally equilibrated compound nucleus.

Several targets in the $f_{7/2}$ shell were chosen to yield a combined system with interesting $C^2S_p^+$ distributions below 10 MeV, including strong, resolvable states. Data have already been obtained for the $^{45}Sc(p,\gamma)^{46}Ti^*$ and $^{51}V(p,\gamma)^{52}Cr^*$ reactions from E_p = 4-15 MeV (E_x = 14-25 MeV) at θ_γ = 90°, in addition to five-point angular distributions for E_p = 7, 11, 15 MeV. The statistical reaction $^{48}Ti(\alpha,\gamma)^{52}Cr^*$ has also been studied at E_α = 24 and 17.2 MeV (E_x = 32 and 25 MeV). We plan to extend the (p,γ) excitation functions up to E_p = 24 MeV (E_x = 34 MeV), and also possibly to study the $^{28}Si(^{18}O,\gamma)^{46}Ti^*$ statistical reaction and the $^{52}Cr(p,\gamma)^{53}Mn^*$ reaction.

Our results indicate that the γ-ray strength distribution does in fact correspond qualitatively with the proton stripping strength. An example is shown in Fig. 3.5-1 for the case of $^{51}V(p,\gamma)^{52}Cr^*$ at E_p = 8 and 15 MeV (E_x = 18.4 and 25.2 MeV). For the higher bombarding energy three distinct regions can be identified and compared to the plot of spectroscopic strength[3] -- a low-lying ℓ=3 ($f_{7/2}$) region, an intermediate ℓ=1 ($p_{3/2}$) section, and a high-lying (E_x^f > 7 MeV) mixed ℓ=1 and ℓ=3 ($p_{1/2}$ and $f_{5/2}$) region. At lower proton energies, statistical contributions are expected to be more apparent, as evidenced by the smoothly rising part below E_γ = 14 MeV in the E_p = 8 MeV

case. It is interesting to note that the observed strength in the region near E_x^f = 3.5-4.5 MeV is in excess of that expected from the spectroscopic information, again qualitatively consistent with strong statistical contributions at low E_p. Another feature present in this spectrum is the enhancement of the highest energy γ rays near E_γ = 18 MeV (close to the peak of the ground state GDR).

Analysis is proceeding on the (p,γ) data using a lineshape deconvolution technique. The states used in the fitting are taken to be those populated strongly in proton stripping. Excitation functions for the various states will be generated, and the integrated $\sigma(\gamma,p_o)$ strengths obtained from these excitation functions will serve to test microscopic schematic model calculations of semi-direct decay strengths (see Sec. 3.1 of this Report). The statistical γ-ray spectra from the heavy-ion fusion reactions are being analyzed with the compound nuclear evaporation code Cascade.

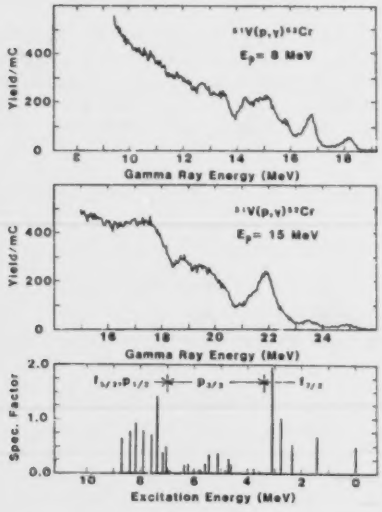

Pig. 3.5-1 Gamma-ray spectra from the $^{51}V(p,\gamma)^{52}Cr^*$ reaction at two different bombarding energies. Below is the spectroscopic strength distribution for E_x<10 MeV in ^{52}Cr obtained from the (^{3}He,d) proton stripping reaction.[3] Values shown are $[(2J_f+1)/(2J_i+1)]C^2S_p^+$. All three plots are shifted so as to align excitation energy in the vertical direction.

References:

1. D.H. Dowell, G. Feldman, K.A. Snover, A.M. Sandorfi and M.T. Collins, Phys. Rev. Lett. 50, 1191 (1983).
2. Nuclear Physics Laboratory Annual Report, University of Washington (1983) p. 17.
3. J.R. Beene, Nucl. Data Sheets 25, 235 (1978).

*****

3.6 Deformation Effects in the Statistical Decay of the Giant Dipole Resonance

J.A. Behr, G. Feldman, C.A. Gossett, T. Murakami, J.L. Osborne, and K.A. Snover

Very little is known about the degree of persistence of nuclear deformation at finite temperature. The effect of static deformation leading to a splitting of the GDR in ground-state photo-induced reactions in deformed rare earth nuclei is well-established. We have begun a study of the radiative emission of γ rays in complex particle collisions in several systems in the deformed rare-earth region. A deformation of excited nuclear states is expected to split or to broaden the GDR strength function required to account for high energy (E_γ > 10 MeV) statistical gamma-ray emission.

A measure of the effects of deformation on excited-state GDR's is obtained by comparing the gamma-ray yields from reactions in which the compound nucleus has low-lying levels which are highly deformed with those in which the compound nucleus has low lying levels which have little or no deformation. In particular, we have studied $^{12}C + ^{148}Sm$ and $^{12}C + ^{154}Sm$ for a ^{12}C incident energy of 63 MeV, in addition to $\alpha + ^{148}Sm$ and $\alpha + ^{154}Sm$ for E_α = 24 and 27 MeV. A comparison of the gamma-ray spectra measured at $\theta_\gamma = 90°$ for the alpha induced reactions is shown in Fig. 3.6-1. The additional structure observed in the high energy gamma yield for the $\alpha + ^{154}Sm$ reaction when compared to $\alpha + ^{148}Sm$ provides evidence of the splitting of the GDR strength function due to nuclear deformation at elevated nuclear temperatures. Results for the spectral shapes from the $^{12}C + ^{148}Sm$ and $^{12}C + ^{154}Sm$ reactions are currently being analyzed. Statistical model calculations from the code Cascade will be compared with the data in order to extract the energy, width and strength parameters for the GDR strength functions. These parameters will then provide quantitative information about the average deformation of excited states in the compound nucleus. Currently, we are looking for the effects of deformation on the angular distribution of emitted γ rays.

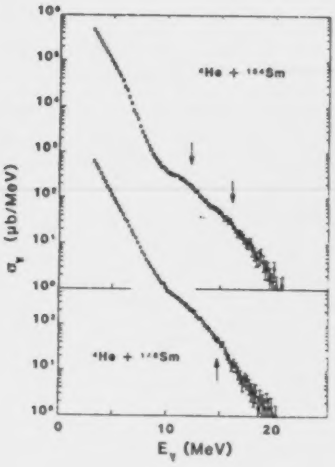

Fig. 3.6-1 Gamma-ray spectra from the α + ^{148}Sm and α + ^{154}Sm reactions for E_α = 27 MeV. Neutron backgrounds were reduced using pulsed beam techniques and the data have been corrected for small (<1% by weight) carbon and oxygen contamination. The arrows indicate the energy locations of the ground state GDR's.

*****

3.7 Excited-State Giant Resonances Observed in the ^{39}K(p,γ)^{40}Ca and ^{40}Ca(p,γ)^{41}Sc Reactions

D.H. Dowell, C.A. Gossett, L. Ricken,* A.M. Sandorfi,† and K.A. Snover

The study of excited-state giant dipole resonances using the (p,γ) reaction has become a new means of examining single-particle strength at high excitation. The nuclear configurations upon which GDR's are built in energetic (p,γ) reactions are those in which a single proton is coupled to the ground state of the target nucleus. The integrated GDR strengths, which are proportional to the proton transfer spectroscopic factors, provide quantitative information on single-particle strength at excitation energies well above those studied in conventional proton stripping reactions.

We have begun a study of excited-state giant resonances in the ^{39}K(p,γ)^{40}Ca and ^{40}Ca(p,γ)^{41}Sc reactions. The excited states upon which one expects GDR's to be built in these reactions are those of relatively simple nuclear configuration. In particular, the states populated in ^{40}Ca(p,γ)^{41}Sc are those which look like a single proton coupled to doubly magic ^{40}Ca, for example the $1f_{7/2}$, $2p_{3/2}$, $2p_{1/2}$, $1f_{5/2}$, and $1g_{9/2}$ single-proton states. States which resemble an f, p, or g proton coupled to the $d_{3/2}$ proton hole in ^{39}K are strongly populated in the ^{39}K(p,γ)^{40}Ca reaction.

We have measured ^{39}K(p,γ)^{40}Ca and ^{40}Ca(p,γ)^{41}Sc cross sections at θ_γ = 90° for E_p = 10-36 MeV using the two-stage and three-stage tandem accelerators

at Brookhaven National Laboratory. Sample gamma-ray spectra for $^{39}K(p,\gamma)^{40}Ca$ at E_p = 18 MeV and for $^{40}Ca(p,\gamma)^{41}Sc$ at E_p = 25 MeV are shown in Fig. 3.7-1. Also illustrated are the proton stripping spectroscopic factors,[1] $C^2S_p^+$. Strong correlation between the structure in the (p,γ) cross section and the distribution of stripping strength is observed. Evidence of a large concentration of single-particle strength at $E_x^f \approx 9.6$ MeV not previously observed in proton stripping is seen in the $^{39}K(p,\gamma)^{40}Ca$ data. We also find a broad concentration of strength near $E_x^f \approx 14.5$ MeV in ^{40}Ca. We observe structure in the final-state single-particle strength distribution in the $^{40}Ca(p,\gamma)^{41}Sc$ reaction up to $E_x^f \sim 10$ MeV, and evidence for excited-state GDR's built upon broad distributions of single-particle strength in ^{41}Sc up to $E_x^f \sim 23$ MeV.

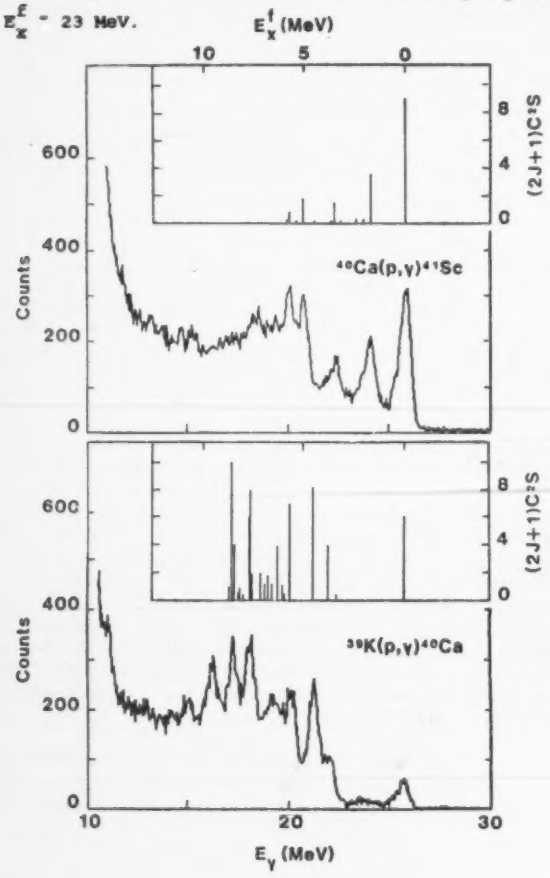

Fig. 3.7-1 Gamma-ray spectra at θ_γ = 90° from $^{39}K(p,\gamma)^{40}Ca$ for E_p = 18 MeV (E_x = 25.9 MeV) and $^{40}Ca(p,\gamma)^{41}Sc$ for E_p = 25 MeV (E_x = 25.5 MeV). Since the ground-state GDR's in ^{40}Ca and ^{41}Sc are located at excitation energies of approximately 20 MeV, one expects to be at the peak of the GDR for final states near E_x^f = 5-6 MeV at these proton energies. The distribution of proton-stripping spectroscopic strengths from Ref. 1 are displayed in the insert above each gamma-ray spectrum.

We are currently analyzing the $^{39}K(p,\gamma)^{40}Ca$ and $^{40}Ca(p,\gamma)^{41}Sc$ spectra in terms of a line-shape decomposition in order to extract (p,γ) strengths. We plan to use the GDR strengths obtained in this analysis to determine single-particle spectroscopic strengths in ^{40}Ca and ^{41}Sc up to $E_x^f \approx 20$ MeV.

References:

* Ruhr-Universität Bochum, West Germany.
† Brookhaven National Laboratory, Upton NY 11973.
1. P.M. Endt and C. Van der Leun, Nucl. Phys. A 310, 1 (1978)

*****

3.8 Forward-to-Backward Asymmetries in the (γ,n) Reactions around the E2 Isovector Giant Resonance

P.T. Debevec,* D.H. Dowell, I. Halpern†, L.J. Morford*, T. Murakami, D.W. Storm, D.R. Tieger, and S.A. Wender†

Compared with our knowledge of the isovector E1 giant resonance, that of the isovector E2 resonance is very limited. Most of the information about E2 has been obtained from inelastic electron scattering data. Because of uncertain backgrounds in the (e,e') spectra, it is desirable to confirm the suggested resonance parameters by using another method. The (γ,n) and (n,γ) reactions are virtually background-free when used to locate the E2 resonance through its interference with the tail of the E1 resonance. Recently Drake et al. found striking evidence for existence and location of the isovector E2 giant resonance, namely a sharp rise in the (n,γ_0) asymmetry in angle seen at ≈23 MeV.[1] Since there are not so many accelerators which can produce neutron beams above 20 MeV, we decided to use the inverse reaction, (γ,n), to continue the same investigation to lighter, higher-resonance-energy targets.

Experiments were performed by using the 39.4 MeV continuous electron beam from the University of Illinois microtron using a superconducting linac (MUSL-2) and the tagged photon facility. The front-to-back asymmetries $[Y(55°)-Y(125°)]/[Y(55°)+Y(125°)]$ for the (γ,n) reaction were measured in three targets as a function of photon energy between 20 and 30 MeV. The neutrons were measured by an NE-213 liquid scintillator which was 30 cm in diameter and 5.1 cm thick. The energies of neutrons were determined by measuring the time interval between the signals from the post-bremsstrahlung electron counters and the neutron detector. Applying a ≈6.5 MeV threshold for the neutron detector, we were able to reduce the number of accidental coincidences between electron and neutron counters. Possible spurious asymmetries of the system were investigated by measuring the known asymmetries of the $^{16}O(\gamma,n_0)^{15}O$ reaction. They turned out to be negligible.

The asymmetry curves for ^{208}Pb and ^{nat}Pb for residual excitations between 0 and 4 MeV in the photon energy range of 20 to 26 MeV were identical within the experimental uncertainties. As seen in Fig. 3.8-1, the asymmetries

were about 0.2 for the lower photon energies and made a transition near $E_\gamma \approx$ 23 MeV to ≈0.6 for the higher energies. For ^{nat}Cd the pattern was similar but the transition region was about 4 MeV higher, consistent with the expected $A^{-1/3}$ dependence of the locations of giant resonances. The detailed analysis of the energy dependence of the asymmetry, using the direct-semidirect model, is in progress.

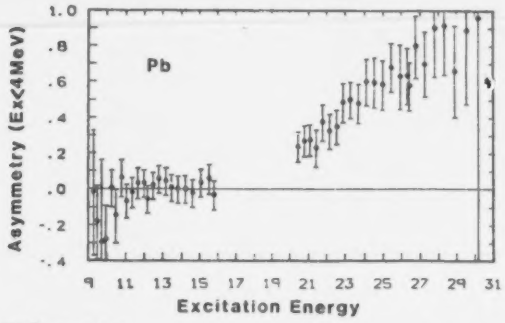

Fig. 3.8-1 Asymmetry curve for ^{nat}Pb for residual excitations between 0 and 4 MeV. The data below E_x = 16 MeV are due to Professor P.T. Debevec.

References:

* University of Illinois, Urbana, IL 61801.

† Los Alamos National Laboratory, Los Alamos, NM 87545.

1. D.M. Drake et al., Phys. Rev. Lett. 47 1581 (1981).

*****

3.9 Determination of a Time Scale for the Emission of High Energy Photons in Heavy Ion Fusion Reactions

D. Habs,* W. Hennerici,* R. Kroth,* A. Lazzarini, V. Metag,† and J.Schirmer*

Recent observations of high energy γ-rays emitted in (HI,Xn) reactions[1-6] have been interpreted as evidence for the existence of highly excited compound nuclear states in the nuclear continuum which are themselves collective excitations.[7] Central to this interpretation are several assumptions. These are that i) the high energy photons originate from electromagnetic transitions between unbound states. The high energy of the photons (10-20 MeV) and their observed emission probability (≈10^{-1}/fusion) both support this assumption. ii) the states of the compound system emitting these photons are collective giant dipole resonance excitations built upon rotational states of high spin. iii) The multipolarity of the gamma transitions is E1. Although these assumptions seem reasonable, there has been no direct experimental verification of their validity. The results of several recent studies indicate that the centroid of the γ-ray enhancement is substantially shifted from its expected value deduced from the GDR of E_γ =

$79A^{-1/3}$.[8] It is not yet clear whether such a shift arises from a change in the interaction leading to the GDR with increasing excitation in the nucleus. High energy transitions in heavy ion reactions have, to date, defied any quantitative analysis. Yet recent (p,γ) studies[9] have produced unambiguous evidence that the collective excitations of lower-lying particle-hole states in nuclei in the s-d shell do exist. It would be enlightening if similar results were found in heavy ion reactions.

The measurement was performed with an 80 MeV ^{16}O pulsed beam from the MPI Heidelberg Tandem Van de Graaff Facility, by bombarding a 400 $\mu g/cm^2$ isotopically enriched ^{58}Ni target. Coincidences were detected between the MPI-GSI 4π Crystal Ball Spectrometer and an array of 4 ΔE-E surface barrier telescopes positioned at angles θ_{lab} = 90°, 120°, 160°, each with typical solid angle $\Delta\Omega$ = 40 msr. 159 of the 162 NaI(Tl) detectors of the Crystal Ball were employed. Once the Crystal Ball trigger was registered, all coincident NaI(Tl) detectors were accepted. Particle energy and angular distributions in coincidence with γ rays detected with the MPI-GSI 4π γ-ray Spectrometer were measured, along with γ multiplicity and angular correlations.

From the particle energy spectra it is possible to estimate the time at which high energy photons are emitted during the compound-nuclear decay. In addition, the multiplicities of both charged particles and γ rays yield information from which details about the spin distribution in the compound nucleus responsible for the energetic photons could be deduced. From the various correlations we have learned the following:

i) The energy spectra of the coincident charged particles reflect the energy lost to the energetic photons. This is evidence for the time-order of the emission process, indicating that the photons are being emitted promptly from the compound system in the first or second step of the decay cascade (see Fig. 3.9-1).

ii) The proton-to-alpha multiplicity, which is a sensitive probe of initial compound nucleus spin, clearly indicates that the spins associated with the emission of energetic photons are about half the mean value of angular momentum brought into the reaction.

iii) The γ multiplicities corroborate our findings in point ii) above, and further indicate that emission of energetic γ rays produces a shift of 7 - 10 ħ in the mean spin of the population of compound nuclei producing them compared to the overall mean for the fusion reaction (see Fig. 3.9-2). Further it is possible to determine the γ-multiplicity dependence of the emission probability for energetic photons. The results are presented in Fig. 3.9-3. The integrated emission probability for E_γ > 14 MeV is 8 × 10^{-4}/fusion.

iv) Particle (observed at 90°)-γ angular correlations are isotropic within error. The isotropy is an expected result arising from the fact that transitions are not expected to be stretched for this case.

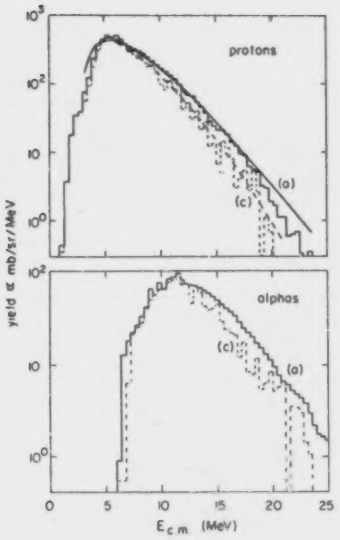

Fig. 3.9-1 Angle summed particle energy spectra in coincidence with γ rays. a) Gate on all γ. c) Gate on events for which E_γ > 14 MeV was observed. Solid curve is Cascade calculation for entire fusion cross section. Dashed curve corresponds to Cascade calculation under conditions similar to experimental gate c) above.

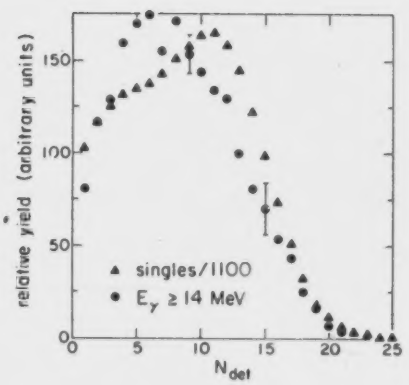

Fig. 3.9-2 γ-ray multiplicity distributions for this experiment. Singles distribution shown in triangles, coincidence with E_γ > 14 MeV shown as circles.

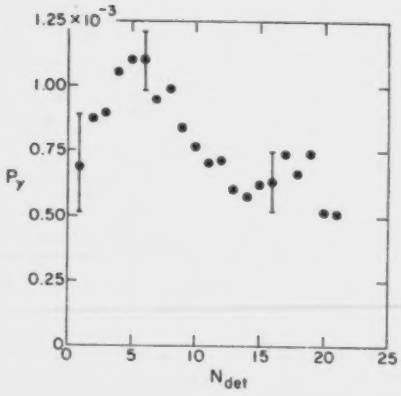

Fig. 3.9-3 Estimates of $\Gamma_\gamma / \Gamma_{tot}$ from data of Fig. 3.9-2.

References:

* Max-Planck-Institut fur Kernphysik, West Germany.

† University of Giessen, West Germany.

1. J.O. Newton, B. Herskind, R.M. Diamond, E.L. Dines, J.E. Draper, K.H. Lindenberger, C. Schück, S. Shih, and F.S. Stephens, Phys. Rev. Lett. 46, 1383 (1981).
2. J.E. Draper, J.O. Newton, L.G. Sobotka, H. Lindenberger, G.J. Wozniak, L.G. Moretto, F.S. Stephens, R.M. Diamond, and R.J. McDonald, Phys. Rev. Lett. 49, 434 (1982).
3. B. Haas, D.C. Radford, F.A. Beck, T. Byrski, C. Gehringer, J.C. Merdinger, A. Nourredine, Y. Schutz, and J.P. Vivien, Phys. Lett. 120B, 79 (1983).
4. A.M. Sandorfi, J. Barrette, M.T. Collins, D.H. Hoffmann, A.J. Kreiner, D. Branford, S.G. Steadman, and J. Wiggins, Phys. Lett., to be published; J. Barrette and A.M. Sandorfi, Comments on Nucl. Part. Phys., to be published.
5. J.J. Gaardhøje, Procoedings of the XX Winter Meeting on Nuclear Physics, Bormio, Italy, (1982).
6. H. Hennerici, V. Metag, H.J. Hennrich, R. Repnow, W. Wahl, D. Habs, K. Helmer, U.V. Helmolt, H.W. Heyng, B. Kolb, D. Pelte, D. Schwalm, R.S. Simon, and R. Albrecht, Nucl. Phys. A 396, 329c (1983).
7. D. Brink, D. Phil. Thesis, University of Oxford, 1955 (unpublished).
8. A. Bohr and B. Mottelson, Nuclear Structure (W.A. Benjamin Inc. Reading, MA, 1975), Vol. II.
9. D.H. Dowell, G. Feldman, K.A. Snover, A.M. Sandorfi, and M.T. Collins, Phys. Rev. Lett. 50, 1191 (1983).

4. HEAVY ION REACTIONS

4.1 Study of Spin-Spin Correlations in Deep Inelastic Collisions

A. Gobbi,* K. Hildenbrand,* J. Kuzminski,* A. Lazzarini, W. Müller,* A. Olmi,* H. Steltzer,* and J. Toke*

The alignment of transferred angular momentum in a deeply inelastic collision is perpendicular to the reaction plane and its magnitude has been shown to be a function of energy loss, scattering angle, and mass transfer. The degree to which these variables are interrelated is still a subject of much discussion and its answer may help to discriminate among several reaction mechanisms for the collision process. In the nucleon exchange model of Randrup and others the interrelationship is straightforward, and the conservation of linear and angular momentum relates the transferred angular momentum to both mass exchange and energy loss. On the other hand a reaction mechanism in which thermal equilbrium is achieved early in the collision and for which the observables simply reflect the thermalization of all intrinsic and accessible degrees of freedom has also had some success in describing the experimental results.

A detailed study of the nucleon exchange model indicates that not only is the transferred angular momentum aligned in a deeply inelastic collision, but also that the spins of the two fragments in such a collision remain very strongly co-aligned during the collision. In fact the co-alignment turns out in many cases to be greater than the alignment of the spin of either fragment relative to the reaction plane. These results can be traced to the conservation of angular momentum, which applies not only to the orbital component, but also to the randomly oriented component arising from the Fermi motion.

We have performed a measurement from which we can infer the spin-spin correlations in a deeply inelastic collision. We have exploited the fact that the angular distribution of fragments produced in the fission of a binary partner in a deeply inelastic collision is highly anisotropic, and that the anisotropy can be used as a tool to probe the alignment and magnitude of the spin of the fissioning system. Here we use a reaction in which both beam and projectile are fissile nuclei. In this manner the bulk of the deep inelastic yield results in final states in which both deeply inelastically scattered fragments have fissioned. The angular correlations of this four-body final state then contain information which may be related to the relative orientation of the spins of the two fragments before they fissioned. We have used the $^{208}Pb + ^{238}U$ reaction at $E_{cm} = 945$ MeV at the GSI Unilac to make our measurements. The four fragments were detected in an array of six avalanche detectors. One array consisted of two detectors on one side of the beam axis. In this manner the two correlated fragments arising from the fission of one nucleus could be observed, thus defining the mass transfer, energy loss and reaction plane for the deep inelastic collision. In addition, we sampled the mass distribution independently using three surface barrier detectors as time-of-flight telescopes. These were arranged on the periphery of the active area of one of the avalanche detectors. On the other side of the beam axis, a

matrix of four position-sensitive avalanche detectors was used to detect the pair of coincident fragments from the other nucleus. The angles of emission of the four fission fragments can be deduced, and these are the relevant quantities which are to be compared with theoretical calculations. By selecting both in-plane and out-of-plane angles on one side of the beam it is possible to observe the variations in the anisotropy of the other two fragments emitted by the other reaction partner. In this manner it is possible to determine the degree of correlation of the spins of the two deeply inelastic fragments.

Work is now in progress to analyze the experimental results.

Reference:

* GSI, Darmstadt, West Germany

*****

4.2 Nuclear Rainbow Scattering with Carbon Isotopes

H.G. Bohlen,* J.G. Cramer, B. Gebauer,* H. Michachaka,* W. von Oertzen,* and Chen Xue-shi*

The phenomenon of nuclear rainbow scattering or "far-side" scattering observed in elastic scattering with projectiles of Z = 1 - 3 has provided valuable insights into interaction potentials and light ion reaction mechanisms. Until recently there had been no evidence that projectiles with Z > 3 could exhibit such nuclear-rainbow/farside scattering effects. However, within the past two years groups at CERN[1] and at the Hahn-Meitner Institute[2] have observed the clear signature of this phenomenon in $^{12}C + ^{12}C$ scattering at laboratory bombarding energies above about 20 MeV/nucleon. It is therefore of considerable interest to determine if heavier systems can also show nuclear rainbow scattering effects.

Using the VICKSI accelerator system at the Hahn-Meitner Institute we have investigated this question for the systems $^{12}C + ^{16}O$, $^{13}C + ^{12}C$, and $^{13}C + ^{14}C$ with a ^{12}C beam at 22 and 25 MeV/nucleon and ^{13}C beam at 18 and 22 MeV/nucleon. Preliminary analysis indicates that the $^{13}C + ^{12-14}C$ systems show clear nuclear-rainbow/farside effects while the $^{12}C + ^{16}O$ system shows little evidence of this phenomenon.

References:

* Hahn-Meitner-Institue fur Kernforschung, Berlin, West Germany.

1. M. Buenerd, et al., Phys. Lett. 102B, 242 (1981).
2. H. G. Bohlen, M. R. Clover, G. Ingold, H. Lettau, and W. von Oertzen, Z. Phys. A 308, 121 (1982).

*****

4.3 Penetrability of the Centrifugal Barrier and the Spin Distribution of the Compound Nucleus

D. Abriola,* P. DeYoung,* S. Gil, A. Lazzarini, D.-K. Lock, R. McGrath,* A. Ray, and R. Vandenbosch

We have continued our studies of the penetrability of the centrifugal barrier and its effect on the spin distribution of the compound nucleus in heavy ion collisions.[1] This year we have performed a series of experiments to measure the total fusion cross section and the first moment of the gamma ray multiplicity M_γ utilizing an experimental technique previously described.[1,2] We used the systems: α, ^{12}C, ^{16}O and ^{28}Si on ^{154}Sm.

The basic motivation of this study is to test experimentally the implication that if the observed broadening of the spin distribution of the compound nucleus at near-barrier energies[2] is due primarily to the penetrability of the centrifugal barrier, then one would expect that this broadening should increase as the reduced mass of the entrance channel increases. The underlying physics of this effect can easily be seen by recalling that the effective potential V_{eff} for the entrance channel can be written as the sum of nuclear, Coulomb, and centrifugal potentials. At the effective interaction distance R_o, where V_{eff} reaches its maximum, we have the condition

$$\frac{\partial V_{eff}}{\partial \ell} = \frac{(2\ell+1)\hbar}{2\mu R_o^2}, \quad \text{where} \quad R_o = r_o\left[A_1^{1/3} + A_2^{1/3}\right]$$

As the mass of the projectile changes, μ and R_o vary. For the cases of α, ^{12}C, ^{16}O and ^{28}Si on ^{154}Sm, the values of μR_o^2 are in the ratio of 1 : 3.5 : 5 : 9 respectively. If the curvature of V_{eff} for the different systems does not change drastically at the effective interaction distance R_o the penetrability T_ℓ should show a slower variation with ℓ for heavier projectiles.

All these experiments were performed using our local facilities, except for the system $^{28}Si + ^{154}Sm$, which was measured using the superconducting booster facility of SUNY at Stony Brook. The data analysis for this experiment has not yet been completed.

The first moment of the spin distribution, the average angular momentum $\langle L \rangle$, is deduced from M_γ as discussed in Ref. 2. Since our experimental technique only allows us to measure the reaction cross section of (HI,xn) for a single residue channel xn, we have used the relative yield predicted for these reactions by the statistical decay code CASCADE[3] to estimate the total fusion cross section. This procedure was tested for the case of $^{16}O + ^{154}Sm$, where the yields are known experimentally[4] and these results are nicely reproduced within a few percent.

In order to be able to compare the results of the different systems studied on the same footing, we found it useful to introduce the concept of

ℓ_{crit} defined as

$$\sigma_{fus} = \frac{\pi}{k^2}\ell_{crit}[\ell_{crit}+1].$$

In the extreme sharp cut-off model, ℓ_{crit} would be the number of partial waves that are required to be removed from the elastic channel in order to obtain the experimental reaction cross section. Within this model one would also have $\ell_{crit} = 1.5\ \langle L\rangle$, corresponding to a triangular distribution.

In Fig. 4.3-1 we present our experimental results for the cases of α, ^{12}C and ^{16}O, together with the fits obtained using a one dimensional parabolic barrier penetration model, including deformation as discussed by Wong.[5] The error bars in ‹L› include both the uncertainties in the measured multiplicities as well as the uncertainties in converting them to angular momentum as described in Ref. 2.

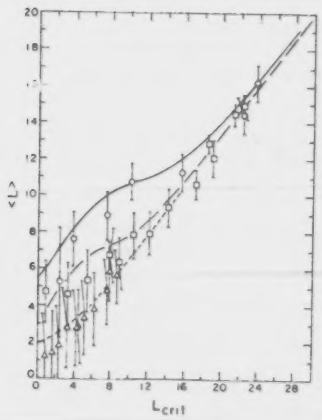

Fig. 4.3-1 ‹L› vs. ℓ_{crit} Experimental results of ‹L› and ℓ_{crit}, obtained from M_γ and σ_{fus} respectively, as described in the text. Full dots correspond to ^{16}O, squares to ^{12}C, and triangles to α. The calculations were all done using a one-dimensional parabolic barrier penetration model including deformation. The full line corresponds to ^{16}O, dashed line to ^{12}C and, dotted line to α. For the sharp cut-off model one expects ‹L› = 1.5 ℓ_{crit}.

Our results clearly reproduce the expected results, namely that the larger the mass of the projectile the larger the deviation from the extreme sharp cut-off model for a given value of ℓ_{crit}, and consequently the broader the spin distribution. Also we see that as the energy increases (and so does ℓ_{crit}), the relation between ‹L› and ℓ_{crit} tends to approach that of the sharp cut-off model.

References:

* Nuclear Structure Laboratory, SUNY Stony Brook, NY 11794.
1. Nuclear Physics Laboratory Annual Report, University of Washington (1983) p. 21.
2. R. Vandenbosh, B.B. Back, S. Gil, A. Lazzarini, and A. Ray, Phys. Rev. C 28, 1161 (1983).
3. F. Puhlhofer, Nucl. Phys. A 280, 267 (1977).
4. R.G. Stockstad, Y. Eisen, S. Kaplanis, D. Pelte, U. Smilansky, and I. Tserruya, Phys. Rev. C 21, 2427 (1980).
5. C.-Y. Wong, Phys. Rev. Lett. 31, 766 (1973).

*****

4.4 Search for High Spin States in ^{32}S

K.J. Davis, S. Gil, M. Hindi,* A. Lazzarini, K.T. Lesko, D.-K. Lock, T. Murakami, A. Ray, and R. Vandenbosch.

Continuing our effort to locate the higher members of the yrast line in ^{32}S, this year we have performed a series of experiments in order to locate the particle unbound members of the band by using a particle-particle coincidence method.

We have explored the possibility of using the following reactions for populating the unbound states in ^{32}S:

a. $^{24}Mg(^{12}C,\alpha)^{32}S$

b. $^{28}Si(^{16}O,^{12}C)^{32}S$

While the first of these reactions did not show the desired selectivity for populating discrete states in the excitation energy region of interest, $E_x \approx 10$-20 MeV, the second reaction did show a good selectivity, and therefore this reaction was chosen for our subsequent experiments.

By means of a preliminary run we found that the main decay mode of these unbound states in ^{32}S was through α emission. We also found that at least two states in ^{32}S, at $E_x = 11.0(\pm 0.4)$ MeV and $12.5(\pm 0.4)$ MeV, strongly decay to the ground state of ^{28}Si.

For the determination of the spins of these states we adopted an angular correlation method[2] which can yield a model-independent spin assignment for the intermediate state in the reaction $^{28}Si(^{16}O,^{12}C)^{32}S^*(\alpha)^{28}Si(g.s.)$. If the ^{12}C is observed along the beam axis, then the angular correlation function between the ^{12}C and α is proportional to the square of a Legendre polynomial $P_\ell(\cos\Theta)^2$, where ℓ is the angular momentum carried out by the α particle, and is equal to the spin J of the excited state in ^{32}S.

In order to observe the ^{12}C at small angles we used our momentum filter[3] (m.f.) and blocked the elastically scattered ^{16}O. For technical reason the m.f. was placed at $\Theta_{m.f.} = 4° \pm 1.5°$ rather than at 0°. A Bragg curve spectrometer[4] was placed at the end of the m.f. for detecting the ^{12}C and operated in coincidence with a position sensitive detector (p.s.d.) for detecting the α particle and its position. The p.s.d. covered an angular range between 95° and 140° (≈40° range in the c.m. system), with an angular resolution of ≈1°. This setup allowed us to detect states with spins $J \geq 5$. For lower spin states the period of the angular oscillations is larger than the angular range of the p.s.d.

The results of the α angular distribution for the states mentioned above did not show any appreciable angular structure. These results are consistent with the fact either that these states are not simple states, i.e., there may be two or more states unresolved at each of these energies, washing out the angular structure, or that these states have spin lower than ≈5, in which case the period of the angular oscillations would be too large to be detected with our set-up. This last possibility would also be consistent with the observed result that for these states, the branching ratio for the decay to the g.s. of ^{28}Si was larger than the corresponding decay to the 2^+ ($E_x = 1.78$ MeV). According to estimates obtained using transmission coefficients from an optical model calculation, this is expected to be the case for low spin states.

Summarizing the results of our studies of ^{32}S, through a particle-gamma coincidence experiment reported previously[1] we have been able to detect the gamma-decay properties of four levels at $E_x = 6.763$, 7.46, 8.3 and 8.5 MeV. The $E_x = 6.763$ MeV level was assigned $J^\pi = 5^-$, $E_x = 7.46$ MeV $J^\pi = (1^-, 2^+)$, $E_x = 8.3$ MeV $J^\pi = (6^+)$ and $E_x = 8.508$ MeV $J^\pi = (3^-, 2^+)$. Two α-unbound levels at $E_x = 11.0(\pm 0.4)$ MeV and $12.5(\pm 0.4)$ MeV are strongly populated with the reaction $^{28}Si(^{16}O, ^{12}C)^{32}S$ at $E_{lab} \simeq 70$ MeV, with an appreciable branching ratio for decay to ^{28}Si(g.s.). Our experiment did not yield a definite spin assignment for them, but suggests overlapping levels or low spin values ($J_\pi < 5$).

References:

* University of Petroleum and Minerals, Dahran, Saudi Arabia.

1. Nuclear Physics Laboratory Annual Report, University of Washington (1983) p. 23.
2. J.G. Pronko and R.A. Lindgren, Nucl. Instrum. Meth. 98, 445 (1972).
3. Nuclear Physics Laboratory Annual Report, University of Washington (1983) p. 75.
4. Nuclear Physics Laboratory Annual Report, University of Washington (1983) p. 82.

*****

4.5 A New Scheme for the Calibration of Sub-Coulomb Heavy Ion Proton Transfer Reactions

K.J. Davis, A. Lazzarini, and T. Murakami

A triad of proton transfer reactions can be used to isolate the product of a spectroscopic factor and the square of the radial wave function for the exchanged proton in the initial and final configurations. Such a set of reactions was described in last year's Annual Report.[1] Only one of those reactions proved to be feasible, so a new triad is being investigated and is shown below.

a. $^{42}Ca + {}^{15}N - {}^{41}K + {}^{16}O$

b. $^{42}Ca + {}^{27}Al - {}^{41}K + {}^{28}Si$

c. $^{27}Al + {}^{16}O - {}^{28}Si + {}^{15}N$

In each case we are planning to use the heavier nucleus as the projectile. We have performed beam development work with the sputter source and have achieved an 80 nA beam of ^{27}Al 6+ after energy analysis and a 52 nA beam of ^{40}Ca 8+. We expect similar results when isotopically enriched ^{42}Ca is used in the source.

The kinematics of these reactions is such that the sub-Coulomb transfer reactions, which are backward peaked in the center-of-mass reference frame, are forward peaked in the lab frame. We intend to use the momentum filter in the vicinity of 10 deg to remove the elastically scattered projectile particles. The Bragg curve spectrometer can be mounted at the final focus of the momentum filter and can be used for particle identification as well as energy determination. This technique has been used in preliminary experiments to investigate reaction c) near the Coulomb barrier. Our results indicate that the ^{15}N can be readily distinguished from other particles hitting the detector and that the peaks corresponding to the first and second excited states of ^{28}Si can be well resolved.

Reference:

1. Nuclear Physics Laboratory Annual Report, University of Washington (1983) p. 27.

*****

4.6 Measurement of Total Reaction Cross Sections at 15 to 35 MeV/A

J.G. Cramer, A. Lazzarini, D.D. Leach, R.A Loveman, W. Lynch,* M.Y. Tsang* and J. Van der Plecht*

We have measured the angular distribution for elastic scattering with the ^{12}C beam of the MSU Superconducting Cyclotron at 15, 25, and 35 MeV/A on

targets of ^{12}C, ^{28}Si, and ^{90}Zr. About twenty points were taken for each target energy in 0.25° to 0.5° steps starting at 1.5°. In addition, similar angular distributions were taken for gold, primarily to monitor the beam stability. From these measurements we will obtain total reaction cross sections and optical model potentials valid for this region.

At low energies the total reaction cross section σ_r for nucleus-nucleus scattering is determined primarily by average collective nuclear behavior, and σ_r is essentially geometrical. As the collision energy is increased the average nuclear behavior becomes less important and individual collisions of nucleons in the target with those in the projectile assume more importance. At the same time, the total cross section for nucleon-nucleon (n-n) scattering decreases dramatically. One can adopt the extreme view that the reaction cross section arises exclusively from scatterings involving individual nucleons in the target and projectile, and that for calculating σ_r the overall average effects can be neglected except as they modify the energies and trajectories of the nucleons in the interacting system.[1] This is essentially the optical limit of the Glauber model.[2]

The method which we have chosen to determine the total reaction cross section is an indirect one: to measure a forward angle portion of the angular distribution and to use these data to deduce σ_r and σ_t. The actual extraction of the cross section can be done in several ways: (1) by using a diffraction model generalization of the "quarter-point recipe"; (2) by employing a parameterized S-matrix analysis of the data and calculating σ_r directly from the resulting S-matrix; and (3) by fitting the data with the optical model and obtaining σ_r from the optical model S-matrix. Our estimates and those of other groups[3] indicate that a combination of these methods should permit an absolute determination of σ_r to better than 2.5%. This error is due to model dependence, and actual errors due to experimental systematics should be less than 1%. Errors in the relative values of σ_r for different energies should also be less than 1%.

The precise angle of the beam relative to the spectrometer is of critical importance in these measurements. Absolute measurement of the scattering angle was obtained by rotating the spectrometer into the beam with a scintillator protecting the detectors at the end of the spectrometer. These measurements were corroborated by cross section measurements on both sides of the measured zero degree point. The error in the absolute angle of the beam was about 0.05°. We monitored the position stability of the beam with pairs of counters mounted symmetrically right-left and above-below with respect to the beam. The monitor counters were also used for beam integration in addition to the Faraday cup.

References:

* Michigan State University, East Lansing, MI 48824.

1. R.M. DeVries and J.C. Peng, Phys. Rev. C 22, 1055 (1980); N.J. DiGiacomo, R.M. DeVries, and J.C. Peng, Phys. Rev. Lett. 45, 527 (1980).
2. W. Czyz and L.C. Maximon, Ann. Phys. (NY) 52, 59 (1982).
3. A.J. Cole, W.D.M. Rae, M.E. Brandan, A. Dacal, B.G. Harvey, R. Legrain, M.J. Murphy, and R.G. Stokstad, Phys. Rev. Lett. 47, 1705 (1981).

*****

4.7 Calculation of Critical Energies as a Function of Nuclear Size

J.G. Cramer and R.A. Loveman

We are beginning a study of critical energies of different systems. For this study we will be using folding model potentials calculated by the same method used by Satchler and Love.[1]

There is a singularity in the classical deflection function of many potentials. In particular, the potentials used to characterize scattering of nuclei fall into this class. There is however a scattering energy above which this singularity in the deflection function disappears. This energy is the critical energy.[2] This energy divides elastic scattering into two regimes. Above the critical energy one might expect to see nuclear rainbows and negative angle scattering. Below it one would expect to see phenomena associated with nuclear orbiting.

We have started studying the critical energy as a function of the initial system. For the calculations of the critical energies we are using both real and complex potentials. For the real part of either potential we are using folding model potentials. For the imaginary part of the complex potential we are using Woods-Saxon potentials which have been used to fit data.

While the calculations are essentially classical there are quantum mechanical analogs to these quantities. The quantum mechanical deflection function is equal to twice the real part of the derivative with respect to ℓ of the phase shifts from the s-matrix. If one uses the single-turning-point W.K.B. approximation to calculate the phase shifts, and then takes twice the derivative with respect to ℓ, one derives the same function as the classical deflection function. There are several approximations used in going from quantum mechanics to classical mechanics, but they all seem to hold up well for heavy ion scattering.

References:

1. G.R. Satchler and W.G. Love, Phys. Rep. 55, 3, 183 (1979).
2. W.H. Miller, J. Chem. Phys. 51, 3631 (1969).

*****

4.8 Projectile Breakup into Coincident Heavy Fragments

T. Awes,* S. Gil, M.N. Harakeh, M.J. Murphy, A. Ray, A.G. Seamster, and R. Vandenbosch

Projectile breakup is a type of reaction mechanism which becomes increasingly important as lab bombarding energies increase above the Coulomb barrier, and ultimately evolves into the high-multiplicity, dissociative reactions observed at relativistic energies. It is a peripheral (large impact parameter) reaction which occurs when the slight damping associated with quasielastic collisions dissipates enough energy in the projectile (or its residue) to cause it to dissociate. The dissociation can take one of several forms: the disintegration of the projectile at contact with the target, the ejection of an excited projectile remnant which decays by particle emission, or perhaps the fission of the projectile or remnant. Our recent investigations have discovered a new version of breakup in which heavy particles ($Z \geq 3$) are emitted by an excited projectile residue.

Our experiment was inspired by the question: does the breakup of a massive projectile ever produce multiple heavy fragments? By heavy we mean larger than the protons, deuterons, and alphas characteristically emitted by excited nuclei. To investigate, we designed a system of four solid-state detector telescopes which was sensitive to coincident heavy ions with energies in excess of several MeV/n. This system was used to observe projectile-like particles emitted in the reaction of ^{35}Cl + Ta at 18 MeV/n.

The measurement was made at the Holifield Facility at Oak Ridge National Lab, and succeeded in detecting projectile breakups into coincident heavy fragments. The results show a broad distribution of coincident events, representing all possible pairings of $Z = 3$ to $Z = 8$ projectile fragments. We obtained coincident energy spectra for all of these fragment pairs, and analyzed their features for information about the reaction mechanism. Most of the analysis employed Monte Carlo simulation of breakup scenarios as viewed by the detector system. We found that the simulation of a sequential breakup mechanism, in which the dissociation of the projectile remnant occurs far from the target, quantitatively reproduced all of the observed characteristics of the kinematic data. In contrast, prompt breakups simulated by introducing the Coulomb field of the target into the fragment final state, produced energy spectra distinctly different from the data, when the target was less than ≈ 40 fm from the fragments. We conclude that the heavy-particle coincidences are produced by the sequential breakup of excited projectile remnants. This can be viewed as either the fission of the remnant, or its decay through the emission of a heavy particle. The observation of such a phenomenon is

surprising - the prevailing wisdom has been that the heavy projectile-like products of sequential breakup are accompanied only by light particles and target products. Our analysis of this experiment is complete, and a letter reporting the result has been prepared and submitted for publication.

Reference:

* Oak Ridge National Laboratory, Oak Ridge, TN 37830

*****

4.9 Reactions of ^{24}Mg With ^{16}O

S. Gil, M.A. Khandaker, D.D. Leach, D.-K. Lock, A. Ray, and R. Vandenbosch

We have recently performed an experiment to measure the angular distribution of the oxygen and carbon particles from the $^{16}O(^{24}Mg,^{16}O)^{24}Mg$ and $^{16}O(^{24}Mg,^{12}C)^{28}Si$ reactions at E_{Lab} = 79.5 Mev at back angles. The motivation[1] for this measurement is to find out whether the large inelastic cross sections observed at backward angles in the carbon and oxygen channels in the $^{28}Si + ^{12}C$ reaction[2] are due to a compound nuclear process. We form a ^{40}Ca nucleus by the $^{24}Mg + ^{16}O$ reaction at the same excitation energy and approximately the same angular momentum (within 5%) as for the $^{28}Si + ^{12}C$ reaction and compare the relative intensities of the carbon and oxygen yields. If we see an entrance-channel effect, then the back-angle yields cannot be attributed to a compound nuclear process.

We used a 200 $\mu g/cm^2$ Al_2O_3 target and about 3 pna of ^{24}Mg beam. We used a gas-ΔE solid-state E telescope and measured the angular distribution of scattered carbon, nitrogen and oxygen particles from Θ_{Lab} = 5.6° to 20° in steps of 3°. We placed a gas absorber cell in front of the telescope at Θ_{Lab} = 14° for normalization and to monitor carbon build-up on the target. We also took measurements at all the angles using a 200 $\mu g/cm^2$ Al target and a 50 $\mu g/cm^2$ carbon target. We finally subtracted out aluminum and carbon backgrounds from the Al_2O_3 spectrum and also corrected for carbon build-up on the Al target and for a layer of 10 $\mu g/cm^2$ of oxygen on the blank aluminum target. We have estimated differential cross sections for scattered oxygen and carbon particles in the (-8.5 MeV $\leq Q \leq$ 0.0 MeV) region. We could not get cross sections at 8° and 5.6° for more inelastically scattered oxygen particles because of absorption and multiple scattering of oxygen particles by the gas cell. The total subtraction due to aluminum and carbon background from the raw counts is not more than 45% in the worst case. We show in Fig. 4.9-1 our angular distribution for energy-integrated (-8.5MeV $\leq Q \leq$ 0.0 MeV) oxygen and carbon particles. The smooth curves show a $1/\sin\Theta$ dependence. In the $^{28}Si + ^{12}C$ reaction,[2] the carbon cross-section is about four times the oxygen cross section. In the $^{24}Mg + ^{16}O$ reaction, we find that the oxygen cross section is about three to four times the carbon cross section in the (-8.5 MeV $\leq Q \leq$ 0.0 MeV) region. Considering the entire spectra also, we find more oxygen particles than carbon particles. So our results clearly

demonstrate an entrance channel effect in the $^{28}Si + ^{12}C$ reaction and these results are consistent with the qualitative picture of the formation of a long-lived orbiting complex in these reactions.

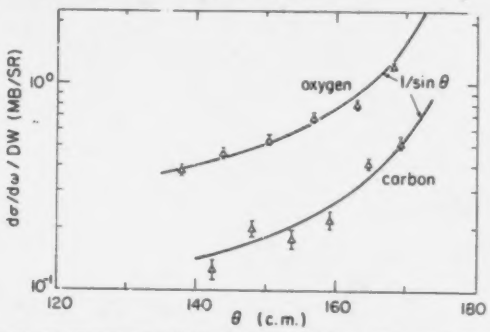

Fig. 4.9-1 Center of mass angular distribution for reaction yield at backward angles. Smooth curves show 1/sinΘ dependence.

References:

1. Nuclear Physics Laboratory Annual Report, University of Washington (1983) p. 26.
2. D. Shapira et al., Phys. Lett. B 114, 111 (1982).

*****

4.10 How is the Excitation Energy Divided in Partially Damped Collisions?

A. Lazzarini, D.D. Leach, D.-K. Lock, A. Ray, A.G. Seamster, and R. Vandenbosch

One of the principal remaining questions concerning quasi- and deeply-inelastic collisions is the division of the excitation energy between the two fragments. The nucleon exchange mechanism leads one to expect rather similar fluxes of exchanged particles in each direction and thus similar excitation energies for each fragment. This should be particularly true for the partially damped events. For more fully damped events the contact time may be sufficiently long that thermal equilibrium can be attained, in which case the excitation energy is expected to divide according to the mass ratio.

These two limiting possibilities lead to a distinguishable difference only when there is a significant mass asymmetry in the exit channel. There are not many experimental observations which bear on this issue, but those that exist tend to indicate that thermalization is reached more rapidly than might have been expected. We have developed a new method for determining the division of excitation energy and applied it to the very mass asymmetric entrance channel system $^{56}Fe + ^{238}U$. We determine the total excitation energy

from the kinetic energy of the projectile-like fragment and the excitation energy appearing in the heavy fragment from the fission mass asymmetry of the coincident sequential fission fragments from the target-like partner. The relative yields of symmetric and asymmetric fission fragments is a very sensitive function of energy for excitation energies below about 60 MeV.

The experiment was performed using a 480-MeV beam of ^{56}Fe produced by the Lawrence Berkeley Laboratory SuperHILAC. The beam was incident on a self-supporting 0.8 mg/cm^2 ^{238}U target, and the projectile-like fragments were detected in a ΔE-E detector telescope located at 45° where there is a good yield over a broad range of inelasticities. The mass distribution of the fission fragments was determined by their time of flight. The mass resolution was very good, with peak-to-valley ratios of over 20 observed at the smallest inelasticities. We have restricted our analysis to those events with Z = 24, 25, and 26, corresponding to Pu, Np, and U complementary fragments. These are fissioning systems for which we have good calibration data on the dependence of the mass asymmetry on excitation energy.[1]

Our results for the ratio of the excitation energy in the heavy fragment divided by the excitation energy in the light fragment are plotted as a function of total kinetic energy loss in Fig. 4.10-1. The upper horizontal

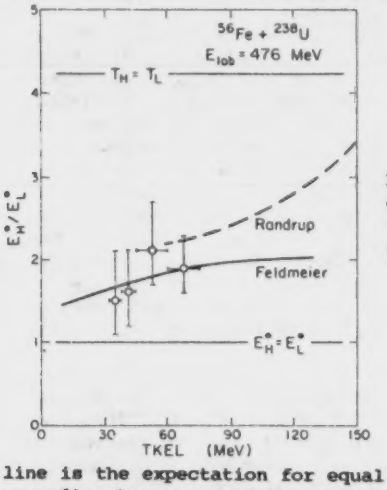

Fig. 4.10-1 Dependence of the ratio of the excitation energy of the heavy fragment to that of the light fragment as a function of the total excitation energy.

line is the expectation for equal temperatures (excitation energy partitioned according to mass ratio) and the lower horizontal line is the expectation for equal division of excitation energies. Our results are intermediate between these two expectations but closer to the latter. It is clear that the present results preclude a division based on thermal equilibrium. Our results are in fact in good agreement with dynamical transport model calculations of Randrup[2] and of Feldmeir.[3] The driving term for equilibration in these calculations is the temperature imbalance resulting from the initial nearly equal division of excitation energy between the two fragments. It is seen that this driving

force is insufficient to equilibrate the temperatures unless the fragments are in intimate contact for an appreciable length of time.

References:

1. See e.g., D. Burnett, UCRL 11006 (unpublished); Z. Frankel et al., Phys. Rev. C 12, 1809 (1975); R.L. Ferguson et al., Phys. Rev. C 7, 2510 (1973); F. Plasil and H.W. Schmidt, Phys. Rev. C 5, 528 (1972).
2. J. Randrup, Nucl. Phys. A 383, 468 (1982).
3. H. Feldmeir, Proceedings of the Nuclear Dynamics Workshop III, Copper Mountain, CO, March 84, and private communication.

*****

4.11 The Effect of Particle Evaporation in the $^{136}Xe + ^{58}Fe$ Reaction and a Reinvestigation of the $^{86}Kr + ^{92}Mo$ System

S. Gil, A. Lazzarini, D.D. Leach, K.T. Lesko, D.-K. Lock, R. Vandenbosch, and A.G. Seamster

The nuclide distributions of Fe-like reaction products from 5.9 Mev/n ^{136}Xe on ^{58}Fe were measured as a function of excitation energy at a laboratory angle of 55.5° using the time-of-flight technique. From the measured distribution of yields the first and second moments were obtained in addition to the correlation coefficients and the isobaric variances. These results were compared with evaporation calculation based on the various complementary primary distributions of light fragments obtained by using the secondary distributions of heavy fragments measured by Schull et al.[1] but corrected for neutron evaporation. Evaporation calculations were also performed on the primary distributions predicted by the nucleon exchange model.[2,3] The comparison between our data and the results of the evaporation calculation shows that our data can be better described by the nucleon exchange model with the inclusion of the effect of particle evaporation. Our mass and neutron variances are consistently smaller that those obtained by Schull et al. after correction for particle evaporation.

The isobaric variances were measured for the 430 Mev $^{86}Kr + ^{92}Mo$ system at 39° in the laboratory using the time-of-flight technique. Our measured variances are smaller than those obtained by Berlanger et al.[4] at low energy losses and are in agreement with the results from the nucleon exchange model. We reproduce the saturation of the isobaric variances observed by Berlanger et al. at large energy losses. We note however that this saturation only occurs at near and sub-barrier total kinetic energies in the exit channel and likely reflect fluctuations in the scission deformation rather than quantal effects.

References:

1. D. Schull, W.C. Shen, H. Freiesleben, R. Bock, F. Busch, D. Bangert, W. Pfeffer, and F. Puhlhofer, Phys. Lett. B 102, 116 (1981).
2. J. Randrup, Nucl. Phys. A 327, 490 (1979).
3. J. Randrup, Nucl. Phys. A 307, 319 (1978).
4. M. Berlanger, A. Gobbi, F. Hanappe, U. Lynen, C. Ngo, A. Olmi, H. Sann, H. Stelzer, H. Richel, and M.F. Rivet, Z. Phys. A 291, 133 (1979).

5. FUNDAMENTAL SYMMETRIES IN NUCLEI: $0^+ - 0^-$ ISOSCALAR PARITY MIXING IN ^{14}N

5.1 Theory of the ^{14}N Parity Mixing Measurement

E.G. Adelberger, B.A. Brown,* and P. Hoodbhoy,†

The general principles of our experiment to measure the $\Delta I = 0$ parity mixing between the $I = 1$ 0^+ and 0^- levels at $E_x = 8.618$ and 8.79 MeV in ^{14}N were given in last year's Annual Report.[1] A paper,[2] to appear in Phys. Rev. C, develops the formalism of longitudinal analyzing power (A_L) measurements over parity mixed resonances and applies this to the example of probing the parity mixing in ^{14}N by detecting A_L over the narrow 0^+ resonance. The formalism utilizes the single-level approximation to Bloch's formulation of reaction theory[3] in order to account for the strong (parity-conserving) reaction amplitudes and is restricted to parity nonconservation associated with the closeness of the two opposite parity resonances. An example of the parity conserving calculation is shown in Fig. 5.1-1 where we compare our calculation to existing[4] unpolarized $^{13}C(p,p)$ data. In order to determine the widths and separation of the 0^+ and 0^- resonances we studied the $^{13}C(p,\gamma_0)$ reaction at $\theta_{lab} = 90°$. Results are shown in Fig. 5.1-2.

Because the PNC A_L is expected to change sign between forward and backward angles we have chosen to detect the observable $A_L(\text{back})-A_L(\text{front})$, where $A_L(\text{back})$ is the longitudinal analyzing power averaged over the angles from 140°-170° while $A_L(\text{front})$ is that averaged over the interval from 33°-37°. Because our observable is a difference of A_L's, effects due to beam intensity modulation or of beam size modulation combined with target nonuniformities cancel to first order.

We estimate the PNC matrix element connecting the 0^+ and 0^- levels using the "best value" PNC NN interaction of Desplanques, Donoghue, and Holstein[5] in a shell model calculation[2] in the ZBM space and obtain $H_{PNC} = -1.39$ eV. Haxton[6] has done a complete $2\hbar\omega$ calculation and obtains a very similar value $H_{PNC} = -1.04$ eV.

When the -1.39 eV matrix element is inserted into our A_L calculations, we discover that an A_L measurement has considerable statistical power (see Fig. 5.1-3). The predicted effect is $\sim 2 \times 10^{-5}$ and counting rates are high enough so that one can achieve a statistical error small enough to give a $\sim 5\sigma$ effect with an integrated beam charge of 1 μA-day. The statistical power of the experiment is due to an enhancement arising from the fact that $\Gamma(0^-) \gg \Gamma(0^+)$ and from the large size of low-energy elastic-scattering cross sections.

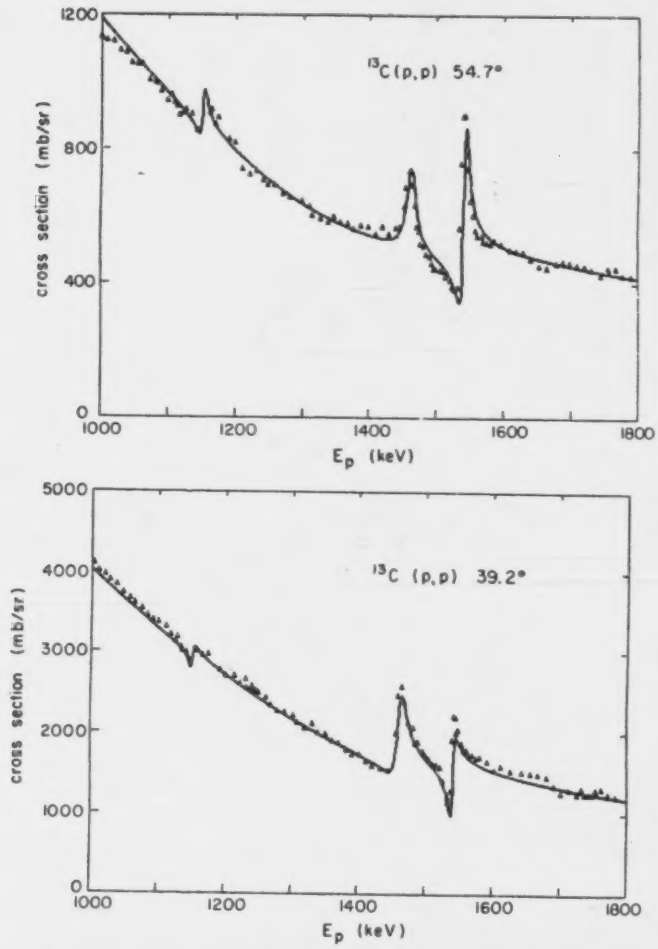

Fig. 5.1-1 Comparison of ^{13}C(p,p) data of Latorre and Armstrong[4] with the parity conserving calculation. Resonance parameters have been taken from the latest compilation and no attempt was made to fit the data by adjusting any parameters.

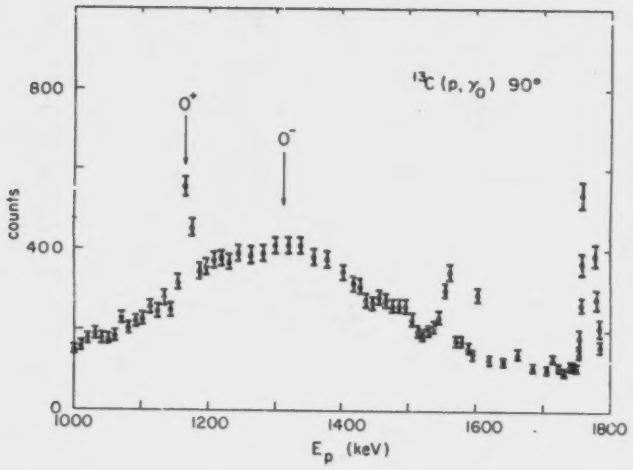

Fig. 5.1-2 Yield of the $^{13}C(p,\gamma_0)$ reaction at Θ_γ = 90°. Gamma rays were detected in the 25 cm × 25 cm NaI spectrometer. The target used was ~20 kev thick to the incident beam and thus, in part, obscures the narrow width of the 0^+ state.

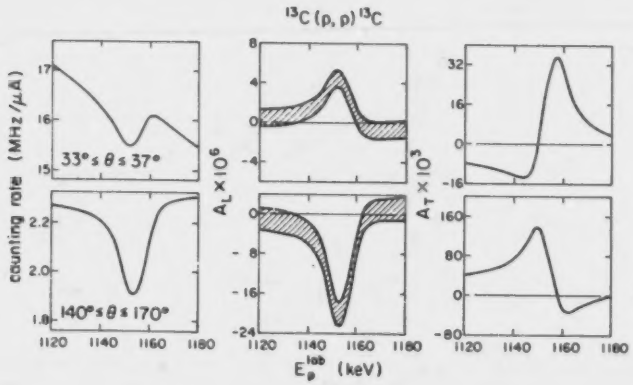

Fig. 5.1-3 Calculated counting rate, longitudinal and transverse analyzing powers over the 0^+ resonance for a 10 kev thick ^{13}C target. We assumed full coverage of the solid angles between 33° and 37° (front counter) and 140° to 170° (back counter). The shaded band on the A_L plot corresponds to ±1 σ, where σ is the statistical error achieved after running with an integrated beam current of 1 μA-day under the above conditions.

References:

* Michigan State University, East Lansing, MI 48824.
† Present Address: Department of Physics, Quaid-e-Azam University, Islamabad, Pakistan.
1. Nuclear Physics Laboratory Annual Report, University of Washington (1983) p. 32.
2. E.G. Adelberger, P. Hoodbhoy, and B.A. Brown, Phys. Rev. C, to be published.
3. C. Bloch, Nucl. Phys. 4, 503 (1957).
4. V.A. Latorre and J.C. Armstrong, Phys. Rev. 144, 891 (1966)
5. B. Desplanques, J.F. Donoghue, and B.R. Holstein, Ann. Phys. (NY) 124, 449 (1980).
6. W.C. Haxton, private communication (1984).

*****

5.2 High Count-Rate Low-Energy Proton Detectors

E.G. Adelberger, M.J. Murphy, J.L. Osborne, H.E. Swanson, and V.J. Zeps

In order to measure a small parity violating effect, we need to count ~1 MeV protons at high rates (~1 MHz/detector). Several requirements determined the proton detection scheme: a) a large solid angle coverage with relative insensitivity to small beam position and angle fluctuations, i.e., large detectors at large distances, b) short pulse width, c) good energy resolution and, d) low background noise.

The method chosen was to mount thin (50 μm) scintillators on 5-cm diameter photomultiplier tubes (PMT's). The detectors cover 32% of the solid angle from 140° to 170°. The scintillators were prepared by Bicron on 3-mm thick, 5-cm diameter lucite substrates with 0.4 μm of Al evaporated on the front surface. The aluminum maximizes the light collection from a proton event, and shields the PMT from seeing the light from the other detectors. The scintillator thickness was chosen to stop the protons in the scintillator, while minimizing background pulses from γ rays and electrons. The scintillators were glued to the PMT's using an optical coupling cement developed by Nuclear Enterprises, Inc. Preliminary tests using some existing RCA 8575(6) and RCA 8850(1) PMT's revealed a substantial amount of low energy noise. This problem was solved by wrapping the PMT's with an Al shield at photocathode potential. Running the PMT's near optimum high voltage, we were able to attain proton pulses of ~0.8 V with 10-nsec pulse widths. The energy resolution varied from 18% to 30%, depending primarily on the photocathode uniformity. This, however, is not a critical factor, since we are interested only in counting the protons, and thus need only to be able to separate the proton peak from the low energy noise. To equalize the counting rate in the front and back counters, the front counters have been further collimated,

exposing only a 1.3-cm diameter hole. This reduces the effects of photocathode nonuniformity, improving the front counter resolution to ~13% (see Fig. 5.2-1). We decided to use the best 4 of 7 RCA PMT's, and to purchase 5 Hamamatsu R239-02 PMT's. The Hamamatsu tubes are equivalent to the RCA 8575's, with the added advantage of a built-in shield at photocathode potential as standard, a better tube wrapping and a much lower price. The PMT's were placed in specially designed holders which mount in the scattering chamber. In order to hold a vacuum, an O-ring seals against the 3-mm edge of the lucite substrate, with the aluminized surface of the scintillator exposed to the target, while the PMT remains outside the vacuum system.

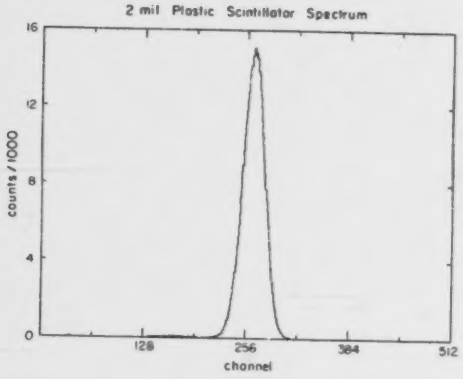

Fig. 5.2-1 Typical energy spectrum of 1.1 MeV protons on a ^{13}C target, as detected in a front counter. The energy resolution is 13%.

PMT bases were built following a standard design.[1] To achieve stability, a large divider chain current (2.2 mA at -2000 V) was employed and zener diodes were used to fix the photocathode to first dynode potential at 480 V.

Reference:

1. R.W. Engstrom, RCA Photomultiplier Handbook, (1980) p. 80.

*****

5.3 ^{14}N Beam Position Stabilization System

E.G. Adelberger, N. Hill, J.L. Osborne, H.E. Swanson, and V.J. Zeps

The incoming proton beam is stabilized to remove position fluctuations. Using four independent control loops, the beam is dynamically steered to pass through the center of both the upstream slits and the Faraday cup. The major elements of the beam sensing and steering system are shown in Fig. 5.6-1 (see

Sec. 5.6). Beam current is measured by pairs of slits (horizontal and vertical) and a Faraday cup split into four quadrants. The physical positions of both slits and Faraday cup can be moved with micrometer adjusting screws. When in operation, these systems serve to maintain the position of the beam along the symmetry axis of the apparatus. Two parameters of the beam are controlled - position and angle at the target location. The upstream magnetic steerer near to the exit of the quadrupole is used to center the beam on the slits. These slits determine primarily the beam's position at the target but beam which was off the z-axis will have acquired an angle with respect to that axis. The steerer near the slit position is used to center the beam on the Faraday cup. This system assures the angle of the beam with respect to the z-axis is minimized.

In order to minimize the loop response times, wide bandwith current preamps were designed and built. These operate in the range of 10 to 1000 nanoamperes with a bandwidth of DC to 40 kHz. Additional operational amplifier circuitry provides sum and difference signals for metering and control. These are displayed on meters to provide visual indication of the beam's intensity and position for tuning diagnostics. These signals are also sent to voltage to frequency converters (V/F's) which are scaled and routed identically to the pulses from the photomultipliers themselves. This allows us to correlate excursions in photomultiplier asymmetries with the beam's position, angle and intensity. Right-left and up-down difference signals are converted to the currents needed to drive the steerers using Kepco BOP operational amplifier power supplies in the case of the upstream steerers, and hybrid high current op-amps made by RCA in the case of the Faraday cup control loops.

The magnetic steerers were constructed by winding coils on each of the four legs of ferrite frames (rectangular toroids). These frames enclose a section of beam tube. Coils on opposite legs of the frames are connected to produce opposing B fields in the ferrite. This causes the field to leave the ferrite and fill the open area in the center of the frame with a very uniform B field. Ferrite has a high permeability and resistivity which allows modulation at rates comparable to the 40 kHz bandwith of the current preamps.

Using a Hewlett Packard Spectrum analyzer, the power spectra of various difference signals were measured. These give an indication of the beam's fluctuations in different regions of frequency space. Over the frequency range of DC to 100 Hz, the stabilization system achieves a 30 dB overall reduction in the power spectrum when compared with an unstabilized beam.

*****

5.4 ^{14}N Data Collection Electronics

E.G. Adelberger, M. Hill, J.L. Osborne, H.E. Swanson, and V.J. Zeps

The data aquisition system uses a somewhat modified version of the Laboratory's singles data taking environment along with external electronics to route the Lecroy scalers. Due to the high data rates produced by the photomultiplier tubes, ADC's cannot be used. All events exceeding a lower level threshold are counted in the 100 MHz scalers, and these provide the peak sums used in the analysis. The Laboratory's polarized ion source controller generates the equal period routing sequence and provides the capability of synchronizing the starting and stopping of data aquisition with the transition to a new routing state. In addition, aquisition is inhibited for a preset time around the state transition to allow for transient effects to damp out.

A typical data aquisition sequence proceeds as follows: The computer, having initialized and cleared the CAMAC scalers, signals the external electronics that all is ready through an ADC test output jack. Data aquisition begins at the transition to the + route state. After a predetermined amount of charge has been collected, aquisition is stopped but only after equal time has been given to each route state. The PDP 11/60 computer is signaled through an ADC input, at which time the scalers are read, cleared, and displayed. This sequence proceeds until the desired number of readings has been acquired.

Presently two scaler banks are used, with the intent to expand to four. Routing is accomplished by sending beam (V/F) and photomultiplier pulses to both banks of scalers, but only gating one bank on at a time consistent with the present ion source state. The assignment of which bank corresponds to the + route state alternates with each sequential readout of the scalers. This was found necessary as the dead times of the individual scalers in each bank are all different. These differential dead times build in an asymmetry unless the individual scaler dead times are averaged over both route states. The analysis software then assumes sequential scaler readings have alternate route assignments and these are unfolded when computing the various asymmetries. The data aquisition system is thus very symmetric in its treatment of the two route states. In order to monitor proper operation of this alternation scheme, the symmetry is broken for one scaler in each bank. A constant frequency oscillator is gated into one physical bank when the assignments are normal and to the other bank when they are inverted. This has the effect of accumulating counts in only one route state. Any counts in the other state indicates a problem with the synchronization and the particular reading sequence could be removed from the totals accumulation.

*****

5.5 Data Acquisition and Analysis Programs

E.G. Adelberger and R.S. Peabody*

The data acquisition program for the ^{14}N parity mixing experiment provides the master control for the data taking cycle, writes all results on tape and provides an on-line measure of the current and cumulative values of all the transverse and longitudinal asymmetries. A single data acquisition cycle consists of:

a. Starting the polarized ion source spin flipper, the Lecroy and NPL scalers, and the ADC used for the 3 × 3 NaI.

b. Stopping the counting after a predetermined beam charge has accumulated.

c. Reading the Lecroy scalers, and clearing them and displaying the results.

d. Starting a new "read cycle."

e. After 40 read cycles the program writes the 40 sets of readings on magnetic tape, and computes the current and cumulative asymmetries. The counting rates and asymmetries are printed out and a new run is begun.

The program is based on the standard Laboratory singles package with the AUTO feature, but it required a number of new programs. The 4 × 12 = 48 Lecroy scaler values for each reading are stored as counts in a spectrum which can be displayed by the standard VT11 routines. Each scaler is labelled by a code denoting its function (i.e., left front counter in the + route). Thus all asymmetries can be based on the function code rather than the physical scaler number. The on-line output of the individual and cumulative counting rates and asymmetries provides an excellent diagnostic and will ultimately be used to control the polarized ion source spin precessor.

The data analysis program computes the various asymmetries and correlations and makes a statistical analysis of the individual values. By allowing us to compare the observed fluctuations of the individual data points with those expected from counting statistics we can determine whether our system is performing as expected.

Reference:

* Present Address: Department of Chemistry, University of Washington.

*****

5.6 Design and Construction of the ^{14}N Parity Experiment Beamline

E.G. Adelberger, C.A. Gossett, M.Z. Iqbal, J.L. Osborne, H.E. Swanson, and V.J. Zeps

As shown in the preceding sections of this report, the measurement of a small (2×10^{-8}) parity non-conserving effect in ^{14}N via the resonant elastic scattering of protons on ^{13}C requires novel designs in the apparatus. The proton counters must cover a large solid angle, yet produce pulses fast enough for the high counting rates. The beam transport system must provide fast automatic stabilization of beam position and angle. The beam line for this experiment must accommodate all of these design considerations while at the same time providing mechanical stability, to reduce asymmetries in the particle counting rates due to translation or vibration of the target chamber, and a clean high vacuum, to reduce carbon buildup on the target.

The final design for the beam line assembly is shown in Fig. 5.6-1. The position of the slits and the target were chosen to provide the optimum focus at the target position. The extent of the apparatus, more than 4 m from the cave quadrupole to the split Faraday cup, precluded its construction on any of the existing beam lines except for the L-30° leg, which is normally used only by the University of Washington Nuclear Medicine Group for the production of short-lived radionuclides (see Sec. 9.3). One prime consideration in the design of the beam line was that it not interfere with this pre-existing usage, therefore removable 30-cm stainless steel bellows and 15-cm section of tube were placed between the quadrupole and the isolation valve to allow their chamber to be re-attached in its usual position.

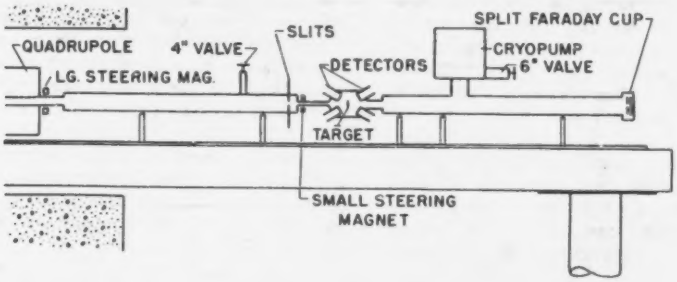

Fig. 5.6-1 A elevation view of the L-30° beamline. There are also an identical pairs of slits, forward-angle counters, back-angle counters and Faraday-cup segments in the horizontal dimension.

The construction of this beam line has now been completed. As shown in Fig. 5.6-1, the beamline components are attached to a 1/2" steel plate supported by two 8" x 2" steel channels. These channels are attached at one end to the quadrupole support and at the other end to a 12" diameter steel pipe which extends through the cave floor to the floor of the basement. The

pumping system chosen for this experiment is a CTI Cryotorr 7 cryopump.

*****

5.7 Studies of System Performances Using an Unpolarized Beam

E.G. Adelberger, C.A. Gossett, J.L. Osborne, H.E. Swanson, and V.J. Zeps

The slit and Faraday cup stabilizing feedback loops reduce the error signal by 30 dB and 10 dB, respectively, at low frequencies, while providing feedback control up to several kHz. A removable quartz viewer has been installed at the target position. This has proved to be both an excellent diagnostic tool and a sensitive way for determining the best beam focus. The best beam spots thus far have been ≈0.5 mm × 0.5 mm. Collimators have been put on the front counters in order to equalize the rate in the front and back counters. This has allowed us to raise the beam current, increasing the rate in the back counters, while maintaining a tolerable rate in the front counters. Because the collimators expose only the central portion of the scintillators to the scattered protons, the resolution in the front counters has improved from ≈25% to ≈13%. At present the back counters can see protons scattered from further down the beamline, creating a continuum of noise that accounts for ≈10% of the total back detector counts. Plans for a cold shroud which should eliminate this problem, are in the shop.

Before we attempt to make measurements using a polarized beam, we must understand possible systematic errors caused by imperfections in our data taking procedure and apparatus. Since the PNC effect is expected to be $\approx 2 \times 10^{-5}$, we would like to reduce systematic errors in A_z to a level of $\approx 2 \times 10^{-8}$. Many sources of systematic error can be probed with an unpolarized beam. Using the control circuit which normally flips the spin of the polarized beam to route the scaler banks, we collect unpolarized beam data exactly as we intend to when running with a polarized beam. Because there is no spin flipping, we expect all asymmetries to vanish. During our first runs, we noticed asymmetries up to 100 times larger than the statistical error. We discovered that the CAMAC scalers read differently, even when all scalers were fed by the same photomultiplier signal. To correct this, we electronically alternated the functions of the two scaler banks after each read, so that each spin state was averaged over the two banks, eliminating the correlation between "spin state" and scaler bank. This dramatically improved A_z(back-front), bringing it to within statistical error. We still found there to be a large analyzing power in the individual A_z(back) and A_z(front) measurements. This was strongly correlated with the asymmetry in the total beam current in each route. We discovered that the computer software would consistantly cut short the positive route at the beginning of each sequence of reads. This caused a fairly consistant negative A_z(back) and A_z(front). After we corrected these known problems in the program and electronics, we observed, in a run with a total charge of 0.25μ A-days, that all asymmetries were consistant with zero, $A_z(\text{front}) = (4.9 \pm 5.0) \times 10^{-8}$, and $A_z(\text{back}) = (5.7 \pm 6.0) \times$

10^{-6}, and A_z(back- front) = (0.9±7.8) × 10^{-6}, with a total of ≈5 × 10^9 counts/detector. Thus, at the present level of accuracy, we are able to measure a null result with unpolarized beam. However more data must be taken to verify the result at the 2 × 10^{-6} level. All-in-all the system seems to be working extremely well, and we are ready to test our apparatus with polarized beam.

6. FUNDAMENTAL SYMMETRIES IN ATOMS: PARITY MIXING IN HYDROGEN AND DEUTERIUM

6.1 Introduction

T.A. Trainor

The object of this experimental program is to measure the weak interaction coupling of n=2 s and p states in hydrogen and deuterium via resonant two-photon s-s transitions induced in a fast atomic beam at 570 G. The sensitivity of the experiment remains, as it was reported last year, at about 1000 times the Standard Model prediction. Our efforts in the intervening period have been directed toward three of the four limitations of the apparatus: magnetic field inhomogeneity, background pressure, and stray electric fields. The fourth problem, motional electric fields due to the fast atomic beam, is indirectly improved by better magnetic field homogeneity.

Although the electric fields which induce the s-s transition amplitudes are generated by highly coaxial precision electrode systems, they are projected on a quantization axis referred to the axial magnetic field of the experiment. This field presently wanders in direction by $\sim 1/10^4$ over the length of the apparatus. The resultant unwanted transverse electric field components complicate the transition amplitudes and mimic the PNC weak interaction. Relative field magnitude variations of the same order also serve to distort the s-s resonance shape. The result is that various techniques used to discriminate against false PNC effects which depend on geometric symmetries and line-shape properties lose their effectiveness below the sensitivity level reported above.

Stray electric fields from various sources other than poor magnetic field geometry also serve to generate spurious amplitudes which make analysis difficult.

Finally, the non-zero residual gas pressure in the system produces collisional 1s-2s transitions which serve to dilute the data acquisition with a non-resonant background yield and reduce the statistical accuracy/time.

A major program has therefore been carried out, consisting of preparation of a new tape-wound solenoid and control system for installation, gold plating all electric field electrodes, and reconditioning the cryopump system, in order to achieve a 100 times improvement in the sensitivity of the apparatus. Progress with the solenoid system and gold plating are reported below. The cryopump system now provides 3-4 times lower operating vacuum than was available during last year's data acquisition runs.

*****

6.2 Cleaning and Plating of RF Cavities:

D.W. Holmgren

The sensitivity of the present H-PNC experiment is limited by the ambient electric field in the RF cavities.[1] As part of the effort to understand and eliminate the stray fields, we cleaned, polished and plated the RF cavities.

The copper cavity sections were cleaned and electropolished in a phosphoric acid solution.[2]

A commercial plater[3] performed further processing, including cleaning in a caustic alkaline and an acidic bath. Cavity sections holding apertures required a sulfuric acid etch to activate the exposed lead-tin solder for plating.

To minimize cost, only those surfaces of the cavity "seen" by the beam were plated. These surfaces, including the coupling loops, received 0.3-0.4 μ electroless nickel, followed by 2.5 μ gold plate.[4]

On return from the plater, the pieces needed further finishing. Stains presumed to be plating salts were removed, and the rough edges of the plated regions were finished with silicon carbide.

The cavities were reassembled and installed in the apparatus. We have not yet determined whether the ambient electric field has been significantly altered.

References:

1. Nuclear Physics Laboratory Annual Report, University of Washington (1983) p. 42.
2. N.V. Cherepnin, Treatment of Materials for Use in High Vacuum Equipment, (Ordentlich, Holon, Israel) p. 182.
3. Criton Hytek Finishes Co., Kent, WA 98032
4. American Chemical Refining solution 258.

*****

6.3 Alignment and Field Scans of the New Solenoid

T.A. Trainor and P. Wong

Several years ago we manufactured an aluminum solenoid consisting of 20 tape-wound pancakes[1] when it was realized that our wire-wound copper solenoid did not produce a magnetic field of sufficient uniformity to permit an experimental sensitivity to the parameter c_{zp} of order unity, our original design goal. In principle it is possible more easily to produce a precision

solenoid with tape-wound pancakes, since jigs can be used to precisely locate the tape on cylindrical forms during the winding process, whereas the wire-wound solenoid is subject to various winding errors as each new layer is wound on the one below. However, in the course of routinely checking the new aluminum pancakes for major faults last year, preparatory to installation, we observed that a number of construction defects were present which would make the new solenoid not significantly better than the old. So we undertook a careful measurement program which determined the mechanical, electrical and magnetic properties of each pancake.

Mechanically, we found that the anodized aluminum cylinders used as forms for the pancakes had become warped, either during the winding process, or later when strains in the pancakes relaxed. The various tape layers also were not perfectly lined up at the outer faces. Shifts of 10-20 mils were observed. Each pancake consists of two layers, one wound inward and one wound outward with an annulus of mylar between, both layers wound from one continuous strip of anodized aluminum tape folded at the center. These halves were observed to have different diameters, as a rule, due to variations in tape thickness, as noted below.

In order to insure an important property of the pancakes, that the windings be lined up and the two outer faces parallel, all the pancakes were pressed between dies with a ten ton press. This had the desired effect on the pancakes, but the forms remained warped. It was decided therefore not to use the forms for axial location of the pancakes as intended but to use insulating spacers which reference to the faces of the pancakes.

Electrically, we found that there were shorts in several of the pancakes and that the aluminum tape varied in thickness in a step-like manner at various points within the windings. These measurements were made with a constant-current source and a 6-1/2 digit DVM to determine the IR drop as a function of position along the tape. Changes in tape thickness, as noted, mean that the effective radii of various pancake halves are different even if the measured outside diameters are the same. Each pancake was therefore surveyed for shorts and mean radii of both halves, as well as total resistance.

Magnetic measurements were made with a Bell 3-axis Hall probe in which the three Hall plates were mutually perpendicular to better than 1/2°. The probe was carried on a precision track referenced to the main coil support jig. Measurements of transverse field components for each pancake were correlated with various physical measurements. Variation in axial magnetic field strength per unit current were correlated with variations in mean radii and known shorts.

At the end of this measurement program the physical, electrical, and magnetic data for each pancake were self consistent at a level of a few parts in 10^5. An assembly scheme was then devised which would produce the most homogeneous magnetic field with the available pancakes. For instance, the effect of two pancake halves having different mean radii is that the effective axial field maximum is displaced with respect to the physical pancake

position. If the pancake is placed in the solenoid at its normal axial position there will be a nonuniformity in the total field which cannot be removed by shunting neighbor pancake currents. Instead, the pancake must be shifted axially a small amount from its normal site by adjusting the axial spacers between pancakes in order to compensate for the radius variation.

The solenoid has been assembled according to the final scheme and awaits completion of the new current control system so that currents will be sufficiently stable to allow total field surveys at the $1/10^5$ level.

Reference:

1. Nuclear Physics Laboratory Annual Report, University of Washington (1981) p. 28.

*****

6.4 Control System for a New Solenoid

P. Wong

Progress is being made on assembling and testing the new solenoid[1] for the H-atom project. The primary components of this solenoid system are 20 "pancakes" of wound aluminum tape, a 20 channel shunt board which determines the relative amount of current flowing in each pancake and a high performance dual current regulator.

One of the major advantages of the new solenoid is that the current through each pancake can be varied individually, allowing variations in B_z to be minimized. To accomplish this a large PVC board with 20 loops of Nichrome wire has been constructed. The resistance of each loop is varied by means of a copper slider. Each pancake field can be continuously varied over a range of ±0.5 gauss and can be set to ±1 milligauss. In addition to having very little noise, the shunts have excellent time and temperature stability. However, there are variations on the order of 20 milligauss/10° C if the temperature of the solenoid changes. If the pancakes are allowed to reach operating temperature before adjustments are made there should be no problem. The shunts will be trimmed using a Hall probe after the pancakes are installed within the flux return.

Because the all-aluminum solenoid has a higher resistance than its copper predecessor, a new power supply configuration capable of higher voltages is required. To reduce the magnetic field "droop" at the ends, the outer three pancakes will be run at a higher current than the remainder. These considerations dictate that a third separate power supply be used to operate the outer pancakes, and a new current controller capable of running all three supplies has been built. It is similar in design to its predecessor[2] and its performance should be the same.

The solenoid should be installed and tested in the next six months.

References:

1. Nuclear Physics Laboratory Annual Report, University of Washington (1980) p. 31.
2. Nuclear Physics Laboratory Annual Report, University of Washington (1983) p. 38.

7. MEDIUM ENERGY PHYSICS

7.1 Inclusive Scattering of Pions from very Light Nuclei at 100 MeV

J.F. Amann,* W. Burger,† K.G.R. Doss,‡ D.H. Dowell, I. Halpern, M.A. Khandaker, D.D. Leach, T. Murakami, D.W. Storm, and D.R. Tieger

Recently we performed an experiment on the inclusive scattering of pions from very light nuclei at 100 MeV. The experiment was motivated by our earlier finding[1,2] that although inclusive pion scattering from elements heavier than ^{12}C appears to be mostly due to quasi-elastic scattering from nucleons, there are some features that cannot be accounted for in this way. We decided to study these features in light elements to avoid multiple scattering effects.

The present measurements were carried out using the QQD spectrometer in the M11 channel at TRIUMF (Experiment 224). Data were collected for π^+ on ^{2}H, ^{3}He, and ^{4}He at several laboratory angles, ranging from 40° to 125°, and for π^- on ^{3}He, and ^{4}He at 60°, 100°, and 125°. For normalization and diagnostic purposes some data were also collected for ^{1}H, ^{14}N, ^{12}C, and ^{208}Pb.

The target was a thin-walled 2 liter gas cylinder. It was run at room temperature and typical pressures of 1500 psi. Data were collected in three momentum bites of the spectrometer in order to cover up to 60 MeV in excitation energy. We had a preliminary run last summer and a final one this February. We are currently in the process of analysing the data. A preliminary set of energy spectra, relatively normalized, for π^+ on ^{1}H, ^{2}H, ^{3}He, and ^{4}He at 60°, is shown in Fig. 7.1-1. The curves here are composites of all three momentum bites.

The main qualitative features of these spectra are as expected: the deuterium spectrum shows a clear quasi-elastic peak in addition to the elastic peak; the ^{3}He and ^{4}He spectra show additional yields at large energy loss, and appropriate gaps next to the elastic line, reflecting the absence of excited states below the particle breakup energy.

It is interesting to compare the ^{3}He and ^{4}He spectra. Quasi-elastic scattering for π^+ (from the two protons) is likely to be more suppressed in ^{4}He than in ^{3}He due to the role of the extra neutron in pion absorption. A preliminary examination of the π^+ data indicates that at forward angles (60°, 75°) the ^{4}He inelastic cross-section, integrated from 24 to 60 MeV excitation energy, is slightly higher than that of ^{3}He, whereas at backward angles (100°, 125°) the cross-section for ^{4}He is slightly lower. Corresponding data for π^- show ^{4}He/^{3}He ratios that are about twice as large. We hope to account quantitatively for our findings in terms of simple models for the absorption and scattering of pions.

The experiment was designed to allow us to compare ^{2}H, ^{3}He, and ^{4}He directly. This should make it possible for us to interpret the observed differences in yields and spectra in terms of the effects of number of nucleon types and mean nucleon separations on the interactions of pions in nuclear matter.

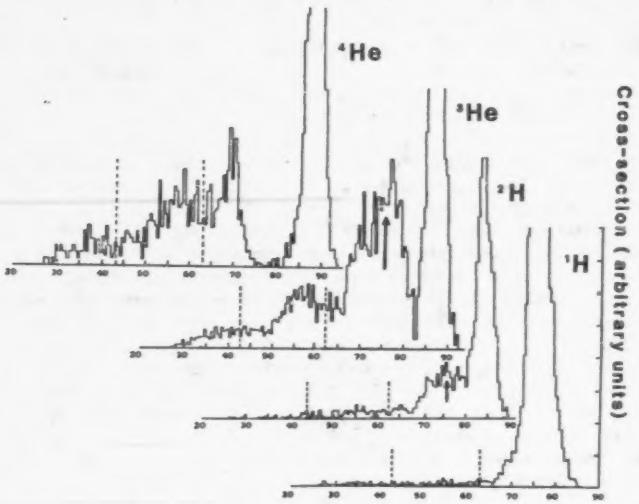

Fig. 7.1-1 Energy spectra for 100 MeV π^{+} on ^{1}H, ^{2}H, ^{3}He, and ^{4}He at θ_{lab} = 60°.

a) No efficiency correction has yet been applied to the spectra.
b) The dashed lines show where the separate spectrometer momentum bites have been joined.
c) The dip in spectra in the range 60–67 MeV is possibly due to fall-off of efficiency at the edges of the spectrometer's acceptance.
d) The small tail on the elastic spectrum has been subtracted using the ^{1}H spectrum.
e) The arrow in the ^{2}H and ^{3}He spectra shows the location of the quasi-elastic peak.

References:

* Los Alamos National Laboratory, Los Alamos, NM 87545.
† Massachusetts Institute of Technology, Cambridge, MA 02139.
+ Lawrence Berkeley Laboratory, Berkeley, CA 94720.

1. Nuclear Physics Laboratory Annual Report, University of Washington (1982) p. 98.
2. Nuclear Physics Laboratory Annual Report, University of Washington (1983) p. 54.

8. ACCELERATOR MASS SPECTROMETRY (AMS)*

8.1 AMS with Carbon and Beryllium: C-14 and Be-10 Radiochronology

D. Balsley, G.W. Farwell, P.M. Grootes,† G.M. Hinn, D.D. Leach, and F.H. Schmidt

Measurements of isotopic fractions in the range of 10^{-11} to 10^{-14} for studies of the variations in ^{10}Be and ^{14}C concentrations in environmental samples have been continued during the past year, and a number of significant technical improvements have been made.

The extremely rapid change in atmospheric ^{14}C concentration caused by the injection of large amounts of ^{14}C, produced in the nuclear weapons tests of the early 1960's, provides an excellent tracer to study the photosynthesis and deposition of carbohydrates as cellulose in tree rings. A better understanding of these processes is important for the use of the isotopic abundance ratios of carbon, oxygen, and hydrogen in cellulose in tree rings as paleoclimatic indicators. Measurements are in progress on ten sequential segments per year for the years 1962 and 1964 of a Sitka spruce from the Olympic Peninsula, Washington. Data for the year 1963, during which the atmospheric ^{14}C content increased dramatically and reached a peak at about 200% of the 1950 value before declining moderately, are nearly complete and it is gratifying to find the atmospheric ^{14}C trends clearly reflected in the single-year tree-ring profile.[1,2] Fig. 8.1-1 shows a comparison of the two ^{14}C profiles. Measurements on the 1962-1964 period are continuing and modelling studies are under way.

A better understanding of the geochemistry of cosmogenic beryllium is needed for its successful use in understanding environmental processes and their chronologies. A study of ^{10}Be concentrations in rain water samples from different northern latitudes in Washington and Alaska is in progress; these measurements will provide information on the latitudinal and temporal variations in natural ^{10}Be deposition rates. We have also begun a series of measurements of ^{10}Be in surface layers of snow from the South Pole.

References:

† Quarternary Isotope Laboratory, University of Washington.

1. G.W. Farwell, P.M. Grootes, D.D. Leach, and F.H. Schmidt, in Proceedings of the Third International Symposium on Accelerator Mass Spectrometry (Zürich, 1984), Nucl. Instrum. Meth. (to be published).
2. R. Nydal, K. Lovseth, and F.H. Skögseth, Radiocarbon 22, 626 (1980).

* Our work has been supported in part by the M.J. Murdock Charitable Trust and the National Science Foundation (Grant EAR-8115994, Environmental Geosciences Program).

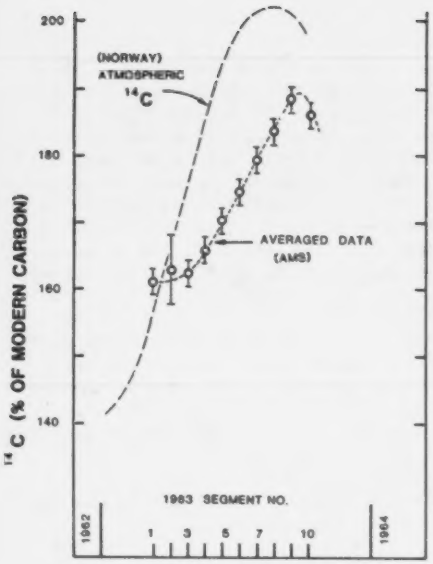

Fig. 8.1-1 Comparison of ^{14}C concentration in sequential segments of a 1963 Sitka spruce tree ring (Olympic Peninsula, Washington) with atmospheric ^{14}C concentrations (Norway and elsewhere, Ref. 2) for the same period.

*****

8.2 AMS: Technical Improvements

D. Balsley, G.W. Farwell, H. Pauska, P.M. Grootes,* D.D. Leach, and P.H. Schmidt

Last year[1] we reported progress on two systems of normalization of the rare isotope beam (particle counting rate, ^{14}C or ^{10}Be) against the stable isotope beam or beams ($^{12,13}C$ or ^{9}Be ion current). In the concurrent monitoring method, the abundant isotope (e.g., ^{12}C) is monitored at the low-energy end of the accelerator while the rare isotope (e.g., ^{14}C) is monitored simultaneously following acceleration and high-energy ion analysis. In the sequential transmission method, the rare and abundant isotopic ion beams are alternated by adjustment of the entire set of accelerator parameters. The recent advent of a two-level, nuclear-magnetic-resonance-controlled isotope alternation system (see below, Sec. 8.3) has greatly enhanced the effectiveness of the sequential transmission method and we experienced little difficulty taking data on carbon from tree-ring segments with about ±2% accuracy for a single measurement. (Our measurements are made by comparison with working standard samples that have been accurately measured by β-counting

in the Quaternary Isotope Laboratory.)

Our low-energy (pre-accelerator) beam handling system has been revised to accommodate the elevation of the sputter ion source to 60 kv accelerating potential and a shift of the ion injection angle from 30° to 45°. (30 kv is the highest accelerating potential actually used to date.) The new sputter ion source-low energy beam system, together with a new particle detector telescope that has a larger aperture and renders our particle counting rates less sensitive to small fluctuations in accelerator terminal voltage, has led to increased stability and higher counting rates for ^{14}C and ^{10}Be. (For example, we recently observed counting rates as high as 3200 ^{14}C ions per minute from a 1964 carbon sample; this is 50% greater than our highest rates observed heretofore.)

The ^{14}C work has been greatly facilitated by the development of a method of direct conversion of carbon to graphite by incapsulating carbon powder in Ta tubing, compressing it to about 14 kilobars, and then heating the capsule to 2,500°C. The capsule is pressed into an aluminum disk, and one end is machined off in a lathe. The samples prepared by this method give beams of the same magnitude as commercial graphite.

Further details of these and related developments are reported elsewhere.[2,3,4]

References:

* Quarternary Research Laboratory, University of Washington.

1. Nuclear Physics Laboratory Annual Report, University of Washington, (1983) p. 122.
2. G.W. Farwell, P.M. Grootes, D.D. Leach, F.H. Schmidt, and M. Stuiver, Radiocarbon 25, 711 (1983).
3. G.W. Farwell, P.M. Grootes, D.D. Leach, and F.H. Schmidt, Radiocarbon 25, 755 (1983).
4. G.W. Farwell, P.M. Grootes, D.D. Leach, and F.H. Schmidt, in Proceedings of the Third International Symposium on Accelerator Mass Spectrometry (ZÜrich, 1984), Nucl. Instrum. Meth. (to be published).

*****

8.3 Isotope Alternation System: Two-Level, NMR-Controlled Rapid Switching

G.W. Farwell, H. Fauska, D.D. Leach, and F.H. Schmidt

In the sequential transmission method of normalization in AMS (Sec. 8.2, above) the magnetic parameters of the accelerator must be alternated between their values for the lighter and the heavier isotopes with as little loss of time as possible. Rapid changing of these parameters has been effected through a combination of computer control and nuclear magnetic resonance (NMR) search and lock control.

In the current applications of the system to ^{14}C and ^{10}Be, the abundant ion (^{13}C or ^{9}Be) is monitored at the image Faraday cup ("flap") and the rare ion (^{14}C or ^{10}Be) at the 24-inch scattering chamber, which is located downstream from the flap and some distance beyond the switching magnet (Fig. 8.3-1). In changing isotopes, then, it is necessary to adjust the low-energy injection magnet ("inflection magnet"), the high-energy 90° analyzing magnet ("90° magnet"), and the high-energy quadrupole magnet, but not the switching magnet. The high-energy quadrupole magnet is computer-controlled[1] to change appropriately as the 90° magnet changes, and it is necessary, therefore, to control directly only the inflection and 90° magnets with the rapid-switching system.

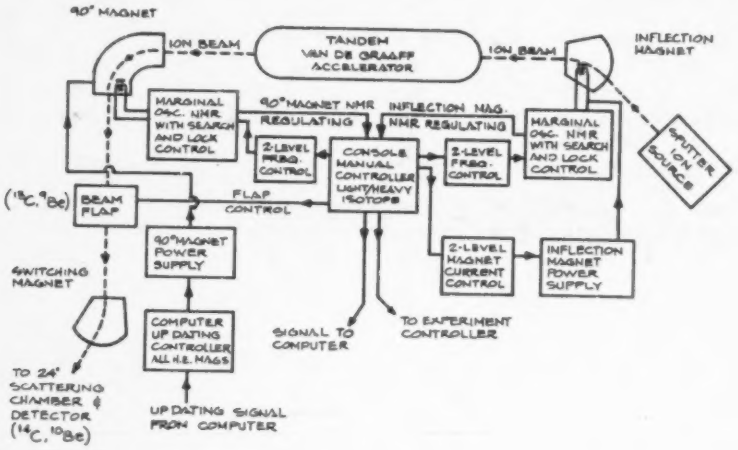

Fig. 8.3-1 Block diagram of two-level NMR-controlled rapid magnet-switching system.

The basic NMR magnet regulator system was described earlier.[2,3]

To assure fast response in the two-level rapid-switching application, we have constructed two NMR marginal oscillator controllers with search and lock features. The NMR regulator fine tuning makes use of Varicaps (voltage variable-capacity diodes); accordingly, the rapid switching circuit generates two voltage levels corresponding to the appropriate NMR frequencies for the lighter and heavier isotopes.

The rapid-switching circuit is interlocked with "in regulation" signals from both the inflection magnet and the 90° magnet; these signals, together with appropriate time delays, are used to protect the rare isotope particle detector from the abundant isotope ion beam and to optimize the actual particle counting intervals.

Because the available NMR-controlled magnetic flux correction is limited, a step current increase is given through the main power supply of each magnet when an isotope shift occurs. In the case of the 90° magnet this is accomplished through computer control, and a corresponding change is imposed on the high-energy quadrupole magnet current.

The total response time for switching between isotopes is typically seven to eight seconds.

While at present the isotope switching control is manual at the operating console, we hope to institute computer-controlled isotope switching and data collection in the near future.

A block diagram of the system is shown in Fig. 8.3-1.

References:

1. Nuclear Physics Laboratory Annual Report, University of Washington, (1981) p. 147.
2. Nuclear Physics Laboratory Annual Report, University of Washington, (1972) p. 16.
3. H. Fauska, in Proceedings of the Third International Conference on Electrostatic Accelerator Technology, edited by J.A. Martin (IEEE, New York, 1981), p. 147.

9. RESEARCH BY OUTSIDE USERS

9.1 Lifetime and Magnetic Moments of States of ^{16}N by the Recoil-into-Vacuum Method

S.S. Hanna,* B.T. Meyer,† and J.L. Thornton,*

The lifetimes and magnetic moments of some of the low lying states of ^{16}N have been measured by means of the recoil-into-vacuum technique.

In this technique the nuclear states under study are produced by a nuclear reaction. The reaction causes the excited nucleus to recoil out of the target at velocities that are several percent of the speed of light. The nucleus is stopped by a stopper (plunger), which can be set at a variable distance from the target. The γ rays that come from a nucleus that decays in flight will be Doppler shifted, while those that come from a nucleus that has stopped in the plunger will be unshifted. By determining the ratio of the shifted to total number of γ rays as a function of distance (and thus time), the lifetime can be determined.

When the nucleus is recoiling in vacuum, its spin also experiences a Larmor precession induced by the hyperfine field of the atomic electrons. For light nuclei the hyperfine field can be calculated exactly, since it is generally due to a single *1s* electron. The effect of the Larmor precession on the angular distribution can be determined by measuring the ratio of the number of γ rays detected at one angle with respect to the number measured at a different angle. The ratio of the number of counts in each detector will undergo an oscillatory pattern as the distance is varied. Since the period of the oscillations is proportional to the magnetic moment of the excited state, the g factor can be extracted.

Lifetime and moment measurements were made on the 297 keV, 3^-_1 state in ^{16}N and lifetime measurements were made on the 397 keV, 1^-_1 state in ^{16}N, with the reaction $d(^{15}N,p)^{16}N$. Measurements detecting the outgoing coincidence proton were made at a beam energy of 34 MeV, while singles measurements were performed at 20 MeV. The preliminary results obtained are (see Fig. 9.1-1):

$$\tau(^{16}N,297,3^-) = 121.2\pm3.5 \text{ psec}$$
$$\tau(^{16}N,397,1^-) = 6.46\pm0.20 \text{ psec}$$
$$g(^{16}N,297,3^-) = 0.499\pm0.025$$

References:

* Physics Department, Stanford University, Stanford, CA 94305.
† Physics Department, Stanford University, Stanford, CA 94305 and Sandia National Labs, Div. 1234, Albuquerque, NM 87185.

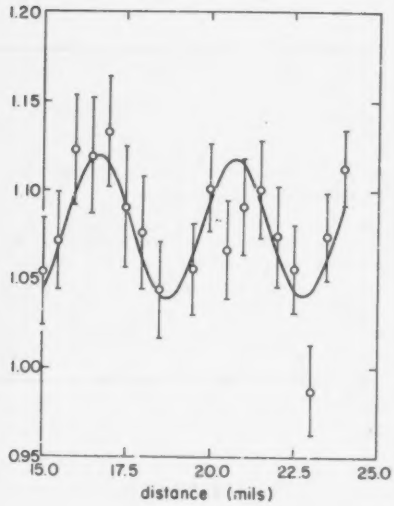

Fig. 9.1-1 Oscillation Curve of the 297 keV, 3^- state of ^{18}N. The ratio of total counts at 0° to total counts at 90°, I, as a function of stopper distance D is shown. The errors shown are statistical.

*****

9.2 Simultaneous Measurement of Nuclear Magnetic Moments by the Transient Field Method

S.S. Hanna,* B.T. Meyer,† and J.L. Thornton,*

In the past year we have completed measurements of the magnetic moments of the first 2^+ states in all even Pd and Te isotopes except ^{130}Te, which was not measured because of its small counting rate. The primary goal of these experiments has been to determine deviations from the predictions of the collective model, g = Z/A. Of particular interest was the exact dependence of the magnetic moments on neutron number N and whether this dependence agreed with predictions of the Interacting Boson Approximation (IBA)[1] and with some previous data.[2,3,4] In this regard special emphasis was placed on modifying the usual transient field method in order to obtain much reduced systematic errors. In this modified method several isotopes were measured at once, instead of the usual one per target and the resulting γ ray lines were separated with Ge(Li) detectors instead of being observed in NaI detectors. Due to the increased resolution of the Ge(Li) detectors this procedure results in a much cleaner extraction of the angular rotations from the data. In addition target dependent errors are virtually eliminated since now beam damage or target fabrication uncertainties will affect all the isotopes equally.

The results of this work are given in the table below where, following the work of Brennan et al.[2] and Dunham,[4] we have taken g(^{106}Pd) = 0.40±0.02, g(^{122}Te) = 0.36±0.02, and g(^{124}Te) = 0.28±0.03 as our calibration points.

These latter values represent averages over various Integral Perturbed Angular Correlation (IPAC) measurements for the relevant magnetic moments. The final g factors have then been determined by doing a least-squares fit to all of our data plus the calibration data for a given isotopic sequence, in which the scale factor relating observed angular rotations to g factors for each target was allowed to vary. These results along with the Z/A and IBA predictions are shown in Fig. 9.2-1.

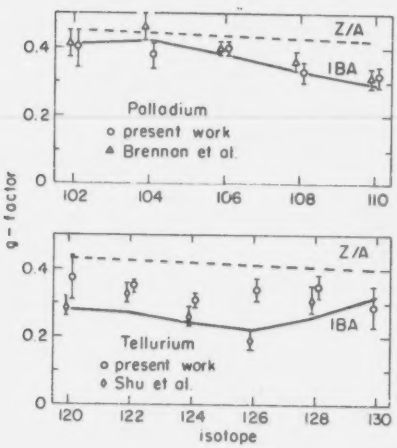

Fig. 9.2-1 Measurements of the 2^+ state g factor for palladium and tellurium isotopes. Dashed line gives Z/A; solid line gives these predictions of the Interacting Boson Approximation.

The results for the Pd isotopes are seen to be reduced somewhat from Z/A and in good agreement with the IBA predictions. They are also in good agreement with the previous measurements of Brennan et al.[2] as might be expected since the Pd targets stand up very well in the beam and thus beam damage errors should be small. For the Te isotopes the measured magnetic moments, while also below Z/A, are seen to be consistently above the IBA predictions. In addition the dip at ^{126}Te predicted by the IBA and exhibited so dramatically in the data of Shu et al.[3] is not observed either here or in the previous work of Dunham.[4] The combined data for ^{126}Te is statistically inconsistent at better than the 99% confidence level and it seems likely that this discrepancy is due to target related error in the data of Shu et al. This is especially true since Te has a very high vapor pressure and we have observed visually dramatic changes in the Te targets even after short exposures to the beam. Thus while the traditional transient field method may be satisfactory in the case of targets that stand up well in the beam, in the case where they do not a simultaneous measurement would seem well warranted.

Table 9.2-1
G-Factors for Pd and Te Isotopes
Measured g-Factors for the First 2^+ States of even Pd and Te Isotopes.

Isotope	G-Factor
^{102}Pd	0.40±0.05
^{104}Pd	0.38±0.04
^{106}Pd	0.40±0.02
^{108}Pd	0.33±0.03
^{110}Pd	0.31±0.03
^{120}Te	0.37±0.06
^{122}Te	0.35±0.02
^{124}Te	0.31±0.02
^{126}Te	0.34±0.03
^{128}Te	0.35±0.03

References:

* Physics Department, Stanford University, Stanford, CA 94035.
† Physics Department, Stanford University, Stanford, CA 94035 and Sandia National Labs, Div. 1234, Albuquerque, NM 87185.
1. M. Sambataro and A.E.L. Dieperink, Phys. Lett. B 107, 249 (1981).
2. Brennan et al., Phys. Rev. C 21, 574 (1980).
3. Shu et al., Phys. Rev. C 24, 954 (1981).
4. J.S. Dunham, Ph.D. Thesis, Stanford University, 1981.

*****

9.3 Short-Lived Radionuclides for Biomedical Research

P. Kremer,* K.A. Krohn,* and J. Link*

This past year we have continued to develop short-lived radioisotopes for biomedical research in the School of Medicine at the University of Washington. ^{18}F is being produced using the Tandem Van de Graaff accelerator by bombarding gaseous ^{20}Ne with 15 MeV deuterons. Added F_2 (1%) reacts with the nucleogenic ^{18}F to produce $F^{18}F$, a useful organic fluorinating agent. We are producing approximately 300 mCi of ^{18}F per 6 μA hours and can transfer 125 mCi from the target to a chemical reaction vessel in a hot cell. The target effluent contains no detectable ^{18}F.

Over the past year, most of the ^{18}F has been used to synthesize 2-fluorodeoxyglucose. The synthesis consists of introduction of the gaseous $F^{18}F$ into a solution of ammonium acetate. The ^{18}F as F^- is ionically complexed with the acetate and ammonium ions. Triacetylglucal (TAG) is added to this mixture and the (^{18}F)-acetylhypofluorite reacts stereospecifically with the two position of TAG. The remaining acetic acid and ammonium fluoride can be conveniently evaporated from the solution. HCl is added and the mixture is heated for 12 minutes to effect hydrolysis of the protective acetyl

groups and yield (^{18}F)-2-fluorodeoxyglucose. The compound is purified by a combination of ion exchange and silica gel flash chromatography and taken to University Hospital for studies in animals. This past year, we have synthesized ^{18}FDG nine times for use in animal studies by three different research groups. Synthesis yields are approximately 20% EOB of the fluorine removed from the target.

Fluorodeoxyglucose is of biomedical interest because it functions in vivo as an analog of glucose. The rate of cellular uptake of the fluorodeoxyglucose is essentially the same as that of glucose as is the rate of intracellular phosphorylation, but the fluorine atom on the second carbon of the hexose prevents further metabolism to fructose and smaller end products. The phosphorylation adds charge to the molecule and prevents it from exiting the cell. Thus the tracer is "metabolically trapped." The 511 keV annihilation photons of ^{18}F are convenient to detect quantitatively by both conventional and positron tomographic nuclear medicine imaging devices. (^{18}F)-fluorodeoxyglucose has been used to study in vivo kinetics and uptake of glucose in both normal and diseased animals by our biomedical collaborators. The purpose of our research is to use this tracer for measurements of tumor energy utilization in rats.

In addition to the production of (^{18}F)FDG, we have made two attempts to fluorinate desmethylimipramine (DMI) using ^{18}F. DMI is an antidepressant drug which interacts in vivo with muscarinic cholinergic, alpha adrenergic, serotoninergic and histaminic receptors. Because interaction of the DMI with these receptors causes the injected DMI to be extracted from the blood and bound to tissues, radiolabeled DMI is potentially useful as an in vivo tracer for blood flow. Thus far, our attempts to label with ^{18}F have produced an unstable compound but work is continuing on this important class of molecules.

In addition to the work with ^{18}F, we are preparing to produce ^{11}C by the reaction of protons on ^{14}N. ^{11}C is of biomedical interest because carbon is a normal component of biochemicals; compounds which are both biologically active and easy to detect quantitatively can be synthesized using this isotope. Nucleogenic ^{11}C will be heated with a catalyst to produce (^{11}C)-CO_2 which will be reduced using $LiAlH_4$ to produce (^{11}C)-CH_3OH, and then refluxed with HI to yield (^{11}C)-CH_3I. Both of these compounds will be used as precursors for synthesis of other compounds of biomedical interest. In particular, the projects which are now in preparation will involve the synthesis of (^{11}C)-fatty acids for the study of cardiac function and (^{11}C)-deoxyuridine from (^{11}C)-CH_3I for the study of DNA synthesis in tumors and surrounding tissues as a function of cytoxic therapy.

Reference:

* Department of Radiology, University of Washington.

*****

9.4 Irradiation of Optical Materials

K.L. Ballou,* C. Gulascik,* G.M. Hess,* and A.R. Tokuda,*

Samples of different optical glasses were irradiated with iodine ions for the Boeing Company. The resulting damage tracks were then etched to form a type of anti-reflecting surface. More work is planned to try to optimize the process.

References:

* Boeing Aerospace Company, Seattle, WA 98124.

******

9.5 Light Ion Irradiation Creep

E.R. Bradley,* C.H. Henager, Jr.,* E.P. Simonen,* and R.G. Stang†

The U.S. Department of Energy, Office of Basic Energy Sciences, supports a Radiation Effects on Metals and Ceramics program at Battelle, Pacific Northwest Laboratory (PNL). A light ion irradiation creep experiment, as part of the PNL research program, is being conducted at the Nuclear Physics Laboratory. Irradiation creep is defined as the time-dependent deformation of a material induced by stress during energetic particle irradiation in excess of that observed in the absence of irradiation. Pure nickel specimens were bombarded with deuterons, using the Van de Graaff accelerator, to further the understanding of low-dose irradiation creep mechanisms.[1,2]

An irradiation creep model developed to explain irradiation creep of nickel[4] has been able to rationalize all the irradiation creep data obtained during this experiment. Specimens of pure nickel with three different microstructures were irradiated at 473° K with 15 or 17 MeV deuterons.[3,4] The effects of irradiation prior to the stress application and the effects of stress increases during irradiation were studied. There was a significant effect due to initial microstructure, predicted by the model, based on the relationship of the applied stress to the yield stress of the particular microstructures.[5] Recently, the irradiation creep model has been used to rationalize low fluence creep data for 316 stainless steel irradiated with either charged particles or neutrons.[6] The model successfully predicted low fluence creep rates and low fluence microstructural evolution in stainless steel. The experiments on pure nickel, therefore, produced results applicable to more complex metal.

References:

* Pacific Northwest Laboratory, Richland, WA 99352.
† Department of Materials Science and Engineering, University of Washington.
1. P.L. Hendrick, Nucl. Instrum. Meth. 161, 345 (1979).

2. C.H. Henager, Jr., J.L. Brimhall, and E.P. Simonen, J. Nucl. Mater. 90, 290 (1980).
3. C.H. Henager, Jr., E.P. Simonen, E.R. Bradley, and R.G. Stang, J. Nucl. Mater. 117, 250 (1983).
4. C.H. Henager, Jr., Ph.D. Dissertation, University of Washington (1983).
5. C.H. Henager, Jr., E.P. Simonen, E.R. Bradley, and R.G. Stang, presented at the 3rd Topical Meeting on Fusion Reactor Materials, Albuquerque, NM, 1983, and accepted for publication in J. Nucl. Mater.
6. C.H. Henager, Jr., and E.P. Simonen, accepted for publication in the Proceedings of the ASTM Twelfth International Symposium on the Effects of Radiation on Materials, Williamsburg, VA 1984.

*****

9.6 Simulation of Cosmic-Ray Upset in Integrated Circuits

C.J. Malone,* L.S. Smith,* and J.A. Zoutendyk*

Cosmic rays are known to cause bit errors (cosmic-ray upset) in digital integrated circuit chips. Heavy ions in the cosmic-ray spectrum are the worst offenders due to their large stopping powers (de/dX). Ionized charge (electron-hole pairs) created along an ion track in a silicon chip is collected at a junction within an integrated circuit in a manner very similar to what occurs in a solid-state nuclear detector. Traversal of a particle through a digital device can cause a bit error to occur provided the collected charge is greater than a critical value (or values) characteristic of that device.

The tandem Van de Graaff accelerator was used to determine experimentally the critical charge values characteristic of a bipolar random-access memory chip. Bromine ions with kinetic energies ranging from 20 MeV to 117 MeV (the latter energy was obtained with a charge state of 12 and a terminal voltage of 9 MV) were used to simulate cosmic-ray upset in the solid-state device. The data obtained for upset cross section as a function of Br-ion energy (collected charge) were in excellent agreement with theoretical modeling done earlier.[1] Structure in the data which was predicted by the theoretical model was observed by selecting twenty-two values of Br-ion energy within the 20-117 MeV range. This experiment is the first one in which the physics governing the interaction of an ion track within a complex integrated circuit has been examined in detail.

References:

* Jet Propulsion Laboratory, California Institute of Technology, Pasadena, CA 91109.

1. J.A. Zoutendyk, IEEE Trans. Nucl. Sci. NS-30, 4540 (1983).

*****

9.7 Fast Neutron Beam Radiotherapy: Medical Radiation Physics*

J. Zenmaa,† J. Kuan,† and P. Wiest†

The Medical Radiation Physics Division continued its routine support of the treatment of cancer patients and neutron beam radiobiology studies. The neutron beam facility has been described in detail in previous reports.[1] No significant developmental or research activity took place during the year.

The facility for treatment of cancer patients was deactivated at the end of February.

References:

* Supported by NCI Grant No CA-12441

† Division of Medical Radiation Physics, Department of Radiation Oncology, University of Washington.

1. Nuclear Physics Laboratory Annual Reports, University of Washington (1972-1981).

*****

9.8 Fast Neutron Beam Radiotherapy: Clinical Program*

G.E. Laramore†

From 4/1/83 through 2/29/84, 26 patients have been placed on RTOG neutron protocols, 5 patients have been entered on an NCI-approved study (SWOG 83-67) to test the feasibility of combining chemotherapy with large dose per fraction neutron radiotherapy for non-small cell lung cancer, and an additional 12 patients have been treated on institutional pilot studies. Of the latter patients, 10 had sarcomas, 1 had a salivary gland tumor recurrent in a previously irradiated region (and, hence, was not protocol-eligible), and 1 had a malignant glioma which was treated with combined chemotherapy and neutron irradiation. The breakdown of the protocol patients is given in Table 9.8-1.

Table 9.8-1
Protocol Patient Distribution

Protocol	Patient Number
RTOG 76-08 (cervix)	1
RTOG 77-04 (prostate)	1
RTOG 79-07 (lung)	5
RTOG 79-21 (pancreas)	1
RTOG 80-01 (salivary gland)	3
RTOG 80-07 (glioma)	11
RTOG 81-10 (bladder)	2
RTOG 82-02 (head and neck)	2
SWOG 83-67 (lung)	5
TOTAL	31

Major New Findings

Lung: As of 6/1/83, protocol RTOG 79-07 had accrued a total of 110 patients. Patients are randomized to receive either conventional photon irradiation, fast neutron irradiation, or mixed beam (neutron/photon) irradiation. This study will likely be closed at the next high LET committee meeting to be held in June 1984. A preliminary analysis of the data seems to indicate a higher complete response rate for the neutron-treated patients but no improvement in median survival. The new SWOG pilot study utilized induction chemotherapy with two alternating cycles of vinblastine/mitomycin-C and vinblastine/cis-platinum prior to neutron irradiation in order to address this problem.

Prostate: Protocol RTOG 77-04 was closed to new patients entry in April 1983. A total of 95 patients were entered. This study compared conventional photon irradiation to mixed beam (neutron/photon) irradiation for patients with stage C adenocarcinoma of the prostate. A preliminary analysis indicated a statistically significant improvement in crude survival at three years in favor of the mixed beam group (82% vs. 49%) but no obvious correlation with clinically-assessed local control or time to the development of distant metastases. The significance of these findings is under study.

Sarcomas: A review of the world's literature on soft tissue sarcomas and bone sarcomas seems to indicate a much higher rate of local control with fast neutrons than would be expected for conventional photon irradiation. A total of 286 patients with large inoperable soft tissue sarcomas have been treated at the various neutron centers with an overall local control rate of 61%. Two review articles of this material are in preparation. We anticipate that sarcomas as well as salivary gland tumors are likely tumor systems to show improved local control with neutron irradiation in the next generation of studies to be carried out on the new clinical treatment facilities.

References:

* Supported by NCI Grant CA-12441.
† Department of Radiation Oncology, University of Washington.

*****

9.9 Neutron Radiobiology in Support of Radiotherapy*

J.S. Rasey†

The Experimental Biology Division of The Department of Radiation Oncology continues to perform radiobiology experiments in support of the radiotherapy of human cancer with fast neutrons. Patient treatment with the 22 MeV d+Be neutron beam from the nuclear physics laboratory cyclotron ceased in February, 1984. Patient treatment will begin shortly with the 48 MeV p+Be neutron beam from the Clinical Neutron Therapy System (CNTS) at the University

Hospital. Our studies in the past year have been directed toward determining the relative biological effectiveness (RBE) of the 22 MeV beam relative to the 48 MeV beam. The RBE for the 22 MeV d+Be neutron beam relative to ^{137}Cs gamma rays has been determined using cell survival in V79 cells *in vitro* and two *in vivo* systems, acute response of mouse skin and survival of mouse intestinal crypt cells. The RBEs obtained with these three systems at various dose levels are summarized in Table 9.9-1. RBE is defined as dose of ^{137}Cs gamma rays required to produce a particular biological effect divided by the dose of neutrons required to produce the same effect. A late responding normal tissue, rat spinal cord, was added to the RBE comparison. It was deemed important to ultimately determine the RBE for 48 MeV p+Be neutrons relative to 22 MeV d+Be neutrons for this dose limiting tissue because neutron RBEs for central nervous system damage have proven to be high.

Table 9.9-1
RBEs for 22 MeV d+Be Neutrons Relative to ^{137}Cs Gamma Rays

System	Endpoint	^{137}Cs Gamma Ray Dose, rads	22 MeV d+Be Neutron Dose, rads	RBE
V-79 cells *in vitro*	0.5 surviving fraction	675	305	2.21
	0.1 surviving fraction	1240	590	2.10
Mouse intestinal crypt cells	50 surviving cells per circumference	1275	640	1.99
	10 surviving cells per circumference	1445	770	1.88
Mouse skin	0.75 average skin response (7-35 days post radiation)	2245	1140	1.97
	1.0 average skin response (7-35 days post irradiation)	3050	1390	2.19
	1.25 average skin response (7-35 days post irradiation)	3760	1600	2.34

The ideal way to determine RBEs between two neutron beams is to irradiate the test system with two radiation sources on the same day. However, the clinical neutron therapy system is not yet available for biological testing. Our approach therefore is to do a gamma ray experiment at the same time as each neutron irradiation, so that experiments with any neutron beam can be normalized to a common photon control. This will ultimately allow determination of relative biological effectiveness for the

new high energy CNTS neutron beam relative to the neutron beam from the Nuclear Physics Laboratory which had been used for patient treatment for over ten years. These studies will facilitate transition of patient treatment from the Nuclear Physics Laboratory cyclotron to the hospital based therapy unit.

References:

* Supported by NIH Research Grant #1 R01 CA35470.
† Department of Radiation Oncology, University of Washington.

*****

9.10 Normal Tissue Neutron Radiobiology*

P.A. Mahler*

The University of Washington is one of three institutions being funded by the National Cancer Institute to examine the efficacy and feasibility of new hospital-based cyclotrons for cancer therapy with neutrons.

Past experience has indicated that central nervous system tissue is the most significant dose limiting normal tissue for neutron therapy.

We are currently conducting experiments to gain information about the new therapy beam by using damage to rat spinal cord as a measure of the beam's relative biological effectiveness (RBE). Using ^{137}Cs gamma rays, 22 MeV d+Be neutrons from the Nuclear Physics Laboratory and 48 MeV p+Be neutrons from the new hospital cyclotron we will determine the doses to produce equal levels of spinal cord damage. The ratios of the doses to produce equivalent effects

$$\frac{^{137}Cs}{p+Be} \quad \text{and} \quad \frac{d+Be}{p+Be}$$

will give measures of the RBE of the new beam compared to the two older beams. The two older beams have a base of human clinical data upon which to draw. Therefore it will be possible to estimate tolerance doses for the new neutron beam based on the experimental RBE's and the human data bases.

Reference:

* Division of Medical Radiation Physics, Department of Radiation Oncology, University of Washington.

*****

9.11 Effect of Antibiotic Decontamination of the GI Tract on Survival Time after Neutron and Gamma Irradiation*

J.P. Geraci,† K.L. Jackson,† and M.S. Mariano†

Antibiotic decontaminated and conventional rats were whole-body irradiated with 8 MeV neutrons (1.5 to 13 Gy) or ^{137}Cs gamma radiation (9 to 20 Gy). The animals were checked for survival at four hour intervals from the second to the seventh day postirradiation and at eight hour intervals on other days. After doses greater than 7.5 Gy of neutrons and 15 Gy of photons median survival time was relatively constant at 4.2 to 4.5 days, indicating death was primarily due to intestinal injury. After doses in the range of 5 to 7 Gy of neutrons and 10 to 14 Gy of photons median survival time was dose dependent and varied from 12 days to 4.5 days, suggesting a changing distribution of deaths due to intestinal injury as opposed to hematopoietic injury. Decontamination of the GI tract increased median survival time 1 to 5 days in this range of dose dependency, whereas the effect of decontamination was negligible for doses that produced mostly intestinal death. These results suggest that sepsis and endotoxin produced by bacteria from the intestinal tract play little role in acute intestinal radiation death.

References:

* Research was conducted according to the principles enunciated in the "Guide for Laboratory Animal Facilities and Care," prepared by the National Academy of Sciences-National Research Council. Work supported by Defense Nuclear Agency contract #DNA001-83-C-0009.

† Radiological Sciences Division, Department of Environmental Health, University of Washington.

*****

9.12 Measurement of Total Body Calcium by Neutron Activation

C.H. Chesnut,* B.L. Lewellen,* and R. Murano*

We have now completed 15 years using neutron activation to measure total body calcium in patients with bone wasting disease.[1] In the past year we performed 88 patient irradiations. Two therapeutic regimes were under test. Under the first regime, patients were treated with 1,25 dihydroxy calciferol (vitamin D).[2] Under the second regime, patients who had been treated with disodium chlodronate[3] were followed after withdrawal of the drug. In both studies, an equal number of untreated control subjects were followed and many other tests were performed as well as neutron activation. Since June, 1982 we have also been measuring the bone mineral in the lumbar spine by the dual photon absorbtion technique developed by Mazess of the University of Wisconsin and applied extensively by Wahner and Riggs of the Mayo Clinic.

References:

* Division of Nuclear Medicine, University of Washington.
1. Nuclear Physics Laboratory Annual Reports, University of Washington (1967-1982).
2. Hoffman-LaRoche Laboratories.
3. Proctor and Gamble.

10. ACCELERATORS AND ION SOURCES

10.1 Van de Graaff Accelerator Operations and Development

J.P. Amsbaugh, J.R. Cromie, H. Fauska, D.J. Hodgkins, D.D. Leach, C.E. Linder, G.E. Saling, F.H. Schmidt, R.E. Stowell, T.A. Trainor, T. Van Wechel, W.G. Weitkamp, and D.I. Will

Major development projects related to the tandem accelerator are described in Secs. 10.3, 10.4, and 10.5. Accelerator modifications required by the radiochronology group are described in Sec. 8.2. In addition to these projects, we have installed a new air cooled high energy cup.

Accelerator maintenance required during the past year has been quite routine. The charging belt presently in the machine seems to be the most long-lived we have had. As of April 15, 1984, this belt had run 10,300 hours.

One rather unexpected maintenance problem was pointed out by the radiochronology group. The calibration of the generating voltmeter on the tandem was found to be erratic. This was traced to deteriorating bearings on GVM motor, which had clogged up with belt dust after more than 100,000 hours of operation.

During the year from April 16, 1983 to April 15, 1984 the tandem operated 4842 hours. Other statistics of the accelerator operation are given in Table 10.1-1.

*****

10.2 Cyclotron Operations and Development

J.R. Cromie, H. Fauska, B.L. Lewellen,* R. Murano,* G.J. Rohrbaugh, R.E. Stowell, W.G. Weitkamp, and P. Wiest†

The 60 in. cyclotron is now in its 34rd year of continuous operation. Maintaining the cyclotron in operating condition required installation of a new oscillator tube, replacement of the variac coils on the main magnet power supply and overhaul of the main magnet oil circulating pump.

The new University Hospital clinical neutron therapy cyclotron is now operating so that cancer therapy operations at the 60 in. cyclotron stopped at the end of February, 1984. (See Sec. 9.7-9.11 for a description of those activities.) Calcium measurements, described in Sec. 9.12, will continue for the near future.

The machine ran 908 hours between April 16, 1983 and April 15, 1984. Other statistics of cyclotron operations are given in Table 10.2-1.

References:

* Nuclear Medicine, University of Washington.
† Medical Radiation Physics, University of Washington.

Table 10.1-1
Tandem Accelerator Operations
April 16, 1983 to April 15, 1984

Activity	Days Scheduled	Percent
A. Nuclear Physics Research		
Light Ions	96	26
Heavy Ions	76	21
Radiochronology	35	9
Total	207	56
B. Outside Users		
Battelle Northwest Laboratories	6	2
The Jet Propulsion Laboratory	6	2
The Boeing Company	4	1
Stanford University	27	7
University of Washington Department of Radiology	4	1
Total	47	13
C. Other Operations		
Accelerator Development	40	11
Accelerator Maintenance	37	10
Unscheduled Time	35	10
Total	112	31
Grand Total	366	100

*****

Table 10.2-1
Statistics of Cyclotron Operations
April 16, 1983 to April 15, 1984

Activity	Days Scheduled	Percent
Department of Radiation Oncology		
Cancer Therapy	98	53
Experimental Oncology	5	3
Neutron Dosimetry	2	1
Division of Nuclear Medicine Total Body Calcium	50	27
Department of Radiological Sciences	4	2
Nuclear Physics Laboratory	2	1
Maintenance	24	13
Total	185	100

10.3 Predicting Tandem Parameters

W.G. Weitkamp

Most modern accelerators are built so that all the beam-optics parameters such as lens and steerer settings can be set automatically by a computer. Some parts of an older machine can be retrofit relatively easily to be automatically set by a computer. An example is the system used to set the high energy magnets on our machine.[1] However, retrofitting all the power supplies of an older tandem accelerator is probably not cost effective. Never-the-less, there are many cases in which an accelerator operator can use the guidance a computer can supply, especially when the operator is inexperienced.

We are developing a program to assist an operator in setting up our tandem accelerator. The program asks a number of questions to determine the ion species and the energy required and the configuration of the machine. It then calculates all beam-optics power supply settings and predicts the beam transmission, using simple algorithms or interpolating between sets of parameters known to give a good accelerator tune. The information is printed out in a form similar to an accelerator log sheet.

The program presently works well for beams from the direct extraction ion source and is soon to be completed for beams from the other ion sources.

Reference:

1. Nuclear Physics Laboratory Annual Report, University of Washington (1983) p. 147.

*****

10.4 Crossed-Beams Polarized Ion Source

J.G. Douglas, C.A. Gossett, S.E. Kellogg, T.A. Trainor, D.I. Will, and V.J. Zeps

This ion source was to be produced by ANAC, Ltd. at Auckland, New Zealand. ANAC went into receivership in December, 1982, with work on the project only partially completed. Attempts early in 1983 to negotiate with the receiver a new contract for completion of the ion source ultimately bore no fruit, although all the interested parties were in agreement on the basic issues. This failure was due in large part to long delays in communication when various University departments acted as third parties in negotiations.

In August, 1983, negotiation turned to establishing terms whereby the the University could claim title to existing hardware. This process was completed in a period of days by telephone. The hardware was received by the University in Auckland and air freighted to Seattle in early October, 1983.

What we have received from ANAC is about 70% of the hardware required to complete the original design. This design calls for a cesium gun, a ground state atomic beam source, an ionizer region, a neutralizer/inflector region and a spin precessor. In addition are required power supplies, racks, support stands, vacuum hardware, and control systems. Although only 30% of the hardware remained to be completed upon shipment, these items usually involved difficult design decisions which had not been made.

In the initial period after shipment these design questions were addressed, and negotiations were carried out with two sub-contractors, one to finish fabrication of some sub-assemblies and furnish specific designs, the other to provide software for the three control computers and to furnish the services of a controls technician to expedite wiring the source. These contracts were in place by the end of February, 1984.

To date, the ion source parts have been uncrated and assembled to the extent possible in an off-line area. Electrical power and cooling water have been delivered to the site. Cable ways have been designed and installed. Missing power supplies and vacuum hardware have been purchased and delivered. The control software has been completed and delivered. The power and control wiring is being installed.

Concurrently a major design effort is in progress. All detailed ANAC designs have been reviewed and significant changes or additions made based on operating experience at this and other laboratories with similar hardware. The goal, in addition simply to providing designs which did not exist, is to produce a device with good electrical and temperature stability and relatively easy maintenance at reasonable intervals. As an example, the cesium gun output beam can contain as much as 2 kW of power. This must be disposed of very carefully within the ion source under all operating conditions. Failure to do this properly will result in thermal instability, sputtering, melting, and outgassing.

In the immediate future, the atomic beam source assembly will be completed. This unit will then be powered up and its performance optimized. In about two months delivery of Cs gun parts should commence. In September, 1984 it should be possible to operate the Cs gun and atomic beam source together and optimize negative polarized beam output. Allowing about two months for this process and two months for installation on the accelerator system we foresee on-line use of the polarized source by end of 1984.

*****

10.5 Sputter Source Elevation

P. James, T.A. Trainor, D.I. Will, and F. Willis

The elevation of our sputter source to improve beam transmission through our FN tandem, as mentioned in last year's annual report,[1] was largely completed and evaluated in the fall of 1983. The original 25 keV source, its frame and vacuum system, associated isolated power supplies, their rack, deionized cooling water lines, light pipe telemetry, the 100 keV Dowlish accelerating tube, and the 10 kVA isolation transformer have all been tested to 60 keV elevation (for a total injected beam energy of 85 keV.) In this test, no detectable corona or sparking was noted and the elevated source appears to be fully capable of operating at this injection energy. However, we have determined that our electrostatic quadrupole triplet injection-lens power supply is incapable of achieving the voltages required to focus and steer an 85 keV beam into our tandem. As a result, we are currently operating at 30 keV elevation for an injection energy of 55 keV, the highest energy beam our quadrupole triplet will focus adequately. Keeping the low energy beam current constant and raising the injection energy from 25 keV to 55 keV results in an increase in high energy beam current to 2.7 times that achievable at 25 keV. The slope of the measured curve of transmission as a function of injected beam energy suggests that operation at the full 85 keV injection energy design point might result in still better transmission. As a result we may upgrade the quadrupole triplet and its power supplies for operation at higher focusing voltages.

Reference:

1. Nuclear Physics Laboratory Annual Report, University of Washington (1983) p. 72.

11. NUCLEAR INSTRUMENTATION

11.1 Design and Construction of Electronic Equipment

H. Pauska, J. LaCroix, R.E. Stowell, T.D. Van Wechel, and M.R. Walker

The following major electronics projects were carried out and are described in detail in the indicated sections of this report.

a. The hardware interface for the laboratory data collection system was rebuilt (see Sec. 12.3).

b. A two-level NMR controlled rapid switching system was built for the radiochronology group (see Sec. 8.3).

c. Design of the electronics for the pre-tandem buncher for the linac has been initiated (see Sec. 13.5).

Several additional electronic projects were undertaken:

a. Two 5 MHz heads were constructed for the deposition monitor in the target laboratory.

b. Four NIM bin power distribution modules were constructed.

c. Two expanded computer terminal patch panels were constructed and installed for the DEC 11/60 and the VAX, featuring LED's to indicate which terminals are active.

d. The number of computer terminal outlets in the laboratory has been expanded.

e. Additional high quality 50 ohm cable systems have been installed between the counting rooms and cave areas.

f. The second set of six beam scanners, partly constructed last year,[1] was completed and installed for cave and beam line areas.

g. A double balanced mixer circuit with gain was constructed for testing the linac cavity.

h. Extensive filtering of critical logic lines on the electronics associated with the momentum filter was installed to prevent spurious and random changes in current settings from occurring.

i. As a result of source elevation (to 30 kV), two channels of lab built light pipe telemetry were added to the sputter ion source. This was accomplished using commercially available Hewlett-Packard light pipes and lab built voltage to frequency converters.

j. The Van de Graaff GVM rotor and stator are being replaced with gold plated units to stabilize the dielectric properties of the suface materials and thus give a more correct voltage output. The plating has been completed but the unit has not been installed or tested yet.

k. Several additional light safety flashers were built for use at various hazardous areas in the laboratory.

Reference:

1. Nuclear Physics Laboratory Annual Report, University of Washington (1983) p. 80.

*****

11.2 Construction and Testing of a Breskin Counter

D.D. Leach

A Breskin type multiwire proportional chamber of 2 × 2 cm has been built and successfully tested. This counter uses two aluminized hostaphan foils operated at ground potential and separated by 6 mm. Midway between these two foils is a harp of 20 μm gold-plated tungsten wires on 1 mm centers. These wires are all connected to a common bus.[1,2] During operation 1-2 Torr of P-10 gas was circulated through the counter and +490 V was applied to the wire harp. The harp signal was amplified with a fast preamp and fed into a constant fraction discriminator. This signal was compared to a signal from a silicon surface barrier E detector. Time resolutions of 220 psec and 240 psec were recorded for 68 MeV ^{16}O and 94 MeV Br respectively.

References:

1. A. Breskin et al., Nucl. Instrum. Meth. 165, 125 (1979).
2. A. Breskin, Invited talk at the Hans Geiger Symposium on Detectors in Heavy Ion Reactions HMI-Berlin, October 1982, to be published in Lectures Notes in Physics, Springer-Verlag.

*****

11.3 Use of the LED-PIN Diode Light Pulser for Gain Stabilization of the 10" × 10" NaI Spectrometer

D.H. Dowell, C.A. Gossett, and K.A. Snover

As interest in studies of the statistical decay of the giant dipole resonance increases (see also Sec. 3.1-3.9), the long term gain stability of the 10" × 10" NaI spectrometer has become particularly important. These studies involve the measurement of gamma-ray spectral shapes which vary by six orders of magnitude over a gamma-ray energy range of ~20-30 MeV, but which have no prominent lines with which to monitor the NaI detector gain. In addition, (p,γ) studies of excited-state giant resonances (see Sec. 3.5), in which the gamma-ray spectra exhibit lines from many closely spaced states, also benefit from improved gain stability and from improved detector resolution resulting from a more stable gain.

We have recently begun routine use of an LED-PIN diode light pulser system for gain stabilization of the NaI spectrometer. The designs of the LED driver circuit and LED stabilization are described in an earlier annual report.[1] A special optical fanout bundle is used to couple a single LED to the seven photomultiplier tubes on the NaI detector. The tubes are "back-illuminated" by shining the LED light through the glass wall onto the rear of the photocathode,[2] and with proper matching of the optical couplings, the light is uniformly distributed among the phototubes. The couplings of the LED to the fiber bundle and to the PIN diode are balanced in such a way as to

allow for a good signal-to-noise ratio in the PIN signal, while operating the LED over a wide dynamic range up to effective gamma-ray energies well above 50 MeV.

Commercial gain stabilization units made by Williams and Harris are used for both the LED and NaI stabilization. The light output of the LED pulser is regulated with the signal from the PIN diode which is processed with a home-built preamp and a Tennelec TC203 BLR amplifier. The LED component of the NaI linear energy signal is used to control the detector high voltage power supply. The shape of the LED pulse[1] is designed to match the pulse shape of true gamma rays in the detector. Detector events from the LED are treated identically to gamma-ray events in the timing and linear signal processing electronics, so that the LED amplitude distribution in the NaI spectrum serves as a realistic indication of pileup.

Our experience with the gain stabilization system over the past few months indicates that the long term regulated stability of the NaI is better than 0.5%. In addition, no short term gain shifts are observed associated with varying detector rates in the range from 2 to 160 kHz, leading also to upper limits of 0.5%. An amazing aspect of our present operation is that the PIN stabilization circuit rarely provides a measurable correction, indicating that the intrinsic LED amplitude stability is very good. Currently we obtain a stabilized NaI detector resolution of 3.3% FWHM for 22.6 MeV gamma rays collimated to illuminate the full detector diameter at a depth of 8". When the collimation geometry is chosen to illuminate ~90% of the rear face of the detector, the resolution is 2.6% for 22.6 MeV. While we are quite pleased with the improved detector performance, further improvements are desirable such as the elimination of a small dependence of the Williams and Harris units on LED rate, and also the incorporation of a zero-level stabilization system.

References:

1. Nuclear Physics Laboratory Annual Report, University of Washington (1982) p. 161.
2. Nuclear Physics Laboratory Annual Report, University of Washington (1983) p. 84.

*****

11.4 Improvement and Testing of the Momentum Filter

J.P. Amsbaugh, K.J. Davis, T. Murakami, and D.W. Storm

During the past year we have made a number of modifications which permit easier and more reliable operation of the momentum filter. Leaks in two welded bellows in the quadrupole vacuum ducts were discovered. In order to replace these it was neccesary to dismantle the quadrupole magnets and completely remove the vacuum ducts so that new bellows could be welded in place. Indium wire seals which had been used in the scattering chamber also

were found to develop leaks after cycling the vacuum. These were replaced by aluminum wire seals except for the 0 degree face of the scattering chamber which now has a rubber O-ring seal to permit easy exchange of the Faraday cup and 0 degree port. We also had to replace the cryopump on the scattering chamber. In addition we devised a technique for mounting the Bragg Curve Spectrometer (BCS) at the final focus without significantly affecting the vacuum throughout the rest of the system. This involves the introduction of a second Mylar window in front of the detector entrance window and using a roughing pump to evacuate the region between the two windows. With the scattering chamber open to the beamline and the BCS mounted and operating we were able to maintain a vacuum of 1×10^{-6} Torr in the scattering chamber, 1×10^{-7} Torr at the dispersed focus and 6×10^{-7} Torr at the final focus.

It was discovered that when the power supply was operated at its maximum current of 400 A, the circuit breaker would trip and fuses in both the primary and secondary circuits would burn out. This problem was corrected by improving the electrical joints by using copper rather than aluminum lugs, using joint compound and by periodically checking the tightness of the connections. We were able to substantially reduce the number of errors in the magnet control by putting filters on the clock lines to the DAC's in the shunt control circuitry. More careful magnetic field measurements were made which allow the fields to be set to an accuracy of a few parts in 10^4. This requires that the magnet currents be set to 400 A and then slowly stepped down to the desired current setting. This procedure is automatically carried out by a new FORTRAN program with which the experimenter interacts. This program allows the option of setting the fields by requesting a particular momentum to change ratio value for the central ray.

By running a particle beam directly into the momentum filter we were able to determine ray trajectories at the dispersed focus by measuring currents on moveable pins and at the final focus by measuring beam positions on a plastic scintillator. These measurements confirm our previous findings that the foci are down-stream of their predicted positions. This situation can be corrected somewhat by reducing the quadrupole currents by between 10 and 15%. A few attempts were made to use the momentum filter at 0 degrees. These proved to be unsuccessful because of an unacceptably large count rate at the final focus resulting from slit scattering from the collimators and charge exchange in the momentum filter. More recently a successful preliminary measurement of the $^{16}O(^{27}Al, ^{28}Si)^{15}N$ reaction was made at 10 degrees (see also Sec. 4.5).

*****

11.5 A Polarimeter for the Momentum Filter

C.R. Christensen, T. Murakami and W.G. Weitkamp

Testing the proton polarimeter for use with the momentum filter described in last year's Annual Report[1] has continued. The polarimeter uses elastic scattering from ^{4}He with vanes to restrict scattering to angles centered around 60°. The detectors are 114 by 6.4 mm disks of NE 102 plastic scintillator viewed by photomultipliers.

We have found that the plastic scintillators are too sensitive to neutrons. A small proportional counter has been installed in front of the polarimeter so we can use coincidence between this counter and the scintillators to reduce neutron induced background. We have also tested other scintillator materials. CsI is about 100 times less sensitive to neutrons than either NE 102 or CaF. CsI scintillators may be installed in the polarimeter in the future.

The focal properties of the momentum filter appropriate to the polarimeter have also been measured. Use of the polarimeter on the momentum filter will require maximum solid angle, minimum spot width at the final focus and minimum deviation between the the average direction of the particles emerging from the final focus and the axis of the polarimeter. To measure these properties, we placed energy absorbers at the final focus in such a way that the particle energy detected in a downstream detector was related to the position at which the particle crossed the final focal plane. We found that both the maxium solid angle and the minimum spot size occur when the magnet is set for a central-ray momentum 9% higher than the actual particle momentum. We also found that the angle between average particle direction and the polarimeter axis is 0.5°, which is within acceptable limits.

Reference:

1. Nuclear Physics Laboratory Annual Report, University of Washington (1983) p. 77.

*****

11.6 Target Preparation

G.M. Hinn

In Table 11.6-1 are listed a few of the more interesting of the 210 targets prepared in the Laboratory last year.

Table 11.6-1

Target	Starting Form	Final Form	Method of Preparation	Backing	mg/cm^2 Thickness
^{9,10}BeO	Ice, Alaska South Pole and carrier ^{9}Be	^{9,10}Be	chelex ion exchange	none	1,5
Ti^{15}N	Ti metal	Ti^{15}N	^{15}N nitriding high temperature	S.S	1
^{28,30}Si	oxide	elemental	reduction E-bombardment	S.S.	1,2.3
^{52}Cr	oxide	metal	H-reduction E-bombardment	S.S.	1.5
^{51}V	metal	metal	E-bombardment	S.S.	0.5
Al_2O_3	metal	oxide	anodization	S.S.	0.2
^{88}Sr	carbonate	oxide	reduction evaporation	100 μg/cm^2 Au	0.05
^{39}KI	salt	salt	evaporation	20 μg/cm^{2}C	0.1
^{238}U	salt	metal	anodization	102 μg/cm^2 Ni	0.3
^{nat}Mn	metal	metal	E-bombardment	S.S.	1

a. Beryllium. We continue to use powdered silver mixed with ^{9,10}BeO to produce souces for accelerator radio dating of Alaskan and South Polar snow. Currently, we are trying to increase production by multiple sample processing.

b. Cracked ethylene stripper foils. We now routinely make 3 μg/cm^2 cracked slacked carbon stripper foils. Most heavy ion experimenters prefer thinner foils because of greater transmission. Experience with stripper foil below 3μg/cm^2 in thickness has shown erratic and poor transmission.

c. Thick 1-2.3 mg/cm^2 ^{28}Si. Research has continued with some degree of success in making enriched ^{28}Si targets starting with the oxide. Further work is being done with electron beam annealing and thermal annealing to extend shelf life beyond 2-3 weeks.

12. COMPUTER SYSTEMS

12.1 Data Acquisition System Enhancements

E.G. Adelberger, R.S. Peabody,* and R.J. Seymour

Our principal data acquisition system consists of a DEC PDP 11/60 computer with two 5 megabyte RL-01 disks, a 1600 bpi 75 ips 9 track tape drive, a Printronix P-300 printer/plotter with a Trilog Tektronix hardcopy board, a DEC VT-11 graphics display, a Tektronix 4006 terminal and a BiRa MBD-11 controlling a CAMAC crate to connect with twelve Tracor Northern TN-1213 ADCs. 15 NPL-built 75 MHz scalers are read via an IEEE-488 bus interface.

New Data Acquisition Hardware

New data acquisition hardware for the DEC 11/60 includes an HP 3582A Spectrum Analyzer and two more LeCroy 2551 CAMAC Scalers.

Additional user control of the SINGLES display was obtained by installing a 20-key keypad to facilitate and extend the control available with the VT-11's light pen. This allows control such as moving the "penned" point in steps smaller than the display's resolution.

New Data Acquisition Software

a. The MBD-11 was reprogrammed to allow snapshots of a LeCroy 2256a Waveform Digitizer into both SINGLES spectra for set-up and MULTI histograms and events for investigating subcoulomb heavy ion proton transfer reactions.

b. Another custom SINGLES MBD program was generated for repetitive reading of the LeCroy scalers for use in the ^{14}N parity experiments (see Sec. 5.4). The SINGLES data structure has been given an additional data type to contain the LeCroy scaler totals. A section of the VT-11 display program was created to display status information and the totalized results of the runs.

c. Another SINGLES MBD program provided selectable routing of one ADC's reading based upon a TAC's output. It made use of coincidence gating of the lab-built ADC interface while running in an overall SINGLES software environment. Although originally used for measurements of the statistical decay of giant dipole resonances, (see Secs. 3.2-3.6), this program has also been used by other experiments.

d. Another SINGLES MBD program provides for 50 microsecond delays and decisions based on multiple ADC "hits" and the resultant readings (see Sec. 1.6). The "decisions" produce "routing" biases placed on some of the ADCs' readings.

An Apparent MBD "Bug"

The heavier use of custom-generated MBD programs has occasionally uncovered hardware bugs in the MBD-11 itself. These involve the MBD-11 processor improperly reading or modifying a minus one (-1) in some locations of its memory. The short-order fix has been to pad programs with zeros to move the -1's to less sensitive areas. Attempts to isolate the problem have been unsuccessful so far.

Programming Considerations

We try to have our experiments run with lab-standard software to avoid "version drift" as features are added or bugs are fixed. The increased control required by newer experiments has forced us to bend this rule on occasion. Some programs, such as the VT-11 display driver, remain lab-standard with additional subroutines for the experiment-specific functions. Others, in particular the MBD-11 CAMAC controller, require completely custom programs, although they are usually developed from the lab-standard programs' skeletons.

As people began to use more customized SINGLES-like software groupings, procedures were created to allow relatively transparent switching from one environment to the next. This was done by providing experiment-specific accounts which established their own environment as a part of the log-in procedure. Thus the computer verb "END" can invoke different results for different experiments, but the people just know that "END" will stop their current data collection cycle.

More use is being made of the inter-computer parallel link. Two experiment groups use it for automatic during-run transfer of intermediate files to the VAX for further processing. This provides both relief from a permanent lack of disk space on the 11/60 and provides access to the advanced environment of the VAX. One of these experiments uses spectra collected by the HP 3582A spectrum analyzer, read over the IEEE bus to the 11/60 and sent to the VAX for analysis.

Control of the Momentum filter has been achieved, and is discussed in Sec. 11.4 of this report.

Reference:

* Present Address: Department of Chemistry, University of Washington.

*****

12.2 Data Analysis System Enhancements

E.G. Adelberger, E.F. Garman, M.N. Harakeh, A. Lazzarini, M.J. Murphy, R.S. Peabody, D.A. Patterson, and R.J. Seymour

Our data analysis system consists of a DEC VAX 11/780 with dual RK-07 disks, a SI Eagle disk, three 9 track and one 7 track tape drives on Western Peripheral controllers, a Printronix P-300 printer/plotter and an AED-512 color graphics display.

Hardware Developments

The principal hardware change was the installation of a Systems Industries Fujitsu Eagle disk system directly attached to the VAX's SBI data path. This replaced the Unibus-attached Systems Industries CDC 9766 system. This raised our user disk space from 256 megabytes to 414. This expansion has allowed more software aids and system programs to be available at all times. It has also speeded up the system by utilizing a much faster datapath between the disk drive and the VAX's memory. It also avoids long searches across the disk for free space.

We had been borrowing a megabyte of VAX memory from the Chemistry Department. When they reclaimed it we lost 40% of our user space, with a consequential slowdown in system speed. We have recently purchased a megabyte of our own to bring us back to 3.25 megabytes. This is fairly closely balanced to our current load.

We have begun the change from VT-52 emulating terminals to VT-100 emulators, some with Tektronix 4010 graphics emulation. This allows more efficient editing and more distributed graphics displays. We had many demonstration units brought in. They all had some bugs somewhere and part of the evaluation procedure was the vendor/manufacturers' response to the problems we had. We bought three Graph-On 140 s and three Micro-Term 301 s.

We have developed informal resource sharing with the UW Physics Department VAX to make use of their 6250-bpi tape drives. This allows us to read tapes generated at the Brookhaven National Laboratory.

We have installed the AED-512's DMA board. We have solicited and received three software drivers from other sites (Jet Propulsion Laboratory, Michigan State University and Oxford University), but lack of programmer time has prevented us from testing or installing any of them.

We have replaced our 300 baud modem with a USR Password 300/1200 baud auto answer/autodial modem. This allows our VAX to call other computers for direct file transfers. We have installed the program HOST to control the modem from a local terminal. This has proved faster and more convenient than transferring tapes.

Software Developments

We have installed Mathematical Sciences Northwest's Superscript word processing package with its requisite Santec Variflex printer. This program was made available to the University by the manufacturer.

We are doing some of the Laboratory's budgeting calculations with a spreadsheet program CCALC. This program was acquired in return for providing some media transfer services and beta-site testing to the authors, Digitec Software Design.

The supported analysis programs were expanded and modified through user request and direct user efforts. The SINGLES analysis program HP has been modified to provide more functions and to handle stripping the SINGLES spectra from MULTI tapes. The two-dimensional analysis program SPAN's display section now asks if the user is on the AED 512 color terminal. If so, the z-axis information is displayed as color instead of variable density pixel patterns used on the Tektronix.

The standard multiparameter sorting program MUSORT has been given more custom "front ends" to read other labs' data tapes. TRIUMF's sorting program MOLLI has begun to gain acceptance, particularly for its ability to selectively display sorted events on a display. MOLLI's display has been modified to use color to show the time sequencing of the displayed events. Also, MOLLI was given MUSORT's front end for reading Laboratory tapes.

To aid users who want to write their own spectrum analysis programs we provide READEM. This subroutine performs all of the esoteric dirtywork needed to untangle any of the known singles-type data structures and tape formats people commonly bring into the Laboratory. It presents the extracted data in a standard form as well as in raw form for quick incorporation of new types as they are generated. Another subroutine READALL can serve as an outer shell for READEM by performing all of the terminal question and answer protocols, calling READEM and finally spliting the results into specific COMMON areas for the user to access. READALL provides the simplest user programming interface for standard operations, while READEM provides the maximum flexibility, yet shields the users from having to understand and coherently handle the linked-list SINGLES data structure and its look-alikes.

Cascades simulates and analyzes compound nuclear decay. It had been brought to the Laboratory before, but last year saw a major revision imported from KVI and modified for running on our VAX.

A general purpose graphics program FIGURE was imported from Oxford and built into DRAW, a command-file driven program for transferring a list of numbers to a well-formed, well-labeled curve.

Another Oxford import AUTOFIT has received work to make it far friendlier and bug-free than it was in its original form. It performs curve fitting on singles spectra.

Reference:

* Present Address: Department of Chemistry, University of Washington.

*****

12.3 Hardware Enhancements to the Laboratory Data Collection System

R.J. Seymour, R.E. Stowell, and T.D. Van Wechel

The core of the laboratory data collection system consist of 12 commercial Tracor Northern 200 MHz ADC's interfaced to a DEC PDP 11/60 computer. The operation of this system has been described in detail in earlier annual reports,[1] but to summarize, the experimenter may select any or all of the 12 ADC's to perform the following:

MODE 0 : ungated singles spectra acquisition.
MODE 1 : gated singles spectra acquisition.
MODE 2 : gated multicoincidence spectra acquisition.
MODE 3 : gated singles spectra acquisition until a multicoincidence occurs whereupon the hardware aborts and clears any singles events that may be in progress, enabling selected ADC's to receive the multicoincidence event.
Mode 4 through Mode 9 : currently ADC lockout. Allows for future expansion.

Modes 0 and 4 through 9 are new to this interface. Selected groups of ADC's may be run in any of the various modes simultaneously.

Enhancement of this data collection hardware consisted of redesigning and constructing a new chassis for the ADC computer interface. This was done to: (1) increase reliability of the system, (2) incorporate all the changes that have occurred over the past four years, (3) provide a system that would allow in-rack diagnosis and board swap repairs, and (4) provide extra room and connector and mode switch capacity for future expansion. This interface also provides a number of monitoring jacks and diagnostic lights to allow quick identification of system malfunctions. Construction has been completed and was accomplished using commercial vector card cages and wire wrap p.c. boards, flat ribbon interconnecting cables and mass terminated connectors. The unit has been installed and tested and has been in operation for the past few weeks. Aside from some required minor modifications, the interface works well and has met its design criteria.

Reference:

1. Nuclear Physics Laboratory Annual Report, University of Washington (1982) p. 178.

12.4 A Continuous-ℓ Optical Model Program

J.G Cramer

In the study of heavy ion scattering it is often of interest to examine in detail the optical model S-matrix and functions derivable from the S-matrix such as the quantal deflection function $\langle\Theta\rangle_\ell$. A problem which immediately arises in investigations is that the independent variable of the S-matrix, the orbital angular momentum ℓ of the scattered system, is quantized in units of $\hbar$. For this reason, the S-matrix cannot be studied as a continuous function, and the deflection function $\langle\Theta\rangle_\ell$ can be approximated only by rather crude numerical differentiation with respect to ℓ.

However, there is a way of dealing with this problem. The orbital angular momentum ℓ appears in three roles in the partial wave numerical solution of the Schroedinger equation: (1) in the Legendre polynomials $P_\ell(\cos\Theta)$ which are the expansion basis of the angular dependence, (2) in the centrifugal potential $\ell(\ell+1)/kr$, and (3) in the regular and irregular Coulomb wave functions $F_\ell(\eta,\rho)$ and $G_\ell(\eta,\rho)$ and the Coulomb phase shift σ_ℓ. For evaluation of the S-matrix, only (2) and (3) are relevant. In the centrifugal potential there is no problem with treating ℓ as a continuous variable. For the Coulomb functions there is also no problem in principle, but the usual way of evaluating these functions employs recursion relations which depend on the unit quantization of ℓ. However, an alternative way of evaluating Coulomb wave functions and phase shifts for arbitrary real or complex values of ℓ has been developed at this Laboratory in connection with the investigation of relativistic dynamic effects in heavy ion reactions.[1] We have employed these relativistic Coulomb routines to de-quantize the orbital angular momentum ℓ and treat it as a continuous variable.

We have developed the computer program DEFL which evaluates the optical model S-matrix and the quantal deflection function in arbitrarily small steps of ℓ. Fig. 12.4-1 shows an Argand diagram of the "continuous" S-matrix calculated for the $^{16}O + ^{16}O$ system at 40 MeV, using the well known Gobbi potential developed at Yale.[2] The kinks in the S-matrix reflect shape resonances generated by the potential.

References:

1. Nuclear Physics Laboratory Annual Report, University of Washington (1977) p. 180.
2. A. Gobbi, R. Wieland, L. Chua, D. Shapiro, and D. A. Bromley, Phys. Rev. C 7, 30 (1973).

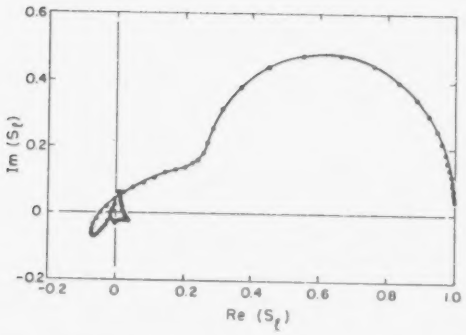

Fig. 12.4-1 A continuous-ℓ Argand diagram of the S-matrix for $^{16}O + ^{16}O$ at 40 MeV, calculated using the Gobbi potential.

13. BOOSTER LINAC PROJECT

13.1 Introduction:

D.W. Storm

During the past year the DOE awarded us a contract to build the superconducting booster proposed in 1982.[1] Although the majority of the funds ($8M) for the project are construction funds included in the DOE contract, part of the project is to be done with state funds ($1.03M) and part with operating funds (3 FTE personnel as well as costs of prototyping the resonators). Therefore it is appropriate to outline the progress in this report. The overall design was changed somewhat from that described in last year's Annual Report. Instead of 12 split ring resonators optimized for beta = 0.10 and 12 for beta = 0.16, we have chosen to use 16 quarter wave resonators optimized for beta = 0.09 and 16 for beta = 0.18. The quarter wave resonators, which have two accelerating gaps instead of the three of the split rings, have a wider transit time factor, which is favorable for accelerating a broader range of particle masses. The quarter wave resonators are to be built of lead plated copper, following the design of Ben-Zvi and Brennan.[2]

The main effort to date, besides planning and design, has been the construction and testing of a prototype low beta resonator and the preparation of and signing of a contract for the helium refrigerator. Following the overall planning and design of the entire project,[3] completed specific planning and design work includes preparation of a design for a plating lab which is under construction, and preparation of specifications for magnets for the part of the beam transport system between the tandem and the LINAC. A mechanical design for a low energy buncher (following the Argonne National Laboratory design[4]) has been completed, and the electronic design is underway. Also, design work for equipping a facility for testing resonators has nearly been completed. In progress are designs which will lead to contracts for production of cryostats and a cryogen delivery system, as well as designs of the control system. The specifics of this work are presented below.

References:

1. Nuclear Physics Laboratory Annual Report, University of Washington (1982) p. 130.
2. I. Ben-Zvi and J.M. Brennan, Nucl. Instrum. Meth. 212, 73 (1983).
3. Conceptual Design Report Superconducting Booster, Nuclear Physics Laboratory, University of Washington (1983).
4. P.J. Lynch, R.N. Lewis, L.M. Bollinger, W. Henning, and O.D. Despe, Nucl. Instrum. Meth. 159, 245 (1979).

*****

13.2 Design and Construction of Superconductor Resonators

I. Ben-Zvi,* T. Goliak, D.W. Holmgren, and D.W. Storm

A low beta resonator was fabricated at the Nuclear Physics Laboratory, then plated and successfully tested at Stony Brook. The basic design (see Fig. 13.2-1) is a quarter wave, cylindrical cavity excited by a magnetic coupling loop. Before the copper prototype was made the exact design parameters were measured by the construction and RF testing of a brass model.

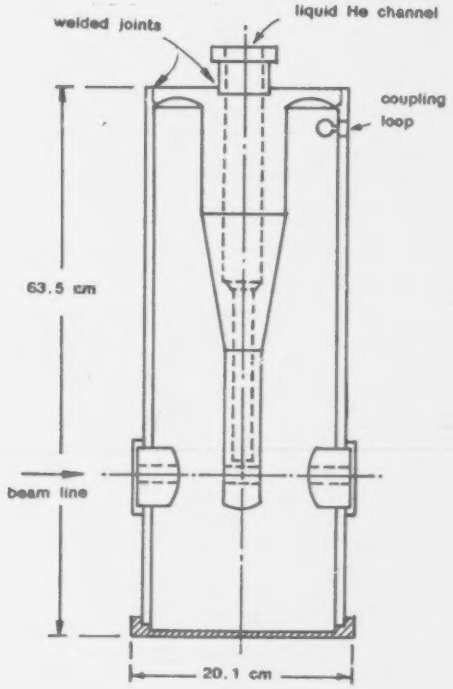

Fig. 13.2-1 Low beta resonator.

When the exact parameters of the design were finalized, the parts of the resonator were fabricated in the NPL shop with the first set of drift tubes made by the Weizmann Institute in Israel. An electron beam welding development program was completed with a contractor in California and the machined parts were then welded into the resonator. The drift tubes were brazed into place and the resonator was ready for polishing, plating, and rf testing at Stony Brook.

The design for the low beta resonator was taken from the Brennan and Ben-Zvi quarter wave resonator design,[1] with a change in the inner diameter of the outer conductor from 16 to 18 cm. The center conductor and drift tube geometry was identical to that used by Ben-Zvi. The extra 1 cm in radius was put into the gap between the center and side drift tubes. It was felt that this would decrease the surface fields on the center conductor. In retrospect, it appears that the gap is not the controlling element for the surface fields. To maintain the same average accelerating field with the larger diameter, the voltage on the center drift tube is increased proportionately. The surface field near the bottom of the drift tube is consequently higher than in Ben-Zvi's version, and that is where the maximum field is probably found.

Essentially, the high beta resonator is the same as the low beta one, except the diameter is twice as big. Since the drift tubes break the cylindrical symmetry, however, some thought must go into their design. Their length along the beam is about double, although the beam hole radius need not be changed. Thus one has the opportunity to change proportions substantially. Furthermore, one has the opportunity to extend the center drift tube somewhat more into the gap than it goes on the low-beta resonator. Finally, one must take into account the fact that the capacitive loading of the resonator will increase proportionately with the radius.

In order to guide the development of the drift tube geometry, we have performed a simple numerical calculation to predict the frequency of a tapered quarter wave resonator with various values of capacitive loading. By comparing with actual results we can determine the capacitive loading. Also, we have developed an electrostatic calculation to determine surface fields in an azimuthally symmetric model. Both calculations agree that the loading of the low beta resonator is 1.6 to 1.7 pF. This corresponds to about 7 degrees of phase angle at the high voltage end of the resonator. The electrostatic model gives guidance regarding the effects of various radii of curvature on the peak surface fields.

For the electrostatic calculation, the resonator is idealized as azimuthally symmetric. The geometry is characterized by the radii (r_i, r_o) of the inner and outer conductors, the longitudinal gap (g) between conductors and the end radius (r_e) of the center conductor. One can chose $r_e > r_i$ to represent the drift tube as part of a sphere. One can also compare results with various r_e smaller than a fixed r_i to learn about the effects of smaller curvatures on the end of a cylindrical structure.

The relaxation procedure solves the Poisson equation for Dirichlet boundary conditions. The volume of interest is bounded by the conductors and the plane at z_{max}, where the potential is set to the logarithmic radial dependence of infinite coaxial cylinders.

The results of the calculations suggest various center drift tube geometries which will provide lower ratios of peak surface field to average accelerating field, without excessive capacitive loading. These options will be tested with a model.

A full scale brass model has been completed for the development of a high beta resonator. As well as helping to optimize the drift tube shape, this model will be used to enable us to obtain parameters for a copper prototype resonator which will resonate at the same frequency as the low beta resonator. When this development effort is completed, the high beta resonator will also be polished, plated, and rf tested as was the low beta resonator.

References:

* Weizmann Institute, Rehovot, Israel.

1. I. Ben-Zvi and J.M. Brennan, Nucl. Instrum. Meth. 212, (1983) 73; and I. Ben-Zvi, private communication.

*****

13.3 Lead Plating of the Low Beta Resonator

J.M. Brennan,* D. Corcoran, R. Coughlin,* T. Goliak, D. Hodgkins, P. James, A.G. Seamster, and J.H. Secora

Plating operations were performed at the lead plating facility at SUNY, Stony Brook. Initial procedures were based on the previous experience of prototype development by Ben-Zvi and Brennan.[1] Several attempts were made to produce satisfactory results, however the lead surfaces were consistently stained and lacked the bright metallic finish routinely achieved with the split loop resonator at SUNY. An unacceptable amount of particulate was also observed on the copper shorting plate, presumably originating at the surface of the lead anode. Two independent cold tests produced results which were below our requirements. The poor performances were attributed to the bulk lead surface as well as the appearance of a crack in the shorting plate.

The development of a new set of procedures was initiated, aided by reports of plating success from Ben-Zvi.[2] Controlled tests were conducted which suggested several changes in the plating parameters. Based on these results and suggestions from the staff at SUNY a new process was defined which was successful in producing the smooth reflective metallic surface known to be necessary for optimum resonator performance.

Following a successful repair of the shorting plate crack, the prototype was plated and chemically polished with the new techniques. The resultant surface was highly reflective and free of stains and particulates. The subsequent prototype cold test was successful.

The following alterations were made to the plating sequence:

a. Increase the temperature of the lead bath to 30-32 °C.
b. Filter the bath during plating through a 5 micron filter
c. Reduce the current density from 10 to 5 mA/in^2.
d. Punch several 0.20" diameter holes in the lead anode.
e. Place the anode inside a polypropylene anode bag.

The following changes were made to chemical polishing sequence:

a. Reduce the polish age time to 12 hours.
b. Etch the lead layer in standing polish for 90 seconds.
c. Fill the resonator rapidly with each processing solution and dump with a fast end-for-end rotation.

References:

* State University of New York at Stony Brook 11794.
1. I. Ben-Zvi and J.M. Brennan, Nucl. Instrum. Meth. 212, 73 (1983).
2. I. Ben-Zvi, private communication.

*****

13.4 Testing of the Low Beta Resonator

J.M. Brennan,* T. Goliak, and D.W. Storm

The low beta resonator was tested three times at Stony Brook between mid February and early April, 1984. The first two tests were unsuccessful in that fields only in the neighborhood of 1 MV/m were obtained with reasonable (less than 10 W) power in the resonator. In both cases the plating was poor. After techniques were developed to give good plating and after drilling out a crack in the bulk material of the resonator, the testing was successful. The techniques used for testing were the standard tests that have been used at Stony Brook for their resonators. The results of their tests typically agree with measurements using accelerated particles to better than 10%. We appreciate the help received and the opportunity to use the test equipment at Stony Brook.

The low beta resonator test consists of four parts. First, a bead test is done to establish the field profile and the ratio of the stored energy U to the square of the average accelerating field $\langle E_a \rangle^2$. For our resonator this ratio is 0.063 Joule/(MV/m)^2. The uncertainty is estimated to be 0.003, based on estimates of the accuracy of frequency shifts in the bead tests and on repeatability.

Second, while superconducting, the voltage probe is calibrated. It delivers a signal whose amplitude V_p is measured with an oscilloscope. This voltage is proportional to the field in the resonator. The calibration is done by first measuring the Q of the resonator by measuring the decay time of the probe voltage when the power into the resonator is turned off. This decay time gives the loaded Q, Q_L, which includes the effects of the amplifier output resistance, and from Q_L the resonator Q, Q_0, is obtained using measurements of reflected power. The variable coupler is either set to give no reflected power during steady state operation (critical coupling), or at the weakest setting if critical coupling is not attainable. The measurement is done at low power so the decay time is purely exponential. We found a value of 2.9×10^8 for Q_0, with a 5% uncertainty.

Once the Q of the resonator is known, the stored energy can be determined by measuring the power P fed into the resonator from the amplifier, ($Q = \omega U/P$). The power supplied the resonator is obtained from the forward minus the reflected power, measured at the directional coupler. Again, the coupling is either set to be critical, or as weak as possible. The accuracy of the power measurement is estimated to be 7%. From the power absorbed and Q_0, we determine the stored energy and (using the bead results) the average accelerating field $\langle E_a \rangle$. The uncertainty in the field resulting from uncertainties in power, in Q_0, and in the bead test results is 5%. Simultaneous measurement of the voltage probe with the oscilloscope give V_p and permits calibration of the probe.

For the third part of the measurement, P_{abs} and V_p are measured at a number of power settings. (The results presented were obtained after "helium conditioning". In this process, helium is introduced into the vacuum of the cryostat and the resonator is pulsed to as high a field as possible. Presumably the discharges and ion bombardment of the high field points of the surface occurring during this process burn the points off and reduce field emission. After helium conditioning, substantially higher fields were achievable without the Q falling and without x-ray emission than before.) The value of $\langle E_a \rangle$ is obtained from V_p, and P_{abs} is obtained from the difference between forward and reflected power at the directional coupler. (If Q_0 falls with power enough that we reach critical coupling, the coupler is adjusted to maintain critical coupling as Q_0 falls further.) At the same time, a value of Q_0 is obtained from the original one measured by decay times using the ratios of V_p^2 and P_{abs}. A graph of those results is shown in Fig. 13.4-1. Those values for Q_0 have been corrected for the contribution of the probe giving V_p. This probe produces an additional Q_{ext} of 1.3×10^9. These corrections amount to a 20% increase at the high values of Q_0, and proportionately less at lower values.

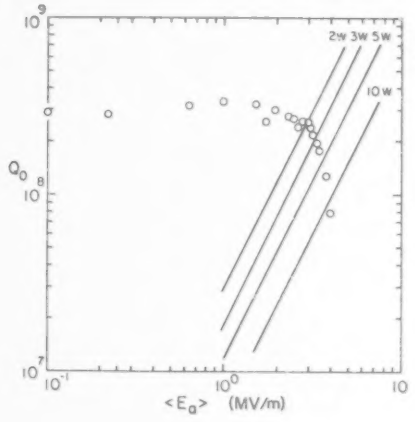

Fig. 13.4-1 Low beta resonator tests. Q of low beta resonator, measured after helium conditioning, plotted vs. $\langle E_a \rangle$, the average accelerating field. The lines show Q vs. E_a for fixed amounts of power absorbed by the resonator.

Finally, we phase lock the resonator and measure the power delivered by the amplifier to achieve lock. In an earlier test, this was done with one of the Stony Brook resonator controllers at a field of 1.1 MV/m. Lock required 4.4 W, 3.7 W of which was required before lock was established, i.e., 3.7 W was consumed in the resonator and 0.7 W reflected back into the amplifier. The coupler was set for critical coupling, and the Q value was fairly low. It was not possible to operate the resonator at 3 MV/m with that plating. However, one can conclude that if one wished to operate a successfully plated resonator with the same Q_L as was the case in the 1.1 MV/m test, then the power required to achieve lock at 3 MV/m would be $(3/1.1)^2$ times 4.4 W (33 W). The coupler would be adjusted to give a sufficiently large Q_{ex} to obtain this Q_L. The fact that lock was achieved without adding much power indicates that Q_L was larger than optimum. In the test with the successful plating, the controller was not operating, but we achieved lock using a voltage controlled oscillator and a phase detector. This lock was done at 50 W. Measurements of the frequency modulation of the resonator resulting from mechanical vibrations indicated maximum modulation of substantially less than 1 Hz.

Reference:

* State University of New York at Stony Brook, NY 11794.

*****

13.5 The Pretandem Buncher

J. Amsbaugh, L. Sima, D.W. Storm, R.E. Stowell, and T. Van Wechel

The LINAC booster will require beam from the tandem Van de Graff bunched to a time width around 100 psec. The direct current beam from the ion sources will be bunched with a single-gap gridded, four-harmonic buncher. After acceleration through the tandem the resulting pulse width will be 1-2 nsec. Beam pulses will then be further bunched by a superconducting quarter wave resonator to the required width.

Several pretandem bunchers of this type have been built and operated successfully.[1,2,3] A 1 mm gap is formed by two aligned grids clamped to copper cones and held in place by a cylinder of MACOR. One cone is driven by an odd harmonic resonant line operating at 50 MHz and 150 MHz. The other is driven by an even harmonic resonant line at 100 MHz and 200 MHz, i.e., a N/2 resonator. The amplitude and phase of each frequency is controlled in a self excited loop. These parameters are adjusted to give a ramp voltage across the grids.

The mechanical design of the buncher box, which follows the new Argonne National Laboratory[4] design closely, has been completed with attention to providing good rf current conduction paths. The design of the resonant lines is also complete. The construction of both designs will be done by September.

The control electronics have been designed copying the original ANL scheme. However the discrete component rf circuitry has been replaced by modern rf modules that are readily available. A 200 W rf amplifier and the associated electronics have been ordered, enabling a prototype of the control board to be built at the fundamental frequency of 50 MHz. The testing of this prototype should be finished by the end of July. This is consistent with our goal to begin beam test in December of 1984.

References:

1. F.J. Lynch, R.N. Lewis, L.M. Bollinger, W. Henning, and O.D. Despe, Nucl. Instrum. Meth. 159, 245 (1979).
2. A.D. Frawley and J.D. Fox, Nucl. Instrum. Meth. 204, 37 (1982).
3. E. Jaeschke, private communication and E. Jaeschke, R. Repnow, and S. Papureanu, Jahresbericht MPI fur Kernphysik Heidelberg, 11 (1978).
4. R. Pardo, private communication.

*****

13.6 Beam Dynamics for the UW Booster Project

J.G. Cramer and D.W. Storm

The beam transport line which injects the booster requires a "dogleg" isochronous transport system which displaces the tandem output beam from the beam axis of the tandem accelerator to a parallel axis 3.6 m to the south of the tandem axis. This transport must be independent (in first order at a given energy) of the path which a given particle takes through the beam transport system. This preserves the time structure quality of the bunched beam from the tandem. The system employs four 45° magnetic dipole bending elements and two pairs of magnetic quadrupole singlet focusing elements.

The characteristics of the dipoles and quadrupoles have been determined using the beam dynamics program TRANSPORT, and a request for information has been mailed to potential suppliers as a part of the UW procurement process. The TRANSPORT calculations have led to the following specifications:

Dipole 1: Deflection angle = 45°; Radius of curvature = 0.600 m; Magnetic rigidity = 1.04 T-m; Effective length = 0.471 m; Maximum B = 1.73 T; Entrance edge angle = +8.0°; Exit edge angle = -15.0°; Gap height in vacuum chamber = 3.8 cm.
(Dipoles 2-4 are either identical to or mirror images of Dipole 1)

Quadrupoles: Aperture diameter = 6.00 cm; Effective length = 0.24 m; Field gradient = 10.0 T/m; Gradient-length product = 2.40 T.

The six-dimensional Monte-Carlo beam dynamics program LYRA written by A. Scholldorf of Stony Brook has been modified so that it can be used to predict the performance of this booster. This has required expansion of the

program array space and modification of the part of the program which deals with resonator performance to describe the performance of quarter-wave resonators as well as split-loop resonators. Several minor bugs have also been corrected. The program is being used to determine the focusing requirements placed on the inter-cryostat quadrupole doublets by various beams so that the specifications for these elements can be determined and procurement initiated. The program is also being modified to make it more interactive and more realistic in its simulation of booster LINAC performance.

*****

13.7 Phase Control System of the Tandem-LINAC System

T.A. Trainor

Successful operation of the tandem-LINAC accelerator combination relies, among other things, on proper control of the relative phases of the time-varying components of the system. In the absence of noise sources it should be possible to adjust each component phase with respect to a master clock according to established criteria. If, in addition, there are sources of phase noise in the system then one or more servo loops are required to reduce the noise to an acceptable level. The result is that correct phases are established and then maintained indefinitely.

Both elements of the phase control problem, establishment of quiescent phase values and dynamic control of relative phases, require some sort of beam phase detector. This detector can be active, as in a sweeper or a driver (accelerating) resonator, in which case subsequent analysis of the beam is required to determine relative phase, or passive, as in a secondary electron pickoff or an undriven (detecting) resonator. These devices vary considerably in sensitively, range, phynical size, band width, etc.

Establishment of quiescent values can be time-consuming. At existing installations manual set up typically requires twelve hours. This lengthy process is unacceptable as a design goal for a new LINAC. The setup procedure should be totally under computer control and take of order one hour to complete. Achievement of such a goal will require careful matching of phase detector properties to the computer control system.

Dynamic phase control is a totally separate problem requiring careful study of phase noise power spectra and response functions of various elements of the phase regulation loop, in order to secure maximum gain-bandwidth product and loop stability over the large range of beam currents anticipated. The transient response of the regulation loop is also critical. Phase transients derived from voltage breakdowns in the tandem or injector cause the regulation system to saturate because of its necessarily limited dynamic range. Recovery time from saturation must be minimized and "phase slip" avoided. That is, beam bunches must be registered in the proper rf cycle, not

prematurely locked into a nearby cycle during recovery from the transient.

To date these general design principles for the phase-control problem have been developed and a number of specific areas have been investigated. A typical phase-noise spectrum from the tandem injector combination has been inferred from voltage stabilities. Properties of various phase detectors have been reviewed. A study of longitudinal phase-space propagation through the dog leg just preceding the LINAC has been made. Some results of this study are for example that an additional transverse waist is desirable between dog-leg output and second stripper, and that both the high-field buncher and a large band-width phase detector should be located at this waist.

The next step is to examine the properties of several prototype phase detectors installed just after the tandem using the existing pre-tandem buncher, and to begin to sketch out a rapid algorithm for computer setup of LINAC phases.

*****

13.8 Resonator Test Facility

R.E. Stowell, H.E. Swanson, and D.W. Storm

Progress on the test facility to date has largely been in the specification and procurement of rf components and test equipment needed for the lab. This facility is required to make measurements of quarter wave resonator (QWR) parameters such as Q and the resonant frequency. It will allow us to operate the QWR's both warm and at superconducting temperatures, at power levels simulating LINAC operating conditions. The first low beta prototype resonator was tested at Stony Brook and that experience was useful in writing specifications to obtain the appropriate capability.

This facility is to be housed here in laboratory space vacated by cyclotron user groups. It should be available for testing the prototype high beta resonator later this year. A list of the major items of equipment follows, with an asterisk showing that the item has been received.

*Tektronics 485 oscilloscope
*Tektronics 2213 oscilloscope
*Hewlett Packard 432B power meter
*Hewlett Packard 5382 frequency counter
*Bird RF power meter (forward/reflected)
*RF Power Labs 100 Watt broadband rf amplifier
*RF Power Labs 200 Watt broadband rf amplifier
*Narda directional couplers
Wavetech 3006 rf signal generator
Wavetech 148A function generator
*Miscellaneous rf components
(Mixers, attenuators, phase shifters, splitters)

13.9 Resonator Control System

C. Stubbs and H.E. Swanson

The amplitude and phase of oscillation of each superconducting resonator in a linear accelerator determines the energy of a particle bunch as it traverses the accelerator. A master frequency synthesizer provides the reference phase for determining the initial bunching of the dc beam from the tandem. It also determines the phase of all subsequent resonators such that the particles appear in the accelerating gap at just the right moment to be accelerated. The amplitude of the oscillation determines the accelerating field seen in the gap.

Control of the resonators is to be achieved in a manner similar to that used on the Stony Brook LINAC. The resonant cavity is made to oscillate by making it part of a self-excited feedback loop. The loop consists of an rf amplifier and an electronic module whose phase shift and attenuation can be controlled. Oscillation occurs at the point where the total loop phase shift is a multiple of 360 degrees. If the phase shift external to the resonator differs from 360 degrees, then the resonator must oscillate off resonance to make up for this phase difference. In this manner control is achieved over the frequency of the resonator and it can be locked to the phase of the master oscillator.

Electronics to provide control of loop phase shift and attenuation has been designed by Ben-Zvi and Brennan at Stony Brook. Their circuit is built around an Olektron part, a complex phasor modulator, which is capable of independent modulation of the in-phase and out-of-phase components of the feedback signal. Using these two components, independent control of both amplitude and phase of the resonators oscillation is achieved. We have obtained schematics and a printed circuit board for this design from Stony Brook and have constructed one of the resonator control modules here. This unit is presently undergoing an evaluation of its operating characteristics.

The controller module requires analog input signals to set its operating parameters. A satellite control computer will provide digital-to-analog and analog-to-digital conversion as well as two way communication with a master control console. A Digital Equipment Corporation Falcon single board computer has been ordered and a prototype satellite controller system is being assembled. The Stony Brook control software has been brought up on the VAX computer and is being evaluated. A Whitesmith's C compiler has also been installed and work is ongoing to modify the software to work with the Falcon based satellite.

*****

13.10 Booster Cryogenics

D.W. Storm, W.G. Weitkamp, and D.I. Will

During this past year we have ordered a helium refrigerator, developed cryostat specifications and come to understand better some of the potential problems to avoid in helium distribution systems. The helium refrigerator consists of a Koch Process Systems 2800HR with three type RS screw compressors. The 2800HR has two dry expansion engines, each with two 3" diameter pistons, and one wet expansion engine with a single 2" diameter piston. It has guaranteed capacities at 4.5°K of 440 W without liquid nitrogen precool and of 510 W with liquid nitrogen precool which compare favorably with our estimated need of 300 W.[1] We are pleased to report that this extra capacity was obtained under budget. At present we have nearly completed material, technique and performance specifications for our cryostats, pending a decision on bayonet design, and we are beginning preliminary specifications for our liquid helium distribution manifold and transfer siphons. We especially wish to thank John Hulbert of Chalk River Laboratory of Atomic Energy of Canada, Ltd., Jack Nixon of Argonne National Laboratory, and Tom Peterson of Fermilab for their assistance in matters cryogenic.

Reference:

1. Nuclear Physics Laboratory Annual Report, University of Washington (1983) p. 94.

*****

13.11 The Plating Laboratory

A.G. Seamster and W.G. Weitkamp

The lead plating of the prototype resonator, described in Sec. 13.3, has been conducted entirely in the plating laboratory at SUNY Stony Brook. Because of the considerable cost and inconvenience in transporting personnel and materials to and from Stony Brook, it is clearly impractical to plate all the resonators there. Furthermore, the high-beta resonator cannot be accommodated at Stony Brook without modifying the set up there. Consequently we are constructing a plating lab in-house.

A suitable plating lab must have the following properties:

a. It must contain a fume hood big enough to hold all the chemicals required for the plating process. Some of the chemicals such as acetone pose a fire hazard, and some such as the lead plating solution are slightly toxic.

b. Safety equipment required in handling the chemicals must be near at hand.

c. Equipment for maneuvering both the high and low-beta resonators as required during the plating process must be available.

d. The lab must be dust-free since dust adhering to the surfaces of the resonator either before or after plating can degrade the electrical properties of the resonator.

e. The lab must contain space and equipment for installing the resonators into the cryostat since it is preferable not to expose freshly plated resonators to the Laboratory environment any more than necessary.

No existing room in the Laboratory had all of the properties required. We found that we could construct such a room by expanding an old hot-chemistry lab adjacent to the high-bay student shop setup area (Room 165) as shown in Fig. 13.11-1. This room will enclose 580 ft^2 including a 90 ft^2 fume hood. A 2600 ft^3/min fan will exhaust air from the hood. A 5 μ filter will remove dust from all incoming air.

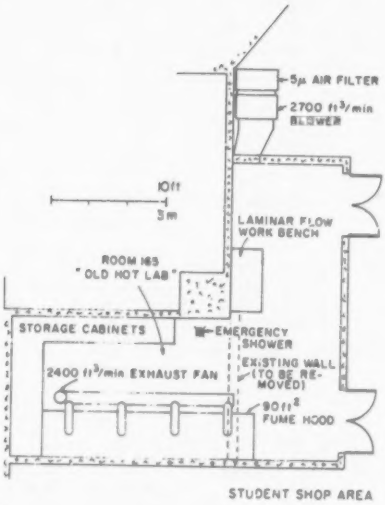

Fig. 13.11-1 The new plating laboratory.

The University Architect's Office has prepared final plans and arranged for a contractor. Work will begin in April; the lab is expected to be ready for occupancy by the end of August 1984.

14. APPENDIX

14.1 Nuclear Physics Laboratory Personnel

Faculty

Eric G. Adelberger, Professor
David Bodansky, Professor; Chairman, Department of Physics
John G. Cramer, Professor; Director, Nuclear Physics Laboratory
George W. Farwell, Professor
I. Halpern, Professor
Albert Lazzarini, Research Assistant Professor
Eric Norman, Research Affiliate Professor[1]
Fred H. Schmidt, Professor
Kurt A. Snover, Research Professor
Thomas A. Trainor, Research Associate Professor
Robert Vandenbosch, Professor
William G. Weitkamp, Research Professor; Technical Director, Nuclear Physics Laboratory

Research Staff

K.G. Radhamohan Doss, Research Associate[2]
David H. Dowell, Research Associate[3]
Elspeth F. Garman, Visiting Scientist[4]
Cynthia A. Gossett, Research Associate
Muhsin N. Harakeh, Visiting Scientist[5]
M. Zafar Iqbal, Research Associate[6]
Tetsuya Murakami, Research Associate
Martin J. Murphy, Research Associate
John L. Osborne, Research Associate
Daniel R. Tieger, Research Associate

Senior Professional Staff

Harold Pauska, Senior Research Scientist[7]
Derek W. Storm, Senior Research Scientist

Predoctoral Research Associates

John A. Behr
Keith J. Davis
Gerald Feldman
Salvador Gil
David W. Holmgren
Stephen Kellogg
Mahbubul A. Khandaker
Steve Lamoreaux[8]
Kevin T. Lesko[9]
Dat-Kwong Lock
Robert A. Loveman
Amlan Ray
Christopher Stubbs
Peter Wong
Valdis Zeps

Professional Staff

John P. Amsbaugh, Research Scientist
Greg Douglas, Visiting Controls Engineer[10]
Thomas Goliak, Research Engineer
Gervas M. Hinn, Research Scientist/Target Maker
David J. Hodgkins, Research Engineer
Donald D. Leach, Research Scientist
H. Pamela McKenna, Computer System Engineer
R. Scott Peabody, Computer System Engineer[11]
Alan G. Seamster, Research Scientist
Richard J. Seymour, Computer System Manager
Rod E. Stowell, Electronics Engineer/Electronic Shop Supervisor
H. Erik Swanson, Research Physicist
Timothy Van Wechel, Electronics Engineer
Douglas I. Will, Research Engineer

Technical Staff

Robert L. Cooper, Instrument Maker
James R. Cromie, Accelerator Technician
Ronald Floyd, Buyer
Louis Geissel, Instrument Maker, Student Shop Leadman
John M. LaCroix, Electronics Technician
Carl E. Linder, Engineering Technician
Georgia J. Rohrbaugh, Accelerator Technician[8]
George Saling, Accelerator Technician[7]
Lawrence Sima, Drafting Technician
Hendrik Simons, Instrument Maker, Shop Supervisor
Allen L. Willman, Instrument Maker[7]

Administrative Staff

William T. Dickie, Office Assistant[8]
Barbara J. Fulton, Administrative Secretary
Margaret M. Nims. Office Assistant
Victoria A. Palm, Accounting Assistant[12]
Maria G. Ramirez, Program Assistant

Part Time Staff

Frederick Bahr
David Balsley
Somjai Boonsripisal[8]
David Chan
Cindy Christensen
Ky Clifford
Dean Corcoran
Jim Davis
Mark DePaccio
Jens Gundlach
Albert Herron
Norman Hill
Steven Holmes
Peter James
Donna Kubik[8]
Kevin McMurry
Margarethe Nelson[8]
David Patterson
Joel Schoen[8]
Michael Walker
Pawn Willis

1. Address: Department of Physics, Seattle University, Seattle, WA 98122.
2. Address: Lawrence Berkeley Laboratory, University of California, Berkeley, CA 94720.
3. Address: Brookhaven National Laboratory, Upton, NY 11973.
4. Address: Oxford University, Oxford, United Kingdom.
5. Address: Kernfysisch Versneller Instituut, Groningen, The Netherlands.
6. Address: Norman Bridge Laboratory of Physics, California Institute of Technology, Pasadena, CA 91125.
7. Retired - part time employee.
8. No longer associated with the Nuclear Physics Laboratory.
9. Completed Ph.D. degree. Present Address: Argonne National Laboratory, Argonne, IL 60439.
10. Group 3 Technology Ltd., Auckland, New Zealand.
11. Department of Chemistry, University of Washington.
12. Department of Computer Science, University of Washington.

******

14.2 Ph.D. Degrees Granted, Academic Year 1983-1984

Kevin T. Lesko - Fusion and Fission Properties of Rapidly Rotating Nuclei

Dat-Kwong Lock - The Effect of Particle Evaporation on the $^{50}Fe + ^{130}Xe$ Reaction and a Reinvestigation of the $^{88}Kr + ^{92}Mo$ Reaction

******

14.3 List of Publications

Published Papers

"The Arrow of Electromagnetic Time and the Generalized Absorber Theory," J.G. Cramer, Found. Phys. 13, 887 (1983).

"Cosmic Clocks," E.B. Norman, McDonald Observatory News, University of Texas, October, 1983, p. 4, (4th Prize Winner in the 1982 McDonald Observatory Science Writing Contest).

"^{182}Hf Chronometer for the Early Solar System," E.B. Norman and D.N. Schramm, Nature 304, 515 (1983).

"On the Half-Life of ^{138}La," E.B. Norman and M.A. Nelson, Nature 306, 503 (1983).

"On the Identification of γ-ray Lines Observed from SS433," E.B. Norman and D. Bodansky, Nature, 308, 212 (1984).

"The University of Washington Superconducting Booster Project," J.G. Cramer R. Vandenbosch, and D.W. Storm, Nucl. Instrum. Methods 220, 204 (1984).

"The g-factor and Lifetime of the 3^-(298 keV) State in ^{16}N," J. Billowes, E.G. Adelberger, O. Avila, N.A. Jelley, and W.R. Kölbl, Nucl. Phys. A, 413, 503 (1984).

"The 1-forbidden Gamow-Teller Decay of ^{39}Ca," E.G. Adelberger, J.L. Osborne, H.E. Swanson, and B.A. Brown, Nucl. Phys. A, 417, 269 (1984).

"Depolarization in Proton Inclusive Inelastic Scattering and in the $(\vec{d},\vec{p})$ Reaction on Medium Weight Nuclei," W.G. Weitkamp, I. Halpern, T.A. Trainor, S.K. Lamoreaux and Z.Y. Liu, Nucl. Phys. A 417, 405 (1984).

"Dynamics of Heavy-Ion Transfer Reactions," B.G. Harvey and M.J. Murphy, Phys. Lett. B 130, 373 (1983).

"Phase Space Constraints on the Momenta of Projectile Fragments," M.J. Murphy, Phys. Lett. B 135, 25 (1984).

"^{7}Be Decay Scheme and the Solar Neutrino Problem," E.B. Norman, T.E. Chupp, K.T. Lesko, J.L. Osborne, P.J. Grant, and G.L. Woodruff, Phys. Rev. C 27, 1728 (1983); Erratum Phys. Rev. C 28, 1409 (1983).

"Proton Capture to Excited States of ^{16}O; M1, E1 and Gamow-Teller Transitions and Shell Model Calculations," K.A. Snover, E.G. Adelberger, P.G. Ikossi, and B.A. Brown, Phys. Rev. C 27, 1837 (1983).

"The Beta Decays of ^{18}Ne and ^{19}Ne and their Relation to Parity Mixing in ^{18}F and ^{19}F," E.G. Adelberger, M.M. Hindi, C.D. Hoyle, H.E. Swanson, R.D. Von Lintig, and W.C. Haxton, Phys. Rev. C 27, 2833 (1983).

"Properties of Fission Induced by Complete Capture of ^{40}Ar by ^{238}U at $E_{C.M.}$ = 291 MeV," K.T. Lesko, S. Gil, A. Lazzarini, V. Metag, A.G. Seamster, and R. Vandenbosch, Phys. Rev. C 27, 2999 (1983).

"Elastic and Inelastic Scattering of Polarized Protons from ^{208}Pb near Isobaric Analog Resonances," N.L. Back and J.G. Cramer, Phys. Rev. C 28, 1040 (1983).

"Penetration of the Centrifugal Barrier in the Fusion of ^{16}O with Heavy Targets," R. Vandenbosch, B.B. Back, S. Gil, A. Lazzarini, and A. Ray, Phys. Rev. C 28, 1161 (1983).

"The Giant Dipole Resonances in the Statistical Decay of ^{63}Cu, ^{78}Kr and ^{127}Cs Compound Nuclei," E. Garman, K.A. Snover, S.H. Chew, S.K.B. Hesmondhalgh, W.N. Catford, and P.M. Walker, Phys. Rev. C 28, 2554 (1983).

"Cross Sections Relevant to Gamma-Ray Astronomy: Alpha-Particle Induced Reactions," A.G. Seamster, E.B. Norman, D.D. Leach, P. Dyer, and D. Bodansky, Phys. Rev. C 29, 394 (1984).

"Current ^{14}C Measurements with the University of Washington FN Tandem Accelerator," G.W. Farwell, P.M. Grootes, D.D. Leach, F.H. Schmidt, and Minze Stuiver, Radiocarbon 25, 711 (1983).

"Technological Advances in the University of Washington Accelerator Mass Spectrometry System," G.W. Farwell, P.M. Grootes, D.D. Leach, and F.H. Schmidt, Radiocarbon 25, 755 (1983).

"Nuclear Probes of Fundamental Symmetries," E.G. Adelberger, Proceedings of the International Conference on Nuclear Physics, Florence, edited by P. Blass and R.A. Ricci, (Tipografia Compositori, Bologna, 1984), Vol. 2, p. 499, (invited paper)

"Breaking of Fundamental Symmetries in Nuclei," E.G. Adelberger, in Symmetries in Nuclear Structure, edited by K. Abrahams, K. Allaart, and A.E.L. Dieperink, (Plenum Press, New York, 1983), p. 55.

"Conclusion and Outlook," R. Vandenbosch, Nuclear Physics with Heavy Ions, edited by P. Braun-Munzinger, (Harwood Academic Publishers, New York, 1984) p. 447, (invited paper).

Papers Submitted or in Press

"On the Half-Life of ^{180}Ta in Stellar Environments," E.B. Norman, S.E. Kellogg, T. Bertram, S. Gil, and P. Wong, Astrophys. J, to be published.

"Giant Dipole Resonances Built on Highly Excited States of Light Nuclei," K.A. Snover, Comments on Nucl. Part. Phys., to be published.

"Production of Thick Elemental Low-Oxygen Content ^{nat,26}Mg from ^{nat,26}MgO," G.M. Hinn, E.B. Norman, T.E. Chupp, and K.T. Lesko, Nucl. Instrum. Methods, to be published.

"Parity Mixing of Elastic Scattering Resonances: General Theory and Application to ^{14}N," E.G. Adelberger, P. Hoodbhoy, and B.A. Brown, Phys. Rev. C, to be published.

"Determination of the Rate of Energy Partition in Deeply Inelastic Collisions," A. Lazzarini and R. Vandenbosch, submitted to Phys. Rev. C.

"Non-Equilibrium Excitation Energy Division in Deeply-Inelastic Collisions," R. Vandenbosch, A. Lazzarini, D. Leach, D.-K. Lock, A. Ray, and A. Seamster, Phys. Rev. Lett, to be published.

"Comment on Fission Fragment Angular Distributions," R. Vandenbosch, Phys. Rev. Lett., to be published.

"Determination of a Time Scale for the Emission of Energetic Photons in Heavy Ion Fusion Reactions," A. Lazzarini, V. Metag, D. Habs, W. Hernerici, and J. Schmirmer, submitted to Phys. Rev. Lett.

"Timescale for Projectile Breakup into Coincident Heavy Fragments," M.J. Murphy, T.C. Awes, G. Gil, M.N. Harakeh, A. Ray, A.G. Seamster, and R. Vandenbosch, submitted to Phys. Rev. Lett.

"Some Methods and Problems Associated with Making Thick (1 Mg/cm^2) ^{28,29,30}Silicon Targets," G.M. Hinn, International Nuclear Target Development Society Workshop, Argonne National Laboratory, September, 1983, to be published, (invited paper).

"The Conceptual Design of the University of Washington Superconducting Booster," W.G. Weitkamp, in Proceedings of the Symposium of Northeastern Accelerator Personnel, 1983, to be published.

"Form Factors and Coupled Channel Analysis of Inelastic Excitations of Low-Lying Collective Bands in Rotational Nuclei," M.N. Harakeh, Kikuchi Summer School, 1983, Kyoto, Japan, to be published, (invited paper).

"Excitation of Low-Lying Collective Bands in Inelastic Hadron Scattering," M.N. Harakeh, Proceedings of RCNP Symposium on Light Ion Reaction Mechanism, 1983, Osaka, Japan, to be published, (invited paper).

"A Review of the Fission Decay of the Giant Resonances in the Actinide Region," M.N. Harakeh, Proceedings of the International Symposium on Highly Excited States and Nuclear Structures, 1983, Orsay, France, Editions de Physique, to be published, (invited paper).

"Giant Resonances Built on Excited States," K.A. Snover, *ibid*, (invited paper).

"Giant Resonances Built on Highly Excited States," K.A. Snover, Proceedings of XV International Summer School in Nuclear Physics, 1983, Mikolajki, Poland, to be published, (invited paper)

Laboratory Reports

"Conceptual Design Report Superconducting Booster," R. Vandenbosch, D.W. Storm, J.F. Amsbaugh, A.G. Seamster, H.E. Swanson, T.A. Trainor, and W.G. Weitkamp.

"Program Management Plan Superconducting Booster," D.W. Storm.

Proceedings of the 11th World Conference of the International Nuclear Target Development Society," edited by G.M. Hinn, Nuclear Physics Laboratory, University of Washington, Seattle, Washington, 1983.

Abstracts

"The Role of Isospin in the Statistical Decay of the Giant Dipole Resonance Built on Excited States," M.N. Harakeh, D.H. Dowell, K.A. Snover, G. Feldman, E.P. Garman, J.L. Osborne, and R. Loveman, Bull. Am. Phys. Soc. 28, 965 (1983).

"Giant Dipole Resonances Built on Excited States," K.A. Snover, Bull. Am. Phys. Soc. 28, 972 (1983), (invited paper).

"Phase-Space Constraints on the Moments of Projectile Fragments," M.J. Murphy, Bull. Am. Phys. Soc. 28, 980 (1983).

"A Search for the β-decay of ^{180}Lu to ^{180}Hf^{m}, S.E. Kellogg and E.B. Norman, Bull. Am. Phys. Soc. 28, 989 (1983).

"Forward-to-Backward Asymmetries in the (γ,n) Reactions around the E2 Isovector Giant Resonance," T. Murakami, I. Halpern, D.W. Storm, P.T. Debevec, L. Morford, D.H. Dowell, and S.A. Wender, Bull. Am. Phys. Soc. 29, 707 (1984).

"The Accelerator Mass Spectrometry Program at the University of Washington," G.W. Farwell, D.D. Leach, P.M. Grootes, and P.H. Schmidt, The Third International Symposium on Accelerator Mass Spectrometry, Zürich, Switzerland, 1984.

"β-Decays of $^{180}Hf^{m}$ and ^{180}Lu and the Origin of ^{180}Ta, E.B. Norman and S.E. Kellogg, Proceedings of the 2nd Workshop on Nuclear Astrophysics, Tegernsee, West Germany, 1983, p. 92.

"Giant Dipole Resonances Built on Excited States of Light Nuclei," K.A. Snover, D.H. Dowell, G. Feldman, A.M. Sandorfi, M.T. Collins, and E.F. Garman, Proceedings of International Conference on Nuclear Physics, Florence, (Tipographia Compositori, Bologna, 1983), Vol. 1, p. 204.

"Searches for Double β^+. β^++EC and Double EC Decays, E.B. Norman and M.A. Nelson, *ibid*, p. 720.

"Possible Non-Quasi-Elastic Events in the Inclusive Inelastic Scattering of Pions from Nuclear," K.G.R. Doss, I. Halpern, M. Khandaker, and D. Storm, *ibid*, p. 368.

"Environmental Studies Using Accelerator Mass Spectrometry Measurements of ^{10}Be and ^{14}C", G.W. Farwell, P.M. Grootes, F.H. Schmidt, M. Stuiver, M.A. DePaccio, and D.D. Leach, *ibid*, p. 752.

"^{182}Hf: A New Short-Lived r-Process Chronometer," E.B. Norman and D.N. Schramm, Meteoritics, 18, 365 (1983).

"The Role of the Giant Dipole Resonance in the Emission of High Energy Gamma Rays from $^{63}Cu^{*}$," E.F. Garman, K.A. Snover, J. Gundlach, D.H. Dowell, M.N. Harakeh, G. Feldman, and R. Loveman, The Spring Meeting of the British Institute of Physics Conference, 1984, Bradford, England.

Other Publications by Members of the Laboratory and Other Laboratory Research

"Calorimetric Beam-Current Integrator," J.L. Osborne and A.J. Howard, Nucl. Instrum. Meth., to be published.

"Determination of the α-induced K-shell Ionization Cross-Sections from the Measured Intensity Ratios of K X-Rays to $(2^{+}\text{-}0^{+})$ γ-rays in Even Deformed Nuclei," M.N. Harakeh, Z. Zujkowski, and D. Chmielewska, Nucl. Instrum. Methods, 219, 111 (1984).

"Low Energy Behavior of the $^{3}He + ^{4}He$ Cross Section," J.L. Osborne, C.A. Barnes, R.W. Kavanagh, R.M. Kremer, G.J. Mathews, J.L. Zyskind, P.D. Parker, and A.J. Howard, Nucl. Phys. A, 419, 115 (1984).

"Structure in the $^{12}C + ^{12}C$ and $^{8}Be + ^{16}O$ Fission Width Distribution of ^{124}Mg Observed via the Reaction $^{12}C(^{16}O,\alpha)^{24}Mg - X+Y$," A.J. Lazzarini, S.G. Steadman, R.J. Ledoux, A. Sperduto, G.R. Young, K. Van Bibber and E.R. Cosman, Phys. Rev. C 27, 1550 (1983).

"Pionic Fission Cross-Sections on Lithium," P.D. Barnes, B. Bassaleck, R.A. Eisenstein, G. Franklin, R. Grace, C. Maher, P. Pile, R. Rieder, J. Szymanski, W.B. Wharton, J.R. Comfort, F. Takeutchi, J.F. Amann, S. Dytman, and K.G.R. Doss, submitted to Nucl. Phys.

"$^{12}C(^{16}O,\alpha)^{24}Mg$ Reaction in the Energy Region $E_{C.M.}$ = 26.6 to 42.9 MeV," M.J. Bechara, A.J. Lazzarini, R.J. Ledoux, and E.R. Cosman, Phys. Rev. C 27, 1540 (1983).

"Inelastic Proton Scattering at 30-40 MeV from ^{12}C," M. Harakeh, R. De Leo, G. D Erasmo, and A. Pantaleo, Phys. Rev. C 28, 1431 (1983).

"Origin of the Structures in the $^{12}C(^{16}O,\alpha)$ Reaction: Dominance of the $^{20}Ne^*$ and $^{16}O^*$ Sequential α-decay Processes," T. Murakami, E. Ungricht, N. Takahashi, Y.-W. Lui, Y. Mihara, R.E. Neese, E. Takada, D.M. Tanner, R.E. Tribble, and K. Nagatani, Phys. Rev. C 29, 847 (1984).

"Inclusive Pion Single Charge Exchange Reactions," D. Ashery, D.F. Geesaman, R.J. Holt, H.E. Jackson, J.R. Specht, K.E. Stephenson, R.E. Segel and P. Zupranski, H.W. Baer, J.D. Bowman, M.D. Cooper, M. Leitch, A. Erel, J. Comuzzi, R.P. Redwine, and D.R. Tieger, submitted to Phys. Rev. C.

Front row: Behr, Adelberger, Amsbaugh, Trainor, Cramer, Fauska, Cooper, Storm, Weitkamp, Fulton

Middle row: Snover, Khandaker, Chan, Kellogg, Gossett, Gil, Loveman, Murakami, Ray, Cromie, Will, Stowell, Ramirez, Holmgren, Swanson, Tieger, Grootes, McKenna, Leach, Schmidt

Back row:. Feldman, Murano, Corcoran, Geissel, Lock, Zeps, Fernandez, Seymour, James, Simons, Floyd, Hodgkins, Osborne, Linder, LaCroix, Van Wechel, Davis, Murphy, Farwell

10.0 Yale University A. W. Wright Nuclear Structure Laboratory Model MP Tandem Van de Graaff Accelerator

1. What new science is being explored by this facility? What scientific opportunities are being exploited?

Answer: The A. W. Wright Nuclear Structure Laboratory at Yale University is characterized by the breadth of its research program and for its educational activities. The research has ranged from the fundamental to the applied aspects of nuclear science and to the interfaces between this and other sciences such as particle physics, atomic physics, condensed matter and materials science, astronomy, and geophysics.

One of the major foci of the research program, which includes both theoretical and experimental research, is the study of new, dynamic symmetries and simplicities in the nuclear many-body system describable within the framework of modern mathematical group theory. As in particle physics, this approach has been very successful not only in correlating a vast amount of existing spectroscopic and reaction data but also in suggesting entirely new families of measurements.

Building upon this work, the first example of an effective supersymmetry--the next step beyond the grand unified theories in that it couples bosons and fermions on an equal footing--in heavy nuclei has been obtained. The apparent breaking of the supersymmetry as one moves away from ^{193}Ir where it appears to be most clearly expressed is now under study.

Another major research focus has been on clustering phenomena and nuclear molecular complexes in the nuclear system. Recently, unexpected, long lived molecular states have been identified at some 70 MeV of excitation in the ^{56}Ni system. These show the well developed structure of two ^{28}Si nuclear clusters orbiting one another with the highest angular momentum (J=44) yet identified unambiguously in any nucleus. This is of particular interest in that simple calculations predict that, at J=50, the system should become unstable against centrifugal fragmentation. Again, using heavy ion beams the detailed quantum states of nuclei in both the lanthanide and actinide regions have been investigated up to 40.5 quantum units of angular momentum. The experimental results have been reproduced with detailed microscopic shell model calculations. Such studies are important to a more fundamental understanding of the new symmetries noted above and to understanding how the nuclear system responds to large centrifugal stresses.

Having demonstrated that molecular states appear to be a ubiquitous aspect of nuclear structure and dynamics, it has now been shown that all the 39 known resonances in the ^{12}C + ^{12}C system can be described within the framework of a simple U(4) symmetry. This is the first successful use of a spectrum generating algebra in an unbound scattering system, as opposed to the usual bound structure system. Extending the U(4) symmetry to nuclear structure, the existence of a new form of nuclear collectivity near closed shells has been predicted and observed in ^{18}O and ^{218}Ra. This dipole collectivity involves an alpha particle cluster outside of an associated core nucleus and has a number of characteristic signatures, including strongly enhanced E1 electromagnetic transitions.

It has been established that in heavy ion collisions the characteristic nuclear and electronic time scales are so different that during the collision the familiar electronic shells form about the collision partners, with $Z_{eff} = Z1 + Z2$, and the corresponding X-radiation and Auger electrons are observable. Currently, the spectroscopy of atomic species with $Z_{eff} > 92$ is being studied. When $Z_{eff} > 170$, the K shell binding exceeds twice the rest mass of the electron and a vacancy in that shell can be filled by a negative energy electron from the Dirac sea leading to ionization of the vacuum and emission of an unaccompanied positron. These positrons have been detected using the very heavy ion beams from the GSI UNILAC in Darmstadt, West Germany in a collaboration between Yale and GSI scientists. This tests quantum electrodynamics in its zero-momentum limit and in a process where it provides the leading terms rather than very small corrections. Moreover, the discovery of totally unexpected sharp positron lines with widths much less than 70 keV, has been interpreted as a signature for the formation of long-lived uranium-uranium and other very heavy nuclear molecular systems. A wealth of open questions, both in nuclear and atomic physics, has been raised by these studies.

In nuclear astrophysics, recent work has focused on determination of precise helium burning cross sections, on redetermination of several of the critical cross sections for solar neutrino astronomy, and on production mechanisms for primordial ^{26}Al whose presence in meteorites serves as a signature for prehistoric nova events in the astronomical neighborhood of the solar system.

Using ultra-sensitive, accelerator mass spectroscopic techniques, we have established a sensitivity of one ^{10}Be in 10^{14} stable ^{9}Be and have used this to show, for example, that manganese nodules from the Pacific abyssal floor grow at a mean rate of about one millimeter per million years. In collaboration with geophysicists, this work is being extended to a wide variety of studies on Pacific sediments, cores, etc. with the intent of providing a much improved determination of prehistoric cosmic ray behavior.

Another applied program concentrates on understanding the physics and application of ion-beam-induced sputtering. As the method of choice for fabrication of the next generation of large scale integrated circuits, it is found that even the crudest sputtering phenomena are not yet understood. A 300 kV ion implanter in conjunction with the MP tandem is being used to establish the underlying physics. In a related activity, in collaboration with Caltech scientists, another new technique is under development--ion-beam-induced adhesion--which is also of great potential use in large scale integrated circuits. It is found that properly chosen ion beam fluxes can make almost any film adhere tenaciously to almost any substrate, e.g. gold on teflon, and that on metals and semiconductors the bonds are, and remain, ohmic as is required for signal contacts to the large scale integrated circuit structures.

2. How does this facility's accelerator (or accelerators) performance compare with any other in the world that are operating, under construction, or planned?

Answer: Currently, the A. W. Wright Nuclear Structure Laboratory houses an MP tandem operating up to terminal potentials of 13.5 MV, a high current 4 MV single-ended Van de Graaff accelerator (acquired as a NASA surplus item during 1983 and currently being reinstalled at Yale) and a high current 300 kV ion implanter accelerator. This combination of facilities provides unique access to phenomena requiring a very broad range of ion-beam energies. As an example, samples for materials science studies can be produced on the 300 kV unit, characterized through Rutherford backscattering and other studies on the 4 MV unit, and finally subjected to entirely new tests using the much higher energy heavy ion beams from the tandem. All this can be accomplished while holding samples at 10-10 torr vacuum throughout. As a second example, there have recently been several occasions to study nuclear systems using radiative alpha-particle capture (using the Brookhaven 3.5 MV Van de Graaff) together with a complementary reaction with high energy lithium beams from the tandem. Thus, all three facilities can be used in complementary fashion; this is particularly important in that it also makes available many more effective hours of beam time for the 30 graduate students currently associated with the Laboratory. No other university laboratory has such a complementary set of accelerator facilities.

The conversion of the tandem to ESTU (extended, stretched, transuranium) status will increase the terminal potential from 13.5 to 22.5 MV, with no extrapolation of current performance parameters. No other electrostatic facility currently operates at this potential, although those at the Holifield Heavy Ion Research Facility at Oak Ridge and the Nuclear Structure Facility at Daresbury, England are designed to do so; both currently operate up to slightly over 20 MV.

The group at the University of Strasbourg has proposed to build a tandem accelerator of entirely new design that will have a terminal voltage goal somewhere between 35 and 50 MV, but it has not yet been funded.

3. **What types of research instrumentation/experimental devices are available at this facility, and what are their capabilities?**

Answer: The answer to Question 2 has already noted the complementary 300 kV and 4 MV accelerators. A state-of-the-art data acquisition and analysis system is also available. Originally utilizing a System 360/44 CPU it now has a 4341 CPU, with correspondingly enhanced capabilities and a variety of DEC buffer and specialized computers.

Yale has one of the two (the other is at MPI-Heidelberg) 23-gap magnetic spectrographs designed for up to 33 MeV tritons and thus still very useful with almost all ESTU beams. A new, large, solid angle, single gap magnetic spectrograph designed in collaboration with Professor Enge of MIT is now under construction.

A very large, high precision, computer controlled goniometer is installed in a special cave constructed entirely from thorium- and potassium-free concrete and covered with 20 feet of earth fill. This powerful instrument is used extensively in spectroscopic studies using large numbers of gamma radiation and particle detectors. A large (1 ft. dia. x 1 ft. deep) NaI crystal with associated cosmic ray shielding is available for study of high energy radiation.

Mentioned above is the interchangeable, ultrahigh vacuum (<10^{-10} torr) target systems for use with all three accelerators. They include electrostatic energy analyzers, quadrupole mass spectrometers, electron diffraction equipment, etc. A cylindrical electrostatic analyzer is also used in the accelerator mass spectroscopy work.

As part of the conversion, beam pulsing and time-of-flight facilities for beams will be installed.

A large solenoidal positron spectrometer designed at Yale is now installed at GSI and will remain there for some time for use in continuing experiments with unique heavy ion beams. It will eventually be returned to Yale or duplicated for continuing use.

4. **What have been the facility's research highlights for the period FY 1981 - present, and what are anticipated for the remainder of FY 1984 and FY 1985?**

Answer: Research highlights since FY 1981 have been the following:

1. Discovery of the first effective supersymmetry in nature in ^{193}Ir.

2. Discovery that all the resonances in the $^{12}C + ^{12}C$ system can be reproduced within the U(4) symmetry framework.

3. Discovery of J = 44 states in ^{56}Ni at approximately 70 MeV of excitation.

4. Discovery of the unaccompanied positrons predicted to occur in supercritical Coulomb fields during heavy ion collisions; zero-momentum test of QED.

5. Discovery of sharp, monoenergetic positron lines superposed on the predicted spectra and now interpreted as possibly reflecting formation of U + U molecular complexes at the nuclear level.

6. Discovery of new effects which increase the ^{26}Al production rate at astrophysical temperatures by five orders of magnitude.

7. Development of one part in 10^{14} sensitivity in ultra mass spectrometry of ^{10}Be and its use in the study of Pacific abyssal features.

8. Development of new adhesion techniques giving ohmic contact on metals and semiconductors.

9. Discovery of a new form of nuclear collectivity near closed shells: dipole collectivity.

10. Demonstration of K X-ray + Molecular X-ray coincidence techniques for the study of transient superatoms, where relativistic and QED effects are pronounced.

5. **What facility changes and additions have occurred or are anticipated for the period FY 1981 - FY 1985?**

Answer: The following are the major facility changes that have occurred in the period FY 1981-present:

1. Installation of a 300 kV high current ion implanter.

2. Installation of a 4 MV Van de Graaff underway.

3. Decommissioning of an obsolete 70 MV electron linac.

4. Replaced the System 360/44 CPU of the data acquisition and analysis system with a 4341 CPU with 16 times the memory and 10 times the speed.

5. Designed and have under construction a split-pole magnetic spectrograph having almost a factor of 10 larger solid angle than any earlier design.

6. Developed ultrahigh vacuum (< 10^{10} torr) targetry for all our accelerators.

7. Designed and built an 80 kV electrostatic separator for use in our accelerator mass spectroscopy program.

8. Designed and had constructed a large-aperture, high-resolution, solenoidal spectrometer.

9. Designed and proposed to DOE the conversion of the MP tandem to ESTU status.

Between now and 1985 we anticipate the following:

10. Installation of the 4 MV accelerator in the vault previously occupied by our 70 MeV electron linear accelerator.

11. Installation of a large solid angle magnetic spectrometer.

12. Begin actual conversion of the tandem as an approved part of the Yale/Washington upgrade project in mid-1985, and have the conversion completed by mid-1986.

13. Increase the number of active beam lines in the facility from 7 to 13 in anticipation of the larger number of collaborators and users following the conversion.

6. **For the period FY 1981 - FY 1985, please provide actual and estimated budget profiles for operations, in-house research, out-of-house research, other operating expenses, Capital Equipment, General Plant Projects, In-House Energy Management, and any other specific construction projects attributable to the facility. Please indicate the source of these funds (i.e., Medium Energy Nuclear Physics, Heavy Ion Nuclear Physics, Low Energy Nuclear Physics, High Energy Physics, Basic Energy Sciences, etc.).**

Answer: The following is the requested funding breakdown:

(B/A in thousands of dollars)

Source of Funding	FY 1981	FY 1982	FY 1983	FY 1984	FY 1985
Heavy Ion Nuclear Physics					
Operations	$565	$600	$615	$675	$705
In-House Research	530	570	560	640	670
Out-of-House Research	30	30	30	35	35
Low Energy Nuclear Physics					
Operations	205	274	345	365	380
In-House Research	210	280	350	370	385
Nuclear Theory	230	240	260	270	280
Capital Equipment	100	25	0	0	0
Construction	0	0	0	4,000	7,000

7. **How much funding for FY 1981 - FY 1985 has been or is expected to be provided by other federal agencies such as the National Science Foundation or by State agencies?**

Answer: None.

8. **For the period FY 1981 - FY 1985, please provide actual and estimated staffing levels.**

Answer: Staffing levels in man years, actual and estimated, for the period FY 1981 - FY 1985 are as follows:

Category	FY 1981	FY 1982	FY 1983	FY 1985	FY 1985
Faculty	19	16	16	16	18
Grad. Students	27	28	31	32	33
Undergrad. Students	12	11	13	11	12
Support Staff	23	23	22	23	25
TOTAL	81	78	82	82	88

9. **What is the actual and estimated facility utilization for the period FY 1981 - FY 1985? What would be defined as "full" utilization of the facility?**

Answer: The tandem accelerator is normally scheduled for 20 8-hour research shifts each week leaving the 21st free for scheduled routine maintenance, and is closed down for 10 days at year end to encompass staff vacations required by the University. Including a minimum of more extensive maintenance leaves approximately 7,500 hours of research time available each year. Full utilization corresponds to 7,500 hours per year of actual research with beam on target.

During the period FY 1981 - FY 1983, utilization averaged 6,200 hours per year or 83%.

During the period from now through FY 1985, it is anticipated that utilization will continue at this rate (83%) up until May 1985 when it is planned to close down the present facility to begin its conversion.

10. **For the period FY 1981 - FY 1985, how many experiments will have been started, continued, and completed?**

    Answer: At any particular time, there are 30-35 different experimental projects in progress at various stages of development. During the period 1981 - 1985 a total of 75 such projects were started and 75 were completed. Each of these projects takes about 2 years to complete and during that time may include up to 10 or 12 separate experiments.

11. **What is this facility's user policy?**

    Answer: As a university facility, Yale has never supported entirely independent user groups. There has been extensive collaboration with scientists from other institutions in this country and abroad who have collaborated with one or more of the Laboratory staff in experimental work.

    On several occasions, letters have been sent to all the nuclear physics groups in the eastern United States and to major groups throughout the entire country inviting them to propose collaborative projects.

    Yale plans to create a Program Advisory Committee with both external and internal members which will consider each research proposal, independent of its origin, on its merits.

12. **For the period FY 1981 - FY 1985, how much reimbursable research has taken place or is estimated to take place? What revenues have been involved?**

    Answer: None.

13. **What is the mechanism by which specific research proposals for experiments at the facility are considered?**

    Answer: At present, the decisions regarding proposed research in the Laboratory are made by the Director and other senior faculty.

14. **How many research proposals have been submitted over the past five years, and how many of these have been approved?**

    Answer: Between 40 and 50 external proposals for experiments have been submitted over the past 5 years. About 70% of them have been approved.

15. **How many university personnel (i.e., faculty and students) have utilized the facility over the past five years?**

    Answer: Over the past 5 years, 44 Yale faculty and 78 Yale students have utilized the facility; over this same period, 22 non-Yale faculty and 13 non-Yale students have used it, for a total of 157 university personnel.

16. **How many industrial researchers have utilized the facility over the past five years?**

    Answer: Over the past five years, eight industrial researchers have utilized the facility.

17. **How many researchers from foreign institutions have utilized the facility over the past five years?**

    Answer: Over the past 5 years, 18 researchers from foreign institutions have utilized the facility.

18. **How many researchers from other agencies have utilized the facility over the past five years?**

    Answer: Over the past five years, nine researchers from non-DOE Federal agencies have utilized the facility. In addition, 13 researchers from other DOE laboratories have also used it.

19. **What are the future development possibilities for this facility (including research instrumentation/experimental devices), what plans are being made to exploit these possibilities, and what are the budgetary implications?**

    Answer: There are many potential future development possibilities for this accelerator facility, but there are currently no approved plans to undertake any of them beyond the activities identified in the FY 1985 budget request. New research instruments and experimental devices will be developed as the physics research program progresses. We intend to give high priority to the exploitation of the facility's unique capabilities.

20. **Please provide a copy of the facility's latest annual report.**

    Answer: The Laboratory does not prepare annual reports. However, each year, as an integral part of their budget proposal to the Department of Energy, Yale's A. W. Wright Nuclear Structure Laboratory includes a general summary of the research underway and that proposed for the coming year (Appendix B, attached).

    Perhaps the best indicator of the Laboratory's productivity in research is to be found in the external publications resulting from work done in it. Attached as Appendix C is a bibliography listing such publications for the five-year period 1978 - 1983.

APPENDIX B

RESEARCH PROGRAM OF THE LABORATORY

GENERAL COMMENTS:

This has been a particularly successful year for the Laboratory in terms of new discoveries, and, of course, a most important development has been the inclusion of our proposed accelerator upgrade in the Department of Energy FY1984 Presidential Budget.

In terms of new discoveries, we have, for example, discovered dipole collectivity, an entirely new mode of behavior of the nuclear many-body system, and this has raised considerable interest, both experimental and theoretical, at other centers; we have also been able to begin a study of the application of supersymmetries to the nuclear system, and have begun to examine the breakdown of supersymmetric predictions as a systematic function of nucleon number in moving away from the region of iridium where the predictions of the models seem to be best fulfilled. We have also measured the highest angular momenta yet determined both in terms of nuclear structure, where we have identified a state with J=81/2 in ^{153}Ho, and in nuclear reactions, where we have identified a structure in the scattering of silicon-silicon with a spin J=42. We have also been involved in some recent work which demonstrates that, in the heaviest systems yet studied, at excitations approaching 100 MeV there still remain sharp structures superimposed on the continuum which appear to have quasimolecular structure. Furthermore, in our studies of the emission of positrons from the supercritical fields brought into being in the collision of uranium on curium, we have observed totally unexpected monochromatic positrons which may signal the formation of quasimolecular complexes even in this very heavy system. In the theoretical program, the interacting boson and interacting boson fermion approach continues to be applied with growing success to the nuclear system, and also to allied fields such as chemistry, atomic physics, molecular physics, and particle physics. We are involved in a fundamental study of the application of group theoretic techniques to the solution of the general quantum mechanical scattering problem and have achieved some substantial success thus far. We have been successful in applying constrained Hartree-Fock techniques to the description of the collisions of complex nuclei with substantially greater detail than has previously been possible, and we may have obtained the first clear evidence of resonant phenomena in such calculations.

The publication listings included in this proposal provide a detailed description of the productivity of the Laboratory during the past year, and augurs well for its continued productivity during the coming year.

We continue to have approximately twenty-five graduate students associated with the Laboratory. We are happy to be able to report that our students remain in active demand and are finding very attractive career opportunities both in and outside of nuclear physics.

If the line item in the Presidential Budget for FY1984 for the upgrading of our accelerator survives the congressional process, as we very much hope it will, then we will be spending an increasing fraction of the time of the senior members of the Laboratory staff over the next several years in implementing the proposed conversion. It is our intention to add a project manager with experience in these matters to the Laboratory's staff to handle the management aspects of the program and, in particular, the detailed interfacing of the conversion program with the Chicago Operations Office and our various subcontractors. It is also our intention, beginning in FY1983, to have Michel LeTournel, who has been spectacularly successful in bringing about the conversion of the Strasbourg tandem to much higher voltage operation, spend significant periods of time here in our Laboratory consulting with us as we finalize details of our conversion. This will enable us to take advantage of all the experience gained at Strasbourg, and we are confident that this will enable us to obtain significantly higher voltages on the completed ESTU structure than we had initially anticipated. We have already entered into detailed discussions with representatives of High Voltage Engineering and with Mr. Jack Danforth, whom we had earlier retained as a consulting engineer on the ESTU structure, concerning details of the mechanical aspects of the conversion. These discussions are continuing and will provide very pertinent input for the Conceptual Design Report required by DOE.

As in previous years, we have augmented our own facilities through extensive use of other facilities at national laboratories and elsewhere. In particular, we have collaborated at various times during the year with personnel at the Lawrence Berkeley Laboratory, at the Lawrence Livermore Laboratory, at Los Alamos, at Argonne, at Oak Ridge, at Brookhaven, at GSI, at Grenoble, at Chalk River and at a variety of universities both in this country and abroad. We consider that these collaborations are extremely important in that they bring new ideas and new capabilities to our program. In a great many instances they allow us to continue programs that we have started on our own facility into other parameter ranges not now accessible to us here at Yale, and, as in the case of the positron studies at GSI, have led to some remarkable results. This has similarly been the case with our heavy ion resonant studies that we have extended beyond our energy range through use of the facilities both at Brookhaven and the Argonne National Laboratory.

In the sections that follow we make no particular attempt at completeness or detail but rather attempt to give an overview of the major thrust of our activity and some feeling for the major areas of research now underway in the Laboratory and continuing into the coming year.

THE EXPERIMENTAL PROGRAM

A. The Search for Symmetries and Supersymmetries in the Nuclear Many-Body System

Professor Cizewski and her collaborators are maintaining a very active program in which the proton beams from the Yale Accelerator and the triton beams from that at Los Alamos are being used in complementary fashion to examine and test the predictions of a whole range of new models that have been developed starting from the work of Iachello and his collaborators and their identification of new families of simple symmetries in the nucleus. During the past year, this program has particularly focused on the possible role of supersymmetries in nuclei, and rather compelling evidence has been found for these new supersymmetries in the iridium region. Cizewski and her collaborators have utilized their reaction studies to move systematically away from the region where the model seems most effective in reproducing the experimental data to search for symmetry breaking. They have succeeded in finding such behavior in systematic fashion and, at least preliminarily, are able to obtain a quantitative reproduction of their results through variation of a single parameter; namely, the strength of coupling of the single valence fermion to the boson core.

It should be emphasized that these studies are in their infancy, but they already show promise of providing entirely new insight into nuclear structure, and the work will certainly continue apace during the coming year.

This work is being supplemented by a wide ranging program directed toward specific structure problems, utilizing both light and heavy ion beams from our accelerator. In particular, for example, $(\alpha,2n\gamma)$ reactions on silver are being studied to populate medium spins states in ^{109}In which are assumed to be based on the $g_{9/2}$ proton orbital in the region of the tin magic number. Here the goal is that of understanding the extent to which this region really does fulfill close shell characteristics. Complementary studies on $(d,^3He)$ and $(^3He,d)$ reactions as well as (t,α) and (α,t) reactions are also in progress.

In addition, heavy ion beams in the range from boron through chlorine from the Yale tandem are being used to study high spin states in rare nuclei in a collaboration involving Professors Cizewski and Parker and collaborators at the University of Strasbourg. This work has lead to a truly remarkable understanding of the structure of the nucleus ^{153}Ho in that the states up to a spin of 67/2 can be understood in terms of the shell model excitations seen in ^{152}Dy, whereas, those between 67/2 and 81/2 appear to result from breaking and excitation of the ^{146}Gd core. As noted above, this spin of 81/2 is the highest that has yet been reported in a level scheme where there is at least reasonable evidence for assignment of the underlying structure.

We are continuing this work aggressively because of the great interest that attaches to understanding how the nuclear system responds to increasing angular momentum, particularly when one reaches values where current theories suggest that the nuclear shape may make the transition from prolate through oblate to triaxial.

This work is being continued up into the actinide region, with detailed studies on elements up to ^{215}Fr reached through the $4n\gamma$ reaction with ^{11}B incident on ^{208}Pb target. The intent here is to examine the extent to which the actinide region shows behavior similar in detail similar to that which is being mapped out in the lanthanide rare-earth region.

Obviously, there is close cooperation and collaboration between our experimental and theoretical activities in this general testing and development of the symmetric and supersymmetric models of nuclear behavior.

B. Dipole Collectivity in Nuclei

It has traditionally been assumed that collective phenomena in nuclei were of quadrupole or higher order. About a year ago, Iachello and Jackson published a brief theoretical paper in which their examination of the level structure of certain heavy nuclei led them to suggest that it might be possible to observe a dipole collectivity in which, in essence, the nucleus splits up into two molecular fragments with the vector separating their centers of mass, giving the dipole degree of freedom.

Professor Bromley and Dr. Gai, as a natural extention of some of the work in which they have been engaged on molecular states in light nuclei collisions, undertook to search for such phenomena both in light nuclei and in heavy ones. In searching for the most suitable system in light nuclei, they hit upon ^{18}O, which might be considered as consisting of the two particularly stiff subclusters ^{4}He and ^{14}C, and undertook a detailed study of the structure of ^{18}O, utilizing radiative α-particle capture on

^{14}C, studied at the lower energy Van de Graaff accelerator at Brookhaven, and the (^{7}Li,t) reaction on the same target utilizing the tandem at Yale. These studies yielded highly complementary information and have provided very strong supporting evidence for the reality of the dipole collectivity that had been proposed. In particular, we found some of the strongest electric dipole transitions that have ever been reported in nuclei, and, in collaboration with Professor George Bertsch at Michigan State, Dr. Gai and Professor Alhassid developed model independent molecular sum rules which have been tremendously useful in understanding the relevance of our detailed measurements.

At the other end of the mass spectrum, we have worked extensively on ^{218}Ra, using ^{208}Pb targets and a ^{13}C beam together with a wide variety of experimental techniques. Here, again, we find rather clear evidence for the coexistence of the quadrupole and dipole collectivity and have high hopes of measuring quantitatively the mixing matrix elements which couple these two types of behavior. We have made measurements on α-particle hindrance factors, on the electromagnetic lifetimes of states, and on the spins and branching ratios of states, and we have been able to construct quite a resonable level diagram for ^{218}Ra up to spins of sixteen and higher.

Now one of our major goals, is to search for equavalent phenomena in the regions of calcium and zirconium. If we are successful in finding evidence for the dipole mode in these intermediate mass nuclei as well as in both light and heavy species, then we may safely conclude that this is a new and ubiquitous degree of freedom for the nuclear system, and one that all future calculations and measurements must deal with.

As an integral part of this program, and working with Mr. Daley of the University of Arizona at Tucson, we are implementing a detailed program on our Laboratory computer which will allow us to do the appropriate calculations for the mixed dipole quadrupole models within the framework of a spectrum generating algebra; this will allow us to make much more detailed and quantitative predictions than any that are available now. This will be a very valuable tool in our general ongoing program.

C. Studies of Resonant Interactions of Heavy Ions

We have been involved in studies of nuclear molecular phenomena since the beginning of this Laboratory, and within the past few years we have been able to demonstrate, for example, that many of the same theoretical techniques that have been so successful in identifying dynamic simplicities in nuclear structure can also be carried over to the explanation of phenomena observed in nuclear interactions as well; i.e., to virtual scat-

of the model rotational bands. This, of course, is not possible in the $^{16}O + ^{12}C$ system because the electric dipole matrix element vanishes in first order because of the self-conjugate nature of the participants. To avoid this difficulty, we have undertaken a detailed study of the $^{18}O + ^{14}C$ system in the hope of first establishing the validity of a U(4) description of the collision system, then identifying specific resonant states with their spins and parities, and, finally, searching for the electric dipole radiation predicted by the group theoretic model. This is probably the most advantageous system available in the light nuclei in terms of providing the greatest potential separation between the centers of mass and centers of charge and, thus, the greatest electric dipole moment. As such, these measurements should provide a stringent test for our understanding of this new approach to resonant phenomena in the light nuclear systems.

Several years ago, while he was still in this Laboratory Betts and his collaborators undertook a detailed study of the $^{28}Si + ^{28}Si$ system and found rather striking structure in the elastic excitation functions at high energy. Since his move to the Chemistry Division at Argonne, he has been continuing this work, in collaboration with Professor Sanders using the Argonne, Brookhaven, and Yale facilities, and has succeeded in showing that each of the broad structures observed in the earlier work were fragmented into very sharp states and that these states show every evidence of being compound states in the compound nucleus ^{56}Ni at excitations of something like 70 MeV.

This is of particular interest inasmuch as any simple model shows that ^{56}Ni would be expected to disintegrate spontaneously under centrifugal stresses at a spin of about 50ħ so that current measurements are approaching the spontaneous disintegration limit.

During the past year, Sanders, and Betts have mounted a detailed series of measurements aimed at understanding this unexpected compound system behavior at such high excitation. In particular, they have demonstrated that the $^{16}O + ^{40}Ca$ interaction, leading to the $^{28}Si + ^{28}Si$ final state, shows resonant structure with a one-to-one correspondence to that observed in the $^{28}Si + ^{28}Si$ elastic scattering. Furthermore, they have been able to show that the reduced widths of these structures, when the quite different penetrabilities in the two systems are removed, are as far as one can tell, identical. This provides very strong supporting evidence that the observed structure does, indeed, correspond to well defined compound states in ^{56}Ni. It is also a very pertinent reminder that fine structure continues to appear at the highest energies at which one has searched with adequate resolution to resolve it, and this augurs well for the future of the higher energy tandems, such as our ESTU.

tering states as well as to bound states. In particular, we have been able to show that a U(4) symmetry appears to describe rather well the lowest thirty-nine resonances that have been studied in detail in the $^{12}C + ^{12}C$ system. This is work in which Dr. Gai and Professor Bromley have been particularly involved with their students and collaborators.

During the past year, this work was extended to the $^{16}O + ^{12}C$ system in the hope of examining the extended validity of this approach in a system where symmetry did not preclude odd parity states. Somewhat to our surprise, it was found that, in this system, only those resonances observed below and in the region of the Coulomb barrier appear to have the dinuclear character to which the U(4) symmetry would apply, while those at higher energies appear to have a more complex character in which it may well be that the α-particle substructure of the participating nuclei plays a much more significant role.

From all the data now available we have begun to glimpse certain systematics in the occurrence of resonances in different systems which point to this special role for the α-particle as one of the molecular clusters. As part of our ongoing program of study of this phenomena, we have arranged to cooperate with Shapira and others at Oak Ridge in a series of studies of the ^{12}C alpha reaction on ^{16}O and ^{20}Ne using the gas-target which has been developed in collaboration with the Oak Ridge group. These gas targets have the advantage of being contaminant free and are not susceptible to burn-up at high current density so that it will be possible for us to study some of the very weak resonances that would otherwise be very difficult to attack. It is our hope that this work will fill in some of the missing data required to establish a more systematic understanding of the resonance phenomena.

In parallel with this work and with the collaboration of Mermaz of Saclay who will be spending part of this coming summer with us, we will be investigating the $^{24}Mg(^{12}C, \alpha)^{32}S$ reaction here at Yale to resolve a number of lacunae in the existing, rather tantalizing data on this reaction.

It is our hope that this series of measurements will provide for the first time a sufficiently complete view of all the resonances in and below the barrier region within the nuclear sd shell to make possible a sensitive search for molecular structures, other than the dinuclear variety, for which there appears to be growing experimental evidence.

Obviously, one of the most sensitive tests for the U(4) approach to these heavy ion interaction resonances would be the observation of the predicted electromagnetic radiation within one

In a very recent collaborative venture, Sanders and Betts have been studying the $^{24}Mg + ^{24}Mg$ system and, here again, find very striking resonant structure. Surprisingly, they find that these resonances typically have spins that are perhaps two units of angular momentum higher than the grazing angular momentum, whereas in the $^{28}Si + ^{28}Si$ case the resonances appear to have the grazing angular momentum. Although this is not yet fully understood, what it may simply reflect is the prolate deformation of ^{24}Mg and the fact that, when two ^{24}Mg happen to collide so that the long ends touch, an additonal angular momentum can be imparted to the system. If this turns out to be the correct explanation, it will be of interest to us not only in this system but also in terms of our possible understanding of the U + Cm molecular complexes that have been postulated to explain the monochromatic positrons that Professor Greenberg and his associates have been observing at GSI.

In order to understand more fully the situation that they have uncovered, Sanders and Betts are continuing their detailed measurements, using different combinations of silicon isotopes and a variety of heavy ion entrance and exit channels involving the same compound nucleus. The results, to date, are extremely interesting in apparently demonstrating that, even at excitations approaching 100 MeV, there can be very sharp states, a very simple configuration superimposed on the nuclear many-body continuum.

We have reached about as far as we can go in these precision studies with existing machines and are awaiting the higher energies with adequate precision and energy variability that will be available with the Yale ESTU, or at HHIRF or Daresbury.

In a different but related series of heavy-ion studies, Sanders and his collaborators have been testing an idea that was originated here several years ago by Ascuitto who noted that, with minor redefinition, the formidable arsenal of particle-hole formalism that had been developed over the years for the treatment of nuclear structure could also be applied to nuclear interactions. In particular, what one needed to recognize was that the particle and hole need <u>not</u> be in the same nucleus so that one could be in the projectile while the other was in the target. Sanders et al. have picked a particularly interesting case involving the $(^{17}O, ^{16}O)$ reaction on ^{48}Ca leading to the 2.02 MeV state in ^{49}Ca, and the inelastic scattering of ^{17}O on ^{48}Ca leading to the 0.87 MeV state in ^{48}Ca. What is being searched for here is the resonant neutron transfer between the $2s_{1/2}$ level in ^{17}O and the $2p_{1/2}$ state in ^{49}Ca--two states having almost identically the same binding energy. Initial measurements were hampered by target contaminants. New targets have been prepared, and the repeat measurements will be run in the very near future. If

this experiment should yield positive results, it will open up an interesting new family of experiments as well calculations utilizing this more general interpretation of the particle hole formalism.

D. Cluster States in Nuclei

Professor Parker and his associates for a number of years, partly because of astrophysical interest and partly because of the intrinsic structure interest, have been systematically examining light nuclei to uncover the extent to which their spectra can be considered as reflecting cluster structure. They have examined alpha particle clusters extensively, as well as multi-alpha particle clusters, and are currently focussing on three nucleon clusters as observed in (^{6}Li,^{3}He) and (^{6}Li,t) reactions. As in the previous work, they are carrying out extensive and kinematically complete coincidence measurements on these reactions and are obtaining a very important body of data with which to confront the very elaborate and extensive calculations that have been produced by the Japanese school in recent years.

E. Nuclear Astrophysics

Because the solar neutrino problem simply refuses to go away, there has been the lingering question of whether the underlying nuclear reaction data were, in fact, correct. For that reason, Professor Parker in collaboration with Professor Howard of Trinity University and a number of colleagues at Caltech, undertook a complete new measurement of the ^{3}He (α,γ) ^{7}Be reaction both by measuring the prompt gamma rays and the resulting ^{7}Be radioactivity. results that their results are entirely in accord with Parker's original thesis measurements and in striking disagreement measurements that have been reported by Rolfs et al., at Munster. The new Caltech results are also supported by several other recent ^{7}Be activity measurement of this reaction, and it therefore appears that the deficit of solar neutrinos cannot be attributed to problems with this nuclear reaction.

One of the nuclides of recent interest in the study of the formation of the solar system is ^{26}Al. In view of the relatively short half-life of ^{26}Al ($t_{1/2}$=7x10^{5} years), the discovery of ^{26}Mg enrichments in ^{27}Al minerals in meteorites has raised questions about the possible origin of this material and the role it may have played in the formation of the solar system. It is therfore essential that we understand the mechanisms whereby ^{26}Al is produced and destroyed. During the past year, Parker, Howard, and their collaborators have undertaken a detailed study of the radiative capture of protons by ^{25}Mg and have located a capture resonance at a center of mass energy of 37 keV. They have estab-

lished all the characteristics of this resonance and demonstrated that it will dominate the low temperature production of ^{26}Al and increase the reaction rate by ten orders of magnitude over previous estimates. What this implies is that there may be substantial ^{26}Al production in the red giant phase of stellar evolution during quiescent proton burning rather than, as was previously assumed, only in supernova explosions. This obviously makes for tremendous changes in the interpretation ^{26}Al in the early solar system. In order to complete the understanding of this situation, however, it becomes necessary to understand the nuclear reactions wherein ^{26}Al, if present, would be destroyed, and Parker and his collaborators are now setting up to study such reactions in order to be able to obtain hard numbers for the net production rate for ^{26}Al in the various temperature domains.

Under the high temperature conditions which can exist during explosive hydrogen burning on the surfaces of accreting white dwarfs and neutron stars, at temperatures greater then are equal to $10^8 K$, proton radiative capture reactions can compete favorably with β - decay . Following proton capture by ^{12}C to produce ^{13}N, the beta decay of ^{13}N in the slow CNO stellar energy generating cycle leads to ^{13}C, whereas, under conditions of very high temperature, before the beta decay can take place the ^{13}N will capture another proton to form ^{14}O, instead. In this production of ^{14}O, the reaction would be expected to be dominated by a low lying s-wave resonance at a center of mass energy of 546 keV in a manner analogous to that in both the ^{12}C and ^{13}C proton radiative capture situations.

Because this new ^{14}O route could have an important impact on our understanding of the energy generation and isotope formation under such conditions, Parker and his collaborators have undertaken an experimental study using the (^3He,n) and (^3He,t) reactions on ^{12}C and ^{14}N, respectively, to study the excited states in ^{14}O and their competing electromagnetic and proton decays.

F. High Energy Atomic Physics

This Laboratory was one of the first to become involved in studying the molecular x-rays which are emitted during heavy ion collisions, and we were successful in demonstrating for the first time that a unique signature could be obtained for the collision broadened molecular X-rays. These studies are continuing under the direction of Professor Greenberg, using both our facilities in this Laboratory and, for the very heavy systems beyond our range, the facilities at the UNILAC accelerator at GSI where we are collaborating with scientists from the University of Frankfurt and from GSI.

One of the important measurements which was completed in this program at Yale during the past year has been the study of

isolated molecular orbital transitions. Whereas, in the past, the measurements have been inclusive ones, we have succeeded in isolating the $2p\sigma$ to $1s\sigma$ molecular orbital X-ray transition from the total yield resulting from 40 MeV Ni + Ni collisions and have measured the emission anisotropy. In terms of the anisotropy predicted by Greiner and his associates, a striking enhancement by a factor of 10 was observed for this selected transition over that previous measured in this Laboratory for the total molecular orbital emission spectrum. These new measurements confirm the theoretical work in striking fashion and also open up a very selective new approach to the measurement of level structures of the quasimolecule and to the determination of the dynamic coupling involved in the heavy ion collisions well below the barrier.

Because of the vital role that vacancy production plays in any of the positron emission studies, we have felt it essential that we understand the process in much more detail than has hitherto been available. In particular, during the past year, we have focused on the formation of multiple vacancies and the extent to which their yield can provide information on the dynamics of the ion atom collisions involved. In particular, we have made detailed measurements on double k-shell vacancy formation in nickel-nickel collisions, utilizing K X-ray, K X-ray coincidence measurements, and have done this as a function of target thickness in order to measure the production cross sections without having to resort to absolute measurements.

Because of the observation of monochromatic positrons in the uranium-curiumm collisions to which we will refer below, there has been widespread theoretical effort devoted to the development of an explanation. Perhaps the most successful of these explanations has been the suggestion that the monochromatic positrons arise from the formation of longlived U + Cm molecular complexes. Because the UNILAC lacks the energy resolution and because targetry problems with uranium are extreme, it becomes exceedingly difficult to search for direct nuclear evidence of molecular formation in these heavy element cases. What we have chosen to do, instead, and Professors Greenberg and Bromley have joined forces on this project, is to try to carry out a detailed study of the nickel-nickel system through both the atomic and nuclear channels simultaneously. Our preliminary measurements have yielded very encouraging results, and we are currently constructing large solid angle gas detectors to enhance our data taking capabilities. If we are fortunate, we will be able to correlate the formation of nuclear molecular complexes in the nickel-nickel system with enhanced yields of quasimolecular X-rays and, thus, obtain a unique handle on both mechanisms.

One of the intriguing questions relevant to the QED of strong fields concerns the behavior of the $1s\sigma$ quasimolecular state of the heavy collision system at small internuclear separation where the binding energy can approach and exceed twice the rest mass of the electron. As input to this study, we recently carried out a measurement of the $1s\sigma$ ionization probability in the Pb + Cm system as a function of the impact parameter of the collision, using a new doppler shift technique developed here. These measurements probe a range of impact parameters from 5-30 fm and show that earlier measurements indicating significant discrepancies between measured and calculated ionization probabilities reflected incorrect measurement.

Although spontaneous positron production reflects the more fundamental aspects of QED and heavy ion collisions, the dynamic atomic processes, themselves, are inherently interesting because they demonstrate the ultra relativistic effects thar are present in superheavy atomic systems and because these effects must be understood before the positron data can be fully analyzed. Using the UNILAC facilities, we have obtained extensive data on the Pb + U, U + U, and U + Cm collisions systems, and, in the U + Pb system, have mapped the entire range of impact parameters that are of significance. These measurements have been essential in pinning down the dynamic processes so that we can focus on the spontaneous ones of greatest interest.

Perhaps the most surprising and gratifying result of the past year has been the observation of a sharp spike in the positron spectrum from U+Cm collision systems and its absence in the Pb+U system where the fields are not supercritical. A number of possible explanations, such as internal pair conversion, can be eliminated. And it is highly probable that we have indeed observed spontaneous positron emission. To improve these measurements, the experimental equipment has been modified to increase its total efficiency by a factor of 3 and to extend the range of positron energies that can be detected with high efficiency and high resolution. In June of 1983, it is planned to carry out experiments to trace the peak structure as a function of $Z1+Z2$, the total number of protons present in the colliding system, an essential ingredient for the unambiguous identification of spontaneous positron production.

The fact that the monochromatic positron peak has a width of less than 80 keV implies that the emitting process has to exist for times greater than 5×10^{-20} seconds. If this peak originates from spontaneous positron emission, then the implication is that we are forming metastable nuclear complexes with Z=186 that live for at least this lifetime. Recent calculations by Greiner and his co-workers on the potentials that can be obtained using realistic internucleon and internucleus forces suggest that, in fact,

there is a possibility of forming relatively long lived nuclear molecules in these heavy element collisions. To the extent that this can happen, the expected result would indeed be the sharp positron line that is observed. And this is a truly exciting new possibility which measurements, beginning in June of this year, will attempt to disentangle.

As in the past, it is our intention to maintain a balanced program using the tandem facilities here at Yale and the GSI facilities in complementary fashion. Thus far, we have found this to be an extremely effective arrangement.

G. Nuclear Geophysics

During the past year, we have continued to perfect our techniques for using our accelerator as an ultrasensitive mass spectrometer using the electrostatic analyzer constructed by Thomas and co-workers. We are collaborating with the Geochemistry group at Yale under Professor Turekian and the Geochemistry group at Rugers University under Professor Herzog and have carried out a wide variety of measurements on ^{10}Be and ^{26}Al from a great many samples. These have included manganese nodules, soil cores, ice cores, rain water, meteoric fragments and the like. Indeed, this has now become a very straightforward program so that we are, in essence, providing a service to our colleagues in geophysics and geochemistry which is enormously valuable to them and excellent science.

We have now become interested in the possibility of being able to focus on ^{53}Mn which has a lifetime of some four million years and which is simply not readily measureable with MP Tandems because we cannot get high enough energy to allow our detection systems to work with reliable sensitivity. With the energies we will have available from the ESTU this will become very readily available as a geochronological isotope, and we foresee a whole new wave of interesting applications studying (1) the production of ^{53}Mn in cosmic-ray induced spellation on interplanetary grains and meteors and (2) its subsequent transport and deposition in terrestrial materials.

H. Surface and Materials Science

During the year, we have succeeded in bringing our ultra-high vacuum lines into service with the tandem and, also, hve fully installed a 300 keV high current iron implanter system which we were fortunate enough to receive from a private donor and which the University installed in a new laboratory immediately adjacent to our second computer room. Professor Weller and his students and associates are engaged in a wide variety of programs using both of these accelerators as well as the 1 MV Van de Graaff in the Yale Sloane Laboratory. We also are looking

forward to the possibility of installing a surplus 4 MV HVEC horizontal Van de Graaff Accelerator in the vault now housing our 70 MeV electron accelerator when it is dismantled and disposed of during the latter part of this coming summer.

Inasmuch as sputtering is becoming a technique of very rapidly growing technical importance in the fabrication of large scale integrated circuits, for example, and in a number of other technological applications, it is surprising to realize how very poorly the process, itself, is understood. It is our goal to correct this situation, and we are undertaking a series of measurements using both accelerators directed toward this end. For example, we will carry out detailed studies on the sputtering of binary alloys, to determine the role of surface segregation assisted by radiation enhanced diffusion in the preferential sputtering of alloys. At the moment, there is no reliable information on the relative yield of alloy components, the topography of the sputtered surface and the like. One aspect of this program will involve detailes measurement of sticking probabilities for sputtered atoms because this information will be critical to much of our further work. We have perfected a technique which allows this to be done rapidly and quantitatively.

Again, because very little information is available on the mass spectrum of sputtered fragments, we have constructed a secondary-ion mass spectrometer and have mounted it for use with beams from the Tandem in an ultra-high vacuum environment. This instrument has only recently been brought into operation, but our initial runs have been entirely successful, and it is now part of the routine instrumentation of the Laboratory. We have for example, measured the energy spectrum of ions in the range from 0-100 eV sputtered by 60-90 MeV bromine ions. The spectrum obtained very closely resembles that of the neutral-atoms sputtered from the same target surfaces by ions in the kilovolt range.

Again, because of the many, important technological applications, we have focused considerable attention on studying the process of radiation enhanced adhesion discovered by Tombrello *et al.* at Caltech within the past two years. In general the sputtering of thin films onto almost any surface leads to very poor adhesion and frequently to the formation of other than ohmic contacts between the sputtered material, and the substrate. This is a matter of crucial importance in the fabrication of everything from semi-conductor nuclear detectors through integrated circuits. What has been found is that, if after the thin gold film has been deposited on the substrate, it is then irradiated with an appropriate beam of alpha particles or heavy ions, the adhesion becomes essentially complete, and the contact becomes purely ohmic in character. We have been focusing, thus far, on the systematic study of the bonding of gold films to quartz sub-

strates using alpha particle bombardments over a wide range of energies. But it has been observed that the technique is applicable to the formation of strongly adhering films applied to metals, semi-conductors and insulators; one can even stick gold films irretrievably to teflon> We believe that this has such potential importance technologically that it deserves intensive study. Measurements that have been made thus far, both here and at Caltech, demonstrate that the radiation enhanced adhesion does not result from diffusion, does not result from local heating, does not result from a variant of ion-beam mixing or, indeed, from any of the normally considered mechanisms. It has been postulated that it may, in fact, result from purely electrostatic phenomena as the very high temperature electron column in the gold film produced by the passage of a heavy ion attempts unsuccessfully to cascade back to its original state, leaving trapped charge and thus residual electrostatic fields. This is an interesting and challenging problem in which one of our graduate students has just now embarked.

In a very real sense, we have spent much of the past year developing the facilities, both at the Tandem and at the ion implanter to proceed with this work. During this coming summer, Professor Tombrello from Caltech will again be spending a month in the Laboratory and at that time we plant to implement the experiment that we discussed a year ago involving sputtering from a horizontal liquid metal surface. The problem in many sputtering experiments is that since we do not know th microscopic topography after sputtering begins, we do not know to what extent the angular characteristics of the yield and the yield itself depend on that microstructure. By doing this sputtering on a molten surface that is intrinsically self-healing, we remove many of the uncertainties and can focus better on the sputtering process itself. This experiment, of course, requires that we deflect the beam from the 300 keV implanter through 90 degrees to impinge vertically on the horizontal molten metal surface.

The combination of facilities that we will have, if we can complete our present plans, ranging from the 300 keV implanter through the 1 MV Van de Graaff to the 4 MV Van de Graaff and then to the large Tandem Accelerator will give us a complement of beam energies and species that will enable us to make an unprecedented attack on the examination of surface and material phenomena.

It is our intent to maintain the level of effort in this program at about its present value, where it is represented by one faculty member, one part-time postdoc and several graduate students.

RESEARCH ACTIVITIES OF THE NUCLEAR THEORY GROUP

A. Composition of the group

The Nuclear Theory Group at Yale is, at present, composed of one Professor (F. Iachello), two Assistant Professors (M. Strayer and Y. Alhassid) and seven Graduate Students (S. Kuyucak, S. Umar, S. Lee, J.S. Wu, J. Zingman, J. Manoyan and J. Engel).

B. Past Activities

The Nuclear Theory Group at Yale has pursued, in FY 1983, several lines of research. The two main areas in which we have concentrated our attention are:

(i) the introduction and exploitation of algebraic techniques in the solution of complex problems in physics and

(ii) the use of many-body techniques in nuclear reaction studies.

Research in these areas has been carried on through work at Yale, involving both Faculty Members and students, and through work performed in collaboration with several other groups and institutions.

In the first area of research, major projects, at least in part completed, are:

B-1. We have introduced a new class of supersymmetry in nuclei. This class deals with complex, multishell, configurations, and extends further the concept of supersymmetries previously introduced by one of us (F. Iachello). This project has been carried on in collaboration with I. Bars (Particle Theory Group, Yale), R. Bijker (University of Groningen,

The Netherlands) and A.B. Balantekin (previously a Graduate Student at Yale and presently at M.I.T.). The introduction of this new class of supersymmetries has led to important developments in the understanding of the structure of medium-and heavy-mass, odd-A nuclei.

B-2. One of us (F. Iachello) has suggested that a new mode of excitation, characterized by a dipole, rather than a quadrupole, nature may exist in nuclei. This mode, described algebraically by the group U(4), is related to the occurrence of clustering phenomena in nuclei. We have started a detailed investigation of the properties of this mode. One of us (Y. Alhassid), together with M. Gai (Nuclear Experimental Group, Yale) and G. Bertsch (Michigan State University), has derived sum rules for the radiative widths of the cluster states. Another of us (F. Iachello) together with A.D. Jackson (SUNY at Stony Brook) and H. Daley (a Graduate Student at the University of Arizona), has analyzed the spectroscopic properties of the newly proposed mode. This study is being carried on in close collaboration with the Nuclear Experimental Group at Yale, who has, recently, found evidence for dipole modes, both in light, ^{18}O, and heavy, ^{218}Ra, nuclei.

B-3. The dipole mode is the fundamental mode of excitation in molecules. One of us (F. Iachello), together with R.D. Levine (The Hebrew University, Jerusalem) has investigated the use of algebraic techni-

ques in the description of atomic molecules, and developed a model, called vibron model, for that purpose. The vibron model promises to play, in molecular physics, the same role played by the interacting boson model in nuclear physics. We have further extended the vibron model to cover triatomic molecules, in collaboration with A.E.L. Dieperink (University of Groningen,The Netherlands) and O. van Roosmalen (Caltech).

B-4. Traditionally, algebraic techniques have been used only for the treatment of bound state problems. Here one considers compact groups, for example U(6) in the interacting boson model and U(4) in the vibron model. Two of us (F. Iachello and Y. Alhassid) together with F. GÜrsey (Particle Theory Group, Yale) have suggested that algebraic techniques may also be used for the treatment of scattering problems and band structure problems in periodic potentials. This suggestion has relayed on the introduction of non-compact groups. We have completed the study of one-dimensional systems, described algebraically by the group U(1,1).

In the second area of research, major projects, again at least in part completed are:

B-5. One of us (Y. Alhassid) has developed, in collaboration with R. Balian (Saclay, France) and H. Reinhardt (Dresden, E-Germany), a geometric approach to dissipation and evolution in many-body systems.

B-6. One of us (Y. Alhassid) has continued the exploitation of path-integral Montecarlo techniques in the calculation of properties of many-body systems. We have calculated, in collaboration with S.E. Koonin and K. Langanke (Caltech) the ground state energy and density of ^{6}Li. We are now in the process of extending path-integral Montecarlo techniques to the calculation of scattering processes.

B-7. One of us (M. Strayer), together with a Graduate student (S. Umar) has used a time-dependent external field model which treats the relative motion classically and the internal excitation quantum mechanically, in order to study inclusive particle emission in heavy-ion reactions. This method will yield particle distributions and multiplicities in terms of nuclear Hartree-Fock potentials.

B-8. A refined classical model of prompt nucleon emission has been studied by one of us (M. Strayer) together with K.T. Davies (ORNL) in order to describe asymmetries in heavy-ion prompt nucleon emission. These asymmetries are sensitive to the time scale involved in the emission process.

C. Future activities

Our planned future activities include the continuation and completion of research programs already started in FY 1983 and the beginning of new projects. Among the programs we intend to continue, we mention:

C-1. The study of clustering phenomena in heavy nuclei using the algebraic approach. Since most heavy nuclei are deformed, this study requires the simultaneous introduction of quadrupole and dipole degrees of freedom. The corresponding model is described algebraically by the product of the two groups U(6) and U(4) of the quadrupole and dipole modes. We plan to investigate in detail the spectra of the actinide nuclei with A≃220. This project will be carried on in collaboration with A.D. Jackson (SUNY at Stony Brook) and H. Daley (University of Arizona).

C-2. We have started a study of shape phase transitions in hot nuclei in collaboration with S. Levit (Weizmann Institute, Israel). Up to now, our study has been limited to a schematic model (the Lipkin model). We now intend to attack more realistic models. This study is being carried on by one of our students (J. Zingman).

C-3. We have started an evaluation of free energy surfaces and level densities in nuclei by a combination of Thomas-Fermi and Strutinski methods at finite temperature, (Y. Alhassid). This work is being carried on by one student (J. Manoyan).

C-4. One of us (M. Strayer), together with a student (S. Lee) is investigating the equation of state of dense nuclear matter in a field theoretic model that includes baryons, scalar and vector mesons. This model will be solved in the 1/N limit and we plan to complete our study

in the course of FY 1984.

C-5. One of us (M. Strayer), together with a student (J.S. Wu), has started an investigation of quasi-periodic molecular vibrations in ^{12}C-^{12}C and α-^{14}C within the framework of the TDHF approximation. The analysis of the different modes is given in terms of generalized correlation functions, and related to the molecular potential energy along the collective path.

A good fraction of our attention will be devoted in FY 1984 to the development of a new project:

C-6. A systematic investigation of heavy ion reactions. We intend here to make use of two different approaches. First, an S-matrix theory, similar to that employed in elementary particle physics for the analysis of collisions between hadrons. We plan to consider most of the available data, including elastic, inelastic and transfer data. In addition, we plan to connect this S-matrix theory with the algebraic approach to scattering problems discussed above in B-4. Here, we plan to extend our present one-dimensional results to three-dimensional cases. This work will be carried on by a new student (J. Engel), together with S.J. Wu and two of us (F. Iachello and Y. Alhassid).

D. Future composition of the group

In the Summer of 1983, one of our Faculty Members (M. Strayer) will leave the group to join ORNL. We plan to use the Assistant Position occupied presently by Strayer, in the coming academic year 1983-84 for a Visiting Professor. Preliminary contacts have been taken with A. Klein (University of Pennsylvania), who has indicated his willingness to come to Yale. A. Klein is presently engaged in the study of the microscopic foundations of the interacting boson model. His visit will thus strengthen that part of our research program devoted to algebraic techniques. In the meantime, we will be actively looking for a replacement for M. Strayer and we expect to fill that position with a new Assistant Professor by the summer of 1984.

In the Summer of 1983 one of our students, S. Kuyucak, will leave. Kuyucak has completed his requirements for a Ph.D. degree. We have already found a replacement for him (J. Engel).

In view of the large number of students, six, present in our group, we would find it appropriate to have a post-doctoral position. We do not have such a position at present, since our budget does not allow it. We would find it very helpful to our research activities if extra funds could be provided to us in order to attract to Yale a post-doctoral fellow.

APPENDIX C

PUBLICATIONS FROM THE WRIGHT LABORATORY, 1978-1983

Sequential Amplitudes in Heavy-Ion Induced Two-Proton Transfer Reactions
P.P. Tung, K.A. Erb, M.W. Sachs, R.J. Ascuitto and D.A. Bromley
Phys. Rev. C18 (1978) 1663.

Role of the Exit-Channel Distorting Potential in Heavy-Ion Induced Reactions
R.J. Ascuitto, J.F. Petersen, and E.A. Seglie
Phys. Rev. Letts. 41 (1978) 1159.

Doppler-Shift Analysis of Continuum X-Radiation from Quasimolecular Systems
P. Vincent, C.K. Davis, and J.S. Greenberg
Phys. Rev. A18 (1978) 1878.

Interacting Boson Model of Collective Nuclear States. III. -The Transition from SU(5) to SU(3)
O. Scholten, F. Iachello and A. Arima
Ann. of Phys. (N.Y.) 115 (1978).

Solar Wind Sputtering of the Martian Atmosphere
P.K. Haff, Z.E. Switkowski and T.A. Tombrello
Nature 272 (1978) 803.

Observation of Positron Creation in Superheavy Ion-Atom Collision Systems
H. Backe, L. Handschug, F. Hessberger, E. Kankeleit, L. Richter, F. Weik, R. Willwater, H. Bokemeyer, P. Vincent, Y. Nakayama and J.S. Greenberg
Phys. Rev. Letts. 40 (1978) 1443.

^{15}N Hydrogen Profiling: Scientific Applications
W.A. Lanford
Nuclear Instr. and Meth. 149 (1978) 1.

An Analysis of Neutron Transfer Between Identical Cores With Applications to the $^{12}C + {}^{13}C$ System
L.T. Chua and D.A. Bromley
Il Nuovo Cimento 47A (1978) 443.

Nuclear Shell Model and Interacting Bosons
T. Otsuka, A. Arima and F. Iachello
Nuclear Physics A309 (1978) 1.

Interference Effects in the Reaction $^{48}Ti(^{16}O,{}^{15}N)^{49}V$
G.B. Sherwood, K.A. Erb, D.L. Hanson, R.J. Ascuitto, D.A. Bromley and J.J. Kolata
Phys. Rev. C18 (1978) 2574.

A Special Mode of Nuclear Motions--The Nature of ^{12}C-^{12}C Interactions
K.A. Erb, D.A. Bromley and J. Weneser
Comments on Nucl. and Particle Physics 8 (1978) 111.

Observation of Striking Shape Differences Between 2_1^+ Angular Distributions for Heavy-Ion-Induced Two-Neutron Stripping and Pickup Reactions in Transitional Samarium Nuclei
C.F. Maguire, D.L. Hendrie, U. Jahnke, J. Mahoney, D.K. Scott, J.S. Vaagen, R.J. Ascuitto and K. Kumar
Phys. Rev. Letts. 40 (1978) 358.

A Study of Resonances in the Sub-Coulomb ^{12}C-^{12}C Reaction from the Viewpoint of Nuclear Molecules
Y. Kondo, Y. Abe and T. Matsuse
Prog. Theor. Phys. 59 (1978) 465.

An Occurrence Mechanism of Molecular Resonances
T. Matsuse, Y. Kondo and Y. Abe
Prog. Theor. Phys. 59 (1978) 1009.

Molecular Resonances in $^{12}C(^{16}O,^{16}O)^{12}C^*$ (2^+,4.44 MeV) Inelastic Scattering by a Band Crossing Model
T. Matsuse, Y. Abe and Y. Kondo
Prog. Theor. Phys. 59 (1978) 1037.

A New Evidence for a Band Crossing Model--Resonances in High Energy ^{12}C-^{12}C Scattering
Y. Abe, Y. Kondo and T. Matsuse
Prog. Theor. Phys. 59 (1978) 1393.

A Band Crossing Model of Resonances in Heavy Ion Reactions--I. Resonances in ^{12}C-^{16}O Scattering
T. Matsuse, Y. Abe and Y. Kondo
Prog. Theor. Phys. 59 (1978) 1904.

Gamma-decay and Band Structures in ^{46}Ti
G.D. Dracoulis, D.C. Radford and A.R. Poletti
Journal of Physics G4 (1978) 1323.

Input Data: Nuclear Reaction Cross Sections
P.D. Parker
Solar Neutrino Conference II (BNL-50879, Volume I) (1978) 77.

Hydrogen Content of Plasma-deposited Silicon Nitride
W.A. Lanford and M.J. Rand
Journal of Applied Physics 49 (1978) 2473.

The Extended Time-Dependent Hartree-Fock Approximation with Particle Collisions
Cheuk-Yin Wong and Henry H.K. Tang
Phys. Rev. Letts. 40 (1978) 1070.

Sensitivity of the T_c of Nb_3Ge to Hydrogen Content
W.A. Lanford, P.H. Schmidt, J.M. Rowell, J.M. Poate, R.C. Dynes and P.D. Dernier
Applied Physics Letters 32 (1978) 339.

Hydration of Obsidian
T. Laursen and W.A. Lanford
Nature 276 (1978) 153.

Location of 0^+ 4p-2h and 6p-4h Configurations in ^{42}Ca
H.T. Fortune, R.R. Betts, J.N. Bishop, M.N.I. Al-Jadv and R. Middleton
Nucl. Phys. A294 (1978) 208.

Multipole Pairing States and the Correspondence Between Two-and Four-Particle Transfer Reactions
R.R. Betts, Nelson Stein, J.W. Somer and C.W. Woods
Phys. Letters 46B (1978) 47.

Study of ^{26}Al by the $^{25}Mg(^3He,d)$ Reaction
R.R. Betts, H.T. Fortune and D.J. Pullen
Nucl. Phys. A299 (1978) 412.

Lifetime Measurements in ^{41}Ar and ^{41}K
D.C. Radford, J.R. Southon and A.R. Poletti
Nucl. Phys. A303 (1978) 134.

Profiling Hydrogen in Materials Using Ion Beams
J.F. Ziegler, C.P. Wu, P. Williams, C.W. White, B. Terreault, B.M.U. Scherzer, R.L. Schulte, E.J. Schneid, C.W. Magee, E. Ligeon, J.L. 'Ecuyer, W.A. Lanford, F.J. Kuehne, E.A. Kamykowski, W.O. Hofer A. Guivarc'h, C.H. Filleux, V.R. Deline, C.A. Evans, Jr., B.L. Cohen, C.J. Clark, W.K. Chu, C. Brassard, R.S. Blewer, R. Behrisch, B.R. Appleton, and D.D. Allred
Nucl. Instr. and Meth. 149 (1978) 19.

Dynamic Symmetries in Nuclei
F. Iachello
Comments on Nuclear and Particle Physics 8 (1978) 59.

The $^{12}C + ^{13}C$ Elastic Transfer Interaction at Intermediate Energies
L.T. Chua, A. Gobbi, M.W. Sachs, D. Shapira, R. Wieland and D.A. Bromley
Il Nuovo Cimento 47A (1978) 430.

Possible Selectivity in $^{12}C(^{10}B,d)^{20}Ne$
H.T. Fortune, R.R. Betts and R. Middleton
Phys. Rev. C17 (1978) 401.

Dynamical Symmetries in Nuclei
F. Iachello
Proc. Int. Conference on Group Theory, Austin, Texas (1978).

The Interacting Boson Model
F. Iachello
Proc. Third International Symp. on Neutron Capture, Gamma-Ray Spectroscopy and Related Topics, Brookhaven, N.Y. Sept. 1978.

Present Status of the Interacting Boson Model
F. Iachello
in Interacting Bosons in Nuclear Physics, Plenum Press, N.Y. (1978).

The Electromagnetic Properties of ^{194}Pt and the Question of its Triaxiality
C. Baktash, J. X. Saladin, J.J. O'Brien and J.G. Alessi
Phys. Rev. C18 (1978) 131.

Precise Determination of B(E2) Values in ^{155}Gd, $^{161,163}Dy$, ^{167}Er and ^{175}Lu
P.F. Brown, C. Baktash, J.J. O'Brien and J.X. Saladin
Phys. Rev. C18 (1978) 666.

Nuclear Molecules
D. Allan Bromley
Scientific American 239 (1978) 58.

Schwere Ionen und Kernmolekule: Quantenelektrodynamik; Gibt es schwarze Locher?
D. Allan Bromley and Walter Greiner
Umschau 78, (1978) 728.

Superheavy Quasiatoms
J.S. Greenberg
McGraw-Hill Yearbook of Science and Technology (1978).

An Interacting Boson-Fermion Model of Collective States in Odd-A Nuclei
F. Iachello and O. Scholten
Phys. Rev. Letters 43 (1979) 679.

$^{12}C + ^{12}C$ Coulomb Barrier Resonances: Direct Determination of Resonance Parameters from Elastic Scattering Measurements
S.K. Korotky, K.A. Erb, S.J. Willett and D.A. Bromley
Phys. Rev. C20 (1979) 1014.

Spectroscopy of High Spin States in ^{16}O and ^{20}Ne Using the $(^{12}C, ^{8}Be)$ (α_0) Reaction
S.J. Sanders, L.M. Martz and P.D. Parker
Phys. Rev. C20 (1979) 1743.

Neutron Time-of-Flight Spectrometers
F.W.K. Firk
Nucl. Instr. and Meth., 162 (1979) 539.

Energy Dependent Structure in $^{28}Si + ^{28}Si$ Scattering
R.R. Betts, S.B. DiCenzo and J.F. Petersen
Phys. Rev. Letters 43 (1979) 253.

Origin of Gross Structure in $^{12}C + ^{12}C$ and $^{16}O + ^{16}O$ Inelastic Scattering
R.L. Phillips, K.A. Erb, D.A. Bromley and J. Weneser
Phys. Rev. Letters 42 (1979) 566.

(^{6}Li,t), (^{6}Li,^{3}He) and (^{7}Li,t) Reactions into the A=19 Nuclei
L.M. Martz, S.J. Sanders, P.D. Parker and C.B. Dover
Phys. Rev. C20 (1979) 1340.

Model for an Effective Q-Value for Heavy-Ion Induced Transfer Reactions
E.A. Seglie, J.F. Petersen and R.J. Ascuitto
Phys. Rev. Letters 42 (1979) 956.

Pair Excitations in Tungsten Nuclei: Pairing Phonons or SU(3) Bosons?
R.R. Betts and M.H. Mortensen
Phys. Rev. Letters 43 (1979) 616.

Positrons from 1.4 GeV Uranium-Atom Collisions
C. Kozhuharov, P. Kienle, E. Berdermann, H. Bokemeyer, J.S. Greenberg, Y. Nakayama, P. Vincent, L. Handschug, E. Kankeleit, H. Bache
Phys. Rev. Letters 42 (1979) 376.

Remeasurement of the Low-Energy Cross Section for the $^{15}N(p,\alpha)^{12}C$ Reaction
J. Zyskind and P.D. Parker
Nucl. Phys. A320 (1979) 404.

The Effect of Cosmic Rays on Computer Memories
J.F. Ziegler and W.A. Lanford
Science 206 (1979) 776.

Rotational-Energy Contributions to the Kinetic Energies of Deep-Inelastic Reaction Products
R.R. Betts and S.B. DiCenzo
Phys. Rev. C19 (1979) 2070.

Application of a Band Crossing Model for Resonances in High Energy $^{12}C + ^{12}C$ Scattering
Yosio Kondo, Yasuhisa Abe and Takehiro Matsuse
Phys. Rev. C19 (1979) 1356.

Intermediate Structure in $^{12}C + ^{12}C$ Elastic Scattering
Yasuhisa Abe, Yosio Kondo, and Takehiro Matsuse
Phys. Rev. C19 (1979) 1365.

The $^{18}O(^{18}O,^{16}O)^{20}O$ Reaction at 52 MeV
S. Kubono, T.K. Li, D. Dehnhard, D.A. Lewis, J.F. Petersen and J.L. Artz
Nucl. Phys. A313 (1979) 434.

The Measurement of ^{10}Be in Manganese Nodules Using a Tandem Van de Graaff Accelerator
K.K. Turekian, J.K. Cochran, S. Krishnaswami, W.A. Lanford, P.D. Parker and K.A. Bauer
Geophysical Research Letters 6 (1979) 417.

Energy-Averaged Angular Distributions for $^{16}O + ^{12}C \rightarrow \alpha + ^{24}Mg$
R. Middleton, R.R. Betts, H.T. Fortune, R.G. Stokstad
Phys. Rev. C19 (1979) 100.

The Erosion of Planetary and Satellite Atmospheres by Energetic Atomic Particles
P.K. Haff and C.C. Watson
Journal of Geophysical Research 84 (1979) 8436.

Interacting Bosons in Nuclear Physics
F. Iachello
Neutron Capture Gamma-Ray Spectroscopy, (eds. R.E. Chrien and W. Kane) (Plenum Press, New York) (1979) 23.

The Angular Distribution of the Polarization of Ground State Photoneutrons from ^{16}O
R. Nath, F.W.K. Firk, and Y.H. Chiu
Neutron Capture Gamma-Ray Spectroscopy
Edited by R.E. Chrien and W.R. Kane, Plenum Press (1979).

N-P Capture and the Photo-Disintegration of the Deuteron
F.W.K. Firk
Neutron Capture Gamma-Ray Spectroscopy
Edited by R.E. Chrien and W.R. Kane, Plenum Press (1979) 245.

A Calculation of Low-lying Collective States in Even-Even Nuclei
F. Iachello, G. Puddu, O. Scholten, A. Arima and T. Otsuka
Phys. Letters 89B (1979) 1.

Two-Particle Two-Hole Configuration in ^{208}Bi and the $^{210}Bi^{m}(p,t)^{208}Bi$ Reaction
K.A. Erb, W.D. Callender and R.K. Sheline
Phys. Rev. C20 (1979) 2031.

Collision Broadening of Continuum Radiation from Ni + Ni Collisions
P. Vincent and J.S. Greenberg
J. Physics C12 (1979).

Two-Step Process (p,^{3}He) (^{3}He,t) in the ^{48}Ca(p,t) ^{46}Ca Reaction
M. Strayer, P.J. Ellis and M.F. Werby
Phys. Rev. C19 (1979) 536.

The State Quadrupole Moment of the First Excited State of ^{30}Si
M.P. Fewell, D.C. Kean, R.H. Spear, T.H. Zabel,
A.M. Baxter and S. Hinds
Phys. Rev. Letters 43 (1979) 1463.

Energy Dependent Structure in Heavy Ion Interactions
A. Gobbi and D.A. Bromley
in Heavy Ion Interactions edited by R. Bock, North-Holland
Publishers (1979) 485-606.

Interacting Boson Model of Collective Nuclear States IV-The O(6) Limit
A. Arima and F. Iachello
Annals of Physics 123 (1979) 468.

Evolution and Use of Nuclear Detectors and Systems
D.A. Bromley
Nucl. Instr. and Methods 162 (1979) 1.

Time of Flight Detectors for Heavy Ions
R.R. Betts
Nucl. Instr. and Methods 162 (1979) 531.

SO_4 Symmetry for Classifications of Dibaryons and Baryoniums
M. Koca and A.B. Balantekin
Nuovo Cimento 52 (1979) 500.

Hydration of Soda-Lime Glass
W.A. Lanford, K. Davis, P. La Marche, T. Laursen,
R. Groleau, R.H. Doremus
Journal of Non-Crystalline Solids 33 (1979) 249.

TDHF Calculation for Nuclear Collisions: Model Studies of Alpha-Alpha Scattering
M. Strayer, K.R. Sandhya Devi and J.M. Irvine
J. Phys. G5 (1979) 281.

Totally Microscopic Description of n-^{16}O Elastic Scattering II
M. Strayer and W.H. Bassichis
Phys. Rev. C20 (1979) 915.

Time-Dependent Hartree-Fock Calculations of ^{86}Kr + ^{139}La at E_{lab}=505,610, and 710 MeV
M. Strayer, K.R. Sandhya Devi and K.T.R. Davies
Phys. Rev. C20 (1979) 1372.

Solar Wind Sputtering of Planetary Atmospheres and Surfaces
C.C. Watson, P.K. Haff and T.A. Tombrello
Lunar and Planetary Science X (1979) 1316.

The Static Quadrupole Moment of the First Excited State of ^{24}Mg
M.P. Fewell, S. Hinds, D.C. Kean and T.H. Zabel
Nucl. Phys. A319 (1979) 214.

Electric Moments of the First Excited State of ^{18}O
M.P. Fewell, A.M. Baxter, D.C. Kean, R.H. Spear and T.H. Zabel
Nucl. Phys. A321 (1979) 457.

Lifetimes of Excited States in ^{54}Mn and ^{53}Cr
D.C. Radford and A.R. Poletti
Journal of Physics G5(1979) 409.

Present Status of the Interacting Boson Model
F. Iachello
Interacting Bosons in Nuclear Physics, (F. Iachello, ed.), (Plenum Press, N.Y.) (1979) 1-16.

Dynamical Symmetries in Nuclear Physics
F. Iachello
The Why's of Subnuclear Physics (A. Zichichi, ed.)
Plenum Press, N.Y.) (1979) 1043-1056.

Dynamic Symmetries in Nuclei
F. Iachello
Group Theoretical Methods in Physics, (W. Beiglbock, ed.)
(Springer Verlag, Berlin) (1979) 420-429.

Science, The Universities and the Federal Government
D.A. Bromley
Science, Technology and Humanities 2 (1979) 205.

The Frontiers of Physics and Their Roles in Society
D.A. Bromley
Physica Scripta 19 (1979) 203.

Nuclear Molecular Resonances in Heavy Ion Collisions
Karl A. Erb and D. Allan Bromley
Physics Today 32-1 (1979) 34.

A Mineral of That Excellent Nature: The Qualities of Silver as a Metal
W.A. Lanford
Silver in American Life, ed. by B. McLean Ward and G.W.R. Ward
(1979) page 3, pub. by the American Federation of Arts, New York.

Energies of the Future
D.A. Bromley
Published by the Communications Department, United Illuminating Company, New Haven, Connecticut (1979).

U.S. Universities and the Federal Government
D.A. Bromley
Published by Vanderbilt University Press (1979).

Superconductors
W.A. Lanford
McGraw-Hill Encyclopedia of Science and Technology (1979).

Nuclear Molecular Phenomena in Nuclei
D.A. Bromley
Published by Vanderbilt University Press (1979).

Superheavy Quasiatoms
J.S. Greenberg
McGraw-Hill Yearbook of Science and Technology (1979).

Dynamical Supersymmetries in Nuclei
F. Iachello
Phys. Rev. Letters 44 (1980) 772.

Search for Fusion Oscillations in the $^{16}O + ^{28}Si$ System
R.R. Betts, M.M. Hindi, S.B. DiCenzo and P.D. Parker
Phys. Rev. C21 (1980) 175.

Finite Range Distorted-Wave Born Approximation Analysis of (p,t) Reactions with a Realistic Triton Wave Function
M.F. Werby, M.R. Strayer and M.A. Nagarajan
Phys. Rev. C21 (1980) 2235.

Classical Limit of the Interacting Boson Model
A.E.L. Dieperink, O. Scholten and F. Iachello
Phys. Rev. Letters 44 (1980) 1747.

$^{210}Bi^{m}$ (d,t) Reaction; $^{210}Bi(9^-)$ Parentage of States in ^{209}Bi
T.P. Cleary, W.D. Callender and R.K. Sheline
Phys. Rev. C21 (1980) 2244.

Resonant and Average Behavior of the $^{12}C + ^{12}C$ Total Reaction Cross Section: $5.6 < E_{c.m.} < 10$ MeV
K.A. Erb, R.R. Betts, S.K. Korotky, M.M. Hindi, P.P. Tung, M.W. Sachs, S.J. Willett and D.A. Bromley
Phys. Rev. C22)(1980) 507.

W(p,t) Reactions: I. Even Targets
M.H. Mortensen, R.R. Betts and C.K. Bockelman
Phys. Rev. C21 (1980) 2275.

W(p,t) Reactions: II. Odd Targets
M.H. Mortensen, R.R. Betts and C.K. Bockelman
Phys. Rev. C21 (1980) 2288.

$^{209}Bi(^{3}He,d)$ ^{210}Po and ^{209}Bi $(^{4}He,t)$ ^{210}Po Reactions and Some Matrix Elements of the Residual Interaction
R. Groleau, W.A. Lanford and R. Kouzes
Phys. Rev. C22 (1980) 440.

Sputter Induced Isotopic Fractionation of Solid Surfaces
C.C. Watson and P.K. Haff
J. App. Phys. 51 (1980) 691.

Measurements of ^{10}Be Distributions Using a Tandem Van de Graaff Accelerator
W.A. Lanford, P.D. Parker, K. Bauer, K.K. Turekian, J.K. Cochran and S. Krishnaswami
N.I.M. 168 (1980) 505.

Nuclear Data Sheets for A=152
C.M. Baglin
Nuclear Data Sheets 30 (1980) 1.

Exactly Central Heavy-Ion Collisions by Nuclear Hydrodynamics
H.H.K. Tang and C.Y. Wong
Phys. Rev. C21 (1980) 1846.

The Interacting Boson-Fermion Model
F. Iachello
Nucl. Phys. A347, (1980) 51.

Observation of Selected Molecular Orbital X-Rays in Coincidence with Separated Atom K X-Rays
J.J. O'Brien, E. Liarokapis and J.S. Greenberg
Phys. Rev. Letters 44 (1980) 386.

TDHF Fusion Calculations for $^{85}Kr + ^{139}La$ and $^{84}Kr + ^{209}Bi$ Collisions
K.T.R. Davies, K.R. Sandhya Devi and M.R. Strayer
Phys. Rev. Letters 44 (1980)23.

New Solar-Neutrino Flux Calculations and Implications Regarding Neutrino Oscillations
J.N. Bahcall, S.H. Lubow, W.F. Huebner, N.H. Maggee, A.L. Merts, M.F. Argo, P.D. Parker, B. Rozsynai and R.K. Ulrich
Phys. Rev. Letters 45 (1980) 945.

Isovector Magnetic Dipole Transition in ^{22}Na
L.K. Fifield, A.R. Poletti and D.C. Radford
Journal of Physics G6 (1980) 723.

Exact Finite-Range Distorted-Wave Born-Approximation Analyses of the Reactions $^{18}O(p,t)\ ^{16}O$, $^{48}Ca(t,p)\ ^{50}Ca$, and $^{90}Zr(t,p)\ ^{92}Zr$ Using Realistic Triton and Nuclear Wavefunctions
D.H. Feng, M.A. Nagarajan, M. Strayer, M. Vallieres and W.T. Pinkston
Phys. Rev. Letters 44 (1980) 1037.

Heavy-Ion Induced Stripping and Pickup Reaction Involving Closed Shell Nuclei
J.F. Petersen, R.J. Ascuitto and E.A. Seglie
Phys. Letters 94B

New Coupling Scheme in the Interacting Boson-Fermion Model: O(6) Spectra in Odd-A Nuclei
F. Iachello and O. Scholten
Physics Letters 91B (1980) 189.

Static Quadrupole Moments of the First Excited States of ^{200}Hg and ^{202}Hg
R.H. Spear, M.T. Esat, M.P. Fewell, D.C. Kean, T.H Zobel, A.M. Baxter and S. Hinds
Nucl. Phys. 345 (1980) 252.

The Dominant Role of the Nuclear Surface in (p,t) Reactions
M.F. Werby, W.H. Bassichis and M.R. Strayer
II Nuovo Cimento 58A (1980) 219.

Surface Sticking Probabilities for Sputtered Atoms of ^{93}Nb and ^{103}Rh
M.R. Weller and T.A. Tombrello
Radiation Effects 49 (1980) 239.

Particles Pair up in the Nucleus
F. Iachello
New Scientist 85, (1980) 390.

Energy Dependence of the Trapping of Uranium by Aluminum Oxide Surfaces
R.W. Weller
Radiation Effects 49 (1980) 195.

Sputtering of Uranium Tetraflouride in the Electronic Stopping Region
R.A. Weller
Radiation Effects 51 (1980) 223.

Evidence for Molecular Resonances in the $^{16}O + ^{16}O$ System
Yosio Kondo, D. Allan Bromley and Yasuhisa Abe
Prog. Theor. Phys. 63 (1980) 772.

Hydrogen Profiles of Anodic Aluminum Oxide Films
C.K. Dyer, R.S. Alwitt and W.A. Lanford
J. of Electrochem. Soc. 127 (1980) 405.

Mass Dependence of the Yrast-Yrare Interaction and Backbending in Light Osmium Isotopes
G.D. Dracoulis, C. Fahlander and M.P. Fewell
Phys. Rev. Letters 45 (1980) 1831.

Application of a Band-Crossing Model for Resonances in $^{16}O + ^{16}O$ Scattering
Y. Kondo, D.A. Bromley and Y. Abe
Phys. Rev. C22 (1980) 1068.

Physics
D. Allan Bromley
Centenary Issure of SCIENCE 209 (1980) 110.

The Ru and Pd Isotopes in the Proton-Neutron Interacting Boson Model
P. Van Isacker and G. Puddu
Nucl. Phys. A348 (1980) 125.

The Interacting Boson Model and Beyond
F. Iachello
Structure of Medium-Heavy Nuclei (ed. by the Demokrites Tandem Group)
(The Institute of Physics, Bristol) (1980) 161.

Nuclear Physics 1980
D. Allan Bromley
1981 Yearbrook of Science and the Future Encyclopedia Britannica (1980) 372.

Nuclear Physics in China
D.A. Bromley and P.M. Perrolle, editors
National Academy of Science Press, (1980).

Polarization Effects in the Small Angle Scattering of Fast Neutrons by Bismuth
M. Ahmed and F.W.K. Firk
Fifth International Symposium on Polarization Phenomena in Nuclear Physics
Edited by G.G. Ohlsen, American Institute of Physics, New York (1981).

Studies of $\vec{n}$-^{6}Li Scattering and the Structure of ^{7}Li
Y.H. Chiu and F.W.K. Firk
Fifth International Symposium on Polarization Phenomena in Nuclear Physics
Edited by G.G. Ohlsen, American Institute of Physics, New York (1981)

Direct Observation of a High Spin ^{12}C-^{8}Be Cluster State in ^{20}Ne
M.M. Hindi, J.M. Thomas, D.C. Radford and P.D. Parker
Physics Letters 99B (1981) 33.

Dimension and Character Formulas for Lie Supergroups
A. Baha Balantekin and Itzhak Bars
Journal of Math. Physics 22 (1981) 1149.

An Investigation of Methods to Reduce the Hydrogen Concentration on Surfaces Useful for Ultra-Cold Neutron Storage
P.H. La Marche, W.A. Lanford and R. Golub
N.I.M. 189 (1981) 533.

U(6/4) Dynamical Supersymmetry in Nuclei
A.B. Balantekin, I. Bars and F. Iachello
Phys. Rev. Letters 47 (1981) 19.

Dynamical Supersymmetries and Single Particle Strengths in Ir
J.A. Cizewski D.G. Burke, E.R. Flynn, R.E. Brown and J.W. Sunier
Phys. Rev. Lett. 46 (1981) 1264.

Higher Order Z_1 Effects in Heavy Ion Stopping Powers and Ranges
J.M. Anthony and Wm. A. Lanford
N.I.M. 186 (1981) 647.

Multilevel Calculations in Odd-A Nuclei
M.A. Cunningham
Phys. Letters 106B (1981)11.

Representations of Supergroups
A.B. Balantekin and I. Bars
Journal of Mathematical Physics 22 (1981) 1810.

The Interacting Boson Model
A. Arima and F. Iachello
Annual Review of Nuclear and Particle Science 31 (1981) 75.

Group-Theoretic Approach to Two-Electron Correlations in Atoms
F. Iachello and A.R.P. Rau
Phys. Rev. Letters 47 (1981) 501.

Rotational and Vibrational Excitations in Nuclear Molecular Spectra
K.A. Erb and D.A. Bromley
Phys. Rev. C23 (1981) 2781.

Algebraic Approach to Nuclear Quasimolecular Spectra
F. Iachello
Phys. Rev. C23 (1981) 2778.

Electron Translation Effects in Heavy Ion Scattering
U. Heinz, W. Greiner and B. Muller
Phys. Rev. A23 (1981) 562.

Proton Hole States in Neutron Rich Nuclei Near A-100
F. Ajzenberg-Selove, R.E. Brown, J.A. Cizewski, E.R. Flynn and J.W. Sunier
Phys. Rev. C24 (1981) 902.

Proton Hole Excitations in $^{201, 203}Au$ from $^{202,204}Hg(\vec{t},\alpha)$ reactions
E.R. Flynn, Ronald E. Brown, J.W. Sunier, J.M. Gursky, J.A. Cizewski and D.G. Burke
Phys. Lett. 105B (1981) 125.

The Electric Quadrupole Moment of the First Excited State of ^{204}Hg
M.T. Esat, M.P. Fewell, R.H. Spear, T.H. Zabel, A.M. Baxter and S. Hinds
Nucl. Phys. A362 (1981) 227.

Elastic and Inelastic Scattering Studies for the Systems ^{12}C + ^{28}Si and ^{16}O + $^{28,29,30}Si$
P. Braun-Munzinger, G.M. Berkowitz, M.Gai, C.M. Jachcinski, T.R. Renner, C.D. Uhlborn, J. Barrette and M.J. Levine
Phys. Rev. C24 (1981) 1010.

Generalized Seniority Scheme for the Systematics of Single Particle States
M. Gai, A. Arima and D. Strottman
Phys. Letters 106B (1981) 6.

High Spin Resonances in ^{28}Si + ^{28}Si Scattering
R.R. Betts, S.B. DiCenzo and J.F. Petersen
Phys. Letters 100B (1981) 117.

Time-Dependent Hartree-Fock Collisions of ^{16}O + ^{93}Nb at E_{Lab} = 204 MeV
K.R. Sandhya Devi, M.R. Strayer, J.M. Irvine and K.T.R. Davies
Phys. Rev. C23 (1981) 1064.

Fusion of ^{28}Si + ^{28}Si
S.B. DiCenzo, J.F. Petersen and R.R. Betts
Phys. Rev. C23 (1981) 2561.

Resonances in ^{16}O + ^{16}O
M. Gai, E.C. Schloemer, J.E. Freedman, A.C. Hayes, S.K. Korotky, J.M. Manoyan, B. Shivakumar, S.M. Sterbenz H. Voit, S.J. Willett and D.A. Bromley
Phys. Rev. Lett. 47 (1981) 1878.

Fusion Excitation Functions for ^{16}O + ^{27}Al and ^{16}O + ^{24}Mg Collisions
K.R.S. Devi, A.K. Dhar and M.R. Strayer
Phys. Rev. C23 (1981) 2062.

Inclusive Reactions of Pions on Nuclei
R.D. McKeown, S.J. Sanders, J.P. Schiffer, H.E. Jackson, M. Paul, J.R. Specht, E.J. Stephenson, R.D. Redwine, and R.E. Segel
Phys. Rev. C24 (1981) 211.

Fusion of $^{24}Mg + ^{24}Mg$
C.M. Jachcinski, D.G. Kovar, R.R. Batts, C.N. Davids, D.F. Geesaman, C. Olmer, M. Paul, S.J. Sanders, and J.L. Yntema
Phys. Rev. C24 (1981) 2070.

Electron Scattering in the Interacting Boson Model
F. Iachello
Nuclear Physics A358 (1981) 89.

The $^{92,94,97,98}Mo$ (t,p) Reaction at E_t=17 MeV
F. Ajzenberg-Selove, R.E. Brown, J.A. Cizewski, E.R. Flynn and J.W. Sunier
Phys. Rev. C24 (1981) 2475.

Mean-Field Approximation for Inclusive Observables
Y. Alhassid, B. Muller and S.E. Koonin
Phys. Rev. C23 (1981) 487.

Mean-Field Approximation to the Many-Body S Matrix
Y. Alhassid and S.E. Koonin
Phys. Rev. C23 (1981) 1590.

A Phenomenological Approach to α-clustering in Heavy Nuclei
F. Iachello and A.D. Jackson
Phys. Lett. 108B (1982) 151.

A Dynamic Algebra for Rotation-Vibration Spectra of Complex Molecules
O. van Roosmalen, A.E.L. Dieperink and F. Iachello
Chem. Phys. Lett. 85 (1982) 32.

Interacting Boson-Fermion Model of Collective States I. The Spin (6) Limit
F. Iachello and S. Kuyucak
Ann. of Physics 136 (1981) 19.

U(6/4) Supersymmetry in Nuclei
A.B. Balantekin, I. Bars, and F. Iachello
Nuclear Physics A370 (1981) 284.

The $^{176}Lu(t,p)^{178}Lu$ Reaction: The Influence of Shell Gaps and Blocking on L=0 Strength
F. Girshick, K. Krien, R.A. Naumann, G.L. Struble, R.G. Lanier, L.G. Mann, J.A. Cizewski, R.E. Brown and J.W. Sunier
Physics Letters 98B (1981) 29.

$^{136,138}Ba$(t,p) and the Systematics of Neutron Pairing Vibrations at N=82
E.R. Flynn, J.A. Cizewski, R.E. Brown and J.W. Sunier
Physics Letters 98B (1981) 166.

Two-Neutron Transfer in Pt Nuclei and the Structure of ^{200}Pt.
J.A. Cizewski, E.R. Flynn, R.E. Brown, D.L. Hanson, S.D. Orbesen and J.W. Sunier
Phys. Rev. C23 (1981) 1453.

Nuclear Structure of ^{161,163}Ho Studied the $(\vec{t},\alpha)$ Reaction
D.G. Burke, G. Lovhoiden, E. Hammaren, E.R. Flynn, J.A. Cizewski and J.W. Sunier
Nuclear Physics A359 (1981) 36.

The ^{159}Tb (tα) ^{158}Gd Reaction with 17 MeV Polarized Tritons
D.G. Burke, E. Hammaren, C.L. Swift, J.A. Cizewski, E.R. Flynn and J.W. Sunier
Nuclear Physcis 1366 (1981) 26.

The Rotational Structure of ^{227}Ra
T. von Egidy, G. Barreau, H.G. Borner, W.F. Davidson, J. Larysz, D.D. Warner, P.H.M. Van Assche, K. Nybo, T.F. Thorsteinsen, G. Lovhoiden, E.R. Flynn, J.A. Cizewski, R.K. Sheline, D. Decman, D.G. Burke, G. Sletten, N. Kaffrel, W. Kurcewicz, T. Bjornstad and G. Nyman
Nuclear Physics A365 (1981) 26.

Elastic and Inelastic Scattering of ^{14}C from Medium Heavy Nuclei
O. Hansen, F. Videbaek, E.R. Flynn, J.C. Peng and J.A. Cizewski
Nuclear Physics A364 144.

Algebraic Methods for Molecular Rotation-Vibration Spectra
F. Iachello
Chem. Phys. Letters 78 (1981) 581.

SU(mn) SU(m)xSU(n) Isoscalar Factors and S(f_1+F_2) S(f_1)xS(f_2) Isoscalar Factors
Jin-Wuan Chen
Journal of Math. Physics 22 (1981) 1.

Prompt Emission of Nucleon Jets in Time-Dependent Hartree-Fock Collisions
K.R.S. Devi, M.R. Strayer, K.T.R. Davies, S.E. Koonin, A.K. Dhar
Phys. Rev. C24 (1981) 2521.

Fusion Behavior in Time-Dependent Hartree-Fock Calculations of ^{86}Kr + ^{139}La and ^{84}Kr + ^{209}Bi Collisions
K.T.R. Davies, K.R. Sandhya Devi and M.R. Strayer
Phys. Rev. C24 (1981) 2576.

Magnetic Moment Measurements in Osmium and Platinum Nuclei
R. Levy, N. Tsoupas, N.K.B. Shu, A. Lopez-Garcia, W. Andreijtscheff, N. Benczer-Koller
Phys. Rev. C23 (1982) 293.

Astrophysically Interesting Nuclear Reactions Involving Radioactive Targets and/or Radioactive Beams
P.D. Parker
Proceedings of the Workshop on Radioactive Ion Beams and Small Cross Sections, Burr Oak (1981) 21.

Two Neutron Transfer in Pt and Os Nuclei and the IBA
J.A. Cizewski
Interacting Bose-Fermi Systems in Nuclei, F. Iachello (Ed.),
Plenum Press (1981) 137.

Tests of Dynamical Supersymmetries via Charged Particle Transfer Reactions
J.A. Cizewski
Interacting Bose-Fermi Systems in Nuclei, F. Iachello (Ed.),
Plenum Press (1981) 389.

Present Status of the Interacting Boson-Fermion Model
F. Iachello
Interacting Bose-Fermi Systems in Nuclei, F. Iachello (Ed.) Plenum Press (N.Y.) (1981) 273.

Bose-Fermi Symmetries in Nuclei
F. Iachello
Interacting Bose-Fermi Systems in Nuclei, ed. by F. Iachello
Plenum Publishing Corp. (1981) 365.

An Introduction to IBM
F. Iachello
Nuclear Structure
Plenum Press (N.Y.) 1981, p.53.

The Other Frontiers of Science
D.A. Bromley
Science 215 (1982) 1035.

The Polarization and Differential Cross Section of Fast Neutrons Scattered from ^{6}Li and an R-Function Analysis of the Interaction Below 4MeV
Y.H. Chiu and F.W.K. Firk
Nucl. Phys. A364 (1981) 43-61.

Standard Solar Models and the Uncertainties in Predicted Capture Rates of Solar Neutrinos
J.N. Bahcall, W.F. Huebner, S.H. Lubow, P.D. Parker, and R.K. Ulrich
Reviews of Modern Physics 54 (1982) 767.

Branching Rules for the Supergroup SU(N/M) from those of SU(N+M)
A. Baha Balantekin, Itzhak Bars
J. Math. Phys. 23 (1982) 1239.

A Nonlinear Boltzmann Equation Calculation of Sputtering From Spikes
R.A. Weller and M.R. Weller
NIM 194 (1982) 573.

Supersymmetry in Nuclear and Particle Physics
F. Iachello
Nucl. Phys. A374, (1982) 635c.

A Phenomenological Approach to α-clustering in Heavy Nuclei
F. Iachello and A.D. Jackson
Phys. Lett. 108B, (1982) 151.

The Stopping Power and Effective Charge of Heavy Ions in Solids
J.M. Anthony and W.A. Lanford
Phys. Rev. A25 (1982) 1868.

Multilevel Calculations in Odd-Mass Nuclei
I. Negative Parity States
M. Cunningham
Nucl. Phys. A385 (1982) 204.

Multilevel Calculations in Odd-Mass Nuclei
II. Positive Parity States
M. Cunningham
Nucl. Phys. A385 (1982) 221.

Radiative Width of Molecular Cluster States
Y. Alhassid, M. Gai and G.F. Bertsch
Phys. Rev. Letters 49 (1982) 1482.

Energy Sharing and Sputtering in Low-Energy Collision Cascades
R.A. Weller and M.R. Weller
Radiation Effects 60 (1982) 209.

A Dynamic Algebra for Rotation-Vibration Spectra of Complex Molecules
O. van Roosmalen, A.E.L. Dieperink and F. Iachello
Chem. Phys. Lett. 85, (1982) 32.

Algebraic Approach to Molecular Rotation-Vibration Spectra. I=Diatomic Molecules
F. Iachello and R.D. Levine
J. Chem. Phys. 77, (1982) 3046.

TDHF Calculation of Nuclear Molecules from $^{12}C + ^{12}C$ to ^{238}U
R.Y. Cusson, H. Stocker, M. Strayer, S. Umar, D.A. Bromley, J.A. Maruhn, and W. Greiner
Time-Dependent Hartree-Fock and Beyond
(ed., K. Goeke and P.G. Reinhard: Springer-Verlog, N.Y.) (1982) 22.

^{10}Be and Th Isotopes in Manganese Nodules and Adjacent Sediments: Nodule Growth Histories and Nuclide Behavior
S. Krishnaswami, A. Mangini, J.Y. Thomas, P. Sharma, J.K. Cochran, K.K. Turekian and P.D. Parker
Earth and Planetary Science Letters 59 (1982) 217.

Fragmentation of L=0 Transfer Strength in the ^{195}Pt(t,p) ^{197}Pt Reaction
J.A. Cizewski, E.R. Flynn, Ronald E. Brown, and J.W. Sunier
Phys. Rev. C26, (1982) 1960.

The 2.102 Mev Level in ^{206}Hg and the Spin Gyromagnetic Ratio of the 3s Proton
J.A. Becker, J.B. Carlson, R.G. Lanier, L.G. Mann, G.L. Struble, K.H. Maier, L. Ussery, W. Stoffl, T. Nail, R.K. Sheline and J.A. Cizewski
Phys. Rev. C26, (1982) 914.

Collective Properties of the Odd Mass I Nuclei: ^{117,119,121}I
M. Gai, D.M. Gordon, R.E. Shroy, D.B. Fossan and A.K. Gaigalas
Phys. Rev. C26 (1982) 1101.

Multiphoton Excitation of Molecules with Realistic Level Structure: An Algebraic Approach
I. Benjamin, R.D. LeVine, O.S. von Roosmalen and F. Iachello
Applied Phys. B28, (1982) 107.

Collective Properties of the odd Mass I Nuclei: ^{123,124,127}I
R.E. Shroy, D.M. Gordon, M. Gai, D.B. Fossan and A.K. Gaiglas
Phys. Rev. C26 (1982) 1089.

Nanosecond Feeding Times: Evidence for High Spin Isomerism Near A=75 and 100
W. Andrejtscheff, M. Senba, N. Tsoupas, Z.Z. Ding, P. Raghavan, A. Lopez-Garcia and R. Levy
Phys. Letters 113B (1982) 209.

The Generalized Centroid Shift Method for Lifetime Measurements in Heavy Ion Reactions
W. Andrejtscheff, M. Senba, N. Tsoupas, and Z.Z. Ding
Nucl. Instru. Meth. 204 (1982) 123.

Magnetic Moment Measurements in Osmium and Platinum Nuclei
R. Levy, N. Tsoupas, N.K.B. Shu, A. Lopez-Garcia, W. Andrejtscheff, and N. Benczer-Koller
Phys. Rev. C25 (1982) 293.

The Interacting Boson Model and Strongly Deformed Nuclei
F. Iachello
Proc. of the 4th International Symposium on Neutron-Capture Gamma-Ray Spectroscopy, Grenoble, T. von Egidy et al. eds.
Inst. Phys. Conf. Ser. 62 15 (1982).

Algebraic and Geometric Properties of the Interacting Boson Model-I
F. Iachello
In "Interacting Bosons in Nuclei", J. Dehesa et al, eds., Springer Verlag, Berlin, 1982, p.1.

Search for the Sparking of the Vacuum
J.S. Greenberg and W. Greiner
Physics today 35 (No.8) (1982) 24.

Supersymmetry in Nuclei
F. Iachello
Am. Scientist 70 (1982) 294.

In Search of Spontaneous Positron Emission
J.S. Greenberg, in X-Ray and Atomic Inner Shell Physics-1982.
Ed. B. Crasemann, American Institute of Physics (1983) 173.

The Other Frontiers of Science
D.A. Bromley
Science 215 (1982) 1035.

TDHF Calculations of Nuclear Molecules from ^{12}C-^{12}C to ^{238}U-^{238}U
M.S. Strayer, R.Y. Cusson, H. Stocker, S. Umar, D.A. Bromley, J.A. Maruhn and W. Greiner
Time-Dependent Hartree-Fock and Beyond
ed. by K. Goeke and P.G. Reinhard
Springer-Verlag, New York (1982) p.22.

Symmetry Laws (Physics)
F. Iachello
In McGraw-Hill Year book of Science and Technology
McGraw-Hill, New York (1982), p. 446.

Development of a Lasar Optically Pumped Polarized Target for use in Heavy Ion Physics
B. Shivakumar, J.R. Beene, C.E. Bemis, K.A. Erb, J.L.C. Ford, Sr., and D. Shapira. Lasers in Nuclear Physics (eds. C.E. Bemis, Sr., and H.K. Carter, Nuclear Science Research Conference Series
Harwood Academic, New York), Volume 3 (1982) 385.

Kernstruktuur Beschreven door Wisselwerkende Bosonen
A.E.L. Dieperink and F. Iachello
FOM Jaarboek 1980, Utrecht (1982) p.183.

Evidence for Nuclear Molecular Orbital Effects in the $^{13}C + ^{13}C$ *
S.K. Korotky, K.A. Erb, R.L. Phillips, S.J. Willett, and D.A. Bromley
Phys. Rev. C28 (1983) 168.

Cluster Structure of 8p - 4h States in $^{20}Ne^{*}$
M.M. Hindi, J.H. Thomas, D.C. Radford and P.D. Parker
Phys. Rev. C27 (1983) 2902.

New Class of Supersymmetry in Nuclei
B. Balantekin, I. Bars, R. Bijker and F. Iachello
Phys. Rev. C27 (1983) 1761.

Dose Dependence in Angular Distributions of Ag and Au Sputtered from an Alloy Target
Martha Riherd Weller
Nim 212 (1983) 419.

The Single Proton Structure of $^{193,195,197}Ir$ and Perturbed Spin (6) Symmetry
J.A. Cizewski, D.G. Burke
Flynn, Ronald E. Brown and J.W. Sunier
Phys. Ref. C27 (1040) 1983.

Potential Scattering, Transfer Matrix and Group Theory
Y. Alhassid, F. Gursey and F. Iachello
Phys. Rev. Letters 50 (1983) 873.

Threshold States in ^{26}Al: II. Extraction of Resonance Strengths
A.E. Champagne, A.J. Howard and P.D. Parker
Nuclear Physics A402 (1983) 179.

Nucleosynthesis of ^{26}Al at Low Stellar Temperatures
A.E. Champagne, A.J. Howard, and P.D. Parker
The Astrophysical Journal 269 (1983) 686.

The Coexistence of Single Particle, Collective Quadrupole and $\alpha + ^{14}C$ Molecular Dipole Degrees of Freedom in ^{18}O
M. Gai, M. Ruscev, A.C. Hayes, J.F. Ennis, R. Keddy, E.C. Schloemer, S.M. Sterbenz, and D.A. Bromley and J.W. Olness and E.K. Warburton
Phys. Rev. Lett. 50 (1983) 239.

Tandem Accelerator Mass Spectrometry of ^{26}Al from an Iron Meteorite
J. Thomas, P. Parker, G. Herzog and D. Pal
NIM 211 (1983) 511.

The Nature of Molecular Resonances and Background in the $^{16}O+^{12}C$ System
E.C. Schloemer, M. Gai, J.F. Ennis, A.C. Hayes, M. Ruscev, B. Shivakumar, S.M. Sterbenz, N. Tsoupas and D.A. Bromley
Phys. Rev. Lett. 51 (881) 1983.

Quantum Electrodynamics of Strong Fields Conference Summary: Experimental Aspects (NATO Advanced Study Institute, June 1981, Lahnstein, W. Germany)
J.S. Greenberg
Plenum, 1983.

Time-Dependent Hartree-Fock Studies of Superheavy Molecules
M.R. Strayer, R.Y. Cusson, H. Stocker, J.A. Maruhn, J.W. Greiner
Phys. Rev. C28 (1983) 228.

Molecular Alpha-Particle Clustering in ^{218}Ra; Dipole Collectivity in The Vicinity of Nuclear Shell Closures
M. Gai, J.F. Ennis, M. Ruscev, E.C. Schloemer, B. Shivakumar, S.M. Sterbenz, N. Tsoupas, and D.A. Bromley
Phys. Rev. Letters 51 (1983) 646.

Neutrons In Science and Technology
D. Allan Bromley
Proc. Symposium Commemorating the First Artifically Produced, Self-Sustaining Nuclear Chain Reaction, University of Chicago, December 1, 1982. Also Physics Today, December 1983, p.31.

Nuclear Physics
D. Allan Bromley
Yearbook on Science and the Future, Encyclopaedia Britannica, 1983.

Spin Alignment and Phase Angles in $^{12}C+^{12}C$ Inelastic Scattering
S.J. Willett, K.A. Erb, S.K. Korotky, R.L. Phillips and D.A. Bromley
Phys. Rev. C28 (1983) 1986.

Group Theory Approach to Scattering
Y. Alhassid, F. Gursey, and F. Iachello
Annals of Physics 148 (1983) 346.

The $^{197}Au(t,p)^{199}Au$ Reaction
J.A. Cizewski, Ronald E. Brown, E.R. Flynn, and J.W. Sunier
Phys. Rev. C28 (1983) 2199.

Algebraic Approach to Molecular Rotation-Vibration
II. Triatomic Molecules
O.S. van Roosmalen, F. Iachello, R.D. Levine, and A.E.L. Dieperink
Journal of Chem. Physics 79 (1983) 2515.

Group Theory of the Morse Oscillator
Y. Alhassid, F. Gursey, F. Iachello
Chemical Physics Letters 99 (1983) 26.

Very High Spin States and Isomerism in ^{153}Ho
D.C. Radford, M.S. Rosenthal, P.D. Parker
J.A. Cizewski, J.H. Thomas, B. Haas, F.A. Beck,
T. Byrski, J.C. Merdinger, A. Nourredine, Y. Schultz
J.P. Vivien, J.S. Dionisio and Ch. Vieu
Phys. Letters 126B (1983) 24.

High Precision Studies with Large Tandem Accelerators
D. Allan Bromley
Prepared for delivery at the International Symposium on
Nuclear Physcis with Large Tandem Accelerators
Legnaro and Padua; March 18, 1983.

Energy and Mass Analysis of Secondary Ions Sputtered from Metallic Targets by MeV Heavy Ions
John P. O'Connor, Patricia G. Blauner, and Robert Weller
NIM 218 (1983) 293.

A Unified Variational Principle for the Information Theoretic Analysis of Data and Their Scatter
J. Manoyan and Y. Alhassid
Chemical Physical Letters 101 (1983) 265.

Nuclear Charge Radii, Nuclear Moments, and Nuclear Structure
F. Iachello
Hyperfine Interactions, Vol. 15/16 (1983) 11.

Alpha-Clustering in Heavy Nuclei
H. Daley, F. Iachello
Physics Letters 131 B (1983) 281.

Positron Emission in Heavy-Ion Reactions
Jack S. Greenberg
Conference on Nuclear Physics with Heavy Ions
April 14-16, 1983 SUNY at Stony Brook

Observation of Peak Structure in Positron Spectra from U+Cm Collisions
J. Schweppe, A. Gruppe, K. Bethge, H. Bokemeyer, T. Cowan,
H. Folger, J.S. Greenberg, H. Grein, R. Schule,
K.E. Stiebing, D. Schwalm, T. Trautmann, and P. Vincent
PRL 51 (1983) 2261.

Group Theoretical Models of Giant Resonance Splittings in Deformed Nuclei
D.J. Rowe, and F. Iachello
Physics Letters, 130B, Number 5, 10/27/83.

Unification of Nuclear Structure Models
F. Iachello
Proc. of Workshop on Collective State in Nuclei, China (Sept. 1983).

Identification and Decay Properties of the Fourth $K^{\pi}=0^{+}$ Band in ^{168}Er
W.F. Davidson, W.R. Dixon, D.G. Burke and J.A. Cizewski
Physics Letters 130B (1983) 161.

D. CONSTRUCTION

1.0 Project 85-R-201, General Plant Projects

1. **Please provide a status report of the FY 1984 GPP activities at the Lawrence Berkeley Laboratory, Los Alamos National Laboratory, and the Massachusetts Institute of Technology as proposed in the FY 1984 budget request.**

Answer: The status of each of the FY 1984 General Plant Projects (GPP) activities under the Nuclear Physics program is shown in the following table:

Lawrence Berkeley Laboratory--Total FY 1984 GPP: $1,500,000

Project	Cost	Status
Bldg. 51 Boiler Replacement	$ 25,000	Complete
Bldg. 69A Foundation	170,000	Engineering 95% complete. Construction scheduled for 3rd QTR FY 1984.
Berkeley Center for X-Ray Optics	360,000	Directive authorization received 3/6/84.
Bldg. 48 Fire Alarm Central Console Improvement	30,000	Engineering complete. Materials requisitioned. Completion scheduled for 4th QTR FY 1984.
Bldgs. 51, 65, and 77 Sprinkler Projects	210,000	Engineering started. Installation scheduled for completion 1st QTR FY 1985.
Bldg. 70 Laboratory Addition Air Conditioning	95,000	Engineering started. Installation scheduled for completion 1st QTR FY 1985.
Bldg. 88 Power Distribution	55,000	Engineering started. Materials on order. Installation scheduled for completion 3rd QTR FY 1985.
Bldgs. 69/74 Area. New 500 kVA Unit Substation	170,000	Final engineering started. Requisitions being prepared for bid and procurement. Construction scheduled for 1st QTR FY 1985.
Bldg. 70. New 750 kVA Unit Substation	160,000	Same as previous item.

Project	Cost	Status
Bldgs. 55/60 Area Transformer	$ 15,000	Engineering completed. Requisitions prepared for bid and procurement. Installation scheduled for 4th QTR FY 1984.
Bldg. 64 Replacement Boilers (2)	50,000	Engineering started. Installation scheduled for 1st QTR FY 1985.
Bldg. 51 Roof Replacement	160,000	Specifications being prepared. Construction scheduled for 4th QTR FY 1984.

NOTE: First two items assigned high priority and approved by DOE San Francisco Operations Office in November 1983 and January 1984 respectively. Other items approved in February 1984.

Los Alamos National Laboratory (LAMPF only)--Total FY 1984 GPP: $500,000

Project	Cost	Status
Tunnel for Beam Stop Neutrino Facility	$400,000	Request for directive pending outcome of Title II review. Construction scheduled for completion 4th QTR FY 1984.
Housing for Helium Liquefier	100,000	Conceptual design completed. Request for directive submitted to the DOE Albuquerque Operations Office.

Massachusetts Institute of Technology (Bates only)--FY 1984 GPP: $200,000

Project	Cost	Status
Lab/Office Space above Utility Bldg.	$125,000	Construction in progress. Scheduled for completion 3rd QTR FY 1984.
Platform and Dump for New Beam Line C	65,000	Conceptual design completed. Request for directive submitted to DOE Chicago Operations Office.
Air Discharge System for Target Areas	10,000	Same as previous item.

2. **Please provide additional information concerning the proposed $950,000 ultra high vacuum processing facility at Lawrence Berkeley Laboratory. What type of research will this facility be used for?**

Answer: The ultra high vacuum (UHV) processing and assembly area at Lawrence Berkeley Laboratory (LBL) will be a general purpose facility and will service a variety of projects supported by several DOE programs. To assure that parts and equipment going into ultra high vacuum systems are suitably prepared to meet UHV requirements and standards, the removal of organics and prevention of recontamination is absolutely essential. Prevention of organic contamination requires a different and higher level of cleanliness than conventional clean rooms that maintain cleanliness by limiting particulate size.

The need for an ultra high vacuum processing and assembly facility is ongoing. Projected requirements for UHV capability are indicated as being needed for projects such as superconducting components associated with the Medical Accelerator, beam line components and assemblies for SPEAR, the Stochastic Cooling Project for Fermi Laboratory, nuclear physics spectrometer projects, and the Mark II End Cap Calorimeter for SLAC. Many parts and assemblies of these projects are required to be put together on tight schedules and with severe specifications for cleanliness. The large detector arrays which will be built for Nuclear Physics and High Energy Physics experiments require clean room capability of this capacity for both fabrication and assembly.

The primary justification for the facility is to have it available for this projected workload. LBL must be able to satisfy the task of cleaning, assembling, and testing subassemblies and assemblies whose ultimate performance and specifications require the precision and cleanliness designed into such a facility. The Laboratory presently lacks a facility of this capability. The schedule to complete the project will require at least 24 months after authorization.

2.0 Project 85-R-203, Continuous Electron Beam Accelerator Facility (CEBAF)

3. When will the CEBAF's total estimated cost (TEC) and construction schedule be available?

Answer: Our present objective is determination of a reliable cost estimate and schedule for the Continuous Electron Beam Accelerator Facility (CEBAF) by July 1984. Office of Energy Research and Oak Ridge Operations Office staff conducted a formal review of the CEBAF project on February 27 and 28, 1984. We plan another formal review in June 1984. In the intervening period, we and Oak Ridge Operations staff will maintain close contact with the CEBAF project.

4. What is the basis for the anticipated TEC of $200 million to $225 million?

Answer: Exact construction costs and project schedule are presently under review. At this time, we estimate that construction costs for the Continuous Electron Beam Accelerator Facility (CEBAF) will not exceed $225 million. This estimate is based upon our review of a draft Conceptual Design Report submitted to us by Southeastern Universities Research Association and a formal review of the CEBAF construction project. This review was conducted on February 27 and 28, 1984, by Department of Energy Headquarters and Oak Ridge Operations Office staff.

3.0 Project 84-R-123, Tandem/AGS Heavy Ion Transfer Line

5. Is this project's December 1983 cost estimate of $10.3 million in FY 1984 dollars, in FY 1985 dollars, or in as-year spent dollars?

Answer: The $10.3 million Total Cost Estimate for the Tandem/AGS Heavy Ion Transfer Line construction project is in as-year spent dollars.

6. What escalation rates were assumed in the December 1983 cost estimate?

Answer: For conventional construction, we assumed 6% per year escalation rates. For accelerator and beam transport components, we assumed 7.5% per year escalation.

4.0 Project 84-ER-110, University Accelerator Upgrade at the University of Washington and Yale University

7. Is the September 1983 cost estimate of $19.0 million in FY 1984 dollars, in FY 1985 dollars, or in as-year spent dollars?

Answer: The September 1983 cost estimate of $19.0 million is in as-year spent dollars.

8. What escalation rates were assumed in the December 1982 estimate? How have the actual escalation rates compared with the December 1982 estimate?

Answer: The December 1982 estimate assumed 9% inflation for the duration of the construction project. A detailed review of the cost estimate and schedule of the project was made in September 1983. Cost estimates for the major components were reexamined; some cost estimates increased while others decreased. The review established a total estimated cost (TEC) of $19.0 million for the project.

9. What shortages or overages have occurred because of the differences in the estimated and actual escalation rates? How have these shortages or overages resulted in changes to the May 1980 estimate?

Answer: The Department's September 1983 detailed cost and schedule review of the project concluded that the total estimated cost (TEC) of the project was $19.0 million.

Examination of the cost estimates of the major components of the project found that some had increased while others had decreased with the net result of no change to the TEC.

10. How do each of these universities rank in the nation with respect to the quality of graduate programs in nuclear physics? Please provide documentation.

Answer: Both Yale University and the University of Washington have long been national leaders in nuclear physics both from the point of view of

producing outstanding young students and of producing good physics research. As mentioned below, Yale University has produced more nuclear physics Ph.D.'s than any other university in the United States, and the University of Washington ranks very high in the production of nuclear physics Ph.D.'s.

Since 1951, the University of Washington has produced over 100 Ph.D.'s in nuclear physics and over half of these have remained in basic nuclear research. Five Washington graduates have become directors of major nuclear accelerator laboratories in the United States--at Brookhaven, Oak Ridge, Indiana, Colorado, and Berkeley. A sixth is a group leader in accelerator technology at Los Alamos. The University of Washington continues to be highly regarded as a trainer of young nuclear scientists.

Of the private universities in the United States, Yale University has the largest commitment to basic nuclear research. A third of the Yale tenured faculty members are nuclear scientists, and over a third of the 700 Ph.D.'s in physics granted by Yale have been in nuclear physics. In the last several years, associate laboratory directors at Argonne and Oak Ridge have been nuclear physics Ph.D.'s from Yale, as are the directors of the physics divisions at Los Alamos and Argonne. The recently named deputy associate director of the Los Alamos National Laboratory is a Yale Ph.D. The Wright Nuclear Structure Laboratory at Yale is one of the largest university-based nuclear physics laboratories in the United States, with a total staff of 75. There are almost always between 20 and 30 nuclear physics graduate students in residence at Yale.

The faculties at Yale and Washington are widely respected in the nuclear physics community and are frequently called to serve on nuclear physics panels. In most of the years of its existence, the membership of the DOE/NSF Nuclear Science Advisory Committee has included representatives from both of these institutions. Finally, in a recent study of physics departments in the United States conducted by the American Council of Education, as reported in Newsweek magazine, the Yale physics department was ranked tenth in the United States and the physics department at Washington was ranked in the top twenty. There is no question that Yale University and the University of Washington continue to rank with the very best nuclear physics programs in the United States by any conceivable criteria.

11. **How many graduate degrees have been awarded from these two institutions over the past ten years? How do they rank in quantity produced compared with other universities which award graduate degrees in nuclear physics, such as the University of Illinois at Urbana-Champaign or MIT?**

Answer: The Manpower Subcommittee of the DOE/NSF Nuclear Science Advisory Committee prepared a report entitled "The 1980 Census of Basic Nuclear Scientists in the United States" (November 1981). The report includes a summary of Nuclear Physics Ph.D.'s produced in the period 1972 to 1980. Those findings should reflect the productivity of various institutions in the last ten years. In the period 1972 to 1980, the total number of Ph.D.'s in nuclear physics produced by each of the four institutions cited in this question are listed below:

Institution	Number of Ph.D.'s from 1972 to 1980
Yale University	42
University of Washington	19
Massachusetts Inst. of Tech.	37
University of Illinois	12

Yale University produced more Ph.D.'s in nuclear physics in the designated period than any other university in the United States.

12. **What was the basis for approving the construction of these two projects at a time when current nuclear physics facilities are being underutilized?**

Answer: This construction project, University Accelerator Upgrade Project at University of Washington and Yale University, will maintain the forefront nuclear research capabilities of two of America's leading universities. These two university facilities are essential components of Nuclear Physics' university-based program.

The vigorous development of a scientific field depends critically on a continuous supply of bright young new researchers and on the availability of forefront facilities. Basic research involves asking the most difficult questions at the very limit of our knowledge, and the answers can only be found with the most up-to-date tools or, indeed, with new tools built for the purpose. The development of such facilities takes much planning and time long before they will be available for research. One is then faced with the problem of establishing a good balance between support of current research efforts and building for the future where there are long lead times required. The decision to proceed with the Yale and Washington construction projects will ultimately provide two forefront heavy ion facilities which are of an optimum size for a university. The presence of these facilities on-site at two outstanding universities will be a strong magnet to attract the desired caliber of student to nuclear physics. The decision to proceed with these construction projects represents an investment in the long term growth and strength of nuclear physics.

APPENDIX II

ADDITIONAL MATERIALS FOR THE RECORD

REPORT OF THE PANEL ON ELECTRON ACCELERATOR FACILITIES

DOE/NSF NUCLEAR SCIENCE ADVISORY COMMITTEE

APRIL 1983

ARGONNE NATIONAL LABORATORY
9700 South Cass Avenue, Argonne, Illinois 60439

Telephone 312/972-4066

April 29, 1983

Dr. James E. Leiss
Associate Director for High
Energy and Nuclear Physics
Office of Energy Research
U.S. Department of Energy
ER-23 GTN
Washington, DC 20545

Dr. Marcel Bardon
Director, Division of Physics
National Science Foundation
1800 G Street, N.W.
Washington, DC 20550

Dear Sirs:

The Nuclear Science Advisory Committee of the Department of Energy and the National Science Foundation herewith transmits, with its endorsement, the report of the Panel on Electron Accelerator Facilities.

This panel was formed at an NSAC meeting on January 12, 1983, and asked "...to review and evaluate electron accelerator facility proposals submitted by Argonne National Laboratory, University of Illinois, Massachusetts Institute of Technology, National Bureau of Standards, and Southeastern Universities Research Association." The essentials of the Panel's recommendations, quoted from the report, are as follows:

> "This Panel finds that the highest priority for new accelerator construction in the U.S. nuclear physics program is for an electron accelerator of high duty factor capable of producing beams at any energy in the range from 500 MeV to 4000 MeV.
>
> "That being the case, we consider the two fully developed proposals for such facilities before us, namely those from the Argonne National Laboratory and from the Southeastern Universities Research Association. It is a measure of the strength of the electromagnetic physics community in the country that two quite different proposals of this scope, magnitude, and quality are available for consideration. The decision between them has been a difficult one. The Technical Subpanel, after a very careful, independent analysis of both designs, has concluded that both designs are feasible ones and that either could very well form the basis for an extremely powerful national facility.
>
> "Our decision between the two proposals then depends upon the relative weightings that we ascribe to the different problems facing the two groups of accelerator designers and to other considerations quite apart from technical ones. With such considerations in mind the Panel recommends:

That the proposal of the Southeastern Universities Research Association (SURA) for the construction of a linac-stretcher ring accelerator system capable of providing high duty-factor beams throughout the energy range from 0.5 to 4.0 GeV be accepted and that this facility be constructed and designated the National Electron Accelerator Laboratory (NEAL)."

The priority NSAC attaches to the construction of an electron accelerator of high duty factor in the few GeV range is the culmination of plans made over the past decade. The role of such an electron accelerator in nuclear research was emphasized in the Long Range Plan for Nuclear Science, presented to and accepted by DOE/NSF in 1979, and in numerous committee reports, starting with the 1977 report of the DOE/NSF Joint Study of Role of Electron Accelerators in U.S. Medium Energy Nuclear Science (the Livingston report).

Nuclear physics is entering a period of expanding horizons; this presents an opportunity to shed new light on problems of long standing and to ask questions that could hardly have been imagined 15 years ago. The support for a 4 GeV CW electron accelerator should not obscure the fact that nuclear physics faces other scientific challenges and opportunities. This Committee shall place these in perspective as part of the new Long Range Plan for Nuclear Science to be completed in 1983.

In recommending a major new facility, it is essential also to recommend measures to ensure the continued growth and vitality of the research community that will use it. What is said here applies not only to the electromagnetic physics community but to the nuclear physics community as a whole. Major facilities in the United States are seriously underutilized, operating because of budgetary constraints at a fraction of full capacity. Much of their instrumentation is in serious need of modernization.

Accordingly, in addition to incremental funding for the construction and operation of the new electron accelerator, there is an immediate need for a significant injection of support to maintain the strength and balance of the nuclear research program. This will require some $20 million per annum in incremental operating and equipment funds.

In conclusion, the Committee sends you the Report of the Panel on Electron Accelerator Facilities with its full endorsement, and recommends that it be implemented without delay.

On behalf of the Nuclear Science Advisory Committee,

John P. Schiffer
Chairman

JPS/bw

Enclosure

DOE/NSF NUCLEAR SCIENCE ADVISORY COMMITTEE

1983

Sam M. Austin (Michigan State University)
Gordon A. Baym (University of Illinois)
Felix Boehm (California Institute of Technology)
D. Allan Bromley (Yale University)
Herbert H. Chen (University of California at Irvine)
Douglas Cline (University of Rochester)
Karl A. Erb (Oak Ridge National Laboratory)
Hermann A. Grunder (Lawrence Berkeley Laboratory)
Cyrus M. Hoffman (Los Alamos National Laboratory)
Arthur A. Kerman (Massachusetts Institute of Technology)
Malcolm H. Macfarlane (Indiana University)
Philip G. Roos (University of Maryland)
John P. Schiffer (Argonne National Laboratory), Chairman
Arthur Z. Schwarzschild (Brookhaven National Laboratory)
Ingo Sick (University of Basel)
Erich W. Vogt (University of British Columbia)

DOE/NSF NUCLEAR SCIENCE ADVISORY COMMITTEE
1983

Sam M. Austin (Michigan State University)*
D. Allan Bromley (Yale University), Chairman of Panel
Joseph Cerny (Lawrence Berkeley Laboratory)
Karl A. Erb (Oak Ridge National Laboratory)*
Hermann A. Grunder (Lawrence Berkeley Laboratory), Chairman of Technical Subpanel*
Ernest M. Henley (University of Washington)
Steven E. Koonin (California Institute of Technology)
Arthur B. McDonald (Princeton University)
Philip L. Morton (Stanford Linear Accelerator Center)*
Richard B. Neal (Stanford Linear Accelerator Center)*
Ednor M. Rowe (University of Wisconsin)*
Ingo Sick (University of Basel)
Arie van Steenbergen (Brookhaven National Laboratory)*

* Members of the Technical Subpanel.

CONTENTS OF THE REPORT

		Page
I.	PRINCIPAL RECOMMENDATION	1
II.	INTRODUCTION	
II A. -	Activities of the Panel	2
II B. -	Criteria Used by the Panel	4
II C. -	Overview of the Scientific Challenges	5
II D. -	Considerations Affecting the Maximum Electron Energy and Duty Factor	10
II E. -	A Major Electron Facility in the Context of the 1979 NSAC Long Range Plan for Nuclear Science	15
III.	GENERAL SCIENTIFIC JUSTIFICATION	18
IV.	CONSIDERATION OF INDIVIDUAL PROPOSALS	
IV A. -	Introduction: Comparison of Electron Acceleration Possibilities	22
IV B. -	Tabular Comparisons of Proposed Accelerator Systems, Costs, and Staffing Levels	29
IV C. -	Discussion and Critiques of Proposals	
	IV-C-1 - Argonne National Laboratory	35
	IV-C-2 - University of Illinois	41
	IV-C-3 - Massachusetts Institute of Technology	46
	IV-C-4 - National Bureau of Standards	51
	IV-C-5 - Southeastern Universities Research Association	55
V.	RECOMMENDATIONS	
V A. -	Argonne and SURA	61
V B. -	University of Illinois	64
V C. -	Massachusetts Institute of Technology	64
V D. -	National Bureau of Standards	65
VI.	ACKNOWLEDGEMENTS	
VII.	APPENDIX	
VII A. -	Experimental Equipment and User Aspects	67

I. PRINCIPAL RECOMMENDATION:

This Panel finds that the highest priority for new accelerator construction in the U.S. nuclear physics program is for an electron accelerator of high duty factor capable of producing beams at any energy in the range from 500 MeV to 4000 MeV. After detailed study and consideration of the proposals for such facilities submitted to it, the Panel **recommends:**

> **That the proposal submitted by the Southeastern University Research Association (SURA) be accepted and funded for the construction of a new National Electron Accelerator Laboratory (NEAL) centering on a 4 GeV linear accelerator-stretcher ring system capable of delivering intense, high duty factor, electron beams in the energy range from 500 to 4000 MeV.**

Additional recommendations relating to this principal one are to be found in the body of this report. As modified by the Panel consequent to its own studies and analyses, the estimated cost (in 1983 dollars) of the accelerator complex is 111.8 million dollars; of the entire laboratory is 146.8 million dollars; and the operating cost averaged over the first five years of operation is 18.1 million dollars per year. The projected 15 year total cost of the project is 418.3 million dollars. The construction period is estimated to be 4.5 years.

The member universities of SURA have already pledged five Commonwealth Professorships, 25 tenure or tenure track positions in experimental nuclear physics and at least five tenure or tenure track positions in theoretical nuclear physics in areas specifically related to the proposed facility. The NEAL Laboratory, from the outset, however, will be constructed and managed as a national rather than a regional facility and will provide the United States with a truly unique facility for research in electromagnetic physics.

II. INTRODUCTION

II-A. Activities of the Panel

The Panel on Electron Accelerator Facilities was established by the DOE/NSF Nuclear Science Advisory Committee (NSAC) during its meeeting on January 12, 1983; the Panel membership is given on the frontispiece to this report. The charge to the Panel was as follows:

> **Within the context of: (1) the December 1979 "Long Range Plan for Nuclear Science"; (2) the scientific discussions of the NSAC Subcommittee on Electromagnetic Interactions report "The Role of Electromagnetic Interactions in Nuclear Science"; and (3) your own best scientific judgment, review and evaluate electron accelerator facility proposals submitted by Argonne National Laboratory, University of Illinois, Massachusetts Institute of Technology, National Bureau of Standards, and Southeastern Universities Research Association. Examine each of the proposed facilities as a possible component of the overall national program of basic nuclear research, and recommend the facility or combination of facilities which will best meet the United States needs for basic nuclear research with electromagnetic probes.**

As an integral part of its review and evaluation of the five listed proposals, each proposing group was requested, by telephone on January 13 and confirming letter dated January 14, to provide the Panel with a listing of its major outstanding concerns relating to each of the other four proposals; such listings of concerns were then circulated to the five groups on January 31 in order that responses might be prepared. In parallel with this, a detailed questionnaire concerning the development of estimates of both construction and operating costs and the structure of, and justification for, such items as contingencies, overhead charges and the like was developed and forwarded to the five groups in order to permit greater intercomparability of the proposals.

A Technical Subpanel was established with membership drawn entirely from within the Panel and was charged with a detailed examination of the technical and accelerator physics aspects of each proposal and an expert evaluation of its feasibility, the adequacy of the R & D already accomplished, the nature of that remaining to be accomplished, and the like. During the period, February 10 - February 15, the Technical Panel scheduled site visits to each of the five proposing institutions; all were accomplished save that to MIT which coincided with the Blizzard of 1983. In its place the Technical Subpanel met with MIT representatives in Washington on February 16 and on February 26 the Chairman of the Subpanel visited MIT.

During a meeting of the Panel held in Washington February 17 - 19, a total of fifteen hours was devoted to public presentation of the five proposals, and responses to concerns raised by other proposing groups, by the technical subpanel, and by members of the Panel. Questions were also invited from the floor and active public discussion of each of the five proposals followed their presentation.

On February 19, the Panel met in closed session to focus on outstanding questions remaining after these presentations, for brief discussions with representatives of several of the proposing groups during which some of these questions were raised, and for preliminary discussion of this report and allocation of drafting responsibilities.

A substantial number of open questions of a technical nature remained and these were addressed by the Technical Subpanel; a further number relating to such topics as management, and to scientific and institutional support were addressed to the groups in question by letter from the Panel Chairman. Each of the five groups was also invited to provide the Panel with any additional information that it felt had been inadequately covered during its public presentation; four groups responded to this invitation and all questions addressed to the groups by the Panel were answered prior to its next meeting, on March 7, in Washington.

Discussions at this March 7 meeting focussed on the accelerator energy and the present requirements of electromagnetic physics, and produced general agreement concerning the needs of the field and the overall scope of the Panel recommendations. Substantial discussion was also devoted to the ancillary research instrumentation requirements of the field if the proposed facilities were to be effectively exploited. On the basis of these discussions and the detailed budgetary analyses of the Technical Subpanel, the Panel chose to recommend increased contingencies to reflect increased R & D requirements and increased equipment budgets for several of the proposals. The proposed budgetary information and the Panel's recommended revisions are summarized in Tables in Section IV-B. A corresponding table listing the characteristics of the accelerators in the five proposals in convenient summary fashion is to be found in Table IV-B-4.

Because there remained unresolved questions concerning the behavior, in particular, of the proposed 4 GeV accelerator facilities at the extremes of their proposed energy ranges, detailed decisions regarding recommendations were deferred until March 30 when the Panel next met, again in Washington.

In the interim, the remaining technical questions were resolved and sections of this report were redrafted in the light of the March 7 discussions and of additional material provided by the proposing groups. In order to avoid misstatements of fact, the Technical Subpanel forwarded draft sections of this report concerning each specific proposal to the corresponding group on March 29 with the request that they be reviewed for accuracy; the opinions stated are, however, those of the Technical Subpanel and were not open to argument or change.

Because the Panel had decided on March 7 to recommend construction of a 4 GeV accelerator as its highest priority, major attention was focussed on a comparison of the two fully developed 4 GeV proposals — those from the Argonne National Laboratory and from the Southeastern Universities Research Association. Prior to the meeting each panel member had undertaken an independent analysis of the advantages and disadvantages of each facility as **the** major national accelerator facility, weighing all considerations as he saw fit and arriving at a choice. The detailed individiual listings of advantages and disadvantages were made available to the Chairman of the Panel, and — as a collection of letters — to all the Panel members at the March 30 meeting, but were not photocopied or distributed. There were no disagreements regarding the actual **facts** of the situation although Panel members differed somewhat in their assignment of different **weights** to these individual facts.

On March 30, the Panel completed discussion of those questions remaining open at the earlier meeting, voted on its final recommendations as included in this report, and devoted substantial time to discussion and review of the contents of this report itself.

While the Panel was not unanimous in its voting, in each case the recommendations included herein received strong majorities.

Drafts of the Panel's completed report were circulated to its members for comment during the week of April 11 and to other members of NSAC during the week of April 18 prior to its formal presentation to NSAC during the scheduled open meeting, in Washington, on April 22.

II-B. CRITERIA USED BY THE PANEL

Clearly, in any panel containing members with as diverse background as does this one, individual members will weigh different factors as having different importance in arriving at their conclusions and votes. We have considered it to be of extreme importance in the present case, however, that there be no uncertainty or disagreement concerning the **facts** — technical, financial, institutional or otherwise — associated with our consideration of each of the proposals. To this end we have felt free to go back repeatedly to the proposing groups for further information or clarification whenever any uncertainty existed. Our Technical Subpanel has carried out an extremely detailed study of the proposed accelerator systems and has among its members internationally recognized experts on the accelerator types involved. Other subgroups of Panel members have examined the research equipment question in considerable detail and have carried out a very detailed analysis of the staffing and budget estimates.

With all these facts in hand, augmented of course by the three hours of public oral presentation and discussion that we arranged for each proposal, what were the criteria that influenced our judgements? As noted above, the exact ordering will be different for different panel members and of course may differ for projects of different scope. Among the criteria most frequently discussed, however, were these:

Importance of the Accessible Physics

Feasibility of the Proposed Accelerator System

Type and Seriousness of Possible Failures to Meet Specifications

Ability of the Proposing Group to Perform — Track Record

Attractiveness to the Scientific Community

Cost Effectiveness

Educational Potential

Potential for Facility Upgrading

Quality and Commitment of Internal Staff

Adequacy of Plant and Support Facilities

Potential Attractiveness to External Users

Provision for, and Experience with, External Users

Adequacy of Management Groups and Structures

Adequacy of Propsed Experimental Facilities

Adequacy of Proposed Staffing Levels

Institutional Support

Quality of Proposal Documentation

Quality of Proposal Presentation

Geographical Location, Access, and Environment

Impact on the Electromagnetic Physics Community

Impact on the Nuclear Physics Community

Advantages and Disadvantages of an Entirely New Laboratory

II-C. OVERVIEW OF THE SCIENTIFIC CHALLENGES

We appear to be on the threshold of much deeper and more extensive understanding of the atomic nucleus. In the face of the remarkable progress that has been made in recent years in understanding the structure and interactions of nuclear systems, the tremendous scope of the remaining open frontiers is often forgotten. Almost all of what we know about nuclei is restricted to energies near the Fermi surface — and to phenomena where nucleons are the overwhelmingly dominant participants. The deep nuclear interior, denied to most available probes by absorption phenomena, is largely unknown territory — as is the nuclear stratosphere. We are only beginning to understand what happens when nuclei are raised to very high temperatures.

It is already well established that even at relatively low temperatures, mesonic effects and effects reflecting the presence of excited nucleons are detectable in modern high resolution nuclear measurements. And at very high energies the quark structure of the nucleons themselves is well established but the effects of this structure on the properties of nuclei remain to be determined.

We are faced with the tantalizing possibility that quantum chromodynamics(QCD) may provide the theoretical framework for the understanding of the strong nuclear interaction that quantum electrodynamics (QED) has so successfully provided for the purely electromagnetic interaction.

And it is surely within the realm of nuclear physics to hope to understand the transitions between those phenomena wherein nucleons are the dominant performers through those dominated by mesons and baryons (excited nucleons) to those wherein quarks play the featured roles. We have no reason to believe that the transitions themselves will be dramatic i.e., low ordered phase transitions. Rather all available (very scanty) evidence points to gradual transitions. In a very crude sense we may think of the nucleons, with increasing available energy, first occupying more complex, more energetic configurations either as independent entities in a shell model sense or collectively as in giant resonances; with increasing energy the nucleons themselves become excited internally to form the Δ, N_1^*, N_2^* etc. and these in turn participate in the overall nuclear configuration; and at still higher energies we may think of the nucleons as **melting** — but melting much more like glass than like ice. Indeed we already have some intriguing evidence from recent deep inelastic muon scattering at CERN that may bear on this point. It has generally been assumed that all nuclei are essentially equivalent and little different from a collection of isolated nucleons as far as deep inelastic scattering at very large four — momentum transfer is concerned. Instead, as shown in Figure 1, the structure functions for deep inelastic muon scattering from iron and from deuterium differ substantially; this difference has been interpreted to imply that a) there is a tendency for quarks to percolate from nucleon to nucleon in iron, b) there is a large increase in the number of "sea" quarks in iron which may reflect pion or other meson-like components in the nuclear wave function, c) the fraction of the momentum per nucleon carried by gluons is significantly less in iron than it is in deuterium and d) there is a small probability for the existence, in iron, of aggregates of more than three quarks. This is clearly an early measurement and interpretation but already it suggests a wealth of nuclear information from the precise determination of nuclear structure functions over extended parameter ranges.

This measurement suggests that we **can** obtain quantitative information regarding these exciting new phenomena — phenomena that in the most fundamental way bridge the artificial and often spurious separation between nuclear and elementary article physics.

This is obviously a high energy illustration, but the situation is scarcely less challenging at low energies. We need to know how the nuclear many-body system responds to an electromagnetic probe and how this response can be understood in the light of microscopic structure, symmetries and simplicities.

Electromagnetic physics at relatively low energy has much to tell us about this critical interplay between particle and collective degrees of freedom. New experimental techniques, pioneered at MIT-Bates, for example, have made possible isolation and study of discrete quantum states of the nuclear system and systematic determinations of the charge $\rho(r)$ and magnetization $\mu(r)$ densities at accuracies better than the 1% level. We have learned, thereby, that the density distribution inside the nucleus is much smoother than we had believed and that the independent particle model is remarkably accurate, even deep in the nuclear interior. These facts pose an outstanding challenge to any detailed microscopic understanding of nuclear structure — as do the new stretched-state particle-hole configurations excited in back angle inelastic electron scattering.

There is a wealth of critically important new information that only relatively low energy electrons can give us. Measurements of the decay modes of the giant electric and

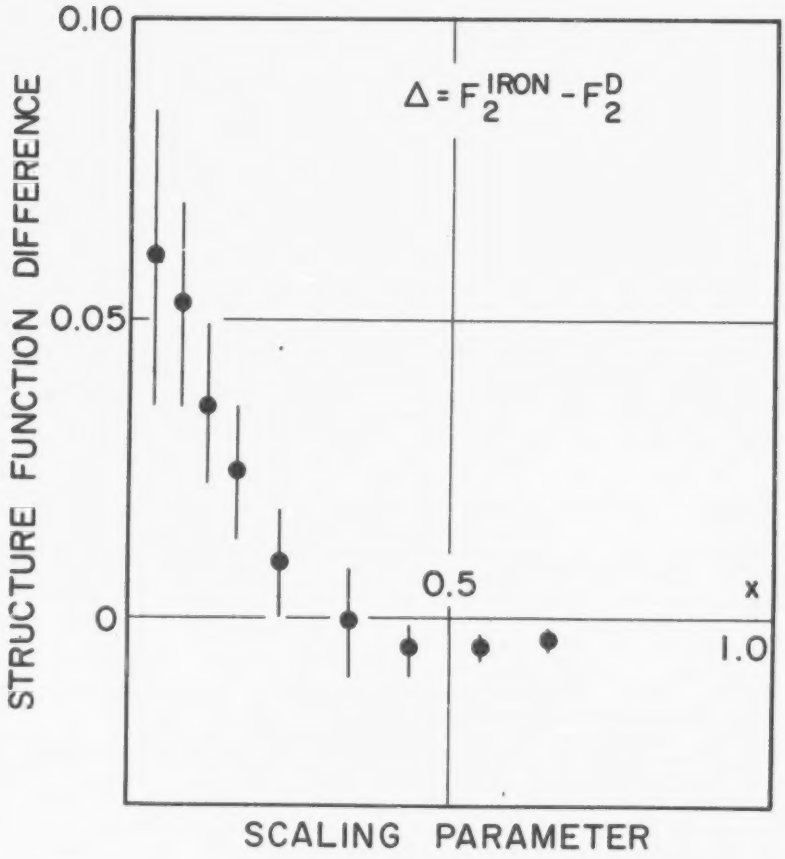
0.10
0.05
0
$\Delta = F_2^{IRON} - F_2^D$
STRUCTURE FUNCTION DIFFERENCE
0.5
x
1.0
SCALING PARAMETER

FIGURE 1

magnetic multipole resonances formed by inelastic electron scattering will tell us much about the structure of these resonances. Particle-knockout experiments will yield information about nucleon momentum distributions and about correlations between nucleons in nuclei. Most of these experiments will require coincidence measurements and these in turn require high duty factor accelerators.

As we move to intermediate energies, both mesonic effects and those reflecting intrinsic excitations of the nucleons themselves are expected to become of increasing importance. This is illustrated in striking fashion in Figure 2 which plots the proton inelastic structure function νW_2 as a function of the four-momentum transfer Q, and the scaling variable $\omega' = 1 + W^2/Q^2$. Here the Δ, N_1^*, and N_2^* isobars appear as peaks corresponding to missing masses of 1.23, 1.50 and 1.65 GeV, respectively. W=2 GeV is shown as a dashed line. It is striking that for large Q and W the isobar peaks essentially fade into the background and the structure function becomes a function effectively of the scaling variable only.

The suggestion is that this is a signature for underlying simplicity with the constituent quarks now responding essentially as free entities in a situation quantitatively describably in QCD terms. Here again we appear to be seeing a smooth transition from nucleon-meson physics to quark-gluon physics. It may well be that the two descriptions are complementary, with QCD being simple and appropriate at high energies, high momentum transfers, and small distances and a meson-nucleon description being the simple and appropriate one at lower energies, smaller momentum transfers, and larger distances.

The details of such a complementarity are simply not discernible from inclusive experiments and if our long history of nuclear experimentation has taught us anything it is that coincidence measurements, wherein particular channels and variables can be isolated for study, provide powerful access to new understanding. It is for this reason that the Panel strongly supports the Barnes Subcommittee recommendation that high duty factor is important at **all** energies.

It would be pointless to attempt any exhaustive coverage of electromagnetic physics here. Section III, which follows, provides a broad overview; the NSAC report **The Role of Electromagnetic Interactions in Nuclear Science** (Barnes Report) provides an up-to-date overview of the field as of mid-1982. This was preceded by the earlier 1977 DOE/NSF Joint Study **Role of Electron Accelerators in U.S. Medium Energy Nuclear Science** (Livingston Report) and by the Report of the Workshop on **Future Directions in Electromagnetic Nuclear Physics** (Stoler Report) of 1981. The reader is referred to these reports for details of the rich spectrum of nuclear physics which a high energy, flexible, electron accelerator facility would make accessible. The proposals under review by the present Panel each present substantial discussion of the part of this spectrum of greatest interest to the proposing group.

What has emerged from all of these reports and studies is a growing consensus within the U.S. nuclear physics community that the time is ripe for an attack, in force, on the new frontiers — at low energies, at high energies, and at all the energies in between — and a similar consensus that an essential component of our national effort in nuclear physics must be a variable energy electron accelerator facility capable of **both** high duty cycle and high energy.

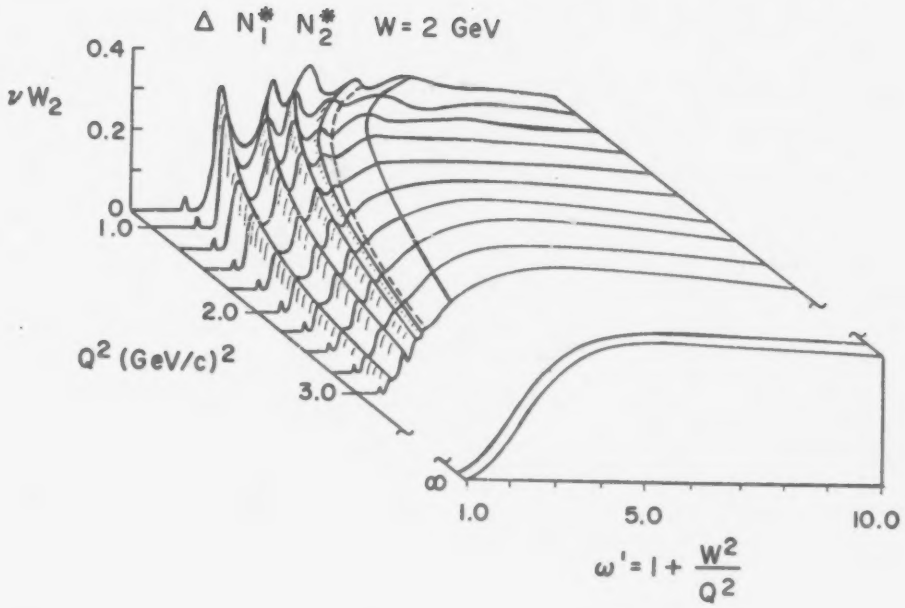

FIGURE

It is worthwhile to quote the recommendation of the NSAC Subcommittee on Electromagnetic Interactions (Peter Barnes, chairman) in its entirety:

> **The Subcommittee strongly recommends the construction of a variable energy electron beam facility capable of operation at both high intensity and high duty factor, and able to achieve an electron energy of about 4 GeV, for the purpose of making coincidence measurements on nuclear targets at large excitation energy and momentum transfer.**

Among its findings, the Barnes Subcommittee also noted the following:

> **The Subcommittee concludes that investigations of complex nuclei with electron beams of 0.1-1.0 GeV, high duty factor, and high intensity would have an important impact on out understanding of nuclear structure and dynamics.**

In short, the Barnes Subcommittee, after detailed study, found a wealth of experimental opportunities for exciting new physics over the entire range from 0.1 to 4 GeV and moreover found that high duty cycle was an important parameter over this entire range.

II-D. CONSIDERATIONS AFFECTING THE MAXIMUM ELECTRON ENERGY AND DUTY FACTOR

But the Barnes Subcommittee was not unanimous in its choice of 4 GeV as the desirable maximum energy of the recommended national electron accelerator facility, and this Panel has received strong arguments both for and against it.

In order to address in a more quantitative way this question of appropriate electron energy, we consider three areas of research: the short-range nucleon-nucleon correlations in nuclei, nucleon resonances and meson exchange currents, and the role of quark constituents for nuclear properties. These topics have high scientific priority; for a given framework used to describe the nucleus, we estimate that the experiments to be discussed impose the most stringent conditions on electron energy. For these areas of research, we first determine limits on the kinematical variables of interest, momentum transfer q and energy loss ν; from these limits on q, ν we then derive the electron energy required. Here we discuss a few of the most relevant arguments only; a much more complete discussion may be found in the Report of the Barnes Subcommittee.

Properties of nuclear wave functions at short range — beyond the region covered by the independent particle model ($K \leq 3$ fm^{-1}) but still in the nucleon-only sector — involve nucleon momenta K=3-5 fm^{-1}. In knockout reactions (e,e' X) the momenta studied are of order $K \approx q$; for single arm experiments, K is somewhat larger than q/2. Taking as a typical value K=(3/4) x q=4 fm^{-1} yields q=5-6 fm^{-1} (1-1.5 GeV/c). The second variable of interest, the energy transferred to the nucleus, is limited by nuclear excitation energies (≤100 MeV) plus nucleon (pair) recoil energies. To minimize final state interactions, the latter should exceed 200 MeV per nucleon, yielding a total energy loss of 500 MeV. This combination of q, ν defines the range that should be accessible if the nucleus is to be investigated within the framework of a picture involving nucleonic constituents only.

The excitation of nucleon resonances (which is inseparable from the question of the short-range nucleon-nucleon interaction) involves initial momenta K somewhat larger than the Fermi momentum; resonances bound in the nucleus (i.e., $\Delta\Delta$ components) have momenta 2-3 fm^{-1}. According to the above criteria, their study requires a momentum transfer of 3-4 fm^{-1}. To excite those resonances that still appear as discrete peaks for the isolated nucleon, an excitation energy up to 800 MeV has to be provided. A total electron energy transfer of $\approx$1.3 GeV allows for appropriate nucleon recoil energies and nuclear excitation.

Most demanding on electron energy is the investigation of the quark/nucleon interface in nuclei. Two types of arguments are general enough to give guidance in the absence of relevant experimental results or detailed theoretical understanding: spatial resolution desired and scaling limit.

From both experiment and theory we expect quark effects to become important at ranges $r \leq 0.5$ fm. The repulsive core of phenomenological nucleon-nucleon interactions, analyzed in terms of meson exchange potentials, occurs at $r \approx 0.4$ fm; the energies of odd-parity nucleon excited states, interpreted in terms of constituent quark models, give a bag-radius $r \approx 0.5$ fm; the little bag models yield radii ≈ 0.4 fm, while the MIT bag model gives somewhat larger values; the nucleon radius, 0.8 fm, corrected for the contribution of the pion cloud, yields a corresponding value of 0.4-0.6 fm. If we want to investigate the effects of quarks - as opposed to the effects of the meson cloud - our electron microscope must have a spatial resolution that is smaller than 0.5 fm by a significant factor. Taking, as a minimal resolving power, 1/3 of the "core" size, we can expect to be able to investigate the effects of quarks on nuclei, and vice versa, with reasonable detail. Given the fact that the electron samples the nucleus via a sin (qr) function, a spatial resolution $\Delta r \approx 0.5$ fm/3 (FWHM) requires momentum transfers $q = 1.5/\Delta r = 10$ fm^{-1}. An energy loss of $\nu = 1.3$ GeV, as discussed above, is required if final states corresponding to discrete nucleon excitations are to be observed.

The scaling arguments start from the detailed investigation of nucleon structure functions performed in the past. Above a certain momentum/energy transfer the structure functions W_2, as illustrated above in Figure 2, become a function of a single variable $X = Q^2/2m\nu$ with $Q^2 = q^2 - \nu^2$. This scaling shows that the physics has simplified, and become uniform. It is taken as proof that, in this regime, the quarks are almost asymptotically free, without interaction. This scaling region can be considered as a possible limit of nuclear physics; in this region nuclear confinement degrees of freedom become unimportant for an understanding of quark wave functions. We can hope that in the reasonably near future this scaling region, where physics is "simple", can be quantitatively understood using QCD. For the investigation of quarks in nuclei, including confinement, experimental studies such as those addressed in this report are required. In order to anchor these studies, points of contact with the scaling region would be most valuable. The experimental data for the nucleon (Figure 3) show that scaling occurs starting at values $Q^2 \geq 1$ $(GeV/c)^2$ and $W^2 = M^2 - Q^2 + 2M\nu \geq 4$ $(GeV)^2$.

Having defined the maximum momentum transfer and energy loss, the derivation of maximum electron energy requires one further consideration. To separate the different structure functions, which contain different physics, experiments must be performed

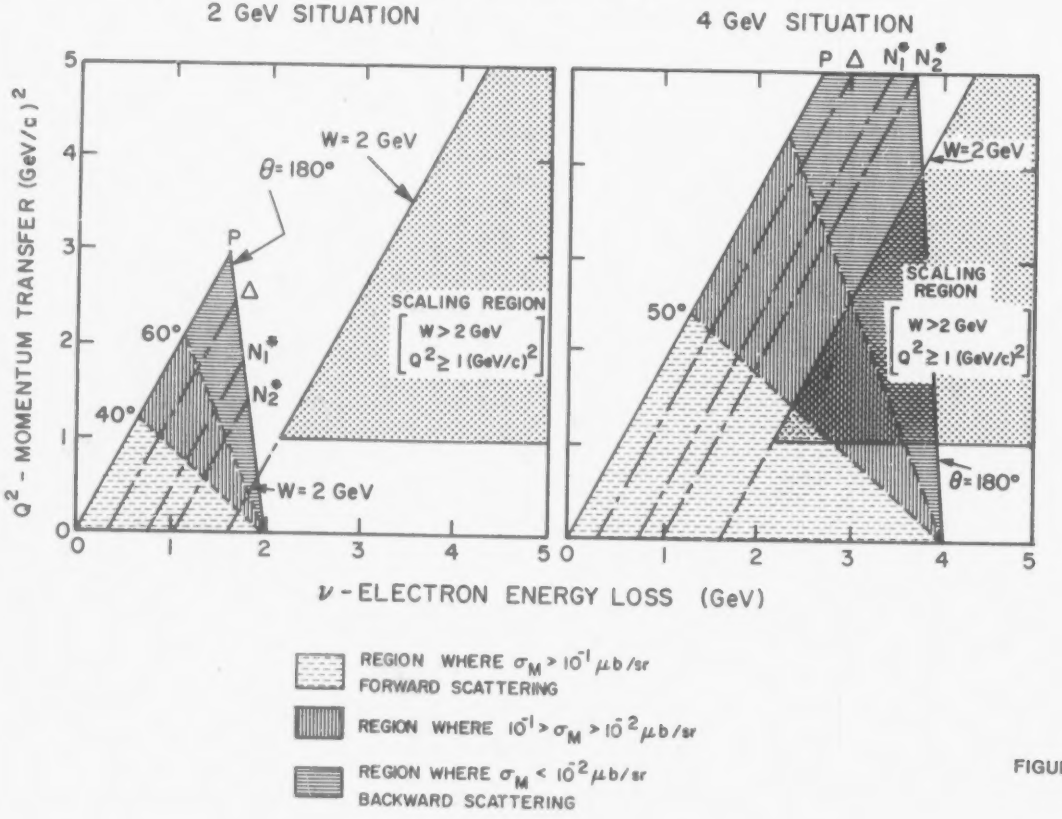
KINEMATICS FOR ELECTRON SCATTERING FROM
A PROTON AT REST
2 GeV SITUATION
4 GeV SITUATION
P Δ N1* N2*
W= 2 GeV
θ= 180°
P
Δ
60°
40°
N1*
N2*
SCALING REGION
[W > 2 GeV
Q2 ≥ 1 (GeV/c)2]
W= 2 GeV
50°
W=2GeV
SCALING
REGION
[W>2 GeV
Q2 ≥ 1 (GeV/c)2]
θ= 180°
Q2 - MOMENTUM TRANSFER (GeV/c)2
ν - ELECTRON ENERGY LOSS (GeV)
0
1
2
3
4
5
REGION WHERE σM > 10-1 μb/sr
FORWARD SCATTERING
REGION WHERE 10-1 > σM > 10-2 μb/sr
REGION WHERE σM < 10-2 μb/sr
BACKWARD SCATTERING

FIGURE 3

at angles θ such that the cross section at a given q can be separated into its longitudinal and transverse components:

$$\sigma(q,\nu) = \sigma_L(q,\nu) + (\tfrac{1}{2} + tg^2(\theta/2))\,\sigma_T(q,\nu)$$

The most demanding constraint results from the fact that, at large q, σ_T heavily dominates σ_L. To separate σ_L, the minimal contribution of σ_T is desirable; $\theta_{max}=50^o$ results in a σ_T contribution 44% larger than the minimal one possible.

Using this constraint, the electron energy needed can be calculated once q,ν are known. From the discussion of q,ν given above, the electron beam energies needed to study the nucleus in terms of nucleonic, mesonic and quark constituents are 1.7, 3 and ~4 GeV, respectively.

As an illustration, Figure 3 gives the kinematical regions accessible for incident electron energies of 2 GeV and 4 GeV. For the study of nuclear wave functions at short range, $q=6$ fm^{-1}, implies $Q^2=2$ GeV/c^2 at $\nu=500$ MeV and this, in turn, requires an incident energy of 1.7 GeV for $\theta=50^o$. A similar incident energy is required for the excitation of nucleon resonances. The investigation of nuclei, with a spatial resolution of one third of the nucleon radius requires $Q^2=2.6$ GeV at $\nu=1.2$ GeV implying an incident energy in excess of 3 GeV. It is apparent, from Figure 3, that essentially no contact with the scaling region is possible with a 2 GeV maximum electron energy whereas with a 4 GeV maximum energy a substantial region of potential study opens up.

We turn then to the question of required duty factor. It has been suggested, for example, that high duty factor is not essential at the higher energies and that the successes already achieved at SLAC with only 0.1% duty cycle are indicative of the kind of exploratory inclusive experiments that should receive major attention in the range where quark-gluon effects might be expected to be of significance.

It is unquestionably true that inclusive (e,e′) experiments have had a great impact on elementary particle physics. The observation of the scattered lepton, only, involves an integration over all hadronic final states, and this greatly simplifies the description of the reaction. Inclusive experimental have been a success, in particular, because of the fact that quarks are asymptotically free. Scattering a lepton from such a quasifree quark leads to an extremely simple and clean reaction mechanism.

In the case of nuclear physics, this simplification does not occur; nucleons in nuclei are not free. In this case we have to, and want to, deal with the complications of the initial and final hadronic states. Even when considering quarks, we are interested primarily by the degree to which quarks are influenced by the nuclear medium. Under these circumstances, the above advantages of inclusive experiments are no longer present. Inclusive experiments as in other branches of nuclear physics, only give very global information that averages over many aspects of the underlying physics. Trivial, prominent processes often cover up the more interesting phenomena; the latter ones are partly accessible only in some corner of kinematical domains (in the case of (e,e′), extremely large momentum transfer, or large momentum and small energy transfer).

In order to understand the strongly interacting system in any detail, we must specify the reaction initiated by the electron in considerable detail. This can be done

only by detecting the products in the final hadronic state. In order to conserve the basic advantage of electrons — variability of the momentum transfer at given energy transfer — this implies coincidence experiments, and hence CW accelerators.

This argument for CW is true at any energy. It becomes the more imperative the more complicated the system we want to study. The most complex (and most interesting) question is the one concerning the nucleon-quark structure of nuclei. In the energy range where this question can be addressed, ~4 GeV, CW becomes a matter of crucial importance.

A most important, but often overlooked, reason for CW concerns future experiments involving parity violation, polarized (recoil) nuclei and hypernucleus production. These topics have high scientific priority, and the relevant experiments are very difficult because of the high statistical accuracy required (parity) or the small cross sections (efficiency of recoil nucleus polarimeter, low production cross section). These important experiments can be carried out if large solid angle detectors are built; these detectors cannot be magnetic spectrometers; the ratio of price to solid angle is simply too large. Less expensive, more sophisticated devices of large solid angle can be utilized provided that the total instantaneous rate of particles, both those of interest and the much more abundant ones from (physical) backgrounds, is not too large. Experience with today's electron-accelerators (duty factor ~1%) clearly suggests the need for the highest duty factor available, i.e., C.W.

On the basis of all such arguments, the Panel has concluded, in agreement with the Barnes Subcommittee, and the arguments presented to it by the Argonne and SURA groups, that the higest priority — in terms of exciting new physics — must be given to a facility spanning the 0.5 to 4.0 GeV energy range with high duty factor. We have also, reflecting past experience in other areas of physics, and in the light of our considerable ignorance of this new higher energy range, given substantial weight in our considerations.

At the same time, and again in agreement with the Barnes Subcommittee, we have been much impressed by the richness of the physics that remains to be done in the 100 MeV - 1000 MeV range, particularly with beams of adequate duty factor to permit coincidence experiments.

Reflecting the relative simplicity of the electron as a probe, we are confident that studies involving electron beams will play an increasingly important role in nuclear physics. And we view it as a very healthy development that the former photonuclear and electronuclear communities are being drawn fully into the mainstream of U.S. nuclear physics.

While we have, as a Panel, given our highest priority to a very large national facility, we have been very mindful of the crucial importance of forging the strongest possible bonds with the university community. Unless some of the very best young graduate students are attracted into work in the electromagnetic field — and with the new facilities — the field will inevitably wither. We consider the maintenance of the highly productive groups at Illinois and at MIT to be extremely important to the national effort in the field. The possibility of drawing a large number of other universities into the field — through provision of tenure and tenure-track positions for both experimentalists and theorists, through active participation at an institutional level in management of the new

facility, that we recommend herein — has also been given very serious consideration in our deliberations.

II-E. A Major Electron Facility in the Context of the 1979 NSAC Long Range Plan for Nuclear Science

When the 1979 Long Range Plan was assembled, it envisaged investments in a small CW electron accelerator in FY1982 as a logical outcome of the joint Stanford-Illinois cavity development program and budgeted three million dollars for it. In part this has already been accomplished through NSF funding of the Illinois program for acquisition of NBS/LANL style end magnets; in part, too, the construction of the 200 MeV CW accelerator at NBS under the NBS/LANL joint program and DOE support contributes to this investment.

As its major project in the electromagnetic field, however, the long range plan envisaged a 1-2 GeV CW electron accelerator costing a total of 50 million ($1979) with funding scheduled to begin in FY1985 and to be completed in FY1987; this would correspond to ~73 million ($1983).

As discussed above, the Panel now recommends construction of a higher energy facility — 4 GeV rather than 2 GeV as a maximum energy. It is appropriate to consider how well the Barnes Subcommittee emphasis on the need for coverage from 0.1 to 4.0 GeV (with which we agree) will be implemented should our recommendations be accepted and followed.

Illinois is currently operating up to about 80 MeV and has already received NSF support for upgrading to 120 MeV with dipole end magnets identical to those under construction at NBS.

NBS is completing a 200 MeV CW accelerator at present.

MIT is currently operating at up to 1.8% duty cycle at ~720 MeV and has received DOE funding for additional radiofrequency power both to increase the maximum energy to 840 MeV and increase the operating reliability.

If constructed as planned, the Panel believes that the SURA facility will operate over the range 0.5-4.0 GeV at greater than 90% duty factor.

We thus find that the entire energy range is indeed covered by our recommendations; however, there is a gap between 200 and 500 MeV where no CW facility will be available. Indeed the Panel believes that a strong scientific case can be made for having some overlap with the lower end of the recommended SURA facility and would hope that in the future it will be possible to obtain CW performance at a second facility in the 200-800 MeV range.

To provide some international perspective, we plot in Figure 4, a modified version of Figure 21 of the Barnes report, the duty factor against maximum beam energy, for a number of the world's electron accelerator facilities. As is evident from this figure the recommended SURA facility will be a unique one which should prove extremely attractive to the entire international as well as the national community of scientists involved

in the use of high energy electromagnetic probes. In Figure 5 we plot the 1983 world distribution of high duty factor electron accelerator projects; this distribution is truly an international one and is a measure of the vitality and challenge of the field.

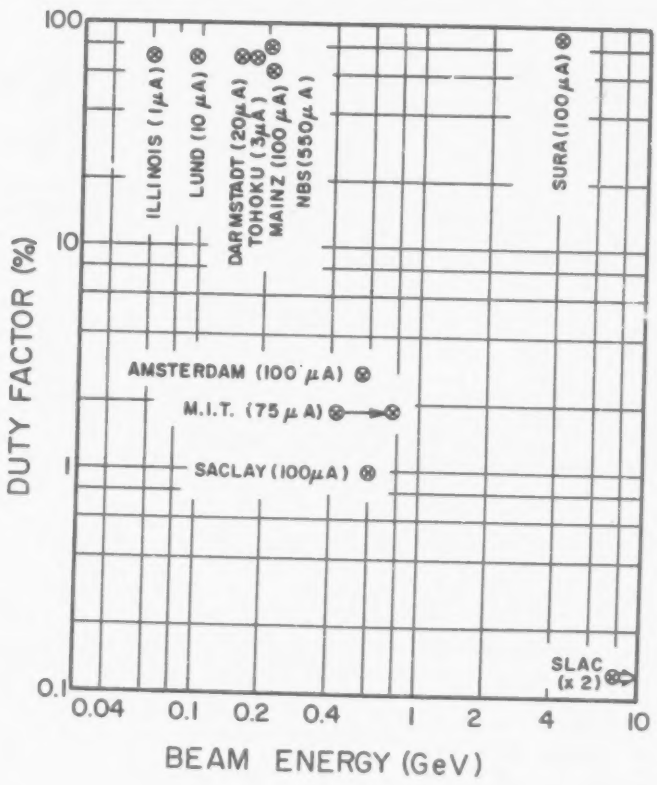

FIGURE 4

WORLD DISTRIBUTION OF HIGH DUTY FACTOR ELECTRON ACCELERATOR PROJECTS - 1983 FIGURE 5

III. GENERAL SCIENTIFIC JUSTIFICATION

As we have noted above, we are approaching fundamental, new understanding of the atomic nucleus from many different points of view. At the simplest level, the nucleus is a system of nonrelativistic nucleons interacting through a two-body potential. Although this "traditional" picture has been very successful in correlating vast amounts of data, it begins to break down at high excitation energies and short distances where nonnucleonic degrees of freedom come into play. For energies from several hundred MeV to several GeV, nuclei are hadronic systems composed of strongly interacting mesons and baryons (nucleons and their excitations). At even higher energies, recent developments in elementary-particle physics strongly suggest that parton degrees of freedom (quarks and gluons) will play a role, although there is as yet little experimental or theoretical understanding of how these properties are manifest, or modified, in multibaryon systems.

The elaboration and integration of these three levels of understanding of the nucleus (nucleons, hadrons, and partons) will be a major task for nuclear science over the next two decades. Our present knowledge is spotty. We are on firmest ground at the nuclear level, although many comparisons between precise data and detailed models must yet be carried out before our understanding is truly complete. Of particular interest are the nature and origin of collective motion and the short-distance behavior of the nuclear wave function. At the hadronic level, we have learned much from the intermediate energy studies with electron, nucleon, and pion beams over the last decade, but many crucial questions are yet to be answered. Finally, the parton level is largely **terra incognita**, although it offers the intriguing opportunity for understanding nuclei as manifestations of the strong interaction in the most fundamental terms.

The electron facilities discussed in this report will allow new experimental studies of nuclei across the whole spectrum of their properties. The electromagnetic interaction provides a unique probe for the study ofthe nucleus. The point-like nature of the electron and the known detailed theory of the electromagnetic interaction make data from this probe readily interpretable, and the penetration of electrons and photons throughout the nuclear volume provides an excellent complement to strongly absorbed hadronic probes. Moreover, the kinematics of electron scattering are such that **the momentum and energy delivered to a nucleus can be varied independently**, so that a broad range of the nuclear response can be studied.

The many scientific opportunities afforded by CW electron beams from 100 MeV to 4 GeV have been fully documented in the five proposals we have considered, in the "Stoler Report" produced by the electromagnetic nuclear physics community, and in the report entitled **The Role of Electromagnetic Interactions in Nuclear Science** (the "Barnes Report"). Below, we mention only a few of the more important studies which address nuclear properties at each of the three levels.

At the nucleon level, much remains to be done in the study of ground state charge and current density distributions and in the study of transition densities for discrete excited states. Elastic and inelastic electron scattering provides precise and otherwise unobtainable information on nuclear wave functions; the continuation of high resolution experiments in this energy region is essential as a complement to intermediate energy hadronic probes. The ability to study $(e,e'\gamma)$ and $(e,e'N)$ processes for discrete nuclear states will provide stringent tests of microscopic nuclear structure calculations. Furthermore, such precision measurements serve as departure points for higher energy experiments aimed at understanding the hadron and parton degrees of freedom.

A major advantage of a high duty-factor/high-current electron beam at an energy of about 1 GeV would be the ability to perform (e,e′ X) coincidence experiments and observe correlations in energy and angle for final state products. The study of giant resonances can be significantly refined through such measurements. Angular correlations at fixed momentum and energy transfer can be studied to determine J^{π} for an observed resonance. The isolation of specific final states provides transition form factors and information on the coupling of the giant resonances to these states; out of plane coincidence measurements can be used to separate charge and current transition densities.

New insights into the nuclear wave function should also result. For example, (e,e′ N) reactions allow the study of deep-lying shell model orbitals and the momentum distribution of nucleons within the nucleus. With the high-resolution tagged photon beams to be available with the new facilities, coincidence experiments can be extended to the real photon limit. In addition, photon beams can be used for elastic photon scattering and quasi-deuteron photon absorption, in which (γ ,np) measurements provide information on relative nucleon momenta in complex nuclei.

At the hadronic level, electromagnetic probes offer different advantages for exploring nuclear structure. Light nuclei ($A \leq 4$) are simple enough that their properties can be calculated from nucleon potentials, e.g., the "exact" three-body approach, and thus the effects of meson exchange currents and isobar degrees of freedom can be isolated with confidence. Interesting experiments include measurements of proton structure functions at high momentum transfers and scattering from the deuteron to obtain the neutron structure functions.

The comparison of electron scattering from light and heavy nuclei should be particularly revealing. In contrast to proton and pion probes, the electromagnetic interaction allows a real or virtual photon to penetrate the entire nuclear volume and create excitations deep within the nucleus. Reactions with real photons, including (γ,π), (γ, πN), (γ, ρ), (γ, ω) and others allow one to probe the relationship of photons to vector mesons and to study the presence, propagation, and interaction of mesons and isobars. At these higher excitation energies, quasi-free nucleon scattering, quasi-production mechanisms dominate the interactions and can be studied effectively through (e,e′ N), (e,e′ π), (e,e′ Nπ). Since the long-range interaction between nucleons is mediated by pions, such experiments are important steps toward understanding nuclei at the hadronic level. Pion production via M1 excitation of the nucleon allows the investigation of most of the energy range where the (3,3) resonance is dominant.

At the parton level, it is generally believed that quantum chromodynamics (QCD) is the basic theory of the strong interaction, i.e., the nuclear interaction. The evidence for quarks and gluons as the basic constituents of mesons, nucleons and nuclei, is now overwhelming. Although the theory predicts asymptotic freedom at very short quark separations, it is dominated by strong color confining interactions at separations relevant to nuclear physics. As stated in the report entitled **The Role of Electromagnetic Interactions in Nuclear Science:** "The study of the transition between standard nucleon-meson degrees of freedom and the subconstituent quark-gluon QCD degrees of freedom is clearly one of the most important future areas of investigation in nuclear physics." The region of interest cannot be described by perturbative QCD and requires many-body approaches familiar to nuclear physics. The physics associated with quark confinement is likely to be important for decisive tests of QCD and also for the understanding of short-distance nuclear phenomena such as internucleon correlations. Thus, experimental investigations with electrons of energies up to 4 GeV will be great assets in developing a

more sophisticated description of confinement and improved theories for short-distance nuclear physics.

An understanding of the transition from hadron to parton degrees of freedom is aided greatly by anchors at both low and at high energies. As mentioned above, the language of hadrons is well suited to energies up to about 1 GeV. For energies above 10 GeV, on the other hand, the scattering of electrons can be described as occurring from essentially free quarks. An electron accelerator providing energies up to about 4 GeV offers exciting opportunities for investigating nuclei and the strong interaction in the region of energies where these two apparently distinct approaches must merge. In this transition region, confinement and possible coherent quark effects (e.g., diquarks) may be important and can be probed. At the high end of the energy region, with energy losses of $\geq$ 2 GeV and at momentum transfers $\geq$ 1 GeV/c, it has been found that the scaling approximation works well. At lower energy losses and/or momentum transfers, deviations from a description in terms of hadrons will give clues to the underlying structure. Common "intuitive" models may not work here.

The electromagnetic study of light nuclei ($A \geq 4$) has particular advantage for exploring and understanding nuclear systems at the parton level. Recoil tensor polarization experiments, polarization transfer measurements, and high momentum transfer quasi-elastic scattering to obtain resolutions of 0.1-0.2 fm are sensitive to the quark substructure. Coincidence experiments with emitted nucleons and mesons will be helpful in studying the transition region between the hadron and parton limits and may help us understand how nucleons deform as they approach each other and how, for example, the three confined quarks in each nucleon merge to form a confined 6-quark deuteron. The dynamics of this transition can be studied with high momentum transfer coincidence experiments, in which an outgoing nucleon is detected with various energies. Measurements of the electric and magnetic structures of the A=3 nuclei have already shown that present models are inadequate. Further coincidence measurements are required to develop adequate theories and models. Polarization information, for instance, on emitted nucleons, provides information on the spin degrees of freedom of the quark distribution functions.

Experiments with photons and electrons for the production of vector mesons may be helpful to our understanding of mesons in terms of quarks and antiquarks. The photo- and electro-production of kaons and hypernuclei explore the "sea" quark distribution in nucleons, since strange quarks are involved. Furthermore, new opportunities in hypernuclear physics can be opened with such experiments. Via the $(e,e' K^+)$ reaction in particular, lambda and sigma hypernuclei can be produced with probes that interact weakly in both the initial and final states. In contrast to the (K, π) reaction, both spin-flip and non-spin-flip transitions can be induced. As a consequence of the momentum mismatch, the (γ, K) reaction can be used to emphasize the excitation of higher angular momentum states.

Quite apart from its potential for studies of nuclei **per se**, an electron accelerator with a polarized beam would have a high potential for the study of fundamental symmetries. Experiments could be performed to test quantum electrodynamics and to search for time reversal violation and $\Delta I=2$ electromagnetic processes. Parity-violating asymmetries reflecting weak neutral currents grow as the square of the momentum transfers and thus become easier to measure at high electron energies and with high current beams. Parity violation measurements could be used to test the weak conserved vector current and pure V, A theory as well as to study the semileptonic and nonleptonic weak

interactions. Semileptonic weak interactions below 1 GeV should be dominated by couplings to protons and neutrons in the target rather than the incoherent quark coupling observed in measurements above 10 GeV. This permits measurements of a different linear combination of electron-quark weak couplings. Measurements of parity nonconservation in discrete nuclear states and in the Δ resonance region will help to determine nonleptonic weak currents and the weak interactions of mesons and resonances. Since the weak interactions are of very short range, parity violation experiments may be particularly helpful in elucidating quark distributions and confinement features.

In summary, there is an unusually broad set of scientific motivations for studying nuclei with high-intensity/high duty-factor electron beams of energy up to 4 GeV. The questions which can be addressed are at the forefront of nuclear science and its interface with elementary-particle physics. The information so obtained will continue the precise studies of the traditional aspects of nuclear structure, and reveal new aspects of nuclei as systems of both hadrons and partons.

IV. CONSIDERATION OF INDIVIDUAL PROPOSALS

In this section we turn to the five proposals that the Panel was charged to review and evaluate. We have not discussed the individual research programs, since to do so would involve substantial repetition of the material summarized in Section III and covered in detail in the Barnes report. Rather, we will here concentrate on the technical aspects of the proposals.

In order to place the discussion in context, however, we begin with a brief overview of the accelerator technology available in the energy range of interest.

IV-A. COMPARISON OF ELECTRON ACCELERATION POSSIBILITIES

With current technology, there are only two methods of achieving GeV-range electron beams with a very high duty cycle (approximately 100%). These are (1) the combination linear accelerator/electron storage ring operated in the "stretcher" mode and (2) the microtron. The former is the more familiar and will be discussed first.

IV-A.1 Linear Accelerator/Electron Storage Ring Method

The linear accelerator/electron storage ring method is quite straightforward: electrons from a high-current pulsed linear accelerator (linac) are injected into a storage ring, from which they are extracted slowly and uniformly during the time intervals between linac pulses. In order to achieve reasonably high **average** beam currents from the stretcher, the linac must provide high **peak** beam currents at a high repetition rate, and injection into the stretcher ring must be very efficient. Because extraction cannot start until after injection is complete, the linac pulse length must be short compared with the time between pulses in order that the duty cycle of the extracted beam be as high as possible. To ensure that the beam from the stretcher is uniform over time, the linac beam quality must be good; this is because there is little time available for "conditioning" the stored beam in the ring if a duty cycle of greater than 90% is to be achieved.

For high peak currents in pulsed linacs, the cumulative beam breakup instability which can degrade beam quality must be considered. This instability occurs when an electron bunch passes off-center through an rf structure and excites transverse deflecting modes. These transverse fields deflect subsequent electron bunches, which in turn excite these modes even more strongly. The severity of this instability depends on the peak current in the linac, the length of the pulse, the length of the linac, and the amount of transverse focusing present.

Once in the ring, the stored beam must be kept free of the myriad longitudinal and transverse instabilities that plague high-current electron storage rings. Although the theory for predicting such instabilities is much better developed now than it was a few years ago, it is still far from complete. In particular, the growth rates of multibunch instabilities are now known, so it is not clear whether these instabilities will manifest themselves in the storage times of the pulse stretcher. Of equal importance is that the extraction process must be very precisely controlled. Finally, because the time between injection and the beginning of extraction must be short, the injection energy must be the same as the extraction energy, i.e., there can be no acceleration in the storage ring. Thus, for example, a 4-GeV stretcher ring requres a 4-GeV injector. Variation of the output energy requires that the energy of both the stretcher ring and its injector be varied and that the injection and extraction systems be retuned. Moreover, only one output energy is possible at a time.

In principle, all of the required techniques have been demonstrated in one way or another during the past two decades, but to date no beam stretcher for electrons (save one relatively low energy test device) has been built. The successful construction of such a machine in the GeV range will require the coordination of a great deal of complicated science and technology.

Beam injection into the stretcher ring is accomplished by means of single-turn fast vertical injection or by three-turn fast horizontal injection operating with a horizontal tune close to a one-third-integer value. With a fast-turn-off orbit perturbation (kicker fall time much less than an orbit time), essentially lossless beam injection is a well-established technique; it has been employed successfully and reliably at a number of proton and electron synchotron facilities.

As stated above, the beam is extracted from the duty-cycle stretcher ring during the interval between beam injection pulses. With a typical injection rate of 1 kHz, the extraction process is achieved by means of a slow resonant extraction mode with a beam-spill duration of 1 msec. In essence, therefore, such a cycle constitutes a rather fast "slow resonant extraction" mode. The total spill occurs in about 1000 orbits for the stretcher rings of relevance here, as compared with the slow extraction cycle of a proton synchrotron, where the total spill occurs typically over 10^6 orbits.

Two modes of resonant extraction are under consideration in the proposals discussed here: the resonance may be excited by operating with the fractional part of the betatron frequency near either a one-half-integer or a one-third-integer value. For either the half-integer or the one-third-integer mode, a perturbing element is used to shift the machine tune to generate a finite-width resonant stopband, after which the particle orbits grow in amplitude at an exponential rate. Nearly lossless beam extraction for either mode of resonant extraction is obtained by intercepting the outward-spiraling particles with an electrostatic wire-septum deflection unit that directs the beam via a thicker septum magnet into the external beam channel. The beam-extraction efficiency is given by the first septum thickness divided by the resonant-growth step size for a particle with a transverse oscillation amplitude equal to the distance of the septum from the equilibrium orbit.

Because the electrostatic wire septum is essentially of "zero thickness" at the beam energies under consideration here, very high beam-extraction efficiences are possible. Both at CERN, where the half-integer resonant mode is used, and at Brookhaven, where the one-third-integer resonant mode is used, beam-extraction efficiencies in excess of 98% have been measured for proton beams. Control over the resonant process, completeness of the beam spill, and the phase space characteristics of the extracted beam are the criteria used to determine the type of resonance chosen for a particular machine.

With single-turn fast injection, as is used in the SURA case, either mode of extraction would be acceptable, whereas with three-turn fast injection, as is used in the MIT-Bates case, the nature of the transverse phase space distribution ("hollow beam") may favor the one-third-integer resonant mode in order to obtain a smaller time averaged transverse phase space of the extracted beam. Note that for the cases relevant here, the lattice synchrotron-radiation damping time is long compared with the beam dwell time, so that a "memory" of the transverse phase space distribution at injection tends to be preserved.

Of great importance is the time structure of the extracted beam. Resonant component excitation and dipole excitation ripple will lead to time modulation of the beam intensity. Beam feedback can be employed, but its response speed is limited because particles bound for extraction remain for tens of turns inside the machine. Experience at the cited proton facilities has shown, however, that with adequate ripple control, fast beam feedback, and the use of a repetitive parameter-correction cycle ("learning cycle"), beam modulation can be kept to less than about 20%. Resonant extraction from a stretcher ring can provide for a CW beam with 90% duty cycle during the "smooth" part of the beam spill, with a macroscopic time structure having approximately 20-μsec gaps every 1000 μ sec and with a microscopic time structure given by the frequency of the rf acceleration system.

In the stretcher ring designs considered here, a racetrack lattice has been adopted in which two long, dispersion-free straight sections are joined to two achromatic arc sections. The use of dispersion-free straight sections for location of the injection and ejection components provides for simpler matched injection and for beam ejection that does not, in first order, couple the beam momentum distribution into the extraction process.

For the use of polarized beams, it is essential to preserve transverse (vertical) polarization in the stretcher ring. Since the stretcher ring operates in a DC mode (beam injection at final energy), avoiding depolarizing resonances is straightforward by choosing a suitable vertical tune for specific ring energy values. Depolarization due to radiative polarization will be no problem for low-energy operation, but—because $\tau_\rho \alpha C \rho^2 \gamma^{-5}$ is approximately 1 hour at 4 GeV — it must be considered at energies above 4 GeV. Nevertheless, external beams with a high degree of transverse polarization can be obtained from these stretcher rings, as can longitudinally polarized beams by means of external transverse-to-longitudinal spin rotators.

IV-A.2 Microtron Method

The microtron, or electron cyclotron, is relatively unfamiliar, although many low-energy pulsed microtrons have been built since the device was first proposed by Veksler in 1945. Essentially, electrons are made to pass through the same accelerating structure, or structures, repetitively by use of a beam transport system that has the property of making each orbit exactly $n\lambda$ longer than the previous orbit, where n is the integral mode number (1,2,3,...) and λ is the wavelength of the accelerating field. Thus, synchronicity with the accelerating wave is maintained, and very efficient use of the accelerating system is achieved. For reasons of phase acceptance, n is generally less than 5.

The beam transport system can be designed for any number of orbits, but 50 is typical. At the end of the last orbit, the electrons are extracted with an energy of $N\Delta E+E_i$, where N is the number of orbits, ΔE is the energy gain per orbit, and E_i is the microtron injection energy. The energy gain per orbit, the magnetic field in the return magnets, B, and the accelerating-field wavelength are related by a simple expression of the form $\Delta E=An\lambda B$, where A is a constant dependent on the geometry of the microtron beam transport system. This expression shows the constraint on the energy gain per orbit that is imposed by technologically feasible magnets.

At lower energies, where quantum excitation is small, the microtron beam quality can be very high because no complicated injection or extraction gymnastics are required. Therefore, low-energy microtrons are conceptually simple and well-suited to

operation at 100% duty cycle with beams in the 100- μA range. Moreover, the individual orbits are separated horizontally, and thus steering on an orbit-by-orbit basis is possible. These accelerators are, in effect, coiled-up transport systems between one or more rf accelerating cavities. Hence the problems of controlling the path length between passes through the accelerating cavities and of obtaining the proper transverse position and angle of the beam are similar to those that must be solved in a typical beam transport system.

For a 100% duty cycle, which is the case of interest here, the accelerating structure will operate at relatively low gradients (by pulsed linac standards), which means that it must be quite long in order to achieve a high energy gain per orbit. In addition, to achieve the high shunt impedance necesary for maintaining the accelerating gradients, the accelerating structure must operate at relatively high frequencies and with a small bore size (compared with accelerating structures in storage rings). This requires very accurate control and correction of errors in the beam transport system, both to maintain the necessary phase between the rf accelerating voltage and the beam bunches passing through the accelerating structure and to maintain the transverse position of the beam relative to the bore of the structure.

Because the total time that electrons spend in the microtron is extremely short compared with the time they would spend in a storage ring, instabilities characteristic of storage rings do not occur in microtrons. Only two types of beam instabilities appear to be of concern. The first, cumulative beam breakup, is the same as that found in linacs and has already been discussed. The second, regenerative breakup, occurs when the transverse modes excited by an electron bunch deflect the same bunch on subsequent passes through the linac structure.

The current passing through the rf structure in a microtron is much lower than the peak current passing through the rf structure of a pulsed linac, but the pulse length is much greater. Thus, the Q of the rf structure plays a more important role for the beam breakup instabilities in a microtron. This may explain why beam breakup has been a major limitation on the intensity in microtrons with superconducting accelerating structures but has not been a problem, at present intensity levels, in microtrons with room-temperature accelerating structures.

Although the effects of synchrotron radiation are important for all electron beams with energies above a few GeV, they are of particular concern for high-energy microtrons. The change in the electron energy due to synchrotron radiation loss in a bending magnet produces a change in the orbit of the electron. The average orbit shift due to synchrotron radiation loss can be corrected by the addition of compensating bending fields. However, because the electrons emit quanta in a random manner, with a spread in the radiated energy, growth occurs in both the transverse and longitudinal phase space emittances. For high-energy microtrons, this effect determines the beam emittance and will be a major factor in choosing the accelerating-structure aperture.

Varying the output energy is relatively simple: electrons can be extracted from any orbit, giving energy variability in steps approximately equal to the energy gain per orbit. Geometries of a microtron beam transport system are possible that make these steps equal to one-half or one-third of the energy gain per orbit. Variation between steps then requires a rather small percentage variation in the excitation of the magnetic elments in the microtron beam transport system and accelerating structure. It is also possible to extract several beam energies simultaneously, by extracting portions of the

beam from different orbits. The macroscopic time structure of the extracted beam is smooth, with a microscopic structure corresponding to the rf acceleration frequency.

To date, one 60-MeV and two 100-MeV pulsed racetrack microtrons have been built and operated successfully. Four CW racetrack microtrons, ranging in energy from 18 to 200 MeV, have also been built and operated successfully, albeit with lower currents than are being considered here. However, because the orbits become very long in multi-GeV microtrons, position tolerances and requirements for the magnetic field quality in the transport system are severe (despite the possibility of steering on each orbit). Therefore, the application of this technique to the multi-GeV energy range is an extension of current accelerator technology and will require a considerable engineering effort.

LINEAR ACCELERATOR/STORAGE RING SYSTEM

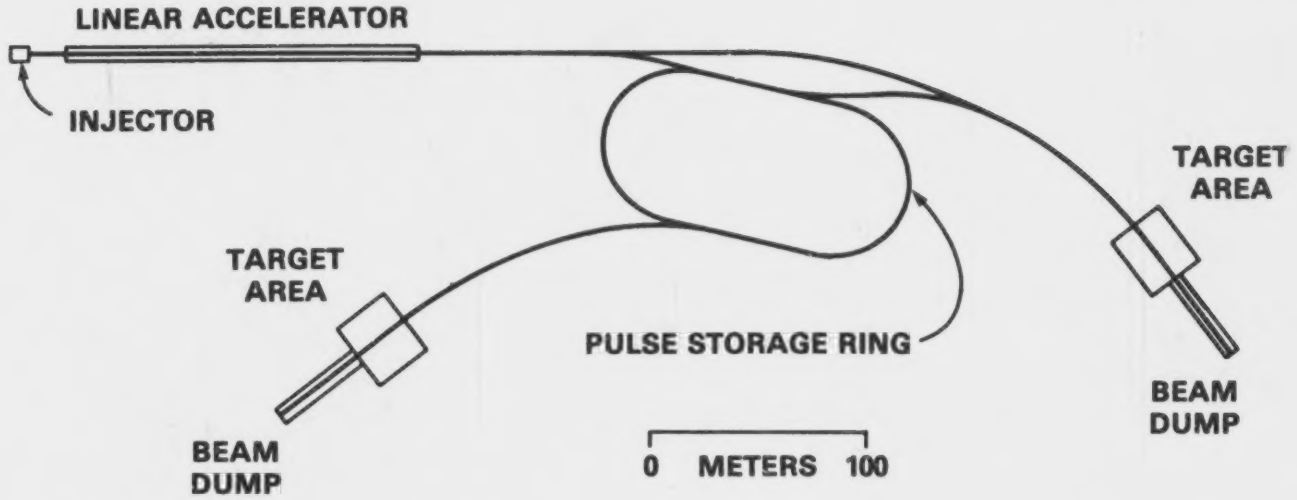

977

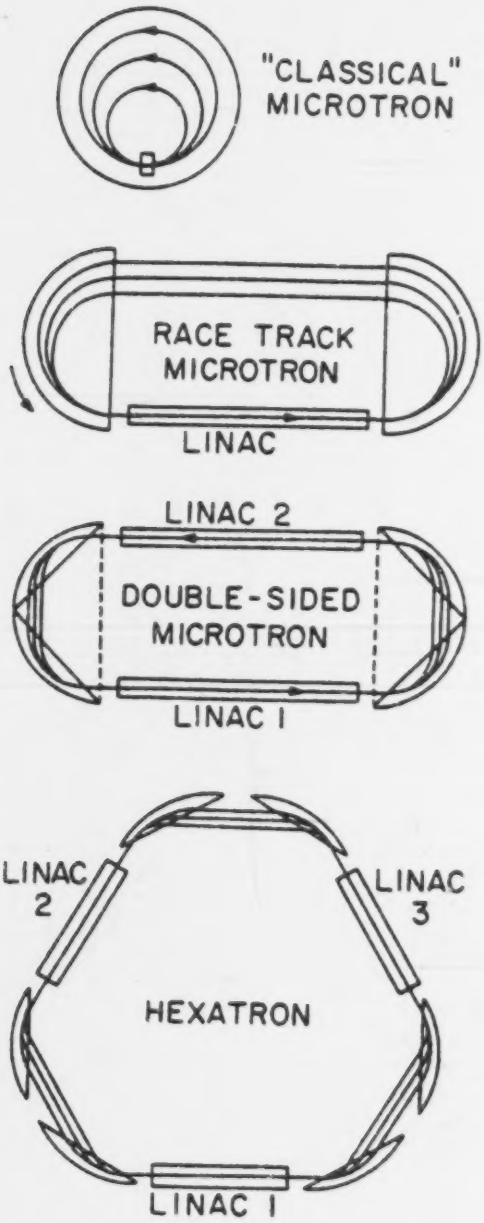

EVOLUTION OF THE MICROTRON

IV-B TABULAR COMPARISON OF PROPOSED ACCELERATOR SYSTEMS, COSTS AND STAFFING LEVELS

To facilitate the evaluation of the five proposals considered by the Panel, we include in this section comparative tables. These tables are largely self-explanatory; they were prepared from material that was included in the proposals themselves, provided by the proposing groups during oral presentations or in response to Panel requests, or, where indicated by appropriate footnotes, developed by the Panel on the basis of its own studies and analyses of the proposals. For example, the Panel has concluded in several instances that inadequate provision was made in the proposals for R&D required prior to the initiation of actual accelerator construction. Appropriate cost increases to cover such recommended R&D (discussed in greater detail below) have been estimated by the Panel and added where indicated in the tables.

For each proposal, the construction costs and annual operating costs are summarized in Tables IV-B-1 and IV-B-2, respectively. All cost data are in FY1983 dollars and must be inflated appropriately for "actual-year" dollars. The proposals are shown in alphabetical order throughout, and a 4-GeV future option for MIT-Bates has been incorporated for reference.

In Table IV-B-1, lines 1-9 reflect the construction costs quoted in the proposal; line 10 shows the manpower requirements quoted by each institution. Lines 4a, 6a, and 8a reflect the additional contingency, R&D, and experimental equipment, respectively, recommended by the Panel. These are included in lines 5a, 7a, and 9a, which correspond to the modified total estimated cost (TEC), total project cost (TPC), and the TPC plus experimental equipment, respectively. Line 9a, therefore, is the total cost that must be requested for construction of a particular facility. Note that the relatively high additional contingency in the SURA column reflects the financial needs arising from: (1) creating a new laboratory; and (2) the substantial additional st' ffing needed for the facility and the related potential time delay.

Table IV-B-2 reflects the annual operating costs of the various proposed facilities. There were numerous discussions between the various groups and the Technical Subpanel, and hence the costs shown here should reflect a fairly accurate and mutually accepted picture. Line 5a (additional capital improvements) has been recommended by the Panel to keep the experimental equipment up-to-date consistent with the standards of a National Facility.

Table IV-B-3 provides estimates of the 15-year total project cost and the initial experimental equipment cost, based on material in Tables IV-B-1 and IV-B-2. There is no new information in Table IV-B-3, but the costs have been combined to facilitate comparison.

The tabular comparisons of the accelerators themselves reflect the data presented in the individual proposals. Summaries of the most salient characteristics of the accelerators and the linac-rf systems are given in Tables IV-B-4 and IV-B-5, respectively. To understand the more intricate details, such as future flexibility, variation in parameters, and interrelation of experimental areas, the original proposals should be studied.

Table IV-B-1 CONSTRUCTION COSTS①

Item	Argonne		Illinois	MIT-Bates			NBS		SURA	
	2 GeV	4 GeV	750 MeV	1 GeV	2 GeV	4 GeV	200 MeV②	1 GeV	2 GeV	4 GeV
1. Conventional construction	$16.2	$17.0	$4.5	$13.0	$23.9	$45.1	$0	$14.1	$26.4	$30.7
2. Accelerator system	48.8	59.4	17.1	5.6	19.1	57.4	0.2	9.8	22.6	41.1
3. Beam transport system	5.2	7.9	1.7	2.7	5.0	8.2	0.8	2.6	9.0	9.9
4. Contingency allowed overall	(20%)	(20%)	(20%)	(20%)	(20%)	(20%)	(20%)	(20%)	(25%)	(25%)
5. Total estimated cost (TEC) (includes contingency)	70.2	84.3	23.3	21.3	48.0	110.7	1.0	26.5	58.0	81.7
4a. Additional contingency recommended by Panel	6.0 (8%)	8.0 (9%)	2.5 (11%)	2.5 (12%)	10.0 (21%)	--	0	2.5 (9%)	10.0 (17%)	15.0 (18%)
5a. Modified TEC (5 + 4a)	76.2	92.3	25.8	23.8	58.0	--	1.0	29.0	68.0	96.7
6. R&D related to construction③	2.2	2.2	1.0	1.4	3.2	5.2	0	5.0	3.0	10.1
6a. Modified R&D recommended by Panel	10.2	16.0	3.5	4.4	8.2	--	0	8.5	7.0	15.1
7. Total project cost (TPC) (5 + 6)	72.4	86.5	24.3	22.7	51.2	115.9	1.0	31.5	61.0	91.8
7a. Modified TPC (5a + 6a)	86.4	108.3	29.3	28.2	66.2	--	1.0	37.5	75.0	111.8
8. Experimental equipment	21.4	21.4	8.0	9.3	24.4	44.4	3.5	20.2	--	12.3
8a. Modified experimental equipment recommended by Panel	25.0	35.0	10.0	10.0	25.0	--	3.5	10.0	25.0	35.0
9. TPC plus experimental equipment (7 + 8)	93.8	107.9	32.3	32.0	75.6	160.3	4.5	51.7	--	104.1
9a. Modified TPC plus modified experimental equipment (7a + 8a)	111.4	143.3	39.3	38.2	91.2	--	4.5④	47.5	100.0	146.8
10. Man-years needed to complete project④	340	414	251	114	290	579	--	141	341	514

① Cost estimates in FY1983 M$ (including EDIA)
② Incremental cost to convert RTM-1 into a nuclear physics research facility
③ Starting in FY1983
④ Including R&D effort; excluding contingency.

Table IV-B-2 ANNUAL OPERATING COSTS[1]

	Item	Argonne		Illinois	MIT-Bates			NBS		SURA	
		2 GeV	4 GeV	750 MeV	1 GeV	2 GeV	4 GeV	200 MeV[2]	1 GeV	2 GeV	4 GeV
1.	Direct personnel cost[3]	$6.0	$6.0	$1.9	$5.4	$5.9	$8.7	$0.4	$2.6	$5.5	$6.3
2.	Indirect costs	1.5	1.5	1.0	4.3	4.7	7.0	0.3	1.6	0[4]	0[4]
3.	Materials and services	3.0	3.0	0.6	2.4	2.7	4.1	0.3	0.7	3.2	3.2
4.	Electric power	1.7	3.6	0.7[5]	1.5	2.0	3.4	0	1.4[5]	1.9	3.6
5.	Capital improvements (AIP/GPP/CE)	2.4	2.4	0.5	3.0	4.2	6.5	0.4	2.9	2.5	3.0
5a.	Additional capital improvements recommended by Panel	1.0	2.0	0.5	0	0	0	0.1	1.0	1.0	2.0
6.	Total operating cost (1 through 5a)	15.6	18.5	5.2	16.6	19.5	29.7	1.5[6]	10.2	14.1	18.1
7.	Direct personnel, FTE[6]	153	153	83	180	204	297	--	75	160	184
8.	Indirect personnel, FTE	39	39	8	0[7]	0[7]	0[7]	--	30	0[7]	0[7]
9.	Total operating FTE	192	192	91	180	204	297	--	105	160	184
10.	PhD research-staff (in-house) FTE included in line 9	19	19	10	9	10	22	--	12	30	35
11.	Experimental-support FTE included in line 9	19	19	19	53	59	97	--	27	46	53

[1] Cost estimates in FY1983 M$.
[2] Incremental cost to operate RTM-1 as a nuclear physics research facility.
[3] Including fringe benefits; excluding indirect charges.
[4] Included in direct costs.
[5] Electric power costs will be paid by the institution.
[6] Number of personnel reporting to the project director.
[7] Included in direct personnel.

Table IV-B-3 FACILITIES COSTS (IN FY1983 M$) FOR 15 YEARS

	Argonne		Illinois	MIT-Bates			NBS		SURA	
Cost	2 GeV	4 GeV	750 MeV	1 GeV	2 GeV	4 GeV	200 MeV	1 GeV	2 GeV	4 GeV
Total project cost plus initial experimental equipment (modified)①	111.4	143.3	39.3	38.2	91.2	160.3④	4.5	47.5	100.0	146.8
Total 15-year operating cost②	234.0	277.5	78.0	249.0	292.5	445.5	22.5	153.0	211.5	271.5
Total 15-year facilities cost	345.4	420.8	117.3	287.2	383.7	605.8	27.0	200.5	311.5	418.3

① From Table IV-B-1, line 9a.
② Not modified; from Table IV-B-1, line 9.
④ From Table IV-B-2, line 6 (× 15).

982

Table IV-B-4 ACCELERATOR CHARACTERISTICS

	Argonne	Illinois	MIT-Bates	NBS	SURA
Type of accelerator	Hexatron microtron fed by racetrack microtron	3 - Stage cascade racetrack microtron	Linac recirculator and pulse stretcher ring	2 - Stage cascade racetrack microtron	Linac recirculator and pulse stretcher ring
Maximum number of recirculations	RTM: 27 Hexatron: 37	RTM-1: 17 RTM-2: 29 RTM-3: 80	Phase 1: 2 Phase 2: 5 Phase 3: 5	RTM-1: 16 RTM-2: 87	2
Duty cycle (beam)	100%	100%	80%	100%	>90%
Output beam energy	RTM: 185 MeV RTM + Hexatron: 500-4000 MeV①	RTM-1: 22 MeV RTM-1 + 2: 83.3-183.3 MeV RTM-1 + 2 + 3: 750 MeV②	Phase 1: 50-1000 MeV Phase 2: 50-2000 MeV Phase 3: 50-4000 MeV③	RTM-1: 15-200 MeV RTM-1 + 2: 200-1000 MeV	500-4150 MeV④
Average beam current	Hexatron: 300 μA	RTM-1 + 2 + 3: 100 μA	Phase 1: 140 μA⑤ Phase 2: 140 μA⑤ Phase 3: 140 μA③,⑤	RTM-1 + 2: 300 μA	Phase 1A: 360 Hz, 278 mA, 120 μA Phase 1B: 1000 Hz, 200 mA, 240 μA③ Phase 2: 720 Hz, 278 mA, 240 μA③
$\Delta E/E$	10^{-4}	10^{-4}	10^{-3}	RTM-1 + 2: 7×10^{-5}	$<10^{-3}$
Beam emittance (at maximum energy)	Vertical: 0.06 π mm mrad Horizontal: 0.15 π mm mrad	0.01 π mm mrad	0.1 π mm mrad	RTM-1 + 2: 0.01 π mm mrad	Vertical: <0.1 π mm mrad Horizontal: 0.3 π mm mrad
Microstructure of beam	0.80 or 2.40 GHz	0.82 or 2.45 GHz	2.856 GHz	0.793 or 2.38 GHz	714 MHz
Beams available	3 CW beams with 2 independently adjustable energies from 0.5 to 4.0 GeV and 0 to 100 μA	Up to 3 CW primary beams of same energy, independently adjustable in current; parasitic beam for tagged-photon experiments	Phase 1 + 2: 1 CW beam; 1 photon beam④ Phase 3: 2 CW beams of different energies; 1 photon beam④	RTM-1 + 2: up to 3 simultaneous beams of different currents: 2 beams up to 200 MeV, 1 beam up to 1 GeV RTM-1: 3 beams up to 200 MeV	2 CW beams of same energy from pulse stretcher ring, 1 photon beam④
Magnetic field in end magnet	RTM: 1.005 T Hexatron: 1.015 T	RTM-1: 0.171 T RTM-2: 0.95 T RTM-3: 1.425 T	--	RTM-1: 1.0 T RTM-2: 1.58 T	--
Number of experimental areas	3	5	9	5 (2 at high energy)	3

① Argonne has also described a 2-GeV option that would have fewer linac sections and klystrons and use less linac and magnet power.
② Lower energies are available by using fewer recirculations.
③ Possible future capability.
④ SURA has also proposed a phased construction program with 2-, 4-, and 6-GeV phases.
⑤ These currents are maximum per beam; the facility current is typically 225 μA.
⑥ The high-intensity pulsed beam from the accelerator with independent energy and intensity can also be used directly.

Table IV-B-5 LINAC-RF SYSTEMS

	Argonne	Illinois	MIT-Bates	NBS	SURA
Linac structure	On-axis coupled[1] (similar to Mainz)	On-axis coupled[1] (similar to Mainz)	Traveling-wave ($2\pi/3$ mode, approx. constant gradient)	Side-coupled (fabricated by LANL)	Traveling-wave ($2\pi/3$ mode, constant gradient)
Frequency	2.40 GHz	2.45 GHz	2.856 GHz	2.38 GHz	2.856 GHz
Beam aperture	1.2 cm	1.4 cm	~2.0 cm (with protection collimator)	1.0 cm	~2.0 cm (with protection collimator)
Shunt impedance	75 MΩ/m	67 MΩ/m	48-58 MΩ/m	82.5 MΩ/m	53-60 MΩ/m
Accelerating gradient	1.54 MV/m at 52 kW/m[2]	1 MV/m at 22 kW/m[2]	~3 MV/m at 40 mA peak beam current	RTM-1: 1.5 MV/m at ~40 kW/m[2] RTM-2: 1.25 MV/m at ~56 kW/m[2]	~19 MV/m at 200 mA peak beam current
Accelerator length	RTM: ~4.5 m Hexatron: 3 linacs, each 25 m long	RTM-1: 1.0 m RTM-2: 5.9 m RTM-3: 8.8 m	Phase 1 + 2: 160 m Phase 3: 270 m	RTM-1: 8 m RTM-2: 8 m	171 m (incl. injector)
RF power source	78 50-kW klystrons (CW)[3]	10 50-kW klystrons (CW)[3]	Phase 1 + 2: 12 5.3-MW pk., 100-kW av. klystrons[4] Phase 3: 21 5.3-MW pk., 100-kW av. klystrons	2 500-kW klystrons (CW)[5]	40 40-MW-peak klystrons[6] Phase 1A: 46 kW av. (360 pps) Phase 1B: 128 kW av. (1000 pps) Phase 2: 92 kW av. (720 pps)

[1] If one of the alterrative structures now under development proves to be superior, it will be used.
[2] Approximately 1/3 to 1/2 of this power is dissipated in the cavities; beam loading consumes the remaining fraction.
[3] Thompson/CSF TH-2075
[4] Varian VA-938
[5] Varian VKS-8270
[6] Similar to SLAC klystrons but with up to 3.2 times higher average power capability.

984

IV-C. DISCUSSION AND CRITIQUE OF PROPOSALS

IV-C.1 Argonne National Laboratory

IV-C.1.1 Concept and Theoretical Analysis

The Argonne Hexatron is a modification of the conventional racetrack microtron (RTM) that allows the microtron concept to be extended to energies not previously considered possible. The design permits a very high energy gain per turn (105 MeV) and a large orbit separation (17 cm) without requiring an accelerating mode number greater than 1, long accelerating field wavelengths, or unreasonably high dipole fields in the microtron beam transport system. The proposed design provides the simultaneous capability of two independent extraction energies from the Hexatron plus a third extraction energy whose value is constrained by the energy gain per orbit and the synchrotron tune. The energy of this third beam can assume values between the injection energy and the maximum beam energy, but with approximately a 500-MeV grid. Finally, the geometry of the Hexatron allows it to be assembled in the existing ZGS ring tunnel; this results in a saving in conventional construction costs. A summary of the machine characteristics can be found in Table IV-B-4.

The size of the Hexatron raises questions as to whether currently feasible guide-field and position tolerances are adequate. The orbit dynamics and components of the Hexatron have been the subjects of studies during the past two years; these studies indicate that guide-field uniformity and position tolerances are marginally state-of-the-art. This is a consequence of the Hexatron geometry, which requires strong focusing but allows the dipoles to operate at the modest field of 1.0 T and allows the beam to reach full energy in only 37 orbits at an accelerating mode number of n=1.

Given that the required field uniformity, in the absence of steering, scales as N^{-2} (where N is the number of orbits), the fields of the 37-orbit Hexatron, despite its size, will in principle not be appreciably more difficult to trim acceptably than those of a conventional RTM with 80 orbits. The large orbit separation (compared with the dipole magnet gap) means that the dipole-edge treatment aimed at achieving exit angles of 90° may be successful. The results of initial computer simulations and magnet modeling are encouraging. The large orbit separation also allows the installation of steering elements to reduce beam-position error.

The effect of quantized synchrotron radiation emission has received intensive study. This is an important effect above 3.5 GeV and may require the use of a larger-bore accelerating structure with lower shunt impedance; the implications of this requirement are still being evaluated. The Hexatron is designed for a maximum energy of 4 GeV, but it would have serious problems of linac aperture demand above 4 GeV because of emittance growth due to quantized synchrotron radiation emission. However, recent high-power tests with side-coupled linac structures have demonstrated that a larger-bore accelerating structure might be feasible.

There are other areas of concern as well. Position tolerances (specified at ± 0.1 mm) may be met initially, but the question remains as to whether they can be maintained against changed in ambient temperature and settling of the foundations. These alignment uncertainties and synchrotron radiation effects give rise to concern as to whether 1.2-cm-diameter beam apertures will be adequate for all 37 orbits. At the power level of the beam in this machine, the damage that it could do to the expensive accelerating

structures would be impressive if no aperture-defining collimators were used. The large number of corrective elements raises questions of machine control and the attendant question of the need for an adequate algorithm for machine operation. Thus, although it is an innovative design, the Hexatron represents a challenging and difficult engineering project.

Argonne seems to have a good and enthusiastic engineering group, which, however, appears to have limited exchanges with those of other laboratories. They are aware of the most important difficulties of their design and are now trying to assess the magnitude of these problems.

The success of this project depends very strongly on the quality and ingenuity of the engineering staff, as well as on the quality and completeness of the correction schemes for alignment and orbit corrections of the accelerator. Unfortunately, if the necessary tolerances cannot be achieved or if the errors cannot be sufficiently corrected, the performance will suffer substantially.

The first stages of the Argonne proposal consist of a linear accelerator to reach 23 MeV and a racetrack microtron to reach 185 MeV. These are rather straightforward designs and should not pose much of a problem.

The Hexatron design is the portion of the proposal that requires the most theoretical study. The Argonne group has already completed much of the theoretical work and has studied questions of tolerances and correction schemes. The difficulty of achieving the necessary magnetic field tolerances is one of the problems facing the Hexatron designers. Theoretical studies have been performed for field errors of $|\Delta B/B| < 10^{-4}$, alignment errors of $|\Delta x| \leq 100\ \mu$m, and rotational errors of $|\Delta\theta| \leq 400\ \mu$rad. It was found that the resulting orbit distortions of a few centimeters could be corrected down to a few millimeters by means of three measuring devices and three correcting magnets per turn. Studies with errors three times larger suggest that they can be corrected for, especially if a larger linac aperture is chosen. More studies are needed, however, before one can fully determine the limits.

Higher-order optics calculations have also been performed for the case of no field errors for the 220-MeV beam orbit. In general, the theoretical problems are being worked on in the proper order and the group is continuing along the appropriate path to perform the remaining required calculations. In particular, many of the effects have been calculated for the "perfect" accelerator but remain to be calculated for the accelerator when errors are present.

IV-C.1.2 Prior R&D Assessment, Technical

The construction-related R&D costs for this project total $2.2 M, or 1.7% of the total (4-GeV) construction cost. Included in this amount are PE&D funds for the accelerator and funds for the design of a superferric magnet-based spectrometer. Although no R&D funds for rf cavity technology are included in the Argonne proposal, ongoing effort in this area is being supported by the joint NBS/LANL accelerator research program. In addition, R&D on sector-magnet design is being supported through separate ANL Program Development Funds. During the period covering FY1980-FY1983, funds have been provided as follows:

Fiscal Year	Amount (K$)	Fiscal Year	Amount (K$)
1980	160	1982	600
1981	520	1983	900

It is the recommendation of the Panel that an additional $13.8 M of R&D funds be used in support of this project. Particular areas to be covered should include:

RF structures (continuing collaboration with LANL)
Model magnet and prototype magnet design
Orbit tracking with measured edge fields and error spectrum
Extraction techniques to permit continuous energy variation
Beam breakup effects with multiple off-axis beams

IV-C.1.3 Technical Components

Linac structures are required for the 23-MeV injector, the 185-MeV RTM, and the 4-GeV Hexatron microtron. Each of these will use an identical biperiodic on-axis coupled structure that is similar to the Mainz design. The lengths of the linacs are 16 m (including capture, pre-accelerator, and accelerator sections of the injector), 4.5 m, and 3x25 m, respectively. As shown in Table IV-B-5, these structures operate at 2.40 GHz, have a beam aperture of 1.2 cm, and a shunt impedance of 75 MΩ/m. There is some concern that the relatively high rf input power (35.2 kW/m for the accelerating fields and 16.8 kW/m for beam loading) will cause detuning of the accelerator cavities and possible frequency separation of the main and coupling cavities of the on-axis coupled structure.

The Argonne group is also considering the use of a side-coupled structure being developed at Los Alamos; they will use that structure if further tests show that it has characteristics superior to those of the on-axis coupled structure. During recent high-power tests of a 1-cm-diameter side-coupled structure at a power level of 32 kW/m and an accelerating field of 1.6 MV/m, no detuning was observed. The cell-to-cell coupling of 4.7% observed in the Los Alamos prototype is adequate for the 2.06-m sections of the Hexatron design, and no modifications of the proposed rf power distribution system are necessary.

The accelerating structures for each of the three linacs of the Hexatron will consist of 11 2.06-m sections. Space is available to add two cells to each section, thereby decreasing the accelerating gradient and power dissipation per unit length, should this prove necessary.

The rf power to the accelerator structures will be provided by 78 50-kW Thompson/CSF TH-2075 klystrons. These tubes are well-proven commercial models with an efficiency of 62% and a lifetime of over 20,000 hours. In the Hexatron, the output of two such klystrons will be combined to feed each 2.06-m accelerating structure.

Probably the most critical design questions associated with the Hexatron have to do with the six sector magnets. The steel yoke and pole pieces for each of these magnets

weigh 673 tons. Each magnet with its power supply and control system will cost approximately $2M. The pole edge of each sector magnet is provided with steps for the first 14 low-energy orbits in order to achieve a beam incidence approximately normal to the field boundary; the remainder of the pole edge is straight. This design is intended to avoid strong vertical defocusing forces resulting from oblique incidence, particularly at low energies. Calculations and measurements at Argonne indicate that the effective edge-field contour of the stepped edge is perpendicular to the beam to within 2°.

The magnetic field integral along each beam orbit must be held constant to within one part in 10^4. Orbit-to-orbit fluctuations of the field integral will induce synchrotron oscillations and increase beam-energy spread. Fluctuations are caused mainly by two factors: (1) errors in the central field strength; and (2) the "softness" of the field edge. Variations in the central field can, in principle, be corrected by means of Purcell filters plus other passive (steel shims, etc.) and/or active (pole-face coils) elements to achieve the desired uniformity. In the Argonne design, the field profile is hardened by the use of magnetic shims along the pole edge and on the inner edge of the pole guard. In addition, magnetic shields are placed between the upper and lower end guards in the regions where the step edges run parallel to the neighboring beam orbits. Measurements indicate that these techniques produce a field that falls off faster than the Enge short-tail edge, for which beam containment has been demonstrated by other calculations.

Despite the apparent success of the sector-magnet design (demonstrated to date by 2-dimensional TRIM calculations and 3-dimensional calculations using steel elements of infinite permeability, as well as by measurements made on a one-step, 2/3-scale-model magnet), the complete achievement of the design field distribution remains to be demonstrated. Argonne has recently begun further studies of the magnet's properties using the Rutherford Laboratory program TOSCA, which performs 3-dimensional magnetostatic field calculations using steel elments with variable permeability. In addition, a 3-orbit prototype of the magnet is being built and will be ready for testing in May, 1983. The results are expected to demonstrate conclusively whether or not the sector-magnet design is satisfactory for its intended use in the Hexatron.

IV-C.1.4 Conventional Facilities

The accelerators, auxiliary equipment, and associated experimental areas would be housed in existing buildings at Argonne. Most of these facilities were used in connection with the now-dismantled ZGS accelerator. Replacement cost of these facilities has been estimated by Argonne to be in excess of $50 M. Their value to the proposed project is undoubtedly less than this amount, because some of the facilities could be built at reduced cost if they were to be designed for the specific needs of the new project. Nevertheless, the availability of these facilities is a great asset to the Argonne proposal.

The principal cost of conventional facilities for the proposed project is for modifications to the existing facilities to make them suitable for housing the Hexatron and the RTM, experimental equipment, and data collection rooms. Three separate experimental areas are planned, each suitable for electron beams of 100 μA in intensity and 4 GeV in energy.

In addition to the buildings, approximately 50 MW of power is available at nearby substations, and 50 MW of water-cooling capacity is also available. These utility capacities are far in excess of the needs of the proposed project ($\sim$14.5 MW). It is estimated that the existing air-conditioning capacity is sufficient for the Hexatron. Ample radia-

tion shielding is also available in the ZGS ring building, the walls of which are constructed of 3.5-ft-thick concrete. Three overhead cranes of 20-ton, 20-ton, and 50-ton capacity are available in the ring building. A control room and many cable trays also exist.

Other required conventional-facilities work entails the construction of beam-line tunnels from the Hexatron to the three experimental areas. The total cost of all conventional-facility modifications and new construction (including EDIA and contingency) is $17.0 M in FY1983 dollars.

IV-C.1.5 Special Situations

A very important "special situation" at Argonne is the availability of numerous buildings and facilities as a result of the dismantling of the ZGS accelerator. These facilities can be used for the proposed project, following necessary modifications that can be made at a small fraction (~15%) of the cost of completely new facilities.

A further asset for Argonne is the availability of a trained design staff and a project management team that is already in place and functioning. Numerous user support services are available, including machine shops, a plastics shop, electronics services, engineering services and graphic arts, computing services, library services, rigging services, an occupational health and safety staff, and a multidisciplinary research staff. Among the general site services provided are fire protection, paramedics, plant security, grounds maintenance, a travel office, and a health and medical office.

Argonne is a half-hour from O'Hare Airport, which provides frequent service to every major airport in the country. The Laboratory has a cafeteria and a visitors' lodging facility that has 112 rooms and apartments on-site.

IV-C.1.6 Capability Assessment

The Argonne group includes a number of senior accelerator physicists and engineers having, collectively, considerable experience. Expansion to the planned level of construction manpower should thus be straightforward. In addition, the project management structure is in place, with H.E. Jackson designated as Project Director and R. Kustom as Associate Project Director.

Besides the present project staff, Argonne National Laboratory has experienced accelerator personnel presently engaged in various areas; this additional staff may be needed, because the Hexatron constitutes a significant technical challenge. The ability to interface with future user group could be strengthened. It appears that the Laboratory management is fully committed to this project and will take the necessary steps to maximize its chances for success.

Further work is in progress on the mechanics of beam extraction from the Hexatron. Basic numerical studies have been carried out that show the feasibility of continuous energy variation (by discrete small steps) of the extracted beam.

Attention is being given to the possibility of regenerative beam breakup, and known scaling laws are being used to compare with operating microtrons elsewhwere. In particular, recent experimental tests carried out in Mainz indicate that regenerative beam breakup should not be a problem for the beam current levels contemplated for the Hexatron. Assuming that the construction commitment is received by January 1, 1985,

there remains a period of 18 months to complete the essential preconstruction R&D work. This is adequate for refining responses to remaining design and technical questions and to prepare for Title I design work.

Support structures for the Hexatron construction project are fully in place, including not only procurement, library, and general laboratory housekeeping organizations, but also substantial shop facilities (mechanical, electronics, plastics) and a superconducting technology group experienced in magnet construction (of direct relevance to spectrometer magnet construction).

The stated duration of construction, 4.5 years, reflects a realistic schedule that includes the period of time available for completing pre-construction R&D work. The group is ready to take on this project from both organizational and skilled-personnel points of view.

IV-C.2 University of Illinois

IV-C.2.1 Concept and Theoretical Analysis

This system consists of three racetrack microtrons (RTMs) operating in cascade. Energy gains — variable at each stage — are limited to factors of less than 10, and the mode number of each stage is n=1. The energy variability of the three stages allows a considerable range of output energies with virtually no retuning of the last stage. Although only one output energy can be obtained at a time, the output beam can be split into three components with high efficiency and can thus serve three experimental halls simultaneously. Another (independent) beam with an energy that is variable between 83 and 183 MeV could be obtained with the addition of a second rf beam splitter between the second- and third-stage microtrons. A summary of the machine characteristics can be found in Table IV-B-4.

Orbit dynamics studies have been carried to an adequate stage of completeness. All components of the system have been studied, and in some cases modeled, either at the University of Illinois or at other laboratories. No technological weakness were found. This is a carefully worked out, conservative design that should achieve its goals. One disadvantage of this design, however, is that it does not allow for energy expansion without considerable redesign or the use of additional microtron stages.

The Illinois group has benefitted from its extensive experience in the design and operation of racetrack microtrons and from close contact with the Mainz and NBS/LANL groups. In making the transition from their present 80-MeV microtron using a superconducting linac to the 750-MeV cascaded microtron of their proposal, they have chosen to incorporate in their design many of the subelements developed at Mainz and NBS/LANL.

IV-C.2.2 Prior R&D Assessment, Technical

There are several areas on which the Illinois group should place R&D emphasis. The work in progress on linac structures will have to be extended substantially. Fortunately, the group should be able to rely at least partially on the results of LANL R&D studies in ths area. Further work in particle tracking should also be undertaken, with inclusion of the full spectrum of errors.

Planned R&D efforts are broken down as follows:

Task	Effort (man-years)
Linac fabrication	10
RF separator system	5
Microtron magnets	2
Microtron optics	5
Spectrometer design	2
	24

Funding for the above construction-related R&D effort is not part of the University of Illinois proposal. The intent is to fund the work (24 man-years, costing $960 K) through the utilization of some of the laboratory's present operating budget.

In terms of the total construction budget of $35.8 M, the $1.0 M for R&D (2.8% of the total cost) is too low. We suggest that a more realistic assessment of R&D costs would raise them to at least 9.8% of the construction cost, or approximately $3.5 M. In addition to placing emphasis on the topics described above, the R&D efforts should include work on the accelerator rf and control systems.

IV-C.2.3 Technical Components

All three stages of the 750-MeV RTM would use room-temperature, on-axis-coupled accelerator structures similar to those used in MAMI-1 and MAMI-2 at Mainz. These well-proven structures have a shunt impedance of 67 MΩ/m and provide an accelerating gradient of 1 MV/m when powered at a level of 15 kW/m. Altogether, the accelerator requires about 20 m of on-axiscoupled structure, mainly in modules about 2m in length. If a superior accelerator structure results from any of the R&D programs now under way at various laboratories, the improved structure could be used; however, the Mainz structure would fully satisfy the beam specifications of the proposed accelerator. Included in the 20 m of on-axis structure required for the cascaded microtron system are a 2-MeV capture section and a 2.5-MeV preaccelerator section that combine to inject a 4.5-MeV beam into the first microtron stage. Table IV-B-5 gives a summary of the linac-rf system characteristics for the proposed accelerator compared with those for the other proposals being considered.

Radio frequency power for the linac structures will be provided by 10, 50-kW CW klystrons (Thompson/CSF TH-2075), each of which will supply power to a single 2-m linac module. These are well-proven commercial tubes with high efficiency (~62%) and long lifetime (over 20,000 hours); they are a good match for the proposed application.

Because of its high cost and critical performance requirements, the power supply system for the Thompson/CSF TH-2075 klystron is one of the most important subsystems of the accelerator. Each of the 10 klystrons requires a 25-kV beam voltage at 3.2 A. With the help of a commercial supplier, the University of Illinois group has developed a preliminary design of the power supply system in which each power supply module will supply three klystrons. Each klystron will be connected to the power supply through a series regulator that will provide 0.1% regulation, current limiting, and fault protection. This design appears to be well conceived and cost-effective. A detailed design study, in collaboration with the Argonne group, is currently in progress.

Other important accelerator systems include the temperature regulation system for the linac, the beam diagnostic devices, and the computer control system. Conceptual designs of these systems have been completed and seem quite adequate for the intended purposes. Much detailed design remains to be done, however.

IV-C.2.4 Conventional Facilities

The University of Illinois proposal includes requests for the following new buildings and site improvements:

Item	Cost (FY1983 K$)
Site development	582
Accelerator vault	1096
Annex building for cooling, power distribution, and klystron power	644
New experimental hall	1143
Beam transport tunnel	242
Modifications to existing experimental hall	70
	3777

The above costs were estimated by architectural and engineering consultants and include EDIA costs but not contingencies; these estimates appear to be reasonable.

IV-C.2.5 Special Situations

The University of Illinois has agreed to contribute an estimated $2 M toward the construction of the proposed facility by limiting its annual collection of indirect costs (for the 5-year period of construction) to the amount received in 1979. In addition, the University has a policy of not including electric power costs as a direct charge to research programs; this policy will save about $750 K/year in operating costs. Finally, the Illinois group intends to provide $8.8 M of the total construction cost and $960 K of the R&D cost by redirecting funds from the operating budget of their present facility during the construction of the new facility.

The physical plant of the existing Nuclear Physics Laboratory (NPL) would be available for the proposed program. Its estimated replacement value is $10.25 M in FY1983 dollars.

Additional available facilities and equipment include the NPL machine shop and electronics shop, related Physics Department facilities, various equipment items from MUSL-2, data acquisition computers (worth approximately $400 K), electronics pool equipment (worth $500-750 K), and existing experimental equipment.

For specialized operations or temporary overloads beyond the resources of the facilities listed above, the new laboratory would have access to various shops within the College of Engineering and other departments of the University.

In addition, a University network of five computers is maintained by the Computer Services Organization and would be available at normal University rates to researchers at the proposed accelerator. The University also has a large library system, including several branch libraries; a nuclear research library is maintained in the NPL site.

Through its indirect budget and/or state funds, the University provides various services and facilities including a business office, a print shop, maintenance of buildings and grounds, janitorial services, utilities, security, fire protection, emergency medical care, safety services, and conference planning and facilities.

The Illinois group is planning two additions to the accelerator facility for user-laboratory, set-up, and office space. The added space would come to 19,000 ft^2 at a total cost of about $900 K. It is likely that the University will contribute a significant fraction of this cost.

Housing, travel facilities, motels, and restaurants are plentiful and convenient to the laboratory. Moreover, the University has agreed to make several of its nearby houses available at modest cost to users for extended visits or to user groups for short visits.

IV-C.2.6 Capability Assessment

Because the cascaded microtrons proposed here do not constitute a significant extrapolation of known technology and because considerable experience exists locally in the construction of experimental hardware, detectors, electronics, etc., there should be little problem in carrying out the construction objectives. A core group of accelerator physicists and nuclear physics experimentalists is in place; with this, enhancement of the staff to the planned level for construction should be straight-forward.

Until recently the preconstruction project management was carried by Professors P. Axel and L. Cardman. The unfortunate death of Professor Axel leaves a leading position unfilled. University search procedures that will result in the appointment of a leading nuclear experimentalist are already under way. Professor Cardman will continue to carry the responsibility for the technical direction of the preconstruction R&D and will subsequently provide the technical direction for construction and operation of the new facility.

Because the design of the cascaded microtrons makes use of linear accelerator structures with modest gradient values (1 MV/m), proven on-axis-coupled accelerator cavities can be used. Collaborations with Chalk Rvier and LANL are in progress, however, and more efficient structures with higher acceleration gradients may be used if appropriate. This issue will certainly be resolved by the time construction begins. Other R&D issues are of a "routine" preconstruction nature (rf separator, microtron magnet, microtron optics, and spectrometer studies) and do not involve critical construction issues.

The basic support organization, in terms of shops, procurement, general laboratory housekeeping, etc., is well established at the Nuclear Physics Laboratory. Consequently, when construction begins there should be no delays associated with the peripheral but essential support structure.

A concern of the Panel is that the existing group has limited experience in managing a project of the magnitude being proposed here. Although the present staff is enthusiastic, bright, and energetic, they are too few in number. The University of Illinois proposes to add 20 people, including seven permanent staff scientists, to the laboratory during the construction phase. An additional eight persons would be added when the new facility becomes operational. The University is committed to maintaining the nine tenured and tenure-track positions currently held by experimental nuclear scientists in the Physics Department. also, the nuclear theory group at Illinois has been augmented by the recent offer of an incremental tenure-track position.

The proposed time scale for construction of this project is 5 years. Based on the present staffing levels, the proposed manpower increments, and the present state of readiness to begin this construction project, it appears that this time scale is realistic.

IV-C.3 Massachusetts Institute of Technology - Bates Laboratory

IV-C.3.1 Concept and Theoretical Analysis

This proposal describes a phased system development based on the existing MIT-Bates 400-MeV, 1.8%-duty-cycle linac and the 720-MeV single-turn recirculator (soon to be upgraded to 462 MeV and 840 MeV, respectively). A further upgrade of the rf system (requiring additional operating funds to refurbish all the klystrons and switchtubes) is being considered that could increase the maximum energy of the recirculated beam to 1080 MeV (unloaded). In Phase 1, the linac (after its energy upgrade) will be used to inject into a 300-m circumference stretcher ring. At this point the system will be capable of providing 300-1080 MeV CW electron beams to the experimental areas now in use at the Bates Laboratory.

For Phase 2, four additional recirculator paths are to be built. Each pass of the five-pass recirculator system travels in its own return transport line. The lengths of these lines are closely matched to the injected-beam pulse length so that the recirculation through the linac is "head-to-tail", in contrast to both the present recirculator scheme and a microtron, where all passes are present in the linac simultaneously. Beams can be switched on a pulse-to-pulse basis (1000 Hz), either to the present recirculator for subsequent transport to the existing experimental areas or to the new recirculator and then to the pulse stretcher ring. Characteristics of the proposed accelerator are summarized in Table IV-B-4.

The beam actually makes five passes through the linac. Thus, for example, at a nominal energy gain of 0.4 GeV, it will be possible to provide 2.0-GeV elctrons to the stretcher ring. The system is expandable in energy by the addition of a 4-GeV storage ring and enough additional linac accelerating structures and rf power to bring the single-pass energy up to 828 MeV (fully loaded).

The design of this system is at present largely conceptual, although the existing single-pass recirculator represents a substantial R&D effort toward the design of the proposed five-pass recirculator. Only modest amounts of R&D on the stretcher ring have been done. It is therefore difficult at this time to make more than general comments and point out possible problem areas. The most serious potential difficulty involves the question of whether the linac will be free from beam-breakup instabilities when operating in the head-to-tail recirculation mode fully loaded. It is not yet possible to calculate this with any certainty. However, empirical tests and use of the Helm-Loew-Panofsky scaling law suggest that the beam-breakup threshold for 2-GeV operation will be above 40 mA.

The proposed three-turn injection scheme inherently leads to a larger transverse phase space in the stretcher ring. However, the use of a properly designed one-third-integer extraction scheme should minimize the loss of beam quality in the external beam. Open-loop operation of the extraction system is proposed, but this slow extraction system may have to include feedback in order to achieve satisfactory intensity-versus-time behavior. This technique has been demonstrated on proton machines, but on much longer (three orders of magnitude) time scales. The time delays inherent in the resonant growth of particle motion that are to be exploited for slow extraction restrict the bandpass of such servo loops to at most a few kilohertz, thereby limiting the efficacy of the feedback system.

The effects of the various transverse and longitudinal instabilities that traditionally plague high-current electron storage rings have not yet been analyzed. These depend quite sensitively on the details of the vacuum chamber envelope and the rf cavity system, which are not available at this time. It is reasonable to state, however, that the high-frequency rf system now proposed (chosen to have the same frequency as that of the linac) will exacerbate any tendency toward longitudinal and transverse instabilities. The instabilities can limit stored beam current and degrade beam quality, thus reducing the performance of the ring as a beam stretcher. In the area of ring instabilities, the MIT-Bates group has relied to a certain extent on the theoretical work of the SURA group. This is clearly only an approximation for those aspects where their design differs from the SURA design.

The MIT-Bates group has designed its low-energy stretcher-ring lattice around surplus Princeton-Penn Accelerator magnets; it is not clear what constraints this implies.

The effects of nonlinear elements in both the transport system and the stretcher ring have been studied in the absence of errors. The effects of errors on the particle dynamics have not been studied, either with or without nonlinearities.

The Bates group plans to use a 2.856-GHz rf system for the stretcher ring; therefore, coupled-bunch instabilities, higher-mode losses, etc., will be considerably different than for the 717-MHz system of SURA.

The success probability of this proposal will be difficult to assess until the design is finished. However, it is probably lower than that of SURA. For example, the average current at 2 GeV might be lower than the 100 μA specified, but it should be easy to reach several tens of microamperes.

IV-C.3.2 Prior R&D Assessment, Technical

In the MIT-Bates proposal, the construction-related R&D costs are \$1.4 M for Phase 1, \$3.2 M for Phase 2, and \$5.2 M for Phase 3. In terms of the construction costs for the three phases, these amounts correspond to 4.1%, 3.9%, and 3.4%, respectively. This level of R&D is insufficient for a project of this degree of difficulty, and the R&D funds should be increased to \$4.4 M in Phase 1 and \$8.2 M in Phase 2 to provide adequate studies of recirculation techniques (including beam breakup) and stretcher-ring design optimization. It will be necessary to add staff to support the increased level of R&D that the Panel suggests. Phase 3 is not well enough defined at this time to provide a basis for an R&D estimate by the Panel.

IV-C.3.3 Technical Components

The existing MIT-Bates accelerator utilizes a traveling-wave structure operating in the $2\pi/3$ mode at 2.856 GHz. To combat beam breakup, the various sections of the accelerator were designed with different HEM_{11} resonant characteristics along the machine in order to reduce the coherent length of the transverse deflecting mode. Thus, a constant $2\pi/3$ phase shift per cavity in the TM_{01} accelerating mode was maintained, but the HEM_{11} resonant frequencies were varied by suitable selection of the iris aperture and the diameter for each cavity. In this manner, a structure with an approximately constant gradient characteristic was achieved that has a high starting current for beam breakup. Because of the dimensional variations, the shunt impedance also varies and has a range of values between 48 and 58 MΩ/m in the accelerator structure. Parameters of the system are given in Table IV-B-5.

The present Bates accelerator has a maximum single-pass energy of about 400 MeV when powered by 10 4-MW peak (100-kW average) klystrons. Beam recirculation has been used to increase the maximum energy to about 720 MeV. The maximum energy will be further increased under present funding to approximately 840 MeV (unloaded) by adding another modulator and two more klystrons.

The mean time between failures (MTBF) of the klystrons has been about 60,000 hours over the last few years, which is excellent. In estimating operating costs, MIT has assumed a more conservative MTBF of 30,000 hours.

In Phase 2, the beam would be recirculated so as to pass through the accelerator five times and thus reach an energy of up to 2.5 GeV at low currents and 2.0 GeV at 100 μ A average current.

In Phase 3, the accelerator length would be increased by 360 ft by adding nine SLAC-type 40-ft girder assemblies, each of which would be powered by an added klystron. The resulting single-pass energy of the accelerator would be increased to 980 MeV unloaded or 830 MeV at 40 mA peak current. With five passes, the maximum output energy would be 4.82 GeV unloaded or 4.07 GeV at 40 mA.

Although the Bates accelerator undoubtedly has a high cumulative beam-breakup threshold, more tests are needed to determine both the maximum achievable value of the beam-breakup scaling variable and the appropriate value of the exponent, n, in the scaling equation that indicates how strongly beam breakup depends on the beam pulse length.

Considering the pressures due to ongoing operations and research programs, it is clear that the present staff would have to be augmented if any part of the new program were undertaken. MIT-Bates proposes an increase of 25 in project staff in FY1984 and an additional staff increase of 39 for Phase 1, if approved. They further propose an increase of about 4 indirect staff members in FY1984 and an additional increase of 5.5 for Phase 1. The Panel agrees that increases of this general magnitude are needed if the proposed program is to move ahead.

IV-C.3.4 Conventional Facilities

Conventional construction costs total $45.1 M for all three phases of the Bates program and amount to approximately 29% of the total construction cost. (These estimates were prepared by the firm of W.B. Merry and Associates, the engineer of record for the recirculator construction recently concluded.) A construction contingency of 10% was included in the base estimates, which were then further increased to include EDIA (10%) and contingency (15%).

Conventional construction to be accomplished during Phase 1 consists principally of the South Hall ring complex, including the ring tunnel, the beam switchyard, the internal target area, the tagging annex, the utility building, the data assembly building, the personnel-utility passageways, and the warehouse. In addition, a research and laboratory building would be constructed. Total cost of conventional construction for Phase 1 is $13.0 M, including EDIA and contingency.

The Phase 2 conventional construction would upgrade the South Hall ring from 1 GeV to 2.5 GeV and would provide a 2.5-GeV recirculator for the linac. Total conven-

tional construction cost for this phase, including EDIA and contingency, is estimated to be $10.9 M.

The Phase 3 conventional construction would provide for accelerator extension to higher energy, conversion of the recirculator from 2.5 GeV to 4.0 GeV, and a high-energy pulse-stretcher ring. The cost of conventional construction for this phase, including EDIA and contingency, is estimaed to be $21.2 M.

IV-C.3.5 Special Situations

MIT has agreed to waive indirect cost charges on the salaries of personnel engaged in the proposed construction project. This would amount to a saving of $731 K for Phase 1, $1373 K for Phase 2, and $2572 K for Phase 3; the total waived for all three phases would be $4676 K.

The replacement cost of the existing Bates Laboratory, accelerator, and research equipment is estimated to exceed $50 M in FY1983 dollars. During the construction period and later during the operating period, additional laboratory, office, shop, and other logistical support space will be available, as well as facilities on the MIT campus.

The extended Bates Laboratory would be operated by MIT as a National Facility and identified as the Bates National Accelerator. Responsibility for the Bates Laboratory and the Laboratory for Nuclear Science has been delegated by MIT to the Dean of Science, who has established two advisory committees: the Bates Policy Advisory Committee and the Bates Management Advisory Committee. The former includes several members from outside MIT.

The Bates Users Group, which was instituted soon after the existing accelerator's completion, was formally incorporated in 1981 with the formation of a Bates Users Corporation structured in accordance with the laws of the Commonwealth of Massachusetts.

The Director of Bates would be advised by three groups: the Director's Advisory Committee, the Program Advisory Committee, and the Technical Advisory Panel.

IV-C.3.6 Capability Assessment

The management structure for the MIT-Bates proposal has been planned, but the Director and other key staff members have not yet been identified. It is planned to separate the management staff of the construction project form that of the ongoing operations and research staffs. Although key management personnel are capable and experienced, the present management structure has not been adequate to the simultaneous demands posed by routine operation, upgrading of the existing facility, and preparation of a proposal for the new facilities under discussion here, at a level of detail that would permit the Panel to assess it properly.

It is simply evident that the MIT group is not adequately staffed at the present time both to carry forth a design study for the proposal prior to construction authorization and to handle the day-to-day demands of their present facility. It was stated, for example, that with present manpower no design work toward the construction proposal will be carried out for the next half-year. If MIT is to maintain even its present level of research activity and machine reliability, quite apart from successful completion of the

upgrading program that has already been approved, the Panel strongly recommends the strengthening of **both** management and operational groups.

The stated duration for Phase 1 construction is three years. This is conditional on the existence of a 15-FTE staff to carry out preconstruction R&D. If this additional effort can be acquired only upon construction approval, a four-year construction period should be assumed for the Phase 1 construction. Successful achievement of stated performance parameters will depend upon the addition to the Bates Laboratory staff of a number of accelerator scientists. Unfortunately, the inability of such scientists, in the past, to attain normal academic status at MIT will make attraction of the most able candidates more difficult than might be the case elsewhere.

Points of major strength for the Bates Laboratory at the present time are, however, its internal groups of outstanding experimentalists, experienced in electromagnetic physics, and leading nuclear theorists as well as its ability to interface with the national experimental users community; in recent years it has been a leading laboratory in the field of experimental nuclear physics.

IV-C.4 National Bureau of Standards

IV-C.4.1 Concept and Theoretical Analysis

The racetrack microtron (RTM) proposed by the National Bureau of Standards is an extension of an R&D project already under way to develop a 200-MeV RTM. It is proposed to build a second RTM — using technologies developed for the first stage — capable of reaching 1 GeV. The mode numbers for the first and second stages are n=2 and n=1, respectively. The second stage requires 87 orbits to reach 1 GeV at the design value of 9.5-MeV energy gain per orbit. Five simultaneous beams at two energies — three at 200 MeV and two at the second-stage extraction energy — would be available. The second-stage extraction energy is variable only in steps corresponding to the energy gain per orbit. A summary of machine characteristics can be found in Table IV-B-4.

All components of the first stage are designed, and, except for the accelerating structure, most are under construction. A preaccelerator section, recently tested at LANL, has exceeded its design goals. It is expected that all components for the second stage will be adequately modeled on RTM-1 and will thus require minimal R&D. Orbit-dynamics calculations have been carried out in great detail for RTM-1 but to a lesser extent for RTM-2.

The overall concept of this system is quite straightforward. However, there are some areas that need attention. Because of its higher mode number, the first-stage accelerating structure operates at 1.5 MV/m. In order to keep the shunt impedance high, the beam apertures in the structure are 1 cm in diameter. This will require careful alignment of the second stage if the same structure is used.

The dipole magnets in the RTM-2 beam recirculator system are to be operated at a gap field of 1.6 T. This is a high value, considering the required field accuracy of $\Delta B/B=10^{-4}$. In principle, the field can be trimmed adequately at one excitation to develop a successful scheme; some R&D will be required to accomplish this.

It is planned to excite the accelerating structure of RTM-2 with one 500-kW klyston; this has the virtue of simplicity. However, the tube selected for this use has not yet been made in large quantity, and operating experience is lacking with regard to service lifetime at full power. Also, phase control at the input ports of the accelerating structure must be carried out at high power levels.

Orbit calculations have been carried out for RTM-2, taking synchrotron radiation into account. Emittance growth due to quantum fluctuations appears to be small, and hence the excellent beam quality is preserved. None of the concerns described above will prevent the machine from reaching its performance specifications.

IV-C.4.2 Prior R&D Assessment, Technical

The present NBS proposal does not include any request for construction-related R&D. However, R&D support is included in the joint NBS/LANL accelerator research program under which RTM-1 is being built. The total cost of the joint NBS/LANL program is approximately $11 M, of which $6 M is the cost of the accelerator.

The Panel feels that an additional $3.5 M (9% of RTM-2 construction costs) is needed for this project. Topics that should be stressed include: (1) orbit tracking with a

full spectrum of errors and (2) linac rf structures (in collaboration with LANL). We note that amounts of $370 K and $2345 K are requested for RTM-1 and RTM-1+2 operations, respectively, for "experimental apparatus modifications, improvements, and replacements."

IV-C.4.3 Technical Components

Present plans call for both stages of the NBS Cascade Microtron System to use the side-coupled linac structure that is currently under development at LANL. This structure has an effective shunt impedance of 80 MΩ/m at 2.38 GHz, a beam aperture of 1.0 cm, and no interfering rf modes. The preaccelerator section of RTM-1 has been fabricated with a design cooling capacity of 28 kW/m at a gradient of 1.5 MV/m. The first high-power tests have obtained an effective shunt impedance of 82.5 MΩ/m and a gradient of 1.6 MV/m at 31 kW/m. Table IV-B-5 gives a summary of the rf system characteristics for the proposed accelerator.

Accelerating structures for both RTM-1 and RTM-2 consist of a pair of 4-m-long side-coupled structures. The RTM-1 structure will operate at a gradient of 1.5 MV/m, whereas the RTM-2 structure will operate at 1.25 MV/m.

Radio-frequency power at 2.38 GHz will be provided by two Varian VKS-8270 klystrons, one each for RTM-1 and RTM-2. Power from each klystron will be split into two equal parts by a high-power splitter and will feed two 4-m side-coupled accelerator structures. High-power phase shifters will also be provided in the waveguide system. The VKS-8270 klystron was designed about 10 years ago for use in the NASA satellite program. Only a few tubes (~10) have been built, so their lifetime is uncertain. NBS has discussed this with Varian and is counting on a lifetime of 10,000 hours; this would require that each tube be replaced about every 2-1/2 years.

If the 200-MeV RTM-1 program is to meet the goal of starting physics research by July, 1985, some additional funding will be necessary to supplement NBS-provided manpower. It is estimated that an additional 7 man-years of design/engineering effort will be needed in FY1984 to ensure that the research equipment is ready to go when the beam is available.

IV-C.4.4 Conventional Facilities

The 15-200 MeV program with RTM-1 will be carried out in three existing experimental areas. Building modifications and additions to permit three low-energy experiments to take place simultaneously are estimated to cost $48 K, including contingency and EDIA.

The high-energy program (200-1000 MeV) will require a new building to house RTM-2 and two new experimental areas and associated data collection rooms. These will be built adjacent to the present laboratory at an estimated cost of $14,022 K, including contingency and EDIA. Together, these additions will permit five experimental programs to be run simultaneously (three electron scattering and two tagged-photon experiments).

The new reinforced concrete building is approximately rectangular, with one side attached to the existing accelerator wing. Its lower floor is 34 ft below ground level. The total floor area of the addition is approximately 35,000 ft^2.

Modifications associated with the 200-MeV program include installation of new beam lines and rearrangement of shielding walls to create Measurement Room 3 at the site of the present linac injector. The 1000-MeV program also requires structural changes to the present building to improve utility access, to install a new fire-suppression system, to improve equipment-handling capability, and to relocate the present RTM klystron power supply.

IV-C.4.5 Special Situations

NBS would provide manpower for the construction project having a value of $2415 K in Phase 1 (200 MeV) and $2645 K in Phase 2 (1000 MeV). In addition, NBS would make a direct contribution of $830 K during Phase 1 for beam transport and building modifications to bring the 200-MeV beam from the accelerator to three existing experimental areas. During Phase 2, NBS would make a direct contribution of $2010 K for modifications of the existing building, installation of 200-MeV beam lines, removal of the old NBS linac, and site preparation for the new building.

Existing structures and facilities that would benefit the new program include: the 200-MeV RTM-1, the building that houses it, and the associated experimental areas; existing beam transport magnets, power supplies, and vacuum systems; existing experimental apparatus, such as the NBS electron scattering spectrometer; and general campus facilities, such as the library, cooling tower, central computer, grounds and access roads, cafeteria, electric power substation, and machine shops. Replacement costs for these structures and facilities are estimated to exceed $27 M.

NBS would contribute $2210 K (62%) of the RTM-1 operating costs and $4290 K (47%) of the RTM-1+2 operating costs. The indirect budget includes the cost of electricity and other utilities based on NBS-wide averages. Although the new microtron facility would clearly use more than its share of electricity, NBS management has agreed that the project will not be charged for the "excess" usage.

IV-C.4.6 Capability Assessment

At the present time, the National Bureau of Standards plans to complete construction of a 200-MeV RTM. They then propose to construct related experimental hardware for this RTM, a cascaded 1-GeV RTM, and additional experimental facilities for use at the 1-GeV electron beam energy. The 200-MeV RTM now under construction is a modest extrapolation from existing racetrack microtron technology (the 175-MeV RTM at Mainz is in an advanced stage of being commissioned), although it makes use of a somewhat higher gradient (1.5 MV/m) standing-wave accelerator structure. Development of the CW rf structure is being carried out in collaboration with LANL, and full-power tests of a side-coupled accelerator structure section have been successful. Consequently, no particular design problems are in evidence for the injector microtron.

The 1-GeV RTM is a scaled-up design from the RTM-1 device, with a larger number of traversals (87 instead of 16). The threshold current for regenerative beam breakup has been calculated to be about 40% above that for the RTM-1 accelerator that will serve as its injector. With earlier completion of the injector unit, regenerative beam-breakup-threshold studies will be carried out, the results of which will be used to guide the choice of final tune for RTM-2. Consequently, RTM-2 is expected to operate well below the beam-breakup threshold. With construction approval anticipated by January 1, 1985, and continuation of the present R&D effort, this project will be ready for construction from a technical point of view.

An explicit management structure for this project has not yet been provided by NBS. Although the present personnel are very experienced, we would consider it prudent to add some senior staff to enhance the depth of project direction.

NBS has proposed that an external organization (i.e., not directly under NBS) be formed, and supported by DOE/NSF, to provide user suppport services. Properly set up, such an organization could provide effective user support and might add to the flexibility of the support structure. It would be important, of course that NBS shop facilities be made available to users for experimental support.

The 4.5-year projected construction period appears reasonable. We would expect NBS to be ready to begin construction by January 1, 1985. The availability of support facilities and staging areas for accelerator and experimental hardware assembly is an asset for construction. Planned manpower over the duration of the construction period appears to be well projected.

IV-C.5 Southeastern Universities Research Association

IV-C.5.1 Concept and Theoretical Analysis

The Southeastern Universities Research Association (SURA) proposes a linac and single-pass recirculator/beam-stretcher ring system. The linac is to be a 2-GeV pulsed machine with single-pass head-to-tail recirculation; it would produce a 4-GeV beam having a pulse length and intensity that allow single-turn injection into the stretcher ring. The charge stored in the ring — extracted uniformly during the time interval before the next injection cycle — would result in a beam current of 240 μA (design specifications) with a duty cycle of about 90%. Characteristics of the proposed machine are summarized in Table IV-B-4.

The ring and injector designs are well matched to their purpose. Schemes for injection and extraction are probably as good as can be proposed now, considering the present state of the art. Extensive particle dynamics calculations have been carried out for the linac, recirculator, and stretcher ring and give confidence in the basic design. However, no component design or modeling has yet been done. Before construction can begin, much R&D must be carried out on critical items, such as the ring accelerating cavities, injection and extraction hardware, magnetic elements, control systems, and vacuum systems.

A more serious problem is the lack of an existing klystron that meets the average power demands of the linac operating at its design specifications in energy, current, and duty cycle. Professional opinion is divided as to the time it would take to develop such a klystron. This uncertainty requires that the performance of the system be downgraded to 120 μA until the design and testing of an appropriate klystron are accomplished.

As pointed out earlier, slow extraction has been a standard procedure at proton accelerators for some time; however, the relevant beam-spill times have so far been measured in seconds rather than milliseconds, as is proposed here. A sophisticated spill-control system must be developed.

Most of the known instabilites that occur in high-current electron storage rings have been considered and found to be tolerable. However, coherent longitudinal coupled-bunch instabilities are expected to be present because the beam is to be injected in highly compressed bunches. Present theory is not capable of predicting precisely the probability of severity of such instabilities. In some storage rings these instabilities constitute an intensity limit; in others they do not. It should be kept in mind that no electron storage ring has achieved the very high injection efficiency or the very large circulating beam specified here. Transverse deflecting modes in the accelerating cavities have not been studied, because the cavities are as yet undefined.

None of the above problems will keep the machine from working, but they may well delay the system from achieving its beam-intensity design goal. Substantial R&D in these areas remains to be done.

The design utilizes a number of parts that either have been tested or are being tested at other laboratories. The SURA group will profit from this work if they are able to put all of these parts together and make them work as a unit. They are trying to push the state of the art in some areas. SURA has some excellent and enthusiastic accelerator physicists who keep in contact with their colleagues around the world. At the present, however, little in-house engineering or technical help is available to them.

39-587 O - 84 - 64

The probability of reaching the full design capabilites of the accelerator at turn-on is uncertain. However, the probability of success at reduced capabilities (200 μA at 1 GeV, 100 μA at 4 GeV) is quite high, assuming that SURA can augment its staff with high-quality personnel.

An electron pulse-stretcher prototype has been built at Sendai, Japan (SSTR), but significant differences between the SURA and SSTR designs make it difficult to use SSTR results to predict the actual performance of the SURA machine. Most of the design differences incorporated into the SURA proposal are to alleviate problems found by SSTR, such as injection losses and coupling resonances crossed by the beam.

Theoretical calculations for the SURA design are well-advanced. This group has spent more than four years performing the calculations, in consultation with many accelerator physicists around the world.

IV-C.5.2 Prior R&D Assessment, Technical

The SURA construction-related R&D amounts to $10.1 M for the 4-GeV project. This amount corresponds to 7.4% of the construction budget. The Commonwealth of Virginia and the SURA universities have promised to provide $6,460 K of R&D funds. Particular aspects of R&D to be covered include:

Klystron development
High-duty-cycle modulator development
Beam breakup in the linac (note that the specified intensity is four times that at SLAC)
High-repetition-rate, fast-injection kickers
Stretcher-ring design (including internal target options)
Stretcher-ring cavity development (including parasitic mode studies)
Stretcher-ring beam instabilities
Resonant extraction studies (including extraction efficiency, time structure, and tolerances)
Extracted-beam parameter studies (including emittance, momentum spread, and stochastic emittance growth due to synchrotron radiation)

IV-C.5.3 Technical Components

SURA proposes to use 40 SLAC-type accelerator sections for its linac structure. Each of these sections is 3.05 m long and is of the traveling-wave, constant-gradient type with an attenuation parameter τ =0.57 Np and an operating frequency of 2.856 GHz. Parameters for the system are given in Table IV-B-5. The value of τ for the structure may need to be further optimized, because SURA plans to use higher beam currents and higher rf power per unit length than SLAC currently uses. This optimization may lead to the adoption of a somewhat lower value of τ. Other types of structures, including standing-wave structures, will also be studied before the final design is selected. Other important parameters of the present SLAC structure are: a shunt impedance of 57 MΩ/m; a Q of 13,200; and a filling time of 0.83 μ sec.

Each of the 40 accelerator sections will be supplied with power by a 40-MW (peak) klystron designed to operate at a pulse length of 3.2 μ sec and a pulse repetition rate of 1 kHz. The resulting duty cycle (0.32%) is 3.2 times that of the present SLAC klystron. This matter has been discussed with klystron experts at other laboratories and in indus-

try, and the SURA group has concluded that the required high-average-power klystron can be built by modifying existing designs to incorporate a more rugged collector and an improved output window.

Important questions arise not only with regard to the technical feasibility of these klystron modifications, but also with regard to the cost and duration of the necessary development program and the lifetime of the production tubes that would result. SURA has received a communication from the Electron Tube Division of ITT giving "budgetary pricing" (in February 1983 dollars) of $500 K for development of the required klystron. Members of the Panel are skeptical of this quotation as regards the cost, the development time (2 years), and the life expectancy (exceeding 20,000 hours).

The SURA group has pointed out that it is not essential for the klystron to produce its full rated average power initially at the accelerator beam turn-on. One-half of the design beam current (i.e., 120 μA) from the stretcher ring could be achieved if the klystron were to operate at a 3.2-μsec pulse length and 360 Hz, which has been achieved at SLAC (although not routinely). However, the lifetime at 360 Hz would be significantly reduced compared with the 15,000-20,000 hours experienced at SLAC. The stretcher ring output would also require that the peak beam current in the accelerator be increased from 200 mA to 278 mA, a nontrivial extension.

Thus, achieving a 40-MW peak output from klystrons — at a duty cycle of 0.1% or higher and with good lifetime — may not be a simple task. Develoment of kystrons with higher ratings has generally taken longer, and cost more, than initially estimated. It is therefore most important to start the klystron development at the earliest feasible moment in the schedule and to expect that operation at reduced levels may be required for a substantial period after the experimental program gets under way.

The SURA project, if approved, would be based at a new laboratory having no established reservoir of scientific, engineering, technical, or administrative staff to begin work on critical aspects of the program. Top priority would have to be given to organizing the laboratory and recruiting the talented people necessary to ensure the success of the project. Experience at other laboratories has amply demonstrated the value of building a strong in-house capability in those technical areas where outside capability is inadequate or limited, or where substantial cost savings can be realized by constructing prototype models.

As soon as possible, the design, procurement or fabrication, and testing of critical components or systems should begin. Backup solutions should be pursued where success of the primary approach appears doubtful. For the SURA project, these maxims would indicate that develoment of components such as the high-power klystrons and modulators for the linac should be started almost immediately. These items are required in large quantity and have a significant impact on both the construction and operating costs, as well as on the overall performance and efficiency of the facility. Other technical items and critical theoretical and engineering issues should be identified and pursued as quickly as possible.

IV-C.5.4 Conventional Facilities

The SURA proposal estimates $30.7 M for the conventional facilities associated with the 4-GeV accelerator project. This estimate in FY1983 dollars includes EDIA and contingency; it amounts to 23% of the total construction cost.

The major conventional facility items are: accelerator housings; beam switchyard housing; end station A, counting house, and beam dump; end station B, counting house, and beam dump; tagged-photon end station and counting house; access and fan buildings; accelerator control building; support facilities; AC power and distribution system; facility cooling system; and site preparation.

Cost estimates for the above items contain the following factors:

Contractor job and bid contingency	**15%**
EDIA	**10%**
Overhead and profit	**15%**
Contingency	**15%**

Building and facility construction costs were compiled by the firm of Hayes, Seay , Mattern and Mattern, which has considerable experience in planning large structures in the Southeast, including tunnels and subway systems.

The item "support facilities" mentioned above in the listing of conventional facilities covers the cost of rehabilitation work in the two large buildings that have been made available to SURA. These buildings are the Virginia Associated Research Center (VARC) and the Space Radiation Effects Laboratory (SREL).

IV-C.5.5 Special Situations

SURA appointed a site committee to evaluate six sites for the proposed accelerator facility. The SURA Board of Trustees reviewed the committee's report and selected the Newport News, Virginia, site, primarily because of the availability at that site of the VARC and SREL buildings.

The VARC building (35,000 ft^2) contains offices, laboratories, classrooms, a machine shop, a technical library, a cafeteria, an electronics shop, and storage areas. The SREL building (70,000 ft^2 floor area) consists of a 130 x 300 x 49-ft-tall high-bay area and a two-story support area. The latter includes offices, conference rooms, laboratories, electrical and mechanical equipment rooms, refrigeration and pump rooms, and a control room with raised computer flooring. The value of these facilities to the proposed laboratory has been estimated as $10.2 M, including $1.0 M for the existing library.

Land for the proposed laboratory (150 acres), including space for future expansion, will be made available by the City of Newport News. The value of the land is estimated to be $0.3 M.

A proposal has been made to the Commonwealth of Virginia for direct support of senior staff positions in the proposed laboratory in the following amounts:

Period	Amount (K$)
1983/84	160
1984/85	332
1985/86	569

The Governor of Virginia has recommended (and the Legislature has approved) $160 K for this purpose in his budget for 1983/84.

During the period 1980-1982, the 23 SURA universities have contributed approximately $600 K in direct and indirect costs toward the development of the National Electron Accelerator Laboratory proposal and the organization of SURA. Continued support of 17 SURA faculty members who will participate in the accelerator and equipment design has also been pledged by the SURA universities.

IV-C.5.6 Capability Assessment

SURA has proposed the construction of the accelerator at the Newport News site formerly occupied by SREL. Except for the impressively large cyclotron building and the VARC laboratory building, this is in essence a "green site" requiring not only the construction of a National Electron Accelerator Laboratory but also a broad spectrum of related facilities that constitute the standard major laboratory infrastructure.

The SURA consortium has brought together a group of collaborators who produced a very substantial design study for the 4-GeV linac/stretcher ring machine. This group has benefited from interactions with respected accelerator scientists elsewhere and has worked closely with the Stanford Linear Accelerator Center.

Present staff members are bright and enthusiastic but have limited experience in accelerator design and construction; they need to be strongly reinforced by professionals from other laboratories if this project is approved.

As mentioned previously, a number of technical issues require further attention. These are not crucial design issues, and most could be resolved with adequate R&D effort before construction begins. However, the current absence of adequate engineering support will limit the pace of the R & D.

The klystrons used for the design of the linear accelerator do not exist, and an unrealistically short development time has been assumed by the SURA group for their production. For this reason, it should be assumed that construction will commence using klystrons with an average power capability (46 kW) equal to that of the SLAC klystrons. The machine would then gradually be upgraded by the subsequent replacement of these klystrons with newly developed, higher-average-power klystrons.

The consequent parameters of the linac/stretcher ring are then as follows:

Parameter	Value	
	Phase 1A	Phase 1B
Linac repetition rate	360 Hz	1000 Hz
Maximum beam energy	4 GeV	4 GeV
Peak intensity	278 mA	200 mA
Average intensity	120 A	240 A
Average klystron power	46 kW	128 kW

This approach constitutes an acceptable and sensible phasing of the construction, eliminating potentially serious delays and permitting the eventual achievement of the original design parameters at acceptable cost.

Essential to the linear accelerator system is early development work on the high-duty-cycle modulators. Beam breakup in the linear accelerator structure should also be of concern, because the maximum beam current in the linac is four times that at SLAC. On the other hand, even with the double-pass design, the effective accelerator length is only 10% of that of SLAC, and the beam pulse length is 75% as long as that at SLAC.

The basic stretcher-ring design is in hand, and its structure has been optimized for fast single-turn injection in vertical-acceptance phase space and slow half-integral resonant extraction from the horizontal phase space. Both modes of beam manipulation are established techniques for proton machines.

It is desirable that computer simulation studies be carried out on the resonant extraction process with relevant component "noise" spectra, in order to optimize extraction efficiency and beam time structure and minimize sensitivity to resonant-growth-driving-term errors. These studies should be done before finalizing the detailed structure of the lattice and the overall resonant-extraction component distribution around the stretcher ring. It is a distinct advantage that extraction takes place from a zero-dispersion straight section of the stretcher-ring lattice, thereby eliminating time-dependent phase space migration of the extracted beam.

The possible beam instabilities that could prevent the stretcher ring from reaching its design intensity were comprehensively assessed. It was correctly realized that the transverse instability due to the high-Q rf cavity could limit the beam current. The required damping of the parasitic modes of the rf cavity by a factor of several thousand is not necessarily straightforward, and early R&D work on the cavity is essential. Furthermore, the longitudinal coupled-bunch instability should be of concern; this could be driven either by the impedance spectrum of the distributed ring elements or, more likely, by the narrowband parasitic impedance spectrum of the rf accelerating cavity. Again, early development work on the rf cavity is needed, and an analysis to assess beam-instability thresholds with a measured rf-cavity "damped" impedance spectrum will be desirable in due time.

Further analytical work is also required to determine the extracted beam parameters (ϵ , $\Delta p/p$) that result from the half integer resonant extraction process, taking into account the stochastic growth of the beam due to quantized synchrotron radiation emission.

With the assumption that the facility is initially downgraded in intensity to the 120-μA level (Phase 1A), there are no crucial design issues that should either prevent a normal transition from preconstruction R&D work to Construction Title I design work by January 1, 1985, or, from a technical point of view, prevent the project from reaching its design goals in due time. A crucial issue at present, however, is the lack of adequate staff to carry forward a vigorous R&D and construction program.

The stated duration of construction is 4 years. However, there is no adequate allowance in the detailed construction schedule for a buildup of staff and support structure. Therefore, a construction schedule of 4-1/2 years should be assumed.

Construction management is not in place at this time. The SURA consortium is in the process of attracting senior project management and is ready to appoint a project director upon approval of the project. The success of the present proposal will indeed depend critically on the choice of this person and his ability to attract a core group of experienced accelerator scientists and engineers.

V - RECOMMENDATIONS:

As noted previously, and in agreement with the Barnes Subcommittee, the Panel recommends that the highest priority for new accelerator facilities in the electromagnetic field be accorded to one having a maximum energy of at least 4 GeV and high duty factor.

V-A - Argonne and SURA

That being the case, we begin our detailed discussion of our recommendations by considering the two fully developed proposals for such facilities before us, namely, those from the Argonne National Laboratory and from the Southeastern Universities Research Association.

It is a measure of the strength of the electromagnetic physics community in this country that two quite different proposals of this scope, magnitude and quality are available for consideration. The decision between them has been a difficult one. The Technical Subpanel, after a very careful, independent analysis of both designs — as discussed in Section IV above — has concluded that both designs are feasible ones and that either could very well form the basis for an extremely powerful national facility. In the Subpanel's considered opinion both designs fall short of the originally proposed specifications — that from Argonne in terms of maximum achievable energy and that from SURA in terms of maximum achievable current. Other questions have been raised concerning both designs in Section IV, but it is the opinion of the Panel that given the normal duration of pre-construction time and the normal R & D that would be expected to continue, in parallel with construction, these can be resolved satisfactorily.

Our decision between the two proposals then depends upon the relative weightings that we ascribe to the different problems facing the two groups of accelerator designers and to other considerations quite apart from these technical ones.

The fact that the SURA group has pulled together the SURA consortium of over twenty universities and that these in turn have pledged five **new** Tenure Commonwealth professorships, 25 **new** tenured or tenure-track experimental nuclear physics faculty positions and at least 5 **new** tenured or tenure-track theoretical nuclear physics faculty positions, should their proposal be approved, has weighed substantially in their favor. Such a combination of collaborating universities and new permanent positions in nuclear physics constitutes a very substantial increment to the total U.S. university involvement in nuclear physics and goes a long way toward providing assurance that there will be the continuing flow of active young scientists required to exploit fully the kind of major new facility that we discuss herein. In the case of Argonne, the University of Chicago has pledged to add two new tenured appointments in nuclear physics to its Physics Department and to arrange adjunct appointments for a number of the permanent staff at Argonne in both nuclear physics and nuclear chemistry in the corresponding university departments.

Important, also, has been the recognition that the SURA design could readily be extended in energy to 6 GeV, or above, should the physics encountered in this new region make such an extension desirable, while the ANL design could not. Although we cannot, with any degree of certainty, tell at this time how important or necessary the higher energies may be, experience has taught us that the option of obtaining them should not be given up lightly. Moreover, we have noted that having constructed the injector for

the 4 GeV stretcher ring, the SURA group would have already available an ideal injector for a 1 GeV or smaller ring which could be added to the facility, at something resembling the cost of a single experiment, to provide CW beams simultaneously in the lower energy range should the national program in electromagnetic physics eventually require it.

And, thirdly, although the Panel has not been unanimous on this point, there is a strong majority belief that the SURA design is a more conservative one once it is agreed, from the outset, to downrate the beam current specifications to more nearly meet present klystron power capabilities. Target beam power limitations convince us that such downrating, at least initially, will not compromise the experimental programs. A number of the Technical Subpanel members still hold significant reservations about the potential beam loss in the ANL accelerator from beam centering errors and quantum fluctuation phenomena at the higher energies as well as about the geometric stability of the large dipoles and other accelerator components to the accuracy required for successful long term operation.

With these, and a large number of lesser considerations in mind the Panel then **recommends:**

> **That the proposal of the Southeastern Universities Research Association (SURA) for the construction of a linac — stretcher ring accelerator system capable of providing high duty factor beams throughout the energy range from 0.5–4.0 GeV be accepted and that this facility be constructed and designated the National Electron Accelerator Laboratory (NEAL).**

Obviously it is a matter of substantial concern that the SURA group has neither the management nor the accelerator construction teams in place nor, realistically, would it have been possible to expect this prior to a decision on their proposal. The Panel is convinced, however, that the ultimate success of this venture depends critically upon the selection and attraction of a strong, dynamic Director at the earliest possible time and the establishment of an accelerator construction team drawn from among the world's most able practitioners. We consider the SURA decision to utilize the five Commonwealth Professorships in attracting the Director and four senior accelerator scientists to be a very wise one.

If this new Laboratory is to fulfill its proper function in the national nuclear physics enterprise, it is essential that its operation and management be truly national in scope and that it draw upon the entire community both for planning and execution of its program. That being so, and because the Panel considers it mandatory that SURA involve the entire community formally and as soon as possible, it **recommends**

> **That SURA management, in consultation with DOE and NSF, appoint a National Advisory Board (NAB) as soon as possible and that the members of this Board be engaged in all major decisions affecting the structure and future of the National Electron Accelerator Laboratory.**

And both because we believe that it is essential to involve the community as soon as possible and because we believe that the SURA group will need detailed assistance from this community in the development, in timely fashion, of experimental facilities for use with the accelerator complex, the Panel further **recommends**

That very soon after formal approval of NEAL, its management, with the advice of its National Advisory Board, announce a formal solicitation of experimental proposals and the creation of a Program Advisory Committee (PAC).

Our reason for what may seem a somewhat premature recommendation is that our experience suggests that external user groups are much more apt to become actively involved in , and take responsibility for, the construction of major pieces or systems of research equipment if they have been formally assured of their subsequent place in the scheduling to use this equipment. Although the tradition of user design and construction of such major equipment is much more highly developed in elementary particle physics there is a rapidly growing number of examples in nuclear physics as well e.g. the spin spectrometer at HHIRF, the 180^{o} spectrometer at Bates, the HRS and EPICS spectrometer systems at LAMPF, etc. As is common practice in particle physics and in these examples in nuclear physics, the Panel believes that the optimum arrangements involve subcontracting via the host Laboratory (here NEAL) rather than direct independent funding of the user groups by the funding agencies.

It also bears emphasis that included in the DOE FY1984 Congressional Budget Request is the new electron source, planned by Arnold **et al.** of American University, for installation at the Stanford Linear Accelerator Center (SLAC) specifically with the intent of making that facility available for nuclear physics research for a fraction of its time — currently estimated at about one month per year. While we recognize that time for nuclear physics research on the SLAC facility will always be severely limited, and in competition with elementary particle physics utilization, we nonetheless **recommend:**

That potentiel users of NEAL be encouraged to develop proposals for utilization of SLAC for consideration by the appropriate Program Advisory Committee, and that DOE/NSF give high priority to provision of the necessary support for those experiments that are accepted, in order that a significantly larger fraction of the U.S. electromagnetic physics community gain access to, and experience from, experimental studies with higher energy electron beams that have hitherto been available to it.

We have addressed, in preliminary fashion, the experimental equipment requirements ancillary to a facility such as NEAL in Appendix VII-A to this report.

Finally, because the Panel believes that convenient access is of major importance to a national facility that will be as unique as NEAL, because it also believes that there are significant advantages in terms of general intellectual ambience, cultural activities, access to libraries and laboratories in widely diverse fields, possible joint use (perhaps even only initially) of facilities and services such as purchasing, personnel, security, health etc, at a site in the vicinity of a major university, and because it understands that the SURA Board was far from unanimous in its selection of the Newport News site proposed for NEAL, it **recommends**

That SURA and NEAL management consider the possible advantages of relocating NEAL to provide improved access to one or more major university campuses and to one or

more major airports, providing that this can be accomplished without significant increase in the total project cost.

Having made these recommendations it is obvious that the Panel does **not** recommend construction of the proposed GEM facility at Argonne. But the Panel wishes to take this opportunity to comment on the excellence of the ANL proposal. The Hexatron is an imaginative new development in accelerator technology and ANL's proposed use of its surplus ZGS facilities to permit a cost-effective proposal is exemplary. Argonne has a very dedicated, able group of scientists and engineers already in place and these, together with the presence of established management and support structures were factors that strongly favored Argonne.

V-B. - University of Illinois

The University of Illinois has a long and very distinguished tradition in electromagnetic physics and an enviable reputation for the education of leaders in this field. It has suffered a grievous loss in the death of one of its leading physicists, Peter Axel, but is fortunate in having a dynamic group of young researchers led by Larry Cardman that is more than capable of carrying forward the Illinois tradition.

The Panel was much impressed by the proposal prepared by the Ilinois group and the presentation of it. We have no doubt that the Illinois group, given their performance in recent years, could, if given the opportunity, move expeditiously to produce the facility that they have proposed.

It is thus with regret that the Panel has concluded that it is **not** possible within a coherent overall national plan for nuclear physics — or indeed for electromagnetic physics — to move forward to the construction of a facility of national scope at the University of Illinois given our decision, above, to recommend construction of the SURA 0.5-4.0 GeV facility.

At the same time, the Panel considers it of great importance that the University of Illinois continue its tradition of excellence in both research and education in this field. To that end we are delighted to learn of the NSF decision, already in place, to fund Illinois for acquisition of microtron dipole end magnets identical to those under construction for the NBS/LANL 200 MeV machine at NBS. This presently approved upgrading of the Illinois facilities, possibly with the further substitution of room temperature linac cavities for the superconducting ones now in use, could result in a CW facility with energies up to a few hundred MeV which could support a very rich spectrum of experimental activities. The Panel, of course, also anticipates that the Illinois group will include very active exploitation of the higher energy SURA facility in their longer range plans.

V-C - Massachusetts Institute of Technology

For more than the past decade, the Bates Laboratory at MIT has been one of the major world centers for electromagnetic physics. This has reflected a unique combination of dedicated, skilled experimentalists who, perhaps more than any others, have demonstrated the potential of truly high resolution measurements with electrons and of equally dedicated, skilled nuclear theorists who have been interested in the electromagnetic physics in detail while ranging broadly over much of theoretical physics.

The Panel considers it essential that this tradition be maintained. It is important not only that MIT experimentalists continue to do the kind of pioneering experiments in electromagnetic physics for which Bates has become justly world famous but also that the MIT theorists, who interact with a much broader national and international community, retain their active interest in, and input to, electromagnetic physics.

It was thus, with considerable disappointment that the Panel learned that the MIT group had not found it possible to carry through a detailed design for a 4 GeV system which would have been considered in parallel with those from Argonne and from SURA. As originally proposed to us, MIT had intended to engage in a phased approach first implementing its currently funded upgrading program to yield a maximum energy of ~ 840 MeV and higher reliability at low duty factor; then adding a stretcher ring to obtain high duty factor at this — or a slightly higher energy ~1 GeV; then moving up to 2-2.5 GeV and finally to 4 GeV. Only conceptual design work has been completed on the later stages of this progression.

Having decided that the time was ripe to move to 4 GeV and to recommend construction of the specific facility proposed by SURA, the Panel now concludes that it would **not** be desirable within the overall national program in nuclear physics for MIT — Bates to plan on significant increase in energy beyond its currently approved upgrading to ~ 840 MeV.

At the same time we recognize that the MIT planning for increase of the duty factor of their facility at this energy was understandably designed as an integral phase of a larger, more ambitious plan directed eventually to 4 GeV and is thus not necessarily optimized for CW operation at 840 MeV.

We would urge the MIT-Bates group, therefore, to complete their currently approved upgrading so that their present research program can be extended to the higher energies to be available and benefit from the higher reliability that the upgrading will provide.

We sense that the demands of the ongoing research program, the current upgrading, and the planning that went into the current proposal have overloaded the management and accelerator groups at Bates and would urge that, as a matter of high priority, these groups be strengthened. Given such internal strengthening, we believe that an optimized design for high duty factor operation of the Bates facility at its upgraded energy will emerge naturally in the course of a few years. We suspect that such an optimized design will be substantially less costly to build and to operate than that included as Phase I of the presently available proposal.

As noted at the outset of this section, MIT-Bates has been one of the leading world centers in electromagnetic physics for more than the past decade; the Panel believes that it has the potential to retain this role in the future. We believe, too, that MIT physicists can and should play important roles in the planning for, and execution of, the NEAL facility.

V.-D. - National Bureau of Standards

The National Bureau of Standards also has a record of accomplishment in electromagnetic physics, over several decades, of which it can be justly proud; included among its achievements is the education of a large number of leading scientists in the field.

Through the currently-in-place, DOE-funded, cooperative program between NBS and LANL, very important contributions have been, and continue to be, made to the technology of electron accelerators. The 200 MeV CW microtron facility has provided, and will continue to provide, an important test bed for new ideas in this area.

Given the continuing and strengthened activities at both MIT and the University of Illinois, and its decision to recommend construction of the SURA 0.5-4.0 GeV facility, the Panel does **not** recommend expansion of the NBS facility to 1 GeV as proposed. Rather the Panel strongly encourages the Department of Commerce to continue to operate the 200 MeV facility as it has NBS facilities in the past, welcoming collaborators from the external scientific community involved in experimental programs with NBS staff. We see it as entirely reasonable that such collaborators, as in the past, would request support for their collaborative activities from NSF or DOE but we do not recommend the establishment of formal mechanisms whereby NSF/DOE would support general user activity through NBS nor do we recommend NSF/DOE provision of major research instrumentation at NBS except insofar as this may evolve naturally as a component of some ongoing collaborative research program.

VI ACKNOWLEDGEMENTS

The Panel wishes to express its appreciation to the many people who have worked long and hard to develop such excellent proposals for new facilities for new electromagnetic physics. In particular, we wish to express our special thanks to Larry Cardman, Peter Demos, Harry Holmgren, Harold Jackson and Sam Penner, the spokesmen for the five proposing groups, for the patience and good humor they have managed to retain in the face of repeated questions, questionnaires, visits, requests for data and the like; they have made our task much easier.

G.E. Brown met with the Panel, at its invitation, on one occasion for discussions of aspects of electromagnetic physics and we are much indebted to him, as we are to all those who have forwarded unsolicited comments and suggestions during the Panel's deliberations.

We would also wish to express our appreciation to Jim Leiss, Enloe Ritter, Bill Rodney and Harvey Willard who, on behalf of the sponsoring agencies, spent long hours with us and provided us with a wealth of fact and insight. Special thanks go to John Erskine who has performed yeoman service in coordinating all Panel activities and in producing its report on an almost impossible schedule.

And, finally, the Panel Chairman, on behalf of his fellow Panel members, wishes to take this occasion to express a special note of thanks to the Technical Subpanel and its Chairman who have spent an enormous amount of time and effort in developing the complete and detailed technical understanding of the five proposed accelerator systems without which the Panel simply could not have functioned responsibly.

VII. APPENDIX

VII-A. EXPERIMENTAL EQUIPMENT AND USER ASPECTS

VII-A1 General Comments

The clarity with which the proposed facility reveals new phenomena will depend as much on the quality and adequacy of the experimental equipment as on the capabilities of the accelerator itself. It is essential that substantial funding be provided for the equipment to carry out the broad-ranging experimental program addressed by this facility. It is also clear that a substantial effort — involving all prospective users of these facilities — will be required to determine the optimum mix and design of the experimental facilities.

For all of the proposals considered here, planning for experimental equipment is less advanced than that for the accelerators themselves. In the main, plans have been carried only far enough to fix the scale and/or layout of experimental areas so they could be reasonably costed. At best, conceptual designs are available; in many cases cost estimates are based on a simple, sometimes large, scaling or earlier designs. Nor are the specified arrays of equipment generally complete, except possibly those for the 1000 MeV facility proposed by the National Bureau of Standards.

This approach can be understood and defended. We are truly entering a new realm of experimentation with energy and beam power increased by a factor of ten and duty cycle by a factor of one hundred. It would be surprising if we could anticipate all of our experimental needs in detail. Furthermore, straightforward extrapolation of earlier spectrometer designs will not necessarily be cost-effective; yet there are no working superconducting spectrometers appropriate to the needs of the proposed research. Nor does one have sufficient experience with large solid angle (4π) photon detectors in this energy range to attempt a cost-effective design.

Nevertheless, it is necessary to have an estimate of total equipment costs, at least through the first five years of operation, so that it is possible to assess rationally the probably cost of the project and its impact on our overall scientific effort. Implicit in this remark is the realization that total equipment costs will be a substantial fraction of the overall cost of the facility.

Although it is difficult to make a detailed estimate at this time, a first approximation has been obtained by combining large items from the various proposals: this yields (see Table A-1) an estimate of $35 M. About one-half to two thirds of this amount should be expended within one year of the completion date of the accelerator, and the remainder during the next three to five years. Substantial uncertainties in the estimate involve the questions of the need to build a high-resolution coincidence-pair spectrometer (included here) or a storage ring for internal target studies (not included), as well as questions relating to the design and cost of 4π detectors. The resolution of these questions and the refinement of the estimates necessarily awaits a final decision on the part of the funding agencies.

The Panel emphasizes again the importance of providing adequate experimental equipment funds early in the project so that the essential research and development work can be completed in a timely fashion. Equally crucial is the early formation of a strong user group to involve the national nuclear physics community in the design ad construction of this equipment.

Table A-1

BASIS OF EQUIPMENT COST ESTIMATE
(for a 4 GeV research program)

Experiment types: High resolution
Moderate resolution
Moderate resolution/photon monochromator

Equipment Item			Total Cost (M$)
(1)	**Computers (on-line and analysis)**		**1.3**
	a) VAX 11/750 (4) = 1.0		
	b) VAX 11/780 (1) = 0.3		
(2)	**Spectrometers**		**25.7**
	a) Photon monochromator	1.6	
	b) High-resolution spectrometer pair	7.0	
	c) Moderate-resolution spectrometer pair (2)	6.8	
	d) Cryogenics	1.9	
		17.3	
	EDIA + contingency (at 49%)	**8.4**	
(3)	**Targets**		**1.0**
(4)	**Polarized targets and recoil polarimeters**		**2.0**
(5)	**Miscellaneous detectors**		**1.0**
(6)	**4π detector(s)**		**3.0**
(7)	**Electronics**		**1.0**
	TOTAL		**35.0**

In the remainder of this appendix we will summarize briefly the experimental equipment requested by those groups submitting proposals for a high duty cycle, high energy electron accelerator. Where relevant, we will also comment here on the means of dealing with users suggested by each facility.

VII-A.2 Argonne National Laboratory

Argonne has proposed a capital equipment construction budget of $21.4 M to outfit the three target areas that receive concurrent beams of independently controlled energy and intensity. Each target area is approximately 24 m in diameter. The experimental equipment consists of a photon monochromator, a high-resolution spectrometer pair, a moderate-resolution spectrometer pair, associated cryogenic facilities, and three data acquisition computers of the VAX 11/750 class. Main characteristics of the spectrometers are summarized below:

SPECTROMETER	p^{max} (GeV/c)	$\Delta p/p$	$\delta p/p$	Ω (msr)
High Resolution Spectrometer A	1.9	10^{-5}	$\pm 5\%$	>20
High Resolution Spectrometer B	1.1	10^{-4}	$\pm 10\%$	>30
Moderate Resolution Spectrometer A	4.0	10^{-3}	$\pm 10\%$	30
Moderate Resolution Spectrometer B	2.0	10^{-3}	$\pm 10\%$	30

The Enge split-pole magnet concept would be used for the photon monochromator to provide tagged photons with an energy resolution of $\Delta E/E \leq 1.5\text{-}5.0 \times 10^{-4}$ without dispersion matching. A superconducting dipole will be used to bend the emerging electron beam into a below-grade beam dump. The distance between radiator and target is 8.0 meters and the photon beam spot on target is ≤ 1.0 cm, FWHM. A moderate resolution spectrometer pair can be used in conjunction with the monochromator.

The Panel concludes that costs for the spectrometers have been estimated carefully, and that considerable thought has been given to their general characteristics. However, no ancillary experimental equipment is requested in the proposal. Argonne expects that items such as cryogenic and other special purpose targets, very large γ, π^0 and neutron detectors, focal plane detectors, Cerenkov detectors, polarized sources, etc., will be provided by users.

The proposed Hexatron facility offers a user-friendly environment. A Program Advisory Committee with a national membership would review proposals and provide rankings and recommendations for scheduling; in addition, a visiting committee would be formed to review annually the facility operations. Argonne has considerable experience in operating user facilities, such as those associated with the ZGS, and has developed a detailed infrastructure for this purpose.

Extensive shop facilities exist at Argonne, and the operating budget allocates $875 K for support of 25 experiments annually ($35 K each). In addition, the proposed operating budget would provide 19 engineering and technical staff people for experimental support. At present, there are relatively few experimentalists on the Argonne staff conducting research in electromagnetic physics, so that the in-house impetus for equipment development must come primarily from researchers with various other backgrounds. Argonne staff members have considerable experience with large magnetic spectrometers, however, which will be invaluable.

Argonne management has stated its intention to reprogram its current LAMPF effort toward the Hexatron, and to add personnel to achieve an in-house complement of 19 experimentalists working at the facility. These 19 scientists would be funded by a separate DOE medium energy physics contract, but would be available for consultation and assistance to outside users of the facility.

VII-A.3 University of Illinois

The experimental equipment listed in the Illinois proposal includes two magnetic spectrometers and photon facilities, with a total cost of ~$5.4M.

In detail, the proposal discusses a 750 MeV/c spectrometer to be used mainly for the detection of scattered electrons. With a 30 msr solid angle and $\pm 10\%$ momentum

acceptance, this spectrometer is expected to yield a momentum resolution of $2\text{-}5\times10^{-4}$. For the detection of pions, a large aperture pion spectrometer is proposed. This QQD spectrometer is intended as a flexible device that can be transported to the pivot when it is needed as coincidence detector. The QQD configuration chosen is expected to give a 10 msr solid angle momentum acceptance of +15% and a 5.3 m flightpath. Tracing the detected pions through the spectrometer by software analysis should permit a momentum resolution of $\pm0.5\%$.

For the production of photons, both a tagged photon facility using a split-pole spectrometer and an untagged bremsstrahlung facility are proposed. The former aims at a +40% momentum bite for the tagging electrons, and an intrinsic resolution of 2×10^{-4}. This facility, when employed using off-axis production of photons, is expected to produce gamma radiation of appreciable (50%) polarization.

For the detection of photons and neutral pions, a spectrometer of two NaI(Tl) detectors (9" x 12") is proposed. This pair of crystals is expected to yield an energy resolution of 2-5 MeV, depending on π^0 energy, and a fairly large (2msr) solid angle.

Extensive experimental equipment, which is already in use in conjunction with the lower energy facility now at Illinois, will be available for the detection of photons and giant resonance decay products. Two large data acquisition computers and an extensive pool of nuclear electronics are also available.

The Illinois laboratory is now primarily a university oriented research facility. Provisions have been made for the use of the new accelerator by a diverse community of outside users, in a way similar to what now occurs at IUCF. The strong tradition of electromagnetic physics research at Illinois represents a definite asset to the development of new apparatus and research programs.

VII-A.4 Massachusetts Institute of Technology - Bates Laboratory

For phase II the Bates proposal discusses experimental equipment, including three magnetic spectrometers, amounting to ~$19 M. These spectrometers are proposed as an addition to the high resolution spectrometer ELSSY and the medium resolution spectrometers MEPS, OHIPS, and BIGBITE and related detectors and computers presently in use.

In detail, the spectrometers discussed include a spectrometer scaled up from the present BIGBITE, which would serve both as a spectrometer with large energy acceptance used in deep inelastic single arm experiments, and as one arm of a coincidence pair. For the investigation of (e,e X) coincidence experiments (X=p,d,α,π,K) a pair of high resolution spectrometers is discussed. These spectrometers, apart from the higher maximum momentum, would be similar to the presently used spectrometer pair at NIKHEF.

SPECTROMETER DESIGN OBJECTIVES

SPECTROMETER	Pmax (GeV/c)	Δ p/p	δ p/p	Ω (msr)
Large acceptance (BIGBITE) QQD	2	5×10^{-3}	±12%	2-3
High resolution QDD	1	$<1\times10^{-4}$	±1%	6
High resolution QDD	1	5×10^{-4}	±5%	17
K-spectrometer	2	2×10^{-4}	±5%	20

For use at 2 GeV, the photon tagging system now already in use would be upgraded by adding a second magnet. This system aims at an energy resolution of 1-2 MeV.

A second photon tagging system is planned using the high intensity electron beam circulating in the stretcher ring. A combination of quadrupole, ring dipole, septum magnet and two additional dipoles would permit the tagging of photons over a large energy range. For electron beam energies of 1-2 GeV, this system is expected to tag photons down to 10% of the circulating electron-beam energy, with an energy resolution of 2-3 MeV.

For (γ ,K) and (e,e′ K) experiments both good energy resolution and short flight path are desirable. As a state of the art spectrometer of this type, the Bates proposal discusses a 2 GeV/c spectrometer with 2×10^{-4} momentum resolution, 20 m flight path and 20 msr solid angle.

In addition, the Bates proposal includes for gamma radiation detection a 16" x 20" NaI(Tl) and a 30 cm x 30 cm BGO detector. A number of cryogenic targets as well as a polarized H source, the beam of which is to be used as internal target in the stretcher ring, are proposed. To run this equipment, a significant upgrade of the present computer facilities, by 3 PDP 11 and 2 VAX-type computers, is envisaged.

The Bates laboratory at present is a facility used approximately 50% by outside users. Beam time is allocated by the director based on recommendations of a Program Advisory Committee which currently has two-thirds of its members from outside the MIT community. Bates has developed considerable experience with the operation of a user facility and in providing outside users with the needed infrastructure. In addition, the expertise of the MIT group would greatly facilitate the development of new apparatus and the early startup of new programs.

With the proposed long-range expansion program of Bates, the laboratory intends to change its relation with the Laboratory for Nuclear Science and MIT, in order to become a more independent national facility. The overall performance of Bates will be monitored by the Dean of Science, who is assisted by a Policy Advisory Committee and a Management Advisory Committee. As the laboratory expands into a national user facility, the membership of the Policy Committee will evolve so as to assure that the interests of the user community are represented. The Program Advisory Committee will operate in the future in its present form.

VII-A.5 National Bureau of Standards

The National Bureau of Standards has proposed equipping its facility with a substantial array of experimental equipment having a total value of $3.5 M for Phase 1

(RTM-1) and $16.6 M for Phase 2 (RTM-2), or a total value of $20.2 M. The proposed operating budget includes $0.37 M/year ($2.3 M/year) during Phase 1 (Phase 2) for modifying, improving and replacing equipment.

Phase 1 equipment, to be housed in three experimental areas, includes magnetic spectrometers (a photon-tagging facility; a large acceptance large solid angle QDD electron spectrometer of moderate resolution; a low energy, 43-137 MeV/c, general purpose spectrometer; a DD spectrometer with Ge detector; and a 180° scattering system); non-magnetic spectrometers (a BGO gamma-ray detector; π^{o} spectrometers; and detectors for neutrons and charged particles including fission fragments); and three on-line minicomputer systems (PDP-11 type). For Phase 2, two more experimental areas will be constructed and furnished with additional equipment including magnetic spectrometers (a photon-tagging facility; a pair of QDD spectrometers for coincidence measurements with large solid angle and high resolution, $\Delta p/p=10^{-4}$; charged-pion and neutron detectors; forward-angle electron spectrometers; a beam swinger for out-of-plane measurements; and a magnetic 4π detector); non-magnetic spectrometers (mainly a BGO crystal ball covering about one-third of 4π ; two on-line minicomputer systems (PDP 11); and a minicomputer (VAX type) for data analysis.

The accelerator is to operate as a national user facility, with NBS reserving less than 20% of the total beam hours for a single 200 MeV beam line, corresponding to perhaps 5% of the capacity of the facility, for mission-oriented research.

All proposals for research in nuclear physics, including those of NBS staff, will be subject to peer review by a Program Advisory Committee (PAC) consisting of outside users and NBS personnel. User activities would be supported by a non-NBS organization, denoted for present purposes as User Services (US). User Services would be funded by DOE/NSF and might operate under the aegis of a university, consortium of universities or a management group of associated universities. The Director of US would be from outside the NBS and would be responsible for purchasing, hiring technical personnel, negotiating contracts, etc. Physicists and technicians would be available to provide liaison with users, and to provide detailed assistance with equipment. The Director of US, and the NBS Research Coordinator would appoint the PAC. The Research Coordinator would be responsible for outside user liaison activities and scheduling of beam time.

VII-A.6 Southeastern Universities Research Association

The table below lists the preliminary designs, costs and locations of the spectrometers requested in the SURA proposal. Costs for these total $8.48 M. The high-resolution spectrometer is not part of the current proposal but is an anticipated future addition. Also requested in the initial experimental apparatus are counting equipment, $1.3 M; electronics, $1.35 M; and a computer, $1.2 M, making a total request of $12.33 M.

SPECTROMETER DESIGN OBJECTIVES

Spectrometer	In Proposal: Moderate Resolution Spectrometers		In Proposal: Large Acceptance Spectrometer	Future Addition: High Resolution Spectrometer
Number	(2)	(1)	(1)	(1)
Maximum Momentum (GeV/c)	4.0	8.0	8.0	1.5
Momentum Acceptance (%)	10	5	10	4
Solid Angle (msr)	10-20	5	15	3
Range of Angular Rotation (degrees)	15-165	20-160	25-155	15-165
Resolution ($\Delta p/p$)	10^{-3}	10^{-3}	10^{-2}	10^{-5}
Cost (M$)	1.61 (ea.)	2.65	2.61	4.2
End Station	A, Tagged photon	B	B	A

The SURA consortium has emphasized that these spectrometer designs may change as they are reviewed by the future user community and has stated its intention to involve users closely in this effort. End station A may receive beam from either the linac or the pulse stretcher ring; as noted in the table it is anticipated to be the location of a moderate-resolution spectrometer and a future high-resolution spectrometer. End station B, which receives beam only from the stretcher ring, is expected to house a moderate-resolution and a low-resolution (large acceptance) pair suitable for coincidence experiments. The tagged-photon facility, adjacent to the stretcher ring, is planned to contain a moderate-resolution spectrometer.

A Program Advisory Committee with broad national and international membership would review requests for laboratory resources and beam time, while an in-house staff of experimentalists, engineers, and technicians would be available to assist outside users. The current extensive involvement of several SURA physicists in ongoing research with electron accelerators indicates that the requisite expertise will be available.

1024

A LONG RANGE PLAN FOR NUCLEAR SCIENCE

A Report by the DOE/NSF Nuclear Science Advisory Committee

DECEMBER 1983

DOE/NSF NUCLEAR SCIENCE ADVISORY COMMITTEE

Sam M. Austin	Michigan State University
Gordon A. Baym	University of Illinois
Felix H. Boehm	California Institute of Technology
D. Allan Bromley	Yale University
Herbert H. Chen	University of California, Irvine
Douglas Cline	University of Rochester
Karl A. Erb	Oak Ridge National Laboratory
Hermann A. Grunder	Lawrence Berkeley Laboratory
Cyrus M. Hoffman	Los Alamos National Laboratory
Arthur K. Kerman	Massachusetts Institute of Technology
Malcolm H. Macfarlane	Indiana University
Philip G. Roos	University of Maryland
John P. Schiffer, Chairman	Argonne National Laboratory .
Arthur Z. Schwarzschild	Brookhaven National Laboratory
Ingo Sick	University of Basel
Erich W. Vogt	University of British Columbia
Liaison:	
Enloe T. Ritter	U.S. Department of Energy
Harvey B. Willard	National Science Foundation

PREFACE

The DOE/NSF Nuclear Science Advisory Committee of the Department of Energy and the National Science Foundation is charged with providing advice on a continuing basis regarding the scientific priorities within the field of basic nuclear research to the Department of Energy and the National Science Foundation. It is in this sense that the Committee was asked (Appendix A) to develop a long range plan for the field, a plan that will serve as a framework for coordinated advancement of the research program over the next decade. This long range plan is the second one since the Committee's establishment in 1977; the 1979 Long Range Plan has guided the priorities of the field over the past several years, and has had a substantial impact on new directions and initiatives.

The Committee started discussing the 1983 Long Range Plan at its meetings in January, February, and April 1983 (Appendix B). The major issues were outlined, and the framework for formulating the Plan were established in April. The detailed substance of the Plan emerged from a week-long workshop in Aurora, N.Y. during the week of July 10 (Appendix C). In this Workshop, the scientific questions confronting nuclear science and the relevant technical issues were thoroughly discussed and drafts of sections of the report were formulated. This workshop involved a larger number of participants (about 30 in addition to the Committee) to ensure a broad representation of expertise and of opinions.

The writing and editing of the Long Range Plan document were carried out during August-October of 1983 and, at the meeting of the Committee on the 15th and 16th of October, the final details were discussed and the Plan was endorsed. Copies of the final draft were mailed to the Committee and to external readers, consisting of G. E. Brown, J. Cerny, H. Feshbach, E. M. Henley, and H. J. Jackson for their comments.

The Committee is indebted to a number of individuals for their help in connection with this task, the names of scientists who participated in the workshop and helped in other ways are listed in Appendix C. The chairman would like to express his particular appreciation to Karen Thayer, whose help during the workshop and in the typing of successive drafts has been invaluable.

TABLE OF CONTENTS

SUMMARY v

I. INTRODUCTION 1

II. THE SCIENCE 3

II.1 ELEMENTARY EXCITATIONS 4

II.2 NUCLEAR SYMMETRIES 8

II.3 HIGH SPIN AND EXOTIC NUCLEI 10

II.4 NUCLEONS AND OTHER HADRONS IN NUCLEI 14

II.5 QUARKS AND QCD IN NUCLEI 18

II.6 STRANGENESS IN NUCLEI 20

II.7 THE ELECTROWEAK INTERACTION AND BEYOND 23

II.8 MACROSCOPIC PHENOMENA 28

II.9 EXTREME STATES OF NUCLEAR MATTER 34

II.10 NUCLEI AND THE UNIVERSE 37

III. APPLICATIONS 41

III.1 CONNECTIONS OF NUCLEAR SCIENCE WITH OTHER FIELDS OF BASIC RESEARCH 41

III.2 SOCIETAL APPLICATIONS OF NUCLEAR SCIENCE AND INSTRUMENTATION 45

IV. RESOURCES 53

IV.1 MANPOWER AND TRAINING 53

IV.2 ACCELERATOR FACILITIES 54

IV.3 INSTRUMENTATION FOR NUCLEAR SCIENCE 63

IV.4 INTERNATIONAL COOPERATION 66

IV.5 BUDGETS 67

V. IMPLICATIONS OF SCIENTIFIC OPPORTUNITIES 73

Appendix A 77

Appendix B 79

Appendix C 85

SUMMARY

In response to the request by the Department of Energy and the National Science Foundation for a Long Range Plan for Nuclear Science, the DOE/NSF Nuclear Science Advisory Committee (NSAC) held a number of meetings and a workshop during 1983 to prepare such a plan. From these discussions and studies, we reaffirm our earlier recommendation for the earliest possible start on the construction of a national electron accelerator laboratory and we make the following recommendations for the future:

1) **The research program in nuclear physics, with the facilities in existence or under construction, faces many challenges and opportunities *now*. To address those opportunities, central to the vitality of our field, it is essential that the $20 million incremental adjustment in operating and equipment funds for the ongoing research program that we recommended earlier this year be forthcoming.**

2) **We identify a relativistic heavy ion collider as the highest priority for the next major facility to be constructed, with the potential of addressing a new scientific frontier of fundamental importance.**

3) **To effectively utilize the national electron accelerator, the relativistic heavy ion collider and the other vital facilities of the nuclear research program, we recommend a level of funding rising to $270 million per year (FY 1983 dollars) by the time the above two major construction projects have been completed.**

The nucleus continues to be a rich source of new and often surprising phenomena. Exploration of many of these lies within the scope of existing accelerators and instrumentation. Nuclear physics both in the U. S. and abroad is in the midst of a renaissance of interest, excitement and optimism. The purpose of this Long Range Plan is to provide the United States with a strong role in the leadership of nuclear physics during the coming decade in which this renaissance is developing.

The major questions facing nuclear physics point to a number of important scientific opportunities beyond the reach of the facilities in existence or under construction. Many of these opportunities may be attained by a variety of possible upgrades and additions to the capabilities of present facilities. Among these are the capability for high resolution continuous (CW) electron operation below 1 GeV, substantially enhanced kaon beams, improved medium energy neutrino capability, antiproton beams, improved proton beams of variable energy between 200 and 800 MeV, and also above 800 MeV, intense neutron sources with energies up to a few hundred MeV, capabilities for accelerating very heavy ions with easily varied energy between 3 and 20 MeV per nucleon, a high intensity pulsed muon facility, and a number of other options. We estimate that a reasonable fraction of these opportunities can be realized within the currently envisioned base program. Decisions on relative priorities should be made at a later time and with more specific proposals in hand.

A high intensity 10-30 GeV proton accelerator (kaon factory), capable of producing intense beams of kaons, neutrinos, and other particles would provide substantial opportunities for physics, in areas that are clearly fundamental and exciting. Given our commitment to the national electron accelerator laboratory and the heavy ion collider discussed above, the financial assumptions of this report preclude a major additional facility. But as circumstances change, we want to keep this important option readily available.

There are fundamental issues in nuclear symmetries, in nuclear excitations, and nuclear dynamics for which the facilities, the instrumentation, the techniques and the theoretical framework are just beginning to come into existence. These major questions facing our science are discussed in the body of the report. We note that in addition to the wide variety of studies of nuclear structure and interactions at lower energies, there is an increasing interest in exploring the nuclear implications of quantum

chromodynamics (QCD), the theory of strong interactions that has emerged from particle physics. Not only are the implications of QCD for nuclear physics profound, but nuclear physics may provide fundamental new information on crucial aspects of QCD, such as quark confinement, by studying the elementary constituents of nucleons within nuclear matter. The 4-GeV electron accelerator of the national electron accelerator laboratory recently recommended by NSAC, will be an ideal instrument for exploring this crucial area and it is eagerly awaited by the nuclear physics community.

Our increasing understanding of the underlying structure of nuclei and of the strong interaction between hadrons has developed into a new scientific opportunity of fundamental importance—the chance to find and to explore an entirely new phase of nuclear matter. In the interaction of very energetic colliding beams of heavy atomic nuclei, extreme conditions of energy density will occur, conditions which hitherto have prevailed only in the very early instants of the creation of the universe. We expect many qualitatively new phenomena under these conditions; for example a spectacular transition to a new phase of matter, a quark-gluon plasma, may occur. Observation and study of this new form of strongly interacting matter would clearly have a major impact, not only on nuclear physics, but also on astrophysics, high-energy physics, and on the broader community of science. The facility necessary to achieve this scientific breakthrough is now technically feasible and within our grasp; it is an accelerator that can provide colliding beams of very heavy nuclei with energies of about 30 GeV per nucleon. Its cost can be estimated at this time only very roughly as about 250 million dollars. ***It is the opinion of this Committee that the United States should proceed with the planning for the construction of this relativistic heavy ion collider facility expeditiously, and we see it as the highest priority new scientific opportunity within the purview of our science.*** The tasks of specifying the detailed characteristics of the accelerator, identifying technical issues, and planning for the necessary instrumentation will have to be taken up by workshops and NSAC subcommittees as soon as is appropriate and practical.

The tools, techniques and concepts of nuclear physics have found wide application in our sister sciences—as indeed we have benefited from advances in other sciences. Many applications have been made to the betterment of society and the nation. Radioisotopes and nuclear detectors, for example, have provided both research and clinical medicine with probes of unprecedented specificity and sensitivity. Nuclear medicine is the most rapidly growing subfield of medicine at the present time. The ion beam technologies developed for nuclear physics have revolutionized many aspects of surface and materials science and of technology. And fundamental concepts such as pairing have been passed back and forth between nuclear and condensed matter physics to the enrichment of both. All these are only isolated examples of the unusually broad impact that nuclear science has had and continues to have on other basic sciences, on technology and on society at large.

The budgetary implications of the Long Range Plan are stated. Comparison to other advanced countries indicates that the relative U. S. investment in nuclear physics is presently substantially lower (by a factor of two to three). In order to respond to the major new opportunities confronting the field with the present facilities we point out the need for the 10% ($20 million) incremental adjustment in operating and equipment funds recommended by our Committee on April 29, 1983.

We see this increment as helping alleviate some of the most urgent needs of the field: (a) supporting long-term developmental work on accelerators and instrumentation; (b) fuller utilization of existing facilities that are funded at subcritical levels of operation, far below their potential to produce outstanding research; (c) support of technical manpower for user groups; (d) support of young investigators; and (e) many opportunities in research where a relatively small investment would have significant impact. Looking further into the future, the budgetary implications of the major new facilities are considered as leading to a total annual budget of about $270 million (FY 1983 dollars) after the completion of the relativistic heavy ion collider.

The opportunities for new research confronting us now are highly promising, a number of them involve changing perspectives and close interactions with other fields of science. Our progress towards meeting the challenges ahead of us is only limited by the resources at hand. Within the framework of this Long Range Plan one can anticipate a decade in which nuclear science will confront key scientific questions and in which the United States will play a leading role.

I. INTRODUCTION

The world in which we live is made mostly of nuclear matter. Though some of the important features of our universe, such as chemical and biological properties, are determined by the fragile shell of atomic electrons surrounding the nucleus, others, such as our sources of energy, are predominantly nuclear in origin. The nuclear fusion reactor that is our sun provides the energy for all life in the biosphere, and this solar energy, as stored in wood, coal and oil, has been the basis for the development of civilization on this Earth. It is also nuclear fission and fusion energy that our society has been attempting to tame during the last four decades as the energy sources for future generations.

The drive to study, understand, and control our environment has been the unique distinguishing characteristic of the human race. This must have been true for many millenia, and has been a crucial element in our evolutionary success. But this pursuit of knowledge based on observation and measurement has been institutionalized by our society only in the very recent past, in the form of systematic support of science.

It is clear that the enormous advances mankind has achieved in the last century in controlling the environment and improving the quality of human life are directly related to prior investments made in very basic, then apparently "useless," science. The pursuit of basic knowledge and of the understanding of our world, this very uniquely human curiosity, pays off in the most unexpected ways, and is the soundest investment our society and our country can make in its future.

We view this Long Range Plan for the future of nuclear science in this spirit. Our perspective is to observe, characterize, and attempt to understand the properties of the atomic nuclei which are the overwhelmingly dominant component of the universe in which we live. Many applications have already sprung from this pursuit of knowledge and understanding—some as techniques, perspectives or insights into other basic sciences—others as direct tools to be used to satisfy the needs of society.

The discovery of the *existence* of atomic nuclei is three quarters of a century old—barely one human lifetime. Our knowledge and characterization of nuclear properties have made enormous advances since that discovery—particularly in the latter part of this century and particularly in the United States

As children are taught now in grade school science classes, the nucleus is made of nucleons: neutrons and protons. There are nuclei with one or two nucleons and nuclei with several hundred. The force that holds nuclei together has been studied and characterized but it is understood only in a very qualitative sense. But the properties of nuclei—simple and isolated many-body systems—show a rich variety of phenomena that are often not sensitively dependent on the details of the nuclear force. Many mathematical techniques of group theory have found their realization in descriptions of the symmetries exhibited by nuclear structure. As it involves the study of a many-body system, nuclear physics shares a common frontier and intellectual overlap with solid-state physics on one hand and atomic physics on the other. In astrophysics, the properties of nuclei and nuclear matter play a crucial and detailed role in stellar evolution and are of critical importance in determining the behavior of supernovae and neutron stars.

The characterization of the symmetries and of the simple excitations and simple modes of motion of nuclei is by no means finished. The interplay between these and the limits where the symmetries change or break down needs to be explored systematically, and there are important lessons to be learned not only for our understanding of nuclei, but also for the applicability of mathematical techniques to the properties of (finite) many-body systems. The limits of nuclear structure symmetries and what lies beyond them are explored in a number of directions: with heavy-ion beams, allowing more and more nucleons within the nucleus to become stirred up from their normally quiescent and relatively inert states; with

simpler probes, which can add more energy and momentum to nuclear excitations; and with more precision, exploring the quantitative limits of our understanding of the nucleus.

A currently very lively frontier of nuclear physics is the one it shares with its younger and precocious sister field—particle physics. The quark-gluon theory of elementary particles that has evolved over the past two decades has been enormously successful in describing the properties of these particles. Since protons and neutrons consist of three quarks each, and the mesons, which are the carriers of the nuclear force, are quark-antiquark pairs, the implications of these new ideas about the structure of nucleons on our understanding of the nucleus must be explored.

The fundamental forces governing the physics of nuclei and all subatomic phenomena have recently been embedded in a consistent theoretical framework involving the basic building blocks—quarks and leptons—and their interactions. It is of paramount importance to determine whether this theory is correct or is in need of modification or extension. This requires experiments at high energies in elementary particle physics and precision experiments at low and intermediate energies using nuclei and the tools of nuclear physics. Nuclear physics has provided a testing ground for many implications of the structure of matter and of the basic forces of nature. Some recent examples are limits on the existence of stable free quarks, of light particles such as axions or light Higgs bosons, of neutrino oscillations and neutrino masses, to name only a few.

The expansion of our horizons and knowledge in nuclear physics has had a unique impact on society. The influence of nuclear fission on the modern age is universally known, as is the continuing search for a major new energy source in the form of nuclear fusion. But the applications of nuclear techniques are much more widespread. Nuclear medicine is the fastest growing subfield in medicine, nuclear accelerators find widespread use in fields beyond medicine, ranging from food preservation to the fabrication of integrated circuits and the measurement of the ages of paleolithic artifacts. Nuclear systems measure environmental contaminants with unprecedented accuracy, and nuclear techniques have given life scientists exquisitely sensitive and selective probes. Most important of all, a good fraction of each generation of U. S. nuclear scientists serve society in industry and government, by applying their skills and training in the techniques of the field to further help solve societal problems. For this contribution to continue, and for the continued scientific vitality of the whole field, it is important that the training of young nuclear scientists receive the high priority that it deserves.

The field of nuclear physics is on the threshold of a new phase in its development. A number of new techniques are in the process of being applied to the investigation of areas of the science where our knowledge is at best fragmentary. The next decade is certain to uncover new results, better understanding and improved insights into this major area of our physical universe.

In 1979 the DOE/NSF Nuclear Science Advisory Committee proposed its first Long Range Plan. It is gratifying to see the extent to which the overall recommendations of that Plan have been and are being implemented, even though the *level* of funding has been severely constrained and some difficult priority decisions have had to be made in order to allow the research programs to continue productively within the available, very limited, resources. The severe lag in accelerator construction of the mid 1970's has been partially corrected and several modest but important construction projects are either underway or just completed. These new capabilities open fresh areas for investigation and should provide us with a new harvest of knowledge over the coming decade.

Especially encouraging is the prospect of a 4 GeV CW electron accelerator which has been a gleam in the eyes of the nuclear physics community for a decade and which was the key goal of the 1979 Long Range Plan. Since 1979, that goal has evolved into specific facility proposals and, in 1983, into the specific recommendation of this Committee for the national electron accelerator laboratory. This facility will play a crucial role in extending the frontiers of nuclear physics to encompass studies of the nuclear dynamics based upon quark degrees of freedom on the interface between nuclear and high-energy physics.

II. THE SCIENCE

In this chapter we formulate some of the basic questions facing nuclear physics today. These questions span a broad range, including both strong and electroweak interactions and the properties of the physical world from the scale of nuclear forces to the large-scale structure of the universe. Nuclear science deals with the many-body aspects of the strong interactions. It also deals with tests of fundamental theories and symmetries. In particular, the limits of the electroweak theory must be explored and nuclear science has important contributions to make to this effort, as it does also in connection with the role of nuclei and nuclear processes in determining stellar structure and in constraining cosmological models.

Our understanding of nuclear structure and nuclear dynamics continues to evolve. Under the impact of improved facilities, new techniques in instrumentation and computing, and fresh ideas we have made substantial progress in the last five years. New simple modes of excitation have emerged, new symmetries are appearing and some completely unexpected new phenomena have been discovered. We may expect this trend to continue in the next decade as new facilities with qualitatively new capabilities will become available for use by nuclear scientists. The identification and characterization of simple modes is a difficult challenge requiring a multiplicity of experimental techniques. But as our knowledge of these modes increases and becomes more complete, it can confirm or alter our understanding of the structure of the atomic nucleus very profoundly. The study of the symmetries inherent in the nucleus has been very rewarding and the insights gained of the nature and the limits of the symmetries have considerable overlap with the study of symmetries in other branches of science. There are many aspects of nuclear symmetries that require further work and hold promise of qualitatively new results, particularly outstanding among these is the pursuit of nuclear structure symmetries in very rapidly rotating nuclei.

Our microscopic approach to a multiparticle system seeks to identify its constituents, to discover and study its elementary modes of excitation, and to describe the elementary excitations in terms of the constituent nucleons and, to some extent, the other hadrons. But as experimental evidence accumulates to confirm quantum chromodynamics (QCD) as the correct theoretical framework for hadronic phenomena, it becomes clear that the basic degrees of freedom in multihadron systems are those of the constituent quarks. The theoretical description of the nucleus in terms of quark dynamics is not yet tractable. Nor is it the whole story. Many-body problems can only be solved approximately and in building such approximate solutions qualitative physical insight is as important to our understanding as numerical prediction. In studying a given mode of excitation, the preferred description reproduces the essential physics in the simplest most readily-visualized way and the selection of the proper degrees of freedom contains a crucial element of qualitative judgment.

In most low-energy nuclear phenomena, the quark dynamics appear to be well approximated in terms of three-quark nucleonic clusters with meson exchanges. The validity of this approximation resides in the fact that in the center of nuclei the typical internucleon separations seem to be substantially larger than the diameters of the nucleon "bags" within which the quarks are confined. The appropriate description here is then in terms of nucleons and the effective interactions between them. This nucleons-only regime is well known and far reaching; the remarkable success of "conventional" nuclear models in correlating nuclear phenomena has profound importance for QCD-based dynamics. The richness and beauty of the excitations and phenomena it encompasses are central to nuclear physics; the pursuit of the detailed characterization and understanding of these nucleonic excitations will remain of crucial importance even as we dig deeper towards the underlying quark structure.

At somewhat higher energies and for high-precision treatment of electroweak and hadron-induced processes, the description in terms of inert, structureless nucleons breaks down, and a level of description intermediate between that based on structureless nucleons and that based

on quarks becomes valuable. At this level, the nucleons (bound states of three quarks) can exist and propagate in their ground and excited states, and their effective interactions are described in terms of the exchange of mesons (bound states of quark-antiquark pairs). This intermediate level of description has had impressive successes, but its place in many-particle strong-interaction physics is still imprecisely defined, although a deeper level of understanding appears to be tantalizingly close. At still higher energies, as the substructures of baryons and mesons become important, so also does the quark content of nuclei, and the basic features of QCD should begin to emerge. It will certainly be of considerable interest to understand such distinctions more precisely as more experimental results emerge.

One of the greatest challenges facing nuclear physics today is to find and follow the implications of quarks and of QCD in nuclei. This challenge is experimental and theoretical in equal measure. We must design experiments that will reveal the relevant degrees of freedom as clearly and unambiguously as possible; we must attempt to find experimental signatures for modes of excitation in which the quark degrees of freedom participate individually, not merely as the underlying structure of nucleons and mesons. The 4-GeV CW electron accelerator recently recommended for funding will play a crucial part in beginning this endeavor.

The more macroscopic approach to nuclei views them as aggregates of nuclear, hadronic or quark matter. Experimental studies focus on the flow of matter and energy in collisions between such aggregates. What matter densities are achieved in such collisions? How much energy can be deposited in regions of high density and over how large a volume is this energy distributed? As answers to those questions are found, it becomes possible to study the nuclear equation of state over a wide range of density and temperature. We may look for phase transitions in which new forms of hadronic matter are produced and the many-body aspects of QCD are realized as they were in the early Universe, new forms in which quarks are no longer confined into individual nucleons and mesons. In this report we identify this physics as presenting a major new opportunity of fundamental significance.

Another interface area with elementary particle physics stems from the fact that nuclear physics can provide tests of the theory of the electroweak interactions which together with QCD forms the "Standard Model." The electroweak theory has been enormously successful. Its prediction and its limits of validity must be explored and understood, and nuclear physics and the tools of nuclear physics can provide some of the crucial experiments for this purpose.

The questions in the subsections of this chapter of our report represent the major current issues in nuclear science. There are certainly other interesting issues that deserve attention, but in this report we have identified these ten questions as being central to future progress in nuclear science.

With the facilities in existence, those under construction, and those recommended previously, the field of nuclear science faces a decade in which our horizons have expanded dramatically and in which we may expect major qualitative progress both in the understanding of nuclear structure and nuclear dynamics and in the elucidation of the foundations of nuclear matter in terms of the basic interactions of nature.

II.1 ELEMENTARY EXCITATIONS

What are the simple modes of nuclear motion? What information do they provide about the properties of the nuclear many-body system, and what constraints do they place on fundamental theories of the nucleus?

A nucleus is a quantal system, built from a number of strongly interacting particles, mainly nucleons, but with important admixtures of pions, other mesons, as well as excited states of the nucleons such as the delta isobar. A consequence is the coexistence and interplay in nuclei of an astonishingly rich spectrum of motions, some involving one or a few nucleons, some involving the coherent motion of many nucleons, and still others involving simultaneously pions, deltas and nucleons. But there is considerable order within this complexity. Studies with a variety of projectiles, targets and energies have led to remarkably successful models of nuclear structure. Two aspects of the nuclear many-body system have made this possible. First, there are simple modes of motion of the nucleus which serve as the elementary degrees of freedom for describing more complex motions; and second, reaction probes are available which selectively excite the simple modes. In the past decade many new elementary excitations have been discovered and their properties characterized. The behavior of these excitations, as a function of mass, proton-neutron ratio, angular momentum and energy provides a controlled laboratory in which to test and develop models of nuclear structure.

The Mean Field

Perhaps the most fundamental and conceptually simple of the elementary modes is the motion of a single nucleon in a nucleus. To a good approximation each nucleon moves almost independently in a mean field created by its average interaction with all other nucleons. The goodness of this approximation is the basis of the shell-model

description of nuclear phenomena. Self-consistent Hartree-Fock calculations have now put this picture on a firm theoretical foundation and predict nucleon densities in nuclei that are extremely accurate, deviating significantly from experiment only deep in the nuclear interior.

A similar picture should describe the interaction of a nucleon scattering from a nucleus, but the mean field, or optical model potential, must now contain an imaginary part to account for absorption of the projectile by the nucleus. Accurate measurements of elastic proton scattering cross sections and spin analyzing powers for energies up to 800 MeV have now been made for many nuclei. New experimental techniques yield similar data for neutrons and permit estimates of the difference in the mean field for neutrons and protons, a difference that affects many nuclear phenomena. These data span a broad range of energy and momentum transfer to provide stringent tests for theories of the mean field.

Progress in the derivation of the mean field from a fundamental theory has been made at three levels: in terms of neutrons and protons alone; in a relativistic theory involving implicitly not only the nucleons but also mesons; and finally at the most fundamental level, in terms of the quarks and gluons of QCD.

It is certainly an oversimplification of the nuclear system to consider only nucleon coordinates. Mesons play a central role for the nuclear force; a more complete theory of the nuclear many-body system must explicitly include them and also include relativistic effects. Many-body and multiple scattering theories based on the relativistic Dirac equation are being considered; they have already provided a simple and accurate description of some nuclear properties and scattering. The spin-orbit interaction, crucial to the success of the nuclear shell model, arises naturally from the relativistic treatment, as it does in atoms.

The detailed implementation of relativistic effects in mean field theories awaits future developments. It will be necessary to understand the status of a relativistic field theory based on composite objects rather than on the presumably fundamental quarks; the origin of certain of the mesonic degrees of freedom in the theory; and the meaning of the implied large decrease in nucleon mass in the relativistic nuclear field. Studies of nuclear structure and reactions within this framework will form a major task for the future.

Single Particle and Collective Excitations

In its simplest form, the shell model describes nucleons moving independently, it is not well suited to the description of more coherent modes. Allowing for a residual pairwise interaction between valence nucleons yields an interacting shell model with greatly increased predictive power. It provides a remarkably accurate description of low-lying nuclear energy spectra in light nuclei and near closed shells where detailed calculations are practical and its predictions have a general validity even for nuclei far from the valley of stability. A recent measurement of the charge density difference between ^{205}Tl and ^{206}Pb determined the shape of a specific proton orbital in the deep interior of the lead nucleus as shown in figure II.1-A; it was found to be well described by the shell model.

These single particle excitations are the basis for the descriptions of more complex phenomena, and must be understood for nuclear excitations to be described on a fundamental basis. At present the location and width of hole states is reasonably well understood only for the two outermost shells, and little is known about deeper lying states. The coming generation of high duty-cycle electron accelerators will allow one to form these in a particularly clean fashion by electron induced knockout of a nucleon, and may even permit definitive studies of short range pair correlations between nucleons. Proton induced knockout reactions provide complementary information through their sensitivity to neutrons and their control of the spin degree of freedom.

The macroscopic collective model is often used to describe phenomena in which large numbers of nucleons move coherently. In this model, the nucleus is treated as a liquid drop, capable of vibrating and rotating. The structure of low lying collective states in most nuclei is dominated by the prolate spheroidal shape. Coulomb excitation is a selective probe for this mode, exciting states with probabilities directly related to this quadrupole deformation. New experimental and analysis techniques involving comparisons of Coulomb excitation with light and heavy projectiles allow an essentially complete determination of the quadrupole structure of nuclei. Other studies have found independent-particle and collective excitations coexisting at low excitation in many nuclei.

New technical developments in gamma-ray spectroscopy involving germanium detectors with anti-Compton shields and many-detector arrays, the so-called "crystal ball" multiplicity filters, should allow extension of these studies to still higher spin and excitation. Unusual new collective modes may be discovered in these unexplored regions. Already there may be some indication of octupole, or pear-shaped deformations for nuclei with mass numbers between 220 and 230. In general one hopes to delineate better the interplay of single particle and collective degrees of freedom, and to determine the limits of the macroscopic collective model.

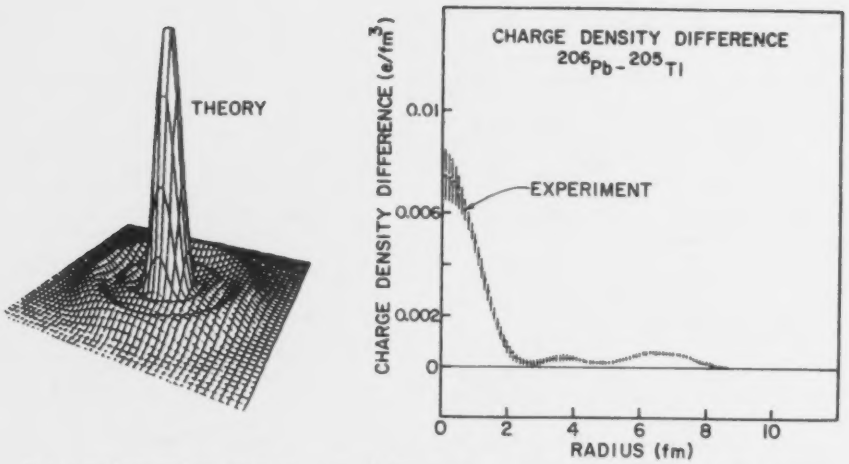

Fig. II.1-A. The density distribution of the least bound proton in ^{206}Pb. The shell model predicts that the last ($3s_{1/2}$) proton in ^{206}Pb should have a distribution with a sharp maximum at the center as shown on the left. Even though there had been considerable skepticism about the validity of the shell model deep inside a heavy nucleus, recent experimental results shown on the right confirm this expectation.

Giant Resonances and Selective Probes

Over the past few years our knowledge of giant resonances has increased dramatically. These resonances are states of the nucleus in which all available nucleons participate coherently. One classifies them into multipoles by the angular momentum L characterizing their vibration (L = 0, monopole; L = 1, dipole; L = 2, quadrupole; etc.). Since the nucleus has four components, protons and neutrons with spin up or down, each multipole vibration can be of four types, neutrons and protons with particular spin orientations moving in or out of phase. These are classified as isoscalar (neutrons and protons in phase), isovector (neutrons and protons out of phase), electric (no spin coherence), and magnetic (spins parallel).

Because these resonances are expected to be broad and often overlapping, it is imperative to use probes which selectively excite the specific modes. The history of the discovery of the giant resonances — the isovector dipole in the mid 1940's, the isoscalar quadrupole in the early 1970's and many others in the past six years — reflects our success in developing such selective probes. Systematic data on the location, width and strength of the electric giant resonances now exist for the isoscalar monopole, quadrupole and octupole and for the isovector monopole, dipole and (possibly) quadrupole. Similar data exist for the spin excitation or magnetic monopole (Gamow-Teller transition) and higher magnetic multipoles. In addition, a variety of data clearly show that the giant dipole resonance exists even when built upon excited states of the nucleus or states with very high spin. The location, width, strength, and systematic variation with nucleus of these simple giant resonance vibrations provide an excellent testing ground for the unification of macroscopic models based on the bulk properties of the nucleus and microscopic descriptions based on the shell model. The location of the isoscalar electric monopole states, in which only radial or breathing motion occurs, provides by far the best measurement of the resistance of nuclear material to compression. This compressibility is important for testing nuclear matter calculations, for understanding shock wave phenomena in heavy-ion collisions and supernova explosions, and for establishing bounds on the sizes of neutron stars.

An important discovery followed from a property of the nucleon-nucleon force around 200 MeV. When a 200-MeV proton projectile knocks a neutron out of a nucleus in a charge exchange (p,n) reaction, it almost always transfers a unit of spin to the nucleus. This process is then a uniquely selective probe for the spin structure of nuclei. A striking application of this probe is the discovery of the giant spin-vibration or Gamow-Teller resonance in

many heavy nuclei as shown in figure II.1-B. The distribution of such spin strength is closely related to the distribution of beta decay strength and is important in a variety of applications in astrophysics (supernova explosions and the rapid-neutron-capture process in the synthesis of the heavy elements) and in the calculation of average fission fragment beta decay spectra in reactors. But perhaps the most important feature of these spin excitations is that their strength is quenched, having only about half the expected value. Evidence is accumulating for a similar quenching in other spin excitations, suggesting that perhaps all spin-dependent phenomena are quenched by about a factor of two. A simple and elegant explanation of this quenching has been proposed in terms of the role of chiral symmetry and the underlying QCD structure in the nucleus. A related simple mechanism is the polarization of the nucleon by the nuclear medium leading to admixtures in the nuclear states of high-lying delta-hole states. However, other phenomena can also affect the transition strength, so that the quantitative importance of this quenching is one of the most interesting open questions involving giant resonances. Further studies of spin excitations offer perhaps the best opportunity for establishing the importance of new degrees of freedom in nuclei. Inelastic scattering and charge-exchange reactions such as (n,p) and (p,n) should play an important role in these studies; new accelerators providing intense beams of polarized protons and neutrons up to a few-hundred MeV will be crucial for such work.

Recent studies of elementary excitations have greatly increased our understanding of a number of the core problems in nuclear physics: the fundamental basis of the nuclear mean field; the importance of relativistic effects on nuclear structure; the interplay of single-particle and collective degrees of freedom in the nucleus and the importance of non-nucleonic degrees of freedom in giant resonance excitations. One expects that further study will further enrich this understanding.

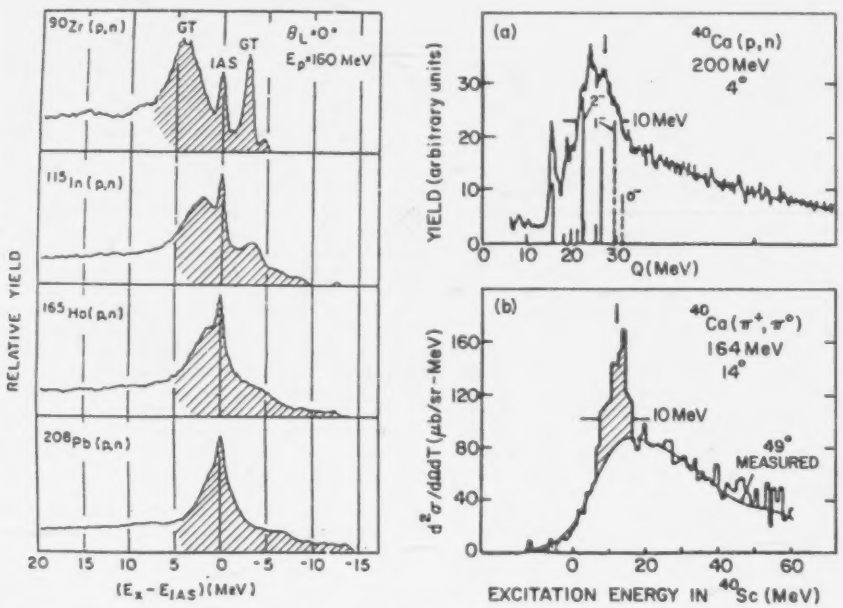

Fig. II.1-B. New giant resonances: evidence for the Gamow-Teller (GT) giant resonance in (p,n) spin flip reactions are shown on the left; on the right recent data from pion charge exchange show evidence for an isovector charge-exchange dipole giant resonance in ^{40}Sc based on ^{40}Ca.

II.2 NUCLEAR SYMMETRIES

How extensively can symmetry considerations be used to describe nuclear properties?

"Symmetry, as wide or as narrow as you may define its meaning, is one idea by which man through the ages has tried to comprehend and create order, beauty and perfection" (H. Weyl). The first serious use of symmetry considerations in physics was in the classification of the shapes of molecules and crystals; the symmetries here are *geometrical*. Later it was realized that the lack of preferred orientations in space-time places severe restrictions on the form and content of physical theories; these are *space-time* symmetries. A third class of symmetry, *dynamic* in character, was first discovered and applied in atomic and nuclear physics around 1930; dynamic symmetries express general properties of the interactions between the constituents of many-body systems (involving the symmetrical interchange of neutrons and protons—isospin invariance—to name but one). Symmetry considerations enable us to identify properties of complex physical systems that transcend the details of their structure and interactions. We concentrate in this section on *dynamic* symmetries. Some milestones in nuclear symmetries are shown in figure II.2-A.

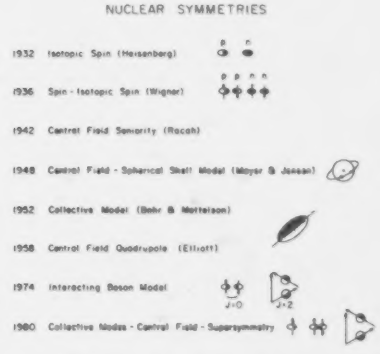
NUCLEAR SYMMETRIES
1932 Isotopic Spin (Heisenberg)
1936 Spin - Isotopic Spin (Wigner)
1942 Central Field Seniority (Racah)
1948 Central Field - Spherical Shell Model (Mayer & Jensen)
1952 Collective Model (Bohr & Mottelson)
1958 Central Field Quadrupole (Elliott)
1974 Interacting Boson Model
1980 Collective Modes - Central Field - Supersymmetry

Fig. II.2-A. Milestones in the development of nuclear symmetries.

Isospin

The symmetry represented by charge independence, expressed by the isospin quantum number, has the mathematical group-theoretic structure of SU(2) and has long been an important tool in the study of nuclear properties. It is now understood in terms of the underlying symmetries in QCD. It relates families of states and giant resonances in nuclei with the same mass number. The energy relations between members of these isobaric multiplets provide exacting tests of our understanding and raise as yet unanswered questions about small charge-dependent components in the nuclear interaction. The relative strengths with which the different multiplet-members are excited in reactions and decays yield precise information about the neutron and proton content of nuclear orbitals.

Isospin considerations have been a fertile source of information about nuclear structure but their application to date has been confined to a restricted class of excitation and to nuclei close to the line of stability. The opportunity now exists to study the isospin properties of new types of nuclear excitation and to push isospin considerations far beyond the line of stability. Detailed study of isobaric multiplets involving low-lying collective excitations may shed light on the elusive relation between the neutron and proton deformations of deformed nuclei.

Isospin symmetry is the simplest of dynamic symmetries; it expresses the fact that nuclear interactions are invariant under interchange of neutrons and protons (charge independence). Spin and isospin symmetries were combined by Wigner in 1936 to fashion a much richer symmetry—supermultiplet [SU(4)] symmetry. The direct impact of supermultiplet symmetry on nuclear physics has been slight; it has been applied only to light nuclei and even there it is strongly broken. There are some prospects for new applications, however. The recently-discovered Gamow-Teller giant resonance involves the simultaneous reversal of the spin and isospin of a single nucleon and it is possible that the supermultiplet symmetry may play a significant role in describing its properties.

Indirectly, of course, supermultiplet symmetry has played a fundamental role in the development of modern physics. A generalization of the symmetry represented by the isospin group [SU(2)] and that of supermultiplet symmetry by [SU(4)] led to the introduction of the Gell-Mann—Ne'eman quark model based on the group [SU(3)]. Indeed, many applications of symmetry considerations in elementary particle physics trace their origins to Wigner's work on supermultiplet theory.

Shell-Model Symmetries

To a surprising extent, nuclear interactions conspire to produce a mean field in which the nucleons move freely. The possibility arises that some of the symmetries of the interactions may achieve simple expression in symmetries of the mean field. Exploitation of this idea started with

20-597 O - 84 - 66

Elliott in 1958. He noted first that the mean nuclear potential is quite similar in shape to a deformed harmonic-oscillator potential, second that this oscillator potential has a dynamical symmetry described by the group SU(3). Systems of nucleons moving almost independently in the mean nuclear potential thus have an approximate SU(3) symmetry. This discovery opened the first fruitful avenue to a microscopic interpretation of nuclear collective properties.

Although Elliott's work is almost 30 years old, much remains to be done before its full implications in nuclear many-body physics become clear. Elliott's early work concerned low-lying modes of excitation, in which valence nucleons populate the levels of the lowest accessible oscillator shells. Consideration of excitations into higher oscillator shells involves enlarging the symmetry group from SU(3) to Sp(6,R). The implications of this group in nuclear physics remains to be explored. Is the symmetry that it carries sufficiently weakly broken to be useful? Can it identify new excitations or families of levels that are of physical interest and are accessible to experimental study? Another interesting property of the harmonic-oscillator potential is that it permits a natural description of another fundamental mode of excitation of nuclei: clustering. The Elliott SU(3) scheme has been extended to describe alpha-particle clustering in nuclei. How accurate is this description?

Pairing and Seniority

The interaction between nucleons in nuclei is particularly strong and attractive between pairs of identical nucleons (neutron pairs and proton pairs) coupled to total angular momentum zero. This pairing property of the interaction between identical nucleons plays a fundamental role in the systematics of both spherical and strongly-deformed nuclei. It is of central importance in studying the effects of rapid rotation on the interaction between nucleons. Nuclear pairing is at bottom a dynamic symmetry of nuclei, the corresponding symmetry label having acquired the name "seniority." Applications of seniority or pairing symmetry to the study of nuclear spectra have been widespread. The main unfinished task, the choice of a physically-motivated generalization to systems involving both valence neutrons and valence protons, has recently come to be viewed from a fresh and promising perspective suggested by work on dynamic symmetries of the collective modes of nuclei.

Collective Models and Symmetry Breaking

The deformation of the mean potential field in a large class of nuclei is an example of a very general phenomenon called spontaneous symmetry breaking. It was applied early in the development of physics to the discussion of ferromagnetism and is now an essential ingredient of modern particle theory. The restoration of symmetry under rotations produces the rotational band, and a new quantum number arises because these nuclei are still axially symmetric. Many nuclear properties can be viewed as a manifestation of this partially broken symmetry of the underlying many-body interactions.

Symmetries of the collective modes can be considered not only from the many-body viewpoint, but also in terms of a phenomenological collective model whose exploration was started by Bohr and Mottelson in the early 1950's and pursued actively since that time. This model possesses three distinct dynamic symmetries, corresponding to special shapes of nuclei: the spherical, the axially deformed, and the axially asymmetric.

Examples of these symmetries abound in the structure of medium and heavy nuclei, although in most cases they are significantly broken. Many important questions remain in the study of this type of symmetry. For example, what are the patterns of symmetry breaking? What is the relation between the dynamic symmetries of the collective modes and the symmetries of the central field? In other words, what is the microscopic origin of the dynamic symmetries of the collective modes?

Interacting Boson Model

Dynamical symmetries of the collective modes have been discovered within the context of a model in which collective features arise because protons and neutrons pair together to form quasi-stable objects (interacting bosons). We have here, on the one hand, the generalization of pairing symmetry alluded to above and, on the other, an opportunity to study from a new viewpoint the microscopic basis of the Bohr-Mottelson collective model. Many open questions remain. In this context, three major threads of nuclear physics meet—the shell-model, the Bohr-Mottelson collective model and new collective dynamic symmetries based on the interacting-boson Hamiltonian. Work in this interface area, with the collective symmetries, and the rich structure of the Bohr-Mottelson model to provide guidance, is bound to yield new insights into the physics of the nucleus.

The Search for Supersymmetries

The concept of symmetry has been further extended in recent years to include a more complex type. Such supersymmetries were originally examined for applications to elementary-particle physics. They apply to mixed systems of bosons and fermions and bring together both bosonic and fermionic states in the same multiplet. Although the

search for supersymmetry has focused on elementary-particle physics, indications of supersymmetry have recently been found in nuclear spectra. The supersymmetry here links the bosonic collective degrees of freedom and the fermionic single-particle degrees of freedom. Numerous interesting questions arise. Can enough convincing examples of supersymmetries be found in nuclei to establish systematic patterns? What is the microscopic origin of supersymmetries in nuclei? What properties of the basic interactions do they express? Since the bosonic degrees of freedom in nuclei are composite, the supersymmetries observed are effective supersymmetries. Is this a general property of all supersymmetries and what implication does it have for supersymmetry searches in elementary particle physics?

Statistical Aspects

In addition to predicting properties of individual levels and excitations, symmetries also affect the statistical properties of physical systems. The relation between statistical properties and symmetries has been systematically investigated in recent years. Techniques have been developed to assess the goodness of symmetries from averaged properties of nuclear spectra. These techniques are being applied to the study of collective symmetries. A problem of great current interest in several branches of physics is the transition between ordered and chaotic behavior, the interplay between statistical properties and those associated with a few selected degrees of freedom. The characterization of this interplay is a profound problem in many-body quantum physics. The nucleus has certain obvious advantages as an arena for such a study. First, the nucleus has an unparalleled richness of dynamic symmetries, stemming from the fact that three levels of fundamental interaction—strong, electromagnetic and weak—play essential parts in determining its structure. Second, the nucleus is a system of precisely the right size (~100 nucleons)—large enough for statistical properties to manifest themselves, not so large that all signs of privileged degrees of freedom are washed out. It will be important to study the interplay between statistical and nonstatistical behavior in nuclei and the role of symmetry considerations in this interplay.

Remarkable though it may seem, the exploitation of dynamical symmetry in nuclei is still, if not in its infancy, not far beyond adolescence. This is due in part to the fact that symmetry considerations, by their very nature, relate data over wide ranges of nuclei and nuclear excitation; data of sufficient quality over sufficient ranges are only now becoming available. The prospects of finding new dynamic symmetries and of finding new uses for those already known, are major challenges for nuclear physics.

II.3 HIGH SPIN AND EXOTIC NUCLEI

How does the nucleus rearrange its shape and structural symmetries under increasingly rapid rotation? What happens to nuclei at the limits of stability?

Nuclei at High Spin

In recent years it has become possible to study nuclei at very high angular momentum under enormous, rotation-induced Coriolis and centrifugal forces. Under these conditions important changes occur in nuclear structure which may still be essentially simple—as long as all the internal energy is concentrated into two macroscopic degrees of freedom, that of collective rotation, and that of particle alignment along the rotation axis.

Changes in pairing and deformation occur as nuclei are subjected to these increasingly strong forces. Do nuclei continue to show both single-particle and collective properties and behavior? When both the temperature and angular momentum are raised, shell effects and pairing effects should disappear; do the nuclei then behave like classical rotating liquid drops, or do new forms of quantal collective motion appear?

The limit to the amount of angular momentum that can be added to a nucleus is provided by the centrifugal force which, in the liquid drop model, is expected to eventually deform the nucleus into a (prolate) triaxial shape before fissioning it into two fragments. The liquid-drop model is based on Coulombic, centrifugal, and nuclear (surface tension) forces, and provides a surprisingly good estimate of the gross limiting angular momentum for fission as a function of neutron and proton number, giving a maximum value of spin of ~70 units for stable nuclei around mass 130. It predicts smaller maximum spin values both for heavier nuclei (due to increasing Coulomb repulsion) and for lighter nuclei (due to the rapid increase in the centrifugal force).

The nucleus carries angular momentum in two ways: by the alignment of the orbital motion of individual nucleons along the rotation axis and, if deformed, by the rotation of the nucleus as a whole. The nucleon alignments tend to destabilize the collective rotation, whereas the centrifugal stretching tends to stabilize the collectivity. Rather extreme examples of these two modes are shown in figure II.3-A. On the right, the levels of ^{212}Rn illustrate particle alignment; the level sequence is quite irregular, with a variety of electromagnetic transitions. On the left, the yrast sequence (lowest energy for each spin) of ^{238}U exhibits features characteristic of a spheroidal rotor, that is, regularly spaced levels connected by

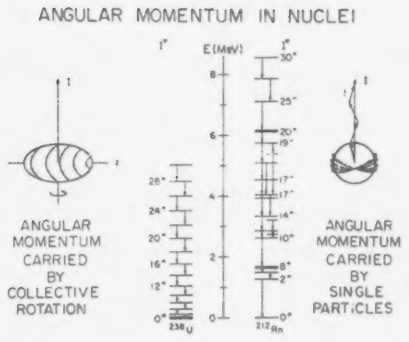

Fig. II.3-A. The sequence of angular momenta in two nuclei. On the left we see the regular level scheme of a nucleus that is a good rotor: ^{238}U. On the right is an example of the irregular pattern that arises as angular momentum increase is being accommodated by the successive alignment of nucleons in single-particle orbitals, in the levels of ^{212}Rn.

enhanced photon emissions. Most nuclei, however, combine both types of motion, and it is this interplay between collective and single-particle motion that makes the behavior of cold nuclei with changing angular momentum so fascinating and so rich in variety.

The nuclear pairing correlations play an important role for spins up to about 30 units. The nucleon orbitals in a static deformed potential can each accommodate two nucleons, corresponding to the two time reversed states. Thus every orbital, whose nucleons have individual angular momenta j, can give rise to a pair of nucleons with total spin zero. The nucleons in a just-filled orbital can scatter as a *pair* into a nearby empty orbital, and the coherent scattering pattern that develops comprises the nuclear pairing correlations. These correlations affect the ability of the nucleus to generate angular momentum and the magnitude of the nuclear moment of inertia.

With high-resolution gamma-ray spectroscopy, we can investigate the changes caused by increased angular momentum as evidenced in the alignments, shapes, and pairing correlations for discrete states up to 20-30 units of spin. These studies have led to an understanding of why the nucleus does not show the nuclear analog of the dramatic phase transition that is seen in superconducting solids where similar pairing correlations occur—the Meissner effect. With increasing angular momentum, the nucleus undergoes a gradual phase transition from the paired to a normal state. Nuclear phase transitions, with only ~100 particles, are less sharp than those in an effectively infinite solid. Because the several pairs of nucleons in the paired phase are made of nucleons with very different j-values and because the Coriolis interaction is stronger the greater the value of j, large irregularities in the nuclear level spacings can occur due to the sudden alignment along the rotation axis of one high-j pair of particles, with all the other (lower-j) nucleons essentially retaining their pairing correlations. An example of the crossing of two bands, the paired and the 2-quasi-particle band, is shown in figure II.3-B. The spectroscopic study of these alignments, or band crossings, is a new endeavor of the last few years and has contributed greatly to our knowledge of the pairing correlations, but has also left unexplained, as yet, a number of changes in behavior at the band crossing. An example of the degree of understanding achieved is illustrated by the fact that the change in the band-crossing frequency (one-half the transition energy) for the first $i_{13/2}$ neutron band-crossing in several odd-mass rare-earth nuclei appears to be well correlated with the deformation (quadrupole moment) of the odd neutron orbital occupied. The blocking effect of the odd neutron on the pairing correlations depends on its configuration; not all orbitals participate equally in the pairing state, as given by the model based on the simplest

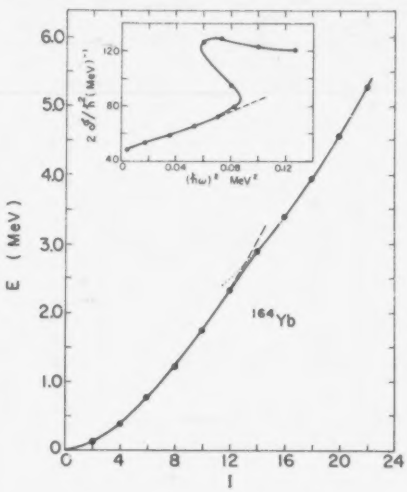

Fig. II.3-B. Plot of excitation energy (E) against spin (I) for the lowest-lying (yrast) levels of ^{164}Yb. The insert shows the same data in a typical backbending plot of the moment of inertia ($2\ \mathcal{J}/\hbar^2$) against the rate of rotation $(\hbar\omega)^2$ deduced from these energies. The dotted and dashed lines show the extensions of the ground and two-quasi-neutron bands that cross to form the backbend.

Bardeen-Cooper-Schrieffer (BCS) theory of superconductivity. There are other interesting and detailed results from measuring the changes in other nuclear properties (such as lifetime and branching ratios) through the first "backbend" discontinuity in the sequence of highest spin states; some of these can be explained, but others are not yet understood.

Discrete-state γ-ray studies may be pushed to spins as high as 40-50 units using newly developed multidetector arrays: "crystal balls" and Compton suppression techniques. But in the foreseeable future, there probably will remain a region of highest spin (up to 60-70 in the rare-earth nuclei), where the discrete transitions become too weak to be observed, and that region can thus only be studied through its continuum γ-ray spectra. Such studies of necessity yield only average properties over a distribution of states. But they still show significant changes with angular momentum, and at these high spins nuclei along the yrast line may still be as individualistic as they are in the ground state. The goal of such studies is not only to determine the persistence of shell effects, but also the role of particle alignments and the importance of collective motion on the properties of nuclei up to the highest spins before fission. Very interesting first steps have been made, both in experimental measurements and in theoretical calculations, to define and measure "kinematic" and "dynamic" moments of inertia. The latter are very sensitive to the local configuration, that is, to changes in alignment and deformation, but have only been available and understood from experiments performed during the past year. In addition, first experiments are being made to measure average lifetimes and magnetic moments in the continuum, and angular distribution measurements have provided evidence in some transitional nuclei of electromagnetic transitions of dipole character, suggesting possible changes in shape at high spin.

Angular momentum may be carried by nuclei in still another, very special way, in the orbital motion of two, almost distinct, nuclear fragments rotating around each other in a transient, molecule-like configuration. Examples of such behavior seem to appear throughout the range of available nuclear systems, but particularly striking examples occur in light nuclei at excitation energies of several tens of MeV above the nuclear ground state. This is a domain where relatively unstructured many-body features of nuclear systems were thought to predominate, but imbedded in this chaotic region are found structures involving simple coherent patterns of motion that have many features in common with atomic molecules, have relatively long lifetimes, and appear in the form of sharp resonances in the yields of heavy-ion reactions. Measurements have shown that in some cases these structures reflect a reorganization of the host nucleus into two massive clusters undergoing an as yet imperfectly understood form of dinuclear molecular motion.

The study of these quasi-molecular and resonance phenomena at high excitation has progressed in step with advances in the ion source, accelerator, and detection apparatus technologies, and has broadened from its original focus on a few nuclei (^{24}Mg and ^{28}Si) to encompass the entire periodic chart. It is clear that the narrowness of these resonances implies a stability that is remarkable at such high excitation energies. We would very much like to know what physical processes underlie this stability.

Molecule-like configurations are also thought to be crucial to understanding the narrow peaks observed in the positron spectra from U + U collisions at around 6 MeV/amu. The positrons reflect spontaneous decay of the e^-e^+ vacuum in the supercritical electromagnetic field of two uranium nuclei in close proximity; the 70-80 keV observed width of the peaks implies the formation of a long-lived giant system in which two uranium nuclei maintain a quasi-stable fixed separation for an extended period of time. The implications of such simple structures at high excitation in the 500 nucleon system are very exciting and have not been fully absorbed.

Future Opportunities

There are many as yet unanswered questions in high-spin nuclear physics. Where and how are the pairing correlations finally quenched by the rotation? What is the detailed nuclear shape and how does it vary as a function of spin in going down an average path through several bands connected by crossings (alignments)? What are the changes in shape induced by excitation above the yrast line holding the spin fixed? Do particle alignments continue as a source of angular momentum all the way to fission, and are the responsible orbitals those of high j from the next shell or even the one above that? What are the appropriate quantum numbers to describe the system at the highest spins? Are there still shell effects along the yrast line at high spin? This is related to interesting questions connected with "superdeformation" and the shape evolution to fission. If there are very large deformations, with the pole-to-pole distance twice that of the diameter at the nuclear equator, what part is played by shell effects and what part by the predicted stretching of a liquid drop before fission? Over a broad range of masses the angular momentum we can study is limited mainly by fission, so it is clear we can reach situations where the centrifugal force produces major changes. How these are influenced by new shell effects or other aspects of the single-particle motion will be fascinating to study. In addition, we still have the problem of the molecule-like resonances to understand. To accomplish this, experiments must be

done with good energy resolution and with highly efficient special-purpose detection apparatus capable of probing specifically the molecular degrees of freedom. Very few theorists have possessed the means of carrying out even remotely realistic calculations and thus the full ramifications of the two-center shell model, the double and multi-resonance coupled channels models, the time-dependent Hartree-Fock approach, and other promising avenues remain largely unexplored. The situation is changing, however, and continued emphasis on modernizing our computing facilities should pay dividends in unlocking the secrets of these quasi-stable configurations found at high excitation energies.

Exotic Nuclei

An important dimension in nuclear structure is that represented by changes in the number of neutrons vs. protons; this clearly yields marked changes in nuclear shapes, structure, and properties. In regions of a great excess of neutrons or of protons, the question arises whether this imbalance affects the relative importance of the effective nn, pp, and particularly the np interactions. This would be reflected in changes in the masses, in different shell closures, and thus in different shapes. Near the proton and neutron drip lines (zero particle binding energy) one has observed in the last few years exotic forms of radioactivity, such as ground-state proton decay, β-delayed two-neutron and two-proton emission, and β-delayed fission.

The production of very heavy elements and the attempts to reach a possible "island of stability" formed by the still heavier "superheavy elements" were pursued in the past by irradiating the heaviest targets with the lowest-Z projectiles that could make the desired nucleus. This method was employed to produce new elements up through 106 at Berkeley, but with decreasing yields. Scientists at Dubna pioneered a new method for making element 106, involving less excitation energy in the compound nucleus, using a closed-shell nucleus, ^{208}Pb or ^{209}Bi, as the target for appropriate heavy-ion projectiles. This technique, coupled with the use of an excellent velocity filter to separate the few product nuclei from the beam particles, enabled the group at G.S.I. to observe ^{262}107 last year and possibly a single atom of ^{266}109 this year. The tentative decay chains of these nuclides are shown in figure II.3-C. Since the single atom of element 109 was produced in 12 days of bombardment, it does not seem likely that one will be able to follow this path to much heavier elements.

Neutron-deficient nuclei far from stability are most frequently studied by using a heavy-ion compound-nucleus reaction (although high-energy proton spallation is also used) and then selecting the desired nucleus with an

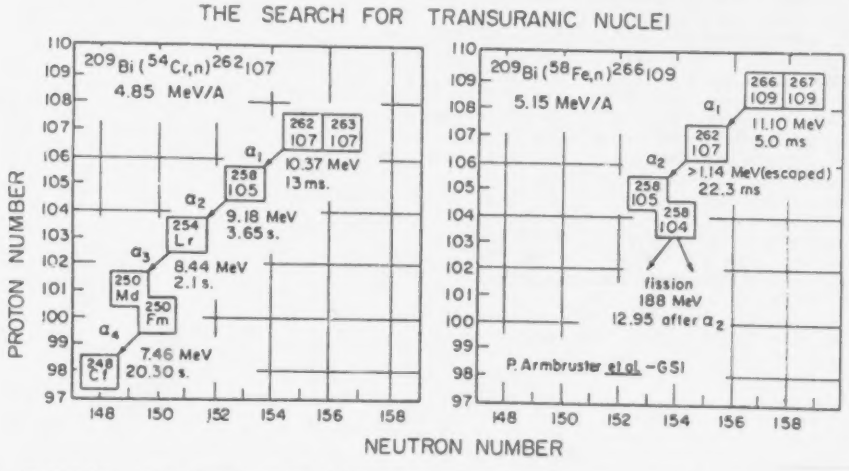

Fig. II.3-C. Evidence for new heavy elements. On the left is the decay scheme for an isotope of element 107 of which several atoms have been identified. On the right is the level scheme suggested for the one atom of element 109 that has been tentatively identified so far, with a lifetime of 5 msec.

isotope separator. Nuclei with a neutron excess are studied by coupling a similar isotope separator to a fissionable target in a reactor or again looking at the products of high-energy spallation or projectile fragmentation. By these methods the systematics of the energy levels of a wide range of isotopes have been obtained in a few cases, and, in still fewer cases, some transition probabilities have been determined. A significant new development has been the increased use of atomic-beam and laser techniques for the determination of nuclear spins, moments, and changes in the mean-square-charge radius. In favorable elements properties can be measured for long sequences of isotopes.

The systematics of energy levels and moments obtained so far show that shell closures depend on the number of the other type of nucleon present; that is, shells are a dynamic variable of the nucleonic makeup and depend on the neutron-proton interactions. Pragmatic tests of various mass formulae can be made by Q-value determinations from transfer reactions or from α decay or from β-decay endpoints. Far from stability β decay may go to highly excited levels; the near continuum of excited states in the daughter nucleus leads to the description of the β-decay rate in terms of an energy-dependent strength function which is crucial to the calculation of stellar production of heavy elements in supernovae. Direct proton radioactivity is also possible in neutron-deficient nuclei and is most likely at the very limits of particle stability. This decay mode was originally observed in a high spin isomer of a nuclide closer to beta stability, but recently was also seen in two rare-earth isotopes, most likely to be ground state decays.

Such radioactivities should become more common as studies extend to the limits of particle stability and even new radioactivities such as direct two-proton emission, should be discovered. The limits of particle stability have been reached only in very light nuclei: future research should greatly increase our knowledge of these exotic decay modes.

II.4 NUCLEONS AND OTHER HADRONS IN NUCLEI

What are the limits for describing the nucleus in terms of nucleons? How do the non-nucleonic, hadronic degrees of freedom manifest themselves? What is the nature of the strong interactions between the hadrons, and how are these interactions modified inside a nucleus?

For most low-energy phenomena, the simplest and therefore the most appropriate description is that in terms of nucleons and the effective interactions between them. As was discussed in Sec. II.1, the main role of the interactions between nucleons inside a nucleus is to establish a smooth mean field in which the nucleons move almost freely. The interaction between nucleons imbedded in nuclear matter is referred to as the *effective* interaction in the nuclear medium. It is qualitatively different from the interaction between free nucleons. In particular, it is not strongly repulsive at short distances; it depends, furthermore, not only on the distance between interacting nucleons but on the ambient matter density of their nuclear environment.

Not all properties of nuclei can be described in terms of protons and neutrons alone. This is not at all surprising since the baryons (of which the proton and neutron are the lightest and most stable) have structure and excitations of their own. These hadronic degrees of freedom are manifest in the spectrum of free baryons and of the mesons which couple them, and reflect the elementary quark composition of strongly interacting particles. These degrees of freedom are at the interface between nuclear and particle physics, with the associated questions spanning the range from hadron dynamics to nuclear structure. The physics of the intermediate and short-range nuclear force clearly involves baryonic excitations, with the role of explicit quark and gluon degrees of freedom still an open question. The propagation of hadronic resonances through the nuclear medium, including modifications arising from multi-nucleon interactions, promises new insights into nuclear forces. The nuclear electromagnetic and weak currents are altered from their "classical" values by the flow of charged mesons and by excitation of nucleon isobars. Even at low energy, spin-isospin modes can couple strongly to modes generated by nucleon excitation. The study of all of these phenomena has begun vigorously in the last few years, with the horizon of "nuclear degrees of freedom" irrevocably enlarged beyond the limited view of nucleons only. The understanding of these phenomena, extrapolation into new regimes such as high density, and the search for qualitatively new nuclear modes based upon the internal degrees of freedom of the nucleon comprise a central program in nuclear science.

The delta (Δ) plays a special role in these considerations. It is the lowest excitation of the nucleon and appears as an isolated resonance dominating the landscape of pion- and photon-nucleon interactions. In quark language, the Δ is a "static" spin-isospin excitation of the nucleon, accounting for its importance in low-energy phenomena. A focus on Δ-nuclear systems will be a unifying element in much of the discussion to follow.

The Two-Baryon System

The most basic arena in which to study the interplay of nuclear and nucleon degrees of freedom is the two-baryon system. Careful investigation of such systems is of crucial importance for the understanding of hadronic effects in nuclei. There has been enormous effort recently in examining the coupled two-nucleon, nucleon-delta, and pion-two nucleon systems at intermediate energy, measuring spin observables in particular. An example of data is shown in figure II.4-A. A major motivation for this program, in addition to refining understanding of the nuclear force, is the search for possible dibaryons associated with the color degree of freedom "hidden" in the study of baryon spectroscopy. Despite considerable theoretical effort, the data have not been reproduced in a unified way with hadronic degrees of freedom alone. Progress in experimental determinations of two-baryon spin amplitudes will provide important further clues.

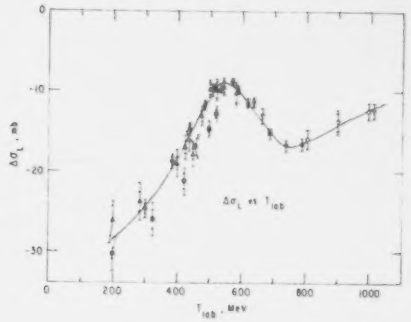

Fig. II.4-A. Compilation of measurements of the polarization parameter $\Delta\sigma_L$ in proton-proton scattering from a number of laboratories. There has been speculation that the sharp energy dependence may be a reflection of exotic 6-quark states.

Studies of antinucleon-nucleon collisions may uniquely complement nucleon-nucleon experiments by highlighting the difference between quark-quark and quark-antiquark interactions. Medium- and long-range meson-exchange contributions to the nucleon-antinucleon force are simply related to the nucleon-nucleon force, but the annihilation of nucleons by antinucleons introduces entirely new features. Some calculations suggest that since the force between a nucleon and an antinucleon is much more attractive than the NN force it may support a number of bound states and resonances, some of which may couple to narrow diquark-antidiquark states.

The nuclear electromagnetic current has been probed to distances small compared with the inter-nucleon separation. The interplay between nucleon and nuclear degrees of freedom is seen clearly here: though the current is a rather simple one-body operator at the quark level, it is decidedly *not* a one-nucleon operator, and the structure of the operator is a measure of the strong-interaction dynamics of the nuclear system. The two-nucleon electromagnetic current recently seen in photodissociation of the deuteron and illustrated in figure II.4-B clearly demonstrates the spectacular failure of using the "classical" one-nucleon current alone and probes a region where the simple exchange currents, based upon the one-pion-exchange potential and charge conservation, must be supplemented by heavier meson and isobar contributions. A key problem of intermediate energy nuclear physics is to develop a quantitative understanding of this question in an underlying QCD description.

Nuclear Matter

It is found that, although individual nuclei may be very different in their low-energy properties, the nature of the nuclear substance in the interior is the same for all but the lightest nuclei. The idea of nuclear matter arose in the attempt to study the material deep inside nuclei free from complications connected with finite size and special "surface" properties. Normal nuclear matter is an idealized infinite system abstracted to allow calculation of properties of the material at the heart of a heavy nucleus.

The crucial problem of calculating the binding energy per nucleon and the density of nuclear matter from a given two-body free-nucleon interaction has been solved. It is now understood why nuclear matter has roughly its observed binding energy and density. A significant residual discrepancy, larger than the errors in the calculation, remains between the observed properties of nuclear matter and those predicted on the basis of the best nucleon-nucleon interaction potentials. At the correct density, nuclear matter is more tightly bound by about 1 MeV per nucleon than the best theoretical estimates. Attempts are now being made to account for the discrepancy in terms of three-body interactions between nucleons or equivalently by explicit reference to the internal structure of nucleons.

Few Body Systems and Forces

The improvement of our microscopic understanding of the three-nucleon systems is a crucial step in the development of a quantitative microscopic theory of nuclear structure. The experimental data to consider for the bound states include binding energies, the ^{3}H-^{3}He mass difference, radial distributions of charge and magnetization, and the interaction and absorption of pions by these

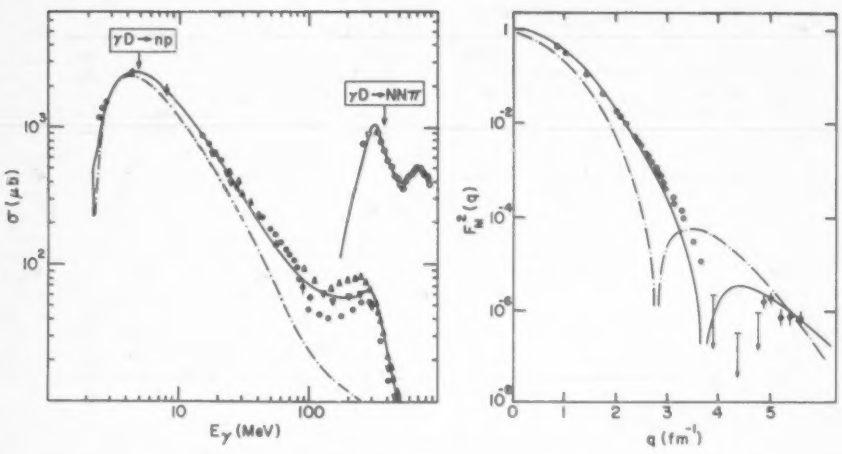

Fig. II.4-8. On the left are data on the photodisintegration of the deuteron and on the right the magnetic form factor for the ^{3}He nucleus. These data demonstrate the limitations of the "nucleons only" description of nuclei. The dashed line represents a calculation with only nucleons included, while the solid line includes mesonic effects and fits the data reasonably.

nuclei. Given a nucleon-nucleon interaction potential fitted to two-nucleon data, it is now possible to calculate the binding energies of three-body nuclei to an estimated accuracy of better than 1%. A significant discrepancy remains between the observed binding energies and those computed from the best two-nucleon interactions; the calculated binding energies are too small by about 1 MeV. This underbinding is consistent with what is found in nuclear-matter studies and presumably is of similar origin.

Three-body nuclei offer the simplest bound system for studying the isospin structure of electromagnetic exchange currents. The ^{3}He magnetic form factor data were shown in figure II.4-B together with the wholly inadequate one-nucleon-current predictions. The analogous data for ^{3}H are awaited eagerly. Our quantitative understanding of exchange currents is still largely restricted to parts of the long-range pion exchange current which are largely independent of dynamical models. For example, the many-body corrections to the nuclear charge operator are bound up with relativistic corrections that must be made in the usual theories of nuclear systems. This problem points to the more general, very important issue of the need for a consistent relativistic theory of nuclei. The pressure for this is provided in many ways, including the probing of nuclei at short-distances with large momentum transfer electron scattering, and the intriguing systematics uncovered in phenomenological relativistic treatments of the nuclear mean field. A substantial theoretical effort is required here.

Great strides have been made recently in our understanding of effective interactions within the nuclear medium. The approximate inclusion in treatments of finite nuclei of the effective interaction resulting from nuclear matter theory has led to a new level of quantitative success and expectations for microscopic many-body calculations of nuclear structure and dynamics. One is now able, for example, to attach significance to systematic small discrepancies between Hartree-Fock calculations and the precise maps of nuclear densities obtained in medium-energy electron- and hadron-scattering experiments. Microscopic analyses of intermediate-energy proton elastic and inelastic scattering data reveal very clearly the role of medium modifications to the internucleon force. Nucleon inelastic scattering and charge exchange transitions initiated at 100-400 MeV have been discovered to provide very useful filters to probe the strength and momentum-dependence of specific terms in the effective interaction. This advance arose from the use of an adequate direct-reaction theory, combined with the selective excitation of states of simple structure (especially involving spin transfer), and with transition densities measured in complementary electromagnetic experiments.

Non-nucleonic Degrees of Freedom in More Complex Systems

In extending these studies to heavier nuclei, it becomes clear that meson contributions play an important role in essentially all large momentum-transfer electromagnetic form factors, particularly for magnetic transitions. Here, the richness of the nuclear spectrum (states of varying angular momentum and isospin transfer and structure) must be utilized to extract systematically the spin, isospin and momentum transfer dependence of the two-body current. The systematics then should lead to the isolation of multi-nucleon contributions to the nuclear current. Such contributions are linked to the fundamental nature of short-range hadron dynamics. The nuclear weak current has been probed far less extensively, partly because of the extreme kinematic restrictions of processes such as muon capture or beta decay.

Spin-isospin modes in nuclei present a particularly good example of possible strong coupling between nucleon and nuclear degrees of freedom at low excitation energy. As indicated above, this possibility arises from the fact that the Δ is a simple spin-isospin excitation of the nucleon. In a series of experiments at Indiana University, the intermediate energy (p,n) reaction proved to be the right tool for locating the nuclear spin-flip response. These experiments, together with electromagnetic studies of transverse magnetic excitations, have systematically found only about half of the expected strength. Qualitatively, some of the strength is expected to be mixed into high-lying Δ-hole excitations with the same quantum numbers. Quantitative resolution of the question will benefit from measurements of the spin-transfer in the continuum region.

Turning to hadron dynamics, the wealth of data from the meson factories has dramatically improved our understanding in the Δ region. The studies at the two-baryon level have been discussed already. Systematic studies of pion reactions with heavier nuclei have included energy and target dependence of pion elastic and inelastic scattering, pion single and double charge exchange, and total pion annihilation. For light nuclei, a rather complete picture of the pion-nucleus reaction, including "competition" between pion scattering and annihilation, has emerged, and is supplemented by electromagnetic data in the corresponding energy region. Much of the data have been described rather concisely in terms of Δ-hole states with a strongly-absorptive, spin and isospin dependent Δ-nucleus interaction. While this theoretical description represents considerable progress, many questions remain open. The Δ reaction processes in heavy nuclei, involving many nucleons, are certainly poorly understood. The important pion annihilation process, which provides a direct link to theories of the strong force, has not been understood microscopically. The role of multi-nucleon absorption processes, analogs of many-body forces at low energy, is an open question, and the rapid fall of the annihilation cross section just above the resonance is not consistent with available models. While we have learned a great deal about the phenomenology of Δ-dynamics in nuclei, fundamental advances in microscopic understanding of the strong short-range force in nuclei remain ahead of us. This progress will depend upon the availability of more data specifically aimed at unraveling the spin-isospin structure and the multibody nature of the Δ-nucleus interaction and the precision nature of the electromagnetic probe must be brought to bear upon these questions more effectively. We note that resonance dominance of meson reaction processes leads in some cases to qualitative tests of nuclear structure. For example, the isospin selection rule implied by Δ dominance leads to a direct measure of isospin mixing in nuclear particle-hole states.

We have focused upon the nuclear interaction of baryon resonances. However, meson interactions not dominated by resonances, such as the low-energy (S-wave) interactions, also pose interesting problems. For example, the origin of the repulsive S-wave pion-nucleus interaction and of the narrow width of deeply-bound pionic atom states has no accepted explanation. These problems are basic to understanding pion propagation in nuclei over a broad range of kinematic conditions and nuclear densities. Experimental reaction studies in this low-energy region have not yet been pushed very far.

The existing key facilities in this area of nuclear physics are LAMPF with its pion, muon and proton beams, and neutrino capabilities, the Bates Laboratory with high-resolution electron scattering, and the Indiana University cyclotron with its proton beams. In the last decade nuclear physics has changed radically under the impact of new research with these intermediate-energy accelerators. The new 4-GeV CW electron accelerator will be an essential forefront facility. However, as was noted in the 1983 Report of our Panel on Electron Accelerator Facilities, CW electron capability up to 1 GeV is likely to play a key role in these areas of nuclear physics. In other areas, upgrading the Indiana cyclotron and its new cooler to higher energies could be an important national program and an improved pion channel deserves serious consideration.

The interpretation of experimental results addressing the fundamental issues of hadron dynamics and large momentum transfer nuclear excitations relies heavily upon theoretical interpretation in terms of strong interaction models and upon assumptions about short-range

nuclear structure. Many of the interesting questions are inextricably tied up with the need for the development of a consistent relativistic theoretical treatment of nuclei.

II.5 QUARKS AND QCD IN NUCLEI

How does the nucleus appear in terms of its quark content and how does the nuclear medium affect quark confinement?

We now believe that hadrons and their interactions have an underlying quark structure whose effects extend beyond the known properties of free baryons and mesons. One of the fundamental questions of nuclear physics is the importance of these quark degrees of freedom for our understanding of nuclei. Models of nuclear structure and nuclear matter have not yet dealt explicitly with this problem. Within nuclei, two complementary questions arise. First, does the fact that the nucleon itself is a composite particle have important consequences for the properties of nuclei? And secondly, how can the effect of the nuclear medium on the nucleon lead us to a better understanding of the manner in which quarks are confined?

On the first question we need to understand better how the observed features of hadrons and their interactions fit into the framework of QCD. QCD is not presently soluble, but in describing hadronic physics it leads to useful approximations in two simple limits. At short distances (high momentum transfer), the "colored" quarks (and gluons) are asymptotically free. At longer distances, the quarks and gluons are confined in "colorless" color-singlet clusters (hadrons), which interact via the exchange of other hadrons (mesons), as in the traditional interpretation of the internucleon potentials. Although the transition between these two regimes has not yet been understood quantitatively, it has been incorporated in existing models by the *ad hoc* introduction of a potential, or "bag," to confine the quarks and gluons. These models have already had significant success in accounting for some properties of hadron structure and hadron-hadron forces, but lead to a number of fundamental questions that remain to be addressed by theory and experiment. Is there a sharp transition between the meson- and gluon-exchange regimes, and if so, what are the characteristic dimensions? What are the relative roles of the constituent quarks and of the meson cloud in hadron structure? How are these roles altered when two hadrons interact? How does QCD produce the observed short-range repulsion between two nucleons? Do the quarks and gluons contribute essentially (e.g., via color excitations of the interacting clusters) to the intermediate-range attraction?

The search for QCD effects in nuclei is very new with only a few but extremely significant results in hand. Most striking is the result from deep inelastic scattering of 250 GeV muons from iron and deuterium which has been beautifully verified by the re-analysis of deep inelastic electron scattering data taken a decade ago at SLAC at lower electron energies between 8 and 20 GeV. These deep inelastic scattering reactions result from a single hard collision of the lepton with a quark within the nucleus. Comparison of the yields from iron nuclei, with 56 nucleons, and deuterium with only two, as a function of the variable x, shows, as seen in figure II.5-A, that for small x the yield from iron is relatively larger by 15%. As x increases the ratio first drops, and then increases again as x approaches one. This latter increase is expected, but the unanticipated behavior at $x < 0.6$ indicates that the quarks in a heavy nucleus have lower average momentum than those in the deuteron. The low-momentum effect may possibly be understood in terms of an increase in the relative number of virtual mesons (mostly pions) in Fe relative to deuterium. The *decrease* in the relative yield for $0.3 \leqslant x \leqslant 0.6$ may indicate a depletion of the higher momentum component of the constituent quarks, which

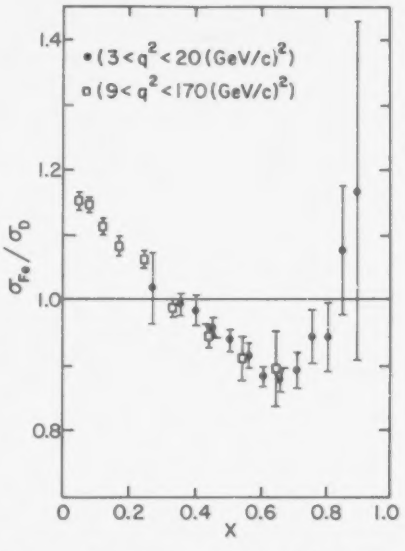

Fig. II.5-A. The observed ratio for the highly inelastic electron scattering cross sections for iron to that for deuterium. The data are a collection of results employing high-energy electrons and muons and are plotted as a function of the scaling variable $x (\equiv q^2/2M_p\nu)$. The unexpected increase in the ratio for x below 0.6 indicates relatively more quarks with lower momenta in the heavy nucleus.

could result from their occupying a larger volume, either due to "percolation" or from 6 quarks sharing a larger "bag." The results of these experiments are potentially very important as they could appreciably alter our ideas on what happens to the nucleon in the nucleus.

All inelastic scattering processes involving very high momentum transfer between leptons and hadronic systems are best understood by treating the process as a hard collision with a single quark. This point has been demonstrated in a host of deeply inelastic scattering experiments which qualitatively can be accounted for within the framework of QCD. In the high momentum transfer limit, QCD predicts a power law falloff of the helicity conserving elastic form factors. Figure II.5-B shows this result applied to the deuterium form factor. This prediction appears to work at momentum transfers less than 1 GeV/c. This is viewed as surprising, insofar as one believes that the non-perturbative effects of QCD would be extremely important at values of momentum transfer, q^2, that small. For an understanding of nuclei in terms of their quark substructure, the result presented in figure II.5-B is most tantalizing.

When considering the directions of future research one should realize that up to the present detailed knowledge of hadronic structure has come almost exclusively from the deep inelastic scattering of high energy leptons and e^+e^- collisions producing hadrons. Electrons, the most accessible leptonic probe, have provided the bulk of the information, although potentially there is further information contained in neutrino scattering. The interactions between the hadrons may be investigated by the scattering of high energy leptons from composite systems as well as direct hadron-hadron scattering.

Further measurements of quark distribution functions from inclusive deep inelastic electron scattering are awaited with great interest. Systematic studies of the dependence of the quark momentum distribution on nuclear size can yield information about how the pion and "6-quark bag" content of nuclear matter depends on nuclear density. Further measurements of the momentum transfer dependence are needed to tell at what wavelength electrons can first resolve individual quarks inside nucleons.

Following the above series of experiments with measurements of exclusive inelastic scattering is an extremely exciting prospect. This research is required to explicitly characterize the modification to the free nucleon by the nuclear medium. Over the range of momenta accessible to a 4-GeV electron accelerator, a systematic program of (e,e'X) coincidence experiments (where X is a nucleon, excited nucleon, pion, light nucleus, or quasi-

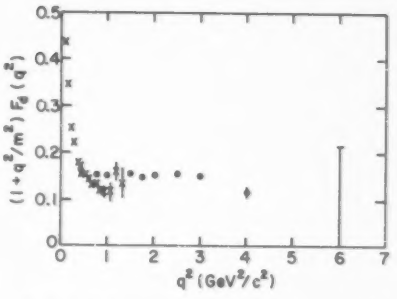

Fig. II.5-B. Product of the deuteron elastic scattering form factor times a kinematic dependence predicted from QCD. The constancy of the results down to $q^2 < 1$ GeV^2/c^2, indicates that certain types of scaling may extend to quite low values of momentum transfer.

two-body state) will provide detailed information which will shed light on the nature of short-range correlations and components of nuclear wave functions. Many of these components can be expressed in terms of hadronic degrees of freedom (N,Δ, higher resonances plus mesons), but others are not. In particular, interactions in which two nucleons exchange quarks, or states in nuclei in which 6 quark configurations are important, are phenomena beyond the conventional description. A very high priority is to quantify the effects of these "hidden color" configurations.

Even for the deuteron, where the dominant configuration, at low (1 fm^{-1}) momenta, is that of colorless protons and neutrons, at higher momenta small components acquire some "color" in the 3-quark bags via gluon exchange. These configurations may couple preferentially to (highly) inelastic channels, and so may be detected in (e,e'N*) experiments. Also, these color degrees of freedom could possibly appear as highly excited dibaryon states with unique decay properties. Unable to decay by pion emission they would have narrow widths, and thus be readily detectable. The search for such states is likely best carried out by exclusive (inelastic) electron scattering. A several-GeV CW electron accelerator is ideal for such searches.

In very deep inelastic electron scattering, a single quark receives a great deal of momentum and attempts to escape from the hadron in which it was confined. The strong force of QCD can be viewed as a string that keeps the quark from becoming deconfined. An individual quark that acquires a large momentum in a collision loses energy as its string stretches by radiating gluons and

creating many quark-antiquark (meson) pairs. While this phenomenon has been studied for free nucleons, it is quite possible that the properties of the extended "string" and the mechanism for losing energy are modified within the nuclear medium. By studying deep inelastic electron scattering on a nucleon imbedded in a heavy nuclear target and comparing the radiations produced with those obtained from a similar process on a free nucleon, one can explore quark propagation in the nuclear medium and the effect of the medium on the "string." The development of QCD at low momenta is of greatest interest to nuclear physics, and conversely the results from nuclear physics are most likely to impact the low-momentum aspects of QCD. Ultimately, analysis of all experiments for evidence of explicit quark-gluon degrees of freedom will depend heavily on the theoretical interpretation, and this requires not only considerable effort directed toward realistic, usable, QCD-based models, but the development of sophisticated relativistic conventional models which can provide a believable standard of comparison.

While much research in this area of quark degrees of freedom of nuclei will involve leptonic probes as discussed above, the properties of baryon and meson spectra plus searches for "exotic" new states predicted by models of QCD will be carried out using hadronic probes. These searches employ polarized protons, pions, kaons and antiprotons in addition to electrons and muons. Unraveling the explicit role of quarks and gluons in nuclei, the integration of nuclear physics with QCD, is one of the most exciting and challenging problems ever faced by nuclear physicists. Its resolution will mean that we have obtained a more fundamental description of hadronic matter, an issue of great impact on nuclear physics, and on both elementary particle and astrophysics.

II.6 STRANGENESS IN NUCLEI

What happens when "strange" quarks, belonging to a different "family" of quarks, are brought into the nucleus? What are the forces, the appropriate degrees of freedom and symmetries?

Nuclei are made of protons and neutrons, with mesons, and isobars (the delta prominent among them) also present. All of these particles are built of quarks that belong to one "family," that of the "up" and "down" (u and d) quarks. Introducing a new quark, from another family, brings a completely different and new degree of freedom into the nucleus, that can test our understanding of nuclear structure and nuclear interactions at a very basic level and strengthen our understanding of the underlying role of QCD. A single "strange" (s) quark, combined with a u and a d quark, forms a baryon called the lambda (Λ), which is sufficiently stable to form long-lived nuclei; the next heavier strange baryons are the sigma (Σ) and the cascade (Ξ). The Λ and Σ can be produced from interactions of the nucleon with the lightest meson containing a strange quark, the kaon (K).

Nuclei containing a strange particle are called "hypernuclei" and were discovered some thirty years ago in emulsion studies. Kaon beam lines and spectrometers for hypernuclear studies have been developed at CERN and Brookhaven National Laboratory (BNL) in the last decade. Because of the low intensity of these K^- beams, the sparse data are of poor resolution and restricted to light hypernuclear systems. Even so, dramatic results determining the small size of the Λ-nucleus spin-orbit force and the tendency to develop dynamical symmetries in hypernuclei have been obtained. The availability of intense kaon beams at some future "kaon factory" would lead to qualitative new insights within nuclear science.

Consider, for example, the question of whether the baryon-baryon interactions can be described in a unified manner, both at the phenomenological and at the fundamental quark levels. Phenomenologically, one must explore the relationship between nucleon-nucleon, lambda-nucleon, and lambda-lambda effective interactions in the context of QCD, where the various quark flavors (u,d,s, ...) are treated on an equivalent footing, and the spectroscopy of hypernuclei is as fundamental as that of ordinary nuclei.

Lambda Hypernuclei

The information available from the early emulsion studies was used to estimate the Λ central potential well depth (some 30 MeV compared to 50-60 MeV for the nucleon) and to determine loose constraints on the lambda-nucleon interaction. With the advent of magnetic spectrometer systems, production of hypernuclei via the strangeness exchange (K^-,π^-) reaction became possible. At a "magic momentum" of about 530 MeV/c, recoilless production of Λ-hypernuclei, in which the 0° reaction produces a Λ at rest in the nucleus, becomes sizeable. These favorable kinematics were first exploited by the CERN group, and a sampling of their results is shown in figure II.6-A. Under these kinematic conditions, the excitation of "substitutional states," in which a neutron is simply replaced by a Λ in the same shell-model orbital, is emphasized. These data led the CERN group to the surprising conclusion that the spin-orbit potential for a Λ is much weaker than that for the nucleon. This fact has subsequently been explained both in the context of meson exchange and of quark models.

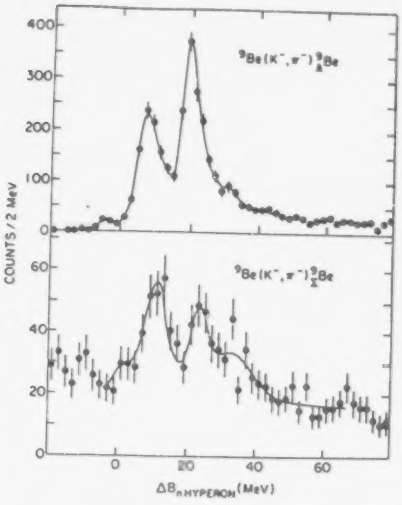

Fig. II.6-A. Evidence for hypernuclei with Λ and Σ hyperons forming $^9_\Lambda$Be and $^9_\Sigma$Be.

The first spectra measured at 0° did not yield quantitative constraints on the residual interaction because of the coarse energy resolution. Subsequently angular distributions were measured with improved energy resolution. Data for ^{13}C at 4° and 15° are shown in figure II.6-B. As the pion angle is varied hypernuclear states of different spin are excited preferentially, relative intensities change, and small but significant energy shifts occur. The data were analyzed in terms of a hypernuclear shell model. The most interesting conclusion is the determination that the spin orbit splitting is an order of magnitude smaller than that for normal nucleons. Despite the weaker central as well as spin orbit interaction, some hypernuclear states show a tendency toward a high degree of spatial symmetry. However, the available energy resolution still does not permit the extraction of quantitative constraints on the ΛN spin-spin and tensor forces. Recently, the feasibility of studying the $(K^-,\pi^-\gamma)$ reaction has been demonstrated at the Brookhaven AGS and electromagnetic transitions between hypernuclear levels were observed. Results for several light nuclei suggest that level splittings due to the spin dependence of the lambda nucleon force are less than 200 keV. Good γ-ray energy resolution permits the precise measurement of energy level differences even when the absolute energies are not accurately known.

Sigma Hypernuclei

The $(K^-,\pi^\pm)$ reactions have also been exploited to produce Σ-hypernuclei. Results for $^9_\Sigma$Be at 0° are included in figure II.6-A and compared with the corresponding excitations in $^9_\Lambda$Be. Figure II.6-C shows similar narrow structure for $^6_\Sigma$H. Presumably, the relatively narrow Σ peaks result again from coherent substitutional transitions. Recently, evidence has also been seen for narrow Σ structure in other light nuclei. There are indications from these data that the Σ central potential is shallower than that of the Λ. The Σ-nucleus spin-orbit potential has not been conclusively determined from the data. In the naive quark model, the Σ-nucleus spin-orbit potential is predicted to be comparable to that of the nucleon, whereas conventional boson exchange models predict it to be about 1/3 as large. Appreciable isospin mixing may occur in contrast to the very small isospin mixings which prevail in normal nuclei. A number of effects have been noted which reduce the Σ widths below simple optical model estimates, but better data are required in order to provide definitive answers.

Future Prospects

The current program should be extended in several directions. High resolution $(K^-,\pi^-\gamma)$ measurements need to be pursued for a variety of targets in order to obtain the systematics necessary for a unique determination of the spin-spin, symmetric and antisymmetric spin-orbit, tensor, and three-body parts of the effective interaction in nuclei. M1 spin-flip transitions between members of the ground-state doublet provide direct information about the Λ-nucleon spin dependence, but their observation requires efficient photon detection below 200 keV. Application of γ-ray methods to heavier hypernuclei is a challenge. One can consider working at higher K^- energy, where the kaon beam intensities are greater and the kaon decay length is longer. Conversely, one could utilize the $(\pi^+,K^+\gamma)$ reaction, which provides access to a wide variety of hypernuclear states with high momentum components. A recent experiment at Brookhaven demonstrated that hypernuclei can be produced in the (π^+,K^+) reaction. The higher pion flux would make possible higher resolution spectrometers for studies of heavier hypernuclei with more complex level schemes. Yet a further opportunity lies in the $(e,e'K^+)$ reaction, which with few GeV electrons from the new 4-GeV electron accelerator will be a very effective tool for producing hypernuclear excitations.

The full exploitation of the structure information available from Λ-hypernuclear spectra clearly requires a considerable improvement in both energy resolution and intensity. Good resolution is particularly important in heavy systems, where level splittings are generally small.

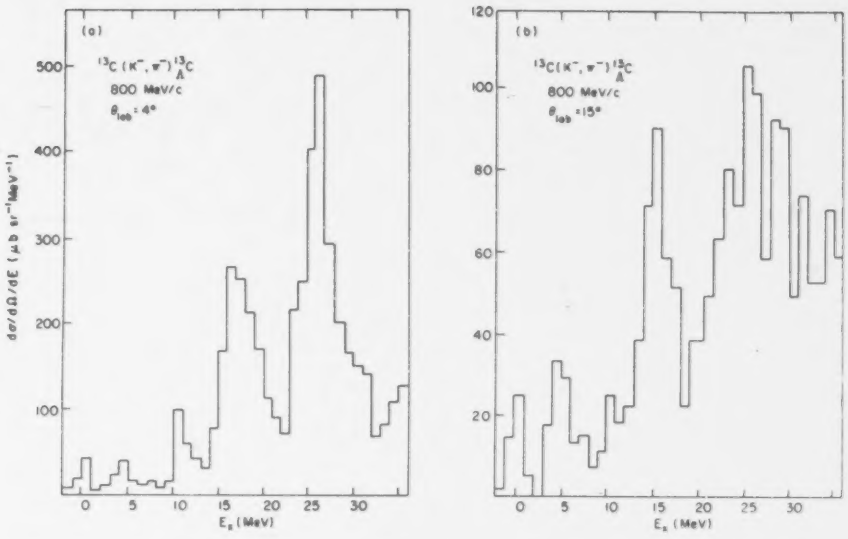

Fig. II.6-B. Production of $^{13}_{\Lambda}C$ at two angles. The variation of intensities with angle enables extraction of crucial spectroscopic information.

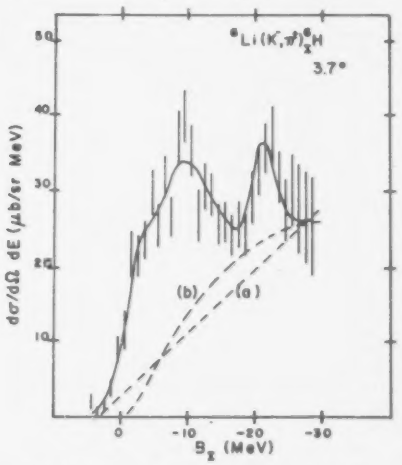

Fig. II.6-C. Evidence for a heavy hydrogen hypernucleus $^6_{\Sigma}H$ produced by the (K^-,π^+) reaction on ^6Li. The peak near a binding energy (B_Σ) of −22 MeV is probably the ground state.

To observe processes with any but the largest of cross sections requires an improvement in intensity. The degree of collectivity in heavy hypernuclei (do "strangeness analog states" exist?) can only be determined with better facilities. Measurement of spins of excited levels, electric and magnetic multipole moments, lifetimes, and disintegration products must also await these improved facilities.

High-resolution work could exploit the Λ as a relatively weakly coupled probe of properties of conventional nuclei. A Λ coupled to a rotational or vibrational nucleus would alter the moment of inertia or effective phonon spectrum of that nuclear core. In superfluid nuclei, the Λ would influence the energy gap. Through core polarization induced by the Λ, one expects changes in the quadrupole moment of a rotational nucleus, and enhanced isoscalar magnetic transitions in the nuclear core. The change in radius due to the presence of the Λ may shed some light on the question of nuclear compressibility. These and other fascinating possibilities for nuclear structure investigations remain totally unexplored.

The study of elastic and inelastic scattering processes induced by K^0 beams or $K_L \rightarrow K_S$ regeneration experiments on nuclei with neutral kaon beams has not yet

been explored in depth. At low momenta, the K^+ has a very long mean free path and is sensitive to neutron as well as proton densities. The K^-, on the other hand, is strongly absorbed and can be considered the strange equivalent of the pion. More intense higher resolution kaon beams with better kaon-pion separation are needed to exploit kaon-induced reactions for these nuclear structure studies. Of course, we must also refine our knowledge of the two-body kaon-nucleon amplitudes, which are only poorly determined at present but which would be critical input for such nuclear structure studies.

The first hypernuclear weak decay experiment was completed recently. More could be done in this particular area with present facilities. Precision measurements of the decay modes of very light hypernuclei, where the nuclear cores are not spin-isospin saturated, are essential in order to unravel the spin and isospin dependence of the $\Lambda N \rightarrow NN$ conversion process. Hypernuclei offer a unique possibility for studying baryon-baryon weak amplitudes. In all but the lightest systems, the weak decay of the Λ hypernuclear ground state proceeds via the $\Lambda N \rightarrow NN$ process which is inaccessible except in the nuclear environment.

The (K^-,π^-) reaction on deuterium or ^{3}He should be thoroughly explored to investigate possible strange dibaryon resonances in the Λp system. Angular distributions are needed to obtain spin assignments; the lowest-lying six-quark bag states which couple to the Λp system require one unit of angular momentum for their excitation (nonzero angle).

The doubly-strange six-quark dibaryon (the "H") is a dramatic prediction of the MIT bag model. A search for such a state requires intense kaon beams in the 1-2 GeV/c range. The "H" particle plays a special role in multiquark spectroscopy because it is predicted to decay only weakly. Two methods for its production have been proposed: the reaction ^{3}He(K^-,K^+n)"H" in which the K^+ and neutron are detected, and the production of a Ξ^- in the reaction $p(K^-,K^+)\Xi^-$ followed by the atomic capture (in say deuterium) leading to the "H" and a neutron, with the monoenergetic neutron being detected.

The study of Σ-hypernuclei would benefit immensely from higher kaon intensity, both for increased counting rate and improved beam purity. A very low-momentum beam (approximately 400 MeV/c is optimum) is required in order to emphasize the production of the narrow substitutional states without large quasi-elastic backgrounds. This is a technically difficult project because of the short decay length and low kaon production cross sections. A basic question is whether narrow states occur only in light nuclei or whether they are representative of a rich, but as yet undiscovered, Σ shell-model spectroscopy of heavier systems.

A subject of much interest in the study of normal nuclei is the role of the Δ resonance in the nucleus. The analogous problem in hypernuclear physics is the production, propagation, and decay of Y^* resonances. The narrow $Y^*(1520)$, with a width of only 15 MeV, is a particularly interesting quark excitation with one unit of internal orbital angular momentum, and thus its study within the nucleus has important unique aspects. Such study also requires a low-momentum K^- beam (400 MeV/c).

Finally, the $(K^-,K^+$ or $K^-,K^0)$ reactions on nuclear targets offer a possible window into the spectroscopy of hypernuclei with two strange quarks, containing a Ξ or two Λ hyperons. Such studies represent a logical next step in the evolution of hypernuclear physics. The spectroscopy of such hypernuclei is potentially rich: narrow Ξ states are likely to exist, just as in the case of Σ's, though their widths will depend on the $\Xi^- p \rightarrow \Lambda\Lambda$ conversion rate as well as other factors, such as the hypernuclear wave function. Cross sections to specific high-spin discrete $\Lambda\Lambda$ states are predicted to be a few nb/sr at 0°, requiring a very intense K^- beam, and providing a formidable challenge to experimenters.

It is remarkable that so much information has already been uncovered from the relatively sparse data now available with strangeness in nuclei. Higher intensity and higher quality kaon beams would help this field toward expanding a more detailed and fascinating new perspective on our understanding of the structure of nuclei.

II.7 THE ELECTROWEAK INTERACTION AND BEYOND

Are there new interactions beyond those of the minimal standard model? Are there new particles of low mass beyond those we know? How can low and intermediate energy nuclear physics contribute to these issues?

The investigation of nuclear processes has always involved to a substantial degree the study of the properties and interactions of elementary particles. Our sister field of particle physics is entirely devoted to this undertaking with its main thrust directed towards the questions which can be probed at higher and higher energy. The study of fundamental interactions has important frontiers in addition to those at high energy. The existence of the weak interaction was one of the early discoveries emerging from the study of nuclei and the existence of neutrinos was inferred from the properties of nuclear decays half a

century ago. Later, the discoveries of many of the critical properties of the weak interaction have come from the study of nuclei and nuclear processes: the confirmation of the existence of neutrinos through their interaction with nuclei; in the late 1950's the discovery of dramatic violations of parity conservation in weak processes, essential to our understanding of this interaction; more recently the demonstration of the conserved vector current relations between weak and electromagnetic processes; and currently some of the most important issues in neutrino physics are being addressed within nuclear physics, such as limits on the neutrino mass and on possible neutrino oscillations. Contributions to these fundamental questions have been made by many branches of physics including atomic physics, astrophysics and cosmology as well as nuclear and high energy physics. These have long been recognized and welcomed as a sign of the coherence and the unity of physics.

Many fundamental questions in both strong and weak interaction physics have been and continue to be investigated with the nucleus as a physical arena. We embrace here, within this long range plan for nuclear science, those questions and aspects of elementary particles which can be effectively addressed within nuclear physics. The pursuit of this subfield of nuclear physics has grown in size and importance because of recent startling developments in our understanding of elementary particles and because of their potential impact on the description of atomic nuclei.

The recent unification of electromagnetic and weak forces is one of the most extraordinary developments in modern physics and it may be compared to the unification of the electric and magnetic forces by Maxwell 100 years ago. The discovery earlier this year of the heavy vector bosons, the W and Z particles, whose large mass is related to the relatively "weak" nature of the weak force, beautifully confirms and reinforces the new theory. These new particles, together with the photon, are responsible for the electroweak force. This theoretical model, with its many experimental triumphs, further challenges us to explore its range of validity and to search for new fundamental interactions and particles.

The two fundamental interactions governing the physics of nuclei as well as of elementary particles (the "strong" and the "electroweak") have recently been embedded in a consistent theoretical framework supported by experiment, the so-called ***Minimal Standard Model*** (MSM). The MSM is a gauge theory (akin to the quantum theory of electricity and magnetism, quantum electrodynamics) and is described by the group theoretical symmetry $SU(2)_L \times U(1) \times SU(3)_C$. [Here the electroweak interaction is represented by $SU(2)_L \times U(1)$ while QCD is contained in the group SU(3).] The known fermions (leptons and quarks) are grouped into three "families" or "generations" each containing two types of quarks and two kinds of leptons; the existence of one hitherto unobserved quark (the top quark) and one unobserved neutrino (the tau neutrino) are predicted. The term "minimal" in MSM refers to the fact that the model contains only the minimal number of ingredients necessary to account for the known facts. For example, MSM does not contain right-handed neutrino fields.

The basic theory has massless particles. In order to generate the masses of the W and Z and the masses of the fermions, the symmetry of the theory is broken through the so-called Higgs mechanism and leads to a hitherto unidentified neutral Higgs particle. This Higgs mechanism is a crucial element of the theory as it is now formulated.

A number of important features are embedded within the MSM framework: baryon number is conserved, as is not only the total lepton number, but also lepton number within each "family" separately. Thus electron number, muon number, and tau number are each conserved leading to the prediction, for instance, that the decay of a muon into a photon and electron is forbidden. The charged-current weak interactions have a vector minus axial vector (V-A) structure. The neutral-current weak interactions are determined by a single new parameter, the Weinberg angle θ_W which determines the ratio of the masses of the Z and the W particles. The neutrinos are massless and there are no neutrino oscillations. The theory contains a CP-(charge conjugation-parity) violating interaction which may account for the observed CP-violation in the neutral kaon system, but there are, in first order, no CP (or time reversal T) violating effects in the leptonic and semi-leptonic weak interactions. The weak and electromagnetic interactions of the leptons e, μ and τ are identical (perfect e-μ-τ universality).

Although all the known physics is consistent with the Minimal Standard Model, it is unlikely to be the ultimate theory. For example, it is described by more than one coupling constant; it provides no clues for the replication of fermion families; the fermion masses and various weak mixing angles are not calculable.

The theoretical possibilities for physics beyond the MSM include: theories which unify the electroweak and the strong interactions (grand unified theories), new interactions which distinguish the fermion families, e.g., the electron and the muon (horizontal gauge interactions), theories which do not require elementary Higgs fields but involve a new strong force and further new interactions (technicolor schemes), a symmetry which relates fermions and bosons (theories with supersymmetry), and theories

39-587 O - 84 - 67

in which the leptons and the quarks are not elementary (composite models). In addition, the electroweak interaction may be described by a group larger than that of MSM (e.g., electroweak theories involving right-handed currents). Also, there may be more than one Higgs particle.

In the presence of any of these possibilities some or all of these quoted features of the MSM will be lost. Thus the major directions of research are, and will likely continue to be: *(a) search for new interactions, and for possible new light particles; (b) further study of the physics of the minimal standard model.* There are important contributions to be made by nuclear physics in both parts of this scientific challenge.

A. ISSUES AND EXPERIMENTAL PROBES RELATING TO PHYSICS BEYOND THE MINIMAL STANDARD MODEL.

Using nuclear processes, or particle beams developed for nuclear physics, a number of issues can be studied which pertain to possible new physics beyond the minimal standard model. Experiments with improved sensitivities may uncover new phenomena, limit proposed theories, or lead to new theoretical possibilities. We shall briefly outline several of these important issues.

CP-Violation. The phenomenon of CP-violation was discovered nearly 20 years ago in the neutral kaon system but, despite considerable effort, its origin is still unknown. It was an unexpected result at the time and to date CP violation has been seen only in this one system. While the data are consistent with the expectation of the MSM, they are also consistent with other possible sources of CP violation that may be present in some of the mentioned extensions of the MSM. The most important experiments to understand the origin of this symmetry violation include: higher precision measurements in the neutral kaon system which require intense kaon beams; searches for CP and T violation outside the neutral kaon system, in particular a sensitive measurement of the electric dipole moment of the neutron, using ultra cold neutrons (the present limit is $D_n < 6 \times 10^{-25}$ e-cm, while 10^{-29}—10^{-32} e-cm is predicted by the MSM); and improved tests of time-reversal invariance in semileptonic kaon decays, muon decay, nuclear beta decay (where present results have sensitivities down to 10^{-3}) and in other leptonic and semileptonic processes.

Conservation of Muon and Electron Number. The relevant processes to study include $\mu \to e\gamma$, $\mu^- \to e^-$ conversion in nuclei, and $K_L \to \mu e$. Meson factories have improved the sensitivity for the branching ratios of the first two processes by two orders of magnitude, to about 10^{-10}. Further improvements are expected from new experiments in progress or proposed on rare kaon decay modes but still higher sensitivity would require better kaon beams. Direct observation of forbidden decays would be of the greatest importance and would signal the existence of new interactions or additional neutrinos. Branching ratios could be just beyond the existing experimental limits. In technicolor schemes, for instance, the branching ratios of $K_L \to \mu e$ and $\mu^- Z \to e^- Z$ are expected to be not far from the present limits.

Conservation of Lepton Number. At present the most sensitive test for the conservation of total lepton number is neutrinoless double beta decay, a process that may occur in many nuclei. Another example is neutrino-antineutrino oscillations which also provide tests of lepton number conservation.

Baryon Conservation. Stimulated by predictions of grand unified models the *decay of the proton* is being studied presently with large-scale detectors. One of these experiments has recently set a lower limit for the lifetime of the decay $p \to \pi^0 e^+$ of 10^{32} years, while theoretical estimates based on the simplest grand unified theory give 10^{28} to 10^{31} years. This crucial confrontation between observation and theory needs to be explored further including sensitive measurements of other decay modes. The search for transitions between neutrons and antineutrons, a process violating baryon number conservation by two units and referred to as a *neutron oscillation* is being conducted at nuclear reactors.

Deviations from the (V-A) Nature of Weak Charged Currents. Precision tests of the space-time structure of the charged-current interaction are important because of the possibility that the standard left-handed (V-A) structure is modified slightly by possible contributions from right-handed currents or charged Higgs exchange. A high-precision search for right-handed currents in muon-decay has just been completed at TRIUMF, and is consistent with V-A. Another relevant muon-decay experiment is in progress at LAMPF. Other tests of V-A come from measurements of helicities and asymmetries of beta particles in nuclear beta-decay. Improvements in the sensitivity of these and other tests are possible with the advent of new techniques for measuring positron polarizations.

The Structure of the Neutral Current Interactions. A powerful probe of possible deviations from the standard model is a set of precise measurements of the neutral current parameters $\sin^2\theta_W$ and ϱ ($\varrho = M_W^2/M_Z^2 \cos^2\theta_W$). In the standard model the parameter $\sin^2\theta_W$ is arbitrary and $\varrho = 1$. In some grand unified models $\sin^2\theta_W$ can be predicted rather precisely; the simplest SU(5) theory agrees well

with the experimental value of 0.224 ± 0.015. The corresponding value of $\rho = 0.992 \pm 0.017$ from semileptonic neutral current processes is consistent with 1.0. Information on ρ and/or $\sin^2\theta_W$ will come from precise determinations of W and Z masses.

One of the important challenges is to also measure, to an accuracy of a few percent, the *purely leptonic* scattering reactions $\nu_\mu e \rightarrow \nu_\mu e$ and $\bar{\nu}_\mu e \rightarrow \bar{\nu}_\mu e$, such studies are under way at present high energy accelerators. One would also want to improve substantially the results for $\bar{\nu}_e e \rightarrow \bar{\nu}_e e$ and to study $\nu_e e \rightarrow \nu_e e$, which are uniquely sensitive to interference between neutral and charged current interactions, and such improvements are not feasible at high energy accelerators. High-intensity neutrino sources, such as those proposed for kaon factories, would be able to achieve substantial improvement in the measurement of these purely leptonic processes.

The scattering of longitudinally-polarized electrons from nuclei offers a way to study the structure of the neutral current interaction. Scattering of polarized electrons on deuterons at SLAC first showed the existence of a parity violating neutral current. An electron accelerator with energies up to 4 GeV, as recently recommended by NSAC, is ideally suited for these pursuits. Precision nuclear excitation and elastic scattering studies with polarized electrons at available electron accelerators (e.g., Bates), and perhaps with eventual neutrino beams, are also useful for testing the isospin structure of neutral hadronic currents and therefore serve as tests of the electroweak theory. The availability of different nuclear targets and variable electron energies is helpful in this regard.

Neutrino Properties. Besides being an important issue in the present theoretical framework, the question of neutrino mass has profound ramifications in astrophysics, and cosmology. Nonzero masses for the neutrinos are strongly suggested by grand unified theories.

From the experimental point of view there are several approaches to pinpoint the neutrino mass. There are *kinematical tests* using low-energy nuclear beta decays such as tritium, or the decay of the pion into a muon and a neutrino. Present sensitivities for the electron neutrino mass are about 35 eV. Several experiments currently in progress with nuclei are expected to resolve an existing experimental controversy concerning the electron neutrino mass, and should be sensitive to a mass as small as 10 eV within the next 2 years. Similarly, the $\pi \rightarrow \mu\nu$ decay should be studied with the aim of obtaining more stringent limits (or values!) of the ν_μ mass whose present limit is only about 500 keV.

For massive neutrinos one expects in general the phenomenon of *neutrino oscillations*, i.e., transitions from one type of neutrino to another. Searches for such processes are currently being carried out with high energy neutrinos from high-energy accelerators, medium energy neutrinos from meson factories, and low-energy neutrinos from fission reactors. To date no evidence has been found for oscillations, but more sensitive tests may yet uncover them. The most sensitive test for $\bar{\nu}_e$ oscillations has been obtained with low-energy reactor neutrinos, and the limits provided by these experiments are shown in figure II.7-A.

The *solar neutrino problem*, the observation of fewer neutrinos from the Sun than expected from the standard solar model is still an unresolved problem despite years of

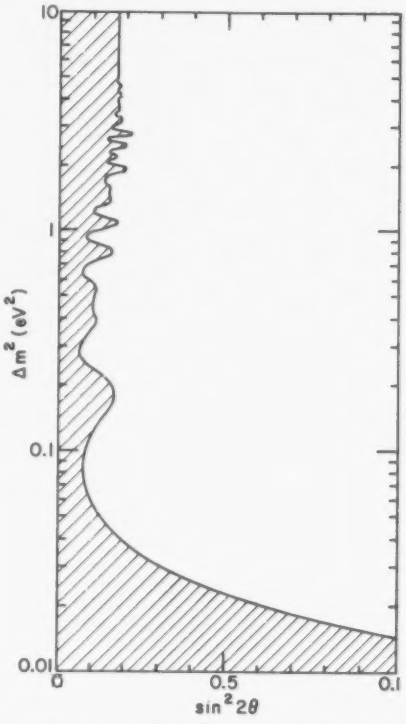

Fig. II.7-A. Present limits on neutrino oscillations. The unshaded region of the plot has been ruled out by reactor experiments. The plot is of the mass difference (between two possible neutrino states) squared, as a function of the phase angle ($\sin^2 2\theta$) that mixes the two states.

studies. This may be related to neutrino oscillations with long oscillation length as discussed in Sec. II.10.

If neutrinos have mass, the question becomes pertinent whether they are *Dirac or Majorana particles*, the latter being particles that are identical to their antiparticle. Neutrinoless double beta decay in nuclei appears to be one of the most sensitive tools to answer this question. Recent studies based on ^{76}Ge set upper limits on the mass parameter of 10-20 eV. New experimental techniques adapted from high-energy physics, such as the time projection chamber, will make these nuclear experiments much more sensitive.

Deviations from e-μ Universality. At present the most sensitive test of e-μ universality in charged current weak interactions is the ratio of the $\pi \to e\nu$ and $\pi \to \mu\nu$ rates. This ratio has recently been measured with an accuracy of about 1.5%, and further improvement is possible. A deviation from e-μ universality would suggest the presence of charged Higgs mesons and/or mixing in the leptonic sector.

New Particles. Experiments possible with nuclear transitions and nuclear physics accelerators or reactors are well suited to search for new particles of low mass. Such particles include the axion (conjectured to explain the apparent absence or smallness of CP violation in QCD), light Higgs bosons, massive neutrinos, and some new particles predicted by supersymmetric theories. Among the processes in which such particles might appear are specific nuclear transitions and rare decay modes of kaons. Sensitive experiments to look for possible massive neutrino states are searches for peaks in the charged lepton momentum spectra from the decay of pions and kaons.

Anomalous Phenomena. An example of anomalous phenomena not permitted in renormalizable gauge theories are *"second-class"* currents. Second-class currents are weak currents which have opposite "G parity" quantum number to that of the usual weak quark currents. Existing experiments on correlations in beta decay are all consistent with no second-class currents, but more sensitive experiments are needed. An interesting new technique involves measuring the electron-neutrino correlation in beta decay, since interpretation of the result does not require knowledge of the weak magnetism form factor.

B. OTHER OPEN AREAS OF RESEARCH IN THE PHYSICS OF THE MINIMAL STANDARD MODEL

Besides the above tests there are other issues bearing on the physics of weak interactions within the MSM.

Weak Form Factors of Hadrons. The weak interaction of hadrons cannot, in general, be predicted directly from the weak interactions of the quarks because of the effects of the strong interactions which induce form factors not present for point particles. It is not known yet how to calculate these effects accurately, although conservation principles (CVC and PCAC) provide some useful relations. Understanding the weak structure of hadrons (especially of the nucleon) complements the studies of the electromagnetic and strong interactions of nucleons. Processes of particular interest, beta decay, parity violating studies in electron scattering, and muon capture, address several issues. CVC can be tested by way of the weak magnetic form factor. Current experiments test this at the ~10% level. It would be valuable to push this down until isospin breaking becomes important. A precision determination is needed of the *axial-vector coupling constant* in the beta decay of the neutron. Aside from its intrinsic importance, this quantity is needed, for example, to predict the amount of ^{4}He produced in the "big bang." At present there are conflicting results on the neutron half-life, however the axial vector coupling constant g_A can probably be better determined from an angular correlation measurement. *The axial-charge form factors in nuclei* are believed to be strongly enhanced by pion-exchange. There is some evidence for this, but more work remains to be done to clarify the issue. There is also evidence for a *quenching of* g_A in a nuclear medium. Further study is needed to shed light on the nature of this effect. Muon capture is particularly sensitive to g_p, the *induced pseudoscalar* form factor. Present results are consistent with the (PCAC) predictions, but the experimental precision should be improved.

The Nonleptonic Weak Interactions. The only strangeness conserving nonleptonic weak interaction which is presently accessible experimentally is the parity-violating nucleon-nucleon force. Parity violation has been observed in both heavy and light nuclei, and also in polarized proton-proton scattering. These experiments provide valuable input for tests of dynamical calculations: for instance, studies of parity-mixed doublets in light nuclei have set constraints on the isospin structure of the parity violating interaction. Parity violating effects in scattering of polarized protons from protons, and in light nuclei are consistent with quark model calculations in the framework of the MSM. Information on this nonleptonic weak interaction can also be obtained from studies of polarized electron nucleus scattering at low momentum transfer.

Study of Higher Order Effects in the Standard Model. Studies of decays forbidden in first order in the standard model are motivated by the desire to test higher order

calculations, to constrain the parameters of the standard model, and to probe for the existence of new interactions. An example is the decay of a charged kaon into a charged pion and neutrino-antineutrino pairs. Calculations lead to the conclusion that a branching ratio significantly above 3×10^{-9} would represent evidence for new physics, while one significantly below 4×10^{-10} would suggest the presence of more than three fermion generations or new interactions. Other examples are precision tests of quantum electrodynamics such as measurements of the anomalous magnetic moment of the muon and the hyperfine splitting in muonium.

Conclusion

In the area of electroweak interactions the lines between particle physics and nuclear physics are especially blurred. Many of the crucial questions in this area can be addressed by nuclear physicists, using nuclei, nuclear processes, or the particle beams developed for nuclear studies. In high energy physics the detailed studies of the decay modes of the W and Z particles as well as many other experiments (searches for the Higgs particle, for evidence of the top quark, for new heavy particles associated with possible extensions of the MSM, etc.) will provide a rich field of study over the coming decade. The combined results of the two scientific communities are likely to lead to a deeper and more thorough understanding in an area of physics which has produced the most quantitative new insights into the nature of matter in the latter half of the twentieth century.

II.8 MACROSCOPIC PHENOMENA

What are the new macroscopic and microscopic phenomena associated with collisions between two nuclei? How and on what time scale is energy absorbed and a new equilibrium established?

Nuclei are many-body systems with many degrees of freedom and with dimensions that are comparable to or often smaller than the mean free paths of their constituents. Exploration of these systems has thus far been limited largely to relatively cold configurations near their quantum ground states. Collisions between nuclei have provided one of the richest sources of information concerning both the microscopic and macroscopic structure and behavior of nuclei; these collisions involving heavier nuclei produce—in controlled fashion—nuclear complexes very different from those encountered in nature and permit study of the phenomena occurring in them under conditions of higher temperature, density, high spin, and high mass-to-charge ratios. Of particular interest are the discovery and understanding of the simple modes of nuclear excitation produced in these damped nuclear collisions, their microscopic foundations, their eventual decay, and the cooperative and relaxation processes responsible for them.

The study of heavy-ion collisions was initiated more than forty years ago by measurements of Alvarez and his collaborators at Berkeley but the full power of heavy-ion studies did not become apparent until the late 1950's with the development of the tandem electrostatic accelerators and the new generation of precision cyclotrons and linacs designed to accelerate all ions in the lower end of the periodic table. This power stemmed from the fact that the heavy-ion collisions, for the first time, gave the experimenter much broader control over collision parameters including charge, angular momentum, linear momentum, number of transferred nucleons, and neutron to proton ratio, than had been possible with more traditional lighter projectiles. Reflecting the very small de Broglie wavelength, these heavy-ion interactions were also amenable to quite simple classical or semiclassical analyses. The early measurements, and indeed, until recently, a very large fraction of *all* studies on the physics of heavy-ion collisions focussed on their macroscopic aspects such as shapes, deformations, and fragment distributions in mass and charge. Only recently has it become possible to focus upon the underlying microscopic behavior of the nucleons responsible for these macroscopic observations; despite this, impressive progress has already been made.

An exception to this rather general rule is the case of Coulomb excitation. These Coulomb-excitation studies were, and remain, one of the most productive sources of information on nuclear collective motion and as such were complementary to light-ion reactions such as deuteron stripping which mapped out much of the single-particle structure of nuclei. The fact that heavy ions could bring large angular momenta into colliding systems, without concomitant energy sufficient to disintegrate them directly, gave access to entire new regimes of hot, high-spin, nuclear configurations and partial answers to the ubiquitous question of how the nuclear many-body system responds to increasing energy and increasing spin. What happened when it was heated?

One of the early discoveries in this field, now thought to be a very general feature of nuclear interactions, was the nuclear molecule—a transient configuration in which the target and projectile retain their identity but are bound together for times long compared to the collision time during which they rotated and vibrated in a fashion familiar from the atomic domain.

Recent discoveries in this field, shown in figure II.8-A, have demonstrated the rather remarkable fact, for example, that at excitations above 70 MeV in the 56 body ^{56}Ni

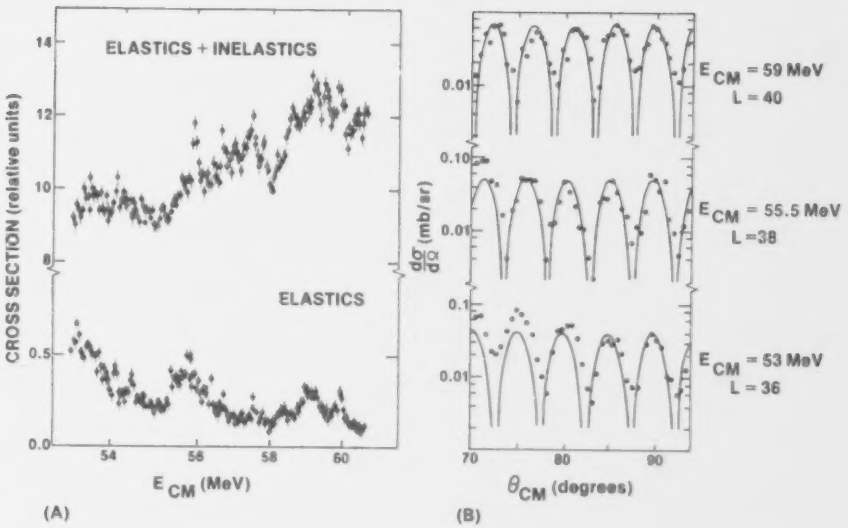

Fig. II.8-A. Scattering of two ^{28}Si nuclei from each other shows sharp energy-dependent structures as seen on the left. On the right are angular distributions of the elastic scattering in this system. These distributions demonstrate that very high angular momenta dominate these "molecular" processes.

system there are sharp states having angular momenta between 40 and 50 units which have very simple structure indeed—two ^{28}Si nuclei bound in a dinuclear molecular configuration.

Damped nuclear collisions are intermediate between the traditional nuclear physics classifications of compound nucleus and direct reactions; they involve the last classical phenomenon to be introduced into the quantum domain—friction; and they show every evidence of presenting entirely new phenomena in nuclear physics. Thus far experimental studies have been extremely limited in scope. Large areas remain unexplored awaiting the availability of new accelerators, new instrumentation and new understanding. Already this class of reactions has provided substantial insight into the behavior of the nuclear many-body quantum system, with some illuminating analogies and connections to other branches of science such as chemical physics and quantum statistics. The possibility of entirely new kinds of nuclear matter—density isomers—of dramatic phase transitions in nuclear matter, and of a wealth of other new phenomena await investigation, as soon as the facilities and instrumentation become available.

It is convenient to divide the energy range into five domains; the critical energies marking their boundaries are roughly 5, 20, 150 and 1000 MeV per nucleon, respectively. The lowest energy is that where Coulomb barrier effects are important; the second is that at which supersonic (i.e., shock wave) effects might first be expected; the third is an effective threshold for mesonic effects and the fourth marks the onset of pronounced relativistic phenomena. We will here discuss the physics near the first three of these boundaries and return to the fourth in Sec. II.9.

Elastic and Inelastic Scattering

Elastic scattering is the simplest interaction between two nuclei dominated, respectively, by electromagnetic and by strong nuclear forces at low and at high energies. The small de Broglie wavelength, comparable to, or smaller than the nuclear size, makes the analogy with optics a very good one and a wide variety of optical phenomena—interference, diffraction, rainbow scattering—are observed dramatically in the nuclear domain.

Passing beyond elastic to inelastic scattering, we have

both Coulomb excitation where the electromagnetic interaction is dominant, and the strong nuclear interactions. In both instances, strong coupling to the nuclear collective modes occurs and has been exploited effectively to provide detailed information concerning the static and dynamic shapes of nuclei.

It is important to note that much of what we know about nuclear quantum states relates to excitations within the pairing gap of the ground state—to cold nuclei. We do not know what happens to collective states when they are superimposed on the continuum, how they spread or dissolve. We do not know in any detail how high in excitation we can hope to follow microscopic behavior and whether we will necessarily turn to macroscopic descriptions. We really do not know in any comprehensive manner how the nuclear many-body system will respond to systematically increased energy and/or angular momentum.

The Nuclear Continuum

The nucleus is one of the few examples of a many-body system which both exhibits statistical behavior and can be studied in sufficient detail to resolve individual energy levels. The behavior of nuclei as a function of excitation energy, angular momentum, and other properties varies dramatically from domains of collective motion and elementary excitations to domains of random motion in which the levels show no correlations between observables. The density of levels is the most basic statistical property of the nucleus, and is usually expressed as a temperature—energy relation. Recent heavy-ion reactions show that the nucleus can maintain its identity at least to temperatures up to 3-6 MeV, but with many properties altered by the large energy the nucleus contains. Experimental data on a much more systematic scale are required to test theory beyond its present rather crude level.

Deep Inelastic Scattering

It has been traditional in nuclear physics to separate nuclear interactions into two broad classes, direct and compound, depending upon the characteristic time scale and the number of degrees of freedom involved. Heavy-ion studies have been unique in that they have included a totally new kind of interaction—deep inelastic scattering, characterized by a massive transfer of kinetic energy into internal excitation as well as limited mass and charge flow. A definite correlation has been postulated between the interaction time and the magnitude of the kinetic energy loss.

The exact mechanism whereby this energy transfer is accomplished remains a matter of some debate and models range from those involving stochastic transfer of individual nucleons between the target and projectile to those based upon excitation of surface vibrational modes. The general characteristics of the deep inelastic process are only just beginning to emerge in broad areas of the periodic table.

Fusion

Enormous impetus has been given to fusion studies by the development of new ion sources, high energy electrostatic accelerators and second-generation linacs in recent years. Once thought to be the consequence primarily of simple one-dimensional barrier penetrability, fusion in heavier systems is now suspected to be strongly dependent on dissipation mechanisms, modes of nuclear excitation, on the dynamics of the collision process, and in general on both the microscopic and macroscopic properties of the colliding nuclei.

With the recent availability of adequate computer capacity, time dependent Hartree-Fock (mean field) TDHF fusion calculations can be extended to very heavy nuclear systems; in these it is found that the flow of matter between the interacting nuclei has a very major influence on the dynamics. Macroscopic calculations, using multidimensional potential energy surfaces have also been applied to the fusion process. They have further elucidated the role of nuclear dynamics and have provided an estimate of the excess energy required to fuse massive nuclei over that anticipated on the basis of simple one-dimensional pictures.

There is a growing suspicion that surface dominated reactions such as inelastic scattering and single and multinucleon transfer can have an appreciable effect on the evolution of the nuclear complex, and that dynamical thresholds for fusion must be tied at least in part to nuclear structure properties. What is badly needed to help clarify these connections is a careful study of quasi-elastic yields in reactions between heavy and moderately heavy nuclei. An example of experimental data showing evidence for fusion, quasi-elastic scattering as well as strongly damped scattering is shown in figure II.8-B.

Fission

The large angular momenta involved in heavy-ion reactions have provided a unique opportunity to extend fission studies beyond their traditional domain. The disruptive nature of the centrifugal force can make any nucleus in the mass table unstable toward fission under experimental conditions readily accessible with the new generation of heavy-ion accelerators. Studies of fission barriers of relatively light systems have provided a testing

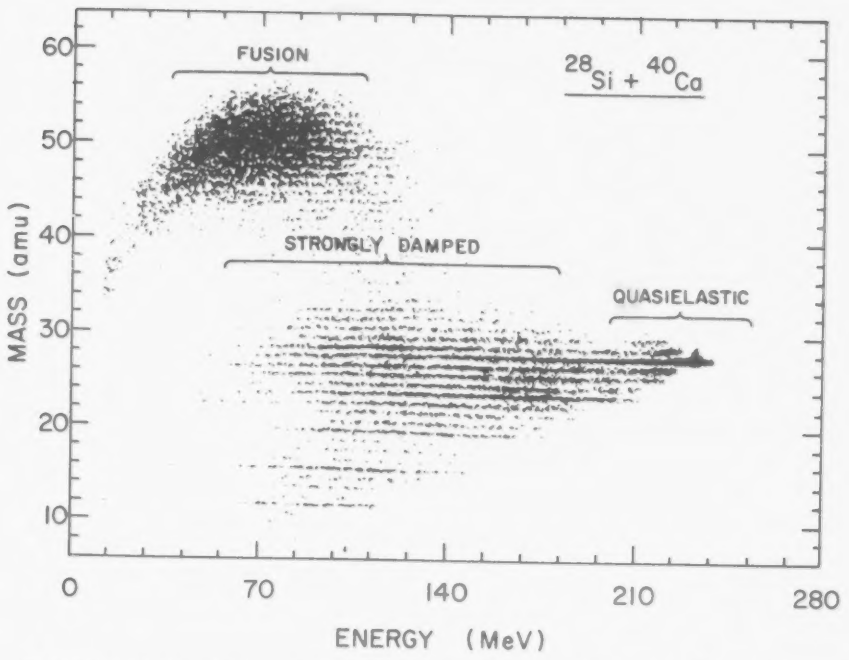

Fig. II.8-B. The particles observed at a forward angle (12°) from the collision between a 250-MeV ^{28}Si nucleus with a ^{40}Ca target. The regions of energies and masses corresponding to three reaction mechanisms discussed in the text are indicated.

ground for the liquid drop model as applied to shapes of extreme deformation. The importance of the diffuseness of the nuclear surface and of the role of the finite range of the nuclear force has been demonstrated, while the effects of shells and other microscopic effects present a challenge for future studies.

In addition to the fission of compound nuclei, a new process, fast-fission, has been identified. The reaction time associated with the process is $\sim 10^{-20}$ sec. Fast fission has been observed under any of the following three conditions: when the energy needed for fusion is just below the threshold; when the compound nucleus is unstable toward fission; and when there is a third body present. While the time involved is intermediate between that of compound nucleus fission and that which characterizes strongly damped reactions, the precise relationship between these processes remains to be explored.

The major challenge here, as yet unanswered, is that of bridging the gap between fission and the fragmentation processes that have been approached via reaction channels.

Collective Phenomena

As we go up in energy can we consider nuclear collisions as just the incoherent sum of a whole range of nucleon-nucleon collisions or rather are there coherent collective phenomena involving all, or a large fraction of, the nucleons present? A number of relatively low energy studies clearly point to such collective effects.

A good example derives from measurements of charged particles emitted in collisions of 400 MeV/nucleon ^{20}Ne beams with heavy targets. The number of protons observed is significantly fewer than predicted and

there is evidence for the existence of a slowly moving source in the laboratory system, suggesting that the projectile appears to be stopped inside the target matter.

These findings all are suggestive of large energy deposition in a small volume, and appear to require a cooperative effect involving many nucleons. Recent work on 86 MeV/nucleon $^{12}C + {}^{12}C$ collisions at CERN provides additional evidence for strong collective phenomena. Finally, and most revealing, the reaction $^{3}He + {}^{3}He \rightarrow {}^{6}Li + \pi$ has been observed using slow beams, well below threshold velocity for the pion production in the free nucleon-nucleon interaction while systematic studies with 35-MeV/nucleon ^{14}N beams on a variety of targets ranging from Al to W have resulted in determination of π^{o} production cross sections. These results demonstrate convincingly that the nuclear many-body environment plays a key role, even in collisions of relatively light nuclei, enabling the almost total conversion of the incident kinetic energy into a coherent nuclear state. Thus high energy densities favorable for the observation of qualitatively new phenomena are achieved in the interactions of nuclei at intermediate energies.

The Nuclear Equation of State

When we consider the equation of state of most materials we examine the appropriate pressure-volume diagrams, searching for phase changes and other singularities or peculiarities.

In the equivalent diagram for nuclei, the nuclear equation of state, only the behavior in the vicinity of the normal nuclear matter minimum has been explored; we do not know whether there are additional local minima which would correspond to density isomers or to entirely new forms of matter. Simple fluid dynamic calculations of the yield of pions expected per nucleon in Ar + KCl and Ne + NaF collisions studied at the Berkeley Bevalac show no evidence for anomalies in the energy range from about 500 to 2000 MeV/nucleon in the laboratory. Hydrodynamic calculations, however, indicate the onset of high densities in collisions above about 80 MeV/nucleon and by 200 MeV/nucleon densities three times normal are expected, albeit for times lasting only 10^{-22} sec. Because of the limited energy range studied, it is entirely possible that measurements to date might have missed such secondary minima if they exist. Moreover, hydrodynamic phenomena may be most fully developed in collisions involving the most massive nuclei; experiments with relativistic uranium beams are just beginning and an early event is shown in figure II.8-C. Just as the collisions give rise to densities above normal in their compression phases, in the subsequent relaxations (or bounces) densities significantly below normal may also occur and it is here that present-day calculations suggest the possibility of another phase transition and the possible coexistence, for brief periods, of both gaseous and liquid phases of nuclear matter. Searches for this transition are planned for the near future.

Localization

A fundamental question concerning the dynamics of nuclear collisions and specifically the energy dissipation mechanisms is that of the possible localization of energy deposition—the formation of hot spots. As we move up in energy the collision times become so short that mean field effects become negligible and only a small fraction of the nucleons present might be expected to participate in the collision, the remainder functioning effectively as spectators.

There are several approaches to the localization question including use of a thermodynamic model for light product emission, of a so-called coalescence model and an interferometric method modelled on that evolved in astronomy for estimation of the size of Sirius. All are crude—but all agree that over the entire range of incident energies from 20-2000 MeV/nucleon, the effective source radius is about 3.5 fm—much smaller than the characteristic dimensions of the interacting systems, and surprisingly constant.

A wide variety of models has been developed for localization in terms of some variation of a participant-spectator situation (e.g., fireball, firestreak, hot spot). In most of these, the overlap region between the two interacting ions is assumed to constitute a very hot source of light particles. Further measurements are needed to determine the extent to which the models present a true picture of interactions between complex nuclei, and particularly, to determine the energy ranges where different phenomena may be dominant.

Fragmentation

As the energy of the projectile increases, the character of the peripheral reaction begins to make a transition at around 20 MeV/nucleon. Just below this energy, the dominant mechanism probably involves the transfer of "participant" nucleons from one nucleus to the other. The momentum distribution of the "spectator" fragment is constrained by the transfer process. With the increase in energy, the angular momentum of these participant nucleons is so large that they cannot be captured by the other nucleus. The momentum distribution of the spectator then attains the fragmentation limit which remains essentially the same up to relativistic energies.

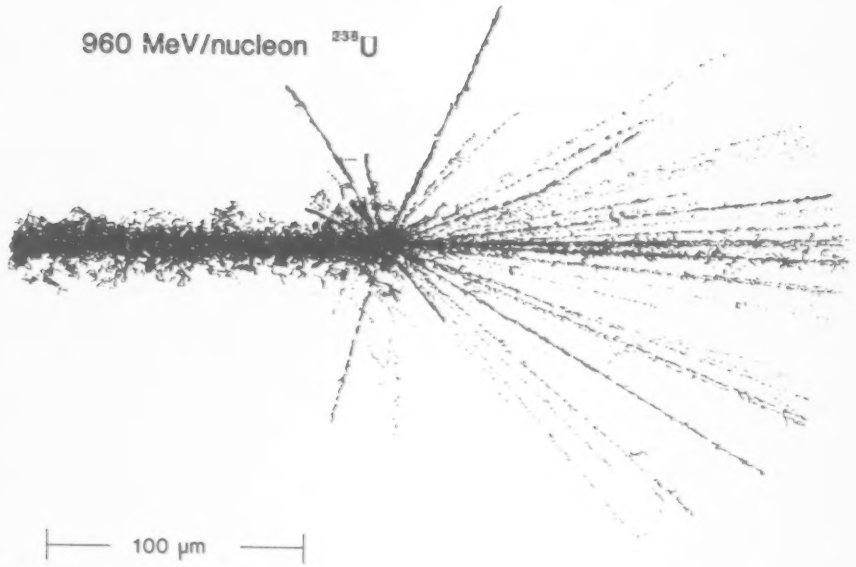

Fig. II.8-C. The pattern of tracks left by a 960-MeV-per-nucleon ^{238}U nucleus colliding with another nucleus in a photographic emulsion.

Supercritical Field Phenomena

In the study of heavy-ion collisions, much attention has been focussed upon the supercritical field phenomena anticipated in the collision of heavy nuclei carrying large mass and charge. In the charge case, the Coulomb field in the neighborhood of the colliding nuclei becomes supercritical in that the electron binding energy exceeds twice the electron rest mass. Under these conditions, a vacancy in the K shell, created in the early phases of the collision, can be filled by a negative energy electron from the Dirac sea with the consequent appearance of an unaccompanied positron. Such positrons have now been observed at GSI in the collisions of uranium beams with uranium or heavier targets, and an example of data is shown in figure II.8-D.

A somewhat analogous strong interaction is that of pion condensation, which may occur at densities several times normal nuclear values and would be characterized by a large pion field and the observation of numbers of pions with unusual correlations. Simple models suggest that such pion condensates might be expected for energies around 200 MeV/nucleon and at densities above about twice the normal density but, as yet, no experimental evidence for the condensates has been obtained. Experiments to date have been very much limited in the range of masses and energy involved. It is not yet clear whether the nuclei studied (e.g., Ne) are simply too small and diffuse to support a pion condensate or whether the effective nuclear correlations are perhaps too strong to permit condensation at the densities achieved.

The search for these pion condensates remains an outstanding challenge in elucidating the phase diagram for nuclear matter.

Nuclear Temperatures

It is rather remarkable that an enormous body of data on the emission of light fragments from heavy-ion collisions can be parameterized for many orders of magnitudes in terms of cross sections depending exponentially on an assumed nuclear temperature. The temperature extracted from such data increases with the available energy, reaching values ~100 MeV for laboratory energies ~1 GeV/nucleon. There appears to be growing evidence for a temperature saturation in nuclei at

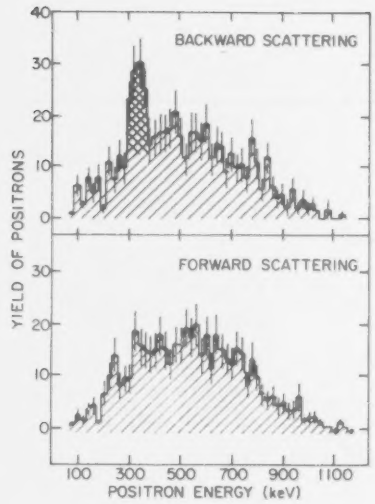

Fig. II.8-D. Positron emission from the "breakdown of the vacuum" in the extremely high electromagnetic fields produced during the collision between a uranium and a curium nucleus. Especially surprising is the presence of a sharp line for backward scattering (close collisions) which could only arise if the combined system were to exist for an unexpectedly long time. Such a long-lived state in the 486 nucleon system would indicate simple structural selection rules of very special character.

about 150 MeV as the available energy is increased. The behavior of the temperature in these high energy heavy-ion collisions may be related rather closely to the nature of the hadronic spectrum at high energies and this in turn could have the most profound consequences in arenas as different as the earliest instants of creation and the final death throes of giant stars, quite apart from its great intrinsic interest as a fundamental aspect of the most basic structure of all matter.

II.9 EXTREME STATES OF NUCLEAR MATTER

What is the nature of nuclear matter at energy densities comparable to those of the early universe? What are the new phenomena and physics associated with the simultaneous collision of hundreds of nucleons at relativistic energies?

Nuclear matter has been explored only over a very limited range of energy and nucleon densities. Probing its equilibrium and dynamic properties further is a problem of deep intrinsic interest in nuclear physics. Beyond needing to map out the gross features of the phase diagram and thermodynamics of nuclear matter, one needs its excitation spectra, and transport properties, such as stopping power for hadronic projectiles, mechanisms of energy dissipation, and particle absorption and emission. Understanding these properties tests our knowledge of the basic forces between nucleons—and at an even more fundamental level, between quarks—and our abilities to derive these properties from first principles in terms of these forces. Exploration of nuclear matter, using existing heavy-ion accelerators, and proposed ultra-relativistic ones, will open experimental and theoretical opportunities at the frontier of physics: most outstanding will be the creation of extended regions of matter at energy densities beyond those ever created in the laboratory over volumes far exceeding those excited in elementary particle experiments and surpassed only in the very early universe. One very exciting possibility at such energy densities is the discovery of new states of matter.

The properties of nuclear matter are of great interest outside nuclear physics as well. In astrophysics they are important to the mechanism of supernova explosions, in which massive stars undergo gravitational collapse to beyond the point where their nuclei are crushed together; to the properties of neutron stars composed in most part of bulk nuclear matter, including their birth and evolution, a determination of their upper mass limit and the transition to black holes; and in cosmology, to the behavior of the early universe in the period from 1 microsecond after the big bang until nucleosynthesis, when space was filled with bulk matter. The study of nuclear matter has direct interplay with the concerns of condensed matter physics, for example, states of broken symmetry, and with those of high energy physics.

Nuclear Matter at Normal Densities

Certain basic properties of nuclear matter are at present well-understood at low excitation energies and nucleon densities very near those found in undisturbed nuclei. While these are reviewed in greater detail in Sec. II-8, we recall salient features here. The "saturation" density ϱ_{nm} of nuclear matter, 0.16 nucleons per cubic fermi (or 1.6×10^{38} per cubic centimeter), and its binding energy, are determined from the properties of static nuclei. Observations on the "breathing modes" (electric monopole giant resonances) of nuclei indicate that nuclear compressibility is close to that of a noninteracting gas at the same density. Current theoretical methods for solving the many-body problem at zero temperature, based on variational techniques, yield results in agreement with these observations, provided two-nucleon forces derived from fits to scattering data are supplemented with many-body forces.

Phase Diagram of Nuclear Matter

On the other hand, the nature of matter under extreme conditions of high compression (or rarefaction) or high energy density remains uncharted experimentally. Calculations of the phase diagram of bulk nuclear matter at finite temperatures and varying densities suggest a very rich structure, as illustrated in figure II.9-A. For example, at particle densities below that of saturation, nuclear matter should undergo a liquid-gas phase transition at low temperatures, similar to the boiling of water, with a critical point. The nuclear medium can greatly modify the properties of particles, such as pions and delta resonances, propagating in it. As a consequence, at densities at least twice the saturation density, bulk nuclear matter is predicted to undergo a transition to a phase said to be "pion-condensed" in which the system should develop a coherent macroscopic pion field, similar to the electromagnetic field in a laser. A charged-pion condensed medium would also be a novel "superconductor," being able to carry electrical current with no resistance, for instance in neutron-star matter. Finally, under conditions of very elevated energy density, nuclear matter will exist in a wholly new phase in which there are no nucleons or hadrons composed of quarks in individual bags, but an extended ***quark-gluon plasma*** within which the quarks are deconfined and move independently. The phase diagram should also exhibit the transitions associated with nuclear pairing which have a low transition temperature. The structure indicated in the figure also depends on the neutron-proton ratio and on the nuclear angular momentum.

The full exploration of this structure of the phases of nuclear matter presents many exciting opportunities. The dynamics and thermodynamics of the liquid-gas phase transition can be studied in heavy-ion experiments that deposit enough energy in the nucleus for it to "boil off" or fragment into smaller droplets; preliminary experiments of this kind have been carried out on heavy-ion accelerators and also at Fermilab and further ones are in progress. Two major avenues currently being pursued promise new access to the nuclear equation of state. The first is study of the dependence on energy of the multiplicity of pions produced in a collision, a measure of the fraction of the total collision energy going into kinetic versus potential energy. The second is global analysis of particle flow in collisions. New observations on collisions of Nb on Nb at 400 MeV per nucleon provide evidence that the particles move in a coordinated or collective flow, suggestive of the behavior of a fluid described by hydrodynamics. Systematic study of the collective flow patterns of matter as a function of particle multiplicity, beam energy, and nuclear size will permit the magnitudes of the pressures generated in such collisions to be extracted.

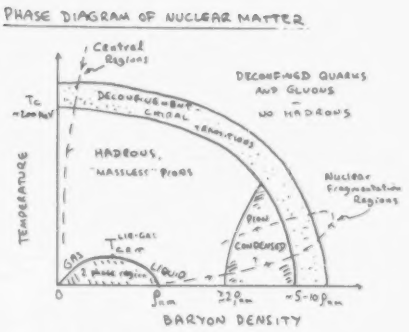

Fig. II.9-A. Expected phases of nuclear matter at various temperatures and baryon (or nucleon) densities, showing the "hadronic phase" including a gas-liquid phase transition region, and the transition region to deconfined quarks and gluons. The dashed lines illustrate trajectories in this phase diagram that can be explored in ultra-relativistic heavy ion collisions.

The effects of nuclear matter on the pion field can be studied in pion absorption and production experiments and possible precursor effects of pion condensation may appear. Temporarily condensed regions may be formed in collisions of heavy ions designed to produce maximum nuclear compression. Pion condensation in the deep interiors of neutron stars would be detectable by satellite x-ray telescopes, such as the proposed Advanced X-ray Astrophysics Facility (AXAF) (likely to be launched in 1991), through the enhancement of the cooling rates via neutrino emission. More generally, the role of non-nucleonic degrees of freedom in nuclear matter is in need of further exploration.

Ultra-High Energy Densities

Ultrarelativistic nucleus-nucleus collisions offer the opportunity of producing high energy-density matter in a controlled laboratory environment, going well beyond the possibilities for study made available by natural laboratories, such as neutron stars, cosmic rays, and the early universe, and providing information complementary to that gained from very energetic scatterings of individual nucleons. With increasing incident energy in a head-on heavy-ion collision the nuclei at first transfer increasing amounts of energy to each other, producing an increasingly compressed and energetic central fireball. Theoretical estimates indicate that the energy densities achievable in collisions of heavy nuclei such as uranium at such energies are up to ~10 times those of ordinary nuclear matter. More importantly, in this regime maximum baryon density is expected. As the bombarding

energy is further increased effects of transparency of nuclear matter set in, and the two nuclei begin to pass through each other, leaving highly excited and compressed remnants, and filling the space between them with a "firetube" of hot matter with relatively low baryon content. These two cases are illustrated in figure II.9-B. In collisions with energies about 30 GeV/nucleon in the center-of mass, the energy densities produced in both the nuclear regions and the central firetube can be at least 10-20 times that of ordinary nuclear matter. The energy densities in these situations are sufficient, by theoretical estimates, to produce a quark-gluon plasma. It is worth stressing that such collisions present a range of different physical systems simultaneously, from the nuclear fragmentation regions in which the initial target and projectile nuclei are broken up, with high baryon density, to the central region with negligibly small baryon density. The plasma that would be produced in the central region has the unusual feature of closely duplicating conditions present in the first few microseconds of the early universe. One should also note that to achieve such energy densities requires using heavy ions, in which many individual nucleon-nucleon collisions take place in the collision volume of many tens and perhaps hundreds of cubic fermis.

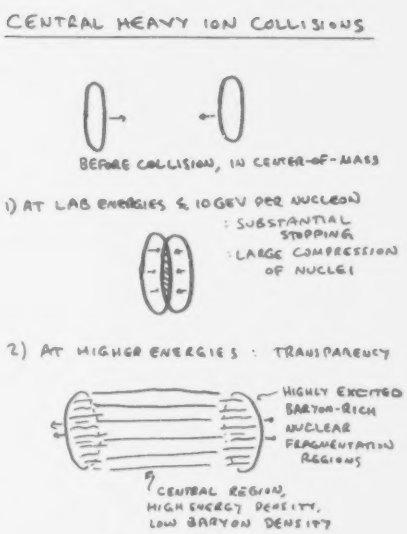
CENTRAL HEAVY ION COLLISIONS
BEFORE COLLISION, IN CENTER-OF-MASS
1) AT LAB ENERGIES ≤ 10 GEV PER NUCLEON
: SUBSTANTIAL STOPPING
: LARGE COMPRESSION OF NUCLEI
2) AT HIGHER ENERGIES : TRANSPARENCY
HIGHLY EXCITED BARYON-RICH NUCLEAR FRAGMENTATION REGIONS
CENTRAL REGION, HIGH ENERGY DENSITY, LOW BARYON DENSITY

Fig. II.9-B. The possible outcome of collisions of heavy-ions at different energies. At lower energies (1) the two nuclei, in a central collision, stop each other producing a high degree of compression, while at higher energies (2), the nuclei pass through and highly excite each other, while at the same time leaving a highly-excited central region composed of matter similar to that in the early universe.

The production and detection of a quark-gluon plasma in ultrarelativistic heavy-ion collisions would not only be a remarkable achievement in itself, but by enabling one to study quantum chromodynamics (QCD) over distance scales as large as 5-10 fm it would make possible the study of fundamental aspects of QCD and confinement unattainable in few-hadron experiments. The deconfinement transition is expected, from numerical computations of the properties of QCD systems as well as other more phenomenological estimates, to take place when the energy density reaches ~0.5-2 GeV/fm^3, some 3-10 times that of nuclei at rest. Such a transition may be first order, with a large latent heat, and with quite dramatic changes in the properties of matter. A second "chiral-symmetry" restoring transition, associated with the underlying mathematical symmetry, is also expected at somewhat higher energy density or perhaps coincident with the deconfinement transition. Such a transition would be heralded by the quarks behaving as massless objects, and low mass pion-like particles no longer being possible excitations in the system.

A further possible outcome of relativistic heavy-ion collisions is the production of stable or metastable exotic composite particles ranging from nuclei far from the valley of beta-stability, to high-density isomers, to quark "droplets" of enhanced strangeness, to objects with unusual stability arising from underlying mathematical or topological structure. Such unusual objects may be related to the observed "Centauro" and "Chiron" cosmic-ray events, and the reported phenomenon of nuclear states with apparently anomalously short mean free paths in matter (anomalons).

Investigations Feasible with Current Probes

Needed investigations, preliminary to embarking on a full-scale experimental study of nuclear and quark matter by relativistic heavy-ion collisions, include experiments that can tell us further the dependence of the energy and baryon densities achieved, on nuclear size and energy. Cosmic ray experiments, such as by the Japanese American Cooperative Emulsion Experiment (JACEE) collaboration, are an excellent source of preliminary information on the gross properties of nucleus-nucleus collisions, indicating that energy densities on the order of 3 GeV/fm^3 are achievable in heavy-ion collisions (an order of magnitude beyond that produced in current heavy-ion accelerators). Such experiments may also provide data on fluctuations, needed for planning accelerator experiments. A continued effort in studying high-energy

cosmic-ray collisions, including balloon and space (e.g., Space Shuttle) flights of detectors will be valuable.

Also important are continuing systematic studies of scattering of protons (as well as pions and other hadrons) with large nuclei. Such experiments, interpreted in conjunction with proton-proton and antiproton-proton scattering experiments, can reveal coordinated or collective behavior of nuclear matter in stopping nucleons, a question of large practical as well as intrinsic interest. Detailed studies of regions of energy and momentum transfer in proton-nucleus collisions not accessible in proton-proton collisions would be very desirable. From proton- and pion-nucleus experiments one will be able to extrapolate to the energy densities and particle multiplicities that will be encountered in nucleus-nuclear collisions. The α-α scattering experiments at the CERN Intersecting Storage Rings (ISR) also provide a first look at the physics of collisions of ultrarelativistic nuclei.

Interactions of anti-nucleons with nuclei are an as yet little explored probe of nuclear matter; annihilation processes can tell us, for example, how nuclei respond to a localized deposition of a large amount of energy.

Much theoretical work is also needed to develop appropriate calculational methods for dealing with relativistic nuclear collisions. In particular, the regimes of validity of nuclear cascade calculations and hydrodynamic descriptions need clearer delineation; a greater understanding of dissipative mechanisms is called for. It is also crucial to learn how the degree of thermalization after a collision depends on the collision parameters, such as nuclear size, energy and impact parameter.

Further theoretical and experimental effort will be required to recognize fully the signals in ultrarelativistic heavy-ion collisions that a deconfined state has been achieved in the collision volume. Measurement of the gross properties of the collision will be needed to determine the energy densities and entropies achieved in early stages of the collision. Correlations of the mean momenta of fragments perpendicular to the collision axis with the mean multiplicities can signal a thermodynamic phase transition. Measurements of nuclear size dependences and fluctuations from the average event are particularly helpful for discriminating between signals arising from a quark-gluon plasma, and backgrounds from pre-equilibrium, or final state dynamics.

Leptons and photons produced in the plasma have long mean free paths, and escape with little interaction. They are also produced most copiously in the early stages of the collision when the plasma is hottest and most dense, and are thus a clean probe of the plasma dynamics. While their signal may be obscured by various backgrounds, the nuclear size and energy dependence should resolve the signal for a plasma from these backgrounds.

Strange-particle production may also provide a signal for a plasma. The equilibrium configuration of a high temperature plasma contains up, down, and strange quark pairs. As such quarks combine into hadrons, a large number of strange baryons and mesons are produced. If there is time and energy for such a configuration of quarks to form, and if the distribution of hadrons survives the expansion and cooling of the plasma, strange hadrons would be copiously produced.

Present heavy-ion accelerators, operating at laboratory energies up to ~2 GeV per nucleon, are providing extensive information on collective behavior and dynamic correlations in heavy-ion collisions. However the energies and particle densities reached are well below the expected thresholds for quark-gluon plasma formation. Injection of ions into existing particle accelerators, such as at CERN, can carry out fixed target experiments in the relatively near future. Such experiments would be at a somewhat higher energy than that of the Bevalac and would begin to uncover further interesting physics of nuclear matter. However, exploration of the qualitatively new physics of nuclear matter will require going to higher energies and using beams throughout the periodic table; this can only be achieved in an ultrarelativistic heavy-ion collider.

II.10 NUCLEI AND THE UNIVERSE

How do the properties of nuclei, of nuclear matter, and of nuclear processes determine the structure and the evolution of stars and affect our understanding of the large-scale structure of the universe?

Nuclear processes and the properties of nuclear matter play a fundamental role in determining the basic structure and evolution of the Universe. Nuclear reactions are responsible for the synthesis of all the chemical elements, are the primary sources of energy driving the evolution of stars, and are, for example, the source of our sun's energy through the fusion of hydrogen into helium. In the near future, we anticipate the production of conditions which existed in the early instants of the big bang, in the collision of ultrarelativistic heavy ions.

The interaction between nuclear physics and astrophysics was initiated by the work of Bethe and has evolved from an interface between two previously

isolated areas of science into the field of nuclear astrophysics, in which both disciplines are combined in the study of important and interesting physics problems. The 1983 Nobel Prize in physics was shared by William Fowler in recognition of his pioneering insights and the key importance of the developments in this field. The astrophysical interest frequently motivates the study of questions which have important nuclear physics content, while nuclear physics discoveries often have profound astrophysical implications. The nucleus provides a microscopic laboratory to study the basic elements responsible for the structure and evolution of the macroscopic Universe. Areas of research where present results point towards important opportunities in the coming decade include the study of high-density nuclear matter in supernova collapse and neutron stars, the study of beta-decay strength functions for decays involving highly excited states in nuclei far from stability, nuclear reactions involving short-lived radioactive nuclei, and the solar neutrino problem.

Creation of the Light Elements

While most of the chemical elements in nature are synthesized in stars, those lighter than carbon are mostly too fragile to survive the conditions found in stellar cores and must have been created at a cooler, or more tenuous, site. A simple description, involving creation in the big bang expansion, and in spallation reactions induced by the galactic cosmic rays, accounts for the abundances of these light elements in an elegant and economic fashion. This description also yields constraints on cosmology, as is illustrated in figure II.10-A, as well as on nuclear and particle physics. Measurements of nuclear spallation cross sections at cosmic ray energies have recently shown that the yields of ^{6}Li, ^{9}Be, ^{10}Be and ^{11}B can be accounted for as the by-products of galactic cosmic rays interacting with the nuclei of heavier elements, such as ^{12}C. The remaining light isotopes ^{2}H, ^{3}He, ^{4}He, and ^{7}Li are the *only* ones whose present abundances are relics of the big bang and must therefore reflect conditions at that time. Their absolute and relative yields are a function of the universal baryonic density, so that one can infer from their yields a value of the present density which is insufficient by itself to close the Universe by about a factor of ten.

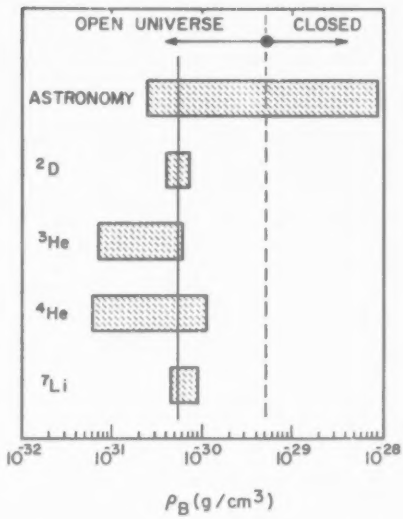

Fig. II.10-A. As determined by nuclear abundances, ours is an "open universe." The fraction of mass that is in the form of very light nuclei is a good measure of the universal density of baryons ρ_B. The values determined from various abundances are shown as shaded bars, the solid vertical line is the best fit to these. The dashed line is the dividing line between the density at which the universe would be closed upon itself, or open.

Supernovae, Neutron Stars, and Nuclear Properties

One outstanding problem in astrophysics is to understand the late stages of evolution of more massive stars, and the physics of their eventual gravitational collapse, their subsequent explosion as supernovae and the formation of neutron stars (highly compressed stars with masses about that of the Sun but with radii of only about 10 km) or of black holes. After massive stars exhaust their nuclear fuel they can no longer resist the inward forces of gravity; their collapse and subsequent rebound is intimately tied to the microscopic properties of the nuclei in their interior. The collapse is initiated by the heating and dissociation of nuclei, and during the collapse the nuclei rebuild into much heavier, more neutron-rich species than are normally found in stars. An exotic aspect of this phase is that neutrinos produced by the capture of electrons in nuclei become trapped in the collapsing core as a consequence of the neutral-current weak interaction between neutrinos and nucleons. This trapping then inhibits further electron captures. The collapse is halted as the nuclei become crushed together, sending out huge pressure waves which form into a very energetic outward-moving shock wave which is believed to be responsible for the ejection of the outer mantle and envelope of the star. The remaining matter condenses rapidly into a neutron star, or if too massive, into a black hole.

Many aspects of this scenario are in need of deeper understanding. The success of the shock in blowing off

the outer layers depends critically on the temperatures, densities, and composition of the star before collapse begins; recent work has shown that these features are in turn highly sensitive to the rates of electron capture by the various nuclei present. Pre-collapse models employing refined electron capture rates are presently being constructed. The determination of the nuclei that are present during collapse requires knowledge, on the one hand, of the level densities and heat capacity of nuclei, and on the other, of the equation of state of hot nuclear matter and the properties of hot nuclear surfaces. As the nuclei are crushed together they form an extended nuclear-matter liquid, and the properties of this nuclear liquid (as it is compressed several-fold) determine the amount of energy transmitted to the outer layers. Although information on the compressibility of nuclear matter has been obtained from studies of the breathing modes of heavy nuclei, in the case of stellar collapse the matter is compressed to extreme conditions where measurements do not presently exist. Data on the behavior of nuclear matter under these conditions can be obtained from laboratory measurements of relativistic heavy-ion collisions. The dissociation of nuclei as the shock wave passes by them is a critical source of dissipation of the shock; present studies of heavy-ion collisions should further illuminate this process.

The shock wave forms outside a central core containing about one solar mass so that the collapse of a massive star leaves behind a highly condensed remnant. If the mass of the remnant is less than about two and a half times that of the sun, the remnant will rapidly evolve into a neutron star; but if a greater mass is left behind the remnant will instead collapse to a black hole. To date, well over 300 neutron stars have been identified, as pulsars and compact x-ray sources, in our neighborhood of the galaxy, and black holes may also have been detected. A knowledge of the nuclear equation of state at high densities is essential to understand these properties of neutron stars and to determine accurately their upper critical mass. Several unusual states of matter may occur at such densities, as is discussed in Sec. II.9, and further studies are needed of the properties of matter at high densities through heavy-ion collisions. Quite generally, the study of supernovae and neutron stars has opened up a new area of nuclear physics, and motivated both theoretical and experimental nuclear research which has led to a deeper understanding of the rich properties of nuclei and nuclear matter.

Two specific weak-interaction processes are of interest in studying the behavior of nuclei under extreme conditions: the beta decay of very neutron-rich nuclei near the neutron drip line and, as mentioned, electron capture at high electron densities and temperatures. Recent work on the beta decay of nuclei far from stability has led to improved calculations of the role of highly excited states of the daughter nuclei in terms of an average energy-dependent strength function. Beta-decay half lives are very sensitive to this quantity, and the recent calculations are in considerably better agreement with measured data than are earlier ones. These half lives are crucial for calculating the production of heavy elements in supernovae, and the refined values yield relative nuclear mass abundances that match observed values extremely well. In addition, the age of the universe obtained by using these half lives and the updated beta-delayed fission rates of heavy elements is now estimated to be about 20×10^9 years, consistent with the largest ages determined from astronomical measurements of the rate of expansion of the universe.

The Sun and the Solar Neutrino Question

Our understanding of hydrogen burning in the sun implies a detailed sequence of processes, with quantitative predictions of the number of neutrinos that should be produced and seen on earth. Since the sun is transparent to neutrinos, solar neutrino experiments sample the entire solar volume. Over the past 15 years, data have been collected from a solar neutrino experiment using ^{37}Cl as the detecting nucleus. There is a persistent discrepancy between the theoretical predictions and the experimental results: only one quarter the expected number of neutrinos is detected. This measurement is fundamental to our understanding of stellar structure, and therefore, the discrepancy has led to critical reexamination of the solar physics, nuclear physics, and particle physics components involved. The interpretation of the experimental result is particularly difficult because the ^{37}Cl detector is primarily sensitive to the high energy ^{8}B neutrinos, which are only produced by a weak (0.01%) branch of the hydrogen burning proton-proton chain. This detector is completely insensitive to the critical p-p neutrinos which comprise 90% of the flux. From another point of view this selective sensitivity for the ^{8}B neutrinos is an important *advantage* since it makes possible the sensitive determination of the conditions at the center of the sun; measurements of the p-p neutrino flux are relatively insensitive to those conditions.

A number of questions have been raised concerning the standard solar model and its predictions—questions involving the optical opacities, the determination of the relevant nuclear cross sections, the distribution of heavy elements and angular momentum in the solar interior, and the possibility of neutrino oscillations. Perhaps the least well understood are the questions on the macroscopic features of the solar interior, opacities and mixing involving angular momentum. But since at the present time no real solution has been found and since

the understanding of our sun is a vital problem, the next logical step in solar physics seems to be the design and construction of alternative neutrino detectors with different sensitivities to the predicted solar neutrino spectrum and the solar interior; these will provide additional independent constraints on our models and the understanding of our sun.

Studies are currently under way to examine the practical feasibility of several proposed radiochemical solar neutrino detectors. Of these the ^{71}Ga detector, based on the ^{71}Ga(ν, e$^-$)^{71}Ge reaction, has been developed the furthest. This detector is sensitive primarily to the p-p neutrinos; most of the ^{71}Ge would be produced by such neutrinos and less than 2% by the ^{8}B neutrinos. Since the flux of p-p neutrinos is determined only by the average solar luminosity and is quite insensitive to the detailed conditions in the solar interior, the ^{71}Ga detector would provide (independent of the details of a solar model) tests of fundamental questions regarding neutrino oscillations and whether or not the Sun is even currently generating energy via nuclear fusion. A pilot project using 1.8 tons of gallium has shown that the recovery of ^{71}Ge is efficient to >95%. A full-scale detector will require 50 tons of gallium, and at the moment its fate is constrained by the high cost of the gallium.

Studies are currently also under way to examine the feasibility of several other solar neutrino detectors. None of them are sensitive to the p-p neutrinos, but they would have different sensitivities to the higher energy parts of the solar neutrino spectrum or average over different production time scales. For example, it has been suggested that suitably shielded geological deposits of ^{98}Mo could be used (because of the long half life of ^{98}Tc) to study the time-integrated solar neutrino flux over the past $\sim 10^6$ years. One might then determine whether the sun is in a transient nonequilibrium phase. A project to measure $\nu + e^-$ scattering in a liquid argon counter is also under development. Such a detector would also provide *directional* information, as well as time and energy, but would be sensitive only to the high-energy neutrinos (^{8}B).

The solar neutrino problem raises a number of important scientific questions, and has to be pursued. At the present time scientific grounds dictate the choice for the next neutrino detector to be ^{71}Ga, on the basis of its demonstrated feasibility and recovery efficiency, but options for alternate detector schemes which could help resolve the present problem should be explored further.

Rapid Proton Capture

In other areas of stellar energy generation and nucleosynthesis, recent interest has been concentrated on hydrogen burning via the MgAl cycle (as possibly in red giants) or the hot CNO cycle and the rapid proton capture process (on the surfaces of white dwarfs). This is illustrated in figure II.10-B. The interest in the MgAl cycle was triggered by the discovery of excess ^{26}Mg in aluminum-rich minerals in meteorites, suggesting that they were originally accreted onto the meteorite as ^{26}Al (with a half life of 700,000 years) produced just before the formation of the solar system. The hot CNO cycle and the rapid proton capture process both involve capture such as ^{13}N(p,γ)^{14}O and ^{15}O(α,γ)^{19}Ne on time scales short compared to beta-decay lifetimes. The study of such reactions presents clear technical challenges, requiring the development of intense secondary beams of radioactive nuclei. At least four different methods have been proposed to produce these beams, and these proposals are still in various stages of design and development. The construction of a full scale facility for short-lived radioactive beams will provide both the information necessary for the understanding of these astrophysical processes as well as the means for studying nuclear reactions that would otherwise be inaccessible.

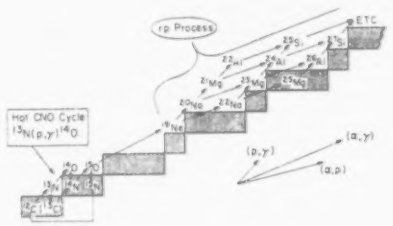

Fig. II.10-B. The path of nuclear reactions in "rapid proton capture" followed in the formation of elements on the surface of white dwarf stars.

39-587 O - 84 - 68

III. APPLICATIONS

III.1 CONNECTIONS OF NUCLEAR SCIENCE WITH OTHER FIELDS OF BASIC RESEARCH

The world we live in is made of atoms, most of whose mass is in the atomic nucleus. The major sources of energy in our world are the end result of nuclear processes in the sun and the stars. So it is that nuclear science has common frontiers with other basic sciences, and that the tools and concepts of nuclear physics have found wide application in other disciplines. The understanding of nuclear forces, structure and interactions, the heart of nuclear science, has profound implications for many branches of physics and chemistry. The machinery of nuclear science: the accelerators, the radioactive species, and the detectors, developed and built specifically for nuclear science, have provided tools and methods applicable to many diverse areas of research from studies of fundamental biological processes, to atomic physics, geology, or astrophysics. The overlap with elementary particle physics in the developments in the quark-gluon structure of QCD and the theory of electroweak interactions is too profoundly interwoven into the fabric of our science to be separately discussed in this section, as is much of nuclear astrophysics, which was discussed in Sec. II.10.

Throughout the last half century radioactive materials as well as beams of particles have been applied to studies in most areas of modern scientific investigation. Radioactive tracer techniques, for example, are used regularly in basic research in chemistry, biology, medicine and metallurgy to name just a few sciences. So too, the use of particle and gamma-ray beams and particle detectors is commonly found within many scientific disciplines. The production and characterization of the radioactivities, the properties of the fundamental interactions of the beams with matter, the development of the detectors and of particle accelerators are all products of nuclear science.

The myriad applications of this knowledge and these techniques cannot be described here. In this chapter we present some of the more exciting new developments on the interface areas with other sciences (some contributions from nuclear science to applied technology areas appear in the next section). The selection is intended to demonstrate the ongoing connections of nuclear science and scientists to other sciences by presenting a few relatively new techniques and fields of study made possible as a result of recent advances or as a result of the suitability of the accelerator equipment and techniques developed in nuclear laboratories.

That nuclear science has profited immeasurably from advances in other sciences—chemistry, solid state, mathematics—pure and applied—to name a few is, of course, understood. In large measure the *interface* areas are two-way communications of enormous benefit to the sciences involved; they are also frequently the areas of greatest excitement and promise. Typical of the two-way benefit is the magnetic interaction of nuclei in crystals discussed below, whose understanding allows unique measurements of nuclear properties as well as the properties of solids.

A. CONDENSED MATTER PHYSICS

Nuclear physics has a deep intellectual unity and interrelation with condensed matter physics, in the varied physical phenomena in each of the fields that arise from the cooperative action of large numbers of interacting particles, in the mathematical techniques and concepts used to describe such phenomena, and in the extensive practical uses of nuclear techniques and concepts in condensed matter research.

Through both fields runs the concept of "dynamical symmetry breaking," in which nuclei as well as solids and liquids often prefer states that are less symmetric, and richer in structure, than might have been expected. The tendency of nuclei to deform spontaneously away from spherical shape is akin to the formation in a magnet, by

the alignment of the fields of the individual particles, of a large scale magnetic field which spontaneously chooses one spatial orientation from among many equivalent ones. Closely related also are the phenomena of superconductivity, in which many metals and alloys at low temperatures lose all resistance to flow of electricity, and pairing phenomena in nuclei, which cause the inner parts of certain nuclei to remain stationary when the rest of the nucleus rotates; underlying these phenomena is the spontaneous breaking of a deep mathematical "phase" symmetry. Techniques for describing interacting particles in nuclei were applied in the development of the theory of superconductivity, and in turn this theory was used to explain nuclear pairing. Recent experiments on rapidly rotating nuclei are exploring phenomena that in many ways parallel the behavior of superconducting materials in a strong magnetic field. Similar pairing effects exist in liquid ^{3}He, and possibly in the nuclear matter of neutron stars.

The interplay between the two fields has been strikingly illustrated in recent studies on the properties of nuclear matter and of helium liquids. Motivated by the desire to derive the properties of nuclear matter in terms of the basic forces between nucleons, theorists have developed very accurate calculational techniques, which have been tested on liquid helium systems, and have yielded greatly improved *ab initio* calculations of the properties of the helium liquids themselves. Furthermore, working in common on both systems they have realized that the behavior of particle "effective" masses in nuclei and that of the heat capacity of liquid ^{3}He involve the same underlying physics, and have exploited this unity to make significant advances on both problems.

At present many further concepts of condensed matter physics, such as energy dissipation and hydrodynamics, are being applied in nuclear physics. Particularly noteworthy are ongoing and planned attempts to search for phase transitions of nuclear matter, such as that from liquid to gas, or the deconfinement or unbinding of quarks—the most elementary building blocks of matter known. Such studies, on the one hand, allow exploration of these phenomena over a range of system sizes and other features not readily available to condensed matter experimentalists, while on the other hand the insights they can give into the question of the fundamental structure of matter has important potential consequences for many branches of physics.

Nuclei are also ideal microscopic probes of the environment in which they find themselves in condensed matter. The ubiquitous hyperfine interaction between nuclei and their host structure results from the interplay between the nuclear moments and the electronic configurations as influenced by crystal structure and dynamics. Short and long range interactions between like ions, or between impurities and hosts are of primary importance, for example, in the preparation of new magnetic compounds and alloys or high ionic conductivity materials required for batteries. The distinct signal produced in nuclear decays allows the study of the behavior of single atoms isolated in matrices. Defects and radiation damage in metals, semiconductors and insulators have been extensively studied.

The hyperfine interaction techniques have been applied to the study of almost every type of magnetic system, to phase transitions and to critical phenomena. Recent studies have pushed the frontiers to the investigation of dynamics of surfaces and to the interaction of fast ions with magnetic solids. The transmission or blocking of fast ions in crystalline channels has greatly extended the intellectual overlap between nuclear physics and condensed matter physics. Channeling and blocking in crystals have yielded detailed descriptions of impurity location, surface conditions, radiation damage, interatomic potentials and electron densities in crystals and have led to direct measurements of the shortest time intervals (attoseconds or 10^{-18} sec and below) yet attained in nuclear physics.

Surface Physics

The surface structure and dynamics of materials can now be probed by new very sensitive microscopic techniques, Mössbauer spectroscopy, perturbed angular correlations and deposition or implantation of polarized heavy ions. The measurement of the electric and magnetic interactions between atoms at surfaces or interfaces is an essential element in the understanding of the chemical absorption processes, and of diffusion and alloying mechanisms that are involved in the preparation of materials.

Perturbed angular correlation techniques have recently been used most effectively to test electric field gradients at the surface of indium metal. It was found that the surface electric field gradient is four times larger than the bulk value and is perpendicular to the surface.

The magnetic properties of the interface between metallic iron and silver have been studied by Mössbauer spectroscopy. The surface magnetic field is smaller than the bulk value at room temperature, but larger at 4°K. The variation of the magnetic hyperfine interaction as a function of depth has been examined for the first time by such techniques, and it was shown that the field reaches the bulk value in only two or three atomic layers.

Extensive theoretical work is in progress to explain the exchange interactions and structural variations that operate in these quasi-two-dimensional systems; the techniques are in their infancy, but as they are uniquely suited to an interesting area of investigation, they are being pursued actively.

Magnetic and Electric Interactions in Solids

Nuclear techniques of angular correlations, Mössbauer spectroscopy, and μ-meson spin rotation (μSR) are very powerful tools for the determination of the magnitude, direction and origin of magnetic and electric interactions in solids. An example is shown in figure III.1-A. Recent technological developments including the extension of pulsed-beam techniques, the discovery of the induced polarization of ions emerging from tilted foils and the very strong magnetic interactions acting on swift ions traversing ferromagnets shown in figure III.1-B, have opened new areas of research. The nucleus provides a very sensitive probe in the investigation of static and dynamic properties of solids, and of ion-solid and ion-surface interactions.

The interest in the μSR technique lies in the fact that a spin-polarized beam of positive or negative muons can be implanted in almost any sample. The time evolution of the polarization then yields information about the muon's local magnetic environment, either at an interstitial or a lattice site in a crystal. As a light interstitial particle, the muon is used to study localization and diffusion phenomena for a particle with mass intermediate between those of the proton which is about ten times heavier, and the electron which is two hundred times lighter. Considering the muon as an ultra light isotope of hydrogen allows one to study non-classical diffusion phenomena unseen in previous experiments using hydrogen.

Finally, muonium (μ^+e^- atoms) centers can be compared with hydrogen in semiconductors, muonium and hydrogen reaction rates can be compared in liquids and gases, and unique information is obtained when hydrogen solubility is low or where no hydrogen paramagnetic states are seen.

Channeling, Blocking and Steering of Charged Particles in Single Crystals

It has been nearly 20 years since the effect of crystal blocking of charged particles was first discovered. It has been applied to the measurement of ultra-short time intervals, to try to determine elementary-particle lifetimes, down to perhaps 10^{-20} sec and even less. An interesting by-product of these experiments was the discovery that by

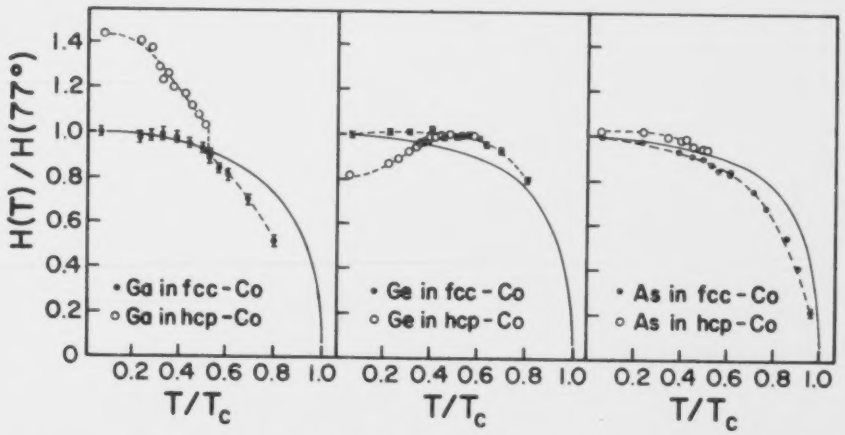

Fig. III.1-A. Measurements of the anomalous magnetic hyperfine field at various substitutional impurities in various (face-centered cubic and hexagonal closed packed) single cobalt crystals. Gallium, germanium and arsenic excited nuclei are implanted using high energy beams and the method of perturbed angular correlations afford the field measurement. The normal field variation as a function of temperature for the host atom (cobalt) is shown as the solid curve. The implanted ions exhibit anomalous fields. These measurements are important for the understanding of material modifications.

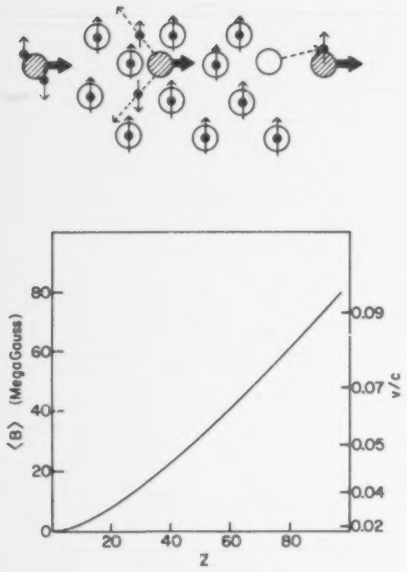

Fig. III.1-B. A schematic representation of a fast ionized atom (shaded circle) traversing a magnetized ferromagnetic material at high speed and exchanging polarized electrons with the medium, is shown on top. The preferential filling of vacancies with electrons of one spin orientation causes very large transient magnetic fields $\langle B \rangle$ at the nucleus of these atoms. The data for ions with a mean effective charge $\langle q \rangle \approx 0.4\,Z$ traversing magnetized ferromagnetic iron at a speed v, in units of v/c, is plotted below.

bending the crystal target mechanically, the charged particles could be made to follow the curvature even at the highest energies—hundreds of GeV—through angles which would require huge superconducting magnets to obtain equivalent deflections. Recent studies on the photons generated by channeled electron or positron beams have demonstrated that there exist exciting possibilities for the production of intense, bright sources of monochromatic x-rays or γ-rays that are tunable in energy.

B. ATOMIC PHYSICS

Ever since the discovery of the isotope effect in optical spectra, nuclei have played an important role in atomic spectroscopy; and in general, much unique information on the properties of nuclei has been extracted from nuclear effects on atomic phenomena. Recently, however, the reverse has happened, as accelerators built for nuclear physics research provide intense beams of ions whose state of ionization and excitation can be varied readily. At these energies two atomic nuclei come very close together and transient atomic configurations not encountered in ordinary systems are formed. Atomic structure calculations can be tested in unique ways on the observed systems. Both experiments and calculations have a bearing on the description of the high temperature stellar environments (as well as those encountered in fusion plasmas for instance in a Tokamak reactor). The production of highly stripped heavy atoms ($Z > 18$) with only one or two bound electrons remaining (hydrogen or helium-like atoms), have afforded systems for study of fundamental atomic physics such as the Lamb shift.

More complicated, but extremely interesting phenomena have recently been accessible to experimentation. The effects of nuclear resonances on K-shell ionization, the details of electron capture by relativistic heavy ions interacting with solid targets, the observation of spontaneous positron creation in superheavy quasi-atoms, and the search for x-rays from superheavy collision systems are only a few of the many problems in "high-energy" atomic physics which have been examined in nuclear physics laboratories and which are controlled by the nuclear reaction rates and energies.

One spectacular example is in collisions between very heavy ionized nuclei, where, for a short time a pseudo-atom with holes in the continuum of negative energy states exists. The filling of these holes results in the emission of positrons, which have indeed been detected. Surprisingly, they exhibit a discrete structure superposed on the continuum spectrum. The origin of the features is not known. Speculations arise as to whether these monochromatic positron lines, which seem to exhibit a distinct collision energy dependence, are due to the formation of giant nuclear complexes or to other new physics.

Rapidly moving atoms, when passed through thin films or low pressure gas, lose much of their complement of atomic electrons. Thus atomic species with reasonably heavy nuclei can be "undressed" and have only the number of atomic electrons characteristic of much lighter atomic systems, but with a much larger positive charge on the nucleus. For example Ar or Cl ions with one electron (hydrogen-like) are produced easily at existing accelerators. Similarly, heavy elements with several tens of electrons can be produced. The study of the atomic spectra of these species both by conventional optical spectrometers and by resonance colliding beam experiments between highly stripped atoms and laser light afford the possibility of stringent tests of theoretical atomic structure calculations. The Lamb shift in one electron Cl, and more

recently in He-like Ne atoms has been measured. Recent experiments to study the structures of the rather simple atomic species H^-, a proton with two electrons, have demonstrated the usefulness of the application of very high-energy (800-MeV) beams to the study of atomic excitation. This atom has "excited states" involving both electrons which are reached by photon absorption in the presence of very high electric fields. In these experiments the highly relativistic beams are passed through magnetic fields which produce very high effective electric fields up to 1.3 million V/cm. Interaction with extreme Doppler shifted laser light in a "crossed beam" experiment, allows a unique detailed study of the fundamental structure and Stark mixing of this simple atom.

Studies on the collisionally-induced dissociation of energetic molecular-ion beams have recently demonstrated in a novel way the interactions ("wake effects") between fast ions and the electron gas that resides in solid targets. Such studies also offer unique methods for determining the stereochemical structures of the molecular projectiles. When fast ions emerge from gaseous or solid targets, there is an associated spectrum of emerging electrons. Recent work on cusp electrons (which are just unbound in the projectile frame) and on emerging Rydberg atoms (where the electron is just barely bound in a high quantum state) have been very fruitful in elucidating the electronic aspects of collisions between fast ions and matter.

C. GEOLOGICAL AND COSMOLOGICAL STUDIES—ACCELERATOR MASS SPECTROMETRY

The revival of high-energy mass spectrometry of nuclides in the 10^{-15} natural abundance range has been accomplished mainly in nuclear physics research laboratories, employing counter telescopes developed for heavy-ion studies and a variety of accelerator types. Cyclotrons and linacs have been used, offering the selectivity of a resonance machine and intrinsic pulsing for time-of-flight particle identification. Tandem Van de Graaff's are widely used and offer their simplicity, economy, and ease of operation, with special advantages for certain ions such as ^{14}C.

Accelerator mass spectrometry is becoming an increasingly important part of the research program in a number of nuclear physics laboratories in the U.S. and other countries. In addition to the possible nuclear science application (so far confined to measurements of half lives, e.g., ^{32}Si and ^{44}Ti) this technique is now widely used in a number of cross-disciplinary fields including archeology, geology, and hydrology, in studies of meteorites, lake and ocean sediments, atmospheric methane, cosmic flux variations, oceanic manganese crust growth, island arc vulcanism, tektites and the growth rate of manganese nodules. Although the field is in relative infancy, the number of other probable applications is increasing rapidly. The importance of the field stems from the small sample sizes required (micrograms to milligrams) and the sensitivity of detection (10^5 to 10^7 atoms per gram in geological samples for example). Several nuclear physics tandem Van de Graaff facilities in this country are involved in the field. Not only can the techniques be used to measure long-lived radioisotopes produced by cosmic rays, but it has also been used to detect stable isotopes such as platinum and iridium in geological samples.

The detection of ^{10}Be atoms with a half-life of 1.5×10^6 years in sea sediments, polar ice, subducted crustal material in volcanic arcs, and meteorites and tektites, has shed understanding on a variety of phenomena that occur on a slow time scale. For instance, growth rate of Mn nodules containing ^{10}Be deposited on the sea floor can be determined as a function of depth and thus some understanding of the formation mechanism for the sea floor is emerging. It has been shown that subducted crustal matter is transported over thousands of years. The composition of tektites has been compared with that of terrestrial and extra-terrestrial rocks, and now it is certain that tektites are of terrestrial origin.

This technique has also been used to search (unsuccessfully) for superheavy elements in various ores. Similarly, several accelerator "mass spectroscopic" experiments with very high sensitivity to possible stable quarks have been carried out or are in progress. Finally, this technique may well offer the best way to measure the small number of atoms of long-lived radioisotopes that are produced by solar neutrinos in suitable geological samples.

III.2 Societal Applications of Nuclear Science and Instrumentation

The direct societal contributions of nuclear physics have been manifold and substantial but not always readily apparent in the complex technological world of recent decades. In fact, one can hardly walk through a hospital without seeing numerous examples of nuclear science—and nuclear scientists—at work. Nuclear energy provides 13% of our electric power, nearly every household is protected by a nuclear smoke detector, and nuclear techniques in the form of ion implantation have revolutionized the semiconductor industry. Food preservation using nuclear techniques offers the possibility of alleviating nutritional problems worldwide, and nuclear defense and the enforcement of nuclear non-proliferation are major elements of our nation's security policy.

A. Nuclear Medicine

The development of nuclear medicine has seen nuclear scientists, physicians, chemists and computer scientists join together in a highly successful attack on some of the most pervasive health problems facing society. In a recent study by the National Research Council, Dr. Richard C. Reba, from the George Washington University Medical Center, stated that

> *"the solution of almost every serious medical problem in patients sick enough to require hospitalization may be facilitated to some degree by a nuclear medicine study."*

Diseases are diagnosed and their treatment monitored with radioactive tracer techniques, and nuclear accelerators and radioisotopes play important therapeutic roles. Radioisotope tracer technology is also important in related health studies involving nutrition, food science, metallobiochemistry and environmental toxicology.

A recent study by the National Research Council has estimated that 5-15 million *in vivo* nuclear medicine procedures were performed in the United States during 1980. A typical diagnostic nuclear medicine procedure involves intravenous administration to the patient of a tissue-specific "radiopharmaceutical" agent, containing a small amount of radioactivity. The gamma-ray emissions, which reflect the tissue distribution of the agent, are recorded by radiation detectors positioned about the patient. These radiopharmaceuticals are designed for selective uptake in a particular organ, region or type of tissue. The detected gamma-rays thus provide a detailed image of the region of interest. Evaluation of the image by a physician specialized in nuclear medicine can reveal abnormalities and lead to more complete diagnoses than might otherwise be possible. The goal in these studies is to evaluate the differences in tissue distribution of radioactivity between normal and diseased tissue. Very recent work on accelerator produced ^{18}F labelled dopamine and on-line PET scans have made possible real time evaluation, for the first time, of the areas in both normal and abnormal human brains engaged in various tasks. In addition, the rates of tissue uptake or loss of radioactivity can be measured with these techniques and differences detected between normal and diseased tissue. Thus, nuclear medicine techniques uniquely measure tissue function and anatomical and structural properties. The principal characteristic of procedures in nuclear medicine is that they are "non-invasive" and require only the intravenous administration of small amounts of radioactive agents; there is generally no trauma, discomfort or danger to the patient. Because of the important clinical information these inexpensive tests can provide, annual sales of radiopharmaceuticals easily exceed 100 million dollars in the U.S. alone.

Nuclear cardiology provides several striking examples of nuclear science at work. One out of every six Americans suffers from heart disease or related cardiovascular disorders, and over 70,000 deaths are reported from heart attacks in the United States each year. Preventative therapy can be of significant value, but symptoms of cardiac and arterial disease can be difficult to detect: many victims are simply unaware of their disease until it is too late for effective treatment. About a decade ago scientists realized that the element thallium, once introduced into the system, rapidly becomes selectively localized in heart muscle; the radioactive isotope thallium-201 could be an effective diagnostic tool for early detection of those diseases if a means could be found to produce the isotope inexpensively at high purity and in commercial quantities. Nuclear physicists and chemists responded to this challenge, with the result that cardiological tests using thallium-201 are now used routinely, and were administered to some 250,000 patients in 1981. A similar example involves the development of the radioactive tracer technetium-99m, the isomer of ^{99}Tc, over the last two decades. A variety of tissue-specific agents labeled with this radioisotope are important for the evaluation of brain, liver, thyroid, lung, skeletal system, kidney, heart, and hepato-biliary disease. Technetium-99m radiopharmaceuticals were used on 5 million patients in the United States in 1981 and involve annual sales of $50 million. Again quoting Dr. Reba,

> *"Clinical nuclear medicine is perhaps the best example of rapid transfer of government supported basic research to the private commercial sector and to the general public."*

Instrumentation for nuclear medicine procedures is another area where nuclear scientists have contributed to improved health care. A recent example is the development of tomographic systems in which gamma-ray emissions are detected by a series of detectors positioned around the patient. These data are reconstructed by computer systems to provide invaluable "pictures" of the patient's internal organs. Alternate techniques involve a single detector that moves around the patient to collect data from different views. In principle, these new "emission" techniques are similar to the well-known reconstruction "transmission" techniques developed for computerized axial tomographic (CAT) scanning using X-ray irradiation of the patient. Emission tomographic techniques can measure the distribution of radioisotopes that decay with the emission of single low-energy photons (e.g., technetium-99m) in a procedure known as single photon tomography. Although these techniques have

been applied successfully to a variety of clinical problems and commercial instruments are available, improvements are required and offer future challenges to nuclear scientists. Methods are needed to correct for the attenuation of photons as they pass through dense tissue such as the chest region, and further improvements are needed in detection systems and computer reconstruction methods.

Similar development is required in positron-emission tomography, where the tomographic reconstruction is accomplished by the coincident detection of the two photons produced by the annihilation of positrons from short-lived radioisotopes such as fluorine-18 and carbon-11. An example is shown in figure III.2-A.

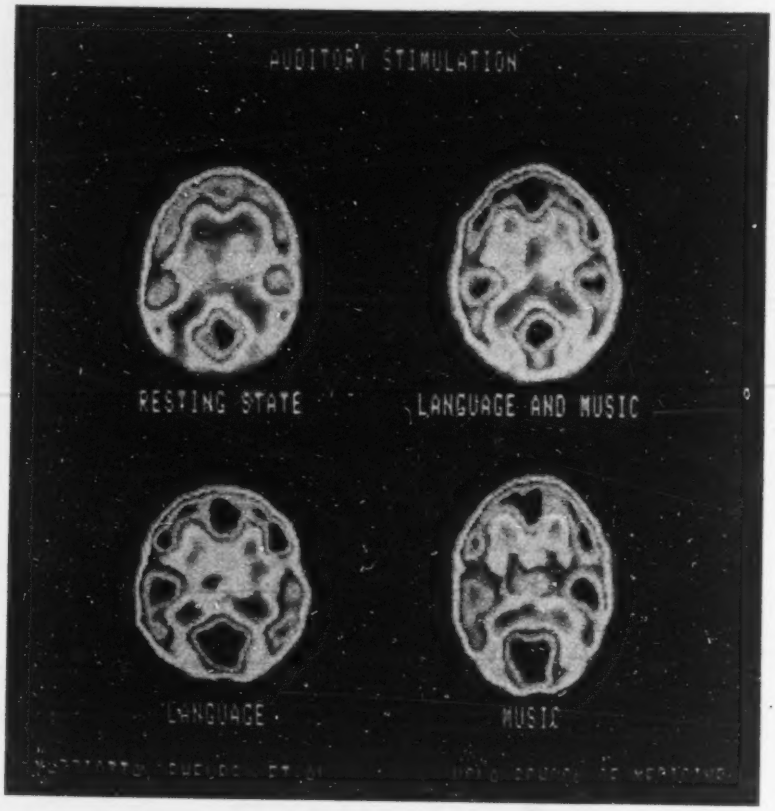

Fig. III.2-A. Radioactive nuclei that emit positrons form the basis for a technique that probes glucose metabolism in the human brain. Shown here are spatially localized responses to various forms of auditory stimulation, as measured by the positron emission tomograph (PET) technique.

The increasing use of diagnostic procedures of nuclear medicine for the evaluation of routine clinical problems has created a corresponding need for dependable, versatile medical cyclotrons for the production of short-lived positron-emitting radionuclides such as carbon-11, fluorine-18, oxygen-15 and nitrogen-13. The short half-lives, less than two hours, of these important radioisotopes require that they be produced at the clinical facility. The only commercial manufacturer of medical cyclotrons in the United States is in difficulties, and medical cyclotrons must be purchased from foreign manufacturers. This certainly represents a unique challenge for U.S. technology to develop economical, dependable and efficient cyclotrons to meet this need. In addition, there is a continuing need for improved target design, for development in cyclotron radioisotope technology, and for future development in the enrichment of stable isotopes for radioisotope production by advanced systems such as laser separation.

In addition to the pervasive role of nuclear techniques in medical diagnosis, nuclear science also plays a key role in the treatment of disease. There are approximately 800,000 new cases of cancer each year in the U.S. and about one half of these receive radiation therapy, either as the main modality or in conjunction with surgery or chemotherapy. The success rate of radiotherapy could be increased further by (1) improving dose localization, thereby sparing normal tissue and (2) improving the biological effect of the delivered dose. Optimization of either of these factors would result in an increased differential between damage to tumor tissue and damage to normal tissues. Dose localization may be improved by using nuclear charged particles heavier than electrons, e.g., protons, heavy ions and negative pions. Biological effectiveness depends, in part, on stopping power and can be increased by using neutrons, heavy ions, and pions in their stopping region. Clinical trials are underway with these nuclear particles to gauge their promise for significantly improved treatment of localized cancers via radiotherapy.

Nuclear science contributes importantly to this research. Nuclear cross-section data and models are being developed to determine the primary beam type and energy, production target material, and shielding requirements, and also to calculate dose distributions. Differences of about 5% in dose can be clinically observable due to the slim margin between tumor control and normal tissue complications, and in some cases better cross-section measurements and nuclear models will be required to permit a closer approach to safe limits with consequent improved tumor control. As in the case of diagnostic nuclear medicine, progress will depend on close collaborations among chemists, physicians and physicists, and coordinated advances in accelerator physics and instrumentation.

Gamma radiation is used in another application of nuclear science to sterilize about 30% of all medical and surgical products used in American hospitals today, and in many cases consumer goods such as talcum powder, milk cartons and cosmetics are routinely sterilized with this procedure. The radiation kills or disables microorganisms, bacteria and insects that otherwise could either spread disease or cause spoilage. Gamma-irradiated foods have been served on the Apollo 17 and space shuttle flights and gamma-treated foods are available to consumers in several countries. The World Health Organization concluded in 1981 that low radiation doses produce no adverse effects on foodstuffs. In the United States, the Food and Drug Administration has proposed new rules that would permit irradiated foods such as spices, fruits and vegetables to be sold to American consumers. Since relief organizations estimate that at least 10% of the crops that are grown in third-world countries are lost either to spoilage or to insects, food preservation via gamma-irradiation may prove to be a significant factor in reducing hunger on a worldwide basis.

Very recent work on the corrosion and wear of surgical alloys used for devices such as artificial hip-joints provides one final example of health benefits made possible by nuclear science. Each year in the United States more than 75,000 total hip joint replacement (THR) operations are performed. This involves surgical implantation of an alloy "ball" working inside a polyethylene "socket." There are several problems associated with this procedure. First, the rubbing wear of this ball and socket in the presence of corrosive body fluids can eventually lead to a poor fit and the failure of the assembly. Second, metallic flotsam is released to the body and can poison and inflame it, leading to undesirable histological effects. These effects have become increasingly serious as the average life span increases, causing many older people to have two THR's in their lifetime. Using ion source and accelerator technology originally developed by nuclear physicists for basic research, materials scientists have found that the ion implantation of nitrogen into the surface of a typical surgical alloy leads to a substantial reduction of this painful problem. By implanting nitrogen over a depth of 1000 angstroms, R. A. Buchanan and J. M. Williams were able to reduce the wear corrosion by a factor of at least 400. The successful clinical application of these very new results could be of enormous benefit to patients requiring artificial articulating joints.

B. Energy

Basic research in nuclear physics has created, and continues to create, a legacy of advanced technology that pervades energy-related research and development. The impact of this legacy extends far beyond the obvious example of nuclear energy into areas as diverse as fossil fuel prospecting and energy conservation.

Nuclear techniques are used by the **drilling industry** to help probe geological formations and to locate hydrocarbons and other substances in strata deep underground. Passive forms of nuclear well-logging employ gamma-ray detectors to distinguish regions containing clean sands and carbonates of low natural radioactivity from the less productive and more radioactive regions containing clays or shaly rock. Gamma-ray and neutron detectors operated in conjunction with neutron sources provide more detailed information. The more sophisticated of such logging techniques generate neutrons with the aid of miniaturized nuclear accelerators that can be lowered into the test bores. The apparatus produces fast neutrons, and the interactions of the neutrons with the surrounding material provide the logging information. In one application gamma rays following inelastic neutron scattering are measured, and the log is inspected for the characteristics that indicate the presence of carbon, a major constituent of oil and gas. In another application, neutron detectors are used to measure the duration of the well-defined slow-neutron pulse that results when the initial fast neutrons from the accelerator encounter hydrogen in the surrounding material. Rapid disappearance of the slow-neutron pulse suggests that the hydrogen in the region is accompanied by chlorine, which has a high efficiency for the capture of slow neutrons, and indicates the presence of salt water. A long-lasting pulse shows that chlorine is not present, and provides a good indication of petroleum deposits. The sensitivity of these and related nuclear techniques helps identify oil or gas-bearing regions that might otherwise be overlooked.

Oil shales are being investigated as a possible source of domestic energy with the aid of small angle neutron scattering (SANS). This technique measures the sizes of pores or voids that might contain petroleum products, thereby identifying shales that could contain potential sources of energy.

Energy conservation results whenever research and development efforts lead to increased efficiencies in existing energy technologies. Examples of nuclear physics contributions are found throughout this area. Nuclear tracer techniques have been used to study friction and wear in gasoline engines by incorporating radioactive carbon in steel piston rings. Ion implantation, initially a by-product of low energy nuclear physics research, is used to modify the surface properties of materials to inhibit friction and wear. Wire-drawing dies, ion implanted with nitrogen at a cost of only a few dollars per die, can be kept in service about five times longer than non-implanted dies, with consequent savings in tooling costs, plant downtime, etc. Ion implantation also shows promise for fabricating corrosion resistant surface alloys while conserving expensive, rare or strategic alloying materials such as chromium, platinum, cobalt and tungsten. The conservation occurs not only through the reduction of corrosion, but also because ion beam accelerators permit the implantation of these scarce elements selectively into the surface of the material—precisely where they are needed for corrosion resistance.

The development of the new alloys and ceramics that would permit fossil fuel power plants to operate at higher pressures and temperatures, with correspondingly higher efficiencies, is another area where nuclear diagnostic techniques such as neutron and charged particle scattering as well as ion beam implantation, with its ability to introduce essentially any element into any substrate, make important contributions. These efforts, aimed at increasing fossil plant steam conditions from the current state-of-the-art 1000°F at 3500 psig to 1400°F at 7000 psig, would result in annual fuel cost savings of 13 million dollars in a typical (800 megawatt) power plant.

The historic role of nuclear physics in the development of **nuclear energy** needs little elaboration, but perhaps less well known are the ongoing research efforts in support of national programs to develop advanced nuclear energy resources. Today, in the United States, approximately 13% of our electrical power is supplied by uranium-fuel thermal neutron spectrum reactors. In some regions of the country, such as Chicago, New England, and the Tennessee Valley areas, the percentage is much higher.

The design of advanced fission and fusion reactors capable of meeting the projected future demand for electricity depends upon detailed knowledge of neutron interactions over a wide range of neutron energies. Even though nuclear-data programs for reactor design have been active for many years and many data requirements have been met, several important ones remain unfulfilled and a few have not been seriously addressed.

Several accomplishments in the last few years can be selected to illustrate the diversity of these neutron data. These are (1) a precise 0.2% measurement of the average number of neutrons per fission from spontaneous fission of ^{252}Cf, used as a standard for all related measurements; (2) capture and fission data on several actinides (Np, Am,

Cm) in the fission reactor waste stream to allow definition of its composition for the various reactor options; (3) resonance data for ^{238}U and to a lesser extent ^{232}Th to permit adequate resonance-capture calculations for thermal light-water and graphite-moderated reactors; (4) the fission cross section of ^{238}U, the fission and capture cross sections in $^{240,241,242}Pu$ and the total cross section of sodium needed for fast reactor design; (5) the neutron total and reaction cross sections to 50-MeV neutron energy of many materials for shield design of the Fusion Materials Irradiation Test Facility, and (6) measurement of the $^{7}Li(n, n\alpha)T$ reaction that will be important for breeding performance in tritium-fueled fusion reactors.

Future needs for the liquid metal fast breeder reactor technology include more accurate data on ^{238}U capture at neutron energies above the resonance region, inelastic neutron scattering for ^{239}Pu and ^{238}U, neutron capture in fission products, and measurements of self-shielded cross sections for ^{238}U and ^{239}Pu in the resonance energy region. Optimal design of thermal reactors requires more accurate knowledge of neutron cross sections at energies through 1 eV on ^{235}U, $^{239,240}Pu$ (and ^{233}U if the thorium cycle is to be thoroughly understood). All fission designs need better-defined neutron spectra from fission, starting with the ^{252}Cf standard. For fusion-energy systems, the higher energy of the primary neutron source at 14 MeV requires extending the energy range of the nuclear-data measurements. Other reactions become important in induced radioactivity in structural materials or in the production of charged particles forming gas inclusions within the structural materials. Adequate nuclear data for shielding materials are yet to be measured. The strongly asymmetric angular distributions, which impact neutron streaming calculations, must be determined.

Intimately intertwined with these ongoing studies are efforts by metallurgists and other materials scientists to understand the effects of intense radiation on the properties of structural materials and to design new materials for service in advanced fission and fusion reactor systems. The nuclear physics and materials science research efforts both depend crucially on the availability of well instrumented, state-of-the-art facilities for nuclear measurements, such as high-flux research reactors and intense-beam pulsed electron and proton accelerators for neutron production.

Low energy Van de Graaff accelerators also contribute in a variety of ways. For example, Rutherford scattering of low energy ions is used to determine the suitability of various nuclear waste containment materials, as well as to characterize the surface properties of new reactor alloys under various conditions. The swelling and other effects that occur when helium is produced in structural reactor materials are being studied under controlled conditions by bombarding the material simultaneously with helium from a Van de Graaff accelerator and with neutrons from pulsed or steady-state sources. Such studies have helped identify metallurgical techniques for trapping the helium in a high concentration of small cavities or bubbles to minimize high temperature swelling and grain-boundary embrittlement.

C. Semiconductor Doping and Ion Implantation

Armed with ion sources, accelerators, and experimental techniques developed in low energy nuclear physics research, investigators in numerous disciplines are discovering that energetic ion beams can be used to alter and study the near surface properties of materials in a selective and often unique manner. When these beams impinge on a solid, ion implantation occurs which can alter or even dominate the electrical, mechanical, chemical, optical, magnetic, or superconducting properties of the material.

The results are often dramatic and several examples have been discussed earlier in this chapter. Perhaps the most impressive application of ion implantation concerns semiconducting materials. Most semiconducting devices require the selective doping of silicon or germanium with impurity atoms and ion implantation has rapidly become the dominant doping technique in the semiconductor industry. Responsible not only for new devices—such as high frequency transistors, improved MOS transistors, and integrated circuits—ion implantation also increases yields of old devices by orders of magnitude during fabrication and permits tremendous miniaturization. As a result, most semiconductor devices and integrated circuits for watches, calculators, computer chips, etc. are fabricated by ion implantation. The billion-dollar-a-year portable calculator industry is but one consequence of ion implanted integrated circuits; other examples ranging from color television to personal computers could be cited in complete analogy.

Ion implantation has been exploited in a myriad of other applications beyond those already mentioned. Controlled ion damage to insulators and semiconductors has been used to alter the index of refraction of materials to fabricate optical waveguides and mixers, and to selectively modify magnetic bubble memory devices. Ion implantation holds promise as a fabrication tool for high temperature superconducting materials, since these involve the formation or stabilization of a metastable phase which need exist only within a few hundred angstroms of the surface. And ion bombardment has proven effective in bonding thin films to substrates via the recently discovered enhanced adhesion phenomenon.

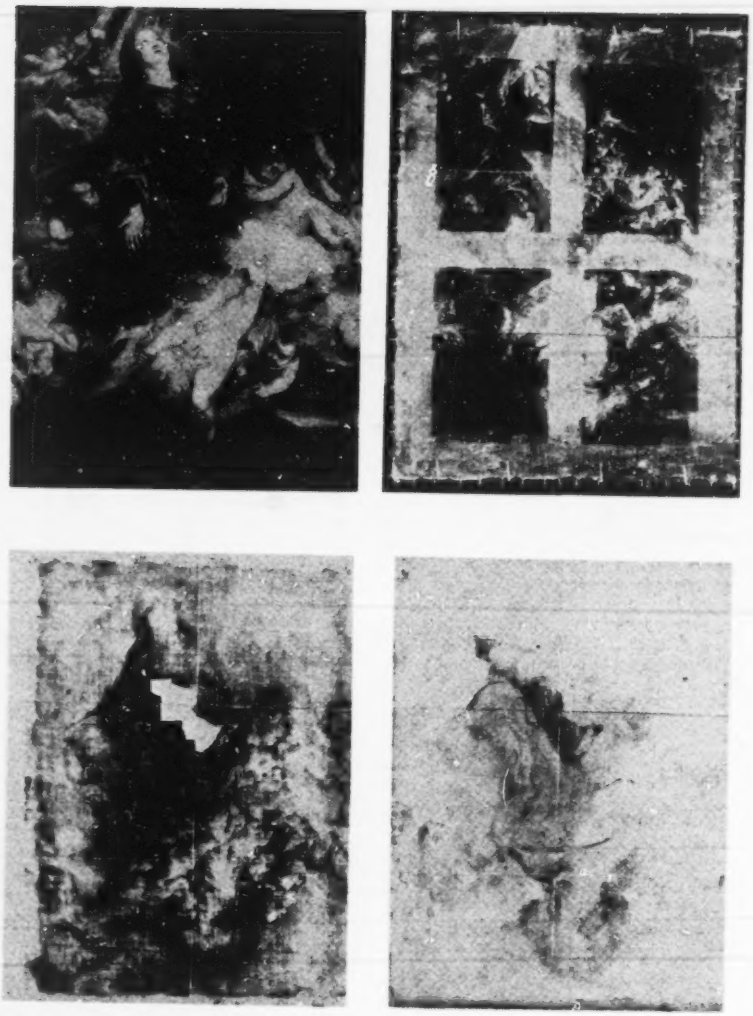

Fig. III.2-8. Neutron autoradiography of the painting *Saint Rosalie Interceding for the Plague-Stricken of Palermo*, by Van Dyck, reveals a hidden underpainting. The painting and its x-ray radiograph are shown in the upper left and right panels, respectively. The neutron radiograph in the lower panels reveal a self-portrait of Van Dyck (upside down, near the bottom of the painting).

D. Fine Arts

Nuclear science even contributes to the study of art history. One technique involves exposing oil paintings to a broadly spread, highly purified, thermal neutron flux of approximately 10^9 neutrons/cm^2/sec for periods up to one hour, generating within these paintings temporary, mild radioactivities. At various periods after activation x-ray film is placed in intimate contact with the painting to record images of the distributions of the radioactivities most predominant during these periods of contact. These images typically show significant differences from one another, as they are the records of radioactivities of quite different half lives. All of them are quite different from the conventional x-ray of the painting, which is largely determined by the distribution of the dense pigment lead white, a material that does not activate strongly with neutrons.

An interesting example of what can be revealed by autoradiography is provided by the study of the painting *Saint Rosalie Interceding for the Plague-stricken of Palermo* by Sir Anthony Van Dyck, which is in the collection of the Metropolitan Museum of Art. A photograph of this painting is shown in the upper left of figure III.2-B and its x-ray radiograph in the upper right. The radiograph reveals details of a hidden underpainting, the face of a man, upside down near the bottom of the picture. It is difficult to interpret this overpainted face in the x-ray as it is masked by many details of the surface painting.

An early neutron activation autoradiograph of this painting, at the lower left taken only a few hours after activation, largely records the distribution of manganese throughout the painting, which is probably present as a component of the dark earth pigment umber. This radiograph shows details of the canvas where it has been filled in by an umber-tinted ground paint layer. Also very noticeable in the upper center are two regions of loss, where original areas of the painting have been replaced by modern repairs, which are free of manganese. The details of the figures in the Saint Rosalie painting can be seen to have the quality of drawings, and indeed are thought by the art historians who have examined this autoradiograph to be the underdrawings, in umber, of the original figures of the painting. It is interesting to note that the angel above and behind Saint Rosalie's head does not appear in the original underdrawing. This angel appears to have been added later in the development of the painting, a change in its initially conceived composition.

A later autoradiograph, started four days after activation, lower right, shows the overpainted man's head in remarkable detail. This autoradiograph is largely from the element phosphorus present in the bone black used in defining the head. Comparison of this autoradiograph with a self portrait of Van Dyck, also in the Metropolitan Museum collection, shows that the overpainted picture was a portrait of Van Dyck himself.

Obviously, this ability to unravel a painting gives the art historians an entirely new dimension of their craft.

IV. RESOURCES

IV.1 Manpower and Training

The crucial element of any science, more important than facilities, instrumentation, or funding, are the people who pursue it. Reflecting a combination of circumstances, historical, economic, and sociological, there has been a substantial decline in the rate at which scientists, physicists and nuclear physicists, in particular, are being trained in the United States. Yet the continued need for nuclear scientists is considerable, with people trained in this discipline carrying out a variety of tasks in nuclear medicine, energy research, in many industrial research tasks and government service, in addition to providing the basic resource for continued research in the discipline.

It is becoming apparent that the rate at which nuclear scientists are being trained will not be adequate to meet the country's needs within the decade. Every year a large number of fresh Ph.D.'s trained in nuclear physics, and particularly in experimental nuclear physics, are hired by industrial laboratories with extraordinary alacrity. Their training in many aspects of advanced technology, the hands-on experience with relatively small-scale experiments where the student gains a measure of self reliance, seem to be factors in this phenomenon. And the forces of the marketplace are such that salaries in basic research positions cannot compete with those offered by industrial laboratories. The training in experimental nuclear science seems to be valued and this skilled manpower represents a major contribution of the field to the nation and to our society.

A healthy program of training nuclear theorists is also vital to the science. With the new construction plans, further upgrades, and fuller use of existing facilities, the theoretical efforts, presently severely limited by manpower, must also be strengthened. We recommend that the trend of the recent past, of increased funding for the buildup of strong theoretical programs be continued.

One reason that the shortage of nuclear scientists is not more acute now is that the condition in a number of countries is the inverse of that in the United States—more scientists are being trained than there are open positions. Some of the best young scientists from abroad come to the United States shortly after getting their doctorates, and either return to their home countries after having spent their most productive years in American laboratories, or sometimes stay on permanently. This influx of young scientists is mutually beneficial, and even healthy--leading to long term international ties—but it is not a viable long term solution to our manpower problems, since the training patterns and needs of other countries are also subject to change.

The reasons for the decline in U.S. graduate student enrollments in physics are complex. The fact that declining college enrollments have led to static and in some cases decreased faculty size at universities has had an especially strong impact on physics departments. For example, the ratio of junior to senior faculty positions in universities is lowest for physics among all the natural sciences. The fact that this has been widely discussed has caused many young people to decide not to take up physics as a profession. It is probably also true that the well-documented deterioration of the secondary school system in the United States is having an especially serious effect on basic training for the physical sciences. Students who have never been exposed to the excitement of science are unlikely to choose physics as a career path. Another effect is more peculiar to nuclear science. Unlike high-energy physics, which has been mostly a "user field" since its inception, university nuclear physics groups usually started with the operation of small in-house accelerators. With much research shifting to the larger facilities, the shutting down of many small university accelerators was inevitable. The psychological impact of having a facility at one's own institution closed down can be devastating and has slowed the momentum of Ph.D. training at the universities thus affected.

While it is important to upgrade science education at

all levels, the following recommendations, if acted on, would make physics in general and nuclear physics in particular more attractive to young people.

1. Programs which involve undergraduates in nuclear science research are extremely important in attracting students to the field. Many outstanding scientists were first attracted to a career in science through participation in such programs. A number of laboratories and universities have programs of this type; efforts should be made to strengthen and expand these, or to start them where they do not exist, if necessary with specific funding from the agencies. Similar programs to involve secondary school students in nuclear science research can also lead to long term benefits, and the involvement of secondary school science teachers in physics research will benefit the field and the nation.

2. Competitive predoctoral fellowships can contribute significantly in encouraging the best young people to study nuclear science. Any increase in the number of NSF Fellowships will naturally help all disciplines and is strongly supported. In addition, we suggest to the Department of Energy that it consider committing funds specifically for fellowships in nuclear science.

3. A competitive program of temporary direct support of new research initiatives by young nuclear scientists should be funded. This would encourage scientists starting in the field to develop new initiatives and an increased measure of independence.

4. Many existing small user groups in nuclear science are so constrained that they put all available funds for manpower into hiring research associates. With no direct technical or engineering staff working with these groups, they either become too dependent for instrumentation development and technical planning on the facility where they are users or an undue burden falls on in-house students and research associates. While clearly some such work should properly be part of a training in nuclear physics, it would considerably strengthen small university user groups to be able to hire their own technical staff, either engineers or scientists specializing in technical problems. The impact on developments of instrumentation, on the style and quality of research and on the attractiveness of doing research as a graduate student in the user mode could be considerable. We recommend that the agencies seriously consider funding supplementary requests for such manpower.

5. Educational aspects, the importance of attracting high caliber graduate students to nuclear physics and giving them the best possible training, should be given consideration in decisions on new facilities.

With the variety of challenging and important research opportunities outlined in Chapter II, both qualitative and quantitative aspects of our manpower and training ultimately determine the viability of the field. The steps outlined here will help the United States to continue to play a leading role in this area of basic research and to continue to train young scientists in skills and techniques which society puts to excellent use in numerous applications.

IV.2 Accelerator Facilities

The particle accelerator is the basic tool of the nuclear physicist and the development of accelerators is tied intimately to the development of nuclear science. Accelerators have also found powerful applications in almost every science ranging from nuclear medicine, through condensed matter and materials research to archeology and geophysics, where use of accelerators as ultra sensitive mass spectrometers has recently had dramatic consequences. The development of accelerators is an essential part of our science that has suffered all too often in times of budget stringencies and manpower shortages. There are major opportunities in the field of accelerator physics, many of them outside the immediate concerns of basic nuclear physics research, and our field must train specialists in this area of applied physics in numbers sufficient to meet the challenges in the future.

During the last decade a number of important advances have been achieved in accelerator physics: the uses of superconducting magnets, of superconducting resonators capable of producing high radiofrequency fields for the acceleration of particles, of beam cooling in storage rings, to mention just a few.

The accelerator facilities of nuclear physics are here separated into two groups. There are nine major national facilities whose operation and research programs account for about 80% of the budgets for experimental nuclear physics. These facilities are used for an important share of the research effort by the national and international community of scientists, with experimental time allocated with the help of Program Advisory Committees. The remaining support is largely for dedicated smaller university research accelerators that play an important role in the education and training of graduate students (along with the major facilities), and in the pursuit of many important research goals.

A. MAJOR NATIONAL FACILITIES

The nine facilities listed here are all "user facilities" in the sense that, because of their unique characteristics, they are generally available to scientists throughout the U.S. and the world, and their experimental priorities are set on the basis of recommendations of Program Advisory Committees. These facilities vary in size from the large U.S. meson factory LAMPF and the one relativistic heavy-ion accelerator in the world the BEVALAC (which between them account for about two-thirds of the above mentioned 80%), to some much smaller and less costly—though still very important accelerators.

For each of these facilities we list present capabilities and future aspirations, without making specific priority recommendations on the implementation of the latter.

1. INTERMEDIATE ENERGY ACCELERATORS

The Los Alamos Meson Physics Facility (LAMPF) is a national facility providing both primary and secondary particle beams for an extensive program of research including nuclear, elementary particle, and condensed state physics. The heart of the facility is a linear accelerator providing a beam of protons of variable energy up to 800 MeV, intensity of 1 mA and a duty factor of 9%. A separate H^- ion source provides the capability of accelerating simultaneously a low current H^- beam with a high current of H^+. The 800 MeV proton beam is used primarily for the production of secondary beams of pions, muons, and neutrinos. Several magnetic channels allow experimentalists to select independently the desired beams of secondary particles. Part of the proton beam is also used for neutron production, and with the completion of the proton storage ring (PSR), will provide an intense pulsed neutron source. H^- beams, polarized or unpolarized, can be obtained at different energies (down to 218 MeV) and used for studies of proton induced reactions. The H^- beam is split between the high-resolution proton spectrometer facility where nuclear structure studies predominate and the nucleon physics laboratory where a comprehensive program of measurements of the two nucleon system is carried out. An extensive program of nuclear structure studies with pions is carried out using the high-resolution pion spectrometer, EPICS. Other major hardware facilities include a π^0 spectrometer capable of measurements with energy resolution of ~1-2 MeV, a time projection chamber, and a large NaI(*Tl*) "crystal box" facility. A new low-energy pion spectrometer, currently under construction, will be installed in the Low Energy Pion Channel to extend the capabilities for high resolution pion spectroscopy to 10-100 MeV.

The LAMPF user group currently has a membership of more than 900 scientists. Approximately 300-400 scientists from ~90 universities are participating in research at LAMPF in any given year.

Future facility plans include an upgrade of the PSR area to provide a pulsed muon facility and a high intensity neutrino source. In addition to numerous planned developments and improvements in the present LAMPF accelerator, a design effort is under way for a major new future accelerator (LAMPF II) that would be based upon a 16-32 GeV synchrotron and stretcher ring injected by LAMPF. This accelerator would provide K-meson beams 100 times as intense as present facilities, as well as improved pion, muon, neutrino and antiproton beams.

The Bates Electron Accelerator Center of the Massachusetts Institute of Technology centers on a high-intensity pulsed S-Band electron linac covering the energy range 50-750 MeV. The typical average current and duty cycle at present are 40 μamp and 0.5%, respectively. This laboratory is recognized worldwide for its leading contributions to high-resolution electron scattering. In the past five years, there has been substantial progress toward expansion of the facilities which includes: (1) increase of the energy to 750 MeV by a single recirculation of the beam through the linac, (2) construction of a second experimental hall (120' x 80'), (3) construction of two large solid-angle spectrometers capable of measurement of momenta up to 400 MeV/c and 1300 MeV/c, respectively, (4) construction of a large opening angle π^0 spectrometer. In addition, a polarized injector will be installed in the immediate future for use in nuclear polarization studies and parity violation experiments.

The further stages of improvement under way are: (1) beam-sharing capability, allowing simultaneous 50 μamp beams in each experimental hall, and (2) the addition of a sixth two-klystron modulator and some increase in the peak-power capability of the existing modulators to achieve both greater reliability and energy capability of at least 900 MeV. In addition, a pulsed stretcher ring to provide ~100% duty factor beams for South Hall experiments is being planned. Provision will be included in the ring design for internal target experiments and for delivery of polarized beams. Bates serves a large community of outside users; about 180 scientists coming from approximately 40 universities and national laboratories. About 50% of the beam time goes to outside users.

The Indiana University Cyclotron Facility provides a variety of light-ion beams over a range of bombarding energies and momentum transfers. The ion beams are generated by a coupled pair of separated sector cyclotrons. Proton currents typically are ~1 μamp and proton energies are in the range 12-210 MeV. Light ions including polarized protons and deuterons are available with

energies up to 220 q^2/A MeV and with pulse widths of 0.35 nsec. Present major experimental facilities include a beam swinger for time-of-flight measurements with path lengths up to 160 m, a QDDM spectrograph, a QQSD spectrograph for low rigidity particles such as pions, two scattering chambers, and a polarized neutron beam. Presently, a dual spectrometer facility, one spectrometer to be high resolution ($p/\Delta p \cong 35{,}000$) is under construction. Accelerator improvements underway include the construction of a storage ring, with electron cooling to reduce dramatically the phase space of the beam and internal targeting, which is to be completed by 1986-1987. Upon completion, three internal target experiments may be carried out simultaneously. Future plans include the possibility of an additional cyclotron to triple the energy, or ramping the energy in the storage ring to 500 MeV, and/or addition of a two-ring collider.

IUCF has been in operation since late 1975 as a national user facility. More than 250 scientists from 47 U. S. institutions have been actively involved in the research program.

A new **4-GeV Electron Accelerator Laboratory** operating at a beam current of 240 μA and a duty cycle of about 90%, to be built by the Southeastern Universities Research Association (SURA), was recommended for construction by NSAC earlier this year. The main components are a 2-GeV pulsed linac with a single-pass recirculator and a beam-stretcher ring system. With double-pass, head-to-tail recirculation, the linac will produce a 4-GeV beam having a pulse length and intensity that allow single-turn injection into the stretcher ring. The accelerator could be upgraded in the future to achieve energies of 6 GeV or higher, should the physics in this region make such an upgrade desirable.

SURA plans to build a tagged-photon facility and two end stations for coincidence experiments and spectroscopy. The designs and specifications for the spectrometers available at each experimental area will be set in close consultation with the user community. As presently envisioned one end station may receive beam from either the linac or the pulse stretcher ring; it will be the location for a moderate-resolution spectrometer with a high-resolution spectrometer to be added later. The second end station will receive beam only from the stretcher ring and will house a moderate-resolution and a low-resolution (large acceptance) pair of spectrometers suitable for coincidence experiments. A tagged-photon facility will include a moderate-resolution spectrometer.

2. HEAVY ION ACCELERATORS

Six of the national user facilities are classified as **heavy-ion facilities**. In most respects, the characteristics of these accelerators are complementary rather than competitive, since none of the technologies are the same and the beam energies and other capabilities of the several machines are quite different, as required by the wide range of research objectives. At all of these facilities, outside users participate actively in much of the research, are involved in the development of new experimental apparatus and, in a variety of ways, influence the accelerator-operating policies. Typically, outsider users are allocated at least 50% of the running time. The total numbers of outside users during a given year varies from about 50 for the smaller facilities to several hundred for the largest.

The **Double MP Tandem Accelerator at Brookhaven**, which came into operation in 1970, covers the low-energy end of the range of heavy-ion projectiles of interest to nuclear physics, providing precise high-resolution beams with energies above the Coulomb barrier for ions in the lower third of the periodic table. Two upgraded model MP tandem electrostatic accelerators can be operated separately or jointly, in several different configurations. The highest energies are obtained with the 3-stage mode in which a negative-ion source is mounted in the high-voltage terminal of the first machine, operated at a negative potential. The heavy-ion performance of this 3-stage system is roughly equivalent to that of a single tandem with 18 or 19 MV on the terminal. The system is also used to accelerate light ions and provides energies as high as 42 MeV for protons.

Brookhaven National Laboratory has proposed major expansion of its present facility by combining it with the AGS (the 30-GeV Alternating Gradient Synchrotron) to accelerate heavy ions to relativistic energies up to ~15 GeV per nucleon. Using direct injection of the AGS, ions up to A = 32 and currents $>10^9$ pps would be available. Construction of a modest intermediate booster accelerator would permit injection of heavier ions, up to about A = 130, into the AGS. This system would provide significantly higher-energy relativistic heavy-ion beams than are now available at the Bevalac. Present studies indicate that beams accelerated in the AGS are suitable for injection into a relativistic collider system which BNL is designing for possible future construction.

The **88-Inch Cyclotron at the Lawrence Berkeley Laboratory** emphasizes nuclear-structure physics with heavy-ion beams in the lower fifth of the periodic table. The accelerator is a variable-energy isochronous cyclotron with spiral sector focusing. Light ions are produced by an internal filament source, polarized protons (up to 55 MeV) and deuterons by an external polarized ion source, and heavy ions by an internal heavy-ion PIG source. One third of the beam time is used for light ions. The high intensity polarized ion source produces a microampere of

39-587 O - 84 - 69

beam on target. A pair of 110° analyzing magnets are dispersion matched for the QSD spectrometer.

The energy range of the 88-Inch Cyclotron will be enhanced considerably and the mass range will be extended to 100 amu by the installation of an electron-cyclotron resonance (ECR) ion source, now under construction. This accelerator improvement is being accompanied by the construction of a major new experimental tool, a compact assembly of 21 Compton-shielded germanium detectors and 44 bismuth-germanate detectors designed to study high-spin nuclear states.

The **Holifield Heavy-Ion Research Facility at Oak Ridge National Laboratory**, completed in 1982, consists of a new 25-MV tandem, the K = 100 Oak Ridge Isochronous Cyclotron (ORIC) which has been modified to serve as an energy booster for tandem beams, and experimental apparatus to utilize beams provided by these accelerators operating both in stand-alone and coupled modes. The beam energy is easily varied in both modes. For ions in the intermediate region of the periodic table (say $40 < A < 110$), the coupled system provides beams in an energy range that is not available at this time elsewhere in the United States for nuclear-structure research. This advantage and an extensive complement of experimental apparatus (4-π, 70-detector gamma-ray spectrometer, on-line isotope separator, two high-resolution magnetic spectrometers, time-of-flight spectrometers, etc.) provide an opportunity for the facility to be especially productive during the next few years.

Two approaches to an extension of the energy and mass range of the Holifield facility have been studied, both involving an improved cyclotron injected by the 25-MV tandem. One approach would increase the beam energy by about 40% and reduce power consumption by using superconducting coils for ORIC. The second option would extend the energy into an entirely new range (200 MeV/nucleon for light ions and 40 MeV/nucleon for uranium) by adding a K = 1200 superconducting cyclotron of the kind under construction at Michigan State University.

A heavy-ion accelerator-collider is being studied as a possibility for a major new facility at ORNL. As now conceived the system would consist of a linac injector, a conventional synchrotron booster, a stacker-stretcher ring, and a pair of superconducting intersecting acceleration-storage rings. For uranium ions the system would provide ~10 GeV/nucleon with a luminosity of $\sim 10^{29}/cm^2$-sec and intensities of 10^{10}-10^{11} particles/sec for fixed target experiments. Straightforward modifications to this design to extend the energies to 30 GeV per nucleon and above are also being explored.

The **Argonne Tandem-Linac Accelerator System (ATLAS)** at Argonne National Laboratory is the world's first successful accelerator to use r.f. superconductivity for the acceleration of projectiles heavier than the electron. It is being built in two phases. The first phase, completed in 1982, consists of a small (9-MV) tandem injecting into a 20-MV superconducting linac which was originally constructed as a prototype machine designed to develop a new technology, but is now used routinely as a research tool. The performance characteristics of the tandem-linac system are similar to those of a very large stand-alone tandem, and consequently the system is most useful for precision nuclear-structure research. Noteworthy features of the performance are the ease with which the energy may be changed and the availability of ultra-short beam pulses.

In the second stage of construction, the present facility is being expanded to form ATLAS. This project will double the size and accelerating power of the linac and add a large, well-equipped experimental area. At the interface between the present prototype linac and the ATLAS addition the beam will be separated into two components, one of which is accelerated to the full energy and the other is directed simultaneously, without further acceleration, into the present experimental area.

Because of the modular character of the tandem-linac system, it can rather easily be modified or expanded. Future options for ATLAS include (a) improving the overall performance of the system by replacing the present FN-model injector by a better machine for the purpose and (b) extending effective acceleration to the heaviest nuclei by modifying and enlarging the linac.

All of the heavy-ion accelerators described above have beam energies that are within an order of magnitude of the Coulomb barrier. The remaining two facilities are designed to provide much higher energies with which to investigate quite different physics.

The accelerators at the **National Superconducting Cyclotron Laboratory** at Michigan State University are two superconducting cyclotrons, which are designed to be operated either as independent machines or in 2-stage acceleration. The phase I machine, the world's first operating superconducting cyclotron, was used to develop a new technology and is now being turned to research. It has a bending-limit parameter of K = 500 and a focusing limit of 80 MeV/nucleon for q = A/2. The first beam was extracted from this prototype machine in 1982, and since then a variety of ion species in the lower part of the periodic table have been developed and used for research. Beams have been extracted at the full K = 500 design limit of the superconducting magnet.

The second phase of the MSU project is now in progress. This work includes the addition of a second, larger superconducting cyclotron (K = 800) and the development of an advanced set of experimental apparatus. In the 2-stage mode of acceleration, this system will provide intense beams with energies up to 200 MeV/nucleon for $A < 40$, thus opening up an unexplored region of energy for investigation.

An attractive option for future improvement of the MSU system is the installation of an external ion source and axial injection; with an ECR source, the coupled facility could yield 80 MeV/nucleon uranium beams.

Bevalac Complex. This is the only facility in the world that can provide relativistic beams of ions over the entire range of the periodic table. It is also at present the only source in the U.S. of very heavy ions with energies above the Coulomb barrier. This unique facility is heavily used by researchers from the U.S. and abroad. One-third of the operating time of the machine is devoted to biomedical research. Major nuclear science facilities include: HISS (Heavy Ion Spectrometer System), a large acceptance spectrometer using a 3 T superconducting magnet in conjunction with an extensive array of detectors to measure many-particle final states associated with projectile fragmentation processes, large momentum transfer processes, and other few particle correlation studies; Plastic Ball/Wall, 4 π electronic detector with approximately 1000 elements for obtaining exclusive charged-particle information on an event-by-event basis; Streamer Chamber, a 4 π visual detector for charged particles allowing full event reconstruction; Low Energy Beam Line, for studying nuclear reactions in the 30-200 MeV/nucleon range. In addition, several smaller detector facilities are available for studying heavy-ion collisions. A dilepton spectrometer (DLS) to study the electron-positron mass spectrum is being planned. Other experimental facility upgrades include (a) modifications to the Low Energy Beam Line (1984) to raise beam intensities; (b) improvements to the Bevalac Switchyard (1985) to enhance operating flexibility and permit delivery of a wide range of rare isotope beams; and (c) installation of a high-resolution system for delivering secondary beams of rare isotopes to the HISS facility.

To increase the intensity of the heaviest ion beams some 10 fold, improvements will be made during 1984 to the transfer line connecting the SuperHILAC to the Bevalac. Another accelerator upgrade project to be completed in mid-1984—replacement of the present Bevatron local injector's pre-accelerator with a radiofrequency quadrupole linac—will enable more efficient switching between the lighter ions (up to silicon) used for biomedical research and the heavier beams needed for the nuclear science programs.

Over the period of the last few years LBL has been studying new machines to provide beams at substantially higher energies than those available at the Bevalac. Present plans center around a two-ring superconducting accelerator complex optimized for acceleration of heavy ions throughout the periodic table which would be capable of both fixed-target and colliding-beam operation. The SuperHILAC will be improved and used as the injector.

B. DEDICATED UNIVERSITY FACILITIES

There are roughly a dozen facilities at universities supported by the agencies for basic research in nuclear physics. These have an important dual role to fulfill. They carry out first-rate basic research within their range of capabilities, often involving the more difficult and time-consuming measurements, and at the same time and most importantly, provide an in-house facility for the training of students in experimental physics. Some of the scientific frontiers of nuclear physics are driving the field to large unique user facilities, but many other important scientific questions are well within the scope of these smaller accelerators. The role of university accelerators in training scientists has been stressed before by the NSAC Subcommittee on University Research and Education in Nuclear Science. These accelerators provide the opportunities for students and young scientists not only to do research and develop their all-around research skills, but to develop the independence and self reliance that is essential in an effective researcher. First-rate scientists can be, and are, effective in the user mode. But the influence of an in-house accelerator within a strong university physics department can be very important in attracting the best graduate students and training them in nuclear physics, in a variety of experimental and technical skills, and most importantly in becoming self-sufficient and strongly motivated researchers.

The "dedicated university facilities" are in general also made available to users from other institutions.

1. CURRENT AND RECENT ADDITIONS AND UPGRADES

A number of the university facilities have been and are in the process of being modified by having major changes or additions implemented.

The **State University of New York at Stony Brook** has recently installed a superconducting linac, based on lead-plated copper resonators (rather than the niobium ones used in the ATLAS project and discussed earlier). This parallel successful development of superconducting radiofrequency technology for accelerators is a major

technical achievement. Operation of the facility at Stony Brook for research started in 1983; the maximum beam energies finally expected are about 10 MeV per nucleon for heavy-ion beams around mass thirty and 5 MeV per nucleon for mass eighty—a qualitative step above the energies of the FN tandem injector.

The continuing development of 100% duty cycle electron microtrons at the **University of Illinois, Urbana** has provided a first-rate research tool with electrons up to 70 MeV. Further developments underway will increase the energy to 100 MeV. An additional microtron stage is planned that will increase the energy to 250-300 MeV.

Major upgrades are under way at **Yale University** and at the **University of Washington.** At Yale the MP tandem is to be rebuilt into an ESTU accelerator—which is expected to operate at almost double the present terminal voltage and greatly increase the research capability of that facility. At Seattle a superconducting linac booster is planned that will provide light ions, including protons up to 37 MeV, as well as heavy ions through 4.3 MeV per nucleon ^{56}Fe.

Florida State University is completing a superconducting linac accelerator-booster based on Nb technology, for their FN tandem. It will provide enhanced heavy-ion capabilities to about ten MeV per nucleon for mass forty. **Texas A & M University** is building, from university and other private funds, a superconducting cyclotron to accelerate lighter ions with mass below twenty, to about 80 MeV per nucleon and heavier ions ($A \approx 100$) to 10 MeV per nucleon. The new 3 MV tandem accelerator at **Caltech** promises to be an interesting facility for low-energy experiments, including measurements important for nuclear astrophysics. All of these upgrading and improvement projects involve a large number of students, undergraduate and graduate, whose participation in the solution of complex problems on the frontier of high technology will have substantial beneficial impact.

We do not mention here all the university facilities, many of which are world renowned for their research and have unique features in the accelerators or associated instrumentation. There are additional university accelerators not listed here that are supported partially for their work in basic nuclear physics.

C. OTHER FACILITIES

Nuclear physicists are making important use of facilities operated primarily for the High Energy Physics Program. The *hypernuclear spectrometer "Moby Dick"* located at the low-energy kaon beam line of the AGS at Brookhaven is the only facility for the study of hypernuclear physics and the science that was outlined in Sec. II.6.

At the Stanford Linear Accelerator Center (SLAC) a new electron injector is being built for nuclear physics experiments. It uses the last six sections of the linac and provides electron beams up to 3.0 GeV of about 20 μA average current, with a duty cycle of 0.04%. The beam is brought into *End Station A* where spectrometers appropriate to electron scattering experiments already exist. This facility is suitable for some of the single-arm measurements that will lead into the physics to be studied at the 4-GeV electron accelerator.

Very interesting pioneering nuclear physics studies with high energy proton beams have been carried out at the *internal gas target facility* of the Fermilab accelerator.

Important studies of nuclear structure severely testing predictions of current models are performed with neutron capture gamma-ray studies at the High Flux Beam Reactor (HFBR) at Brookhaven. The on-line isotope separator *TRISTAN*, on another HFBR port supports an active user program studying nuclei far from stability, produced in the fission of uranium.

Although the large majority of facilities for basic nuclear research are supported by DOE (Office of Energy Research) and the NSF, there are some smaller accelerators (e.g. various machines at the Lawrence Livermore National Laboratory, Los Alamos National Laboratory and including the new 200 MeV microtron soon to be completed at the National Bureau of Standards) that receive their support for basic nuclear research from other federal sources. There are many other accelerators that are funded from a variety of federal programs, in atomic physics, in materials science, or for measurements of cross sections needed in the nuclear energy programs, that often contribute significantly to nuclear physics research. Indeed, sources of slow neutrons at research reactors and pulsed neutron sources are among these.

D. ACCELERATOR TECHNOLOGY DEVELOPMENT

The vitality of nuclear physics as a discipline depends critically on the continuing refinement of its experimental tools, and for most of the subject the primary tool is now the particle accelerator. The immense changes during the past two decades in the nature and the scale of the accelerators required for forefront nuclear-physics research, demonstrate graphically the speed with which the subject is advancing. In the 1960's, the typical nuclear-physics projectiles were electrons, protons, neutrons, deuterons, and α particles with maximum energies of a few tens of

MeV. It was the era of the Van de Graaff, small cyclotron, and small electron linac, of which there were a large number, mostly similar in character and commercially built. In contrast, now the number of active accelerators is much smaller, the range of projectiles includes all stable nuclei, GeV electrons and secondary mesons, many individual accelerators are an order of magnitude larger and more complex, beam energies are being expressed in GeV rather than MeV, and there is a strong emphasis on uniqueness of performance characteristics.

Clearly, accelerators are increasingly important to nuclear physics and, as a consequence, nuclear physics is becoming more important to accelerator technology, as is evident from the changing subject matter presented at the biannual National Accelerator Conference. These trends are almost sure to continue and to require nuclear physics as a discipline to have a more systematic approach to the development of accelerator technology.

It has been the experience in the past that advances in the technology of basic-research accelerators soon found their way into more practical applications. Chapter III of this report discusses a number of such applications—ion implantation, the generation of medical isotopes, radiation therapy, numerous materials-diagnostic techniques, and so on. Undoubtedly, some of the recent advances in accelerator technology mentioned below will be the basis for future applications that have not yet been realized.

This section attempts to give a brief overview of the technical developments that are now important to nuclear-physics accelerators; the treatment is intended to be illustrative rather than comprehensive. A few of the more clearly foreseen needs for the future are also mentioned.

1. Examples of Past and Present Developments

a. Ion Sources

Progress in the development of ion sources has been very rapid during the past decade. Sources have been developed for almost all elements of the periodic table through uranium, at up to fully stripped charge states, and with steadily improving current, quality and reliability. There are numerous source development programs at present. For example, at the University of Wisconsin-Madison, improvements are being made in the colliding beam source of polarized negative ions and in SNICS, an unpolarized heavy negative ion source. Development of an intense laser driven polarized negative ion source is also under way. Particularly important developments in negative ion sources have been made at the University of Pennsylvania. At ORNL, new versions of the Aarhus and axial-geometry cesium plasma sources and a new universal Li-vapor charge-exchange negative-ion source for Group IA and IIA elements are being tested.

The development of intense polarized electron sources producing a high degree of polarization will be important in order to exploit the polarization observables; a promising new opportunity that becomes realistic with the CW-electron beams available in the future.

At LBL, an electron-cyclotron resonance (ECR) source under construction will axially inject highly stripped heavy ions into the 88-Inch Cyclotron, providing increased energies and 100 percent duty factor. Most of the early development of this source occurred in Europe, as is the case also with the electron beam ion source (EBIS). These sources, various ideas for laser-driven sources, and polarized ion sources will be important elements of future nuclear physics programs. A final example of source work is the interesting area of radioactive ion-beam production, under active development at Ohio State University and at other facilities.

b. Electrostatic Accelerators

Electrostatic accelerators were the earliest accelerators used to study the nucleus, and the Van de Graaff has been the yeoman performer since its invention. Improvements were constantly made. These machines were relatively inexpensive, and form a backbone of research and teaching facilities to this day. It is also interesting to note that the market stimulated commercial suppliers.

Even though the Van de Graaff has been worked on throughout several decades, there is still worldwide interest in the technology. A novel new approach, developed at the University of Strasbourg, could, if successful, lead to the construction, at a moderate cost, of a 35 megavolt tandem Van de Graaff which would be able to accelerate ion species up to uranium to energies exceeding 5 MeV per nucleon. A more modest development now in progress is a method first used in Japan for cleaning accelerator tubes by means of a glow discharge. This technique is exciting interest because it promises to increase the maximum voltage of accelerating tubes by as much as 20%, a large increase in the mysterious business of high-voltage technology. Another notable development is the demonstration at Brookhaven that a tandem Van de Graaff can be used to accelerate exceedingly intense pulses (200 μA) of highly-stripped ions, a technique that may prove useful for the production of intense beams of relativistic heavy-ions.

c. Linear Accelerators - Microtrons

The need for higher energies and intensities required larger machines. LBL pioneered development of accelerator technology in linacs and circular machines that has been used worldwide. In the 1960's, the very large LAMPF project produced firsts in a number of important areas—particularly in automatically controlled rf fields, and in basing its operation from startup on a computer control system. Aspects of these innovations had a wide influence in both private and public sectors; for example, the accelerator structure developed for the high-beta section formed the basis for most of the electron linacs used in medical x-ray machines today.

A few years ago, a fundamentally new type of accelerator for low-velocity ions, the radiofrequency quadrupole (RFQ), was pioneered at Los Alamos following theoretical concepts developed in the USSR. This structure, now under development at many laboratories, allows adiabatic bunching and acceleration, resulting in very efficient capture (>90%) and high beam quality. This device is ideal for many applications that require the acceleration and bunching of relatively slow-moving ions, particularly as the initial stage of an accelerator system. An RFQ for ions as heavy as silicon is being built at LBL to replace a Cockcroft-Walton preaccelerator at the Bevatron. The structure has passed its high-power tests, and preparations for beam tests are proceeding.

The need for electron accelerators resulted in extensive development of the rf-efficient microtron. The University of Illinois Nuclear Physics Laboratory has pioneered use of the superconducting linac in microtrons. Higher energy and intensity requirements spurred development of room-temperature technology in Europe and in an NBS/Los Alamos collaboration, and this approach is a candidate for CW electron machines in the GeV range.

For several decades, one of the most challenging tasks for the future has been to harness the remarkable characteristics of superconducting materials. This goal is now being achieved. Superconducting resonators operating at radiofrequencies have a reputation for being especially perverse, but by now they have developed into an established technology, with numerous applications to heavy-ion acceleration and beam bunching and to electron acceleration. The pioneering recent work at Argonne on niobium accelerating structures shown in figure IV.2-A demonstrated the practicality and the power of the technology for heavy ion acceleration. In an alternate approach, an effort involving Cal Tech, Stony Brook, and the Weizmann Institute has used lead plated on copper to form superconducting accelerating structures that are relatively easy to fabricate. These various devices are now being used or seriously considered for use in at least 9

Fig. IV.2-A. Niobium resonator developed for the acceleration of heavy nuclei. These resonators operate at very low temperatures as superconducting radiofrequency cavities. Surface fields as high as 36 million volts per meter, and accelerating fields as high as 8 MV/m have been attained in resonators very similar to this one. Such devices are now being used routinely in accelerators.

linacs in 6 countries. The next step, already under way, is to extend the velocity range for which the superconducting accelerating structures are effective.

d. Superconducting Cyclotrons

Another advanced application of superconductivity is the superconducting cyclotron. This effort, started in the mid-1970's at Chalk River and at Michigan State University, has now been taken up by about a dozen groups around the world. The advantage of this approach is that the immense magnetic field obtainable with superconductors reduces the size, the power requirements, and hence cost of the cyclotron. The cryostat for the $K = 500$ cyclotron at Michigan State is shown in figure IV.2-B. The small size is also the main developmental challenge; successful operation of the cyclotron at Michigan State shows that the challenge of developing accelerator hardware consistent with this small size can be met.

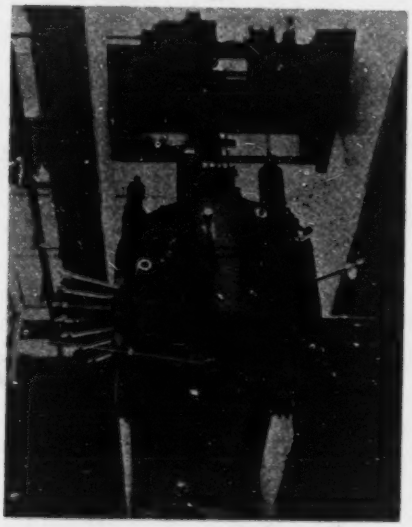

Fig. IV.2-B. Cryostat containing the superconducting magnet of the K500 superconducting cyclotron at Michigan State University being lowered into position in the magnet iron.

e. Superconducting Magnets for Beam Transport

Superconducting magnets have to date played little role in the beam-transport systems and spectrometers associated with nuclear-physics accelerators. This will soon change, however, since such components will be used extensively at the Michigan State cyclotron; and some superconducting beam-line elements, including a beam splitter, are also being developed for the Argonne heavy-ion linac. The requirements for nuclear physics are in some respects more challenging than the corresponding work for high-energy physics, since the beam must often be bent through large angles and also because the cost effectiveness of the superconducting approach is less clear cut.

f. Beam Cooling — Target Development

The need by experimentalists for increasing beam intensity and beam quality refinement provides a strong stimulus for progress in accelerator development. What appears to be a major new departure is an effort to couple the Indiana cyclotron to a storage ring in which the energy spread of the stored beam will be greatly reduced by "cooling" the beam. This circulating beam will pass through an internal target that is thin enough to preserve the exceptional beam quality of the cooled beam, thus providing a previously-untouched level of precision for experiments with energetic protons. Clearly, an internal target is the cost-effective way to achieve unusual capabilities at other accelerators also, and the technique is likely to be extensively developed during this decade. A big step in this direction is the plan by an Argonne group to develop an internal polarized-deuteron target for the electron storage ring Aladdin.

2. Future Needs

The accelerators in current use for nuclear physics research will continually require additional development to meet new research needs. All of the areas discussed above will see further evolution. Beyond that will be a new set of accelerator development needs specifically associated with new major facility plans. These might include, for example: the development of larger superconducting magnets for cyclotrons that provide ion focusing and bending capability well beyond that of the MSU K-800 now under construction; development of superconducting bending and focusing magnets, new relativistic heavy ion accelerators, which may require magnets with good magnetic field quality over a wide range of magnetic fields and capable of fast cycling. Larger, high current proton accelerators may require development of efficient fast cycling magnet systems much larger than built heretofore, high power accelerating stations, and fast beam switching systems for injection, extraction, and external beam manipulation. The NEAL electron accelerator will require the development of new high power klystrons. These needs for the next

generation of facilities will require significant new investment in accelerator development.

New accelerator systems that would provide new levels of experimental capability will require an extensive development in accelerator technology. This program must include research on techniques which are not needed for a specific project but which could lead to dramatic advances in accelerator capabilities. It is hoped that such a program would encourage more scientists and engineers to work in this crucial endeavor. This is necessary to assure that new accelerators be successful and completed in a timely and cost-effective fashion.

IV.3 INSTRUMENTATION FOR NUCLEAR SCIENCE

Nuclear physics rests on a triad of resources: manpower, whose collective knowledge, wisdom and drive for understanding is the motive force; accelerator facilities that provide the essential probes for investigation of the physics of the nucleus; and instrumentation that detects and characterizes the physical processes as they occur. The rate of progress in any scientific area is in large measure fixed to the rate at which hypotheses can be tested and refined or unexpected results uncovered. By its very nature experimental research involves the investigation of new phenomena or the observation of known phenomena with new techniques.

As measurements become more difficult and complicated, the overall design of the experiment becomes increasingly critical. In addition to more advanced detectors capable of handling more information at a faster rate, the methods of data collection and analysis have to be well planned. It is not at all unusual to find the real computer time required for the analysis of data to be twenty times longer than the time for data acquisition. With the advent of higher-energy machines and more sophisticated detector systems, it is evident that instrumentation for data acquisition and data handling must be optimized and make full use of the latest applicable developments in computer technology, otherwise we face a major bottleneck that could absorb huge fractions of the available skilled manpower.

With constrained budgets, the investment in instrumentation and in the expert manpower required for its long-term development has lagged in U.S. nuclear science. This lag was identified in the 1979 Long Range Plan and has been corrected in some measure since then. This is not an isolated problem in nuclear science and "Revitalization of Laboratory Instrumentation" was a subject of a recent workshop by NRC-NAS where the general problem and its possible solutions were discussed. There are major needs and opportunities within nuclear science and it is difficult to establish firm budgetary quotas. Certainly some fraction of the enhancement that has been recommended to the Operating Budgets for FY 1985 should be devoted to instrumentation, to the development of instrumentation, and to manpower associated with it.

A. INSTRUMENTATION TO BE APPLIED TO PRESENT RESEARCH

Modern computing facilities are at the heart of every nuclear physics laboratory. They are essential to the recording, sorting and analysis of data. The computer industry continues to provide a stream of products that allow one to deal ever more effectively with the complexity of energetic nuclear reactions. The newer 32-bit super minicomputers have become the accepted standard at most laboratories and most recent developments are built around such systems. Memory size is no longer an obstacle (at 2 K$/MB) and 500 MB discs are available at 20 K$. As the CAMAC dataway rate can be pushed to 400 kHz with suitable hardware, it appears to be able to handle most experiments for the next 5 years. Those few experiments requiring higher rates can avail themselves of either parallel CAMAC systems or the new FASTBUS system. This system is 10 times faster than CAMAC, operates on a 32-bit structure and allows for more efficient and modern circuit design. FASTBUS with intelligent processors will be especially useful for experiments requiring fast complex triggers. Every effort should be made to keep these data acquisition systems up to date since the new technology permits the basic sharing of software and ready assimilation of technological advances.

Spin polarized projectiles and targets have played an important role in the study of nuclear phenomena. Significant increases have been obtained in polarized hydrogen beam currents and the incorporation of these advances into facilities using polarized beams can provide a 10-fold increase in current. Further work in developing these polarized sources will be actively pursued, partly because of the potential gain they can provide to the thermonuclear fusion process.

Very considerable progress has been made in obtaining increased performance from large NaI photon detectors. Resolution of 2% at 20 MeV has been achieved and an $E^{-1/2}$ dependence of the resolution has been observed from 15 to 45 MeV. These detectors now routinely achieve 2 to 3 times better resolution than was the case just a few years ago. Large arrays of photon detectors subtending nearly 4π are now possible to construct and operate; one is shown in figure IV.3-A. These systems are seen to be essential tools in dissecting the gamma ray

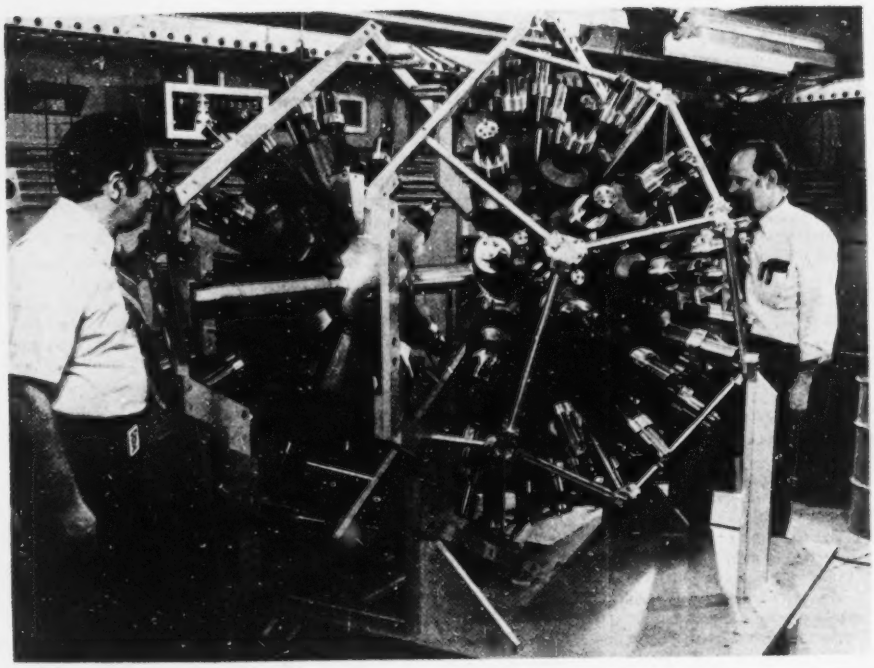

Fig. IV.3-A. An array of NaI photon detectors consisting of 72 elements used at the Holifield Heavy Ion Facility.

cascades in the decay of very high spin ($J \geq 40$ units) nuclear states. Many interesting systems which combine features of the very high resolution of Ge with the high efficiency of NaI or BGO have been proposed. The best of these proposals should be funded. If coupled with appropriate systems for analyzing the resulting multiparameter data, they offer unsurpassed power for extracting the properties of nuclei at high excitation energy and particularly, at high angular momentum.

B. PROMISING AREAS FOR NEAR TERM INSTRUMENTATION R&D

Very real opportunities exist to aggressively push certain important areas of instrumentation development that offer high hope for success. The following is not meant to be exhaustive but to indicate the nature of the opportunities.

The complexity of many nuclear reactions now under study and envisioned for the future requires that many parameters be simultaneously recorded to obtain sufficient characterization of the process. Such multiparameter data is not readily analyzed in conventional mainframe computers which function as serial or vector processors. In addition to the analysis of multiparameter data, several classes of problems in a variety of scientific areas would benefit greatly from employing multiple processing elements operating in parallel on the same problem. A development project at LBL using this notion has been able to demonstrate a system with the data analysis capability of a CDC 7600 at 1/20 the cost. Such systems seem capable of extension at modest cost to achieve the order of 100 times the data analysis capability of the 7600. For such systems to be broadly useful, they should be readily transferable and highly interactive. The development of such systems and their widespread use by physicists over the next few years will allow for the timely and effective analysis of the experiments required to further deepen our understanding of nuclear processes.

Polarized beams and targets can be further developed to produce more than a ten fold increase in yield. Particularly exciting and new is the possibility of using polarized gas or vapor in targets. Increases in densities of these targets up to 10^{14} atoms/cm^2 would be highly desirable. In fact, a development program to produce unpolarized jet targets of a variety of materials would greatly enhance the utility of stored circulating beams for nuclear research.

Effective use of the intense neutrino beams produced at LAMPF requires detection of electrons in the energy interval 20-200 MeV. Electrons of this energy have a propensity to readily radiate photons with the attendant problem that it is difficult to measure the energy and direction of the electron. In order to produce high event rates in detection, it is desirable to use inert and inactive material to increase the mass of the detector at low cost. Therefore a careful study should be made of the proper balance between the amount of inert material versus active scintillator that allows adequate determination of the electron energy and direction.

The development of noble liquid ionization detectors offers a real opportunity for breakthroughs in detector technology. They could serve both as high resolution (100 keV at 100 MeV) photon detectors and if operated as time projection chambers, as extremely fine grained detectors (1 mm × 1 mm × 1 mm) with extremely good differential energy loss resolution. The problem to be solved is how to produce large volumes of noble liquids with high enough purity to allow full charge collection.

C. AREAS IN NEED OF DEVELOPMENT

The physics to be done in the future with higher energy beams and particularly with heavy ions requires the development of detection systems far beyond any that have been used in nuclear physics to date. For example, as discussed in Sec. II.5 the search for hidden color via exclusive channels in deeply inelastic electron scattering will involve detection of the decay of excited baryonic states. Such experiments would be very difficult to carry out with present-day spectrometers, which have solid angles of 50 msr, and magnetic systems with acceptances on the order of steradians would be very important. To achieve such a large solid angle requires an extensive R&D program, first to identify the background sources in order to determine how to adequately shield the detector systems, then to design appropriate magnets and particle detection systems, and construct prototypic devices.

The challenges presented to detector physics by relativistic heavy ion collisions are impressive. The extremely high multiplicity, on the order of a thousand or more of final particles, requires a finely segmented detector with a wide dynamic range (10^3). In order to obtain good mass resolution detectors, large area detectors with fast timing properties will be required and again the difficulties presented by the large dynamic range must be dealt with. Potential candidate detectors to perform these tasks exist, but they must be developed, tested and engineered before they become components in the large, expensive detection system that will have to be constructed if we are to efficiently extract the exciting physics from these spectacular collisions.

In general, fine-grained detectors can facilitate whole classes of experiments in which background rejection is a principal concern. In nuclear research, fine-grained detectors with much greater sensitivity are required than are employed in high energy experiments because of the lower energy of the radiations characteristic of nuclear processes. Fine-grained detectors for position measurement and simultaneous good (10%) energy determination would greatly impact experiments such as the search for double beta decay, or neutrino scattering, especially from nuclei, where determining the final state greatly enhances the information content from the experiment.

Thus we are entering a new phase in experimental nuclear physics which requires development of new detector components and their integration into large-scale detection systems. This subject will have to get much more attention over the next ten years than it received in the past decade.

Finally, important areas of our science in which U.S. nuclear theorists require capabilities for large-scale computations are being dangerously impeded by lack of adequate access to Class VI computers.

D. ENRICHED ISOTOPES

The need for enriched isotopes is a continuing one for basic research in the nuclear sciences. It is ironic that the tremendous success of nuclear techniques and the use of special isotopes in medicine and other applied fields has created such heavy demand on the facilities which produce them that the broader inventory of enriched isotopes for sale to basic researchers has been severely depleted. In almost all aspects of nuclear science the need for enriched isotopes is akin to the need of a chemist for pure chemicals. Without them the interpretation of results often becomes less clear and precise. The United States is effectively the world's only supplier of most of the enriched stable isotopes. Users should pay for the replacement cost of the isotopes they consume, and an adequate inventory must be reestablished and maintained.

E. NUCLEAR DATA COMPILATIONS

The ready availability of up-to-date information on the properties of individual nuclides and on nuclear transitions and reactions is an essential resource to our science. The compilation of such data is crucial in making such information generally available to scientists in useful form. It is a matter of some concern that, while experimental data are certainly being obtained and published at a continuing rate, the *compilation* of new data in the areas of interest to basic research activities in nuclear science has slowed down very substantially. While this matter has not been studied by NSAC in some time, it is one of serious concern and should receive more systematic attention in the future.

IV.4 INTERNATIONAL COOPERATION

The benefits from international cooperation arise both from access to unique facilities not available at home and also from the mix of people and ideas at the highest international levels of excellence.

A long-range plan for nuclear science in the U.S. must be viewed in a worldwide context. Nuclear research is an international enterprise carried out at a network of laboratories in the developed countries of Europe, in Canada, Japan and in the U.S.A. The evolution in style of nuclear research toward concentration in a small number of large facilities is also a global phenomenon. The U.S. basic nuclear research program is substantially the largest national program in the world, both in manpower and resources; it leads the world in many important areas of the field. Yet the U.S. program cannot and should not attempt to dominate across the entire spectrum. Our long-range plan must maintain balance between two competing requirements. On the one hand, it must be sufficiently broad in scope and rich enough in new initiatives to ensure internal viability. On the other hand, it must avoid weakening itself by trying to cover all eventualities, duplicating in the process major facilities that exist elsewhere.

The development of a worldwide network of facilities is relatively recent in the history of nuclear physics. After the Second World War, when the field began to grow rapidly, much of the work was carried out with small low-energy accelerators—cyclotrons, electron linacs, and Van de Graaff accelerators. The United States was in a position of world leadership and, by the late 1960's, developed a system of over 100 such accelerators, many of them university based. This program was followed by the development of many similar accelerators elsewhere in the world. In the pursuit of nuclear structure and nuclear reactions, much was gained by competition between similar laboratories in different countries and by the free exchange of ideas and of people.

Building on the knowledge of the nucleus established with smaller accelerators, new directions in nuclear physics were initiated in the 1970's as nuclear physics developed a number of large user facilities, which brought the need for international cooperation into sharper focus. These large facilities cannot encompass all of the possible experimental facilities important for basic nuclear research. In a number of cases, the facilities in the United States are (or will be) unique and attract considerable interest from abroad. In other cases, facilities abroad are complementary to those in the United States and attract American users.

The new experimental facilities—the 4-GeV CW electron accelerator previously recommended by this Committee and the colliding-beam relativistic heavy-ion accelerator—identified here as major opportunities for the future, are unique; they will attract users from all over the world. The Bevelac, too, is unique and has attracted long-term user groups from Germany and Japan who have brought with them millions of dollars for ancillary instrumentation. LAMPF has unique features in energy and intensity, and attracts users from around the world, even though there are two other "meson factories" in Switzerland (SIN) and Canada (TRIUMF) operating at lower energies and beam currents, though with higher duty cycle. The new injector of SLAC will be unique for nuclear physics in the world, and will surely attract scientists from abroad. Many other facilities have significant international user groups.

On the other hand, many American groups and individual scientists are carrying out nuclear research at various installations outside the United States, at facilities which have capabilities unmatched within this country. Examples of such capabilities are the energetic uranium beams at the German heavy-ion facility (GSI), the polarized proton and deuteron beams up to 3 GeV/c at Saturne II in France, the good duty cycle pion and muon beams at TRIUMF and SIN, the low-energy antiproton storage ring LEAR at CERN in Switzerland, the intense thermal, cold, and ultracold neutron beams at ILL in France, and the separated kaon beams at KEK in Japan. Approximately three to four million dollars were spent on such work in FY 1983.

Another important aspect of the international nature of our science is the investment by one country in equipment placed at unique research facilities of another country. Examples are the plastic ball detector at the Bevalac (built largely by GSI, Germany), the π^0 spectrometer at LAMPF (built with major participation from Tel Aviv

University, Israel), and major new detectors at the Bevalac (built by the INS, Japan), the possible participation by the Max Planck Institute (Germany) in the construction of the gallium solar neutrino detector, and the participation by the U.S. in heavy-ion acceleration by the PS and the SPS at CERN. Such international collaborations should be encouraged. They enable scientists in a country to play a major role in an area of physics in which their country has no existing facility. In addition, they also can help ease the financial burden of instrumentation on the country constructing a new facility. Nevertheless, one must be careful that the construction schedule and useful implementation of such a facility not be unduly delayed by the vagaries of international negotiations.

As more large facilities come into existence, their unique properties have to be considered not only as a national but as a worldwide scientific resource. At present, exchange arrangements are handled on a person-to-person or laboratory-to-laboratory basis. We believe that these arrangements are working well and see no present need for a more formal administrative structure.

Visits by American scientists to foreign laboratories and by foreign scientists to the U.S. should be encouraged in whatever ways are feasible. This is an important and cost-effective part of scientific activity, especially with the recent advances in the scientific importance of many European laboratories. The costs are low and the beneficial impact can be enormous. The worldwide network of nuclear laboratories and the international participation of scientists in research at American laboratories is a vital resource for nuclear science in the United States.

IV.5 BUDGETS

The sociology and economics of science is a complicated matter. How much should a society spend on basic research? How does the long-term development of high technology, of technically skilled and innovative manpower, of industrial development in general, of the standard of living and of the quality of life depend on a society's investment in basic research? This broad and complex subject cannot be treated here in detail. The scientific questions confronting the field of nuclear science at this juncture represent a major opportunity for an increase in our knowledge and understanding of the physical world and a potential source of many societal benefits. The role of the United States as a technological and scientific leader among advanced nations is an important one and the financial support of this basic research effort is crucial for our country's future productivity. The primary economic resources for the pursuit of basic nuclear research in the United States are the budgets allocated by the Federal Government annually through the Department of Energy and the National Science Foundation.

In this section we summarize the past and present funding levels, compare the United States budget to that of other countries, and then present our recommended budget projections for the next decade.

A. PAST AND PRESENT FUNDING OF BASIC NUCLEAR RESEARCH IN THE UNITED STATES

As a standard of comparison for the funding of basic nuclear research, we show the history of funding in the U.S. in two ways. In figure IV.5-A, we see the combined DOE/NSF budgets for basic nuclear physics research, converted into 1983 dollars by the Consumer Price Index. It is certainly true that the cost of research, particularly in instrumentation, has risen more sharply than the consumer price index—we have not attempted to correct for such effects here. But even so, the total level of funding of basic nuclear research averaged about 210 million FY 1983 dollars annually in a five year period centered about 1970 and declined to 170 million FY 1983 dollars in the five

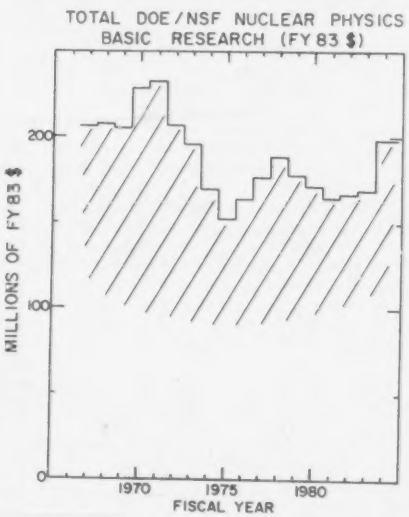

Fig. IV.5-A. The total DOE/NSF budget for basic research in Nuclear Science since 1967, in constant FY 1983 dollars, as measured by the Consumer Price Index. The eventual value for the FY 1984 budget will be somewhat lower than shown since the 1983 CPI was used for the value shown in this plot.

year period centered on 1980, a 25% decline for the decade.

But should basic research be maintained at a fixed level of dollars? Or should a nation and a society invest in its future by putting at least a constant fraction of its effort, the Gross National Product, into basic research. Figure IV.5-B shows the combined nuclear physics budgets as a fraction of our Gross National Product and the decline of the early 1970's becomes even more dramatic.

While each way of analyzing these budgets is open to some criticism—the qualitative impression from both is correct—that the United States investment in basic nuclear research decreased substantially about ten years ago and has remained at this lower value until recently. This puts it considerably below both the *absolute* level of investment of a roughly comparable unit, the European Economic Community, and also substantially below Europe in the *relative* fraction of GNP in this investment, as we will see later.

The vitality of science rests on a delicate combination of factors: historical, social, psychological and economic. There is no question that the real decreases in funding of a decade ago had a depressing impact on U.S. science, out of proportion to the strict economic impacts of the cuts. This impact manifests itself in a number of aspects, such as the attractiveness of the field to graduate students and the incentive to invest in new instrumentation rather than make do with existing equipment. Yet training of skilled manpower and challenging technological frontiers with advanced instrumentation are important by-products of basic research.

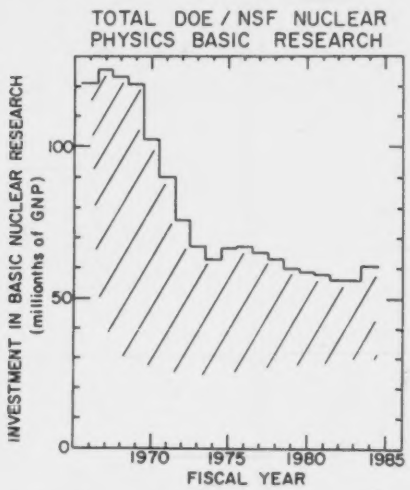

Fig. IV.5-B. The total DOE/NSF budget for basic research in Nuclear Science since 1967 as a fraction of the Gross National Product. The FY 1983 and FY 1984 budgets are likely to be somewhat lower than shown here since the Gross National Product was not yet known for those years.

B. INTERNATIONAL COMPARISONS

Since the rate of investment in basic research for a society is poorly defined, we compared the U.S. investment in nuclear physics to that for countries with similar levels of technology and standards of living: some of the major countries of Western Europe and Canada. Such a comparison is obviously complicated by significant differences in methods of funding and accounting systems. The numbers quoted below have been compiled with some effort to eliminate bias resulting from such differences.

In Europe we obtained data for Belgium, Germany, France, Italy, the Netherlands, Switzerland and the United Kingdom, which between them account for over 85% of the population and of the gross national product of western Europe.

The support for research in nuclear physics abroad is generally from two sources: 1) DOE/NSF-like agencies that support both national laboratories and university-based research groups. Such support accounts typically for about 80% of expenditures for basic nuclear research and fairly reliable numbers are available. 2) University support to research groups, mainly the salaries of physicists and technical support staff. Direct support of research other than salaries is, in general, small. In certain countries there are major university contributions to the operation of experimental facilities; these have been included. For the salaries of university-based researchers, we used, as a rule, 50% of their estimated salary, with the other half assumed to be for teaching. The cost for university administration and overhead has not been included since it is largely directed towards education rather than research. The budgets were extracted from the reports of agencies, long-range plans of individual countries, national studies giving the breakdown of support from different sources, and estimates of the university salaries prepared by either faculty members in the individual countries or by the agencies. For the countries with the larger fraction of the expenditures, Germany, France, Switzerland and the United Kingdom, the relevance of the numbers extracted, corrections and consistency checks were established by

discussions with scientists experienced in the funding patterns of the individual countries; these checks indicated that the numbers are reasonably accurate.

The budgets for the U.S. were obtained from the DOE and NSF, with the university contribution estimated from the number of DOE/NSF supported university-based physicists and the average salaries deduced from DOE/NSF summer salaries. The budgets for Canada were obtained in a similar fashion.

The numbers on manpower result from a recent survey carried out by the European Science Foundation (ESF), which, in 1982, determined for all European countries the number of Ph.D. physicists, technicians and graduate students working in basic nuclear research.

The budgets for 1982 were related to the gross national product also for 1982, to avoid fluctuations in exchange rates. The results are summarized in Table IV.5-1.

TABLE IV.5-1
Comparison with Other Countries

	U.S.	Other Advanced Countries[a]
Population (millions)	233	284
1982 GNP (Billions of 1982 US$)	3059	2377[b]
Per Capita GNP (Thousands of 1982 US$)	13.1	8.4[b]
1982 Investment in basic nuclear research (Millions of 1982 US$)	170	305[b]
Ratio of 1982 investment in basic nuclear research to 1982 GNP (Millionths)	56	129[c]

[a] Includes Belgium, Canada, Germany, France, Italy, Netherlands, Switzerland, and United Kingdom.
[b] Currency conversion rates for 1982 from U.S. Statistical Abstracts, Dept. of Commerce 1983.
[c] Ratio computed in country's own currency to avoid fluctuations in exchange rates. Averaged by weighting each ratio by the 1982 GNP for that country.

As may be seen, an average of ***129 millionths*** of the GNP was invested in basic research in nuclear physics in 1982 for Canada and the European countries considered, while for the United States, this fraction is about ***56 millionths,*** more than a factor of two lower. Since for the different countries the total investments in basic research in nuclear physics vary greatly, we also considered this investment as a function of *per capita GNP*. This is shown in figure IV.5-C. For Europe and Canada, the investment, as a fraction of GNP, is described by a roughly linear function of the per capita income, with the scatter of points not very much larger than the uncertainties and the arbitrariness introduced by fluctuating exchange rates. The U.S. is almost exactly a factor of three below this line, considering its per capita GNP.

As may be seen in figure IV.5-C. a high level of economic productivity is closely related to substantial investment in basic research. This effect goes in two directions: (1) Research in basic and applied science and the related education in the development and use of frontier technology leads to the broader application of high technology and an increase in productivity and the standard of living. (2) Conversely, a country with a higher level of technology both *needs* to invest in research to maintain its lead, and can also afford to invest an increasing fraction of its national effort in basic research with long-term payoffs.

Comparison between the U.S. and Europe and Canada, demonstrates that the U.S. effort and investment in basic nuclear research is significantly and substantially lower. This is probably also true of other areas of physical research for which we do not have the detailed data available.

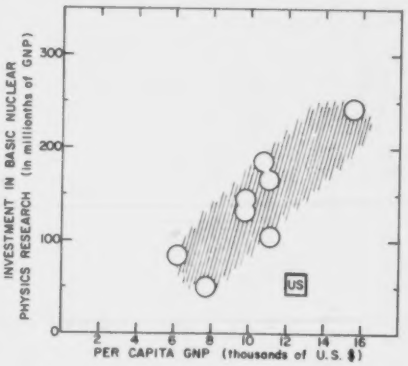

Fig. IV.5-C. Comparison of the level of investment in basic research in Nuclear Science with per capita income in 1982 in various advanced countries listed in the text. There appears to be a systematic trend of higher investment for the wealthier countries, but the U.S. is conspicuously low.

A comparison can also be made of the number of Ph.D. physicists working in basic nuclear research. Again, there is a rough correlation with the GNP per inhabitant, although the scatter is larger. There are about six nuclear physicists per million inhabitants in the U.S. compared to ten in European countries with similar per capita GNP.

Quite apart from all such quantitative data, visits to European laboratories give an even more compelling picture. The judicious investment by many European nations over the past decade in instrumentation and technical support has paid off: these laboratories are characteristically better equipped for frontier research in nuclear physics than are their U.S. counterparts, and this difference is evident to even the most casual observer. Moreover the number of students involved in nuclear physics in Europe is relatively much higher than in the U.S. and their level of commitment, of excitement and of dedication is impressive. That these things are so is no accident, they reflect more than a decade of severe constraints and slow starvation of nuclear science in the U.S. and a corresponding period of well-considered investment in Europe.

C. BUDGET PROJECTIONS

The major incremental elements entering into our budget considerations are as follows:

1) The level of funding for nuclear science has been very severely constrained in the past decade. The strong recommendation of NSAC to increase the operating and capital equipment funds by a $20 million step was transmitted in a letter of April 29, 1983. This was our estimate of the *minimal funds* required to bring the field of nuclear physics to a level of funding commensurate with the challenges confronting it by adequate utilization of the relevant facilities in existence and under construction. We recommended that these incremental funds be used for instrumentation programs associated with major scientific opportunities, for better utilization of facilities, and for programs to encourage user groups and young investigators. *We strongly recommend that this total of about $220 million (FY 1983 dollars) per year, be maintained as a minimal level of support for the continuing program of research with facilities in existence and now under construction in order to face up to some of the opportunities discussed in Chapter II.* In our plan we assume this level to constitute the base program.

2) We assume the NEAL 4-GeV electron accelerator will be constructed, as discussed in the report of the NSAC Panel on Electron Accelerator Facilities, and that the concomitant budget for operating this facility will be incremental to the base program, in accordance with the transmittal letter of April 29, 1983. Since the 4-GeV electron accelerator is at one of the most exciting frontiers of our science, and will be a national user facility, it will require incremental support for user groups in addition to the resources allocated for the operation and in-house research efforts of the NEAL facility. We estimate these incremental costs for user support to reach their full level of about $6 million in FY 1989, the scheduled start up year for NEAL, but to begin gradually at least three years earlier.

3) Finally we estimate, very roughly, the cost of a new colliding beam, relativistic heavy-ion facility at about $250M (FY 1983 dollars) including initial major detection apparatus. A similar rough estimate for the operating and in-house research costs is about $35M (FY 1983 dollars) annually. The detailed refinement of specifications for this facility and for the associated instrumentation, and thus of cost, will have to be the subject of more careful future study.

The projected funding we recommend for basic nuclear science research is shown in figure IV.5-D. After construction of the relativistic heavy ion collider the equilibrium budget level we estimate at $270M per annum in FY 1983 dollars.

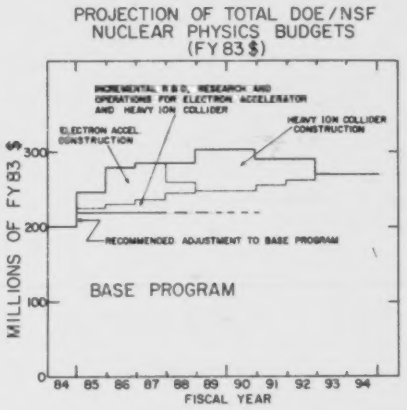

Fig. IV.5-D. Projected DOE/NSF budgets for basic research in Nuclear Science through 1994 in FY 1983 dollars. The present base program and the increment recommended by NSAC is shown for FY 1985. The estimated construction budgets for the 4-GeV electron accelerator facility and for the Heavy Ion Collider are shown as well as the incremental levels of operating funds.

D. TRENDS WITHIN THE BASE PROGRAM

The budgetary implications of pursuing the most important scientific goals will have to be considered carefully over the next decade in the context of specific decisions and programs. A comparison of major categories between FY 1977 and the average of the last three years (1982-1984) is shown in Table IV.5-II. The fraction of the budget in construction projects in 1982-1984 was about 9%—we recommend for the coming decade that a similar fraction of the base program be used for the most attractive new smaller construction and upgrade projects. The fraction of the total budget for instrumentation is approaching 10%, including not only the Capital Equipment budgets in DOE but also estimates of DOE operating funds used toward this goal and the fraction of operating funds used for instrumentation within the NSF budget. We comment on long term instrumentation development and planning needs elsewhere in this report—both DOE and NSF appear to be sensitive to the crucial importance of these activities.

TABLE IV.5-II
Fractional Distribution of Expenditures

	FY 1977	Average of FY 1982, 1983 1984
Theoretical Research	5.3%	6.2%
Experimental Research	35.3%	35.6%
Facility Operations	42.3%	39.8%
Instrumentation	8.2%	9.3%
Construction	8.9%	9.1%

The fraction of the nuclear physics budgets devoted to theory has increased by ~20% since 1977. The 1979 Long Range Plan stressed the need for increased support of nuclear theory. It is gratifying to see that this recommendation has been implemented even under the very stringent budgets of the past years, but we certainly recommend that opportunities for supporting strong theory programs not be neglected and that resources be made available as suitable opportunities present themselves. A strong theory program is an important component in the national effort in nuclear science.

V. IMPLICATIONS OF SCIENTIFIC OPPORTUNITIES

Many important and challenging scientific opportunities are confronting our field, as is apparent from the Scientific Questions posed in Chapter II. We here wish to present the major implications of these opportunities in terms of resources.

Recognition of some of the simplicity and symmetries underlying nuclear structure has enabled us to begin to work toward a new level of correlation of nuclear data and an understanding of the microscopic origins of that structure. The discovery of entirely new structural phenomena such as the observation of spin-flip giant resonances, have been matched by the observation of entirely new reaction mechanisms, such as deep inelastic scattering, that are not yet fully understood. New classes of accelerators are beginning to permit study of the structure of the nuclear continuum and of how the nuclear many-body system responds to increasing energy and angular momentum. Whole new parameter ranges are being opened for the first time to precision study.

There are interesting and vital open questions in nuclear physics that require investigation and understanding in nuclear structure and in the dynamics of nuclear interactions that hitherto were inaccessible. We will be able to address these now or in the near future with new or newly upgraded facilities, or ones that are presently under construction. These provide advanced new capabilities for the study of electromagnetic interactions at energies below 1 GeV, of nucleus-nucleus collisions with improved capabilities in the regime of normal nuclear dynamics and in the transition region around the nuclear "sonic barrier," and of light-ion reactions using the high resolution capabilities of stored and cooled beams. Exploitation of these capabilities holds great promise for scientific advances in the near term.

A new theme in nuclear physics that emerges in this report concerns the implications of *QCD*, the fundamental framework for our characterization of the strong interaction, in the nuclear many body system. This theme shines through a number of the topics that are discussed in Chapter II. In particular, the 4-GeV electron accelerator recently endorsed by NSAC is an important tool to address these questions. Both in this field and in the domain of electroweak interactions, traditional dividing lines between nuclear physics and particle physics are shifting. This is certainly healthy; the divisions are perhaps somewhat historical and sociological in origin, but there are also real, important differences in intellectual perspectives, particularly in the appreciation by nuclear physicists of the importance of many-body dynamics and the real possibilities that collective phenomena contain new physics and qualitatively new insights into the fundamental nature of matter.

The facilities and instrumentation needed to confront a variety of important opportunities in the future are discussed below by classifying them according to the types of particle beams.

Relativistic Heavy Ion Collider

In this Long Range Plan, we identify the scientific opportunities presented by an accelerator that can provide colliding beams of very heavy ions at about 30 GeV per nucleon and recommend that it be the next major construction project for nuclear science.

Having made the above recommendation, we note that this will be a project of unusual magnitude for our field. Both the accelerator ideas and the underlying physics concepts of this recommendation were pioneered in the United States. Considerably more R&D will have to be expended, both prior to formal proposals and during the construction phase of the accelerator. Although the design of the accelerator is within the framework of existing technology, many problems and alternative solutions will have to be studied. Various possible ion sources, techniques of injection and acceleration of the heavy ion

39-587 O - 84 - 70

beams, and the design of the appropriate magnet structures are among the features that need attention.

The detector problems will be formidable. Although multiplicities (the number of particles produced in a single collision, that will have to be detected simultaneously) will, in general, be substantially higher than in nucleon-nucleon collisions at very high energies, the requirements on spatial resolution of detectors, or granularity, may not be much greater. Important physics may be signalled by the number of strange particles relative to ordinary hadrons, by di-lepton pairs, or simply by the flow pattern in the thousands of reaction products. Detector systems for all these experiments will have to be thought out, designed and built with the same amount of care as the main facility. Since the scale of these detectors will be comparable to those used in high energy physics, that experience will have to be used as a basis of further R&D efforts.

The only present facility for research with relativistic heavy ions in the U.S. is the Bevalac, and with the variety of beams and energies available, it is a unique facility anywhere. Some beams at higher energies will probably be available sporadically at CERN over the next few years. In order to begin to understand the problems associated with the physics of the future colliding beam accelerator, it would be desirable to carry out experiments in the U.S. with heavy ions at energies significantly higher than those of the Bevalac. Such measurements would provide needed data concerning nuclear stopping power, particle multiplicities and detector technology. Exploratory experiments at energies that will begin to test our ideas about nuclear compressibility and attainable nuclear densities can attract the new generation of scientists, as well as provide the experience that will be essential to the development of the physics program over the next decade at this new collider facility.

In the preconstruction phase it is especially important that NSAC and suitable workshops and subcommittees be charged with giving advice periodically on the best course for the physics program, accelerator characteristics, and detector needs associated with this major scientific endeavor. Since this is a border area, of close interest to high energy physicists, some attention should be given to including leading members of that community in the process of helping specify the course of this new undertaking.

Pions, Kaons, Muons, Neutrinos, and Antiprotons

The pion capabilities of LAMPF are being utilized in a strong program of experimental studies. The use of pions in nuclear structure physics, exploiting their sharp spin-isospin selectivity in the delta region, is an outstanding and unique opportunity. There is a possibility for enhancing our present capabilities through a new pion channel, allowing access to higher energy pions as well as improved resolution, counting rate, and possibly duty factor. Such a new pion beam should be coupled to a new high resolution pion spectrometer. The characterization and understanding of the behavior of the delta (the simplest nonnucleonic excitation) in the nucleus is an important element in much of hadronic nuclear physics. A large solid-angle multiparticle spectrometer may be important for this work.

The electroweak theory of Glashow, Salam, and Weinberg has had spectacular confirmation with the discovery of the intermediate vector bosons, the $W^{\pm}$ and Z° at CERN. This theory and QCD constitute the Standard Model which forms the basis of nuclear interactions. Numerous opportunities exist for probing the validity of this model. Improved kaon beams can be used to search for decays and other processes not present in the Minimal Standard Model. Better neutrino beams coupled with high granularity, high mass, tracking detectors can search for new interactions beyond those of the standard model, and for neutrino oscillations. Muon beams with improved duty factor can be used, for instance, to search for muon number nonconserving processes. Neutrino-nucleus scattering could further probe the structure of the weak neutral current. Such reactions also provide a tool to probe new aspects of nuclear structure.

Improved kaon facilities could provide much better counting rate and better resolution for important studies of hypernuclei. Higher energy kaon beams and spectrometers would allow searches for the as yet unobserved doubly strange states of hypernuclei. These same facilities would make possible the use of kaons for inelastic scattering and for studies of strange resonances in nuclear matter.

Antiprotons can provide a unique tool for probing the foundations of the strong interaction, for studying possible exotic quark configurations, and for producing a very hot small region within nuclear matter. A new source appears to be beyond the resources of our community. However, an antiproton storage ring, or possibly a new time separated antiproton beam, at an existing facility may provide a unique opportunity for cost-effective experimentation with antiprotons.

A major new "Kaon Factory," a 10-30 GeV proton accelerator with 10^{14}-10^{15} protons per second, would provide substantial opportunities for physics in all of these areas. This physics is clearly very fundamental, important, and exciting. Given our commitment to the construction of the National Electron Accelerator Laboratory and the

heavy ion collider discussed above, the financial assumptions of this report preclude a major additional facility. But as circumstances change, we want to keep this important option readily available: it clearly presents many unique opportunities.

In the meantime we have many opportunities for physics which can be done without such a major new accelerator. Among these opportunities are new experiments on solar neutrinos, experiments on nuclear beta decay and double beta decay, and opportunities to take advantage of new kaon beams, new muon facilities, new neutrino beams and detectors, and new pion beams and spectrometers at existing accelerators.

Electromagnetic Facilities

It is clear that electromagnetic probes will play an increasingly important role in many areas of nuclear physics. Questions about the nucleon-nucleon interaction, about connections to QCD and the quark structure, about the hadronic structure of nuclei, elementary excitations and nuclear-structure symmetries, all require electromagnetic probes. The **new 4 GeV electron facility at NEAL is clearly the major near-term new initiative in nuclear physics**. Its completion is awaited eagerly by our community. The cost of this accelerator and that of its first generation of experimental facilities was discussed and estimated in the report of the NSAC Panel on Electron Facilities, which also noted that a strong scientific case can be made for CW electron capability with high resolution below 1 GeV. We see such a lower-energy capability as a major opportunity for the field in studies on the deuteron, on hadronic degrees of freedom, particularly in the delta regime, on many aspects of the elementary excitations and structural symmetries of nuclei and, with longitudinally polarized electron beams, on the structure of semileptonic neutral weak currents.

Light Ion Facilities

Light ions are the oldest probes of nuclear structure. Yet as the scientific questions show, refinement of these probes has yielded qualitatively new discoveries of fundamental importance, and holds great promise for the future. Scientific opportunities call for the upgrade of existing facilities to yield variable energy protons in the energy range from 200-500 MeV, polarized protons in this region and below with substantially improved intensity and reasonably intense polarized proton beams at variable energies up to several GeV. They also call for secondary polarized neutron beams of useful intensities with energies to at least 200 MeV (up to perhaps 60 MeV this can be accomplished with upgrades of existing facilities, but the higher energy neutrons may require a new facility).

Heavy Ion Facilities

With energies below 200 MeV per nucleon, the facilities that exist or are under construction have many of the features that are required to study the key scientific problems in the area. The completion of the National Superconducting Cyclotron Laboratory and of ATLAS will be major innovative technical achievements and provide important new capabilities. One still needed is the ability to obtain very heavy (up to uranium) beams of variable energy between 3 and 20 MeV per nucleon, a capability that is important in nuclear structure studies, and that could become critically important if present indications of long-lived nuclear molecules in very heavy systems are confirmed. There are needs for larger detector systems in heavy-ion physics, in arrays of photon detectors and in large area systems for charged particles, all requiring adequate data handling systems.

Manpower

The importance of having sufficient skilled and innovative scientists is evident, especially in view of the new initiatives considered here. This is not an issue readily amenable to administrative action. In Sec. IV.1 we identified a number of measures that should be taken to assure adequate training of new manpower, though the intellectual vitality of the problems facing us is likely to be the most important advantage in attracting a new generation of physicists.

The support for nuclear theorists has increased since the last Long Range Plan from 5 to 6% of the total nuclear physics budgets. This is a necessary trend, since much of the physics confronting us requires careful prior theoretical thought and substantial theoretical interpretation of the results. We recommend that this trend be continued.

International collaborations are becoming of increasing importance to nuclear physics around the world, and we are pleased that the funding agencies are doing their best to facilitate these. An important issue is the ease with which foreign travel can be arranged, both for U.S. scientists abroad and for arranging visits by foreign scientists in the U.S. The easy interchange of people and ideas is essential to a healthy science and should be facilitated.

Budgets

The U.S. investment in basic nuclear research in FY 1984 will be close to 200 million dollars. This can be compared with the trend in other highly developed countries, as shown in figure IV.5-D, which would correspond to a budget of $400-600 million per year. Such comparisons merit serious consideration, not only in nuclear

physics but in all areas of basic research in the physical sciences. Enormous benefits to the nation, direct and indirect, would accrue from a major long term initiative to upgrade American investment in basic science to a level approaching that abroad.

It is beyond the scope of this Committee to recommend such an overall initiative. But it *is* our responsibility to recommend what we consider a *minimal* budget to maintain the vitality of nuclear science in the United States and to address some of the most urgent and important current issues. We thus reaffirm our recommendation of April 29 this year, that as a base program, the 200 million dollars of the 1984 budget be augmented by 20 million dollars as soon as practical to improve the utilization of our existing resources for research in nuclear science. We also reaffirm our endorsement of the recommendation for a 4-GeV electron accelerator facility. In the longer term, we identify a new opportunity to explore the behavior of matter at extremely high energy densities, densities which hitherto have occurred only in the early moments of the creation of the Universe, and recommend construction of an ultra-relativistic heavy-ion collider to address this opportunity. These studies have great potential for fundamental discoveries.

There are profound and challenging scientific issues confronting nuclear physics. With the requisite scientific manpower, facilities and budgets, nuclear science in the United States will be in a strong position to lead the international process of scientific discovery and of increased knowledge and understanding of the world we live in.

APPENDIX A

Department of Energy
Washington, D.C. 20545

June 23, 1983

John P. Schiffer, Chairman
DOE/NSF Nuclear Science Advisory
Committee
Physics Division
Argonne National Laboratory
9700 South Cass Avenue
Argonne, Illinois 60439

Dear John,

This letter is to request that the DOE/NSF Nuclear Science Advisory Committee (NSAC) conduct a study of scientific opportunities and priorities in U.S. basic nuclear research and that NSAC develop a long range plan which will serve as a framework for coordinated advancement of the Nation's basic nuclear research programs over the next decade. The 1979 Long Range Plan is an appropriate and important reference document for the long range plan which you will be formulating. However, because our field has evolved so rapidly over the past four years, you should naturally expect to identify exciting scientific opportunities not cited in the 1979 Plan and, alas, should expect some of the bright hopes of 1979 to have proved to be blind alleys. Please submit your report to the Department of Energy and National Science Foundation by September 1, 1983.

The requested NSAC study comes at a most interesting and critical time in the history of American basic research. While the United States has a distinguished record of accomplishment and leadership in basic nuclear research, we face formidable challenges from Western Europe, Japan, Canada, and other nations. These countries have enormously strengthened their basic nuclear research programs over the past decade. The new long range plan should discuss both the steps needed to maintain America's position of leadership and also identify opportunities for cooperation with other countries on projects of mutual interest.

The new long range plan must first and foremost attempt to identify the most important nuclear physics questions to be attacked in the next decade. Having identified the scientific opportunities, the long range plan should tell us what resources are required to pursue these opportunities. The resources to be discussed include capabilities of nuclear physics facilities, instrumentation, manpower, and funding. The discussion of manpower requirements must include examination of ways in which some of the best minds may be attracted to nuclear physics.

We admire and appreciate your courage as you begin this task. The effort will be considerable, but the importance of this work to basic nuclear research in the United States will also be considerable. We look forward to your advice.

Sincerely,

James E. Leiss
U. S. Department of Energy

Marcel Bardon
National Science Foundation

APPENDIX B

Agendas for the 1983 Meetings of the Nuclear Science Advisory Committee

DOE/NSF Nuclear Science Advisory Committee

January 12, 1983
Room 338
National Science Foundation
1800 G Street, NW.
Washington, DC

Tentative Agenda

9:00 a.m. - Opening remarks by the Chairman (Schiffer)

9:30 a.m. - Remarks by representatives of the funding agencies (Leiss/Bardon)

10:00 a.m. - Discussion of DOE and NSF budget situations for FY 1983 (Ritter/Willard)

* 10:30 a.m. - Status of the Long Range Plan (Schiffer/Feshbach)

11:00 a.m. - Discussion of procedure for proposal evaluation (Schiffer/Leiss/Bardon)

12:30 p.m. - LUNCH

1:30 p.m. - Continuation of discussion of procedure for proposal evaluation (Schiffer/Leiss/Bardon)

* 2:30 p.m. - Discussion of procedure for developing the new Long Range Plan (Schiffer)

3:00 p.m. - Discussion of subcommittee reports and other business (Schiffer)

4:30 p.m. - ADJOURN

The items on the agendas where the Long Range Plan was discussed are marked with an asterisk.

REVISED
February 8, 1983

DOE/NSF Nuclear Science Advisory Committee

February 16, 1983
Room 8E-089
Forrestal Building
1000 Independence Avenue, SW.
U.S. Department of Energy
Washington, D.C.

Tentative Agenda

9:00 a.m. -- Discussion of DOE and NSF budgets for FY 1983 and FY 1984 (Ritter/Willard)

* 9:30 a.m. -- Presentation and discussion of scientific plans at Lawrence Berkeley Laboratory

* 11:00 a.m. -- Presentation and discussion of scientific plans at Brookhaven National Laboratory

12:30 p.m. -- LUNCH

* 1:30 p.m. -- Presentation and discussion of scientific plans at Los Alamos National Laboratory

3:00 p.m. -- Discussion with Alvin W. Trivelpiece

3:30 p.m. -- Discussion of draft report of the Subcommittee on University Research and Education in Nuclear Science (Huizenga)

* 4:00 p.m. -- Discussion of the Long Range Plan

6:00 p.m. -- ADJOURN

The items on the agendas where the Long Range Plan was discussed are marked with an asterisk.

Tentative Agenda for NSAC Meeting

U.S. Department of Energy
Room 1E-245, Forrestal Bldg.
1000 Independence Ave., SW
Washington, D.C.

April 22 and 23, 1983

April 22 — Friday:

9:00 - 12:00		Discussion of the Draft Report of the Electron Facilities Panel D. A. Bromley
* 1:30		Discussion of Long Range Plan
Working Group Reports:		
* 2:00	Theory	G. E. Brown
* 2:30	Light Ions	S. M. Austin
* 3:00	Heavy Ions (non-relativistic)	D. A. Bromley
* 3:30	Eletromagnetic Probes	J. D. Walecka
* 4:00	Pions, Kaons	E. W. Vogt
* 4:30	Weak Probes	F. Boehm
5:00	Relativistic Heavy Ions	G. A. Baym

April 23 -- Saturday:

* 9:00	Information on Facilities and Accelerator Techniques H. Grunder
* 9:45	Relationship to Other Basic Sciences A. Schwarzschild
* 10:00	Application to Societal Needs K. A. Erb
* 10:15	Instrumentation

The items on the agendas where the Long Range Plan was discussed are marked with an asterisk.

* 10:30	Other Aspects of Long Range Plan Budgets Manpower Training Scope Organization Mechanics of Workshop D. Cline
* 1:00	Synthesis of Scientific Questions
* 5:00	Adjourn

The items on the agendas where the Long Range Plan was discussed are marked with an asterisk.

DOE/NSF Nuclear Science Advisory Committee

DATE AND TIME:	October 15, 1983 9:00 am -- 6:30 pm October 16, 1983 9:00 am -- 5:30 pm
PLACE:	Room R-150 Building 203 (Physics) Argonne National Laboratory Lemont, Illinois
TYPE OF MEETING:	Open
AGENDA:	October 15, 1983 9:00 am -- 6:30 pm Discussion of the 1983 Long Range Plan for Nuclear Science October 16, 1983 9:00 am -- 5:30 pm Continuation of the discussion of the 1983 Long Range Plan for Nuclear Science

APPENDIX C

LONG RANGE PLAN WORKSHOP, Wells College, Aurora, New York (July 11-15, 1983)
Preliminary Agenda

Monday	Morning (9:00--12:30)	
	Discussion of Procedures	
	Elementary Excitations	S. Austin
	NN, Hadron-hadron Force (free and effective)	S. Vigdor
	Many-Body Forces and Currents	
	Afternoon (2:00 - 5:00)	
	Nuclear Symmetries	F. Iachello
	Accelerator Facilities	J. Martin
	Evening (7:30 -)	
	General Discussion and/or Working Group Meetings	
Tuesday	Morning (9:00 - 12:30)	
	High Angular Momenta, Extreme States	R. M. Diamond
	Dissipative, Statistical and Quasistatistical aspects	D. A. Bromley
	Afternoon (2:00 - 5:00)	
	Non-nucleonic, Hadronic Degrees of Freedom	E. Moniz
	Non-nucleonic, Quark Degrees of Freedom	G. T. Garvey
	Evening (7:30 --)	
	General Discussion (Budgets, Manpower)	

Wednesday	Morning (9:00 - 12:30)	
	Nuclear Matter and Equation of State: Quark Gluon Matter	G. A. Baym
	Strange Quarks (in nuclei)	C. B. Dover
	Afternoon (2:00 - 5:00)	
	Fundamental Symmetries and Interactions (in nuclei)	F. H. Boehm C. Baltay
	Societal Applications	K. A. Erb
	Evening (7:30 -)	
	General Discussion (International Aspects), Working Group Meetings	
Thursday	Morning (9:00 - 12:30)	
	Instrumentation	G. T. Garvey
	Ties to Other Scientific Disciplines	A. Schwarzschild
	Evening	
	General Discussion	
Friday	Discussion of Revised Drafts of Sections of the Long Range Plan	

Participants in Long Range Plan Workshop

E. G. Adelberger	University of Washington, Seattle
*S. M. Austin	Michigan State University
C. Baltay	Columbia University
*G. A. Baym	University of Illinois
W. Bertozzi	Massachusetts Institute of Technology
G. Bertsch	Michigan State University (Amer. Phys. Soc., Div. of Nucl. Phys.)
*F. H. Boehm	California Institute of Technology
*D. A. Bromley	Yale University
J. Cerny	Lawrence Berkeley Laboratory
*H. H. Chen	University of California, Irvine
*D. Cline	University of Rochester
P. T. Debevec	University of Illinois, Urbana
R. M. Diamond	Lawrence Berkeley Laboratory
C. B. Dover	Brookhaven National Laboratory
*K. A. Erb	Oak Ridge National Laboratory
G. T. Garvey	Argonne National Laboratory
D. F. Geesaman	Argonne National Laboratory
F. L. Gross	College of Wm. and Mary
*H. A. Grunder	Lawrence Berkeley Laboratory
M. Gyulassy	Lawrence Berkeley Laboratory
P. E. Haustein	Brookhaven National Laboratory (Am. Chem. Soc., Div. of Nucl. Sci.)
J. Heisenberg	University of New Hampshire
P. Herczeg	Los Alamos National Laboratory
*C. M. Hoffman	Los Alamos National Laboratory
F. Iachello	Yale University
G. J. Igo	University of California, Los Angeles
*A. K. Kerman	Massachusetts Institute of Technology
N. B. Koller	Rutgers University
S. E. Koonin	California Institute of Technology
T. W. Ludlum	Brookhaven National Laboratory
*M. H. Macfarlane	Indiana University
M. J. Martin	Oak Ridge National Laboratory
R. D. McKeown	California Institute of Technology
L. D. McLerran	University of Washington, Seattle
E. Moniz	Massachusetts Institute of Technology
P. D. Parker	Yale University
R. P. Redwine	Massachusetts Institute of Technology
R. G. H. Robertson	Los Alamos National Laboratory
*P. G. Roos	University of Maryland
*J. P. Schiffer	Argonne National Laboratory, Chairman
L. S. Schroeder	Lawrence Berkeley Laboratory
*A. Z. Schwarzschild	Brookhaven National Laboratory
*I. Sick	University of Basel
S. Vigdor	Indiana University
*E. W. Vogt	University of British Columbia

*Member of Nuclear Science Advisory Committee

Agency Representatives:

H. C. Britt	Department of Energy
H. L. Crannell	National Science Foundation
J. R. Erskine	Department of Energy
J. B. McGrory	Department of Energy
C. R. Richardson	Department of Energy
E. T. Ritter	Department of Energy
W. S. Rodney	National Science Foundation
H. B. Willard	National Science Foundation

Chairmen of Working Groups:

Nucleons in Nuclei	S. Vigdor
Non-nucleonic, Hadronic Aspects	E. Moniz
Non-nucleonic, Quark Aspects	G. T. Garvey
Nuclear Matter and Equation of State	G. A. Baym
Elementary Excitations	S. M. Austin
High Angular Momenta	R. M. Diamond
Nuclear Symmetries	F. Iachello
Macroscopic Aspects	D. A. Bromley
Fundamental Symmetries	F. H. Boehm
Strange Quarks in Nuclei	C. B. Dover
Nuclear Astrophysics	P. D. Parker
Connections with Other Sciences	A. Z. Schwarzschild
Societal Applications	K. A. Erb
Accelerator Facilities	M. J. Martin
Instrumentation	G. T. Garvey
International Aspects	E. W. Vogt

Participants in Working Groups who did not attend Workshop

B. R. Appleton	Oak Ridge National Laboratory
L. M. Bollinger	Argonne National Laboratory
J. N. Bradbury	Los Alamos National Laboratory
G. E. Brown	SUNY at Stony Brook
R. Eisenstein	Carnegie-Mellon University
J. A. Harvey	Oak Ridge National Laboratory
R. A. Jameson	Los Alamos National Laboratory
F. F. Knapp, Jr.	Oak Ridge National Laboratory
F. Plasil	Oak Ridge National Laboratory
P. Thieberger	Brookhaven National Laboratory
J. D. Walecka	Stanford University

DEPARTMENT OF ENERGY

FISCAL YEAR 1985 CONGRESSIONAL BUDGET REQUEST

GENERAL SCIENCE AND RESEARCH

VOLUME 4

TABLE OF CONTENTS

Appropriation Language 19

Summary of Estimates by Major Category 20

Program Overview 21

High Energy Physics 27

Nuclear Physics 79

General Science Program Direction 129

39-587 O - 84 - 71

Department of Energy

Proposed Appropriation Language

General Science and Research Activities

For expenses of the Department of Energy activities including the purchase, construction and acquisition of plant and capital equipment and other expenses incidental thereto necessary for general science and research activities in carrying out the purposes of the Department of Energy Organization Act (Public Law 95-91), including the acquisition or condemnation of any real property or facility or for plant or facility acquisition, construction, or expansion; purchase of passenger motor vehicles (not to exceed [12] 4 for replacement only); [$638,250,000] $746,105,000, to remain available until expended. (Energy and Water Development Appropriation Act, 1984)

DEPARTMENT OF ENERGY

FISCAL YEAR 1985 CONGRESSIONAL BUDGET REQUEST

SUMMARY OF ESTIMATES BY APPROPRIATION BY MAJOR ACTIVITY

GENERAL SCIENCE AND RESEARCH

BUDGET AUTHORITY IN THOUSANDS OF DOLLARS

	FY 1983 Actual	FY 1984 Estimate	FY 1985 Request
High Energy Physics	$430,985	$480,000	$561,000
Nuclear Physics	136,975	159,000	183,600
High Energy and Nuclear Physics Program Direction	1,413	2,250	2,205
Subtotal, General Science and Research	569,373	641,250	746,805
Adjustments	-11,520	---	---
Savings from Management Initiatives.	---	---	-700
Total, General Science and Research.	$557,853	$641,250	$746,105

DEPARTMENT OF ENERGY
1985 CONGRESSIONAL BUDGET REQUEST
PROGRAM OVERVIEW

High Energy and Nuclear Physics

The Department's General Science programs are concerned with basic research to discover and understand the fundamental constituents of matter and energy and the basic forces in nature. These constituents, the forces between them, and the physical laws governing their interactions form the basis for all of the physical sciences. Understanding of the laws of nature and the basic components from which matter and energy, in all their varied forms are composed, forms the foundation upon which all of modern science and technology rests. Deeper understanding correspondingly contributes, sometimes in spectacular ways, to all of the scientific disciplines and to our Nation's technological base.

The Department's General Science programs are organized into two interrelated scientific programs, High Energy Physics and Nuclear Physics. While these programs are not directly associated with energy technology in the near or mid-term, they support basic research whose aim is to provide new knowledge which is expected to have long-term scientific and technological impacts on energy development and utilization and on other aspects of our society. The salaries, benefits and associated costs of the staff of the High Energy Physics and Nuclear Physics programs are also included in the General Science category as a separate program, called General Science Program Direction.

The purpose of the High Energy Physics and Nuclear Physics programs is to perform exploratory forefront research on the structure, constituents and properties of submicroscopic matter, to study the basic forces of nature and their relationship, and to study the transformations of matter and energy at the most elemental level. History has shown that this type of basic research has significant long-term benefits, e.g., the discovery of both fission and fusion of nuclei resulted from the kind of basic research undertaken in these programs earlier in the century. The Department, along with its predecessor agencies, has a history of effectively managing and operating the large, high technology facilities and research activities which characterize high energy physics and nuclear physics. The Department serves as the lead agency for these programs.

Matter is made up of substances known as the chemical elements. The smallest distinguishable unit of an element is the atom. Within the atom, there is a central part called the nucleus which contains most of the mass of the atom. The constituents of the nucleus are neutrons and protons, which in turn are now believed to be made up of more elementary particles, called quarks. The Nuclear Physics program strives to attain a deeper understanding of the structure and properties of atomic nuclei and the forces governing their motion and interactions. The High Energy Physics program delves even deeper. It strives to reach the ultimate description of matter and energy through discovering and studying the properties of the most basic constituent building blocks of matter (quarks), and the nature and relationship of the four known basic forces acting among them.

High Energy Physics is an exploratory field of basic research in which experimental and theoretical studies are conducted on the fundamental constituents of matter and the fundamental forces of nature in an attempt to understand energy and matter and their most elemental transformations. In recent years outstanding progress has been made toward the unification of the forces of nature and toward understanding the ultimate structure of matter in terms of basic constituent quarks and leptons. In achieving these levels of knowledge, United States high energy physicists have won or shared in three Nobel prizes during the last five years.

A major current objective of High Energy Physics is the unification of the basic forces into a single comprehensive theoretical framework. Part of the recent great progress in science has been a reduction in the apparent number of basic forces through the

conceptual unification of the weak nuclear and electromagnetic forces into a single force -- the electroweak force. The recent experimental evidence for the existence of the W and Z^0 particles, together with experimental discoveries during the past decade of neutral weak currents and of particles with charmed quark and even heavier quark constituents, confirm this conceptual unification. The electromagnetic and weak nuclear forces can now be viewed in a natural way as different aspects of one electroweak force. There is now increasing anticipation that the unification of the strong nuclear and electroweak forces into one "grand unified" force may be possible, thereby reducing the apparent number of basic forces in nature to only two. The basic experimental technique used is to study the results of violent collisions of very high energy particles with fixed targets or with other particle or antiparticle beams. In these collisions many entirely new forms of matter can be produced in an energy/matter interchange, and the study of the interactions reveals properties of the underlying building blocks and basic forces involved.

Nuclear Physics is an exploratory field of basic research in which experimental and theoretical studies are conducted on the structure and behavior of atomic nuclei and the understanding of the behavior of nuclei in terms of the fundamental constituents of matter and laws of nature. Atomic nuclei are especially fruitful for fundamental physics studies since only in nuclei do three of the forces of nature, electromagnetic force, weak nuclear force, and strong nuclear force, come into play simultaneously. Nuclear physics research is strongly coupled to high energy physics research. Not only are the experimental and theoretical tools similar, but also the progress in the two fields interact synergistically. For example, developments in understanding of the laws of nature and theoretical projections have led to development of a new theoretical framework, quantum chromodynamics (QCD), which promises to allow understanding of the strong nuclear force on a fundamental basis. Experiments in nuclei will allow tests of these theoretical developments and will provide guidance for future development of the theory.

High energy and nuclear physics research requires the use of large particle accelerators, colliding beam facilities and particle detectors. These few large scientific facilities are available to qualified scientists on the basis of the merit of their scientific proposals. Approximately 75% of the research in high energy physics is done by university-based scientists who usually form collaborations with scientists from other universities or laboratories. Proposals from university and laboratory user groups for accelerator research time are evaluated by scientific program advisory committees which recommend those proposals with the greatest scientific promise. The High Energy Physics program operates almost exclusively in this mode, while Nuclear Physics, in addition to national facilities, also supports dedicated accelerator facilities located on the campuses of four leading universities. To complement, interpret, and guide the experimental work, each program supports a vigorous theoretical research effort at universities and at the national laboratories.

The FY 1985 High Energy Physics budget request addresses the funding requirements for utilization of present facilities at about the 55% level, for continued progress on construction projects, for R&D in support of projects presently underway, and for initiation of preliminary R&D studies on the Superconducting Super Collider project.

A major feature of the FY 1985 High Energy Physics program will be the operation of the Energy Saver/Tevatron superconducting synchrotron at Fermilab for research in the 1000 GeV energy range. Priority is also given to operation and research utilization of the PEP facility, and of the AGS with its new polarized proton beam and excellent low energy neutrino capabilities. The overall utilization level of the DOE High Energy Physics accelerator facilities will be about 55 percent, somewhat above the FY 1984 level, and about equal to the FY 1983 level. The request provides continuing support for university based research groups including accelerator user group efforts, non-accelerator experiments, and theoretical research efforts. There will be continuing accelerator R&D efforts at Fermilab and SLAC in support of on-going construction efforts. The FY 1985 program of preliminary R&D studies for the SSC project will focus on development and evaluation of technical options for magnets and other accelerator

components, development and validation of cost saving designs and fabrication techniques, consideration of accelerator design alternatives, and trade-off and cost optimization studies. The program request includes a substantial increase in capital equipment in order to meet the highest priority needs associated with implementation of research programs using the major new research capabilities being provided by the Tevatron I and Tevatron II projects at Fermilab and the Stanford Linear Collider at SLAC. This major new thrust in FY 1985 is essential to minimize delays in implementing these research programs which are critical for effective utilization of the U.S. High Energy Physics facilities and for the health of the U.S. High Energy Physics program for the remainder of the 1980's. The budget requests construction funds for the continued construction of the SLC project at an optimum pace at SLAC, for completion of the Tevatron II project at Fermilab and for continued construction of Tevatron I at Fermilab.

The FY 1985 Nuclear Physics budget request addresses the funding requirements to maintain the overall utilization of the national accelerator facilities at 90% of the FY 1984 utilization levels. In FY 1985, emphasis will continue to be given to exploitation of new research capability provided by successful completion of construction projects in FY 1984 and FY 1985. These include: (1) the Argonne Tandem/Linac Accelerator System (ATLAS) to provide precise energy and time structured heavy ion beams for investigations of the mechanisms by which colliding nuclei exchange mass, energy, and angular momentum; (2) the completion of the Bates Electron Accelerator recirculator project (MIT) which provides electron beams for precision electron-nuclear scattering studies at higher energies than previously available; and (3) a new injector at SLAC to provide high energy, very sharply pulsed electron beams for examination of the magnetic properties of nuclei and for exploratory experiments into the ways in which quarks influence the makeup and behavior of nuclei.

A major feature of the FY 1985 Nuclear Physics program is the initiation of construction of the Continuous Electron Beam Accelerator Facility project at Newport News, Virginia. This will be a major facility centering on an electron linear accelerator/stretcher ring complex capable of delivering intense, continuous beams in the energy range from 500 to 4,000 MeV. The intensity of the beam in combination with multi-GeV energy and unique high duty factor will make this facility unmatched in the world. The facility will have the capability of addressing a crucial class of problems facing nuclear physics today, namely the understanding of the relationship between the traditional and emerging descriptions of nuclear dynamics. The aim is to synthesize into a unified description of the traditional picture--based on nuclear, meson, and isobar degrees of freedom--and the emerging view of an underlying structure of quarks and gluons. The budget also provides for the conduct of R&D to support the Continuous Electron Beam Accelerator Facility construction.

The FY 1985 Nuclear Physics budget also requests funds for the ongoing construction of the University Accelerator Upgrade Project at the University of Washington and Yale University. The FY 1985 request completes funding for this construction project.

Nuclear knowledge, techniques, instruments, and applications pervade modern American society. These serve as the basis for our national defense strategy, for therapeutic and diagnostic medical applications, for generation of electricity with nuclear processes to serve our economy, and for a large and diverse array of applications in industry and other areas of science. Pursuit of the High Energy and Nuclear Physics programs yields an ever deeper understanding of the constituents of matter and energy and their role in the physical universe, and provides a national base of knowledge, techniques, instrumentation, and skilled manpower in critical technologies.

These decision units reflect $-5,300,000 for savings resulting from management initiatives in the areas of administrative systems and administrative processes/field structure.

DEPARTMENT OF ENERGY
1985 CONGRESSIONAL BUDGET REQUEST
PROGRAM OVERVIEW
HIGH ENERGY AND NUCLEAR PHYSICS
GENERAL SCIENCE AND RESEARCH
(Tabular dollars in thousands. Narrative material in whole dollars.)

	1983 Appropriation	1984 Appropriation	1985 Base	1985 Request
High Energy Physics				
Physics Research				
Operating Expenses	$ 90,278	$ 99,500	$ 99,500	$107,700
Subtotal	$ 90,278	$ 99,500	$ 99,500	$107,700
Facility Operations				
Operating Expenses	145,400	161,000	161,000	182,100
Capital Equipment	47,500	51,500	51,500	55,400
Construction	57,707	86,000	86,000	114,000
Subtotal	250,607	298,500	298,500	361,500
High Energy Technology				
Operating Expenses	90,100	82,000	82,000	91,800
Subtotal	90,100	82,000	82,000	91,800
Total				
Operating Expenses	325,778	342,500	342,500	381,600
Capital Equipment	47,500	51,500	51,500	65,400
Construction	57,707	86,000	86,000	114,000
High Energy Physics	$430,985	$480,000	$480,000	$561,000
Nuclear Physics				
Medium Energy Nuclear Physics				
Operating Expenses	$ 58,548[a/]	$ 65,000[a/]	$ 65,000[a/]	$ 72,000
Subtotal	58,548	65,000	65,000	72,000
Heavy Ion Nuclear Physics				
Operating Expenses	$ 39,910	$ 47,000	$ 47,000	$ 49,800
Subtotal	39,910	47,000	47,000	49,800
Low Energy Nuclear Physics				
Operating Expenses	$ 12,257[b/]	$ 13,000	$ 13,000	$ 13,500
Subtotal	12,257	13,000	13,000	13,500
Nuclear Theory				
Operating Expenses	$ 8,150	$ 9,000	$ 9,000	$ 9,300
Subtotal	8,150	9,000	9,000	9,300
Capital Equipment	10,410[c/]	11,300	11,300	13,700
Construction	7,700	13,700[d/]	13,700[d/]	25,300
Total				
Operating Expenses	118,865	134,000	134,000	144,600
Capital Equipment	10,410	11,300	11,300	13,700
Construction	7,700	13,700	13,700	25,300
Nuclear Physics	$136,975	$159,000	$159,000	$183,600

	1983 Appropriation	1984 Appropriation	1985 Base	1985 Request
General Science Program Direction				
Operating Expenses	$ 1,413[e]	$ 2,250	$ 2,250	$ 2,205
Program Direction	1,413	2,250	2,250	2,205
Total				
Operating Expenses	446,056	478,750	478,750	528,405
Capital Equipment	57,910	62,800	62,800	79,100
Construction	65,407	99,700	99,700	139,300
General Science and Research	$569,373	$641,250	$641,250	$746,805[f]
Staffing Total FTE's	33	35	35	35

Authorization: Section 209, P.L. 95-91

[a] Includes $3,000,000 in FY 1983 and $3,000,000 in FY 1984 which were provided under Defense Programs for LAMPF facility operations.
[b] Budgeted under the Nuclear Sciences subprogram of Basic Energy Sciences in FY 1983.
[c] Includes $510,000 in FY 1983 which was budgeted under the Nuclear Sciences subprogram of Basic Energy Sciences.
[d] Does not include $5,000,000 proposed reprogramming from High Energy Physics for the Tandem/AGS Heavy Ion Transfer Line project (84-R-123).
[e] Includes $272,000 transferred from Policy and Management.
[f] These decision units reflect $-5,300,000 for savings resulting from management initiatives in the areas of administrative systems and administrative processes/field structure.

DEPARTMENT OF ENERGY
1985 CONGRESSIONAL BUDGET REQUEST
LEAD TABLE
HIGH ENERGY PHYSICS
GENERAL SCIENCE AND RESEARCH
(Tabular dollars in thousands. Narrative material in whole dollars.)

	1983 Appropriation	1984 Appropriation	1985 Base	1985 Request
High Energy Physics (ER)				
Physics Research				
Operating Expenses	$ 90,278	$ 99,500	$ 99,500	$107,700
Subtotal	90,278	99,500	99,500	107,700
Facility Operations				
Operating Expenses	145,400	161,000	161,000	182,100
Capital Equipment	47,500	51,500	51,500	65,400
Construction	57,707	86,000	86,000	114,000
Subtotal	250,607	298,500	298,500	361,500
High Energy Technology				
Operating Expenses	90,100	82,000	82,000	91,800
Subtotal	90,100	82,000	82,000	91,800
Total				
Operating Expenses	325,778	342,500	342,500	381,600
Capital Equipment	47,500	51,500	51,500	65,400
Construction	57,707	86,000	86,000	114,000
Total High Energy Physics	$430,985	$480,000	$480,000	$561,000[a/]

Staffing
FTP/Total FTEs..... (Reference General Science Program Direction Decision Unit)

Authorization: Section 209, P.L. 95-91.

a/ This decision unit reflects $-4,000,000 for savings resulting from management initiatives in the areas of administrative systems and administrative processes/field structure.

DEPARTMENT OF ENERGY
1985 CONGRESSIONAL BUDGET REQUEST
SUMMARY OF CHANGES
HIGH ENERGY PHYSICS
GENERAL SCIENCE AND RESEARCH
(In thousands of dollars)

1984 Appropriation enacted	$480,000
Built in increases and decreases	0
1985 base	$480,000
Program increases and decreases:	
o Funding required to maintain constant level of program activity	+ 33,600
o Planned increment for SLC construction	+ 26,260
o Facility operation at about a 55 percent utilization level (slightly above FY 1984 level, taking into account new capabilities at Fermilab)	+ 9,830
o Physics research matched to the planned utilization level, including needs for 1000 GeV experiments at Fermilab and U.S. commitments to LEP experiments	+ 1,240
o Increment for advanced technology R&D, including R&D for SSC	+ 4,050
o Capital equipment to meet needs at Fermilab for Tevatron I and II and at SLAC for SLC detectors	+ 10,300
o Tevatron I and Tevatron II construction as planned	- 2,010
o Terminate CBA construction	- 5,350
o Increment for improved level of Accelerator Improvement Projects	+ 370
o Increase General Plant Projects to improve maintenance of the Brookhaven National Laboratory physical plant	+ 2,710
1985 Budget Request	$561,000

High Energy Physics

The High Energy Physics program supports basic research which seeks to discover the fundamental constituents of matter and to understand the laws of nature that govern the fundamental behavior of matter and energy. Discoveries and knowledge resulting from this activity in the past have made possible the highly technological world in which we live today. In this century, scientific investigation has focused on understanding the relationships between ever more fundamental constituents of matter, with the research frontier moving from the study of molecules to atoms, to nuclei, to the constituents of nuclei (protons and neutrons), and recently to even more elemental subnuclear constituents called quarks and gluons. The Department of Energy provides over 90% of the Federal support for this most basic scientific endeavor and serves as the Executive agent for the national program. The Department has responsibility for planning for the national program, with the goals of maintaining a comprehensive and productive national program and a competitive world leadership position for the United States.

The framework for comprehending natural phenomena has, until recently, rested on the belief that all occurrences in nature could be described in terms of just four fundamental forces and a set of basic constituents of matter. The "electromagnetic" force describes how atoms and molecules are formed and is the cornerstone to understanding chemistry, electronic communication and biological processes. The "weak nuclear" force describes processes such as the radioactive decay of nuclei and the relative abundances of the chemical elements. The "strong nuclear" force describes how the sun and stars produce so much energy. The "gravitational" force describes falling objects, orbiting celestial bodies, the formation of black holes, and the large scale features of the universe.

Part of the recent great progress in science has been a reduction in the apparent number of basic forces through the conceptual unification of the weak nuclear and electromagnetic forces into a single force -- the electroweak force. Recent experimental evidence for the existence of the W and Z^0 particles, together with experimental discoveries during the past decade of neutral weak currents and of particles with charmed quark and even heavier quark constituents, confirm this conceptual unification. The electromagnetic and weak nuclear forces can now be viewed in a natural way as different aspects of one electroweak force. The 1979 Nobel Prize in Physics was awarded to three theoretical high energy physicists (two from the U.S.) for their work toward this unification.

There is increasing anticipation that the unification of the strong nuclear and electroweak forces into one "grand unified" force is possible, thereby reducing the apparent number of basic forces in nature to only two. The enormous energy scale at which this grand unification occurs can be derived from basic contributions which led to the award of the 1982 Nobel prize in physics to a U.S. theoretical physicist. Early theoretical predictions of grand unification give possible explanations for the observed imbalance of the abundance of matter to antimatter in our universe. The 1980 Nobel Prize in Physics was awarded to two U.S. experimental high energy physicists for research which indicated that certain elemental processes are not exactly reversible. This lack of exact reversibility could explain the observed imbalance of matter and antimatter in the universe. Other predictions of the grand unification models are that protons, which were previously thought to be absolutely stable, do eventually decay; and that neutrinos, which were previously thought to be massless, may in fact have a small mass. Special emphasis in the experimental program is focused on testing these predictions of the grand unified theories. If these predictions are verified by the experiments currently in progress, this would be a major scientific breakthrough. These new concepts have profound implications for astrophysics also, where they help provide an understanding of how the universe evolved from the proposed primordial big bang beginning to its present state and whether the universe will expand forever or perhaps contract again in the distant future to another fireball.

The goal is to eventually incorporate the gravitational force into a super-grand unification scheme, which brings all of the basic forces into a single unified framework. Exactly what will follow from the stages of unification cannot be predicted in any detail. However, one can certainly anticipate profound and practical impacts, analogous to those which followed the unification of electricity and magnetism by Maxwell late in the 19th century and the unification of matter and energy by Einstein early in this century.

Progress in high energy physics research is based on a complex and continuing interplay of advancements in experiment, theory and technology. Each is strongly dependent for its progress on the advancement of the others. High energy physics experiments expand the horizons of theoretical and technical knowledge, and the range of possible experiments is determined by technological as well as conceptual capabilities and limitations. Physicists frequently have to invent new and unique apparatus and novel techniques in order to carry out the experiments of greatest interest, thereby contributing directly and immediately to the technology resources of the country.

To probe deeper into the depths of matter, into the domain of quarks, gluons, and other new particles, it is most effective to use intense beams of very energetic particles which are only available from high energy particle accelerators. Through studying the results of the violent collisions of these accelerated particles with other particles in a dense fixed target or in another beam, information is acquired about the constituents of those particles and about the forces which act within and between them. The high energy particle accelerator and colliding beam facilities to be operated by the Department in FY 1985 include: the 30 GeV (billion electron volt) proton synchrotron, Alternating Gradient Synchrotron (AGS), at Brookhaven National Laboratory (BNL); the 1000 GeV superconducting magnet proton synchrotron at Fermi National Accelerator Laboratory (Fermilab); and the 32 GeV linear electron accelerator at the Stanford Linear Accelerator Center (SLAC). SLAC also has two electron-positron colliding beam facilities for which the linear accelerator acts as an injector: the Stanford Positron Electron Asymetric Ring (SPEAR) (4 GeV x 4 GeV) and the Positron-Electron Project (PEP) (15 GeV x 15 GeV). Each of these DOE accelerator centers provides a unique set of experimental capabilities, complementary to the others. As an ensemble they provide capabilities essential for a comprehensive forefront national research program in high energy physics.

A major part of high energy physics funding is required to meet the direct needs of the accelerator laboratories to develop, maintain and operate the major accelerator and detector facilities. The facilities at these laboratories provide the data source for accelerator-based high energy physics research, of which more than 75% is carried out by university-based user scientists. In this sense, as much as three-quarters of the funding provided to the accelerator laboratories can be considered as indirect support of the university program.

At Fermilab the Energy Saver, the world's first high energy accelerator using superconducting magnets, is now in operation delivering beam to a number of experiments. Extensions are being made under the Tevatron I and Tevatron II construction projects. The Tevatron I project, initiated in FY 1981 and scheduled for completion in FY 1986, has already provided the RF and cryogenic upgrades to increase the beam energy capability of the Energy Saver from 500 GeV to about 1000 GeV. The major thrust of Tevatron I is to provide the capability for operating the superconducting synchrotron as a 1000 GeV on 1000 GeV proton-antiproton colliding beam storage ring. A key element of Tevatron I, the intense source of antiprotons, is scheduled to begin first operating tests in FY 1985. The project remains on schedule and within cost for completion and first research utilization at low luminosity by the end of FY 1986.

The Tevatron II project at Fermilab, begun in FY 1982 and scheduled for completion in phases from late FY 1983 through FY 1985, has already provided the capability to extract accelerated protons from the Energy Saver/Tevatron at energies up to 1000 GeV, and to transport them through the switchyard to the external target stations. Several of the upgraded secondary beam lines will come into operation in FY 1984. The new Tevatron II beam enclosures and experimental halls will be completed by the end of FY 1985. The project is on schedule and within cost.

Funds were provided in FY 1984 to initiate construction of the SLAC Linear Collider (SLC). The SLC has, as a primary goal, the development and demonstration of the fundamental technical feasibility of using linear accelerators with precisely controlled, high intensity and micron-sized beam pulses to provide a reliable source of high luminosity electron-positron collisions. The successful demonstration of the SLC capabilities is a critical step toward future electron-positron colliders at energies far beyond those which would be affordable with circular colliders. SLC construction is planned on a three year schedule. This will give the U.S. a 50 GeV x 50 GeV electron positron collider and earliest access to the scientifically exciting physics associated with the anticipated copious production of the Z^0 boson in high energy electron-positron collisions.

HEPAP and its 1983 Subpanel on New Facilities unanimously recommended as highest priority "the immediate initiation of a multi-TeV high luminosity proton-proton collider project with the goal of physics experiments at the earliest possible date" and stressed that project preparation must begin as soon as possible in order to meet the goal of completion in the first half of the 1990's. The new facility, designated as the Superconducting Super Collider (SSC), is envisioned as a proton-proton collider with an energy of 20 TeV per beam and high luminosity, up to 10^{33} cm^{-2} sec^{-1}. Recent rapid progress in physics understanding and technology, including the great success of the CERN laboratory in their successful construction and operation of a proton-antiproton colliding beam capability and the subsequent discovery of the W and Z particles, has emphasized the importance of physics experiments in the several trillion electron volt (TeV) mass range where new phenomena, including new forms of matter with unique properties are firmly expected. The SSC would have immense physics potential for truly major advances in understanding the fundamental nature of matter in an energy domain where there are no existing or planned facilities in the world and would assure a world competitive U.S. high energy physics program from the mid-1990's into the next century. Such a project lies within the reach of present technology and has been made possible by the recent outstanding successes resulting from the substantial U.S. investment in superconducting magnet technology. The physics importance of exploration of the TeV mass scale coupled with the technical feasibility, leads to the conclusion that the limited U.S. resources in manpower and funds are best utilized by concentrating on this highest priority project with its crucial physics importance. Thus it was decided not to continue the CBA effort which would have compromised the achievement of this goal.

The preliminary R&D for the SSC project would consist of critical R&D and conceptual design studies to answer key questions needed to define any future construction effort. Currently planned activities would include R&D to investigate various superconducting magnet designs to determine which would lead to best performance at least cost, and studies to integrate physics objectives into design criteria for the facility, to define the scope of the facility, to develop a cost-optimized design, to develop realistic cost and schedule estimates, and to establish site criteria. R&D preliminary to the SSC is being carried out in FY 1984 (primarily via a reprogramming of CBA funds) and in FY 1985. Specifically, in FY 1985 the advanced accelerator R&D effort would focus on providing the necessary engineering and technical inputs for a cost optimized design which will identify performance/cost choices among technical alternatives, integrate technical requirements with cost effective fabrication techniques, establish site criteria, and provide realistic cost and schedule estimates.

In addition to research carried out using the U.S. high energy accelerators, the Department's high energy physics program supports some experiments which use the capabilities of unique foreign accelerators and some experiments, such as proton decay experiments, which involve techniques not requiring accelerators. The research carried out at facilities overseas takes advantage of unique research opportunities offered by foreign accelerator facilities which have capabilities not available in the U.S. The research using nonaccelerator sources of particles includes studies of very rare processes which are critical to verifying force unification theories. Included among the processes studied are the predicted decay of the proton and the spontaneous conversion of matter to anti-matter.

This decision unit reflects $-4,000,000 for savings resulting from management initiatives in the areas of administrative systems and administrative processes/field organizations.

The budget request addresses the funding requirements for utilization of present facilities at about the 55% level, for continued progress on current construction projects, for R&D in support of projects presently underway, and for initiation of preliminary R&D studies on the SSC project.

The FY 1985 request for operating expenses is $381,600,000. A major feature of the program in FY 1985 will be the operation of the Energy Saver/Tevatron superconducting synchrotron at Fermilab for research in the 1000 GeV energy range. Priority is also given to operation and research utilization of the PEP facility and of the AGS with its new polarized proton beam and excellent low energy neutrino capabilities. The overall utilization level of the DOE HEP accelerator facilities will be about 55%, somewhat above the FY 1984 level, and about equal to the FY 1983 level. The request provides continuing support for university based research groups including accelerator user group efforts, non-accelerator experiments, and theoretical research efforts. There will be continuing accelerator R&D efforts at Fermilab and SLAC in support of on-going construction efforts. The FY 1985 program of preliminary R&D studies for the SSC project will focus on development and evaluation of technical options for magnets and other accelerator components, development and validation of cost saving designs and fabrication techniques, consideration of accelerator design alternatives, and trade-off and cost optimization studies.

The FY 1985 capital equipment request of $65,400,000 provides a substantial increase above the FY 1984 level in order to meet the highest priority needs associated with implementation of research programs using the major new research capabilities being provided by the Tevatron I and Tevatron II projects at Fermilab and the Stanford Linear Collider at SLAC. This major new thrust in FY 1985 is essential to minimize delays in implementing these research programs which are critical for effective utilization of the U.S. High Energy Physics facilities and for the health of the U.S. High Energy Physics program for the remainder of the 1980's. The request gives priority to Fermilab for the new secondary beam lines and detector systems needed to implement the 1000 GeV research program associated with the Tevatron II program and for work on the colliding beam detectors needed for the Tevatron I research program; to SLAC for work on detectors for SLC research; and to the university program for needs of experiments at the U.S. Laboratories and at the Large Electron Positron (LEP) facility, and for non-acccelerator experiments.

The request for construction funds is $114,000,000. The major features are the continued construction of the SLC project ($60,500,000) at SLAC, completion of the Tevatron II project at Fermilab ($12,000,000), and continuation of Tevatron I ($21,300,000) at Fermilab. Funds are also requested for Accelerator Improvement Projects (AIP) ($10,000,000) taking into account the needs of the recent new facilities being operated and for an improved level of General Plant Projects (GPP) ($10,200,000) with particular emphasis on the needs at BNL, where this program provides

for the full needs of this multipurpose laboratory. The accelerator improvement projects are essential on an annual level of effort basis for maintaining the reliability and efficiency, as well as the scientific effectiveness of the existing accelerator facilities. GPP projects are required to keep the general plant of the laboratories, including building, utilities and roads, in a viable operating condition.

The High Energy Physics program may be considered to consist of three subprograms: Physics Research, Facility Operations and High Energy Technology. Although the three functions within the program are discussed as separate subprograms, they are not independent. Each is coupled to the other two and cannot exist separately by itself. The close interaction and dynamic nature of these three subprograms make it imperative that some adjustments in the distribution of funding among the subprograms be permitted during the year in order to ensure the most effective program and the best use of overall program funds.

	FY 1983	FY 1984	FY 1985 Request
Physics Research			
Operating Expenses.....	$ 90,278	$ 99,500	$107,700

The Physics Research subprogram includes the direct support of university- and laboratory-based research groups both for the planning, preparation and execution of experiments, and for the measurement analysis, interpretation and dissemination of experimental results. It also supports experimental high energy physics research using data sources and facilities other than accelerators, and the research of university-and laboratory-based theoretical physicists in both phenomenological and formal areas of theoretical study.

The goal of high energy physics research is to determine the fundamental nature of matter and energy. Experiments in high energy physics generally require the use of large particle accelerators together with complex detection apparatus to study the products of collisions of high energy particles. The DOE-supported accelerators and experimental facilities are located at three central laboratories where they are accessible to qualified scientists on the basis of the scientific merit and promise of their proposed research. Although the experiments are performed using the accelerators at the national centers, 75 percent or more of the research is done in a user mode by university-based physicists. Because of the size and complexity of a typical high energy physics experiment, users from a number of institutions frequently collaborate on a given experiment. The resultant research teams typically include a mix of physicists, engineers, technicians, and graduate students. There is usually significant interaction and assistance from laboratory staff and support facilities in each experiment. The research teams provide manpower for the experiment during the data-taking phase at the laboratory. The recorded data is generally taken back to the home institutions for analysis, interpretation and publication of results. This entire process from conception of the experiment to publication of results usually takes three to five years. U.S. user group involvement in unique experimental opportunities at foreign laboratories such as DESY and CERN is also supported.

Studies of some of the important fundamental problems in high energy physics are now being carried out in experiments which do not involve the use of high energy accelerators. The new grand unified theories predict some phenomena whose direct observation requires energies far above those presently available from accelerators, but they also predict some effects that can best be observed in high precision experiments at very low energies. While experiments to search for proton decay currently represent the largest of the non-accelerator experimental efforts, there are other experiments, both proposed and operational, including: searches for free quarks, magnetic monopoles, and neutrino mass; measurement of neutrino-less double beta decay; investigation of extensive air showers; and studies of cosmic ray neutrino interactions. In FY 1985 about $7,000,000 is expected to be devoted to non-accelerator experiments promising important results.

Theoretical research provides a framework for understanding the results of experimentation and provides suggestions for new measurements important for advancement of understanding. Experiments test existing theory, and experimental results and discoveries often provide the basis for extensions, revisions and modifications of the theoretical framework and understanding. There is thus a strong interaction and interdependence of experimental and theoretical research. Because of this, experimental and theoretical research groups work closely together. High energy theoretical research presently has a strong focus on developing a unified description of the forces in nature through generalized gauge-invariant field theories. An increasing trend in theoretical research is the use of large computing facilities to explore numerical solutions of candidate theories which are not amenable to analytic methods, along with the development of more powerful numerical and analytical techniques.

The Physics Research Subprogram provides support for the Outstanding Junior Investigator program which provides research support for outstanding untenured high energy physicists who might otherwise have to leave the field due to lack of permanent positions. This small program is very important for encouraging some of the best young scientists to enter and to remain in this kind of research and thus bears importantly on the long range vitality of the field.

The FY 1985 budget requests $107,700,000 for Physics Research which will support a somewhat improved level of effort relative to FY 1984. The funds requested are necessary to maintain the capability of the university and laboratory research groups to participate effectively in today's more complex experiments, to provide an appropriate match with the planned level of facility utilization and to allow continuation of the substantial theoretical research and non-accelerator high energy physics research programs.

Distribution by Facility

Physics Research	FY 1984 Appropriation	FY 1985 Request
Fermi National Accelerator Laboratory (Fermilab).....	$ 9,000	$ 9,700
Brookhaven National Laboratory (BNL).....	6,900	7,500
Stanford Linear Accelerator Center (SLAC).....	10,500	11,100
Argonne National Laboratory (ANL).....	4,500	4,900
Lawrence Berkeley Laboratory (LBL).....	7,800	8,400
Universities and other agency Laboratories.....	60,800	66,100
Total Physics Research.....	$ 99,500	$107,700

Fermi National Accelerator Laboratory

$9,700,000 is required in FY 1985 for the support of the Fermilab in-house research effort, compared to $9,000,000 in FY 1984. This would permit physics research activity by Fermilab scientists, focusing on the new physics opportunities available with completion of the final phases of Tevatron II and the preparation for Tevatron I research efforts the following year. Most of the research of the Fermilab scientists is done in collaboration with university-based groups from across the country where they simultaneously provide a crucial support and liason function for the many university users of Fermilab. The major lines of research to be pursued by Fermilab scientists in FY 1985 will be searches for new particles, studies of nucleon constituents, and exploration of the electroweak force through neutrino interactions. The 1000 GeV capability resulting from operation of the Energy Saver/Tevatron superconducting synchrotron in conjunction with upgraded and new experimental facilities provided by the Tevatron II project, will offer many highly promising new opportunities for research advances.

The constituents of the nucleon will be probed by studying the properties of jets of particles produced with high transverse momentum and by studying the dimuon spectrum resulting from energetic proton collisions with a fixed target. Experiments will also be conducted using the higher energy neutrino beam available from completion of elements of the Tevatron II project. A major study of the substructure of the nucleons is planned using the superconducting "Chicago Cyclotron" magnetic spectrometer, as well as continuation of investigation of the creation of charmed and heavier quark states by photons in photoproduction experiments at new higher energies. The requested funds also include support for the Fermilab theoretical physics research programs.

Brookhaven National Laboratory

$7,500,000 is required in FY 1985 for the BNL in-house research program, compared to $6,900,000 in FY 1984 to permit about the same level of research as in FY 1984. The research capabilities at the AGS are unique, since no other accelerator covers this range of beam energies. A major emphasis during FY 1985 is an analysis of data from experiments on interactions of polarized beams on polarized targets utilizing the polarized proton beam capability at the AGS, neutrino oscillations and neutrino-electron elastic scattering, and rare K decays. A complementary program of theoretical analyses of experimental results and other theoretical studies will also be pursued.

Stanford Linear Accelerator Center

$11,100,000 is required for FY 1985 compared to $10,500,000 in FY 1984 for support of SLAC physics research groups at about the same level of effort as in FY 1984.

In FY 1985, PEP is expected to operate at a record high luminosity and, with an improved set of detectors, provide excellent opportunities for new discoveries. New particle searches will continue with better sensitivity, and, higher precision experiments including measurements of electroweak asymmetries and particle lifetimes will be emphasized. The SPEAR detector (Mark III) will continue taking data concentrating on states in the Psi region to obtain a better understanding of the charmed quark. Increased linac energy, combined with the improved SLAC hybrid spectrometer, will give a unique opportunity for observing the creation of new particles with short decay lifetimes and increased accuracy in measuring such lifetimes. The theoretical program at SLAC includes a variety of phenomenological studies, as well as studies of fundamental issues concerning properties of the basic forces, the constituents of matter and the unification of forces.

Argonne National Laboratory

$4,900,000 is requested for the ANL physics research program in FY 1985 compared to $4,500,000 in FY 1984. ANL scientists are primary participants in the operation of the High Resolution Spectrometer (HRS) at PEP, in the data-taking and analysis phases of experiments with HRS, and in the upgrading of this facility. They are involved in preparation for experiments to study 1000 GeV x 1000 GeV proton-antiproton collisions at Fermilab when the Tevatron I comes into operation and are participants in a Fermilab experiment to study jets produced from hadron collisions, which is expected to give information on the quark-gluon interaction. In addition, they will be part of a major effort to observe neutrino oscillations at the Los Alamos Meson Physics Facility; they are leading a novel search for free quarks; and they are major participants in a nucleon decay experiment. The ANL physicists collaborate closely with university research groups in these activities and together with unique ANL laboratory capabilities provide an important technical service base for these groups. The high energy theoretical physics group at ANL focuses on the study and formulation of phenomenological models for strong interactions.

Lawrence Berkeley Laboratory

The request provides $8,400,000 in FY 1985 for the LBL research program compared to $7,800,000 in FY 1984 to maintain about a constant overall level of activity. These funds are required for participation of the LBL research groups in experiments at PEP, Fermilab and the TRIUMF facility in Canada. LBL will continue to play a major role in experiments at PEP including use of the Time Projection Chamber and the Mark II Magnetic Detector, which will be modified to be the first SLC detector. Detailed study by LBL physicists of muon reactions at Tevatron energies at Fermilab should lead to a better understanding of the electroweak force at highest energy available with lepton probes. The LBL experiment at TRIUMF, which uses polarized muons to search for the effects of a possible new type of vector boson whose existence would invalidate the standard theory of electroweak interaction, will yield its first high precision results in FY 1985.

An important part of the LBL program is the Particle Data Center, which is the only such U.S. capability and which provides a valuable service function for the entire high energy physics community. Support for high energy astrophysics experiments in 3 degree Kelvin background radiation, supernovae detection and observation, and studies of compact stellar objects is expected to continue. These experiments provide important data on elementary processes which complements that of other high energy physics experiments. Theoretical physics at LBL will continue to emphasize the investigation of the basic particle interactions, the fundamental structure of matter, and topics in advanced accelerator physics.

Universities and other Agency Laboratories

The Physics Research request for FY 1985 provides $66,100,000, compared to $60,800,000 in FY 1984, for university-based groups and for research programs at Ames, Los Alamos National Laboratory (LANL), Oak Ridge National Laboratory (ORNL) and Pacific Northwest Laboratories (PNL). This amount is required to permit university-based research groups to participate effectively as users at U.S. accelerator laboratories and unique foreign facilities; to mount new forefront non-accelerator experiments; to contribute the development of innovative research instrumentation required for the next generation of experiments, such as solid state detectors and laser streamer chambers; and to make available some new opportunities for outstanding junior investigators to do independent research.

University physics departments provide important intellectual leadership and are a source of young physicists for the nation. Physics research in the high energy physics program is carried out both by university-based groups and by laboratory-based groups. There is a synergistic institutional relationship between the universities and laboratories, and between their respective personnel, which has resulted in a highly productive national program and is highly beneficial to its sustained progress. The Department supports approximately 115 experimental and 65 theoretical high energy physics research groups at 90 leading universities across the nation, as well as the efforts at Ames, LANL, ORNL and PNL. The record of success of the program indicates that universities are outstanding centers for developing the innovative and creative ideas required for the success of the program. The subjects of research in the university program run the gamut of high energy physics from the most abstract theoretical studies to phenomenological studies, elementary particle experiments and instrumentation development.

DOE University-based high energy experimental groups are engaged in a great variety of forefront experiments (more than 200) in various stages of progress, in which the data are collected mainly from U.S. accelerators at BNL, Cornell, Fermilab, or SLAC, from European accelerators at the European Center for Nuclear Research (CERN) and the Deutsches Elektronen - Synchrotron (DESY), and from non-accelerator settings (e.g., deep mines for proton decay). Such well-conceived and carefully executed experiments provide

the basis for progress in the field. University-based high energy theorists generate much of the body of advanced literature in the field. Especially important recently are the conceptual advances leading to the unification of the forces of nature and a better understanding of the basic constituents of matter.

	FY 1983	FY 1984	FY 1985 Request
Facility Operations			
Operating expenses	$145,400	$161,000	$182,100
Capital equipment	47,500	51,500	65,400
Construction	57,707	86,000	114,000
Total facility operations	$250,607	$298,500	$361,500

Facility Operations

Facility Operations supports all of the many activities required to operate, maintain, equip, and construct the high energy accelerators, colliding beam storage ring facilities, experimental areas, secondary beams, large multi-user detector facilities, and support facilities required for the pursuit of experimental high energy physics research.

Operating expenses	$145,400	$161,000	$182,100

The operating expenses portion of Facility Operations provides the accelerator and experimental facility operating crews and support personnel, the electric power, and the expendable materials and services required for these activities, which are concentrated in the three high energy accelerator centers at BNL, Fermilab and SLAC. These accelerator facilities provide the beam time needed for the research work of the DOE-supported high energy physicists, and of most of the National Science Foundation (NSF) supported high energy physics experimental research groups as well. The required accelerator and detector facilities are large, complex and expensive; hence, they are few in number and are operated as national centers made available to those qualified physicists whose research proposals are of the highest scientific promise and merit.

The complementary capabilities at the three centers provide the essential variety in types of particle beams, particle energy and beam intensity for a productive U.S. high energy physics program. At Fermilab, the superconducting magnet proton synchrotron provides intense beams of protons with energies up to about 1000 GeV and also provides various types of secondary particle beams with the high energies and high intensities needed for fixed target experiments. At BNL, the AGS provides protons with energies up to 30 GeV in the primary beam, high energy polarized proton beams and a variety of secondary beams and neutrino beams for use in fixed target experiments. At SLAC, the two-mile linear accelerator delivers electrons up to 32 GeV, positrons at 21 GeV and secondary particle beams for use in fixed target experiments. Also at SLAC, the PEP colliding beam facility stores electrons and positrons for collisions at 15 GeV on 15 GeV and the SPEAR facility provides similar capabilities for collision energies up to 4 GeV on 4 GeV.

The funding request in FY 1985 will provide an average utilization level in the 55 percent range, including operation of the 1000 GeV program at Fermilab with the Energy Saver/Tevatron and the completed portions of the Tevatron II project.

Operating Expenses

Distribution by Facility

Facility Operations	FY 1984 Appropriation	FY 1985 Request
Fermilab	$ 73,100	$ 86,700
BNL	34,200	37,800
SLAC/PEP	48,000	52,900
LBL	700	700
Other	5,000	4,000
Total Facility Operations	$161,000	$182,100

Fermi National Accelerator Laboratory

The FY 1985 requirement for Facility Operations at Fermilab is $86,700,000 compared to $73,100,000 in FY 1984. The superconducting magnet Energy Saver/Tevatron accelerator will be operated in the fixed target research mode during the first seven months of FY 1985 at energies ranging up to about 1000 GeV. Operations for preliminary tests of the antiproton beam related to the Tevatron I project is scheduled at the end of this running period. The liquid helium cryogenic plant will remain in operation for the full year to keep the superconducting magnets cold. Operation of the entire expanded sequence of five accelerators at Fermilab (Cockroft-Walton Preaccelerator, Linac, Booster, Main Ring and Superconducting Energy Saver/Tevatron Ring) will require $54,300,000, with another $32,400,000 needed for operation of the laboratory's extensive complex of secondary beams experimental detectors and research facilities. When the accelerator is operating for fixed target experiments, about a dozen secondary beam lines will provide a variety of intense high energy particle beams for research use, and about 15 different experiments are expected to take data during FY 1985. This is a major increase over FY 1984 and is a major source of the requested increase in funding for Facility Operations. Major experimental facilities to be operated will include the 15-foot bubble chamber, two major neutrino detectors, the tagged photon spectrometer and the multiparticle spectrometer, a calorimeter to study the production of jets of particles at high transverse momenta, and a massive magnetic spectrometer with high resolution to search for new kinds of heavy particles which decay into pairs of muons.

Brookhaven National Laboratory

In FY 1985, $37,800,000 is requested for operation of the AGS and associated experimental facilities compared to $34,200,000 in FY 1984. Of this amount, $18,400,000 is needed for accelerator operations and $19,400,000 is needed for experimental facility operations for about a 35-week level of machine operation. The FY 1985 operating program is expected to include 15 weeks of slow extracted beam operation, 10 weeks of fast extracted beam operation for neutrino experiments, and 10 weeks of polarized proton beam operation. The new high energy polarized proton beam will be an important and unique capability not available anywhere else in the world. The BNL neutrino beams are also unique.

Stanford Linear Accelerator Center/Positron Electron Project

$52,900,000 is required in FY 1985 for operation of the SLAC linear accelerator, the PEP and SPEAR colliding beam rings, and their associated experimental facilities compared to $48,000,000 in FY 1984. Of that sum, $28,400,000 is for the operation of the linear accelerator, the SPEAR storage ring, and PEP. This should make it possible to operate the linear accelerator for about 30 weeks, providing a substantial program of colliding beam physics with PEP and SPEAR. The delivery rate of electron pulses, which primarily affects the fixed target research program, would be about 20% of maximum capability. (The facility operating levels will be considerably lower at this funding level if SLAC

loses its withdrawable electric power allocation from WAPA.) SPEAR storage ring operations will continue to be half-time for high energy physics research and half-time for the Stanford Synchrotron Radiation Laboratory, which is supported by the Basic Energy Sciences Program. The high energy physics portion of SPEAR operation will focus on the use of the improved Mark III general purpose magnetic detector for studying properties of the charmed particles. Operation of PEP, which is expected to be at a high level of productivity with a record high luminosity and an improved set of improved detectors, will be given high priority.

The remaining $24,500,000 for SLAC is required to support operation of the experimental areas, detector facilities and the central computer facility. A full complement of PEP detectors will be operating in FY 1985. Other facilities to be operated during FY 1985 include the Mark III detector at SPEAR and an improved spectrometer for fixed target experiments.

Lawrence Berkeley Laboratory

The request provides $700,000 for support of LBL's participation in operation of the Time Projection Chamber (TPC) facility at PEP. LBL provides engineers, computer scientists, technicians, and physicists who are primarily responsible for reliable operation of the TPC.

Other

In FY 1985, $4,000,000 is required for special process spares, common use stores and other specialized activities to meet requirements at the accelerator laboratories. An adequate complement of spares and specialized replacement parts is essential to avoid unnecessary disruptions to the operating schedule in the event of component failures. These very complex and advanced technology facilities require many components that are custom made and are not off-the shelf items, and thus, are not rapidly available when a problem occurs.

	1983	1984	1985 Request
Capital Equipment.....	$ 47,500	$ 51,500	$ 65,400

Capital Equipment funding is required to provide the secondary beam line components, particle detection apparatus, portable shielding, and data analysis systems essential to do high quality experiments in high energy physics. It also is required for replacement of components that have worn out or become obsolete. Capital equipment funds are absolutely essential for effective utilization and operation of the major high energy physics research beam facilities.

To maintain a world leading research program which is capable of advancing the frontiers of knowledge and consistently making new discoveries, the timely introduction of improved beam and detector capabilities and the regular upgrading and modification of existing capabilities is essential. The large scale of the high energy facilities for which capital equipment funding is needed is illustrated by the fact that a typical secondary beam line can range from several hundred feet to a mile or more in length, with many beam transport, beam shaping and control elements; the portable shielding required around detectors and targets can involve arrays of hundreds of shielding blocks weighing as much as 10 Tons each; the analysis magnets incorporated in detection systems weigh many tons; large calorimeters with weight of 100 tons or more are not uncommon; electronics systems with hundreds of thousands of data channels can be required. These large and complex beam and detection facilities often involve a time span of as much as five years from design, through fabrication and installation, to checkout and operation for research. Specific examples of items of equipment needed include beam transport magnets, precision large volume analysis magnets for detector systems, precision regulated power supplies, particle beam diagnostic and control systems, electronic and optical detectors with improved spatial and time resolution, high speed and large volume

data processing systems, special cryogenic components for liquid hydrogen targets and superconducting devices, and a host of specialized electronics and laboratory support equipment items.

$65,400,000 is required in FY 1985 to meet the capital equipment needs of the program, with the major needs being at Fermilab and SLAC. At Fermilab the needs are related primarily to completing the new secondary beams and detectors required to implement the 1000 GeV fixed target program made possible by the Tevatron II project, and for fabrication of detectors for 1000 GeV on 1000 GeV proton-antiproton colliding beam experiments with Tevatron I. At SLAC major new needs are related to upgrading an existing PEP detector (Mark II) for use at the SLC, to upgrading of the existing PEP detectors for second generation experiments, and to work on a second SLC detector. There are also major needs of university users for non-accelerator experiments and for experiments at the European LEP facility.

High Energy Physics
Summary of Capital Equipment by Laboratory

	FY 1984 Appropriation	FY 1985 Request
Fermilab	$ 25,000	$ 32,100
BNL	,400	4,300
SLAC	7,500	10,900
LBL	1,100	1,600
ANL	500	600
Other DOE laboratories	280	50
Universities	10,220	11,950
General Purpose Equipment (BNL)	3,500	3,900
Total capital equipment	$ 51,500	$ 65,400

Fermi National Accelerator Laboratory

In FY 1985, $32,100,000 is required for capital equipment. A major need ($14,500,000) is for the new and improved secondary beam lines and detectors which are essential for effective utilization of the Fermilab accelerator complex at the 1000 GeV level, as the Tevatron II project approaches completion in FY 1985. Another major need ($12,500,000) is for effort on two detectors necessary to the 1000 GeV on 1000 GeV proton-antiproton colliding beam experiments at the B-Zero and D-Zero intersection regions of Tevatron I ($11,000,000 and $1,500,000, respectively).

Summary of Capital Equipment Request for Fermilab

	FY 1985 Estimate
Detectors for 1000 GeV fixed target experiment	$ 6,500
Secondary beam line components and shielding	8,000
1000 GeV on 1000 GeV colliding beam detectors	12,500
Research Services Department	1,800
Accelerator related equipment items	1,900
General computing equipment	900
Technical support and site operations equipment	500
Total	$ 32,100

Much of the capital equipment funding requested is needed to fabricate detection equipment for new experiments and to upgrade existing facilities for higher energy operation. This work contributes directly to meeting the research needs of university users. The emphasis in FY 1985 will be on implementing experiments at 1000 GeV as the last elements of Tevatron II become operational. The requested $6,500,000 includes $3,250,000 for approved experiments in the Neutrino Area, $1,000,000 in the Proton Area, $2,000,000 in the Meson Area and $250,000 for new experiments and general support equipment.

The large scale of the Fermilab fixed target experimental areas and their great distances from the accelerator dictated by their high operating energy require unusually long secondary beam transport lines with associated magnets, control systems and shielding, all of which are provided from capital equipment funds. This need is particularly essential in FY 1985 so that the new opportunities provided by the completion of Tevatron II can be exploited. In addition to upgrading several existing beamlines, a number of major new secondary beam enclosures provided by Tevatron II project need to be equipped. A total of $8,000,000 is requested for secondary beam equipment. The major efforts on new beams in FY 1985 will include work on the broad band photon beam ($900,000), prompt neutrino beam ($2,800,000), polarized proton beam ($1,300,000) the new high energy pion beam in the Meson Area ($1,600,000), the P-West hadron beam ($500,000) and the Meson Area neutral beam ($700,000). The remaining $200,000 is for a number of smaller upgrades and modifications.

The major detector for the study of 1000 GeV on 1000 GeV proton-antiproton interactions at the B-Zero interaction region of the Tevatron I facility was started in FY 1981 with DOE funds and substantial support from Japanese and Italian collaborators. In FY 1985, this detector will require about $11,000,000 in DOE funds in addition to an anticipated $2,000,000 contribution from Japanese and Italian participants. The detector is scheduled for completion in FY 1986 to be ready for operation when the 2000 GeV reaction energy becomes available upon completion of Tevatron I. The $11,000,000 included here is intended to cover the full FY 1985 funding for all U.S. participants in the detector project, including funds which may be assigned directly to collaborating U.S. laboratories and universities. The second detector needed for research using Tevatron I capabilities at the D-Zero interaction region will require about $1,500,000 in FY 1985.

The Research Services Department effort in FY 1985 will focus on fabrication of large aperture analysis magnets and the prompt neutrino shield magnets. Capital equipment items are required for maintaining the scientific effectiveness of the numerous and complex accelerator systems and the Central Helium Liquifier at the laboratory, and for replacement of worn out and obsolete units of the operating accelerator facility. These include components of the control, RF, vacuum and cryogenic systems. Also needed is equipment in support of the R&D needs related to the Tevatron I project including RF instrumentation, stochastic cooling instrumentation, magnet measurement equipment, vacuum components and control instrumentation.

The Fermilab central computer complex requires the addition of peripheral equipment, both to improve the data acquisition capability and to improve access by users. Small additions to the central computer system to maintain its effectiveness are also included. Technical support and site operations equipment items include machine tools, vehicles, office equipment, and site maintenance equipment.

Brookhaven National Laboratory

The FY 1985 request of $4,300,000 for BNL includes $3,400,000 for needs of the ongoing AGS and physics program. This includes $900,000 for the major experiment to study rare kaon decays, $700,000 for equipment to improve the polarized proton beam capability; $600,000 related to AGS intensity improvements; $400,000 for improved AGS controls and beam instrumentation; $500,000 for improved beam line power supplies and $300,000 for additions to the experimenters' equipment pool.

The remaining $900,000 is for the Accelerator and Facility R&D programs. This includes $350,000 for magnet test instrumentation, $300,000 for the cryogenic equipment, and $250,000 for minicomputers for monitoring and data collection applications.

Stanford Linear Accelerator Center

The request of $10,900,000 is required in FY 1985 to meet equipment needs related to the SLAC linear accelerator, the SPEAR and PEP storage rings, the associated experimental detection facilities, upgrading of the Mark II detector and beginning work on a new detector for use at SLC, and the SLAC accelerator research and development programs.

Of the $10,900,000 requested for SLAC, $800,000 is for the Linac and SPEAR programs including improvements to the Mark III Detector ($600,000), completion of the micro-beta modification of the SPEAR lattice for increased luminosity ($200,000). $1,200,000 is required for equipment to support PEP and its detectors; the effort is expected to include the upgrading of one of the major detectors. The $300,000 required in support of SLAC's accelerator research and development effort includes equipment needs for improvements in the linac beam, for work on surface physics and superconductivity and for the research and development leading to the possibility of a linear collider. There are also needs for $300,000 for on-line data acquisition equipment addition and $300,000 general laboratories support equipment.

$4,700,000 of the request for SLAC is required for the upgrade of an existing PEP detector (Mark II) to operate effectively at the higher SLC energies to provide a quantitative test of the success of the linac collider concept in providing high luminosity collisions at 100 GeV and to explore physics in the new energy region, concentrating on production of the Z^0. In addition $3,300,000 is provided for work on a new SLC detector designed and scoped to include calorimetry for more detailed study of Z^0 physics.

Lawrence Berkeley Laboratory

A total of $1,600,000 is requested for capital equipment needs at LBL. The physics research program requires $1,000,000 for the support of ongoing experiments at PEP, Fermilab and TRIUMF, and for general purpose equipment and instrumentation. The advanced accelerator R&D effort requires $600,000 in equipment for further investigations related to LBL's effort on the Fermilab antiproton cooling ring and for supporting the R&D program on very high field superconducting accelerator magnets.

Argonne National Laboratory

A total of $600,000 is required for ANL capital equipment needs in FY 1985. This is for support of the physics research program, including the polarized proton beam experiment at Fermilab, a VAX type computer, and detector needs for the neutrino oscillation and proton decay experiments.

Other Laboratories

The FY 1985 request for equipment funding for high energy physics also includes $50,000 for Ames Laboratory for detector components for experiments at Fermilab and the European Center for Nuclear Research (CERN).

Universities

The $11,950,000 requested for university programs is required for experimental detection and data analysis equipment. These funds primarily support the major apparatus needs of the experimental research programs of the university users for experiments at U.S. and foreign national accelerator laboratories, and for the needs of non-accelerator experiments such as nucleon decay, neutrino oscillations, double beta decay, high energy astrophysics, and magnetic monopoles. There are major equipment needs associated with user equipment which will be used in experiments using the 1000 GeV Tevatron capability

at Fermilab for both fixed target experiments and proton-antiproton colliding beam experiments; for utilization of the high intensity capability of the AGS at BNL for neutrino oscillation and kaon rare decay experiments; for electron-positron colliding beam experiments at SLAC: for participation of U.S. universities in major LEP electron-positron colliding experiments presently in the preparation stage; for participation of U.S. universities in the TRISTAN colliding beam experimental program at KEK; and with non-accelerator experiments such as the proton decay searches which are operated in deep mines. On-line computer equipment, interfacing components and peripherals, which are an integral part of experimental detector systems, and small computer systems used in scanning, measuring, and data analysis, are to be provided to university experimental groups. In addition, theoretical groups based at universities have a requirement for computing capability for some types of calculations such as lattice gauge calculations. For these purposes consideration will be given to funding computers and computer peripherals at California Institute of Technology, University of California-Los Angeles, University of California-Riverside, Carnegie Mellon University, Columbia University, University of Florida, University of Illinois, Institute for Advanced Study, Massachusetts Institute of Technology, Ohio State University, University of Oklahoma, University of Pennsylvania, Purdue University, Stanford University, and Yale University.

Other Capital Equipment

The High Energy Physics program provides for all the general purpose equipment requirements at BNL. In FY 1985, $3,900,000 is required for this multipurpose equipment, which is essential to the proper, day-to-day operations at the Laboratory. Included are all the needs of the Laboratory's service and support divisions, central scientific computing facility and central shops, as well as equipment required to respond to health, safety, security and environmental needs. It is important that obsolete and worn-out equipment be replaced in order to promote efficient laboratory operations, to increase productivity, and to avoid high maintenance costs.

	FY 1983	FY 1984	FY 1985 Request
Construction.....	$57,707	$ 86,000	$114,000

A total of $114,000,000 in construction funding for high energy physics projects is requested in FY 1985. The projects are listed below:

Project	Project No.	FY 1985 Request	Total Estimated Cost
Tevatron I (Fermilab).....	81-E-218	$ 21,300	$ 82,500
Tevatron II (Fermilab).....	82-E-206	12,000	49,000
Stanford Linear Collider (SLC).....	84-ER-133	60,500	112,000
Accelerator Improvement Projects (AIP).	85-R-100	10,000	10,000
General Plant Projects (GPP).....	85-R-101	10,200	10,200
		$114,000	

The construction request includes funding for the continuation of Tevatron I and the completion of Tevatron II at Fermilab, and for continuation of the SLC project at SLAC. These line item projects will provide new experimental capabilities and research opportunities which are vital to the long-range productivity, strength and competitiveness of the United States' program. Also included are funds for improvements and modifications to the existing accelerators, experimental facilities and general laboratory plants which are needed on an annual basis to maintain the efficiency, reliability and scientific effectiveness of the laboratories.

Tevatron I

The Tevatron I project at Fermilab, initiated in FY 1981, will provide the facilities needed for a 1000 GeV on 1000 GeV proton-antiproton colliding beam capability. This will be accomplished by producing intense counter-rotating beams of protons and antiprotons which, when brought into collision, will interact with about 2000 GeV of reaction energy, the highest available in the world. Specifically, the project includes: 1) additional refrigeration and radiofrequency accelerating structures so that the Energy Saver ring can operate at 1000 GeV for proton-antiproton colliding beams; 2) an anti-proton source; and 3) two experimental areas suitable for detectors to study the results of very high energy proton-antiproton collisions. The $21,300,000 required in FY 1985 is for continued work on the antiproton source technical components and final civil construction of the project. Additional details are provided in the construction project data sheet.

Tevatron II

The Tevatron II project at Fermilab, initiated in FY 1982, will provide the facilities needed for a 1000 GeV fixed-target experimental program. Specifically, these include: 1) a 1000 GeV beam extraction system; 2) the upgrade of the external beam switchyard to 1 TeV; 3) the provision for 1 TeV beam transport and targeting; and 4) new secondary beam enclosures and support facilities. This project will allow the experimental exploitation of the 1 TeV energy of the superconducting accelerator for fixed target experiment, and will provide unique capabilities for producing a variety of secondary particle beams at higher energies and intensities than anywhere else in the world. Final completion is anticipated, as scheduled, in FY 1985. The $12,000,000 required in FY 1985 will allow completion of enclosures for the four new secondary beam lines (the muon, broad-band photon, polarized proton and prompt neutrino beams) and conventional construction in the three existing experimental areas. Funding for the experimental detectors and secondary beam line components is included under Capital Equipment. Additional details are provided in the construction project data sheet.

Stanford Linear Collider (SLC)

The SLC project at SLAC, initiated in FY 1984, will provide: 1) systems for producing intense electron and positron bunches; 2) a small storage ring and pulse compressor to increase the density of the electron and positron bunches; 3) two semicircular arcs of small aperture magnets, housed in appropriate enclosures to bring the electron and positron beams into head-on collisions; 4) special focusing systems near the interaction point, including the necessary housing and associated experimental hall and staging area; and 5) the instrumentation and control system for both the Linac and Collider arcs.

The SLC project will accelerate beams of electrons and positrons simultaneously in the linear accelerator, separate them and transport them through two semicircular arcs at the end of the linac and then bring them into head-on collision. It will provide an essential technology demonstration of the technical feasibility of the new linear collider concept which is a critical step toward future extension of electron-positron reaction energies in a cost effective way beyond the maximum that is practical with circular colliders such as PEP and LEP. In addition, when completed in 1986, the SLC will be the first electron-positron colliding beam system in the world capable of achieving an energy of 100 GeV in the center-of-mass system and, as a consequence, should be capable of producing copious quantities of the recently discovered Intermediate Vector Boson (Z^0), one of the carriers of the electroweak force. The study of the Z^0 is one of the major and most exciting areas of physics research indicated by present theories. The project benefits in a major way from the use of the existing 2-mile linac and supporting facilities. The estimated TEC for the project remains at $112,000,000 and the estimated completion date the end of FY 1986. The $60,500,000 requested in FY 1985 will allow completion of the beam line enclosures, progress on other conventional facilities and procurement of many of the technical components. Additional details are provided in the construction project data sheet.

Accelerator Improvement Projects

A total of $10,000,000 is required for Accelerator Improvement Projects (AIP), to be distributed as follows: Fermilab ($5,300,000); BNL ($2,000,000); and SLAC ($2,700,000). AIP funds are required on an annual basis to provide essential modifications and upgrades of the existing accelerators and colliding beam facilities in order to maintain their scientific effectiveness and to improve their operating economy and efficiency. For an annual cost much less than 1% of the U.S. Government's total capital investment in these facilities, AIP funds provide necessary improvements to enhance scientific performance, reliability and efficiency of operation, and to avoid early obsolescence. It is frequently necessary to provide new or modified research capabilities on short notice in order to accommodate the varying needs of high priority experiments. These changes are often required on a time scale much shorter than the normal, two-three year Federal budget cycle. AIP funds are essential to permit the rapid and flexible response essential to meet the most urgent of such needs.

There are special needs for AIP funds at Fermilab because of the very large scale and scope of the superconducting Energy Saver/Tevatron accelerator and its extended cryogenics facilities, experimental facilities and beam lines, and because of the need to adjust to the new 1000 GeV capabilities being brought into final operation for research. Additional details on the AIP needs at each of the three accelerator facilities are provided in the construction project data sheet.

General Plant Projects

General Plant Projects (GPP) funds are for maintenance, modification, and improvement of the general laboratory plant at BNL, Fermilab and SLAC. GPP funds are required for projects such as service utilities, support buildings, roads, shops, etc., and, although small compared to the capitalized value of the plant, are essential to keeping it in good and viable operating condition. The FY 1985 request totals $10,200,000 for GPP at the following laboratories: Fermilab ($3,000,000), BNL ($5,700,000), and SLAC ($1,500,000). There is a major increase to meet serious needs at BNL where the High Energy Physics Program provides all of the GPP funding needs for the needs of this multipurpose laboratory. Additional details are provided in the construction project data sheet entitled, "General Plant Projects, Various Locations (Project No. 85-R-101)."

	FY 1983	FY 1984	FY 1985 Request
High Energy Technology			
Operating Expenses	$90,100	$ 82,000	$ 91,800

Forefront experiments in high energy physics require the largest, most complex and advanced research facilities that mankind has ever built. The extent of the physical world which can be explored by these facilities is frequently determined by the limits of available technology. Since advances in high energy physics research proceed at a rapid pace and the development of applicable supporting technology must proceed not only in response to the needs of the research but also in anticipation of them, the DOE program in High Energy Physics supports a broad subprogram in advanced technology R&D. This subprogram has the specific goals of providing the technological base for improving the scientific effectiveness, reliability, and efficiency of existing facilities on a day-to-day basis and for extending the scientific capability of experimental high energy physics research in a cost effective manner through the design and construction of advanced facilities. As a byproduct, work carried out under the advanced technology R&D program frequently pushes forward or opens up new technological frontiers.

In order to sustain an effective advanced technology R&D program which is both responsive to and stimulates the basic physics research, it is necessary to: a) pursue a vigorous theoretical research effort into the physics and engineering principles underlying the concepts and operation of the instrumentation, detectors and accelerators; b) conduct forefront research and development in selected, promising areas of applicable technology; c) develop and prove emerging new ideas and concepts; and d) transform these ideas and concepts into the devices and techniques to be used in the physics research.

The High Energy Technology activity is subdivided into two major areas: accelerator R&D and experimental facility R&D. These reflect the two functional roles of instrumentation supporting high energy physics. Accelerator R&D provides new concepts and techniques for accelerating particle beams which form the technological basis for improving the performance of accelerators and enhancing their capability. Experimental facility R&D develops the highly sophisticated apparatus that measures, records and analyzes the phenomena resulting from the interactions of the particle beams with matter. A strong program of advanced technology R&D properly balanced between the two subactivities is essential for the continued progress and vitality of the basic research effort in high energy physics and for ensuring that the optimum research capability and productivity are achieved.

Accelerator R&D is concerned with the science and technology fundamental to accelerators, colliding beam systems, and beam transport systems. Its goal is to develop new and improved concepts, techniques and devices of direct application to the acceleration, storage, and transport of particle beams to be used for probing the innermost depths of matter and energy. The end products are particle beams of higher energy, increased intensity, longer stored lifetime, greater brightness (more particles per unit transverse beam area), and greater diversity.

Experimental facility R&D is concerned with the targets, secondary beam transport systems, detection apparatus, and data processing systems directly involved in the physics experiments. It focuses on developing new and improved means for generating, splitting, and transporting secondary particle beams; on inventing new types of instrumentation required for detecting and studying the characteristics of particle interactions produced in experiments; and on devising advanced processing techniques for the collection and analysis of data gathered in experiments.

While the purpose and thrust of the technology R&D subprogram is to ensure and extend the technology base vital to the progress of high energy physics research, the results of the advanced R&D effort frequently find critical application in other scientific and engineering disciplines. The following examples illustrate a few of the beneficial spin-offs from technology supported primarily for the furtherance of high energy physics research.

The two mile electron linear accelerator at SLAC is wholly dependent on the efficient and reliable operation of narrow band klystron tubes which act as very high power radiofrequency amplifiers to provide the time varying voltage pulses that accelerate electrons to 30 GeV. Consequently, SLAC has become a leading center of expertise for this highly specialized technology. As another example, nuclear medicine and cancer diagnostic and therapy work have drawn frequently on particle detection techniques and on experts in high energy physics to produce instrumentation that is more effective, safer, more accurate, and reliable. Recent examples are Computer Assisted Tomography (CAT) scanning and Nuclear Magnetic Resonance (NMR) imaging techniques. Standardized electronics instrumentation systems have also been developed which have been accepted on a worldwide basis both inside and outside high energy physics. Examples of such standardized electronics systems include CAMAC and the recently developed FASTBUS.

The technology R&D effort is concentrated primarily at the five DOE supported national laboratories; however, a small but significant part is also carried out at universities and industrial firms. The FY 1985 request of $91,800,000 would provide a strong R&D effort at SLAC in support of linear collider development and preliminary R&D for the

SSC. A natural reduction in effort is planned for Fermilab as its Tevatron program approaches completion. Also included in this category is the $3,812,000 assessment for the SBIR program. The following table summarizes the funding requests for the Technology R&D Subprogram.

High Energy Technology	FY 1984 Appropriation	FY 1985 Request
Fermi National Accelerator Laboratory	$ 28,000	$ 26,000
Brookhaven National Laboratory	20,100	21,200
Stanford Linear Accelerator Center	15,000	16,700
Argonne National Laboratory	1,200	1,400
Lawrence Berkeley Laboratory	7,100	7,500
Other	10,600	19,000
	$ 82,000*	$ 91,800**

* Distribution by contractor includes allocation of $19,000,000 for preliminary R&D for SSC.

**The indicated allocation of funding to contractors includes a tentative assignment of program responsibilities and allocation of $20,000,000 in R&D resources for the SSC in FY 1985. This distribution is subject to modification pending R&D results in FY 1984 and decisions to be made in FY 1985.

Fermi National Accelerator Laboratory

A total of $26,000,000 is required by Fermilab in FY 1985 for technology R&D compared to $28,000,000 in FY 1984. Accelerator R&D needs for Fermilab facilities are decreasing in FY 1985 as the Tevatron I construction nears completion and final elements of Tevatron II are brought into operation. Of the FY 1985 request, $18,500,000 is for accelerator R&D and $7,500,000 is for experimental facilities R&D.

A major focus of the accelerator R&D program will be work in support of the completion of Tevatron I. Substantial effort is needed for continued studies to optimize the performance of stochastic cooling systems required to obtain an intense source of antiprotons, including the installation and testing of hardware for the accumulator ring, and studies of antiproton production and collection techniques to ensure the optimal performance of the facility.

In FY 1985, the R&D associated with the effort to improve the performance of the base accelerator complex will include studies of methods for enhancing the accelerated beam intensity and stability in the superconducting ring, and will address any technical difficulties which might arise in the early period of operation. R&D studies will also be pursued on the performance of superconducting magnets in a high radiation environment and on beam stability in a cold vacuum system. Theoretical and experimental studies which directly impact the performance of the colliding beams for Tevatron I and the extracted beams for Tevatron II will continue in order to improve the understanding of the basic accelerator physics of the superconducting ring.

The Fermilab effort on SSC R&D in FY 1985 is expected to be about $4,000,000. This program will focus primarily on the development and evaluation of 5-6 T superconducting magnets using NbTi conductor in a design which places two coils in a single cryostat (2-in-1 design) using magnetically unlinked iron. Also included will be studies of accelerator design, beam dynamics, and other technical systems critically coupled to the superconducting magnets.

In the experimental facilities R&D program, as Fermilab begins to exploit the 1000 GeV research capability made available by Tevatron II, there will be continuing work on the development of higher performance beam transport, targeting and beam splitting apparatus and on improved particle detectors for experiments to effectively utilize the higher energy fixed target research capabilities. Research and development in support of the detectors for Tevatron I colliding beam experiments will continue in FY 1985.

Brookhaven National Laboratory

The FY 1985 request includes $21,200,000 for technology R&D at BNL, compared to $20,100,000 in FY 1984. This includes $17,500,000, for accelerator R&D and $3,700,000 for experimental facilities R&D.

The accelerator R&D will include efforts to maintain the operating effectiveness and to improve the scientific capability of the AGS. This will include studies directed toward achieving a major increase in AGS accelerated beam intensity and improvements to the polarized beam capability.

The BNL effort on SSC R&D in FY 1985 is expected to be about $9,000,000. This program will focus on development and evaluation of Nb_3Sn conductor suitable for very high field superconducting magnets (greater than or equal to 8T) and of superconducting magnets which use the 2-in-1 design with magnetically linked iron. BNL will also collaborate with LBL on its development of 5-6T superconducting magnets using improved NbTi conductor in a 2-in-1 design using magnetically linked iron. The program is also expected to include associated studies of cryogenic systems and accelerator physics.

The experimental facilities R&D will focus on new detector and beam line developments aimed primarily at improving the unique capabilities of the AGS for polarized beam experiments, low energy neutrino studies and rare kaon processes.

Stanford Linear Accelerator Center

A total of $16,700,000 is required for FY 1985 for technology R&D at SLAC, compared to $15,000,000 in FY 1984. Of this amount, $12,900,000 is for support of accelerator R&D and $3,800,000 is for experimental facility R&D. In FY 1985, a major part ($7,000,000) of the accelerator R&D at SLAC will be used for work in support of the SLC construction effort. There will also be work on development of advanced aspects of the linear collider concept. The balance of the R&D funds will be directed toward improvements in performance, reliability, and operating efficiency of the linear accelerator and the SPEAR and PEP colliding beam devices.

The FY 1985 accelerator R&D studies will bear heavily on issues connected with the SLC, which requires accelerating very intense micron-sized pulses of electrons and positrons simultaneously in the linear accelerator, and then bring them into collision in a manner that would provide very high interaction energies and luminosities. Special areas of study include developments to increase the energy of the linear accelerator; methods for enhancing positron beam intensity; problems of stability of high current micron-sized beam pulses in the linear accelerator during acceleration; beam transport in the two semi-circular arcs of magnets to be used to bring the electrons and positrons into head-on collision; and methods to control the collisions of the very high intensity micron-sized electron and positron pulses.

Ancillary R&D activities at SLAC will include development of higher gradient accelerating structures, development of very high power pulsed klystrons, theoretical and experimental studies of new and advanced concepts of linear accelerator systems, development of sophisticated beam instrumentation and control devices, and development of special new beam transport systems.

Experimental facility R&D at SLAC in FY 1985 will be directed primarily toward design of advanced detectors for future experiments at the SLC and PEP. Some R&D supporting continued research on the SPEAR electron-positron storage ring, and on development of underlying detector technologies are also included.

Lawrence Berkeley Laboratory

A total of $7,500,000 is required in FY 1985 for technology R&D at LBL, compared to $7,100,000 in FY 1984. Of this amount, $5,600,000 is to be used to support advanced accelerator R&D, which consists predominantly of R&D related to the SSC and collaborative studies with Fermilab and others on stochastic cooling techniques and development of beam cooling hardware to be used in the Fermilab Tevatron I project. The LBL accelerator R&D program also includes work in support of aspects of the PEP and SLC facilities at SLAC.

The LBL effort on SSC R&D in FY 1985 is expected to be about $2,000,000. This program will focus on the development and evaluation of 5-6T superconducting magnets using improved NbTi conductor in a 2-in-1 design with magnetically linked iron. (This effort is in collaboration with BNL and makes use of the magnet fabrication facilities at BNL.) The program will also include participation in accelerator design and beam dynamics studies.

The experimental facilities R&D request of $1,900,000 is required to support experimental facilities R&D at LBL in FY 1985. R&D tasks covered include development of a new hadron calorimeter for a major proton-antiproton experiment at Fermilab; studies of advanced detectors for use with linear colliders in collaboration with SLAC; work to improve the performance of experimental apparatus at SLAC/PEP and Fermilab; and long range instrumentation and detector development.

Argonne National Laboratory

A total of $1,400,000 is required for High Energy Technology for ANL for FY 1985, compared to $1,200,000 in FY 1984. Of that amount, $600,000 is for accelerator R&D and $800,000 is for experimental facilities R&D.

The high energy accelerator R&D at ANL for FY 1985 is expected to be directed primarily towards collaborative work with Fermilab on design and development for the Tevatron I proton-antiproton capability, including particle cooling techniques and beam transport and on studies of advanced accelerator concepts.

Experimental facilities R&D is expected to concentrate on research and development for new types of particle detectors; further improvements to the High Resolution Spectrometer at PEP; contributions to the colliding beam detector for the Fermilab Tevatron I project; and the development of new types of polarized targets.

Other Advanced Technology Program

In FY 1985, $19,000,000 is requested to support programs in advanced technology R&D in universities and industry and the portions of the SSC R&D not described previously.

The work carried out in universities and industry under this part of the technology R&D subprogram will require $10,184,000. This program is expected to include contracts with about 20 institutions in FY 1984. The work covers a very broad range of topics including instrumentation standards, new particle detector concepts, theoretical studies in charged particle beam dynamics, and new accelerator concepts. In recent years a significant part of this effort has been directed at basic studies related to new accelerator concepts. The need to develop new accelerator techniques, derives from the need to optimize the cost of large, modern accelerator and colliding beam facilities. While there are no known physics or technology reasons why present acceleration techniques can't be pushed to much higher energies than any now contemplated, the size and associated cost produce severe constraints. Because of this, resources are being

directed toward discovering and developing new concepts of charged particle acceleration that are more cost effective and give higher final particle energies in a device that is smaller and more energy efficient than existing devices. Representative lines of research include collective methods of particle acceleration, laser acceleration of electrons, theories of nonlinear dynamics, collective effect and space charge induced phenomena, very high frequency and high power radio frequency sources, and very high field superconducting magnets. A major effort in this area is critical for providing the required future HEP facility capabilities in a cost effective manner, and is essential for the U.S. to remain competitve on a world basis in this frontier field of research.

Included in the Other Advanced Technology Program is $5,000,000 for SSC R&D. This covers the funding for participants other than the three major DOE laboratories already discussed and for the technical and management activities of the SSC R&D center. It also includes funding not yet allocated to specific participants pending results of FY 1984 R&D and decisions to be made during FY 1985. The R&D program is presently pursuing four superconducting magnet approaches. Two of these options will be eliminated during FY 1985 and efforts concentrated on the two remaining options. The work being pursued outside of BNL, Fermilab, and LBL is expected to include the study of the superferric magnet option by a consortium with participants from Texas A&M, University of Texas, Rice University, University of Houston Area Research Center, University of Wisconsin, Argonne National Laboratory, Brookhaven National Laboratory, and Lawrence Berkeley Laboratory; and accelerator design efforts at Argonne National Laboratory.

Management Initiative

This decision unit reflects $-4,000,000 for savings resulting from management initiatives in the areas of administrative systems and administrative processes/field organizations.

DEPARTMENT OF ENERGY
1985 CONGRESSIONAL BUDGET REQUEST
CONSTRUCTION PROJECT DATA SHEETS
GENERAL SCIENCE AND RESEARCH - PLANT AND CAPITAL EQUIPMENT
GENERAL SCIENCE AND RESEARCH
HIGH ENERGY PHYSICS
(Tabular dollars in thousands. Narrative material in whole dollars.)

1. Title and location of project: Accelerator improvements and modifications, various locations

2. Project No.: 85-R-100

3. Date A-E work initiated: 1st Qtr. FY 1985

3a. Date physical construction starts: 3rd Qtr. FY 1985

4. Date Construction ends: 2nd Qtr. FY 1987

5. Previous cost Estimate: none
Less amount for PE&D: none
Net cost estimate: none
Date:

6. Current cost estimate: $10,000
Less amount for PE&D: 0
Net cost estimate: $10,000
Date: 5/83

7. Financial Schedule

Fiscal Year	Authorization	Appropriations	Obligations	Costs
1985	$10,000	$10,000	$10,000	$ 6,000
1986	0	0	0	3,500
1987	0	0	0	500

8. Brief Physical Description of Project

The following are examples of the major items of work to be performed at the various locations:

Brookhaven National Laboratory..... $2,000,000

Funds are requested for modifications, improvements and additions to the Alternating Gradient Synchrotron (AGS) and its related experimental facilities. Items planned include: replacement of the present flywheel and uninterruptible power source with a modern solid state supply ($200,000); addition of an accumulator ring between the linac and AGS to improve polarized proton beam intensity ($1,400,000); consolidation of three control rooms and provision for new computer hardware to improve utilization of operating personnel ($400,000).

1. Title and location of project: Accelerator improvements and modifications, various locations

2. Project No.: 85-R-100

8. Brief Physical Description of Project (continued)

Fermi National Accelerator Laboratory..... $5,300,000

Funds requested are for modifications, improvements and additions to the Fermilab accelerator facilities (which includes the linear accelerator, booster synchrotron, main ring, and energy saver ring) and to the switchyard, beam lines, target facilities and experimental areas.

Modifications to the accelerator facilities are expected to include: accelerator control computer improvements, including faster computers and increased capacity to improve monitoring and control of beam parameters throughout the complex of accelerators ($850,000); modifications to correction package spoolpieces to improve beam intensity in the Saver and improve extraction efficiency and reliability ($550,000); power supply and quench protection improvements ($450,000); installation of superconducting magnets with higher quench currents at selected locations in the lattice ($500,000); higher current power feedcans and power spools to permit operation with longer flattop on the magnet cycle ($200,000); and implementation of second generation process control systems, expansion of helium liquefaction and refrigeration capacity and improved cryogenic feed systems to increase reliability and operational stability ($650,000).

Modifications to the experimental facilities are expected to include: installation of additional refrigeration capacity in the experimental areas to serve the additional superconducting beam line and analyzing magnets ($500,000); replacement of low conductivity water heat exchangers ($600,000); enhanced earth berms and other shielding to maintain acceptable radiation levels with higher energy operation ($300,000); modifications of experimental area structures to accommodate special purpose beamline equipment ($600,000); and, enhancements to experimental area control systems to increase diagnostic capability, reliability and responsiveness ($100,000).

Stanford Linear Accelerator Center (SLAC)..... $2,700,000

Funds are requested for modifications, improvements and additions to the SLAC linear accelerator, to the SPEAR and PEP colliding beam facilities, and to the associated experimental facilities. Items now planned for FY 1985 include: linac control improvements to include upgrade of the linac instrumentation, RF system and beam line components in sectors 11 through 20 to handle highly confined very intense beam pulses ($2,200,000); upgrade of PEP control system with new microprocessors ($300,000); installation of new beam diagnostic instrumentation (beam position, current and profile monitors and emittance measuring components) to provide for suitable transport of beam pulses for colliding beam operations ($200,000). This subproject will be constructed at the Stanford Linear Accelerator Center on non-Government owned property.

CONSTRUCTION PROJECT DATA SHEETS

1. Title and location of project: Accelerator improvements and modifications, various locations

2. Project No.: 85-R-100

9. Purpose, Justification of Need for, and Scope of Project

Accelerator improvements are essential on an annual basis to maintaining the short term operating efficiency and reliability, and the research flexibility of the high energy accelerators, colliding beam systems and related experimental facilities, thereby maintaining or enhancing their level of scientific effectiveness and productivity. Research advances and facility requirements in high energy physics occur at a rapid pace; further, each research facility is a unique assemblage of very specialized, high technology components. Consequently, there is a continuing need to modify facilities frequently on a short time scale in response to research needs and to respond to problems that can affect the reliability, efficiency and economy of operation on a time scale shorter than the normal two-year budget cycle. The requested accelerator improvements and modifications will provide greater flexibility for experimental setups during operations. By capitalizing upon the ability to operate at increased performance level and by increasing serviceability and, thereby decreasing facility downtime, they will improve the productivity, and scientific effectiveness and cost effectiveness of the U.S. program in High Energy Physics.

Since needs and priorities may change, other subprojects may be substituted for those listed and some of these may be located on non-Government owned property.

10. Details of Cost Estimate

a. Engineering, design and inspection and component assembly and installation	$10,000
Total Estimated Cost	$10,000

The estimated costs of specific sub-projects are preliminary and, in general, indicate the magnitude of each program.

11. Method of Performance

Design will be by contractor staff. To the extent feasible, construction and procurement will be accomplished by fixed-price subcontracts awarded on the basis of competitive bidding.

GENERAL SCIENCE AND RESEARCH
HIGH ENERGY PHYSICS
(Tabular dollars in thousands. Narrative material in whole dollars.)

1. Title and location of project: General Plant projects, various locations

2. Project No.: 85-R-101

3. Date A-E work initiated: 1st Qtr. FY 1985

3a. Date physical construction starts: 2nd Qtr. FY 1985

4. Date Construction ends: 2nd Qtr. FY 1987

5. Previous cost Estimate: none
Date: none

6. Current cost estimate: $10,200
Less amount for PE&D: 0
Net cost estimate: $10,200
Date: May 1983

7. Financial Schedule

Fiscal Year	Obligations	Costs FY 1983	FY 1984	FY 1985	After FY 1985
Prior Year Projects	XXXXXXX	$ 2,688	$ 2,200	$ 0	$ 0
1983	6,500	2,338	2,600	1,562	0
1984	7,000	0	1,900	2,800	2,300
1985	10,200	0	0	2,800	7,400
		$ 5,026	$ 6,700	$ 7,162	$ 9,700

8. Brief Physical Description of Project

The following are examples of the major items of work to be performed at the various locations:

Brookhaven National Laboratory $5,700,000

Requirements include: Additional building required to house a 2nd Neutrino Oscillation Experimental Facility ($400,000); installation of automatic duplex strainers and a water treatment system on three cooling towers serving the Alternating Gradient Synchrotron (AGS) Linac, and development facility to eliminate sludge contamination, electrolytic corrosion and reduce scale in the systems ($300,000); additional building space for Biology ($300,000); building alterations at the Central Scientific Computer Facility required for installation of a new class V computer system ($350,000); building additions for NSLS ($300,000); power improvements to provide an additional 5 MW of power

1. Title and location of project: General plant projects, various locations 2. Project No.: 85-R-101

8. Brief Physical Description of Project (continued)

for the installation of new experimental areas at the AGS ($400,000); a new accumulator tunnel to connect the existing 200 MeV Linac with the former 50 MeV Linac building and house the accumulator ring equipment ($550,000); experimental building to provide for expansion of the I-10 Test Beam Facility at the AGS ($250,000); building alterations and expansion to provide a facility for coal-water slurry technology and cleaning ($300,000); upgrade cooling tower system to provide more efficient energy, equipment and system utilization ($350,000); construct a new assembly building to house the neutrino power supply controls ($150,000); provide addition to an existing office building for Nuclear Energy Program expansion ($150,000); construct a second 13.8 KV electric feeder to serve as an alternate power source for the LINAC ($300,000); addition of a second floor to provide additional office space for the Center of Structural Biology research ($250,000); construct radiation storage building to store all the high radiation equipment and experimental devices for the AGS ($300,000); provide addition at the NSLS facility to serve as a target room for development of the high-energy gamma-ray beam ($350,000); addition to the Physics building to provide additional office and conference room space for visiting scientists working in the various AGS and NSLS program areas ($250,000); and miscellaneous smaller projects ($450,000).

Fermi National Accelerator Laboratory $3,000,000

Requirements include: specialized parts storage facility ($200,000); additions to service buildings and improvements to the utility corridor around the main ring to facilitate maintenance ($500,000); additional feeders and switchgear for improved reliability and recovery in event of local or extended power failure ($700,000); upgrade of refrigeration power and cooling water systems to improve stability and reliability of operations ($500,000); additional office and light laboratory space ($200,000); experimental area electric power distribution improvements ($200,000); repair of existing buildings in Village area ($250,000); gas and flammable liquid storage facility ($150,000); additions to receiving and storage facility, and interconnection of industrial buildings ($300,000).

Stanford Linear Accelerator Center $1,500,000

Requirements include: additional pumps, heat exchangers and a cooling tower to increase capacity of PEP LCW system ($700,000); third floor addition to central laboratory annex ($700,000); additional storage space for cafeteria and auditorium ($50,000); and a new air compressor and dryer installation for PEP-2 region ($50,000). This subproject will be constructed at the Stanford Linear Accelerator Center on non-Government owned property.

CONSTRUCTION PROJECT DATA SHEETS

1. Title and location of project: General plant projects, various locations 2. Project No.: 85-R-101

9. Purpose, Justification of Need for, and Scope of Project

General plant projects are required for the general maintenance, modification and improvement of the overall laboratory plant and include minor new construction, capital alterations and additions, and improvements to buildings and utility systems. These are short-term projects whose timely accomplishment is essential for maintaining the productivity, increasing the operational cost effectiveness, and ensuring that necessary support services are available to the research program at the DOE-owned facilities. Since it is difficult to detail the most urgently needed items in advance, a continuing evaluation of requirements and priorities may result in additions, deletions, and changes to the currently planned subprojects. No significant R&D program is anticipated as a prerequisite for design and construction of the subprojects under consideration.

The funds requested for FY 1985 are estimated as follows:

Brookhaven National Laboratory	$ 5,700
Fermi National Accelerator Laboratory	3,000
Stanford Linear Accelerator Center	1,500
Total Estimated Cost	$10,200

Since needs and priorities may change, other subprojects may be substituted for those listed and some of these may be located on non-Government owned property.

10. Details of Cost Estimate

See description, item 8. The estimated costs are preliminary and, in general, indicate the magnitude of each program. These costs include engineering, design and inspection.

11. Method of Performance

Design will be by contractor staff or on the basis of negotiated architect-engineer contracts. To the extent feasible, construction and procurement will be accomplished by firm fixed-price contracts and subcontracts on the basis of competitive bidding.

DEPARTMENT OF ENERGY
1985 CONGRESSIONAL BUDGET SUBMISSION
CONSTRUCTION PROJECT DATA SHEETS
GENERAL SCIENCE AND RESEARCH - PLANT AND CAPITAL EQUIPMENT
GENERAL SCIENCE AND RESEARCH
HIGH ENERGY PHYSICS
(Tabular dollars in thousands. Narrative material in whole dollars.)

1. Title and location of project: Stanford Linear Collider (SLC)
Stanford Linear Accelerator Center (SLAC)
Stanford, CA

2. Project No. 84-ER-133

3. Date PE&D initiated: 2nd Qtr. FY 1980

3a. Date physical construction starts: 1st Qtr. FY 1984

4. Date Construction ends: 4th Qtr. FY 1986

5. Previous cost estimate: $113,957,000
Less amount for PE&D: 1,957,000
Net cost estimate: $112,000,000
Date: May 1982

6. Current cost estimate: $114,272,000
Less amount for PE&D: 2,272,000
Net cost estimate: $112,000,000
Date: October 1983

7. Financial Schedule:

Fiscal Year	Authorizations	Appropriations	Obligations	Costs
1984	$ 32,000	$ 32,000	$ 32,000	$ 23,000
1985	60,500	60,500	60,500	52,000
1986	19,500	19,500	19,500	37,000
Total	$112,000	$112,000	$112,000	$112,000

8. Brief Physical Description of Project

The SLAC Linear Collider (SLC) is a new type of electron-positron colliding beam facility which is an important step toward reducing the cost of very high energy colliding beam devices for extending the upper limit in energy above that which is at present technically and fiscally feasible. The SLC will be constructed on non-government owned property at the Stanford Linear Accelerator Center (SLAC) which is located on Stanford University property. Its operation is based on the acceleration of an intense positron bunch and an intense electron bunch to energies of approximately 50 GeV each. At the end of the linac, the two bunches are injected in opposite directions into two arcs of magnets, arriving at a collision point where an effective interaction energy of approximately 100 GeV is achieved. After the collision, the particles are disposed of and not used again. Because the beam is used only once, the magnets in the ring can have small aperture and, hence, low cost. Compared to storage rings, the single pass collider system operates at a relatively low repetition rate (180 Hz in the system proposed here) but makes up for the low collision frequency by the extremely high current densities which can be tolerated at the collision point.

1. Title and location of project: Stanford Linear Collider (SLC)
Stanford Linear Accelerator Center (SLAC)
Stanford, CA

2. Project No. 84-ER-133

8. Brief Physical Description of Project (continued)

The main components of the SLC are the energy upgrade of the SLAC linac; a transport system from the end of the linac to the small aperture magnet arcs; the magnet arcs themselves which includes the special focusing systems required near the interaction point; the necessary beam housing; an experimental hall and staging area; a high power positron production target; a positron booster; a transport system from the positron target at the 2/3rd point of the linac back to the injection end of the linac; a new high peak current electron gun; two small storage rings to reduce the emittances of the electron and positron beams by radiation damping; pulse compressors to reduce the length of the bunches in the storage rings before injection back into the linac; and the necessary instrumentation and control systems for both the linac and the collider system.

Since the SLC involves a new type of colliding beam system, its operation and the function of the various components are described below. A bunch of positrons containing approximately 5×10^{10} particles is injected into the SLAC linac. The SLAC linac is to be upgraded as part of this project to give a final energy of approximatley 50 GeV. A single intense electron bunch, also of 5×10^{10} particles, is injected into the linac approximatley 20 meters behind the positron bunch. A second electron bunch is injected behind the first intense electron pulse. This second electron bunch is used for the production of a new positron bunch. The first two bunches are accelerated in the linac to an energy of about 50 GeV. At the end of the linac a splitter takes the leading intense positron and electron bunches and starts them around the final arcs in opposite directions. After each bunch travels halfway around the ring, they come to the collision area where a collection of special lenses focuses the beams to spots of about 2 micron radius at the collision point. After the beams pass through each other at the collision point they are disposed of and not used again.

The second electron bunch, which travels down the linac behind the intense electron-positron bunches is deflected out of the linac at the 2/3rd point and is directed onto a positron production target. Positrons from this production target are boosted to an energy of around 0.2 GeV by a short section of linac and transported back to the injector end of the main linac. There they are boosted to an energy of approximately 1.2 GeV and put into a damping ring. In the damping ring the size of the beam decreases by synchrotron radiation damping to the appropriate value for re-injection into the main linac. The damping time will be longer than the approximately 5 milliseconds between pulses of the collider system and, therefore, this ring must store two bunches of positrons. The bunch which has been stored for the longest time is the one which is ejected from the damping ring and injected into the linac for the next pulse. The electron gun is pulsed slightly later than the time at which the positron beam arrives at the injector. The first 100 meter section of the linac accelerates both electron bunches to 1.2 GeV for insertion into the electron damping ring. At the time of the next main linac pulse, the electron and positron bunches are ejected from their damping rings, compressed to a bunch length of 1 to 2 mm and injected into the linac. The cycle repeats at 180 Hz.

CONSTRUCTION PROJECT DATA SHEETS

1. Title and location of project: Stanford Linear Collider (SLC)
Stanford Linear Accelerator Center (SLAC)
Stanford, CA

2. Project No. 84-ER-133

9. Purpose, Justifictaion of Need for, and Scope of Project

The SLC has two goals. First, it will develop and serve as the first test of a new colliding beam technique, which is a critical step toward achieving electron-positron collisions at much higher center-of-mass energies at lower cost per GeV than the technology used up to now -- that of the Colliding Beam Storage Rings (CBSR); and second, the SLC will increase the center-of-mass energy available for physics experiments with the electron-positron system by a factor of about three above that now available at existing electron positron CBSR's. The lower cost of the SLC itself is achieved by virtue of the fact that it uses the existing 2-mile linac.

The highest energy electron-positron colliding beam storage rings now in existence are the PEP Project at Stanford and PETRA at Hamburg, West Germany with center-of-mass energy of around 30-40 GeV. The next step in circular colliders is the LEP machine, now being built by CERN physicists and engineers, which will achieve a maximum center-of-mass energy of about 100 GeV initially with conventional radio frequency (RF) and perhaps as high as 240 GeV with superconducting RF, if that technique should prove practical. The version with conventional RF is estimated to cost about 1,000 million Swiss Francs in 1981 value not including labor costs.

In order to make use of the single existing linac at SLAC, the SLC has two arcs of magnets to guide the bunches from the linac to the collision point. At the planned 50 GeV energy level the synchrotron radiation emitted in these magnets has a negligible effect on the total power required to operate the facility, while allowing the facility to be based on a single linac rather than two linacs. This project will not only pioneer a new accelerator technology which promises to reduce costs for future generation of e+e machines, but will also contribute to a better under standing of the physical world through the experiments to be done using it.

From recent research, a new theoretical concept has emerged which interprets both the weak and electromagnetic forces as different manifestations of one basic force. This concept is known as the gauge theory, the simplest form of which is the "standard model" of Weinberg and Salam. All of the variants of the gauge theory have one or more heavy particles which interact with the electron-positron system in the same basic way as does the ordinary zero mass photon. It is the interaction of this heavy guage particle (a^0) and its charged companions (w^+ and w^-) that is responsible for the properties of what is called the weak interaction. The gauge theories have had such success in explaining apparently unrelated facts that they are generally believed to be correct.

1. Title and location of project: Stanford Linear Collider (SLC)
Stanford Linear Accelerator Center (SLAC)
Stanford, CA

2. Project No. 84-ER-133

9. Purpose, Justification of Need for, and Scope of Project (continued)

The SLC is designed to have a total energy large enough to copiously produce the neutral gauge particles, resulting in many hundreds of events per hour. The decay of these Z^0's into quarks, leptons, and perhaps other more exotic particles, will give a vast amount of information about a broad spectrum of basic physics questions ranging from the number of elementary building blocks which make up our world, to the possible relation of the strong interaction to the weak and the electromagnetic to the conditions in the early universe when it was only a few seconds old. The first evidence for the gauge particles has been found at the CERN antiproton-proton collider, but experiments on this and similar machines can give only a small fraction of the important detailed information which can only be obtained from an electron-positron machine.

Funds for detection apparatus to be used for high energy physics experiments with the SLC will be included in the capital equipment budget. Equipment funds will be used to upgrade an existing detector (Mark II) previously used for lower energy experiments at PEP and to initiate work on a second detector.

10. Details of Cost Estimate

	Item	Total Cost
A. ED&I (Excludes previously funded Plant Engineering & Design ED&I) @ 18% of construction costs, item B.		$ 14,100
B. Construction Cost:		$ 77,200
1. Site Work, Utilities, and Structures including a) Experimental Hall; b) Collider Housing, and c) Linac-Collider Connection Tunnels.....	23,900	
2. Accelerator components: a) Electron and Positron Sources; b) Energy Upgrade; c) Collider Arcs; and d) Focusing, Damping and Control Systems	53,300	
C. Standard Equipment (Cranes)		$ 400
D. Contingency @ approximately 22% of above cost		20,300
E. Total		$112,000

CONSTRUCTION PROJECT DATA SHEETS

1. Title and location of project: Stanford Linear Collider (SLC)
Stanford Linear Accelerator Center (SLAC)
Stanford, CA

2. Project No. 84-ER-133

11. Method of Performance

Design of conventional facilities will be accomplished by subcontracts. Design of technical components will be by the operating contractor (SLAC). To the extent feasible, construction procurement and installation will be accomplished by fixed-price subcontracts awarded on the basis of competitive bidding.

12. Funding Schedule of Project Funding and Other Related Funding Requirements

	Prior Years	FY 1984	FY 1985	FY 1986	Total
A. Total Project Costs:					
1. Total Facility Costs:					
(a) Construction Line Item	$ 0	$23,000	$52,000	$37,000	$112,000
(b) PE&D	2,272	0	0	0	2,272
(c) Expense Funded Equipment	0	0	0	0	0
(d) Inventories	0	0	0	0	0
Total Direct Costs	2,272	23,000	52,000	37,000	114,272
2. Other Project Costs:					
(a) R&D Necessary to Complete Construction	0	9,700	7,500	5,300	22,500
(b) Other Project Related Costs:					
(1) R&D Related Capital Equipment & Plant	0	500	400	250	1,150
Total Other Project Funding	0	10,200	7,900	5,550	23,650
Total Project Costs (Items 1 & 2)	$ 2,272	$33,200	$59,900	$42,550	$137,922

CONSTRUCTION PROJECT DATA SHEETS

1. Title and location of project: Stanford Linear Collider (SLC)
Stanford Linear Accelerator Center (SLAC)
Stanford, CA

2. Project No. 84-ER-133

12. Funding Schedule of Project Funding and Other Related Funding Requirements

B. Other Related Annual Costs (Estimated life of project: 10 years)

1. Facility operating costs (including incremental power costs)	$ 9,600
2. Programmatic operating expenses directly related to the facility	5,200
3. Capital equipment not related to construction but related to the programmatic effort in the facility	500
4. GPP or other construction related to programmatic effort in the facility	400
Total related incremental annual costs in FY 1985 dollars	$15,700

13. Narrative Explanation of Total Project Funding and Other Related Funding Requirements

A. Total Facility

(a) Construction Line Item (no narrative required)

(b) PE&D - The SLC is a totally new kind of colliding beam system, and although the technology involved is well understood, the project has benefited immeasurably from Plant Engineering and Design (PE&D) funding to more firmly establish component costs and conventional facility costs and schedules. The project was provided with $300,000 of PE&D funding in FY 1980, $750,000 in FY 1981, $907,000 in FY 1982, and $315,000 in FY 1983. The FY 1980 PE&D money funded a preliminary geological study of the site, preliminary tunnel and experimental hall design, and the study of alternative site layouts. The FY 1981 PE&D funding was allocated to more detailed structural design (Title I) of the linac/collider and connecting tunnels. In June 1981, SLAC retained the services of Tudor Engineering as an A/E firm to perform Title I and Title II design on the SLC project. The FY 1982 and FY 1983 PE&D funding supported completion of Title I and partial Title II design for SLC conventional facilities.

1. Title and location of project: Stanford Linear Collider (SLC)
Stanford Linear Accelerator Center (SLAC)
Stanford, CA

2. Project No. 84-ER-133

13. Narrative Explanation of Total Project Funding and Other Related Funding Requirements (continued)

(c) Expense Funded Equipment - none anticipated for this project.

(d) Inventories - no inventories are anticipated for this project.

2. Other Project Funding

(a) R&D Necessary to Complete - funds provided in High Energy Physics Research, Accelerator Research and Development.

(b) Other Related Funding Provide the capital equipment and plant funding needed in support of the R&D effort.

B. Total Related Funding Requirements:

The programmatically useful lifetime of the facility is estimated to be about 10 years.

1. Facility operating costs include the incremental costs of accelerator operations, experimental area operations, and related research and development efforts. These costs are for salaries, electric power, materials and supplies, with the dominant cost element being the electric power charges.

2. Programmatic Operating Expenses Directly Related to the Facility - this estimate is for high energy physics research to be performed by SLAC in-house physicists or physicists from the user community.

3. Capital Equipment Related to the Programmatic Effort in the Facility - this estimate is for general capital equipment needed to support research at the facility. It will provide for research detector apparatus, data recording and analysis instrumentation and miscellaneous laboratory instruments. It does not provide for any major new detection system.

4. GPP or Other Construction Related to Programmatic Effort - this estimate is a general "level of effort" which would provide for minor structures and utility extensions for the research area, as well as modifications and improvements (AIP) of the facility to maintain its scientific effectiveness and productivity.

5. Other Costs - no narrative required.

DEPARTMENT OF ENERGY
1985 CONGRESSIONAL BUDGET REQUEST
CONSTRUCTION PROJECT DATA SHEETS
GENERAL SCIENCE AND RESEARCH - PLANT AND CAPITAL EQUIPMENT
GENERAL SCIENCE AND RESEARCH
HIGH ENERGY PHYSICS
(Tabular dollars in thousands. Narrative material in whole dollars.)

1. Title and location of project: Tevatron II, Fermi National Accelerator Laboratory, Batavia, Illinois

2. Project No.: 82-E-206

3. Date A-E work initiated: 2nd Qtr. FY 1982

3a. Date physical construction starts: 3rd Qtr. FY 1982

4. Date Construction ends: 4th Qtr. FY 1985

5. Previous cost estimate: $49,800
Less amount for PE&D: 800
Net cost estimate: $49,000
Date: 9/82

6. Current cost estimate: $49,800
Less amount for PE&D: 800
Net cost estimate: $49,000
Date: 7/83

7. Financial Schedule:

Fiscal Year	Authorization	Appropriations	Obligations	Costs
1982	$ 6,000	$ 6,000	$ 6,000	$ 2,439
1983	18,000	18,000	18,000	17,149
1984	13,000	13,000	13,000	16,500
1985	12,000	12,000	12,000	12,912

8. Brief Physical Description of Project

This project completes the program to upgrade Fermilab's accelerator and experimental facilities for 1000 GeV research capability. It provides necessary facilities for 1 TeV (1000 GeV) fixed target experimental program in existing areas to fully exploit the higher energy of the superconducting accelerator, the Tevatron. The element of this project are:

a) The construction of an extraction system for 1 TeV protons.

b) The upgrade of the external beam switchyard to 1 TeV and the provision for 1 TeV targeting in the present external experimental areas.

c) The construction of new secondary beam enclosures and support facilities in each external experimental area in order to exploit the fixed target physics opportunities of the Tevatron. Some of these new beam lines will replace existing beams.

CONSTRUCTION PROJECT DATA SHEETS

1. Title and location of project: Tevatron II, Fermi National Accelerator Laboratory, Batavia, Illinois 2. Project No.: 82-E-206

8. Brief Physical Description of Project (continued)

This project provides for the installation of the electrostatic septa, septum magnets, kicker magnets and other specialized components needed to extract the 1000 GeV protons into the beam branching switchyard. Provision will be made for slow resonant extraction (1 to 10 secs.) which is required for electronic detector systems and for the fast resonant extracted beam (1 to 3 milliseconds), which is preferred for neutrino experiments.

Additional septa, bending magnets, focusing magnets and ancillary components which are necessary to transport the 1 TeV protons to the three external experimental areas are also included. The target stations and experimental facilities of all three areas will be modified to optimize the handling of the 1 TeV proton beams and to exploit the unique physics opportunities they present. Ancillary storage and materials handling capability will be provided for the improvement of efficiency and flexibility in the conduct of experiments. The requisite secondary beam line equipment and experimental detectors will be provided through the capital equipment budget.

The Fermilab 1 TeV accelerator will provide a unique opportunity for producing secondary particle beams at higher energies and intensities than anywhere else in the world. The Tevatron fixed target program will give Fermilab international leadership in hadron physics for many years. It will be possible for scientists to use this facility to study many new phenomena involved in the fundamental interactions of matter. Study of these phenomena is at the heart of increasing our understanding of the most basic processes of matter. The components for the new secondary beam lines and the new and upgraded research detectors required to implement the initial Tevatron II research program will be acquired as capital equipment items during FY 1983 through FY 1985.

9. Purpose, Justification of Need for, and Scope of Project

The collisions of 1 TeV protons with nuclear targets will provide intense sources of muons, electrons, neutrinos, mesons, and baryons with which to study the emerging pictures of the weak, electromagnetic and strong interactions of the fundamental constituents of matter. In each of the three existing external experimental areas at Fermilab, many new research opportunities will be possible at 1 TeV. The gain in the event rate of energetic interactions, and the increased energy and intensity of the planned muon bem, will allow detailed measurements of the quark structure functions of protons and neutrons and sensitive tests of predictions of energy dependencies according to the theory of quantum chromodynamics. The careful measurement of high energy neutrino interactions will test the unified description of the weak and electromagnetic interactions of leptons, including the predicted damping of the total cross sections due to the intermediate vector boson.

CONSTRUCTION PROJECT DATA SHEETS

1. Title and location of project: Tevatron II, Fermi National Accelerator Laboratory, Batavia, Illinois 2. Project No.: 82-E-206

9. Purpose, Justification of Need for, and Scope of Project (continued)

The production and study of heavy quarks is greatly enhanced at higher energies. The combination of high energy and advanced detector technology makes it possible to study particle lifetimes as short as 10^{-13} seconds. The studies of the strong interaction dynamics of quarks will be enhanced by the increased energies available in hadronic interactions, as well as the improved duty cycle of the Tevatron which permits greater average secondary beam intensities. Better measurements of fundamental hadron properties, including those related to particle jets and polarization, can be made at higher energies. The increased fluxes open new domains in the study of high transverse momentum interactions. These studies of high transverse moments, which probe the structure of subnuclear matter at very small distances, will be crucial to the determination of the detailed dynamics of quarks and gluons. The Tevatron fixed target program can be expected to uncover new subnuclear phenomena.

10. Details of Cost Estimate:

	Item Cost	Total Cost
a. Engineering, design and inspection at approximately 18% of conventional construction costs (special facilities EDIA included in special facilities construction costs item b. 2)		$ 3,400
b. Construction costs:		42,100
1. Conventional Construction of Beam Enclosures, Laboratories, etc.	$19,200	
2. Special Facilities	22,900	
a. Switchyard Area Upgrade	6,100	
b. Meson Facilities Upgrade	6,000	
c. Neutrino Facilities Upgrade	6,000	
d. Proton Facilities Upgrade	4,800	
c. Contingency at approximately 8% of the above costs		3,500
Total Project Cost		$49,000

11. Method of Performance:

Design of facilities will be by the operating contractor and subcontractor as appropriate. To the extent feasible, construction, procurement and installation will be accomplished by fixed-price subcontracts awarded on the basis of competitive bidding.

CONSTRUCTION PROJECT DATA SHEETS

1. Title and location of project: Tevatron II, Fermi National Accelerator Laboratory, Batavia, Illinois

2. Project No.: 82-E-206

12. Funding Schedule of Project Funding and Other Related Funding Requirements

	Prior Years	FY 1982	FY 1983	FY 1984	FY 1985	Total
a. Total project funding						
1. Total Facility Costs						
a. Construction line item	$ 0	$ 2,439	$17,149	$16,500	$12,912	$49,000
b. PE&D	800	0	0	0	0	800
Total Facility Costs	$ 800	$ 2,439	$17,149	$16,500	$12,912	$49,800
2. Other Project Funding						
a. Direct R&D operating costs necessary to complete construction	3,672	3,505	2,759	2,835	2,194	14,965
b. Other project related costs	35	634	806	800	760	3,035
Total Other Project Funding	$3,707	$ 4,139	$ 3,565	$ 3,635	$ 2,954	$18,000
Total Project Funding (Items 1 & 2)	$4,507	$ 6,578	$20,714	$20,135	$15,866	$67,800

b. Total related incremental annual funding requirements (estimated life of project: 20 years)	
1. Facility operating costs	$ 2,000
2. Programmatic operating expenses directly related to the facility	3,000
3. Capital equipment not related to construction but related to the programmatic effort in the facility	4,000
4. GPP, AIP programmatic costs	1,000
Total Other Related Annual Funding Requirements	$10,000

CONSTRUCTION PROJECT DATA SHEETS

1. Title and location of project: Tevatron II, Fermi National Accelerator Laboratory, Batavia, Illinois 2. Project No.: 82-E-206

13. Narrative Explanation of Total Project Funding and Other Related Funding Requirements:

a. Total project funding

1. See details of cost estimate, item #10.
2. Other project funding

a. R&D operating costs: A program of development is underway to adapt Energy Saver dipole and quadrupole magnets and refrigeration systems to the existing physical plant in the Meson, Neutrino and Proton areas. The target handling and muon shielding requirements associated with 1 TeV energies are also being studied. Further studies are being undertaken to increase the intensity capabilities of the Tevatron accelerator in order to further improve the research potential of the 1 TeV fixed target program.

b. The items included in these costs are magnets, power supplies, cryogenics, and electronics which are general equipment to support the R&D referred to above.

B. Total related incremental annual funding requirements - The more complex character of experiments at high beam energies and intensities will result in increased programmatic R&D and experimental facility operating costs. The Tevatron fixed target program will require an increase in the annual equipment budget to accommodate its greatly increased secondary bem energies, requiring more extensive and complex beam line equipment as well as larger new research detectors and experimental facilities. GPP and AIP funds needed will follow closely the experience of the existing 400 GeV program, with consideration of the increased scale and complexity of a 1000 GeV operating facility.

DEPARTMENT OF ENERGY
1985 CONGRESSIONAL BUDGET REQUEST
CONSTRUCTION PROJECT DATA SHEETS
GENERAL SCIENCE AND RESEARCH - PLANT AND CAPITAL EQUIPMENT
GENERAL SCIENCE AND RESEARCH
HIGH ENERGY PHYSICS
(Tabular dollars in thousands. Narrative material in whole dollars.)

1. Title and location of project: Tevatron I, Fermi National Accelerator Laboratory, Batavia, Illinois

2. Project No.: 82-E-218

3. Date A-E work initiated: 1st Qtr. FY 1981

3a. Date physical construction starts: 3rd Qtr. FY 1982

4. Date Construction ends: 4th Qtr. FY 1986

5. Previous cost estimate: $82,500
Less amount for PE&D: 0
Net cost estimate: $82,500
Date: 5/82

6. Current cost estimate: $82,500
Less amount for PE&D: 0
Net cost estimate: $82,500
Date: 10/83

7. Financial Schedule:

Fiscal Year	Authorization	Appropriations	Obligations	Costs
1981	$ 2,000	$ 2,000	$ 2,000	$ 1,211
1982	18,000	14,100	14,100	4,182
1983	18,000	18,000	18,000	11,845
1984	20,000	20,000	20,000	26,400
1985	21,300	21,300	21,300	24,000
1986	3,200	7,100	7,100	14,862

8. Brief Physical Description of Project

This project provides for:

1. the modification of the superconducting Tevatron accelerator ring so that it can be used as a 1 TeV proton on 1 TeV antiproton colliding-beam storage ring;

2. two experimental areas to provide facilities for simultaneous high energy physics experiments; and
3. the construction of an antiproton production, cooling and accumulation system.

CONSTRUCTION PROJECT DATA SHEETS

1. Title and location of project: Tevatron I, Fermi National Accelerator Laboratory, Batavia, Illinois 2. Project No.: 82-E-218

8. Brief Physical Description of Project (continued)

To operate the superconducting Tevatron ring near the full energy of 1 TeV requires additional satellite refrigerators because superconductors, as they approach full magnetic field, will make the transition from the superconducting to normal state with decreasing amounts of energy deposited in them. Thus, extra cooling will prevent quenches of the superconducting ring at full energy. To simultaneously accelerate and store protons in one direction and anitprotons in the opposite direction, and to optimize the collision configuration, requires additional rf cavities and other special devices.

Two experimental areas to house high energy physics colliding beam detectors will be an integral part of the Fermilab Main Ring tunnel. The design of the experimental areas will allow the rapid efficient introduction of large detectors into the beams. To accomplish this, there will be separate detector assembly areas. The project also provides an overpass for the conventional magnet ring, to deflect it over the detector at one of the experimental areas.

The Fermilab scheme for production and collection of antiprotons uses the present accelerators plus two additional new storage rings. The first of these is the debuncher ring, operating at about 8 GeV energy, which will have a large acceptance for antiprotons and will be used to debunch the beam as it comes from the antiproton production target. The second ring is the accumulator which will be used for cooling of the antiproton beam after it emerges from the debuncher, and for accumulating the antiprotons. The term "cooling of a particle beam" means reducing the energy spread of the beam. This cooling is particularly important for producing an accelerator quality beam from the dilute beam of secondary particles emerging from the antiproton production target. The accumulator will collect the antiprotons from about ten thousand targeting cycles. It then increases their density by stochastic cooling until the antiproton bem is intense enough to transfer into the Tevatron ring, where it will be accelerated and brought into collision with a counter-rotating proton beam. The project includes construction of the debuncher ring, the enclosures for the two rings, associated beam transport enclosures and the target station.

The research detectors required for experiments will be funded as capital equipment items. The major detector for the B-Zero Area is being fabricated over the five-year period from FY 1981 through FY 1985. Substantial participation and financial assistance is being contributed by the Japanese, under the United States-Japan Implementing Agreement of Cooperation in High Energy Physics and also by Italian collaborators. The DOE funding contribution for this detector over the five years is currently planned to be about $30,000,000. Work on a second, smaller detector for the D-Zero Area is expected to begin in FY 1984.

CONSTRUCTION PROJECT DATA SHEETS

1. Title and location of project: Tevatron I, Fermi National Accelerator Laboratory, Batavia, Illinois 2. Project No.: 82-E-218

9. Purpose, Justification of Need for, and Scope of Project

When protons and antiprotons are stored in the superconducting ring and brought into collision, the reaction energy available for particle production will be about 2000 GeV. This is almost 50 times greater than the reaction energy which is available at Fermilab when 1000 GeV protons strike a fixed target, although the interaction rates of the colliding beams are much lower than those of the fixed target program. This reaction energy will be sufficiently high to produce the W and Z intermediate vector bosons which are the carriers of the weak nuclear force, and to study their properties. The data from experiments done at Fermilab and at other high energy accelerators have shown that the proton behaves as though it were made up of constituents. Extending particle physics investigations into new, much higher reaction energies has proven to be of immense scientific value in the past. The most compelling scientific expectation is the likelihood of discovering totally unexpected phenomena at this new world record reaction energy.

10. Details of Cost Estimate

		Item Cost	Total Cost
a. Engineering, design and inspection at 17% of construction costs..			$10,100
b. Construction costs.....			58,600
1. Conventional construction.....		$22,800	
a. Experimental areas.....	$10,100		
b. Ring and beam line housing.....	12,700		
2. Special facilities.....		35,800	
a. Antiproton source.....	23,500		
b. Accelerator components.....	12,300		
c. Contingency at 20% of above costs.....			13,800
Total.....			$82,500

11. Method of Performance

Design of facilities will be by the operating contractor and subcontractors as appropriate. To the extent feasible, construction and procurement will be accomplished by fixed-price contracts awarded on the basis of competitive bids.

CONSTRUCTION PROJECT DATA SHEETS

1. Title and location of project: Tevatron I, Fermi National Accelerator Laboratory, Batavia, Illinois 2. Project No.: 82-E-218

12. Funding Schedule of Project Funding and Other Related Funding Requirements

	FY 1981	FY 1982	FY 1983	FY 1984	FY 1985	FY 1986	Total
a. Total project funding:							
1. Total facility costs:							
(a) Construction line item.....	$1,211	$ 4,182	$11,845	$26,400	$24,000	$14,862	$ 82,500
Total facility costs.....	$1,211	$ 4,182	$11,845	$26,400	$24,000	$14,862	$ 82,500
2. Other project funding:							
(a) Direct R&D operating costs necessary to complete construction.....	2,221	3,337	15,600	17,500	3,240	1,500	43,398
(b) Capital equipment in support of R&D	621	368	500	700	500	200	2,889
Total other project funding.....	$2,842	$ 3,705	$16,100	$18,200	$ 3,740	$ 1,700	$ 46,287
Total project funding (Items 1 & 2)	$4,053	$ 7,887	$27,945	$44,600	$27,740	$16,562	$128,787

b. Total related incremental annual funding requirements (estimated life of project: 20 years)

1. Facility operating costs.....	$- 3,000*
2. Programmatic operating expenses directly related to the facility.....	2,500
3. Capital equipment not related to construction but related to the programmatic effort in the facility.....	3,000
4. GPP, AIP programmatic costs.....	500
Total other related annual funding requirements.....	$ 3,000

13. Narrative Explanation of Total Project Funding and Other Related Funding Requirements

a. Total project funding:

1. Total facility costs

(a) Construction line item - explained in items 8, 9 and 10.

*Reference item 13.b. for explanation.

CONSTRUCTION PROJECT DATA SHEETS

1. Title and location of project: Tevatron I, Fermi National Accelerator Laboratory, Batavia, Illinois 2. Project No.: 82-E-218

13. Narrative Explanation of Total Project Funding and Other Related Funding Requirements (continued)

2. Other Project Funding:

(a) Direct R&D operating costs - Studies of stochastic cooling techniques will continue. R&D on the antiproton production target system and the accumulator ring are now in progress. R&D on other elements of the project, to optimize performance and minimize the costs of various subsystems, will continue through the late stages of construction.

(b) Other project-related costs - The items included in these costs are magnets, power supplies, electronics and other general equipment to support a.2(a) above.

b. Total related annual funding requirements - It is assumed that after Tevatron I comes into operation approximately one-half of Fermilab accelerator operations time will be for colliding beams. This means that the fixed target experimental areas will not be operating one-half of each year. During the colliding beam operating period, there will be a net reduction of power consumption at Fermilab of about 15 Megawatts compared to running full time for fixed target experiments, which corresponds to a savings of about $3,000,000 over six months at current power rates. The programmatic effort in the facility will require approximately 30 additional people, and additional material and supplies are required to effectively operate the facility. The acquisition of research detectors for Tevatron I will be made with capital equipment funds. In the future, it is anticipated that major detector upgrades will be required about every three years, each with an estimated capital equipment cost of about $9,000,000. GPP and AIP funds will be required as experience in operating the new antiproton source and utilizing the Tevatron as a storage ring indicates specific areas where improvements would be more beneficial.

DEPARTMENT OF ENERGY
1985 CONGRESSIONAL BUDGET REQUEST
LEAD TABLE
NUCLEAR PHYSICS
GENERAL SCIENCE AND RESEARCH
(Tabular dollars in thousands. Narrative material in whole dollars.)

	1983 Appropriation	1984 Appropriation	1985 Base	1985 Request
Nuclear Physics				
Medium Energy Nuclear Physics				
Operating Expenses	$ 58,548[a]	$ 65,000[a]	$ 65,000[a]	$ 72,000
Subtotal	58,548	65,000	65,000	72,000
Heavy Ion Nuclear Physics				
Operating Expenses	39,910	47,000	47,000	49,800
Subtotal	39,910	47,000	47,000	49,800
Low Energy Nuclear Physics				
Operating Expenses	12,257[b]	13,000	13,000	13,500
Subtotal	12,257	13,000	13,000	13,500
Nuclear Theory				
Operating Expenses	8,150	9,000	9,000	9,300
Subtotal	8,150	9,000	9,000	9,300
Capital Equipment	10,410[c]	11,300	11,300	13,700
Construction	7,700	13,700[d]	13,700[d]	25,300
Total				
Operating Expenses	118,865	134,000	134,000	144,600
Capital Equipment	10,410	11,300	11,300	13,700
Construction	7,700	13,700[d]	13,700[d]	25,300
Total Nuclear Physics	$136,975	$159,000	$159,000	$183,600[e]
Staffing				
FTP/Total FTE's	(Reference General Science Program Direction Decision Unit)			

Authorization: Section 209, P.L. 95-91.

a/ Includes $3,000,000 in FY 1983 and $3,000,000 in FY 1984 which were provided under Defense Programs for LAMPF facility operations.
b/ Budgeted under the Nuclear Sciences subprogram of Basic Energy Sciences in FY 1983.
c/ Includes $510,000 in FY 1983 which was budgeted under the Nuclear Sciences subprogram of Basic Energy Sciences.
d/ Does not include $5,000,000 proposed reprogramming from High Energy Physics for the Tandem/AGS Heavy Ion Transfer Line project (84-R-123).
e/ This decision unit reflects $-1,300,000 for savings resulting from management initiatives in the area of administrative processes/field structure.

DEPARTMENT OF ENERGY
1985 CONGRESSIONAL BUDGET REQUEST
SUMMARY OF CHANGES
NUCLEAR PHYSICS
GENERAL SCIENCE AND RESEARCH
(In thousands of dollars)

1984 Appropriation enacted	$159,000
Built in increases and decreases	0
1985 Base	$159,000
Program increases and decreases:	
o Maintain overall research and instrumentation activities at 95% of FY 1984 levels and operate national accelerator facilities at 90% of FY 1984 levels[a/]	+ 7,605
o Operate new SLAC injector for nuclear research	+ 995
o Continue on schedule with the University Accelerator Upgrade Project at University of Washington and Yale University; complete funding for this construction project in FY 1985	+ 3,000
o Complete construction phase of Tandem/AGS Heavy Ion Transfer Line project and provide instrumentation for initial experiments	+ 7,000
o Initiate Continuous Electron Beam Accelerator Facility construction project and conduct supporting R&D for the Continuous Electron Beam Accelerator Facility construction project	+ 5,000
o Increase General Plant Projects to improve maintenance of the Lawrence Berkeley Laboratory physical plant	+ 1,000
1985 Budget Request	$183,600

[a/] Assumes continuation of Defense Programs' partial support of LAMPF facility operations; Defense Programs provided $3,000,000 in FY 1984 and $3,000,000 in FY 1983.

OVERVIEW

Introduction

Nuclear knowledge, techniques, instruments, and applications pervade American society. These serve as the basis for our national defense strategy, for therapeutic and diagnostic medical applications, for generation of electricity with nuclear reactors (fission now and fusion in the future), and for a large and diverse array of applications in industry. The behavior of nuclei and nuclear matter determine the physical properties of our universe--from its creation from a primordial mix of energy and elementary particles to the reactions which power our sun to the makeup of our planet. Thus, basic nuclear research is both a central component in America's long term investment in its technological future with nuclear processes and is also essential to any basic understanding of the world about us.

The Nuclear Physics program is a comprehensive program of interdependent experimental and theoretical investigations of atomic nuclei. Long range goals are an understanding of the interactions, properties, and structures of atomic nuclei and nuclear matter at the most elementary level possible and an understanding of the fundamental forces of nature by using nuclei as a proving ground. Basic ingredients of the program are talented and imaginative scientists and a diversity of facilities to provide the variety of probes, instruments, and computational equipment needed for modern nuclear research. Approximately 80% of the total Federal support of basic nuclear research is provided through the Nuclear Physics program; almost all of the remaining 20% is provided by the National Science Foundation. Thus, the Department of Energy has a unique responsibility for this important area of basic science and its role in high technology.

Experimental and theoretical investigations are leading us to conclude that a new level of understanding of atomic nuclei is achievable. This optimism arises from evidence that: (1) the mesons, protons, and neutrons which are inside nuclei are themselves composed of quarks and gluons and (2) quantum chromodynamics (QCD) can be developed into a theory which both describes correctly the interaction among quarks and gluons and is also an exact theory of the strong nuclear force. These concepts will be important drivers of basic nuclear research in FY 1985 and years beyond.

Long Range Planning

Long range planning, scientific community input, and coordination of Department of Energy work with National Science Foundation (NSF) activities take place through a variety of channels. The most important of these channels are external and internal review of specific research areas, frequent staff contact with counterparts at NSF, and the work of the DOE/NSF Nuclear Science Advisory Committee (NSAC). In cooperation with the Department of Energy and NSF, NSAC has developed a long range plan for basic nuclear research in the United States -- "A Long Range Plan for Nuclear Science" (December 1983). This long range plan is based upon a comprehensive review of scientific advances and opportunities which have emerged since development of the previous long range plan -- "A Long Range Plan for Nuclear Science" (December 1979).

The 1983 Long Range Plan reaffirms NSAC's April 1983 recommendation that construction of a 4 GeV, continuous electron beam facility be initiated as soon as possible, and it identifies a longer term, high priority need for a relativistic heavy ion collider facility. From very different aspects, both the electron facility and the heavy ion collider share the common scientific goals of understanding quantum chromodynamics as an exact theory of the strong nuclear force and understanding the ways in which the quarks inside protons and neutrons determine the behavior and makeup of nuclei. Also, in the interaction of very energetic colliding beams of nuclei, extreme conditions of energy density will occur, conditions which hitherto have prevailed only in the early instants of creation of the universe. The energy densities will be so great that transitions to new phases of nuclear matter seem likely. If these bright prospects can be realized, a new level of knowledge of atomic nuclei will be achieved. The FY 1985

request provides for initiation of construction of a 4 GeV, continuous electron beam facility at Newport News, Virginia and for a significant advancement in our capability for heavy ion nuclear research at Brookhaven National Laboratory.

Accelerator Facilities

Success of the Nuclear Physics program depends upon the existence and effective operation of large and complex accelerator facilities. These facilities provide the variety of projectile beams which are required for forefront nuclear research. Their capabilities determine which experiments can be performed and which cannot.

Seven existing accelerator facilities are operated by the Nuclear Physics program as national facilities whose beam time is made available to all the Nation's scientists on the basis of scientific merit and technical feasibility. The national facilities are: the Clinton P. Anderson Meson Physics Facility (LAMPF) at Los Alamos National Laboratory (LANL); the Bates Linear Accelerator Center at Massachusetts Institute of Technology (MIT); the SuperHILAC/Bevalac at Lawrence Berkeley Laboratory (LBL); the Holifield Heavy Ion Research Facility at Oak Ridge National Laboratory (ORNL); the 88-inch Cyclotron at LBL; the Tandem/Linac Facility at Argonne National Laboratory (ANL); and the Double MP Tandem Van de Graaff facility at Brookhaven National Laboratory (BNL).

Each of the national facilities accommodates major university-based user group research programs. Typically, an outside user group plans experiments and fabricates detectors and other instrumentation at the home institution, executes and partially analyzes experiments at the national facility, and completes analyses and publication of results at the home institution. Nuclear Physics directly supports 75 university-based user groups who conduct most or all of their research at these national facilities. To complement the national facilities, the Nuclear Physics program supports dedicated on-campus accelerators at Yale University, Duke University, University of Washington, and Texas A&M University.

In FY 1985, $73,760,000 of Operating Expenses is needed for operation of the existing national and dedicated accelerator facilities in order for them to achieve 90% of the overall levels of utilization experienced in FY 1984; an additional $1,090,000 is required for operation of the new SLAC injector discussed below. (The statement of 90% overall operation of existing facilities assumes continuation of Defense Programs' partial support of LAMPF facility operations costs.) Also, in the FY 1985 Operating Expenses request, $60,450,000 is planned for experimental research and $9,300,000 for theoretical research. Of the total FY 1985 Operating Expenses request, 26% is planned as direct support to universities--university-based users of American and international facilities, operation of Bates and the four dedicated on-campus accelerator facilities, research at on-campus facilities, research and development work on the 4 GeV, continuous electron beam facility by the Southeastern Universities Research Association, and research by university theorists. University support in an amount almost equal to the direct support is also provided through the accelerator centers in the form of services in support of experiments by university scientists and delivery of particle beams to these experiments.

New Capabilities

Over the last decade, active scientists within the basic nuclear research community identified a need for high energy, continuous electron beam accelerator capability. The 1979 NSAC Long Range Plan specifically projected initiation of construction in Fiscal Year 1985. By January 1983, five institutions responded to the identified need and the FY 1985 projection for start of construction with formal submission of unsolicited proposals.

DOE and NSF requested that NSAC establish an ad hoc panel to review and evaluate the five proposals and recommend the facility or combination of facilities which would best meet the United States needs for basic nuclear research with electromagnetic probes (i.e., electrons and photons). This "Panel on Electron Accelerator Facilities" was chaired by Professor D. Allan Bromley of Yale University. Following public presentations, site visits, and written critiques during February, March, and April of 1983, this Panel completed its work and reported its findings to the parent DOE/NSF Nuclear Science Advisory Committee at a public meeting of NSAC on April 22 and 23, 1983. In a letter of April 29 to DOE and NSF, the Chairman of NSAC transmitted the Panel report to the Department with NSAC's full endorsement and recommendation that the report be implemented without delay.

As its principal recommendation, the Panel on Electron Accelerator Facilities recommended "that the proposal submitted by the Southeastern Universities Research Association (SURA) be accepted and funded for the construction of a new National Electron Accelerator Laboratory (NEAL) centering on a 4 GeV linear accelerator-stretcher ring system capable of delivering intense, high duty factor, electron beams in the energy range from 500 to 4000 MeV." To start work on this high priority requirement for basic nuclear research, the FY 1985 request provides for initiation of the Continuous Electron Beam Accelerator Facility construction project (85-R-203) and for supporting research and development work. Work in FY 1985 will include research and development on key accelerator components, architect/engineer studies, minor site work, and detailed design beyond conceptual design. Southeastern Universities Research Association is expected to serve as contractor for both construction and later operations phases of this project.

Upon completion of the Continuous Electron Beam Accelerator Facility (CEBAF) project, American scientists will have a unique opportunity to investigate the ways in which the quarks bound in neutrons and protons influence the makeup and behavior of nuclei, to determine how quarks interact while imbedded within nuclear matter, and to test quantum chromodynamics as the fundamental theory of the strong nuclear force. Experiments in which electrons knock protons, neutrons, or even excited states of protons and neutrons out of nuclei will yield information about how energy and momentum is distributed among the nucleons (generic name for protons and neutrons) bound inside nuclei and will tell us about correlations among nucleons in nuclei. At energies above the CEBAF maximum energy, high energy physics experiments are, to a good approximation, only sensitive to effects of electrons scattering from individual quarks within the nuclei. Under these circumstances nuclei can be described as a loose collection of free quarks. At energies below 1 GeV, electron scattering from nuclei can accurately be described as electrons scattering from the protons, neutrons, and mesons known to be in nuclei. Thus, the 0.5 to 4 GeV capability of CEBAF permits quantitative examination of the transition between two diverse, but likely complementary, descriptions of nuclei. The experiments described above require coincidence measurements and thus require the unique continuous beam capabilities of CEBAF.

In FY 1985, $5,000,000 in Operating Expenses is requested for research and development in support of the CEBAF project. To initiate the CEBAF construction effort, $2,000,000 in Construction funds is requested.

At Brookhaven National Laboratory, $5,300,000 in FY 1985 Construction funds is requested for completion of the Tandem/AGS Heavy Ion Transfer Line construction project (84-R-123). The objective of this project is to transport beams of nuclei as massive as sulfur (32 atomic mass units) from the existing Double MP Tandem Facility to the Alternating Gradient Synchrotron (AGS) for acceleration to energies of 15 billion electron volts per atomic mass unit. The research that this project will make possible is an important first step towards experiments with the NSAC-recommended heavy ion collider and is an excellent complement to Bevalac's existing lower energy (1 to 2 billion electron volts per atomic mass unit) but much higher mass (up to uranium at 238 atomic mass units) beams. Bevalac research shows that concentrations of mass and energy do occur in enegetic collisions of massive nuclei. Tandem/AGS Heavy Ion Transfer Line beams will extend our capabilities into regions in which the quarks inside nuclei will

be violently forced together possibly producing a transition of nuclear matter into new forms. Start of the Tandem/AGS Heavy Ion Transfer Line construction project (TEC=$10,300,000) is planned in FY 1984 by reprogramming of $5,000,000 of ISABELLE construction project (78-10-b) funds from the High Energy Physics Program. Also, $1,700,000 in FY 1985 Capital Equipment funds is requested for experimental area equipment.

During FY 1985, two smaller projects--Argonne Tandem/Linac Accelerator System (ATLAS) and a new injector at the Stanford Linear Accelerator Center (SLAC)--will reach completion and be put into research use. ATLAS will provide heavy ion beams for investigations of the mechanisms by which colliding nuclei exchange energy, mass, momentum, and angular momentum. The new SLAC injector will provide high energy, very sharply pulsed electron beams for examination of the magnetic properties of nuclei and for exploratory experiments into the ways in which quarks influence the makeup and behavior of nuclei. The new SLAC injector experiments are a very important introduction into the research which will be possible upon completion of the Continuous Electron Beam Accelerator Facility project. Experiments begin in FY 1985 with beam from the new injector; $1,090,000 of FY 1985 Operating Expenses is needed for operation of the new injector and for setup and maintenance of magnets and other instruments in the experimental area in which nuclear research is to be conducted.

The FY 1985 Request also provides $11,000,000 in Construction funds for completion of upgrade of on-campus accelerator facilities at Yale University and University of Washington (84-ER-110). This construction project, University Accelerator Upgrade Project at University of Washington and Yale University, will maintain the forefront nuclear research capabilities of two of America's leading universities.

This decision unit reflects $-1,300,000 for savings resulting from management initiatives in the area of administrative processes/field structure.

	FY 1983	FY 1984	FY 1985 Request
Medium Energy Nuclear Physics	$ 58,548	$ 65,000	$ 72,000

The Medium Energy Nuclear Physics subprogram supports operations and research at accelerator facilities with sufficient primary beam energy to produce pi mesons (pions) using projectiles no more massive than alpha particles. In addition, the subprogram supports nuclear physics experiments at accelerators operated by other DOE programs (e.g., High Energy Physics and Basic Energy Sciences) and at other unique domestic or foreign facilities.

Two national accelerator facilities are operated under the Medium Energy subprogram the Clinton P. Anderson Meson Physics Facility (LAMPF) at Los Alamos National Laboratory and the Bates Linear Accelerator Center operated by the Massachusetts Institute of Technology. These accelerator facilities serve a nationwide community of scientists from over 100 American institutions, of which over 90% are universities. Nearly all of the "outside user" groups receive direct project support for their research activities from either the Department of Energy or the National Science Foundation. Starting in FY 1985, the accelerator at the Stanford Linear Accelerator Center (SLAC) will be operated for nuclear physics research for one to two months of the year using the new off-axis source and injector installed during FY 1984. These operations will be supported under the Medium Energy subprogram.

In FY 1985, $72,000,000 in Operating Expenses is requested for the Medium Energy Nuclear Physics subprogram. The costs of operations at the LAMPF, Bates, and SLAC (nuclear physics component) facilities require 60% ($43,320,000) of the FY 1985 Medium Energy Nuclear Physics request. In addition to supporting the operation of the accelerators themselves, these operations costs also provide for the maintenance and operation of secondary beam lines, major spectrometer systems, and other permanently installed experimental equipment. The remaining 40% of the budget supports costs directly attributable to executing individual experiments, support of participating research scientists, R&D in support of the Continuous Electron Beam Accelerator Facility construction project, and advanced accelerator physics studies. Of the $72,000,000 request in FY 1985, $21,223,000 will be for direct support of universities, including the Southeastern Universities Research Association.

Medium energy nuclear physics research activities range over an extremely broad selection of topics, including studies of: the fundamental symmetries of nature; distribution of electric charge and magnetic fields inside nuclei; interactions of protons, mesons, and neutrons with nuclei; neutrino oscillations and the neutrino mass; interactions between nucleons; and nuclear structure. Some recent accomplishments in medium energy research in these areas and plans for the next steps are summarized in the following paragraphs.

One of the most fruitful methods of improving our understanding of physical phenomena and forcing refinements to scientific theories is to perform experimental tests of the validity of fundamental hypotheses, such as: the conservation of parity; time reversal invariance; and charge conjugation invariance. The invariance of physical laws under inversion of the spatial coordinates (the conservation of parity) has long been known to be violated by the weak force, which is responsible for nuclear beta decay. Medium energy experiments are determining the extent to which the force between nucleons contains a component of the weak force. Such a component would cause a violation of parity conservation in the interaction between two protons. In very difficult experiments with polarized proton beams of 15 MeV and 800 MeV, a small violation of parity conservation has been observed. These impressive results have sparked much theoretical interest in the study of the weak component of the force between nucleons. Parity nonconservation due to the weak force in the scattering of electrons from nuclei will be studied in FY 1985 at the Bates accelerator using beams of polarized electrons.

A second concept of fundamental importance is that the laws of physics are invariant under time reversal. This hypothesis can be tested by comparing the scattering of polarized beam particles from a target with the polarization of initially unpolarized particles scattered from the same target. In a LAMPF experiment studying the interaction between neutrons and protons at 800 MeV, a new limit of sensitivity was established for comparison with theories of the strong nuclear force. A new measurement, five times more sensitive than previous measurements, is planned for the near future.

Neutrinos are particles of enormous importance in nuclear astrophysics and cosmology. The measurement of the flux of solar neutrinos on earth provides a test of our understanding of the nuclear reactions that are the source of the sun's heat. A very large number of neutrinos are believed to occupy the intergalactic space. Thus if neutrinos have even a very small mass, they would contribute in an important way to the total mass of the universe. The value of that total mass determines whether the universe will continue to expand indefinitely or will eventually begin to contract. Measurements of the solar neutrino flux on earth have obtained a value that is about four times less than that calculated from current theories. This dilemma can possibly be resolved by accepting the hypothesis that neutrinos are a mixture of two or more of several different varieties and that the amplitudes of the separate components in the mixture oscillate in time and, therefore, in distance from the source. However, these oscillations can occur only if there is a difference in mass among the different neutrino components, and that is not possible if the neutrino mass is exactly zero. Indeed, some Grand Unified Theories allow for neutrinos with nonzero rest mass. The Medium Energy subprogram is supporting an experiment at the Goesgen power reactor in Switzerland, where experimenters are looking for oscillations of the antineutrinos that arise from the beta decay of fission products in the reactor core. By measuring the antineutrino flux at two different distances from the reactor core, the analysis of this experiment is independent of the energy spectrum of the neutrinos emitted by the reactor core. There is no evidence from this elegant experiment that neutrino masses are other than zero, and the solar neutrino discrepancy remains without explanation. Two major new searches for neutrino oscillations are in preparation at LAMPF.

Nucleons (protons and neutrons) interact with one another through the strong force, another of the four fundamental forces of nature. It is the strong force that is responsible for the binding together of protons and neutrons to make nuclei. A full understanding of this force is not only important in its own right, but it is also an essential ingredient in the understanding of nuclear structure and nuclear reactions. The strong force is very complex. Its strength depends on the distance between the two colliding nucleons, their relative velocity, and the orientations of their spins with respect to each other and with respect to the velocity vectors of each nucleon. The force between two protons is not identical with that between two neutrons or between a proton and a neutron. Eventually, perhaps, all these complications will be understood at a deeper level in terms of the quark substructure of the nucleons. Any acceptable theory of the interactions among quarks must quantitatively describe the scattering of nucleons by other nucleons. For the moment, though, such quantitative understanding is far from possible. Experiments must therefore be made in which spin-oriented (polarized) protons and neutrons of various energies are scattered from polarized proton targets. This is a lengthy program of difficult experimental research that will require several more years for full completion and subsequent theoretical analysis. The detailed study of medium energy nucleon-nucleon scattering is now being pursued very actively at LAMPF, TRIUMF (Canada), SIN (Switzerland), KEK (Japan), and Saclay (France). Challenging experiments have produced a precise and detailed set of proton-proton data up to 800 MeV. These data have conclusively shown that widely accepted amplitude analyses were incorrect and have defined a more reliable set of phase shifts. There are some data at nearby energies, but not nearly enough to define the amplitudes conclusively. Medium energy research has greatly improved this essential data base over the past decade. However, much improved data are still needed on the important and even more difficult neutron-proton process. These fundamental but difficult nucleon-nucleon

experiments require major technological advances in polarized targets and polarized ion sources. This need has resulted in a close and mutually productive interaction among medium energy physicists and atomic, low temperature, high energy, plasma, and accelerator physicists.

While the more detailed study of the interaction between nucleons is providing one of the ingredients essential to the understanding of nuclear structure and nuclear reactions, new probes and improved experimental methods are yielding new and more precise information about the properties of nuclei that will both guide and challenge the theorists. These include electron scattering experiments, comparison of experiments using different probes, and studies of muonic atoms.

As a probe of nuclear structure, the electron occupies a very special position because the relative weakness of its interaction facilitates the interpretation of experimental results. The scattering of electrons from nuclei allows very precise measurements to be made of the radial distributions of electric charge, of electric currents, and of magnetism in nuclei. The doubly closed shell nucleus lead-208 and several other nuclei have been studied in detail. The quenching already observed in transitions involving the nuclear magnetic fields was also observed in transitions involving the transverse electric fields. This quenching is so far not understood. Theorists are exploring the possibility that it comes from the coupling of nucleons with nuclear vibrations, from the polarization of the core of the nucleus itself, from the effect of certain excitations, or from correlations between nucleons in the ground state of the target nucleus. The wealth of high precision experimental results from these and many other electron scattering studies, primarily at Bates, are making an important impact on theories of nuclear structure.

The electron interacts electromagnetically with the charges, currents, and magnetic fields inside nuclei. Hadronic probes, on the other hand, interact through the strong force with the neutrons as well as with the protons of the target. A comparison of electron and hadron scattering therefore yields more nuclear structure information than can be obtained by the use of a single probe. Such intercomparisons constitute a most important new direction for nuclear structure studies. In this work, the High Resolution Spectrometer (HRS) at LAMPF is an invaluable tool for the study of proton scattering. Experiments with pions depend on the Energetic Pion Channel and Spectrometer (EPICS) facility at LAMPF. An example of the value of the comparison of probes is provided by a study of electron, proton, and pion scattering by oxygen-16. The electron and proton scattering experiments were done at Bates and the Indiana University Cyclotron Facility (a national facility whose operations is supported by NSF) and the pion scattering was done at LAMPF. The inelastic pion scattering excited three oxygen-16 states of the same spin and parity. By electron scattering, two of these three states are excited but not the third. However, a previously unobserved state with the same spin and parity is observed in electron scattering. All four states were observed in the inelastic scattering of 135 MeV protons. On the basis of the electron and proton scattering data alone, the newly observed state would have been incorrectly classified. Data from all three probes was necessary for the correct interpretation. Moreover, comparison of the electron, proton, and pion results shows that these particular states are excited in proton and pion scattering by a simple one-step process.

In many current medium energy research activities, precise data and refined concepts point to areas of investigation which could be fruitfully explored beyond the capability of presently available facilities. Some examples include: nucleon structure and few-body form factors; discrete states, giant resonances and single nucleon-hole states in complex nuclei; nucleon excitation in nuclei; hypernuclei; deep inelastic scattering on few-body and complex nuclei; and tests of electroweak interaction theories. In the Medium Energy subprogram, several approaches to these unexplored areas are being undertaken, each of which makes use of unique properties of electromagnetic probes: an off-axis injector at SLAC will provide moderate current, pulsed electron beams at

energies up to about 6 GeV; polarized beams of tagged photons will be produced at the National Synchrotron Light Source at BNL by backscattering laser light; and approval is being requested for the Continuous Electron Beam Accelerator Facility construction project which will provide high quality, high current, continuous beams of electrons in the energy range of 500 to 4000 MeV.

Of the three accelerators for which operations support is provided under Medium Energy, the largest nuclear physics program is carried out at LAMPF. The facility is centered around a linear accelerator which is capable of accelerating very intense beams of protons to 800 MeV. The ability to provide ten or more simultaneously operating beams of protons, neutrons, pions, muons, or neutrinos enables LAMPF to be a highly cost-effective basic nuclear research facility. In addition to providing beams for nuclear research, LAMPF provides beams for basic materials research and weapons development at the Weapons Neutron Research (WNR) facility.

To operate LAMPF in FY 1985, $36,480,000 is required. This total will permit LAMPF to operate 2850 beam hours for research if Defense Programs continues to provide partial support of LAMPF facility operations costs. In addition to these operations costs, $13,000,000 is required for the conduct of research at LAMPF by Los Alamos scientists and by outside user groups, including university groups.

The other accelerator facility entirely supported under the Medium Energy subprogram is the Bates accelerator facility. The accelerator is capable of producing electron beams of excellent quality at energies up to 750 MeV. Since 1974, with the first results of the Bates experimental program, a major part of the program has been high resolution nuclear structure studies with electrons. Over that period, Bates has been the premier facility in the world for nuclear structure studies involving high resolution electron scattering. Achromatic transport of the beam to the spectrometer focal plane allows energy-loss spectroscopy to be done using the full beam current of the accelerator and with excellent energy resolution. Bates has recently brought into operation a new set of spectrometers which dramatically broaden the scope of the Bates research program. The polarized electron source now being installed will provide yet another valuable dimension to the Bates capability, as mentioned above.

To operate Bates in FY 1985, $5,750,000 is required, and in addition, $3,300,000 is required for the conduct of research at Bates by MIT scientists and outside user groups. Operation of the new SLAC injector and associated experimental area requires $1,090,000 in FY 1985, with an additional $300,000 being budgeted for support of research groups using the facility. R&D activities in support of the CEBAF project will require $5,000,000 in FY 1985.

Medium energy nuclear physics research using kaons from a separated beam at the Brookhaven AGS will continue as an important component of this subprogram. AGS accelerator and facility operations are supported by the High Energy Physics program. Other Medium Energy activities for FY 1985 include: research at unique foreign facilities; research using polarized, tagged photons at the National Synchrotron Light Source (NSLS); and advanced accelerator research. For these research activities, $7,080,000 is requested in FY 1985.

	FY 1983	FY 1984	FY 1985 Request
Heavy Ion Nuclear Physics	$ 39,910	$ 47,000	$ 49,800

The Heavy Ion Nuclear Physics subprogram supports a broad range of facilities at national laboratories and major universities. In combination, these facilities provide beams of atomic nuclei ranging in mass from lithium to uranium and in energy from a few MeV to several hundred thousand MeV. In general, each facility provides beams and

experimental facilities for research groups centered both at the host institution and at other institutions. The "outside user" groups include many based at universities. The research programs make use of unique properties of heavy ion beams or heavy ion reactions as a tool to open new research opportunities in such diverse areas as microscopic nuclear properties, macroscopic nuclear interactions, and searches for predicted exotic phases of nuclear matter. At the lowest energies and with the lightest masses, heavy ion nuclear research interleaves with low energy nuclear physics. At the highest energies, many of the goals and techniques adjoin those of medium energy nuclear physics and high energy physics.

Upon completion in FY 1986, the Tandem/AGS Heavy Ion Transfer Line construction project (84-R-123) will provide beams up to 15 billion electron volts per atomic mass unit (GeV/AMU) for atomic nuclei up to masses of approximately 32 (sulfur). This capability, which will be unique in the world, offers the possibility that for the first time scientists may be able to create, for brief periods, exotic new states of nuclear matter which have never before been observed in the laboratory. This project at Brookhaven National Laboratory represents a limited but important initiative into the field of relativistic heavy ion collisions that was identified in NSAC's 1983 Long Range Plan for Nuclear Science as one of the most promising new research directions for the future. Work in FY 1985 will emphasize preparation for and design of experiments with relatvistic heavy ion beams.

At LBL the Bevalac, which is also unique in the world, provides heavy ion beams up to 2.1 GeV/AMU and can accelerate atomic nuclei of any mass up to 238 (uranium). Thus, Bevalac and the new Tandem/AGS capabilities are complementary in both mass and energy. The recent upgrade of this facility to provide beams as massive as uranium has opened research directions which are yielding new insights into properties of relativistic heavy ion collisions. The capability to create nuclei at very high temperatures and greater than normal densities utilizing these heavy ion beams will remain a unique property of this facility until the mid 1990's when the relativistic heavy ion collider identified in the 1983 Long Range Plan as the highest major new priority would become operational. Both Bevalac and the new Tandem/AGS are fixed target facilities (with no colliding beam capability) and have center-of-mass energies 10 to 100 times less than the collider recomended by NSAC.

Very active research programs utilizing lower energy heavy ion beams (5-25 Mev/AMU) are supported by complementary facilities at several national laboratories. The ANL Tandem/Linac provides medium mass projectiles with beams that can be controlled very accurately in energy or with sharply pulsed structure for timing experiments. Upon completion in FY 1985, the ATLAS construction project (82-E-223) will significantly extend ANL capabilities to higher mass and higher energy. The Holifield Heavy Ion Research Facility (HHIRF) is a recently-completed, state-of-the-art tandem accelerator designed to achieve 25 million volts (MV) on the terminal and is well equipped with many new detection devices. Used alone or coupled with the Oak Ridge Isochronous Cyclotron (ORIC), it will provide the highest energy precision beams and widest variety of projectiles. The LBL 88-inch Cyclotron presently supplies beams of the lighter heavy ions (up to 40 AMU). Completion of a new Electron Cyclotron Resonance (ECR) ion source at LBL will provide a broad selection of heavy ion species which is complementary to that of the tandem facilities. Each of the national laboratory-based accelerators is operated as a national facility. Access to machine time and experimental equipment is open to all qualified scientists on the basis of proposals reviewed for scientific merit and technical feasibility.

In addition to the national laboratory accelerators, forefront facilities are also maintained at three universities -- Yale University, University of Washington, and Texas A&M University. The University of Washington and Yale University facilities are being upgraded (84-ER-110) so that they can continue to maintain a forefront research capability in a university setting. These facilities complement the research done at the larger national laboratory facilities while at the same time providing high quality training to their graduate students. An additional upgrade is underway at Texas A&M using State of Texas funds and private Welch Foundation funds.

In FY 1985, $49,800,000 is requested for Heavy Ion Nuclear Physics. Operation of the national facilities and three university laboratories requires $28,660,000 of which $17,625,000 is planned for operation of the Bevalac (providing for operation for approximately 3600 beam hours in FY 1985). A total of $11,035,000 is requested for heavy ion operation of the Holifield Heavy Ion Research Facility, Argonne Tandem/Linac, LBL 88-inch cyclotron, Brookhaven Double MP, and the three on-campus university accelerators.

The remaining $21,140,000 supports the heavy ion research program, the major fraction of of which is based at DOE-supported facilities. A small fraction of the research is performed at NSF-supported accelerators and at unique foreign facilities. Of the research funds, $5,798,000 will go directly to university-based research programs. Additional university support is provided through the national laboratories in the form of services in support of experiments and provision of beam time.

Research in FY 1985 will emphasize implementation and utilization of new and unique research capabilities. The physics addressed by heavy ion nuclear research spans a wide range of interests. However, the problems can be divided into major areas, characterized roughly by the amount of overlap of the nuclei during the collision (e.g. violent head-on collisions versus more gentle grazing collisions) and by the velocity of the colliding nuclei relative to the velocities of neutrons and protons inside those nuclei.

At energies of a few MeV/AMU, heavy ion reactions are dominated by fusion processes (the colliding nuclei fuse together) and peripheral reactions (the colliding nuclei sideswipe each other). Such collisions lead to highly excited projectile and target-like fragments. Heavy ion fusion provides a unique opportunity to observe the properties of equilibrated nuclear systems with large excitation energies over a wide range of angular momenta. Current research in this area includes studies of the alpha decay of aligned nuclei using the spin spectrometer at Holifield where new and more detailed information on changes in nuclear shapes is sought as more and more angular momentum is added to the nuclei under study. At sufficiently high angular momentum centrifugal forces become so great that excited nuclei predominately decay by fission. Recent experiments using facilities at ORNL, ANL, BNL, and LBL have led to major advances in our understanding of the deformed potential energy surfaces that regulate the fission process at high angular momentum. More complex experiments involving emission of light particles (e.g. protons, neutrons, helium nuclei) now show considerable promise for study of the dynamics of a fissioning system. Similar studies of light particles emitted in peripheral collisions have led to a more detailed understanding of mass exchange and energy damping in heavy ion collisions.

At intermediate energies of a few tens of MeV/AMU, nuclear collisions become more violent and begin to involve the emission of neutrons, protons, and even more complex bits of nuclear matter in the early stages of the reaction process. Experiments at Holifield and the Low Energy Beam Line at Bevalac are just beginning to investigate this interesting new area by studying peripheral reactions where the projectile is sometimes shattered into a few large pieces. A puzzling new phenomenon that has appeared in this energy regime (and also in high energy collisions of protons with nuclei) is the emission of medium mass fragments (e.g. masses of 10 to 40 AMU) with rates that are much greater than is characteristic for evaporation from an equilibrated system. Energies of these medium mass fragments are also much lower than normal for projectile shattering processes. These results may provide signatures for the properties of nuclei in the transition region between a liquid-like phase which dominates the low energy regime and a gas-like phase which becomes increasingly important at high energies.

At energies of hundreds of MeV/AMU, the Bevalac provides the only research tool in the world. Highlights of recent progress include the first experimental determination of the compressibility of nuclear matter by studying the emission of pions from a variety of nuclear systems and the development of interferometry techniques to study the evolution of the hot "fireball" formed in high energy head-on collisions. In this latter case the size of the region from which pions and protons are emitted is determined from

two particle correlation studies by a method similar to optical techniques used in astronomy to measure the size of stellar systems. It is found that particles with different energies probe the collision process at different characteristic times with the pions being emitted earliest at the hottest, most dense stage of the process whereas low energy protons appear to come from a later stage from a cooler, less dense system. In this area experiments are continuing to provide more rigorous tests of the theoretical models which are being used as a basis for predicting the exciting new properties of nuclear matter which are expected to become important at higher energies.

At the highest Bevalac energies and beyond, theories predict that heavy ion central collisions will create a quark and gluon plasma, which rapidly expands and decays into observable protons, electrons, muons, mesons, and neutrons. The pressures and temperatures of nuclear matter for these brief instants simulate the nature of the universe during a fraction of a second after creation. Intense efforts and new instrumentation will be dedicated to exploring this phenomenon.

A broad variety of intense theoretical effort is being expended to specify the signatures of various possible exotic states of nuclear matter that may be created in high energy heavy ion collisions. This will guide the experiments in distinguishing desired events from more prolific background processes. Augmented instrumentation at Bevalac's Heavy Ion Spectrometer System (HISS) and construction of a new spectrometer for detection of electron-positron pairs from quark-gluon plasmas will be major experimental factors in the subtle process of identifying distinguishing characteristics of exotic events. These new experimental and theoretical efforts will provide the basis needed for the pursuit of research at even higher energies when beams from the BNL Tandem/AGS Heavy Ion Transfer line project become available.

While the central objective of the Heavy Ion subprogram is basic nuclear research, heavy ion accelerators have important applications in atomic physics research, astrophysics, fusion energy technology, biomedical research, and human cancer therapy. Bevalac heavy ion beams are used to evaluate the effectiveness of heavy ions in destroying human cancer cells while doing minimum damage to intervening healthy cells. This research is supported and managed by the National Cancer Institute and the Department's Nuclear Medicine Applications subprogram in the Biological and Environmental Research program. All facility operations costs of Bevalac, including those for biomedical research, are supported by the Heavy Ion Nuclear Physics subprogram. Heavy ion accelerator facilities are also unique sources of atomic ions found only in interstellar space and in the very hot plasma of a working fusion reactor. Atomic data from heavy ion accelerator facilities will be increasingly important for diagnosis of fusion reactor operation as those reactors reach the working prototype stage. The use of heavy ion beams to identify the motion of inner-orbit electrons under conditions of strong perturbations is growing rapidly and is providing valuable results to both nuclear physics and atomic physics programs.

	FY 1983	FY 1984	Request
Low Energy Nuclear Physics.....	$ 12,257	$ 13,000	$ 13,500

Beams of low energy light ions, neutrons, and gamma rays are essential for continuing detailed studies of nuclear structure and reaction mechanisms. The pursuit of low energy research is also well suited for university research in view of the relatively small size of the accelerators and detection apparatus required. This has been well demonstrated by the successful ongoing research programs at universities supported by the Low Energy Nuclear Physics subprogram.

The FN tandem accelerator complex at the University of Washington has been used for a decade and a half in a wide range of low energy light ion and heavy ion nuclear research. The University Accelerator Upgrade Project (84-ER-110) provides a post-tandem superconducting linac booster. This booster accelerator has been designed to optimize the acceleration of the lighter heavy ions, including protons. To exploit this feature,

the upgraded facility will be equipped with a new high intensity proton-deuteron polarized ion source. The increase in ion energies will permit the study of reaction mechanisms above the energies where the more ordinary compound nuclear effects dominate. Higher energies will also permit new parity violation studies exploiting longitudinal analyzing power measurements in fundamental systems like protons interacting with protons and neutrons interacting with protons. Radiative capture studies of giant resonances built on highly excited states will also be facilitated. With higher energies, a broader range of heavy ion projectiles will be useful, and higher energy heavy ions can also impart larger amounts of angular momentum, which permits tests of current ideas about the behavior of rapidly rotating nuclei.

The University Accelerator Upgrade Project also extends both energy and mass ranges of the Yale electrostatic accelerator. These planned improvements will increase significantly the research potential of the Wright Nuclear Structure Laboratory. Heavy ion induced single-nucleon transfer reaction studies to test recent theoretical predictions of certain high-spin nuclear states will be facilitated. Recent research results at Yale include the discovery of a new dynamical mode of the nuclear many-body system -- dipole collectivity.

At another premier university nuclear physics facility, the Triangle Universities Nuclear Laboratory (TUNL), located at Duke University, a new cryogenic polarized target facility has been brought into operation. This new capability permits the study of the reactions of polarized neutrons with polarized nuclei, from which new knowledge of the spin-spin interaction in nuclear reactions will be gained. Meanwhile, polarized neutrons have been used to determine the analyzing power for the scattering of neutrons from deuterons. These very precise measurements, when compared with measurements of the scattering of protons from deuterons, give convincing evidence for differences in the reactions for these charge symmetric three-body systems.

A large superconducting cyclotron, which will act as an ion injector for the existing cyclotron at Texas A&M university, is being built with State of Texas and private Welch Foundation funds. While construction continues, the existing cyclotron is being heavily used for research with both light and light-heavy ions. Light ions, in particular the tightly bound alpha particles, have proven to be very effective in the study of the effect of nuclear deformation on giant resonance reactions. Recent measurements of the inelastic scattering of alpha particles from the deformed nucleus samarium-148 demonstrate strong mixing of the giant quadrupole and monopole resonances, a behavior that is still not fully understood.

University users have proven to be essential to the exploitation of the on-line isotope separator, TRISTAN, at the Brookhaven High Flux Beam Reactor. These include scientists from Clark University, Cornell University, Georgia Institute of Technology, Iowa State University, the University of Maryland, Oklahoma University, and Texas A&M University. Scientists from several of the national laboratories also are taking advantage of this unique facility for the study of the very neutron-rich, unstable, fission-product nuclei available from the separator. The research has been paced by the ion-source development being carried out at BNL. Several successful sources have been developed which, together, provide an array of separated isotopes that can be studied. In this way, systematic trends in level structure can be studied as neutrons are added one by one to a given element, to produce nuclides successively farther and farther from the stability line.

Studies of light nuclei far from stability are also being conducted at the Berkeley 88-inch cyclotron. An on-line mass analysis system, has been used to search for nuclei near the proton and neutron drip lines that may decay by new or exotic radioactivities. Most recently, helium-3 beams were used to produce the unstable nuclei aluminum-22 and phosphorus-26; observation of their beta-delayed two-proton decay is the first experimental confirmation of this theoretically predicted decay mode. Light ion beams are also being used to investigate the advent of fission-like phenomena in deep-inelastic collisions.

The FY 1985 Request for Low Energy Nuclear Physics is $13,500,000, which will permit the maintenance of low energy nuclear physics activities at about 95% of levels attained in FY 1984. Of this total request, $10,630,000 is budgeted for research activities; $2,870,000 is budgeted for facility operations costs.

	FY 1983	FY 1984	FY 1985 Request
Nuclear Theory	$ 8,150	$ 9,000	$ 9,300

The nucleus is unique in physics in that it is a many body system which must be treated quantum mechanically and can be treated in a microscopic many-body theory. Traditionally the constituents of the many-bodied nucleus have been assumed to be the hadrons, i.e. neutrons, protons, and mesons. In recent years, elementary particle physics has revealed that there is a substructure of the hadrons made up of quarks and gluons. It would be a major physics achievement were it possible to understand quantitatively the interactions between hadrons in terms of the coordinates of and interactions between the quarks and gluons. To this end there is now a growing overlap of activity in theoretical nuclear and particle physics. The many body expertise of nuclear physics is being combined with field theory concepts of particle physics to construct more fundamental descriptions of the many different interactions among neutrons, protons, and mesons. Recent experimental evidence suggests that the quark structure of nucleons is different when the nucleons are free and when they are bound in nuclei. More sophisticated models of nuclei are being developed to allow a detailed study of these differences.

Almost all evidence suggests that quarks only exist in nature in groups of two, three, or more, confined within the boundaries of hadrons. Nuclear theorists have conjectured that if one can cause two massive nuclei, such as two uranium nuclei, to collide at very high energies (greater than 10,000 MeV/AMU) a hot dense plasma will be formed in which the quarks and gluons are freed from their hadronic confinement and a totally new form of matter is created. Nuclear theory and particle theory are again being combined to predict the properties of this new matter and to define experimental signals that such matter exists.

The opportunities to unite nuclear and particle physics at these new boundaries have brought much new excitement to nuclear physics. The CEBAF project is designed to study many of these new questions. Nuclear theorists are increasingly active in astrophysics, another exciting overlap area. One particular question here is "why do supernovas explode?". The evolution of a supernova is described by a classical hydrodynamics equation. The calculation depends critically on the equation-of-state of the stellar medium. The experience developed in the study of the nuclear matter equation-of-state is now being introduced to the calculation of the stellar matter equation-of-state in an attempt to understand these cataclysmic events. Quark phenomena are of major significance in very high energy processes; in supernova, stellar matter is a hot, dense form of nuclear matter.

There remains a large area of nuclear physics where the traditional picture of interacting hadrons remains appropriate, and in this area there remain many unanswered questions. Some of these areas, and questions being asked there are briefly listed here.

Intermediate Energy--The scattering of intermediate energy protons (200 MeV to 800 MeV) from nuclei is usually treated within the framework of the nonrelativistic Schroedinger equation. Within this framework, the nuclear potential varies as a function of the proton energy in a manner which is not easily understood. Recently, such scattering processes have been analyzed in terms of a phenomenological relativistic Dirac equation. In this new picture, the energy dependence of the nuclear potential is more easily understood, and complex proton polarization effects are well described. Nuclear

theorists are now trying to calculate this effective Dirac potential from "first principles," so that one might have a consistent picture of such a simple process as the scattering of a proton from a nucleus over a very wide range in incident proton energies.

Nuclear Structure--Experiments with low energy heavy ions have provided much new quantitative information on the behavior of nuclei as they rotate faster and faster. Nuclear structure theorists have recently made detailed studies of the energy levels of single particles (neutrons, protons) moving around a rapidly rotating deformed nucleus. The motion of these particles is a sensitive probe of the shape of the nucleus. The new calculations suggest ways to directly measure the triaxial deformation degree of freedom with much more precision than has been previously possible.

Heavy Ion Reactions--During the collision of two heavy ions at low energies (less than 50 MeV/AMU), there is a rapid exchange of energy and particles between the two colliding nuclei. The time averaged effects of this kind of nuclear reaction are described by mean-field theories such as Time Dependent Hartree Fock theory, but even the grossest details of these reactions are poorly understood. Can one start from a mean-field theory, and add corrections so as to successfully describe these reactions?

The Nuclear Theory subprogram is very diverse in character. Programs are supported at five national laboratories (Argonne, Berkeley, Brookhaven, Los Alamos, and Oak Ridge), where major experimental facilities are operated. Approximately 55% of the theory program is carried on at 27 American universities. Major theory efforts are supported at Massachusetts Institute of Technology, Yale University, State University of New York at Stony Brook, University of Maryland, and University of Washington, while smaller programs (1-2 senior investigators) are supported at the 22 other universities. The overall budget request for Nuclear Theory operating expenses in FY 1985 is $9,300,000. This budget request will allow nuclear theory work to proceed at about 95% of FY 1984 levels of activity.

	FY 1983	FY 1984	FY 1985 Request
Capital Equipment.....	$ 10,410	$ 11,300	$ 13,700

As the various nuclear physics research programs move into new scientific areas, there is a continuing need to develop new detection instrumentation, upgrade the capabilities of existing instruments, improve the efficiency and sophistication of data acquisition and analysis systems, and improve the performance and beam characteristics at the major Nuclear Physics accelerator facilities. In general, the emphasis is to try to address more definitive questions about nuclear reactions and properties of nuclei by means of more complex and precise experiments and by the development of entirely new techniques.

At Brookhaven National Laboratory $1,700,000 is requested for equipment to be used in the first heavy ion experiments at the AGS. These experiments will be made possible by the line-item construction project, Tandem/AGS Heavy Ion Transfer Line (84-R-123). Two complementary spectrometer systems are needed: (1) a new Multi-Function Spectrometer to measure precisely properties of emitted particles under well-defined trigger conditions and to observe rare events and (2) an upgrade of the existing AGS Multi-Particle Spectrometer to do measurements with complete reconstruction of events with 100 or more fragments coming from a single nuclear collision.

Two major equipment projects at BNL and LBL will establish important new experimental capabilities. At Brookhaven National Laboratory, a new, unique capability will be established which can provide intense beams of monochromatic and polarized gamma rays with energies up to 300 MeV by using laser light backscattered from the circulating electron beam at the National Synchrotron Light Source. At the Lawrence Berkeley Laboratory, the start of construction of a major new instrument, the Dilepton Spectrometer, is planned for FY 1985. This spectrometer is designed to detect electron-positron pairs in attempts to gather information concerning quark deconfinement and the quark-gluon plasma that may be created during the collision of relativistic heavy ions.

At Oak Ridge National Laboratory and Argonne National Laboratory, capital equipment funds are needed to exploit the capabilities of the Holifield and new ATLAS facilities. A multielement gamma-ray detector (a "spin spectrometer") has been very successful at Holifield in giving new insights into fundamental properties of heavy ion reactions and the properties of nuclei at high angular momentum. An expansion of this system to include high resolution germanium detectors with bismuth germanate (BGO) shields will provide an even more powerful and unique tool for a new generation of experiments. At the ATLAS facility a different kind of multielement gamma ray detection array, having 56 BGO elements and 10 Compton-suppressed spectrometers, will become a major part of the new apparatus needed to equip the experimental areas.

The increasing complexity of nuclear physics experiments requires more powerful data acquisition and analysis systems. Initiatives in this area include $1,000,000 for the expansion of data handling capabilities at LAMPF and at several other laboratories.

At Bates, the upgrade of a beam line which feeds three magnetic spectrometers will provide new capability and increased efficiency. At ATLAS and Holifield, the development of new beam lines is also an important part of the instrumentation needed to exploit the diverse capabilities of these new facilities.

The Nuclear Physics program has responsibility for providing for all of Lawrence Berkeley Laboratory's general purpose equipment. For efficient operation of the Laboratory plant and for personnel safety, obsolete equipment must be replaced on a continuing basis. In FY 1985, $800,000 is requested for all capital equipment that cannot be identified with specific programs. Some examples are: two-dimensional color computer aided design (CAD) units to aid circuit board design and layout, a numerically controlled heavy duty lathe, and two air-ride semitrailers for transporting delicate experimental equipment.

In FY 1985, $12,900,000 in programmatic Capital Equipment funds is required for the research initiatives discussed above and for maintenance of the overall productivity of the Nuclear Physics program. In addition, $800,000 is required for general purpose equipment at Lawrence Berkeley Laboratory.

	FY 1983	FY 1984	FY 1985 Request
Construction	$ 7,700	$ 13,700	$ 25,300

The total FY 1985 request for construction funds for Nuclear Physics is $25,300,000 as indicated in the table which follows:

Nuclear Physics
Summary of Construction
(Dollars in Thousands)

Project Name	Project Number	1985 Request	TEC
Continuous Electron Beam Accelerator Facility	85-R-203	$ 2,000	Under Review
Tandem/AGS Heavy Ion Transfer Line	84-R-123	5,300	10,300
University Accelerator Upgrade Project at the University of Washington and Yale University	84-ER-110	11,000	19,000
Accelerator Improvement Projects	85-R-200	3,500	3,500
General Plant Projects	85-R-201	3,500	3,500
Total		$ 25,300	

Authorization and appropriation are requested to initiate the Continuous Electron Beam Accelerator Facility construction project. The heart of the proposed facility is an accelerator complex that produces an intense, continuous beam of electrons at an energy intermediate between the conventional nuclear physics regime and the particle physics regime. This capability is needed for the study of the largely unexplored transition between the nucleon-meson and quark-gluon descriptions of the nuclear force. The Tandem/AGS Heavy Ion Transfer Line project allows the rapid realization of a unique relativistic heavy ion capability having beam energies approximately a factor of seven times greater than those available elsewhere in the world for nuclei as massive as sulfur (32 atomic mass units). The University Accelerator Upgrade Project is designed to strengthen the nuclear research capabilities of two of America's leading universities. Authorization and appropriation are requested in FY 1985 for funds to complete this project and the Transfer Line project. Accelerator Improvement and General Plant funds are required in FY 1985 in order to meet the changing demands of frontier nuclear research, improve efficiency of facility operations, and provide for personnel safety.

Continuous Electron Beam Accelerator Facility

In FY 1985, $2,000,000 is requested to initiate construction of an electron accelerator complex capable of delivering intense, continuous beams in the energy range from 500 to 4000 MeV. The intensity of its beams in combination with multi-GeV energy and high duty factor will make this facility unmatched in the world. The facility will have the capability of addressing a crucial class of problems facing nuclear physics today, namely the understanding of the relationship between the traditional and the emerging descriptions of nuclear forces. The aim is to synthesize into a unified description the traditional picture which is based on nucleon, meson, and isobar degrees of freedom and the emerging picture of an underlying structure of quarks and gluons.

The electron accelerator complex will consist of a 2000 MeV pulsed linac; the beam transport system to recirculate the electron pulses for a second pass of acceleration through the linac to attain the full 4000 MeV maximum energy; the pulse stretcher ring, in which the short, intense electron pulses are smoothed into a continuous stream; the beam transport system to take the pulses from the linac either to the pulse stretcher ring or directly to an experimental hall; the beam transport system to deliver the electrons from the pulse stretcher ring to the experimental halls; and instrumentation and control systems for the accelerator complex. The accelerator will service three independent experimental areas--two buildings for experiments using electron beams and a smaller area for experiments using photon beams.

The conventional construction needed for the facility will include tunnels for the linac, recirculator path, and stretcher ring, buildings for general office space, experimental areas, RF galleries, beam dumps, and utilities. General office, laboratory, and shop space will also be provided by rehabilitation of and additions to existing structures.

In addition to the accelerator complex and buildings to house the accelerator and research activities, this project will also provide an initial complement of experimental equipment to exploit the capabilities of the accelerator. This equipment includes several large magnetic spectrometers and data acquisition and analysis computers.

The FY 1985 construction funds will be used for architectural and engineering work, for minor site work, and for design beyond the conceptual level in order to establish a reliable cost estimate for the project. Activities will include detailed design of the accelerator housing, experimental areas, and support facilities; engineering design studies of accelerator components; and geotechnical investigations of the site in order to find the best location for the accelerator.

Tandem/AGS Heavy Ion Transfer Line

This project creates a unique, heavy ion research capability at Brookhaven National Laboratory through the construction of a beam transfer line which connects the Double MP Tandem Facility with the Alternating Gradient Synchrotron (AGS). Beams of nuclei with mass up to 32 atomic mass units can be generated with energies of 15 GeV per atomic mass unit. This seven-fold increase in energy over existing Bevalac capability will permit experiments which focus on a fundamentally new form of matter. Head-on collisions of heavy nuclei are expected to create hot, high density regions of nuclear matter. Under these conditions hadronic matter is expected to undergo a phase transition to a deconfined state in which quarks and gluons interact in asymptotic freedom.

The Transfer Line project consists of: (1) a 2000 foot tunnel to connect the Tandem Facility and the AGS, (2) a beam transport system, (3) modifications of the tandems to improve voltage stability and source performance, and (4) modifications to the RF and injection systems of the AGS to provide for heavy ion acceleration.

The Total Estimated Cost of the Tandem/AGS Heavy Ion Transfer Line project is $10,300,000. In FY 1985, $5,300,000 is requested to complete the construction phase of this project ($5,000,000 in FY 1984 funds are expected to be available for the project by reprogramming funds from the High Energy Physics ISABELLE construction project).

University Accelerator Upgrade Project at the University of Washington and Yale University

This project will greatly enhance the research capability of two key university accelerator facilities. At the University of Washington a superconducting linac booster capable of 25 million volts of accelerating power is being added to an existing FN tandem Van de Graaff. At Yale University the MP tandem Van de Graaff accelerator is being upgraded by increasing the length of the insulating columns to increase the maximum voltage available for acceleration of nuclei and by increasing the size of the pressure vessel which surrounds the accelerator.

These upgrades extend the energies and range of ion species of the available beams and thus enable significant advances in the research programs of the two laboratories. This work includes studies of fundamental aspects of the nucleon-nucleon interaction, radiative capture, the nuclear force symmetry problem, search for dynamic symmetries and simplicities underlying nuclear structure and reactions, and studies of the response of nuclear systems to extreme centrifugal stress.

In FY 1985, $11,000,000 is required to complete this project. These funds will be used for fabrication, installation, testing and procurement of resonators, cryostats, high voltage column structures, beam transport magnets, and control computers.

Accelerator Improvement Projects

Accelerator facilities have continuous need during their operating life for small modifications or additions which improve their performance and enhance their usefulness to the research program. In FY 1985, a total of $3,500,000 is required for these kinds of facility upgrades under Accelerator Improvement Projects.

At Argonne National Laboratory, $660,000 is needed for a testbed section for the superconducting linac. This will permit off-line maintenance of RF resonators, thereby maximizing performance of the resonators and reducing accelerator downtime.

At the Lawrence Berkeley Laboratory, $1,400,000 is needed for an upgrade of the Bevalac switchyard. This project will significantly enhance the beam delivery flexibility, reduce beam tuning time, and, moreover, provide the capability of delivering a broad range of beams of rare isotopes.

At Los Alamos National Laboratory, $1,100,000 is needed for two efforts: (1) the completion of an improvement program at the LAMPF main beam stop, which corrects existing operational problems and provides for new research programs and (2) the rebuilding of approximately half of the quadrupole doublets on LAMPF's side-coupled linac in order to correct overheating problems of the quadrupole power coils and to improve the magnetic field quality.

At the Bates Linear Accelerator Center, $340,000 is needed for an upgrade of the switch tubes on four transmitters. This will improve operational reliability of the electron accelerator and provide the option to increase the maximum energy of the Bates beam to approximately 1 GeV.

General Plant Projects

The construction request includes $3,500,000 for General Plant Projects (GPP) at the Lawrence Berkeley Laboratory, the Bates Linear Accelerator Center, and the LAMPF facility at Los Alamos National Laboratory. At these laboratories, the Nuclear Physics program has responsibility for GPP funds which provide for minor conventional construction such as building additions, alterations, and improvements as well as improvements to land and utility systems. A total of $2,500,000 is requested for projects at the Lawrence Berkeley Laboratory, including office and laboratory space additions, upgrade of buildings to withstand earthquakes and to improve their usefulness to research programs, electrical and mechanical utility upgrading, an equipment and construction materials storage area, a PCB and radioactive materials storage area, and road projects. At the LAMPF facility, $950,000 is requested for an office and laboratory building to house health physics monitors, physicists, engineers, and service personnel connected with day-to-day operation of the experimental areas. At Bates, $50,000 is required for minor building and roadway projects to assure continuation of high safety standards at the Middleton, Massachusetts site.

Management Initiative

This decision unit reflects $-1,300,000 for savings resulting from management initiative in the area of administrative processes/field structure.

DEPARTMENT OF ENERGY
1985 CONGRESSIONAL BUDGET REQUEST
CONSTRUCTION PROJECT DATA SHEETS
GENERAL SCIENCE AND RESEARCH - PLANT AND CAPITAL EQUIPMENT
GENERAL SCIENCE AND RESEARCH
NUCLEAR PHYSICS

(Tabular dollars in thousands. Narrative material in whole dollars.)

1. Title and location of project: Accelerator improvements and modifications, various locations

2. Project No. 85-R-200

3. Date A-E work initiated: 1st Qtr. FY 1985

3a. Date physical construction starts: 2nd Qtr. FY 1985

4. Date construction ends: 2nd Qtr. FY 1987

5. Previous cost estimate: None
Less amount for PE&D: None
Net cost estimate: None
Date:

6. Current cost estimate: $3,500
Less amount for PE&D: 0
Net cost estimate: $3,500
Date: 5/83

7. Financial Schedule:

Fiscal Year	Authorizations	Appropriations	Obligations	Costs
1985	$ 3,500	$ 3,500	$ 3,500	$ 2,000
1986	0	0	0	1,000
1987	0	0	0	500

8. Brief Physical Description of Project

This project provides for additions, modifications, and improvements to major research accelerators and ancillary experimental facilities. The requested funds are necessary to maintain and improve reliability and efficiency of operations and to provide new experimental capabilities as required for execution of the planned research program.

Listed below are the laboratories and a description of each subproject:

Argonne National Laboratory ..... $ 660

This subproject provides an accelerator testbed consisting of a cryostat, six resonators, and three focusing solenoids, for use in conjunction with the Argonne superconducting linac. The testbed is the essential component required for a new system of linac maintenance.

1. Title and location of project: Accelerator improvements and modifications, various locations 2. Project No. 85-R-200

8. Brief Physical Description of Project (continued)

Lawrence Berkeley Laboratory ..... $ 1,400

A two-part subproject is planned for the Bevalac: the first part is aimed at increasing the acceptance of the beam lines for primary and secondary beams, and the second part is aimed at improving the flexibility of the External Particle Beam (EPB) system for ease in switching beam lines and making rapid momentum changes as required by experimenters.

Increasing the acceptance of the EPB system will be accomplished by rebuilding portions of this beam transport system, including the removal of aperture restrictions, relocation of optical elements, and installation of production targets for secondary beams at positions optimized for large acceptance.

Flexibility will be gained by replacing critical solid-core steering magnets with laminated switching dipoles, by adding magnet power supplies, and by improving control and instrumentation systems to allow rapid switching among beam lines and fast momentum changes within a particular beam line. This subproject will be constructed at the Lawrence Berkeley Laboratory (Berkeley, California) on non-Government owned property.

Los Alamos National Laboratory (Anderson Meson Physics Facility) ..... $ 1,100

This subproject completes a program of major improvements at the main LAMPF beam stop. The overall upgrade will provide collimators, current monitors, profile monitors, guard rings, a beam window, and a water degrader at the beam stop. Several new proton and neutron irradiation ports will be added.

This subproject also includes the upgrade of approximately 60 of the 104 quadrupole doublets which provide radial focusing in LAMPF's side-coupled linac. These magnets now display compelling evidence that they are nearing the end of their useful life. They will be replaced with magnets of improved design.

Massachusetts Institute of Technology (Bates Linear Accelerator Center)..... $ 340

Modifications will be made to the Bates RF system so that Transmitters 2-5 will be capable of delivering a peak power of 5.4 MW per klystron. The major modification required is a change of the magnetic confinement field for the Litton switch tubes from permanent magnets to solenoids. Thus this upgrade will require the retrofit installation of a solenoid and power supply in the sixteen switch tubes which are in use in the present modulators (4 per modulator). This subproject will provide 18 such units including two spares. This subproject will be constructed at the Bates Linear Accelerator Center (Middleton, Massachusetts) on non-Government owned property.

39-587 O - 84 - 76

CONSTRUCTION PROJECT DATA SHEETS

1. Title and location of project: Accelerator improvements and modifications, various locations

2. Project No. 85-R-200

8. Brief Physical Description of Project (continued)

9. Purpose, Justification of Need for, and Scope of Project

Argonne National Laboratory

The testbed to be provided by this subproject is expected to substantially improve the operating efficiency of the Argonne superconducting linac, increasing both the running time and the accelerating voltage by at least 15%.

The existing superconducting heavy-ion linac is a complete machine that is operated intensively for research. The primary remaining problem in its use is that the accelerating structures cannot be maintained at the performance levels of which they are capable without being taken off-line and thus losing several months of operating time each year.

The testbed will eliminate this problem by allowing the implementation of a maintenance system in which the performance of a linac section is perfected off-line and then, when convenient, this unit is quickly interchanged with an on-line unit that needs maintenance. In this way, it is planned that the linac as a whole will be systematically rejuvenated on a continuing basis without extended periods of accelerator downtime.

Lawrence Berkeley Laboratory

This improvement project will significantly enhance the beam delivery flexibility of the Bevalac and reduce beam tuning time. Moreover, the project will provide the capability--presently not available at any other accelerator--of delivering to nuclear physics experiments a broad range of beams of rare isotopes at energies from 40 to 2100 MeV/AMU. Thus, beams of both stable and unstable (lifetimes greater than 1 microsecond) rare isotopes will be available for experiments in any Bevalac experimental area.

Recent experimental demands for improved beam quality (i.e., minimum ion contamination and absence of halo) and for the production and transport of exotic secondary beams are unfulfilled because the External Particle Beam system is in urgent need of upgrading. The present transport system, which has not been changed (except for vacuum improvements) since the days of proton running, is inadequate for many experimental needs. Crucial shortages of magnet power supplies, controls, and instrumentation presently limit easy switching to only some selected beam lines; others require the manual recabling of magnets to change beam lines.

CONSTRUCTION PROJECT DATA SHEETS

1. Title and location of project: Accelerator improvements and modifications, various locations — 2. Project No. 85-R-200

9. Purpose, Justification of Need for, and Scope of Project (continued)

Los Alamos National Laboratory

This improvement project at the LAMPF beam stop will correct existing operational problems, reduce down time and provide for potential new research programs. The new design of the beam stop will allow quick access for repair, easier maintenance, improved shielding and provide new irradiation space.

Some of the quadrupole doublets on LAMPF's side-coupled linac have failed in service, probably due to the high operating temperature of the present design. Further, it has been found that the magnetic field quality of the present magnets is marginal at best. The rebuilt magnets will have adequate field quality and are expected to have long lives.

Massachusetts Institute of Technology (Bates Linear Accelerator Center)

This project will provide the option of increasing the maximum energy of the Bates accelerator to approximately 1 GeV and will increase reliability in achieving lower beam energies in the 600 to 840 MeV range by operating the RF system at less than maximum capacity. Since a significant fraction of the research program will use these lower beam energies, being able to achieve them with less than the maximum installed RF power both increases the lifetime of components and improves the likelihood that a scheduled beam will be achieved.

Since needs and priorities may change, other subprojects may be substituted for those listed and some of these may be located on non-Government owned property.

10. Details of Cost Estimate

a. Engineering, design, inspection, construction, procurement, component assembly, and installation ...	$ 3,500
Total Estimated Cost	$ 3,500

11. Method of Performance

Design will be by contractor staff. To the extent feasible, construction and procurement will be accomplished by fixed-price subcontractors awarded on the basis of competitive bidding.

DEPARTMENT OF ENERGY
1985 CONGRESSIONAL BUDGET SUBMISSION
CONSTRUCTION PROJECT DATA SHEETS
GENERAL SCIENCE AND RESEARCH - PLANT AND CAPITAL EQUIPMENT
GENERAL SCIENCE AND RESEARCH
NUCLEAR PHYSICS
(Tabular dollars in thousands. Narrative material in whole dollars.)

1. Title and location of project: General plant projects, various locations

2. Project No. 85-R-201

3. Date A-E work initiated: 1st Qtr. FY 1985

3a. Date physical construction starts: 2nd Qtr. FY 1985

4. Date construction ends: 2nd Qtr. FY 1987

5. Previous cost estimate: None
Less amount for PE&D: None
Net cost estimate: None
Date:

6. Current cost estimate: $3,500
Less amount for PE&D: 0
Net cost estimate: $3,500
Date: 5/83

7. Financial Schedule:

Fiscal Year	Obligations	Costs FY 1983	FY 1984	FY 1985	After FY 1985
Prior Year Projects	$ 0	$ 3,405	$ 400	$ 0	$ 0
1983	2,200	407	1,000	600	193
1984	2,200	0	600	1,000	600
1985	3,500	0	0	800	2,700
		$ 3,812	$ 2,000	$ 2,400	$ 3,493

8. Brief Physical Description of Project

This project provides for minor new construction, other capital alterations and additions, and for improvements to land, buildings, and utility systems. Where applicable, the request also includes the cost of installed capital equipment integral to a subproject. No significant R&D program is anticipated as a prerequisite for design and construction of the subprojects under construction.

Lawrence Berkeley Laboratory..... $ 2,500

1. Title and location of project: General plant projects, various locations 2. Project No. 85-R-201

8. Brief Physical Description of Project (continued)

Requirements include: Ultra high vacuum processing facility ($950,000); a yard for storage of plant engineering and construction equipment and materials ($490,000); a PCB and radioactive materials storage area ($120,000); experimental area and building rehabilitation and renovation ($590,000); utilities upgrade ($225,000); roads, walks, pathways ($125,000). This subproject will be constructed at the Lawrence Berkeley Laboratory (Berkeley, California) on non-Government owned property.

Los Alamos National Laboratory (Anderson Meson Physics Facility): ..... $ 950

Requirements include a 7000 square-foot two-story building with a full basement which contains thirteen offices, two laboratories, a conference room, drafting room and several basement work areas. The building will replace antiquated trailer offices for health physics monitors, physicists, engineers, and service personnel connected with day-to-day experimental area operations.

Massachusetts Institute of Technology (Bates Linear Accelerator Center):..... $ 50

Minor building and roadway improvements are required to assure continuation of high safety standards at the Middleton, Massachusetts site. This subproject will be constructed at the Bates Linear Accelerator Center (Middleton, Massachusetts) on non-Government owned property.

9. Purpose, Justification of Need for, and Scope of Project

Projects at the Lawrence Berkeley Laboratory, at the LAMPF facility at Los Alamos National Laboratory, and at the Bates Linear Accelerator Center at the Massachusetts Institute of Technology are needed to improve efficiency and productivity of these installations and to assure continuation of safe and reliable operations for both personnel and instrumentation.

The distribution of funds requested for FY 1985 is as follows:

Lawrence Berkeley Laboratory	$ 2,500
Los Alamos National Laboratory (Anderson Meson Physics Facility)	950
Massachusetts Institute of Technology (Bates Linear Accelerator Center)	50
Total Estimated Cost	$ 3,500

Since needs and priorities may change, other subprojects may be substituted for those listed and some of these may be located on non-Government owned property.

CONSTRUCTION PROJECT DATA SHEETS

1. Title and location of project: General plant projects, various locations 2. Project No. 85-R-201

10. Details of Cost Estimate

See description, item 8. The estimated costs are preliminary and, in general, indicate the magnitude of each program. These costs include engineering, design, and inspection.

11. Method of Performance

Design will be on the basis of negotiated architect-engineer contracts. To the extent feasible, construction and procurement will be accomplished by firm fixed-price contracts and subcontracts on the basis of competitive bidding.

DEPARTMENT OF ENERGY
1985 CONGRESSIONAL BUDGET REQUEST
CONSTRUCTION PROJECT DATA SHEETS
GENERAL SCIENCE AND RESEARCH - PLANT AND CAPITAL EQUIPMENT
GENERAL SCIENCE AND RESEARCH
NUCLEAR PHYSICS

(Tabular dollars in thousands. Narrative material in whole dollars.)

1. Title and Location of Project: Continuous Electron Beam Accelerator Facility, Newport News, Virginia

2. Project No. 85-R-203

3. Date A-E work initiated: 1st Qtr. FY 1985

3a. Date Physical Construction Starts: a/

4. Date Construction Ends: a/

5. Previous Cost Estimate: None
   Less amount for PE&D: None
   Net cost estimate: None
   Date:

6. Current cost estimate: $2,000a/
   Less amount for PE&D: 0
   Net cost estimate: $2,000a/
   Date: 12/83

7. Financial Schedule:

Fiscal Year	Authorizations	Appropriations	Obligations	Costs
FY 1985	$ 2,000	$ 2,000	$ 2,000	$ 1,500
FY 1986	0	0	0	500

8. Brief Physical Description of Project:

The Continuous Electron Beam Accelerator Facility (CEBAF) is a new facility to be located in Newport News, Virginia on a site including the land and buildings once occupied by the Space Radiation Effects Laboratory (SREL). Southeastern Universities Research Association (SURA) is expected to be the operating contractor during both construction and later operations phases of this project. It is currently planned that the site for this facility will be Federally owned land. Real estate discussions are in progress with the City of Newport News, the State of Virginia, and SURA. Electric power will be provided under direct contract with the Department of Energy.

a/ The FY 1985 request provides for architect-engineering work, detailed design beyond conceptual design, and preliminary site work. The total estimated cost of this project and exact construction dates are under review.

CONSTRUCTION PROJECT DATA SHEETS

1. Title and location of project: Continuous Electron Beam Accelerator Facility
Newport News, Virginia

2. Project No. 85-R-203

8. Brief Physical Description of Project (continued):

The accelerator facility will include a 4 GeV high intensity, continuous beam electron linear accelerator/pulse stretcher storage ring complex; experimental areas and equipment to conduct basic nuclear research; and buildings to house the accelerator complex and its research activities. The facility will possess a full complement of experimental equipment and supporting facilities to exploit the capabilities of the accelerator.

a. Conventional Construction

New construction needed to house the accelerator and the experimental areas consists of the following structures: linac tunnel, recirculation path tunnel, beam transport tunnel, ring tunnel, klystron gallery, ring gallery, two end stations, two beam dumps, and access and fan buildings.

Support facilities, including research offices and laboratories, administrative offices, conference and meeting rooms, and some shop space will be housed in both new construction and existing structures. An existing building of 70,000 square feet will be modified to provide a high-bay heavy assembly area; machine, vacuum plating, cryogenics, klystron and electronics shops; and general maintenance and equipment storage area.

Improvements to the site include grading, drainage, paving, lighting and roadways, and the extension of existing utilities, including electrical power, water, sewage, and communications.

b. Accelerator System

The centerpiece of CEBAF is the electron accelerator. It will consist of a 2 GeV pulsed linear accelerator (linac), the beam transport system to return the electron pulses for a second pass of acceleration through the linac to attain maximum energy of 4 GeV, the pulse stretcher ring in which the short, intense electron pulses are smoothed into a continuous stream, the beam transport system to take the pulses from the linac either to the pulse stretcher ring or directly to an experimental hall, an energy compression system, the beam transport system to deliver the electrons from the stretcher ring to the experimental halls, and the instrumentation and control systems for the accelerator.

The linac will consist of forty accelerating sections, each three meters long. After being accelerated through the linac once the electrons will be returned to the upstream end and reinjected into the linac between the fifth and sixth accelerating sections. After the second traversal of the linac the beam will be extracted. The intensity and energy of the electron beam will be variable on a pulse to pulse basis. Immediately following the linac will be the energy compression system wherein the energy spread of the beam will be reduced. Following the energy compression system will be a switching magnet with which the beam can be directed either to an experimental area or to the pulse stretcher ring.

CONSTRUCTION PROJECT DATA SHEETS

1. Title and location of project: Continuous Electron Beam Accelerator Facility 2. Project No. 85-R-203
Newport News, Virginia

8. Brief Physical Description of Project (continued):

The pulse stretcher ring will have a race track shape, approximately 370 m in circumference. Each electron pulse will be injected into the closed, central orbit of the stretcher ring during a single turn. Slow extraction of the beam will be achieved using half-integral resonant extraction where the tune of the machine will be moved onto the resonance by pulsing focussing elements in the ring. Vertically polarized electrons may be injected into and extracted from the ring with minor loss of polarization. Beams may be extracted at two points located on opposite sides of the ring. The beam lines will be configured to permit energy dispersed and/or longitudinally polarized beams at the targets.

c. Experimental Facilities

The accelerator will service three independent experimental areas: two buildings for experiments using electron beams and a smaller area for experiments using photon beams. Nationwide users of the new facility are now participating in detailed studies of CEBAF research equipment. These studies indicate that the equipment will need to include: a pair of moderate resolution magnetic spectrometers, an out-of-plane spectrometer, target monitor spectrometers, nonmagnetic spectrometers, detectors that are simultaneously sensitive to all scattering angles, high power targets, polarized targets, miscellaneous detectors and electronics, and a set of computers for data acquisition and analysis.

9. Purpose, Justification of Need for, and Scope of Project:

The Continuous Electron Beam Accelerator Facility meets the highest priority need for new accelerator construction in the U.S. nuclear physics program. CEBAF's electron linac/stretcher ring accelerator complex, with its continuous beam and its capability of providing beams at any energy in the range from 500 MeV to 4,000 MeV, offers the opportunity to study the largely unexplored transition between the nucleon-meson and the quark-gluon states of nuclear matter. Recent experiments have established that nucleons and mesons are composed of quarks and gluons, which are believed to interact according to the laws of Quantum Chromodynamics (QCD). The crucial problems facing nuclear physics today are, therefore, to understand to what extent this clustering of quarks and gluons into nucleons and mesons breaks down in the nuclear medium, giving rise to new states of matter and to learn how these new states of matter, which are the most visible manifestation of the presence of quarks and gluons and the laws of QCD, can be used to understand the structure of nuclei and the nature of the effective force between nucleons and mesons. CEBAF will possess the unique facilities necessary to address these questions with an unprecedented degree of precision.

CONSTRUCTION PROJECT DATA SHEETS

1. Title and location of project: Continuous Electron Beam Accelerator Facility 2. Project No. 85-R-203
Newport News, Virginia

9. Purpose, Justification of Need for, and Scope of Project: (Continued)

Measurements of the electric charge distribution of the neutron, pion, and kaon, which will be possible at CEBAF, promise to reveal much about the distribution of quarks in simple bound systems. Electro- and photoproduction of hypernuclei via the (e, e'K^+) reaction inserts strange quarks into nuclei and thus provides ideal opportunities to study selectively valence quark distributions. Polarized beams at CEBAF will make possible studies of fundamental symmetries of nature and will permit the direct measurement of many amplitudes which are particularly sensitive to details of nucleon structure that cannot be measured otherwise.

Detection of a scattered electron at a given angle and with a particular energy could result from a wide variety of electron-nucleus interactions. To accurately determine the dynamics of the event often requires that one or more reaction products be detected in coincidence with the scattered electron; this dictates that the incident beam have a high duty factor, that is, be a continuous beam rather than the sharply pulsed beams presently available at existing accelerators. The necessity for a continuous beam is essential at all energies and it becomes even more imperative as the numbers and complexity of the possible final states increase, which happens at the higher energies.

CEBAF will be the only facility in the world capable of producing electron beams which meet the necessary criteria of energy, duty factor and beam intensity. Other accelerators can deliver beams of similar or higher energies and others can match the high duty factor, but CEBAF's combination of polarized beams of multi-GeV energy, with high intensity and high duty factor, is unmatched. The unique combination of beam parameters available at CEBAF will make it a facility of unparalleled capability and the research will enable the U.S. to maintain its preeminence in this important area of nuclear science. The broad spectrum of physics accessible at CEBAF ensures that it will become and remain one of the important scientific centers in the world.

The FY 1985 construction funds will be used for architectural and engineering work, design beyond the conceptual level, and preliminary site work in order to establish a reliable cost estimate for the project. Activities will include detailed design of the accelerator housing, experimental areas, and support facilities; engineering design studies of accelerator components; and geotechnical investigations of the site in order to find the best location for the accelerator.

CONSTRUCTION PROJECT DATA SHEETS

1. Title and location of project: Continuous Electron Beam Accelerator Facility 2. Project No. 85-R-203
Newport News, Virginia

9. Purpose, Justification of Need for, and Scope of Project (Continued)

10. Details of Cost Estimate:

The project provides funds for architect-engineering work and detailed design beyond conceptual design during FY 1985. Early studies have been completed, and it is anticipated that the TEC will be $200,000,000 to $225,000,000.

11. Method of Performance:

Design and inspection will be by the Operating Contractor and by negotiated A-E contract. To the extent feasible, construction, procurement and installation will be accomplished by fixed-price contracts and subcontracts awarded on the basis of competitive bidding.

DEPARTMENT OF ENERGY
1985 CONGRESSIONAL BUDGET REQUEST
CONSTRUCTION PROJECT DATA SHEETS
GENERAL SCIENCE AND RESEARCH - PLANT AND CAPITAL EQUIPMENT
GENERAL SCIENCE AND RESEARCH
NUCLEAR PHYSICS
(Tabular dollars in thousands. Narrative material in whole dollars.)

1. Title and location of project: Tandem/AGS Heavy Ion Transfer Line, Brookhaven National Laboratory, Upton, N.Y.

2. Project No. 84-R-123

3. Date A-E work initiated: 2nd Qtr. FY 1984

3a. Date physical construction starts: 3rd Qtr. FY 1984

4. Date construction ends: 1st Qtr. FY 1986

5. Previous cost estimate: None
Less amount for PE&D: None
Net cost estimate: None
Date:

6. Current cost estimate: $10,300
Less amount for PE&D: 0
Net cost estimate: $10,300
Date: 12/83

7. Financial Schedule:

Fiscal Year	Authorizations	Appropriations	Obligations	Costs
1984	$ 5,000[a/]	$ 5,000[a/]	$ 5,000[a/]	$ 3,000
1985	5,300	5,300	5,300	5,000
1986	0	0	0	2,300

a/ Proposed reprogramming from ISABELLE construction project (78-10-b).

8. Brief Physical Description of Project

A beam transfer line will be constructed to connect the Double MP Tandem Facility with the Alternating Gradient Synchrotron (AGS). This transfer line will transport beams of heavy ions initiated with the Tandems to be further accelerated in the AGS to energies of approximately 15 GeV/nucleon. With minimal modification to the AGS and Tandems, intensities of oxygen beams of 4×10^{10} particles per pulse (ppp) and intensities of sulfur beams of 6×10^{8} ppp can be anticipated with beams of higher mass up to calcium possible at reduced intensity. These beams will have energies approximately a factor of seven greater than those presently available elsewhere in the world. The Transfer Line project includes: (1) bending and focusing magnets and vacuum pipe to transport heavy ion beams from the Double MP Tandem Facility to the AGS, (2) a tunnel to house these magnets and vacuum pipe, and (3) necessary, minor modifications of the Tandem Van de Graaff and the AGS accelerators.

CONSTRUCTION PROJECT DATA SHEETS

1. Title and location of project: Tandem/AGS Heavy Ion Transfer Line, Brookhaven National Laboratory, Upton, N.Y. 2. Project No. 84-R-123

8. Brief Physical Description of Project

a. Transfer Line Tunnel

The tunnel will be about 2000 feet long and 10 feet in diameter. The location of the transfer line was determined by selecting the most suitable entry point for the AGS ring, C-20 straight section, while minimizing the number of beam bends and site modifications.

The tunnel will be bored below grade in the area next to the Tandem Facility; cut-and-fill methods will be used for the rest of the tunnel. The tunnel will be connected to the Tandem Facility at the east end of the north wall, will run parallel to the north wall for about 1000 feet and will bend 48^{0} north to meet the AGS ring. Emergency exits and necessary structures for electrical, mechanical and environmental equipment are included in the tunnel design.

Work due to the reconfiguration of the site will include modifications to existing roadways and parking lots, as well as grading and seeding. Additional primary utilities will be extended from present main utility systems. Construction will be non-combustible throughout. The tunnel will have a steel liner and a concrete floor.

The environment within the tunnel will be controlled by an energy-efficient ventilating and heating system with humidity controls designed to optimize energy conservation. Day and night control set-back systems and equipment turnoff to reduce energy consumption during off hours when experiments are not running will be installed. The entire facility will be fire protected by a dry pipe pre-action sprinkler system and detectors. Power will be distributed by 115/208/460 volt, 3 phase system. Lighting levels and equipment will be designed to meet the latest energy conservation requirements and to ensure low maintenance costs.

b. Beam Transport System

Heavy ion beams from the Double MP Facility are of very high quality and are thus not difficult to transport to the AGS. The beam line has been designed around modular 200 foot sections each requiring a quadrupole doublet and a small steering magnet. A double 90^{0} bend is needed to turn the beam into the tunnel at the Tandems; a 48^{0} bend is needed part way to direct it to the appropriate straight section of the AGS; and a double 69^{0} bend is needed at the AGS. A 10^{-9} Torr vacuum is required in order to reduce the charge changing collisions of heavy ions with the residual gas.

CONSTRUCTION PROJECT DATA SHEETS

1. Title and location of project: Tandem/AGS Heavy Ion Transfer Line
Brookhaven National Laboratory, Upton, N.Y.

2. Project No. 84-R-123

8. Brief Physical Description of Project (continued)

c. Tandem Modification

The Double MP Tandems require only minor modifications to perform as an injector for the AGS. A new high intensity ion source and pulsing system are needed for the high voltage terminal of MP-6. A portico-intershield will be installed in MP-7 to improve the voltage stability of the terminal.

d. AGS Modification

Because the heavy ions from the Tandem Facility will have low velocity the RF system of the AGS must have a new acceleration stage. The beam is to be accelerated first by a "pre-conversion" AGS cavity which will be provided with a new RF amplifier and bias system to sweep in frequency from 0.55 to 2.2 MHz. The remainder of the acceleration cycle will be handled by the present RF system. A new electrostatic inflector is required to inject the beam into the AGS ring. Also, the AGS control system will be extended to the new equipment in the AGS and to the transfer line using standard modules developed in part for the AGS polarized proton program.

9. Purpose, Justification of Need for, and Scope of Project

The most exciting of the experiments to be performed at the AGS with the 15 GeV/nucleon probes will focus on phenomena associated with a fundamentally new form of matter. This research opportunity stems from the realization that the conditions for creating an energy density greater than that of the proton can be obtained in head-on collisions of heavy nuclei at large center-of-mass energies. In such central collisions high densities are expected to be created over regions with size of the order of nuclear dimensions, through the cooperative action of the many nucleons involved. As a result, the bags confining the constituents of normal hadrons are expected to disappear, giving way, instead, to a large bubble within which large numbers of quarks and gluons interact in asymptotic freedom. While there seems to be agreement among theorists that such a deconfined state will exist given the right physical conditions, it remains problematical what these "right physical conditions" exactly are, and, precisely in which way this new matter-phase will manifest itself. It is the major object of the experimental program to answer these questions.

Heavy-ion beams with energies approximately seven-fold increased over existing capabilities will surely produce conditions in the nuclear medium that have not been accessible before. Aside from the search for quark matter, there are many other important subjects to address that have arisen through both experimental results and theoretical hypotheses, among them; pion condensates, nuclear transparency, density isomers and anomalons.

CONSTRUCTION PROJECT DATA SHEETS

1. Title and location of project: Tandem/AGS Heavy Ion Transfer Line
Brookhaven National Laboratory, Upton, N.Y.

2. Project No. 84-R-123

a. Transfer Line and Tunnel

The transfer line connecting the AGS and the Tandems is the most expeditious way of obtaining heavy ions at AGS energies. The Tandem Facility is a proven source of heavy ions at energies, charge states and intensities useful for AGS injection. Both accelerators have run for many years and have well known, predictable operating characteristics. The transfer line poses no technical problems because of the small transverse emittance and the small energy spread of the Double MP Tandem beam. Building a new heavy ion injector for the AGS would be much more expensive than the transfer line and would take much longer to construct. It is indeed the fortuitous circumstances of the Tandem Facility and the AGS both being available that allows the rapid realization of a unique relativistic heavy ion facility simply through the construction of a transfer line.

b. AGS Modifications

There are two essential modifications of the AGS which are needed to accelerate the heavy ions injected by the Tandems. At present the AGS is injected by using negative ions and stripping them to their positive charge state in order to capture them. This procedure is not suitable for positive heavy ions from the Tandems. An electrostatic inflector is required. In addition, heavy ions from the Tandem are moving at much lower velocity than the protons now used for AGS injection. Consequently, a new AGS acceleration stage is required to raise the heavy ions to velocities sufficient for acceleration by existing AGS systems. Also, control systems linked to the AGS must be extended to the new equipment.

c. Tandem Modifications

Injection of heavy ion beams from the Tandem Facility into the AGS puts heavy demands on the Tandem ion source and requires excellent voltage stability of the Tandems. The ion source problems have been solved by pulsing a Mark VII Middleton ion source; the beam intensities quoted for the AGS are based on those already obtained for two-stage acceleration. A second source is requested for installation in MP-6 to permit three-stage operation and thereby develop the highest possible currents for fully stripped ions with mass greater than A=16.

This project also includes the construction of a portico intershield for MP-7 (the tandem with the positive terminal), as has already been done at Strasbourg, France on a similar machine. The intershield, which provides better electrostatic field distribution in the insulting gas, will allow an increase in terminal voltage to 18

1. Title and location of project: Tandem/AGS Heavy Ion Transfer Line
Brookhaven National Laboratory, Upton, N.Y.

2. Project No. 84-R-123

c. Tandem Modifications

million volts, and of more importance to the AGS research program, will increase the stability and reliability at the terminal voltages used for injection.

10. Details of Cost Estimate*

	Item Cost	Item Subtotal	Total Cost
a. Engineering, Design and Inspection			$ 1,630
1. Conventional construction at approximately 13% of items b.1 and b.2		$ 420	
2. Technical components at approximately 30% of items b.3		1,210	
b. Construction Costs			$ 7,230
1. Improvements to land		60	
2. Conventional Construction		3,140	
a) Tunnel, miscellaneous structures	$ 3,020		
d) Mechanical and electrical utilities	120		
3. Special Facilities		$ 4,030	
a) Beam transport system	2,680		
b) AGS modifications	910		
c) Tandem modifications	440		
Subtotal			8,860
c. Contingency at approximately 16% of above costs			1,440
Total Estimated Cost			$ 10,300

*Based on a completed conceptual design.

11. Method of Performance

This type of construction is unique and therefore the conceptual design, preliminary design (Title I), construction supervision, assembly and testing will be done by the staff of the Brookhaven National Laboratory (with the assistance of an architectural-engineering firm). Component parts wherever possible will be fabricated by industry under fixed-priced, competitively obtained procurement actions. Some components may be fabricated in the shops at

CONSTRUCTION PROJECT DATA SHEETS

1. Title and location of project: Tandem/AGS Heavy Ion Transfer Line
Brookhaven National Laboratory, Upton, N.Y.

2. Project No. 84-R-123

11. Method of Performance (continued)

BNL. It is also anticipated that other laboratories, private consultants and industrial firms will be used for advice on specific problems. Final building design and construction will be by a competively obtained, design-build, lump sum contract. Because of its unique design, it is anticipated that the portico intershield will be purchased from the French company that manufactures this item.

12. Funding Schedule of Project Funding and Other Related Funding Requirements

	FY 1984	FY 1985	FY 1986	Total
a. Total project cost				
1. Total facility cost				
a) Construction line item	$ 3,000	$ 5,000	$ 2,300	$ 10,300
b) PE&D	0	0	0	0
Total facility costs	3,000	5,000	2,300	10,300
2. Other project costs				
a) R&D necessary to complete construction	700	1,000	0	1,700
b) Experimental equipment costs	0	1,700	3,300	5,000
Total other project costs	700	2,700	3,300	6,700
Total project cost	$ 3,700	$ 7,700	$ 5,600	$ 17,000

b. Other related annual funding requirements (in FY 1985 dollars)

1. Facility operating costs	
a) Incremental costs for AGS operation	$ 5,600
b) Incremental costs for transfer line operation and AGS research	1,800
2. Programmatic operating expenses directly related to the facility	
a) Cost of the existing research program and accelerator operations at the Double MP Tandem Facility	3,500

1. Title and location of project: Tandem/AGS Heavy Ion Transfer Line
Brookhaven National Laboratory, Upton, N.Y.

2. Project No. 84-R-123

3. Capital equipment not related to construction but related to the programmatic effort
   a) Incremental cost of equipment acquisition at the AGS..... $ 250
   b) Costs of base program equipment acquisition at the Tandems.... 250

Total other related annual funding requirements..... $ 11,400

13. Narrative Explanation of Total Project Funding and Other Related Funding Requirements

a. Total project cost
   1. Total facility cost
      Explained in Items 8, 9, and 10

   2. Other project costs

      R&D necessary to complete construction - includes engineering and design effort by Tandem and AGS staff.

      Experimental equipment - includes two complementary spectrometer systems: (1) the Multi-Particle Spectrometer to study global event structure with nearly complete measurement of individual events in a large solid angle and (2) the Multi-Function Spectrometer for the detailed, microscopic measurement of foward-angle charged and neutral production from the central fireball and projectile fragments.

b. Other related annual funding requirements
   1. Facility operating costs
      a) Incremental cost associated with operating the AGS for 10 weeks per year.
      b) Incremental cost of operation and maintenance of the transfer line and research at AGS.

   2. Programmatic operating expenses directly related to the facility.
      a) This includes costs of the ongoing research program and is equal to the present Tandem Research and Operations budget for FY 1984 (escalated to FY 1985).
   3. Capital equipment not related to construction but related to the programmatic effort

      a) These equipment funds will provide utilization growth of the facility through the acquisition of: new detectors, detector improvement, and general capital items for the research program.
      b) Ongoing capital equipment funding for the Tandem Facility to provide for new research efforts at the AGS.

DEPARTMENT OF ENERGY
1985 CONGRESSIONAL BUDGET REQUEST
CONSTRUCTION PROJECT DATA SHEETS
GENERAL SCIENCE AND RESEARCH - PLANT AND CAPITAL EQUIPMENT
GENERAL SCIENCE AND RESEARCH
NUCLEAR PHYSICS

(Tabular dollars in thousands. Narrative material in whole dollars.)

1. Title and location of project: University Accelerator Upgrade Project at University of Washington and Yale University Seattle, Washington and New Haven, Connecticut

2. Project No. 84-ER-110

3. Date A-E work initiated: 1st Qtr. FY 1984

3a. Date physical construction starts: 3rd Qtr. FY 1984

4. Date construction ends: 3rd Qtr. FY 1987

5. Previous cost estimate: None
Less amount for PE&D: None
Net cost estimate: None
Date:

6. Current cost estimate: $19,000
Less amount for PE&D: 0
Net cost estimate: $19,000
Date: 9/83

7. Financial Schedule:

Fiscal Year	Authorizations	Appropriations	Obligations	Costs
1984	$ 8,000	$ 8,000	$ 8,000	$ 2,000
1985	11,000	11,000	11,000	8,000
1986				6,000
1987				3,000

8. Brief Physical Description of Project

This project consists of two subprojects which provide for the addition of a superconducting linac booster to the University of Washington FN tandem Van de Graaff accelerator and the upgrade of the MP tandem Van de Graaff accelerator at Yale University.

University of Washington

Principal additions and modifications are: (a) fabrication and installation of superconducting linac sections which provide about 25 million volts (MV) of accelerating power; (b) improvement of the ion source system of the tandem accelerator; and (c) installation of a beam transport system to convey the beam from the tandem to the booster and from the booster into an existing experimental area. The main components of the proposed superconducting linac consist of an array of lead-plated copper quarter-wave resonators. A prototype for these

CONSTRUCTION PROJECT DATA SHEETS

1. Title and location of project: University Accelerator Upgrade Project at University of Washington and Yale University Seattle, Washington and New Haven, Connecticut

2. Project No. 84-ER-110

8. Brief Physical Description of Project (continued)

resonators has been developed jointly by the State University of New York at Stony Brook and the Weizmann Institute of Science. Most aspects of the radiofrequency control and cryogenic systems will be copied from the Stony Brook superconducting linear accelerator, incorporating improvements developed for the Weizmann Institute accelerator. The iinac will fit entirely within existing shielded building space.

The booster will more than double the range of energies of ions available for nuclear research--for example, protons and deuterons from 18 million electron volts (MeV) to 36 MeV and oxygen ions from 88 to 240 MeV. New beams of heavier ions will be possible, for example, silicon ions at 350 MeV and calcium ions at 370 MeV.

The University of Washington has agreed to provide up to $1,030,000 of support for refrigeration and cryogenic distribution systems, building modifications, and for technical personnel.

The superconducting booster will be housed on non-Government owned land within the Nuclear Physics Laboratory which is located on University of Washington property.

Yale University

Principal additions and modifications are: (a) extension of the acceleration tubes and insulating column structure; (b) replacement of the pressure tank; (c) upgrade of terminal charging and mechanical power systems; and (d) improvement of beam transport and analysis systems. With these changes, based on operational experience at well above 13.5 million volts (MV) on terminal, terminal potentials in the proposed configuration can conservatively be anticipated at 20 MV with 22 MV as a realistic goal. Heavy ions having atomic masses as high as 120 will have energies exceeding the Coulomb barrier on a uranium target; heavy ions up to uranium itself will have energies in excess of 2.5 MeV per nucleon. Light ion beams will be available in the energy ranges up to 44 MeV for hydrogen ions, 66 MeV for helium ions, and 88 MeV for lithium ions. The desirable characteristics of electrostatic accelerators, namely, excellent beam energy resolution, rapid variabiltiy of beam energy over a wide energy range, and the continuous beam, will not be compromised by the additions and modifications to the accelerator.

The existing structure uses four eight-foot long accelerating tube sections on either side of the high voltage terminal. This number will be increased to five by adding an additional section at each end of the acclerator. Furthermore, each tube section will be increased in length from 72 to 88 inches by extension into former intertube

CONSTRUCTION PROJECT DATA SHEETS

1. Title and location of project: University Accelerator Upgrade Project at University of Washington and Yale University Seattle, Washington and New Haven, Connecticut

2. Project No. 84-ER-110

8. Brief Physical Description of Project (continued)

dead spaces. The existing pressure tank has an internal diameter of 18 feet in the terminal region and a pronounced taper to small diameter at its ends; this tank will be replaced with one having a 25 foot internal diameter in the terminal region and much reduced taper.

Certain additional changes to the accelerator will be required. Because addition of new components such as foil strippers, cyropumps, and electrostatic quadrupole lenses to the existing terminal would overcrowd the available space in the eight-foot long present structure, the terminal length will be increased by two feet during the conversion. This increase, together with the two additional column sections, implies a new tank some 20 feet longer than the current one, i.e., 100 rather than 80 feet. The existing electrostatic column and its associated hardware, resistors, etc., will be transferred directly to this new tank with the addition of the new column extension. To provide greater lateral mechanical stability to the longer column, insulating braces will be added to the dead sections closest to the tank ends. In addition, a Letournel portico-intershield will be installed to provide better electrostatic field distribution in the insulating gas. In order to ensure adequate charge carrying capacity by the existing charging chains at higher terminal potentials, the chains will be freed of their current function of transmitting some 6 KW of mechanical energy to the terminal. For this purpose, a rotating shaft mechanical power system will be installed in parallel with the chains.

Since this subproject will provide substantially improved energy performance for all ions, particularly in mass regions above those now in use at Yale, the primary 90^{o} momentum analyzing magnet, the high energy magnetic quadrupole lens and the switching magnet will be replaced with units appropriate to the higher magnetic rigidities which will become available.

The new tank will fit within the existing laboratory vault so that the only building modifications required are the opening and closing of one of its corners to permit exchange of the pressure tanks and the provision of new footings and pads for the larger tank. All of the modifications and improvements that have been made to the MP accelerator since its commissioning in 1966, and such ancillary units as the injector and gas handling system, will be directly transferred to the upgraded accelerator.

A further enhancement of the accelerator facility will be provided by the addition of facilities for bunching and pulsing the accelerator beam. New beam lines and a switching magnet will also be provided for the second target room.

The upgraded tandem Van de Graaff accelerator will be housed on non-Government owned land within the A.W. Wright Nuclear Structure Laboratory which is located on Yale University property.

CONSTRUCTION PROJECT DATA SHEETS

1. Title and location of project: University Accelerator Upgrade Project at University of Washington and Yale University Seattle, Washington and New Haven, Connecticut

2. Project No. 84-ER-110

9. Purpose, Justification of Need for, and Scope of Project

This project will greatly strengthen the research capabilities at the Nuclear Physics Laboratory of the University of Washington and at the A. W. Wright Nuclear Structure Laboratory of Yale University. The increased beam energies and expanded range of ion species will enable forefront nuclear physics experiments to be performed in these university laboratories, which have a history of training high quality nuclear science graduates.

University of Washington

The new superconducting booster facility will open new areas of research in light ion nuclear physics. This subproject will be constructed at the University of Washington on non-Government owned land. The factor-of-two greater energy, high beam quality, variable energy of the beam, and availability of a high intensity polarized ion source will enable expansion of the present work of the University of Washington laboratory. Emphasis will be placed on light ion reaction studies, radiative capture, and studies of fundamental aspects of the nucleon-nucleon interaction. High quality polarized beams will be used for improved nuclear structures studies, for nuclear force symmetry problem studies, and for parity violation studies exploiting longitudinal analyzing power measurements in systems such as proton + proton and neutron + proton. The characterization of the symmetry properties of the strong part of the nuclear force and the parity violating component of the weak part of the nuclear force are two of the leading contemporary problems in understanding nuclear forces.

The new linac booster will also provide light heavy-ion beams for the exploration of a projectile energy domain where a large fraction of the total reaction cross section goes into noncompound nuclear reactions. The domain is fertile ground for learning about the dynamic behavior of nuclear matter under extreme conditions. The availability of light heavy ions in the 10-15 MeV/nucleon range enables exploration of the energy region where there are indications of a transition from the predominantly two-body exit channels of low energy reactions to the fragmentation mechanisms characteristic of very high energy nuclear collisions. It is in this energy region where the projectile velocity becomes comparable to the velocity of sound in nuclear matter. It will thus be possible to assess the relevance of this transition in determining the dynamical behavior of nuclear matter.

Yale University

The proposed conversion of the MP tandem accelerator will greatly increase the research potential of the Wright Nuclear Structure Laboratory. This subproject will be constructed at Yale University on non-Government owned land. The upgraded accelerator will be capable of doing transfer reactions with heavy ion beams using, for example, the reaction which converts oxygen-18 to oxygen-17 by "transferring" a neutron to the target nucleus.

CONSTRUCTION PROJECT DATA SHEETS

1. Title and location of project: University Accelerator Upgrade Project at University of Washington and Yale University Seattle, Washington and New Haven, Connecticut

2. Project No. 84-ER-110

9. Purpose, Justification of Need for, and Scope of Project (continued)

The enhanced heavy ion capability of the upgraded facility will also permit extensions of the Laboratory's long established program in quasi-molecular resonance studies. For the first time, Yale scientists can extend the measurements to systems such as Si + Si, which has shown surprising oscillatory cross sections even though the silicon nucleus is known to be oblate in its lowest energy state. Higher energy resonance investigations of oxygen systems have given hints of cluster structure. For example, silicon plus alpha particle structures are detected in the decay of the compound system. Use of very heavy systems, such as Ni + Ni, will extend the pioneering work of Yale investigators on atomic-nucleus coupling. Yale scientists will attempt to determine the time scale of compound nucleus formation by identifying the K X-rays ejected as the nuclear reaction proceeds to completion.

In addition to providing unique probes of nuclear structure and dynamics in regions inaccessible to facilities of lesser precision and flexibility, the upgraded accelerator will permit continuation of the very broad program of study that has characterized the Wright Laboratory since its founding. Augmenting the core nuclear physics studies, this program includes nuclear astrophysics, high energy atomic and molecular physics, as well as programs in the interfaces between nuclear and materials science and between nuclear and surface science. The Yale program has spanned a range of studies from those on the fundamental natural forces, through nuclear structure and dynamics, to very applied ones on such topics such as the behavior of hydrogen in inner wall materials of possible fusion reactors and the hydration of possible glasses to be used in nuclear waste isolation. In all of these studies, the unique beam properties and flexibility of the Van de Graaff beam have been essential. These experiments have raised new and interesting questions which require higher energies and intensities for their solution.

10. Details of Cost Estimate*

	Item Cost	Total Cost
University of Washington Subproject		
a. Engineering, design and inspection at approximately 13% of item b.....		$ 730

CONSTRUCTION PROJECT DATA SHEETS

1. Title and location of project: University Accelerator Upgrade Project at University of Washington and Yale University Seattle, Washington and New Haven, Connecticut

2. Project No. 84-ER-110

10. Details of Cost Estimate* (continued)

	Item Cost	Total Cost
b. Construction and special equipment costs.....		5,550
1. Acceleration structures.....	$1,180	
2. Cryostats.....	990	
3. RF system and control.....	1,000	
4. Cryogenic distribution system.....	280	
5. Beam bunching and transport.....	1,520	
6. Tandem injection upgrade.....	580	
c. Contingency at approximately 27% of above cost		1,720
Total estimated cost (University of Washington Subproject).....		$8,000
Yale University Subproject		
d. Engineering, design and inspection at approximately 10% of item e.....		$ 840
e. Construction and special equipment.....		8,360
1. Pressure tank.....	$2,235	
2. Column sections, power drive shaft, acceleration tubes, resistors and assembly hardware.....	3,360	
3. High voltage terminal modifications, charging chain extension, and insulating gas.....	760	
4. Pulsing and bunching systems.....	235	
5. Beam transport equipment.....	890	
6. Installation.....	880	

CONSTRUCTION PROJECT DATA SHEETS

1. Title and location of project: University Accelerator Upgrade Project at University of Washington and Yale University Seattle, Washington and New Haven, Connecticut

2. Project No. 84-ER-110

10. Details of Cost Estimate* (Continued)

f. Contingency at approximately 20% of above cost	1,800
Total estimated cost (Yale University Subproject)	$11,000
Total estimated cost for both subprojects.....	$19,000

* Cost estimate based on completed conceptual design reports

11. Method of Performance

For the subproject at the University of Washington, to the extent feasible construction and procurement will be accomplished by fixed-price contracts awarded on the basis of competitive bids.

For the subproject at Yale University, the major fraction of the components required will be procured on a fixed-price basis from High Voltage Engineering Corporation which is the sole source for these components. The remaining components will be procured on a competitive fixed-price basis. Many aspects of the installation will be subcontracted by Yale on a competitive basis. High Voltage Engineering Corporation will provide installation supervision (including guarantee of the mechanical integrity of the converted electrostatic structure).

12. Funding Schedule of Project Funding and Other Related Funding Requirements

	Prior Years	FY 1984	FY 1985	FY 1986	FY 1987	FY 1988	Total
a. Total project cost							
1. Total facility costs							
a) Construction line item	$ 0	$ 2,000	$ 8,000	$ 6,000	$ 3,000	$ 0	$19,000
b) PE&D	0	0	0	0	0	0	0
Total facility Costs	$ 0	$ 2,000	$ 8,000	$ 6,000	$ 3,000	$ 0	$19,000

CONSTRUCTION PROJECT DATA SHEETS

1. Title and location of project: University Accelerator Upgrade Project at University of Washington and Yale University Seattle, Washington and New Haven, Connecticut

2. Project No. 84-ER-110

12. Funding Schedule of Project Funding and Other Related Funding Requirements (continued)

	Prior Years	FY 1984	FY 1985	FY 1986	FY 1987	FY 1988	Total
2. Other project costs							
a) R&D necessary to complete construction	$ 0	$ 120	$ 180	$ 200	$ 130	$ 0	$ 630
b) Capital equipment costs	0	0	0	0	500	500	1,000
Total other project costs	$ 0	$ 120	$ 180	$ 200	$ 630	$ 500	$ 1,630
Total project costs	$ 0	$ 2,120	$ 8,180	$ 6,200	$ 3,630	$ 500	$20,630

b. Other related annual funding requirements (in FY 1984 dollars)
1. Programmatic operating costs directly related to the facilities $ 1,000

Total other related annual funding requirements $ 1,000

13. Narrative Explanation of Total Project Funding and Other Related Funding Requirements

a. Total project cost
1. Total facility costs
Construction line item explained in items 8, 9 and 10
2. Other project costs
R&D necessary to complete construction - includes engineering and design effort by laboratory staff.
Capital equipment costs - includes ancilliary equipment needs.

b. Other related annual funding requirements
The estimated incremental annual cost of performing physics research by the University of Washington and Yale University faculty, graduate students, and postdoctoral fellows is $500,000 in FY 1984 dollars at each institution.

DEPARTMENT OF ENERGY
1985 CONGRESSIONAL BUDGET REQUEST
LEAD TABLE
GENERAL SCIENCE PROGRAM DIRECTION
GENERAL SCIENCE AND RESEARCH
(Tabular dollars in thousands. Narrative material in whole dollars.)

	1983 Appropriation	1984 Appropriation	1985 Base	1985 Request
General Science Program Direction				
Operating Expenses	$ 1,413	$ 2,250	$ 2,250	$ 2,205
Total	1,413*	2,250	2,250	2,205
Staffing Total FTE's:	33	35	35	35

*Reflects comparability adjustment of $272,000 from Policy and Management - Energy Research for support associated with the programs.

Authorization: Section 209, P.L. 95-91.

DEPARTMENT OF ENERGY
1985 CONGRESSIONAL BUDGET REQUEST
SUMMARY OF CHANGES
GENERAL SCIENCE PROGRAM DIRECTION
(in thousands of dollars)

1984 Appropriation enacted	$ 2,250
Built in reduction	- 45
1985 budget request	$ 2,205

General Science Program Direction

The FY 1985 request for General Science Program Direction is $2,205,000, a decrease of $45,000 from the FY 1984 level. These funds are required to provide for the salaries, benefits, travel and other expenses associated with 35 full-time equivalents in the Office of the Associate Director for High Energy and Nuclear Physics, the Division of High Energy Physics, the Division of Nuclear Physics, and associated ER support staff required to administer these programs. The funding reduction represents some management savings while at the same time absorbing the increased personnel costs related to continuation of the FY 1984 staffing level. The increased workload resulting from continued program growth will require an increase in staff productivity and more efficient management and coordination activities among the Headquarters, field, and contractor staffs.

This staff is responsible for providing effective management, planning and direction to ensure that a viable, high quality national program of basic research is carried out in the fields of high energy physics and nuclear physics. To carry out these responsibilities, the staffs assess the basic research needs in these areas with advice from the appropriate advisory committees, High Energy Physics Advisory Panel (HEPAP) and DOE/NSF Nuclear Science Advisory Committee (NSAC). The DOE staff provides administrative support for operation of HEPAP and participates actively in both HEPAP and NSAC meetings and special subpanel studies. This staff develops and coordinates, with appropriate agency and external communities, a coherent policy and long-range plan for support of balanced national programs in high energy and nuclear physics; develops budget requests and justification for funding to implement program plans; optimizes the allocation of resources to the laboratories and universities supported by the Department to achieve maximum research productivity, cost effectiveness and efficiency of operation; and provides technical oversight for high energy and nuclear physics research programs at 15 major laboratories and for about 200 university contracts and 7 major construction projects. The staff also participates extensively in international cooperative efforts, which involve the development and management of activities under three formal agreements for cooperation, including participation of U.S. scientists both in experiments at foreign facilities with unique capabilities not available in the U.S. and in conferences and workshops abroad. Coordination of high energy and nuclear physics activities is assisted by staff participation in on-site program reviews of contractors; semiannual on-site review of major projects; meetings of laboratory program advisory committees; special facility and research planning meetings; and regional, national, and international research meetings, and technical workshops.

The high energy physics staff oversees the operation of three large, complex high energy accelerator centers at BNL, Fermilab, and SLAC which are used on a national basis by qualified physicists. The staff will provide technical oversight for three major ongoing construction projects, including at Fermilab the Tevatron I ($82,500,000) with scheduled completion in FY 1986 and Tevatron II ($49,000,000) with scheduled completion in FY 1985 and at SLAC the Stanford Linear Collider ($112,000,000) with scheduled completion in FY 1987. Technical oversight of the operation of the completed portions of Tevatron II and preparation for and participation in new 1,000 GeV Tevatron experiments will be required. The staff also oversees an extensive program in advanced technology R&D including efforts in support of ongoing construction projects, efforts related to enhancing scientific capability and operating effectiveness of existing facilities and studies of advanced concepts. The staff manages over 100 university research tasks.

Success of the Nuclear Physics program depends upon effective operation of seven large and complex national accelerator facilities. Nuclear Physics staff will oversee high priority, new research capabilities at LBL (Uranium Beams Project), ORNL (Holifield Heavy Ion Research Facility), and ANL (ATLAS Construction Project). This staff will continue to oversee the University Accelerator Upgrade Project at the University of Washington and Yale University to strengthen university research capabilities. New initiatives include the start of nuclear physics experiments at both the new SLAC injector and BNL's National Synchrotron Light Source. In addition, this staff will be

responsible for R&D and construction of a major new facility, the Continuous Electron Beam Accelerator Facility. It will be built by a consortium of universities unfamiliar with Departmental construction procedures. More than normal staff work will be required for success of this construction project. The staff will also be responsible for construction of a new nuclear physics facility at BNL, a heavy ion beam transfer line to the Alternating Gradient Synchrotron from the Double Tandem Facility (Tandem/AGS Transfer Line construction project). Nuclear Physics program staff also manage the Nuclear Data activity which is budgeted under Basic Energy Sciences.

The High Energy and Nuclear Physics staff also manages the Heavy Ion Fusion Accelerator Research program budgeted under Basic Energy Sciences to develop heavy ion accelerator technology and perform appropriate ion-beam experiments to the point where an adequate data base exists for future decision-making. FY 1984 and FY 1985 activities involve overall policy and program planning and management, as well as review and evaluation of the first stage of research and development activities carried out under laboratory projects. This will include site visits to evaluate progress toward development of heavy ion accelerator technology, responding to inquiries, attending appropriate national and international conferences, and developing and maintaining a communications network with other interested parties.

○